

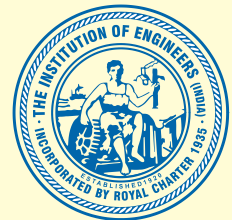
35th Indian Engineering Congress

Technical Volume



December 18-20, 2020

Engineering for Self Reliance and Sustainable Goals



The Institution of Engineers (India)

8 Gokhale Road, Kolkata

Technical Volume



35th

Indian Engineering Congress

December 18-20, 2020

Theme

Engineering for Self-reliance and Sustainable Goals



The Institution of Engineers (India)

Copyright Information

For Authors

As soon as an article is accepted for publication, authors will be requested to assign copyright of the article (or to grant exclusive publication and dissemination rights) to the organizer. This will ensure the widest possible protection and dissemination of information under copyright laws. More information about copyright regulations for this Technical volume is available at: www.ieindia.org

For Readers

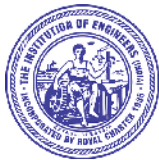
While the advice and information in this Technical Volume is believed to be true and accurate at the date of its publications, neither the authors, the editors nor the publisher can accept any legal responsibility for any errors or omissions that may have been made. The publisher/organizer make no warranty, express or implied, with respect to the material contained herein. All articles published in this Technical Volume are protected by copyright, which covers the exclusive rights to reproduce and distribute the article (e.g, as offprint), as well as all translation rights. No material published in this Technical Volume may be reproduced photographically or stored on microfilm, in electronic data bases, on video disks, etc, without first obtaining written permission from the organizer (respective the copyright owner). The use of general description names, trade names, trademarks, etc, in this publication, even if not specifically identified, does not imply that these names are not protected by the relevant laws and regulations. For permission for reuse our content please send request addressed to: The Director (Technical), The Institution of Engineers (India), 8 Gokhale Road, Kolkata 700020 (Tel. 033-40106213 or Email: technical@ieindia.org)

Copyright

As per By-Law 118, Copy right of each paper published in the Institution journals or proceedings in full or in abstract at its Centres shall lie with the Institution.

© The Institution of Engineers (India) 2020

The Institution of Engineers (India) has exclusive rights and license to publish and distribute the print as well as online edition of proceeding worldwide. The views expressed in this publication do not necessarily reflect those of the Institution. All rights reserved. No part of this publication may be reproduced, stored in a retrieval system or transmitted in any form or by any means, without prior written permission of The Institution of Engineers (India).



The Institution of Engineers (India)

AN ISO 9001 : 2015 CERTIFIED ORGANISATION

(ESTABLISHED 1920, INCORPORATED BY ROYAL CHARTER 1935)

8 GOKHALE ROAD, KOLKATA - 700 020

A Century of Service to the Nation

Er Narendra Singh, FIE
President



It is a pleasure for me to recognize the efforts of all concerned who have meticulously planned and worked hard to bring out this wonderful 'Technical Volume' on the occasion of the 35th Indian Engineering Congress held online during 18 – 20 December 2020 on the theme "Engineering for Self-reliance and Sustainable Goals".

The Indian Engineering Congress is the apex activity of the Institution enjoying a special status amongst the engineering fraternity. This is organized every year where professionals and engineers from all the disciplines of the engineering gather to share their knowledge and experience. This year due to the unprecedented scenario of nation-wide lockdown to control the pandemic, we had no other way but to organise it on virtual mode. We are really overwhelmed by the response from all over the country and abroad.

This volume comprises of the articles by engineering professionals with rich experience in their discipline. I am sure that the articles in this technical volume will benefit scientist, engineers, technologists, policy makers, academicians and all concerned.

A handwritten signature in black ink, consisting of a stylized 'N' followed by a horizontal line and a small dot.

Er Narendra Singh
President, The Institution of Engineers (India)

Composed by

Technical Department

The Institution of Engineers (India)

8 Gokhale Road, Kolkata 700020

Published by

The Institution of Engineers (India)

8 Gokhale Road, Kolkata 700020

Publisher

Dr H R P Yadav

Secretary and Director General for The Institution of Engineers (India)

ISBN 978-81-950662-0-9

Technical Volume of 35th Indian Engineering Congress



The Institution of Engineers (India)

AN ISO 9001 : 2015 CERTIFIED ORGANISATION

(ESTABLISHED 1920, INCORPORATED BY ROYAL CHARTER 1935)

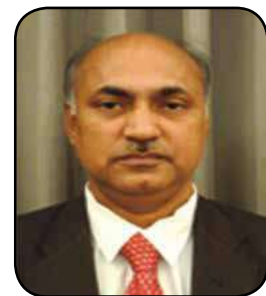
8 GOKHALE ROAD, KOLKATA - 700 020

A Century of Service to the Nation

Prof (Dr) Swapan Bhaumik, FIE

Chairman

Committee for Advancement of Technology and Engineering (CATE)



On behalf of the Technical Committee, I am honoured and delighted to present the prestigious Technical Volume of the 35th Indian Engineering Congress, which was held in virtual mode during 18-21 December 2020. The major theme of this Congress was “Engineering for Self-reliance and Sustainable Goals”. I am excited that despite pandemic, there were huge responses to attend the Mega Event of IEI. On the first day of 35th Indian engineering Congress, there are eight parallel Technical Sessions on virtual mode. Out of 230 papers received, 192 papers were accepted after review. We are thankful to the Reviewers for their kind evaluation of the papers received for 35th IEC, Session Chair and Co Chair of all technical sessions for their relentless effort to conduct the sessions successfully.

I also thank Director (Technical) of The Institution of Engineers (India) and his team for their relentless effort to make the event successful and bringing out this Technical Volume.

A handwritten signature in black ink, appearing to read 'Swapan Bhaumik'.

Swapan Bhaumik
Chairman CATE



The Institution of Engineers (India)

35th Indian Engineering Congress

President

Er Narendra Singh

Chairman, Technical Committee

Prof Swapan Bhaumik

Secretary & Director General

Dr H R P Yadav

Editorial Team

Technical Department, IEI

Dr N Sengupta, Dr S Ghosh, Mr K Sen, Mr T Chakraborty, Ms A Dutta,
Ms H Roy, Mr S Bagchi, Mr P Chakraborty, Ms P Nath, Mr P Mukhopadhyay, Mr S Misra

Agricultural Engineering

AG/087/01	Optimization of the Growth of Microalgae <i>Sprulina Platensis</i> - Full Factorial Experimental Approach <i>Mir Shariful Islaml, Bidyut Baran Saha</i>	23
AG/088/02	Timer Based Automatic Family Drip System (FDS) - A Sustainable Technology for Increased Vegetable Production in Urban Sector <i>Chithra G, Jyothi Rachel Varghese, Dr Binu John Sam</i>	33
AG_105_04	Experimental Investigation of Double Collector Solar Dryer for Agricultural Products <i>G S Divya Laxmi I, D Sakthivadivel, P Ganesh Kumar, S Iniyan</i>	39
AG_106_05	Performance Study of Manually Operated Drum Seeder for Sowing of Jute <i>R K Naik, S K Jha, S Sarkar, A K Ghorai</i>	45
AG_125_06	Development of Track Width and Ground Clearance Enhancing Platform and Matching Implements for Low Horse Power Tractor <i>B Sanjeeva Reddy, Ashish S Dhimate, I Srinivas, R V Adake, V R Mallikarjuna, G Karthik</i>	51
AG_176_07	IoT Based Smart Agriculture Monitoring System <i>G Roja, M Ramesh</i>	59
AG_208_08	Design of Multipurpose Harvesting Machine for Lowland Areas for The Upliftment of Farmers <i>Niloy Laskar, Umar Faruk Bhuiya, Krishna Chakraborty, Dr Arindam Majumder</i>	65

Architectural Engineering

AR_089_01	Fractal Geometry as an Adaptive Technique for Human Capital Development: A Review based on Indian Temple Architecture <i>Shyru R V</i>	75
AR_090_02	2BHK Dignity Housing Programme in Greater Hyderabad Municipal Corporation <i>K Suresh Kumar, P Saroja Rani, B Venkateshwarlu, K Varalakshmi</i>	81
AR_181_03	Advanced Tool for Green and Energy Efficient Building Design <i>Ankur Mittal, Ashutosh Saxena, B N Mohapatra</i>	87

Aerospace Engineering

AS_014_01	Transformation of Rectangular Parallelepipeds into Fighter Jets & Airborne Missile Launching Platforms <i>Rajarshi Mukherjee</i>	95
AS_103_02	Activating Atmospheric Boundary Condition Inside the Subsonic Wind Tunnel using Passive Turbulence Grid <i>E Livya, S Nadaraja Pillai</i>	99
AS_126_03	Aerodynamic Characteristics of Grooved Rotating Circular Cylinder <i>Kirthika N, MadhuMadhan, Lokesh U, S Nadaraja Pillai</i>	105
AS_127_04	Optimum Satellite Access Techniques "TDMA / SCPC or PSMA" For Next Generation VSAT Networks <i>Y S Rayudu</i>	113
AS_229_05	Electromechanical Behavior of Graphene-based Composite Plate with Flexoelectric Effect <i>K B Shingare, S Naskar</i>	119

AS_230_06	Influence of the Pivot Locations on the Aerodynamic Performance of a 2D Flapping Elliptic Airfoil at Close Proximity of the Ground <i>Jit Sinha, Sunil Manohar Dash</i>	127
Chemical Engineering		
CH_005_01	Recovery of Technology Metals from Oceans <i>T L Prasad</i>	137
CH_128_03	Effect of Microwave Radiations on Germination and Minerals Content of <i>Arachis hypogaea</i> L. <i>S J Wagh, M S Patwardhan, R N Dhawale</i>	143
CH_224_05	Design Optimization of Heat Exchanger by Old and New Generations Metaheuristic Optimization Algorithms: Insights and Comparisons <i>Boyina Venkata Akhil, Prashanna Sharma, Sandip Kumar Lahiri</i>	149
CH_225_06	Thermal and Performance Analysis of Bio Gas Digesting System <i>S Babu, C Gajendran, B Bhuvaneshwari, T Nandhini</i>	157
CH_226_07	A New Generic Methodology for Modelling and Optimization of Running Commercial Chemical Plant to Balance Profit and Negative Environment Impact with Cumene Production Plant as Case Study <i>Somnath Chowdhury, Sandip Kumar Lahiri</i>	163
CH_227_08	Artificial Intelligence based Modelling and Multi-objective Optimization of Vinyl Chloride Monomer (VCM) Plant to Strike a Balance between Profit, Energy Utilization and Environmental Degradation <i>Sucharita Pal, Bipul Jha, Sandip Kumar Lahiri</i>	169
CH_228_09	Artificial Intelligence Modelling for Real Time Prediction of Melt Flow Index In Commercial HDPE Plant <i>Annasha Dey, Rhythm Aich, Dr Sandip Kumar Lahiri</i>	177
Computer Engineering		
CP_003_02	Low Latency Low Power Encryption-decryption Method for Securing Memory Operations <i>Nageswararao Yelleswarapu, Dr Sajal K Das</i>	187
CP_064_06	Application of Artificial Intelligence for Intent Determination in Threat Evaluation <i>Rahul Mahajan, Atul Sethia, Manoj Tyagi</i>	193
CP_065_07	IT Infra Capacity Upgrade: IT Infra Monitoring with Smart Trend Analysis for Determining 'New Size' <i>Rahul Yadav, Brajesh Kumar, Shakti Manchanda</i>	199
CP_066_08	Implementation of an Artificial Intelligence based Predictive Maintenance for Fire Control System <i>Ajay Kumar Singh, Navya K M, S Arun, Abhishek Kumar</i>	205
CP_067_09	Leveraging Various Technologies for Tracking of Logistics in Steel Plants <i>Ayan Goswami, Shyamalesh Saha</i>	213
CP_080_11	Post-surgery Recovery using Deep Learning <i>Kuldeep Hule, Arjun Dashrath</i>	219
CP_129_13	Development of a Deep Learning Model for Analysis and Prediction of Sepsis condition <i>Melvin M, Banu Rekha B</i>	223

CP_130_14	Facial Expression based Pain Monitoring in Hospital Environment using Compact Convolutional Network <i>Ashish Semwal, Narendra D Londhe</i>	229
CP_174_19	Secured Approach for One Umbrella Management System for Improving Healthcare Services <i>Dr S Tamil Selvi, B Ganapathy Ram, V S Preethashree</i>	237
CP_218_21	Miniscule Payload Location in Least Significant Bit Stego Images using Transform based Image Denoising Cover Estimators <i>S Arivazhagan, E Amrutha, W Sylvia Lilly Jebarani, S T Veena, S Ananthi Roy</i>	245
Civil Engineering		
CV_004_01	Geopolymer Concrete: A Pathway to Sustainable Manufacturing in the Indian Concrete Industry <i>Jyotirmoy Mishra, Bharadwaj Nanda, Sanjay Kumar Patro</i>	259
CV_012_02	A Geotechnical Study on Properties and Uses of Shales of the Dharwar System, Karnataka, India <i>Dr Udayashankar D Hakari</i>	265
CV_015_03	Maintenance of PMGSY Roads in India <i>Sandeep K Shrivastava</i>	273
CV_016_04	Way Forward to Enhancing Skills for Betterment of Indian Economy through Construction Industry <i>Sekar Kumbeswara</i>	275
CV_017_05	Fibre Reinforced Geopolymer Concrete as a Repair Material for Rigid Pavements-A Review <i>Peter Cibi, Karthi Lathi</i>	281
CV_019_07	Emerging Trends in Affordable Housing – GFRG Technology for Self Reliance and Sustainable Growth <i>K B Agarwal</i>	291
CV_020_08	Managing the Risk and Uncertainty in Coastal Residential Building Codes <i>Gino Hosein, Indrajit Ray</i>	297
CV_032_09	Analysis and Affine Transformation of Skew Slab <i>M Ravindra</i>	305
CV_033_10	Prediction of Mechanical Characteristics of Concrete Containing GSA, GGBS and WF <i>R Murugaboopathy</i>	319
CV_034_11	An Experimental Study on Self Repairing Concrete to Improve Strength and Sustainability <i>S Ramesh Kumar, D Sakthivel, E Vellaingiri</i>	329
CV_043_14	Energy Efficient Building to Fight Against Covid-19 <i>Sushovan Sarkar, Gargi De</i>	337
CV_049_15	Impact of GGBS as Partial Substitution of Cement and Replacement of Robo Sand to Fine Aggrigate on M50 Grade of High Performance Concrete <i>L Sai Indra Sena Reddy, Dr M M Vijalakshmi Nataraj</i>	343
CV_054_16	Effective Quality Management for Sustainable Roads <i>Kishor Kumar Pahuja</i>	353
CV_055_17	Feasibility Study of Ferrochrome Slag as an Alternative to Natural Aggregates <i>P N Ojha, Abhishek Singh, Brijesh Singh, B N Mohapatra</i>	361

CV_059_18	Artificial Intelligence Techniques to Predict the Compressive Strength of Sustainable Eco-friendly Strain-hardening Concrete Composites <i>K K Yaswanth, J Revathy, P Gajalakshmi</i>	371
CV_068_19	Risk Assessment in an Infrastructure Project <i>Dr K Srinivas, Dr K R Ramana</i>	377
CV_075_20	Sustainable Alternative to External Curing: Use of Superabsorbent Polymer in Concrete <i>Jyoti P Bhusari, Akhilesh A More</i>	383
CV_076_21	A Case Study on Stabilized Shallow Foundation for a Large Oil Storage Steel Tank on Soft Soil <i>Somdev Pakrashi</i>	395
CV_098_23	Theoretical Calculation of Crack Width in Pile for Tension and Lateral Loading <i>Md Arshad Jamal, Vaishali Sharma, Deepak Singh, Ayan Khan</i>	403
CV_099_24	Condition Assessment of Structural Components using Internet of Things (IoT) <i>C Harshitha, Mallika Alapati</i>	409
CV_100_25	Comparison of GSA 2003 and 2016 Guidelines for Evaluating Progressive Collapse Potential of Steel Moment Resisting Frame Building <i>Parthav P Patel, Digesh D Joshi</i>	415
CV_101_26	PSWC-BAR for Sustainable Concrete Construction <i>Anil K Kar</i>	423
CV_102_27	Planning, Analysis and Design of G+5 Cyclone Resistant Administrative Building at Kovalam, Chennai <i>Amjad Latif, Shweta Devekar</i>	431
CV_107_28	Study on Comparative Advantages of E350 vs. E250 Grade Steel in Industrial Structures <i>Amresh Kumar, Saptadip Sarkar, Anurag Sinha</i>	447
CV_108_29	Design and Development of Floating Structure for Solar PV plant using Numerical Analysis <i>Harsh V Chudasama, Ashish M Vajir</i>	457
CV_109_30	Correlation between Ground Motion and Structural Response of Multi-storied Buildings in the Performance Based Seismic Design <i>Soumyan K, Deepa Balakrishnan S</i>	465
CV_110_31	Preliminary Results of Concrete with Shredded Disposable Face Masks <i>Soham Parija1, Dhanada K Mishra2, 3, Christopher Y K Leung</i>	473
CV_111_32	A Technical Paper on "RCC Blanket Wall" <i>H M Viswanatha Sastry</i>	479
CV_112_33	Wind Pressure Distribution over Solar PV Panels Mounted on Pitched Building Roofs <i>Ashish Agarwal, Hassan Irtaza, Azhar Jameel</i>	485
CV_113_34	Design and Construction of Irregularly Shaped Cut & Cover Box Tunnel as an Innovative Solution for Space Restriction at Site <i>Chiranjib Sarkar, Anant Mehendale, Harsha G M</i>	497
CV_114_35	1D Flood Model to Retrace the July 2018 Flood in Lower Reaches of Pampa River, Kerala <i>Dr T K Drissia</i>	505

CV_131_36	A Comprehensive Review on the usage of Waste Materials in Flexible Pavements and their Impact <i>Pala Gireesh Kumar, Abhirami Priyanka Pathivada</i>	509
CV_133_38	Developing Self-Compacting Concrete as per IS 10262: 2019 by Utilizing C and D Waste as Aggregates and Fines <i>Ajay N, Ashwin M Joshi, Namratha Bharadwaj, Girish S</i>	515
CV_134_39	Analytical Estimation of Boundary Layer Thickness for Flow Over Spillways <i>Suresh Kumar N, Prasanna S V S N D L</i>	527
CV_136_41	Application of VH Polarization Sentinel-1 Imagery for Flood Mapping of Bhagalpur, Bihar <i>Deepak Kumar, Kumar Yuvraj</i>	533
CV_137_42	Performance based Design of Shear Ductile Wall with Custom Openings <i>Mohammad Suhail Saifi, Dr Khalid Moin</i>	539
CV_138_43	Design of Framed Foundation for Absorber in Flue Gas Desulphurization System <i>R L Dinesh, Ranjit P Kangralkar, Sandhya Krishnamurthy, Rohit Pantoji</i>	551
CV_139_44	Simulation of Earthquake Forces for Equipment Supported on Structure <i>Papia Mandal, K Madhavalatha, Anurag Sinha</i>	555
CV_188_45	Review on Limestone Calcined Clay Cements (LC3) <i>S M Gunjal, B Kondraivendhan</i>	561
CV_189_46	Bolted Shear Connections: A Comparative Study on Effect of Eccentricity and Other Design Criteria as Per International Codes <i>Saptadip Sarkar, Papia Mandal, Anurag Sinha</i>	573
CV_190_47	An Analytical Study on Wind Pressure Distribution on Rectangular Tall Building with Setback and Twist using Computational Fluid Dynamics <i>Vigneshwaran Rajendran, Prabavathy Shanmugasundaram</i>	579
CV_191_48	Selection of suitable Quantity of Fly Ash and Water to Achieve Desired Workability and Strength of Geopolymer Concrete <i>Subhash V Patankar, Sanjay S Jamkar, Yuwaraj M Ghugal</i>	589
CV_192_49	A Sustainable Approach to Flood Damage Repair of Hill Roads in Tripura using Soil Filled Gabions – A Case Study <i>D Roychowdhury</i>	597
CV_193_50	Analysis of Access Control & Traffic Bottleneck on Western Express Highway using PTV Vissim <i>Shrivastav Laxman Sutar, Siddharth Deepak Gondhale</i>	605
CV_209_51	A Comparative Study of MLP and MLP-FFA Models for Flood Prediction <i>Sandeep Samantaray, Abinash Sahoo, Siddhartha Paul</i>	615
Electrical Engineering		
EL_010_02	Analysis of Wireless Power Transfer Compensation Topologies for EV Battery Charging <i>Amarjeet S Pandey, D B Pardeshi</i>	625
EL_011_03	Power Electronic Interfaces on Renewable Energy System <i>Sanjeev Kumar Bhatnagar, Priyabrata Pradhan</i>	631
EL_072_06	Review on Solar Powered Hydrogen Fuel Cell: A Promising Alternative for Future Energy Sustainable Development <i>Rajesh Bodkhe, Rakesh Shrivastava, Vinod Kumar Soni, Kshitij Shrivastava</i>	637

EL_073_07	Next Generation Advanced Core Material for Reluctance Machine <i>K Vijayakumar, A Joseph Basanth, R Karthikeyan, S Kannan</i>	645
EL_086_10	Solar Energy and Hydropower Complementing Each Other – A Global Trend for Achieving SDGs <i>Jnan Ranjan Pal</i>	651
EL_123_11	Renewable Energy Sources & Smart Grids Integration <i>Sangeeta Deb Barman, Dr Kumari Namrata, Dr S M Ali</i>	657
EL_145_12	Source Side Energy Management of Hybrid Renewable Energy System by Intelligent Control <i>Hemlata Joshi, Ekta Mishra, Ganesh H Patil</i>	663
EL_147_13	Improved Adaptive Controller Based Speed Estimator at Low Speeds for Sensorless Vector Controlled Induction-Motor <i>Meghraj S Morey, Vasudeo B Virulkar</i>	669
EL_148_14	Affordable Energy for Civilization: A Global Programme to Provision Collective Clean Energy Admittance <i>Chilukuri Bala Venkata Subbarayudul, Dr Katikala Premalatha, Dr Mohd Iliyas</i>	679
EL_178_15	Solution of Single Objective and Multi-Objective Optimal Power Flow Problem using Chicken Swarm Optimization <i>Saket Gupta, Narendra Kumar, Laxmi Srivastava</i>	685
EL_184_16	An Enhanced Power Conditioning Unit Enabling Reduction in DC Link Voltage Fluctuation for a Grid Connected Photovoltaic System during FRT <i>Nishij G Kulkarni, Vasudeo B Virulkar</i>	693
EL_200_17	Tidal Power Generation – Prospects in India and Challenges for Engineers <i>Kirit B Trivedi</i>	701
EL_201_18	Net Zero: Emission vs Employment: The Transition in Indian Power Sector <i>Shreya Karmakar, Joy Chakraborty</i>	707
EL_202_19	ANN Based Adaptive SOGI-FLL Controller for Multifunctional Grid Tied Solar Energy Conversion System <i>Dinanath Prasad, Narendra Kumar</i>	713
Environmental Engineering		
EN_037_01	Modular Air Purifier for Metropolitan Cities <i>Sreekala P</i>	727
EN_045_02	Sustainable Infrastructure Management: Recovery and Reuse of Resources and Energy in Landfills <i>Dr Anumita Mishra, Prof Rao Y Surampalli</i>	733
EN_116_03	Green Hydrogen: A Perspective <i>S Sakthivel, Shireesh S Swami, Atul Choudhari</i>	739
EN_117_04	Green Multi-Storey Society Concept for Urban Area of India <i>Kapil Kukreja, Manoj Kumar Soni, Bibekananda Mohapatra</i>	747
EN_155_05	Effluent Treatment & Wastewater Recycling-Copper Smelter Perspective <i>Mary Sarker</i>	753
EN_156_06	Conservation of Topsoil at Construction Sites <i>Krishna Nirmalya Sen, Gollapalli Muralidhar</i>	765
EN_157_07	GIS-based Well Water Monitoring of Gunjalwadi and Velhale Villages, Maharashtra, India <i>Navale V B, Mhaske S Y</i>	771

EN_166_08	Sewage Pollution of Ground Water <i>Maresh Patnaik</i>	781
EN_168_09	Energy Audit of Waste Heat Recovery System in Indian Cement Plants - Case Studies <i>Prateek Sharma, M V Ramachandra Rao, Ashutosh Saxena, B N Mohapatra</i>	785
EN_179_11	Wealth from Waste <i>Bhalchandra B Bhalerao</i>	793
EN_204_12	Design Algorithm: Solar Powered Water Supply System for Municipalities & Rural Area <i>Dilip Yewalekar, Manisha Kinge</i>	803
EN_211_13	Master Plan for Drought Mitigation at Jhargram District of West Bengal to Ensure Sustainable and Reliant Drinking Water Supply <i>P Roy Chowdhury</i>	807
Electronics and Telecommunication Engineering		
ET_021_01	Design and Analysis of Converters for Hybrid Electric Vehicle <i>Dr K Balachander</i>	815
ET_023_03	IoT based Smart Energy Meter Tracking using ZigBee <i>Dr Belsam Jeba Ananth M, Dr Revathi KG</i>	823
ET_046_04	Innovative Slope Stability Monitoring Instrument for O/C <i>S P Singh</i>	829
ET_062_05	Source and Effects of Conductive Emission in the Frequency Range 2.5 to 150 kHz and Its Measurement <i>Y Dhayaneswaran, Dr A Amudha, Dr L Ashokkumar, Y Umamaheswari</i>	833
ET_063_21	Text Recognition of Embossed Metadata Obtained from Live Video of UAVs <i>Gagan Kumar Nigam, MGR, Sumit Srivastava, SE</i>	841
ET_070_06	Mitigate Challenges of Co-location Interference for SDR applications <i>Sandeep Singla, Sidharth Sarawat, Radheshyam Kumawat, Deepa Bajpai</i>	853
ET_071_07	EMI/EMC (MIL-STD) Compliant Design for 12V/28VDC Bus to Meet Ground based Military SDR Systems <i>Sandeep Singla, Radheshyam Kumawat, Vikas Arora, Deepa Bajpai</i>	861
ET_081_08	Design and Development of Forced Air Cooled Dip-brazed Chassis for Safety Critical Electronics <i>Prashant, A Karthikeyan</i>	869
ET_095_09	Low Power ADC Design for Biomedical Implantable Devices <i>Aneesh K, Manoj G</i>	877
ET_096_10	Study on Electro Magnetic Interference and Compatibility Across Various Levels and Mitigation Technique using Software <i>Y Uma Maheswari, Y Dhayaneswaran, Dr A Amudha, Dr L Ashokkumar</i>	885
ET_097_11	Comparison between Different Wavelet Transform Techniques for Indoor Optical Wireless Communication System Employing Pulse Position Modulation & On-OFF Keying <i>Ankita Aggarwal, Dr Gurmeet Kaur</i>	893
ET_121_22	Streaming Video Data from Remote Sites to Command Center under Bandwidth Constrained Environment <i>Anitha K M, Sampath Kumar R, Prabha Gupta, Sonu Shreshtha</i>	907

ET_122_12	Design of Charge Pump PLL using 180nm CMOS Technology Ashwini Desai, Uma Kulkarni	913
ET_146_18	A Brief Study of Optical Flip-flops based on Microring Resonator <i>Kankana Debnath, Srikanta Das, Arka Roy Bin, Bishanka Brata Bhowmik</i>	919
ET_149_13	Cybernation of Home Appliances using Raspberry PI <i>Yerramsetti Jaswanth, Bathina Venkateswara Rao, Kalagara V V R S Vishnu Thejavathu Thirumalarao</i>	925
ET_150_14	Data Interoperable on DVB-S /S2 “Digital Video Broadcast” Compliant Systems <i>Y S Rayudu</i>	931
ET_151_15	ML-based Constellation-rotation Correction of QPSK Signal in Optical Fiber Communication <i>Nitish Sinha, Satyabrata Singha, Mohua Chakraborty, Bishanka Brata Bhowmik</i>	937
ET_152_16	Wavelength dependent Configurable optical AND to OR Gate based on Micro Ring Resonator loaded on Mach–Zehnder Structure <i>Arka Roy Bin, Srikanta Das, kankana Debnath and Bishanka Brata Bhowmik</i>	941
ET_153_17	Soil Humidity Measurement using Microstrip Interdigital Capacitor (IDC) and Rectangular Slotted Fingers Interdigital Capacitor (RSFIDC) <i>Jayant Gajanan Joshi, Mandar P Joshi, Balwinder Singh Dhaliwal, Shyam S Pattnaik</i>	947
ET_167_20	Integrated Communication Interface with Configurable Dual Active Cellular Data Connection, Navigation and PAN Options as Generic IoT Hardware <i>Kiran Rawal, Harmandeep Singh, Ashish Gupta, Gurjeet Singh, Mohan Lal, Deepa Bajpai</i>	955
Mechanical Engineering		
MC_013_01	Designing a Proper Hoe towards Zero Loading Losses to Achieve 100% Productivity with Reduced Fuel Consumption <i>Rajarshi Mukherjee</i>	963
MC_027_02	Disaster Management over Indian Railways- Reliability, Operation & Safety of 140t Gottwald Crane <i>Narendra Kumar Verma</i>	967
MC_051_03	Experimental and Prediction Analysis of the Screening Performance of Coal in Linear and Circular Vibratory Screen <i>Bharath Kumar Shanmugam, Harsha Vardhan, Govinda Raj M, Harish Hanumanthappa</i>	981
MC_058_04	Satyan King-Pin-Drive for Electric Vehicles <i>Dr Sathyanesan T N</i>	985
MC_077_05	Efficiency Improvement of Concentrated Photovoltaic Module by way of Various Active and Passive Cooling Techniques – a Review <i>Yogesh Nandurkar, R L Shrivastava, Vinod Kumar Soni</i>	991
MC_078_06	CFD Analysis of an Automotive Cabin Air Filter <i>Koyal V Sadaphal, Dr A S Mohite</i>	997
MC_079_07	Study and Analysis of Asphalt Hot Mixing Plant <i>Vishal K Patel, Dr A S Mohite</i>	1003
MC_092_08	Sustainability Adaptation by Retrofitting Volatilizer in Thermal Power Plant for Co-generation of Cement and Power <i>C Prabhakar Reddy, Amiya P Goswami</i>	1009
MC_093_09	Optimization of Cross Flow Forced Draft Air Cooled Tubular Heat Exchanger (FDAC-HE) of Fumes Extraction System in Steel Melting Plant <i>Vijay S Kumavat, Dr Arvind Mohite, Manish Khanna, Hemant Chaudhary</i>	1013

MC_094_10	Effect of Different Cooling Mediums on Friction Stir Welded AA6061 Alloy <i>Dinesh Chaudhary, Dr A S Mohite</i>	1025
MC_118_11	A Vibrational Test for Chaos using 0-1 in a Vertical Axis Wind Turbine <i>C B Maheswaran, R Gopal, S Nadaraja Pillai</i>	1033
MC_119_12	Development of Prototype of Thermal Air Sterilizer to Combat COVID-19 <i>Sunil Kumar Thamida1, Srikumar V R, Mohith K S, Amarendra Kumar Gupta, Vasudharani Devanathan, Harshini Chakravarthy</i>	1039
MC_120_13	Design of a Centrifugal Impeller for Lean Supercharging of Motorcycle Engines <i>Harishankar S, Aswin A Asokan, Madhav Murali, Rejath R S, Rajesh T N</i>	1045
MC_203_16	Effect of Varying Surface Thickness on Wetting Delay and Rewetting Velocity through CFD Analysis <i>Monika Siyal, Chitranjan Agrawal, B L Salvi, S Jindal</i>	1051
MC_213_17	Energy Efficient Surfaces for Improved Performance of Heat Exchanger Through Enhanced Pool Boiling Heat Transfer: A Review <i>Anil S Katarkar, Biswajit Majumder, Swapan Bhaumik</i>	1059
MC_214_18	Finite Element Structural Analysis of Inflatable Semicircular Air Beam <i>K Hans Raj1, Akash Jain, Ravi Kumar, Arun Kumar Saxena</i>	1067
MC_219_19	Performance Characteristics of External Gear Pump with the use of Burnt Oil <i>Aditya Anurag Bal, J Randhari</i>	1073
MC_221_20	Explosive Welding-The Need of Industry 4.0 for Atmanirbhar Bharat <i>Prabhat Kumar, Subrata Kumar Ghosh, John Deb Barma, S Saravanan</i>	1079
MC_222_21	Analysis of Latent Heat Based IC Engine Exhaust Waste Heat Recovery System <i>Dr S Babul, S A Ravi Varman, R Santhosh Mugil</i>	1085
Materials and Metallurgical Engineering		
MM_007_01	Salvaging used Reformer Tubes for Conserving Nickel <i>Satish Bhagwan Kunte</i>	1093
MM_026_02	Spinel Magnesium Aluminate by Sol-gel Assisted Combustion Process and Its Characterization <i>Soumya Mukherjee</i>	1099
MM_050_03	Mitigating Covid-19 induced disruption to Steel use in Construction through Engineering Solutions <i>Manos Kumar De, Pratip Bhattacharya</i>	1103
MM_052_04	Effect of Vanadium on the Tensile Strength as a Function of Austenitizing Temperature on LHB Wheels <i>Smeeta Kujur, P P Sarkar, Asha Bajpai</i>	1111
MM_053_05	Challenges for using Iron-ore as Coolant in BOF Steelmaking <i>Sanjay Kumar Gupta</i>	1117
MM_162_06	Hydrothermal Synthesis and Characterization of Nanocrystalline Zinc Orthovanadate($Zn_3V_2O_8$) on Graphene Oxide Scaffolds <i>Lakshmana Naik R, H Seshagiri Rao, Pernapati Nagaraja, Bala Narsaiah T</i>	1125
MM_163_07	Study of Mechanical and Thermal Properties of ABS Reinforced with Fly Ash by using Maleic Anhydride as Coupling Agent <i>Bulti Kandar, Deepshikha Datta</i>	1131
MM_180_08	Development and Applications of Forged Microalloyed Steels in India <i>P K Mandal</i>	1139

MM_205_09	Study and Development of Graphene Oxide based Hybrid Polymer Nanocomposites <i>Geetha Rajamani, Jawahar Paulraj</i>	1147
MM_206_10	Determination of Critical Temperature for Austenite to Ferrite Transformation During Hot Rolling of Low Carbon Nb-V-Ti Steel <i>Santosh Kumar, B Sunita Minz, N Mondal, Dr K Mukherjee</i>	1155
MM_207_11	Ag@CuO Decorated Tailored Nanostructures based CO ₂ Sensors: Role of n-type Semiconductors in Enhancing Heterostructured Sensor Efficiency <i>Shravanti Joshi</i>	1165
Mining Engineering		
MN_158_01	Retrospection of the Longwall Mining for Mass Production of Coal from Indian Underground Mines <i>K Nageswara Rao, G Budi, P K Mandal, A J Das, J Vinod Kumar</i>	1173
MN_215_02	Innovative Methodologies of Carbon Sequestration for Sustainable Development of Unmineable Coal Seams <i>Singam Jayanthu, Singam Jayadarshana, Chandramohan</i>	1183
MN_223_03	Application of Recent Guidelines of 2020 For TARP Vis-À-Vis Design of Stable Slopes in Opencast Coal Mines-A Case Study <i>Singam Jayanthu, Pritiranjana Singh, K Sridhar Reddy, Rishabh Lala</i>	1191
Marine Engineering		
MR_028_01	Design and Engineering for a Self-reliant Society in Marine Engineering <i>Sandeep Kumar</i>	1199
MR_039_02	Sustainable Shipping <i>N M C Nair</i>	1209
MR_040_03	Water Dependency Test on a Novel Method of Water Transportation at Static Conditions <i>Arulanantha Samy Santhiyagu, Jaikumar Mayakrishnan</i>	1215
MR_044_04	IoT based Oil and Gas Survey <i>B Kannan</i>	1221
MR_056_05	An Overview Study of Ocean Energy Potential and Technologies in India <i>Geetam Saha, Dipesh Majumdar</i>	1229
Production Engineering		
PR_001_01	Sustainable Manufacturing: Principles, Applications and Directions <i>Ashok Kumar Panda</i>	1241
PR_036_03	Preparing for Post Covid-19 Sustainable Manufacturing Ecosystem <i>Dr Goutam Sengupta</i>	1245
PR_048_04	The Advancement of 3DBioPrinting Technology uses as Bio-Manufacturing Process <i>Ranjit Barua, Sudipto Datta, Pallab Datta, Amit Roy Chowdhury</i>	1253
PR_061_06	Challenges & Way Forward in Integration of Remote based Working Environment for a Multi-Disciplinary Engineering Design Centre <i>Anirban Datta, Gautam Gangopadhyay, Sushmita Choudhury</i>	1259
PR_091_07	Principles, Applications and Directions of Sustainable Manufacturing: A Case of Indian Micro, Small and Medium Enterprises (MSMEs) <i>Dr Om Parkash Mehta</i>	1267
PR_115_08	Unforeseen Risks in Project Execution – A Case Study <i>Balakrishnan Nair</i>	1275

PR_135_12	Engineering Solution as Sustainable Manufacturing for Protection in Pandemic Regime <i>A A Panja, M S Patwardhan</i>	1281
PR_161_11	The Sustainable Manufacturing in Chennai Plastic Sacks Cluster <i>Dr E Bhaskaran</i>	1289
PR_183_16	Application of AI based Models on 3D Printing Technology : Future Prospects for Additive Manufacturing <i>Shivam Raj, Sanjit Kumar Rajak, Ganta Sai Rahul, Rajat Gupta</i>	1303
PR_185_13	Possible Mitigation Measures for Various Hazards Associated with Cement Factories of Assam- A Discussion <i>Dr Sanjoy Kumar Dey, Dr Rajat Gupta</i>	1309
PR_186_14	Framework for Skill-Based Teaching Pedagogy for Computerized Numerical Control (CNC) Machine Programmer Course <i>Dr Charudatta Pathak, Rajkumar Baghel, Sumit Dubal, Yogendra Jain, Dr Hrushikesh B Kulkarni</i>	1315
PR_187_15	The Future of Industrial Training and Simulation <i>Dr Sathyanarayana A</i>	1321
Textile Engineering		
TX_009_01	Potential of Jute & Banana Blended Engineered Fabric for Technical Application <i>S N Chattopadhyay, N C Pan, A N Roy, Kartick K Samanta</i>	1327
TX_060_02	Tensile, Impact & Dynamic Properties of Jute/E-Glass Composite by Adding Shear Thickening Fluid <i>Abhishek M R, Dr Suresh P M</i>	1337
TX_082_03	The Effect of Flow Rate on the Electrospun PEG-PVA/ CNF/NCG Nano-composite Fibres <i>Arpita Priyadarshini Samantaa, Jonathan Tersur Orasughab, Dipankar Chattopadhyay Swapna Kumar Ghosh</i>	1345
TX_164_04	Sustainability of Handlooms and Textiles for A Self Reliant India <i>Dr Sasmita Panda, Dr P L Panda</i>	1351
TX_165_05	Development of Portable Water Tank for Retting of Jute Ribbons and Root Cuttings <i>A K Thakur, V B Shambhu, A Singha</i>	1357
Interdisciplinary		
ID_083_04	Engineering Institution for Self-reliance and Sustainable Goals <i>Dr S Swapna Kumar</i>	1365
ID_124_05	Skilling India through NSQF - A Way Forward to Atmanirbhar Bharat <i>Dr Anil Kumar, Suneel Grover</i>	1369
ID_140_06	Self Reliance and Sustainability : An Environment Perspective <i>Seema Garg, Navita Mahajan</i>	1375
ID_142_08	Self Reliance: A Context of Sustaining Indian Automobile Industry <i>Rohit Radhakrishnan, Vaisakh V, Dr Nidhi M B</i>	1381
ID_143_09	Flamingo: Labour Management Interface System <i>Kushal Vilas Datrange, Pankit Rajesh Rana, Dr Anil Achyut Kunte</i>	1387
ID_144_10	The Technical Efficiency of Unemployed Youth Employment Generation Programme in Tamil Nadu <i>Dr E Bhaskaran</i>	1391

ID_182_11	Role of Consulting Engineers in Mechanical Engineering on the way to Self-Reliant India <i>Anirban Datta, Tarun Kumar Ray Chaudhury</i>	1397
ID_194_12	Innovations, Incubation and Entrepreneurship is a Driving Force for the National Economic Development <i>Dr C Sendil Kumar</i>	1403
ID_196_14	Exploring Nexus of Socio-economic-environmental Aspects for High Speed Rail Corridors Development in India <i>Dheeraj Joshi, Shikha Saini, Vivek Joshi</i>	1407
ID_197_15	Prediction and Assessment of Environmental Impacts (Effects) on the Design and Arts Environment for Industry 3.0 Cotton Roller Ginning Process <i>Dr Vijayan Gurumurthy Iyer</i>	1413
ID_198_16	Protocol Analysis for Intrusion Detection System on IoT Based Network Communication <i>S Ponmaniraj, Dr Amit Kumar Goel</i>	1425
ID_216_17	Upliftment of Indian Economy through Sustainable Development <i>Vaibhav Gupta, Sudershan K Popli</i>	1433
ID_217_18	Education's New Normal: Some Challenges and Much Opportunity <i>Dr Shilpa Tripathi</i>	1435

Agricultural Engineering



Optimization of the Growth of Microalgae *Spirulina Platensis* - Full Factorial Experimental Approach

Mir Shariful Islam^{1,2,3}, Bidyut Baran Saha^{*1,2}

Mechanical Engineering Department, Kyushu University, 744 Motoooka, Nishi-ku, Fukuoka 819-0395, Japan¹

International Institute for Carbon-Neutral Energy Research (WPI-I2CNER), Kyushu University, 744 Motoooka, Nishi-ku, Fukuoka 819-0395, Japan²

Department of Oceanography, University of Dhaka, Dhaka-1000, Bangladesh³

✉ saha.baran.bidyut.213@m.kyushu-u.ac.jp*

ABSTRACT

Owing to an increased demand for dietary food and the reduction of arable land, an alternative solution such as microalgae is recently being exploited. One such viable microalgae candidate for high-value food and protein production is *Spirulina platensis*. The present work reports on the optimum growth, protein and fatty acid content of *Spirulina platensis*. A 23 full factorial central composite design (CCD) was used to estimate the culture involvement variables initial concentration of nitrogen, initial inoculum concentration, and cultivation time to optimize the biomass concentration, protein, and fatty acid extraction from *Spirulina platensis*. This study illustrates that the most influential factor is the cultivation time for optimum biomass and protein content growth. The results found using full factorial CCD indicate that 15 days, 0.1 g/l of inoculum concentration and 0.015 M of initial nitrogen concentration are optimal working parameters to attain a maximum biomass yield of 2.21 g/l.

Keywords : Cultivation; Full factorial design; Microalgae; Protein; *Spirulina*.

ABSTRACT

Algae have allured global attention in the last two decades due to high-value proteins, commercially potential natural products, polyunsaturated fatty acid, coloring agents, which can be used in diversified fields [1–4]. Algae can be categorized as either microalgae (micrometers to tens of micrometers) or macroalgae (large, a few millimeters to plants up to 4 m high). Microalgae studies have been performed since the 1950s: particularly *Spirulina* sp., *Dunaliella* sp., and *Chlorella* sp. are used for the production of valuable chemical elements, protein, lipids, vitamins, antioxidants, fuel production, and wastewater treatments[5–8]. Microalgae are extremely adaptable due to their distinctive capacity to grow under different environmental conditions, such as wastewater, saline water, brackish water, as well as freshwater[9]. The microalgae biomass growth curve shows the sigmoidal growth shape phenomena [10–14].

The blue-green cyanobacterium microalgae *Spirulina platensis* are the simple microscopic and primordial life forms on earth. It may be 10 micrometers in diameter and 60–300 micrometers long. Generally, it is available in tropical and subtropical areas living alkaline waters, lakes and ponds. *Spirulina* grows very well in basic water (pH 9–11) since other microbes did not survive in an alkaline environment [15]. The tribes of Chad lake in Central Africa used *Spirulina* as functional food from ancient times [3,16–19]. *Spirulina* contains high protein (approximately 60% – 70 %), essential fatty acid, vitamin contents, lipids, carbohydrates, minerals such as zinc, iron, calcium, magnesium, sodium and potassium [20]. *Spirulina* based products, such as powder, tablet or capsule and supplements, are manufactured in Japan, Israel, Thailand, India, Taiwan, Mexico, the USA for the food market [8,21]. *Spirulina* has been effective for cholesterol-lowering, anti-cancer, anti-allergic, anti-viral, antioxidant, anti-inflammatory, and the treatment of arsenic poisoning. *Spirulina* is called the future food of the earth and named as “Superfood” by the World Health Organization. It was effectively used for astronauts on space missions, according to the European space agency, Japan Aerospace Exploration Agency (JAXA), and NASA [22]. Besides, this research work on microalgae related topic matches the 9 of 17 goals of the United Nations SDG. These goals are SDG—1: Zero poverty, SDG—2: Zero hunger, SDG—3: Good health and wellbeing, SDG—7: Renewable energy, SDG—8: Good Jobs and economic growth, SDG—9: Innovation and infrastructure, SDG—12: Responsible consumption, SDG—14: Life below water, and SDG—13: Climate action.

Spirulina platensis biomass production depends on many factors such as high pH values (9–10), light, temperature, nutrient concentration, magnetic field, light, speed, length of cultivation, solar radiation, season and inoculum cell concentration[23–26]. Nitrogen is the key nutrient that contributes to the cultivation of *Spirulina* biomass. In this research, one of our targets is to find the answer to the question: How these environmental factors affect the growth rate of *Spirulina* and its protein content and amount of fatty acid?

The objective of this study was to illustrate the influential factors of the fast cultivation of *Spirulina platensis*. In this analysis, (I) duration of cultivation, (II) initial nitrogen concentration, and (III) initial inoculum concentration of algae are considered predicted factors during the cultivation time. We also analyzed the growth development of biomass concentration of *Spirulina platensis* and the amount of protein and fatty acid content.

METHODS

In this study, a full factorial central composite technique is employed for the growth of *Spirulina* sp. High and low levels are studied regarding primary experiments [27]. This study evaluates three factors, such as the length of cultivation, initial nitrogen concentration and initial inoculum concentration for the biomass concentration, protein (%), and fatty acid (%) content. The upper and lower level of cultivation time is 20 to 15 days, initial nitrogen concentration is 0.03 to 0.015 M, and initial biomass concentration is 0.2 to 0.1 g/l.

Design of Experiments for 2³ Factorial

A full factorial technique is an eminent procedure to establish the effects of variables on a particular response. This method can be applied to minimize the number of trials in which several variables must be studied simultaneously. Furthermore, it can be used to three main effects (independent factors), three two-way interaction effects, and a three-way factor interaction and a constant term. A 2³ full factorial design with maximum and minimum levels and three factors were performed using statistical software Minitab to observe the factors for biomass concentration, protein and fatty acid content.

A full factorial design demonstrates the assessment of all possible combinations. So, the full factorial method is best for a small number of parameters. To analyze the parameters a mathematical model was used, which determines the correlation between the response and the main factors (C, N, I). This mathematical model can be expressed by a polynomial equation model, as shown below:

$$Y = \alpha_0 + \alpha_1 N + \alpha_2 C + \alpha_3 I + \alpha_{12} NC + \alpha_{13} NI + \alpha_{23} CI + \alpha_{123} NCI$$

Where Y is the response, α_0 is the constant; α_1 , α_2 and α_3 are coefficients of the main variables N, C and I, respectively; α_{12} , α_{13} and α_{23} are coefficients of the effects of the two-way interaction; α_{123} is the coefficients of three-way interaction effects. Let, N, C, and I are three variables at two levels N_0 , N_1 ; C_0 , C_1 ; I_0 , I_1 , respectively. The all possible combination of predicted variables can be written as:

Table 1: Possible combination of a factorial experiment

(I)	(N)	(C)	(I)	(NC)	(NI)	(CI)	(NCI)
$N_0 C_0 I_0$	$N_1 C_1 I_1$	$N_0 C_1 I_0$	$N_0 C_0 I_1$	$N_1 C_1 I_0$	$N_1 C_0 I_1$	$N_0 C_1 I_1$	$N_1 C_1 I_1$

RESULTS AND DISCUSSION

In this research, a 2³ factorial experimental technique was employed to find the consequences of the variables cultivation length (days), initial concentration of nitrogen (M), and inoculum concentration and their interaction effects on the production of biomass concentration, protein and fatty acid content.

Pareto Chart of the Effect of Variables

Pareto diagram shows the magnitude and significance of the effect of variables. It describes the absolute value of the effects and depicts the reference line (red line in Fig.) on the graph. The horizontal bars that cross the red reference line are statistically important. Bar chart 1(a) shows that the interaction CI and factors I and C are most significant for fatty acid content. In Fig. 1(b) and 1(c), factor C is the most prominent factor for biomass concentration and protein content. Moreover, the three-way interaction effect NCI (Initial nitrogen concentration, cultivation time, and initial inoculum concentration) are not statistically significant, which is shown in Fig. 1(c).

Main and Interaction Effect of Variables

The main effect plot is used to evaluate the relative strength of the effects of individual factors. The magnitude describes the strength of the effect, and the sign of the main effect explains the direction of the effect. Fig. 2(a) and 2(c) describes the same relation for the biomass concentration and protein content between the factors of nitrogen concentration and cultivation time. Interactions effect plot illustrates the response of two variables at all probable arrangements of their settings. In Fig. 2(b) and

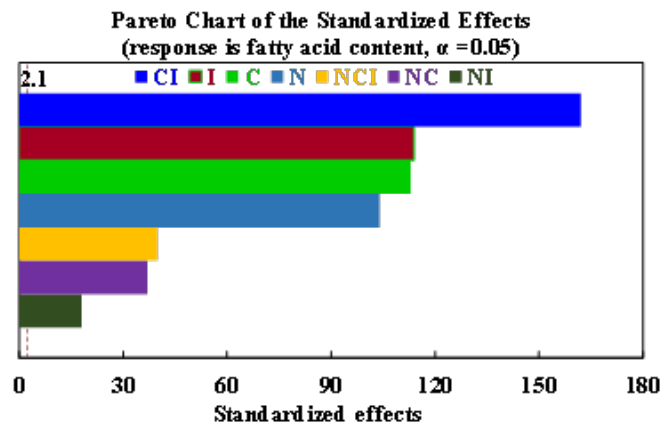


Fig.1(a): Standardized effect on the fatty acid content

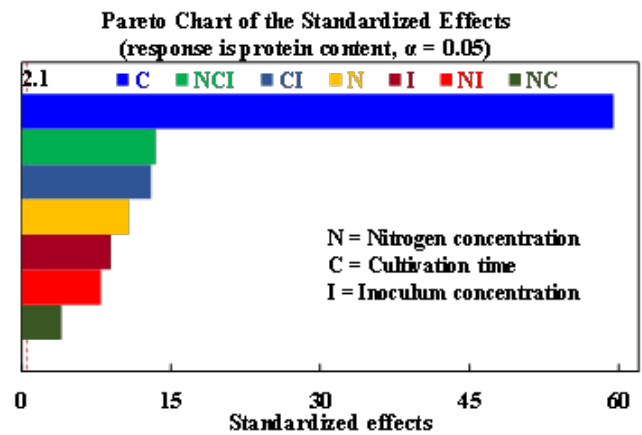


Fig.1(b): Standardized effect on protein content

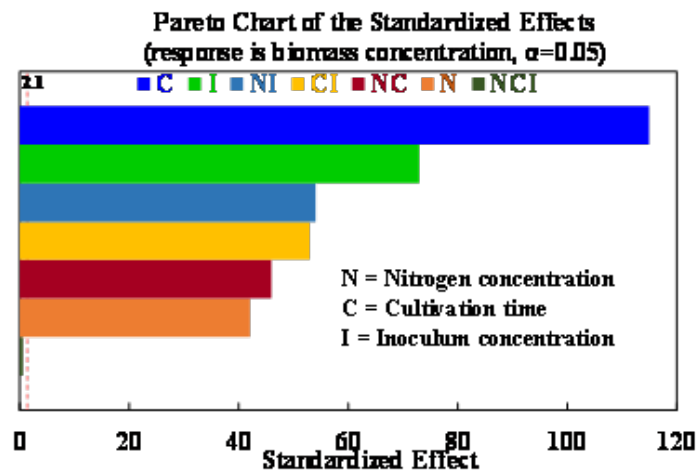


Fig.1(c): Standardized effect on biomass concentration

2(d), it shows that the interaction effect between nitrogen and inoculum concentration for biomass and protein content is greater than fatty acid content (Fig. 2(e)).

Residual Plot

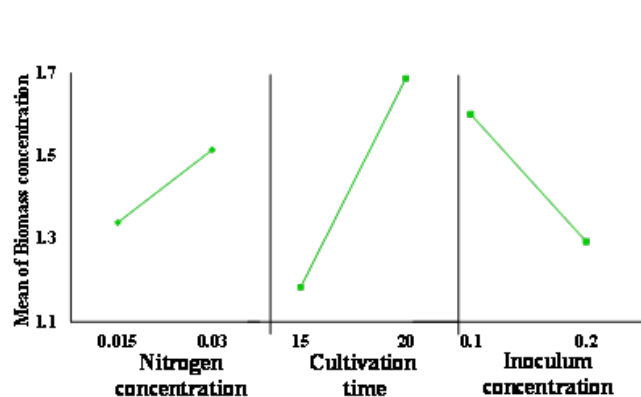


Fig.2(a): Main effect of biomass concentration

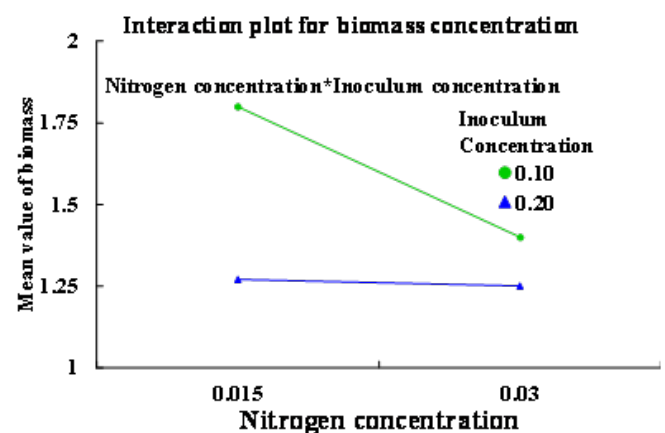


Fig.2(b): Interaction effect of biomass concentration

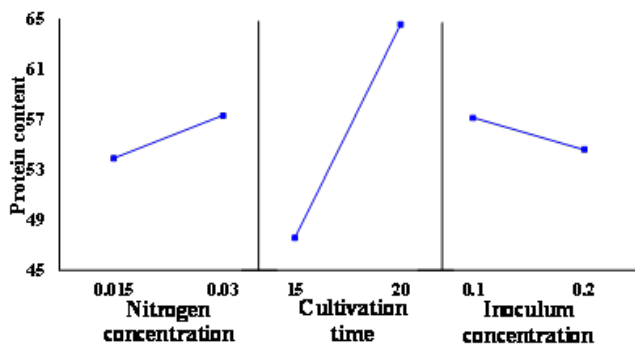


Fig. 2(c): Main effect of protein extraction

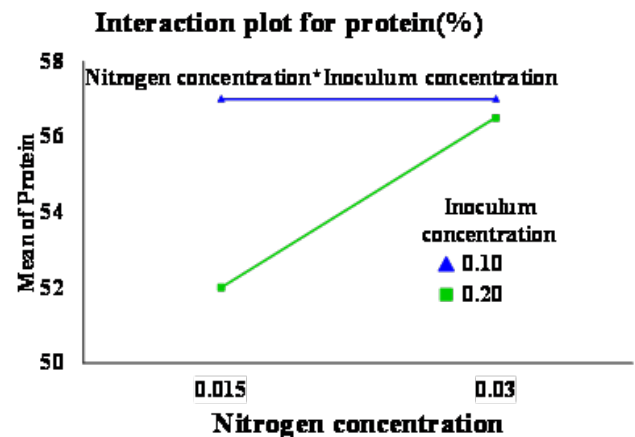


Fig. 2(d): Interaction effect of protein content

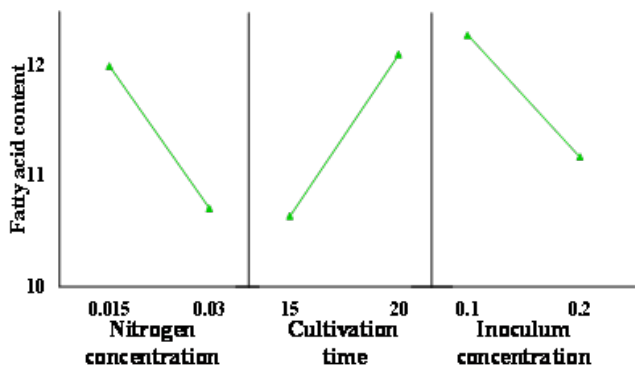


Fig. 2(e): Main effect of fatty acid content

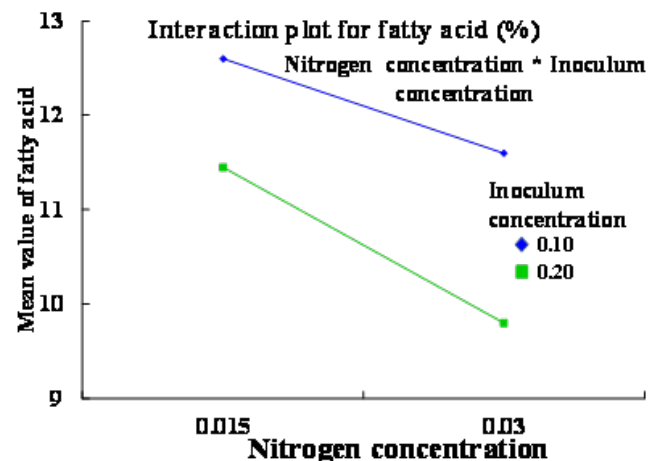


Fig.2 (f): Interaction effect of fatty acid concentration

Fig. 3(a), 3(b), and 3(c) are residual plots for biomass concentration, protein and fatty acid content, which are suitable tools for model justification. To find the standardized residual, we use the following equations:

Residual = observed value - predicted value.

The normal probability plot of residuals shows that all the points in Fig. 3 fall on a straight line approximately. So, the residuals for the response variables almost fitted the normal distribution.

Analysis of Variance (ANOVA)

The influence of each parameter is a key element in the production of biomass concentration, protein content and, the amount of fatty acid. Analysis of variance was employed to investigate the results of the research and to estimate how much deviation was promoted by each factor. Different level of variables acknowledges the main factors and their interaction impacts.

Protein and fatty acid contents, which are affected by various factors from the ANOVA technique, were shown in Table 2.

The impact of variables is statistically significant if the p-value less than 0.01. To have a better understanding of the variables, computer-generated main and interaction effects were investigated since any individual element possibly interacts with any or all the factors. From Table 2, it is explored that all linear, 2-way interaction effects and 3-way interactions effects are statistically significant for fatty acid and protein content. It is also studied that all effects are statistically significant for biomass concentration (data not shown). It is illustrated that the adjusted sum of squares of cultivation length (C) is the highest (1752.07)

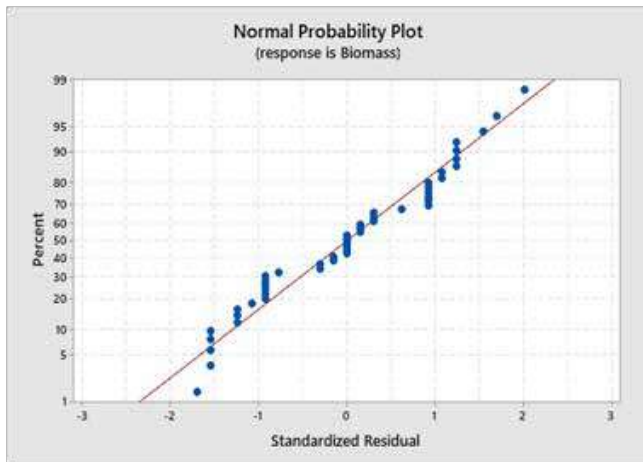


Fig.3 (a): Normal probability plot of residuals of biomass concentration

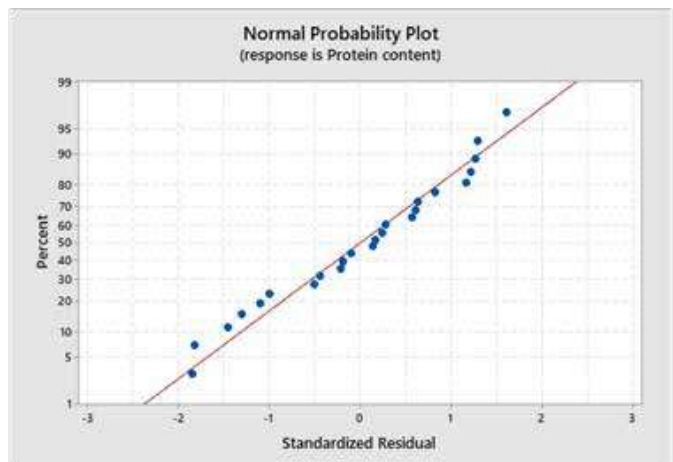


Fig.3 (b): Normal probability plot of residuals of fatty acid content

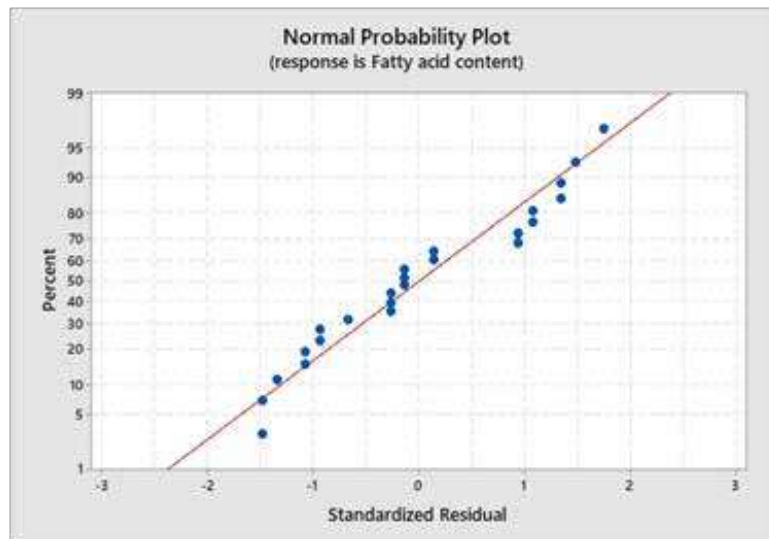


Fig.3 (c): Normal probability plot of residuals of protein content

for protein content. But for fatty acid content, inoculum concentration (I) and cultivation time (C) have the same adjusted sum of squares (approximately 11.7). For two-way interaction effects, cultivation time, and Inoculum concentration (CI) has the most adjusted sum of squares on the production of fatty acid (24.32) and protein content (85.05). The consequence of each coefficient determined by p-values are listed in table 2. All the parameters are significant for linear, 2-way interactions, and 3-way interactions model: the smaller the p-value, the more influential the corresponding coefficient.

The production of biomass was modeled employing the following equation:

$$\text{Biomass (g/l)} = -1.400 - 28.67 * N + 0.11600 * C + 19.300 * I + 4.800 * N * C - 313.3 * N * I - 0.9000 * C * I + 1.33 * N * C * I$$

Adjusted and predicted R-squared values computed for protein content were 0.9945 and 0.9913, and for fatty acid content was 0.9997 and 0.9995, respectively. These values are rational for each other.

Contour Plot for the Biomass Concentration, Protein and Fatty Acid Content

In this work, the contour plot illustrates the correlation between the independent (initial nitrogen concentration (M), duration of cultivation (day), and initial inoculum concentration (g/l)) and dependent (biomass concentration (g/l), fatty acid (%), and


Table 2: The least-squares fit and coefficient estimates for the production of protein content by using the ANOVA technique

Source	DF	Adj SS	Adj MS
Model	7	2054.30	293.47
Linear	3	1845.06	615.02
Nitrogen concentration	1	60.93	60.93
Cultivation time	1	1752.07	1752.07
Inoculum concentration	1	32.06	32.06
2-Way Interactions	3	119.23	39.74
Nitrogen concentration* Cultivation time	1	6.96	6.96
Nitrogen concentration* Inoculum concentration	1	27.22	27.22
Cultivation time*Inoculum concentration	1	85.05	85.05
3-Way Interactions	1	90.02	90.02
Nitrogen conc.*Cultivation time*Inoculum conc.	1	90.02	90.02
Error	16	7.95	0.50
Total	23	2062.25	
Source	F-Value	P-Value	
Model	590.62	0.000	
Linear	1237.74	0.000	
Nitrogen concentration	122.62	0.000	
Cultivation time	3526.08	0.000	
Inoculum concentration	64.53	0.000	
2-Way Interactions	79.98	0.000	
Nitrogen concentration* Cultivation time	14.00	0.002	
Nitrogen concentration* Inoculum concentration	54.78	0.000	
Cultivation time* Inoculum concentration	171.17	0.000	
3-Way Interactions	181.16	0.000	
Nitrogen conc.* Cultivation time*Inoculum conc.	181.16	0.000	
R-sq	R-sq(adj)	R-sq(pred)	
99.61%	99.45%	99.13%	

protein content (%) factors. Contour maps are a method to describe a 3-dimensional surface on a 2-dimensional plane. In this method, x and y-axes represent the predictor variables and response variable z as contours. It is a technique to illustrate a 3-dimensional surface on a 2-dimensional plane. In Fig. 4(a), 4 (b), and 4(c) shows the contour plot for biomass concentration, 4(d), (e), and (f) shows the fatty acid content, and 4(g), (h) and (i) depicts the protein content in the same set of axes. Biomass concentration is more than 1.75 g/l when inoculum concentration at a minimum level (0.10 g/l) and duration cultivation is

maximum level (20 days). Biomass concentration is increasing when the duration of cultivation time and nitrogen concentration increasing.

CONCLUSIONS

The 23 full factorial technique gives easy and feasible results for the three variables at two levels. This study is allowing not only the main effects of initial nitrogen concentration, cultivation time, and inoculum concentration, but also providing clarifications of the 2- way and 3-way interactions, including these variables. The major effects of the three variables are examined from ANOVA tests. The most potential variable is the length of cultivation for the maximum growth of *Spirulina platensis*. The interaction between cultivation time and inoculum concentration is significant for the synthesis of fatty acid.

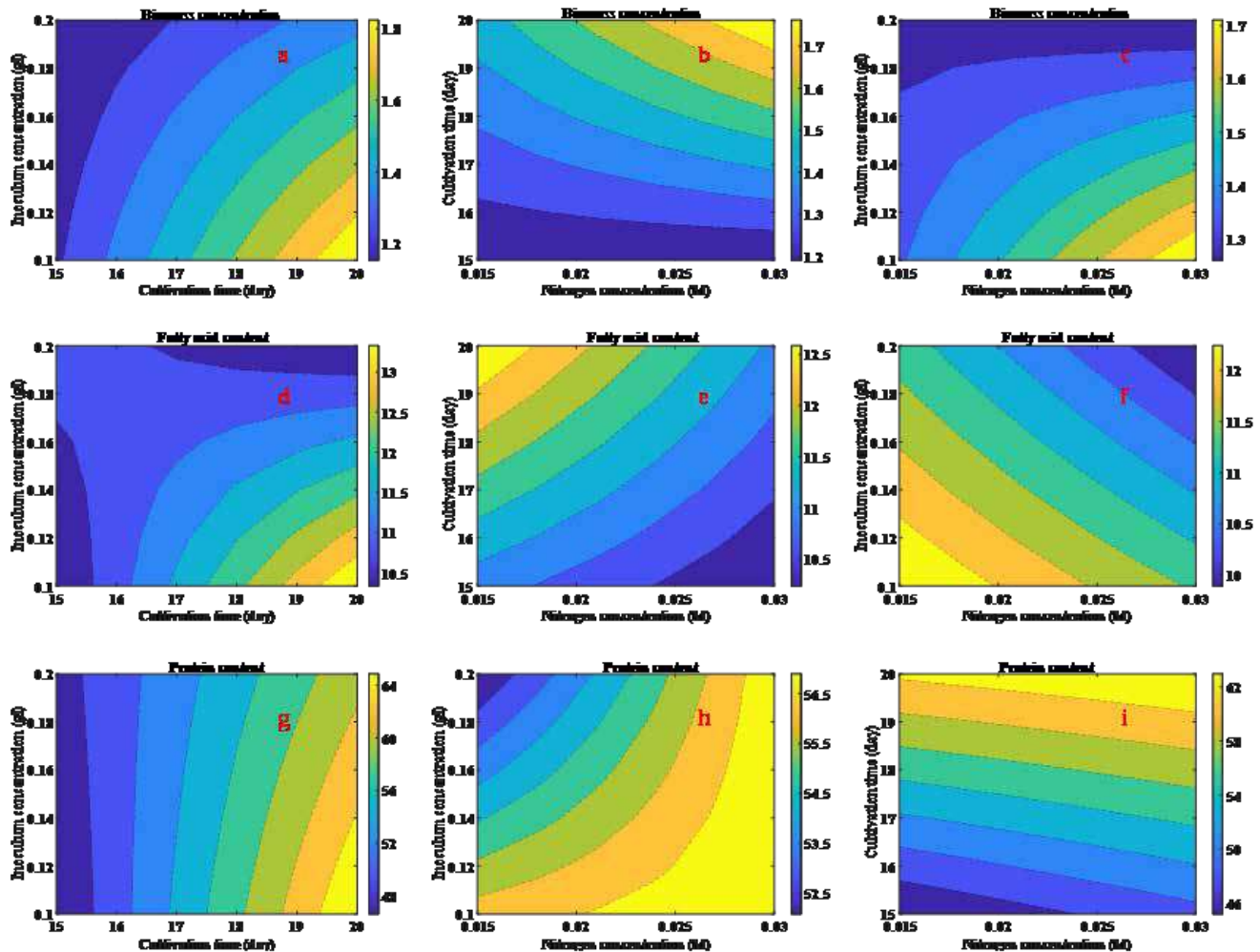


Fig4. Contour plot of (a) inoculum concentration and cultivation time, (b) nitrogen concentration and cultivation time, (c) nitrogen concentration and inoculum concentration for biomass concentration (g/l), (d) inoculum concentration and cultivation time, (e) nitrogen concentration and cultivation time, (f) nitrogen concentration and inoculum concentration for fatty acid content (%), (g) inoculum concentration and cultivation time, (h) nitrogen concentration and inoculum concentration, and (i) nitrogen concentration and cultivation time for protein content.

REFERENCES

1. Subhaschandra T, Rajak U, David O. Optimization of performance and emission parameters of direct injection diesel engine fuelled with microalgae *Spirulina* (L.) – Response surface methodology and full factorial method approach. *Fuel* 2021;285:119103. doi:10.1016/j.fuel.2020.119103.



2. Bleakley S, Hayes M. Algal Proteins: Extraction, Application, and Challenges Concerning Production. *Foods* 2017;6. doi:10.3390/foods6050033.
3. Wayne CK, Wayne K, Ying J, Loke P, Hui N, Ching J, et al. Microalgae biorefinery : High value products perspectives Bioresource Technology Microalgae biorefinery : High value products perspectives. *Bioresour Technol* 2017;229:53–62. doi:10.1016/j.biortech.2017.01.006.
4. Güven KC, Coban B, Özdemir O. Pharmacology of Marine Macroalgae. *Encycl. Mar. Biotechnol.*, 2020, p. 585–615.
5. Ogbonda KH, Aminigo RE, Abu GO. In X uence of temperature and pH on biomass production and protein biosynthesis in a putative *Spirulina* sp . *Bioresour Technol* 2007;98:2207–11. doi:10.1016/j.biortech.2006.08.028.
6. Pane L, Solisio C, Lodi A, Luigi G, Converti A, Xv VB, et al. Effect of extracts from *Spirulina platensis* bioaccumulating cadmium and zinc on L929 cells \$. *Ecotoxicol Environ Saf* 2008;70:121–6. doi:10.1016/j.ecoenv.2007.05.019.
7. Chisti Y. Biodiesel from microalgae. *Biotechnol Adv* 2007;25:294–306. doi:10.1016/j.biotechadv.2007.02.001.
8. Vigani M, Parisi C, Rodr E, Barbosa MJ, Sijtsma L, Ploeg M. Food and feed products from micro- algae : Market opportunities and challenges for the EU. *Trends Food Sci Technol* 2015;42:81–92. doi:10.1016/j.tifs.2014.12.004.
9. Rajvanshi M, Limited RI, Sagaram US, Limited RI. *Biomolecules from Microalgae for Commercial Applications*. Taylor and Francis; 2019. doi:10.1201/9780429027970-1.
10. Islam MS, Islam MS, Khan AFMK, Bangalee ZI. A Procedure to Fit an Interpolating Curve to a Set of Logistic Data. *Dhaka Univ J Sci* 2017;65:103–5.
11. Gompertz B. On the nature of the function expressive of the law of human mortality, and on a new mode of determining the value of life contingencies. *Philos Trans R Soc London* 1825.
12. Richards FJ. A flexible growth function for empirical use. *J Exp Bot* 1959. doi:10.1093/jxb/10.2.290.
13. Islam MS, Saha BB. Study on biomass models : Opportunities for microalgae growth. *Int. Conf. Earth Environ. Sci. Technol.*, 2020, p. 711–73.
14. Islam MS, Rahman MM, Saha BB. Full Factorial Experimental Design for Growth of *Spirulina Platensis* and Valuable Products Enhancement Mir Shariful Islam. *Proc. Int. Exch. Innov. Conf. Eng. Sci.*, vol. 6, 2020, p. 299–304.
15. Shi W, Li S, Li G, Wang W, Li Y, Ling X. Investigation of main factors affecting the growth rate of *Spirulina*. *Opt - Int J Light Electron Opt* 2016;127:6688–94. doi:10.1016/j.ijleo.2016.04.125.
16. Ciferri O. *Spirulina*, the edible microorganism. *Microbiol Rev* 1983. doi:10.1128/mmbr.47.4.551-578.1983.
17. Spolaore P, Joannis-cassan C, Duran E, Isambert A, Génie L De, Paris EC. Commercial Applications of Microalgae. *J Biosci Bioeng* 2006;101:87–96. doi:10.1263/jbb.101.87.
18. Khatun R, Noor P, Akhter N, Jahan MAA, Hossain M, Munshi JL. *Spirulina* Culture in Bangladesh XI Selection of a Culture Medium , Suitable for Culturing a Local Strain of *Spirulina*. *Bangladesh J Sci Ind Res* 2006;41:227–34.
19. Vonshak A, Richmond A. Mass production of the blue-green alga *Spirulina*: An overview. *Biomass* 1988;4565:233–47. doi:10.1016/0144-4565(88)90059-5.
20. Arora R, Sudhakar K, Rana RS. Trends in Food Science & Technology *Spirulina* e From growth to nutritional product : A review. *Trends Food Sci Technol* 2017;69:157–71. doi:10.1016/j.tifs.2017.09.010.
21. Khan MI, Shin JH, Kim JD. The promising future of microalgae : current status , challenges , and optimization of a sustainable and renewable industry for biofuels , feed , and other products. *Microb Cell Fact* 2018;1–21. doi:10.1186/s12934-018-0879-x.
22. Karkos PD, Leong SC, Karkos CD, Sivaji N, Assimakopoulos DA. *Spirulina* in Clinical Practice : Evidence-Based Human Applications. *Evidence-Based Complement Altern Med* 2011;2011:4–7. doi:10.1093/ecam/nen058.
23. Fadel F, Kamil AE. Production and nutritive value of *Spirulina platensis* in reduced cost media. *Egypt J Aquat Res* 2012;38:51–7. doi:10.1016/j.ejar.2012.09.003.



24. Vonshak A, Abeliovich A, Boussiba S, Arad S, Richmond A. Production of Spirulina Biomass: Effects of Environmental Factors and population Density. *Biomass* 1982;2:175–85.
25. Carolina A, Piazzzi F, Veiga C, Oliveira L, Vieira A, Kuhn C, et al. Modeling the growth of microalgae *Spirulina* sp . with application of illuminance and magnetic field. *J Chem Technol Biotechnol* 2019;94:1770–6. doi:10.1002/jctb.5942.
26. Senaha I, Nagamatsu K. Development of macroalgal onshore cultivation system utilizing Carbon dioxide. *J Japan Inst Energy* 2017;96:393–9. doi:10.3775/jie.96.393.
27. Alberto J, Costa V, Linde GA, Ibraim D, Atala P. Modelling of growth conditions for cyanobacterium *Spirulina platensis* in microcosms Modelling of growth conditions for cyanobacterium *Spirulina platensis* in microcosms 2000. doi:10.1023/A.



Timer Based Automatic Family Drip System (FDS) – A Sustainable Technology for Increased Vegetable Production in Urban Sector

Chithra G, Jyothi Rachel Varghese, Dr Binu John Sam

Mitraniketan Krishi Vigyan Kendra – ICAR, Velland, Thiruvnanthapuram, Kerala

✉ gchithramitra@gmail.com

ABSTRACT

A comparative study was conducted to evaluate the performance of time based automatic drip irrigation system and manual hose irrigation in okra. Irrigation time optimized at 15 minutes provided 250 ml of water per plant. Based on the growth stage of the crop water requirement of vegetables was estimated to be 0.6 to 2 litre/day. To meet this water requirement, irrigation was done at 4 intervals i.e., twice in the morning and twice in the evening twice in such a manner that 1 litre water was irrigated per grow bag. Thus drip irrigation conserved 50% water compared to manual hose irrigation. It was found that drip irrigation gave 70% higher yield than the yield obtained with the manual irrigation system. Automatic DIS increased irrigation efficiency up to 95% than that of conventional method of irrigation.

Keywords : DIS; Water use Efficiency; Crop yield.

INTRODUCTION

Kerala, blessed with lot of rivers and good rains, gets an average annual rainfall of 3000 mm per year. During the South West monsoon Kerala receives 90% of rains; bulk of which is not utilized due to surface runoff owing to undulating topography. Urbanisation, which has resulted in shrinkage of cultivated area, together with unavailability of water during off seasons has led to shortage of quality produce in the state. Shortage of local produce leads to import from nearby states.

In India good volume of agricultural produce occurs. About 500 million tons of vegetables need to be produced by 2050 (As per survey of Government of India, 2001). In order to meet the target, agriculture has to be taken up in a big scientific way and in this process, water demand goes up. It would be as high as about 85-90% of the total available water. The demand for water from other sectors too would increase multiple folds due to which water allocation for farming may come down to only 75% of what would be required (Sivanappan, 1987). In our country, while irrigation resources are limited, the water use efficiency is very low. In this context, the best approach is implementation of drip irrigation system wherever possible, that makes use of providing optimum quality of water to the plant root thereby enhancing the water use efficiency along with reduction in its wastage. In India, drip irrigation technologies were introduced in the 1970s from countries like Israel and the USA, where it is widely used in large farms. Micro irrigation system has become popular in India and it has been adopted on 400,000 ha. Maharashtra leads in area under drip irrigation covering almost half the total area, followed by Andhra Pradesh, Karnataka and Tamil Nadu. The extent of drip irrigation has increased from almost zero in 1970 to 1000 ha in 1985 and to about 400000 ha in 2002 covering about 30 crops in India.

Owing to high cost of vegetables in the market and general awareness on use of organic produce, a new breed of urban farmers have emerged who have started using their house's roof top for cultivation with plants in grow bags. Many urban farmers are either old and have great difficulty in using the stairs to reach the terrace for watering their plants or are severely short of time owing to their hectic office schedule. Irrigation method used for grow bag cultivation is either hose irrigation or bucket irrigation in which there is large wastage of water. In order to improve the water use efficiency, plant irrigation may be carried out through drip system with the help of micro tubes, though the technology is slightly costly.

Micro irrigation is an expensive venture. The social acceptability is also a decision making factor. Its large scale adoption involves a crucial question of economic viability. In recent times, farmers have been compelled to opt for this advanced method of irrigation, due to limited availability of water resources and high demand for water from all sectors. In spite of the technical and economic feasibility of drip irrigation, its adoption on large scale is not so encouraging in India. There are some limitations in the prevailing methods of drip irrigation like economic investment, clogging of drippers, low awareness level (16%) and inadequate knowledge about its application, utility, method of operation and maintenance.



Keeping in view of the above few facts, a field experiment was conducted on automatic drip irrigation for grow bag cultivation to evaluate yield, water-use- efficiency and economic feasibility of a commonly used vegetable, okra. Comparison was done with the manual hose irrigation for grow bags.

REVIEW OF LITERATURE

In micro irrigation sector, manual interventions are automated to perform all operations, starting from watering to fertigation as per prescribed schedule. Development of automated system has resulted in lot of developments in crop production like improvement in water saving, increase in crop yield, enhancement in water as well as fertilizer use efficiencies and greater benefit cost ratio as well, in comparison to general micro irrigation system (Suresh, 2010). Automated timer based system is comparatively cheaper and hence gaining more popularity than the volume based system (Rajkumar et al, 2008).

In one study on tomato crop (Carpena, et al. 2003), automated irrigation system with feedback from soil moisture sensors resulted in 73% reduction in water use, when compared with standard commercial practices, without any effect on the yield.

Drip irrigation also gave the highest yield with 319 mm of water use as compared to surface irrigation and drip irrigation system with LLDPE plastic mulch increased yield by 57 % over surface irrigation with same quantity of irrigation water. Similar results have been obtained by Tiwari et al. (1998a) for okra crop at Kharagpur, West Bengal. Paul et al. (2013) conducted a study on drip irrigation with plastic mulching; this system increased yield by 57% and net seasonal income by 54%. Sivanappan et al.(1987) conducted a study on drip irrigation for okra and the result revealed that water saved was as high as 84.7% and noted a slight increase in yield by 7.6%.

MATERIALS AND METHODS

This study was conducted for two years (2016 and 2017). About 150 units of drip irrigation system (DIS) had been installed at different locations in the urban areas of Thiruvananthapuram Corporation. This was indeed a turning point for agriculture in urban and peri-urban areas. Nowadays urban people take due care by cultivating vegetables in their roof – top, because of high pesticide residues in market produce. But urban farming initiatives lack supervision and guidance in cultivation practices especially in irrigation. Here comes the role of low cost drip irrigation to solve acute water shortage and labor problem.

Automated DIS helps to irrigate plants in an automated manner. In drip irrigation, water is applied drop by drop to the root zone area of the plant for its effective utilization. This is a precise form of irrigation and helps to manage water resources in an efficient way. Main advantage of this system is that the time and duration of the irrigation sequence can be programmed with very little or no manual intervention. The benefits of embracing this technology are less dependency on labour, smooth operation and energy savings. Each plant will get 1ltr.of water in 1 hour. Dripper discharge rate is 4ltr. / hr. The system contains screen filter that ensures that the emitter does not get clogged. The advantage of this system is that its durability is at least five years and enormous savings in water use as only required water will be used for irrigation and that wastage of water can be minimized.

In summer, plants face severe water stress and water shortage and this will lead to them to permanent wilting point. Absence of irrigation affects vegetative growth which directly influences the crop yield. The closure of stomata is the first symptom of plant water stress. This is followed by plant wilting and finally damage of the plant through overheating. Crop loss occurs once plant wilting occurs. In order to avoid such situations, part time cultivators and aged people can easily adopt the DIS technology for irrigation. Being a labour enhancing technology, automatic drip irrigation avoids man power utilization for watering the plants at the right time, right quantity, right place and right manner. **Table 2** show the cost of the equipments used for the drip irrigation

1) Drip kit :- Drip kit consists of 16mm LLDPE lateral (15 m length), dripper / emitter (4 LPH), stake 4 way assembly with micro tube, screen filter (100 μ efficiency), fittings and accessories.

2) Automatic digital timer:- The mainstay of an automated DIS is the operating time. Automatic timer is a lifesaver in a DIS. Battery powered timers let you to set the frequency and duration of watering schedules for different applications. With automatic shut-off, you can set the timer and be at peace. We can pre -set eight programmes in a timer for all days of the week. Out leads from Timer must be connected to switch board and in leads to the Timer to the pump. Installation and maintenance of the system is simple and easy to use. Water requirement decides the operation time. The controller clock is set for the current day and time. While in operation, as the controller clock time coincides with the start time of the programme, signals are sent to the valves and the sequence of operation is initiated and accordingly the pump gets switched on and off at the specified time. Timer is basically 230VAC with 8 on/off provision having an output rate of 2Amperes.

3) Booster pump:- Pump is essential when the tank is kept on the terrace floor. In order to obtain the necessary discharge, a minimum pressure of 1 kg/cm² is necessary. A 35W submersible pump can lift water up to 3m with a maximum discharge rate of 500 lph. If the tank is above the ground level at a height of more than 2m, having a pump is optional as water flows down due to gravity alone. If pump is used, a 16mm lateral may be connected to the pump to obtain the sufficient pressure.

Drip kit, Digital timer and pump typically used in a DIS is given in **Fig. 1**.



Fig. 1: Dripkit, Timer and Pump of DIS

Fig. 2 gives the schematic of installation of DIS. Submersible pump must be immersed in water tank and timer connected to the circuit. The main line Φ 16mm LLDPE pipe is directly connected to a 35 watts pump to lift the water from the tank. The main unit is connected to a screen filter and control valve. The lateral is provided with on line turbokey dripper of 4 ltr/hr discharge capacity. Four-way assembly with 4 micro tubes are fitted on dripper and tubes were inserted into the 4 grow bags. Fifteen drippers can irrigate 60 grow bags with a discharge rate of 1LPH / Poly bag when the grow bags are arranged side by side. If they are arranged 45cm apart an additional 10m lateral is needed to cover 60 grow bags. Screen filter, filter the water efficiently @ 700 litre per hour. Drip kit will last for more than five years without any fail.

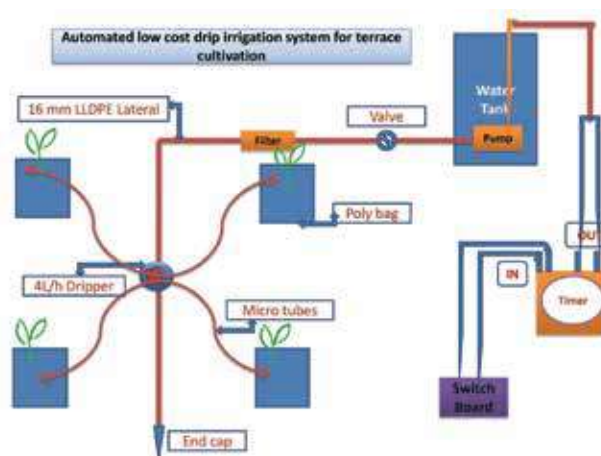


Fig. 2: Schematic of Automated DIS

4) Operation procedure:- Irrigation rate was 250ml of water per plant for 15 minutes. Since the crop water requirement of vegetables is 0.6- 2 ltr./day, irrigation was applied daily for 1 hour. Drip irrigation was applied more frequently in 4 irrigation intervals due to the slower water delivery rate of the drip system.

5) Crop yield:- The yield was recorded for three crop seasons. Weight of vegetables obtained from 60 grow bags has been measured as the total crop yield.

6) Water use efficiency:- Water use efficiency was determined using (1),

$$Eu = C/Wc \quad (1)$$

Where C= Crop yield in Kg/Wc

Wc = Water consumed by the crop in ha cm per Unit area

Since the drip irrigation was used for grow bag vegetable cultivation; based on the experimental study conducted by Babu.G.R,

et.al (2015), the consumptive water use for okra was fixed as 309.8 mm for drip irrigation and for manual irrigation 535 mm based on the study of Sivanappan et.al (1987).

7) Irrigation Scheduling:- The crop requires adequate moisture in the soil during summer months for faster growth. Drip irrigation is most suitable to the crop as it provides uniform moisture throughout the season. The daily water requirement of okra crop is 2.4 l/day/4 plants during early growth stage and 7.6 l/day/4 plants during the peak growth stage. The irrigation system should be operated daily for 75 minutes during initial growth stage and for 228 minutes during peak growth of the crop with an emitter capacity of 2 lph. Irrigation on each day or on alternate days with On-line type of drippers is preferred. (Tiwari, 2015)

8) Economic analysis:- Benefit-Cost ratio and net profit were carried out to determine the economic feasibility of the crop using surface and drip irrigation as suggested by Tiwari et al. (1998a). The fixed cost of the drip irrigation system was Rs.3750/unit. The useful life of the drip system was considered to be 5 years. The system cost was evaluated by distributing the fixed cost of system over life period of drip irrigation set. In addition to this the cost of cultivation includes expenses incurred for grow bags, porting mixture, intercultural operation, fertilizer, crop protection measures, irrigation water and harvesting with labour charge.



Fig. 3: Automated DIS after installation at terrace of farmers

RESULTS AND DISCUSSIONS

Experiments were conducted to study the crop response and growth of vegetables under automated drip irrigation at 5 plots. **Fig. 2** shows the automated DIS installed at two houses. Water was applied equally in all bags. Germination was highest in grow bags that were irrigated through DIS. Plants responded to DIS so much so that flowering in drip irrigated bags started a month earlier than controlled bags (those being watered manually using hose). The yield was recorded for three crop periods. The yield obtained per plant, for okra, was 215kg in drip compared to hose irrigation.

1) Water use efficiency:- On an average, water consumption was observed to be 50 % less compared to conventional irrigation. The amount of water required was further less during rainy seasons. Irrigation was programmed for 15 minutes duration at four different timings to meet the per day water requirement of 1ltr/ plant. **Table 1** gives the water use and yield for drip irrigated and control methods for cultivation of okra (average of two year period).

Table 1 : Water use and yield in drip irrigated and control method

Plot no.	Water use efficiency (t/ha ^{-cm})		Yield (Kg/60 nos. of polybags)		% increase in yield
	Control	Drip	Control	Drip	
1	2.34	6.62	125	205	64
2	2.30	6.29	123	195	51
3	2.06	6.08	110	188	70
4	3.08	6.94	165	215	30
5	1.77	6.10	95	189	98

It may be observed that maximum water use efficiency was observed to be 6.94 t/ha-cm at plot 4 compared to hose irrigation. The water use efficiency between conventional and drip irrigation is given in **Fig. 4**.

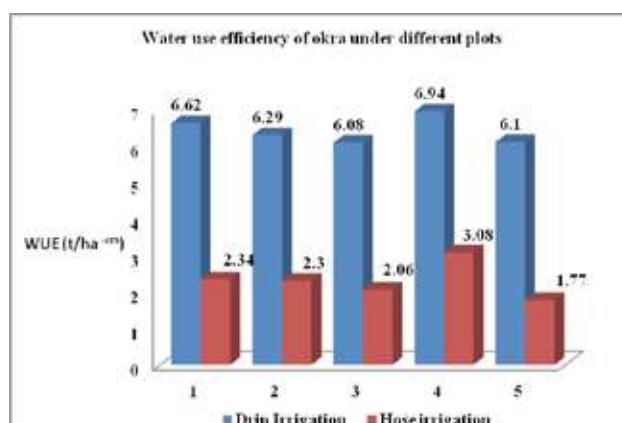


Fig. 4: Water use efficiency of DIS and hose irrigation during cultivation of okra at five terraces

2) Irrigation efficiency:- During manual irrigation, about half the amount of water supplied is lost by leakage, overflow and also thorough evaporation. The irrigation efficiency is only 50%. Using timer based automated DIS, water saved was as high as 95%. Quantity of water used for 4 drip irrigations was 1-2 litres/plant against 5 - 10 litres in conventional method.

3) Yield:- As observed from Table 1, maximum yield obtained was 215kg for 60 numbers of poly bags compared to conventional irrigation for three crop seasons. As the discharge rate increases, crop yield also increases substantially (Fig.8). The yield of okra under drip irrigation gave 30 -98% more yield compared to conventional method of irrigation by overcoming severe moisture stress.

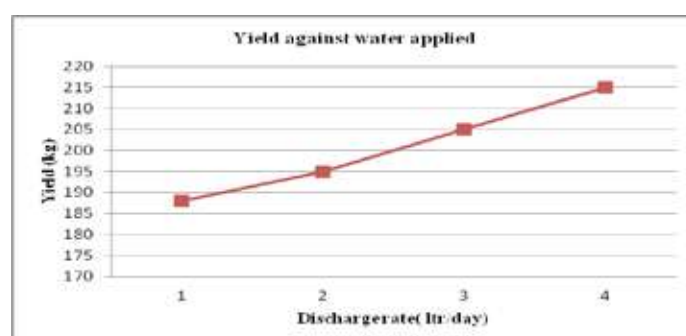


Fig. 5: Crop yield with water discharge

4) Water savings:- It was observed that there was substantial water saving ranging from 70 to 90 per cent compared to conventional hose irrigation.

5) Economic feasibility:- Maximum net return of Rs.3425 for 60 grow bags with B:C ratio of 1.54 was recorded at P4 and lowest net profit of Rs.1845 for 60 grow bags with B:C ratio of 1.25 in P1 (Table 3). At the same time for conventional irrigation net income varies from Rs. 250 – 575 for 60 grow bags with B:C ratio 1.04 to 1.08. The lower B.C ratio is attributed to lower yield as a result of improper irrigation and thereby low gross income.

Table 2 : Water use and yield in drip irrigated and control method

Plots	Drip				Control			
	Gross cost	Gross income	Net income	BCR	Gross cost	Gross income	Net income	BCR
P1	7380	9225	1845	1.25	5200	5625	425	1.08
P2	6680	9750	3070	1.45	6150	5800	350	1.06
P3	6000	9400	3400	1.56	5500	5250	250	1.04
P4	6250	9675	3425	1.54	7425	6850	575	1.08
P5	6500	9450	2950	1.45	4750	4500	250	1.05



CONCLUSION

Timer based Automatic Family Drip System (FDS) is observed to be user friendly, economical and cost effective as compared with conventional hose irrigation for farming on terraces in cities. 70% increase in yield was obtained against 6.08 t/ha-cm water use efficiency. Water savings to the tune of 50% was observed for drip irrigation by avoiding the wetting of terrace with overrun water loss. Time savings, low energy consumption and low pressure low cost DIS had been widely accepted among urban farmers to promote vegetable cultivation in their own houses.

REFERENCES

1. Babu, G. R. Bhaskara Rao, I. Raj Kumar, K. N, "Response of okra to different levels of drip irrigation on growth, yield and water use efficiency". International Journal of Agricultural Engineering, 2015, Vol 8 (1):pp47-53.
2. Carpena, M. R., Bryan, H. and Klassen, W, "Automatic soil moisture - based drip irrigation for improving tomato production", Proc. Fla. State Hort. Soc, 2003, Vol 116:pp0-85
3. Paul, J. C. Mishra, J. N. Pradhan, P. L. and Panigrahi, B, "Effect of drip and surface irrigation on yield, water- use -efficiency and economics of capsicum (capsicum annum 1.) grown under mulch and non-mulch conditions in eastern coastal india" European Journal of Sustainable Development, 2013, Vol 2(1):pp99-108.
4. Rajkumar, D. Raamah, K. Rathika S and Thiyagarajan, G, "Automation in Micro irrigation. Science tech Entrepreneur, 2008
5. Sivanappan, R. K. Padmakumari, O. and Kumar, V, "Drip Irrigation", Keerthi Publishing house (P) Ltd., Coimbatore, 1987
6. Suresh, R, "Micro irrigation". First Edition. Standard Publishers Distributors. New Delhi, 2010
7. Tiwari, K. N, "Technical bulletin on okra", 2015 NCPAH. (www.ncpahindia.com)
8. Tiwari, K. N. Mal, P. K. Singh, R. M. and Chattopadhyaya, A., ".Response of Okra to drip irrigation under mulch and nonmulch conditions", Agricultural Water Management, 1998, Vol 38, pp91-102.



Experimental Investigation of Double Collector Solar Dryer for Agricultural Products

G S Divya Laxmi¹, D Sakthivadivel^{1,*}, P Ganesh Kumar², S Iniyan³

School of Mechanical Engineering, Vellore Institute of Technology, Vellore, Tamil Nadu¹

School of Mechanical Engineering, Yeungnam University, Gyeongbuk, Republic of Korea²

Department of Mechanical Engineering, Anna University, CEG Campus, Chennai, Tamil Nadu³

✉ sakthi2energy@gmail.com*

ABSTRACT

Drying of agricultural products is an important unit operation in the post-harvest phase. It is a thermo-physical and Physico-chemical operation by which the excess moisture in a product is removed. It makes the product suitable for safe storage and protects them against attacks of insects, molds, and other micro-organisms during storage. However, the absence of appropriate preservation techniques and non-renewable energy sources can cause significant production losses that would be prevented by the execution of solar drying devices. The objective of the study is to construct, develop, and validate a double collector solar dryer with improved drying performance. In this present work, the solar dryer was designed based on the design consideration for the Chennai location. The system consists of a primary collector with a V-Corrugated absorber plate which is attached to a drying chamber and the secondary collector is placed on the roof of the drying chamber. And this collector gives an extra thermal source, which indirectly transfers heat to the chamber through a metal plate. This also compensates for the thermal energy loss in the drying chamber. The double collector solar dryer achieved the collector efficiency of 38.23% with an average drying rate of 1.55 g/min for *Andrographis paniculata* (Nilavembu).

Keywords : Solar drying; V-Corrugated absorber plate; Double Collector; *Andrographispaniculate*.

INTRODUCTION

Every year tonnes of agricultural produce gets blemished due to the lack of infrastructures such as cold chain, transportation, storage facility, and inadequate food processing. The study conducted by the Central Institute of Post-Harvest Engineering and Technology (CIPHET) reports that 16% of produced fruits and vegetables in India are being wasted every year [1]. To avoid agricultural losses, preservation techniques must be adopted. Drying of agricultural products is an important unit operation under the post-harvest phase[2] and it should be chosen in such a way that it should be energy-efficient, economically viable, and eco-friendly. Thus, food processing through solar energy helps in the food supply for the growing population.

Solar energy is radiation emitted by the sun that can produce heat and if harnessed, it has the potential to satisfy the world's energy needs. This energy is a form of renewable energy because of its inexhaustible nature, and it can be a substitute for fossil fuels. It can be utilized for applications like solar- water heating, space heating, distillation, pumping, drying, cooking, power generation, etc. Since the price of fossil fuel was not fixed and it has environmental concerns, it creates the users to switch to renewable energy.

Open sun drying is the traditional method of food drying but it has negative impacts such as slow drying rate, dust contamination, and susceptibility to insects and birds. To overcome these impacts, advanced drying technologies were developed and one that kind is drying in a closed chamber by supplying hot air. The solar dryer is preferred over other conventional dryers due to more energy consumption. It can be classified based on the airflow and the solar radiation received by the product. And the main three categories are direct, indirect, and mixed mode of drying. In direct solar drying, the products are exposed to solar radiation through a transparent cover. In the indirect modes of solar drying, the product is not directly exposed to solar radiation. For this, the hot air required for drying is provided through an air heater. In some instances, a solar dryer combines both direct and indirect mode of drying as a single system and that type of drying is known as a mixed mode solar dryer. In this, the product receives heat from the indirect sources (air heater) and the radiation falls through the transparent cover.

Andrographis paniculata also known as Kalmegh or “King of Bitters” is used in traditional medicines[3]. This herb helps to treat chronic and infectious diseases. The aerial parts of the plant (leaves and stems) are used to extract the active phytochemicals and thus used for its medicinal importance.

Srisittipokakun N, Kirdsiri K et.al.,(2012)[4]conducted solar drying experiments of *Andrographis paniculata* (AP) in Nakhon Pathom, Thailand using a newly designed parabolic-shaped solar tunnel dryer which consist of a flat-plate solar collector and a drying tunnel. The total area of the collector was 108 m². The performance of the dryer was investigated by drying 100 kg of *Andrographis paniculata*. The dryer used the leaves of 75% (wb) moisture content, and they dried for 2-3 days to reach safe moisture level of 7% (wb) with a drying air temperature in the range of 35 - 75°C which depends on the weather conditions. The products being dried in the dryer got the heat from both the sunlight and the collectors.

Md Azharul Karim et.al.,(2005)[5] developed a v-groove solar air collector for drying applications and their experimental results indicated that, it is 12% more efficient compared to a flat plate collector. Considering the efficiency of the collector and the outlet temperature, author recommended a flow rate of 0.035 kg/m²s for most drying uses.

Shahrbanou Shamekhi-Amiri et.al., (2018)[6] investigated the thin-layer drying behavior of lemon balm leaves in an indirect-mode solar dryer with forced convection. To enhance the heat gain of the air heater, a counter- flow double-pass packed bed wire mesh layer was configured. The outlet temperature of the collector varied from 38°C to 68°C. While increasing the flow rate from 0.006125m³/s to 0.01734m³/s, it improved the collector thermal efficiency by ~ 20%; further increasing the flow rate to 0.034378m³/s had an undesirable effect on the collector efficiency.

El-Sebaai A A, and Shalaby S M, (2013)[7]designed and fabricated an indirect-mode forced convection solar dryer using double pass v-corrugated plate solar air heater and the thermal performance of the solar dryer was experimentally investigated. Drying experiments were performed for thymus and mint at an initial temperature of 29°C and the final moisture contents for thymus and mint were reached after 34 and 5 hr, respectively. The maximum temperature of the thymus and mint was 51°C and 47°C, respectively.

Hee, Y.Y. and Chong, G.H (2015)[8]Hempedu bumi (*Andrographis paniculata*, AP), also noted as king of bitters. It is commonly found in Asian countries and used for medicinal purposes. In this study, the drying behaviour of AP was investigated at a different temperature of 40, 50, and 60°C with vacuum pressures of 10 and 30 kPa. From the results, it is revealed that the drying time is significantly altered by temperature and pressure. The moisture diffusion's effective diffusivity and active energy were 10-13 m²/s and 33.4 kJ/mol, respectively.

The work on solar drying of *Andrographis paniculata* is less and to improve this, a double collector solar dryer with V-Corrugated absorber plate was developed. The performance of the dryer was experimentally evaluated and presented.

MATERIALS AND METHOD

Experimental Setup

A double collector solar device was designed for Chennai, Tamil Nadu, (13.0827°N, 80.2707°E). This device has two collectors (primary and secondary collectors),that is made up of mild steel. The primary collector is a single pass air- heater with a top glass cover of 5 mm thick and has a V-Corrugated absorber plate with an area of 1 x 2 m and inclined based on the latitude of the region, i.e., 13degrees. The absorber plate fabricated was using aluminium. The outlet of the solar air heater was attached to the bottom of the drying chamber. The chamber consisted of three trays where the products to be dried are kept. And the chamber was insulated by glass wool to avoid heat losses. The dimensions of the drying chamber are 0.530 x 0.355 x 0.9m.

The performance of the solar dryer is based on the heat transfer characteristics of the air heater. The heat transfer characteristics is relied on the absorber plate.

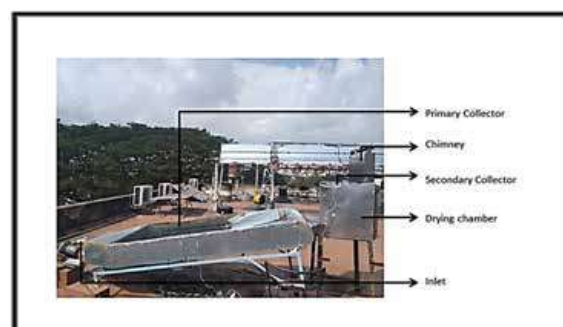


Fig. 1: Experiment setup of Double Collector Solar Dryer



Thus, the area of the absorber plate of the primary collector was increased with the limited space by using V-Corrugated absorber plate ($\theta=60^\circ$). According to this concept, the heated air from the outlet of the primary collector enters the bottom of the drying chamber and moves to the successive trays of the chamber. While doing so, it removes the water content from the products and at the same time the hot air that moves to the further trays will have reduced temperature and this causes uneven drying. To avoid so, the roof of the drying chamber was conceived with a secondary collector. This absorbs the radiation through a glass cover and transfers the heat to the metal plate of the collector. Thus, it indirectly transfers the heat to the products and by this additional heat, the temperature of the chamber can be maintained in all the trays and therefore even drying can be obtained.

Product Characteristics

The product used in this study is the *Andrographis paniculata*, a medicinal herb. This plant is widely found in Asian countries and it is used to cure many infectious and chronic diseases. For the experiment, fresh leaves of about 189g were used for each test. In the morning, the leaves were loaded manually in the trays and during the experiment the leaves were weighed at an interval of time and the temperature in each tray was measured by Thermocouple Type T (range -270 to 370°C).

ANALYSIS

Thermal performance of solar collector

The useful heat gained by the collector is given by,

$$Q_u = m \dot{\square} \times C_p \times \Delta T \quad (1)$$

Where Q_u is useful heat gain (W), $\dot{\square}$ is mass flow rate (kg/s), C_p is specific heat capacity of air (J/kgK), and ΔT is temperature difference (K).

The collector efficiency can be calculated by using following equation,

$$\eta = \frac{Q_u}{I \times A} \quad (2)$$

Where η is the efficiency of the collector, I is solar insolation (W/m^2), and A is the area of the collector (m^2).

B. Drying curves

Moisture content on the wet basis which is the weight of water per unit initial weight of matter is given by,

$$\text{MC} = \frac{w_i - w_f}{w_i} \times 100 \quad (3)$$

Where MC is moisture content on wet basis, w_i is the initial weight of the product (kg), w_f is the final weight of the product (kg).

Drying Characteristics are given in terms of weight at regular intervals of time and drying rate at an interval of time. As mass remains conserved, the drying rate is given by the difference in weight at regular interval of time. Mathematically, drying rate shall be written as,

$$\text{DR} = \frac{w_t - w_{t+\Delta t}}{\Delta t} \quad (4)$$

Where DR is the drying rate (g/min), w_t is the weight of the product at time, t (kg), $w_{t+\Delta t}$ is the weight at regular interval of time (kg), and Δt is the time interval (min).

RESULTS AND DISCUSSION

The experiment was conducted at Anna University, Chennai, Tamil Nadu during the month of February and March of the year 2020 and the drying characteristics of *Andrographis paniculata* (Nilavembu) was investigated. The thermal performance of the collector and the drying characteristics such as moisture content and drying rate of different samples were calculated.

Temperature Profile of the Solar Collector

The temperature profile of the solar collector such as the inlet, outlet and the drying temperature was plotted with respect to the solar radiation is shown in **Fig. 2**. As the solar radiation increases the temperature increases and once the radiation falls the temperature tend to decrease. From the **Fig. 2** it has been observed that the outlet and drying temperature are almost maintain the same range and thus temperature loss is minimum, therefore the drying rate can be increased. The average temperature difference between the inlet and the outlet was 16.3°C . The maximum drying temperature achieved in the drying chamber was

plotted with respect to the solar radiation is shown in **Fig. 2**. As the solar radiation increases the temperature increases and once the radiation falls the temperature tend to decrease. From the **Fig. 2** it has been observed that the outlet and drying temperature are almost maintain the same range and thus temperature loss is minimum, therefore the drying rate can be increased. The average temperature difference between the inlet and the outlet was 16.3°C . The maximum drying temperature achieved in the drying chamber was 64°C at 1079 W/m^2 .

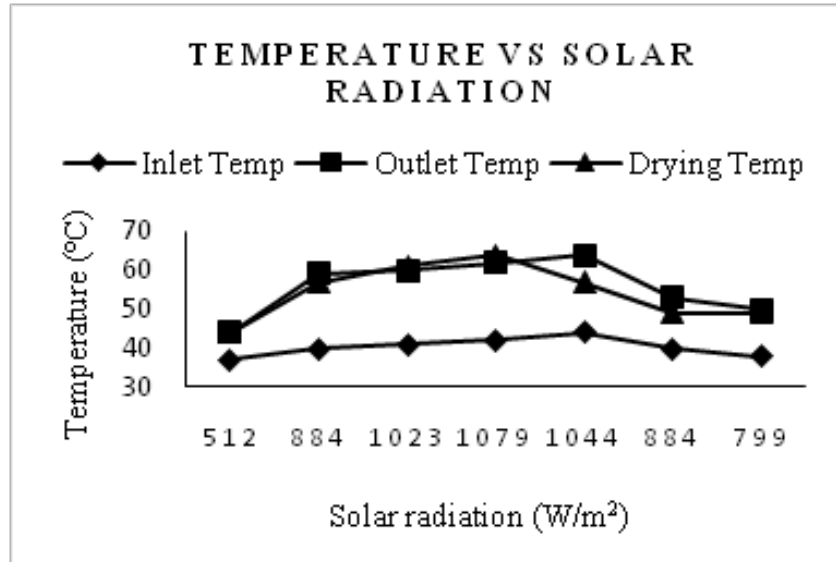


Fig. 2: Variation of Temperature vs Solar Radiation

The temperature profile of the drying chamber was plotted in **Fig. 3**. From the **Fig. 3**, T_1 , T_2 , and T_3 represents the lower, middle, and upper tray of the drying chamber and T_{in} indicates the inlet temperature. Initially the temperature of the three trays were varied and latter, the temperature was almost remained same in the trays due the addition of the secondary collector and this has compensated the temperature loss in the chamber. The highest temperature was obtained in the lower tray because of the primary collector effect.

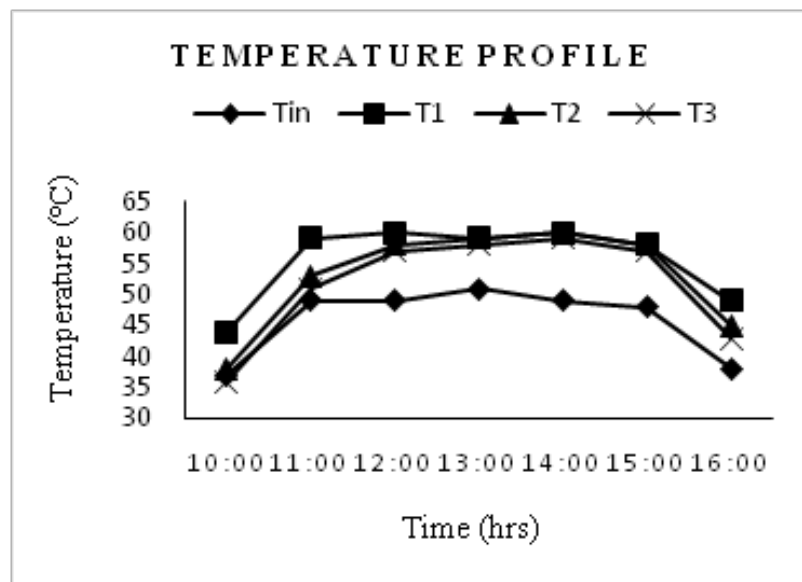


Fig. 3: Temperature profile of the drying chamber

Drying Characteristics

The fresh *Andrographis paniculata* leaves of about 189 g was placed in the trays of drying chamber. The reduction in the weight was observed at a regular interval of time during the day. The weight of leaves in the chamber was reduced to 21g in 3 hours during this solar drying. The initial moisture content of the leaves was 78.12% and that of the final moisture content was 11.11 %.



Fig. 4: Fresh Vs Dried *Andrographis paniculata* leaves

The variation of drying rate with respect to time was shown in the Fig. 5. Initially, the rate of drying was faster due to the rapid fall of moisture content and this starts to decrease as the sample loss more moisture and thus the drying rate was slower at the final state. The average drying rate of *Andrographis paniculata* was 1.55 g/min and that of maximum drying rate was 2.5 g/min at the temperature of 52°C.

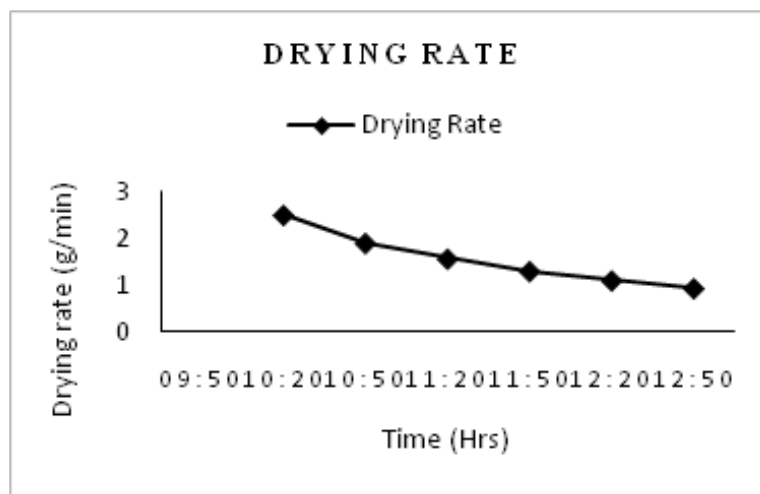


Fig. 5: Variation of Drying Rate Versus time for *Andrographis paniculata* leaves

CONCLUSION

Drying is an ancient technique that has been used to preserve agricultural products. The solar drying system utilizes solar energy to heat the air and to dry any food substance, which is not only beneficial, but also it reduces the wastage of agricultural products and helps them in preservation. It also makes the transportation of such dried products easier and promotes the health and welfare of the people. During this study, the fabrication of a double collector solar dryer was done based on the calculated geometry. The main aim of the project was to develop a solar dryer to reduce the drying time and improve the efficiency of the solar dryer.

The following are the deliberations made by conducting the performance evaluation of the double collector solar dryer with V-corrugated absorber plate:



- Efficiency of the double collector solar dryer with V-Corrugated absorber plate was 38.23%
- The addition of secondary collector on the roof of the drying chamber, improved the drying process and maintained the even drying in the chamber.
- Further the addition of secondary collector on the roof of the drying chamber reduced the space required for drying and hence with limited space more drying process can be carried out.
- The average outlet temperature and the drying air temperature obtained was 56.8°C and 55°C, respectively.
- The sample of fresh *Andrographis paniculata* leaves of about 189 g were placed in the drying chamber and it reduced to a weight of 21g in 3 hours with an average drying rate of 1.55 g/min. and thus the drying rate was improved, and the time taken for drying also reduced.
- This type of dryer is more efficient than that of the normal flat plate collector solar dryer.

REFERENCES

1. <https://www.financialexpress.com/economy/india-wastes-up-to-16-of-its-agricultural-produce-fruits-vegetables-squandered-the-most/1661671/>
2. A. S. Mujumdar and C. L. Law, "Drying Technology: Trends and Applications in Postharvest Processing," *Food Bioprocess Technol.*, vol. 3, no. 6, pp. 843–852, 2010, doi: 10.1007/s11947-010-0353-1.
3. S. K. Mishra, N. S. Sangwan, and R. S. Sangwan, "Phcog Rev. : Plant Review *Andrographis paniculata* (Kalmegh): A Review," *Rev. Lit. Arts Am.*, vol. 1, no. 2, pp. 283–298, 2007.
4. N. Srisittipokakun, K. Kirdsiri, and J. Kaewkhao, "Solar drying of *Andrographis paniculata* using a parabolicshaped solar tunnel dryer," *Procedia Eng.*, vol. 32, no. February 2016, pp. 839–846, 2012, doi: 10.1016/j.proeng.2012.02.021.
5. M. A. Karim and M. N. A. Hawlader, "Performance evaluation of a v-groove solar air collector for drying applications," *Appl. Therm. Eng.*, vol. 26, no. 1, pp. 121–130, 2006, doi: 10.1016/j.applthermaleng.2005.03.017.
6. S. Shamekhi-Amiri, T. B. Gorji, M. Gorji-Bandpy, and M. Jahanshahi, "Drying behaviour of lemon balm leaves in an indirect double-pass packed bed forced convection solar dryer system," *Case Stud. Therm. Eng.*, vol. 12, no. August, pp. 677–686, 2018, doi: 10.1016/j.csite.2018.08.007.
7. A. A. El-Sebaili and S. M. Shalaby, "Experimental investigation of an indirect-mode forced convection solar dryer for drying thymus and mint," *Energy Convers. Manag.*, vol. 74, pp. 109–116, 2013, doi: 10.1016/j.enconman.2013.05.006.
8. Y. Y. Hee and G. H. Chong, "Drying behaviour of *Andrographis paniculata* in vacuum drying," *Int. Food Res. J.*, vol. 22, no. 1, pp. 393–397, 2015.



Performance Study of Manually Operated Drum Seeder for Sowing of Jute

R K Naik, S K Jha, S Sarkar, A K Ghorai

ICAR-Central Research Institute for Jute and Allied Fibres, Barrackpore,
Kolkata-700121, West Bengal

✉ ranjanagrieng@gmail.com

ABSTRACT

Jute is one of the important cash crops grown in India by small and marginal farmers of Eastern and North Eastern states. Among several natural fibre crops, jute comes next to cotton in use and trade. Sowing of jute is the most important farm operation for getting healthy and dieses less crop for higher fibre production. Based on spatial characteristics of jute seed and considering the social and economic aspects of jute farming community, a light weight manually operated drum seeder was designed and developed. The transparent drums are having 12 nos. of seed metering orifices or holes at equal interval of 30.0 mm to achieve plant to plant distance of 50-70 mm and row spacing of 250 mm as per the agronomic recommendation. From the experiments, it was found that the seed requirement was 2.8-3.0 kg/ha against 6-7 kg/ha in broadcast sowing. The effective field capacity at mean speed of 1.6-2.0 km/h was 0.18-2.0 ha/h i.e. about 6 hours per hectare with field efficiency of 90-95 per cent. The sowing of jute with drum seeder followed by mechanical weed control using cycle weeder/ nail weeder showed 60 % reduction in manual labour requirement compared to broadcast sowing with increase in fibre yield of 20-22 per cent.

Keywords : Jute; sowing; drum seeder; performance evaluation; effective field capacity; field efficiency.

INTRODUCTION

Jute is an important environment friendly fibre producing crop and its fibre is the second most important textile fibre next to cotton [1]. It provides direct or indirect employment to small and marginal farm families and also jute industry workers. The total area under jute cultivation in India is about 8 lakh hectare and it is mainly grown as a rainfed crop followed by paddy. Due to suitability of climate and soil, the crop is cultivated mainly by small and marginal farmers of Eastern states of India. Method of sowing is the most important farm operation in jute farming for getting healthy and dieses less crop for higher fibre production. The crop yield is affected by type and variety of seed, their emergence and plant density in the field [2]. Jute is mostly sown at the advent of pre-monsoon showers in the month of March and April. To utilize the limited soil moisture availability due to summer rainfall, the farmers follow mostly broadcast method of sowing. In practice farmers use a higher seed rate (6-7 kg/ha) than recommended seed rate due to small size seeds. The weeding and plant protection measures are major problem due to scattered and higher plant density [3]. To maintain optimum plant population in the field, excess 75-80% of the emergent seedlings are removed during weeding and thinning operation at 21-45 DAE. About 15 % of total energy of 10904.1 MJ/ha and about 30-35 % of total cost of production is consumed in the weeding and thinning operation. Further, due to uneven plant population and higher plant density, the overall fibre yield reduces about 10-15 per cent. The line sowing of small seeds using seed drill saves precious seed, ensures depth of placement, germination and reduced cost of sowing and weeding [4]. The seed drills available commercially for small seeds, use sophisticated pneumatic metering mechanism and are costly [5]. Farmers being poor with minimum land holding do not permit them to have seed drills. They are therefore bound to follow the traditional practice of broadcast sowing and face difficulty in intercultural operations and overall management of their crop. As the yield rate is low, farmers derive marginal benefit out of their produce [9]. Considering the socio-economic condition, nature of land holding of farmers, a low cost and light weight manually operated four row drum seeder for sowing jute and other small seeded up-land crops has been designed and developed at ICAR-Central Research Institute for Jute and Allied Fibres (ICAR-CRIJAF), Barrackpore, Kolkata. The developed implement is able to reduce drudgery in seed sowing operation and reduction in cost of cultivation with higher productivity. The present study was undertaken to evaluate the seed pattern characteristics of seed rate deviation, seed distribution and economics of developed manual drum seeder.

MATERIALS AND METHODS

The physical and morphological characteristics of the promising variety, JRO-204 (Suren) jute seed of were measured in the laboratory. Using these seed characters and other agronomic information, shape and capacity of seed drum, no. of seed

dispensing orifices of metering mechanism and distance between metering orifices were determined [6]. The wall thickness of seed drum was determined by the bulk density of the seed. The shape and size of seed dispensing orifice were determined by trial and error method taking seed rate into account for obtaining plant population.

The average length, breadth and thickness were found to be 2.07 mm, 1.20 mm and 1.10 mm, respectively. The test weight, bulk density and angle of repose were measured to be 1.92 g, 0.74 g/cc and 27.25 degree, respectively.

Description of the drum seeder

The manually operated drum seeder mainly consists of seed drum-cum-dispenser, main shaft, ground-cum-transportation wheels, frame, furrow openers and covering device “**Fig. 1**”. The conical frustum shaped seed drum is fabricated with light weight, durable and transparent material for visibility of seed. Drilling of seed on the furrow happens during the movement of implement through the seed dispensing orifices on the seed drum at equal interval of 30.0 mm to achieve desired plant to plant distance of 30-50 mm in the field [7]. The hoe type furrow openers are present ahead of seed box at equal spacing of 250 mm [8]. The bigger size ground wheels of ϕ 304.8 mm fabricated with mild steel flat with 12 nos. pegs are used for easy movement of implement without slippage on tilled soil. A single chain made of mild steel is attached besides the seed drums for covering the drilled seeds on the furrow. The implement consists of a compacted and height adjustable handle. It can be adjusted according to the height of operator for easy operation and reducing the drudgery during operation. The drive shaft is attached with two sealed bearings for easy movement during operation. The technical specifications of the implement have been presented in **Table 1**.



Fig. 1: Drum seeder for jute

Laboratory test of drum seeder

The drum seeder was calibrated in the laboratory as per BIS test code for seed rate. Seeding uniformity was tested on a bed of 5 m x 1 m size prepared in the field with a thin white cloth lying on the top. A thin layer of grease was applied on the cloth to prevent displacement of seeds from line while falling from seed box. The drum seeder was operated on the prepared seed bed using plain ground wheels of same dimensions like spiked ground wheel at walking speed of 1.6-2 km/h. Number of seeds per meter of bed was counted and uniformity of seed distribution along the line was calculated using “(1)”.

$$S_e = 100 (1 - \frac{Y}{D}) \quad (1)$$

Where,

S_e = Seed distribution efficiency of drum seeder;

Y = Average numerical deviation of number of seeds per meter from average number of seeds per meter length;

D = Average number of seeds per meter length.

Table 1: Technical specifications of drum seeder

Parameter	Values
Overall dimensions	
Length	1046 mm
Width	1000 mm



Height	1000 mm
Weight	14 kg
Ground drive details	
No. of wheels	Two (m.s. flat)
Effective diameter	304.8 mm
Lug height	45 mm
Seed metering	Gravity fall
Drum capacity	Vol. 0.001 m ³
Row spacing	25cm
No. of rows	4
Suitability of crop	Jute, mustard and sesame
Seed covering mechanism	Chain type (L=1680 mm)

Field performance test of drum seeder

The field experiment for sowing of jute seed (JRO-204) using manual drum seeder was conducted in the ICAR-CRIJAF experimental field as per BIS test code. The soil at the experimental site was sandy loam having sand, silt and clay in the ratio of 74.8, 13.2 and 11.8 per cent, respectively. The tests were replicated thrice in plot size of 20 m x 10 m. The field observation like speed of operation, depth of seed placement, effective field capacity and draft were recorded and mean observations were taken. A direct reading type spring dynamometer was used to measure the pull of drum seeder. Draft of the drum seeder was computed taking angle of pull. The power required to pull the implement was calculated using “(2)”.

$$\text{Horse power (hp)} = \frac{D \times S}{75} \quad (2)$$

Where,

D = Draft of the implement, kg;

S = Speed of operation, m/s.

Labour requirement, field efficiency and power requirement were computed from the observed field data as per BIS standard. The seed pattern characteristics were observed after germination of the seed under field condition and compared with broadcast sowing.

RESULTS AND DISCUSSION

Laboratory test of drum seeder

The calibration of the drum seeder was carried out in laboratory for jute. There was variation in seed rate at different seed drum conditions i.e. full filled (400 g), $\frac{3}{4}$ filled (300 g) and $\frac{1}{2}$ filled (200 g) due to unequal size of seeds. The minimum 2.61 kg/ha and maximum seed rate of 4.37 kg/ha was observed with full filled and $\frac{1}{2}$ filled seed drum. The optimum seed rate of 3.48 kg/ha was observed at $\frac{3}{4}$ filled seed drum, which was significantly lower than the recommended seed rate of 6-7 kg/ha for broadcast sowing. Thus, around 50 per cent reduced seed rate may help in reducing the cost of cultivation in terms reduction in labour cost for weeding and thinning operations.

No mechanical damage was observed due to absence of mechanical metering mechanism and gravity flow of seeds from seed drum. Minimum and maximum number of seeds dropped per meter was 55 and 73. The seed distribution efficiency varied from 60 to 70 per cent and found decreased with increase in speed of operation.

Field performance test of drum seeder

The field performance of the drum seeder was carried out at the ICAR-CRIJAF Farm, Barrackpore “Fig 2” and results are presented in Table 3. During the test the mean actual seed rate was found to be 2.8-3.0 kg/ha. The lower seed rate obtained may be due to skidding of ground wheel during operating in the field. The depth of seed placement was varied 10 mm to 15 mm. The operational speed of implement in the field varied from 1.6 -2.0 km/h. Effective field capacity (EFC) of drum seeder varied from 0.18 to 0.20 ha/h, thus one hectare could be sown in 5-6 hours only. Average field efficiency was found to be 90-95

per cent. Draft of the implement was calculated taking height of the handle from ground during the operation. The angle of pull was found to be 39.350. The draft was varied from 72.71 N to 95.35 N with an average of 85.02 N. The power requirement was varied from 37.3 W to 46.56 W with an average of 41.93 W, which could be easily pulled by a man or women for 2-3 hours continuously. The overall performance of the manually operated drum seeder was found satisfactory.



Fig. 2: Field performance test of drum seeder

The seed pattern characteristics were observed after germination of seeds under field condition. The average number of plants per hill was found to be 1-2. The plant growth characters like plant height and basal diameter were compared with broadcast method of sowing and depicted in “**Fig. 3**”. The jute plants were harvested at 120 DAS and retted in water for fibre extraction. The fibre yield of about 28.6 q/ha was obtained in line sowing; against yield of 22.3 q/ha in broadcast method of sowing.

Table 3: Field performance of drum seeder

Parameters	Observed values
Crop	Jute
Variety	JRO-204 (Suren)
Type of soil	Sandy loam
Size of plot	20m x 10m
Soil moisture, % (db)	22.55
Mean weight dia. of clods, mm	0.35
Speed of operation, km/h	1.6-2.0
Coverage width, m	1.0
Depth of seed placement, mm	10-15
Seed rate observed, kg/ha	2.8-3.0
Average draft, N	85.02
Power requirement, W	41.93
Effective field capacity, ha/h	0.18-2.0
Field efficiency, %	90-95
Seed distribution efficiency, %	60-70
Average number of plants/hill	1-2
Seed pattern observed	Drilling
Fibre yield, q/ha	28.6

CONCLUSION

Sowing of small seeds like jute in rows is very much desirable to save seed, to reduce the cost cultivation by cutting the cost involvement in weeding and thinning. The developed manual drum seeder for jute and other small seeded crops distributed seeds uniformly along the rows. Mechanical intercultural operations in line sown crop using cycle weeder/ nail weeder showed 60 % reduction in manual labour requirement and cost for weeding and thinning by more than 50 per cent. Due to evenly and healthy plant population, the overall yield increases fibre yield about 20-22 per cent.

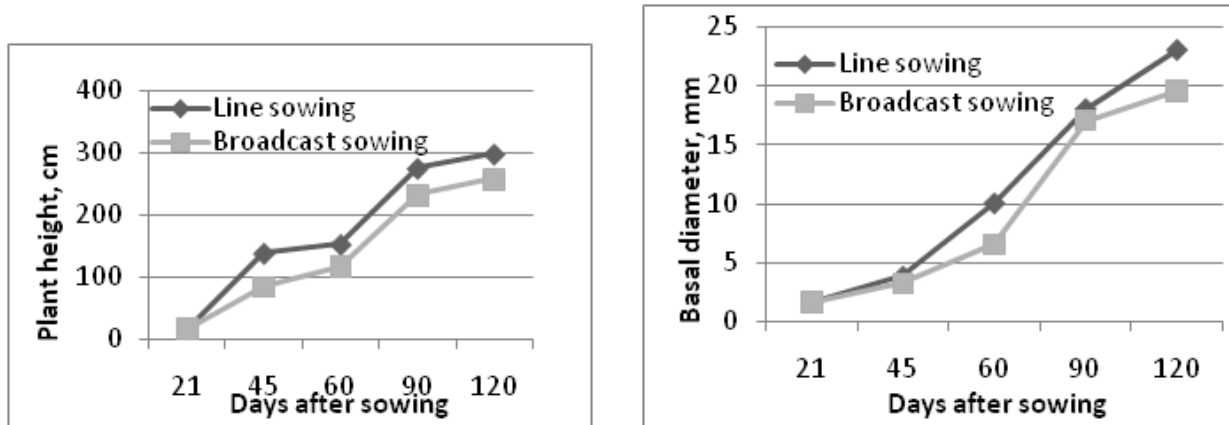


Fig. 3: Comparison between line sowing and broadcast sowing

REFERENCES

1. D.L. Smith and C. Hamel, "Crop yield physiology and processes", Springer Verlag Berlin Heidelberg, pp. 271-286, 1999.
2. T.P Ojha and A.M. Michel, Principles of Agricultural Engineering, Vol. 1, Jain Brothers, New Delhi, 1987.
3. J. Herbek and L. Murdock, "Planting and drill calibration", A comprehensive Guide to Wheat Management in Kentucky, Vol. 4, pp. 20-24, 2009.
4. N.S. Chandel, V.K. Tewari and K.P. Vidhu, "Engineering innovation in developing rural load carrier operated jute seed drill for farm workers", African J. of Agric. Res., Vol.9, No.8, pp. 797-805, 2014.
5. M.K. Ghosal and S.C. Pradhan, "Performance study of a low cost manually operated cup feed metering seed drill for sowing green gram", Agril. Engg. Today, Vol. 37, No. 1, pp. 37-41, 2013
6. M.D. Goswami, "A laboratory set up for testing planters and seed drills", J of Agril. Engg., Vol. 38, No. 4, pp. 69-72, 2001.
7. S.Rahman, M.R.Khan, "Effect of plant characteristics of jute varieties on incidence of pests in West Bengal, India", Archives of Phytopathol. Plant Protect. Vol.45, No.5, pp.608-619, 2012.
8. S.M.Masum, M.H. Ali, M.S. Islam, S. Sultana, "Influence of plant spacing and post emergence herbicide on the yield of white jute (*Corchorus capsularis*)", Int. J. Sustain. Agric. Vol.3, No. 3, pp. 82-87, 2001.
9. V.B. Shambhu and A.K. Thakur, "Functional performance of a manually operated seed drill for jute", Int. J. urr. Microbiol. App.Sci., Vol. 7, No. 6, pp.52-59, 2018.



Development of Track Width and Ground Clearance Enhancing Platform and Matching Implements for Low Horse Power Tractor

B Sanjeeva Reddy, Ashish S Dhimate, I Srinivas, R V Adake, V R Mallikarjuna, G Karthik

ICAR-Central Research Institute for Dryland Agriculture, Hyderabad, Telangana

✉ Bs.Reddy@icar.gov.in, ✉ ashish.dhimate@icar.gov.in

ABSTRACT

A high ground clearance platform for low horse power tractor with matching weeding and spraying implements was developed. This new development will increase effective use of tractor for weeding and spraying operations in tall growing crops like maize, castor, red gram, cotton, etc. The developed platform basically consists of three components (i) Front wheel axle (ii) Rear drive wheel axle and (iii) Reworked steering set system for enhanced track width. The developed prototype of high clearance platform fitted to a mini tractor of 18.5 hp. The matching rotary weeder developed for high clearance platform is tested in castor and pigeon pea at two different speeds and two growth stages. The weeding efficiency, plant damage and fuel consumption were determined. The developed boom sprayer unit basically consists (i) Base frame to give support / fix various components (ii) Pump with manifold for flow control and pressure regulation (50 lpm & 30kg /cm² rating) (iii) Boom with height adjustable frame work and (iv) High pressure hose pipes. The standard nozzles on the boom were fitted with spacing adjustable provision to use for different types of rainfed crops. The weeding efficiency of rotary machine varied 74 to 86.8% for castor and 78.98 to 85.43% for pigeon pea, respectively at different speed and growth stage. The boom sprayer was operated in cotton crop and pigeon pea. The operator can steer the tractor comfortably and sprayer worked satisfactorily. The field capacity of the boom sprayer ranged from 0.77 to 1.15 ha/h. The newly developed implements showed significant advantage in monetary terms when compared with traditional practices.

Keywords : High clearance platform, low hp tractor; weeding; spraying..

INTRODUCTION

In Indian farming system, the weed control and intercultural operations used to taken care by a well set system of traditional sowing implements and matching intercultural tools combinations till recent past. But, due to introduction of new crop varieties, high yielding hybrids, farmers focus shifting more towards commercial crops. With varying crop row spaces in different soils and agro-climatic conditions, the traditional set of tools not able to meet the present days crop cultivation requirements.

Though mechanization and use of power operated equipment is picked up since last two decades, it is confined to mostly certain crops and specific operations in dryland system. For ex. in maize seeding and cobs threshing combine; in red gram sowing and grain removal using multicrop thresher. The cotton crop though present in considerable acreage in dryland system, one of the least mechanized crop in Telangana and Andhra Pradesh.

In addition to these factors, the relay cropping practice which is confined to irrigated crops like wheat in cotton [1], also slowly picking up in rainfed system due to climate variability and effectively utilizing the late rainfalls and to compensate kharif season crop loss if any occurred. The crops like gram, horse gram, cowpea are relay cropped in long duration crops red gram and cotton. Such practices enhance the overall farm income of dryland system besides generating considerable fodder biomass for livestock. The major portion of farm holders is small and marginal category in the country compounded by resource poorness in drylands. Hence, the government departments are promoting low horse power or mini tractors to decrease initial investment on power source and matching machinery. However, availability of matching implements and machinery is a problem for lower horse power tractors.

To address some of these problems, ICAR - Central Research Institute for Dryland Agriculture (CRIDA), Hyderabad has developed various matching implements such as cultivator, seed planter, Slasher etc. to name few. In spite of these efforts, utility of farm tractors are limited in dryland crop production operations like weeding and plant protection operations due constraints in crop row configurations even in wide row spaced crops like cotton, castor and red gram. So, to increase the

utility of low horse power tractor in these operations, development of high under ground clearance and enhanced track width platform for mini tractors in the range of 18 - 22 horse power was thought off. This gives an extend service opportunity for tractors with crop based specific operational capability with matching implements and machinery. To address these problems, ICAR - CRIDA developed a prototype of high under ground clearance and track width platform for low hp tractors in the range of 18 - 22 horse power to suite to red gram and cotton crops.

MATERIAL AND METHODS

The high ground clearance platform and matching implements i.e. rotary weeder and boom sprayer for low horse power tractor were developed to address the present constraints as enumerated in instruction part of these paper, in tall growing crops like cotton, pigeon pea, maize.

Development of prototype of high under ground clearance and track width platform for mini tractors

The newly developed platform basically consists of three components (i) Front wheel axle (ii) Rear drive wheel axle and (iii) Reworked steering set system for enhanced track width **Fig. 1**. The reworked-out axle length selected such a way that, the tyres centre to centre distance was 166 cm and ground clearance 90 cm. In setting the front axle, all original features were retained while replacing axle spindle, spindle housing and steering set. The rear axle length was extended using additional step cut spindle lengths at top and lower portions. The extension spindles of rear axle were properly secured in position with the support of appropriate length bushes and pedestal bearings. The rear axle extension portions were fitted in position using a frame made of 50X5mm mild steel angle iron. The power transmission was provided from top rear drive axle to lower tyre axle using sprocket and chain system. While designing the above three basic mechanisms, all commercially available readymade parts and few reworked out components were used to reduce fabrication costs and interchange ability from one model to other model of tractor of same make within the selected horse power range. To cover the rear and side portion of the rotor shaft assembly half portion of the blades, an inverted D shape supported sheet metal structure was fabricated and fitted to the rotary weeder machine. The overall dimensions of rotary weeder are 1000 mm length, 800mm width and 120 mm height. The brief specification of high clearance platform for low horse tractor given in **Table 1**.

Table 1: Brief specification of high ground clearance platform

S No	Particulars	Specifications
1	Tractor Manufacturer	Mitsubishi Shakti
2	Make	MT 180D
3	Power, hp	18.5
4	Rear tyre track width, cm	166
5	Front tyre track width, cm	151
6	Total weight, kg	980
7	Ground clearance, cm	90
8	Turning radius, m (without brake)	5.2
9	Overall dimension, L*W*H, cm	250*199*197
10	Safety aspects	provided



Fig. 1: CAD model of high ground clearance platform for mini tractor



Fig. 2: High ground clearance platform for mini tractor

Development of a prototype of rotary weeding tool for interrow weeding

To utilize the high clearance platform effectively a rotary weeder was fabricated and attached to the power unit (**Fig 3**).



Fig. 3: Weeding operation in pigeon pea crop

The rotary weeder matching to high clearance platform consists of a main frame with hitch mast, gear box housing with power transmission, rotor shaft assembly with soil working tools. The rotary weeder was developed by considering the crop row geometry and machine parameters. The machine main frame consists of a 760 x 400mm rectangular shaped tubular frame made from two numbers of hollow square bars of 760mm length which are set from a 50x50x5mm M.S. angular iron welded bar. To give enough strength and rigidity to the frame 5mm wall thick and 50x50mm size tubular rectangular bar support pieces of length 30cm were welded at the centre portion of the frame. The frame thus fabricated was provided with a standard three point hitch mast. A proper seating arrangement at the middle portion of frame provided and a gear box fitted. A 35 mm output shaft that runs perpendicular to the input shaft of gear box was provided with a heavy-duty sprocket. Power to the soil working rotor blades shaft was drawn through sprocket and chain arrangement.

The rotor shaft assembly basically consists of a solid shaft, working blades, sprockets for power transmission and end bearing blocks fitted over the mounting end support brackets. The dimensions of the rotor blades and shafts were determined on the basis of speed of operation, width, depth of cut during operation and soil conditions. The overall dimensions of rotary weeder are 1000 mm length, 800mm width and 120 mm height. The L shaped blade gives better performance index as compare to other, therefore L shape blade was selected [2]. The brief specification of rotary weeder given in **Table 2**.

Table 2: Specification of developed rotary weeder

S No	Particulars	Specifications
1	Length x Width x Height (mm)	1000X800X120
2	Number of flanges per unit	4
3	Number of blades per flange	3
4	Total blade	12
5	Theoretical width of cut, mm	760



6	Diameter of rotor, mm	200
7	Shape of blade	L
8	Outer width of cover of rotor assembly, mm	76
9	Speed ratio (PTO to rotor shaft)	1.8
10	Safety aspects	provided

Performance parameter for rotary weeder

The performance of high clearance tractor operated rotary weeder tested in castor and pigeon pea crop. The weeder was tested for weeding efficiency, plant damage and fuel consumption at two forward speed, one blade shape and two growth stages i.e. Days After Sowing (DAS) as per standard test procedure [2], [3].

Development of a prototype of boom sprayer for high ground clearance platform

Among cotton growing farmers of the country, nearly 96% use Bollgard (BG)-II Bt in various states. India is the only Bt cotton-growing country in the world facing the problem of resistance of pink bollworm (PBW) infestation to the toxins produced by Bollgard II. The target pests becoming resistant to Bt cotton has now emerged as a new problem in parts of major cotton growing states such as Gujarat, Andhra Pradesh and Maharashtra. The available information suggests the need for proactive six-pronged insect resistance management (IRM) on Bt cotton fields. Otherwise the development of insect resistance to Bt cotton can significantly diminish the returns and benefits that are currently being derived from the technology. In fact, Integrated Pest Management (IPM) practices for Bt cotton is equally important, in which spraying equipment play a major role. Keeping this point in view, the boom sprayer matching to high clearance fitment attached tractor was developed.

The developed boom sprayer unit basically consists (i) Base frame to give support / fix various components (ii) Pump with manifold for flow control and pressure regulation (50 lpm & 30kg.cm⁻³ rating) (iii) boom with height adjustable frame work and (iv) high pressure hose pipes. The pump gets the required power from tractor PTO. The nozzles on the boom were fitted with spacing adjustable provision to use for different types of rainfed crops. In fabrication of the boom sprayer all the standard commercially available components were procured and reworked for tight fitments to avoid fluid leakages. The row crop sprayer was tested in the laboratory for 4-5 hours for inspection of discharge and proper working of all functional components before field trials in the cotton crop. The preliminary adjustments were made in the sprayer to avoid air lock and liquid leakage from the pipe lines. The brief specification of developed boom sprayer for high clearance tractor given **Table 3**.

Table 3: Specification of developed boom sprayer

S. No	Particulars	Specifications
1	Type of boom	Foldable
2	No. of nozzles	8
3	Nozzle spacing, mm	90, adjustable
4	Type of nozzles	Solid cone type
5	Type of pump	Piston type
6	Pump pressure, kg/cm ²	10-30
7	Type of pump drive	V-belt and pulley
8	Tank capacity, litres	150
9	Boom height, mm	Adjustable
10	Ground clearance, mm	900

Performance parameter for boom sprayer

The performance of high clearance tractor mounted boom sprayer tested in cotton and pigeon pea field (**Figs. 4, 5**). The lab testing of sprayer nozzle was conducted with nozzle discharge, nozzle spray angle, swath width at different pump pressure (**Table 4**). The actual field efficiency, theoretical field efficiency and field efficiency were calculated as per standard procedure [3].



Fig. 4: Spraying operation in cotton crop



Fig. 5: Spraying operation in pigeon pea

Table 4: Dependent and independent parameter

S. No	Independent parameter	Levels	Dependent parameter
1.	Nozzle type	1. Solid cone nozzle 2. Flat fan type	1. Discharge rate
2.	Pressure	10-30 kg/cm ²	2. Swath width
3.	Nozzle height, cm	1. 126 2. 146 3. 166	3. Spray angle

RESULT AND DISCUSSION

Performance of rotary Weeder

The developed rotary weeder was tested in castor (90cm row to row and 45cm plant to plant spacing) and pigeon pea (90cm row to row and 20cm plant to plant spacing) crops after 25 and 45 Day After Sowing (DAS). The field trials were taken up in sandy loam soil and respective crops were planted using tractor operated mechanical planter. The operator was able to steer the tractor at much ease with the new developments and no considerable plant damage observed while in operation.

The data presented in the **Table 5** shows that as the days after sowing increases, the operator has to exercise some caution (due to plant height and growth increase) to avoid plant damage. The weeding efficiency of rotary machine varied from 82.5% to 74.0 and 85.43% to 80.91 for castor and pigeon pea, respectively as speed changes from 2.0 km/h to 2.5 km/h at 25DAS. Moreover, at 45 DAS, the weeding efficiency of rotary machine decreased from 86.8 to 78.5 % and 82.56 to 78.98 % for castor and pigeon pea, respectively as operating speed changed from 2.0 to 2.5 km/h. This may be due to variation in bite length of blade due to speed. Slight variation in weeding efficiency from crop to crop may be due to moisture level variation in soil.

The plant damage during rotary weeding increased from 2.15 to 3.10% and 2.26-2.39% for castor and pigeon pea, respectively when forward speed increases from 2 to 2.5 km/h. After 45 DAS, in weeding the plant damage was varied 2.49 to 3.47% and 3.22 to 3.82% for castor and pigeon pea, respectively when forward speed increased from 2 to 2.5 km/h. It was observed that as plant height and forward speed increases damages also increases. Slight variations in plant damage may be due to difference in crop canopy spread.

Table 5: Result for rotary weeder

S. N0	Crop and growth stage	Day after sowing, DAS	Machine forward speed, kmph	Weeding efficiency, %	Plant damage, %	Fuel consumption, l/h
1	Castor	25	2.0	82.5	2.15	1.39
			2.5	74.0	3.10	1.79
		45	2.0	86.8	2.49	1.29
			2.5	78.5	3.47	1.81

2	Pigeon pea	25	2.0	85.43	2.26	1.45
			2.5	80.91	2.39	1.77
		45	2.0	82.56	3.22	1.40
			2.5	78.98	3.82	1.60

The Fuel consumption during rotary weeding increased from 1.39 to 1.79 l/h and 1.29-1.81 l/h for castor after 25 and 45 DAS, respectively when forward speed increases from 2 to 2.5 km/h. In case of pigeon pea, after 25 DAS and 45 DAS, the fuel consumption was varied 1.45 to 1.77 l/h and 1.40 to 1.60 l/h when forward speed increases from 2 to 2.5 km/h respectively. From result, it was observed that as forward speed increases fuel consumption also increases. The variation in fuel consumption with respect to other parameter may be due to difference in soil type and soil moisture status.

Performance of boom sprayer

The boom sprayer mounted on high clearance platform fitted tractor was evaluated under laboratory and field conditions in tall growing crops. Two types of nozzles i.e. solid cone and flat fan nozzles were tested to determine the discharge rate, swath width and spray angle at different combinations of nozzles height and pressure. The observations were presented in **Table 6, 7 and 8**, respectively.

From the **Table 6**, it was observed that solid cone nozzle gave slightly more discharge rate as compare to flat fan nozzle. However, use of nozzle type depends on type chemical to be used and pest to be controlled. It was also observed that as the pressure increases discharge rate also increases. The discharge rate for solid cone nozzle varied from 0.350-0.510 l/min, whereas for flat cone it varies from 0.360 to 0.486 l/min as the pressure changes from 2.5 to 3.5 kg/cm². The similar trends were also observed for flat cone nozzle as in [4].

Table 6: Discharge rate at various pressures

Nozzle type	Pressure, kg/cm ²	Discharge rate, l/min
Solid cone	2.5	0.350
	3.0	0.389
	3.5	0.510
Flat fan	2.5	0.360
	3.0	0.381
	3.5	0.486

The swath width at different pump pressures and height of nozzle was given in **Table 7**. As inferred from the data, the flat fan type nozzle gives better swath width when compare to solid cone nozzle.

Table 7: Swath width (mm) at different pressure and height of nozzle

Nozzle type	Pump pressure, kg/cm ²	Height of nozzle, mm		
		350	450	550
		Swath width (mm)		
Solid cone	2.5	210	280	340
	3.0	265	340	420
	3.5	350	460	540
Flat fan	2.5	315	400	470
	3.0	360	450	540
	3.5	410	530	630

The nozzle spray angle data indicates that as pressure increases spray angle increases (**Table 8**). When pressure varied from 2.5 to 3.5, the spray angle changes from 34-53 degree for solid cone nozzle and the same is varied from 47-61 degree in case of flat fan nozzle.

**Table 8:** Nozzle spray angle at various pressure

Nozzle type	Pressure, kg/cm ²	Average Spray angle
Solid cone nozzle	2.5	34
	3.0	42
	3.5	53
Flat fan nozzle	2.5	47
	3.0	53
	3.5	61

The developed boom sprayer was tested in pigeon pea and cotton crop at forwarding speeds of 1.5, 2.0 and 2.5 km/h. The average theoretical field capacity of 0.9, 1.2 and 1.5 ha/h were observed at forwarding speeds of 1.5, 2.0 and 2.5 km/h, respectively. The corresponding average effective field capacity of 0.77, 0.97 and 1.15 ha/h was observed for respective forward speed. Whereas the field efficiency of 0.84, 0.80 and 0.76% for pigeon pea was observed. Almost similar field capacity was observed for cotton crop. Most of the time lost in tank filling due to small capacity. The good coverage was observed at 2 km/h with solid cone nozzle. The operator is able to steer the tractor comfortably and sprayer worked satisfactorily. The cost of spraying operation worked out is Rs 600/-per ha.

CONCLUSIONS

1. A high ground clearance platform for low horse power tractor was observed to be perfect solution for intercultural operation in tall growing crop.
2. Developed high clearance boom sprayer avoid direct contact of operator with chemical which reduces the health risk.
3. Multi utility platform helps to reduce cost of cultivation and drudgery involved in various operation.
4. The maximum weeding efficiency of 82.5% and 85.43% was observed for castor and pigeon pea at 2 km/h forward speed.
5. The average effective field capacity of 0.77, 0.97 and 1.15 ha/h was observed at forward speed of 1.5, 2 and 2.5 km/h, respectively for boom sprayer.
6. It can be concluded that the recommended quantity of spray liquid can be sprayed by adjusting forward speed and pressure setting.

REFERENCES

1. Manpreet-Singh, J. S. Mahal, H. S. Sidhu, G. S. Manes, M. L. Jat, and Yadvinder-Singh, "Development and feasibility of innovative relay Seeders for seeding wheat into standing Cotton using a high clearance tractor In cotton-wheat system". Applied Engineering in Agriculture, Vol. 32, no. (4), pp.341-352.
2. Srinivas I, et al, Comparative performance of different power weeders in rainfed sweet sorghum crop. Indian Journal of Dryland Agriculture Research and Development, 2010, vol 25, no.2, pp. 63-67.
3. Mehta ML, Verma SR, Mishra SR, Sharma VK (2005) Testing and evaluation of agricultural machinery. Days Publ House, Delhi.
4. Dash Bhabani Shankar, Development and performance evaluation of self-propelled boom sprayer for intra canopy spraying in row crops. 2016, Unpublished Thesis, G.B. Pant University of Agriculture and Technology, Pantnagar - 263145 (Uttarakhand).



IoT Based Smart Agriculture Monitoring System

G Roja, M Ramesh

*Department of Electronics and Communication Engineering, Periyar Centenary Polytechnic College,
Periyar Nagar, Vallam Thanjavur, Tamilnadu*

✉ shanthiparthiban1977@gmail.com

ABSTRACT

Agriculture is done in every country from ages. Agriculture is the science and art of cultivating plants. Agriculture was the key development in the rise of sedentary human civilization. Agriculture is done manually from ages. As the world is trending into new technologies and implementations it is a necessary goal to trend up with agriculture also. IOT plays a very important role in smart agriculture. IOT sensors are capable of providing information about agriculture fields. we have proposed an IOT and smart agriculture system using automation. This IOT based Agriculture monitoring system makes use of wireless sensor networks that collects data from different sensors deployed at various nodes and sends it through the wireless protocol. This smart agriculture using IOT system is powered by Arduino, it consists of Temperature sensor, Moisture sensor, water level sensor, DC motor and GPRS module. When the IOT based agriculture monitoring system starts it checks the water level, humidity and moisture level. It sends SMS alert on the phone about the levels. Sensors sense the level of water if it goes down, it automatically starts the water pump. If the temperature goes above the level, fan starts. This all is displayed on the LCD display module. This all is also seen in IOT where it shows information of Humidity, Moisture and water level with date and time, based on per minute. Temperature can be set on a particular level, it is based on the type crops cultivated. If we want to close the water forcefully on IOT there is button given from where water pump can be forcefully stopped.

Keywords : Arduino, Temperature sensor, Moisture sensor, water level sensor, GPRS module, Humidity.

INTRODUCTION

Agriculture uses 85% of available freshwater resources worldwide, and this percentage will continue to be dominant in water consumption because of population growth and increased food demand. There is an urgent need to create strategies based on science and technology for sustainable use of water, including technical, agronomic, managerial, and institutional improvements. There are many systems to achieve water savings in various crops, from basic ones to more technologically advanced ones. For instance, in one system plant water status was monitored and irrigation scheduled based on canopy temperature distribution of the systems can also be automated through information on volumetric water content of soil, using dielectric moisture sensors to control actuators and save water, instead of a predetermined irrigation schedule at a particular time of the day and with a specific duration. Through a timed temperature threshold, automatic irrigation was triggered once canopy temperatures exceeded the threshold for certain time accumulated per day. Automatic irrigation scheduling consistently has shown to be valuable in optimizing cotton yields and water use efficiency with respect to manual irrigation based on direct soil water measurements.

LITERATURE REVIEW

As of today, some 1.1 billion planetary inhabitants do not have access to clean drinking water, and 2.6 billion do not have sanitation services. Agriculture is by far the leading user of freshwater worldwide, accounting for almost 85% of global consumption. Because of growing demand, we will need to raise food production by nearly 50% in the next 50 years to maintain our present per capita supply, assuming that the productivity of existing farmland does not decline. The latter portion of this chapter discusses ways in which this emerging crisis may be mitigated [1]. Evapotranspiration based irrigation controllers, also known as ET controllers, use ET information or estimation to schedule irrigation. Previous research has shown that ET controllers could reduce irrigation as much as 42% when compared to a time-based irrigation schedule. The objective of this study was to determine the capability of three brands of ET based irrigation controllers to schedule irrigation compared to a theoretically derived soil water balance model based on the Irrigation Association Smart Water Application Technologies (SWAT) protocol to determine the effectiveness of irrigation scheduling. Five treatments were established, T1–T5, replicated four times for a total of twenty field plots in a completely randomized block design. The irrigation treatments were as follows: T1, Weather matic SL1600 with SLW15 weather monitor; T2, Toro Intelli-sense; T3, ET water Smart Controller 100; T4, a time-based treatment determined by local recommendations; and T5, a reduced time-based treatment 60% of T4. All treatments utilized rain sensors

set at a 6 mm threshold [2]. A prototype system was developed and constructed for automating the measurement and recording of canopy, soil, and air temperature, and soil moisture status in cropped fields. The system consists of a microcontroller-based circuit with solid-state components for handling clock/calendar, sensor power, and data storage and retrieval functions. Sensors, including an analog soil moisture sensor, analog and digital temperature sensors, and a digital infrared thermometer, are widely available and inexpensive [3]. Systems were built and tested during the 2009 growing season in a corn field to evaluate performance and suitability under local conditions. The sensors performed according to manufacturers' specifications, with accuracies of $\pm 0.4^\circ\text{C}$, $\pm 1.4^\circ\text{C}$, and $\pm 0.3^\circ\text{C}$ for air-, soil-, and canopy-temperature measurements, respectively. Soil moisture sensors were calibrated and provided measurements within ± 2 kPa of the manufacturer's values. Reliability of data collection and storage averaged 91%, with most bad or missing data occurring during periods of inclement weather and electrostatic interference [4]. Efficient automated irrigation systems, which can irrigate the substrate of potted plants to a desired level and supply those plants with just the amount of water required for normal plant growth are currently not available [5]. These systems, if developed, could reduce wastage of irrigation water due to excess application. This subsequently could reduce leaching and run-off, and aid growers to cope with increasing regulations of water-use by state governments in the US. Here we describe an irrigation controller that irrigates a substrate to a set-point (volumetric water content, θ) and maintains θ close to that set-point for several weeks. The controller uses calibrated, dielectric moisture sensors, interfaced with a data logger and solenoid valves, to measure the θ of the substrate every 20 min. [6].

SYSTEM ANALYSIS

India's major source of income is from agriculture zone and 70% of farmers and general people depend on the agriculture. So the agricultural system in India should be advanced to reduce the manual efforts of farmers. Various operations are performed in the agriculture field like seed sowing, weeding, cutting, pesticide spraying etc by the farmers manually. In India most of the seed sowing process are operated manually. These manual technique are replaced with automated techniques. The fabrication of ground nut sowing machine is reasonable and low cost effective for agricultural production. The basic requirements for small scale cropping machines are, they should be suitable for small farms, simple in design and technology and versatile for use in different farm operations. IOT plays a very important role in smart agriculture. IOT sensors are capable of providing information about agriculture fields. We have proposed an IOT and smart agriculture system using automation. This smart agriculture using IOT system is powered by Arduino, it consists of Temperature sensor, Moisture sensor, water level sensor, DC motor and GPRS module. When the IOT based agriculture monitoring system starts it checks the water level, humidity and moisture level.

BLOCK DIAGRAM

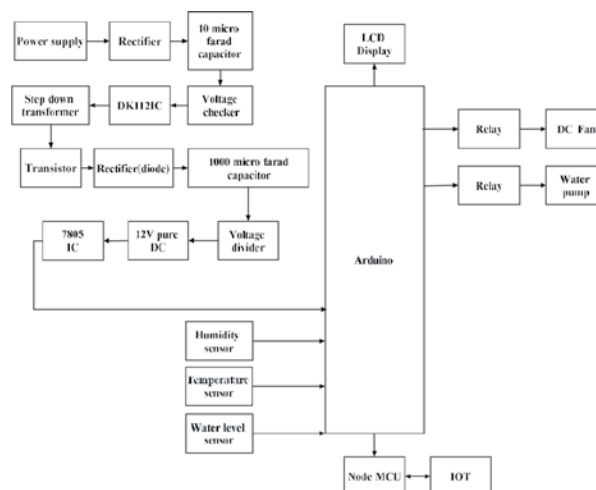


Fig. 1: Block diagram of IoT based smart agriculture monitoring system

Fig. 1 shows the block diagram of IOT Based Smart Agriculture Monitoring System. This IOT based Agriculture monitoring system makes use of wireless sensor networks that collects data from different sensors deployed at various nodes and sends it through the wireless protocol. A robot is a mechanical, artificial agent and is usually an electromechanical system, because of software programming it makes complicated tasks easy to perform. Applying automation to agriculture its advancements to



the industry while helping farmers to save money and time. In this system automatic seed sowing is done which aims to drop seeds at particular position with specified distance between two seeds and lines while sowing by using PIC Microcontroller. This smart agriculture using IOT system is powered by Arduino, it consists of Temperature sensor, Moisture sensor, water level sensor and DC motor. Our project model includes wheel, Rod, Digging rod. Solenoid Valve is used as Seed Feeder, where we have to keep the seeds. It is closed by default. While the system activates, the solenoid valve does opens and closes based on the programmatic time. Seed falls in to the land. It sends SMS alert on the phone about the levels. Sensors sense the level of water if it goes down, it automatically starts the water pump. If the temperature goes above the level, fan starts. The main focus of this system is its Automatic way of sowing the seeds. The seeds are been sowed in a proper sequence which results in proper germination of seeds. This automatic way of sowing seeds using a robot reduces the labor requirement. Here the wastage of seeds is also been reduced to a greater extent. This system has been developed for the sowing of seeds in an automatic way. Here with the help of a robot the seeds are been dispensed in the soil in a proper sequence hereby reducing the wastage of seeds.

HARDWARE REQUIREMENT

Power Supply

A power supply is an electronic device that supplies electric energy to an electrical load. The primary function of a power supply is to convert one form of electrical energy to another and, as a result, power supplies are sometimes referred to as electric power converters. Some power supplies are discrete, stand-alone devices, whereas others are built into larger devices along with their loads.

SMPS

SMPS transfers electric power from a source (AC mains) to the load by converting the characteristics of current and voltage. SMPS always provide a well regulated power to the load irrespective of the input variations. SMPS incorporates a Pass transistor that switches very fast typically at 50Hz and 1 MHz between the on and off states to minimize the energy waste. SMPS regulates the output power by varying the on to off time using minimum voltage so that efficiency is very high compared to the linear power supply.

Input rectifier

The AC input from mains is first rectified in the SMPS using a rectifier to convert it into DC. The rectifier consisting of a full wave diode bridge or module that produces an unregulated DC voltage to the Smoothing capacitor. The input AC passing into the rectifier has AC voltage pulses that may reduce the power factor. So control techniques are used to force the average input current to follow the sine wave.

Inverter

This stage converts the rectified DC into AC using a power oscillator. The power oscillator has a small output transformer with a few windings at the frequency 20-100 kHz. Switching is controlled by a MOSFET amplifier. The output AC voltage is usually isolated optically from the input AC by using an Optocoupler IC for safety reasons.

Voltage regulator IC 7805

7805 is a voltage regulator integrated circuit. It is a member of 78xx series of fixed linear voltage regulator ICs. The voltage source in a circuit may have fluctuations and would not give the fixed voltage output. The voltage regulator IC maintains the output voltage at a constant value as shown in Fig. 2.



Fig. 2: Voltage Regulator IC 7805

PIC Microcontroller 16F877A

The PIC microcontroller PIC16f877a as shown in **Fig.3** is one of the most renowned microcontrollers in the industry. This controller is very convenient to use, the coding or programming of this controller is also easier. One of the main advantages is that it can be write-erase as many times as possible because it use FLASH memory technology. It has a total number of 40 pins and there are 33 pins for input and output. PIC16F877A is used in many pic microcontroller projects. PIC16F877A also have many application in digital electronics circuits.



Fig. 3: PIC 16F877A Microcontroller

Sensors

Temperature sensor is a device, to measure the temperature through an electrical signal it requires a thermocouple or RTD (Resistance Temperature Detectors). If the difference in voltage is amplified, the analogue signal is generated by the device and it is directly proportional to the temperature. The coolant temperature sensor, also known as the coolant temperature switch, is an engine management

System sensor that is used to monitor the temperature of the engine's coolant. Most coolant temperature sensors operate using electrical resistance to measure the temperature of the coolant.

A humidity sensor as shown in **Fig. 4** (or hygrometer) senses, measures and reports both moisture and air temperature. The ratio of moisture in the air to the highest amount of moisture at a particular air temperature is called relative humidity. Relative humidity becomes an important factor when looking for comfort.

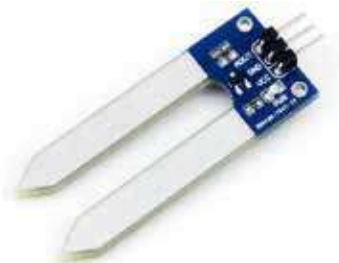


Fig. 4 : Humidity sensor

therefore, while selecting a strong and consistent one, one should think about the requirement.

LCD display

LCD (Liquid Crystal Display) screen as shown in **Fig. 5** is an electronic display module and find a wide range of applications. A 16x2 LCD display is very basic module and is very commonly used in various devices and circuits. These modules are preferred over other multi segment LEDs. The reasons being: LCDs are economical; easily programmable; have no limitation of displaying special & even custom characters (unlike in seven segments).





ARDUINO

Arduino as an open source hardware and software company, project and user community that designs and manufactures single board and microcontroller kits for building digital devices and interactive objects that can sense and control both physically and digitally. Its products are licensed under the GNU Lesser General Public License (LGPL) or the GNU General Public License (GPL), permitting the manufacture of Arduino boards.

SOFTWARE REQUIREMENT

Proteus Software

Proteus is software for microprocessor simulation, schematic capture, and printed circuit board (PCB) design. It is developed by Lab center Electronics. The XGame Station Micro Edition was designed using Lab center's Proteus schematic entry and PCB layout tools.

Embedded C

Embedded C is a set of language extensions for the C Programming language by the C Standards committee to address commonality issues that exist between C extensions for different embedded systems. Historically, embedded C programming requires nonstandard extensions to the C language in order to support exotic features such as fixed point arithmetic, multiple distinct memory banks, and basic I/O operations. In 2008, the C Standards Committee extended the C language to address these issues by providing a common standard for all implementations to adhere to. It includes a number of features not available in normal C, such as, fixed-point arithmetic, named address spaces, and basic I/O hardware addressing.

CONCLUSION

This IOT Based Smart Agriculture Monitoring System save time and reduce human effort. In most of the agriculture we need a separate person to sowing seeds. This is a long time process. In rush hours workers will be in hurry to do such workers. This system will overcome this problem.

REFERENCE

1. S.U. Zagade, R.S. Kawitkar (2012) "Wireless Sensor Network for Greenhouse" International Journal of Science and Technology, Volume 2 No.3, ISSN 2224- 3577.
2. Kiran Sahu, Susmita Mazumdar (2012) "Digitally Greenhouse Monitoring and Controlling of System based on Embedded System" International Journal of Scientific & Engineering Research, Volume 3, Issue 1, ISSN 2229-5518.
3. Alausa Dele W.S, 2Keshinro Kazeem Kolawole, "Microcontroller Based Green House Control Device" Volume 2, Issue 1,1 ISSN 2319 – 1813.
4. Thomas, Andrew L. and Richard J. Crawford, Jr. (2001) "Performance of an energy-efficient, solar heated greenhouse" in southwest Missouri. Southwest Missouri Agricultural Research and Education Center 2001 Research Report. University of Missouri-Columbia.
5. Akshay C., Nitin Karnwal, Abhfeeth K.A., Rohan Khandelwal, Tapas Govindraj, Ezhilarasi D and Sujan Y., "Wireless sensing and control for precision Greenhouse management", 978-1- 4673-2248-5/12/\$31.00 ©2012 IEEE.
6. Orazio Mirabella and Michele Brischetto "A Hybrid Wired/Wireless Networking Infrastructure for Greenhouse Management", in IEEE Transactions on Instrumentation and Measurement, Vol. 60, No. 2, February 2011.
7. J. Burrell et al. Vineyard "computing: sensor networks in agricultural production", IEEE Pervasive Computing, 3(1):38–45, Jan-Mar 2004.



Design of Multipurpose Harvesting Machine for Lowland Areas for The Upliftment of Farmers

Niloy Laskar^{1*}, Umar Faruk Bhuiya¹, Krishna Chakraborty¹

Dr Arindam Majumder²

M.Tech scholar^{1}, Assistant Professor², Department of Mechanical Engineering*

National Institute of Technology Agartala, Jirania, Agartala, West Tripura

✉ niloylaskar3@gmail.com

ABSTRACT

This paper addresses a Multipurpose Harvesting Machine for lowlands which is fabricated with very simple mechanisms at a very low cost. Cutting and gathering of the crop are important agricultural operations which demand a considerable amount of labor. The availability and cost of labor during harvesting season is a problem. The shortage of labor during harvesting season and sudden variation of the weather condition causes a great loss to the farmers it is, therefore, essential to adopt the mechanical methods so that the timeliness in the whole operation could be ensured. The use of mechanical harvesting devices has been increased in recent years. To harvest crops, farmers are usually using reapers or combines. But these are very costly, thus making it unaffordable to most of the small farmers. Although, some manual operated reapers were developed. But as because of the limitations of manual power, none of them become popular among farmers as the power available for transportation of the machine as well as cutting and conveying of the crop was not sufficient. In this research, we have studied and fabricated a Multipurpose Harvesting Machine at a very low cost and techniques were carried out.

Keywords : Multipurpose harvesting machine; Crop cutter; Crank and slotted quick return mechanism; Pulley; Gears.

INTRODUCTION

India is an agricultural country. About 70% of our population depends on agriculture. One-third of our national economy comes from agriculture. Our agriculture remains underdeveloped for a long time. We did not produce enough food for our people because of the manual harvesting of crops. But things are now changing by the replacement of machines to do the necessary harvesting works. Still, lowlands are facing a major problem in handling those heavy machines. There comes the idea of manufacturing a multipurpose harvesting machine for lowland where the main aim is to reduce the weight of the machine as well as the cost so that the poor farmers of our country can afford such machines ultimately leading to higher production in less time.

METHODOLOGY

Basically, our study is mainly focused on our native state Tripura. Tripura being a hilly state, the amount of plain land is very limited. So, mostly agriculture is done in lowland areas. The property of the lowland is such that it cannot withstand the load of heavier machines (more than 100kg). So, to overcome this and eliminate labor dullness, an affordable machine of limited weight needs to be introduced. The major problem occurs during the harvesting season. So, our main approach is focused on the cutting and gathering of crops. So, for the fulfillment of our aim, we followed some steps. We had visited various agricultural lands and from there we got to know the problems faced by our farmers. What are the machines they are using, how much the existing machinery cost, whether these machines are feasible for lowlands, what are the existing traditional techniques, and the price of labor?

LITERATURE REVIEW

The model has been designed utilizing our own ideas & knowledge, but still we have taken some inspiration from the papers listed below:

Moheb (2006) designed a self-propelled machine suitable for cutting crops. The actions of this machine involve cutting, reeling, conveyor belts, and transmission systems. We used this as a guide and replaced the conveyor belt mechanism in reducing the overall weight of our machine.[1]

Yuming Guo's paper (2016) explains the relations between the stalk strength and cutting force that is require for cutting the soybean. This paper was supportive in guiding the calculations front for rice harvesting.[2]

WORKING PRINCIPLE

This machine consists of a quick return Mechanism for reciprocation of cutter blade over stationary cutter blade and this mechanism is also used to convert rotary motion into linear motion. This machine is run by 9.5HP, 6000rpm 2 stroke petrol engine. One end of the output shaft is connected to the Crank and slotted lever mechanism which converts the rotary motion of the shaft into reciprocating motion of the cutter blade. Reciprocating cutter blade slides over the fixed blade and creates scissoring action responsible for cutting the crop and another end is connected to the collecting mechanism and hence helps in gathering of crops.

CAD MODEL OF PARTS OF THE MACHINE

The drawing of the crop cutting machine will be presented by using CATIA drawing software and the pictorial views are presented below:

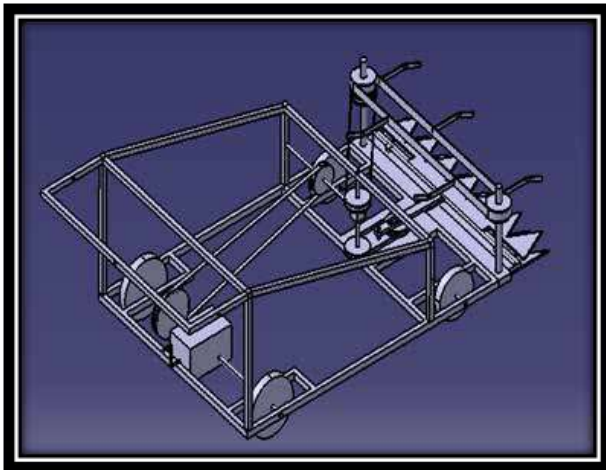


Fig 1: Isometric view

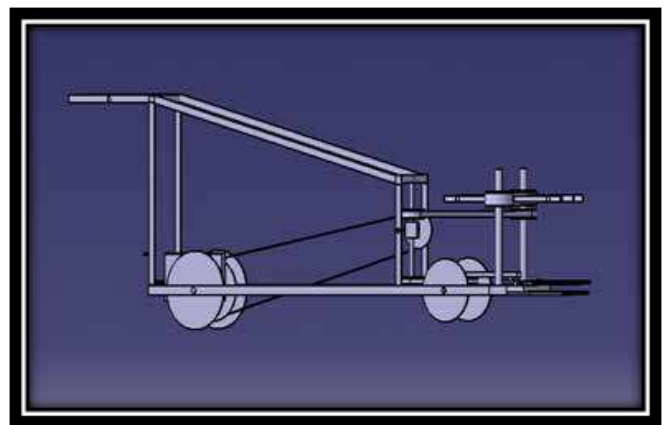


Fig 2: Side view

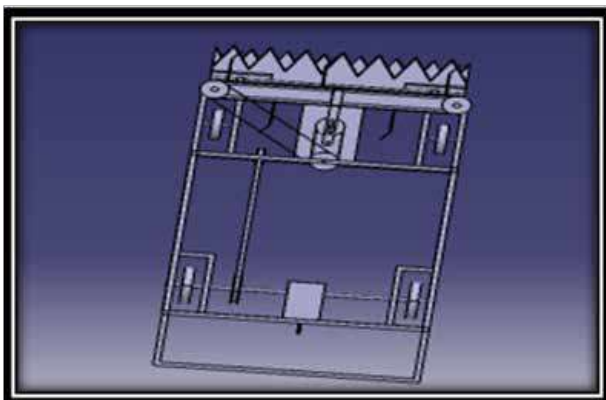


Fig 3: Top view

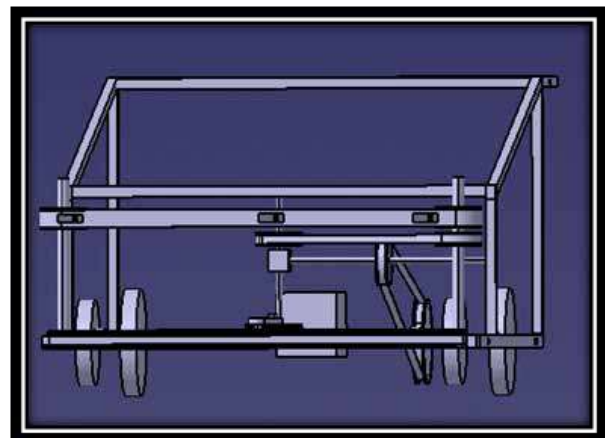


Fig 4: Front view

CONSTRUCTION

The machine mainly performs two functions 'Harvesting and collecting'. The machine consists of mainframe, petrol engine, cutter mechanism, collecting belt mechanism, bevel gear mechanism and crank slotted lever mechanisms and the details are given below:

Mainframe: - The mainframe is designed in such a manner that it must be lightweight and also able to carry the load of the petrol engine and other accessories. The machine will have dimensions of 30x50 inches as width and length.

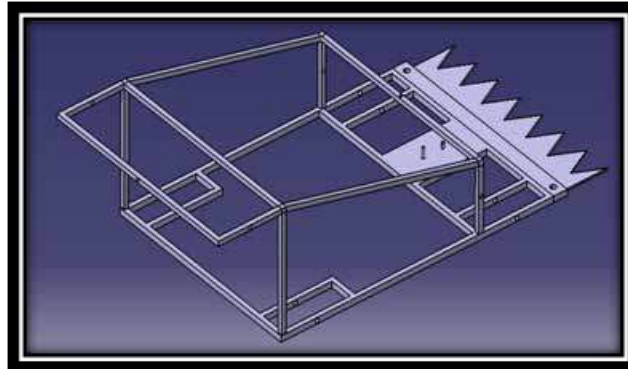


Fig 5: Mainframe

Petrol Engine: - A two-stroke engine is used because of more power strokes and lightweight. The engine will be run by a 9.5 H. P 6000 rpm petrol engine. We choose petrol because of the small size engine.



Fig 6: A two-stroke engine

Cutter mechanism:- Cutter assembly consists of both sliding and stationary cutting blade. Along with the cutting, the collection of crops is also done from the same power source with the help of three different belt pulley attachments. The upper blade follows a quick return mechanism while the lower blade remains stationary and moves along the motion of the vehicles thus providing a scissoring action.

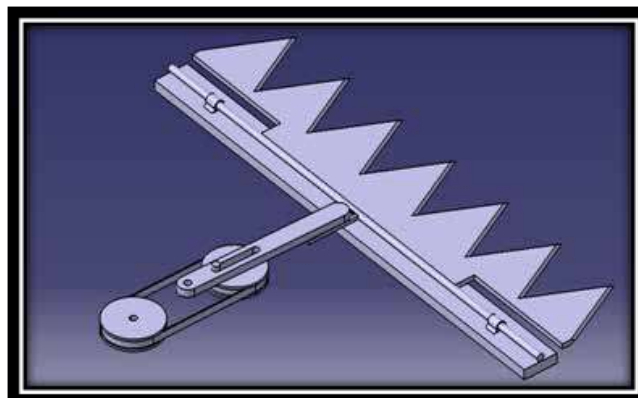


Fig 7: Cutter assembly

Bevel Gear Mechanism:- It is required to transmit power to two mechanisms – the quick return mechanism and the collecting mechanism by diverting the motion by 90°.



Fig 8: Bevel gear

Collecting Belt mechanism:- In this mechanism, the transmission of power takes place between the parallel shafts. Consists of two pulleys over which an endless belt is passed encircling both and Rotary motion is transmitted from driving pulley to driven pulley.

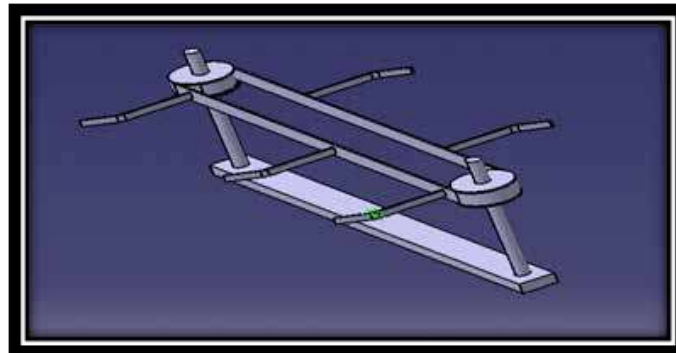


Fig 9: Collecting Belt mechanism

Crank and slotted lever quick return mechanism:- This is the mechanism basically used in shaping machines, where the rotational motion of the crank will be converted to the linear mechanism of the slider.

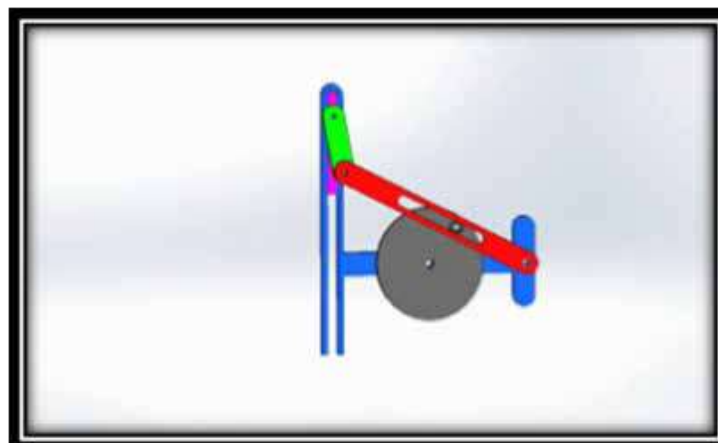


Fig 10: Crank and slotted lever mechanism

MATERIAL USED

Various materials are used for various components of the harvesting machine which are given below:

- Carbon steel is used for Bevel gear because of its high toughness and high strength.



- ii. Mild steel is used for angle because mild steel is preferred for the structural framework and bearing stresses.
- iii. Mainframe is mainly made of Iron.
- iv. Cast iron is used for pulley because of its low cost.
- v. Assynthetic rubber is flexible to bend, so it is used for V-belt.
- vi. Because of high weldability and machinability of mild steel, it is used for shafts.

DESIGN OF MACHINE

Calculation is a vital element of designing. For designing of the machine, the calculations for finding the wheel RPM & for finding the RPM of driver & driven pulley is given below:

Calculation of Wheel RPM

Diameter of the Wheel (D) = 16 inch

$$= 16 \times 25.4 = 406.4 \text{ mm}$$

Diameter of driver Pulley (d1) = 7 inch

$$= 7 \times 25.4 = 177.8 \text{ mm}$$

Diameter of driven Pulley (d2) = 4 inch

$$= 4 \times 25.4 = 101.6 \text{ mm}$$

Perimeter of wheel = $\pi D = \pi \times 406.4 \text{ mm}$

$$= 1276.54 \text{ mm}$$

Speed of vehicle = 10 km/hour

$$= 10 \times (5/18) = 2.78 \text{ m/sec} = 2777.8 \text{ mm/sec}$$

Revolution of wheel/ sec = $(2777.8/1276.54)$

$$= 2.176 \text{ Rev/sec} = 130.56 \text{ Rev/min} [3]$$

Calculation for driver and driven Pulleys

RPM of driver Pulley = RPM of Wheel

$$= 130.56 \text{ RPM}$$

$$(d_1/d_2) = (N_2/N_1)$$

$$N_2 = (d_2 \times N_1) / d_1 = (177.8 \times 130.56) / 101.6$$

RPM of driven Pulley (N_2) = 228

Blade reciprocation in 1 revolution of driven Pulley = 2 Total blade reciprocation in 1 min. = 228×2

$$= 456$$

Total reciprocation of blade in 1 sec = $456/60$

$$= 7.6 \cong 7 [3]$$

Forces and Energy calculation required to cut the Crop:

Area of the wheat straw to cut by 1 teeth of blade

$$= 2 \times (50 \cos 60^\circ) \times 5 = 250 \text{ mm}^2$$

Area of wheat straw cut by the 7 teethes

$$= 7 \times 250 \text{ mm}^2 = 1750 \text{ mm}^2 \text{ A} = 0.00175 \text{ m}^2$$



Shear strength of the wheat straw (τ_{ult})

$$= 10 \text{ MPa} = 10 \text{ N/mm}^2$$

Required cutting force (F) = $\tau_{ult} \times A$

$$= 10 \times 1750 \text{ N} = 17500 \text{ N} = 17.5 \text{ kN} [4]$$

Calculation for the velocity of collector mechanism belt

$$\text{RPM of 2nd driven pulley} = \text{RPM of 1st driven pulley} = 228$$

COST ESTIMATION

Cost estimation is the approximate cost of the product that will be required for the manufacturing of the product. The total cost of our machine depends on the following aspects:

- Raw Material Cost (Includes angles, shaft, engine, wheel, sheet metal, paint, petrol)
- Standard item cost (Includes nut, bolt, bevel gear, pulley & belt, bearing, grinding & cutting blades, drill bit)
- Machining Cost (Includes turning, drilling, milling cost)
- Transportation cost.

Item	Materials	Total cost (Rs)
Wheels	MS	$500 \times 4 = 2000$
Engine	9000
Cutter blades	Stainless steel	4000
Pulley	$400 \times 7 = 2800$
Body frame	Cast iron	8000
Machining cost	3000
Other accessories including transportation cost	3200

Total Cost: Rs 32000

WEIGHT ESTIMATION

In the lowland area, the maximum weight that can allow running the harvesting machine is 100 kg. If the weight goes beyond that limit, then it will be difficult to operate the machine. So, we try to estimate the approximate weight of the machine:

Parts name	Weight
Mainframe	35kg
Engine	8kg
Pulley	6kg
Belt	5kg
Cutter	4kg
Wheel	20kg
Accessories	6kg

Total Weight: 84 kg

ADVANTAGES

The multipurpose harvesting machine is mainly designed to uplift the farming section of our country. This machine plays a vital role in agriculture and some of its advantages are given below:

- Reduce the human effort- Crop harvester is mainly designed to reduce the human effort in which only one operator can



handle the machine.

- ii. Reduce the cost- In agriculture for cropping and ploughing, it can do work at the cheapest prices because it saves the worker cost.
- iii. Reduce the time- By using this machine, they increase the capacity of the working and cutting and it can possible the maximum cutting within minimum time.
- iv. Easy to handle- This machine is easy to handle and we can easily start the machine.
- v. Efficient in crop cutting- Adjustable blades are arranged at ground level leaving minimum residues and hence it will help to reduce the pollution due to the burning of residues mainly in northern India.

RESULTS AND DISCUSSION

Since the main concentration of our design is to reduce the weight as well the cost keeping in mind the standard of mechanism, so the comparison between cutting time of 1 Kani land by machine & by labor is as follows:

FOR MACHINE

- i. The machine is working in 1 Kani (1600 sq. feet) area = the fuel consumption is 1.5 liters/hour.
- ii. Total cost = Fuel cost (Rs. 150) + labor cost (Rs. 350) + M/C cost (Rs. 50) = Rs.550
- iii. Time for cutting of 1 Kani area = 2 hours.

FOR LABOR

- i. Cutting time for 5 labor in 1 Kani area of farm = 6 hours.
- ii. Labor Working in 1 Kani area the associated cost = Rs. 350/head
- iii. Total cost = Rs. 350*5 =Rs. 1750

So, from above we can see that the harvesting time of 1Kani land takes 6 hours for labor & 2 hours for the machine. Our model is $(6 - 2) * 100/6 = 66.67\%$ better than the traditional model in saving time and $(1750 - 550) * 100/1750 = 68.57\%$ better in saving money. Hence in the above comparison, it is clear that the cost of working by machine in the farm for said application is less as compared to labor cost. Further we are using a single power source for both scissoring action as well as for motion of wheels and hence we can eliminate the motor as used in some existing machines. Also, we are using removable cutters and can increase the number of cutters if needed. So, our design is more efficient as compared to manual processes.

CONCLUSION

The main concentration of our design is to reduce the weight as well the cost keeping in mind the standard of mechanism. For the development of this harvesting machine, we are utilizing all the past techniques and concepts. We also tried to create a simple mechanism for this machine so that everyone can handle it easily. Our model is 66.67 % better than the traditional model in saving time and 68.57 % better in saving money. We have reduced the weight to almost half compared to existing machines. Thus, we can conclude that by using this machine in lowland areas and other agricultural lands, we can increase the production rate. The market share will also increase, contributing more to the economy of our country.

REFERENCES

1. Ogunlowo, Q.O. and Olaoye J.O, Development and performance evaluation of a guided horizontal conveyor rice harvester, Agrosearch (2017) 17 No. 1: 66– 88.
2. Liang L. and Guo Y., Relationship between Stalk Sheer Strength and Morphological trait of Stalk crops, International Journal of Advance Engineering and Research Development Volume 3, Issue 12, December -2016.
3. Bhandari V.B, Design of Machine Element, Publication Tata Mc-Graw-Hill Ltd. Edition (2007)
4. Khurmi R.S. and Gupta J. K., Machine Design, Publication S. Chand (2018)

Architectural Engineering



Fractal Geometry as an Adaptive Technique for Human Capital Development: A Review based on Indian Temple Architecture

Shynu R V

*Department of architecture, APJ Abdul Kalam Technological University,
TKM College of Engineering, Kollam*

✉ shynurobert@gmail.com

ABSTRACT

Architecture design configuration is an incredible and powerful medium that enhance performance over society. The conduct and capital development of humankind rely on the sort of environment which they perceive. This writing survey endeavours to research fractal-based social practice through the instance of the ancient Indian temple built environment. Sensible assessment pack investigating the concept of built environment in sanctuary design. Additionally, specialists have been investigating the realities with respect to the impact of geometrical patterns over sanctuary design. Sanctuary configuration is a mechanism of communication, and critical to recognize its importance in the social system, since fractal designs align with visual attention and structural efficiency. Indian sanctuary designs have a basic part in attention engagement and cognition, it is appropriate to find the centrality of social impact that dependent due to the manufactured temple environment. Ancient social data was polished as Vedas in which patterns has a basic work. Pros have been exploring the real factors concerning the effect of numerical models over the constructed environment of sanctuary buildings. Temple design development dependent on numerical calculations and discoveries show that the customary culture has a significant part to direct Fibonacci gathering for legitimate practice. The cognition of human over such fractal-based visual data must be confirmed experimentally for additional understandings in the domain of human capital development.

Keywords : Communication; Fractal; Social system; Environment; Cognition.

INTRODUCTION

The design principle is a crucial element in the theory of architecture. An efficient design can deliver information for communication and visual information is considered as an element of communication in the architectural design. The formation of a social system depends upon the communication medium. So built environment as a medium reflects the communication quality of the social system. Each social system depends upon the communication system. Society is only possible where communication is possible [1]. Luhman the German sociologist and a prominent thinker in system theory state that communication can be considered as the basic unit of observation for the assessment of the operation of the social system. The limit of modern society is the limit of communication [2]. Individuals do not participate in society unless they engage in communication [3]. Luhman states that social system uses communication as their particular mode of autopoietic reproduction. Autopoietic systems are a system that reproduces themselves from within the system. This statement refers that such system based practices improves the productivity and performance. This autopoietic system represents as fractal geometry because of fractal exhibit self-similarity [4]. Luhman considered media as a vehicle to communicate. Similarly architectural built environment is a medium of the vehicle to communicate for its user. The vehicle increase the reachability of addresses and the probability that addresses will receive information 'but they do not guarantee the success of the information' [5]. These data demonstrate the probability of delivering information more effectively based on fractal pattern through the built environment.

BACKGROUND STUDY

Initial investigations will focus on the fractal patterns. The concept of clarifications regarding the examples in nature and investigating the Fibonacci arrangement to comprehend its effectiveness [6]. The examination shows human visual information process capacity restricted to enormous amount of data, so conventional practices as temple architecture addressed such data perception through three-dimensional environments for faster information processing [7]. Patterns displayed on the built environment of temple design. Exceptional bona fide records open on old temple form practices, the assessment acknowledged that temple structure responded reliant on the exacting show [8]. Indian temple form development has a fantastic customary history of the practice. The investigation expected that the Harappan human advancement related to the Vedic period and shows



that the Vedic period has begun before 2000 B.C [9]. This information shows the period of customary assembled practice. Vastu is an assessment structure which has used in Indian built practice [10]. Studies show that during antiquated time creators chronicle a decent manufactured structure, with the guide of plan and height through the use of Vastupurusamandala is thought of [11]. Collectors perceived that a bit of the Vedas works formed during the fifteenth to fifth century B.C. From the seventh and eighth century, A.D. Chalukya line disengaged into two general classes, the Nagara style and the Dravida style. The study clearly shows the point by point change information on the manufactured type of both Nagara and Dravida sanctuary engineering [12]. Likewise, the geometry dependent on Vastupurushamandala clarified the evolutionary advancement of Nagara style and Dravidian style [13]. These styles are the most refined cases which show the social characteristics to the extent Golden proportion and Fibonacci sequence over the temple built environment [10].

METHODOLOGY

The literature review contains a thematic investigation to find subjects inside the data. A snowball analysing approach used to recognize relevant wellsprings of information. Individuals who may move toward disseminated or unpublished work concerning Fibonacci groupings in social practice also considered. It was sensible to discover this data through both formal and easy-going courses. Also, a couple of investigation specialists had reached to discover this data. Finally, institutions and schools having data concerning open educational documentation are added to the review furthermore. The information were then ordered into different sorts as per arrangement rules as appeared in **Table 1**. The papers were then isolated by the subjects. A specific code had created for reference. For many years it has seen an extending examination of composting volume focused in on the capacity of fractal in designing and visual perception. Overall assessment dispersions from various countries show worldwide enquiry reliant on the fractal. Regardless, the assessment data isn't explaining the fractal models' prompt relationship with the built environment because of temple design and its association with social practices.

Table 1: Classificatory category and definitional criteria

Category	Definitional criteria
Group 1	Clear fractal centre. Solid proof, clear outcome
Group 2	Fractal related. Solid proof, clear outcome
Group 3	Clear Vedic culture centre. Some proof
Group 4	Not limited to Vedic culture. Some proof
Group 5	Clear structural core interest
Group 6	Not limited to measurable data
Group 7	Published reports
Group 8	Unpublished reports
Group 9	Institutional documents

ANALYSIS

The disclosures emerge from the composition on Fractal progressions can be summed up under a couple of headings.

Fractal and Temple Architecture

The property of self-similarity recursive geometry insinuated Fractal pattern. Obsolete Indian mathematicians are capable at the count. They applied their knowledge into math in the different terrain also. They saw and grasped the principles of emphasis, accentuation and self-similarity from trees, water and ground cover that keep the fractal norms. Temple design painstakingly adhered to the Vastu norms, which depict self-similarity of its number related class. The temple rise influences the fractal design, by controlling a two-dimensional structure plan to the course of action by three-dimensional portrayal. **Fig. 1** illustrates the sample of fractal based built form in south India. The investigation recognized that visitors and voyager's thought influenced by these self-similarity parts [14].

The investigation evaluated to understand sanctuary designing arrangement guidelines over the count of the early Nagaracella (especially in the curvilinear Shikhara of the northern Indian Nagara culture). Consistently lessening groupings of self-similarity structures recognized outwardly of the superstructure [15]. These explain the presence of fractal-based practice in Indian show all throughout the north and south zones. Basically, fractal features are recognized on KandariyaMahadev temple at

Khajuraho as fractal count [16]. This information points out that the outdated Hindu religion has a strong numerical perspective over their collected characteristic practices. The examination addresses self-similarity that progresses the fractal speculation through Indian sanctuary configuration practice [14]. Therefore, a reasonable affiliation chose in fractal and social symbolism. As demonstrated by Indian masters of Vedic period they don't authentically reflect the character of nature in their speciality anyway make comparing with nature [17]. This preparation is on the grounds that ordinary people have not progressed to follow such an astounding character of nature around them, so they duplicate simply its property.



Fig. 1: Brihadisvara Temple, Thanjavur, Tamil Nadu

Fractal and Nature

History perceived that the central content in the out of date library is the Vedas since it is the important Indian Heritage. To the information, this heritage primarily perceived as the basic human advancement that is the Vedic Aryan turn of events. Vedic data particularly followed reliant on the points of view towards nature and life. Additionally, Aryans were known as the posterity of nature, since they are thinking about nature minutely [18]. That is the Vedic period may have been the utilization of nature guidelines subject to human-based preliminary or discernment revelations. Since the sanctuary design practices are painstakingly kept subject to the Vastu norms and show the self-similarity character over its natural arranging and keep the developed standards reliant on human degrees. The examination by Dutta and Adane in 2014 shows the evidence of replication in self-similarity, various accentuations, components and unusualness. The different scales are the ones that express the crudeness of Hindu sanctuary fractal designs. The best occasion of the model is the Shikhara of Khajuraho sanctuary design were the repetition of apexes notice explicit degrees and rules similarly as numerical properties [19]. Advanced reproduction strategy is utilized for structures to portray antiquated temple engineering for understanding its shape grammar, and its correlation with manufactured structures from the coding point of view [20]. All these examination examinations propose the conceivable outcomes that sanctuary configuration utilized dependent on parametric structure generative standards. A study led with 3D scanned models with the guide of computational CAD-based environment to clarify few parameters [21]. Again these revelations express the effect of the fractal design over the manufactured structure, since fractal mirror the properties of nature.

Fractal and Built Environment

The examination recognized that the Golden proportions and Fibonacci numbers were utilized in the design development for aesthetical just as utilitarian purposes. The sequential Fibonacci numbers or arrangement has numerical ideas which lead to the Golden proportion. Studies show Egyptians utilized the Golden proportion for the development of pyramids [22]. At the point when we notice nature can recognize the Fibonacci number. The example of the petals on blossoms, a course of action of leaves in the stem of a plant, the pineapples scales shows the presence of Fibonacci number. Also, the examination led by Omotehinwa and Ramon in 2013 demonstrates that Fibonacci groupings are sorted out in the human body parts. Additionally, it is distinguished that numerous human body parts have been proportioned by the brilliant proportion [23][24]. Since architectural practices are concern with human scale, it is pertinent to adhere to these design standard to chronicle subjective spaces. Akhtaruzzaman and Shafie in 2011 express that Golden Proportion cadence is additionally figured in the human pulses [26] likewise it is distinguished that Penrose tiling have numerous regular highlights identified with the pentagon and consequently to the Golden Ratio [25]. Since Penrose is associated with fractal and Fibonacci numbers, this data will prompt further enquiry in researching the productivity of the Golden proportion as a design arrangement. All these information demonstrate connote

the connection among fractal and configuration impact over various domains. According to the mathematical explanation, the Fibonacci square shape can be imagined as the course of action of square shapes in which the sides are two reformist Fibonacci numbers long. This clarifies that it is made through squares with sides having Fibonacci progression. Moreover, it is known as a Golden square shape when a square shape's sides are identical to the Golden extent [27]. It additionally distinguished that the Golden Ratio is outwardly satisfying and restricted to feel as well as nature and human body extents [25]. This mirrors the affiliation and association among nature and human wisdom in the space of the Fibonacci progression. Also, the twisting has a type of an example on nature that is known for its self-similarity that creates or fills fit as a fiddle without changing its profile. The shell of snails and the shell shows comparable winding shapes. This implies the presence of fractal designs in nature. One can outwardly follow them easily as a result of the satisfying character of the twisting shape because of the presence of these fractals. All these data reflects the efficiency of a fractal based profile on its form for productivity and performance. Essentially, **Fig. 2** speak to fractal-put together Indian social practice concerning the socially constructed environment. This training exhibits fractal calculation adjusted to its social framework because of its natural characteristics.



Fig. 2: The Royal Palace, Thanjavur, Tamil Nadu

CONCLUSION

This research might be an underlying examination concerning the Fibonacci course of action dependent on old social practice and its effect on the built environment for human resources improvement. Through a wide composing overview and examination of existing subjects reveals fractal-based regular practice and made constructed association. The effect of Fibonacci over the built environment of sanctuary design through abstract publication concerning ordinary practices so far recognized. This investigation is inciting the route for exploring the character of fractal nature-based Indian custom and its foundation of data, which has a colossal effect over visual communication based practices. Investigation maintains that the fractal estimation progresses more record in settling on a choice about the wonderfulness than visual complexity [28]. This result suggests fractal properties sway in visual acknowledgement that must moreover analyse to appreciate fractal-based arrangement practices over the amassed environment for choosing successful characteristic communication. Basically, the examination discusses the visual elegant acumen by virtue of the fractal-based arrangement in the streetscape. The created information will have the option to comprehend whether fractal math can proceed as a vehicle of the design for compelling communication as a versatile procedure for human capital development. While coordinating the information in the field of design investigation, these outcomes may be giving the diagnostic assertion about how an individual gets and comprehends data for social execution. Indian sanctuary engineering utilized fractal on its built form, it is anticipated that such pattern language upgrades the view of the user for social



execution. Since fractal designs are incorporated over sanctuary structure for its auxiliary proficiency just as data liberation. The sanctuary structure itself is a three-dimensional historical data representation through its surface for human capital development on a social system. The study anticipated that solitary solace environment can ensure the compelling communication on the part of human perception. So further research examinations must be utilized for seeing how effective environment can be worked for better data trade for human capital development.

REFERENCES

1. Mattheis, Clemens. "The system theory of NiklasLuhmann and the constitutionalization of the world society." Goettingen J. Int'l L. 4 (2012): 625.
2. Halsall, Francis. "NiklasLuhmann and the body: Irritating social systems." The new bioethics 18.1 (2012): 4-20.
3. Luhmann, Niklas, and William Rasch. Theories of distinction: Redescribing the descriptions of modernity. Stanford University Press, 2002.
4. Seidl, David, and Kai Helge Becker. "Organizations as distinction generating and processing systems: NiklasLuhmann's contribution to organization studies." (2006): 9-35.
5. Pleshkevich, E. A. "NiklasLuhmann's concept of social communication and documentary information theory: Cross points." Automatic Documentation and Mathematical Linguistics 51.1 (2017): 1-5.
6. Garg, Ankit, Akshat Agrawal, and Ashish Negi. "A review on natural phenomenon of fractal geometry." International Journal of Computer Applications 975 (2014): 8887.
7. Ferschlin, Peter, and Andreas Gramelhofer. "Architecture as information space." Proceedings. Eighth International Conference on Information Visualisation, 2004. IV 2004.. IEEE, 2004.
8. Sinha, Ajay J. "Architectural Invention in Sacred Structures: The Case of Vesara Temples of Southern India." The Journal of the Society of Architectural Historians 55.4 (1996): 382-399.
9. Kak, Subhash. "Early Indian architecture and art." Migration & Diffusion-An International Journal 6.23 (2005): 6-27.
10. Oijevaar, K. J. "The South Indian Hindu temple building design system." Unpublished essay sourced online at <http://www.oijevaar.eu/hindu.pdf> (accessed 01 June 2013) (2007).
11. Thakur, Laxman S. "Application of Vāstupuraśamaśāla in the Indian Temple Architecture: An Analysis of the Nāgara Temple Plans of Himachal Pradesh." ArtibusAsiae (1990): 263-284.
12. Hardy, Adam. "Tradition and Transformation: Continuity and ingenuity in the temples of Karnataka." The Journal of the Society of Architectural Historians 60.2 (2001): 180-199.
13. Vardia, Shweta. Building science of indian temple architecture. Diss. 2008.
14. Sardar, Dhrubajyoti, and S. Y. Kulkarni. "Role of Fractal Geometry in Indian Hindu Temple Architecture." International Journal of Engineering Research & Technology 4.5 (2015): 532-537.
15. Datta, Sambit. "Infinite sequences in the constructive geometry of tenth-century Hindu temple superstructures." Geometries of Rhetoric. Birkhäuser, Basel, 2010. 471-483.
16. Rian, IasefMd, et al. "Fractal geometry as the synthesis of Hindu cosmology in KandariyaMahadev temple, Khajuraho." Building and Environment 42.12 (2007): 4093-4107.
17. Dutta, Tanisha, and V. S. Adane. "Shapes, Patterns and Meanings in Indian Temple Architecture." American Journal of Civil Engineering and Architecture 6.5 (2018): 206-215.
18. Tiwari, Shashi. "Origin of Environmental Science From Vedas." (2016).
19. Dutta, Tanisha, and Vinayak S. Adane. "Symbolism in Hindu Temple Architecture and Fractal Geometry-'Thought Behind Form'." International Journal of Science and Research (IJSR) 3.12 (2014): 489-497.
20. Das, Vinay Mohan, and Yogesh K. Garg. "Digital reconstruction of pavilions described in an ancient Indian architectural treatise." Journal on Computing and Cultural Heritage (JOCCH) 4.1 (2011): 1-16.



21. Rao, Kailash, and B. S. Bhooshan. "Parametric Design Principles Found in Ancient Indian Temple Architecture-Case Examples of Columns of KalyaniChalukya Period of Karnataka." *International Journal of Architecture and Infrastructure Planning* 1.1 (2015): 37-42.
22. Debnath, Lokenath. "A short history of the Fibonacci and golden numbers with their applications." *International Journal of Mathematical Education in Science and Technology* 42.3 (2011): 337-367.
23. Omotehinwa, T. O., and S. O. Ramon. "Fibonacci numbers and golden ratio in mathematics and science." *International Journal of Computer and Information Technology (ISSN" 2279-0764) Volume* (2013).
24. Safran, Charles. "The Fibonacci Numbers." *CHANCE* 5.1-2 (1992): 43-46.
25. Akhtaruzzaman, Md, and Amir A. Shafie. "Geometrical substantiation of Phi, the golden ratio and the baroque of nature, architecture, design and engineering." *International Journal of Arts* 1.1 (2011): 1-22.
26. Ciucurel, Constantin, LuminitaGeorgescu, and Elena IoanaIaconaru. "ECG response to submaximal exercise from the perspective of Golden Ratio harmonic rhythm." *Biomedical Signal Processing and Control* 40 (2018): 156-162.
27. Salingaros, Nikos A. "Applications of the golden mean to architecture." Keenan P.(editor, 2012), *Meandering Through Mathematics* (2012).
28. Forsythe, Alex, et al. "Predicting beauty: fractal dimension and visual complexity in art." *British journal of psychology* 102.1 (2011): 49-70.



2BHK Dignity Housing Programme in Greater Hyderabad Municipal Corporation

K Suresh Kumar, P Saroja Rani, B Venkateshwarlu, K Varalakshmi

*Public Health & Municipal Engineering Department, Municipal Administration & Urban Development
Government of Telangana*

✉ saroja2829@gmail.com

ABSTRACT

2BHK Dignity Housing Programme is a unique initiative of Government of Telangana for constructing Double Bedroom houses for shelter less poor people below Poverty line (BPL) with an objective of achieving Slum-free cities. The Programme aims to provide Double Bedroom houses free of cost to the beneficiaries and avoids them from getting into debt trap. The programme intends to provide dwelling unit (DU) with plinth area of about 52 sq.m. with two bedrooms, hall, kitchen and two bath-cum-toilets. Civic infrastructure such as Cement Concrete roads, Storm Water Drains, Underground Drainage System, Protected Water Supply, Electrification Works and Socio Infrastructure such as Primary Health Centers, Community Centres, Schools, Bus Stands, Parks, Play Grounds, Tot-lots etc., are provided. Vertical construction strategy is adopted to accommodate more beneficiaries as the available land is minimal. Planning of these structures was done carefully keeping balance between safety and economy. Promotion of State of Art technologies like Shear wall technology and Pre-cast technology to complete the Project in a short time with higher precision and reduction of labour compared to conventional practise.

Keywords : Dignity Housing; Beneficiary; Technologies; Infrastructure; Self-Reliant Society.

INTRODUCTION

Pradhan Mantri Awas Yojana (PMAY) Mission launched on 25th June 2015 intends to provide Housing For All (HFA) by the year 2022. The Government of Telangana have formulated the Double Bed Room Housing Scheme in the month of October 2015 with an objective to provide dignity to the poor. There is no beneficiary contribution under this scheme, which is one of its kind. In rural areas, beneficiaries solely depend on seasonal conditions for their earnings, the 2BHK housing helped in protecting them from debt traps.

Greater Hyderabad Municipal Corporation (GHMC), an Urban Local Body notified in 2007 is spread over 625 sq.km having a population of 6.81 million (Census 2011) is divided into 6 zones and 30 circles. The Government of Telangana has given One-lakh 2BHK Housing units as target for GHMC in the first phase.

The 2BHK Housing Scheme in Urban areas is dovetailed with PMAY (Urban) under Affordable Housing in Partnership (AHP) vertical, wherein the Mission provides Central Assistance to the implementing agencies through States/Union Territories (UTs) and Central Nodal Agencies (CNAs) for providing houses to all eligible families/ beneficiaries. The Central Sanctioning and Monitoring Committee (CSMC) of Government of India (GOI) has accorded sanction for these houses in their 4th, 6th, 26th and 51st CSMC Meetings.

As per PMAY (Urban) guidelines, the size of a house for Economically Weaker Section (EWS) could be up to 30 sq. mt. carpet area, however States/UTs have the flexibility to enhance the size of houses in consultation and approval of the Ministry. 2BHK Programme of the Government of Telangana intends to provide dwelling unit with plinth area of about 52 sq.m comprising two bedrooms, hall, kitchen and two bath-cum-toilets.

The GHMC adopted two-pronged strategy to achieve the target. One is the development of in-situ slums and the other is construction of Housing Projects in vacant lands. All the layouts under the Project are approved by Town and Country Planning Department and a Single window cell formed for this purpose with official from Hyderabad Metropolitan Development Authority (HMDA), Revenue, Aviation and Fire Departments. Based on the availability of sites, the houses are being taken up in Cellar+Stilt+9, Stilt+5 and G+3 Floors with a unit cost of Rs.8.65 Lakhs, Rs.8.50 Lakhs and Rs.7.75 Lakhs respectively for housing and infrastructure. Lifts and Generators are provided in Cellar+ Stilt+9, Stilt+5 floor structures. Fire fighting arrangements are covered for Cellar +Stilt+9, Stilt+ Stilt+9 floor structures.



The Construction of One Lakh Houses under 2BHK Housing Programme is taken up with a Project Cost of Rs.8598.58 Crores. GOI provides Central Assistance for an amount of Rs. 1.50 Lakhs per DU under PMAY which contributes to around 18% of the Project Cost. The balance 82% of the Project Cost is being borne by the Govt. of Telangana.

DEMAND SURVEY

Area specific demand assessment is carried out in the GHMC duly consulting the stake holders/ slum dwellers/ beneficiaries.

Necessary Demand Survey for 2BHK housing in GHMC limits has been conducted as part of the State Government's Samagra Kutumba Survey (Comprehensive Household Survey) in the year 2014. Based on parameters like Own Thatched Shelter, Rent-Thatched Shelter, Rent-Tiled Shelter, Temporary Thatched Shelter & Temporary Tiled shelter etc., it was estimated that there is a demand for 4.57 lakh families with housing requirement in GHMC limits.

Demand Validation is being done by Regional Centre for Urban and Environmental Studies (RCUES), Hyderabad and the beneficiary data is uploaded in PMAY Website.

LAND POOLING- TSUNAMI CONVERGENT MODEL

Tsunami Convergent Model is an innovative Land pooling technique used to acquire land required for the project within short period by involving all the Department Officials and Public Representatives duly analyzing that microscopic minority holding significant land tried to stall the process.

Counselling and awareness regarding the benefits of the programme created by the vibrant and robust network of SHGs of GHMC and a NGO SRACO (Society for Rehabilitation and Counselling Organization) with a proven expertise in social engineering and family/community counselling issues has been roped in. With extensive interaction with the stakeholders and IEC activities like Street plays by SRACO, "Chetana" awareness programme by Media, Counselling by Public Representatives all their apprehensions about the life in newly developed colonies from completion of project, allocation of dwelling units, management of the colonies etc., have been alleviated.

To reinforce confidence in the slum communities, a single and Common Possession Certificate is issued by the Revenue Department, wherein all the names of families evacuated from a slum for taking up 2BHK Housing project is enumerated in a single order. All these helped in convincing the citizens.

The construction of 2BHK housing units was initially proposed in in-situ slums and vacant / open lands within GHMC area. As a first priority, all the Government lands within the City have been enumerated. Construction of 2BHK housing units in peripheral areas of the City was also considered, which could help meeting the target.

All this made possible to pool up the land to an extent of 667.50 acres for implementing the Dignity Housing Project in GHMC.

DESIGNS, INNOVATIVE TECHNOLOGIES AND GREEN INITIATIVES ADOPTED

A well-engineered structure greatly minimizes the possibility of costly failures. Simply one can't make a building architecturally superb without a deep understanding about its structural planning and behavior. Structural elements in building are like skeleton in human that gives the strength as well as proper shape to make it perfect. Proper structural planning for a building makes it strong and cost effective.

Planning of structures being constructed under 2BHK Programme was done carefully keeping balance between safety and economy. Vertical construction strategy is adopted to accommodate more beneficiaries nearer to city as the available land is minimal.

Different plans/layouts are adopted at various locations based on the site conditions and availability as detailed below:

- i) Cellar+Stilt+9 floors (C+S+9) with 24 Dwelling Units per floor, 12 Dwelling Units per floor, 8 Dwelling Units per floor and 6 Dwelling Units per floor.
- ii) Stilt + Stilt +9 floors (S+S+9) with 12 Dwelling Units per floor, 8 Dwelling Units per floor.
- iii) Stilt +5 floors (S+5) with 24 Dwelling Units per floor, 12 Dwelling Units per floor, 8 Dwelling Units per floor and 6 Dwelling Units per floor.
- iv) Ground +3 floors (G+3) with 24 Dwelling Units per floor, 12 Dwelling Units per floor, 8 Dwelling Units per floor, 6 Dwelling Units per floor, 4 Dwelling Units per floor and 2 Dwelling Units.

The Expertise of Jawaharlal Nehru Architecture & Fine Arts University (JNAFAU), has been utilized for the designs of 2BHK housing at Kollur Site where 15,660 DUs are proposed.



Fig. 1: 15660 DUs at Kollur II of Patancheru in S+10/S+11 Pattern

The structures are analyzed as Space frames using STAAD Pro/ETABS software. The appropriate loads and loads combination as per the relevant clauses in IS Codes are chosen for analysis and designs.

These structures are taken up with different technologies of constructions as detailed below:

i) Conventional Method

Most of the structures are constructed using Conventional Method. The columns and beams are analyzed as a space frame structure using STAAD Pro and designed for M25 Grade of concrete and Fe500 reinforcement.

ii) Shear Wall Technology

Shear wall technology (Construction of Walls and Slab using MIVAN Form work/ Tunnel form work).

MIVAN form work:

This technology is adopted at Dundigal site. Designs are proof checked by JNTU. The structure is analyzed using ETABS as a space frame considering the wall as a spandrel and pier and designed for M35 Grade of concrete and Fe500 reinforcement. Construction speeds are achieved faster due to lighter form work and less labor required for carrying the form work. Production cycle of 3 days can be achieved with higher precision in production of walls and slab units. However, 7-Day cycle was adopted for stripping of Form work. Plastering is not necessary because of the finish obtained.



Fig. 2: Construction of 864 DUs in S+S+9 Pattern at Dundigal using Shear wall Technology - Mivan Form Work

Tunnel form work

This technology is adopted at Rampalli site. Designs are proof checked by IIT Madras. The walls and slabs are monolithic to each other and accordingly the structure is analyzed using ETABS and designed for M40 Grade of concrete and Fe500 reinforcement. The use of rapid hardening concrete was proposed as it attains a compressive strength of 12Mpa within 24 Hours which allows faster de-shuttering and requires no plastering because of the finish obtained. Hence higher construction speeds are achieved. However, 3-Day cycle was adopted for stripping of Form work.



Fig. 3: Construction of 6240 DUs in S+10 Pattern at Rampally with Shear wall Technology - Tunnel Form Work

iii) Precast Technology

The structure is analyzed using ETABS as a space frame considering the wall as a spandrel and pier and designed for M35 Grade of concrete and Fe500 reinforcement.

The usage of precast technology in building construction is relatively new in our country. At present only IS 15916:2010 and National Building Code 2016 (Part 6 -Section 7) are the available Indian standards related to building design and erection using this technology. Designs are proof checked by NIT, Warangal.

The joints between precast elements i.e. the wall-wall joints, the wall-slab joints, the slab-slab joints are important for transmitting the loads coming on to the structure to the ground safely. Columns are casted upto parking floor levels and then Pre-stressed hollow core slabs with M40 grade are erected. As all the elements are prefabricated, higher construction speeds are achieved.



Fig. 4: Construction of 1512 DUs in S+S+9 Pattern at Dundigal using Precast Technology

In addition to the above said technologies, the following Green/Eco friendly initiatives were taken:

- i) Use of natural timber or wood is avoided.
- ii) Raw materials such as Fly-Ash bricks, fly-Ash blended PPC cements, Crushed Stone sand (Robo Sand) are used.

IMPLEMENTATION OF THE PROJECT

i. Policy Initiatives

- a. Relaxations of payment of EMD (1%) & FSD (3%) against 10% for other works.
- b. Supply of cement at subsidized rate of Rs.230/- per bag
- c. Sand is supplied at free of cost by TSMDC (Telangana State Mineral Development Corporation)
- d. Other State / Central Government registered contractors also made eligible to participate in tenders.
- e. Existing GHMC licensed Builders made eligible to participate in tenders.
- f. To accept the single tenders in the 1st call

ii. Physical & Social Infrastructure

Provision of physical infrastructure like adequate Drinking Water, Road Connectivity, Electricity supply, efficient Drainage and Sewerage systems are linked to existing schemes of the State Government.



Bus stops integration with Telangana State Road Transport Corporation (TSRTC), Fire stations to colonies, Open Air Gyms, Sports complexes, ATMs, CC Camera surveillance with support from Police Department. School Buildings, Primary Health Centers, Anganwadi centers, Public Distribution system centers, DWACRA buildings, Markets, Burial grounds, Cremation centers are planned to be developed along with Tree Plantation. Spaces have been earmarked for the above and these will be taken up under respective Government programs.

MAINTENANCE MECHANISM

Layouts are planned with revenue generating features like shopping malls or shops at stilt floor in order to partially meet the recurring maintenance expenditure towards lift, security, and housekeeping of common facilities making the Dignity Housing Project a self-sustainable model.

AWARDS & ACCOLADES

- i. Prime Minister's Award for Excellence in Public Administration 2018, for Excellence in Implementing Pradhan Mantri Awas Yojana".
- ii. Telangana Excellence Award, 2018 to the Commissioner, GHMC and team for the project "Land Pooling for 2BHK" by the Government of Telangana.
- iii. HUDCO Award, 2018 for Outstanding Contribution by GHMC in Housing Sector through various Innovative Initiatives.
- iv. HUDCO Award, 2019-2020 for Best Practices to improve living Environment under Housing, Urban Poverty and Infrastructure for 2BHK Dignity Housing at Kollur II in GHMC.

CONCLUSION

The Dignity Housing Project reached its culmination in the creation of better living standards by constructing 2BHK Houses with Civic and Social Infrastructure. The Houses completed are handed over to the eligible beneficiaries.

Tangible benefits of the projects are providing a spacious ventilated house with all amenities like piped water lines, sewerage system, community center, schools, etc. This leads to intangible benefits of improving the life style of the individuals and in turn achieving a self-reliant society.

REFERENCES

1. PMAY Guidelines from GOI.
2. G.O.Ms. No. 10 Housing (RH&C.A1) Department, Government of Telangana, Dated: 15.10.2015.
3. G.O.Ms. No. 12 Housing (RH&C.A1) Department, Government of Telangana, Dated: 26.11.2015.
4. G.O.Rt. No. 849, MA & UD Department, Government of Telangana, Dt.13.12.2016.
5. G.O.Rt. No. 107, MA & UD Department, Government of Telangana, Dt.28.02.2017.
6. G.O.Rt. No. 380, MA & UD Department, Government of Telangana, Dt.01.07.2017.
7. G.O.Ms. No. 03 Housing (RH&C.A1) Department, Government of Telangana, Dated: 06.11.2020.
8. IS-875 (Part 1)- 1987, Code of Practice for Design loads (other than earthquake) for buildings and structures – Unit weight of building materials.
9. IS-875 (Part 2)-1987, Code of Practice of Designs loads (other than Earthquakes) for buildings and structures – Imposed Loads.
10. IS-875 (Part 3)-1987, Code of Practice of Designs loads (other than Earthquakes) for buildings and structures – Wind Loads.
11. IS:1893 -2002 & 2016, Criteria for Earthquake resistant design of Structure.
12. IS:456 -2000, Code of Practice for design of Plain and Reinforced Concrete structures.
13. SP 34, Hand book on concrete reinforcement and detailing



Advanced Tool for Green and Energy Efficient Building Design

Ankur Mittal, Ashutosh Saxena, B N Mohapatra

National Council for Cement & Building Materials (NCB), Ballabgarh (Haryana)

✉ ankurmittal82@gmail.com

ABSTRACT

Current projections indicate that 66 percent of the world's population will live in cities by 2050. Population equivalent to 7 (seven) "New Delhi" size cities is added per year to world's urban population. According to the data published by The Energy and Resources Institute (TERI), urban share of GDP in India will rise to 75% in 2030-31. Buildings represent around 40% of world's primary energy consumption. They are, therefore, directly responsible for increase in greenhouse gases and can play a key role in climate change adaptation. To achieve an energy efficient building regime, governments, businesses and individuals must transform the way buildings are designed, built and operated. Energy efficient buildings (new constructions or renovated existing buildings) can be defined as buildings that are designed to provide a significant reduction of the energy need for heating and cooling, independently of the energy and of the equipments that will be chosen to heat or cool the building.

The area of study is to develop understanding of high performing building envelope and drive adoption of energy efficient built to investigate and quantify the energy impact from the expected proliferation of important energy efficient solutions.

INTRODUCTION

Construction of building uses land, energy, water, and natural resources, and produces construction waste and releases greenhouse gases causing ecological imbalance. The buildings can develop the capacity to curtail GHG emissions and reduce the carbon footprint by incorporating building codes or rating systems in India. In a building. Energy audit reports and literature review indicates a typical break up of electrical energy consumption in Built Environment of commercial buildings is indicated in **Table 1**.

Table 1: Energy consuming areas in commercial building

Area of Consumption	Percentage Break-up
HVAC System	55%
Lighting	25%
Office equipments	15%
Other auxiliaries	5%

Heating, Ventilation and Air Conditioning system (HVAC) are energy guzzlers in any air conditioned commercial building. The purpose of a HVAC system is to create a comfortable environment by adjusting the four parameters of indoor air - temperature, humidity, air flow, and cleanliness, for the person inside the room/facility or product/process to meet requirement. Another high energy consuming section in building is lighting systems. Lighting not only provide a basic visual environment for occupants, but also have a significant impact on human health, work efficiency, and building energy consumption. Today, many people spend most of their day indoors. Therefore, it is important to create a comfortable visual environment to improve the living environment of the occupants and improve the efficiency of work.

Indoor environmental quality (IEQ) is the quality of a building's environment directly linked to health and comfort of occupants using that space. IEQ is determined by many factors including lighting, air quality, and damp conditions. Indoor environmental quality (IEQ) is a general indicator of the quality of conditions inside a building. It can also include functional aspects of space, for example whether the layout provides access to equipment when needed and whether the building has sufficient space for its occupants. In this regard it is necessary to address for thermal comfort, visual comfort and air quality etc. and their role in IEQ improvement.



Thermal Comfort

Thermal comfort in environment is important because discomfort in thermal conditions are potentially life-threatening for humans if the core body temperature reaches conditions of hyperthermia ($> 37.5\text{--}38.3\text{ }^{\circ}\text{C}$ or $99.5\text{--}100.9\text{ }^{\circ}\text{F}$) or hypothermia ($< 35.0\text{ }^{\circ}\text{C}$ or $95.0\text{ }^{\circ}\text{F}$). Buildings modify the conditions of the external environment and reduce the effort that our body needs to do in order to stay stable at a normal human body temperature, important for the correct functioning of our physiological processes.

Six primary factors that directly affect thermal comfort are defined as

- Metabolic rate
- Clothing insulation
- Air temperature
- Mean radiant temperature
- Air speed
- Relative humidity

Visual Comfort

Visual comfort is usually defined through a set of criteria based on the level of light in a room, the balance of contrasts, the colour ‘temperature’ and the absence or presence of glare.

Visual comfort is a reaction to the quantity and quality of light within any given space at a given time. It depends on our ability to control the light levels around us. Inadequate as well excessive light can cause visual discomfort. Changes in light level or sharp contrast can cause stress and fatigue due to human eye permanent adaption to light levels. It can vary depending on the following factors:

- Time of exposition,
- Type of light,
- Color of the eyes/ age of the person

Working in a window-less office, even under adequate light conditions, and working in an office with a view, are totally different experiences. Abundant scientific studies show positive impacts of the latter on mood and job satisfaction. A well-designed lighting system must provide adequate illumination to ensure safety and enable movement, contribute to visual comfort and facilitate visual performance and color perception. Monitored parameters include quantitative physical measures of the luminous environment (illuminance, luminance, daylight provision and glare) and qualitative aspects of vision (distribution, uniformity, color rendering, the spectral composition of radiation).

Air Quality

Indoor Air Quality (IAQ) directly affect over occupant health, comfort, and productivity significantly. Serious health impacts resulting from poor IAQ include Legionnaires’ disease, lung cancer from radon exposure, and carbon monoxide poisoning. More widespread health impacts include increased allergy and asthma from exposure to indoor pollutants (particularly those as associated with building dampness and mold), colds and other infectious diseases that are transmitted through the air and “sick building syndrome” symptoms due to elevated indoor pollutant levels as well as other indoor environmental conditions.

The two fundamental connections include the impact of ventilation on indoor pollutant levels and the impact on heating and cooling energy (sensible and latent). Given equation expresses the relationship between the outdoor air ventilation rate Q and the indoor pollutant concentration C_{in} for a single zone under steady-state conditions.

$$C_{in} = C_{out} + \frac{S}{Q} - \frac{R_{fac}}{Q}$$

Where C_{out} is the outdoor pollutant concentration, S is the indoor contaminant source strength, and R_{fac} is the rate at which the contaminant is removed by filtration or air cleaning.

This relationship shows that as the ventilation rate increases, the indoor concentration decreases (assuming $S > R_{fac}$).



The amount of energy E required to heat (or cool) and move the ventilation air is expressed as

$$E = \rho C_p Q \Delta T + \rho C_l Q W + E_{fan} - E_{hr}$$

where ρ is the air density, C_p is the specific heat of air, C_l is the air latent heat factor, ΔT is the temperature difference between indoor and outdoor air, W is humidity ratio difference. E_{fan} accounts for the energy associated with equipment used to move the ventilation air (e.g., fans), and E_{hr} is the energy recovered by heat recovery equipment.

Equation shows that as the ventilation rate increases, the energy required to heat (cool) the outdoor air also increases, but it also implies flexibility in how the air is delivered and through the use of heat recovery.

BUILT ENVIRONMENT AND ENERGY EFFICIENCY

Thermal comfort, indoor air quality and visual comfort have to be taken into consideration while designing an energy efficient and healthy building environment, as the overall goal is not just the deployment of such environments but also their overall acceptance by their occupants. The objective of developing low energy consuming or low carbon buildings is to increase the sustainability of the built environment while ensuring the long-term well-being of occupants. However, for an existing it is challenging to modify and redesign a building to meet thermal comfort, visual comfort and indoor air quality for low energy consumption. The field case study findings for energy use implications and adaptive models are discussed to develop clear depiction. There have been a number of studies investigating the energy use implications in the built environment. In this paper, we are briefly discussing measures focusing on performance assessment and approaches to improve energy efficiency of HVAC system in facility.

Sustainability of the Built Environment

Sustainable planning for a commercial building derived from thermal modeling of a particular site and the built environment. Several factors taken into account; sunlight path analysis, orientation of building, climatic conditions. The building shape and orientation are optimised reduce the heat to minimise the delta temperature outside and inside of the building thereby minimizing overall HVAC requirement. In a new building, planned and designed external cladding, insulation and glazing minimizes heat gain/ loss, increase natural ventilation and day light saving in and around the building.

To stop solar heat gain from roof, reflective coating material or installing light-colored roofing materials capable of absorbing, and not transferring, solar radiation should be provide. No other data available.

The energy performance of chiller systems depends on the heat rejection medium, ambient conditions, compressor efficiency and the load carried by each operating chiller. Instead of operating chillers at the same part load ratio, it is recommended to properly accounting for their part load performance characteristics, which maximize the entire system performance.

In an existing building, modifying and improving the chilled water lines, replacing the single glazed glasses with double glazed glass, improving the thermal insulation, is complicated and challenging. It is always advised to consider building envelope design, materials, thermal comfort with overall energy consumption during the construction phase of the building.

The behavioural change for setting higher indoor temperatures in summer-time lead to less prevalence of cooling systems. In situations/locations where air conditioning is unavoidable, a wider range of indoor thermal environment would mean less cooling requirements and hence less electricity consumption for the air conditioning systems.

Energy Efficiency of Built Environment

Maximum energy is consumed by HVAC systems and other chilling units. Some of the reasons for high power consumption and low efficiency are: Operating at low set temperature, Wrong selection of system (oversize or under size equipment), manual control of system, aged system and poor maintenance, choked filters. The poor insulation of the chilled water tank leads to heat gain in summer and more loads on chiller. With proper insulation, the heat gain from the storage tank can be reduced up to 2-5% based upon the ambient conditons.

Energy Conservation Act 2001 support the uptake of energy conservation practices for equipments and appliances announced under energy conservation building code, the adoption of energy efficient appliances and technologies and several rating system in India. The changeover to energy efficient appliances leads to lower energy consumption (reduction of up to 23% in households) and lower instantaneous electric demand.



Energy Efficiency and Recent Developments

Advanced IEQ control systems use learning-based methods, Rule-Based Control (RBC), Model based Predictive Control (MPC) and agent-based control systems. The application of Artificial Intelligence (AI) techniques and smart metering systems create intelligent buildings to improve energy efficiency, comfort, health and productivity of occupant in facility units. Recent domains of AI that are widely used in buildings are Computational Intelligence (CI) or soft computing and Distributed Artificial Intelligence (DAI). Selection of building climate control strategy is highly dependent on the available computational capacity. Appliances equipped with motion sensors or connected to an automatic centralized control system based on occupancy or utilization, bring higher reduction than conventional appliances and can result in a 10% reduction in energy consumption compared to appliances without any power control system or equipped with a standby mode.

Buildings equipped with recent lighting system like LEDs through out in their campus can lead to optimized use of lighting however, in the less occupied spaces there is a need of motion sensors. Buildings with centralized chiller plants may be provided with thermal storage facility for chilled water in the basements or in underground holes. Most of the commercial complexes require the HVAC system during day time so the buildings with thermal storage can operate their chiller plants during non peak hours and store the chilled water and same could be utilized during day time.

Sensors are used to collect data on environmental conditions to manage and operate a facility. These are distributed through the monitored spaces to collect relevant data. Wireless Sensor Networks (WSNs) are a promising technology that will upgrade the data collection and convenient to monitor. The sensors are coupled with actuators which are responsible for the system operation (blinds, lightings and heaters). Indoor environmental climate controls can be linked to immediate occupancy information.

DISCUSSION AND CONCLUSIONS

We have defined the factors that limit the interactions between occupants, IEQ and building design. It is crucial to respect the interdependencies in a human-built environment system for a successful design of healthy, energy efficient and comfortable indoor environment.

Energy consumption, conservation, and the impact of climate change are the upcoming challenges for the future IEQ research. The flexibility and adaptability on smart energy saving measures can be achieved through better built design during construction stage, automated building parameter control, behavioural change and tangible energy conservation measures. However, substantial uncertainties still exist in operation and maintenance, usage and monitoring. There is a need to create a structure enabling continuous training and awareness in the field of building technology and operation for users. The future building environment will be highly automated, based on artificial intelligence and prediction methods. It is believed that highlighted points in this paper will be relevant, especially concerning the emerging markets when it comes to building automation and that they will contribute to more human-centric and environmentally-conscious building initiatives.

REFERENCES

1. ASHRAE. 2005. ANSI/ASHRAE/ACC Standard 180-2008, standard practice for inspection and maintenance of commercial building HVAC systems. Atlanta, GA: American Society of Heating, Refrigerating, and Air-Conditioning Engineers, Inc.
2. ASHRAE. 2009d. Fundamentals Handbook, Indoor environmental health, chap. 10. Atlanta, GA: American Society of Heating, Refrigerating, and Air-Conditioning Engineers, Inc.
3. ASHRAE. 2010b. ANSI/ASHRAE Standard 55-2010, thermal environmental conditions for human occupancy. Atlanta, GA: American Society of Heating, Refrigerating, and Air-Conditioning Engineers, Inc.
4. Baird, G. 2005. User perceptions of indoor air quality in a range of large-scale facilities, with natural and mixed-mode ventilation-field studies in Australia, Germany, New Zealand, and Singapore. Proceedings of the 10th International Conference on Indoor Air Quality and Climate, Beijing, China, 1:6–1.
5. DHHS. 2005. Report of the Surgeon General's workshop on healthy indoor environment. Department of Health and Human Services, Rockville, MD.
6. EPA. 2008. National primary and secondary ambient air quality standards. Washington, DC: U.S. Environmental Protection Agency. www.epa.gov/air/criteria.html.
7. Fisk, W. 2009. Climate change and IEQ. ASHRAE Journal 51(6):22–3.



8. Fisk, W.J. 2000. Health and productivity gains from better indoor environments and their relationship with building energy efficiency. *Annual Review of Energy and the Environment* 25:537–66.
9. GBI. 2010. ANSI/GBI 01-2010, green building assessment protocol for commercial buildings. Portland, OR: Green Building Initiative.
10. Grosskopf, K.R., P. Oppenheim, and T. Brennan. 2008. Preventing defect claims in hot, humid climates. *ASHRAE Journal* 50(7):40–52.
11. Howard-Reed, C., J.C. Little, E. Marand, S.S. Cox, S.J. Nabinger, and A.K. Persily. 2008. *IAQ 2007—Healthy and Sustainable Buildings, Improving the reliability of voc emissions testing of building products*. Baltimore, MD: American Society of Heating, Refrigerating and Air-Conditioning Engineers, Inc.
12. Samet, J.M. 1993. Indoor air pollution: A public health perspective. *Indoor Air* 3(4):19–226.
13. SMACNA. 2007. *IAQ guidelines for occupied buildings under construction*. Chantilly, VA: Sheet Metal and Air Conditioning Contractors' National Association.
14. USGBC. 2009. *LEED 2009 for new construction and major renovations rating system*. Washington, D.C.: U.S. Green Building Council.
15. Weschler, C.J. 2000. Ozone in indoor environments: Concentration and chemistry. *Indoor Air* 10(4):269–88.

Aerospace Engineering



Transformation of Rectangular Parallelepipeds into Fighter Jets & Airborne Missile Launching Platforms

Rajarshi Mukherjee

A-5/5 Uttarayan Housing Estate, 102, B T Road, Kolkata

✉ rajarshi.mukherjee@myworldmail.org

Keywords : Rectangular Parallelepiped, Drilling, Boring, Rotary Cam Milling, Tungsten Electrode Welding, Mild Steel Electrode Welding, Laser Beam Welding, Fighter Jets, Air-Borne Missile Launching Platforms, Single Turbine Aircraft, Twin Turbine Aircraft, Auxiliary Fuel Tank, Shortest Possible Time (SPT).

INTRODUCTION

This paper analyzes some of the Fighter Jets available in the world and in conjunction, discusses, if Rectangular Parallelepipeds can be turned, through simple machining and welding, into a mass production system, in the shortest possible time – SPT, of making Fighter Jets and Airborne Missile Launching Platforms.

This paper delves on simplistic manufacturing practices and an analysis of turning out a futuristic, simplified and alternative approach to design and manufacturing, leading to mass production systems for Fighter Jets and Airborne Missile Launching Platforms.

BODY

India should look at the Fighter Jets available with it, like, examples of MIG series Aircrafts which are a little nose down, Mirages we are not sure of and not too many India has, Sukhois have noses pointed more downwards compared to MIGs, HAWKS have noses pointed more downwards compared to Sukhois, the new induction Rafiels have the base flat and in a straight line but the nose a little pointed downwards. The basic design enlightens us to think of Air-to-Air combats, no fighter jet amongst these have a machine gun on the nose, every one of them has an electro-probe, and in the ATA combats, it is a motion like to keep the beaks straight in a Hen fight, the aircrafts will form a triangle in the motion and will crash into each other at some top-end of the triangle, the formed triangles varying from Aircraft to Aircraft, based on positioning of the noses.

This paper delves in simple manufacturing processes like drilling and boring and cam-milling to turn rectangular parallelepipeds into the structures' of Fighter Jets and Airborne Missile Launching Platforms and in the shortest possible time – SPT, with an idea of creating Mass Production Systems for the future. Some other manufacturing processes, simplistic of them, are involvement of Laser Beam Welding and Laser Cutting.

The processes are and can be broken down into some parts, like one set of drilling, boring and cam milling and the other set, die punching and then laser cutting, finally leading to laser beam welding.

We are dealing with the formation of the structures first, and hence we are moving to the process of rectangular parallelepipeds getting turned in Airframes, with limited operations and finally the wings on them.

SINGLE TURBINE AIRCRAFT

A rectangular parallelepiped, shown sideways and from the front.



Fig. 1: The schematic view of a rectangular parallelepiped

A rectangular parallelepiped first drilled and then bored. It actually resembles the frame of a single turbine aircraft.



Fig. 2: Drilling & boring a rectangular parallelepiped

Rotary Cam-milled after drilling and boring. The shape becomes circular on the outside.



Fig. 3: External Surface Rotary Cam-Milled

The cam-milled rectangular parallelepiped will look like a cylinder. This will house the turbine engine and the oil tank. It will form the structure for a single turbine aircraft.



Fig. 4: Rotary cam-milled surface

The top of the single turbine can be cam-milled whole length, or a portion left out any side, to laser beam weld the Cabin portion with the nose holding the machine gun. If cam-milled partially, the object will look like so.



Fig. 5: Semi-cam-milled into two sections of different diameters

The cabin portion can be shaped as below, in a triangular form. The smaller side of the trapezoid holding the machine gun while the bigger side holding the Pilot(s) cabin. It can be Die Punched or Cone Casted.



Fig. 6: The cabin & machine gun section

Once the Cabin and the Basic turbine holding structure is formed, can be laser beam welded on the front, un-cam-milled portion.

TWIN TURBINE AIRCRAFT

The below diagram represents the basic shape of a twin turbine aircraft.



Fig. 7: twin turbine drilling & boring

SINGLE AUXILIARY TANK AND TWIN AUXILIARY TANKS

A single auxiliary tank or a twin auxiliary tank covers more distance.



Fig. 8: Auxiliary tanks for fuel

TWIN MISSILE CHAMBERS OR FOUR MISSILE CHAMBERS ON A SINGLE TURBINE WITH ONE AUXILIARY TANK

Depending upon Turbine weight towing capacity and wing span, the rectangular parallelepiped can be drilled and bored to carry two or four missiles, with one turbine one auxiliary tank or twin turbine two auxiliary tanks and wings laser welded to the sides.



Fig. 9: Twin or four missile chambers on single turbine & single auxiliary tank

TWIN MISSILE CHAMBERS OR FOUR MISSILE CHAMBERS ON TWIN TURBINES AND TWIN AUXILIARY TANKS



Fig. 10: twin or four missile chambers on twin turbine and twin auxiliary tanks

The above diagrams are a schematic view of what from the front, a single turbine or a twin turbine will look like, how a single or a twin auxiliary tank(s) will fill in, and how each one of them can carry a twin or a four missile system will look like. They are all born off simple machining processes like drilling, boring, cam-milling to get the round outer surface, simple laser cutter to put the machine gun on the nose and simple laser beam welding to add the cabin portion to the structure, noting it will be a single piece design with welded, and laser, cabin and wings. Laser welding is mentioned as it is better to Tungsten and Mild Steel conventional welding and the single piece structure forms the right airframe when speed and wind circulation in the atmosphere are concerned.

CONCLUSION

We hope this paper successfully discusses the simplest of manufacturing processes when used properly, can come out with complex objects like Fighter Jets and Airborne Missile Launching Platforms, a futuristic, simplified and alternative approach, and if thought out properly, can cause, mass production systems in shortest possible time – SPT, for India to be self-reliant in mass producing Fighter Jets and Airborne Missile Launching Platforms.

We hope we are not rubbing off shoulders of people currently involved in Fighter Jet designs, but we are trying to develop a futuristic, simplified and alternative thought process on if can be done, then we can try and evolve for the future of India where skies can be filled with too many of them and in too short a time, bordering on simplicity on mind and efficient work habits, inculcated through the maturity of thinking leading to some experimentations in practical.

We need to note the above discussion is on the formation of the structure without discussing on the wings for the Fighter Jets and the Air-borne Missile Launching Platforms, just laser beam welding the wings on the sides do.

LIST OF REFERENCES

None. (An Alternative Thought Paper Towards Mass Production In Shortest Possible Time -- SPT).



Activating Atmospheric Boundary Condition Inside the Subsonic Wind Tunnel using Passive Turbulence Grid

E Livya, S Nadaraja Pillai

*Turbulence and Flow control Lab, School of Mechanical Engineering,
SASTRA Deemed University, Thanjavur, Tamil Nadu, India*

✉ nadarajapillai@mech.sastra.edu

ABSTRACT

The main objective of this paper is to induce a huge mass of turbulence intensity (T.I) in the test section of a low-speed wind tunnel using a passive turbulence grid. Inducing turbulence inside the wind tunnel is necessary to match the climatic boundary condition of airflow during testing. The rectangular frame of the grid is designed with the reference of the test section inner dimension. The different diameter tube with an alternative grid number is utilized to predict the possibility of generating a higher level of turbulence. In this manner, higher-order turbulence intensity ranging from 4% to 11% can be attained in the test section. Concern has also been given to the flow uniformity that has been verified using rake probe. The flow consistency is a required parameter for developing immense turbulence level. Details of the designed grid structure and outcome of turbulent intensity for various grid arrangement and grid location length scale are conferred in this paper.

Keywords : Turbulence intensity; Boundary layer stimulation; Passive grid; Wind tunnel; Pressure transducer.

ABBREVIATION

T.I -Turbulence Intensity in %

T.G. - Turbulence Grid

U_{∞} - freestream velocity in m/s

P_0 - Total pressure in N/m²

P_s - Static pressure in N/m²

h, b, w - height, base, a width of the designed T.G in cm

H, L, W – Height, Length and width of the tunnel test section in cm

T_u – turbulence level

n – Number of grid

l – Grid location length in cm.

INTRODUCTION

During stormy, the effect of shear stresses are considered at the height of 300m to 400m from ground level will be merely turbulent. This is called viscous sub-layer, a representation of very high wind shear. The earth surface with roughness components like grass, house, trees etc., makes flow with some swirls. Based on this intensity of swirl the velocity, temperature and all other properties of the flow are represented by entropy, momentum and velocities. Due to this purpose, while performing experiments inside the wind tunnel to calculate aerodynamic forces and other air properties, wind tunnel should have the capacity to generate the flow condition as nearly as possible to earth sub-layer, where the frictional velocity is nearly constant. This work is aimed to implement similarity theory using some turbulence generating grids to develop turbulent boundary layer wind tunnels. Several flow conditions are considered by a vast level of turbulence intensity. For the sample, the turbulent intensity level of 20% is gained in turbo machinery flows. Similar wind tunnel experiments are carried to trigger identical turbulent intensity, to reflect the turbulent induced flow rationally. Indistinct, the transition of the laminar-turbulent transition and heat transfer is largely indigent on the free stream level of turbulence.

The determination of the growth of boundary layer enhancement and aerodynamic performance criteria is strongly based on the transition effects. This flow transition depends on merged effects of more turbulence intensity and nearly less Reynolds number as common of high-speed turbo machinery flow. As a result, the replication of achieving similar turbulence levels is of most important for wind tunnel experiments. The perfectly constructed wind tunnel will reflect a very low level of turbulence in a free stream wind speed. Accordingly, a passive mode of turbulence generating grid is utilized to induce the posterior turbulence and change the mean-velocity distribution. Based on the action, the turbulence generators are clustered into two categories.

Passive Turbulence Generator

Generally, passive kind of turbulence generator, are used for raising the level of turbulence inside the wind tunnel test section. In this work, a frame with cylindrical pipe arranged in a grid manner act as a turbulent inducer. From the survey, introducing an appropriate combo of grid criteria (shape of the grid element, grid element width, etc.) helps to achieve a high level of turbulence reported by S. Arunvinthan et al. [1]. Passive kind of turbulent generator are the easiest way of inducing turbulence in wind tunnels. Grid with cylindrical tube produces eddies and the formation of vortices and these vortex effects to add turbulent energy to the flow at the downstream in the wind tunnel. The energy generated by the vortex comparatively has high frequency and breaks the large scale eddies to small scale. The rapid decay of energy in the downstream will takes place. The flow faraway behind the grid is described adequately by good uniformity and isentropic by Thorben Aufderheide et al. [2].

Active Turbulence Generator

The flow injection or introducing rotating parts or an array of winglets placing on a shaft are introduced behind the grid in an active mode of turbulence generator. These add-on parts generate a high swirl isentropic flow in the test section of a wind tunnel. With the aid of the active grid, developing shear turbulent and triggering turbulent boundary layer can be achieved. The active mode of the turbulence generator is complex for generating turbulence. The familiar technique to dominate the turbulence intensity in the wind tunnel is jet injection. The amount of turbulence generation depends on the injection ratio and direction. Review shows that a new method of the active mode of increasing turbulence is endless in research.

RESEARCH METHODOLOGY

Subsonic Wind Tunnel

The Low-speed wind tunnel of the aerodynamics laboratory at SASTRA Deemed to be University is utilized for inducing turbulence at the test section with and without the grid. The wind tunnel motor is rotated with the maximum horsepower of 10HP. The maximal free stream velocity is about free stream velocity $U_\infty = 60$ m/s. The freestream velocity of the airflow is controlled by the RPM regulator. The basic turbulence intensity at the test section of the tunnel is as $T.I \approx 0.1\%$.



Fig. 1: Subsonic wind tunnel facility in SASTRA Deemed to be University.

Pitot Static Tube

The pitot static tube fixed at the downstream of the wind tunnel test section approximately 125 cm away from the test section inlet collects the parallel (P_0) and perpendicular (P_s) direction of incoming flow in the test section used to predict the turbulence level of the flow.

Pressure Scanner

64 channel pressure scanner is used to sense the pressure from the pitot-static tube. The connecting tubes are used to link the Pitot static tube and the scanner. The data was captured with the transient recorder with the sampling frequency of 700 HZ.



Fig. 2: 64-Channel Pressure transducer

Turbulence Generating Grid

The frame of the grid is designed with the dimension of $h*b*w = 30\text{cm}*30\text{cm}*2.5\text{ cm}$. Cylindrical PVC pipe of 2 cm and 2.5 cm in a count of five and six are fitted to the frame. Giulio Vita [4] figured out, if the velocity distribution rear to the grid is not homogeneous, this is due to the impact of turbulence generated by the bars. While choosing the number of the pipe some parameters like solidity factors play an important role. The empirical formula for designing a turbulence grid helps to construct perfect T.G. The ratio between the interference of bars and cavity of the screen is maintained to reduce the solidity factor. The huge solidity grid is not considered and for this reason in this paper, the porosity of the grid is limited within 40%.

The solidity factor of the grid is calculated by using (1)

$$\varepsilon = \left(1 - \frac{d}{g}\right)^2 > 0.5 \quad (1)$$

Where d is the diameter of the grid pipe and g is the distance between the bars.

The turbulence intensity can be theoretically predicted using the grid parameter using Ref. [4] as

$$T.I = 100 \frac{\sqrt{u'^2}}{\bar{u}} \quad (2)$$

Here, T.I turbulence intensity is the deviated velocity in the test section and \bar{u} is the mean velocity measured from the test section.

In this paper, a parallel-mesh grid is designed and tested by placing in vertical directions. This arrangement achieves aimed turbulence magnitude of about 12% with 25 mm diameter pipe with 6 tubes. The experiment carried by placing 5-6 number of tubes separated with an equal distance of $l/n=30/5$ and $l/n = 30/6$.

RESULT AND DISCUSSION

Wind tunnel calibration with and without grid

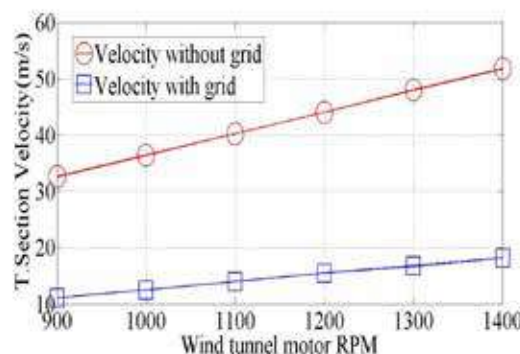


Fig. 3: Wind tunnel motor RPM vs velocity in the test section

The calibration carried out with and without placing the turbulence grid. The mean-flow velocities are measured 90% far away from the test section inlet using Pitot - static tube connected to the pressure scanner. From **Fig. 3**, after introducing the

turbulence grid the velocity inside the test section has been reduced 65% of the free stream velocity, this is stated theoretically in (2). This is due to the formation of turbulence generation by the grid placed at the test section inlet.

Effect of the number of grid

The Intensity of turbulence has been calculated by arranging a PVC pipe in a parallel mode in the vertical direction. To increase the level of turbulence the grid number is increased from 5 to 6, separated by an equal spacing of $L/n=30/5$ cm, $30/6$ cm.

Table 1 : Variation of velocity and turbulent intensity based on grid number and grid size

S.No	The grid at test section inlet	T.S Velocity(m/s)	T.I %
1	5 G, 2 cm Dia.,	23	3
2	6 G, 2 cm Dia.,	14.5	7.14
2	5 G, 2.5 cm Dia.,	14	6.8
4	6 G, 2.5 cm Dia.,	11	12

From **Table 1**, it can be stated from increasing the number of the grid the turbulence level has been increasing twice but the velocity at the test section is reduced half a time of free stream velocity. Even, increasing the diameter of the grid pipe results in increase 60% more T.I.

Location of Grid

The Turbulence grid with 5 and 6 number of pipe are placed at various length ratio (l_r), $l_r=l/L$. Where L is the test section length (150 cm), l is the grid location from the test section inlet. The value of l is varied by placing by placing T.G at 5cm, 10cm, 15 cm, 20cm, 25cm and 30cm.

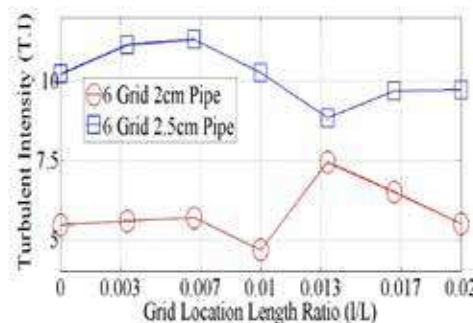


Fig. 4: Variation of the intensity of turbulence along with the grid location with various grid diameter

Fig. 4, gives a detailed view for the results of passive turbulence grid, the results pointed out that turbulence intensity does not vary much only when placing the grid at various location along the test section length. This is because on placing grid at $l/L=0$, results in 5.2% turbulence intensity the same 5.4% of T.I is obtained when placing the grid at $l/L = 0.02$. The placement of the grid is not a considerable parameter in turbulence generation technique. However, increasing the grid pipe diameter from 2 cm to 2.5 cm, the maximum turbulence intensity level of 11.5 % is achieved. Hence the T. I depend strongly on pipe diameter.

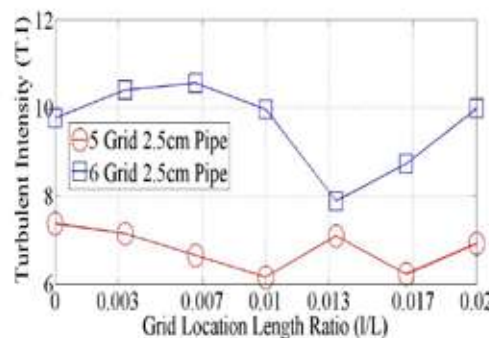


Fig. 5: Variation of the intensity of turbulence along with the grid location with varying number of the grid.



Predicting T.I by increasing number of grid pipe from 5 to 6 count separated by equal spacing, the intensity of turbulence increases to 25%. Thus increasing number of grip pipe results to increase turbulence intensity to 35% from Fig. 5, while choosing several pipes, solidity factor should be considered.

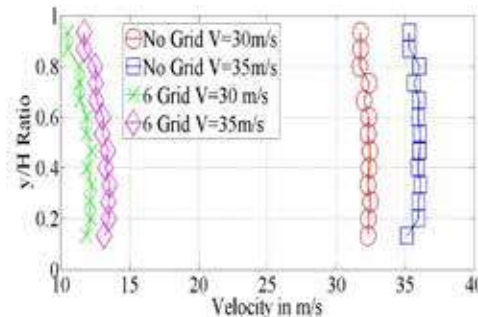


Fig. 6 Flow uniformity check with and without grid along the y-direction

Commonly, the airflow inside the wind tunnel test section is homogeneous throughout, the flow is aligned to the test section and has fully laminar by Junsik Lee et al. [5]. Though the quality of airflow is to be checked, hence the regulation of flow is checked out to measure the amount of irregularity in the airflow. The velocity along the y-direction of the tunnel is measured using the Rake tube. Fig. 6, shows the velocity seems to be equal throughout the height H of the tunnel before and after introducing the turbulence generator grid. This result favours well for the future work for predicting aerodynamic properties for any model under this predicted turbulence intensity generated using this designed turbulence generator grid.

CONCLUSION

A passive mode of generating turbulence by designing a turbulence grid acts as a disturbance to the incoming free stream flow results to a greater quantity of turbulence. This consequences to stimulate atmospheric boundary condition inside the test section of the wind tunnel. The tested turbulence generating method achieves a maximum of 11.5% of maximum intensity. The intensity of turbulence completely depends on the freestream velocity. From increasing grid number from five to six, the T. I is raised to $\Delta T.I = 25\%$. From rake tube, the velocity distribution test result proves the proper homogeneity of the flow in the test section. The tried design of wind tunnel with turbulence generation grid will be perfectly suitable for future construction of boundary layer wind tunnel.

ACKNOWLEDGEMENT

This experimental work was supported by “Research and Modernization fund, SASTRA Deemed to be University” grant number R&M/0035/SoME-008/2015-17. The authors thank SASTRA Deemed to be University for their financial assistance in carrying out this research work.

REFERENCES

1. S. Arunvinthan, S. Nadaraja Pillai, “Aerodynamic Characteristics of unsymmetrical aerofoil at various turbulence intensities”, Chinese Journal of Aeronautics, 32(11): 2395-2407, December 2018.
2. Thorben Aufderheide, Christoph Bode, Jens Friedrichs and Dragan Kozulovic, “The generation of higher levels of turbulence in a low-speed cascade wind tunnel by pressurized tubes”, 11th world Congress on Computational Mechanics (WCCM XI).
3. B. Manshoor, I. Zaman, M.F. Othman and Amir Khafid, “ Experimental study of circle grid fractal pattern on turbulent intensity in pipe flow”, 2nd International Conference on Mechanical Engineering Research, IOP Conf. Series: Material Science and Engineering, 2013.
4. Giulio Vita, “Generating turbulence in wind tunnel experiments: use of passive grid”, Final report, Short-Term Scientific Mission (STSM), COST-STSM-TU1304-35490, February 2016.
5. Junsik Lee and Jae-Hak Lee, “Study on turbulence intensity behaviour under a large range of temperature variation”, processes, November 2020.



Aerodynamic Characteristics of Grooved Rotating Circular Cylinder

Kirthika N, MadhuMadhan, Lokesh U, S Nadaraja Pillai*

*Turbulence and Flow control Lab, School of Mechanical Engineering,
SASTRA Deemed University, Thanjavur, Tamil Nadu*

✉ nadarajapillai@mech.sastra.edu

ABSTRACT

Flow past a grooved rotating circular cylinder placed in a uniform stream is investigated via numerical simulations. The Reynolds number based on the cylinder diameter and the free stream velocity is 0.4×10^5 . The effect of grooves on the cylinder is analysed on various Groove Ratio GR ((no. of grooves)*perimeter of groove/circumference of cylinder) and Spin Ratio α (surface speed of the cylinder/free stream velocity). The cylinder is rotated for 100 rpm and 200 rpm. The C_D and C_L are plotted with different Groove Ratio for two Spin Ratio. The variation of C_D and C_L with Flow time are also plotted. The results are compared with the Smooth (no groove) cylinder on same conditions. The study revealed that the presence of grooves on the cylinder considerably reduces C_D and increases C_L . As the Groove Ratio decreases, C_D decreases for both Spin Ratio. The C_D remains almost same for both Spin Ratio. Furthermore, pressure contours and velocity streamline have been plotted to understand the flow for smooth and grooved rotating circular cylinder on various Groove Ratio and Spin Ratio.

Keywords : Groove Ratio; Spin Ratio; Circular grooves; Groove Depth Ratio.

INTRODUCTION

Flow past a rotating circular cylinder placed in a fluid flow finds many engineering applications. Due to periodic fluid flow, the shear layer separates from either side of the cylinder and develops vortex shedding in the downstream of a cylinder. This vortex shedding causes fluctuating forces on the cylinder which would result in structural vibrations. So, it is essential to control these effects in order to effectively implement it in engineering applications.

The variation of coefficient of drag (C_D) and lift (C_L) of a rotating circular cylinder in a uniform flow have been reported widely in the literature [1]. Unlike smooth stationary cylinder, the smooth rotating cylinder modify flow patterns and reduces flow-induced oscillation from vortex shedding in a viscous uniform flow. However, the Spin Ratio has a great effect on flow separation and formation of vortex shedding. The vortex shedding activity occurs from $\alpha = 0$ to $\alpha \sim 1.95$, after which it is suppressed [2]. Surprisingly, it again resumes in the range $4.34 < \alpha < 4.70$ [1]. In addition to Spin Ratio, Reynolds number is found to have a strong effect on wake morphology behind the cylinder. The presence of grooves on the cylinder has a significant effect on controlling the vortex shedding pattern. The coefficient of drag is reduced when the grooves are made on the cylinder [3]. Due to presence of grooves, the shear layer remain contact on either side of the cylinder and helps in controlling the flow separation. The aerodynamic performance of grooved rotating cylinder is higher than the smooth rotating cylinder. The variation of C_D and C_L with different groove depth have been reported in the literature. However, the aerodynamic characteristics of grooved rotating cylinder with different Groove Ratio have not yet been reported. Therefore, in the present study, the aerodynamic characteristics of grooved rotating cylinder with different Groove ratio are studied via numerical simulation.

The current work is aimed to study the variation of coefficient of drag and lift with different Groove Ratio for Spin Ratio $\alpha=0.03, 0.06$ corresponding to the cylinder rotation 100 rpm and 200 rpm. The pressure and velocity contours are plotted for GR to understand the flow and wake morphology. The results from the grooved rotating cylinder are compared with the smooth cylinder to obtain the aerodynamic characteristics.

NUMERICAL METHODOLOGY

Geometry

We have modelled cylinder with circular grooves on its cross-section by varying no. of grooves. The Groove Ratio (GR) is defined based on the number of grooves, perimeter of the groove and cylinder. Different models have been made according to GR. **Table 1** shows the geometry of cylinder with different GR. For present study, the Groove Depth Ratio GDR (depth

of groove/radius of cylinder) of 1:7.5 is chosen which turns out the depth of the groove to be 4 mm. The specification of the cylinder is illustrated in **Table 2**.

The Smooth Cylinder (no groove) of same diameter and length is used as reference model. For smooth cylinder, GR is zero. The variation of C_D and C_L have been measured and compared the results with the grooved cylinder of different GR. The two parameters C_D and C_L have been computed with variation in GR = 0, 0.8, 1.067, 1.2, 1.3, 1.6 corresponding to the no. of grooves 0, 6, 8, 9, 10, 12. These conditions are measured for Spin Ratio $\alpha = 0.03, 0.06$. The following are the new parameters defined for this paper.

1. Groove Ratio GR = (no. of grooves)*(perimeter of groove/circumference of cylinder)
2. Groove Depth Ratio GDR = depth of groove/radius of cylinder
3. Spin Ratio α = surface speed of the cylinder/free stream velocity

Mesh and Boundary Conditions

ANSYS FLUENT has been used for the computational study and the post processing analysis of the model. The rectangular domain has been generated with 500 mm along x-axis, 300 mm along y-axis and 188.49 mm along z-axis. The model is placed at 170 mm from inlet and 180 mm. The generated mesh for different grooved cylinder ranges from 3×10^5 to 8×10^5 mesh elements. Tetrahedral elements have been used for all models so as to maintain uniformity. The meshing is done in such a way that the mesh is extremely fine near the cylinder and the mesh size increases gradually away from the cylinder. The mesh independence is checked before running the simulation. **Table 3** shows the boundary conditions for the flow simulation.

Table 1: Geometry of cylinder

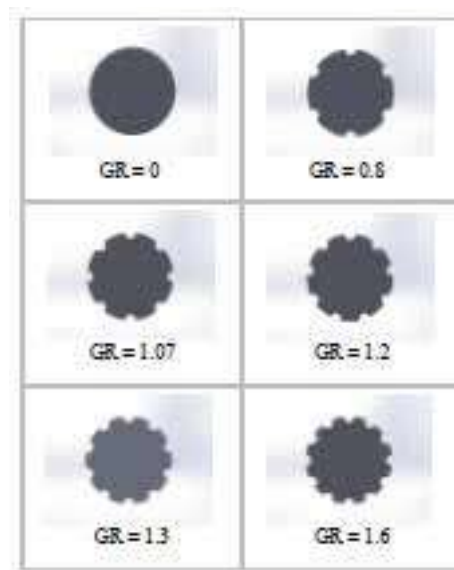


Table 2: Specification of cylinder

Parameter	Value
Cylinder diameter	D = 60 mm
Cylinder length	L = $\pi D = 188.49$ mm
Groove depth ratio(GDR)	1:7.5
Groove depth	d = 4mm

Table 2 : Boundary conditions

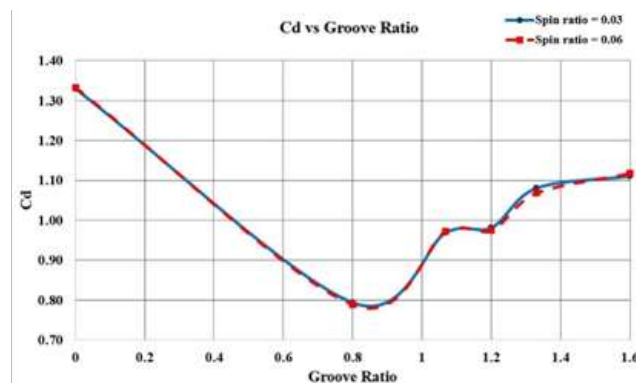
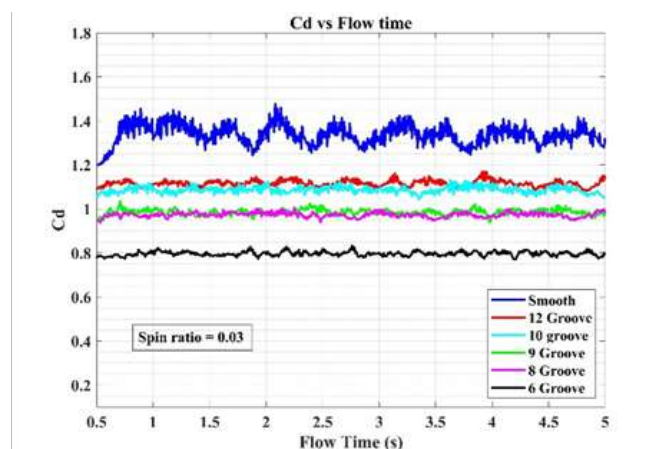
Position Condition	
Inlet Uniform velocity inlet (velocity magnitude = 10.413 m/s)	
Outlet Pressure outlet	
Moving wall Speed of rotation = 10.4719 rad/s (100rpm) = 20.9439rad/s (200 rpm)	
Model	Viscous
Frontal area	$LD = \pi D^2 = 11309.7 \text{ mm}^2$

RESULTS AND DISCUSSION

The variation of drag and lift coefficient with Groove Ratio for two Spin Ratio has been studied. The results of the grooved cylinder are compared with smooth cylinder. This helps in gaining a better understanding of the aerodynamic performance of the different models.

Coefficient of Drag(C_D)

The variation of coefficient of drag is plotted with $GR = 0, 0.8, 1.07, 1.2, 1.3, 1.6$ for $\alpha = 0.03, 0.06$. It is inferred from the graph that C_D remains almost same for both α . For both Spin Ratio, C_D is maximum for smooth cylinder and least for $GR = 0.8$ grooved cylinder. As the GR increases from 0.8, C_D increases for both $\alpha = 0.03, 0.06$. The C_D for all grooved cylinder is less than the smooth cylinder. **Fig 1, Fig 2 and Fig 3** shows the variation of C_D with different GR and Flow time for both Spin Ratio.

**Fig. 1:** Coefficient of drag vs Groove Ratio**Fig. 2:** Coefficient of drag vs flow time

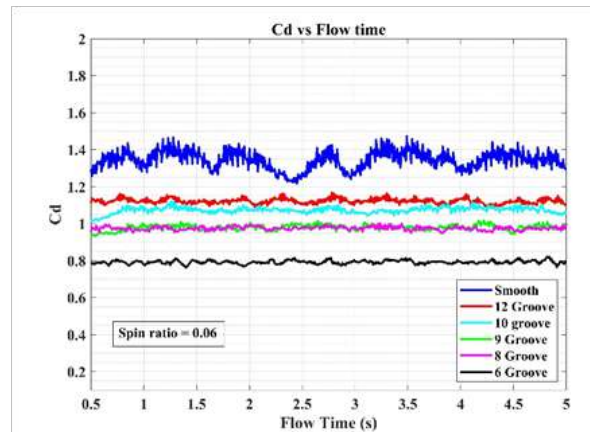


Fig. 3: Coefficient of drag vs flow time

Coefficient of Lift (C_L)

The variation of coefficient of lift is plotted with $GR = 0, 0.8, 1.07, 1.2, 1.3, 1.6$ for $\alpha = 0.03, 0.06$. It is inferred from the graph that C_L increases with increase in α for smooth and grooved cylinder. For both Spin Ratio, C_L is maximum for grooved cylinder with $GR = 1.2$ and least for smooth cylinder. The C_L for all grooved cylinder is more than the smooth cylinder. The variation of C_L with Flow time is also plotted for different GR which follows the same.

Therefore, these reduced C_D and increased C_L imply a better aerodynamic performance compared to the reference model (smooth). The presence of grooves makes the grooved cylinder models a better one compared to the smooth cylinder. **Fig 4**, **Fig 5** and **Fig 6** shows the variation of C_L with different GR for both Spin Ratio.

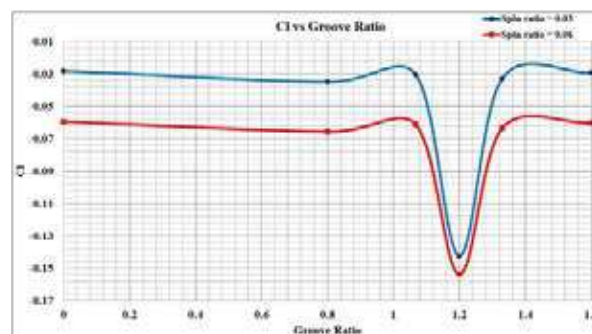


Fig. 4: Coefficient of lift vs Groove ratio

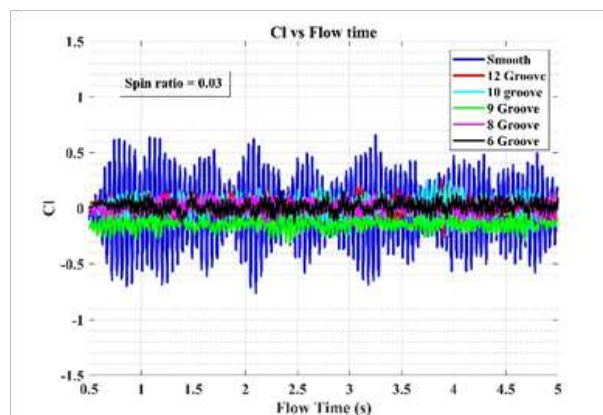


Fig. 5: Coefficient of lift vs flow time

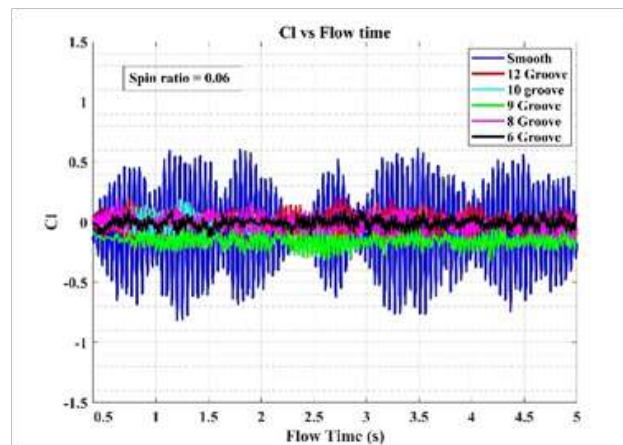


Fig. 6: Coefficient of lift vs flow time

Pressure Contour ($\alpha = 0.03$)

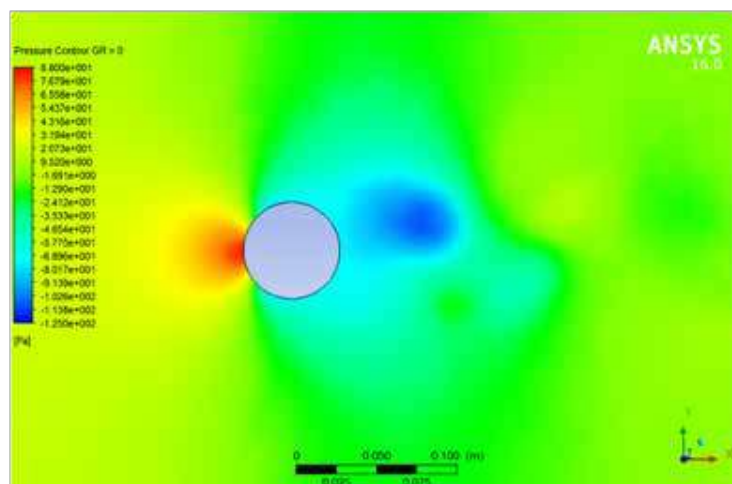


Fig. 7: Pressure contour of smooth cylinder

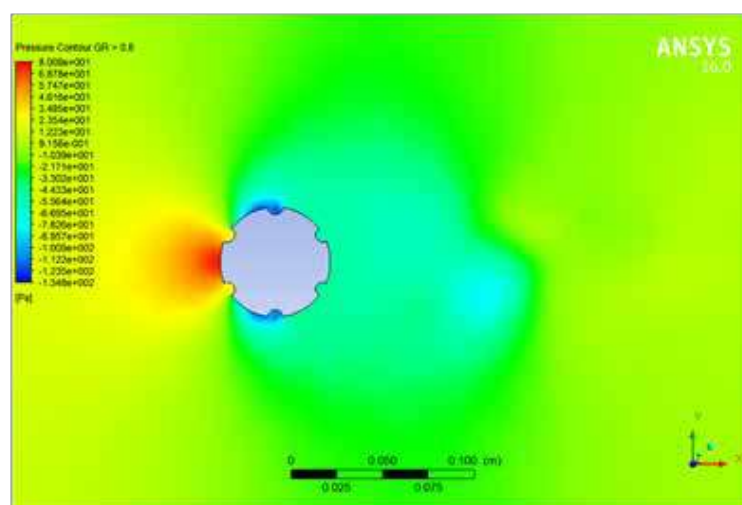


Fig. 8: Pressure Contour of 6 groove cylinder

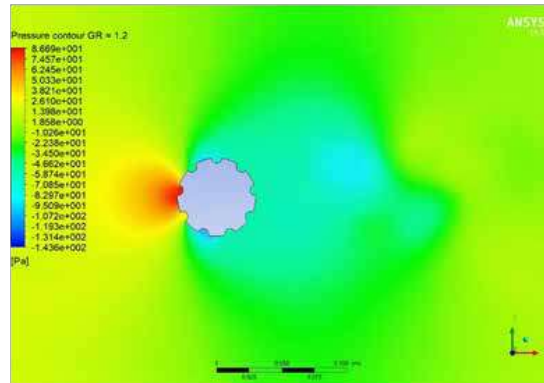


Fig. 9: Pressure contour of 9 groove cylinder

Velocity Streamline ($\alpha = 0.03$)

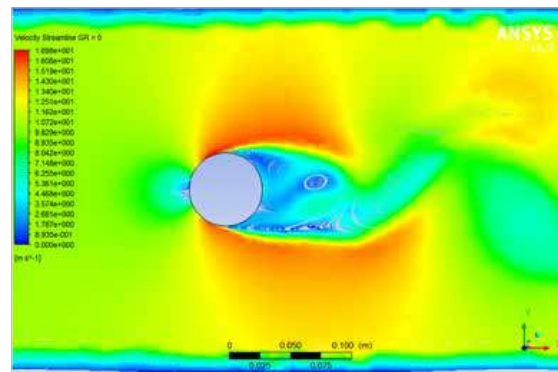


Fig. 10: Velocity streamline of smooth cylinder

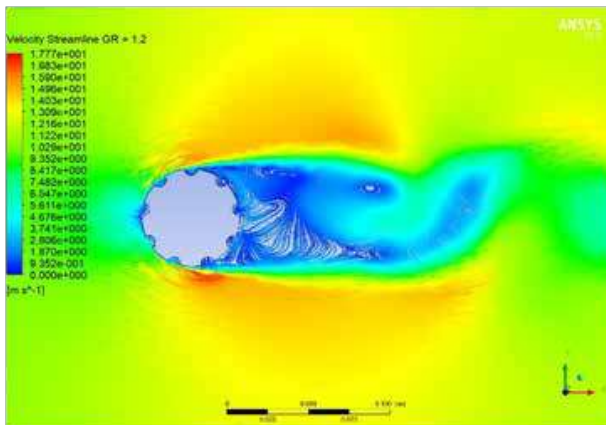


Fig. 11: Velocity streamline of 6 groove cylinder

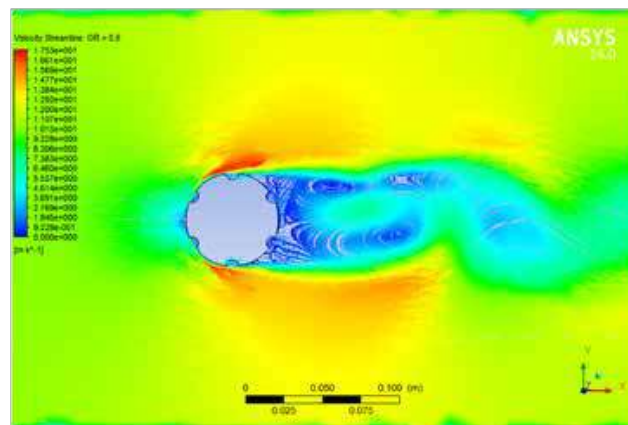


Fig. 12: Velocity streamline of 9 groove cylinder

CONCLUSION

The simulation results for a Grooved and Smooth Cylinder revealed the following:

1. The drag coefficient remains almost same for both Spin Ratio.
2. The drag coefficient is maximum for smooth cylinder and minimum for grooved cylinder with $GR = 0.8$
3. The lift coefficient increases with increase in Spin Ratio.



4. The lift coefficient is minimum for smooth cylinder and maximum for grooved cylinder with $GR = 1.2$
5. For all grooved cylinder, drag coefficient is less and lift coefficient is more than the smooth cylinder for a subcritical Reynolds number 0.4×10^5 .

The results have proved that the presence of grooves on the cylinder led to an increase in aerodynamic performance. Further studies have to be done to understand the aerodynamic characteristics based on different Reynolds number, Groove Depth Ratio and Type of Groove for several Spin Ratio.

REFERENCES

1. Sanjay Mittal and Bhaskar Kumar “Flow past a rotating cylinder” J. Fluid Mech. (2003), vol. 476, pp. 303-334.
2. S Kumar, C. Cantu and B. Gonzalez “Flow Past a Rotating Cylinder at Low and High Rotation Rates” Journal of Fluids Engineering APRIL 2011, Vol. 133 /041201-5
3. Takayama, S and Aoki, K. “Flow Characteristics around a Rotating Grooved Circular Cylinder with Grooved of Different Depths “, Journal of Visualization, Vol. 8, No. 4 (2005)295-303
4. Monalisa Mallick, A Kumar and Anta Murmu “Flow Modelling in various cylindrical surfaces”, Aquatic Procedia 4(2015) 834-840
5. Cetin Canpolat “Characteristics of flow past a circular cylinder with a rectangular groove”, Flow Measurement and Instrumentation 45(2015)233–246
6. Badr, H. M. & Dennis, S. C. R. 1985 Time-dependent viscous flow past an impulsively started rotating and translating circular cylinder. J. Fluid Mech. 158, 447–488.
7. Sangamo Kang, Haecheonand, Sangsan Lee “Laminar flow past a rotating circular cylinder”, Phys. Fluids(Vol. 11, No.11, November 1999.
8. Bo Zhou, Xikun Wang, Wei Guo, Wie Min Gho and Soon Keat Tan,” Control of flow past a dimpled circular cylinder”, Experimental Thermal and Fluid Science69(2015)19-26.
9. Cetin Canpolat and Besir Sahin, “Influence of single rectangular groove on the flow past a circular cylinder”, International journal of Heat and Fluid Flow64(2017)79-88
10. Adnan M. El-Makdah and Ghanem F. Oweis, “The flow past a cactus-inspired grooved cylinder”,Exp Fluids (2013) 54:14.



Optimum Satellite Access Techniques “TDMA / SCPC or PSMA” For Next Generation VSAT Networks

Y S Rayudu

Dy General Manager, D&E-Coastal Surveillance System/NS-2, Bharat Electronics Ltd., Bangalore

✉ rayuduys@bel.co.in

ABSTRACT

In this paper multiple Satellite Access technologies discussed in detail with respect to protocol over heads, and its salient features, for next generation Satcom networks ie Coastal Surveillance VSAT network is considered as case study. The misconception of “Time Division Multiple Access (TDMA) for IP data, Single Channel Per Carrier (SCPC/MCPC) for serial data” existed earlier in Satcom industry studied quantitatively. This misconception existed earlier, due to SCPC manufacturers’ were offering Serial interfaces as default and IP Interface as add-on card, but Nowadays all Non TDMA systems such as SCPC and MCPC (Multi Channel Per Carrier)/PSMA(Packet Switching Multiple Access) based modem equipment manufacturers are offering Modems with IP interface as default interface due to wide acceptability of IP applications’. SCPC and TDMA systems treat user data as series of bit streams without carrying any routing information in its packets. PSMA is true IP based VSAT network technology in which Data packets also carries information about the connection and services including Source and Destination addresses, Priority, Security, and Applications. PSMA processes the connection information and forward each packet over the sky to the required destination modem. As CSS (Coastal Surveillance Services) VSAT network is multi hierarchical hybrid network with bursty, fluctuating user traffic, PSMA with Adaptive Bandwidth on Demand (ABOD) with Capability of Connectivity Management will be the ideal choice.

Keywords : CSS VSAT Network, PSMA , TDMA, SCPC.

INTRODUCTION

It has been for quite a number of years since Ethernet interfaces and IP transport have been available on most, if not all base band satellite communication equipment’s in the industry, there was a misconception of “Time Division Multiple Access (TDMA) is for IP data, Single Channel Per Carrier (SCPC/MCPC) is for serial data .In this paper it is attempted to clarify this misconception by taking one typical case study of Coastal surveillance VSAT network.

This misconception was due to, earlier SCPC manufacturers’ were offering Serial interfaces as default and IP Interface as add-on card, but Nowadays all Non TDMA-TDMA systems like SCPC and MCPC/PSMA based modem equipment manufacturers are also offering Modems with IP interface as default interface due to wide acceptability of IP applications.

TDMA and SCPC can carry IP data traffic, but both the technologies treat user traffic packets as bit streams and do not use any information carried in IP packets.

Packet Switching Multiple Access (PSMA) is the only true IP based VSAT network technology in which Data packets carries rich information about the connection and services including Source and Destination addresses, Priority, Security, and applications. PSMA processes the connection information and forward each packet to different modem accordingly, similar to the function of a IP route.

CASE STUDY: CSS VSAT NETWORK

Coastal Surveillance VSAT network is the integrated real time Chain of Static Sensors project established to safe guard entire Indian coast including Andaman Nichobar and Lakshadweep Islands. CSS network established in the form of Remote Radar Stations (RS) with Electro-optic Surveillance Systems at close to 100 remote locations, 15 ROS’s (Radar operating Station) stations, Five ROC (Regional Operating Center) and Control Center. ROS will be receiving data from the connected RS stations. After processing (correlation) the data will be further linked to the Coast Guard Regional Headquarter (RHQ) known as (ROC). All ROCs will be further connected to the main control center.

VSAT network at the main land locations served as backup network for primary leased line network and surveillance data will be transported through VSAT automatically without user intervention when leased line fails. VSAT network at Island

locations served as primary connectivity network and surveillance data will be transported through VSAT. In order to make VSAT connectivity availability on 24x7 basis, technology required to choose with state of art technology with multi nodes , multi hierarchal and multi technologies which has sufficient link margins as some of the sites are very remote and at the places where satellite foot prints are weak .

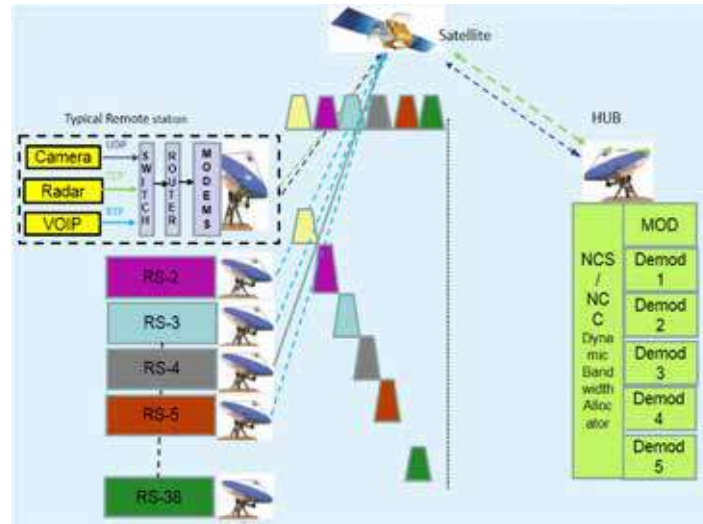


Fig . 1: Typical TDM/TDMA or TDMA/TDMA based VSAT Network

Table 1: Bandwidth requirement at remote station

Sl. No	Description	Bandwidth required (Mbps)
1.1	Data Rate required for Radar sensor	0.5
1.2	Data Rate required for EO/camera System	1.0
1.3	Data Rate required for VHF,MET data sensors	0.2
1.4	Overhead (Protocols, Encryption etc)	0.2
Total Bandwidth required from Remote Radar station		2.0

1. Data rate from each RS Radar station is 2 Mbps.
2. 50 % of Data at ROS need to uplink to ROC
3. 50 % data at ROC need to uplink to CC (25 % of RS sites data)
4. Multi layer architecture with Echelon feature ie when intermediate ROS station fails, RS data required to reach ROC station using over the air dynamic routing protocols.

Typical ROS station with five RS stations as shown in fig 1 is considered for case study in order to identify optimum technology for CSS Network by listing pros and cons of each system. In order to utilize the full advantages of TDM /TDMA offerings i.e. multiple remote sites utilizing same carrier by bursting (Transmitting) at higher rate i.e. 4 to 5 times than actual data rate required by the remotes. This feature will enable other sites to use same carrier at different time slots yet seamless data transfer is ensured.

For example if the data rate required from a typical remote (R1) is 0.4 Mbps then five (5) such remotes can transfer data seamlessly by bursting at 2 Mbps by each remote at different time slots. Remotes (R1, R2, R3, R4 and R5) will burst at next time slots i.e.

$$T1=T0,$$

$$T2= T1+T/5,$$

$$T3=T2+T/5,$$

$T_4 = T_3 + T_5$,

$T_5 = T_4 + T_5$ respectively.

Any VSAT network with such data requirements i.e. sub 1 Mbps data rate exists, user can comfortably utilize the advantages offered by TDM / TDMA technology like bank ATMs etc where data requirement from each ATM machines/ SCADA based remotes will be in the order of few Kbps.

But data rate required from each remote station of Surveillance system will be typically in the order of 2 Mbps due to presence of bandwidth hungry signals like cameras etc. So in order to utilize TDM / TDMA full advantage, user required to configure modem to burst at 10 Mbps though the data rate required per remote is 2 Mbps.

Nowadays most of the applications are demanding carrier rates in the order of 2Mbps/4 Mbps /8Mbps/10 Mbps due to user content is IP centric with video, Audio and Data services.

Whether TDMA technology for such high carrier data rate is appropriate? One must analyze quantitatively instead of qualitatively before choosing appropriate (right) technology.

It may be noted that DOT guideline does not permit to transmit more than 2 Mbps data from the remote sites with 2.4 Mt/ 3.8 Mt Antenna. It may be noted that accommodating bigger size antennas at remote places is not feasible due to cost implications and non-availability required real estate at remote places is real issue to accommodate bigger antennas at proposed (RS sites). So with the proposed antenna sizes at remote RS stations, user cannot take the advantages of TDM/TDMA Access mechanism systems for CSS kind of traffic.

MULTIPLE SATELLITE ACCESS MECHANISMS

Data through put efficiency of TDMA / SCPC or PSMA Systems are studied in detail and same is tabulated , shown in **Fig.2** which enable user to adapt appropriate technology based upon applications.

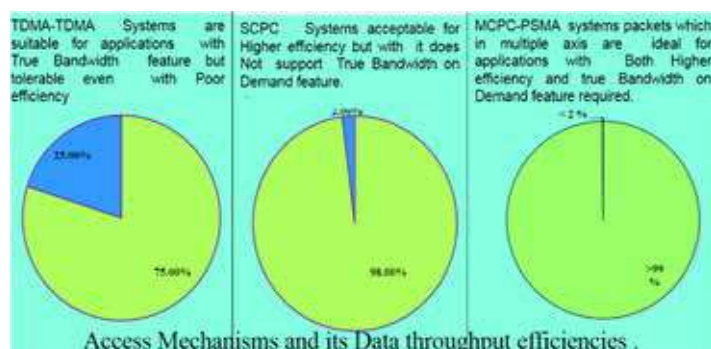


Fig. 2: TDMA / SCPC or PSMA systems

TDMA-TDMA, TDM/TDMA Systems

Efficiencies offered by TDMA-TDMA Systems (Typically around 75 %) which can be tolerable, where user data to be transported per Node is in the order of sub 1 Mbps (64 Kbps/128 Kbps/512 Kbps i.e. less than 1 Mbps) with true Bandwidth On Demand (BOD) feature i.e. burst demodulation. With this TDMA access mechanism precious 25 % satellite bandwidth forced to utilize for framing overheads which are inevitable with TDMA systems. This inefficiencies can be tolerable, if the user IP data rate required from the remotes are sub 1 Mbps, then one can think of TDMA

SCPC Systems

SCPC systems will be suited for applications where user data to be transported per Node is high but number of nodes in the network are limited and no true native Band width on demand feature is required.

MCPC/PSMA (Packet Switching Multiple Access) Systems

Such systems are very efficient true Bandwidth on Demand satellite access mechanism which will transport user payloads with near zero or bare minimum over heads, (< 2%). In other words PSMA (Packet Switching Multiple Access) is the true IP based VSAT network technology with efficiencies better than 98 % and in which Data packets also carries information about

the connection and services including Source and Destination addresses, Priority, Security, and applications. PSMA processes the connection information and forward each packet over the sky to the required destination modem accordingly. PSMA based satellite modem will act like a switch in the Sky (True IP based layer 3 Switch in the Sky), unlike most of existing VSAT networks are layer-2 networks WAN side .

SALIENT FEATURES OF PSMA TECHNOLOGY

This next generation Technology realize, True bandwidth on demand feature by a mere 48 Kbps signaling channel for entire network and each site is assigned by NCS . a carrier which is transport to user pay load data with zero overheads which enable to realize ~99% overall data throughput efficiencies. This feature will help in saving precious satellite bandwidth over 30 to 50 % over existing TDMA-TDMA technology.

Adaptive Bandwidth on Demand (ABOD) feature with Connectivity Management which improve bandwidth efficiency by Streamlining burst and fluctuating user traffic which is very much applicable for CSS type of traffic. Tighter Roll-off factors of 5 % compared with existing modems which are with 20 % roll offs will further reduce satellite bandwidth by another 15%.

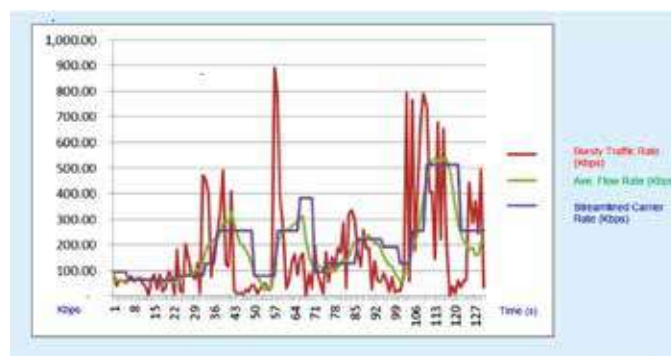


Fig. 3: Adaptive bandwidth on demand (ABOD)

PSMA Modems with LDPC Forward Error Codes will require 2.5 to 3 dB lower E_b/N_0 than the existing MFTDMA modems which are with TPC(Turbo Product Code) Forward Error Codes for the same BER (Bit error rate) of 1×10^{-8} . This additional 2.5 to 3 dB advantage in E_b/N_0 will further increase link margin which will help in maintaining VSAT remote sites where satellite foot prints are poor.

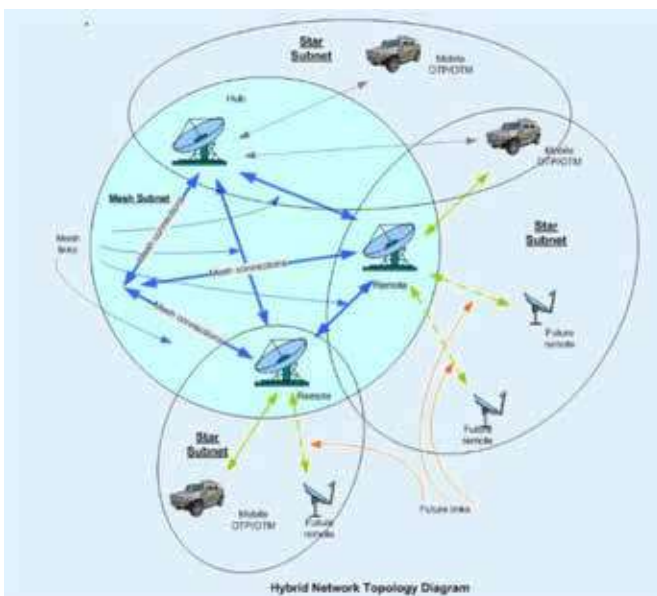


Fig. 4: Hybrid Network Topology with connectivity control Diagram



Proposed modem technologies supports, higher modulation like 16QAM / 32QAM. Use of Higher modulation like 16QAM compared with QPSK/8PSK will further saves bandwidth by 50 to 100 % at places where 7.5 Mt antennas are used will save satellite bandwidth by another 100 % from QPSK to 16 QAM.

The following are the advantages of next generation VSAT systems using PSMA multiple access techniques:

1. Continuous wave carriers with zero multiplexing overheads results in higher overall efficiencies up to 99%
2. Lower carrier spacing's (Tighter Roll off) up to 5 % instead of existing 20 %.
3. ABOD (Adaptive Bandwidth on Demand) feature further improves efficiency more than 30 %
4. Packet compression feature further reduce data rate requirement which is yet another Bandwidth efficiency feature
5. Connectivity control feature added network flexibility.
6. Dynamic Routing over Satellite (True Switch in Sky)
7. User Configurable network structure for dynamic connectivity which enable to accomplish mission critical , dynamic war scenario situations where technology should not become limiting factor.
8. As PSMA technology has bare minimum (less than 2 %) overheads on the user data rate, Total data rate requirement will reduce drastically which enable to use lower Power BUC (Block up converters) from remotes. Lower Power BUCs are more reliable and over cost of VSAT network can come down.
9. By adapting latest Forward Error codes such as LDPC(Low Density Parity Check) , advanced features such as AUPC (Automatic uplink power control) and ACM (Adaptive Coding modulations) will enable to achieve higher link margins which will help to maintain network 24X7 even during signal degradations due to pointing inaccuracies developed over period of time and atmospheric variations.
10. Smaller remote antennas can suffice, for user BER (Bit Error Rate) requirements which avoids requirement of complex Antenna control units.
11. As this next generation SATCOM modem require lesser bandwidth more number of VSAT nodes for given Bandwidth (More Concurrency) can serve through VSAT within allocated Bandwidth or it can reduce the satellite Bandwidth typically by 40 % to 50 % for same number of concurrency requirements.

COMPARISON OF PSMA WITH EXISTING TDMA SYSTEMS

Table 2: Comparison of psma & existing vsat

Features	PSMA VSAT	Existing TDMA VSAT
No. of Carriers	One carrier per site	One shared among multi-sites results higher data rate per site
Carrier Rates	Vary and On-Demand, from 8 kbps to 22/40 Mbps	Pre-Fixed at rates 256/ 612.5 kbps / 1.25 / 2.5 / 5 Msps.
Data Throughput	Same as Carrier Rates.	Only Fraction of carrier rates
Carrier Activation	On-Demand and Continuous and adaptive Bandwidth on demand	Frequent Bursts in the order of milliseconds
FEC (Forward Error Correction)	Supports LDPC which require 2 to 2.5dB lesser Eb/No	Supports Turbo FEC only by existing MFTDMA systems which does not support LDPC.
Channel Efficiency	Near to 99%, throughput=carrier rate	50-75% (Sometimes lower than 50% avg.)
MCPC Multiplexing	Layer 2 & 3 Routing	TDMA Mux
Latency	Typical 500 ms round trip delay	Typical 650 ms round trip delay
Connectivity	Unlimited supports Star / Mesh / Hybrid)	Single Topology (Star or Mesh)
Network Expansion	Unlimited	Limited by TDMA Carrier Rate
BUC and Antenna Size	Smaller Antenna sizes with lower power BUC can provide comfortable Link margins.	Higher antenna sizes are required in order to maintain same BER(Bit Error Rate) which add additional cost.



CONCLUSIONS

Next generation VSAT networks such as CSS (Coastal surveillance system require multi hierarchical, multi node complex hybrid network unlike simple Star or mesh alone network. Due to its complexity, CSS VSAT network, ideally will be requiring high efficiency technologies like PSMA with Adaptive Bandwidth on Demand feature with connectivity control feature. Selection of optimum satellite access technology for CSS will be very much important, in view of number of nodes are 125 + nodes and needing satellite bandwidth in excess of 2 + transponders.

Lastly , the total cost (Capital & Operational expenditure i.e. CAPEX & OPEX) of each solution with respect to precious satellite bandwidth, System reliability and ease of maintenance will play vital role in selecting right technology for given user requirements.

REFERENCES

1. ETSI TS 101545-3 V1.3.1 (2020-0) Digital Video Broadcasting (DVB- RCS) pp 9-20.
2. ETSI EN 301790 V1.5.1 (2009-05) pp 14-63.



Electromechanical Behavior of Graphene-based Composite Plate with Flexoelectric Effect

K B Shingare, S Naskar*

Department of Aerospace Engineering, Indian Institute of Technology Bombay, Powai, Mumbai

✉ susmitanaskar@iitb.ac.in*

ABSTRACT

In this paper, the derivation of an exact analytical solution of nanoplate using Navier's method and Kirchhoff's plate theory is investigated. The electromechanical behavior of simply supported graphene-reinforced composite plates accounting the influence of size-dependent properties under the uniformly distributed load is investigated. So, the analytical results obtained from the present study show that the influence of size-dependent properties such as piezoelectric and flexoelectric effect on the nanoplates' piezoelectric response is substantial with respect to thickness of plate. The electromechanical response including maximum deflection and resonant frequency of graphene-reinforced composite plates shows significant enhancement when compared to the conservative composite plate. Outcomes of present results reveal that effect of flexoelectricity on static and dynamic characteristic of composite plate is noteworthy and cannot be neglected.

Keywords : Graphene, Flexoelectric effects, Nanocomposite, Nanoelectromechanical.

INTRODUCTION

In the past few decades, the discovery of piezoelectric composite structures has paid huge interest in the research communities to predict their properties and possible use such as nanoelectromechanical systems (NEMS) application such as sensors [1], actuators, electric switches, nano-generators, transistors, energy harvester, and distributors [2] for the active control of high-performance lightweight smart structures subjected to static and dynamic loading [3]. The effect of piezoelectricity was first observed in 1880 by P. Curie and J. Curie [4]. Piezoelectric material has the property to generate electrical polarization in response to the homogeneous strain and vice versa. Whereas, in 1957, Mashkevich and Tolpygo observed the effect of flexoelectricity [5] and defined as the spontaneous polarization to an applied strain gradient can be called as direct flexoelectric effect, which is coupling between the electric response (in terms of polarization or electric field) and gradient of mechanical responses. Numerous studies were carried out so far to explore the effect of piezoelectricity in bulk materials and recently, exploitation of nanomaterial has attracted the researchers interest significantly to study the effect of the piezoelectricity in the different materials. However, due to the homogeneous strain, the piezoelectric effect unable to improve the size-dependent characteristics of piezoelectric nanostructures, in such cases by breaking the inversion symmetry, non-piezoelectric dielectrics nanostructures can also be polarized this phenomenon of breaking inversion symmetry to polarized non-piezoelectric dielectrics is named as flexoelectricity [6]. The recent advancement of nanoscale technologies has captivated the attention in flexoelectricity since the large strain gradients frequently exist at the nanolevel may cause to flexoelectric effect.

The ground-breaking experimental analysis concerning to 2D single layer of graphene by Novoselov et al. [7] has engrossed massive response from researchers and scientists because of its distinctive mechanical strength, electrical conductivity, thermal conductivity. Recently, Shingare and co-authors [8]–[12] studied the electromechanical response of graphene-based nanocomposite (GNC) and its structures such as beam, plate, shell and wire by incorporating piezoelectric nanoscale graphene fiber in polyimide matrix. In this, they assumed graphene as nanoscale fiber and found effect of size-dependent properties such as piezoelectricity, flexoelectricity and surface effect on these GNC structures. They have predicted the piezoelectric and dielectric properties of GNC using analytical and numerical models. They showed the significant enhancement in static, dynamic and electric response of GNC structures due to incorporation of these size dependent properties. Garcia-Macias et al. [15] also shown GNPs in the composite are superior to carbon nanotubes (CNTs) while considering the load-bearing capacity and stiffening effects. Naskar and co-authors [16]–[19] proposed a new micromechanical analysis for predicting the effective properties of fiber-reinforced composite and functionally graded material (FGM) by using a novel approach of stochastic representative volume element (SRVE) considering spatial distribution with stochastic analysis and uncertainty quantifications. They have also carried out static and dynamic characteristics including sensitivity and frequency analysis of laminated composite and FGM by using a probabilistic uncertainty quantification approach.

Liu and Rajapakse [20] integrated the effect of surface parameters for determining the deflection and vibration of nanoplate. To the authors' knowledge, a flexible piezoelectric graphene-based nanoplate with consideration of effect of flexoelectricity offers various opportunities for developing NEMS. Therefore, in the present study, we develop an analytical model based on Navier's method and Kirchhoff's plate theory for SS nanoplates with considering the effects of flexoelectricity. Obviously, a closed-form solution is developed for nanoplates with uniformly distributed loading (UDL) was evidently absent from the earlier literature.

GOVERNING EQUATIONS FOR PIEZOELECTRIC PLATE

In this, the governing equations for graphene-reinforced composite (GRC) plate subjected to the uniformly distributed mechanical load (q_0) are derived from investigating its static bending and dynamic behavior considering the flexoelectric effect.

Fig. 1 shows the schematic of simply-supported (SS) GRC nanoplate having thickness h , length a and width b . A Cartesian coordinate system is used to describe the nanoplate with a thickness along the z -axis and the midplane of the unperformed nanoplate that coincides with the x - y plane.

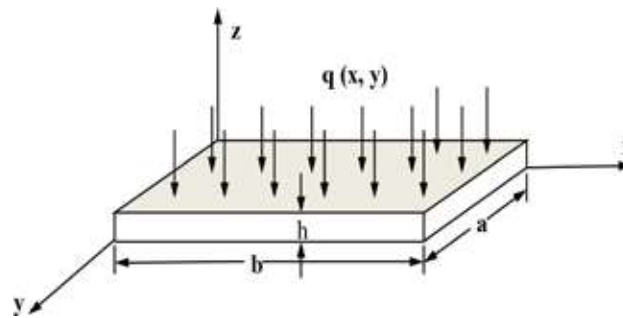


Fig. 1: Representation of a SS GRC nanoplate under UDL

Assumptions of Kirchhoff's Plate Theory

- Straight lines normal to the mid-surface (i.e., transverse normals) before deformation remain straight after deformation.
- The transverse normals are inextensible (i.e., do not experience elongation).
- The thickness of the plate does not change during deformation.
- The transverse normals rotate such that they remain normal to the middle surface after deformation. The first three assumptions signify that transverse displacement is independent of transverse (or thickness) coordinate and transverse normal strain is zero. The last assumption indicates zero transverse shear strain.

As per Kirchhoff's plate theory, the in-plane displacement of the plate in terms of transverse displacement $w(x,y,t)$ can be expressed as [21]:

$$u(x, y, z, t) = -z \frac{\partial w(x, y, t)}{\partial x};$$

$$v(x, y, z, t) = -z \frac{\partial w(x, y, t)}{\partial y};$$

$$w(x, y, z, t) = w(x, y, t) \quad (1)$$

where u and v are displacement components with respect to x and y directions, and t is the time. Considering the infinitesimal deformation, by assuming the coupling between electric field and strain gradient, the constitutive Eq. for the energy density function U is expressed as [22]:

$$U = -\frac{1}{2} \epsilon_{kl} E_k E_l + \frac{1}{2} C_{ijkl} \epsilon_{ij} \epsilon_{kl} - e_{ijk} \epsilon_{ij} E_k - \mu_{ijkl} E_i \eta_{jkl} + r_{ijklm} \epsilon_{ij} \eta_{klm} + \frac{1}{2} g_{ijklmn} \eta_{ijk} \eta_{lmn} \quad (2)$$

in which, ϵ_{kl} , C_{ijkl} , e_{ijk} , μ_{ijkl} denote the permittivity, elastic, piezoelectric, and flexoelectric coefficient, respectively; ϵ_{ij} , E_i , and

η_{jkl} indicate the component of strain, electric field, and the strain gradient, respectively; r_{ijklm} are the coupling amongst the strain and strain gradient and g_{ijklmn} are the components of nonlocal elastic effects which are neglected for simplicity. Here, for convenience, we consider the flexoelectric coefficient can be presented such as $\mu_{31} = \mu_{3113} = \mu_{3223}$ [23]. Using the equation of Gauss' law of electrostatics ($\nabla \cdot D = \rho_s$), in the absence of free electric charge (ρ_s), the electric displacement for the thin nanoplate can be written as:

$$\frac{\partial D_z}{\partial z} = 0 \quad (3)$$

The governing equations for the SS nanoplate problem can be derived using dynamic version of Hamilton's variational principle, such as [24]:

$$\delta \int_0^t (U + W - K) dt = 0, \quad (4)$$

Boundary conditions considered for SS rectangular GRC nanoplate on all four edges are prescribed and can be deduced as [24]:

at $x = 0$ and $x = a$:

$$w = 0, M_{xx} = 0. \quad (5)$$

at $y = 0$ and $y = b$:

$$w = 0, M_{yy} = 0. \quad (6)$$

By virtue of Eqs. (5-6): M_{xx} , M_{xy} , M_{yx} and M_{yy} indicate the bending moments, N_{xx} and N_{yy} are the axial force across the thickness and is presented as:

$$\begin{aligned} M_{xx} &= \int_{-\frac{h}{2}}^{\frac{h}{2}} \sigma_{xx} z dz, \quad M_{yy} = \int_{-\frac{h}{2}}^{\frac{h}{2}} \sigma_{yy} z dz, \\ M_{xy} &= M_{yx} = \int_{-\frac{h}{2}}^{\frac{h}{2}} \tau_{xy} z dz \end{aligned} \quad (7)$$

$$N_{xx} = \int_{-\frac{h}{2}}^{\frac{h}{2}} \tau_{xx} dz, \quad N_{yy} = \int_{-\frac{h}{2}}^{\frac{h}{2}} \tau_{yy} dz \quad (8)$$

By using values of M_{xx} , M_{xy} , M_{yx} , M_{yy} , N_{xx} and N_{yy} into Eq. (5 and 6), the governing expression for the transverse deflection w is given as:

$$\begin{aligned} F_{11} \left(\frac{\partial^4 w}{\partial x^4} + \frac{\partial^4 w}{\partial y^4} \right) + 2(F_{12} + 2F_{66}) \frac{\partial^4 w}{\partial x^2 \partial y^2} + \\ \rho h \frac{\partial^2 w}{\partial t^2} = q_0 \end{aligned} \quad (9)$$

with

$$\begin{cases} F_{11} = \left(C_{11} + \frac{e_{31}^2}{\epsilon_{33}} \right) \frac{h^3}{12} + \frac{\mu_{31}^2}{\epsilon_{33}} h \\ F_{12} = \left(C_{12} + \frac{e_{31}^2}{\epsilon_{33}} \right) \frac{h^3}{12} + \frac{\mu_{31}^2}{\epsilon_{33}} h \\ F_{66} = C_{66} \frac{h^3}{12} \end{cases} \quad (10)$$

It can be concluded that bending stiffness of the GRC nanoplates is influenced by flexoelectricity i.e., in case of F_{11} and F_{12} it will increase but will not change in case of F_{66} . From the above formulation, it is observed that the flexoelectric effect has a significant influence on the bending stiffness of nanoplate.

Derivation for Static Response

The governing equation (9) in terms of static mechanical bending behavior of the GRC nanoplates can be re-expressed as:

$$F_{11} \left(\frac{\partial^4 w}{\partial x^4} + \frac{\partial^4 w}{\partial y^4} \right) + 2(F_{12} + 2F_{66}) \frac{\partial^4 w}{\partial x^2 \partial y^2} = q_0 \quad (11)$$

It should be revealed that in the absence of the flexoelectric effect, considering linear piezoelectricity, the above governing equation can follow the conservative Kirchhoff plate theory. Hence, to derive the governing Eq. (11) of the SS GRC plate, the Fourier series is expressed for $w = w(x, y)$ are as follows:

$$w(x, y) = \sum_{m=1}^{\infty} \sum_{n=1}^{\infty} A_{mn} \sin \alpha x \sin \beta y \quad (12)$$

where $\alpha = \frac{m\pi}{a}$, $\beta = \frac{n\pi}{b}$ and A_{mn} are the coefficients to be evaluated for each m and n should be satisfied everywhere in the domain of the plate. By making use of Fourier series, the uniformly distributed load $q_0(x, y)$ is expressed as:

$$q_0(x, y) = \sum_{m=1}^{\infty} \sum_{n=1}^{\infty} Q_{mn} \sin \alpha x \sin \beta y \text{ and } w(x, y) = \frac{Q_{mn}}{d_{mn}} \quad (13)$$

where

$$Q_{mn} = \frac{16q_0}{mn\pi^2} \quad m, n = 1, 3, 5, \dots$$

$$d_{mn} = \quad (14)$$

$$\left(\frac{\pi}{b} \right)^4 \left\{ F_{11} \left(\frac{m}{a} \right)^4 + F_{12} \left(\frac{n}{b} \right)^4 + 2(F_{12} + 2F_{66}) \left(\frac{mn}{ab} \right)^2 \right\} \quad (15)$$

By putting Eqs. (14 and 15) into Eq. (13), to derive transverse deflection, one can acquire the solution for the SS plate.

Numerical outcomes validate that the transverse deflection series has a quick convergence rate, and the first term with respect to $m = 1$ and $n = 1$ is far higher compared to the other factor. Thus, taking the first term from the above equation, one can derive the approximate solution.

Derivation for Dynamic Response

The dynamic behavior of GRC nanoplates can be expressed by using Eq. (10) as follows:

$$F_{11} \left(\frac{\partial^4 w}{\partial x^4} + \frac{\partial^4 w}{\partial y^4} \right) + 2(F_{12} + 2F_{66}) \frac{\partial^4 w}{\partial x^2 \partial y^2} + \rho h \frac{\partial^2 w}{\partial t^2} = 0 \quad (16)$$

Analogous to the conservative model for plate, the periodic solution for $w(x, y, t)$ is obtained as:

$$w(x, y, t) = \sum_{m=1}^{\infty} \sum_{n=1}^{\infty} B_{mn} \sin \frac{m\pi x}{a} \sin \frac{n\pi y}{b} e^{i\omega_{mn}t} \quad (17)$$

in which B_{mn} , m , n and ω_{mn} represent the mode shape amplitude, the half wave numbers, the resonant frequency, respectively, and $i_2 = -1$.

Substituting Eq. (17) into Eq. (16), the plate resonant frequency written as follows:

$$D_{11} \left[\left(\frac{m\pi}{a} \right)^4 + \left(\frac{n\pi}{b} \right)^4 \right] + 2(F_{12} + 2D_{66}) \left(\frac{m\pi}{a} \right)^2 \left(\frac{n\pi}{b} \right)^2 - \rho h \omega_{mn}^2 = 0 \quad (18)$$

From above, it is clear that if flexoelectric effects are neglected, then the resonant frequency will be evaluated through the



conservative theory of piezoelectricity. In this study, we only consider the mode (1,1) resonant frequency ω_{11} (i.e., fundamental frequency) with a variation of aspect ratio and thickness of the plate in the subsequent section.

RESULTS AND DISCUSSIONS

In this section, to examine the influence of size-dependent properties on the static and dynamic behavior of GRC nanoplates, we considered the effective properties of GRC accounting the graphene volume fraction as 10% and are summarized in **Table 1**.

Table 1: Effective properties of GRC

Material	C_{11} (GPa)	C_{12} (GPa)	C_{66} (GPa)	e_{31} (C/m ²)	ϵ_{33} (10 ⁻¹¹ F/m)
Graphene	9.99	6.66	1.67	-0.0002	3.815

The density of the GRC, ρ_{nc} , graphene, ρ_g , and polyimide, ρ_m is 1417 kg/m³, 2200 kg/m³ and 1330 kg/m³, respectively. The uniformly distributed load is considered as $q_0 = 0.05$ MPa. Zubko et al. [25] confirmed by using the experimental methods and to more specific, it is experimentally validated for polymers that the flexoelectric coefficient is ranges from (10⁻⁸–10⁻⁹ C/m). Henceforth, we assumed the flexoelectric coefficient $\mu_{31} \approx 10^{-8}$ C/m for our calculations.

Static and Dynamic Response

Figs. 2 and 3 represent the maximum deflection of GRC nanoplates with and without flexoelectricity effect and the normalized maximum deflection (i.e. w/w_0) of the nanoplate against the thickness of the plate at the fixed in-plane dimension ($a=b=45h$ and $55h$). It can be seen from figure 2 that the flexoelectric effect is size-dependent, i.e., the smaller the plate's thickness better the result. Where w and w_0 is a maximum deflection of the GRC plate with and without considering the flexoelectricity effect, respectively. It is obvious that the consideration of influence of flexoelectricity results in the lower deflection of a GRC nanoplates over that of classical plates.

As expected, from figure 3, it may be concluded that the influence of the flexoelectric effect is most effective for smaller thickness, it becomes negligible when the plate thickness increases. Figs. 4 and 5 illustrate the influence of size-dependent characteristics on the dynamic behavior of piezoelectric GRC plates for the resonant frequency and the normalized fundamental frequency of mode (1,1), respectively, against the corresponding thickness.

From **Fig. 4**, it can be determined that as the plate thickness is smaller (< 30 nm), the resonant frequency is lower for the plate without flexoelectric effect as that of the flexoelectric nanoplate. Also, it may be seen that the resonant frequency is dependent on the dimension of the plate, as the in-plane dimension increases the resonant frequency diminishes. The resonant frequency ratio ($\omega_{mn}/\omega_{mn}^0$) is the ratio of frequency of flexoelectric SS plate ω_{mn} and conventional plate ω_{mn}^0 . From **Fig. 5**, it can be concluded that the results for the ratio of resonant frequency diminishes progressively as the plate thickness increases, and it lastly reaches unity for both cases considering in-plane dimension ($a = b = 45h$ and $55h$). Concisely, the effect of size-dependent properties becomes more pronounced as the plate thickness decreases. The ratio of resonant frequency is near about ~ 5.5 times the frequency without considering flexoelectricity.

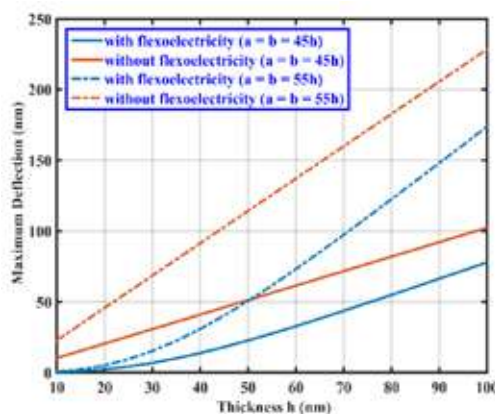


Fig. 2: Maximum deflection against the thickness of plate (h) under UDL with in-plane dimension

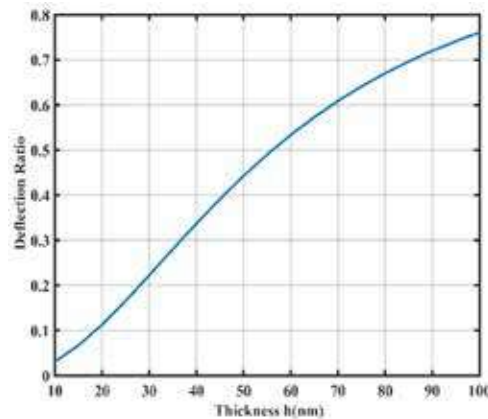


Fig. 3: Normalized deflection against the thickness of plate under UDL

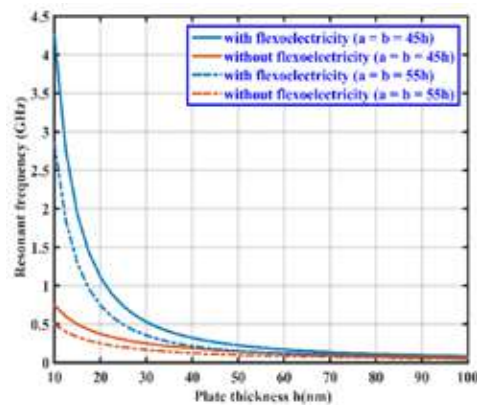


Fig. 4: Resonant frequency against the thickness of plate with in-plane dimension

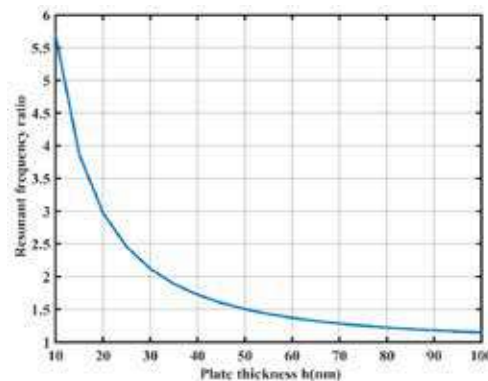


Fig. 5: Resonant frequency ratio against the thickness of plate

CONCLUSIONS

In this novel work, the flexoelectric plate model based on the Navier's method and Kirchhoff's plate theory are developed to explore the static and dynamic behavior of simply supported GRC plates including the deflection and frequency analysis. The numerical outcomes reveal the influence of effect of flexoelectricity on the static and dynamic behavior of GRC nanoplates is significant for nanoplates with a smaller thickness while the influence diminishes with the rise of the plate thickness. The current study might provoke the investigators to build this novel GRC and aid the purpose of validating the experimental approximations. We expect that some of the enhancements outlined in the current work will guide the pathway for exploring the different structural health monitoring and energy harvester in NEMS application.



ACKNOWLEDGMENT

KBS acknowledges Institute Post-doctoral Fellowship received from IIT BOMBAY. SN acknowledges the Initiation Grant received from IIT BOMBAY.

REFERENCES

1. Y. Sapsathiarn and R. K. N. D. Rajapakse, "Static and dynamic analyses of nanoscale rectangular plates incorporating surface energy," *Acta Mechanica*, vol. 228, no. 8, pp. 2849–2863, 2017.
2. Q. Deng, L. Liu, and P. Sharma, "Flexoelectricity in soft materials and biological membranes," *Journal of the Mechanics and Physics of Solids*, vol. 62, no. 1, pp. 209–227, 2014.
3. M. C. Ray, K. M. Rao, and B. Samanta, "Exact analysis of coupled electroelastic behaviour of a piezoelectric plate under cylindrical bending," *Computers and Structures*, vol. 45, no. 4, pp. 667–677, 1992.
4. J. Curie and P. Curie, "Development by pressure of polar electricity in hemihedral crystals with inclined faces," *Bull. soc. min. de France*, vol. 3, no. 1, p. 90, 1880.
5. V. Mashkevich and K. . Tolpygo, "Electrical, Optical and Elastic Properties of Diamond Type Crystals. I," *Soviet Physics JETP*, vol. 5, pp. 435–439, 1957.
6. R. Maranganti, N. D. Sharma, and P. Sharma, "Electromechanical coupling in nonpiezoelectric materials due to nanoscale nonlocal size effects: Green's function solutions and embedded inclusions," *Physical Review B - Condensed Matter and Materials Physics*, vol. 74, no. 1, 2006.
7. K. S. Novoselov et al., "Electric field effect in atomically thin carbon films.," *Science (New York, N.Y.)*, vol. 306, no. 5696, pp. 666–9, 2004.
8. K. B. Shingare and S. I. Kundalwal, "Flexoelectric and surface effects on the electromechanical behavior of graphene-based nanobeams," *Applied Mathematical Modelling*, 2019.
9. K. B. Shingare and S. I. Kundalwal, "Static and dynamic response of graphene nanocomposite plates with flexoelectric effect," *Mechanics of Materials*, vol. 134, pp. 69–84, Jul. 2019.
10. K. B. Shingare, M. Gupta, and S. I. Kundalwal, "Evaluation of effective properties for smart graphene reinforced nanocomposite materials," *Materials Today: Proceedings*, Jul. 2020.
11. S. I. Kundalwal and K. B. Shingare, "Electromechanical response of thin shell laminated with flexoelectric composite layer," *Thin-Walled Structures*, vol. 157, no. April, p. 107138, 2020.
12. S. I. Kundalwal, K. B. Shingare, and M. Gupta, "Flexoelectric effect on electric potential in piezoelectric graphene-based composite nanowire: Analytical and numerical modelling," *European Journal of Mechanics, A/Solids*, vol. 84, no. May, 2020.
13. E. García-Macías, L. Rodríguez-Tembleque, and A. Sáez, "Bending and free vibration analysis of functionally graded graphene vs. carbon nanotube reinforced composite plates," *Composite Structures*, vol. 186, no. November 2017, pp. 123–138, 2018.
14. M. Kandpal, V. Palaparthi, N. Tiwary, and V. R. Rao, "Low Cost, Large Area, Flexible Graphene Nanocomposite Films for Energy Harvesting Applications," *IEEE Transactions on Nanotechnology*, vol. 16, no. 2, pp. 259–264, 2017.



15. E. García-Macías, L. Rodríguez-Tembleque, and A. Sáez, “Bending and free vibration analysis of functionally graded graphene vs. carbon nanotube reinforced composite plates,” *Composite Structures*, vol. 186, no. November 2017, pp. 123–138, 2018.
16. S. Naskar, T. Mukhopadhyay, S. Sriramula, and S. Adhikari, “Stochastic natural frequency analysis of damaged thin-walled laminated composite beams with uncertainty in micromechanical properties,” *Composite Structures*, 2017.
17. S. Naskar, T. Mukhopadhyay, and S. Sriramula, “Probabilistic micromechanical spatial variability quantification in laminated composites,” *Composites Part B: Engineering*, 2018.
18. S. Naskar, T. Mukhopadhyay, and S. Sriramula, “Spatially varying fuzzy multi-scale uncertainty propagation in unidirectional fibre reinforced composites,” *Composite Structures*, 2019.
19. P. K. Karsh, T. Mukhopadhyay, S. Chakraborty, S. Naskar, and S. Dey, “A hybrid stochastic sensitivity analysis for low-frequency vibration and low-velocity impact of functionally graded plates,” *Composites Part B: Engineering*, 2019.
20. C. Liu and R. K. N. D. Rajapakse, “A size-dependent continuum model for nanoscale circular plates,” *IEEE Transactions on Nanotechnology*, vol. 12, no. 1, pp. 13–20, 2013.
21. M. Zhao, C. Qian, S. W. R. Lee, P. Tong, and H. Suemasu, “Electro-elastic analysis of piezoelectric laminated plates,” vol. 3046, 2012.
22. S. Hu and S. Shen, “Electric Field Gradient Theory with Surface Effect for,” vol. 13, no. 1, pp. 63–87, 2009.
23. L. Shu, X. Wei, T. Pang, X. Yao, and C. Wang, “Symmetry of flexoelectric coefficients in crystalline medium,” *Journal of Applied Physics*, vol. 110, no. 10, 2011.
24. J. N. Reddy, “Mechanics of Laminated Composite Plates and Shells: Theory and Analysis, Second Edition -,” Book, vol. 2003, p. 858, 2003.
25. P. Zubko, G. Catalan, and A. K. Tagantsev, “Flexoelectric Effect in Solids,” *Annual Review of Materials Research*, vol. 43, no. 1, pp. 387–421, 2013.



Influence of the Pivot Locations on the Aerodynamic Performance of a 2D Flapping Elliptic Airfoil at Close Proximity of the Ground

Jit Sinha, Sunil Manohar Dash*

Department of Aerospace Engineering, Indian Institute of Technology, Kharagpur, West Bengal

✉ smdash@aero.iitkgp.ac.in

ABSTRACT

In this paper, the ground effects on a two-dimensional flapping elliptic airfoil is investigated at three different pivot locations. The numerical simulations are conducted using a finite volume solver at a fixed Reynolds number of 5000. Five different ground clearances between $1c$ to $5c$ are considered to investigate the transient and time-averaged aerodynamic force performance of the flapping airfoil. Here, c is the chord length of the airfoil. We found that the thrust and lift performance of the airfoil is significantly enhanced when the ground clearance is less than $2c$; otherwise, their variations are minimal. Additionally, we have observed that the pivot location near the trailing edge produces a better thrust force than the other two pivot locations at least in the considered parametric space. However, when it comes to the lift force the center pivot location shows a better performance.

Keywords : Flapping elliptic airfoil; Pivot point location; Ground effect; Low Reynolds number; Ansys-Fluent.

INTRODUCTION

In the last few decades, the use of flapping wing-based propulsion mechanism in the Unmanned Under Water Vehicles (UUWVs) and Micro Aerial Vehicles (MAVs) has gained popularity since it produces better manoeuvrability compared to the fixed and rotary wing type propellers (Platzter et al. [1]). Often these UUWVs operate near the ground or shallow water environments. Previously, researchers have tried to understand the wing in the ground effect (WIG). However, they mainly considered conventional fixed-wing or airfoil configurations (Wu et al. [2]). Note that the analysis of the fixed-wing in WIG configuration may not be applicable for the corresponding flapping-wing cases since in the latter the unsteady wake dynamics are more pronounced. Nevertheless, the benefits of fixed-wing in WIG configuration have been already explored in WIG crafts, race cars, etc (Qu et al. [3]). Whereas the studies and engineering applications involving flapping wing in WIG configuration is still in the budding phase. In the following, we have reviewed some of the relevant studies with the flapping wing in WIG configuration.

Liang et al. [4] have performed analytical studies on a sinusoidal heaving of NACA 0012 airfoil over a flat and wavy surface. They have found that for a particular reduced frequency the time-averaged lift coefficient is enhanced when the gap ratio between the airfoil and ground surface is decreased. A similar study was done by Wu and Zhao [5] using the immersed boundary-lattice Boltzmann method (IB-LBM) for the heaving of NACA0012 airfoil near the ground surface. They have observed that the critical Strouhal number (or the non-dimensional flapping frequency) to be around 0.3 to generate thrust or positive lift for the airfoil heaving near the ground. Additionally, they have reported for higher flapping frequency and smaller ground clearance distance, the magnitude of generated lift and thrust force gets enhanced. Ahmed and Sharma [6] and Luo and Chen [7] have experimentally investigated the effect of varied angle of attack (AOA) and ground clearance. They have observed that at close proximity to the ground, a high-pressure region is formed on the bottom surface of the airfoil which favours the extra lift and thrust force generation. This phenomenon is otherwise known as the “Ramming Effect” or “Convergent-Divergent Channel Effect”. Furthermore, they noticed the pressure distribution on the upper surface of the airfoil is more dependent on the AOA than the ground clearance whereas the pressure variation on the lower surface of the airfoil is equally dependent on both. A similar observation was reported by Qu et al. [3]. In another study, Wu et al. [8] have investigated the ground effect on the energy harvesting aspect of the flapping NACA 0015 airfoil using IB-LBM simulations. They have reported that superior power extraction efficiency can be achieved in the case of low ground clearances. A similar observation was postulated by Wu et al. [9] when the flat ground was replaced by a wavy ground. Furthermore, Wu et al. [10] have conducted numerical simulations to determine the scope of the power extraction of the flapping wings between the two parallel walls or grounds. At low $Re = 150$, using IB-LBM simulations Wu et al. [2] have investigated flapping of NACA 0012 airfoil with varied ground clearances and flapping frequency (or St). They found that close to ground drag coefficient increases whereas the lift coefficient reduces.

Also, they have further observed that at high Strouhal numbers, the shed vortices and ground induced vortices interact with each other and propagate obliquely in the wake. Mivehchi et al. [11] have performed experiments in a towing tank on high aspect ratio flapping airfoil and showed that the flapping kinematics can be adjusted to capture the positive effect of ground without sacrificing thrust. Apart from the symmetric flapping cases, Lin et al. [12] have investigated flapping airfoil with asymmetric heaving motion. They found the thrust coefficient increases when the duration of upstroke is reduced and the lift coefficient increases when the duration of down stroke is reduced.

We noticed that the above-cited flapping wing in WIG configurations studies are limited to a particular pivot location on the flapping airfoil. Therefore they fail to explain the significance of pivot-point locations on the flow physics of the near wake region, and transient and time-averaged thrust and lift performance of the flapping airfoil in close proximity to the ground. To bridge the knowledge gap, in this study, we have performed a systematic numerical investigation of the two-dimensional flapping elliptic airfoil. Three different pivot locations on the airfoil are considered. Furthermore, we have assessed the effect of the ground clearance on the aerodynamic performance of the flapping airfoil at five different mean heights of the airfoil from the ground.

METHODOLOGY

Problem Statement

The down stroke and upstroke motion of a flapping elliptic airfoil near the ground is depicted in **Fig. 1(b)**. The sinusoidal heaving $h(t)$ and pitching $\theta(t)$ motion profiles follow the (1) and (2). Here, the phase angle (ϕ) difference between heaving and pitching profile is considered as 90° since at this phase angle generally maximum propulsive efficiency is obtained for the flapping airfoils (Sinha et al. [13]; Anderson et al. [14]).

$$h(t) = h_0 \cos(\omega t) \quad (1)$$

$$\theta(t) = h_0 \cos(\omega t - \phi) \quad (2)$$

$$\alpha(t) = \arctan\left(\frac{h'(t)}{U_\infty}\right) - \theta(t) \quad (3)$$

$$\theta_0 = \left(\frac{\omega h_0}{U_\infty}\right) - \alpha_0 \quad (4)$$

In the present study, the induced geometric effective angle of attack profile $\alpha(t)$ is expressed in (3) where U_∞ is the incoming free stream flow ($U_\infty = 0.125$ m/s). To obtain the pitching amplitude θ_0 , for a fixed maximum amplitude (α_0) of $\alpha(t)$, two scenarios are evaluated. For the low flapping frequency ($St < 0.2$), (4) is used which is a linearized approximated form of (3). For $St \geq 0.2$, the maxima of (3) are used to calculate θ_0 . Here, $h_0 = 0.75c$ and $\alpha_0 = 10^\circ$ are the heaving and effective angle of attack amplitude, respectively and $c = 0.04$ m is the chord length of the flapping airfoil. h_m is the mean distance of the airfoil from the ground which is varied from $1c$ to $5c$ at an interval of $1c$. f and ω is the flapping frequency and angular flapping frequency, respectively. Moreover, to investigate the thrust performance of the flapping airfoil, three pivot points A, B and C at locations $0.25c$, $0.5c$ and $0.75c$ from the leading-edge are considered, respectively, as shown in **Fig.1(b)**. Additionally, for the present analysis, two non-dimensional numbers, Reynolds number, $Re = U_\infty c/\nu$ and Strouhal number $St = fA/U_\infty$ are defined. Here, ν is the kinematic viscosity of the fluid and A is the width of the wake (= maximum excursion of the trailing edge of the airfoil, i.e $2h_0$). The transient thrust and lift coefficient is defined using a generic force coefficient expression, $CF = \left(\frac{F}{0.5\rho U_\infty^2 S}\right)$, where F can be thrust or lift force, ρ is the density of the fluid and $S=1.0$ is the planform area of the airfoil.

Numerical Solver Details

In the present study, a finite volume method (FVM) based commercial software package, ANSYS FLUENT

is utilised to simulate the transient incompressible flow over a flapping elliptic airfoil at $Re = 5000$ and $St = 0.3$ with a laminar viscous flow model. The effectiveness of the ANSYS FLUENT solver in simulating flapping airfoil problems has been thoroughly verified and documented in the literature (Dash et al. [15]). Using the dynamic mesh principle, the conservative form of the governing equations shown in (5) is solved in an inertial frame of reference on an arbitrary control volume cv with moving control surface cs .

$$\begin{aligned} & \frac{\partial}{\partial t} \int_{cv} \rho \psi dV + \oint_{cs} \rho \mathbf{n} \cdot (\mathbf{v} - \mathbf{v}_g) \psi dS - \oint_{cs} \rho \Gamma_{\psi} \mathbf{n} \cdot \nabla \psi dS \\ & = \int_{cv} S_{\psi}(\psi) dV \end{aligned} \quad (5)$$

Here, the variables \mathbf{v} , \mathbf{v}_g , Γ_{ψ} , S_{ψ} , and ρ are the flow velocity, moving mesh velocity, diffusion coefficient, source term of ψ per unit volume and fluid density, respectively. \mathbf{n} is the unit vector normal to the control surface. Pressure and velocity coupling are done using the Pressure-Implicit with Splitting Operators (PISO) algorithm. We have used the PISO skewness correction for highly-distorted meshes and the under-relaxation factors for the momentum and pressure are defined as 0.3 and 0.7, respectively. Spatial and temporal discretization of the momentum equation is carried out using the second-order upwind scheme and first-order implicit scheme, respectively. A double-precision solver setting is followed to approximate the computer-generated round off errors. The convergence criterion for the iterative method for both momentum and mass residuals are kept to $O(10^{-5})$.

Computational Domain, Mesh and Validation

A semicircle type computational domain as shown in **Fig. 1(a)** is adopted in the present simulations. The domain is subdivided into three zones with a deforming inner zone Ω_2 and a stationary outer zone Ω_3 . Ω_1 is moved as a rigid body along with the airfoil wall (Γ_0). Between the two zones Ω_2 and Ω_3 , an interior boundary condition (Γ_1 and Γ_2) is applied. The inner (Γ_2) and outer (Γ_3) boundaries are located at a radius of $15c$ and $30c$, respectively, so that the far-field boundary effects on the airfoil wall are negligible. At the start of the flapping stroke, the center of the elliptic airfoil is located at a distance of H ($H = h_m + h_0$) from the ground wall. On the inlet section, a uniform free-stream velocity (U_{∞}) in the X-direction is assigned. No-slip velocity condition on the airfoil wall and solid ground (Γ_4) is implemented. Atmospheric pressure condition on the outlet boundary is applied. Standard initialization is adopted for computing the result from the inlet. To obtain the flapping motion profile shown in (1) and (2), a C-programming based user-defined function (UDF) is written and compiled in ANSYS FLUENT.

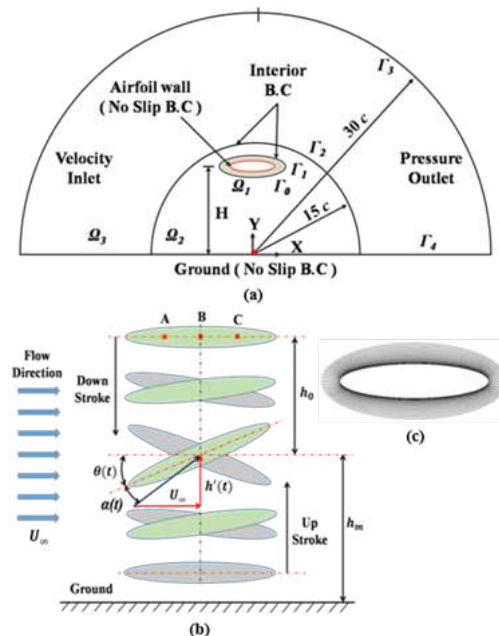


Fig. 1: (a) Represents the semicircle type computational domain and (b) shows the flapping cycle of the elliptic airfoil near the ground. The pivot points A, B and C on the airfoil are located at a distance of $0.25c$, $0.5c$, and $0.75c$, from the leading-edge, respectively. (c) close up view of the mesh around the elliptic airfoil which will move as a rigid body along with the airfoil.

Grid Independency Test and Validation

A structured mesh with quadrilateral elements has been generated in the computational domain using face meshing. A close-up view of the mesh around the airfoil is shown in **Fig. 1(c)**. Here, keeping the outer domain stationary, diffusion smoothing based dynamic mesh technique was incorporated only in the inner zone to minimize computational time. To perform the grid independence study, five different mesh sizes as shown in **Table 1** are selected. Since for the mesh size M3, the error percentage of time-average CT is below 0.1%, therefore it is chosen for the rest of the simulations. Additionally, we have validated the numerical solver by performing a simulation similar to that of Wu et al. [8] and compared the time-averaged CL (refer **Fig. 2**). The results obtained in the present solver are found to match excellently.

Table 1: Grid independency test

Grid name	No of nodes	CT value	$\% \text{Error} \left \frac{C_{T\text{new}} - C_{T\text{old}}}{C_{T\text{old}}} \right \times 100$
M5	93,422	0.2409	0.3320
M4	81,422	0.2401	0.1249
M3	69,422	0.2398	0.0834
M2	57,422	0.2396	0.0417
M1	45,422	0.2395	-

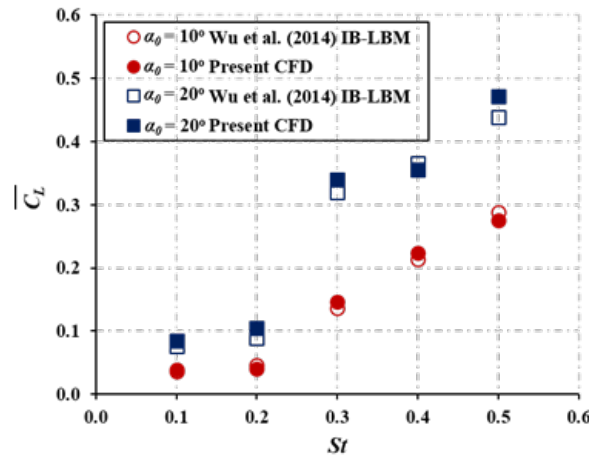


Fig. 2: Comparison of time-averaged CL values obtained in the present solver with that of the Wu et al. [8]

RESULT AND DISCUSSION

In **Fig. 3**, the numerical results of the time-averaged thrust and lift coefficient as functions of ground clearance (h_m/c) are plotted at three different pivot locations of the flapping airfoil. Notice in **Fig. 3** that at all pivot locations, with decreasing ground clearance, a negligible amount of increment in time-averaged C_T is observed till $h_m/c = 2$. On the other hand when $h_m/c < 2$, a substantial enhancement of the time-averaged C_T is observed. A similar trend is also found for the time-averaged C_L . Furthermore, between the pivot locations, pivot A and C are found to have superior thrust performance compare to pivot B irrespective of ground clearance. But in the matter of lift, generally, the pivot locations near the leading (pivot A) and trailing (pivot C) edge under perform than that of the center pivot location (pivot B). It is worth highlighting here that at a sufficiently large ground clearance, both time-averaged thrust and lift coefficients attain a value same as that of the infinite domain case (i.e. in absence of ground effect).

To better understand the time-averaged C_T and C_L variation at different pivot locations of the flapping airfoil we have further investigated the transient C_T and C_L profile over one flapping cycle for only one representative case of $h_m/c = 1$ at three pivot locations. It is noticed that the transient C_T and C_L plots distinctively vary at different pivot locations (compare in **Fig. 4**) and

their trends were asymmetric between the two flapping strokes (i.e. upstroke and down stroke).

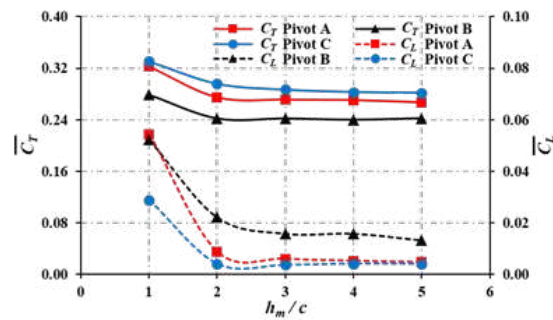


Fig. 3: Shows the numerically obtained time-averaged CT and CL values at three different pivot locations (namely A, B and C) with varied ground clearances

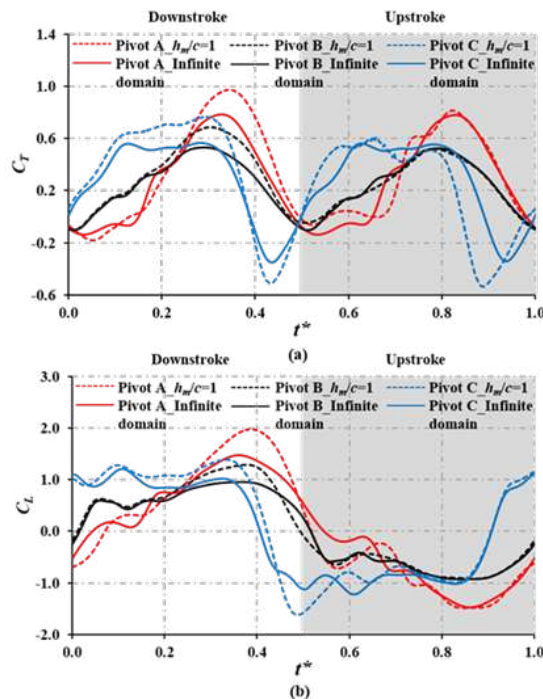


Fig. 4: Shows the comparison between numerically obtained transient (a) C_T and (b) C_L for $h_m/c = 1$ and infinite domain case for pivot A, pivot B and pivot C

Moreover, higher transient C_T and C_L peaks are observed in the case of downstroke i.e. when the airfoil is moving towards the ground. This improved aerodynamic performance in the downstroke is because of the ramming effect (Luo & Chen [7]) in which a favourable high-pressure region is formed between the airfoil and ground (see in **Fig. 5**). In general, the transient force profiles follow a parabolic pattern. Here, due to page limitations, the details of the flow physics associated with different types of transient C_T and C_L profiles are not discussed which can be found elsewhere (Sinha et al. [16]). Further notice that between three pivot locations the transient C_T peak is found to be lower for pivot B, which may have led to reducing time-averaged thrust performance compare to pivot A and C cases. However, when it comes to the lift performance pivot B attains a higher region of the transient C_L with a positive value than pivot A and C that may have attributed to its greater time-averaged lift performance. Additionally, in **Fig. 4**, we have compared the transient C_T and C_L values for the infinite domain case. It can be clearly seen in **Fig. 4** that the favourable aerodynamic effects have produced improved transient C_T and C_L performance in the presence of ground.

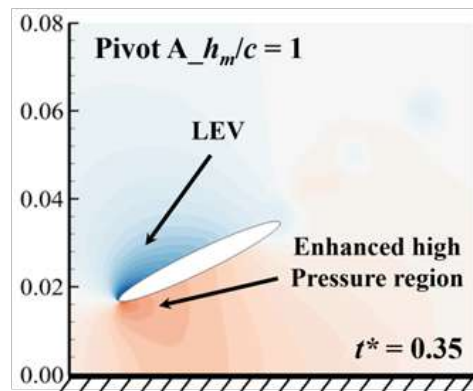


Fig. 5: Depicts the favourable high-pressure region under the airfoil due to the ramming effect

CONCLUSION

In the present numerical study, the effect of solid ground on a two-dimensional flapping elliptic airfoil is investigated at three different pivot locations for Reynolds number of 5000, $St = 0.3$ and $\alpha_0 = 10^\circ$. Five different ground clearances between $1c$ to $5c$ are considered at an interval of $1c$. Here, only the transient and time-averaged aerodynamic force coefficients are evaluated. We observed that the thrust and lift performance of the airfoil is enhanced when the ground clearances less than $2c$. This is because of the formation of the high-pressure region around the airfoil due to the ramming effect. Additionally, we have observed that in terms of the thrust performance, the pivot location near to trailing edge (i.e pivot C) performs better than other pivot locations at least for the range of parameters investigated here. Whereas the center pivot location (i.e pivot B) shows a better lift performance.

ACKNOWLEDGMENT

The authors are immensely grateful to IIT Kharagpur for the computational support and SERB (Science and Engineering Research Board) and ARDB (Aeronautical Research and Development Board) for financial support.

REFERENCES

1. Platzer, M. F., Jones, K. D., Young, J., Lai, J. C. S., "Flapping wing aerodynamics: Progress and challenges", AIAA J, 46, 2136, 2008.
2. J. Wu, Y. L. Qiu, C. Shu, N. Zhao, "Fluid Dynamics of Flapping Insect Wing in Ground Effect", J. Bionic Engineering, 11, 52-60, 2014.
3. Q. Qu, W. Wang, P. Liu, R. K. Agarwal, "Airfoil Aerodynamics in Ground Effect for Wide Range of Angles of Attack," AIAA J, Vol. 53, No. 4, 2015.
4. H. Liang, X. Wang, L. Zou, Z. Zong, "Numerical study of two-dimensional heaving airfoils in ground effect", J. Fluids and Structures, 48, 188-202, 2014.
5. J. Wu, N. Zhao, "Ground effect on flapping wing", 7th Asian-Pacific Conference on Aerospace Technology and Science, 67, 295-302, 2013.
6. M. R. Ahmed, S. D. Sharma, "An investigation on the aerodynamics of a symmetrical airfoil in ground effect", Experimental Thermal and Fluid Sciences, 29, 633-647, 2005.
7. S.C. Luo, Y.S. Chen, "Ground effect on flow past a wing with a NACA0015 cross-section", Experimental Thermal and Fluid Sciences, 40, 18-28, 2012.
8. J. Wu, S.C. Yang, C. Shu, N. Zhao, W. W. Yan, "Ground effect on the power extraction performance of a flapping wing biomimetic energy generator", J. Fluids and Structures, 2014.
9. J. Wu, Y. L. Qiu, C. Shu, N. Zhao, "An adaptive immersed boundary-lattice boltzmann method for simulating a flapping foil in ground effect", Computers and Fluids, 2014.



10. J. Wu, Y. L. Qiu, C. Shu, N. Zhao, “Pitching-motion-activated flapping foil near solid walls for power extraction: A numerical investigation”, *Phys. Fluids*, 26, 083601, 2014.
11. A. Mivehchi, J. Dahl, S. Licht, “Heaving and pitching oscillating foil propulsion in ground effect”, *J. of Fluids and Structures*, 63, 174–187, 2016.
12. X. Lin, S. Guo, J. Wu, J. Nan, “Aerodynamic Performance of a Flapping Foil with Asymmetric Heaving Motion near a Wall”, *J Bionic Eng*, 15, 636–646, 2018.
13. Sinha, J., Sreedharan, N., Dash, S.M., “Effect of the pivot point locations on the wake dynamics and thrust performance of a flapping elliptic airfoil : A numerical study”, 46th National Conference on Fluid Mechanics and Fluid Power (FMFP-2019), Coimbatore, India, 2019.
14. Anderson, J., Streitlien, K., Barrett, D., Triantafyllou, M.S., “Oscillating foils of high propulsive efficiency”, *J. Fluid Mech*, 360, 41, 1998.
15. Dash, S.M., Lua, K. B., Lim, T. T., Yeo, K. S., “Enhanced thrust performance of a two dimensional elliptic airfoil at high flapping frequency in a forward flight”, *J. Fluids and Structures*, 76, 37-59, 2018.
16. Sinha, J., Dash, S.M., “Effects of the Pivot Locations on the propulsive performance of a 2D Flapping Elliptic Airfoil at a Close Proximity of Solid Ground”, Unpublished.

Chemical Engineering



Recovery of Technology Metals from Oceans

T L Prasad^{1,2}

Chemical Engineering Group¹, Homi Bhabha National Institute², Bhabha Atomic Research Centre, Mumbai

✉ tlpasad63@gmail.com

ABSTRACT

Economic needs as well as ecological demands are major driving forces in improving the chemical processes and developing of alternative or secondary resources. Oceans contain around eighty elements of periodic table and some of the elements are very scarce on land and/or very expensive, elements such as uranium, vanadium are also a few among them. With its lean but clean resource, oceans can serve as constant potential source of valuable technology elements for a long run. India with a large coastline has a large stake in exploiting the valuable elements locked in seawater. The greatest of the scientific and technological challenges in extracting technology metals from seawater are lying in finding a technology that gives a net positive energy balance in terms of electricity produced from the so recovered uranium and the other is the cost of production. The Indian efforts in addressing these issues and pilot scale demonstrations based on lab-scale field trials being carried out are presented in this paper.

Keywords : Oceans; Radiation processing; Tidal energy; technology metals; Secondary sources.

INTRODUCTION

With merits of high energy density and nearly zero greenhouse gas's emissions, the nuclear power serves as an important energy resource worldwide. To this day, uranium is the major ingredient for the most nuclear power stations. The booming growth in the demand of the nuclear energy is stimulating exploitation of uranium ores. The process of mining, metallurgy, and especially in situ leaching and disposing tailing of uranium ore often releases uranium nuclides in the formation of uranyl into the aqueous environment. Furthermore, due to incredibly diffuse electrons in 5f orbital the element uranium is prone to coordinate with various ligands containing electron-donor atoms such as nitrogen, phosphorus, sulfur and oxygen etc. through coordination bonds. It is such coordination interaction that makes uranium highly mobile in aqueous environments. Literature and publications point out the large resources of valuable elements in the world's oceans with remarkably uniform concentrations [1, 2, and 3]. In addition, 8500 tonnes per year enter the oceans through rivers and submarine eruptions [4, 5]. Oceans contain around eighty elements of periodic table and some of the elements are very scarce on land and/or very expensive, uranium and vanadium are also few elements among them with relative abundance factors of 23 & 24 respectively. Uranium subsists in the environment due to leaching from mine tailings, natural deposits, use of uranium-containing phosphate fertilizers, emissions from the nuclear industry. With its lean but clean resource, oceans can serve as constant potential source of uranium and other valuable elements for a long run. Based on an average seawater salt content of about 3.5%, the salt concentration is 106 – 107 times larger than the concentrations of trace elements like U, V, Fe, Ni, Cu, Zn, Li and Au. In the last century uranium has universally gained acceptance as primary energy source. Currently it caters to ~17% of the electricity generation globally. Uranium has been projected as the main workhorse of future when the fossil energy reserves dwindle by the middle of this century. The terrestrial distribution of uranium ore occurrence is grossly uneven. With a large coastline, India, Japan, Korea and a few other nations have a larger stake in exploiting the 4.5 billion tonnes of uranium locked in seawater [4, 5 and 7]. Also the electricity produced from nuclear energy with uranium extracted from oceans has the advantage of No mill tailings; No fly ash and No carbon dioxide generation. The recovery of valuables from seawater requires the processing of large amounts of water, depending on the efficiency of adsorption and elution processes. The problems to be addressed as a part of R&D activities are to develop most effective and most selective extraction system and associated chemical engineering and to develop economic method of contacting large amounts of water with such extraction system. The uranium concentration in various secondary sources and corresponding reserves are as given in following **Table 1**.

Uranium bearing substances	Avg. Concentration (mg/L)	Reserves (10 ⁶ tU)
Conventional uranium ores	350-5000 and more	4-5
Phosphates	100-200	5-10

Bauxite	8-12	0.09-0.1
Lignite	0.1-1	0.15-1.5
Granite	4	4×10^3
Manganese modules	4-7	10-14
Shelf sediments	1-4	$3-4 \times 10^5$
Seawater	0.003	4.5×10^3

The granite source containing 4 ppm of U concentration with total reserves of 4 billion tones has the drawback being in solid form and technology demonstration is not available. But in case of seawater, the uranium is present in ionic form in liquid phase and which is easier to process with the technology being developed. This article deals with the Indian efforts on these issues and highlighting the demonstration of pilot scale “RUSWapp~100g “facility. Also large quantity of seawater being pumped into the facilities, either for condenser cooling at power plants or for desalination purposes and thus opportunity for co-generation of technology metals.

PROCESS MECHANISM

During seventies and eighties the Initial investigations on the possibilities of recovery of uranium from seawater have been done using inorganic adsorbents [5, 6 and 7]. The inorganic adsorbents suffer limitations of adsorption rate and insufficient mechanical stability. Since early nineties extensive investigations are being carried out on organic adsorbents. Polyacrylo Amid Oxime (PAO) has been picked up as the best bet for our studies. It preferentially extracts heavy metal ions by chelating mechanism [7, 8]. A polypropylene fiber substrate is irradiated with electron beam to create grafting sites on the polymer chain and then treated with acrylonitrile to graft cyano groups on those sites. Then the cyano groups are reacted with hydroxylamine to convert them into amidoxime groups. These amidoxime groups trap the loosely bonded uranyl ion from the uranyl tricarbonate present in the ionic form i.e. $\text{UO}_2(\text{CO}_3)_3^{4-}$ in seawater. The adsorption mechanism is given in the Fig. 1.

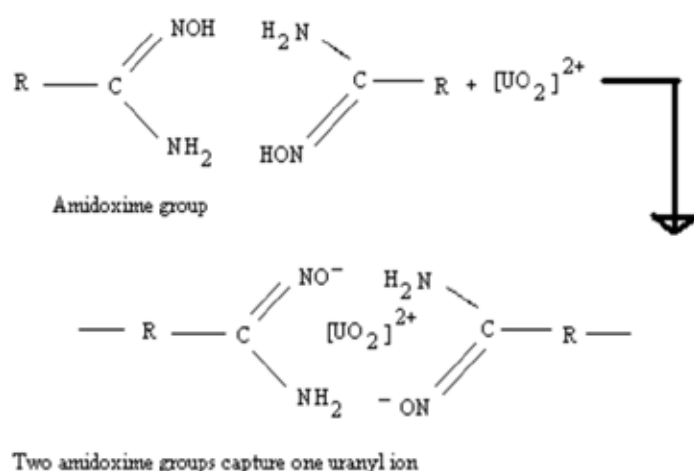


Fig. 1. Adsorption Mechanism of uranyl ion

Thus for each pair of two molecules of polyacrylo amidoxime (PAO), one uranium atom is captured. Stoichiometrically PAO will have an extraction capability of 3600 g U/kg PAO.

DESCRIPTION OF THE LAB-SCALE EXPERIMENTS

Substrate: During lab-scale experiments, many types of fiber cross-sections and geometries were evaluated for establishing efficacy of grafting. Polypropylene fiber of 1 to 2 Denier cross-sections as stem material in non-woven felt form was used. Electron Beam Radiation induced grafting of acrylonitrile was carried out with optimized parameters [9, 10, and 11]. The solution viscosity and temperature were also found to be important factors. Then the cyano group was converted to PAO as shown in Fig. 2.

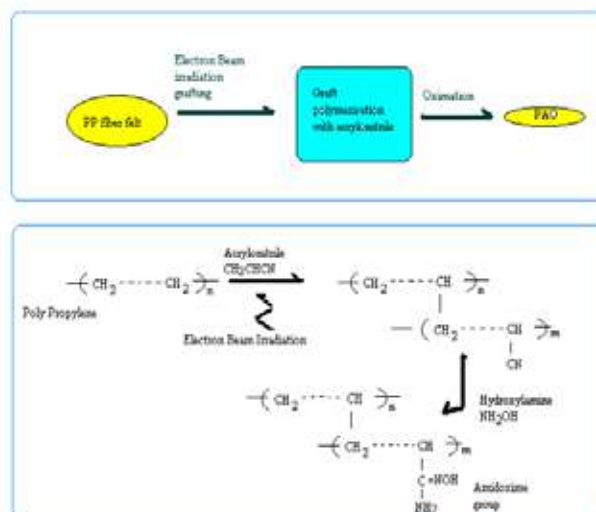


Fig. 2. Cyano group conversion to PAO

The substrate was then reacted with alkaline solution to impart hydrophylicity and adsorption characteristics. The tokens of size 75x75x2 mm thick and 150x150x2 mm thick were used in the lab scale field trials.

Experimental results: The summary of the experimental results in terms of concentration factors evaluated for different field trials conducted at various sites is shown in **Table 2**. Corrosion, bio fouling and their combined effect on the adsorption kinetics and mechanical properties of the materials used in the suspension assembly and the substrate were studied. Their compatibilities with seawater and process chemicals were established. The optimum submergence periods for various locations were also studied. The liquid samples are analysed using advanced nuclear analytical technique for estimating lean concentrations of technology metals [12].

Table 2. Summary of the lab scale experimental results

Sl. no	Location	Concentration Factors achieved		Remarks
		Uranium	Vanadium	
1	CIRUS jetty Trombay	300	200	For submergence period of 12 days
2	NPP Intake/Out fall canals Tarapur	600	500	For submergence period of 14 days
3	Andoman & Nicobar Islands	700	Not analysed	For submergence period of 23 days

Process flow sheet for 100gU/year semi pilot scale facility

Based on initial success of extracting micro grams and milligrams of uranium at lab scale by harnessing the tidal wave using PAO adsorbent, a process flow sheet for a facility to extract 100gU/year has been developed. Compared to lab scale, a surface area scale up factor of 1200 has been maintained in pilot scale facility. The process flow sheet of RUSWapp~100g facility was evolved, designed, installed and commissioned at Trombay for demonstration trials. The process block diagram is as shown in **Fig. 3** below. The holdup volumes of process reactors are 2000 litres and 2 bar steam is used as heating medium. The required mixing and turbulence is maintained in the process using continuous recirculation of the solution mixture. The adsorbent is used in the form of leaflets of size 1mx1mx1m with 27 of sheets per contactor assembly and a gap of 30 mm is maintained between the sheets for achieving optimal hydrodynamics. The material of construction for contactor assembly is polypropylene, which is compatible for both hot alkali and acid solutions. The scaled up facility has given pick up rate of 0.6 g of Uranium per kg of adsorbent material against the reported literature of 1 g of Uranium per kg of PAO for the first A-S-E cycle. The preferential fractional elution for technology metals of interest is demonstrated with this facility.

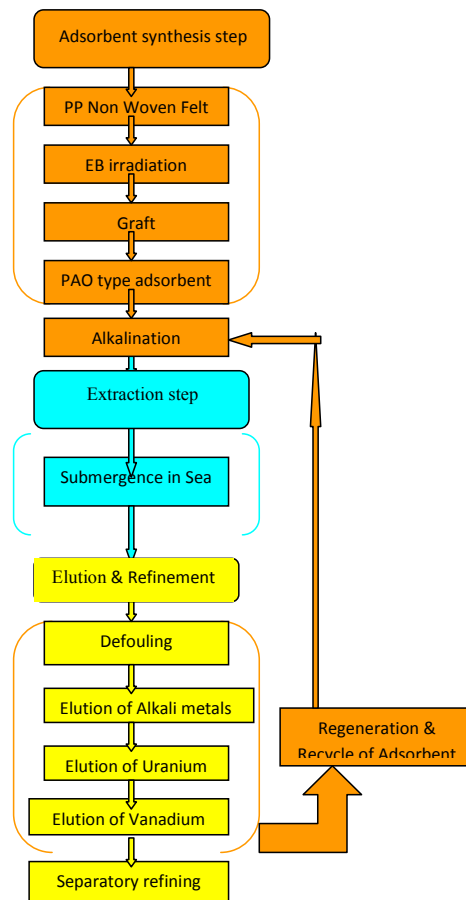


Fig. 3. Block diagram for uranium extraction from

Fig. 4 below shows the details of semi pilot scale RUSWapp~100g facility for the A-S-E (Alkalinization-Submergence-Elution) cycle and arrangements for De-fouling of 1Mx1Mx1M contactor assemblies. Each A-S-E cycle consumes duration of approximately 20 days including defouling time.



Fig. 4. Semi pilot scale RUSWapp~100g facility

The technological scenario assumed for the design is having a global information base as well as the strength of in house experiments. A full gamut of more than 24 inorganic and organic possible adsorbent materials has been screened. The choice has been zeroed on Polyacrylamid Oxime (PAO) adsorbent with a reasonable and achieved performance of 1g of uranium per kg of PAO as reported in literature. Instead of the postulated peak performance of 3.6g of uranium per kg of PAO in laboratory conditions, our report assumes the performance reported by literature as reasonably achievable by us as well. The life of



substrate and adsorbent material is considered as 25 cycles. The plant basically consists of two on-shore units viz. one for synthesis of adsorbent and the other for elution and further processing. The third component is an offshore unit for mooring of seawater contactor assembly carrying adsorbent. The contact technique is based on floating body method utilizing the tidal rise and fall of the seawater level coupled with the large water body movements due to the tidal changes in the seawater levels.

A conceptual process design and cost benefit analysis is carried out for a 100 Te per year 'uranium from seawater' plant. It includes the costs for off shore and on shore civil works, major process equipment and consumption of chemicals, substrates etc. About 18,000 contactor assemblies of size 4m x 4m x 4m will be used with total load of 6050 Tonne of PAO adsorbent. The project land area requirement for the on shore units is approximately 250m x 250m having the plant area of 60m x 120m for PAO synthesis and 150mX120m for elution and allied services. For the offshore segment the area requirement is 500m x 1000m with water depth >20m at lowest tide conditions. The PAO synthesis unit will have a dedicated electron beam irradiator. The estimated capital outlay is Rs. 1226 Crores for fixed capital, Rs. 240 Crores for working capital. The Annual Operating cost is estimated to be Rs. 260 Crores. Direct manpower requirement is ~310 persons at various levels of operation. The cost of production including depreciation works out to around Rs. 27,600/- per kg of product uranium based on the current status of technology. The project implementation period will be 220 weeks. Thus it is likely to be competitive with the current Indian mining costs.

CONCLUSIONS

The recovery of uranium and other technology metals from seawater has been an area of significant interest since at least the early 1950s. Numerous materials have been examined during the nearly 7-decades-long period since then.

- The contactor assembly loaded with specially developed organic adsorbent PAO has shown promising results for recovery of technology metals from seawater.
- Harnessing tidal waves has the advantage of positive electricity gain.
- The extent of energy gain ratio will depend much on the site selection.
- Feasibility studies on various sizes of pilot scales will help in optimization of process design parameters of adsorbent synthesis and improving the yield of recovered heavy metals.
- Various configurations of contactor array designs are being developed to facilitate the operational flexibility for the offshore unit of the plant and utilization of tidal energy/waves more efficiently.
- Further brine mining aspects are being planned to facilitate value addition to desalination plants in future through the concept of CRUDE (Coupling of Recovery of Uranium and other metals from Desalination Effluents).
- These technological developments will open up indigenous secondary sources for the country in meeting up technology metal requirements.

ACKNOWLEDGEMENTS

Special thanks are due to Director Chemical Engg Group, BARC; Head RTDD/BARC; Head Planning Section CIRUS, BARC and NRG, BARC for their technical suggestions, discussions and infrastructure support. Authors would like to thank all the RUSWapp team members and members of 'DAE-Collective Vision 2004' proposals. Thanks to Homi Bhabha National Institute Mumbai for identifying doctoral research area in this programme.

REFERENCE

1. Davies, R.V., Kennedy, J., Mciloy, R.W., Spence, R., Hill, K.M., "Extraction of uranium from seawater", *Nature*, 203 (1964) 1110-1115
2. Alexander I. Wiechert, Austin P Ladshaw, Li-Jung Kuo, Horng-Bin Pan, Jonathan E. Strivens, NicholasJ Schlafer, Jordana R. Wood, Chien M. Wai, Gary A. Gill, Sotira Yiaccoumi, and Costas Tsouris., "Uranium recovery from seawater using Amidoxime based braided polymers synthesized from acrylic fibers" *Ind Eng Chem Rse.*, DOI: 10.1021/acs.iecr.0c01573 publication Date (web) 10 Jul 2020
3. A. P. Ladshaw, S. Das, W.-P. Liao, S. Yiaccoumi, C. J. Janke, R. T. Mayes, S. Dai, and C. Tsouris., "Experiments and Modeling of Uranium Uptake by Amidoxime-Based adsorbent in the Presence of Other Ions in Simulated Seawater" DOI: 10.1021/acs.iecr.5b03456 *Ind. Eng. Chem. Res.* 2016, 55, 4241–4248



4. Kelmers, A.D., ‘ Status of Technology for the Recovery of uranium from Seawater’, Separation Science and Technology, 16 (1981) No 9 1019-1035
5. Kakodkar A, “Chemical Engineering perspectives in Indian Atomic Energy Programme”, HL Roy memorial lecture delivered at CHEMCON-2000, Organised by Indian Institute of Chemical Engineers, Kolkata, December 19-22, 2000.
6. Best, R., PhD Dissertation on “ Recovery of uranium from seawater’ Massachusetts Institute of Technology, Boston, January 1980
7. Generation IV Roadmap – cross cutting fuel cycle R&D scope report, issued by Nuclear Energy Research Advisory committee and the Generation IV International forum, December 2002
8. Saxena, A K, “Uranium from seawater: a new resource for meeting future demands of Nuclear reactors”, Indian Chemical Engineer, Section C, Vol 43, No. 3, July –September 2001
9. Tomomi Kawai, Kyochi Saito, Kazuyuki Sugita, Akio Katakai, Noraiaki Seko, Takanobu Sugo, Jun-ichi Kanno, Takashi Kawakami, “ Comparison of amidoxime adsorbents prepared by co-grafting Methacrylic acid and 2-hydroxy methacrylate with acrylonitrile onto polyethylene” Ind Eng Chem Res, 39 (2000) 2910-2915
10. Saxena, A.K., Prasad, T.L., Tewari, P.K., “ Radiation processing for super speciality adsorbent preparation for Uranium extraction from seawater“ Presented at Biennial Trombay Symposium on Radiation and Photochemistry (TSRP-2006) held at BARC Mumbai, January 5-9 2006
11. Prasad TL Tewari PK “Recovery of Uranium and other valuables from Seawater/Brine” was made under Indo French Collaboration on Integrated Nuclear Desalination Systems during 3rd Technical meeting at BARC (Trombay) India on 3rd March, 2008.
12. Kalsi, P.C., Pramila, D.S., Ramaswami, A., Manchanda, V.K., “ Track etching characteristics of polyester detector and its application to uranium estimation in seawater samples“ Journal of Radio analytical and Nuclear Chemistry, 273 (2007) No.2 473-477.



Effect of Microwave Radiations on Germination and Minerals Content of *Arachis hypogaea* L.

S J Wagh¹, M S Patwardhan², R N Dhawale¹

Department of Bio Chemistry, NAC& S college, Ahmednagar¹, FSRE, MPKV, Rahuri², Rahuri

✉ *waghshalini27@gmail.com*

ABSTRACT

This study was undertaken to enhance seed germination as well as minerals contents in Groundnuts. Groundnut seeds were subjected to microwave field treatments. It was found that its germination was sensitive to microwave irradiations. The power level of 60 % i.e. 540 W for 20 sec duration was found best with 100% germination in comparison with 76% germination for untreated. The seed relationship between minerals and power applied along with time of operation was developed using statistical approach. It was observed that due to microwave treatment with 60% power at 20 sec duration significant improvement in minerals. Thus this methods can be adopted for improvement of immunity among whole population to fight against any pandemic situation.

Keywords : Groundnut germination; Microwave field; Regression model; Minerals.

INTRODUCTION

The effect of this electromagnetic treatment on groundnut seed will be more impactful. This non invasive, cheap and eco-friendly process will help the world to get recover from pandemic covid-19 situation. We all are this situation where we should improve our immune system, we should focus on our foods nutritional values to maintain our health. We have to focus on this friendly research which will lead towards sustainable environmental development. Advantages of this electromagnetic treatment as follows, This treatment help to give the protection to plant. It helps to reduce use of more fertilizer and as we said earlier it will ease to store it for more days. Electromagnetic method will help to use for seed disinfection treatment which will improve plants quality and automatically it helps to increase nutritional value of plant. according to health experts, adequate nutrition and hydration are the cornerstones to build a robust immune system and keep infections in this covid era. People who eat a wholesome diet tend to be healthy with a strong immune system and lower risk of chronic disorders and infectious diseases. Hence it is pivotal to eat a varied diet rich in fresh natural produce to get your daily dose of vitamins, minerals, fibre, proteins and antioxidants. So all these vitamins, minerals, fibre, proteins, antioxidants will boost immunity as early as possible if we do effective research on this electromagnetic seed treatment. This will help to recover easily in pandemic situation and will help to tackle it. The right kind of food you eat plays a key role in determining overall well-being and immunity. To combat deadly coronavirus it is important to eat a well-balanced diet thats why this method will be beneficial.

Recently world population has been accelerating its growth rapidly and will greater than nine thousand million in 2050. however it is difficult to obtain farmland due to urbanization. Thus food storage may become serious issue in near future hence there are requirement of bioresearch to improve the harvest efficiency of food plant.

Many researchers are done electromagnetic treatment on seed like cucumber[9], maize[11], tomato[4][11], and soyabean [5] and give positive result in germination seedling growth & enzyme activity also increases as compare to control (untreated seed). So we can select groundnut seed which contain high nutritional value so we can find out there nutritional parameter experimentally.

Microwave radiation is physical method of stimulation are considered as an innovative area of research and we have emerged as magic tool which could improve the yield of crops. When the rational use of agricultural production space is promoted, pre-treatment of seed with physical factor become more important (Phirke et.al., 1996; Pistruszewski, 1993; Podlesny, 2001)[12] The purpose of investigation non availability of quality seed is one of the major drawbacks. In order to enhance the productivity of groundnut, the seed quality can be maintained either by storing in contorted condition or by seed treatment. Storing the seed under controlled condition [12] is a costly affair and hence seed treatment like electric field application need to be practiced for improving viability and vigour of seed before sowing. Pulsed electromagnetic field showed could replace hormones in



vegetative propagation of oregano stimulating rooting process in stem cutting[9] In view of above circumstances the present research was taken to study the effect of electric field application on growth yield and seed quality parameter of groundnut.

MATERIALS AND METHODS

The present investigation entitled “Effect of electric field application on germination and nutritional content and seed quality of groundnut (*Arachis hypogaea* L.) was conducted during kharif 2017-18, season at Post Graduate Institute of Department of Biochemistry, New Arts, Commerce and Science college, Ahmednagar and MPKV, Rahuri, Ahmednagar.

Laboratory Equipment

The equipment viz. microwave oven was utilised from electrical engineering laboratory, Dr. Annashaeb Shinde College of Agricultural Engineering and double door germination chamber, hot air oven, electrical conductivity meter, weighing balance, measuring scale etc were utilized from seed technology research unit. The laminar air flow, incubation room, petridish, forceps, microscope etc. were made available by seed health testing laboratory.

Chemicals

The chemicals required for bio chemical analysis viz, sulphuric acid, potassium sulphate, mercuric oxide, copper sulphate, sodium hydroxide, sodium thiosulphate, boric acid, hydrochloric acid, monobasic potassium phosphate, dibasic potassium phosphate, hydrogen peroxide, EDTA, was made available by Department of Bio Chemistry, New Arts, Commerce and Science College, Ahmednagar. One year old seeds of groundnut (variety Phule Unnati) were obtained from M.P.K.V Rahuri, Maharashtra.

Treatment details

Groundnut seeds were treated with different electrical power intensities for different duration of exposure by microwave which rated total electric power intensity.

Application of electric field treatment

Microwave oven was setup for 3 desired power level 100%, 80%, 60% each for three time 10sec, 20sec, 30sec. respectively seed were treated for combination of each power level and time period.

Treatment Combination

Table 1. Treatment combination electric field intensities to exposure timing respectively seed were treated

Electric field intensities (%)	Exposure timing (sec)
P1- 100 (900w)	T1 - 10
P2- 80 (720w)	T2 - 20
P3 – 60 (540w)	T3 - 30

P = Power, T = Time

The treatment combination take place as follows, P_1T_1 , P_1T_2 , P_1T_3 , P_2T_1 , P_2T_2 , P_2T_3 , P_3T_1 , P_3T_2 , P_3T_3 Untreated Controlled.

METHODOLOGY

Sample Collection Fresh and One year old ground nut variety, Phule Unnati were obtained from mahatma Phule Krushi Vidyapeeth Rahuri. Ground nut seed were treated with different electric power intensities for different duration of exposure of microwave.

Germination Test

Germination test were carried out immediately after one day of electrostatic field exposure. Seed were sown kept in germinator where the temp. and humidity were controlled as per ISTA standard at 25oc. 80% respectively. Final count was measure on 8th day given in table.

Root shoot Length

Ten normal seedling from each of the replication of germination test were randomly selected and root shoot length was measured



in cm. The average length was calculated and recorded in cm.

Ash and Moisture Content

Sample of 2 gm was used in analysis of ash content ground nut was final grind using grinder before carry out ash analysis sample are high in moisture often dried to prevent spattering during ashing. Muffle furnace was used for determine ash content at the pre ground substance to be examined weighted into inclination tray. The tray is placed into muffle furnace at specified 600°C Temp. Where it inserted and then weighted again.

$$\% \text{Total ash} = (\text{Ash wt} / \text{Wt of Sample}) \times 100$$

Sadashivam practical book of Biochemistry [] Moisture Content was determined by hot air oven method. by Drying 2gm of groundnut seed at 103°C for 17 hrs in hot air oven. The percentage of moisture content was calculated on the wet weight (w/w) basis.

Biochemical Study

The estimation of minerals carried out by different method by practical book [2] of biochemistry by sadashivam by the different method and tests

Calcium – by volumetric method (pink colour)

Calcium precipitate as calcium oxalate and is treated with standard potassium permanganate which also act as self indicator.

Phosphorus – by spectrophotometric method (bluish colour)

For the determination of total phosphorus the sample in which organic matter has been destroyed by tri acid mixture, is used. The phosphate containing solution is treated with sulphomolybdic acid to produce phosphomolybdic acid. This is then reduced by stannous chloride giving a blue coloured complex whose colour intensity is proportional to the amount of phosphate in the preparation Iron – by colorimetric method (pink colour) Iron is determine the in food stuff after either dry or wet ashing of the food sample. A suitable aliquot of the mineral extract containing 0.1-0.5 microgram of iron is made to react with alpha alpha dipyrindyl in the presence of hydroxylamine hydrochloride to give a pink colour with absorbance maxima at 520 nm.

Germination Study

Three replication of seeds from each treatment were kept for germination at 25±2 degree temp and 90% relative humidity for 10 day using between paper method (BP) in germination chamber. The germination percentage was expressed on the basis of normal seedling only as described in ISTA rule (Anonymous 1999).

$$\text{Germination \%} = \frac{\text{No of Normal Seeding Germinated}}{\text{Total No of Seed Place for germination}} \times 100$$

RESULTS

Table 2. Effect of microwave Radiation on groundnut treated as well as control seed minerals by therotically

Treatment	Minerals		
	Calcium (µg)	Iron (µg)	Phosphorous (µg)
P ₁ T ₁	0.040	1.5	0.0045
P ₁ T ₂	0.360	1.5	0.0048
P ₁ T ₃	0.200	1.5	0.0036
P ₂ T ₁	0.240	1.5	0.045
P ₂ T ₂	0.12	1.0	0.036
P ₂ T ₃	0.240	1.5	0.005
P ₃ T ₁	0.160	1.5	0.0030
P ₃ T ₂	0.120	2.0	0.0026
P ₃ T ₃	0.080	1.5	0.005
Untreated Control	0.080	1.5	0.0058

The above value of minerals were practically done in laboratory from above value we can see normal change in minerals value with respect to treatment combination.

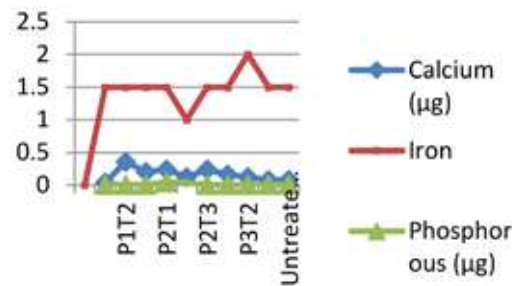


Fig.1. Graphical representation of minerrals content calcium ,iron, phosphorus treated as well as control seed of groundnut

RESULTS

Germination: With reference to several filter trails the parameter for voltage applied and duration of time of exposure were selected based on statistical requirement the experimental was planned for factorial randomized block design. There were nine treatment combination with three replication and one control all sample were kept in germinator on 8th Day. Germination count was made and fresh weight and root shoot length were measured. After that as ISTA international seed testing association recommendation the sample put in oven for 17hr at 60oC for measurement of dry mater content then weight at all sample were noted using these results. Germination study were calculated.

Table 3. Effect of microwave radiation on germination and root shoot length(cm)

Sr. No	Sample	Average Germination	Root Shoot Length (cm)
I.	P ₁ T ₁	44.5	20.05
II.	P ₁ T ₂	33.5	16.5
III.	P ₁ T ₃	38.5	17.7
IV.	P ₂ T ₁	45.0	17.4
V.	P ₂ T ₂	37.5	17.4
VI.	P ₂ T ₃	58.0	16.9
VII.	P ₃ T ₁	56.5	21.3
VIII.	P ₃ T ₂	43.5	15.7
IX.	P ₃ T ₃	31.5	14.2
X.	Untreated Control	39.5	15.2

From the observation table there is large different in germination average and root shoot length due to microwave radiation effect. Easily showed the observation table there is rate of average germination is greater than control.

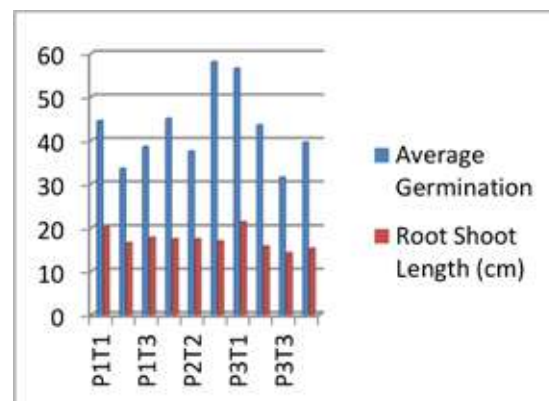


Fig 2. Graphical representation of Germination and Root Shoot length in cm Vs treated seed and control



DISCUSSION

The effect of microwave power level and exposure timing on germination on groundnut studied and data present in Graph no.1 present investigation the seed quality parameter decline progressively with increasing storage period it has been believe that biological process including free radicals, excite the activity of protein and enzymes which emergence, growth rate and seed vigour, which might have resulted better germination of onion seed during storage that untreated control. Shivare et al. (1971) reported the high seed germination could be maintained by using microwave power levels 0.25 w.g for seed of corn. However, Moon and chung (2000) recorded that the inhibitory effect of germination when electric field intensities exceeded 12 kv/cm for exposure time greater than 60 sec/in tomato. In Pea cultivator it has been found that the magnetic field presowing seed treatment can be used practically to enhance the growth and yield[7]

Root Shoot length

The effect of microwave power level and exposure timing root shoot length present in graph no. 1 electric field exposure of seed may result in breaking of hydrogen bounding in ultra structural elements of cell. This structural alternation may increase enzymes activity depending on the strength of electric field and exposure timing. This might have resulted increase in seed germination , seedling length and dry matter content which also increase the seed vigour than untreated control.

The seed recorded higher root shoot length dry matter content as compare with control the seed were treated with microwave power level 60% (P3) recorded root shoot length. Dry matter contain the seed which is untreated at exposure timing 10 sec(T1) recorded higher root shoot length than (T2) 20sec. T3(30 sec.).

CONCLUSIONS

- i. Exposure to action of high intensity AC electric field can be effective tool for the enhancement of germination and maintain the nutritional value.
- ii. The seed recorded significantly higher germination as compared to control. The seeds were treated with 80% microwave power level (p2) recorded higher germination percentage than 60(P3) and (100%) the seed were treated with exposure timing of 30 sec. (T3) and also give better germination result in 60% (p3) and time exposure to 10 sec.
- iii. The seed recorded higher root shoot length dry matter content as compare with control the seed were treated with microwave power level 60% (P3) recorded higher root shoot length . Dry matter contain the seed which is treated at exposure timing 10 se (T1) recorded higher root shoot length than (T2) 20 sec, (T3) 30 sec.
- iv. The seed recorded higher mineral contain as compared to control the seed which were treated with microwave power 60% P3 recorded higher mineral content than the seed which is treated and uncontrolled .There is no change in Phosphorous content. Iron content 100% time exposure to 20 sec. Gives better result.

ACKNOWLEDGMENT

The Authors are pleased to acknowledge Agricultural Engineering Department of Mahatma Phule Krishi Vidyapeeth, Rahuri and Chemistry department of New Arts Commerce and Science College Ahmednagar, for providing research facilities. Authors thank Prof. S. P Salave and D.S. Thanage for their help and support.

REFERENCES

1. M. S. Patwardhan, W. Z. Gandhare, "High Voltage Electric Field Effect On Germination rate of tomato Seed", Acta Agrophysica, Vol. 20, no.2, pp. 403 -413, 2013
2. S. Sadashivam, A. Manickam "Biochemical Methods Newage International Publisher, Delhi. ISBN No. 9788122421408
3. Aspasia Efthimiadou, Nikolas Katesenios, Anestis Karkanis, "Effect of Presowing Pulsed Electromagnetic Treatment of Tomato seed on Growth, Yield and Lycopene Content" Hindawi Publishing Cor. The Scientific World Journal, <http://dx.doi.org/10.1155/2014/369745>.



4. Alessandro de Lucca e braccini, Mucio silvareis, “Biochemical Changes Associated to Soybean Seeds Osmo Conditioning during Storage” *pesq.agropec. bras., brasil* vol. 35, no.2, pp. 433 -447, 2000.
5. Elizabeth Isaac A, Claudia Hernadez A, Aururo Dominguez P, and Alfredo Cruz, “ Effect of Pre sowing Electromagnetic Treatment on Seed Germination and Seedling Growth in Maize (*Zea Mays L.*)” *Agronomia Colombiana* vol.29, no.2, pp. 213-220, 2011.
6. Bhaskara M.V, G.S.V. Raghvan, A.C> Kushalappa and T.C. Paulitz, , “Effects of Microwave Treatment on Quality of Wheat Seed Infected with *fusarium graminearum*”. *Journal of Agricultural Engineering Research*, 2010.
7. M.Iqbal, M.RAhemad, S.M.Hussain, R.A.Khera,T.H.Bokhari, and M.A.Shehzad, ‘optimization of pre-sowing magnetic field does through RSM in pea.’ *International Agrophysics*, Vol.27, pp265-274,2013
8. Kasetsart J.“Change in Antioxidant Enzyme Activity, Lipid Peroxidation and Seedling Growth of Cucumber Seed Induced by Hydropriming and Electric Field Treatments.” *Nat. Sci.*pp.825-834, 2006.
9. D. Bilalis, N. Katsenios A. Ethimiadou P and A. Karkanis, ‘pulsed electromagnetic field effect in organo rooting and vegetative prapogation; a potential new organic method, *Acta Agriculturae scandinavica B:soil and plant science*, Vol.62,no1,pp94-99,2012
10. Effect of pre-sowing electromagnetic treatment on seed germination and seeding growth in maize (*Zea mays L.*) *Agronomia Colombiana* 29(2), 213-220,2011
11. Effect of seed osmopriming on seed germination behavior and vigor of soyabean (*Glycine max L.*) *ARPJ Journal of agricultural and biological science*. Vol. 6, no.1,pp.39-43, Jan. 2011,ISSN 19902- 6145.
12. Phirke P S, A B Kubde, S P Umbarkar, 1996. The influence of magnetic field on plant growth. *seed. Sci. Techol.*24,375-392.



Design Optimization of Heat Exchanger by Old and New Generations Metaheuristic Optimization Algorithms: Insights and Comparisons

Boyina Venkata Akhil, Prashanna Sharma, Sandip Kumar Lahiri*

Department of Chemical Engineering, National Institute of Technology, Durgapur, West Bengal

✉ sandipkumar.lahiri@che.nitdgp.ac.in

ABSTRACT

This study compares the performance of 3 old generation algorithms namely Genetic Algorithm, Particle Swarm Optimization and Differential Evolution with two new generation algorithms namely Firefly Algorithm and Symbiotic Organism Search in optimization of heat exchanger. The optimization procedure involves the selection of the major geometric parameters such as tube diameters, tube length, baffle spacing, number of tube passes, tube layout, head type, baffle cut, etc., as per TEMA standard and minimization of total annual cost is considered as the design target. The methodology takes into account the geometric and operational constraints typically recommended by design codes. Three different case studies are presented to demonstrate the comparative effectiveness and accuracy of proposed five algorithms. From the results of all the three case studies, it is concluded that DE performed the best in terms of capturing the lowest value of total cost and minimum execution time. The new generation algorithm, SOS performed the second-best as it captures the lowest values of total cost every time, honours the constraints every time in reasonably low execution time. The final optimized heat exchanger comply TEMA standard, having lowest cost and obey all geometry, velocity and service constraints.

Keywords : Heat Transfer; Mathematical Modelling; Heat Exchanger Design; Firefly Algorithm (FA); Symbiotic Organism Search (SOS); Differential Evolution (DE); Constrained Optimization.

INTRODUCTION

Heat exchanger (HE) remains as the most widely used heat transfer equipment in chemical process industries. Major chemical industries around the globe are facing unprecedented challenges due to shrinking profit margin and cut-throat global competition. Chemical industries are now looking for new ways to reduce their capital and operating expenditure (CAPEX and OPEX). Due to large numbers of HEs available in industries, a slight reduction of cost in heat exchanger (both CAPEX and OPEX) has multiplication effect. Hence, improvements in HE design methodology has attracted many researchers over the decades to minimize cost. HE design remains as potential area which can have a huge impact on the plant's profitability.

The traditional design of STHE involves heat transfer area and tube and shell side pressure drop calculations. Traditional design approaches does not take into account the cost of HE as main design target. It involves trial and error approach and does not guarantee the lowest cost HE. Detail design of HE involves thermodynamics, heat transfer and fluid dynamics calculations, strength calculations and last but not the least cost estimation. Various commercial software packages like HTRI, HTFS, ASPEN automates the thermal design and rating of STHE. In this software, designer needs to specify a priori various design decision variables like tube diameter, tube length, tube pitch, shell type, baffle spacing, baffle cut etc. from the standard values given in drop-down menu. Based on the user inputs, these software calculate various constraints like pressure drop, velocity through tubes etc. and check for any violation based on some industry-specific criteria. If any constraint gets violated, based on his experience, designer assumes new values of above geometric variables to explore the possibility of reducing the heat transfer area while obeying all the constraints. This type of trial and error approach is time-consuming and does not guarantee minimum cost design as cost minimization is not considered as design target.

Many gradient-based optimization techniques are tried in past by several researchers to minimize total cost. Researchers applying the gradient descent based traditional cost minimization techniques to STHE problem did not get encouraging results as most of the time, solution gets trapped in local optima. Hence, traditional optimization techniques are not proven to be very efficient and also, they have limited applications in complex heat exchanger optimization.

The second objective of the present study is to integrate the optimization algorithm of STHE with TEMA (Tubular Exchanger

Manufacturers' Association) standard. TEMA standards are followed by industry all over world to design and fabricate heat exchanger. From the literature survey, it was found that TEMA standard is not considered in the majority of published papers during the optimization of STHE. Hence, the resultant optimum STHE found in the literature does not comply with TEMA standard sizes and thus makes the fabrication cost higher. This makes the lowest cost heat exchanger with standard dimensions and easy for fabrication.

The third objective of the paper is to incorporate the best practices followed by different industries in HE design. In the actual shop floor of the industry, the lowest cost HE may not be always the best exchanger. Maintainability, less fouling tendency, less flow-induced vibration, ease of cleaning of tubes and shell, less floor space requirement, compactness of design are some of the criteria which must be considered during design of STHE. In the present study, we have incorporated those geometric and hydraulic constraints during the design optimization phase and thus ensure all these constraints are obeyed.

The optimal HE design problem

The calculation sequence of the optimum HE design has the following steps:

- 1) Assume a set of seven design variables like tube diameter, tube length, Ratio of baffle spacing to shell diameter, Number of tube pass, Type of pitch, Head type, Baffle cut %. These are the free optimization variables which need to be optimized to attain a lowest cost exchanger.
- 2) Estimate the heat transfer area based on required duty and assuming the values of design variables in Step 1.
- 3) Evaluate the shell and tube side pressure drop.
- 4) Based on the heat transfer area and pressure drop, calculate the capital cost, operating cost, and total cost.
- 5) Evaluate different constraints like velocity constraint, pressure drop constraint, geometric constraint, hydraulic constraint, and see whether all constraints are obeyed.
- 6) Iterate and select new set of values for design variables within their upper and lower bounds to minimize the cost.

Continue iteration until total cost is minimized and all the constraints are obeyed.

An attempt has been made in this work to apply different optimization techniques such as GA, PSO, DE, FA and SOS to design the lowest cost heat exchanger with TEMA dimensions (Table 1) and satisfying all of the constraints.

Table 1: Design variables and their options

Optimization variable	Variable Notation	Optimization variable	Options Available
x_1	d_o	Tube diameter	[0.00635, 0.009525, 0.0127, 0.01905, 0.022225, 0.0254, 0.03175, 0.0381, 0.04445, 0.0508, 0.05715, 0.0635]
x_2	L	Tube length	[1.2192 1.8288 2.4384 3.048 3.6576 4.8768 6.096 6.7056 7.3152]
x_3	R_b	Ratio of baffle spacing to shell diameter	[0.2, 0.25, 0.3, 0.35, 0.4, 0.45, 0.5, 0.55, 0.6, 0.65, 0.7, 0.75, 0.8, 0.85, 0.9, 0.95, 1]
x_4	N_{pass}	Number of tube pass	[1, 2, 4, 6, 8]
x_5	P_t	Type of pitch	Triangular or Square
x_6	Head type	Head type	Fixed tube sheet or U tube, outside packed head, split ring floating head, and pull through floating head
x_7	Baffle Cut	Baffle cut, %	[15, 25, 35, 45]

Objective Function

The capital investment (C_i) can be obtained from Hall's correlation, which involves the C_i as the function of the HE surface area. The expression is as follows [21]:

$$C_i = a_1 + a_2 S^{a_3}$$

If the material of construction of the HE is stainless steel, the values of a_1 , a_2 and a_3 are 8000, 259.2, and 0.93, respectively.

The total discounted operating cost (C_{od}) can be computed by the following expression:

$$C_{od} = \sum_{x=1}^{ny} \frac{C_o}{(1+i)^x}$$

C_o is the annual operating cost formulated as below:

$$C_o = PC_e H$$

Where C_e is the energy cost and P is the pumping cost which can be expressed as below:

$$P = \frac{1}{\eta} \left(\frac{m_t}{\rho_t} \Delta P_t + \frac{m_s}{\rho_s} \Delta P_s \right)$$

The total cost (C_{tot}) is the summation of C_i and C_{od} and thus formulated as follows:

$$C_{tot} = C_i + C_{od}$$

Constraints

Table 2: Geometric, velocity and service constraints

Constraints description	Remarks
Geometric Constraints	
$3 \leq L/D_s \leq 5$	-
$0.2 \leq R_b \leq 1$	-
Velocity Constraints	
$v_t^{min} \leq v_t \leq v_t^{max}$ $1 \leq v_t \leq 2$ (in this case study)	Process fluids: 1 to 2 m/s, maximum of 4 m/s if it is required to reduce fouling; water: 1.5 to 2.5 m/s
$v_s^{min} \leq v_s \leq v_s^{max}$ $0.3 \leq v_s \leq 1$ (in this case study)	shell-side: 0.3 to 1 m/s
Service Constraints	
$\Delta P_t \leq \Delta P_t^{max}$ $\Delta P_t \leq 35000 Pa$ (in this case study)	For fluids having viscosity less than 1 mNs/m ² maximum pressure drop is 35 kN/m ² and for fluids having viscosity 1 to 10 mNs/m ² maximum pressure drop is 50-70 kN/m ²
$\Delta P_s \leq \Delta P_s^{max}$ $\Delta P_s \leq 35000 Pa$ (in this case study)	Shell side also has the same conditions as the tube side.

Optimization Algorithms

Symbiotic organisms search (SOS), Firefly algorithm and Differential evolution is given to understand their working principle. GA and PSO algorithm are also used in the present study but their working principle are not given here for the sake of brevity. More details of all the algorithms can be found in reference Yang [10].

Symbiotic Organisms Search (SOS): SOS is a nature-inspired metaheuristic optimization technique proposed by Cheng and Prayogo [11]. This method basically imitates the relationship among different organisms.

Firefly optimization (FA): Firefly optimization algorithm (FA), proposed by Yang [13] mimics the periodic flashing behaviour of fireflies.

Differential Evolution (DE): DE is one of the old metaheuristic optimization methods and has been proved to be very effective in solving many real-life optimization problems.

Testing of algorithms against heat exchanger optimizations through a case study:

The data as shown in **Table 3** were supplied as input to the different optimization algorithm. This case study is taken from Kern [6]. Each optimization algorithm was run 100 times due to the stochastic nature of such algorithm and the best out of 100 runs was taken as the final optimum value for that algorithm. One distinctive feature of the present study, which differs from the earlier research work, is that in the present study, the optimization algorithm is forced to take discrete standard values as per TEMA standard. It cannot take any other values, which are not standard. This ensures that the final design obtained after optimization complies with TEMA standard. For other optimization variables also discrete values as per TEMA standards are taken, and those values are given in **Table 1**. All the values of discounted operating cost are computed with $n_y = 10$ years, annual discounted rate $i = 10\%$, energy cost (C_e) = 0.12 €/kW h. Annual amount of work hours (H) = 7000 h/year.

Table 3: Process parameters and physical properties of the case study

Condition	Mass flow (kg/s)	T_{input} (°C)	T_{output} (°C)	ρ (kg/m ³)	C_p (kJ/kg K)	μ (Pa.s)	K (W/m K)	$R_{fouling}$ (m ² K/W)
Shell side: methanol	27.8	95	40	750	2.84	0.00034	0.19	0.0003
Tube side: sea water	68.9	25	40	995	4.20	0.0008	0.59	0.0002

Table 4 shows the optimum HE results of 5 metaheuristic algorithms, namely GA, PSO, DE, SOS, and FA, along with their original design solutions given by the referenced authors.

Based on the performance to capture the minimum value and execution time, the following sequence can be made:

- 1) DE (Capture the lowest value and the lowest execution time)
- 2) SOS (Capture the lowest value and the second-best execution time)
- 3) PSO (Capture the lowest value, execution time is very high)
- 4) FA (Did not capture the lowest value, however reasonably low execution time)
- 5) GA (Did not capture the lowest value and reasonably low execution time)

We also observed that the total cost has increased from 37064.04 € to 38687.15 € when the constraints are imposed. Therefore, the difference of 1623.11 € is due to the imposing constraints mentioned in Table 2 but it ensures the best performing HE.

Table 4: Results of optimization

Parameter	Literature	GA	PSO	DE	SOS
d_0 (m)	0.02	0.0191	0.0191	0.0191	0.0191
L (m)	4.83	3.658	3.658	3.658	3.658
R_b	0.39	0.8	1	1	1
N_{pass}	2	2	2	2	2
P_{type}	-	Square	Square	Square	Square
Head type	-	Split Ring Floating head	Outside packed head	Outside packed head	Outside packed head
Baffle Cut	-	35%	15%	15%	15%

N_t	918	694	677	677	677
D_s (m)	0.894	0.8101	0.7754	0.7754	0.7754
v_t (m/s)	0.75	1.0936	1.1210	1.1210	1.1210
v_s (m/s)	0.58	0.3530	0.3083	0.3083	0.3083
h_t (W/m ² K)	3812	5297.47	5403.56	5403.56	5403.56
h_s (W/m ² K)	1573	15863.2	22025.9	22025.9	22025.9
U_{calc} (W/m ² K)	615	1143.37	1172.06	1172.06	1172.06
S (m ²)	278.6	151.89	148.17	148.17	148.17
ΔP_t (Pa)	6251	10366	10844	10844	10844
ΔP_s (Pa)	35789	3866.01	2407.19	2407.19	2407.19
C_1 (€)	51507	33051.1	32492.4	32492.4	32492.4
C_{od} (€)	12973	6349.34	6194.71	6194.71	6194.71
C_{tot} (€)	64480	39400.4	38687.2	38687.2	38687.2
Run Time (s)	-	1.89062	57.2031	1.89062	2.3125
Constraints					
L/D_s	*5.4027	4.5149	4.7173	4.7173	4.7173
v_t (m/s)	*0.75	1.0936	1.1210	1.1210	1.1210
v_s (m/s)	0.58	0.3530	0.3083	0.3083	0.3083
ΔP_t (Pa)	6251	10366	10844	10844	10844
ΔP_s (Pa)	*35789	3866.01	2407.2	2407.2	2407.2

*Did not obey the constraints

Observations

The optimization algorithms are able to reduce the total cost from 64480 € (literature) to 37064€ i.e., 43 % decrease in total cost when no constraints were imposed. However, when constraints were imposed, minimum total cost was achieved 38687 € i.e., equivalent to 40% reduction in total cost. In other words, the cost of imposing constraints is around 1623 €.

From the results, we can conclude that DE performed the best among all algorithms in terms of capturing the lowest value of total cost and minimum execution time. The new generation algorithm, SOS performed the second-best as it captures the lowest values of total cost every time, honours the constraints every time in reasonably low execution time. PSO captures the lowest values every time, but its execution time is excessively high as compared to DE and SOS. FA has reasonably well execution time, but it fails to attend the lowest values of total cost in all three cases. Therefore, as observed from the results of three case studies, SOS is the most promising new generation algorithm, and DE being old generation classical algorithm, still performs the best among all the five algorithms.

The major advantages of these type of case studies are as follows:

- It helps the designer to locate the minimum cost HE very quickly without trial and error.
- Use of different algorithms enables the designer to validate the final optimum results as the most of the algorithms converge to same minimum value. Agreement of final results by five different algorithms increase the confidence of designer about his calculations
- The imposition of different constraints in optimization algorithms enables the HE maintainable, robust, and compact.

Use of discrete decision variables ensures that the final optimized HE would comply with TEMA standard, which is followed by the industry globally.

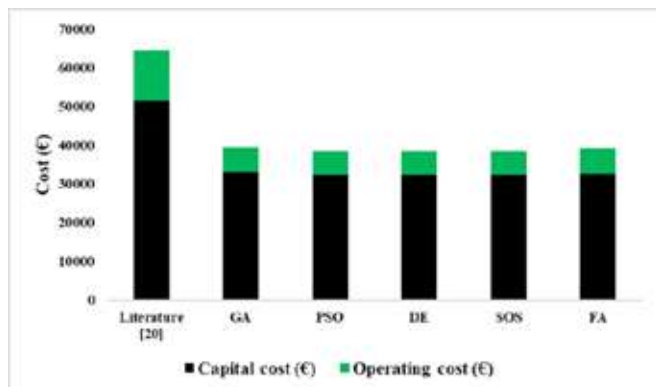


Fig 1: Comparisons of total cost, capital cost and operating cost obtained from different algorithms for case study

CONCLUSIONS

This study applies 5 metaheuristic algorithms on heat exchanger optimization problems and able to find out the lowest cost heat exchanger automatically. From the comparative study results, it is concluded that SOS has great potential among new generation algorithms. However, DE performs best in heat exchanger optimization problem. Instead of picking up any random value between lower and higher bound, this study enforced picking up only TEMA specified discrete values for tube diameter, tube length etc and thus ensure that the resultant heat exchanger coming out from algorithms comply with TEMA standard. Also, various best practices in heat exchanger design followed by industry is incorporated in the design algorithm in terms of geometry and hydraulic constraints so that optimum heat exchanger performs best in the shop floor in spite of its lowest cost.

NOMENCLATURE

a_1 = numerical constant (€)

a_2 = numerical constant (€/m²)

a_3 = numerical constant

Baffle_cut = Baffle cut

C_e = energy cost (€/kWh)

C_i = capital investment (€)

C_o = annual operating cost (€/yr)

C_{od} = total discounted operating cost (€)

C_{ps} = Cp of shellside fluid (kJ/Kg K)

C_{pt} = Cp of tubeside fluid (kJ/Kg K)

C_{tot} = total annual cost (€)

D_s = shell inside diameter (m)



d_i = tube inside diameter(m)
 d_o = tube outside diameter (m)
 ΔP_s = shellside pressure drop (Pa)
 ΔP_t = tubeside pressure drop (Pa)
 F = temperature difference correction factor
 H = annual operating time (h/yr)
 h_s = convective coefficient shellside (W/m²K)
 h_t = convective coefficient tubeside (W/m²K)
 i = annual discount rate
 j_h = Parameter for Baffle Cut
 K_1 = numerical constant
 K_s = thermal conductivity shell side (W/m K)
 K_t = thermal conductivity tube side (W/m K)
 L = tube length (m)
 $LMTD$ = mean logarithmic temperature difference (°C)
 m_s = shell side mass flow rate (kg/s)
 m_t = tube side mass flow rate (kg/s)
 μ_t = viscosity at tube wall temperature (Pa s)
 n_1 = numerical constant
 n = Number of passes
 N_t = tubes number
 η = overall pumping efficiency
 n_y = equipment life (yr)
 P = pumping power (W)
 P_t = tube pitch (m)
 P_{type} = Pitch type
 Q = heat duty (W)
 R_b = Baffle Spacing / Shell Diameter Ratio
 R_{fs} = conductive fouling resistance shellside (m²K/W)
 R_{ft} = conductive fouling resistance tube side (m²K/W)
 ρ_s = fluid density shellside (kg/m³)
 ρ_{ts} = fluid density tubeside (kg/m³)
 S = heat exchange surface area (m²)
 S_a = Crosssectional area normal to flow direction
 T_{hi} = inlet fluid temperature shellside (K)
 T_{ci} = inlet fluid temperature tube side (K)



T_{ho} = outlet fluid temperature shellside (K)

T_{co} = outlet fluid temperature tubeside (K)

U = overall heat transfer coefficient (W/m^2K)

v_s = fluid velocity shellside (m/s)

v_t = fluid velocity tubeside (m/s)

REFERENCES

1. P. D. Chaudhuri, M. D. Urmila, & S.L. Jefery, An automated approach for the optimal design of heat exchangers, *Ind. Engng. Chem. Res.* (1997) 36, 3685 – 3693. <https://doi.org/10.1021/ie970010h>.
2. A.C. Caputo, P.M. Pelagagge, P. Salini, Heat exchanger design based on economic optimisation, *Appl. Therm. Eng.* (2008). <https://doi.org/10.1016/j.applthermaleng.2007.08.010>.
3. B. V. Babu, S.A. Munawar, Differential evolution strategies for optimal design of shell-and-tube heat exchangers, *Chem. Eng. Sci.* (2007). <https://doi.org/10.1016/j.ces.2007.03.039>.
4. V.K. Patel, R. V. Rao, Design optimization of shell-and-tube heat exchanger using particle swarm optimization technique, *Appl. Therm. Eng.* (2010). <https://doi.org/10.1016/j.applthermaleng.2010.03.001>.
5. A. Hadidi, A. Nazari, Design and economic optimization of shell-and-tube heat exchangers using biogeography-based (BBO) algorithm, *Appl. Therm. Eng.* (2013). <https://doi.org/10.1016/j.applthermaleng.2012.12.002>.
6. D.Q. Kern, *Process Heat transfer*, McGraw-Hill, New York (1950)
7. R.K. Sinnott, *An introduction to chemical engineering design* Chemical engineering series by J.M. Coulson and J.F. Richardson, 6, Pergamon Press, Oxford (1989)
8. N. Khalfe, K. Lahiri, K. Wadhwa, Simulated annealing technique to design minimum cost exchanger, *Chem. Ind. Chem. Eng. Q.* (2011). <https://doi.org/10.2298/ciceq110204027k>.
9. A.H.L. Costa, E.M. Queiroz, *Appl. Therm. Eng.* 28 (2008) 1798-1805
10. X.S. Yang, *Nature-inspired metaheuristic algorithms*, Luniver Press (2010)
11. M. Y. Cheng, D. Prayogo, Symbiotic organisms search: a new metaheuristic optimization algorithm. *Computers & Structures* 139, 98-112 (2014)
12. T. Dokeroglu, E. Sevinc, T. Kucukyilmaz, A. Cosar, A survey on new generation metaheuristic algorithms, *Comput. Ind. Eng.* (2019). <https://doi.org/10.1016/j.cie.2019.106040>.
13. X.S. Yang, Firefly algorithm, stochastic test functions and design optimization, *Int. J. Bio-Inspired Comput.* (2010). <https://doi.org/10.1504/IJBIC.2010.032124>.
14. S.K. Lahiri, N. Khalfe, Improve shell and tube heat exchangers design by hybrid differential evolution and ant colony optimization technique, *Asia-Pacific J. Chem. Eng.* (2014). <https://doi.org/10.1002/apj.1772>.
15. M. Serna, A. Jimenez, A Compact Formulation of the Bell–Delaware Method for Heat Exchanger Design and Optimization, *Chem. Eng. Res. Des.* 83(A5) (2005) 539-550. <https://doi.org/10.1205/cherd.03192>



Thermal and Performance Analysis of Bio Gas Digesting System

S Babu¹, C Gajendran², B Bhuvaneshwari, T Nandhini³

Associate Professor, Dept. of Mechanical Engineering, PSG College of Technology, Coimbatore, Tamil Nadu¹

Associate Professor, Dept. of Civil Engineering, Karunya Institute of Technology and Sciences, Coimbatore, Tamil Nadu²

M E Energy Engineering, Dept. Of Mechanical Engineering, PSG College Of Technology, Coimbatore, Tamil Nadu³

✉ sjsham@gmail.com, gajendran@karunya.edu

ABSTRACT

India has committed to have 40 per cent of its electricity capacity from non-fossil fuel sources. Biogas is one among the major source of renewable energy. In this research an attempt is made to provide heat to the bio mass in the digester in a passive manner so that no energy is spent in generating and transferring heat. Solar energy is harvested and transported to the digester through helical coil and the performance of bio-digester is studied. Initially the digester was started without heat source and experiments are conducted with cow dung followed by food waste and solid waste. The same experiment is repeated with heat source. It can be analyzed clearly that addition of heat source enhances the generation of bio gas.

Keywords : Bio mass, Helical coils, Solar water heater.

INTRODUCTION

Biomass is organic material that comes from plants and animals, and it is a renewable source of energy. India is very rich in biomass and has a potential of 16,881MW (agro-residues and plantations), 5000MW (bagasse cogeneration) and 2700MW (energy from waste). Biomass power generation earns investments of over Rs.600 crores every year, generating more than 10 million man-days in the rural areas. It briefly explains about anaerobic digestion process, steps involved and the parameters affecting the digestion process[1]. Methanogenesis is a critical step in the entire anaerobic digestion process, as it is the slowest biochemical reaction of the process[2,3]. It is severely influenced by operation conditions. Composition of feedstock, feeding rate, temperature, and PH are examples of factors in methanogenic process. Carbon and nitrogen concentration are essential constituents for the optimal growth of bacteria in anaerobic digester[4,5]. Universally adopted carbon nitrogen range is 25:1 to 30:1. Deviation from this ratio will slow down the process. Thus biomass has a greater advantage in the production of energy as they are easily available[6], economically cheap and environmentally friendly[7]. There are various technique and methods for the biomass conversion[8]. This project uses biogas digester to produce methane which is the main portion of biogas which can be converted to other form of energy such as heat and electricity. The outcome of the research is to analyse the digester performance using the passive heat source.

METHODOLOGY

The design of anaerobic digester with solar water heater and develop a heat exchanger coil. A technique is developed for measuring the quantity and quality of biogas and various experimental results are obtained with and without heat source.

Design of the anaerobic digester with solar water heater

Anaerobic digester plant is used to produce the digestion process where the organic matter is converted in to useful gases. The design and technology of biogas plant differs from country to country, depending on climatic conditions and national frameworks, energy availability and affordability. Many types of digesters were designed and the few categories are listed, 1.fixed dome 2.floating drum 3.bag digesters 4.plug flow digester 5.anaerobic baffled reactors.

Among these, nano gas digester is selected because the volume of gas produced can be found in this digester and size of plant. Dimensions of the digester is,

Height of digester (h1) = 65 cm

Height of gas dome(h2) = 28.5cm

Dia of digester (d_1) = 46 cm

Diameter of dome (d_2) = 44 cm

Volume of digester and gas holder is 105 litres and 45 litres.

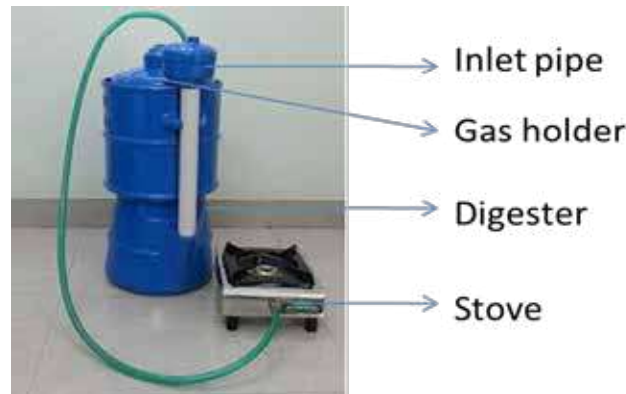


Fig 1. Bio Gas Digester

Selection Of Heat Source

Heat energy is given to the biomass in the digester to increase the temperature of the slurry. Solar energy is used as heat source where it is abundant in nature, it is the renewable source of energy. These radiations are converted to other forms of energy such as heat and electricity. Some types and apparatus are used to do this conversion and main conversion types are solar electric energy and solar thermal energy. Here, in order to improve the performance of a collector it is necessary to reduce the heat loss by convection on the top side of the collector as in **Fig. 1**. This is done by having vacuum above the absorber plate i.e., evacuated tube collector using thermosyphon effect. As a consequence, it becomes to use a glass tube as the cover because only a tubular surface is able to withstand the stresses introduced by the pressure difference. The dimensions of the solar collectors are,

Inner tube diameter (d_1) = 35mm

Outer tube diameter (d_2) = 45mm

Tube length (L) = 600mm

Diameter of the tank = 130mm

Length of the tank = 600mm

Volume of tank = 30liters

Design and Fabrication of Heat Exchanger Coil

Heat exchanger is a device used to transfer heat energy from one fluid to another generally from hot fluid to cold fluid. They are used in many applications for both heating and cooling. In our project these coils are used to heat the slurry in the digester.

The software used for designing the heat exchanger coil is “BS Solid works 2015”. In that various coils were designed such as helical coil, spiral coil, spherical coil and S-shape coil. Among these helical coil with the tapering side is selected because it fits inside the digester exactly and large amount heat transferring area is achieved in this design as shown in **Fig. 2**.

The specifications of the coil is,

Diameter of the coil = 1.2cm

Length of coil = 750cm

Height of the coil = 21cm

Number of turns = 11turns

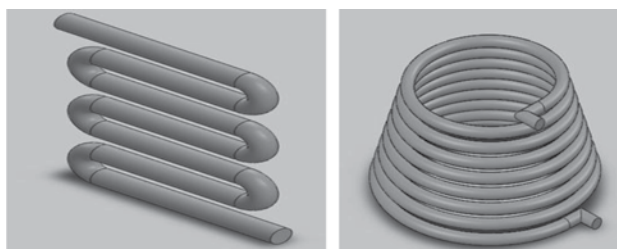


Fig 2. S-Shape Coil And Spiral Coil

Material used for the coil is copper because of its good heat transfer properties. Copper has the thermal conductivity of 386W/mK which is a good conductor.

EXPERIMENTATION

The biogas digester, solar water heater which acts as heat source and the heat exchanger coil is brought into a single setup. Heat exchanger coil is placed inside the digester and it is made leak proof so that hot fluid does not mix with the slurry in the digester at any situation. At first the digester is drilled and two holes were made for outlet and inlet entry of fluid. The heated water from the tank enters the top of the coil and the heat transfer takes place from the oil to the slurry as the water moves downwards the temperature is reduced and reaches the outlet and enters into tank, the process is repeated. As the slurry gets heated, the decomposition and microbial generation becomes faster and bio gas is produced quickly. They are collected in the gas holder and the quantity is measured with the help of scale in gas holder. To test the quality of the bio gas Zakaria tube is used. The quality of biogas depends upon the presence of methane in it. Zakaria tube is a U-tube structure made up of glass with markings up to 5ml and internal dia 12mm. Saturated solution of potassium hydroxide solution (KOH) is prepared by dissolving pellets and poured into a tube. This solution is capable of absorbing all carbon di oxide in biogas. The biogas produced from digester is collected in 5ml syringe and injected into a tube .the value of methane and carbon dioxide is noted in a table which is used for analysing the quality of biogas.

RESULT AND DISCUSSION

The experiments were conducted with and without heat source and the results are displayed in graphical form for the easy understanding and comparison that includes the specific biogas yield, specific methane yield, retention time and quality of biogas. Specific biogas yield is the ratio of total volume of gas produced to the total mass of feed stock added for digestion. As biomass is feed in to the digester, the digester starts to digest the food waste and produce the biogas. The gas produced form the biomass which we use cow dung, food waste and municipal solid wasted are listed below.

Methane gas produced from the biomass is the result of methation process and the percentage of methane produced is measured using zakaria tube. The total amount of gas produced for 15 days these values are added up and it is the total volume of gas produced. The total mass of biomass for every process is 50kg. total volume of gas produced is divided by mass and it is the Specific Gas yield. In terms of methane volume of divided by the mass. The values are tabulated and graphs are drawn.

Quality of biogas

From the below table and figure that blue bar indicates the quality of the biogas when there is no heat supplied and it is found 70% for cow dung, 62% for food waste and 55% for MSW and they are in good quality as in **Table 1**.

Table 1. Relationship between Net Calorific Value and Percentage of Methane

S.no	Methane content (%)	Net Calorific Value (Mj m^3)
1	50	20
2	65	22
3	70	25

The biogas produced from the feedstock is in good quality for combustion, among that the biogas produced from the cow dung

has high quality with methane percentage of nearby 70% and it has the calorific value nearby 25 Mega joules per meter cube. The percentage of methane in the biogas before and after the applying of heat source heat source is tabulated in **Table 2**, the values marked here is the percentage of methane in the stable region of biogas yield.

Table 2. Percentage of Methane (%) for 15 Days

S.NO	Biomass	Percentage of Methane (%)	
		Without heat	With heat
1	Cow dung	70	64
2	Food waste	62	55
3	MSW	55	52

UNCERTAINTY ANALYSIS

- In the open test there are some variation in the results and the percentage of uncertainty is about 10%.
- From Zakaria tube the uncertainty in the results about 5%.
- Due to fouling and scaling of the heat transfer coil the uncertainty is about 3%.
- The temperature indicator has its uncertainty about 3%.
- The total uncertainty of the project is about 21%.

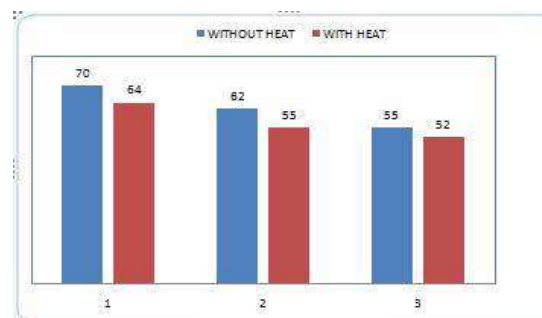


Table 3. Quality of bio gas

The red bar indicates methane quality with heat source and it is 64% for cow dung there is reduction of 6% percentage, food waste shows 55% and it also has some reduction 8% and for MSW it is 52% and it reduces from 55% though the quality reduces they are in combustible zone where biogas 50% of methane is combustible.

Specific Biogas Yield 15 Days



Fig 3. Specific Biogas Yield for 15 Days

The Fig. 3 is drawn for Specific biogas yield for the period of 15 days. In this chart blue bar indicates the specific biogas yield without heat source and the red bar indicates the specific biogas yield with the heat source. The cumulative biogas yield from Cow dung, Food waste and MSW without heat source is 316 liters, 232 liters and 174 liters respectively. The specific gas yield is 6.3 liters for Cow dung, 4.6 liters for Food waste and 3.4 liters for MSW. The red bar indicates the biogas yield with heat source and the cumulative gas produced by applying heat is 437 liters, 399 liters and 345 liters for Cow dung, Food waste and MSW. The specific gas yield is 8.7 liters for Cow dung, 7.9 liters for Food waste and 6.9 liters for MSW. It is clearly seen that the when heat is supplied the specific gas yield increases from 6.3 liters to 8.7 liters for Cow dung. Food waste shows a variation in biogas yield from 4.6 liters to 7.9 liters and MSW shows a good production in biogas from 3.4 liters to 6.9 liters that is it is almost doubled.

Specific Methane Yield 15 Days

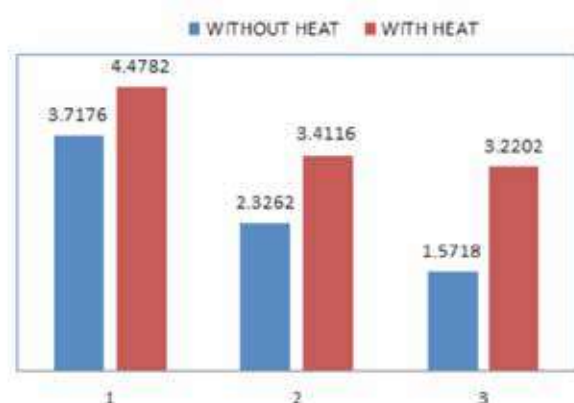


Fig 4. Specific Methane Yield for 15 Days

The Fig. 4 is drawn for Specific methane yield for the period of 15 days. In this chart blue bar indicates the specific methane yield without heat source and the red bar indicates the specific methane yield with the heat source. The cumulative methane yield from Cow dung, Food waste and MSW without heat source is 185 liters, 116 liters and 78 liters respectively. The specific methane yield is 3.7 liters for Cow dung, 2.3 liters for Food waste and 1.5 liters for MSW.

The red bar indicates the methane yield with heat source and the cumulative methane produced by applying heat is 223 liters, 116 liters and 78 liters for Cow dung, Food waste and MSW. The specific gas yield is 4.4 liters for Cow dung, 3.4 liters for Food waste and 3.2 liters for MSW. It is clearly seen that the when heat is supplied the specific gas yield increases from 3.7 liters to 4.4 liters for Cow dung. Food waste shows a variation in methane yield from 2.3 liters to 3.4 liters and MSW shows a good production in methane from 1.5 liters to 3.2 liters that is it is almost doubled.

CONCLUSIONS

In this project a hybrid digester with solar water heater has been designed, fabricated and experiments were successfully carried out. The result show the performance of digester has increased by applying heat energy. A passive mode of heat transfer is achieved by thermo syphon effect, thus the cost of the system is reduced. The fabricated model is a successful one and it can be converted into large scale. Additives and be developed for digesting solid waste.

REFERENCES

1. Sumit Sharma, Rajendra Meena, Amit Sharma, Pawan Kumar Goyal. "Biomass Conservation Technologies for Renewable Energy and Fuels. A review note" Volume 11, Issue 2 Ver. 111 March 2014), PP-35.
2. V.Nallathambi Gunaseelan, "Anaerobic Digestion of Biomass for Methane Production: A review" journal of Biomass and Bioenergy.
3. Jae Kyoung Cho, Soon Chul Park, "Biochemical Methane Potential and solid-state anaerobic digestion of Korean food wastes", Bioresource Technology 2(1995) 245-253.



4. Cunsheng Zhang, HaijiaSu, JanBaeyens, TianweiTan, “Reviewing the anaerobic digestion of food waste for biogas production”, journal of Renewable and Sustainable energy reviews 38(2014) 383-392.
5. ChunlanMaoa, YongzhongFeng, XiaojiaoWang, GuangxinRen. “Review on research achievements of biogas from anaerobic digestion”, journal of waste Management 31(2011) 1737-1744.
6. Azeem Khalid, Muhammad Arshad, MuzammiAnjum, Tariq Mahmood, Lorna Dawson. “The anaerobic digestion of solid organic waste”, journal of Waste Management 31(2011) 1737-1744.
7. Yebo Li, Stephen Y. Park, Jiying Zhu “Solid-state anaerobic digestion for methane production from organic waste” journal of Renewable and Sustainable Energy Reviews 15(2011) 821-826.
8. Yadvika, Santhosh, T.R.Sreekrishnan, SangeetaKohli, VineetRana.” Enhancement of biogas production from solid sub rates using different techniques---A review” journal of Bioresource Technology 95(2004) 1-10, March 2004.



A New Generic Methodology for Modelling and Optimization of Running Commercial Chemical Plant to Balance Profit and Negative Environment Impact with Cumene Production Plant as Case Study

Somnath Chowdhury, Sandip Kumar Lahiri*

Department of Chemical Engineering, National Institute of Technology Durgapur, West Bengal

✉ sandipkumar.lahiri@che.nitdgp.ac.in*

ABSTRACT

The research work mainly emphasizes on the establishment of a methodology that will help to delicately balance the negative environmental impact created by the industries and profitability of the plants. A case study of cumene manufacturing plant is considered. At first, Aspen simulation of the cumene plant was performed. After that, the sensitivity analysis of the key parameters was carried out to generate data which was used for the development of artificial neural network (ANN) model. This model was used to generate Pareto optimal solutions of three pairs of variables viz. vent flow & product flow, reboiler heat duty & product flow, reboiler heat duty & vent flow. Besides these, another Pareto optimal solution of Profitability vs. Eco-indicator 99 was also generated. Eco-indicator 99 reflects the negative environmental impact of a product starting from its production to its consumption. To obtain these Pareto solutions, multi-objective firefly optimization (MOF) was applied. The developed methodology is generic and can be applied to any running process plant on real-time basis.

Keywords : Modelling; Optimization; Aspen Plus; ANN; Multi-objective Firefly; Eco-indicator 99.

INTRODUCTION

Due to rapid industrialization in last three decades and the negative impact on environment created by oil, gas, chemical, mineral processing, and metal industries, the time has come to relook the way these industries are running. Cutthroat global competition forces these industries to run the plant at maximum capacity ignoring the negative environmental impact and higher energy consumption. Due to the devastating negative impact on health and environment in the last decade, these companies are now looking for sustainable solutions which will fulfill the following three objectives: (i) maximize production and profit, (ii) minimize environmental impact, and (iii) maximize energy efficiency. As these three objectives are contradictory with each other, there is a need to develop a methodology which will optimize the running plants by properly balancing these three contradictory objectives. In this work, a methodology involving Artificial Intelligence (AI) based modelling, and metaheuristics-based optimization technique has been developed which will evaluate the optimum operating conditions of running plant so that all the three contradictory objectives are simultaneously optimized.

In this work, cumene plant was considered as a case study to demonstrate step-by-step methodology of modelling and optimization of running plants. Cumene is produced by the reaction between benzene and propylene. Fig. 1 illustrates a simplified schematic of cumene plant, where benzene and propylene are fed into a reactor and cumene is produced. The outlet of the reactor is fed to a Flash Drum (FD) to remove the inert propane, which comes as an impurity in propylene feed. Top of the FD consist of propane and unreacted benzene is either vented off or burnt as fuel and have a significant negative environmental impact. The bottom of the FD essentially consists of unreacted benzene, cumene, heavier compounds are fed to a distillation column, Benzene Recovery Column (BRC) where benzene is separated as top product and is recycled back to reactor. The bottom product consists of cumene, and heavier compounds is fed to another distillation column namely Cumene Recovery Column (CRC), from where pure cumene (99.5% w/w) is separated as top product. The bottom product consists of heavier compounds is considered as low-value product or waste. The main objectives of this study is to develop an optimization framework which can be used in real-time in plant environment to find out the optimal reactor condition (temperature, pressure, benzene, and propylene flow ratio), FD temperature, and pressure so that the following objectives are met: (i) Maximization of cumene product flow (to maximize profit), (ii) Minimization of the vent from the FD (to minimize environmental impact) and

(iii) Minimization of summation of heat duty of reboilers of two distillation columns (to maximize energy efficiency). Since the reaction is exothermic, the maximum reactor heat removal capacity was put as a constraint.

This methodology utilized the first principle-based Aspen simulation to develop the base case simulation model of the whole cumene plant. A large number of operating data is generated from the Aspen model with a sensitivity analysis. These simulation results were used to develop an Artificial Neural Network (ANN) based model so that it can be utilized in real-time basis in the plant. Once an accurate ANN model is developed, operating conditions were optimized by recent Multi-Objective Firefly (MOF) algorithm, which generated Pareto diagram that can be used by the plant personnel to get the best suited optimum result as per their priority [1]. The scientific novelty of this work is as follows: (i) This developed methodology is generic and can be applied to any process plant which has a significant environmental impact, (ii) It contains first principle-based and data-driven AI-based modelling technique for the development of a correlation which can be readily used to predict the plant output from its operating condition, (iii) It utilizes MOF algorithm to solve a real-life multi-objective problem and found delicate balance between profit and environment impact.

METHODOLOGY

Aspen-based modelling of commercial cumene plant

Aspen Plus is a powerful software package used for the design and simulation of a variety of processes [2]. Aspen Plus uses mainly first principle-based phenomenological modelling technique and that is why the models have the explainability of their own. In this study, Aspen Plus V8.8 was used for the simulation of cumene production plant, the schematics of which has been illustrated in **Fig. 1**. For the REACTOR, built-in reactor model namely RGIBBS was used. RGIBBS model is generally used where the reaction kinetics are unknown. RGIBBS actually solves the model by minimizing the Gibb's free energy. The detail of process simulation input has been depicted in Table. At first, a base case simulation was executed. In the Flowsheet analysis of Aspen plus, there is a feature, namely Design Spec. If a particular output variable is set by iterative method, Aspen Plus changes the input variables in such a manner that the particular output reaches the target value. In this study, three Design Specs were applied to the base case simulation wherein the targets were fixed as follows:

- 99.9 % (w/w) purity of benzene at BRC top
- 99.5 % (w/w) purity of cumene product at CRC top
- 99.9% recovery of cumene as top product.

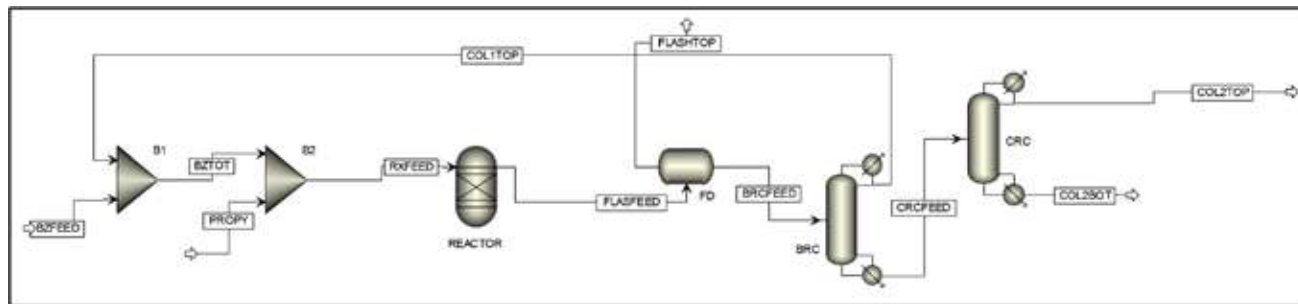


Fig. 1. Process flow diagram of cumene production

Sensitivity analysis of base case Aspen model

Sensitivity analysis is another model analysis tool of Aspen Plus. Using this tool, user can visualize the variation of target output variables by changing the manipulated variables in a given range of values. Operating parameters/ decision variables viz. Feed flow of benzene, propylene, reactor, FD temperature and FD pressure were varied with $\pm 25\%$ from their base case values. Cumene flow, FD vent flow and summation of heat duties of two reboilers were considered as outputs. The main aim of performing this sensitivity analysis is to form a large database of input and output variables so that using this database, the ANN model can be developed.

ANN Modelling

ANN, an effortless data-driven modelling technique has gained a vast popularity thanks to the advent of artificial intelligence



applications in diverse fields. The strength of ANN lies in its capability to handle noise in the data, performing efficiently with multiple output system, efficacy to learn non-linearity and complex relationship [3]. ANN uses multi-layer perception in its network architecture.

In this study, the database developed from sensitivity analysis was used for building up of ANN based model. ANN based modelling was developed because of the following reasons:

- (i) It is not possible to integrate and run the Aspen model in real-time due to its longer execution time.
- (ii) With the Aspen model, multi-objective optimization is difficult to execute.
- (iii) Aspen Plus in-built optimization process has a large possibility to be stuck in local optima, whereas since metaheuristic optimization technique undergo random search in the search space, its possibility to be stuck in local optima is comparatively less.

Here, to build-up the network architecture, 10 number of hidden neurons were used. Different activation functions were tried among which tan-sigmoid activation function gave the best predictability. For training the network, Levenberg-Marquardt back propagation technique was applied. To evaluate the performance of the ANN model, two statistical parameters, namely, coefficient of determination (R²), and Average Percentage Error (APE) were used.

Multi-objective firefly algorithm: at a glance

Multi-objective optimization problems are more complicated in comparison to single-objective optimization as unlike single-objective, a multi-objective optimization problem has no single unique solution, but it has multiple non-dominated solutions, and this set of solutions is called Pareto optimal solutions.

Firefly optimization algorithm is inspired by the flashing characteristics of the firefly. The following rules have been applied in this algorithm [1]:

- (i) Regardless the sex, one firefly attracts others by generating flashes
- (ii) The attractiveness is essentially measured by the brightness of the flashes. Obviously, the more the brighter is the flash, the other fireflies will be attracted more.
- (iii) So, in the search space of the optimization, the brightness of the firefly is determined.

The brightness of the flash of firefly $I(x)$ is proportional to the objective function $f(x)$ but the attractiveness β is relative and adjudged by the brightness of others. The β can be represented by the following equation (1):

$$\beta = \beta_0 + e^{-\gamma r^2} \quad (1)$$

Where r is the distance between two fireflies, β_0 denotes brightness at $r = 0$, and γ represents the absorption coefficient. The attractiveness varies in the range of $\beta_0 - \beta_0 e^{-1}$. If positions of two fireflies, namely i and j are represented by x_i and x_j respectively, then the distance between them is $r_{ij} = \|x_i - x_j\|$. Due to more attractiveness, the movement of i towards j can be expressed as follows (2):

$$x_i^{t+1} = x_i^t + \beta_0 e^{-\gamma r_{ij}^2} (x_j^t - x_i^t) + \alpha_i \varepsilon_i^t \quad (2)$$

Where the second term and third term at right-hand side of (2) represents the attraction and randomization, respectively. In each iteration, the location of the fireflies is updated. With the principle stated above, multi-objective firefly (MOF) optimization was developed to find out the set of Pareto optimal solutions. The Pareto optimal is defined as: “ x^* is Pareto optimal if there exists no feasible vector of decision variables which would decrease some criterion without causing a simultaneous increase in at least one other criterion” [4].

To obtain $Pbest_i^*$, the $\psi(x)$ has to be minimum. The $\psi(x)$ is the weighted combination of the two objective functions, the expression of which is mentioned below (3):

$$\psi(x) = w_1 f_1(x) + w_2 f_2(x) \quad (3)$$

where w_1 and w_2 are the weights, the summation of which is equal to 1.

If a firefly is not dominated by others, then it takes a random walk, which can be expressed as below (4):

$$x_i^{t+1} = Pbest_i^t + \alpha_i \varepsilon_i^t \quad (4)$$

In this study, after the development of reliable model, it was subjected to optimization. MOF was applied as an optimization tool to generate optimum operating condition, which can balance the contradictory objectives, which are:

- (i) Maximization of product flow and minimization of FD top vent flow,
- (ii) Maximization of product flow and minimization of summation of heat duties of two reboiler,
- (iii) Maximization of FD top vent flow and minimization of summation of heat duties of two reboiler.

Here, maximum heat recovery from reactor was put as constraint.

Environment impact through Eco-indicator 99

In this research work, Eco-indicator 99 (Eco 99) has been used as a key indicator of the environmental impact. In a holistic approach, Eco-indicator 99 measures the total environment and health impact of the chemical production process, based on the methodology of the Life Cycle Analysis (LCA) [5]. Eco 99 includes all the negative impacts such as Carcinogens, Climate change, Ionizing radiation, Ozone depletion, Respiratory effects, Acidification, Ecotoxicity, Land occupation, Fossil fuels, Mineral extraction, etc. and quantify them with realistic numbers [5]. Every chemical product has a negative impact on the environment. The impact starts from raw material processing, followed by product manufacturing, distribution, and packaging. Furthermore, additional environmental impact occurs during the product's usage as the product consumes energy and material. If environmental damage caused by the product has to be measured, then the inclusion of its whole life cycle phases has to be carried out, and this analysis is called Life Cycle Analysis (LCA). For a designer, performing an LCA is a difficult and time consuming task. The Eco 99 has resolved this problem in the following manner:

- (i) Eco 99 uses the LCA method and comes out with a single numerical score, which represents the total environmental impact caused by the particular product.
- (ii) Data has been collected in advance for the most common material, and processes and the eco indicator scored has been assigned from this.

In holistic approach, minimization of Eco 99 automatically imitates the minimization of FD vent flow and heat duties of the reboilers. This is also a fact that Eco 99 minimization affects the profitability of the plant. Therefore, in this study MOF was again applied with two contradictory decision variables viz. Eco 99 and profit to obtain Pareto optimal solutions.

RESULTS AND DISCUSSION

A. Accuracy of ANN model The predictability of the ANN model was adjudged by determining R^2 and AEP. The values of R^2 was found to be 0.99, and the AEP was obtained as 0.5%. Looking at the R^2 values to be close to 1 and reasonably low values of AEP, it can be inferred that the ANN model is quite accurate and reliable to be used for optimization study.

Optimization

By applying MOF on the developed ANN model, the Pareto solutions were generated, which have been plotted in **Fig. 2** and **Fig. 3**. **Fig. 2a** clearly shows that if product flow is increased, then the heat duty of the reboilers has to be increased, which results in a rise in negative environmental impact. It is because the rising heat duty of reboilers means an increment in steam consumption. **Fig. 2b** indicates that if vent flow is kept at the lower side, the reboiler heat duty will be at the higher side as there will be more feed to the BRC and CRC. Increment in vent flow or in reboiler heat duty, in any case, more negative impact on the environment will be there. **Fig. 2c** depicts that if vent flow increases, there will be a decrease in product flow.

Fig. 3 illustrates the Pareto diagram of the Profit vs. Eco 99. From this plot, it can be seen that if profit is increased, negative impact on environmental will also increase, which is always the case for most of the chemical industries. Increasing the profit means running the plant with higher capacity and higher production of cumene. In **Fig. 3**, it can be visualized that profit is the highest at point C, but there the Eco-99 is also the highest, which essentially means that a very high profit can be achieved only by hampering the environment. At point A, both profit and Eco-99 are on the lower side. But if we go from A to B, profit has been increased drastically, but Eco-99 does not increase much. So, it is better to operate the plant in such a manner that the vent flow, heat duty of the reboilers and product flow remain at corresponding to the point B because in this condition, profit would be obtained is reasonably high, but the environmental impact will remain at a lower side.

SCIENTIFIC NOVELTY

This work developed an ANN-based model of cumene manufacturing unit using data developed by the sensitivity analysis employing Aspen Plus simulation of the same plant. The model can be utilized on a real-time basis in a running process plant. Operating conditions were optimized by recent MOF. The scientific novelty of the current work is as follows:

- (i) A generic methodology has been developed which addresses the core issue of chemical plants i.e., how to maintain a delicate balance between profitability and environmental impact. The developed methodology generic and can be applied to any process industries which have a significant environmental impact. The methodology is applicable in those running plants where designing modification is not possible.
- (ii) In this work, the concept of Eco- indicator 99 is introduced to take into account all the negative health and environmental impact a manufacturing process can produce during its operation. This holistic approach to accounting environmental impact can be a reliable methodology to optimize the process parameters of running the commercial chemical plant.
- (iii) It has utilized a recently developed MOF algorithm, which was able to solve real-life optimization problem and found a delicate balance between profit and environmental impact.

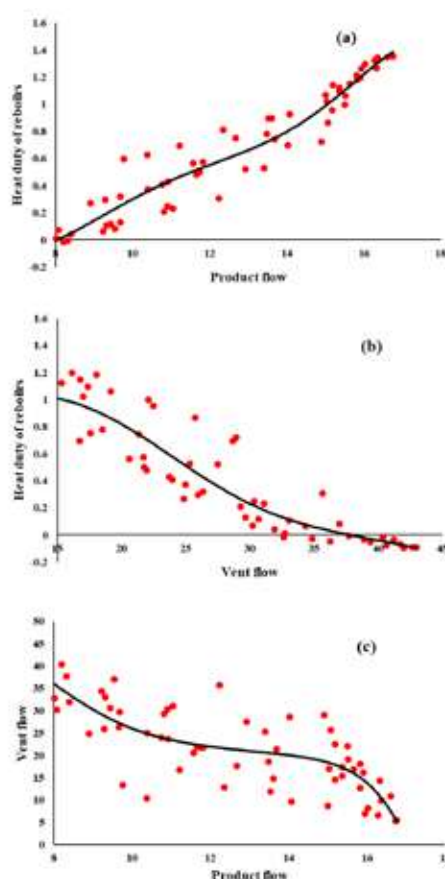


Fig. 2. Pareto diagrams of (a) heat duty of reboilers vs. product flow, (b) heat duty of reboilers vs. vent flow, (c) vent flow vs. product flow

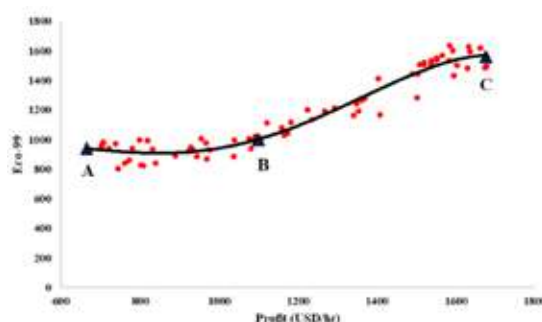


Fig. 3. Pareto diagram of profit vs. Eco-99

CONCLUSION

This work developed a new modelling and optimization methodology, which can be used by commercial chemical plants to quantify their environmental impact and find a delicate balance between profit and environmental impact. This work shows an easy way to use Aspen Plus and ANN modelling methodology for commercial plants. Multi-objective hybrid ANN and firefly algorithm has been used in the present study to find a delicate balance between profit and environmental impact. The effectiveness of the proposed methodology is shown through a case study of commercial cumene manufacturing process. The proposed methodology develops a Pareto optimal solutions platform to gain insights into the balance between profit and environmental impact. These insights may be very useful to the plant management to take informed decision regarding plant operations.

The developed methodology utilized the Aspen simulation, latest AI based modelling and nature-inspired optimization technique and is generic, which can be extended to any other running plant. The optimizer can be run on a real-time basis, and the optimal conditions can be evaluated in the ever-changing dynamic environment of the plant. The developed methodology balances between profit and environmental impact in totality for running a chemical plant.

REFERENCE

1. Yang, X. Multiobjective firefly algorithm for continuous optimization. *Engineering with Computers*, vol. 29, pp. 175–184, [2013]
2. Abdelouahed, L et al., “Detailed Modeling of Biomass Gasification in Dual Fluidized Bed Reactors under Aspen Plus”. *Energy Fuels* vol. 26, 6, pp. 3840–3855 [2012]
3. Chowdhury S, Halder G, Mandal T, Sikder J (2019) Cetylpyridiniumbromide assisted micellar-enhanced ultrafiltration for treating Enrofloxacin-laden water. *Sci Total Environ* 687:10–23
4. Jaimes, AL, Coello, C (2008) “Multi-objective evolutionary algorithms: A review of the state-of the-art and some of their applications in chemical engineering”. In: Rangaiah, G. (ed.) *Multi- Objective Optimization: Techniques and Applications in Chemical Engineering*: pp. 61–86. World Scientific, Singapore [2008]
5. Geodkoop, M, Spriensma, R., “The eco-indicator 99. A damage oriented for life cycle impact assessment. Methodology report and manual for designers”. Technical Report, Amersfoort, the Netherlands: PRe Consultants [2001].



Artificial Intelligence based Modelling and Multi-objective Optimization of Vinyl Chloride Monomer (VCM) Plant to Strike a Balance between Profit, Energy Utilization and Environmental Degradation

Sucharita Pal, Bipul Jha, Sandip Kumar Lahiri

Department of Chemical Engineering, National Institute of Technology, Durgapur, West Bengal

✉ sandipkumar.lahiri@che.nitdgp.ac.in

ABSTRACT

The present work emphasizes the development of a generic methodology that addresses the core issue of any running chemical plant, i.e., how to maintain a delicate balance between profit and environmental impact. Here, commercial vinyl chloride monomer (VCM) production plant has been taken as a case study. This work developed a new modelling and optimization methodology, which can be used by commercial chemical plants to quantify their environmental impact and find a delicate balance between profit and environmental impact. This work shows an easy to use Aspen and ANN modelling methodology for commercial complex reactors. Multi-objective hybrid ANN and genetic algorithm has been used in the present study to find a delicate balance between profit and environmental impact. The effectiveness of the proposed methodology is shown through a case study of commercial VCM manufacturing process. The proposed methodology generates optimum operating conditions of VCM reactor, which can be implemented in commercial plants to boost profit. Moreover, the proposed methodology develops a Pareto optimal solutions platform to gain insights of the balance between profit and environmental impact. These insights may be very useful to the plant management to take informed decision regarding plant operations.

Keywords : Aspen simulation; Multiobjective Genetic Algorithm; ANN, sensitivity analysis; Pareto.

INTRODUCTION

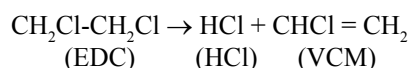
For the last three decades, chemical industries have produced a lot of chemicals with the sole objective of profit maximization. On operating a plant with a philosophy of profit maximization, the chemical industries have damaged the environment drastically. Lately, the industries have realized that the industries cannot succeed in the long run by damaging the environment and hence there is a thrust to find a sustainable solution. The main hindrance chemical industries are facing today in their journey to reduce their negative environmental impact is that it hits their bottom line and reduce their profit margin. Last decade giant chemical industries across the globe have operated their plants with maximum capacity in order to maximize the profit and to survive in the global business competition. While running those plants at the highest capacities, these industries have also maximized the environmental damage. To reduce the environmental impact, these companies either have to reduce their capacities or have to install pollution control equipment, both of which hit the bottom line of the profitability.

Vinyl chloride monomer (VCM) is one of the world's most important and largest commodity chemicals. VCM is used primarily for the production of polyvinyl chloride (PVC) homo-polymer and copolymer resins. PVC has the advantage of being utilized in conversion and fabrication processes with great flexibility, such that end products cover a wide range, including pipe and fittings, profiles and tubes, siding, wire and cable, windows, doors, floorings, film and sheet, and bottles.

In this study, our objective was to find a sustainable solution for the VCM plant. Finding a sustainable solution is a multi-objective optimization problem where we increase the product (VCM) flowrate and simultaneously reduce the energy consumption and environmental damage by venting. This industrial case study has developed a modelling and optimization framework which can be deployed in a commercial plant for simultaneous achievement of three contradictory objectives, such as profit maximization, energy conservation and reduce environment damage.

Problem Description

In this study, we have considered the production of vinyl chloride monomer from ethylene dichloride, by following the reaction:



In the VCM plant flowchart, 1000 kmol/hr of pure EDC feed, at 20°C and 30 bar is entering a reactor, where the cracking reaction takes place at 500°C and 30 bar. The reactor outlet stream is let to a cooler with a 10 degrees sub-cooling with a 0.5 pressure drop. The stream from the cooler outlet is fed to the first distillation column with 15 stages. A reflux ratio of 1.082 and a distillate to feed ratio of 0.34 is maintained in this distillation column. The feed enters above stage 8 and a column pressure of 25 bar is maintained. The distillate of this column which is HCl is vented out, while the bottom stream is fed to another distillation column of 10 stages. A reflux ratio of 0.969 and a distillate to feed ratio of 0.55 is maintained in this column. The feed enters the second distillation column above stage 7 and a column pressure of 8 bar is maintained. The distillate is the product stream containing VCM while the bottom stream is recycled back via a pump of 30 bar outlet pressure to the reactor to enhance the conversion.

The product flow rate determines the economy of the running plant and, hence this factor is responsible for profit maximization in the plant. Reboiler heat duties of the two distillation columns determine the total energy consumption of this plant and hence minimizing this is important to save energy. Minimizing venting is equally important in a plant to reduce environmental damage. Our objective is to determine the operating conditions, which will simultaneously maximize product flowrate, minimize reboiler heat duty and, also minimize the vent flow rate.

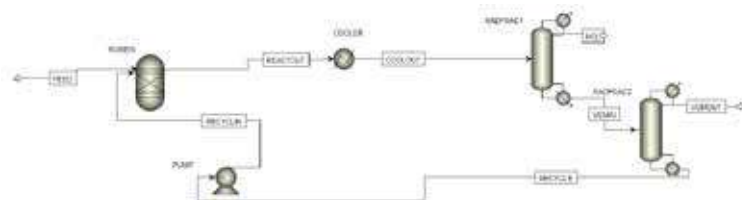


Fig 1. The VCM plant flowchart

Initial Simulation

The base case simulation was performed using the Aspen Plus software. Three components (ethylene dichloride, hydrogen chloride and vinyl chloride monomer) were defined in the Component-Specifications sheet. RK-Soave property method was selected in the Methods-Specifications sheet to represent the vapor–liquid equilibrium. This information was sufficient to run the properties test. In the simulation section, the VCM flowsheet is defined. ARGibbs module was selected from the Reactors module, in order to explore the dependence of the product yield on reactor temperature and pressure. The feed and product streams were also inserted. A Heater model is inserted from the Exchangers module and the reactor outlet stream is fed to it. The heater outlet stream is fed to a RadFrac unit from the columns module, the bottom product of which is fed to another Radfrac unit. The product streams are inserted and the bottom product stream of the second RadFrac is recycled back to the reactor with a Pump unit from the Pressure Changers module. The reactor and temperature and pressure was optimized at 300K and 3 bar respectively. The feed composition and the operating conditions are specified as per the problem statement. (Refer to Fig. 1) The next sheet to be completed was the Reactions sheet. Nevertheless, no available reactions were selected because they were defined in the Reactions folder. Once the Reactions folder is opened, a new reaction pack is defined, and an ID was assigned to it. Once the reaction has been defined, the reaction was now selected and sent to the Selected reaction sets box. After loading all the required information, the Run button is pushed to start the simulation. The VCM yield achieved for the base case simulation was 85%.

Table 1. Sensitivity analysis- parametric optimization

VARY in Sensitivity Module	Base Case Value	Lower Limit	Upper Limit
COOLER (DEG SUBCOOL) (°C)	10	5	15
RADFRAC1 (MOLE RR)	1.082	0.8115	1.3525
RGIBBS (TEMP) (°C)	500	375	625
RGIBBS (PRESS)(BAR)	30	22.5	37.5

Analysis

During a sensitivity analysis (or design spec) Aspen iterates its calculation sequence through a range of values provided for an independent variable, in order to obtain a specified result for a dependent variable (within a certain tolerance). A complete sensitivity analysis was done using the 'Sensitivity' module of Aspen Plus to find out the impact of temperature and pressure of the cracking reactor, degree of sub-cooling of the cooler, reflux ratio of both the distillation tower on product flowrate, heat duty of reboiler and HCl vent flow. Parametric optimization was performed by changing the parameters to $\pm 50\%$ of its base case value. A design spec was also introduced to maintain the product purity of VCM to 99% (more than requirement), so that product purity is not compromised in any of the cases. The reflux ratio of the first RadFrac was selected as a manipulated variable for the Design Spec, and its value was varied by $\pm 50\%$ of its base case value. At the same time, three contradictory objectives were tried to be met: (i) Maximizing product flowrate; (ii) Minimizing total heat duty; (iii) Minimizing vent. For each manipulated variable, five number of data points were chosen at equispaced intervals. A total of 625 data sets were generated using sensitivity analysis in Aspen Plus. Plant data was not available and hence sensitivity analysis of Aspen simulation was used to generate the required data. The varying of parameters took into account the various process disturbances in an actual plant. A table showing the range of manipulated variables in the Sensitivity module is depicted in **Table 1**.

Artificial Neural Networking Modelling

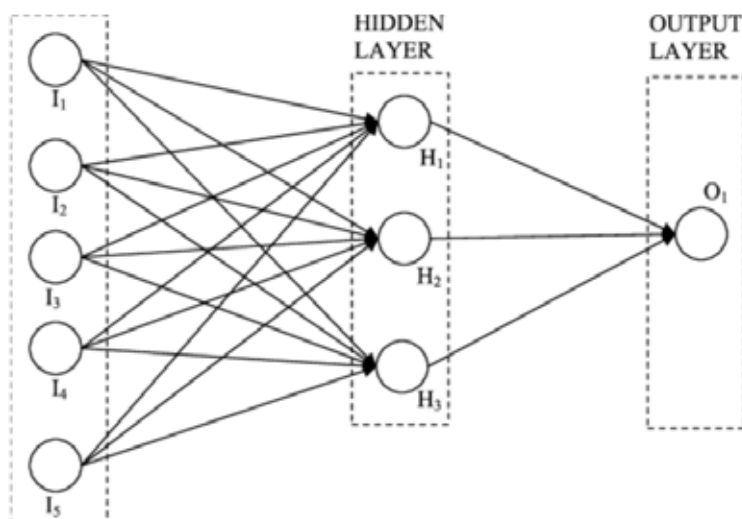


Fig 2. Schematic of Artificial Neural Network structure

Artificial Neural Networks (ANN) are biologically inspired computer programs designed to simulate the way in which the human brain processes information. ANNs gather their knowledge by detecting the patterns and relationships in data and are trained through experience, not from programming (black box). ANN is formed from hundreds of single units, artificial neurons or processing elements (PE), connected with coefficients (weights), which constitute the neural structure and are organized in layers. As of now, no mathematical model of an industrial VCM plant is available. It is not possible to deploy a first principle based model as a real-time application with varying industrial conditions as it is time-consuming. However, a black box model is dependent on the quality of data. Only accurate measurements will ensure effective model. So, here we have used the data generated by sensitivity analysis in Aspen Plus to develop our model. Using the application tool of Artificial Neural Networking in MATLAB software, a model is developed which consists of four input layers, ten hidden nodes and three output layers. The input matrix consists of the manipulated variables in sensitivity analysis, namely, degree sub-cooling of the cooler, reflux ratio of the first distillation column, reactor's operating temperature and the reactor's operating pressure. The output layer consists of our target variables namely product flowrate, total reboiler heat duty and HCl vent flowrate. The developed calculation model will be used in real time plant control.

From the graphs of actual vs predicted values (**Figs 4,5,6**), we can see that ANN has accurately predicted the value of the objective variables.

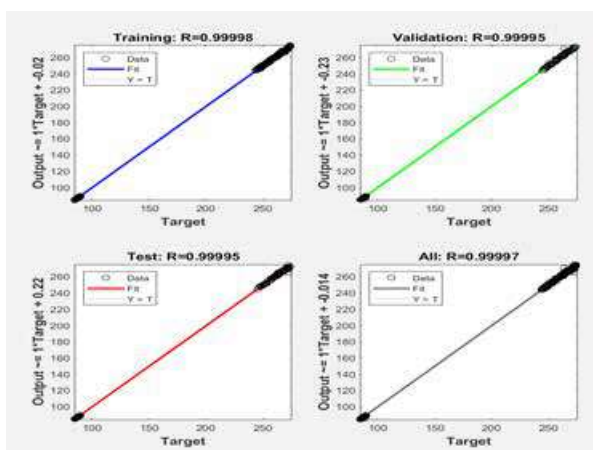


Fig 3. The regression coefficient of the developed ANN model

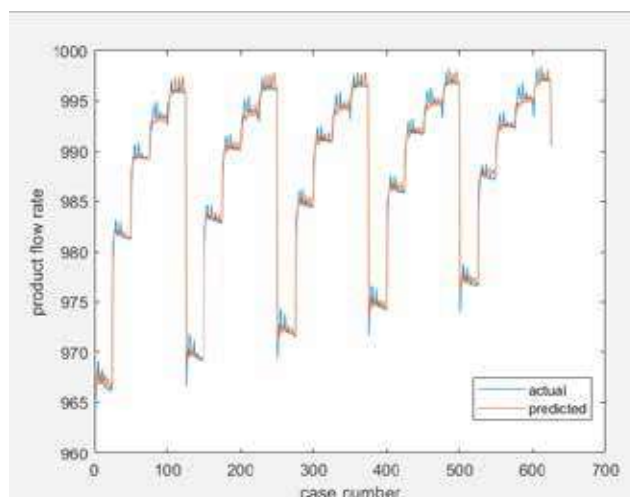


Fig 4. Validation of ANN model's predicted product flowrate

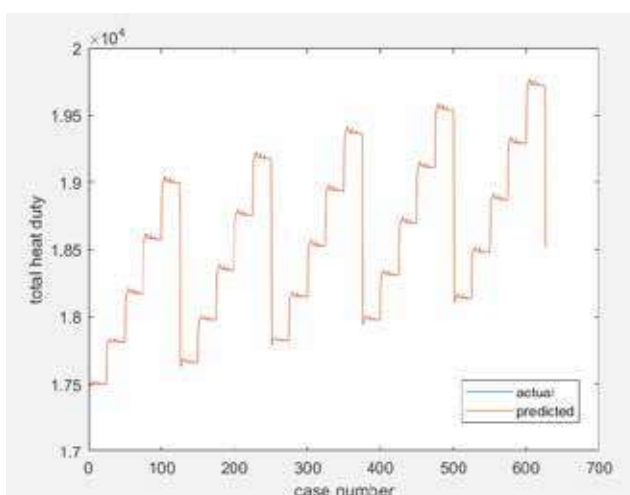


Fig 5. Validation of ANN model's predicted total heat duty

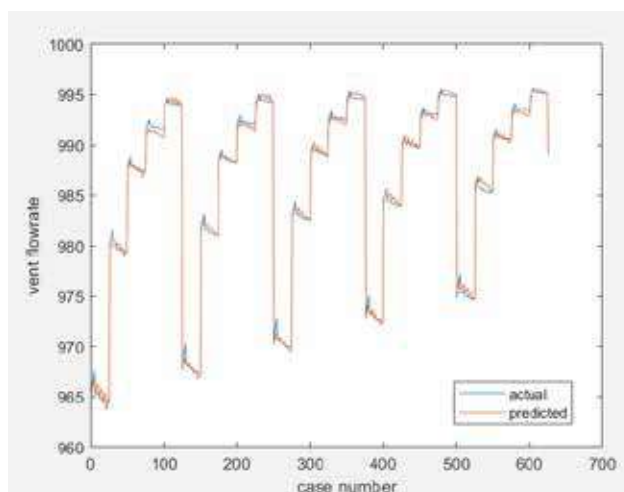


Fig 6. Validation of ANN model's predicted vent flow rate

Five arbitrary cases were chosen within the range of the manipulated variables and the predicted values of the ANN model was compared to that obtained by Aspen simulation. The analysis is depicted in **Table 2**.

Table 2. Analysis of the developed model's results

Description of Manipulated variables		
TARGET OBJECTIVES	Mean Square Error (%)	R2
Value		
Product (VCM) flowrate	0.06	0.995
Total reboiler heat duty	0.01	0.999
Vent (HCl) flowrate	0.035	0.998

The mean square error percentage obtained for each of the objective variable is less than 0.1%. The R squared value obtained for each of the objective function is above 99%. Thus, the model developed is highly accurate and reliable.

Multi-objective Genetic Algorithm Optimization

In computer science and operations research, a genetic algorithm is a metaheuristic inspired by the process of natural selection, which belongs to the larger class of evolutionary algorithms. Multi-objective Genetic Algorithm (MOGA) is a guided random search method. It is suitable for solving multi-objective optimization related problems with the capability to explore the diverse regions of the solution space. Here MOGA tool of the MATLAB software is used to optimize the VCM plant operation, which is modelled by using ANN, where the objective function is to increase product flow rate and simultaneously decrease total reboiler heat duty and HCl vent flow rate. Thus, we aim to find out the optimum operating conditions that will simultaneously meet the three contradictory objectives. The upper and lower limit of each target objective was set to the minimum and maximum value of the variable in the dataset generated. Through the conflicting objective functions a set of optimal solutions can be produced, and they are known as Pareto-Optimal solutions. These optimal solutions can't say which one is better than the other with respect to all objective functions and the reason is that there are many optimality solutions. Also Pareto optimal set known as solution to multi objective optimization represent a collection of points. These solutions are also termed as non-inferior, admissible, or efficient solutions. There is no single optimum solution as the objectives are contradictory. This gives rise to multiple optimum solutions for simultaneously maximizing product flowrate, and minimizing heat duty and vent flowrate. It can be left to the operator's discretion on which operating variable should be given more preference.

The trade-off between three contradictory objectives is depicted in the Pareto diagram (**Fig. 7**).

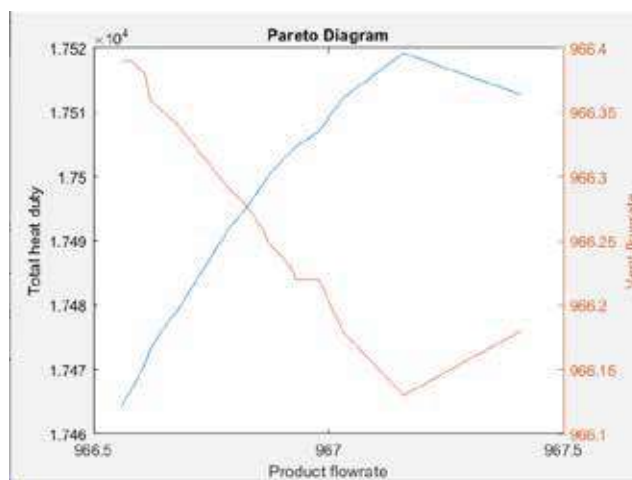


Fig 7. Pareto diagram depicting the optimal solution of the multi-objective optimization problem

The modelling and optimization framework developed can be deployed in a real time commercial plant to optimize the process parameters.

The optimum operating conditions obtained by the multi- objective Genetic algorithm optimization are depicted in **Table 3**.

Table 3. Optimal Operating conditions

S. No	Cooler Deg Sub-cool	Radfrac1 RR	RGibbs Temp (K)	RGibbs Press (bar)
1	5	0.81	375	22.5
2	5	0.81	425.03	22.5
3	5	0.81	425.02	22.5
4	5	0.81	425.02	24.6
5	5	0.81	378.14	22.6
6	5	0.8115	375	22.5
7	5	0.811501	382.82	22.5
8	5	0.811512	400.21	22.5
9	5	0.811501	405.3	22.5
10	5	0.811522	408.43	22.7
11	5	0.811506	376.33	22.5
12	5	0.811505	384.55	22.5
13	5	0.811505	414.74	22.5
14	5	0.811509	396.55	22.5
15	5	0.8115	380.46	22.5
16	5	0.811502	401.42	22.5
17	5	0.811503	405.99	22.5
18	5	0.8115	394.48	22.5

CONCLUSIONS

The developed modelling and optimization framework can be deployed in a commercial plant. The developed methodology is generic and can be extended to any other chemical plant. For the last few decades chemical industries have functioned with a single objective of profit maximization. On operating a plant with the philosophy of profit maximization, the chemical industries have damaged the environment drastically. It is only in the recent past, that the realization has dawned upon the industries



that they cannot survive in the long run by damaging the environment and there is a quest for finding a sustainable solution. Our study aims at finding a sustainable solution such that the profit is maximized and at the same time the environmental damage and energy consumption is reduced. Thus, finding a solution is a multi-objective optimization problem where we maximize the product flowrate but simultaneously reduce energy consumption and environmental damage by venting. This industrial case study has developed a modelling and optimization framework which can be deployed in a real, commercial plant for simultaneous achievement of three contradictory objectives such as profit maximization, energy consumption and environmental damage.

The developed methodology utilized the latest AI based modelling and nature-inspired optimization technique and is generic, which can be extended to any other running plant. The optimizer can be run on a real-time basis, and the optimal conditions can be evaluated in the ever-changing dynamic environment of the plant.

REFERENCES

1. Valceres V.R. Silva, Peter J. Fleming, Jungiro Sugimoto, Ryuichi Yokoyama, "Multiobjective optimization using variable complexity modelling for control system design", *Applied Soft Computing*, Volume 8, Issue 1, 2008, Pages 392-401, ISSN 1568-4946, <https://doi.org/10.1016/j.asoc.2007.02.004>.
2. A. G. Borsa. Industrial plant/laboratory investigation and computer modeling of 1,2-dichloroethane pyrolysis. PhD thesis, Colorado School of Mines, 1999.
3. A. G. Borsa, A. M. Herring, J. T. McKinnon, R. L. McCormick, S. Yamamoto, Y. Teraoka, and Y. Natori. Characterization of Coke Formed in Vinyl Chloride Manufacture. *Ind. Eng. Chem. Res.*, 35(11):4259–4267, 1999.
4. A. G. Borsa, A. M. Herring, J. T. McKinnon, R. L. McCormick, and G. H. Ko. Coke and Byproduct Formation during 1,2-Dichloroethane Pyrolysis in a Laboratory Tubular Reactor. *Ind. Eng. Chem. Res.*, 40(11):2428–2436, 2001.
5. B.-S. Choi, J. S. Oh, S.-W. Lee, H. Kim, and J. Yi. Simulation of the Effects of ccl4 on the Ethylene Dichloride Pyrolysis Process. *Ind. Eng. Chem. Res.*, 40(19):4040–4049, 2001.
6. A. C. Dimian and C. S. Bildea. *Chemical Process Design: Computer-Aided Case Studies*, chapter Vinyl Chloride Monomer Process, pages 201–230. Wiley–VCH, 2008.
7. E.-L. Dreher, T. R. Torkelson, and K. K. Beutel. Chloroethanes and Chloroethylenes. In *Ullman's Encyclopedia of Industrial Chemistry*. Wiley–VCH, 2012.
8. G. F. Froment and K. B. Bischoff. *Chemical Reactor Analysis and Design*. Wiley–VCH, second edition, 1990.
9. H. C. Hottel and A. F. Sarofim. *Radiative transfer*. McGraw–Hill, 1972.
10. K. E. Howlett. The pyrolysis of 1,2-dichloroethane. *Transactions of the Faraday society*, 48:25–34, 1952.
11. J. A. Incavo. A Detailed Quantitative Study of 1,2-Dichloroethane Cracking to Vinyl Chloride by a Gas Chromatographic Pyrolysis Device. *Ind. Eng. Chem. Res.*, 35:931–937, 1996.
12. D. Jo, J. Bae, J. Kim, B. Oh, and S. B. Ha. Method of inhibiting coke formation in ethylene dichloride pyrolysis cracker, Nov. 2006. Patent no. US 7,132,577 B2.
13. T. H. Kaggerud. Modeling and EDC Cracker using Computational Fluid Dynamics (CFD). Master's thesis, Norwegian University of Science and Technology, June 2007.
14. F. Benyahia. VCM process design. *Chemical Engineering Education Journal*, 39(1):62–67, 2005
15. A. Lakshmanan, W. C. Tooney, and L. T. Biegler. A case study for reactor network synthesis: the vinyl chloride process. *Computers and Chemical Engineering*, 23:479–495, 1999.
16. K. Y. Lee. Numerical Simulations of the Pyrolysis of 1,2-Dichloroethane. *KSME International Journal*, 16(1):102–108, 2002.
17. C. Li, G. Hu, W. Zhong, H. Cheng, W. Du, and F. Qian. Comprehensive Simulation and Optimization of an Ethylene Dichloride Cracker Based on the One-Dimensional Lobo–Evans Method and Computational Fluid Dynamics. *Ind. Eng. Chem. Res.*, 52:645–657, 2012.



18. C. Li, G. Hu, W. Zhong, W. Du, and F. Qian. Coke Deposition Influence Based on a Run Length Simulation of a 1,2-Dichloroethane Cracker. *Ind. Eng. Chem. Res.*, 52:17501–17516, 2013.
19. D. T. T. Limited. PVC markets of Europe and South-East asia: analysis of profitability and production cost. http://www.deloitte.com/assets/DcomRussia/Local%20Assets/Documents/Energy%20and%20Resources/dttl_PVC-markets-of-Europe-and-SouthEastAsia_EN.pdf, October 2014.
20. D. Ma and G. Shahani. Improve the cracking of ethylene dichloride. *Hydrocarbon Processing*, pages 61–62, April 2014.
21. L. S. Marks, T. Baumeister, E. A. Avallone, and T. Baumeister III. *Marks' Standard Handbook for Mechanical Engineers*. McGraw–Hill, 1996.
22. I. Mochida, T. Tsunawaki, C. Sotowa, Y. Korai, and K. Higuchi. Coke Produced in the Commercial Pyrolysis of Ethylene Dichloride into Vinyl Chloride. *Ind. Eng. Chem. Res.*, 35(10):3803–3807, 1996.
23. P. Mullinger and B. Jenkins. *Industrial and Process Furnaces - Principles, design and operation*. Butterworth–Heinemann, first edition, 2008.
24. R. H. Perry, D. W. Green, and J. O. Maloney. *Perry's Chemical Engineers' Handbook*. McGraw–Hill International Editions, seventh edition, 1997.
25. R. C. Reid. *Parameters of the properties of gases & liquids*. McGraw–Hill, fourth edition, 1988.
26. R. Schirmeister, J. Kashnitz, and M. Trager. Influence of EDC Cracking Severity on the Marginal ~ Costs of Vinyl Chloride Production. American Chemical Society, 2009.
27. R. P. Tewarson. Sparse Matrices. In *Mathematics in Science and Engineering*, volume 99. Academic Press Inc., 1973.
28. Y. Tong. Phosphine coke inhibitors for EDC–VCM furnaces, Sep. 2002. Patent no. US 6,454,995 B1.



Artificial Intelligence Modelling for Real Time Prediction Of Melt Flow Index In Commercial HDPE Plant

Annasha Dey, Rhythm Aich, Dr. Sandip Kumar Lahiri

Department of Chemical Engineering, National Institute of Technology, Durgapur, West Bengal

✉ sandipkumar.lahiri@che.nitdgp.ac.in

ABSTRACT

In commercial HDPE plants, Melt flow index (MFI) is the most important quality parameter of the final polymer product. Usually, MFI is measured by lab analysis which takes 4-6 hours based on which, production engineers change the operating parameters to regulate the MFI. Due to this time lag, when product goes off-spec, tons of polymers are produced with undesired MFI value and industry incurs huge losses. In this work, a data driven model is developed from commercial plant data which can predict the MFI on real-time basis. Both of them are AI-based modelling methodologies. Improvements have been made to their basic algorithms to make them effective for accommodation of industrial plant data. Commercial plant data and plant operating experience has been utilised to identify the input parameters and train the models. The developed models are very accurate and reliable as evident from very high R² value and very low prediction error percentage on unseen data (test data). The operating conditions obtained from both models have been compared against each other for further validation. These models can be deployed in plant DCS to indicate MFI of HDPE product in real-time basis which helps the production engineer to take easy corrective and preventive action to avoid losses from off-spec polymer product.

Keywords : Soft Sensor; Melt Flow Index; Artificial Intelligence; Artificial Neural Networks; Genetic Programming; High-density polyethylene.

INTRODUCTION

In our daily life, the usage of plastic in its various shape and size has become inevitable. The number of commercial plants for polymer production is increasing rapidly to meet the demand for plastic consumption. In a situation where the chemical industries are constantly providing for a gigantic consumer market, production of undesired products due to lack of knowledge, expertise or efficiency is highly unacceptable. Unfortunately, in most of the polymer industries around the globe, plants are run on the basis of experience only due to non-availability of reliable phenomenological model. The plant operator changes the value of operating parameters based on past experience which often doesn't lead to the most optimum conditions for production. This results in the production of undesirable products which eventually adds up to the waste generated resulting in huge losses for the industry.

One such major problem is faced by the operators working in commercial High Density Polyethylene (HDPE) plants. In the process of producing HDPE polymer, Melt Flow Index (MFI) is the most important quality parameter of the final product. Usually, this is measured using specially designed MFI apparatus in the laboratory. The lab analysis for calculating MFI of a polymer takes 4-6 hours for a certain range of temperature. Based on the results, the production engineers change the operating parameters to regulate the MFI. The major drawbacks of the lab analysis are it is highly time consuming and it only takes temperature as the variable eliminating the weightage of other variables that can be controlling the value of MFI.

The main objective of this project is to overcome this problem of inefficient testing procedures. Hence, an alternative way to calculate the value of MFI followed by the optimal range of variables responsible for governing it is desirable. Here, we have opted for data driven modelling so that it is possible to predict the value of MFI without a first-principle based model. The second objective of this study is to compare two different data driven modelling technique, namely Genetic Programming and Artificial Neural Network. Both of them are AI-based modelling methodologies and give results within a few minutes. The basic algorithm has been improved to accommodate the data of a HDPE plant and predict the value of MFI. The plant data will be used to train both the models and compare with the actual value of MFI. It is to see that which model is more accurate and reliable in calculating the MFI value. The R² value and the error percentage of these models will be compared with each other.

The third objective of this work is to incorporate the best model in any HDPE plant and test its efficiency on real time basis



instead of waiting for lab results. The developed model can be deployed in plant DCS to indicate MFI value in real-time basis. It will be much easier for the plant operator to change the values of the input variables in order to produce polymer of the desired MFI value. This will save a lot of time and prevent losses to the plant caused by off-spec product.

AI-based modelling of MFI

The following steps were followed in developing the best model for predicting the MFI value.

1. Cleaning of the industrial data. It is important to clean the industrial data as the chances of anomaly due to reasons like malfunctioning of any instrument is very common. If those data are fed to any AI-based model, the model will not be accurate. So, the first step for preparing any data-driven model is to clean the data and get rid of dataset will abnormally low or high value of any input variable. There are total eight input variable and one output variable.
2. Preparing the Genetic Programming algorithm for feeding the data. This step is carried out in MATLAB. The entire dataset is divided into two parts, training and testing dataset. The training dataset is used to develop the model and the testing dataset is used to check the accuracy of the model.
3. MATLAB was used to build and train the ANN model. The Neural Network Toolbox is used to train, test, and validate the data. The user can manually change the number of hidden layers for this process and check the fitness for each of them.
4. After creating the models individually by GP and ANN, the result is compared. Trend of each variable is studied both for GP and ANN. The predicted value of MFI by GP and ANN is compared against the actual industrial value of MFI. Error percentage and accuracy of each model are considered.
5. Conclusions are drawn on which AI-based technique deemed to be the fittest for developing the MFI value.

Both the techniques are hit and trial method. So, the program is rerun several times until the fitness of the model (R^2) is maximized and the percentage error is minimized.

The details of all the input variables considered are given in the Table.

Table 1. Name of input variables

Input variable	Name of input variable
x_1	Hydrogen concentration
x_2	Reactor pressure
x_3	Ethylene concentration
x_4	Reactor Temperature
x_5	Reactor H ₂ to feed ratio
x_6	Reactor density
x_7	hydrogen flow
x_8	Reactor ethylene flow

Building the MFI model using Genetic Programming

Genetic programming is a biologically inspired machine learning method that evolves computer programs to perform a task. Genetic programming achieves this goal of automatic programming (also sometimes called program synthesis or program induction) by genetically breeding a population of equations using the principles of Darwinian natural selection and biologically inspired operations. It does this by randomly generating a population of computer programs (represented by tree structures) and then mutating and crossing over the best performing trees to create a new population. This process is iterated until the population contains programs that (hopefully) solve the task well. It is a hit-and-trial method but at the end of each run, we get an equation that helps us to understand both the structure and parameters of the mathematical model.

In this work, the Genetic Programming system is built in a way such that it is compatible with taking the industrial input, run



the program, and gives a set of equations as an output along with their complexities.

There are five preparatory steps of Genetic Programming. They are as follows:

1. The set of terminals for each branch of the to-be-evolved program.
2. The set of primitive functions for each branch.
3. The fitness measure
4. Certain parameters for controlling the run
5. The termination criteria and method for designating the result of the run.

There are three execution steps of Genetic Programming. They are as follows:

1. Randomly create an initial population (generation 0) of individual equations composed of the available functions and terminals.
2. Iteratively perform the following sub-steps (called a generation) on the population until the termination criterion is satisfied:
 - (a) Execute each equation in the population and ascertain its fitness (explicitly or implicitly) using the problem's fitness measure.
 - (b) Select one or two individual equation(s) from the population with a probability based on fitness (with reselection allowed) to participate in the genetic operations.
 - (c) Create a new individual program(s) for the population by applying the following genetic operations with specified probabilities:
 - (i) Reproduction: Copy the selected individual program to the new population.
 - (ii) Crossover: Create new offspring program(s) for the new population by recombining randomly chosen parts from two selected programs.
 - (iii) Mutation: Create one new offspring program for the new population by randomly mutating a randomly chosen part of one selected program.
 - (iv) Architecture-Altering operations: Choose an architecture-altering operation from the available repertoire of such operations and create one new offspring program for the new population by applying the chosen architecture-altering operation to one selected program.
3. After the termination criterion is satisfied, the single best program in the population produced during the run (the best-so-far individual) is harvested and designated as the result of the run. If the run is successful, the result may be a solution (or approximate solution) to the problem.

To develop the MFI model based on Genetic Programming, the training and test dataset is divided. In this work, $80 \pm 5\%$ of the total data has been taken as a training dataset and the remaining dataset was fed into the program as a test dataset. The dataset is chosen randomly. This step is comparatively time-consuming than ANN method as the two different dataset needs to be fed manually. After each run, the value of R^2 for training and testing data is received along with an equation with the best accuracy. The value of the input variables in the test dataset is then put in the equation to find the value of the predicted MFI. The error percentage is calculated for the MFI value. The program is rerun several times to and the best model is chosen. The best model gives the highest value of R^2 and the least error percentage.

Building the MFI model using Artificial Neural Networks

Neural networks are computer algorithms inspired by the way information is processed in the nervous system. An important difference between neural networks and standard regression is their ability to learn. This learning property has yielded a new generation of algorithms. An ANN paradigm is composed of several highly interconnected processing elements, analogous to biological neurons that are tied together with weighted connections analogous to synapses.

Training a network consists of an iterative process in which the network is given the desired inputs along with the correct outputs for those inputs. It then seeks to alter its weights to try and produce the correct output (within a reasonable error margin). If it succeeds, it has learned the training set and is ready to perform on previously unseen data. If it fails to produce the



correct output it rereads the input and again tries to produce the correct output. The weights are slightly adjusted during each iteration through the training set (known as a training cycle) until the appropriate weights have been established. Depending upon the complexity of the task to be learned, many thousands of training cycles may be needed for the network to correctly identify the training set. Once the output is correct the weights can be used with the same network on unseen data to examine how well it performs.

Neural learning is considered successful only if the system can perform well on test data on which the system has not been trained. This capability of a network is called generalizability. Given a large network, it is possible that repeated training iterations successively improve network performance on training data, e.g., by “memorizing” training samples, but the resulting network may perform poorly on test data (unseen data). This phenomenon is called “over training”. The proposed solution is to constantly monitor the network performance network on the test data.

MATLAB was used to build and train the ANN model for this project. The software has a feature called Neural Network Toolbox which is equipped to generate Artificial Neural Networks with custom specifications for training the model set by the user.

On being provided with a set of input and corresponding output data in the form of a matrix, the tool divides up the data into training, test and validation sets. In the case of this study, the data was divided in the following composition-

Training – 70%

Test – 15%

Validation – 15%

Then the user is asked to provide the number of hidden layers that are to be introduced in the ANN model. The method to be used for the training can also be set by the user. In this case, all training can be done by the Levenberg-Marquardt method.

After that is determined, on hitting the ‘Train’ button, the tool trains an ANN model. The Training, Testing and Validation graphs are also displayed, along with the R^2 value. The closer the average R^2 value is to 1, the higher is the accuracy of the training. The trend lines on the graphs also give significant indications as to the preparedness of the model.

Now for this case, we have searched for the model with the highest R^2 value and the lowest percentile error. We have also tried to minimize the number of nodes, as a lower number ensures a simpler and cleaner model.

The error was calculated by comparing the model and the results it produced against a previously unseen set of data. A piece of code was written within MATLAB itself to compare the two, find the percentile error and generate graphs representing the error.

After a large number of trials and errors, by changing the number of nodes and training multiple models, multiple times, a satisfying value was reached in all these categories.

This particular ANN model was selected for further testing and comparison against the model mode using Genetic Programming.

Results and Observation

For ANN, after a large number of trails and errors, by changing the number of nodes and training multiple models, multiple times, a satisfying value was reached. The given tables show the best result obtained by training the ANN.

To obtain the error percentage a code has been written within MATLAB itself which determines the error according to the following formula:

$$\text{Error \%} = ((\text{actual MFI value} - \text{predicted MFI value}) / \text{actual MFI value}) * 100$$

ANN modelling result is shown in **Table 2**.

From very high R^2 value and low MSE, it is concluded that developed model is very accurate and learn the relationship between MFI and reactor operating parameters.

Table 2. ANN modelling result

No of nodes in the hidden layer	Best R2 value	Least percentage error	Algorithm used for training	Transfer function
6	0.998	2.36	Levenberg-Marquardt	Sigmoidal

For GP, the best run parameters, the best model, performance metrics for the model and the model properties has been obtained. The formula used is same as used for calculating error percentage for ANN model. The least percentage error has been calculated for the test set which is 3.8%.

The following tables shows the results obtained for the GP model.

Table 3. Run parameters for GP

Population size	250
Max. generations	150
Generations elapsed	21
Input variables	8
Training instances	336
Tournament size	
Elite fraction	25
Lexicographic selection pressure	0.7
Probability of pareto tournament	On
Max. genes	0.7
Max. tree depth	6
Max. total nodes	4
ERC probability	Inf
Crossover probability	0.1
Mutation probabilities	0.84
Complexity measure	0.14
Function set	Expressional
	TIMES MINUS PLUS SQRT SQUARE EXP ADD3 MULT3 RDIVIDE

Overall model

$$y = 0.00353x_2^2 - 1.52x_2x_5 + 96.75^2 - (3.58x_3x_5^3)/x_4 + (5.41e15x_3x_4^2x_5)/(2.31e18x_4 - 2.31e18x_7) + (1.1e-4x_3x_4x_5)/(x_4 - 1.0x_7)^2 + 2.28$$

Table 4. Parameters for evaluating model performance

Parameters	Training Data	Test Data
R2	0.93763	0.98022
RMSE	0.20504	0.22901
MAE	0.071581	0.11212
SSE	14.1263	4.0909
Max. abs. error	3.2903	1.1558
MSE	0.042042	0.052448

Table 5. Model properties

Description	Value
Genes	6
Nodes	36
Expressional Complexity	100
Depth	4
Inputs	5
Inputs used	x2, x3, x4, x5, x7

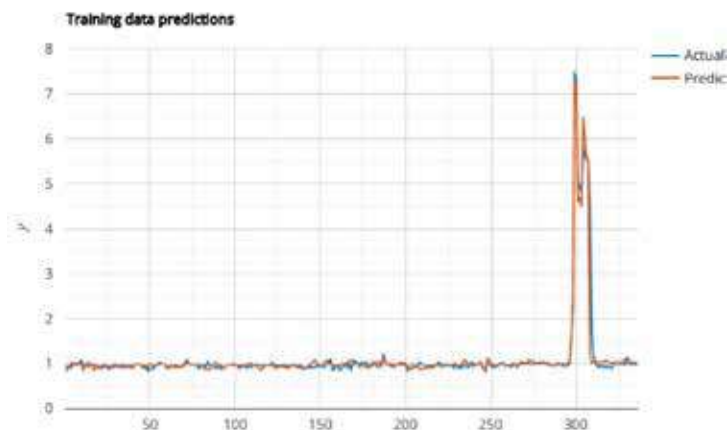


Fig 1. Comparison of the actual vs. the predicted MFI for training dataset in GP

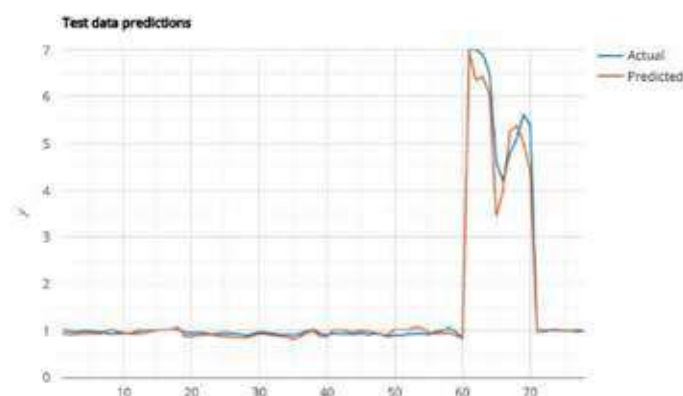


Fig 2. Comparison of the actual vs. the predicted MFI for test dataset in GP

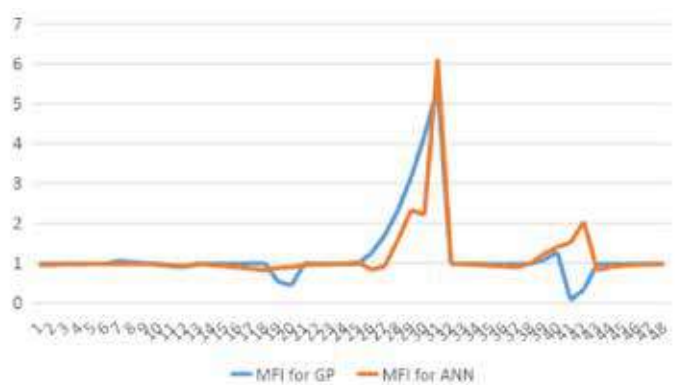


Fig 3. Comparison between the predicted MFI data for GP and ANN model

CONCLUSION

This paper develops artificial intelligence based modelling strategy to develop a relations between MFI and reactor operating parameters in running commercial plant. Such data driven methodology is easy to build and very accurate and very effective in scenario where phenomenological model is difficult to build or time consuming., ANN shows a better prediction accuracy than GP.

However, Genetic Programming has an advantage in the form that it produces a specific equation of the algorithm it has created



which can be further analyzed to understand the weightage of each variable in the process. This feature is unavailable in ANN as the closed form of equation is not available.

Developing model independently by two different algorithms (ANN and GP) increase their prediction reliability and reduce the false negative phenomena.

This complete methodology, when deployed in plant DCS, can almost instantaneously predict and show which variables to change and by how much to maintain MFI at its target range. This helps production engineer to understand to take necessary steps to maintain the desired MFI value and thus cut down on the losses due to off-spec product.

REFERENCE

Lahiri, S. K. (2020). Profit Maximization Techniques for Operating Chemical Plants. John Wiley & Sons.

Computer Engineering



Low Latency Low Power Encryption-decryption Method for Securing Memory Operations

Nageswararao Yeleswarapu, Dr Sajal K Das

Intel Technology, Bangalore

✉ yeleswarapu.nageswararao@intel.com; ✉ sajal.k.das@intel.com

ABSTRACT

A simple time, resource, power and cost-effective solution is proposed for encryption and decryption of data block and the same method is proposed to be used for instruction encryption, which is stored in external RAM or cache memory. As this method is very simple to implement, so it can be easily implemented in software with single cycle operation e.g. no time delay and no extra HW resource is needed. The power consumption, processing power requirement and delay involved in this encryption-decryption process is close to nil, compared to other existing methods. These existing methods involve lot of delay, power and resource consumptions. So, the proposed method can be implemented in many applications, where data security is a concern without sacrificing the system performance.

Keywords : Cache memory, computer memory, embedded system, RAM, CPU, Hardware, Software .

INTRODUCTION

Today, due to widespread usage of data processing systems, there exists an inherent risk of misuse of confidential information. So, efforts have been made in the field of information security to improve the confidentiality, integrity, and availability of information.

A programmable computing unit is typically designed to process a sequence of instructions, which is referred to as program code to perform a certain task. In most common architecture, the program code is typically stored in a memory and supplied to the computing unit at runtime via cache memory. For information security purpose, it may be desired to protect the instructions from being analyzed while they are stored in the memory or transmitted from the memory to the computing unit. On the other hand, errors or malfunctioning may occur during an execution of the program code if the instructions reaching the computing unit differ from desired instructions. Differences between the instruction actually processed by the computing unit and the desired instructions may have a random cause or could be deliberately provoked by an intruder. So, it is desirable to store the data in encrypted form outside the CPU on the external RAM to avoid attacks.

There are two main kinds of attacks: snooping on a live RAM bus or modifying data on the bus and dumping the RAM content.

So, data encryption-decryption is always desirable for protecting data including the instruction in RAM. But the problem is most of time, the decryption process takes lot of processing power and imposes lot of delay in the process because of the reason as described below. So, today, most of time it is not feasible to apply encryption-decryption due to delay and extra processing overhead.

Generally, (as shown in **Fig. 1**) in each block encryption method, a secure key K_c (which is of N bit) is ExclusiveORed (XOR) with binary data block (D) which needs to be encrypted and produces a resultant data stream R . So, $R = D \oplus K_c$. On the decryption side, the reverse process is followed, e.g. the resultant data block is ExclusiveORed with the secure key (K_c) and the D is retrieved back. $R \oplus K_c = [D \oplus K_c] \oplus K_c = D$.

Where, \oplus denotes the exclusive OR (XOR) operation. This operation is sometimes called modulus 2 addition. The XOR operator is most commonly used as a component in more complex ciphers operations.

PROBLEM ASSOCIATED WITH THE EXISTING METHODS

Now, the ExclusiveOR operation- over N bits (N is key length), is very processing cycle expensive operation. As it imposes lot of delay in the system and consumes battery power and consumes lot of processing power. So, it is most commonly implemented in dedicated Hardware block. This makes the system expensive, difficult to interface with software, power hungry and slow (e.g. delayed). So, in many cases, though system designers wish to implement a secure mechanism for data protection

at every stage in data/information flow, but due to this above issue it is not feasible to implement.

As a reference- in one research paper [1], it is mentioned that - "...In principle, the entire encryption process for any given character requires 20 microcontroller clock cycles. Hence for the microcontroller running at 48MHz the time required for the encryption of a character is $0.42\mu s$"

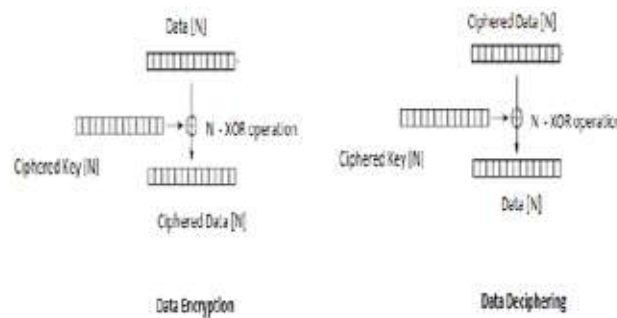


Fig 1. ExclusiveOR operation for Encryption / Decryption

DESCRIPTION OF THE PROPOSED METHOD

This solution proposes a simple, processing power, battery power effective, and resource effective method to encrypt and decrypt data.

In the encryption and decryption side there will be one random number generator, which will generate sequence of numbers $[s_1, s_2, s_3, \dots, s_M]$. The random number sequence generator is initialized with a SEED, which will be same as encryption side and decryption side and kept secret to both the parties. If the same SEED is fed in encryption side and decryption side random sequence generator, then they will generate same sequence of random numbers e.g. $[s_1, s_2, s_3, \dots, s_M]$ Encryption_side will be same as $[s_1, s_2, s_3, \dots, s_M]$ Decryption_side.

Now, in the encryption side, different bits located at different positions of the input data block (or instruction) are inverted based on the random number value. That means, if first number in the random number sequence is 6, (say, $s_1=6$) then encryption block will change the bit value from 0 to 1 (or vice versa) at the 6th location of the 1st input data block. So, based on the random number, it just inverts the respective bit positions in the input data block (or instruction). Now, after the specific bit inversion, the input data pattern (or instruction) is changed, and which bit is changed that remains unknown to the eavesdropper/hacker. Repeat the same process over other input data block stream (e.g. instruction-2, instruction-3, ... etc.) for encryption of the whole data stream (or whole program).

In the decryption side, it also generates random numbers using same SEED and that will provide the same random numbers (sequence of numbers) as produced in the encryption side. Here also, invert those specific bit values in the received encrypted data block (or instruction) at those specific bit positions, as indicated by that random numbers. That means, here also, the first generated random number will be 6 ($s_1=6$), so invert the bit (0 to 1 or 1 to 0) at the 6th position of the received data block (or instruction). This will help to get the original data (or instruction) back. Repeat the same for other encrypted data blocks (or instructions) to decrypt and get back the whole data stream. Please find the details in next section.

This process does not require any XOR operations, neither requires any complex cycle intensive operations. It just invert the bit value (1 to 0 or vice versa) at some specific (secretly random way) bit positions, so it does not requires any resources – so offers very low cost, simple, power effective encryption-decryption solution with the same level of robustness as in existing with complex methods.

Fig. 2, proposed method of simple cost and resource effective data encryption and decryption.

Data Encryption Module

The following steps are performed at the data encryption side to encrypt the input data block (or instruction, e.g. one data block is considered as one input instruction). This is depicted in **Fig. 2**.

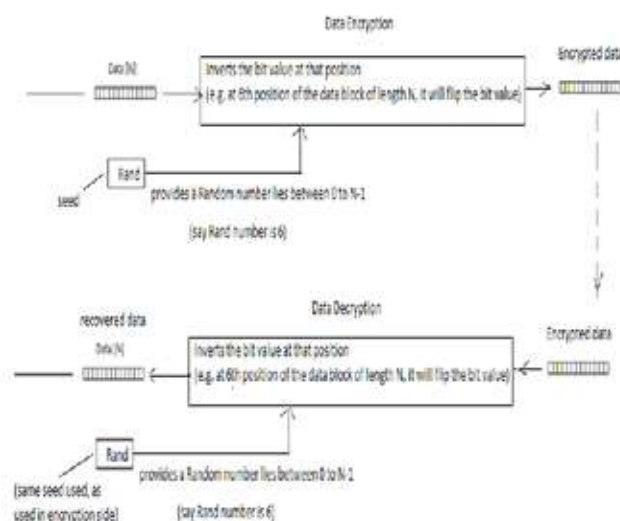


Fig. 2. Proposed method of simple cost and resource effective data encryption and decryption

Random Number generation

A pseudorandom number generator (PRNG) is an algorithm for generating a sequence of random numbers. This generates random number sequence based on the small set of initial values, called the SEED. A random seed (SEED) is a number (or vector) used to initialize a pseudorandom number generator. Two or more systems using matching pseudorandom number algorithms and matching seeds can generate matching sequences of random numbers which can be used to synchronize remote systems.

Here, we propose to use Rand () function, which is already available in the software and very simple to implement. The seed used here is also known to the decryption side, so that it also uses the same seed during reverse operation and generate the same sequence of random numbers.

In the encryption side, a Rand-1 () function is called and it provides a random number RN (from 0 to N) e.g. [s1,s2,s3,...,sM] Encryption_side . That means, the generated random numbers are: s1 is the first sequence, then s2 is the second sequence etc. till sM. Each random number lies in-between 0 to N value. Where N is the length of the input data sequence (or instruction max length).

Here, we assume that the first time generated random number is $s1 = 6$ (for example). Then '6' (e.g. s1) number is passed to the next unit (data ciphering unit) for ciphering first input block (or first instruction).

Data ciphering unit

The input to this unit is: a random number from the rand-1 () and a data block of length N (or instruction). Now, based on the random number RN (say s1), the bit value of the Data [N] at location 's1' is flipped. For example, say, the random number is 6 (say) and the data sequence is of length 8 ($N = 8$) is – 1010-1100. So, according to random number value 6, the 6th bit of the data sequence (1010-1100) will be flipped. Here, at 6th location the bit value is 0, so, this will be inverted, and the new value will be 1. So, the encrypted data block will be – 1110-1100.

Here, no exclusiveOR operation is performed, rather a random bit position is determined, and that bit is inverted. This operation can be done very easily without any processing load in software or CPU or HW.

One single bit change (inversion) over a data block (or instruction) is enough to protect that block, as the whole data block becomes garbled and cannot be recovered by a single bit change over a single block. If the data block size ($0, \dots, N-1$) is large enough, then instead of one bit position, several other positions can also be inverted using more rand() functions and then flipping those bit positions (in the same way).

This same process repeats over the other data blocks (or instructions) over the entire data sequence. That means, every time the rand function is called, which returns a number and based on that number the bit value at that specific bit location number of



the input data block is inverted as shown in Fig. 2.

Data De-Encryption Module:

The following steps are performed at the data decryption side to decrypt the data block.

Random Number generation

The decryption side also uses the same random number sequence generation mechanism that means it uses matching pseudorandom number algorithms and matching SEED. So, it calls the Rand-1() function and gets the same number as output ([s1,s2,s3,...,sM] Decryption_side) as it was in the encryption side. That means, here also the Rand() will generate first number as 6 (say). This is passed to the next unit which is decryption unit.

Data deciphering unit

This unit receives the random number and the ciphered data block of length N (0,1,...,N-1) as an input. Then it just does the reverse operation e.g. it just inverts the bit at the random number given position. For, example, here the input to the deciphering unit will be- the random number generated at first time which is 6 and the first input ciphered block data is 1110-1100. So, this unit will invert the bit value at the 6th position, which is now 1, that will be '0' once it is inverted. So, the de-ciphered data block will be 1010-1100. Which is the original bit sequence. So, we recover the original data block (or instruction).

Like this, the same will be repeated over the loop for the entire data sequence decryption.

ADVANTAGES OF THIS PROPOSED METHOD

The existing methods of data encryption-decryption uses XOR operations and are very complex to implement. Whereas this one proposes a new simple method which is not used earlier.

- (1) The proposed method of encryption and decryption is very simple to implement
- (2) It does not require any extra HW for doing ExclusiveOR operations, whereas the legacy methods require dedicated HW block for doing N XOR operations per data block, which makes the system more complex, resource intensive.
- (3) As the present method just inverts the required bit at a specific position (as indicated by rand) so, it is just a very simple operation and does not add any delay for encryption or decryption.
- (4) It does not take any extra cycles to implement the encryption/decryption.
- (5) It can be implemented by software only as it does not require any extra cycle intensive operations.
- (6) It can be used in several places to protect the data as using this process data encryption-decryption becomes very easy on both Encryption side as well as in the decryption side. So, transmitter and receiver encryption become very cost and resource effective.

POTENTIAL APPLICATIONS

It can be used in many blocks inside embedded and communication systems. Some examples are:

- (1) Secure code execution: The software/firmware code can be encrypted using this method (each instruction will be encrypted using this method). Then during execution, after fetching these instruction or data from external RAM or Flash memory, the processor will decrypt very easily using this proposed method without any cycle overhead and pass it to the decoder unit (in CPU). So, the instruction will be decrypted one by one (may be every block could be one instruction) and then passed to the instruction decoder unit in the CPU and then executed accordingly. This method will not impose the processing delay or power consumption overhead.
- (2) Communication system: In bus level transactions or data communication via wireless or wired channels can also use this same method for simple, resource, power consumption effective data protection.
- (3) Data storage security: The same also can be used for storing the encrypted data in memory and then later recover stored data using decryption.

CONCLUSION

Continuous efforts are made in the field of information security to improve the confidentiality, integrity, and availability of



information. But one major challenge is to implement a method which is simple, processing power, battery power, and resource effective to encrypt and decrypt data. But proposed method does not require any XOR operations, neither requires any complex cycle intensive operations. It just inverts the bit value (1 to 0 or vice versa) at some specific (secretly known random way) bit positions, so it does not require any hardware resources and offers very low cost, simple, power effective encryption-decryption solution.

REFERENCES

1. “Design of Circuit System-Based Cryptography”, F. C. Akinwonmi, B. K. Alese, F. M. Dahunsi, F. A. Osuolale, Proceedings of Informing Science & IT Education Conference (InSITE) 2015.



Application of Artificial Intelligence for Intent Determination in Threat Evaluation

Rahul Mahajan, Atul Sethia, Manoj Tyagi

Development and Engineering, Network Centric System, Bharat Electronics Limited, Ghaziabad

✉ rahulmahajan@bel.co.in

ABSTRACT

The ability to identify intent of a threatening hostile aerial target is an important component of threat evaluation. Most of the current systems that have the capability of threat assessment employ mathematical models, which primarily compute threat on the basis of proximity and heading of a threatening track against a vulnerable asset. This approach proves quite reasonable as well as useful for these systems in intent determination [4, 8]. But sometimes an attacking aircraft may deceive the system by following a path that seems to be non threatening. This aircraft might be following an attack pattern before actually attacking its target. There is necessity to determine such threats following a predefined or new kind of attack pattern/profile along with its final target (vulnerable asset).

Keywords : Threat Evaluation, Machine Learning, Hidden Markov Model, Attack Profiles.

INTRODUCTION

Real time threat evaluation plays a vital role in a typical air defense scenario. In a tactical environment, an early and accurate threat assessment is vital to the defense of vulnerable assets. There has been a multi dimensional growth of air threats in recent times. A great amount of complexity in the environment is introduced due to presence of multiple targets and multiple attack profiles followed by these attacking aircrafts, and also multiple assets that are to be defended. [2-3].

As of now, Threat evaluation methodology adopted by systems has been mainly a rule based approach. The threat evaluation basically evaluates the hostile tracks in a real time environment for engaging these targets in a prioritized manner. Generally a set of rules are defined for determining the list of priority targets for engagement. These set of rules are limited to target kinematics and computations with respect to the defended assets. This approach has been used by many threat assessment systems [4] and has provided immense support to the ground operators in their decision making process to neutralize the hostile targets.

In recent years there has been a major shift from rule based systems to systems that involve intent determination aspects due to several limitations in rule based methods [1, 5, 6, 9]. These systems fail to incorporate the attacker's intent and tend to ignore different attack patterns adopted by the enemy aircraft for damaging vital assets. The need of the hour is to correlate the air track trajectory with attack profiles and find the defended assets for which the attack profile is being followed. System should have the capability to automatically learn from the three dimensional threat attack trajectory, identify patterns and predict the hidden intent which might not be perceivable in a real time air situation picture. This identification of attack profile is the core of Intent determination process. Profile matching in real time and efficiently in a dynamic environment for a large data set is the primary challenge in current scenario.

HMM APPROACH IN THREAT ASSESSMENT

In the current work we tackle the challenge of identifying attack profiles from track data based on HMM or Hidden Markov Model. HMM is a statistical model in which the state relationships between instants of time series are depicted by the hidden states transition

and the probability distribution between the hidden states and observations [9]. The modeling object in this approach is the track data consisting of feature vector with three attributes, namely speed, heading, and pitch. The main intent of the approach is to mine a reasonable description for parameter of the Hidden Markov model from the given dataset.

HMM contains the following parameters:

$$\theta = \langle O, H, A, B, \pi \rangle$$

Where $O = \{o_1, o_2, \dots, o_T\}$ is an observation sequence.

T is the total length of the time series, which in our work is the number of update cycles.

A hidden state set H consists of a finite number of discrete states. There is always a hidden state h_t belonging to H , corresponding to a certain observation o_t at time t , and all the hidden states are formed as a hidden state sequence. Matrix A consists of the transition probability between every two hidden states. The state transition probability matrix.

$$A = \begin{pmatrix} a_{11} & \dots & a_{1N} \\ \vdots & \ddots & \vdots \\ a_{N1} & \dots & a_{NN} \end{pmatrix}$$

Where $a_{ij} = p[h_i(t+1)|h_j(t)]$

i.e. probability of transition from hidden state i at time step t to hidden state j at time step $t+1$. Again

$$\sum_{j=1}^N a_{ij} = 1, \quad \text{for all } i.$$

If the observation distribution of a given hidden state is discrete, B is the measurement probability matrix. Otherwise, it is a conditional probability distribution function:

$$b_{jk} = p[o_k(t)|h_j(t)]$$

i.e. probability of emission of visible symbol o_k from hidden state h_j at time step t . Again

$$\sum_{k=1}^M b_{jk} = 1, \quad \text{for all } j$$

i.e. sum of the probabilities of emission of ' M ' visible symbols from a given state ' j ' is equal to 1.

We observe extracted feature vector in the target (track) dataset. The hidden state in our model denotes the motion trend of the aircraft. It cannot be directly observed through the saved flight trajectory. HMM solves this issue by computing the relationship between hidden states and observations. Obviously, the observation sequence is the feature vector in polar coordinates in this model. The hidden state set should be a finite set, and it needs to be manually specified.

The approach for identifying attack profiles can be summarized as shown in (Fig. 1).

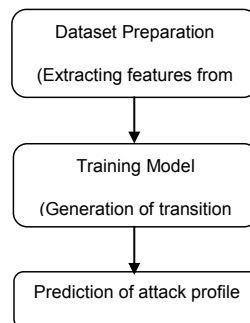


Fig. 1. Determination of attack profile(s)

Dataset Preparation

The dataset preparation involves capturing of real-time track data following some attack pattern. The attack profiles that are to be used shall be labeled or shall contain metadata indicating a specific profile. Model shall use this data (and metadata) to learn characteristics of the profile. However one sample of each profile may not be enough. Multiple samples of each attack profile shall be required for the model. The real time track data mainly contains track information i.e. speed, heading and height.

The motion trend can be classified into three types (Fig. 2):

Speed

- Constant acceleration (A)
- Constant velocity (C)

- Constant deceleration (D)

Heading

- Turn left (L)
- Go straight ahead (N)
- Turn right (R)

Pitch

- Climb (U)
- Cruise (X)
- Descent (W)

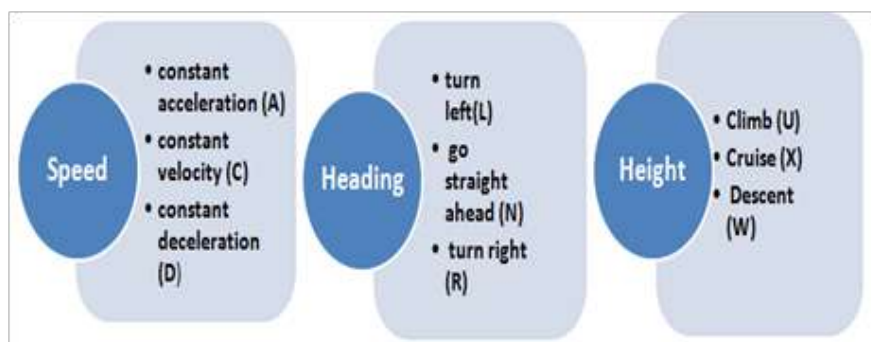


Fig. 2. Motion Trend

The approach uses these parameters from track data set namely, speed (constant, acceleration, deceleration), heading (left, right, straight), and pitch (climb, descent, or cruise). Based on track data set, sequence of trends (hidden state) i.e. <acceleration, straight, climb>, <acceleration, straight, cruise>, . . . , <deceleration, left, descent> are calculated as shown in figure 3.

These hidden state sequence are used for making transition probability matrix.

Let the speed unit be m/s, and the speed difference between two neighboring prediction time instants be $\Delta s = s(t+1) - s(t)$.

The trend of speed would be estimated by Δs ,

Δs – zero means constant velocity(C),

Δs – positive means acceleration (A), and

Δs - negative indicate deceleration (D).

The heading is also calculated in similar manner as Δv ,

Δv – zero means no change (N),

Δv – positive means right turn(R), and

Δv - negative indicate left turn (L).

The pitch is calculated as $\Delta \square$,

$\Delta \square$ - zero means cruse(X),

$\Delta \square$ - positive means climb (U), and

$\Delta \square$ - negative indicate descent (W).

Speed	Heading	Height	Speed (ΔS)	Heading (ΔV)	Height ($\Delta \Theta$)	Speed	Heading	Pitch
168.518	92.4441	9997	-44.059	11.3747	8001	D	R	U
212.577	81.0694	1996	8.417	-3.1563	0	P	L	X
204.16	84.2257	1996	14.045	-8.7523	0	P	L	X
190.115	92.978	1996	0	0	0	C	N	X
190.115	92.978	1996	6.033	2.6632	0	P	R	X
184.082	90.3148	1996	4.718	-3.8701	0	P	L	X
179.364	94.1849	1996	0	0	0	C	N	X

Fig. 3. Design of State Transitions

Training Model

Based on the hidden state sequences, a transition probability matrix is generated. The final hidden state set of the motion trends has 27 members, each of which corresponding to one combination of speed, heading, and pitch from 3 speed \times 3 heading \times 3 pitch types. The hidden states are labeled as 1 to 27 corresponding to the indices of the elements in the hidden states transition probability matrix, so the dimensionality of the transition probability matrix is 27 \times 27 since there are 27 hidden states in our model as shown in Fig. 4.

	ARU	ALW	DNW
ARU	A(1,1)	A(1,2)	.	.	A(1,26)	A(1,27)
ALW	A(2,1)					.
.	A(3,1)					.
.	.					.
.	.					.
.	A(26,1)	A(26,27)
DNW	A(27,1)	A(27,27)

Fig. 4. Transition Probability Matrix

Also, generation of emission probability matrix shall be done from the track data (Fig. 5). The probabilities describe the relationship between the hidden states and the observations provided by input data.

	Accelerat ion(I)	Decele ration(II)	Consta nt(III)	Right (IV)	Left (V)	Straigh t(VI)	Climb (VII)	Desce nt(VIII)	Cruise (IX)
1									
2									
3									
.									
+									
27									

Fig. 5. Emission Probability Matrix

Once both the above matrix is generated, HMM model shall ingest them as an input for predicting the next or future sequence of activities (or states) from its previously predicted state as shown in Fig. 6.

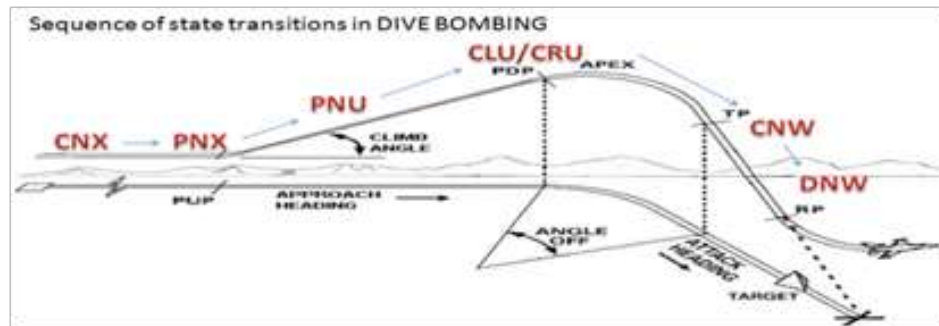
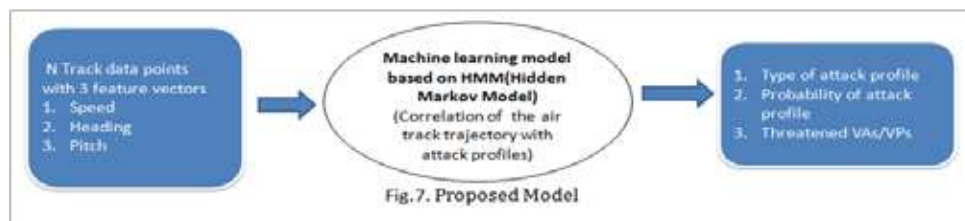


Fig 6. Sequence of State Transitions in Dive Bombing

Profile generation and Matching

For predicting the most likely sequence of hidden states a dynamic programming algorithm shall be used. The efficient generate a path which is a sequence of states that generated the observations. In the profile generation phase, Concatenation of existing and predicted activities (future 50 activities) shall be performed to generate a new profile. This generated profile shall either match with some existing profile or treated as a new profile for the model. In this approach for performing matching of generated profile with existing profiles. The model shall accurately predict the attack type, probability of attack profile and the threatened defended asset (Fig. 7).



Validation

This trained model shall be applied to test the real time target environment which have not been used for training purpose and shall validate the performance of the model. The model shall be tested against multiple attack profiles that can exist in a real time environment.

SUMMARY/CONCLUSION

The approach used in this paper is capable of monitoring the air traffic and detecting out the anomalistic behavior indicating that deep learning models such as Hidden Markov models and rule-based classification may be a way forward in the automatic detection of attack profile of the aerial targets.

We have broken our central dynamic problem into several feature vectors to determine which state transitions are possible. This method can be used to describe the forms of relationships between speed, heading and pitch. All possible states in a system can be identified while offering a complete parameterization of all possible tactical maneuvers. Additional information can be used to establish which of the several alternative behaviors will actually take place. Performance of HMM based classification model may be enhanced by augmenting the existing training dataset with huge number of target profiles corresponding to each type of attack. Aircraft attack profile classification may be extended to various aircraft categories by training the model with the real or simulated track data corresponding to each category.

ACKNOWLEDGEMENT

The authors would like to acknowledge Gp Capt R K Dhir (Rtd), Arvind Kumar (DGM), Sandeep Kumar (Mgr), Rupin Chaudhary(Mgr) and ,IITDM Jabalpur for their consistent support and motivation.



REFERENCES

1. Azak, M. and A.E. Bayrak. "A New Approach for Threat Evaluation and Weapon Assignment Problem, Hybrid Learning with Multi-Agent Coordination." in 23rd International Symposium on Computer and Information Sciences (ISCIS), 2008, pp-1-6.
2. Roux JN and Van Vuuren JH, 2007, Threat evaluation and weapon assignment decision support: A review of the state of the art, Orion, 23(2), pp. 151-187
3. Roux JN, 2005, Real-time threat evaluation of fixed wing aircraft in a ground based air defence environment, MSc Eng Thesis, University of Stellenbosch, Stellenbosch.
4. Fredrick Johansson, 2010, Evaluating the performance of TEWA systems
5. Xin-de Li, Jin-dong Pan and Jean Dezert, Automatic aircraft recognition using DSMT and HMM
6. Ervin Y. Rodin and S. Massoud Amin, Maneuver prediction in air combat via artificial neural networks (July 1991)
7. E Y. Rodin and S. M. Amin, Prediction and identification of tactical air combat maneuvers: neural network implementation of a qualitative approach presented at the Fifth AAAI Conference, Dayton, OH, (Oct 1989)
8. Seckin Unver and Tuncay Gurbuz, Threat Evaluation in Air Defense Systems Using Analytic Network Process (Volume 19, Issue 4), Journal of Military and Strategic Studies
9. Soham Deshmukh, Rahul Rade, and Dr. Faruk Kazi, Department of Electrical Engineering, VJTI, Attacker Behaviour Profiling using Stochastic Ensemble of Hidden Markov Models.



IT Infra Capacity Upgrade: IT Infra Monitoring with Smart Trend Analysis for Determining ‘New Size’

Rahul Yadav¹, Brajesh Kumar², Shakti Manchanda³

Deputy Engineer¹, Senior Engineer², Deputy Manager³, Bharat Electronics Limited, Ghaziabad

✉ rahulyadav@bel.co.in; ✉ brajeshkumar@bel.co.in; ✉ shaktimanachanda@bel.co.in

ABSTRACT

For large scale enterprises with multi-geographical presence changing their enterprise-wide applications is a daunting task, especially if the enterprises and their applications have been operating for decades. The application software having gone through test of time, passing through the hands of several developers have finally graduated to a level of maturity. The feature set enhancements, support to statutory and regulatory compliances and ensuring information security however necessitates continuous update and upgrades of the applications which also warrant the change in operating systems and middleware which further have a cascading effect requiring change of the underlying infrastructure. What becomes more challenging than update or migration of the applications is, to ensure that all these parameters are compatible with each other and that the applications availability is not hampered. To ensure that underlying infrastructure is capable of handling not just the sustained load but should be capable of handling the peaks as well. Some may out rightly propose ‘Cloud’ as the solution to the problem. However, establishing cloud too requires planning the underlying hardware. And, any miscalculation not only results in CAPEX loss but also results in OPEX when one seriously looks at the time and effort spent in managing the servers, storages, load balancers, operating systems and application. This paper proposes a data collection and analysis system for monitoring existing infrastructure, applications, resource utilization and database parameters to furnish real-time performance statistics & trend analysis to assist and simplify decision-making processes on capacity additions, upgrades of application & system.

Keywords : IT infrastructure monitoring, trend analysis, network monitoring, application Monitoring, System upgrades, etc..

INTRODUCTION

New features, regulatory compliances, threat intel feeds, middleware and database upgrades, Operating System updates and upgrades are some of the critical factors which force enterprises to update their enterprise wide applications. Similarly, as demand for the service increases, the need to enhance the capacity of their systems increases as well with view to have a well maintained and managed environment. Large scale applications have encountered resource problems when the load on the overall system becomes very large. Large levels of load can expose bugs (from application to operating system to hardware) that are only caused under these conditions. Multiple faulting components can destabilize the entire environment.

This seemingly simple action becomes mind boggling for those who actually have to perform these.

The major challenge which the system owners face is that at no point in time a situation of significant downtime is permissible. The applications should be available at time of need irrespective of the fact whether the applications are operating at 20%, 50%, 75%, 100% or even 150% load. The underlying infrastructure should be provisioned to provide necessary compute for all expected situations.

And, these are the question which the administrators, the architects as well as the developers struggle to answer. What are the expected situations wherein the applications are expected to operate? What should I size the infrastructure to meet the application requirement?

There is no readymade answer to these queries. Rather, the industry intuitively works on the experience of their best resources to size the hardware. And, this is what leads to resource crunch in few cases and over provisioning in most of the cases.

This paper provides a strong foundation for sizing the capacity upgrades. It proposes monitoring of existing IT infrastructure with smart trend analysis for determining the new size. The continuous monitoring of the applications, databases, operating systems, CPU, RAM and memory of the endpoints provides data whose analysis over a period of time in correlation with multiple events provides insight into the actual computational requirements of the applications at different loads and also forms the basis for predicting the compute required for an extrapolated loads.



BACKGROUND

Monitoring capabilities in health & performance tool keep a vigilant eye on the abnormalities occurring within the IT infrastructure. The server and application monitor allows one to set threshold limits for vital parameters that are important to maintain server uptime and to get instant notifications if the thresholds are violated. In addition, one can automate remedial actions such as starting or stopping a server or drill down to the root cause of the issue to understand and resolve them thoroughly.

Integrated health & performance tool's server performance monitor offers numerous analytically capabilities to measure and track resource utilization and their performance trends of infrastructure. While Trend Analysis reports [1][2] allows admin to understand the performance trends of different parameters in a end points. The health and application monitor enables one to plan load distribution and resource allocation adequately by providing capacity planning reports [3] that facilitates admin in identifying servers that are over-utilized or underutilized. Additionally, one can create custom reports and schedule automatic report generation based on set intervals.

Web-server-performance monitoring is an increasingly important field of research. Our review focuses mostly on existing soft-ware tools. One can find several techniques and methodologies to improve performances of Web servers by an appropriate software and hardware design in relevant textbooks. Monitoring a Web server is usually performed by analyzing its log files, which hold information about each single HTTP request and the consequent response and errors. According to the Common Log File Format, where the fields are filled with data coming from the request and the response. Given the high workload for popular Web servers, log file sizes can quickly grow to hundreds of megabytes. Log analyzers must present aggregated data so that they effectively represent a snapshot of the server's behavior and functioning over a given time interval. Several popular monitoring tools [4] exist, including Stephen Turner's Analog, Boutell. Com's Wusage and Maher Consulting's Access Watch provide a variety of parameters and statistics that are visualized using graphical interfaces. They aggregate monitoring data to inform Webmasters, for example, which pages in the Web site are the most popular, which countries (domains) are accessing the site, which pages outside the site contain broken links to pages in the Web site, and so on. The need for integrating several views of the log file motivated researchers to add a third dimension to graphical representation. Developed three different display metaphors for performance data time tunnels, scatter cubes, and geographic displays.

Currently various type of end point monitoring and performance analyzer tool [5] [6] were used for performance & health monitoring. In these tools monitoring may be configure either in agent based or agent less, but in large organization both type of monitoring is required. For monitoring of all end points, the separate monitoring tool was implemented. Both type of system have their own fault detecting and resolving technique which is completely different and management of each system is unique. There were no single integrated trend analyzer tool is available which may cater the trend analysis for computing resource utilization and application availability analysis.

SOLUTION APPROACH

In this paper we propose integrated trend analyzer of applications and computing resource of IT infrastructure which helps in system and application upgrade. In this approach we are monitoring IT infrastructure entity, end points resource utilization, applications & database health that helps to analyze real-time performance statistics & trend analysis. The monitoring of IT infrastructure may be done through agent based and agent less (SNMP based). It may track critical metrics, availability of end points & identify the root cause of issues, and resolve them using IT work flow automation. The historical data helps to analyze performance and utilization trends. On the base of resource trends on CPU utilization, memory utilization, packet loss, availability, response time, and disk utilization which assists for decision-making. **Fig. 1** depicts the overall view of proposed solution. Figure 1 shows the there are different component in the proposed solution. Agent less monitoring server, Agent based monitoring server, custom event adapter, performance & event Data store & trend analyzer Server.

Agent less monitoring server collect health data through SNMP based monitoring. It collect the data as per the provided management information base(MiB). The monitoring parameter may be configuring with the threshold breach condition, fault generation criteria and polling interval on server for monitoring. The health data as per configured parameter is collected through the SNMP walk and the fault generated on these devices will forward to the event processor.

Agent based monitoring server collect the health data & performance matrix through agent installed on end points. Server may also monitor the process/service & Log for generation the fault. For monitoring the services/process admin have to make a policy to define the threshold breach condition, fault generation criteria and error details. The performance matrix contains the resource utilization of CPU, Memory, Disk, Network etc. he fault generated on these device will forwarded to the event processor further processing.

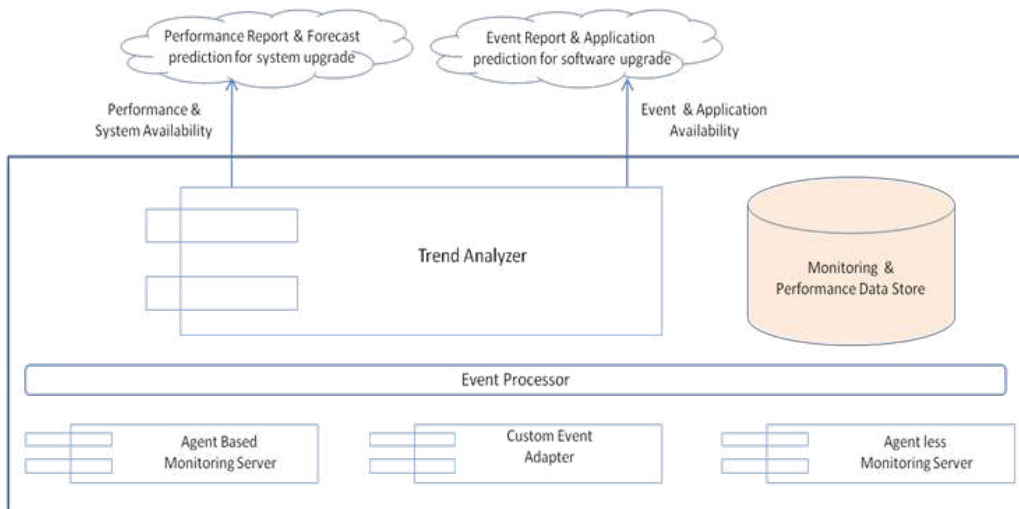


Fig. 1. Architecture of proposed Solution

Custom event adapter is used to integrate the event & performance data collected by other monitoring tools, which is seamlessly integrated and forwarded to event processor.

Event Processor is used for event categorization, de- duplication, event co-relation, alert generation, root cause analysis on monitoring data received from agent base monitoring server, agent less monitoring server & custom event adapter.

Monitoring & Performance data store keeps the data received from multiple monitoring source and forward all the data to trend analyzer.

Trends analyzer is the main component of the solution which collects the event generated from all the end points and the compute resource analysis data. These data are analyzed on the basis of different threshold, criteria and policies defined for application/system monitoring. The trend analyzer generates availability, performance and system utilization trends which helps in generating historical system performance, availability report and suggest/forecast on system resource usage for system upgrade/downgrade. The trend analyzer also generate the multifactor based application availability report and historical events trends for decision making for application upgrade.

EXPERIMENTAL RESULT

The solution is configured for more than 5000 agent based and agent less end points. these end points are different types, In agent based device servers, work station, laptop, tablet etc. and in agent less devices are radios, UPS, switch, UTM etc. these devices are configured in this environment for health status and fault resolution. In this experiment, an application is deployed on a server with recommended compute resource running 24*7. Here we have multiple cases for the trend analysis:

Case 1 : Trend analyzer shows that application has crashed 25 times in 1 month, when memory utilization has reached to more than 95%. So trend analyzer suggest to upgrade the system.

Case 2: Trend analyzer shows the compute resource utilization is not more than 50% but application has crashed more than 35 time in 1 month. So trend analyzer suggest to upgrade/downgrade the software version.

Case 3 : Trend analyzer shows the compute resource utilization is not more than 30% and application has not crashed in 6 month. So trend analyzer suggest to downgrade the system compute resource.

Case 4 : Trend analyzer shows the disk utilization is increasing at the rate of 5% per 20 days. In last six month disk space has crossed 60%(15% initial Use + 45 % incremental data). So trend analyzer forecast that in next 5 month disk will full so plan for upgrade the disk.

The trend analyzer also shows the multiple factor base health status & availability. The health status of end points shows the hardware status, utilization and trends as shown in **Figs 2-5**.

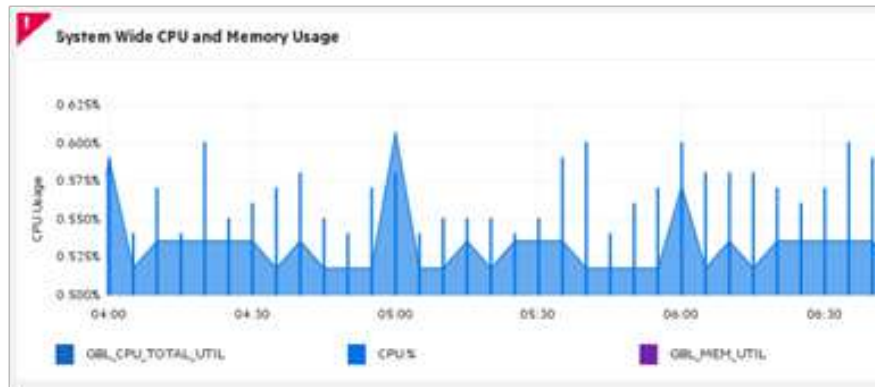


Fig. 2. CPU utilization and memory utilization trends

In the **Fig. 2** it shows that for a particular server the current CPU utilization trends which helps the administrator to decide that system should be upgrade/downgrade for a particular application.

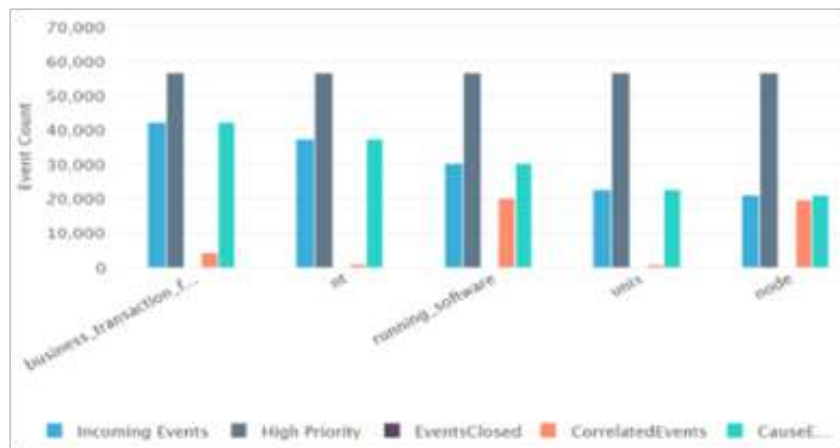


Fig. 3. Application wise CPU utilization

Fig. 3 shows the monitoring policy wise event count, which depicts the incoming events, high priority, closed event, and other parameter based events of different category.

Fig. 4 shows the application wise memory utilization, in which it depicts the usage percentage of memory trends for an interval for understand the usage pattern of memory consume by an application.

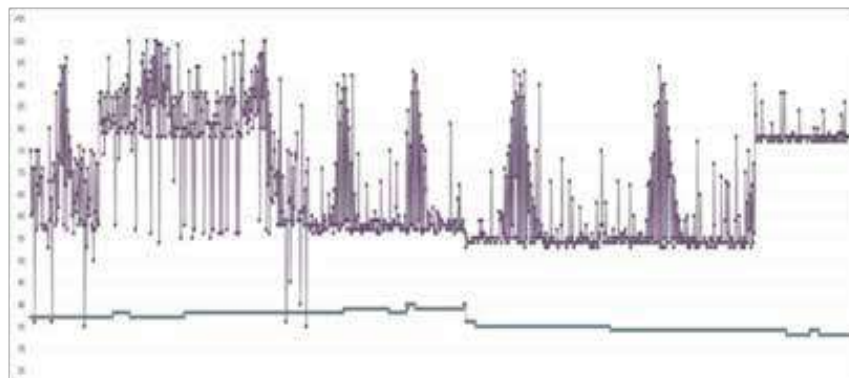


Fig. 4. Application wise Memory utilization

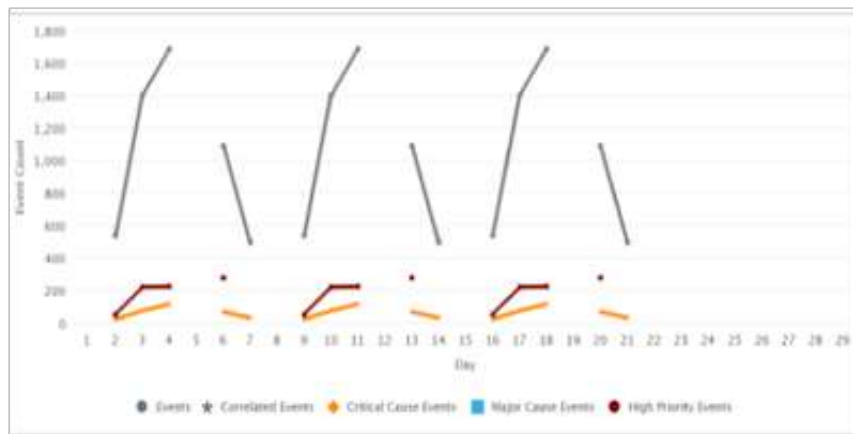


Fig. 5. Event distribution over time

Fig. 5 shows the event distribution over a time for analysis an application for resolving the faults and improve the up time or plan for new version of application.

CONCLUSION

This solution provides the performance metrics, Up & down time of end points & identify the fault issues. It also provides the historical data which helps to analyze performance and utilization trends. On the basis of the resource utilization, it assists and simplifies decision-making processes on capacity additions, upgrades, or maintenance schedules. It also provides the historical & forecasting trends for system and application availability with performance for deciding the system/application upgrade/downgrade.

Additionally, the future work may be entailed to include an AI module to predict application and / or hardware failures based on the historical data and watching the trends.

ACKNOWLEDGMENT

We would like to thank our Organization Bharat Electronics Ltd, our Unit Head and Executive Director, Mr Joydeep Majumdar and our Divisional Head Gp. Capt R K Dhir for giving us an opportunity to establish and work on the solution for IT infrastructure monitoring and for motivating and inspiring us. We would also like extend our gratitude to Mr. Amit Gupta and Mr. Manoj Tyagi for their unwavering support and guidance. We would also like to thank other members of our department for providing support in implementation of IT infrastructure as and when required.

REFERENCES

1. W. H. Scullin, T.T. Kwan, and D.A. Reed, "Real-Time Visualization of World Wide Web Traffic," Proc. Symp. Visualizing Time-VaryingData, 1995.
2. Brajesh Kumar, Shakti Manchanda, " Way to Industry 4.0: Integrated IT monitoring with auto-identification of root cause for heterogeneous environment"
3. Alain Mouttham, Liam Peyton, Ben Eze, Abdulmoteleb El Saddik, Event-Driven Data Integration for Personal Health Monitoring, Journal Of Emerging Technologies In Web Intelligence, Vol. 1, No. 2, 2009.
4. Chris A. Otto, Emil Jovanov, and Aleksandar Milenkovic, A WBAN-based System for Health Monitoring at Home, CSE journal 2010
5. A E Aktany, A J Helmicki and V J Hunt Issues in health monitoring for intelligent infrastructure, Smart Mater. Struct. 7 (1998) 674–692.
6. D. A Menasce and V. A. F. Almeida, Capacity Planning for Web Performance: Metrics, Models, and Methods, Prentice Hall, Upper Saddle River, N.J., 1998.



Implementation of an Artificial Intelligence based Predictive Maintenance for Fire Control System

Ajay Kumar Singh, Navya K M, S Arun, Abhishek Kumar

Software, BEL-BG

✉ ajaykumar.singh@bel.co.in; ✉ navyakm@bel.co.in; ✉ aruns@bel.co.in; ✉ abhishek_kumar@bel.co.in

ABSTRACT

Predictive Maintenance applications are gaining traction over the traditional preventive maintenance or run to failure maintenance activities in high availability mission critical systems. The advantage Predictive Maintenance has over the traditional methods is that it is trained on historical data related to a machine's state, operational behaviour and efficiency. Thus, a Predictive Maintenance application helps in carrying out effective maintenance activities, reducing maintenance costs and unexpected downtimes. This in turn helps in effective product lifecycle management. The Predictive Maintenance for Fire Control Systems is piloted in accordance with Defence Ministries' initiative to incorporate Artificial Intelligence (AI) in defence applications that aid the operator in effective Product Maintenance.

Keywords : AI; Machine Learning; Predictive Maintenance; Preventive Maintenance; Run to failure Maintenance.

INTRODUCTION

Equipment reliability and availability have been key cost drivers in manufacturing, especially when it comes to mission critical systems. For Defence Manufacturing industries, Product Support Lifecycle often extends up to a period of around 15 years. The traditional methods of maintenance such as run to failure maintenance, or preventive maintenance are based on Mean Time between Failures (MTBF) or Mean Time to Failure (MTTF) values for the devices during normal operating conditions. They do not take into account any abnormalities in the system. These typical maintenance activities can sometimes incur costs in the form of unplanned system downtime, high labour costs, high spare management cost. The method of Predictive Maintenance tries to overcome the shortfalls of traditional maintenance activities by constantly monitoring the equipment's operational behaviour and efficiency and estimate the maintenance period of the machine/system when needed[1]. A Predictive Maintenance method involves deploying a learned ML Model based on historical data to analyse the behaviour of the system, and warning the user of anomalous behaviour or predicting system/subsystem failure with reasonable accuracy. It also helps in just in time maintenance scheduling, thus avoiding unnecessary maintenance cost [2]. This paper describes the AI based Predictive Maintenance Piloted for the Fire Control Systems for Indian Navy.

PROBLEM STATEMENT

The Fire Control System is deployed in various ships of the Indian Navy. BEL has indigenously manufactured many systems/sub-systems/components for the Fire Control System. These assets need to be maintained for a period of over 10 to 15 years. There is a need to implement a maintenance method that shall further improve the systems' Reliability, Availability and Maintainability, and help achieve the goal of zero-defect performance.

SOLUTION

The proposed AI based Predictive Maintenance method consists of the following features to aid the operator in maintaining the system with minimal downtime.

- Real-time logging of operating hours and indication for the PCBs against the MTBF values.
- Provision to log PCB or item failures.
- Warnings and Anomaly Detection based on model prediction.

Given below is the flow chart of the steps involved from fetching of data to presenting the data on user dashboard.

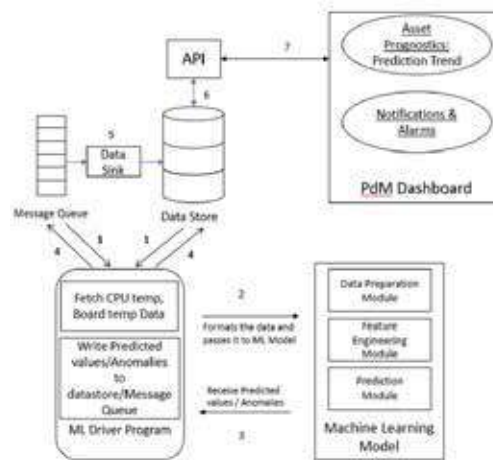


Fig. 1. Predictive Maintenance Flow Diagram

Step 1. Fetching data from Message Queues and Data Stores

The live data is fetched from Kafka Message Queue, and historical data is fetched from the Data Stores like Open Time Series Database (OpenTSDB).

Step 2. Data Formatting and input to ML Models The data fetched from Message Queue and Data Store is fed to the ML Model for further processing.

Step 3. Receive Predicted Measurements/ Anomalies The predictions from ML Model are fetched by the ML Driver program.

Step 4,5. Write Predictions to Data Sources.

The Predictions are written back to the Kafka Message Queue and OpenTSDB by the ML Driver Program

Step 6. Read Predictions, Notifications, Alarms from Data Stores

The Python API reads Predictions, Notifications and generated Alarms from the Data Store (OpenTSDB, Redis).

Step 7. Present Predictions, Notifications, Alarms on User Dashboard.

The Predictions, Notifications, Alarms fetched by the Python API are presented on the User Dashboard.

a) Real-time logging of operating hours and useful life remaining information for the PCBs against the MTBF values.

The proposed solution has a comprehensive HMI where the operator is made aware of the running systems with real-time logging and visualization of operating hours for MTBF based and life-limited based PCBs or items. The solution also incorporates user warnings based on percentage of useful life remaining for the PCBs.



Fig. 2. Dashboard depicting system health

b) Provision to log PCB or item failures

The operator is provided with an option to manually log the PCB or item failure. This logging aides in training AI/ML models for failure prediction.



Fig. 3. Failure Report Page

c) Warnings based on AI/ML models

Data was collected for various PCBs within the Fire Control System over a period of one year. The data was logged for the following subsystems: 1) Weapon data for large calibre gun mount. 2) Weapon data for low calibre gun mount (up to maximum of five gun-mounts) 3) Reference Voltages 4) Line to Line Voltages 5) Ship household data (Roll, Pitch, Speed) 6) Power Meter. This dataset was used to train and test the ML models for prediction and anomaly detection. We have used regression models for Prediction and supervised classification and unsupervised clustering models for Anomaly Detection. Given below is a brief explanation of the Regression and Classification approaches used for Predictive Maintenance of the systems/subsystems.

c1) Decision Tree Regression: Decision Tree Regression has been used to predict PCB temperature and warn user of anomaly in PCB temperature for various subsystems of the Fire Control System. The following are the steps followed:

Step 1. Feature Selection

We derived Start temperature as a feature for the PCBs board and CPU temperature variables. Start temperature is taken as the average of first 10 temperature values in each run.

Step 2. Model Selection

Decision tree regressor is used to predict Board/CPU temperature (continuous variable) using two other continuous variables (predictors) i.e. Message Send Count & Start CPU/Board Temperature. The hyperparameters used for Decision tree regressor are:

```
{
  "presort": "deprecated",
  "ccp_alpha": 0.0,
  "max_features": null,
  "max_leaf_nodes": null,
  "min_samples_split": 2,
  "min_impurity_decrease": 0.0,
  "min_weight_fraction_leaf": 0.0,
  "splitter": "best",
  "criterion": "mse",
  "max_depth": 10,
  "random_state": null,
  "min_samples_leaf": 1,
  "min_impurity_split": null
}
```

Step 3. Model Training and Validation

The model is trained on dataset after removing the abnormal data points, outliers and runs with less than 10 mins of total operating time. For training, the decision tree regression model has been fitted on 80% of historical dataset (2,68,654 observations). Cross-validation score is used to come up with optimum depth of decision tree model (10 in our model). By re-sampling the data multiple times, splitting them into training and validation sets, fitting trees with non-identical sizes on the training set and

looking at the classification accuracy on the validation set, the optimum tree depth has been decided, which gives the best bias-variance trade-off. One variable Message Send Count and one feature CPU/Board start temperature are used to predict CPU/Board temperatures respectively in the ML model as these predictors are highly correlated with response variable.

Step 4. Model Testing

The trained model has been tested on the remaining dataset (20% of whole dataset). For data splitting, train test split method of data splitting has been used which randomly splits the data frame into train and test subsets. The prediction accuracy of the Board & CPU temperatures is more than 97% and 95% respectively on the test dataset.

A smoothening factor has been added into the prediction data by calculating the exponential moving average (ema) of actual predictions. Given below is a sample graph of actual and predicted values for the PCB against vs Message Send Count.

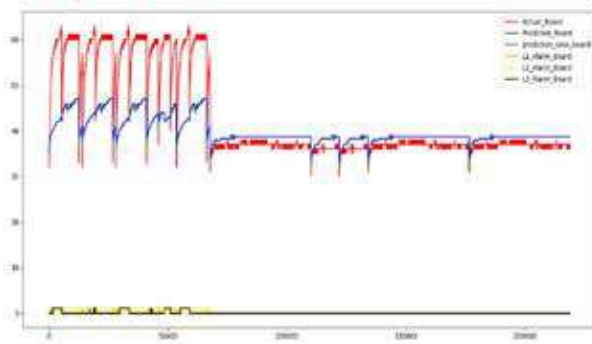


Fig. 4. Board Temperature (Actual, Predicted, Predicted ema) vs Message Send Count

Step 5. Model Evaluation

R-squared (r^2) & RMSE methods of ML model evaluation has been used in this model. R-squared (coefficient of determination) estimates distribution of data points around the fitted regression line. A higher R-squared values represent smaller differences between the observed data and the fitted values. R-squared is the percentage of the dependent variable variation that a linear model explains. RMSE is a measure of the differences between predicted values by a model or an estimator and the values observed. Following is the model accuracy for CPU and Board temperature prediction:

Table 1. Model accuracy for CPU Temperature prediction

Alarm Level	Condition
RMSE	0. 8362605514574895
R2_SCORE	0. 9543043184746002

Table 2. Model accuracy for Board Temperature prediction

Alarm Level	Condition
RMSE	0. 5636338851667885
R2_SCORE	0. 9765438198557354

c2) Support Vector Machine: Support Vector Machine (SVM) has been used to classify and detect anomaly from input data for Power Meter. The Power Meter device provides the voltage, current and power values for various sub-systems of the Fire Control System. The scenarios identified for flagging anomalous behaviour are Lower and Upper Control Limit breaches, sudden jump in Power Meter values. The steps followed are:

Step 1. Feature Selection

A set of seven features was selected from a set of 200 parameters.

Step 2. Model Selection

The objective of our model is to classify a data as anomalous or normal. For this purpose, we have used SVM. The hyperparameter used are:



SVC(C=1.0, cache_size=200, class_weight=None, coef0=0.0, decision_function_shape='ovr', degree=3, gamma='auto_deprecated', kernel='linear', max_iter=-1, probability=False, random_state=None, shrinking=True, tol=0.001, verbose=False)

Step 3. Model Training, Testing and Validation

SVM Model was trained on 70% dataset and Testing done on rest 30% dataset. The logged data had more than 4 lacs data points. We resampled the data in batches of 600 seconds interval, and selected 95% of quantile to generate meaningful data (around 756 data points), out of which 530 data points were used for training, and remaining for testing the Model.

Step 4. Model Evaluation

SVM Model was evaluated by Kfold validation which gave accuracy of more than 95%. Given below is the validation measure and confusion matrix for the model:

Table 3. Model Validation Measure

F1 Score	0.9946
TPR	0.9985
TNR	0.95
PPV	0.9957
NPV	0.9827
FPR	0.05
FNR	0.0014
FDR	0.0042
Overall accuracy ACC	0.9947

Table 4. Confusion Matrix

Predicted Results	Ground Truth Table		
		0	1
	0	53	3
	1	1	695

C3) Clustering:

K-Means Clustering algorithms is used to flag anomalous behaviour for the Discrete and Synchro PCBs. The Discrete and Synchro PCBs control the gun movement of the Fire Control System. The model flags anomalous behaviour whenever it identifies faulty sequences in the operation of systems and sub-systems. The faulty sequences are identified on the basis of patterns, sudden spikes and deviations from the ideal operating conditions. The steps followed are:

Step 1. Feature Selection

We selected 7 features from a set of 180 parameters. By using Principal Component Analysis (PCA) we reduced the dimensionality to 3.

Step 2. Model Selection

We applied multiple clustering algorithms to the dataset for identifying the most suitable algorithm [3]. First, the K-Means clustering was performed on raw dataset. The inertia value was very large due to high-dimensionality. Second, we performed K-Means after PCA. We plotted our PCA components to look for segregation. The clusters were overlapping. Third, we attempted Density Based Spatial Clustering Algorithm (DBSCAN) as data points were densely packed together. The hyperparameters Epsilon(eps) and minPoints were set to 0.3 and 10 respectively. The number of labels generated by the algorithm on 70 % train data was very large. Fourth, we attempted K-Means after PCA with normalisation. Based on the output of Elbow curve and Silhouette score, an optimum number of five clusters was selected. The model performance was found to be satisfactory.

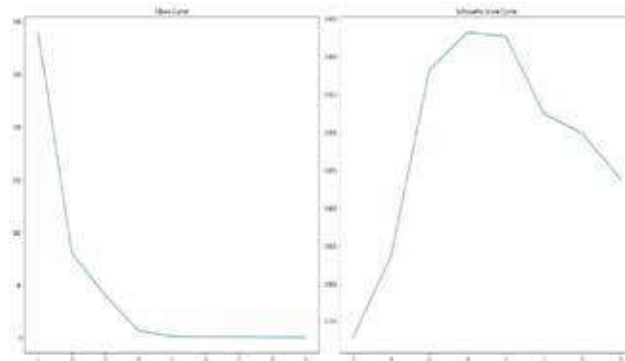


Fig. 5. Optimized Clustering selection

Step 3. Testing validation and Results.

The model was trained on 70 % dataset and tested with rest 30 % dataset. Given below is the model accuracy in the form of Confusion Matrix and validation measure tables. The data visualisation in 5 clusters is also shown below.

Table 5. Confusion Matrix

Predicted Results	Ground Truth Table		
		0	1
	0	21	1
	1	3	36

Table 6. Model Validation Measure

F1 Score	0.9473
TPR	0.9230
TNR	0.9545
PPV	0.9729
NPV	0.875
FPR	0.04545
FNR	0.0769
FDR	0.0270
Overall accuracy ACC	0.9344

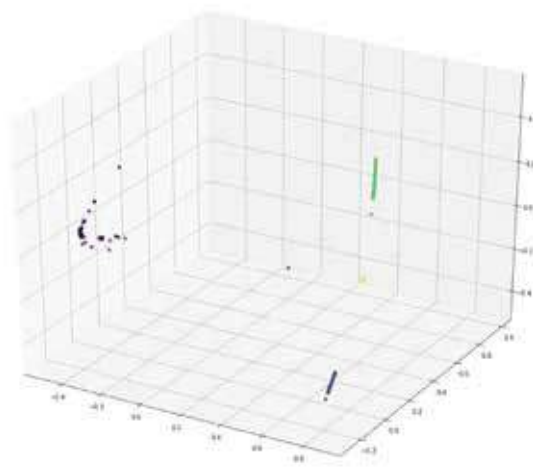


Fig 6. Data visualization in 5 clusters



RESULTS AND FUTURE SCOPE

The above results using a mixture of historical and simulated test data show the model accuracy for all the models to be greater than 90 %. As a Proof of concept, this Predictive Maintenance System will be installed in one of the Indian Naval ships. Further improvements shall be incorporated based on feedback from Navy and from our experience during integration with the actual Fire Control System.

CONCLUSION

Incorporating Industry 4.0 concepts such as Predictive Maintenance can help us in achieving higher Reliability, Availability and Maintainability (RAM) and thus a better Product Lifecycle Support for our Systems. Further, as BEL invests more and more in indigenisation of defence systems, extending the Predictive Maintenance to various projects can help in predicting failures and minimising downtime of these indigenous systems.

REFERENCES

1. Arnab Naskar, “Predictive Reliability Modelling of an Industrial System”, in International Journal of Science and Research (IJSR), Volume 9 Issue 9, September 2020, 1361 – 1364.
2. Cavalieri, S., & Salafia, M.G. (2020), “ A Model for Predictive Maintenance Based on Asset Administration Shell ,” in Sensors (Basel, Switzerland), Volume 20 .
3. L. Chen and H. L. Tang, “Improved computation of beliefs based on confusion matrix for combining multiple classifiers,” in Electronics Letters, vol. 40, no. 4, pp. 238-239, 19 Feb. 2004, doi: 10.1049/el:20040176.



Leveraging Various Technologies for Tracking of Logistics in Steel Plants

Ayan Goswami*, Shyamalesha Saha

Research & Development Centre for Iron & Steel (RDCIS), SAIL, Ranchi, Jharkhand

✉ ayangoswami@sail.in*

ABSTRACT

In recent years, a rapid stride has been made in various technologies for tracking of logistics. Now-a-day various industries are increasingly employing these cutting edge technologies to track vehicles as well as materials to increase efficiency and production. During last decade, steel industry are extensively using latest technologies like GPS based, RFID based, Barcode and QR code based tracking solutions to track materials like slabs, coils, sheets etc. as well as transports like locomotives, dumpers, trucks etc. These has resulted in significant jump in efficiency of various operations in Steel Plants and minimised errors resulted from manual based tracking. The prime objective of this paper is to discuss various tracking solutions employed in Steel Industry for tracking of logistics whether it is raw materials, finished products as well as transports. This paper will emphasise on the various technologies, their usage and their applications in Steel Plant scenario.

Keywords : GPS; GPRS; Vehicle tracking system; RFID; QR Code; Logistic tracking.

INTRODUCTION

The importance of logistic tracking and tracing of raw materials, semi-finished products and end products are considered quite high for manufacturing firms like steel plants to ensure better customer service and also essential for managing logistics networks efficiently. Logistic tracking is one of the major problems faced by global industries both from tracking and tracing in their logistics supply networks, that creates huge coordination problems in the overall product development process[1]. Today's multi-supplier environments, manufacturing firms are looking for the appropriate solution to track their logistics, equipments, input & output materials, delivery shipment on real-time environment. In the last decade, rapid strides have been made in the field of various logistic tracking technologies. There has been an exponential growth in usage of these technologies for tracking logistics by various industries be it transports, railways, steel, mining etc. In today's world, there are several tracking technologies available to manufacturing industries through GPS, RFID, Barcode, QR Code etc.

Heavy industries like iron and steel industries are widely using these tracking technologies for tracking of logistics, be it raw materials, in-process products, finished products, in plant transports, locomotives etc. Each of the technologies mentioned above have its own merits and de-merits. All these technologies are finding wide applications in various areas of iron and steel making starting from raw material handling to dispatch of finish products.

The objective of this paper is to discuss application of various tracking solutions in the Indian steel sector. This paper will further emphasize on diverse usage of various solutions for tracking of logistics in steel plants.

GPS BASED TRACKING

GPS (Global Positioning System) is a radio-navigation system based on a network of orbiting satellites that send precise details of their position in space back to earth. The GPS devices on ground act as a receivers to the signals, and are used to calculate the exact position, speed and time at the vehicles location. The unique feature of this system is that it allows users to determine their three dimensional position, velocity and time anywhere in the world, be it land, sea or air. Like many other applications initially developed for military purpose, it is now being increasingly used for civilian purposes[2].

Integrated steel plants are heavily dependent on various modes of transportation like rail and road transport to ferry goods inside the plant. Generally, this transportation network covers the entire plant connecting all its major shops and locations, stockyards and dealers. Managing such a huge infrastructure poses a huge challenge to the plant. Smooth functioning of such distributed facility has a substantial impact on overall productivity of the plant. This traffic management can be eased and made more efficient and productive through the installation of a GPS-based vehicle tracking system. The vehicle tracking system employed in Steel Industry and in general have two major components:

- a) Vehicle tracking hardware
- b) Vehicle tracking software

Vehicle Tracking Hardware

In order to track vehicle in real-time, vehicle tracking system comprises of an in-vehicle device comprises of a GPS receiver and a communication module. The GPS receiver can be easily installed into the vehicle to be tracked. Its captures the GPS location information as well as other vehicle information at regular intervals and sends the information to a central server in remote location. Apart from geo-location, other vehicle information which can be send comprises of fuel quantity status, temperature of engine, altitude, door open/close, pressure of tire, ignition off status, headlight on status, taillight status, battery status, GSM area code, number of GPS satellites in view, emergency button status, total idling and movement status, odometer readings, engine RPM and vehicle speed, etc. to name a few. The efficiency of the GPS devices determines the effectiveness of the whole tracking system.

Most vehicle tracking systems, in addition to providing the vehicle's location data, also provides a wide range of communication ports that can be easily hooked up with various controls available on board, allowing to check their status and control and help in automate their operation. **Fig. 1** shows the schematic of a GPS based locomotive tracking system.



Fig. 1. Schematic of GPS / GPRS based vehicle tracking hardware

Vehicle Tracking Software

The Vehicle tracking software essentially processes the data generated by GPS in terms of latitude, longitude, velocity and time for any given location. Huge amount of data is generated during tracking operation, which is transformed into relevant information. The vehicle tracking software can be broadly categorized into three modules, namely

- (a) Communication module,
- (b) Geographical Information System (GIS) module
- (c) Database Module.

The job of the communication module is to collect desired vehicle data either in real time or at a periodic intervals. GIS module relates to the digital map of the site, decode the latitude and longitude of the location received from the device and depict it over the digital map on the screen of the user in picto-graphical manner. Additionally, mapping of working location based on latitude and longitude can be saved into a database, which can be referred to draw display / mimic diagrams. The objective of the database module not is to stores positional information and also to manage other information about vehicles, drivers, trips, GPS data loggers etc.

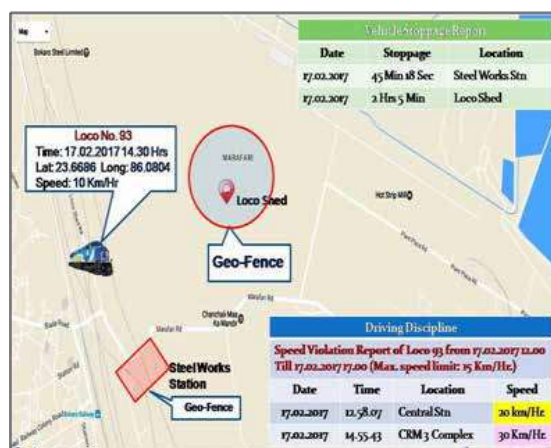


Fig. 2. GPS based vehicle tracking application software

Application of GPS based Tracking in Steel Plants

Now-a-day, GPS based vehicle tracking are increasingly finding its usage in steel plants. Some of the application areas are discussed here:

- Deployment of such a system in Blast Furnace (BF) zone of steel plant is briefly presented here. The tapping of hot metal from blast furnaces are done at pre-defined intervals. The liquid hot metal is transported to the steel melting shops in huge ladles called hot metal ladles. The ladle circulation time is a very important factor and on an average, it varies between 4 hrs to 7 hrs due to various operational constraints. Any deviation in turn-around time may eventually result in an increase in demand for more number of hot metal ladles and locomotives in circulation to compensate for the deviation. The GPS-based tracking system implemented for such hot metal ladles which are pulled by locomotives continuously provides the exact location of ladles inside the steel plant. This helps to plan the ladle movement from a central location. The major benefits due to such tracking systems are a reduction in ladle circulation time, lesser loco-run-hour, less amount of heat losses during the transfer of hot metal to mixer, etc
- GPS based locomotive tracking is increasingly being used for tracking locomotives in steel plant. locomotive tracking and fleet management of locomotives always pose a stiff challenge to the Traffic Department in Steel Plants. In-efficient fleet management results in significant delays resulting in high demurrage charges. Also, effective delay analysis becomes difficult and time-consuming without the availability of real-time data of locomotive movement. Hence, tracking of locomotives through GPS based tracking system is progressively being employed for managing a fleet of locomotives in steel plants.

RFID BASED TRACKING

Radio frequency identification (RFID) is a state-of-the-art radio wave based technology that enables simultaneous and automatic identification without the need for a line-of-sight. Based on the advantages of this technology, usage of RFID is spreading in various fields, such as smart card, localization, supply chain management, and so on[4].

Though various types of RFID exist, but broadly, we can divide RFID devices into two different classes: active and passive. Active tags generally require a power source. Active tags are either connected to a powered infrastructure like power supply or use energy stored in an integrated battery. For the second category of tags, the tag's lifetime is limited by the stored energy and depends on the number of read operations the device has undergone.

Passive RFID is very popular as the tags don't require batteries and are absolutely maintenance free. The tags also have a very long operational life. These tags are small and can be easily fit into an adhesive label and stick to the surface. A passive tag basically comprises of three parts (a) an antenna (b) a semi-conductor chip attached to the antenna, and (c) some form of encapsulation. It is the responsibility of the tag reader to power and communicate with a tag. The antenna of tag reader captures the energy and transfers the tag's unique identification. The entire operation is coordinated by the tag's chip. The encapsulation maintains the tag's integrity and protects the antenna and chip from environmental conditions, dust, chemical or reagents prevalent in harsh environment such as in steel plants.

In order to communicate, RFID tags and RFID tag readers have to be on to the same frequency. The most common frequencies an RFID system can use are as follows:

- Low frequency, or LF, (125 – 134 kHz)
- High frequency, or HF, (13.56 MHz)
- Ultra-high frequency, or UHF, (433, and 860-960 MHz)

Frequency Range	< 135 KHz (LF)	13.56 MHz (HF)	860-960 MHz (UHF)
Read Range	< 0.5 m	~ 1 m	~ 4-5 m
Tag Type	Passive Inductive Coupling		Passive or Active
Applications	Access control, Animal tagging, Immobilizer	Smart cards, Item-level tagging, Libraries	Supply chain pallet- box-level tagging, Toll collection

Table 1. Comparison of LF, HF, and UHF RFID

Application of RFID based tracking in steel plants

RFID based tracking is one of the most used technologies employed for tracking of materials / logistics in steel plants. Some of the applications are mentioned here:

- After manufacturing, the coil like HR or CR is packaged, banded, and kept in storage until delivered to the customer. Coils are generally very heavy, weighing over several tons. Therefore, cranes are used in plant for the coil movement. The coil information is being managed in following ways. First, a coil-storing map is used. When a crane moves a coil, information of the movement is captured and updated. Second, if there is a problem on the map, the operator have to check it by reading the marking or barcode labels attached to the coils. However, in case coils are marked manually or bar-coded, the workers have to come close to the coils to read the marking or the barcodes one by one. Therefore, the checking process is time intensive and can be very dangerous within the crane-operating boundary.

To address this problem, an RFID-based steel coil identification system is widely used these days. Unlike the barcode system, an RFID reader can read distant tags simultaneously without the need for an optical line of sight. Therefore, RFID tags are generally added to the label and attached on the coil which can be scanned without human intervention.

- The ladle running costs comprise not only the refractory costs, preheating fuel costs, and related labor costs, but also the cost of additional heating in ladle furnace due to lower than optimum ladle temperatures, consequently additional process delays incurred in delivering steel at the right temperature to the downstream unit, metallurgical disadvantages of receiving steel at caster at too low or too high temperature and the occasional costs of ladle breakout due to inability to judge the residual life of the ladle.

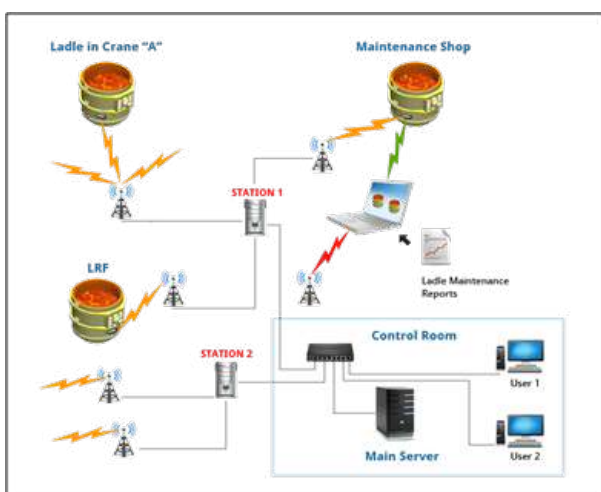


Fig. 2. Schematic of RFID based ladle management system



The RFID based Ladle Management is usually used to manage the complete ladle logistics in the most optimum manner in terms of energy loss, utilization factors. This has led to better planning of lining refractory which in turn results in a just-in-time supply of refractory materials. The temperature modeling has helped in better planning of target temperatures at various units (BOF, LF etc.).

BAR CODE & QR CODE BASED TRACKING

A barcode comprises of bars and spaces of varying width. It is basically an optical, machine-readable, representation of data wherein the data usually describes something about the object. The barcodes may be referred to as linear or one-dimensional (1D).

Similarly, a QR code is a type of matrix bar code or two-dimensional code that can store data information and designed to be read by smartphones and QR code readers. The QR stands for “Quick Response” which indicates that the content of the QR code can be decoded at high speed on the fly. The QR code comprises of black colored marks arranged in a square pattern on a white background. The information encoded may be text, URL, information, or any other data. The capability to put a huge amount of information in a small area and the ability to quickly decode the data has increased the popularity of QR codes. Its applications are growing rapidly all around the world.

Nowadays, barcodes and QR codes are increasingly finding their applications in tracking materials and logistics in the steel industry. Bar code or QR code stickers are attached to the coils, plates, etc. to identify them during different stages of its processing. Bar code readers and smart-phones are used to read these codes to determine the coil number. The readers are connected to the coil information system.

CONCLUSION

Various cutting edge technologies are increasingly being used for tracking of logistics as well as materials in steel plants now-a-day. These technologies have not only helped in accurately tracking of materials but also in effective planning and decision making in the steel plants. In recent times, machine vision, OCR based tracking etc. are also making its roadway into the logistic tracking and in future will change the way materials are tracked in steel plant.

REFERENCES

1. Real-time Tracking and Tracing System: Potentials for the LogisticsNetwork, AHM Shamsuzzoha and Petri T Helo. Proceedings of the 2011 International Conference on Industrial Engineering and Operations Management, Kuala Lumpur, Malaysia, January 22 – 24, 2011
2. GPS solutions for tracking applications in steel industry, R. K. Jha, K. K. Mallik, S.Jha & S M Mohanty, M S Sharma, T Ravindran.
3. Optimisation of logistics operations using GPS technology solutions: a case study, Dr Roula Michaelides.
4. RFID Technology Principles, Advantages, Limitations & Its Applications, Mandeep Kaur, Manjeet Sandhu, Neeraj Mohan and Parvinder S. Sandhu, International Journal of Computer and Electrical Engineering, Vol.3, No.1, February, 2011, 1793-8163.



Post-surgery Recovery using Deep Learning

Kuldeep Hule, Arjun Dashrath

Department of Computer Engineering, Army Institute of Technology, Pune, Maharashtra

✉ hulekuldeep@gmail.com; ✉ arjunsumant_19256@aitpune.edu.in

ABSTRACT

The objective of this research was to deploy a Deep learning, pose estimation algorithm by implementing an application that would analyze imperfections caused in fixing joints during orthopedic surgeries and provide corrective physical suggestions to fix improper joint placement/posture caused as a consequence of surgery. The application provides guidelines for optimal posture of multiple joints and prompts the user to imitate the movements consciously in order to physically fix the errors over time.

Keywords : Deep learning, Orthopedic, Post surgery recovery, Tensorflow, Pose estimation, PoseNet.

INTRODUCTION

Every year the world sees 22 million orthopedic surgeries. In India, 67% of the total orthopedic patients fall under 21-60 years of age, a significant part of the working population. 33% of these suffer from trauma that require corrective measures [3].

The most prevalent of orthopedic surgeries are:

1. Joint replacement surgeries (Shoulder, Knee, Hip)
2. Surgeries as a result of fractures, dislocations and muscle tears.
3. Spinal surgeries.

These surgeries usually have a long rest period for proper recovery but cause certain complications almost every time that require physical corrective methods for mobility and stance correction. The complications can be majorly divided into two categories:

1. The longer rest periods and prolonged usage of casts and braces often hinder the correct placement and structure of the injured joints.
2. Slight imperfections caused during surgery procedures that may deviate from the optimal joint placement angles.

For example, during an ankle surgery recovery, over or under pronation of the foot might occur due to the lack of pressure on the ankle due to long rest, weakened muscles due to long usage of casts and braces or incorrect attachment/positioning of the joint during surgery. This may have a permanent negative impact on the joint causing suboptimal physical capabilities of the joint or severe impairment.

The solution devised is to use deep learning algorithms to develop an application that analyses the joint placement and angles, compares it to the optimal structure from the existing dataset of optimal cases depending upon different body types and structures, finding the deviation from the optimal case and thereby recognizing incorrect surgery outcomes (incorrectly fixed joints) and incorrect stances (e.g. drooping of fixed shoulder) and suggesting corrective and medical solutions thereby making it ideal for professional and home usage. The corrective measure consists of guided stance correction that the user can consciously try to imitate to improve stance by strengthening muscles around the joints and getting habitual to it. For example, a spinal surgery may cause a patient's back muscles to be weakened due to bed rest causing a bad spinal posture, the application would point out the problem and suggest optimal corrective postures that the patient can imitate to correct their posture over time. Thus, the application can greatly contribute in post-surgery recoveries and incorrect surgery detection.

LITERATURE REVIEW

Pose estimation algorithms from various packages like Tensorflow and PyTorch have been extensively used in the past mainly for augmented reality, gait analysis and CGI techniques in movies.



A research was conducted in November 2017 by a group of American authors on NCBI USA on Artificial intelligence for analysing orthopedic trauma radiographs that used deep learning algorithms for diagnosing joint fractures and dislocations in radiographs. The results showed the algorithm predicting fractures with an accuracy of 83% [4].

Another research was conducted in April 2019 on Deep learning prediction on hip fracture using confounding patient and healthcare variables. Also, they were used statistical learning algorithms for finding a hip fracture [5].

Another research was conducted in March 2020 on PLOS ONE that deployed deep learning for analysis of bone quality in fractured osteoporotic patients. To investigate teriparatide action on parameters of bone quantity and quality and on Bone Strain Index (BSI), also derived from DXA lumbar scan, based on the mathematical model finite element method. [6]. In this research, Artificial Neural Network algorithm used for analyzing the various bone quality parameters.

TECHNOLOGY USED

Tensorflow

Tensorflow is an open source python library containing machine learning models that can be modified and redeployed. The applications will be based on the Tensorflow core version for x86 computers(windows/linux/macOS) and Tensorflow Lite for mobile phone platforms (Android/iOS) and arm-based computers/IOT devices (Raspberry Pi) [1].

Some examples of implementations of tensorflow are:

1. Google uses Tensorflow Machine learning models to optimize search engine results, mails etc.
2. PayPal uses Tensorflow implementations for fraud detection.
3. Coca-Cola uses Tensorflow to implement mobile proof-of-purchase

PoseNet

PoseNet is a tensorflow based vision model used for pose estimation, the algorithm used in the application would be similar to PoseNet with some extra additions to enhance the accuracy and the speed of the algorithm.

POSENET WORKING PROCEDURE

PoseNet detects human stances and connects multiple keypoints that can be used to detect angles between multiple key points [2]. The pose estimation happens in the following phases:

1. An input RGB picture is put through a convolutional neural network
2. A single pose algorithm using the bottom up approach returns a list of keypoints and its pose confidence score (the confidence of detecting a person/body part correctly). The algorithm detects multiple keypoints like elbows, shoulders etc. and returns their keypoint confidence score (the confidence of the key point being accurate)

PoseNet currently detects just 17 keypoints like shoulders, hips, wrists etc. which is insufficient for the application. Therefore, the implemented algorithm would contain more keypoints for each body part for higher accuracy and more recognition processes for poses of individual body parts along with the pose of the entire individual.

METHODOLOGY AND IMPLEMENTATION

Fig.1 showing application working flow.

The application would be connected to an optimal body angle data set (containing normal, healthy images of different body parts along with their angles to keypoints) for different categories of people (fit, healthy, etc.) and an issue data set (containing examples of errors caused due to incorrect surgeries or commonly occurring imperfections post-surgery) via cloud (AWS, Azure etc) and would be implemented as follows :

1. The RGB input picture will be selected or taken from the camera sensor and the user will select the body part to analyse (wrist, knee, spine etc)
2. The first process of the algorithm would be to detect similar body types to the user. For example, some users may be skinny while others may be healthier, the joint angles in the skinny users would be sharper due to less body fat while the healthier users would have softer joint angles

3. The algorithm would process recognition of the selected body part until a threshold confidence score is crossed
4. The algorithm will then determine multiple important key points that will be selected on the basis of the curvature of the body part and the goal will be to include maximum curve spots on that part until threshold confidence score is achieved to maximize the accuracy
5. The algorithm will then plot lines between the keypoints and store the angles between the indexed keypoints
6. The algorithm will then predict if the issue can be resolved by self-correction or will require surgical methods, it would inform the user of the latter and will state out the issues comparing to the issue dataset and terminate in that case
7. If the issue can be resolved by self-correction, the program will compare the angles to the optimal angles from the data set
8. The program will display a different coloured line indicating the optimal stance and will prompt the user to coincide the user's joint line to the optimal joint line until the lines are coincided thereby correcting the stance/joint posture.

Application will prompt to the users by reminding them to do this task frequently in order to the users for become habitual to the postures & develop muscle strength to maintain it, thereby improving the joint placement over time.

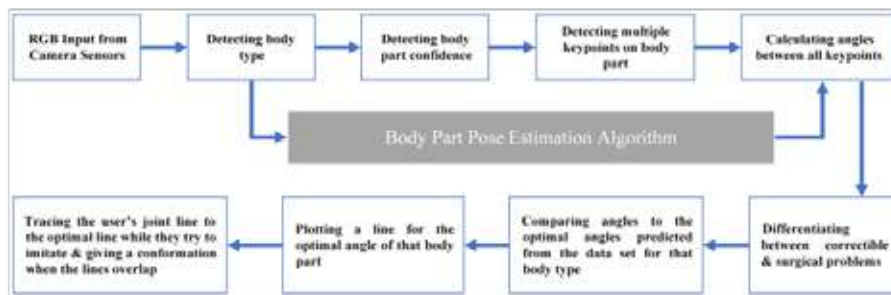


Fig.1. Application Flow Diagram

Figs 2, 3 & 4 will show some of the examples of application UI, in Fig 4 the green line signifying the optimal joint line to be coincided for correct posture(drooping shoulder).

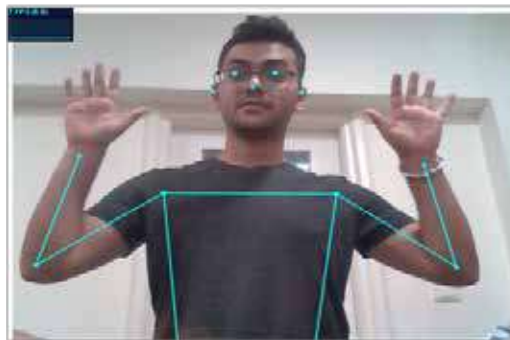


Fig. 2. Example of keypoint mapping using PoseNet

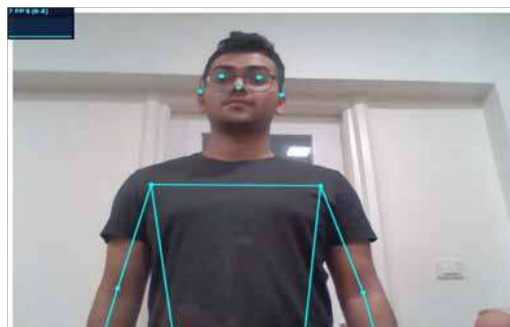


Fig. 3. Optimal joint angles(shoulder)

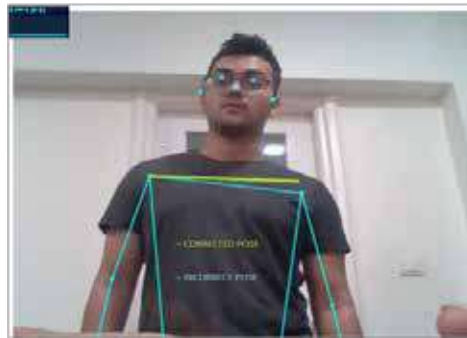


Fig. 4. Optimal joint line to be coincided for correct posture

COSTING

Since there is no requirement for specific hardware, and the architectures being open sourced, no cost is required to develop the application. Storing the datasets in the cloud may require some additional costs. The most part of the expenses would come from developing the data sets according to the medical standards as it would require a lot of people to volunteer to help contribute to the images of the dataset.

FEASIBILITY AND CHALLENGES

Due to the vast support of Tensorflow over various platforms, the models are fairly simple to run on most devices and can be easily integrated on most application development interfaces/architectures. The challenge would be to develop such large datasets covering such vast categories of people and adhering to the optimal medical standards. The massive involvement of test subjects and medical professionals would require a great amount of effort. Moreover, storing and preparing such quantities of data would prove to be a challenging task.

CONCLUSION

Post-surgery recoveries have a bigger role in the patient's health than the surgery itself as the effects of an incomplete recovery can be severe and permanent like restricted physical capabilities, hampering movement or in worst cases, impairment. This study was focused mainly on modelling an accurate solution that could be used by the patients as well as medical professionals to avoid complications post-surgery and correcting the after effects of surgeries. The solution concluded from the study was to leverage such a deep learning algorithm to build a program that analysed the operated body parts and suggested physical and surgical corrective measures. The patients can self-diagnose their conditions and can consciously try to correct it with the aid of the application thereby reducing the risks of incorrect joint postures and positions due to weakened muscles. Moreover, doctors can confirm successful surgeries using the application by analysing minute imperfections that may go unnoticed to the eye and basic tests. Although it would be challenging to develop the datasets for the algorithm, implementation and usage of the application would greatly contribute to the field of surgery recovery and positively affect millions of lives all over the world.

REFERENCES

1. The statistics of Tensorflow were taken from Tensorflow.org
2. The PoseNet algorithm structure was referred from PoseNet's official git repository <http://github.com/tensorflow/tfjs-models/tree/master/posenet>
3. Indian orthopaedic statistics were referred from <https://hhbc.in/orthopaedic-market-scenario-of-india/>
4. "Artificial intelligence for analyzing orthopedic trauma radiographs. Deep learning algorithms—are they on par with humans for diagnosing fractures?" by Jakub Olczak, Niklas Fahlberg, Atsuto Maki, Ali Sharif Razavian, and others.
5. Deep learning predicts hip fracture using confounding patient & healthcare variables by Marcus A. Badgeley, John R. Zech, Luke Oakden-Rayner, & others. <https://www.nature.com/articles/s41746-019-0105-1>
6. Artificial neural network analysis of bone quality DXA parameters response to teriparatide in fractured osteoporotic patients by Carmelo Messina, Enzo Grossi, Luca Petruccio Piodi, Maria Luisa Bianchi and others. <https://doi.org/10.1371/journal.pone.0229820>



Development of a Deep Learning Model for Analysis and Prediction of Sepsis condition

Melvin M, Banu Rekha B*

Department of Biomedical Engineering, PSG College of Technology, Peelamedu, Coimbatore, Tamil Nadu

✉ banurekha.cbe@gmail.com

ABSTRACT

Sepsis occurs while the body's internal fighting mechanism is activated against infections but it attacks the internal organs. It is a life threatening condition that can lead to localised or system-wide infection. Sepsis is difficult to identify at early stages, challenging the emergency and intensive care department. In this work, a Deep learning model is developed to predict sepsis condition before 11 hours of onset, that can aid the clinicians in early diagnosis and treatment planning. The dataset has been obtained from a public domain. The greatest challenge in this prediction model is the large number of missing data available in the dataset and the timing of prediction. While six hours or less is considered to be a golden standard for the prediction of sepsis, in this work, we have attempted to get the best possible accuracy for our method of data preprocessing. This foundational work can be explored and expanded with deep learning approaches to reduce the time window of prediction.

Keywords : Deep Learning; Sepsis; Long Short Term Memory; Imputation; Sequential classification.

INTRODUCTION

Sepsis is body's extreme reaction to an infection causing tissue damage, organ failure or death. It is estimated that globally, 31.5 million septic conditions arise every year [1]. While sepsis coexists with the existing medical conditions, it is necessary that sepsis is detected as early as possible to initiate antibiotic treatment. Hypotension is one of the outcome of septic condition and with hypotension conditions, the risk of mortality increases around 7% with every passing hour. Traditional clinical routines are ineffective in identifying the onset of septic conditions. Current research works carried out on vital signs data using machine learning techniques have explored the early identification of sepsis conditions.

In this work, the open source dataset of the clinical data collected from patients who underwent sepsis condition is considered. Due to the volume of data available, a deep learning method is attempted to predict the septic condition. The initial part of the research work focuses on detecting the missed data and performing the imputation. Using the data thus generated, we aim to develop a model to predict sepsis condition 12 hours ahead of its occurrence.

EXPLORATORY ANALYSIS OF DATA

The data was obtained from by Physionet repository. The Computing in Cardiology Challenge 2019 [2] was based on the database collected from patients who underwent sepsis condition. The dataset consists of 40,336 records with 40 various parameters of vital signs, laboratory test values and demographics. The exploratory data analysis performed on the dataset shows that the data is imbalanced with 7% of patient data labelled as sepsis and the remaining data labelled as healthy. The analysis of data also revealed the occurrence of a large number of missing data. Out of the 40 attributes, only 4 attributes, viz., Age, gender, HospAdmTime and ICULOS were void of any missing data. **Fig. 1** shows the percentages of missing data in the various attributes.

METHODOLOGY

The methodology followed in this research work is as follows:

- Exploration of the dataset
- Identification of missing data
- Imputation of missing data
- Training of deep learning model
- Validation of the trained model

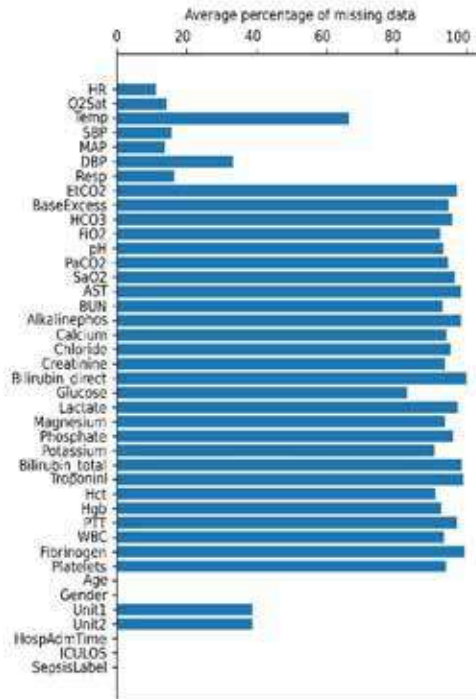


Fig. 1. Visualization of missing data in the CinC2019 Sepsis dataset

Pre-processing of Data

The dataset is prone to missing values (NaN). To process and model the data, The features with less percentage missing data, less than 92% is taken. **Table 1** represents the count of missing data. This leads to reduction in dimension of data from 40 dimension to 10 dimensions, Heart rate, oxygen saturation, temperature, systolic blood pressure, diastolic blood pressure, mean arterial pressure, respiration rate, age and gender are considered. To process the missing data in the extracted features random sampling imputation is performed. Using mean or median imputation can distort the normal distribution of the data when a feature has more missing values. To predict sepsis before 11 hours of onset, the 11 data points before the diagnosis of sepsis condition are considered. The significance of random sampling imputation is illustrated on a patient sample with highest recordings.

Table 1. Features with number of missing value

Features	Number of NaN
HR	8
O2Sat	11
Temp	227
SBP	10
DBP	10
MAP	10
Temp	71

Handling of Imbalanced data

Data imbalance can be addressed in several methods such as Over-sampling, Under-sampling, SMOTE method. Oversampling leads to overfit the data resulting in high variance. Undersampling can sometimes lead to information loss and underfit the model.

Synthesized Minority Class Oversampling Technique (SMOTE) learns [3] the topological properties of the neighbourhood of those data points in the minority class. It generates the virtual training records by linear interpolation for the minority class.

These synthetic data are generated randomly selecting one or more K- nearest neighbours for each data point in minority class. The following plots is a scatter plot between two most correlated features with and without SMOTE.

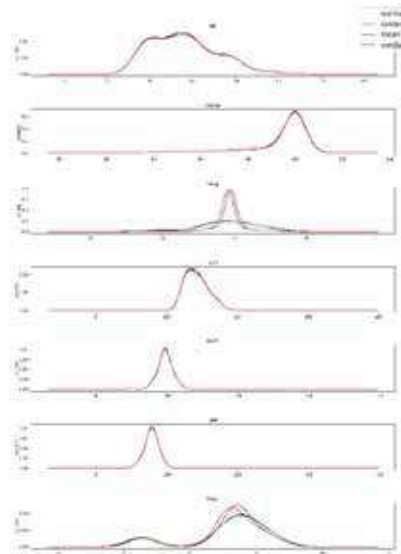


Fig 2. Comparison with various imputation methods

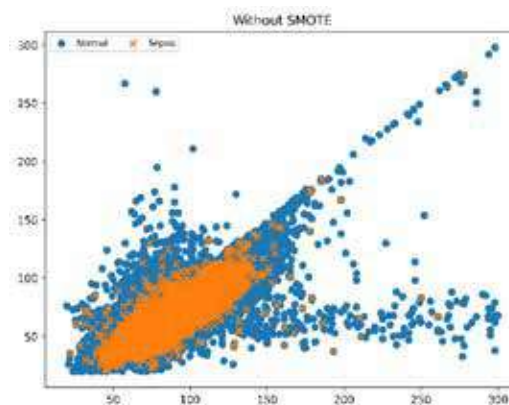


Fig 3(a). Scatter plot of SBP and DBP before SMOTE

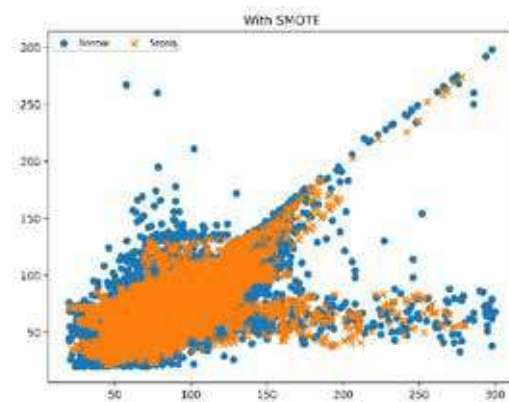


Fig 3(b). Scatter plot of SBP and DBP after SMOTE

SMOTE keeps the majority class (normal) data as much and over samples the minority class (sepsis) to the number of majority class by selecting the K neighbour data points in minority class, so the algorithm is less likely to over fit. **Fig 3** provides the effect of SMOTE on the data.

Architecture of the Learning Model

After pre processing and data augmentation the data is up-sampled to 59,740 files. The data was split as 80:20, 80% training: validation split. The input matrix of shape (47792,11,9) is fed to the model. Table II provides the features of the deep learning model.

Table 2. Model architecture

Layers	Nodes	Input shape	Output shape
LSTM	32	(None,11,9)	(None,11,32)
Dropout (probability=0.1)		(None,11,32)	(None,11,32)
LSTM	32	(None,11,32)	(None,11,32)
Dropout (probability=0.1)		(None,11,32)	(None,11,32)
LSTM	64	(None,11,32)	(None,11,64)
LSTM	64	(None,11,64)	(None,11,64)
Conv1D (kernel size=11)	64	(None,11,64)	(None,1,64)
Flatten		(None,1,64)	(None,64)
Dense	32	(None,64)	(None,32)
Dense	10	(None,32)	(None,10)
Dense	5	(None,10)	(None,5)
Dense	1	(None,5)	(None,1)

A combination of Recurrent Neural Networks and Convolutional Neural Network is used to train the data. The Recurrent Neural Network consists of 4 layers of LSTM stacked to fetch the temporal features in the time series data. The hyperbolic and sigmoid are used for activation and recurrent activation function respectively. Convolutions are useful to extract features with less trainable parameters. One dimensional convolution are used to reduce and extract information from each time step, ReLu activation is used. Three layers of Dense neurons are stacked followed by the convolutional layer. To avoid vanishing gradient ReLu is preferred as activation function. To predict the sepsis condition a neuron with sigmoid activation function is used.

Training of the Model

To avoid over fitting, two Drop outs each with dropping probability of 0.1 is inserted between the RNN. Kernel L2 regularization

is performed on all layers except the last neuron with regularizing parameter = 0.001.

The model was trained on 70,000 epochs with mini batch size of 64 samples, The model uses RMSprop optimizer with learning rate 0.000001 for optimization. The binary cross entropy is the loss function to be optimizer during training. Figure 4 provides the Training and validation accuracy and the corresponding loss.

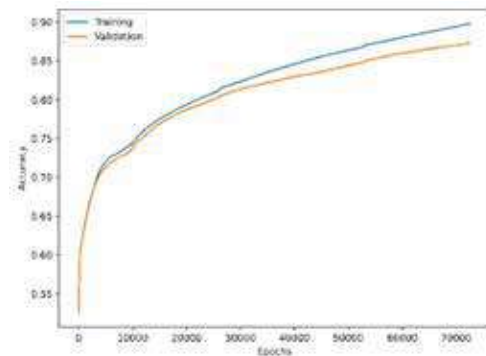


Fig 4(a). Training and Validation accuracy

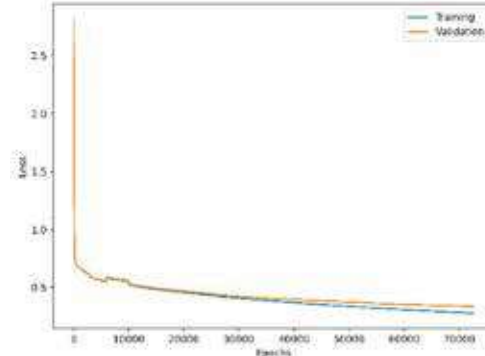


Fig 4(b). Training and Validation loss

RESULTS AND DISCUSSION

In this work, a total of 59,740 samples are augmented from 40,336 patients from which 47,792 samples were used as training set and 11,948 samples were used as validation set. The model achieves 92% of training accuracy and AUROC 0.92 for training set. **Table 3** shows the metrics for the test data at the end of 70,000 epochs.

Table 3. Test data metrics at the end of 70000 EPOCHS

Accuracy	0.87
Loss	0.33
Precision	0.83
Recall	0.95
AUROC	0.87
F1 Score	0.88
Specificity	0.80

Recurrent Neural Networks can be useful in extracting features from time series data and Convolutional Neural Networks are useful in feature extraction. Instead of ensemble learning using different net within the same architecture yields good results. **Fig 5** provides the performance of the deep learning model through the ROC and Precision-Recall values.

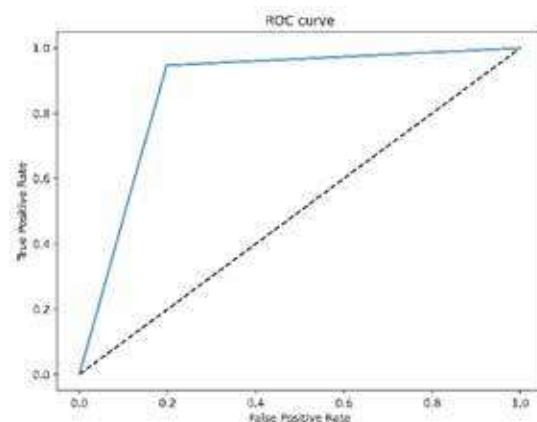


Fig 5(a). Receiver operating characteristic curve(ROC)

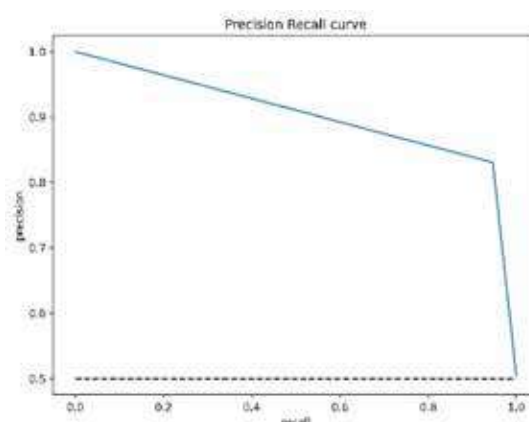


Fig 5(b). Precision recall curve



CONCLUSION

In this paper a model is developed which can predict the onset of sepsis before 11 hours. The model predicts good results even with uncleaned environment (missing values). The data processing pipeline can handle missing data and can predict sepsis in real time environment for early diagnosis and treatment. The model can be further optimized by hyper parameter tuning for better results.

REFERENCES

1. Fagerström, J., Bång, M., Wilhelms, D. et al. LiSep LSTM: A Machine Learning Algorithm for Early Detection of Septic Shock. *Sci Rep* 9, 15132 (2019). <https://doi.org/10.1038/s41598-019-51219-4>
2. Seyna, M., Josef, C., Jeter, R., Shashikumar, S., Moody, B., Westover, M. B., Sharma, A., Nemati, S., & Clifford, G. (2019). Early Prediction of Sepsis from Clinical Data -- the PhysioNet Computing in Cardiology Challenge 2019 (version 1.0.0). *PhysioNet*. <https://doi.org/10.13026/v64vd857>.
3. Blagus, R., Lusa, L. SMOTE for high dimensional class-imbalanced data. *BMC Bioinformatics* 14, 106 (2013). <https://doi.org/10.1186/1471-2105-14-106>

Facial Expression based Pain Monitoring in Hospital environment using Compact Convolutional Network

Ashish Semwal, Narendra D Londhe*

Department of Electrical Engineering, National Institute of Technology, Raipur, Chhattisgarh

*✉ nlonche.ele@nitrr.ac.in

ABSTRACT

Pain is a feeling of physical discomfort, and its assessment is known to be a crucial factor for medical diagnosis and pain management. Presently, subjective methods are used for pain assessment such as self-report which might provide inconsistent results. Therefore, several automated techniques have been proposed by the researcher in the recent past for pain assessment using facial expressions. However, current techniques for pain assessment utilizes very deep neural networks. Utilizing deep networks are prone to overfitting and computationally expensive. Therefore, in this study, a Compact Pain Assessment Network (C-PANet) has been proposed. To enhance the model performance first a VGG based deep model has been trained using an online pain dataset. Moreover, the knowledge of this network has been transferred to a much compact network. The compact network is consists of the Global Average Pooling (GAP) layer. Further, various data augmentation techniques are used to enhance the generalization of the implemented model. Further, we have also carried out extensive experiments to validate the proposed system. The proposed pain assessment system has been validated on a self-generated pain dataset of 10 patients recorded in the hospital. The experimental results demonstrate that the proposed method has achieved F1-score of 0.88 and AUC of 0.98.

Keywords : Patient monitoring; Deep learning; Computer vision; CNN; Fully Connected Network; network pruning..

INTRODUCTION

Pain is an unpleasant feeling and its assessment is very crucial for pain management and diagnosis of diseases. At present, subjective techniques are used for pain detection and assessment such as self-report and expert observation. However, such techniques are highly subjective and required proper communication between healthcare experts and patients. Hence, pain assessment based on self-report may provide inconsistent outcomes. Furthermore, in the case of infants and impaired patients self-report is not feasible. Therefore, in the recent past techniques based on objective methods are gaining more attention. In objective approaches, facial expression based automated pain assessment has been explored widely by researchers. This is because the facial expressions convey rich information related to pain[1]. However, previous pain assessment systems are trained on the dataset recorded in a highly constrained lab environment. Pain assessment based on facial expressions is still a challenging computer vision problem due to poor lighting conditions, variability in facial expressions, and partially occluded faces. Moreover, the current pain assessment systems are trained on the face images from the UNBC MacMaster dataset [2] which is collected in lab settings as shown in Fig. 1 (a). It can be observed that the dataset contains high-resolution frontal face images. Moreover, the head pose is almost constant. The 2nd sequence represents the dataset collected in a hospital environment. Form the 2nd sequence it can be observed that there are high variations in head pose, illumination conditions. Moreover, the faces are not frontal. Because of the above-mentioned challenges pain detection is one of the challenging tasks in wild.



Fig. 1. Some of the images from a) the UNBC dataset b) self-created dataset. The yellow and red bounding box represent the corresponding head-pose

Literature Survey

Various research work has been carried out for pain detection using facial expression in the recent past. In this regard, the first work reported by Lucey et al. with the release of the UNBC-McMaster pain dataset[2]. They have trained an SVM classifier by utilizing landmark-based features. Further, Irani et al. [3] used separable steerable filters for pain detection. Further, Pedersen et al. [4] used a technique in which first faces are warp into frontal faces using AAM [5] and then a linear SVM has been trained. Nesov et al. [6] used SIFT features and trained SVM classifier for pain detection. Most of the previous approaches have utilized handcraft features with conventional machine learning techniques. Conventional machine learning requires carefully selected hand-engineered features which is time-consuming task. Therefore, recent works have utilized deep learning-based techniques for pain assessment due to their success in various computer vision applications[7, 8]. Given that, Zhau et al. has utilized RNN based network to learn temporal dependencies for pain assessment. A VGG-16 and LSTM based network is used for pain detection by Pau et al.[9]. Further, Bargshedy et al. [10] used a technique based on CNN-BiLSTM to classify pain intensities. The problem with the above-mentioned deep learning approaches is that they utilize a very deep network with a large number of trainable parameters. It has been observed that the deeper network has two main drawbacks; 1) problem of overfitting 2) computationally expensive. It has been observed [8] that a model with a large number of trainable parameters leads to overfitting. Moreover, the fully connected layer in VGG-Net increases the number of trainable parameters [11] which might affect the network performance. network pruning has been utilized widely in the recent past to compress the deeper model[12]. The layer-wise pruning is a technique in which the redundant layers are removed empirically. Therefore, in this study, a layer-wise pruning approach is utilized to compress the deep model. For this purpose, the author has proposed a GAP [13] based technique that can reduce the number of parameters in a CNN model. GAP based techniques are used in fully convolution network for localization[11]. It helps to reduce the parameters by taking the average of each feature. The compact networks might be useful for pain diagnosis in mobile devices.

The methodology has been described in Section I. Further, experimental details are presented in Section II. Section 3 described the results and discussion. Finally, the paper has been concluded in Section 4.

METHODOLOGY

In this section, we have presented the overall methodology of the proposed C-PANet for pain assessment. The overall methodology of the proposed pain monitoring system is depicted in Fig. 2.

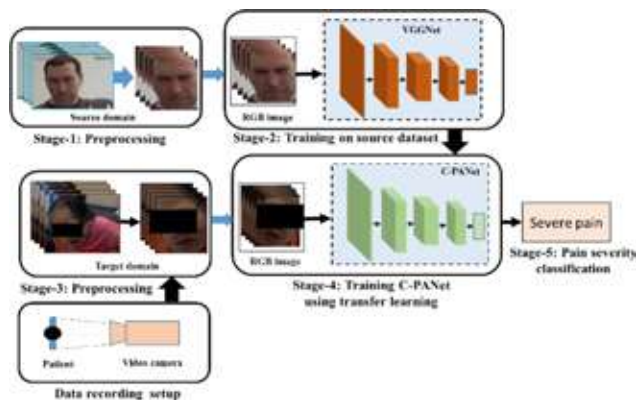


Fig. 2. The methodology of the proposed pain monitoring system

The methodology of the proposed system is consists of 5 stages. In the 1st stage, the face has been localized and cropped to remove the unwanted region. Further, a VGG-16 based network has been trained using the source dataset namely, the UNBC-McMaster dataset. In the 3rd stage, the face has been localized and cropped to remove the noise from the self-generated dataset. Moreover, the cropped faces are provided to a GAP based network by utilizing pre-trained VGGNet weights. Once the network has been trained the pain has been classified in the final stage. Note that the mode of training has been completed offline. However, pain monitoring can be accomplished using a trained C-PANet model.

Dataset Details

In this study, we have utilized 2 datasets. The first dataset is called the UNBC-McMaster dataset which consists of pain images of 25 patients suffering from shoulder pain. Moreover, a second dataset has been utilized which has been acquired at DKS

hospital Raipur C.G. India. The patient data is recorded by a Sony AX700 video camera. Before starting the video recording patient consent form and information sheet have been given to each patient. After that, the video of patients has been recorded for about 3 minutes duration. Moreover, the videos are annotated based on self-report and observation of the medical expert. All the video frames are then categorized into 4 classes namely, no pain, moderate pain, severe and very severe pain as shown in **Table 1**.

Table 1. Class-wise data distribution

Class label	Class name	Number of samples
0	No pain	11321
1	Moderate	3158
2	Severe	1460
3	Very severe	571

Preprocessing

In this work, we have employed face detection and cropping based preprocessing before training the proposed system. In order to detect face from input images, a multi-task CNN [14] based pre-trained model has been utilized. After detecting the face from input images each face has been cropped using their coordinate values (i.e., bounding box data).

Pain severity assessment using transfer learning

Deep neural network-based networks are generally trained using similar data distribution. However, in some cases, training data might be collected in different scenarios (i.e., using distinct sensors, different environments). This leads to a domain shift in the collected data which causes variations in the target dataset. Additionally, to train a neural network model large dataset is required to improve the model generalization. Transfer learning-based techniques are utilized widely in the recent past to alleviate such problems[9, 15]. Therefore, in this study VGG-CNN based source model has been trained on a larger dataset namely, UNBC-McMaster. Once the model has been trained the best weights are saved to utilize for transfer learning. For the second dataset, we have implemented a compact network namely C-PANet based on GAP. The C-PANet is a modified version of the VGG-16 network. In order to make this network compact some of the redundant FC layers have been removed. The Fully Connected (FC) layer at the output of the VGGNet has been replaced with the Global Average Pooling (GAP) Layer. It is worth noticing that the neurons in the FC layer are connected to a global region instead of the local region. As a result, the number of parameters in the GAP base network is significantly lower than FC based network. The architectural details of the proposed model are described in the subsequent section. The layer-wise values are presented in **Table 2**.

Table 2. Architecture details of proposed C-PANET

L. No.	Layer	Filter size	Output shape
L ₀	Input layer	-	(128,128,3)
L ₁	Conv1_1	(3,3)	(128,128,64)
L ₂	Conv1_2	(3,3)	(128,128,64)
L ₃	MaxPool-1	(2,2)	(64,64,64)
L ₄	Conv2_1	(3,3)	(64,64,128)
L ₅	Conv2_2	(3,3)	(64,64,128)
L ₆	MaxPool-2	(2,2)	(32,32,128)
L ₇	Conv3_1	(3,3)	(32,32,128)
L ₈	Conv3_2	(3,3)	(32,32,128)
L ₉	Conv3_3	(3,3)	(32,32,128)
L ₁₀	MaxPool-3	(2,2)	(16,16,256)
L ₁₁	Conv4_1	(3,3)	(16,16,512)
L ₁₂	Conv4_2	(3,3)	(16,16,512)
L ₁₃	Conv4_3	(3,3)	(16,16,512)
L ₁₄	MaxPool-4	(2,2)	(8,8,512)
L ₁₅	Conv5_1	(3,3)	(8,8,512)
L ₁₆	Conv5_2	(3,3)	(8,8,512)
L ₁₇	Conv5_3	(3,3)	(8,8,512)
L ₁₈	MaxPool-5	-	-
L ₁₉	GAP	-	(512)
L ₂₀	Dense	-	(4)

Convolutional layer

The implemented model for pain assessment consists of 20 layers. The 1st layer of the proposed network is consists of a convolutional layer which has been represented by L1 as shown in Table II. A stack convolutional operation has been used along with ReLU and maxpooling to extract rich features related to pain. The convolution operation is calculated as follows:

$$Cn_{ij} = f \left(b_{ij} + \sum_{m=0}^{l-1} \sum_{n=0}^{l-1} (X_{i+m,j+n}) * W_{mn} \right) \quad (1)$$

where; Cn_{ij} = output of the first layer. b_{ij} = bias term, X = input matrix, W_{mn} = weights.

The stacked convolution has been performed for other layers by using (1). In our implemented network the number of filters has been doubled for each convolutional block. Note that convolutional operation with max-pooling extracts hierarchical features while the final layer (i.e., FC layer) is used for classification purpose.

Global Average Pooling (GAP)

Previous studies have shown that a network with huge parameters has the problem of overfitting[11]. Moreover, each node in the FC layer is connected to previous nodes. This leads to an increment in trainable parameters. Therefore, in this study, we are using the global average pooling (GAP) layer. GAP layer simply takes the average of each feature map and then the output is directly fed to the FC layer followed by the softmax layer. The problem of overfitting can be reduced using GAP since there is no parameter to optimize in this layer. Therefore, if there are spatial translations of the activations the GAP layer is more robust for that scenario. Once the network has been implemented the weight of the network has been updated using the backpropagation algorithm. The output of the softmax function provides different probability values for the final classification task. Since we have four classes a vector of four probabilities has been obtained. Suppose the probabilities are defined by p_1 , p_2 , p_3 , and p_4 for four classes. The pain intensities can be obtained as follows:

$$Y_{cls} = \text{argmax}(P_1, P_2, P_3, P_4) \quad (2)$$

EXPERIMENTAL SETUP

In this work, to train the deep learning model Keras [16] library is used. Data loading and preprocessing has been done by the OpenCV [17]library. All the experiments are carried out in an HP workstation with an NVIDIA graphics card with 32 GB of RAM. In this work, 2 experiments are carried out. In the first experiment, the source model has been trained using the UNBC dataset. Moreover, in the second dataset, the C-PANet has been trained using transfer learning.

Before training the proposed networks for pain assessment, first, the images are resized to 128×128. Furthermore, the dataset has been normalized between 0 and 1. Further, the dataset has been categorized into training and testing. For this purpose, 80 % of the data has been used for training and 20 % of the data is used for testing. Moreover, each model has been fine-tuned with 80 % of the training dataset using the stratified k-fold cross-validation technique. Finally, the held-out 20 % testing dataset is used to validate the generalization of the trained model. Note that after fine-tuning only the best weights have been utilized for the final prediction for the held-out test dataset. The learning rate of 0.0008 has been used for all the networks. Moreover, the batch size of 64 is used and networks have been trained for 30 epochs. Note that data augmentation such as rotation and horizontal flipping is used during training to improve generalization.

RESULTS AND DISCUSSION

In this section, we have presented the results of carried of experiments for pain assessment. Each implemented model has been validated using various metrics such as Precision, recall, and F1-score. F1-score is utilized to evaluate the model because it provides a better evaluation if the dataset is imbalanced. From **Table 3** it can be observed that the proposed C-PANet for pain assessment has achieved an average precision of 0.91 recall of 0.86 and F1-score of 0.88. From the evaluation metrics, it can be observed that the model has achieved encouraging results even in the challenging unconstrained hospital environment.

Table 3. Evaluation metrics for proposed C-PANET

Average	Precision	Recall	F1-score
Macro	0.91	0.86	0.88

Furthermore, to observe the effect of each class on the average performance, we have analyzed the class-wise performance of

the proposed system. From **Table 4** it can be observed that the class “0” which is no pain class has achieved Precision of 0.91 recall of 0.98 and F1-score of 0.94.

Table 4. Class-wise performance metrics of C-PANET

Class	Precision	Recall	F1-score
0	0.91	0.98	0.94
1	0.90	0.69	0.78
2	0.97	0.80	0.88
3	0.85	0.96	0.90

Further, we have analyzed the Precision-recall (PR -curve) curve for the proposed pain assessment system as depicted in **Fig. 3**.

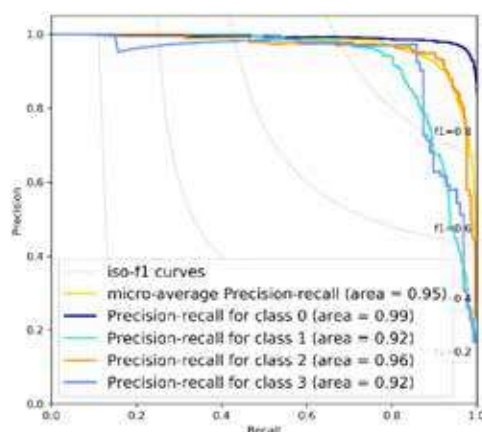


Fig. 3. Precision recall curve of the proposed pain assessment system

The PR-curve is a useful metric in the case of an imbalanced dataset. The trade-off between Precision and Recall can be represented by a PR curve using different threshold values. If the area under the PR-curve is high it represents high precision and recall. From **Fig. 3** it can be observed that for class 1 model has achieved PR value of 0.99. This indicates that the model can detect the no pain class accurately. However, the PR value for both moderate and very severe class the model has achieved lower PR values. The lower values of PR indicates that moderate and very severe class have less discriminative features.

Comparative analysis between GAP and FC based Network

To analyze the effect of GAP based model a comparative analysis has been carried out. To validate the effect of layer pruning two experiments are carried out. In the first experiment, the model has been trained using the FC layer. From **Table 5** it can be observed that the model trained with the FC layer has achieved a Precision of 0.92 recall of 0.86 and F1-score of 0.88. In our second experiment, the 2 FC layers have been removed and replaced by the GAP layer. As a result, the Precision of the network has been reduced slightly. However, the model has achieved comparable results. Additionally, it has been observed that the model trained with the GAP layer has reduced network parameters up to 14 %. Currently, the FC based network takes around 43 seconds to complete one training epoch, while the GAP based network takes around 39 seconds. This demonstrates that the implemented GAP based pain assessment model maintains a trade off between network complexity and performance.

Table 5. Comparison of FC and GAP based network

Class	Precision	Recall	F1-score
0	0.91	0.98	0.94
1	0.90	0.69	0.78
2	0.97	0.80	0.88
3	0.85	0.96	0.90

Comparative analysis with existing approaches

This section presents a comparative analysis of the proposed pain assessment system with existing approaches. Note that only recent works have been included in this study, for comparative analysis. To the best of our knowledge, the proposed system based on GAP based pruning has not been implemented previously for pain assessment. From **Table 5** it can be observed that

the work done by the researcher [2] have been used conventional machine learning technique which might fails if data size increase. Our proposed method has been trained using a fully automated method for pain assessment. Further, deep learning-based methods are used by [9, 10], but their implemented model has a large number of trainable parameters which might lead to overfitting and computation burden. From Table V it can be also observed that previous approaches are trained using the lab collected dataset. Such models might not work in unconstrained hospital settings for pain monitoring. Contrary, to previous work our pain assessment model, has been trained on challenging datasets acquired in hospital settings. Moreover, the proposed model has achieved F1- score of 0.88 and an AUC of 0.98. The encouraging results demonstrate the usefulness of the proposed pain assessment system in hospital settings for pain monitoring purposes.

Table 5. Comparative analysis of proposed method with existing approaches for pain assessment

Approach	Dataset	Metrics
SVM[2]	Lab collected	AUC: 0.83.9
CNNLSTM[9]	Lab collected	ACC:
BiLSTM[10]	Lab collected	F1: 0.89
C-PANet (ours)	Hospital dataset	F1: 0.88 AUC: 0.98

CONCLUSION

This work presents a fully automated pain monitoring system which can assess pain from face images. For this purpose, a compact CNN model has been proposed which utilized a pooling-based pruning strategy. The work demonstrates that the GAP based model not only reduces the computational burden but maintain the network performance of pain assessment. Further, we have also utilized a transfer learning approach to improve network generalization for the pain assessment task. The experimental results demonstrate that the model has reduced up to 14 % with about 1.0% loss in Precision on the self-created pain dataset. For the future other pain behavior parameters such as body movements and sound can be utilized with facial expression to improve the robustness.

ACKNOWLEDGMENT

The author would like to thanks the doctors at DKS Super Speciality Hospital Raipur for their valuable guidance during data recording. The author acknowledges the Science and Engineering Research Board (SERB), Government of India, for financial support vide Reference No. EEQ/2017/000470 to carry out this work.

REFERENCES

1. Prkachin, K.M., Solomon, P.E.: 'The structure, reliability and validity of pain expression: Evidence from patients with shoulder pain' Pain, 2008, 139, (2), pp. 267–274.
2. Lucey, P., Cohn, J.F., Prkachin, K.M., Solomon, P.E., Matthews, I.: 'Painful data: The UNBC-McMaster shoulder pain expression archive database', in 'Face and Gesture 2011' (2011), pp. 57–64
3. Irani, R., Nasrollahi, K., Moeslund, T.B.: 'Pain recognition using spatiotemporal oriented energy of facial muscles' IEEE Comput. Soc. Conf. Comput. Vis. Pattern Recognit. Work., 2015, 2015-Octob, pp. 80–87.
4. Pedersen, H.: 'Learning appearance features for pain detection using the unbc-mcmaster shoulder pain expression archive database', in 'International Conference on Computer Vision Systems' (2015), pp. 128–136
5. Cootes, T.F., Edwards, G.J., Taylor, C.J.: 'Active appearance models' Lect. Notes Comput. Sci. (including Subser. Lect. Notes Artif. Intell. Lect. Notes Bioinformatics), 1998, 1407, (6), pp. 484–498.
6. Neshov, N., Manolova, A.: 'Pain detection from facial characteristics using supervised descent method' Proc. 2015 IEEE 8th Int. Conf. Intell. Data Acquis. Adv. Comput. Syst. Technol. Appl. IDAACS 2015, 2015, 1, (September), pp. 251–256.
7. Szegedy, C., Liu, W., Jia, Y., et al.: 'Going deeper with convolutions', in 'Proceedings of the IEEE Computer Society Conference on Computer Vision and Pattern Recognition' (2015)
8. Dash, M., Londhe, N.D., Ghosh, S., Semwal, A., Sonawane, R.S.: 'PsLSNet: Automated psoriasis skin lesion segmentation using modified U-Net-based fully convolutional network' 2019, 52, pp. 226–237.



9. Rodriguez, P., Cucurull, G., Gonalez, J., et al.: 'Deep Pain: Exploiting Long Short-Term Memory Networks for Facial Expression Classification' IEEE Trans. Cybern., 2017, pp. 1–11.
10. Bargshady, G., Zhou, X., Deo, R.C., Soar, J., Whittaker, F., Wang, H.: 'Enhanced deep learning algorithm development to detect pain intensity from facial expression images' Expert Syst. Appl., 2020.
11. Tekchandani, H., Verma, S., Londhe, N.D.: 'Mediastinal lymph node malignancy detection in computed tomography images using fully convolutional network' Biocybern. Biomed. Eng., 2020.
12. Chen, S., Zhao, Q.: 'Shallowing Deep Networks: Layer-wise Pruning based on Feature Representations' 2018.
13. Zhou, B., Khosla, A., Lapedriza, A., Oliva, A., Torralba, A.: 'Learning deep features for discriminative localization', in 'Proceedings of the IEEE conference on computer vision and pattern recognition' (2016), pp. 2921–2929
14. Zhang, K., Zhang, Z., Li, Z., Qiao, Y.: 'Joint face detection and alignment using multitask cascaded convolutional networks' IEEE Signal Process. Lett., 2016, 23, (10), pp. 1499–1503.
15. Dou, Q., Ouyang, C., Chen, C., Chen, H., Heng, P.A.: 'Unsupervised cross-modality domain adaptation of convnets for biomedical image segmentations with adversarial loss', in 'IJCAI International Joint Conference on Artificial Intelligence' (2018)
16. Chollet, F., others: 'Keras: The Python Deep Learning Library. 2015' 2019.
17. Bradski, G., Kaehler, A.: 'Learning Open CV: Computer vision with the OpenCV library' (' O'Reilly Media, Inc.', 2008).



Secured Approach for One Umbrella Management System for Improving Healthcare Services

Dr S Tamil Selvi, B Ganapathy Ram, V S Preethashree

Department of Electronics and Communication Engineering, National Engineering College, Kovilpatti, Tamilnadu

✉ stsece@nec.edu.in

ABSTRACT

People living all over the world are directly or indirectly connected with health care services for monitoring and maintaining their health care records. In case of emergencies, patients are required to get the hospital services through doctors, pharmacy and clinical laboratories. Sometimes patients need to know the availability of doctors, availability of medicines in a pharmacy and their clinical records after doctors' validation in a secured manner. Sometimes patients need to carry their previous clinical reports while consulting with doctors. With the deployment of One umbrella Management system (OUMS), it is possible to integrate the various stakeholders such as doctors, patients, pharmacy, healthcare industry to meet out their requirements. The proposed OUM system facilitates the patient and doctor to visualize the history of medical records at anytime, anywhere in the world with two layer security. Only the authenticated user could able to access their data with the help of secured encryption and decryption techniques. The proposed architecture enables the patients to access the various services offered by hospital management system, pharmacy and clinical laboratories with their digital signatures and certificates in a cost effective manner.

Keywords : Health care information system, Two layer data security, Data access control, OUMS.

INTRODUCTION

COVID-19 pandemic has thought the human about the significance of maintaining stable and good health condition to tackle and to combat with the viruses. Maintenance of health condition requires periodic health checkups, analyzing the health records and undergoing proper medication/treatment during unhealthy conditions. All the above-said processes are taken care of by hospitals or health care centres. One of the most traditional methods followed for maintaining health record is a manual method, which includes paper and files. It is a very difficult and high time-consuming process which often requires large storage space. Electronic health record (EHR) replaced paper-based record creation and maintenance by storing the patient's health information (PHI) in the database. The patient's health records need to be accessed easily at any time from any location and also make patient's to analyze their health conditions to lead a healthy life.

A healthcare management system should not only be computer software that provides facilities to manage the hospitals but also to support increasing the efficiency of healthcare services. The main characteristics of online HIS comprise many important decisions which may need artificial intelligence. Decision-making process in the healthcare management system should be fast and accurate.

EHR is a large amount of data, which is very sensitive and affects patients' privacy and security if misused. Digitizing patient health records is having a danger on another hand, which may be stolen or misused by various intruders like organ smugglers, insurance agencies, employers, any entity intended in exploiting the data for personal gain. Exchanging health records of patients between various stakeholders of the healthcare system by connecting digital technologies existing in the healthcare management system, which brings major concerns to maintain confidentiality and privacy on the patient's record. Security and privacy are more important in EHR as important as Quality of service (QoS).

As technology is growing fast and the penetration of information and communication facilities in the healthcare sector, the HIS is facilitated through mobile devices. Healthcare service providers as well as patients are using mobile devices, which causes security breaches on both sides of PHI. A security breach can be done in two different ways that are attacking the network and brute force attack on data related to HIS. Network attacking is controlled by installing and maintaining the strongest cyber security infrastructure, which may incur a large cost. Data access control solutions are only a smart move to keep health data as secure as possible. Hence, in this paper, the PHI is accessed with strong double-layer encryption using public and private keys, along with digital signature and certificate for secured data access control over the internet.



Rest of this paper is organized as follows. Section 2 deals with studies and analysis of healthcare information system developed or portrayed in various literatures. Proposed methodology is explained in the section 3. Experimentation with detailed specifications are represented in the section 4. Section 5 portrays the results and discussion on the research done for implementing the proposed data access control mechanism. In the section 6, conclusion is arrived and future scope is predicted.

LITERATURE SURVEY

In [1], a secured EHR system is developed to track and monitor the health condition of the patient in order to make prior decision to avoid chronic disease. In addition, it reduces the patient's time to consult with healthcare providers. The ultimate objective of this paper is to provide quality of care in better way where patient is allowed entering their personal data and it can be seen at the time of hospital visit and real time basis. Depending on the data, the report is generated and stored in secure manner. Cloud based patient health record (PHR) system by creating clinical document architecture (CDA) is analyzed in [2]. CDA is developed to make decision to cure major disease for a clinical support system and it is designed as a mobile application. In this paper, both PHR and EHR are integrated as per the medical standards such as HL7 and ICD-9-CM. Static CDA is developed to store permanent data such as personal information, contact detail, blood types, etc, and dynamic CDA is developed to store temporary data such as blood pressure and sugar level. Cloud based real time storage of health record for Indian healthcare needs is described in [4]. Clinical record of outdoor patient record is maintained for 5 years and indoor patients record is maintained for 10 years therefore EHR is used to maintain for once own life time. This paper mainly focusses on to ensure security and privacy into mobile network based on cloud management system. Healthcare data is encrypted and stored in a third party server.

Literature [6] addresses the practical implementation of EHR Server framework for Open EHR standard and its support in the clinical treatment of Chikungunya by the Brazilian Government and health service non-public providers. Electronic Patient Record (EPR) in the Health Information Systems (HIS) of a sanatorium is accessible whenever and wherever required by considering various measures like proprietary systems engineered with different design, business rules, info technologies and models, additionally to incompatible clinical language. [8] deals with smart healthcare monitoring system via internet of things to collect and to monitor health information. Authors designed this system to collect data of health via wearable devices through application programming interface (API) technology using open source front end web application development technologies such as Hyper Text Markup Language (HTML), JavaScript, back end hypertext preprocessor and MySQL database management systems. The health information is retrieved using application programming information (API) and it act as healthcare advice system. Monitoring the continuous patient's health care after discharge from hospital is briefed in the research article [10]. The internet based electronic medical record (EMR) is designed with assorted functions such as template function, log and medical record query function, record writing function, system configuration function and quality control function. A platform is developed to establish communication between patients and healthcare experts where information is stored in database and can be viewed whenever it requires for further treatment.

The information shared between doctor and patient is very sensitive there is in need of security to keep data very confidential and private. The essentials of maintaining confidentiality, privacy and security of patient's EHR are studied in [13]. A system is developed to allow doctors to upgrade data in database through their authentication credentials and to allow patients to see their data by private key through digital signature. In the paper [14], block chain-based Personal health record (PHR) system is developed with the system components like Ethereum, proxy re-encryption, trusty oracles, reputation systems, and Inter Planetary File System (IPFS). It allows patients to have a control over their medical records with certain authentication to maintain privacy and security access. The accuracy and correctness of maintaining PHR using Ethereum block chain –smart contracts is also validated. [15] addresses to demonstrate the use of simulation tool to balance the hospital resources to reduce waiting time of patients through interfacing graphical features for decision making.

PROPOSED METHODOLOGY

In this paper one umbrella approach is proposed to share the data pertaining to healthcare information services with various stakeholders of Healthcare industry such as doctors, nurses, patients, hospital management, authorities of clinical laboratory/ diagnostic Centre, and pharmacy in a secured manner under one umbrella infrastructure[3,5]. Special care is taken to develop one umbrella approach by not altering the existing infrastructure of the healthcare services to save the huge installation and operational cost of the healthcare service providers.

One Umbrella Architecture

The existing information and communication facilities in the hospital to implement HIS are computer systems, network

switches/routers for wired communication and Wi-Fi access points for wireless communication. The stake holders may have digital tablets, smart phones which are connected with internet through gateway. These infrastructures can be utilized in an efficient way to form one-umbrella architecture to integrate the stake holders. The one umbrella architecture is illustrated in Fig. 1.

EHR is very essential in tracking and monitoring the patients health conditions continuously in order to make prior decision making in diagnostic process or therapeutic process. The requirements must be taken into account such as,

- 1) Smart Devices: Smart devices generally connected to another platform via wired and wireless protocols such as Ethernet and Wi-Fi.
- 2) Gateway: It is a networking hardware used for communication that allows the data to transfer. It allows connecting huge network for multiple access either through wired or wireless protocol.

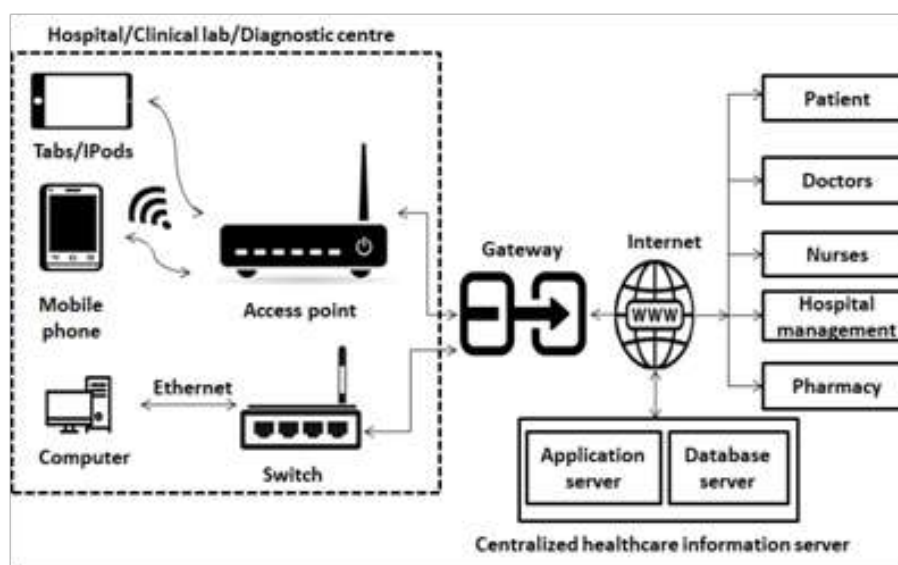


Fig. 1. One Umbrella Architecture

- 3) Server: Server, which provides data to other device and to serve data via local area network (LAN) through switches/access points and wide area network (WAN) over the internet via gateway.
 - Application Server: It is a server which consists of both hardware and software to run OUMS web application. It is served by the HTTP protocol with secured digital signatures and certificates. It compiles the application server side scripts and generate client machine understandable HTML format which can be viewed in web browser. Application Programming Interfaces (APIs) are installed in the server to transact the data with the relational database management system (RDBMS). The performance of the application server is ensured with various hardware configurations such as processor, random access memory (RAM), etc. Also server side scripts run on this application server should be optimized to reduce the processing time.[7,9].
 - Database Server: It is a server software which runs a RDBMS. This server is used to store, update and retrieve the patient's information and health records in a secured manner.

Flow of Web Application

Web application is an open framework where the patient, physicians and other health care providers can communicate each other on real-time whenever necessary by simply registering. Based on patient medical report digital prescription is given to the patient depending on the health problems. The process of flow for the operation designed for web application is shown in Fig. 2.

HTML is a standard markup language which is used for the front end for developing web application. It is assisted by CSS and scripting languages such as Bootstrap and JavaScript to create attractive web pages. On other hand .NET web framework is used as back-end framework as a web application.

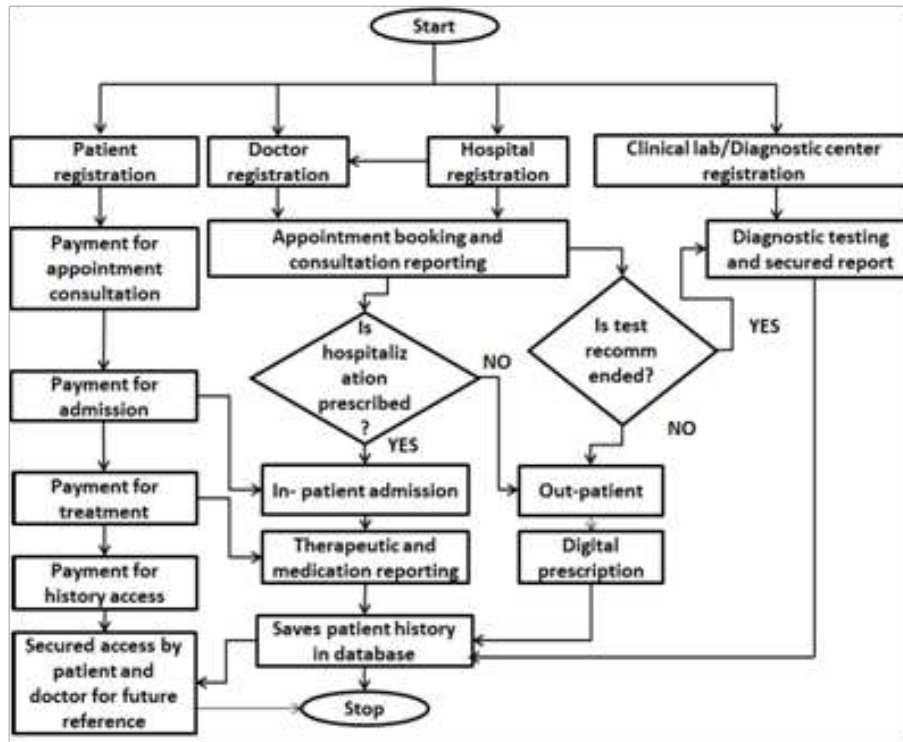


Fig. 2. Process flow for web application

Security and privacy

Advancement in technology security and privacy is most important in the EHR. The system can be accessed through a web portal by health care providers where it requires confidential information. So it can able to keep safe from unauthorized access. The security and privacy system is developed as shown in Fig. 3.

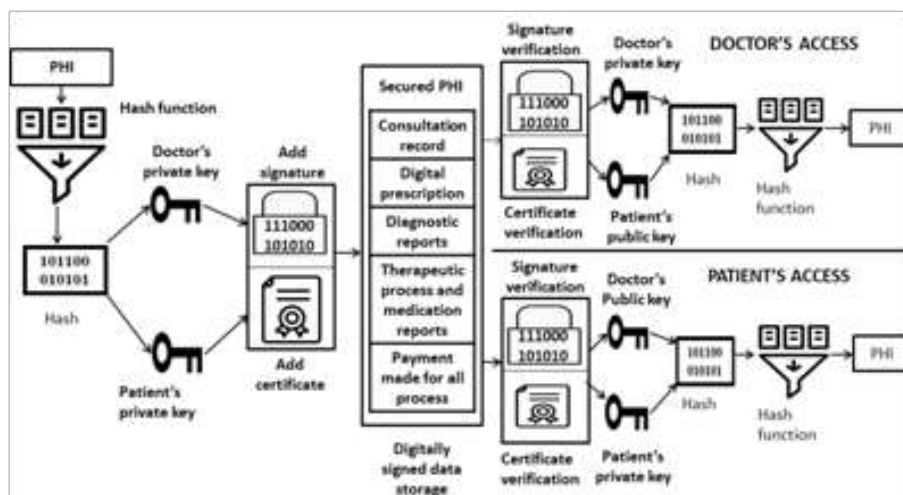


Fig. 3. Security and privacy structure

Security and privacy requirements must be taken into account such as,

- 1) PHI: Protected health information (PHI) is about any information regarding health conditions, the provision of health care status or payment regarding health care created by health institutions.[12]



2) Sign In

- Hash Function: It is one of the methods to encrypt the data. The arbitrary size of data is mapped in the form of the bit array in order to require fixed size.
 - Private Key: Both encrypted and decrypted data is allowed to share between patient's and health care providers of encrypted data.
 - Add Signature and Certificate: Signature act as secure lock and it requires a certificate. Both are compared to provide a digitally signed data.
- 3) Data Storage: Information regarding the patient's health status is stored in digitally signed data for secure manner. It consists of consultation record, digital prescription, the therapeutic process and medication reports, diagnostic report and payment made for all process.
- 4) Verification: Doctor's and patient's can access once digitally secured data by following the process as,
- Doctor's Access: A Public key is accessed by the patients and private key by doctors which is shared between two parties only are compared. Where encrypted data is converted into its original form known as decryption. If decrypt and encrypt are equal authorized person can access.
 - Patient's Access: A Public key is accessed by doctors and private key by the patients which is shared between two parties only are compared. Where encrypted data is converted into its original form known as decryption. If decrypt and encrypt are equal authorized person can access.

EXPERIMENTATION

The front end web application designing languages such as HTML, bootstrap styles, cascaded style sheets and java scripts are used to design graphical user interface for doctors and patients. ASP.net technology is used as the back end programming language to do data access control in the application server. MySQL RDBMS is used to store and retrieve the encrypted data .

Base64 is a MIME encoding scheme that encode binary to text, which represents binary data in an ASCII strong format. Translation is done through radix 64 for hashing the PHI.

Data encryption and secured storage algorithm for OUMS

- | | | |
|----------|---|--------------------------------------------------------------------------------------------------------------------------------------|
| Step (1) | : | First layer encryption is done on the patient health information using base 64 based hashing function |
| Step (2) | : | Second layer encryption is done using doctor's private key and patients private key to offer strong protection against data attacks. |
| Step (3) | : | Include digital signature and digital certificate for storing PHI in the secured data storage system. |

Data decryption and secured accession algorithm for OUMS

- | | | |
|----------|---|--------------------------------------------------------------------------------------------------------------------------------------------------------------------------------------------------------------------------------------------------------------------------------------------------------|
| Step (1) | : | Verify the digital signature and digital certificate for accessing the secured data storage in OUMS |
| Step (2) | : | Second layer decryption is done using doctor's private key and patients public key to read the base 64 encrypted hashed PHI if it is read by a doctor.

If the decryption is done by a patient, the doctor's public key and patients private key are used to decrypt and read base 64 hashed PHI |
| Step (3) | : | First level decryption is done using base 64 to binary data in order to recognize PHI for decision making in medication process. |

QR code based encoding and decoding procedure is used in the second layer encryption and decryption process to understand the public key of the patient during the doctor's access and the public key of the doctor using the patient's PHI data access.

RESULTS AND DISCUSSIONS

Table 1 shows the original PHI of a patient during the hematology test and the corresponding hashed value given to the second level encryption using private keys.

Table 1. Base 64 encrypted hash table for first level encryption

S. No.	PHI			hashed PHI
	Hematology Parameters	Observed Value	Units	Encoded HASH value
1	Hemoglobin	175	g/L	MTc1
2	Platelet count	350	$10^9/L$	MzUw
3	White cell count	10	$10^9/L$	MTA=
4	Red blood count	5.5	$10^{12}/L$	NS41

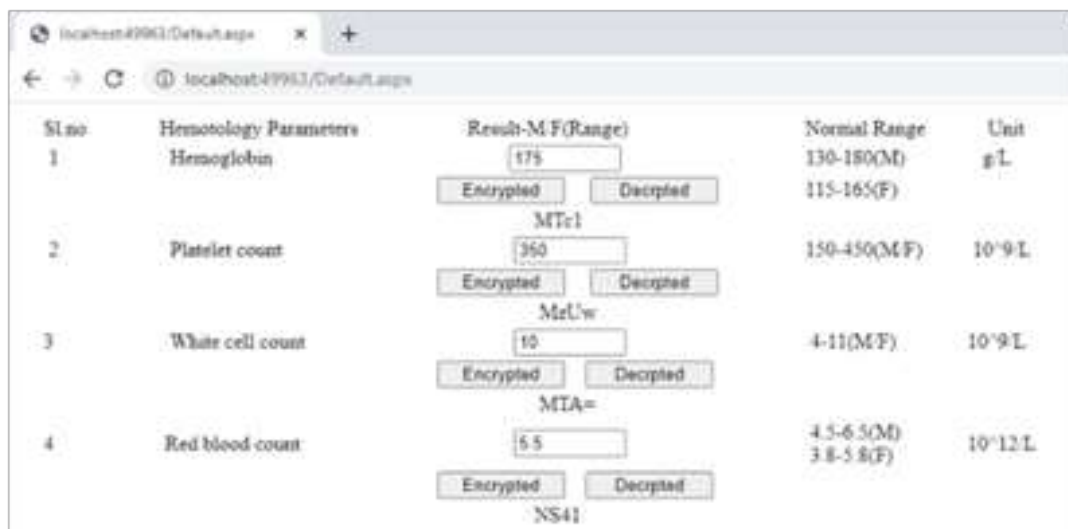


Fig 4. Screen shot of first level encryption and decryption

The public key of the patient and the public key of the doctors are encoded as QR codes which may be scanned by both the parties to provide high level of data security. It is portrayed in **Fig. 5**.



Fig 5. Screen shot for reading patient's public key

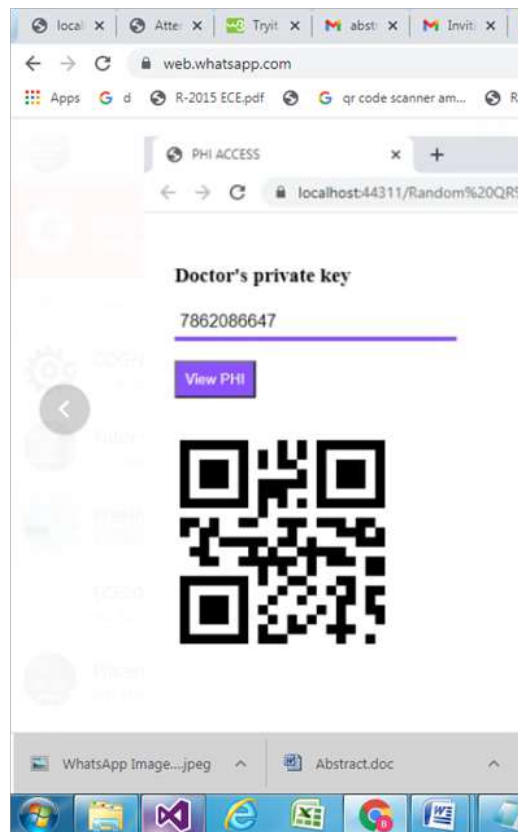


Fig 6. Screen shot for reading doctor's public key

CONCLUSION

The proposed one umbrella system has been established, implemented, and tested with private and public keys in a secured manner. In this paper, both patient and doctor could be able to send their data using their public and private keys. It is ascertained that unknown persons were not allowed to enter and view or manipulate the medical records of the intended user and thereby high confidentiality is maintained in the healthcare management services. Further the research will be extended to have HIS for healthcare imaging modalities also.

ACKNOWLEDGMENT

Thanks to National Engineering College Business Incubator for offering an Incubation support and funding to develop smart health care management system. This paper is a part of the above said startup program.

REFERENCES

1. Khan, Imran A. "Personalized electronic health record system for monitoring patients with chronic disease." In 2013 IEEE Systems and Information Engineering Design Symposium, pp. 121-126.
2. Yeong-Tae Song, Sungchul HonJ and Jinie Pak "Empowering patients using cloud based personal health record system." In 2015 IEEE/ACIS 16th International Conference on Software Engineering, Artificial Intelligence, Networking and Parallel/Distributed Computing (SNPD), pp. 1-6.
3. Hangaw Qader Omar, Abdulqadir Khoshnaw and Wrya Monnet. "Smart patient management, monitoring and tracking system using radio-frequency identification (RFID) technology." In 2016 IEEE EMBS Conference on Biomedical Engineering and Sciences (IECBES), pp. 40-45.
4. R. Kavitha, E. Kannan and S. Kotteswaran. "Implementation of cloud based Electronic Health Record (EHR) for Indian healthcare needs." Indian Journal of Science and Technology 9, no. 3 (2016): 1-5



5. Iuliana Chiuchisan, Doru-Gabriel Balan, Oana Geman, Iulian Chiuchisan and Ionel Gordin. "A security approach for health care information systems." In 2017 E-Health and Bioengineering Conference (EHB), pp. 721-724.
6. Fabio Gomes, Joao Paiva, Arthur Bezerra, Cesar Moura, Mauro Oliveira and Odorico Andrade. "MARCI: applied clinical record management: eletronic health record applied with EHRServer." In 2018 IEEE 20th International Conference on e-Health Networking, Applications and Services (Healthcom), pp. 1-6.
7. Day Nicole Jillian B., Karmelo Antonio Lazaro R. Carranza, Lawrence Matthew S. Lin, Albert R. Ponce, Wilbur Rex O. Reyes, Nilo T. Bugtai, and Renann G. Baldovino. "Design of a Web-based and Electronic Health Record Management System for Medical Teleconsultation." In 2018 IEEE 10th International Conference on Humanoid, Nanotechnology, Information Technology, Communication and Control, Environment and Management (HNICEM), pp. 1-5.
8. Siriwan Kajornkasirat, Napat Chanapai and Benjawan Hnusuwan. "Smart health monitoring system with IoT." In 2018 IEEE Symposium on Computer Applications & Industrial Electronics (ISCAIE), pp. 206-211
9. Wang Shuai, Jing Wang, Xiao Wang, Tianyu Qiu, Yong Yuan, Liwei Ouyang, Yuanyuan Guo, and Fei-Yue Wang. "Blockchain-powered parallel healthcare systems based on the ACP approach." IEEE Transactions on Computational Social Systems 5, no. 4 (2018): 942-950.
10. Xiaolan Hea, Lei Cai, Shiju Huang, Xiaoju Mac and Xueling Zhoua. "The design of electronic medical records for patients of continuous care." Journal of infection and public health (2019).
11. Harshini V M, Shreevani Danai, Usha H R and Manjunath R Kounte. "Health Record Management through Blockchain Technology." In 2019 3rd International Conference on Trends in Electronics and Informatics (ICOEI), pp. 1411-1415.
12. Okami, Suguru, and Naohiko Kohtake. "Transitional complexity of health information system of systems: managing by the engineering systems multiple-domain modeling approach." IEEE Systems Journal 13, no. 1 (2017): 952-963.
13. Saleem Waad Y. Bin, Hanan Ali, and Nouf AlSalloom. "A Framework for Securing EHR Management in the Era of Internet of Things." In 2020 3rd International Conference on Computer Applications & Information Security (ICCAIS), pp. 1-5.
14. Madine, Mohammad Moussa, Ammar Ayman Battah, Ibrar Yaqoob, Khaled Salah, Raja Jayaraman, Yousof Al-Hammadi, Sasa Pesic, and Samer Ellahham. "Blockchain for Giving Patients Control over their Medical Records." IEEE Access 8 (2020): 193102-193115.



Miniscule Payload Location in Least Significant Bit Stego Images using Transform based Image Denoising Cover Estimators

S Arivazhagan, E Amrutha, W Sylvia Lilly Jebarani, S T Veena, S Ananthi Roy

Centre for Image Processing and Pattern Recognition, Department of Electronics and Communication Engineering, MepcoSchlenk Engineering College (Autonomous), Sivakasi, Tamilnadu

✉ amrutha@mepcoeng.ac.in

ABSTRACT

Miniscule payloads are minute secret information in the form of binary bits hidden inside any cover image for the purpose of undercover communication by steganography. Steganography when misused by unlawful entities can pose a great threat to law enforcement agencies. Detection of such low volume payloads from a stego image is the very challenging task of steganalysis when there is no evidence of steganography method or any steganography tool used. Location of minuscule payloads is possible through sophisticated cover estimators and need not be necessarily in their logical order. In this paper an extraction technique is proposed, in which multiresolution transform based cover estimation is combined with weighted residual based location estimation to recover low volume payloads from stego images created with Least Significant Bit (LSB) steganographic schemes such as LSB-Replacement (LSBR), LSB-Matching (LSBM), LSBM-Revisited (LSBMR) and 2 bit LSBR (LSBR2). Among the various multiresolution transforms analysed, such as discrete wavelet, dual tree complex wavelet, ridgelet, curvelet, contourlet, shearlet, wavelet packet, and tetrolet, the dual tree complex wavelet transform is identified as the best transform to produce an accurate cover estimate of stego image and results in 85 % accuracy in locating payloads from stego image. Experimental results show that in order to locate payloads, lesser number of stego images containing payload in same locations are needed while using DTCWT for cover estimation.

Keywords : Image steganalysis; Wavelet Transform; Bivariate Shrinkage; Residual Extraction; Least Significant Bit Steganography; Payload Location.

INTRODUCTION

In digital image steganography, a cover image is used to hide a secret (or payload) through the use of embedding techniques namely Least Significant Bit (LSB) schemes, group-parity steganography, and matrix embedding to get a stego image. While embedding the payload, pixels in the cover image are modified in such a way that the modifications are imperceptible to a human eye. The job of a steganalyst becomes very difficult in a blind environment i.e., only suspicious stego images are at hand and no knowledge regarding the source of cover or size or location of payload. In such conditions, steganalysts assume a clairvoyant scenario [1]. Provided that the naive steganographer reuses the embedding key in order to locate payload in same pixel location and a large number of such stego images are available for a steganalyst, location of payload can be detected reliably without the knowledge of the original cover source. To achieve this goal, several steganalytic methods are developed to extract the hidden information.

The work was sponsored by Directorate of Extramural Research & Intellectual Property Rights (ER & IPR), Defence Research Development Organization (DRDO), Ministry of Defence, Government of India under Grant No. ERIP/ER/201702007/M/01/1733.

The first approach [2] is the identification of location of payloads with determined stego keys by brute force method (dictionary attack) with a trace from the image header. Fridrich et al. [3] proposed a chi-square based method to find the stego key by an exhaustive search of the de-noised image beside portions of the embedding path. When textured or noisy images having a large key space is used as cover, their method was not successful. Also, it required the embedding scheme to be known in advance.

The work was sponsored by Directorate of Extramural Research & Intellectual Property Rights (ER & IPR), Defence Research Development Organization (DRDO), Ministry of Defence, Government of India under Grant No. ERIP/ER/201702007/M/01/1733.

Ker [4] deployed a novel method of using weighted stego filters to determine the locations of payload for LSBR steganographic algorithm. This method requires large number of stego images (say 500 images) embedded with same stego key. Later, Ker and Lubenko [5] redeveloped the weighted averages residuals using Wavelet Absolute Moments (WAM) in the spatial domain to estimate locations of payloads for LSBM algorithm. For their work, several databases created using different camera sources were used for validation purposes. Luo et al. [6] proposed the residual method of identifying location of payload for LSBM with 2 and weighted l2 residuals. Though, only the sections of images and smaller images were considered in order to locate the payloads in low volume (1%). Then, Quach [7] developed a new method of estimating payload location using cover estimation techniques by Maximum likelihood A Priori (MAP) decoding and second-order statistical cover model to compute residuals for both LSBR and LSBM algorithms. Later, Quach [8] improved his work by tree pruning method to obtain an accuracy of 99.39% for LSBR and 92.34% for LSBM with 1000 images. Gui et al. [9] suggested a trivial modification to the earlier work, where estimation of cover was done in eight different directions instead of one for LSBM algorithm. Quach [10] proposed Markov Random Field (MRF) and MRF+MAP methods to estimate locations with fewer images and with higher precision for simple LSB and group parity steganographic schemes. But, all these methods required the knowledge of the cover source and needed a few thousand cover images to train the steganalyser to find the prior probabilities for cover estimation. Veena et al. [11] proposed an improved method of identifying location of payload using enhanced weighted residuals extracted from the stego and its estimated cover. The cover image is estimated from the stego image by a locally weighted bivariate shrinkage function in transform domain (Discrete Wavelet Transform (DWT) and Dual Tree Complex Wavelet Transform (DTCWT)). This method required only prior knowledge of relative payload size and only a few hundred stego images embedded with the same stego key. This method was extended to five spatial LSB variant schemes for five different payloads.

The success of payload location depends on the accuracy of the cover estimators. Various methods are used to estimate cover from the stego in a blind steganalysis process, the predominant being spatial domain filtering, wavelet filtering, Markov modeling and locally weighted bivariate shrinkage function using Wavelet transforms (DWT and DTCWT). The enhanced weighted residuals ensure that the transform domain method is universally applicable for detecting payload locations in spatial least significant bit stego images. The added advantage of this method is that it does not require any prior knowledge of the cover source or the embedding algorithm to determine the exact locations.

In this paper, performance of various cover estimators with multiresolution transforms such as discrete wavelet, dual tree complex wavelet, ridgelet, curvelet, contourlet, shearlet, wavelet packet, and tetrolet are analysed. From the estimated covers, payload location estimation is carried out using weighted residual extraction process.

The rest of the paper is organized as follows: Section 2 explains the proposed methodology; Section 3 provides the experimental setting and Section 4 presents the results and discussions. Section 5 concludes the research work with future scope.

PROPOSED METHODOLOGY FOR COVER ESTIMATION AND PAYLOAD LOCATION

The proposed block diagram for cover estimation and payload location is depicted in **Fig. 1**. The first step in the proposed method is to estimate cover image from a given stego image.

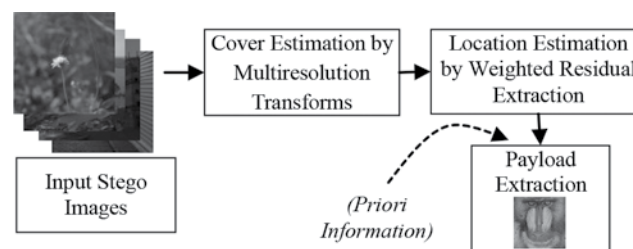


Fig. 1. Block Diagram of the Proposed Method

This process is similar to image denoising since steganography is purposefully adding a stego noise to an innocent cover. Image denoising is performed using multiresolution transforms to obtain a cover estimate. Under the Clairvoyant scenario, several stego images with same embedding key to hide payloads at same location are taken and their cover estimates are obtained. After the estimation of cover images, weighted residuals are calculated from stego and estimated cover images. From the weighted average residuals, locations of payload are identified that correspond to the estimated secret message length. Making use of a priori information i.e., stego key, from the extracted locations' pixels the least significant bits are retrieved and the hidden payload is obtained.

Cover Estimation by Image denoising Technique using Multiresolution Transforms

The estimation of cover from stego images is vital in order to extract payload locations. The process of cover estimation using locally weighted bivariate shrinkage function is depicted using a flow chart in **Fig 2**. Cover estimation can be considered as image denoising process since hidden payload is characterised as additive noise.

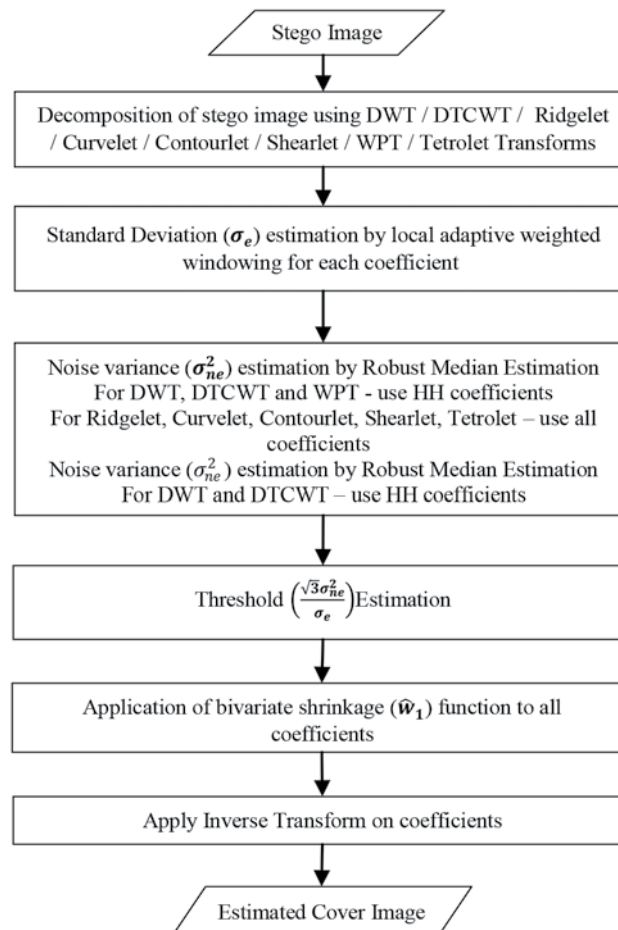


Fig. 2. Flow chart for Cover Estimation in the Proposed Method

In this paper, the stego images are subjected to different wavelet transforms (Discrete Wavelet Transform (DWT), Dual Tree Complex Wavelet Transform (DTCWT), Ridgelet, Curvelet, Contourlet, Shearlet, Wavelet Packet Transform (WPT) or Tetrolet) and the image pixels in spatial domain are converted into transform domain coefficients. DWT [12] is implemented as a set of high-pass and low-pass filter banks. At the cost of approximate shift-invariance, Kingsbury introduced the DTCWT [13], which has the added characteristic of Perfect Reconstruction and implemented as two separate two-channel filter banks. Ridgelet transform [14] effectively maps line singularity to point singularity using Radon transform. Curvelet transform [15], one of the multiscale geometric transforms, attempts to overcome the inherent limitations of traditional multistage representations such as wavelets and provides the options to analyze an image with different block sizes, by using with a single transform. Contourlet transform [16] is a directional transform which is capable of capturing contour and fine details in an image. Shearlet [17] decomposition procedure is initiated by separating the image into its high pass and low pass components, which is accomplished using Laplacian pyramid. WPT [18] applies the DWT decomposition to both the low pass and the high pass resultants. Tetrolet Transform [19] is a geometric adaptive transform having tetromino support and the potential to adapt to the directional features of an image. In [11], the authors have relied on DTCWT for cover estimation, whereas in this work an extension of [11] is carried out by studying the performance of seven other transforms and the best cover estimator is identified. Then, a locally weighted bivariate shrinkage function is applied on these coefficients. Then appropriate inverse transform is

applied on the denoised coefficients which results in the estimated cover image pixels. According to Zong [22], there exist strong dependencies between neighbour coefficients such as between a coefficient, its parent (adjacent coarser scale locations) and siblings (adjacent spatial locations) in transform domain. In the basis of an orthogonal wavelet transform, a stego image S in transform domain can be represented using equation (1).

$$y_k = w_k + n_k \quad (1)$$

where, y and w are the k^{th} wavelet coefficients of the stego (S) and cover (C) images respectively. Let w_{2k} represent the parent of w_{1k} . w_{2k} is the wavelet coefficient at the same position as the k^{th} wavelet coefficient w_{1k} , but at the next coarser scale. Let y_{1k} and y_{2k} be noisy observations of w_{1k} and w_{2k} and n_{1k} and n_{2k} are noise samples. It is formulated as $y_{1k} = w_{1k} + n_{1k}$ and $y_{2k} = w_{2k} + n_{2k}$ to take into account the statistical dependencies between a coefficient and its parent. Hence, $w_k = (w_{1k}, w_{2k})$, $y_k = (y_{1k}, y_{2k})$ and $n_k = (n_{1k}, n_{2k})$. The joint shrinkage function [23] is given by equation (2).

$$\hat{w} = \frac{\left(\sqrt{y_1^2 + y_2^2} - \frac{\sqrt{3}\sigma_{ne}^2}{\sigma_e} \right)_+}{\sqrt{y_1^2 + y_2^2}} \cdot y_1 \quad (2)$$

where, g_+ is soft thresholding. This function is used for wavelet transforms like DWT, DTCWT and WPT. This estimator requires the prior knowledge of the noise variance σ_{ne}^2 and the marginal variance σ_e for each wavelet coefficient. σ_{ne}^2 estimated by robust median estimator given by equation (3).

$$\sigma_{ne}^2 = \frac{\text{median}(|y_i|)}{0.6745}, y_i \in \text{subband HH} \quad (3)$$

The marginal variance for the k^{th} coefficient will be estimated using neighboring coefficients proposed by Sendur et al. [24] in the region $N(k)$. From the observation model, $\sigma_y^2 = \sigma_e^2 + \sigma_{ne}^2$ where σ_y^2 is the marginal variance of noisy observations y_1 and y_2 .

An average filter is used to locally estimate the signal's standard deviation. A weighted local window mentioned in [11], $f = \frac{1}{13} \begin{bmatrix} 1 & 3 & 1 \\ 3 & 6 & 3 \\ 1 & 3 & 1 \end{bmatrix}$ is used for estimating the standard deviation, σ_e . This weighted filter is especially useful for LSB steganography where the minute changes of embedding have to be removed while preserving the other information details. Since y_1 and y_2 are modeled as zero mean, σ_y^2 can be found empirically by equation (4).

$$\sigma_y^2 = \frac{1}{M} \sum_{y_i \in N(k)} f \times y_i^2 \quad (4)$$

where, M is the size of the neighborhood $N(k)$. Then, σ_e can be estimated by equation (5),

$$\hat{\sigma}_e = \sqrt{\left(\sigma_y^2 - \sigma_{ne}^2 \right)_+} \quad (5)$$

After calculating $\hat{\sigma}_e$ and $\hat{\sigma}_{ne}^2$, using equation (5) each coefficient is estimated. Unlike DWT, DTCWT and WPT, the Ridgelet, Curvelet, Contourlet, Shearlet, Tetrolet and QWT transforms do not have parent and siblings relationship. So, the computation of the joint shrinkage function [25] is given by equation (6).

$$\hat{w} = \frac{\left(y - \frac{\sqrt{3}\sigma_{ne}^2}{\sigma_e} \right)_+}{y} \cdot y_i \quad (6)$$

where, y represents coefficients of Ridgelet, Curvelet, Contourlet, Shearlet, Tetrolet and QWT transform decomposition. The calculation of noise variance and signal standard deviation are same as equations (3-5). The output of the above filtering excavates high residual values at the embedding points, while preserving the nature of the image at other locations. Thus, the locally weighted bivariate shrinkage using DWT and DTCWT coefficients are perfectly reconstructable and provide the estimated cover in spatial domain ($\hat{C} \square$).

Location Estimation by Weighted Residual Extraction

After the estimation of cover images, weighted residuals are calculated from stego and estimated cover images. From the



weighted average residuals, locations of payload are identified and the count of these locations correspond to the estimated secret message length. In the residual extraction, the first step is to find the difference between the stego image and its estimated cover image. In general, the residual (r_k) is obtained by equation (7).

$$r_k = |S_k - \hat{C}_k| \quad (7)$$

where S_k and \hat{C}_k are the k^{th} stego and estimated cover images respectively. However, using weighted residual boosts varying levels of confidence in the predictor by a weight, which is local variance dependent. In a local 3×3 window of the residual matrix centered at (i, j) , a weight $w_{i,j} = \frac{1}{5000 + \sigma_{i,j}^2}$ is applied. Since the residuals are minuscule for a single image, it is customary to accumulate residuals of a few hundred to thousand images to identify the locations precisely and hence, the weighted mean residual \bar{r} obtained over N images is given by equation (8).

$$\bar{r} = \frac{\sum_{k=1}^N r_k \times w_k}{N \times \sum_{k=1}^N w_k} \quad (8)$$

The residual is taken as such and a prior knowledge of relative payload (M) is obtained from a quantitative steganalyzer [11]. The highest M non-zero magnitude residual coordinates are identified as the spatial locations. This method uses only the relative payload (M) information to find the locations for all algorithms with no other prior information of cover.

EXPERIMENTAL SETTING

The evaluation of the proposed work is carried out on the stego images created using Least Significant Bit algorithms and their variations. The Least Significant Bit (LSB) variant algorithms are non-content adaptive i.e., the payloads are hidden in a random fashion throughout the image without considering image contents like edges and textures. The algorithms considered are LSB-Replacement (LSBR), LSB-Matching (LSBM), LSBM-Revisited (LSBMR) and 2 bit LSBR (LSBR2). In LSBR, the LSB of a cover image is replaced by random secret bit to produce the stego image, whereas in LSBR2, the last two LSBs are altered with random secret data. The main principle of LSB embedding is the inherent asymmetry with even values either unchanged or increased by 1 and odd values either unchanged or decreased by 1. With this idea, LSBM [20] (also known as ± 1 embedding) embeds the secret bit randomly by either by adding or subtracting from cover image, if the secret data bit does not match the LSB of cover image. In LSBMR [21], the embedding of random secret data is achieved using a pair of pixels as a unit so that lesser pixel change rate is achieved than LSBM. The cover database for generating stego images is taken from Bossbase v1.01 which consists of 10,000 grayscale images of size 512×512 . Stego images are generated with six different very low volume relative payloads such as 0.01 bpp, 0.02 bpp, 0.03 bpp, 0.04 bpp, 0.05 bpp and 0.1 bpp using the four LSB algorithms. The embedding is done in such a way that the bit change rate remains the same. So, for a fixed payload of 0.1 bpp, 0.05 bpp, 0.04 bpp, 0.03 bpp, 0.02 bpp and 0.01 bpp, the single-bit schemes such as LSBR, LSBM, LSBMR embed in 26214, 13105, 10484, 7863, 5243 and 2621 pixels respectively, 2 bit LSBR (LSBR2) being multibit scheme embed in 13107, 6554, 5423, 3932, 2621 and 1311 pixels respectively using the same stego key. However, the payload is random and no two images have the same payload embedded in them. For this purpose, random N images are chosen and residuals are computed, where N assumes values of 1, 10, 100, 500 and 1,000.

EXPERIMENTAL RESULTS AND DISCUSSIONS

The accuracy of correctly identified pixels for different LSB stego images using DWT, DTCWT, Ridgelet, Curvelet, Contourlet, Shearlet, WPT and Tetrolet transforms is presented in this section. The accuracies for Payload Location Estimation in LSBR and LSBM stego images using Different Transforms for different N values such as 1, 100 and 1,000 are provided in a graphical format in **Fig. 3**.

From Fig. 3, it can be observed that, the proposed method of payload location by using cover estimation with DTCWT reigns supreme in all experiments. When the number of stego images considered to locate payloads is increased, the detection accuracy is also increased and vice versa. In the case of stego images created using LSBR algorithm, by using DTCWT cover estimation, even for a single known stego image ($N = 1$), the identification of pixel location is high in very low volume payload (0.01 bpp) i.e., 774 pixels are located and for 0.1 bpp payload, 9461 pixels are located with an accuracy of 29.53 % and 36.09 %

respectively. Using DTCWT, it is also inferred that for $N = 1000$, the accuracy is about 99.95 % and 97.9 % for 0.1 bpp and 0.01 bpp respectively. DTCWT is able to provide a better result due to its directional selectivity and shift invariance property. On comparing DWT, Ridgelet, Curvelet, Contourlet, Shearlet, WPT, Tetrolet and QWT transforms, Contourlet performance is better due to its Laplacian pyramid transformation along with directional filter banks.

From Fig. 3, it can also be observed that, for LSBM, by using DTCWT cover estimation, for a single known stego image the accuracy of locating payload is about 11.5 % for 0.1 bpp and 1.53 % for 0.01 bpp. But, when N is increased, the accuracy is also increased to 97.89 % (25661 pixels) and 97.25 % (2549 pixels) for 0.1 bpp and 0.01 bpp respectively. In case of Contourlet transform, for 0.1 bpp when $N = 1000$, 97.25% (25492 pixels) accuracy is achieved and for 0.01 bpp, 92.4 % (2428 pixels) accuracy is achieved. There is only 0.64 % accuracy increase between DTCWT and Contourlet transforms for $N = 1000$ (0.1 bpp). This is because of embedding pattern of LSBM algorithm. In case of DWT and Curvelet transforms, DWT performs better and its accuracy of identifying of locations of payload (0.1 bpp and 0.01 bpp) when $N = 1000$ is 88.16 % (23109 pixels) and 76.34 % (2001 pixels).

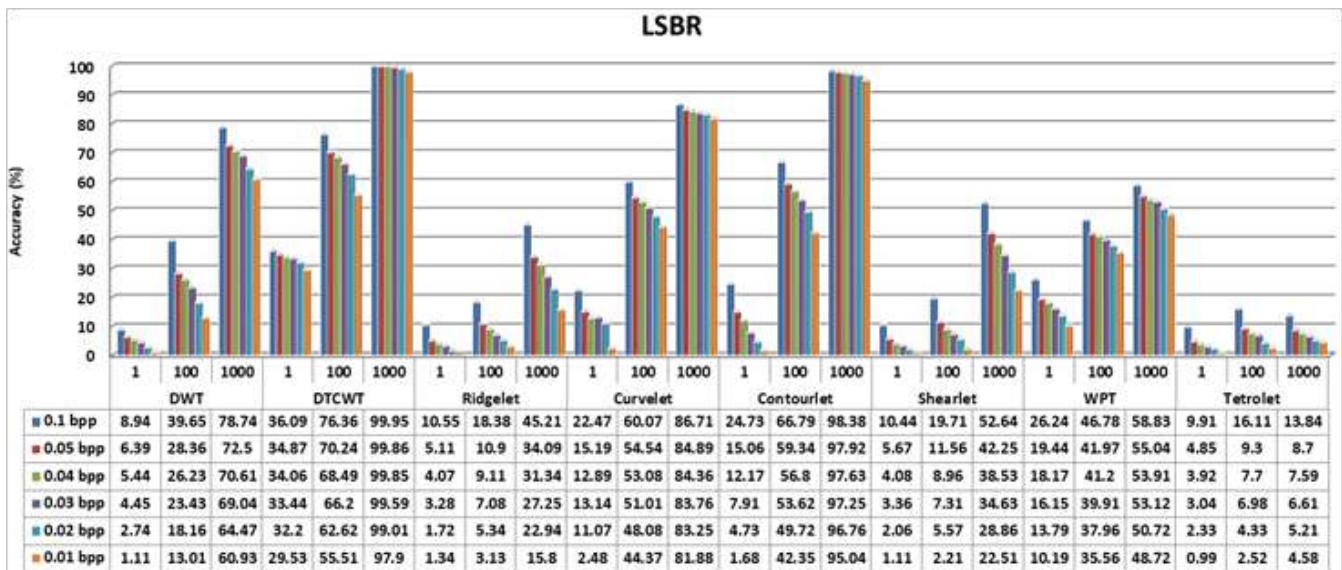
The accuracies for Payload Location Estimation in LSBR and LSBM stego images using Different Transforms for different N values such as 1, 100 and 1,000 are provided in a graphical format in Fig. 4.

From Fig. 4 it can be inferred that, DTCWT performs better than other transforms. In the case of LSBMR algorithm, For $N = 1$, the accuracy of locating payload is 14.2 % (3781 pixels) for 0.1 bpp and 1.79 % (47 pixels) for 0.01 bpp. When $N = 1000$, the accuracy is increased to 87.08 % (22826 pixels) and 78.9 % (2068) for 0.1 bpp and 0.01 bpp respectively. In the case of LSBR2 algorithm, for $N=1$, accuracy of correctly identified pixels for very low volume payload of 0.01 bpp is 33.64 % and 36.74 % for 0.1 bpp. As N increases (200 to 500), the accuracy also increases to about 97 % for 0.1 bpp and when $N = 1000$, the accuracy is of 99.2 % (13002 pixels) which is only 105 pixels less to the total number of pixels (13107) embedded.

From Fig. 4, it can be concluded that the proposed method using DTCWT and Contourlet perform better in the identification of the location of payloads in all LSB algorithms for varying payloads (0.01 bpp, 0.02 bpp, 0.03 bpp, 0.04 bpp, 0.05 bpp and 0.1 bpp) with high accuracy.

Fig. 5 provides a comparison for payload location estimation accuracy using DTCWT for all the algorithms. From Fig. 5, it is observed that the correctly identified payload pixels are less in LSBMR algorithm than the other algorithms. This is due to the embedding pattern of LSBMR algorithm which makes the steganalysis task difficult.

Table 1 - 4 provides the extracted payload from these locations when considering stego images from all the LSBR algorithms.



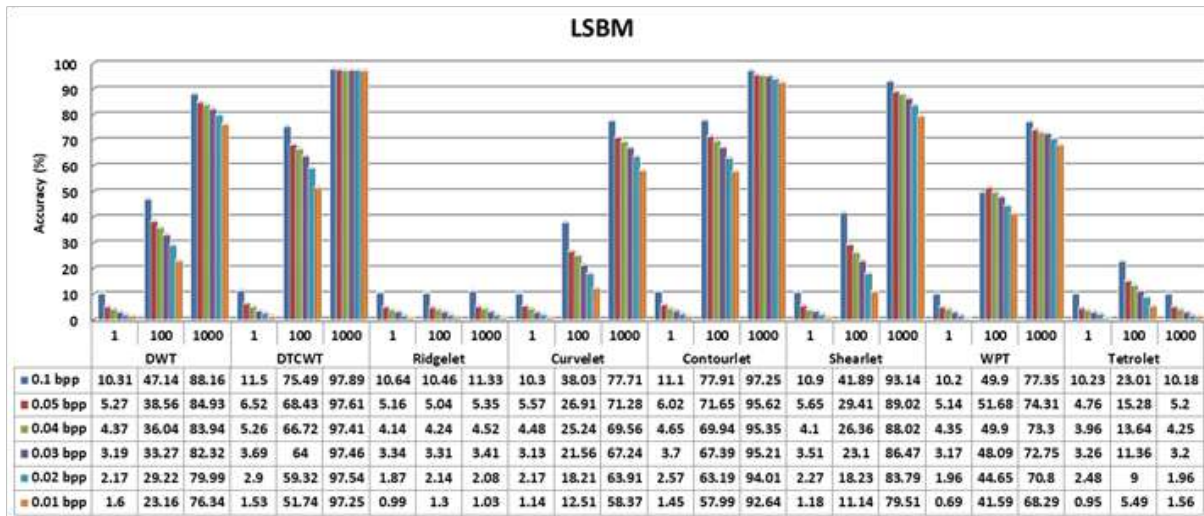


Fig. 3. Accuracy (%) for Payload Location Estimation in LSBR and LSBM stego images using Different Transforms

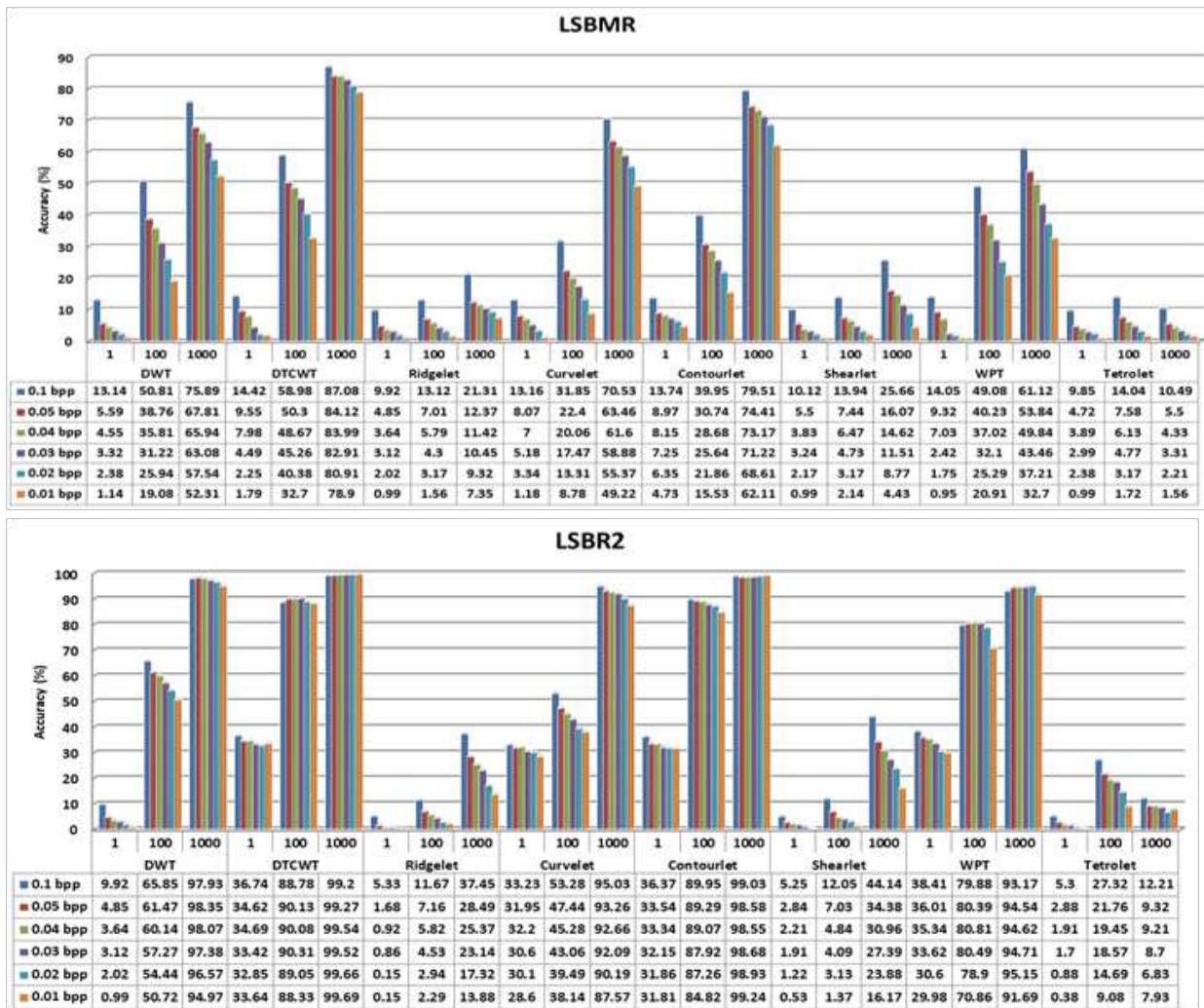


Fig. 4. Accuracy (%) for Payload Location Estimation in LSBMR and LSBR2 stego images using Different Transforms

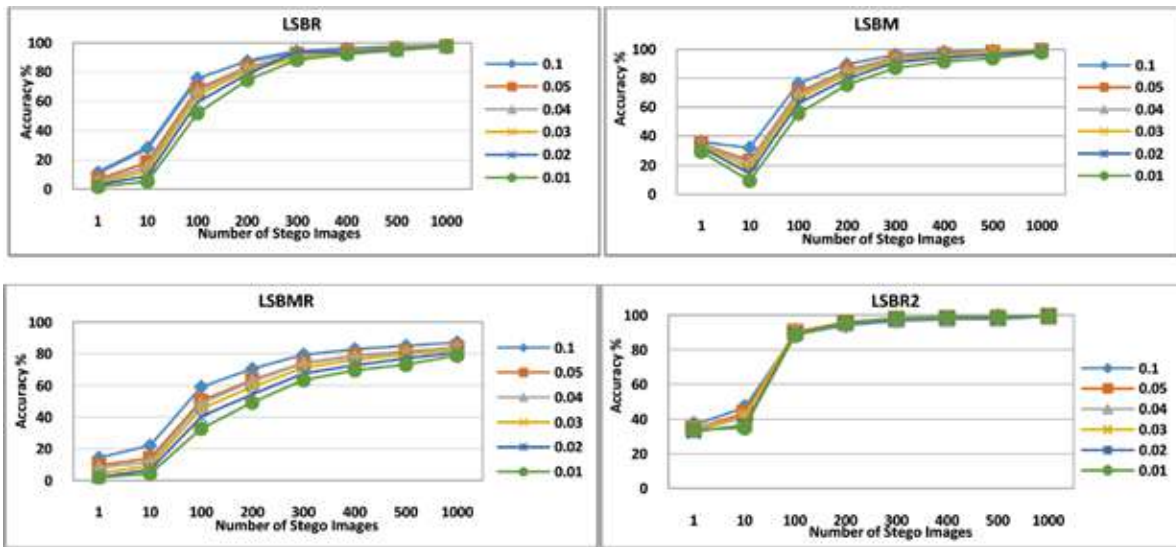


Fig. 5. Accuracy of correctly identified payload pixel locations using DTCWT based cover estimation

Table 1. Extracted payload from LSBR stego images using proposed DTCWT method based cover estimation

























Payload	N = 1	N = 100	N = 500	N = 1000
0.01bpp				
0.02bpp				
0.03bpp				
0.04bpp				
0.05bpp				
0.1bpp				

Table 2. Extracted payload from LSBM stego images using proposed DTCWT method based cover estimation

























Payload	N = 1	N = 100	N = 500	N = 1000
0.01bpp				
0.02bpp				
0.03bpp				
0.04bpp				
0.05bpp				
0.1bpp				

Table 3. Extracted payload from LSBMR stego images using proposed DTCWT method based cover estimation

















































Payload	N = 1	N = 100	N = 500	N = 1000
0.01bpp				
0.02bpp				
0.03bpp				
0.04bpp				
0.05bpp				
0.1bpp				

Table 4. Extracted payload from LSBR2 stego images using proposed DTCWT method based cover estimation

Payload	N = 1	N = 100	N = 500	N = 1000
0.01bpp				
0.02bpp				
0.03bpp				
0.04bpp				
0.05bpp				
0.1bpp				

From **Table 1-4** it is clearly seen that, when N is increased, the payload can be extracted with minimum errors across all payload bins. The quality of the reproduced secret is of the order LSBR2, LSBR, LSBM and LSBMR. The reason is that LSBR2 has double embedding pattern, LSBR and LSBM becomes nearly the same with same key embedding and LSBMR is difficult than these because of its embedding change rate and pattern. It is evident that, more the availability of stego images that too in a clairvoyant scenario the embedded secret can be extracted. At least a 100 stego images are required to have a clue of the embedded secret, but in case of LSBR2, the embedded secret begins to be visible with only 10 stego images since the embedding bit is twice compared to other algorithms.

CONCLUSION

In this paper, comparative analysis of various multiresolution transforms in cover estimation of stego images for payload location estimation is thoroughly studied. From the experimentation done, DTCWT is chosen to be the best cover estimator. In addition to DTCWT, Curvelet and Contourlet based cover estimation also detects the locations with better accuracy because of their efficiency to decompose the stego images while preserving the edges and contours. DTCWT performs better than DWT since it accounts for the positive and negative frequencies and hence it results in providing increased level of directional sensitivity and perfect reconstruction of stego images. Based on the experimentation, the order of transforms that are able to locate the payload with high accuracy is found to be DTCWT, Contourlet, DWT, Curvelet, WPT, Shearlet, Ridgelet and Tetrolet for all algorithms. It is observed that, payload location in LSBMR stego images is somewhat difficult compared to other LSB algorithms since in LSBMR, pixel change rate is very less. Under the Clairvoyant scenario, secret is also extracted from the stego images of all the four LSB algorithms.

Since, in this proposed method a greater number of stego images embedded using same stego key are needed to get a high accuracy for payload location, the work can be extended in future with a minimum number of stego images.



ACKNOWLEDGMENT

The authors would like to thank ER & IPR - DRDO New Delhi, Management and Principal of MepcoSchlenk Engineering College, Sivakasi for providing the necessary facilities and support to carry out this research work.

REFERENCES

1. AD. Ker, I.Lubenko: 'Feature reduction and payload location with WAM steganalysis', IS&T/SPIE Electronic Imaging, 2009, pp 7254–13
2. N.Provos, P. Honeyman: 'Detecting steganographic content on the internet'. Tech. rep., Center for Information Technology Integration, 2010
3. J. Fridrich, M. Goljan, D. Soukal: 'Forensic steganalysis: determining the stego key in spatial domain steganography', Electronic, 2005, pp 631–642
4. AD. Ker: 'Locating steganographic payload via WS residuals', Proc. of the 10th ACM workshop on Multimedia and security, 2008, pp 27–32
5. I. Lubenko, AD. Ker: 'Steganalysis using logistic regression', IS&T/SPIE Electronic Imaging, 2011, pp 7880–7880–11.
6. Y. Luo, X. Li, B. Yang: 'Locating steganographic payload for LSB matching embedding', Proc. of the IEEE on Multimedia and Expo, 2011, pp 1-6
7. TT. Quach: 'On locating steganographic payload using residuals', Proc. Media Watermarking, Security, and Forensics XIII, 2011, pp 7880–7880–7
8. TT. Quach: 'Optimal cover estimation methods and steganographic payload location', IEEE Trans Inf Forensic Secure, 2011, 6, (4), pp 1214–1222
9. X. Gui, X. Li, B. Yang: 'Improved payload location for LSB matching steganography', Proc. Int. Conf. on Image Processing, 2012, pp 1125–1128
10. TT. Quach: 'Cover estimation and payload location using Markov random fields', IS&T/SPIE Electronic Imaging, 2014, pp 9028–9028–9
11. S.T. Veena, S. Arivazhagan: 'Universal secret payload location identification in spatial LSB stego images', Annals of Telecommunications, 2018, 10.1007/s12243-018-0676-x
12. M. Kimlyk, S. Umnyashkin: 'Image denoising using discrete wavelet transform and edge information', IEEE Conference of Russian Young Researchers in Electrical and Electronic Engineering, 2018, pp. 1823-1825
13. N.G. Kingsbury: 'The dual-tree complex wavelet transform, a new efficient tool for image restoration and enhancement', Proc. EUSIPCO 98, September, 1998, pp 319-322
14. S. Arivazhagan, L. Ganesan, T.G. Subash Kumar: 'Texture classification using ridgelet transform', Pattern Recognition Letters, 2006, 27, (16), pp.1875–1883
15. J.L. Starck, E.J. Candes, D.L.Donoho: 'The curvelet transform for image denoising', IEEE Transactions on Image Processing, 2002, 11, (6), pp. 670–684
16. M. N. Do, M.Vetterli: 'Contourlets: a Directional Multiresolution image representation', Proc. IEEE International Conference on Image Processing, 2002, 1, pp 357-360
17. T. S.Anju, N.R.Nelwin Raj: 'Denoising of Digital Images Using Shearlet Transform', IEEE Int. Conf. On Recent Trends In Electronics Information Communication Technology, May 20-21, 2016



18. Rajni, Inderbir Kaur, Anutam,: 'Image Denoising using Wavelet Packet Transform and Optimal Wavelet Basis', Proc. National Conference on Computing, Communication & Electrical Systems, 2016
19. Krommweh, Jens: 'Tetrolet transform: A new adaptive Haar wavelet algorithm for sparse image representation', Journal of Visual Communication and Image Representation, 2010, 21. 364-374
20. T. Sharp: 'An implementation of key-based digital signal steganography', Springer Moskowitz I (ed) Information Hiding, Lecture Notes in Computer Science, 2001, 2137, pp 13–26
21. J. Mielikainen: 'LSB matching revisited', IEEE Signal Processing Letters, 2006, 13, (5), pp 85–287
22. H. Zong, F.L. Liu, X.Y. Luo: 'Blind image steganalysis based on wavelet coefficient correlation', Digit Investig, 2012, 9, (1), pp 58–68
23. L. Sendur, I.W. Selesnick: 'Bivariate shrinkage functions for wavelet-based denoising exploiting interscale dependency', IEEE Transactions Signal Processing, 2002, 50, (11), pp 2744–2756
24. L. Sendur, I.W. Selesnick: 'Bivariate shrinkage with local variance estimation', IEEE Signal Processing Letters, 2002, 9, (12), pp 438-441
25. Q. Guo, S. Yu: 'Image denoising using a multivariate shrinkage function in the curvelet domain', IEICE Electronics Express, 2010, 7, (3), pp 126–131.

Civil Engineering





Geopolymer Concrete: A Pathway to Sustainable Manufacturing in the Indian Concrete Industry

Jyotirmoy Mishra*, Bharadwaj Nanda, Sanjay Ku Patro

Department of Civil Engineering, Veer Surendra Sai University of Technology, Burla

*✉ jmishra0805@gmail.com

ABSTRACT

Manufacturing has been an essential component of the Indian economy which fosters self-reliance. One of the top manufacturing industries in India in the present scenario is the concrete industry whose core ingredient is cement. Potential problems associated with the concrete industry include the generation of carbon dioxide due to the production of cement that in turn, leads to exhaustion of limestone reserves. Therefore, it is critical to find sustainable manufacturing methods for the production of concrete and move towards sustainable development. In this paper, the authors stress the importance of adopting geopolymer concrete as an alternative to traditional cement. From the available literature, the compressive strength properties of various industrial waste-derived geopolymer concrete have been highlighted and tabulated. Besides, the paper also explores the implications of using geopolymer concrete on the environment, thus promoting its use, as an effective method of sustainable concrete manufacturing.

Keywords : Geopolymer concrete; Sustainable development; Cement production; Sustainable manufacturing.

INTRODUCTION

Sustainable manufacturing refers to the type of manufacturing which improves the environmental performances of the end products while reducing production costs, waste generation, consumption of natural resources, and carbon emissions as well. The chief driving force of the economy is the manufacturing sector which also has the ability to shape the society into a more sustainable one. The last decade witnessed a rapid growth in the infrastructure sector in India and the demand for concrete has increased manifold. However, the traditional concrete that is widely used for infrastructure development requires cement for its production and thus responsible for 7-8% of the total greenhouse gas emissions (CO₂) and global warming [1]. Further, the manufacturing of cement consumes natural reserves of limestone and is an energy-intensive process that requires high thermal energy for calcination of limestone and combustion of fossil fuels for clinker production. Apart from this, there is generation of solid wastes such as kiln dust and other solid particulates. To address this growing concern of unsustainability in the concrete manufacturing sector, it is high time to escalate the pursuit of alternative binders and concrete and out of these alternatives, geopolymer concrete seems to be an ideal choice from the perspective of sustainable development.

Geopolymer concrete is a cement-less construction material which is produced from alkali activation of industrial aluminosilicate solid wastes, for instance - fly ash (FA), ground granulated blast furnace slag (GGBFS), rice husk ash (RHA), Palm oil fuel ash (POFA), silica fume (SF), ferrochrome slag (FS) and ferrochrome ash (FCA) etc. The alkali activators are usually a mixture of sodium hydroxides and silicates. The manufacturing of geopolymer concrete is considered to be more sustainable than traditional cement-based concrete as there is less energy requirement and carbon emissions are reduced by 70-80% - in the absence of cement. Moreover, it provides a pathway for the implementation of circular economy in the construction sector i.e. conversion of wastes to wealth. It can be prefabricated easily and the literature suggests that the strength and durability properties are outstanding when compared to the cement-based concrete [2,3].

The primary motivation for this study includes the overview of the compressive strength properties of various types of geopolymer concrete made out of different industrial wastes in the last decade. This paper also strives to promote green and sustainable manufacturing of concrete, thus serving to reduce environmental impacts caused due to the traditional method of manufacturing concrete.

PREPARATION OF GEOPOLYMER CONCRETE

Although the preparation of geopolymer concrete is similar to the preparation of cement-based concrete, there is a slight difference in the type of ingredients used. The ingredients of geopolymer concrete essentially include the source materials

(aluminosilicate industrial wastes), alkaline solutions, and conventional aggregates – presented in **Fig. 1**. The chemical composition of source materials plays a significant role in the strength development of the geopolymer concrete samples. Higher the Si/Al ratio of the source materials, the greater is the rate of geopolymerization i.e. stronger covalently bonded -Si-O-Al- framework. The alkaline solutions are generally taken as a mixture of solutions of sodium hydroxide and silicate at a fixed mass/volume ratio. Interestingly, the geopolymer concrete does not necessarily require any additional water during the mixing process, instead, water is expelled during the reaction process, which is very helpful in maintaining the fluidity of the mixtures. Moreover, the need for water curing is also eliminated due to the absence of cement. However, the temperature is the principal governor of strength development over the ages. Researchers have therefore adopted the method of ambient curing [4] for in-situ casting purposes and the elevated temperature curing [5] for prefabrication requirements. Currently, ambient cured geopolymer concrete is more preferred, to enable its wide acceptance and implementations.

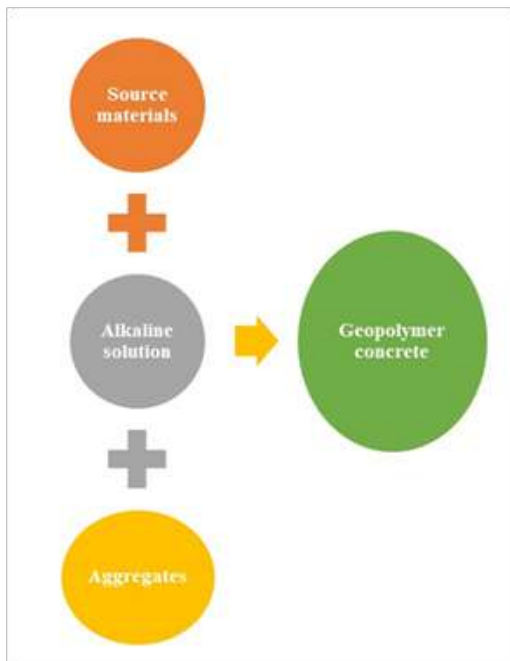


Fig. 1. Manufacturing of geopolymer concrete

COMPRESSIVE STRENGTH PROPERTIES OF VARIOUS INDUSTRIAL WASTE-DERIVED GEOPOLYMER CONCRETE

The compressive strength is considered to be the most vital mechanical property of any given concrete. In the case of cement-based concrete, the strength development is due to the generation of calcium silicate hydrate (C-S-H) gel whereas the formation of calcium aluminate silicate hydrate (C-A-S-H) and sodium aluminate silicate hydrate (N-A-S-H) gels are responsible for strength development in geopolymer concrete [6]. Since geopolymerization is a set of rapid and complex reaction mechanisms, the chemical composition of the source materials, therefore, is a crucial parameter to focus upon. For this reason, different source material composition exhibits a unique set of mechanical and durability properties. Besides, the compressive strength also depends on the concentration of sodium hydroxide, the ratio of sodium hydroxide and silicate solution (by weight or volume), temperature conditions among other factors – which are beyond the scope of this paper. Therefore, based on past literature (2010-2020), the present study highlights some of the source material compositions and their corresponding compressive strength results achieved under different curing regimes; presented in **Table 1**.

Table 1. Compressive strength properties of different source material combinations based geopolymer concrete

Authors	Source material combination	28-day Compressive strength (MPa)	Type of curing regime	References
Sreevidya et al. 2010	100% FA	24.4	Ambient	[7]
Pan et al. 2011	100% FA	69.8	Elevated temperature	[8]



Rajamane et al. 2012	50% FA + 50% GGBFS	51	Ambient	[9]
Rashad et al. 2013	85% FA + 15% GGBFS	55	Ambient	[10]
Usman et al. 2014	85% FA + 15% RHA	21.32	Elevated temperature	[11]
Hussin et al. 2015	70% FA + 30% POFA	35	Elevated temperature	[12]
Venkatesan et al. 2016	90% GGBFS + 10% RHA	48.44	Ambient	[13]
Islam et al. 2017	50% GGBFS + 50% POFA	27.69	Ambient	[14]
Elchalakani et al. 2018	50% FA + 50% GGBFS + 3% SF	71.6	Ambient	[15]
Özcan et al. 2019	75% GGBFS + 25 % FS	59.48	Oven	[16]
Mishra et al. 2020	80% FCA + 20% GGBFS	32.6	Outdoor	[17]

*FA – fly ash; GGBFS – ground granulated blast furnace slag; POFA – palm oil fuel ash; SF– silica fume; RHA – rice husk ash; FS - ferrochrome slag; FCA -ferrochrome ash

FERROCHROME ASH BASED GEOPOLYMER CONCRETE

The authors of this study recently prepared geopolymer concrete by blending FCA and GGBFS as source material combination, cured under outdoor conditions [17]. FCA is a waste obtained from ferroalloy industries while GGBFS is a by-product of the steel industry; their disposal is a great concern. The compressive strength achieved after 28 days of curing was found to be 32.6 MPa (as shown in **Fig. 2**) that could be used for general construction purposes. As a result, it serves as a potential alternative to cement-based concrete. The study also discussed the microstructure – scanning electron microscopy (SEM), fourier transform infrared spectroscopy (FTIR) analysis, of the resulted FCA based geopolymer concrete samples. Further, the authors highlighted the importance of the circular economy and elucidated its basic features.

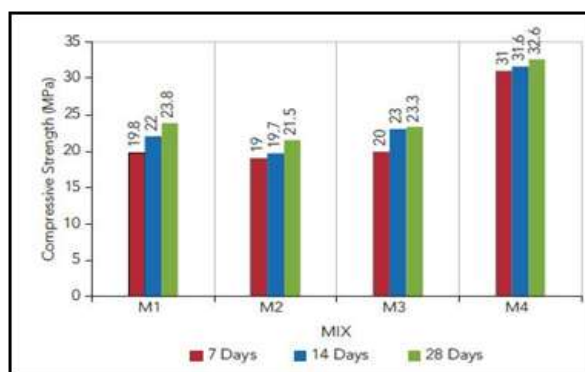


Fig. 2. Compressive strength of FCA based geopolymer concrete with GGBFS [17]

IMPLICATIONS OF SUSTAINABLE MANUFACTURING OF GEOPOLYMER CONCRETE

The geopolymer concrete is relatively a new construction material being adopted worldwide. Its conceptualization began in the 1970s by the French scientist, J. Davidovits who termed this as “geopolymer technology”. However, the durability and serviceability data require time, and almost after five decades of research, the data suggests that geopolymer concrete shows outstanding potential in comparison to the traditional cement-based concrete. In many parts of the world, especially in U.K and U.S.A, the geopolymer concrete has been rapidly adopted to address the concerns of the environment such as global warming, water shortages, exhaustion of natural reserves, and industrial waste disposals. Implementation of this green manufacturing in India may be considered to be the first step towards a sustainable future.



In the meantime, India faces challenges such as global warming, climate change, and acute water shortages. As discussed earlier, the issue of greenhouse gas emissions can be effectively addressed by the implementation of cement-less geopolymers. Simultaneously, it is also observed that there are considerable changes in the timing of wet and dry seasons with a disturbed hydrological cycle. In 2019, India witnessed major rainfall accompanied with floods in its northern part which is contrary to the issue of acute water shortage in the southern part at the same time. Chennai became the first city to face an acute water shortage. The National Institution for Transforming India (NITI Aayog) report clearly states that India has been suffering from a significant water crisis for which economic growth, livelihoods, human well-being as well as ecological sustainability is at stake, and 21 major cities including New Delhi will run out of groundwater by 2020 [18]. These issues cannot be solved unless there is a focus on sustainable development and manufacturing. As the infrastructure demand rises in India, the demand for concrete will rise simultaneously. The traditional method of concrete manufacturing requires a huge amount of water for mixing and curing purposes, hence, sustainable manufacturing of geopolymers, which essentially does not require any water, seems to be a prudent decision. This could save our natural water reserves from depletion and recover the groundwater table.

Another major advantage of adopting geopolymers is that it helps mass utilization of industrial solid wastes and could lead to a circular economy. This model of economy may involve the construction sector and the concrete manufacturing sector to convert the wastes into the economy. The industrial wastes such as FA, GGBFS, RHA, FS, FCA are viable candidates for geopolymerization as they contain a significant amount of aluminum oxides and/or silicon dioxides. Presently, there has been some progress in the utilization of these wastes as pozzolanic materials for the production of blended cement-based concrete manufacturing in the construction sector. However, the full utilization of these wastes in the construction sector seems to be a challenge. Therefore, the implementation of geopolymers could certainly enhance the utilization rate of these wastes and provide an alternative pathway for sustainable manufacturing thereby enabling the circular economy into the current scenario.

CONCLUSIONS

The carbon-conscious market drives the demand for the development of alternative sustainable ways of manufacturing. The research carried out so far has successfully established geopolymers as an alternative to cement-based concrete. This paper elucidated the importance of sustainable manufacturing of geopolymers. The traditional method of manufacturing concrete has become unsustainable, therefore it is high time to focus on the commercialization of geopolymers, to build a smart and sustainable future. The core challenge, however, is the mutual participation of industry stakeholders, research agencies, and government policymakers.

ACKNOWLEDGMENTS

The authors are grateful to Dr. S. M. Mustakim, Mr. Shaswat Ku. Das, Mr. R. S. Krishna for the needful motivation during the manuscript preparation.

REFERENCES

1. C.R. Meesala, N.K Verma, S. Kumar, "Critical review on fly-ash based geopolymers concrete". Structural Concrete. 2020, 21, 1013–1028
2. Y. M. Amran, R. Alyousef, H. Alabduljabbar et al., "Clean production and properties of geopolymers concrete; A review". Journal of Cleaner Production. 2020, 251, 119679.
3. S. K Das, S. M. Mustakim, A. Adesina et al., "Fresh, strength and microstructure properties of geopolymers concrete incorporating lime and silica fume as replacement of fly ash". Journal of Building Engineering. 2020, 32, 101780.
4. A. Hassan, M. Arif and M. Shariq, "Structural performance of ambient-cured reinforced geopolymers concrete beams with steel fibres". Structural Concrete. 2020.
5. H. Y Zhang, G. H. Qiu, V. Kodur, et al., "Spalling behavior of metakaolin-fly ash based geopolymers concrete under elevated temperature exposure". Cement and Concrete Composites. 2020, 106, 103483.
6. S. K. Nath, "Fly ash and zinc slag blended geopolymers: Immobilization of hazardous materials and development of paving blocks". Journal of hazardous materials, 2020, 87, 121673.
7. V. Sreevidya, R. Anuradha, and R. Venkatasubramani, "Study on fly ash geopolymers concrete to reduce global warming



- gases". *Nature, Environment and Pollution Technology*, 2010, 9(2), 383-387.
8. Z. Pan, J. G. Sanjayan. and B. V. Rangan, "Fracture properties of geopolymer paste and concrete". *Magazine of concrete research*. 2011, 63(10), 763-771.
 9. N. P. Rajamane, M. C. Nataraja, J. K. Dattatreya et al., "Sulphate resistance and eco-friendliness of geopolymer concretes". *Indian Concrete Journal*, 2012, 86(1), 13.
 10. A. M. Rashad, "Properties of alkali-activated fly ash concrete blended with slag". *Iranian Journal of Materials Science and Engineering*, 2013, 10(1), 57-64.
 11. M. K. Mohamed Usman, M. Senthil Pandian, "Study on Fly Ash and Rice Husk Ash Based Geopolymer Concrete with Steel Fibre". *Civil Engineering Systems and Sustainable Innovations*. 2014, 179-183.
 12. M. W. Hussin, M. A. R., Bhutta, Azreen, et al., "Performance of blended ash geopolymer concrete at elevated temperatures". *Materials and Structures*, 2015, 48(3), 709-720.
 13. R. P. Venkatesan, K. C. Pazhani, "Strength and durability properties of geopolymer concrete made with ground granulated blast furnace slag and black rice husk ash". *KSCE Journal of Civil Engineering*, 2016, 20(6), 2384-2391.
 14. A. Islam, U. J. Alengaram, M. Z. Jumaat et al., "Influence of steel fibers on the mechanical properties and impact resistance of lightweight geopolymer concrete". *Construction and Building Materials*, 2017, 152, 964-977.
 15. M. Elchalakani, M. Dong, Karrech, A. et al., "Development of fly ash-and slag-based geopolymer concrete with calcium carbonate or microsilica". *Journal of Materials in Civil Engineering*, 2018, 30(12), 04018325.
 16. A. Özcan, and M. B. Karakoç, "Evaluation of sulfate and salt resistance of ferrochrome slag and blast furnace slag-based geopolymer concretes". *Structural Concrete*. 2019, 20(5), 1607-1621.
 17. J. Mishra, S. Das, R.S. Krishna, B. Nanda, "Utilization of Ferrochrome Ash as a Source Material for Production of Geopolymer Concrete for a Cleaner Sustainable Environment". *The Indian Concrete Journal*, 2020, 94(7), 40-49.
 18. N. I. T. I. Aayog, Composite water management index, National Institution for Transforming India, GOI. 2019.



A Geotechnical Study on Properties and Uses of Shales of the Dharwar System, Karnataka, India

Dr Udayashankar D Hakari

Associate Professor, Department of Civil Engineering, S.D.M. College of Engineering and Technology, An Autonomous Institute under Visveswaraya Technological University, Dharwad, Karnataka

*✉ uday.hakari@gmail.com

ABSTRACT

Shales are fine-grained, laminated or fissile classic sedimentary rocks with predominance of clay and silt as the detrital components. They may be classified as clayey, silty or sandy shales on the basis of texture. Other criteria used in the classification of shales include mineralogical composition, cementing materials, organic matter content, depositional environment and strength. Generally, shales have moderate to high clay content, low strength, low permeability and are water sensitive. Apart from many uses, the shales are important to the petroleum industry because of their usefulness as source rocks in extraction of oil and natural gas, use as seals in petroleum traps and reservoirs. In the present paper, it is attempted to present the properties and uses of shales of the Dharwar system which is 4–1 billion years old and has special distinction of being the first and oldest metamorphosed sedimentary rock system in India. Because of its unpredictable behaviour, shales are found to be difficult rocks to classify, sample and obtain reliable test data for engineering purposes. The origin, distribution, classification, properties and the possible uses of shales of Dharwar system are briefly discussed and their engineering evaluation for construction also has been presented.

Keywords : Shales; Classification; Dharwar system; Composition; Oil and natural gas.

INTRODUCTION

Shale is a fine-grained sedimentary rock that forms from the compaction of silt and clay-size mineral particles which makes it fissile and laminated. This composition places shale in a category of sedimentary rocks known as mudstones. In fact, the shale can be considered as boundary material between soil and rock; which makes it typical for characterising its engineering properties. Hence Shales are considered as one of the problematic rock types for their applications in engineering domains (Farrokhrrouz and Asef, 2013). In general, the shale is composed of quartz, feldspar and minerals. The major minerals in shale are kaolinite, illite, and smectite. Other minor constituents normally found are organic carbon, carbonate minerals, iron oxide minerals, sulfide minerals, and heavy minerals. Shales are the most abundant of all sedimentary rocks constituting about 60%, and are distributed over wide range of geologic ages. Their colours may range from white through green to grey and brown to black depending on their composition and environment of deposition (Boggs, 2009). The organic material of the shale offers prospects of oil and natural gas if pressured and properly heated after burial.

In this paper, the composition, classification, properties and uses of shales are presented with emphasis on their engineering evaluation. The shales of Dharwar system are considered in particular while illustrating the importance of this rock class.

Origin and composition of shales

Shales may form in any environmental condition in which sediment is abundant and water energy is sufficiently low to allow settling of suspended fine silt and clay (Porter et al, 1980). Silts and clays when newly deposited from suspension in water undergo compaction due to continuous accumulation of other sediments above them. The silt and clay percentage in the shales may vary but however at least 50% of their material is finer than fine sand. The transformation of soil into shale rock and the subsequent formation of metamorphic rocks depending on the mineral composition of the shale and degree of metamorphism is schematically indicated in **Fig. 1**.

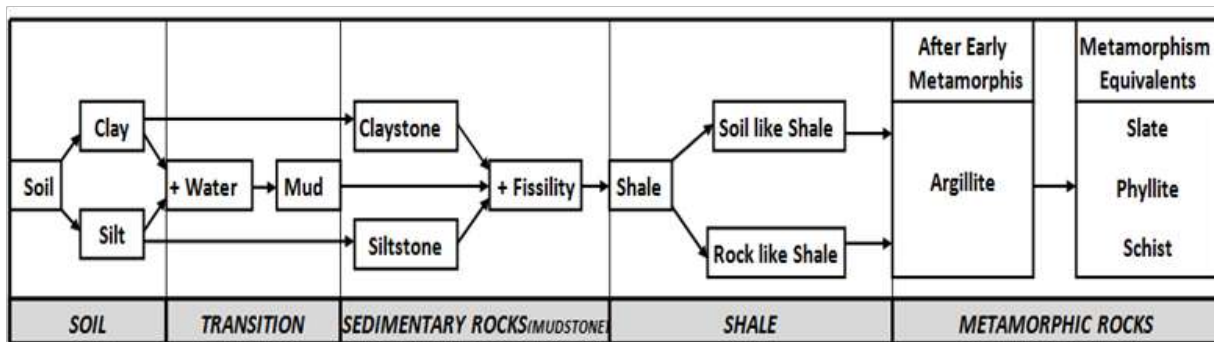


Fig. 1. Transformation of soil into shale and subsequent metamorphic rocks

Classification of Shales

Shales are fissile clastic sedimentary rocks formed from transportation, deposition and compaction of detrital materials of silt and clay. Fissility (the property of a rock to split easily along thin closely spaced [$< 10\text{mm}$] parallel layers) of the clay is the main characteristic of the shales which distinguish them from other sedimentary rocks. Shales can thus be classified based on the observable features and environment of deposition such as texture, mineralogical composition, type of cementation/cementing materials, depositional environment, organic matter content and strength (Boggs, 1995). Brief discussion on the classification of shales is presented below.

Texture

Shales characteristically contain fine-grained silt and clay particles. They are therefore classified as silty shale or clayey shale, depending on whether silts or clays dominate in the constituents of the rock. Silty shale and clay shale may collectively be called argillaceous shales.

Mineralogical composition

Shales may be classified as quartzose, feldspathic or micaceous shales depending on the predominant presence of minerals viz. quartz, feldspar or mica, respectively in the rock (Pettijohn, 1957).

Type of cementation/cementing materials

Shales like other sedimentary rocks are cemented by some minerals or elements after deposition and compaction. The cementing material may be used in the classification of the shales since the type of cementing material may affect the properties or performance of the shale when used as an engineering material. The cementing materials commonly found are silica, iron oxide and calcite or lime. Accordingly, the shales may be classified as siliceous, ferruginous or calcareous depending upon the predominance of the presence of silica, iron oxide and calcite or lime, respectively.

Environment of deposition

The environment in which sediments are accumulated and later get transformed into rock is a natural geographical process which can be considered as another valid base for classifying the shales (Reineck and Singh, 1980). Three sedimentary environments of deposition namely, continental, transitional or marginal and marine are prominently observed. Shales are generally deposited in lacustrine (continental), deltaic (transitional) and marine depositional environments and may accordingly be classified as lacustrine, deltaic and marine shales (Boggs, 1995). Lacustrine deposits are characterized by mixture of clay, silt, sands, inorganic carbonate precipitates and various fresh water invertebrate organisms as well as various plant deposits. Deltaic deposits are generally paralic i.e. consisting of orderly sequences of shales and sandstones. These deposits are also characterized by shallow depth and concentration of clay minerals such as kaolinite, illite and montmorillonite. Marine deposits are non-paralic and are characterized by homogenous rock sequences, great depth, oxygen deficiency, concentration of illite/montmorillonite, dark colour and considerable presence of marine fossils.

Organic matter content

Shales may be classified as carbonaceous or bituminous on the basis of their organic matter content (Krumbein and Sloss, 1998). The carbonaceous and bituminous shales generally contain more than 10% of organic matter which in fact induces black



or grey colour to the shales. When the dominant organic matter content in shales is from plant fragments such as pollen grains, stems and leaves, the shales are then classified as carbonaceous. When the dominant organic matter content in the shales is from animal fragments such as fossils, such shales are classified as bituminous. It is worth-noting here that, both carbonaceous and bituminous shales are important source rocks for generation of petroleum oil and gas.

In addition to the above criterion, the rock strength may be considered for classifying the shales, which can be fairly useful in evaluation of strength of shales. Likewise, colour of the shales, which in fact may be quite useful in understanding the composition of the materials forming the shales and suggesting its usefulness, may also form a base for classifying the shales. This is evident from the fact that, colour of the shale is often derived by the presence of specific materials composing it; for example, just a little presence of organic material or iron can significantly alter the colour of the shale.

The summary of the classification of shales is presented at **Table 1**.

Table 1. Criterion wise classification of shales

Sl.no.	Criterion	Classification
1	Texture	Silty shales, Clayey shales, Sandy shales
2	Colour	Black and Grey shales, Red, Brown, Yellow shales
3	Mineralogical composition	Feldspathic shales, Quartzose shales, Micaceous shales
4	Cementing materials	Calcareous shales, Ferruginous shales, Siliceous shales
5	Organic matter content	Carbonaceous shales, Bituminous shales
6	Depositional environment	Lacustrine shales, Deltaic shales, Marine shales
7	Strength characteristics	Soil-like or rock-like shales, Weak or Strong shales, Low strength or High strength shales, Low/ High modulus ratio shales, Soft/Plastic or Hard/Brittle shales

THE DHARWAR SYSTEM SHALES – LITHOLOGY AND DISTRIBUTION

Lithology

The term Dharwar has been derived from Dharwad district of Karnataka where these rocks were first discovered. The geological name for the crystalline schist near Dharwad is known as 'Dharwar System', the name being given by Robert B.F. who identified them way back in 1886. The Dharwar system is formed by lava, dust and other particles of volcanic origin and is made up of sedimentary rocks. This sedimentary system was believed to have been formed after granitoid gneiss rocks broke upon due to tectonic changes resulting in disturbance of sedimentation and formation of metamorphic rocks. These rocks are not found in their original horizontal manner, rather these have been greatly deformed by tectonic activities may be such as folding, faulting, tilting etc. And as such they have lost many traces of their sedimentary nature and have acquired crystalline and schistose structure. The weathering of the pristine Archaean gneisses and schists yielded the earliest sediments which were deposited on the bed of the sea, and formed the oldest sedimentary strata called the Dharwar system (Wadia, 1975). There are four types of rock system in this rock formation viz. (a) Igneous rocks, (b) Crystalline sedimentary rocks (c) Disfigured sedimentary rocks and (d) Intruded Igneous rocks. The rocks of Dharwad schists are spread in north south direction as bands in different sizes. Surrounding this are found granite and gneiss rocks.

The Dharwar system shales are thus a complex of rocks- like classic sediments, chemically precipitated rocks, volcanic and plutonic rocks-which have been highly metamorphosed. The main rocks are schist, phyllites and slates. The schists are of various types: horn-blende schist, chlorite schist, magnetite schist, haematite schist, feldspathic schist which are interbedded with quartzites, marbles, ophalcites, banded jaspers, beds of steatite, iron ores etc. These rocks are very much intruded by plutonic masses like nepheline-syenites, sodalite-syenites, tourmaline-granites, dunites etc. They occur in narrow elongated synclinal outcrops and are rich in minerals. The structure of the Dharwar rocks shows no layerings and these are mostly found in tabular form.

Distribution

The Dharwar system of rocks occur in scattered patches in: (i) Southern Deccan, (ii) Central and Eastern parts of the Peninsula, (iii) The north-western region, and (iv) The Himalayan region. The distribution of the Dharwar system shales in India is shown at **Fig. 2**. A brief description of these are presented in the following sections.

Southern Deccan

This includes the Dharwar region (presently called as Dharwad) of Karnataka state where these rocks have been found in abundance. These rocks occupy 15,540 sq. km. of area in Dharwad and Bellary districts of Karnataka and extend up to the Nilgiris, Madurai and Sri Lanka. Five prominent areas of occurrence of shales of Dharwar system have been identified (Naha et.al. 1993). They are Eastern, Eastern-central, Western-central, Central and West-ern belts. These rocks are divided into lower, middle, upper and post-Dharwar strata. Amongst these the lower Dharwar system are largely igneous, varying from acidic to basic. These are overlain by middle Dharwar system rocks consisting of quartzites, slates, conglomerates, horn-blende-schist, talc-schist, chart, iron-stone, marble and also some granite and porphyries. Numerous veins of quartz traverse these rocks. The rocks of upper Dharwar are predominantly sedimentary rocks, ferruginous, calcareous, siliceous and argillaceous, containing large quantities of iron and manganese ores. Rocks belonging to the Dharwar system are also found in Andhra Pradesh (Hyderabad, Guntur, Nellore), and Tamil Nadu (Arcot, Tiruchchirappalli).

Central and Eastern Peninsula

This is a large area spreading over the parts of the country in the states viz. Madhya Pradesh, (Balaghat, Chhindwara, Jabalpur), Maharashtra (Nagpur, Bhandara), Jharkhand (Ranchi, Singhbhum, Hazaribag), Orissa (Sambalpur, Keonjhar, Mayurbhanj) and West Bengal. The rock system here consists of main series viz. Chilpi Series, Sausar Series, Sakoli Series, Khondalite Series and Iron Ore Series.

North-Western Region

The Dharwar system rocks are found to occupy a wide surface area in Rajasthan and Gujarat states including the Aravalli Hills. These consist of the Aravalli system, the Raialo series and the Champaner series.

Extra-Peninsula

Outside Peninsula, the outcrops of the Dharwar system rocks are also found in the Meghalaya Plateau (the Shillong series in Khasi and Jaintia hills), the Himalayas (the Salkhala series in Gilgit, Baltistan, Ladakh, Karan and Kishtwar consisting of carbonaceous and graphitic shales, slates, phyllites, quartzites, schists, gneisses and marble).

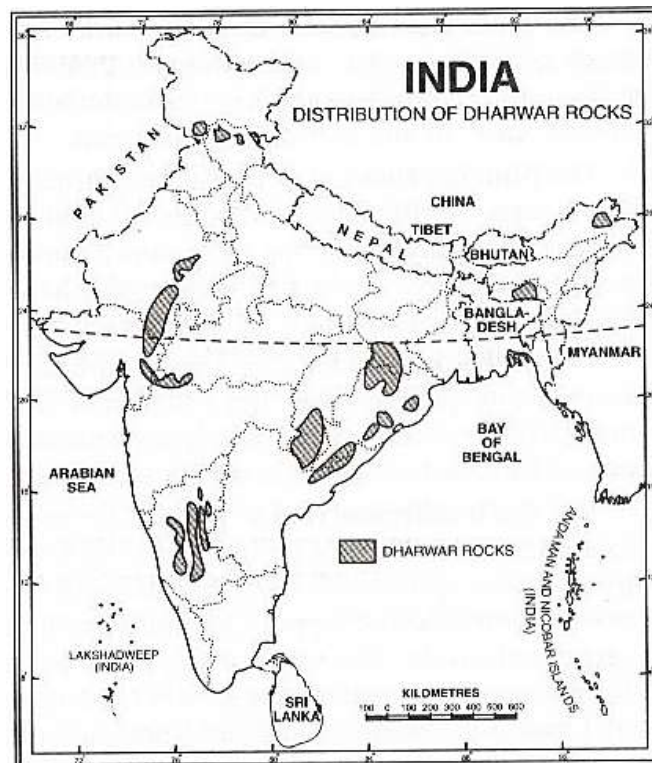


Fig. 2. Distribution of the Dharwar system shales over India



PROPERTIES OF SHALES OF DHARWAR SYSTEM AND THEIR EVALUATION FOR CONSTRUCTION

Shale in general is of interest with respect to its mechanical properties (Josh et al., 2012; Sondergeld et al., 2010). Deformation of soil and strength are critical for various stability problems. Horsrud (2001) noted the fact that the shales have certain characteristic features that make them difficult to handle correctly. The critical characteristics which make the shales problematic are low strength, high clay content, low permeability and sensitivity to contacting fluids.

Due to the varied nature of shales, the properties also vary for different shales. The index and geotechnical properties which are useful in the evaluation of shales as engineering material for construction have been determined. Table-II gives typical range of values of these properties. The desirable range of values of these parameters for the shales of Dharwar system are also given in the table along with their engineering evaluation (Waltham, 1994). The values indicated are based on the respective tests conducted as per the relevant IS codes for these tests. The evaluation offers further scope as well, for conducting few more tests viz. slake index test, slake durability index test, jar slake index test, point load test etc. and considering the values of these indices also for the evaluation.

Shales of Dharwar system and the soils derived from them are considerably problematic materials from the point of view of construction upon them. They are subject to changes in volume and competence that generally make them unreliable construction substrates. As can be seen from the Table-II, the shales of Dharwar system exhibit moderate to poor geotechnical characteristics to be considered as engineering material for construction. The clay minerals in some shale-derived soils have the ability to absorb and release large amounts of water. This change in moisture content is usually accompanied by a change in volume which can be as much as several percent and hence they exhibit the nature of expansive soils. When these soils become wet they swell and when they dry out they shrink. Buildings, roads, utility lines or other structures placed upon or within these materials are likely to get weakened or damaged by the forces and motion due to volume change. Owing to their poor shear strength, these shales are often associated with landslides. Weathering transforms the shale into a clay-rich soil which normally has a very low shear strength - especially when wet. When these low-strength materials are wet and on a steep hillside they can slowly or rapidly move down slope. Overloading or excavation by humans may also often result in failure. Shales of Dharwar system are hence considered to be one of the bedrocks that give potential problems for construction. As the overburdened load is removed during excavation, the rebound of the sides and bottom of the excavation in the bed shales causes the problem which is commonly faced. Swelling during monsoon deforms structural members or structural elements of engineering works in shale mass. Swelling of shales is a common problem for highways constructed in cut and fill situations. Shrinkage develops fractures along existing micro-cracks, thus degrading shear strength, and increasing hydraulic conductivity in rock mass. From the hydraulic conductivity point of view, these shales are impermeable except where silt or sand occurs in alternating layers within the shale mass. When these shales are weathered, it breaks and slakes easily. They slake almost immediately when exposed to air, which causes a problem during construction of tunnel and other underground openings in shale mass. The shales of Dharwar system and the soils derived from them, thus exhibit nearly similar behaviour as that of clayey or black cotton soils. There are some properties of these shales which are desirable even though these rocks are problematic for engineers and designers. For example, these shales can govern the hydraulic conductivity that controls movement of ground water by acting as a barrier. From excavation point of view, it is easily excavated and seldom requires ripping and almost never requires drilling and blasting.

USES OF SHALES OF DHARWAR SYSTEM

Shales of Dharwar system exhibit certain special properties that make them useful resources. Some of the possible uses of these shales are briefly mentioned below, which may open up scope and prospects even for exploring oil and natural gas, apart from yielding certain minerals

Clay Products

Shales of Dharwar system prove useful in forming the clay. As it is known, many products such as bricks, tiles, pots etc. are normally made from natural clay. However, such enormous and incessant use has resulted in depletion of most of the clay deposits, necessitating the need for a new source of similar raw material. Mixing finely ground shale with water would produce clay that often had similar or superior properties as that of natural clay. As a result, many of clay products that were once produced from natural clay have been replaced by almost identical items made from clay manufactured by mixing finely ground shale with water.



Table 2. Range of values of index and geotechnical properties of Shales of Dharwar system shales and their engineering evaluation

Sl. no.	Parameter	Typical Range of values for shales	Desirable range of values for construction	Average value of Shales of Dharwar System	Evaluation of Shales of Dharwar System as engineering material for construction
1	Natural moisture content (%)	20 - 34	5 - 20	18	Marginally acceptable.
2	Dry density (kN/m ³)	1.12 - 1.78	1.8 - 2.5	1.60	Marginally acceptable / Indicative of moderate strength.
3	Activity ratio	0.75-2.0	0.35 - 0.75	0.65	Highly Plastic. Acceptable but high volume change is expected
4	Predominant clay mineral	Illite/ Montmorillonite	Kaolinite / Chlorite	Montmorillonite	Unfavourable / High swell-shrink character expected.
5	Swell potential (%)	3 - 15	1 - 3	4.2	Unfavourable / High swell potential
6	Coefficient of Permeability (cm/sec)	1x10 ⁻⁵ - 1x10 ⁻¹⁰	>1x10 ⁻⁵	0.85x10 ⁻⁵	Marginally acceptable / Poor drainage property expected.
7	Angle of internal friction (degrees)	10 - 20	20 - 45	18	Unfavourable/ Indicative of low shear strength and low bearing capacity.
8	Cohesion (kN/m ²)	35 - 700 kN/m ² (3.5-70 t/m ²) (35-700 KPa)	700 - 10000	32	Critical / Indicative of low bearing capacity.
9	Unconfined Compressive Strength (UCS) (kN/m ²)	340-2070 kN/m ² (0.34-2.07 MPa)	2000 - 35000	3600	Marginally acceptable but critical / Indicative of poor strength characters.

Cement

These shales offer scope to produce cement as well, by crushing the shale and lime stone and then heating to a temperature that is high enough to evaporate off all water and break down the limestone into calcium oxide and carbon dioxide. The carbon dioxide is lost as an emission but the calcium oxide combines with the heated shale and results in a powder which is similar to cement and which gets hardened when mixed with water and allowed to dry. Such cement can be used to make concrete and many other products for the construction industry. This is another area that offers scope for the possible commercial exploitation of the abundant deposits of shales of Dharwar system.

Hydrocarbons

Liquid and gaseous hydrocarbons can be extracted from oil shale which contains significant amounts of organic material in the form of kerogen (a mixture of hydrocarbons from deceased plants and animals). But the rock requires to be heated and/or treated with solvents. This is usually much less efficient than drilling rocks that will yield oil or gas directly into a well. However,

extracting the hydrocarbons from such oil shales produces emissions and waste products that cause significant environmental concerns and this fact may be the reason for

the world's extensive oil shale deposits not being aggressively utilized.

Oil and natural gas

The black organic shales of Dharwar system are the source rocks for oil and natural gas deposits. These black shales obtain their black colour from tiny particles of organic matter that were deposited with the mud from which the shale formed. As the mud



was buried and warmed within the earth, some of the organic material was transformed into oil and natural gas, which then get migrated out of the shale and move upwards through the sediment mass because of its low density. The oil and gas are often trapped within the pore spaces of the rock unit which then easily flow into the extraction well as in case of a conventional oil/gas reservoir. Although large amounts of oil and natural gas can be extracted unconventionally from the reservoir rock by way of drilling, much of it remains within the shale and this oil and gas is very difficult to remove because it exists trapped within tiny pore spaces or adsorbed onto clay mineral particles that form the shale.

In the late 1990s natural gas drilling companies developed new methods for liberating oil and natural gas that is trapped within the tiny pore spaces of shale, and this was significant achievement which led to unlocking of some of the largest natural gas deposits in the world. However, steps in the direction to explore oil and natural gas from the shales of Dharwar system are yet to be initiated and their importance to the petroleum industry is yet to be established. Large scope thus exists to carry out the explorative works on shales of Dharwar system.

CONCLUSIONS

In the literature only a few studies are available that have been focussed and exclusively carried out on Dharwar system shales. Based on the limited horizon of the study carried out in this work, following broad conclusions are drawn. It may be noted that, the Dharwar system rocks offer a great scope further for elaborate studies particularly pertaining to their possible commercial exploration.

- i) Shales of Dharwar system are fine-grained laminated sedimentary rocks with silt and clay as predominant detrital particles. Other major constituents include organic matter and cementing materials. The minerals contained in these shales are distributed in the silts, clays, cementing materials and organic matter.
- ii) Clays and quartz are the main minerals constituting these shales. The other common minerals of these rocks include feldspars, calcite, mica, pyrites, iron oxides and organic carbon.
- iii) Texture, mineralogical composition, cementing materials, organic matter content, depositional environment and strength criteria can be considered for classifying these shales. They are found to vary in colour ranging from white through red and green to grey and black depending on mineralogical composition and depositional environment. They are water sensitive with low strength and low permeability.
- iv) The Dharwar system shales exhibit poor to moderate geotechnical properties and their engineering evaluation indicates that these rocks as well as their derived soils are considerably plastic in nature, weak in strength and hence are considered as problematic substrata for construction.
- v) The occurrence of black shales of Dharwar system can be found as source rocks, and reservoir rocks for prospecting oil and gas. These rocks may also offer prospects for being explored to manufacture clay products, cement and gaseous hydrocarbons.

REFERENCES

1. Farrokhrouz M. and Asef. M.R.. Shale Engineering: Mechanics and Mechanisms, CRC Press (Taylor & Francis), Florida, USA. 2013.
2. Boggs S.. Petrology of Sedimentary Rocks, Cambridge University Press. UK. 2009.
3. Porter, P.E., Mynard, T.B. Pryor, W.A. Sedimentology of Shale, Springer -Verlag, New York, USA. 1980.
4. Boggs, S.J. Principles of Sedimentology and Stratigraphy. Prentice Hall, New Jersey, USA. 1995.
5. Pettijohn, F.J. Sedimentary Rocks, Harper and Row Publishers, New York, USA. 2001.
6. Reineck, H.E. and Singh, I.B. Depositional Sedimentary Environments. Springer- Verlag, New York. 1980.
7. Krumbein, W.C. and Sloss, L.C. Stratigraphy and Sedimentation, W.H. Freeman and Company, San Francisco, USA. 1998.



8. 8.Wadia, D.N. Geology of India,Tata McGraw-Hill Publishing Co., New Delhi. 1989.
9. 9.Naha K., Srinivasan R.,Gopalan K.,Pantulu G., Subbarao M.V.,Vrevsky A. and Bogomolov Y. The nature of the basement in the Archaean Dharwar craton of southern India and the age of the Peninsular Gneiss, Earth Planet Science,Indian Academy of Science, Vol. 102, No. 4, pp. 547-565, 1993.
10. Josh M.,Lionel E., Claudio D. and Jole S Laboratory characterisation of shale properties, Journal of Petroleum Science and Engineering, Vol.6, pp.107–124. 2012.
11. Sondergeld C., Newsham K., Comisky J. and Rice M. Petrophysical Considerations in Evaluating and Producing Shale Gas Resources ,Unconventional Gas Conference, Pittsburg Pennsylvania, USA, Feb 2010, pp.23-25, 2010.
12. Horsrud P. Estimating Mechanical Properties of Shale From Empirical Correlations, Journal of Drilling & Completion, Vol.16(2): pp.68-73, 2001.
13. Waltham, A.C. Foundations of Engineering Geology, Blackie Academic and Professionals, London, UK., 1994.

Maintenance of PMGSY Roads in India

Sandeep K Shrivastava

Professor and Head, Civil Engineering Department, OIST, Bhopal

✉ joisthodce@oriental.ac.in

ABSTRACT

PMGSY is a nationwide plan with a view to provide all weather connectivity to remote rural villages which are unconnected to main road so far. This centrally sponsored scheme has launched by the PM Late Shri A. B. Vajpayee in 2000, 20 years ago with the aim to provide roads to all villages in rural India and by 2020 it is expected hundred percent connectivity will be achieved. Looking to the huge stock of rural roads the roads needs proper maintenance for smooth traffic facility to rural habitat to have optimum service in roads. This is in general the maintenance of roads are done by government Agencies but introduction of private contractors needed in present situation. The ownership of PMGSY road cluster connected to main road of particular chainage/KM awarded to private contractors for maintenance of roads for specified period.

Keywords : Agencies, maintenance, PMGSY, service, scheme, ownership.

INTRODUCTION

Maintenance of roads continues to be responsibility of Government agencies in India. The quality of road network remains as a subject of concern not only to Government department but also to as well road users. Proper maintenance of PMGSY road network & construction to adduces the long sharing public demand involves large investment & public money and are one of the most important public utility. There is a need to use better road construction & maintenance techniques and as well as ensuring accountability by the agencies involved in this existing conventional system of road maintenance by Government agencies should be worked and remained to explore the possibilities of introducing novel avenues such as innovative contracting procedure term contract to wide a few to treasure these possibilities near long lengths of time.

Aspects of Maintenance

The maintenance of PMGSY Road can be broadly classified in the following subheads

1. Ordinary Repairs
2. Renewal and Resurfacing
3. Special Repairs such relates to curves or of damaged CD works
4. Emergency repairs due to natural calamities such as floods, landslide and so on.
5. Routine Repairs



Fig. 1. PMGSY Road – Poor Maintenance



Contract Maintenance Procedure

PMGSY scheme can take up some pilot level projects for the maintenance of roads by involving private entrepreneurs. The task of maintenance of given roads connected between Chainage of main highways. The design and minimum levels of serviceability can be given on contract. It is suggested that an innovative contracting procedure be prepared for the maintenance of such PMGSY roads connected between chainage of NH and highways with minimum serviceability period fixed between 5 to 10 years. Before bidding the agency has to evaluate the structure and functional condition of pavement, condition of shoulders, drainage measures should bid for the contract to maintain the routes. It is suggested that a single contract incorporating all maintenance items should be feasible. This method of contracting would significantly reduce the contract administration cost.

Issues

Majority area of pavement section in PMGSY roads have inadequate crust thickness and poor subgrade and surface drainage facilities under these making it is very difficult to predict the future performance level of pavement.

There are uncertainties regarding the budget allocation for maintenance of PMGSY roads.

The roads of five years or so old there is a absence of maintenance record of road i.e. maintenance history of PMGSY roads are not known.

Due to heavy traffic and overloading the point is that why roads would fail much earlier than the anticipated design traffic.

Advantages of contract management

The firm which has to maintain a minimum level of serviceability has to use better materials, better methods or Constructions, employing the staff available for the maintenance and machinery. The private firm taking the responsibility of preventing premature failure of roads due to overloading and heavy rains. The PMGSY roads will become more safer as there will be proper sign boards markings and will be maintained by firm. May firm will be responsible of mainting the riding quality of during its serviceability time. There are number of problems of maintenance such as minor changes, rain water drains and repairs of CD works.

On the project maintenance contract for which the contractor established an appropriate quality system the PMGSY department engineer has to perform the audits of system like inspection of work and random sampling of materials used in maintenance of roads there by limiting the role of PMGSY engineers, there will be an objective evaluation of road condition in terms of riding quality, problems of subjective assessment are eliminated such as condition of road surface physical condtion of culverts & minor bridges condition of shoulders etc.

CONCLUSIONS

The problem of poor condition of PMGSY roads in India cannot be solved by enhanced allocation of funds for maintenance alone, effective utilization of funds can be realizes by the inclusion of private sectors and by innovative contract procedures.

The problem of higher maintenance cost of PMGSY roads can be managed by private entrepreneurs to develop commercial establishments at the suitable junctions of NH to PMGSY road of government land generate funds from shops, from stipulated time period of 5 to 10 years and maintain the PMGSY roads cluster under these particular Chainage of NH there by reducing the budget allocation of maintenance of roads.

The NGO of young engineers can be involved in the maintenance of PMGSY roads to reduce the unemployment. The promotion of self help groups of locals comprising of team of Engineers willing to undertake maintenance of PMGSY Road can be improve their proposals.

An innovative contract procedure of professional employment can result in lower overhead costs and direct cost to the government.

In the end it could be summarised at the maintenance of PMGSY roads through contracts 5 to 10 years needs to be tried on extensive scale in their of privatization where large role is contemplated for private entrepreneurs

REFERENCES

- Pateriya & Indresh. Maintenance of Rural Roads under Pradhan Mantri Gram Sadak Yojana(PMGSY) in India.
- K.C. Manjunath. PMGSY and Rural Development in India; Economic Financial and Maintenance Issues, Indian Journal of Applied Research, VOL-1, Issues 5.



Way Forward to Enhancing Skills for Betterment of Indian Economy through Construction Industry

Sekar Kumbeswara

Chief Engineer & Administrator, ALHW (Retd.) Ministry of Shipping, GOI

✉ ksekar_alhw@yahoo.com

ABSTRACT

The construction industry in India is one of the prime contributors towards the economic development of India. There has been inordinate delays in project implementation thereby resulting in cost-over-run. Reasons behind such delays, solutions and way forward are discussed in this paper.

Keywords : Project management; Ease of doing business; Factors delaying projects; Self-reliant India; Unfair clauses.

INTRODUCTION

The Construction industry of India is an important indicator of the development of India as it creates investment opportunities across various related sectors. With a share of around 9%, the contribution of construction industry to the national GDP at factor cost in 2011–12 is estimated as ₹670,778 crores (US\$ 130 billion).

In the report of Ministry of Statistics and Program Implementation, Government of India it is stated that out of 782 construction projects in India monitored by it, a total of 215 projects are delayed from 1 to 261 months of time-overrun. The primary causes which are noted are delays in land acquisition, obtaining forest/environment clearances, tie-up of project financing, finalization of detailed engineering, tendering, ordering and equipment supply, lack of infrastructure support and linkages, ordering and equipment supply, changes in scope, geological surprises, delay in tendering, , law and order problems, and contractual issues.

Major impact of delays

1. Delays in projects causes a direct impact on the overall cost of project. For example, from 2010 to 2015, the cost of cement (per bag) increased by 74%, steel increased by 34%, bricks increased by 69%, sand increased by 240% and skilled labor (on a per day basis) increased by 96%. It is therefore, understandable, that the cost overrun in delayed projects has resulted in approx. 24.77% increase in the original cost of the projects, amounting to Rs. 1, 09,359crores.
2. The likelihood of disputes between the parties in a contract increases multifold and these disputes may derail the project. A statistics show that the average duration for settlement of disputes is more than 7 (seven) years in India.[1]

Over the past few decades, there has been several big-ticket infrastructure projects launched in India, investing billions into the country's aviation, industrial development, railways, roads, smart cities and energy sectors. The most recent available Flash Report of September 2018 published by the Ministry of Statistics and Planning

states that out of 1,420 central-sector infrastructure projects worth Rs 1.50 billion and above, 385 are on schedule, 366 projects delayed, 358 projects reported cost overrun, and 136 projects are both time and cost overrun. Around 32 mega projects have reported additional delays vis-à-vis their date of completion. [2] The predominant reasons for delays in project completion are:

- 1) Lack of expertise in project planning and management by the project authorities
- 2) Environment issues
- 3) Insufficient data collection and analysis before formulation of detailed Project report
- 4) Change in Government laws
- 5) Bureaucracy of the Government officials and Corruption
- 6) Frequent Change Orders



- 7) Poor estimation without consideration of steep escalating costs
- 8) Inadequate funds flow for the project
- 9) Lack of knowledge of updated technology by project authorities which leads to wrong planning and varying costs
- 10) Unfair and one sided substandard contract clauses

Prime Minister Narendra Modi's administration has drawn up a plan for an estimated cost of \$1.5 trillion of such projects over five years. But delays in land acquisition, environment clearances, and financing are among issues that have held up projects over the years -- a big worry for multilateral investors when it comes to funding projects in India. [3]

The reason for this worry is quite justifiable as the investors are worried about the unfair clauses in the construction contracts, especially those executed by departments under state or union governments in India.

It is highly imperative that India needs to move faster on the reforms front and to lure global investments. The available data suggests that the resources required for starting a business can be considerably higher in the lower income economies. Improving the conditions for "Ease of Doing Business" (EoDB) rankings have been a great opportunity to improve India's internal processes and structural changes and make them business-friendly. This could give an edge of benchmarking India, on common parameters, with the rest of the world. In fact, with competition among countries hotting up, EoD Rankings have become the sole biggest value proposition to attract investment.

Sectors like rail, road, transport, steel and cement are crying for such reforms. The priority reforms which are demanding are enforcing contracts, registering property, starting a business, and paying taxes. For example, for enforcing contracts during the year 2019, India's rank was 163rd among 190 economies which implies much time and cost overruns in resolving commercial disputes, which is certainly not conducive for a thriving business environment. [4] The way forward is to carry out long pending reforms of judicial systems in India. A slew of small, but bold, decisions, which may not even be politically fashionable, offer a great opportunity to make a lasting difference.

Recently, as a part of the government's economic stimulus package announced under AtmaNirbhar Bharat Abhiyan, the Government of India has decided to bring various amendments to Insolvency and Bankruptcy Code and Companies Act, 2013 to enhance ease of doing business in the country. The vital areas where India should invariably do a lot of progress and to improve score on Ease of Doing Business are the six parameters- enforcing contracts (163rd), resolving insolvency (52nd), starting a business (136th), registering property (154th), paying taxes (115th) and trading across borders (68th) where it has been scoring very low. [5] Though it is a tough job to improve on these pointers, it is a must that stringent actions are to be taken to regulate them through judicial reforms.

Project related activities-Problems and Solutions

It is very important to identify and spot the project failures before they actually happen. The following are the indicators to such disasters.

- 1) When the stake holders show lack of interest by not turning up for meetings and discussions. If stakeholders stop caring about a project, it is high time to 'hold a sit-down' to determine the current perceived value of your project to the organization.
- 2) When there is poor communication. The best Project manager spends 90% of his time on communication with his team, stake holders and project authorities. Fast, automated and efficient communication system should be ensured.
- 3) When honesty about the velocity is lost. There cannot be any delay in approvals or decision making on problems. The Project Managers should be so capable of facing the bottleneck at lightning speed and hence they should have proper training, education, will and drive to face the situation daringly.
- 4) No-Bad News Situation shall prevail. This is possible only if a proper and instant tracking system of all activities is in place and monitored closely by the monitoring team of the Project manager.
- 5) Minimize Scope Change. This is possible only when proper investigations are done before formulation of the project by abundant data collection, analysis. When this is done stupendously, the design of project becomes near perfect which renders almost correct estimation. A good project Manager with the support of a good management can draw a balanced tender document which is the key for completion of project without time or cost-over run.

It is high time to see certain examples of poor planning and lack of project management ideas.



- 1) Gujarat International Finance Tec (GIFT) City that is planned on 886 acres of land near the Ahmedabad airport as a 50:50 joint venture between International Leasing and Financial Services (ILFS) and a state government firm. The 78,000 crore project is caught in red tape.[6] Several buildings being left incomplete with power supply yet to be made available due to lack of clearances. In addition to this delay, permission to lay the underground power cables to the city has not been obtained from the National Highways Authority of India (NHAI). And to top it all, due to lack of norms of operating procedures, the project has not been able to attract a single client to set up operations. This is a clear example where the project is announced first and clearances applied for later.
- 2) In Sept 2011, Delhi received a massive amount of rainfall as a result of a cloudburst. As a result, a part of T3, the spanking new airport terminal, was under ankle deep water, parts of the roof leaking profusely, the underpass leading to the airport under 4 feet of water. Basically, the brand new airport was in a state of partial shutdown and a total mess. This is a glaring case of poor vision, poor planning, bad design and poor execution.

Way Forward to improve Project Management Techniques

An area of project management that requires the greatest improvement is the definition of explicit, realistic, immediate, and long-term development objectives. The success for any project is possible only when objectives are understood and accepted by all participants in project administration. Knowledge in proactive risk management associated with the scope, schedule and cost of the project is extremely demanding for the entire project management team.

Developing countries like India require two types of trained and expert project administrators:

- i) who can plan and coordinate the entire project cycle as an integrated process and
- ii) who can manage the project as an organizational entity once it is selected and approved.

Most importantly, the needs of the “client” should be kept in mind on priority while improving project management techniques. Any new designs that violate the social, cultural, political and organizational traditions of developing countries simply will not work. Techniques must be developed which are sensitive to national needs, available resources, constraints and opportunities. These techniques must take advantage of the experience of local officials who know best what will work or will not work in their own countries.

Need for Fair Conditions in Construction Contract Documents

The most important reason for the poor response of global tendering in India is that in most of the tenders, the vital conditions are one sided and unfair. They are mostly a “Take it or Leave it” type of documents. Such tenders and contracts invariably lead to disputes and end up with arbitration and litigation thereby the parties are put to heavy loss apart from inordinate delays in project completion and cost overrun.

Some examples of unfair clauses in the contracts are elucidated below:

- 1) Clause (22) Conditional/ Incomplete tender will not be accepted. (Tender Ref. No: WBPWD/EE/BED/41/e-IT of 2019_20_3rd call)

It is understandable to reject incomplete tenders but not conditional tender. Conditions arise only when details or data provided in the tender documents are truncated or insufficient. This means that the project authorities have not done proper home work to collect all relevant data to suffice requirements.

- 2) “No claim for interest or damages will be entertained by the Government with respect to any money or balance which may be lying with the government or may become due owing to any dispute, difference or misunderstanding between the Engineer-in-charge on the one hand and the contractor on the other hand or with respect to any delay on the part of the Engineer-in-charge in making periodical or final payment or in any other respect whatsoever” which is unfair.
- 3) Under the general law of contracts, once the contract is entered into, any clause giving absolute power to one party to override or modify the terms of the contract at his sweet will or to cancel the contract – even if the opposite party is not in breach, would amount to interfering with the integrity of the contract.
- 4) A clause in a contract debarring the contractor from claiming escalation in rates has been construed to be limited only up to the stipulated period of contract and not beyond.
- 5) One sided clauses providing for unlimited variation in quantities and unfair interpretation of variation clauses have been set



aside by the Courts by holding that the Engineer-in-charge cannot require a contractor to execute additional work without any limit and that a reasonable limit should be placed on the quantity of additional work, which the contractor may be required to execute at the rate stipulated for the main work under the contract.

The Standard form contracts of the government departments and PSUs are usually pre-printed contracts that are only “contracts” in name. The standard terms and conditions unilaterally prepared by one party are offered to the other on a take it or leave it basis, rather, the terms are forced on the other party. When the party having greater bargaining position has introduced exemption clauses unilaterally in its own favor, the courts have no other option but to give full effect to those unreasonable or unconscionable clauses which have been agreed upon and signed by both parties in accordance with the current laws in force.

With a view to reform this lacuna, the Law Commission of India in its 103 Report suggested that an additional Section 67A be added to the Indian Contract Act, which reads as follows:

“67A. (1) Where the Court, on the terms of the contract or on the evidence adduced by the parties, comes to the conclusion that the contract or any part of it is unconscionable, it may refuse to enforce the contract or the part that it holds to be unconscionable.

(2) Without prejudice to the generality of the provisions of this Section, a contract or part of it is deemed to be unconscionable if it exempts any party thereto from – (a) the liability of willful breach of contract, or (b) the consequences of negligence.”[7]

The 199th Report of Law Commission of India on UNFAIR (PROCEDURAL & SUBSTANTIVE) TERMS IN CONTRACT submitted to Government of India during August, 2006 states as, “Our business and commerce will be put to serious disadvantage if we do not have a law regulating unfair terms of contract.....Therefore, it has become necessary to provide additional provisions in India for redressal against unfair terms of contracts”. [8] The highlight of this Report is the consideration of Unfair Terms of Contract by separating the ‘procedural unfairness’ and the ‘substantive unfairness’ in the matter of contracts or their terms and strengthening the recommendations of the Law Commission report 103.

What is proposed in this Report and the Bill is to provide additional provisions of ‘procedural unfairness’ and ‘substantive unfairness’ and remedies for removing such types of unfairness. These new remedies can be granted by the Civil Courts, arbitral tribunals and the consumer fora under the Consumer Protection Act, 1986 in addition to what has already is provided for in The Indian Contract Act, 1862.

“Section 16 ‘Undue influence’ of Indian Contract Act, 1862 defines: (1) A contract is said to be induced by ‘undue influence’ where the relations subsisting between the parties are such that one of the parties is in a position to dominate the will of the other and use that position to obtain an unfair advantage over the other.

(2) In particular and without prejudice to the generality of the foregoing ..., a person is deemed to be in a position to dominate the will of another –

(a) When he holds a real or apparent authority over the other or where he stands in a fiduciary relation to the other; or

(b) Where he makes a contract with a person whose mental capacity is temporarily or permanently affected by reason of age, illness or mental or bodily distress.”

(ii) Subsection (3) of sec 16: The other relevant provision is sub-section (3) of section 16 which refers to the aspect of burden of proof in ‘unconscionable transactions’ induced by ‘undue influence’. Sub section (3) of section 16 and illustration

(c) Are reproduced as under:-

“16(3) Where a person who is in a position to dominate the will of another, enters into a contract with him, and the transaction appears, on the face of it or on the evidence adduced, to be unconscionable, the burden of proving that such contract was not induced by undue influence shall be upon the person in a position to dominate the will of the other.

Nothing in sub section shall affect the provisions of section 111 of the Indian Evidence Act, 1872.”

Though countering and beating of these unfair clauses in the contract is being pushed for approval of the government for more than two decades, it is unfortunate that no fruitful results have emerged yet. It is high time that this should be taken up by competent forums with the Government which will go a long way in achieving the goals of the country in reaching to top slots in the global survey of “Ease of Doing Business” which will create tremendous potential of FDI, thereby uplifting the economy.



RECOMMENDATIONS

- 1) The contract documents for infrastructure projects should be standardized in line with FIDIC MODEL contract forms for all major contracts. This should be enforced in all construction departments of Governments.
- 2) Lack of Project Management techniques with the project authorities and construction agencies is a major problem and bottleneck causing delays in completion of projects. Hence, it is imperative that all such authorities should be trained suitably in Project Management techniques through workshops, seminars, training programs etc.
- 3) Project Management should be introduced as a part of core subject in the curriculum of under graduation streams with special post-graduation stream for the same including Risk Analysis and management so that there is no dearth of Project Management expertise in this country.
- 4) The recommendations contained in the Law Commission Report of 2006 in this regard of unfair clauses should be passed and promulgated without further delay.
- 5) Red tapism in bureaucracy should be curbed to the maximum extent and transparency brought in.
- 6) All clearances to be under single-window- system.
- 7) Necessary and adequate judicial reformation should be brought in expeditiously. Promotions to Engineering cadre to Group A positions in government departments shall be made on selection basis by scrutiny of their integrity, attitude, aptitude, knowledge, shrewdness to tackle unexpected situations by way of test, examination and personal interview etc. without any favoritism or politics.

CONCLUSION

For achieving the ultimate goal of raising the country as a leading economy in the world, it is essential that proper and sincere introspection by each and every citizen of this country, especially Engineering and project Management fraternity is a must. The government, having committed to reforms, should work in the directions suggested in this paper by giving a serious consideration. As per the proverb, “If there is a will there is a way”, what is all the more desired now is the “WILL” to enhance the skills, quality and safety to promote India as a self-reliant country.

REFERENCES

- 1) India: Delays In Construction Projects, 24 January 2017, by Khyati Rathod and Niharika Dhall
- 2) Shrial Sethumadhavan and Rahul Kamat, How India is losing Rs 3 trillion in infrastructure projects! 02 Jan 2019
- 3) India’s crawling infrastructure projects to be delayed further by Covid and lockdown, Vrishti Beniwal 31 July, 2020
- 4) P K Vasudeva, | November 4, 2019, Business India
- 5) World Bank’s ease of doing biz: DPIIT focusing on 6 parameters to push India’s ranking.
https://economictimes.indiatimes.com/news/economy/policy/world-banks-ease-of-doing-biz-dpiit-focusing-on-6-parameters-to-push-indias-ranking/articleshow/73106380.cms?utm_source=contentofinterest&utm_medium=text&utm_campaign=cppst
- 6) Vikas Dhoot, The Economic Times, Nov., 10, 2014
- 7) <https://indiankanoon.org/doc/107622101/>
- 8) The 199th Report of Law Commission of India on Unfair (Procedural & Substantive) Terms in Contract submitted to Government of India during August, 2006.



Fibre Reinforced Geopolymer Concrete as a Repair Material for Rigid Pavements-A Review

Peter Cibi*, Karthi Lathi

Department of Civil Engineering, TocH Institute of Science and Technology, Kochi, Kerala

*✉ peter.cibi@gmail.com

ABSTRACT

Concrete is a durable construction material, yet it is susceptible to distresses and deterioration. Numerous concrete repair systems are available with repair materials comprising of either cementitious types or polymer-modified cementitious types. The focus on sustainability in present times makes the use of cementitious based repair materials undesirable and hence the search for a sustainable and durable repair material is very relevant. Geopolymer concrete repair materials have gained considerable interest in this regard. Geopolymer is relatively a new construction material which could be produced by the chemical action between alumino-silicate material such as fly ash or blast furnace slag and alkaline solutions like sodium silicate or sodium hydroxide. They generate 70-80% less carbon dioxide than concrete made with ordinary Portland cement, making them ideal in aspects of both sustainability and durability for repair. In this paper, the focus is on the use of geopolymer based repair materials for rigid pavements. Concrete pavements undergo various types of distresses and damages during its lifetime such as damages in joints, shrinkage cracking, corner breaks, punch out, linear cracking, durability cracking and so on. Fibre reinforced geopolymer concrete which have proved useful as a repair material for different construction purposes due to its improved tensile characteristics and crack control properties are promising sustainable and economical solution to pothole repair for both flexible and rigid pavements. The enhanced bonding between the concrete substrate and better durability properties of fibre reinforced geopolymer concrete are ideal properties to be considered as repair material for rigid pavement. This paper reviews the literature related to the various studies conducted on fibre reinforced geopolymer concrete and the repair materials for rigid pavements with the purpose of finding common ground in both.

Keywords : Geopolymer concrete; Alumino-Silicate; Rigid pavements; Alkaline solution; Polypropylene.

INTRODUCTION

Deterioration in infrastructure and its repair and rehabilitation is one of the major challenges of modern construction industry that civil engineers face nowadays. The deterioration of concrete includes the loss in compressive strength, cracks formation and increase in porosity. Repairing concrete is one of the emerging sectors in construction industry. There are numerous methods and techniques for concrete repair and a wide variety of repair materials are available in the construction field. The two types of materials for concrete repair are cementitious and polymeric. The cementitious materials include materials based on portland cement, blended cement and rapid hardening cement. Among polymeric materials, one type is polymer modified concrete, in which latex, water soluble polymer or liquid polymer are mixed with an ordinary portland cement (OPC). Another type is polymer concrete which makes use of a polymer binder for the aggregates without using OPC. The selection of repair materials depends on factors like rapid setting, high flexural and compressive strengths, bond strength to the substrate, low drying shrinkage and similar modulus of elasticity as the substrate and low compressive creep. The major draw backs in selecting cementitious repair materials are low tensile strength and low durability problems like chemical attacks such as alkali -silica reaction, acid attack and sulphate attack, which in turn lead to corrosion and deterioration of the concrete structure. They are also not sustainable due to the fact that the major component is cement and manufacturing 1 ton of OPC releases around one ton of carbon dioxide (CO₂).

The focus on sustainability in present times motivates research in sustainable repair material. Geopolymer concrete (GPC), first introduced by Joseph Davidovits [15] is desirable in this regard. It is created by the reaction of alumino silicate binders such as fly ash (FA)/ground granulated blast furnace slag (GGBFS)/metakaoline (MK) with the alkaline solutions like Na₂SiO₃ /sodium hydroxide (NaOH). Geopolymer cements cure more rapidly than portland cement based concrete. Most of the compressive strength is gained within a day. Geopolymer binder production releases 80-90 % less CO₂ than OPC and usage of waste



industrial byproducts such as fly ash and ground granulated blast furnace slag make geopolymer a green material. Though the cost of producing geopolymer binder is higher than that of manufacturing OPC, it can be reduced by selecting the nearest source of feedstock thereby reducing the cost of transportation of raw materials. This paper reviews the use of geopolymer based repair materials for rigid pavements.

There are two types of pavements based on design considerations i.e. flexible pavement and rigid pavement. Difference between flexible and rigid pavements is based on the manner in which the loads are distributed to the subgrade. Flexible pavement can be defined as the one consisting of a mixture of asphaltic or bituminous material and aggregates placed on a bed of compacted granular material of appropriate quality in layers over the subgrade. A rigid pavement is constructed from cement concrete or reinforced concrete slabs. The rigid pavement has rigidity and high modulus of elasticity to distribute the load over a relatively wide area of soil.

Rigid pavements undergo various types of distresses and damages during its life time such as spalling, shrinkage cracking, corner breaks, punch out, linear cracking, durability cracking etc. The main techniques used for rigid pavement repairs are full depth repair, partial depth repair, diamond grinding and retrofitting dowels. Partial depth repairs are performed if the deterioration is within $(1/3)$ rd of pavement slab thickness. It is deployed if the patch is of size 300mm X 100mm in area. The repair materials used are either normal setting plain cement concrete (PCC), high early strength PCC, rapid strength developing materials such as epoxy resin mortar or epoxy concrete. A “green” alternative for the rigid pavement repair could be fibre reinforced geopolymer concrete (FRGPC).

FRGPC has excellent flexural properties, crack control and toughness. There are numerous fibres compatible with geopolymer binder. Poly vinyl alcohol (PVA) fibres are highly stable in alkaline environment and show good bond to geopolymer binders but cost of PVA fibres are high. Steel fibres are relatively cheaper and exhibit excellent toughness. Addition of polypropylene (PP) fibre up to a limit of 2.5% by volume of binder increases the mechanical properties of GPC. For instance, adding PP fibres to Fly ash based GPC increases the ductility of the resulting compound. The presence of fibre in the geopolymer matrix makes the mix stiffer but this could be well compensated with addition of suitable super plasticizer. FRGPC excels in fire resistant properties and resistance to sulphate attack. It is used for constructing underground structures with outstanding mechanical, durability and shrinkage properties compared to OPC concrete with 70 % less carbon emissions.

In summary, the enhanced mechanical properties, less shrinkage and durability properties of FRGPC make it an excellent contender as a repair material in the current market. The addition of calcium compounds or slag based geopolymer can reduce the setting time. The incorporation of PP fiber in to GPC resulted in improved tensile characteristics, crack control, bond strength to the substrate and increased durability properties particularly with outdoor heat exposure (OHE) cured composites. Geopolymer cement is widely used for the construction of rigid pavements in North America for the last three decades under the brand name Pyrament© [14]. Thus FRGPC could be used as a sustainable and economical solution to pothole repair for both flexible and rigid pavements.

LITERATURE REVIEW

Turner L K et al. [37] compared the carbon dioxide equivalent ($\text{CO}_2\text{-e}$) emissions between GPC and OPC concrete. They found that 76.4 % $\text{CO}_2\text{-e}$ for the OPC concrete. GPC shows comparatively 9 % less emissions than that of GPC. If the GPC is made with blended binders such as GGBFS and fly ash, $\text{CO}_2\text{-e}$ emissions could be reduced by 19%-29 %.

Palomo A et al. [7] studied about the alkali activated fly ashes as a “cement for the future”. Class F fly ash was used for the experiment. The activators used are 12M NaOH, 18M KOH, $\text{Na}_2\text{SiO}_3 + \text{NaOH}$ pellets and $\text{Na}_2\text{SiO}_3 + \text{KOH}$ pellets. The alkali activation reaction of fly ash takes place as an exothermic process of dissolution, during which the breakdown of the covalent bonds Si-O-Si and Al-O-Al in the silicon and aluminum then pass into the solution. The reaction results in a poorly ordered structure with good mechanical strength. The curing temperature influences the gain in strength of the compound. Alkaline solutions containing soluble silicates increase the rates of reactions than solutions containing hydroxide. The binder to activator ratio was not so significant in strength development of the compound.

M Komljenovic et al. [25] studied about the mechanical and micro structural properties of alkali-activated fly ash geopolymers. The investigation made use of class F fly ash and the alkaline activators used were $\text{Ca}(\text{OH})_2$, NaOH, Na_2CO_3 , KOH, $\text{Na}_2\text{O} \cdot n\text{SiO}_2$ (Aqueous solution of Na_2SiO_3 – water glass, $n = \text{SiO}_2/\text{Na}_2\text{O} = 3.04$). The highest compressive strength was found when Na_2SiO_3 was used as the activator.

Ren X et al. [39] studied experimentally about the properties of GPC from waste concrete. The initial setting time was found to



be varying between 21 to 151 minutes and it was affected by the binder to aggregate ratio as well. It was also seen that the high calcium fly ash-based geopolymer paste/concrete has a shorter initial setting time than the class F fly ash-based geopolymer paste/concrete in general.

Ding Y et al. [41] studied the fracture properties of fly ash/slag based GPC cured in ambient temperature. It was found that the increase in alkali concentration from 3% to 5% increased the compressive strength of slag/fly ash GPC by 83. 6%. Increase in slag content also increases the compressive strength due to the presence of calcium. The splitting tensile strength of fly ash/slag based GPC increased by 32.3%, when the alkali concentration increased from 3% to 5%.

Jithendra C et al. [22] studied the role of super plasticizer on GGBFS based GPC under ambient curing. GPC was made up of 100% GGBFS, Na_2SiO_3 to ratio of 2.5, alkaline activator to binder ratio of 0.5, super plasticizer (2% to 6%) and the concentration of 12M NaOH. The workability of concrete was increased with increase in percentage of super plasticizer. It was found that the compressive strength slightly decreased with increase in percentage of super plasticizer.

Chindaprasirt P et al. [9] investigated the basic properties like workability and strength of geopolymer mortar made from coarse lignite high calcium fly ash. The geopolymer was activated with NaOH, Na_2SiO_3 and heat. The results revealed that, increase in NaOH and Na_2SiO_3 concentrations reduced the flow of mortar. The workable flow of geopolymer mortar was in the range of $110 \pm 5\%$ – $135 \pm 5\%$ and was dependent on the ratio by mass of Na_2SiO_3 to NaOH and the concentration of NaOH. The obtained compressive strength was in the range of 10–65 MPa. Improvements in the workability of the mortar could be achieved with addition of water or super plasticizer. However, the use of super plasticizer had an adverse effect on the strength of geopolymer. The optimum Na_2SiO_3 to NaOH ratio to produce high strength geopolymer was 0.67–1.0. The concentration variation of NaOH between 10 M and 20M was found to have a small effect on the strength.

S.K.Saxena et al. [34] investigated the fire resistant properties of geopolymer cement mortars. Fly ash, GGBFS, calcined clay and silica fume were used as the different alumino silicate materials. The alkaline solution was a combination of 8 % NaOH and 10% Na_2SiO_3 . The presence of silica fume increased the development of compressive strength as it increases the geopolymerization and decreases the porosity. Geopolymer mortars made from all the raw materials were quite fire resistant up to 600°C but after that the fire resistant property decreased. Fly ash based geopolymer mortar containing silica fume had the maximum fire resistant property at 800°C and 1000°C.

Saha S et al. [35] studied about the addition of GGBFS to enhance the properties of fly ash based GPC. In this study, GGBFS is added 10%, 20%, 30%, 40% and 50 % of the total binder. NaOH to Na_2SiO_3 ratio is kept as 1.0 and alkali solution to binder as 0.4. It was found that addition of GGBFS reduced the initial and final setting time of GPC. Initial setting time of geopolymer paste was found to be reduced by 73%–94% and final setting time was reduced by 77%–92% with the addition of GGBFS from 10% to 50% in the mixes when compared to the setting time of geopolymer paste mixes without GGBFS. Compressive strength showed an increasing trend when the concentration of NaOH and the percentage of GGBFS were increased.

Bakharev T. [8] studied about the geopolymeric materials prepared using class F fly ash and cured at elevated temperature. Fly ash was mixed with sodium NaOH and Na_2SiO_3 solutions, providing up to 10% Na in mixtures and water/binder ratio of 0.3. The samples did not harden after 1 day curing at room temperature. The sodium % of sodium (Na) in the alkaline solution had significant role in the compressive strength development of GPC. It was found that keeping the geopolymer samples at room temperature and application heat curing increases the strength significantly. It was found that fly ash activated by Na_2SiO_3 with 6 hour heat curing is better than 24 hour curing for the strength development.

Chindaprasirt P et al. [10] investigated the effect of calcium-rich compounds on setting time and compressive strength development of alkali-activated fly ash (FA) pastes. Three calcium rich compounds viz., Portland cement (PC), $\text{Ca}(\text{OH})_2$ and calcium CaO were used as additives to replace FA at the dosages of 5, 10, and 15% by weight basis. NaOH and Na_2SiO_3 solutions were used as alkali activator liquids in all mixtures. Alkali activator liquid/solid binder (FA and calcium-rich compound) ratio of 0.60, Na_2SiO_3 -to- NaOH ratio of 2.0 and curing at ambient temperature (25 °C) were used for all mixes. Test results showed that the setting time and compressive strength of alkali-activated FA depended on the type and content of calcium-rich compound. The incorporation of all three calcium additives resulted in the acceleration of setting time. Alkali-activated FA with $\text{Ca}(\text{OH})_2$ and PC could improve the strength development; however, the use of CaO resulted in the compressive strength reduction. The 28-day compressive strengths of alkali-activated FA with 15% PC and 5%, 10% and 15% CH met the strength requirement for repair material as specified by ASTM standard. The alkali-activated FA with additives can thus be used as an alternative repair binding material.



Phoo-ngernkham T et al. [36] developed a low cost and sustainable repair material made from alkali activated high calcium FA with calcium carbide residue (CCR). It was found that the setting time decreased with both (CCR) replacement and Na_2SiO_3 to NaOH ratio. As the CCR contains around 89.2 % CaO, the heat generated by CaO helped the geopolymerization. The high Na_2SiO_3 -to-NaOH ratio reduced the setting time also. This was because the reactive SiO_2 from Na_2SiO_3 solution reacted with CaO from high calcium FA and CCR. The fast setting of alkali activated mortar is advantageous for repair material. As per ASTM C881/C881M-14 the required initial setting time for repair material must be less than 30 minutes. Up to 30 % increment in CCR replacement with FA, the compressive strength tended to increase. The maximum was 64.6 MPa for 20% where the control mix had 51.8 MPa. The Na_2SiO_3 to NaOH ratio had also an impact on strength increment, the maximum strength showed on when the ratio was 2.0. The 28-day shear bond strength between repair mortar and concrete substrate tended to increase with increasing CCR replacement and Na_2SiO_3 -to-NaOH ratio up to an optimum level. For example, the shear bond strengths for 100FA- Na_2SiO_3 /NaOH = 2.0 and 80FA/20CCR- Na_2SiO_3 /NaOH = 2.0 were 9.0 and 15.0 respectively.

Laskar S M et al. [33] studied about the mechanical properties of ultra-fine slag based geopolymer (UGGBS) as a concrete repairing agent. It was found that the GPC mix containing only UGGBS had very poor workability of 25 mm. Addition of FA increases the workability and polyether based super plasticizer efficiently increased the workability. Addition of Fly ash in UGGBS based GPC decreased the compressive strength of the GPC. The mixes without any FA content or low FA content (less than 40%), could attain high strength at early ages. About 50, 80 and 90% of 28 days strength were attained by these mixes at 1, 3 and 7 days respectively. It is evident that the bond strength (pull out) of mix with 30% FA content is highest compared to others.

Huseien G F et al. [20] evaluated the performance of alkali activated mortars containing industrial wastes as a surface repair material. It was found that the increase in FA content reduced the workability (Flow test). The mix containing GBFS and FA in 50:50 ratios exhibited the maximum flow percentage of 56. A steady increment in compressive strength also found with the increased percentage of GGBS in mix. An enhancement in the GBFS content lead to the formulation of the higher amount of C-A-S-H gel in the mixtures containing up to 30% of GBFS than the other mixtures. An increase in the GBFS content could cause the formation of more C-S-H and C-A-S-H gels beside the N-A-S-H gel, which in turn increased the bond strength and improved the microstructures of the GPC mortars especially after the 28 days of age.

Sharkawi A et al. [2] compared geopolymer and high strength grout as repair material for reinforced cement concrete. Two phases of geopolymer mortars have been used; namely plain geopolymer mortar (GPM) and fiber reinforced geopolymer mortar (FRGPM). PP short fibers having 1% volume fraction were used in the FRGPM mix. The results of rebar pull-out test, using geopolymer and grout mortars for anchorage of steel reinforcement should be implemented by surrounding thickness not less than 5 mm. PP fiber reinforced geopolymer repair mortar represents high performance flexural repair material from the ultimate capacity, toughness and crack control points of view.

Koenig A et al. [6] studied the flexural behavior of steel and macro-PP fibre reinforced concretes based on alkali activated binders. The 28 day compressive strength is found to be similar for OPC sample and the Alkali Activated Slag sample. The sample with FA showed the lowest compressive strength even though with the heat curing. The addition of PP fibre and steel fibre had 10% of strength increment in OPC concrete and around 13% decrease for slag based and fly ash based geopolymer sample. No clear trend was found for split tensile strength with addition fibre but the ductility had been improved beyond the maximum load.

Albidah A et al. [1] studied the bond strength between concrete substrate and MK geopolymer repair mortars at ambient and elevated temperatures. Control mortars were cementitious and polymer-modified (PM) mortars. Three plain and three fibres (PVA) reinforced GP mortars were used in this study. The pull of test was conducted according to ASTM 4541-17. The plain and PVA reinforced GP mortars cured at ambient temperature displayed excellent repair potentials in terms of their bond and compressive strengths. The test results indicate that GP mortars are the promising alternative of the cementitious repair mortars.

Ranjbar N et al. [26] studied the mechanisms of interfacial bond in steel and PP fibre reinforced geopolymer composites. As the fibre content increased, a reduction in flow was found both for steel and PP fibre added geopolymer composites. Steel fibre mix was found to be stiffer than the PP fibre mix. Inclusion of 3% steel fibre by volume of binder (Low calcium FA) shows the maximum flexural strength at 7 days and 28 days. Addition of PP fibre had negligible influence on the flexural strength of the composites. Addition of steel fibre up to 3% increased the early development of compressive strength but PP fibre addition had negligible impact on the compressive strength.

Patil et al. [28] investigated the effect of PP fibre on the strength parameters of GPC. The results showed that the compressive



strength, splitting tensile strength and flexural strength of PP fibre reinforced GPC increased with respect to increase in percentage volume of PP fibres from 1.5% of 12mm, 1.5% of 20 mm and 1.5% of hybrid PP fibre. Addition of 1.5% volume fraction of PP fibres of 20mm showed maximum increase in compressive strength, split tensile strength and flexural strength. The effects of volume fraction of PP fibre other than 1.5% on the mechanical properties of GPC were not considered in this study.

Mohseni E [17] assessed the impact of ratio of Na_2SiO_3 to NaOH on the performance of PP fibre -reinforced MK based geopolymer composites. It was seen that compressive strength of samples with Na_2SiO_3 to NaOH ratio 3 has 10 % increment that with that of ratio 2. The specimens with Na_2SiO_3 to NaOH ratios of 2, 2.5 and 3 and 0.3 percent of polypropylene showed flexural strengths of 7.03, 7.51 and 7.69 respectively while 1% PP fibre showed the strengths 9.02, 9.36 and 9.87 respectively. This shows that addition of PP fibres can control cracks and reduce the number of cracks and their width.

Sukontasukkul P et al. [29] studied about the toughness and flexural properties of hybrid steel and PP fibre reinforced geopolymer. The compressive strength of plain geopolymer was 40 MPa. When steel fibres were added in 0.5% and 1%, the compressive strength increased to about 56.6 and 61.7 MPa respectively. For PP fibre, the compressive strength for 0.5% PFRG is found to be higher than that of plain geopolymer. In the case of a hybrid fibre GPC when the base fibre (1.0% polypropylene) is replaced by steel fibre at a 0.2% increment in volume fraction, compressive strength started to increase. The highest strength of this type of hybrid fibre geopolymer is 56.8 MPa with 0.2% polypropylene +0.8% steel fibre. But the compressive strengths of all hybrid GPC samples are lower than that of 1.0% steel fibre GPC. A comparison among the fibre reinforced GPC showed that steel fibre geopolymer has higher flexural strength than the PP fibre reinforced GPC. Regardless of the fibre type, the toughness is found to be increased in increase in percentage of fibre content.

Reed M et al. [30], this research was aimed at investigating the effect of heat curing by comparing the mechanical properties such as compressive strength and ductility of ambient cured and heat cured FRGPC samples. This research investigated the effects of PP fibres in GPC using 0.05 and 0.15 % fibres (by weight). There were two test variables namely the amount of PP fibres used and the curing method/duration. Three levels of PP fibres (0, 0.05 and 0.15 % by weight) and three levels of curing (ambient cured for 24 hours, oven cured for 3 and 6 hours) were investigated. The results reveal that, compressive strength of GPC is not affected by the curing method for low-strength concrete and the majority of the strength of GPC is reached in 21–28 days. Heat curing can speed up the initial strength development. The addition of PP fibres improved the compressive strength from 28MPa to 33MPa and ductility of GPC. Better compressive strength and ductility was found when fibre content was kept at 0.15%.

Zhou J et al. [21] studied about the cement hydration and micro structure in concrete repairs with cementitious repair materials. For unsaturated substrate deceleration in hydration of repair material occurs and reduces the porosity and leads to a dense pore structure. The interface and repair material have high bond strength and tensile strength. When the substrate is saturated water flows from substrate to the repair material, there by increases the hydration in the repair material and leads to a dense structure.

Cabrera J G et al. [23] studied the mechanical properties of different repair materials for concrete structures like OPC, cementitious repair materials (CRM), polymer modified cementitious repair material (PMC) and pulverized fuel ash (PFA). It was found that the CRM showed the highest compressive strength and bond strength and the failure occurred through interphase meaning failure in cohesion.

A.S.E. Belaidi et al. [3] studied the mechanical properties of cementitious repair mortar, silica fume with synthetic fibre and silica fume without fibre. It was found that the silica fume with synthetic fibre shows the highest compressive strength. Flexural strength also showed the same properties. The shrinkage of synthetic fibre added with silica fume showed the least value. The bond strength calculated from the pull out test was more in the case of synthetic fibre added silica fume. It was also noted that water absorption is increased by the addition of fibres.

Feng S et al. [32] compared the microstructure and interfacial bond properties of normal concrete and ultra-high performance concrete repair materials. The compressive strength and split tensile strength of UHPC repair concrete are 127.61 and 13.65 MPa respectively compared to 45.5 MPa of normal concrete (C45). For a given substrate it was found that UHPC materials have more cohesion and shear bond strength.

Banthia N et al. [27] studied the permeability under stress and the bond strength between old concrete with the fibre reinforced cement concrete. The fibres used were cellulose and Poly vinyl alcohol (PVA). It was found that permeability under stress value equal to half of the ultimate strength, less than that of unstressed specimen. Three fibre volume fractions were studied, 0%, 0.5% and 1%. The bond strength increases according to the increment in the fibre content.



Lei F et al. [19] investigated about sustainable phosphate based rapid repairing material and their mix proportions. The raw materials used to make the repair material are circulating fluid bed (CFB) fly ash and Magnesium oxide (MGO)-containing by products and potassium dihydrogen phosphate (KDP (P))- industrial grade white crystalline powder with 98% monopotassium phosphate (KH_2PO_4). The utilization of LG-MgO can reduce the exploitation of natural high-purity MgO.

Litina C et al. [12] developed a sustainable concrete repair material through microencapsulated agents. Five repair mortars from Fosroc Ltd were selected for this project and the self healing microcapsules contained a solution of mineral oil and Na_2SiO_3 (40% weight in water). Three different percentages, 8%, 16% and 32% of microcapsules were selected for the study. The experiments proved the repair materials showed improved crack width and crack depth reduction and permeability improvement.

Stanaszek-Tomal E. [18] investigated about bacterial concrete as a sustainable building material. A self-healing process (Autogenous) takes place with the use of products formed in the presence of carbon monoxide dihydrate and water. Calcium carbonate or hydration products such as C-S-H are formed in order to cause crack healing. Directly introduced magnesium oxide and bentonite can cause the crack healing. Another method, (Autonomous) by the use of bacteria, organic compounds and encapsulated materials with pozzolan. In this treatment, chemical factors such as calcium lactate and biological factors, i.e., bacteria are distinguished. Their coupling enables better end results to be obtained. Recycled concrete aggregate 50% FA as bacterial immobilizers showed the most effective repair of cracks up to 1.1mm wide and allowed to recover the compression strength of 85%.

Micro concrete are repair materials consists of a mixture of graded sand , cement and water to have properties of cement which could be used for small scale works especially repair works. Micro concretes are available in pre packed bags where cement and sand are mixed in dry conditions. Different forms of micro concrete in pre packed bags are available for the patch works or repair of concrete pavements.

In their work, Jonbi j et al. [24] found that addition of PP fibre does not have effect on setting time of micro concrete repair material yet it increases the flexural strength and compressive strength of by 2.9 % .The addition of 1 % of super plasticizer (Polycarboxylate Ether, PCE) increases the compressive strength by 24.3 % after a day. The flexural strength increments are 9.7 % for PP fibre addition and 22.6 % for PP fibre plus PCE addition.

Krishnamurthy R R et al. [31] replaced coarse aggregate and clean river sand (Fine aggregate) with shredded rubber and grinded plastic bottles (Polypropylene, PP) in different percentages in OPC concrete for the repair work. 6mm of shredded tyre and 5 mm grinded plastic bottles were used for the replacement with different percentages which are 10%,20%,30%,40% and 50 % by weight of coarse (12 -14 mm) and fine aggregate. They found that both recycled materials were able to replace either coarse or fine aggregate and the optimum percentage for the maximum indirect split tensile strength was found to be 10 %. Even if the percentage of replacement is 50 %, still the indirect split tensile strength was found to be more than that of the site sample of highest tensile strength.

Guan Y et al. [40] studied about application of Calcium sulfoaluminate cement for the rapid repair of concrete pavement. 70 % of 28 days strength was found to be achieved in a day for these types of cement. The result could make way to open the repaired area for traffic even 4 hrs after repairing. The shrinkage volume change also 38 % less than conventional cement.

Arora A et al. [4] studied about the possibility of using Magnesium phosphate cement as a pavement repair material. The compressive strength increased by 75 % from 1 hr to 1 day curing period when the phosphate magnesium ratio is 1:2. Though the flexural strength was more in the initial 28 days of curing but as the curing period reached 90 days the flexural strength was found to be less than that of OPC .The water resistivity is MPC is not as so great , the strength decreases by 42.34 % for 28 days when it is engrossed in water.

CONCLUSION

The following conclusions were made from the literature review,

- Use of geopolymers with blended binders such as FA and GGBFS, the CO₂ emissions can be reduced by 19-29 % compared to OPC Concrete.
- The type of alkaline solution has a significant influence in the development of compressive strength in GPC Na_2SiO_3 .
- For the blended geopolymer composite materials, the increase in slag content and increase in concentration of alkali solution increases the mechanical properties such as compressive strength and split tensile strength.



- The presence of calcium compound in the binder of GPC reduces the setting time of concrete.
- Addition of super plasticizer in to geopolymers increases the workability of GPC but it has a slightly inverse effect on the compressive strength. Increase from 2% to 6% of super plasticizer increases the workability to 40.7%.
- Geopolymers prepared with high calcium FA has optimum strength when the NaOH to Na₂SiO₃ is from 0.67 to 1.00.
- Geopolymers show good fire resistance up to 6000C, and then the fire resistance compound is getting reduced.
- Addition of GGBFS from 10-50% in to FA based GPC reduces the initial setting time by 73-94% and final setting time by 77-92 %
- Long pre-curing at room temperature is beneficial for strength development of geopolymeric materials utilising fly ash and cured at elevated temperature and if the activator is Na₂SiO₃, 6 hours heat curing is more beneficial than 24 hours curing.
- Alkali activated FA with addition of calcium rich compounds like OPC, CaO or Ca(OH)₂ resulted in accelerated setting time but CaO addition reduced the compressive strength.
- Addition of Calcium carbide residue up to 20 % in the fly ash based GPC increases the shear bond strength of the material. The CaO present in Calcium carbide decreases the setting time of the repair mortar.
- Addition of FA in to UGGBS based geopolymer repair improves the workability of the mix but adding more than 40% of FA reduces the compressive strength. The bond strength is maximum when the FA content was 30%
- GPC concrete containing FA and GGBFS as binders shows better compressive strength and splitting tensile strength as the percentage of GGBFS increases in the binder mix.
- Addition of PP fibre does not have any effect on the fibre reinforced concrete but 1% addition increases the compressive strength by 24.3% after day.
- Addition of PCE based super plasticizer along with PP fibre increases the flexural strength of fibre reinforced concrete by 22.6%
- PP fibre reinforced geopolymer repair mortar represents high performance flexural repair material from the point of view of ultimate capacity, toughness and crack control comparing with to plain geopolymer mortar.
- The PVA fibre reinforced MK based GP mortars cured at ambient temperature display excellent repair potentials in terms of their bond and compressive strengths.
- Addition of fibres (Steel or PP) reduces the flow of the GPC and addition of steel fibre up to 3% by volume of binder gives the maximum flexural strength at 7 days and 28 days
- Addition of 1.5% volume fraction of PP fibres of 20mm in GPC showed maximum increase in compressive strength, split tensile strength and flexural strength.
- Addition of 1% PP fibre by volume of binder and with Na₂SiO₃ to NaOH ratio 3 shows excellent flexural strength properties and crack control in MK based GPC
- Comparison among the fibre reinforced GPC showed that steel fibre reinforced geopolymer has higher flexural strength than the PP fibre reinforced GPC.
- The majority of the strength of GPC is reached in 21–28 days and compressive strength of GPC is not affected by the curing method for low-strength concrete.
- Heat curing can speed up the initial strength development. The addition of PP fibres improved the compressive strength by 18% and the ductility of GPC.
- Among the repair mortars, cementitious repair mortar (CRM) showed the highest compressive strength and bond strength consider other repair materials like PMC, PFA and OPC.
- The compressive strength and split tensile strength of UHPC repair concrete are higher that of normal concrete repair material. For a given substrate it was found that UHPC materials have more cohesion and shear bond strength.
- The permeability of the fibre reinforced concrete repair materials at ultimate stress is less than half of that of unstressed OPC repair materials.



- Use of calcium sulfoaluminate cement proved to be a very good option as a rigid pavement repair material due to its early strength gain and shrinkage properties
- Magnesium phosphate cement has good early strength development but the flexural strength after a 90 days period is less than that of OPC and the water resistivity also not so good to be used a repair material for rigid pavements.
- Replacement of coarse and fine aggregates with shredded tyre and grinded plastic bottles in OPC concrete showed an optimum 10% replacement gives the maximum indirect split tensile strength.

In summary, the paper explores the suitability of FRGPC as a sustainable alternative to repair material in rigid pavements. The paper also provided an overview of the various research performed using FRGPC and GPC for different types of application showing its advanced mechanical properties. It is evident that FRGPC will provide a sustainable solution to not just pavement repair but also in all facets of construction.

REFERENCES

1. Abdulrahman Albidah, Aref Abadel, Fahed Alrshoudi, Ali Altheeb, Husain Abbas, Yousef Al-Salloum, "Bond strength between concrete substrate and metakaolin geopolymer repair mortars at ambient and elevated temperatures" *Journal of Materials Research and Technology*, Vol. 9, pp 10732-10745, 2020.
2. Aladdin Sharkawi, Mohamed Taman, Hamdy M. Afefy, Yasmeen Hegazy, "Efficiency of geopolymer vs. high-strength grout as repairing material for reinforced cementitious elements" *Structures*, Vol. 27, pp 330-342, 2020.
3. Akram Salah Eddine Belaidia, Benchaa Benabeda and Hamza Soualhib., "Physical and mechanical properties of concrete repair materials in dry and hot-dry environment". *Journal of Adhesion Science and Technology*, Vol.29(6), pp 543–554, 2015.
4. Amit Arora, Birpal Singh, Parampreet Kaur, "Novel material i.e. magnesium phosphate cement (MPC) as repairing material in roads and buildings" *Materials Today: Proceedings*, Vol. 17, pp 70–76, 2019.
5. Arumugam V, Bhagavathi Pushpa T., Basanth Babu K M., (2018) "Effect of Polypropylene Fibers in Geopolymer Concrete". *International Journal of Engineering Science and Computing*, Vol. 8(6), pp 18125-18131, 2018.
6. Andreas Koenig, Annemarie Wuestemann, Federico Gatti, Laura Rossi, Florian Fuchs, Dustin Fessel, Felix Dathe, Frank Dehn, Fausto Minelli, "Flexural behaviour of steel and macro-PP fibre reinforced concretes based on alkali-activated binders". *Construction and Building Materials*, Vol. 211, pp 583-593, 2019.
7. A. Palomoa, M.W. Grutzeckb, M.T. Blanco, "Alkali-activated fly ashes A cement for the future". *Cement and Concrete Research*, Vol.29, pp 1323–1329, 1999.
8. Bakharev T., (2005) "Geopolymeric materials prepared using Class F fly ash and elevated temperature curing". *Cement and Concrete Research*, Vol. 35, pp 1224–1232, 2005.
9. Chindaprasirt P., Chareerat T., Sirivivatnanon V., (2007) "Workability and strength of coarse high calcium fly ash geopolymer" *Cement and Concrete Composites* Vol. 29, pp 224-229, 2007.
10. Chindaprasirt P., Phoo-ngernkham T., Hanjitsuwan S., Horpibulsuk S., Poowancum A., Injorhor B., "Effect of calcium-rich compounds on setting time and strength development of alkali- activated fly ash cured at ambient temperature" *Journal of construction materials*, Vol. 9, pp 1-8, 2018.
11. Chindaprasirt P., Rattanasak U., "Synthesis of polypropylene fiber/high-calcium fly ash geopolymer with outdoor heat exposure" *Clean Technologies and Environmental Policy*, Vol. 19(7), 2017.
12. Chrysoula Litina and Abir Al-Tabbaa., "Development of sustainable concrete repair materials via microencapsulated agents". *Concrete Solutions: MATEC Web of Conferences*, Vol. 289, 11002, 2019.
13. Davidovits J., "Geopolymer Cement a review" *Geopolymer Science and Technics*, Technical Paper #21, Geopolymer Institute Library, 2013.
14. Davidovits J., *Geopolymer Chemistry and Applications*, Institut Géopolymère, Saint-Quentin, France, 5th Ed. 2011.
15. Davidovits J., "Geopolymers: inorganic polymeric new materials" *Journal of Thermal Analysis and Calorimetry*, Vol. 37, pp 1633–1656, 1991.



16. Davidovits J., "Properties of geopolymer cements" Proceedings First International Conference on Alkaline Cements and Concretes, Vol. 1, SRIBM, Kiev, Ukraine, pp 131 – 149, 1994.
17. Ehsan Mohseni., "Assessment of Na₂SiO₃ to NaOH ratio impact on the performance of polypropylene fiber-reinforced geopolymer composites" Construction and Building Materials, Vol. 186, pp 904-911, 2018.
18. Elzbieta Stanaszek-Tomal, "Bacterial Concrete as a Sustainable Building Material" Sustainability, Vol.12(2): 696, 2020.
19. Feng Lei, Chen Xi-qing, Wen Xiao-dong, Zhang Zheng-ya, Shou Lv-yan, "Investigating and optimizing the mix proportion of sustainable phosphate-based rapid repairing material". Construction and Building Materials Vol.204, pp 550-561, 2019.
20. Ghasan Fahim Huseien, Kwok Wei Shah, "Performance evaluation of alkali-activated mortars containing industrial wastes as surface repair materials" Journal of Building Engineering, Vol.30, pp 101234 (1-15), 2020.
21. Jian Zhou, Guang Ye, Klaas van Breugel, (2016) "Cement hydration and microstructure in concrete repairs with cementitious repair materials" Construction and Building Materials, Vol.112, pp 765-772, 2016.
22. Jithendra C, Elavenil S, "Role of Superplasticizer on GGBS based Geopolymer Concrete under ambient curing" Materials Today: Proceedings, Vol.18, pp 148–154, 2019.
23. J. G. Cabrera and A.S. Al-Hasan, "Performance properties of concrete repair materials "Construction and Building Materials, Vol. 11, Nos 5-6, pp 283-290, 1997.
24. Jonbi Jonbi, A. R. Indra Tjahjani, Nuryani Tinumbia, A. M. Pattinaja, and Bambang. S. Haryono, "Repair of rigid pavement using micro concrete material". ICRMCE: MATEC Web of Conferences, Vol. 195, 01014, 2018.
25. Komljenovic M., Z. Bascarevic, V. Bradic, "Mechanical and microstructural properties of alkali-activated fly ash geopolymers" Journal of Hazardous Materials, Vol. 181 pp 35–42, 2010.
26. Navid Ranjbar, Sepehr Talebian, Mehdi Mehrali, Carsten Kuenzel, Hendrik Simon Cornelis Metselaar, Mohd Zamin Jumaat, "Mechanisms of interfacial bond in steel and polypropylene fiber reinforced geopolymer composites" Composites Science and Technology, Vol.122 pp 73-81, 2019.
27. Nemkumar Banthia, Cristina Zanotti, Manote Sappakittipakorn, "Sustainable fiber reinforced concrete for repair applications" Construction and Building Materials, Vol. 67, pp 405-412, 2014.
28. Patil. S.S., Patil. A. A., "Properties of Polypropylene Fibre Reinforced Geopolymer Concrete" International Journal of Current Engineering and Technology, Vol. 5, pp 2909-2912, 2015.
29. Piti Sukontasukkul, Phattharachai Pongsopha, Prinya Chindaprasirt, Smith Songpiriyakij, "Flexural performance and toughness of hybrid steel and polypropylene fibre reinforced geopolymer". Construction and Building Materials Vol. 161, pp 37-44, 2018.
30. Reed M., Lokuge W., Karunasena W., "Fibre-reinforced geopolymer concrete with ambient curing for in situ applications", Journal of Material Science, Vol. 49, pp 4297–4304, 2014.
31. Renga Rao Krishnamoorthy, Dr. Thevaneyan Krishta David, En.Noor Azman Bin Mastor, Ir. Kuganeswaran Nadarasa, "Repair of Deteriorating Pavement Using Recycle Concrete Materials" Procedia Engineering, Vol. 142, pp 370 – 381, 2016.
32. Shuo Feng, Huigang Xiao, Hui Li, "Comparative studies of the effect of ultrahigh-performance concrete and normal concrete as repair materials on interfacial bond properties and microstructure" Engineering Structures, Vol. 222, pp 111122(1-15), 2020.
33. S.K.Saxena, Mukesh Kumar and N.B.Singh, "Fire Resistant Properties of Alumino Silicate Geopolymer cement Mortars". Materials Today: Proceedings, Vol. 04, pp 5605–5612, 2017.
34. Sulaem Musaddiq Laskar, Sudip Talukdar, "Preparation and tests for workability, compressive and bond strength of ultra-fine slag based geopolymer as concrete repairing agent" Construction and Building Materials, Vol. 154, pp 176-190.
35. Suman Saha C., Rajasekaran, "Enhancement of the properties of fly ash based geopolymer paste by incorporating ground granulated blast furnace slag", Construction and Building Materials, Vol. 146, pp 615-620, 2017.



36. Tanakorn Phoo-ngernkham, Chattarika Phiangphimai, Darrakorn Intarabut, Sakonwan Hanjitsuwan, Nattapong Damrongwiriyanupap, Long-yuan Li, Prinya Chindapasirt P, “Low cost and sustainable repair material made from alkali-activated high-calcium fly ash with calcium carbide residue” *Construction and Building Materials*, Vol. 247 pp 118543 (1-12), 2020.
37. Turner L K., Collins F G., (2013) “Carbon dioxide equivalent (CO₂-e) emissions: A comparison between geopolymer and OPC cement concrete”, *Construction and Building Materials*, Vol. 43, pp 125–130.
38. Wen-Ten K., Ming-Yao L., Chuen-Ui J., “Bonding Behavior of Repair Material using Fly-Ash/Ground Granulated Blast Furnace Slag-Based Geopolymer” *Materials*, Vol .12(10): 1697, 2019.
39. Xin Ren and Lianyang Zhang, M.ASCE., “Experimental Study of Geopolymer Concrete Produced from Waste Concrete”, *Journal of Materials in Civil Engineering*, Vol.31(7), pp 04019114(1-14), 2019.
40. Yanhua Guan, Ying Gao, Renjuan Sun, Moon C. Won, Zhi Ge, “Experimental Study and Field Application of Calcium Sulfoaluminate Cement for Rapid Repair of Concrete Pavements”, *Frontiers of structural and Civil Engineering*, Vol.11, pp 338–345, 2016.
41. Yao Ding, Cai-Jun Shi, Ning Li, (2018) “Fracture properties of slag/fly ash-based geopolymer concrete cured in ambient temperature”, *Construction and Building Materials* ,Vol.190, pp 787-795, 2018.



Emerging Trends in Affordable Housing – GFRG Technology for Self Reliance and Sustainable Growth

K B Agarwal

Ex GM, ITR Co. Ltd., Bareilly

✉ uday.hakari@gmail.com

BACK GROUND

Engineering for 'Self reliance & sustainable growth' denotes new or improvised Engineering with raw material & technology available in India. Adequate shelter for all people is one of the pressing challenges faced by the developing countries. India is currently facing a shortage of about 20 million houses. It is found that up to 30% of the construction cost, including material and labour cost, can be saved by using the new technologies in comparison with the traditional construction methods. In rapidly urbanizing areas land has become a scarce commodity. Many governments aim to improve the situation by investing in infrastructures renewal. For sustainable growth rapid & mass construction will bring improvement in economy in general.

DIFFERENT CONSTRUCTION TECHNOLOGIES

- Conventional Load bearing wall structure.
- RCC Framed structure.
- Precast Technology
- Glass Fiber Reinforced Gypsum Panel Technology (GFRG).
- 3D Technology.

3D Technology in building construction is still in experimental stage. It is new, jazzy and cost-effective. 3D printing is part of a wider technological concept known as 'building printing' that uses 3D printing to develop buildings. As construction is still a conservative process in India, this technology will take long time to take off. Its ability to construct buildings of any shape and size in remarkably less time makes it the future of the construction industry.

GLASS FIBER REINFORCED GYPSUM PANEL TECHNOLOGY

GFRG Panel Technology or rapid wall technology has fast emerged as leading technology of future and is fit for mass scale Affordable Housing. A GFRG Panel is basically Calcined Gypsum plaster, reinforced with glass fibers which when filled with reinforced concrete in an appropriate proportion becomes strong enough to act as a local bearing and sheer wall.

GFRG panels made of high quality gypsum plaster reinforced with special glass fibers were first introduced in Australia in 1990. This technology replaced the traditional method of construction where use of blocks and bricks was popular for the structure of a house.

These panels are prefabricated and manufactured at factories and brought to the construction site directly. Once the foundation is laid, these panels are erected on the foundation with the help of cranes. These panels do not need plastering and painting.

GFRG Panel can resist the lateral loads due to earthquakes and wind. Not only the walls, but the roof, floors, sunshades and the boundary walls can be made using GFRG panels. Looking at its success and innumerable advantages, the technology is spreading like wildfire and is being adopted heavily throughout the construction industry.

The typical dimension of a GFRG building panel is 13x3x0.127 m. which weighs around 1.6 tons. It is provided with 4 cavities within 1 meter of the panel.

It is possible to design such buildings up to ten stories in low seismic zones (and to smaller elevation in high seismic zones).

GFRG Panel are originally white in color (due to gypsum) and have a smooth finished surface, they can be whitewashed or painted without cement plastering the walls, therefore, providing some scope of creativity for the client.



PANEL MANUFACTURING

- I. The manufacture of GFRG Panels is done in a semi-automatic plant using the slurry obtained by heating the Calcined Raw Gypsum.

The Calcined Raw Gypsum (plaster) is mixed with water, white cement and certain chemicals like D50 (retarder) and BS94 (water repellent) in a mixer.

Different layers of slurries are then spread over a table and are interspersed with glass fibers cut, spread & imbedded uniformly in to the slurry with help of screech roller. Aluminum plugs (for creating hollow cavities) are also imbedded.

After half hour or so, the aluminum plugs are removed and the panels are sent to a dryer. Panels are dried at temperature of 275 degree centigrade. The wall panels can be cut as per dimensions and requirements of planned building.

- II. Mechanical Properties of panels (nominal values, based on test results): Unit weight 0.433 kN/m², Modulus of elasticity EG 7500 N/mm², Uni-axial compressive strength Puc 160 kN/m (4.77 mPa) (Strength obtained from longitudinal compression / tension tests with ribs extending in the longitudinal direction), Uni-axial tensile strength Tuc 34 – 37 kN/m, Ultimate shear strength, Vuc 21.6 kN/m, Out-of-plane moment capacity, (Rib parallel to span), Muc 2.1 kNm/m, Out-of-plane moment capacity, (Rib perpendicular to span), Muc , perp 0.88 kNm/m, Mohr hardness 1.6 (Out-of-plane), flexural rigidity, EI, (Rib parallel to span) 3.5 x 10¹¹ Nmm² /m, Out-of-plane flexural rigidity EI (Rib perpendicular to span) 1.7x10¹¹Nmm² /m, Coefficient of thermal expansion Cm 12x10⁻⁶mm/mm/o C, Water absorption 1.0% : 1 hr 3.85% : (24 hrs Average water absorption by weight % after certain hours of immersion), Fire resistance : Structural adequacy / integrity / insulation 140/140/140 minutes CSIRO, (Australia/ IS 3809:1979), Sound transmission class (STC) 40 dB ISO 10140-3:2010* * ISO 10140-3:2010,

APPLICATION OF GFRG PANELS

- As a light-weight bearing wall.
- As high-capacity vertical and shear load bearing wall.
- As partition wall.
- As roof slabs / horizontal floor.
- As compound wall / Security wall.
- As pitched roofing.
- As cladding in industrial structures.

METHOD OF CONSTRUCTION WITH GFRG PANELS

The construction process up to the plinth level remains similar as in the conventional method. No special foundation is required for the installation of GFRG Panels.

Concrete belts are built at the plinth area with protruding iron rods which are meant to strengthen the interlocking with the cells of the panel.

GFRG Panels are placed at the appropriate positions using mechanical means, preferably a crane and external supports are provided to maintain the verticality. Necessary cuts for doors, windows, sanitary fittings, vents etc. are made as per the design.

The hollow cavities are filled with concrete and reinforcement as per the requirement to strengthen the panels. Generally, concrete is filled in every third cavity of the panel and the remaining cavities can be filled with waste materials like quarry dust.

Finally, waterproofing treatment is carried out for the roofs and floors of the building.

The basic arrangement of GFRG Panel Building System is as follow:



BUILDING A HOUSE WITH GFRG

IIT Madras has built G+1 House using GFRG technology Panels , timeline goes like this:

❖ Pre Construction Phase

1. Excavation & Foundation
2. Waterproofing of Foundation
3. Plinth construction.
4. Concrete Flooring.
5. Starter Bars for Panel Erection.
6. Erection of Panels.

❖ Construction Phase

7. Superstructure - Day 1
8. Water proofing for Joints.
9. Concrete filling in Cavities (Wall panels).
10. Placement of First Floor Slab - Day 8.
11. Instrumentation for Structural Performance.
12. Reinforcement cage for Embedded Beams.
13. Screed Concreting on First Floor slab.
14. GFRG panel for stair case.
15. Erection of panels for First Floor - Day 11.
16. Placement of Panels for Roof slab - Day 15.
17. Slab Reinforcement & Concreting of Roof slab.
18. Filling concrete in GFRG Panels.
19. Water proofing in Toilet area.
20. Strain Gauging for structural performance .
21. Flooring

❖ Finishing Phase

22. No need to Plastering and go direct to Painting.
23. Painting.
24. Electrical and Plumbing Works.
25. Sanitary Ware and CP fittings.

G.F - 1 BHK + 2 BHK.

F.F - 1 BHK + 2 BHK.

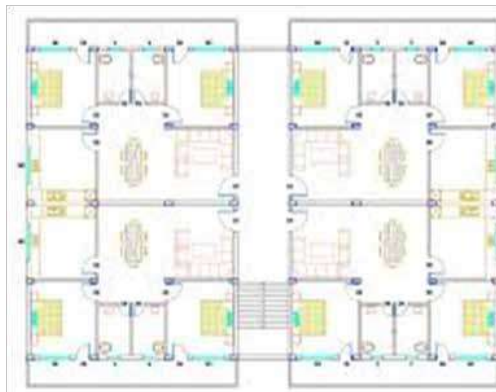
We need crane to erect the GFRG panels on plinth. G.F + F.F – completed Appox within 40 days.

COST ESTIMATION AND ANALYSIS

In parapet = 265.55 Sq. Mt.
In stairs = 26.24 Sq. Mt.
In openings = 341.28 Sq. Mt.
Total = 6061.72 Sq. Mt.
Total cost of panels = Rs. 67.89 Lakhs

Table -1: Cost Comparison of GFRG Building with Load Bearing Wall Structure and Framed Structure

Description	Types of Building			Savings/Benefits in GFRG when compared to	
	GFRG building	Load bearing wall Str.	RCC Framed Str.	Load bearing wall Str.	RCC Framed Str.
Dwelling units	16	16	16	-	-
Carpet Area	122.19 SqM	116.02 SqM	119.02 SqM	5.32%	2.66%
Total Build up area	2341.36 sqm	2341.36 sqm	2341.36 sqm	-	-
Excavation	Rs. 74,560	Rs. 83,987	Rs. 95,025	11.22%	21.54%
Steel	Rs. 16,21,540	Rs. 11,91,679	Rs. 21,54,550	-36.07%	24.74%
Cement	Rs. 14,22,490	Rs. 24,46,373	Rs. 33,20,647	41.85%	57.16%
Bricks	-	Rs. 25,33,360	Rs. 15,45,745	-	-
Panels	Rs. 67,89,126	0	0	-	-
Course Aggregate	Rs. 13,47,046	Rs. 13,52,470	Rs. 23,42,706	0.40%	42.50%
Fine Aggregate	Rs. 4,09,045	Rs. 10,52,702	Rs. 12,05,517	61.14%	66.07%
Shuttering cost	Rs. 0	Rs. 4,85,590	Rs. 8,13,477	100%	100%
Labour	Rs. 6,24,271	Rs. 27,71,050	Rs. 28,91,952	77.47%	78.41%
Sub Total	Rs. 1,22,88,078	Rs. 1,19,17,211	Rs. 1,42,74,596	-	-
Miscellaneous	Rs. 13,41,690	Rs. 37,45,862	Rs. 41,68,461	-	-
Total	Rs. 1,36,29,679	Rs. 1,56,63,073	Rs. 1,84,43,057	12.98%	26.10%



(Typical Floor Plan)

Standard size of the panel = 12m x 3m x 0.124 m

Rate of GFRG panels (per square meter) = Rs. 1120

Quantity of panels required for G+3 building

In slab = 2883.41 Sq. Mt.

In walls = 3217.80 Sq. Mt



BENEFITS OF USING GFRG TECHNOLOGY

- I. Economical:- GFRG can save up to 30% of total construction cost.
- II. Rapid construction:- Houses, specially large no. of houses can be built faster than conventional buildings. No beams & columns are needed.
- III. Eco- friendly:- GFRG saves tons of cement & sand reducing carbon foot prints & global warming due to use of eco friendly material. Building industry accounts for 40% of world's carbon foot print.
- IV. Cooler Houses:- GFRG keeps homes cooler up to 4 degree centigrade compared to normal buildings, thus reducing use of ACs.
- V. Fire Resistant:- GFRG can withstand 1000 degree centigrade for 4 hours, giving enough time to residents to escape during fire accident.
- VI. Earthquake Resistant:- Major cities like Delhi, Bombay, Kolkata are in Zone IV. GFRG resist earthquake in buildings up to Zone V.
- VII. Light & Strong: – GFRG is light in weight (43 kg/m²) resulting in less load transfer to foundation. However it is 5 times stronger than conventional building, lasting 80 years life without deterioration (conventional building 50 years).
- VIII. Water resistant:- GFRG repels water, hence deterioration of structure due to water seepage from roof or walls and growth of bacteria & vegetation is saved. There is no water leakage during floods. GFRG floor slabs do not bulge due to water.
- IX. More Carpet area with less Maintenance Cost:- Maintenance cost of GFRG houses is less while carpet area is more as thickness of GFRG panels is only 5 inches.

SHORT COMINGS OF GFRG

Following are disadvantages in the use of GFRG Technology:

1. More space needed for crane movement
2. Complicated design makes it uneconomical for making less houses.
3. Skilled labour needed.
4. GFRG panels should be handled with care in transportation and erection.
5. Need specific machinery for cutting GFRG panels at site.
6. Erection and placing of GFRG panels are a bit difficult & crane is needed.

SELF RELIANCE & SUSTAINABILITY

'Since Gypsum is available in plenty at economical price In India, hence this type of construction is self reliant, economical & is sustainable.

ACKNOWLEDGEMENT

Indian Institute of Technology, Madras

Google Search Engine



Managing the Risk and Uncertainty in Coastal Residential Building Codes

Gino Hosein*, Indrajit Ray

*Department of Construction Engineering and Management, University of the West Indies,
St. Augustine, Trinidad and Tobago*

*✉ ginohosein@yahoo.co.uk

ABSTRACT

Because of the frequency of natural disasters occurring in the Caribbean over the last 20 years, damage has been inflicted on the small island developing states (SIDS) coastal residential buildings in particular. This is in part to do with the apparent low resistance of residential buildings, as compared to public buildings, to the different types of oceanic disasters. Generally only buildings being constructed in the urban areas are regulated because of their close location to the regulatory agencies. As a result of this, the rural residential buildings mainly in the proximity of the coastline of the islands, are being designed, constructed and even renovated in an unregulated manner. These are the ones at risk from possible destruction by natural disasters due to non-building code compliance. This research is therefore based on identifying the main risks that are associated with non compliance of coastal residential building codes via a literature review, and identify the gap for further improvements by comparing the main risks with international standards.

Keywords : Building code; Oceanic natural disasters; Coastal residential buildings; Risk; Non compliance.

INTRODUCTION

Because of the frequency of natural disasters occurring in the Caribbean over the last 20 years, damage has been inflicted on the Caribbean islands coastal residential buildings in particular. This is nothing new to the Caribbean [20]. It is in part to do with the apparent low resistance of residential buildings, as compared to public buildings, to the different disasters. People in Small Island developing States (SIDS) are three times more likely to be displaced by disasters as compared to other disaster zones. One reason for this is that there is no policy in place in the Caribbean to mitigate against this risk. The gap between the Caribbean and other zones is not that wide, as the problem is a global one [1]. The natural disasters outlined in this research are: Earthquakes and Hurricanes relating to oceanic origins.

Regionally, in Barbados it was concluded that construction professionals and Government needs to take more responsibility for building code adherence. It was recommended that adherence to the building code minimum standards be law [2]. Case studies done in Naples and Guadeloupe highlighted technical and institutional capacities should be simultaneously developed. An example of this is developing natural hazards maps for areas and also considering institutional architecture for the area as well [3]. This architecture has to be designed and built by relevant natural disaster compliant building codes. Building codes are essentially provisions for health and safety and structural sufficiency [18].

On an international scale, particularly the United States of America (USA), it was found that due to climate change, more frequent natural disasters are predicted for the future. With this in mind it was deduced that building codes were not as effective in the USA as they could be [4]. Globally, over the past 40 years, approximately USD 40 trillion dollars have been lost due to natural disasters. Natural disasters such as earthquakes and tsunamis account for USD 1.1 trillion [16]. In Mexico there have been failures of mid-rise dwellings because of earthquakes [21]. Bangladesh is, considered by historical data as, one of the most natural disaster affected country in the world. Natural disasters include earthquakes and flooding. Research done on developing a disaster zoning map confirmed that the majority of the county was classed as either high or medium zones [5]. They share coastlines, in part, along the Bay of Bengal with India. The Sendai framework [6] aims to reduce disaster losses in lives, livelihoods, and health adopted in March 2015 in Sendai, Japan by 187 United Nations (UN) member states [19]. This is important as 15 out of the 25 most costly insured global catastrophes has occurred since 2001 to 2011. 80% of these were weather related [17].



RESEARCH FOCUS

The aim of this research is to improve the compliance of coastal building codes.

The objectives are identified as follows:

- To identify and evaluate the existing building code risk inputs for coastal residential building structures regionally.
- To compare these risk inputs to international standards to determine the code compliance gap.

LITERATURE REVIEW

This section addresses the reason for research between residential building codes and coastal natural disasters and identifies the associated risks. Based on the preliminary search, it can be concluded that works have been carried out into this area of research by various organizations. Research organizations considered for this section are:

- Federal Emergency Management Agency (FEMA),
- National Institute of Building Sciences (NIBS), and
- International Building Code (IBC).

The reason for the three organizations is that their research is applicable to the Caribbean Small Island Developing Countries (SIDS). This is because of the geography of the coastlines exposed to coastal natural hazards. We all share relationship with regions above and below the Tropic of Cancer, this is applicable for the Caribbean SIDS, USA in the North Atlantic Ocean and India in the Indian Ocean as well.

Federal Emergency Management Agency (FEMA)

The Recommended Residential Construction for Coastal Areas [7] document by FEMA outlines a number of recommendations and designs for home construction. It was written that while risk cannot be totally eliminated, the intention of the document was to significantly reduce the risk of life and damage to property. These, as also stated can be achieved by designing and building less vulnerable homes.

The document was broken up into a number of sub sections as follows:

Types of Hazards

This section essentially lists and explains the different types of hazards that coastal residential structures are vulnerable too.

- High Winds – This is important as it must be considered when designing as well as building. With respect to hurricanes, the wind speeds are classed into categories as recommended by Saffir -Simpson scale.
- Storm Surge – This is an increase of the sea level by as many as 20-30 feet in some area. It was stated that the surge occurs with a combined force of lower barometric pressure and wind driven waves advancing to the shoreline.
- Flood Effects – This as explained can be as a result of storms and hurricanes. If the surface water has nowhere to drain, it becomes backed up and causes flooding. This coupled with additional water being introduced from the ocean due to storm surge increases the flooding.
- Hydrostatic Forces – Stagnant or very slow moving flood waters cause this effect. It is basically when floodwater forces on opposite sides of a structure are not equal. One result from this is floatation.
- Hydrodynamic Forces – Moving flood waters cause this effect. This moving water can destroy structures as well as move them depending on how much of the structure is submerged and the flow rate of the water.
- Waves – Breaking waves are the ones described as being disastrous. Structures can resist the force from an isolated wave easily, however wave forces are cyclic in nature which results in repetitive force. This is what causes destructions.
- Floodborne Debris – These are produced as a result from the hurricanes and tropical storms.
- Erosion and Scour – This includes the washing away of sand and soils.

These are some of the risks from hazards that can be used in the research.



The Coastal Construction Guide [8] by FEMA also lists out some pertinent risks:

a). Flood Hazards – General Design Considerations

- Erosion.
- Rising sea levels.
- Deposition of sediments.
- Land subsidence.
- Failure of levees.

b). Wind Hazards – General Design Considerations

- Straight line wind- Normally generated by thunderstorms.
- Thunderstorm – These normally move through an area rapidly, generating high winds and heavy rains for a couple minutes on average.
- Downburst – This is a powerful downdraft emanating from a thunderstorm. As the downdraft makes contact with the ground it spreads horizontally, typically 6,000 - 12,000 feet across. Added to this is the vortex ring, typically 2,000 feet above the ground. This generates high winds and heavy rains usually for 15-20 minutes.
- Tornado – These are massive rotating columns of air starting from the base of a thunderstorm to the ground. This can generate winds over 200 mph center.
- Hurricane – These are massive spiraling winds coming together with increasing speeds towards the storm or the eye of the hurricane. They form over warm waters and the diameter of the hurricane can be anywhere from 50 miles to 600 miles. Winds speeds can be over 155 mph as seen in figure 2 above.

c). Other Hazards

- Earthquake and seismic events – These events can cause liquefaction, landslides and tsunamis.
- Tsunamis – These are large waves generated in the ocean and sustained over a long period of time. They can travel great distances in deep water and grow quite large in shallow coastal waters.
- Indoor air quality- Mold grows in the absence of proper air flow in moist areas in the household. A main location is the HVAC systems. After a storm, generally there is usually long term power outages. Therefore the mold would have time to grow.

National Institute of Building Sciences (NIBS)

The Natural Hazards Mitigation Saves Report [9] was geared to considering the benefits of the following economic risks identified:

- Deaths, injuries and post-traumatic stress disorder.
- Property repair costs for buildings and its contents.
- Additional living expenses: sheltering costs for displaced households.
- Direct business interruptions; loss of revenue etc.
- Indirect business interruptions: loss of economic activity etc.
- Loss of service to the community when public buildings are destroyed. E.g. hospitals, fire stations etc.
- Urban search and rescue costs.
- Environmental losses.

These are also some of the risks from hazards that can be used in the research.

International Building Code

This is used as a template to guide a countries' specific code. An example of this is Bangladesh. The country has no official

building code, and relies on a draft code. The draft code[10] provides a comprehensive commentary on the rules for proper residential housing construction. However no relevant code compliance model was proposed for the complete adherence of the code from end users. Overall, in the listing by the Coasts at Risk report [11], Bangladesh ranked as the 7th country most at risk to coastal threats. 29% of the population comprising of 32 million people live in the coastal zone of the country [12]. The coastal zone is entirely in the Bay of Bengal with the length of the coastline being 580 km. Natural hazards include droughts; cyclones; much of the country routinely inundated during the summer monsoon season. Most of the country is situated on deltas of large rivers flowing from the Himalayas: the Ganges unites with the Jamuna (main channel of the Brahmaputra) and later joins the Meghna to eventually empty into the Bay of Bengal [13]. Risks outlined are consistent with those stated above in the FEMA list.

These are also some of the risks from hazards that can be used in the research.

DISCUSSION

Arising from the literature review, the following **Table 1** can be derived.

Table 1. Risk inputs for coastal residential building structures

Risk Considerations	FEMA	NIBS	IBC
High Winds	X	X	X
Storm Surge	X		X
Flood Effects	X		X
Hydrostatic Forces	X		X
Hydrodynamic Forces	X		X
Waves	X	X	X
Erosion And Scour	X		X
Flood Borne Debris	X		X
Hurricanes	X		X
Earthquakes	X		X
Deaths And Injuries		X	
Cost Of Repairs		X	
Environmental Losses		X	
Economic Losses		X	
Cost For Displaced Households		X	

Table 1 illustrates the international risk inputs considered for this research. These are considerations put in place by the international regulatory agencies used in the literature review. Specific to the Caribbean Small Island developing States (SIDS), the standards that are used as base documents are primarily from the usage of I-Codes. They are the IBC, IMC, IPC and IECC. These are managed by the Caribbean Regional Organization for Standards and Quality (CROSQ) (ICC, 2020). Each country also has their local standards and quality agencies. Based on research, the following **Table 2** can be realized.

Table 2. Caribbean countries exposed to coastal risks from natural disasters& their building code regulatory status

Item	Country	Existing Building Code	Legal Status	Regulatory Status
1.00	High Risk			
1.10	Antigua and Barbuda	Yes	No	No
1.20	St Kitts and Nevis	Yes	No	No
1.30	Guyana	Yes	No	No
1.40	Jamaica	Yes	No	No
1.50	Grenada	Yes	No	No



1.60	St. Lucia	Yes	No	No
1.70	St Vincent and the Grenadines	Yes	No	No
2.00	Medium Risk			
2.10	Trinidad and Tobago	Yes	No	No

Trinidad and Tobago by way of a license agreement, have adopted from the ICC A117.1-2009, 2015 IBC, IRC, IMC, IFGC, IPC and IgCC as the basis for the national code mainly for structural requirements. These in conjunction with the TTS 599 [14] for small residential buildings make up the required building code standards. The TTS 599 is regulated by the municipal corporations. The country's population is 1,389,860 and the coastline is 362 km. The closeness of the country to the South American mainland makes it outside usual path of hurricanes and other tropical storms. Although there is still a medium level of risk. The population on Trinidad is concentrated in the western half of the island, on Tobago it is in the southern half. Trinidad is bordered by the North Atlantic Ocean in the West, South and East. The Caribbean Sea borders the North, East and South coasts of Tobago. With the East coast bordered by the North Atlantic Ocean.

The Guyana standard code of practice for buildings, GCP 9-1:2005 [15], is the only code in the country. This code is ultimately regulated by the Guyana National Bureau of Standards. Guyana's population is 779,000 with a coastline of 459 km that is bordered by the North Atlantic Ocean on the East. Some of the main natural hazards are flash flood threat during rainy seasons. The population is heavily concentrated in the northeast coast in and around Georgetown, with notable concentrations along the Berbice River to the east; the remainder of the country is sparsely populated.

Grenada's population is 111,450 with a coastline of 121 km. The country lies on edge of hurricane belt; with the hurricane season lasting from June to November each year. Volcanism is also a threat. Approximately one-third of the population is found in the capital of St. George's; the island's population is concentrated along the coast. The island is located between the Caribbean Sea and the Atlantic Ocean.

St Vincent and the Grenadines has a population of 110,210 with a coastline of 84 km. The main natural hazard threat are hurricanes and the La Soufriere volcano on the island of St Vincent is a constant threat. Most of the population is concentrated in and around the capital of Kingstown. The islands are located between the Caribbean Sea and the Atlantic Ocean.

St Lucia's population is 181,890 with a coastline of 158 km. The main natural hazard threat is hurricanes. Most of the population is found on the periphery of the island, with a larger concentration in the north around the capital of Castries. The island is located between the Caribbean Sea and the North Atlantic Ocean.

St Kitts and Nevis population is 52,440 with a coastline of 135 km. The main natural hazard threat is hurricanes. Population clusters are found in the small towns located on the periphery of both islands. The islands are located between the Caribbean Sea and the North Atlantic Ocean.

Jamaica has adopted the 2009 I-Codes as the basis for their standards. The country has a population of 2,934,860 with a coastline of 1,022 km. The main natural hazard threat is hurricanes. The population density is high throughout, but increases in and around the capital city of Kingston, Montego Bay, and Port Esquivel. The island is surrounded by the Caribbean Sea.

Antigua and Barbuda's population is 96,290 and the coastline is 153 km. The island of Antigua is home to approximately 97% of the population; nearly the entire population of Barbuda lives in Codrington. Natural hazards include hurricanes and tropical storms (July to October); periodic droughts. The islands are located between the Caribbean Sea and the North Atlantic Ocean.

Similar to the Caribbean countries, a similar table derived from the same source, [11], for international countries is as follows:

Table 3. International countries exposed to coastal risks from natural disasters& their building code regulatory status

Item	Country	Existing Building Code	Legal Status	Regulatory Status	Gap
1.00	Top Tier				
1.10	Bangladesh	No	No	No	Only a draft code exists
1.20	India	Yes	Yes	Yes	Latest edition was in 2016
1.30	Japan	Yes	Yes	Yes	Up to date



1.40	Netherlands	Yes	Yes	Yes	Up to date
1.50	Madagascar	Yes	No	No	Needs to be regulated.
2.00	Middle Tier				
2.10	Brazil	Yes	Yes	Yes	Up to date
2.20	Denmark	Yes	Yes	Yes	Up to date
2.30	United States	Yes	Yes	Yes	All states are based on the International Residential code (IRC).
2.40	Mexico	Yes	Yes	Yes	Not up to date
2.50	China	Yes	Yes	Yes	Up to date
3.00	Bottom Tier				
3.10	Russian Federation	Yes	Yes	Yes	Up to date
3.20	South Africa	Yes	Yes	Yes	Up to date
3.30	Portugal	Yes	Yes	Yes	Up to date
3.40	Ghana	Yes	Yes	Yes	Up to date
3.50	Israel	Yes	Yes	Yes	Up o date

CONCLUSION

While all of the countries analyzed have existing building codes in use, it can be seen that the international countries have a better regulatory process and legal status to ensure better building code compliance. This is something lacking in the Caribbean as a whole.

All of the countries selected are exposed to different levels of coastal risks. However Brazil, Denmark, US, Mexico and China are all exposed to medium risks just like Trinidad and Tobago. What makes Trinidad and Tobago unique in this grouping is the fact that it is the only country here that is an island. Which, theoretically makes the both islands entirely exposed to coastal risks.

The lack of legal and regulatory status regionally makes it impossible to ensure building code compliance. This further justifies the need for a risk compliance model evaluating coastal residential building codes in the Caribbean with respect to natural disasters.

REFERENCES

1. Hamza, Mo, Ida Koch, and MaltePlewa. "Disaster induced displacement in the Caribbean and the Pacific." 2017. www.fmreview.org/latimamerica-caribbean. Pg 62 – 64.
2. Chmutina, Ksenia, and Lee Boshier. "Construction in Barbados: keeping natural hazards in mind?" *Disaster Prevention and Management*; Boston Vol. 23, No. 2. Pp 175 – 196. 2014. DOI 10.1108/DPM-07-2013-0111.
3. Scolobig, Anna., NadejaKomendantova, Anthony Patt, Charlotte Vinchon, Daniel Monfort-Climent, Mandy Begoubou-Valerius, Paolo Gasparini, and Angela Di Ruocco. "Multi Risk Governance for Natural Hazards in Naples and Guadeloupe." *Springer Science and Business Media Dordrecht*. 73:1523-1545. 2014. DOI 10.1007/s11069-014-1152-1.
4. Shapiro, Shari. "The realpolitik of building codes: overcoming practical limitations to climate resilience." *Building Research and Information*. Vol. 44: Nos 5-6. 490-506. 2016. DOI 10.1080/09613218.2016.1156957.
5. Barua, Uttama, M.Shammi Akhter Mehedi, and Ahmed Ansary. "District wise multi hazard zoning of Bangladesh." *Nat Hazards* 82: 1895-1918. 2016. DOI 10.1007/s11069-106-2276-2.
6. United Nations (UN). "Sendai Framework for Disaster Risk Reduction 2015-2030". Accessed online November 2020. https://www.preventionweb.net/files/43291_sendaiframeworkfordrren.pdf. 2015.
7. Federal Emergency Management Agency (FEMA). "Recommended Residential Construction for Coastal Areas. Building on Strong and Safe Foundations." FEMA P-550, Second Edition/December 2009.



8. Federal Emergency Management Agency (FEMA). "Local Officials Guide for Coastal Construction. Design considerations, regulatory guidance, and best practices for coastal communities." FEMA P-762 / February 2009.
9. National Institute of Building Sciences (NIBS). "Natural Hazards Mitigation Saves – 2019 Report." 2019.
10. Bangladesh National Building Code (BNBC). <https://policy.asiapacificenergy.org/node/3520>. 2015
11. US Aid, Coastal Resources Centre, The Nature Conservancy, United Nations University, and The University of Rhode Island, USA. "An Assessment of Coastal Risks and the Role of Environmental Solutions. Coasts at Risk. 2014.
12. Ahmad, Hafez. "Bangladesh Coastal Zone Management Status and Future Trends." *Journal of Coastal Zone Management*. 22:1. 2019. doi:10.24105/2473-3350.22.466.
13. Central Intelligence Agency. *The World Fact Book*. Access online November 2020. <https://www.cia.gov/library/publications/the-world-factbook/geos/bg.html>.
14. Trinidad and Tobago Building Code. "Guide to the Design and Construction of Small Building." TT 599:2006.
15. Guyana National Bureau of Standards c/o National Standards Council. "Code of Practice for Buildings – Part 1: Enforcement." GCP 9-1:2005.
16. Holzeu, Thomas., and Ginger Turner. "The Natural Catastrophe Protection Gap: Measurement, Root causes and ways of addressing underinsurance for extreme events." *The Geneva Papers*. Vol 43:37-71. 2018. DOI 10.0157/s41288-017-0075-y.
17. Kunreuther, Howard, and Erwann Michel-Kerjan. "Insuring future climate catastrophes." *Climate Change*. 118:39-354. 2013. DOI 10.1007/s10584-102-0625-z.
18. Arlani, A.G., and A.S. Rakhra. "Building Code Assessment Framework." *Construction Management and Economics*. Vol. 6 No. 2. 117-11. 1988.
19. Aitsi-Selmi, Amina., Virginia Murray, Chadia Wannous, Chloe Dickinson, David Johnson, Akiyuki Kawasaki, Anne-Sophie Stevance, and Tiffany Yeung. "Reflections on a Science and Technology Agenda for 21st Century Disaster Risk Reduction." *International Journal of Disaster Risk Science*. 7:1-29. 2016. DOI 10.1007/s13753-016-0081-x.
20. Martin, Marcus L., Hulannie A., Beth B. Mehring, and A. Cong Ma. "All hazards, all communities: An approach to Disaster Preparedness and Policy." *Journal of Race and Policy*. 2012.
21. Reinoso, Eduardo., Miguel A Jaimes, and Marco A. Torres. "Evaluation of building code compliance in Mexico City: mid-risedwellings." *Building Research and Information*. Vol. 44, No. 2, 202-213. 2016. DOI 10.1080/09613218.2014.991622.



Analysis and Affine Transformation of Skew Slab

M Ravindra

Department of Architecture, Andhra University College of Engineering (A), Andhra University, Visakhapatnam, Andhra Pradesh

✉ dr.ravindra.mudunury@gmail.com

ABSTRACT

Generalised equations are derived for reinforced concrete skew slabs for regular and irregular failure patterns using Yield Line Theory. The variation of strength of a skew slab compared to strength of a rectangular slab for different reinforcement details is studied. Orthogonal skew slabs can be transferred to isotropic skew slabs similar to rectangular slabs using affine transformation by modifying the coefficient of orthotropy. The strength of a skew slab is directly proportional to the strength of rectangular slabs at a particular aspect ratio. If the strength of skew slab is known at an aspect ratio, we can find the strength of the skew slab at any aspect ratio at a particular skew angle. In this paper the skew angle is limited to 35° . The strength of the skew slab is increasing with increase in skew angle at any aspect ratio irrespective of the edge condition. The strength of simply supported slab is half the strength of Continuous Slab.

Keywords : Aspect ratio; Affinity theorem; Orthotropic reinforced concrete skew slabs; Orthotropy; Virtual work equations; Yield line theory.

INTRODUCTION

Skew slabs are the requirement of present situation to satisfy the architectural need, optimum utilization of space etc. Also, in order to cater greater speed and more safety of present-day traffic, the modern highways are to be straight as far as possible. This requirement along with obstacles, complex intersections, or mountainous terrain is responsible for provision of increasing number of skew deck slab. Many bridge decks slabs have been built on skew alignment.

Skew slabs are defined as a four-sided slab having equal opposite angles other than 90° . Skew angle is usually measured clockwise from vertical line perpendicular to the support line of the skew slab. The analysis and design of a skew slab is very complicated due to its shape.

The ultimate strength of such slabs may be conveniently determined by using the yield-line theory

The ultimate strength of such slabs may be conveniently determined by using the yield-line theory proposed by Johansen [1, 2]. Many design codes [3–5] recommend Yield-Line theory as one of the possible methods of slab design. Park and Gamble [6] presented in detail the work/research work done on two-way rectangular slabs for uniformly loaded, point load and line loads along with work equations. Limited literature is available on Balcony slabs [7], Trapezoidal slabs [7, 8], Skew slabs [9, 10]. Major work is limited to simply supported (SS) and continuous slab (CS) edge conditions. Rajesh Kumar et al. [10] derived work equations for all the edge conditions separately and presented moment coefficient tables for skew slabs. In this paper generalized virtual work equations are derived for the predicted possible admissible failure yield line patterns (refer Fig. 1 and Fig. 2) which are applicable to all edge conditions.

METHODOLOGY

The generalized virtual work equations for continuous edge (CS) condition of slab are derived for the predicted possible admissible failure yield line patterns using the virtual work method. Let δ be the virtual displacement at E & F (Fig. 1), for the considered failure Pattern-1 of a slab. Three unknown dimensions C1, C2, & C3 are necessary to define the yield line propagation completely. To get the equations for other edge conditions of the slab, modification should be carried out in the numerators of the equations of each failure patterns. For Two Adjacent Side Continuous (TAC) slab $I_c = I_d = 0$, or $I_a = I_b = 0$.

In skew concrete slabs the reinforcement may be placed parallel to the edges of the slab, and hence the plate is not orthotropic [11]. Let the reinforcement be placed in the X direction and in the Y direction so that the plate is orthotropic. The bending resistance, of a yield line making an angle θ with the Y-axis is $K'_x m_{ult} \cos^2 \theta + K'_y m_{ult} \sin^2 \theta$ if the yield line is positive

(sagging) and $I_1 m_{ult} \cos^2 \theta + I_2 m_{ult} \sin^2 \theta$ or $I_3 m_{ult} \cos^2 \theta + I_4 m_{ult} \sin^2 \theta$ if the yield line is negative (hogging).

Generalized equations are derived for both the failure patterns considered. A sample derivation is presented for the continuously supported skew slab Yield line pattern-1 (Refer Appendix-B).

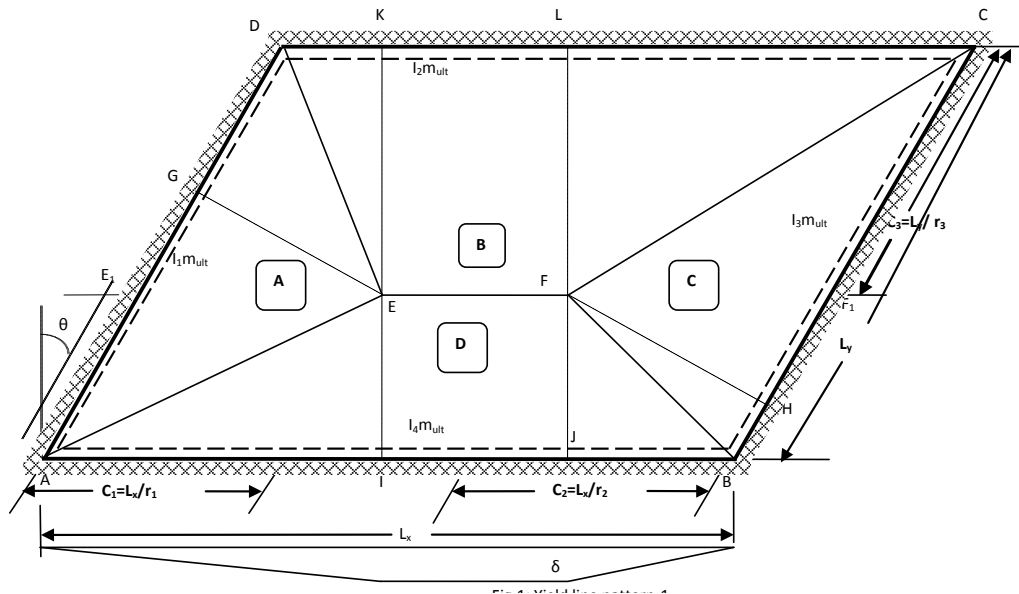


Fig. 1. Yield line pattern-1

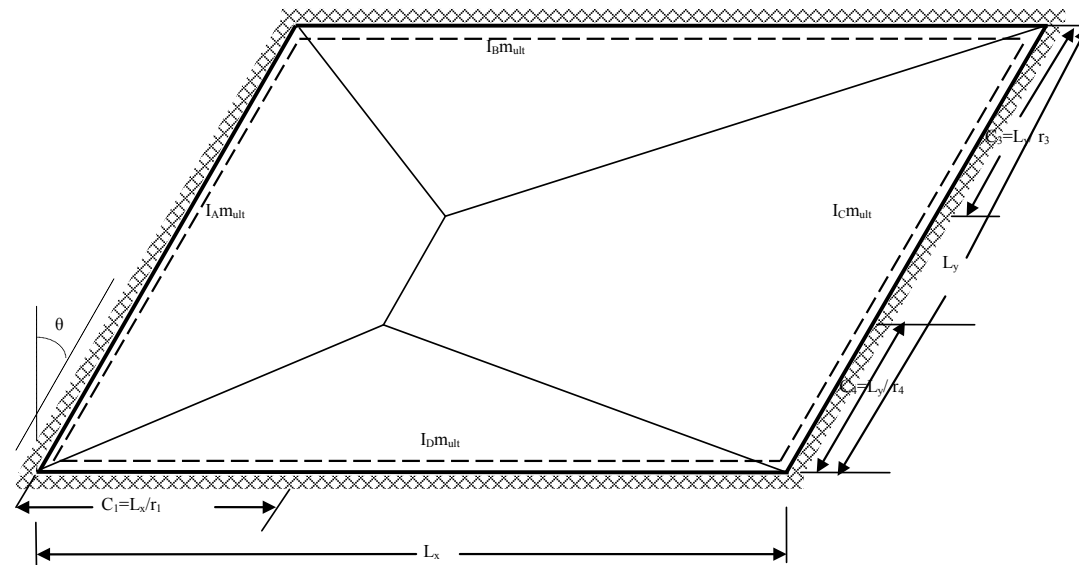


Fig. 2. Yield line pattern-2

Minimization of Virtual Work Equations

The equations of $W_{ult} L_y^2 / m_{ult}$ of the two failure patterns consist of the unknown non dimensional parameters r_1 , r_2 , r_3 and r_4 which define the positions of the yield lines. A computer program has been developed in FORTRON for various values of the non-dimensional parameters r_1 , r_2 , r_3 and r_4 within their allowable ranges in order to find the minimum value of $W_{ult} L_y^2 / m_{ult}$ for the yield line failure patterns considered. In this computer program at different aspect ratio and skew angle, θ of the slab the values of r_1 , r_2 , r_3 and r_4 were varied at increments of 0.01 in order to find the minimum value of $W_{ult} L_y^2 / m_{ult}$ and the failure pattern. Using the above equations, one can develop useful charts basing on orthogonality which may be used either for design or analysis in general.



Affine transformation of a skew slab

'Affine transformation' based on theorems VI and VII of Johansen [1] is a technique that transforms an orthogonal slab into that of an equivalent isotropic slab, whose strength is same as that of original orthotropic slab. The transformation of orthotropic slab to that of related isotropic slab is presented with specific examples for different edge conditions. In order to perform the transformation, charts are required and these charts are prepared using isotropic (affine) reinforcement (coefficients), which means that in each direction the reinforcement is same and unity i.e. $K_x^1 = K_y^1 = I_1 = I_2 = I_3 = I_4 = 1.0$. These charts show the minimum value of $W_{ult} L_y^2 / m_{ult}$ versus aspect ratio of slab for various skew angles. A computer program is developed in FORTRAN which gives the least value of $W_{ult} L_y^2 / m_{ult}$ for orthogonal moment coefficients.

According to theorems VI and VI of Johansen [1], any orthogonal slab can be transformed into an equivalent related isotropic slab provided that the ratio of negative to positive moments in the slab is same and unity. When the ratio of negative to positive moment in the orthogonal slab is same and unity, then such a slab can be transformed into an equivalent isotropic slab directly as shown in **Fig. 3**, which means that the given orthogonal slab solution can be obtained by analysing the isotropic slab with modified dimensions in the X-direction.

When the ratio of negative to positive moment in the orthogonal slab is not unity, then such a slab can be transformed into an equivalent isotropic slab directly as illustrated in Example 2.

In order to transform an orthotropic continuous skew slab to an equivalent isotropic slab in which the ratio of Negative moment to positive moment in both directions is same and unity using the affine theorem, the length of the slab in X – direction should be divided with $\sqrt{(\mu \times \cos^2 \theta) + \sin^2 \theta}$. The new aspect ratio is calculated and the value of $W_{ult} L_y^2 / m_{ult}$ is read from affine charts (Appendix-C).

Example 1: Transform a Continuous slab 3m X 3m with $K_x' = I_1 = I_3 = 0.25$, $K_y' = I_2 = I_4 = 1.0$, $\theta = 5^\circ$.

For the given data, we get $W_{ult} L_y^2 / m_{ult} = 28.678$ from computer program.

Since $I_1/K_x' = I_2/K_y' = 1.0$, the given orthotropic skew slab is transformed to an equivalent isotropic slab by dividing the length of the slab in X – direction with $\sqrt{(\mu \times \cos^2 \theta) + \sin^2 \theta}$.

The modified value of $\mu^* = ((\mu \times \cos^2 \theta) + \sin^2 \theta)$

$\mu^* ((0.25 \times \cos^2 5^\circ) + \sin^2 5^\circ) = 0.256$. The new aspect ratio is

$$r^* = \frac{L_x}{L_y} = \frac{L_x / \sqrt{(\mu \times \cos^2 \theta) + \sin^2 \theta}}{L_y} = \frac{r}{\sqrt{(\mu \times \cos^2 \theta) + \sin^2 \theta}} = \frac{1.0}{\sqrt{0.256}} = 1.977 \text{ and the value of } W_{ult} L_y^2 / m_{ult} \cong 28.67 \text{ (from Chart No.1).}$$

This principle is illustrated in **Fig. 3** using the above methodology.

Example 2: Find the strength of continuous skew slab 4.5m X 3m with skew angle 15° if the orthogonal moment coefficients are: $K_x' = I_1 = 0.6$, $K_y' = I_2 = 0.9$.

Solution: For $K_x' = I_1 = 0.6$, $K_y' = I_2 = 0.9$, $\theta = 15^\circ$ and $r = 1.5$, we get $W_{ult} L_y^2 / m_{ult} = 28.94$ from computer program.

Since $I_1/K_x' = I_2/K_y' = 1.0$, the given orthotropic skew slab is transformed to an equivalent isotropic slab by dividing the length of the slab in X – direction with $\sqrt{(\mu \times \cos^2 \theta) + \sin^2 \theta}$.

The modified value of $\mu^* = ((\mu \times \cos^2 \theta) + \sin^2 \theta) = ((0.667 \times \cos^2 15^\circ) + \sin^2 15^\circ) = 0.689$. The new aspect ratio,

$$r^* = \frac{r}{\sqrt{(\mu \times \cos^2 \theta) + \sin^2 \theta}} = \frac{1.5}{\sqrt{0.689}} = 1.807$$

The new aspect ratio is 1.807 and the value of $W_{ult} L_y^2 / m_{ult} \cong 32.166$ (from Chart No.1). Since $K_y' \neq 1.0$, the value of $W_{ult} L_y^2 / m_{ult}$ obtained from chart should be multiplied by K_y' in order to get the actual value of $W_{ult} L_y^2 / m_{ult}$, i.e. $32.166 \times 0.9 = 28.940$. Few numerical examples are presented in Table 1.

The COS20 PRINCIPLE

If the strength of SLAB is known at an aspect ratio, we can find the strength of the slab at any aspect ratio using the COS20 PRINCIPLE.

The principle of COS²θ states that the product of the difference in strength between two aspect ratios and square of the Cosines is constant for any skew angle.

$$i. e. \left[\left(\frac{W_{ult} L_y^2}{m_{ult}} \right)_{r_1} - \left(\frac{W_{ult} L_y^2}{m_{ult}} \right)_{r_2} \right] \cos^2 \theta = C, \text{ where } r_1 < r_2. \quad (1)$$

In other words, if the strength of SLAB is known at an aspect ratio, we can find the strength of the slab at any aspect ratio using the COS²θ PRINCIPLE and this principle is illustrated in Example 3 shown below. COS²θ PRINCIPLE is applicable to all edge conditions provided both the positive moment coefficients and negative moment coefficients are equal to each other. The constants given in **Table 2** for different edge conditions are for isotropic moment coefficients. The constants change if the moment coefficients change. In case of CS, OSD, OLD and TAC edge conditions we can find the strength of the slab at other aspect ratios even though the positive moment coefficients change, as we can find the strength of the slabs for these edge conditions using Affine Transformation. First, we can perform affine transformation and find the aspect ratio of the slab at which $K_x' = K_y' = 1.0$. Then by using the COS²θ PRINCIPLE we can find the strength of the skew slab (approximately) using the constants given in **Table 2** without using charts.

Table 1. Affine transformation examples for skew slabs

Sl.No.	Slab	Orthogonal Moment Co-efficients	r	θ	μ*	r*	Strength $W_{ult} L_y^2 / m_{ult}$	Actual Strength $W_{ult} L_y^2 / m_{ult}$	Refer Chart No.
1	CS	$K_x^1=0.25, K_y^1=1.0, I_1=0.25, I_2=1.0, \mu=0.25, \sum K=2.5$	1.0	5°	0.256	1.978	28.678	28.678	<u>1</u>
2	CS	$K_x^1=0.6, K_y^1=0.9, I_1=0.5, I_2=1.0, \mu=0.667, \sum K=3.0$	1.5	15°	0.689	1.807	32.166	28.940	<u>1</u>
3	CS	$K_x^1=1.0, K_y^1=2.0, I_1=1.0, I_2=2.0, \mu=0.5, \sum K=4.0$	1.5	10°	0.515	2.09	28.400	56.800	<u>1</u>
4	TAC	$K_x^1=1.0, K_y^1=1.0, I_1=1.0, I_2=1.0, \mu=1.0, \sum K=4.0$	2.0	15°	1.0	2.0	22.084	22.084	<u>4</u>
5	TAC	$K_x^1=1.333, K_y^1=0.667, I_1=1.333, I_2=0.667, \mu=2.0, \sum K=4.0$	1.6	25°	1.821	1.186	36.285	24.203	<u>4</u>
6	OSD ($I_c=0.0$)	$K_x^1=0.667, K_y^1=1.0, I_1=0.667, I_2=1.0, \mu=0.667, \sum K=3.334$	1.4	10°	0.667	1.701	29.215	29.215	<u>2</u>
7	OSD ($I_c=0.0$)	$K_x^1=1.5, K_y^1=2.0, I_1=1.5, I_2=2.0, \mu=0.75, \sum K=5.0$	1.6	20°	0.779	1.812	31.010	62.020	<u>2</u>
8	OLD ($I_b=0.0$)	$K_x^1=2.0, K_y^1=1.0, I_1=2.0, I_2=1.0, \mu=2.0, \sum K=6.0$	1.7	15°	1.933	1.223	35.93	35.93	<u>3</u>
9	OLD ($I_b=0.0$)	$K_x^1=1.5, K_y^1=0.5, I_1=1.5, I_2=0.5, \mu=3.0, \sum K=4.0$	2.0	30°	2.5	1.265	43.28	21.64	<u>3</u>

NOTE: $\mu^* = ((\mu \times \cos^2 \theta) + \sin^2 \theta), r^* = r/\sqrt{\mu^*}, \text{Actual Strength} = \text{Strength} \times K_y'$

Table 2. Constants(C) for r = 1.0 to find $W_{ult} L_y^2 / m_{ult}$ at different aspect ratios for different edge conditions

Edge Condition Aspect Ratio, r_2	CS	OSD	OLD	TAC	TLC	TSC	OLC	OSC	SS
1.1	4.216	3.220	4.050	3.072	2.369	3.868	2.233	2.930	2.108
1.2	7.507	5.749	7.201	5.469	4.241	6.877	3.987	5.209	3.753
1.3	10.138	7.781	9.709	7.386	5.756	9.266	5.399	7.020	5.069
1.4	12.283	9.446	11.743	8.949	7.003	11.200	6.557	8.488	6.141
1.5	14.061	10.832	13.422	10.245	8.048	12.788	7.522	9.700	7.031
1.6	15.557	12.004	14.828	11.335	8.935	14.111	8.337	10.714	7.778
1.7	16.831	13.005	16.021	12.263	9.696	15.228	9.035	11.573	8.416
1.8	17.929	13.870	17.044	13.062	10.356	16.183	9.639	12.310	8.964
1.9	18.882	14.625	17.931	13.757	10.935	17.006	10.165	12.947	9.441
2.0	19.718	15.289	18.705	14.366	11.445	17.723	10.629	13.504	9.859

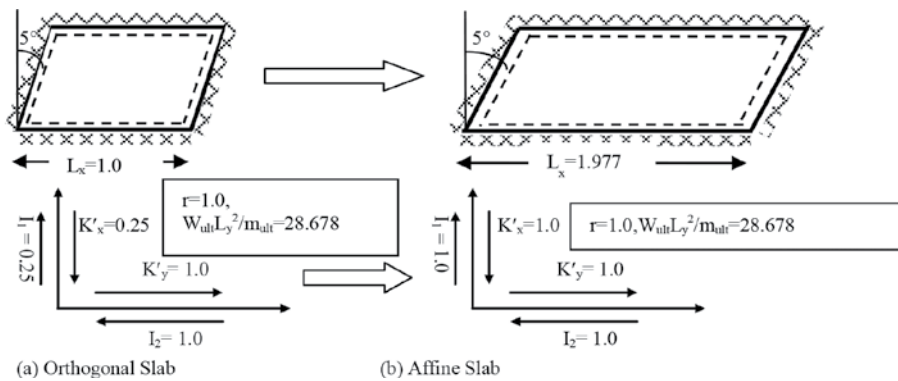


Fig. 3. Affine Transformation

Example 3: In Example 2 affine transformation was done and the strength of the slab was found referring charts. The same thing can be done by using the COS²θ PRINCIPLE.

Using expression (1),

$$\left[51.407_{r=1.0} - \left(\frac{W_{ult} L_y^2}{m_{ult}} \right)_{r=1.807} \right] \cos^2 15^\circ = 1.793 \cong 1.8;$$

for $r=1.8$, $C=17.929$ for CS (from Table 2).

$$\therefore \left(\frac{W_{ult} L_y^2}{m_{ult}} \right)_{r=1.8} \cong 32.191$$

Since $K'_y \neq 1.0$ and $K'_y = 0.9$, the value of $W_{ult} L_y^2 / m_{ult}$ obtained from the COS²θ PRINCIPLE should be multiplied by K'_y in order to get the actual value of $W_{ult} L_y^2 / m_{ult}$ i.e. $32.191 \times 0.9 = 28.971$, which is approximately equal to the value obtained from Affine Transformation in Example 2.

Table 2 shows the constants using which we can find the strength of a skew slab at any aspect ratio, r , using the strength of the slab at aspect ratio, $r = 1.0$.

Example 4: Find the strength of the Continuous skew slab at aspect ratio 1.5, if the strength of the Continuous skew slab at $r = 1.0$ is 64.0 for skew angle of 30°.

From the principle of COS²θ,

$$\left[\left(\frac{W_{ult} L_y^2}{m_{ult}} \right)_{r=1.0} - \left(\frac{W_{ult} L_y^2}{m_{ult}} \right)_{r=1.5} \right] \cos^2 \theta = C$$

From Table 2, for CS, Constant, $C=14.061$.

$$\therefore \left[\left(\frac{W_{ult} L_y^2}{m_{ult}} \right)_{r=1.0} - \left(\frac{W_{ult} L_y^2}{m_{ult}} \right)_{r=1.5} \right] \cos^2 \theta = 14.061$$

$$\therefore \left[64.00 - \left(\frac{W_{ult} L_y^2}{m_{ult}} \right)_{r=1.5} \right] \cos^2 30^\circ = 14.061$$

$$\Rightarrow \frac{W_{ult} L_y^2}{m_{ult}} = 45.253 \text{ (Refer Chart no. 1)}$$

Few numerical examples are presented in **Table 3**.

The strength of skew slab is directly proportional to the strength of the rectangular slab at a particular aspect ratio.

$$\text{i.e. } \left[\left(\frac{W_{ult} L_y^2}{m_{ult}} \right)_{\theta} \propto \left(\frac{W_{ult} L_y^2}{m_{ult}} \right)_{\theta=0.0} \right]_r$$

$$\left[\left(\frac{W_{ult} L_y^2}{m_{ult}} \right)_{\theta} = \frac{1}{\cos^2 \theta} \left(\frac{W_{ult} L_y^2}{m_{ult}} \right)_{\theta=0.0} \right]_r \quad (2)$$

Statements I and II are valid if both the positive moment coefficients and negative moment coefficients are equal to each other, i.e. $K_x' = K_y'$, $I_1 = I_2$.

Example 5: The strength of a 2.5m X 1.25m two adjacent side's continuous rectangular slab is 20.605. Find the strength at a skew angle of 15° .

Using expression (2) we can write,

$$\left[\left(\frac{W_{ult} L_y^2}{m_{ult}} \right)_{15^\circ} = \frac{1}{\cos^2 15^\circ} \left(\frac{W_{ult} L_y^2}{m_{ult}} \right)_{\theta=0.0^\circ} \right]_{r=2.0}$$

$$\Rightarrow \left(\frac{W_{ult} L_y^2}{m_{ult}} \right)_{15^\circ} = 22.084 (\text{Refer Chart 4}).$$

Preparation of Charts

Design charts (Charts1-9) have been prepared for SKEW slabs and are shown in Appendix-C. Charts1-9 are plotted for $W_{ult} L_y^2 / m_{ult}$ versus skew angle, θ for various values of aspect ratio, r and different edge conditions. The skew angle, θ is limited to 35° and is varied in increments of 5° . The aspect ratio, r is taken between 1.0 and 2.0. While preparing the design charts, the least value of $W_{ult} L_y^2 / m_{ult}$ given by the two failure patterns is considered. Using these charts one can directly design or do analysis of a skew slab. These charts are prepared using isotropic (affine) reinforcement (coefficients) (refer **Table 4**), which means that in each direction the reinforcement is same and unity i.e. $K_x' = K_y' = I_1 = I_2 = I_3 = I_4 = 1.0$ (refer **Table 4**).

Analysis and Design Problems

Analysis Problem

A continuous skew slab 4.5m X 3.0 m with skew angle of 10° is reinforced with 10 mm diameter bars @163 mm c/c perpendicular to long span and 8 mm diameter bars @ 250 mm c/c perpendicular to short span. Two meshes are used one at top and one at bottom. Thickness of the slab is 120 mm. Concrete grade is M20.

Two meshes are used one at top and one at bottom. Thickness of the slab is 120 mm. Concrete grade is M20.

Table 3. Examples based on constants(C) given in Table 2

Sl. No.	Slab	θ	Strength $\frac{W_{ult} L_y^2}{m_{ult}}$ at $r = 1.0$	r^*	Constant C	Strength $\frac{W_{ult} L_y^2}{m_{ult}}$ at $r = r^*$	Refer Chart No.
1	CS	5°	48.368	1.6	15.557	32.692	<u>1</u>
2	OSD ($I_c=0.0$)	15°	44.322	1.3	7.781	35.982	<u>2</u>
3	OLD ($I_b=0.0$)	10°	42.638	1.7	16.021	26.120	<u>3</u>
4	TAC	20°	39.604	1.2	5.469	33.411	<u>4</u>

Table 4. Affine coefficients

SLAB (edge condition)	K_x'	K_y'	I_1 or I_3	I_2 or I_4	μ	$\sum K$
CS	1.0	1.0	1.0	1.0	1.0	4.0
OSD($I_3 \neq 0.0$)	1.0	1.0	1.0	1.0	1.0	4.0
OLD($I_4 \neq 0.0$)	1.0	1.0	1.0	1.0	1.0	4.0
TAC ($I_3 = I_4 = 0.0$)	1.0	1.0	1.0	1.0	1.0	4.0
TLC	1.0	1.0	0.0	1.0	1.0	4.0
TSC	1.0	1.0	1.0	0.0	1.0	4.0
OLC($I_4 = 0.0$)	1.0	1.0	0.0	1.0	1.0	4.0
OSC($I_3 = 0.0$)	1.0	1.0	1.0	0.0	1.0	4.0
SS	2.0	2.0	0.0	0.0	1.0	4.0

Solution

According to IS 456:2000[5], $m_{ult} = 0.87 f_y A_{st} z$, where $z = d (1 - (f_y A_{st} / f_{ck} bd))$ (3)

Taking Effective depth of slab in short span direction=100 mm.

Effective depth of slab in long span direction = 90.00 mm.

Area of the steel perpendicular to long span and short span are 481.45 mm² and 201.06 mm² respectively.

The ultimate moments in short and long span directions can be found using expression (3).

Therefore, m_{ult} parallel to long span = 6.956 kNm/m,

m_{ult} parallel to short span = 13.908 kNm/m.

For aspect ratio of slab (r) = 4.5/3.0 = 1.5 and taking $m_{ult} = 6.956$ kN-m/m, the orthogonal coefficients (**Fig 6**) will be $K'_x = I_1 = I_3 = 1.0$ and $K'_y = I_2 = I_4 = 2.0$. With these orthogonal coefficients and for skew angle of 10°, $r = 1.5$; two predicted failure patterns are evaluated by using computer program to find the governing failure pattern and the final results are as follows:

$W_{ult} L_y^2 / m_{ult} = 56.944$, $r_1 = 3.165$, $r_2 = 3.150$, $r_3 = 2.01$ and the failure pattern is 1.

Alternatively, by performing affine transformation, the modified value of r is 2.09 and $W_{ult} L_y^2 / m_{ult} \cong 28.4.4$ from Chart 1.

Since $K'_y = 2.0$, actual value of $W_{ult} L_y^2 / m_{ult} = 2.0 \times 28.4 = 56.8$.

$W_{ult} = (56.944 \times 6.956) / (3.0^2) = 44.011$ kN/m²

W_{dl} = (dead load including finishing)

$W_{dl} = (0.12 \times 25) + 1.0 = 4.0$ kN/m²

$W_{ll} = (44.011 - 4.0) = 40.011$ kN/m²

Safe $W_{ll} = 40.011 / 1.5 = 26.674$ kN/m²

The intensity of safe uniformly distributed live load on the slab is 26.674 kN/m².

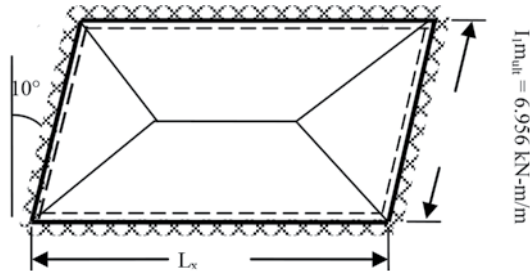


Fig. 4(a). Analysis problem

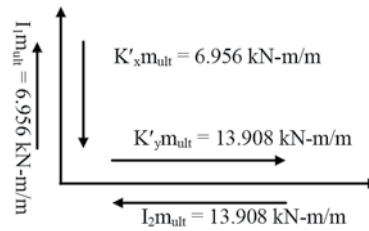


Fig. 4(b). Orthogonal moments

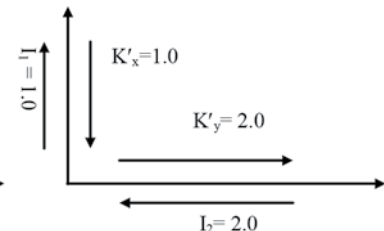


Fig. 4(c). Orthogonal moment coefficients

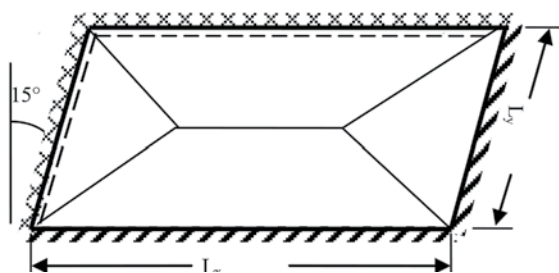


Fig. 5(a). Design problem

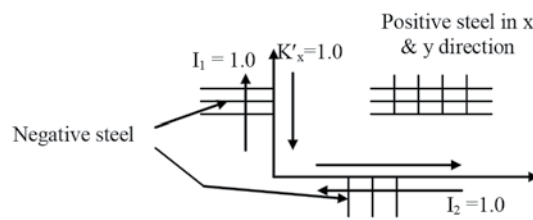


Fig. 5(b). Orthogonal moment coefficients

Design Problem

Design Two adjacent sides continuous skew slab of span 8.0 m X 4.0 m to carry imposed load of 2.5 kN/m². The skew angle of slab is 15° and it is 130 mm thick. Use M20 grade concrete and Fe415 grade steel.

Given: Aspect ratio of slab = $L_x/L_y = 8.0/4.0 = 2.0$, skew angle of 15°

Assuming $K'_x = I_1 = 1.0$, $K'_y = I_2 = 1.0$, $r = 2.0$ (refer **Fig. 5**) and skew angle of 15°, We get $W_{ult} L_y^2 / m_{ult} \cong 22.084$ and failure pattern is 1. (From Chart-4 for skew angle of slab is 15° and $r = 2.0$ we get $W_{ult} L_y^2 / m_{ult} \cong 22.084$).



Overall thickness of slab = 130.0 mm (say)

Dead load of slab = $0.130 \times 25.0 = 3.25 \text{ kN/m}^2$

Dead loads including finishing's = 4.25 kN/m^2

Imposed load = 2.5 kN/m^2 .

Total design ultimate load = $(1.5 \times (4.25 + 2.5)) = 10.125 \text{ kN/m}^2$, i.e. $W_{ult} = 10.125 \text{ kN/m}^2$

$$\therefore m_{ult} = \frac{10.125 \times 4.0^2}{22.084} = 7.336 \text{ kNm/m} \\ \cong 7.34 \text{ kNm/m}$$

The orthogonal moments are

$$K_x' m_{ult} = I_1 m_{ult} = 1.0 \times 7.34 = 7.34 \text{ kN-m/m}$$

$$K_y' m_{ult} = I_2 m_{ult} = 1.0 \times 7.34 = 7.34 \text{ kN-m/m}$$

According to IS 456:2000[5], $m_{ult} = 0.87 f_y A_{st} z$, where $z = d (1 - (f_y A_{st} / f_{ck} bd))$, (3)

Short span reinforcement:

Positive reinforcement 10 dia bars @ 300c/c = 9.88 kN m/m

Negative reinforcement 8 dia bars @ 260c/c = 7.46 kN m/m

Long span reinforcement:

Positive reinforcement 10 dia bars @ 300c/c = 9.88 kN m/m

Negative reinforcement 8 dia bars @ 260c/c = 7.46 kN m/m

Adopt effective depth as 110 mm and overall depth as 130 mm.

CONCLUSIONS

1. The strength of the skew slab is directly proportional to the strength of a rectangular slab at a particular aspect ratio if both the positive moment coefficients and negative moment coefficients are equal to each other.
2. If the strength of SLAB is known at an aspect ratio, we can find the strength of the slab at any aspect ratio using the $\text{COS}^2\theta$ PRINCIPLE for all the edge conditions if both the positive moment coefficients and negative moment coefficients are equal to each other.
3. Strength of Slab can be found by using affine transformation to find the ratio at which the orthogonal moment coefficients are equal to one and find the strength of the slab at that particular aspect ratio using the $\text{COS}^2\theta$ PRINCIPLE without using affine charts at any skew angle.
4. It has been observed that the strength of CS and SS Slabs are same.
5. It has been observed that the strength of OSD, OSC, OLD and OLC Slabs approximately same for lesser skew ($\theta \leq 10^\circ$) angles.
6. The strength of TAC Slab is lesser than other edge conditions irrespective of the aspect ratio and skew angle.
7. Strength of the slab is increasing with increase in skew angle irrespective of the aspect ratio.
8. Strength of the slab is decreasing with increase in aspect ratio irrespective of the skew angle.
9. For TSC both regular and irregular patterns are governing at aspect ratio 1.4 irrespective of the skew angle.
10. The strength of Simply Supported slab is half the strength of Continuous Slab.

REFERENCES





1. Johansen, K. W., "Yield-line theory", Cement and Conc. Assoc., London, 1962.



2. Johansen K. W., "Yield-Line formulae for slabs", Cement and Conc. Assoc., London, 1972.
3. ACI 421.3R-15, "Guide to Design of Reinforced Two-Way Slab Systems," American Concrete Institute, pp 11.
4. BS 8110-1, "The structural use of concrete – Part 1, Code of practice for design and construction." BRITISH STANDARDS INSTITUTION, BSI, 1997.
5. IS 456:2000, "Indian Standard Plain and Reinforced Concrete-Code of Practice", Bureau of Indian Standard's, BIS New Delhi, India.
6. Park, R. and Gamble, W. L., "Reinforced concrete slabs", John Wiley & sons, New York, 2000.
7. KUANG-HAN CHU and RAM B. SINGH, "Yield Analysis of Balcony Floor Slabs", ACI Journal, Title No.63-28, May 1966, 571-586.
8. Sudhakar, K.J., and Goli, H B., "Limit State Coefficients for Trapezoidal- Shaped Slabs Supported on Three Sides", Journal of Structural Engineering, Chennai, India, Vol.32, No.2, June-July 2005, 101-108.
9. Prakash Desai and K.U.Muthu, "A brief review on strength, deflection and cracking of rectangular, skew and circular reinforced concrete slabs", J. Indian Inst. Sci., Mar-Apr. 1988, 68, pp91-108.
10. Rajesh Kumar, S.Mandal and Veerendra Kumar, "Yield line analysis of reinforced concrete skew slabs", Journal of Structural Engineering, Chennai, India, Vol.41, No.2, June-July 2014, 97-114.
11. D. Bauer And R. G. Redwood, "Numerical yield line analysis", Computers and Structures, Vol. 26, No. 4, 1987, 587-597.

APPENDIX-A

Notation:

	Continuous edge
	Simply supported edge
	Positive yield line
	Negative yield line
CS	A slab supported on all sides continuously (restrained)
I_1, I_2, I_3 and I_4	Negative moment coefficients in their corresponding directions
I_A, I_B, I_C and I_D	Total Negative moment coefficients of their corresponding segments
$I_1 m_{ult}$ and $I_3 m_{ult}$	Negative ultimate yield moment per unit length provided by top tension reinforcement bars placed parallel to X-axis.
$I_2 m_{ult}$ and $I_4 m_{ult}$	Negative ultimate yield moment per unit length provided by top tension reinforcement bars placed parallel to Y-axis.
$K_x^1 m_{ult}$	Positive ultimate yield moment per unit length provided by bottom tension bars placed parallel to X-axis
$K_y^1 m_{ult}$	Positive ultimate yield moment per unit length provided by bottom tension bars placed parallel to Y-axis
L_x	Slab dimensions in X direction
L_y	Inclined Slab dimensions
m_{ult}	Ultimate Yield moment per unit length of the slab
OLC	A slab restrained on one long edge and other three sides simply supported
OLD	A slab restrained on three edges and one long side simply supported
OSC	A slab restrained on one short edge and other three sides simply supported

OSD	A slab restrained on three edges and one short side simply supported
r	Aspect ratio of slab defined by L_x/L_y .
r_1, r_2, r_3, r_4	Non dimensional parameters of yield line propagation
SS	A slab simply supported on all sides
TAC	A slab supported on two adjacent sides continuously (restrained)
TLC	A slab restrained on two long edges and other two sides simply supported
TSC	A slab restrained on two short edges and other two sides simply supported
Udl	Uniformly Distributed Load
W_{dl}	Dead load
W_{ll}	Live load
W_{ult}	Ultimate uniformly distributed load per unit area of slab.
θ	Skew angle
μ	Coefficient of orthotropy

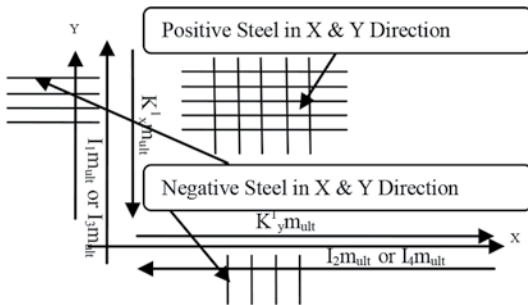


Fig. 6. Orthogonal moments and reinforcement notation

APPENDIX-B

Derivation of Virtual Work Equations of Yield line pattern-1(Fig.1) and Yield line pattern-2(Fig.2)

Yield line Pattern-1(refer Fig.1):

$$DK = C_1 - C_3 \sin \theta, CL = C_2 + C_3 \sin \theta, AE_1 = L_y - C_3, FH = C_2 \cos \theta, EG = C_1 \cos \theta, EK = C_3 \cos \theta, DI = EJ = (L_y - C_3) \cos \theta, BJ = C_2 - (L_y - C_3) \sin \theta, EF = IJ = L_x - C_1 - C_2$$

$$\text{Let } (I_1 m_{ult} \cos^2 \theta + I_2 m_{ult} \sin^2 \theta) = I_A, I_2 = I_B, (I_3 m_{ult} \cos^2 \theta + I_4 m_{ult} \sin^2 \theta) = I_C \text{ and } I_4 = I_D$$

The external work done by segment A:-

$$= \left[\frac{1}{2} (AD)(GE) \frac{W_{ult}}{3} \right] = \left[\frac{1}{2} L_y C_1 \cos \theta \frac{W_{ult}}{3} \right] = \frac{C_1 L_y \cos \theta W_{ult}}{6}$$

The external work done by segment B:-

$$= \left[\frac{1}{2} (DK)(EK) \frac{W_{ult}}{3} + (EK)(EF) \frac{W_{ult}}{2} + \frac{1}{2} (CL)(FL) \frac{W_{ult}}{3} \right]$$

$$= \left[\frac{1}{2} (C_1 - C_3 \sin \theta)(C_3 \cos \theta) \frac{W_{ult}}{3} + (L_x - C_1 - C_2)(C_3 \cos \theta) \frac{W_{ult}}{2} + \frac{1}{2} (C_2 + C_3 \sin \theta)(C_3 \cos \theta) \frac{W_{ult}}{3} \right]$$

The external work done by segment C:-

$$= \left[\frac{1}{2} (CB)(FH) \frac{W_{ult}}{3} \right] = \left[\frac{1}{2} L_y C_2 \cos \theta \frac{W_{ult}}{3} \right] = \frac{C_2 L_y \cos \theta W_{ult}}{6}$$

The external work done by segment D:-

$$= \left[\frac{1}{2} (AI)(EI) \frac{W_{ult}}{3} + (IJ)(EI) \frac{W_{ult}}{2} + \frac{1}{2} (BJ)(FJ) \frac{W_{ult}}{3} \right]$$

$$= \left[\frac{1}{2} (C_1 + (L_y - C_3) \sin \theta) ((L_y - C_3) \cos \theta) \frac{W_{ult}}{3} + (L_x - C_1 - C_2)(L_y - C_3) \cos \theta \frac{W_{ult}}{2} + \frac{1}{2} (C_2 - (L_y - C_3) \sin \theta) ((L_y - C_3) \cos \theta) \frac{W_{ult}}{3} \right]$$

$$= \left[\frac{(L_y - C_3) \cos \theta W_{ult}}{6} (C_1 + C_2) + (L_y - C_3) \cos \theta \frac{W_{ult}}{2} (L_x - C_1 - C_2) \right]$$

Total work done = work done by segment's (A+B+C+D)

$$= W_{ult} L_y^2 r \left[\frac{C_1 L_y \cos \theta W_{ult}}{6} + \frac{1}{2} (C_1 - C_3 \sin \theta) (C_3 \cos \theta) \frac{W_{ult}}{3} + (L_x - C_1 - C_2) (C_3 \cos \theta) \frac{W_{ult}}{2} \right. \\ \left. + \frac{1}{2} (C_2 + C_3 \sin \theta) (C_3 \cos \theta) \frac{W_{ult}}{3} + \frac{C_2 L_y \cos \theta W_{ult}}{6} + (L_y - C_3) (C_1 + C_2) \cos \theta \frac{W_{ult}}{6} \right. \\ \left. + (L_y - C_3) (L_x - C_1 - C_2) \cos \theta \frac{W_{ult}}{2} \right] \\ = W_{ult} L_y^2 r \cos \theta \left[\frac{1}{2} - \frac{1}{6} \left(\frac{1}{r_1} - \frac{1}{r_2} \right) \right] \quad (4)$$

Energy absorbed yield lines: -

$$= \left[(K'_x m_{ult} \cos^2 \theta + K'_y m_{ult} \sin^2 \theta) \frac{L_y}{C_1 \cos \theta} + (I_1 m_{ult} \cos^2 \theta + I_2 m_{ult} \sin^2 \theta) \frac{L_y}{C_1 \cos \theta} + K'_y m_{ult} \frac{L_x}{C_3 \cos \theta} \right. \\ \left. + I_2 m_{ult} \frac{L_x}{C_3 \cos \theta} + (K'_x m_{ult} \cos^2 \theta + K'_y m_{ult} \sin^2 \theta) \frac{L_y}{C_2 \cos \theta} + (I_3 m_{ult} \cos^2 \theta + I_4 m_{ult} \sin^2 \theta) \frac{L_y}{C_2 \cos \theta} \right. \\ \left. + K'_y m_{ult} \frac{L_x}{(L_y - C_3) \cos \theta} + I_4 m_{ult} \frac{L_x}{(L_y - C_3) \cos \theta} \right] \\ = \left[(K'_x m_{ult} \cos^2 \theta + K'_y m_{ult} \sin^2 \theta) \frac{L_y}{C_1 \cos \theta} + I_A m_{ult} \frac{L_y}{C_1 \cos \theta} + K'_y m_{ult} \frac{L_x}{C_3 \cos \theta} \right. \\ \left. + I_B m_{ult} \frac{L_x}{C_3 \cos \theta} + (K'_x m_{ult} \cos^2 \theta + K'_y m_{ult} \sin^2 \theta) \frac{L_y}{C_2 \cos \theta} + I_C m_{ult} \frac{L_y}{C_2 \cos \theta} \right. \\ \left. + K'_y m_{ult} \frac{L_x}{(L_y - C_3) \cos \theta} + I_D m_{ult} \frac{L_x}{(L_y - C_3) \cos \theta} \right] \\ = \frac{m_{ult}}{\cos \theta} \left[(K'_x \cos^2 \theta + K'_y \sin^2 \theta) \frac{L_y}{C_1} + I_A \frac{L_y}{C_1} + K'_y \frac{L_x}{C_3} + I_B \frac{L_x}{C_3} \right. \\ \left. + (K'_x \cos^2 \theta + K'_y \sin^2 \theta) \frac{L_y}{C_2} + I_C \frac{L_y}{C_2} + K'_y \frac{L_x}{(L_y - C_3)} + I_D \frac{L_x}{(L_y - C_3)} \right] \\ = \frac{m_{ult}}{\cos \theta} \left[(K'_x \cos^2 \theta + K'_y \sin^2 \theta) \frac{r_1}{r} + I_A \frac{r_1}{r} + (K'_y + I_B) r r_3 \right. \\ \left. + (K'_x \cos^2 \theta + K'_y \sin^2 \theta) \frac{r_2}{r} + I_C \frac{r_2}{r} + \frac{(K'_y + I_D) r r_3}{(r_3 - 1)} \right] \quad (5)$$

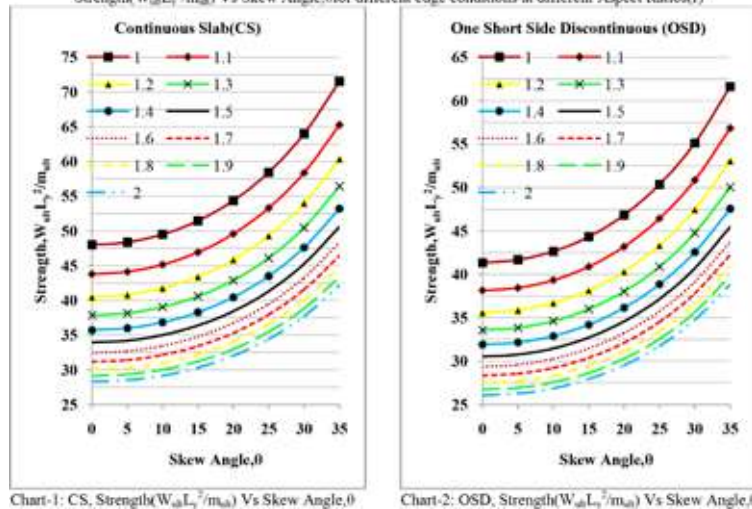
Equating total work done by the segments to energy absorbed by yield lines we get

$$W_{ult} L_y^2 r \cos \theta \left[\frac{1}{2} - \frac{1}{6} \left(\frac{1}{r_1} - \frac{1}{r_2} \right) \right] = \frac{m_{ult}}{\cos \theta} \left[(K'_x \cos^2 \theta + K'_y \sin^2 \theta) \frac{r_1}{r} + I_A \frac{r_1}{r} + (K'_y + I_B) r r_3 \right. \\ \left. + (K'_x \cos^2 \theta + K'_y \sin^2 \theta) \frac{r_2}{r} + I_C \frac{r_2}{r} + \frac{(K'_y + I_D) r r_3}{(r_3 - 1)} \right] \\ \frac{W_{ult} L_y^2}{m_{ult}} = \frac{(K'_x \cos^2 \theta + K'_y \sin^2 \theta + I_A) \frac{r_1}{r} + (K'_y + I_B) r r_3 + (K'_x \cos^2 \theta + K'_y \sin^2 \theta + I_C) \frac{r_2}{r} + \frac{(K'_y + I_D) r r_3}{(r_3 - 1)}}{r \cos^2 \theta \left[\frac{1}{2} - \frac{1}{6} \left(\frac{1}{r_1} - \frac{1}{r_2} \right) \right]} \quad (6)$$

$$\text{Yield line pattern-2: } \frac{W_{ult} L_y^2}{m_{ult}} = \frac{(K'_x \cos^2 \theta + K'_y \sin^2 \theta + I_A) r_1 + (K'_y + I_B) r r_3 + (K'_x \cos^2 \theta + K'_y \sin^2 \theta + I_C) r_2 + (K'_y + I_D) r r_3}{r \cos^2 \theta \left[\frac{1}{2} - \frac{1}{6} \left(\frac{1}{r_3} - \frac{1}{r_4} \right) \right]} \quad (7)$$

APPENDIX-C

Strength ($W_{ult} L_y^2 / m_{ult}$) Vs Skew Angle, θ for different edge conditions at different Aspect Ratios (r)



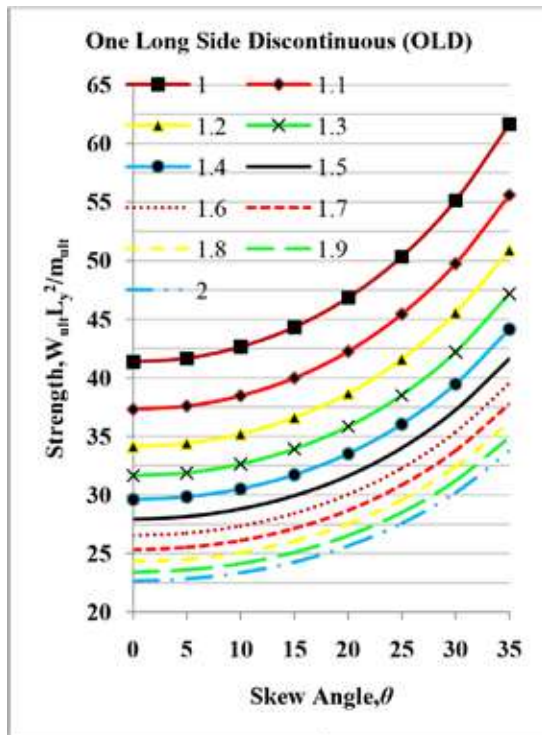


Chart-3: OLD, Strength($W_{ult} L_y^2 / m_{ult}$) Vs Skew Angle, θ

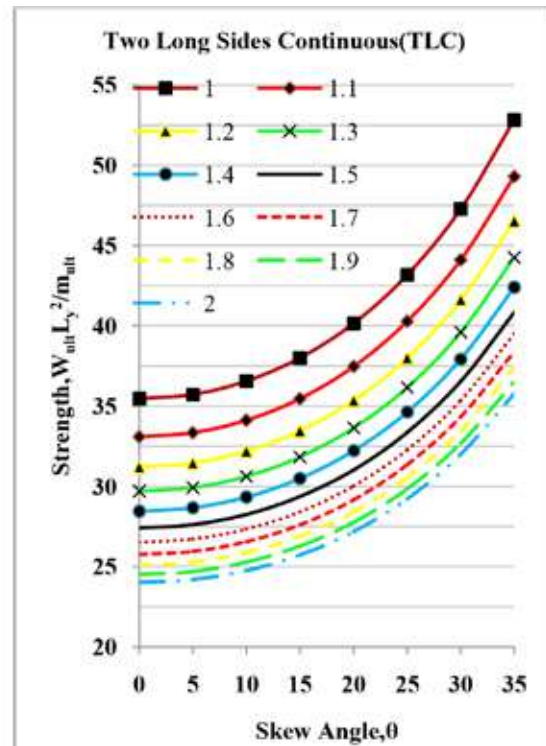


Chart-5: TLC, Strength($W_{ult} L_y^2 / m_{ult}$) Vs Skew Angle, θ

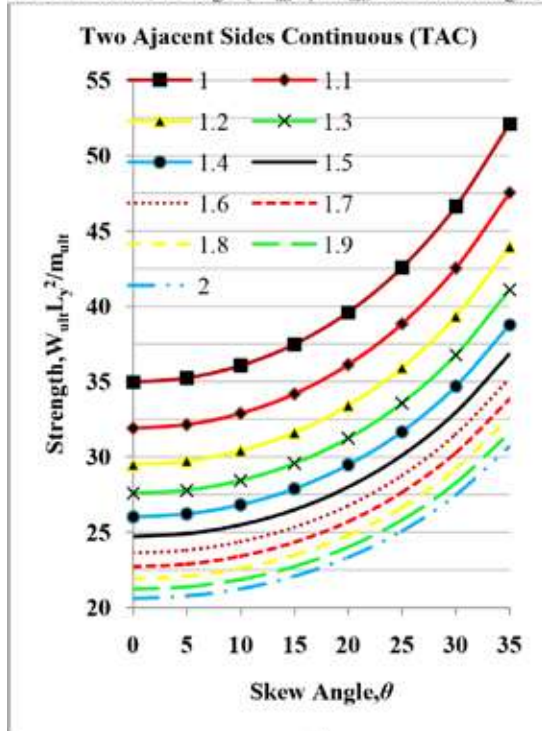


Chart-4: TAC, Strength($W_{ult} L_y^2 / m_{ult}$) Vs Skew Angle, θ

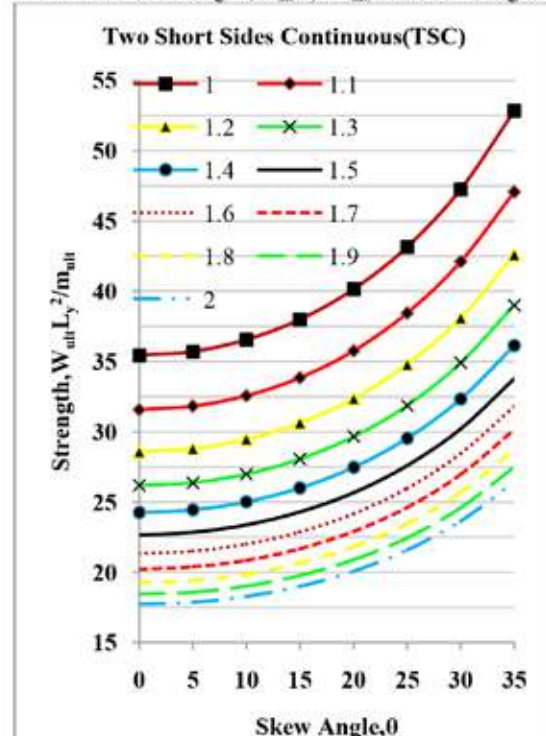


Chart-6: TSC, Strength($W_{ult} L_y^2 / m_{ult}$) Vs Skew Angle, θ

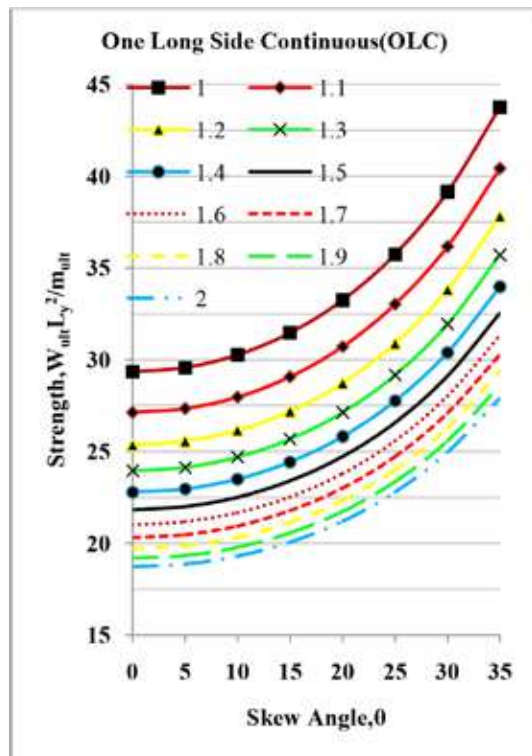


Chart-7: OLC, Strength($W_{ult} L_y^2 / m_{ult}$) Vs Skew Angle, θ

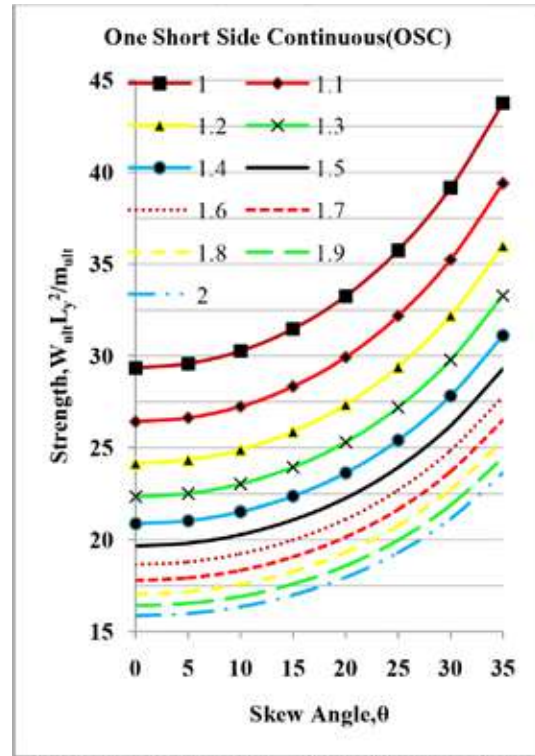


Chart-8: OSC, Strength($W_{ult} L_y^2 / m_{ult}$) Vs Skew Angle, θ

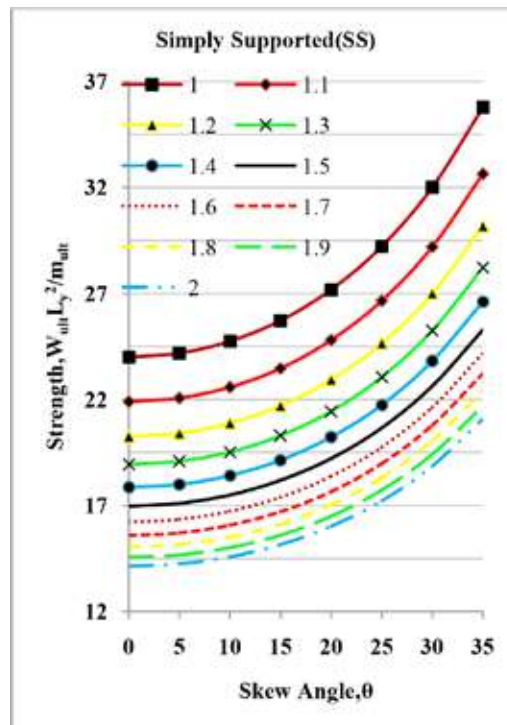


Chart-9: SS, Strength($W_{ult} L_y^2 / m_{ult}$) Vs Skew Angle, θ



Prediction of Mechanical Characteristics of Concrete Containing GSA, GGBS and WF

R Murugaboopathy

Department of Civil Engineering, PAC Ramasamy Raja Polytechnic College, Rajapalayam, Tamil Nadu

✉ murugaboopathy2k9@gmail.com

ABSTRACT

In the modern construction industries the utilization of cement plays vital role in the production of concrete and hence the needs of cement is crucial in the construction of Civil Engineering structures, such as building, bridge, dam, and road, etc., The cost of cement is enormous, therefore it is difficult to construct the own building by the poor people in the locality. On the other hand, the production of cement is increased in the cement plant due to increasing the demand of cement in the construction field. While manufacturing of cement in dry process produce the emission of CO₂. The range of CO₂ emission is 0.8 to 1.3 tonne per tonne of cement manufacturing. The CO₂ emission might be increase earth temperature and leads to global warming. The global warming is very dangerous to earth, health and plants. The earth climate will be changed due to increasing the global temperature. It will affect the health of human being and plant life. On focusing these issues, it is proposed to carry out this research work to examine the precise way to partial replacement of cement using waste materials, like, Groundnut Shell Ash (GSA), Ground Granulated Blast Furnace Slag (GGBS) and Wool Fibre (WF). The specimens replaced with GSA (8%), GGBS (35%) and WF (0.3%) has better mechanical properties, such as cube compressive strength, cylinder splitting tensile strength and prism flexural strength of concrete.

Keywords : Cement; Groundnut shell ash; Ground granulated blast furnace slag; Wool fibre.

INTRODUCTION

In current scenario, lot of waste materials are disposed, like, groundnut shell, GGBS, fly ash, maize combs, saw dust, rice husk, millet husk, coconut shell etc., and making environmental hazard. Tonnes of waste materials are disposed on the land with minor effective method of waste recycling only. Some of these disposed waste materials are not fully decomposed and thus making the people as illness [1]. The ash which is obtained from groundnut shell, maize combs, saw dust, rice husk, millet husk, coconut shell, GGBS and fly ash have been used as secondary cementing materials. These supplementary materials help to reduce the permeability of concrete by altering their pore structure and thus improve the durability [2]. The groundnut shell is usually used to cook by burning or dumped or left to decay naturally. It will create nuisance to the people and environment, when it is disposed on the field without doing any recycling process [3-4]. Therefore it is proposed to incorporate the by-product agricultural waste of groundnut shell in the form of ash for the partial replacement of OPC for the preparation of concrete to safeguard the land and people from serious environmental hazards and to achieve the economy in the construction industry by minimizing the cost of construction. When the percentage of GSA level is increasing from 8% of the replacement the compressive strength and splitting tensile strength of concrete is decreased for all the age of concrete. The workability of concrete is also decreased while increasing the GSA replacement level for all water cement ratio when compared with control concrete [5].

Hence, it is decided to utilize another one pozzolanic materials obtained from iron industries, that is, Ground Granulated Blast Furnace Slag (GGBS) in order to enhance the strength and workability performance of concrete incorporated with GSA. The GGBS is a by-product obtained from blast-furnace of iron and steel industries [6-7]. It contains large amount of silicates and alumina silicates of calcium. It is a good replacement for OPC because of it consists of important chemical components such as lime, calcium sulphate and alkalies to activate the slag with OPC [8-10]. The replacement level of GGBS is ranges from 20 to 50% at the interval of 5% by weight of OPC in addition with GSA replacement ranges from 6 to 10%. The adopted concrete mix is M20 and water cement ratio is 0.55. The result shows that the compressive strength of concrete cube is increased when the GGBS is blended with GSA and it is suddenly decreased when the GGBS replacement level is more than 35%. But there is no any improvement in the splitting tensile strength and prism flexural strength of concrete when the cement is replaced with GSA and GGBS. Then, it is planned to improve the splitting tensile and flexural strength of concrete by adding fibre. The fibres can

be classified as artificial fibres and natural fibres. Carbon fibre, steel fibre, metallic fibre, boron fibre, polypropylene fibre, glass fibre, etc., are available in the market as artificial fibre and bamboo fibre, banana fibre and wool fibre are available naturally is called as natural fibre [11-12]. The addition of randomly distributed fibres to brittle cement based materials can increase their fracture toughness, ductility and impact resistance [13]. The wool fibres obtained from Scottish sheep has been used in the soil to get the soil matrix. In his research, the untreated and straight wool fibre was used. The amount of wool fibre used is 0.25% to 0.5% by weight of soil. Tests showed that adding alginate increases compression strength from 2.23 to 3.77 N/mm² at 69%. The addition of wool without alginate (maybe due to its hard workability) does not improve performance so much: adding only wool also increases compression strength at 37%, from 2.23 to 3.05. But the addition of both, wool and alginate improves significantly (doubles) ERROL soil resistance up to 4.44 N/mm². Better results were obtained with a lower quantity of wool [14]. Hence, the wool fibre obtained from sheep (WF) from 0.1% to 0.5% is used in this research work in addition with GSA and GGBS to enhance the splitting tensile and flexural strength of concrete.

MATERIALS AND THEIR PROPERTIES

The materials used in the research work are: Ordinary Portland Cement (OPC), Fine Aggregate, Coarse Aggregate, Groundnut Shell Ash (GSA), Ground Granulated Blast Furnace Slag (GGBS), Wool Fibre (WF), and Super plasticizer.

Cement

The properties of cement used are given in the **Table 1**. The cement contains large amount of Oxides of Calcium, Silicon, Aluminium and Iron.

Table 1. Physical properties of cement

Sl. No.	Physical Properties of Fine Aggregate	Properties
1	Specific gravity	3.13
2	Standard consistency	31%
3	Fineness	312m ² /kg

Fine Aggregate

The river Sand is a naturally occurring granular material composed of finely divided rock and mineral particles. The size of sand used in this research work is varying from 600 μ to 4.75mm. The physical properties of sand used in this research are given in the **Table 2** and tested in accordance with IS: 2386.

Table 2. Physical Properties of Fine Aggregate

Sl. No.	Physical Properties of Fine Aggregate	Properties
1	Specific gravity	2.67
2	Fineness modulus	2.9
3	Unit Weight	1558kg/m ³
4	Absorption of water	2.0%

Coarse Aggregate

The Coarse aggregate used is crushed from granite of size varying from 4.75mm to 20mm. The physical properties of crushed stone used in this work are given in the **Table 3** and tested in accordance with IS: 2386.

Table 3. Physical Properties of Coarse Aggregate

Sl. No.	Physical Properties of Fine Aggregate	Properties
1	Specific gravity	2.74
2	Unit Weight	1684kg/m ³
3	Absorption of water	0.5%
4	Crushing value	24.24%



Groundnut Shell Ash (GSA)

The groundnut shell is collected from oil manufacturing industries, was then thoroughly cleaned, dried and burned at a temperature of 500°C to 600°C for a period of 4 hours to get the ash. The size of GSA is varying from 10 to 75 μ . The physical properties of GSA are tabulated in the **Table 4**.

Table 4. Physical Properties of GSA

Sl. No.	Physical Properties of Fine Aggregate	Properties
1	Size of GSA	10 to 75 μ
2	Specific gravity	1.93
3	Fineness modulus	4.96
4	Unit weight	1090kg/m ³
5	Fineness	329m ² /kg

GGBS

The physical properties of GGBS are tabulated in the **Table 5**.

Table 5. Physical properties of GGBS

Sl. No.	Physical Properties of Fine Aggregate	Properties
1	Size of GGBS	10 to 45 μ
2	Specific Gravity	2.75
3	Unit weight	1172kg/m ³
4	Final Setting Time	289 min
5	Fineness	342m ² /kg

Fibre

Wool fibre is the natural hair grown on sheep and is composed of protein substance called as keratin. Wool is composed of carbon, hydrogen, nitrogen and this is the only animal fiber, which contains sulfur in addition. The wool fibers have crimps or curls, which create pockets and give the wool a spongy feel and create insulation for the wearer. The physical properties of wool fibre are tabulated in the **Table 6**.

Table 6. Physical Properties of WF

Sl. No.	Physical Properties of Fine Aggregate	Properties
1	Size of the fibre	0.05mm
2	Length of fibre	25 mm
3	Unit weight	350kg/m ³

Superplasticizer

In this investigation, super plasticizer Conplast SP 430, based on sulphonated naphthalene polymers, complies with IS 9103-1999, BS: 5075 part 3 and ASTM C – 494, Type F was used. Commercially available high performance superplasticizing admixture, Conplast SP430, conforming to ASTM C 494 (1992) was used to maintain the slump of the concrete. The properties, supplied by the manufacturer, are given in **Table 7**.

Table 7. Properties of superplasticizer

Sl. No.	Physical Properties of Fine Aggregate	Properties
1	Composition	Sulphonated naphthalene formaldehyde
2	Appearance	Brown liquid



3	Specific gravity	1.20 at 20°C
4	Chloride content (%)	Nil
5	pH value	7.0- 8.0

MIX DESIGN

Mix ratio of concrete

The mix design for concrete (M20) with the water-cement ratio of 0.55 is carried out by adopting IS 10262-2009 and the details of mix design is listed in **Table 8**. A very lesser volume of Super plasticizer at 1% volume on weight of cement has been used to cause good workability. The proportions of fine aggregate, coarse aggregate, and water are fixed constant throughout the research work. The cement is only replaced with GSA and GGBS. Also the WF is used to increase the tensile strength of concrete.

Table 8. Mix ratio of concrete

Sl. No.	Materials	Mix Proportions	
		In weight	In parts
1	Cement	344.68kg	1
2	Fine Aggregate	616.97kg	1.79
3	Coarse Aggregate	1158.12kg	3.36
4	Water	189.57lit	0.55

Mix Proportions

In this research work, totally 12 mixes were casted to predict the cube compressive strength, cylinder splitting tensile strength and prism flexural strength of concrete at the period of 7 days and 28 days of curing by replacing the cement with GSA, GGBS and WF. The specimen prepared without replacement of waste materials is assigned as control specimen (C). The specimens (P1 to P5) prepared by replacing the cement using GSA from 2% to 10%, the specimens (P6 to P8) prepared by replacing the both cement using GSA from 6% to 10% and GGBS from 20% to 50% and the specimens (P9 to P12) prepared by replacing the all the waste materials, such as, cement using GSA from 6% to 10%, GGBS from 20% to 50% and WF from 0.1% to 0.5%. The details of specimens prepared for this study are shown in **Table 9**.

Table 9. Mix proportions

S. No.	Sample ID	Cement	GSA	GGBS	WF
		(%)	(%)	(%)	(%)
1	C	100	0	0	0
2	P1	98	2	0	0
3	P2	96	4	0	0
4	P3	94	6	0	0
5	P4	92	8	0	0
6	P5	90	10	0	0
7	P6	74	6	20	0
8	P7	57	8	35	0
9	P8	40	10	50	0
10	P9	73.9	6	20	0.1
11	P10	56.5	8	35	0.3
12	P11	39.5	10	50	0.5

Table 10. Test results of Cube Compression, Cylinder Splitting Tension and Prism Flexural Strength of hardened concrete

Sample ID	Compressive Strength in N/mm ²		Splitting Tensile Strength in N/mm ²		Flexural Strength in N/mm ²	
	CCS 7 days	CCS 28 days	CSTS 7 days	CSTS 28 days	PFS 7 days	PFS 28 days
C	13.63	24.57	1.58	2.74	2.14	3.87
P1	12.16	21.87	1.02	2.08	1.53	2.65
P2	11.36	19.18	0.83	1.46	0.94	1.59
P3	11.55	19.57	0.92	1.58	1.13	2.16
P4	13.31	23.97	1.04	2.25	1.35	2.14
P5	11.89	20.39	0.68	1.19	0.78	1.35
P6	14.69	24.67	1.34	2.41	1.63	2.93
P7	15.25	25.63	1.54	2.73	1.87	3.27
P8	13.93	24.98	1.22	2.25	1.32	2.47
P9	15.67	25.89	1.76	2.89	2.29	4.12
P10	16.53	26.84	1.93	3.07	2.56	4.97
P11	14.87	24.71	1.69	2.81	2.19	3.95

RESULTS AND DISCUSSIONS

Cube Compression Test

A cube moulds made up of cast iron of size, 150 mm × 150 mm × 150 mm were used to prepare the concrete cubes to examine the cube compressive strength of concrete at 7 days and 28 days curing period. Three numbers of concrete cubes were casted for each proportion and tested. A Compression Testing Machine (CTM) of 200tonnes capacity were engaged to evaluate the compression of concrete cube as per IS 516-1959 standard. The cube specimen was kept over the middle of the lower plate of CTM and the compression load was applied on the cube till the specimen was failed. The testing arrangement of compression test of cube specimen is shown in **Figure 1**. The compressive strength can be calculated using the following formula.

Where,

Cube compressive strength = P/A

P = Ultimate compressive load of concrete (kN)

**Figure 1.** Testing arrangement of compression test of cube specimen

The test results of compressive strength of concrete cube at the age of 7 days and 28 days of curing were shown in **Table 10**. From the test results, it was examined that the cube compressive strength of concrete for control specimen (C) at the curing age of 7 days and 28 days were 13.63N/mm² and 24.57N/mm² respectively. The cube compressive strength of concrete at the age of 7 days and 28 days was nearly close with the control specimen with a replacement level of 8% of GSA for cement (P4), whereas, it was reduced for other percentage of substitution of GSA (P1, P2, P3 and P5). The cube compressive strength of concrete for all the specimens (P6, P7 and P8) at the age of 7 days and 28 days were higher than that of control specimen, when the cement is replaced with both GSA and GGBS. It was also examined that the cube compressive strength for all the specimens (P9, P10 and P11) at the age of 7 days and 28 days were higher than that of control specimen, when the cement is replaced with

both GSA and GGBS incorporated with WF. The maximum cube compressive strength of concrete is obtained for specimen P10, which is replaced with 8% of GSA, 35% of GGBS and 0.3% of WF. The cube compressive strength of specimen (P10) at 7 days and 28 days of curing were 16.53N/mm² and 26.84N/mm² respectively. The variations of cube compressive strength of concrete specimens are shown in **Figure 2**.

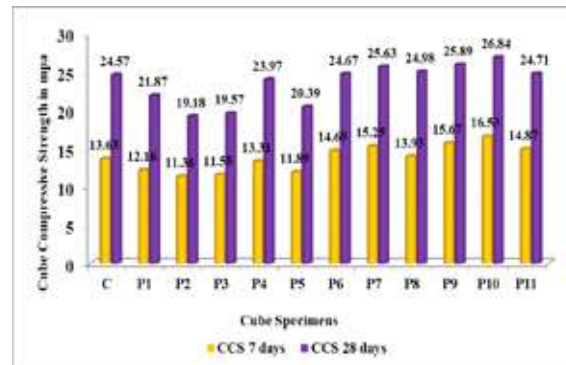


Figure 2. Variations of cube compressive strength

Cylinder splitting tension test

A cylinder moulds of 150mm in diameter and 300mm in height made up of cast iron was engaged to prepare the concrete cylinder to predict the splitting tensile strength of concrete cylinder at 7 days and 28 days curing periods. Three numbers of cylinder specimens were casted for each mix proportion and tested. The concrete cylinder specimens were compressed to evaluate the splitting tensile strength of concrete using Compression Testing Machine (CTM) with a capacity of 200tonnes according to IS 5816-1999 standard. The cylinder specimen was kept over the middle of the lower plate in between the plywood strips and the load was applied on the strip until the specimen was failed. The testing arrangement of splitting tensile strength of cylinder specimen is shown in **Figure 3**. The splitting tensile strength can be calculated using the following formula.

$$\text{Splitting tensile strength} = 2P / \pi DL$$

Where:

P = Ultimate splitting tensile load in kN

D = Diameter of the cylinder specimen in mm

L = Length of the cylinder specimen in mm



Figure 3. Testing arrangement of splitting tensile strength

The test results of splitting tensile strength of concrete cylinder at the age of 7 days and 28 days of curing were shown in **Table 10**. From the test results, it was observed that the cylinder splitting tensile strength for control specimen (C) at the age of 7 days and 28 days were 1.58N/mm² and 2.74N/mm², respectively. It was examined that the cylinder splitting tensile strength at the age of 7 days and 28 days was lower than that of control specimen for the all cylinder specimens partially replaced using GSA for cement (P1 to P5) in various mix proportions. The cylinder splitting tensile strength of concrete specimen (P7) substituted with 8% of GSA and 35% of GGBS at 7 days and 28 days of curing were 1.54N/mm² and 2.73N/mm² respectively. It was understood that the splitting tensile strength of concrete at the curing period of 7 days and 28 days were very near to the control specimen (C) with a replacement level of 8% of GSA and 35% of GGBS (P7). At the same time, it was declined for other specimens replaced with GSA and GGBS (P6 and P8). The cylinder splitting tensile strength of concrete for all the specimens (P9, P10

and P11) at the age of 7 days and 28 days were higher than that of control specimen, when the cement is replaced with both GSA and GGBS incorporated with WF. The maximum splitting tensile strength of concrete is obtained for specimen P10, which is replaced with 8% of GSA, 35% of GGBS and 0.3% of WF. The prism flexural strength of specimen (P10) at 7 days and 28 days of curing were 1.72N/mm² and 2.89N/mm², respectively. The variations of cylinder splitting tensile strength of concrete specimens at the age of 7 and 28 days are shown in **Figure 4**.

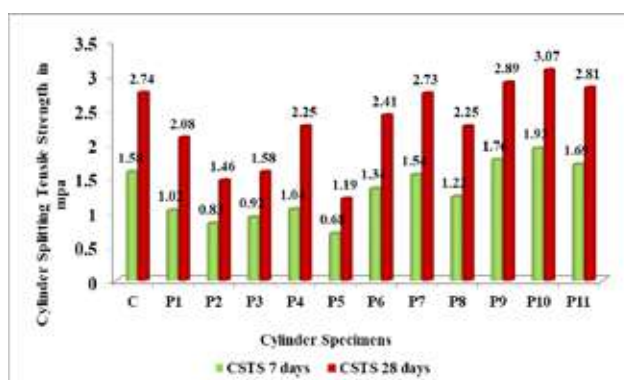


Figure 4. Variations of cylinder splitting tensile strength

Prism Flexural |Test

A prism mould of 150mm × 150mm × 700mm size made up of cast iron was utilized to prepare the concrete prism to determine the prism flexural strength of concrete at 7 days and 28 days curing periods. Three numbers of concrete prisms were casted for each proportion and tested. A Universal Testing Machine (UTM) with a capacity of 60tonnes was engaged to test the concrete prism as per IS 9399-1979 standard. The testing arrangement of prism flexural strength of concrete specimen is shown in **Figure 5**.

The flexural strength of concrete prism of size 15cm × 15cm × 70cm was calculated using the following equation 4.4 and 4.5, Prism Flexural Strength in N/mm²,

$$F_c = \frac{3P_p a}{b_p d_p^2} \quad (\text{When } a = 20 \text{ cm to } 30 \text{ cm})$$

$$F_c = \frac{P_p l}{b_p d_p^2} \quad (\text{When } a = 17 \text{ cm to } 20 \text{ cm})$$

Where, P_p = maximum flexural load at failure in N,

a = distance between the line of fracture and the nearest support in mm,

b_p = measured breadth of prism in mm at the point of failure,

d_p = measured depth of prism in mm at the point of failure, and

l = length of span in mm on which the specimen was supported.



Figure 5. Testing arrangement of prism flexural strength

The test results of flexural strength of concrete prism at the age of 7 days and 28 days of curing were shown in **Table 10**. From the test results, it was notated that the flexural strength of concrete prism for control specimen (C) were 2.14N/mm² and 3.87N/mm², respectively. From the experimental investigation, it was predicted that the prism flexural strength at the age of 7 days and 28 days was lesser than that of control specimen for the all prism specimens partially replaced with GSA for cement (P1 to P5). The prism flexural strength of concrete specimen (P7) substituted with 8% of GSA and 35% of GGBS at 7 days and 28 days of curing were 1.87N/mm² and 3.27N/mm², respectively. It was realized that the prism flexural strength of concrete at the curing period of 7 days and 28 days were somewhat lesser than that of control specimen (C) with a replacement level of 8% of GSA and 35% of GGBS (P7). But, it was abruptly declined for other specimens replaced with GSA and GGBS (P6 and P8). The prism flexural strength of concrete for all the specimens (P9, P10 and P11) at the age of 7 days and 28 days were higher than that of control specimen, when the cement is replaced with both GSA and GGBS incorporated with WF. The maximum prism flexural strength of concrete is obtained for specimen P10, which is replaced with 8% of GSA, 35% of GGBS and 0.3% of WF. The prism flexural strength of specimen (P10) at 7 days and 28 days of curing were 2.56N/mm² and 4.97N/mm², respectively. The variations of flexural strength of concrete prism specimens are shown in **Figure 6**.

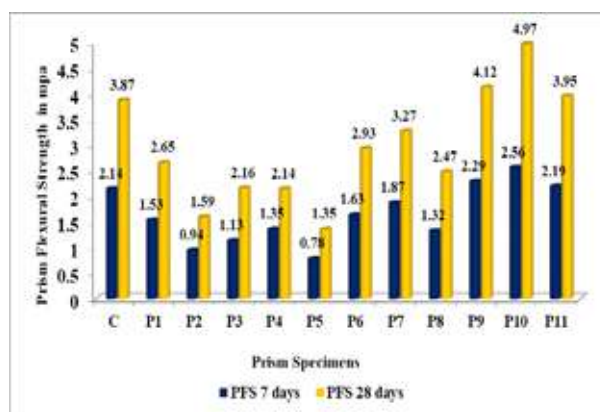


Figure 6. Variations of prism flexural strength

CONCLUSION

1. The results obtained in this study signified that when the GSA (From 0% to 10%) alone substituted for the partial replacement of cement, the cube compressive strength of concrete blended with 8% of GSA (P4) at all the 7 days and 28 days curing periods was very nearer to the control specimen (C) and the compressive strength of concrete were decreased for other specimens partially replaced with GSA for cement (P1, P2, P3 and P5) than that of specimens C and P4.
2. On the other hand, the splitting tensile strength of cylinder and flexural strength of prism specimens (P1, P2, P3, P4 and P5) at all the curing periods were declined than that of control specimens. Hence, it is suggested utilize the GGBS (From 20 to 50%) in addition with GSA (From 6 to 10%) for the replacement of cement to enhance the compressive strength of concrete.
3. It was observed that while replacing the cement by 35% of GGBS along with 8% of GSA (P6,P7 and P8), there was an improvement in compressive strength of concrete at all the curing age as compared to control mix. At the same time, the cylinder splitting tensile strength and prism flexural strength of concrete at 7 days and 28 days were reduced than that of control concrete specimen for all the mixes.
4. Subsequently, it is recommended to include a small size (0.05mm diameter and 25mm length) of randomly distributed WF (From 0.1 to 0.5%) in addition with GSA (From 6 to 10%) and GGBS (From 20 to 50%) (P9, P10 and P11) to enhance the cylinder splitting tensile as well as the prism flexural strength of concrete specimens.
5. As a result, it is observed that the specimen (P10) replaced with GSA (8%), GGBS (35%) and WF (0.3%) has better mechanical properties, such as cube compressive strength, cylinder splitting tensile strength and prism flexural strength of concrete.



REFERENCES

1. Raheem, S., Oladiran, G., Olutoge, F. and Odewumi, T. (2013) 'Strength properties of groundnut shell ash (GSA) blended concrete', *Journal of Civil Engineering and Construction Technology*, Vol. 4, No. 9, pp.275–284.
2. Olutoge, F.A., Buari, T.A. and Adeleke, J.S. (2013) 'Characteristics strength and durability of groundnut shell ash (GSA) blended cement concrete in sulphates environment', *International Journal of Scientific and Engineering Research*, Vol. 4, No. 7, pp.2122–2134.
3. Patel, S. and Balakrishna, D.H. (2014) 'Flexural behaviour of reinforced concrete beams replacing ggbs as cement and slag sand as fine aggregate', *International Journal of Civil and Structural Engineering Research*, Vol. 2, No. 1, pp.66–75.
4. Alabadan, B., Olutoge, M., Abolarin, M. and Zakariya, M. (2005) 'Partial replacement of ordinary Portland cement (OPC) with bambara groundnut shell ash (BGSA) in concrete', *Leonardo Electronic Journal of Practices and Technologies*, No. 6, pp.43–48.
5. Buari, T.A., Ademola, S.A. and Ayegbokiki, S.T. (2013) 'Characteristics strength of groundnut shell ash (GSA) and ordinary Portland cement (OPC) blended concrete in Nigeria', *IOSR Journal of Engineering*, Vol. 3, No. 7, pp.1–7.
6. Escalante, J., Gomez, L., Johal, K., Mendoza, G., Mancha, H. and Mendez, J. (2001) 'Reactivity of blast-furnace slag in Portland cement blends hydrated under different conditions', *Cement Concrete Research*, Vol. 31, No. 10, pp.1403–1409.
7. Guettala, S., Mezghiche, B. and Mellas, M (2012) 'Influence of addition dune sand powder to cement, on the properties physical-mechanical and deformability of concrete', *Asian Journal of Civil Engineering (Building and Housing)*, Vol. 13, No. 6, pp.765–781.
8. Arivalagan, S. (2014) 'Sustainable studies on concrete with GGBS as a replacement material in cement', *Jordan Journal of Civil Engineering*, Vol. 8, No. 3, pp.263–270.
9. Murugaboopathy Rajagopal & Ganesan Karuppiyah (2019), 'Green environmental sustainability development in construction industry using response surface methodology', *International Journal of Environment and Sustainable Development (IJESD)*, Vol. 18, No. 1, pp. 13 – 44.
10. Murugaboopathy Rajagopal (2018), 'Durability Characteristics of Concrete Incorporated with Groundnut Shell Ash and Ground Granulated Blast Furnace Slag', *Journal of Computational and Theoretical Nanoscience*, Vol. 15, No. 11/12, pp. 3237 – 3247.
11. Wang, Y., Backer, S. and Li, V.C. (1987) 'An experimental study of synthetic fibre reinforced cementitious composites', *Journal of Material Science*, Vol. 22, No. 12, pp.4281–4291.
12. Banthia, N. and Nandakumar, N. (2003) 'Crack growth resistance of hybrid fiber reinforced cement composites', *Cement Concrete Composites*, Vol. 25, No. 1, pp.3–9.
13. Kakooei, S., Akil, H.M, Dolati, A. and Rouhi, J (2012) 'The corrosion investigation of rebar embedded in the fibers reinforced concrete', *Construction and Building Materials*, Vol. 35, pp.564–570.
14. Galen-Marin, C., Rivera-Gomez, C., and Petric, J., (2010), 'Clay-based composite stabilized with natural polymer and fibre', *Construction and Building Materials*, Vol.24, pp.1462–1468.



An Experimental Study on Self Repairing Concrete to Improve Strength and Sustainability

S Ramesh Kumar¹, D Sakthivel¹, E Vellaingiri²

Assistant Professors, Dept. of Civil Engineering, Velalar College of Engineering and Technology, Erode¹

Under Graduate Student, Dept. of Civil Engineering, Velalar College of Engineering and Technology, Erode²

✉ ramesh070792@gmail.com

ABSTRACT

The aim of this research project is the development of a new type of concrete in which integrated bacteria promote self-healing of cracks. Traditional concrete does usually show some self-healing capacity what is due to excess non-hydrated cement particles present in the material matrix. These particles can undergo secondary hydration by crack ingress water resulting in formation of fresh hydration products which can seal or heal smaller cracks. However, the integration of excess cement in concrete is unwanted from both an economical and environmental viewpoint. Cement is expensive and, moreover, its production contributes significantly to global atmospheric CO₂ emissions. In this study we developed a two-component self-healing system which is composed of bacteria which catalyze the metabolic conversion of organic compounds to calcite. Both components are mixed with the fresh cement paste, thus becoming an integral part of the concrete. Experimental results show that ingress water channeled through freshly formed cracks activates present bacteria which through metabolic conversion of organic mineral-precursor compounds produce copious amounts of calcite. This new bio-based two-component system may represent a new class of self-healing mechanisms which can be applied to cement- based systems. The self-healing capacity of this system is currently being quantified what should result in an estimate of the materials durability increase. A self-healing concrete may be beneficial for both economic and environmental reasons. The bacteria based concrete proposed here could substantially reduce maintenance, repair and premature structure degradation what not only saves money but also reduces atmospheric CO₂ emissions considerably as less cement is needed for this type of self-healing concrete. The recent research shows that specific species of bacteria can actually be useful as a tool to repair cracks in early stage of already existing concrete structures. A highly impermeable calcite layer formed over the surface of an already existing concrete layer, due to microbial activities of the bacteria (*Bacillus subtilis*) seals the cracks in the concrete structure and also has excellent resistance to corrosion.

Keywords : Self-Healing; Bacterial concrete; Calcite; *Bacillus subtilis*; Calcium carbonate.

INTRODUCTION

Concrete can be considered as a kind of artificial rocks with the properties similar to that of some kinds of rocks. As it is strong, durable and relatively cheap, concrete is since, almost two centuries, the most used construction materials worldwide, which can easily be recognized as it has changed the physiognomy of rural areas. Normally the concrete as we all know is good in compression but weak in tension. The most of the crack which forms initially is due to tension. Cracks can form at any stage of its life and mostly begin internally where they cannot be seen for years until major repairs are needed. Damage is caused by freeze/thaw cycles, corrosion, extreme loads, chemical attacks and other environmental conditions. Consequently, maintenance to concrete structures is frequent and costly. Billions of dollars are spent every year on buildings, bridges and highways for maintenance, making materials requiring less frequent repairs very appealing. The production of concrete is an energy pensive process when mining, transportation and processing is considered. Its production level lies more than 2.35 billion metric tons per year and contributes an astonishing 10% of CO₂ emissions into the atmosphere. Here the self-healing would enables the fewer repairs works or even failure of a structure through which the production level can even be decreased along with the reduced CO₂ emission.

Tiny cracks on the surface of the concrete make the whole structure vulnerable because water seeps in to the cracks and degrade the concrete and corrode the steel reinforcement, greatly reducing the lifespan of a structure. Repairs can be particularly time consuming and expensive because it is often very difficult to gain access to the structure to make repairs, especially if they are underground or at a great height. High figures of CO₂ emission, energy and materials consumption, structural failures and huge indirect costs are anything but a sign of sustainability. From an environmental viewpoint, the latter concrete types are preferred



as less cement per concrete volume is used contributing to lower CO₂ emissions. Although high strength concrete allows building of more slender structures than ordinary concrete and thus need less concrete volume, the total amount of cement used is still significantly higher due to the inherent high percentage of non- or partially hydrated cement particles in the material matrix. The development of a self-healing mechanism in concrete that is based on a potentially cheaper and more sustainable material than cement could thus be beneficial for both economy and environment. The main goal is to develop a type of self –

BIOMINERALISATION IN SETTING TIME

Healing concrete using a sustainable self-healing agent, i.e. limestone-producing bacteria. Although bacteria, and particularly acid-producing bacteria, have been traditionally considered as harmful organisms for concrete, recent research has shown that specific species such as ureolytic and other bacteria can actually be useful as a tool to repair cracks or clean the surface of concrete. Self-repairing concrete biologically produces calcium carbonate crystals to seal cracks that appear on the surface of the concrete structures. Specific spore forming alkaliphilic bacteria genus *Bacillus*, supplied with a calcium-based nutrient are incorporated in to the concrete suspended in mixing water. These bacteria based self-healing agent is believed to remain hibernated within the concrete for up to 200 years. When cracks appear in a concrete structure and water starts to seep in through, the spores of the bacteria starts microbial activities on contact with the water and oxygen. In the process of precipitating calcite crystals through nitrogen cycle the soluble nutrients are converted to insoluble CaCO₃. The CaCO₃ solidifies on the cracked surface, thereby sealing it up. It mimics the process by which bone fractures in the human body are naturally healed by osteoplastic cells that mineralize to reform the bone. The consumption of oxygen during the metabolic biochemical reactions to form CaCO₃ helps in arresting corrosion of steel because the oxygen is responsible to initiate the process of corrosion thereby increasing the durability of steel reinforced concrete structures.

USING BACTERIA TO SELF-HEAL CRACKS IN CONCRETE

Bacteria added to concrete mix in suspension state must meet certain criteria. Concrete is a highly alkaline building material, so bacteria used as self-healing agent should be able to survive in this high alkaline environment for long durations and be able to form spores (highly resistant structures) withstanding mechanical forces during concrete mixing. In the concrete technology laboratory, a bacterial concrete mix is prepared using alkali-resistant soil bacteria *Bacillus subtilis* along with nutrients from which the bacteria could potentially produce calcite based bio-minerals. It was found that strains of the bacteria genus *Bacillus* were found to thrive in this high-alkaline environment. Such gram positive bacteria have extremely thick outer cell membrane that enables them to remain viable until a suitable environment is available to grow. They would become lively when the cracks form on concrete surface allowing water to ingress into the structure. This phenomenon will reduce the pH of the concrete environment where the bacteria incorporated become activated.

A peptone based broth medium supplied along with bacteria in suspension helps in producing calcite crystals. It is found that this biomineralisation process will not interfere with the setting time of the concrete. The most expensive ingredient in developing bacterial concrete is nutrients. So any inexpensive alternative for laboratory growth media would potentially bring down the cost of the bacteria based self-healing sustainable concrete. Only factor need to be checked is the effect of nutrients media on the setting time of cement. So this needs proper study while using suitable medium.

MECHANISM OF SELF-HEALING USING BACTERIA

The microorganism used for manufacturing of microbial concrete should be able to possess long-term effective crack sealing mechanism during its lifetime serviceability. The principle behind bacterial crack healing mechanism is that the bacteria should be able to transform soluble organic nutrients into insoluble inorganic calcite crystals which seals the cracks. For effective crack healing, both bacteria and nutrients incorporated into concrete should not disturb the integrity of cement sand matrix and also should not negatively affect other important fresh and hardened properties of concrete. Only spore-forming gram positive strain bacteria can survive in high pH environment of concrete sustaining various stresses. It was reported that when bacteria is added directly to the concrete mix in suspension, their life-time is limited due to two reasons; one is continuing cement hydration resulting in reduction of cement sand matrix pore diameter and other is due to insufficient nutrients to precipitate calcite crystals. However, a novel method of protecting the bacterial spores by immobilization before addition to the concrete mixture appeared to substantially prolong their life-time.

BACILLUS SUBTILIS

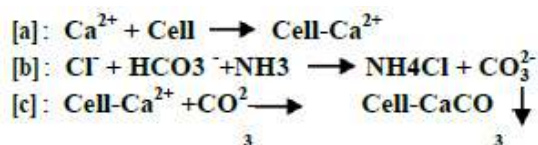
This strain isolated from soil has characteristics of high level urease activity, incessant precipitation of dense insoluble calcite crystals and has high negative zeta-potential. Potential applications of biological mineral precipitation are wide such as in sand



consolidation and stabilization, remediation of cracks in concrete, preservation and restoration of historic heritage structures, areas where it is not possible to shut down the plant or hazardous for human beings to reach for repair work such as nuclear power plants, repair of waste water sewage pipes etc. These are the most bacteria to use for self-healing purposes since these are alkaliphillic spore forming bacteria. The bacteria, from this genus *Bacillus subtilis* is adopted for present study. The bacteria are cultured in the broth medium of artificial brothextract.

PRINCIPLE OF SELF-HEALING PROCESS

Specially selected types of the genus *Bacillus*, along with a calcium based nutrient and nitrogen and phosphorus in presence of oxygen, the soluble calcium source is converted to insoluble calcium carbonate by ureolytic activity. The calcium carbonate solidifies on the cracked surface, thereby sealing it up. It mimics the process by which bone fractures in the human body are naturally healed by osteoblastic cells that mineralize to reform the bone. MICP occurs via far more complicated processes than chemically induced precipitation. The bacterial cell surface with a variety of ions can non-specifically induce mineral deposition by providing a nucleation site. Ca^{2+} is not likely utilized by microbial metabolic processes; rather it accumulates outside the cell. In medium, it is possible that individual microorganisms produce ammonia as a result of enzymatic urea hydrolysis to create an alkaline micro environment around the cell. The high pH of these localized areas, without an initial increase in pH in the entire medium, commences the growth of CaCO_3 crystals around the cell. Possible biochemical reactions (vide Eq. a, b & c) in Urea- CaCl_2 medium to precipitate CaCO_3 at the cell surface can be summarized as follows



VIABILITY OF BACTERIA IN CONCRETE

Growth of bacteria in concrete is a most questionable factor because of concrete's high alkalinity which is a restricting aspect for the survival of the bacteria. Only specific alkaliphillic bacteria can survive in such hostile environment of concrete. Therefore, it is necessary to immobilize the bacterial cells and to protect them from the high pH in concrete. Polyurethane (PU) has been widely used for immobilization of nutrients and bacterial cells even silica gel was used to protect the bacteria against the high pH in concrete. Several studies show that the bacteria can survive for several hundred years if spores remained unaffected.

MORPHOLOGY OF NATURALLY PRECIPITATED CALCIUM CARBONATE CRYSTALS

CaCO_3 is available in three different crystal structures but with same chemical formula in the form of Calcite, aragonite and vaterite. Most stable form of CaCO_3 , Calcite is rhombohedra in shape. It is formed due to the presence of magnesium, manganese and orthophosphate ions. Aragonite is a orthorhombic shaped crystal form of CaCO_3 and geologically changes into calcite over time at high temperature or low temperature in the presence of magnesium ions and pH less than 11. Vaterite mineral is rarely found in nature. It is produced in the pH range from 8.5 to 10, low Ca^{2+} concentration or low temperature and high Ca^{2+} concentration. The morphology of vaterite depends on the pH value and temperature. It was morphology of the crystals does not depend on calcium source only.

The study of M V SeshagiriRao (15) showed that using SEM analysis it was proved that the rhombohedra shape to calcite crystals is due to the presence of chloride ions where as spherical shape to crystals is due to the presence of acetate ions.

EXPERIMENTAL PROGRAM

The main aim of the present experimental program is to obtain the specific details of the crack healing of the concrete incorporated with the bacterial species of specific kind. This experimental program involves

Phase 1: Culture and growth of *Bacillus subtilis*.

Phase 2: Evaluation of the compressive strength of the concrete incorporated with the bacteria.

Phase 3: Healing mechanism of the self-repairing concrete.

MATERIALS USED

Following are the details of the materials used in this investigation:

Cement OPC of 53 grade locally available is used in this investigation. The Cement is tested for various properties as per the IS : 4031 – 1988 and found to be confirming to various specifications of IS: 12269 – 1987 having specific gravity 3.0.

Fine aggregate locally available clean, well graded, natural river sand having fineness modulus of 2.89 conforming IS: 383 – 1970 was used as the fine aggregate.

Coarse Aggregate crushed angular aggregate of size 20 mm nominal size from the local source with specific gravity of 2.7 was used as coarse aggregate.

Water locally available potable water conforming to IS 456 is used.

Microorganisms *Bacillus subtilis*, a model laboratory soil bacterium which is cultured and grown at Biotech Laboratory was used at a total cell concentration of 105 cells per ml by serial dilution.



Mix Design The mix proportion for the ordinary grade concrete and standard grade concrete are designed using IS 10262 – 1982. Materials required for 1 cubic metre of concrete in ordinary grade concrete (M 20) is

Ordinary Grade Concrete (M 20)	Mix proportion 1: 2.43: 3.31: 0.55
-------------------------------------------	-----------------------------------------------

RESULTS AND DISCUSSION

The strength characteristics of the standard cubes (100mm x 100mm x 100mm) with and without the bacteria were casted and tested as per the IS code. The several cubes were tested for the compressive strength and remaining for the healing phenomenon analysis i.e. the self-repairing phenomenon by calcite precipitate formation. The standard results of the compressive strength are tabulated in **Table 1**. The increased in the compressive strength in bacteria induced specimen is nearly 19.4% as in **Table 2** than the controlled specimens. For the crack healing study the bacteria induced concrete is allowed to develop the first crack by loading and then the crack healing phenomenon is studied by allowing the ingress water and atmospheric air to pass through the developed crack. The study reveals that the crack is healed to some extent by means of the calcite layer formation, i.e. microbiologically induced calcite precipitation. The **Table 1 & 2** shows the compressive strengths of concrete cube and percentage increase with the days.

Figures depict the comparative results of compression strengths of concrete.

Table 1. Effect of *Bacillus Subtillus* bacteria addition on Compressive strength

Nature of concrete	Compressive Strength of Concrete Cube (MPa)		
	7 days	14 days	28 days
Controlled concrete	14.18	21.61	28.18
Self Healing Concrete	17.01	24.11	32.86

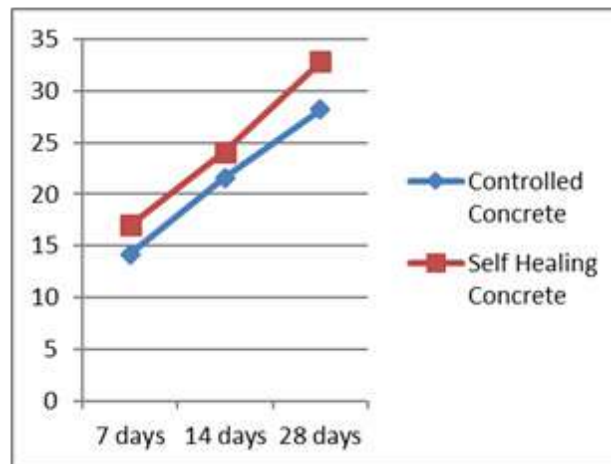


Figure 1. Comparison of compressive strength of Controlled and Self healing concrete

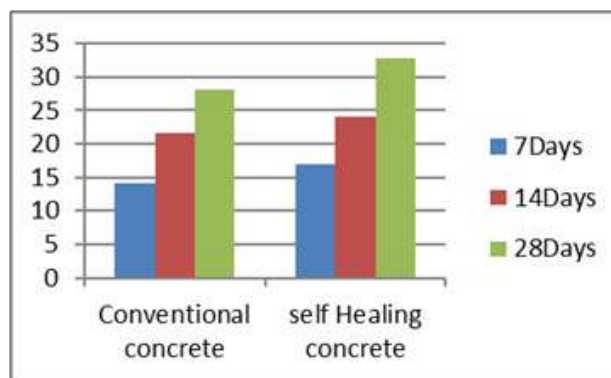


Figure 2. Effect of bacillus Subtillus bacteria on compressive strength

Table 2. Effect of bacillus Subtillus bacteria addition on Compressive strength

% Increase of Compressive Strength of Concrete Cube (MPa)		
7 days	14 days	28 days
19.95 %	11.57 %	16.61 %

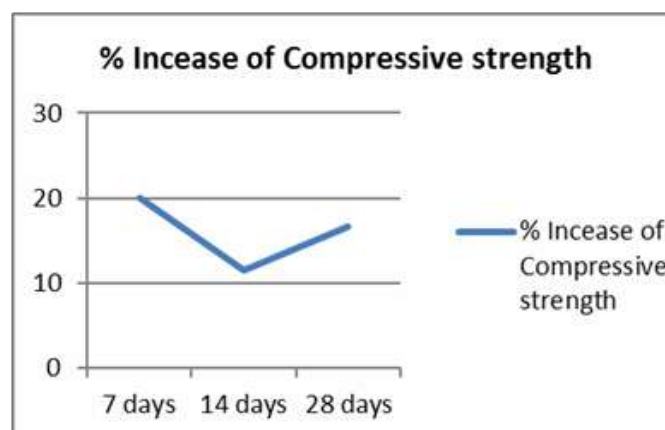


Figure 3. % Increase in Compressive strength of self healing concrete with ages

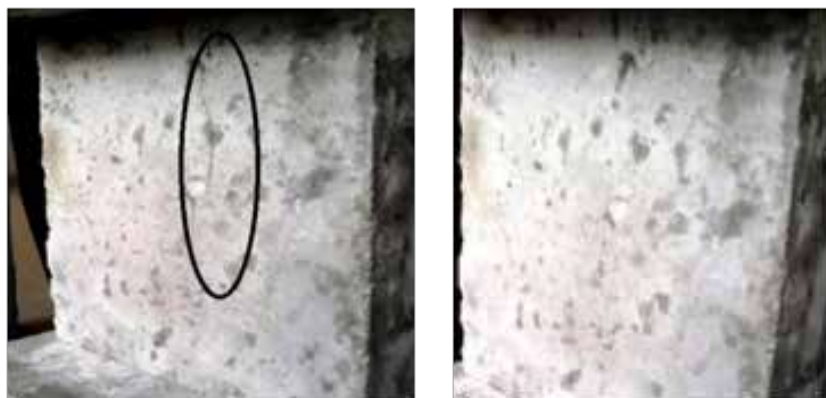


Figure 4. Crack healed concrete specimen With crack (left) & Healed Specimen (right)

CONCLUSION

Microbial mineral precipitation resulting from metabolic activities of some specific microorganisms in concrete to improve the overall behavior of concrete has become an important area of research. The following are the summary of research outcomes done at the final project

The alkalliphillic aerobic microorganism bacillus subtilus is induced into cement mortar samples at cell concentration of 105 cells per ml in suspension along with the mixing water. The greatest improvement in compressive strength occurs at cell concentrations of 105 cells/ml for all ages.

The study showed that a 16.61 % increase in 28 day compressive strength of cement mortar was achieved. The strength improvement is due to growth of filler material within the pores of the cement–sand matrix. Different cell concentrations were derived from the bacterial growth culture by serial dilution method.

SCOPE OF FUTURE RESEARCH

Bacterial concrete has improved microstructure and permeation properties than controlled concrete. Studies showed that bacterial concrete has better acid resistance in aggressive environments. So, this study can be extended to evaluate the durability performance of the bacterial concrete in terms of acid attack, chloride penetration, porosity, elevated temperature studies and corrosion resistance studies.

REFERENCES

1. Ramachandran S.K., Ramakrishnan V. and Bang S.S., Remediation of concrete using microorganisms, *ACI Materials Journal* 98(1), 3-9 (2001)
2. De Muynck W., Cox K., De Belie N. and Verstraete W. Bacterial carbonate precipitation as an alternative surface treatment for concrete, *Constr Build Mater*, 22, 875 -885(2008)
3. Jonkers H.M., Self healing concrete: A biological approach. In *Self healing materials – An alternative approach to 20 centuries of materials science* (ed. S. van der Zwaag), 195– 204 (2007) Springer, the Netherlands
4. De Belie N. and De Muynck W., Crack repair in concrete using bio-deposition, in Alexander et al. (eds.) *Concrete Repair, Rehabilitation and Retrofitting II*, Proceedings of an International Conference, Cape Town, November, 2008 (Taylor and Francis Group, London, 777-781(2009)
5. Jonkers H., Self healing concrete: a biological approach, in S. van der Zwaag (ed.) *Self Healing Materials: An alternative approach to 20 centuries of materials science* (Springer, Dordrecht, 195-204 (2007)
6. Jonkers H.M. and Schlangen H.E.J.G., Bacteria- based selfhealing concrete, *Restoration of Buildings and Monuments* 15(4) 255-266(2009)
7. De Muynck W., De Belie N. and Verstraete W., Microbial carbonate precipitation in construction materials: A review , *Ecological Engineering* 36(2), 118-136(2010)



8. Raijiwala D.B., Bacterial Concrete: A Self- Healing Concrete” The ICFAI University Journal of Structural Engineering, I(2), 56-63(2008)
9. Li, V., University of Michigan, Self-healing concrete for safer, more durable infrastructure, Science Daily, 22 Apr. 2009. Web. 28 Feb.(2012)
10. SalwaMutlaq Al-Thawadi, Ureolytic Bacteria and Calcium Carbonate Formation as a Mechanism of Strength Enhancement of Sand, Journal of Advanced Science and Engineering Research 98- 114 (2011)
11. Ehrlich H.L., Geomicrobiology: Its significance for geology. Earth-Science Reviews, 45, 45-60 (1998)
12. Castanier S., Le Métayer-Levrel, G. and Perthuisot J.P. Carbonates precipitation and limestone genesis—the microbiologist point of view. Sedimentary Geology, 126(1-4), 9-23(1999)
13. Castanier S., Le Metayer-LevrelG. and Perthuisot J. P., Bacterial roles in the precipitation of carbonate minerals. In Riding, R.E., Awramik and S.M. (Eds.), Microbial Sediments, 32-39(2000)
14. Stocks-Fischer S., Galinat J.K., and Bang S.S., Microbiological precipitation of CaCO_3 . Soil Biology and Biochemistry, 31(11), 1563-1571 (1999)
15. Bioengineered Concrete - A Sustainable Self- Healing Construction Material M.V. SeshagiriRao, V. Srinivasa Reddy, M. Hafsa, P. Veena and P. Anusha Department of Civil Engineering, JNTUH College of Engineering Hyderabad, INDIA . Research Journal of Engineering Sciences ISSN 2278 – 9472 Vol. 2(6), 45-51, June (2013)
16. International Journal of Advances in Engineering & Technology, IJAET ISSN: 2231- 1963 Bio MineralisationOf Calcium Carbonate By Different Bacterial Strains And Their Application In Concrete Crack Remediation Jagadeesha Kumar B G, R Prabhakara, Pushpa H. Mar.(2013)
17. Sanchez-Moral S., Canaveras J.C., Laiz L., Saiz-Jimenez C., Bedoya J., and LuqueL..Biomediated precipitation of calcium carbonate metastable phases in hypogean environments: A short review, Geomicrobiology Journal, 20(5), 491- 500(2003)
18. IJAETA Biological Approach To Enhance the Strength and durability in Concrete Structures Vol 2 Issue 2 Sept(2012).
19. J L Day, A V Ramakrishnan, and S S Bang, “Microbiologically Induced Sealant For Concrete Crack Remediation,” Quality Assurance, pp. 1–8. (2003).



Energy Efficient Building to Fight Against Covid-19

Sushovan Sarkar^{*1}, Gargi De²

*Department of Civil Engineering, Dr Sudhir Chandra Sur Institute of Technology and Sports Complex, Kolkata¹
Amity University, Newtown, Kolkata²*

*✉ sushovan.sarkar@dsec.ac.in

ABSTRACT

Energy efficient building to fight against COVID -19 is found a very relevant research work in the development of building technology taking into account energy efficiency, water efficiency, environment protection, indoor air quality and innovation of the building. In the energy efficiency, main focuses are kept on building orientation, building envelope design, HVAC and lighting system design, renewable energy like solar photovoltaic, biofuel, wind power, hydro power etc. , system commissioning, measurement and verification. Water efficiency is done considering design with minimum water usage and efficient irrigation system, rain water harvesting, recycling of water, minimizing water usage in cooling tower. Under the environment protection weightage has been given on the site material like low VOC for the building, proximity of the location to public transport, minimum heat island effect, minimum light pollution, building reused material, usage of material with recycling, usage of rapidly renewable energy material, usage of regional material etc. Indoor air quality in the building is mainly dealt with proper design of ventilation system, controllability of lighting and thermal comfort.

Keywords : Energy efficiency; Building envelope; Renewable energy; Environment protection; Water efficiency.

INTRODUCTION

The COVID-19 pandemic has highlighted the necessity of access to affordable, sustainable energy. Wellness oriented design and development strategies have therefore become the new determinants of market competitiveness and investment appeal, according to sustainable development demands. To contain this pandemic, residents have to remain indoors. Therefore, energy efficient buildings now play a significant role. Community and building-based prevention and control measures namely natural ventilation, indoor disinfection and cleaning, avoiding gathering; waste management, controlling the exhaust backflow of kitchens and bathrooms; setting up effective water seals to reduce the risk of virus transmission through drainage pipes and stools; controlling the concentration of indoor particulate matter; controlling air-conditioning system by zones; well-designed site wind environment for dissipation of viruses and harmful gases; air and water quality monitoring; changing the room function when necessary into medical rooms, transitional residential rooms, isolation and observation rooms, storage rooms, enable energy efficient buildings to contain the virus effectively and provide quick access to medical facilities. Energy efficient buildings using energy efficient building material with anti-bacterial function have been designed to control indoor air pollutants like ammonia, formaldehyde, benzene, total volatile organic compounds, radon, PM2.5 and PM10; moisture condensation on the inner surface of this building to prevent the growth of pathogenic bacteria; prohibiting smoking; ensuring water safety; and having gyms to promote physical movement and thereby boost immunity. Since most of the development is directly linked to energy resources available in a country, every nation ought to pay attention towards creation of new energy sources or towards conservation of energy. So, a large percentage of GDP is actually going towards the energy resources. Around one third of total energy is consumed in building and built environment.

METHODOLOGY OF CONSTRUCTION

One of the major construction materials used in buildings is cement, but its manufacture consumes a lot of energy and leaves a significant carbon footprint. This can be reduced by using RCC, anti-corrosion and anti-cracking concrete. Carefully selecting construction materials ensures lesser impact on environment and optimized recycling of the materials. Accumulation of industrial waste like fly ash, silica fumes, granulated blast furnace slag can be considerably reduced by incorporating them into concrete mixes as cement substitutes. Utilising locally acquired materials can reduce energy consumptions due to transportation. Fly ash has become an important substitute for bricks. Fly ash bricks are cheaper than conventional bricks. Eco-friendly tiles are an improvement on the conventional ones. They are less expensive and consume less energy in their production. For low maintenance, water proof yet washable paint, coloured lime is suitable. For better insulation and improved



cooling, glazed windows maybe used. Argon and krypton may substitute for air, to fill up the cavity between the glass panes. Glazing also provides privacy. Placement of hollow bricks with a gap in between provides insulating effect. Solar heat can be used for generating electricity by installing solar photovoltaic devices. This reduces energy consumption. The system consists of using solar panels containing solar cells which have photovoltaic materials. Rain gardens can not only be used for rain water harvesting for domestic use, but the collected water may also be used to run micro hydro turbines to generate energy. To reflect or absorb solar heat certain finishes and paints can be used. Windows and doors can also be designed in order to reflect heat. All of this in combination reduces cooling load. Solar heat gain coefficient (SHGC) is a ratio that measures the amount of heat passing through all windows of a building to the total heat that actually falls on them. Visible transmittance is a ratio of the visible light that gets transmitted through the glazing. Lower values of SHGC means reduced heat transfer to the building and lower values of VT. A proper balance is required between lighting and heating requirements. Roofs are made cooler by applying reflective coating. An optimum window to wall ratio ensures maximum daylight into the building.

BUILDING ENVELOPE AND ANALYSIS OF RELEVANT BUILDING MATERIALS

Opaque Building Envelope

1) Insulation Materials: The most commonly used insulation materials based on physical characteristics [9] and their respective thermal conductivities (λ) [1] are: mineral fiber blankets and loose-fill products like fiberglass [λ : 0.035 W/(m*K)], rock wool; mixed or poured-in with concrete materials like perlite [λ : 0.04-0.055 W/(m*K)], vermiculite [λ : 0.069-0.071 W/(m*K)], cellulose [λ : 0.04-0.045 W/(m*K)]; foams like polyethylene foam [λ : 0.035-0.05 W/(m*K)], extruded polystyrene (XPS) [λ : 0.03-0.04 W/(m*K)], polyurethane (PUR) [λ : 0.02-0.04 W/(m*K)] etc.

2) Insulation Types: It includes vacuum insulation panels (VIPs) and structurally insulated panels (SIPs). VIPs have excellent thermal efficiency, high performing, with a low thermal conductivity of 0.003 W/(m*K) to 0.02 W/(m*K) [9].

3) External Wall: It plays a key role in the building envelope and their R-value i.e. their thermal resistance has a significant impact on energy consumed by the building during its life-cycle, especially true in case of buildings having high wall to envelope ratio [9]. A few advanced wall systems are as follows:

- Light Weight Concrete Walls (LWC)-low in their density as well as thermal conductivity and mixed with light weight aggregates to improve their thermal resistance;
- Ventilated walls are walls with air cavities enclosed within two layers and are mainly needed for passive cooling. Increasing air cavity width increases performance but only up to 0.15m. Approximately 40% cooling energy can be conserved during summer [2];
- Walls with latent heat storage use PCM technology (phase change material). Their heat storing capacity is dependent on the percentage weight of PCM material present within the wall. They help decrease the temperature by 4.2K within a room [6]; For wall insulation exterior walls should have high thermal resistance. Materials used should be Fibreglass, Styrofoam etc. to be placed on the inner side and an optimal thickness is required for proper energy conservation.

4) Roofs: The roofs of buildings receive a very high percentage of the solar heat and thus play a key role in the building envelope. Various roof systems are given below:

- Masonry Roofs: These are usually concrete roofs, which absorb tremendous amount of sunlight and heat. An increase in the outside temperature during daytime heats up the roof leading to rising indoor temperature. For such roofs, radiation reflectors and thermal insulation work together as compound roof structures, reduce heat gain during the day.
- Lightweight Roofs: LASRS (lightweight aluminium standing seam roofing systems) have poor thermal characteristics, which can be improved through insulation and coating. The use of light coloured coating along with insulation materials like polyurethane on outer roof surface conserved around 53.8% of peak cooling load compared to a dark coating [4;9].
- Ventilated Roofs: Have ducts placed between slabs to allow free movement of air to conserve the cooling load during summer. This air flowing through the ducts may be natural/passive) or active.
- Vaulted and Domed Roofs: It lowers the indoor temperature considerably during the day in comparison to flat roofs. More energy is released by such roofs at night through thermal radiation and convection, in comparison to flat roofs.
- Solar-Reflective Roofs: Due to high infrared emittance and high solar reflectance (SR) it decreases surface temperature. Solar reflective coatings like aluminium coating can raise the SR value to 0.6 and more.



- Thermal Roof Insulation System: It uses various insulation materials like fibreglass, polystyrene etc. to reduce the high heat gain or the heat lost through the roof. This insulation in combination with a reflective surface can reflect infrared radiation.

Transparent Building Envelope:

1). Windows: Another key part of the building envelope that regulate the movement of air, light and heat to and from the building. The main concern of the modern window systems is to provide a spectrally selective glazing for an improved visible transmittance while maintaining a lower SHGC(Solar Heat Gain Coefficient) and contributing to reduced energy consumption in the building.

- Single Glazing: Windows with tinted glazing absorb more solar radiation than clear windows which gets transformed into heat inside the glass increasing its initial temperature. This however leads to discomfort within short range and a reduction in visible transmittance more so than that of SHGC; Windows with reflective glazing are coated with the likes of metal oxides to improve their reflective properties. They give better room heat gain and SHGC values but a low visible transmittance value; Windows with low-emissivity glazing give improved U-value and SHGC value but lead to rising glass temperatures. However this temperature can be reduced by applying low e-coating to the outer surface, but in turn will lead to rising room heat gain[3].
- Double Glazing: To improve the energy performance of windows it may be doubly or triply glazed, whereby an air or gas filled cavity is enclosed between two glass panes which give low U-values and SHGC values. In comparison to single glazed windows, here the room temperature and inner glass temperature are considerably reduced. This technique limits the presence of condensation in a room and acts like a barrier against moisture.

BUILDING DESIGN CONCEPTS AND BUILDING SYSTEM

The design of a building takes into consideration various conflicting factors like aesthetics, climate, structure, budget etc. The design also has impact on the sources of energy consumed by the building and the unwanted heat trapped inside.

Passive Building Design Guidelines

It envisages the use of the natural environment to meet the heating and cooling demands of the building. The design should be focused on natural ventilation and shading along with appropriate building materials to make efficient use of the natural sun light and air. The key elements of passive building design are:

- 1) Window Sizes and Ventilation: Regulate air circulation as well as insulation and temperature within a room. By increasing the velocity of air within the room in hot climates generates cooler temperature without requiring air- conditioners. The use of low absorption coatings on roofs and other shading devices on the exterior helps maintain optimal temperature. For a higher rate of airflow window sizes with vertical fins are useful. For optimum natural ventilation the aperture arc should be 20% of the entire floor area[10;7].
- 2) Infiltration and Airtightness: Accidental introduction of air within a building through leaks and cracks in the building envelope is known as infiltration, whereas leakage of air to the outside is known as exfiltration. To maintain moisture level, and increase the thermal comfort, while also reducing energy consumption infiltration must be minimized. This increases building efficiency. For this leaks and cracks must be sealed which however may lead to a problem of air-tightness thereby deteriorating the quality of air(International Energy Agency[5]. Studies reveal that buildings in different climates have saved around 5 to 40% energy on heating and cooling by reducing leakage of air[9;5].
- 3) Orientation: The positioning of a building according to the direction of winds and seasonal variations of the sun's rays is an important aspect of passive building design in tropical climates. The orientation should allow maximum air flow while restricting direct sunlight. Windows and vents should be on opposite walls for optimum air circulation. Some vents should be located at the top of building for expelling the rising hot air on the inside. The longer side of the building should be aligned along north and south with width to length ratio of 1:1.7, to reduce heat gains and prevent conflict between solar and wind alignment.
- 4) Daylighting: To combat rising climate change concerns, we must cut down on energy consumption. We may reduce electricity consumption by utilizing sunlight for all insulation and lighting needs. A combination of artificial lighting with natural light can efficiently meet all the requirements. To reduce the use of electric lighting, windows with high shading coefficients glazing along with a high VT is the best[8]; also maximum savings on electricity consumed by lighting is possible by using clear glazing, electrochromic, and finally tinted and reflective glazing[8].



5) Shading and Micro-Climate Modification: Shading devices reduce heat gains, need for air-conditioners, glare problems etc. It also improves thermal insulation and comfort within both ventilated and non-ventilated buildings, though it reduces natural light. Shading can be provided by natural landscaping or overhangs, etc. Though increasing the length of the shading devices reduces cooling load, the heating load is increased. Energy consumption in warmer climates may thereby be reduced. Reducing the energy consumption of the building is another option - micro-climate modifications using plant, trees which provide better shading, and water bodies. Evaporation from a nearby pool helps lower temperature during summer and the high heat capacity of water helps maintain constant temperatures during winter. Introducing a green roof may help reduce the surrounding temperature and the heat within the building, since roofs absorb a lot of heat, though the introduction of vegetation reduces heat flow from the roof into the building. Energy consumption of the building is thus reduced and so is the need for cooling devices.

6) Thermal Mass: The correct usage of thermal mass reduce the temperatures within the room by averaging out the day and night extremes. Building elements like roof, floors, walls absorb heat during the day and release it when the temperature falls, reducing the need for using cooling /insulation devices. In tropical areas, the difference between day and night temperatures is negligible and thus light weight construction materials are more suitable. For effective use of thermal mass proper shading devices should be used in combination with glazing faces in the proper direction.

BUILDING HVAC SYSTEM AND ENERGY CONSUMPTION

HVAC systems of buildings are responsible for at least half the energy consumed in buildings. So, it is necessary to analyse the energy consumed and find ways to reduce the consumption without compromising on the comfort of the residents. Air-conditioning, heating and ventilation constitute the HVAC system. In tropical climates however the major energy consumers are air conditioning and ventilation.

Air-Conditioning, Cooling and Dehumidification

In tropical climates cooling and dehumidification is an important factor. Compression cooling is one such way. The common methods of cooling include single-split or multi-split air conditioners. Some newer technologies include thermal, district and PV- driven cooling. The widely used electricity driven air-conditioner is the single-split. The energy efficiency ratio of air-conditioners must be high for better efficiency and more energy savings. Multiple splits are used in larger homes to reduce cost and space required for installation. Different temperatures can be achieved in different rooms. The PV system generates the electricity and stores it in a battery storage for future use. Thermal driven coolers can save more energy because it utilises the solar heat stored by the system for running the cooling system.

Ventilation

Indoor air quality is crucial for the well-being of the occupants of the building. An efficient ventilation system helps to filter the air supply and expel unwanted heated up air outside. Ventilation system can affect its occupants as follows:

- 1) Hygrothermal comfort: The temperature of the air inside, the relative humidity and air velocity should be homogenous.
- 2) Indoor air quality: To maintain the indoor air quality the inlets and outlets should be far away from each other to prevent intermingling of fresh and stale air.
- 3) Acoustics: Noise from the ventilation system should be kept to a minimum.

CONCLUSION

Design and construction of energy efficient buildings have always been a priority of the building sector but with the alarming climatic changes and a worldwide pandemic, has highlighted the need for creating social awareness about the growing need of designing and constructing green and energy efficient buildings and their benefits. Hereafter buildings will need to take into consideration the obstacles as well as the opportunities brought about by technological, environmental and various societal and architectural changes. This is where smart buildings which have automated systems that can adapt and communicate with its occupants will gain prominence. The construction industry must recognize and incorporate them into their designs and practices. A few of the green technologies that must be incorporated are photovoltaic systems or solar panels to reduce consumption of electricity and fuel which can save around 40% of the load. Use of skylights can reduce requirement of artificial lighting. Low flow fixtures and sensors can reduce water wastage. Rain water harvesting can help store and use of water for domestic purposes including running mini hydro turbines for generating energy. Appropriate ventilation and glazing will reduce



energy consumed for insulation and air-conditioning. Reuse and recycling of construction wastes and incorporating waste as construction components will reduce landfill accumulation. Natural landscaping and planting of trees and other flora will contribute to a sustainable living environment. Smart buildings can therefore bring down energy consumption by at least 40% in comparison to normal buildings.

REFERENCES

1. Bürger, V., Hesse, T., Quack D., Palzer, A., Köhler, B., Herkel, S., Engelmann P., 2016 KlimaneutralerGebäudebestand
2. Ciampi, M., et.al 2003. Ventilated facades energy performance in summer cooling of buildings. *Solar Energy* 75(6).
3. Chow, T.-t., Li, C., Lin, Z., 2010. Innovative solar windowsfor cooling-demand climate *Solar Energy Materials and Solar Cells* 94(2).
4. Han, J., Lu, L., Yang, H., 2009. Investigation on the thermal performance of different lightweight roofing structures and its effect on space cooling load. *Applied Thermal Engineering* 29.
5. International Energy Agency(IEA), 2013. Technology Roadmap. Energy efficient building envelopes.
6. Kuznik, F., Virgone, J., 2009. Experimental assessment of a phase change material for wall building use. *Applied Energy* 86(10).
7. Liping, W., Hien, W.N., 2007. The impacts of ventilation strategies and facade on indoor thermal environment for naturally ventilated residential buildings in Singapore. *Indoor Air 2005 Conference* 42(12).
8. S. Chungloo, B. Limmeechokchai, S. Chungpaibulpatana, 2001. Energy Efficient Design of Side-Window for Daylighting Application in Thailand.
9. Sadineni, S.B., Madala, S., Boehm, R.F., 2011. Passive building energy savings: A review of building envelope components. *Renewable and Sustainable Energy Reviews* 15(8).
10. Tantasavasdia, C., Srebric, J., Chenc, Q., 2001. Natural Ventilation Design for Houses in Thailand. *Energy and Buildings* 33(8).



Impact of GGBS as Partial Substitution of Cement and Replacement of Robo Sand to Fine Aggrigate on M50 Grade of High Performance Concrete

L Sai Indra Sena Reddy¹, Dr M M Vijalakshmi Nataraj²

Research Scholar, Sathyabama Institute of Science and Technology, Chennai¹

Professor, Civil Engineering, Faculty of Building and Environment, Sathyabama Institute of Science and Technology, Chennai

✉ Indra.reddy521@gmail.com; ✉ Vnat12345@gmail.com

ABSTRACT

The present evaluation focuses on optimal utilization of GGBS on M50 grade of concrete with various proportions mixes (0%, 10%, 20%, 30%, 40%) and replacement of RoboSand as fine aggregate which was maintained at 30% constant, along with addition of 1% of steel fibre by volume of concrete. For this various cubes, prisms, cylinders were casted and tested for different ages (3, 7, 28 days). To assess the mechanical properties of concrete some test were performed. Mix-3 emerges as the optimal replacement with enhanced value of compressive, split and flexural strength. Addition of steel fibre demonstrates the enhancement of flexural and split properties. Further, Acid attack test was conducted to assess the durability characteristic for optimal mix.

Keywords : GGBS; RoboSand; Steel fibre; Mechanical properties; Durability test (Acid Attack).

INTRODUCTION

Concrete is an ingredient material used in the construction industry it consists of chemically inert particulate substances like as an aggregate (fine aggregate and coarse aggregate) which is bonded with a cement and portable water. As per WHO concrete is a second broadest material consumption by human resources after food and water. The concrete is prepared by the proper mixing of cement, fine aggregate, coarse aggregate and water as per the mix proportions. Later the mix is allowed to cure and finally it is hardened like as stone. The hardening process is takes place just because of present chemical activities between water and cement for this concrete became strong with age. The concrete strength, durability, and many other properties are mainly dependence on the properties of the concrete ingredients, mix proportions, type of method of compaction and many other controls at the time of mixing, compaction, placing, and transportation and at the end curing at the end. Minimum of two proportions of an elevation amount as much compared to the standard materials. GGBS is a by-product material which is obtained from a steel manufacture industry which may be a replaceable material partially with the cement because

of it reduces the ecologically burden with associating with the concrete at both stages like the hardened state and fresh state of the concrete. RoboSand have be proposed for an alternate material for the river sand as it gives an additional strength and profit to concrete and also improves strength in concrete. RoboSand is well-known to enlarge the

potency of concrete. More over it may concrete through up of with a one and the same quantity of river sand. The strength of RoboSand concrete attention ally continues in raise with era for every proportion of RoboSand content in concrete. The proper use of a RoboSand as a fine aggregate it may twirl this desecrate matter. This cause discarding difficulty in nature into a more precious resources the perfect using of RoboSand may reduce the stain problem of supply of natural Fine aggregate and in turns helps cost reduction of concrete.

OBJECTIVES

1. To find out the optimum percentage of GGBS replacement to cement in high strength concrete.
2. To assess concrete's compressive strength with a various proportions of GGBS(10%,20%,30%,40%) to the cement, with the fine aggregate is partially replaced with RoboSand as maintain 30% constant and addition of steel fibre it is also maintain 1% constant by weight of volume of concrete.
3. To assess the concrete's Flexural strength and the Split tensile strength having various proportions of GGBS with constant



materials RoboSand and Steel Fibres.

4. To investigate durability characteristics of GGBS content concrete using HCL solution.

LITERATURE REVIEW

1. M. Adams Joe et.al [1] This current paper focus on investigation of features of M40 grade concrete of with a range of proportional for GGBS with cement and addition of 1% of steel fibre. Maintain water cement ratio 0.35. In the present work GGBS is varied in 0%, 10%, 20%, 30%, 40% & 50% and 1% steel fibre is used for getting the better results. At the end of experimental work it is concluded that 40% replacement of GGBS with cement & 1% of steel fibre are help to increase the force of concrete compare to standard design mix concrete.

2. S.P.Sangeetha et.al [2] For the determination of flexural performance of reinforced concrete beams the cement is replaced by GGBS. This experimental work mainly focuses on flexural force of beam. In this work M30 grade of concrete were used. For cement replacement GGBS are used in the proportion of 0%, 30%, 40%, 50%, 60% tested for 56 days also considering 28 days. Finally this experimental study explains that 40% of GGBS can be a replacement for cement which will be used for reinforced concrete beams. The strength increases about 21% at 56 days as compared to 28 days.

3. B Vidivelli et.al [3] Has investigated the mechanical & durability characteristics of concrete with GGBS & steel fibre for this grade maintained as M30. In this work maintain the GGBS as 20% & steel fibre about 1% the tests are conducted of for specimen 98, 56 & 28 days of all compressive, flexural force & 28 days test for elastic modulus. Along with this work simultaneously we have carried out the durability tests of sulphate attack, acid attack and water absorption. At the end of this experimental investigation we have concluded that GGBS with 20% replacement & 1% steel fibre addition gives better compressive, flexural & elastic modulus of concrete results of about 47.58, 4.5, 32.18 of about 90 days curing and also sulphate attack, acid attack are tested for about weight loss in respect to 7.94 & 10.45 and water absorption test results are 13.56 of about 20 % of GGBS replaced with cement & 1 % of steel fibre addition.

4. Suchita Hirde et.al [4] Through the present experimental work is to determine the mechanical properties of GGBS with adding up of steel fiber. For this GGBS is replaced with cement in the proportion of 0%, 10%, 20%, 30%, 40% by mass of cement and steel fiber are kept unvarying 1.5 % the specimens are cured for 28 & 56 days tested under compression & flexural strength along this flexural toughness indices are also determined. Finally the experimental investigation conclude that 20 % replacement of GGBS which maintains 1.5% steel fiber gives good results of compressive strength. This work is mainly concentrated by varying the GGBS content is varied in size of aggregate of about 10mm, 20mm, 12mm which results of about 61.09 MPa, 61.91 MPa, and 61.01 MPa. Along with this 20mm aggregate with 20% replacement of GGBS gives better flexural results of about 10.26% compare to other size of aggregate.

5. G. Balamurugan et.al [5] In this work variations are considered in the grade of concrete M20& M35. For this the RoboSand is replaced with natural sand. In the proportions of 0% to 100% of about 7 days and 28 days curing. But the test results give a clear image of about RoboSand. In this work finally concluded that 50% replacement of RoboSand material can be replaced to natural sand gives better results of strength achieve in nature beyond this decreases in strength.

6. S.Azhagarsamy et.al [6] The work is to find out the high performance concrete strength by using RoboSand material as replacement material for sand. For considering M60 grade concrete the RoboSand is replaced to natural sand directly i.e. maintained constant & steel fiber are varied in the percentage of 0.5%, 1%, & 1.5% the test were conducted 3, 7, 28 days . Finally the work is concluded that 60% of RoboSand and 1% of steel fiber gives better comfortable results of high performance concrete.

7. R.Rasika Priya et.al [7] In this work the normal sand is replace by RoboSand in this the variations of 10%, 20%, 30%, 40%, 50% & 60%with maintaining 1% of steel powder. At the end of experimental work conclude that 40% of RoboSand With 1% of steel powder gives an optimum strength.

8. Santosh Kumar Karri et.al [8] In this prescribed work explain the GGBS is partially replaced to cement for the grade of concrete M20 and M40 in the range of 30%, 40%, 50%.cubes, cylinders, prisms are casted for determining the compressive, tensile and flexural force of concrete along this durability tests are also conducted like acid tests sulphuric acid and hydrochloric acid used to conduct the work. This experiment finally concluded that for both M20 and M40 grade concrete the GGBS material can be replace of cement up to 40% optimum results for all strengths. In durability properties comparing the H2SO4 with HCL. The compressive strength value GGBS concrete effect of HCL more compare to H2SO4.

MATERIALS

Cement

In this present investigation we use OPC (ordinary Portland cement) as a binding material.

The test results are tabulated in a below table.

Table 1. Shows the Preliminary Test Results of Cement

Particulars of cement	Normal consistency	Specific gravity	Fineness	Initial setting time	Final setting time
Test out comes	33%	3.14	5%	44 min	398 min

Fine Aggregate

In this present project work fine aggregate used is naturally available river sand which is under zone-II as per IS 383:1970. The preliminary experimental outcomes of FA are as shown in the below table.

Table 2. Shows the Preliminary Test of Fine Aggregate

Particulars of FA	Specific gravity	Water absorption	Fineness modulus	Silt content
Test out comes	2.66	1.4%	3.42	2.32%

Coarse Aggregate

In this present project work crushed angular stone size is about 10mm and 20mm were used. Table below shows the properties of Coarse aggregate.

Table 3. Shows The Preliminary Test Results of CA

Particulars of CA	Specific gravity	Water absorption	Fineness modulus
Test out comes	2.73	1.1%	2.24

Ground Granulated Blast Furnace Slag

The slag is a through invention material from iron manufacturing industry. It is mainly composed of 30% to 40% of silicon dioxide (SiO_2) and also 40% Cao which is also similar as the chemical composition of cement. The GGBS as a replacing material for cement it says that the compressive strength can be high as much as possible. It gives a good workability, durability characteristics in nature and also a cost effective construction material. Test results are shown in **Table 4**.



Figure 1. Shows sample of GGBS

Table 4. Shows the Test Results of GGBS

Particulars	Specific gravity	Fineness (Kg/m^2)	45 Micron (Residue) %
Test out comes	2.88	382	7.40

RoboSand:

RoboSand is used for the present investigation work it is partial replacement material for fine aggregate which was collected from stone brick manufacture in khammam dist. Telangana. The test results are shows in below Table below.

Table 5. Shows the Preliminary Test Results of RoboSand

S.No	Particular	Test results
1	Specific gravity	2.57
2	Fineness modulus	3.10



Figure 2. Shows sample of RoboSand

Steel Fibres

In this experiment to enhance the tensile strength of concrete we are going to add the steel fibre. The steel fibres are hooked at end it is of 1mm diameter and Aspect ratio 50mm. The steel fibres were collected from Maruthi steel suppliers, Bangalore. **Fig 3** shows steel fibres sample and **Table 4** shows the property of Hooked End SF.

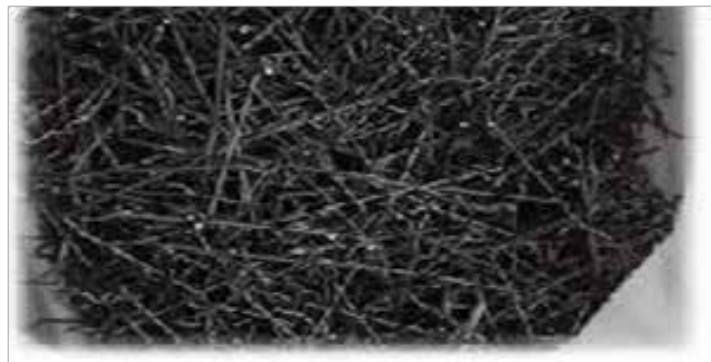


Fig. 3. Shows sample of steel fibres

Table 6. Properties of Steel Fibres Used

Properties of SF	Length	Diameter	Aspect ratio	Specific gravity	Tensile strength	Density
Approved values	50mm	1.0 mm	50	7.80	1200 MPa	7860 Kg/m ³

Chemical Admixture

Fosroc auramix 300-plus is used as a chemical admixture and its specific gravity is about 1.06.

Potable Water

In this experimental work water is used for concrete mixing and curing. water used as clean, clear & free from acid content and portable water used which is referred from IS - 456 2000 are used.

MIX DESIGN BY ABSOLUTE VOLUME METHOD:

According to IS: 10262-2009 mix design was done for the purpose of concrete casting of various mixes with the help all above preliminary investigation test outcomes. The mix design was done for M50 grade. From the mix design conventional trial mix was prepared and it having mix ratio is 1:2.38:3.10 and the w/c of 0.40.

Table 7. Mix Proportions of Concrete

Material	Quantity (Kg/m ³)	Proportion
Cement	342	1
FA	816.12	2.38
CA	1061	3.10
Water	131.42	0.40
Chemical admixture	4.5	1.2%

EXPERIMENTAL PROGRAM

In this present experimental investigation involves casting of 45 cylinders, 45 cubes and 45 prisms and testing is conducted after curing period of 3, 7, 28 & 90 days to assess compressive strength, split-tensile strength & flexural-strength of casted concrete. In this work there are five mix proportions to study the variation of strength and to conclude with optimum percentage of the GGBS. The below table VIII represents the different mix proportion details and their percentage. To determine the durability characteristics of concrete, 3 conventional cubes and 3 cubes having an optimum percentage of GGBS, ROBO SAND and Steel fibres are casted.

Table 8. Shows Mix Proportions were Involved in this Present Work

Mix	Cement (%)	GGBS (%)	ROBO SAND (%)	Steel fibre (%)
Nominal mix	100	-	-	-
Mix - 1	90	10	30	1
Mix - 2	80	20	30	1
Mix - 3	70	30	30	1
Mix - 4	60	40	30	1

PROCEDURE FOR CONCRETE CASTING

As per design mix the material are weighed and mixed in tray by hand mixing. The water cement ratio is maintained for this work is 0.40. The specimens are will be casted uniformly distributed & randomly the specimen used trowel with in one hand & in other hand is will be taken by the concrete which it helps to fill the concrete in the specimen. Conventional concrete is casted without any replacement for the purpose of comparing the strength. To get high strength in concrete the variations are made of the GGBS material. With the help of the tamping rod the concrete is tamped in the specimen with 3 layers the casting will be done by hand mixing method. The cylinders & prisms are casted same as that of the cube casting. After casting the specimen is kept it for 24 hours after this the specimen are de molded & kept it in curing tank. Maintain normal temperature the specimens are kept in curing tank for the purpose of curing to getting the high strength. The specimen are keeping it for 3, 7, 28 days respectively. After 3, 7, 28 days curing the testing process are conducted on specimen and note down the all the readings and calculations are done for determination of compressive, split, flexural strength as per our Indian force values.



Fig. 4. Shows freshly casted specimens



Fig 5. Shows the casted Cured specimens

RESULTS AND DISCUSSIONS

Slump Cone |Test

In the fresh state of concrete the test is conducted is slump test for the purpose of checking of the workability of concrete with many trials are conducted. The slump test shows the workability which may increase by rising in proportion partially replaced of GGBS in OPC.



Fig. 6. Shows Slump cone test

Table 9. Represents Slump Test Results

S.No	% of GGBS added	Slump value in mm
1	0%	45
2	10%	58
3	20%	63
4	20%	68
5	40%	59

Compaction Factor Test

For the determination of fresh concrete workability compaction factor test also conducted.



Fig. 7. Shows compaction factor test

Table 10. Represents Compaction Factor Test Results

S.No	% of GGBS added	Slump value in mm
1	0%	0.91
2	10%	0.95
3	20%	0.96
4	20%	0.97
5	40%	0.92

Compressive Strength

From the below Graph and table, we can say that there will be a considerable increase in strength of replacement concrete compare to the conventional concrete. Mix 3 i.e., GGBS 30%, RoboSand 30% and 1% of Steel fibre shows the superior strength compare to other mix.

Table 11. Shows the Compressive-Strength Results

Mix	Compressive strength in N/mm ²			
	3 days	7 days	28 days	90 days
Nominal mix	23.4	37.86	57.86	60.85
Mix - 1	23.95	30.96	43.62	62.78
Mix - 2	24.12	33.47	55.18	64.65
Mix - 3	26.45	37.92	59.96	65.78
Mix - 4	28.54	36.29	53.69	68.39

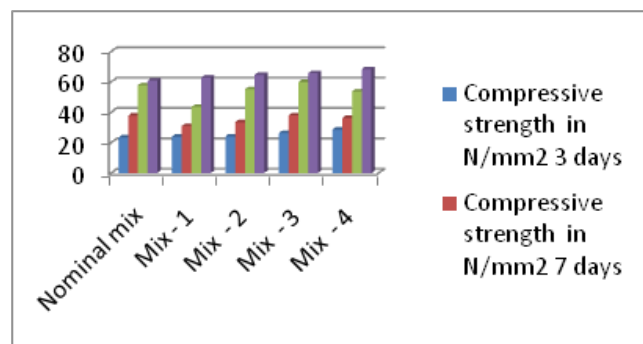


Fig. 8. Shows the Compressive-Strength results

Split-tensile Strength

From the below graph and table we can say that there is a great influence of presence of chemical admixtures, Mix 3 i.e., GGBS 30%, RoboSand 30% and 1% of Steel fibre shows the better split tensile strength of concrete compare to other mix.

Table 12. Shows the Split-Tensile Strength Results

Mix	Split-Tensile Strength in N/mm ²			
	3 days	7 days	28 days	90 days
Nominal mix	2.26	3.54	4.33	4.99
Mix - 1	2.8	2.68	3.95	4.54
Mix - 2	2.26	2.99	4.29	4.65
Mix - 3	3.13	3.62	4.95	5.03
Mix - 4	3.03	3.44	4.71	4.99

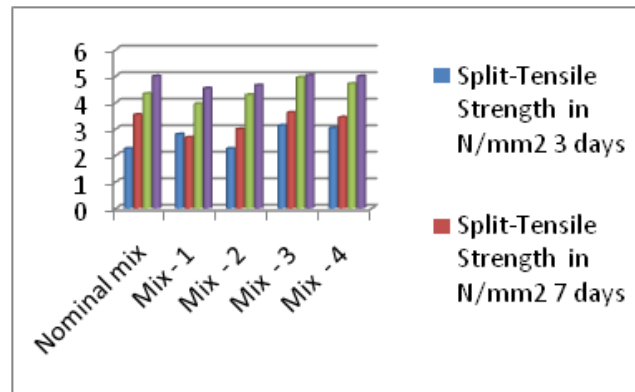


Fig. 9. Shows the Split-Tensile Strength results

Flexural Strength

The flexural prism having size is about 700mm×150mm×150mm were casted and tested under two point load testing machine to assess the flexural-strength. The results show that, the integration of SF shows the good ductility to flexural force. The Mix 3 i.e., GGBS 30%, RoboSand 30% and 1% of Steel fibre shows the extraordinary flexural strength of concrete compare to other mix.

Table 13. Shows the Flexural-Strength Test Results

Mix	Flexural-Strength in N/mm ²			
	3 days	7 days	28 days	90 days
Nominal mix	3.96	5.62	6.03	6.54
Mix - 1	4.36	6.16	6.51	6.87
Mix - 2	4.83	6.13	7.16	7.25
Mix - 3	5.86	7.23	7.43	7.58
Mix - 4	5.06	6.23	6.33	6.98

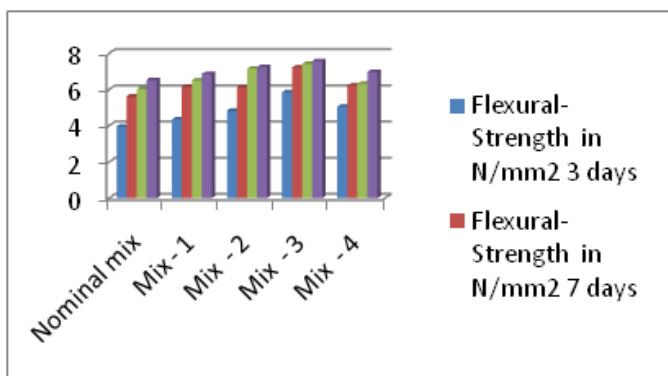


Figure 10. Shows the Flexural Strength results

Acid Test

- To check the durability characteristics of concrete we considered the optimum mix3 i.e. GGBS 30%, RoboSand 30% and 1% of Steel fibre. The cubes were casted and immersed in 5% concentrated hydro choric acid [HCL] solution for 28 days to examine the weight loss in concrete which shows the resistance of concrete against the acid attack environment.
- The resistance to acid for the Mix3 integrated concrete was superior to the CC. From the HCL solution water was absorbed by cubes and forms black whitish film appears on the concrete surface.

- The below Table represents the results for the weight loss in percentage. The presence of GGBS in concrete improves the resistance against the acid attack.
- The average percentage loss in weight was 3.40% whereas GGBS, ROBOSAND and steel fiber content concrete i.e. MIX3 was 1.15%.

Table 13. Shows the weight loss in cubes during due to acid effect

S.No	Mix	Weight of cubes after 28 days	Weight of cubes before 90 days	% of weight loss in cubes	Average weight loss
1	Nominal mix	8.76	8.40	4.1	3.4
		8.77	8.46	3.5	
		8.76	8.53	2.6	
2	Optimum mix (mix -3)	9.45	9.16	3.0	1.18
		9.36	9.12	0.24	
		9.43	9.21	0.23	

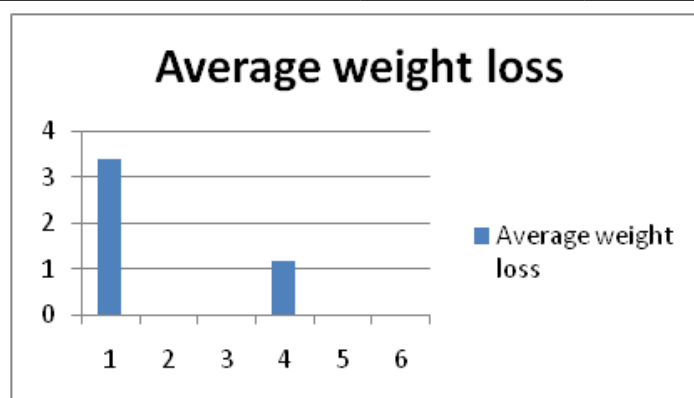


Figure 11. Represents average %age weight loss

CONCLUSIONS

- The workability is to be improved markedly by fresh concrete up to 30% replacement of GGBS to cement above this percentage workability decreases.
- The Compressive Strength increases with the use of GGBS material as replaceable material for cement. The maximum strength achieved in concrete having 30% GGBS, 30% ROBOSAND and 1% SF i.e., Mix 3. the strength increased 2.1% as compare to CC.
- The adding up of steel fibers also improves the split tensile strength of concrete. The maximum strength achieved in concrete having 30% GGBS, 30% ROBOSAND and 1% SF i.e., Mix 3. the strength increased 0.65% as compare to normal concrete.
- The Flexural-Strength also shows the enhancing in strength of concrete with the presence of GGBS, The maximum strength achieved in concrete having 30% GGBS, 30% ROBOSAND and 1% SF i.e., Mix 3. the strength increased 1.4% as compare to normal concrete.
- Hence for the above experimental investigation has concluded that cement with GGBS, sand with RoboSand for 30% partial replacement with addition of steel fiber gives a optimum good results of forces and also helps in improving the strength & durability properties of high strength concrete
- The % of weight loss in GGBS is less as compared to normal concrete i.e. MIX3 (30% GGBS, 30% ROBOSAND, 1% SF) the average weight loss in CC is about 3.4% and in Mix3 the average weight loss is 1.154%.



REFERENCES

- A Maria Rajesh M. Adams Joe, M. Adams Joe “An Experimental Investigation on the Effect of GGBS & Steel Fibre in High Performance Concrete” International Journal of Computational Engineering Research||Vol, 004||subject, 004|| April 2014.
- P.S Joanna, S.P.Sangeetha “Flexural Behavior of Reinforced Concrete Beams with Partial Replacement of GGBS” American Journal of Engineering Research (AJER) e-ISSN: 2320-0847 P-ISSN: 2320-0936 Volume-03, Issue-01, pp-119-127 www.ajer.org. 2014.
- D. Dhanalakshmi, B Vidivelli et.al “Study On Mechanical And Durability Properties Of Concrete With GGBS & Steel Fibre” International Journal Of Engineering Research & Technology (IJERT), ISSN 02319-05991 Vol. 05, No. 03, August 2016.
- Suchita Hirde et.al “Effect Of Addition Of Ground Granulated Blast Slag Furnace (GGBS) On Mechanical Properties Of Fiber Reinforced Concrete “International Journal Of Current Engineering And Technology E-ISSN 02277 – 04106, P-ISSN 02347 – 05161 Vol.5, No.3 (June 2015)
- Dr. P.Perumal & G.Balamurugan “Use Of RoboSand To Replace Sand In Concrete An Experimental Study” International Journal Of Scientific And Research Publications, Volume no. 03, Issue no. 012, December, 2013.

Effective Quality Management for Sustainable Roads

Kishor Kumar Pahuja

Superintending Engineer UP PWD

✉ pahujakishore1@gmail.com

ABSTRACT

Construction industry in India accounts for about 10% of GDP of the country. Out of this the share of roads and highways which form an important part of infrastructure is about 30%. The journey of road development has been a long one. Now we are in an age which facilitates fast moving vehicles reducing travel time and to sustain high and heavier volumes. For sustainability roads are to be built with good quality. Good quality gives consistency in performance and induces reliability giving rise to increase in the confidence level of the system. It is very important for the highway engineers to develop a self-sustaining and reliable system of construction methodology which can integrate quality management to produce sustainable road network. Construction industry and more particularly the projects in the highway sector are of varied nature and require a large number of parameters to be controlled and the end product is produced in a rather open and relatively uncontrolled environment. This gives rise to a big challenge to produce an acceptable quality product. IRC has put in place codes and manuals to guide the requirements in this field. To stay in competition consistent improvement in quality is essential. It is felt that there need to look at and deal with the issue of quality in a comprehensive way and to introduce the concept, ethos and practice of Total Quality Management to get sustainable road system and self-reliance.

Keywords : Words: Sustainability; Consistency; Reliable system; Total Quality Management; Self-reliance.

INTRODUCTION

A good and efficient network of roads is a pre requisite for development and very important element affecting the quality of life of the people. In a country like India with a very large population, road projects constitute a large part of Government investments be it for the improvement of National Highways, Expressways or other category of roads. All road projects have three essential elements. They are scope, time and cost. Scope is decided based on the requirement or the mandate given for the improvement of the existing facility. Scope is something which cannot be squeezed unilaterally by the construction agency. On the other hand there is always a tendency by the contracting agency to reduce the cost they have to incur and at the same time the agency wants to reduce the time as well. Schematically the three elements form three sides of the triangle as shown in **Fig 1**. In addition to these there is an element of quality which is delicately balanced. Hence quality is central to the scheme of things and should maintain its place and should not suffer.

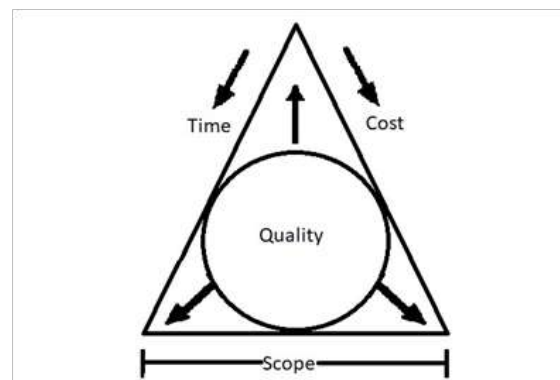


Fig 1. Relation of Quality with Scope, Cost & Time in a Project

Our Prime Minister has recently given a very ambitious call for “AtmaNirbhar Bharat”. This can only be achieved by producing good quality roads which can sustain through their design lifecycle. If the domestic contracting agencies excel in the quality work then they can truly capture larger share in the major projects to bring out a change towards self-reliance as shown in **Fig 2**.

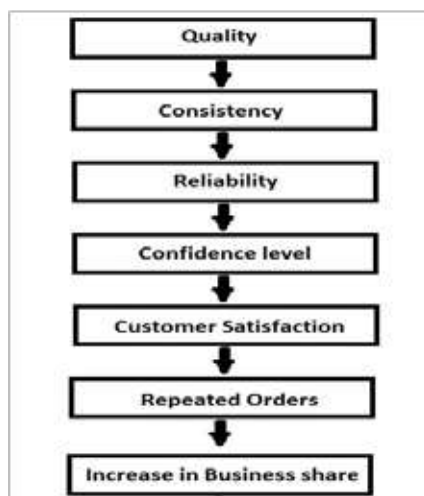


Fig 2. Quality-Consistency Flow Chart

OBJECTIVES OF THE STUDY

- This study has been done mainly to understand issue of quality and to explore potential to improve it.
- To understand the effect and role of quality in the highway sector in the fast developing infrastructure scenario.
- To understand how quality issue is handled in the projects with the guiding principles laid down MoRTH and IRC.
- To see if quality can be continuously improved using concepts like Total Quality Management.

METHODOLOGY

The methodology adopted in this study is through literature survey of the work done in the area of quality improvement in the construction and highway sector. Specifications for Road and Bridge Works by MoRTH and the Manual for Quality Control in Road and Bridge Works IRC:SP 112-2017 has been compared with the practices of Total Quality Management and current practices in Human Resource Management.

CONCEPTS AND DEFINITION OF QUALITY

The word quality has come up from the latin word “qualis” which means “what kind of” . Here the word what kind of has got inherent in it “how good”. Although quality has been defined by many experts but the general sense in which it is used in the organizations is that good quality is that which is acceptable among the customers. So the quality is relative. It is also good as well as bad in different cases. Juran has defined the quality as “the fitness for use therefore quality products should meet or exceed customer requirements”. Crosby has defined quality as “quality is conformance to requirement. Thus requirement must be clearly stated so that these cannot be misunderstood”. Whenever there is mention of quality the two attributes which are quite inseparable from it are consistency and reliability. This implies that the acceptable work or product should not deviate from the acceptable level and it should have high reliability of achieving the standards. High reliability factor means high degree of confidence

PROVISIONS FOR QUALITY IN IRC CODE AND MANUALS

Codal provisions for quality existed before the year 1998 through the MorTH detailed specifications for roads and bridges and the Manual for Quality Control 1984. But after 1998 with the construction of 4 laning of Golden Quadrilateral and expressway construction there was a need to inculcate quality right from planning to construction to operation and maintenance. Thus quality assumed greater importance so that the constructed roads could serve throughout their design life cycle giving safe and comfortable riding facility reducing vehicular operating cost and travel time. Thus the IRC codes namely IRC SP:11-1984 Handbook for Quality Control for Construction of Roads and Runways, IRC SP:57-2000 Guidelines for Quality Systems for Road Construction and IRC SP:47-1998 Guidelines for Quality Systems for Road and Bridges were merged to form IRC SP:112-2017 Manual for Quality Construction in Road and Bridge Works. This manual is an extensive and detailed document listing guidelines from the preparation of road project and through the post construction maintenance. Now this manual in



conjunction with MoRTH Specification for Roads and Bridges is the basis for guiding and controlling the quality of works. Further Guidelines and standard operating procedures for quality control/Assurance in construction of National Highways and other centrally sponsored projects have been issued vide order RW/NH-34066/01/2020-QCZ Dated 01.10.2020. In line with the importance given to the quality by BS 7580-1:1992, Transport Research Board, American Society for Quality Control and American Society for Testing and Materials (ASTM-E699) Total Quality Management has been adopted and various road works have been divided into classes as shown in **Table 1**.

Table 1. Class Nomenclature and QA (Source: IRC SP 112-2017)

Classes of Quality Assurance	Class Nomenclature	Road Classes/Categories Covered
Nominal QA	Q1	Rural Roads in Remote areas
Normal QA	Q2	Rural Roads average size/MDR
High QA	Q3	National Highways& State Highways, Coastal Roads, Roads in High altitude, Roads in high rainfall areas & Large size Projects on Major District Roads
Extra High QA	Q4	Tunnels, Elevated Highways

Though the construction of roads is taken up through various modes like Build Operate and Transfer (BOT), Engineering Procured Contract (EPC), Hybrid Annuity Mode (HAM) in addition to the conventional contract systems the contractor is primarily responsible for construction of quality but role of other stakeholders like engineer and the client is also important. The contractor has to ensure quality assurance plans incorporating organizational duties, responsibilities, procedure, inspection, tests frequencies, acceptance criteria, internal audit etc. The contractor has to get the approval of the Authority or independent engineer for the executed work. The desired quality can only be achieved by adequate and appropriate quality personnel deployed by the contractor at the project. The deployment of personnel required depends on the size of the project as shown in **Table 2**.

Table 2. QC of Personnel of Contractor (Source: IRC SP 112-2017)

Size of Project	Details of Key & Sub Professional
<Rs 300 Crore	Material Engineer-1, QC/ Assistant QC Engineer-2, Lab Technician-4
≤ Rs 300 Crore	Material Engineer-1, QC/ Assistant QC Engineer-3, Lab Technician-6

The duties of personnel shown in **Table 2** are listed in the manual. Similarly for the control and check of quality created by contractor number and duties of personnel to be available with the engineer are also detailed as shown in **Table 3**.

Table 3. QC Personnel of Engineer (Source: IRC SP 112-2017)

Size of Project	Details of Key & Sub Professional
<Rs 300 Crore	Material Engineer-1, QC/ Assistant QC Engineer-1, Lab Technician-2
≤ Rs 300 Crore	Material Engineer-1, QC/ Assistant QC Engineer-2, Lab Technician-4

As per guidelines laid down by IRC SP 112-2017 all materials and finished items and levels etc. have to be checked with the stipulated frequency at all stages of the work. The establishment of laboratory for material testing is a necessary pre-requisite in projects.

As already discussed in section 4 about the concept of quality, it is always the end user, customer or the client whose requirement has to be met with. It is not the builder who is going to use the facility. Builder and user thus stand on the two opposite sides so quality aspect has to be pushed by the user. Also quality just can not be subjective only. Quality has to be evaluated on “measurable” basis. Statistical analysis for assessment of quality is necessary since variability is a reality in road construction. Variability occurs in materials and processes and at different stages in road construction. Under such circumstances statistical analysis helps in taking informed decisions about acceptance. Physical quantities that are expected to be the sum of many independent processes often have distributions that are nearly normal. Normal distribution curve is flatter if variation of data is more from mean and vice versa as shown in **Fig 3**.

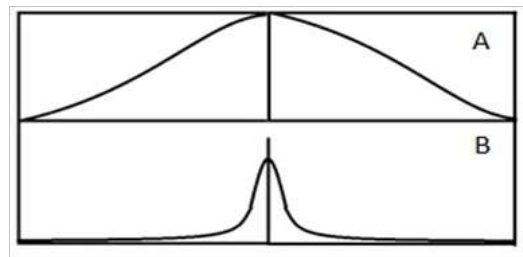


Fig 3. Normal Distribution

A With large Dispersion from mean

B With small Dispersion from mean

Depending upon the confidence limits set out for the specific works individual upper or lower specification limits are set, called USL and LSL. There can be single specification limit talking any one of these or taking double limits. Generally different items in road works are specified for 90% confidence level meaning thereby that out of every 100 in the selected lot 90 values will come under the specified limits and 10 values can be accepted to be out of these limits.

QUALITY CONTROL AT DIFFERENT LEVELS

A multi-layer approach is adopted in the case of highway projects. The basic and the first layer is at the level of the contractor where the quality is controlled at the execution level. This is either “in process” or the ongoing controls and can also be “after process” checks when the item gets completed. The second layer of checks is at the level of the engineer or the supervision consultant. There may be higher level inspections from the client side. The third layer is the independent “third party” checks. There may be post construction checks or audits.

Despite these mechanisms to ensure quality the most important level is at the initial first level itself. It is at the level of the contractor that the importance of quality and its role in the building up of the reputation of the firm and the long term advantage has to be stressed. It is with this perspective that total quality planning, organizing; staffing etc. has to be undertaken.

TOTAL QUALITY MANAGEMENT

The Concept Of TQM

Total Quality Management has been adopted in the manufacturing sector. It was developed in post war Japan under the aegis of William Edwards Deming. It has been successfully used in our country also. To achieve self reliance in the field of highway sector companies have to adopt high standards of quality so that they can face the tough competition within the country as well as outside to edge out competitors and win contracts. For this they have to adopt Total Quality Management and approaches like “Six Sigma”. Total Quality Management is different from quality assurance or quality control. In fact TQM encompasses both quality assurance and quality control and is more comprehensive. TQM starts at the planning and project preparation stage. It goes through the implementation and execution and operation phase. There are continuous checks and controls, different tools and management techniques are deployed. The process is refined and the focus is on continuous improvement and to achieve practically “zero defects” output. Some of the features of TQM are:

- It involves everyone in the organization in producing products and services to match the customer’s needs and expectations.
- It is not fixed but a dynamic process involving effectiveness and efficiency of all elements of a business.
- It uses set of tools and techniques and process output which yields customer satisfaction.
- It also integrates functions and processes within the organization to achieve continuous improvement of quality of goods and services.
- Teamwork is practiced.
- Formal system of education and training is adopted.
- Suppliers and customers are integrated into the involvement process.

Three Levels of Total Quality Management:

This is done at all the 3 management stages-Strategic, Tactical and Operational. Fig 4 shows how broad policy, procedure and execution are related to different levels. Policy dictates how the construction company deals with the strategic long term goals and how project work progress is managed which includes the level of importance given to quality. Depending upon the policy initiative, the procedures are formed at the middle level and the requirement about staffing is managed. At the execution stage endeavour is make best use of the personnel and other resources.



Fig 4. 3 Levels vs Policy/Procedure & Execution

Fig 5. Shows how Quality Models, standards and tools are related to different levels.

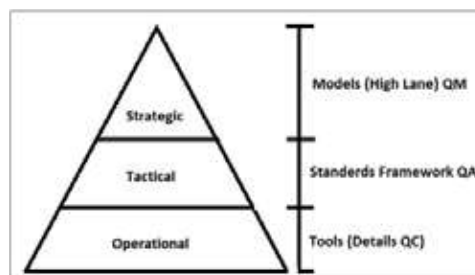


Fig 5. Models, Standards & Tools for QM

Generally the planning and control activities are related to strategic, tactical and operational level as shown in **Fig 6**.



Fig 6. Strategic/Tactical & Operational level vs Planning & Control Activities

Fig 7. shows a generalized model of organization chart from Strategic perspective which can be adapted. This model integrates needs of the customers and focuses on the continuous improvement principle to achieve quality.

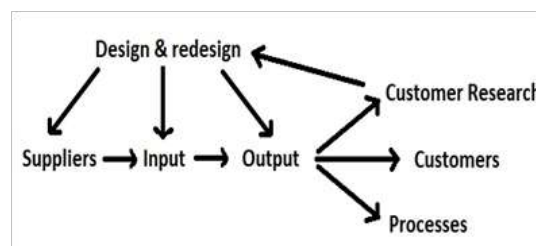


Fig 7. Model of Organization from Strategic Perspective



Human Asset Management approach to Quality

Human Asset Management is the key to achieve quality and to move towards the goal of Total Quality Management. Though the input of machinery has increased in construction yet the controlling of machine output and quality depends on the expertise and intent of the human factor controlling it hence the role of human resource management continues to be important and has become even more comprehensive in the form of Human Asset Management. Some of the important points to be considered are:

- Right number of personnel deployment.
- Appropriate personnel deployment at the appropriate place.
- Exchange of ideas and sharing of information for continuous control and assessment of work quality.
- Retention of expert personnel.
- Continuous Training and up gradation required.
- Keeping the team motivated to achieve best quality.
- Improving group dynamics to achieve larger goal.
- Introducing concepts like Quality Circle in large projects.

Tools and Techniques for Quality Management:

- Cause and Effect Diagram. Any process when analysed in parts by breaking down can reveal major causes of a particular problem.
- Flow Charts show all steps and stages in a process and help in identifying problem.
- Check Lists make checks systematic.
- Control Charts as “in process” controls to check whether a process is statistical control.
- Scatter Diagrams show relationship of two variables.
- Pare to Charts to identify causes and prioritize solution.
- Histograms showing graphical representation of individual measured values.

CHALLENGES IN IMPLEMENTING QUALITY MANAGEMENT:

- Nature of work which involves many parties and stake holders makes the implementation difficult.
- Highways projects and road works are different from the manufacturing industry where bulk lots are produced in the relatively more controlled factory settings. Road projects comprise of a variety of items which are produced in the field. There is large input of different raw material resources which are always liable to vary. Although checks and controls can be put at different levels but the basic level where actual execution initially takes place is extremely important. It has been a long time observation that the quality depends on the attitude and inclination of the contractor towards quality hence it is quite individual- centric.
- Bringing change is difficult due to rigid attitudes and is slow and incremental.
- Lack of will to learn new things.
- Lack of system to have formal trainings.
- The guidelines to quality as already discussed are extensive and detailed. But following these guidelines is not easy if the constructing agencies are not quality oriented then complete enforcement by the supervision engineer is not easy.
- It is a known fact that there is tough competition for works among the contractors. This drives contractors to bid for works at lower rates. Sometimes these rates are not workable and the quality suffers. There is lack of support for rejection of unworkable below par rates.
- As per the provisions of the codes in practice there can only be acceptance or rejection.



- There is no sound framework for incentive based work. The contractors completing works with good quality are treated at par with other contractors in the bidding process. There needs to be a comprehensive grading system for completed works.
- There is no system in place to connect performance with payment.

SUGGESTIONS AND RECOMMENDATIONS:

- Each and every project is unique with its size, scope, time of completion and other constraints. In addition to this the items covered in the scope of work in each infrastructure project are much varied hence it is suggested that each project needs a quality management model based on the specific nature and needs.
- The acceptance criteria of 90% confidence level as per specifications generally set out for different items of work is difficult to achieve without good quality work. Moving towards TQM which also includes approach like quality circle for major works will improve human factor very vital for change.
- There is always a lot to learn from failures. There should be no attempt to hide non-conformance either in “in process” checks or “after process” checks. All cases of non-conformance should be examined and reviewed to implement changes. Quality management is a dynamic process.
- It is imperative to increase the defect liability period to make the contractors quality oriented.
- Contracts should have clear conditions for reduced pay factor in case of sub standard work and the reduction should be substantial.
- Periodic post construction performance audits after 5 or 10 years can be considered linking incentives to the contractor based on the performance. This audit is suggested to take a comprehensive view after considering all the design parameters and the traffic growth also in the project reach.

REFERENCES

1. Ministry of Road Transport and Highways Specifications for Road and Bridge Works (Fifth Revision) Published by IRC on behalf of Government of India MoRTH.
2. Manual for Quality Control in Road and Bridge Works IRC:SP:112-2017
3. Government of India MoRTH (Quality Control Zone) Order no. RW/NH-34066/01/2020-QCZ Dated 01.10.2020
4. Statistics for management (seventh edition) by Richard I. Levin and David S. Rubin.
5. Business statistics (second edition 2019) by Naval Bajpai.
6. Peter Hoonakker, Pascale Carayon and Todd Loushine (Total Quality Management vol. 21 No. 9 Sept. 2010): Barriers and benefits of quality management in the construction industry- an empirical study.
7. Algan Tezel, Lauri Koskela, Patricia Tzortzopoulos, Saeed Talebi and Luciana Miron (26th Annual Conference of the International Group for Lean Construction 2018): Continuous improvement cells in the highway sector.
8. Ajinkya D. Upawar, R.D. Shinde (IRJET Vol. 7 issue 8 Aug. 2020): Application of Six Sigma Quality Control Tool at Construction site.



Feasibility Study of Ferrochrome Slag as an Alternative to Natural Aggregates

P N Ojha, Abhishek Singh, Brijesh Singh, B N Mohapatra

National Council for Cement and Building Materials, Faridabad, Haryana

✉ brijeshsehwagiitr96@gmail.com

ABSTRACT

The utilization of waste generated from any industrial process and conservation of natural resources is one of the main objective of sustainability goal. Ferrochrome slag is waste material obtained from manufacturing of high carbon ferrochromium alloy. Depending upon cooling process, two types of ferrochrome slag are produced i.e. Air cooled by letting molten slag cooled down under normal temperature and water cooled ferrochrome slag by quenching molten slag. Presence of chromium in Cr^{+3} and Cr^{+6} state in ferrochrome slag is an area of concern towards its feasibility to be used as a constituent material in concrete. In this study characterization of both types of slags has been carried out to check the feasibility of replacing natural fine aggregates with water cooled ferrochrome slag and natural coarse aggregates with air cooled ferrochrome slag. In concrete mix designs, natural aggregate has been replaced with ferrochrome slag at percentage of 30%, 60% and 100%. Mixes were prepared at two w/c ratios and fresh & hardened properties of concrete were evaluated. It was concluded that 60% replacement of natural coarse aggregate with air cooled ferrochrome slag and 60% replacement of natural fine aggregate with water cooled ferrochrome slag in concrete is feasible.

Keywords : Ferrochrome slag; characterization; aggregates; leaching.

INTRODUCTION

The Ferrochrome slag is an important byproduct of ferrochromium industries and generated during the manufacturing of ferrochrome alloy. Ferrochrome alloy is manufactured in a submerged electric arc furnace by physiochemical process at the temperature of 1700°C . The main constituents of ferrochrome slag are SiO_2 , Al_2O_3 and MgO with minor traces of ferrous/ferric oxides and CaO . Chromium is generally present in the form of partial altered chromite and entrapped alloy. Quartzite is added as fluxing material to reduce the melting temperature of slag. The slag production is 1.1-1.6 t / t Ferrochrome alloy depending on feed materials.

Depending upon the cooling process, two types of ferrochrome slag are produced i.e. Air cooled by letting the molten slag cooled down under normal temperature and water cooled ferrochrome slag by quenching the molten slag. Due to particle size being in the range of coarse fraction, the air cooled ferrochrome slag can be used as replacement of natural coarse aggregate in concrete. Since, the particle size of water cooled ferrochrome slag is in the range of fine fraction, the water cooled ferrochrome slag can be used as replacement of natural fine aggregate in concrete. However, presence of chromium as Cr^{+3} which is not soluble in water (when oxidized turns into Cr^{+6}) and Cr^{+6} which is soluble in water (hazardous), makes ferrochrome slag a potent threat to environment.

In both water cooled and air cooled ferrochrome slag as determined by Nilamadhaba et.al [1], chromium is present in stable spinel phase and in the form of entrapped metallic granules. In molten slag, Cr is mainly in Cr^{+2} , which is not stable at room temperature and therefore solidifies in most stable oxide i.e. Cr_2O_3 or Cr^{+3} which is insoluble in water and also not expected to oxidize at atmospheric temperature to highly soluble and carcinogenic Cr^{+6} form. The Cr present in entrapped metallic granules is in dispersed state and therefore not expected to leach out when in contact with water. However, many researchers addressed the oxidation of Cr^{+3} to Cr^{+6} in the presence of strong oxidants which results the possibility of slowly releasing Cr^{+6} to environment in the long run. Leachability of heavy metals is the main environmental concern due to possible impacts on human health and environmental pacts.

Lind et. Al [2] investigated that “leaching tests with salt seawater and PH adjusted water reveal low leachability from the slag for most elements. It was also reported that in road construction, there was a low migration of particles from the slag to the under lying soil and that the leaching from the Ferrochrome slag to the groundwater was low for the elements analyzed,

with the exception of potassium. Al Jabri et al. [3] investigated the combined effects of fly ash as cement replacement and ferrochrome slag as aggregate substitute. Cement was replaced with fly ash at the ration of 10, 20, and 30% whereas coarse limestone aggregates were replacing with coarse ferrochromium aggregate at the ratio of 25, 50, and 75%. The results from the study revealed that ferrochromium aggregates increase the strength of concrete and also the abrasive wear resistance while it has negligible influence on the porosity and water absorption of concrete.

Panda et.al [4] investigated the environmental and mechanical properties of concrete. The concrete made with ferrochrome slag shows increased strength as compared to control sample. The standard leaching experimental results showed that the leachable chromium remains well immobilized in the cement and concrete matrix with very low to non-detectable level of chromium leaching. Sathwik et. Al [5] investigated the utilization of ferrochrome slag as replacement of coarse aggregate in concrete. Researcher done the study on M50 grade of concrete. Studies reveal that up to 75% replacement of ferrochrome slag with natural aggregates the compressive and flexural strength are comparable with that of control sample. Zyranov et.al [6] investigated the possibility of low carbon ferrochrome slag into a dry slag and further recycling it into commercial product. Study concludes that strength of concrete under normal condition is less than the strength of concrete under steam curing as high temperature activates the process of slag hydration.

EXPERIMENTAL WORK

Characterization of ferrochrome slag and other concrete making materials was done as per relevant standards. Ferrochrome slag (both water cooled and air cooled) were evaluated for different physical characteristics as per IS: 2386 [7] (as applicable for manufactured sand and manufactured coarse aggregates). Both water and air cooled ferrochrome slag samples were subjected to chemical analysis for evaluation of loss on Ignition, major constituents (Cr_2O_3 , Al_2O_3 , Fe_2O_3 , CaO , SiO_2 , reactive silica and MgO) and minor constituents (Na_2O , K_2O , SO_3 , Cl^- , TiO_2 etc.). Total alkali content as Na_2O equivalent, total sulphate content as SO_2 , acid and water soluble chloride content and total sulphur as S. Elemental analysis and leaching study as per TCLP procedure for heavy metals was carried out for both ferrochrome slag samples. Other concrete making materials such as cement, natural aggregate and admixture were meeting the criteria as mentioned in relevant Indian Standards.

Two control concrete mixes were prepared using OPC along with 100% natural fine aggregates and 100% natural coarse aggregates at two different water-cement ratios of 0.65 and 0.40. Then, mixes were prepared by replacing natural fine aggregates with water cooled ferrochrome slag at 30, 60 and 100% along with 100% natural coarse aggregates at both the water cement ratios. Further, mixes were prepared by replacing natural coarse aggregate with air cooled ferrochrome slag at 30, 60 and 100% along with 100% natural fine aggregates at both the water cement ratios. Thus, a total number of 14 concrete mixes were prepared. All the mixes were studied for fresh properties of concrete such as workability (in terms of slump at 30, 60, 90 and 120 minutes) and air content of concrete as per IS: 1199 [8]. Mixes were also evaluated for compressive strength, flexural strength, split tensile strength, densities, drying shrinkage of concrete and modulus of elasticity of concrete at various ages.

STUDY ON FUNDAMENTAL PROPERTIES OF AIR COOLED FERROCHROME SLAG AND WATER COOLED FERROCHROME SLAG

Physical Characterization of Ferrochrome Slag

Sieve analysis of Water Cooled Ferrochrome slag ferrochrome slag ($< 4.75\text{mm}$), Air Cooled Ferrochrome slag (20 mm and 40 mm) samples was carried out as per IS 383:2016 [9] and the results are given in Table 1.

Table 1. Sieve analysis of ferrochrome slag samples

IS Sieve Size	Water Cooled Ferrochrome slag ($< 4.75\text{mm}$) % Passing	Air Cooled Ferrochrome slag, 20mm, % Passing	Air Cooled Ferrochrome slag, 10mm, % Passing
40mm	-	100	-
20mm	-	100	-
12.5	-	-	100
10 mm	100	28	100
4.75 mm	100	1	23
2.36 mm	98	-	5



1.18 mm	79	-	-
600 μm	46	-	-
300 μm	28	-	-
150 μm	15	-	-

The results of physical characterization of Ferrochrome slag samples are given in **Table 2** below.

Table 2. Results of physical characterization of Ferrochrome slag samples

Test Carried out	Water Cooled Ferrochrome slag (<4.75mm)	Air Cooled Ferrochrome slag, 20mm	Air Cooled Ferrochrome slag, 10mm
Specific gravity	2.87	2.99	2.98
Water absorption, %	0.74	0.33	0.31
Material finer than 75 μm % (wet sieving)	3.97	0.10	0.1
Soundness, MgSO_4 %	2.68	1.28	1.91
Organic impurities %	Nil	Nil	Nil
Clay Lumps %	Nil	Nil	Nil
Total deleterious material, % (excluding coal & lignite)	Nil	Nil	Nil
Loose Bulk Density, Kg/lit	1.09	1.61	1.43
Compacted Bulk Density, Kg/lit	1.21	1.71	1.56
Accelerated Mortar Bar, ASTM C1260, %	0.02	0.09	0.09
Abrasion value	-	14	-
Crushing Value	-	19	-
Impact Value	-	15	-

The physical properties of water cooled and air cooled ferrochrome slag meets the various requirements of IS: 383-2016. The specific gravity of slag samples was observed to be higher than that of natural aggregates. Water absorption and material finer than 75 μm were found to be comparable with natural aggregates. The water cooled ferrochrome slag lies in zone 2 of grading as per IS: 383-2016. The low values of abrasion, crushing and impact reflects the stronger nature of air cooled ferrochrome slag.

Chemical Characterization of Ferrochrome slag samples.

Both type of ferrochrome slag samples (water cooled and air cooled) were characterized for several chemical parameters. The results of chemical characterization of ferrochrome slag sample are tabulated in **Table 3** below.

Table 3. Results of chemical characterization of ferrochrome slag samples

Test Carried out	Water Cooled Ferrochrome slag (<4.75mm), %	Air Cooled Ferrochrome slag, (>4.75mm), %
Gain on Ignition, %	+1.51	+0.93
Silica	25.73	31.54
Iron Oxide	3.59	5.23
Alumina	35.3	28.67
Calcium Oxide	2.8	3.68
Magnesium Oxide	22.36	19.22

Sulphuric Anhydride	0.12	0.06
Chloride	0.015	0.01
Alkalies Equivalent as Na ₂ O	0.23	0.55
Titanium Dioxide	1.06	1.44
Reactive silica	21.49	25.24
Water soluble chloride	0.001	0.0018
Total Sulphur	0.25	0.44

The prescribed limit of total alkali content is given as 0.3%. The observed value of alkalis equivalent is 0.23% in case of water cooled ferrochrome slag which lies within the limit specified. However, the value obtained in case of air cooled ferrochrome slag is higher than the prescribed limit. The observed values of chloride content, calcium oxide, iron oxide and total Sulphur are well within the limits.

Elemental Analysis of Ferrochrome slag samples.

Both water cooled and air cooled ferrochrome slag samples were subjected to elemental analysis. The results of elemental analysis of ferrochrome slag samples are tabulated in **Table 4** below.

Table 4. Results of elemental analysis of ferrochrome slag samples

Element	Water Cooled Ferrochrome slag (<4.75mm), %	Air Cooled Ferrochrome slag, (>4.75mm), %
Barium	0.027	0.098
Beryllium	0.001	0.0005
Bismuth	Below detection Limit	Below detection Limit
Cadmium	0.002	0.001
Cobalt	0.012	0.012
Chromium	8	8.86
Copper	0.175	0.42
Gallium	Below Detection Limit	Below Detection Limit
Manganese	0.219	0.185
Molybdenum	0.011	0.008
Nickel	0.032	0.04
Lead	0.013	0.008
Selenium	Below Detection Limit	Below Detection Limit
Strontium	0.088	0.008
Tellurium	Below Detection Limit	Below Detection Limit
Thallium	Below Detection Limit	Below Detection Limit
Zinc	0.029	0.061
Vanadium	0.012	0.013
Chromium, Cr ⁺³	-	-
Chromium, Cr ⁺⁶	0.0002	0.0003

Table 11 of IS: 383-2016 quotes limits for environmental safety and quality standards for using iron, steel and copper slag aggregates. The values obtained for cadmium, lead, selenium and hexavalent chromium are within limits.

Leaching study for heavy metals on ferrochrome slag samples

Leaching study on air and water cooled ferrochrome slag has been conducted as per TCLP procedure. The results of concentration

of heavy metals in slag sample have been tabulated in **Table 5** below.

Table 5. Results of leaching study on ferrochrome slag and natural aggregates

Sl No.	Constituents	Water cooled FS Slag FA	Air-cooled FS Slag CA	Limits as per TCLP procedure
1	Chromium	0.486	0.727	5
2	Copper	0.005	*BDL	25
3	Manganese	1.298	1.215	10
4	Nickel	0.831	0.774	20
5	Lead	0.020	BDL	5
6	Zinc	0.208	0.209	250
7	Iron	45.37	53.93	-
8	Titanium	0.012	0.011	-

As per the leachable concentration limits given in ministry of environment [10], forest and climate change guidelines, the observed values are lower than the prescribed limits.

STUDIES ON FRESH, HARDENED AND DURABILITY PROPERTIES OF CONCRETE MIXES

Concrete mixes containing water cooled Ferrochrome slag as replacement of Natural fine aggregate

Two control concrete mixes (M4 and M0) were prepared using OPC along with 100% natural fine aggregates and 100% natural coarse aggregates at two water-cement ratios of 0.65 and 0.40. Then, mixes were prepared by replacing natural fine aggregate with water cooled ferrochrome slag at 30, 60 and 100% along with 100% natural coarse aggregates at both the water cement ratios

Therefore, a total of 8 mix designs (2no. of control mixes + 3 x 2 = 6 number of mixes containing water cooled ferrochrome slag as fine aggregate) were carried. The concrete mixes were designed for initial slump value of around 150mm. Mix design details of concrete mixes are tabulated in **Table 6**.

Table 6. Concrete mix design details of mixes containing water cooled Ferrochrome slag as replacement of Natural fine aggregate

S. No.	Mix	Ferrochrome slag as fine Aggregates (%)	Cement (Kg/m ³)	Water (Kg/m ³)	Ferrochrome slag as fine Aggregates (%)	Natural Fine aggregate(Kg/m ³)	Natural Coarse Aggregate (10 mm) (Kg/m ³)	Natural Coarse Aggregate (20 mm) (Kg/m ³)	Admix (%)
1	M4	0	300	195	0	874	414	623	0
2	M1	30	300	195	287	611	413	622	0.2
3	M2	60	300	195	573	349	413	621	0.7
4	M3	100	300	195	957	0	413	622	0.2
5	M0	0	425	170	0	773	439	661	0.2
6	M5	30	425	170	254	541	439	661	0.3
7	M6	60	425	170	507	309	439	660	0.5
8	M7	100	425	170	847	0	439	661	0.2

Fresh Concrete Properties

Fresh concrete properties such as workability (in terms of slump at 0 minutes, 30 minutes, 60 minutes and 120 minutes after preparation of mix) and air content were evaluated for all the 8 mixes and test results are given in **Table 7**.

Table 7. Fresh Concrete Properties of mixes containing water cooled Ferrochrome slag as replacement of Natural fine aggregate

S. No	W/c Ratio	Mix ID	Ferrochrome slag as fine Aggregates (%)	Natural Sand	Workability of concrete (mm)				Air Content, %	Remarks
					0 Min	30 Min	60 Min	120 Min		
1	0.65	M4	0	100	145	135	125	100	1.8	Homogeneous mix
2	0.65	M1	30	70	150	120	100	55	1.9	
3	0.65	M2	60	40	160	110	85	30	2	
4	0.65	M3	100	0	140	120	90	40	2.1	Segregation and bleeding
5	0.4	M0	0	100	150	140	120	90	1.7	Homogeneous mix
6	0.4	M5	30	70	150	110	80	40	1.9	
7	0.4	M6	60	40	145	100	60	30	2.1	
8	0.4	M7	100	0	150	110	80	40	2.4	Segregation and bleeding

Concrete mixes containing Ferrochrome slag showed significantly higher slump loss after 60 and 120 minutes in comparison to the control concrete mixes. Air content of all 8 mixes were similar and comparable (around 2%). It was observed that when replacement of natural coarse aggregate with air cooled ferrochrome slag goes beyond 60%, mixes showed signs of segregation and bleeding due to high specific gravity of ferrochrome slag.

Hardened Concrete Properties

Hardened concrete properties were evaluated for the eight concrete mixes. Compressive strength test was conducted on concrete cubes (size 150 mm) as per IS: 516 [11]. Flexural strength test was conducted on concrete beam (size 500mm x 100mm x 100mm) as per IS: 516. Split strength test and Modulus of Elasticity were conducted on concrete cylinder (150mm diameter and 300mm height) as per IS:5816 [12] and IS:516 respectively. Drying shrinkage test was conducted on concrete beam (75 x 75 x 300 mm) as per IS:1199. The test results are in **Table 8**.

Table 8. Hardened Concrete Properties containing of mixes containing water cooled Ferrochrome slag as replacement of Natural fine aggregate

W/c	Mix ID	Ferrochrome slag as fine Aggregates (%)	Compressive Strength, MPa				Flex Strength, MPa		Split Tensile Strength, MPa	Dry Density Kg/m ³	Drying Shrinkage	MOE (N/mm ²)
			1 Day	3 Day	7 Day	28 Day	7 Day	28 Day				
0.65	M4	0	4.54	12.5	18.1	26.22	4.07	5.05	2.42	2450	0.0171	28204
0.65	M1	30	6.33	14.5	20.2	30.14	4.4	5.3	2.67	2470	0.0168	30651
0.65	M2	60	7.38	16.5	22.95	38.05	5.07	5.37	2.72	2550	0.0164	32982
0.65	M3	100	8.67	18.8	24.46	41.89	5.45	6.01	3.21	2502	0.0179	34876
0.4	M0	0	15.95	32	41.86	49.79	6.4	8.07	4.51	2478	0.0191	37144
0.4	M5	30	19.05	27.2	43.01	46.75	6.37	9.77	4.75	2494	0.018	38013
0.4	M6	60	20.84	29.3	42.89	53.08	7.17	10.3	5.1	2520	0.0175	38885
0.4	M7	100	23.76	27.8	44.78	56.89	8.5	11.4	5.26	2560	0.0173	40016

Compressive, flexural and split tensile strength at age of 28 days for experimental mixes (containing water cooled ferrochrome slag as replacement of fine aggregates) at both w/c were found to be either higher or comparable to their control mix. Due to higher specific gravity of ferrochrome slag, dry density of the concrete mixes containing water cooled ferrochrome slag were higher than control mixes. The drying shrinkage values for all the concrete mixes were found satisfactory and comparable with their corresponding control mixes. Modulus of Elasticity (MOE) of the concrete mixes containing ferrochrome slag as



replacement of natural fine aggregates were found to be either higher or comparable to corresponding control mixes

Concrete mixes containing air cooled Ferrochrome slag as replacement of Natural coarse aggregate

Along with two control concrete mixes (M4 and M0), mixes were prepared by replacing natural coarse with air cooled ferrochrome slag at 30, 60 and 100% along with 100% natural fine aggregates at both the water cement. Thus, six experimental mixes (containing air cooled Ferrochrome slag) were prepared along with two control mixes. All the concrete mixes were designed for initial slump value of around 150mm. Mix design details of concrete mixes are tabulated in **Table 9**.

Table 9. Concrete mix design details of mixes containing air cooled Ferrochrome slag as replacement of Natural coarse aggregate

Mix	Ferrochrome slag as coarse Aggregates (%)	Cement (Kg/m ³)	Water Kg/m ³	Natural Fine aggregate (Kg/m ³)	Ferrochrome slag as coarse Aggregate (10mm) (Kg/m ³)	Ferrochrome slag as coarse Aggregate (20mm) (Kg/m ³)	Natural Coarse Aggregate (10 mm) (Kg/m ³)	Natural Coarse Aggregate (20 mm) (Kg/m ³)	Admix (%)
M4	0	300	195	874	0	0	414	623	0
M8	30	300	195	863	116	217	286	431	0
M9	60	300	195	863	233	433	164	246	0
M10	100	300	195	862	387	721	0	0	0.6
M0	0	425	170	773	0	0	439	661	0.2
M11	30	425	170	759	123	229	302	454	0.3
M12	60	425	170	759	245	457	172	260	0.3
M13	100	425	170	759	409	762	0	0	0.3

Fresh Concrete Properties

Fresh concrete properties such as workability and air content were evaluated for all the 8 mixes. Test results are given in **Table 10**.

Table 10. Fresh Concrete Properties of mixes containing air cooled Ferrochrome slag as replacement of Natural coarse aggregate

S. No	W/c Ratio	Mix ID	Ferrochrome slag as fine Aggregates (%)	Natural coarse aggregates	Workability of concrete (mm)				Air Content, %	Remarks
					0 Min	30 Min	60 Min	120 Min		
1	0.65	M4	0	100	145	135	125	100	1.8	Homogeneous mix
2	0.65	M8	30	70	150	140	120	80	1.7	
3	0.65	M9	60	40	150	130	110	50	1.8	
4	0.65	M10	100	0	150	120	70	50	2	Segregation and bleeding
5	0.40	M0	0	100	150	140	120	90	1.7	Homogeneous mix
6	0.4	M11	30	70	150	135	110	70	1.6	
7	0.4	M12	60	40	140	125	90	40	1.9	
8	0.4	M13	100	0	145	90	60	50	2.1	Segregation and bleeding

Concrete mixes containing air cooled ferrochrome slag showed significantly higher slump loss after 60 and 120 minutes in comparison to the control concrete mixes. Air content of all 8 mixes were similar and comparable (around 2%). It was observed that when replacement of natural coarse aggregate with air cooled ferrochrome slag goes beyond 60%, mixes showed signs of segregation and bleeding due to high specific gravity of ferrochrome slag.

Hardened Concrete Properties

Hardened concrete properties were evaluated for all the six concrete mixes (M8 to M13) along with the control mixes (M4 and M0). Specimen size, test method and age of testing for all the tests were kept same as discussed in 4.1.2. Test results have been tabulated in **Table 11**.

Table 11. Hardened Concrete Properties containing of mixes containing air cooled Ferrochrome slag as replacement of Natural coarse aggregate

W/c	Mix ID	Ferrochrome slag as fine Aggregates (%)	Compressive Strength, MPa				Flex Strength, MPa		Split Tensile Strength, MPa	Dry Density Kg/m ³	Drying Shrinkage	MOE (N/mm ²)
			1 Day	3 Day	7 Day	28 Day	7 Day	28 Day				
0.65	M4	0	4.54	12.5	18.1	26.22	4.07	5.05	2.42	2450	0.0171	28204
0.65	M8	30	4.91	16.7	19.11	27.96	4	4.83	2.41	2470	0.0175	28508
0.65	M9	60	3.61	9.93	16.01	24.69	3.87	4.73	2.17	2460	0.0159	26588
0.65	M10	100	6.57	16.4	21.68	28.55	3.89	4.97	2.54	2580	0.0170	28486
0.4	M0	0	15.95	32	41.86	49.79	6.4	8.07	4.51	2478	0.0191	37144
0.4	M11	30	14.42	30.9	33.04	47.44	5.67	7.03	3.46	2490	0.0174	34140
0.4	M12	60	9.58	29.6	38.19	45.44	5.87	7.7	3.57	2515	0.0171	34395
0.4	M13	100	11.92	29.9	37.18	45.39	4.73	6.93	3.87	2560	0.0167	33854

Compressive, flexural and split tensile strength at age of 28 days for experimental mixes (containing air cooled ferrochrome slag as replacement of coarse aggregates) at both w/c were found to be similar and comparable to their control mix. Due to higher specific gravity of ferrochrome slag, dry density of the concrete mixes containing air cooled ferrochrome slag were higher than control mixes. The drying shrinkage values for all the concrete mixes were found satisfactory and comparable with their corresponding control mixes. Modulus of Elasticity (MOE) of the concrete mixes containing ferrochrome slag as replacement of natural coarse aggregates were found to be similar and comparable to corresponding control mixes.

Leaching Studies on Selected Concrete Mixes

Leaching study was also conducted on few selected concrete samples made with replacement of natural aggregates with corresponding ferrochrome slag aggregates, as per Toxicity Characteristic Leaching Procedure (TCLP) to detect the presence of different heavy metals constituents. The results of concentration of heavy metals ions leached out from concrete samples are given in **Table 12**.

Table 12. Results of Leaching study on concrete samples

SI No.	Constituents	M0	M1	M4	M5	M6	Limits as per TCLP procedure
1	Chromium (Cr)	0.010	0.119	0.1341	0.169	0.187	5
2	Copper (Cu)	0.006	0.047	0.009	0.12	0.007	25
3	Manganese (Mn)	0.002	0.025	0.002	0.002	0.002	10
4	Nickel (Ni)	BDL	0.023	0.013	0.007	BDL	20
5	Lead (Pb)	BDL	BDL	BDL	BDL	BDL	5
6	Zinc (Zn)	0.035	0.053	0.039	0.028	0.034	250
7	(Fe) Iron	0.048	0.032	BDL	0.010	0.001	-
8	Titanium (Ti)	0.003	0.92	0.054	0.028	0.053	-

As per the leachable concentration limits given by ministry of environment, forest and climate change guidelines, the observed values of heavy metal ions are lower than the prescribed limits.



CONCLUSIONS

Based on the results and observations of above mentioned studies following conclusions can be drawn:

- a) Physical properties of water and air cooled ferrochrome slag meets the various requirements of IS: 383-2016. Specific gravity of slag samples was observed to be higher than that of natural aggregates. Water absorption and material finer than 75 μm were found to be comparable with natural aggregates. The low values of abrasion, crushing and impact reflects the stronger nature of air cooled ferrochrome slag.
- b) The results of elemental analysis of ferrochrome slag samples showed that concentrations of elements are within limits.
- c) Concrete mixes were prepared at two w/c ratios by replacing natural fine aggregates with water cooled ferrochrome slag and natural coarse aggregates with air cooled ferrochrome slag. Concrete mixes containing Ferrochrome slag showed significantly higher slump loss after 60 and 120 minutes in comparison to the control mixes. It was observed that when replacement of natural aggregates with ferrochrome slag goes beyond 60%, mixes showed signs of segregation and bleeding due to high specific gravity of ferrochrome slag. Hardened properties of concrete mixes containing ferrochrome slag were found to be higher or comparable to their corresponding control mixes at the age of 28 days.
- d) Leaching study was conducted on water and air cooled Ferrochrome slag as per Toxicity Characteristic Leaching Procedure (TCLP) to detect the presence of different heavy metals constituents such as Cr, Fe, Zn, Cu, Mn, Ni, Pb and Ti. The observed values of heavy metal ions are lower than the prescribed limits. Leaching study was also conducted on few selected concrete samples made with replacement of natural aggregates with corresponding ferrochrome slag aggregates and the observed values of heavy metal ions are lower than the prescribed limits.

Based on the above conclusions, following recommendations are being made:

Water cooled Ferrochrome slag can be used as replacement of natural fine aggregate up to 60% by weight along with 100 % with natural coarse aggregates for making concrete. Air cooled Ferrochrome slag can be used as replacement of natural coarse aggregate up to 60% by weight along 100 % with natural fine aggregates for making concrete.

REFERENCES

1. Nilamadhabha Sahu, Arijit Biswas & Gajanan U Kapure (2016). "A short review on utilization of ferrochromium slag." Mineral Processing and Extractive Metallurgy Review.
2. B.B.Lind, A.M. Fallman & L.B. Larsson (2001). "Environmental impact of ferrochrome slag in road construction." International Conference on the Science and Engineering of Recycling for Environmental Protection
3. S. Al-Jabri & Khalifa. (2018). "Research on the use of Ferro-Chrome slag in civil engineering applications." MATEC Web of Conferences
4. C.R. Panda, K. K. Mishra, C.R. Panda, B.D. Nayak, B.B. Nayak (2013). "Environmental and technical assessment of ferrochrome slag as concrete aggregate material." Construction and Building Materials.
5. S. R. Sathwik, J. Sanjith & G. N. Sudhakar (2016). "Development of high strength concrete using ferrochrome slag aggregate as replacement to coarse aggregate." American Journal of Engineering Research
6. F. AZyranov, A.B. Bukreev & O.O. Zyranova, (2016). "Heavy Concrete on Cement with slag of low carbon ferrochrome." Electric Journal of Structural Engineering
7. IS: 2386 - 1963 (Reaffirmed 2002), Methods of Test for Aggregates for Concrete
8. IS: 1199 - 1959 (Reaffirmed 2004) Methods of Sampling and Analysis of Concrete
9. IS: 383-2016 Coarse and Fine Aggregate for Concrete – Specification (Third Revision)
10. Government of India, Ministry of Environment, Forest and Climate Change, published in the gazette of India, extraordinary, part II, section 3, sub-section (i)
11. IS: 516 - 1959 (Reaffirmed 2004), Methods of test of strength of concrete
12. IS: 5816 - 1999 (Reaffirmed 2004), Splitting Tensile Strength of Concrete - Method of Test



Artificial Intelligence Techniques to Predict the Compressive Strength of Sustainable Eco-friendly Strain-hardening Concrete Composites

K K Yaswanth, J Revathy, P Gajalakshmi

Department of Civil Engineering, B S Abdur Rahman Crescent Institute of Science & Technology, Chennai, Tamil Nadu

✉ yaswanthkkphd@gmail.com

ABSTRACT

A novel building material that breaks the frailty criteria of the brittle nature of concrete, comprises of eco-friendly sustainable materials as ingredients is called as “Engineered Geopolymer Composites (EGC).” In the scenario of the material development stage of EGC, researchers need to focus on the application of various sustainable materials that are locally available, in the production of EGC, without compromising the mechanical performance. A prediction tool, that helps to forecast the performance of the designed material with the mix-design criteria, would help the researchers for more advanced research; and practicing engineers to decide upon structural applications in the field. ANN and ANFIS have been used in this study to develop the predictive models to estimate the compressive strength performance of EGC. Totally 110 data sets have been prepared from EGC material researches with 6 mix-design influences as inputs, to facilitate the training and validation process of the predictive models. The validated results are analyzed. The research study reveals that the ANN model has predicted the compressive strength of EGC with the accuracy of 78% with RMSE 3.3 whereas ANFIS showed a prediction of about 86% accuracy with RMSE 3.03.

Keywords : ANFIS; ANN; Engineered geopolymer Composites; Flexible concrete; Prediction; Strain hardening composites.

INTRODUCTION

Interdisciplinary research has become popular in almost all kinds of research fields. Especially the usage of electronics and Information technology in accounting, material design, machine designs, labour managements, navigation etc., The most notable thing in the field of the construction industry is the application of artificial intelligence in concrete material design. The development of predictive models with various soft-computing techniques (SCT) or machine learning models have helped various researchers and practicing engineers to prejudge the outcome of design or research progress without actually experimenting it. Significant SCTs include Neural Networks, Fuzzy logic, Genetic algorithm etc., that facilitated to predict the mix-design, strength and workability parameters in various kinds of special concrete composites.

Artificial Neural Networks (ANN) and Adaptive Neuro-Fuzzy Inference System (ANFIS) are the most popular tools among AI, particularly in the application of concrete technology from the early 2000s. These are based on real-life concepts, generated artificially, to solve problems on optimization, prediction, forecast etc. ANN works on the principle of interconnected neurons in the human brain. ANN network consists of an input layer, hidden layer and an output layer, interconnected with neurons. Speaking mathematically, starting with an input variable across the hidden layer bridged with ‘weights’ towards output variable forms an empirical equation. During the training process, the weights upon the variables keep on changing continuously until a suitable equation with maximum accuracy will be obtained. With that established equation, prediction can be done. ANFIS is a combination of ANN and Fuzzy logic (FL). FL works on the principle of ‘IF-THEN’ rule sets. FL has various types and numbers of membership functions (MF), based on which it forms different ‘rule sets’, e.g., “IF input-1 is very low, input-2 is medium and input-3 is high; THEN the output is very low”

Thus, based on the number of inputs; the number of MF and the type of MF, the ANFIS system generates large ‘rule sets’ from which the output values will be predicted.

Researchers focus on two major drawbacks in cement concrete in terms of environmental and material strength aspects. Usage of cement binder in concrete affects the environmental conditions near the manufacturing unit of cement, as it releases huge greenhouse gases like carbon-di-oxide into the atmosphere, when raw materials are burnt at very high temperature in the clinker. In ‘strength of materials’ point of view, concrete is weak upon tensile force due to its brittle nature, because of which the deformation in concrete occurs instantly thereby giving least warning to the occupancies.

A recent novel building material that is tailored to overcoming aforesaid drawbacks of the conventional concrete is popularly known as ‘Engineered Geopolymer Composites’ (EGC). EGC is the hybrid combination of Engineered Cementitious Composites (ECC) and Geopolymer Concrete (GPC). ECC is a kind of ultra-high ductile fiber reinforced cementitious composites that uses a special synthetic fiber called Polyvinyl alcohol fiber (PVA) that enhances the ductility of the material. The material ingredients of ECC are tailored in such a way that the fiber bridging capacity is greater than the matrix toughness post-first crack, thereafter leads to the formation of multiple cracks (micrometer crack width) thereby enhances strain-hardening criteria. Because of this peculiar property, the concrete composite attains flexible nature, thus it is also known as “Flexible concrete”.

Replacing the cement in ECC with Geopolymer binder which is 100% eco-friendly sustainable materials, is called as EGC. Thus, EGC, which comprises of 100% eco-friendly material ingredients that overcome the brittle failure of conventional concrete, serving both environmental and technical aspects. The recent researches on ECC and EGC material behaviour have been summarized in the literature review section. This paper attempts to apply artificial intelligence tool(s) that would facilitate the researchers around the world for advanced EGC material research.

Literature Review

Material research on EGC has started a decade back. Researches tried to develop EGC material with various industrial by-products in mixed proportions. Kan et al [1] have used Metakaolin and Flyash in mixed proportions and obtained the maximum strain capacity of 6.8%. 100% Metakaolin was used by Ekatpuri et al [2] with varying volume fractions of PVA fiber and it reveals that 0.6% Volume fraction was optimum. Ling et al [3] used slag along with ash i.e., Ground Granulated Blast furnace Slag (GGBS) and Flyash in mixed proportions and the optimum was 80% flyash with 20% GGBS. Some notable variations on PVA fibers and fine aggregate have also been carried out by the researchers which include lightweight fillers like expanded perlites [4]; and some micro-fibers like polypropylene fibers are added along with PVA fibers [5].

Initially, in the early 2000s, ANN has been used to predict the compressive strength of concrete [6] and prejudge the workability by estimating the slump of concrete. [7]. Later, keeping the strength and/or workability as inputs, researchers have analyzed the mix-design contents, thereby engineers can alter the material proportions to obtain the desired strength. Generally, the literature reveals that ANN gives maximum accuracy in prediction to the range 80-95%. Similarly, the ANFIS tool has also been used in similar applications as that of ANN. Sadrmomtazi et al [8] have predicted the compressive strength of lightweight concrete using ANN and ANFIS models it is concluded that bell-shapes membership function has produced the accuracy level of 98%. Vakhshouri et al [9] have estimated the compressive strength of high strength self-compacting concrete and they reveal that ANFIS established a strong correlation between mix-factors and strength.

Need for Study

The main fact to be analysed before involving the usage of GPC in construction is the ‘local availability’ of concrete ingredients. GPC uses any kind of alumino-silicate based industrial by-products like Flyash, GGBS, Metakaolin, Silica fume etc., as a binding material; where each material has its peculiar merits and demerits on mechanical properties of the GPC composites. For instance, Flyash based GPC is known best for its better mechanical and workability performances, whereas GGBS based GPC gives excellent strength parameters. In such a case, practising engineers might need to have a preliminary decision making upon the usage of those locally available alumino-silicate material(s) that suits for the mix-design purpose, structural applications and site conditions. For any mix-design process of concrete composites, compressive strength is the prior criteria that need to be satisfied. Predicting the minimum compressive strength that can be obtained, with the available ingredients and the predefined mix design criteria, would help the practising engineers to make decisions on using those locally available concreting ingredients in mix-design of GPC. In this paper, based on the application of AI tools, suitable predictive models are needed to be developed with higher accuracy which would enhance the above-mentioned decision-making criteria to the practising engineers in the field. It also facilitates various researchers on material EGC to select the concreting ingredients for advanced materials research on EGC, thereby reducing the cost and time for experimental procedures.

Preparation of Database & Development of Predictive models

Based on the literature survey, it is clear that, among the SCTs, ANN and ANFIS perform greater in predicting the compressive strength of concrete composites particularly when the mix-design influencing parameters are lesser. This paper tries to attempt the usage of AI tools – ANN and ANFIS in developing the predictive models to anticipate the magnitude of compressive strength of the material EGC.

1) Database: Initial database is required for training the predictive models and thereby validating the models to check the accuracy of prediction. The database is collected from various research publications around the world. These researches are based on PVA fibre-reinforced GPC with binding materials as Class F flyash and/or Metakaolin based Geopolymer paste (no

fine aggregate contents are involved in those material research). Sodium based alkali activators with the combination of sodium hydroxide and sodium silicate has been used in those literatures. The specimens are treated under elevated temperature for a few hours before ambient curing (for a certain number of days) before testing.

Totally, 110 data set has been prepared from various literatures [1-5,10-12] with aforesaid testing conditions, for training and validation of the predictive models. Among which 90 data set has been used for training the models and the subset of the 20 data set has been used for validating the models. To ensure the accuracy of prediction, the literatures have been selected in such a way that no additional parameters (includes additional binding materials other than flyash and metakaolin; additional admixtures or fine aggregate contents) have been included in the testing of the literatures. The mix-design factors which are selected as input parameters to the prediction, along with mean, standard deviation, maximum-minimum range is summarized in Table I. The input parameters mentioned in **Table 1** is described as follows, FFA - Class F flyash content (kg/m³), MK - Metakaolin content (kg/m³), PVA - volume fraction of PVA fiber in %, ACT- activator to binder ratio, CT - temperature of heat curing (°C), ACD - Ambient curing temperature duration in days; SD - standard deviation.

Table 1. Inputs for training and validation

Input Parameters	Training				Validation			
	Min	Max	Mean	SD	Min	Max	Mean	SD
FFA	0	1029	85.1	235	0	850	126	256
MK	0	890	761	312	0	890	702	362
PVA	0	3	0.7	0.7	0	2	0.8	0.7
ACT	0.27	0.89	0.8	0.2	0.27	0.89	0.8	0.2
CT	25	80	53.9	19.9	25	80	50.5	22.7
ACD	3	56	19.8	16.7	3	56	22.6	19.2

2) Creating ANN & ANFIS models: ANN and ANFIS predictive models have been developed using MATLAB application software. The functions involved in MATLAB for creating and analyzing the ANN and ANFIS models are 'nntool' and 'anfisedit' respectively. For creating ANN & ANFIS models, few preliminary design-data are needed to be specified, that suits best intended for the purpose of creating the models. For instance, specifying the number of hidden neurons, type of ANN network, no. of epochs etc., are needed to be specified initially. For creating ANN models, the following design-data parameters are specified, (considered based on literatures) such as Levenberg-Marquardt (trainlm) type ANN network, one layer of hidden neurons, Feed-forward Back Propagation type, Number of epochs-10000, Max fail-10000. A tedious task here is to select the number of hidden neurons. The number of hidden neurons in the hidden layer is always influenced by the number of input parameters. Since the number of input parameters is 6, the number of hidden neurons is varied from 4 – 10 and the best number has been identified based on trial and error method. Here, regression function during the training process has been used to analyze the ANN models and the best ANN model has been chosen as ANN-5 (which indicates ANN network with 5 hidden neurons in the hidden layer) which is also represented as ANN [6:5:1] (no of inputs: no. of hidden neurons: no of outputs). The software randomly takes 70% of the training dataset for self-training, 15% of the data for self-testing and 15% of the data for self-validation. The overall regression and best validation performance of the ANN-5 model during the training process have been illustrated in **Fig. 1**. After this training process, the outputs for validation has been simulated.

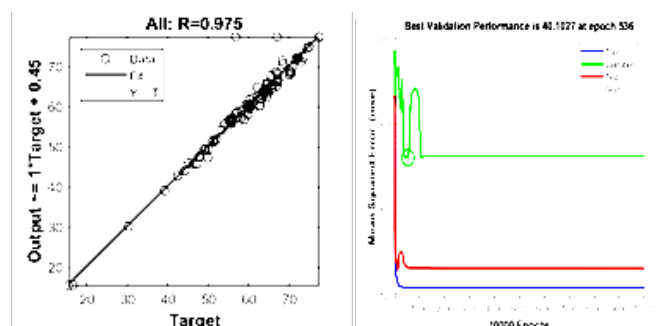


Fig. 1. Regression during training process and Best validation performance

Similarly, while creating the ANFIS model in MATLAB the following design-data are specified which includes, 'Grid partition' type of FIS, 3 numbers of MF, 'Triangular' type of MF, 'hybrid' optimization method and 10 number of epochs. The accuracy of the progress can be viewed during the training process through the chart shown in **Fig. 2**. Blue circles indicate the actual values and Red star indicates the predicted values, overlapping of those two indicates the greater accuracy in the training process of ANFIS. Validation outputs can then be obtained using 'evalfis' function.

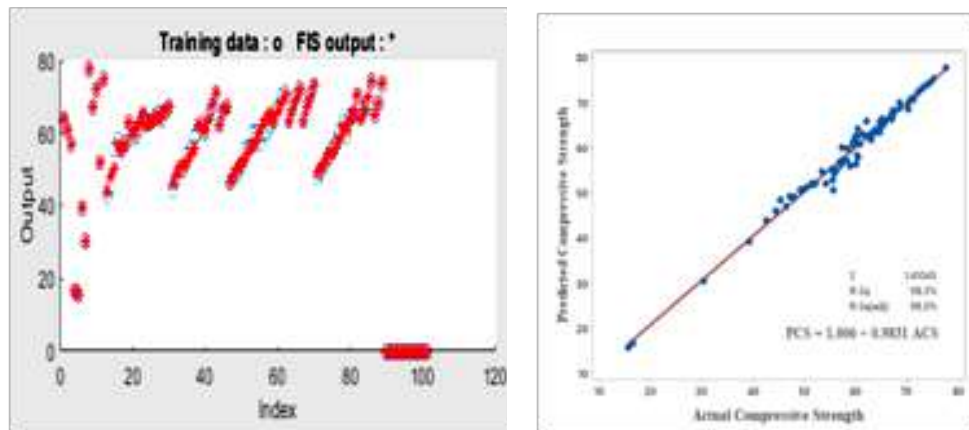


Fig. 2. Accuracy plot & R2 during training of ANFIS

RESULTS AND DISCUSSIONS

1) Validation of ANN and ANFIS: **Table 2** gives the predicted output results of compressive strength of Engineered geopolymer composites with ANN and ANFIS tools, compared to the actual compressive strength values from the literature, with the results of the coefficient of determination, Magnitude of residue and the Root mean squared error.

As it is clear from table II that, ANN and ANFIS had shown excellent potential in predicting the compressive strength of EGC. The overall accuracy obtained can be inferred from the co-efficient of determination (R2) value. **Fig. 3** shows the plot between the actual compressive strength and the predicted compressive strength of ANN and ANFIS models with the regression line of fit and co-efficient of determination during the validation process. It is observed that the ANN model has shown 97% accuracy in the training process (**Fig. 2**) and 78% accuracy in prediction during validation (**Fig. 3**).

Table 2. ANN and ANFIS predicted outputs of validation with R2 and RMSE

Ref	ACS	ANN		ANFIS	
		PCS	Error	PCS	Error
[10]	73.00	64.13	8.87	78.63	-5.63
[11]	41.00	34.84	6.16	39.20	1.80
[1]	56.80	62.78	-5.98	60.70	-3.90
[12]	67.80	68.52	-0.72	66.93	0.87
[12]	68.40	69.84	-1.44	69.36	-0.96
[12]	74.40	71.09	3.31	73.16	1.24
[12]	64.70	68.64	-3.94	63.05	1.65
[12]	67.80	69.18	-1.38	65.44	2.36
[12]	60.00	68.20	-8.20	55.67	4.33
[12]	60.80	61.04	-0.24	59.14	1.66
[12]	43.60	50.07	-6.47	45.80	-2.20
[12]	56.70	56.23	0.47	53.00	3.70
[12]	64.10	65.24	-1.14	64.84	-0.74

[12]	59.30	59.28	0.02	61.18	-1.88
[12]	47.30	54.23	-6.93	52.24	-4.94
[12]	54.80	51.31	3.49	48.40	6.40
[12]	60.20	59.01	1.19	55.29	4.91
[12]	55.40	56.33	-0.93	58.65	-3.25
[12]	70.70	68.62	2.08	65.90	4.80
	R ²	0.78		R ²	0.86
	RMSE	3.31		RMSE	3.01

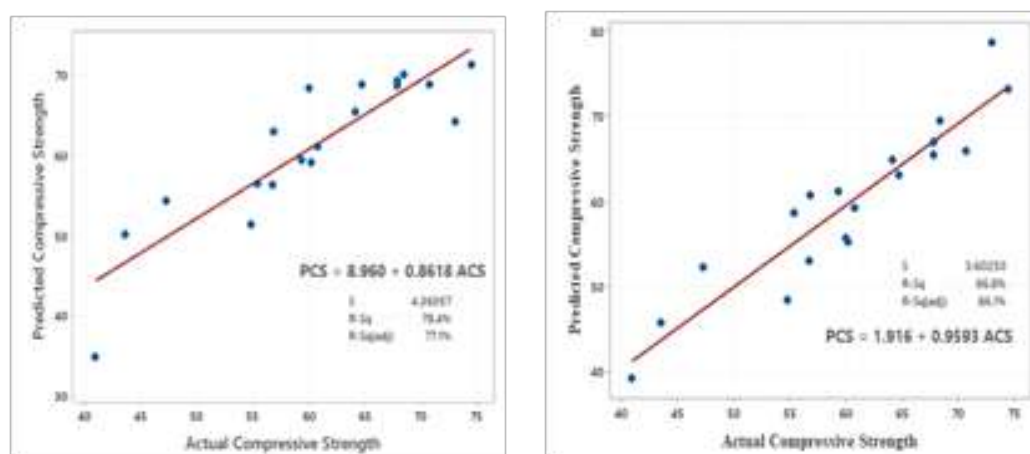


Fig. 3. Coefficient of determination of ANN and ANFIS models

The foremost thing to be considered during the prediction of compressive strength of concrete composites is the magnitude of residue between the actual and predicted values. During the mix-design process of concrete, it is mandatory to achieve the minimum compressive strength required, whereas the maximum strength achieved by the design is secondary. Thus, during the prediction process, the number of positive residues to be given prior importance than the number of negative errors. It is observed that 42% of the validation data set have shown positive errors, but it is also to be noted that the range of those positive error lies within 0 to 2, and the RMSE obtained is 3.31 which is phenomenal. The maximum positive error obtained from the ANN model validation is 8.8, which is quite not acceptable for sensitive parameters like compressive strength of EGC. The overall accuracy obtained during the validation of the ANN model is 78%, which is comparatively less accurate than ANN predictive models of other special concrete of estimating the compressive strength. Generally, there are no restrictions on the number of input parameters for ANN models, therefore all the mix-design influences affecting the compressive strength can be taken into account as inputs and it is also to be noted that, more the number of inputs and database more will be the accuracy of the prediction of ANN models.

ANFIS tool has also shown the excellent potential of predicting the compressive strength of EGC, since the RMSE has obtained as 3.01 i.e., the ANFIS tool has the ability to predict the compressive strength with the approximate error of ± 3 . **Fig. 3** shows the comparative plot between the actual compressive strength of the experimental results from the literatures and the predicted values from the ANFIS of validation data set by which the coefficient of determination R^2 value is computed. Here, the 'test data' represents the prediction of output with the input data that were used to train the ANFIS model (**Fig. 2**) whereas the 'validation data' represents the output predicted for the inputs from the validation data set (**Fig. 3**). Thus the 'test data' indicates the accuracy of the training process and the 'validation data' indicated validation accuracy of ANFIS model. The coefficient of determination values shows that with 90 training data set, the ANFIS tool can able to train itself to the accuracy of nearly 98% ($R^2 = 0.9831$). The trained ANFIS model can now be able to predict the compressive strength of the validation data set (19 data set) with the accuracy of about 86.4%. The magnitude of residues obtained within the range of 0 to 2 is about 57% and the maximum positive residue obtained is 6.4 which is comparatively acceptable. As far as the ANFIS tool prediction is concerned, the grid-partition type FIS accepts a limited number of input parameters and the prediction accuracy can be obtained around 90%.



CONCLUSIONS

N and ANFIS models have been created, trained and validated with the databases prepared from various literature. ANN [6:5:1] model and Grid-partition based FIS model has been used in this study and the following conclusions are made.

- The ANN model with one hidden layer with 5 number of hidden neurons was the best among other ANN models (with other hidden neurons) and the model has shown 78% accuracy in the validation, based on the coefficient of determination with RMSE 3.3.
- Grid-partition based ANFIS model has shown the accuracy of 86% based on R2 during the validation process with RMSE 3.03.
- With the limited number of input parameters (fewer mix influences), ANFIS can predict the compressive strength of EGC with greater accuracy, whereas, ANN can produce maximum accuracy when the number of input parameters are more with a large database.

REFERENCES

1. L. Kan, W. Wang, W. Liu, and M. Wu, "Development and characterization of fly ash based PVA fiber reinforced Engineered Geopolymer Composites incorporating metakaolin," *Cement and Concrete Composites*, vol. 108, p. 103521, Apr. 2020
2. J. J. Ekaputri, S. Junaedi, and Wijaya, "Effect of Curing Temperature and Fiber on Metakaolin-based Geopolymer," *Procedia Engineering*, vol. 171, pp. 572–583, 2017
3. Y. Ling, K. Wang, W. Li, G. Shi, and P. Lu, "Effect of slag on the mechanical properties and bond strength of fly ash-based engineered geopolymer composites," *Composites Part B: Engineering*, vol. 164, pp. 747–757, May 2019
4. B. Nematollahi, R. Ranade, J. Sanjayan, and S. Ramakrishnan, "Thermal and mechanical properties of sustainable lightweight strain hardening geopolymer composites," *Archives of Civil and Mechanical Engineering*, vol. 17, no. 1, pp. 55–64, Jan. 2017
5. M. Farooq, A. Bhutta, and N. Banthia, "Tensile performance of eco-friendly ductile geopolymer composites (EDGC) incorporating different micro-fibers," *Cement and Concrete Composites*, vol. 103, pp. 183–192, Oct. 2019
6. J. I. Kim and D. K. Kim, "Application of neural networks for estimation of concrete strength," *KSCE Journal of Civil Engineering*, vol. 6, no. 4, pp. 429–438, Dec. 2002
7. J. Bai, S. Wild, J. A. Ware, and B. B. Sabir, "Using neural networks to predict workability of concrete incorporating metakaolin and fly ash," *Advances in Engineering Software*, vol. 34, no. 11–12, pp. 663–669, Dec. 2003
8. A. Sadrmomtazi, J. Sobhani, and M. A. Mirgozar, "Modeling compressive strength of EPS lightweight concrete using regression, neural network and ANFIS," *Construction and Building Materials*, vol. 42, pp. 205–216, May 2013.
9. B. Vakhshouri and S. Nejadi, "Prediction of compressive strength of self-compacting concrete by ANFIS models," *Neurocomputing*, vol. 280, pp. 13–22, Mar. 2018.
10. M. Ohno and V. C. Li, "An integrated design method of Engineered Geopolymer Composite," *Cement and Concrete Composites*, vol. 88, pp. 73–85, Apr. 2018.
11. B. Nematollahi, J. Sanjayan, and F. U. A. Shaikh, "Matrix design of strain hardening fiber reinforced engineered geopolymer composite," *Composites Part B: Engineering*, vol. 89, pp. 253–265, Mar. 2016.
12. M. Zahid and N. Shafiq, "Effects of Sand/Fly Ash and the Water/Solid Ratio on the Mechanical Properties of Engineered Geopolymer Composite and Mix Design Optimization," *Minerals*, vol. 10, no. 4, p. 333, Apr. 2020.



Risk Assessment in an Infrastructure Project

Dr K Srinivas¹, Dr K R Ramana²

Senior Faculty, National Academy of Construction, Hyderabad¹

Adjunct Professor, National Academy of Construction, Hyderabad²

✉ k_srinivas@nicmar.ac.in; ✉ kr.ramana@gmail.com

ABSTRACT

Infrastructure spurs the economic growth of any nation. All over the world, infrastructure projects are known for their cost and time overruns and India is no exception. Owing to plethora of risks, infrastructure projects get bogged down and in the absence of proper risk management mechanism, most of the project plans go haywire. This leads to such a situation wherein the project would have taken a substantially long period to reap the benefits by which time the financial calculations would have gone awry. Ultimately majority of the infrastructure projects become a drag on a nation by way of substantial investment with returns not fructifying in a timely manner. This paper analyses the risk mitigation mechanisms that were undertaken in a Thermal Power Project in the state of Andhra Pradesh that led to success of the project in terms of cost and time under run.

Keywords : Risk management; Risk mitigation.

INTRODUCTION

The role of infrastructure in spearheading economic development of a country and also setting its pace can hardly be over emphasised. The economic growth of a country progresses with the development of its infrastructure. A sound infrastructural foundation is the key to the overall socio-economic development of a state. Infrastructure encompasses the whole spectrum of vital services such as roads, railways, civil aviation, shipping, power generation transmission, telecommunications, postal facilities and urban development. Infrastructure facilities act as a catalyst for rapid achievement of sustainable economic growth. Infrastructure has a two-way relationship with economic growth i.e infrastructure promotes economic growth, and economic growth brings about changes in infrastructure. The management of risks in infrastructure projects becomes all the more important given the propensity of an infrastructure project to experience plethora of risks. The more effective risks management mechanism is in place, to that extent an infrastructure project is insulated from risks.

LITERATURE SURVEY

- 1) Abhishek V Jadhav et al (2010)on “A Study of Risk Involved in Execution and Management of Thermal Power Station – A Case Study” have investigated on the various risks in the project taken up for study and concluded that construction and operational risks pose the highest risks in a thermal power project and hence suitable identification and mitigation of these risks can bring down the cost of the project to a substantial extent
- 2) Akintoye et al (1997) in their study on “ Risk Analysis and Management in Construction” has revealed that risk analysis and management in construction industry is dependent on three factors i.e 1) Experience 2)Judgement and 3)Intuition of team members. Unfortunately, formal activities to analyse and manage risk are rarely used in construction industry. This main reason for this is the ignorance of project teams towards such techniques and the associated myths that these techniques are unsuitable for use in construction industry
- 3) Avinash Bogale et al (2006) on “Risk Management – A Comparative Study of Power Generating Resources and Technology” have researched on similar risk parameters in Thermal/Hydel/Nuclear power stations and concluded that construction and operating risks contributed to nearly 65% of risks in a thermal power plant.
- 4) Astak et al(2000) conducted a study in which they made broad categories of construction risks i.e Project, Market and Country level risks. Country risks are associated with macroeconomic stability of the country and are linked with the monetary and fiscal policy of the country and the resistance of the country against economic viability. Market risks involve technical advantage of the firm over local competitors, availability of construction related resources and Government support at both local and foreign level towards construction industry. Project level risks are specific to the project activities and they include improper project



design, safety measures for construction site, constraints of logistics, improper control of quality and environmental protection etc They developed a model named ICRAM for assessment of risks.

5) Divya Gupta et al (2015) on “Risk Management in Construction Projects of Developing Countries” have analysed the levels of risk factors in construction industry and concluded that financial risk, defective design, delayed payment on contracts and preparation of feasibility report were the risk factors which had influence in the projects.

6) Eweline Gajewska et al (2011) on “Risk Management Practices in a Construction Project- A Case Study” in Sweden have researched on application of risk management in early stage of life cycle of a construction project have concluded that unstructured risk management is used in construction sector and knowledge and attitude is the missing factor in organisations for implementing risk management and adhoc risk mitigations practices were widely practiced.

7) Kolhatkar M J et al (2014) in the paper on “Risk Management in Construction Projects”, studied the construction industry’s perception of risk associated with the activities and the extent to which industry uses risk analysis and management techniques with the help of questionnaire survey of general contractors and Project Managers. The authors concluded that risk management is essential in construction activities in minimising losses and enhancing profitability. They found that Risk Analysis and Management depends on intuition, judgement and experience and formal risk analysis and management techniques are rarely used due to lack of knowledge and because of doubts over the suitability of these techniques for construction industry activities.

9) Lei Bing et al (2001) in a survey on “Risk Management of International Construction Joint Ventures”, three main groups were made to identify risk factors namely external, internal and project specific. The study examined some cases where risk mitigation measures were used effectively by construction professionals in East Africa. An international survey of contractors revealed that the most critical risk factors existed in the financial aspects of joint ventures, Government policies, economic conditions and project relationships.

10) Shahid Iqbal et al (2015) on “Risk Management in Construction Projects” have dealt on the various risks faced in construction industry and the study revealed that financial issues, accidents at site, defective design are the most significant risks affecting the construction projects and that preparation of proper schedule , good coordination during the implementation stage and suitable preventive risk management techniques are the most effective techniques of risk management.

11) Uher et al(1999) researched cases from Australian construction industry where risk management was used in the conceptual phase of project development. They found that although a majority of respondents had familiarity with risk management processes and techniques and inspite of their willingness to adapt these techniques, risk management was rarely used in the conceptual phase of construction projects

14) Walke R C et al (2011) on “ An Approach to Risk Quantification in Construction Projects Using Expected Monetary Value (EMV) Analysis” have investigated on effective system for risk quantification in construction projects based on EMV analysis and concluded that even though the system does not give a detailed quantitative analysis of risks, it can be fairly used for decision making at commencement of every phase of the project. This technique is sparingly used for quantification of risks

15) Zhen-Yu Zhao et al (2009) in their paper titled “Risk Management of Thermal Power Construction Projects in China – A Case Study” have spelt the increasing need of risks identification and management during the development and construction process of power projects. Using expert investigation method, the preliminary project risk list was obtained and key risks were identified. To deal with the identified high risk factors, a batch of risk controlling and monitoring measures and strategies were proposed. They concluded that a comprehensive and a systematic study of risk management during feasibility study stage will help reduce risk probability and the losses due to these risks. This enhanced the effectiveness of risk management

RISK MANAGEMENT IN CONSTRUCTION PROJECTS

Risk Management is the identification, assessment, and prioritisation of risks followed by coordinated application of resources to minimise, monitor, and control the probability and/or impact of unfortunate events / to maximize the realization of opportunities. Risk management is a systematic way of looking at areas of risk and consciously determining how each should be treated. It is a management tool that aims at identifying sources of risk and uncertainty, determining their impact, and developing appropriate management responses. Risk management consists of 1) risk identification 2) Risk assessment and 3) Risk Mitigation.

DATA COLLECTION

Data for this study was collected by way of questionnaires administered to various stakeholders in a project i.e Client, Contractors



and Consultants. The questionnaires were sent to 500 respondents and the response received was 220 (44%). The respondents were asked to identify the likely risks in various phases of the project i.e pre-investment phase, investment phase, execution phase and closing out phase and also qualitative opinion regarding the contribution of each risk to delay in each phase of the project.. Total of 30 such risks were identified. The qualitative opinion to be given by each respondent were 1) Strongly Agree 2) Agree 3) Disagree 4) Strongly Disagree. The Research analysis was carried out subsequently with the help of collected data.

DATA ANALYSIS

The details of the responses received from the respondents are presented in the following Tables. The values in table indicate the opinion of respondents in percentage.

Table 1. Perception of respondents for risks in pre-investment phase

Sl.No	Risk	Strongly agree (%)	Agree (%)	Disagree(%)	Strongly Disagree (%)
1	Land acquisition	33	45	20	3
2	Obtaining Statutory Clearances/ Approvals	22	35	30	13
3	Reliability of Feasibility report	35	23	31	11
4	Resettlement and Rehabilitation	30	41	22	7
5	Delay in decision making	17	25	40	18
6	Environmental Concerns	35	37	18	10
7	Reliability of Detailed project Report	30	32	24	14
8	Accessibility to site	40	39	15	6
9	Legal issues	35	25	22	18
10	Project manager with inadequate skills	39	33	21	7

Table 2. Perceived Severity of Risks in Pre-investment Phase in descending order

Sl.No	Risk	Respondents who have agreed (%)
1	Accessibility to site	79
2	Land acquisition	78
3	Project Manager with inadequate skills	72
4	Environmental Concerns	72
5	Resettlement and Rehabilitation	71
6	Reliability of DPR	62
7	Legal Issues	60
8	Reliability of Feasibility report	58
9	Statutory Approvals	57
10	Statutory Approvals	42

Table 3. Perception of respondents for risks in Investment phase

Sl.No	Risk	Strongly agree (%)	Agree (%)	Disagree(%)	Strongly Disagree (%)
1	Experience of the team	22	42	26	10
2	Faulty design	30	49	15	6
3	Continuity of the team	21	32	30	17
4	Practicality of concept	26	39	27	8



5	Clauses of contract in unambiguous manner	11	25	40	24
6	Availability of contractor on quoted terms and conditions	25	34	31	10
7	Release of drawings in time by client	17	30	33	20
8	Scope of work not defined properly	24	45	21	10
9	Availability of funds	31	40	22	7
10	Delay in decision making	20	35	33	12

Table 4. Perceived Severity of Risks in Investment Phase in descending order

Sl.No	Risk	Respondents who have agreed (%)
1	Faulty Design	79
2	Availability of Funds	71
3	Scope of Work not Defined Properly	69
4	Practicality of Concept	65
5	Experience of Design Team	64
6	Availability of Contractor on Quoted terms	59
7	Delay in Decision making	55
8	Continuity of team	53
9	Release of Drawings in Time	47
10	Clauses of contract in an unambiguous manner	36

Table 5. Perception of respondents for risks in Execution Phase

Sl.No	Risk	Strongly agree (%)	Agree (%)	Disagree (%)	Strongly Disagree (%)
1	Design/Scope change	36	40	15	9
2	Inadequate availability of skilled resources	42	45	10	3
3	Deviation in site parameters	25	39	20	16
4	Geological Surprises	35	33	22	10
5	Coordination issues with vendors/project team	30	35	25	10
6	Ineffective project monitoring	42	44	12	2
7	Non-availability of funds in time	35	38	15	12
8	Legal Restrictions	24	30	32	14
9	Contractual issues	27	47	17	9
10	Delay in grant of approvals for commissioning	20	35	28	17

Table 6. Perceived of Risks in Execution Phase in descending order

Sl.No	Risk	Respondents who have agreed (%)
1	Inadequate availability of skilled resources	87
2	Ineffective project Monitoring	86
3	Changes in scope and Design	76



4	Contractual Issues	74
5	Unavailability of funds in time	73
6	Coordination issues with vendor/ project team	65
7	Deviation in Site Parameters	64
8	Delay in Grant of Approvals for commissioning	55
9	Legal Restrictions	54
10	Geological Surprises	48

RISK MITIGATION

- The primary source of risk i.e land acquisition was done in a smooth manner by paying an amount 5 times the market price. Thus the risk was suitably mitigated.
- Finalisation of consultants which is a time consuming activity was completed quickly and the consultants were selected based on their technical capacity
- Good accessibility to site ensured that there was no hindrance in movement of materials and equipments to site
- High quality Techno-Economic Feasibility Report and Detailed Project Report infused confidence in lenders because of which the process of funding was an easy affair
- Drawings was released in time which meant that contractors need not had to wait for the same
- Scope of work was defined very precisely giving no room for changes/ modifications at a later date
- Evaluation process of bids were done in a transparent manner
- There was proper dispute resolution mechanism which meant that project was not halted because of disputes between the parties
- Contract was enforced in letter and spirit
- Afforestation was done in and around the plant to take care of environmental problems subsequent to construction of project
- As there was a consensus on construction of this project between the various political parties, political risk was minimised
- Concerned stakeholders were taken into confidence prior to commencement of project
- Pre-bid meeting with contractors minimised the apprehensions of the contractors regarding the project to a very great extent
- Timely release of mobilisation funds enabled the contractors to mobilise the resources to the site well in advance of commencement of project
- Agreement with contractors on variations/ deviations arising subsequently out of execution of contract minimised the contractual risks considerably.
- There was a three tier planning and monitoring system which ensured that the cost performance index and schedule performance index at any point of time did not exceed the limits
- Design of all major structures was carried out by an experienced team who had indepth understanding of the subject
- Proper technical investigations were carried out and action was taken accordingly to strengthen the soil bearing capacity
- Frequent checking of quality of materials/ construction infused confidence in the quality of the work that was executed.
- For foreseen and unforeseen risks, proper insurance was taken to mitigate the impact in the event of occurrence of any risk
- Insistence on usage of Personal Protective Equipment by workers enhanced safety aspects at site and thus chances of accidents was almost nil but for minor incidents.
- Proper supervision by the top management and contractor side during the erection of boiler/turbine/ generator ensured that there was no mishaps at site



- Continuous follow up regarding milestone of each activity
- Preparation of proper manuals/checklists for erection and commissioning
- Dedicated project team for each of the functional areas
- Insuring of materials at site against theft/ pilferage which indemnified the contractor in the event of loss of materials at site
- Emergency Diesel Generator (DG) facility in the event of failure of supply and one standby DG set was provided so that work was not hampered.
- Use of flyash bricks which preserved the environment and conserved top soil
- Proper work permit system was in place and strictly followed

CONCLUSION

This project highlights one of the best risk management practices that was adopted in the construction of any infrastructure project in India and because of effective project management, the project was completed substantially ahead of schedule and at 10% lesser than the projected cost. Hence, it can be concluded that risk management plays a vital role for a project to be successful.

REFERENCES

1. Abhishek V jadhav, Deepak D Tole and Shubham Keserwani ,(2010), A Study of Risks Involved in Execution and Management of Thermal Power Project- A Case Study, (PGPACM Thesis, NICMAR), Accession No :1255
2. Akintoye, Mcloed(1997), Risk Analysis and Management in Construction, International Journal of Project Management, 15(1), pp 31-38
3. Bogale,A., Pranay,R. and Sharma ,V.,(2006), Risk Management – A Comparative Study of Power Generating Resources and Technology , (PGPACM Thesis,NICMAR),Accession No::750
4. Aaslak.M, Shaked.A (2000), ICRAM-Model for International Construction Risk Assessment, Journal of Management in Engineering, 16(1), pp 59-67
5. Divya Gupta, Manoj Sharma and Dr.Ashutosh Shankar Trivedi(2015), International Journal of Engineering Research and Applications,6(11), pp 154-156
6. Ewelina Gajewska, Mikaela Ropel (2011), Risk Management Practices in a Construction Project- A Case Study , (Master's Thesis, Chalmers University of Technology, Sweden) retrieved from <https://www.scribd.com/doc/298944330/Risk-Management-Practices-in-a-Construction-Project-a-case-study>
7. Kolhatkar.M.J ,Amit Bijon Dutta, (2014), Study of Risk Management in Construction Projects, International Journal of Management, 5(6), pp 32-39
8. Li Bing, Tiong R.L.K, Wong.W.F, Chow.D (2006), Risk Management of International Construction Joint Ventures, Journal of Construction Engineering and Management, American Society of Civil Engineers, 125(4), pp 277-284.6
9. Shahid Iqbal, RafiqM.Chaudhry, KlansHolschemacher, Ahsan ali and Jolanta Tamosaitiene (2015), Journal of Technological and Economic Development of Economy, 21(1), pp 65-78
10. Uher.T.E,Toakley A.R (1999), Risk Management in Conceptual Phase of project management, International Journal of Project Management, 17(3), pp 161-169
11. Walke R.C, Tokar V.M, (2011), An Approach to Risk Quantification in Construction Projects using EMV Analysis, (Ph.D Thesis, VJTI, University of Mumbai) retrieved from http://www.idc-online.com/technical_references/pdfs/civil_engineering/AnApproach.pdf
12. Zhen Yu Zhao, Zheng-Hao Yun and Jian Zuao, (2009), Risk Management of Thermal Power Construction Projects in China- A Case Study, International Conference on Management and Service Science, Beijing (China).



Sustainable Alternative to External Curing: Use of Superabsorbent Polymer in Concrete

Jyoti P Bhusari, Akhilesh A More

Department of Civil Engineering, Sinhgad College of Engineering, Pune, Maharashtra

✉ jpbhusari.scoe@sinhgad.edu

ABSTRACT

External water curing is one of the traditional and conventional method used for curing the concrete at site which uses substantial amount of water. In the scenario of paucity of water, the new alternative to curing is use of Super Absorbent Polymers (SAP) that can absorb large amount of liquid and swell substantially to form a soft and insoluble gel. The property of SAP to absorb water and release the water when required makes it ideal material for internal curing agent. SAP promotes autogenous healing by releasing the absorbed water during hydration process and thereby is helpful to control autogenous shrinkage of concrete at early age. This provides a new alternative way to control early age cracking of concrete. This paper presents the results of the extensive experimentation carried out to assess the potential use of super absorbent polymer to mitigate early age shrinkage cracking and its use as an internal curing agent. This is done by conducting water absorption test, sorptivity test, early age shrinkage cracking test and mechanical tests viz; compression, split tensile and four-point bending tests. For the experimental program, specimens of M30 grade of concrete is considered with 0%, 0.5%, 1% & 1.5% of superabsorbent polymer by weight of cementitious material in concrete. Two sets of specimens are cast for mechanical tests viz; air cured and water cured. The experimental results for compressive, split tensile and flexural strength of concrete showed super absorbent polymer up to 1% dosages in concrete is most effective in both air and water curing. Its use in air cured condition has maintained the designed strength whereas its strength has increased by 65% in water cured condition as compared to strength of controlled specimen. Early age shrinkage cracking test results showed the concrete cracking area highly reduced when super absorbent polymer with 1% dose as an internal curing agent was used in concrete. With this dosage of SAP, the time of occurrence of initial surface crack of concrete was delayed by more than 10 hours as compared to controlled specimen and area of the cracks was very minimal as compared to controlled specimen.

Keywords : Super absorbent polymer; Autogenous healing; Internal curing agent; Shrinkage.

INTRODUCTION

Curing insures proper hydration of cement thereby insures achievement of the desired strength and durability of concrete. Proper curing helps to reduce shrinkage. In high strength concrete, where the water cement ratio is kept very less, plastic shrinkage, drying shrinkage and thermal cracks can occur in concrete. There is also a higher risk of autogenous shrinkage at the early stage, when the concrete is still unmaturing [9, 17]. Internal curing (IC) of concrete is one of the remedial measures to this problem. IC helps for hydration process in concrete which maximize its potential in a simple, economical and sustainable way. IC till now is done using pre-wet expanded shale, clay and lightweight aggregate. Now, researchers have come up with a new material called as super absorbent polymer (SAP) as an internal curing agent which exploits its property to absorb large amount of water, sustain it during mixing process and make it available during the hydration process [6,18]. It is made from lightly cross-linked and partially neutralized poly acrylic acid and available in powdered and gel form. The abilities of SAP is to absorb and retain large volumes of water and aqueous solutions. They can swell to a rubbery gel form when immersed in water [10]. This property of SAP can very well be exploited in concrete technology by considering the application of SAP as an internal curing agent [7, 8]. Didier Snoeck et al., used a cross-linked potassium salt polyacrylate which showed a substantial effect on the water permeability of cracked specimens of concrete as the overall permeability was reduced by a factor 104. The smaller copolymer of acrylamide and sodium acrylate proves not to be efficient to seal a crack, mainly due to its size. The small size of sodium acrylate is inappropriate for total sealing of the cracks as they are not able to bridge a crack effectively and are possibly washed out [7]. B J Olawuyi et al. observed the absorption capacity of SAP in both water and cement pore solution to increase as the time of immersion increases [4, 21]. Addition of SAP in concrete increases the compressive strength, flexural and tensile strength as compared with the conventional concrete [3, 20].

This paper tries to assess the potential use of SAP to mitigate early age shrinkage cracking and hence its use as an internal curing agent. The absorption properties of SAP are studied beforehand. The effect of SAP on various mechanical properties of concrete is studied by conducting compressive, split tensile and flexural strength tests on concrete performed for two curing conditions viz; air cured and water cured condition. Water absorption test and sorptivity test on concrete are conducted to understand the absorption characteristics of SAP. Early age shrinkage cracking test is performed to understand the potential of SAP to mitigate early age shrinkage cracks in concrete.

MATERIAL PROPERTIES AND MIX DESIGN

The properties of the materials used in the experimental program and mix design of the concrete used are as follows.

Materials

Materials conforming to IS 12269:2013 [13] was used throughout the work. Specific gravity of cement was 3.15. Locally available fine aggregate and coarse aggregate conforming to IS 383-1970 [11] specifications are used. The specific gravity of both the aggregate is 2.81. Water absorption and fineness modulus of fine aggregate was 1.023 % and 4.26 respectively. Coarse aggregate of size 20 mm and less is used. Water absorption and fineness modulus of coarse aggregate was 0.2% and 5.94 respectively. The water used was potable, colorless and odourless that is free from organic impurities of any type. Super plasticizer Auramix 400 conforming to the specifications IS 9103:1999 [12] is used to improve workability of concrete. Potassium polyacrylate based super absorbent polymer in powdered form was used.

Mix Design

Mix design is carried out for M30 grade of concrete using IS 10262:2009 [14]. The mix proportion of 1:2.24:2.86 with water cement ratio of 0.44 is used. The Super absorbent polymer in the dosage of 0.5%, 1% and 1.5% by weight of cementitious materials is used along with appropriate dosage of super plasticizer to maintain the desired workability (slump value of 70-80 mm). Two sets of specimens are casted for mechanical tests viz; air cured and water cured. The experimental tests for compressive, split tensile and flexural strength of concrete are carried for variation in SAP dosages. The compressive strength is found at the end of 7-,14- and 28- days whereas other tests are conducted at the end of 28- days.

TESTING METHODS

Water Absorption Test on Super Absorbent Polymer

Water absorption test on super absorbent polymer is conducted using a specimen in a cylindrical plastic mould of 100 mm diameter. The mould is supported by means of two metallic rods as shown in **Fig. 1**. The empty weight of whole assembly is taken as initial reading W_1 . Super absorbent polymer in powdered form having weight 2 gm (W_2) is spread evenly at the bottom of the cylinder which is formed using plastic net is having very fine mesh. Now the assembly is placed over a bath of water in a tray in such a way that the bottom of mould immerses by 1 mm from the free surface of water.

Weight of whole assembly is taken after 5 minutes, 30 minutes and 1 hour as the SAP absorbs the water and designated as W_3 .

The water level in the tray was constantly maintained by replenishing the water absorbed by SAP.

Total water absorbed by SAP will be $W_3 - W_2 - W_1$ (gms)



Fig 1. Experimental setup for water absorption test on super absorbent polymer

Water Absorption Test on Concrete

The absorption test conforming to ASTM 642-06 [2] was conducted on specimens cast in 150 x 150 x 150 mm cubical moulds. The specimens were water cured specimens for 28_days with variation in SAP dosages.

Sorptivity Test:

The sorptivity test is conducted as per the specifications laid down in ASTM 1585 [1]. The schematic diagram for sorptivity test and actual test set up is as shown in Fig. 2 & Fig. 3.

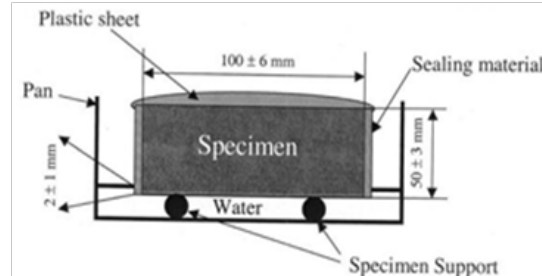


Fig. 2. Schematic of test procedure [1]



Fig. 3. Setup for sorptivity test

The specimens with 100 mm diameter and 50 mm length are preconditioned to 80% relative humidity and 50°C temperature in humidity-controlled chamber for 4 days and then kept in a sealed container for at least 15 days. The sides of the concrete sample are sealed. The initial mass of the sample has taken and specimens are immersed to a depth of 1-3 mm in the water. Readings in terms of gain in mass are noted at required time intervals. The gain in mass per unit area over the density of water is plotted versus the square root of the elapsed time. The slope of the line of the best fit of these points is reported as the sorptivity.

Early Age Shrinkage Cracking Test:

The test is based on the China Structural Building Society standard CCES 01[5], which has suggested flat panel test technique for testing the crack resistance of concrete. The size of mould used in this test for a slab specimen is 600 mm × 600 mm × 63 mm. The side plates of the mould are welded with 10 mm diameter rods protruding for length of 100 mm. Total 14 rods are provided on each face in two layers in staggered fashion as shown in Fig.4. This facilitates the concrete to be restrained enabling the process for restrained shrinkage.

The fresh concrete is poured in flat-panel mould and is kept in environmental chamber (Refer Fig. 5) where the temperature is maintained at 30±2°C and the relative humidity is maintained at 60%. The wind speed of 4.5 m/s blowing over the concrete surface is maintained by providing a fan in the chamber. Concrete surface is observed at every 30 minutes interval. Once the 1st surface crack is visible the observations are then taken at an interval of 1 hour. The number of cracks, crack length, initial cracking time and crack width are recorded for a period of 24 hours. The development of cracks on concrete specimen are drawn progressively as cracks developed and the crack area is found out using equation as follows:

$$S = \left(\frac{1}{2N} \sum_i^N W_i \cdot L_i \right) \frac{N}{A} \quad (1)$$

where,

W_i = maximum width of the i^{th} crack (mm);

L_i = length of the i^{th} crack (mm);

N = total number of cracks;

A = surface area of the slab (m^2).



Fig.4. Slab specimen for restrained shrinkage test



Fig. 5. Setup for environmental chamber



Fig. 6. Concrete specimen for early age shrinkage cracking test

Compression Strength Test

Compression test performed on 150 x 150 x 150 mm cubical specimens as per IS: 516–1959 [15]. 7, 14- and 28-day compressive strength is found.

Tensile Strength Test

This test is carried out on cylinder of size 150 mm diameter and 300 mm height as per IS: 5816-1999 [16].

Flexural Strength Test

The two point flexural test is conducted on the beam specimen of size 150 x 150 x 700 mm conforming to IS: 516–1959 [15].

RESULTS AND DISCUSSIONS

Water Absorption Test on Super Absorbent Polymer

Water absorption test carried on 2 grams of superabsorbent polymer and result is recorded at the end of 5 min, 30 min and 1 hour. Results of absorption test showed that 85% of water is absorbed by SAP in just 5 minutes as compared to its full absorption capacity. After 30 minutes 98% of full absorption capacity was achieved. Full absorption condition is achieved in an hour. The weight of the sample did not increase thereafter. The results show that SAP is able to absorb water 331 times its original weight.

Water Absorption Test on Concrete

As per the results of the water absorption test on concrete as shown in **Fig 7**, it is observed that there is increase in the water absorption with increase in amount of super absorbent polymers in concrete.

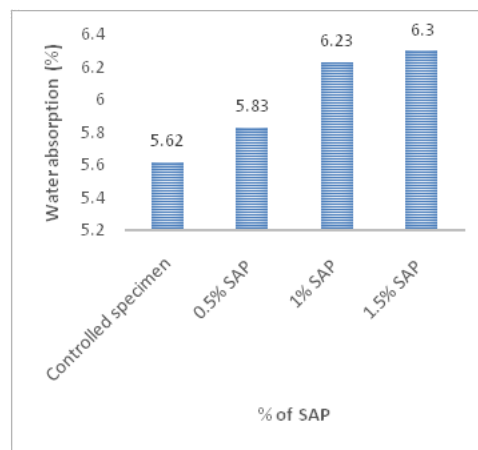


Fig. 7. Water absorption of concrete for different dosages of SAP

Controlled specimen absorbed 5.62% of water by the weight of specimen. For specimens with 0.5%, 1% and 1.5% of SAP absorbed 5.83%, 6.23% and 6.30% of water by the weight of specimens. This increase is not so significant because the average increase of water absorption is hardly 0.4%.

Sorptivity Test

The results of sorptivity test is represented by the graph shown in **Fig. 8** which shows plot of the water absorbed by the specimens vs. square root of time. The rate of absorption of water given by slope of the curve is obtain in two parts to get initial (up to 6 hrs. of experiment) and secondary (after 6th to 8th day of experiment) rate of absorption, which are represented in **Fig. 9** and **Fig.10** respectively for different dosages of SAP.

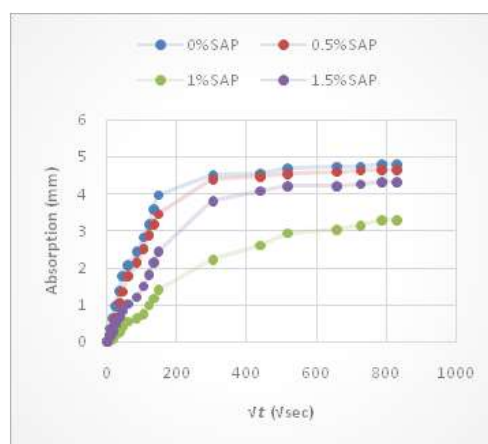


Fig. 8. Water absorption vs square root of time for sorptivity test

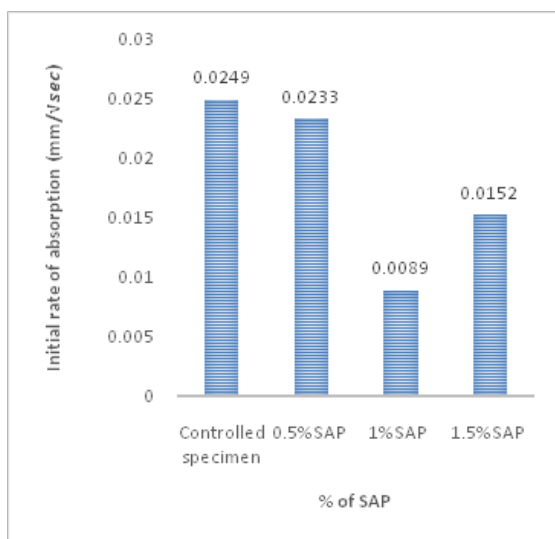


Fig. 9. Initial rate of absorption for different dosages of SAP

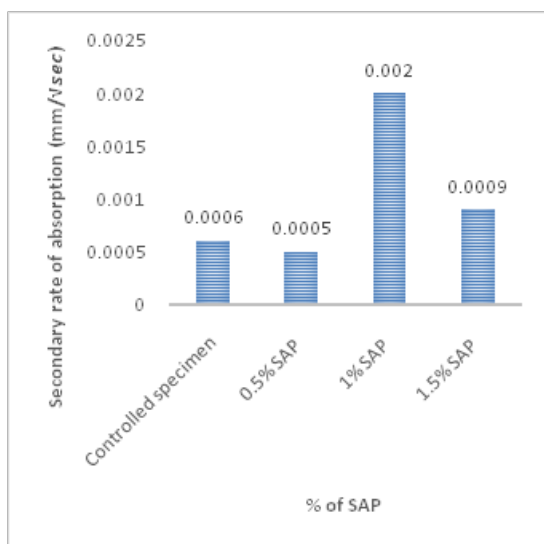


Fig. 10. Final rate of absorption for different dosages of SAP

With increase in amount of SAP from 0% to 1%, the value of initial rate of absorption is reduced. The minimum value is observed for 1% addition of SAP i.e. 0.0089 mm/√sec which increases to 0.0152 mm/√sec for 1.5% addition of SAP. The maximum value of secondary rate of absorption observed for 1% of SAP i.e. 0.002 mm/√sec and for controlled specimen and specimen with 0.5% SAP it is observed to have nearly same values i.e. 0.006 and 0.005 mm/√sec respectively.

Early Age Shrinkage Cracking Test

In this test, the initial cracking time, crack width, crack length, the final number of cracks, and the cracking area of specimens at 24 hours were recorded and given in **Table 1**. The average wind speed was 4 m/s. The temperature and relative humidity conditions were respectively 35 °C and 26%. The control specimen shows the first crack at 45 min, which is much earlier than the specimens with SAP. The amount and the length of cracks as well as the cracking area decreased significantly for the specimens with SAP as compared to the controlled specimen. Control specimen had 35 cracks with cracking area of 147170 mm²/m². For specimen with 1% of SAP only four cracks could be found. The number of cracks decreased by 88.59% and the cracking area decreased greatly to 0.15 mm²/m² in case of 1% SAP. When the SAP dosage was increased from 1% to 1.5%, the initial cracking time was decreased by 90 min. Also, the crack width for 1.5% SAP specimen was wider than that of the 1%

SAP specimen. The measured cracking area decreased with the increase of SAP dosage except in the 1.5% SAP specimen. This suggests that SAP dosage of 1% can be considered as suitable dosage. When this amount is exceeded, the additional SAP as internal curing agent does not help to mitigate the shrinkage cracking of concrete. This is because when the SAP dosage exceeds what the concrete needs, it leaves excessive water and capillary voids in the hardened concrete that reduces the tensile strength.

Table 1. Observations of early age shrinkage cracking test

% SAP	Time in which First crack appeared (mins)	Ave Crack width (mm)	Crack length (mm)	Number of cracks	Cracking Area (mm ² /m ²)
0	45	0.5	1730	35	147170
0.5	630	0.2	195	7	2.65
1	870	0.1	68	4	0.15
1.5	780	0.1	79	6	0.40

Compressive Strength Test

The test results of 7_day, 14_day and 28_day compressive strength for controlled specimen and air cured specimens with 0%, 0.5%, 1% and 1.5% of SAP content in **Fig. 11** and corresponding results for water cured specimens are given in **Fig. 13**.

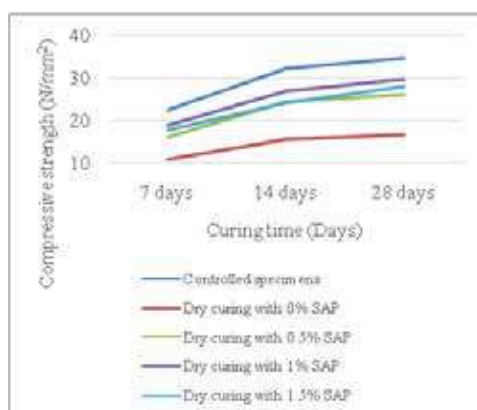


Fig. 11. Compressive strength vs curing days graph of controlled specimens with dry air cured specimens of varied SAP contents

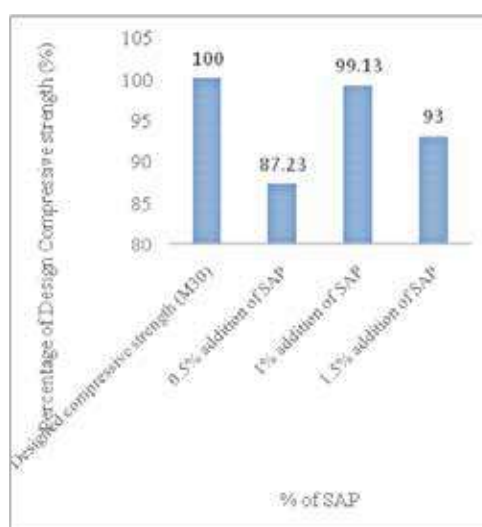


Fig. 12. Achieved compressive strength for air cured specimens by addition of various dosages of SAP to design strength

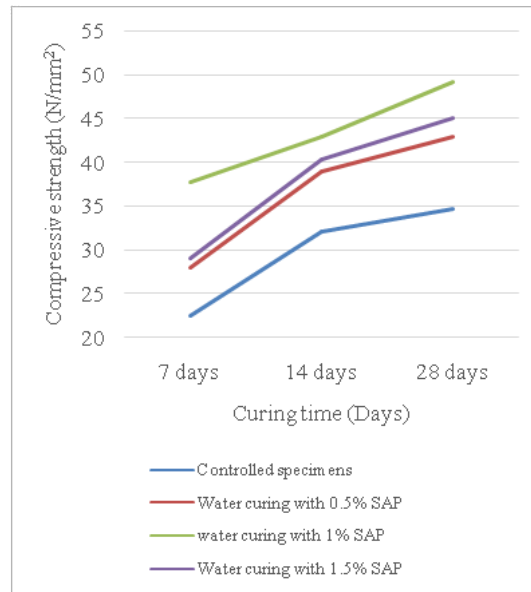


Fig. 13. Compressive strength vs curing days graph of controlled specimens with water cured specimens of varied SAP contents

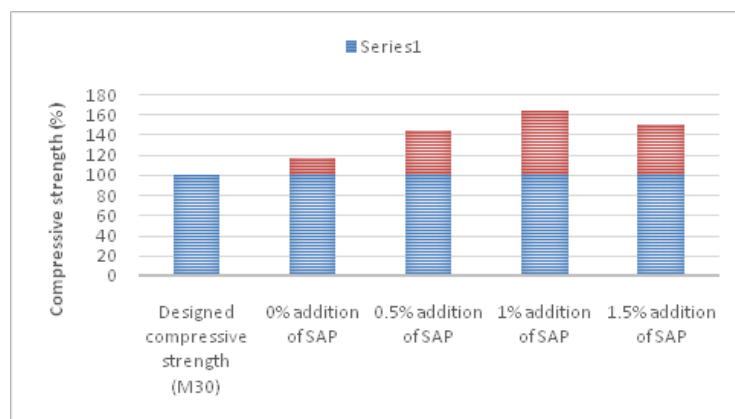


Fig. 14. Additional compressive strength for water cured specimens by addition of various dosages of SAP to design strength

50% reduction in compressive strength of air cured specimen with 0% SAP is observed when compared to controlled specimens (water cured). Increase in strength for air cured specimens with addition of super absorbent polymer in concrete is observed. The specimens with 0.5% and 1% addition of SAP in concrete has achieved by about 87.23% and 99.13% respectively of design compressive strength. Specimens with 1.5% addition of SAP in concrete achieved 93% design strength. These observations are shown in **Fig. 12**. In case of 1.5% addition of SAP, strength is reduced due to formation of excessive voids in concrete. Dosage of 1% addition of SAP in concrete proves to be suitable again.

The compressive strength of water cured specimens for 28 days with 0.5% and 1% addition of SAP in concrete has increased by about 43.1% and 64% respectively of design compressive strength. In case of specimens with 1.5% addition of SAP in concrete the compressive strength increased by only 50.4% of design strength which is again proves the suitable dosage of SAP as 1 %. (**Refer Fig. 14**).

Flexural Strength Test

Flexural strength for different dosages of SAP with air cured specimens and water cured specimens is recorded and plotted in **Fig. 15** and **Fig. 16** respectively. Reduction of 31% flexural strength of air cured specimens at the end of 28 days as compared to controlled specimens (water cured) is observed. The air cured specimens with 0.5% and 1% addition of SAP in concrete has

achieved by about 85.71% and 100% flexural strength as compared to controlled specimen. The flexural strength of water cured specimens with 0.5% and 1% addition of SAP in concrete has increased by about 28.07% and 63.3% respectively as compared with the controlled specimens as shown in **Fig. 16**.

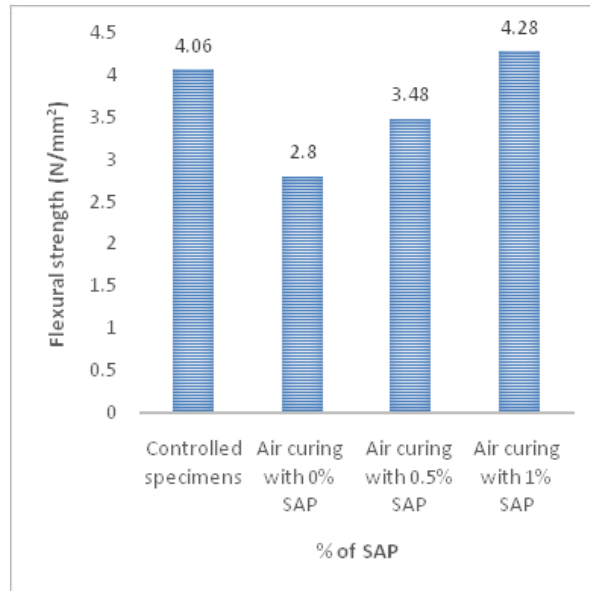


Fig. 15. Flexural strength for different dosages of SAP with air cured specimens

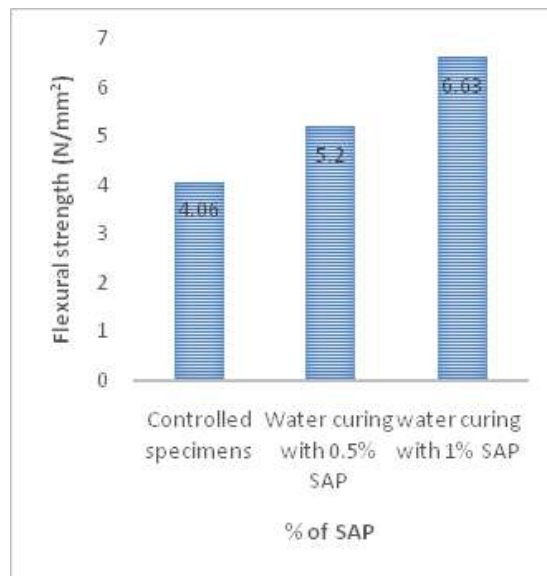


Fig. 16. Flexural strength for different dosages of SAP with water cured specimens

Split Tensile Strength Test

Split tensile strength for different dosages of SAP with air cured specimens and water cured specimens is recorded and plotted in **Fig. 17** and **Fig. 18** respectively. It is observed that almost 59% of reduction in split tensile strength of air cured specimens for 28 days with 0% SAP takes place when compared to controlled specimens i.e. water cured for 28 days.

The air cured specimens with 0.5% and 1% addition of SAP in concrete achieved about 43.29% and 75.77% split tensile strength of controlled specimen. The tensile strength of water cured specimens for 28 days with 0.5% and 1% addition of SAP in concrete has increased by about 19.32% and 51.8% split tensile strength of controlled specimens respectively.

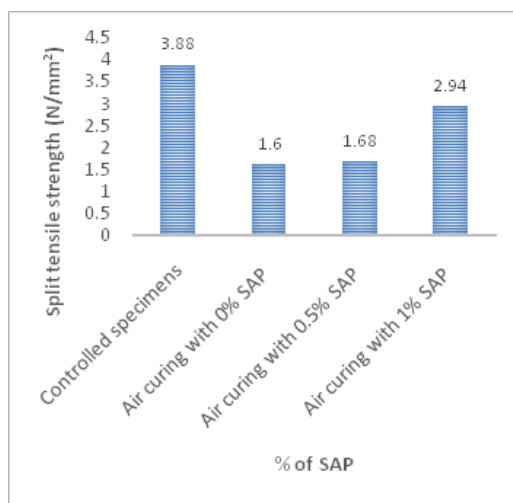


Fig. 17. Split tensile strength for different dosages of SAP with air cured specimens

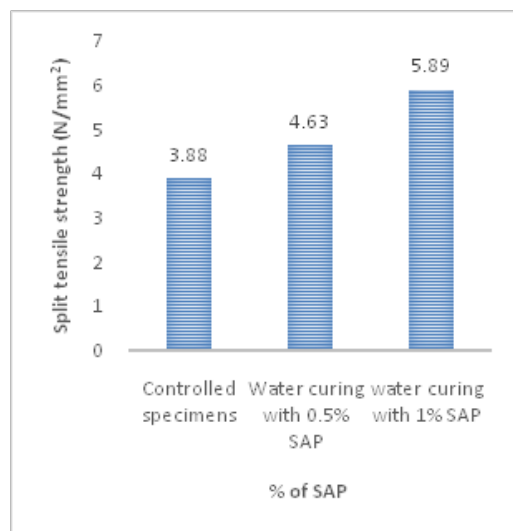


Fig. 18. Split tensile strength for different dosages of SAP with water cured specimens

CONCLUSIONS

Various tests were carried out on super absorbent polymer to verify its properties and on concrete with different dosage of super absorbent polymers to study its effect on mechanical properties such as compressive strength, tensile strength and flexural strength as well as shrinkage test along with durability tests such as water absorption test and sorptivity test. The conclusions made from the interpretation of the test results are given as follows:

- 1) It is observed from the water absorption test on SAP that full absorption capacity of super absorbent polymer is achieved within an hour. It is observed that weight of water absorbed by SAP is about 330 times the weight of SAP.
- 2) Controlled specimen of concrete absorbed 5.62% of water by the weight of specimen. The specimens with 0.5%, 1% and 1.5% of SAP absorbed 5.83%, 6.23% and 6.30% of water by the weight of specimens which is just 0.4% more. Thus, it is observed that increase in amount of super absorbent polymers in concrete does not increase water absorption capacity significantly.
- 3) The air cured specimens with 0.5% and 1% addition of SAP in concrete has achieved by about 85% and 99% respectively of design compressive strength. Specimens with 1.5% addition of SAP in concrete achieved 93% design strength which is slightly reduced as compared to 1% addition of SAP.



Super absorbent polymer as an internal curing agent promotes self-curing in concrete, hence the strength is maintained, but as the proportion of the SAP increases, the proportions of voids generated in concrete after the water in SAP is used increases and hence there is decreasing trend in compressive strength.

- 4) The compressive strength of water cured specimens for 28 days with 0.5% and 1% addition of SAP in concrete has increased by about 45% and 65% respectively of design compressive strength.
- 5) The air cured specimens with 0.5% and 1% addition of SAP in concrete has achieved by about 85% and 100% flexural strength as compared to controlled specimen. The flexural strength of water cured specimens for 28 days with 0.5% and 1% addition of SAP in concrete has increased by about 30% and 65% respectively as compared to flexural strength of controlled specimens.
- 6) The air cured specimens with 0.5% and 1% addition of SAP in concrete has achieved by about 50% and 75% split tensile strength as compared to controlled specimen. The split tensile strength of water cured specimens for 28 days with 0.5% and 1% addition of SAP in concrete has increased by about 20% and 50% respectively flexural strength of controlled specimens.
- 7) The initial rate of absorption for controlled specimen observed, has much higher value i.e. $0.0249 \text{ mm}/\sqrt{\text{sec}}$ than specimens with SAP. As increase in amount of SAP from 0% to 1% the value of initial rate of absorption reduced. The minimum value of initial rate of absorption observed for 1% addition of SAP i.e. $0.0089 \text{ mm}/\sqrt{\text{sec}}$. For 1.5% addition of SAP value of initial rate of absorption slightly increased to $0.0152 \text{ mm}/\sqrt{\text{sec}}$. On the other hand, maximum value of secondary rate of absorption observed for 1% of SAP i.e. $0.002 \text{ mm}/\sqrt{\text{sec}}$. The value of secondary rate of absorption for controlled specimen and specimen with 0.5% SAP observed nearly same values i.e. 0.006 and $0.005 \text{ mm}/\sqrt{\text{sec}}$ respectively. It is observed that water ingress in controlled specimen is highest in case of initial rate of absorption. But for secondary rate of absorption, water ingress is highest for specimen with addition of 1% SAP which is nearly similar to results of water absorption of concrete.
- 8) The concrete cracking area was highly reduced when super absorbent polymer as an internal curing agent was used in concrete up to dosage of 1%. With a dosage of SAP up to 1% the time of occurrence of initial surface crack of concrete was delayed by more than 10 hours as compared to controlled specimen.

Thus, SAP has a potential use in concrete as an internal curing agent and it is a sustainable alternative to external curing which can save substantial amount of water. Its inclusion in concrete improves the performance of concrete against early age shrinkage phenomenon. It also improves the mechanical properties of concrete if used as an admixture in normal concrete.

REFERENCES

1. ASTM C 1585-04, "Standard test method for measurement of rate of absorption of water by hydraulic cement concrete." ASTM Committee C09. Published on 2004.
2. ASTM 642-06, "Standard Test Method for Density, Absorption, and Voids in Hardened Concrete."
3. Autade Pankaj and Anbhule Sachin, "Effect of Super Absorbent Polymer in Concrete." International Research Journal of Engineering and Technology, Vol. 04 Issue: 07, pp3520-3525, 2017.
4. B J Olawuyi and W P Boshoff, "Compressive Strength of High-Performance Concrete with Absorption Capacity of Super-Absorbing-Polymers." Research and Applications in Structural Engineering, Mechanics and Computation – Zingoni (Ed.). Taylor & Francis Group, London, ISBN 978-1-138-00061-2. pp 1679- 1685, 2013
5. Chinese Civil Engineering Society standard CCES 01, "Guide of Design and Construction to Durability of Concrete Structures", Chinese Building Industry Press (2005).
6. Dejian Shen, Xudong Wang, Dabao Cheng, Jinyang Zhang and Guoqing Jiang, "Effect of Internal Curing with Super Absorbent Polymers on Autogenous Shrinkage of Concrete at Early Age." Construction and Building Materials, 106, pp. 512–522, 2016.
7. Didier Snoeck, Peter Dubruel and Nele De Belie, "How to Seal and Heal Cracks in Cementitious Materials by Using Superabsorbent Polymers." Application of Superabsorbent Polymers and Other New Admixtures in Concrete Construction, V. Mechtcherine, C. Schroeﬂ (eds.), RILEM Publications S.A.R.L., Proceedings PRO 95, 2014.



8. Jingyun Han, Xuyan Song, and Ruyuan Xu, "Influence of Different Varieties of Water Reducing Agent on the Early Cracking of Concrete." 2nd International Conference on Electronic & Mechanical Engineering and Information Technology (EMEIT), 2012.
9. H.X.D. Lee, H.S. Wong and N.R. Buenfeld, "The Potential of Superabsorbent Polymer for Self-Sealing Cracks in Concrete.", *Advances in Applied Ceramics* 109, 5, pp. 296-302, 2010.
10. Heesup Choi, Masumi Inoue, Sukmin Kwon, Hyeonggil Choi, and Myungkwan Lim, "Effective Crack Control of Concrete by Self-Healing of Cementitious Composites Using Synthetic Fiber." *Materials* (Basel, Switzerland) vol. 9 (4), 248. 30 Mar. 2016, doi:10.3390/ma9040248
11. Indian Standard Specification for Coarse and Fine Aggregates from Natural Sources for Concrete, IS: 383-1970, Bureau of Indian Standards, New Delhi.
12. Indian Standard Specification for Concrete Admixtures, IS: 9103 (1999), Bureau of Indian Standards, New Delhi.
13. Indian Standard for Ordinary Portland Cement, grade 53, IS: 12269-2013, Bureau of Indian Standards, New Delhi.
14. Indian Standard Guidelines for Mix Design, IS: 10262-2009, Bureau of Indian Standards, New Delhi.
15. Indian Standard Methods of Tests for Strength of Concrete, IS: 516-1959, Bureau of Indian Standards, New Delhi.
16. Indian Standard Methods of Splitting Tensile Strength of Concrete, IS: 5816-1999, Bureau of Indian Standards, New Delhi.
17. J. S. Kim and E. Schlangen, "Super Absorbent Polymers to Stimulate Self-Healing in ECC.", *Proceedings of the 2nd International Symposium on Service Life Design for Infrastructure* (Eds. K. van Breugel, Guang Ye, and Yong Yuan), Delft, Netherlands, pp. 849-858, Oct. 4-6, 2010.
18. Juntao Dang, Jun Zhao and Zhaohua Du, "Effect of Superabsorbent Polymer on the Properties of Concrete." *Polymers*, 9, 672, 2017.
19. K. Mahendra and P. Bala Krishna, "To Study the Strength Characteristics of Concrete by Replacing Curing Water with Self-Curing Compounds." *International Research Journal of Engineering and Technology*. Volume: 05 Issue: 03, 2018.
20. Kenneth Sequeira and B.H.V. Pai, "Effect of Small Percentage Additions of Superabsorbent Polymer on Mechanical Properties of Concrete." *International Journal of Scientific & Engineering Research*, Volume 6, Issue 6, 2015.
21. M. Manoj Kumar and D. Maruthachalam, "Experimental Investigation on Self-Curing Concrete." *International Journal of Advanced Scientific and Technical Research*, Issue 3 volume 2, 2013.



A Case Study on Stabilized Shallow Foundation for a Large Oil Storage Steel Tank on Soft Soil

Somdev Pakrashi

Managing Partner, Consultants Engineers & Builders (Geotechnical Engineering Consultancy Firm), Kolkata

✉ s_pakrashi@rediffmail.com

ABSTRACT

Soft clayey subsoil was encountered at shallow depths, during geotechnical investigation, at the site for one large diameter oil storage steel tank in Singur, Hooghly, West Bengal, India. Bearing pressure from the tank was observed to be greater than the net safe bearing capacity of the subsoil below traditional sand pad. A usual solution by piled sand pad foundation construction was not considered first the same being costly and time consuming. Instead, a number of trial analyses were taken up considering compacted coarse sand layer of different thickness by replacing the existing soft sub soil below the sand pad to check if a suitable thickness of compacted coarse sand course could achieve necessary ground improvement to increase bearing capacity of the stabilized soil along with required reduction of net bearing pressure and settlement values, below stabilized sand course, to provide a safe stabilized foundation base at shallow depth for the large storage steel tank. Thus, by utilizing the use of a stabilized shallow foundation base, a safe and economic foundation system could be achieved for the large oil storage steel tank on soft soil.

Keywords : Stabilization; Sand pad; Oil storage steel tank; Net bearing pressure; Differential settlement; Soft soil.

INTRODUCTION

A geotechnical investigation work in respect of foundation for one 32m dia. x 15m ht. tar oil storage tank was taken up in Mahishtickry, Singur, Hooghly. Subsoil profile up to (-) 1.7m (layer 1) was a locally compact fill of soft silty clay, in general. It was followed by soft to medium silty clay becoming stiff at places, at lower reaches, upto (-) 6.25m overlying a 1.25m thick stratum of loose to moderately dense silty fine sand. Bearing pressure from the large tank was too high to consider a suitable foundation base at shallow depths containing soft clayey soil. Usually such foundation problems can be solved by a piled foundation or piled raft foundation system. But a shallow sand pad foundation on improved ground in the form of a compacted coarse sand layer of required thickness by replacing existing soft soil is a cheaper and less time consuming solution if it can provide adequate factor of safety against shear and settlement failures. Different case studies in connection with large storage steel tanks on soft soil have also concluded that ground improvement has the most appropriate potential to provide a solution to a foundation problem for storage steel tanks. Nowadays, a large number of tank foundations have been treated with different ground improvement techniques and many such cases have been presented in journals or conference publications [1, 2, 3, 4] was thought, therefore, necessary, to try to utilize the concept of stabilization of the foundation base with the use of compacted coarse sand in layers by replacing existing poor subsoil up to the required shallow depth. A considerable number of references made it clear, as well, that stability and settlement are two major aspects to design a safe shallow oil storage steel tank foundation [5,6]. In reality, uniform settlement does not pose dangerous problems. Differential settlement, which is the vertical difference of two points at the foundation structure interface, initiates distress of the tank foundation, if it is excessive, and may lead to complete tank rupture [7, 8]. Differential settlement occurs due to non-homogeneity and compressibility of the subsurface deposit as well as non-uniform distribution of load on to the foundation base. This paper presents the use of ground improvement by filling and compaction of coarse sand by replacing soft soils at shallow depth leading to the increase in bearing capacity of the foundation base along with control of differential settlement for stability and prevention of damage of the tank structure components. Analyses were made to find out the required thickness of the stabilized course of sand as foundation base and finally a safe and economic stabilized shallow foundation system for the tank was achieved.

OBJECTIVE OF THE STUDY

It has been observed that although a piled foundation is the usual solution for a safe foundation system for large oil storage steel tanks on weak soils, a necessary consideration for a cheaper solution, where ever possible, should be made in the form of stabilized shallow foundation system where compacted layers of coarse sand replacing the existing poor subsoil to the required



depth below ground level may provide a safe shallow foundation base. A safe stabilized shallow sand pad foundation base would save a lot of construction cost and time, in comparison to the same required for a piled sand pad foundation. This paper focuses on sharing the experience of such an economic solution in terms of ground improvement for a large oil storage tank foundation on soft soil and brings about the lead for the subject of the study.

ASSUMPTIONS

- Evaluation for settlements, loads on the foundation base, effect of foundation load on the next stratum etc. have all been carried out according to the provisions of applicable clauses of IS8009-1,1976 , IS1892,1979, IS 6403,1981, IS1904,1986, as well as other relevant books and codes of practice.
- Soil Investigation & testing works at site and laboratory have all been conducted following the provisions of applicable clauses of SP 36-1,1987, SP 36-2,1988 and other relevant IS codes.
- Centre of gravity of excavation and the installed structure coincide.

STUDY AREA AND SUB SOIL PROFILE

The site that was earmarked for the 32 m Dia. x 15m ht. tar oil storage tank at Mahishtickry, Singur,

Hooghly, West Bengal was found to be a flat terrain. Subsoil profile as obtained by necessary site investigation and laboratory tests, contains the following layers:

Layer	Range	Thickness (m)	Description
1	0.0 -1.70	1.70	Locally compacted fill having silty clay mixed with sand and some brick pieces followed by silty fine sand, at places, at lower reaches. N=3-6, G = 2.69-2.71 Least c =2.86 t/m ² , Av.mv = 0.0024 m ² /t 10 – 20 t/m ² .
2	1.70 - 6.25	4.55	Soft to medium silty clay being clayey silt at places. N= 4 - 5, G =2.7 - 2.71 Least c = 3.29t/m ² , Av.mv= 0.00185m ² /t 10 – 20 t/m ²
3	6.25 -7.50	1.25	Loose silty fine sand mixed with little clay, at places. N=4 - 8, G=2.69 c= nil, ϕ = 29.5o - 30.5o, mv = nil, sc = nil
4	7.50-24.75	17.25	Medium to stiff silty clay becoming very stiff clayey silt/silty clay with kankar at lower reaches. N=7 – 26, G =2.7 -2.72 Av. c = 7.60 t/m ² , Av.mv = 0.0009m ² /t 2.5 -5 t/m ²
5	24.75 – 48	23.75	Very stiff to hard clayey silt to silty clay. The layer contains some sand and kankar mixed with clay, at places, at lower reaches-up to termination depth. Av. c =15.3 t/m ² , G =2.7-2.72 N=30 - 66, Av mv= 0.00022m ² /t 0.0 - 2.5 t/m ²

DISCUSSION

It is usual to provide a sand pad below oil storage steel tanks in order to raise the bottom plate to a desired level above the existing ground surface to prevent corrosion of steel plates by accumulation of surface or subsoil water around the tanks .The sand pad also provides resilience to the surface and transfers the load without causing local stress concentration at the tank bottom and allows the plates to move radially or circumferentially with varying conditions of temperature and stress [9].Thickness of the sand pad, above ground surface, had already been fixed by the client as 0.9m. Considering 0.5 m thick excavation and removal of top soil for usual preparation of base for the sand pad, total thickness of sand layer below tank bottom including sand pad works out to (0.9+0.5) m =1.4m and depth of foundation becomes 0.5m below ground level. It was observed from necessary analysis that net bearing pressure at 0.5m, below usual sand pad, worked out to 14.77 t/m² and ultimate bearing capacity of layer 1, ranging from ground level up to a maximum depth of (-) 1.7m, was 19.17 t/m². Obviously, F.S. =

$19.17/14.77 = 1.30$ was less than allowable limits i.e. 1.7 [10]. Therefore, a shallow foundation base at (-) 0.5m in layer 1 is not suitable for the large storage tank. Piled foundations are usually provided to prevent large differential settlements in very poor subsoil conditions [9]. Therefore, solution to the foundation problem could be safely achieved by piled foundation system to transfer the oncoming load from the large tank bottom to layer 4 having stiff to hard silty clay. But it is an expensive and time consuming affair. It is also essential to achieve economy in construction in respect of oil storage tanks for depots and other purposes as those are usually provided in large numbers on any given site [9]. In the present case, therefore, it was considered first to study the results applying ground improvement technique and check whether the large oil storage tank could be safely placed on a shallow stabilized base. Stabilization of soil by mechanical process has been in practice for hundreds of years. It results in improving the density of soil along with its other related engineering properties like settlement, cohesion, internal friction etc.[10]. Compaction is a major type to bring about soil stabilization the process requiring, in general, a heavy weight to drop repeatedly to compact the soil at optimum moisture content. This is usually the cheapest method of improving site soils [10]. In the present case vibratory portable compactor of required capacity was used to compact coarse sand in 0.15m layers at optimum moisture content after excavation and removal of soft soils up to the required depth below ground level (**Fig. 2**). A number of necessary trial analyses were carried out using different thickness of compacted sand course in replacement of the soft subsoil below ground level to check if a possible solution can be achieved in the form of a shallow stabilized foundation. It was finally observed that the net bearing pressure below a stabilized/compacted sand base at (-)2.1m worked out to 12.43 t/m^2 and ultimate bearing capacity of layer 2 (from (-)1.70m to (-) 6.25m) was 22.23 t/m^2 . Therefore, F.S. achieved $=22.23/12.43 = 1.79$ which was more than allowable limits [10]. It was also clear from settlement calculations that necessary settlement parameters were below allowable limits. It was thus observed that soil stabilization by excavation and removal of existing sub soil below ground level and replacing the same with 2.1m thick coarse sand free from dirt or fine sand compacted in 0.15m layers at optimum moisture content could provide a safe shallow sand pad foundation base for the large dia. oil storage steel tank providing adequate factor of safety. Compaction in confined condition according to necessary procedures as well as checks to ascertain required density, quality and standard of compaction were also adhered to in order to achieve best results.

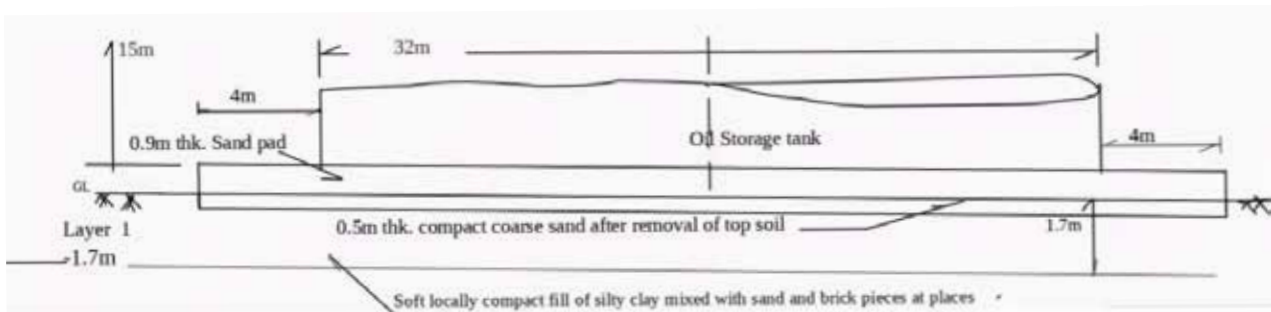


Fig. 1. The oil storage steel tank on sand pad

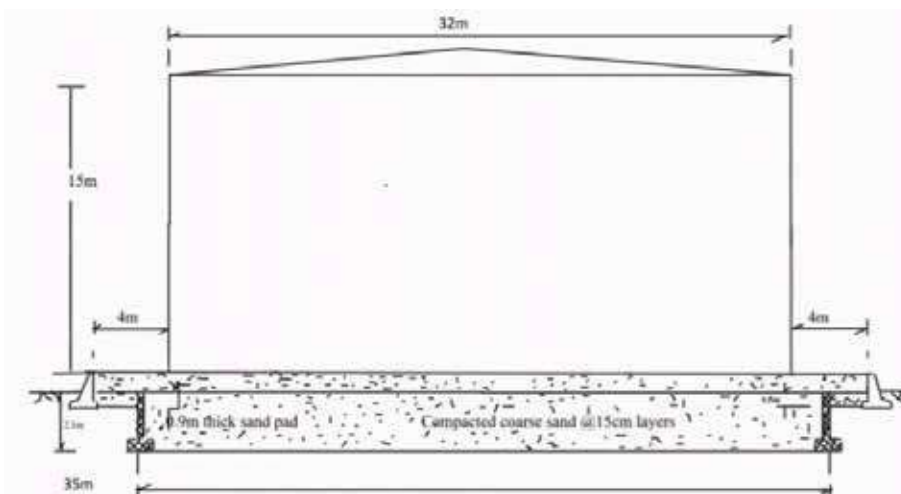


Fig. 2. Stabilized foundation base for the oil storage steel tank

CONCLUSIONS

Large oil storage steel tanks transferring heavy load pose problems in respect of a safe shallow foundation system especially on soft soil. In such cases a piled sand pad foundation is considered to transfer the heavy load safely on to a sufficiently strong stratum at deeper depth although it is a costly and time consuming affair. Present study in respect of a large dia. heavily loaded oil storage steel tank shares the experience where stabilization of foundation in the form of compacted coarse sand in replacement of existing poor soil up to required depth was taken up and it was observed that compacted coarse sand layer of required thickness could adequately improve the foundation base for the large steel storage tank in i) providing adequate factor of safety against shear failure and in ii) reducing necessary settlement values below allowable limits. As a result a safe shallow stabilized sand pad foundation system for the large oil storage steel tank could be used successfully. Utilization of the concept of soil stabilization by replacing the existing soft subsoil with compacted coarse sand of required thickness and density can thus be very effective and beneficial, wherever possible, to provide a safe shallow sand pad foundation base for large oil storage steel tanks on soft subsoil as it negates the use of a piled sand pad foundation system and consequently saves a lot of construction cost and time.

APPENDIX

Calculations

Bearing Capacity

I. Check for a safe shallow foundation base at (-) 0.5m : Consider a shallow foundation when the tank bottom is on $(0.9\text{m} + 0.5\text{m}) = 1.4\text{m}$ thick compact sand course placed at 0.5m below ground level (**Fig. 1**).

Bearing pressure at tank bottom, considering hydrostatic test $= 15 \times 1 + 360 \times 4 / [\pi \times (32)^2] = 15.45 \text{ t/m}^2$. Considering 45° spread of load, bearing pressure at (-) 0.50m .

i) Load from the tank and its content $= 15.45 \times 322 / (32 + 2 \times 1.4)^2 = 13.06 \text{ t/m}^2$

ii) Load from 0.90m thick sand pad $= 0.9 \times 2 \times 40^2 / \{40 + 2 \times 0.5\}^2 = 1.71 \text{ t/m}^2$

Total $= 14.77 \text{ t/m}^2$

Ultimate bearing capacity, qult at (-) 0.50m, $= cN_c s_c d_c i_c [11] = 2.86 \times 5.14 \times 1.3 \times 1.0029 \times 1 = 19.17 \text{ t/m}^2$ F.S $= 19.17 / 14.77 = 1.3 < 1.7$. Not o.k.

Least $c = 2.86 \text{ t/m}^2$, $s_c = 1.3$, $\gamma_{\text{sand}} = 2 \text{ t/m}^3$ $d_f = 0.5\text{m}$, $N_c = 5.14$ $d_c = 1 + 0.2 \times d_f / B = 1 + 0.2 \times 0.5 / 34.8 = 1.0029$, Self wt. of tank $= 360 \text{ ton}$, Permissible F.S $= 1.7$ [10]

II. Check for a safe shallow sand pad foundation on 2.1m thick stabilized base (**Fig. 3**).

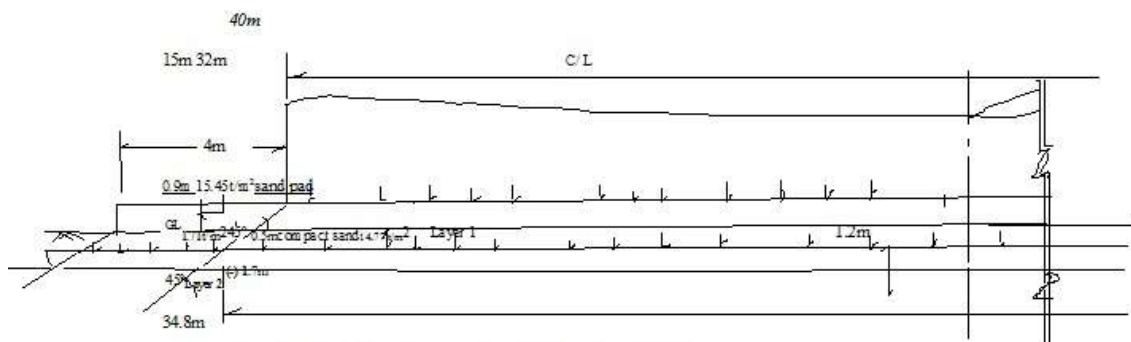


Fig. 3. Load transfer from the oil storage tank to virgin soil at (-) 0.5m

Bearing pressure at tank bottom, considering hydrostatic test $= 15.45 \text{ t/m}^2$.

Considering 45° spread of load, net bearing pressure at 2.1m below G.L.:

i) Load from tank and its content $= 15.45 \times 32^2 / \{(32 + 2 \times (0.9 + 2.1))\}^2 = 10.956 \text{ t/m}^2$

ii) Load from 0.90m thick sand pad $= 0.9 \times 2 \times 40^2 / (40 + 2 \times 2.1)^2 = 1.474 \text{ t/m}^2$

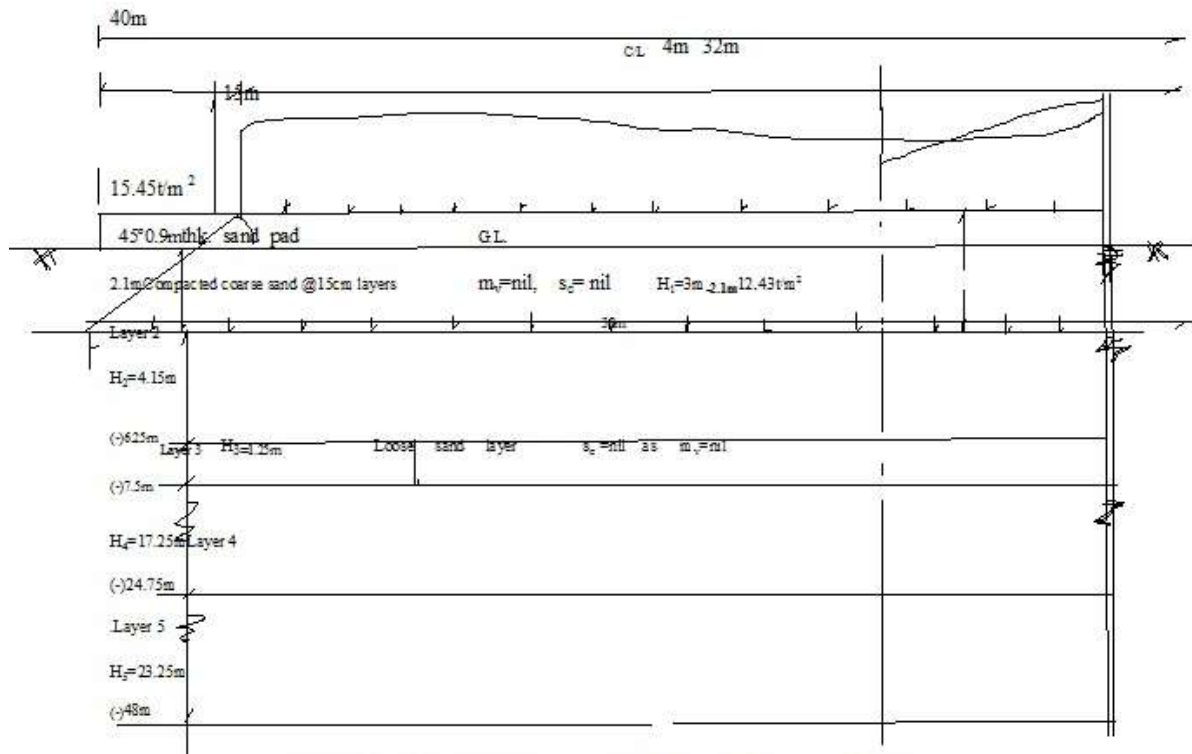


Fig. 5. 2.1 m thick stabilized course underlain by subsoil layers up to (-) 48m

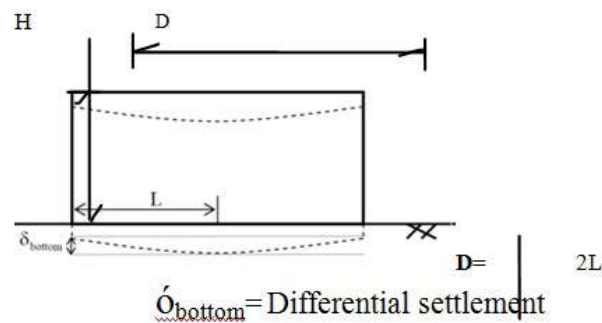


Fig. 6. a: Bottom – center differential settlement for steel tanks

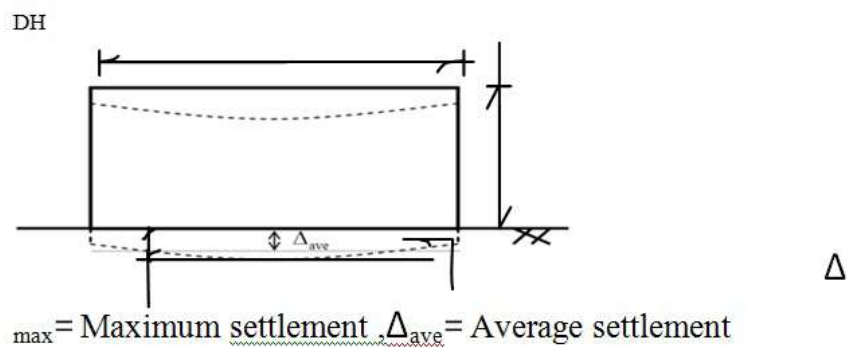


Fig. 6. b: Maximum and average settlements for steel tanks



REFERENCES

1. J.M. Cognon, I. Juran and S. Thevanayagam, Vacuum consolidation technology – principles and field experience, Proceedings of the Conference on Vertical and Horizontal Deformations of Foundations and Embankments, College Station, TX, USA, (Yeung AT and Felio GY (eds.)). ASCE New York, NY, USA, Geotechnical Special Publication, 40, 1994, pp. 1237–1248
2. M. S. Hendy and I. C. Muir Proceedings of the Third International Conference on Ground ... Experience of dynamic replacement on a 40m deep reclamation in Hong Kong.75, 1997
3. Kul Bhushan, Ashok Dhingra, Curt Scheyhing and Endi Zhai, Ground Improvement by Stone Columns and Surcharge at a Tank Site ,2004, International Conference on Case Histories in Geotechnical Engineering
4. J.M. Debats, G. Scharff, J. Balderas and S. Melentijevic, Proceedings of the Institution of Civil Engineers - Ground improvement efficiency and back- analysis of settlements,166 (3) ,2013,,pp.138-154
5. R.A. Bell, and J. Iwakiri Settlement comparison used in tank-failure study. Journal of the Geotechnical Engineering Division, ASCE, 106(2), 1980, pp.153-169.
6. P. A. Green and D. W. Height, The failure of two oil storage tanks caused by differential settlement. Proceedings, British Geotechnical Society Conference on Settlement of Structures, Pentech Press, London, England, 1975.
7. T. B. D’Orazio and J.M. Duncan, Differential Settlements in Steel Tanks. ASCE, Journal of Geotechnical Engineering, 113(90),1986, pp. 967-983
8. W. A. Marr, J.A Ramos and T. W. Lambe, Criteria for settlement of tanks Journal of Geotechnical Engineering, ASCE 108(8), 1982, pp.1017-1039.
9. M. J. Tomlinson , Foundation Design and Construction, Fourth Edition, The English Language Book Society and Pitman, ELBS edition reprinted ,1981, p.106,127,128, 131.132.252 – 254.
10. J. E. Bowles, Foundation Analysis and Design, Fourth Edition, McGraw-Hill Book Company, New York, USA, 1988,p.99, 232, 259, 276,288,289.
11. IS: 6403 – 1981, Indian Standard Code of Practice for Determination of Bearing Capacity of shallow Foundations, Indian Standards Institution, Manak Bhavan, 9, Bahadur Shah Zafar Marg, New Delhi 110002,November 1981
12. S. N. Klepikov, Performance criteria-allowable deformation of building and damage-general report /discussion,28, 1989.
13. API 1998, 1-API 653, Appendix-B. Tenth Edition, November 1998.

Theoretical Calculation of Crack Width in Pile for Tension and Lateral Loading

Md Arshad Jamal, Vaishali Sharma, Deepak Singh, Ayan Khan

Department of Structural Design, Quality Austria Central Asia, New Delhi

✉ jamal@qacamail.com; ✉ vaishali@qacamail.com

ABSTRACT

The cracks likely to initiate on a tension and lateral loaded pile and would causes greater tension load and deflection at the pile head however, there is lack of investigation on the cracking response due to tension and lateral loaded piles. In this article, a full scale calculation of crack width on circular pile shaft under tension and lateral load is done. Although the explicit calculation of flexural crack width in rectangular section of beam and slab can be found widely in varies textbooks. A design and calculation procedure for a circular section crack width calculation in tension and lateral load have not been documented.

Keywords : Tension; Lateral loaded; Pile; Crack width.

INTRODUCTION

When pile foundation is design for GBT (Ground Base Tower) or GBM (Ground Base Monopole) tower, tension and lateral load act on it. That's why it is required to check the permissible tension stress limit in bars and the crack width due to tension and lateral loading. Deep foundation design for GBT or GBM in tension and lateral load is predominantly in design prospective. Tension and lateral loads develop the cracks in pile shaft. Generally deep foundation is design wherever water table is below 1.0m from ground level or soil bearing capacity is very low. Because pile in water table, cracks in pile shaft is harmful for the reinforcement of pile shaft.

According to the IS456:2000 in the member where cracking in the tensile zone is harmful either because they are exposed to the effects of the weather or continuously exposed to moisture or in contact with soil or ground water, an upper limit of 0.2mm is suggested for the maximum width of cracks. Cracking due to direct tension is of serious concern than flexural cracking, it cause a clear separation in the concrete through the entire section of the member. At the crack location, the reinforcement is required to resist the entire tension and the width and spacing of cracks are governed primarily by the reinforcement detailing. If minimum percentage of reinforcement is provided then steel may yield and result in wide crack width. However, crack width can be significantly controlled by maintaining number of bars in circular cross section with relatively low tensile stress and strain in the steel at service loads. As in the case of eccentric tension the concrete in between the cracks resists some tension (tension stiffening effects). The axial stiffness of the member can be greatly reduced by the presence of wide cracks but this reduction is mitigated by the tension stiffening effects. The Indian Standard code does not have any recommendation to calculate crack width of the member subjected to direct or eccentric tension. However, such recommendation is given in the British code BS8110. BS8110 permits the extension of the procedure prescribed for crack width prediction under pure flexure to situation of flexural to situation of flexural combined with axial tension. When axial tension is predominates, the entire section is likely to be under tension with the neutral axis lying outside the section. This is the extreme case of pure tension, here $X \rightarrow -\infty$. It is suggested that if f sufficient to consider $x = -D$

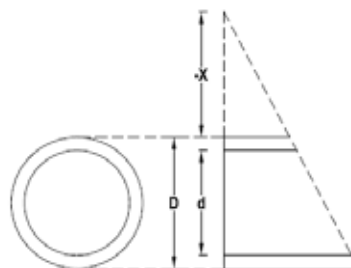


Fig. 1. Pile shaft section and x is the neutral axis

PROPOSED METHOD OF CALCULATION

Assuming pile of diameter D , tension load on pile is T , and moment acted on pile due to the lateral load is M .

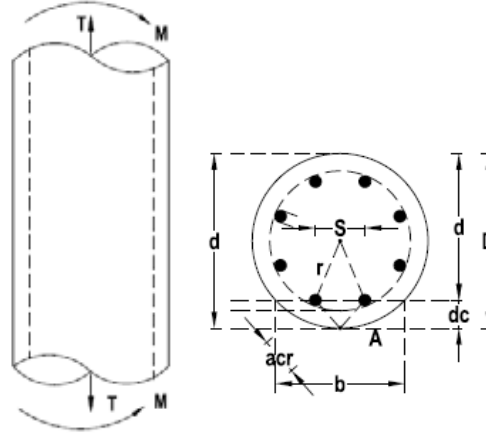


Fig. 2. Pile shaft action of tension and moment

According to **Fig. 2**, S is the center to center spacing between the main longitudinal reinforcement, C_{min} is the minimum clear cover, r is the radius of camber of main reinforcement, ϕ is the radius of main reinforcement, ϕ_{tr} is the radius of secondary reinforcement, n is the number of longitudinal reinforcement, a_{cr} is the diagonal distance to main longitudinal reinforcement and outer edge of concrete surface (the calculation point of crack width), b is the width of the section at the longitudinal reinforcement level, a' is the distance between outer most surface to the crack calculating point and d is the effective depth of the section.

Radius of camber of main reinforcement

$$r = \frac{(D - 2C_{min} - 2\phi_{tr} - \phi)}{2}$$

Spacing of main reinforcement

$$S = 2r \sin\left(\frac{\pi}{n}\right)$$

Effective cover

$$d_c = \frac{D}{2} - r \cos\left(\frac{\pi}{n}\right)$$

Shortest distance between main longitudinal reinforcement and at calculation point of crack width

$$a_{cr} = \sqrt{\left(\frac{S}{2}\right)^2 + d_c^2} - \left(2\phi_{tr} - \frac{\phi}{2}\right)$$

Crack width in any section depends on the stress distributed on the longitudinal main bars, Indian standard code permit the limit of stress in main longitudinal bars (at cracked location) is $0.8f_y$, where f_y is the yield stress of main longitudinal reinforcement.

The average steel strain ϵ_m may be calculated on the basis of basic of following assumption.

The concrete and steel are both consider to be fully elastic in tension and compression. The elastic modulus of the steel may be taken as 200 kN/mm^2 . Whereas, elastic modulus of the concrete is as derived by the equation

$$E_s = 5000\sqrt{f_{ck}}$$

The code allow to an approximation for computing ϵ_m which involves only conventional 'cracked' section analysis using modular ratio concept.

$$\epsilon_m = \epsilon_1 - \epsilon_2$$

These assumption are illustrated in Fig. 3.

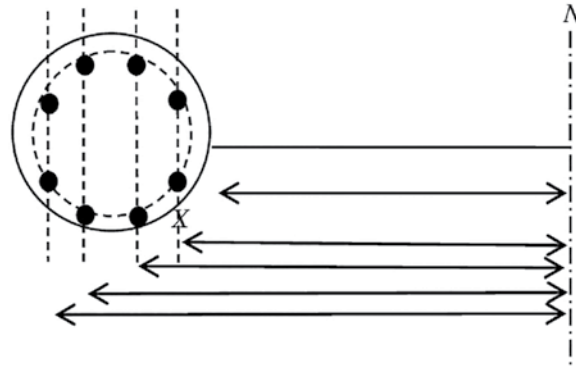


Fig. 3. Location of NA

Whereby x (depth of neutral axis) and the 'apparent' strain ϵ_1 at the extreme fiber of concrete is calculated. Assuming the tensile strength of concrete is zero.

$$\epsilon_1 = \frac{f_{st}}{E_s} \frac{a' - x}{d - x}$$

The strain ϵ_2 corresponds to a reduction in tensile stress in reinforcement suggest a reduction in tensile force in reinforcement, equal to the force generated by the triangular distribution of tensile stress in concrete.

$$\epsilon_2 = \frac{b(D-x)(a'-x)}{3E_s A_s (d-x)}$$

If the value of calculated value of ϵ_2 is exceed by ϵ_1 (ie $\epsilon_m < 0$) then it should be constructed that the section is un cracked.

Calculation of ϵ_1 and ϵ_2 for circular section as below.

$$f_{st} = f_{st1} + f_{st2}$$

Where f_{st} is tensile stress in steel in outer most steel and f_{st1} , f_{st2} is stress due to axial and moment in section respectively, A_{st} is the total area of reinforcement

$$f_{st1} = \frac{T}{A_{st}}$$

$$M = f_{st2} \cdot A_{st} \cdot y' + f_{st2}'' \cdot A_{st}'' \cdot y'' + f_{st2}''' \cdot A_{st}''' \cdot y''' + f_{st2}'''' \cdot A_{st}'''' \cdot y'''' + \dots$$

Where f_{st2} is the stress in outer most reinforcement due to bending moment.

$$f_{st2}' = f_{st2}$$

$$y' = x + \frac{D}{2} + r \cos \frac{\pi}{n}$$

$$y'' = x + \frac{D}{2} + r \cos \frac{3\pi}{2n}$$

$$y''' = x + \frac{D}{2} - r \cos \frac{3\pi}{2n}$$

$$y'''' = x + \frac{D}{2} - r \cos \frac{\pi}{n}$$

Stress in reinforcement at different level

$$f_{st2}'' = \frac{f_{st2}}{y'} y''$$

$$f_{st2}''' = \frac{f_{st2}}{y'} y'''$$

The expression for predicting crack width.

$$w_{cr} = \frac{3a_{cr}\epsilon_m}{1 + \frac{2(a_{cr} - C_{min})}{(D - x)}}$$

PROPOSED METHOD OF CALCULATION

After analytical calculation of crack width, we observed that value of x and f_{st2} is depend on each other, where the location of neutral axis is outside the section and if neutral axis is more far from the section then the stress in reinforcement due to bending in minimum. Although according to BS code BS 8110 Part 2, for cases where the whole section is in tension, an effective value of neutral axis can be estimated by interpolation between the following limiting conditions:

- where the neutral axis is at the least compressed face,
- for axial tension, Neutral axis location = $-D$

But if we calculate by the conventional section analysis method , then we found the neutral axis location is between the compressed face and depth of the section.

Some numerical example are solved and observed the variation with the parameter as graph given below, and the factors Influencing crack-widths as mentioned below.

Tensile stress in the steel bars;

Thickness of concrete cover;

Diameter and spacing of bars;

Depth of member and location of neutral axis; and

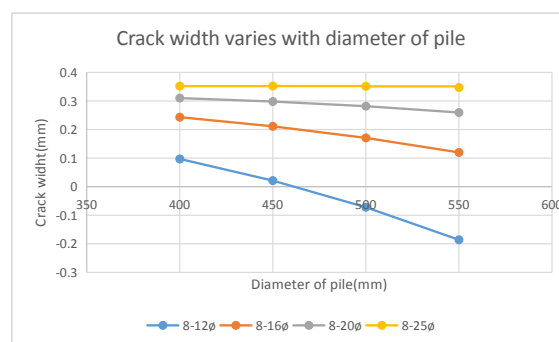
Bond strength and tensile strength of concrete.

Crack width varies with diameter of pile

The variation of crack width with the diameter of pile, and in calculation acting tensile load, moment is constant, but the number of reinforcement is same and the diameter of bars is varies, for the study of the crack width.

Where ,

$T_u = 100\text{kN}$ and $M_u = 25\text{kNm}$



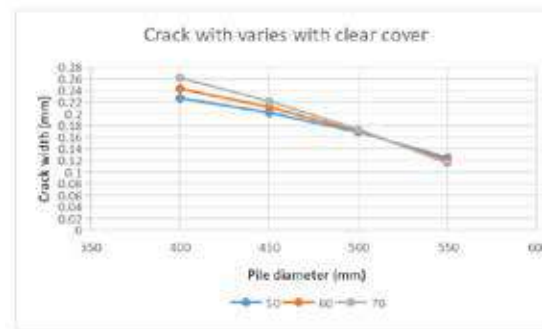
Graph 1. Crack width with varies with diameter of pile



Crack width varies with clear cover in pile shaft

The variation of crack width with the clear cover in pile shaft, and in calculation acting tensile load, moment, number of reinforcement, diameter of reinforcement is constant for the study of the crack width.

Where, $T_u = 100\text{kN}$ and $M_u = 25\text{kNm}$, Reinforcement is $16\phi-8\text{No's}$



CONCLUSION

Crack width in pile shaft is minimized with increasing the diameter of pile shaft, but when diameter of main reinforcement is increased then the value of crack width also increases. Crack width also increases with the increasing of clear cover.

ACKNOWLEDGMENT

The author is indebted to the company of Quality Austria Central Asia Pvt.Ltd, New Delhi. Thanks for their support.

REFERENCES

1. R Wynne Edwards, "Technical Note. Cracks in Reinforced Concrete Piles," Proceedings of the Institution of Civil Engineers, E-ISSN 1753-7789, Volume 39 Issue 1, JANUARY 1968, pp. 133-134
2. Zhijun Yang, Qing Fang, Bu Lv, Can Mei, and Xudong Fu "An Investigation into the Effect of Cracking on the Response of Drilled and Postgrouted Concrete Pipe Pile under Lateral Loading," Hindawi Advances in Materials Science and Engineering Volume 2020, Article ID 5373958, 12 pages [https://doi.org/10.1155/2020/5373958]
3. Indian Standard PLAIN AND REINFORCED CONCRETE - CODE OF PRACTICE (Fourth Revision) IS456:2000.
4. British Standard STRUCTURAL USE OF CONCRETE BS 8110-2: 1985



Condition Assessment of Structural Components Using Internet of Things (IoT)

C Harshitha^{*1}, Mallika Alapati²

PG Student, Department of Civil Engineering, VNRVJIET, Telangana¹

Professor, Department of Civil Engineering, VNRVJIET, Telangana²

*✉ bkharshitha97@gmail.com

ABSTRACT

Structural Health Monitoring (SHM) has gained a lot of importance in today's scenario. Significant reduction in the cost of sensors and connectivity, made remote data collection possible to monitor the structures and perform critical analysis so that actions can be taken to assess and enhance the residual life of the structures. Internet of Things (IoT) is the network of smart sensors that combines sensing and transmission of various responses of the structures to distant servers which continuously processes and monitors these responses. The present paper proposes an integrated platform of IoT for damage detection using Wi-Fi module, Raspberry Pi, (Piezoelectric) PZT sensors along with Digital to Analog (DAC) and Analog to Digital converters (ADC). Signatures are extracted from PZT sensors and an algorithm is proposed to identify and quantify the damage comparing with base line signatures of healthy structural component. The algorithm is executed using python. In the present work, tests are conducted on simply supported aluminium beam surface bonded with two PZT transducers, one acts as an actuator and the other acts as a sensor. Beam is actuated by a sinusoidal vibration through a python program. DAC converts this digital wave into analog form and sends it to actuator which excites the aluminium beam. Initially signatures from healthy beam are recorded for a specified time duration. The sensor receives the response from aluminium beam which is in analog form and this response is converted to digital form using ADC. Damage is induced in the form of crack in aluminium beam signatures data is collected from piezoelectric sensor and communicated to Raspberry Pi. An algorithm is proposed to quantify the damage using cross correlation (CC).

Keywords: SHM; IoT; Raspberry Pi; Cross correlation index; PZT.

INTRODUCTION

From the past few years, there have been many advancements in various fields using the Internet of Things (IoT). Many innovative ways are proposed to make human life easier especially in the fields of electronics, industrial machines, aircraft, etc. Structural Health Monitoring (SHM) is one process where IoT is yet to be used for the real-time purpose. SHM is a process of detecting incipient damages in a structure, with the help of sensors and data acquisition systems, we can monitor uninterruptedly to detect and estimate the residual life of the structure. Sensors are more sensitive and accurate than any other equipment used for health monitoring. They play a significant role in capturing responses and sending continuous data from the host structure. IoT in SHM comes into the picture when we want to store this huge data into a wifi module or cloud. IoT also helps to monitor any type of structure remotely without human inspection at the structures. It helps to analyze the responses using various signal processing techniques and mathematical models.

The present project aims on detecting the extent of damage on a smart aluminium beam using PZT transducers and Raspberry Pi. Two PZT transducers are surface mounted on aluminium beam where one acts as an actuator while the other is a sensor. Harmonic analysis is done by inducing sinusoidal excitation into the beam. PZT sensor receives these responses and sends them to thingspeak which is a cloud platform for storing data.

LITERATURE REVIEW

Although SHM using sensors is applied to various fields, very few works were done on Structural Health Monitoring using the Internet of Things (IoT). Scantly available journal papers mainly include crack detection of various specimens with the help of different sensors using Raspberry Pi. Carmelo Scuro et al. [1] have used the acoustic emission technique to monitor reinforcements in structural components. Ultrasonic waves are generated and received through the emitter and receiver. In case any damage is detected in the structural reinforcement, an alert message is sent to the server through remote control and

service room. Alex Myers et al. [2] have used ABAQUS software to generate guided longitudinal waves on steel plate. They have proposed a mathematical model to find the size and location of the damage. Md Anam Mahmud et al. [3,4] have proposed a signal processing technique on aluminium sheet. Two PZT transducers are mounted on aluminium sheet and the output of these transducers is stored in oscilloscope. The output data is further analyzed using MATLAB where a simple cross correlation index is used and to remove noises from extracted data, Butterworth filter is used.

Ahmed Abdelgawad and Kumar Yelamarthi [5] have conducted both experimental and analytical studies on steel plate to find damage location and size. The results of both studies are compared and percentage error is calculated. In [6], NRF module and Pro-Trinket microcontroller are used to send data to Raspeberry Pi. Hongyang Zhang et al. [7] have conducted SHM using IoT to remove environmental effects from the data obtained from the sensor, principal component analysis is conducted. After removing the environmental effects, Hilbert Huang Transformation (HHT) is used for signal analysis. Amira Zrelli et al. [8] have proposed IoT based SHM to detect the location of damage using wireless sensor network. “Mean Normalized Curvature Difference of Waveform Jerk Energy” (MCDWJE) and “Curvature Difference Probability waveform Jerk” (CDPWJE) methods are used to detect damage in bridges. Byung Wan Jo et al. [9] have combined IoT with blockchain technology to monitor underground structures. In [10], Lin-sheng Huo et al. have done damage detection based on Cross Correlation Function Amplitude (CCFA) and Support Vector Machine (SVM). This consist of two stages, in the first stage, data is extracted from the sensors using CCFA from dynamic responses of the host structure and in the second stage, this data is sent to SVM to classify the damage of the structure. Seunghee Park et al. [11] have proposed instantaneous baseline signatures using Digital Signal Processing (DSP) module where the damages are detected based on Wavelet Transform (WT) and Cross Correlation (CC) index. Shao-Fei Jiang et al. [12] have proposed Fuzzy Neural Networks (FNN) and data fusion techniques for detecting the damage in structures. These methods are useful when the output data is vast and inaccurate. Victor Giurgiutiu and Giola Santoni-Bottai [13] have used piezoelectric wafer sensors for monitoring composite structures from that of the metallic structures. F.Lamonaca et al. [14] have used MQTT protocol to avoid the waiting time of the receiving signal. They have shown the importance of synchronization of signals. Apoorva Jindal and Mingyan Liu [15] have shown the significance of network computing using wireless sensor networks. The present work aims at identifying and quantifying the damage in smart beams using PZT Transducers.

EXPERIMENTAL STUDY

Methodology

As the actuator excites the host structure with a sinusoidal wave, while receiving the response from the sensor, noises are observed. To remove these noises caused by environmental effects or external vibrations, the Butterworth filter is used. The CC value is calculated for the excitation signal and the filtered signal. The CC value obtained is 0.971.

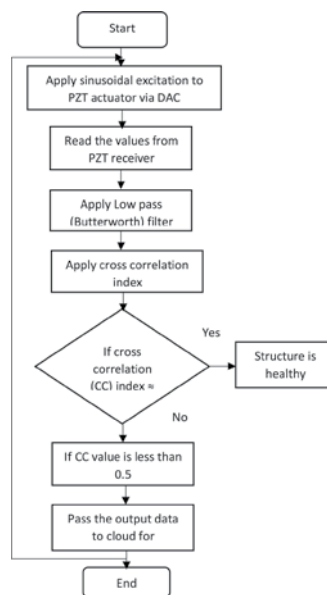


Fig. 1. Flow chart of proposed SHM



Hardware Required

The proposed IoT experimental work consists of Raspberry Pi, Analog to Digital converter (ADC), Digital to Analog converter (DAC), PZT, breadboard and jumper wires. Breadboard is used for temporary connections where soldering is not required. Jumper wires are used for connecting Raspberry Pi to PZT transducers via DAC and ADC.

Raspberry pi 4. Raspberry Pi 4 Model B is the new generation of Raspberry Pi single board computer which supports more RAM (2GB). It is a 64bit quad core ARM-Cortex A72 with a clock speed of 1.5GHz. With the help of the New Out of Box software (NOOBS), operating system of Raspberry Pi (Raspbian) is installed. It contains 5V and 3.3V GPIO pins and the current it draws is around 3.4 watts. It is used to send the excitation signal, store the receiving data, analyze the data, and send the data to the cloud.

DAC. As the PZT transducers accept only analog signals, we use a digital to analog converter (DAC) to send the sinusoidal wave to the actuator. MCP4725 is used for converting the signal into analog form. It is a 12 bit, low power, and high accuracy converter. Its power supply ranges from 2.7V to 5.5V. It has an I2C interface at a rate standard, fast and high speed with 100KHz, 400KHz, and 3.4 MHz respectively.

ADC. ADC is used for converting an analog signal received from the PZT sensor to a digital signal and send it to Raspberry Pi. In the present work, ADS1015 is used which is a 12bit resolution with a sample rate of 3.3 kSPS. Its power supply ranges from 2.0V to 5.5V. It has got four channels i.e., with one ADC we can connect up to four sensors.

Piezoelectric Transducers. When mechanical strain is induced it produces an electric field and vice versa. Therefore, it acts as both an actuator and a sensor. In the present work, two PZT transducers are surface mounted on either side of the specimen. One excites the signal and the other receives the signal.

Proposed Damage Quantification Metric

The damage is identified from the results, signatures, or responses obtained by various sensors used for monitoring the structures. The most commonly used damage metrics are the Root Mean Square Deviation (RMSD) method, Cross-Correlation (CC) method and Covariance method. In the present work, Cross-Correlation is used for identifying and determining the extent of the damage. The PZT actuator excites the host structure with a sinusoidal wave towards the sensor. The PZT sensor receives the wave and sends it to Raspberry Pi. An algorithm is proposed to compare the similarity of two signals. The CC value is used as a damage index which is defined as

$$CC = \frac{\left(\frac{1}{N}\right) \sum_{i=1}^N (E_i - \bar{E})(R_i - \bar{R})}{\sigma_E \sigma_R} \quad (1)$$

Where E and R are excitation and receiving signals respectively. A structure is said to be healthy when the excitation and receiving signals are similar whose CC value is 1. The structure is said to be damaged if the CC value is other than 1. The value of CC ranges from -1 to 1.

EXPERIMENTAL SETUP

A simply supported smart aluminium beam of 33cm length, 2.5cm width and 0.2cm thick is considered. The effective length of the beam is 30cm and the actuator and sensor are surface mounted at a distance of 10cm and 18cm respectively from the left support. Since the PZT transducers send and receive only analog data, ADC and DAC are used for converting the signals from analog to digital and vice versa. The actuator is connected to DAC (digital to analog converter) and the sensor is connected to ADC (analog to digital converter). Through a python driven program, a sinusoidal wave of 16kHz frequency is sent to the actuator via DAC towards the sensor. This actuator excites the host structure and sensor receives the signal. An algorithm is written to apply the Butterworth filter to remove noises from the received signal. A low pass filter of order 5 is used whose cutoff frequency (normalised) is 0.5. Cross correlation index is applied on the excitation signal and received filtered signal. The CC value obtained for a healthy beam after applying the Butterworth filter is 0.9714. Now, cracks are induced at increase in percentages between actuator and sensor. CC value is observed for different crack percentages and a graph is plotted to compare the damaged beam with the healthy beam.

Since the main aim of using the internet of things platform is to store the output data in the cloud, the output of CC values is sent to thingspeak in the form of graphs. These graphs are seen using a mobile app which helps us to monitor from any place.

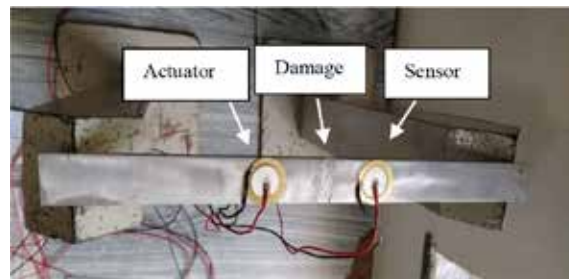


Fig 2. Damaged specimen

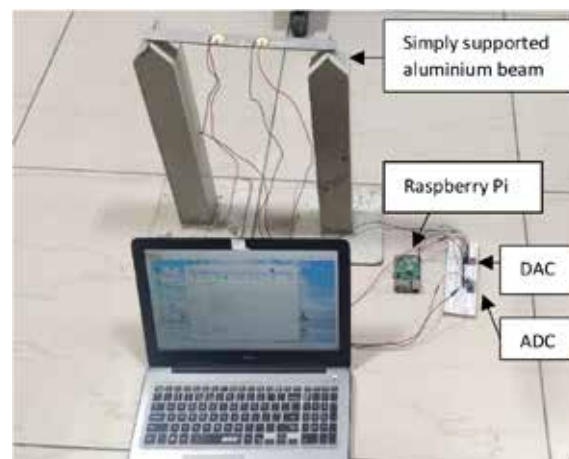


Fig 3. Experimental Setup

RESULTS AND DISCUSSION

Cracks of different widths are induced in the aluminium beam and the CC value is obtained using the mathematical model in python. The values of CC are

Table 1. CC values for different crack widths

Damage percentage	0% (Healthy)	1.25%	2.5%	3.75%	5%
Cross correlation (CC) index	0.9714	0.656	0.1013	-0.6123	-0.9341

The samples of the received signals are taken for all the cases and graphs are plotted to compare with the healthy samples.

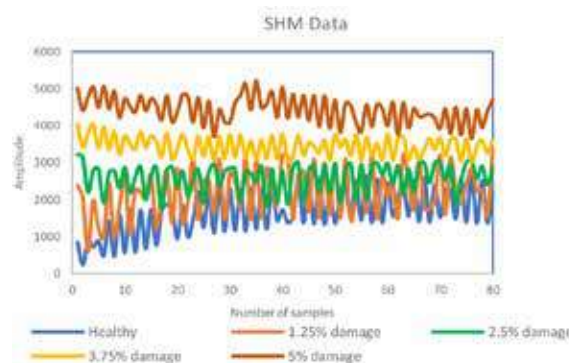


Fig. 4. Variation in amplitudes at different crack widths



Fig 5. A snapshot of Thingspeak's web page

CONCLUSION

- In this study, IoT based SHM platform is designed to detect damages (cracks) in simply supported aluminium beam.
- An algorithm is proposed to identify the damage extent using python.
- CC index values are extracted through the python program from the received signal from ADC after the application of filters.
- It is observed with the increase in the percentage of damage width, there is a decrease in CC index which varies between -1 to +1.
- The main aim of IoT is to store the data in the cloud therefore the values are stored in thingspeak and are used for further analysis.
- The CC values are viewed through a mobile application and a threshold limit is set. The mobile application gives an alarm signal whenever the CC value is reduced below 0.5.

REFERENCES

1. Carmelo Scuro, Paolo Francesco Sciammarella, Francesco Lamonaca, Renato Sante Olivito, and Domenico Luca Carni, "IoT for Structural Health Monitoring," IEEE Instrumentation and Measurement Magazine, 2018.
2. A. Myers, M. A. Mahmud, A. Abdelgawad and K. Yelamarthi, "Toward integrating Structural Health Monitoring with Internet of Things (IoT)," IEEE International Conference on Electro Information Technology (EIT), Grand Forks, ND, 2016, pp. 0438-0441, 2016.
3. Md Anam Mahmud, Ahmed Abdelgawad, Kumar Yelamarthi and Yasser A. Ismail, "Signal Processing Techniques for IoT-based Structural Health Monitoring," 29th International Conference on Microelectronics (ICM), 2017.
4. Md Anam Mahmud, Kyle Bates, Trent Wood, Ahmed Abdelgawad, Kumar Yelamarthi, "A Complete Internet of Things (IoT) Platform for Structural Health Monitoring (SHM)," 2018.
5. A. Abdelgawad, K. Yelamarthi, "Internet of Things (IoT) Platform for Structure Health Monitoring," Wireless Communications and Mobile Computing, vol. 2017, Article ID 6560797, 10 pages, 2017. doi:10.1155/2017/6560797.
6. A. Abdelgawad and K. Yelamarthi, "Structural health monitoring: internet of things application," in Proceedings of the 59th IEEE International Midwest Symposium on Circuits and Systems (MWSCAS '16), Abu Dhabi, United Arab Emirates, October 2016.
7. H. Zhang, J. Guo, X. Xie, R. Bie, Y. Sun, "Environmental Effect Removal Based Structural Health Monitoring in the Internet of Things" Seventh International Conference on Innovative Mobile and Internet Services in Ubiquitous Computing, pp:512 – 517, Taichung, 2013.
8. Amira Zrelli, Hacen Khlaifi and Tahar Ezzedine, "Application of Damage Detection for Bridge Health Monitoring," IEEE, 2017.



9. Byung Wan Jo, Rana Muhammad Asad Khan and Yun-Sung Lee, “Hybrid Blockchain and Internet-of-Things Network for Underground Structure Health Monitoring,” *Sensors*, 2018.
10. Lin-sheng Huo, Xu Li, Yeong-Bin Yang, and Hong-Nan Li, “Damage Detection of Structures for Ambient Loading Based on Cross Correlation Function Amplitude and SVM,” Hindawi Publishing Corporation, Volume 2016, 12 pages, 2016.
11. Seunghye Park, Steven R. Anton, Jeong-Ki Kim, Daniel J. Inman, and Dong S. Ha, “Instantaneous Baseline Structural Damage Detection Using a Miniaturized Piezoelectric Guided Waves System,” *KSCE Journal of Civil Engineering*, Volume 14, pp: 889-895, 2010.
12. S. Jiang, C. Zhang and S. Zhang “Two-stage structural damage detection using fuzzy neural networks and data fusion techniques”, Elsevier- *Expert Systems with Applications*, vol. 38, pp- 511–519, 2011.
13. V. Giurgiutiu and G. Santoni-Bottai, “Structural health monitoring of composite structures with piezoelectric-wafer active sensors,” *AIAA Journal*, vol. 49, no. 3, pp. 565–581, 2011.
14. F. Lamonaca, C. Scuro, P. F. Sciammarella, D. L. Carni, and R. Olivito, “Synchronization of IoT layers for structural health monitoring” in *Proc. IEEE Int. Workshop on Metrology for Industry 4.0 and IoT*, Apr. 2018.
15. A. Jindal and M. Liu, “Networked Computing in Wireless Sensor Networks for Structural Health Monitoring,” *IEEE/ACM Transactions on Networking IEEE/ACM Trans. Networking*, vol. 20, no. 4, pp. 1203–1216, 2012.



Comparison of GSA 2003 and 2016 Guidelines for Evaluating Progressive Collapse Potential of Steel Moment Resisting Frame Building

Parthav P Patel, Digesh D Joshi

Department of Civil Engineering, Institute of Technology, Nirma University, Ahmedabad, Gujarat

✉ 19mclcl3@nirmauni.ac.in

ABSTRACT

Progressive collapse is a situation in which failure of primary load bearing element leads to failure of adjoining members progressively which is disproportionate to initial event. In this paper, progressive collapse potential of 9-storey steel moment resisting frame building is evaluated using Alternate Load Path Method (APM) as specified in GSA 2003 and 2016 guidelines. Analysis results obtained from linear static, non-linear static and non-linear dynamic analysis are compared for middle column removal scenario from longitudinal bay. Demand Capacity Ratio (DCR) for beams and columns located adjacent to removed column are determined from linear static analysis. Load carrying capacity of building is found out using non-linear static analysis. Displacement time history is plotted at the location of removed column from non-linear dynamic analysis. Also, ductility demand and plastic hinge rotations obtained from non-linear analysis following GSA 2003 and 2016 guidelines are compared. From the analysis, it is observed that if structure is designed following to GSA 2003 guidelines then its vulnerability against progressive collapse will be higher compared to design following to GSA 2016 guidelines.

Keywords: Progressive collapse; Steel building; Alternate load path method; Demand capacity ratio; Displacement time history.

INTRODUCTION

Progressive Collapse due to loss or failure of local load carrying element which leads to partial or total collapse of structure. The extent of damage or collapse disproportionate to initial event. It is a dynamic failure mechanism in which loss of one or more local load carrying element propagates through a system causing widespread collapse progressively. It is caused by abnormal loads like gas explosions, vehicular impacts, blast loading etc. The design/protection of structure against progressive collapse becomes a concern after Ronan Point apartment tower collapse (London, 1968) due to gas explosion. Also, after collapse of World Trade Centre (New York 2001), many government and private agencies worked on the development of guidelines for progressive collapse resistant structure. The U. S. General Services Administration (GSA) and Department of Defense's Unified Facility Criteria (UFC) employ the Alternate Load Path Method (APM) to ensure the resistance of structure against progressive collapse. Marjanishvili [1] compared the four analytical methods – linear static, linear dynamic, non-linear static and non-linear dynamic analysis to evaluate progressive collapse potential of structure. Marjanishvili et al. [2] evaluated the progressive collapse potential of 9-storey steel building using SAP2000 following to GSA 2003 guidelines. Kim and Kim [3] assessed the progressive collapse resisting capacity of 3, 6 and 15 storey steel moment frames using GSA 2003 and DoD 2005 guidelines. Progressive collapse of 4 and 8-storey moment resisting frame was assessed by Kiakojoury et al. [4] using static and dynamic incremental analysis following to GSA 2013 guidelines. Authors concluded that static analysis predicts larger capacity compared to dynamic analysis against progressive collapse. Tavakoli and Alasthi [5] evaluated progressive collapse potential of 5 and 15 storey steel buildings under lateral loading. Authors concluded that, as number of bays and stories increase, progressive collapse potential of building increase.

In this paper, comparative study of GSA 2003 and GSA 2016 guidelines for progressive collapse is carried out by analyzing 9-storey steel moment resisting frame building. Linear static, non-linear static and non-linear dynamic analysis are carried for middle column removal scenario to evaluate the progressive collapse potential of steel building. The results obtained based on GSA 2003 and GSA 2016 guidelines are compared.

GSA GUIDELINES

The U. S. General Services Administration issued the guidelines for analyzing and evaluating the resistance of structure against progressive collapse. The guidelines are applicable to new and renovated federal buildings with the aim to reduce the potential for progressive collapse by utilizing Alternate Path Method (APM). The GSA guidelines were first published in November 2000 which primarily focused on reinforced concrete structures [6]. These guidelines were updated in June 2003 in order to address the progressive collapse potential of steel frame structure also. After thorough research on the available guidelines for progressive collapse, certain inconsistencies were identified and revised guidelines were published on October 2013 with 1st revision in January 2016.

Table 1. Comparison of GSA 2003 and GSA 2016 guidelines

Parameter	GSA 2003 Guidelines	GSA 2016 Guidelines
Type of approach	Threat Independent	Threat Dependent in conjunction with Interagency Security Committee (ISC)
Type of member end action	No differentiation	Force Controlled and Deformation Controlled
Preferred Analysis Methods	Linear Static (LS), Linear Dynamic (LD), Non-linear Static (NS), Non-linear Dynamic (ND)	
Load combination for LSA	2 (DL + 0.25LL)	$\Omega_L(1.2DL + 0.5LL)$ Where, Ω_L depends on governing m-factor
Load Combination for NSA		$\Omega_N(1.2DL + 0.5LL)$ Where, Ω_N depends on yield and allowable plastic hinge rotation
Load combination for LDA and NDA	(DL + 0.25LL)	(1.2DL + 0.5LL)
Irregular building analysis	DCR ≤ 1.5 for linear analysis	DCR ≤ 2 for LSA DCR > 2 – LSA not allowed
Acceptance criteria for LSA	DCR ≤ 2 , for beam-flexure DCR ≤ 1 , for column	DCR \leq Governing m-factor for beam-flexure DCR ≤ 1 for column

So, it is important to identify the major differences between these guidelines. The GSA 2016 guidelines were developed with the aim to reduce the inconsistencies between the GSA and Department of Defense (DoD) methodologies [7]. **Table 1** shows the comparison of GSA 2003 and GSA 2016 guidelines.

METHODOLOGY

The 9-storey steel moment resisting frame building is considered for the study. The beams, columns are designed as per IS 800: 2007 [8] composite slab is designed as per IS 11384: 1985 [9]. The progressive collapse potential of the building is evaluated using GSA 2003 and GSA 2016 guidelines for middle column removal scenario from ground floor and results obtained are compared. For modelling and progressive collapse analysis, SAP2000 software is used.

Description of Model

The 9-storey steel building considered for study has 6-bays in longitudinal direction and 3 bays in transverse direction [2]. The uniform spacing of column is 8.25 m in longitudinal direction and 9.75 m in transverse direction. The typical storey height is 4.3 m. The plan and elevation view is shown in **Fig. 1** and **Fig. 2**. All the beam column connections assumed as fully restrained and support condition of column to ground is considered as fix.

Loading on Building

There are total four load cases considered in SAP2000 which includes dead load, slab load, live load, and wall load. The dead load case includes the self-weight of beams and columns. The thickness of composite concrete slab is considered as 90 mm. Slab load is applied as an area load by considering density of concrete as 25 kN/m³. The live load is considered as 1.9 kN/m² on

all floors. The wall load is considered as 19.7 kN/m and applied on perimeter beams except on roof. The seismic load applied on building as per IS 1893:2016 [10] by considering building in zone III. The designed section of primary beam is ISMB500 and ISMB450 for all floors. Column section is designed as built-up column with 550 mm depth, 400 mm flange width, 30 mm flange thickness and 25 mm web thickness.

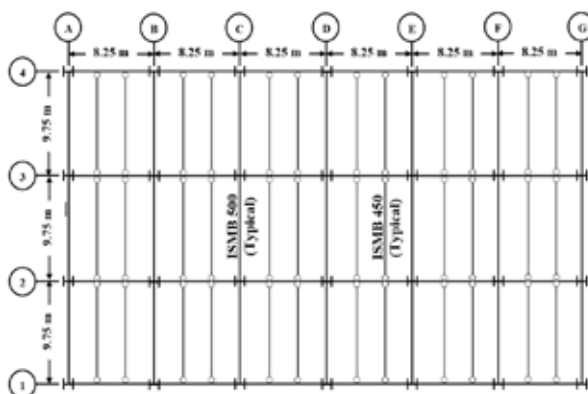


Fig. 1. Plan view of building [2]

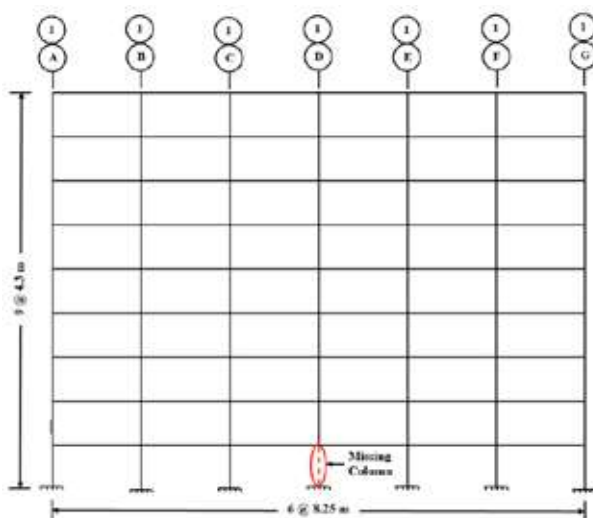


Fig. 2. Elevation view of building

LINEAR STATIC ANALYSIS

The Linear Static Analysis (LSA) is performed to evaluate the progressive collapse potential of the building. This analysis gives an indication whether the building is vulnerable to progressive collapse or not by calculating Demand Capacity Ratio (DCR). The load combination for LSA is given in **Table 1**. As per GSA 2003 guidelines, the load increase factor is considered as 2 but as per GSA 2016 guidelines, load increase factor is depends on force-controlled and deformation-controlled action. For present study, the moment and shear in beam is classified as deformation and force-controlled respectively.

For column, moment can be force-controlled or deformation-controlled which depends on ratio of P/P_{CL} . If $P/P_{CL} > 0.5$ then moment and axial force is considered as force-controlled action, but for $P/P_{CL} \leq 0.5$, moment is considered as deformation controlled action and axial force is considered as force-controlled. P_{CL} is lower bound axial compressive strength of column.

Determination of Load Increase Factor

In GSA 2016, the different load increase factors are given for force controlled (Ω_{LF}) and deformation-controlled actions (Ω_{LD}). For force-controlled action, the Ω_{LF} is considered as 2 and for deformation controlled action Ω_{LD} is determined as per equation (1).

$$\Omega_{LD} = 0.9m_{LF} + 1.1 \quad (1)$$

Where m_{LF} is smallest of 'm' for any primary beam or girder which is denoted as 'm-factor' or 'Demand Modifier'. Demand modifier need to find out for steel component as well as for connections and the smallest value of m is considered as m_{LF} . The m-factor for flexure in beam is depends on ratio of flange width to twice flange thickness and depth of web of beam to thickness of web. GSA 2016 guidelines suggests Table 9-4 of ASCE 41-13 to find m-factor for beam and for connections for Collapse Prevention (CP) criteria [11]. But for certain type of connections, the Table 10 of GSA 2016 should be used. For ISMB 500 beam, the value of Ω_{LD} is estimated as 3.8.

Calculation of Demand Capacity Ratio (DCR)

From linear static analysis, Demand Capacity Ratios of members adjacent to removed column are calculated. DCR for beam is calculated by considering bending moment. The axial force and bending moment are used to calculate DCR in column.

DCR for Flexure in Beam

It is the ratio of actual moment (M_{actual}) to plastic moment capacity (M_p) of the section. Mathematical expression for DCR for beam is given in equation (2).

$$DCR (\text{Beam-Flexure}) = M_{actual} / M_p \quad (2)$$

Where $M_p = Z_p f_y$

Z_p = Plastic section modulus

f_y = Yield stress of the material

DCR for Column

There are certain equations given in ASCE 41-13 to calculate the DCR for column. The type of equation used is depends upon ratio of P/P_{CL} . P_{CL} is the lower bound axial compressive strength of column. P is the axial force acting on the column after application of increased gravity load. If GSA 2016 guidelines used then value of 'P' should be taken from the model generated for deformation-controlled action. Equations (3) to equation (5) is used to calculate DCR in column [11].

$$\frac{P}{P_{CL}} > 0.5; DCR = \frac{P_{UF}}{P_{CL}} + \frac{M_x}{M_{CLx}} + \frac{M_y}{M_{CLy}} \quad (3)$$

$$0.2 \leq \frac{P}{P_{CL}} \leq 0.5; DCR = \frac{P_{UF}}{P_{CL}} + \frac{8}{9} \left[\frac{M_x}{m_x M_{CEx}} + \frac{M_y}{m_y M_{CEy}} \right] \quad (4)$$

$$\frac{P}{P_{CL}} < 0.2; DCR = \frac{P_{UF}}{2P_{CL}} + \frac{M_x}{m_x M_{CEx}} + \frac{M_y}{m_y M_{CEy}} \quad (5)$$

Where, P_{UF} = Axial compressive force on column

M_x = Bending moment in section about x-axis

M_y = Bending moment in section about y-axis

M_{CLx} = Lower bound flexural strength of the member about x-axis

M_{CLy} = Lower bound flexural strength of the member about y-axis

M_{CEx} = Expected flexural strength of member about x-axis

M_{CEy} = Expected flexural strength of member about y-axis

m_x or m_y = value of m-factor for column bending about x or y-axis respectively

In the present study, DCR calculated for flexure in beams is located between gridline C1 and E1 for all stories. DCR for column is calculated for columns located at gridline C1 and at gridline E1 for all stories. C1 means the intersection point of gridline C and gridline 1. DCR for beams and columns are calculated for GSA 2003 and GSA 2016 guidelines and results are compared. The acceptance criteria for flexure in beam is governing m-factor, which is estimated as 3. **Fig. 3** shows the comparison of DCR for column. The acceptance criteria column DCR is 1.

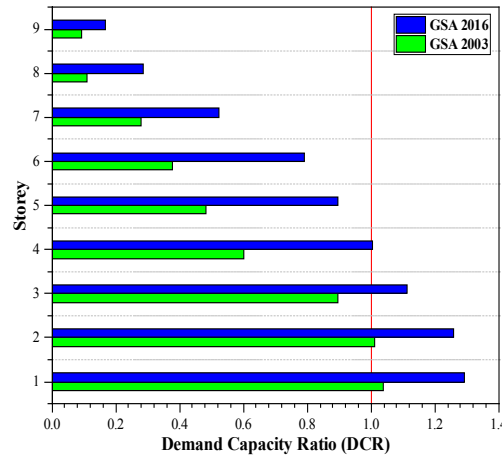


Fig. 3. DCR for Column at grid C1 or E1

From the Fig. 3, it is clear that there is a difference between the results of DCR calculated for GSA 2003 and GSA 2016 guidelines. The DCR calculated as per GSA 2016 guidelines are on a higher side than DCR calculated as per GSA 2003 guidelines.

NON-LINEAR STATIC ANALYSIS

The main advantage of non-linear static analysis is that it considers the material and geometric non-linearity. For progressive collapse it can be termed as ‘Vertical Pushover Analysis’ in which increased vertical load is applied stepwise until the structure collapses. In Table 1, the load combination is given for non-linear static analysis as per GSA 2003 and GSA 2016 guidelines. The dynamic increase factor (Ω_N) is considered as 2 as per GSA 2003 guidelines, but GSA 2016 guidelines suggest that Ω_N should be less than 2 and it depends on support yield rotation (θ_y) and allowable plastic rotation angle (θ_{pra}) for collapse prevention criteria. The Ω_N can be calculated from the equation (6) given below.

$$\Omega_N = 1.08 + \frac{0.76}{\left(\frac{\theta_y}{\theta_{pra}} + 0.83\right)} \quad (6)$$

The ratio θ_y/θ_{pra} is the smallest ratio for any primary element, component or connection in the model within or touching the area with increased gravity load. From, the equation (6), the Ω_N is obtained as 1.36.

The geometric non-linearity is considered in SAP200 by selecting P-delta option for non-linear static load case. To include the material non-linearity the plastic hinges are assigned in the beams and columns ends. From non-linear static analysis, the collapse load of structure can be find out.

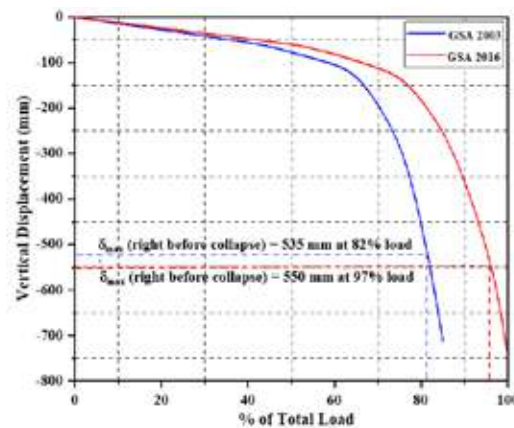


Fig. 4. Non-linear static curve at column removal location

Fig. 4 shows that comparative graph of % of total load v/s vertical displacement for GSA 2003 and GSA 2016 guidelines. From the **Fig. 4**, it is evident that estimation safe load carrying by the building is different for both the guidelines. Also, the vertical displacement at column removal location is different. **Table 2** shows the comparison of % of load taken by building and plastic hinge rotation between GSA 2003 and GSA 2016.

NON-LINEAR DYNAMIC ANALYSIS

Progressive collapse is highly dynamic and non-linear phenomenon. Non-linear dynamic analysis is an efficient method of progressive collapse analysis because it includes the dynamic effect along with material and geometric non-linearity. The load combination for non-linear dynamic analysis is given in **Table 1**. In non-linear dynamic analysis, the simulation of sudden column removal is very important. In the present study, the sudden column removal is simulated using initial conditions. Obtain the reacting force in the column to be removed from linear static analysis. Then delete the column from the model and apply the upward reacting force at column removal location obtained from equilibrium model as joint load.

Table 2. Comparison of non-linear static analysis results

Parameter	GSA 2003	GSA 2016
Total load taken by SAP	85%	99.69%
Safe Load	82%	97%
$\theta_{\text{safe load}}$ at support (from SAP)	3.74 degrees	3.86 degrees
$\theta_{\text{collapse load}}$ at support (from SAP)	5.14 degrees	5.28 degrees
$\theta_{\text{allowable}}$ (for CP criteria, ASCE 41-13)	4.97 degrees	4.97 degrees

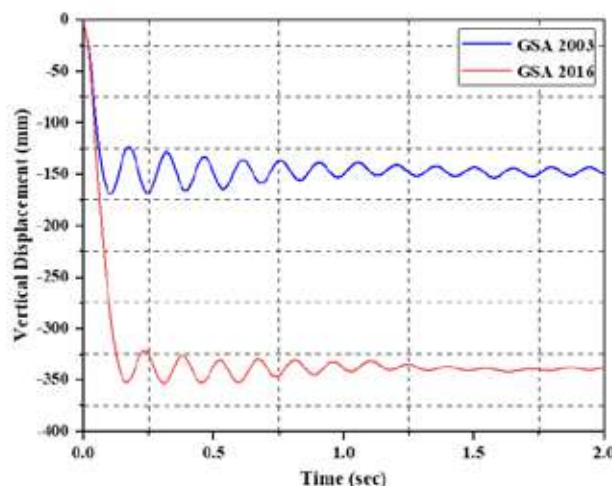


Fig. 5. Displacement time history at column removal location

The non-linear static load case includes all gravity loads defined as an initial condition. After model reach to its equilibrium condition, the column is removed by ramping down the upward reacting force. For dynamic analysis Rayleigh damping is used with 2% damping ratio. The plot displacement time history at joint exactly above removed column is shown in **Fig. 5**. There is a significant difference observed between maximum dynamic displacement obtained following to GSA 2003 and 2016 guidelines. From **Table 3**, it is evident that the ductility demand and plastic hinge rotation is significantly higher followed to GSA 2016 guidelines compared to GSA 2003 guidelines.

CONCLUSIONS

In this study, GSA 2003 and 2016 guidelines for evaluating progressive collapse potential are compared by analyzing 9-storey moment frame building. Linear static, non-linear static and non-linear dynamic analysis are carried out for middle column removal scenario from longitudinal bay and results obtained are compared. Based on the comparative study, following conclusions are derived:

**Table 3.** Comparison of non-linear dynamic analysis results

Parameter	GSA 2003	GSA 2016
Ductility ($\mu = \delta_{\max}/\delta_{\text{yield}}$)	168.9/61.55 = 2.74	353.5/56.96 = 6.21
$\theta_{\max, \text{ support}} = \tan^{-1}(\delta_{\max}/\text{span of beam})$	1.17 degrees	2.45 degrees
$\theta_{\max, \text{ support}}$ (from SAP)	0.951 degrees	2.34 degrees
$\theta_{\text{allowable}}$ (for CP criteria, ASCE 41-13)	4.97 degrees	4.97 degrees

- The DCR for beams and columns obtained per GSA 2016 guidelines are significantly higher compared to DCR obtained as per GSA 2003 guidelines. DCR of some of the columns satisfying the acceptance criteria as per GSA 2003 guidelines but the same columns exceed the acceptance criteria as per GSA 2016 guidelines.
- The load carrying capacity of the building from non-linear static analysis is accurately identified following to GSA 2016 guidelines. Because from analysis, the almost 100% load is taken by the building safely whereas GSA 2003 guidelines estimate 82% load taken by the building. This difference occurs due to the magnitude of dynamic increase factor (Ω_N).
- The maximum dynamic displacement is very high followed to GSA 2016 guidelines compared to GSA 2003 guidelines. Also the ductility demand is very high when building is analyzed as per GSA 2016 guidelines compared to GSA 2003 guidelines.
- The comparison of analysis results indicates that, vulnerability of the building against progressive collapse will be high if it is designed following to GSA 2003 guidelines compared to designed following to GSA 2016 guidelines.

REFERENCES

1. S. Marjanishvili "Progressive analysis procedure for progressive collapse analysis", Journal of Performance of Constructed Facilities, vol. 18, pp. 79-85, May 2004.
2. S. Marjanishvili, E. Agnew, "Comparison of various procedures for progressive collapse analysis", Journal of Performance of Constructed Facilities, vol. 20, pp. 365-374, November 2006.
3. J. Kim, T. Kim, "Assessment of progressive collapse resisting capacity of steel moment frames", Journal of Constructional Steel Research, vol. 65, pp. 169-179, 2009.
4. F. Kiakojouri, M. Sheidaii, V. Biagi, B. Chiaia, "Progressive collapse assessment of steel moment-resisting frames using static and dynamic incremental analyses", Journal of Performance of Constructed Facilities, vol. 34, March 2020.
5. H. Tavakoli, A. Alasthi, "Evaluation of progressive collapse potential of multi-storey moment resisting steel frame buildings under lateral loading", Scientia Iranica, vol. 20, pp. 77-86, 2013.
6. U. S. General Services Administration (GSA – 2003), "Progressive Collapse Analysis and Design Guidelines", June 2003.
7. U. S. General Services Administration (GSA – 2016), "Alternate Path Analysis and Design for Progressive Collapse Resistance", January 2016.
8. IS 800: 2007, "Code of Practice for General Construction in Steel", Bureau of Indian Standards, New Delhi, India.
9. IS 11384 – 1985, "Code of Practice for Composite Construction in Structural Steel and Concrete", Bureau of Indian Standards, New Delhi, India.
10. IS 1893 – 2016, "Code of Practice for Earthquake Resistant Design of Structures", Bureau of Indian Standards, New Delhi, India.
11. ASCE/SEI 41 – 13, "Seismic Evaluation and Retrofit of Existing Buildings", ASCE.

PSWC-BAR for Sustainable Concrete Construction

Anil K Kar

Engineering Services International, Salt Lake City, Kolkata

✉ dr.anil.kar@gmail.com

ABSTRACT

Reinforced concrete is the number one medium of construction. Such constructions with plain round bars of mild steel proved to be durable. Following the use of ribbed bars of carbon steel, concrete structures have shown signs of decay and distress early. This is due to the susceptibility of ribbed bars to excessive corrosion due to the provision and presence of ribs, and the consequent loose rust on the surface of such bars before concreting. This can not only reduce the load-carrying capacity of concrete elements, reinforced with ribbed bars, it can also lead to failures during vibratory loadings. Moreover, loose rust on the surface of ribbed bars will prevent any possible passivation of rebars, thereby hastening the process of corrosion in rebars and distress in reinforced concrete constructions. The use of PSWC-BAR, characterized by its plain surface and wave-type configuration, can not only solve the problems of excessive corrosion in rebars of high strength carbon steel and the consequent early distress in concrete structures, it makes concrete constructions sustainable by lowering the life cycle cost of constructions to a fraction of what it is today, and the adverse impact of construction on the environment and the global climate.

Keywords: Corrosion; Deformed bar; Durability of concrete Constructions; PSWC-BAR; Ribbed rebar; Reinforcing bar.

INTRODUCTION

Reinforced concrete is the most common medium of construction. Bridges, buildings, dams, stadiums, roadways and runways are all constructed with reinforced concrete.

Strength, easy formability, relatively easy availability of the component materials of construction and durability of the constructed projects have led concrete constructions to this pre-eminent position.

Reinforced concrete constructions with ribbed rebars of carbon steel (**Fig. 1**) since the mid-nineteen sixties in western countries and since the mid-nineteen seventies in India have, however, reached states of distress fairly early in life (**Fig. 2**).



Fig. 1. Fresh ribbed bars showing start of corrosion at damaged ribs

The ribbed rebars in India are required to conform to the provisions in the Indian Standard IS 1786 [1].

The worldwide problem, created by the use of ribbed bars, whether of the cold twisted deformed (CTD) or thermo mechanically treated (TMT) type, has been aptly summed up in Ref. [2] wherein it was observed : “The last two decades have seen a disconcerting increase in examples of the unsatisfactory durability of concrete structures, specially reinforced concrete ones.”



Fig. 2. Distress in staging of overhead water reservoir due to corrosion in rebars

Sixteen years later, it was remarked in Ref. [3] that “the most direct and unquestionable evidence of the last two/three decades on the service life performance of present constructions and the resulting challenge that confronts us is the alarming and unacceptable rate at which the infrastructure systems all over the world are suffering from deterioration when exposed to real environments.”

In the midst of persistent claims of tremendous advances in the manufactured materials of construction, viz., cement and rebars, a surprise was expressed in Ref. [3] thus: “What is most surprising is that this massive and horrendous infrastructure crisis has occurred in spite of the tremendous advances that have been made in our understanding of the science engineering and mechanics of materials and structures.”

There had to be reasons.

RIBS TO BLAME FOR EARLY DISTRESS IN REINFORCED CONCRETE CONSTRUCTIONS

The surprise in Ref. [3] emanated from the fact that, probably except for the writer [4] and metallurgists/engineers in Russia [5], no one wanted to see what was in front of their eyes, no one wanted to hear about it, and no one wanted to talk about it (**Fig.3**).

If they did, they would have seen all around them examples of excessive corrosion in ribbed CTD bars and ribbed TMT bars (**Fig. 1**), the use of which led to early decay and distress in reinforced concrete constructions (**Fig. 2**).

This pitiable condition of infrastructure, that has led to worldwide concern, has emanated from a failure to recognize that rebars of carbon steel, with ribs on the surface, are intrinsically susceptible to corrosion at accelerated rates.

The reasons for this intrinsic susceptibility of ribbed bars of carbon steel to corrosion at accelerated rates have been provided by in Ref. [4]. The reasons in short are :

1. residual stresses develop at the bases of ribs during the manufacture of rebars
2. cracks, which trigger corrosion, may develop at the edges of ribs at the time of manufacture, during transportation and handling (**Fig. 1**).
3. inside structures under load, nominal stresses in ribbed rebars are enhanced in keeping with the phenomenon of stress concentration due to the presence of ribs or cracks.



Fig. 3. Manufacturers, design engineers and constructors would like not to see, not to hear and not to talk about the problems inherent in high strength deformed rebars of carbon steel

4. additional stresses develop in ribs due to wedge action of such ribs against surrounding concrete
5. the sum-total of stresses and strains in 1 to 4 approach or reach yield stress or strain levels
6. rate of corrosion increases with increasing stress levels; the rate accelerates as the stress or strain approaches yield levels, and the surface becomes unstable once beyond yield, whereupon the process of corrosion becomes unstoppable
7. alkaline solution of $\text{Ca}(\text{OH})_2$ in the pores inside concrete cannot passivate the unstable steel surface at an yield state and thus cannot guard ribbed steel rebars inside concrete against corrosion
8. even without the additional stresses, which ribbed bars under service load conditions can be subjected to, the rate of both micro corrosion and macro corrosion are higher in the case of ribbed bars than in the case of plain bars
9. the rate of corrosion increases with an increase in the yield stress level of the steel material in rebars, apparently because of higher carbon contents.
10. The problem of corrosion is magnified when the strength in rebars is increased by taking recourse to cold twisting, as in the case of CTD bars, or to thermomechanical treatment, i.e., quenching as in the case of TMT bars, as it was/is done in India.
11. by the time of concreting, ribbed bars of carbon steel in many or most cases are covered with a layer of loose rust (**Fig. 4**), essentially making such bars unsuitable for use as rebars (see Subsection 5.6.1 in Ref. [7]), as decreased bond can lower load-carrying capacities [8], or even to failures, especially during vibratory loads
12. besides preventing bond between rebar and concrete, a layer of loose rust on the surface of rebars before concreting (**Fig. 4**) prevents passivation of rebars by the alkaline solution of $\text{Ca}(\text{OH})_2$ in the pores inside concrete.



Fig. 4. Ribbed bars coated with products of corrosion even before concreting, leading to a total loss of bond with concrete

SOLUTIONS

An obvious solution to the world-wide problem of early decay and distress in reinforced concrete constructions would be :

- (a) going back to the old days and use plain round bars of mild steel or use PSWC-BAR, with its plain surface and wave-type configuration, as in Ref. 4,8,9,10, 11, 12], and ordinary portland cement (OPC) of appropriate quality, or
- (b) providing surface protection systems in the nature of waterproofing [13, 14, 15, 16, 17, 18, 19], a concept that has been adopted in Subsection 8.2.1 of Ref. [21], and which is today widely used in the surface protection of concrete bridges.

PSWC-BAR FOR SUSTAINABLE CONCRETE CONSTRUCTION

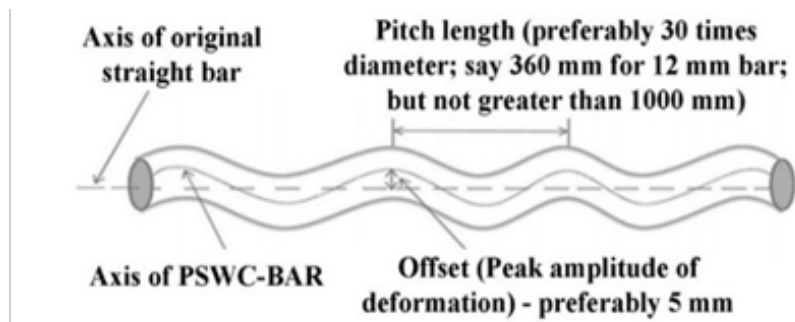
References[9, 10, 11,12] offered the use of PSWC-BAR (**Fig. 5**) (initially named as C bar), in lieu of ribbed bars, whether of the CTD or TMT type or not, as a solution to the problem of early distress in reinforced concrete constructions.

In the absence of ribs or any other surface feature of any type, PSWC-BARs are free from the ill effects which bedevil today's conventional rebars of high strength steel (**Fig. 1, Fig. 2 and Fig. 4**).

PSWC-BARs are preferably hot rolled, say as in Ref.[20]. The wave pattern in a PSWC-BAR is created with the help of a pair of gear rollers at the last stand of the rolling mill process [9]. If desired, PSWC-BAR can also be cold rolled [9].



(a) typical PSWC-BARs of steel, characterized by plain surface and gentle wave-type configuration



(b) schematic view of a typical PSWC-BAR

Fig. 5. PSWC-BAR

Unlike CTD bars, PSWC-BARs are not twisted. Though PSWC-BARs are preferably hot rolled, such bars can also be quenched as in the TMT process.

For purposes of standardization, the pitch length (**Fig. 5(b)**) has been suggested to be 30 times the diameter of the rebar and the peak amplitude of deformation has been recommended to be 5 mm. Five millimeter is not a sacrosanct number. Tests on numerous concrete flexural (beam) and compression (column) elements at different universities have shown that a peak amplitude of deformation of 6 mm generally leads to better structural performances of concrete structures [8].

Tests have shown that compared to concrete elements, reinforced with conventional rebars, viz., plain, ribbed TMT and ribbed epoxy coated bars, such structures, when reinforced with PSWC-BARs, show best performances under load [9].

Besides increased load-carrying capacities, there is several fold enhancement of ductility as well as energy-absorbing capacity when flexural concrete elements are reinforced with PSWC-BARs in lieu of conventional bars [9].

Observations of rebars at site [**Fig. 1, Fig. 4, Fig. 5**] and analysis of test results have shown that there is a total misconception among engineers about “bond” between rebars and concrete, whereas in the context of reinforced concrete, “bond” is as important an element as concrete and rebars are.

In Ref. [9], three terms have been suggested, viz., bond, effective bond, and engagement to replace “bond” engineers loosely refer to.

In the case of a plain bar, it is the pure “bond”, which may be totally absent in the case of ribbed bars which, because of excessive corrosion, may be covered with a layer of loose rust (Fig. 4). In the case of ribbed bars, as in Fig. 1, there is no “bond” between such bars and the surrounding concrete, the bars are not passivated inside concrete, with attendant low life span, under-performance under static load and susceptibility to local or total structural failure under vibratory loads.

Structures with highly corroded ribbed rebars perform under load because of certain levels of “effective bond” or “engagement”.

Structural elements, reinforced with PSWC-BARs, perform the best, as because, in the absence of loose rust, the competent adherent rust on the surface of such bars aid the development of “bond”, and additionally the gentle wave-type configuration



provides additional “engagement” between rebars and concrete, leading to the best “effective bond” or “engagement” between such bars and concrete.

In the case of a PSWC-BAR, “effective bond” and “engagement” are synonymous.

With the focus on durability and thus greater sustainability of infrastructure construction, the desirable mechanical properties of PSWC-BARS have been selected as shown in **Table 1**. The reasons for the selection of the different quantities have been explained in Ref. [11], wherein it has been explained why bars of steel of 650 MPa and 700 MPa yield strength can lower the load-carrying capacities of flexural elements of reinforced concrete.

The use of PSWC-BARS as rebars can do wonders to reinforced concrete construction, and, on a long term basis to individual and national wealth, to the environment and the global climate.

BENEFITS OF USING PSWC-BARS

At no additional cost or effort, the use of PSWC-BARS, in lieu of conventional plain or ribbed bars, leads to the following benefits :

a) several-fold longer life span of concrete structures at no added effort or cost

Sl. No.	Property	Fe 415	Fe 500	Fe 550
i)	yield stress, Min, N/mm ²	415.0	500.0	550.0
ii)	yield stress, Max, N/mm ²	500.0	600.0	660.0
iii)	Y/Y _{specified} ratio ¹	1.02 -1.2	1.02 -1.2	1.02 -1.2
iv)	TS/ Y _{specified} ratio ²	≥ 1.15 - ≤ 1.40	≥ 1.15 - ≤ 1.40	≥ 1.15 - ≤ 1.40
v)	Elongation, percent, Min. on gauge length $5.65\sqrt{A}$, where A is the cross-sectional area of the test piece	20.0	16.0	12.0

Note :

¹)Y/Y_{specified} ratio refers to ratio of actual yield strength to specified yield stress of the test piece

²)TS/ Y_{specified} ratio refers to ratio of tensile strength to specified yield stress of the test piece

Additional Note :

¹)The steel shall be suitable for welding processes

- b) lowering the life cycle cost of reinforced concrete constructions by at least fifty percent; leading thereby to great savings in individual and national wealth.
- c) several-fold increase in ductility and energy-absorbing capacity of concrete flexural elements
- d) greater load-carrying capacities of reinforced concrete elements; with the potential to prevent catastrophes during earthquakes
- e) greater safety during earthquake events
- f) greatly diminished damages to the local and global environments
- g) greater sustainability on many counts, viz., greatly reduced life cycle cost, greater safety during earthquakes, reduced disruption to the society, greatly reduced demand on nature resources, and approximately 5% reduction in the total global emission of CO₂ from all sources.

There have been many publications in India and in the UK on PSWC-BAR since 2010. The three articles in References 10, 11 and 12 should provide an overall picture about the capabilities of PSWC-BAR.

SUMMARY

Reinforced concrete is the number one medium of construction. Besides strength, easy formability and availability of the constituent materials, trouble-free long term performance, i.e., durability of concrete structures, constructed with plain round



bars of mild steel, having yield stress of around 250 MPa to 280 MPa had helped reinforced concrete attain this position.

With time, the use of medium strength (yield stress of about 350 MPa) and high strength (yield stress of about 415 MPa and higher) adversely affected the time-dependent performance of reinforced concrete constructions, leading to worldwide concern about the poor health of infrastructure.

The use of PSWC-BAR, characterized by its plain surface and wave-type configuration, at no added effort or cost, can solve the worldwide problem of early distress in reinforced concrete construction.

Besides several-fold enhancement of life span, with many added benefits, like greatly reduced life cycle cost, the use of PSWC-BAR may prevent catastrophes during earthquakes.

In consideration of additional requirements for survivability under seismic forces, the yield stress of steel in PSWC-BAR is recommended to be limited to 550 MPa, and preferably to 500 MPa.

Recommended mechanical properties of PSWC-BAR for durable concrete constructions are provided.

The several—fold enhancement of life span of concrete structures, reinforced with the use of PSWC-BAR, can prevent staggering financial losses to individual property owners and to national economies of all countries as well as great harm to the environment and to the global climate.

REFERENCES

1. Bureau of Indian Standards, “Indian Standard 1786:2008 - High Strength Deformed Steel Bars and Wires for Concrete Reinforcement --- Specification,” Amendment No. 3 (Fourth Revision).
2. Papadakis, V.G. et al, “Physical and Chemical Characteristics Affecting the Durability of Concrete,” ACI Materials Journal, American Concrete Institute, March – April, (1991).
3. Swamy, R. N. “Infrastructure Regeneration : the Challenge of Climate Change and Sustainability — Design for Strength or Durability,” The Indian Concrete Journal, The ACC Ltd., Vol. 81, No. 7, July , (2007).
4. Kar, A. K. “Concrete Structures – the pH Potential of Cement and Deformed Reinforcing Bars,” Journal of The Institution of Engineers (India), Civil Engineering Division, Volume 82, Kolkata, June 2001.
5. Alekseev, S. N., “Corrosion of Steel Reinforcement,” Durability of Reinforced Concrete in Aggressive Media, Oxford & IBH Publishing Co. Pvt. Ltd., (Translation of : Dolgovechnostizhelezobetona v aggressivnikhsredakh, Chapter 7, pp. 164-247, Stroiizdat, Moscow, 1990.
6. Mohammed, T.U., Ottsuki, N., and Hisada, M., “Corrosion of steel bars with respect to orientation,” ACI Materials Journal, American Concrete Institute, March-April 1999, pp. 154-159.
7. Bureau of Indian Standards, IS 456:2000, “Indian Standard Plain and Reinforced Concrete --- Code of Practice.”
8. Kar, A. K., “A Theory on the Performance of Reinforced Concrete Elements,” Proceedings of the Institution of Civil Engineers – Journal of Construction Materials, <https://doi.org/10.1680/jcoma.18.00019>.
9. Kar, A. K., “Improved Rebar for Durable Concrete Constructions,” New Building Materials & Construction World; New Delhi; Vol. 16, Issue-1, July 2010, pp. 180-199.
10. Kar, A. K., “A Reinforcing Bar for Durable Concrete Constructions and Much More,” The Masterbuilder, Vol. 20, No. 9, Chennai, September 2018.
11. Kar, A. K., “The Search for an Ideal Rebar for Durable Concrete Construction Leads to PSWC-Bar,” International Journal of Technical Innovation in Modern Engineering & Science (IJTIMES), Volume 5, Issue 09, September 2019.
12. Kar, A. K., “Mitigation of GHG Emission and Assault on the Climate and the Environment with the use of PSWC-Bar – an Ideal Rebar for Durable Concrete Construction,” The Masterbuilder; Vol. 21, No. 9, Chennai; September 2019.



13. Kar, A. K., "Protection of Structures as a Means to a Long Life for Bridges," Indian Highways, Vol. 28, No. 7, The Indian Roads Congress (IRC), New Delhi, July 2000.
14. Kar, A. K., "Waterproofing of Structures : Challenges and Solutions," New Building Materials & Construction World, New Delhi, Vol. 11, Issue 10, April 2006.
15. Kar, A. K., "Durability of Concrete Bridges and Roadways," New Building Materials & Construction World, New Delhi, Vol. 13, Issue 3, September 2007.
16. Kar, A. K., and Vij, S. K., "Enhancing the Life Span of Concrete Bridges," New Building Materials & Construction World, New Delhi, Vol. 15, Issue 6, December 2009.
17. Kar, A. K., and Vij, S. K., "Waterproofing of Structures for Durability," New Building Materials & Construction World, New Delhi, Vol. 15, Issue-10, April 2010.
18. Kar, A. K., "Making Concrete Bridges Durable Through Surface Protection by Waterproofing," The Masterbuilder; Vol. 18, No. 6, Chennai; June 2016.
19. Kar, A. K., "Surface Protection Waterproofing of Segmental Concrete Bridges and Viaducts," The Masterbuilder; Vol. 21, No. 6, Chennai; June 2019.
20. Bureau of Indian Standards, IS 2062:2011, "Indian Standard Hot Rolled Low, Medium and High Tensile Structural Steel".
21. Bureau of Indian Standards, Section 8.2.1 IS 456:2000, "Indian Standard Plain And Reinforced Concrete — Code of Practice (Fourth Revision)".



Planning, Analysis and Design of G+5 Cyclone Resistant Administrative Building at Kovalam, Chennai

Amjad Latif, Shweta Devekar

Department of Civil Engineering, National Institute of Construction Management and Research, Pune

✉ Shweta.25devekar@gmail.com

ABSTRACT

The main objective of the project work is to plan, analyze and design of administrative building. The building is constructed at Kovalam, Chennai. This deals with the planning analysis and design of G+5 cyclone resistant administrative building. An attempt has been made for planning and analyzing the structure. Modelling is done for both circular and Square buildings using STAAD.PRO and AUTOCAD. The analysis of the structure with addition of lacing will be carried out using STAAD.PRO. Major design such as design of slab, design of beam, design of columns and foundation will be done. The design of cyclone evacuation shelter will be carried out using Indian standards and in accordance with National Disaster Management policies. Load calculations will be done considering dead load, live load & wind load. The necessity of the building is to provide a facility for the basic medical relief during and after disaster to safe guard basic assets needed by people to survive after disaster and to save human lives during cyclone.

Keywords: Cyclone; Shelter; (G+5); Design; STAAD.PRO.

INTRODUCTION

Instances of cyclones have been increasing in recent years owing to various reasons such as global warming and human activities. Almost every year during the period of April-May and September-December, cyclones brew in seas along Indian coastline. These cyclones are followed by strong storm surge which can enter land up to distance of 10kms. People living adjacent to coastline are most affected as storm water can stay up to several days in their homes. Further, the tidal surge accompanying the cyclone is a major cause for the loss of lives and property. It is essential to provide accommodation to the vulnerable population living along the coast during any eventuality or disaster due to natural calamities such as cyclones and associated tidal waves and storm surges. These efforts should provide robust buildings and enduring towards such calamities and should be economically viable.

Literature Review

B. S. Mashalkar et al., (2017) deals with the development of buildings and flexible structural systems which are prone to wind action. It gives effect of cyclones on various framed structures such as V, C and K which are not symmetric along both axes. In this paper two plans are taken into consideration and based on drifts results are compared for two buildings. It's found that circular building can resist maximum wind load due to the fact area exposed to wind is very less compared to rectangular and square plans. Ankush Agarwal (2013) provides information on how cyclones damages building and how the risk of loss of property and lives can be minimised. His method for construction of cyclone resistant structures is unique and leads to structural and experimental investigation & recommended protecting house by various methods like proper planning of house, use of roof truss, lacings, and vertical bracing. Jonathan Ochshorn et al (2014) Demonstrated by his work that the effect of wind on any structure will be dependent on various factors like its location and obstructions near the structure which may cause any change in air flow and the properties of the structure itself. He proved that plus shape and Non-uniform shape were the most stable shapes whereas L-shape and U-shape was the less stable of all the considered shapes. Shreyas Ashok keot (2012) Instances of cyclones have been increasing in recent years owing to various reasons such as global warming. Cyclones cannot be stopped; hence various methods are needed to reduce risk associated with it. There is a great need to make changes to buildings in present to reduce the collateral losses to these structures. Planning and design of new construction requirements for buildings are recommended to reduce the risk of structural damage in future. Dhanendra kumar et al (2015) says wind is most powerful force effecting a tall building. He presented a brief introduction to the design of different structural parts of a building to be safe in coastal areas such as roof, foundation, walls, etc. is given. In this paper various methods to alter path of cyclone are elaborated.



Thus in this study various advancement in developing a cyclone shelter are provided in most simple way and findings indicate towards effect of shape plan on drag force and wind effective pressure.

Prof. M. R. Wakchaure (2016) this paper shows the buildings having same gross area but constructed with different shapes are compared. Wind loads are determined based on gust effectiveness factor method. The critical gust loads are found. Amount of area exposed to wind in case of Circular buildings is very less, thus the wind pressure is less, square shaped buildings are less stable against wind load than circular buildings on basis of this study. Hence it is concluded that wind load is reduced with circular plan.

V. Rajesh et.al., (2016) aims to provide economical section based on geometry, cross section supports and stability of rc structure. First loads are calculated based on specific location and then analysis is carried out. It insists in providing more reinforcement in areas of high deflection and shear to improve lateral load carrying capacity of building.

Details of the proposed structure

Plan and dimension of the openings are taken from clause 12 of cyclone building and the planning and designing of the structure is built according to the MOEFC (Ministry of environment, forest and climate change) as stated in the environment constrains.

Type of building: Rectangular & circular building

Number of storeys: G+5

Total Gross area for rectangular building: 1296 m²

Total Gross area for circular building: 1256 m²

The building consists of

- Office rooms
- Bath rooms
- Storage room
- Waiting rooms
- Reception
- Pantry rooms
- Rest rooms
- Administrative office

Figures and Tables

Plan for rectangular building

- a) The ground floor plan of the G+5 rectangular building was prepared in AutoCAD as mentioned below in the **Fig. 1** and the total gross area is 1296 m².

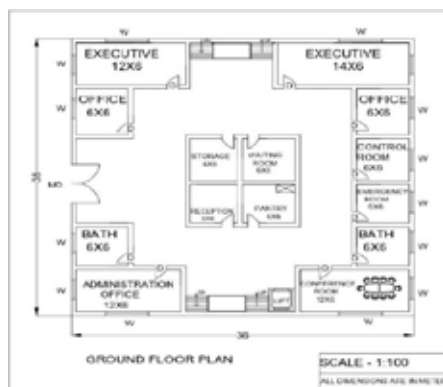


Fig. 1 Ground floor plan for rectangular building

The **Fig. 1** illustrates that the Dimensions of openings is taken from clause 12 of cyclone resistance building architecture prepared under GOI – UNDP, Disaster Risk management Programme.

The plan for the rest of the floors was also made using Auto CAD as shown in the **Fig. 4**.

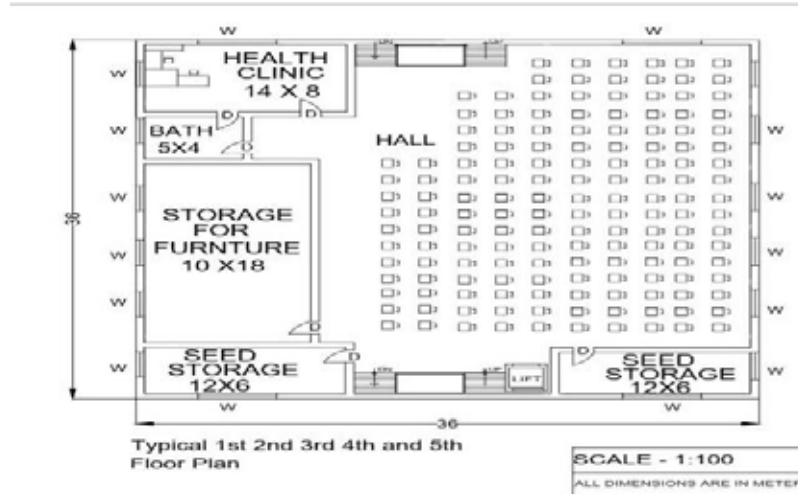


Fig. 2. Plan for first to fifth of the rectangular building

The **Fig 2** is the plan for the first to fifth floor which mainly consist of Hall, health clinic and bath rooms etc. It consists of two way stairs and lift so that the people may use both in case of emergency.

Plan for Circular Building

The ground floor plan of the G+5 circular building was prepared in AutoCAD as mentioned below in the figure 4.1 and the total gross area is 1256 m².

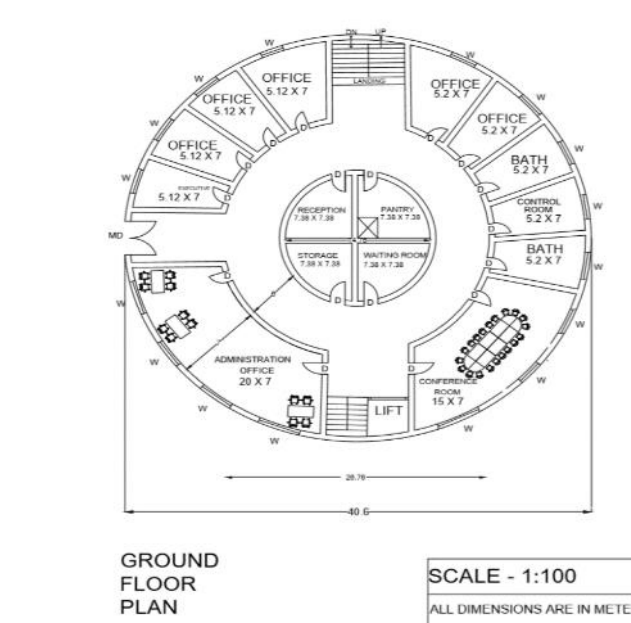


Fig. 3. Ground plan for circular building

The **Fig. 3** illustrate the arrangement of the conference room, administrative room, office rooms and the Dimensions of openings is taken from clause 12 of cyclone building architecture prepared under GoI – UNDP, Disaster Risk management Programme.

The plan for the rest of the floors was also made using Auto CAD as shown in the **Fig. 4**.

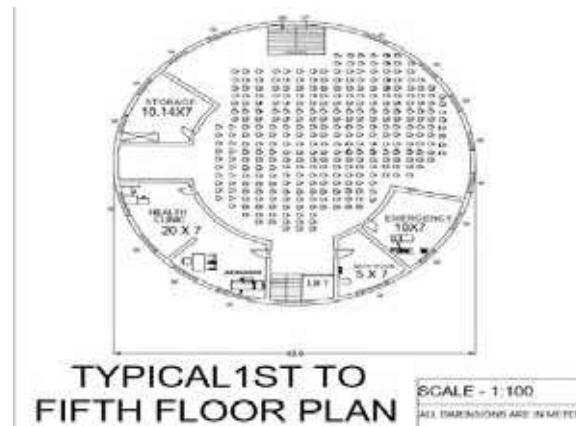


Fig. 4. Plan for first to fifth floor for circular building

The **Fig. 4** is the plan for the first to fifth floor which mainly consist of Hall, health clinic, bath rooms and emergency room. It consists of two way stairs and lift so that the people may use both in case of emergency and the Dimensions of openings is taken from clause 12 of cyclone building architecture prepared under GOI – UNDP, Disaster Risk management Programme.

Analysis wind load for circular and rectangular building

The **Figs 5 and 6** shows that the wind load acting on the rectangular and circular building.

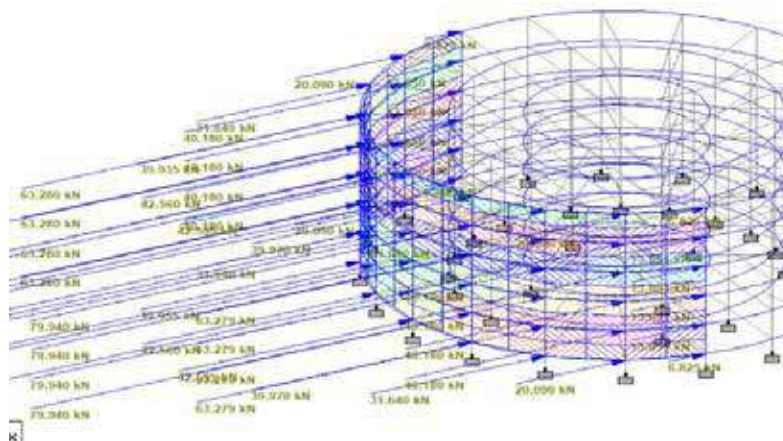


Fig. 5. Wind load for Circular Building

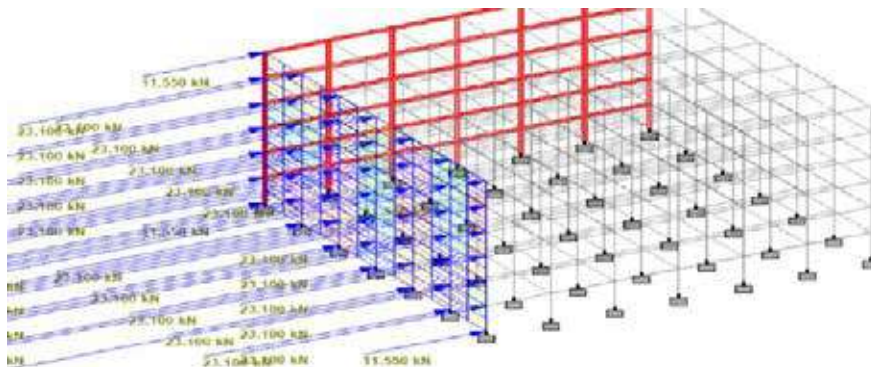


Fig. 6. Wind load for Rectangular Building

Analysis of rectangular structure

The 3D Rendered view was prepared by using STAAD.Pro and is shown below in **Fig 7**.

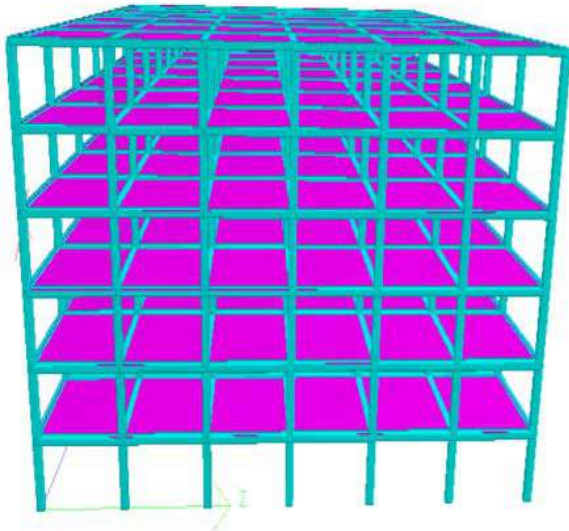
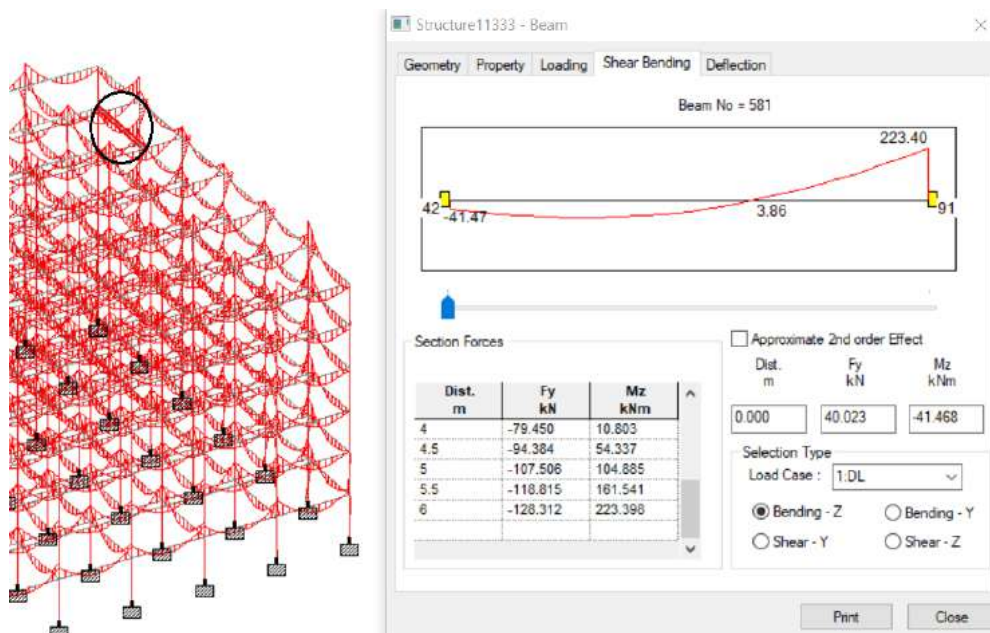


Fig. 7. 3D Rendered view for rectangular building



The Maximum bending moment =918kNm

Fig. 8. Bending moment of the Rectangular Building

Fig.8 the bending moments for rectangular building developed by using STAAD.Pro. These values can be further used for manual calculations and safety purposes.

Design Calculations

Design of Slab

1) **Given data:** Slab size = 6.0 x 7.0



Width of support = 600 mm

Depth of slab = 210 mm

Clear span = 6.0 m

Fe 415 and M20 grade

$F_{ck} = 20 \text{ N/mm}^2$, $F_y = 250 \text{ N/mm}^2$

Sides of ratio

$$L_y / L_x = 7.0 / 6.0 = 1.16 < 2$$

[Hence Two way slab]

Thickness of slab

Overall depth $D = 210 \text{ mm}$

Effective depth $d = 210 - 15 - 8 = 185 \text{ mm}$

Effective span

Effective span = Clear span + effective depth

$$= (6.0 + 0.185) = 6.185 \text{ m}$$

Load analysis

Consider 1m width of slab

Self-weight of slab = $B \times D \times \text{unit weight of concrete}$

$$DL-1 = 1 \times 0.210 \times 25 = 5.25 \text{ kN/m}^2$$

Finishes DL-2 = 1 kN/m^2

Live Load = 4 kN/m^2

Total service load = 10.25 kN/m^2

Ultimate load (W_u) = $1.5 \times 10.25 = 15.375 \text{ kN/m}^2$

Ultimate design moment and Shear force

$$\frac{L_y}{L_x} = \frac{7.185}{6.185} = 1.16$$

From the code book IS 456:2000 refer table 9.2 and read out the moment coefficients for 1.16

$$\alpha_x = 0.065$$

$$\alpha_y = 0.056$$

$$M_{ux} = (\alpha_x W_u L_x^2) = 0.065 \times 15.375 \times 6.185^2 = 38.23 \text{ kN-m}$$

$$M_{uy} = (\alpha_y W_u L_x^2) = 0.056 \times 15.375 \times 6.185^2$$

$$= 30.996 \text{ kN-m}$$

$$V_u = (0.5 W_u L_x) = 0.5 \times 15.375 \times 6.185$$

$$= 46.125 \text{ kN}$$

Check for depth

$$M_{max} = 0.138 f_{ck} b d^2$$

$$D = \sqrt{\frac{30.996 \times 10^6}{0.138 \times 20 \times 1000}} = 105 < 210 \text{ mm}$$

Hence, the effective depth selected is sufficient to resist the design ultimate moment.

$$(A_{st})_{\min} = (0.0012 \times 1000 \times 210) = 252 \text{ mm}^2$$

Reinforcement (short and long span)

Along shorter span in X – direction (middle strip)

$$\text{width of middle strip} = \frac{3}{4} L_y = 5.38 \text{ m}$$

$$M_{ux} = 0.87 A_{st} F_y d \left[1 - \frac{A_{st} F_y}{b d f_{ck}} \right]$$

$$38.23 \times 10^6 = (0.87 \times 250 A_{st} \times 185) \left[1 - \frac{250 A_{st}}{1000 \times 185 \times 20} \right]$$

$$A_{st} = 1020 \text{ mm}^2 > A_{st \min}$$

Provide 16 mm diameter bars at 200 mm centre to centre spacing in middle strip of width 5.3 m.

Along longer span in Y – direction (middle strip)

$$\text{width of middle strip} = \frac{3}{4} L_x = 4.6 \text{ m}$$

$$\text{Effective depth} = (185 - 4 - 4) = 177 \text{ mm}$$

$$M_u = 0.87 A_{st} F_y d \left[1 - \frac{A_{st} F_y}{b d f_{ck}} \right]$$

$$30.996 \times 10^6 = (0.87 \times 250 A_{st} \times 177) \left[1 - \frac{250 A_{st}}{1000 \times 177 \times 20} \right]$$

$$A_{st} = 856 \text{ mm}^2 > A_{st \min}$$

Provide 16 mm diameter bars at 230 mm centre to centre spacing in middle strip of width 4.6m

Reinforcement in edge strips:

$$A_{st \min} = 0.12 \text{ percent of cross-sectional area} = (0.0012 \times 1000 \times 210) = 252 \text{ mm}^2$$

Provide 10 mm diameter of bars at 300mm centres.

Check for shear stress

$$\tau_v = \left[\frac{V_u}{b d} \right] = \left[\frac{46.125 \times 1000}{1000 \times 185} \right]$$

$$= 0.249 \text{ N/mm}^2$$

$$P_t = \left[\frac{100 A_{st}}{b d} \right] = \left[\frac{100 \times 1020}{1000 \times 185} \right]$$

$$= 0.508 \%$$

$$K \tau_c = (1.23 \times 0.249) = 0.306 \text{ N/mm}^2 > \tau_v$$

Hence the shear stress are within safe permissible limits

Check for cracking:

Steel provides is more than the minimum percentage of 0.12 percent





Design of Circular Beam

GIVEN DATA

Radius = 7.38

No of columns = 4

Factored load = 14.06 kN/m

$F_{ck} = 20 \text{ N/mm}^2$

$F_y = 415 \text{ N/mm}^2$

Moment and Shear force

$$\Theta = \frac{\pi}{4} = 0.785 \text{ radians}$$

$$\begin{aligned} M_u &= W r^2 \left(\frac{\Theta}{\sin \Theta} \cos \Theta - 1 \right) \\ &= 14.06 \times (7.38)^2 \left(\frac{0.785}{\sin(45)} \cos 45 - 1 \right) \\ &= 164.64 \text{ kN/m} \end{aligned}$$

$$\begin{aligned} V_u &= W_u \times R \times \Theta \\ &= 14.06 \times 7.38 \times 0.785 \\ &= 81.4 \text{ kN} \end{aligned}$$

Max Torsion

$$\begin{aligned} T_u &= W_u R^2 \left(\frac{\Theta}{\sin \Theta} \sin \phi - \phi \right) \\ \phi_m &= \cos^{-1} \left(\frac{\sin \Theta}{\Theta} \right) \\ \phi_m &= \cos^{-1} \left(\sin \frac{45}{0.785} \right) = \cos^{-1}(0.9) = 0.45 \\ T_u &= 14.06 \times (7.38)^2 \left(\frac{0.785}{0.707} \times \sin(25.783) - 0.45 \right) \\ &= 25.23 \text{ kN/m} \end{aligned}$$

Limiting moment of resistance

$$\begin{aligned} M_{u \text{ lim}} &= 0.36 \times f_{ck} \times b \times x_m \times (d - 0.42 x_m) \\ &= 0.36 \times 20 \times 300 \times 216 (450 - 0.42(216)) \end{aligned}$$

$$M_{u \text{ lim}} = 150604120 \text{ N-mm}$$

As $M_u > M_{\text{lim}}$ section is designed as doubly reinforced beam.

$$M_{u2} = M_u - M_{u \text{ lim}} = 14395880 \text{ N-mm}$$

$$A_{st1} = \frac{M_{\text{lim}}}{0.87 \times 250 \times (450 - 90.72)} = 2111 \text{ mm}^2$$

$$A_{st2} = \frac{M_{u2}}{0.87 \times 415 \times (450 - 50)} = 150 \text{ mm}^2$$

$$A_{st} = 2261 \text{ mm}^2$$

Provide 5 bars of 25 mm diameter at bottom.

$$A_{sc} = \frac{M_{u2}}{f_{sc}(450 - 50)} = 230 \text{ mm}^2$$

Provide 2 bars of 12 mm diameter at top.

Provide 2 bars of 12 mm diameter at top.



Check for Shear:

$$\tau_v = \left[\frac{Vu}{bd} \right]$$

$$= \frac{81.4 \times 1000}{300 \times 450} = 0.60$$

$$P_t = \frac{100 A_{st}}{bd} = 1.81$$

$$\tau_c = 0.77 \text{ (Table 19 IS 456)}$$

$$\tau_v < \tau_c$$

Hence no shear reinforcement is to be provided, however provide 12mm Ø stirrups.

Spacing = $113 \times 4150.4 \times 300 = 300$ mm centres < 0.75d Adopt spacing 300 mm

Check for Torsion

$$\text{Equivalent shear } V_e = V_u + 1.6 \left[\frac{T_u}{b} \right]$$

$$V_u = W_u \times R (\phi - \phi_m)$$

$$= 14.06 \times 7.38 (0.785 - 0.45)$$

$$= 34.76 \text{ kN}$$

$$V_e = 34.76 + 1.6 \times \frac{25.23}{300}$$

$$= 134.594 \text{ Kn}$$

$$\tau_v = \frac{134.594 \times 10^3}{300 \times 450}$$

$$\tau_v = 0.996 \text{ N/mm}^2$$

$$P_t = \frac{100 A_{st}}{b \times d} = \frac{245400}{300 \times 450} = 1.81$$

$$\tau_c = 0.77 \text{ (Table 19 IS 456)}$$

$\tau_v > \tau_c$ hence shear reinforcement is to be provided.

Shear Reinforcement

Transverse reinforcement:

$$A_{sv} = \frac{T_u \times S_v}{bd \times (0.87) f_y} + \frac{V_u \times S_v}{2.3 d_1 (0.87) f_y}$$

Provide 12mm Ø stirrups – 2 legged

$$2 \times \frac{\pi \times 12^2}{4} = \frac{25.23 \times S_v}{300 \times 500 \times (0.87) \times 415} + \frac{34.76 \times S_v}{2.3 \times 500 \times (0.87) \times 415}$$

$$S_v = 420 \text{ mm centre to centre}$$

2. Longitudinal Reinforcement

$$\frac{A_{sv}}{b \times S_v} = \frac{0.4}{0.8 \times f_y}$$

$$\frac{75058}{0.4 \times 300} = S_v$$

$$S_v = 550 \text{ mm}$$

7) Equivalent Bending Moment

$$M_e = M_u + \frac{T_u \left(1 + \frac{d}{b}\right)}{1.7}$$

$$M_u = W_u \times R^2 \left(\frac{1.7}{\sin \theta} \times \cos \theta - 1 \right)$$

$$M_e = 164 + \frac{25.23 \left(1 + \frac{450}{300}\right)}{1.7}$$

$$M_e = 201 \text{ kN-m}$$

$$M_u = 0.87 \times f_y \times A_{st} \times (d - 0.42x_u)$$

$$A_{st} = 3342 \text{ mm}^2$$

Extra reinforcement = $3342 - 2261 = 1181 \text{ mm}^2$ Use 12 bars of 16 mm diameter

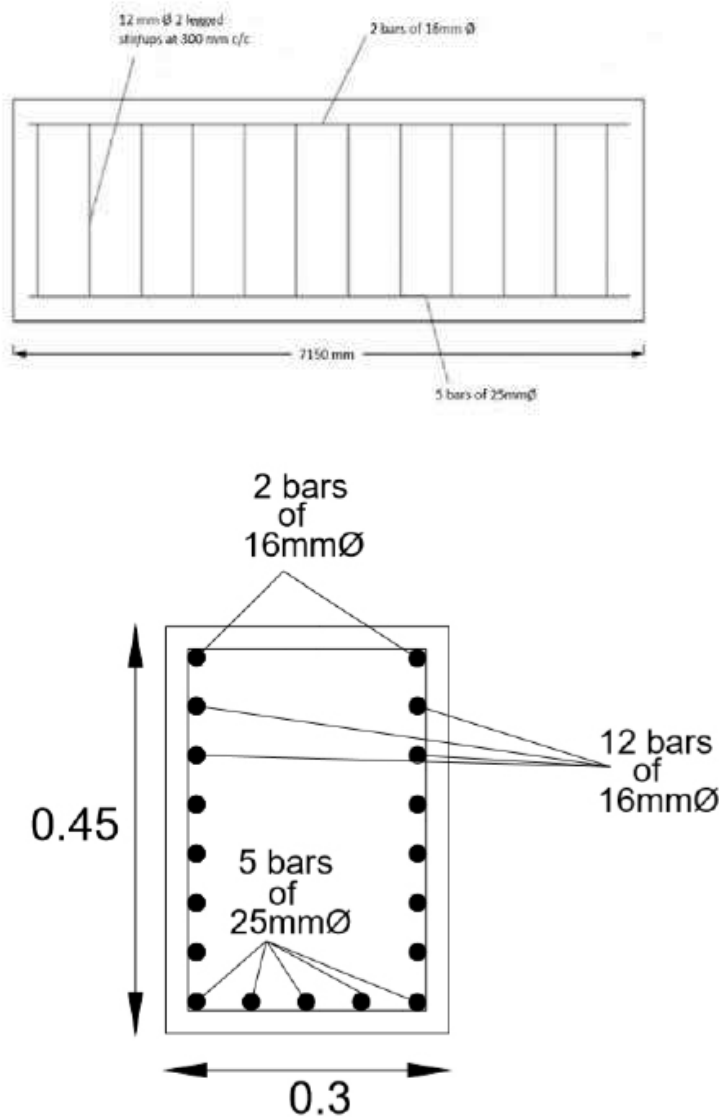


Fig. 10. Reinforcement detailing of beam

Design of Footing

Vertical load (w) = 3578 kN

Self-Weight of footing @10%=357.8 kN

Total load = 3935.8 kN

Base of footing = (300×500) mm



Safe bearing capacity of soil = 250 kN/m²

Size of footing = 3935.8/250 = 15.7 m²

Let ratio of length to width be equal to 2, $y = 2x$

So area = $2x^2 = 15.74 \text{ m}^2$

$x = 2.80 \text{ m}$ and $y = 5.60 \text{ m}$

Pressure due to column load only, = $3578/5.60 \times 2.80 = 228.1 \text{ kN/m}^2$

Factored soil pressure $p_0 = 1.5 \times 228.1 = 342.28 \text{ kN/m}^2$

Calculation of depth of footing

Depth based on one-way shear

Shear force in longer direction = $p_0 \times Y (0.5(x-a)-d)$

$$= 342.28 \times 5.60 (0.5(2.8-0.3)-d)$$

$$= 2395.96 - 1915.12 \times d$$

Shear force in shorter direction = $p_0 X (0.5(y-b)-d)$

$$= 342.28 \times 2.80 (0.5(5.6-0.5)-d)$$

$$= 2443.76 - 958 \times d$$

Shear force resisted by concrete = $\tau_c X d$

$$= 0.32 \times 10^3 \times 2.80 \times d$$

$$= 896d$$

Equating above equations we get

$$2443.76 - 958 \times d = 896d$$

$$\text{Depth} = 1.318 \text{ m}$$

Depth based on two-way shear

For two way shear section critical section lies at $d/2$ from the column face all around:

Shear force at critical section = $p_{0(xy-(a+b) \times (b+d))}$

$$= 342.28 (15.53 - 0.8d - d^2)$$

$$= 5315.6 - 273.82 - 342.28 d^2$$

Punching shear resisted by section = $\tau_c \times A$

$$= \tau_c = 0.25\sqrt{20}$$

$$= 0.25\sqrt{20}$$

$$= 1.11 \text{ N/mm}^2$$

Area of critical section = $((0.3 + d) + (0.6 + d)) \times d$

$$= 0.9d + 2d^2$$

Shear force resisted = $1.118 \times 10^3 \times (0.9d + 2d^2)$

$$= 1006.2d + 2236d^2$$

Equating above equations we get

$$5315.6 - 273.82 - 342.28 d^2 = 1006.2d + 2236d^2$$

$$2578d^2 + 1006.2d - 5589.42 = 0$$

$$d = 1.29 \text{ m}$$

Depth of Footing by Bending Moment Criterion

Critical section is at the face of column so Bending Moment at the critical section is:

$$\begin{aligned} M_{ux} &= \frac{P_u}{8} (x - a)^2 \\ &= 42.785 \times (2.8 - 0.3)^2 \\ &= 267.40 \text{ kN-m} \end{aligned}$$

$$\begin{aligned} M_{uy} &= \frac{P_u}{8} (Y - b)^2 \\ &= 42.785 \times (5.6 - 0.5)^2 \end{aligned}$$

= 1112.83 kN-m, Hence moment in larger direction is more

Moment of resistance in longer direction,

$$\begin{aligned} M_r &= 0.138 \times f_{ck} b d^2 \\ &= 0.138 \times 20 \times 2800 \times d^2 \\ &= 7728 d^2 \end{aligned}$$

Now,

$$1112.83 \times 10^6 = 7728 d^2$$

$$d = 380 \text{ mm} = 0.380 \text{ m}$$

Hence, the highest value of 'd' is adopted as: 1.318 m

Overall depth, $D = 1318 + 50 + 8 = 1350 \text{ mm}$

$$d = 1292 \text{ mm}$$

Area of reinforcement

$$M_u = 0.87 F_y A_{st} d \left[1 - \frac{A_{st} F_y}{b d f_{ck}} \right]$$

a) For longer direction

$$1112.83 \times 10^6 = 0.87 \times 250 \times A_{st} \times 1292 \left[1 - \frac{A_{st} \times 250}{2800 \times 1292 \times 20} \right]$$

$$A_{st} = 4505 \text{ mm}^2$$

$$\text{Spacing} = \frac{201}{4505} \times 2800 = 140 \text{ mm}$$

Use 16 mm ϕ bar @120 mm spacing

For shorter direction

$$267.40 \times 10^6 = 281010 A_{st} - 1.727 A_{st}^2$$

$$A_{st} = 953 \text{ mm}^2$$

$$A_{st \text{ min}} = (0.0012 \times 1292 \times 2800) = 4341 \text{ mm}^2$$

$$A_{st} < A_{st \text{ min}}$$

As per codal provisions, $\frac{\text{reinforcement in central band}}{\text{total reinforcement in short direction}} =$

$$\frac{2}{\beta + 1}$$

Where $\beta = 2$

Reinforcement in central band = $4341 \times \frac{2}{3} = 2894 \text{ mm}^2$

Reinforcement shall be distributed in central 2.8 width

Spacing of 16mm ϕ bars = $\frac{201}{2894} \times 2800 = 194 \text{ mm}$

Use 16 mm ϕ bar @194 mm spacing in central band

Balanced area of steel to be distributed in outer bands = 3388 mm^2

Spacing = $2013388 \times 2800 = 160 \text{ mm}$

Use 16 mm ϕ bar @160 mm for the outer bands

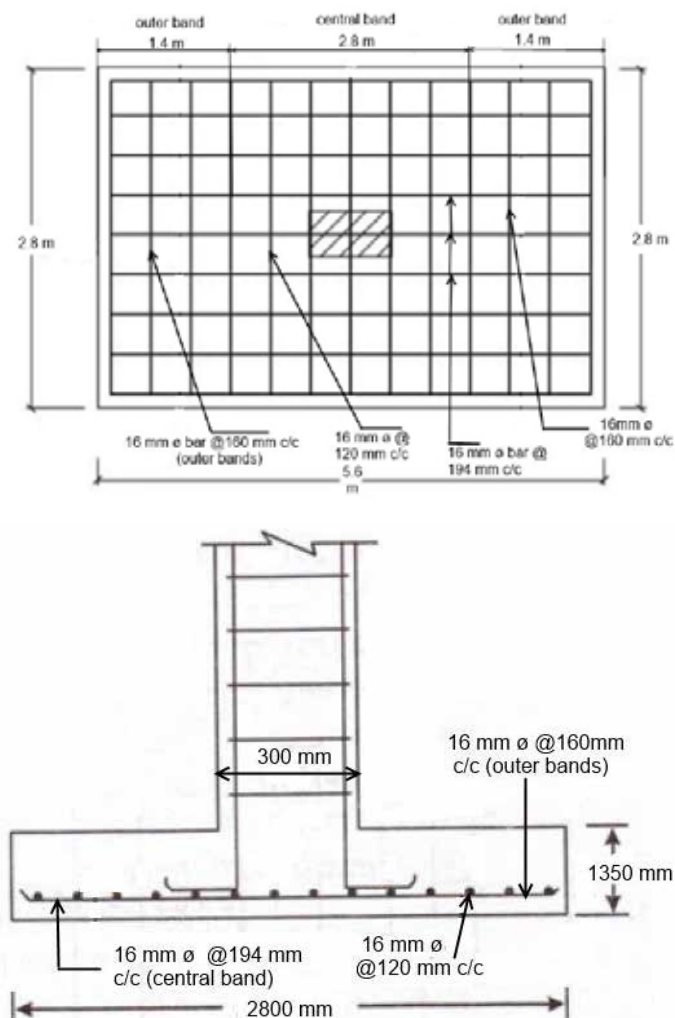


Fig. 11. Reinforcement detailing of footing

Design of Column

Given data

$P_u = 5660 \text{ kN}$

$L = 3.5 \text{ m}$

$f_{ck} = 20 \text{ N/mm}^2$

$$f_y = 415 \text{ N/mm}^2$$

$$D_y = 300 \text{ mm}$$

$$D_x = 500 \text{ mm}$$

$$M_u = 135 \text{ Kn-m}$$

|Slenderness ratio

$$\left(\frac{L}{D_y}\right) = 11.6 < 12$$

Hence, it is a short column.

Minimum eccentricity

$$E_{x \min} = \left(\frac{L}{500}\right) + \left(\frac{D_x}{30}\right) = 24 > 20 \text{ mm}$$

$$E_{y \min} = \left(\frac{L}{500}\right) + \left(\frac{D_y}{30}\right) = 17 < 20 \text{ mm}$$

As $\frac{e_{\min}}{d} < 0.05$ Hence, the column is designed as

Axially Loaded Short Column

Non dimensional parameters

$$\left(\frac{P_u}{f_{ck} b d}\right) = \frac{5660 \times 1000}{20 \times 300 \times 500} = 0.864$$

$$\left(\frac{M_u}{f_{ck} b d^2}\right) = \frac{135 \times 10^6}{20 \times 300 \times 500^2} = 0.09$$

Longitudinal reinforcement

Chart 32 SP: 16

Cover = 50 mm

$$d/D = 0.10$$

$$\frac{P}{f_{ck}} = 0.04$$

$$P = 0.04 \times 20 = 0.8$$

$$A_{sc} = \frac{P b D}{100} = \frac{0.8 \times 300 \times 500}{100} = 1200 \text{ mm}^2$$

$$A_{st} = 490.625 \text{ mm}^2$$

$$\text{Number of bars} = \frac{1200}{\frac{\pi}{4} \times d^2} = \frac{1200}{490} = 6 \text{ bars}$$

Provide 6 bars of 25 mm diameters with 4 bars distributed on longer face.

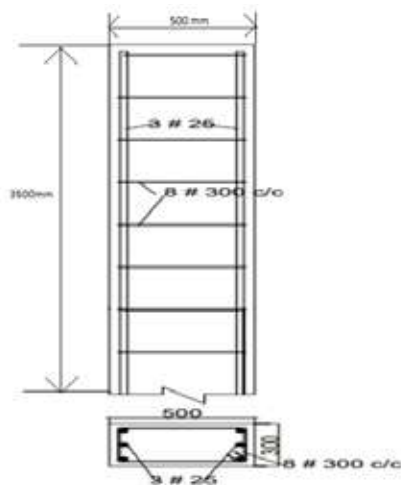


Fig. 12. Reinforcement detailing of column



CONCLUSION

- The process described has been assessed under the environmental impacts of all elements of the cyclone resistant evacuation shelter.
- The plan of the building is prepared using AutoCAD while considering all the requirements as per Disaster Risk Management Programme.
- The cyclone resistant evacuation shelter was analysed for various loads such as dead load, live load and wind load as per the guidelines of the Indian Standards. The analysis was carried out using STAAD.Pro.
- The cyclone resistant evacuation shelter has been designed for all the loads applicable and the loads have been calculated as per Indian Standards.
- Whereas the maximum bending moment in circular cyclone resistant evacuation shelter was found to be 809 KNm while as that of rectangular cyclone resistant evacuation shelter was found to be 918 kNm. Hence due to less bending moment in circular cyclone resistant evacuation shelter it is more effective in cyclone prone areas.
- The structure which is found to be safe and designed according to Indian standards is also found to be a substitute to the cyclone resistant evacuation shelter and has been found to be much more efficient and economical. Hence can be implemented in cyclone prone areas and serve in a much efficient way.

REFERENCES

1. IS: 456 (2000) Criteria for design of plain and reinforced concrete structures, Bureau of
2. IS:875 (Part1) (1987), “Code of Practice for Dead Loads (other than earthquakes) for Building and Structures”
3. IS:875 (Part2) (1987) , “Code of Practice for Imposed Loads (other than earthquakes) for Building and Structures”
4. IS:875 (Part3) (2015) , “Code of Practice for (other than earthquakes) Wind Loads for Building and Structures”
5. IS:15498-(2004) , “Guidelines for improving the cyclonic resistance of low rise houses and other buildings/structures”
6. Park R. and Paulay T (1975), Reinforced Concrete Structures, John Wiley & Sons. New York, 769 p
7. Selvi Rajan (2013) , Design of Cyclone Shelters Based on Wind Tunnel Studies□, The
8. Eighth Asia-Pacific Conference on Wind Engineering, December 10–14, 2013, Chennai, India
9. Anderson, C. E., Burns, D. J. and Reid, J. S. (2003). “The Next Evolutionary Step for circular buildings



Study on Comparative Advantages of E350 vs. E250 Grade Steel in Industrial Structures

Amresh Kumar*, Saptadip Sarkar, Anurag Sinha

Structural Division, Engineers India Limited, New Delhi

*✉ amresh.kumar@eil.co.in

ABSTRACT

Use of structural steel of grade E350 conforming to IS 2062 has seen an increase in India specially, in industrial structures. The reasons for this increased use is essentially high mechanical strength, good tensile strength, easy formability, good ductility, high shear strength etc. However the limitations on easy availability and higher cost of E350 than E250 Grade steel it raises the doubts about impact on overall cost to the project. Therefore, it is imperative to perform a comparative analysis of these two most used steel grades in Indian structural engineering on basis of design strength and steel quantity requirements, to enable the designers to select the appropriate grade, fitting the functional requirements and economics of the project. This study summarizes the comparative benefits of using E350 instead of E250 grade steel by presenting a theoretical comparison as well as a case study of two industrial technological structures in hydrocarbon industry.

Keywords: E350 grade steel; E250 Grade steel; Yield strength; IS 2062; Industrial structures; Cost Benefits.

INTRODUCTION

E350 grade structural steel (conforming to IS 2062) is gaining popularity in industrial structures in India due to its higher mechanical strength and tensile strength, easy formability, good ductility, higher shear strength etc. However, the availability of E350 grade is not easy for full spectrum of hot rolled sections especially when required in small quantities and in remote areas. This adds transportation and delay costs in already higher prices of E350 grade steel as compared to E250 steel. Further, designers are usually asked to replace the structural member of one grade to another in order to expedite the procurement, which is mostly (and sometimes wrongly) done increasing or decreasing the design properties in ratio of yield strength, ignoring the effect of other important factors such as section size, effective length and slenderness etc. This study attempts to study the comparative benefits of using E350 grade steel in place of E250 grade steel from the strength and cost advantages point of view.

OBJECTIVE

The study is designed to examine the following w.r.t. the use of E350 grade steel instead of E250 grade-

- I. Extent of gain in design capacities and the relation of the same with section size and slenderness
- II. Change in overall quantity of structural steel in technological structures
- III. Extent of variation in cost of structure
- IV. Other qualitative and operational/functional benefits.

METHODOLOGY

To establish the aforementioned objectives, this study is designed in following parts-

Comparison based on theoretical design capacities

This part contains calculation of ultimate bending and axial capacities of hot rolled I- and channel sections as per relevant sections of IS 800-2007 (Limit State Design) by varying the slenderness and grade of steel to establish the relation between relative gain when steel grade is changed from E250 to E350.

This is done in following steps

- Comparison of allowable bending moments of Indian Isections for varying effective lengths (1.25 m, 2.5 m & 3.75 m) for lateral torsional buckling,
- Comparison of allowable bending moments of Indian Channel sections for varying effective lengths (1.25 m, 2.5 m & 3.75 m)for lateral torsional buckling,
- Comparison of allowable axial force of Indian Isections for varying effective lengths (2.0 m, 4.0 m & 6.0 m)for slenderness,

Comparison based on actual design

To access how far the difference in capacities achieved in first part, translate into reduction in required steel quantity for actual structures, a comparison of structural steel quantity required in technological structures in a refinery is presented considering the grade of steel as E250 and E350. For getting the idea of dependence of variation in quantity on section sizes used, one lightly loaded non-equipment supporting structure and one heavily loaded equipment supporting structure (**Fig. 1**) is selected and design is performed in STAAD Pro Select series v8i using IS 800-2007 (LSM) as design code. For ease of identification following nomenclature is adopted-

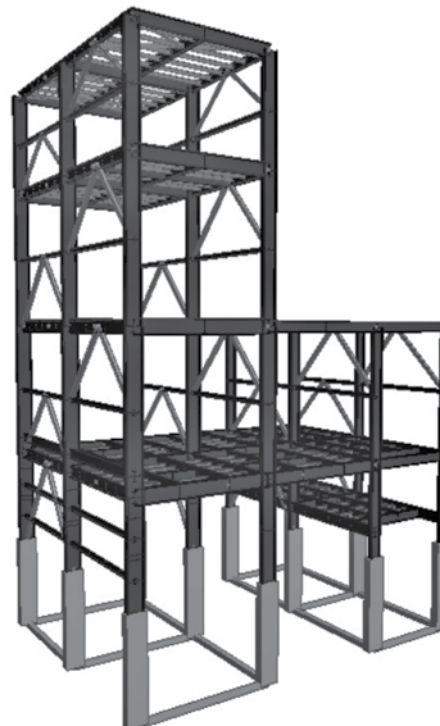
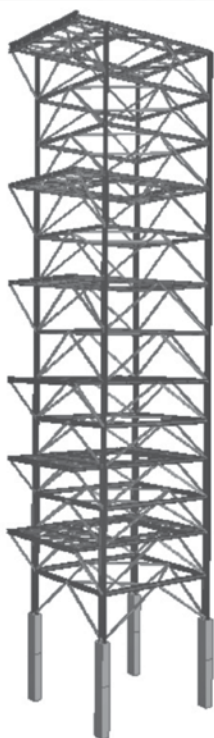
TS_L_E250: Lightly loaded Technological Structure designed for optimum sections using E250 grade steel TS_L_E350: Lightly loaded Technological Structure designed for optimum sections using E350 grade steel

TS_H_E250: Heavily loaded Technological Structure designed for optimum sections using grade E250 steel

TS_H_E350: Heavily loaded Technological Structure designed for optimum sections using Grade E350 steel

Table 1. Gives the details of the structures used for this comparative analysis

Based on analysis and design of above structures, a comparison of structural steel quantity required for TS_L_E250 and TS_H_E250 vis-à-vis TS_L_E350 and TS_H_E350, respectively, is presented to estimate the reduction in steel requirement in actual structures.



1(a)-Structure considered for TS_L_E250 and TS_L_E350

1(b)-Structure considered for TS_H_E250 and TS_H_E350

Fig. 1. Structures considered for structural steel quantity and cost calculation

Table 1. Details of technological structures

STRUCTURE NAME	STRUCTURAL DIMENSIONS			DETAILS OF LOADING			STEEL GRADE USED IN DESIGN
	LENGTH (IN M)	WIDTH (IN M)	HEIGHT (IN M)	LIVE LOAD (KN)	PIPING LOAD (KN)	EQUIPMENT LOAD (KN)	
TS_L_E250	8	8	38	336	768	0	E250
TS_L_E350	8	8	38	336	768	0	E350
Ts_H_E250	22	16	30	2976	1984	2389	E250
Ts_H_E350	22	16	30	2976	1984	2389	E350

Analysis of Qualitative Benefits

Benefits of using E350 grade from operational and durability point of view are highlighted.

RESULTS AND DISCUSSION

A direct comparison of yield strength of E350 grade and E250 grade indicates that a 40% gain is expected ($350/250=1.4$) and as a misconception usually it is followed that when replacing E350 steel member with E250 steel member, design properties shall be increased by 40% and vice-versa. This idea completely ignores the effect of section size and effective length of the member. This fact needs to be examined with respect to the findings based on design capacities of individual members as discussed below. Comparison of design moment capacities for commonly used hot rolled I-section beams is presented in **Fig. 2** and for hot rolled channel beams in **Fig. 3**. Similar comparison of design axial compression capacities for I-section columns is shown in **Fig. 4**. A. Effect on Bending capacity of I-beams:

Fig. 2(a), (b) & (c) show that for all three L_{eff} (i.e. 1.25m, 2.5m and 3.75m), design moment capacities increase with change of yield strength from E250 to E350, which is obvious. But interestingly, the increase in moment capacities is dependent on section size and as the section size increases, percentage gain in capacity also increases. When the gain in moment capacity is averaged for all sections, average percentages are 35.63% for $L_{eff} = 1.25m$, 30.00% for $L_{eff} = 2.5m$ and 22.82 for $L_{eff} = 3.75m$. It indicates that if the member unrestrained lengths are large, the relative gains due to use of higher grade steel are lost to some extent. **Table 2** presents the summary of findings for I-sections in form of percentage change in design capacities. From the table, an important fact to be noted is that gain in moment capacity is almost constant (in the range of ~30-38%) for all wide flange sections (with exception of WPB600x300x128.79) for all three values of L_{eff} and is very close to the increase in yield strength (i.e. 40%). The increase in moment capacity of ISMB sections is also in the same range but only for $L_{eff} = 1.25m$ and as L_{eff} increases moment capacity decreases sharply.

Table 2. Summary of increase in capacity of I-sections of e350 vs. e250 grade steel

EFFECTIVE LENGTH (M)	INCREASE IN BENDING MOMENT CAPACITY			INCREASE IN AXIAL COMPRESSION CAPACITY		
	1.25	2.5	3.75	2	4	6
SECTION SIZE	% DIFF	% DIFF	% DIFF	% DIFF	% DIFF	% DIFF
MB300	36.19	22.29	9.90	24.02	3.67	1.66
MB400	36.11	21.72	9.44	23.72	3.60	1.64
MB450	36.54	23.75	10.55	26.36	4.23	1.83
MB500	37.34	28.17	13.80	31.22	6.50	2.43
MB 600	35.63	30.56	19.41	32.42	10.68	3.39
WPB 600@128.79	23.30	21.61	17.83	37.67	29.16	12.42
WPB 600@177.77	36.99	35.17	32.62	35.64	29.90	15.67
WPB 700@149.89	38.80	36.75	32.03	37.56	28.21	11.35
WPB 700@204.48	36.78	35.04	32.18	35.56	29.24	14.42
WPB 700@240.51	36.83	35.09	32.46	35.57	29.34	14.60
WPB 800@262.33	36.63	34.95	31.98	35.49	28.68	13.48
WPB 900@291.45	36.46	34.84	31.59	35.42	28.10	12.61
AVERAGE	35.63	30.00	22.82	32.55	19.28	8.79

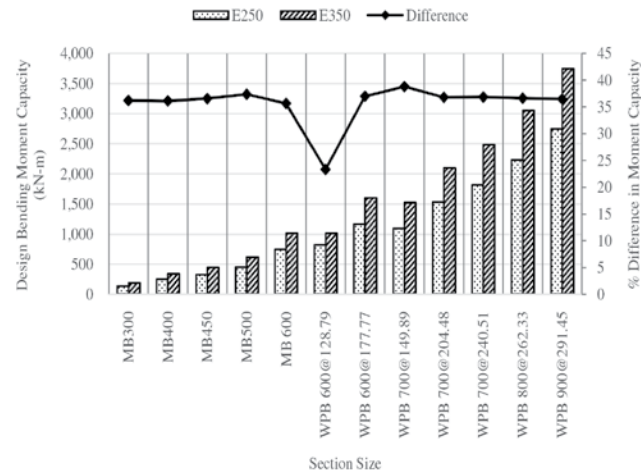


Fig. 2(a) Design bending moment capacity of I-section beams of $L_{eff} = 1.25m$

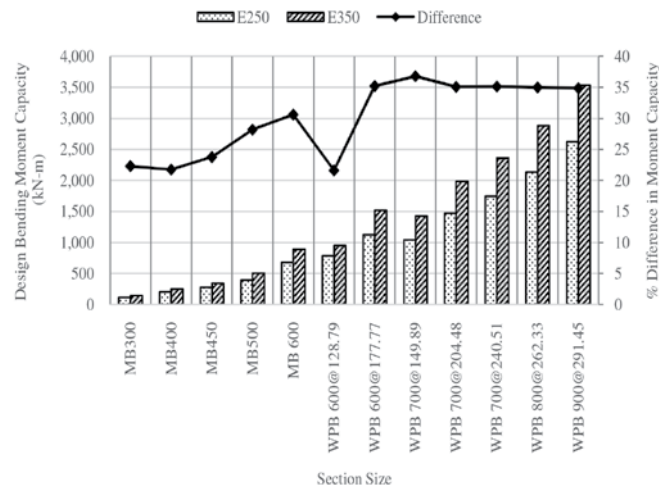


Fig. 2(b) Design bending moment capacity of I-section beams of $L_{eff} = 2.5m$

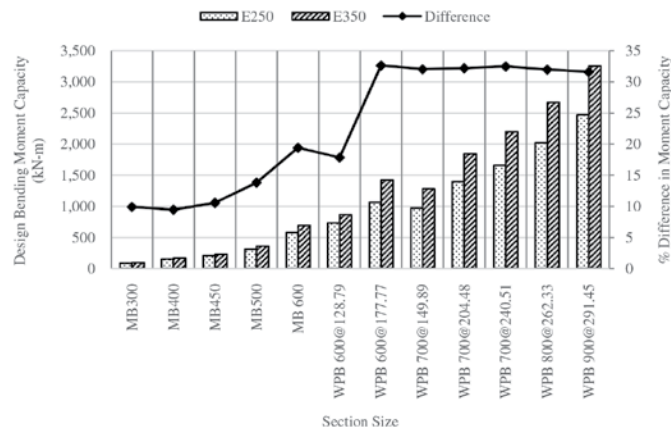
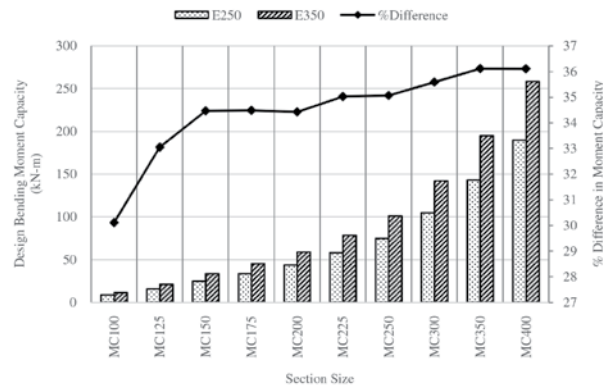


Fig. 2(c) Design bending moment capacity of I-section beams of $L_{eff} = 3.75m$

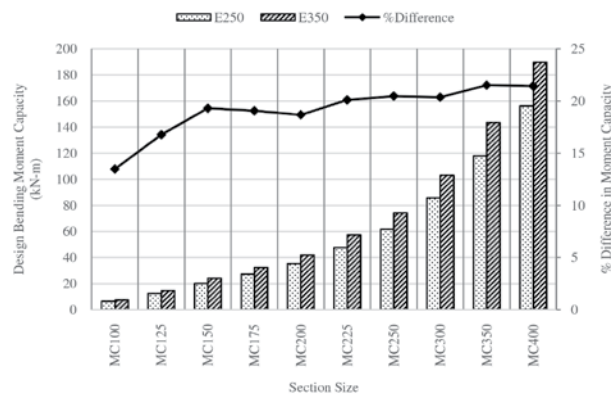
Fig. 2. Design bending moment capacity of I-section beams

Effect on Bending Capacities of Channel beams

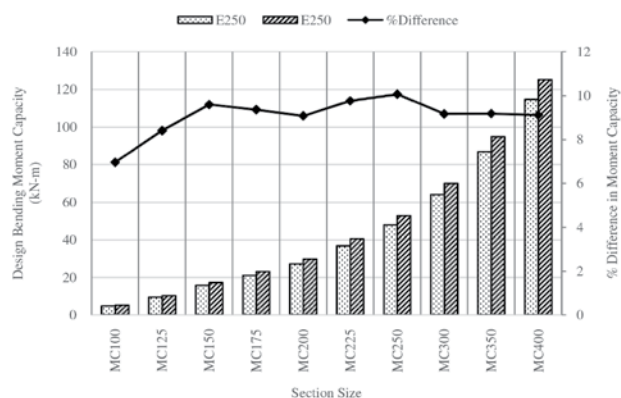
Fig. 3(a), (b) & (c) show that for all three L_{eff} , design moment capacities increase with change of yield strength from E250 to E350, and like I-beams, the increase in moment capacities is dependent on section size. As the section size increases, percentage gain in capacity also increases. When the gain in moment capacity is averaged for all sections, average percentages are 34.45% for $L_{eff} = 1.25m$, 19.12% for $L_{eff} = 2.5m$ and 9.07% for $L_{eff} = 3.75m$. Thus for channel sections also, the benefits in terms of increased moment capacity are more prominent when unrestrained lengths are small. Gain in smaller channel sections is not much as compared to larger sections and as effective length, and consequently slenderness, increases the gain in capacity decreases.



3(a) Design bending moment capacity of channel beams of $L_{eff} = 1.25m$



3(b) Design bending moment capacity of Channel beams of $L_{eff} = 2.5m$



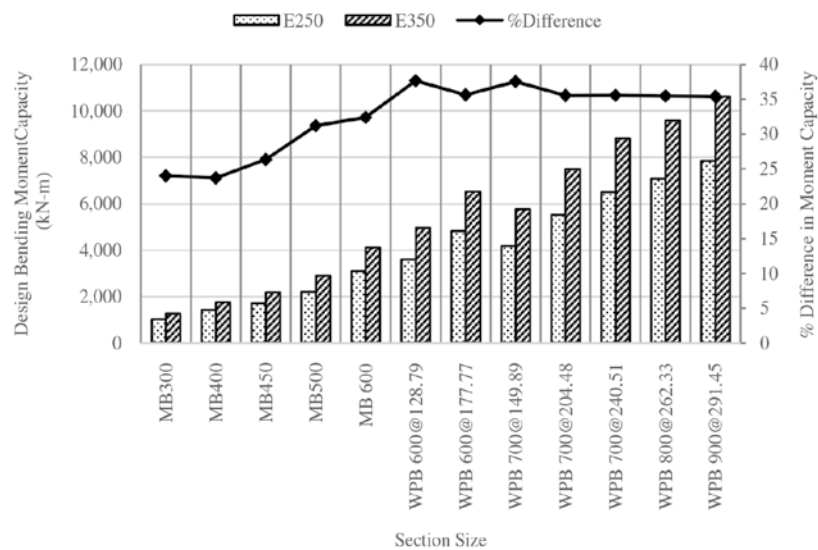
3(c) Design bending moment capacity of Channel beams of $L_{eff} = 3.75m$

Fig. 3. Design bending moment capacity of Channel beams

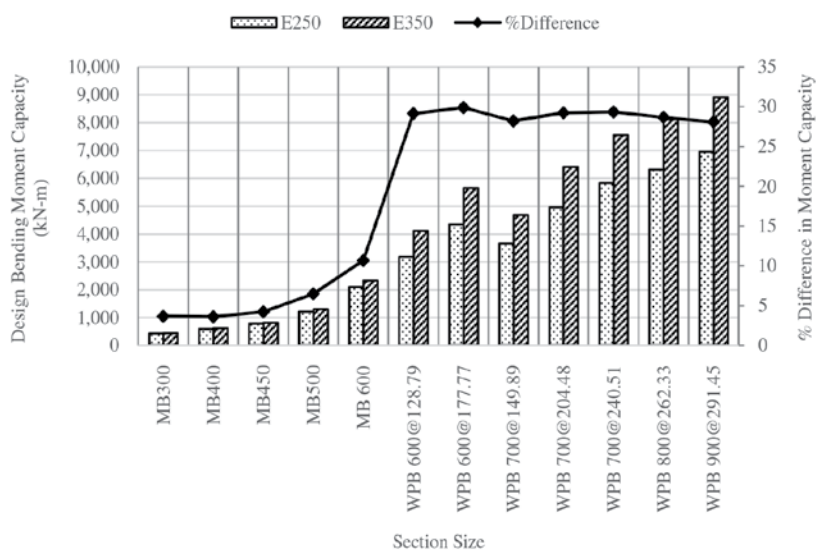
Effect on Axial compression capacities of I-columns

Fig. 4(a), (b) & (c) show that for all three effective lengths (i.e. 2.0m, 4.0m and 6.0m), like design moment capacity, design axial compression capacity also increases with change of yield strength from E250 to E350 and increase in axial capacity is dependent on section size and effective length of column section. Percentage gain in axial capacity, averaged for all sections, are 32.55% for $L_{eff} = 2.0m$, 19.28% for $L_{eff} = 4.0m$ and 8.79% for $L_{eff} = 6.0m$. It indicates that if the member unrestrained lengths are large, the relative gains due to use of higher grade steel are lost to some extent. Table 2 indicates that as L_{eff} increases, the average gain is reduced because due to increase in slenderness, reduction in allowable stress as per IS800-2007 becomes prominent irrespective of the steel grade.

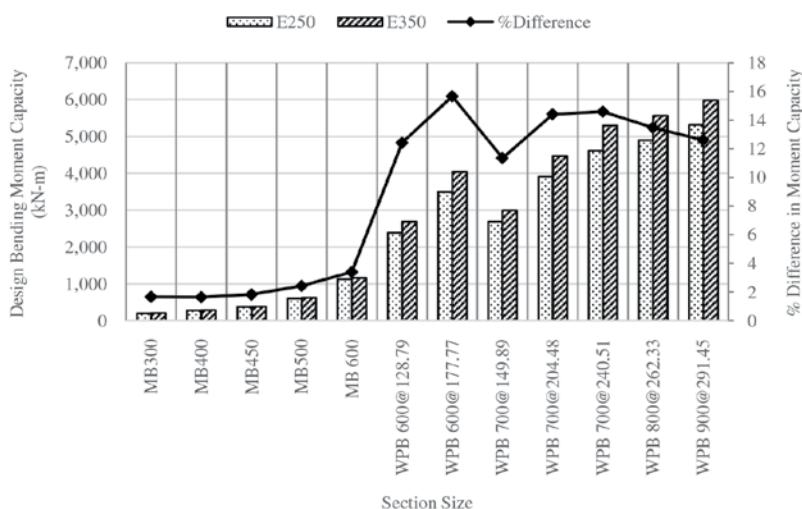
Further Table 2 and Fig. 4 indicate, that gain in axial capacity is almost constant for one value of L_{eff} for all wide flange sections (e.g. 35.42-37.67% for $L_{eff} = 2.0m$, 28.10-29.90% for $L_{eff} = 4.0m$ and 11.35-15.67% for $L_{eff} = 6.0m$) however the gain sharply reduces with increase in L_{eff} . In case of $L_{eff} = 4.0m$ average increase in axial capacity is 28.95% for wide flange sections and only 5.74% for ISMB sections. These values are much lower than increase in yield strength (i.e. 40%).



4(a) Design axial compression capacity of I-section columns of $L_{eff} = 2.0m$



4(b) Design axial compression capacity of I-section columns of $L_{eff} = 4.0m$



4(c) Design axial compression capacity of I-section columns of $L_{eff} = 6.0m$

Fig. 4. Design axial compression capacity of I-section columns

Effect on Structural Steel Requirement and overall cost in Technological structures

Structural steel quantities for the technological structures selected for study are presented in Table-III. Structural steel required for TS_L_E350 is 8.80% less than that of TS_L_E250, while for TS_H_E350 it is only 5.46% less than that of TS_H_E250. It shows that actual gain in terms of reduced structural quantity by using E350 grade steel instead of E250 are 8.80% and 5.46% for light and heavy structure, respectively.

Thus actual gain in overall structures is much less than as expected based on individual member capacities. The reason for this is that in actual structure each member can't be provided the optimum section arrived by design because it will result in large variety of sections. Instead, for ease of procurement, some standard sections only are used and members having similar behavior are grouped and are provided largest size required by any members of that group. Further, for some members (e.g. tie members) slenderness becomes the governing criteria and even though the smaller section is sufficient from stress point of view, larger section is provided to achieve required slenderness. Hence, even if E350 grade steel is used, section size for these members can't be reduced as minimum radius of gyration (r_y) is required to be maintained.

Section sizes required in heavier structure are large than those required for lighter structure. Hence the percentage reduction in structural quantity in heavier structure is expected to be more than that for lighter structure. However, values in **Table 3** are not in line with this. The reason for this may be that due to standardization of section sizes and grouping of members, some members are always underutilized so even if yield strength is reduced, the section size is not required to be increased due to already available reserved capacity. Further, the reduction in overall steel quantity for a structure will depend on the percentage of heavier and lighter sections in the structure. Therefore further study with large number of structures and varying percentage of members used as beams and columns may be required to establish this point.

While designing the structures, only allowable stresses and slenderness ratio have been considered for determining the required section size. If the stricter deflection requirements in industrial structures and shear capacity of connections are also considered, it may be possible that section sizes can't be reduced even if smaller section of E350 grade is sufficient by bending moment criteria. Thus, the comparative gain is further reduced. But as the deflection requirement and shear capacity of connection requirements are usually the governing criteria for beams supporting very heavy equipments only, the effect may not have much impact on steel requirement for overall structural.

Effect on overall Cost of Steel Structure

Cost of structural steel works includes mainly three components: material cost, fabrication cost and erection cost. Material cost of E350 grade steel is approximately 5-7% higher than E250 grade steel. As per code requirement, welding material shall be of same or better grade than the base metal. Hence, for grade E350 steel, use of E70 rods is compulsory whereas for E250 steel, E60 rods can be used. As former is found to be at least 25% costlier and welding cost contributes to approximately 10% of the

total fabrication cost, fabrication cost for E350 steel can be said to 2.5% more than E250. Erection cost can be assumed not to be directly affected by grade of material used.

Table 3. Summary of change in overall quantity and cost of structures

STRUCTURE NAME	STEEL QUANTITY (KN)	% DIFFERENCE IN QUANTITY	STEEL COST (INR/KG)	FABRICATION COST (INR/KG)	ERECTION COST (INR/KG)	TOTAL COST (INR/KG)	% DIFFERENCE IN COST PER KG	TOTAL COST (IN M INR)	% DIFFERENCE IN OVERALL COST
TS_L_E250	489.04	-8.80%	45	35	20	100.00	4.03%	48.90	-5.13%
TS_L_E350	445.99		48.15	35.875	20	104.03		46.39	
TS_H_E250	2362.78	-5.46%	45	35	20	100.00	4.03%	236.28	-1.65%
TS_H_E350	2233.88		48.15	35.875	20	104.03		232.38	

Based on these, a cost comparison is presented in **Table 3** for the technological structures. As exact price of steel works vary depending on various factors, a normalized value of 100 INR/Kg is assumed for E250 grade with 45%, 35% and 20% weightage for material, fabrication and erection costs respectively.

Table 3 shows even though the material cost and fabrication cost for E350 grade are higher, it results in reduction in overall cost of the structure. However this reduction is only 5.13% for lightly loaded structure and 1.65% for heavy structure which is not very significant considering the increase in yield strength and design capacities of individual members. This is an important point to be kept in mind while finalizing the tender quantities and cost estimation for structural steel works.

Qualitative benefits of E350 grade steel

Other than increased yield and ultimate strength E350 grade steel possesses some better qualitative properties, owing to its higher carbon equivalent value, such as resistance to acids in elevated temperature, resistance to pitting and crevice corrosion, and resistance to oxidation, chloride stress and cracking corrosion. E350 grade steel works at high temperature and shows hardness and toughness at the cryogenic to high temperature. Due to these reasons, E350 grade steel is well preferred for using in nuclear plants, refineries, petro-chemical plants and fertilizer plants.

CONCLUSION

Summarily, present study highlights following points regarding the use of E350 grade steel-

- The use of 1.25 m as unrestrained length of beams is an ideal condition where in maximum capacity of the beams can be utilized. It gives a benefit of up to 36% in moment capacity if E350 grade steel is used instead of E250 grade.
- For columns, effective length of 4.0 m, which is the most commonly used length as per industry practices; use of E350 grade steel gives a benefit of 10.67% in axial compression capacity against E250 grade steel.
- The benefits of using E350 grade steel is more prominent in wide flange sections and members with smaller unrestrained lengths.
- The benefits in increased design capacity by using E350 grade instead of E250 grade are not directly proportional to ratio of yield strengths and are largely dependent on slenderness ratio. Structural engineers should always keep this in mind while suggesting section replacements.
- The impact of using E350 grade instead of E250 grade on overall structural steel quantity of structures is very limited due to section standardization and grouping. Hence, it is suggested that at the time of tendering, structural steel quantities shall not be reduced on account of using E350 grade.
- Even though E350 grade steel being costlier, the extra cost is mostly balanced by reduced quantity. However, the impact of reduced quantity is found to be approximately ~5% or less, hence this cost reduction may be ignored while finalizing the costing of the entire project especially in LSTK contracts.

Thus, this study establishes that benefits of E350 grade vs. E250 grade steel are very limited considering the overall project. However, this study doesn't discourage the use of it but only warns against overestimating the benefits merely looking at the increased yield strength.



On one hand, use of E350 can save a lot of fabrication time as the quantity of built-up sections can be reduced. Also, hidden advantages in material handling and transportation are also there. But on the other hand; E350 grade steel is not very easily available especially if smaller quantity distributed over large variety of sections is required. The problem of availability is more severe for wide flange sections because the availability is subjected to minimum quantity of ordering and number of producers is also limited. Further, it is suggested that for projects where in very heavy loads and very tall structures are anticipated, use of E350 is preferred whereas in minor structures and temporary structures use of E250 may be preferred.

REFERENCES

1. Bureau of Indian Standards, IS 800: General Construction in Steel-Code of Practice, 3rd rev. New Delhi: Bureau of Indian Standards, 2007.
2. Bureau of Indian Standards, IS 2062: Hot Rolled Low, Medium and High Tensile Structural Steel, 6th rev. New Delhi: Bureau of Indian Standards, 2006.



Design and Development of Floating Structure for Solar PV plant using Numerical Analysis

Harsh V Chudasama, Ashish M Vajir

Department of Structural Engineering, Civil Department, Birla Vishvakarma Mahavidhyalay, Anand, Gujarat

✉ chudasamaharsh182@gmail.com; ✉ ashish@elitecengg.com

ABSTRACT

This paper highlights the concept of floating solar PV plant and deals with the floating solar photo voltaic design, development using numerical analysis. Floating components are made up of HDPE which show superior performance and are cost effective. CFD analysis is executed on the structure for the study of flow and assessment of wind pressure on the developed model using Indian environmental conditions. The CFD results have been compared and validated with the analytical calculations obtained through IS 875 codes part 3 for wind pressure. Also, Structural FE analysis is carried out to ensure structural stability for the given environmental conditions.

Keywords: Floating solar PV plant; Green energy; High Density Polyethylene (HDPE), FEA analysis; CFD Simulation; IS 875- part 3.

INTRODUCTION

In recent times, solar energy usage is growing rapidly as it is considered as one of the most promising energy alternatives due to its sustainability and eco-friendly nature. All over the world solar energy is available to a large extent. Frequent use of solar energy is through Photovoltaic (PV) system. The main difficulty for the same is the availability of land. Ground-Mount type installation has the pressure of land requirement, which is an expensive resource. Hence to overcome the cost of solar projects and make it economically feasible, installation of Solar Power Plant on water bodies can become a very logical alternative.

This concept of installing solar power plant on water bodies will not only boost the economic viability of the solar projects but will also increase the efficiency of the plant as the operating temperature is less underneath the panels. [1] Additionally, it also reduces water loss due to evaporation and inhibits algae growth due to shading of water. [2] We identify the possible design solutions for the floating structure addressing the key challenges and established a solar farm model in CAD.

The most normally used floating platforms are template type platforms made of Steel, Fiber- reinforced plastic FRP, High density polyethylene (HDPE) and used in marine, aerospace etc. industries. [4] The design and analysis of these floating structures must be made in accordance with layout of water bodies and in assistance with anchoring and mooring system. The design and analysis of floating platforms must be done taking into consideration many factors, including the following important constraints:

- Environmental conditions and undesirable disruptions like wave load, fatigue load.
- Water bodies characteristics for suitable choice of material.
- Code requirements (e.g. Indian Standard Codes “IS” codes)
- Intensity level of consequences of failure.

The entire design, installation, and operation must be approved by the client. Important features of the components are as follows.

- Environmentally friendly, easy installing and dismantling, Safety, Maintenance free and cost effective.
- Design Versatility, No Sharp Corner.
- High Load Capacity, UV Resistant.

The floating platforms are made up of High-Density Polyethylene (HDPE) which can withstand ultraviolet rays and corrosion.

Pontoons made up of heavy molecular weight high density polyethylene and other additive's as raw material are strong, tough and durable, resistant to UV rays, salt water and oil, chemical corrosions.

Concept of floating solar PV plant

A Floating Solar technology results from a combination of PV plant technology and floating technology. A Floating body consists of connecting Structure and Floats. Floaters are the components that float on water bodies with buoyancy enough to mount PV modules. An array of such floaters forms a solar farm and is designed as per the requirement. Structures are the supporting system which connects the Floats and the PV modules. According to research, having this effective cover of Floating Structure and PV Modules has caused a reduction in evaporation of water from the reservoir. [2] Floaters consist of pontoons, connectors, solar panels, and cables.

Pontoon is a floating component of the floatation system with the required buoyancy to float with a heavy load to maintain stability. The Platform is designed as per the required number of panels. Solar PV crystalline panels are widely used for floating solar PV systems. As any metal corrodes with time, the polymer made frame must be used.

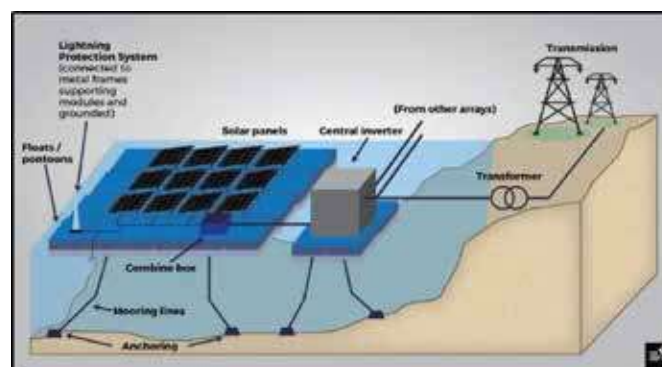


Fig 1. Floating solar plant working Schematic [16]

Cables and Connectors – The power through solar modules can be stored in solar batteries or fed to the grid. To transfer power to the distribution line, robust and waterproof cables are used to provide a long Service. India today is fastest growing market for renewable energy in the world. India visions a renewable energy target of 175 Gigawatt by year 2020 in which energy from solar sources is 100 GW. The country has been building rapid advances in this area. As such, it is obvious that floating solar would become a technology for consideration by policymakers in the country.

LITERATURE REVIEW

Alok Sahu et al [2] highlights the concept of the floating PV system and compares it with the land-based Installation. In India, Source of water bodies are easily available and thus this technique serves as a complementary advantage. In addition to all positive aspects, proper design consideration such as wind, water stability, temperature limit, snow load, cyclone, and typhoon, etc. should be considered. Also, proper azimuth tilt and angle as per geographical location should be considered. It is found to produce 1.2 times the current production of PV on lands. Luyao Liu et al [11] studied the power generation effectiveness of the floating solar PV plant and analyzed the capacity of a floating solar PV system with respect to terrestrial solar PV system. It was estimated that floating PV system is almost increased by 2% in comparison with the land-based PV system.

Young-Geun Lee et al [4] designed and constructed a floating PV generation system with actual construction. Composition of Unit structure and process of large scale floating system was suggested. As per material cost, a brief analysis was performed of the structural system fabricated with different materials. It was found that the structural system with FRP is the most cost-effective due to the lightweight. Overall, the above example was a positive experience for the construction of large scale floating system in the near future. Sun-Hee Kim et al [3] showed that in comparison to conventional constructing materials, FRP and HDPE has good mechanical properties and also corrosion– resistance.

Girma T. Bitsuamlak et al [8] Studied different cases for various wind angle of attack on standalone ground mounted solar panels. The solar panel experienced the highest overall wind loads for 0°degree wind angle of attack i.e. upwind case. Veysel Emre Uslu et al [7] concluded that panel length has a major impact on solar panels. Also, spacing factor is an important factor for designing a solar farm. First row panels are subjected to higher wind loads when panel length increases. Wael Charfi

[10] showed that Solar PV system performance is enhanced due to its open design which facilitates natural ventilation. A 3D CFD model describing the performance of the system is developed and compared with the experimental data. Paturi Lakshmi Prasanna Kumar et al [5] concluded the angle of attack of wind on surface plays an important role to study the mean pressure distribution. It was observed that pressure was maximum at 0° and 180° . Puneeth kumaar HP [6] studied variations of lift and drag force with the change in the angle of attack. It was found that at 30° , the lift force is higher than the drag force.

GEOMETRIC MODEL

Design Consideration

The concept of installing Solar PV modules on water bodies is complex and requires proper planning, construction and hence key design factors must be taken into account carefully. The factors taken into account were the Layout of the pond, Floating structure geometry, Orientation of PV panel [2]. The floating solar power plant is constructed by connecting pontoons using connection pin/bolts to minimize the bending moment induced by unstable movement of water surface [3]. As per the geographical location, tilt angle was kept at 10 degrees.

The model designed was optimized enough to minimize weight by eliminating unnecessary material and at the same time should sustain environmental conditions. The location of installation was India and therefore wind speed was kept at a maximum speed of 60m/s considering coastal region effect. (IS875).

Design of Unit Structures and Formation of Solarfarm

A unit structure consisting of solar module, Main Float and Walkway Float (Floating System which is composed of HDPE) and connecting members are as shown in below figure. Additional members are aluminum purlin which connects the PV module and the main floats using bolts to maintain stable contact. Connection pin devices bring into line the lug to lug connection of floats and customs a solar panel farm. All the components were modelled in CAD platform. The HDPE Float members are optimized enough to provide the buoyancy for heavy load and at the same time withstand forces on it. HDPE being cost-effective is also lightweight, provides high strength.

The length of all the members is kept within an assortment for ease in handling and maintenance. The Floating PV generation system consists of several Floats as per the desired power output. Each panel has a capacity of 330W, in which panels arranged in rows and columns with the dimension of 1962×992 mm per panel are installed. The total plant capacity depends on the space and panel arrangement. The solar farm formed by array of solar panels is as per the layout of water bodies and supported by the anchoring system which retains.

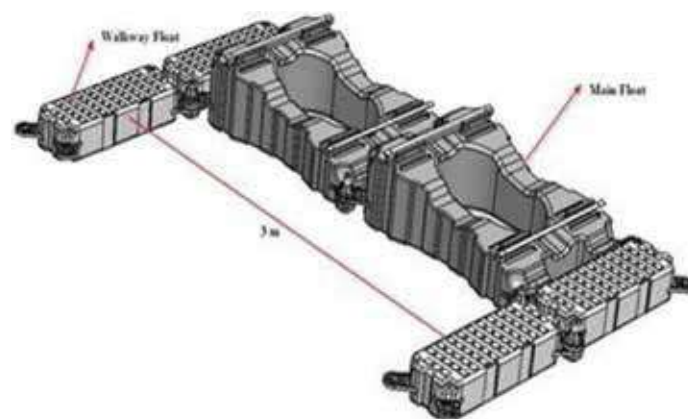


Fig 2. Unit Structure displaying Main and Walkway Float

the position of the structure when subjected to any wave disruption. The anchoring and mooring system is firm enough to maintain the steadiness of assembly for the subjected wind speed and wave disturbance.

CFD ANALYSIS

A 3D CFD models interpreting the solar PV system is developed. A grid dependency test was carried out and we selected a mesh size of 710587 cells. The mesh type was cut cell method. The generated mesh is shown in **Fig 3**.

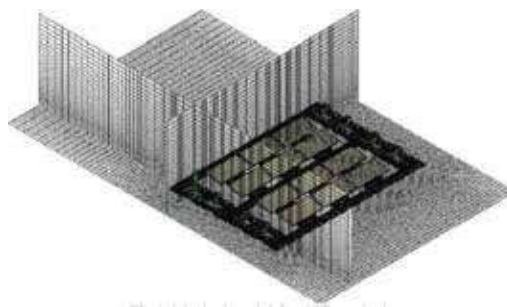


Fig 3. Meshed model for CFD analysis

As the system is subjected to load due to the wind, the forces acting on the panel is computed by CFD analysis. In the mentioned analysis, CFD methodology is used to figure out the force and pressure developed by wind on the Solar panels to wind incident angle of 0° , 90° and 180° for wind flow. Solar panels at 10° angle of orientation are studied at 60 m/s wind speed. The CFD model is developed with a fixed wind speed under the steady state condition. The information of input data is given in **Tables 1 and 2**.

Table 1. CFD data

Analysis Type	External
Closed Cavities	Exclude cavities without flow, Exclude include space
Gravity	9.8 m/s ²
Basic Wind Speed	60 m/s
Fluid	Air
Flow type	Laminar and Turbulent
Environmental Pressure	101325 Pa
Temperature	293.2 K
Turbulence intensity	5%

Table 2. Air property

Specific heat ratio(Cp/Cv)	1.399
Molecular mass	0.02896 kg/mol
Dynamic viscosity	1.85e-05 Pa.s (at 293.2 K)
Density	1.225 kg/m ³

Load Combinations:

Following three load cases have been considered for design for serviceability:

1. WINDWARD- 0°
2. LEEWARD- 180°
3. SIDEWIND- 90°

The modeling process consists of first taking the real world fluid characteristics and imitating this in the simulated environment. From here, a mesh is created to divide the fluid volume into discrete sections. In this CFD Domain, anything that doesn't have a flow condition applied to the volume is excluded i.e. cavities without flow are excluded. Boundary conditions are then entered into the model to term parameters such flow inlet/outlet, type of fluid to be taken, details of any solid edges, domain dimensions etc. The domain for CFD simulation is shaped so as to develop a high flow on stationary surfaces. The free exposure of Structure with panels to wind is studied. Domain Size is $20 \times 5 \times 8$ for all conditions. The CFD simulation computed the forces on various panel surfaces is shaped so as to develop a high flow on stationary surfaces and wind pressure was evaluated from the forces. As a result, maximum pressure is considered for steady state analysis.

As computed, the maximum lift generated force due to wind flow for windward condition is 1120 N and for leeward condition is 940.5 N and hence accordingly, analysis for the same load condition needs to carry out for respective load conditions. It is clear enough from CFD analysis that high pressure is observed for upwind condition due to high variation in flow and hence a certainty factor should be taken into account to calculate design wind Pressure.

STRUCTURAL ANALYSIS FOR UPWIND

To examine the magnitude of induced stresses arising from various design loads, a design-by analysis approach using finite element methods has been necessary because of the absence of suitable design-by-rule methods for the design features requiring assessment. In order to get wind pressures, CFD on 5Cx4R Floating solar farm was done, which is then used in following FEA, so as to check the strength and stability of component. The site location is India with a basic wind speed of 60m/s.

Material data

Table 3. Material data

Material	HDPE
Density	960 kg/m ³
Youngs Modulus	1450 MPa
Proof Strength	29 MPa
Poissons Ratio	0.4
Allowable stress	14.5 MPa

Note:

- 1) Material Data is taken from [12].
- 2) Allowable Stress is S_y / FOS ; where $\text{FOS} = 2$ for all components.

Boundary Condition and Loads

The analysis aims to provide the verification of structural stability considering dead load, wind and wave loads for the Floating solar farm by means of the structural FE analysis. The system which constitutes a photovoltaic array(s) is designed to withstand the extreme fair wind (positive pressure) and adverse wind (negative pressure) on design tilt angle of solar photovoltaic array(s).

- a) For individual strength checks, inner faces (hole) of lugs are constrained in all directions.
- b) Wind force on the panel due to wind loading is applied on the Panel face as normal force. Wind pressure for Load due to fair wind direction on design tilt angle of panel, Load due to adverse wind direction on design tilt angle of panel and Load on side face of components is considered. All the values are obtained as per CFD see Section III.
- c) Self-weights are directly taken by FEA software from given densities.
- d) Since Geometry and loading is symmetrical, it is convenient to solve the problem by considering Symmetry in FEA. Thus, in fig all the models are shown in halves, because of Symmetric boundary condition.



Fig 4. Boundary conditions and load for upwind

Design Wind Pressure

Maximum Force is computed through CFD analysis and is used for evaluation of Wind Pressure for the worst load condition as shown below

As, Pressure = Force/Area

Panel Exposed Area to wind = $1962 \times 992 = 1946304 \text{ mm}^2$

Thus,

Upwind pressure through CFD analysis = $1120 / (1.946304) = 575.44 \text{ Pa}$

To account for uncertainties

Design upwind pressure = $1.5 \times 575.44 = 863.174 \text{ Pa}$. Here factor 1.5 is used to consider a Gust safety factor.

Stress Plot

As per the above analysis, the induced stress in all the component are within the permissible limit and hence the designed components for the given material with required additives is safe for the given load condition.

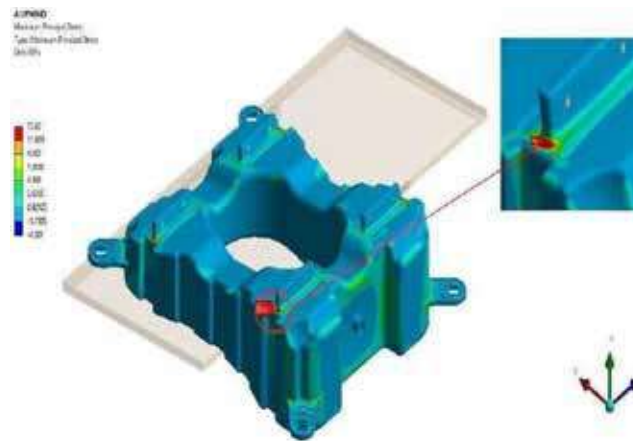


Fig 5. Equivalent stress plot for upwind

FATIGUE ANALYSIS

As floats of solar mounting floating system are subjected to alternate stresses due to waves and other varying external disturbance, fatigue analysis is important to evaluate actual life of the system. To avoid fatigue failure, fundamental requirements during design and manufacturing phase is a must. Hence the following work addresses the same and analyzes the components for fatigue loading.

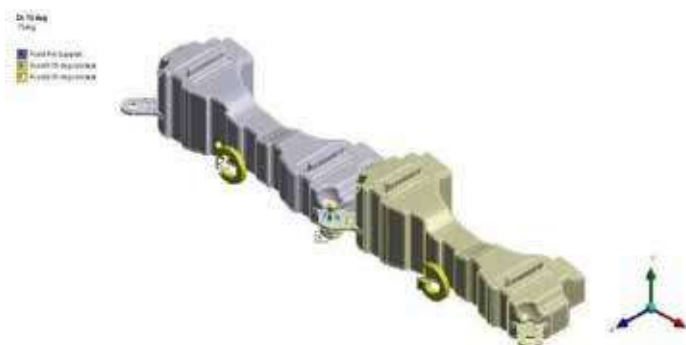


Fig 6. Boundary conditions and load for 5° load condition

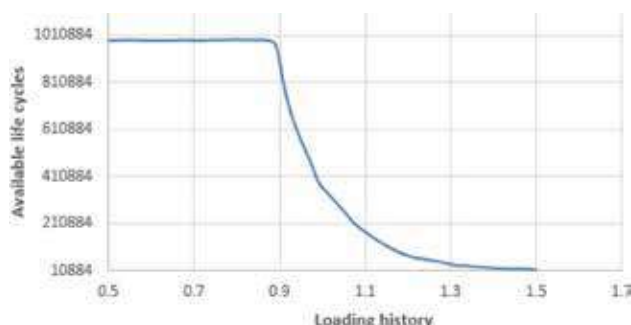


Fig 7. Fatigue sensitivity plot for 5°

Note: This plot shows % loading on X axis and Life cycle on Y axis. On X –axis, 0.5 corresponds to 50% of load applied.

The floats are fixed at connection point and allowed to rotate about z axis for different load combination (**Fig 6**). In the same way, other rotations were assigned the boundary conditions. The available load combination is chosen as per standard target set for floats i.e. safety check design life of 360000 cycles for 15°, 10° and 5°. Safety factor plot and Fatigue sensitivity plot for the described load condition is studied and analyzed accordingly. It can be clearly interpreted from the graph that increasing number of life cycles for respective load condition is more safer for 5° and then for 10° and then ultimately for 15°. Hence, the developed model is more suitable for calm and less wavy.

RESULT SUMMARY

Table 4. Stress assessment for upwind condition

Component	Induced Stress(M Pa)	Allowable Stress (M Pa)
Main Float	13.69	14.5
Walkway Float	14.35	14.5
Dead load for unit system + 100kg Live Load	9.84	14.5

Table 5. Wind pressure comparison

Wind Pressure (Pa)	Method	
	CFD Simulation	Analytical analysis (IS 875)
Upwind	863.174	838.44
Downwind	724.83	503.064

As understood from above table 4, it can be concluded that stress in upwind condition which is worst case as per CFD simulation is within permissible limit and is safe for desired service for the HDPE material. Also, from **Table 6**, can be concluded that the CFD results are approximately similar to the analytical approach using IS codes 875 part 3. Fatigue analysis concludes that the developed model is more safer for 5° Load condition for design life of 360000 cycles, whereas for 10° and 15° load condition the components fails at minute regions for the available life cycle.

CONCLUSION

This paper highlights the concept of Floating Solar Technology, develops a design and CFD model and discusses the important results and outcomes.

Maximum wind speed, the heavy load should be considered in the analysis. A proper study of factors like the layout of a water body, Orientation and Geometry of structure, tilt angle, etc. must be carried out for better results. Although HDPE shows superior performance and is reliable, FRP can also ascertain to be a worth replacement.

CFD simulation indicates that high wind pressure is subjected near panel region during the upwind load condition and hence the probability of failure at this condition is high and hence accordingly maximum lift force is considered for Structural analysis. Upwind load condition should be taken as the worst case and design and analysis should be done for the same case.



Static structural analysis was carried in FEA software for the upwind condition and the work demonstrates that stresses arising in the specified areas are within allowable limits and that the floating solar farm is therefore satisfactory for the intended service. Fatigue check for number of cycles to failure as per standard guidelines for float was studied and the system for the given material is safe and more reliable for less intense wavy water bodies. Wind pressure from CFD analysis was close to analytical analysis as per the IS code (Analytical analysis). Compared to land based installation, almost 42% installation cost is saved in floating PV plant. Also, the payback period is less in floating solar PV system..We hope that this article will assist researchers to address issues in near future in the area of Floating solar installation and development.

REFERENCES

1. V. Arun Kumar, , M Rashmitha, B. Naresh ,V. Rajagopal and J Bangararaju, "Performance analysis of different Photo Voltaic technologies," in International Conference on Advance Electronics system, 2013.
2. Neha Yadav, K.Sudhakar, Alok Sahu, "Floating photovoltaic power plant:A review," Elsevier, p. 10, 2016.
3. Wonchang Choi, Soon-Jong Yoon, Sun-Hee Kim, "Design and Construction of 1 MW Class Floating PV Generation Structural System Using FRP Members," Enegies, p. 14, 2017.
4. Hyung.-Joong Joo, Soon-Jong Yoon, Young-Geun Lee, "Design and Installation of Floating Type Photovoltaic energy generation system using FRP members," Solar Energy, p. 13, 2014.
5. Paturi Lakshmi Prasanna Kumar, K Gowri Sankar, " CFD Analysis of wind loading in Solar Panels"
6. Puneeth Kumar HP, Dr SB Prakash, " CFD analysis of wind pressure over solar panels at different orientations of placement"
7. Oguz Uzol. Afsin Saritas. Veysel Emre Uslu, "Wind Loading acting on solar panels in a row by CFD analysis," ACEM 16, p. 14, 2016.
8. Agerne. K. Dagnew, James Erwin, Girma T. Bitsuamlak, "Evaluation of wind loads on solar pnaels modules using CFD," CWE (Cpomputation Wind Engineering), p. 9, 2010.
9. H Fouad, "Characrezation and processing of High Density Polyethylene/carbon nano- composites," Materials and Design, p. 7, 2010.
10. Monai Chaabane, Hatem Mhiri, Phillippe Bournot, Wael Charfi, "Performance evaluation of a solar photovoltaic system,"Energy Reports, p. 7, 2018.
11. Qinxing Wang, Haiyang Lin, Hailong Li, Ronald wannersten, Luyao Liu, "Power Generation Efficiency and prospects of Floating Photovoltaic Systems," Energy Procedia, p. 7, 2017.
12. Z. Chuntao and M. D. Ian, "Nonlinear mechanical response of high density polyethylene. Part II: Uniaxial constitutive modeling," Polymer Engineering and Science, vol. 37, no. 2, pp. 414- 420, 1997
13. N. S. Gokhale, S. S. Deshpande, S. V. Bedekar and A. N. Thite, Practical Finite Element Analysis, Pune: Finite to Infinite, 2008.
14. Antaryami Mishra, "Stress Analysis of Glass/HDPE Composite Rocker Arm by Finite Element Method" International Journal of Engineering Science and Innovative Technology (IJESIT) Volume 3, Issue 3, May 2014
15. IS 875 part 3 : 2015 DESIGN LOADS FOR BUILDING AND STRUCTURES-CODE OF PRACTICE [16] www.livemint.com/Industry/saGIF4VEwvv38rf208tUAM/Solarpower.



Correlation between Ground Motion and Structural Response of Multi-storied Buildings in the Performance Based Seismic Design

Soumyan K¹, Deepa Balakrishnan S²

Assistant Professor, Department of Civil Engineering, College of Engineering Vadakara, Kozhikkode, Kerala¹

Professor, Division of Civil Engineering, School of Engineering, Cochin University of Science & Technology, Kochi, Kerala²

✉ soumyanchd58@gmail.com

ABSTRACT

The basic concept of the Performance Based Seismic Design (PBSD) is to provide engineers with the capability to design buildings that have a predictable and reliable performance in earthquakes. The main time consuming step in the evaluation of performance of the building due to earthquake ground motion is the procedures to be followed in the Nonlinear Dynamic Analysis. So the identification of ground motion parameters having good correlation with the structural response and development of Structural Response Functions are significant in the performance assessment of multi-storied buildings. This paper describes the basic concepts of the PBSD and the findings of various researchers on this area. The major steps in the development of Structural Response Functions include collection of strong motion data, evaluation of ground motion parameters, Nonlinear Dynamic Analysis on various buildings, calculation of structural response parameters and multivariate regression analysis of ground motion parameters on the structural response parameters. The complexity of the analysis can be simplified by developing the response functions.

Keywords: Performance based seismic design; Ground motion; Structural response; Nonlinear dynamic analysis, Multivariate regression analysis.

INTRODUCTION

The Performance Based Seismic Design (PBSD) process explicitly evaluates how a building is likely to perform, given the potential hazard it is likely to experience, considering uncertainties inherent in the quantification of potential hazard and the assessment of the actual building response. The basic concept of the PBSD is to provide engineers with the capability to design buildings that have a predictable and reliable performance in earthquakes. It is a design methodology done on the probable performance of the building under input ground motions. Due to the recent advances in seismic hazard assessment, PBSD methodologies, experimental facilities, and computer applications, Performance Based Seismic Design has become increasingly more attractive to developers and engineers of buildings in seismic regions. The seismic design of buildings typically was developed using performance-based capacity design procedures in which the engineer proportioned the building for intended nonlinear response and then used nonlinear structural analysis to verify that the structure's performance would be acceptable when subjected to various levels of ground shaking. So the strength based design is slowly giving way to the performance based design. The guidelines for PBSD are given in FEMA 356, FEMA 445, ATC 40, ATC 58 etc.

Severe damages of multi-storied buildings due to the earthquakes lead the engineers and seismologists to investigate the ground motion characteristics and structural seismic effects. The structural responses are correlated with simple ground motion parameters viz., peak ground or spectral response acceleration at fundamental period of the structure for predicting the seismic response of structures. These measures of ground motion intensity are chosen because they correspond to existing seismic hazard models. Other ground motion characteristics or parameters need to be identified that correlate better with seismic performance, particularly for the cases when the structural systems becomes nonlinear and its dynamic properties change with ground motion intensity. The identification of the ground motion characteristics or parameters will drive the development of corresponding seismic hazard data and models that can be combined with structural response or damage data and models serving to a good prediction in the performance assessment process. This study focuses mainly in correlating the ground motion parameters and the structural response of the multi-storeyed reinforced concrete buildings.

GROUND MOTION PARAMETERS

Ground motion parameters are essential for describing the important characteristics of strong ground motion and to develop



Ground motion prediction equations. S. L. Kramer [12] explains the main characteristics of earthquake ground motion as follows:

- 1) Amplitude
- 2) Frequency Content
- 3) Duration

Amplitude Parameters

- 1) *Peak Ground Acceleration (PGA)*: the largest absolute value of horizontal acceleration obtained from the accelerogram of that component.
- 2) *Peak Ground Velocity (PGV)*: the greatest speed of shaking recorded at particular point during an earthquake.
- 3) *Peak Ground Displacement (PGD)*: the greatest distance moved by the ground at particular point during an earthquake.
- 4) *Effective Acceleration*: the acceleration which is most closely related to structural response and to damage potential of an earthquake.
- 5) *Sustained Maximum Acceleration (Velocity)*: The lower peaks of the accelerogram is used to characterize strong motion by defining the Sustained Maximum Acceleration (Velocity) for three or five cycles as the third or fifth highest absolute value of acceleration(velocity) in the time history.
- 6) *Effective Design Acceleration*: the peak acceleration that remains after filtering out accelerations above 8 Hz.

Frequency Content Parameters

1) *Ground Motion Spectra*: Any periodic function can be expressed using Fourier analysis as the sum of a series of harmonic terms of different frequency, amplitude and phase. Using the Fourier series, a complete description of the ground motion can be provided since the motion can be completely recovered by the inverse Fourier spectrum as:

$$x(t) = c_0 + \sum_{n=1}^{\infty} (c_n \sin(\omega_n t + \phi_n))$$

Where c_n and Φ_n are the amplitude and phase angle, respectively of the n th harmonic of the Fourier series.

2) *Fourier Spectra*: Fourier transform brings a motion in the time domain to the frequency domain. A plot of Fourier amplitude versus frequency is known as Fourier amplitude spectrum.

3) *Power Spectra*: The frequency content of a ground motion can be described by a power spectrum or power spectral density function. The total intensity of a ground motion of duration T_d is given in the time domain by the area under the time history of squared acceleration as:

$$I_0 = \int_0^{T_d} [a(t)]^2 dt$$

4) *Response Spectra*: describes the maximum response of a Single Degree of Freedom (SDOF) system to a particular input motion as a function of the natural frequency or natural period and damping ratio of the SDOF system.

5) *Predominant Period*: the period of vibration corresponding to the maximum value of the Fourier Amplitude Spectrum.

6) *Bandwidth*: the range of frequency over which some level of Fourier amplitude is exceeded.

7) *Shape Factor*: indicates the dispersion of the power spectral density function about the central frequency.

8) v_{max}/a_{max} : Because peak velocities and peak accelerations are usually associated with motions of different frequency, the ratio v_{max}/a_{max} should be related to the frequency content of the motion

Duration Parameters

1) *Bracketed duration*: the interval between the points in time where the acceleration amplitude first and last exceeds a prescribed level.



2) *Significant duration (T_d)*: the time trace required to build up from 5% to 95% of the integral for the total duration of the recorded motion.

Other Parameters

1) *rms Acceleration*: a single parameter that includes the effects of the amplitude and frequency content of a strong motion record.

$$a_{rms} = \sqrt{\frac{1}{T_d} \int_0^{T_d} [a(t)]^2 dt}$$

2) *Arias intensity*: a parameter closely related to the rms acceleration.

$$I_a = \frac{\pi}{2g} \sqrt{\frac{1}{T_d} \int_0^{T_d} [a(t)]^2 dt}$$

3) *Cumulative absolute velocity*: the area under the absolute accelerogram.

$$CAV = \int_0^{T_d} |a(t)| dt$$

4) *Response spectrum intensity*: The area under the pseudo-velocity response spectrum between periods of 0.1 and 2.5 seconds.

5) *Effective peak acceleration*: the average spectral acceleration over the period range 0.1 to 0.5 seconds divided by 2.5.

6) *Effective Peak Velocity*: the average spectral velocity at a period of 1 second divided by 2.5.

7) *Damage potential*: a parameter incorporates the effects of strong motion duration on the response of medium rise buildings and is expressed as:

$$I = PGV T_{d0.25}$$

8) *Cosenza-Manfredi metric*: a dimensionless duration metric expressed as:

$$CMM = \frac{\int_0^{t_{max}} a^2 dt}{PGA \times PGV}$$

Where

t_{max} = Length of the accelerogram

STRUCTURAL RESPONSE PARAMETERS

The output from Nonlinear Time History analysis includes peak values of displacement, nonlinear deformation demands and component forces. From these demand sets following key response parameters are developed to represent the structural and non-structural damage of the buildings due to earthquake shaking [11].

A. *Interstory Drift Ratio*: ratio of interstory displacement to story height. It depends on several factors including structure's mass, stiffness, strength, damping and the ground motion record.

B. *Park-Ang Index*: a damage index combining both ductility and cumulative hysteretic energy demand [10].

$$D_{PA} = \frac{d_m}{d_u} + \frac{\hat{a}}{V_y d_u} \int dE_h$$

Where

d_u = ultimate deformation capacity under monotonic static loading

d_m = maximum deformation demand under dynamic loading



dE_h = incremental hysteretic energy demand

V_y = yield strength

β = a non-negative non-dimensional parameter

C. *Floor Acceleration and Velocity* : represented for the estimation of damage of non-structural elements. Floor velocity is calculated by numerical differentiation which consists of dividing the difference in the floor at adjacent time steps by the size of the step. Floor acceleration is obtained by taking a second numerical differential which consists of dividing the difference in floor velocities at adjacent time steps by the size of the time step [11].

D. *Residual Drift Ratio*: highly sensitive to component modelling assumptions related to post-yield hardening/softening slope and unloading response and is evaluated by the following equations:

$$\Delta_r = 0, \text{ for } \Delta < \Delta_y$$

$$\Delta_r = 0.3(\Delta - \Delta_y), \text{ for } \Delta_y < \Delta < 4\Delta_y$$

$$\Delta_r = (\Delta - 3\Delta_y), \text{ for } \Delta > 4\Delta_y$$

Where

Δ = maximum storey drift ratio

Δ_y = median storey drift ratio calculated at yield

LITERATURE REVIEW

The US Federal Emergency Management Agency (FEMA) published the guidelines for the Performance Based Seismic Design (PBSD) from time to time. According to FEMA-445 [7] PBSD is an iterative process and the major steps in the procedure are as follows:

- 1) Select performance objectives
- 2) Develop preliminary building design
- 3) Characterization of ground shaking hazard
- 4) Select a desired yield mechanism and target drift for the design earthquake hazard
- 5) Perform analysis of the structure
- 6) Conversion of base Shear – displacement curve to ADRS Spectra
- 7) Revise design

The FEMA-356 [8] identifies the following performance levels and adopts roof-level lateral drift at the corresponding load levels as a measure of the associated behaviour states of the building

1) *Operational (O)* : very light damage, no permanent drift, structure substantially retains original strength and stiffness, minor cracking of facades, partitions, and ceilings as well as structural elements, all systems important to normal operation are functional.

2) *Immediate Occupancy (IO)* : no permanent drift, structure substantially retains original strength and stiffness, minor cracking of facades, partitions, and ceilings as well as structural elements, elevators can be restarted, fire protection operable.

3) *Life Safety Level (LS)*: moderate, some residual strength and stiffness left in all stories, gravity-load bearing elements function, no out-of-plane failure of walls or tipping of parapets, some permanent drift, damage to partitions, building may be beyond economical repair.

4) *Collapse Prevention Level (CP)*: severe, little residual stiffness and strength but load-bearing columns and walls function, large permanent drifts, some exits blocked, infills and unbraced parapets failed or at incipient failure, building is near collapse.

A K Chopra [13] and ATC-40 [9] described the general procedures adopted for analysis of multi-storied buildings in the performance based seismic design process. They are linear static, linear dynamic, nonlinear static, and nonlinear dynamic



analyses. Linear static analysis can only be used for regular structure with limited height. The main disadvantage of linear static analysis is that it will not consider the inelastic behaviour of the structure. The static nonlinear analysis or pushover analysis allows the inelastic behaviour of the structure and provides reasonable estimation of the global deformation capacity of the structure and so is more efficient than linear static analysis. The dynamic analysis is classified as Response Spectrum and Time History Analyses. The Response Spectrum Analysis is an elastic dynamic analysis of a structure utilizing the peak dynamic response of all modes having a significant contribution to total structural response. The Time History Analysis is the analysis of the dynamic response of a structure at each increment of time when the base is subjected to a specific ground motion time history. It is performed with pairs of appropriate horizontal ground motion time history components that are selected and scaled from minimum three recorded events. The Nonlinear Time History Analysis (NTHA) is performed when high degree of accuracy is desired for obtaining the structural response of the multi-storied buildings during earthquake ground motion. In the case of inelastic systems the lateral resisting forces are dependent on the prior history of motion and a numerical integration method is used to solve the differential equations of motion to obtain the time history of the response. By selecting the Nonlinear Time History Analysis nonlinear inelastic response and the time-history of the seismic response of the structure are obtained. So this method is more accurate than linear static, response spectrum, and nonlinear static or pushover analyses.

As a result of the development work by the ATC-58 project of the US Federal Emergency Management Agency (FEMA) three series of volumes referred to as FEMA P-58 [11] was published in 2012. These volumes describe the methodology for seismic performance assessment of individual building that properly accounts for uncertainty in the ability to accurately predict the structural response. The inputs of this methodology include the development of basic building information, response quantities, fragilities and consequence data. The FEMA P-58 procedures are probabilistic, uncertainties are explicitly considered and the seismic performance of buildings followed by earthquake ground motion is expressed as the probable consequences in terms of human losses, direct economic losses and indirect losses. The methodology is applicable for all types of buildings if basic data on structural and non-structural damageability are available.

A Massumi and F Gholami[1] conducted a study of correlation between the ground motion and structural response by selecting 85 far-field ground motion records from 17 earthquake events with magnitudes in the range 5.9-7.6 from the PEER strong motion database. Non-linear dynamic analyses of four reinforced concrete frames were performed using IDARC-20 software. Principal Component Regression Analysis was performed by taking time-dependent and frequency-dependent ground motion parameters as dependent variables and inter-storey drift, roof drift and Park-Ang Index as dependent variables. It was observed that frequency-dependent parameters were better correlated than time-dependent parameters to predict the structural damage during an earthquake.

G Molas, M Rahnema and P Seneviratna[2] performed the Time History Analyses by selecting 480 records from the 7 earthquakes on 3 and 9 storied steel frame structures using DRAIN-2DX software. The maximum inter-storey drift was obtained as output and is converted into the Mean Damage Ratio (MDR) which was taken as dependent parameter. The Peak Ground Acceleration (PGA), Peak Ground Velocity (PGV), and Acceleration Response Spectra amplitudes (S_a) for the periods 0.3 and 1 seconds were taken as the ground motion parameters or independent variables. A Neural Network Model is used to find the relation between the ground motion and structural response parameters. It was observed that better correlation is attained when the full set of input ground motion parameters are used.

A Elenas [3] developed a procedure to evaluate the post seismic damage of multi-storied buildings. 400 records of past earthquakes were selected and evaluated 20 ground motion parameters. Non-linear dynamic analysis was performed on various models of multi-storied buildings and Overall Structural Damage Indices (OSDIs) such as Park and Ang, Maximum Interstorey Drift Ratio (MISDR) and Maximum Softening Index of DiPasquale and Cakmak were selected as damage indices. Multilinear regression analysis and Discriminant analysis were performed to find the correlation between the ground motion parameters and the damage indices. Also a structural response function was developed combining the effect of all the ground motion parameters and the structural response. The accuracy of the equation is tested by creating another set of artificial accelerograms.

M Elassaly [4] conducted Non-linear dynamic analyses on a two dimensional model of a 12 storey RCC building using the computer program IDARC2D V.6.1 subjected to 21 earthquake records. The study was focused on the effect of the Peak Ground Acceleration (PGA) and frequency contents on the structural response due to the ground motion. The frequency content was represented by the A/V ratio where A is the Peak Ground Acceleration (PGA) and V is the Peak Ground Velocity (PGV). Park and Ang Index and Interstory Drift Ratio were selected as damage indices. The records were classified into LFC, MFC and HFC for low, medium and high frequency contents. It was concluded that when the A/V ratio increases both Park and Ang Index and Interstory Drift Ratio of the buildings decreases.



K Kostinakis, M Papadopoulos, A Athanatppoulou and K Morfidis[5] conducted a study on the correlation between structure-specific ground motion intensity measures and the damage indices. The intensity measures were evaluated by the Pushover Analysis on RCC buildings by selecting 20 pairs of earthquake ground motions from the PEER strong motion database with magnitudes between 5.5 and 7.8. Then Nonlinear Time history Analyses was performed on four 5-storey buildings for each of the ground motions using the computer programme Ruaumoko. The Maximum Interstory Drift Ratio (MIDR) and Overall Structural Damage Index (OSDI) were taken as the structural response parameters. The Pearson correlation coefficient is taken as the indicator to evaluate the correlation between the intensity measures and the seismic performance parameters. And it was observed that the spectral acceleration at the fundamental mode period is having good correlation with the structural damage of the buildings compared to other intensity measures.

S Chakroborty and R Roy[6] studied the role of important ground motion characteristics on the demand of a plan asymmetric system by using a number of records with widely varying characteristics but adjusted to a common spectral shape. Because ground motion components are generated from the same earthquake source and seismic waves that travel through the same medium, strong dependence between the temporal and spectral characteristics of the two components was expected. Orientation of the ground motion axis with respect to the structural axis had been shown to play an important role in regulating response. A change in the orientation of ground motion components was associated with a corresponding change in ρ_{xy} which had been considered an important parameter for record selection in bidirectional analysis. It was also concluded that significant duration (T_d), frequency content, mean period (T_m) and the correlation coefficient (ρ_{xy}) between two horizontal earthquake components of a record might be chosen as characteristic ground motion parameters. Also the relevance of the energetic length scale (L_e) on the inelastic responses of irregular systems was explored.

CONCLUSION

The significance of the Performance Based Design and the studies on the correlation between ground motion parameters and the structural response parameters are reviewed. By developing Structural Response Functions the complexity of Nonlinear Dynamic Analysis can be avoided in the evaluation of seismic performance of the buildings during ground motion. The effect of various ground motion parameters and its effects on the response of buildings, considering many geometrical and structural parameters are to be investigated in future for simplifying the procedures in the Performance Based Seismic Design process.

REFERENCES

1. Ali Massumi and Fatemah Gholami, "The influence of seismic intensity parameters on structural damage of RC buildings using principal components analysis," *Applied Mathematical Modelling* 40 (2016), Elsevier, 2016, pp.2161-2176.
2. Gilbert Molas, Mohson Rahnama and Pasan Seneviratna, "On the correlation of ground motion indices to damage of structure models," 13th World Conference on Earthquake Engineering, Vancouver, B.C., Canada, August 1-6, 2004, Paper No.1074.
3. A. Elenas, "Seismic-Parameter-Based Statistical Procedures for the approximate assessment of structural damage," *Mathematical Problems in Engineering*, Hindawi Publishing Corporation, February 2014, Article ID 916820.
4. M. Elassaly, "Effects of ground motion characteristics on damage of R C buildings: A detailed investigation," *International Journal of Civil and Environmental Engineering*, vol.6, No.6, 2015.
5. Konstantinos Kostinakis, Manthos Papadopoulos, Asimina Athanatppoulou and Konstantinos Morfidis, "Correlation between structure-specific ground motion intensity measures and seismic response of 3D R/C buildings," Second European Conference of Earthquake Engineering and Seismology, Istanbul, August 25-29, 2014.
6. Suvonkar Chakroborty and Rana Roy, "Role of ground motion characteristics on inelastic seismic response of irregular structures," *Journal of Architectural Engineering*, American Society of Civil Engineers, January 2016.
7. Federal Management Emergency Agency, "Next-generation performance based seismic design guidelines program plan for new and existing buildings, FEMA 445," Applied Technology Council, California, August 2006.
8. Federal Management Emergency Agency, "Prestandard and commentary for the seismic rehabilitation of buildings, FEMA 356," Applied Technology Council, California, November 2000.
9. ATC-40, "Seismic evaluation and retrofit of concrete buildings, Volume 1," Applied Technology Council, California, November 1996.



10. Sidharth Ghosh, Debarati Dutta and Abhinav A. Katakdhond, “Estimation of Park-Ang damage index for planar multi-storey frames using equivalent single-degree systems,” *Engineering Structures*, Elsevier, June 2011, pp.2509-2524.
11. Federal Management Emergency Agency, “Seismic performance assessment of buildings, Volume 1, Methodology, FEMA P-58-1,” Applied Technology Council, California, September 2012.
12. Steven L. Kramer, *Geotechnical earthquake engineering*, Prentice-Hall International Series in Civil engineering and Engineering Mechanics, New Jersey, 1996.
13. Anil K Chopra, *Dynamics of structures, theory and applications to earthquake engineering*, Fourth edition, Prentice-Hall International Series in Civil engineering and Engineering Mechanics, New Jersey, 2012.



Preliminary Results of Concrete with Shredded Disposable Face Masks

Soham Parija¹, Dhanada K Mishra^{2,3}, Christopher Y K Leung²

Department of Mechanical Engineering¹, Department of Civil and Environmental Engineering, Hong Kong University of Science and Technology (HKUST), Clear Water Bay, Hong Kong SAR

KMBB College of Engg and Tech, Biju Patnaik University of Technology (BPUT), Odisha

✉ dhanadam@ust.hk

ABSTRACT

Hong Kong discards between 4-6 million disposable face masks every day. The global figure is estimated in the billions. The bulk of the discarded face masks are sent to the landfill along with Municipality Solid Waste (MSW). Based on the estimation that each face mask weighs two to three grams, the face masks disposed of at landfills every day weigh at least 10 to 15 tonnes. But a significant number end up polluting the environment. In this paper, we describe a method to sanitize the used facemasks and also recycle them into useful concrete products. It involves the collection of used facemasks, sanitizing the same using ozone treatment, shredding them, and mixing them in a suitably designed cement-based composite to make products like bricks, tiles, slabs, etc. The paper describes the results of preliminary experiments that establish the feasibility of the approach as concrete mixes with a range of densities and compressive strengths are produced.

Keywords: PPE; Face mask; Covid19; Papercrete; Recycling; Concrete.

BACKGROUND & INTRODUCTION

The building construction sector is one of the main components of the global economy directly accounting for 6% of global GDP [1]. Concrete is arguably the most widely used construction material in the world. At about 20 billion metric tons or around 2.5 metric tons per person on an annual basis in 2013 [2] it is being consumed at an ever-increasing rate. For example, between 2011 and 2013, China consumed 6.6 gigatons of concrete¹ – more than what the US used in the entire 20th century. The consumption of materials in general and construction material in particular has driven the growth of the economy. An indicator of this growth is the consumption of cement². Since 2010, China's consumption has increased from 2.05 billion tons per year to 2.35 billion tons with a high of 2.7 billion tons³ in 2014. In the same period, the world consumption of cement has increased from 3.64 billion tons to 4.65 billion tons. Construction is also one of the largest employment generators in most countries –being highly labor-intensive. In a world where developed countries like the USA, Canada, Europe, Japan, and Australia, etc have more or less reached a point of saturation, the future growth in construction is bound to come from fast-developing economies of countries like China, India, south-east Asia, South America, and Africa. In the developed world, the investment in repair and replacement of existing infrastructure will outpace new construction. With the growing threat of climate crisis, the construction sector is going to face the challenge of reducing its carbon footprint of about 25-40% emission out of which 7-8% is contributed by the manufacturing of cement alone. There are efforts to make the entire construction sector achieve net-zero carbon by 2050 by way of the use of green materials in construction and renewable energy in the operation of buildings. [3]

Overall municipal solid waste (MSW) generation will increase to 3.40 billion metric tons by 2050 from around 2.01 billion tonnes currently as per a World Bank report⁴. In 2016, the world produced 242 million tonnes of plastic waste which was

¹ <https://www.forbes.com/sites/niallmccarthy/2014/12/05/china-used-moreconcrete-in-3-years-than-the-u-s-used-in-the-entire-20th-century-infograp hic/#3493a5ed4131>

² <https://www.globalcement.com/magazine/articles/858-defining-the-trendcement-consumption-vs-gdp>

³ <https://www.statista.com/statistics/1042516/chinese-cement-consumption/>

⁴ <https://www.wastedive.com/news/world-bank-global-waste-generation-2050/533031/>



12 percent of all municipal solid waste. It is estimated that only 13.5% of today's waste is recycled and 5.5% is composted. Plastic waste is choking our oceans, yet our consumption of plastics is only increasing [4]. The Covid19 pandemic has added significantly to this crisis by a sudden increase in the consumption of Personal Protective Equipment (PPE). An estimated 1.6 billion tonnes of carbon dioxide-equivalent (CO_2 -equivalent) greenhouse gas emissions were generated from solid waste in 2016, which is about 5 percent of global emissions. Without improvements, solid waste-related emissions are anticipated to increase to 2.6 billion tonnes of CO_2 -equivalent by 2050. Hong Kong discards between 4-6 million disposable face masks every day. The bulk of the discarded face masks are sent to the landfill along with the general waste. Based on the estimation that four to six million face masks are used in Hong Kong daily and each face mask weighs two to three grams, the face masks disposed of at landfills every day will weigh some 10 to 15 tonnes. But a significant number end up polluting the environment including the drains, streams, beaches, and end up in the sea⁵. Panda et al. have provided a comprehensive global scenario as far as plastic waste recycling is concerned.

BRIEF REVIEW OF PRIOR RESEARCH

Fuller, B., et al. [6] have conducted a study to determine the mechanical and physical properties of Papercrete using laboratory tests for the commonly used sample mixes and compared them with anecdotal evidence. The stress-strain curve obtained suggests that papercrete is ductile and resists permanent deformations. The study conclusively states that with the proper mix design, papercrete can be safe for 2-story residential home constructions, but indicates the scope for better testing to gather more information in order to generate more conclusive evidence for it to be used for heavy-duty applications as well.

Almeshala et al. [7] have investigated the effects of using PET as a partial substitute for sand in concrete and studied their physical and mechanical properties. They crushed PET bottles to 4-0.075 mm and used in the concrete mix in different proportions to attain the desired percentage of substitution. It has been observed that the density, tensile strength, compressive strength, and workability of concrete decreases with an increase in PET in the mix. Additionally, the flexural strength is also shown to be reduced and can be explained by the low strength of plastic aggregates and low bond strength between the cement mix and the plastic aggregates due to the hydrophobic nature of plastic. It has been hence concluded that this form of substitution can be used for mechanically less intense structures and lightweight applications.

Alqahtani et al [8] have produced recycled plastic aggregate (RPA) using waste plastic and red sand filler and conducted a comparative study with respect to lightweight aggregate (LWA). It is noted that the use of plastic reduced the compressive strength of the concrete due to lower bond strength with the cement mortar and the RPA. While the permeability of LWA decreased with an increase of the Water to Cement Ratio, it remained unaffected for the RPA concretes. The concrete ion permeability of RPA concrete was observed to be much lower than the corresponding LWA concrete since plastic aggregates blocked the transfer of chloride ions. Thus this kind of concrete is recommended to be used in applications that demand low strength and inertness to chemical attacks.

Okeyinka et al. [9] have reviewed the use of solid wastes in building construction materials. The use of plastic in form of aggregates in the concrete has shown improved compressive and flexural strength but are poorly bonded to the concrete and thus require surface roughening treatment. The use of paper has been found to increase the weight to strength ratio, insulation properties, and toughness characteristics of concrete materials. However, the tensile and compressive strength is found to be reduced based on experimental tests.

Sharma and Bansal [10] have reviewed the use of different forms of waste plastic in concrete. They have also emphasized the various additives that can help in assuaging the drawbacks of plastic addition to the mix. It has been observed that the workability of the concrete reduces adding waste plastic, but the performance can be improved using a chemical treatment such as alkaline bleach treatment. They have also reported the increase in tensile strength of the concrete on plastic addition, which is attributed to the bridging action of fibers in the concrete. The flexural strength has also been observed to improve since the plastic acts as a crack arrestor. The review suggests that more research has to be done on the process of mixing, the shape, percentage ratio, and surface properties of the plastic fiber in order to ensure adherence to the mix. Durability is considered to be a major concern and hence the use of plastic is recommended to be used in relatively light-duty applications.

Shermale and Varma [11] have done a study on the compressive strength and mass density by producing papercrete with different ingredients such as fly ash, sand, and glass fiber. It has been observed that the compressive strength of the concrete is

⁵ <https://uk.reuters.com/article/uk-health-coronavirus-hongkong-enviromne/discarded-coronavirus-masks-clutter-hong-kongs-beaches-trails-idUKKBN20Z0PI>



directly proportional to the amount of cement in the mix and inversely dependent on the amount of waste paper pulp added to the mixture. The density of the concrete reduces with the increase in the amount of paper in the mix. Thus the study suggests using papercrete for lightweight components and construction materials that are not subjected to heavy loads.

Dalhat and Wahhab [12] have evaluated the thermal and mechanical properties of recycled polystyrene (rPS) and polypropylene (rPP) concrete. Based on the testing conducted the rPP showed higher compressive strength than rPS and AC (Asphalt Concrete), almost equivalent to PCC (Portland Cement Concrete). The rPS shows high bending resistance than PCC, AC, and rPP. The rPP showed very high flexural strength whereas the rPS showed higher flexural strength than rPP and rPS. Both rPP and rPS show better moisture resistance and thermal sensitivity than AS.

Malek et al. [13] have studied the effect of the addition of recycled polypropylene on the mechanical properties of concrete. The comparison is made between three different mixing ratios (0.5%, 1%, and 1.5% wt. of cement) and two different forms of recycled PP fibers (White polypropylene fiber (PPW) and green polypropylene fiber (PPG)). A significant increase in compressive strength, flexural strength, and split tensile strength was observed on adding each type of fiber with PPG giving better results for the two.

SIGNIFICANCE OF THE RESEARCH

It is possible to sanitize the used facemasks⁶ alongside mixed waste plastics to recycle them into useful concrete products. It involves the collection of used facemasks, sanitizing the same using ozone treatment, shredding them, and mixing them in suitably designed cement-based composite mixes to make products like bricks, tiles, slabs, etc. Such an approach can help ease the burden of safe and sustainable disposal of waste plastic including PPEs.

EXPERIMENTAL PROGRAM

Materials

A preliminary experimental program was carried out to test whether shredded used sanitised face masks can be effectively incorporated in papercrete as a strategy for its recycling. Disposable face masks were collected and sanitised using ozone treatment (**Fig. 1**). They were shredded manually and using a paper shredding machine. The shredded facemasks are shown in **Fig. 2b**. The paper pulp was obtained by soaking shredded paper from the concrete laboratory office and mixing them after 3 days using a mortar mixer. The moisture content of the pulp was measured to be 94% in undrained condition and 82% after draining excess water in the pulp. A photograph of the paper pulp is shown in **Fig 2a**. The Ordinary Portland cement, local fly ash, and river sand along with tap water were used in all mixes. The mix proportions are shown in **Table 1**. The objective was to test a range of mixes with properties ranging from low strength lightweight concrete for non-structural applications to normal density and medium strength concrete for load-bearing applications.

Table 1. Mix proportions (by weight)

Sl. No.	Components	Mix I	Mix II	Mix III
1	Cement	1.0	1.0	1.0
2	Fly Ash	1.0	1.0	1.0
3	Paper (%)	50	15	0.0
4	Sand	0.0	2.0	2.0
5	Shredded face mask (%)	0.0	2.0	10
6	Water	8.4	1.4	0.8

Sample Preparation and Testing

Small quantities of material adequate to cast several 40 mm cubes were mixed by a hand mixer. All the dry ingredients were mixed first followed by mixing of water and superplasticizer as required to make a flowable mortar before adding the shredded face masks. All samples were demoulded after 2-4 days of drying as required and air-cured until testing at 28 days. A photograph of the samples is shown in **Fig. 3**.

⁶ A Hong Kong company - Zero Impact will assist in sanitising facemask using Ozone treatment - <https://zeroimpact.com.hk/>



Fig. 1. Ozone treatment machine from Bio3Gen distributed by ZeroImpact Limited (www.zeroimpact.com.hk)

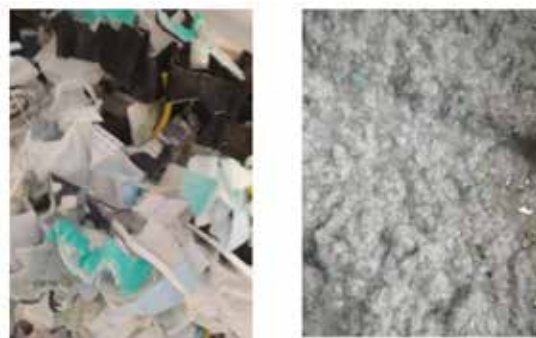


Fig. 2. (a) Shredded sanitised face masks and (b) paper pulp used in the experiments

RESULTS AND DISCUSSION

The density of the three mixes was monitored as evaporation of excess water took place. **Table 2** shows the change of weight with the time of the three mixes. It also shows the average compressive strength at 28 days. The density of the papercrete (Mix I) is 0.35 g/cc while the mix with both paper and shredded face mask (Mix II) is 1.56 g/cc and the third mix with face mask only is 1.8 g/cc.

Table 2. Density (G/CC) and 28 day comp strength (MPa)

Sl. No.	Age	Mix I	Mix II	Mix III
Density (g/cc)				
1	1	0.43	1.86	2.08
2	3	0.36	1.67	1.89
3	7	0.35	1.56	1.80
Compressive Strength (MPa)*				
4	28	1.14	9.46	19.45

*Average of three test results.



Fig. 3. (a) cube samples cast in plastic moulds, and (b) samples after demoulding, air curing and testing

Fig. 4 shows the cut section of a sample each from Mix II and III. They show the microstructure with paper and face mask and with face mask alone respectively.

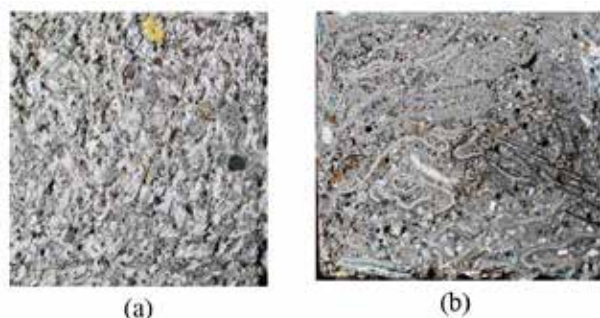


Fig. 4. (a) Section of a Mix II sample with paper and face mask, and (b) Section of a Mix III sample with only face mask.

Future Work

The work presented in the paper represents a very preliminary experimental exploration of concrete mixes incorporating waste paper pulp and shredded disposable face masks. Based on these preliminary results it is demonstrated that recycling PPE waste plastic such as disposable used face masks in concrete to make a variety of useful products of different densities and strengths is feasible. A comprehensive experimental program will help optimise the mix proportions and characterise the material properties suitable for different structural and non-structural applications. Other approaches to the recycling of mixed waste plastics such as converting liquid fuel through catalytic thermolysis [5], manufacture of lightweight aggregates, using melted plastic as a binder to produce bricks, blocks, paving/roofing tiles, etc can also be explored.

SUMMARY AND CONCLUSIONS

The following conclusions can be drawn based on the information presented in this paper.

1. Disposal of waste plastics is a global challenge that has become even more critical with the pandemic generating a multitude of disposable PPEs such as face masks that need an urgent solution.
2. A preliminary experimental study shows that using shredded facemasks in concrete is a feasible approach to recycling.
3. A range of properties such as density (0.35 g/cc to 1.8 g/cc) and compressive strengths (1.14 - 19.45 MPa) are achievable.
4. Further research should be carried out to explore other approaches to recycling such as conversion to fuel, lightweight aggregate, or plastic products to manage the global menace of burgeoning waste plastics.

ACKNOWLEDGMENT

Dhanada K Mishra gratefully acknowledges KMBB College of Engineering and Technology, Bhubaneswar, India for permitting and HKUST for supporting his sabbatical as a visiting research scholar. We thank Federico Galimberti and Massimiliano Martinello of Zero Impact Limited for their support.

REFERENCES

1. T.A. Boden, G. Marland, and R.J. Andres, Global, Regional, and National Fossil-Fuel CO₂ Emissions, Carbon Dioxide Information Analysis Center, Oak Ridge National Laboratory, U.S. Department of Energy, Oak Ridge, Tenn., U.S.A., 2017.
2. P.J.M. Monteiro and S.A. Miller, A. Horvath, Towards sustainable concrete, *Nature Materials*, 16, 2017. 698-699.
3. D.K. Mishra, "Moving to a Circular Economy Model is Vital for the Planet, 3rd July 2020, <https://earth.org/circular-economy-model> .
4. S. Kaza, L. C. Yao, P. Bhada-Tata, and F. Van Woerden, "What a Waste 2.0 : A Global Snapshot of Solid Waste Management to 2050," Urban Development, Washington, DC: WorldBank.2018.<https://openknowledge.worldbank.org/handle/10986/30317> License: CC BY 3.0 IGO.



5. A.K. Panda, R.K. Singh, and D.K. Mishra, “Thermolysis of waste plastics to liquid fuel A suitable method for plastic waste management and manufacture of value-added products - A World Perspective”, *Renewable and Sustainable Energy Reviews*, 14 2010. 233–248. (<https://doi.org/10.1016/j.rser.2009.07.005>).
6. B. Fuller, A. Fafitis, and J. Santamaria, “Structural Properties of a New Material Made of Waste Paper”, *Architectural Engineering Conference (AEI) 2006* DOI: 10.1061/40798(190)10
7. I. Almeshal, B. A. Tayeh, R. Alyousef, H. Alabduljabbar, and, A.M. Mohamed, “Eco-friendly concrete containing recycled plastic as a partial replacement for sand,” 2020. *jmaterrestech*2020(<https://doi.org/10.1016/j.jmrt.2020.02.090>)
8. F. Alqahtani, G.S. Ghataora, and S. Dirar “Lightweight Concrete Containing Recycled Plastic Aggregates”, *International Conference on Electromechanical Control Technology and Transportation (ICECTT 2015)*
9. M. Oriyomi, D.A. Okeyinka, and J.M.K Oloke,, “A Review on Recycled Use of Solid Wastes in Building Materials”, *Open Science Index, Civil and Environmental Engineering* Vol:9, No:12, 2015 waset.org/Publication/10003128
10. R. Sharma and P.P. Bansal, “Use of different forms of waste plastic in concrete - a review,” *Journal of Cleaner Production* 112 2016.
11. Y. Shermale and M.B. Varma “Properties of Papercrete Concrete: Building Material”, *IOSR Journal of Mechanical and Civil Engineering (IOSR-JMCE)* e-ISSN: 2278-1684,p-ISSN: 2320-334X, Volume 14, Issue 2 Ver. VII, Mar. - Apr. 2017, PP 27-32 www.iosrjournals.org
12. M.A. Dalhat and H.A. Wahhab, “Properties of Recycled Polystyrene and Polypropylene Bounded Concretes Compared to Conventional Concretes”, *Journal of Materials in Civil Engineering*, · September 2017.
13. M. Małek, M. Jackowski, W. Łasica, and M. Kadela, “Characteristics of Recycled Polypropylene Fibers as an Addition to Concrete Fabrication Based on Portland Cement”, 2020.DOI: 10.1002/suco.201800336



A Technical Paper on “RCC Blanket Wall”

H M Viswanatha Sastry

Director (Technical), Department of Civil, Bhamys Constructions Pvt. Limited, Lakshmipuram, Mysore, Karnataka

✉ sastry.hmv@bhamys.com

ABSTRACT

In the hilly and mountainous terrain many types of structural methods are used to withstand high earth pressure and also prevent soil erosion and hold the earth surface intact. The generally used techniques include building retaining walls, soil nailing, reinforced earth retaining wall (RERW) etc. These types of construction methods not only consume high quantity of steel and concrete but also increase labour and time of construction. This technical paper on “Blanket wall” for the ‘safe Protection’ of the cut & exposed/Natural surfaces of the hilly terrains will provide an alternative innovative method of construction which will reduce cost of construction, save time and re-sources without compromising on the quality, safety and intent of construction. This particular article exemplifies one of NMDC mining projects at Bailadila, Chhattisgarh.

In the course of this study a lot of innovative engineering ideas and thoughts have studied before arriving at general layout and its technological requirements. Following factors are considered while planning and designing Blanket Wall:

- Space constraints
- Type of terrain
- Soil conditions
- Area subjected to heavy rainfall, thick fog considerations
- Transportation of heavy machineries & equipment
- Time factors with respect to project schedule achieving the cost economy & various related aspects.

Keywords: Terrain; Protection; Innovative; Quality; Safety & Economy.

INTRODUCTION

The ‘RCC Blanket Wall’ is required to be constructed for the protection and ‘safety’ of the adjoining existing structures. This type of structure is mainly constructed for the existing elevated natural terrain conditions or series of mountainous hilly area ranging to a high altitude/ +1800 meters.

The blanket wall can be easily constructed without any deep excavation.

In case of conventional construction methods retaining walls are constructed to withstand the earth pressure in the hilly terrain. The foundation part of the retaining wall is deeper & base width as per required design governed by the soil conditions. It would be difficult to design and construct a retaining wall with space constraints specially to accommodate foundation depth due to terrain condition. In the Course of this larger area of space provision to be planned, this may impact on cost & time.

Irrespective of the terrain/profile conditions, the blanket wall can be adopted to safe guard the existing terrain. In case of steep slopes at an angle up to 70 degree the blanket wall shall be adopted after trimming/dressing the profile wherever necessarily called for benches forming to a minimal bare width depending on the profile availability.

The Blanket wall is an art of design and the peripheral end need to be provided with key beams (also called as grip/anchor beams.) At the bottom most level of the blanket wall a conventional drainage system is provided. The thickness of RCC blanket wall varies between 50 mm to 100mm with nominal reinforcements. Weep holes are provided depending on the site conditions especially at lower elevations. The weep holes are located at road drainage and formation level to a height of at least 4meters.

The embedded ‘U’ shaped reinforcement bars are provided to enable access for maintenance activities during emergency situations.

To quote as an example, the blanket wall shown in the pictures has been designed and constructed in a hilly terrain to an altitude of +1120 meters with respect to primary crusher at +1090 meters (30 meters height.)

This blanket wall was constructed 22 years ago and is structurally firm/intact and stable even today. The Blanket Wall has its own merits and advantages compared to vertical walls/retaining walls/reinforced earth retaining wall(RERW)/Soil nailing/other such methods. Most suitably implemented for natural slopped surfaces. It has more advantages than limitation, the cost aspects are also dealt with comparatively very economical to above said methods.

Figures 1, 2, 3, 4, 5 & 6 be referred.



Figure 1. Front view of Blanket wall



Figure 2. Front view of Blanket wall benches



Figure 3. view of Blanket wall at primary crusher entry



Figure 4. Side view of Blanket wall



Figure 5. Side view of blanket wall with key beam & drain



Figure 6. NMDC Project office, Protection Works

Purpose of Blanket wall

‘Blanket Wall’ serves as surface protection to the ad-joining existing units, keeping in view its vicinity to hill, elevated altitudes, space restrictions to provide retaining wall, cost aspects due to wider spread area with close proximity to varying site profile & other many such related. The blanket wall is generally treated as one of the protections to hilly terrains instead of other methods.

Procedure adopted

The ‘Blanket Wall’ is usually spread at a single stretch of length 50 meters&sloping height of 70 meters.

Considering the existing/prevaling site conditions in a hilly terrain area, where crushing plant was built to a height of 30meterswith respect to the start of downhill conveyor. The Dumper Platform (DPF)is at an elevation of +1120 meters. The mountainous terrain in between dumper platform and start off downhill conveyor; was retained/undisturbed (For which the blanket wall protection was adopted.)

The existing contours of the hill have been physically-surveyed and plotted on the drawing in **Fig. 7** as shown below.



Fig. 7. Plan of blanket wall

Based on the contours the location of the dumper Plat-form,primary crusher,secondary crusher,transfer houses, downhill conveyors,silos, screening plant (wet circuit system),loading plant, road/approaches and all the concerned units connectivity requirements have been marked;to accommodate the required size of the plant buildings based on technology of the mining process right up to loading plant.

The level from DPF (Dumper platform) at +1120 meters to loading plant at +550 meters being RHT (Rail Head Top.)that is units are housed to a height of 570 meters in mountainous strata.

Keeping in view the ‘safety’ of all technological units;a decision has been taken to protect the road leading to entry at primary crusher/start of downhill conveyor system.

The base for blanket wall is designed along with the road drain to induce gravity by weight in the form of a beam, to enable blanket wall spring from the beam top. The cross section of the blanket wall shown in **Fig. 8**.

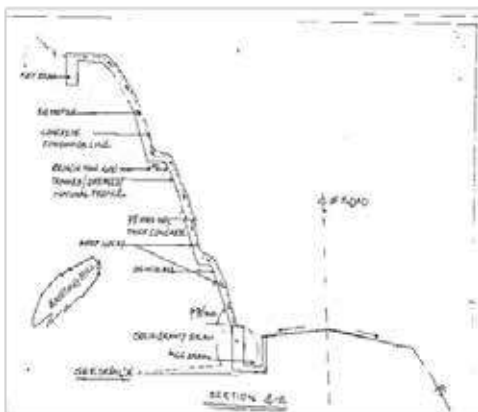


Fig. 8. Cross section of blanket wall

The design of creating gravity beam is to serve the following multiple purposes:

- As a structural member & a part of drain.
- Solid coverage & protection between road & hill part.
- To enable safe movement of heavy moving trolleys/equipment/machinery/other such.
- Envisage Kerb on the outer drain wall supplementing mines safety.
- Also to cater branch to blanket wall.

Key/edge beams: This shall be provided all along the periphery of the blanket wall. The size of key beams generally ranges with width between 200 mm to 250 mm and depth around 400mm. Refer **Fig. 9** for further details.

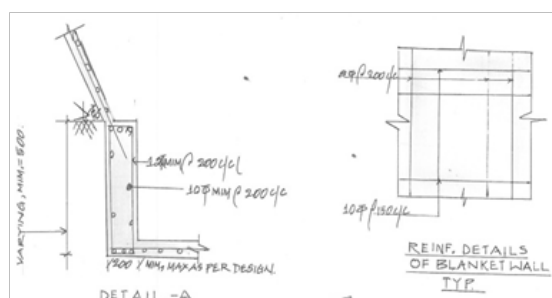


Fig. 9. Reinforcement details of gravity beam & Blanket wall

At the exterior end of the key beam; fill the extreme cut portion, adjacent to key beam with available boulders & interstices with good earth/morrum. At the meeting point of two different stretches of the blanket walls an expansion joint of width 30mm to be provided. This gap of 30mm is filled with twisted jute impregnated in hot bitumen.

While making blanket wall the trees of any girth can be retained. The required space around the tree is provided with key beams. Before laying the blanket wall the 'construction paper/polythene sheet' is provided on the hill profile surfaces before placing the reinforcement. The uniform top surface to the extent possible need to be maintained while laying the concrete.

The thickness of blanket wall concrete due to the existing hill profile varies. Maintain minimum of 50mm thick at any given cross sectional point.

Provide 10mm diameter or 12mm diameter reinforcements in the blanket wall including the key beams to enable flexibility while matching existing terrain/profile conditions. U-shaped bars with 10mm diameter are reinforced as steps which will be used for maintenance activities or at emergency situations.

Quality & Safety Aspects

Quality: Best efforts required to be exercised in all respects to quality aspects, strength of concrete, grade of cement, grade of steel all such related as per IS.

Safety: All precautionary and care need to be implemented as the hilly terrain contours may abruptly vary during construction activities. Prolific experience & expertise will be an added advantage in handling such challenging works.

Cost Aspects

In General with all aspects & considerations no comparison for a blanket wall is drawn with respect to retaining wall/Soil nailing/reinforced earth retaining wall (RERW)/other such. All the said methods are heavily reinforced. However on a broad concept considering the use of nominal reinforcement (excepting the gravity beam), the blanket wall is around 25 percent of other said methods.

Benefits & Limitations of Blanket Wall

Benefits: It has many advantages in comparison with other types of protection works. The listed below are the advantages.

- Faster commencement of work.



- Less involvement of materials, labourers and earth equipment.
- Minimum involvement of the vegetation removal, bigger girth of trees can be retained; unless otherwise demanded by safety considerations.
- Helps in retaining trees and thus partly contribute towards environmental protection.
- Protection to natural drain in valley spots.
- Envisage easy making of benches suiting to site conditions.
- The gravity beam is clubbed along with drainage part.
- Less utilization of steel & minimum grade of concrete.
- Retention of natural terrains without much disturbance.
- 'U' shape rings/steps provided for safety to-wards the maintenance to reach at top point of elevations, also; it will be further useful for works continuity.
- Less maintenance.

Limitations: The listed below are the limitations.

- The Protection is extended for slopes less than/within 70 degree angle of inclination to natural hill.
- This can be adopted as protection to valleys portion where natural water stream flow all time.
- Protection to downstream check dams.
- Effectively made use for capping methods.

ACKNOWLEDGMENT

The Author would like to thank:

- (i) "MECON Limited & NMDC Limited". The Blanket Wall was designed at project Deposit No.10 & 11A, Bailadila Chhattisgarh, Suited to Project requirement, client NMDC got this executed by renowned executing agencies under the challenging situations; keeping in view the safety of all adjacent existing structures/units during the year 1992 to 2001.
- (ii) M/s Bhamys Construction Pvt. Limited., Dr M D Raghavendra Prasad, Managing Director & Mr D S Mallikarjuna, Chief executive officer.



Wind Pressure Distribution over Solar PV Panels Mounted on Pitched Building Roofs

Ashish Agarwal*, Hassan Irtaza, Azhar Jameel

Department of Civil Engineering, Zakir Hussain College of Engineering & Technology, Aligarh Muslim University, Aligarh

*✉ ashishagarwal.ce@gmail.com

ABSTRACT

In the 21st century, transition from non-renewable to renewable energy sources taking place at rapid pace. Within last few years major world economies have shifting to solar and wind energy sources at large scale to meet their energy demand. The government of India has also aimed to reach 100 GW of solar energy installation by 2022 under National Solar Mission, out of which 40 GW is to achieve through rooftop solar. A significant portion of rooftop solar will be installed over pitched building roofs. The pitched roofs are most widely used for buildings in the mountainous region and for industrial buildings. Solar PV arrays are vulnerable under wind-induced loads, and several damaging incidents of have been reported in recent years. Due to the lack of design guidelines and standards, for safe design, wind pressure coefficient over solar arrays mounted on the pitched roof cannot be predicted accurately. In this study, wind pressure coefficients have been determined for solar arrays mounted on hip and saw type building roof subjected to normal (90°) and inclined (45°) wind incidences. Pitch angle considered for hip type and saw type building roofs were 20°, 30°, and 40°. Computation Fluid Dynamics (CFD) technique has been used to determine wind pressure coefficients over solar PV arrays mounted on low rise pitched roof buildings. Reynolds Averaged Navier Stokes (RANS) equations were incorporated in the second-order RNG k- ϵ turbulence model to predict the airflow behaviour through pitched roof buildings and solar arrays mounted on it.

Keywords: Pitched roof; Hip type building roof; Wind pressure; CFD; RANS.

INTRODUCTION

With the technological advancement in the last two decades of the 21st century, the cost per watt installation of solar panels has reduced drastically. Both developed and developing countries are shifting towards solar energy at a rapid pace. Recently, in China and India, Solar energy installation overtook other new installation of renewable or non-renewable energy generation units. India has aimed to reach 100 GW solar installed capacity by 2022 and further raised target to achieve 450 GW of total renewable installed capacity by 2030. As of October 2020, the total installed capacity of solar energy has reached 36 GW, out of which rooftop solar is just 6 GW [1]. Under National Solar Mission, India has aimed to reach 40 GW installed rooftop solar by 2022. The ambitious aim to achieve 40 GW rooftop solar can be done by the installation of solar arrays over unused rooftops of industrial units, factories, and mills. With the cost reduction of solar panels and Li-ion batteries for energy storage, major industries are moving ahead to install rooftop solar systems for energy cost reduction. [2]. India lies between equator and tropic of cancer, and blessed with high solar irradiation throughout the year. Solar array mounting over pitched roof in mountainous region can impart huge potential since pitched roof are common practice in large region in India including Himalayan region and western ghat region. Target to achieve the 40 GW roof mounted solar installation, mountainous buildings with pitched roof can play important role in roof-top solar installation. This ambitious target would incur high capital resources, and any flaw in the solar system at large scale would lead to a huge investment at stake. Solar arrays are vulnerable in wind-induced loads and many past incidents showed damages of rooftop solar arrays at large scale. One such incident was in which wind gust blew off rooftop solar panels mounted on the pitched roof in Buetzow, Germany at wind speeds of up to 119 km/h (6 May 2015) as shown in **Fig. 1** [3].

Cyclone Hudhud has blown away the rooftop solar PV panels in Visakhapatnam at approximate wind speed 160 km/h (October 12, 2014). 12 kW rooftop solar PV array system consisting of 120 panels, out of which 65 were damaged. While solar arrays are vulnerable under wind loads, but still there are very few or no guidelines in any international design codes, including ASCE/SEI 7-10 [4]. Most of the manufacturers and designers rely on conventional codes to determine wind-induced forces on solar array while considering solar array as a mono-slope roof. This approach could not precisely predict the wind load acting on solar arrays/panels and would cause damage to PV panels under wind-induced loads.

Aerodynamic behaviour of solar arrays has been studied both in wind tunnel experiments and numerical simulations by various researchers. The study of PV arrays by various researchers can be divided into three sub-groups, ground-mounted PV arrays, flat roof-mounted PV arrays, and pitched roof-mounted PV arrays. Kopp et al. (2002) [5], Chung et al. (2008) [6], Shademan & Hangan (2010) [7], Bitsuamlak et al. (2010) [8], Jubayer et al. (2011, 2014) [9], [10] and Irtaza et al. (2018) [11] worked on ground-mounted arrays using wind tunnel experiment or CFD simulation or both. Kopp et al. (2012) [12] and Stathopoulos et al. (2014) [13] worked both on flat roof-mounted and ground-mounted arrays. Most of the previous roof-mounted studies were focused on PV arrays mounted on flat roof (Banks (2013) [14]; Geurts et al. (2002) [15]; Kopp (2014) [16]; Stathopoulos et al. (2014) [13]; Wood et al. (2001) [17]).



Fig 1. Damaged solar panels due to high wind over the hipped roof [3]

Ginger et al. (2011) [18] performed wind tunnel tests on flat roof and gable roof buildings (1:20 scaled models) in the wind tunnel test facility at James Cook University, Australia. Pitch angles of gable roof considered were 7.5° , 15° , and 22.5° . The findings from this study were adopted by AS/NZS 1170.2:2011 (AS/NZS, 2012). PV panels of size 1 m x 1.7 m were installed parallel to the gable roof surface and number of tests were performed by changing the size of array (1.7 m x 7 m & 3.4 m x 7 m), location of array on the roof, clear distance between panel and roof surface (0.1 m and 0.2 m) and wind incidence angle. It was observed that the roof pitch angle, panel tilt angle and location of the panel on roof considerably affect the wind pressure over the PV arrays, whereas clear distance and size of the array do not have any significant effect on wind forces over the arrays.

Erwin et al. (2012) [19] investigated wind pressure over PV panels mounted on low rise building roof using full-scale test at Wall of Wind (WoW) research facility, Florida International University, and 1:12 scaled tests were performed using boundary wind tunnel test at RWDI. In this study, single PV panel of dimension 0.95 m x 1.58 m was mounted on the flat roof having tilt angle 0° , 15° , and 45° , and gable roof model at 0° and 15° tilt angles. A good agreement between the small and full-scale results was found for 45° tilted panels.

Geurts and Blackmore (2013) [20] performed field tests on 1 m x 1.5 m single PV panel mounted parallel on the pitched roof of an actual building having pitch angle 42° and compared findings with 1:100 scaled model using wind tunnel tests. Five different clearance distances (0.025 m, 0.05 m, 0.1 m, 0.2 m, and 0.3 m) were tested for a scaled model in a wind tunnel. Relatively small effects on wind pressures over the PV panel was observed on varying the clearance distance.

Aly and Bitsuamlak (2014) [21] performed wind tunnel tests on 1:15 scaled gable roof models having pitch angle 14° (1:4) and 18.3° (1:3). Building dimensions considered were 18.20 m x 9.05 m in plan and 4.27 m roof height, at full-scale. Three different panels of full-scale size 1.5 m x 0.9 m, 1.5 m x 2.4 m, and 1.5 m x 2.7 m were used in wind tunnel experiments. PV panels were mounted parallel with a pitched roof on both sides of the gable. From the results, it was found that wind pressure over PV panels affected both by pitch angle of gable roof and location of the panel on the roof.

Stenabaugh et al. (2015) [22] investigated the aerodynamic effect on PV arrays mounted on a 1:20 scaled model of low-rise buildings having a flat roof and gable roof, using wind tunnel tests at the University of Western Ontario. Several combinations of clearance distances and the gap between modules were examined. The effect of the solar PV panel tilt angle was not considered in this study. From this study, it was found that the small clearance distance and the large gap between panels lead to a smaller net force coefficient on PV panels.

Model Configurations & CFD Simulation

The objective of the current study is to determine wind pressure coefficients over PV panels mounted parallel to hip-type and saw-type industrial building roof having a varied pitched angle from 20° to 40° at an interval of 10° . CFD simulations were incorporated using ANSYS Fluent 18 software [23]. The dimension of hip type building in the plan was 7 m x 14 m. Solar PV

panels are mounted on both side of pitched roof along longer dimension of building in plan. 12 PV panels were mounted in both windward and leeward pitched roof as shown in **Fig. 2**. The dimension of saw type building in the plan was 8 m x 20 m and the height of the building at the windward face was 6 m. Solar arrays mounted over saw type industrial building roof consisting of 6 PV panels (1 m x 2 m) over each 4 pitched roofs of saw type building, as shown in **Fig. 3**. Building and solar arrays mounted over its pitched roof were subjected to the turbulent wind having wind incidence angles of 45° and 90°, as shown in **Fig. 3**. Reynolds's average Navier Stokes equations were incorporated in the Renormalization Group (RNG) k- ϵ turbulence model. The following are the governing equations used in the RNG k- ϵ turbulence model.

$$\frac{\partial(\rho k)}{\partial t} + \text{div}(\rho k U) = \text{div}[\alpha_k \mu_{\text{eff}} \cdot \text{grad}(k)] + \tau_{ij} \cdot S_{ij} - \rho \epsilon$$

$$\frac{\partial(\rho \epsilon)}{\partial t} + \text{div}(\rho \epsilon U) = \text{div}[\alpha_\epsilon \mu_{\text{eff}} \cdot \text{grad}(\epsilon)] + C_{1\epsilon}^* \frac{\epsilon}{k} \tau_{ij} \cdot S_{ij} - C_{2\epsilon} \rho \frac{\epsilon^2}{k}$$

$$\text{and, } \tau_{ij} = -\rho \overline{u'_i u'_j} = 2\mu_t S_{ij} - \frac{2}{3} \rho k S_{ij}$$

$$\text{where, } \mu_{\text{eff}} = \mu + \mu_t, \quad \mu_t = \rho C_\mu \frac{k^2}{\epsilon}$$

$$\text{and } C_\mu = 0.0845, \quad \alpha_k = \alpha_\epsilon = 1.39, \quad C_{1\epsilon} = 1.42, \quad C_{2\epsilon} = 1.68$$

$$\text{and } C_{1\epsilon}^* = C_{1\epsilon} - \frac{\eta(1 - \eta/\eta_o)}{1 + \beta\eta^3}, \quad \eta = \frac{k}{\epsilon} \sqrt{2S_{ij} \cdot S_{ij}},$$

$$\eta_o = 4.377, \quad \beta = 0.012$$

1:50 scaled industrial building model with PV panels placed parallel over a pitched roof, within the computational domain was modeled in Gambit 2.4.6., commercial modeling and meshing software. The core domain having building was discretized using unstructured mesh by 3D tetrahedral elements, whereas the outer domain was structurally meshed using hexahedral 3D elements. The atmospheric boundary layer was used as a velocity inlet in the computational domain. The inlet velocity profile considered was based on field data of Texas Technical University. Log law atmospheric boundary layer equation taken is as follows.

$$U_z = \frac{u^*}{k} \log\left(\frac{z + z_o}{z_o}\right)$$

where, u^* = friction velocity, k = von Karman constant = 0.41, z_o = roughness length

Friction velocity u^* considered 0.539 m/s and roughness length 10 mm at full scale. Inlet velocity at height 10 m was 10 m/s in the ABL velocity profile. The turbulent intensity and length scale provided in the simulation was 15% and 0.45 m based on field data from Texas Technical University [24]. The base of the computational domain was defined as a rigid wall, and standard boundary function was provided with prismatic elements. Pressure outflow was provided at the outlet of the computational domain.

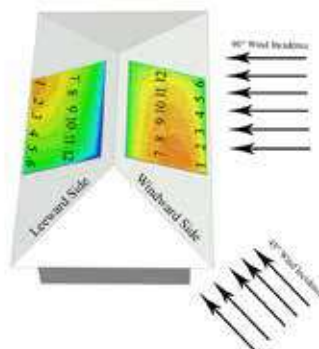


Fig. 2. Wind incident (90° and 45°) on solar array mounted on hipped roof building

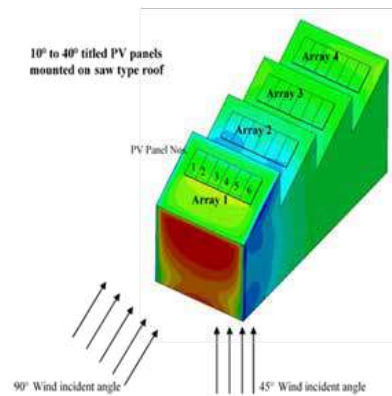


Fig. 3. Wind incident (90° and 45°) on solar array mounted on industrial building with saw type roof

RESULTS & DISCUSSION

Variation on net pressure coefficients over each PV panels mounted over hip type building roof in both windward and leeward roof slopes and subjected to 45° and 90° wind incidences, are shown in **Fig 4**. Pressure coefficient contours over top surface of PV panels mounted on windward and leeward sides of hipped roof are shown in **Figs 7** and **8** for each roof pitch angle in both 45° and 90° wind flow directions, respectively.

Similarly, variation of pressure coefficients over PV panels mounted over saw type industrial building roof in **Fig 5** subjected to 45° wind incidence are shown and in Figure 6 subjected to 90° wind incidence are shown for each roof pitch. Pressure coefficient contours over top surface of PV panels mounted on saw type industrial building roof are shown in **Figs 9** and **10** for each roof pitch angle in both 45° and 90° wind flow directions, respectively.

PV panels subjected to 90° wind incidence, maximum suction pressure found to be increasing with the increase in roof pitch angle for both hip type and saw type building roofs.

Maximum suction observed on PV panels in array 2 for each roof pitches for the saw type buildings. Suction pressure over array 1 decreases with the increase in pitch angle. For 45° wind incidence, maximum suction occurred at panel 1 (near leeward longer side of the building) in array 2 and 3 for all 4 roof pitch angles considered.

Variation in pressure over PV panels with the change in pitch angle does not show any definite pattern when arrays are subjected to 45° wind incidence. For the 40° pitched roof, positive pressure was observed along with PV panels in array 1, when subjected to both 45° and 90° wind incidences. On increasing roof pitch angle, the first sloped roof of saw type building crossed the wake region above it formed by hindrance provided by the windward wall.

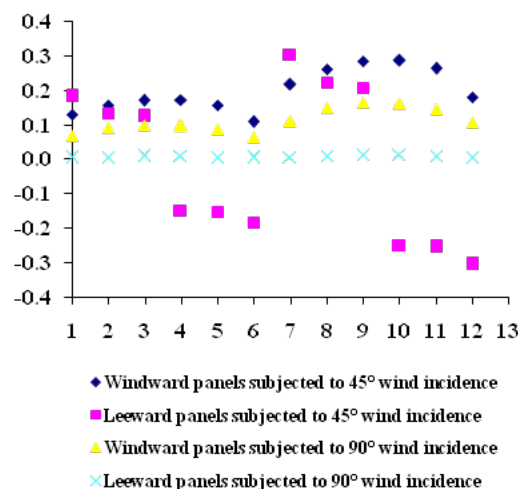


Fig. 4(a). Pressure coefficient of solar panels mounted over 20° pitched hipped roof building

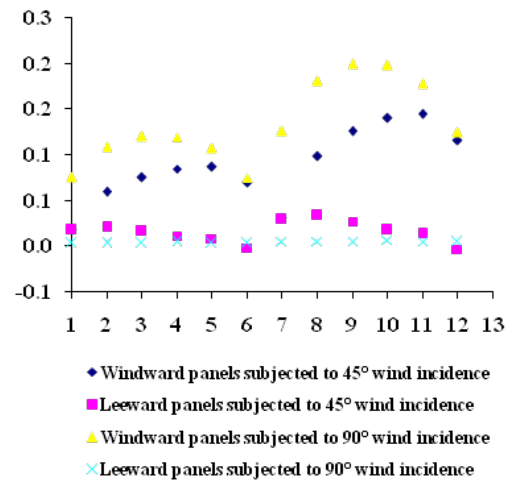


Fig. 4(b). Pressure coefficient of solar panels mounted over 30° pitched hipped roof building

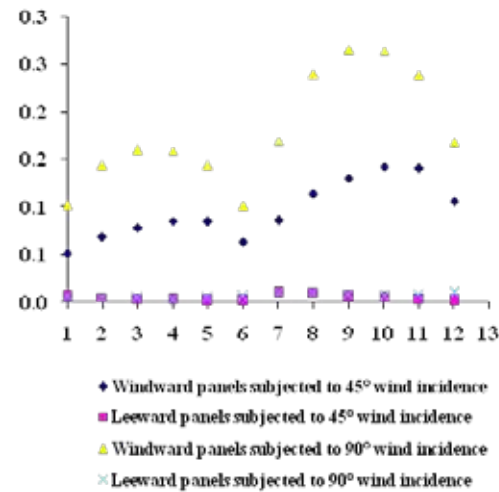


Fig. 4(c). Pressure coefficient of solar panels mounted over 40° pitched hipped roof building

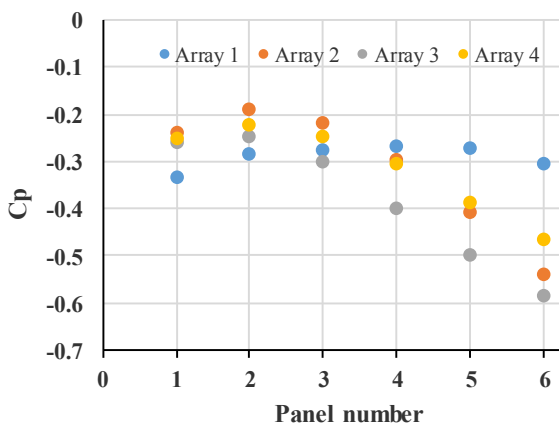


Fig. 5(a). Pressure coefficient of solar panels mounted over 20° pitched saw type industrial building roof subjected to 45° wind incidence

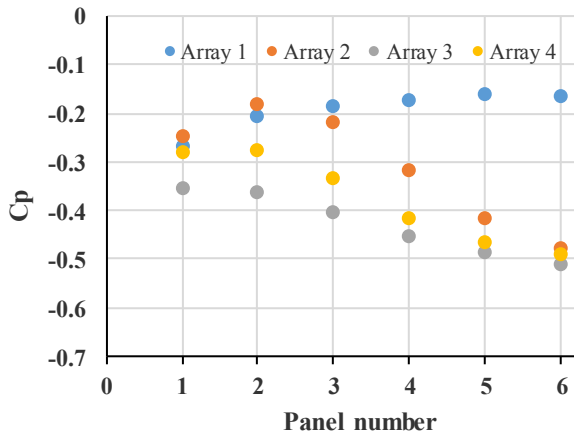


Fig. 5(b). Pressure coefficient of solar panels mounted over 30° pitched saw type industrial building roof subjected to 45° wind incidence

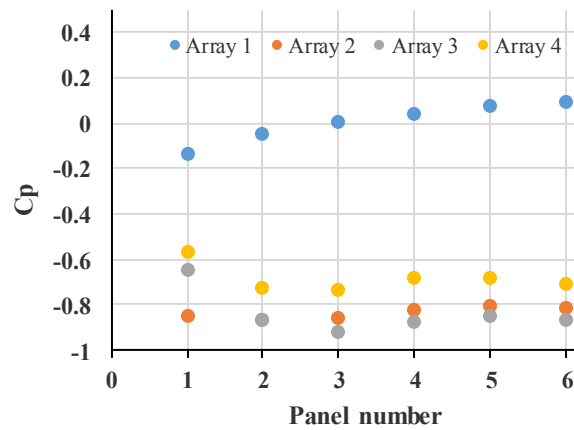


Fig. 5(c). Pressure coefficient of solar panels mounted over 40° pitched saw type industrial building roof subjected to 45° wind incidence

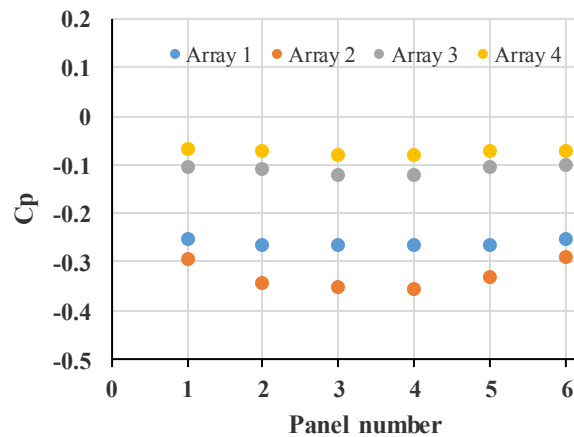


Fig. 6(a). Pressure coefficient of solar panels mounted over 20° pitched saw type industrial building roof subjected to 90° wind incidence

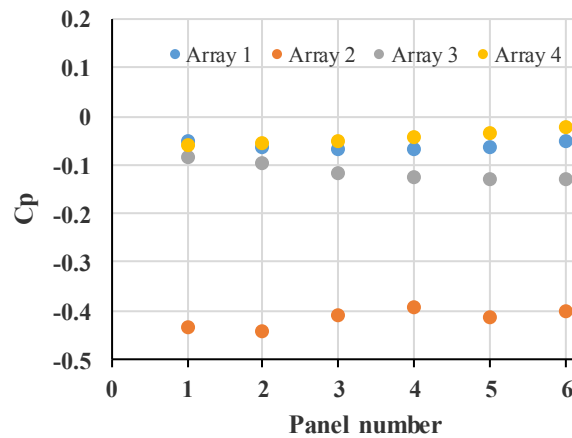


Fig. 6(b). Pressure coefficient of solar panels mounted over 30° pitched saw type industrial building roof subjected to 90° wind incidence

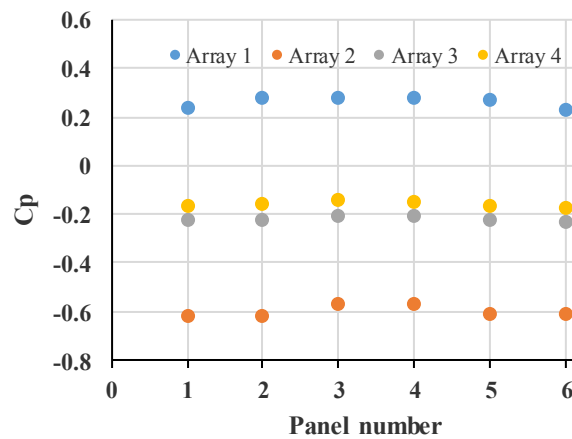


Fig. 6(c). Pressure coefficient of solar panels mounted over 40° pitched saw type industrial building roof subjected to 90° wind incidence

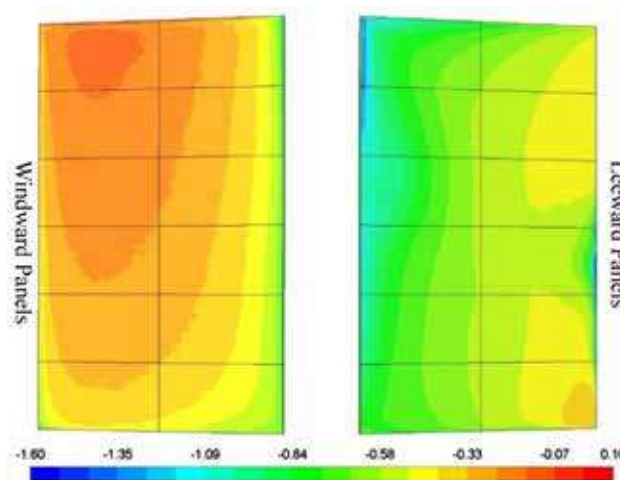


Fig. 7(a). Pressure contour over solar PV panels mounted on 20° pitched hip type building roof subjected to 45° wind incidence

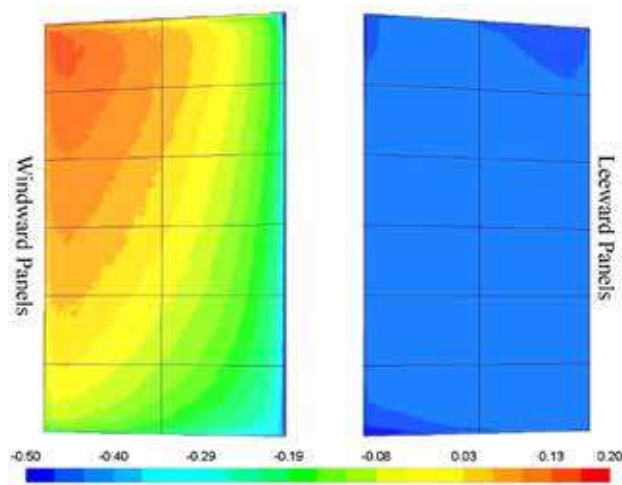


Fig. 7(b). Pressure contour over solar PV panels mounted on 30° pitched hip type building roof subjected to 45° wind incidence

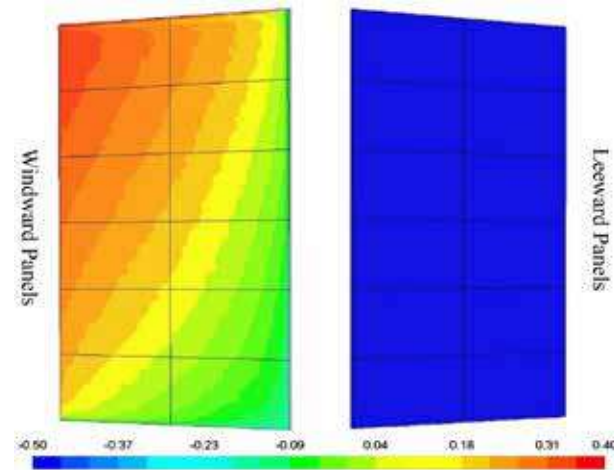


Fig. 7(c). Pressure contour over solar PV panels mounted on 40° pitched hip type building roof subjected to 45° wind incidence

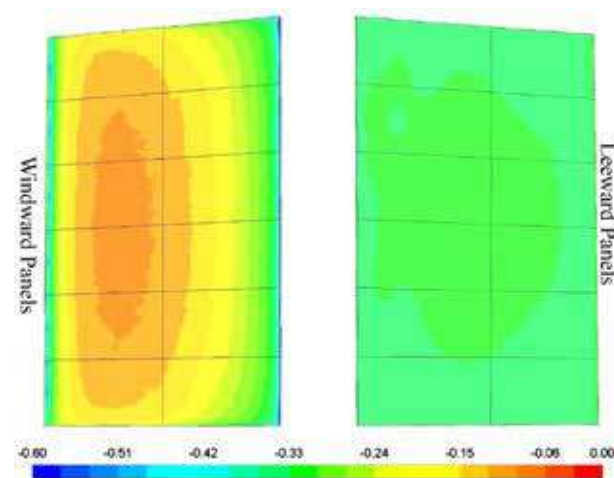


Fig. 8(a). Pressure contour over solar PV panels mounted on 20° pitched hip type building roof subjected to 90° wind incidence

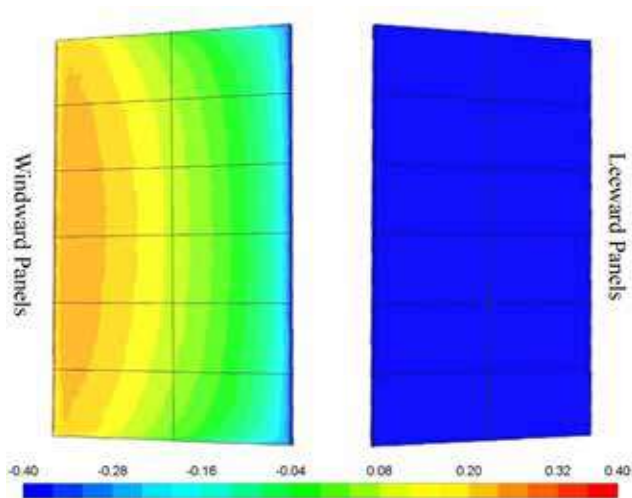


Fig. 8(b). Pressure contour over solar PV panels mounted on 30° pitched hip type building roof subjected to 90° wind incidence

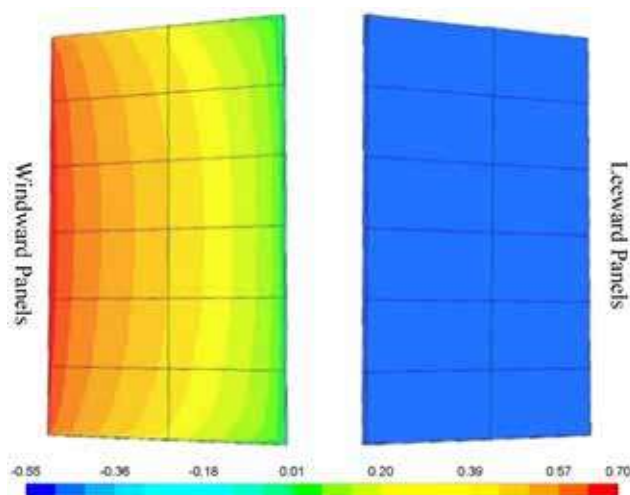


Fig. 8(c). Pressure contour over solar PV panels mounted on 40° pitched hip type building roof subjected to 90° wind incidence

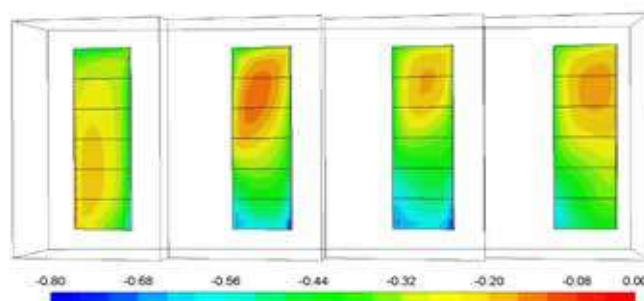


Fig. 9(a). Pressure contour over solar PV panels mounted on 20° pitched saw type industrial building roof subjected to 45° wind incidence

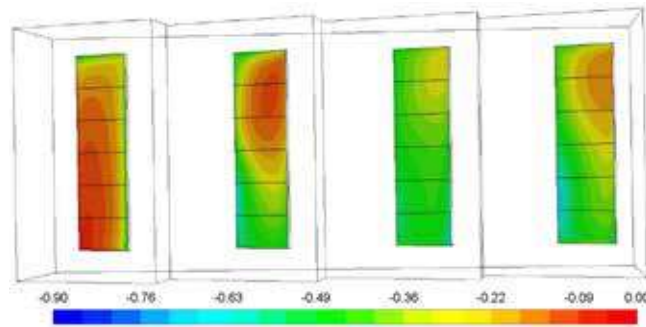


Fig. 9(b). Pressure contour over solar PV panels mounted on 30° pitched saw type industrial building roof subjected to 45° wind incidence

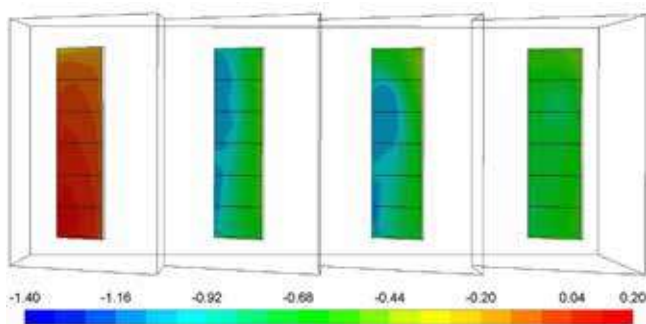


Fig. 9(c). Pressure contour over solar PV panels mounted on 40° pitched saw type industrial building roof subjected to 45° wind incidence

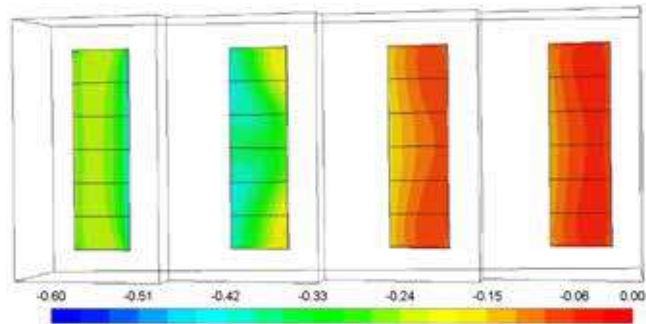


Fig. 10(a). Pressure contour over solar PV panels mounted on 20° pitched saw type industrial building roof subjected to 90° wind incidence

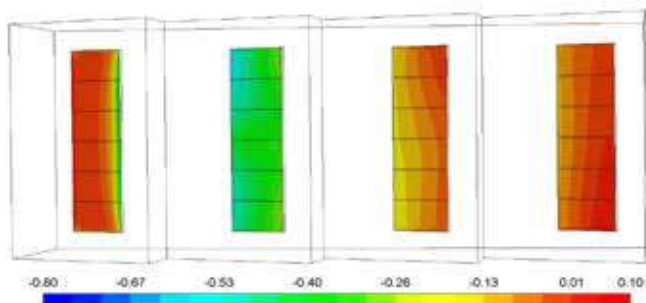


Fig. 10(b). Pressure contour over solar PV panels mounted on 30° pitched saw type industrial building roof subjected to 90° wind incidence

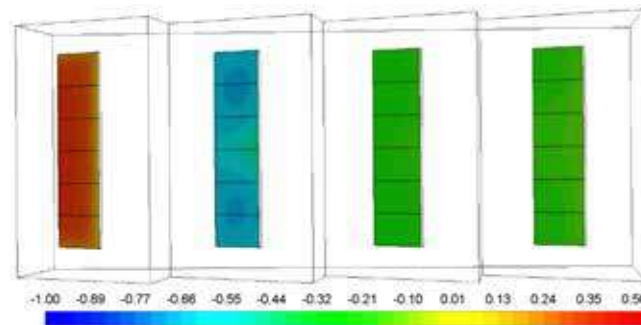


Fig. 10(c). Pressure contour over solar PV panels mounted on 40° pitched saw type industrial building roof subjected to 90° wind incidence

CONCLUSION

- Pressure coefficient over PV panels, mounted over windward pitched roof for hip type building and first array for industrial saw type building, increases with an increase in roof pitch angle subjected to both 45° and 90° wind incidence.
- Pressure coefficients of PV panels mounted over leeward roof in hip type and saw type roof, decrease to higher suction with the increase in roof pitch angle in both 45° and 90° wind incidence.
- On varying wind incidence for 30° pitched roofs, maximum suction was observed over panels in array 3 and array 4 under 45° wind incidence.
- Maximum suction pressure was found over PV panels in array 2 when subjected to 90° wind incidence for all three pitch angles of saw type roof building.
- Solar PV panels mounted on pitched building roof, wind load advisable to design for maximum pressure observed on the individual PV panel mounted over the building roof.

ACKNOWLEDGEMENT

The authors wish to express their gratitude for the financial support received from the Ministry of New & Renewable Energy, Govt. of India sponsored project and Senior Research Fellowship (09/112(0628)2K19 EMR-I) awarded to the corresponding author by the Council of Scientific and Industrial Research (CSIR) under Ministry of Human Resources Development, Govt. of India.

REFERENCES

1. “Monthly Report on Installed Capacity, October 2020”, Central Electricity Authority, India. (Accessed on: 20.11.2020)
2. “The roadmap to 40 GW rooftop solar” PV Magazine India, 27 September 2019.
3. <http://www.cythelia.fr/2015/05/21/maitrise-doeuvre-pour-une-installation-photovoltaique-sur-toiture-industrielle-100-kwc/> (Accessed on: 09.11.2020)
4. ASCE, “Minimum Design Loads for Buildings and Other Structures,” American Society of Civil Engineers, Virginia, USA, 2010.
5. Kopp, G. A., Surry, D. and Chen, K. (2002), “Wind loads on a solar array,” Wind Structure, 5, 393–406.
6. Chung, K., Chang, K. and Liu, Y. (2008), “Reduction of wind uplift of a solar collector model,” Journal of Wind Engineering & Industrial Aerodynamics, 96, 1294–1306.
7. Shademan, M. and Hangan, H. (2010), “Wind loading on solar panels at different azimuthal and inclination angles,” Proceedings of the Fifth International Symposium on Computational Wind Engineering, Chapel Hill, North Carolina, USA.
8. Bitsuamlak, G. T., Dagneu, A. K. and Erwin, J. (2010), “Evaluation of wind loads on solar panel modules using CFD,” in Proceedings of the Fifth International Symposium on Computational Wind Engineering, Chapel Hill, North Carolina, USA.



9. Jubayer, C. M. and Hangan, H. (2012), "Numerical Simulation of Wind Loading on Photovoltaic Panels", in Structures Congress ASCE.
10. Jubayer, C. M. and Hangan, H. (2014), "Numerical simulation of wind effects on a standalone ground-mounted photovoltaic (PV) system," *Journal of Wind Engineering & Industrial Aerodynamics*, 134, 56–64.
11. Irtaza, H., and Agarwal, A. (2018), "CFD simulation of turbulent wind effect on an array of ground-mounted solar PV panels", *Journal of Institution of Engineers India - Series A (Springers Publications)*, 99(2), 205–218.
12. Kopp, G. A., Farquhar, S., and Morrison, M. J. (2012), "Aerodynamics mechanisms for wind loads on tilted roof-mounted solar arrays", *Journal of Wind Engineering and Industrial Aerodynamics*, 111, 40–52.
13. Stathopoulos, T., Zisis, I., and Xypnitou, E. (2014), "Local and overall wind pressure and force coefficients for solar panels", *Journal of Wind Engineering and Industrial Aerodynamics*, 125, 195–206.
14. Banks, D. (2007). "How to calculate wind loads on roof-mounted solar panels in the US." <http://www.cppwind.com/support/PDF/HowToCalculateWindLoads.pdf> (Sep. 19, 2019).
15. Geurts, C. P. W., and Van Bentum, C. A. (2007). "Wind loads on solar energy roofs", *Heron*, 52(3), 201–222.
16. Kopp, G. A. (2014), "Wind loads on low-profile, tilted, solar arrays placed on large, flat, low-rise building roofs", *Journal of Structural Engineering*, 140(2), 04013057.
17. Wood, G. S., Denoon, R. O., and Kwok, K. C. S. (2001), "Wind loads on industrial solar panel arrays and supporting roof structure." *Wind Structures*, 4(6), 481–494.
18. Ginger, J., Payne, M., Stark, G., Sumant, B., and Leitch, C. (2011), "Investigations on wind loads applied to solar panels mounted on roofs." Report No.TS821, Buildings Codes Queensland, School of Engineering and Physical Sciences, James Cook Univ., Townsville, Australia.
19. Erwin, J., Chowdhury, A.G., Bitsuamlak, G., and Guerra, C. (2011), "Wind effects on photovoltaic panels mounted on residential roofs", 13th International Conference on Wind Engineering, July 11-15, Amsterdam, The Netherlands.
20. Geurts, C., and Blackmore, P. (2013), "Wind loads on stand-off photovoltaic systems on pitched roofs", *Journal of Wind Engineering and Industrial Aerodynamics*, 123 (A), 239-249.
21. Aly., M. A., and Bitsuamlak, G. (2014) "Wind-Induced Pressures on Solar Panels Mounted on Residential Homes", *Journal of Architectural Engineering*, 20(1).
22. Stenabaugh, S.E., Iida, Y., Kopp, G.A., and Karava, P. (2015), "Wind loads on photovoltaic arrays mounted parallel to sloped roofs on low-rise buildings", *Journal of Wind Engineering and Industrial Aerodynamics*, 139, 16-26.
23. ANSYS FLUENT 18 User's Guide, ANSYS Inc., (2017).
24. Tieleman, H. W. (1996), "Model/full scale comparison of pressures on the roof of the TTU experimental building", *Journal of Wind Engineering and Industrial Aerodynamics*, 65,133–142.



Design and Construction of Irregularly Shaped Cut & Cover Box Tunnel as an Innovative Solution for Space Restriction at Site

Chiranjib Sarkar¹, Anant Mehendale², Harsha G M³

Senior Structural Engineer, AECOM India Pvt Ltd, New Town, Kolkata¹

Assistant General Manager, Tata Projects Ltd, Mumbai²

Former Sr. Engineer, Tandon Consultants (P) Ltd, Delhi³

✉ chiranjibsarkar.civil@gmail.com; ✉ anantmehendale@tataprojects.com; ✉ 24x7civilconsultant@gmail.com

ABSTRACT

Tunnels and underground structures are playing significant role in solving space congestion problem of urban-transportation and sustainable development of the city. The increasing need of underground structures in transportation system is the main reason for studying design and construction methodology of underground structures in very rapid and cost-effective way. Therefore, it is necessary to have an innovative practice on design/construction methodology with realistic consideration of actual site conditions. Also, an innovative technical solution in design/construction might save a project from a deadlock condition arising due to site constraints and other issues. A cut & cover box tunnel section of Lucknow Metro project has been taken for present case study. As per alignment plan, some portions of tunnel infringed with few columns of the portico of a building existing at site. Due to site restriction, an alternative unconventional design/construction methodology was adopted by introducing pile, strut-waler and lattice-girder support systems to construct the cut & cover box tunnel partly irregular in shape without dismantling the existing portico structure. Structural Design/stability and ground deformation have been checked by developing numerical model compared with available analytical solutions. Concept of the present case study may be helpful for the practising engineers in the design of cut & cover tunnels.

Keywords: Underground Structure, Cut & Cover Box Tunnel, Construction Methodology.

INTRODUCTION

The tunnelling and underground structures are nowadays gaining popularity in urban transportation system and other utilities due to the limitations in movement of transportation as well as the restriction in wide expansion of surface infrastructure. Almost every developing city in our country is currently planning to construct tunnels and underground structures for rails, roads, metros, subways and other utilities as well as sustainable development of the city. The growing necessity to expand the urban transportation networks is the main motive for studying the construction and design methodology of underground structures in a very rapid and cost-effective way. And, therefore, it is essential to have an innovative practice on construction and design methodology for such underground structure with realistic consideration of actual site-specific conditions. Also, an innovative technical solution for site-specific design and construction methodology might save a project from a deadlock condition arising due to site constraints and other unwanted issues.

In the present study, a cut & cover box tunnel section of Lucknow Metro North – South corridor has been considered for analysis and discussion purpose. As per tunnel alignment plan of North – South corridor, some portions of a cut & cover box tunnel had infringed with four columns and foundation of building-portico existing at site. Due to site and space constraint, an alternative unconventional design and construction methodology were adopted by introducing RCC Pile, structural steel member strut-waler and lattice girder support with shotcrete systems to construct the cut & cover box tunnel partly irregular in shape without removing and dismantling the existing portico structure at site. Structural stability of the proposed structure and safety of the existing adjacent structures were main key purpose of these innovative and unconventional methodology. Design and construction concept of the present case study may be helpful to practising engineers in the design of tunnels and cut & cover structures.

LOCATION, SITE DETAIL SAND SUB SOIL PROFILE

The line LKCC-06 of Lucknow metro extends from underground ramp (near Charbagh Metro Station) to end of underground

ramp (near K D Singh Babu Stadium metro station) on North – South corridor of Lucknow MRTS, Phase-1A project at Lucknow, Uttar Pradesh, India. Entire project corridor is situated on busy road and clustered building area. As per tunnel alignment, some portions of a cut & cover box tunnel had infringed with four columns and foundation of the portico of a building existing at site. A plan illustrating the cut & cover Box Tunnel (Diaphragm Wall Panels) affected due to infringement of column and foundation of existing portico is shown in **Fig. 1**.

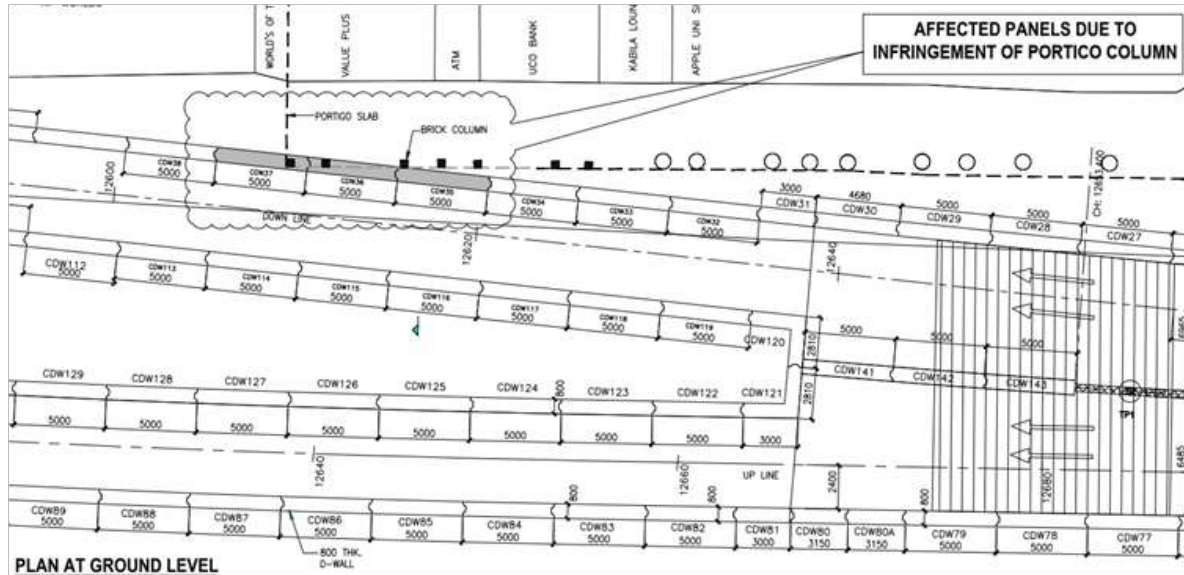


Fig. 1. Plan showing cut & cover Box Tunnel (Diaphragm Wall Panels) affected due to infringement of column and foundation of existing portico of a building

Sub-soil data of concerned location with description for different stratum is shown in **Table 1**. During sub-soil investigation actual water table was observed at 28m below ground level. Also, water level was not encountered during excavation for the entire cut and cover box structure.

Table 1. Geotechnical parameters for different stratum

Ground Condition	Soil Type	Depth, m	SPT Value (Avg.)	Φ' (Avg.) deg	Bulk Density (Avg.) kN/m ³
Top Soil	Made up Ground	0 – 3	-	26	18.0
Stratum - I	Loose to medium silty fine sand	3 – 8.5	20	30	19.0
Stratum - II	Medium to dense silty sand	8.5 – 10.5	35	32	19.0
Stratum - III	Hard Sandy Clayey silt	10.5 – 30.0	30	30	19.0

METHODOLOGY

Due to site constraints and other unwanted issues, partial dismantling or removal of the existing portico structure was not possible during casting of cut & cover box tunnel. Hence, an alternative unconventional construction methodology had been adopted to execute the cut & cover box tunnel without removing / dismantling the existing portico structure. To avoid infringement with column and footing of the portico, cut & cover box tunnel had been cast partly irregular in shape with the help of RCC pile, structural steel members like strut-waler and lattice girder support (steel ribs) systems. **Fig. 2** shows the rearrangement of four Diaphragm wall (D-Wall) panels due to infringement of Portico column-footing. Few D-walls are laterally connected and supported by longitudinal and transverse beams. Cross Section of the rearranged portion of cut & cover box tunnel and a typical portion of cut & cover box tunnel are shown in **Fig. 3**.

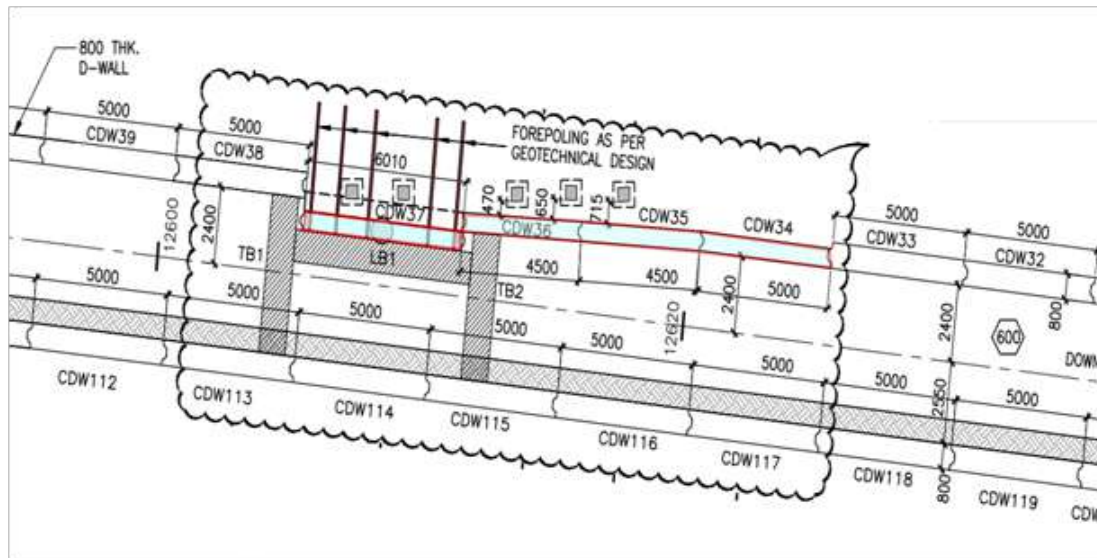


Fig. 2. Plan showing the rearrangement of four D-Wall panels due to infringement of Portico column-footing.

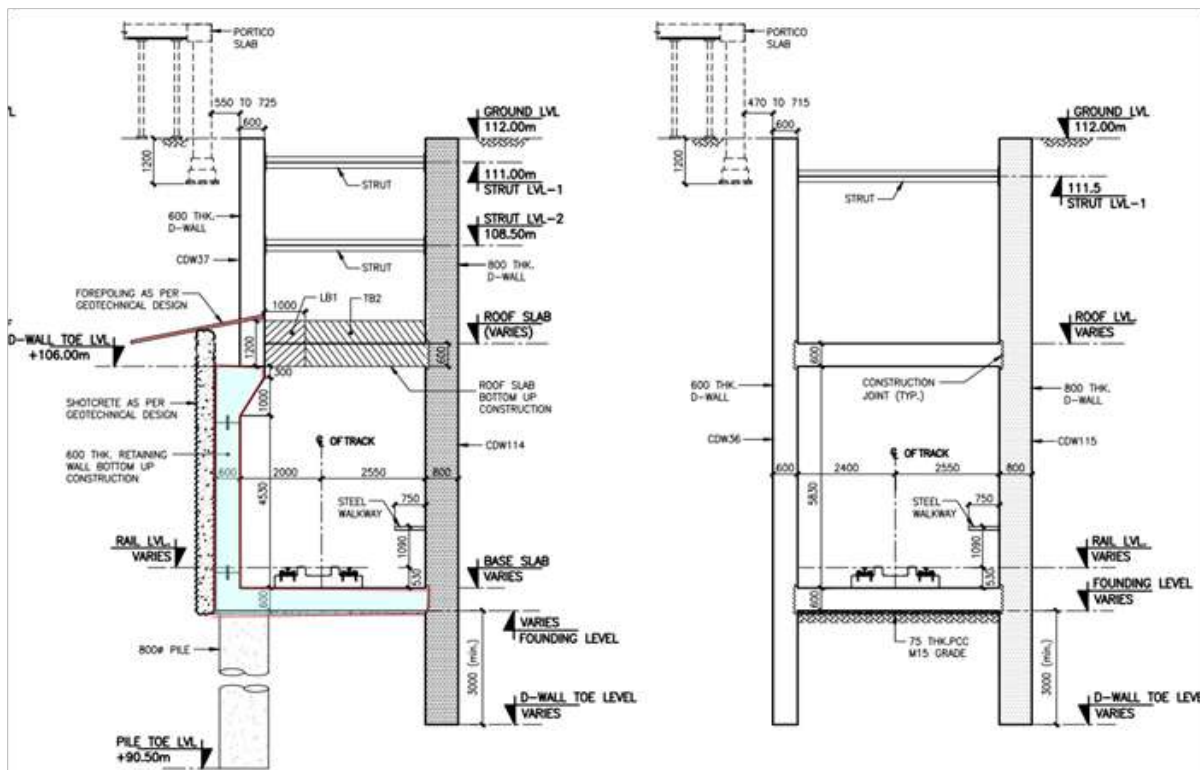


Fig. 3. Cross Section showing the rearranged portion of cut & cover box tunnel (left side) and a typical portion of cut & cover box tunnel (right side).

Stability of the proposed structure and safety of the existing adjacent structures were the main concern of this unconventional methodology and it had been ensured at every stage of the entire construction period.

Construction Methodology

As per construction sequence, the entire casting period had been sub-divided into four different stages of construction which

is partially top-down and partially bottom-up. In first stage, one full-height Diaphragm wall (D-Wall) and one half-height Diaphragm wall (resting on RCC bored pile with a diameter of 800mm) had been cast to serve the purpose of temporary as well as permanent earth retaining structure. Two level of temporary steel strut-waler had been used for supporting excavation till the soffit of top slab of the box tunnel. In second stage, two transverse beams and one longitudinal beam had been further cast along with casting of top slab of box tunnel. These beams ensured the lateral stability and interconnectivity between all rearranged D-Wall panels. Forepoling system had been provided through the half-height D-Wall well before the starting of further excavation below top slab of box tunnel. **Fig. 4** shows excavation done till the soffit of top slab of box tunnel and casting of beams along with top slab of box tunnel.

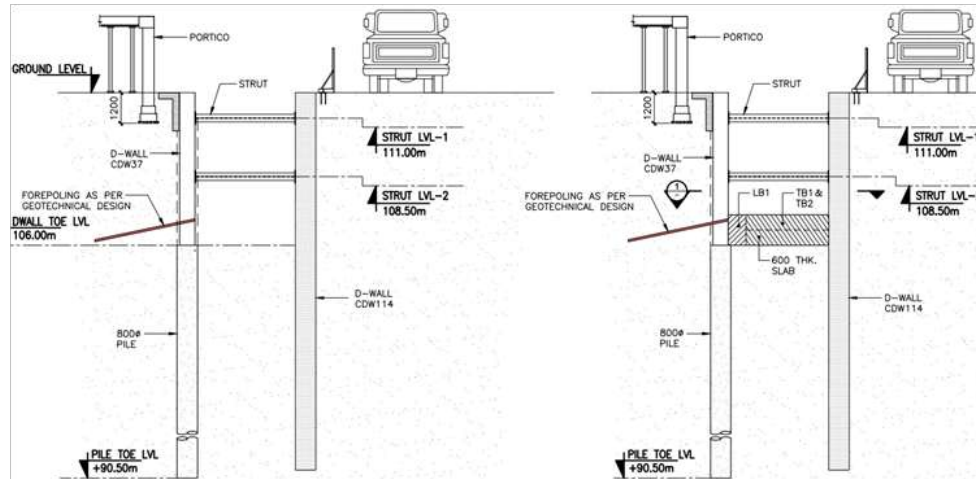


Fig. 4. Cross Section showing excavation done till the soffit of top slab of box tunnel (left side) and casting of beams along with top slab of box tunnel (right side).

In third stage, excavation had been continued till soffit of bottom slab of box tunnel. A lattice girder support (steel ribs) with shotcrete systems had been provided as part of earth retaining system till the casting of bottom slab and RCC wall. In final stage, bottom slab and connecting RCC wall had been cast. Backfilling and reinstating of road surface had been done after removal of temporary steel strut-waler. **Fig. 5** shows the excavation below top slab of box tunnel and reinstating of road surface after casting and backfilling done.

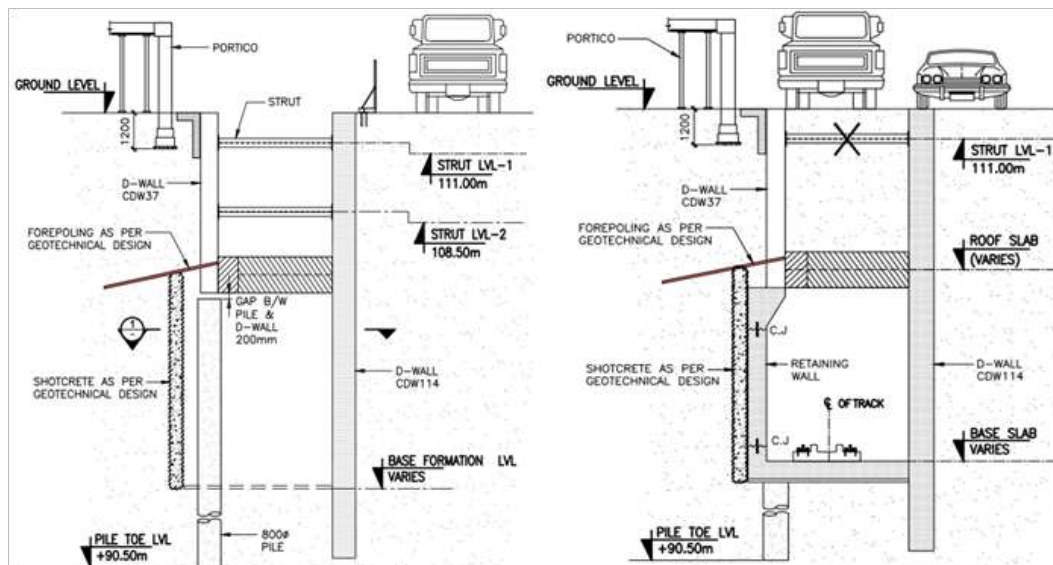


Fig. 5. Cross Section showing the excavation below top slab of box tunnel (left side) and reinstating of road surface after casting and backfilling done (right side).

Design Methodology

Design methodology has been sub-divided into construction stage analysis, service stage analysis and stability analysis. The structure analysis was done for different loads and combination to obtain the most severe combinations and envelopes of forces (moments, shear force, etc.) on every component of the structure.

Construction Stage Analysis

Construction stage analysis of diaphragm wall was done by using WALLAP [6] & STAAD Pro. [3] software to obtain the effects of lateral load during sequential excavation. Effect due to vertical construction load was obtained by using STAAD Pro [3]. Construction of D-Wall and top slab of cut & cover box tunnel was done by top-down sequence with two level of temporary strut-waler support. Bending moment, shear force and displacement envelope of the D-wall from WALLAP analysis are shown in Fig. 6.

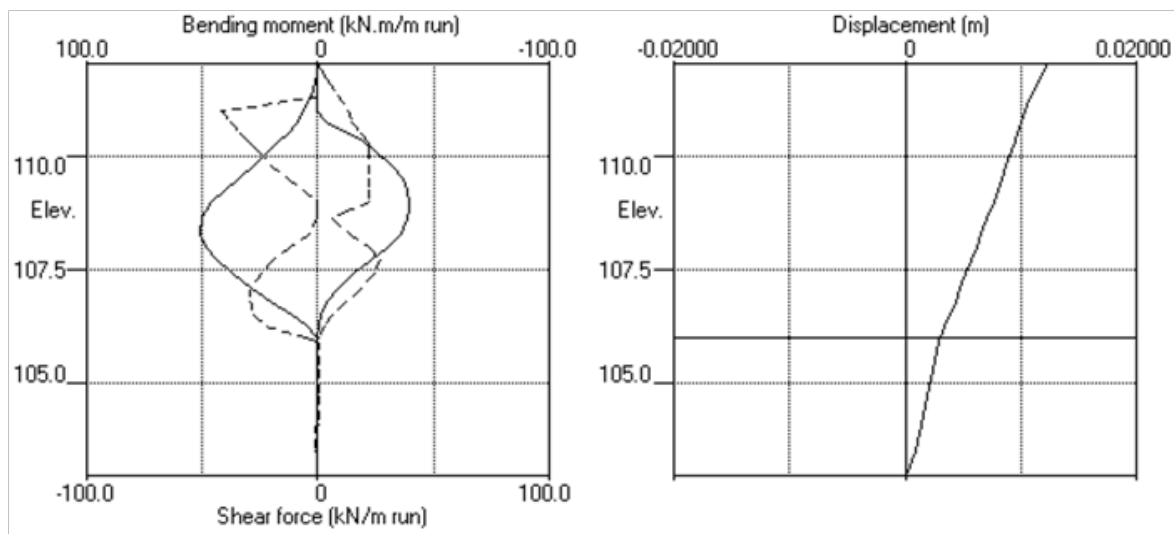


Fig. 6. Bending moment, shear force and displacement envelope of the D-wall from WALLAP analysis

Isometric view of the STAAD Pro. Plate 3D model with two levels of strut support and bending moment contour are shown in Fig. 7.

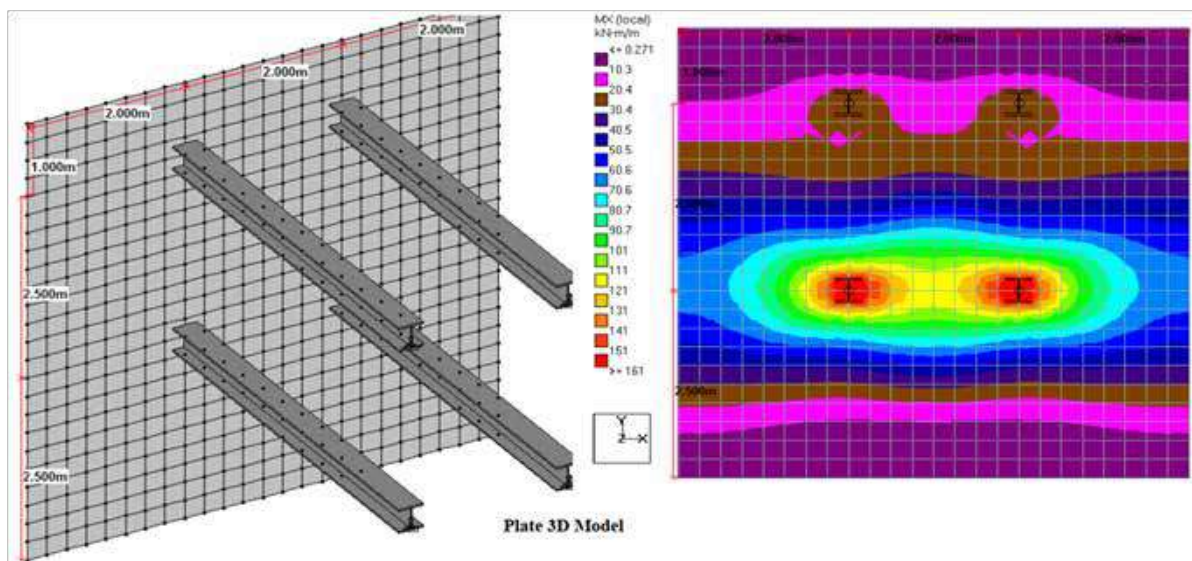


Fig. 7. Isometric view of the STAAD Pro. Plate 3D model (left side) and bending moment contour (right side)

Service Stage Analysis

Service stage analysis for lateral and horizontal loads was done by using STAAD Pro. software. All service stage loads like Dead Load, Superimposed Deal Load, Live Load, Water Pressure and Earth Pressure were considered and suitably combined as per load combination to obtain the most severe combinations and envelopes of forces [2]. Seismic racking analysis with 0.12g(DBE) and 0.24g(MCE) was also performed for the service stage [1].

Stability Analysis

The complete structure was checked against flotation with water table at ground level. Capacity of RCC pile below half-height D-Wall was checked with respect to vertical load at D-Wall tip. A numerical model (finite element method) was further developed to check the ground stability. Input for numerical model (finite element method) with full excavation is shown in **Fig. 8**.

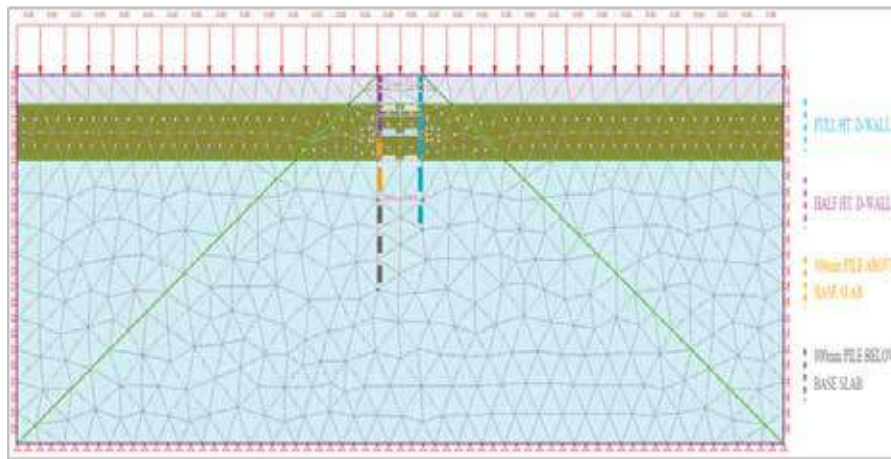


Fig. 8. Input of numerical model (finite element method) with full excavation.

DISCUSSION ON ANALYSIS

As outcomes of numerical model (with full excavation), vertical settlement of ground surface and D-wall along with horizontal displacement of D-Wall were estimated. Ground stability and safety to adjacent structure were ensured by checking ground deformation with respect to its limiting value. Apart from theoretical values, actual site-based ground settlements were recorded and checked during the entire excavation and casting procedure at site. Vertical settlements of ground surface, pile and D-Wall are shown in **Fig. 9**. Horizontal displacements of D-Wall and pile are shown in **Fig. 10**. As an additional precaution, a detailed building condition survey (BCS) on adjacent existing structures was done prior to excavation. Additional protection to the existing adjacent structure had been further provided based on BCS report.

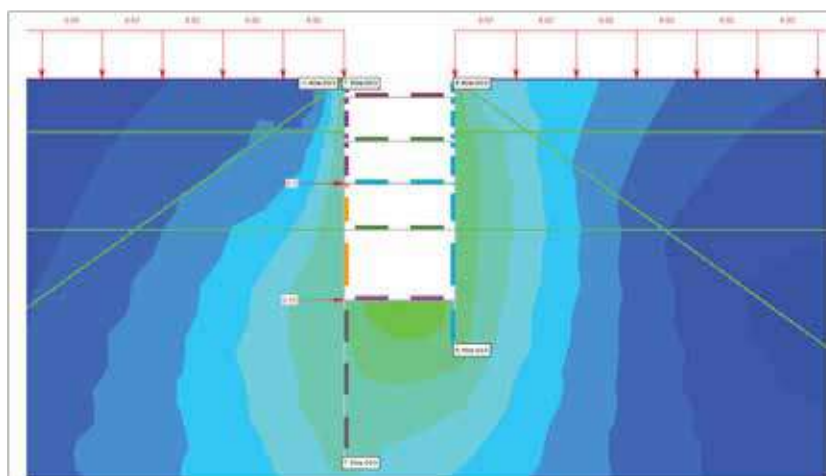


Fig. 9. Vertical settlement of ground surface, pile and D-Wall.

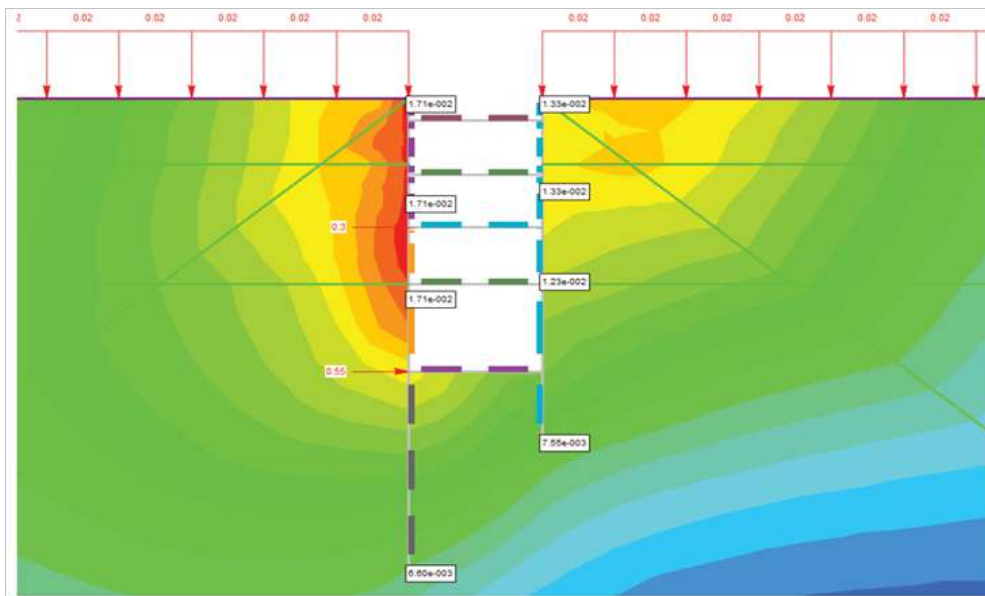


Fig. 10. Horizontal displacement of D-Wall and pile.

Schedule of dimension check for Kinematic envelope and structure gauge was also done for irregular shape of cut & cover box tunnel. Fig. 11 shows schedule of dimension check for Kinematic envelope and structure gauge.

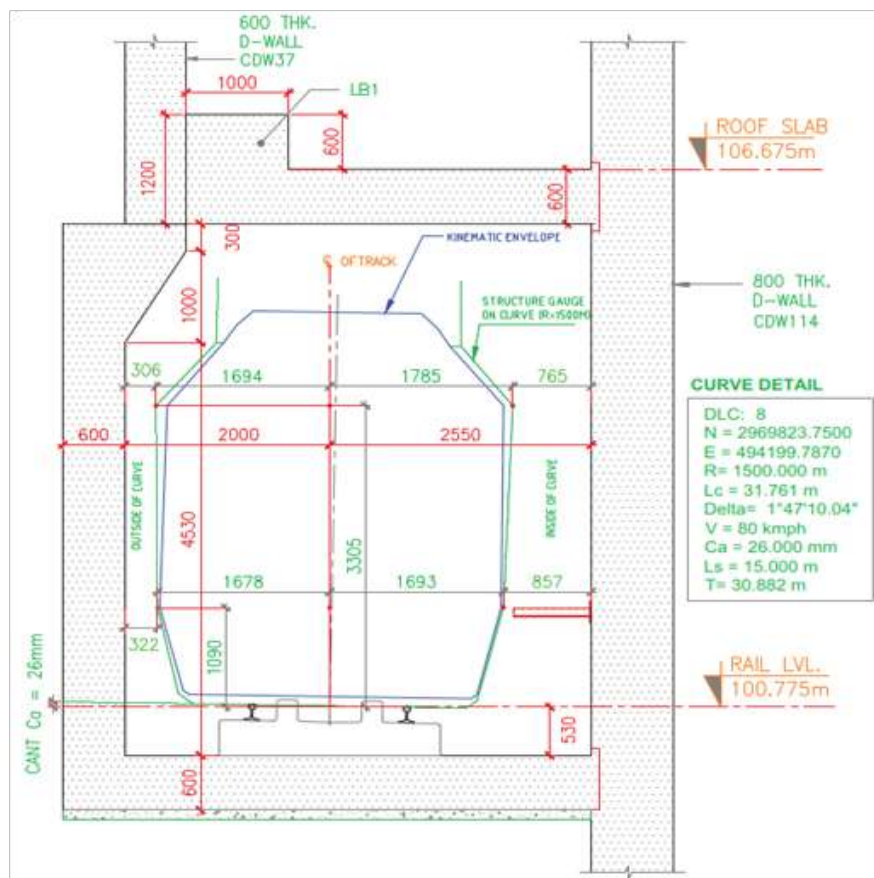


Fig. 11. Schedule of dimension check for Kinematic envelope and structure gauge.



CONCLUSIONS

The present paper describes an alternative unconventional design and construction methodology to construct a cut & cover box tunnel without removing/dismantling the portico of an existing building at site. To avoid infringement with existing building-portico, cut & cover box tunnel had been cast partly irregular in shape with the help of RCC Pile, structural steel members such as strut-waler and lattice girder support (steel ribs) systems. Present innovative solution had been conceptualised, analysed and finalized after exploring of various options related to structural stability of the proposed structure and safety of the existing adjacent structures. Unconventional and innovative technical solution for site-specific issues may save a project from a deadlock condition arising due to site constraints and other unwanted issues. The entire concept of the present case study may be helpful for the researchers and practising engineers in the design of tunnels and cut & cover structures for rails, roads, metros, subways and other utilities.

ACKNOWLEDGMENT

The authors acknowledge the support from the entire team involved in Lucknow Metro Rail Corporation project LKCC-06.

REFERENCES

1. Youssef M.A. Hashash, Jeffrey J. Hook, Birger Schmidt, John I-Chiang Yao: Seismic Design and Analysis of Underground Structures. Tunnelling and Underground Space Technology 16 (2001) 247–293.
2. Lucknow Metro Railway Corporation, Technical Specification: LMRC Out line Design Specification for Underground Structure.
3. STAAD.Pro V8i (SELECT Series 6) 20.07.11.33.
4. IS: 456 -2000, Plain and Reinforced Concrete.
5. IS: 2911 (Part I)-2011, Design and Construction of Pile Foundations.
6. WALLAP Version 6.05 Revision A44.B58.R48.



1D Flood Model to Retrace the July 2018 Flood in Lower Reaches of Pamba River, Kerala

Dr T K Drissia

Surface Water Division, Centre for Water Resources Development and Management, Kozhikode, Kerala

✉ drissia@cwrwm.org

ABSTRACT

Devastating floods occurs every year at some regions of the world, in Indian also. The year 2018 witnessed severe flood in Kerala. This study attempted to retrace the flood event during July 2018, though severe flood occurred is during August 2018, due to the non-availability of observed data. This study used MIKE HYDRO River for developing a hydrodynamic model for the lower reaches of Pamba during the period 1/6/2018 to 14/08/2018. The river stretch considered for the study is the between the Kalloopara in Manimala River, Malakkara in Pamba River and Thumpamon in Achenkovil River and Thottapally spillway. The model calibration was carried out by changing manning's coefficient. At the Pamba, Manimala and Achenkovil gauging stations, the correlation coefficient between the simulated and observed water level is 0.949, 0.879 and 0.799. The flood model give a spatial variation of the flood depth during July 2020. This study helps to understand the flood dynamics and initiates further study on the August 2018 flood.

Keywords: 1D flood model; MIKE HYDRO River; Pamba; Kerala.

INTRODUCTION

Extreme events are frequently occurring in recent years, which destroy life and property. The Kerala Flood 2018 is one such event; the earlier experience of flood in this region is in 1924, almost 100 years back. A one-dimensional model is the simplest way of representing river dynamics, assuming the river along the center line of the river. Literature reported various 1D model for hydrodynamic models. TUFLOW Classic1D, Flood ModellerPro 1D solver, OBEK Suite, MIKE11/MIKE HYDRO River, HEC-RAS are few to name [1]. The one-dimensional hydrodynamic model uses Saint Venon's equation to simulate the flood [2; 3]. The flood vulnerability area of Damodar River, India is studied using MIKE HYDRO River. The model was calibrated with Manning's coefficient and validated with ground data [4].

With these short literature discussed, it is to say that in the past, the flood was not a frequently occurring phenomenon in Kerala, except the Kuttanad region. Because of this, flood-related studies in Kerala is not available much. In this regard, this study evaluates the flood occurred during July 2018 in Pamba river Kerala. Though devastating flood occurred during August 2018, the discharge data is not available. Therefore, to understand the dynamics of the flood, initially, the model was developed for the flood occurred during July 2018.

STUDY AREA

Pamba is the third-longest river in Kerala, with 176km). Manimala River drains in the north of Pamba and Achenkovil converges in the south before joining the Arabian Sea through Thottapally spillway. The annual average rainfall in the catchment of Pamba is 3771 mm, Manimala is 3516 mm, and Achenkovil is 2933 mm (CWRDM, 2017). This study considered the lower reaches of the Pamba River in Kerala, the river stretch between the Malakkara to the Thottapally spillway in Pamba, the river stretch in Manimala River from Kalloopara until it joins Pamba, the river stretch in Achenkovil between the Thumpamon until the confluence point with Pamba **Fig 1**.

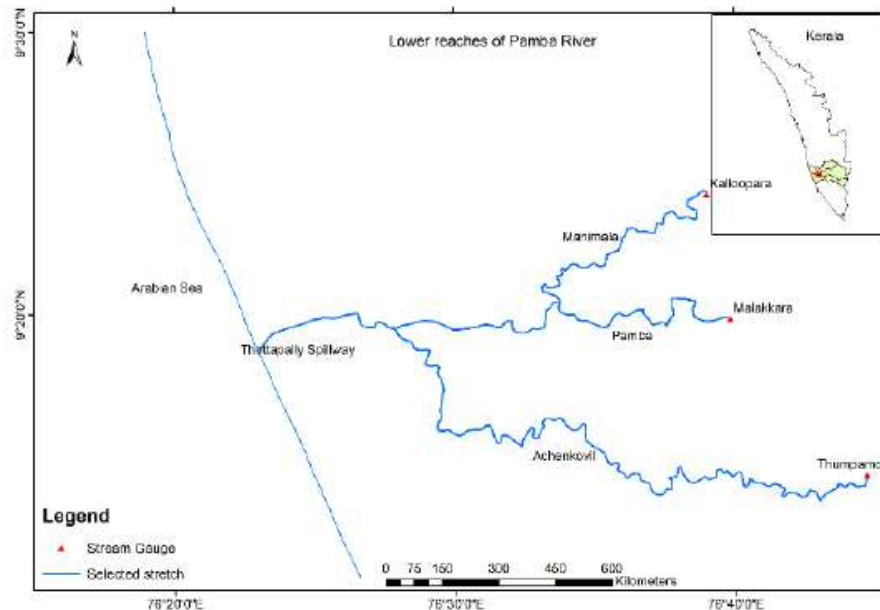


Fig. 1. Location of lower reaches of Pamba

MATERIALS AND METHOD

For the analysis, this study utilised the discharge and water level data of three gauging stations, Malakkara, Kallioopara and Thumpamon maintained by Central Water Commission (CWC), India. These are the upper bound of

the study area, the lower bound being the level at Thottapally Spillway. The water level near Thottapally spillway is obtained from the Water Resources Department, Kerala. For developing the flood model, another input required is the river cross-sections. Hydrographic Survey Wing (HSW), Government of Kerala carried out the bathymetry and topographical survey to extract the cross-sections of the streams from the mean sea level. The period analysed were from 1/6/2018 to 14/8/2018, though the most severe flood occurred from 14th to 16th August 2018, as the observed discharge is not available.

The 1D flood model was developed using MIKE HYDRO River developed by DHI. The main governing equation in fluvial hydraulics is saint Venon's equation, finite difference method. Saint Venon's equation works on the conservation of mass and momentum. The assumptions in the governing equations are the flow is one-dimensional i.e. velocity is constant. Flow is assumed to be gradually varying along the channel. The bottom slope is small, so the effect of scouring and deposition is negligible. The differential form of the equations is as follows.

$$\frac{\partial A}{\partial t} + \frac{\partial Q}{\partial x} = 0 \quad (1)$$

$$\frac{\partial Q}{\partial t} + \frac{\partial}{\partial x} (uQ) + gA \left(\frac{\partial h}{\partial x} - S_o \right) + gAS_f = 0 \quad (2)$$

where Q is discharge, A is cross-sectional wetted area, u is longitudinal flow velocity, h is flow depth, S_o is bed slope, and S_f is friction slope (Chow, 1988). The flood model developed for 1/6/2018 to 14/8/2018 using surveyed cross section.

RESULTS

The 1D model developed using MIKE HYDRO River was for the period 1/6/2018 to 14/8/2018. The MIKE HYDRO River has four modules, network module, cross-section module, boundary condition module and hydrodynamic parameters module. The network module was created, by delineating the river stretch from the CWC gauging stations to Thottapally spillway, after that, chain ages generated for the river stretch. In the cross-section module, we entered the river cross-sections. Boundary condition module requires the upper boundary and lower boundary; the upper boundary condition is the observed discharge at Kallioopara, Malakkara and Thumpamon gauging station. The lower boundary condition is the water level near the Thottapally.

In the hydrodynamic- parameter module, we selected the fully hydrodynamic option. Initially, the model is run by taking the default Manning's coefficient. Then, for the calibration of the model, in the Manimala stream, the Manning's coefficient changed to 0.03 until chainage 14070m and the remaining 0.035, in Pamba stretch of river, from 0 to 4414, m is taken as 0.04 and remaining is 0.03, in Achenkovil, from chainage 0 to 44261, m is 0.02, until 63130 is 0.03.

The model was calibrated by changing Manning's coefficient; the evaluation is carried out by the water levels at the three gauging stations. **Figs. 2 to 4** show the calibration graphs of Kalloopara, Malakkara and Thumpamon. In Achenkovil, the flows are under predicted. The simulated water level at Kalloopara and Malakkara show good agreement with the observed data with R-value as 0.959 and 0.973, respectively.

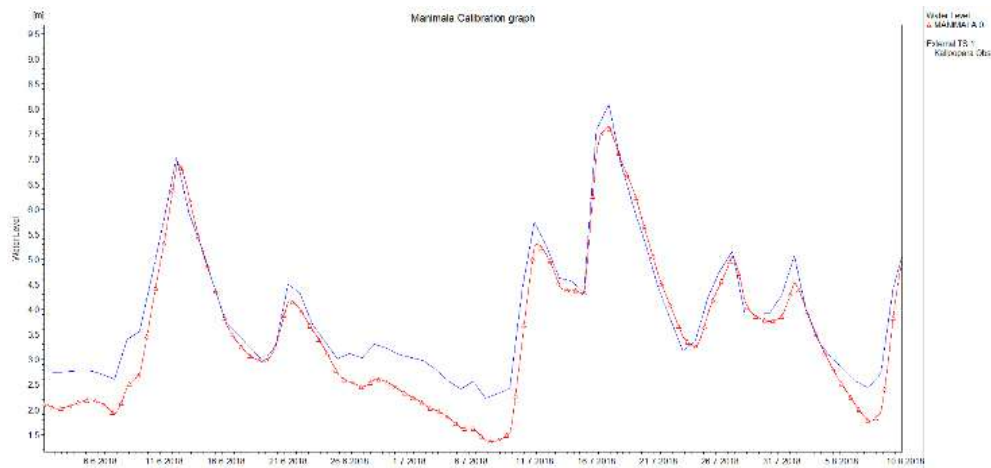


Fig. 2. Calibration graph at Kalloopara gauging station in Manimala

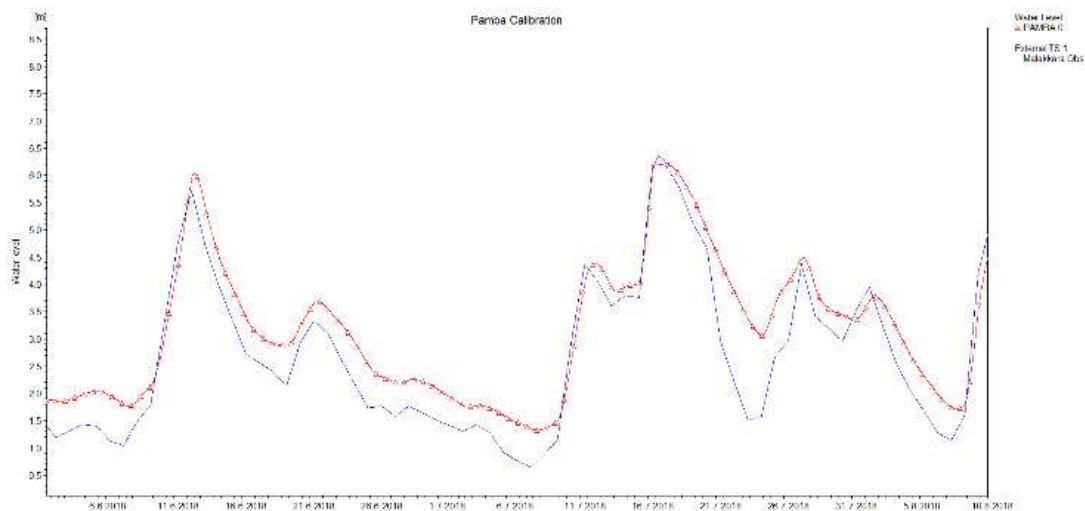
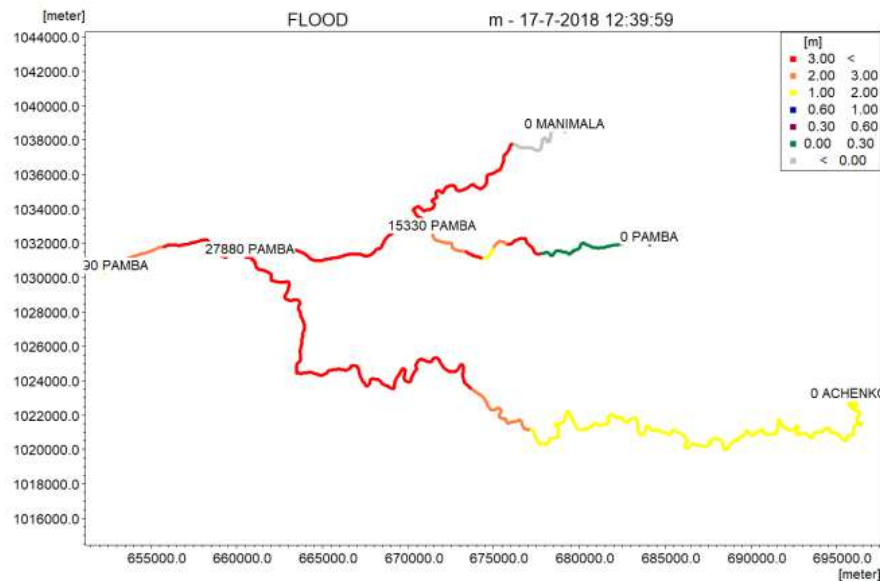


Fig. 3. Calibration graph at Malakkara gauging station in Pamba

Preceding August 2018 flood, a flood occurred during 16-17 July 2018, the peak water level observed is 8.1 m at Kalloopara on 17th July, but the simulated value is about 11 m. In Malakkara, the observed peak water level is 6.215m on 16th July, whereas the simulated water level is around 11 m. The maximum water level observed in Thumpamon during July is 10.76m, in the place of simulated water level of about 10.5m. It is evident from the **Table1**, with peak error as -0.341m and -0.436m and 0.006, respectively for Manimala, Pamba and Achenkovil. The spatial representation of the flood depth at various location between the gauging stations and Thottappally spillway is analysed. **Fig. 5** presents the spatial representation of flood depth. The flood depth at the downstream of Pamba is higher than 3 meter as per the model output on July 17th, 2018. The upper reaches of Pamba and Manimala are not much affected. The model shows the upstream of Achenkovil has a flood depth of 1-2m, but the model prediction has a maximum positive difference of 1.672m (Table 1), and hence the actual flood depth may be less than this.

Table 1. Performance evaluation of the model

Statistical indicators	Manimala	Pamba	Achenk ovil
Correlation coefficient	0.949	0.877	0.799
Peak error	-5.525%	-23.232%	-4.756%
Volume error	-9.34%	-19.329%	5.549%
Max. positive difference	0.342m	0.212m	1.672m
Max. negative difference	-1.072m	-1.882	-1.292m


Fig. 4. Spatial presentation of flood depth on 17/7/2018

CONCLUSIONS

The July 2018 flood in the lower reaches of Pamba River Kerala is retraced using MIKE HYDRO River. The calibration with the observed water level at the three CWC gauging stations shows good agreement with the observed values. The peak difference is less than one in Manimala and Pamba River, though slightly more than one in Achenkovil River. This study helps to understand the flood occurred in July 2018 and aids in the further study of August 2018 flood occurred in Kerala.

ACKNOWLEDGMENT

The author thank The Hydrographic Survey Wing, Government of Kerala for carrying out survey work. The Central Water Commission is acknowledged for sharing the data.

REFERENCES

1. Tenga, J., Jakemanb, A.J., Vazea, J., Crokeb, B.F.W., Duttaa, D., and Kim, S. (2017) Flood inundation modelling: A review of methods, recent advances and uncertainty analysis, *Environmental Modelling & Software*, 90, 201-216.
2. Paiva, R. C. D., Collischonn, W. & Tucci, C. (2011) Large scale hydrologic and hydrodynamic modeling using limited data and a GIS based approach. *J. Hydrol.* 406, 170-181.
3. Jahandideh-Tehrani, M., Helfer, F., Zhang, H. et al. Hydrodynamic modelling of a flood-prone tidal river using the 1D model MIKE HYDRO River: calibration and sensitivity analysis. *Environ Monit Assess* 192, 97 (2020). <https://doi.org/10.1007/s10661-019-8049-0>.
4. R. K. Singh, V. G. Kumar Villuri, S. Pasupuleti et al., Hydrodynamic modeling for identifying flood vulnerability zones in lower Damodar River of eastern India, *Ain Shams Engineering Journal*, <https://doi.org/10.1016/j.asej.2020.01.011>.



A Comprehensive Review on the usage of Waste Materials in Flexible Pavements and their Impact

Pala Gireesh Kumar¹, Abhirami Priyanka Pathivada²

Associate Professor and Head, Department of Civil Engineering, Shri Vishnu Engineering College for Women (Autonomous), Vishnupur, Bhimavaram, Andhra Pradesh¹

U G Student, Shri Vishnu Engineering College for Women (Autonomous), Vishnupur, Bhimavaram, Andhra Pradesh²

✉ palagireeshk@gmail.com; ✉ abhiramipriyanka4@gmail.com

ABSTRACT

This propounded literature paper emphasizes a cardinal focus on the elaborative research work proffered on the impact of assorted waste materials in flexible pavement construction. From numerous pieces of literature, it is evident that the neoteric materials fashioning flexible pavements are coir geotextiles, rubber, marble dust, nylon tire cord fibers, which pitch-up to strengthen the soil and also improvising the life span of the pavements, with minimal rutting and cracking distress problems causing a surge in CBR value, and thereby, ameliorating the tensile strength of the bituminous concrete mixes (BC). Furthermore, crumb rubber (CR), Polypropylene, and eco-friendly asbestos fibers, pile up to the genre of enhancing the bitumen binder properties besides being cost-effective. Therefore, this study catalogues the hefty scope in the usage of a differential combination of waste materials in acquiring a high performing sub grade.

Keywords: Geotextile; Crumb rubber; Polypropylene fibers; Tensile strength.

INTRODUCTION

A pavement can either be a flexible or rigid pavement. Flexible pavement comprising of sub grade, sub-base, base, and surface course pavement has lower flexural strength [1] and is pliable in structural action under a higher volume of traffic and load relays the vertical or compressive stresses by grain to grain transfer to the lower layers of soil [2]. An ideal flexible pavement yields elastically to traffic loading. In general, the flexible pavement is devised with a treated bituminous surface or with a fairly thin hot- matrix asphalt surface (HMA) on the sub grade where one or more unbounded base courses rest [3]. The load-distributing characteristics of a layered pavement derive its strength delineated to protect each layer from compressive shear failure in the sub grade. In the present study, combinations of various waste materials used to improve the flexible pavement sub grade are quoted.

STATE OF THE ART

An extensive literature survey has put forth on the use of sundry waste materials in all categories and its effects on flexible pavement construction.

Raji A.K et al (2011) discussed the inclusion of coir geotextile and fly ash in black cotton soil of low CBR value and high pavement distress. An amalgamation of fly ash (5%), cement and reinforced with geotextile (2.5%) at 1000 repetitions is 5.72 mm given as rut behavior. With 28%, CBR has proven to be extraordinary for the soil with improvised design life [4].

Adebayo V.B and Mohammed H (2016) have scrutinized the asphaltic concrete with pulverized coconut fiber (PCF) containing surplus quantity of lignin makes it tougher and stiffer. The Marshall Stability test is done for Asphaltic concrete with PCF in the quantity of 0%, 4%, 6%, 8%, 10%, and 12% by weight. From the results, an optimum rise of 8% is noted in the stability and flow properties of the pavement [5].

Narendra Goud G et al (2017) quoted the inclusion of coir pith and lime in soil, making it a suitable sub grade material by reducing the free swell index (FSI). The Unconfined Compressive Strength (UCS) and the California Bearing Ratio (CBR) tests for soil in combinations of coir pith contents (1%, 2%, and 3%) and lime contents (2%, 3%, and 4%) resulted in a rise of UCS



value by 300KPa to 380KPa after 3 days and 470KPa to 570KPa after 7 days of curing & a rise in the CBR value by 1.04% to 9% [6].

Vijayan A et al (2016) scrutinized composites (coir fiber- latex, woven coir mat, and woven coir mat- latex) as a separator in flexible pavements for its high mechanical strength deliberated by CBR value. It was heeded that the 28th day CBR value of woven coir mat- latex composite was examined to be three times higher than the coir fiber- latex composite and ten times exorbitant than woven coir mat [7].

Nithin S et al (2012) asseverated coir geotextile (CGT) inclusion in the wet macadam mix as a reinforcing material to strengthen the sub grade and witnessed an advancement by 1.61 times in Ultimate Bearing Capacity and have evinced the improvement of greater footing settlement in the load settlement characteristics [8].

Singh R. R and Shelly M (2014) study expounded the effect of coconut coir on soil stabilization with the help of unsoaked, soaked CBR and UCS tests. It is clearly seen that the unsoaked and soaked CBR values have exhibited an increase of 8.72% to 13.55% and 4.75% to 9.22% with an increase in the fiber content. As per the observations, the maximum improvements in UCS values are achieved with an inclusion of 1% of coir to the soil [9].

Mahabir P et al (2013) unraveled the incorporation of VG 30 bitumen, CRMB 60 (modified binder), and non-conventional coconut fiber (natural fiber) which resulted in the huge improvement of the toughness of mixture but the biodegradable nature of these fibers made them inappropriate for longer reinforcement life. Therefore, from the performed analysis, it has been obvious that annexation of 0.3% fiber can overshadow the fatigue life of the mix [10].

T A Balqis (2020) affirmed the inclusion of crumb rubber it is ratified that pavement with CR is found to exhibit lesser tensile strain by 20.6 % and compression strain by 2.9%. Besides the decrease in strain, CR inclusion in the pavements is proven to have enhanced the performance of flexible pavements along with an increased life [11].

Sigit Pranowo Hadiwardoyo et al (2018) discussed the stratagem of revamping the strength characteristics and also truncating building materials in composite materials by the wield of synthetic and natural fibers. As avowed, the tensile strength of fibers is high, and they also have the flair to enhance the asphalt mixture's cohesive nature. In this study, the preferred additives are shortly decorticated pulp coconut fibers. 60/70 asphalt content was taken to which 0.5-1.25cm of short coconut fibers were mixed anticipating 0%, 0.75%, and 1.5% yield. The skid number of asphalt mixture has risen by 19% with the appendage of 0.75% coconut fiber when analogized with virgin asphalt mixture. But the inclusion of fibers did not show any acceptable increase in the resistance criteria with changes in temperature, thereby proving that with a hike in the vehicular count of passes, the resistance falls off [12].

Suresh T et al (2016) manifested that the usage of waste materials in the bituminous pavement is out of harm's way with a more ecological binder for escalating properties of road. This paper deals with the study of the influence of waste materials in the bituminous pavement performance. In appraising the study, bitumen is combined with 1%, 2%, 3%, 4%, and 5% of coir fibers. Marshall Stability test was performed on both normal and modified bitumen. Consequently, it is observed that bitumen with coir fibers intended better durability. Also, the supreme concern of a bituminous modifier is to proliferate the resistance of the asphalt against perennial deformation at high road temperatures besides, maintaining the original bituminous properties unmoved. The inclusion of plastic waste in the modified bitumen has shown a surpassed binding property along with enhanced stability, and density. Therefore, it is writ large that the stability enhancement is more in the case of modified bitumen rather than in the regular bitumen mix. The value of softening also exhibited a slight decrease in the modified bitumen mix [13].

Saravana Selvam V et al (2016) studied the usage of coir fiber (natural fiber) and nylon tyre-cords (synthetic fiber) in pavements. The full-length experimental work was categorized as Phase-1: Index properties determination. Phase-2: Determination of engineering properties. Phase-3: Designing of subgrade pavement thickness as per IRC 37-2001. The fibers are used in the soil sample as additives in the percentage of 0.1%, 0.2%, 0.3%, and 0.4%. Not only the optimum traditional fiber mix but also the expansive clays were also treated with non-traditional bio-enzyme stabilisers. Utilization of Coir fiber, Tyre cord fiber and bio-enzyme in the stabilisation of expansive soil thereby increases strength and reduces the thickness of subgrade. Bio-enzyme is available as a concentrated liquid and is to be diluted with water before mixing with soil which produces cementation action. The dosage of the enzyme is 200ml for 1m³ of soil. The use of bio-enzyme reduces pavement thickness [14].

Priya K. V (2016) discussed the coir fiber reinforced bituminous mixes. To avoid cracking and to improve stability, the



bituminous mix is reinforced with coir fiber along with the inclusion of an anti-stripping agent. Silicon-based Nano-technology termed as the Wet bond is the preferred anti-stripping additive in the asphalt whose thermal resistivity is considerably high, thus making it suitable for hot and warm road designs. One more crucial pronouncement in the area of complex modulus is that the value is noted to have an increase with the rise in content of modified binder and vice versa in the case of the phase angle. The addition of coir fibers has resulted in a two-times more increase in the value of stability. Inclusion of anti-stripping agent “wet bond-SP+” improves the bonding between aggregate and bitumen in the pavement, thus avoiding the stripping problems even in heavy rainy conditions. Polypropylene (PP) fibers were also used in fiber reinforced bituminous concrete for escalating the Marshall Stability value. Eventually, PP fibers abated the flow values [15].

Leema Peter (2020) instigated the use of coir waste as a subgrade material for strengthening the flexible pavements. Soft soil alone is inappropriate material for pavement construction as the occurrence of failure can be noted at the premature age itself. As a counteract, coir waste material is taken into consideration to resist the volume changes of the subgrade soil. Coir waste material, when mixed with soil subgrade, becomes resistive in nature. Consequently, the engineering properties of coir waste material need to be balanced. Thus, the inclusion of lime along with coir waste material as a subgrade filler is introduced. Lime plays the role of a stabilizer with coir waste to balance the low behaviour of soil in terms of compression, undrained shear strength, and deformation criteria. From the experimental analysis, it is evident that the inclusion of coir waste along with lime is handy in constructing a sustainable pavement with reduced thickness and with a cost cut-down [16].

M.C. Jayachandran (2019) exclusively dealt with the study of coir geotextile (CGT) in the flexible pavement as a reinforcing material. CGT is a natural fiber with more cost-effectiveness due to its availability in abundance. This study has given an intelligible comparison between the reinforced and unreinforced CGT pavements. The strength of the pavements is determined using the Dynamic Cone Penetrometer (DCP), and the visual evaluation is done for performance functionality. As per the study, four pavements are tested for strength with a subdivision of pavement with coir reinforcement and pavement without coir reinforcement in each pavement. From the results of DCP, the observed values exhibited the coir reinforced pavement to have retained its stability even after 6 years without any pavement distress. The coir reinforced pavement exhibited a reduction of 20% to 30% in the indices of DCP for a span of six long years provided the strength and stability are comparatively high in the pavement with CGT. Concerning the visual evaluation, the pot-holes were located on the pavement without CGT but for the same time, those are accounted to be absent in CGT pavement. Therefore, conclusions drawn from the experimental analysis states that the life span of coir reinforced pavement is way longer than the conventional type with lessened distresses and deformations [17].

Hayder K. Shanbara et al (2020) emphasized the supreme focus on deterioration of flexible pavements due to lack of significant tensile strength of bituminous mixtures. To achieve the desired strength, incorporation of polypropylene fibers in the bituminous mix is made and thereby, tests are carried out for performance evaluation experimentally. 100/150 penetration grade bitumen binder is employed for mix. Polypropylene fiber of 0.1 mm diameter of unit weight 900 kg/m³ were added to the binder of 1.02 g/cm³ density. For a more accurate outlook, various tests akin to Indirect tensile stiffness modulus, Four-point bending fatigue, Three-point bending tests were performed. Fibers in the percentage of 0.2, 0.3, 0.35 and 0.4 were added to the binder resulting in the development of stiffness modulus by 30%. In addition to the stiffness, polypropylene fiber has lowered the fatigue by 41 % and finally makes the mixture the most desired one than the conventional mix [18].

WASTE PRODUCTS IN THE CONSTRUCTION OF ROADS

The following tabular forms indicate the usage of various industrial waste products used in flexible pavement construction.

Table 1. Industrial waste products suitability in the construction of roads

Waste Product	Source	Possible Usage
Slag from Blast Furnace	Steel industry	Filler material in Base and Sub-base course, Binders for soil stabilization (ground slag)
Dust from Cement kiln	Cement industry	Base Stabilization & Modified binder in bituminous mix
China clay	Bricks and tile industry	As bituminous mix aggregates & Bulk-fill
Colliery spoil	Coal mining	Bulk-fill
Sands of Foundry	Foundry industry	Bulk-fill, filler for Concrete, crack-relief layer



Glass waste	Glass industry	Reinforcement of Glass-fiber, bulk fill
Fly ash	Thermal power station	Bulk fill, filler in bituminous mix, artificial aggregates
Marble dust	marble industry	Filler in bituminous mix
Waste tyres	Automobile industry	Rubber modified bitumen, aggregate

(Source: Javed et al., 1994 [19]; Sherwood 1995 [20]; Okagbue et al., 1999 [21]; Mroueh et al., 2002; Hawkins et al., 2003 [22]; TFHRC 2004)

Table 2. Advantages and disadvantages of utilization of industrial waste products in the field of road construction

Materials	Highlights	Challenges
Fly ash	Light weight, its pozzolanic properties made it a good choice as a binder to stabilise base/sub-base	Non-homogeneous, development of strength is a time taking process
Steel Slag	Resistance to skid is relatively high	incompatible for fill work beneath slabs as well as for concrete works
Slag of Blast Furnace	Plays a key role in the manufacturing of cement and granular fill	Leachate formation makes it undesirable and effects groundwater in the form of pollution, used as unbound aggregates
Colliery Soil	-	
	Inevitable unburnt coal combustion, Impact of sulphate attack on concrete roads is not desirable	
Spent oil shale	-	Burning of combustible materials
Cement kiln dust	Hardening can be achieved when moisture exposure is provided. Also a good stabilization material	Percentage of alkalis provokes Corrosion effect on metals (used in concrete roads)
Used engine oil	Makes a better air entraining material that can be utilized in the works dealing with concrete	System of collection of used engine oil is slightly complicated
Non Ferrous Slag	Light weight	May show inconsistent properties
Tailings of Mills	Pozzolanic nature makes it worthy	Presence of undesirable poisonous materials

(Source: Javed et al., 1994[19] ; Sherwood 1995[20]; Nunes et al., 1996[22] ; Hawkins et al., 2003[22]; TFHRC 2004)

CONCLUSION

From The Performed Studies, It Is Evident That The Modified Bituminous Concrete Mixture Of Marble Dust And Coir Fiber Exhibits A High Rise In Tensile Strength When Compared To Neat Mix. The Improvement In The Predominant Strength Property Concerning CBR And Rut Depth Is Determined Through Experimental Analysis Of Soil With The Inclusion Of Waste Materials Like Fly Ash, Cement, And Coir Geotextiles In The Selected Sub Grade. Also From The Investigation, It Is Proven That The Inclusion Of Pulverized Coconut Fiber Can Increase The Marshall Stability Value Of Asphaltic Concrete. Likewise, The Enhancement Of CBR Value By 8% Or More Can Be Achieved By Modifying Expansive Soil With The Addition Of Lime And Coir Pith In The Sub Grade Of Highways. From The Inference, It Is Known That The Pavement Distress Can Be Kept Under Check With The Inclusion Of Additives Like Crumb Rubber, Natural Rubber, And Polymers. Besides These, The Frequently Used Fiber Reinforcing Materials Of Bituminous Concrete Are Coir, Polypropylene, Polyester, And Glass Fibers. Bio-Enzyme, Tyre Cord Fibers, Asbestos Fibers Are Also Used As Additives In The Stabilization Of Expansive Soils. After All The Possible Scrutiny, We Can Conclude That There Is More Exposure In The Area Of Research Concerning The Better Performance Of Pavements With The Usage Of Waste Materials In Terms Of Increasing The Lifespan And Reducing The Pavement Distress Problems Thereby Making The Pavements Sustainable And More Economical.



REFERENCES

1. Milind V., Mohod Kadam K. N., "A Comparative Study on Rigid and Flexible Pavement: A Review", IOSR Journal of Mechanical and Civil Engineering (IOSR-JMCE), e-ISSN: 2278-1684, p-ISSN: 2320-334X, Volume 13, 2016.
2. Amit G. and Animesh D., "Emerging road materials and innovative applications." National Conference on Materials and their Application in Civil Engineering, 2004.
3. Roberts F. L., Kandhal P. S., Brown E. R., Lee D-Y., Kennedy T. W., "Hot Mix Asphalt Materials, Mixture Design and Construction", National Asphalt Pavement Association Research and Education Foundation, Transportation Research Board, 1991.
4. Raji A.K., Karthika R., Amruthalekshmi G.R., Anju K., Peter M. Mohamed Sajeer., "Study of Rut Behavior of Coir Reinforced Black Cotton Soil using Wheel Tracking Apparatus", Indian Geotechnical Conference, Paper No. J- 258, 2011.
5. Adebayo V. B. and Mohammed H., "Pulverized Coconut Fiber as an Additive in Asphaltic Concrete". International Journal of Materials, Methods and Technologies. Vol.4, No. 1, pp.1-10, ISSN: 2327-0322, July 2016.
6. Narendra Goud G., Hyma A., Shiva Chandra V. and Sandhya Rani R., "Expansive Soil Stabilization with Coir Waste and Lime for Flexible Pavement Subgrade", IOP Conf. Series: Materials Science and Engineering, doi:10.1088/1757-899X/330/1/012130, 2017.
7. Vijayan A., Peter L., Jayasree P. K., Balan., "Long Term Strength Studies On Natural Fiber Composite (N-F-C) Sheets for Use as Separator in Flexible Pavements in Terms of CBR Values", Indian Geotechnical Conference, 15-17, 2017.
8. Nithin S., Sayida M. K., Sheela Evangeline, Y., "Experimental Investigation on Coir Geotextile Reinforced Subgrade". Indian Geotechnical Conference, Paper No. B 269, December 2012.
9. Singh R. R., and Shelly Mittal Er., "Improvement of Local Subgrade Soil for Road Construction by the use of Coconut Coir Fiber". International Research Journal of Engineering and Technology, Vol. 3(5), 2014.
10. Mahabir P., Suchismita A., and Jyothi Prakash G., "Utilization of Ripe Coconut Fiber in Stone Matrix Asphalt Mixes". International Journal of Transportation Science and Technology, Vol.2, No. 4, 2013.
11. T. A. Balqis and S. Suherman, "The Effect of Using Crumb Rubber on Fatigue and Rutting Lives in Flexible Pavement", IOP Conf. Ser.: Mater. Sci. Eng. 732 012030, 2020.
12. Pranowo Hadiwardoyo S., "Contribution of Short Coconut Fibre to Pavement Skid Resistance", January 2018.
13. Suresh T., Vijay T.J., Chandrasekar A., "Modelling Marshall Stability of Coir Fibre Reinforced Asphalt Concrete". International Research Journal of Engineering and Technology, Vol. 3(11), 2016.
14. Saravana Selvam V., Sivaraja M., Raja K., Navaneethan K. S., Dheeran G., "Minimization of Subgrade Thickness using Natural and Synthetic Additives in Roads". Journal of Mechanical and Civil Engineering. Vol. 13(5), pp 66-72, 2016.
15. Priya K.V., Brammananadham G. G., Sri, Gnana Prakash P., Vinoth Kumar G., Santha Kumar G., "Study of Coir Fiber Reinforced Bituminous Mixes with Anti- Stripping Agent". International Journal of Science and Innovative Engineering and Technology, Vol.1 ISBN 978-81-904760-8-9, 2016.
16. Leema Peter P., Jayasree K. & Balan K., "Optimization, Quantification of Strength and Design Benefits of Flexible Pavements Resting on Soft Soil Subgrades Treated with Coir Waste and Lime", Journal of Natural Fibers, DOI: 10.1080/15440478.2020.1788490, 2020.
17. M.C. Jayachandran, Y. Sheela Evangeline, G. V. Rao, M. K. Sayida, Ajn Krishna & Akhila Vijaya., "Study on the coir geotextile reinforced flexible pavements using DCP", Recent Advances in Materials, Mechanics and Management – Evangeline, Rajkumar & Parambath (Eds)©2019 Taylor & Francis Group, London, ISBN 978-0-8153-7889-1, 2019.



18. Hayder K. Shanbara, Sarah S. Musa and Anmar Dulaimi, "The Effect of polypropylene fibres on the tensile performance of asphalt mixtures for road pavements", 2020 IOP Conf. Ser.: Mater. Sci. Eng. 888 012082, 2020.
19. Javed S., Loveell C.W., Wood W., "Waste foundry sand in asphalt concrete", Transportation Research Council, TRB, National Research Council, Washington, D. C, 1437, 27-34, 1994.
20. Sherwood P.T., "Alternative materials in road construction", 1995.
21. Okagbue C. O., and Onyeobi T. U. S., "Potential of marble dust to stabilise red tropical soils for road construction", Engineering Geology, 53, 1999.
22. Hawkins G. J., Bhatta J. I., O' Hare A. T., "Cement kiln dust production, management and disposal", Portland Cement Association, PCA, R&D, Report No. 2737, 2003.
23. Nunes M.C.M., Bridges M.G., Dswson D.G., "Assessment of Secondary Materials for Pavement Construction: Technical and Environmental Aspect. Waste Management, Vol.16, No. 1-3, 87-96, 1996.

Developing Self-Compacting Concrete as per IS 10262: 2019 by Utilizing C and D Waste as Aggregates and Fines

Ajay N¹, Ashwin M Joshi¹, Namratha Bharadwaj², Girish S³

Infrastructure Construction and Management, RASTA- Centre for Road Technology, VCE Campus, Peenya, Bangalore¹

Department of Architecture, B M S College of Architecture, Bull Temple Road, Bangalore²

Department of Civil Engineering, B M S College of Engineering, Bull Temple Road, Bangalore³

✉ drajaynagaraj.2019@gmail.com; ✉ ashwinmjoshi@gmail.com

ABSTRACT

Self-compacting concrete (SCC) referred to as a type of special concrete” offers economical and technical advantages over the normal concrete. So far, the design and development of SCC mixes were carried out as per established design methods. For the first time Bureau of Indian Standards has come out with guidelines for SCC mixes through IS 10262: 2019 revision.

The present study attempts to develop SCC mixes as per the revised IS guidelines utilizing marginal materials such as RMC sludge and granite sludge as fines (particle size less than 125 microns); recycled concrete aggregate as coarse and fine aggregates and GGBS as a filler material. The powder content, cement content and water content were maintained at 550 kg/m³, 334 kg/m³ and 200 lt/m³, respectively. The developed SCC mixes satisfy the requirements of hardened & fresh properties. The morphology of the microstructure of developed SCC mixes were also analyzed through Scanning Electron Microscopy (SEM).

Results indicate the RMC sludge and granite sludge may be utilized in developing SCC mixes. SCC mixes with granite sludge has shown better performance as compared to SCC mixes with RMC sludge as fines.

Keywords: C&D waste; Granite Sludge; IS: 10262-2019; RMC sludge; Self-compacting concrete.

INTRODUCTION

Self-Compacting Concrete (SCC) was first developed in Japan” [1]. It has become a well-accepted innovation in concrete industry, and is widely adopted, especially for important structures where strength, serviceability and speed of construction are of prime importance. SCC has advantages over normal concrete (NC). It provides better surface finishes, thinner concrete sections, enable easier placement of concrete, faster construction, eliminate the vibration, improved durability, and reduction in site manpower and so on [2,3,4]. In pre-cast industry, where the speed of placing concrete and removal of the elements from the forms at the earliest is essential while also ensuring the surfaces are free from defects [5,6]. **Fig. 1** shows a general comparison between mix proportions of SCC and NC [5,6].

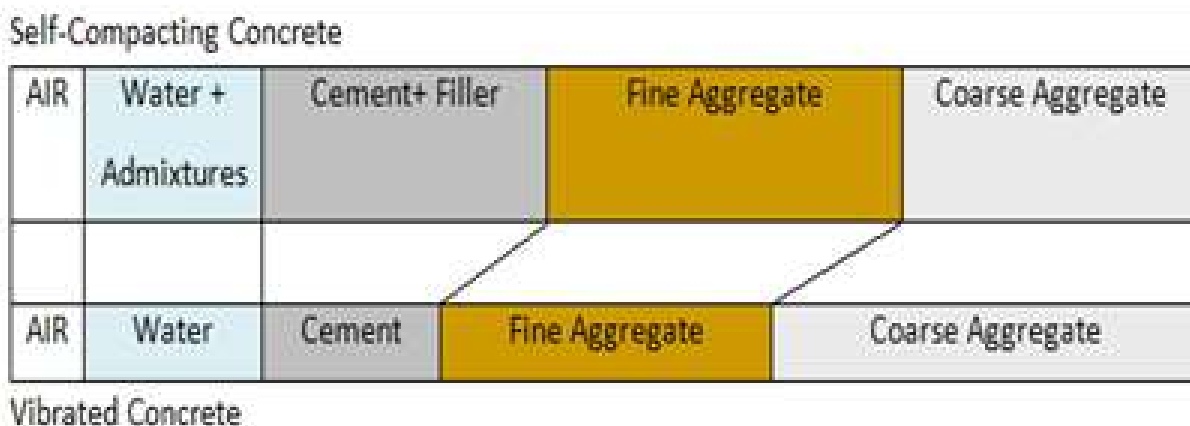


Fig. 1. Comparison of mix proportioning between SCC and NC [1]

SCC has the following property (fresh) requirements viz: filling ability, passing ability & segregation resistance (**Fig.2**).

<p>Flowing Ability:</p> <p><i>"The ability to flow into and fill completely all spaces within the formwork, under its own weight". This property is a combination of total flow capacity and flow rate</i></p>	
<p>Passing Ability:</p> <p><i>"The ability of SCC to flow through tight openings such as spaces between steel reinforcing bars without segregation or blocking"</i></p>	
<p>Segregation resistance;</p> <p><i>"The ability of SCC to remain homogenous in composition during transport and placing"</i></p>	

Fig. 2. Fresh property requirements of SCC [1]

The requirements for workability of SCC are mainly depend on the applications. Before producing SCC mixes, it is important to understand and measure the fresh properties of SCC. The interpretation of test results with respect to the field applications is also important. SCC is one of the complex types of concrete mix to design. The mix-proportioning process of SCC is more complex as compared to that of NC because the constituents of SCC include rounded or crushed aggregates, ordinary Portland cement or blended cements; different types of mineral admixtures; superplasticizer (SP) and sometimes even Viscosity Modifying Admixture (VMA).

There are number of mix design methods were developed and/or adopted by many researchers, which are based on different principles [7]. While SCC has passed the stage of laboratory practice to field implementation, there are no systematic standards or requirements to be followed in its mix proportioning [7]. Effective proportioning and control of SCC mixes necessitate an authoritative guideline relating the effect of constituent characteristics and corresponding mix proportions.

In India during early 1990's, the public knowledge about the SCC was limited and there are always doubts about the performance. Gradually researchers worked on developing self-compacting concrete, including specifications on fresh and hardened properties. Currently, there are hundreds of technical articles and on SCC has moved from laboratory research to field application. However, the Bureau of Indian Standards (BIS) committee has revised the guideline IS: 10262-2019 [8] which includes SCC mix design method.

RESEARCH SIGNIFICANCE

The construction activities generate large amount of construction and demolition (C&D) waste materials through aggregates, excavated soil, masonry and mortar debris, RMC sludge, marble powder, granite sludge etc. These debris, especially the finer materials are disposed of unscientifically through landfills, lakebeds etc., affecting the environment. It is estimated, in India alone the construction industry generates up to 716 million tons of C&D waste and as per 2016 estimates the city of Bengaluru alone generates about 3600 T/day [9]. Significant attempts have been made to utilize masonry debris, concrete debris and other marginal materials in different construction materials [10,11,12]. Granite sludge (GS) and RMC sludge (RS) (**Fig. 3**) which are obtained from granite polishing industry and ready-mix concrete plants respectively can be part of C&D waste. Unscientific disposal of these in landfills impacts health, environment, and ecology [13,14]. The best way of disposal of such materials is to utilize them as construction materials, especially in concrete, which is the most widely consumed construction material currently.

Developing SCC mixes using alternatives to natural resources is important in environmental protection and achieving sustainability in construction. Developing SCC mixes using alternatives or other marginal materials is certainly most challenging as compared to developing the other types of concretes. This is due to the complexities involved in achieving equilibrium amongst different constituent materials used in proportioning SCC mixes.

In the revised guidelines IS 10262: 2019 [8] the fines of about 8% (in fine aggregate) is recommended in proportioning SCC mixes and these fines content (8%) is pivotal in determining the fine aggregate content. It is impractical for specific percentage of fines either to be present in fine aggregate; (or) procure fine aggregate with specified value of fines (particle size < 125 μ); nor

assume fine aggregate to have specific fines content irrespective of its gradation characteristics and zonal classification. Even fine aggregates belonging to any particular zone as per IS 383: 2016 [15] shall consists of fines content (%) in a broad range of values and not a specific value. Also, there are no specific recommendations regarding the possible measure which one has to adopt under such circumstances i.e., when percentage of fines is more than or less than a specific value. This is evident in current case, especially when the percentage of fines in procured fine aggregate is less than specific value ($< 8\%$). To attain the required fines content in fine aggregate, it may be necessary to add fines in addition to existing fines content in fine aggregate, thereof to calculate fine aggregate content and estimate the coarse aggregate content for given SCC mix.

The present study attempts to develop SCC mixes using IS 10262: 2019 [8] along with different fine materials (particle size $< 125 \mu$) and filler material. The study primarily focuses on developing the SCC mixes as per IS guidelines and exploring the possibilities of utilizing marginal materials as fines.



(a)



(b)

Fig. 3 (a) RMC sludge; (b) Granite sludge

EXPERIMENTAL METHODOLOGY

Materials

The list of constituent materials and their corresponding properties are tabulated in **Table 1**.

Table 1. Properties of material

Sl. No.	Materials	Specific gravity	Specific Surface (m ² /kg)	Water absorption (%)
1	Cement – “(OPC-53 grade) conforming IS:12269-2013”[16]	3.14	280	-
2	Fine aggregate – (RFA) “confirming” to Zone-II as per IS 383-2016” [15]	2.58	-	6.00
3	Coarse aggregates –(RCA) 20mm maximum size of aggregate	2.78	-	5.83
4	“Ground Granulated Blast Furnace Slag (GGBS) - IS 12089-2018”[17]	2.85	425	-
5	Superplasticizer (SP) - Polycarboxylic Ether (PCE) based conforming to IS: 9103-1999 [18]	1.09	-	-
6	RMC Sludge (RS)	2.14	435	-
7	Granite Sludge (GS)	3.65	365	-
8	Water - Conforming to IS 456 - 2000 [19]	1.00	-	-

Mix Design Method

The “SCC mixes were developed” based on IS code recommendations. The details are presented through the flow chart (**Fig. 4**) and brief discussion below.

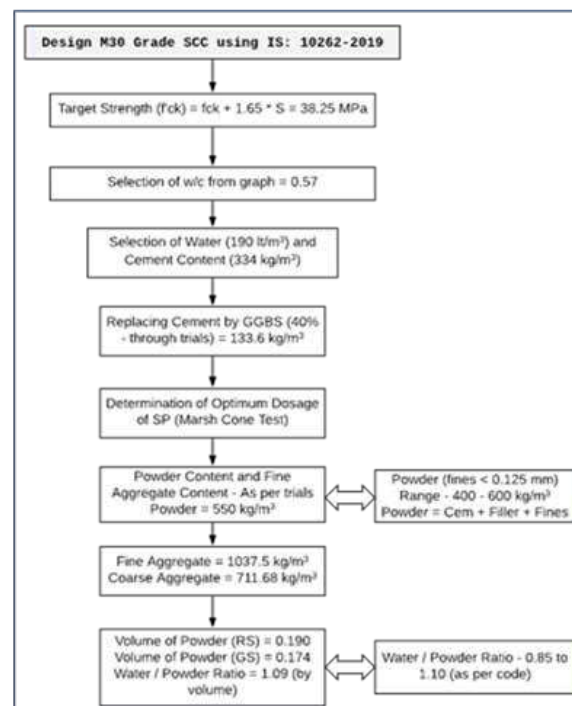


Fig. 4. Flow chart representing the mix design adopted (M30 grade SCC)



The target strength was calculated based on the equation recommended. The selection of water content was based on the graph of water content v/s compressive strength (which dependson the grade of cement) as suggested in IS code. The recommended water content range was 150 - 210 lt/m³. About 190 lt/m³ was chosen based on trials and practical field application. The cement content was calculated on basis of water content chosen and the percentage replacement of filler by weight. After trials, about 40% GGBS by weight of cement was added as filler since replacing 25-50% by weight of cement by filler not yielded required flow for SCC trials. Marsh cone test was performed to decide on optimum dosage of SP.

The recommended powder content range as per IS 10262 2019 [8] is 400 to 600 kg/m³. The powder content constitutes of cement, filler, and the fines (content) in the fine aggregate. It is required to determine the powder content to decide on mixes. Though exact procedure is not stated, the powder content was established through trials in the present study and the values were verified against the ratio of w/p by volume recommended (0.85 to 1.10) under a note in section E-7.5 of IS code. This value of powder content is important since the fine aggregate content can be established only using the fines content of the fine aggregate. The relation is given by:

Total powder content = cement + filler + 10% fines of zone II fine aggregate.

Fine = Powder – (cement + filler)

The fines present in fine aggregate was considered to be 8%, to calculate the fine aggregate proportion. The mass of coarse aggregate for the mix is then determined from the volume of coarse aggregate. The “volume of coarse aggregate” is determined by deducting the volume of air content, water, cement, filler, admixture, and fine aggregate from per meter cube of concrete. The w/p ratio determined must lie between 0.85 and 1.10.

Trials Mixes

To begin with, the trials were conducted with lower powder content. The fine aggregate confirms to zone–II, however it consisted of 1.40% fines. The remaining, fines content to achieve 8% fines was externally added by utilizing various marginal materials having particle size <0.125 mm. Natural river sand fines (NF), marble powder (MP), fly-ash fines (FF), RMC sludge (RS) and granite powder (GS) were utilized as the substitute for fine aggregate fines. The IS code recommends the powder content in the range of 400 to 600 kg/m³. More than 30 trials are reported, which the powder content in the recommended range. Details of trials are tabulated in **Table 2**.

Table 2. Detail of trial mixes

Mix No	Cement	GGBS	Fine aggregate (FA)	Coarse aggregate (CA)	Fines	Powder	Water	SP (%)	w/p	Slump flow (mm)	Result
	kg/m ³	kg/m ³	kg/m ³	kg/m ³	kg/m ³	kg/m ³	lit/m ³				
Powder Content (400 kg/m³)											
1	255	85	810	1082	80	340	180	0.35	1.26	-	segregation
2	255	85	810	1082	80	340	200	0.40	1.40	-	
3	237	79	1050	834	84 (6.6 NF+1.4 RS)	400	180	0.20	1.33	400	
4	237	79	1050	834	84 (6.6 NF+1.4 RS)	400	190	0.35	1.40	505	bleed
5	237	79	1050	834	84 (NF fines)	400	180	0.35	1.33	-	segregation
6	237	79	1050	834	84 (NF fines)	400	200	0.80	1.48	-	
7	237	79	1050	834	84 (6.6 NF+1.4 RS)	400	180	0.40	1.33	-	



8	237	79	1050	834	84 (6.6 NF+1.4 RS)	400	200	0.60	1.48	-	
9	237	79	1050	834	84 (NF fines)	400	180	0.35	1.33	-	
10	237	79	1050	834	84 (NF fines)	400	220	0.60	1.62	-	
11	237	79	1092	792	84 (NF fines)	400	180	0.20	1.33	-	
12	237	79	1092	792	84 (NF fines)	400	200	0.60	1.48	-	
13	237	79	1092	792	84 (FF)	400	180	0.20	1.36	-	
14	237	79	1092	792	84 (FF)	400	265	0.70	2.00	525	bleed
Powder Content (400 to 520 kg/m ³)											
15	255	85	1000	817	80 (GS)	420	180	0.35	1.35	-	segregation
16	255	85	1000	817	80 (GS)	420	195	0.60	1.46	-	segregation
17	384	111	975	351	78 (GS)	500	190	0.60	1.04	-	segregation
18	287	155	975	680	78 (RS)	520	190	0.20	1.05	100	segregation
19	287	155	975	680	78 (RS)	520	300	0.50	1.66	540	bleed
20	287	155	975	680	78 (GS)	520	190	0.20	1.13	320	No mix
21	287	155	975	680	78 (GS)	520	200	0.90	1.19	500	No mix
Powder Content (> 520 kg/m ³)											
22	287	155	975	680	78 (RS)	520	190	0.20	1.05	200	No mix
23	287	155	975	680	78 (RS)	520	300	0.50	1.66	-	segregation
24	287	155	975	680	78 (GS)	520	190	0.20	1.13	620	bleed
25	287	155	975	680	78 (GS)	520	200	0.90	1.19	-	segregation
26	384	128	475	709	38 (RS)	550	220	0.50	1.22	-	segregation
27	325	97	963	869	77 (FF)	500	175	0.48	0.91	595	stable mix
28	335	100	963	849	77 (FF)	512	180	0.46	0.92	615	stable mix
29	345	103	950	817	76 (FF)	525	185	0.44	0.92	635	stable mix
30	352	105	963	818	77 (FF)	535	190	0.42	0.92	690	stable mix
31	362	108	938	824	75 (FF)	545	195	0.38	0.93	715	stable mix

Table 3. Details of “SCC mix Proportions”

Mix Designation	Cement (kg/m ³)	GGBS (kg/m ³)	Fines (kg/m ³)	Powder (kg/m ³)	Water (lt/m ³)	FA (kg/m ³)	CA (kg/m ³)	SP (%)	Remarks
M1 – Control Mix (CM)	334	133	83 (Natural fine)	550	200	1038	683	0.4	Natural Aggregates
M2	334	133	83 (RCA fine)	550	200	1038	578	0.6	Recycle aggregates
M3	334	133	83 (RS fines)	550	220	1038	578	0.8	Recycle aggregates
M4	334	133	83 (GS fines)	550	200	1038	578	0.8	Recycle aggregates



M1- Control mix



M2-RCA fines



M3-RS fines



M4-GS fines

Fig.5. Final reference mixes

The results indicate the SCC mixes were not achieved at lower powder content (about 400 kg/m^3) these mixes also exhibit lower cement content ($< 250 \text{ kg/m}^3$). SCC mixes showed segregation and bleeding, when the powder content was in range of 400 to 520 kg/m^3 . It is also interesting to note, the w/p ratio was achieved in some of the mixes and the value was near to the upper limit of 1.10 in the mix (mix no.19) which achieved maximum flow of 500mm. The upper limit of 1.10 also finds its mention in literatures of EFNARC [20]. The SCC mixes were only achieved when powder content was above 550 kg/m^3 . IS code recommending the value of powder content between $400 - 600 \text{ kg/m}^3$; though EFNARC [20] allows up to 650 kg/m^3 . Thus, 550 kg/m^3 (powder) was considered for further study.

The control mixes were developed based on these criteria. Further, the 8% fines content was achieved with four different types of materials viz., natural fines (CM-M1). For remaining mixes, NF was replaced by RCA fines, RS fines and GS fines for same mix proportions (CM-M1). The adopted mixes in current study (**Fig. 5**) are tabulated through **Table 3**.

Test Details

Fresh properties of SCC mixes studied were established through slump flow test by recording flow diameter in mm; difference in height between outer and inner sides of J-Ring apparatus was recorded in mm and time for flow through V funnel was

recorded in seconds. These tests values were ascertained as per EFNARC guidelines as recommended in IS code [8]. As far as mixing sequence is concerned, a modified procedure where water along with SP followed by cement, filler, FA and CA was adopted [21,22]. For each of SCC mixes, specimens were subjected to compression, split tensile and flexural strength tests at 28 days ageing and were determined as per IS 516 [23].

RESULTS AND DISCUSSIONS

Fresh Properties

Fresh properties of SCC ascertained, are tabulated through Table IV. Slump flow was recorded to check the mobility of SCC. Passing ability to verify ability of the mixes to get through narrow or congested areas of rebars. The stability and homogeneity of SCC was evaluated via resistance to segregation.

Table 4. Fresh properties

Mix Designation	Slump flow (mm)	T50cm (sec)	J-ring (mm)	V-funnel (sec)	
				V0	V5
M1	615	3.0	6.0	7.2	10.8
M2	615	4.6	5.5	8.6	11.4
M3	620	5.3	10.0	7.1	10.7
M4	605	4.3	6.5	7.4	10.5

The developed SCC mixes satisfied the requirements of fresh properties as the values recorded were within the recommended range [20]. The slump flow values recorded range from 605 to 620 mm, T50cm from 3.0 to 5.3 sec, J-ring 5.5 mm to 10 mm and V-funnel at zero minute from 7.1 to 8.6 sec. This shows SCC mix may be developed by using revised IS code with some modification in the mix design procedure and with marginal materials as fines. The viscosity of the mix was ascertained through T50cm and the segregation resistance was assessed through V-funnel.

Hardened properties

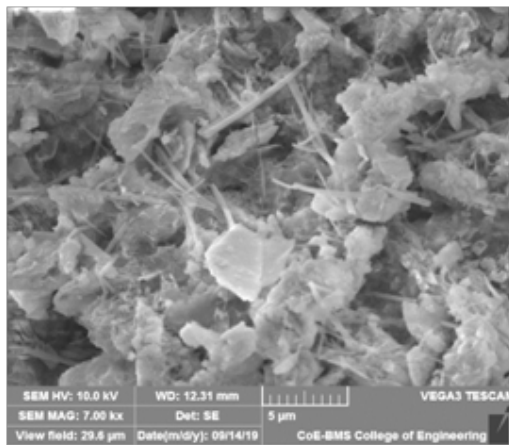
Strength properties of SCC viz., compressive strength, flexure and split tensile strengths were tested for 28-day ageing and are tabulated in Table 5 against their corresponding SCC mixes. Fig. 7 shows the Scanning Electron Microscope photograph (SEM) of SCC mixes. A similar microstructure was reported by Sequeria et. al [24] while exploring mud concrete mixes by utilizing other forms of C&D waste.

Table 5. Hardened properties

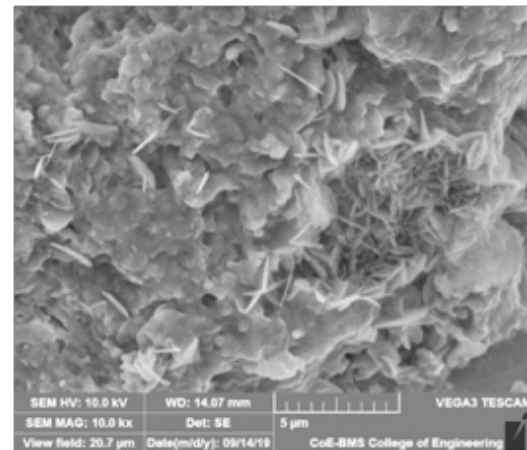
Mix Designation	Compressive Strength (MPa)	Split Tensile Strength (MPa)	Flexural Strength (MPa)
M1	36.2	3.5	6.8
M2	30.0	2.3	6.6
M3	25.0	2.7	5.0
M4	31.3	2.5	3.8

The increase in strength linearly to increased powder content (for all water contents) may be attributed to higher paste content coating aggregates through continuous matrix of hydrated cement paste. A well-defined cement paste matrix may have also resulted in better packing. In certain instances, but not all, an apparent optimality of powder with respect to compressive strength was noted, though the number of mixes is limited. CM in comparison, with the SCC mix consisting of granite dust as fines has given the satisfactory result.

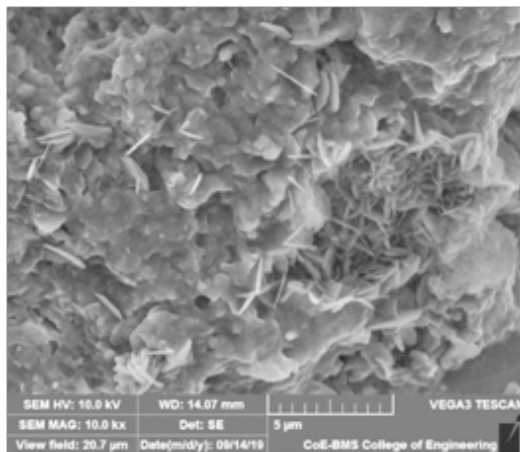
The water demand for mix M3, consisting of RS fines has increased by about 10% as compared to other proportions with slight increase in SP dosage to achieve similar slump flow values. an increased w/p ratio, which may reflect increased specific surface as compared to other mixes. Understandably, the highest strength characteristics were observed in proportions containing natural aggregates and natural fines (M1-CM); least strength characteristics were observed in mixes M3 & M4, having RS and GS as fines. However, mix proportions different constituents for each series (M1 to M4) are quite similar, in addition to fresh characteristics.



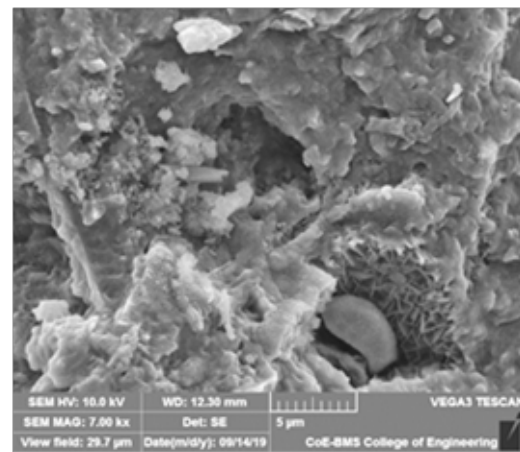
Natural + CM – M1 – CM



M2 – RCA



RCA + RMC



RCA + GD

Fig.7. Scanning Electron Microscope photograph (SEM) of SCC mixes

CONCLUDING REMARKS

IS 10262:2019 guidelines may be considered for utilizing fines ($<125\mu$) in SCC mixes. The study also reveals that powder plays a major role in achieving SCC mix. The 8% fines in powder content plays a major role in constituting fine aggregate content. The fines ($<125\mu$) in fine aggregate may vary from 0 - 10% (Zone II – IS 383-2016); if the fines present is less than (or even greater than) 8%, the type of material which should be added to fulfill 8% fines is not suggested in the guidelines. When the powder content was less than 550 kg/m³ the desired SCC mixes were not achieved. The SCC with RS fines demands more water content; the mix was sticky (cohesive) as compared to mixes with GS fines. However, mix containing GS fines exhibited better results in fresh and hardened state.

ACKNOWLEDGMENT

The authors would wish to acknowledge KSCST, Bengaluru for their monetary support for this research work and RASTA – Center for Technology, Bengaluru for their support for conducting experiments. Mr. Karthik and Mr. Zeeshan Ahmed, former M.Tech Students, CIM, RASTA – Center for Road Technology in conducting experiments.

REFERENCES

1. H.Okamura, and K.Ozawa, "Mix design for self-compacting concrete," Concrete Library of JSCE, vol.25, pp.107-120, 1995.



2. S.Girish, N.Ajay and Sasha Azimi, "Development of self- compacting concrete using construction and demolition waste as an alternative to natural coarse aggregate with emphasis on sustainability," The Indian Concrete Journal, vol.94,no.8,pp.40-50,2020.
3. N.Ajay, S.Girish and M.S.Sindhu, "Comparative studies on fresh and compressive strength properties of SCC by modified is 10262-2009 method and volume fraction method," I-manager's Journal on Structural Engineering, vol.8, no.3,pp.44-49, 2019. doi.org/10.26634/jste.8.3.16575.
4. S.Girish, "Influence of powder and paste on SCC using recycled concrete aggregates,"Bonfring International Journal of Industrial Engineering and Management Science, ISSN 2277-5056, vol.02, no.04, pp. 68-75, 2012.
5. S.Girish and H.R.Arjun, "Development of SCC with crushed rock fines as filler," Journal of Structural Engineering, vol.38, no.01, pp.60-66, 2011.
6. S. Girish and G.N.Mallikarjun, "Influence of volume of paste on the fresh and hardened properties of SCC using recycled aggregates," 6th international RILEM, Symposium on SCC, Montreal, Canada, pp.275-284,September 2010.
7. Caijun Shi, Zemei Wu, KuiXiLv, Linmei Wu, "A review on mixture design methods for self-compacting concrete," Construction and Building Materials, vol.84, pp.387-398,2015.
8. IS: 10262:2019, "Guidelines for design and development of different types of concrete mixes," Indian Standards, New Delhi, 2019.
9. Joshi A.M., Basutkar S.M., Jagadish K.S. "Stabilized Mud Concrete for Sustainable Construction". In: Delgado J. (eds) Sustainable Materials in Building Construction. Building Pathology and Rehabilitation, vol 11, pp. 135-147, Springer, Cham, 2020.https://doi.org/10.1007/978-3-030-46800-2_6
10. N. Ajay., Joshi, A.M., Girish, S., Harshitha, M.R., "Experimental studies on rheological properties of conventional vibrated concrete using direct shear box", Indian Concrete Journal, vol.92, no.8, pp. 19-28, 2018.
11. Joshi, A.M., Raghunath, S., Keshava, M., Jagadish, K.S., "Stabilized Adobe using Demolished Brick Masonry Waste", National Seminar on Emerging Building Materials and Construction Technologies, New Delhi, 2018. DOI: 10.13140/RG.2.2.24096.84481
12. A.M.Joshi, S.M.Basutkar, M.Keshava, S.Raghunath, and K.S.Jagadish, "Performance of masonry units prepared using construction and demolition waste as fine aggregates," In: 10th International Masonry Conference, IMC, Milan; Italy, pp.1176-1185, July 2018. DOI: 10.13140/RG.2.2.22838.55364.
13. Joshi, A.M., Basutkar, S.M., Ahmed, M.I., Keshava, M., Raghunath, S., Jagadish, K.S., "Performance of stabilized adobe blocks prepared using construction and demolition waste", Journal of Build Rehabilitation,vol.4, no.13, 2019. <https://doi.org/10.1007/s41024-019-0052-x>.
14. S.Girish, N.Ajay N, Ishani Nimbargi, D.M.Chaitra and M.Hrushikesh, "Development of innovative green self-compacting concrete with partial replacement of fine and coarse aggregate by using slag,"D.K.Ashish et al. (eds.), RILEM Bookseries, V.29, pp 49-62, 2020. doi.org/10.1007/978-3-030-51485-3_5.
15. IS: 383-2016, "Coarse and fine aggregate for concrete – specification," Indian Standards, New Delhi, 2016.
16. IS: 12269:2013, "Ordinary Portland cement – 53 grade specification," Indian Standards, New Delhi, 2013.
17. IS:12089-2018, "Ground Granulated Blast Furnace Slag for Use in Cement, Mortar and Concrete – Specification," Indian Standards, New Delhi, India, 2018.
18. IS:9103-1999, "Concrete Admixtures – Specification," Indian Standards, New Delhi, 1999.
19. IS: 456-2000, "Plain and reinforced concrete - code of practice," Indian Standards, New Delhi, 2000.



20. EFNARC, "The European guidelines for self-compacting concrete - specification, production and use," European guidelines, 2005.
21. S.Girish, "Importance of volume of paste on the compressive strength of SCC - A parameter to be considered in mix design," The Indian Concrete Journal, vol.91, no.4, pp.51-62, 2017.
22. S.Girish S., N.Ajay, T.Soumya T, "Sorptivity as a durability index for service life prediction of self-compacting concrete," In: Narasimhan M.C., George V., Udayakumar G., Kumar A. (eds.) Trends in Civil Engineering and Challenges for Sustainability, Lecture Notes in Civil Engineering, Springer, Singapore, vol.99, pp.295-309, 2021. doi.org/10.1007/978-981-15-6828-2_23.
23. IS:516-1959, "Method of test for strength of concrete," Indian Standards, New Delhi, 1959.
24. Sequeira V.L., Joshi A.M., Kerekoppa M.D., Bharadwaj N., "Physical and Microstructural Properties of Construction and Demolition Waste Based Masonry Units", In: Ashish D.K., de Brito J., Sharma S.K. (eds) 3rd International Conference on Innovative Technologies for Clean and Sustainable Development. ITCSD 2020. RILEM Bookseries, vol 29, pp.411-428, Springer, Cham., 2021 https://doi.org/10.1007/978-3-030-51485-3_27

Analytical Estimation of Boundary Layer Thickness for Flow Over Spillways

Suresh Kumar N, Prasanna S V S N D L

Department of Civil Engineering, College of Engineering (A), Osmania University, Hyderabad

✉ nsksdr@yahoo.co.in

ABSTRACT

The Spillways provide a safe passage for the excess water or flood water in the reservoir. The present study was emphasized towards estimation of boundary layer thickness, wall shear stress, and skin friction coefficient for flow over spillways. These parameters are helpful in estimating the flow resistance over the spillway and can be made use of in the design of energy dissipators. Analytical estimates were made for the above parameters making use of equations available in the literature. The boundary layer thickness was evaluated for four different discharges.

Keywords: Boundary layer thickness; Velocity; Depth of flow.

INTRODUCTION

A boundary layer is a very thin layer close to the surface where viscous forces and rotationality are considered. The boundary layer will form on the spillway flow, beginning from the crest of the spillway. The thickness of the boundary layer (δ), will grow with the distance from the profile of the spillway crest. The region of transition from laminar to turbulent boundary layer develops far upstream. An increase in the surface roughness will result in faster boundary layer growth. Hence, it will result in reduction of zone of flow development length. The boundary layer thickness will become equal to the depth of flow over the spillway at some point, provided the required length of spillway is available. The flow over the spillway crest is similar to the flow over a streamlined object. As the flow over the spillway will be accelerating, the flow may have a favourable pressure gradient. Hence, the chances of flow separation are not likely to occur till the head over the crest is substantially large (greater than three times the design head) [1].

Review of Literature

For the computation of turbulent boundary layer, Chow adopted a practical method as detailed in the “equation (1),” for the boundary layer growth over the profile of the spillway. This procedure is applicable to channels with mild slope wherein flow is either uniform or accelerating, or channels having steep slopes. The region of transition from laminar to turbulent boundary layer develops far upstream from the zone of consideration. An increase in the surface roughness will result in faster boundary layer growth. Hence, it will result in reduction of zone of flow development length [2].

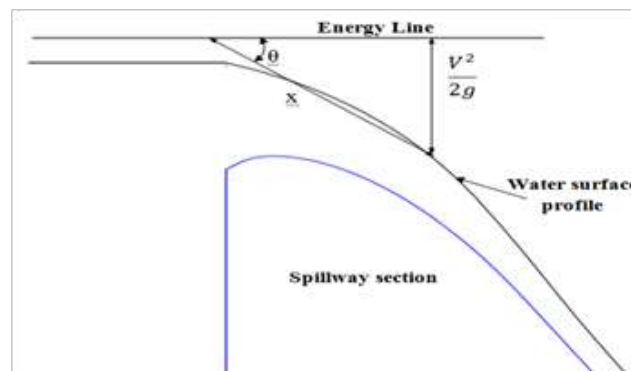


Fig. 1. Boundary Layer Growth

$$\left. \begin{aligned} \frac{\delta}{x} &= \frac{0.024}{\left(\frac{x}{k}\right)^{0.13}} \\ \frac{V^2}{2g} &= x \sin \theta \end{aligned} \right\} \quad (1)$$

Case Study

The present investigations were carried out for Nagarjuna Sagar project. It is built at 2.4 km downstream of Nandikonda village of Miryalaguda Mandal of Nalgonda District in Telangana State. It is located at 79°18' 47" E longitude and 16°34'23" N latitude. The project comprises of 124.66 m (409 ft) high masonry dam with total volume of 199 million cu ft. The salient features of the case study are highlighted in **Table 1** [3].

Table 1. Salient feature of NS dam

Description of Parameters	Details
Maximum Water Level (MWL)	181.100 m
Full Reservoir Level (FRL)	179.832m
Discharge (Q)	58,340m ³ /s
Top of the Dam (TOD)	184.40 m
Crest level of Spillway	166.421 m
Height of the spillway	166.421 – 67.06 = 99.361m
Maximum height of the dam	124.66 m
Length of spillway	470.916 m
Pier thickness	4.572m
Average River Bed Level	184.40 – 124.66 = 59.74 m
Size of each bay of crest gates	13.716 x 13.41m
Constants	Kp = 0.01 and Ka = 0.1

METHODOLOGY

The present investigation adopts standard ogee shaped spillway profiles developed by U.S. Army Corps of Engineers at Waterways Experiment Station (WES). The study adopts “equation (2),” for the spillway crest upstream profile with origin at the crest of the spillway and uses “equation (3),” for downstream spillway profile [4]. The curve extends 0.270H_d (X_c) on upstream and 0.125H_d (Y_c) below the crest point of the spillway as shown in the **Fig. 2**.

$$Y = \frac{0.724(X + 0.27H'_d)^{1.85}}{H'_d} + 0.126H'_d - 0.4315H'_d{}^{0.375} (X + 0.27H'_d)^{0.625} \quad (2)$$

$$X^n = K.H'_d{}^{n-1}.Y \quad (3)$$

The analytical values of boundary layer thickness (δ) for hydraulically smooth surface were estimated by the “equation (4) to (7),” [5]. The boundary layer thickness values were evaluated for four different discharges viz., 58,340 cumec, 43,755 cumec, 29,170 cumec and 14,585 cumec.

$$\frac{1}{\sqrt{C_f}} = 3.85 * \log \left(\frac{\delta U}{\nu} \right) + 3.67 \quad (4)$$

$$C_f = \frac{b_s}{(\log R_x)^{2.38}} \quad (5)$$

$$b_s = 0.32 + 8.15 * k_s^{0.47} \quad (6)$$

$$\tau_w = \frac{0.0315 * \mu^{1/7} * \rho^{6/7} * U^{13/7}}{x^{1/7}} \quad (7)$$

where

X, Y = coordinates of the upstream and downstream profile (m)

n, K = variable parameters which depend on the inclination of the upstream face of the dam, n = 1.85 and K = 2.0

H_d = Design head (m)

V is the velocity at 'x', m/s

θ is the angle w.r.t the total energy line above the crest of the spillway, degrees

δ is the boundary layer thickness, m

C_f is local loss coefficient

b_s empirical coefficient accounting for sand grain roughness

x is the point of interest on the WES profile of spillway, m

k_s is the surface roughness height, m

τ_w is the wall shear stress, Pa

μ is the dynamic viscosity, Ns/m²

ρ is the mass density of water, kg/m³

U is the stream velocity at the point of interest, m/s

The point, at which boundary layer thickness coincides with the free surface, is the location at which flow is fully developed. The plots for the point of intersection of boundary layer thickness and depth of flow for various flow conditions are shown in Fig. 3 (a) to (d).

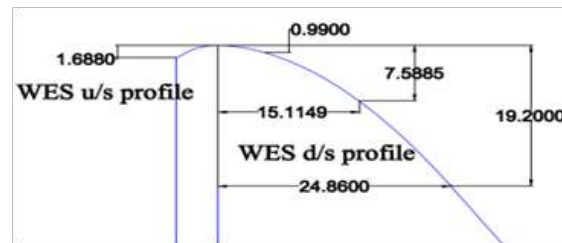
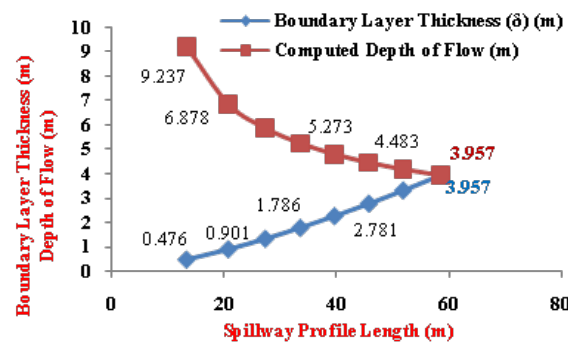
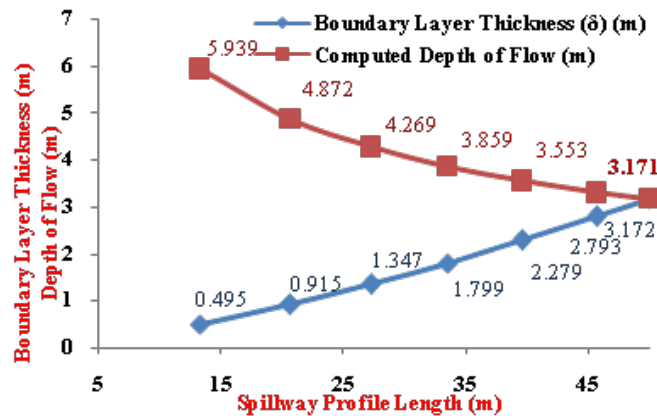


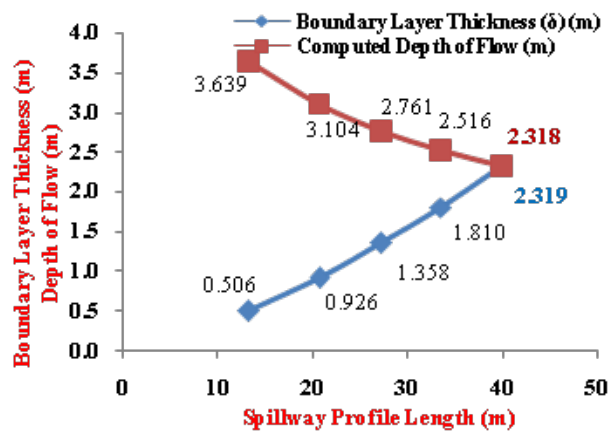
Fig. 2. WES Profile of Spillway



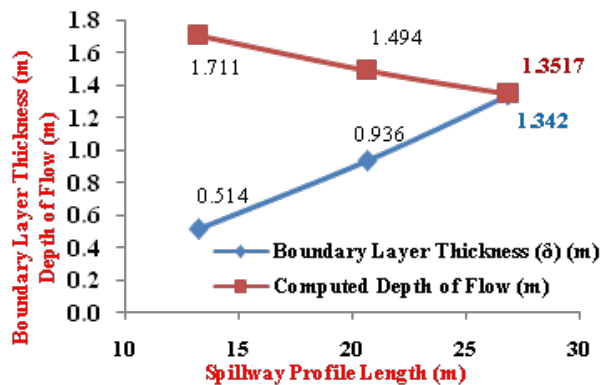
(a) Plot of 58,340 cumec



(b) Plot of 43,755cumec



(c) Plot of 29,170cumec



(d) Plot of 14,585cumec

Fig. 3. Intersection point of Boundary Layer and Depth of flow

It can be seen from the Table 2 that the distance of flow development is decreasing with the reduction in the design discharge over the spillway. Moreover, it is also observed that, even the thickness of boundary layer is decreasing for the reduced flow rates. This is due to the fact that, as the lead distance from the crest of the spillway is decreasing, the Reynolds number is decreasing. As a consequence of this, the thickness of boundary layer is decreasing.

Table 2. Boundary layer thickness values

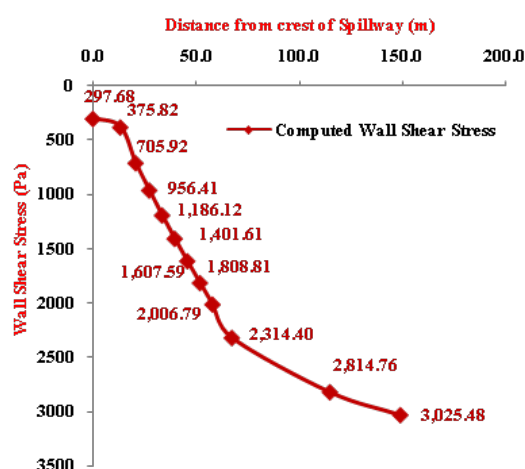
Discharge	Spillway Profile Distance	Velocity	Reynolds Number (R_x)	Boundary layer thickness (δ)	Depth of flow on the profile of spillway (y)
cumec	m	m/s	$\times 10^8$	m	m
58,340	58.755	31.144	18.38	3.978	3.978
43,755	49.926	29.301	14.57	3.172	3.171
29,170	39.888	26.710	10.62	2.319	2.318
14,585	26.848	22.913	6.13	1.342	1.352

The analytical estimations of wall shear stress were evaluated from the “equation (7)”. The values of computed wall shear stress are detailed in **Table 3**. The graph detailing the variation of wall shear stress from the crest of the spillway to the lip level of the bucket is shown in **Fig. 4**. Velocity reduction away from the boundary layer will be dependent on the magnitude of shear stress and is independent of how it arises.

The skin friction coefficient (C_f) is a component of profile drag, which is a resistant force exerted (on the spillway) and is useful in estimating total frictional drag exerted (on the spillway). The flow resistance over the spillway can be made use of in the design an energy dissipator, at the downstream end of the spillway.

Table 3. Computed wall shear stress values

Spillway Profile Distance (m)	Velocity (m/s)	Reynolds Number ($\times 10^8$)	Computed Wall shear stress (Pa)
13.232	13.412	1.77	375.8154
20.646	18.012	3.70	705.9213
27.231	21.019	5.70	956.4057
33.433	23.494	7.82	1186.1176
39.534	25.671	10.10	1401.6097
45.636	27.638	12.6	1607.586
51.737	29.450	15.2	1808.8093
57.838	31.144	18.2	2006.7861
67.154	34.743	23.2	2314.3997
114.584	43.753	49.9	2814.7607
148.661	44.345	65.7	3025.4808

**Fig. 4.** Analytical variation of wall shear stress



RESULTS AND DISCUSSIONS

The present study was carried out for Nagarjuna Sagar project.

- Analytical estimates were carried out to evaluate the intersection point of boundary layer thickness and depth of flow over the profile of the spillway.
- It is proved from the calculations that the thickness of boundary layer is decreasing with the reduction in the design discharge as well as with the lead distance from the crest of the spillway.
- The results of wall shear stress and skin friction coefficient are useful for the estimation of flow resistance that can be adopted in the design energy dissipators.

REFERENCES

1. Chadwick Andrew and John Morfett, Hydraulics in Civil and Environmental Engineering, E & FN Spon an imprint of Routledge, London, 1998, pp.415-430.
2. Chow, Ven Te, Open-Channel Hydraulics, McGraw Hill Book Company INC, New York, 1959, pp. 192-212
3. Gopal Rao M, Nagarjuna Sagar – The Epic of A Great Temple of Humanity, Bharatiya Vidya Bahvan, Bombay, Chapter-7, Design and Instrumentation, 1979, pp.137–140.
4. Stephen T. Maynard, General Spillway Investigation (Hydraulic Model Investigation), Technical Report, HL-85-1, Department of Navy, Waterways Experiment Station, U.S. Army Corps of Engineers, Mississippi, pp.4-10.
5. Falvey, H.T., Air-water flow in Hydraulic Structures, USBR Engineering Monograph, 41, 1980, pp.16-19.



Application of VH polarization Sentinel-1 Imagery for Flood Mapping of Bhagalpur, Bihar

Deepak Kumar*, Kumar Yuvraj

Department of Soil & Water Conservation Engineering, College of Technology, GBPUA&T Pantnagar, Pantnagar, Uttarakhand

*✉ deepak.swce.cot.gbpuat@gmail.com

ABSTRACT

Flood is generally a natural disaster which has a everlasting consequences in terms of loss of life and property. It is world's most pervasive hydrological threat that affects the conservation of resources, wildlife, economic activities etc. In this paper, flood mapping has been done for a very flood prone region of Bihar. Bhagalpur, which is situated on the southern bank of river Ganga. Sentinel-1 SAR (Synthetic Aperture Radar) images has been used for mapping the study area. The Sentinel-1 SAR imagery has been use for the month of September-October 2019. Sentinel-1 satellite operating in C-band is the major breakthrough in the development of SAR application. Vertical-Horizontal (VH) polarization configuration and Lee filtering 7×7 window sizes has been used and image processing has been done using SNAP. Two methods were applied to flood maps from Sentinel-1 SAR images: RGB (Red, Green, Blue colour model) composition based on the differences between the pre- and post-event images; and the calibration threshold technique or binarization based on histogram backscatter values. The result suggested that out of 2100 km² region selected for study, 907 km² areas was severely affected by flood.

Keywords: Sentinel-1; Flood mapping; SAR imagery; VH polarization; Bihar.

INTRODUCTION

With rapid urbanization, global warming, and growing demand on present services, infrastructures are now falling into the hazard-prone areas. Bihar susceptibility to floods can be understandable from the ongoing situation that floods in Bihar become an annual feature. Some or the other districts face flooding situations almost every year. Bhagalpur district is under severely affected flood prone district in Bihar which face flood every year. In present study, Sentinel-1 imagery is used to develop flood map of study area. Several researches has been done on using sentinel-1 imagery for flood study (Twele et al. 2016; Clement et al. 2018; Li et al. 2018; Uddin et al. 2019; Liang and Liu 2020). Bazi et al. (2005) used SAR images obtained from ERS-2 satellite to detect the flooded areas in the City of Pavia and City of Bern during the flood event of October 2000. Further, Borah et al. (2018) analysed the use of Sentinel-1 SAR images for flood inundation monitoring and mapping of the Kaziranga National Park (KNP) during the monsoon period in 2017. Dual polarized (VH, VV) SAR images were used to generate inundation map. The investigation observed that out of the total area within KNP, an area of 23,487.8 ha (61%) was under land features, 2270.31 ha (6%) under permanent water bodies and 12,660.28 ha (33%) was under monsoon flood. Hakdaoui, S. et al (2019) presented a technique to supervise wetland areas after the flash flood event in Laayoune city (Southern Morocco) situated in the arid region of Sahara Desert. The proposed method uses multi-sensor images i.e. SAR images and optical images to find the inundated land. The overall accuracy of the land cover map and flood inundation mapping was found to be 87.51% and 96.44% respectively. The total flooded area for April, June and August 2017 corresponded to 2.01%, 4.53% and 7.01% respectively. Similarly, Nasirzadehdizaji, R., et al (2019) mapped the flood event in Lake Urmia, Golestan Province and Khuzestan province of Iran during 2019. The GRDH Sentinel 1 C-Band SAR images with VH and VV polarization in Interferometric Wide (IW) swath mode were used for flood mapping. In the present study, the flood mapping.

STUDY AREA DESCRIPTION

Bhagalpur is the district in Bihar known as silk city of India (Kingsley 1897; Tannen 1986). The Bhagalpur district has population more than 30 lakhs with density closer to 1200 people per square kilometers (Minister of Home Affairs 2011).

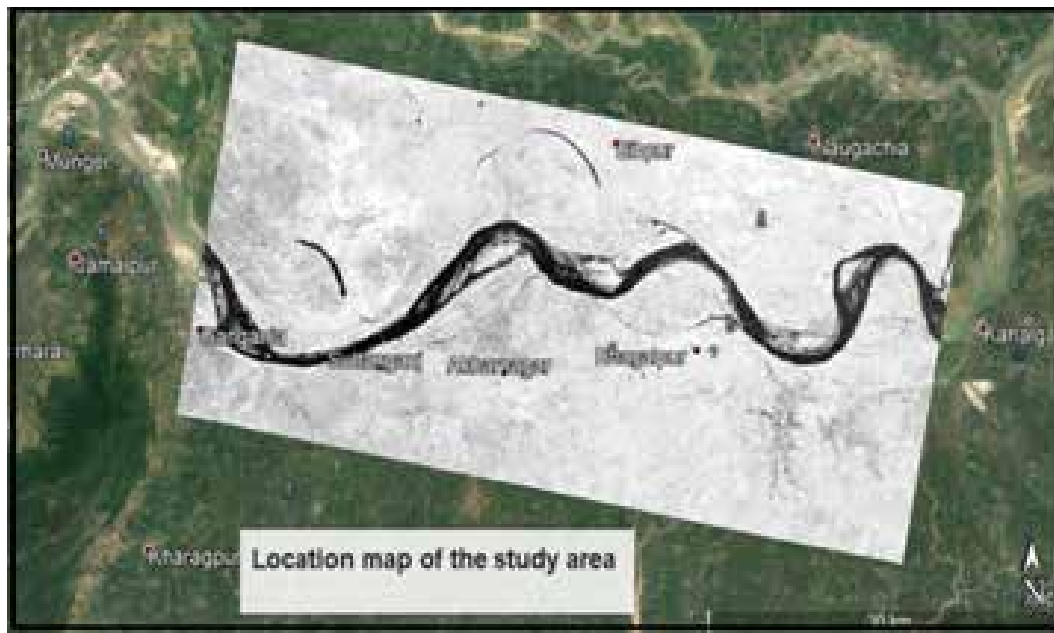


Fig. 1. Sentinel 1 imagery for Bhagalpur region

The river Ganga has been the lifeline of Bhagalpur (Bihar) (Agrawal 1994; Singh et al. 2003). The present study area is situated between 25.1070 – 25.4560 N latitude and 86.5720 – 87.2210 E longitude.

The study area is shown in **Fig. 1**. The Sentinel image has been taken for 2019. The processing of Sentinel 1 imagery has been done using SNAP (Sentinel Application Platform).

TOOLS USED FOR IMAGE PROCESSING

The processing of Sentinel 1 imagery has been done using SNAP (Sentinel Application Platform).

SNAP is a set of executable software and application programming interfaces (APIs) designed to enable the use, display and, analysis of a range of remotely sensed data. In this study, Sentinel-1 SAR images has been used because of their features, configuration, and the free data set available online from Earth Observation (EO) data resources. The Sentinel-1 sensor is part of an ESA (European Space Agency) satellite constellation. It is composed of Sentinel-1A, launched on 3 April 2014, and Sentinel-1B, on 22 April 2016. Both satellites have a useful life of 7 years and a 12-day orbital repetition cycle (6 days between them). These temporal limitations of image capture mean that we did not have images of the day of the highest level of the Ebro at the study points. The available image that was closest to the moment of maximum flood was from 13 April 2018 and it was the one used for the development of the study. Each image has a coverage range of 250 km with a 5×20 m resolution. The images are Level-1 Ground Range Detected (GRD) products; this means that they were detected, multi-looked, and projected to the ground range using an Earth ellipsoid model. The acquisition mode is Interferometric Wide Swath, and the images have a high resolution; the sensor pass is ascending, with incidence angles between 29° and 46° , and dual polarization, VV (Vertical-Vertical) and VH (Vertical-Horizontal). The study area is covered by VV and VH only according to the observation scenarios shown in Earth Observation Data Center for Water Resources Monitoring (EODC).

The pre-processing of sentinel 1 GRDH SAR images was performed in SNAP software using the Sentinel 1 toolbox. The flow chart for the same has been shown in Fig. 2. The post processing steps are done in QGIS software. Final flood mapping for this study area were obtained using VH polarization configuration and Lee filtering 7×7 window sizes. Two methods were applied to flood maps from Sentinel-1 SAR images: RGB (Red, Green, Blue colour model) composition based on the differences between the pre- and post-event images; and the calibration threshold technique or binarization based on histogram backscatter values.

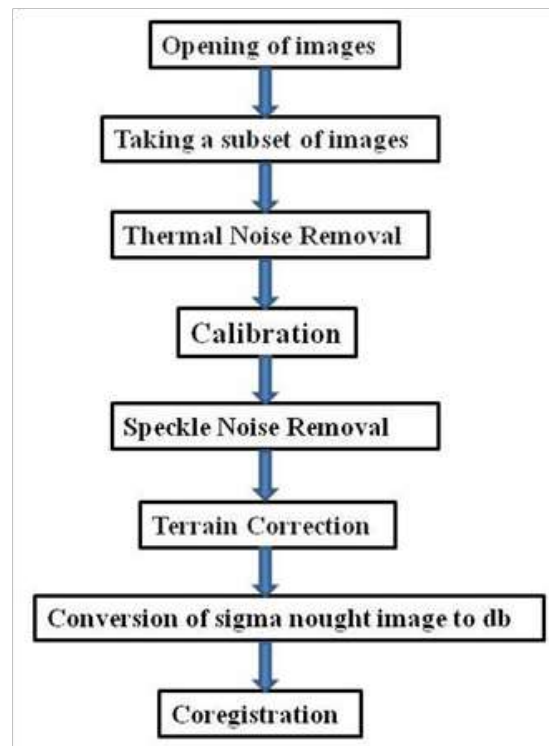


Fig. 2. Flow chart of image processing using SNAP

RESULTS AND DISCUSSIONS

For extracting the pixel having flood area, VH polarization Sentinel-1 image has been used. The histogram of pixel information has been shown in **Fig. 3**. To further specify the boundary point between the areas with water and without water, a water mask was generated on the VH polarization image. This layer was created by randomly capturing some flooded areas within zone 1 and subsequently generating a histogram. In this way, intensity values were obtained in which only areas with water or flooded areas are shown, independent of the frequency or number of pixels taken.

It should be noted that this layer serves only to confirm and verify the suitability of the threshold taken with the total histogram of the zone. It has been observed that most representative values of the presence of the water range mostly between -6.06 to -15 dB, so -6.06 dB was considered. The threshold taken was therefore set to -6.06 dB.

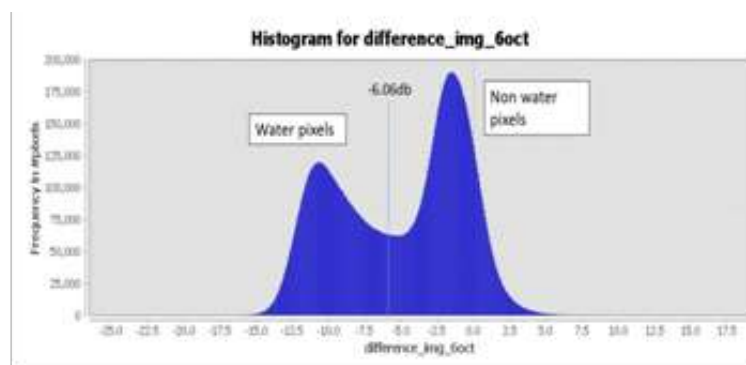


Fig. 3. Histogram of frequency of pixels

RGB flood map after image processing is shown in **Fig. 4**. The RGB composition is an appropriate method to visualize multi-temporal modifications and facilitates the detection of changes on the terrain surface through a temporal colour image. It is a

method based on the differences between the pre- and post-event images, and in which a combination of bands is set for these differences to become visually remarkable. These differences are defined by the change in the intensity value for the same pixel on different dates. The result is a multi-temporal image to which a band is assigned to each of the primary colours to form an image of RGB composition For **Fig. 4**, those areas, with intermediate intensity values and in which there have been hardly any variations, are consolidated in blue tones. The light pink tones are characteristic of areas with high humidity while the red ones represent the flood surfaces in which the water has completely flooded.

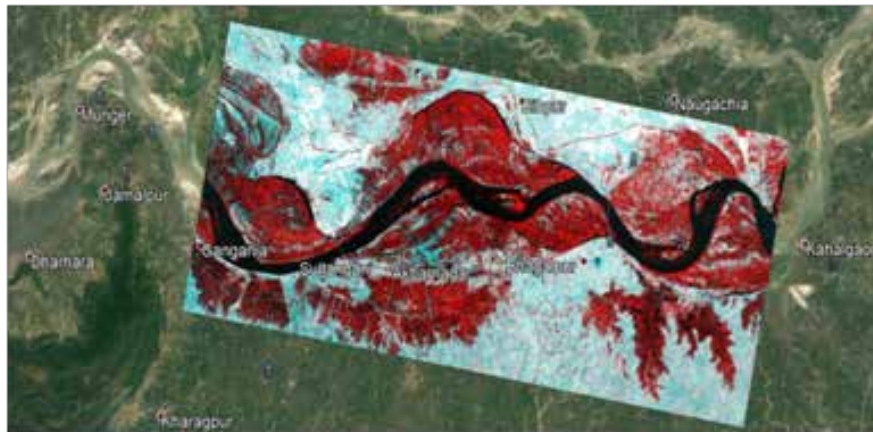


Fig. 4. RGB flood map

After conducting the pixel calculation on the study area, total number of image pixels under study were 772456 in which image pixels inundated with water or flood were 353762. Thus, in terms of area, study area comprises of 2100 km². The total inundated areas under flood were 907 km². Thus approximately 43% of the total area were under flood in Bhagalpur during the flood of 2019 in Bhagalpur.

Table 1. Estimated pixel count and representative area

S. No	Field	Pixel Count	Total area (km ²)
1	Total Study area	772456	2100 km ²
2	Flooded area	353762	907 km ²

CONCLUSIONS

Flood map of Bhagalpur has been done in study area for Bhagalpur region of Bihar. Bhagalpur is situated on the bank of Ganga river and usually in rainy season, it remain affected with flood. Sentinel-1 SAR data has been used for 2019 to study the severity of flood in this region. It has been estimated that out of 2100 km² of study area, 907 km² area was under flood.

REFERENCES

1. Tvele, A., Cao, W., Plank, S., and Martinis, S. (2016). Sentinel-1-based flood mapping: a fully automated processing chain. *International Journal of Remote Sensing*, 37(13), 2990-3004.
2. Clement, M. A., Kilsby, C. G., and Moore, P. (2018). Multi-temporal synthetic aperture radar flood mapping using change detection. *Journal of Flood Risk Management*, 11(2), 152-168.
3. Li, Y., Martinis, S., Plank, S., and Ludwig, R. (2018). An automatic change detection approach for rapid flood mapping in Sentinel-1 SAR data. *International journal of applied earth observation and geoinformation*, 73, 123-135.
4. Uddin, K., Matin, M. A., and Meyer, F. J. (2019). Operational flood mapping using multi-temporal sentinel-1 SAR images: a case study from Bangladesh. *Remote Sensing*, 11(13), 1581.
5. Liang, J., and Liu, D. (2020). A local thresholding approach to flood water delineation using Sentinel-1 SAR imagery. *ISPRS Journal of Photogrammetry and Remote Sensing*, 159, 53-62.



6. Bazi, Y., Bruzzone, L. and Melgani, F., 2005. An unsupervised approach based on the generalized Gaussian model to automatic change detection in multitemporal SAR images. *IEEE Transactions on Geoscience and Remote Sensing*, 43(4): 874-887.
7. Borah, S. B., Sivasankar, T., Ramya, M.N.S. and Raju, P.L.N., 2018. Flood inundation mapping and monitoring in Kaziranga National Park, Assam using Sentinel-1 SAR data. *Environmental monitoring and assessment*, 190(9), p.520.
8. Hakdaoui, S., Emran, A., Pradhan, B., Lee, C.W. and Nguemhe Fils, S.C., 2019. A collaborative change detection approach on multi-sensor spatial imagery for desert wetland monitoring after a flash flood in Southern Morocco. *Remote Sensing*, 11(9), p.1042.
9. Nasirzadehdizaji, R., Akyuz, D.E. and Cakir, Z., 2019. Flood mapping and permanent water bodies change detection using sentinel sar data. *International Archives of the Photogrammetry, Remote Sensing & Spatial Information Sciences*.
10. Kingsley, M. H. (1897). *Travels in West Africa: Congo Français, Corisco and Cameroon*, Macmillan.
11. Tannen, D. (1986). "That's Not. What I Meant! How Conversational Style Makes or Breaks Relationships." New York: Ballantine.
12. Agrawal, P. (1994). "Ganga Pollution Control." *Environment Protection and Pollution Control in the Ganga*, 99.
13. Singh, M., Müller, G., and Singh, I. (2003). "Geogenic distribution and baseline concentration of heavy metals in sediments of the Ganges River, India." *Journal of Geochemical Exploration*, 80(1), 1-17.



Performance based Design of Shear Ductile Wall with Custom Openings

Mohammad Suhail Saifi¹, Dr Khalid Moin²

PhD Student, Department of Civil Engineering, Jamia Millia Islamia , New Delhi¹.

Professor, Department of Civil Engineering, Jamia Millia Islamia, New Delhi²

✉ er.suhail.civil@gmail.com

ABSTRACT

High rise buildings now a days have become a common trend to accommodate the increasing population in the country. Executions of the shear walls along the exterior perimeter of high rise buildings enhance the efficiency of such buildings to resist the seismic excitations. But uncertainties in the locations of shear walls are very high because of the demandable architectural openings for door or windows in the exterior views of such buildings. So, this study presents a considerable interest in establishing design guide lines for numerical investigation of seismic response of shear walls taking into account such openings and their locations. Six models of different configurations of the openings in the frame structure are chosen and compared to figure out the best installation of custom openings having more efficiency on the performance of shear walls under seismic excitation.

The objective of this research is to compare the impact of shear wall in frame structure. To evaluate the performance of frames with shear wall and shear wall with openings, Response Spectrum Analysis and Non Linear Static Analysis (Pushover Analysis) performed. Parameters that are compared are Modal Time Period, Storey Displacement, , Base Shear, Maximum Displacement by using Response spectrum analysis, and parameters like Target displacement, and maximum displacement by Nonlinear Static Analysis i.e. Push over analysis. For the accomplishment of this study six different 10 storey shear wall RC frame models (Model 1 to Model 6) are considered with variable size of openings area of 7%, 13%, & 27% respectively. Analysis is carried out using standard package SAP 2000v.18.0.1. The comparative study of these models for different parameters are presented here.

Keywords: R C shear wall; Response spectrum analysis; Pushover analysis; Hinge formation; Performance point.

INTRODUCTION

Seismic design of structures is essential to improve the performance of buildings subjected to dynamic earthquake loads. In the last decades, seismic design has become more rational due to new knowledge provided by comprehensive research and the development of more efficient analysis techniques [1]. Many destructive earthquakes have been reported in past historical records that have devastated different parts of the world in different times. Earthquake is one of the hazard which results in the loss of properties and the human lives. It poses a unique engineering design problem for civil engineers. An intense earthquake constitutes severe loading to which most of the structures may possibly be subjected. The number of earthquakes occurs in the past history which causes the huge loss of life and economy.

The shear walls in structure may have openings for the windows, doors and duct spaces for functional reasons. The number, location and size of openings affects the behavior of a structure as well as stresses in the shear wall. It is necessary to use a fine mesh finite element model for an accurate analysis of a shear wall with openings. Research on efficient analyses of shear wall with openings has been undertaken [2-5].

OBJECTIVES

In general practice shear walls are provided at the sides or at the corners of buildings. Sometimes, the shear walls are arranged in the form of core. Core walls are generally used in staircases and lifts. In high rise buildings, shear walls to be located at different positions to fulfill the requirements. Therefore shear walls may have one or more openings depending upon the position of walls and purpose to be served. In Residential type of building, openings size and location in the shear wall are often decided without anticipating their negative impact on the system. Thus, the principal objectives of the present research are:



1. To conduct seismic analysis of building models with various types of lateral force resisting systems.
2. To compare the results of Response spectrum analysis for different parameters like displacement, time period and base shear.
3. To carry out non-linear static analysis to evaluate different building frames and to determine the possible location of plastic hinges/damages.

The scope of this study was limited to the following:

This study is to be done on 10 Story 5 X 5 bays frame-shear wall Residential buildings with 5-m span in X and Y Direction and floor to floor height is 3 meters, by using Response Spectrum Analysis and Non-Linear Static (Pushover) analysis.

1. Typical floor plan with same dimensions 25 m X 25 m is used for all model buildings.
2. Shear wall of 5 m X 3 m X 0.25 m is taken for evaluating the results for all the different building models using finite element methods.
3. For the research purpose, opening size is changed in shear wall and location is changed for same opening size.
4. Size and concrete grade used for all structural elements are same for all structural models.

In this study five Models of building created. All have a plan dimension of 25m X 25m, in each floors of 10 storey buildings. Floor height of each floor was to considered 3 m.

The standard package of SAP2000.V.18.0.1 [6]. is employed to investigate the effect of openings in the models considered in this study. Primarily building model analyzed by Response spectrum analysis, after passing of all structural members by using IS codes, we go ahead for Pushover analysis.

Performance point of the structure is to be obtained by superimposing the capacity spectrum on demand spectrum, the intersecting point of these curves is known as the Performance Point. The performance point is the point where the capacity and demand of the structure are equal. We can obtain the performance level of the structure and formation of plastic hinge at performance point [7].

Six structural models considered to study the effect of opening are summarized below in tabular form. In each model shear wall is assigned by meshing it into small area of size 0.5m x 0.5m. From this meshed shear wall area opening is created by deleting small fragmentation of meshed area of required size.

Table 1. Models consider for analysis

Model No.	Opening Size (m)	Opening Percentage	Horizontal eccentricity In storey & above storey (m)
M-1	0	0%	0
M-2	1×1	7%	0
M-3	1×2	13%	0
M-4	1×2	13%	1.5 & -1.5
M-5	2×2	27%	0
M-6	2×2	27%	1 & -1

The above table describes the structural models considered for analysis with increase in opening size in shear wall. The openings are created in the centre of wall and with horizontal eccentricity in opening is provided.

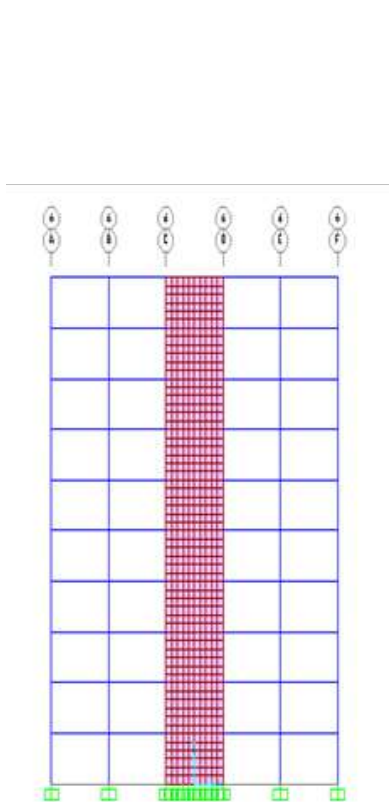


Fig 1 (a) : Front view of 1st Model

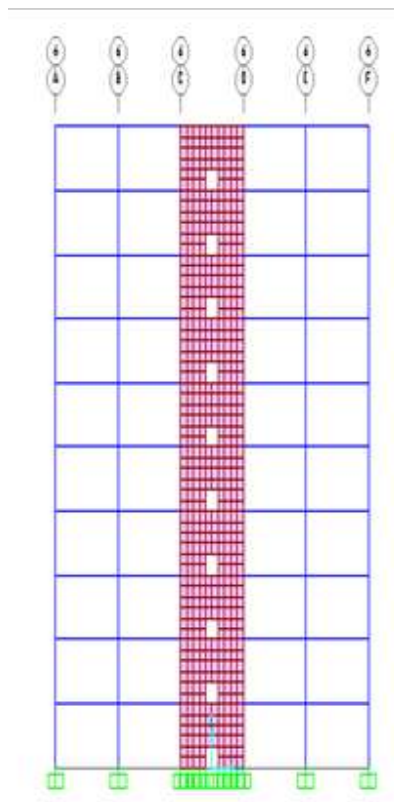


Fig 1 (b) : Front view of 2nd Model

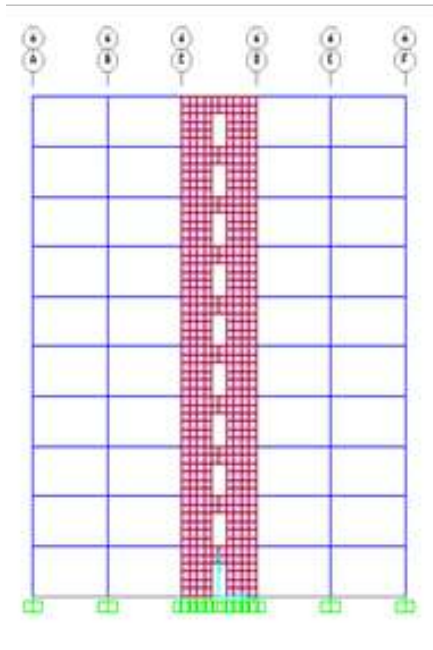


Fig 1 (c) : Front view of 3rd Model

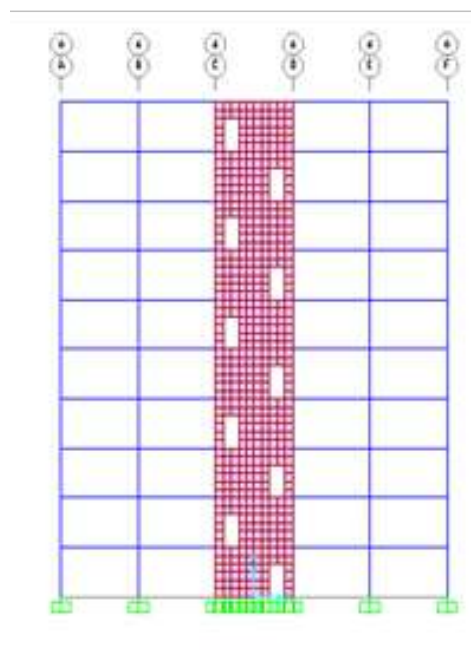


Fig 1 (d) : Front view of 4th Model

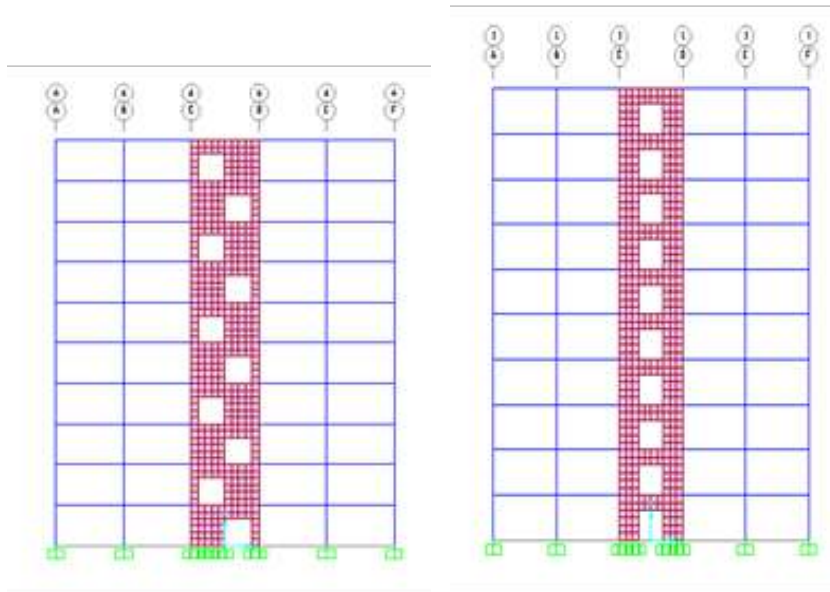


Fig 1 (f) : Front view of 5th Model

Fig 1 (e) : Front view of 6th Model

Since the type of building taken in this study was Residential with dual system (shear wall and special moment resisting frame) located IVth zone of Quake,

Zone factor (Z) = 0.24, Response reduction factor (R) = 5 and Importance Factor (I) = 1, and as given in IS code (Appendix A) were used for lateral load calculations. Assuming hard type of soil on which the foundations rest and the damping ratio of 5% for concrete structure [8].

Material Property

The material properties of any member consists of its mass, modulus of elasticity unit weight, shear modulus, and Poisson's ratio. Various material properties considered for the analysis are given below:

1. Grade of concrete for beams and columns = M30
2. Grade of concrete for slabs and shear walls = M30
3. Grade of Steel = Fe500
4. Modulus of Elasticity of Concrete (E) = 2.5×10^4 N/mm² for M25 grade of concrete.
5. Modulus of elasticity (E) = 2.738×10^4 N/mm² for M30 grade conc.
6. Poisson's ratio taken as (ν) = 0.2

Unit weight of Concrete (γ) = 25 kN/m³

Structural Members

Beams and columns are modeled by 3D frame elements. Beam-Column joints are considered to be rigid. The column end at foundation level assumed to be Restrained in all directions for the models considered in this study. To utilized the effect of in-plane stiffness rigid diaphragm assigned on each floor level.

Section properties considered for various elements of the structure are as follows:

1. Column size: 0.5 m \times 0.7 m
2. Beam size: 0.30 m \times 0.45 m
3. Slab thickness: 0.150 m
4. Shear wall thickness: 0.25 m

Base shear of the structure is also calculated manually to verify the analytical results by using the formula [8].

$$V_B = A_h \times w$$

where A_h is a horizontal seismic coefficient and w is the seismic weight of the building. Seismic weight for Model-1, Model-2 and Model-5 manually calculated as 109680KN, 109555KN and 109180KN respectively.

Horizontal seismic coefficient expression is given as

$$A_h = ZIR/2R_g$$

value of A_h is calculated as per the seismic definitions for the considered zone, structural system and importance of building is 0.034. Now the base shear can be calculated by above formula as 3729.1 KN, 3724.9 KN & 3712 KN which is approximately equal to the base shear obtained by the software result as tabulated in table no-3.

Base shear distributed along the height of the building can be calculated by the expression is given here.

$$Q_i = V_B \times \frac{W_i h_i^2}{\sum W_i h_i^2}$$

After analyzing models in SAP2000 using response spectrum analysis for zone IV for various load combinations given in IS 1893 (Part 1), final dimensions mentioned above for the structural elements for further analyses of the buildings were obtained. The maximum percentage of reinforcements for columns and walls was limited to 4% of concrete gross area as per IS 456: 2000 [9]. Maximum story drift due to design lateral force with partial load factor of 1 was limited to 0.004 times the story height as given in IS 1893 (Part 1). Similarly, the maximum nominal shear stress in shear wall due to factored loads was limited to $0.2f_{ck}$ for wall with largest opening area used for this study. Then, the developed models were analyzed for each size and location of openings in shear walls to evaluate the effects of openings in shear wall on stiffness as well as on seismic responses of the frame-shear wall structures.

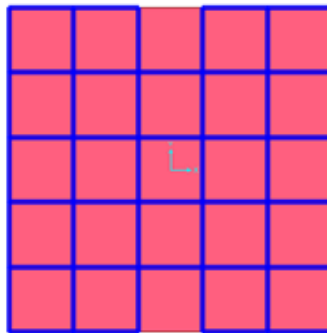


Fig. 2. Typical plan (25×25) of building models of RC frame shear wall structures

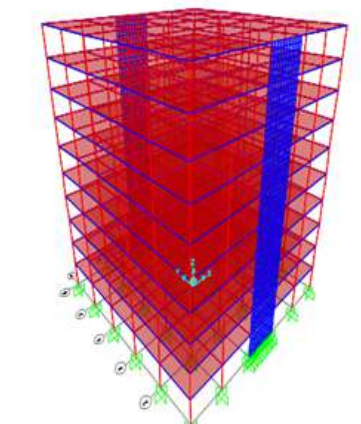


Fig 3. 3D view for 10-story building with frame-shear wall structures

RESULTS AND DISCUSSIONS

Various structural parameters such as storey displacement, base shear, modal time period, target displacement of the structures are presented here in tabular and graphical form and compared between six different structural models considered for analysis. Results of non linear static analysis (pushover analysis) are also compared for different models and plot of capacity curve is shown.

RESPONSE SPECTRUM ANALYSIS RESULTS

Table 2. Storey Displacement for different models

Storey Displacement (mm) in X-direction						
Storey Level	M-1 U1 (mm)	M-2 U1 (mm)	M-3 U1 (mm)	M-4 U1 (mm)	M-5 U1 (mm)	M-6 U1 (mm)
10th	37.12	37.50	38.38	40.16	42.8	44.60
9th	33.7	34.09	35.13	36.56	38.80	40.32
8th	29.74	30.15	31.26	32.53	35.04	36.28
7th	25.46	25.88	27	28.08	30.74	31.76
6th	20.95	21.35	22.41	23.31	25.0	26.84
5th	16.34	16.70	17.70	18.34	21.3	22.68
4th	11.80	12.13	13	13.38	16.02	18.50
3th	7.58	7.84	8.52	8.7	9.06	10.54
2nd	3.96	4.14	4.58	4.60	6.55	7.15
1st	1.27	1.34	1.5	1.48	1.65	1.89
Base	0	0	0	0	0	0

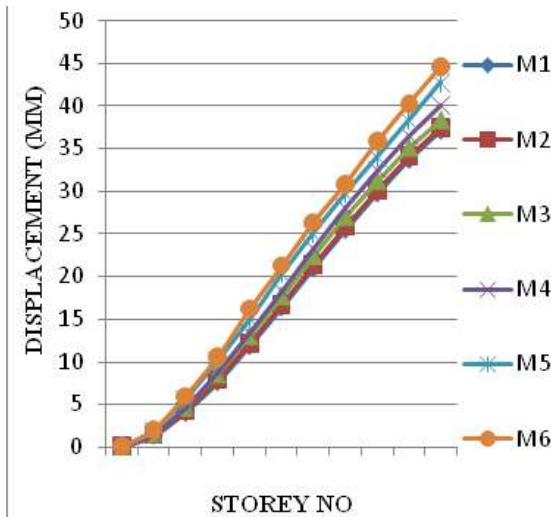


Fig 4. Storey displacement plot for different models

Table 3. Parameters like Time period, Base shear and maximum Displacement for Response Spectrum Analysis is shown below in tabular form

S. No	Parameters		M-1	M-2	M-3	M-4	M-5	M-6
1	Time Period (T) sec	Mode 1	1.638	1.638	1.639	1.639	1.638	1.649
		Mode 2	1.189	1.198	1.222	1.2458	1.2807	1.279
		Mode 3	1.101	1.110	1.133	1.157	1.192	1.192

2	Base Shear (KN)	In X Dir.	3731	3725	3720	3720	3709	3709
		In Y Dir.	3731	3725	3720	3720	3709	3709
3	Max Displacement (mm)	In X Dir.	37.1	37.5	38.3	40.1	42.8	44.6
		In Y Dir.	58.3	58.3	58.4	58.6	58.6	58.7

Base shear shows a decreasing pattern as the size of the opening increases in both the directions. This may be due to the decrease in gravity load due to reduction in size of shear wall. The maximum displacement of top storey of building structure increase in x-dir. as the size of opening increase. To confirm the accuracy of the results base shear for Models M1, M2 and M5 were manually calculated and approximately equal to the results of software model.

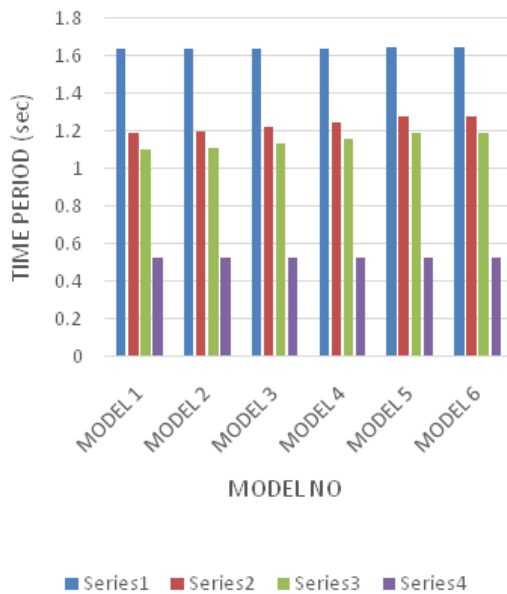


Fig 5. Bar chart of time period for different models

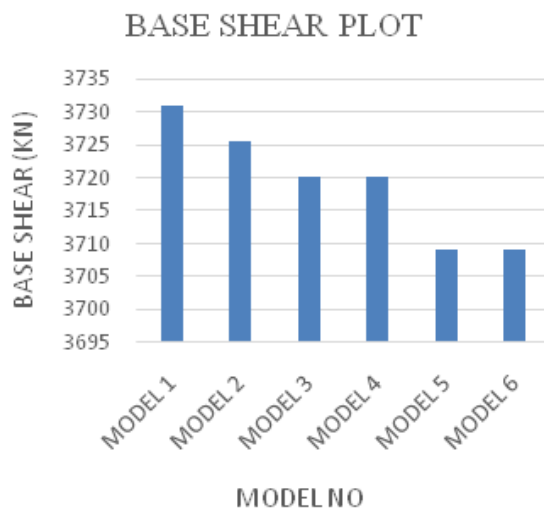


Fig 6. Bar chart of Base Shear for different models

PUSHOVER ANALYSIS RESULTS

A Nonlinear Pushover analysis carried out on these six considered building model as per IS standard by putting the values of C_a (coefficient of acceleration) and C_v (coefficient of velocity) equal to $Z/2$ (where Z is zone factor).

The Pushover curve obtained by analyzing the building models by static pushover analysis is shown below.

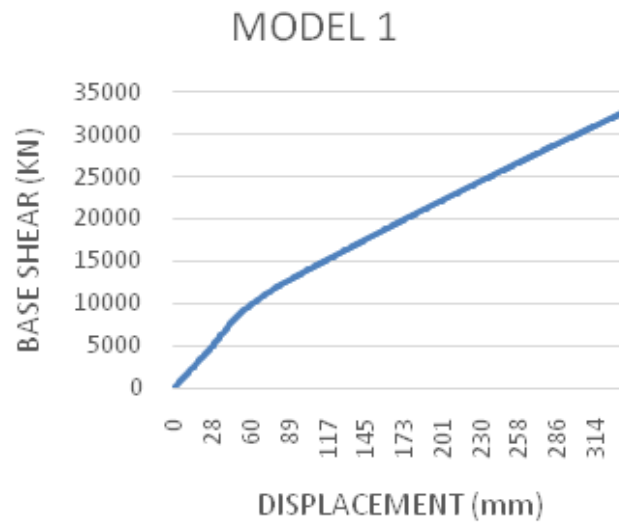


Fig 7(a). Pushover curve for 1st model

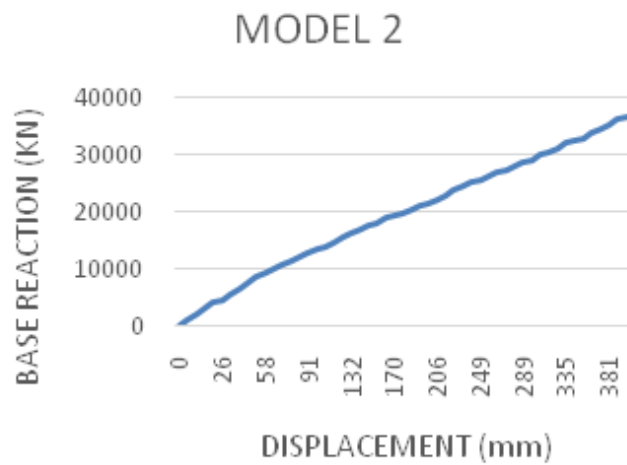


Fig 7(b). Pushover curve for 2nd model

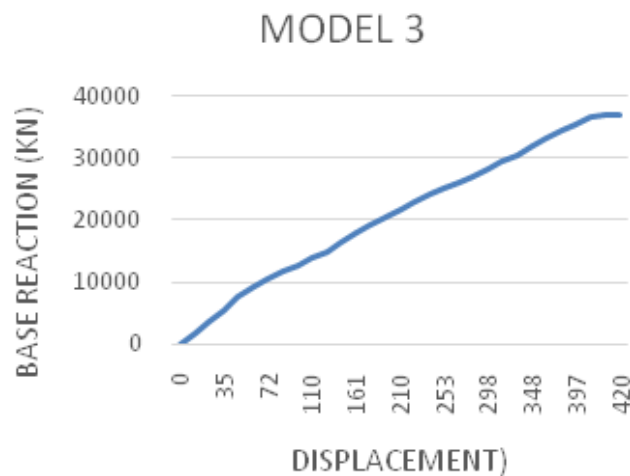


Fig 7(c). Pushover curve for 3rd model

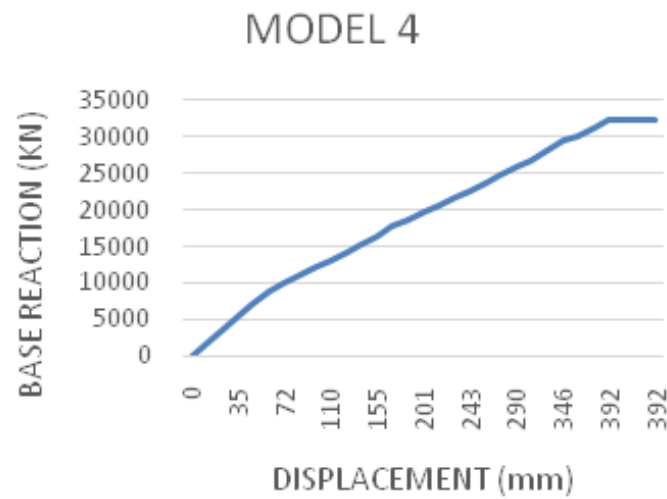


Fig 7(d). Pushover curve for 4th model

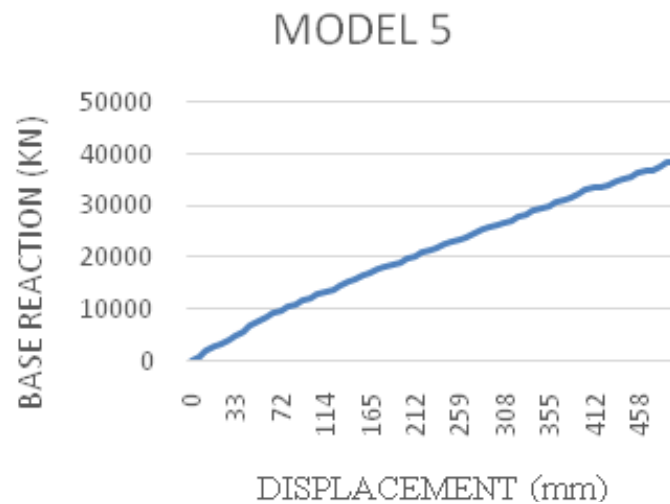


Fig 7(e). Pushover curve for 5th model

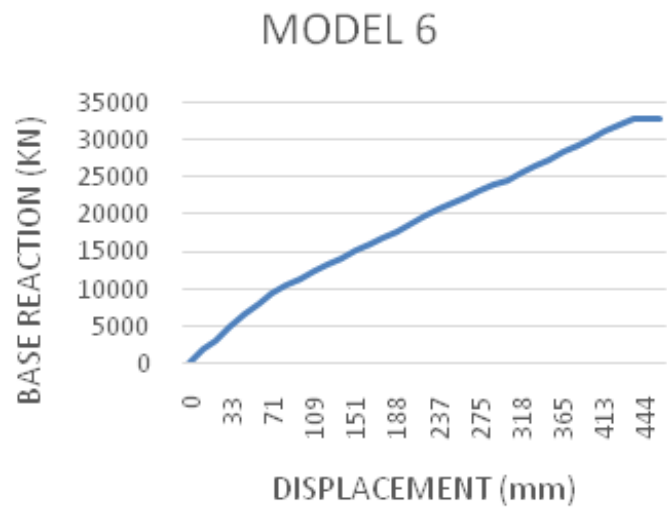


Fig 7(f). Pushover curve for 6th model

The Pushover curve for different structural model shown in **Fig.7** depicts that the ultimate displacement for the top storey in building models keeps on increasing with the increase in opening size and base shear shows a decreasing pattern with the increase in size of openings.

HINGES FORMS AT PERFORMANCE POINT IN DIFFERENT BUILDING MODELS BY PUSHOVER ANALYSIS

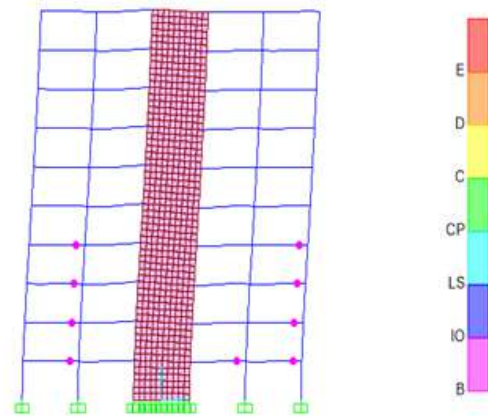


Fig 8(a). Hinges forms at Performance point in 1st model

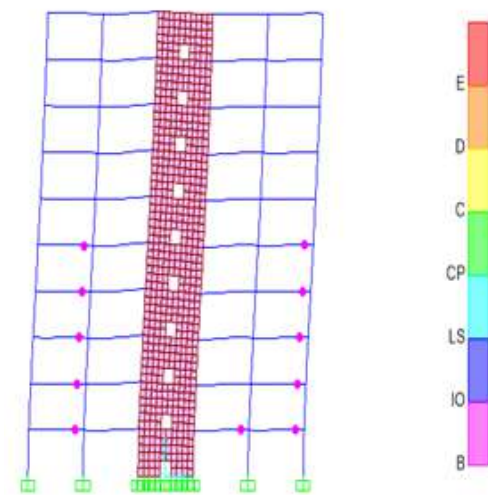


Fig 8(b). Hinges forms at Performance point in 2nd model

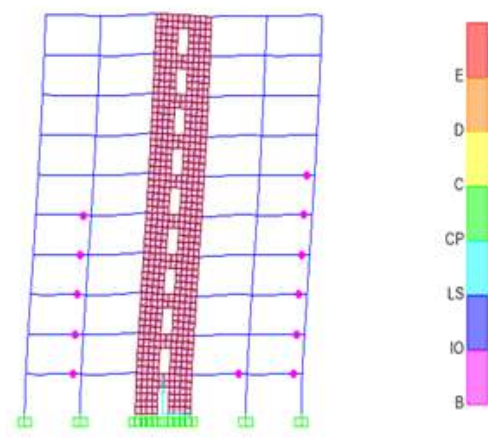


Fig 8(c). Hinges forms at Performance point in 3rd model

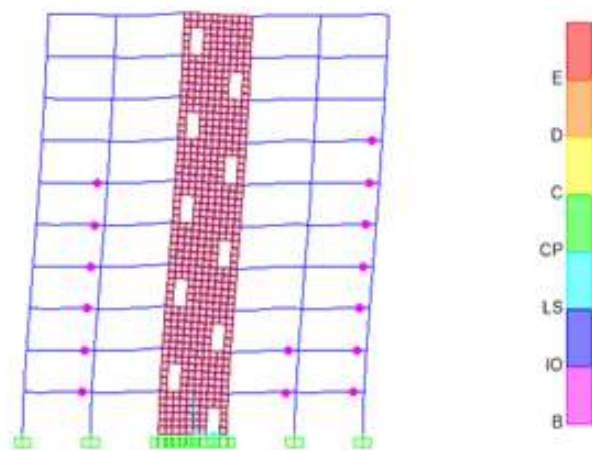


Fig 8(d). Hinges forms at Performance point in 4th model

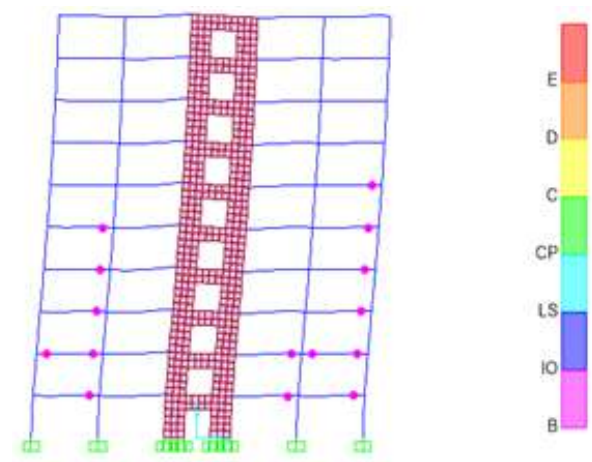


Fig 8(e). Hinges forms at Performance point in 5th model

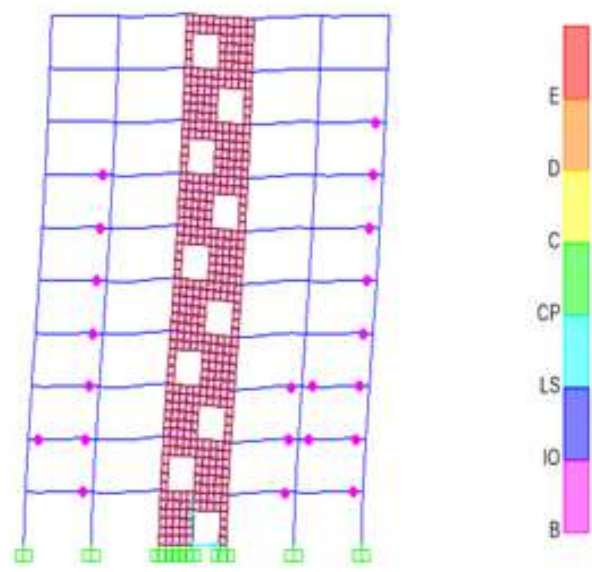


Fig 8(f) : Hinges forms at Performance point in 6th model.



DISCUSSION AND CONCLUSION

In this work, Response Spectrum analysis and non linear static analysis (Pushover analysis) is performed on a 10 storey building models to see the effects of openings in RC shear wall frame structure. It has been found that increase in opening size has big effect than by changing the position of opening area in the shear wall. Increasing size of openings also affects the strength of wall in big proportion.

The following Conclusions are summarized on the basis of numerical results.

1. The RC shear wall has high in-plane stiffness and strength, which can be utilized simultaneously to resist large horizontal forces and supports gravity load.
2. Symmetrically placed shear walls reduces the ill effect of Torsion in the building.
3. The observed maximum displacement of top storey in case of response spectrum analysis is found 20.15% more in case of 27% opening area of shear wall than the shear wall without an opening. This change in maximum displacement of top storey is 32.65% in case of pushover analysis.
4. Similarly the displacement value increases to 6% when we provide an opening area of 13% at a horizontal eccentricity of 1.5m from centre of wall as compared to no horizontal eccentricity. This change in maximum displacement of top storey is 8.5% in case of pushover analysis.
5. It is to be recommended that the opening in shear wall should be at center of the shear wall or with a very small eccentricity for the better performance of the structure under the seismic excitation.
6. It has been seen that no. of hinges forms at Performance point going to increase as well as the size of opening in shear wall increases. The hinge formation shows the weak members of the structure.

REFERENCES

1. David Ugalde, Diezo Lopez-Garcia "Behaviour of Reinforced concrete shear wall buildings subjected to large earthquakes". Procedia Engineering (Elsevier) 199 (2017)3582-3587.
2. Amaruddin M. "In-plane stiffness of shear walls with openings". Building and Environment 1999;34:109–27.
3. Choi CK, Bang MS. Plate element with cutout for perforated shear wall. Journal of Structural Engineering 1987;133(2):295–306.
4. Tham LG, Cheung YK. Approximate analysis of shear wall assemblies with openings. The Structural Engineer 1983;61B(2):41–5.
5. Ali R, Atwall SJ. Prediction of natural frequencies of vibration of rectangular plates with rectangular cutouts. Computers & Structures 1980;12:819–23.
6. Computers and Structures (2003). "SAP2000: Integrated Software for Structural Analysis and Design", Computers and Structures, Inc. (<http://csiberkeley.com>), Berkeley, CA, U.S.A.
7. Chopra A K., (2001). "Dynamics of Structures-Theory and Application to Earthquake Engineering", Prentice Hall of India Pvt. Ltd.
8. IS 1893 (part1). "Indian Standard Criteria for Earthquake Resistant Design of Structures", Fifth Revision, Bureau of Indian Standards, New Delhi.
9. IS 456:2000 "Indian Standard Plain and Reinforced Concrete Code of Practice", Fourth Revision, Bureau of Indian Standards, New Delhi.

Design of Framed Foundation for Absorber in Flue Gas Desulphurization System

R L Dinesh, Ranjit P Kangralkar*, Sandhya Krishnamurthy, Rohit Pantoji

Civil Department, TATA Consulting Engineers Limited, Bangalore

*✉ rpkangralkar@tce.co.in

ABSTRACT

Flue Gas Desulphurization (FGD) system is required to be provided for all operational thermal power plants and the new plants being operational in future for meeting the new guidelines laid by Ministry of Environment Forest and Climate Change. FGD system provides the “Environmental Sustainability” by reducing the SO₂ gas liberated to the atmosphere which is a health hazard causing respiratory infections, eye irritation, breathing difficulty, asthma, etc. Absorber (scrubber) is the heart of the FGD system wherein the SO₂ reacts with lime and the concentration of SO₂ emission reduces from the flue gas. Absorber structure needs to be supported on a rigid foundation. This paper describes a case study for the selection of type of foundation for absorber structure with a view to provide a cost effective and eco-friendly sustainable solution.

Keywords: FGD; Absorber; Scrubber; Rigid foundation; Ash.

INTRODUCTION

Flue Gas Desulphurization (FGD) system is required to be provided for all operational thermal power plants and the new plants being operational in future for meeting the new guidelines laid by Ministry of Environment Forest and Climate Change (MOEF & CC) [1]. The FGD system being a retrofit to the existing power plants and is to be provided within the available space; for old power plants there is a space constraint to locate various structures within the available area. It is experienced in most of the power plants that space for this retrofit is identified in ash filled areas which is leading to deep foundations with removal of ash deposition. For better performance to FGD system, it is necessary to support the structure on a rigid foundation system with very low displacement of soil below the Absorber base slab.

DESIGN REQUIREMENTS

- 1) The OEM [2] requirement was a rigid base slab which can support bottom structural steel plate of 16.3m diameter with a complete contact so that the bottom plate will not deflect due to the lime/gypsum slurry load.
- 2) The EPC specification from owner did not have any specific requirement for absorber foundation. However, it was specified that any storage tank resting on ring foundation shall have a compacted sub base made with layers of sand with concrete base slab to support the bottom plate.

DESIGN APPROACH

A conventional foundation for the absorber is with the similar concept of the large tanks supported on the ring wall as shown in **Fig 1**. The area within the ring wall is backfilled with well compacted natural sand. This backfilling is done in layers so that the required relative density is achieved and there is no settlement of the bottom plate due to large dead load intensity arising from the lime slurry weight inside the absorber.

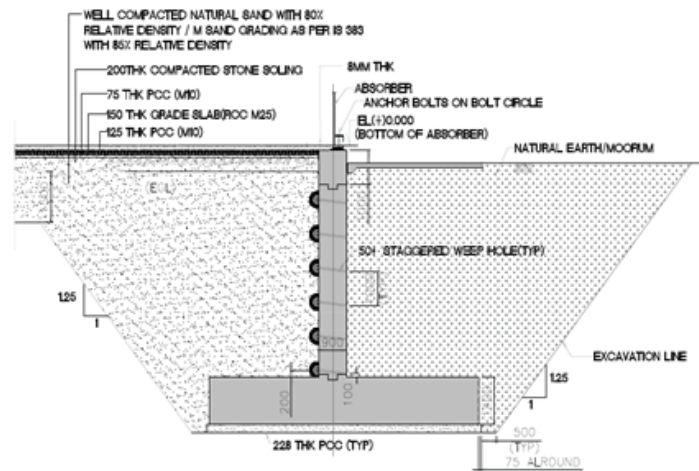


Fig. 1. Conventional design as ring wall foundation

The arrangement considered by the client during bidding was rigid pile cap (2m thick) at ground level with 100 piles per unit for this foundation. The location of the structure is in the ash filled area of nearly 6m depth. Proposed RC Chimney of height 200m is adjacent to the Absorber structure and excavation up to 7m depth was required for Chimney pile cap. This would result excavation in the Absorber area and subsequent backfilling. As the proposed piles of Absorber foundation would be in backfilled material there would be drastic reduction in lateral capacity of the piles. So, there was a requirement of alternative solution which would be cost and time effective.

Considering the requirement of the rigid base at the bottom of the absorber a framed foundation was conceptualized. It was suggested to adopt open foundation with underground framed structure to support absorber as the required bearing capacity was available at nearly 9m below ground level as shown in **Fig 2**. The conceptual sketches were submitted to the OEM and Owner. The detailed analysis and design were further carried out after the acceptance of the concept.

A 3-dimensional model using plate elements and beam elements was created for analysis using FEM analysis tool (Refer **Fig 3**).

Concrete of grade M25 is considered based on the exposure condition as per IS:456 [3] and Reinforcement of Grade Fe500 conforming to IS:1786 [4] is considered for the design.

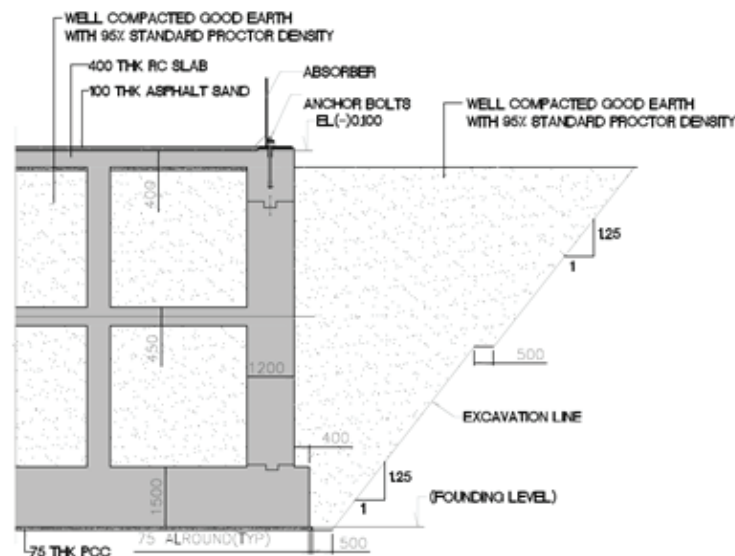


Fig 2. Rigid framed foundation – structural configuration

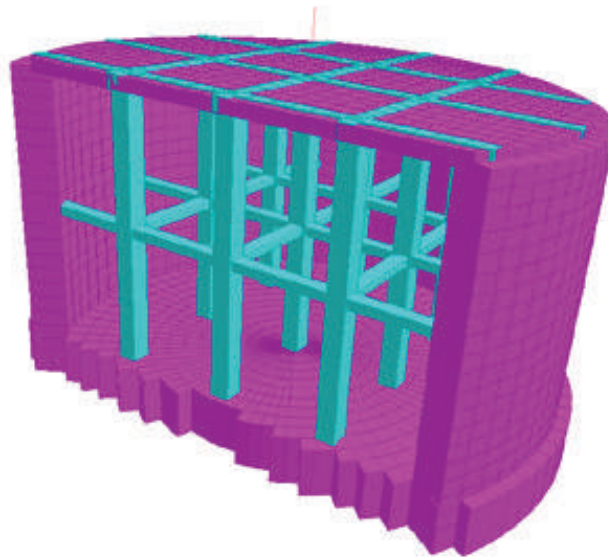


Fig 3. Rigid framed foundation – analysis model

LOADS ON THE FOUNDATION

All the loads provided in the Load Data [6] by the absorber manufacturer are considered for the analysis and design of the foundation.

- 1) Dead Load – This load includes the load due to self-weight of the structure along with its various platforms.
- 2) Imposed load – This load is arising due to the live load on the platforms & roof of absorber
- 3) Gypsum Slurry Load – This load is generated from the Gypsum Slurry present inside the absorber. The intensity of this load is 87.5kN/m² over the top slab of the foundation system.
- 4) Wind Load – This is the load acting on the surface of the absorber structure
- 5) Seismic Load – This load is generated due to the seismic effect on the structure. Gypsum load in liquid and solid conditions have been considered in two separate load cases.
- 6) Load generated on the anchor bolts due to internal pressure & internal suction have been considered in the design

LOAD COMBINATIONS

Absorber foundation was analysed for following load combinations

- 1) Foundation sizing- Load combinations as specified in IS: 875 Part-5 [5] with unit load factors
- 2) Load combinations and load factors for Limit state method as per IS: 456 [3]

CONCLUSION

The rigid framed foundation does not require sand filling within the ring wall as the absorber will be supported on a structural system and only well compacted good earth/ash is used for filling to overcome the uplift due to ground water table. This design has saved usage of 5000 cubic meter of natural resources like river sand (for four units) leading to an eco-friendly solution. The concept adopted meets the requirement of OEM, Contract Specification and the Codal Provisions with a considerable saving of construction time and cost in installation of 400 piles. The concept has saved concrete material, which has not only directly contributed to saving of natural resources like aggregates, water and sand but also contributed indirectly to reduction of carbon foot print because of lesser usage of cement.

ACKNOWLEDGMENT

We are thankful to our organization TATA Consulting Engineers Ltd., for encouraging us to adopt this innovative approach. We



are grateful to our customer for adopting this new approach for such important structure like absorber by taking appropriate approvals from various stakeholders of the project.

REFERENCES

1. Norms for installation of FGD for new environmental regulations - 7th December-2015 – Notification by Ministry of Environment Forest and Climate Change (MOEF & CC) Government of India.
2. Original Equipment Manufacturer (OEM) & the technology partner for the project.
3. Indian standard code for Plain and Reinforced concrete: Code of practice, IS 456: 2000(R2016), Bureau of Indian Standards, New Delhi.
4. Indian standard code for High strength deformed steel bars and wires for concrete reinforcement - Specification, IS 1786: 2008(R2018). Bureau of Indian Standards, New Delhi.
5. Indian standard code for Code of practice for design loads (other than earthquake) for buildings and structures: Special Loads and Combinations, IS 875 (Part 5): 1987 (R2018). Bureau of Indian Standards, New Delhi.
6. Data sheet, general arrangement and foundation load data for Absorber.
7. Indian standard code for Criteria for earthquake resistant design of structures: General Provisions and Buildings, IS 1893 (Part 1): 2016. Bureau of Indian Standards, New Delhi.
8. Indian standard code for Criteria for earthquake resistant design of structures: Industrial structures including Stack -like structures, IS 1893 (Part 4): 2015. Bureau of Indian Standards, New Delhi.
9. Indian standard code for Code of practice for and construction of foundations in soils: General Requirements, IS 1904: 1986 (R2018). Bureau of Indian Standards, New Delhi.



Simulation of Earthquake Forces for Equipment Supported on Structure

Papia Mandal, K Madhavalatha, Anurag Sinha

Structural Division, Engineers India Limited, New Delhi

✉ papia.mandal@eil.co.in

ABSTRACT

Heavy vertical equipments are supported on structures, in many process units of hydrocarbon plants. Apart from the operating weights of the equipments, earthquake forces acting on the equipments become critical for structural design. For the purpose of structural design, earthquake forces of equipments are taken from the mechanical data sheet. As a general practice, during mechanical design, equipments are assumed to be resting on fixed base support, whereas structures that support the equipments have certain amount of flexibility. Further structural designs are performed by 3D analysis of structures with various equipment loads including earthquake forces. Thus, boundary conditions considered for mechanical design of equipment and load transfer mechanism for structural design are contradictory. This results in over design of structure including the foundation system. Ideally, earthquake forces on equipment should be determined by the method of floor spectra, i.e. generating an alternate spectral curve at the structural floor level, supporting the equipment. Spectral curve on the structural floor and earthquake forces thereof is expected to be more relaxed due to flexibility of the supporting structure. Due to complex nature of analysis involved in generating floor spectra, and interface issues of equipment-structure integrated analysis, presently this method is not in common industry practice. The aim of the study presented in this paper, is to estimate actual earthquake forces for the equipments supported on structure, in absence of floor spectra and its further implications on structural design

Keywords: Earthquake forces; Floor spectra; Equipment supporting structures; Equipment-structure integrated analysis.

INTRODUCTION

In process units of hydrocarbon plants, heavy equipments are supported on structures. Along with the heavy operating weight of the equipment, huge earthquake force acting on the equipment becomes critical for designing the structure as well as the foundation system.

Sometimes, mechanical design of the equipments is done considering equipment supporting base to be fixed. However, in reality equipment being supported on the structures with certain amount of inherent flexibility, equipment supporting bases are also flexible to some extent. This conceptual difference in boundary condition of equipment causes additional amount of earthquake forces/ moments at equipment base level. Thus results in over design of equipment along with the structure and the foundation system.

The aim of this paper is to explore alternate methods of analysis to estimate the actual earthquake force on the equipments. Further implications of the earthquake forces, obtained from various analysis methods, and on structure and foundation system are studied. The focus of analysis shall be on two aspects, firstly, estimating earthquake base shear of equipment along with supporting structure and secondly, cost implication on the supporting structure and foundation system. Though there are few papers available on seismic design of equipments [1] or earthquake forces on equipments [2], above mentioned aspects are not covered in the studies.

STUDY DESIGN

Following approach of analysis is adopted to estimate the earthquake base shear of equipment including supporting structure. Details of equipment and supporting structure are tabulated in **Table 1**.

Approach-I: Earthquake forces, as per Mechanical Data Sheet are applied on the structure (**Fig. 1a**) for analysis.

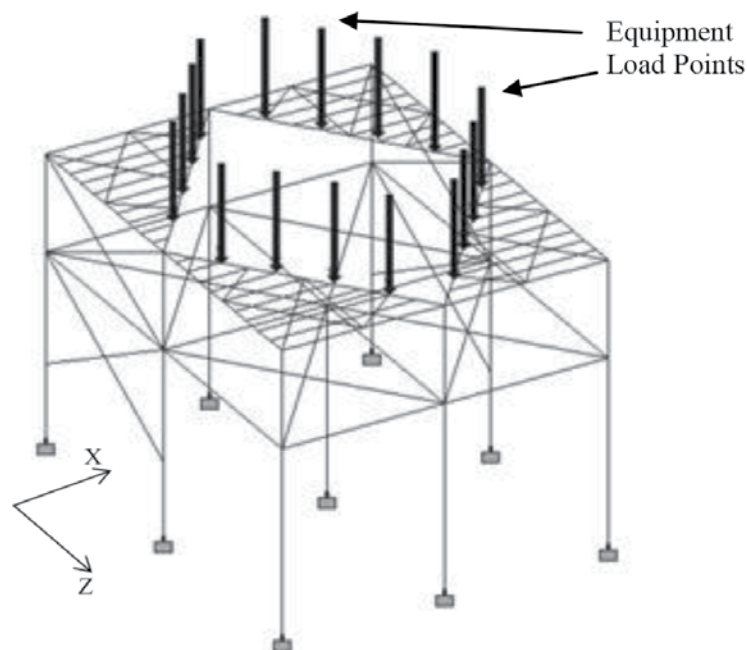
Approach-II: Equipment operating weight is lumped at the C.G. of the equipment and connected to the structure through rigid link at anchor bolt locations (**Fig. 1b**) for further analysis.

Approach-III: FEM modeling of equipment is performed through plate element. Segment-wise thickness of the plate elements are assigned to get equivalent operating weight of the equipment maintaining its C.G. (**Fig. 1c**) for integrated analysis.

Table 1. Equipment-structure details

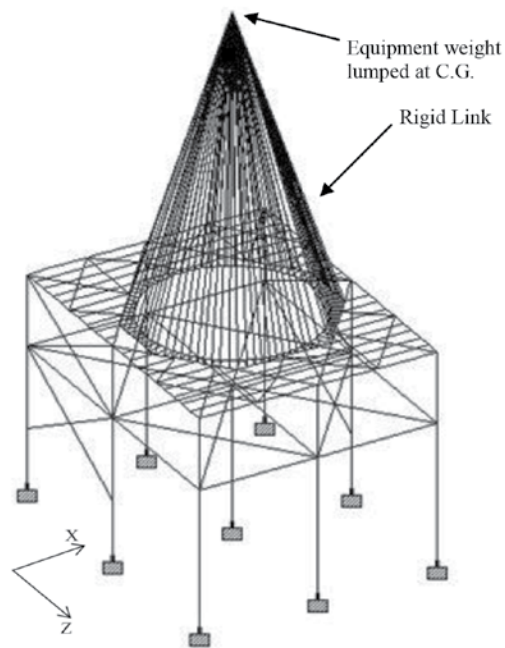
Configuration of the Structure		
Description	Direction-X	Direction-Z
No of Bays	2	2
Bay Length	8 M	10 M
Frame Type	Moment Frame	Braced Frame
Equipment Supporting	11M Above Grade Level	
Detail of the Equipment:		
Overall Height	56 M	
Inner Diameter	11 M	
Operating Weight	3146 Mt	

For this purpose, earthquake response spectrum analysis is performed on a 3D-framed structure. Base shear is obtained at the foundation level. Thus, base shear includes effect of earthquake forces on both of the equipment as well as the supporting structure.

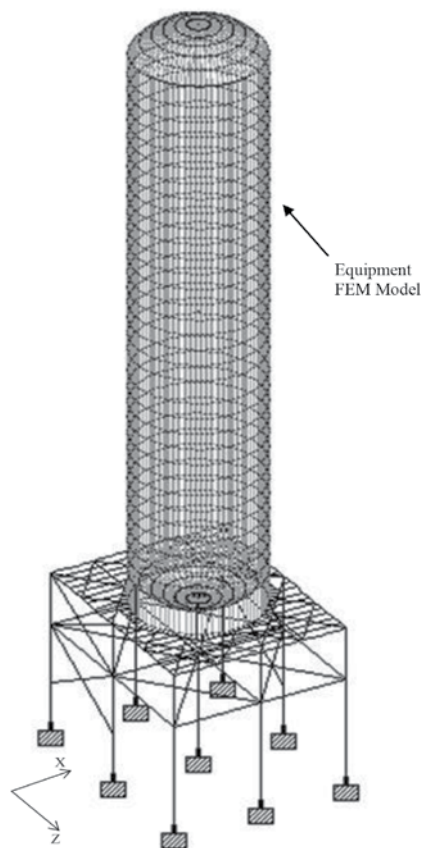


(1a): Analytical Model – Approach-I

Structure along with the foundation, are designed for all the approaches against corresponding earthquake forces. Cost comparison of the structure and foundation system for all the three approaches (Fig. 1) are carried out.



(1b): Analytical Model – Approach-II



(1c): Analytical Model – Approach-III

Fig. 1. Analytical 3D Models

Earthquake parameters:

Analysis Method: Response Spectrum (**Fig. 2**)

Importance factor, $I = 2.0$

Redundancy Factor, $R = 5$

$I/R = 0.4$

As per IS: 1893 (Part 4) **Table 5**, Process columns on elevated structures are categorized as Category-1. Accordingly, Importance factor of 2 has been considered for the structure. Response reduction factor of 5 corresponding to Special Moment Resisting Frame has been considered as per IS: 1893 (Part-4) **Table 3**.

RESULT AND DISCUSSION

Time Period of Equipment along with Supporting Structure

From site spectra as shown in **Fig. 2**, maximum value of spectral acceleration, S_a/g lies in the range of time period of 0.1 to 0.55 sec. Thus, as the time period of the system increases and goes beyond this range, S_a/g value reduces substantially.

Time periods tabulated in **Table 2** against Approach-I and II are 0.20 and 1.17 sec respectively; the same are for the supporting structure along with equipment weight modeled as lumped mass. Whereas, time period of 1.97 sec against Approach-III, is the combined time period for both of the equipment and the supporting structure. From the values mentioned in **Table 2**, against all the approaches, it is evident that, time period increases drastically when flexibility of equipment or the supporting structure is taken into consideration. (**Fig. 3**).

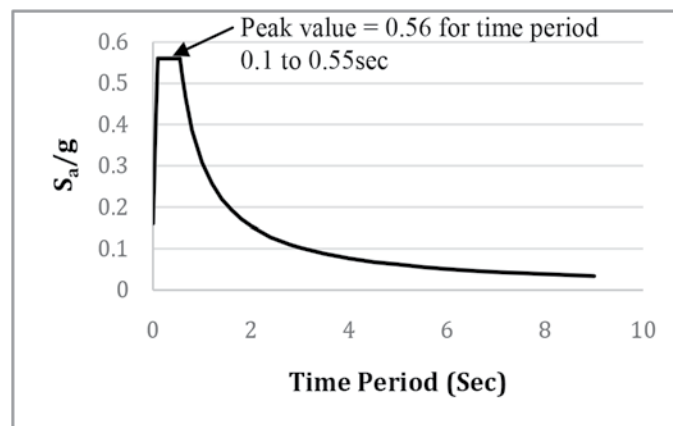


Fig. 2. Site Spectra – 2% Damping

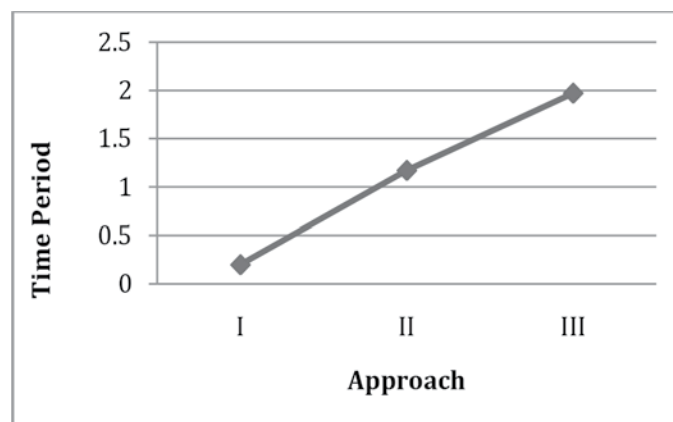


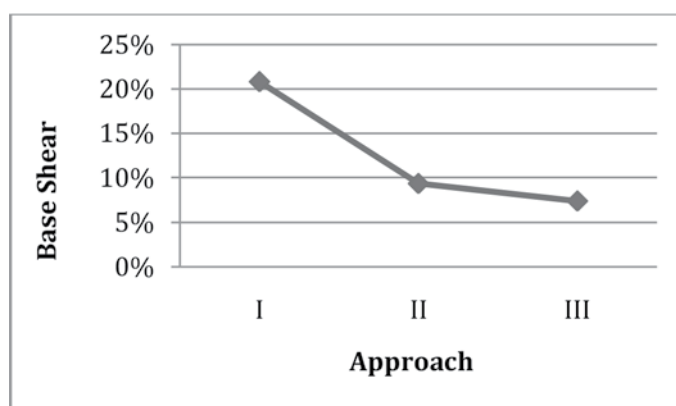
Fig. 3. Time period for Approach – I, II & III

Table 2. Time period & base shear for various approaches

Approach No.	Time Period	Earthquake Force On Equipment (Mt)	Base Shear (Mt)	% Base Shear
I	0.20	As Per Mechanical Data Sheet	719	21%
Ii	1.17	From Response Spectrum Analysis	325	9%
Iii	1.97	From Response Spectrum Analysis	256	7%

Earthquake Base Shear of Equipment along with Supporting Structure

Base Shears from earthquake for equipment along with the supporting structure obtained from response spectrum analysis against various approaches are tabulated in **Table 2**. Base shear percentages with respect to total vertical load, (i.e. Self weight of structure + 50% of Live load + Equipment operating weight), are tabulated in **Table 2**. From the values it can be clearly understood that, base shear against Approach-II is quite less than that of Approach-I and the same reduces drastically against Approach-III (**Fig. 4**).

**Fig. 4.** Base shear (% age) for approach – I, II & III

Cost of Supporting Structure along with Foundation

Earthquake force on equipment has major impact on structural design. With reduction in the force as shown in **Fig. 4**, structure as well as foundation cost reduces significantly. Quantities of structural steel, RCC along with their respective approximate costs against all the approaches are tabulated in **Table 3**.

RCC cost includes cost of associated items such as reinforcement bars, excavation, shuttering, admixtures, PCC below foundation etc. Overall cost of structure including foundation system against all the approaches are presented in **Fig. 5**.

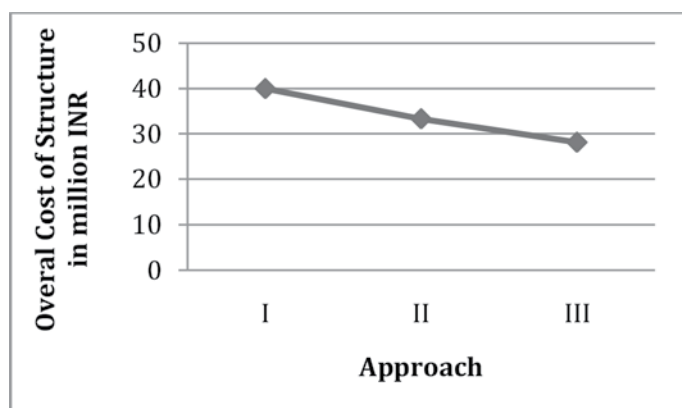
**Fig. 5.** Overall Cost of Structure for Approach – I, II & III



Table 3. Quantities & cost of foundation & super-structure for various approaches

Approach No.	Foundation (RCC)		Super Structure (Steel)		Overall Cost (Inr Million)
	Quantity (Cum)	Cost (Inr Million)	Quantity (Mt)	Cost (Inr Million)	
I	570	13.55	249	26.39	39.95
Ii	495	9.96	220	23.32	33.28
Iii	400	8.05	189	20.04	28.09

CONCLUSION

On the concluding note, findings from the present study can be summarized as below –

1. For equipments supported on structures, earthquake force on the equipment majorly depends on the boundary condition of the supporting base. Time period of the Equipment along with supporting structure may vary up to a range of 0.2 to 1.97 seconds (Table 2).
2. Along with the increase of time period, the system becomes flexible and as a result attracts less earthquake force. Base shear percentage with respect to total vertical load of the system varies maximum of 21% to minimum of 7% against system time period 0.2 and 1.97 respectively.
3. With proper estimation of earthquake force of the equipment, structural design can be optimized to a great extent (Table 3). Overall cost of the structure against Approach-I is 39.95 million INR (Approx.) and the same against Approach-III is 28.09 million INR (Approx.). Therefore, saving in overall structural cost may be as high as around 30%.
4. However, there will be no implication on mechanical design of the equipment. Equipment and the equipment supporting members have no redundancy like structural frame members. Hence, equipment and the supporting members should be designed with an earthquake force as per Mechanical datasheet. So, design of equipment and the supporting members against Approach-II & III will remain same as in Approach I.
5. Generation of earthquake force on equipment through floor-spectra is not in common industry practice. So in absence of floor-spectra, earthquake force on heavy equipments should be derived through equipment structure integrated analysis to rationalize the forces as well as for cost optimization of system.

This study, thus suggests a concept, which may be adopted for other heavy equipments and supporting structures of the industry. Further, values mentioned here are relevant for this case study only and the same should not be used for other systems without analytical backup. However, extent of rationalization should be judicially decided by keeping in view the importance of the equipment.

REFERENCES

1. U. Yuceoglu, “Seismic Design of Equipment, supports and Connections in Industrial Installations – Preliminary Study” - December 1978 LEHIGH/FL/424--3
2. Asadour H. Hadjian, (A.M.ASCE), Engrg. Specialist; Bechtel Corp., Vernon, CA, “Earthquake Forces on Equipment in Nuclear Power Plants” - Journal of the Power Division, 1971, Vol. 97, Issue 3, Pg. 649-665.



Review on Limestone Calcined Clay Cements (LC³)

S M Gunjal^{a,b}, B Kondraivendhan^c

Department of Civil Engineering, Sanjivani College of Engineering, Savitribai Phule Pune University, Kopergaon, Maharashtra^a

Applied Mechanics Department, S V National Institute of Technology, Surat, Gujarat^{b,c}

✉ gunjalsachin20@gmail.com

ABSTRACT

Limestone calcined clay cement (LC³) is low budget, eco-friendly creative ternary blended cement. It is made by using the combination of low grade calcined clay, limestone and gypsum. It can be replaced by 50% of clinker which is beneficial for reduction of carbon dioxide (CO₂) emission at the time of production of cement. In the existing literature the physical and chemical characteristics, sources of raw clay, methods used for calcination, temperature effect on raw clays, mechanical properties of LC³ i.e. compressive strength is checked with respect to the portland pozzolana cement (PPC) and ordinary portland cement (OPC). Durability properties by different researchers were studied such as rapid chloride penetration test, permeability and sorptivity. Production cost and field application of this blended cement were checked. An Industrial trial was carried out in India, Cuba and Switzerland which shows significantly good performance of all the above mentioned properties. In the present study, a review of literature on limestone calcined clay cement carried out for the purpose of future research.

Keywords: Calcined clays; Limestone; Blended cement; Compressive strength; durability.

INTRODUCTION

Day by day demand of concrete is increasing due to industrialization, globalization and infrastructure development. Developing countries require a large quantity of concrete. Concrete is the homogenous mixture of cement, coarse aggregate, fine aggregate, and water. For the production of 1 ton of cement, it emits nearly 1 ton of carbon dioxide (CO₂) into atmosphere [1]. As compared to the world, India is second highest cement producer, in which near about 280 million tons of cement is produced in India [2]. Annually from cement production nearly about 1.35 billion tons of greenhouse gas releases, which is represented in the 2013 World Business Council for Sustainable Development Energy Agency (WBCSDEA) [3]. Clinkers contain nearly about 20% of the supplementary cementitious material (SCM). These are fine limestone, granulated blast-furnace slag (GBFS) and coal fly ash (FA). The GBFS and FA sources are limited globally to only about 15–25% of cement consumption. Metakaolin is also used as a partial substitution for cement in concrete [4]. A combination of metakaolin to limestone as 2:1 in portland cement (PC) and the mixture was prepared, in addition of 15, 30, 45 and 60% of quartz in PC by Antoni et al. [5] blended cement and calcined clay are used up to 30% obtained from low-grade kaolinite clay and limestone (addition of limestone in cement ranges of 0-10%) cement are produced and the filler effect and pozzolanic effect on compressive strength, hydration phases and pore size distribution were studied [6]. A recently developed alternative low-CO₂ SCM system uses optimized combinations of calcined clays with ground lime.

Utilization of Cement in India and Other Industrial Nations

According to International Energy Agency (IEA), the future cement consumption for other industrial nations will increase day by day up to 2050 [7]. Growth in cement production is higher in developing countries where the population increases. Cement production in the whole world 10 years ago which is nearly equal to today's production in China. In India demand of cement has increase but consumption per capita is only 1/6th that in China [3] as shown in **Fig. 1**.

The utilization of other building materials such as glass, asphalt, iron, ceramic, wood etc. is very less as compared to cement and other cementitious materials as shown in **Fig. 2**.

Limestone Calcined Clay Cement (LC³)

LC³ is an innovative blended portland cement contains clinker, calcined clay, low grade limestone and gypsum [8]. In which clinker, calcined clay, limestone and gypsum are 50%, 30%, 15% and 5% respectively are as shown in **Fig. 3**. The main

invention in LC³ is to mix the easily found low-quality (percentage of kaolin content is less) kaolinite clay with the substitution of 15% limestone without deduction in mechanical properties [9]. Scrivener et al.[10] Studied the reaction of metakaolin and limestone in which alumina present reacts with limestone, to make a low permeable material giving same compressive strength when higher replacement of clinker.

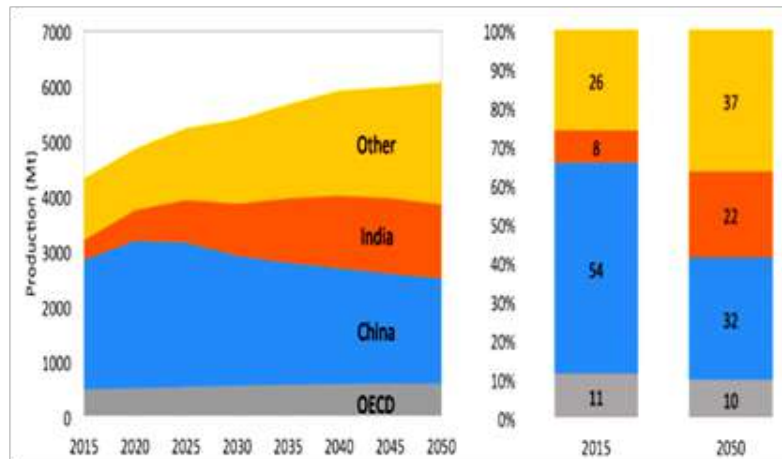


Fig. 1. Utilizations for future cement by region [3] .The lower section shows the evolution of cement production distribution among different regions

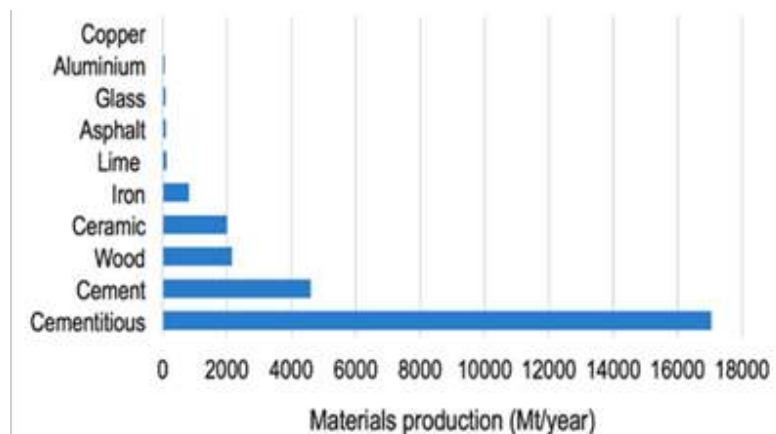


Fig. 2. Estimated utilization of common materials 2001-2005. Data from [7] except from ceramics asphalt and cementitious, all other materials are shared with other industries

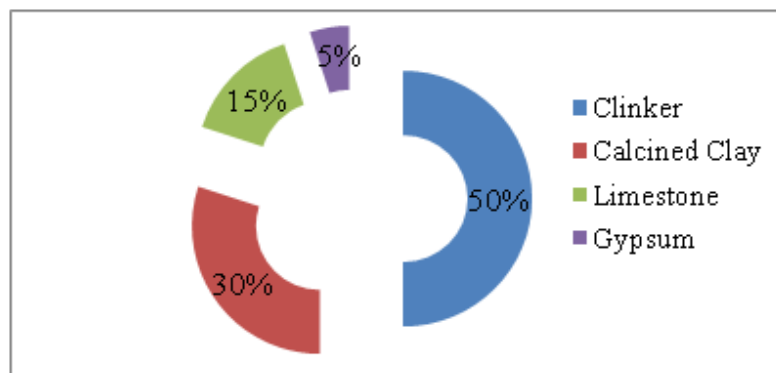


Fig. 3. Percentage of LC3 content



Temperature Effect on Raw Clays

One of the SCM i.e. raw clays is abundantly available worldwide. Clays have sufficient proportion of kaolinite and becomes highly pozzolanic if calcined between 700°C to 850°C. A very reactive material is added in cement known as metakaolin produced by calcining high purity kaolinitic clays [11]. Raw kaolinite clays produced an excellent pozzolanic activity when clay is calcined at a temperature of 500°C to 800°C due to the creation of the active amorphous phase called metakaolin [12]. Similarly, the calcination of good kaolinitic clays at temperature of 550°C to 900°C develops an amorphous silica compound aluminosilicate which is a highly reactive pozzolana. Tironi et al. [13] investigated temperature required for calcination of clay A2, A3, A4, and A5 at 700°C to complete conversion of kaolin to metakaolin and A1 clay required the temperature of 800°C for the calcination. Where A1 and A2 contain high kaolinite poor kaolinite i.e. 16% before calcination of clay.

The methods used for calcination of calcined clay are either by rotary and vertical shaft kiln for the small production of cement. An oil fired shuttle kiln was used for the calcination process [14]. The two clays A1 and A2 were used for calcination using laboratory furnace fixed bed technique, the complete kaolinite conversion of clay was checked by X-ray diffraction (XRD) [12]. Depending on sources of clay the chemical composition may vary. The calcined clay which is used in making LC³ the chemical composition, calcination process and origin of clay used by different authors are as listed in **Table 1**. The tests carried out on calcined clay such as pozzolanic activity, mineralogical composition, and microstructural properties are as shown in **Table 2**.

Comparison of LC³ with Ordinary Portland Cement

Production Process

Limestone and raw material are taken from quarry then broken into small pieces and fed into the rotary kiln to burn up to 1450°C to create clinker which is after crushed and blended with gypsum to form OPC. For fly ash based portlandpozzolana cement, is fly ash added in the preparation of cement. By using same technology LC³ is produced. The substitution of calcined clay and low quality of limestone blending together with clinker to form LC³. The typical production process of ordinary portland cement (OPC), fly ash based portlandpozzolana cement (PPC) and limestone calcined clay cement (LC³) are as shown in **Fig. 4**.

Following are the advantages of LC³

1. Emissions of CO₂ in LC³ are considered to be 20-30% less than ordinary portland cement because of decreased in clinker content leads to less emission of carbon dioxide in the atmosphere. Crushing of limestone takes less energy than burning it. Calcination of clay takes place at 800°C. Total 55% of the energy required for clinkerisation at 1450°C.
2. LC³ can be manufactured with presently available equipment, leading to only marginally additional investments for calcination of clay.
3. Low cost of production, less clinker content, reduced fuel consumption for calcination contributes to smaller production costs.

Table 1. Chemical composition of Calcined clay, Calcination process and origin of clay

Sr No	Chemical Composition (%)	SiO ₂	Al ₂ O ₃	Fe ₂ O ₃	CaO	MgO	Na2O	K2O	TiO2	LOI
1	Tironi et al.,2012									
	A1(94% Kaolinite clay)	45.9	37.0	0.77	0.08	0.12	0.06	0.40	0.99	13.30
	A2(76% Kaolinite clay)	51.4	31.3	0.92	0.40	0.19	0.36	0.38	1.42	12.15
	A3(65% Kaolinite clay)	59.4	27.1	0.76	0.15	0.12	0.14	0.41	0.26	9.65
	A4(48% Kaolinite clay)	65.7	21.1	0.85	0.26	0.22	0.07	0.68	0.43	7.77
	A5(16% Kaolinite clay)	74.8	14.8	1.10	0.30	0.26	0.92	3.71	0.18	3.44
	Calcination Process	Laboratory furnace fixed bed techniques								
	Origin of Clay	Argentina (La Rioja,Chubut and Santa Cruz)								
2	Antoni,Rossen,Martirena, & Scrivener, 2012									
	Metakaolin	50.62	46.91	0.38	0.02	0.09	0.28	0.18	1.29	0.00
	Calcination Process	Flash								
	Origin of Clay	Burgess								



3	Tironi et al., 2014									
	A1(94% Kaolinite clay)	45.9	37.0	0.77	0.08	0.12	0.06	0.40	0.99	13.30
	A2(76% Kaolinite clay)	51.4	31.3	0.92	0.40	0.19	0.36	0.38	1.42	12.15
	Calcination Process	Laboratory furnace fixed bed techniques								
	Origin of Clay	Argentina (La Rioja,Chubut and Santa Cruz)								
4	Bishnoi et al., 2014									
	70 to 80% kaolinite clay	43.30	36.35	2.26	0.46	-	-	-	-	13.94
	20 to 30% kaolinite clay	55.78	17.46	8.89	4.84	-	-	-	-	9.49
	Calcination Process	Oil fired shuttle kiln								
	Origin of Clay	West Bengal (eastern India)								
5	(Vizcaino-Andrés et al., 2015)									
	Sample 1	54.7	27.8	12.1	1.7	0.9	0.3	1.5	0.8	10.4
	Sample 2	54.2	28.2	12.3	1.7	0.9	0.3	1.6	0.8	10.3
	Sample 3	55.0	26.0	13.4	1.8	1.0	0.3	1.6	0.8	9.8
	Calcination Process	Wet process Rotary Kiln								
	Origin of Clay	Pontezuela,Cuba								
6	Anders L et al., 2015									
	Calcined Clay	48.4	29.5	16.5	0.4	1.0	0.0	0.7	0.6	1.5
	Calcination Process	Laboratory Oven								
	Origin of Clay	Pontezuela, Cuba								
7	Hollanders, Adriaens, Skibsted, Cizer, & Elsen, 2016									
	Kaolinite clay 1	45.82	38.79	0.56	0.01	0.05	0.03	0.20	0.42	14.12
	Kaolinite clay 2	46.24	40.03	0.27	0.03	0.04	0.03	0.02	1.59	11.76
	Kaolinite clay 3	44.77	38.45	1.12	0.02	0.06	0.05	0.01	2.23	13.29
	Kaolinite clay 4	44.85	38.62	0.17	0.04	0.04	-	-	0.01	16.27
	Calcination Process	Fixed bed electrical furnace								
	Origin of Clay	Capim and Halloysite Industrial supplier								
8	Emmanuel et al., 2016									
	Kaolinite clay 1	63.44	24.47	0.68	0.1	0.11	0.22	0.12	1.44	9.21
	Kaolinite clay 2	54.67	27.69	4.93	0.06	0.13	0.25	0.12	1.68	10.28
	Kaolinite clay 3	44.59	37.59	0.817	0.034	0.09	0.04	0.15	3.01	13.46
	Kaolinite clay 4	43.95	36.92	1.29	0.1	0.13	0.03	0.23	3.44	13.66
	Kaolinite clay 5	41.1	37.13	1.39	0.1	0.14	0.09	0.47	4.67	14.37
	Calcination Process	Rotary kiln								
	Origin of Clay	Kutch Gujarat,India								
9	Tironi, Scian, & Irassar, 2015									
	Kaolinite clay	65.7	21.1	0.85	0.26	0.22	0.07	0.68	0.43	7.77
	Calcination Process	Laboratory Oven								
	Origin of Clay	Santa Cruz, Argentina.								
10	Dhandapani&Santhanam, 2017									
	Calcined Clay	58.43	24.95	5.08	0.09	0.19	0.05	0.21	1.41	9.58
	Calcination Process	Rotary kiln								



	Origin of Clay	Bhuj, Gujarat, India								
11	Dhandapani, Sakthivel, Santhanam, Gettu, & Pillai, 2018									
	Calcined Clay	58.43	24.95	5.08	0.09	0.19	0.05	0.21	1.41	9.58
	Calcination Process	Rotary kiln								
	Origin of Clay	Bhuj, Gujarat, India								

Table 2. Different test carried out on calcined clay

Sr. No	Authors	Pozzolanic activity	Mineralogical composition	Microstructural Properties	Properties of LC ³
1	Tironi et al., (2012)	Fratini Test Electrical Conductivity	X-ray diffraction Fourier transformed infra-red spectrometry (FTIR)	Mercury intrusion porosimetry (MIP)	Compressive strength of Mortar. Blaine Fineness
2	Tironi et al., (2014)	Fratini Test	X-ray diffraction Scanning Electron Microscopy	Mercury intrusion porosimetry (MIP) Scanning electron microscopy (SEM)	Compressive strength of Mortar Blaine Fineness
3	Scrivener, (2014)	Pozzolanic reactivity	----	Mercury Intrusion Porosity (MIP)	Compressive strength Chloride Penetration
4	Bishnoi et al., (2014)	Lime reactivity test (IS 1727-1967)	X-ray diffraction Fourier transformed infra-red spectrometry (FTIR)	----	Standard consistency Initial setting time Compressive strength of Mortar Blaine Fineness
5	Vizcaino-Andrés et al., (2015)	Pozzolanic reactivity	X-ray fluorescence X-ray diffraction	Mercury Intrusion Porosity (MIP)	Compressive strength of mortars.
6	Anders L et al., (2015)		X-ray fluorescence X-ray diffraction	Mercury Intrusion Porosity (MIP) Isothermal Calorimetry	Compressive strength of mortars.
7	Hollanders et al., (2016)	Chapelle Test (French norm NF-P 18-513)	X-ray fluorescence X-ray diffraction Fourier transformed infra-red spectrometry (FTIR)	----	Blaine Fineness
8	Emmanuel et al., (2016)	Lime reactivity test (IS 1727-1967)	X-ray fluorescence X-ray diffraction	Mercury intrusion porosimetry (MIP) Scanning electron microscopy (SEM) Isothermal Calorimetry	Standard consistency Initial setting time Final setting time Compressive strength of Mortar Blaine Fineness Specific gravity
9	Tironi, Scian, & Irassar, (2015)	Fratini Test	X-ray fluorescence X-ray diffraction	Mercury intrusion porosimetry (MIP) Scanning electron microscopy (SEM)	Compressive strength of Mortar
10	Dhandapani & Santhanam, (2017)	Lime reactivity test	X-ray fluorescence X-ray diffraction	Mercury intrusion porosimetry (MIP) and electrical impedance spectroscopy (EIS).	Compressive strength of Mortar
11	Avet & Scrivener, (2018)	Pozzolanic reactivity	X-ray fluorescence X-ray diffraction	Mercury intrusion porosimetry (MIP) and Scanning electron microscopy (SEM).	Compressive strength of Mortar
12	Dhandapani et al., (2018)	Lime reactivity test	X-ray fluorescence X-ray diffraction	Oxygen permeability, rapid chloride penetration, chloride migration, resistivity development and water sorptivity	Compressive strength of Mortar and concrete. Standard consistency, Initial setting time, Final setting time, Blaine Fineness, Specific gravity.

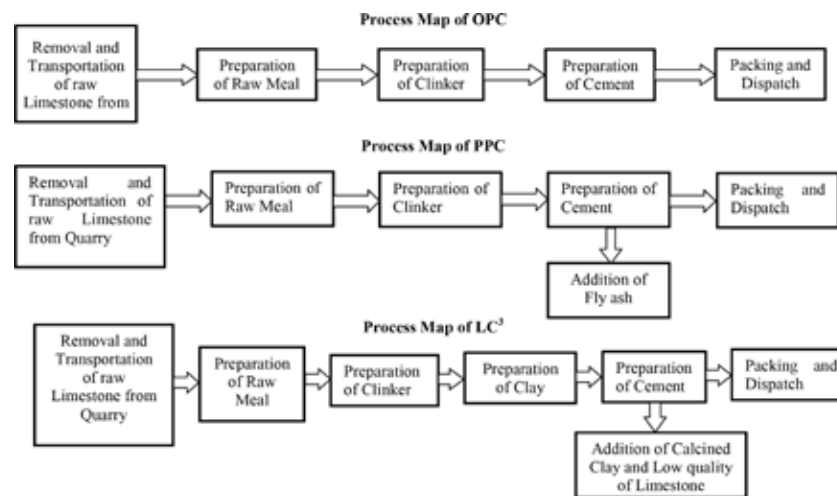


Fig. 4. Process Map for a Typical Cement Plant in India, OPC, PPC and LC³

Clay Minerals Occurrence in India and World Soil Map

In India, kaolinite clays commonly known as china clays according to Indian Bureau of Mines in 22 states are available [15]. India has estimated clay resources of about 2803 Million tons as per Indian Bureau of Mines report (2014-2015 Mineral Year Book), as is given in **Table 3**.

Table 3. Clay Stock in India Category Wise (Indian Bureau of Mines report (2014-2015 Mineral Year Book))

Type of Clay	Existence Stock in Million Tons	Probable stock in Million Tons	Possible stock in Million Tons	Total stock in Million Tons
China Clay	124	53	2527	2704
Ball clay	12	4	67	83
Shale	15	0.5	0.5	16
Total	151	57.5	2594.5	2803

The reserve constitutes only about 7% of resources out of 208.5 Million tons in terms of proved and possible reserve estimation system as per UNFC classification. China clay available in the state of Kerala is 25% similarly in West Bengal, Rajasthan and Orissa States is 16% and Karnataka state is 10%. In case of Ball clay resource from Andhra Pradesh Contributes 60% & 38% from Rajasthan state. World Soil Map is as shown in **Fig. 5**.

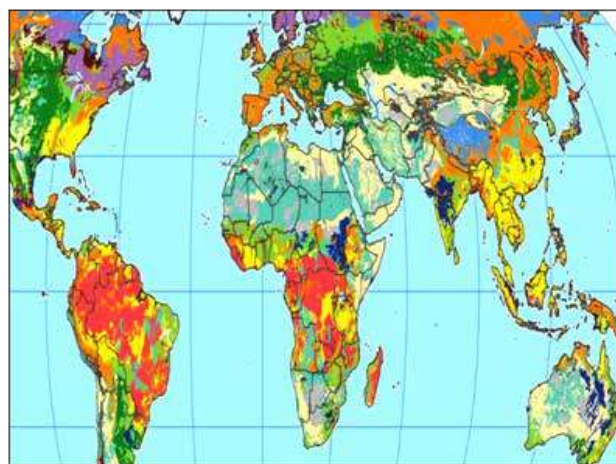


Fig. 5. World Soil Map. Kaolinite clays are yellow and pale green region likely occur on top surface [9]



Kaolinite clay most likely occurs near the top surface in the yellow and pale green region, Alfisols (pale green) and Ultisols (yellow) as on the map. Clay is the weathering product from all type of rocks which are abundantly available near the earth surface. Particularly kaolinite clay is available in plenty in India and South East Asia.

Compressive Strength of LC3 as Compared to Other Cement

LC³-50 contains 50% of clinker, 30% of calcined clay, 15% of limestone and 5% of gypsum which give same mechanical properties as compared to ordinary portland cement. The compressive strength of mortar (cement to standard sand 1:3) with water to the cement ratio of 0.50 give good compressive strength than portland cement [8,13]. As the percentage of kaolin in calcined clay increases the growth of compressive strength varies accordingly at 7 days and 28 days than the OPC. The early stage of compressive strength i.e. 1 day is smaller because of pozzolanic reaction is slow at an initial stage and same behavior through a graph of compressive strength as shown in **Figs. 6 and 7**. In India [14] first trial production of LC³-50 was carried out in the state of West Bengal (Eastern India) due to the availability of clay. Clay 1 and 2 contain 70 to 80% and 20 to 30% of kaolinite content respectively. The limestone A and B contain 36.29% and 42.84% of CaO was used in this study. The four blends of LC³, A, B, C, and D (blend A contain clay 1 and limestone A, blend B contain clay 1 and limestone B, blend C contain clay 2 and limestone A, blend D contain clay 2 and limestone B.) were prepared and compared with OPC and PPC with a slight change in water-cement ratio.

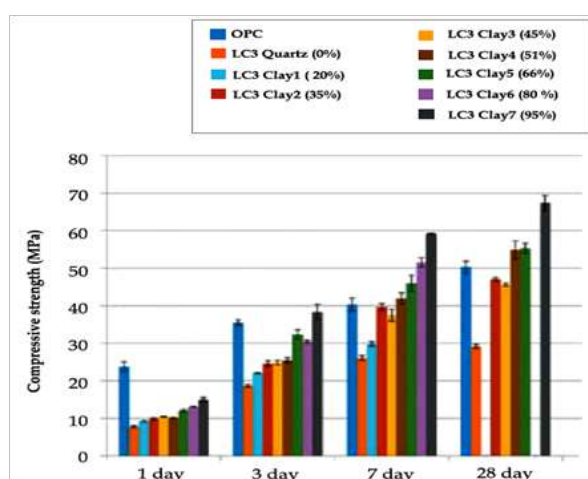


Fig. 6. Compressive strength of OPC and LC³ Cement ranging from lower clay content to higher clay content. The calcined clay originate from India, Brazil, Thailand and Cuba [9].

The blend A and B have highest compressive strength than OPC and PPC while blend C and D has more compressive strength than PPC at 3, 7 and 28 days. The compressive strength of concrete at the water-cement ratio of 0.45, the LC³ A has the highest strength than all other blends, such as OPC and PPC at 3, 7 and 28 days [14]. An Industrial trial was carried out in Cuba to form an LC³ in which clinker is replaced by 50% of SCM. Such as calcined clay and limestone. Andres et al. [16] studied the compressive strength of new production cement is more than OPC at 3, 7 and 28 days. Second trial production of LC³ was carried out in India at Gujarat. The clay which contain 58% kaolin content was used for the production of LC³. The colour of this clay is reddish because it contains high iron. Compressive strength of mortar containing LC³, water to cement ratio (w/c) taken as 0.35, 0.40, 0.45 and 0.50 as compared to OPC. The Initial strength of LC3 at 3, 7, 28 days are higher than that of OPC, while the strength gain later age 56 days is less than OPC [17].

Compressive strength of LC³ at 28 days as compared to ordinary portland cement and 30% fly ash used in OPC i.e. FA30 was higher result [18]. Mechanical properties and durability properties were studied [19] on OPC, FA30 and LC³ with the addition of clinker 50%, calcined clay 31%, limestone 15% and gypsum 4% respectively. The compressive strength of mortar at 28 days of OPC, FA30, and LC³ is 61.0, 46.0 and 43.7 MPa. The compressive strength of Concrete OPC-M30, OPC-M50, FA30-M30, FA30-M50, LC3-M30 and LC3-M50 was also checked.

Tironi et al. [13] studied compressive strength on mortars taking cubes (Size 25x25x25 mm) made with standard sand (1:3) and w/c ratio of 0.50. The 5 clay A1, A2, A3, A4 and A5 were used having kaolinitic content 94, 76, 65, 48 and 16% respectively. The Clay A2 strength is higher than OPC at 7, 28, and 90 days. Similarly, clay A1 compressive strength nearly equal to OPC

and other clay has less compressive strength than OPC. Tironi et al. [12] for blended cement two clay A1 and A2 replaced by 15% and 30% by mass of cement. Clay A2 has highest compressive strength at 30% replacement than other clay at 2, 7 and 28 days because of clay A2 has a high pozzolanic activity which was carried out by Frattini test [20]. Antoni et al. [5] taken has metakaolin to limestone ratio 2:1 and prepared four mixes using the combination of portland cement, limestone and metakaolin B15, B30, B45 and B60 such that the replacement of portland cement 15, 30, 45 and 60% and adding metakaolin to limestone ratio 2:1. The compressive strength of mortars compared to with reference portland cement The B15 has highest compressive strength than other mixes and reference concrete at 1, 7, 28 and 90 days. The calcium carbonate reacts with alumina present in metakaolin making important amounts of hemicarboaluminate and less amount of monocarboaluminate at early as 1 day. Similarly, limestone and metakaolin absorb calcium hydroxide in the blends which could be completely missing with the high level of substitution at past ages.

Durability of LC³

Durability is an important property to measure performance life of a structure. The detailed study on durability of LC³ is going in Switzerland, Cuba and India [9]. The phase compositions of LC³ are very similar to Portland and blended cement. Calcium silicate hydrate (C-S-H) is principal products after reaction, also forms aluminate phases monohemicarbonate and ettringite in limestone cement. LC³ has a small porosity as compare to other blended cement as shown in Fig. 8 [9] by using mercury intrusion porosimetry. Similarly, LC³ kept in 0.5M NaCl solution shows good resistance to penetration of chloride ion after two years of ponding as shown in Fig. 9 [9].

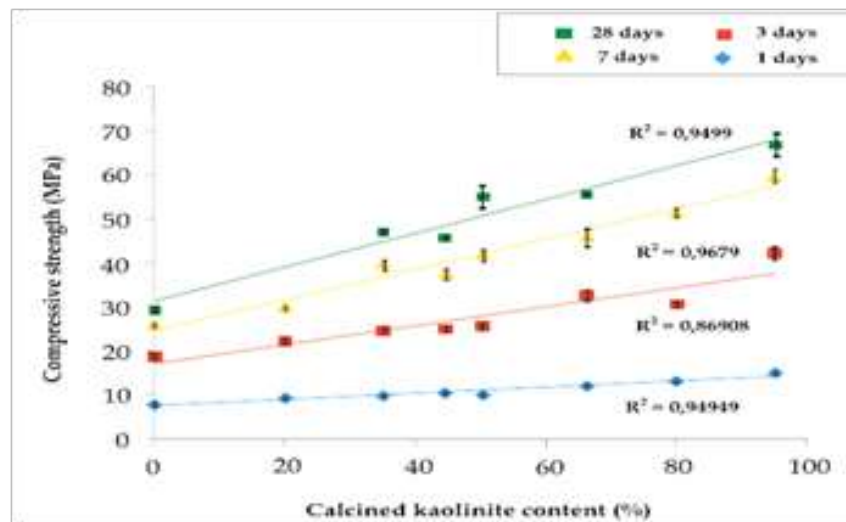


Fig. 7. Relation between calcined kaolinite content and compressive strength [9]

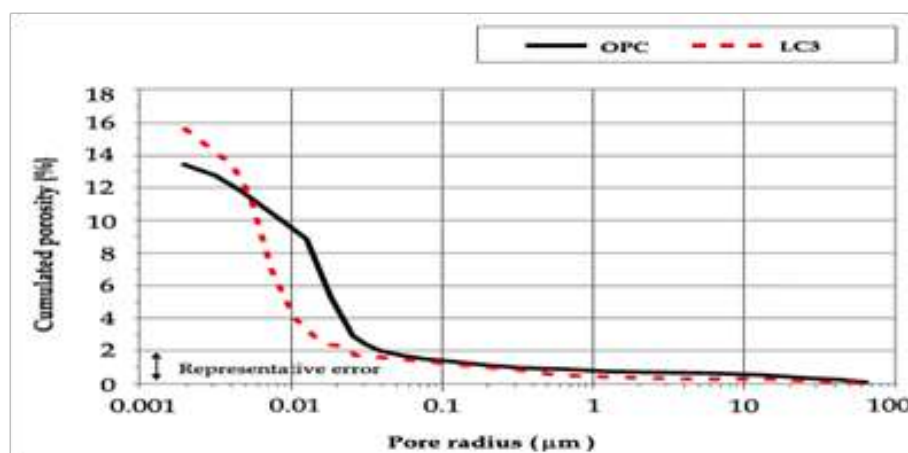


Fig. 8. Mercury Intrusion Porosity results for LC3blend and reference Portland cement [9]

Dhandapani and Santhanam studied pore structure development by using mercury intrusion porosimetry (MIP) as compared to Portland cement, FA30 and LC³. In that LC³ binder has significantly improved pore structure. Also, rapid chloride permeability test (as per ASTM C1202) for LC³ binder was done and observed that reduced permeability as compared to OPC and FA30. Similarly, LC³ system has critical pore size evaluation and conductivity greater improvement was in 7 days. X-ray diffraction prove that at early age calcium hydroxides consume due to the sensitivity of calcined clay monocarboaluminate and hemicarboaluminate phases were seen at early age beneficial to microstructure development which reduces the porosity [18].

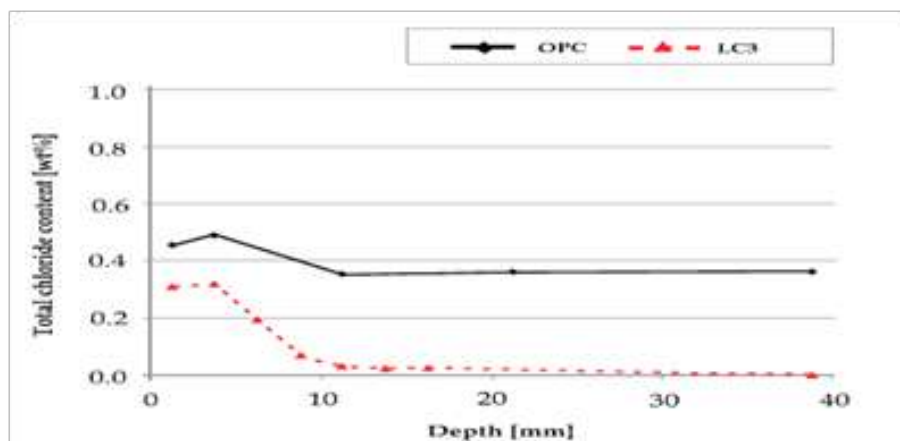


Fig. 9. Chloride profiles after 2 years ponding in 0.5 NaCl solutions [9]

Field Application of LC³

Using LC³ first trial production carried out in India for testing of concrete in the laboratory as well as in the field. The various application is such as micro cracking roofing tiles, RCC door and window frame, hollow concrete blocks, low duty paving blocks and construction of two storey houses[14] are as shown in **Figs. 10 and 11**. Industrial trials were carried out in Cuba for the manufacture of hollow concrete blocks, many cubic meters of 25MPa concrete used under standard condition[16].



Fig. 10. Micro concrete roofing tiles produced using different blends of LC³ [14]

Production cost of LC³

Last few years various studies have been going on LC³ [7, 12]. It is observed that LC³ is more economical than fly ash based portland pozzolana cement in India [21]. Following point is to be considered for economical production of LC³:

1. Using combination of limestone and calcined clay 50% of reduction in clinker is possible and lower energy is required for burning.
2. Crushing limestone takes lower energy than burning it
3. At 800°C calcination takes place and nearly 55% of energy required for clinkerisation.

4. Existing equipment can be used.

In India high kaolin content clay known as china clay available at least in 22 states [22]. Economical production of LC³ with respect of OPC and PPC depends upon the cost, availability and quantity of fly ash used.



Fig. 11. Construction of two story house using LC³ [14]

CONCLUDING REMARKS

With low capital investment, alternative cement production is possible in developing country which faces an increase in population, infrastructure development and greenhouse gas emissions. This article tries to present a review of sources of raw clay, calcination methods, compressive strength, durability properties, chemical composition, field application and physical performance of limestone calcined clay cement.

The most of the work in LC³ is going on to study durability, transport properties, corrosion due to carbonation and chloride ingress, alkali-silica reaction, sulphate attack and leaching also, mechanical properties, flexure strength, compressive strength, tensile strength and creep and shrinkage. However there is no work on high performance concrete (HSC) and ultra-high performance concrete (UHPC), reported in the literature. Therefore, there is a lot of scope for studying these properties of HSC and UHPC in near future.

REFERENCES

1. Gartner, E.: Industrially interesting approaches to 'low-CO₂' cements. *Cem. Concr. Res.* 34, 1489–1498 (2004). doi:10.1016/j.cemconres.2004.01.021
2. Planning Commission. Low Carbon Strategies for Inclusive Growth. Government of India, 2011. http://planningcommission.gov.in/reports/genrep/index.php?preps=report_carbon.html
3. Initiative, WBCSD Cement Sustainability Getting the Numbers Right, Project Emissions 2014, Report, 2016
4. Sabir, B., Wild, S., Bai, J.: Metakaolin and calcined clays as pozzolans for concrete: A review. *Cem. Concr. Compos.* 23, 441–454(2001). doi: 10.1016/S0958-9465(00)00092-5
5. Antoni, M., Rossen, J., Martirena, J., Scrivener, K.: Cement substitution by a combination of metakaolin and limestone, *Cem. Concr. Res.* 42, 1579–1589 (2012). doi:10.1016/j.cemconres.2012.09.006
6. Tironi, A., Scian, A.N., Irassar, E.F.: Blended Cements with Limestone Filler and Kaolinitic Calcined Clay: Filler and Pozzolanic Effects. *J. Mater. Civ. Eng.* 29, 195–201(2017). doi:10.1007/978-94-017-9939-3_24
7. IEA, Energy Technology Perspectives 2015 Mobilizing Innovation to Accelerate Climate Action, Energy Technol., 2015. <http://www.iea.org/etp/etp2015>
8. Scrivener, K., Martirena, F., Bishnoi, S., Maity, S.: Calcined clay limestone cements (LC₃), *Cem. Concr. Res.* (2017). doi:10.1016/j.cemconres.2017.08.017
9. Scrivener, K.L.: Options for the future of cement. *Indian Concr. J.* 88, 11–21(2014). http://www.lc3.ch/wp-content/uploads/2014/09/0851_ICJ_Article.pdf



10. Limestone Calcined Clay Cements. <https://www.lc3.ch>
11. Fernandez, R., Martirena, F., Scrivener, K.L.: The origin of the pozzolanic activity of calcined clay minerals: A comparison between kaolinite, illite and montmorillonite. *Cem. Concr. Res.* 41, 113–122(2011). doi:10.1016/j.cemconres.2010.09.013
12. Tironi, A., Castellano, C.C., Bonavetti, V.L., Trezza, M.A., Scian, A.N., Irassar, E.F.: Kaolinitic calcined clays - Portland cement system: Hydration and properties. *Constr. Build. Mater.* 64, 215–221(2014). doi:10.1016/j.conbuildmat.2014.04.065
13. Tironi, A., Trezza, M.A., Scian, A.N., Irassar, E.F.: Kaolinitic calcined clay: Factors affecting its performance as pozzolance. *Constr. Build. Mater.* 28, 276–281(2012)
14. Bishnoi, S., Maity, S., Mallik, A., Joseph, S., Krishnan, S.: Pilot scale manufacture of limestone calcined clay cement : The Indian experience, *Indian Concr. J.* 88, 22–28(2014)
15. Indian Minerals Handbook, Ministry of Mines, Government of India, 2011, 2011
16. Vizcaíno-Andrés, L.M., Sánchez-Berriel, S., Damas-Carrera, S., Pérez-Hernández, A., Scrivener, K.L., Martirena-Hernández J.F.: Industrial trial to produce a low clinker, low carbon cement, *Mater. Construcción.* 65, e045 (2015). doi:10.3989/mc.2015.00614
17. Arun, S.B., Emmanuel, C., Haldar, P., Maity, S.: Second pilot production of limestone calcined clay cement in India: The experience. *Indian Concr. J.* 90, 57–64(2016)
18. Dhandapani, Y., Santhanam, M.: Assessment of pore structure evolution in the limestone calcined clay cementitious system and its implications for performance. *Cem. Concr. Compos.* 84, 36–47 (2017). doi:10.1016/j.cemconcomp.2017.08.012
19. Dhandapani, Y., Sakthivel, T., Santhanam, M., Gettu, R., Pillai, R.G.: Mechanical properties and durability performance of concretes with Limestone Calcined Clay Cement (LC3). *Cem. Concr. Res.* 107, 136–151 (2018). doi:10.1016/j.cemconres.2018.02.005
20. BS EN 196-5:1995, British Standard Methods of testing cement Part 5: Pozzolanicity test for pozzolanic cements
21. Maity, S., Joseph S., Bishnoi, S.: An economic analysis of the production of limestone calcined clay cement in India, *Indian Concr. J.* 90, 22–27(2016)
22. Indian Bureau of Mines. Indian Minerals Yearbook 2012, Part-III: Mineral Reviews, Government of India. 2011.



Bolted Shear Connections: A Comparative Study on Effect of Eccentricity and Other Design Criteria as Per International Codes

Saptadip Sarkar, Papia Mandal, Anurag Sinha

Structural Division, Engineers India Limited, New Delhi

✉ Saptadip.sarkar@eil.co.in

ABSTRACT

Bolted shear connections are widely used internationally, however, in India its application is primarily confined in few industries only. But recently, bolted shear connection being best suited for stick built construction approach, has been rightly adopted and proved successful with incomparable schedule advantages. Shear connections are covered and discussed in details in various international codes with a degree of difference in the design concept. In this study, a comparison is made between the American code, Indian code and Euro code. Also the paper aims to highlight the availability and importance of guidelines for connection configurations along with various design and practical consideration, which are not elaborated in Indian code.

Keywords: Simple connection; Indian code; Design; Steel; Bolted connection.

INTRODUCTION

This paper focuses on highlighting the difference of design criteria for bolted joints for eccentricity and other criteria considering American [ANSI/AISC 360-16 (AISC 2016)], Indian [IS800:2007, IS 1367 (Part 3)] and European [BS EN 1993-1-8 along with its accompanying National Annex, BS EN 1993-1-1 along with its National Annex and Publication P358], for evaluating and then subsequently highlighting similarities and differences among them. A few authors have compared building codes for the United States and Europe, focusing their attention on strength limit states related to basic materials only, without considering steel connections. This work intend to draw comparison of criteria related to eccentricity from various established codes. Further this paper also highlights the international guidelines regarding connection configurations, having significant impact on design which are missing in Indian code. The study also present actual design cases as per American, Indian and Euro Code.

OBJECTIVE

The study is designed to examine the following as per Euro Code, American Code and Indian Code–

- I. Reduction in bolt numbers due to eccentricity.
- II. Bolts stresses due to combined Shear and Tension.
- III. Strength of bolt materials

METHODOLOGY

The design considerations are broadly divided into four different categories where in each of them are evaluated. Subsequently similarities and differences among them are highlighted.

In the first section, reduction in bolt numbers due to eccentricity is discussed briefly. In the second shear and tension interaction of bolts is discussed. In the third section, yield strength and ultimate strength of bolt material as per different codes are mentioned briefly. In last section, actual design capacities for different cases are compared. The meaning of symbols are mentioned separately at the end for simplicity.

Reduction In Bolt Numbers Due To Eccentricity

The effective number of bolt in shear and bearing are reduced due to eccentric loading. The instantaneous centre of rotation method is an accepted method as per International Codes to attain the effective number of bolts.

The reduction factors in terms of coefficients C (for reduction of actual number of bolts) for eccentrically loaded bolt groups are directly mentioned in STEEL CONSTRUCTION MANUAL, AISC. Direct values for different combination of pitch, eccentricity and number of bolts are given.

The equivalent reduction factor to C as mentioned earlier can be obtained as per Euro Code as per the formulae below:

$$x = \sqrt{(1 + \alpha n)^2 + (\beta n)^2}$$

Where n = Number of Bolts

For a single vertical line of bolts:

$\alpha = 0$ and

$$\beta = \frac{6e_2}{n(n+1)p_1}$$

[Joints in Steel Construction: SIMPLE JOINTS TO EURO CODE 3] (Refer **Fig. 1**)

Specific guidelines in line with international codes are not available in Indian Code.

- From **Fig. 2**, for any configuration of a connection, the effective number of bolts as per American code is always higher than that obtained as per Euro Code.
- For same Pitch (P_1) and Eccentricity (e_2), the difference between the effective number of bolts as per American code and Euro code decreases with the increase of number of bolts
- The difference between the effective number of bolts as per American code and Euro Code increases with the increase in the eccentricity.
- For practical configuration of bolt numbers following recommended geometry (pitch and eccentricity), the bolt numbers are reduced by as much as 40 %.

With a single vertical line of bolts, the connection shear resistance is in the range of 25% to 50% of the beam shear resistance. Using two vertical lines of bolts, the resistance can be increased, but as the eccentricity of the load also increases due to two lines of bolt, the benefit does not double and the best that can be achieved is around 75% of the full beam shear resistance.

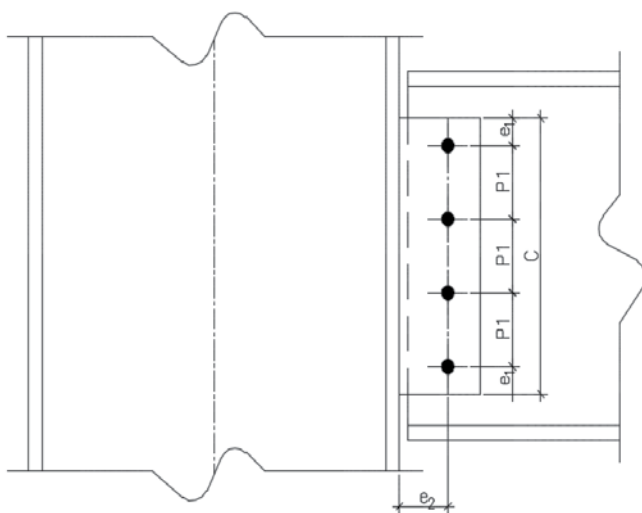


Fig. 1. Connection configuration

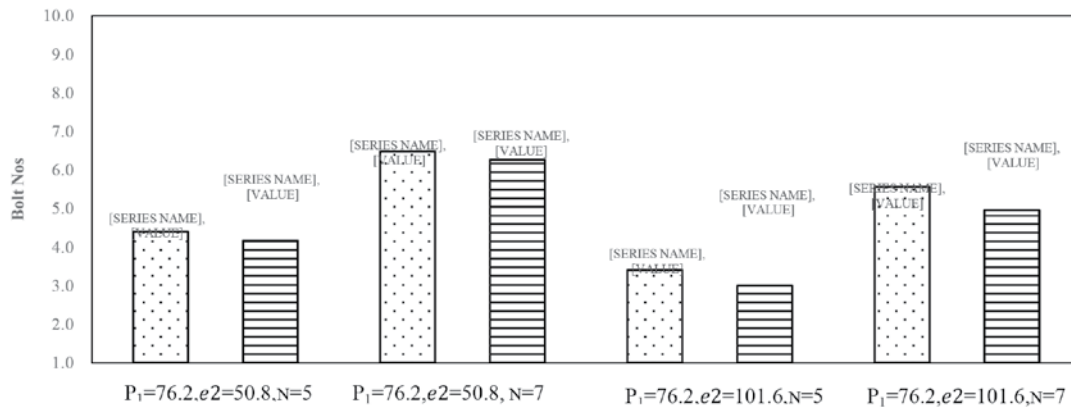


Fig. 2. Effective Number of Bolts

Bolt Subjected to Combined Shear and Tension

The equation for design resistance for individual fasteners subjected to shear and/or Tension as per International Codes are as below:

$$\frac{F_{bs}}{1.3\phi F_{ubs}} + \frac{F_{bt}}{1.3F_{ubt}} \leq 1, \phi = 0.75$$

[ANSI/AISC 360-16 (AISC 2016)]

$$\left(\frac{F_{bs}}{F_{ubs}}\right)^2 + \left(\frac{F_{bt}}{F_{ubt}}\right)^2 \leq 1 \quad [\text{IS800:2007}]$$

$$\frac{F_{bs}}{F_{ubs}} + \frac{F_{bt}}{1.4F_{ubt}} \leq [\text{BS EN 1993-1-1, BS EN 1993-1-8}]$$

From Fig. 3, for a bolt subjected to combined shear and tension, permissible value of stress ratio for tension is higher for Indian code in comparison to American and Euro Code for F_{bs}/F_{ubs} greater than 0.3.

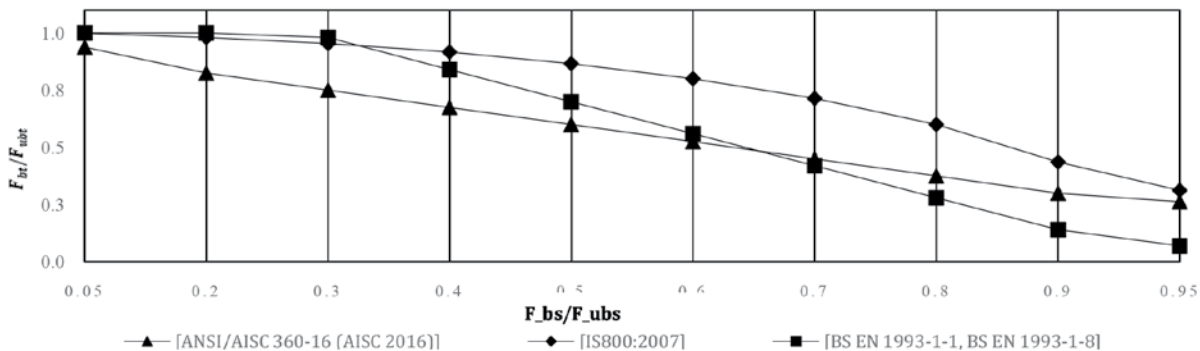


Fig. 3. Permissible stress ratio in Shear v/s Tension

Strength of Bolt Material

Nominal values of the yield strength F_y and the ultimate tensile strength F_u for bolts as per various international codes are as below:

Table 1. Nominal values of yield strength & ultimate tensile strength for bolts [ANSI/AISC 360-16 (AISC 2016)]

Bolt Class	A307	A325	A490	F3043
$F_{yb}(\text{N/mm}^2)$	310	620	780	1040



Table 2. Nominal values of yield strength & ultimate tensile strength for bolts [IS800:2007])

Bolt Class	3.6	4.6	4.8	5.6	5.8
$F_{yb}(N/mm^2)$	180	240	320	300	400
$F_{ub}(N/mm^2)$	330	400	400	500	500

Bolt Class	6.8	8.8	9.8	10.9	12.9
$F_{yb}(N/mm^2)$	480	640	720	900	1080
$F_{ub}(N/mm^2)$	600	800	900	1100	1200

Table 3. Nominal values of yield strength & ultimate tensile strength for bolts [BS EN 1993-1-1, BS EN 1993-1-8]

Bolt Class	4.6	4.8	5.6	5.8	6.8
$F_{yb}(N/mm^2)$	240	320	300	400	480
$F_{ub}(N/mm^2)$	400	400	500	500	600

Bolt Class	8.8	10.9
$F_{yb}(N/mm^2)$	640	900
$F_{ub}(N/mm^2)$	800	1000

From **Table 1**, **Table 2** and **Table 3** the nominal values of yield strength & ultimate tensile strength for bolts against grade of bolts are same for Indian code and Euro code. The grade of bolt is different as per American Code.

Actual design capacities for different configurations

In this section, capacities of actual simple connection configurations are compared. The configurations compared are as per **Table 4**, with bolts of Grade 8.8 and cleat angle welded.

The design capacities against each configurations are mentioned in **Table 5**.

Table 4. Design configuration

CONFIGURATION	ANGLE SIZE	NO OF BOLTS	DIA OF BOLTS	P_1 (MM)	E_2 (MM)	C (MM)
C1	200X200X20	7	30	76.2	102	580
C2	150X150X16	6	30	76.2	76.2	560
C3	150X150X16	5	30	76.2	76.2	480
C4	150X150X16	6	30	76.2	76.2	560
C5	150X150X16	5	30	76.2	76.2	480
C6	150X150X16	5	30	76.2	76.2	480
C7	150X150X16	5	24	76.2	76.2	420
C8	130X130X12	4	24	76.2	76.2	340
C9	130X130X12	4	24	76.2	50.8	300
C10	90X90X10	3	20	76.2	50.8	230

Table 5. Design capacity

CONFIGURATION	DESIGN CAPACITY AS PER ANSI/AISC 360-16 (MT)	DESIGN CAPACITY AS PER IS800:2007 (CONSIDERING BOLT REDUCTION AS PER EURO CODE)(MT)	DESIGN CAPACITY AS PER IS800:2007 (CONSIDERING BOLT REDUCTION AS PER AMERICAN CODE)(MT)	DESIGN CAPACITY AS PER BS EN 1993-1-1 (MT)
C1	103.55	101.30	113.79	104.80
C2	92.75	93.23	101.92	96.45
C3	72.64	72.36	79.82	74.85
C4	92.75	93.23	101.92	96.45
C5	72.64	72.36	79.82	74.85
C6	72.64	72.36	79.82	74.85
C7	46.49	46.31	51.08	47.91
C8	33.49	33.54	36.81	34.70
C9	39.57	40.91	43.49	38.85
C10	18.46	19.30	20.28	19.96

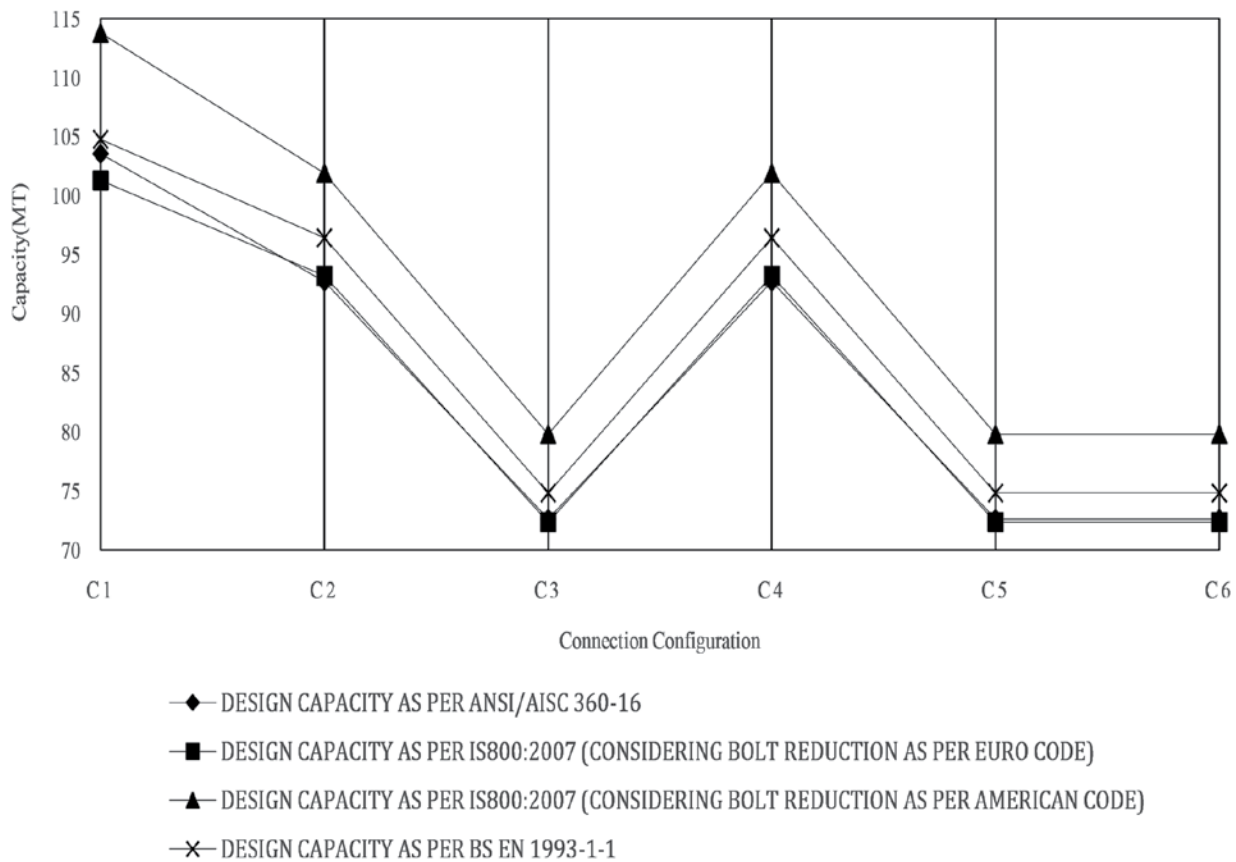


Fig. 4. Capacity of connection configurations as per various codes

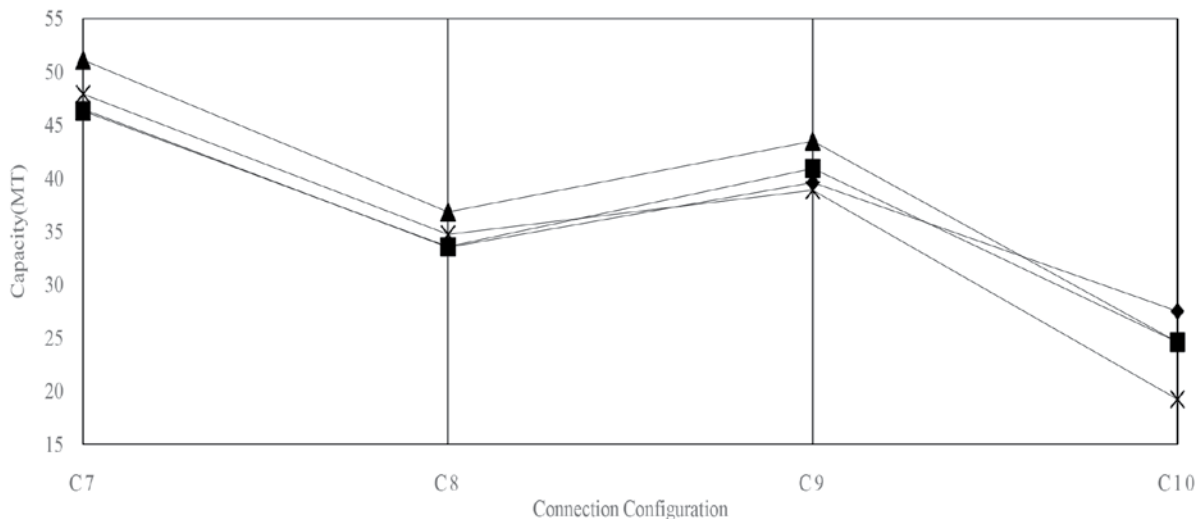


Fig. 5. Capacity of connection configurations as per various code

From **Fig. 4** and **Fig. 5**, if bolt numbers are reduced as per Euro code, then the connection capacity obtained following relevant clause of per Indian code is slightly lower or comparable to values obtained as per Euro Code and if bolt numbers are reduced as per American code connection capacity obtained following relevant clause of per Indian code is higher than American Code. In view of this, reduction of bolts numbers as per Euro code is suggested.



GENERAL NOMENCLATURE

The following definitions apply, as these variables are used in this paper.

F_u = Ultimate Stress of the member material

F_{yb} = Yield Stress of the Bolt material

F_{ub} = Ultimate Stress of the Bolt material

F_{bs} = Actual Shear stress in Bolt

F_{bt} = Actual Tensile stress in Bolt

F_{ubs} = Nominal Shear stress in Bolt

F_{ubt} = Nominal Tensile stress in Bolt

ϕ = Reduction Factor

CONCLUSION

Reduction of number of bolts due to eccentricity is discussed briefly in Indian code without any reference or guiding formula. The reduction is mentioned in tabular form in American code (Steel Construction Manual) and relevant formulas as per Euro Code (Joints in Steel Construction: Simple Joints to Euro Code 3) are readily available. The capacity of a connection achieved as per Indian code when reduced by a factor due to eccentricity of bolts as per Euro code gives comparable results. In view of this, reduction of bolts numbers due to eccentricity as per Euro code is suggested.

Actual capacity of connection obtained as per Indian code will be very high in comparison to that obtained from American and Euro code, if the combined shear/tension interaction of bolt is taken into consideration and reduction of bolt numbers due to eccentricity is ignored.

Prequalified tested connection configurations are available in American code. Also, as per Euro Code, recommended detailing practices are readily available (Joints in Steel Construction: SIMPLE JOINTS TO EURO CODE 3), which are tested and can be considered equivalent to Pre-qualified connections of American code. Provision of Prequalified connection is required to be added as per Indian Code.

REFERENCES

1. AISC Committee on Specifications, 2016, Specification for Structural Steel Buildings, 2016, ANSI/AISC 360-16
2. European Committee for Standardization (CEN), 2004, Eurocode 3: Design of steel structures -Part 1-8: Design of joints, BS EN 1993-1-8:2005
3. Structural Engineering and Structural Sections Sectional Committee, CED 7, 2007, Indian Standard General Construction In Steel - Code of Practice (Third Revision), IS800:2007
4. The Steel Construction Institute, The British Constructional Steelwork Association Limited, Joints in Steel Construction: SIMPLE JOINTS TO EURO CODE 3
5. American Institute of Steel Construction, INC., STEEL CONSTRUCTION MANUA.



An Analytical Study on Wind Pressure Distribution on Rectangular Tall Building with Setback and Twist using Computational Fluid Dynamics

Vigneshwaran Rajendran, Prabavathy Shanmugasundaram

Department of Civil Engineering, MepcoSchlenk Engineering College, Sivakasi, Tamil Nadu

✉ vignesh.rajen.93@gmail.com

ABSTRACT

Due to lack of land availability in cities there is a great demand for tall buildings. These tall buildings are highly subjected to predominate wind loads. For the present study four building models are chosen such as Square Building (SB), Twist Square Building at 45° (TSB), Building with Setback (BS) on all sides and Twist Square Building with setback (TSBS) on all sides. The investigation of wind loads on tall buildings are made possible with the help of Computational Fluid Dynamics (CFD) available in ANSYS Fluent software. The simulation is carried for a particular 0° wind angle at a wind velocity of 10 m/s. From the results the pressure coefficient (C_p) on each face of the building are calculated. Further formation of wake regions behind the building, flow pattern are studied.

Keywords: Turbulence model; Wake regions; Computational Fluid Dynamics (CFD); Wind flow.

INTRODUCTION

For tall buildings, wind load is the dominant load criterion to be considered in construction. Since the buildings are cantilever structure to the ground, a large base moment is generated, the base moment is larger when the structure is slenderer and subjected to lateral loads. Hence there is a need to investigate the actual wind load loads on buildings. The pressure coefficient value for the regular plan shaped building is available in various wind Engineering codes such as AS/NUS 1170-2; ASCE 7-10; BS 6399-2 (1997); IS 875 (Part 3) 2015. For unconventional and irregular plans there is no proper Pressure Coefficient (C_p) values. The study of actual wind load on buildings is carried out by analytically and Experimentally. An experimental study is carried out using wind tunnel but it is costlier and time-consuming. The analytical study is done numerically using Computational Fluid Dynamics (CFD) incorporated using ANSYS Software. The overall strength of the structure depends upon strength, durability and risk of failure of the structure under extreme loads such as wind and cyclone. Many previous literatures carried out wind pressure distribution around the buildings. Chitra Ganapathi et. al (2017) investigated the upstream terrain characteristics for rectangular plan shape tall building is studied. The models are scaled to 1:2:3 and simulated through a wind tunnel. The results of mean pressure and force coefficient are compared with international codes of standards. Biswarup Bhattacharyya and Sujit Kumar Dalui (2018) studied the pressure distribution around E plan shape tall building for different wind angles such as 0° to 180° at an interval of 30°. Validation of the results is done by both numerically and experimentally. Finally, the wind pressure at various different faces is computed. Monalisa Mallick et al. (2018) investigated the modeling of wind pressure coefficient on C-Shaped building models. A wind velocity of 12.9 m/s is applied to investigate the wind pressure distribution for different angles 0° to 180° at an interval of 30°. Hence from the result of previous work, there is a need to investigate the wind pressure distribution for different plan shape tall building and hence this paper studies the wind flow around square building and compared with the square building of twist 45° from the base.

Input Parameters

In order to study the wind flow around the building, the actual load 50 m/s is scaled 1:5 ratio and 10 m/s is given at the inlet of the computational domain. Free slip is considered at the side wall of the computational domain and No-slip is consider at the floor of the computational domain. Wind velocity of 0 m/s is given at the outlet. Usually, wind velocity varies with height and so adjacent to the earth's surface is almost zero. The velocity of the wind increases eventually at every gradient height. Wind speed is nearly unaffected by surface friction and the movement of the wind is mostly by local and seasonal winds. Since the

wind speed is affected by topography it is called an atmospheric boundary layer. Wind speed within the layer is given as

$$V_z = V_g \left(\frac{Z}{Z_g} \right)^{1/\alpha} \quad (1)$$

Where V_z is the mean wind speed at height Z from the ground, V_g assumed constant above the ground level, Z represents the height above the ground and α represent power law of 0.087 for open terrain and 0.20 for buildup urban. **Fig. 1** shows the details of the models used for CFD simulation.

Computational domain size and Meshing

In order to study flow simulation in ANSYS, the computation domain is built based on certain guidelines given by Franke (2004). From the building rear side, top, right, and left 5H and 15H in the leeward side of the building. Where H represents the height of the building. The size of the domain is fixed such that the flow should not be disturbed, at the time of computation. Figure 1 (a) shows the side view of the size of the computational domain and **Fig. 1 (b)** shows the elevation view of the computational domain. Meshing is done in the form of a grid and a very fine mesh is applied for building. **Fig. 2 (a)** shows the meshing details of square building (SB) of nodes 40,371, Element 2,11,104, **Fig. 2 (b)** shows the meshing details of Square Building with Twist (SBT) of nodes 40,205 and element 2,09,709, **Fig. 2 (c)** shows the meshing details of Isolated building with setback (IBS) of nodes 8,83,279 and element 50,71,797 and **Fig. 3 (d)** shows the meshing details of Isolated twist building with setback (ITBS) of nodes 8,83,151 and element 50,70,203.

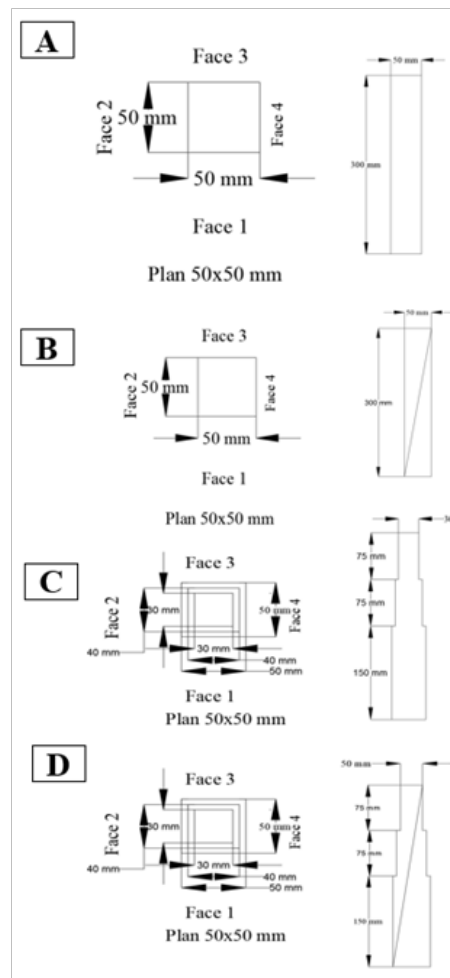


Fig. 1. Plan and elevation for building models (A) Square Building (SB), (B) Twist Square Building at 45° (TSB), (C) Building with Setback (BS) on all sides, (D) Twist Square Building with setback (TSBS)

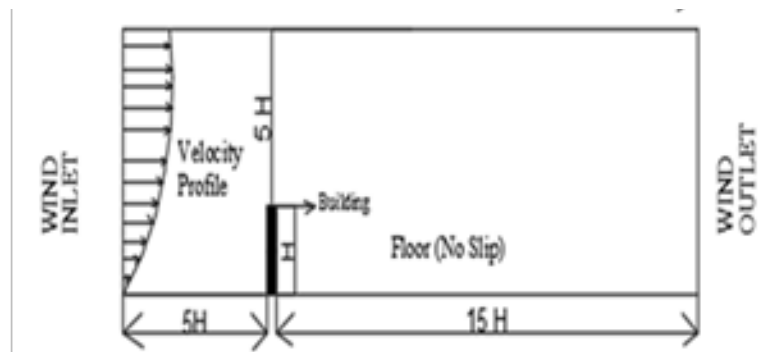


Fig 1. Size of the Computational domain (a) side view of the domain (b) Plan view of the domain

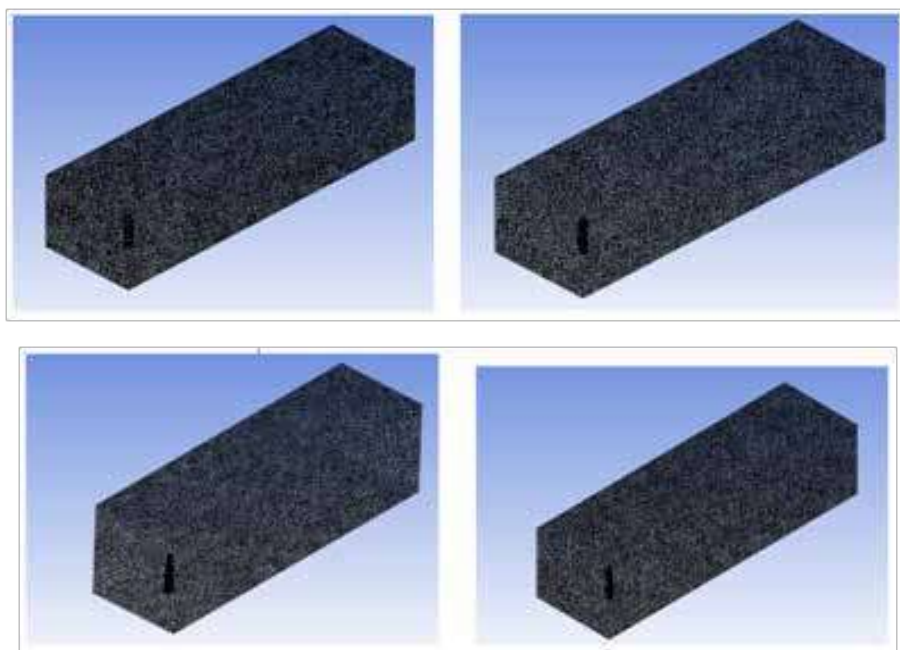


Fig 2. Meshing of Computational domain (A) Square Building (SB), (B) Twist Square Building at 45° (TSB), (C) Building with Setback (BS) on all sides, (D) Twist Square Building with setback (TSBS)

Validation

Before starting the CFD analysis validation is done for a square building of plan 50 mm X 50 mm and of height 300 mm. Turbulence k- ϵ is applied for flow simulation because its convergence factor is faster. The obtained pressure Coefficient C_p is compared with wind Engineering code IS 875 Part-3 (2016). **Table 2** shows the validation of Pressure Coefficient with wind Engineering Codes.

Table 2. Validation of the pressure coefficient with wind engineering codes

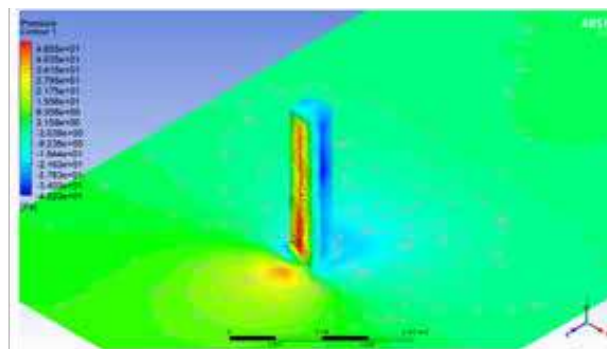
Wind loading code	Face A (C_p)	Face B (C_p)	Face C (C_p)	Face D (C_p)
ANSYS Fluent	0.9	-0.20	-0.86	-0.85
IS 875	0.8	-0.25	-0.8	-0.8

RESULTS AND DISCUSSION

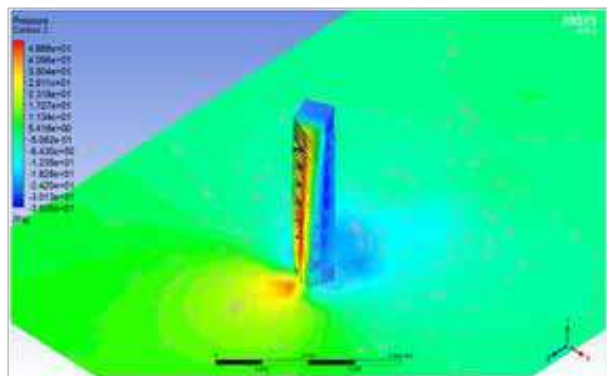
To study the wind flow around the building the simulation is carried out for Square Building (SQ) and Square Building with twist 45° from the base. The result discusses the pressure distribution, flow pattern, Identification of wake regions.

Pressure Distribution

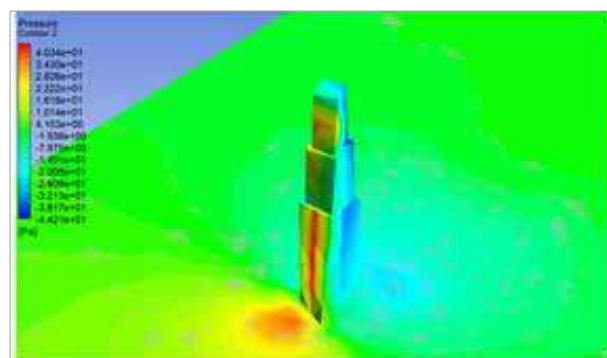
When the wind flows around the building, high positive pressure is obtained in the upstream side of the building and negative pressure occurs in the downstream of the building. The wind pressure distribution in the building surface is not constant it varies continuously. Pressure variation varies from point to point on the building surface. The analysis is carried out for 0° wind angle for various buildings such as Square Building (SQ) and Square building with twist 45° from the base (SQT), Isolated Building with Setback (IBS) and Isolated twist square building with setback (ITBS). **Fig. 3** shows the wind pressure distribution along the Square Building (SB). From the contour of **Fig. 3** indicates the pressure distribution red color in the figure indicate high pressure which occurred in the windward face of the building and building experience low pressure in the leeward face of the building indicated in blue color. **Fig. 3 (a)** SB (b) SQT (c) IBS (d) ITBS shows the wind pressure distribution. Pressure variation on the building is directly influenced by the wind flow patterns. **Table 3** shows the pressure coefficient on various face of the building. **Fig. 4** shows the graphs for wind pressure distribution on various faces of the building for Square Building (SB) and for Square building with twist 45° (SQT). **Fig. 5** shows the graph for wind pressure distribution for Isolated square building with setback (IBS) and Isolated twist square building with setback (ITBS).



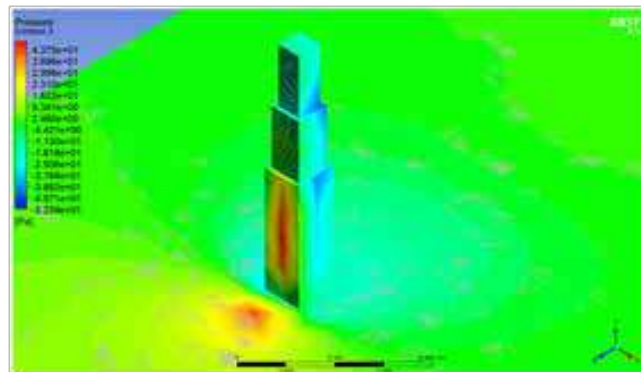
(a)



(b)



(c)



(d)

Fig 3. Wind pressure distribution (a) SB (b) TSB (c) BS (d) TSBS

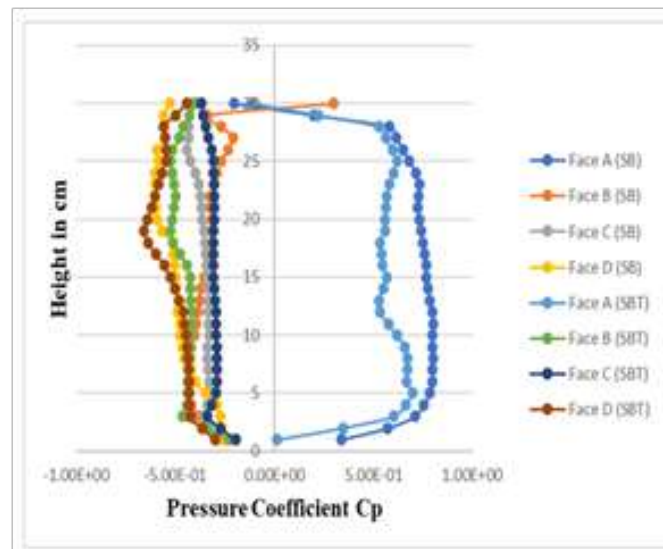


Fig 4. Graph of wind pressure on various faces of the buildings

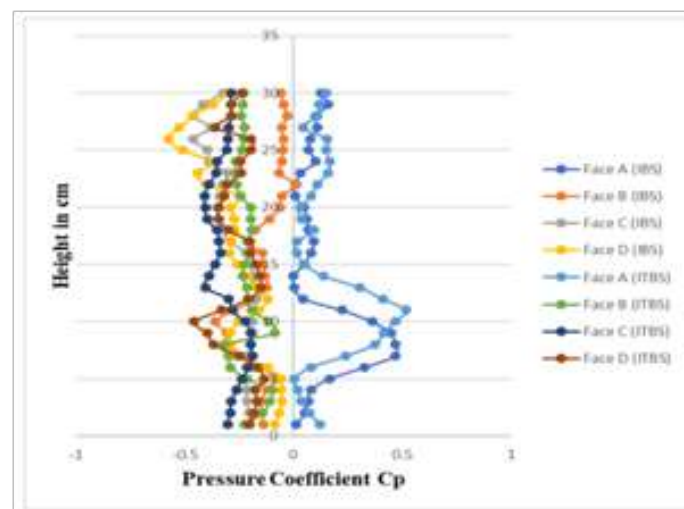


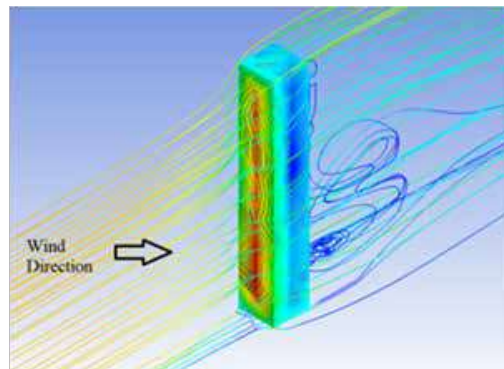
Table 3. Pressure coefficient on various faces of the building

Building Model	Face A	Face B	Face C	Face D
SB	0.9	-0.20	-0.86	-0.85
TSB	0.51	-0.22	-0.25	-0.34
BS	0.579	-0.13	-0.27	-0.27
TSBS	0.412	-0.21	-0.30	-0.25

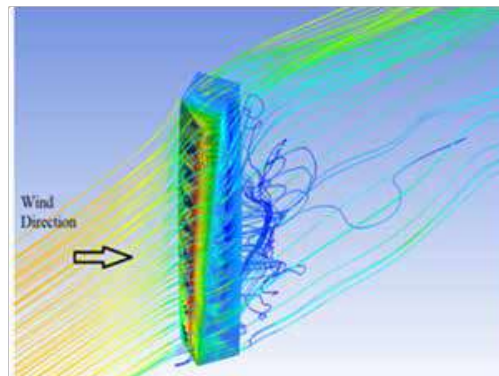
From **Table 3** display the pressure coefficient on various faces of the buildings. On Face A of the SB there is 43% reduction in pressure coefficient (C_p) when compared to SQT followed by 35.7% when compared to IBS and 51.3% reduction on ITBS when compared to SB. On face B of SB 10% increase C_p when compared to SQT, followed by 15% decrease in C_p when compared to IBS and 5% increase in pressure when compared to ITBS. On Face B experiences negative sign since it lies in the leeward face of the building. On face C there is 29% decrease in pressure coefficient when compared to SQT followed by 68.7 reduction in C_p when compared with IBS and 66% reduction when compared to ITBS. On face D experiences 60% reduction in C_p when compared to SQT followed by 68.5% reduction in C_p when compared with IBS and 70.6% reduction in C_p when compared with ITBS. From the results it is clear that modification of shape and orientation of the building significantly reduces the wind load on buildings. Reduction of wind load on building significantly improves the comfort of the occupancy inside the building. For building with twist there is a change of positive and negative pressure on the windward face of the building i.e in face A, Due to the twisting nature of the building, wind gets diverges and change of positive and negative pressure are occurred.

With the regard to pressure distribution on building depends on side and aspect ratio. Side ratio is defined as depth to the Width and aspect ratio is defined as height to the square root of the product of depth and width. Side ratio has very little influences in the distribution of wind pressure along vertical directions. When the wind incidence on the large frontal area there is reduction in stiffness in the along the direction of the wind force.

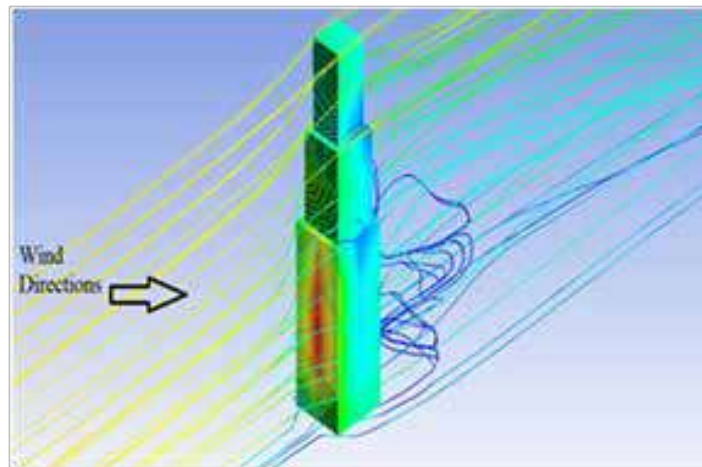
Flow Pattern



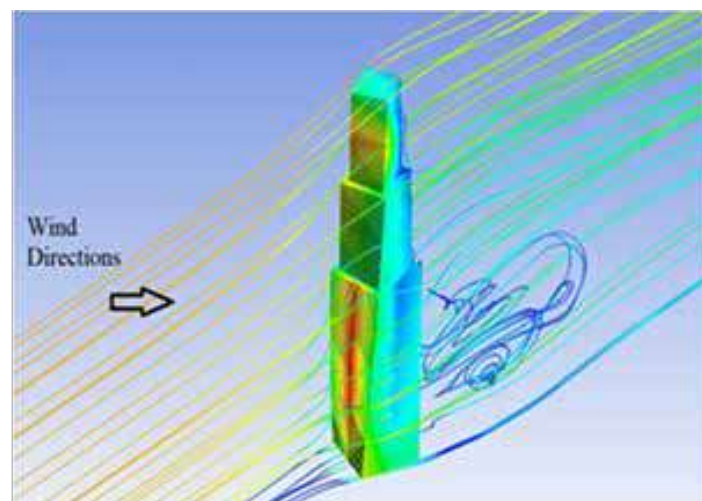
(a)



(b)



(c)



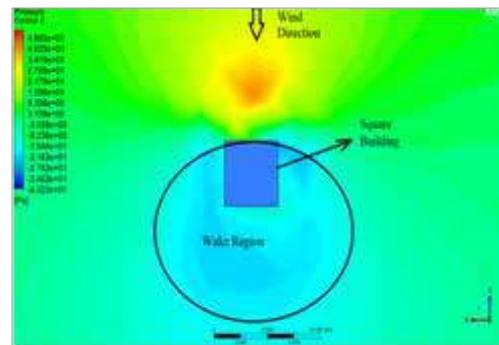
(d)

Fig 6. Streamline generation along buildings(a) SB (b) TSB (c) BS (d) TSBS

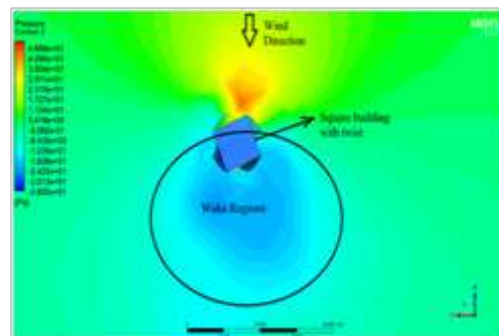
The wind flow pattern is different for different shape building. Depending upon the building shape the formation of the vortex will be varying. For bluff bodies such as building the vortex shedding frequency should not matches with the frequency of the building when both the frequency matches then failure will occur. The failure of the Tacoma narrows bridge is of this type. **Fig. 6 (a)** Shows the streamline generation for Square Building (SB) and **Fig. 6 (b)** shows the Streamline generation for Square Building with Twist (SQT). **Fig. 6 (a)** observed that steady streamlines are developed at the base of the building and from **Fig. 6 (b)** observed that disturbed streamlines are developed in Square building with a twist at 45° .

WAKE REGIONS STUDY

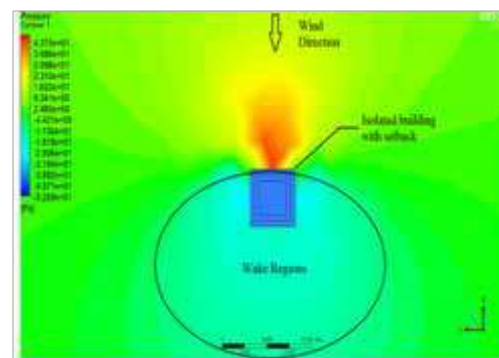
The study of wake regions is essential to improve the occupancy comfort inside the building and to have a proper wind flow pattern. Usually, wake regions are formed in the regions of the leeward side of the building i.e in the downstream of the bluff body and in the regions of low velocity. For bluff bodies such as buildings the region of wake formation will be larger but for streamline body, i.e for aerodynamically modified buildings, the formation of wake regions will be thin. Wake is generally the separated body behind the bluff body such as buildings. **Fig. 7 (b)** shows the identification of wake regions for Square Building (SB), **Fig. 7 (b)** shows the identification of wake regions for square building with twist 45° (SBT), **Fig. 7 (c)** shows the identifications of wake regions for Isolated square building with setback (IBS) and **Fig. 7 (d)** shows the identification of wake regions for Isolated twist square building with setback (ITBS). The regions of formation of wake is larger for SQT and less for IBS.



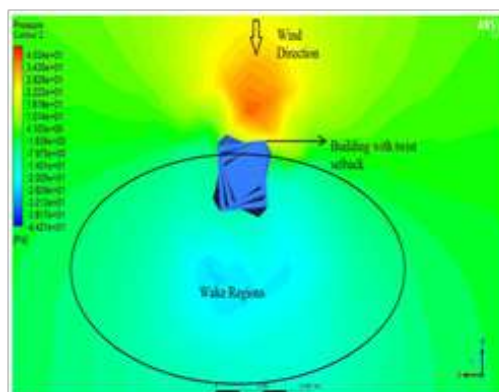
(a)



(b)



(c)



(d)

Fig 7. Identification of wake regions for (a) SB (b) TSB (c) BS (d) TSBS



CONCLUSIONS

The present study, the following are the conclusions are made drawn

- On Face A of the SB there is 43% reduction in pressure coefficient (C_p) when compared to SQT followed by 35.7% when compared to IBS and 51.3% reduction on ITBS when compared to SB. On face B of SB 10% increase C_p when compared to SQT, followed by 15% decrease in C_p when compared to IBS and 5% increase in pressure when compared to ITBS.
- Present study proves that the building with minor modifications such as setbacks, twist leads to reduction of wind loads on buildings.
- From the distribution of pressure, it is observed that windward face of the building experiences positive pressure coefficient because of solid wind and because of frictional flow wind separations and vortex formations leeward faces experiences negative pressure, but even in the windward face's experiences negative pressure because of separation of low uplift, side and backwash due to wind.
- There is no certain direct value available in any wind Engineering codes for predicting the pressure coefficient (C_p) for building with irregular shape and twisting nature. Computational Fluid Dynamics is the robust tool in predicting the wind flow around bluff body such as buildings.

ACKNOWLEDGMENT

The research is conducted in Department of Civil Engineering of Mepco Schlenk Engineering College, Sivakasi, Tamil Nadu, India and special thanks to Institute of Engineers (IEI) for their financial support under Grant in aid Scheme (Project Id: DR2020004).

REFERENCES

1. R. E. Britter, S. R. Hanna, "Flow and Dispersion in Urban areas", Annual Review of Fluid Mechanics 35: 469-496, 2002.
2. Biswarup Bhattacharyya, Sujit Kumar Dalui. "Investigation of mean wind pressures on E plan shaped tall building". Wind and Struct 26 (2): 99-114, 2018.
3. Bert Blocken, StafRoels, Jan Carmeliet, Modification of pedestrian wind comfort in the Silvertop Tower passages by an automatic control system. Journal of Wind Engineering and Industrial Aerodynamics 92:849-873, 2004.
4. B. Blocken, P. Moonen, T. Stathopoulos and J. Carmeliet. "Numerical Study on the Existence of the Venturi Effect in Passages between Perpendicular Buildings". Journal of Engineering Mechanics Vol. 134, No. 12, 2008.
5. S. Chitra Ganapathi, P. Harikrishna, S. Selvi Rajan. "Effect of upstream terrain characteristics on aerodynamic coefficient of structures". Archives of Civil and Mechanical Engineering 17:776-785, 2017.
6. J. Franke, C. Hirsch, A. G. Jensen, "Recommendations on the use of CFD in wind engineering, in proceedings of International conference on urban Wind Engineering and building Aerodynamics: COST C14: Impact of wind and storm on city life and built Environment", Rhode-saint- Genese, Belgium, May 2004.
7. Fluent User Guide: 19.2. 2019.
8. IS:875 – 2015 (Part 3). Indian Standard Code of Practice for design loads. Wind loads
9. JimingXie, "Aerodynamic optimization of super tall building and its effectiveness assessment". Journal of wind Engineering and Industrial Aerodynamics. 130: 88-98, 2014.
10. S. Lamb, K. C. S, Kwoka, "The fundamental human response to wind-induced building motion". Journal of Wind Engineering and Industrial Aerodynamics, 165:79-85, 2019.
11. Monalisa Mallick, Abinash Mohanta, Awadhesh Kumar, Vivek Raj. "Modelling of wind pressure coefficients in C-Shaped Building Models". Modelling and Simulation in Engineering, 2018.
12. Norasikin Mat Isa, Nurul Fitriah Nasir, Azmahani Sadikin, Janil Ariff, Hairul Bahara, Investigation of wind behavior around high rise building. IOP Conference Series: Material Science Engineering 243, 012037, 2017.
13. Shi Zhang, Xiaoda Xu, "Pedestrian level wind around super tall building: Effect of podium" International conference Series: Earth and Environment Science, 218:012036, 2019.
14. Yukio Tamura, Xiaoda Xu, Qingshan Yang, "Characteristics of pedestrian-level Mean wind speed around square buildings: Effects of height, width, size and approaching flow profile". Journal of Wind Engineering and Industrial Aerodynamics 192:74-87, 2019.



Selection of suitable Quantity of Fly Ash and Water to Achieve Desired Workability and Strength of Geopolymer Concrete

Subhash V Patankar¹, Sanjay S Jamkar², Yuwaraj M Ghugal³

Department of Civil Engineering, Sanjivani College of Engineering, Kopergaon, Savitribai Phule Pune University¹

Department of Applied Mechanics, Government College of Engineering, Aurangabad, Maharashtra²

Department of Applied Mechanics, Government College of Engineering, Karad, Maharashtra³

✉ sypatankar11@gmail.com

ABSTRACT

This paper presented the effect of quantity of fly ash and total quantity of water in the design of geopolymer concrete on the basis of fineness of fly ash to achieve desired workability and compressive strength. Sodium silicate solution containing Na₂O of 16.45%, SiO₂ of 34.35% and H₂O of 49.20% and sodium hydroxide solution with concentration of 13 Mole were used as alkaline activators. Geopolymer concrete mixes were prepared by maintaining solution to fly ash ratio of 0.35. Workability of freshly mixed geopolymer concrete was measure by flow table apparatus. Geopolymer concrete cubes of 150 mm side were cast and tested for compressive strength after heated in oven at 900C for specified period of heating and rest period. Test results show that the fineness of fly as plays vital role in selecting quantity of fly ash in the design mix to achieved desired strength. Similarly quantity of water plays important role in balancing workability but compressive strength reduces with increase in quantity of water similar to cement concrete.

Keywords: Geopolymer concrete; Fly ash fineness; Water, Flow; Strength.

INTRODUCTION

Concrete is one of the most important civil engineering material and its consumption is next to water. It might be due to ease in construction, low cost, strength and durability as compared to other construction materials and most important is the availability of cement used as binding material. Every year the production of Portland cement is increasing with the increasing demand of construction activities. Therefore the rate of production of carbon dioxide released to the atmosphere is also increasing. World production of hydraulic cements is close to one thousand million tons per year. The climatic change due to global warming is one of the major issue concerning with the environmental pollution. The global warming is caused by the emission of greenhouse gases like CO₂ to the atmosphere by various industries. Cement industry is also one of the major contributors for the emission of greenhouse gasses which is about 1.35 billion tons annually [1, 2].

On the other side, fly ash is the waste material of coal based thermal power plant, available abundantly but creates disposal problem. Several hectors of valuable land is required for disposal of fly ash and bottom ash. In terms of fuel, coal-fired plants account for 56% of India's installed electricity capacity, compared to South Africa's 92%; China's 77%; and Australia's 76%³. For every ton of fly ash used in place of Portland cement saves about a ton of carbon dioxide emission to the atmosphere [4]. As fly ash is light in weight and easily flies, creates severe health problems like asthma, bronchitis, etc. According to the survey, the total fly ash production in the world is about 780 million tons per year [2, 6]. In India, more than 280 million tons of fly ash is produced annually, out of which 50-65 % fly ash is used in the production of Portland Pozzolana Cement, partial replacement of cement and workability improving admixture in concrete and also in the production of cellular blocks, bricks and in soil stabilization [6]. With silicon and aluminium as the main constituents, fly ash is an effective cement replacing material. The concrete made with fly ash is eco-friendly and can be made to replace more than 50% cement to produce high volume fly ash concrete [7, 8, 9].

For full utilization of fly ash, Davodevits [3, 4] suggested the activation process in which cement is totally replaced by pozzolanic material and activated by alkaline solutions known as geopolymer. The development of geopolymer concrete can provide a solution to produce greener concrete for sustainable development. Davidovits [5] highlighted the global warming

impact due to CO₂ emission from Portland cement production and also explained the development of Geopolymeric Chemistry and applications of geopolymer cement and concrete. Talling et al. [10] studied the use of alkalis in geopolymer binder systems. The effect of the molar composition of the oxides present in the mixture and the water content used on the polymerization process has been studied by Barbosa et al. [11]. Jaarsveld et al. [12] observed that the water content have a substantial effect on the final properties of the geopolymer while solution-to-fly ash ratio is not a relevant parameter as observed by Palomo and Fernandez [13]. Djwantoro et al. [14] found water content alone did not have any significant influence on the compressive strength provided the water-to-geopolymer solids ratio by mass remained constant. Hardjito et al. [15] studied the effects of the mixing time and the rest period while Wu and Sun [16] investigated the effect of amounts of chemical activator and various curing conditions using light weight aggregate. Ranganath and Saleh [17] highlighted the effect of fly ash, water content, sodium silicate-to-sodium hydroxide ratio and the duration of elevated temperature curing on the properties of geopolymer concrete whereas Al Bakri et al. [18], Jamkar et al. [19] observed the increase in compressive strength with increase in fineness of fly ash. Rangan [20] have proposed the mix design procedure for production of fly ash based geopolymer concrete whereas Anuradha et al. [20] have presented modified guidelines for Mix design of geopolymer concrete using Indian standard.

In the present investigation, an experimental investigation is carried out to study the effect of fineness of fly ash and quantity of water on workability in terms of flow and degree and duration of heat curing on the compressive strength of fly ash based geopolymer concrete after a specified rest period.

EXPERIMENTAL PROGRAM

Materials

In the present experimental work, low calcium fly ash obtained from coal based Thermal Power plant at Eklahare, Nasik was used as source material. **Table 1 and Table 2** show the Physical properties and chemical composition of five different types of fly ash used in the investigation. Coarse aggregates of 20mm, 12.5mm and locally available Godavari river sand as fine aggregate were combined in proportions 43.55%, 23.45% and 33% respectively for making geopolymer concrete. The fineness modulus of combined aggregates is reported as 5.64. **Table 3 and Table 4** show the grading of fine aggregate and coarse aggregate samples. The laboratory grade sodium hydroxide in flake form and sodium silicate solution were used as alkaline activators. Concentration of sodium hydroxide solution was maintained at 13M as per past research [19, 22].

Table 1. Physical properties of different types of fly ash

Physical properties	Processed Fly ash			Unprocessed fly ash	
	F-1	F-2	F-3	UF-1	UF-2
Specific surface area, (m ² /kg)	542	430	367	327	252
Specific gravity	2.25	2.25	2.25	2.3	2.35

Table 2. Physical properties of different types of fly ash

Chemical Composition	Processed fly ash, (%)			Unprocessed fly ash, (%)	
	F-1	F-2	UF-3	UF-1	UF-2
SiO ₂ + Al ₂ O ₃ + Fe ₂ O ₃	93.82	91.66	91.66	91.74	92.14
SiO ₂	59.24	56.38	57.24	56.73	57.30
MgO	2.4	2.09	1.90	1.37	1.48
SO ₃	0.98	0.88	1.02	1.34	1.34
Na ₂ O	0.42	0.39	0.66	0.69	0.79
Total chloride	0.033	0.026	0.027	0.027	0.023
Loss of ignition.	0.90	1.00	1.30	2.30	2.50

**Table 3.** Grading of fine aggregate

Sr. No.	IS Sieve size Designation (mm)	Cumulative Percentage Passing for River Sand	Remark
1	10	100	Confirming to grading zone –II as per IS 383
2	4.75	92	
3	2.36	84.80	
4	1.18	59.90	
5	0.600	35.30	
6	0.300	10.60	
7	0.150	0.60	
8	0.075	0.10	

Table 4. Grading of coarse aggregates

Sr. No.	IS Sieve size Mm	Cumulative Percentage Passing for			
		CA-I 20mm	CA-II 12.5mm	Combined Aggregate CA-I : CA-II 65 : 35	Required grading as per IS 383:1970
1	40	100	100	100	100
2	25	100	100	100	--
3	20	84.40	100	89.86	90-100
4	16	06.80	100	39.42	--
5	12.5	0.40	96.50	34.04	--
6	10	0.00	76.40	26.74	25-35
7	4.75	0.00	0.90	0.32	0-10
8	2.36	0.00	0.00	0.00	--

Preparation of Geopolymer Concrete Mixes

Quantities of ingredients of geopolymer concrete are calculated by considering solution-to-fly ash ratio of 0.35 and sodium silicate-to-sodium hydroxide ratio by mass of 1. Moreover, concentration of sodium hydroxide in terms of molarity of 13, and concentration of Sodium silicate solution with Na₂O of 16.37%, SiO₂ of 34.35% and H₂O of 49.28% were maintained constant as per past investigation [22]. Preparation of geopolymer concrete is similar to that of cement concrete. Two types of coarse aggregates, sand and fly ash were mixed in dry state. Then add prepared mixture solution of sodium hydroxide and sodium silicate along with extra water based on water-to-geopolymer binder ratio and mix thoroughly so as to give homogeneous mix. It was found that the fresh fly ash-based geopolymer concrete was viscous, cohesive and dark in colour. After making the homogeneous mix, workability of fresh geopolymer concrete was measured by flow table apparatus similar to cement concrete as per IS:1199-1959. As freshly mixed geopolymer concrete is very viscous and water comes out during polymerisation reaction, slump cone test is not suitable to measure the workability. Similarly, compaction factor apparatus is also not suitable as concrete fall very slowly and most of concrete stick to the top and bottom hoppers. So, for geopolymer concrete, it is recommended to use flow table apparatus to give comparatively good idea about workability of geopolymer concrete. After measuring the workability, concrete cubes of side 150 mm were cast in three layers and compacted similar to cement concrete. After 24 hours of casting, all cubes were demoulded and then placed in an oven for thermal curing (heating). To avoid the sudden variation in temperature, the concrete cubes were allowed to cool down up to room temperature in an oven itself. Three cubes were cast for each mix and tested for compressive strength after heating in oven for specified period and thereafter 1, 2, 3, 7 and 28 days of rest period.

RESULT AND DISCUSSIONS

Effect of Quantity of Water on Workability of Geopolymer Concrete

As per past research [22, 23], the suitable quantity of water required for making geopolymer concrete is up to 160 kg/m^3 for water-to-geopolymer binder ratios (0.25, 0.30, 0.35, 0.40, 0.45 and 0.50). Similarly beyond solution-to-fly ash ratio of 0.35, rate of gain of strength is not much significant. So to find minimum quantity of water to achieve desired degree of workability, 100 to 150 kg/m^3 quantity of water is taken with a difference of 10 kg/m^3 for solution-to-fly ash ratio of 0.35. Five different samples of fly ash were considered with different fineness as mentioned in **Table 1**.

Fig. 1 shows the effect of quantity of water on workability of geopolymer concrete for water-to-geopolymer binder ratio of 0.35, solution-to-fly ash ratio of 0.35 with different fly ash fineness. It is observed that the workability in terms of flow decreases with increase in fineness of fly ash for same quantity of water. Workability in terms of flow increases with increase in quantity of water but reduces with higher fineness. It is observed that the low degree of workability can be achieved when the quantity of water is in between 100 to 110 kg/m^3 for all types of fly ashes. Similarly for higher degree of workability, more quantity of water is required for same fly ash fineness. So, depending on fineness of fly ash, it is possible to choose quantity of water for design of geopolymer concrete mixes.

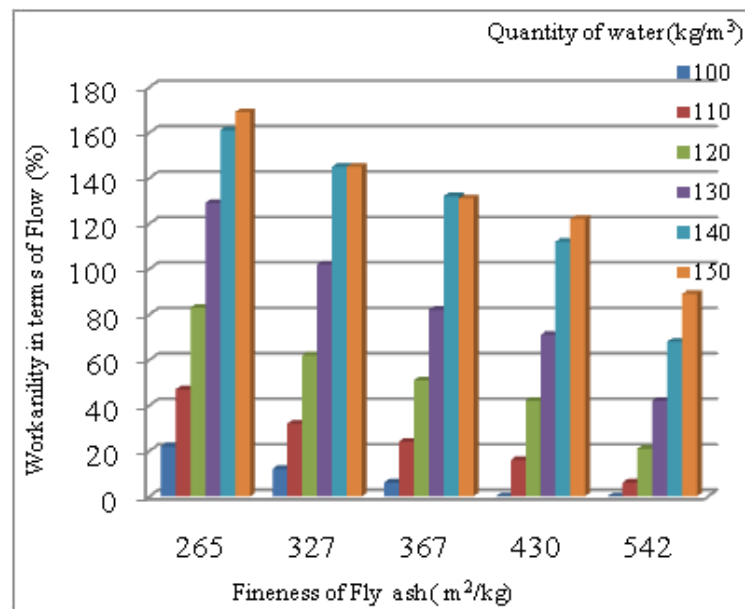


Fig. 1. Effect of fineness of fly ash on workability of geopolymer concrete for different quantities of water at W/GPB of 0.35

Effect of Degree of Heating

For the development of geopolymer concrete, temperature and duration of heating plays an important role in the activation process which is accelerated at and above 30°C temperature as mentioned by Rangan [20]. Water curing is required to maintain moisture during the process of hydration in cement concrete while, in polymerisation process, heat is required. So for oven heating process, instead of heat curing or oven heating, we may call 'degree of heating'. In the present investigation, cubes were demoulded after 24 hours of casting and then place in oven for heating. After specified degree of heating, oven is switched off and cubes are cooled down to room temperature in oven itself. Then after 24 hours of heating, cubes are removed from oven and place under normal room temperature for specified period and then compression test is carried out similar to cement concrete.

Figs. 2 to 4 shows the effect of temperature, duration and test period on compressive strength of geopolymer concrete. Test period is the time elapsed between the cubes remove from the oven and place in the normal atmosphere to the time of testing for compressive strength. Compressive strength test is carried out after test period of 1, 2, 3, 7 and 28 days after oven heating. This was done when room temperature is in between 30 to 35°C . For that, the quantity of fly ash is considered as 400 kg/m^3 having fineness of $430 \text{ m}^2/\text{kg}$ at water-to-geopolymer binder ratio of 0.35 and solution-to-fly ash ratio of 0.35. To check the degree of heating, 40 , 60 , 90 and 120°C temperature were considered each for heating period of 8, 12 and 24 hours in oven and

also natural sunlight curing was carried out in summer season with average day time temperature of 39 to 44°C to check the possibility of natural curing of geopolymer concrete.

Figs. 2 and 3 shows the effect of test period on compressive strength of fly ash based geopolymer concrete for various degree of heating for duration of 8 hours and 12 hours respectively by maintaining W/GPB ratio of 0.35

It is observed that the compressive strength of geopolymer concrete increases with increase in degree and duration of heating. But there is no large variation in compressive strength of geopolymer concrete beyond degree of heating at 90°C. But more than 90% strength is achieved just after one day test period at 120°C. But for higher duration of heating at 120°C temperature, hair cracks are developed on cube surface. It might be due to fast evaporation of water from geopolymer concrete cubes in oven. Similarly to achieved approximately same compressive strength of geopolymer concrete at 60°C, need 28 days of rest period. If duration of heating increases rate of gain of strength is also increase as observed in **Figs. 2, 3 and 4**. But at degree of heating at 40°C, duration of heating should be 24 hours and also achieved nearly same strength after rest of 28 days. Similarly slightly lower but considerable compressive strength is achieved at natural sunlight curing at rest period of 24 hours. It might be due to variation in day and night time temperature in natural curing. That means geopolymer concrete can be to produce without heating and best alternative to cement concrete specifically in summer season where Government not allowed the construction activities due to scarcity of water. That means desired strength can be achieved by increasing temperature with less duration of heating and rest period. From **Figs. 2, 3 and 4**, it is possible to select degree and duration of heating to achieve desired strength of fly ash based geopolymer concrete.

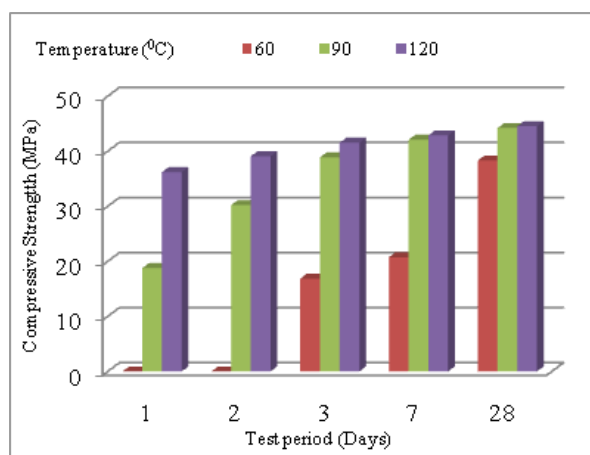


Fig. 2. Effect of test period on compressive strength of geopolymer concrete for various degree of heating for 8 hours at W/GPB ratio of 0.35

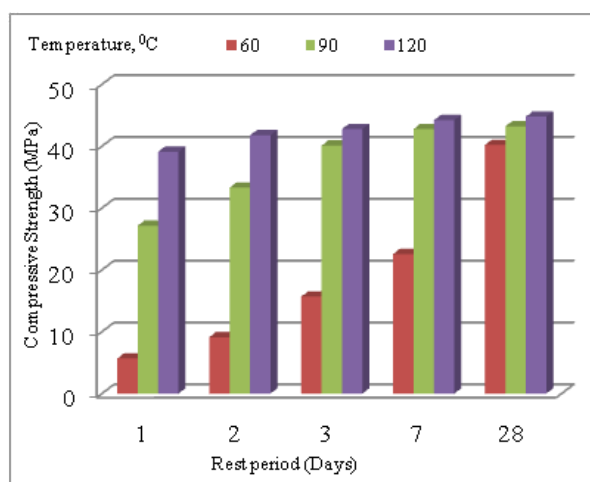


Fig. 3. Effect of test period on compressive strength of geopolymer concrete for various degree of heating for 12 hours at W/GPB ratio of 0.35

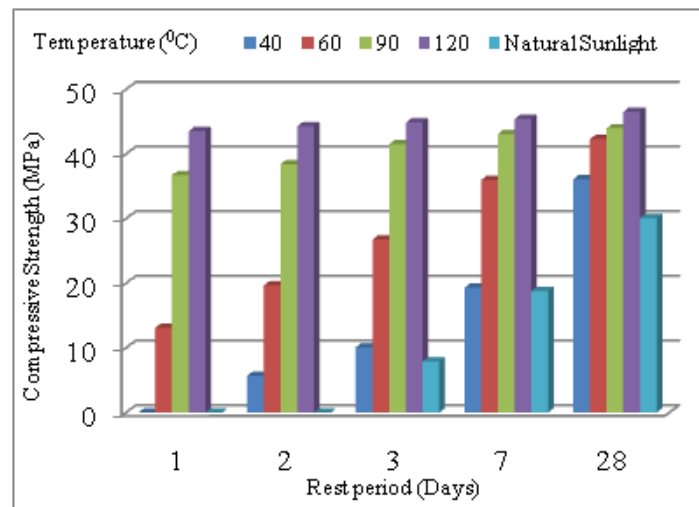


Fig. 4. Effect of test period on compressive strength of geopolymer concrete for various degree of heating for 24 hours at W/ GPB ratio of 0.35

Effect of Quantity of Fly Ash

Fig. 5 shows the effect of quantities of fly ash for different fineness on compressive strength of fly ash based geopolymer concrete at solution-to-fly ash ratio of 0.35 with all other test variables were held constant. Compressive strength test is carried out on three cubes cured in an oven at 90°C for 8 hours of duration and tested after test period of three days for each quantity of fly ash with different fineness. It is observed that the compressive strength of geopolymer concrete increases with increase in quantity of fly ash for same fineness. The rate of gain of strength is linear for all the quantities of fly ash with Blains fineness of 265 and 327 m²/kg, while fly ash with higher fineness shows linear variation in strength up to 550 m²/kg quantity of fly ash. But there is no appreciable change in compressive strength beyond quantities of fly ash of 550 kg/m³. It might be due to large volume occupied by fly ash with lower density and produced highly viscous mix due to which the concrete is not properly compacted. That means the suitable quantity of fly ash used for making geopolymer concrete is in between 250 kg/m³ to 550 kg/m³. It is also observed that the compressive strength can be increase by increasing fineness of fly ash. So, both, quantity and fineness of fly ash are considered in the development of proposed mix proportioning procedure.

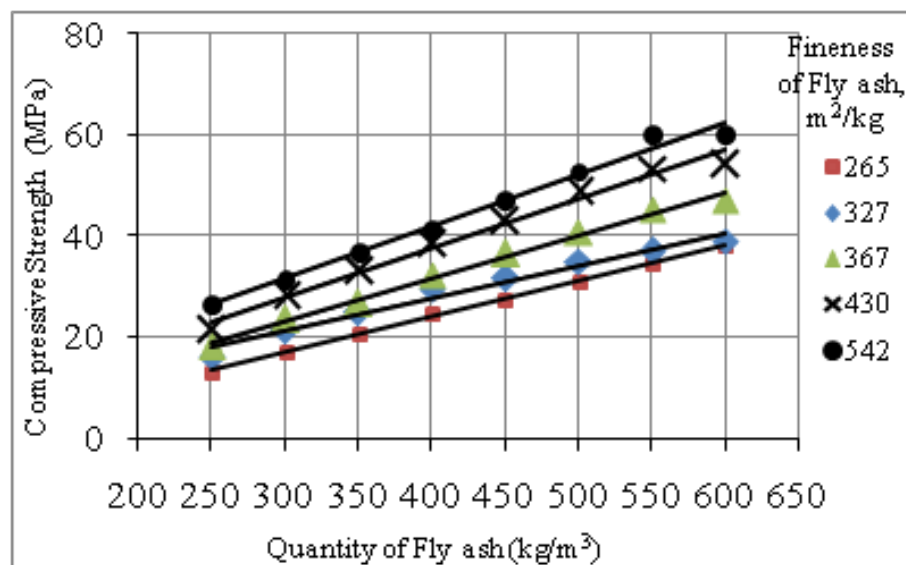


Fig 1. Effect of quantity of fly ash for different fineness on compressive strength of geopolymer concrete at solution-to-fly ash ratio of 0.35 [19]



CONCLUSIONS

This paper presented the effect of quantity of fly ash, total quantity of water, degree and duration of heating and test period on compressive strength on the basis of fineness of fly ash. Based on the experimental work, following conclusions are drawn;

- Fineness of fly ash plays vital role in the development of geopolymer concrete.
- Higher fineness required more quantity of water to achieved desired degree of workability.
- While the compressive strength of geopolymer concrete decrease with increase in quantity of water for same fineness of fly ash.
- Degree and duration of heating and test period also plays important role to achieve desired compressive strength.
- To achieved desired strength geopolymer concrete cured in oven at 40°C for 24 hours and tested after 28 days while nearly same strength can be achieved when heated in oven at 60°C for 24 hours and tested after 07 days. Similarly for 90°C and 120°C required only 8 hours of heating and tested after 3 days and 1 day respectively.
- But there is no large variation in compressive strength after 90°C temperature heated in oven for 8 hours and tested after 3 days as compared to 120°C heat curing.

REFERENCES

1. D. Hardjito, S.E. Wallah, D.M.J. Sumajouw and B.V. Rangan, "On the development of Fly ash-Based Geopolymer Concrete", ACI Materials Journal, November-December 2004, pp 467-472.
2. D. Hardjito, S.E. Wallah, D.M.J. Sumajouw and B.V. Rangan, "Fly ash-Based Geopolymer Concrete, Construction Material for Sustainable Development", Invited paper, Concrete World: Engineering and Materials, American Concrete Institute, India Chapter, Mumbai, India, 9-12 December 2004.
3. J. Davidovits, "Geopolymers: Inorganic Polymeric New Materials", Journal of Thermal Analysis, vol. 37, 1991, pp. 1633-1656.
4. J. Davidovits, "Geopolymers: Man-Made Geosynthesis and the Resulting Development of Very Early High Strength Cement", J. Materials Education, vol. 16 (2&3), 1994, pp. 91-139.
5. J. Davidovits, "Global Warming Impact on the Cement and Aggregate Industries", World Resource review, vol. 6, no. 2, 1994, pp. 263-278.
6. Vimal Kumar, Mukesh Mathur, Shashank Shekhar Sinha and Sagar Dhattrak. 2005. "Fly Ash: an Environmental Saviour", Fly Ash Utilisation Programme (FAUP), TIFAC, DST, Fly Ash India, 2005, New Delhi, pp. IV 1.1-1.4.
7. A.K. Mullick, "Use of Fly ash in Structural Concrete: Part I – Why?", The Indian Concrete Journal, May 2005, pp 13-22.
8. A.K. Mullick, "Use of fly ash in Structural Concrete: Part II – How Much?", The Indian Concrete Journal, June 2005, pp 10-14.
9. Malhotra V. M. and Ramezani-pour A. A., "Fly ash in Concrete", Canada Centre for Mineral and Energy Technology (CANMET) September 1994, pp.1-253.
10. Bob Talling, Renotech, Turku and Finlande, "Blast-Furnace Slag, the Ultimate Geopolymeric Binder", Proceedings of the 2nd International Conference Geopolymere- 99, France, 30 June to 02 July 1999, pp. 109-110.
11. V.F. Barbosa, K.J. MacKenzie and C. Thaumaturgo, "Synthesis and Characterisation of Materials Based on Inorganic Polymers of Alumina and Silica: Sodium Polysialate Polymers", International Journal of Inorganic Materials, vol. 2, no. 4, 2000, pp. 309-317.
12. Jaarsveld J. G. S Van, Deventer J. S. J Van, and Lukey G. C, "The Effect of Composition and Temperature on the Properties of Fly Ash and Kaolinite-Based Geopolymers", Chemical Engineering Journal, 2002, Vol. 89, No. 1-3, pp. 63-73.
13. A. Palomo and A. Fernandez-Jimenez, "Alkaline Activation of Fly Ashes. Manufacture of Concrete Not Containing Portland Cement", Conference in Institute Eduardo Torroja (CSIC), Madrid, Spain, 1999, pp. 1-8.



14. Djwantoro Hardjito, Steenie E. Wallah, Sumjouw D. M. J. and B. V. Rangan, “Brief Review of Geopolymer Concrete”, Invited paper, George Hoff Symposium, American Concrete Institute, Los Vegas, USA, 25 May 2004, pp.1-14.
15. D. Hardjito, S.E. Wallah, D.M.J. Sumajouw and B.V. Rangan, “Geopolymer concrete: Turn Waste into Environmentally Friendly Concrete”, Proceedings of International Conference on Recent Trends in Concrete Technology and Structures (INCONTEST). 2003. Coimbatore, India, pp129-140.
16. Wu Hwai-Chung and Sun Peijiang, “New Building Materials from fly Ash-Based Lightweight Inorganic Polymer”, Construction and Building Materials, 2007, vol. 21, pp. 211-217.
17. Ranganath R.V. and Mohammed Saleh., “Some Optimal Values in Geopolymer Concrete Incorporating Fly Ash”, The Indian Concrete Journal, October 2008, vol. 82, No. 10, pp. 26-34.
18. Al Bakri Mohd. Mustafa, Mohammed H., Kamarudin H., Niza I. Khairul and Zarina Y., “Review on Fly ash Based Geopolymer Concrete Without Portland Cement”, Journal of Engineering and Technology Research, 2011, vol. 3, No.1, pp. 1-4.
19. Jamkar S.S., Ghugal Y.M., and Patankar S.V., Effect of fly ash fineness on workability and compressive strength of geopolymer concrete, The Indian Concrete journal, vol. 87, No.4, pp. 57-62, April 2013
20. Rangan B.V., “Mix Design and Production of Fly Ash Based Geopolymer Concrete”, The Indian Concrete journal, pp 7-15, May 2008.
21. Anuradha R, Sreevidya V, Venkatasubramani R, Rangan BV (2012) Modified guidelines for geopolymer concrete mix design using Indian standard. Asian J Civ Eng (Build Hous) 13 (3):353–364
22. Subhash V. Patankar, Yuwaraj M. Ghugal, Sanjay S. Jamkar, “Selection of Suitable Quantity of Water, Degree and Duration of Heat Curing for Geopolymer Concrete Production, Proceedings of 3rd International Conference on Recent Trends in Engineering & Technology (ICRTET’2014), Elsevier, pp.1-4. 2014
23. Patankar SV, Jamkar SS, Ghugal YM, “Effect of solution-to-fly ash ratio on flow and compressive strength of geopolymer concrete”, Proceedings of 8th biennial conference on structural engineering convention (SEC–2012) at S.V.N.I.T., Surat, 2012, pp 161–166.
24. IS: 1727, “Methods of test for pozzolanic materials”, Bureau of Indian Standards, New Delhi, 1967.
25. IS: 3812, “Specification for fly ash for used as Pozzolana and admixture”, Bureau of Indian Standards, New Delhi, 1981.
26. IS: 5512, “Specification for flow table for use in tests of hydraulic cements and pozzolanic materials”, Bureau of Indian Standards, New Delhi, 1983.



A Sustainable Approach to Flood Damage Repair of Hill Roads in Tripura using Soil Filled Gabions – A Case Study

D Roychowdhury

Chief Engineer, Central Public Works Department, Kolkata

✉ debjyotiroychowdhury@gmail.com

ABSTRACT

The roads in north eastern parts of India suffer from rain cuts and landslides due to high rainfall and subsequent loss of road connectivity. Traditionally, bamboo piles and mats, brick masonry retaining walls, or random rubble masonry walls are used to retrofit such flood damage of the subgrade. Use of rock fill wire mesh gabion retaining and breast walls are gaining popularity due to their ease of construction, better structural performance, better dissipation of pore water and better quality control of components. In this study, rock fill is substituted in some part of the wall with local soil / landslide debris, filled in geotextile bags placed in the gabions. This sustainable innovation can be of immense use for decision makers, while choosing between various engineering solutions in a given location. A qualitative sustainability assessment framework is introduced incorporating environmental, social and economic indicators for selection of best alternatives.

Keywords: Gabion; Geotextile; Landslide; Flood damage; Sustainable.

INTRODUCTION

The Indo-Bangladesh Border states of West Bengal, Assam, Meghalaya, Mizoram and Tripura have high rainfall and silty soil of the Indo Gangetic and Brahmaputra plains. This leads to considerable flood damage to the roads in this region during the monsoon season. It is therefore a challenge to maintain connectivity of the roads, especially those along the international borders which are strategically important and have been built over the years with considerable investment. Some of the states among these also have the additional drawback that there is a dearth of stones/rocks. This makes use of rubble masonry and gabion structures expensive. Therefore, it is desirable to look for technological innovation to manage the situation.

Flood induced landslide retrofitting works in the North-Eastern states typically adopt construction of breast walls / retaining walls where there are landslides, reconstruction of washed away culverts coupled with construction / renovation of roadside drains. Out of these, the construction of retaining walls is the most time consuming and costly affair. In the hilly areas of the North-Eastern states, retaining walls are usually constructed with random rubble masonry, except in the state of Tripura, where stones are not naturally available and conventional retaining walls are made of burnt clay bricks. This case study deals with the construction of soil filled gabions in the state of Tripura, but similar solution may be used in other locations where stones are scarce or expensive.

TRIPURA – CLIMATE AND TOPOGRAPHY

Tripura has a tropical climate and receives rain fall during the monsoons. The average annual rainfall of the state is 2100 mm. The maximum summer temperature is around 36°C and minimum winter temperature is around 2°C. Tripura has about 839 kms. of international border with Bangladesh [6]. The terrain is plain in the northern parts and hilly in the central and southern parts. The dominant soil types available in Tripura are the red loamy soil, reddish yellow sandy soil and silty alluvial soil. Soil structure is granular and amenable to erosion. There is heavy soil erosion due to high rainfall as well as reducing forest cover.



Plate 1 : Extensive damage to IBB road in Tripura – The soil subgrade has been totally eroded and rain water has made deep channels on the road side. Inset : Damage to random rubble masonry retaining wall.

MITIGATION AND REPAIR OF FLOOD DAMAGE – EXISTING PRACTICES

The hills of Tripura are largely devoid of rocks and consist of soil with forest cover. They are prone to raincuts and often lead to road subgrade damage. It seriously affects the connectivity of roads and also causes silting and blockage of rivers/streams. The following practices exist in this region for taking care of flood damage during the rainy season.

Brick masonry gravity retaining walls

The usual practice is to opt for burnt clay brick masonry gravity retaining walls and breast walls. Drainage of water is achieved by providing sufficient number of weep holes in the wall. A layer of 150-200 mm thick lean concrete is provided below the retaining wall, which is generally constructed in cement mortar 1:6 (1 Cement : 6 Coarse sand). The base width is kept as 0.6 to 0.7 times the height and the structure checked for sliding and overturning. The locally available soil itself is used as backfill

The common problems with brick masonry retaining walls are rigidity of the structure, requirement of deeper foundations (1.2m to 1.5m), poor drainage due to clogging of weep holes. Remoteness of site makes it difficult to ensure quality of construction materials like bricks, sand and water as well as process quality control like soaking of bricks, quantity of cement in mortar, curing of brickwork, etc.

Bamboo Piling with bamboo mat backing

The use of closely driven bamboo piles with split bamboo mats has also been a traditional practice in the North Eastern states in India for retaining earth for making check dams, diverting water stream, etc. The bamboo piles of 65 to 80 mm diameter and 3 to 4 m. in length are driven into the ground at close spacing upto around half their length in a zig-zag manner to receive bamboo runners. The runners made of half split bamboo, 65 to 75 mm diameter, are placed horizontally between the piles and tied together to maintain alignment. Inclined stays are provided at 1 m. intervals with bamboo of same size as used for piling. A mat made of 50 mm wide bamboo strips is sometimes placed behind the walling and tied to the walling with binding wire to keep in place. Local earth is filled and compacted behind the mat. Sometimes stone filling is also used for good drainage. While this can be an excellent bio-engineering method, indiscriminate usage and improper installation often renders it ineffective.



Plate 2 : Bamboo / wooden piles with inclined stays and bamboo mat behind them to retain the earth. A brick masonry retaining wall is also seen in the background.

Use of Gabion Structures with Rock Fill

Retaining wall structures erected by filling stone boulders in wire mesh gabions are a good substitute for masonry or concrete retaining walls. The gabion walls can take some movement (good for seismic zones, weak foundation soil, etc.) and are suitable for heights of 4-6 m. [3,4]. These are designed as gravity retaining walls. The gabion walls generally have a backing of non woven geotextile filter that allows water to pass through but retains the soil. The drainage properties of boulder filled gabions with geotextile backing is much superior compared to conventional weep holes with PVC pipes in conventional retaining walls. Most importantly, it allows in-plane drainage within the geotextile and effectively dissipates water pressure build-up in case of local clogging.



Plate 3 : A rock fill gabion wall with geotextile backing under construction. Inset : Gabion boxes being prepared for placement.

The gabions are factory manufactured in accordance with ASTM-A-975-1997 (Re-approved 2016) [1] and IS and MoRTH Specifications [5,7]. These are made of galvanized wire mesh with or without PVC coating. The geotextile is provided as per the requirements of filtration use in accordance with AASHTO-288-05 (Revised 2017) [2] and MoRTH Specifications [7]. The grain size distribution of back fill soil is important for determining the filtration/retention properties of the geotextile.

At locations where the toe of the gabion wall is in wet soil, additional measures like using bamboo or wooden piles are adopted, which increase the sliding and overturning resistance of the wall.

The design of the gabion walls is done as per standard practice for gravity retaining walls – for sliding and overturning modes of failure. The safe bearing capacity of the soil at the base of the wall is also a consideration. The factor of safety against sliding is kept as 1.5 and that against overturning is kept as 2.0. The minimum base pressure should not be less than 0 and maximum should not be more than allowable bearing pressure [4].

Another important aspect here is the ease of quality control in gabion retaining walls given the fact that all the components i.e. gabions, boulders and geotextile are easily accessible for QC check at any time. It is easy to install and does not require skilled labour. On the contrary, in case of brick/concrete walls, issues like cement content, quality of bricks/sand/water, water cement ratio, curing, workmanship, quality of shuttering, etc are critical and need to be supervised.

USE OF SOIL FILLED GABIONS AS RETAINING WALL – A CASE STUDY

The non-availability of rocks in the state of Tripura leads to increased use of bricks. The requirement of stone aggregates for roads, buildings and other infrastructure works, is imported from nearby Assam, Mizoram, etc. The practices therefore have adapted to this shortage and road construction is often done with broken over-burnt brick aggregates (jhama bricks), except the weathering course (top layer), for which stone aggregates are brought in from neighbouring states.

Retaining walls are conventionally made of bricks. The problems usually encountered while constructing brick masonry structures include deeper foundations, quality control of bricks, mortar, water and workmanship.

Rock filled Wire mesh Gabion retaining walls have been the traditional solution to this problem. The drainage properties of boulder filled gabions with geotextile backing is much superior compared to conventional weep holes.

In this case, two walls were constructed – one at a lower level above the river stream and the other above the first at road level – both are 4m high with 0.5m embedment for foundation.



USING GEOBAGS (SOFT ROCK) INSTEAD OF ROCK IN GABIONS

In this type of system, the 1mx1mx1m gabion boxes are filled with locally stitched non-woven geotextile bags which are filled by local sandy soil. The weight of a sand filled gabion compares well with that of a rock filled gabion and hence can be used as a retaining structure [9].

The gabions are filled with rock/stones of 200 mm average size whereas the soil from the slide debris is filled in geotextile bags and tamped with wooden mallet.

The density of fill material, and hence the earth pressure, are calculated as :

$$\gamma = [(G_s + S_r \cdot e) \cdot \gamma_w] / (1 + e), \text{ and } e = n / (1 - n),$$

where

γ = Density of fill material (t/m³),

G_s = Specific gravity of fill material

γ_w = Density of water (=1 t/m³)

e = void ratio of fill material (V_v/V_s)

S_r = Degree of Saturation (%)

n = porosity of fill material (V_v/V)

V_v = Volume of voids

V_s = Volume of solids

V = Total Volume

Table 1. Comparison of densities of rock & soil filled Gabions

<u>Rock filled Gabion</u>	<u>Soil filled Gabion</u>
Here $G_s = 2.7$ $\gamma_w = 1 \text{ t/m}^3$ $S_r = 0\%$ (free draining)	Here $G_s = 2.6$ $\gamma_w = 1 \text{ t/m}^3$ $S_r = 100\%$ (saturated soil)
$n = 0.2$ as per CPWD Specs Vol I para 1.27	$n = 0.08$ as per CPWD Specs Vol I para 1.27
Therefore $e = 0.25$	Therefore $e = 0.09$
Hence Density of fill material (γ) = 2.16 t/m^3	Hence Density of fill material (γ) = 2.47 t/m^3
	Under dry conditions ($S_r=0$), $\gamma = 2.39 \text{ t/m}^3$

It can be seen that the bulk weight of the soil filled gabion is more than the bulk weight of the rock filled gabion. As such its performance with regard to sliding as well as overturning will be superior. However, the foundation level stresses as well as the bursting stresses on the geotextile need to be checked. For low height walls around 4m to 6m height, foundation level stresses are within usual limits. If the subgrade is weak, additional corrective measures will be required.

The nonwoven geotextile used here was Terram1000© for drainage and filtration function. The engineering properties (as provided by the manufacturer) are :

Strip Tensile strength	:	8 kN/m at 60% peak elongation.
Mass per unit area	:	125 grams / sq.m.
CBR Puncture Resistance	:	1500 N
Apparent Opening Size (AOS)	:	0.15 mm
Permeability	:	90 litres/m ² s

The fill soil was non plastic and %age passing 0.075mm sieve was in the range 15 to 50. As such all parameters required by Section 700 of the MoRTH Specs for Road and Bridge Works [7] are met.

Geotextile provides excellent engineering performance, but is suspect for its longevity; especially given the fact that exposed geotextile is destroyed by UV radiation over a period of 2-3 years. However, some manufacturers claim UV stability over 20-25 years for some specialty products.

In the instant case, bamboo mats are used to protect the geotextile, to prevent exposure to UV radiations. Bamboo mats are also a local product.



Plate 4 : Soil filled Gabion wall provided with HDPE drainage pipe as an additional drainage measure. Inset : Use of bamboo mat for UV protection

A trial panel in the walls was executed with Non-woven geotextile bags, alongside rock filled gabions. The bags were locally stitched by hand, and placed inside 2m x 1m x 1m gabions of 2.7mm zinc coated wire (without PVC coating) and 10x12 mesh opening size. This work was carried out in December, 2011 and monitored till February 2015.

Limitations of the use of locally available soil filled gabions

Soil filled gabions suffer from the following problems in execution :

- The geotextile tends to bulge out of the gabion openings if the mesh opening is too large. The burst strength of the textile needs to be higher in such cases, especially for larger wall heights. The choice of smaller mesh size and special geotextile is a matter of cost economics and availability.
- Fixing of bracing wire, especially when bamboo mats are placed between the geotextile and gabion wall, is cumbersome. It also damages the geotextile.
- The soil tends to settle down after some time, especially as upper layers put load on the bottom layers. Hence the filling is required to be slightly on the higher side, with proper tamping and compacting.
- The lead time for transportation of gabions and geotextiles is high for remote locations. However, with increasing use of these materials, the lead time is coming down.
- More field trials are required to gain confidence in this application, as soil filled gabions in retaining applications are few and unreported.



Plate 5:[A] May 2012 – Some green cover is seen over the gabion walls [B] March 2013 – Green cover has increased [C] March 2013 – Soil fill gabion panels are holding fine [D] February 2015 – No subsidence is seen at wall location. Vegetation growth is abundant



SOIL FILLED GABIONS – THE SUSTAINABILITY PARADIGM

Sustainability of a particular technological alternative is measured in terms of its potential to promote economic development, social well being and environmental protection. It is therefore a multidisciplinary optimization problem with soft constraints and objectives. In addition, the time scale on which the performance is to be evaluated extends over decades instead of months and years [8]. It is also pertinent to mention that since environmental and social factors come into play, the sustainability parameters have local dimensions and there is no “one size fits all” formulation of the problem.

A key step in the move towards sustainability is the freezing of the indicators for measuring sustainability, which may often be qualitative measures, often requiring a trade-off amongst them. For example, energy use, land use, noise pollution, water pollution, air pollution etc. are common environmental indicators for infrastructure projects. Similarly, local employment generation, protection to cultural heritage, service benefits to the project vicinity, change in land value, etc. are some important social indicators of infrastructure projects. Economic indicators include technical superiority, project cost, financial risk, maintenance and operation costs and paybacks over the life cycle, etc. [9].

Soil filled Gabions – Sustainability Indicators

The relative qualitative indicators for sustainability relevant to flood damage rehabilitation work, for the conventional brick gravity retaining wall construction and for the soil filled gabion retaining walls, are given in **Table 2** in Annexure A, which is self explanatory. Qualitative Gradings have been given as Excellent, Very Good, Good, Moderate and Poor. The qualitative gradings have been selected by the author from his own experience. More sophisticated qualitative assessment methods are available.

The new system is found to be superior on most sustainability indicators, whereas on some other aspects it is neutral with respect to the conventional brick masonry retaining wall system.

Inhibitors for Adoption of Sustainable Measures

The following factors can be considered as the major inhibitors in the present context :

1. The status quo is beneficial to the contractors who also invested in brick kilns. They tend to lose their established profitable activities. Hence there is local resistance.
2. Triple bottom line is not an established norm in decision making, which remains anchored to cost economics alone.

Policy level decisions towards sustainable development are not translated to operational methodologies due to subjectivity and complexity of the processes involved.

CONCLUSIONS AND THE ROAD AHEAD

It is seen that the use of soil filled gabions with geotextile bags and bamboo mat UV protection is a practicable and eco-friendly solution for small height retaining walls and breast walls, as a repair scheme for small landslide locations. It uses locally available landslide debris and does not entail stone/sand mining. It is also quite fast and does not require much specialized labour.

As brought out above, it is a sustainable technology for areas having dearth of rock formations or where the environmental responsibilities dictate a non-invasive methodology for flood damage mitigation and repair.

Considering these few panels of soil filled gabions as a technology demonstration, there is a need to take up larger walls with this method.

ACKNOWLEDGEMENTS

I would like to acknowledge the inputs and support provided by Shri A K Gupta, EE (Civil, P&A, CPWD, Silchar) (Retd.), Shri P Panneer Selvam, EE (Civil, CPWD, Silchar) (Retd.) and Shri V K Verma, EE (Civil, CPWD, Agartala) along with their team of Assistant Engineers and Junior Engineers, who have supported this endeavor with their inputs from the field.

REFERENCES

1. ASTM-A-975-1997 (Re- approved 2003)
2. Indian Standard 14458 (Part-1) : 1998 - Retaining Wall for Hill Area - Guidelines (Part 1 : Selection of Type of Wall)



3. Indian Standard 14458 (Part-2) : 1997 - Retaining Wall for Hill Area - Guidelines (Part 2 : Design of Retaining / Breast Walls)
4. Website of Govt. of Tripura (<https://tripura.gov.in/know-tripura>) accessed on 22.05.2019
5. Specifications for Road and Bridge Works (5th Revision) (2013), Ministry of Road Transport and Highways.
6. Beena, K.S. and Jayasree, P.K. (2009), Gabion Retaining Walls with Alternate Fill Materials, Proc. of the Indian Geotechnical Conference, Guntur, 2009, pp - 472 to 475.
7. Brundtland, G.H., Report of The World Commission of Environment and Development : Our Common Future, 1987.
8. Sahely, H.R., Kennedy, C.A. and Adams, B.J. (2005), Developing Sustainability Criteria for Urban Infrastructure Systems, Canadian Journal of Civil Engineering, Vol. 32, pp- 72 to 85.
9. Shen, L., Wu, Y. and Zhang, X. (2011), Key Assessment Indicators for the Sustainability of Infrastructure Projects, Journal of Construction Engineering and Management, Vol. 137(6), ASCE pp - 441 to 451.
10. Rodriguez, S.I., Roman, M.S., Sturhahn, S.C. & Terry, E.H. (2002) "Sustainability Assessment and Reporting for the University of Michigan's Ann Arbor Campus", Report No. CSS02-04.

Table 2. Conventional Masonry Retaining Walls Vs. Soil Filled Gabions – Sustainability Indicators

S. No.	Indicator	Qualitative Assessment		Remarks
		Conventional System (Brick masonry R/Wall)	New System (Soil filled Gabion R/Wall)	
A..	Economic Indicators			
1.	Capital Cost per cu.m. of retaining wall	Moderate	Excellent	Cost per cu.m. for brickwork in the instant location works out to approx. Rs. 6000/- per cu.m. whereas for new system it is Rs. 4000/- (At 2011 prices)
2.	Maintenance cost	Moderate	Good	Low maintenance cost of gabions compared to brick work requiring plaster, whitewash, etc.
3.	Engineering performance	Moderate	Excellent	Brick structure - rigid structure, poor long term drainage, Quality Assurance problematic. Gabion structure - Flexible with superior drainage properties, factory made components ensure better Quality Control.
B.	Social Indicators			
1.	Local employment generation	Moderate	Moderate	The labourers in both cases are locals and there is not much difference in the quantity of labour. However, in the conventional system, local contractors benefit from supply of materials much more than in the new system
2.	Lesser road blocks / landslides	Good	Very Good	Better performance of the new system leads to better safety & accessibility in hilly areas.



3.	Conservation of agricultural land	Low	Very Good	The large scale demand for bricks lead to mushrooming of kilns and consequent loss of agricultural land, thus lowering local food grain availability.
C.	Environmental Indicators			
1.	Energy Usage	Poor	Excellent	The gabions and geotextile come in better packaging, i.e. each truck load brings material for large volume of work, with little wastage at site. For bricks, truckability is moderate. Also wastage in bricks is much higher at around 5%. The embodied energy of brickwork is very high, especially due to kiln burning.
2.	Land usage	Good	Moderate	Brick retaining walls take up lesser space than gabions in plan area, for usual heights of 4 to 6m.
3.	Construction material usage	Moderate	Moderate	The volume of construction materials is almost same, however brickwork inputs are costlier than gabion filled with sand / soil.
4.	Conservation of top soil	Moderate	Moderate	The top soil loss at the site of work is almost similar, as in case of gabions, the plan area is higher, however, the top soil is partly put back over the gabions for greening.
5.	Green Surfacing of Structure	Poor	Very Good	The soil filled gabions grow local vegetations, especially in hot and humid conditions, which binds the silty / sandy soil.

Source: Reference [10]



Analysis of Access Control & Traffic Bottleneck on Western Express Highway using PTV Vissim

Shrivastav Laxman Sutar, Siddharth Deepak Gondhale

Department of Transport and Communications, Mumbai Metropolitan Region Development Authority, Mumbai, Maharashtra

✉ shrisutar10@gmail.com; ✉ siddharth.gondhale@mailmmrda.maharashtra.gov.in

ABSTRACT

The Mumbai City renowned to be a vertical city surrounded by water on its three sides is witnessing loss of time in traffic queues which results into an extended trip time for every commuter in peak hours. Our research is based on the western express highway (WEH) which ranked sixth among worlds metropolitan regions & fourth traffic Congested highway as per TomTom index in the world. This highway is directional lifeline of the heart of Southern Mumbai. All the commuters using WEH are in traffic for at least 20 minutes daily. Considering this issue, this paper aims to lessen the reduction in travel time & traffic congestion for every commuter to his destination using traffic flow rates, speed, lane utilization and other traffic characteristics with simulating it in PTV Vissim software to result into better traffic pattern. An attempt has been made in this research to result WEH more mobilized highway for which in present it conveys 23266 PCU's/Hr. The entire WEH corridor is studied with traffic surveys considering the traffic congestion pattern & delay locations on it.

Based on these surveys an alternative access controlled concept plan will be designed which does consists of ease to accesses points and reduction in access point densities to enhance safety & easy manoeuvring for commuters. Finally the results are compared using PTV Vissim software in the terms of traffic characteristics, lane utilization, traffic congestion and flow rate.

Keywords: Traffic bottlenecks; Ravel time, Traffic density; |Traffic queue; Lane management.

INTRODUCTION

Mumbai Metropolitan Region (MMR) is ranked as the sixth largest metropolitan region in the world by population densities & one of the fastest growing metropolises in India with a population of about 22.8 million based on 2011 censuses (estimated population of MMR was 24.6 million based on 2016 Draft Regional Plan Report). Mobility is an engine of growth and transportation systems have to be dynamic to meet the growing requirements of an urban area. Peak-hour traffic jams are a fundamental consequence of the workings of metropolises where highways play a significant role in the transport network providing high-capacity routes connecting people, employment, industry and other transport nodes. Urban highways are critical road assets which are expensive to provide and maintain. They represent significant public investment to support community and economic activity.

The population of vehicles of the city and the length of the roads are comparable for the average space on road & its capacity. The compound annual growth rate (CAGR) of registered motor vehicles increased by 10.11% during the period from 2007 to 2017. Among the various types of vehicles, the highest CAGR was reported by two-wheelers between 1981-1991 (18.4%) and cars, jeeps and taxis (9.6%), followed by freight vehicles (9.4%), other vehicles (10.9%) and buses (7.4%). This increase in vehicle population against the space or road lengths available in urban area gives you the area index which decides your city's level of space availability.

When the demands are exceeding its carrying capacity this will result in flow breakdown and congestion reducing productivity (Flow x Speed) by as much as 50%, which occurs typically on urban highways for increasingly longer periods of the day, along with an increasing number of fatal and serious casualty crashes. This is because of high number of factors creating bottlenecks on the roads. Historically, the lack of control on entries and exit's of urban highways allows flow breakdown to occur. When saturation flow is more than unity (temporal – sub one-minute flows) they must be managed to have safety and economic outcomes for the community. There is need of trails and error strategies on WEH to control utmost traffic.

LITERATURE REVIEW

The literature of this study is a review of earlier works that has been carried to control the access of highway and to provide controlled traffic systems all over the world. Queue always forms when vehicles are stopped at the service area. When the demand exceeds the capacity at an approach, a queue forms (Highway Capacity Manual, 2000). When these queue forms certainly there is need of volumetric control analysis which denies traffic jam issue into controlled highway system. (Bing HUANG, 2013) et.al. studied the impacts of access density against the access points within given distance. The study finds the solution that speed variation & access density can directly positively affect the traffic volume, SSD & thereby negatively affect the number of lanes. Prior to queue formation about 10% of flow forming a queue on motorway. (Robert L. Bertini & Monica T. Leal, 2005) Using statistical error analysis methods, the proposed algorithm and the design methods were calibrated and evaluated using field data collection from two distinct freeway corridors (US 12/14 and I-894) in the U.S. state of Wisconsin.

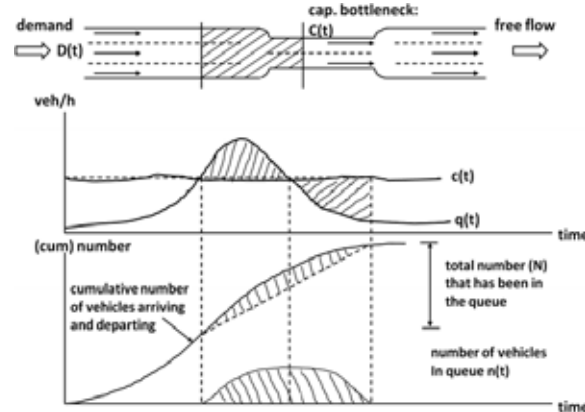


Fig. 1. Bottleneck theory & free flow traffic impact w.r.t. time

The Urban Corridor Concept Plan seeks to improve the landscape amenity and provide improved connections to re-establish its relationship with the Swan River. The city of Belmont study by Taylor on urban development of Great Eastern Highway is about all the impact management techniques are covered in this research. (TRB; NCHRP Report 420 1999) Corner clearances, signal spacing, median alternatives, left turn lanes, easy U turns, ramp access were studied.

PROBLEM IDENTIFICATION

The time one should take to travel from Dahisar Check Naka to Mahim Junction on the WEH, a distance of 25 km, should be about 1 hour 5 minutes if one considers an average vehicle speed of 60kmph, however, at present it takes two hours and even more in peak four hour congestion timings.

1. The measure reason for bottleneck is the capacity of vehicles at entry are greater than exit,
2. Land Encroachments,
3. RoW used by the Metro Line 7 and Line 3 connectivity's and its construction work,
4. Lane changing behaviour of users and it is single option for North-South connectivity for commuter to transit.
5. Lack in uniformity of signage's with no headway and gap controls on highway.

Currently, both local traffic and long-distance traffic gets mixed on WEH. Therefore, it is important that long term measures are taken to segregate the local traffic movement and the long-distance traffic. Vehicle management for their access to WEH is greater issue with mixed types of vehicles which create large shockwave & queuing on WEH.

OBJECTIVES

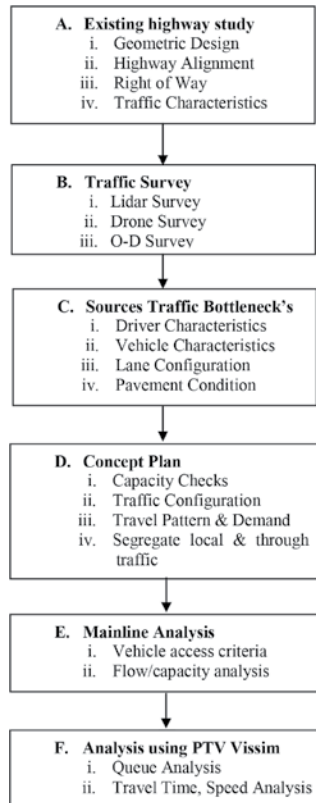
To achieve a time efficient, jam free and smoother highway following objectives are considered.

1. To collect & analyse the traffic volumes at every access points on highway.
2. To identify crash rates, land use, travel pattern & congestions points.
3. To identify critical traffic location with bottlenecks & queue spill backs particularly at on and off ramps.

4. To segregate the local & through traffic.
5. To propose new alignment over existing design fulfilling above traffic conditions and safety.
6. To analyse merging & demerging of traffic between lanes w.r.t. travel time.
7. Simulate and analyse results discussion for before and after conditions.

METHODOLOGY

The methodology describes the process of analysis of traffic flow for existing and after simulation conditions of the WEH. The whole highway corridor has been studied as per the following methodology from A to F.



Existing Highway Study

WEH is a major north-south 8-10 lane arterial road in Mumbai, India, stretching from the suburb of Dahisar to Bandra. The 25.33 km highway begins near the Mahim Creek and extends to the Mira-Dahisar toll booth in the northern limit of the city. Beyond the city limits, it continues as the Delhi-Bengaluru National Highway 48. The road serves the city of Mumbai to its western suburbs, including the Chhatrapati Shivaji International Airport. The Western Expressway starts from Mahim Junction to Dahisar Check Naka. The total length of this highway is 25.33 Kms.



Fig. 2. WEH corridor @ segment Goregoan

The Western Expressway has, at most of the stretch, 5+ 5 lane main carriageways and 2+2 lane service road. The total length of service road is 24.800 Kms. The present P.C.U. on this highway is 23266 per hour. There are 12 flyovers, 2 major bridges, 11 minor bridges, 12 pedestrian underpasses, 10 vehicular underpasses and 10 foot over bridges & 1 ROB's on this road. It was very difficult to capture the traffic characteristics of the WEH and carried out by drone survey as in **Fig. 2** i.e. heterogeneous traffic conditions.

As per methodology considered geometric details of the WEH are studies and note it down for the existing situation. The traffic manoeuvring is very important part of analysis that can be stated and concluded by the traffic surveys.

Traffic Survey

Traffic survey started at the Kalanagar Junction ended up at Dahisar Toll Post. In the survey it is found that the traffic density at every section is different due to surface conditions, vehicle characteristics & user perception. Time saving qualitative & quantitative design of non-conflicting geometric model of highway deficiencies were found. Hence in the todays date this paper studied the behaviour and demand with entry & exit of highway as per their travel purpose as shown in **Fig. 3**. The x-axis has day time on WEH whereas the Y-axis defines the number vehicles of PCU per hour from morning 6am to evening 10pm IST.

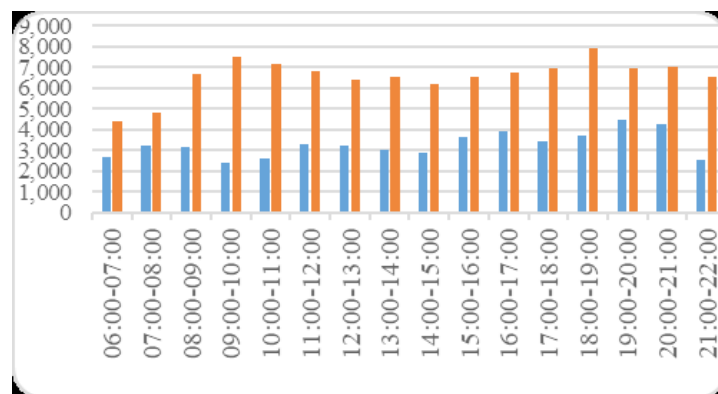


Fig. 3. Monday traffic volume on WEH.

In the O-D survey it was clear that most of the traffic congestion occur due to high volume to capacity/demand. The policy has to be set up for the same as per demand. The various modes of traffic can direct impact the regular and smooth movement of long-distance traffic. For considering the traffic bottlenecks vehicle composition are also important factor. Following chart vehicle composition of vehicles along the western express highway. With the traffic volume count at entry point and exit point of western express highway it is analysed that following percentage of vehicle distribution is along WEH as shown in **Fig 4**.

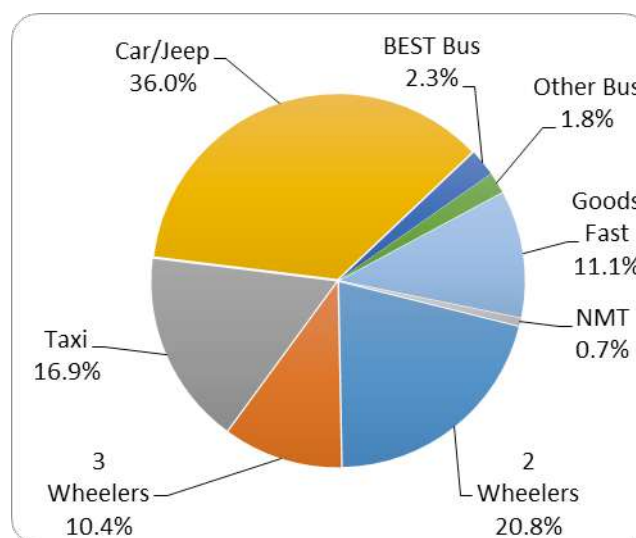


Fig 4. Traffic share modes of travel



The distribution & comparison made on the basis of traffic volume count with traffic survey as shown in the following **Table 1**. The directional split of ADT showed that the flow in both the directions was evenly distributed on the section. The directional split ranged between (52%) to (48%) at all locations.

Table 1. Directional Split of traffic flow

Location	Directional Split Ratio	Direction
Kalanagar	51.2 : 48.8	Kalanagar to Dahisar : Dahisar to Kalanagar
Vakola	50.2 : 49.8	
Santacruz	51.6 : 48.4	
Gundavali	51.7 : 48.3	
Dahisar Toll	47.2 : 52.8	

Source of Traffic Bottlenecks

It was very difficult to differentiate the sources that contributes to the traffic congestion in the context of bottleneck analysis. Further study introduces the factors lead to the bottleneck & congestion of traffic on WEH as below.

Driver Characteristics

One of the problems that traffic and transport engineers encounter when considering driver characteristics in terms of design is categorized by the range of highway driver's various skills and sensory abilities, including the ability to hear, see, evaluate, and react to information. Studies have shown that these abilities can also vary in a person under different conditions such as alcoholism, fatigue and time of day.

Vehicle Characteristics

The geometric design criteria of highways are partly based on the static, kinematic and dynamic characteristics of the vehicles. Static features include the weight and size of the vehicle, while dynamic features include the speed of the vehicle regardless of the forces that cause the motion. Dynamic features include the force that causes the movement of vehicles. Since almost all highways are both passenger-vehicle and truck traffic, the design criteria must take into account the characteristics of different types of vehicles. A thorough knowledge of these characteristics will aid the highway and/or traffic engineer in designing highways and traffic-control systems that allow the safe and smooth operation of a moving vehicle, particularly during the basic manoeuvres of passing, stopping, and turning.

Merging & Diverging

In these cases, a higher level / intensity of mandatory lane changing for some vehicles is required as well as lane changing to balance traffic across the available through lanes. fig. 4 shows an example where ramp and mainline flows are assumed and angled arrows are shown to demonstrate the typical nature and magnitude of lane changes required for entry / exit manoeuvre and to balance volumes across the carriageway. Fig. 5 sorted on a segment entering 3 lanes of flyover at Vakola which describes the lane inter-movement of merging & diverging of vehicles done by manual observations for 100m segment. Most of the merging & diverging are observed at flyover starts & end, entry ramps, exit ramps, interchanges and junctions. JVLR junction & Milan Flyover area has the most traffic bottlenecks issues found in the study. The concept plan for avoiding all the above sources are mentioned in concept planning.

Road Condition

WEH road conditions are recently under development by the authority in a bituminous layer. There is lack in uniformity of pavement surfaces and are found in rigid, flexible pavements and in zigzag paver blocks at some part of segments on WEH. This leads to unevenness of surface by external effects & loading conditions.

Concept Plan

The concept plan has 3 flyover lanes, 2 lanes for slip roads & 2 lanes for service roads on each side of upstream & downstream. The vehicular movements for u/s & d/s are managed by separating the traffic patterns as per their destination points from O-D surveys. All the highway traffic is segregated as service/local traffic flow, slip road/diverging traffic flow & through traffic flow. Most of the Indian scenario are heterogeneous traffic in compare to other metropolises and hence need to control the actual lane

movement. Traffic flow can be controlled such that no conflict movement will occur at the overall entries and exits on WEH. The intersections are best managed in phases and ramps created to cater the all bound traffic volumes. In this paper we design for through & lane separation traffic movements that finds suitable for better understanding of lane importance to users. The following Fig. explains the movement of the vehicles between lanes i.e. merging & diverging.



Fig. 5. Concept plan WEH

The **Fig. 5** simulated in the Vissim Software for no conflict between vehicular movements. In this design concept the local traffic and through traffic were segregated with their travel demands. Where a vehicle from Bandra to Dahisar can continue the flyover lanes to reach at minimum travel time. Whereas the middle segments are joined with slip lanes to service roads and mainline flow.

But it is very difficult to find out practically that where a vehicle does entering from and demanding to go. Hence we considered here the bridge as a through or fast travelling lanes then slip roads to enter or exit flyover and a service lane to manoeuvre to their destinations. Therefore using PTV Vissim software we are analysing the existing situation to be a better part of future or not! We studied that in results and discussions chapter.

SOFTWARE ANALYSIS AND ITS MEASURES

All micro-simulation models are static in nature, so there is some degree of randomness associated with all distributions. The random seed parameter controls the generator of random numbers in the simulation. Therefore, the micro-simulation model must be run with different random seed values to average the stochastic variation in the model. For the purpose of analysis, the base model is run five repetitions, from which the results are drawn before the presentation and the average is increased. The simulation model is set to simulate 1:15 hours (4500 seconds) of peak period operation. The first 15 minutes of the simulation represent the 'warm-up' period. The network is loaded to peak hour traffic volumes during these first 15 minutes. The next 1 hour represents the peak time operation.

Driving Behaviour

Driving behaviour has been coded based on the A typical driving behaviour typology for motorized traffic with the corresponding parameters. Based on road categories different types of driving behaviour topologies are used to reflect the driving behaviour on roads.

Network Coding

The actual road geometry has been matched to the best possible extent while coding links. All the roads included in the network inventory/ base network plan was coded. Based on the road categories, driving behaviour attributes such as lane changing and vehicle following behaviour are allocated to each link.

Static Routing

In the case of static assignment in VISSIM, the travel demand is specified by using vehicle inputs on the links with a given volume. The base model uses static assignment for the distribution of traffic. For this purpose, all entry and exit links have been identified and coded as per the traffic movement.

Coding of Conflict Points and Priority Rules

All junctions and traffic merging areas have been coded with conflict points and priority rules as required. Priority rules have

been set to look for a minimum gap in terms of distance and time headways separately. Conflict points to avoid both vehicle-vehicle conflicts.

Static Assignment in VISSIM

The static assignment procedure was designed to model the route choice behaviour of drivers using a vehicle flow input. This static assignment where the travel demand is specified by using vehicle inputs on the links with a given volume.



Fig. 6. Modelling of highway in PTV Vissim

The above software inputs were given in Vissim which represents some results and analysis in terms of queue length, travel time, speed, flow or volume per kilometre and delay that we discuss in results and discussions.

RESULT AND DISCUSSION

It can be clearly seen that the volume of highway increased by 9 % than before in **Table 2**. Per lane vehicle gets increased due to segregated traffic movements. The service flow rate for this highway with an interchange considering as the starts of flyovers i.e. merging-diverging conditions the fully managed highway shown in Fig. are within 5500 to 6000 vehicles per hour which is 10% increase in the previous onsite practical survey. Partially managed highway does not include the lane management which resulting into the decrease of nearly 1000 vehicles per hour per lane. There is increase in 2 number of lanes as service road to enter in slip lane from residential or commercial access.

Table 2. Results after simulation in Vissim

	October 2019	Simulation	Difference
No. of Lanes	5x2	7x2	+40%
Avg. Daily traffic	23500	25500	+9%
Avg. daily u/s traffic	66500	72800	+9.4%
Avg. daily d/s traffic	63580	70560	+11%

The following **Fig. 7** explains us the condition on WEH after simulation on Y-axis with traffic count in vehicle per hour & on X-axis the traffic inter-counts. The fully managed Maximum Service Flow Rate (MSFR) can be achieved with the 5800 vehicle per hour whereas in practice on site nearly 4000 vehicle per hour are moving. Previously the flow rate of vehicles increased by 2000 vehicle per hour. There are two options were studied in simulation that is considering access point densities. The fully managed road comes with all ITS, traffic signage's and road guiding installations. The above simulation is description of fully managed MSFR.



Fig 7. MSFR at an interval of entries

For a lane wise control analysis of traffic volume the **Figs. 8, 9, 10** are found to be suitable and increase in their volume traffic flow per hour. It is found that there is an improvement in simulation model for segregated to local and through traffic in a day. After modelling in vissim with the all inputs following results are obtained. The following figures analysed per minute per lane volume of WEH. The red line is minimum traffic volume whereas the blue indicates the maximum traffic volume per minute per lane.

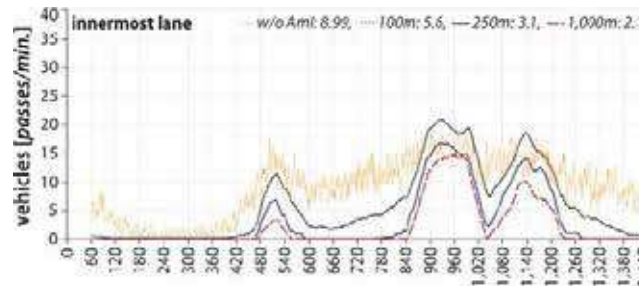


Fig. 8. Rightmost lane of highway

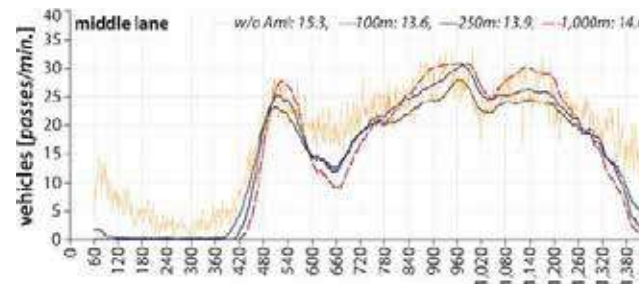


Fig. 9. Middle lane analysis of highway

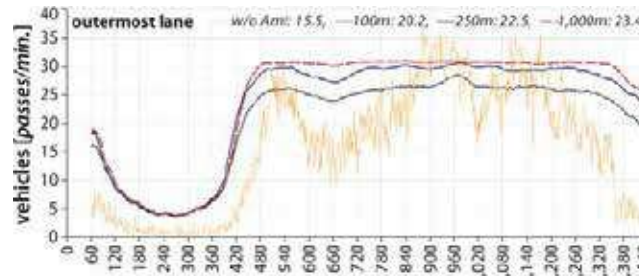


Fig. 10. Leftmost lane analysis of highway

Queue length has been decreased by 40m, delaying of vehicles reduced up to 40sec and speed is increased i.e. vehicular manoeuvring set to best level of service. Traffic flow rate also get increased in terms of capacity from 5x2 lanes to 7x2 lanes which is now 1000 PCUs per hour per lane. Speed we kept as constant term to identify the exact bottleneck positions in simulation and practices. The traffic characteristics are also compared to the new design and existing condition on WEH.

Table 3. Comparison of results Before & After conditions.

	Existing	Simulation	Remark
Queue Length	236.67m	191.66m	19% decrease
Delay	185.33	66.39	36.83% less
Travel Time	105min	65min	38% less
Speed	50kmph		-
Flow	850 pcu/hr/ln	940 pcu/hr/ln	9.5% increase

The last queues of the highway extend beyond the upstream exit, where the signals collected by the road meter help to manage the outflow flow. From the above findings it is concluded that the highways when accessed well and with controlled traffic entry & exit must increase in overall productivity i.e. flow x cost of area & reduces the travel time for commuters. The **Fig. 11** clears an idea of our future WEH network.

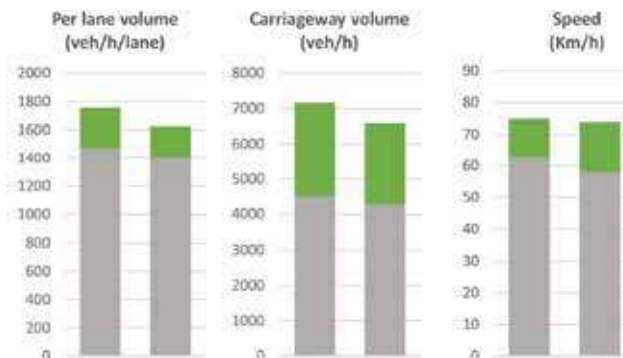


Fig. 11. Speed, Volume and Flow after simulation



Fig. 11. Architectural picture of WEH network after simulation

ACKNOWLEDGMENT

Overall work has been carried out with the guidance and involvement of MMRDA professionals and the team. I thanked and acknowledge them all who did supported and helped me for the research work on WEH. This paper is part of research in MMRDA on redesign & redeveloping of WEH network.

REFERENCES

1. Bing HUANG, Y. Z., "A Simulation Study for Minimizing Operating Speed Variation of Multilane Highways by Controlling Access", Volume No. 1394-1402, 2013.
2. Highway Capacity Manual 2000, Transportation Research Board.
3. Impact of Access Management Techniques NCHRP Report 420, 1999. Transportation Research Board.
4. Leal, R. L., "Empirical Study of Traffic Features at a Freeway Lane Drop", Volume 131, 397-407, Journal of Transportation Engineering, 2005.
5. Mohammad Alauddin Ahammed, & Yasser Hassan, a. T., "Modelling Driver Behaviour and Safety on Freeway Merging areas", Volume 134, 370-377, Journal of Transportation Engineering, 2008.
6. Peter (Jing) Jin, P., "Freeway Recurrent Bottleneck Identification Algorithms Considering Detector Data Quality Issues", Volume 138, 1205-1214, Journal of Transportation Engineering, 2012.
7. Xu, H. F.-J., "The Access Delay Model under High Access Volume", CITCP Conference, Page No. 2802-2812, 2019.



A Comparative Study of MLP and MLP-FFA Models for Flood Prediction

Sandeep Samantaray, Abinash Sahoo, Siddhartha Paul

Department of Civil Engineering, National Institute of Technology Silchar, Assam

✉ samantaraysandeep963@gmail.com

ABSTRACT

Accurate flood forecasting is crucial for flood prevention, flood damage mitigation, development of flood warning systems, soil conservation and reduction of soil erosion. Objective of present study is to employ a hybrid model to forecast flood events and study its accurateness. 30 years of monthly historical flood data was utilised for evaluating performance of proposed model. Statistical performance indicators such as the RMSE and the WI are applied for evaluating model performance. Results obtained from present research reveal that integrated ANN model with FFA outperforms the classical ANN method making better forecasts during training and testing periods in all input cases improving effectiveness of proposed models. Results also reveal that integration of optimization algorithm and ANN model can be a potential tool to forecast flood discharge in proposed gauge stations more precisely.

Keywords: Flood; MLP; MLP-FFA; Prediction.

INTRODUCTION

Flood is a widespread extreme hydrologic event that results in substantial damages to environment and property along with loss of life around the world. Forecasting flood events is one of the most important non-structural measures for flood control for protecting human lives and properties. It is also important for water resource design, planning and management. An accurate and reliable long term flood forecasting model gives least error, and it enables decision makers for achieving minimal flood risks, optimal reservoir operations and allowing adequate time for preparing about hazard management.

In the last decade, neural networks have been progressively applied in water resources management, for example stream flow forecasting (Sridharam et al. 2020; Mohanta et al. 2020; Sahoo et al. 2019; Haddad et al. 2005; Cigizoglu 2003), rainfall runoff modeling (Samantaray and Sahoo 2020 a, b; Samantaray et al. 2020; Sattari et al. 2012; Shamseldin 2010; Dawson and Wilby 2001; Rajurkar et al. 2002), prediction of flood events (Sahoo et al. 2020a, b) and prediction of reservoir inflow (Sentu and Regulwar 2011; Othman and Naseri 2011). Application of various ANN methods have also been supported in recent studies as an effective alternate approach for real time river stage forecasting (Kisi 2007; Chang et al. 2007; Dawson et al. 2002). Cigizoglu (2003) investigated the extrapolation and forecasting capability of ANN for multi-step forecasts utilizing daily flow data and showed that MLP network was able to generalize the structure of entire data set and capture nonlinear dynamics. A concept of applying ANN has been broadly studied, and was revealed as an alternate modeling approach in hydrological field of study (ASCE Task Committee 2000a; b).

Different conventional data driven models were employed at various watersheds to predict flood events for different time interval (Piotrowski et al. 2006 and Rezaeianzadeh 2013). Hoai et al. (2011) employed MLP technique for downscaling precipitation from global Numerical weather prediction (NWP) outputs to an average scale of basin for predicting flood runoff at Thu Bon River Basin, located in Central Vietnam. Kim and Singh (2013) developed and applied MLP, self-organizing maps (SOM) and generalized regression neural network (GRNN) for flood forecasting at Sangye station of Bocheong watershed located in Republic of Korea. Results revealed that SOM provided more accurate flood discharge compared to MLP and GRNN. Latt and Wittenberg (2014) examined the performance of stepwise multiple linear regression (SMLR) and MLP model for multi-step flood forecasting of River Chindwin in northern Myanmar. In their study, MLP model provided best performance compared to simple linear regression model.

Training of ANN models can be done with conventional training algorithms namely descent gradient technique and back-propagation. Conventional training algorithms may play local minima. Additionally, speed of convergence of simple ANN

techniques may not be high. Hence, instead of conventional training algorithms newly developed optimization algorithms can be utilised (Al-Jamimi et al. 2019; Alade et al. 2019). Optimization algorithms have high ability and high flexibility to find preeminent architecture of ANN tools. For addressing these challenges, it is essential for defining new integrated ANN models with novel optimization algorithms, so that they can improve accuracy and computational time of ANN models.

Hybrid models were applied for forecasting flood occurrences at Bocheong stream located in South Korea and their accuracy was investigated for different lead times (Seo et al. 2014). Khatibi et al. (2017) applied integrated MLP with Levenberg–Marquardt (LM) and FFA for studying stream flow predictions of Bear River located in U.S.A. Results indicated that MLP-FFA outperformed MLP-LM hybrid model with significant improvement in model output. Naganna et al. (2019) investigated the hybridization of MLP with FFA and gravitational search (GSA) for modeling Dew point temperature of semi-arid and humid areas in India. Dtsisibe et al. (2020) used MLP for designing a flood forecasting model using discharge as input–output variables. Findings from their study showed that proposed model was very effective with a good forecasting capacity. Shamshirband et al. (2020) used simple MLP, SVM and integration with FFA i.e. MLP-FFA and SVM-FFA for modelling soil temperature of Ahar and Tabriz weather stations situated in East Azerbaijan region, Iran. The researchers reported that proposed hybrid models performed more efficiently and reliably compared to classical MLP and SVM models.

Even though FFA has been successfully used in various field of study, to the author's best knowledge, application of MLP-FFA for flood forecasting problems is yet to be done. Present research investigates potential of hybrid MLP-FFA approach to predict flood events and comparing the performance of developed hybrid model with its corresponding simple ANN model for flood forecasting at River Mahanadi, India.

STUDY AREA

Like many other seasonal rivers of India, Mahanadi is a major river with draining area 1,41,589 sq. km. flowing in east central India. It drains into Bay of Bengal off the coast of Odisha. It lies between 80°30' and 86°50' E longitude and 19°20' and 23°35' N latitude originating at a height of about 442m above average sea level near Pharsiya village of Raipur, Chhattisgarh. Total river length from its place of origin to convergence at Bay of Bengal is around 851 km, of which 494 km flows in Odisha and 357 km in Chhattisgarh. The basin extends over states of Odisha and Chhattisgarh and comparatively small parts of Madhya Pradesh, Maharashtra and Jharkhand. Mean annual precipitation fluctuates from 1200 to 1400 mm in the entire basin. It receives nearly 90% of annual rainfall from June to October (monsoon periods). The highest temperatures are registered in April and May varying between 39 °C to 40 °C whereas coldest months have a minimum temperature of 12 °C in December and January. Kesinga and Jondhra gauge stations were considered in present study for flood prediction.

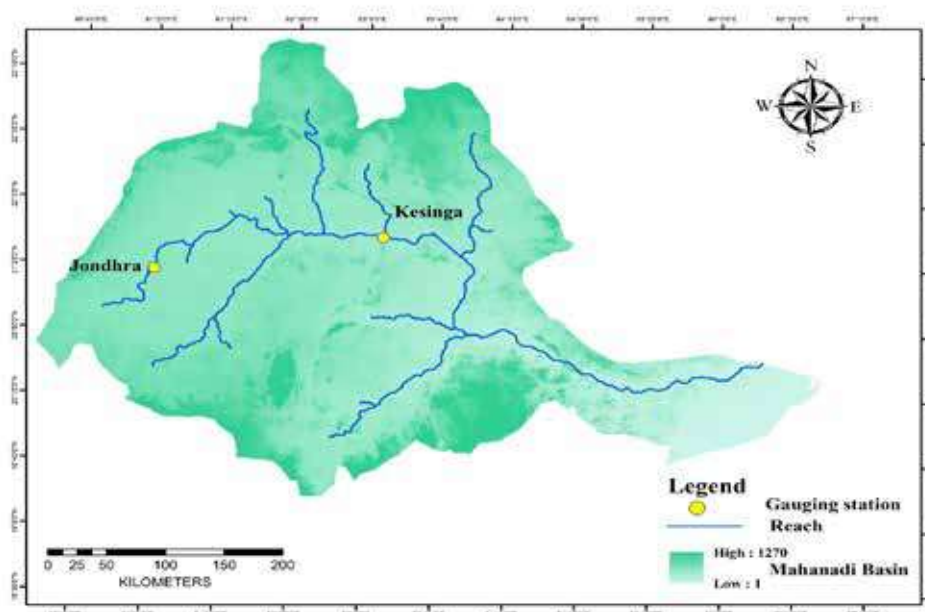


Fig. 1. Proposed study area



METHODOLOGY

MLP

Mcculloch and Pitts first presented the ANN in 1943 (McClelland & Rumelhart, 1988). Haykin in 1994 introduced a branch of ANN called MLP. In general, a basic MLP structure consist of input, output and hidden layers. Number of neurons is different in each layer. Number of layers required is associated with nature of problem considered, and using trial and error method number of hidden layers is selected to minimize error in prediction (Firat & Gungor, 2009; Ustaoglu et al., 2008). Moreover, by providing a weight to each input layer neuron, effect of each variable can be determined (Ghorbani et al., 2016) and Logarithmic sigmoid function, hyperbolic-tangent sigmoid function, and Linear function were used as activation function respectively as given in equation 1–3

$$f(x) = \frac{1}{1 + e^{-x}}$$

$$f(x) = \frac{2}{1 + e^{-2x}} - 1$$

$$f(x) = x$$

It is an entrenched technique in field of soft computing, where interconnected weights link each layer to next layer. A hypothesis is made in MLP model that number of neurons in input layer is n_i , in hidden layer is n_h and in output layer is n_o . Neurons are positioned in different layers. For computation of final output, activation functions are responsible in hidden and output layer. The weight connection links each layer to the next layer.

MLP-FFA

Based on social movement of fireflies, Yang (2010) presented a new nature-inspired optimization algorithm called the FFA (Yang, 2010; Ghorbani et al., 2017). It gives a great hybridization flexibility with MLP for any type of time-series analysis to make an effective implementation. It is derived from attraction and flashing behavior of fireflies. Metaheuristic property of MLP enables users for searching optimum parameters of the model. Degree of attractiveness and light intensity distinguishes each firefly. In this framework, FFA is integrated with MLP for updating bias, weights, and number of hidden neurons of NN. Training process of MLP continues up until meeting the stopping criterion. Regardless of their sex, each brilliant firefly can attract its neighborhood fireflies, and attraction is based on its brightness, making assessment of optimum search space increasingly useful (Zhang et al. 2016).

In present study, computation of optimum weight values for MLP was done using a flowchart as shown in **Fig. 2**. The figure demonstrates modelling process by utilising MLP for formulating problems related to prediction and by utilising FFA for serving as an optimization problem for identifying required weights of MLP. Light intensity emanated from fireflies reduces due to absorption by the media and with distance from its source. In mathematical terms, intensity of light ' I ' varies exponentially with light absorption coefficient γ and distance r . It is signified as follows (Iztok et al. 2013):

$$I = I_o \cdot e^{-\gamma r^2}$$

where I_o is initial light intensity at distance $r = 0$. As it is presumed that firefly attractiveness is directly proportional to intensity of light I , light attractive coefficient β of firefly is defined as:

$$\beta = \beta_o \cdot e^{-\gamma r^2}$$

where β_o is initial light attractiveness at $r = 0$. Cartesian distance amid any two fireflies i and j at x_i and x_j is specified by:

$$r_{ij} = \|x_i - x_j\|_2 = \sqrt{\sum_{k=1}^d (x_{i,k} - x_{j,k})^2}$$

where k signifies constituent in spatial coordinate and d is number of dimensions.

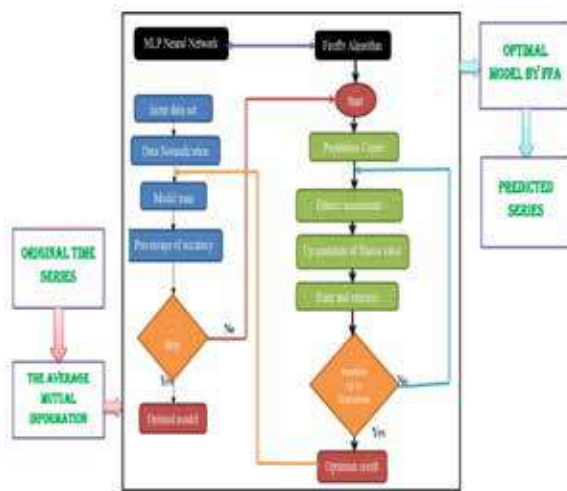


Fig. 2. Flowchart of proposed hybrid MLP-FFA model

RESULT AND DISCUSSION

Performance of MLP model for two proposed gauging sites with different inputs are given in **Table 1**. Two evaluation indices RMSE, WI is used for training and testing periods as given below.

Table 1. Results of MLP model for flood prediction

Station	Models	Input Scenarios	Training		Testing	
			RMSE	WI	RMSE	WI
Kesinga	MLP1	P_{t-1}	92.88	0.9046	93.91	0.8937
	MLP2	P_{t-1}, P_{t-2}	92.37	0.9077	93.7	0.8976
	MLP3	$P_{t-1}, P_{t-2}, P_{t-3}$	91.96	0.9109	93.24	0.9002
	MLP4	$P_{t-1}, P_{t-2}, P_{t-3}, P_{t-4}$	91.37	0.9143	92.59	0.9068
	MLP5	$P_{t-1}, P_{t-2}, P_{t-3}, P_{t-4}, P_{t-5}$	90.53	0.9172	92.21	0.9084
Jondhra	MLP1	P_{t-1}	93.52	0.8987	94.22	0.8905
	MLP2	P_{t-1}, P_{t-2}	93.18	0.9013	94.06	0.8931
	MLP3	$P_{t-1}, P_{t-2}, P_{t-3}$	92.45	0.9073	93.33	0.8991
	MLP4	$P_{t-1}, P_{t-2}, P_{t-3}, P_{t-4}$	91.65	0.9126	92.97	0.9043
	MLP5	$P_{t-1}, P_{t-2}, P_{t-3}, P_{t-4}, P_{t-5}$	90.86	0.9168	92.73	0.9066

Amongst five models, MLP5 model specifies preminent result having WI value 0.9172 for training and 0.9084 for testing period when $P_{t-1}, P_{t-2}, P_{t-3}, P_{t-4}, P_{t-5}$, as input parameter for Kesinga gauge station. For Jondhra station MLP5 model provides paramount WI value of 0.9168 and 0.9066 respectively for both phases out of five simulations. Outcomes of MLP-FFA approach based on RMSE, WI in training and testing phases is provided in **Table 2**.

Table 2. Results of MLP-FFA model for flood prediction

Stations	Model	Input Scenario	Training period		Testing period	
			RMSE	WI	RMSE	WI
Kesinga	MLP1-FFA	P_{t-1}	85.768	0.9477	86.362	0.9349
	MLP2-FFA	P_{t-1}, P_{t-2}	81.664	0.9502	82.899	0.9388
	MLP3-FFA	$P_{t-1}, P_{t-2}, P_{t-3}$	76.089	0.9546	77.864	0.9435
	MLP4-FFA	$P_{t-1}, P_{t-2}, P_{t-3}, P_{t-4}$	72.487	0.9599	84.584	0.9468
	MLP5-FFA	$P_{t-1}, P_{t-2}, P_{t-3}, P_{t-4}, P_{t-5}$	67.884	0.9641	74.996	0.9584
Jondhra	MLP1-FFA	P_{t-1}	87.116	0.9419	88.934	0.9356
	MLP2-FFA	P_{t-1}, P_{t-2}	83.656	0.9485	84.067	0.9368
	MLP3-FFA	$P_{t-1}, P_{t-2}, P_{t-3}$	78.995	0.9526	80.523	0.9407
	MLP4-FFA	$P_{t-1}, P_{t-2}, P_{t-3}, P_{t-4}$	74.811	0.9589	76.337	0.9443
	MLP5-FFA	$P_{t-1}, P_{t-2}, P_{t-3}, P_{t-4}, P_{t-5}$	69.058	0.9626	75.645	0.9553

Here five varying scenario models are utilised for estimating RMSE and WI value for two gauge station. When $P_{t-1}, P_{t-2}, P_{t-3},$

P_{t-4} , P_{t-5} , is utilised as input scenario, it provides the most excellent WI value. For Kesinga station best value for WI is 0.9641 in training and 0.9584 in testing period. In the similar manner, WI value of training and testing period is 0.9626, 0.9553 for Jondhra gauge station respectively.

Comparison of Models

The performances of flood prediction are compared using MLP and MLP-FFA approaches. The values of performance indices are provided in **Tables 1 and 2**, which shows that performance of each model on flood prediction is acceptable and these approaches are applicable for modeling flood series data. The results of Kesinga station for MLP and MLP-FFA models are 0.9084 and 0.9584, respectively. Similarly the values of WI are 0.9066 and 0.9553 for MLP and MLP-FFA models during testing phase at Jondhra gauge station. Appraisal of MLP and MLP-FFA models during training and testing periods for all proposed gauging stations are represented in **Fig. 3 and Fig. 4**, respectively. It was concluded that outcomes of MLP-FFA models are better compared to MLP model. Present study illustrates that the way forward is to have a proper understanding regarding the performance of individual models and utilise as many models as possible for gathering more evidence for selected models.

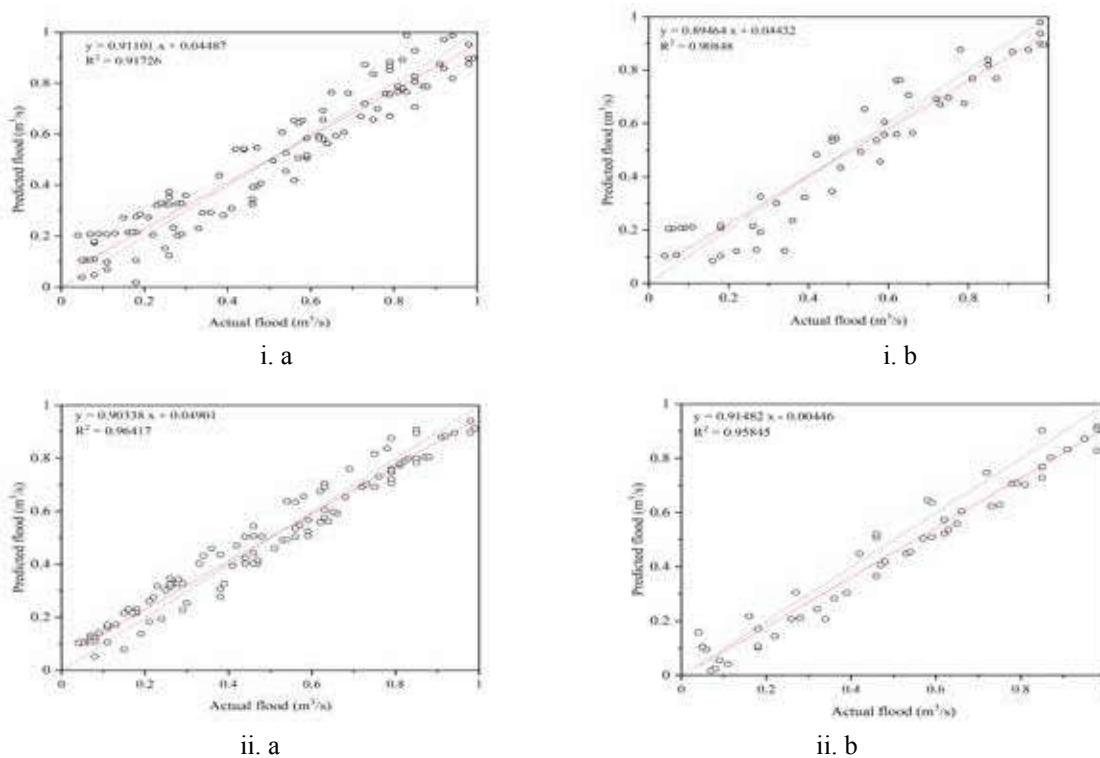
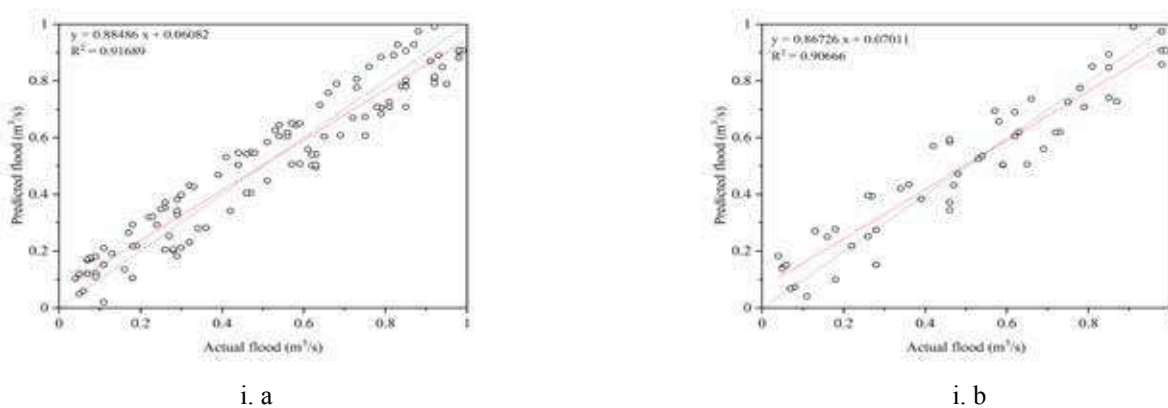


Fig. 3. Actual verses predicted flood using (i) MLP, (ii) MLP-FFA during (a) training and (b) testing phase at Kesinga station



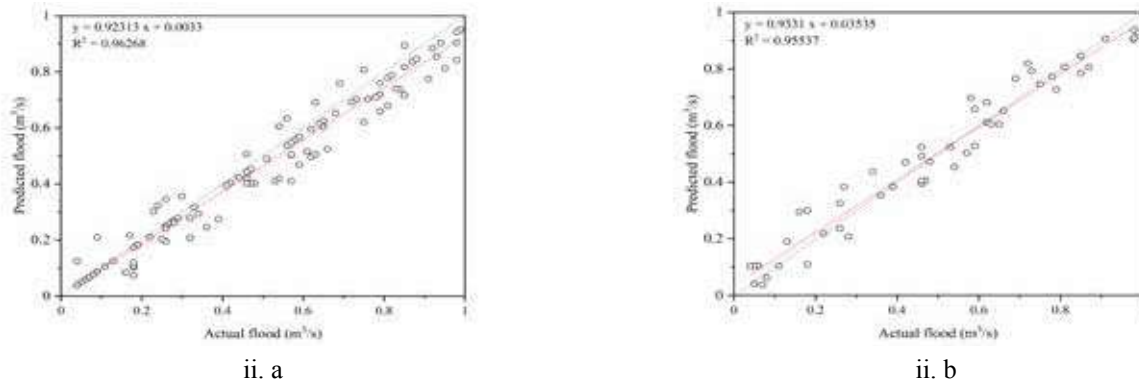


Fig. 4. Actual verses predicted flood using (i) MLP, (ii) MLP-FFA during (a) training and (b) testing phase at Jondhra station

Linear scale plots of actual versus predicted flood for proposed models at proposed sites are displayed in **Fig.5**. Outcomes show that estimated peak flood discharge is 3623.505m³/S, 3822.612m³/S for MLP and MLP -FFA against actual peak 3988.536m³/S for the station Kesinga. The approximated peak flood is 3477.086m³/S and 3664.134m³/S for MLP, MLP-FFA adjacent to actual peak 3835.304m³/S for Jondhra division.

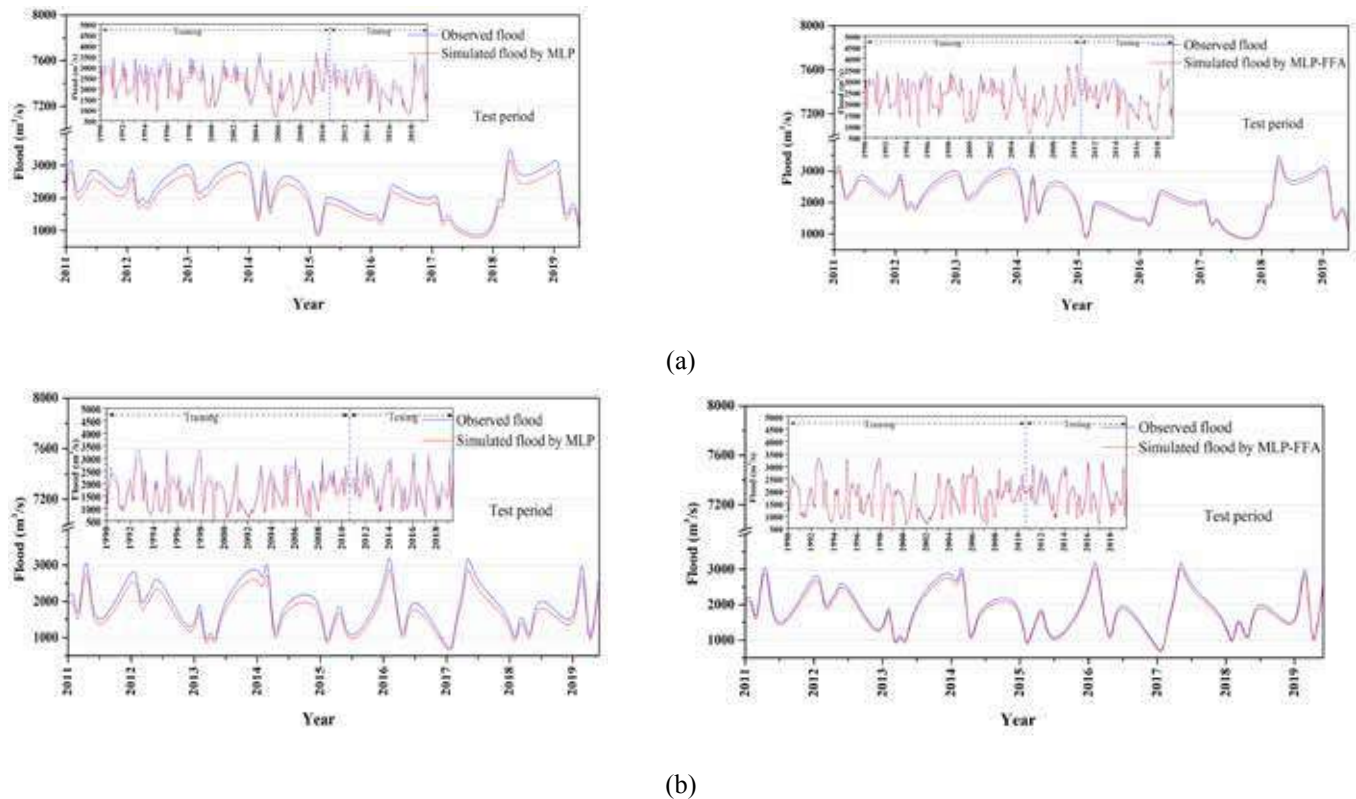


Fig. 5. Deviation of actual and predicted flood at (a) Kesinga, (b) Jondhra stations

CONCLUSION

A novel integrated model combining FFA algorithm and MLP, was proposed for predicting flood events in Mahanadi river basin. The demand for adaptation and evolutionary strategies for configuring artificial neural networks is due to real-world applications in modeling non-stationary environments. FFA was used to optimize search parameters of MLP and then compared it with simple MLP model for performance evaluation. Results revealed that, combination of MLP model with FFA were proven to be more effective and accurate than customary MLP.



REFERENCE

1. Naganna, S.R., Deka, P.C., Ghorbani, M.A., Biazar, S.M., Al-Ansari, N. and Yaseen, Z.M., 2019. Dew point temperature estimation: application of artificial intelligence model integrated with nature-inspired optimization algorithms. *Water*, 11(4), p.742.
2. Seo, Y., Kim, S. and Singh, V.P., 2015. Multistep-ahead flood forecasting using wavelet and data-driven methods. *KSCE Journal of Civil Engineering*, 19(2), pp.401-417.
3. Rezaeianzadeh, M., Tabari, H., Yazdi, A.A., Isik, S. and Kalin, L., 2014. Flood flow forecasting using ANN, ANFIS and regression models. *Neural Computing and Applications*, 25(1), pp.25-37.
4. Piotrowski, A., Napiorkowski, J.J. and Rowiński, P.M., 2006. Flash-flood forecasting by means of neural networks and nearest neighbour approach—a comparative study. *Nonlinear Processes in Geophysics*, 13(4), pp.443-448.
5. Mohamadi, S., Ehteram, M. and El-Shafie, A., 2020. Accuracy enhancement for monthly evaporation predicting model utilizing evolutionary machine learning methods. *International Journal of Environmental Science and Technology*, pp.1-24.
6. Latt, Z.Z. and Wittenberg, H., 2014. Improving flood forecasting in a developing country: a comparative study of stepwise multiple linear regression and artificial neural network. *Water resources management*, 28(8), pp.2109-2128.
7. Kim, S. and Singh, V.P., 2013. Flood forecasting using neural computing techniques and conceptual class segregation. *JAWRA Journal of the American Water Resources Association*, 49(6), pp.1421-1435.
8. Khatibi, R., Ghorbani, M.A. and Pourhosseini, F.A., 2017. Stream flow predictions using nature-inspired firefly algorithms and a multiple model strategy—directions of innovation towards next generation practices. *Advanced Engineering Informatics*, 34, pp.80-89.
9. Dtissibe, F.Y., Ari, A.A.A., Titouna, C., Thiare, O. and Gueroui, A.M., 2020. Flood forecasting based on an artificial neural network scheme. *Natural Hazards*, 104(2), pp.1211-1237.
10. Do Hoai, N., Udo, K. and Mano, A., 2011. Downscaling global weather forecast outputs using ANN for flood prediction. *Journal of Applied Mathematics*, 2011.
11. Shamshirband, S., Esmailbeiki, F., Zarehaghi, D., Neyshabouri, M., Samadianfard, S., Ghorbani, M.A., Mosavi, A., Nabipour, N. and Chau, K.W., 2020. Comparative analysis of hybrid models of firefly optimization algorithm with support vector machines and multilayer perceptron for predicting soil temperature at different depths. *Engineering Applications of Computational Fluid Mechanics*, 14(1), pp.939-953.
12. Al-Jamimi HA, Bagudu A, Saleh TA (2019) An intelligent approach for the modeling and experimental optimization of molecular hydrodesulfurization over AlMoCoBi catalyst. *J Mol Liq* 278:376–384.
13. Alade IO, Rahman MAA, Saleh TA (2019) Predicting the specific heat capacity of alumina/ethylene glycol nanofluids using support vector regression model optimized with Bayesian algorithm. *Sol Energy* 183:74–82.
14. Had Haddad OB, Sharifi F, Alimohammadi S (2005) ANN in river flow forecasting. *Proceedings of the 6th WSEAS Int. Conf. on Evolutionary Computing*. Lisbon, Portugal: 316–324.
15. Sattari NT, Apaydin H, Ozturk F (2012) Flow estimations for the Sohu stream using artificial neural networks. *Environ Earth Sci* 66(7):2031–2045.
16. Shamseldin AY (2010) Artificial neural network model for river flow forecasting in a developing country. *IWA J Hydroinformatics* 12(1):22–34.
17. Othman F, Naseri M (2011) Reservoir inflow forecasting using artificial neural work. *Int J Phys Sci* 6(3):434–440.
18. Sentu D, Regulwar DG (2011) Inflow prediction by different neural network architectures: a case study. *Int J Earth Sci Eng* 4(6):225–230.
19. Dawson CW, Wilby RL (2001) Hydrological modelling using artificial neural networks. *Prog Phys Geogr* 25(1): 80–108
20. Rajurkar MP, Kothiyari UC, Chaube UC (2002) Artificial neural networks for daily rainfall-runoff modeling. *Hydrol Sci* 47(6):865–877.



21. ASCE Task Committee on application of artificial neural networks in Hydrology (2000a) Artificial neural networks in hydrology. I: Preliminary concepts. *J Hydrol Eng* 5(2):115–123.
22. ASCE Task Committee on application of artificial neural networks in Hydrology (2000b) Artificial neural networks in hydrology. II: Hydrologic applications. *J Hydrol Eng* 5(2):124–137.
23. Cigizoglu HK (2003) Estimation, forecasting and extrapolation of river flows by artificial neural networks. *Hydrol Sci* 48(3):349–361.
24. Kisi Ö (2007) Streamflow forecasting using different artificial neural network algorithms. *J Hydrol Eng* 12(5): 532–539.
25. Chang F, Chiang Y, Chang L (2007) Multi-step-ahead neural networks for flood forecasting. *Hydrol Sci* 52(1): 114–130.
26. Dawson CW, Harpham C, Wilby RL, Chen Y (2002) Evaluation of artificial neural network techniques for flow forecasting in the River Yangtze, China. *Hydrol Earth Syst Sci* 6(4):619–626.
27. McClelland, J., & Rumelhart, D. (1988). *Explorations in parallel distributed processing: A handbook of models, programs, and exercises*. MIT Press.
28. Ustaoglu, B., Cigizoglu, H. K., & Karaca, M. (2008). Forecast of daily mean, maximum and minimum temperature time series by three artificial neural network methods. *Meteorological Applications*, 15(4), 431–445.
29. Ghorbani, M. A., Ahmadzadeh, H., Isazadeh, M., & Terzi, O. (2016). A comparative study of artificial neural network (MLP, RBF) and support vector machine models for river flow prediction. *Environmental Earth Sciences*, 75(6), 476–490.
30. Firat, M., & Gungor, M. (2009). Generalized regression neural networks and feed forward neural networks for prediction of scour depth around bridge piers. *Advances in Engineering Software*, 40(8), 731–737.
31. Zhang, L.; Liu, L.; Yang, X.S.; Dai, Y. A Novel Hybrid Firefly Algorithm for Global Optimization. *PLoS ONE* 2016, 11, 1–17.
32. Ghorbani, M.A.; Deo, R.C.; Karimi, V.; Yaseen, Z.M.; Terzi, O. Implementation of a hybrid MLP-FFA model for water level prediction of Lake Egirdir, Turkey. *Stoch. Environ. Res. Risk Assess.* 2017, 32, 1683–1697.
33. Yang, X.S. Firefly algorithm, stochastic test functions and design optimisation. *Int. J. Bio-Inspired Comput.* 2010, 2, 78–84.
34. Iztok, F.; Iztok, F.J.; Xin-She, Y.; Janez, B. A comprehensive review of Firefly algorithms. *Swarm Evol. Comput.* 2013, 13, 34 – 46.
35. Sahoo, A., Samantaray, S. and Ghose, D.K., 2019. Stream Flow Forecasting in Mahanadi River Basin using Artificial Neural Networks. *Procedia Computer Science*, 157, pp.168-174.
36. Samantaray, S. and Sahoo, A., 2020a. Appraisal of runoff through BPNN, RNN, and RBFN in Tentulikhunti Watershed: A case study. In *Frontiers in Intelligent Computing: Theory and Applications* (pp. 258-267). Springer, Singapore.
37. Samantaray, S. and Sahoo, A., 2020b. Estimation of runoff through BPNN and SVM in Agalpur Watershed. In *Frontiers in Intelligent Computing: Theory and Applications* (pp. 268-275). Springer, Singapore.
38. Sahoo, A., Samantaray, S., Bankuru, S. and Ghose, D.K., 2020a. Prediction of Flood Using Adaptive Neuro-Fuzzy Inference Systems: A Case Study. In *Smart Intelligent Computing and Applications* (pp. 733-739). Springer, Singapore.
39. Mohanta, N.R., Patel, N., Beck, K., Samantaray, S. and Sahoo, A., 2020. Efficiency of River Flow Prediction in River Using Wavelet-CANFIS: A Case Study. In *Intelligent Data Engineering and Analytics* (pp. 435-443). Springer, Singapore.
40. Sridharam, S., Sahoo, A., Samantaray, S. and Ghose, D.K., 2020. Assessment of Flow Discharge in a River Basin Through CFBPNN, LRNN and CANFIS. In *Communication Software and Networks* (pp. 765-773). Springer, Singapore.
41. Sahoo, A., Singh, U.K., Kumar, M.H. and Samantaray, S., 2020b. Estimation of Flood in a River Basin Through Neural Networks: A Case Study. In *Communication Software and Networks* (pp. 755-763). Springer, Singapore.
41. Samantaray, S., Sahoo, A., Mohanta, N.R., Biswal, P. and Das, U.K., 2020. Runoff Prediction Using Hybrid Neural Networks in Semi-Arid Watershed, India: A Case Study. In *Communication Software and Networks* (pp. 729-736). Springer, Singapore.

Electrical Engineering



Analysis of Wireless Power Transfer Compensation Topologies for EV Battery Charging

Amarjeet S Pandey, D B Pardeshi

Sanjivani College of Engineering / Savitribai Phule Pune University / Sanjivani College of Engineering, Kopargon

✉ tnpamarjeet@sanjivani.org.in; ✉ pardeshidipeshselect@sanjivani.org.in

ABSTRACT

This paper provide comprehension of compensation topologies encountered and foreseen issues, enabling technologies considering compensation network. To have the appropriate designing procedure the compensation tank for both CC and CV mode charge. The design approach focuses on the required measures to ensure power transfer over the complete operating range of the system. This paper gives insight to research entities, industry professionals as ready reference information for the resonant topologies with research gap.

Keywords : Inductive power transfer (IPT); Compensation network; Electric vehicle; Resonance.

ABSTRACT

In recent years, it has been adopted an electric vehicle (EV) Charge to bring convenience Complement of power appendage. Currently, the most conventional method is plug-in charging, where a copper connected cable forms the power link. It usually takes an overnight charge to bring a depleted battery up to full charge. There are several disadvantages to this method, which have led to the investigation of inductive charging technology. IPT is a contactless power supply system that would allow electrical energy to be safely supplied to vehicles without any mechanical contact. IPT works by the same principle

as a transformer. With IPT the air gap is large but the operating frequency is raised to 15 000 Hz to compensate. With the large air gap the system becomes insensitive to positional tolerances of the pick-up on the track. Multiple loads may also be operated at the same time. The track power supply generates the high frequency alternating current in the track cable. The special shape of the pick-up is most effective at capturing the magnetic field generated by the track conductors. The captured AC magnetic field produces electrical energy in the pick-up coil and the pick-up regulator converts the high frequency AC power to DC while regulating the power to the load.

The main features of the IPT system are:

Efficiency: the track power supply and vehicle pick-up work with an efficiency of up to 96%. Both track and pick-up systems are resonant so that losses and harmonics are minimised. Power: hundreds of kW may be transferred. Power ranges of 30–1000kW are possible. Large Airgap: power may be transferred across air gaps of 100mm and more. Multiple Independent Loads: using intelligent control, any number of vehicles may be operated independently and simultaneously on a system. Safety: all components are fully enclosed and insulated. Hence the system is fully touch-proof. Speed: with conductor bar, festoon or cable reel systems, speed is a limiting factor Ref.[1] With IPT speed of operation is unlimited. Inductive charging (or Inductive Power Transfer [IPT]) uses time varying magnetic fields to jump the air gap of a car chassis and wirelessly recharge a vehicle parked over a transmitter. The fundamental principles of such systems are identical to well-known closely coupled electromechanical devices such as transformers and induction motors, where the leakage inductance is much lower than the mutual inductance. The compensation tank is an important part

That contributes to a reduction in the reactive power, and an improvement in power transfer capability and overall efficiency. The primary winding (stationary track or coil) is normally compensated in order to minimize the VA rating of the supply. Compensation is often required for the secondary winding (movable pickup) to enhance the power transfer capability. A switched-mode controller may be used to control the power flow from the pickup to the load. In more complex systems many individual pickups can exist, supplied by a single track. Depending on how the compensation capacitors are added to the primary and secondary coils.

Basic Topologies

Four basic topologies labelled as SS, SP, PP, and PS are shown in **Fig.1**, where the first S or P stands for series or parallel compensation of the primary winding and the second S or P stands for series or parallel compensation of the secondary winding.

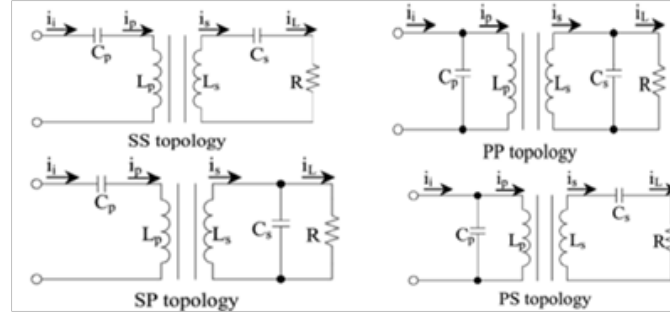


Fig. 1. four basic IPT topologies (a) SS. (b) SP (c) PS. (d) PP

Here, the subscripts “i”, “p”, “s”, and “L” stand for “inverter”, “primary”, “secondary”, and “load”, respectively. The resistance represents the load on the secondary. Using a mutual inductance coupling model, each of these topologies can be modelled. The induced and reflected voltages in this model are specified in terms of the mutual inductance “M”, the operational frequency “ ω ”, and the primary and secondary currents. The mutual inductance is related to the magnetic coupling coefficient by

$$k = \frac{M}{\sqrt{L_p L_s}}, \quad (1)$$

Single Pickup

The reflected impedance from the secondary to the primary Can be found as:

$$Z_r = \frac{\omega^2 M^2}{Z_s} \quad (2)$$

where Z_s is the impedance of the secondary network and depends on the selected compensation topology. The power transferred from the primary to the secondary is given by

$$P = (\text{Re} Z_r) I_p^2 \quad (3)$$

where the operator “Re” represents the real component of corresponding variable. The current flowing through the secondary winding is

$$I_s = \frac{j\omega M I_p}{Z_s}, \quad (4)$$

The voltages across the primary and secondary windings are,

$$V_p = j\omega L_p I_p - j\omega M I_s \quad (5)$$

Therefore, given by V_p and V_s respectively in eqn. (5) and (6) respectively

$$V_s = j\omega M I_p - j\omega L_s I_s, \quad (6)$$

The secondary impedance is given in Table I(a) for series and parallel-compensated networks. The load voltage and current are also given in the same table. The reflected resistance and reactance calculated from (2) at the secondary resonant frequency are also given in Table I(b) and depend on the compensations used. The secondary quality factor defined at the secondary resonant frequency is also given in the same table. Here, the quality factor is the ratio between reactive and real power. The series-

compensated secondary resembles a voltage source, while the parallel-compensated secondary looks like a current source. Ref. [2]

TABLE 1
SECONDARY IMPEDANCE, LOAD VOLTAGE/CURRENT, AND PROPERTIES AT THE
SECONDARY RESONANT FREQUENCY. (a) SECONDARY IMPEDANCE
AND LOAD VOLTAGE/CURRENT. (b) PROPERTIES AT THE SECONDARY
RESONANT FREQUENCY ω_0

(a)		
Compensation	Series	Parallel
Secondary impedance Z_s	$j\omega L_s + \frac{1}{j\omega C_s} + R$	$j\omega L_s + \frac{1}{j\omega C_s + \frac{1}{R}}$
Load voltage V_L	$I_s R$	V_s
Load current I_L	I_s	$\frac{V_s}{R}$
(b)		
Compensation	Series	Parallel
Reflected resistance	$\frac{\omega_0^2 M^2}{R}$	$\frac{M^2 R}{L_s^2}$
Reflected reactance	0	$-\frac{\omega_0 M^2}{L_s}$
Secondary Quality factor Q_s	$\frac{\omega_0 L_s}{R}$	$\frac{R}{\omega_0 L_s}$

$$\omega_0 = \frac{1}{\sqrt{C_s L_s}} = \frac{1}{\sqrt{C_p L_p}} \quad (7)$$

LCL Converter Design

The LCL load resonant converter shown in **Fig. 2** is chosen in this application because of the following advantages.

- The inverter bridge only has to supply the real power required by the load and any losses in the resonant tank. The high track currents are constrained to self-circulate in the resonant tank. For example, in most practical applications.

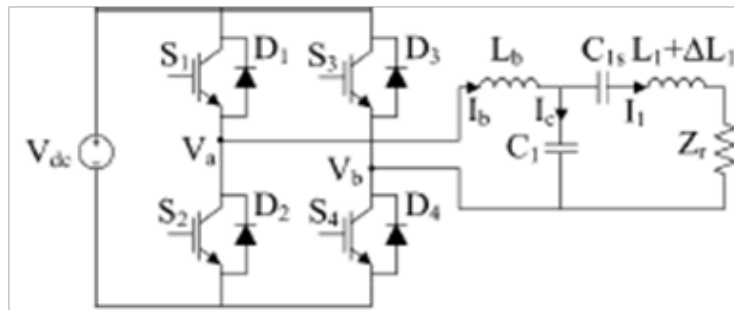


Fig. 2. A LCL load resonant converter

Where $Q_1 > 1$, $I_b > I_1$, (**Fig.2**) the switches have low conduction losses and a high converter efficiency is achieved.

- The output current is independent of load, making it a constant current source ideal for IPT applications. The primary pad I_1 current is only dependent on one control variable and hence the power output, or uncompensated power (SU) in [3], is directly controlled.

To design the LCL converter, the reactance of each branch is tuned by the conventional equation in (8) and hence the power output, or uncompensated power (SU) in (1), is directly controlled. Here, is a series tuning capacitor to reduce the reactance of the pickup to a desired operating value. For this system, phase-shift control or symmetric voltage cancellation (SVC) [4] is used to directly control the track current (I_1) with one control variable. To determine the track current under SVC, and assuming fundamental mode analysis, the following equation is used:

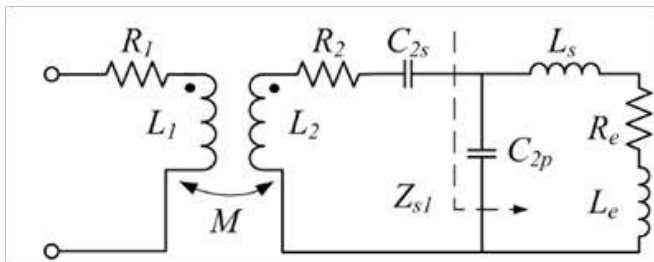
The maximum obtainable track current can be determined when is set to 180. For the LCL converter, the specifications in **Table 2** are calculated according to the design equations.

Table 2. Design parameters for LCL converter

Parameter	Value	Parameter	Value
V_{dc}	400V	C_{1s}	663nF
X_l	9.21 Ω	L_1 (Figure 3)	177-188uH
$I_{l \max}$	39A	$L_{1 \text{ short}}$	161-172uH
L_b	73.3uH	ω	1.257x10 ⁵ rad/s
C_1	885nF		

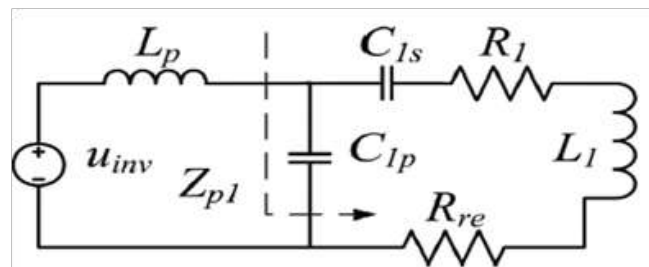
LCC Compensation

As per Compensation networks which act as special for EV WCS Performance, and can match the barriers between Coil and inverter source or rectifier load. There are specifically two WCS type of compensation network Compensation, including series capacitor (SC) compensation Parallel capacitor compensation, etc; The other is complicated compensation, of which a specific inductor capacitor-capacitor (LCC) compensation has put more attention due to its convenient feature for WCS. SC compensation is selected as the example of single device compensation, and compared with LCC compensation to discuss the interoperability of WCS compensation networks. WCS equivalent models with secondary side SC and LCC compensation networks are shown in Fig.4. Where, L_1 and L_2 are self-inductances of the transmit coil and receive coil; M is mutual-inductance between them; R_1 and R_2 are self-resistances of the transmit coil and receive coil; C_2 is secondary side SC compensation; C_{2s} , C_{2p} and L_s constitute the secondary side LCC compensation network; rectifier equivalent load is expressed by series equivalent resistance and inductance R_e and L_e . Ref. [5].


Fig. 3. Secondary side with LCC compensation

Compensation Network Interoperability Operation

WCS has good interoperability means system performance does not change much, when different types of compensation networks are adopted in the secondary side. So, firstly, we will discuss system performance in this section, taking system power and inverter load inductance as examples. Here, primary LCC compensation network is used for discussion. Equivalent circuit of WCS primary side is shown in Fig. 4.


Fig. 4. Primary side equivalent circuit of wireless charging system, considering the secondary side as a reflected resistance R_{re}

Where, u_{inv} is inverter output equivalent voltage source; R_{re} is reflected resistance of the secondary side; C_{1s} , C_{1p} and L_p constitute the primary side LCC compensation network; Z_{p1} is defined as the impedance after the primary side of Z_{p1} is given by (8). Where, $X_{pe} = \omega L_1 - 1/(\omega C_{1s}) - 1/(\omega C_{1p})$; $\text{re}(Z_{p1})$ means the real part of Z_{p1} ; $\text{im}(Z_{p1})$ is the imaginary part of Z_{p1} . So, the expression of system power and inverter load Inductance can be given by (10).

$$P_{out} = \left| \frac{u_{inv}}{Z_{p1} + j\omega L_p} \right|^2 \frac{Re(Z_{p1})}{R_{re} + R_t} \quad (10)$$

$$L_{inv} = \text{Im}(Z_{p1}) + L_p$$

Equations (10) suggest system power and inverter load inductance are both decided by reflected resistance R_{re} , when primary side parameters are fixed. So, system performance of the primary side will not change much, if the reflected impedances of different types of compensation networks are similar. Finally, we can think that different types of compensation networks can have good interoperability, if their reflected Impedances are similar. Hence, reflected resistance R_{re} can be used to evaluate the interoperability between different secondary side compensation networks. In view of SC and LCC compensation networks, they can have well Interoperability, if $R_{re_sc} \approx R_{re_lcc}$, which means $R_e \approx R_{opt,Ref}$. [6]

Analysis of the Double-Sided LCC Topology

Fig. 5(a) shows the double-sided LCC compensation topology. The circuit consists of a full-bridge inverter, a LCC compensation tank in sides, a bridge rectifier, and a load network with an output capacitor.

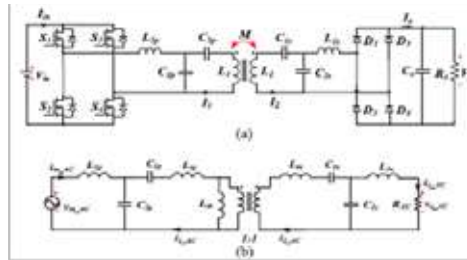


Fig. 5 (a) Double-sided LCC compensation topology.(b) AC equivalent circuit of double-sided LCC compensation topology.

The T model equivalent circuit in **Fig. 5(b)** is analysed in the frequency domain based on the First Harmonic Approximation (FHA) for the sake of simplicity [7]. To get the maximum fundamental output voltage, each switch conducts with almost a 50% duty ratio. The primary compensation tank is composed of a resonant inductor (L_{1p}) and two resonant capacitors (C_{1p} and C_{2p}). Here, C_{1p} and C_{2p} are connected in series and in parallel with the primary coil, respectively. Similarly, the secondary compensation tank is composed of L_{1s} , C_{1s} , and C_{2s} . To simplify the analysis and design of the IPT system, it is assumed that the number of turns of the primary side coil is equal to that of the secondary side coil. The coil is modelled by a T model. The relationships among the self-inductances L_1 and L_2 , the leakage inductances L_{rp} and L_{rs} , and the coupling coefficient k can be expressed as follows:

$$k = \frac{M}{\sqrt{(L_m + L_{rp})(L_m + L_{rs})}} = \frac{M}{\sqrt{L_1 L_2}} \quad (11)$$

Where M and L_m are the mutual inductance and the magnetizing inductance between the two coils, respectively. The first harmonic components, based on the equivalent circuit in **Fig. 5(b)**, can be written as

$$\begin{aligned} L_{rp} &= (1-k)L_1, \quad L_{rs} = (1-k)L_2 \\ v_{uAC}(t) &= \frac{4}{\pi} V_{in} \sin(2\pi ft), \quad v_{uAC}(t) = \frac{4}{\pi} V_o \sin(2\pi ft + \theta) \\ i_{oAC}(t) &= \frac{\pi}{2} I_o \sin(2\pi ft + \theta), \quad R_{AC} = \frac{8}{\pi^2} \frac{V_o}{I_o} = \frac{8}{\pi^2} R_o \end{aligned} \quad (12)$$

V_{in} , V_o , and I_o represents the values for input dc-link voltage, required output voltage for the battery, and required output current for the battery, respectively. The first harmonic components are subscripted by "AC". θ is the phase difference between v_{inAC} and v_{oAC} . In the following analysis V_{in} , V_o , I_{in} , I_1 , I_2 , and I_o are used to depict the complex form of the corresponding variables.

It can be easily deduced from (11) that the voltage conversion ratio of the double-sided LCC topology $|V_o/V_{in}|$ is identical to V_o/V_{in} . In the following sections, the load-independent characteristics of the double-sided LCC compensation topology are analysed to show how to implement the CC/CV mode charge. Ref. [8]



CONCLUSION

The paper objective is to highlight the most advanced modification in the compensation topologies with respect to the conventional one. The technical points discussed are: 1) Equivalent compensation topologies parameter; 2) Primary resonance design for the resonant topologies; 3) approach to implement the CC/CV charge with innovative topology is introduced to achieve both load independent current and voltage characteristics. The research gaps for sustainable points of view: 1) Implementation of Compensation network with novel topology which will give the optimal solution to match the impedances between the coils and inverter source or rectifier load. 2) CC/CV charge with novel topology for the wide range of load variations.

ACKNOWLEDGMENT

This work was supported by Department of Electrical, Sanjivani College of Engineering, Kopargon.

REFERENCES

1. James Larminie Oxford Brookes University, Oxford, UK John Lowry Acenti Designs Ltd., UK "Electric Vehicle Technology Explained" Copyright © 2003 John Wiley & Sons Ltd.
2. C. W. Wang, O. H. Stielau, and G. A. Covic, "Design considerations for a contactless electric vehicle battery," *IEEE Trans. Power Electron.*, vol. 52, no. 5, pp. 1308–1314, Oct. 2005.
3. M. Borage, S. Tiwari, and S. Kotaiah, "Analysis and design of an LCL-T resonant converter as a constant-current power supply," *IEEE Trans. Ind. Electron.* vol. 52, no. 6, pp. 1547–1554, Dec. 2005.
4. H. H. Wu, A. Gilchrist, K. Sealy, P. Israelsen, and J. Muhs, "Design of Symmetric voltage cancellation control for LCL converters in inductive power transfer systems," in *Proc. IEEE Int. Electric Machines Drives Conf. (IEMDC'11)*, 2011, pp. 866–871.
5. Yanjie Guo, Lifang Wang, Yuwang Zhang, Shufan Li, and Chenglin Liao, "Rectifier load analysis for electric vehicle wireless charging system," *IEEE Trans. Ind. Electron.*, vol. 65, no. 9, pp. 6970–6982, Sep. 2018.
6. Yanjie Guo, Yuwang Zhang, Bingrong Yan "Interoperability Analysis of Compensation Network in Electric Vehicle Wireless Charging System," *IEEE* ©2018.
7. R. W. Erickson and D. Maksimovic, *Fundamentals of Power Electronics*, 2nd ed. New York, NY, USA: Academic, 2001.
8. Van-Binh Vu, Duc-Hung Tran, and Woojin Choi, "Implementation of the Constant Current and Constant Voltage Charge of Inductive Power Transfer Systems With the Double-Sided LCC Compensation Topology for Electric Vehicle Battery Charge Applications," *IEEE Trans. Power Electronics*, vol. 33, no. 9, pp. 7398–7408, Sep. 2018.
9. Plugless Power, Plugless Power vehicle compatibility. [Online]. Available: www.pluglesspower.com/go-plugless/wireless-evcharging/supported-evs/
10. J.M. Miller, "Wireless Plug-in Electric Vehicle (PEV) Charging," Oak Ridge National Laboratory, Tech. Rep., 2012. [Online]. Available: http://www1.eere.energy.gov/vehiclesandfuels/pdfs/merit_review_2012/veh_sys_sim/vs_s061_miller_2012_o.pdf

Power Electronic Interfaces on Renewable Energy System

Sanjeev Kumar Bhatnagar, Priyabrata Pradhan

Hindustan Petroleum Corporation Limited

✉ skbhatnagar@hpcl.in; ✉ priyabratap@hpcl.in

ABSTRACT

Steady rise in the consumption pattern of global energy, has created a consistent need to increase the capacity to generate power. Sustainable energy is the need of the hour. In this paper we have tried to analyze available resources and technologies to address the challenges of the future and their role thru the usage of power electronics in the various segments of power transmission, distribution and finally end –user applications. With the vital role on the integration of grids being done thru Power Electronics Grids, the interface by converter based on Power Electronics in renewable energy systems is destined to increase, including in the photovoltaic (PV), wind and fuel cell applications.

Keywords : Turbines; Photovoltaic; MPPT; PWM.

ABSTRACT

The energy consumption is increasing gradually and with the deregulation of electricity, the production capacity of installed high power stations will not be able to suffice to the demand in future..Thus investing in the alternate energy sources e.g. wind turbines, photovoltaic systems, and fuel cell systems is highly essential. Renewable energy technologies have almost negligible environmental impact than conventional energy technologies .Of the two main trends in the development of power systems, the first one involves wide utilization of power sources involving renewable energy. The second includes decentralization of power generation.

This paper includes some of the requirements of the power electronic interface applicability with respect to wind, photovoltaic, and fuel cell power generation units.

TURBINE SYSTEMS (WIND)

Wind power is the conversion of wind energy into a very useful form of energy which includes wind turbines. **(Fig 1)** Air pressure, Wind speeds, air pressure, earth surface temperature atmospheric temperature, etc., are highly inter- linked parameters. The speed of the wind is the most vital factor which influences the total production of energy from a wind turbine. With increase in the velocity of the wind, it increases the amount of air passing the rotor, which gradually increases the output of the wind system as shown in **Table 1**.

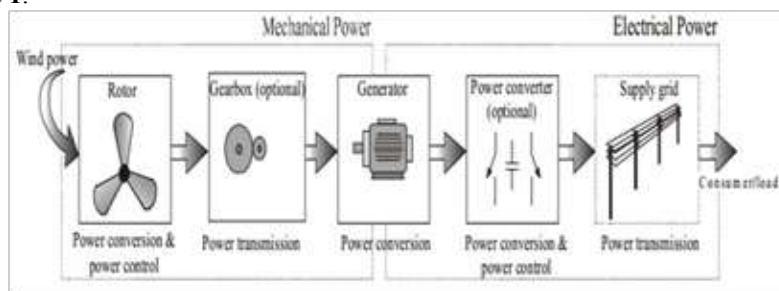


Fig. 1. Basic Power Conversion Principle in Wind Energy System

Table 1. Basic Power Conversion Principle in Wind Energy System

Average Wind Speed Km/h(mph)	Suitability
Up to 15(9.5)	No good
18(11.25)	Poor

22(13.75)	Moderate
25(15.5)	Good
29(18)	Excellent

The popular machines and power electronics in the large wind turbines include:

- Synchronous generators along with rectifiers&inverter (power) for grid interconnection [1].In this case inverter and rectifier need to be kept at the same power level as the generator.
- Doubly fed induction generator with an ac-to-ac power converter for rotor frequency and power control. In this case the converter is required only up to 30% of the power from the generator.

As per the basics of wind energy the generation of wind energy can be summarized as below. The power that can be extracted from the wind is

$$P_W = \frac{1}{2} \pi R^2 \rho v^3 C_p(\lambda)$$

Where,

R = blade length

ρ = density of air

v = wind velocity

λ = tip speed ratio

C_p = power coefficient

The tip speed ratio is defined as the ratio of the tip speed to wind speed.

$$\lambda = \frac{R\Omega}{v}$$

Presently with the focus on the variable speed and horizontal wind turbines, power electronic circuits do play a vital role in variable speed based wind energy conversion systems. Wind turbines with fixed speed are reliable, simple and robust which maintain the grid frequency constantly with respect to rotor. The maximum attainable efficiency for wind energy conversion is 0.59. As a consequence of which we are not able to obtain the optimal aerodynamic efficiency point C_{pmax} . In case of wind speeds which are varying, wind turbines with fixed speeds are not able to trace the optimal power extraction point C_{pmax} . In case of the wind turbines with variable speed, to enable variable speed operation, power electronic circuit partially or completely decouples the rotor mechanical frequency from the grid electrical frequency. To understand the difference between the characteristics of fixed speed vs variable speed is depicted in **Fig 2**.

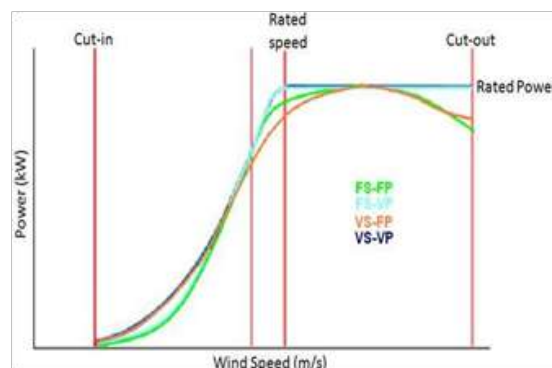


Fig 2. Characteristics of fixed speed vs variable speed

The wind Turbines are connected to the utility grid feeding the produced energy to the grid either directly or through power

electronics,. On this type of Wind turbine (WT) efforts are made to increase the size and efficiency of the machines. Studies have been made on the controlling of the speed part and on finding ideas on how to get reduction in the cost of the unit.

Several types of inverters are used on wind turbine installations, such as the bi-directional converter Pulse Width Modulation(PWM) – Voltage Source Inverter (VSI) converters and less used matrix converters. The bi-directional PWM-VSI power converter has two no's of PWM – VSI inverters [2]. Conversion of AC waveform to another AC waveform is done by a solid-state AC-AC converter and the setting of the frequency and output voltage can be done arbitrarily. A rotor side ac-dc converter, a dc link capacitor, and a dc-ac inverter connected to the grid do form the main parts of the power converter system.

The power converter system comprises of as shown in **Fig 3**. An AC-AC converter is with a bidirectional power flow and sinusoidal input currents. It is comprehended by coupling a pulse-width modulation (PWM) rectifier and a PWM inverter to the DClink. The DC-link quantity is then impressed by an energy storage element that is common to both stages, which is a capacitor C for the voltage DC-link or an inductor L for the current DC-link. The controlling of the Pulse width modulation rectifier ensures drawing of a sinusoidal AC line current, which is in phase or anti-phase (for feedback of energy) with the corresponding AC line phase voltage.

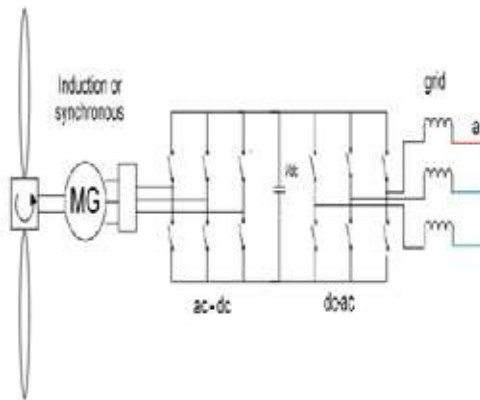


Fig.3. Fully variable wind energy conversion system

The DC-link storage element provides the advantage of both converter stages to a large extent is decoupled for control purposes. In addition to the above, for the Pulse width modulation inverter stage a constant AC line input quantity exists which is independent in nature, which results in high utilization of the converter's power capability. On the other hand, the DC-link energy storage element has a larger physical volume, and when electrolytic capacitors are being used, in the case of a voltage DC-link, there is potentially a reduction in system lifetime.

Inversion is inherently a step down converter hence the turbine side AC-DC converter ensures sufficient voltage level is obtained in order to integrate with the grid. If additional boosting of the voltage is required, an additional dc-dc boost converter can to be employed as a result of which the overall cost and complexity is increased. To avoid this a Z-source inverter based conversion system is employed which is depicted as per **Fig 4**.

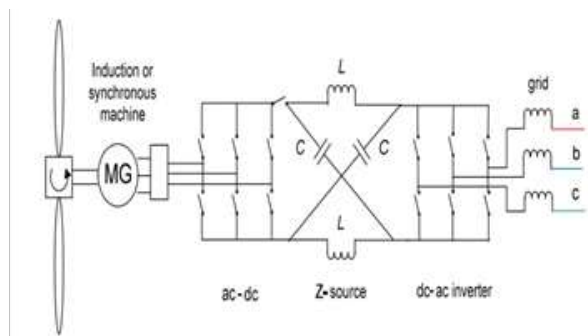


Fig. 4. Z-source based variable speed wind energy conversion system

The Summary of the Wind Energy Conversion is as per **Table 2**.

Table 2. Wind Energy Conversion Systems Summary

WEC based on	Generator	Grid integration	Key points
Fixed speed system	Induction generator	Direct	Constant speed Simple Low controllability
Partially variable System	Doubly- fed induction generator	ac-dc- ac voltage source converter	Highly controllable Vector control of active and reactive power
Fully variable system	Induction generator or Synchronous generator	ac-dc- ac voltage source converter or potentially Z-source converter	Highly controllable Wide range of speeds. For Z-source, Short circuit protection Improved EMI feature

PHOTOVOLTAICSYSTEMS

Solar Photovoltaic (SPV) technology has a gradual increasing trend in demand both in grid-connected as well as off-grid stand-alone modes. One of the major drawbacks of solar PV system is its high installation cost for producing desired power level of electricity which attributes to the high cost of manufacturing of solar modules in addition to the low conversion efficiency. With the target of making solar PV system commercially operable, the cost of unit generation of electricity needs to be reduced which, requires development of a low cost, high efficient power conversion systems. Thus it is very important to critically design the most appropriate power converters and assess their performance to ensure maximum power capture from solar modules in addition to impeccable power quality, reliability and efficiency.

It comprises a method of using semiconductors that exhibit the photo voltaic effect resulting in Photovoltaic power generation solar panels generating electrical power by converting solar radiation into direct current electricity. The formation of PV panels are by connecting a number of solar cells in series. Since the cells are connected in series to build up the terminal voltage, the current flowing is determined by the weakest solar cell. The PV system mainly consists of three blocks i.e. the PV array, DC/DC converter and DC/AC inverter.

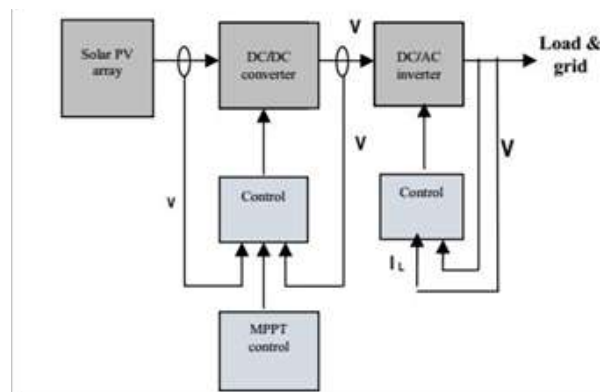


Fig. 5. Experimental setup of the solar PV system

The system converts the output voltage from solar module to DC power (using a DC-DC converter) and then, to the required AC power (using a DC-AC inverter) for operating most of the conventional appliances. A major challenge that needs to be attended by the DC-DC converters is to take the nonlinear output characteristic of the solar PV. It varies with isolation of temperature and solar. On the similar fashion, shaping the current and voltage into a sinusoidal waveform and maintaining the maximum power factor is an challenge for the DC-AC inverter. In order to maximize the performance of the panel, a maximum power point tracker (MPPT) controller [3] is employed in SPV system as shown in **Fig. 5**. The MPPT applies heuristic algorithms to track array voltage resulting in maximum power, given a solar irradiance level as shown in **Fig. 6**. The efficiency of modern MPPTs is in the range of 90-96%. The input resistance of the converter is similar range to the output resistance of the PV cell/module.

Thus the relationship between the resistance (output) of the PV cell and the actual load for having maximum power transfer using buck-boost converter can be acquired as:

$$R_{OUT(Module)} = R_{O(Load)} \cdot \frac{(1 - D_{mp})^2}{D_{mp}^2} \quad (3)$$

Here,

$R_{OUT(Module)}$ = PV cell resistance

$R_{O(Load)}$ = Load resistance

D_{mp} = Duty Cycle at MPPT

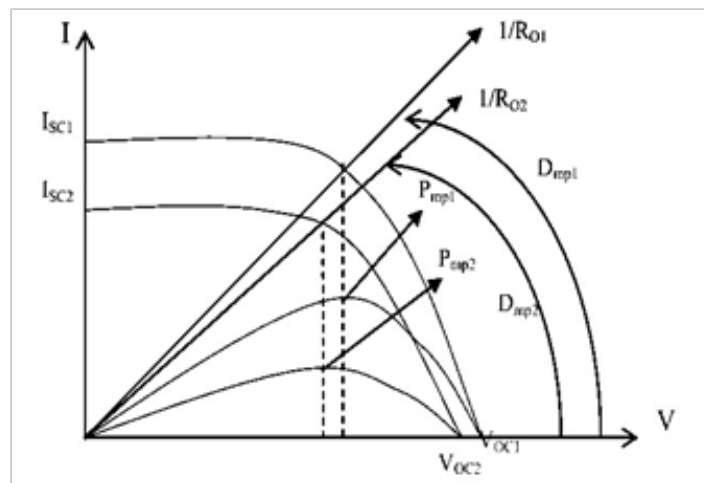


Fig 6. Maximum Power Point Tracking

Maximum power point tracking system (MPPT) tracks the maximum power point of the PV module and adjusts D_{mp} from the feedback network based on the current and voltage of the PV cell/module to match with the load. Maximum power point tracking can be ensured in a number of ways. The first step is to define $K = \frac{V_{mp}}{V_{oc}}$ where $0 < K < 1$. In the block diagram shown, reference cell is supposed to be an identical cell that is being used in an application. The V_{mp} of this cell is compared with the voltage of the actual cell. The V_{mp} of the reference cell is obtained by multiplying V_{oc} with K . When V_{module} matches with V_{mp} , there will be zero error and the module is delivering maximum power. If error is not zero, then the error signal will be fed into a controller that would create a rectangular pulse of appropriate duty cycle which is fed to the power conditioner circuit (in present case it is a DC-DC converter).

FUEL CELL SYSTEM

A fuel cell is an electro-chemical device which results in production of electricity without any intermediate power conversion stage. The most significant benefits of fuel cells are low emission of greenhouse gases and high power density. The efficiency of a fuel cell is also high, in the range of 40% to 60%.

Fuel cells are very similar to PV systems in that they produce DC power. Inverters and DC-DC converters which forms the vital components of Power conditioning systems are often required to supply normal customer load demand or for sending electricity into the grid. Cascaded DC-AC and DC-DC converters (DC-link) and cascaded AC-AC and DC-AC converters are the two topologies that can be used with fuel cells for supplying consumer loads and for utility connection include

The drawing shown in figure 7 consists of a fuel system stack followed by the DC-AC converter. In case the isolation or a high ratio of the voltage conversion is required, a transformer is usually integrated [4]. The main drawback for this type of configuration is the bulkiness and expensive nature which is caused due to the low-frequency transformer placed at the output of the inverter.

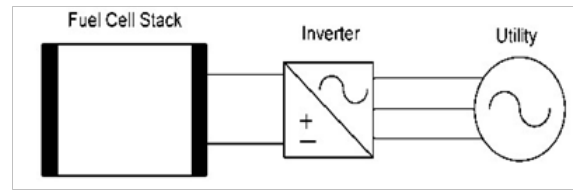


Fig. 7. Fuel cell system configuration with a single inverter

A converter (DC-DC) is put between the fuel cell and the inverter. Two functions are performed by the DC-DC converter: 1) it acts as the DC isolation for the inverter; and 2) production of sufficient voltage for the inverter input so that the required production of the voltage (AC can take place [5]. The inverter can be a single-phase or three-phase depending on the utility of the same. For e.g. a fuel cell system with interfacing of power electronics into a three-phase utility system, where an isolated bridge converter(DC-DC) and a three-phase hard switching voltage-source inverter (VSI) are used. The main disadvantage of Voltage Source Inverter is that its operation is a step down operation. Z-source inverter presented adds the boost into the Voltage Source Inverter without any alteration in the inherent features of the VSI. This appears to be useful for fuel cell and other applications involving renewable energy.

CONCLUSION

In view of promising renewable energy sources for generation of electricity, this paper provides an overview detailing upon the power electronic interfaces upon the renewable energy sources comprising of wind, solar-PV and fuel systems. This paper describes upon integrating doubly fed induction generator wind system (DFIG) into Turbines for getting useful power at varying rotor speeds, getting maximum power from photovoltaic system using Maximum power point tracking (MPPT) controller and fuel system using two inverters (Z-source and Voltage Source Inverter (VSI)) for higher efficiency to the grid, thus demonstrating the crucial role of power-electronics interface in the research and development of renewable energy systems.

REFERENCES

1. C. Cecati, C. Citro, A. Piccolo, and P. Siano, "Smart operation of wind turbines and diesel generators according to economic criteria," *IEEE Trans.*
2. S. Chakraborty, M. D. Weiss, and M. G. Simoes, "Distributed intelligent energy management system for a single-phase high-frequency AC microgrid," *IEEE Trans. Ind. Electron.*, vol. 54, no. 1, pp. 97–109, Feb. 2007.
3. J. M. Carrasco, L. G. Franquelo, J. T. Bialasiewicz, E. Galvan, R. C. P. Guisado, M. A. M. Prats, J. I. Leon, and N. Moreno-Alfonso, "Power-electronic systems for the grid integration of renewable energy sources: A survey," *IEEE Trans. Ind. Electron.*, vol. 53, no. 4, pp. 1002–1016, Aug. 2006.
4. Xu, H.; Kong, L.; Wen, X. (September 2004). "Fuel Cell Power System and High Power DC– DC Converter." *IEEE Transactions on Power Electronics*; Vol. 19.
5. G. M. Masters, *Renewable and Efficient Electric Power Systems*. New York, NY, USA: Wiley 2004.



Review on Solar Powered Hydrogen Fuel Cell: A Promising Alternative for Future Energy Sustainable Development

Rajesh Bodkhe^{1*}, Rakesh Shrivastava², Vinod Kumar Soni³, Kshitij Shrivastava⁴

Department of Mechanical Engineering, Yeshwantrao Chavan College of Engineering, Nagpur¹

Consultant and Trainer, Nagpur²

Sr. Section Engineer, Central Railways, Nagpur³

PhD research Scholar at Indian Institute of Technology, Kharagpur⁴

*✉ rgbodkhe37@gmail.com

ABSTRACT

Electricity generation and supply through power transmission lines, installation of solar power plant needed greater investment especially in hilly or remote areas. Power backup arrangement such as battery can be use for limited period of time. A single power generation system is not efficient and has its own limitations. A solar energy is available in abundant form in the nature. The utilization of solar energy in different ways is the need of hours for the sustainable energy development worldwide. Renewable hydrogen production through water electrolysis process is the cheap way to find the efficient energy storage device. This hydrogen fuel can be use to run the fuel cell to generate electricity in the sunshine and non sunshine hours. The integration of renewable resources with hydrogen fuel cell technology will play an important role in today's scenario to meet the new energy demands worldwide. Many of the researchers reported their work on this topic have covered various methods of electrolysis for hydrogen fuel production and conversion of the same into electricity. They have discussed the individual approach in detail. The work reported by worldwide researchers has been referred and appreciated. Still, some research gaps need to be studied and it is the very objective of the present work.

Keywords : Green house gas emissions; Solar PV panel; Water electrolysis; Hydrogen; Fuel cell; Electricity.

ABBREVIATIONS

PV - Photovoltaic

DC - Direct current

AC - Alternating current

NG – Natural Gas

DLFC - Direct Liquid Fuel Cell

DEFC - Direct Ethanol Fuel Cell

DMFC - Direct Methanol Fuel Cell

MCFC – Molten carbonate Fuel Cell

PAFC – Phosphoric Acid Fuel Cell

NASA – National Aeronautics Space Administration

GHG – Green House Gas

PEM – Polymer Electrolyte Membrane

PEMFC – Polymer Electrolyte Membrane Fuel Cell,

NaOH – Sodium hydroxide

C₂H₅OH – Ethanol



URFC – Unitized Regenerative Fuel Cell

HFC – Hydrogen Fuel Cell

CFC – Carbon Fuel Cell

ABSTRACT

In our country, today the stationary systems, transport systems, industry operation, household operation depends on fossil fuel based combustion power generation system. Due to this the air quality issues rising in day to day life. It affects the human respiratory system, plant, animals, environmental conditions, pollution and climate changes etc. We are realizing all three seasons in a day or week. At present, in remote areas, hilly areas still power transmissions grid lines are not reached due to heavy investment. This investment is not affordable to any government. Since two decade, the solar PV panels are used to generate the electric power directly. But there are some limitations of solar panels such as efficiency of solar panel is less about 15 – 18 %. Weather predictability issues arises while using solar panel for power generation directly especially in remote or hilly areas. Many Researchers are focusing on the improvement of efficiency of solar panel. A Very few researchers performed the analysis for the alternate ways to harness the solar energy for the generation of hydrogen or any kind of renewable fuel. This is the better alternative. And this renewable fuel can be use to run the fuel cell.

Energy demand in day to day life rapidly increasing worldwide. At present, the power that comes from coal, electricity, and gas is used for charging mobile phones, laptops, transportations, automobiles, electric cars, machines, and producing heat. Most of the time there is a mismatch between available energy and demands. Currently, major power generated through fossil fuels but these fuels are exhausted by their use and it is limited in nature. Fossil fuels may not be available shortly. Fossil fuels have a bad impact on the environment due to combustion product gases such as carbon dioxides, nitrogen, sulfur which leads to global warming. The hydrogen is known as alternative clean energy that can be overcome the fossil fuel depletion [1]. These fossil fuels are the major contributor to the greenhouse effect which leads to global warming. Everyday pollution is increasing rapidly. This is harmful to everyone. Today major problem facing by every human being is that unable to get quality of air in the atmosphere. Fuel cells are compatible with hydrogen composed of renewable energy sources for sustainable energy development. The output is pure water and heat if pure hydrogen is used as a fuel. It produces clean energy. The fuel cell is a technology that are increasingly turning to both primary and backup power such as telecommunication towers, hospitals, airports, banks and data centers, traffic signal, water, and sewage pumps.

Fuel cell technology is the state of the art technology. The principle of working is similar to battery. But the difference between the battery and fuel cell is that battery discharges once it is use. Then again we have to keep for charging. Battery may get overheated due to excessive use. In cold region, difficult to start the engine. Currently battery operated vehicles are manufacturing by automobile industry such as Hyundai, Honda, Mahindra etc. Currently very few charging stations are available in India and cost of the electric vehicle is higher than petrol or diesel vehicle. To reducing the cost of electric vehicle is the challenge remains.

In remote or hilly areas, difficult to charge the battery once it is discharged. Life span of battery is maximum 5 years. While fuel cell requires fuel and oxidant to generate electric power continuously. The thermodynamic efficiency of fuel cell is about 93 %. Advantage of fuel cell is that no moving part compared to internal combustion engine, diesel generator set. The life span of fuel cell is about 20 years except electrolyte membrane and catalyst material in fuel cell.

The main objective of this study is 1) To utilize the maximum amount solar energy for the generation of fuel this is available in abundant form 2) To generate the renewable fuel to drive the fuel cell for electric power generation. 3) To supply the electric power in remote areas and hilly areas. 4) To reduce the green house gases from the atmosphere this leads to global warming. 5) To improve the atmospheric air quality 6) To replace the internal combustion engine by fuel cell transport system 7) To replace fossil fuel based combustion power generation system by renewable fuel cell system. 8) To make hybrid power system which makes use of solar, fuel cell and battery for day and night application. This paper covered the comprehensive review on comparison between fossil fuel based combustion fuel generation methods and through renewable source fuel generation method such as solar energy. The role of hydrogen and fuel cell in the global energy system for electricity generation, transport, heat, industry, and low carbon energy storage system presented in this study. This review shows that challenges related to cost, performance and considerable improvements are still required for hydrogen to become a clean energy carrier in this competitive world. But such competitiveness required for the long term prospect of hydrogen in the global energy system which fully justifies the growing interest and policy support for these technologies around the world. [2].



The first fuel cell was demonstrated by scientist Sir William Grove a Welsh physicist, a patent lawyer in the middle of the 19th century. Sir William Grove considered being a father of fuel cell due to his series of experimental demonstrations. F. T. Bacon, British engineer successfully developed the 5 KW Alkaline Fuel cell in the year 1939. W. T. Grubb, a chemist in 1955, modified an original fuel cell design and uses sulfonated polystyrene ion-exchange membrane as the electrolyte. He was worked with General Electric (GE) Company. Also, L. Niedarch, GE chemist, devised a way of depositing platinum on to the membrane. GE worked with NASA to develop this technology. This PEMFC technology was used in the Gemini space program. , NASA uses AFC technology as per Bacon's work in its Apollo space program. G. H. J. Broers and J.A.A. Ketelaar developed MCFC technology. G. V. Elmore and H. A. Tanner developed and demonstrated on the PAFC technology. DuPont introduces the polymer electrolyte membrane material Nafion in 1968. Worldwide researchers extensively research on all fuel cell types with PEMFC technology. Jet propulsion laboratory-developed DMFC technology in 1992.

Hydrogen can be extracted from both renewable and non-renewable resources. All efforts taken by researchers around the World to produce hydrogen. The current energy conversion systems such as heat engine are using combustion-based power generation technologies are very harmful to the environment that produces noise, vibration and pollution and predominantly to many global concerns such as climate change, global warming, air quality issue, ozone layer depletion, acidic rains, On the other hand, fuel cell technology provide a clean and efficient mechanism for energy conversion process with no pollution. Very few researchers conducted the experimental research on single fuel cell at laboratory scale. Further scope of research and development in fuel cell stack is remaining to reduce the cost, increasing the durability and to optimize and improve the performance. Researchers should study carefully the current trends of the fuel cell industry to overcome the obstacles and challenges to commercialize hydrogen fuel cell technology for power generation at a large scale.[3]

The recent advancement in polymer electrolyte membrane fuel cell, advanced materials for the fuel cell membrane, physical properties, structure and performance of different polymer electrolyte membranes, prospects of the metal-organic framework for fuel cell, the key factors for commercial applications of fuel cell technologies reviewed by author. Further research is required for scaling up the technologies, however, application of materials in fuel cell remains promising.[4]. A fuel cell is a promising candidate as a renewable energy source. Fuel cells generally operate on pure hydrogen and air. It requires a continuous supply of fuel and oxidant to produce D.C. electricity. Hydrogen can combust like fossil fuels but the only products are water vapour and heat, making it zero-emission fuel. This cell can be used during non-sunshine hours. It does not depend on crude oil like an internal combustion engine. These are in modular construction and their efficiency is independent of size. Thermodynamic efficiency is about 80 %. These are quiet, have no moving parts, longer life, no need to replace like batteries, efficient and preferred because they never run down or never need charging like a battery. It does not affect climate change [5].

In India, at present conventional thermal power plants generating the power using fossil fuels such as coal at large scale, Heat engine uses petrol and diesel to produce the power and transport, but it increasing the greenhouse gas emissions daily. Very few electric cars are running on the road because the cost of investment is high, very few charging stations are available and the limitation of this car is only running within the city after charging. Batteries stores the electricity but are sensitive to extreme heat and cold, particularly in tribal areas, remote areas or hilly areas where electricity source is not available easily, the battery can be used there but it is discharging in 3 to 4 hours. It may be overheated due to their excessive use continuously and hence every few years due to declining performance need to be replaced. Limitations of battery are major concerns. [6]. Hydrogen has been considered as future renewable energy source expected to be used at large scale to generate electricity and transportation in the world. Hydrogen is the highest clean energy carrier [7].

The potential substitutes of waste to energy routes that do not cause a negative societal impact on human life on this earth planet for their daily energy needs through the use of solar energy, wind energy, wave energy, tidal energy for sustainable energy development. It can reduce the conflict globally regarding energy reserves. It will provide opportunities for new technologies development through waste to energy routes [8]. The experimental results on solar photovoltaic cells coupled with electrolyzer to generate hydrogen gas for residential applications presented in this study. This system would be cost-effective compared to the conventional energy system. For PV systems one of the big challenges remains that matching the sun's diurnal and intermittent power supply with the dynamic and non-coincident power demand of the house. One of the solutions is given to the problem that the PV array should be operated in parallel. Some energy devices must be employed if the PV array is operated independently from the grid. This device must deliver power at the desired rate and time and also must store excess energy. Today the most common energy storage device with PV systems is rechargeable lead-acid battery [9]. One of the promising new energy storage devices is regenerative fuel cells are similar to the batteries. It is possible to implement such a system design by integrating the regenerative fuel cells and batteries to become a hybrid power source.



The Hydrogen production technologies based on fossil and non fossil fuels including steam reforming, gasification reviewed by the author. Recently Plasma technology is an important method to produce hydrogen using hydrocarbons or alcohols. It was mentioned that, the renewable energy source can be utilized for hydrogen production through water electrolysis to get eco-friendly technology but which renewable source specifically is not covered here. Researcher envisaged that to develop the best hydrogen production technologies, more research and development is needed in the field of hydrogen production [10].

Currently, the global carbon dioxide emissions produced from fossil fuel combustion-based power generations. About 90 % of carbon dioxide emission reductions are possible through the use of renewable sources and energy efficiency. Also, GHG emissions are required to reduce substantially from sectors such as industry, power, direct heat, transport, buildings. It is necessary to transform the present energy system into an efficient and renewable low carbon energy system. It is expected that these emissions can be reduced rapidly if the contribution of renewable energy sources increases up to 41 % in transport and buildings. Additionally 13 % through electrification and 40 % through energy efficiency in power and industries. To achieve this goal, the share of global energy consumption needs to increase from 18 % today to 65 % in 2050. [11].

Hydrogen is a promising alternative to meet the new energy demand and help to reduce the greenhouse gas effect which leads to global warming. It can be presented as a commercially mature technology that can be applied at low costs and get high efficiencies. Currently, fossil fuels are the main source of hydrogen production. It is essential to increase hydrogen production using renewable energy sources on a large scale around the world [12].

To install the solar system on a large scale, technology needs to be cost-effective compared to fossil fuel-based power generation. Due to large intermittency in power generation and predictability challenges of weather, the deployment of solar energy technologies for electricity generation was a major concern [13].

Hydrogen fuel cell and solar photovoltaic hybrid renewable energy system (HRES) for stand-alone applications for academic research building were proposed in this study. This system arrangement consists of a hydrogen tank, battery, and electrolyzer was used as energy storage. The result of this study shows that HFC and battery bank was the most significant modules of the HRES to meet load demands early day and late-night hours. [14].

Modeling of an integrated power cycle consists of natural gas decarburization in collaboration with a hydrogen fuel cell and a carbon fuel cell was analyzed. However, the author mentioned that the present development in CFCs is limited due to little demonstrations. The more research and development is required in the CFC. By using pure carbon from the NG decarbonization feed, the development of CFC will be accelerated. Some chemical, mechanical and engineering issues will be solving if HFC development will be applied to CFC [15].

The approaches for integrating hydrogen energy technology into hybrid energy systems, emphasizing electricity generation using a hydrogen fuel cell, integration of energy storage, sizing methodologies, energy flow management reviewed carefully[16].

The problem with the use of hydrogen at large scale is that it is an expensive form of energy and also it requires considerable energy for producing hydrogen. This work is under research and development. Many studies have been developed to evaluate the hydrogen economy challenges of transition [17-18].

DLFC is divided into two types: DEFC and DMFC. Ethanol is a hydrogen-rich fuel. In the absence of hydrogen generation through the solar photovoltaic electrolysis process, hydrogen can be replaced by Ethanol fuel. This is an alternate option to operate the fuel cell system. It is revealed that ethanol is a sustainable, carbon-neutral transportation fuel than methanol. It has higher energy density and ease of transportation, storage, and handling compared to hydrogen and methanol. The ethanol fuel can be used instead of hydrogen in the direct ethanol fuel cell to generate electrical energy. The main problem with the DLFC at present is the higher cost of catalyst. This issue is important to find the catalyst for both the anode and the cathode at the cheaper cost and to improve the membrane electrolyte assembly fabrication and to promote better utilization of fuel cells [19].

The technical status of hydrogen and direct ethanol fuel cell technologies, progress towards research in solar hydrogen, DEFC, focused on energy storage applications and comparisons between the hydrogen, methanol, ethanol for fuel cell with respect to theoretical specific energy, electrical energy density, boiling point, vapour pressure, availability, infrastructure facility, simplicity of handling, flammability, explosiveness and toxicity were presented in this study[20]. In DEFC, to avoid ethanol crossover through the membrane is a major concern reported by the many researchers. Ethanol should be transported through the proton exchange membrane without taking part in the electrochemical reaction. However, It is interestingly to know the effect of cell voltage, current density, and efficiency of the cell and its overall performance under the working condition. Researchers also revealed that the rate of crossover decreases the current through direct ethanol fuel cell; however, it is not yet



clear that the current density is reduced due to incomplete oxidation of ethanol crossover. This is the remaining challenge for the researchers [21- 24].

The new sustainable hydrogen clean energy with zero emissions and the potential to be more cost-effective by using renewable energy represents in all regards a superior solution to the carbon fossil fuel systems [25]. Electricity generation using renewable energy sources such as solar, wind, biomass, hydro tidal energy, ocean thermal and geothermal energy is the best possible option to overcome these challenges. As solar energy is the abundant form is available in the nature free of cost. At present, solar energy playing a very important role in meeting energy demands globally [26]. Some crucial energetic, environmental and sustainability issues and the role of hydrogen and fuel cell technologies as one of the potential solutions to these issues. Assessments of the sustainability of processes and systems, and efforts to improve sustainability should be based in part upon thermodynamic principles, and especially the insights revealed through exergy analysis [27]. A techno-economic analysis of an autonomous power system integrating with hydrogen technology shows that the autonomous system is costlier but helps to reduce the greenhouse gas emissions compared to PV –diesel system [28].

DISCUSSION AND CONCLUSION

Based on literature studied, the use of any single power generation system has its own limitations. The present study covered the two promising alternative energy sources such as solar energy and hydrogen gas in a fuel cell as a renewable source to meet new energy demand worldwide. Fuel cell utilizes the hydrogen as a fuel with no polluting emissions making hydrogen the clean energy carrier. Both are the trust area for study worldwide. Major parameters related to solar photovoltaic technologies such as deployment of solar energy technologies for electricity generation, main barriers, efficiency & Performance of PV technologies, limitations of automobile sector, battery, generators, inverters, hydrogen production methods, storage and fuel cell types the electrolyzer types, fuel cell types, its applications and recent developments in hydrogen fuel cell technologies, advances in fuel cell, electrode, material for membranes, comparison of fuels like ethanol, methanol with hydrogen, its properties, comparisons study of fuel cell with battery, generator set, potential applications and limitations. the technical and economic growth of hydrogen fuel cell technologies globally, progress towards commercialization, role of industry and Indian government towards the development of hydrogen fuel cell technology reviewed carefully. Very few researchers focused on the material issues, fuel cell charge transport and mass transport issues, behavior of system before, during and after electrochemical reaction, gas diffusion layer, catalyst layer etc. Finding the good membrane and catalyst material, bipolar plate, fuel and oxygen flow channels flow structure, water and thermal management for the improvement fuel cell performance is the challenge remains.

Hydrogen is a promising clean, efficient and sustainable energy that can sufficiently cover the global energy demand and decrease the total energy cost [29]. Integration of the Fuel Cell system using hydrogen through renewable sources will play an important role and become a hybrid power source to meet new energy demands soon worldwide [30]. The integration of photovoltaic and fuel cells for sustainable power generation were proposed in this study which consists of fuel cell, photovoltaic's array and the battery. This hybrid power system can work in three modes such as fuel cell and battery, photovoltaic's array and battery, fuel cell, photovoltaic's array, battery, and fuel cell. [31].

ACKNOWLEDGEMENT

The authors gratefully acknowledge the researchers for their efforts taken in the field of hydrogen fuel cell technology. However lot of scope is still available for research and development in the near future.

REFERENCES

1. Hübert, T., Boon-Brett, L., Black, G. and Banach, U. (2011) Hydrogen Sensors—A Review. *Sensors and Actuators B: Chemical*, 157, 329-352. <https://doi.org/10.1016/j.snb.2011.04.070>
2. Iain Staffell, Daniel Scamman, “Anthony Velazquez Abad, et al., “The role of hydrogen and fuel cells in the global energy system”, *Energy & Environmental Science*, 12, pp. 463—491, 2019
3. Omar Z. Sharaf, Mehmat F. Orhan, “ An Overview of Fuel Cell Technology: Fundamentals and applications”, *Renewable and Sustainable Energy Reviews*, 32, pp. 810 -853, 2014.
4. Abhishek Dhand, Srinidhi Suresh, Aman Jain et. al., “Advances in Materials for Fuel Cell Technologies-A Review”, *International Journal for Research in Applied Science & Engineering Technology (IJRASET)*, ISSN: 2321-9653; IC Value: 45.98; SJ Impact Factor:6.887, 9(5), pp. 1672-1682 , 2017.



5. Joan M. Ogden, "Prospects for Hydrogen In The Future Energy System", research report, Institute of Transportation Studies, University of California, its.ucdavis.edu, pp. 1-31, 2018
6. Schmidt-Rohr, K., "How batteries store and Release energy: Explaining Basic Electrochemistry", *J. Chem. Educ.*, 95: 1801 – 1810, 2018
7. Dincer, I. and Acar, C. (2018) Smart Energy Solutions with Hydrogen Options. *International Journal of Hydrogen Energy*, 43, 8579-8599. <https://doi.org/10.1016/j.ijhydene.2018.03.120>
8. Richa Kothari et. al., "Waste to energy: A way from renewable energy sources to sustainable development", *Renewable and Sustainable Energy Reviews*, 10, pp. 3164 – 3170, 2010
9. Maclay J. D., Brouwer J., et. al., "Experimental results for hybrid energy storage systems coupled to photovoltaic generation in residential applications", *International Journal of hydrogen energy* 36(19), pp. 12130 – 12140, 2011
10. Mostafa El-Shafie, Shinji Kambara, Yukio Hayakawa, "Hydrogen Production Technologies Overview", *Journal of Power and Energy Engineering*, 7, 107-154, 2019, <http://www.scirp.org/journal/jpee>
11. Emanuele Taibi et. al., Hydrogen from renewable power: Technology outlook for the energy transition, International Renewable Energy Agency (IRENA), ISBN 978-92-9260-077-8, PP. 1-52, 2018, www.irena.org/publications,
12. Baykara, S.Z. (2018) Hydrogen: A Brief Overview on Its Sources, Production and Environmental Impact. *International Journal of Hydrogen Energy*, 43, 10605-10614. <https://doi.org/10.1016/j.ijhydene.2018.02.022>
13. Mohamed EL-Shimy, Taha Abdo, "PV technologies: History, technological advances, and characterization", In *Encyclopedia of Energy Engineering and Technology*, Second Edition. Taylor and Francis: New York, <http://www.tandfonline.com/doi/book/10.1081/E-EEE2>, pp. 1397-1424, 2015
14. Anandsingh, Prashany Baradar, Bhupendra Gupta, "Techno-economic feasibility analysis of hydrogen fuel cell and solar photovoltaic hybrid renewable energy system for academic research building", *Energy Conversion and Management*, 145, pp. 398 – 414, 2017
15. Quan Zhuang*, Philip Geddis, Allan Runstedtler, Bruce Clements, "An integrated natural gas power cycle using hydrogen and carbon fuel cells", *Fuel*, 209, pp. 76 – 84, 2017
16. E.L.V. Eriksson, E. MacA. Gray, "Optimization and integration of hybrid renewable energy hydrogen fuel cell energy systems - A critical review", *Applied Energy*, 202, pp. 348 – 364, 2017
17. Gahleitner, G. (2013) Hydrogen from Renewable Electricity: An International Review of Power-to-Gas Pilot Plants for Stationary Applications. *International Journal of Hydrogen Energy*, 38, 2039-2061. <https://doi.org/10.1016/j.ijhydene.2012.12.010>
18. Balta-Ozkan, N. and Baldwin, E. (2013) Spatial Development of Hydrogen Economy in a Low-Carbon UK Energy System. *International Journal of Hydrogen Energy*, 38, 1209-1224. <https://doi.org/10.1016/j.ijhydene.2012.11.049>
19. B.C. Ong, S.K. Kamarudin, S. Basri, Direct liquid fuel cells: A review, *Int. J. Hydrogen Energy*, 42, pp. 10142-10157, 2017
20. Helena Berg, Joakim Nyman, et al., Direct Ethanol Fuel Cells: Ethanol for our future fuel cells? , Swedish Hybrid Vehicle Centre, ENERGIFORSK, ISBN 978-91-7673-137-6, 2015
21. J.P. Pereira, D.S. Falcão, et al., Performance of a passive direct ethanol fuel cell, *Journal of Power Sources*, 256, pp. 14-19, 2014
22. L. An, T.S. Zhao, R. Chen, Q.X. Wu, A novel direct ethanol fuel cell with high power density, *Journal of Power Sources* 196, pp. 6219–6222, 2011
23. S.P.S. Badwal, S. Giddey, A. Kulkarni, J. Goel, S. Basu, "Direct ethanol fuel cells for transport and stationary applications – A comprehensive review", *J. Of Applied Energy*, 145, 80 -103, 2015



24. Z. Zakaria, S. K. Kamarudin, et al., “Membranes for Direct Ethanol Fuel Cells: An overview”, J. Of Applied Energy, 163, pp. 334- 342, 2016
25. Alvin G. Stern, “A new sustainable hydrogen clean energy paradigm”, Int J. Of Hydrogen Energy, xxx, pp. 1-12, 2018
26. M. A. Suárez González, A. M. Blanco Marigorta, and J. A. Peña Quintana, “Review on hydrogen production technologies from solar energy,” Renew. Energy Power Qual. J., vol. 1, no. 9, pp. 347–351, 2017
27. Dincer and C. Zamfirescu, “Sustainable Energy Systems and Applications”, springer science, DOI 10.1007/978-0- 387-95861-3_13, 2011
28. G. Tzamalīs, E.I. Zoulias, et al., “Techno-economic analysis of an autonomous power system integrating hydrogen technology as an energy storage medium”, Renewable Energy 36, pp.118-124, 2011
29. D. Graf, N. Monnerie, M. Roeb, et al., Economic comparison of solar hydrogen generation by means of thermochemical cycles and electrolysis, Int. J. Hydrogen Energy, 33 (17), pp 4511–4519, 2008
30. E. L. V. Eriksson, E. MacA. Gray, “Optimization and integration of hybrid renewable energy hydrogen fuel cell energy systems – A critical review”, Applied Energy, 202, pp. 348–364, 2017
31. Lourdes Laura A., “Compact Hybrid Power Source using Fuel Cell a PV Array”, International Journal of Scientific and Research Publication, 11(4), pp. 2250 – 2153, 2014.



Next Generation Advanced Core Material for Reluctance Machine

K Vijayakumar^{1*}, A Joseph Basanth², R Karthikeyan³, S Kannan⁴

Electrical Engineering, SSMIET¹, AU Dindigul Campus², SVCE³ and GESS⁴, Dindigul, Chennai, Tamilnadu and Puducherry

*✉ k.vijaymec@gmail.com

ABSTRACT

The field of manufacture of electrical machines has advanced significantly in recent years due to the introduction of new materials. New electrical steels have reduced losses and rare-earth permanent magnet materials have provided a 'lossless' source of magnetic flux. The soft magnetic materials most predominately used in electrical machines are silicon steels and ferrites. In the world of Permanent magnet materials (PM) the choice of laminated stack is Soft Magnetic Composite (SMC) iron powder. Here it is the iron powder grains which are separated from one another by electrically insulating layer using phenolic or silicone resin. As compared with laminated stacks, SMC materials offer a greater resistance to eddy current formation, as well as presenting designers with the advantage of magnetic properties which are isotropic in nature, instead of being confined to two dimensions as within the case of laminates. This reveal exposes the possibility of creating complicated 3-D flux paths, which would be impossible or prohibitively expensive to fabricate from conventional laminated sheet. This paper presents option of research the SMC iron powder as core material in a switched reluctance machine that might run as a motor or generator mode of operation. Results of in-depth finite element analysis and experimentation of the proposed prototype are delineated.

Keywords : Switched reluctance motor; Switched reluctance generator; Pre-form blanks; Finite element analysis; Prototype.

INTRODUCTION

Soft magnetic composite material (SMC) comprises particles of iron powder wherein every particle is insulated by an oxide layer. Compaction of iron powder particles with a binder and a lubricant, at high pressure results a bulk

material [2]-[3]. Lubricant ease compaction and the ejection of component. The binder strengthens the material. The insulation between particles is rendered by the lubricant and the binder. Internal stresses generated during compaction can be relieved through the heat treatment process of curing. Compared to lamination material lower permeability (850(SMC)) and higher iron losses are major shortcomings of SMCs [2]. Even though the SMC material has inferior permeability it has the following advantages: Improved overall thermal loading of the motor, reduced vibration due to the cushioning nature of insulation (lubrication) binder between the iron powder particles of the material and a prospect for greatly reduced production cost.

SMC materials find application in the design and fabrication of complex geometry electrical machines such as claw pole alternator and transverse flux motor. Switched Reluctance Machines are characterized by simple and rugged construction, high power density, wide speed range and high speed operation owing to lack of magnets and winding on the rotor [1]. The switched reluctance motor (SRM) can be a feasible substitute to generate high torque or thrust and power density at relatively low speeds, thereby eliminating the need for a speed reducer between the motor and the washer or pump drive applications. Switched reluctance generator (SRG) can be a cost effective alternative in variable speed wind generating systems that normally employ permanent magnet generators or field wound synchronous generators. The SRG is also characterized by maintenance free and highly reliable operation [4]. This paper work delineates the fabrication of a switched reluctance machine using pre-form soft magnetic composite material Somaloy 1000 3P and along with the presentation of some of the test results.

SWITCHED RELUCTANCE MACHINE

The switched reluctance machine is a doubly salient but singly excited machine wherein the stator carries the winding while the rotor is simply made of stacked silicon steel laminations [1] as evidenced from the Computer Aided Design (CAD) model of a 6/4 switched reluctance generator shown in Fig. 1.



Fig. 1. CAD Model of 6/4 (3phase) SRM

DEVELOPMENT OF SMC RELUCTANCE MACHINE

Powder metallurgy process the backbone behind the fabrication of machine parts using soft magnetic composite has been explained coherently [3] – [14]. Soft Magnetic Composite (SMC) materials consist of metal particles where every particle is coated with a continuous insulate oxide layer. The particles are compacted, together with an addition of lubricant and possibly a binder, at high pressure into a bulk material. There are a number of combinations (Table 1) between the soft magnetic powders for electromagnetic application, the binders and the possible compression molding techniques. The variety of resin additives and lubricants influences the particle insulation, compressibility and the mechanic and magnetic properties of the core [11]. They are chosen according to the complexity of the core, the need for post-processing in order to get the final shape, the application orientation in magnetic loading vs. frequency domain and according to the other properties emphasized. High compressibility and warm compaction increases the permeability and saturation induction [12]. The addition of a binder attains higher strength. The heat treatment and purity reduces the strains and static core losses in the SMC core. It is important that the compaction process and the heat treatment allow getting a good homogeneous core with the low eddy current loss coefficient. The press ready mix, which contains lubricating binder (0.6%LB1), is selected to be treated under warm compaction process at 800 MPa+130°C and heat treatment at 275°C. This combination Soft magnetic composite gives higher strength [5], [12] and improves post-processing, when the final shape of the claw-pole structure is formed. Using Kenolube gives a more brittle composite material, which is more difficult to tool. Generally, the SMC premix with 0.5% Kenolube is better adapted for the use in electromagnetic design purposes. It has a higher permeability and lower static core losses. The bulk resistivity is lower due to the higher filling rate.

Table 1. Soft magnetic powders, binders, lubricants and production methods

Magnetic powder	Lubricant/Binder	Production method
• Somaloy500	• Kenolube	• Cold compaction
• Somaloy550	• LBI	• Warm compaction
• Somaloy1000	• 3P lube	• Steam compaction

The machine structure is divided into a two major components (stator and rotor) that are produced one after another and after inserting the coils these are assembled together. In order to machine larger components, the three circular shape blanks (Diameter 120 mm and Height 20 mm) as shown in **Fig. 2** are glued together using an epoxy glue and then process of milling as the machining methods such as CNC machining, Wire cutting technique are not suitable for machining of SMC core [10]. After milling, surface grinding on the stator and rotor ensures a smoother finish. **Fig. 3** shows the assembled stator and rotor core.

The key parameters of the structure include: Stator outer diameter: 96 mm, Stator inner diameter: 77.9 mm, Length of stack: 59.99 mm, and Air gap: 0.5 mm. The prototype can operate at 5000 rpm, developing mechanical output power of 682 W. In traditional machining the use of cutting fluid which would destroy insulation between the iron particles and the material behavior gets changed [8] - [9]. The most challenging aspect in the development of these prototype components is dry machining. It means no cutting fluid is used, but only vacuum cleaning methods are preferred. Dry machining process causes size variation due to increase in temperature [6]. During machining pre-form blanks get hotter and expands. After cooling, it can be undersized. This is the biggest practical issue of machining of pre-fabricated SMC blanks [7] which has been circumvented by meticulous milling and surface grinding process.



Fig. 2. Pre-form SMC blanks



Fig.3. Stator and rotor of a prototype motor.

SWITCHED RELUCTANCE MACHINE AS GENERATOR

A prime mover that provides mechanical energy input, to the fabricated SMC-SRG is required. This can be achieved using an electric system comprising a motor, with a coupling and bearings for the SR machine.

A suitable prime mover has to be selected in order to couple with the fabricated SMC switched reluctance machine. The power capability of the prime mover motor must be higher than the switched reluctance machine that it drives. In this work a simple permanent magnet DC motor has been selected as the prime mover. The motor specifications are, 180V DC, 1500 rpm and 5.2 A. A base frame has been fabricated and the two machines are laid on the base and fitted to the base frame through suitable U shaped clamps. The shafts of the two machines are then level coupled through LOVE-JOY coupling. In order to control the operation of the prime mover DC motor an autotransformer and rectifier unit has been employed. The voltage generation capability of SMC-SRG has been studied through the developed prototype test platform as shown in **Fig. 4**.

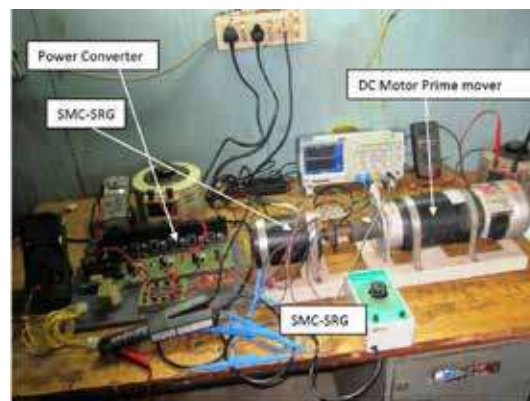


Fig. 4. SMC-SRG prototype test platform

The SMC-SRG has been coupled to a DC motor which acts as the prime mover whose speed can be varied through variation of its applied voltage. A load of 50 ohm, 1kW has been connected across the DC bus. A digital storage oscilloscope with completely isolated channels along with a high resolution current probe has been employed to capture the waveforms. In a singly excited machine such as a switched reluctance machine, at the time of starting there is no residual flux in stator winding. Therefore the switched reluctance machine is prone to draw large initial excitation current for a small applied voltage. Hence the excitation voltage has been kept at very small value of 5.8V, the switched reluctance machine has drawn a current of 3.9A, one of the main drawback of armature excited small reluctance type machine, and then the prime mover DC motor is made to run at a speed of 1200 rpm. At this speed the voltage across load increased to 8.3V thus demonstrating the generating capability of the SMC-SRG as shown in **Fig. 5**.

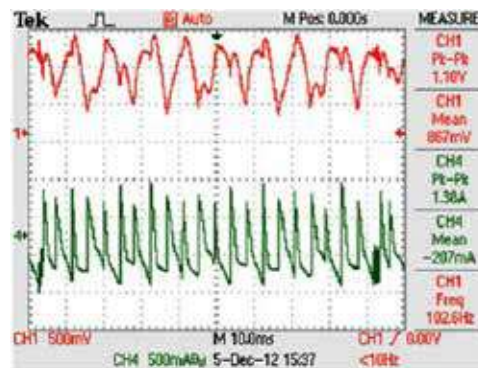


Fig. 5. Output voltage and Current waveforms at $V_{exc}=5.8V$, $N=1200$ rpm

The top wave form is the generated voltage exhibiting voltage ripple while the bottom waveform is the current through the load which also exemplify the ripple in it. The steady state generated voltage waveform of SMC-SRG from transient analysis is shown in **Fig. 6**, which correlates with the experimental result obtained.

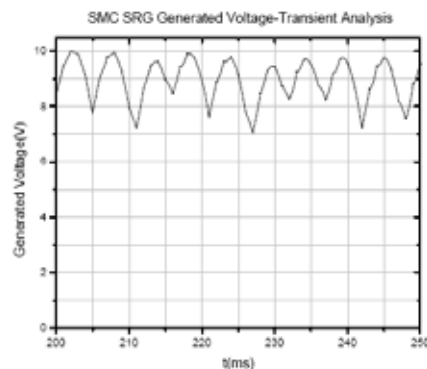


Fig. 6. Transient analysis of SMC-SRG - Steady state generated voltage

The current waveforms of the phases also exhibits different peak values reflected in the bus capacitor current waveform. The peak phase current waveform is 0.6A for the excitation voltage chosen while that from simulation is 2.7A for the simulation excitation voltage. Again the manufacturing imperfections in SMC-SRG accounts for the discrepancy between simulation and test results. The phase voltage waveform, gate pulse, capacitor voltage waveform along with load current waveform is shown in **Fig. 7**.

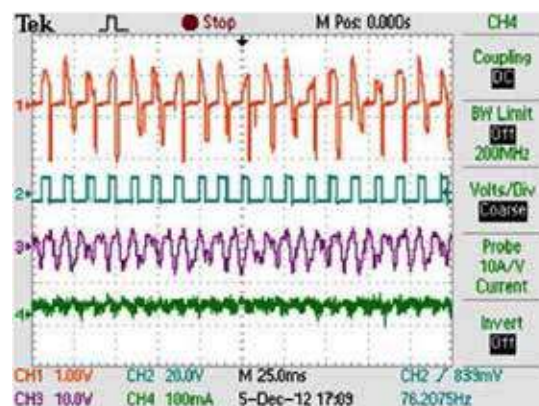


Fig. 7. Phase voltage waveform, Gate pulse, Capacitor voltage waveform and the Load current waveform for the condition: $V_{exc}=5.8V$, $I_{exc}=4A$, $R_L=50$, $N=1200$ rpm, $V_{gen}=8.3V$, $I_{dlink}=1.9A$

It is evident that the generated voltage contains ripple but at a magnitude less than the conventional SRG. In any type of SRG, nevertheless these ripples have to be removed through suitable means before deploying SRG for specific application.

SWITCHED RELUCTANCE MACHINE AS MOTOR

Prototype motor parameters have been verified through experimentation. The SMC-SRM prototype is coupled with a dynamometer as shown in **Fig. 8**. A load cell is mounted on a dynamo which is directly connected to high speed dynamo controller in order to measure shaft torque and speed. **Fig. 9** shows the mechanical characteristics, i.e., the motor speed vs. the dc link voltage of power converter. The motor torque of 1.2 Nm at 3000 rpm with a dc link voltage of 85V has been measured. **Fig.10** shows current in stator phase and stator temperature rise comparison of measured and FEA calculated. The phase current waveform of FEA seems to be closer to ideal current wave shape as ideal material properties are incorporated in the electromagnetic FEA while measured waveform is due to imperfections in the fabricated machine geometry and variations in the material property of SMC pre-form blanks employed in the fabrication. The comparison of measured and FEA predicted hot spot temperature rise in stator core of SMC prototype is given in **Table 2**.



Fig. 8. Experimental setup

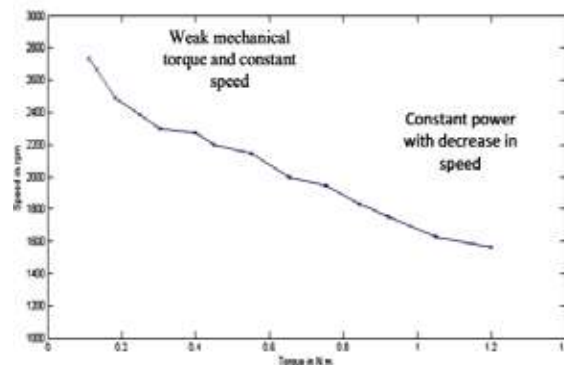


Fig. 9. Measured torque versus speed curve

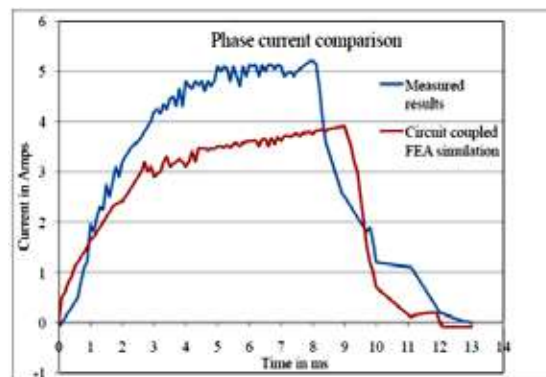


Fig. 10. Measured and simulation results comparison of phase current

Table 2. Comparison of experiment and simulation results

Time (s)	Stator Core temperature (°C)		Winding temperature (°C)	
	Simulation	Experiment	Simulation	Experiment
1000	44.17	39.7	47	47.6
2000	52.1	44.55	55.7	52.5
3000	55.9	47.85	59.8	56.12
4000	57.1	50.15	61.95	58.6
5000	58.83	53.26	63.47	60.12

CONCLUSION

In a nutshell, it can be concluded that this paper pursuit identified the advantages and disadvantages of the use of SMC in switched reluctance generator for the first time, through extensive simulation, fabrication and experimental avenues. The thermal performance and vibration behavior fared well in the prototype SMC-SRG while it exhibited poor performance on the electromagnetic front. It has the potential of reduced weight and voltage ripple which may promise a reliable, low cost switched reluctance generator in standalone wind energy conversion systems meant for rural and remote area electrification scheme. The relative weakness of the powder material in terms of electromagnetic performance of the machine can be partially compensated by an increase in current density level within the designed structure without the risk of overheating of the machine. In a SMC-SRM front, it has raised strengths to be a serious candidate for the pump drive and washer applications.

REFERENCES

1. R. Arumugam, D. A. Lowther, R. Krishnan and J. F. Lindsay, — Magnetic field analysis of a switched reluctance motor using a two dimensional finite element model, IEEE Trans. Magn., vol. MAG-21, no. 5, pp. 1883-1885, Sep. 1985.
2. M. Persson, P. Jansson, A. G. Jack, B. C. Mecrow, —Soft Magnetic Composite Materials – Use for Electrical Machines, 7th International Conference on Electrical Machines and Drive at Durham, England, Sep. 1995.
3. A.G. Jack, —Experience with the Use of Soft Magnetic Composites in Electrical Machines, International Conference on Electrical Machines, Istanbul, Turkey, 1998, pp. 1441-1448.
4. A.V. Radun, and Y. Q. Xiang, “Switched reluctance starter/generator system modeling results,” Trans. SAE, J. Aerosp., vol. 104, sec. 1, pp. 257-266, 1995.
5. P. Jansson, —Soft magnetic materials for AC applications, Powder Metallurgy, Vol. 35, No. 1, pp.63-66, 1992.
6. Graham, D. “Dry Out.”, Cutting Tool Engineering, Vol. 52, No. 3, March 2000, pp. 56 – 65.
7. Narutaki, N., Yamane, Y., Tashima, S. and Kuroki, H. “A New Advanced Ceramic for Dry Machining”, Annals of the CIRP, Vol. 16, No. 1, pp. 43 – 48, 1997.
8. The latest development in soft magnetic composite technology, SMC Update, Reports of Höganäs AB, Sweden, 1997-2007. Available at <http://www.hoganas.com/>, see News then SMC Update.
9. Somaloy prototyping material (SPM), Hoganas, 2016
10. R. Kobler, D. Andessner, G. Weidenholzer, and W. Amrhein, “Development of a compact and low cost axial flux machine using soft magnetic composite and hard ferrite,” in 11th International Conference on Power Electronics and Drive Systems (PEDS), Jun. 2015.
11. Krings, A.; Boglietti, A.; Cavagnino, A.; Sprague, S. “Soft magnetic material status and trends in electrical machines. IEEE Trans. Ind. Electronics, 2017, 64, 2405–2414.
12. Pennander, L.O., Jack, A., “Development of iron powder SMC materials and the application in electrical machines”, Electrical machines symposium, Dept. of Electrical Engineering, KTH, Stockholm, June, 2001.
13. K. Vijayakumar, R. Rajendirakumar, Y. Thiagarajan, A. Joseph Basanth, R.Karthikeyan and S. Kannan, “Development of an Iron Powder Metallurgy Soft Magnetic Composite Core Switched Reluctance Motor”, Elsevier Journal of Materials Today: Proceedings, Article in Press (<https://doi.org/10.1016/j.matpr.2020.10.346>), 2020. .
14. K. Vijayakumar, A. Joseph Basanth, R.Karthikeyan and S. Kannan, “Influence of iron powder core on the switched reluctance motor performance enhancement”, Elsevier Journal of Materials Today: Proceedings, Article in Press (<https://doi.org/10.1016/j.matpr.2020.04.082>), 2020.



Solar Energy and Hydropower Complementing Each Other – A Global Trend for Achieving SDGs

Jnan Ranjan Pal

Chief Engineer (Retd.), Irrigation Department, Lucknow, Uttar Pradesh

✉ jrpal0909@gmail.com

ABSTRACT

Renewable energy is a clean and sustainable source of energy derived from nature and it has potential to provide solutions to the vulnerable energy problems being faced by India. India has the continuous supply of solar energy, which can be utilized for producing electricity. World's largest single location solar energy plant is being established in India in the beautiful mountainous landscape of Ladakh. In its first assembly in New Delhi in March, 2018, International Solar Alliance (ISA), was formed by solar- resources rich countries to undertake joint efforts to reduce cost of finance and technology for deployment of at least 1000 GW, solar energy world wide by 2030. Hydro-electric power is a renewable source of energy, which has immense potential in India, which can be harnessed to mitigate electricity shortage in India and even out the variability added to the grid system, due to solar and wind power generation. The 193 member states of the united Nations adopted 17 new Sustainable Development Goals (SDGs) as a unanimous commitment to end poverty, fight inequalities and injustice and tackle climate change. The goals are to be achieved by 2030. Target 7.1 and Target 7.2 ensure universal access to affordable, reliable and modern energy services, by increasing substantially the share of renewable energy.

Keywords : Solar energy; Hydropower; Renewable energy; Water; Environment; Pollution; Conservation; Dam; Electricity; Generation.

INTRODUCTION

Recent trend in Power Sector is the concept of water energy nexus refers to the relationship between the water used for energy production and the energy consumed to extract, purify, deliver, treat and dispose of water and waste water. AS the treatment of waste water in western countries is a significant component of energy consumption, different technologies have been developed to invest less or recover more from the treatment processes. Furthermore, the use of solar energy generation can serve as an alternative to the use of fossil fuels for water pumping.

Out of 17 SDGs adopted to transform the World water finds a role in ending poverty in all its forms everywhere; ending hunger, achieving food security and improved nutrition, and promoting sustainable agriculture; ensuring healthy lives and promoting well being for all at all ages; ensuring availability and sustainable management of water and sanitation for all; ensuring access to affordable, reliable, sustainable and modern energy for all; taking urgent action to combat climate change and its impacts; and conservation and sustainably using the oceans, seas and marine resources for sustainable development.

Renewable energy is a clean and sustainable source of energy derived from nature and it has potential to provide solutions to the vulnerable energy problems being faced by India. It is time to make collaborative efforts to extract naturally gifted sources of energy to meet our long-term energy demands and to ensure sustainable growth of our nation.

Renewable energy solutions do come with their own limitations when compared with the conventional mass production power generation measures. The limitations have to be addressed with the counterbalancing measures for managing the power consumption at all times and in all areas.

Renewable Energy, initially driven by concerns on climate change and supported with subsidies. RE has now gained substantial momentum with technological advancement and declining cost. Following the Paris Agreement on climate change, Prime Minister Shri Narendra Modi has laid out ambitious plan to build 175 GW of RE by 2022. Advent of opportunistic generation measures have led to requirement of augmentation in the fields of energy storage and load balancing. Correlation with demand, energy storage capability such as Pumped Storage Projects and grid prioritization etc. will have to be integrated into the development plan and policies for sustainable development goals. Power being a dynamic commodity which has to be consumed as soon as it is produced, provides us with challenges of its management when the non conventional resources are employed.

WORLD'S LARGEST SOLAR ENERGY PLANT IN INDIA

Ladakh, known for its pristine natural beauty and colorful mountains towering over vast swathes of desolate land, is set to add another feature to its fame – the world's largest single-location solar photo-voltaic plant. Some 200 km to the south in Kargil, another mega project will join forces to light up the plains, keep glaciers cool by saving 12750 tons of carbon emission a year, remove dependence on diesel generator sets and create livelihood for the local population that remains cut off for 6-8 months in a year.

SECI (solar energy corporation of India) under the renewable energy ministry is promoting the projects in Union Territory of Ladakh on a scale matching the grandeur of their locations- 5000 MW for the Ladakh unit and 2500 MW for Kargil- to be completed by 2023 at an estimated investment of Rs 45000 crore. The following table shows the top PV Solar Power Projects already implemented and to be implemented in future around the world as per June 2017 statistic.

Table 1. Biggest solar projects of the World

S. No.	Top 5 Solar PV Projects (single location)	Present capacity (MW)	Projected capacity (MW)	Location
1.	Tengger Desert Solar Park	1547	-	Ningxia, China.
2.	Bhadla Solar Park	1365	2255	Rajasthan, India.
3.	Datong Solar Power Top Runner Base	1000	3000	China.
4.	Kurnool	1000	2000	Andhra Pradesh, India
5.	Longyanxia Dam Solar Park	850	-	Eastern Zhejiang, China
6.	Ladakh Project	-	5000	Ladakh, India
7.	Kargil Project	-	2500	Kargil, India



Fig. 1. Solar Panel

The Ladakh Project will be located at Hanle-Khaldo in Nyoma, a strategically important area 254 km from Leh. The Ladakh project will still be the world's largest, even after others complete their planned capacities. The Kargil Project will be built at Suru in Zaskar, 254 km from the District HQ. Power from the Ladakh project will flow to Kaithal in Haryana. For which a 900 km transmission line will be connected with the grid at New Wanpoh near Srinagar.

Another positive development is that the Leh and Kargil administrations have designated 25000 and 12500 acres of non-grazing land, respectively at prices, remunerative for the hill councils. The council will also earn around Rs 1200 per hectare per annum as rent with 3% annual escalation. The projects are expected to spur development in the remote border regions and empower the local population through skilling for jobs such as cleaning of solar panels and maintenance of transformers etc.

INTERNATIONAL SOLAR ALLIANCE (ISA)

OPEC countries in the list of ISA potential members include UAE, Saudi Arabia, Venezuela, Libya, Nigeria and Algeria, among others. India also proposed that ISA membership be thrown open to all UN members apart from 121 who are fully or partially between the Tropics of Cancer and Capricorn as initially envisaged by ISA. ISA, an inter-governmental treaty-based



organization, was formed by Solar-resource-rich nations to undertake joint efforts to reduce cost of finance and technology, and mobilize more than \$1 trillion investment needed by 2030 for the deployment of at least 1000 GW of solar energy worldwide.

The first assembly of ISA in New Delhi on March, 2018 has laid the foundation for a global solar agenda. The assembly as the supreme decision-making body of ISA, will steer the process to significantly harness solar energy for achieving universal energy access at affordable rates. 70 countries had signed the framework agreement on the alliance and of these 44 had ratified it.

The occasion also saw the inauguration of the Indian ocean Rim Association (IORA) renewable energy ministerial meeting and the second Global Renewable Energy investment summit. IORA was set up with the objective of strengthening regional co-operation and sustainable development within the Indian Ocean Region, with 21 member countries and seven dialogue partners. Its first meeting was held in Abu Dhabi in January 2014.

DEVELOPMENT OF HYDRO POWER IN INDIA.

Hydro power is cheap, clean and pollution free renewable energy and requires almost negligible running and maintenance cost. For this reason, all over the world, the developed nations harnessed all the hydro potential available to them. Unfortunately, though India is the 7th largest hydroelectric power producer in the world and has a high potential for hydro power generation i.e. 148701 MW, out of which 93876.9 MW is yet to be taken up for development. Moreover, many hydro-power projects with capacity of nearly 6000 MW are stalled due to a variety of reasons- from lack of funds to environmental reasons. Hydropower is the second largest contributor of energy consumed in the Indian power sector. The most significant hydropower potential in India exists in the three major transboundary river basins i.e. Ganges, Indus and the Brahmaputra. However, all these basins have experienced substantial changes in precipitation and air temperature that affected water availability for hydropower generation. India's installed hydro capacity at the end of 2018 was around 45400 MW, an annual growth of just 1%, the lowest since 2009. The power generation in India has registered a significant progress since the 5 Year planning started from 1951. In the year 1947 the total installed capacity was 1360 MW. And now it is about 358 GW, which is dominated by thermal power with around 63% share. Hydropower, with an installed capacity of 45 GW, has a share of only 13%, coming down from 46% in 1966 and 25% in 2008.



Fig. 2. Bakhra Dam

India with surging population, increased industrialization and associated high demand for fresh water, food and energy becomes highly vulnerable. India shares nearly 17.5% of the global population, but has only 4% of the total fresh water sources. In our country, the rain fall occurs only in few months of monsoon and that too in a few spells of intense and heavy rains. If surplus water is not stored, it will go waste, most of the time causing damage en-route by floods. Conservation of water is one of the principles enshrined in our National water policy which was adopted in 1987, which means converting as much as available water into utilizable water. Therefore, there is need that every river basin is provided with a major dam, so that a major portion the water derived from rainfall in monsoon period is stored for beneficial use for irrigation, water supply, hydropower generation, flood control, besides tourism and fisheries as additional benefits.

From the technical considerations, the dams, whether large, medium, or small not be constructed at any place as the selection of it depends upon consideration of a number of technical aspects like, suitability of site, topography, geology, physical properties of foundation, seismicity, extent of area to be commanded, availability of water and climate condition etc. besides scheme

being economically viable. Replacement of a single large dam by a number of small dams, to generate equivalent benefits, is not always possible as alternative sites are not available in river course. Moreover, with a single storage dam and with regulated releases from this storage, the power availability gets doubled compared to a series of down- stream diversion projects. The detailed studies have also revealed that cost of 1 KW of installed capacity increases three-fold in a small dam as compared to the large dam.

Major dams like Bakhra and Nangal dam has provided enormous economic progress and prosperity in the state of Punjab and Haryana. Tehri Hydro Power Plant with a 260.5 m high, Earth & Rock fill dam and Underground Power House of installed capacity of 1000 MW (4*250 MW) is fully operational from 2006-07 and producing much needed power to the northern grid. The command area is availing irrigation benefits from the project and drinking water is being supplied to Delhi and Uttar Pradesh. For a developing country like India, having very few oil and gas resources but having very vast and largely undeveloped Hydro resources, need to be fully harnessed for economic benefits and development.

The result of studies shows that the installed capacity in India by the end of 2029-30 will be 831502 MW, which includes Hydro 64 GW contributing only 8% in comparison to RE sources with 350 GW at 40% and a Battery Energy storage capacity of 34000 MW/136000 MWh. Further the sensitivity analysis for contingency scenarios show that with the base installed capacity along with envisaged battery energy storage capacity, the demand is likely to be fully met with increase in availability of coal-based power plants by 1% to 1.5%. Wide variations in solar/wind availability can only be mitigated through large hydro/conventional PHS. Some estimates suggest that 300 GW of additional wind energy requires 50 GW of conventional resource to account for the variability added to the grid system.

Prime Minister Shri Narendra Modi laid out ambitious plans to build 175 GW of renewable power generation by 2022, with the addition of 100 GW of solar, including 40 GW from solar roof tops, 60 GW of wind, 10 GW of biomass and 5 GW of small hydro. This will be done for reducing carbon emission and tackling the climate change. However, these variable and intermittent power to the Grid system which if not balanced properly, have the potential to destabilize the whole Indian power system.



Fig. 3. Nagarjuna Sagar Dam

Fluctuation in the electricity Grid working on renewable energy is obvious. Hence with the help of Pumped Storage Hydropower Plants it is possible to even out frequent changes between electricity shortages and surpluses. Pumped storage hydropower plants are power storage devices which can be used during off-peak hours and power supply can be resumed during peak demand, thus curtailment of renewable energy can be prevented. The role of Pumped Storage Hydropower Plants become vital in this scenario as these plants are capable of balancing the grid for demand driven as well as generation driven fluctuations at a high ramp up/down rate.

The revised pump storage potential in the country is about 82419 MW. Presently, 9 Pumped Storage Projects (PSPs) with an aggregate capacity of 4785.6 MW are constructed in the country. It is worth to mention here that a unique Pump Storage Hydropower project at Tehri Dam, involve construction of an underground Machine Hall housing four reversible pump turbine units of 250 MW each on the left bank of river Bhagirathi. The Tehri Dam reservoir shall function as the upper reservoir and Koteshwar reservoir as the lower balancing reservoir with a large head variation of about 90m. The project would provide 1000 MW peaking power to Northern Region with an annual generation of 1268 million units. Work on the project commenced from 27th July 2011. Project is scheduled to be commissioned in the year 2019-2020.



CONCLUSION

Solar power is now available in India for Rs 4-5 per unit. Other renewables continue to follow the trend. Wind power become competitive with coal around two years ago, and prices have continued to reduce. In 2008, the cost of industrial batteries was \$1000 per KWH of energy stored in USA; by 2015, it had fallen to \$268. Now this may be down to \$111. The price drop and related efficiency increases won't stop. These are forming a virtuous cycle: as the price drops, installations double, and as installations double, the price drops. Power usage will keep increasing, so this is a moving target. Taking that into account, solar can potentially provide more power than the world needs in less than 20 years.

While adopting the 17 SDGs, it is indicated that now is the time to take global action for the global resources and move the people and planet towards sustainable future. Water being the prime natural resource for sustaining lives and economies, finds an indirect implication in other goals as well.

In countries where governments have undertaken various initiatives including policy, regulatory, fiscal, financial measures, the renewable energy generation increases many folds. In 2009 Scotland sourced just 27% of its energy from renewables. Just a decade later, that figure now stands at 70%, making it a world leader. The incredible boom follows a major program by the Scottish government to develop its onshore wind and hydroelectric capacity. Scotland plans to reach its target of 100% consumption from renewable sources by 2020. What wind did for Scotland, solar can do for India.

So far as Hydropower is concerned, it is argued at many fora that the development of a Hydropower plant can cost from about 7 crores to 9 crore per MW, which is relatively higher when compared with that of thermal power or for solar energy, and that the gestation period is also relatively more. However, the hydropower has distinct advantages. Apart from the fact that water used for hydropower generation is non-consumptive in nature and is used for many purposes in the downstream of the project, such as irrigation, forestation, drinking water supply etc. The running and maintenance cost of hydropower plant is very low, and it is most suited for generation of power needs for meeting the peak time requirement as discussed earlier. Therefore, such energy source is most suited for securing energy security in the long run. Hence hydro power generation is to be promoted.

REFERENCES

1. Reference taken from seminar conducted by NWDA New Delhi in 'India water week' 2019.
2. Reference taken from seminar conducted by NWDA, New Delhi in 'India Water Week' 2016
3. Reference taken from Souvenir published for seminar on 'Hydropower Development in Uttarakhand and Adjoining Himalayan Region', organized by The Institution of Engineers (India), Dehradun Local Center, February, 7-8, 1997.
4. Scotland details and battery prices taken from column written by Prof. Vivek Wadhwa in Times of India 2019.



Renewable Energy Sources & Smart Grids Integration

Sangeeta Deb Barman¹, Dr Kumari Namrata², Dr S M Ali³

Department of Electrical Engineering, PhD Scholar, NIT, Jamshedpur¹

Department of Electrical Engineering, Associate Professor, NIT Jamshedpur²

Director (Membership), The Institution of Engineers (India), Kolkata³

✉ meghadb13@gmail.com; ✉ namrata.ee@nitjsr.ac.in; ✉ drsma786@gmail.com

ABSTRACT

Smart grid technology is the key for a well-organized consumption of dispersed energy resources. The smart grid is the future adaptation for the methods and policies of manufacture and the collaboration of all the constituents of power grid. Observing the weather change becomes a significant matter of anxiety, the entire ecosphere is presently facing the ever growing value of petroleum products, coal etc. and also the lessening in rate of renewable energy power schemes, giving prospects for renewable energy schemes to address electricity generation. However, to accomplish this assignment, an effective energy organization system needs to be addressed. In this context, the concept of smart grid plays a vital part and can be fruitfully applied to the power systems. This paper presents the study of assimilating renewable energy in smart grid system. The preliminary part deliver the role of renewable energy and dispersed generation in smart grid system. The perception of smart grid renewable energy system and its applications along with the PV smart grid system are also been deliberated and studied.

Keywords : Introduction; Smart grid technology; Role of renewable energy sources in smart grid.

INTRODUCTION

In latest ages, the operation of renewable energy sources in smart grid scheme has been growing. The mission for cleaner, green and more consistent energy sources has considerable allegations to the present power transmission and distribution arrangement. Conventionally the power is produced in majority and dispersed to the excessive load hubs via the transmission lines. The allocation of power was constantly one method, which is from the services to the customers. Nowadays in the instant future, renewable energy sources cannot support the whole network by themselves. So they have to be linked to the main network acting as secondary power sources thus dropping the global weight on the main power generation units. They might also be employed to assist load units completely inaccessible from the leading grid. A power system having wind powered turbines, micro generators, fuel cell based system and PV systems supplementing the core power lines will found a dispersed power generation (DG) system. In a DG system final users need not only be inert clients, but they can be active dealers to the grid. Distributed generation (DG) is an substitute which is

not only gathering motion but can also playing an significant character in meeting the eternally cumulative power burdens by means of an marginal source of energy such as photovoltaic, wind, fuel cells, etc. The necessity of assimilating the renewable energy into power system is to diminish the ecological influence on conservative plant. Smart grid plays a key role here. The basic objective of smart grid is to indorse active customer contribution and decision making as well as to make the operation environment in which both utilities and consumers can intermingle with each other. In smart grids, users can influence efficacies by providing DG sources such as photovoltaic units or energy storage devices at the point of use, and responding pricing indications. Additionally, utilities can recover dependability through the request response programs, adding DG or energy storage at substations, and providing control mechanization to the grid.

SMART GRID TECHNOLOGY

Smart grid lacks a standard definition but enters on the use of progressive of technology to increase the dependability and productivity of the grid, from transmission to distribution. The Smart Grid is a dream of a better electricity delivery organization. Smart Grid application dramatically increases the amount, quality, connectivity, automation and coordination between the suppliers, customers and networks, and use of data obtainable from progressive sensing, computing, and communications hardware and software.

Smart grid has different aspects and can be categorized as follows:-

- Collaborating with users and markets
- Adaptive and climbable to variable situations
- Optimized to make the best use of resources and equipment
- Pro-active instead of reactive to prevent emergencies
- Self-healing grids with advanced mechanization
- Integrated, merging monitoring, control, protection,
- Maintenance, EMS, DMS, AMI, etc.
- Having plug-and-play –features for network equipment and ICT solutions
- Secure & consistent
- Cost effectual
- Delivers real time data and monitoring



Fig. 1. Features of smart grid

Outmoded grid includes regional power generation, and at the distribution level unidirectional power flow and weak market integration. Smart grids include regional and distributed power generation produced significantly by renewable energy sources. They integrate distributed and active resources (i.e. generation, loads, storages and electricity vehicles) into energy markets and power systems. Smart grid is nothing but the power network that briskly assimilates creators and consumers to efficiently deliver electricity which is satisfactorily accomplished and coverage area accessible, safe, economic, reliable, efficient, and supportable. Smart grid development tends to be driven by one of the two principal visions for enhancing electric power interactions for both utilities and end use customers.

The quickly mounting installations of non-conventional energy resources require a synchronized and joint exertion from the planning stage all the way down to the electronic devices basically used for power generation, distribution, storage purpose and feeding.

ROLE OF RENEWABLE ENERGY SOURCES IN SMART GRID

Around the ecosphere slight alteration in generation of power is obligatory in order to Figurant climatic variations and to rise energy safety. Subsequently, renewable energy resources and DG's are getting provision and their bonds in electricity generation are quickly growing. The rising renewable generation in an unbending scheme is the important challenge for designers and practitioners of smart grid system. The addition of DG to the electrical distribution scheme has been the key driver in the development of dispersed system; though DG barely gets any market signals nor contributes in system organization for two reasons. Firstly, DG is often from renewable energy sources and therefore pre-planned on the basis of importance under fixed feed-in prices and not obliged from market prices. Also, generators in distribution systems are often too small and not prepared with skill. Furthermore, one of the difficulties skilled is that the increasing renewable stocks may cause mobbing in distribution systems. While erection new organizations, smart grid technologies can also help efficacies to improve grid congestion and to exploit the potential of our current construction.



Fig. 2. Role of Renewable Energy Sources in Smart Grid

As smart grid knowledge's become more popular, the electrical grid will be completed more efficient, subsequent in decrease of matters of overcrowding. Lots of Sensors and controls will help logically, redirect power to other lines when compulsory, helpful energy from renewable sources, so that power can be transported to a larger distance, where it is desired. Smart grid transports electricity from suppliers to clients using digital technology through control mechanization, continuous monitoring and optimization of distribution system, in order to save energy, reduce consumer cost and expand consistency.

RENEWABLE ENERGY SOURCES

Renewable energy sources are accessible in numerous forms. Major renewable energy sources are listed below:

- A. Solar energy
- B. Wind power
- C. Hydro energy
- D. Biomass / Biofuel
- E. Geothermal energy
- F. Other sources (ocean energy, tidal power, ocean thermal energy)

Solar Energy

Healthy light and heat from the sun, has been harnessed by hominids since primeval periods using a variety of ever- evolving knowledges. Solar energies, along with subordinate solar-powered resources such as wind and wave power hydroelectricity and biomass, interpretation for most of the obtainable renewable vigor on earth.

Only a minute portion of the accessible solar energy is used India is both thickly tenanted and has high solar insolation, providing an ideal assortment for solar power in India. The Karnataka Power Corporation Limited (KPCL) has mounted India's largest solar photovoltaic power plant at Yalesandra village in Kolar district of Karnataka.



Fig. 3. Role of Solar Energy in Smart Grid

Wind Power



Fig. 4. Wind Energy

The growth of wind power in India started in the 1990s, and has meaningfully enlarged in the last few years. Although a comparative newcomer to the wind trade associated with Denmark or the US, India has the fifth biggest mounted wind power capability in the world. The universal fitted capability of wind power grasped 157,899 MW by the end of 2009. USA (35,159 MW), Germany (25,777 MW), Spain (19,149 MW) and China (25,104 MW) are ahead of India in fifth place.

Hydro Energy



Fig. 5. Hydro Energy

India is gifted with thriftily useable and feasible hydro potential measured to be around 84,000 MW at 60% load factor (1,48,701 MW installed capacity). In addition, 6780 MW in terms of installed volume from Small, Mini, and Micro Hydel arrangements have been measured. Also, 56 sites for pumped storage arrangements with a total installed size of 94,000 MW have been recognized. However, only 19.9% of the potential has been yoked so far. Hydroelectricity is the term mentioning to power produced by hydropower; the manufacture of electrical power finished the usage of the gravitational force of dwindling or graceful water. It is the maximum widely used method of renewable energy.

Biomass

Biomass has been a key performer in energy generation even in the bygone. Biomass, indistinct as all terrestrial and water-based flora as well as carbon-based wastes, satisfied almost all of human kind's energy essential prior to the industrial revolution. In current day scenario, once again its use for generation of energy has increased impetus because of limited accessibility of the conservative energy goods as well as ecological concern due to GHG emissions. In the past decade there has been transformed attention in the biomass as a renewable energy source universal.



Fig. 6 Biomass Energy

Geo-Thermal

Geothermal energy is the earth's natural heat obtainable privileged the earth. This thermal energy delimited in the stalwart and watery that filled up fractures and pores in the earth's coating can lucratively be used for several resolves. This energy is retrieved by boring water or steam shafts in a procedure similar to boring for oil. Geothermal energy is a vast underused heat and power source that is fresh (emits little or no greenhouse gases), consistent (average system availability of 95%), and homespun (making us less dependent on foreign oil). India has sensibly good budding for geothermal; the prospective geothermal backwaters can harvest 10,600 MW of power.

CONCLUSION

In this paper, the important knowledge's of smart grid have been deliberate and revised. The main significance of renewable energy, renewable energy centered energy conversion systems, and distributed power generation has been repeated. It can be determined that with the progressions being prepared in the zone of renewable energy and distributed power generation, smart grid has a challenging and critical role in the future of well-organized power generation and distribution. With Renewables, impending as vast source of electric energy and due to its high abilities, predominantly in the zones of wind and solar power, in the years to come it will form substantial part of generation feeding the grid.

Conversely, as it originates with random and mutable influence, while assimilating smart grid exploiting progressive skills of digital computing and communication has to activate and regulate the power scheme within the satisfactory varieties of parameters. Controlling mechanism in India, some previously in rage and others progressively coming to be in force inspires to endorse Dispersed Generation and Renewables and defends the disturbed Green Energy Sources to encounter the power demand at each instantaneous of time along with integrated conventional thermal or nuclear generation. But at the same time stringent events need to be fulfilled with in operation while connected to grid, of course taking benefit of improvement in technologies as accessible to the smart grid which over the years has altered from what it was in the past in terms of process and control.

REFERENCES

1. National Renewable Energy Laboratory (NREL), "Using distributed energy resources". Available: <http://www.nrel.gov/>
2. EPRI White Paper, "Integrating distribution resources into electric utility distribution system", Technology Review, 2011.



3. P. Mazidi and G. N. Sreenivas; “Reliability assessment of a distributed generation connected distribution system”. International Journal of Power System Operation and Energy Management (IJPSOEM), 2011.
4. Math H. Bollen and Fainan Hassan “Integration of distributed generation in the power system”, John Wiley & Sons, 2011.
5. Shahid, A., “Cyber-physical modeling and control of smart grids – A new paradigm”, IEEE PES Innovative Smart Grid Technologies (ISGT), 2016.
6. Tugrul Atasoy, Hulya Erdener Akinc, Ozden Ercin, “An analysis on smart grid applications and grid integration of renewable energy systems in smart cities”, 4th International Conference on Renewable Energy Research and Applications (ICRERA), 2015.
7. Lo, C.H., Ansari, N., “The progressive smart grid system from both power and communications aspects”, Communications Surveys & Tutorials, IEEE, 14(3), 799-821, 2012.
8. Shahid, A., “Event based reduction of power fluctuation using cyberphysical control-communication network in smart grids”, Power Systems Conference, 2016.
9. H. Bevrani, “Microgrid control: a solution for penetration of renewable power”, International Conference on Green Energy and Applications, 2017.
10. Shahid, A., “A preliminary communication-assisted hybrid control strategy for maximum reliability and efficiency in smart grids”, IEEE PES Transmission and Distribution Conference (T&D), 2016.
11. Shahid, A. “An overview of control architecture for next generation smart grids”, 19th International Conference on Intelligent System Application to Power (ISAP), 2017.



Source Side Energy Management of Hybrid Renewable Energy System by Intelligent Control

Hemlata Joshi, Ekta Mishra, Ganesh H Patil

Department of Electrical Engineering, JSPM's Rajarshi Shahu College of Engineering, Tathawade, Pune

Dr. D. Y. Patil Institute of Technology, Pimpri, Pune

✉ hemlatamungikar@gmail.com; ✉ ektamishra0707@gmail.com

ABSTRACT

To meet the increasing energy demand and continue depletion of fossil fuel hybrid renewable energy technologies gaining more importance to fulfil power demand of today's world. The Hybrid Renewable Energy Systems (HRES) can be described as a set of loads, renewable generation and storage units that can operate in standalone mode or connected to the main grid. However intermittent behaviour of RES and trade-off between capital investment and system reliability, an optimum sizing of all HRES components and reliability analysis is needed. This paper deals with the source side energy management using PV solar system, wind turbine. Energy management insures by intelligent control for intermittent nature of renewable energy sources. A relative study of hybrid model solar, wind. Modelling and simulation are carried out in MATLAB/Simulink. Easy simulation model is implemented with intelligent control to extract maximum power from hybrid renewable energy system.

Keywords : Hybrid Renewable Energy Systems (HRES); Intelligent control; Energy management.

INTRODUCTION

The renewable energy sources are becoming of utmost important throughout the world in the past decade due to constant usage of conventional resources and environment issues[1]. Renewable energy is the most promising form of energy; it is an efficient way of solving scarcity of energy demand and mitigation of energy issues related to environment. But due to unpredictable and intermittent nature of renewable sources only one source is not sufficient to fulfil the demand of energy in present scenario. In order to make the continuous use of renewable energy sources two or more sources are combined together to meet the demand, so combination of two or more sources like solar, wind, hydro and batteries are classified as hybrid renewable energy system (HRES)[2]. Renewable energy has three inherent challenges. 1) It relies on intermittent sources, producing energy only when the sun is shining, or wind is blowing 2) Its output is constrained to specific hours of the day 3) Its use leads to lower utilization of transmission lines, this can create issues in matching peak power demand with renewable output (e.g. in evening hours when solar energy is not available), and raise costs of transmission. Multiple energy management control strategies are incorporated for smooth and efficient energy and power management of HRES. Real time control environment with MATLAB/SIMULATION has been done. The Stand-alone hybrid system is used to supply isolated areas interconnected to a weak grid. Energy generation hybrid system is used to meet the power demand depends on the atmospheric condition[3]. The excessive power can lead to the over-voltage in the dc bus and affects the reliability of the system. To prevent reliability and prevent over-voltage issues during excessive generation, the adaptive control strategy is used. It is archived by monitoring the DC bus voltage. MATLAB environment for simulation, optimization and sensitivity analysis of small power generating systems based on renewable energies is used in this paper. Regen Sim library along with MATLAB Sim Power Systems library is used to validate HRES model with solar and wind system. Basic components of RegenSim library are: Wind generators, PV generators, Hydro generators and Storage devices.

The energy management system with intelligent control reduces the computational time and easy to manage stand-alone system. There are different types of controllers used in the hybrid system. The most commonly used controller is PID controller. Fractional-order proportional-integral-derivative (FOPID) controller is used for the control of frequency deviation in fractional-order power generation and energy storage systems [4]. PID controller is used to improve the transient response and oscillations are reduced at the output response. PID controller is used to reduce the settling time of the frequency deviation. The primary objective of this paper is to satisfy load power demand integrating solar and wind hybrid renewable sources.

This paper is organized as follows. Section II introduces the proposed architecture of Intelligent controller-based hybrid system. In Section III Simulation results are analysed and discussed. Finally, the summary of the proposed system is concluded in section IV.

SOLAR-WIND HYBRID SYSTEM ARCHITECTURE WITH INTELLIGENT CONTROLLER

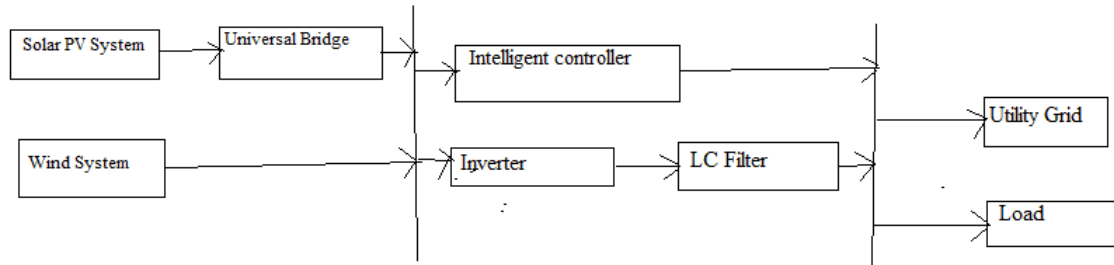


Fig.1. Block diagram of hybrid renewable energy system with intelligent controller

Above is the block diagram of hybrid renewable energy system with intelligent controller. This architecture is used to model hybrid renewable system with two or more renewable sources. Power from solar and wind is fed to the intelligent controller through universal bridge. LC filter is used to mitigate harmonics and ripples to ensure power quality at output side[5,6].

Intelligent controller ensures power management and continuous supply of energy on the availability of power from solar and wind system. MATLAB function programming is done in controller in which logic is designed to get the maximum output from solar and wind hybrid system, due to their intermittent nature.

The photovoltaic cell transforms the sunlight energy into electrical energy. Photovoltaic cells are connected either in series or parallel to generate higher voltage and power. The nature of current obtained is direct current (DC). Electricity generated from solar power is an integral step towards clean energy production. Maximum power from PV system is tracked by using MPPT technique. The wind turbine generator (WTG) is used to generate electricity from the wind by converting the kinetic energy into mechanical energy. Later the mechanical energy is converted into electrical energy. The current obtained from wind turbine is alternating current (AC). The output of wind turbine is directed to rectifier, which converts AC to DC.

SIMULATION RESULTS AND ANALYSIS

Behaviour of solar wind hybrid system is analysed using MATLAB/Simulink. **Fig 2** shows the simulation model of solar wind hybrid system with intelligent controller. Simulation is done under different circumstances and different configuration.

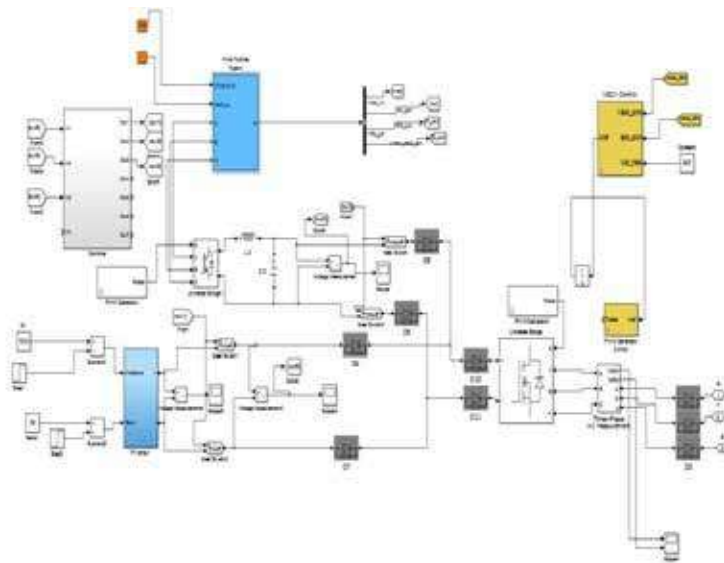


Fig. 2. Simulation model of solar wind hybrid system with intelligent controller

The simulation model of the proposed system consists of a PV module, wind module, battery, Luo converter and fuzzy logic controller. The photovoltaic system generates a current in DC form. Maximum power can be obtained from PV by using MPPT technique. The output of wind turbine is in AC form. A rectifier is used to convert AC to DC. The power from wind and PV is fed as input to the DC-DC Luo converter. Now the output of the Luo converter is DC, which is converted to AC by means of PWM inverter. The ripples and harmonics in the output signal is reduced by LC filter.

The solar module generates a DC voltage of 85V. The output voltage generated by wind turbine is 90V. The solar and wind voltages are fed to the intelligent controller and based on the maximum power generated by the source controller is designed to give that power to load. Based on controller logic simulation result of solar, wind hybrid system is shown in **Figs 3(a), 3(b), 3(c), 3(d), 3(e), 3(f)**.

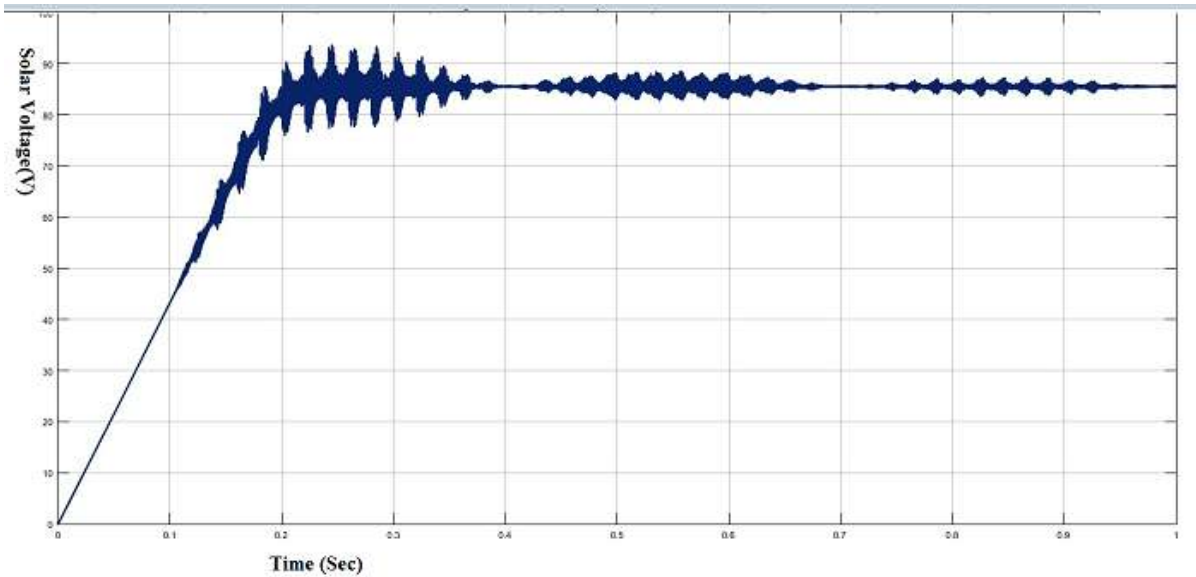


Fig. 3(a) Solar voltage

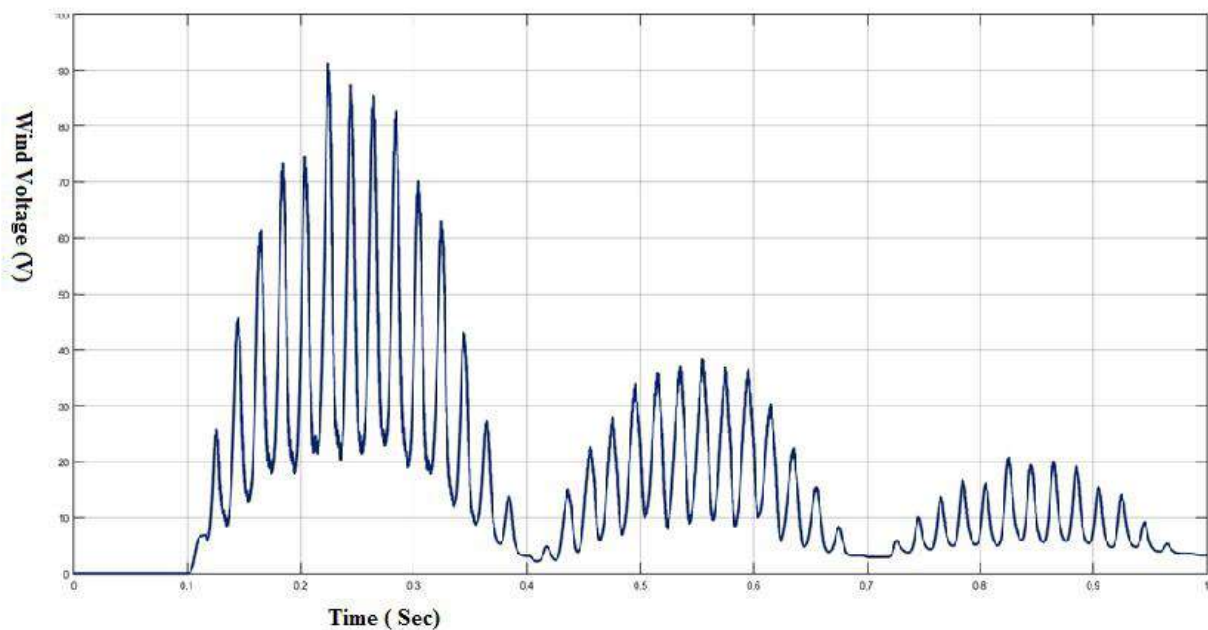


Fig.3(b) Wind Voltage

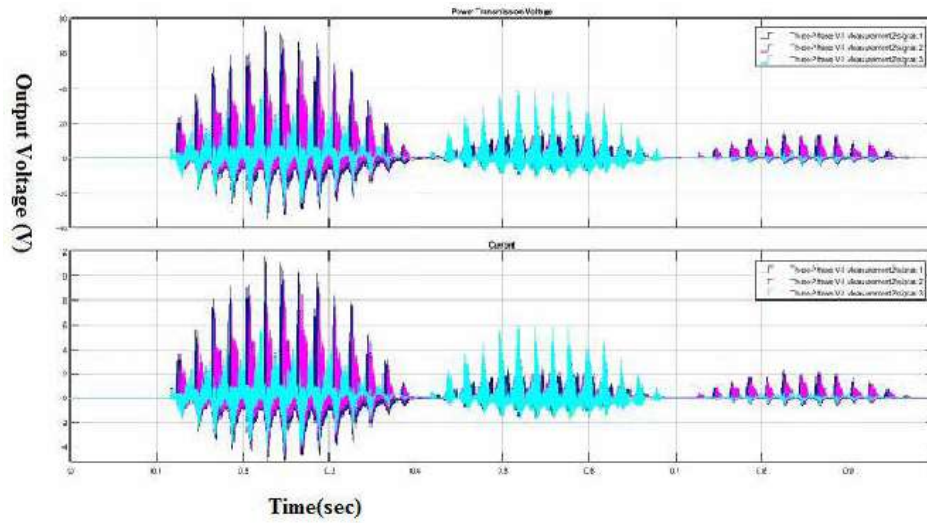


Fig. 3(c) Output voltage when wind gives more output

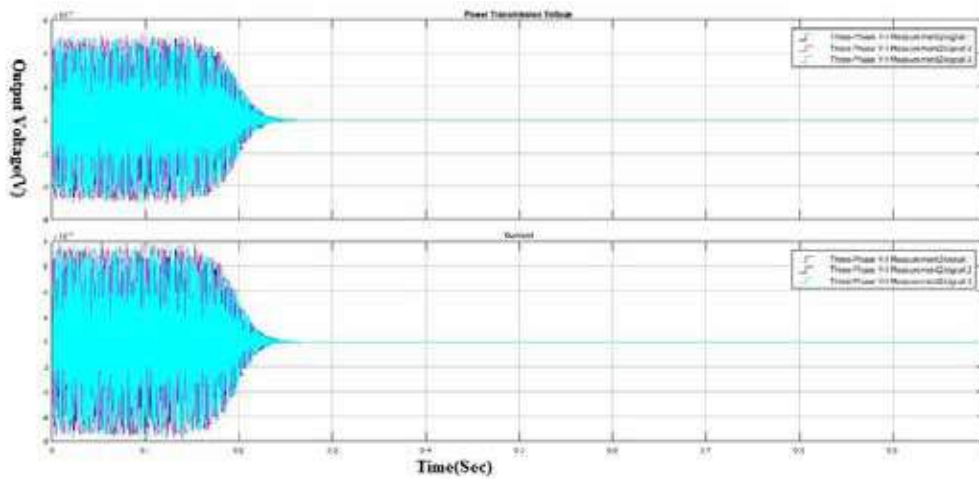


Fig. 3(d) Output voltage when Solar gives more output

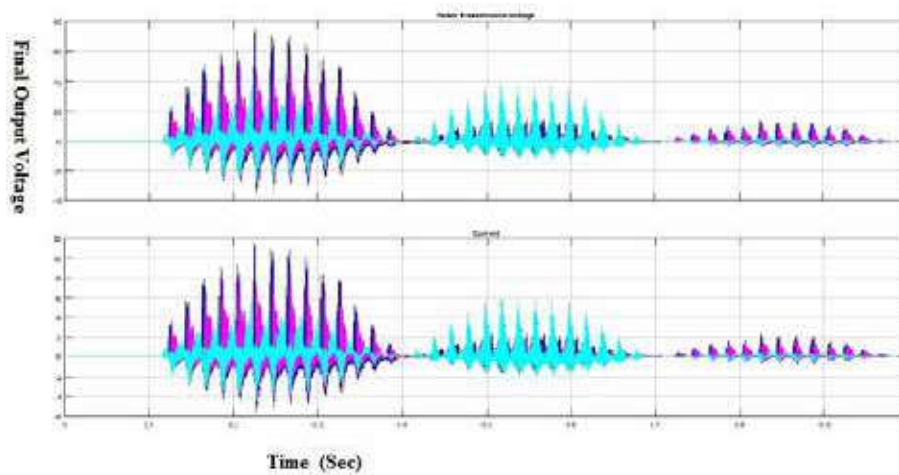


Fig. 3(e) Output voltage when Solar gives more output

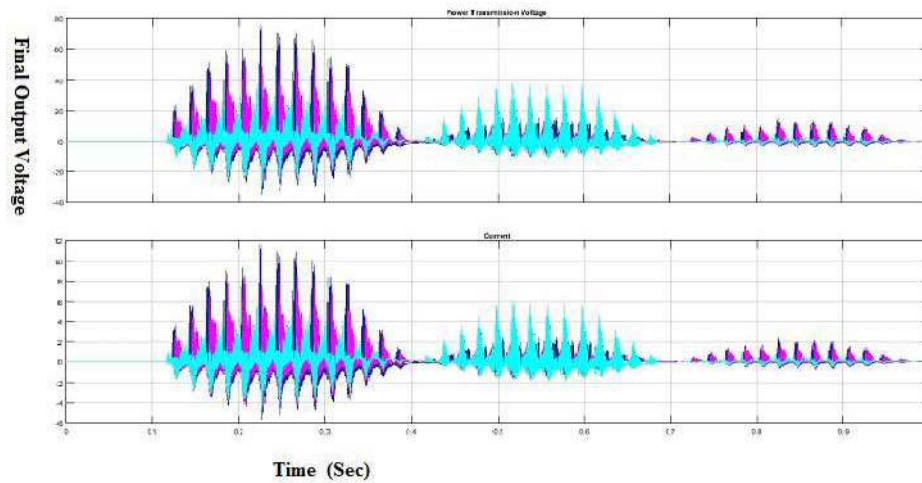


Fig. 3(f) Final output voltage

CONCLUSION

In this paper, an intelligent controller is designed for solar, wind hybrid renewable energy system. Matlab/Simulation library with RegenSim library along with Sim Power System library is used to validate and ensure maximum power and energy management at load side. This simulation work is useful in present scenario to allowing research going on hybrid renewable energy system. Performance of system has been analysed by changing source parameter of solar irradiance and wind pitch angle.

The future work is oriented to connect more renewable sources with existing system to improve performance of the system.

REFERENCES

1. S. M. Shyni , R. Ramadevi “Fuzzy Logic Controller Based Energy Management (FLCBEM) for a Renewable Hybrid System” 978-1-7281-5286-8/19,2019 IEEE.
2. S. Saib, A. Gherbi, “Simulation and Control of hybrid renewable energy system connected to the grid” 978-1-4673-7172-8/15,20 IEEE
3. B. Kanagasakthivel, Dr D Devaraj, “Simulation And performance analysis of solar pv-wind hybrid energy system using matlab/Simulink” 978-1-4799-7623-2/15, 2015 IEEE
4. Anjali Rana, Mohammad Ilyas, “Implementation of a Wind/PV Hybrid System using MATLAB/Simulink” Vol. 4, Issue 7, July 2015.
5. Junzhi Yu, Chunxia Dou, and Xinbin Li, “MAS-Based Energy Management Strategies for a Hybrid Energy Generation System” 0278-0046 , 2015 IEEE.
6. Z. Sabiri, N. Machkour, K. El Majdoub, M. Bezza, Elm. Kheddioui,” Management Strategy of a Hybrid Renewable Energy System.



Improved Adaptive Controller Based Speed Estimator at Low Speeds for Sensorless Vector Controlled Induction-Motor

Meghraj S Morey*, Vasudeo B Virulkar

Department of Electrical Engineering, Government College of Engineering Amravati, Amravati, Maharashtra

*✉ meghraj01@gmail.com

ABSTRACT

This paper proposes an modified rotor flux space vector, model following adaptive controller based rotor speed observer in speed encoder less vector-controlled induction motor drives. The proposed scheme mainly focuses on improving the speed performance of these drives around and through zero-speed regions. A conventional rotor flux MRAS speed estimator—associated with the disadvantage of poor performance near zero-speed regions, where the error of rotor flux state vector is used as the tuning signal—is driven by the adaptation mechanism to generate the estimated speed. In the proposed speed observer, the error of electromagnetic torque vector is used simultaneously with that of rotor flux state vector for speed estimation. Also, the adaptation algorithm in a conventional adaptive control based speed observer, which consist of PI controller, for tuning the rotor flux error vector, is reformed to a new adaptation algorithm by introducing the torque error vector operated by a low pass filter and added with classical rotor flux based adaptation system. Computer simulations are shown to verify proposed scheme in SIMULINK MATLAB at different speeds especially, low speeds including regeneration and load torque profiles.

Keywords : Induction motor drives; Estimation, MRAS; Rotor flux; Sensorless vector control.

NOMENCLATURE

$\bar{\psi}_{dr}, \bar{\psi}_{qr}$ = d and q-axis rotor flux

$\hat{\bar{\psi}}_{dr}, \hat{\bar{\psi}}_{qr}$ = estimated d and q-axis rotor flux

$\bar{v}_{ds}, \bar{v}_{qs}$ = d and q-axis stator voltages

$\bar{i}_{ds}, \bar{i}_{qs}$ = d and q-axis stator currents

R_s, R_r = stator and rotor winding resistance

L_s, L_r = stator and rotor winding self inductance

M = mutual inductance

$\sigma = 1 - \frac{M^2}{L_s L_r}$, leakage factor

$T_r = \frac{L_r}{R_r}$, rotor time constant

INTRODUCTION

Sensorless control of induction motor (IM) is favorite in the industry due to its good dynamic response [1]. The speed sensorless has the vast industrial applications such as domestic appliances, robots, electric vehicle, water pumping for agricultural purpose where submersible induction motor are preferred, railway traction applications. In conventional speed-sensor IM drives, rotor speed is measured using a sensor, which is an encoder or a tachogenerator, Eliminating the speed sensors has many advantages of cost reduction, reducing the space for motor system and reduce the fault caused by failure of speed sensors and increase the drives reliability. Therefore, sensorless drives have an upper edge over traditional speed-sensor IM drives. Researchers have developed many speed estimation schemes based on model-based and signal injection-based approaches. The latter approach of rotor speed estimation, which involves signal injection, has been proposed in [2]-[5], and gives better performance in low and through zero-speed regions. However, this method requires extra circuitry hardware for signal injection, which has an erroneous effect of the injected signal on motor dynamics, and hence, the performance of the drive. The model-based approach,

which mainly includes Kalman filter (EKF) [6]-[8], observer-based methods (ELO) [9]-[12], has gathered significant research interest in the last two decades. However, Kalman filter based speed estimation are robust to parameter sensitivity and noise in the system involves large computation. Observer-based methods require the information of several machine states. Predictive control methods [13, 14] use the combination of switching states for increasing the speed estimation accuracy.

Another solution among the model-based methods is the model reference adaptive system (MRAS) principle for speed estimation, in which a state error vector is formed from the difference between the outputs of two models, both dependent on different states and then adjusted to zero through tuning of the parameter on which one of the model performance depends upon. The MRAS approach has advantages such as high speed of adaptation, less computation, and ease of implementation as compared to ELOs or EKFs. Thus, they can be easily implemented and have direct physical interpretation. Depending upon signal used for formation of error vector, the adaptive controller based speed observer developed so far are : 1) The rotor flux error-based MRAS scheme, developed by Ohtani [15] and Schauder [16], called the classical MRAS speed observer (CMRAS); 2) the back electromotive force error-based MRAS scheme, where the tuning signal is obtained from the difference of the measured and estimated back EMFs [17,18]; 3) the reactive power-based speed estimator, which uses either instantaneous reactive power [19] or steady-state reactive power [20]; 4) the electromagnetic torque MRAS-based speed estimator [21]; and 5) the stator current error-based MRAS [22, 23].

Study available in the literature shows that speed estimation using model-based methods are mostly affected by on the machine's parameter which varies with operating conditions, mainly stator resistance at low speed; in addition, speed observer involves pure integration, causes the problem of initial conditions and dc offset, and restricts operation of the drive near zero-speed regions [24]. Many strategies have been applied to enhance the accuracy and parameter dependency of these methods, such as online updating of stator resistance and online estimation of stator resistance along with rotor speed [25, 26]. To enhance the estimation response at low speed, the pure integrator is replaced by a low-pass filter (LPF) [27] and a programmable cascaded LPF is used as reported in [28].

This paper proposes a classical MRAS-based rotor speed observer modification for improving the performance of speed-sensorless vector control of IM drives. In the proposed speed observer, the error of electromagnetic torque vector is used simultaneously with that of rotor flux state vector for speed estimation. Also, the adaptation algorithm in a conventional model following adaptive control based speed observer, which is proportional-integral for the tuning the rotor flux error vector, is reformed to a new adaptation algorithm in which the electromagnetic torque error vector operated by a low pass filter added with the rotor flux based adaptation system. Proposed scheme is verified in SIMULINK using MATLAB at different speeds and low speeds including regeneration and at different load torque conditions.

Induction Motor Modelling

The IM mathematical model in a synchronous command frame is expressed by the following machine's voltage model equations.

$$\begin{cases} \bar{v}_{ds} = R_s \bar{i}_{ds} + \sigma L_s \frac{d\bar{i}_{ds}}{dt} + \frac{M}{L_r} \frac{d\bar{\psi}_{dr}}{dt} - \omega_e \frac{d\bar{i}_{ds}}{dt} - \omega_e \frac{M}{L_r} \bar{\psi}_{dr} \\ \bar{v}_{qs} = R_s \bar{i}_{qs} + \sigma L_s \frac{d\bar{i}_{qs}}{dt} + \frac{M}{L_r} \frac{d\bar{\psi}_{qr}}{dt} + \omega_e \frac{d\bar{i}_{ds}}{dt} - \omega_e \frac{M}{L_r} \bar{\psi}_{qr} \end{cases} \quad (1)$$

$$\begin{cases} 0 = \frac{1}{T_r} \bar{\psi}_{dr} - \frac{M}{T_r} \bar{i}_{ds} + \frac{d\bar{\psi}_{dr}}{dt} + \omega_r \bar{\psi}_{qr} \\ 0 = \frac{1}{T_r} \bar{\psi}_{qr} - \frac{M}{T_r} \bar{i}_{qs} + \frac{d\bar{\psi}_{qr}}{dt} - \omega_r \bar{\psi}_{dr} \end{cases} \quad (2)$$

The motion equation is given by

$$C_e - C_l = j \frac{d\omega_m}{dt} + f \omega_m \quad (3)$$

$$\text{where, } C_e = \frac{3}{2} \frac{P}{2} \frac{M}{L_r} (\bar{i}_{qs} \bar{\psi}_{dr} - \bar{i}_{ds} \bar{\psi}_{qr}) \quad (4)$$

In the above equation, j is the rotor moment of inertia, ω_m is the mechanical speed of the rotor, f is the viscous coefficient.

Assuming load torque and the viscous coefficient together, (3) can be written as,

$$C_e - C = j \frac{2}{P} \frac{d\omega_r}{dt} \quad (5)$$

Where, $C = C_l + f \omega_m$

Proposed MRAS-Based Estimator

Speed Estimation Using CMRAS

An MRAS approach calculates the same quantity in two ways, using two models. The output of these two models then drives the adaptation mechanism, whose output is the estimated quantity. A typical block diagram utilized for speed estimation by the CMRAS technique is shown in **Fig. 1**. In which machine stator voltages either measured or reconstructed and the machines current signals are measured, and is composed of the command (voltage) and the adjustable (current) model.

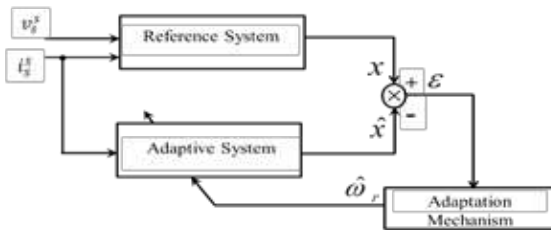


Fig. 1. Structure for speed estimation by CMRAS principle

The IM model in a stationary command frame is represented as

$$\begin{cases} \bar{v}_{ds} = R_s \bar{i}_{ds} + \sigma L_s \frac{d\bar{i}_{ds}}{dt} + \frac{M}{L_r} \frac{d\bar{\psi}_{dr}}{dt} \\ \bar{v}_{qs} = R_s \bar{i}_{qs} + \sigma L_s \frac{d\bar{i}_{qs}}{dt} + \frac{M}{L_r} \frac{d\bar{\psi}_{qr}}{dt} \end{cases} \quad (6)$$

Equation (6) calculates the rotor flux vector using stator voltage and current, usually referred as voltage model flux observer, whereas in (7) rotor flux is calculated using stator current and rotor speed knowledge, referred as current model flux observer. These can be expressed as

$$\begin{cases} \frac{d\bar{\psi}_{dr}}{dt} = \sigma L_s \frac{d\bar{i}_{ds}}{dt} + \frac{L_r}{M} (\bar{v}_{ds} - R_s \bar{i}_{ds}) \\ \frac{d\bar{\psi}_{qr}}{dt} = \sigma L_s \frac{d\bar{i}_{qs}}{dt} + \frac{L_r}{M} (\bar{v}_{qs} - R_s \bar{i}_{qs}) \end{cases} \quad (7)$$

$$\left\{ \begin{aligned} \frac{d\bar{\psi}_{dr}}{dt} &= \frac{M}{T_r} \bar{i}_{ds} - \frac{1}{T_r} \bar{\psi}_{dr} - \omega_r \bar{\psi}_{qr} \\ \frac{d\bar{\psi}_{qr}}{dt} &= \frac{M}{T_r} \bar{i}_{qs} - \frac{1}{T_r} \bar{\psi}_{qr} + \omega_r \bar{\psi}_{dr} \end{aligned} \right\} \quad (8)$$

Equation (8) can be written in the estimated form as

$$\left\{ \begin{aligned} \frac{d\tilde{\psi}_{dr}}{dt} &= \frac{M}{T_r} \tilde{i}_{ds} - \frac{1}{T_r} \tilde{\psi}_{dr} - \hat{\omega}_r \tilde{\psi}_{qr} \\ \frac{d\tilde{\psi}_{qr}}{dt} &= \frac{M}{T_r} \tilde{i}_{qs} - \frac{1}{T_r} \tilde{\psi}_{qr} + \hat{\omega}_r \tilde{\psi}_{dr} \end{aligned} \right\} \quad (9)$$

Proposed MRAS Speed Observer

In the proposed method, two error vectors are used: conventional rotor flux and torque developed by the motor. The electromagnetic torque of the motor in terms mathematically can be represented as,

$$C_e = \frac{3}{2} \frac{P}{2} \frac{M}{L_r} (\bar{i}_{qs} \bar{\psi}_{dr} - \bar{i}_{ds} \bar{\psi}_{qr}) \quad (10)$$

The above equation can be written in the estimated form as,

$$\hat{C}_e = \frac{3}{2} \frac{P}{2} \frac{M}{L_r} (\tilde{i}_{qs} \tilde{\psi}_{dr} - \tilde{i}_{ds} \tilde{\psi}_{qr}) \quad (11)$$

writing (3) in the estimated form as,

$$\hat{C}_e - C_l = j \frac{2}{P} \frac{d\hat{\omega}_r}{dt} + f \hat{\omega}_r \quad (12)$$

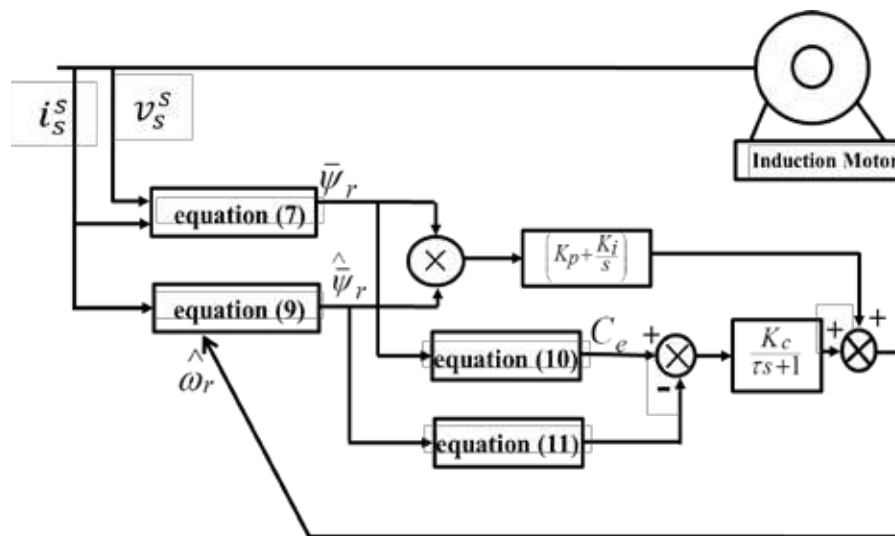


Fig. 2. Proposed MRAS speed observer

and subtracting (12) from (3), we obtain the following

$$\varepsilon_c = C_e - \hat{C}_e = \frac{2}{P} \frac{d(\omega_r - \hat{\omega}_r)}{dt} + f \omega_m \quad (13)$$

Then, for correct speed estimation, the following two conditions are considered:

$$\left(\frac{d\varepsilon_d}{dt} = -\frac{1}{T_r} \varepsilon_d - \omega_r \varepsilon_d - (\omega_r - \hat{\omega}_r) \tilde{\psi}_{qr} \right) \quad (14.1)$$

$$\left(\frac{d\varepsilon_q}{dt} = -\frac{1}{T_r} \varepsilon_q - \omega_r \varepsilon_q - (\omega_r - \hat{\omega}_r) \tilde{\psi}_{dr} \right) \quad (14.2)$$

$$\varepsilon_c = C_e - \hat{C}_e = \frac{2}{P} \frac{d(\omega_r - \hat{\omega}_r)}{dt} + \frac{2}{P} f(\omega_r - \hat{\omega}_r) \quad (15)$$

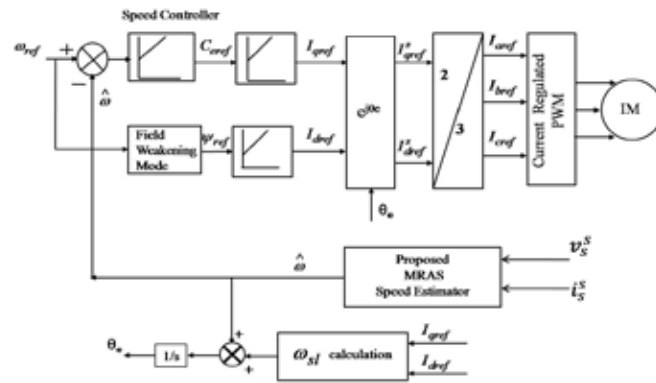


Fig. 3. Proposed MRAS speed estimator using indirect vector control of IM

Thus, combining the previously derived adaptation law with the error of the electromagnetic torque, the new adaptation law defined as;

$$\hat{\omega}_r = \left(K_p + \frac{K_i}{s} \right) (\tilde{\psi}_{qr} \tilde{\psi}_{dr} - \tilde{\psi}_{dr} \tilde{\psi}_{qr}) + \varepsilon_c \frac{K_c}{\tau s + 1} \quad (16)$$

In this scheme, rotor speed is estimated by adding the classical adaptation law and placing an LPF after the motor torque error. The modified MRAS speed observer is as shown in **Fig. 2**.

Verification of Proposed MRAS-based Speed Estimation

Fig. 3. shows a block diagram indicating the proposed speed estimator for a speed-sensorless vector-controlled IM drive, where the actual speed-sensor signal is replaced by the proposed speed estimator. Simulation using Simulink/MATLAB software is conducted to verify the drives' operation with proposed scheme for various command speed signal pattern under varying load condition. The parameters of the IM used are

Comparison of classical and proposed speed estimator

A comparison study between the speed response of a conventional rotor flux based and the proposed MRAS speed estimator is carried out and presented in **Fig. 4**. **Fig. 4(a)** shows the reference speed, conventional MRAS estimated speed, and proposed MRAS estimated speed tracking response. **Fig. 4(b)** shows the zoomed-in plot of the conventional and proposed MRAS estimated speeds tracking the reference speed.

The results comparing the performances of the conventional and proposed MRAS speed estimator for sequence of reference speed in the low speed regions at 15 rad/s, 10 rad/s, 5 rad/s and finally at zero speed and load is held constant throughout the operation of the drive. Due to the combined effect of the conventional adaptation law and LPF speed estimates, the proposed speed estimator tracks the reference speed satisfactorily with a very small error as compared to the conventional speed estimator

and reaches to its steady state very fast. The conventional speed estimator shows the significant errors in the rotor speed before the rotor speed settles to the reference speed.

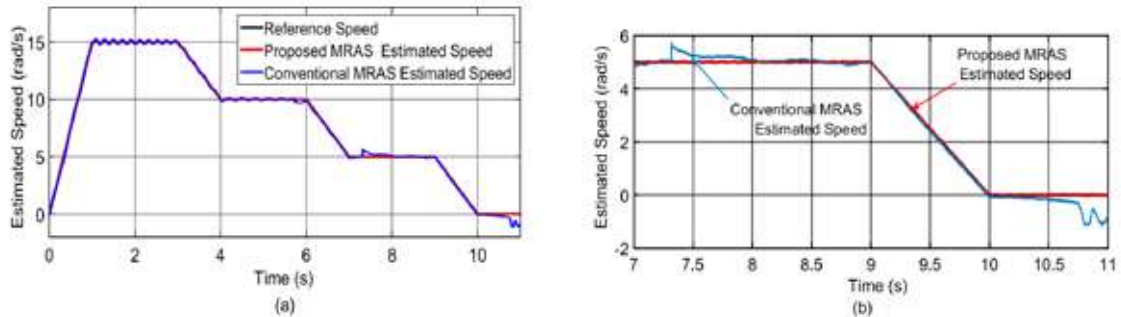


Fig. 4. Response of conventional MRAS estimated speed and proposed MRAS speed estimator

Drive's response to step change in rotor speed operation

Performance of the drive using the proposed MRAS estimator for staircase change in the command speed is presented in **Fig. 5**. **Fig. 5(a)** shows change in command speed from zero to 5 rad/s to 10 rad/s to 15 rad/s and 15 rad/s to 10 rad/s to 5 rad/s. The estimated speed tracks the command speed satisfactorily with very low error, as shown in **Fig. 5(b)**. The d- and q-axis stator currents appear as dc quantities in the synchronously rotating frame in **Fig. 5(c)**. During the entire operation of the drive, undisturbed field orientation is achieved as shown in **Fig. 5(d)**. The torque developed by the machine is shown in **Fig. 5(e)**. The drive is operated at 2 Nm for the first 5 s, and then, at no load for the remaining duration. In the proposed tested sensorless-drive, both the estimated and actual speeds, are close to each other not only for the steady-state operation but also under sudden change of reference speed and load torque and with speed tracking errors tends to zero.

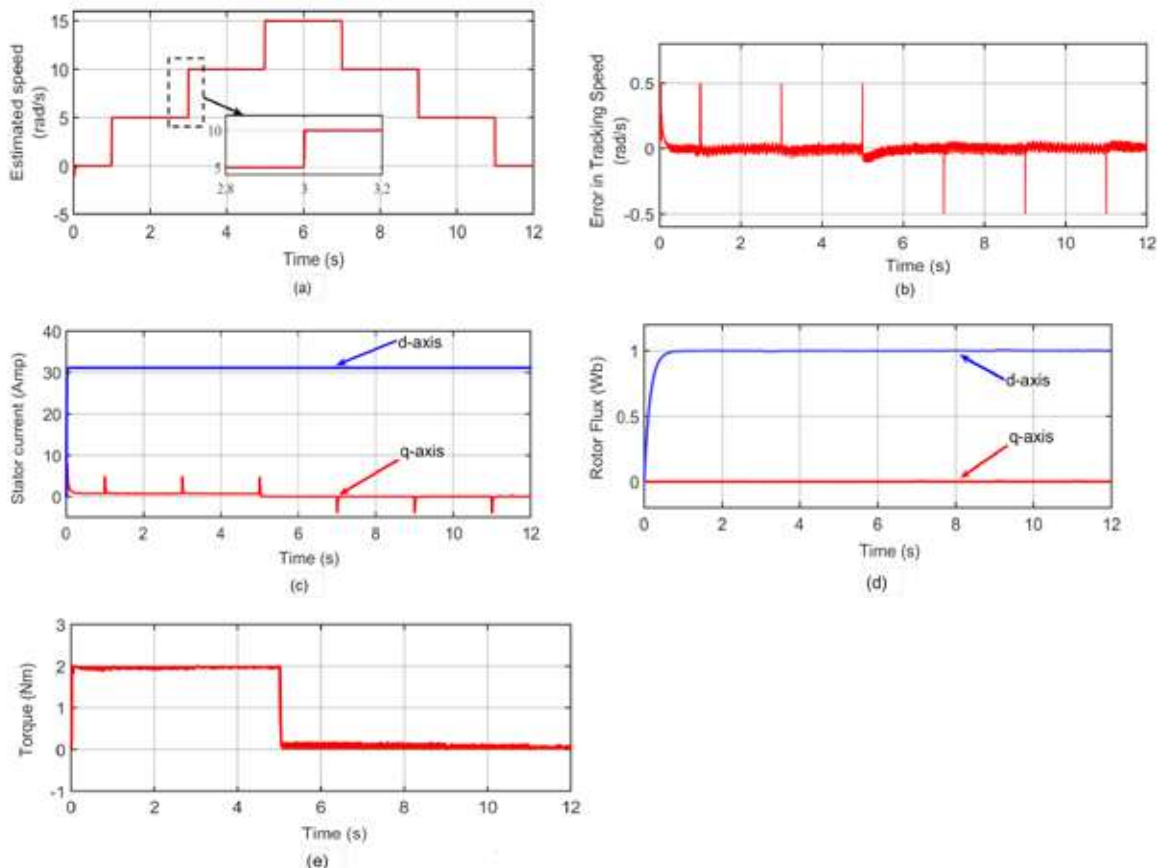


Fig.5. Response of the proposed MRAS speed estimator for the staircase speed pattern reference and estimated speed

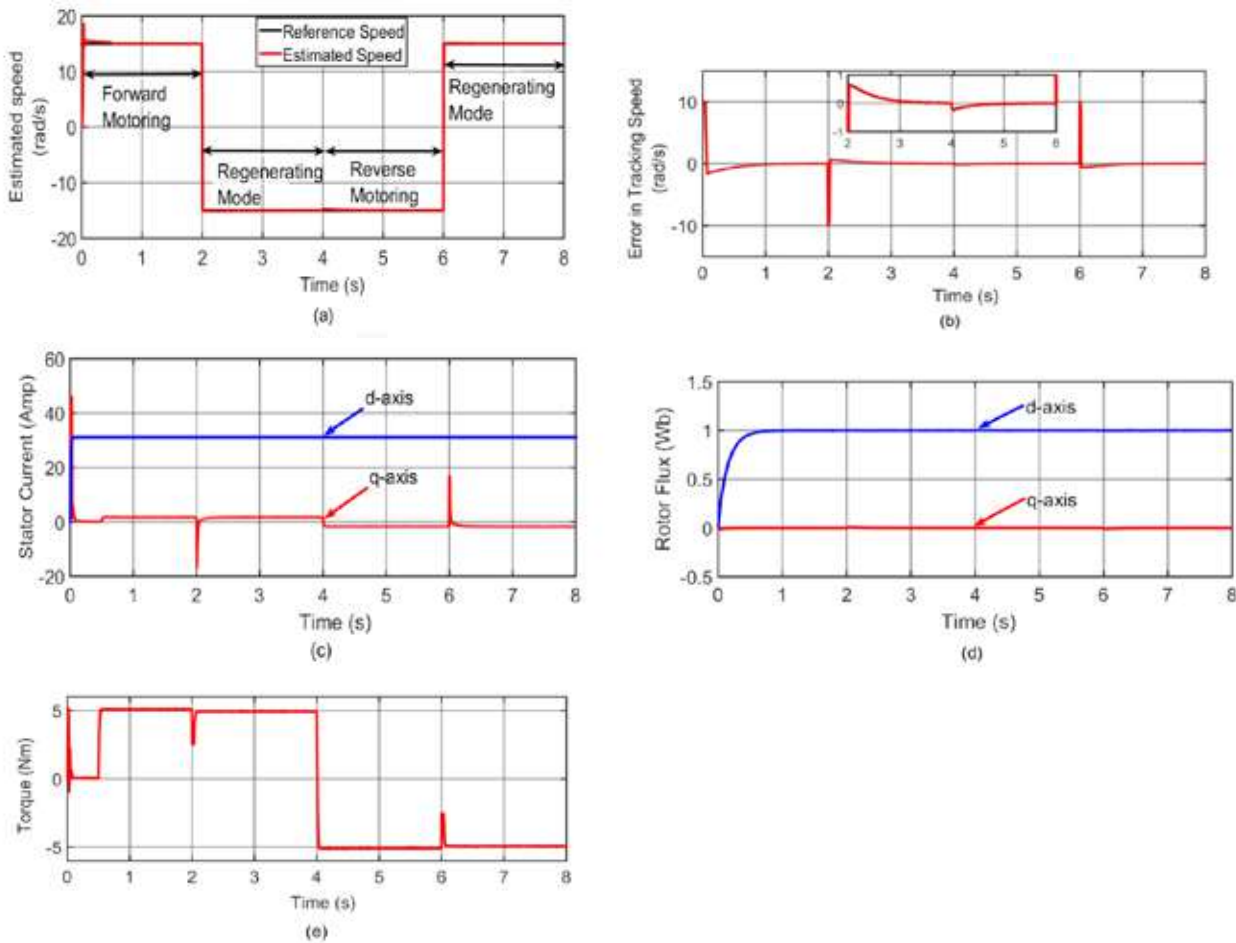


Fig.6. Four-quadrant operation of the drive using the proposed speed estimator

Proposed speed estimator performance during four-quadrant operation of the drive

During an initial period of 2 s, the drive operates in the forward motoring mode, where both the speed (15 rad/s) and torque applied (5 N-m) are positive. After 2–4 s, the regenerative mode of operation is presented. Then, during 4–6 s, the drive operates in the reverse motoring mode, where both speed and torque applied are negative. Finally, during 6–8 s, the regenerative mode of operation is demonstrated. In all modes of drive operation, the estimated speed tracks the reference speed with a very small error. **Fig. 6(c)** presents the d-q axis stator current in a synchronously rotating frame. Field orientation control is maintained during the entire operation shown in **Fig. 6(d)**. **Fig. 6(e)** shows the torque response of the motor. The rotor flux and stator current responses show the proposed speed estimation scheme capability of operating the drive for both, motoring and regenerative regions of operation.

CONCLUSION

This paper proposes an improvised rotor flux MRAS rotor speed observer for improving the performance of a sensorless vector controlled induction motor drive. Simulated results for different speed and load torque profiles show better performance of the proposed speed observer in low- and through zero-speed regions. These results prove that the combined effect of LPF to the conventional adaptation control algorithm has solved the problem of classical MRAS speed estimator performance in these regions. The proposed rotor speed observer is robust to wider variation of load torque, insensitive to the stator resistance variations at low speeds and also, allowing the correct field orientation. The proposed estimator also gives the good performance in all the four quadrants of the drive unlike classical MRAS for IM drive.



APPENDIX

Induction motor parameters

3.7 kW, 160 V, 60 Hz three phase, 4 pole stator winding resistance $R_s = 0.3831\Omega$, rotor winding resistance $R_r = 0.2367\Omega$, mutual inductances $M = 48.08$ mH, stator and rotor winding self-inductance $L_s = L_r = 33.34$ mH.

REFERENCES

1. L. Gou, C. Wang, M. Zhou, X. You, "Integral Sliding Mode Control for Starting Speed Sensorless Controlled Induction Motor in the Rotating Condition", IEEE Trans. Power Electron., vol. 35, no. 4, pp. 4105 - 4116, Apr. 2020..
2. Wei Sun, X. Liu et al., "Zero Stator Current Frequency Operation of Speed-Sensorless Induction Motor Drives Using Stator Input Voltage Error for Speed Estimation", IEEE Trans. Ind. Electron., vol. 63, no. 3, pp. 1490 – 1498, 2016.
3. P. Zhang, Y. Du, T. G. Habetler, and B. Lu, "Magnetic effects of DC signal injection on induction motors for thermal evaluation of stator windings," IEEE Trans. Ind. Electron., vol. 58, no. 5, pp. 1479–1489, May 2011.
4. M. Pucci and M. Cirrincione, "Neural MPPT control of wind generators with induction machines without speed sensors," IEEE Trans. Ind. Electron., vol. 58, no. 1, pp. 37–47, Jan. 2011
5. Y. D. Yoon and S.-K. Sul, "Sensorless control for induction machines based on square-wave voltage injection," IEEE Trans. Power Electron., vol. 29, no. 7, pp. 3637-3645, July 2014.
6. F. Alonge, F. D'Ippolito and A. Sferlazza, "Sensorless Control of Induction-motor drive based on robust Kalman filter and adaptive speed estimation," IEEE Trans. Ind. Electron., vol. 61, no. 3, pp. 1444-1453, March 2014.
7. F. Alonge, T. Cangemi, F. D'Ippolito, A. Fagiolini and A. Sferlazza, "Convergence analysis of extended Kalman filter for sensorless control of induction motor," IEEE Trans. Ind. Electron., vol. 62, no. 4, pp. 2341-2352, April 2015.
8. M. Habibullah and D.-C. Lu, "A speed-sensorless FS-PTC of induction motors using extended Kalman filters," IEEE Trans. Ind. Electron., vol. 62, no. 11, pp. 6765-6778, Nov. 2015
9. S. Yin, Y. Huang, et al. , "Improved Full-Order Adaptive Observer for Sensorless Induction Motor Control in Railway Traction Systems Under Low-Switching Frequency" , IEEE Journal of Emerging and Selected Topics in Power Electron., vol. 7, no. 4, pp. 2333 – 2345, Dec. 2019.
10. M. Hinkkanen and J. Luomi, "Parameter sensitivity of full-order flux observers for induction motors," IEEE Trans. Ind. Appl., vol. 39, no. 4, pp. 1127–1135, Jul./Aug. 2003.
11. B. Chen, W. Yao, F. Chen and Z. Lu, "Parameter sensitivity in sensorless induction motor drives with the adaptive full-order observer," IEEE Trans. Ind. Electron. , vol. 62, no. 7, pp. 4307-4318, May, 2015.
12. E. Etien, C. Chaigne, and N. Bensiali, "On the stability of full adaptive observer for induction motor in regenerating mode," IEEE Trans. Ind. Electron., vol. 57, no. 5, pp. 1599–1608, May 2010.
13. P. Alkorta, O. Barambones, J. A. Cortajarena and A. Zubizarreta, "Efficient multivariable generalized predictive control for sensorless induction motor drives," IEEE Trans. Ind. Electron., vol. 61, no. 9, pp. 5126-5134, Sept. 2014.
14. Y. B. Zbede, S. M. Gadoue, D. J. Atkinson, "Model Predictive MRAS Estimator for Sensorless Induction Motor Drives" IEEE Trans. Ind. Electron., vol. 63, no. 6, pp. 3511 – 3521, June 2016.
15. T. Ohtani, N. Takada, and K. Tanaka, "Vector Control of Induction-Motor without Shaft Encoder," IEEE Trans. Ind. Appl., vol. 28, pp. 157-164, Jan-Feb 1992.
16. C. Schauder, "Adaptive speed identification for vector control of induction motors without rotational transducers," IEEE Trans. Ind. Appl., vol. 28, no. 5, pp. 1054–1061, Sep./Oct. 1992.
17. F. Z. Peng and T. Fukao, "Robust speed identification for speed-sensorless vector control of induction motors," IEEE Trans. Ind. Appl., vol. 30, no. 5, pp. 1234–1240, Sep./Oct. 1994.
18. M. Rashed and A. F. Stronach, "A stable back-EMF MRAS-based sensorless low speed induction motor drive insensitive to stator resistance variation," IEE Proceedings Electric Power Applications, vol. 151, no. 6, pp. 685-693, 7 Nov. 2004



19. Ta, C.-M., Uchida, T., Hori, Y., “MRAS-based speed sensorless control for induction motor drive using instantaneous reactive power,” *Int. Conf. Rec. of the IEEE-IECON*, pp. 1417–1422, (2001).
20. S. Maiti, C. Chakraborty, Y. Hori, and M. C. Ta, “Model reference adaptive controller-based rotor resistance and speed estimation techniques for vector controlled induction motor drive utilizing reactive power,” *IEEE Trans. Ind. Electron.*, vol. 55, no. 2, pp. 594–601, Feb. 2008.
21. Smith A. N., Gadoue S. M., Finch J. W., “Improved Rotor Flux Estimation at Low Speeds for Torque MRAS-Based Sensorless Induction Motor Drives,” *IEEE Trans. Energy Convers.*, vol. 99, pp. 1-13, 2015.
22. Chul-Woo Park, Woo-Hyen Kwon, “Simple and robust speed sensorless vector control of induction motor using stator current based MRAC,” *Electric Power Systems Research*, vol. 71, pp. 257–266, 2004.
23. T. Orłowska-Kowalska, M. Dybkowski, “Stator Current-based MRAS Estimator for Wide Range Speed-Sensorless Induction Motor Drive,” *IEEE Trans. Ind. Electron.*, vol. 57, no. 4, pp. 1296-1308, Apr 2010.
24. T. Kikuchi; Y. Matsumoto; A. Chiba, “Fast Initial Speed Estimation for Induction Motors in the Low-Speed Range,” *IEEE Trans. on Ind, Appl.*, vol. 54, no. 4, pp. 3415 – 3425, Aug. 2018.
25. V. Vasic, S. N. Vukosavic, and E. Levi, “A stator resistance estimation scheme for speed sensorless rotor flux oriented induction motor drives,” *IEEE Trans. Energy Convers.*, vol. 18, no. 4, pp. 476–483, Dec. 2003.
26. M. S. Zaky, M. M. Khater, S. S. Shokralla, and H. A. Yasin, “Wide speed-range estimation with online parameter identification schemes of sensorless induction motor drives,” *IEEE Trans. Ind. Electron.*, vol. 56, no. 5, pp. 1699–1707, May 2009.
27. M. Hinkkanen and J. Luomi, “Modified integrator for voltage model flux estimation of induction motors,” *IEEE Trans. Ind. Electron.*, vol. 50, no. 4, pp. 818–820, Aug. 2003.
28. B. Karanayil, M. F. Rahman, and C. Grantham, “An implementation of a programmable cascaded low-pass filter for a rotor flux synthesizer for an induction motor drive,” *IEEE Trans. Power Electron.*, vol. 19, no. 2, pp. 257–263, Mar. 2004.

Affordable Energy for Civilization: A Global Programme to Provision Collective Clean Energy Admittance

Prof Chilukuri Bala Venkata Subbarayudu¹, Dr Katikala Premalatha², Dr Mohd Ilyas³

Department of Electrical and Electronics Engineering, Shadan Women's College of Engineering and Technology, Khairatabad, Hyderabad¹

Department of Electronics and Communication Engineering, Shadan Women's College of Engineering and Technology, Khairatabad, Hyderabad²

Department of Electronics and Communication Engineering, Shadan College of Engineering and Technology, Peerancharu, Hyderabad³

✉ cbvsubbarayudu@ieee.org; ✉ premalatha.katikala@gmail.com, ✉ ilyas.ece@gmail.com

ABSTRACT

Strong measures are important to achieve clean energy security by addressing the imminent problem of global energy demand in line with the UN Sustainable Expansion Goal – by the end of this decade. This determination calls for a duty to support novel ventures. Ensuring of widespread energy admission- besides better-quality life time superiority; as a priority need, has eluded strategy producers, and what's more, governments in the recent past. Moderateness of energy administration for each worldwide resident, spreading over numerous distinct districts and their neighbourhoods, requires a change of strategy and massive dissemination of advancements that offer “purpose of energy utilization” alternatives combined with new plans of action. Predetermination of social advancements and flexible administration methods are likewise essential for incorporation through systemic and mechanical improvements. The degree and size of determinative change range from huge scope framework frameworks to decentralized conveyed assets at network levels to the family units. We suggest a worldwide organization of “energy access advancement focus” devoted to giving a dynamic “augmentation administration” that supports the global energy system and ensures its flexibility.

Keywords : Affordable electricity; Universal energy access; Energy poverty; Life Quality; Social value creation; Clean technology innovation.

INTRODUCTION

The assessed speculation required around the world to accomplish universal energy admission remains in the range of \$0.5–\$1 trillion or a yearly venture of \$50 billion [1]–[3]. On behalf of one billion individuals, due to deformities of the monetary pyramid providing no entrance by any means, or exceptionally lacking efficacious administration, this converts into a venture duty of \$50 per individual yearly, until 2030. Performance of undertakings on this gauge can be correctly measured. Yet, the organizational framework must be completed with a vision providing limelight on the organization, plan of action and developments. Plans ranging from constructive to accessible are cultured by the best, reasonable and particular information accessible through various channels. They will help in the choice of quality that fulfils the most noteworthy guidelines of frankness and expertise. In this paper, we investigate the assorted trials towards widespread contact. Assuming the size of progress essential and the requirement on behalf of critical activity [4]–[6], we centre round the requirement on behalf of organization and heading of aggregate endeavours to develop an organization of “energy access advancement focuses” (EAICs). We depict the apparition, targets as also yields, sequential plan also gauge, significant capacities, and operative necessities used for these EAICs. Theoretically, the EAICs are like the territorial exploration and effort hubs of the Consultative Group for Inter-public Agricultural Research (CGIAR) and the undertaking advancement models of the World Bank's Climate Innovation Centre (CIC). Central to this exercise is the help for a planned approach at this point with an appropriated network zeroed in on research, limit fabricating, and supporting another age of business visionaries. The EAICs represent the requirement for and the estimation of “utilization roused essential examination” to quicken the advancement of livelihoods and admission arrangements scheduled on a worldwide scale, through boundary working towards development of the futuristic age of pioneers; and change specialists needed for and fast scale-up of fruitful pilots and neighbourhood business as the essential conveyance technique for inventive arrangements.

In the current global energy scenario, the individuals who are expected to contribute towards vitality at a maximum level, recompense the greatest per element of the energy management [4] dependent on petroleum product assets. This paper, on behalf of mankind reacts to the dire requirement aimed at enormous organization of fresh and dynamic arrangements that are adaptable, accessible easily, and dependent on a manageable level of low-Carbon fuel foundations. Furthermore, developments that can be portrayed as “advancement arrangements” will assume a significant job whenever planned as “fit-for-reason” answers for an assorted scope of neighbourhood and social settings. The mechanical developments when joined with new plans of action conveyed by another age of business people, little to-medium undertakings (SMEs), and neighbourhood change specialists can possibly yield greatest advantage to networks. The misuse of cooperative energies will stay a basic element for progress. In the event that we are to exploit the limit with regards to expansion that exists inside college and industry investigation labs, there is essential to fabricate additional stranded spans between nearby implementers of arrangements and worldwide information organizations. Energy destitution is a human advancement trap. Dependence on conventional fills, for example, kindling and lamp fuel, loots the liveliness deprived of their most noteworthy asset period. Dependence on fills, for example, lamp oil, requires the continuous acquisition of fuel that turns out to be essentially expensive over the long haul; while offering support. These powers additionally cause critical antagonistic well being impacts from respiro-conservative sickness. Indoor air contamination identified with indoor cookery utilizing these fills; kills roughly 4,000,000 people yearly, surpassing the cost of jungle fever and AIDS joined [7].



Fig 1. Energy admittance as a multiplier of UN SDGs

CHALLENGE

Importance of Energy Admittance

As portrayed in **Fig. 1**, energy admittance remains an incredible multiplier of for altogether intents and purposes the entirety. Energy administrations stand complicatedly connected towards the arrangement of sufficient well being and instructive administrations that rely upon a solid foundation. Conveyance of spotless water besides water system for horticulture, the ability to ship harvest to business sectors without waste, cooking through cleaner fuel sources, diminishing labour also pod nook on ladies aimed at basic family unit undertakings, and financial strengthening of people through work sparing gadgets all depend on reasonable energy administrations. All inclusive energy access is presently close enough yet requires fast dissemination of spotless liveliness alternatives.

Energy admittance stands considered through the International Energy Agency (IEA) by way of “a domestic consuming rock-hard also bear accomplished admission to together spotless cookery headquarters, also to electricity, which is adequate towards elegantly a mound of energy welfares at first, and subsequently an increasing level of control ended the extensive run towards attain at the regional standard” [2]. The “heap of energy administrations” contains a degree of negligible energy prerequisites fundamental on behalf of light and correspondence. Family units deprived of admittance to spotless cookery offices or the characterized insignificant degree of liveliness administrations continue to live in the hope of seeing light at the end of the tunnel.

Energy admittance remains one key path for the decrease of widespread worldwide energy imbalance. However it will require systemic advancements which lead to the improvement of logical and mechanical arrangements that can convey critical upgrades in execution. Admittance of energy turns into the driver of high-esteem impressions of global excellence.

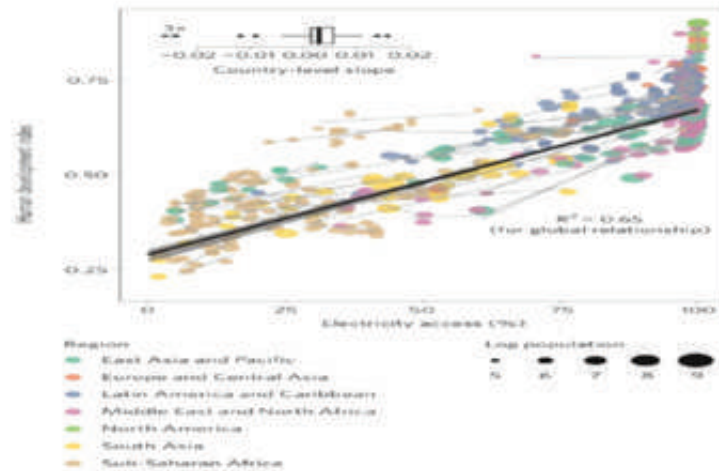


Fig. 2. Association amongst admittance to electricity and HDI for the decade 2000–2010[8].

Fig. 4 demonstrates the connections of per capita power furthermore, chose humanoid improvement markers. [8].In reality;evidence exists that there are together the financial and social advantages of mounting up energy admittance. In a progression of education that had undergone transformations over the long run and as more information opened up, a powerful connection between the power utilization per capita was established. An entire scope of measurements of advancement have been investigated (see Fig. 3) from proficiency [see Fig. 3(a)], to instructive achievement [Fig. 3(b)], to measurements of neediness.

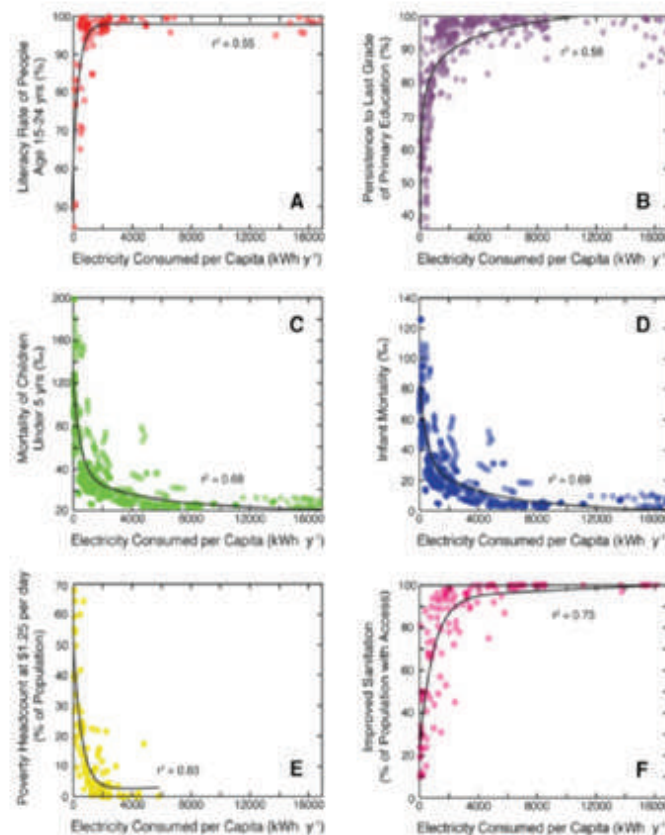


Fig. 3. Association between energy admittance and key metrics of expansion. Source:[8].

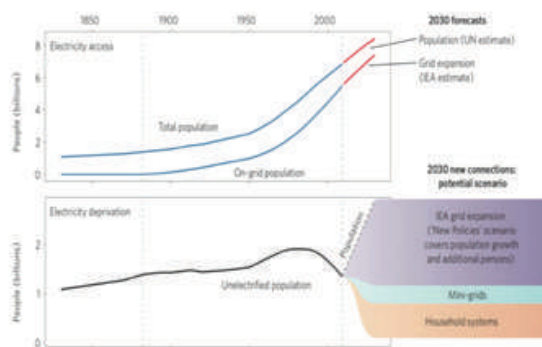


Fig. 4. Two centuries of historical trends. Source:[8]

POWERFUL SOLUTION ON: A MOVEMENT TO CREATE AN “ENERGY ACCESS EXTENSION SERVICE FOR THE PLANET”

The desperation and ground breaking monetary, social, as also ecological compensations of creation of energy admission, a top-level worldwide essential, suggests that we must zero in correspondingly on information development, social and conduct change. The requirement for arrangements that are financially as well as earth economical makes the objective of moderate all inclusive admittance to clean energy, steady with environmental change objectives. It is proposed to make energy destitution a commentary of history; and if we accept that if this issue gets the logical, specialized, money related, and social consideration it merits, energy neediness can be destroyed by 2030.

The novelty of our solution

Our answer assembles existing organizations and assets so as to address an unpredictable test. Current worldwide interests in meeting energy access objectives are insignificant, being regularly summed up as “two lights and a fan.” Our point is to grow long haul methodologies that will lead, after some time, to full admittance- to present day energy administrations for improved life quality and monetary independence.

Current methodologies are centred barely around conveying “pre-decided” innovation arrangements that emphasize on energy access; in seclusion to more extensive endeavours to empower financial development. Our methodology depends on both the acknowledgment of the size of the issue and the advantages

Requirements

The World Bank’s Access Investment Model gives intelligent base up evaluations of the expenses- of arriving at general access- in nations with enormous electricity access shortages. These nations reflect contrasts in populace and topography just as neighbourhood unit expenses, and they can be utilized to give a worldwide gauge of access venture needs [3]. The model, in light of the multi-tier system, permits clients to pick the level of access, which would be utilized to meet the general access target, and shows how drastically this influences the expenses of jolt.

To arrive at general access at Tier 5 (full 24×7 framework power), one would require ventures of \$500 billion more than ten years [1]. This is a significant level gauge that means a dedication at a degree of \$50 per individual every year. Ventures on this scale help in providing an anchor to a thought of the degree of financing, fitting to bring to realization of an operational idea of a worldwide augmentation administration connected to an organization of EAICs.

ENERGY ACCESS INNOVATION CENTERS

Our proposal for the foundation of a connected organization of EAICs as “worldwide augmentation administration” is like the CGIAR and the fresher endeavour advancement models of the World Bank’s CIC and the European Institute of Innovation and Technology’s Knowledge Innovation Communities (KICs). To build up an organization, for instance, each EAIC with a notional financial plan of \$5 million every year more than ten years would require a dedication in the request for \$50 million for each middle or \$250 million for five territorial EAICs.

A “College Movement” committed to the production of new information and arrangements explicit to the destruction of energy neediness is one facet of the solution. There is a developing need to fill the missing gaps gracefully and strengthen the chain that underpins information creation, improvement and sending of targeted arrangements; and expeditious initiation of restorative

activities; based on the outcomes from exercises in the past. We have seen the emergence of various universally powerful movements tending to worldwide difficulty, in the past. The food emergencies and starvations of the 1950s and 1960s prompted the scale-up—with an unobtrusive introductory speculation—of a worldwide food exploration and expansion exertion [12].

The EAIC model encapsulates energy benefits that essentially recreate the best exercises from the worldwide agri-social expansion administrations of the CGIAR exertion with the current energy and clean innovation endeavours that the CICs centre around, supporting. The current CIC network gives a significant operational organization today; that unites specialized, market, and social developments with forthcoming business people and local gatherings.

EAICs are places where change specialists—yearning entrepreneurs and pioneers in the energy access area—get everyday help to help them in creating arrangements that will serve the provincial market of their EAIC. The EAIC is analogous to a conventional hatchery, in which it gives mentorship, budgetary, specialized, and provincial statistical surveying guidance to support the change specialists that it has

Program Design

The key help elements of the EAIC's program plan and a couple of examples that give the inspiration to help a worldwide movement on the side of widespread energy access are discussed herewith. We feature the part of exploration, limit building, and business person transport. As a primary advancement, the most proper areas of EAICs—considering convincing necessities—would be three in Africa (South, East, and West Africa), one in Latin America, and one in Asia. When operational, the recharging commands of the EAICs and the foundation of the extra new EAICs- can be assessed, based on the experience and a fruitful evaluation, of the estimation of commitments to the progression of the all-inclusive energy access. Over the long run and expanding on effective results, our objective is to make (EAICs the central points for mixing research contributions into programs that enlist and backing promising business people. This exertion brings research straightforwardly to the requirements of energy administration objectives and identifies the entrepreneurs in direct contact inside accomplice foundations everywhere on the world. This group based methodology will empower both the examination and augmentation specialists to create ventures that are co-designed with accomplices for revolutionary enhancements in the moderateness of clean energy arrangements in immature business sectors.

Research

The essential goal is to support and quicken the “utilization propelled fundamental exploration” for energy access on a worldwide scale. To overcome any barrier between driving exploration labs and effect arranged associations that work in the field, the examination centre is to create and test solid and financially savvy procedures for arriving at the objective of giving moderate, fair, and clean admittance to energy supplies. Improving moderateness through mechanical advancement is especially significant in addressing the requirements of the most devastated markets. For new advancements to be satisfactory, they should be planned with a profound comprehension of their utilization.

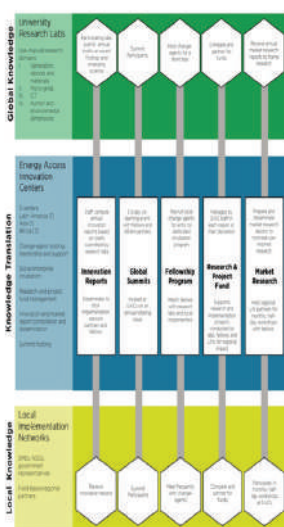


Fig.5.Transitions From global knowledge to knowledge translation and then to the use of local knowledge

CONCLUSION

We presume that the test to meet the twin objectives- of meeting decrease focuses for environmental change and arrangement of all inclusive energy access- moderate and open to an extremely huge extent of the worldwide populace- will require a huge speculation, generally assessed in the request for \$50 billion for each annum. To guarantee that the venture on such a scale stays compelling—considering the fast development of arising information—it requires an interesting accentuation on coordinating new arrangements with an inside and out comprehension of the neighbourhood setting. The quintessential test is to make continue capable upgrades to the personal satisfaction without undermining the reason for ventures.

We propose “A Global Movement to Support Universal Clean Energy Access” to be actualized through the foundation of five EAICs worldwide. For clean conveyed energy answers for becoming realities for those at the lower part of the pyramid, “Use-Inspired Basic Research” must motivate the advancement of the up and coming age of advances and plans of action for adoption at the nearby level. The essential objective is to convey information on the guarantee of reasonable admittance to energy benefits and the management capacity of off-lattice arrangements, where they are required most; and where they have the best potential for improving life quality.

REFERENCES

1. State of Electricity Access Report (SEAR), IBRD/WB, World Bank, Washington, DC, USA, 2017, p. 7.
2. Energy Outlook 2017-From Poverty to Prosperity, World Energy Outlook Special Report, OECD/IEA, 2017.
3. Sustainable Energy for All 2017 Progress Towards Sustainable Energy, IEA/Worldbank, Washington, DC, USA, 2017.
4. Electrifying Africa—Lights, Power, Action in Dept Follow- Upto APP Report—Power, People, Planet
5. Power for all—Electricity Access Challenge in India, State of Electricity Access Report (SEAR), World
6. IEA, Financing Energy Access—International Energy Agency. World Energy Outlook (WEO), 2011, Ch. 13, p. 469.
7. WHO. (2016). Factsheet, Household Air Pollution and Health.[Online]. Available: <http://www.who.int/mediacentre/factsheets/fs292/en/>
8. P. Alstone, D. Gershenson, and D. M. Kammen, “Decentralized energy systems for clean electricity access,” *Nature Climate Change*, vol. 5, pp. 305–314, Mar. 2015. doi: 10.1038/NCLIMATE2512.
9. C. E. Casillas, and D. M. Kammen, “The energy-poverty-climate nexus,” *Science*, vol. 330,
10. Towards a Sustainable Energy Future, Energy Access for Development, Cambridge Univ. Press, Cambridge, U.K., 2012, ch. 19.
11. M. Bazilian et al., “Accelerating the global transformation to 21st century power systems,” *Electr. J.*, vol. 26, no. 6, pp. 39–51, 2013. doi: 10.1016/j.tej.2013.06.005.
12. M. R. Dove and D. Kammen, *Science, Society and the Environment: Applying Anthropology and Physics to Sustainability*. Boca Raton, FL USA: Taylor and Francis, 2015.
13. D. Stokes, *Pasteur’s Quadrant: Basic Science and Technological Innovation*. Brookings Inst. Press, 2011.



Solution of Single Objective and Multi-Objective Optimal Power Flow Problem using Chicken Swarm Optimization

Saket Gupta¹, Narendra Kumar¹, Laxmi Srivastava²

Electrical Engineering Department, Delhi Technological University, Delhi¹

Madhav Institute of Technology and Science²

✉ sguptamits@gmail.com; ✉ dnk_1963@yahoo.com

ABSTRACT

This work presents application of recently developed algorithm namely Chicken Swarm Optimization (CSO) algorithm for solving constraint optimal power flow (OPF) problem. CSO is a new algorithm for optimization inspired by nature. The hierarchy of the swarm and the behaviors of the swarm of chicken are imitated to address the global optimization. The Algerian-59 bus system was used for the solution of the OPF problem to check the efficiency of the proposed CSO algorithm. The comparison between numerical outcome obtained by CSO algorithm and the results produced by other Swarm Intelligence (SI) and Evolutionary Computing (EC) techniques as reported in the recent literature has been carried out. Based on comparative analysis, the results obtained by the proposed algorithm provide admirably better and feasible solution.

Keywords : Chicken swarm optimization (CSO); Evolutionary computing; Swarm intelligence; Multi-objective optimal power Flow.

NOMENCLATURE

x	Dependent variable
u	Control variable
$Z(x, u)$	Objective function
$g(x, u)$	Equality constraint
$h(x, u)$	Inequality constraint
P_{gi} and Q_{gi}	Active and reactive power generations
N_{bus}	Number of buses
N_{LB}	is the number of load buses
N_{tl}	is the number of transmission lines
N_{GN}	Numbers of generators, and
N_C	Numbers of VAR compensation units
N_{TR}	Numbers of regulating transformers
P_{di} and Q_{di}	Active and reactive load demand
P_{gi} and Q_{gi}	Active and reactive power generations
P_{Loss} and Q_{Loss}	Real and reactive power loss
V_{gk}^{max} and V_{gk}^{min}	Maximum and minimum bus voltage limit of the k^{th} generator bus
Q_{gk}^{max} and Q_{gk}^{min}	Maximum and minimum limit of reactive power output of k^{th} generator bus
P_{gk}^{max} and P_{gk}^{min}	Maximum and minimum active power limit of the k^{th} generating units



T_k^{Min} and T_k^{Max}	Minimum and maximum tap setting of k^{th} transformer
V_{Lk}^{Min} and V_{Lk}^{Max}	Minimum and maximum voltage limit of k^{th} load bus
S_{lk}^{Max}	Maximum MVA flow in k^{th} transmission line
A_i , B_i , and C_i	Fuel cost coefficients of the i^{th} Generator units
PD	Real load demand
NB	Total number of buses
C_1 , C_2 , C_3 and C_4	Penalty factors corresponding to limit violations
$\text{Randn}(0, \sigma^2)$	Gaussian distribution with a mean of 0 and a standard deviation of σ^2
ϵ	Very small constant used to avoid the division by zero error
k	Roosters index which is randomly selected from the roosters group
f_i	Fitness value of the rooster
Rand	Uniformly distributed random number between 0 and 1
r_1	Rooster index
r_2	Chicken index (rooster or hen)
X_{mj}^i	Position of the mother of the i^{th} chick's

INTRODUCTION

In the early 1960's Carpentier [1] presented the optimal power flow problem for the first time in history as an extension of economic load dispatch problem. Later the problem was solved by Dommel and Tinney [2] and defined as OPF. Modern power systems operate under high stress conditions because of continuous growth in load demand and transmission expansion and generation capability is not capable of meeting such load requirement. The utilities face a large number of problems such as increase in operating costs, power losses, poor voltage profile, voltage instability problems, transmission line overloading. In order to deal with these problems, the OPF methodology is required by power engineer / utility companies as the key tool for network planning, operation and management [3].

Main motive of the OPF problem, to adjust controllable variables setting so as to optimize the chosen target function while ensuring that all the physical and functional limits, the power flow equation etc are taken into account. In general, OPF problem is a complex constraint optimization problem which has a large number of equality and inequality constraints [4].

Many classical optimization techniques (COT's) [5] such as Linear Programming, Non-Linear Programming, Interior Point Method etc. were employed during the early decades to resolve OPF problem, while some COT's have outstanding convergence properties, many of them are often used in the industry and have certain deficiencies. Their disadvantage includes the following: they are unable to guarantee global optimality, i.e. converge to local optimum, they can't manage binary or integer variables and they are facing the problem to deal with system having non-convex, non-differentiable, multi-modal optimization function and constraint. Also, conventional optimization method required initial point so the COT's are not appropriate for solving OPF problem. Evolutionary Computing technique is an alternative to COT's to overcome this drawback and manage these difficulties [6-7]. These techniques were successfully applied to problem of optimization that are multi-modal, non-convex, non-linear optimization [8].

Problem Formulation

The objective function along with constraint of OPF problem selected in this paper is mathematically formulated as follows:

$$\text{Optimize } Z(x, u). \quad (1)$$

Subject to the constraints:
$$\begin{cases} g(x, u) = 0 \\ h(x, u) \leq 0 \end{cases} \quad (2)$$

Here, x can be expressed as



$$x^T = [P_{g1}, V_1, \dots, V_{NLB}, Q_{g1}, \dots, Q_{gNGN}, S_1, \dots, S_{Ntl}] \quad (3)$$

while, u can be expressed as

$$u^T = [P_{g2}, \dots, P_{gNGN}, V_{g1}, \dots, V_{gNGN}, Q_{C1}, \dots, Q_{CNC}, T_1, \dots, T_{NTR}] \quad (4)$$

Constraints

The equality constraints are combination of active and reactive non-linear power flow equations. In Eq. (2), $g(x, u)$ is a set of equality constraint and is describe as:

$$0 = P_{gi} - P_{di} - P_{Loss} \quad (5)$$

$$0 = Q_{gi} - Q_{di} - Q_{Loss} \quad (6)$$

The inequality constraints $h(x, u)$ are represent system operating limit of various power system equipment, which are describe as:

$$V_{gk}^{min} \leq V_{gk} \leq V_{gk}^{max} \quad k = 1, \dots, NGN \quad (7)$$

$$P_{gk}^{min} \leq P_{gk} \leq P_{gk}^{max} \quad k = 1, \dots, NGN \quad (8)$$

$$Q_{gk}^{min} \leq Q_{gk} \leq Q_{gk}^{max} \quad k = 1, \dots, NGN \quad (9)$$

$$T_k^{min} \leq T_k \leq T_k^{max} \quad k = 1, \dots, NTR \quad (10)$$

$$Q_{Ck}^{min} \leq Q_{Ck} \leq Q_{Ck}^{max} \quad k = 1, \dots, NGN \quad (11)$$

$$V_{Lk}^{min} \leq V_{Lk} \leq V_{Lk}^{max} \quad k = 1, \dots, NLB \quad (12)$$

$$S_{lk} \leq S_{lk}^{max} \quad k = 1, \dots, ntl \quad (13)$$

Objective Function

Fuel cost minimization (FCM)

$$Z_{FCM} = \sum_{i=1}^{NGN} A_i + B_i P_{gi} + C_i P_{gi}^2 \quad (\$/h) \quad (14)$$

Voltage profile improvement (VPI)

$$Z_{VPI} = \sum_{i \in NLB} |V_i - 1| \quad (15)$$

Voltage Stability Enhancement (VSE)

$$Z_{VSE} = \max [L_j] \quad j = 1, 2, \dots, NLB \quad (16)$$

Real power losses minimization (RPLM)

$$P_{Loss} = \sum_{i=1}^{NB} P_i = \sum_{i=1}^{NB} P_{Gi} - \sum_{i=1}^{NB} P_{Di} \quad (17)$$

Incorporation of Constraints

The inequalities are incorporate into the objective function in order to find a feasible solution and the extended objective function can be defined as:

$$Z_{aug} = Z + C_1 \cdot h(x_1) + C_2 \sum_{i=1}^{NGN} h(Q_{Gi}) + C_3 \sum_{i=1}^{NLB} h(V_{Li}) + C_4 \sum_{i=1}^{Ntl} h(S_{li}) \quad (18)$$

Chicken Swarm Optimization (CSO)

CSO is a recently developed optimization algorithm inspired by nature. In order to address global optimization, it imitates hierarchy and the behavior of the chicken swarm. There are three sections of the population, namely the roosters, the hens and

the chicks. These three sections learn, compete and show the sociality of swarm intelligence in their entirety. CSO essentially utilizes the following four guidelines to idealize chickens swarm behaviour [7-8]:

1. There are several groups of chicken swarm, each with the dominant rooster, a few hens and chicks.
2. The identity of each chicken (chick, hen and rooster) depends on the fitness of the chicken itself in every group of chicken swarm. The chickens are recognized as rooster with the highest fitness values. Each one is in a group ahead of roosters. The chickens would be recognized as chicks with worse fitness values. The rest are the hens.
3. Following every number (G) of steps, hierarchical, dominance and relationship between the child- mother must be completely change.
4. The chickens are looking for food to follow their rooster-mate. We presume that chick randomly steal the good food that others already have. The chicks are looking for food around their mothers. In food competition rooster has benefit.

We differentiate the following numbers in a chicken's swarm of N individuals: MN, RN, CN and HN, which represent the number of mother hens, of roosters, of chicks, and of hens, respectively. The location of each chicken within D dimensional space is depicted by $x_{i,j}$ ($i \in [1, \dots, N]$, $j \in [1, \dots, D]$) in each place. CSO contains three kinds of chicken. Every kind has its own equation of movement:

Rooster Movement

Having best levels of fitness value, the rooster can find food in a wider range of places than those with poorer fitness level. They are described their movement in Eqs. (19) and (20) respectively.

$$x_{i,j}^{t+1} = x_{i,j}^t * (1 + \text{Randn}(0, \sigma^2)) \quad (19)$$

$$\sigma^2 = \begin{cases} 1 & \text{if } f_i \leq f_k \\ \exp\left(\frac{(f_k - f_i)}{|f_i| + \epsilon}\right) & \text{otherwise} \end{cases} \quad k \in [1, N], k \neq i \quad (20)$$

$$x_{i,j}^{t+1} = x_{i,j}^t + S_1 * \text{Randn} * (x_{r1,j}^t - x_{i,j}^t) + S_2 * \text{Randn} * (x_{r2,j}^t - x_{i,j}^t) \quad (21)$$

$$S_1 = \exp\left(\frac{(f_i - f_{r1})}{|f_i| + \epsilon}\right) \quad (22)$$

$$S_2 = \exp(f_{r2} - f_i) \quad (23)$$

r_2 is randomly selected from the swarm ($r_1 \neq r_2$).

Chick Movement

Chicks are exploring their mother to find food. Chick movement has been formulated in Eq. (24)

$$x_{i,j}^{t+1} = x_{i,j}^t + \text{FL} * (x_{m,j}^t - x_{i,j}^t) \quad (24)$$

To take into consideration difference between various chicks, FL is randomly selected in the range [0, 2].

The solution algorithm for solving OPF using CSO algorithm can be summarized in following steps:

Step 1: Input Data: population size 'P', maximum iteration counts It_{\max} and control variables 'D'.

Step 2: Initialize the load flow data and system parameters.

Set count $I = 0$, generate population of N individuals randomly with uniformly distributed amongst $[X_{\min}, X_{\max}]$. For each individual, run NRLF program (Newton Raphsonload flow) and evaluate the fitness of objective function defined in Eq. (18).

Step 3: Arrange individuals according to the value of their fitness value.

Step 4: Use Equations (19), (21) and (24) to update the position of roosters, hens, and chicks. Then, Evaluate fitness of individuals.

Step 5: If new solution found is superior then previous solution accept the new solution otherwise keep previous solution.

Step 6: If $I < I_{max}$, increase iteration by 1 i.e. $I = I + 1$ and go to step 3. Else go to step 7.

Step 7: Stop and Display fitness value of best results.

OPF RESULTS AND DISCUSSION

In this work, an efficiency assessment of the proposed CSO algorithm will be carried out in Algerian 59 bus system. The simulation outcomes after optimization are represented in this section. The numerical outcomes of the proposed CSO algorithm are compared to the outcomes of the recent literature by other EC/SI techniques

The control variables limit, line data, bus data along with their initial settings are taken from [9]. For this system, 30 runs were taken using CSO algorithm to solve the different objective functions of OPF problem and best results are given here.

Case 1 # (FCM): The minimum fuel cost acquired from CSO algorithm after optimization is 1688.7848 \$/h. The numerical results obtained after optimization were compared with other reported results in **Table 1**. Appendix-A provides the decision variables setting of present case. Table 1 it is clear seen that results produced by the CSO algorithm are excellent as compared to existing algorithms in literature. The convergence characteristics obtained by the proposed method is depicted in **Fig. 1**.

Table 1: Comparison of OPF results obtained by CSO and other algorithm for Case 1 of Algerian 59 bus system

Algorithm	FC (\$/h)
CSO	1688.7848
LCA [9]	1689.0768
ESDE [10]	1692.0624
ESDE-MC [10]	1688.5586
ESDE-EC [10]	1690.3171
SKH [11]	1688.5742
BHBO [12]	1710.0859

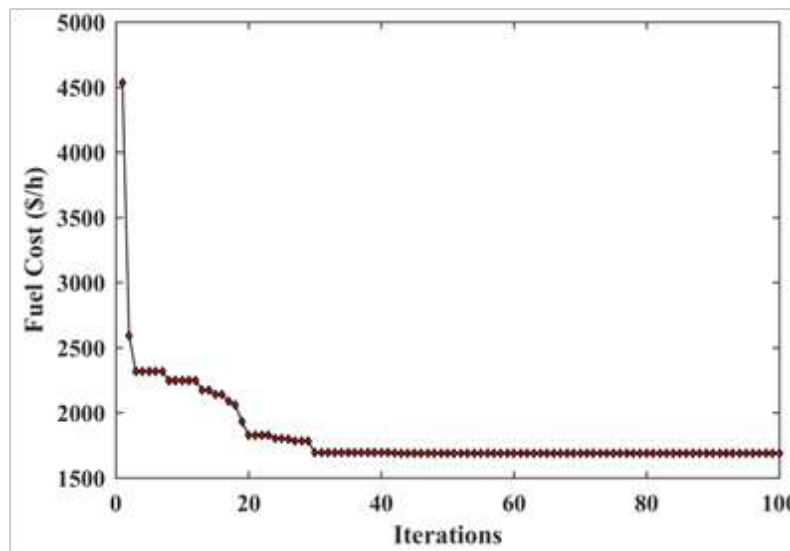
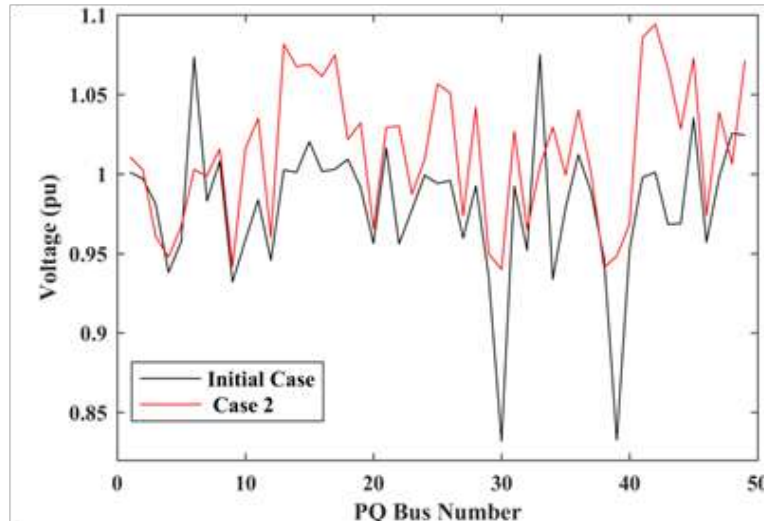


Fig. 1. Convergence of CSO algorithm for Case 1

Case 2 # (FCM +VPI): The minimum voltage deviation as 1.8837pu, and total fuel cost as 1719.9957\$/h were found by proposed CSO algorithm. The voltage profile is significantly improved in case 2. As earlier in case 1 the total voltage deviation (TVD) was 1.9981pu which is reduced to 1.8837pu. The control variables settings are given in Appendix-A. The optimized OPF results are compared with other EC based algorithm in **Table 2**, while, in **Fig. 2**, the voltage profile is shown in case 2 and initial case.

Table 2. Comparison of OPF results obtained by CSO and other algorithm for Case 2 of Algerian 59 bus system

Algorithm	FC (\$/h)	TVD
CSO	1719.9957	1.8837
LCA [9]	1755.5775	1.8404


Fig. 2. Convergence of CSO algorithm for Case 2

Case 3 # (FCM+VSE): In this case (Case 3), the VSE is considered in addition to fuel cost for Algerian 59 bus system. The suggested CSO algorithm offered minimum value of the L-index 0.2163. **Table 3** provides the comparison of outcomes for L-index with other EC/SI based methods. The results produced by the CSO algorithm are excellent as compared to existing algorithms in literature. Appendix-A shows the control variables setting of present case.

Table 3. Comparison of OPF results obtained by CSO and other algorithm for Case 3 of Algerian 59 bus system

Algorithm	FC (\$/h)	L-Index
CSO	1688.7848	0.2163
LCA [9]	1693.5788	0.2164
ESDE-EC [10]	1692.2421	0.2163
ESDE-MC [10]	1691.4891	0.2163
ESDE [10]	1692.5818	0.2164

Case 4 # (FCM + RPLM): The optimized results found after optimization is compared with other reported result in **Table 4**. In present case CSO algorithm gives 11.8827 MW after optimization. The control variable setting is given in Appendix-A. The convergence characteristic is represented in **Fig. 3**.

Table 4. Comparison of OPF results obtained by CSO and other algorithm for Case 4 of Algerian 59 bus system

Algorithm	Power Loss(MW)
CSO	11.8827
SKH [11]	11.9833
KH [11]	12.2491

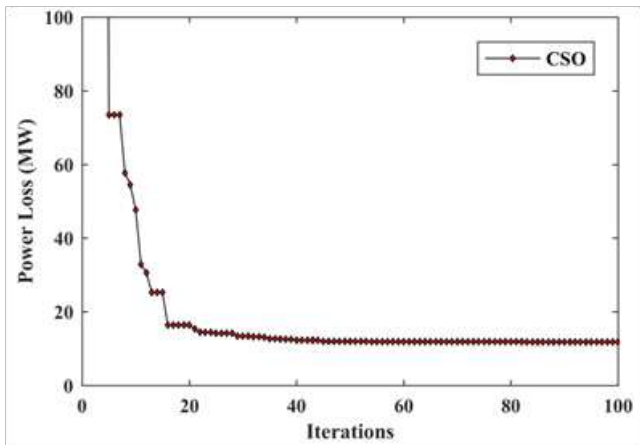


Fig. 3. Convergence of CSO algorithm for Case 4

CONCLUSIONS

In this work, the OPF problem was solved by recently proposed Chicken swarm algorithm. Different objectives functions were considered for solving OPF such as: Fuel cost minimization, total voltage deviation, voltage stability enhancement and real power loss minimization. In order to evaluate its efficiency and superiority, the proposed CSO algorithm it has been applied to Algerian 59-bus system. The numerical results comparison has been carried out between the outcome acquired from the suggested CSO algorithm and other well-known optimization techniques lately published in recent literature. The comparison of results clearly demonstrate that the proposed CSO algorithm is highly efficient and robust over other popular algorithm which are reported in recent literature.

REFERENCES

1. J. Carpentier. Contribution a l'etude du dispatching économique", Bulletin de la Société Française des Electriciens, Vol. 3, Ser. 8, August 1962.
2. H. W. Dommel and W. F. Tinney. Optimal Power Flow Solutions. IEEE Transactions on Power Apparatus and Systems, vol. PAS-87, no. 10, pp. 1866-1876, Oct. 1968.
3. Gupta S., Kumar N., Srivastava L. Bat Search Algorithm for Solving Multi-Objective Optimal Power Flow Problem. Applications of Computing, Automation and Wireless Systems in Electrical Engineering. Lecture Notes in Electrical Engineering, vol 553. Springer, Singapore, 2019.
4. Biswas, P. P., Suganthan, P. N., Mallipeddi, R., & Amaratunga, G. A. J. Optimal power flow solutions using differential evolution algorithm integrated with effective constraint handling techniques. Engineering Applications of Artificial Intelligence, Vol. 68, pp. 81-100, 2018.
5. J. A. Momoh, R. Adapa and M. E. El-Hawary. A review of selected optimal power flow literature to 1993. I. Nonlinear and quadratic programming approaches. IEEE Transactions on Power Systems, vol. 14, no. 1, pp. 96-104, Feb. 1999.
6. Al Rashidi, M. R., & El-Hawary, M. E. Applications of computational intelligence techniques for solving the revised optimal power flow problem. Electric Power Systems Research, Vol. 79, No. 4, pp. 694-702, April 2009.
7. Meng X., Liu Y., Gao X., Zhang H. A New Bio-inspired Algorithm: Chicken Swarm Optimization. In: Tan Y., Shi Y., Coello C.A.C. (eds) Advances in Swarm Intelligence. ICSI 2014. Lecture Notes in Computer Science, vol. 8794. Springer, Cham, 2014.
8. A. Aziz, K. Singh, W. Osamy and A. M. Khedr. Optimising compressive sensing matrix using Chicken Swarm Optimisation algorithm. IET Wireless Sensor Systems, vol. 9, no. 5, pp. 306-312, 2019.
9. Boucekara, H. R. E. H., Abido, M. A., Chaib, A. E., & Mehasni, R. Optimal power flow using the league championship algorithm: A case study of the Algerian power system. Energy Conversion and Management, Vol. 87, pp. 58-70, 2014.



10. Pulluri, H., Naresh, R., & Sharma, V. An enhanced self-adaptive differential evolution based solution methodology for multi-objective optimal power flow. *Applied Soft Computing Journal*; Vol. 54, pp.229–245, 2017.
11. Pulluri, H., Naresh, R. & Sharma. A solution network based on stud krill herd algorithm for optimal power flow problems. *Soft Comput*; Vol. 22, pp. 159-176, 2018.
12. H.R.E.H. Boucekara. Optimal power flow using black-hole-based optimization approach. *Appl. Soft. Comput.*, Vol. 24, pp. 879–888, 2014.

Appendix-A

S. No.	Control variable	Initial Case	Case-1	Case-2	Case-3	Case-4
Generator active power output						
1	PG2	0.7	0.2286	0.2042	0.2286	0.22954
2	PG3	0.7	1.00765	1.0215	1.00765	1.00266
3	PG4	1.15	1.08989	1.2285	1.08989	1.11246
4	PG13	0	0	0	0	0
5	PG27	0.4	0.25448	0.3284	0.25448	0.25784
6	PG37	0.3	0.50756	0.49	0.50756	0.50539
7	PG41	1.1	0.96848	0.72	0.96848	0.96937
8	PG42	0.7	1.42318	1.4761	1.42318	1.41109
9	PG53	2	1.06514	1.1569	1.06514	1.03472
Generator voltage						
10	VG1	1.06	1.1	1.0995	1.1	1.1
11	VG2	1.04	1.1	1.075	1.1	1.08152
12	VG3	1.05	1.1	1.0994	1.1	1.09979
13	VG4	1.0283	1.09796	1.0429	1.09796	1.0905
14	VG13	1	1.09894	0.9794	1.09894	1.09673
15	VG27	1.0266	1.09761	1.0397	1.09761	1.09058
16	VG37	1.0273	1.1	1.0281	1.1	1.09961
17	VG41	1.0966	1.1	1.0108	1.1	1.1
18	VG42	1.034	1.1	1.1	1.1	1.1
19	VG53	1	1.1	1.1	1.1	1.1
Fuel Cost (\$/h)		1943.70103	1688.7848	1719.9957	1688.7848	1922.1785
Total Voltage Deviation(pu)		1.5757	2.8314	1.8837	2.8314	2.9978
L-Index		0.2767	0.2165	0.2189	0.2163	0.2167
Real Power Loss (MW)		29.1409	27.5683	27.6289	27.5683	11.8827
P_{GI}		8.2409	57.1703	49.1706	57.1703	21.3179



An Enhanced Power Conditioning Unit Enabling Reduction in DC Link Voltage Fluctuation for a Grid Connected Photovoltaic System during FRT

Nishij G Kulkarni¹, Vasudeo B Virulkar²

Department of Electrical Engineering, M.B.E. Society's, College of Engineering, Ambajogai, Maharashtra¹

Department of Electrical Engineering, Government College of Engineering, Amravati, Maharashtra²

✉ nishij1@yahoo.co.in; ✉ vbvirulkar@yahoo.com

ABSTRACT

This paper presents the control strategy for reducing the dc link voltage fluctuation of power conditioning unit (PCU) of a grid connected photovoltaic (PV) system during fault ride through (FRT) period. This is achieved by incorporating the reactive power and real power corrections to satisfy power quality prerequisite of minimum variation in dc link voltage without outpacing current limits of PCU. Power conditioning system for integrating the solar PV system to grid comprises of high gain boost converter (HIBC) as maximum power point tracker (MPPT) and three phase inverter. During FRT period, dc link voltage increases and when it exuberances limit of presetting value, controller changes MPPT mode to a voltage control mode. Voltage command is given to reduce dc link voltage. During FRT period, dc link voltage increases speedily at start of voltage drop and afterwards comes back to normal quicker than supplying reactive current only. A Matlab / simulation had carried out to check efficacy of a suggested strategy.

Keywords : Fault ride through; Power conditioning unit; Fluctuation; Voltage sag; Minimum reactive current; Reactive power.

INTRODUCTION

More endeavours have been made recently on integration of PV networks or systems into grid, to take care of basic demand of a clean and reliable power generation. Generation of electric power from solar energy resources is one of the most efficient, environment friendly and cost effective techniques [1]-[3]. Integration of electricity generated from PV energy into conventional power network has necessitated power network administrators to modify grid codes for ensuring reliable and quality power supply to the customers. FRT ability of PV network ensures controller of PCU to stay associated with grid during the anomalous operating condition and provide voltage support during and after unusual operating condition of grid. FRT ability is characterized as PV network should remain associated with grid at the time of failure of grid and can inject reactive power to support grid during fault [4].

It is required from PV network to supply a reactive current to improve stability inconformity with grid code for PV network, during fault. For FRT requirement, **Fig. 1** displays E.ON Netz GmbH code (E. ON code) voltage profile as suggested by Germany [5]. Furthermore, for grid recovery, grid connected PV system is reached that transfers reactive power in extent with reactive current interjected to grid as shown in **Fig. 2**. For E.ON as appeared in **Fig. 1**. PCU should remain associated with grid when voltage falls to 0 V for 0.15 seconds and inject a small amount of reactive current into grid. **Fig. 2** demonstrates desired rate of reactive current during FRT.

As specified, line voltage falls suddenly during FRT and then part of real power developed from PV panel transferred to grid. Exclusively, for a three phase grounded fault, no real power can be transmitted then dc link voltage raised rapidly. Earlier studies proposed some remedies to accord with FRT position [6]-[8]. Symmetric component system was used to confront with FRT issues. But this system prospects high current stress on irregular and diminished grid voltage [9]. Real and reactive current components analogous to positive and negative sequence components were taken into consideration during FRT and control way could reduce unbalanced grid voltages without outpacing maximum current limit of PCU [10].

Three phase line voltage indicates unbalanced conditions in amplitudes and phase angles both during FRT. To handle unbalanced

conditions, positive and negative synchronous frame method is trendy method. Normally positive, negative and zero sequence components can be obtained here by using above method. Three phase three wire system have only first two terms.

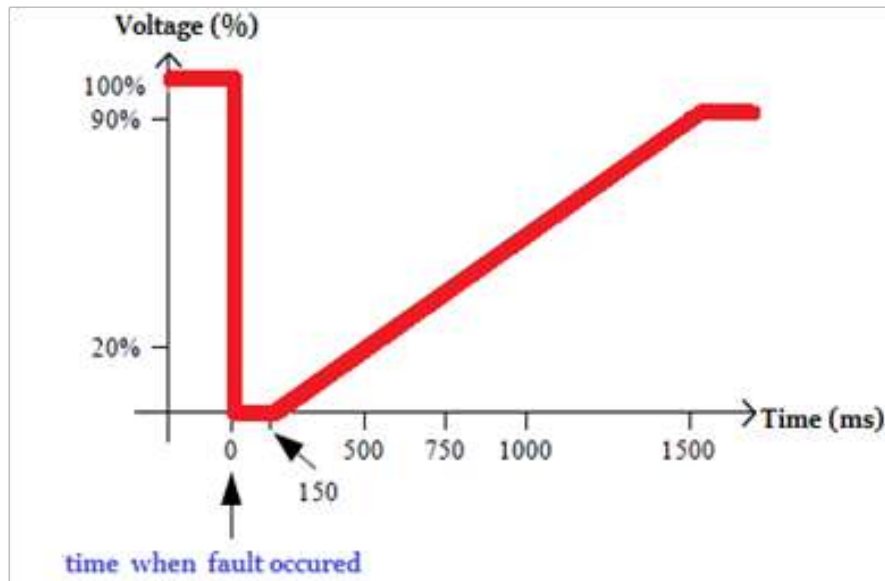


Fig. 1. E.ON code voltage profile for FRT requirement

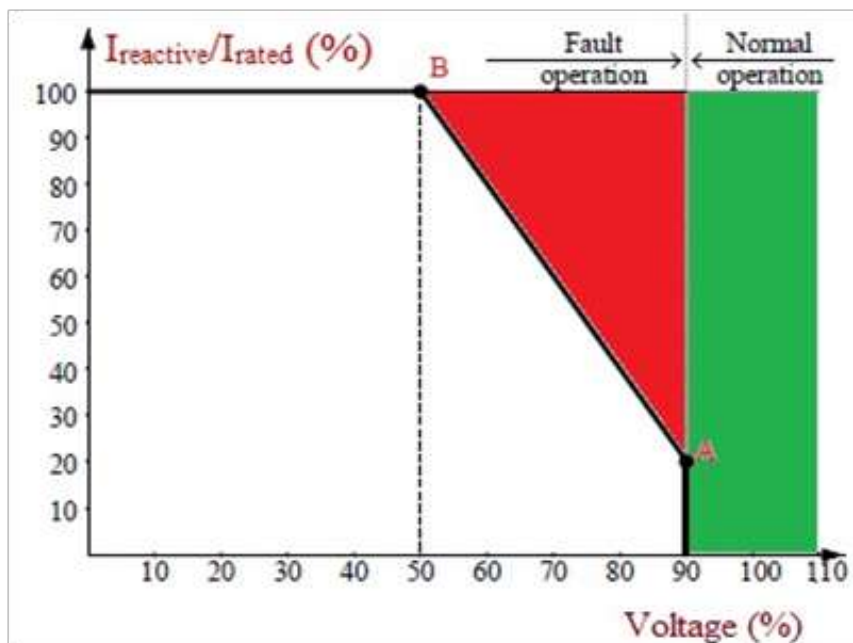


Fig. 2. Desired rate of reactive current during FRT

Two stage power structure comprises of dc-dc HGBC and a PCU as shown in **Fig. 3**. Here, PCU connected to a three phase three wire system, hence line voltages contains only positive and negative components, that is used to calculate needed current commands [11][12].

The control strategy suggested here for reducing dc link voltage fluctuation during FRT, which maintains minimal desired reactive current and when there is continuation of a current capacity; suggested method delivers active power to grid as much as desirable, definitely without exuberance of PCU current. Therefore, dc link voltage increases speedily to normal quicker than supplying reactive current only.

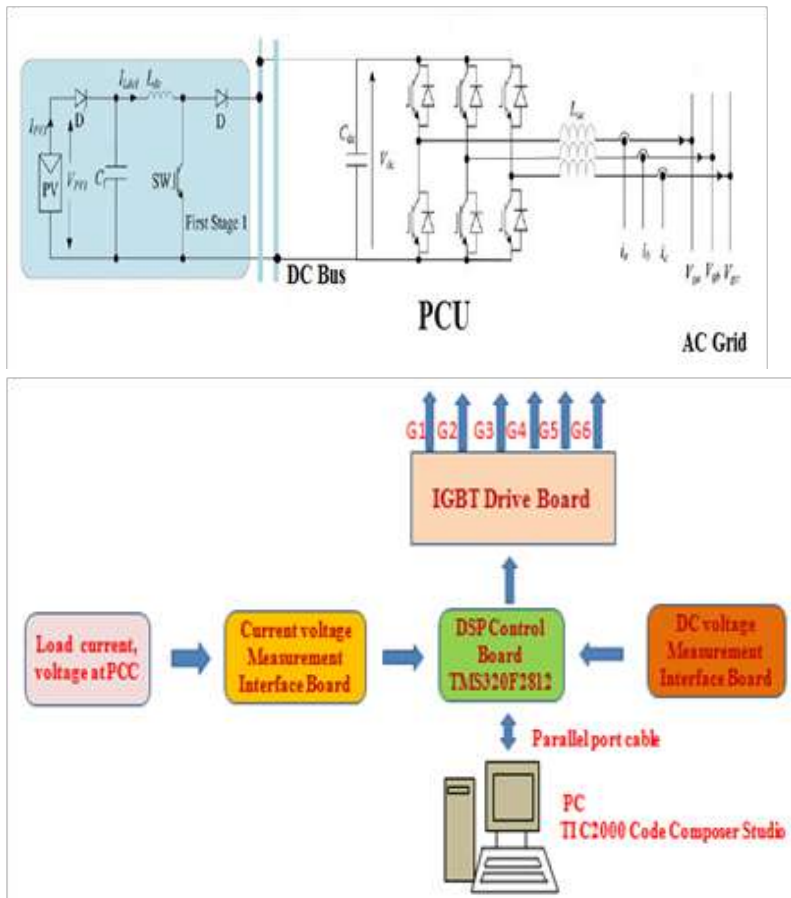


Fig. 3. Power conditioning system comprising PCU

To check efficacy of a suggested strategy, a three phase grounding fault scenario is explored by Matlab/simulation.

The proposed control strategy with power stages is explained in section II and III. Simulation results of three phase grounding fault case is displayed in section IV and paper concluded in section V.

GRID TIED PCU

Power stage consists of a HGBC as MPPT and a three phase PCU, as shown in **Fig. 3**. MPPT operation is performed in front stage or appropriate real and reactive powers are transferred in front stage as per grid regulation and grid interfacing is done via three phase low pass filter in second stage. A power conditioning system comprises of PCU is indicated in **Fig. 3**. DC link voltage is controlled to recover maximum value of power from supply source with outside voltage regulator. Controller suggests real power generated reference which is interjected to grid.

Even, components exploited in HGBC like condensers, diodes and switches are double in comparison to traditional BC, hence this topography has two main merits such as required voltage rating of main switches as low and low ripple in inductor current [13][14]. Furthermore, three terminal output is a desirable structure to PCU, which provides similar advantages of HGBC and is relevant to high power applications [15][16].

During normal working condition, MPPT and a power management blocks accomplished to convey real and reactive powers to grid. Grid line voltage is observed for system controller need. The variation in dc link voltage is monitored and then a criterion is set to reduce fluctuation in dc link voltage of PCU.

PROPOSED FRT CONTROL STRATEGY

Fig. 4 shows flowchart of proposed FRT control strategy and **Fig. 5** shows control block diagram of proposed FRT inverter. **Figs. 5 (a) and (b)** shows that controller has two segments. Initial segment executes MPPT by controlling duty ratio of switch

in HGBC and supplies real power command to next segment. During FRT period, dc link voltage increases and when it exuberances limit of presetting value, controller changes the mode from MPPT to voltage control as indicated in **Fig. 5 (a)**. Voltage command (V_{DC}^*) given for reducing dc link voltage. DC link voltage before FRT is nice contestant for voltage command which furnishes less MPPT transient period when voltage of grid turns to normal.

Fig. 5(b) indicates another segment of controller, which supplies real power to grid, confers to power command of MPPT in regular condition. When voltage sag is observed, power management shifts to one of other two blocks for mitigation of sag. Positive and negative synchronous references are used here [4] and value of d-axis positive sequence voltage component e_{dp}^e is used for FRT occurrence. The current commands are as follows, if e_{dp}^e reverts to 90% of V_r

$$\begin{bmatrix} i_{dp}^* \\ i_{qp}^* \end{bmatrix} = \frac{2P_{3\phi}^*}{3(e_{dp}^{e2} + e_{qp}^{e2})} \begin{bmatrix} e_{dp}^e \\ e_{qp}^e \end{bmatrix} + \frac{2Q_{3\phi}^*}{3(e_{dp}^{e2} + e_{qp}^{e2})} \begin{bmatrix} e_{qp}^e \\ -e_{dp}^e \end{bmatrix} \quad (1)$$

Where V_r is normal grid voltage. $P_{3\phi}^*$ and $Q_{3\phi}^*$ are real and reactive power commands rendered by MPPT controller. i_{dp}^* and i_{qp}^* are d and q axis positive sequence current component commands respectively.

The current commands, if $e_{dp}^e < 0.5 V_r$ are:

$$\begin{bmatrix} i_{qp}^* \\ i_{dp}^* \end{bmatrix} = \begin{bmatrix} I_r \\ 0 \end{bmatrix} \quad (2)$$

Where I_r is rated output current of PCU. The rated value of only reactive current is injected to grid, in this mode.

When $0.5V_r < e_{dp}^e < 0.9V_r$, desired reactive current is lower than I_r , thus PCU supplies some of active current so as total current not outpacing rated current. The minimum prerequisite for reactive current for this position is:

$$i_{dp}^* = 2I_r \left(1 - \frac{e_{dp}^e}{V_r}\right) \quad (3)$$

For not outpacing rated current, residual current capacity must be finding first. If residual current is more than peak power current of photovoltaic panel, then MPPT mode is continued. Moreover, only residual segment is designated to active current command, which is as follows:

$$i_{dp}^* = \begin{cases} I_{mp} & , I_{mp} < \sqrt{(I_r)^2 - (i_{qp}^*)^2} \\ \sqrt{(I_r)^2 - (i_{qp}^*)^2} & , I_{mp} > \sqrt{(I_r)^2 - (i_{qp}^*)^2} \end{cases} \quad (4)$$

Where I_{mp} is current at maximum power.

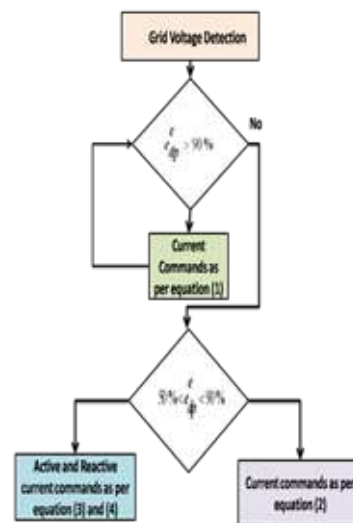


Fig. 4. Flowchart of proposed FRT control strategy

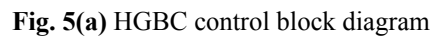


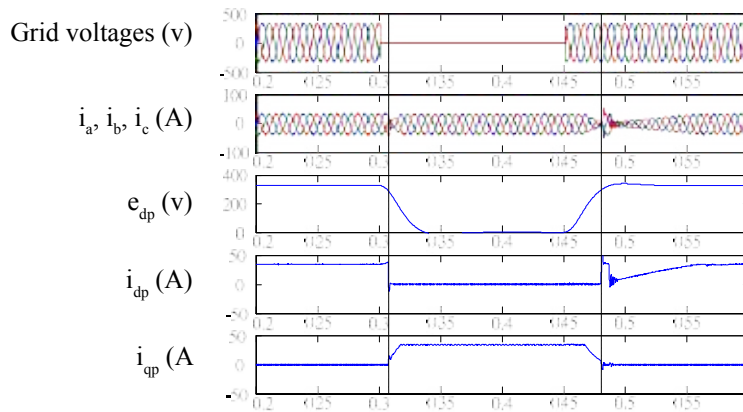
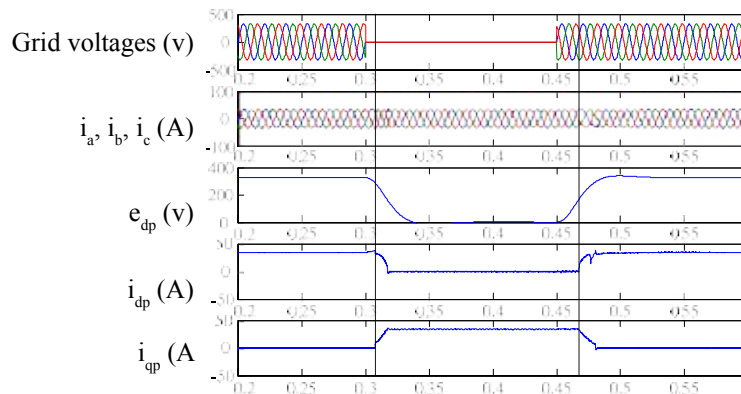
Table 1. Parameters used for system

Quantity	Symbol	Value
Grid voltage	V_g	440 V
Rated Current	I_{Rated}	12.8 A
DC Link Voltage	V_{dc}	650 V

SIMULATION RESULTS

To check efficacy of a suggested strategy, a three phase grounding fault scenario along with profiles is shown in Fig. 1 is explored by Matlab/simulation. Parameters used for system simulation are for a 17 kW PV system. Table I displays major parameters for simulation. Waveform results of suggested method are as discussed as follows.

In three phase grounding fault, grid three phase voltages fall to nearly zero symmetrically for 150 ms, recovered to its normal value. A fault is noticed when a specific delay triggered by controller time. Controller gives response to the fault. **Fig. 6(a)** shows major parameter waveforms by injecting only reactive current to grid for three phase grid voltages, phase currents, d axis positive sequence voltage component e_{dp} , d and q axis positive sequence current components i_{dp} and i_{qp} are shown respectively from top to bottom. Simulation waveforms of proposed FRT strategy are mentioned in **Fig. 6(b)**. Fault happens at time $t = 0.3s$ and grid come back to normal at time $t = 0.45s$. As per e_{dp} , fault is observed at time $t = 0.31s$, some transient response of it is observed from three phase current results. Then i_{dp} restrains to zero because no real power supplied to grid and i_{qp} increases to its rated value to fulfil FRT prerequisite. After comparison it is found that suggested method gives steady results for phase currents, i_{dp} and i_{qp} respectively. Furthermore, dc link voltage suddenly increases as shown in **Fig.7** for both the methods. It is also observed that, suggested method reduces dc link voltage quickly; even dc link voltages of both cases reach its peak value.


Fig 6(a). Injecting only reactive current during FRT simulation waveforms

Fig 6(b). Simulation waveforms of proposed FRT strategy

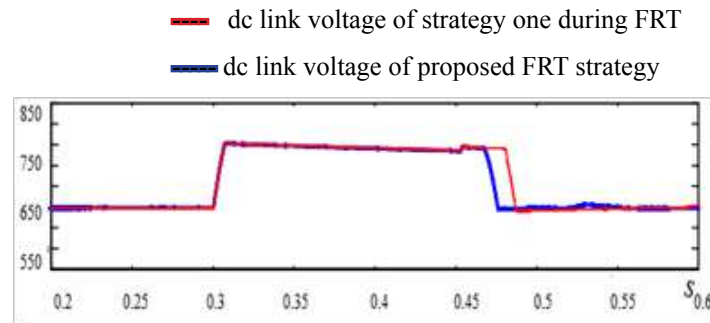


Fig 7. DC link voltage waveform during three phase grounding fault

CONCLUSION

A control strategy is proposed in this paper to restrain dc link voltage under FRT period and by using it, minimum needed reactive current is supplied and sufficient amount of real power to grid also delivered without exuberance of PCU current. DC link voltage fluctuation of a PCU during FRT reduces fastly in comparison to method of injection of reactive current to make it an enhanced PCU; is the main contribution of this paper. Three phase grounding fault voltage sag scenario is investigated with simulation and results show that proposed method accomplished control objective.

REFERENCES

1. EPIA - European Photovoltaic Industry Association "Global Market Outlook for Photovoltaic 2014-2018", 12 June 2014, Available at <http://www.epia.org>
2. Aslan Mojallal, Saeed Lotfifard, "Enhancement of Grid Connected PV Arrays Fault Ride Through and Post Fault Recovery Performance", IEEE Transactions on Smart Grid, Vol.10, 2019.
3. Amir Taghvaie, Md. Enamul Haque, Md. Apel Mahmud, "A New Step-Up Switched- Capacitor Voltage Balancing Converter for NPC Multilevel Inverter-Based Solar PV System", IEEE Access Journal Article, Volume 8, 2020.
4. Y Yang, and F. Blaabjerg, "Low-voltage ride-through capability of a single-stage single-phase photovoltaic system connected to low-voltage grid." International Journal of Photo energy 2013.
5. Grid Code High and Extra High Voltage, E. ON Netz GmbH, Bsyreuth, Germany, Apr. 2006.
6. Xiangyang Lin, Yang Han, Ping Yang, Congling Wang, Jingqi Xiong, "Low-Voltage Ride-Through Techniques for Two Stage Photovoltaic System under Unbalanced Grid Voltage Sag Conditions", IEEE 4th Southern Power Electronics Conference (SPEC), Singapore, 2018.
7. S Raja Mohamed, P Aruna Jeyanthi, D Devaraj, Mounir Bouzguenda, "Performance Comparison of Active and Passive Passive LVRT strategies for Grid Connected PV Systems", IEEE International Conference on Intelligent Techniques in Control, Optimization and Signal Processing (INCOS), India, 2019.
8. Naresh P.; V. Seshadri; Sravankumar, "Analysis of Low Voltage Ride Through Techniques for Grid Connected Photovoltaic Systems", IEEE International Conference on Power Electronics, Smart Grid and Renewable Energy (PESGRE2020), India 2020.
9. L. Chia-Tse, H. Che-Wei and C. Po-Tai, "A Low -Voltage Ride through Technique for Grid-Connected Converters of Distributed Energy Resources," IEEE Transactions on Industry Applications, vol. 47, pp.1821-1832, July/August 2011.
10. S. Alepuz, S. Busquets-Monge, J. Bordonau, J. A. Martinez- Velasco, C. A. Silva, J. Pontt, and J. Rodriguez, "Control Strategies Based on Symmetrical Components for Grid- Connected Converters Under Voltage Dips," IEEE Transactions on Industrial Electronics, vol. 56, pp. 2162-2173, 2009.
11. S. Raja Mohamed, P. Aruna Jeyanthi, D. Devaraj, M. H. Shwehdi and Adel Aldalbahi, "DC-Link Voltage Control of a Grid-Connected Solar Photovoltaic System for Fault Ride-Through Capability Enhancement", Article published in MDPI, Appl. Sci. 2019.



12. Yiwen Geng, Ke Yang, Zou Lai, Pengfei Zheng, Haiwei Liu and Renxiong Deng, “A Novel Low Voltage Ride Through Control Method for Current Source Grid-Connected Photovoltaic Inverters”, IEEE Access Journal Article, 2019.
13. J R Pinheiro, D L R Vidor, H A Grundling, “Dual output three-level boost power factor correction converter with unbalanced loads, ” in Proc .PESC Conf., 1996, vol.1, pp. 733- 739.
14. Ehsan Afshari, Gholam Reza Moradi, Ramin Rahimi, Babak Farhangi, Yongheng Yang, Frede Blaabjerg and Shahrokh Farhangi, “Control Strategy for Three-Phase Grid Connected PV Inverters Enabling Current Limitation under Unbalanced Faults’, IEEE Transactions on Industrial Electronics, Issue 99, 2017.
15. S Jae Hyeong, C. Chang Ho, and H. Dong Seok, “A new simplified space-vector PWM method for three – level inverters,” IEEE Transactions on Power Electronics, vol. 16, pp. 545-550, 2001.
16. Ntare, R.; Abbasy, N. H.; Youssef, K.H.M., “ Low Voltage Ride through Control Capability of a Large Grid Connected PV System Combining DC Chopper and Current Limiting Techniques”, J Power Energy Eng. 2019, Vol.7, pp. 62–79.



Tidal Power Generation – Prospects in India and Challenges for Engineers

Kirit B Trivedi

Deputy Executive Engineer (Mech.)- Retired, N.W.R.W.S. & K. Department, Government of Gujarat, Gandhinagar

✉ kbtrivedi27@gmail.com

ABSTRACT

The rapid growth in all the field of lives of human being is electricity, which is primarily obtained using the once abundant & affordable fossil fuels like coal, oil and gas. The alarming situation is that the once abundant and affordable fuels were depleting rapidly and would soon become expensive to use. As per a report by the International Energy Agency (IEA), the world would need a total of 28,141 Terra Watt Hour of electricity in 2030 against 20,757 TWh generated in 2015. All this demanded for another source of power generation, which we now generally call as renewable energy. One of system to generate electricity is known as tidal power. A variety of different technologies are under development throughout the world to harness the energy of Tidal waves. Tidal Power makes use of 50+ years of technology development pioneered by the sub-sea oil & gas industry and most recently the amazing development made by the offshore industry in efficient power transmission back to the shore.

The basic advantages are- (i) Zero Greenhouse Gas Emission, (ii) may be useful for at least 2 billion years, (iii) it is predictable and constant, ensure a relatively steady power supply. (iv) The cost of a Tidal Power system is a double-edged sword. The initial costs are extremely high. but, the systems are mostly maintenance free over a life span of about 30-40 years.

India is not only blessed with about 7500 km long coast line, but is also one of the 20 places worldwide where the height of the high tide is over 5 m higher than the low tide, needed to capture the Tidal Power potential about 8000 MW of tidal energy, with 7,000 MW in the Gulf of Kambhat, 1,200 MW in the Gulf of Kutch in Gujarat, and about 100 MW in the Gangetic delta in Sunderbans in West Bengal. Though there is good potential for tidal power Government has recently decided not to go forward with the proposed tidal power plant developments in states of Gujarat and West Bengal on financial challenges in implementation of these projects, because of high capital cost ranging from Rs 30 crores to 60 crores per MW.

Here the challenge comes for engineers of India to show their talent to become a path giver for other countries in this field of Tidal Power Generation. Technology is already there, world is using it, but we are somewhat lagging, in various ways. As an engineers, we must have to show our talent and give some innovative ideas for cheaper technologies to combat this pity situation. Though India is going to create many Solar, Wind and bio-gas plants to generate electricity, but the Tidal is waiting for all the Indians to get some power from them. If we have to follow our Hon'ble Prime Minister Vision of "Atma-Nirbhar Bharat", we have to develop our indigenous technologies and fruitful planning for the new vision of Tidal Power Generation. Indian Engineers will certainly make some new technology and instruments to generate the Tidal power in a very different way, for the betterment of all the human kind, who actually starving for electricity in their day to day life. Jai-Hind.

Keywords : Renewable energy; Tidal power; Dynamic tidal power system; Tidal barrage and stream generator system; Advantages & Disadvantages; Atma nirbhar Bharat.

INTRODUCTION

Along with the rapidly accelerated development of the human civilization in the past couple of hundred years, there has been an equally rapid growth in the basic needs & desires of humans. The key enabler of this growth was electricity; primarily electricity obtained using the once abundant & affordable fossil fuels like coal, oil and gas. But in the latter half of the last century, not only did we realize the alarming harm that these fossil fuels had done to our environment but also that the once abundant and affordable fuels were depleting rapidly and would soon become expensive to use.

As per a report by the International Energy Agency (IEA), the world would need a total of 28,141 Terra Watt Hour of electricity in 2030 against 20,757 TWh generated in 2015. For India it may be from 893 to 1935 TWh. The world definitely needs to move towards developing & adopting the non-conventional, renewable sources of energy in order to meet these demands and to grow sustainably.

The Government of India is on its way to achieving 500 GW target for installed Renewable Energy capacity by 2030, India is one of the countries with large production of energy from renewable sources. As of 27 November, 38% -including large hydro- of India's installed electricity generation capacity is from renewable sources, which is about 136 GW out of 373 GW. In the Paris Agreement, India has committed to an Intended Nationally Determined Contributions target of achieving 40% of its total electricity generation from non-fossil fuel sources by 2030. The country is aiming for even more ambitious target of 57% of the total electricity capacity from renewable sources by 2027 in Central Electricity Authority's strategy blueprint. According to 2027 blueprint, India aims to have 275 GW from renewable energy, 72 GW of hydroelectricity, 15 GW of nuclear energy and nearly 100 GW from "other zero emission" sources.

This is why the technology for renewable energy generation and its feasibility is an important area of active research over the last few years. A relative new comer to this renewable world is Tidal Energy- the energy captured from the tides of the oceans & seas. Though Tidal Energy is still considered to be in a nascent stage, but still a lot of research has been going on in this field in the past few decades and has shown promising results.

In this paper I will try to share some aspects of Tidal Energy, its present status and future prospects and the biggest challenges for engineers to develop economical generation.

WHAT IS TIDAL POWER

Historically, tide mills have been used both in Europe and America. The earliest occurrences date from the Middle Age or even from Roman Times. Tidal Power/Energy is a form of hydropower that converts the energy obtained from tides into useful forms of power-mainly electricity. In a simple manner we can say that this is the energy harnessed from ocean tides.

As Tidal Power draws on the energy inherent in the orbital characteristics of the Earth-Moon system, it makes power generation very predictable, unobtrusive and reliable. In fact it is the only form of power generation that makes use of this Earth-Moon system.

A variety of different technologies are under development throughout the world to harness the energy of Tidal waves. Tidal Power makes use of 50+ years of technology development pioneered by the sub-sea oil & gas industry and most recently the amazing development made by the offshore industry in efficient power transmission back to the shore.

GENERATION OF TIDAL POWER

There are about 4 basic mechanisms with several variations for harnessing Tidal Energy:

Tidal Barrage

This is more like traditional hydro-power- In that it uses potential energy that results from the difference in height between high & low tide. The system works by creating a pool that fills during high tides and then drains through a turbine as the tide goes out. These involve the creation of huge concrete dams with sluices.

The bottom of this barrage dam is located on the sea floor with the top of the tidal barrage being just above the highest level that the water can get too at the highest annual tide. The barrage has a number of underwater tunnels cut into its width allowing the sea water to flow through them in a controlled way by using "sluice gates" on their entrance and exit points. Fixed within these tunnels are huge tidal turbine generators that spin as the sea water rushes past them either to fill or empty the tidal reservoir thereby generating electricity.

Flood Generation

In which the tidal power is generated as the water enters the tidal reservoir on the incoming tide.

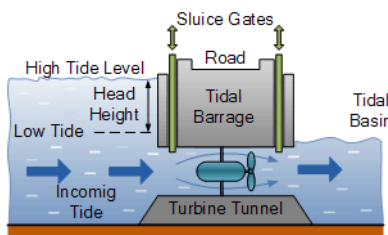


Fig 1. Tidal power – flood generation

Ebb Generation: in which the tidal power is generated as the water leaves the tidal reservoir on the ebb tide.

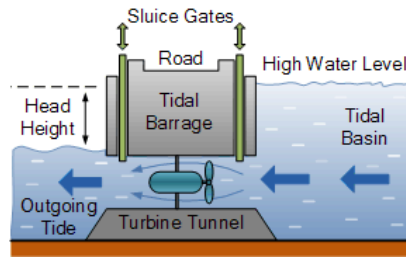


Fig 2. Tidal power – Ebb generation

Two-way Tidal Barrage Scheme uses the energy over parts of both the rising tide and the falling tide to generate electricity.

Tidal Stream Generator

The tides contain both potential and kinetic energy. Potential energy is the energy stored or available when water is available at an elevation higher than normal. This is possible during flooding tides and energy will be available during the ebbing phase. The energy available from barrage depends on the area of the water surface impounded by the barrage and the corresponding magnitude of the tidal range. The tidal generators connected with stream turbine-immersed in sea- make use of kinetic energy of the water stream which in turn spins the turbine and drives the generator to produce electricity. It is very similar in many ways to the principles of wind power generation. Horizontal turbine generators called “tidal turbines” or “marine current turbines” are placed on the ocean floor, the stream currents flow across the turbine blades powering a generator much like how wind turns the blades of wind power turbines.

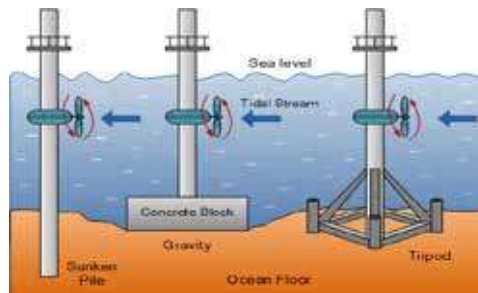


Fig 3. Tidal stream generator supports

Dynamic Tidal Power

It is a technology that uses the difference between the potential energy and kinetic energy of tides. Long dams are built from coasts straight out into the sea or ocean - meaning that the tides in the areas where these systems might be implemented usually flow parallel to their respective coasts. During the movement of tides, water on one side of the dam is at a higher level than the other side. As this water flows through the dam it drives a series of turbines installed within the dam and generates electricity. Furthermore, these dams are designed with bi-directional turbines, which flip 180° after each tide in order to generate power both when the tide comes in and goes out. The added output from having bi-directional turbines is a huge advantage for these types of systems, they allow the power output to basically double.

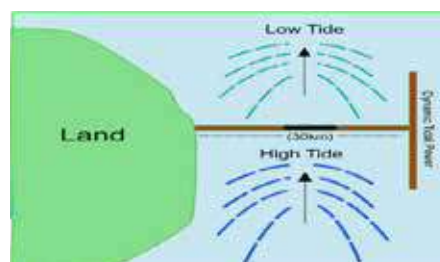


Fig 4. Dynamic Tidal power generation



Tidal Lagoon

A new tidal energy design option is to construct circular retaining walls embedded with turbines that can capture the potential energy of tides. The pumping power could be provided by excess to grid demand renewable energy from for example wind turbines or solar photovoltaic arrays. Excess renewable energy rather than being curtailed could be used and stored for a later period of time. The proposed Tidal Lagoon Swansea in Wales, United Kingdom would be the first tidal power station of this type once built.

ADVANTAGES OF TIDAL POWER GENERATION

- (1) One of biggest advantages of Tidal Power generation is Zero Greenhouse Gas Emission.
- (2) Tidal Power may be useful for at least 2 billion years, making tidal power as renewable as wind and solar, but the major problem is maintenance over the long term.
- (3) Unlike solar or wind, the tides are predictable and constant. The tides can be predicted 100s of years into the future and hence we can ensure a relatively steady power supply.
- (4) The initial costs are extremely high. but, the systems are mostly maintenance free over a life span of about 30-40 years.
- (5) Barrage system can protect coastal towns and ports from flood, and it can double as a bridge or other connection route, so this facilitates for transportation too.
- (6) The tidal stream generators are probably the most eco-friendly of all tidal power schemes. They operate at all times. Because tidal stream generators can be designed to work no matter what direction the tide is flowing, they can generate power up to 20 hours per day, making them more practical as a standalone system.

DISADVANTAGES OF TIDAL POWER GENERATION

- (1) Disruption of the life cycles of certain marine life. They can also prevent access to rivers and cut off shipping. They are costly to build and locations are highly limited.
- (2) Spinning blades of Stream Generators can kill marine wildlife. Their acoustic disturbances can affect migration and other aspects of marine life. They can interfere with shipping channels and are more prone to damage by high waves and rough water than other systems.
- (3) Dynamic Tidal Power schemes are very costly, are untested yet and more impacts of the system in various things cannot be judged at present.

CURRENT GLOBAL STATUS

Tidal power is not yet widely used around the world, though it has the potential for future electricity generation. Many recent technological developments and improvements - both in design and turbine technology indicate that the total availability of tidal power may be much higher than previously assumed. Most of them utilize Tidal Barrage Technology.

Table 1. List of existing tidal power plants in the world

Sr. No	Name of Tidal Power Station	Country	Capacity in MW	Commissioned
1	Rance Tidal Power Station	France	240	1966
2	Kislaya Guba Tidal Power Station	Russia	1.7	1968
3	Jiangxia Tidal Power Station	China	3.2	1980
4	Annapolis Royal Generating Station	Canada	20	1984
5	Strangford Lough Sea Gen	U.K.	1.2	2008
6	Uldolmok Tidal Power Station	South Korea	1.5	2009
7	Sihwa Lake Tidal Power Station	South Korea	254	2011
8	Bluemull Sound Tidal Stream Array	U.K.	0.5	2015
9	Meygen Tidal project	U.K.	398	2016



CURRENT STATUS OF TIDAL ENERGY IN INDIA

India is not only blessed with about 7500 km long coast line, but is also one of the 20 places worldwide where the height of the high tide is over 5 m higher than the low tide, needed to capture the Tidal Power potential. The Gulf of Khambhat and the Gulf of Kutch in Gujarat on the west coast have the maximum tidal range of 11m and 8m with average tidal range of 6.77m and 5.23m respectively. The interest in Tidal Energy comes in the backdrop of India's growing energy demand.

Table 2. Tidal Potential along Indian Coastline

Coastal Region	Ideal Range (m)	Typical Tidal Current (m/s)	Average Available Potential Energy (MW/sq. km)	Average Available Kinetic Energy (MW/sq. km)	Potential Options / Technologies
Kutch	4-9	3.0	7.2	4500.2	Barrage/Stream Turbine
Khambhat	5-11	2.5	10.9	2604.3	Barrage / Stream Turbine
Sundarbans	4-7	2-3	7.2	2604.3	Barrage
South Gujarat	2-4	2.0	1.5	1333.4	Barrage
Orissa Coast	2-4	1.5	1.5	562.5	Barrage
Maharashtra	2-4	1.5	1.5	562.5	Barrage
Karnataka	1-1.5	1.5	0.2	562.5	Barrage
Kerala	1-1.5	1.5	0.2	562.5	Barrage
Andhra Coast	1-2	1.0	0.2	166.7	Barrage

According to Indian Institute of Technology, Chennai, total identified potential of tidal energy is approximately 12,455 MW. Based on the studies, there is an estimated potential of about 8000 MW of tidal energy, with 7,000 MW in the Gulf of Kambhat, 1,200 MW in the Gulf of Kutch in Gujarat, and about 100 MW in the Gangetic delta in Sunderbans in West Bengal.

THE CHALLENGES

As we are aware that India has reportedly decided not to go forward with the proposed tidal power plant developments in states of Gujarat and West Bengal on financial challenges in implementation of these projects, because of high capital cost ranging from Rs 30 crores to 60 crores per MW. Though there are plenty of potential for Tidal Power generation of electricity, considering as a new source of renewable power energy, India is lacking behind to develop a economical system, which can produce electricity at some reasonable amount per unit of power as compare to some developed countries.

Here the challenge comes for engineers of India to show their talent to become a path giver for other countries in this field of Tidal Power Generation. Technology is already there, world is using it, but we are somewhat lagging, in various ways, because, the Government of India is not finding tidal power generation as a viable for Gujarat and W. Bengal, it is a challenge for us, as an engineers, we must have to show our talent and give some innovative ideas for cheaper technologies to combat this pity situation. Though India is going to create many Solar, Wind and bio-gas plants to generate electricity, but the Tidal is waiting for all the Indians to get some power from them.

If we have to follow our Hon'ble Prime Minister Vision of "Atma-Nirbhar Bharat", we have to develop our indigenous technologies and fruitful planning for the new vision of Tidal Power Generation, as there are plenty of potential, considering the longest coastal area. I hope in the coming years, Indian Engineers will certainly make some new technology and instruments to generate the Tidal power in a very different way, for the betterment of all the human kind, who actually starving for electricity in their day to day life. As world is going to manufacturing Electrical Cars, the Electricity will have its own power.

CONCLUSION

The Ministry of New and Renewable Energy (MNRE) has taken several steps to fructify Prime Minister Shri. Narendra Modi's dream of a clean energy future for the 'New India'. The largest renewable capacity expansion programme in the world is being taken up by India. The government is aiming to increase share of clean energy through massive thrust in renewable. Core drivers for development and deployment of new and renewable energy in India have been Energy security, Electricity shortages, Energy Access, Climate change etc.



The Government is also planning an active role in promoting the adoption of renewable resources by offering various incentives, which includes-generation based incentives (GBIS). Capital and interest subsidies, Viability gap funding, concessional finance and fiscal incentives. All these leads for better India in field of renewable energy.

Tidal energy has the potential to play a valuable part in the sustainable energy future. Now-a-days and in coming years, increased attention is being given to the tidal current energy development all over the world. Research by University of Technology (LUT)-in Finland, expounds that India has a huge potential to move into fully renewable electricity system by 2050, owing to an abundance of renewable resources.

Though, there is still a need for re-assessment of Tidal Power potential in India, in terms of scientific evaluation and strategic planning. Jai-Hind.

REFERENCES

1. The international journal of ocean & climate system-2017, Vol-8/2.
2. Official web site-Ministry of New & Renewable Energy-GOI.
3. Article published in Times of India, Jan-2011, Gujarat aims for Asia's biggest Tidal Power plant".
4. Damon Lapping-energy management consultant-South Africa-Article-July-2018.
5. Information from the website of Atlantis Resources Corporation.(UK).



Net Zero: Emission vs Employment: The Transition in Indian Power Sector

Shreya Karmakar¹, Joy Chakraborty²

A Senior Designer of Grid Connected Solar PV Systems, Serving for a Solar EPC and a final semester M.Tech student on Power Systems in IIT, Dhanbad¹

A Working Professional on Renewable Energy Systems²

✉ shreya03karmakar@gmail.com; ✉ joychakro19@gmail.com

ABSTRACT

In 2015, India had fixed up the target to add 175 GW of Renewable Energy [RE] in its grid by 2022. By October, 2020, India has achieved 89.63 GW from Renewable. [RE Invest: Govt. Of India: November, 2020] So, India has to achieve 85 GW further of Renewable Energy to reach at its 'intended nationally determined RE contribution goal' of 175 GW by 2022. For accomplishing this target, Indian Corporate Sector has already formulated different strategies which include the concept, known as: Net Zero. The Coal India has declared a plan to be a Net Zero company in respect of its power consumption by 2022-23. In the meantime, Solar PV has emerged as the cheapest energy source in India. These developments put pressure on Coal Sector. These result the closure of coal mines and joblessness to people, attached with coal mining etc. So, in Indian Energy Sector, it is the transition phase. Here, attempt is made to formulate strategy to achieve sustainable goals through self-reliance or energy independence using the positive vibes created for RE sector in this transition, with policy analysis, case studies and recommendations of alternative policy road map.

Keywords : RE transition; Net zero.

INTRODUCTION

Climate Change has emerged as the worst threat to human civilization. The Paris Climate Accord, as signed in 2015 targets: 'non-fossil fuel share of cumulative power generation capacity of 40% by 2030 [conditional]' to limit the global temperature rise within 1.5 degree Celsius by 2100.

In last few years, India has witnessed steady growth in Solar and Wind Energy sectors. In recent biddings, Solar PV has become the cheapest source of electricity in India; tariff varies in between Rs. 2.01 to Rs.2.12 per kWh. It is almost half of the cost of producing electricity from coal from recently installed thermal power stations. In September, 2020, the United Nations has recommended for not allowing any further Thermal Power Station in India, after 2021.

The said developments and automation have noticeable impact on Indian Coal Industry. In the initial days of human civilization, people were energy independent. Now he scope has come again. Here, this transition for Renewable Energy [RE] sector in India is addressed in such a manner, that it can be compatible for supplying most of the nation's electricity requirement both in self-reliant and sustainable manner with a special focus on employment.

THE TRANSITION AT A GLANCE: STORAGE IS INEVITABLE

It is noticed in June, 2020 data of the Central Electricity Authority [CEA], Govt. of India that India's overall installed power generation capacity has reached [May, 2019 to April, 2020] from 357 GW to 371 GW. Out of this total 14 GW of capacity addition, conventional sectors have contributed [from 278 to 283 GW] 5 GW and the Renewable have contributed [from 78 to 87 GW] 9 GW. In percentage contribution to grid, presently RE stands for 10 % +. This is one side of the 'story'.

On the other hand, coal mines become rapidly unprofitable. Say, in Jharkhand, 50% of coal mines are presently closed. Among presently operational mines, half are incurring huge operational losses. In Bokaro, 16, out of 25 mines are already closed. In Jamtara, all five coal mines, in Ramgarh, 50% of the mines are closed. In these areas, 25% of entire population [10, 83,802 people] are directly dependent on coal industry for their income, mostly in informal sectors associated with coal mining. [The CEO, FOREST, TOI, 28.11.2020]



In the said background, coal and coal based electricity companies have already planned for investing in large for increasing its Renewable Energy portfolio to make such companies as Net Zero Company by 2022-23. Obtaining enthusiastic achievements, the Govt. of India is planning to upgrade its RE target from 175 GW to 220 GW by 2022. [Inauguration of World Solar Technology Summit: Speech of the Hon'ble Prime Minister of India: 8th September, 2020] The further target is 450 GW of RE by 2030 which is co-terminus with India's goal to enhance its non-fossil fuel contribution to its total power generation capacity to 40% by 2030.

In the Economic Times webinar on 20th November, 2020, the NitiAyog has uttered that Indian Power Sector infrastructure, at present, is enough to accommodate upto 17 % grid penetration from RE. But, the rapid growth in capacity addition from RE sources indicates that 17 % limit is not enough. In such a position, reducing the peak demand through Energy Efficiency measures and propagation of large scale advanced and efficient storage has become inevitable.

NET ZERO FOR INCREASING NON-FOSSIL FUEL BASED POWER GENERATION CAPACITY

For accomplishing Paris Accord, more contribution of non-fossil fuel based energy sources in respect of cumulative power generation capacity is required. Co-terminus with Paris accord, the nationally pre-determined target is 175 (or 220) GW RE by 2022. Accordingly, Indian Corporate have taken initiatives to extend its RE portfolio by 2022 and so on. It serves multiple purposes like making that company into a Net Zero company through reducing its electricity bill into Zero or near Zero. It also kicks start the diversification exercise of the company in respect of its core business activities, so far. Here, Net Zero stands for making the fossil fuel based power consumption into zero by reducing the consumption level and then meeting the consumption through non-fossil fuel based power generation.

The CIL is one of top 20 global companies responsible for highest amount of GHG emissions during 1965-2017. Roughly 55% of electricity in India comes from CIL's coal. The CIL's aggregated annual loss is 16,000 crores. In this background, the Coal India Limited [CIL] has planned to invest Rs.5, 650crores by 2023-24 to install 3,000MW of Solar Power Plants as part of reaching their target to become a Net Zero Company by 2023-24. These Solar projects are expected to reduce CIL's annual electricity bill of Rs,3,400 crores which is more than 4% of revenue expenses of CIL in 2019-20. This Net Zero initiative of CIL will also serve some other important purposes like initiation of CIL's diversification plan for shifting from a coal company to an energy company [like the California Oil, Gas and Solar Company in the USA.], contribution for meeting India's 175 (220) GW RE target and reducing CIL's carbon (emission) footprint significantly. [According to the United Nation's Framework Convention on Climate Change, one Million Unit of Solar Power generation corresponds to avoidance of 700 tons of CO₂ emission to the atmosphere.]

The State owned Thermal Generator, NTPC has also taken similar aggressive RE plan by adding 10,000 MW of Solar Power by 2022 to make NTPC a Net Zero (auxiliary energy) company. A separate subsidiary company: NTPC Renewable Energy has been created to build NTPC's RE portfolio.

Recently, Adani Greens have bagged a 45,000 crores order from the Maharashtra Government for 8GW of Solar Power. With 15 GW of present Renewable Portfolio Assets, Adani Green is inching closer of becoming the world's largest Renewable Energy company (as well as a Net Zero power company) by 2025. They have Solar Module manufacturing facility, EPC business, Solar Generation in Solar Parks etc.

Fossil Fuel to Non-Fossil Fuel Transition in Indian Power Sector: A graph

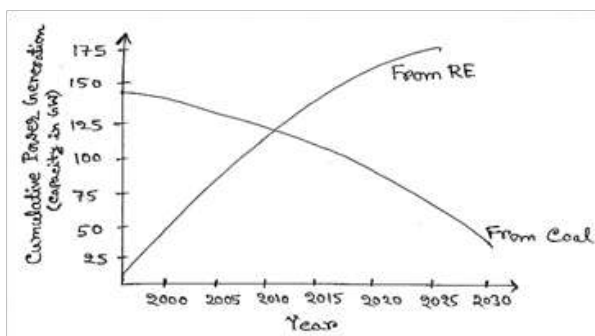


Fig. 1. Fossil Fuel to Non-Fossil Fuel Transition in Indian Power Sector



IMPACT OF NET ZERO INITIATIVES: 'NEW POOR' FOR DECAY IN COAL SECTOR

Net Zero initiatives on one hand reduce our carbon footprint, inching towards meeting India's ambitious RE target by 2022. On other hand, it results closure of coal mines in India, especially in Jharkhand. It has already become a huge threat for the very existence of nearly 11 lacs of population in three districts [Bokaro-Jamtara-Ramgarh] in Jharkhand. Here, the CIL has planned to install 800 MW of Solar power [within its total aggregated target of 3000 MW Solar capacity addition] plants. If we consider the present employment market for Solar Power, these upcoming Solar power Plants in Jharkhand, are not at all enough to provide alternative income source to those people who have either already lost their jobs or going to lose it in near future. So, the writing on the wall is clear now.

Now, question comes that whether Sustainable Goal can be achieved through huge job loss and making a large section of marginalized population as jobless. Unless it is addressed now, with appropriate policy alternatives, jobless New Poor will create negative impact on sustainable growth. In this critical juncture, alternatives are explored and analyzed from available information and future trend in Indian Power Sector.

New Road Map for inclusive growth with Self-reliant and employment friendly alternatives: enhancing the manufacturing capacity for RE and extending RE EPC activities

Even in the recent pandemic due to Covid 19, the Renewable Energy has emerged as the Sunrise Industry and the Coal Energy is the decaying industry now, in India. From recent studies of the International Renewable Energy Agency [IRENA], Ministry of New & Renewable [MNRE], TERI [The Energy & Resources Institute], ILO [international Labour Organisation], it appears that the workforce requirement in the Indian Power sector may reach 35 lac by 2050. RE technologies tend to be more labour intensive than conventional. Distributed renewables like small-scale hydro, rooftop solar and biomass can create maximum employment for every MW of installed capacity. It is estimated that Rooftop solar employs 24.72 persons, small hydro employs 13.84 persons and biomass employs 16.24 persons for constructing and running a one-megawatt plant. So, a business friendly RE EPC Policy is the need of the hour.

IRENA estimates that Some 3, 80,000 people were employed in RE sector in India in 2015 which is increased to 8, 24,000 in September, 2020 and it is expected that some 20 lac people will be working in Indian RE sector by 2030. Presently, employed people in Solar energy: 2, 04,000. The employee strength of CIL [Coal India Limited] was 5, 10,671 in 2015, which has reduced to 2, 72,445 in September, 2020. During 2000 to 2015 in CIL 1, 05,000 jobs were lost and the figure for 2015-2020 is 2, 38,225.

From the said analysis, it is evident that for a proper balance in respect of energy independence and sustainable growth, rapid increase of manufacturing facility is inevitable to meet the employment requirement to ensure the inclusive growth in Indian power sector.

Sl. No	Item	Govt. Policy /Present trend	Employment Scenario
1	EPC Business in RE	Large corporates and Small & Medium Enterprises [SMEs] are very keen on diversifying to become a Solar EPC. Other small businesses are vertically integrating to the EPC business. Employment opportunity in informal sector is also there.	Presently 5, 60,000 people are working. It can be nearly 13lac people in 2030
2	Solar Cell, Module Manufacturing	Present indigenous manufacturing capacity for cells is 2GW annually and it is nearly double for Modules. New MNRE Solar Cell Manufacturing Policy is there for cutting edge technology for large scale upgrading indigenous manufacturing capacity. Scope of indirect employment is also there.	Presently 2, 52,000 people. It can be enhanced upto 6 lac people by 2030.
3	(advanced storage) Battery Manufacturing	The advanced chemistry cell battery manufacturing policy of the Government of India is in the final stage.	Presently 16,480 people. It can be enhanced upto 1 lac people by 2030

MANUFACTURING OF SOLAR PV CELL AND MODULE: THE 'MARUTI STORY' CAN BE REPEATED:

In India's total RE capacity, now Solar PV is nearly 35 GW. Present indigenous manufacturing capacity for Solar cells is 2GW annually and it is nearly double for Modules. So, for the sake of Self Reliance or to make India 'Atmanirbhar' in Solar Energy Sector, India's indigenous cell and module manufacturing facility requires rapid capacity addition. These new manufacturing units can create larger employment opportunity, both in formal and informal sectors. This can ensure the re-creation of earning sources to the distressed people, till recent past who were totally dependent on coal mining for their income.

So, from above analysis, the proposal is, like the AdaniGreen; the CIL, NTPC can start manufacturing (may be a new joint venture company / consortium) of Solar Cells, Solar modules, Smart Batteries or so at their existing semi or unutilized facility.

Such recent initiatives of Adani Green, Tata, Vikram, Loongietc can be compared with that of India's top car maker. For Maruti, along with the car maker an entire range of ancillary industry also comes into reality. Here, for Solar also, elevating local manufacturing can create an ecosystem of suppliers for solar cells and modules. This can open scope for more employment in both formal and non-formal sector.

Manufacturing of smart storage batteries: To reduce our emissions to meet the un-conditional goal of Paris Accord, India has introduced National Hybrid Mobility Mission where time bound more penetration of Electric Vehicle is coming as a reality. Almost 40 % of total cost of an EVehicle goes to its battery. Presently, both these batteries are coming mostly from China. In this context, the Govt of India is preparing the advanced chemistry cell battery manufacturing policy .It is now in the final stage. Here also, a growth of ancillary industry is expected which can create more employment.

Change in no of people employed in Coal and Re Sector in India 2015 vs2020 : a table

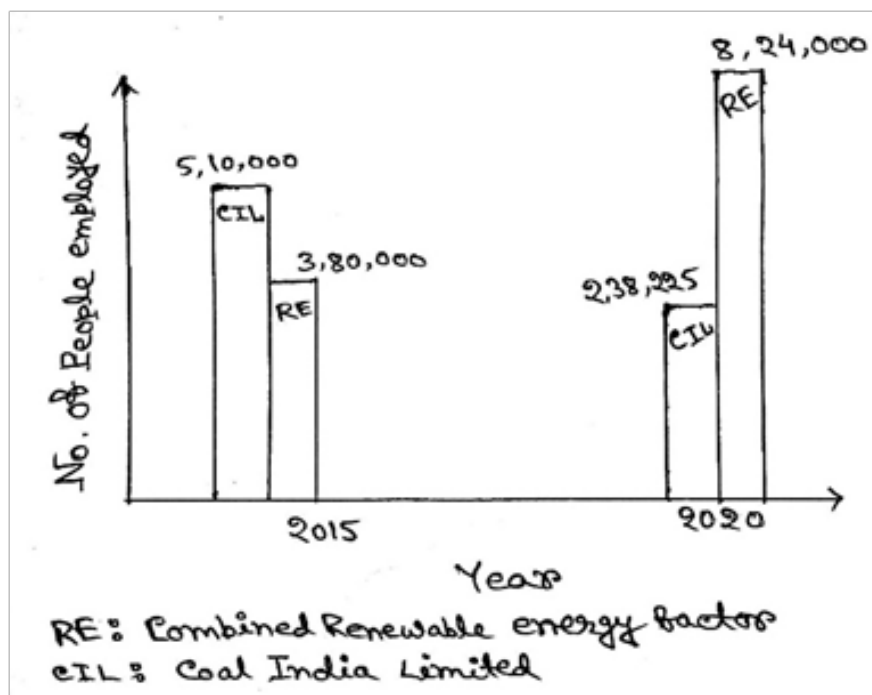


Fig. 2. Transition in Indian Power Sector: Employment

EXTENDING NET ZERO EXERCISES IN NON-CORPORATE SECTOR: BHALOPAHAR: A CASE STUDY

In Purulia, a charitable trust has created Bhalopahar which is mainly a huge plantation initiative of cultivation of 10 lacs of trees and for sustainable health and livelihood practices for the local marginalized population. In recent days, they are suffering from huge amount of electricity bill. In this background, a technical proposition is made and now in implementation in phased manner there with following details.



SL. No	Building type/ name	Present energy use pattern	Changed pattern towards net Zero	Present status
1.	Office cum dispensary	Light, Fan, Pump, Computer, Refrigerator	Rooftop PV with battery backup, Solar Pump	Estimate is prepared.
2.	School	Light, Fan	Grid Connected Rooftop PV	Plant is installed
3.	Guest House	Light, Fan, Geyser	Solar Water Heating System	Installed
4.	Dairy	Light, Fan, Pump	Rooftop PV with battery backup, Energy Efficient Pump, Biomass based electricity	Pump is installed

The journey towards Near Zero at Bhalopahar is like:

December, 2019	No change in energy use pattern	Rs.38,000 per month
July, 2020	Grid Connected PV installed	Rs.26,000 per month
September, 2020	Energy Efficient Pump installed	Rs.17,000 per month
October, 2020	Solar Water Heating System installed. Fan is closed as winter is settled	Rs.6,300 per month
January, 2021	New Solar Plant with battery will be installed	Rs.4,500 per month (expected)
December, 2021	Electricity from cow-dung and biomass will start producing	Near Zero (expected)

CONCLUSIONS

A Greener and cleaner world is the common dream of all dreamers in this universe. This clean and green scenario can only be achieved in environment friendly and self-reliant manner. The RE push in Indian Power Sector creates a scope of greener environment. But at the same time it eats the income opportunity of the marginalized people associated with coal mining. So far, the Net Zero exercises are limited with corporate sector only. An integrated and alternative approach through elevating indigenous RE manufacturing capacity and extending Net Zero exercises in non-corporate sector, can ensure propagation of RE Sector in India more sustainable and inclusive. This will reduce the GHG emissions, enhance RE penetration and will provide new scope of employment to the youth, jobless and other marginalized population.



ANN Based Adaptive SOGI-FLL Controller for Multifunctional Grid Tied Solar Energy Conversion System

Dinanath Prasad, Narendra Kumar

Department of Electrical Engineering, Delhi Technological University, Delhi

✉ dnk_1963@yahoo.com

ABSTRACT

This paper presents Artificial Neural Network (ANN) based adaptive second order generalized integrator frequency locked loop (SOGI-FLL) control technique for grid-tied solar photovoltaic (SPV) system. The system includes boost converter, the duty ratio of which is regulated by maximum power point tracker (MPPT) system. An incremental conductance based MPPT controller is incorporated for maximum power extraction from SPV system. The three-leg voltage source converter (VSC) is connected with SPV array via DC link capacitor. Proposed ANN based adaptive SOGI-FLL control scheme is designed to generate reference grid currents. The proposed system exhibits multifunctional applications such as, power quality enrichment, balancing of load, reactive power compensation, voltage regulation etc. ANN based controller is utilized for maintaining DC link voltage. The PV feed-forward technique is incorporated in proposed controller for dynamic performance enhancement. The proposed system is implemented in Matlab/Simulink environment and the simulation results exhibit the high value performance for microgrid applications.

Keywords : Power quality; SPV; Array; MPPT; Adaptive SOGI-FLL.

INTRODUCTION

In the present scenario, energy requirements are increasing day to day, along with conventional resources such as coal, natural gas and oil are in a limited amount. Therefore, various researches are going on to find alternate energy sources to maintain the gap between generation and demand with higher efficiency, greater power, and minimal pollution [1]. Renewable based energy resources having sustainable alternative energy resources and it attracts the world energy economy and improves energy security apart from a clean and continuous generation system [2]. The solar photovoltaic system (SPV) is one of the renewable energy resources which having wider solutions such as grid-connected, off-grid, industrial, commercial as well as in residential operations. Moreover, the price of the SPV system is decreased and due to large installations, some market analysts proposed that its installation could be 25% of the total generated power by 2050 [3]. Single and double configurations for the grid-tied SPV system interfaced inverter are incorporated in the literature [4]. Single-stage SPV system having greater efficiency, less complexity, and it requires fewer components as compared to the double-stage SPV system. In the literature [5], single-stage, single-phase for abnormal grid interfaced SPV system is proposed. Additionally, a double-stage grid interfaced PV system having higher power loss and insignificant due to the maximum power point tracker (MPPT) used [6]. To extract the maximum amount of power from SPV it is desirable to operate at maximum power point (MPP) at every instant of time irrespective of the fluctuation by solar intensity and temperature. Several MPPT techniques are reported with the advantages and disadvantages and tabulated in the literature [7, 8]. Moreover, coordinated control of the SPV generator system with MPPT and battery storage control during micro-grid operation are reported in the literature [9].

The role of power electronic converters has been addressed for optimal power flow, grid synchronization, and reactive power control, as well as many more developments in the field of renewable energy systems, which are reported in the literature [10, 11]. With such large developments of power electronics devices, the utilization of power electronics-based loads is increased which causes numbers of power quality problems such as voltage and current related harmonics are arisen [12]. Moreover, various power quality problems, and their solutions are mentioned in the literature [13]. the major power quality issues due to integration of renewable energy, and their various compensation technique such as local loads, point of common coupling point (PCC), grid impedance variations, DC line current harmonic generation-based schemes are reported [14].

The application of shunt active power filter (AF) in conjunction with the SPV module system showing filtering capability and reactive compensation is reported in the literature [15]. Moreover, compensation of reactive power and load balancing,

distribution static compensator (DSTATCOM) with different controllers such as instantaneous reactive power (IRP), Adaline and synchronous reference frame (SRF) based technique for reference current generation signal for voltage source converter (VSC) are presented in the literature [16]. However, SRF based technique possesses bad dynamic performance because of the low pass filter used. Various control schemes are demonstrated in the literature as of now, but an accurate and robust strategy is required for the generation of switching pulses for VSC so that it can perform multifunctional tasks such as power quality enrichment, load balancing, reactive power compensation and fundamental components of load current extraction. Therefore, for the above-mentioned functions, various literatures [17-22], such as SOGI, ILST, UVT, LMF, DSOGI, and ISOGI based control algorithm are reported for the reference current generation.

The phase-locked loop (PLL) technique is widely utilized in the power system for grid synchronization purposes. However, the applications of the PLL technique were found in the communications field such as frequency modulation track or synchronization of different frequencies and many more. The concept behind the use of PLL in a grid interfaced system is utilized for fast and accurate detection of the phase angle of the utility voltage as well as synchronization between the distribution grid and power generating sources [23]. The PLL technique is utilized with the SPV system, also various technique classifications such as SRF-PLL enhanced EPLL, Quadrature-phase QPLL, Second-order generalized based integrator SOGI-PLL and Dual SOGI-PLL reported for single-phase system [24, 25]. Although, the SRF-PLL technique detected unwanted ripples due to the notches in utility voltage, which can be eliminated by the adaptive based SRF-PLL technique [26]. Likewise, For the fixed-parameter SOGI-PLL based controller is implemented in [27], for minimum settling time by utility voltage variations as well as the design of PLL for power quality enhancement are reported in respected literature [28, 29]. A dual (DSOGI-FLL) control technique based on a frequency locking application is utilized instead of phase locking for grid synchronization purposes [30]. Although, in DSOGI-FLL in-phase signal is utilizing to synchronizing with phase voltage but in the literature [31], 90° shifted namely the SOGI-QSG concept is used for high order harmonics attenuation. Moreover, SOGI-QSG having some limitations such as sub-harmonics components is present in the fundamental component of load current, this limitation can overcome by technique SO-SOGI based controller reported in the literature [32]. In literature [33], multi-second-order generalized integrator (MSOGI-FLL) is utilizing for higher harmonics cancellations.

In the proposed work adaptive SOGI filter structure and frequency locking concept is utilized for grid synchronization. The ANN technique is used for loss calculation for VSC as, PI controller is used in many literatures [16], [18-22], they require proper tuning of PI gains (K_p and K_i), which is observationally determined. Therefore, by utilizing ANN controllers, limitations of conventional PI controller has been eliminated. Moreover, this paper aims to provide a robust controller design for power quality enhancement, load compensation, and reactive power compensation. The goal of the proposed work, are presented below.

1. An adaptive SOGI-FLL based controller is implemented to provide getting pulses to VSC as well as for fundamental components of current extraction from the load currents.
2. The feed-forward component is incorporated in the solar PV system, which improves the dynamic performance of the system.
3. An incremental conductance-based MPPT algorithm is utilized for maximum power extraction from the solar PV system.
4. The ANN controller is proposed to maintain the DC bus voltage constant.
5. The performance of the proposed controller is simulated in MATLAB SIMULINK environment with non-linear load and it ensures that the total harmonic distortions (THD) fall under the IEEE-519 standard.

System Layouts

Fig. 1 presents the proposed configuration system. The system contains SPV array for source of renewable energy. The proposed SPV system is interfaced to 3-phase grid along with non-linear load. Voltage source converter (VSC) and ripple filters are coupled at point of common coupling point (PCC). The VSC is utilized for supplying power to the distribution system and ripple filters are used for elimination of switching ripples. The SPV system includes SPV array, DC-DC boost converter for step the DC voltage, maximum point tracking (MPPT) unit for utilization of maximum power from SPV array.

Control Algorithm

The control algorithms are applied for boost converter of SPV as well as for voltage source converter (VSC). However, pulses of SPV boost converter is regulated by the incremental conductance (INC) based MPPT controller. The energy of SPV is feed to

DC-link capacitor of VSC. Furthermore, fuzzy logic controller (FLC) is utilized for maintaining constant DC-Bus voltage and loss computation for VSC. The pulses of VSC are extracted by SOGI-FLL based controller. The function of VSC is to power quality improvement as well it can be utilized to power conversion. Parameters of the SPV system are mentioned on appendix.

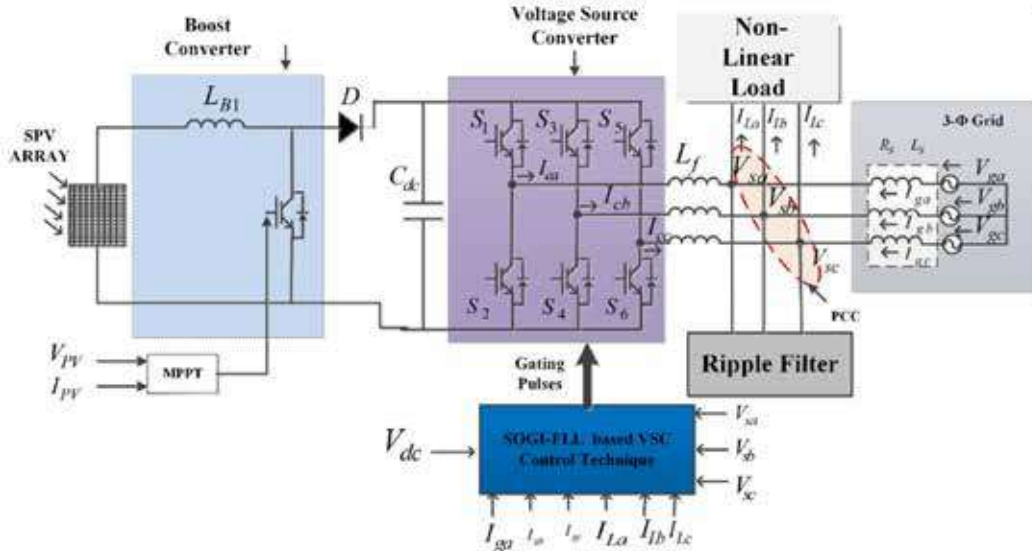


Fig. 1. System Configuration

Incremental Conductance-based MPPT Controller

The incremental conductance (InC) based maximum power point tracker (MPPT) is utilized to extract maximum power from the solar array. It is easier to implement, fast maximum tracking capability, and good dynamic behaviour kind of attracting features to choose as an MPPT controller [7]. Therefore, InC based controller is applied to extract maximum power from the proposed SPV array. The basic mathematics describe the operation of this MPPT controller as,

$$P = V_{PV} \times I_{PV} \quad (1)$$

$$\begin{aligned} \frac{\partial P}{\partial V} &= \frac{\partial (V_{PV} \times I_{PV})}{\partial V} \\ &\approx I_{PV} + V_{PV} \frac{\partial I_{PV}}{\partial V} \end{aligned} \quad (2)$$

Now, comparing the array conductance with increment conductance to find the maximum power point.

$$\begin{aligned} \text{left of MPP when, } \frac{\partial I_{PV}}{\partial V_{PV}} &> \frac{-I_{PV}}{V_{PV}} \\ \text{Right of MPP when, } \frac{\partial I_{PV}}{\partial V_{PV}} &< \frac{-I_{PV}}{V_{PV}} \\ \text{\& at MPP when, } \frac{\partial I_{PV}}{\partial V_{PV}} &= \frac{-I_{PV}}{V_{PV}} \end{aligned} \quad (3)$$

Hence, eq. (3) concludes that the maximum power point is tracked when incremental conductance will be equal to the array conductance.

Adaptive SOGI-FLL Control Scheme

The proposed controller is presented in Fig.2(a). The applied control scheme is utilized for accurate generation of switching pulses for VSC. In this section step by step procedure are presented for generation of switching pulses. Moreover, various silent signals are utilized for generation of switching pulses for VSC, the signals are:

1. Magnitude of terminal voltage

2. In-phase and quadrature-phase unit template
3. Feed-forward component of current
4. Loss component of current
5. Equivalent component of current
6. Net active component of current

1. Magnitude of terminal voltage (V_{tm}):- The magnitude of terminal voltage is computed as,

$$V_{tm} = \sqrt{\frac{2(V_{ga}^2 + V_{gb}^2 + V_{gc}^2)}{3}}$$

Where, V_{ga} , V_{gb} , V_{gc} are the phase voltages

2. In-phase and quadrature-phase unit template:- The quadrature unit template (α_{q1} , α_{q2} , α_{q3}) and the in-phase unit template signals (α_1 , α_2 , α_3) are utilized for VSC switching algorithm [17].

In-phase unit templates are,

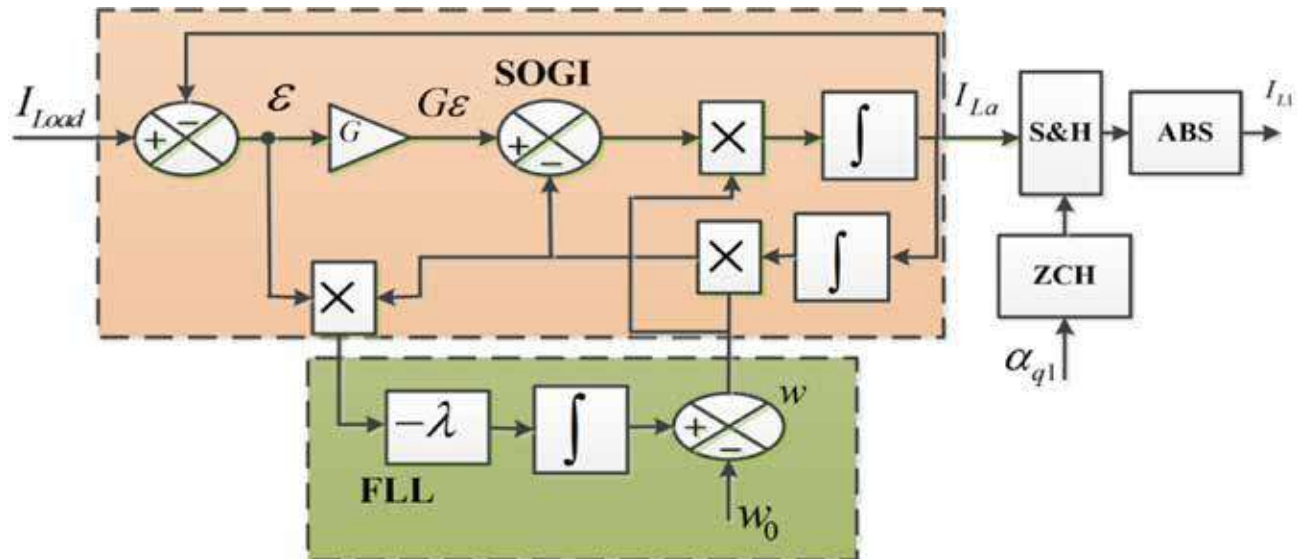
$$\alpha_1 = \frac{V_{ga}}{V_{tm}}, \alpha_2 = \frac{V_{gb}}{V_{tm}}, \alpha_3 = \frac{V_{gc}}{V_{tm}} \quad (4)$$

The quadrature unit template is estimated as,

$$\alpha_{q1} = \frac{\alpha_3 - \alpha_2}{\sqrt{3}}, \alpha_{q2} = \frac{\alpha_1 - \alpha_3}{\sqrt{3}}, \alpha_{q3} = \frac{\alpha_2 - \alpha_1}{\sqrt{3}} \quad (5)$$

3. Feed-forward component of current: The feed-forward loop is utilized for the reference current generation (I_{pf}), which helps in dynamic response improvement. The PV based feed-forward component is estimated as,

$$I_{Pvq} = \frac{2}{3} * \frac{P_{pv}}{V_{tm}}$$



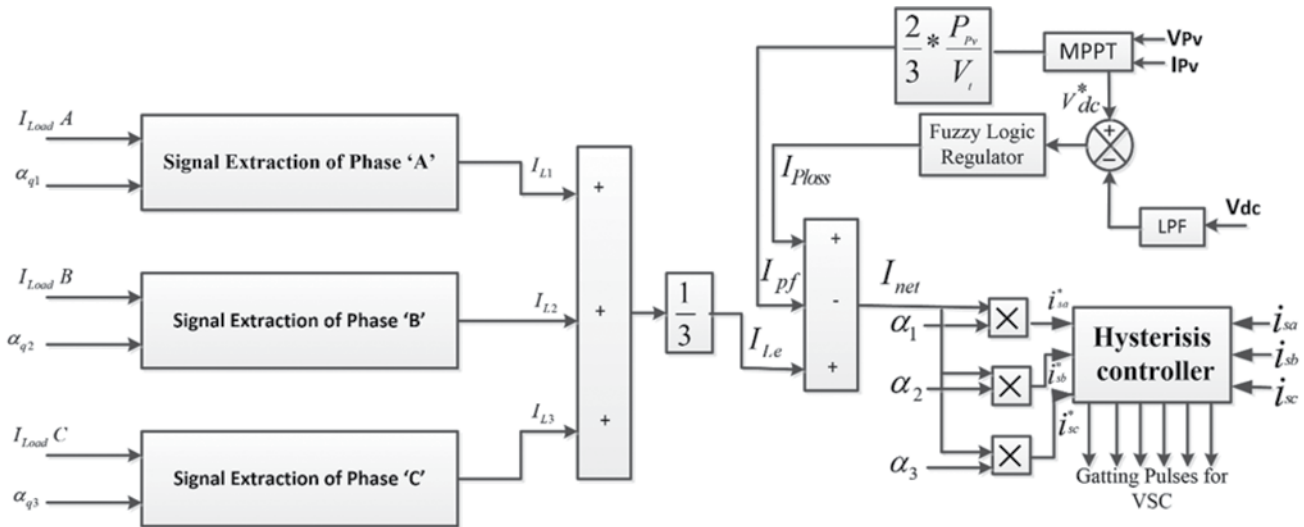


Fig. 2. (a) Adaptive SOFI-FLL control scheme for fundamental component of load current extraction from phase 'A', (b) Adaptive SOGI-FLL control scheme for reference current generation

4. Loss component of current :- The artificial neural network (ANN) based controller is utilized to maintain the DC bus voltage constant as well as for loss component of current estimation. As efficient and fast it maintains the constant value as minimizes the losses in converter. This technique is measured to be the latest tool to improve the dynamic performance design control circuits of adaptive SOGI-FLL. Moreover, ANN is a mathematical model motivated through biological neural networks. It comprises an interconnected collection of artificial neurons.

Here, V_{dc}^* is the reference DC bus voltage and V_{dc} is the sensed DC bus voltage. So, error in voltage ($V_e(n)$) is represented as, $V_e(n) = V_{dc}^* - V_{dc}(n)$. Moreover, the loss component of voltage error $y(n)$ is represented as,

$$y(n) = V_0(n) - V_0(n-1) \quad (6)$$

Here, $V_0(n)$ is the output to compute the loss component of current.

The following procedure algorithm is adapted for ANN to regulate the DC-bus voltage.

- Initialize neural network toolbox
- Define input and target parameters with the help of PI controller
- Import input and target data from MATLAB workspace
- Create a network
- Define data into the network as input data, target data, training function, performance function, number of layers, and number of the transfer function.
- Train the network
- Check performance
- If training regression value is near to one then import the network otherwise update the weights and do again training up to when performance gets the satisfactory result.

To improve the performance, a feed-forward network of a single layer (trained by backpropagation method) is used. This network comprises two layers with their respective neuron interconnections. The input layer has 1 neuron for receiving input and the hidden layer has 20 neurons which are fed by each processed input. The activation functions are designated to every layer for training purposes. The artificial neural network block is shown in **Fig. 3** for the intervals of 'n' and 'n-1', the huge data of DC link voltage is collected and stored in MATLAB workspace from the PI controller. Using this data, training of ANN is performed and the training algorithm is used for retrieving the stored data from the workspace. The neurons of input layer and

output layer are almost in a fixed quantity, whereas the accuracy of ANN operation is dependent on the number of neurons in the hidden layer.

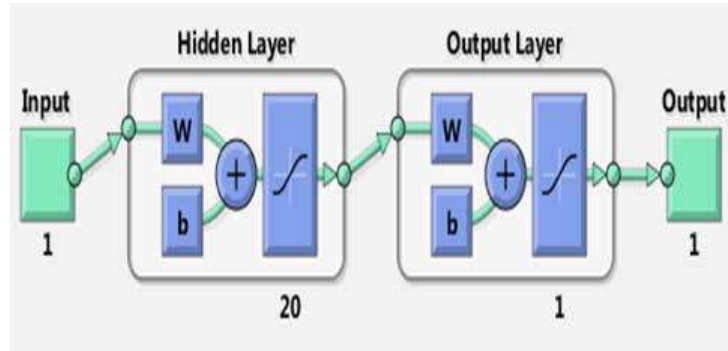


Fig. 3. Artificial Neural Network block

5. Equivalent component of current:- The equivalent component of in-phase and quadrature-phase current is calculated as follows

$$I_{Le} = \frac{I_{L1} + I_{L2} + I_{L3}}{3} \quad (7)$$

Where, I_{L1} , I_{L2} , and I_{L3} in-phase component of load currents.

6. Net active component of current:- The net active component of current is computed as,

$$I_{net} = (I_{Ploss} - I_{pvq} + I_{Le}) \quad (8)$$

Where, I_{Ploss} = loss component of current

I_{pvq} = feed-forward component of current

I_{Le} = Equivalent component of current

Furthermore, reference grid currents are compared with the source currents (I_{sa} , I_{sb} , I_{sc}) by using hysteresis current controllers. A not gate logic is used to convert these three-reference grid current to six gating pulses to control the grid-tied IGBT's based VSC.

RESULTS AND DISCUSSION

The simulation is carried out with varying operating condition to illustrate the behaviour of proposed methodology using Matlab/Simulation software. The results have been carried out by considering linear as well as non-linear loads at point of common coupling. For the performance analysis of the proposed system, simulation results includes, solar irradiance (G), DC link bus voltage (Vdc), SPV current (Ipv), SPV power (Ppv), feed-forward current (Ipvq), AC grid voltage (Vgabc), AC grid current (Igabc), compensating current (Ica), load current (iLa), AC grid active power (Pg), AC grid reactive power (Qg), terminal voltage (Vtm) and frequency (wr).

Behavior of system under nonlinear load

Figs. 4 (a), (b) present the behavior of Solar PV system under non-linear load at variable insolation. **Fig. 4 (a)** shows the waveforms of G, Vdc, Ipv, Ppv, and Ipvq. **Fig. 4 (b)** shows the waveform of Vgabc, Igabc, Ica, iLa, Pg and Qg at step insolation increase from 700 W/m² to 1000 W/m² at t = 0.4s. The grid current (Igabc) and voltage (Vgabc) are perfectly sinusoidal. It is notice that as solar insolation increase at t = 0.4 s, SPV array power (Ppv) and SPV current (Ipv) are increased. The DC link voltage is maintained constant and very minute oscillation is observed in it. The feed-forward current is also increased, because of the increment in SPV power. Therefore, it causes low oscillations are observed in grid current. Moreover, it is observed that as insolation increases at t=0.4s, the power generation from solar power system is increased and therefore, active power flow and grid current are decreased because of load power is constant in this operation. The system is carry on at unity power factor, as reactive power (Qg) is zero as shown in **Fig.4 (b)**.

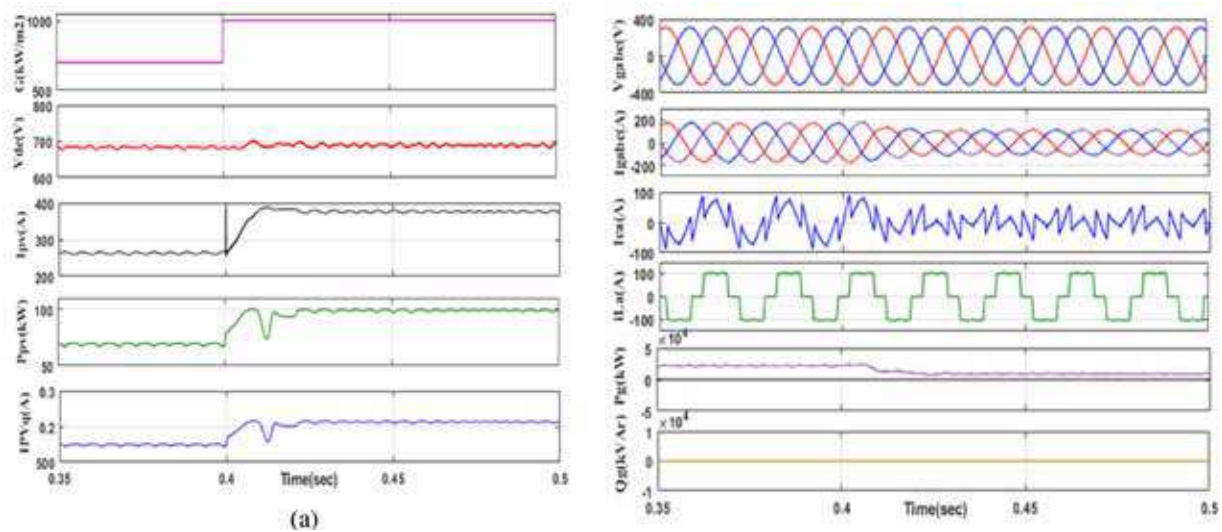


Fig. 4. Behaviour of the system (a), (b) nonlinear load under variable irradiance

Fig. 5 (a) presents the behaviour of Solar PV system for intentionally load unbalancing of one phase under load non-linear load condition. **Fig. 5 (a)** shows the waveform of G , V_{gabc} , I_{gabc} , i_{La} , I_{ca} , V_{dc} , P_g and V_t . In this case, assume that solar array is constantly operates at 1000 W/m^2 insolation but, phase 'a' intentionally removed at ($t = 0.4 - 0.5\text{s}$). The grid currents are observed balanced and perfectly sinusoidal in both steady state condition (before $t = 0.4\text{s}$ and after $t = 0.5\text{s}$), as well as in unbalanced condition at ($t = 0.4-0.5\text{s}$). During unbalancing period the active power demand and load balancing criterion are fulfilled by Solar PV generating system. However, with this unbalancing condition the DC bus voltage of VSC is maintained constant at 700 V .

Fig. 5 (b) presents the dynamic behaviour of solar PV system for varying system frequency 49.5 Hz to 50.5 Hz . **Fig. 5 (b)** depicts the waveform of V_{gabc} , I_{gabc} , i_{La} , I_{ca} , I_{pvq} , V_{dc} and w_r . With the system frequency variation, it is observed that the grid current and voltage are balanced and sinusoidal. The DC link voltage and feed-forward current are remains unaffected irrespective of system frequency variations.

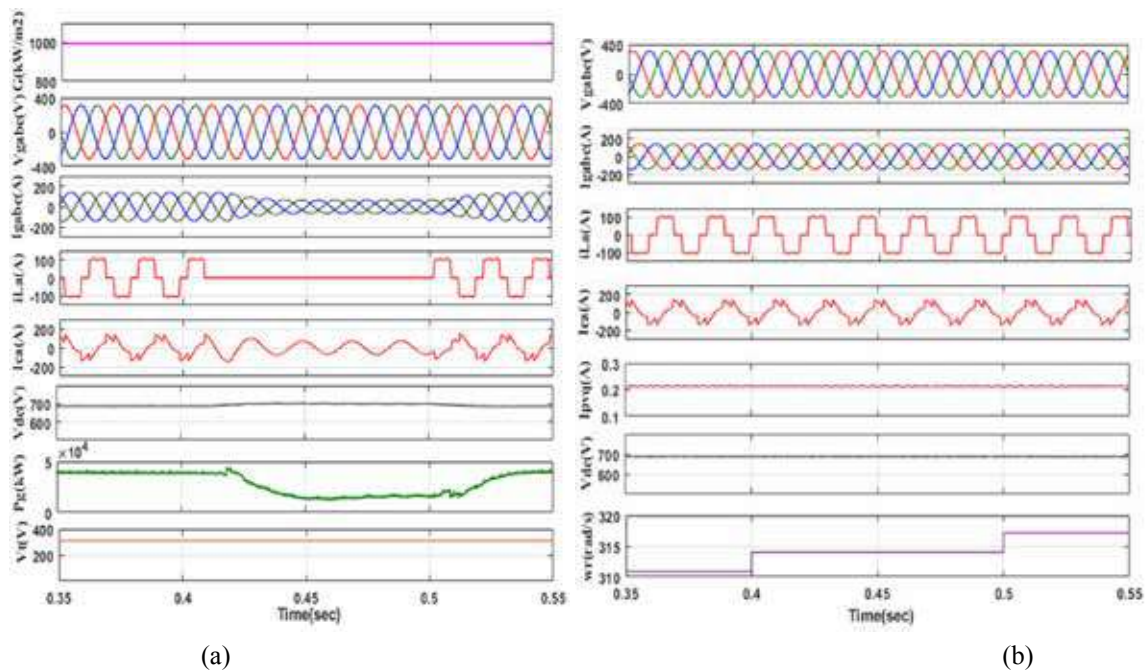


Fig. 5. Behaviour of system (a) under load unbalancing, (b) under variable system frequency

Figs. 6 (a), (b) present the behaviour of Solar PV system under linear load at variable insolation. **Fig. 6(a)** shows the waveforms of G , V_{dc} , I_{pv} , P_{pv} , and I_{pvq} . **Fig. 6(b)** shows the waveform of V_{gabc} , I_{gabc} , I_{ca} , i_{La} , P_g and Q_g at step insolation increase from 700 W/m^2 to 1000 W/m^2 at $t = 0.4 \text{ s}$. The grid current (I_{gabc}) and voltage (V_{gabc}) are perfectly sinusoidal. It is notice that as solar insolation increases at $t=0.4 \text{ s}$, SPV array power (P_{pv}) and SPV current are increased. The DC link voltage is maintained constant and very low oscillation is observed in it. The feed-forward current component is also increased, because of the increment in SPV power. Therefore, it causes low oscillations are observed in grid current. Moreover, it is observed that as insolation increases at $t=0.4 \text{ s}$, the power generation from solar power system is increased and therefore, active power flow and grid current are decreased because of load power is constant in this operation. The system is carry on at unity power factor, as reactive power (Q_g) is zero as shown in **Fig. 6(b)**.

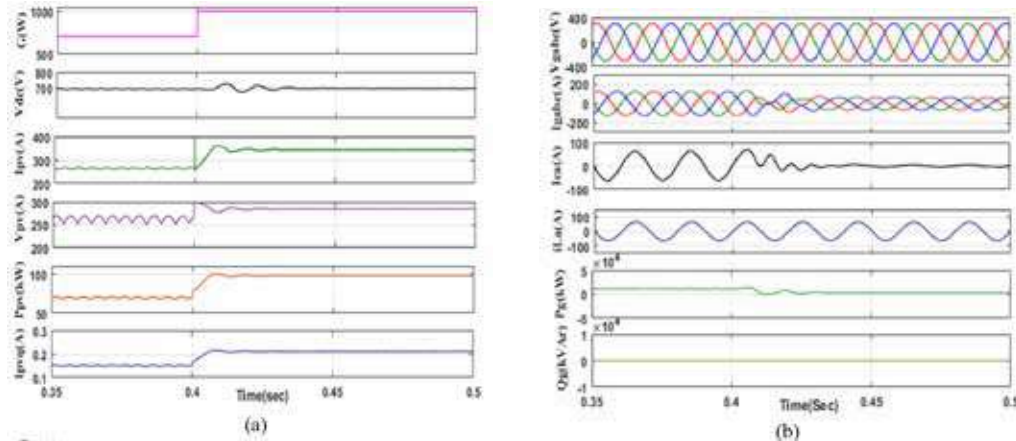


Fig. 6. Behaviour of system (a), (b) under linear load under variable irradiance

Fig. 7 (a) presents the behaviour of Solar PV system for intentionally load unbalancing of one phase under load non-linear load condition. **Fig. 7(a)** shows the waveform of G , V_{gabc} , I_{gabc} , i_{La} , I_{ca} , V_{dc} , P_g and V_t . In this case, assume that solar array is constantly operates at 1000 W/m^2 irradiance but, phase 'a' intentionally removed at ($t = 0.4 - 0.5 \text{ s}$). The grid currents are observed perfectly sinusoidal in both steady state condition (before $t=0.4 \text{ s}$ and after $t=0.5 \text{ s}$), as well as in unbalanced condition at ($t = 0.4-0.5 \text{ s}$). During unbalancing period, the active power demand and load balancing criterion are fulfilled by Solar PV generating system. However, with this unbalancing condition the DC link voltage of VSC is maintained constant with small oscillations.

Fig. 7(b) presents the behaviour of solar PV system under varying system frequency 49.5 Hz to 50.5 Hz. Fig. 13(b) depicts the waveform of V_{gabc} , I_{gabc} , i_{La} , I_{ca} , I_{pvq} , V_{dc} and w_r . With the system frequency variation, it is observed that the grid current and voltage are perfectly sinusoidal. The DC link voltage is approximately constant to its reference value.

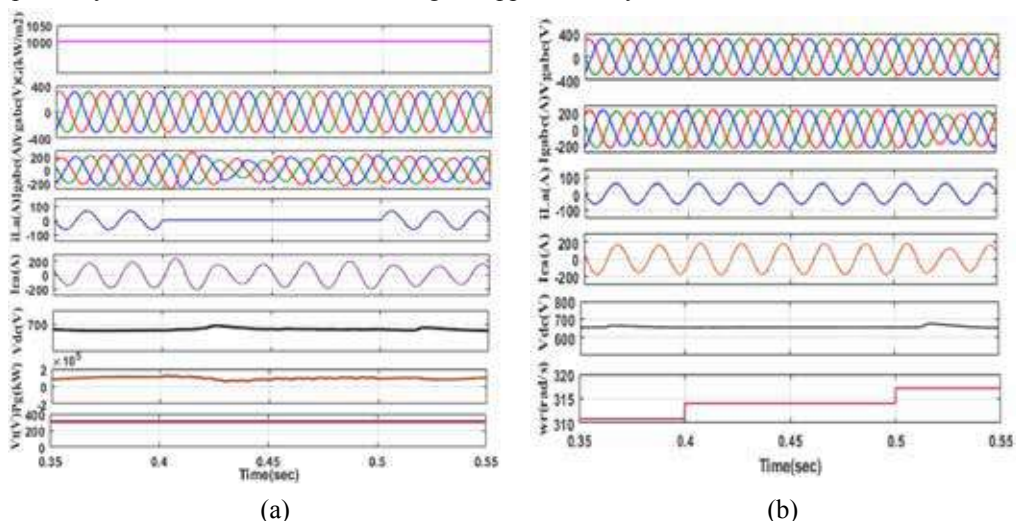


Fig. 7 (a) behaviour of system under load unbalancing, (b) system under variable frequency



CONCLUSION

A three-phase grid interfaced solar photovoltaic system (SPV) has been implemented and controlled by using SOGI-FLL based adaptive control scheme. This scheme has been effectively used for extraction of reference currents and providing gating pulses to VSC. The performance of control scheme for SPV system has been found satisfactory under linear and nonlinear loads as well as in load unbalancing conditions under varying system frequency. The proposed system along with ANN based adaptive control scheme has shown better performance in power quality enhancement. The effectiveness of feed-forward component has been presented for dynamic performance improvement. ANN controller is incorporated accurately with adaptive control scheme for converter loss component estimation. The THD has been reduced much better using ANN controller ensuring decent operation of shunt active power filter thus resulting in improved power quality. The proposed system has been simulated using Matlab/simulink software and the results demonstrate the harmonic free source current.

REFERENCES

1. Renewable Energy Policy Network for the 21st Century, Global Status Report 2014, <http://www.ren21.net/ren21activities/globalstatusreport.aspx>.
2. Omar Ellabban and Haitham Abu-Rub and Frede Blaabjerg, "Renewable energy resources: Current status, future prospects and their enabling technology", *Renewable and Sustainable Energy Reviews*, vol.39, pp. 748- 764, 2014.
3. M. Malinowski, J. I. Leon and H. Abu-Rub, "Solar Photovoltaic and Thermal Energy Systems: Current Technology and Future Trends," in *Proceedings of the IEEE*, vol. 105, no. 11, pp. 2132-2146, Nov. 2017, doi: 10.1109/JPROC.2017.2690343.
4. A. K. Barnes, J. C. Balda and C. M. Stewart, "Selection of converter topologies for distributed energy resources," 2012 Twenty-Seventh Annual IEEE Applied Power Electronics Conference and Exposition (APEC), Orlando, FL, 2012, pp. 1418-1423, doi: 10.1109/APEC.2012.6166006.
5. C. Jain and B. Singh, "Single-phase single-stage multifunctional grid interfaced solar photo-voltaic system under abnormal grid conditions," in *IET Generation, Transmission & Distribution*, vol. 9, no. 10, pp. 886-894, 27 2015, doi: 10.1049/iet-gtd.2014.0533.
6. T. Wu, C. Chang, L. Lin and C. Kuo, "Power Loss Comparison of Single- and Two-Stage Grid-Connected Photovoltaic Systems," in *IEEE Transactions on Energy Conversion*, vol. 26, no. 2, pp. 707-715, June 2011, doi: 10.1109/TEC.2011.2123897.
7. T. Esum and P. L. Chapman, "Comparison of Photovoltaic Array Maximum Power Point Tracking Techniques," in *IEEE Transactions on Energy Conversion*, vol. 22, no. 2, pp. 439-449, June 2007, doi: 10.1109/TEC.2006.874230.
8. B. Subudhi and R. Pradhan, "A Comparative Study on Maximum Power Point Tracking Techniques for Photovoltaic Power Systems," in *IEEE Transactions on Sustainable Energy*, vol. 4, no. 1, pp. 89-98, Jan. 2013, doi: 10.1109/TSTE.2012.2202294.
9. E. B. Ssekulima and A. A. Hinai, "Coordinated voltage control of solar PV with MPPT and battery storage in grid-connected and microgrid modes," 2016 18th Mediterranean Electrotechnical Conference (MELECON), Lemesos, 2016, pp. 1-6, doi: 10.1109/MELCON.2016.7495332.
10. Haitham Abu-Rub, Mariusz Malinowski, Kamal Al-Haddad, *power electronics for renewable energy systems, Transportation and industrial applications*, IEEE press and John Wiley & sons Ltd., UK, 2014.
11. J. M. Carrasco et al., "Power-Electronic Systems for the Grid Integration of Renewable Energy Sources: A Survey," in *IEEE Transactions on Industrial Electronics*, vol. 53, no. 4, pp. 1002-1016, June 2006, doi: 10.1109/TIE.2006.878356.
12. H. Akagi, "New trends in active filters for power conditioning," in *IEEE Transactions on Industry Applications*, vol. 32, no. 6, pp. 1312-1322, Nov.-Dec. 1996, doi: 10.1109/28.556633.
13. B. Singh, A.Chandra and K. Al-Haddad, *Power quality: problems and mitigation techniques*, John Wiley & Sons Ltd., United Kingdom, 2015.



14. X. Liang, "Emerging Power Quality Challenges Due to Integration of Renewable Energy Sources," in IEEE Transactions on Industry Applications, vol. 53, no. 2, pp. 855-866, March-April 2017, doi: 10.1109/TIA.2016.2626253.
15. Nak-gueon Sung, Jae-deuk Lee, Bong-tae Kim, Minwon Park and In-keun Yu, "Novel concept of a PV power generation system adding the function of shunt active filter," IEEE/PES Transmission and Distribution Conference and Exhibition, Yokohama, Japan, 2002, pp. 1658-1663 vol.3, doi: 10.1109/TDC.2002.1176849.
16. B. Singh and J. Solanki, "A Comparison of Control Algorithms for DSTATCOM," in IEEE Transactions on Industrial Electronics, vol. 56, no. 7, pp. 2738-2745, July 2009, doi: 10.1109/TIE.2009.2021596.
17. L. Coluccio, A. Eisinberg, G. Fedele, C. Picardi and D. Sgro, "Modulating functions method plus SOGI scheme for signal tracking," 2008 IEEE International Symposium on Industrial Electronics, Cambridge, 2008, pp. 854-859, doi: 10.1109/ISIE.2008.4677143.
18. B. Singh, C. Jain and S. Goel, "ILST Control Algorithm of Single-Stage Dual Purpose Grid Connected Solar PV System," in IEEE Transactions on Power Electronics, vol. 29, no. 10, pp. 5347-5357, Oct. 2014, doi: 10.1109/TPEL.2013.2293656.
19. B. Singh, C. Jain and S. Goel, "A UVT based control for single-stage grid interfaced SPV system with improved power quality," 2014 6th IEEE Power India International Conference (PIICON), Delhi, 2014, pp. 1-6, doi: 10.1109/POWERI.2014.7117612.
20. R. K. Agarwal, I. Hussain and B. Singh, "LMF-Based Control Algorithm for Single Stage Three-Phase Grid Integrated Solar PV System," in IEEE Transactions on Sustainable Energy, vol. 7, no. 4, pp. 1379-1387, Oct. 2016, doi: 10.1109/TSSTE.2016.2553181.
21. B. Singh, S. Kumar and C. Jain, "Damped-SOGI-Based Control Algorithm for Solar PV Power Generating System," in IEEE Transactions on Industry Applications, vol. 53, no. 3, pp. 1780-1788, May-June 2017, doi: 10.1109/TIA.2017.2677358.
22. Vineet P. Chandran Shadab Murshid Bhim Singh, "Design and analysis of improved second order generalized integrator-based voltage and frequency controller for permanent magnet synchronous generator operating in small-hydro system feeding single-phase loads", doi.org/10.1002/2050-7038.2827, February 2019.
23. L. Coluccio, A. Eisinberg, G. Fedele, C. Picardi and D. Sgro, "Modulating functions method plus SOGI scheme for signal tracking," 2008 IEEE International Symposium on Industrial Electronics, Cambridge, 2008, pp. 854-859, doi: 10.1109/ISIE.2008.4677143.
24. A. Nagliero, R. A. Mastromauro, M. Liserre and A. Dell'Aquila, "Monitoring and synchronization techniques for single-phase PV systems," SPEEDAM 2010, Pisa, 2010, pp. 1404-1409, doi: 10.1109/SPEEDAM.2010.5545057.
25. A. Nicastrì and A. Nagliero, "Comparison and evaluation of the PLL techniques for the design of the grid-connected inverter systems," 2010 IEEE International Symposium on Industrial Electronics, Bari, 2010, pp. 3865-3870, doi: 10.1109/ISIE.2010.5637778.
26. F. Gonzalez-Espin, E. Figueres and G. Garcera, "An Adaptive Synchronous-Reference-Frame Phase-Locked Loop for Power Quality Improvement in a Polluted Utility Grid," in IEEE Transactions on Industrial Electronics, vol. 59, no. 6, pp. 2718-2731, June 2012, doi: 10.1109/TIE.2011.2166236.
27. A. Kulkarni and V. John, "A novel design method for SOGI-PLL for minimum settling time and low unit vector distortion," IECON 2013 - 39th Annual Conference of the IEEE Industrial Electronics Society, Vienna, 2013, pp. 274-279, doi: 10.1109/IECON.2013.6699148.
28. F. D. Freijedo, J. Doval-Gandoy, O. Lopez and J. Cabaleiro, "Robust phase locked loops optimized for DSP implementation in power quality applications," 2008 34th Annual Conference of IEEE Industrial Electronics, Orlando, FL, 2008, pp. 3052-3057, doi: 10.1109/IECON.2008.4758447.
29. F. Gonzalez-Espin, E. Figueres and G. Garcera, "An Adaptive Synchronous-Reference-Frame Phase-Locked Loop for Power Quality Improvement in a Polluted Utility Grid," in IEEE Transactions on Industrial Electronics, vol. 59, no. 6, pp. 2718-2731, June 2012, doi: 10.1109/TIE.2011.2166236.



30. P. Rodríguez, A. Luna, R. S. Muñoz-Aguilar, I. Etxeberria-Otadui, R. Teodorescu and F. Blaabjerg, "A Stationary Reference Frame Grid Synchronization System for Three-Phase Grid-Connected Power Converters Under Adverse Grid Conditions," in IEEE Transactions on Power Electronics, vol. 27, no. 1, pp. 99-112, Jan. 2012, doi: 10.1109/TPEL.2011.2159242.
31. P. Rodriguez, A. Luna, M. Ciobotaru, R. Teodorescu and F. Blaabjerg, "Advanced Grid Synchronization System for Power Converters under Unbalanced and Distorted Operating Conditions," IECON 2006 - 32nd Annual Conference on IEEE Industrial Electronics, Paris, 2006, pp. 5173-5178, doi: 10.1109/IECON.2006.347807.
32. Z. Xin, X. Wang, Z. Qin, M. Lu, P. C. Loh and F. Blaabjerg, "An Improved Second-Order Generalized Integrator Based Quadrature Signal Generator," in IEEE Transactions on Power Electronics, vol. 31, no. 12, pp. 8068-8073, Dec. 2016, doi: 10.1109/TPEL.2016.2576644.
33. P. Rodriguez, A. Luna, I. Etxeberria, J. R. Hermoso and R. Teodorescu, "Multiple second order generalized integrators for harmonic synchronization of power converters," 2009 IEEE Energy Conversion Congress and Exposition, San Jose, CA, 2009, pp. 2239-2246, doi: 10.1109/ECCE.2009.5316279.

APPENDIX

SPV power =32 kW, open circuit voltage= 32.9 V, short circuit current= 8.21A, V_{mp} = 26.3, cells per module= 96, parallel string (N_p)= 6, series module (N_s)= 27, Parameters:- AC grid voltage, $V_{gabc}(V) = 415V$; DC bus voltage $V_{dc}(V) = 700V$; ripple filter:- $R = 5\Omega$, $C = 50 \mu F$; interfacing inductor= 2.5 mH; nonlinear load, $R = 5 \Omega$, $L = 8 \text{ mH}$

Environmental Engineering



Modular Air Purifier for Metropolitan Cities

Sreekala P

Assistant Professor, Department of Electrical and Electronics Engineering, Amal Jyothi College of Engineering, Kottayam, Kerala

✉ psreekala@amaljyothi.ac.in

ABSTRACT

Air pollution is one of the major problems the world is facing today. According to an American study about 5.5 million people are killed each year as a result of air pollution and developing countries like India and China are responsible for half of these deaths. The Great Smog of Delhi is one of the worst scenarios of how bad air quality has become in Delhi and adjoining areas. Installation of modular air purifier to filter the air of harmful pollutants during peak hours can be used to reduce air pollution and provide clean air to the public. Air from surrounding is drawn inside a chamber, which is filled with water and the smoke and dust particles are forced to settle down. The air is then flown along an activated carbon bed, which removes the remaining harmful gases by means of adsorption. An air ionizer too is used to prevent air from getting trapped inside the tank. The purified air is then released to the surroundings.

Keywords : Air pollution; Water chamber; Activated carbon bed; Negative air ionizer.

INTRODUCTION

In India, air pollution is a grave issue with fuel adulteration, traffic congestion, vehicular emissions, suspended dust, industrial and construction materials and fuel wood burning being the major sources of pollution. Developing countries like India and China are responsible for about two-thirds of the mortality rates in Asia. Air pollution also accounts for the increasing global warming rates and climatic condition variations. In India, the air quality is extremely poor with 54% of the citizens living in cities not meeting NAAQS standards on fine particulate matter and with no city meeting the prescribed WHO standards.[1]

On 1st to 9th November 2016 air pollution has reached a peak level on both PM 2.5 and PM 10 levels. It was reported as one of the worst levels of air quality in Delhi since 1999. Common ill effects of smog on health are shortness of breath, wheezing, coughing, and discomfort while breathing. These lead to reduced lung capacity and can cut down the life expectancy of people breathing in the Delhi smog. Particulate matter can cause plaque in the arteries, which causes them to harden and eventually leads to heart attack. With the dangers of Delhi smog, the state government has ordered schools to be shut down for three days. Citizens have been warned to stay at home and two Ranji Trophy matches have been cancelled over the smog, which the Delhi environment minister called an emergency.

Table 1. Present air quality status in Indian cities[1]

City	SO ₂			PM ₁₀		
	Annual average $\mu\text{gm-3}$	I	R	Annual average $\mu\text{gm-3}$	I	R
Agra	7	L	L	186	C	C
Delhi	5	L	L	222	C	C
Ludhiana	11	L	L	221	C	C
Kanpur	8	L	L	184	C	C
Chennai	12	L	L	65	M	M
Bangalore	16	L	L	94	M	H



Industry, R-Residential, L-Low, M-Moderate, H-High, C-Critical

Table 1 shows that in Agra, Delhi, Ludhiana and Kanpur PM10 levels are critically high. If the pollutant levels are higher than 1.5 times the standards specified by CPCB then it is classified as critical and if the levels reach 50 percent of the standards then they are labeled as moderate. [1]

A lack of intra-city divided lane highways and inter-city expressways has contributed to the increase in traffic congestion in India. This results in the transmission of air pollutants about four to eight times higher than if the congestion was less severe. This also makes the vehicles consume more carbon footprint fuel per trip. In many Indian cities including Delhi, the traffic gridlock is quite severe. The Central Pollution Control Board of India now monitors 4 pollutants namely, suspended particulate matter (SPM), oxides of sulphur (SO_x), oxides of nitrogen (NO_x) and respirable particulate matter.

The causes responsible for the altered composition of air can be classified as natural causes and anthropogenic or man-made causes. The natural sources of air pollution consist of dust, fires, volcanic activities etc. Emission from industries, waste disposal landfills and mobile sources such as vehicular emission, marine vessels and airplanes are the main anthropogenic sources. On the basis of origin sulphur -dioxide, carbon-monoxide ammonia etc are called primary air pollutants as they are directly emitted to the atmosphere from the source. Ozone, peroxyacetylenitrates (PAN), smog etc are the secondary pollutants as they are formed as a result of the chemical reactions between normal atmospheric constituents and primary air pollutants.[2]

Various technologies have been used to filter air and reduce pollution levels. Most of these technologies have been employed to filter and improve the quality of indoor air.

HEPA stands for high efficiency particulate air filter. HEPA filter removes about 99.97 per cent of particulate matters having a size of more than 0.3 microns greater surface area for the air to be pushed in through the filter. These filters are made of very thin threads of glass having diameter which is less than a micron. The fibre like material is arranged in the form of an accordion by folding it back and forth. This creates a HEPA filter which is commonly used in hospitals as they are highly efficient in removing bacterial viral particles. Particles get trapped via interception, impaction and diffusion. They have a life span ranging from two to four years. However, these filters are not widely used as the pores tend to get clogged easily and have a tendency to hold moisture forming moulds. They also do not help in eliminating odors and other chemical gases. The purity of air increases with each time the air flows through the filter. When the filter becomes completely loaded with particles air will not further pass and the filter will need a replacement. Carbonaceous materials have been used since the 1700s for the removal of contaminants such as for filtering raw sugars. During World War I carbon was used in gas masks for purification of air. In the modern era carbon has been highly processed to improve its mechanical and thermal stability levels, tolerance levels and to increase its surface area.[3] UV or ultraviolet technology employs the use of ultraviolet rays to kill the germs and microorganisms using an ultraviolet lamp. It is used in collaboration with particulate filter systems. When the microbes are passed through the UV rays, cellular or genetic damage occurs and as a result the micro-organism gets destroyed. This is an excellent method to purify air from harmful microbes and to kill germs. The effectiveness of this technology depends upon the duration of exposure to the rays and its wattage. However, the use of ultraviolet rays results in the production of ozone as they convert the oxygen and water molecules found in air to ozone and hydroxyl. It is commonly used in the final stage of filtration.

TECHNOLOGIES USED IN MODULAR AIR PURIFIER

The modular air purifier proposed uses water, activated charcoal and air ionizer to purify the air in public places such as roadsides and construction areas to improve the quality of breathing air

Activated Carbon

Activated carbon is an extremely porous form of carbon. Carbon is processed so as to increase its surface area for adsorption. These molecular sized pores have excellent adsorbent ability.

Pure carbon is extracted by a procedure known as pyrolysis. Sources of carbon such as coal, peat or any other carbonaceous material are carbonized by heating in this method. The carbonized material is then oxidized by treating it with oxygen, steam, carbon-dioxide or by means of a chemical treatment. This process of converting a carbonaceous material into pure carbon through heating is called carbonization. Highly dense carbon is used as a raw material and heated at a temperature about 200 degree Celsius. The resultant material consists of highly porous carbon having a weight of 20-30 percent of initial raw material and a small amount of inorganic gas. This carbon is activated by means of gas or chemical treatment. In gas treatment the carbon is heated in the presence of a gas. In chemical treatment the material is immersed in a bath of acid, base or other chemicals.

This mixture is then heated to a temperature range between 450-900 degree Celsius. The end activated carbon product is then processed depending upon the uses into granular activated carbon, powdered activated carbon, impregnated carbon etc.

Air Ionizer

An air ionizer is a device that ionizes the air molecules by means of a high voltage. A negative air ionizer releases negative ions into the air. Under Standard temperature and pressure conditions (STP) conditions the air from activated carbon molecules are electrically neutral.[4] The released negative ions repel and hence flows around. These high velocity ions when colliding with pollutant particles near the ionizer pass on their charge. As the particles drift around pollutants such as dust, cigarette smoke and aerosol propellants are attracted to these ions. Hence the particle become heavy and settles down. For an increased efficiency commercial products provide earthed conductors such as wall and ceilings for the de-ionisation of the ions.

Water

Insoluble particulates such as dust can be filtered using water. The air containing these pollutants is bubbled through water. The insoluble particles remain suspended in the water column. By adding alum these particles may be made to settle down at the bottom. Alum chemically is hydrated double sulphate salt of aluminum. The particulates clump together because of London Dispersion Force which are part of the Van der Waals forces to the alum increasing its size. As the particles grow heavier it settles down at the bottom.

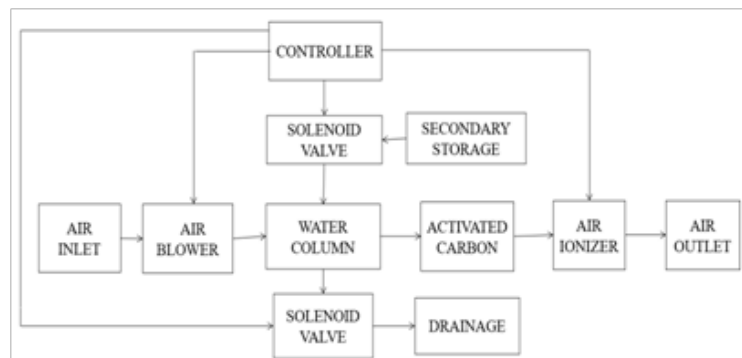


Fig 1. Block diagram representing different air purification layers

SCHEMATIC DIAGRAM

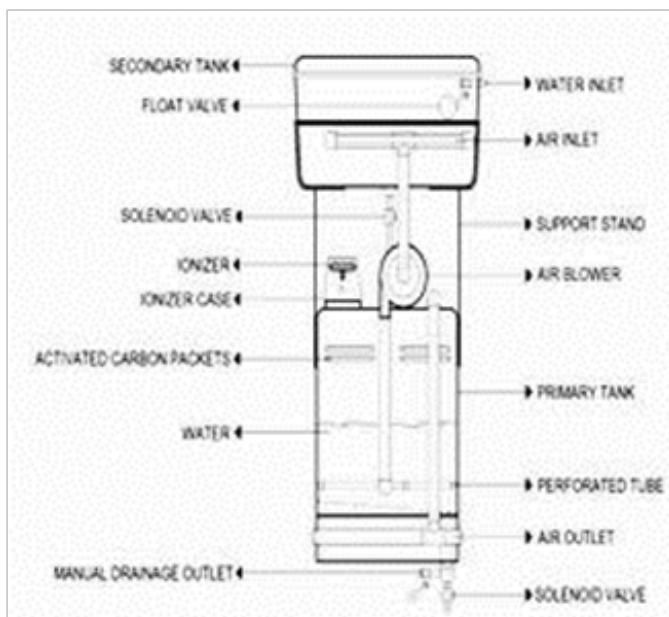


Fig 2. Diagram of natural air purifier



WORKING METHODOLOGY

The modular air purifier consists of a blower, primary water chamber, secondary water storage tank, a column of water, a bed of activated carbon and an ionizer. Relays are used to control the solenoid valves which regulate the flow of water.

Air is drawn into the primary water chamber by means of the blower. An air inlet opening is kept facing the road or direction of released polluted air at a height of 1.5 to 6 metres. The drawn air passes through a section of water by means of a perforated tube. A perforated tube is used to increase the flow time of air allowing the dust particles time to settle. These dust particles accumulate in the water overtime. Addition of Alum helps the dust particles to clog together. The bottom of the water chamber has a slope and the pollutants accumulate at the end of the slope. Turbidity sensors may be used to check the suspension of dust particles. These sensors pass a ray of light through the medium. The intensity of the received light is evaluated to determine the contamination level of water. The intensity of the perceived light decreases as the amount of dust particles in the water increases. As the quality of water becomes poor the primary water is discharged and refilled from the secondary water storage tank.

Table 3. Removal of gaseous pollutants by activated carbon[4]

Flow rate (L/min)	Bed Height (cm)	CO removal (%)	SO ₂ removal (%)
5	5	11	100
5	15	73	100
5	30	75	100
10	30	63	96
15	30	49	98

The bubbled air is then passed through a layer of activated carbon of 15cm thickness. The gaseous air pollutants such as oxides of sulphur, nitrogen and carbon get adsorbed on the activated carbon and do not recirculate. It is experimentally proven that palm shell activated carbon under optimum condition can adsorb about hundred percent of sulphur dioxide gas and 75 percent carbon-monoxide gas at a bed height of 15cm and a flow rate of 5 litres per minute.

An air ionizer is also added to further remove the circulating pollutants. The purified air is then released into the surrounding atmosphere

RESULT

The prototype of the modular air purifier was tested in the “Integrated Environmental Solutions” which is a laboratory approved by the Kerala State Pollution Control Board. The pollutants tested were dust particles, SO₂ and NO₂. It is seen that the output air has reduced quantities of these pollutants compared to the input air.

Table3. Test results

SI NO.	Pollutants	Amount in atmospheric air (mg/Nm ³)	Amount in output air (mg/Nm ³)
1.	SO ₂	60	47
2.	NO ₂	72	53
3.	Dust	90	13

The percentage reduction of SO₂, NO₂ and dust particles obtained from the test results are calculated as follows:

$$\text{Reduction of SO}_2 = \frac{(60-47)}{60} \times 100 = 21.66\% \quad (1)$$

$$\text{Reduction of NO}_2 = \frac{(72-53)}{72} \times 100 = 26.38\% \quad (2)$$



$$\begin{aligned}\text{Reduction of dust} &= \frac{(90-13)}{90} \times 100 \\ &= 85.55\%\end{aligned}\tag{3}$$

Thus, the purified air that was released from the modular air purifier had 85% less dust particles compared to the atmospheric air. The other two pollutants measured that is, SO₂ and NO₂ were also lowered by 21% and 26%, respectively

CONCLUSION

A prototype of the proposed modular air purifier was developed. Based on experimental results it is seen effective to remove the pollutant gases present in the atmosphere and make atmosphere air suitable for inhaling. These modular air purifier if placed at sufficient intervals can limit the amount of pollutants in the air. Use of activated carbon of higher efficiency will increase the output by a larger scale. It will be high need in metropolitan cities like Delhi were due to the high levels of air pollutants schools and factories have been shut down leading to disruption of human activities and economic loss

ACKNOWLEDGMENT

The work was completed with help of technical staff from Amaljyothi College of Engineering. Thankful to all officers from integrated environment at solutions approved laboratory by Kerala pollution control board Kottayam for test of our work.

REFERENCES

1. Pratima Gupta, Ranjit Kumar, Shalendra Pratap Singh, Ashok Jangid, "A study on monitoring of air quality and modeling of pollution control."
2. ENVIS Centre CPCB, "Air pollution in Delhi", 2016.
3. P G Gray, "A fundamental study on the removal of air pollutants(sulphur dioxide, nitrogen dioxide and carbon dioxide) by adsorption on activated carbon" Gas separation and purification, vol. 7, no. 4, 1993.
4. Ralina Shirin Akbar, Christopher M K Chew, Nurhazwani Ismail, TVN Padmesh, "Adsorption of gaseous pollutants(SO₂ & CO) onto palm shell activated carbon", EURECA 2013
5. Aghighi, A., & Haghighat, F. (2015). Evaluation of nano-titanium dioxide (TiO₂) catalysts for ultraviolet photocatalytic oxidation air cleaning devices. Journal of Environmental Chemical Engineering, 3, 1622–1629.



Sustainable Infrastructure Management: Recovery and Reuse of Resources and Energy in Landfills

Dr Anumita Mishra^{*1}, Prof Rao Y Surampalli²

Department of Civil Engineering, Indian Institute of Technology Roorkee, Uttarakhand¹

Global Institute for Energy, Environment and Sustainability, Lenexa, Kansas, USA²

*✉ anumita.mishra@ce.iitr.ac.in

ABSTRACT

The world is witnessing ever expanding urbanization of their cities where a lot of solid waste is generated continuously. The environmental laws are stringent and the environmental engineer has a tough task of planning construction and operation of landfills with limited land and money. Under the circumstances, there has been a paradigm shift in the perception of managing landfills. The scientists and engineers are now looking at the landfills as valuable resources of compost and energy and the landfill site as a factory where municipal solid waste enters as input raw material, gets processed and the valuable outputs are compost and methane gas. This paper revisits the different phases of biochemical processes and presents the related emerging technologies like enhanced landfill mining, semi aerobic landfill, bioreactor landfill and semi mechanized trench technique. This paper reviews the challenges of efficient biodegradation of solid wastes, management of leachate and landfill gases and also the procedure of proper closures of landfills.

Keywords : Solid waste; Landfill; Bioreactor landfills; Biological degradation; Leachate recycle; Resource reuse.

INTRODUCTION

The solid waste disposal system in municipalities are often in the form of landfills which are engineered and constructed to contain the wastes [1, 2]. The wastes are buried between the soil layers and allowed to stabilize by the action of bacterial biological degradation or decomposition. A liner system is provided at the bottom to prevent leachate from entering into the soil and aquifer beneath. The top of the landfill is covered with soil and rain water or storm water is suitably disposed-off by providing drainage arrangements. All these arrangements are provided with the intention of converting wastes into usable products (e.g., methane and stabilized solid waste as fertilizer), with little or minimum damage to the environment. But, municipalities have limited land and money and the generation of solid waste is continuous. Therefore, planners are often worried about finding newer sites of disposal. There has been a paradigm shift from this perception recently and the landfills are now being constructed as a reusable resource of compost and energy apart from getting rid of the municipal solid wastes.

CLASSIFICATION OF LANDFILLS

Landfills may be classified based on the type of waste material which are required to be managed, such as: Municipal Waste Landfill, Industrial Waste Landfill, Demolition Waste Landfill and Hazardous Waste Landfill. They may also be classified based on the type of stabilization process such as: anaerobic type, aerobic type and the hybrid type in which both aerobic and anaerobic processes take place.

LANDFILL COMPONENTS AND THEIR DESIGN REQUIREMENTS

Depending on the depth of water table during rainy season, the landfills may be located either above the ground or partially underground. The former is provided when ground water table is high and the latter is provided when ground water table is low [3, 4]. The site may be flat or slightly sloping, therefore, the design of some components would depend on the type of site. Typically, the landfill has the following components [5, 6] shown in the **Fig. 1**.

Liner System

It consists of compacted low permeability soil layer profiled and graded in such a way that piping system laid over it would facilitate collection of leachate under gravity. A strong waterproof geosynthetic membrane is laid between profiled subgrade and the piping system with the objective of containing pollutants.

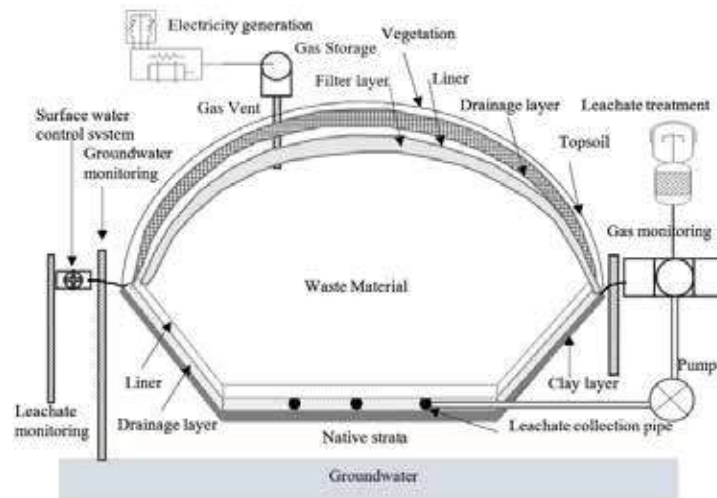


Fig. 1. Cross-section of a modern containment landfill with on-site leachate treatment facilities and electricity generation from landfill gas facilities

Pipe network and pumps to collect Leachate

Sometimes the leachate collection system may require pumping. The leachate is highly concentrated and toxic and has high BOD and COD. It is collected and stored in suitably designed storage tanks. The leachate quality is continuously monitored.

Collection of Landfill gases

The perforated piping system with vents are suitably installed which collect and release gases into the atmosphere. The piping network has horizontal and vertical pipes both. Sometimes vacuum pumps, extraction wells and header pipes are also installed to collect gases.

Soil layers to cover the solid municipal waste on daily basis

The whole site of landfill is divided into numerous cells and the sorted municipal waste is dumped into these cells one by one. The sorted solid waste is inspected for non biodegradable materials and the truck loads detrimental to the biodegradation process are not allowed to dump into these cells. The municipal waste is evenly spread and compacted with the help of heavy machinery to reduce in volume and then covered with a soil layer on daily basis. As a result of compaction, the moisture present in the municipal solid waste trickles down into the leachate collection system.

Final layers of soil after closure

After the landfill site has been loaded with designed amount of solid waste, the site is closed. Covering layers are constructed on the top of the landfill after closure within 180 days. Layers of compacted clay or geosynthetic materials are applied over the entire landfill surface to prevent migration of gas and entry of surface water into the landfill as a final cover or cap. The final cover typically consists of a vegetation layer followed by a protective soil layer, drainage layer, hydraulic barrier, gas control layer, and a foundation layer. The surface or vegetation layer is to provide suitable soil for plant growth. The protective layer prevents the roots of the plants from penetrating the hydraulic barrier. The drainage layer facilitates easy flow path to a grid of perforated pipes. The hydraulic barrier prevents the movement of water into the landfill. The gas control layer acts as a vent to carry the gases to the surface. The foundation layer or the grading layer provides a stable foundation to build upon rest of the cover layers. All these layers may not be needed in some cases.

Storm water collection

The rainfall occurring over the landfill site is suitably collected into the drainage ditches leading to the natural stream. The ditches are designed for maximum rainfall of 25 years of recurrence interval [7].

Stable slopes

The landfill site should not be sloping at steeper slopes that are not stable under saturated conditions. Suitable horizontal stretches known as berms are constructed in between. The berms also serve as service roads.



PHASES OF BIOLOGICAL PROCESSES

Phase one starts immediately after placing the wastes in landfill. The aerobic bacteria becomes active in surface layers and starts degrading the waste. Oxygen is continuously consumed by the aerobic bacteria and carbon dioxide is released in the process. In the second phase, anaerobic bacteria also become active in deeper layers and starts releasing methane, little amount of ammonia, hydrogen sulphide and carbon dioxide. The end of second phase is marked when all the oxygen is depleted. The decomposition further continues in the third phase and brings down the pH value to its lowest and the leachate is very acidic which dissolves some inorganic matter as well. In the fourth phase, a lot of methane is generated and pH value of leachate rises. In the final phase, also called maturation phase, almost all of the organic matter has been stabilized and thus, the landfill gas production reduces considerably. Some oxygen and nitrogen also starts reappearing in the landfill gases.

MICROBIAL GROUPS PARTICIPATING IN ANAEROBIC REACTIONS

The solid waste contains a variety of organic and inorganic matters. The discussion is about the different chemical substrates and the respective microbes involved in the biodegradation process in absence of oxygen. There are various complex organic polymers in the waste which are broken by a different class of bacteria called hydrolytic bacteria and fermenting bacteria into simple monomers. The simple monomers are further degenerated by acetogenic bacteria. The acetic acids and volatile fatty acids are degenerated by acetoclastic methanogenic bacteria and methanogenic archaea, respectively. The cellulose and hemicellulose are attacked by cellulolytic and hemicellulolytic bacteria, respectively. The sulphates are reduced by sulphate reducing bacteria and hydrogen is oxidized by hydrogen oxidizing methanogenic bacteria.

THE LANDFILL RELATED ENVIRONMENTAL ISSUES

The degradation of solid wastes by bacteria produces leachate and numerous odorous gases which may pollute the soil, water bodies and air so there are issues and environmental laws related to proper management of these pollutants.

Landfill Leachate

This is a highly toxic liquid with very high values of BOD and COD. It trickles down to the bottom of the landfill, thus, it is not allowed to come in contact with the soil and groundwater bodies below [8]. The bottom liner and the pipe network is installed at the bottom of the site to collect it safely and is taken to the storage tanks. From the storage tanks, it may be taken to the treatment facility directly or recirculated back into landfill in case of bioreactor type landfills for moisture addition to increase the biological degradation. The leachate in young landfill is acidic in nature and its oxygen demand is high, but as the waste stabilizes, its pH value rises and the oxygen demand decreases gradually.

Landfill Gases

The gases produced in the biodegradation process are mainly methane (50-60%) and carbon dioxide (40-50%). Traces of hydrogen sulphide (less than 5%), carbon monoxide, ammonia and nitrogen are also produced. Methane is combustible and can be harnessed as a resource [9] if collected and managed suitably by proper design of the landfill site [10]. Hydrogen sulphide and ammonia have unpleasant odors and thus may create nuisance if not removed properly prior to use of methane. Most of the landfill gases are also greenhouse gases, thus, their proper management is bound by environmental laws [11].

PROPER CLOSURE OF LANDFILL SITE AND ITS END USE

After the landfilling is done to its designed capacity, the closure activities start within 30 days and the site needs to be properly closed within six months. For preparing a closure plan, a number of factors are considered such as: the final cover thickness, overall grade for slope stability and possible final settlement. Proper closure implies placing a final cover of soil of appropriate thickness and profile, installing rain water collection system, planting of vegetation, proper monitoring and collection of leachate and landfill gases, and also the ground water quality and air quality in the vicinity. Aftercare plan is also prepared judiciously and inspections are done for a specified period of time. The soil cover and methane gas generation is constantly monitored and repairs are immediately done wherever required. Post closure monitoring is conducted for a specified period of time. Properly managed closed sites can be used as parks, playground, agriculture and forestry purposes and also for storage. Converting closed landfills into parks is very common practice in many countries.

INNOVATIVE TECHNOLOGIES OF SOLID WASTE MANAGEMENT

Recent perception in management of solid wastes has changed from getting rid of unwanted garbage to recovery of useful resources and energy contained in the solid waste. Some of these technologies are briefly described below.

Enhanced Landfill Mining (ELFM)

The environmental engineer faces a tough task of designing an economical solid waste management project under various stringent social and ecological norms [12]. The enhanced landfill mining (ELFM) envisages a system in which the landfill is designed, constructed and operated using most advanced technologies to yield usable resource materials and energy from solid wastes. It looks like an efficient and continuous process as in a factory in which municipal solid waste is the prime input and usable materials and energy are the prime outputs [13].

Semi-aerobic Landfill

In this system, the leachate is removed and natural air is injected, thereby making it a semi-aerobic type stabilization process, as shown in **Fig. 2**. Under such an environment, the stabilization process is relatively faster. The aerobic bacteria converts carbon into mostly carbon dioxide and it does not generate foul odor since hydrogen sulfide and methane production are limited [14, 15].

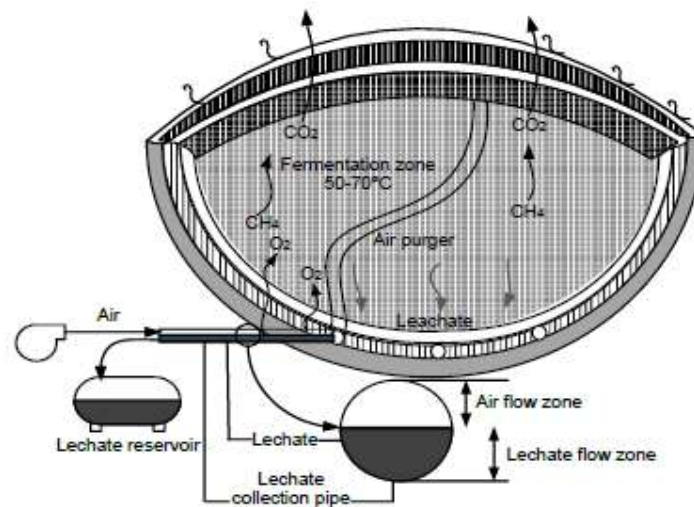


Fig. 2. The schematic diagram of a semi-aerobic landfill

Bioreactor Landfill

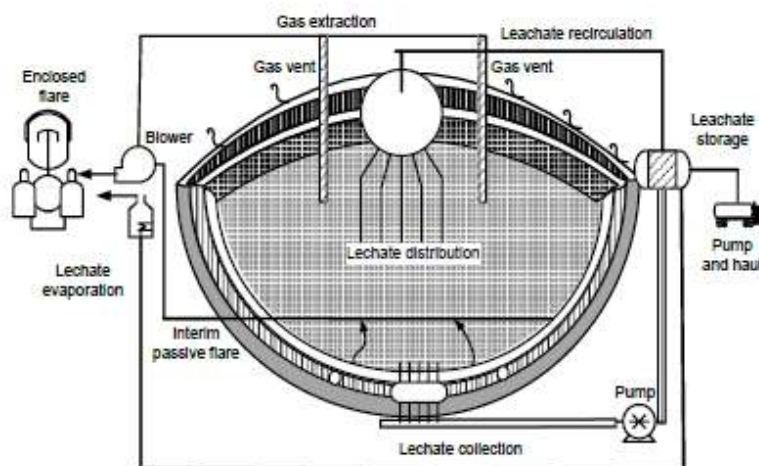


Fig. 3. The schematic diagram of a bioreactor landfill

This technology utilizes mostly anaerobic biological degradation through activation of anaerobic bacteria. The leachate and some makeup liquid is recirculated in the landfill to keep solid waste moist and which promotes faster stabilization of wastes, as shown in **Fig. 3**. The optimum moisture level is about 40 to 60% of field capacity. The distribution of moisture is done evenly to the entire landfill mass through lateral or vertical pipes and the same pipes can also be used for gas collection. For this



purpose, drip irrigation tubing, surface spraying, horizontal trenches or vertical injection needles may be employed. Sometimes, pressurized air is also injected. The biodegradation takes place at a faster rate and the landfill mass reduces in volume rapidly, thus providing additional capacity of about 20 to 40%. The leachate handling cost and post closure cost is also greatly reduced in this type of landfill [16]. The production of methane is maximum but it requires careful monitoring and controls over the process. The methane is utilized as an energy source since it is combustible.

The Semi Mechanized Trench Method

Sometimes the municipalities have enough land but limited money to spend on garbage disposal. In such situations, this method of waste disposal may be used. Trenches are dug and the excavated material may be partly used elsewhere [17]. These excavated trenches receive the municipal wastes. The wastes stabilized in semi-aerobic conditions get compacted under its own overburden. Thereafter, they are covered with a layer of previously excavated soil on daily basis. This method is useful in small cities.

CONCLUSIONS

The urban areas are fast expanding all over the globe in the present times and lots of solid wastes are being generated. The municipalities are often facing the challenge of managing landfills under stringent environmental regulations. They have to manage with limited land and limited money. This paper presents the recent innovations in the landfill management which envisages the landfills as resources and energy source rather than burden on municipalities. The scientific processes involved in different technologies have been discussed. The approach of enhanced landfill mining has been explained and several other technologies like semi-aerobic landfill, bioreactor landfill, and semi-mechanized trench have been discussed briefly in this paper. The full-scale implementation of these innovations is governed by regulations, cost analysis, technical feasibility and sustainability.

REFERENCES

1. K-R. Kim and G. Owens, Journal of environmental management, vol. 91, pp. 791-797", 2010.
2. P. Frändegård, J. Krook, N. Svensson and M. Eklund, Journal of Cleaner Production, vol. 55, pp. 24-34, 2013.
3. P. White, M. Dranke and P. Hindle, Integrated solid waste management: a lifecycle inventory, Springer Science & Business Media, 2012.
4. M.L. Davis and D.A. Cornwell, Introduction to environmental engineering, McGraw-Hill Companies, 2008.
5. R.E. Marshall and K. Farahbakhsh, Waste Management, vol. 33, pp. 988-1003, 2013.
6. G. Tchobanoglous, H. Theisen and S. Vigil, Integrated solid waste management: engineering principles and management issues, McGraw-Hill Science/Engineering/Math, 1993.
7. A. Bagchi, Design of landfills and integrated solid waste management, John Wiley & Sons, 2004.
8. M. Rawat, U.K. Singh, A.K. Mishra and V. Subramanian, Environmental monitoring and assessment, vol. 137, pp.67-74, 2008.
9. H.R. Amini and D.R. Reinhart, Waste Management, vol. 31, pp. 2020-2026, 2011.
10. J.W. Wong, R.Y. Surampalli, T.C. Zhang, R.D. Tyagi and A. Selvam, Sustainable Solid Waste Management, American Society of Civil Engineers, 2016.
11. G. Emmi, A. Zarrella, A Zuanetti and M. De Carli, Energy Procedia, vol. 101, pp. 352-359, 2016.
12. P.T. Jones, D. Geysen, Y. Tielemans Y, S. Van Passel, Y. Pontikes and B. Blanpain, Journal of Cleaner Production, vol. 55, pp. 45-55, 2013.
13. S. Van Passel, M. Dubois, J. Eyckmans, S. De Gheldere, F. Ang and P.T. Jones, Journal of Cleaner Production, vol. 55, pp. 92-102, 2013.
14. J.E.S. Center, Minister's Secretariat Waste Management and Recycling Department, Nagoya Google Scholar, 2012.
15. O.P. Karthikeyan, S.Y.M. Jane and R. Balasubramanian, Bioresource Technology, vol. 217, pp. 205-209, 2016.
16. S.K. Khanal, R.Y. Surampalli, T.C. Zhang, B.P. Lamsal, R. Tyagi and C. Kao. Bioenergy and biofuel from biowastes and biomass, American Society of Civil Engineers, 2010.
17. S.M. Oakley and R. Jimenez, Waste Management, vol. 32, pp. 2535-2551, 2012.

Green Hydrogen: A Perspective

S Sakthivel*, Shireesh S Swami, Atul Choudhari

Technology Group, TATA Consulting Engineers Ltd, Mumbai

*✉ ssakthivel@tce.co.in

ABSTRACT

Hydrogen is a clean-burning and emission free fuel, which can produce locally any primary energy source, be it fossil or renewable. It has highest energy density (120 MJ/kg), which compared gasoline (45 MJ/kg) and which ensures energy security (i.e., produced from a variety of domestic sources). Hydrogen is an alternative clean fuel, particularly for hydrogen vehicles, alternative industrial feedstock, power generation and energy storage etc. Furthermore, hydrogen is involving new applications for example vehicle fuel, DRI process, and energy storage. In this context, to understand entire hydrogen value chain includes production, storage, transportation and distribution to end user. This article focuses on overview of green hydrogen production methods, landscape of electrolyser technology, cost analysis.

Keywords : Electrolysis; Green hydrogen; Cost Analysis; Applications.

INTRODUCTION

Presently, global economy is based on fossil fuel economy, which is referencing the global hydrocarbon industry. The energy used mostly comes from fossil fuels like crude oil, natural gas and coal. Problems of using these fossil fuels are emission of greenhouse gases (GHGs), price fluctuation, issues with supply /distribution network, etc., These problems can be minimized by adopting clean energy or alternative clean fuel such as Hydrogen. Hydrogen economy relies on use of hydrogen as a low carbon commercial fuel in transportation sector, alternative industrial feedstock, power generation and energy storage etc., [1].

At present, worldwide hydrogen production is around 70 MMtpy. Currently there are four main sources for commercial production of hydrogen such as natural gas (48%), crude oil (30%), coal (18%) and water electrolysis (4%) [2]. In this context, the energy transition is a pathway towards transformation of the global energy sector from fossil-based fuels to zero/ low-carbon emission fuel. Hydrogen could transform the global energy production leveraging 'a more natural and sustainable substitute' for fossil fuels. Solar PV, wind, hydro power, nuclear, geothermal, biomass, and tidal energy can be used in the production of hydrogen at commercial-scale. Hydrogen is finding applications in a fuel cell electrical vehicle, industrial feedstock for ammonia production, power generation and stationary power generation, making the process sustainable and cleaner. A typical Hydrogen economy value chain is shown in Fig 1.

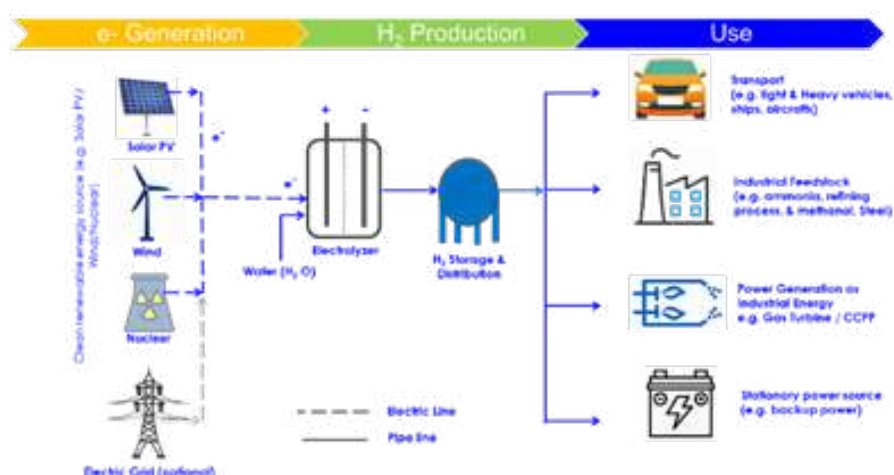


Fig. 1. Flow scheme of green production via renewables and their applications

Overall annual hydrogen demand is estimated to increase eightfold by 2050. Hydrogen is being used in steel and special steel production as a reducing agent and semiconductor industry as a carrier gas. **Fig. 2** depicts that global hydrogen demand will increase due to increased demand from existing and newer industrial applications. In 2020, global demand for hydrogen in various industries stood at 0.7 MMT (million metric ton) for transportation, 1.4 MMT for Industrial Energy, 1.4 MMT for building heat and energy, 0.7 for new feedstock (CCU, DRI) and 1.4 MMT for power generation.

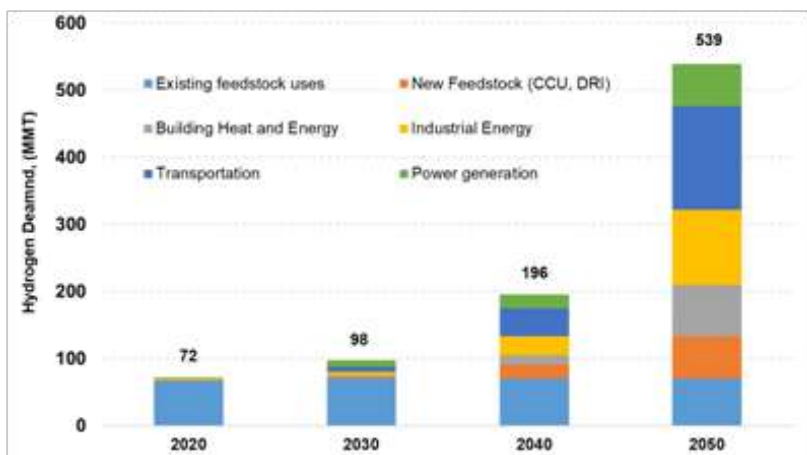


Fig.2. Hydrogen demand projection

Role of Hydrogen

Hydrogen is expected to play a crucial role in several industrial segments as discussed in the following paragraphs.

Transport: Hydrogen can be utilized in transport sector by either directly combusting it in Internal Combustion (IC) engines or by replacing the IC engines by fuel cells (FC) as in electric vehicles. The fuel cell systems are relatively more energy efficient when compared to IC engine (hydrogen fuelled) based systems. While few automotive manufacturers (like BMW) in the past decade concentrated on hydrogen fuel-based IC engines rather than fuel cells, other leading automobile manufactures (like Toyota, General motors, Hyundai, Mercedes Benz etc.) have shown greater affinity towards the fuel cell technology. Typically, the IC engines operating on ‘Carnot cycle’ have efficiency in the range of 25% to 33%, while the system efficiency of fuel cells ranges between 45% to 65% depending upon the technology in use and the end application. Hydrogen powered fuel cell electrical vehicles (FCVs) received much revelation during the 2000s, but lack of commercial models and technological maturity, contributed to growth of battery electric vehicles. However, hydrogen FCVs will now be approaching maturity considering developments in hydrogen technology and infrastructure.

Stationary power generation: Hydrogen is one of the foremost options for production of electricity and thermal energy using fuel cell. Hydrogen is used as an energy carrier as well as energy storage medium. Stored hydrogen being used for off-grid sites for back-up power applications. Stationary fuel cells are now emerging energy system, which produces electrical power and co-generation of a thermal energy. Stationary fuel-cell power stacks are used for office, home and large-scale power plants to offer emergency power and supplemental power for on-site service, which reduces carbon emissions. It has several applications such as reliability, power quality, remarkably higher system efficiency and quiet source of power.

Hydrogen will be playing a notable role for building heating purposes, which has potential to replace up to 50 % of natural gas consumption used for building heating requirements in cold countries. Hydrogen can also be blended in building’s existing natural gas network. Generally, use of fuel cells for building heating purpose is gaining momentum in cold countries like European region, Japan, Korea etc. Fuel cells are proving to be the best fit for buildings as they are having low space heating requirement. Recently, more than lakhs of houses are using fuel cells for heating purpose in Japan. In addition, Fuel cell is also used to provide emergency backup power and primary power in computer data centers, where continuous power supply is a mandatory requirement for proper functioning.

Industry Feedstock: Hydrogen is a common industrial feedstock and it is being used in refinery operation, ammonia and methanol production processes, steel making process of direct reduction of Iron ore and other industries like inert or protective gas in producing flat glass, food processing, electronics, metal alloying. If hydrogen produces from clean energy sources, it



could be used to make green-ammonia. Ammonia can be used as hydrogen carrier. For example, ammonia can provide high hydrogen storage densities.

Currently hydrogen is used in desulfurization process in refinery for removing contaminants, such as Sulphur, from gasoline/diesel fuels. Approximately 75% of hydrogen is presently used in various sectors such as refinery, hydrogenation, coolant, fertilizer- ammonia, and semiconductor industry, which is produced from conventional energy source by burning fossil fuel like natural gas/naphtha/coal.

These fuels are responsible for higher carbon emission. Hydrogen economy propose to use sustainable energy source for hydrogen production and its use as industrial feedstock. Renewable energy from solar /wind can be stored in efficient manner by converting it into hydrogen using electrolysis. The same hydrogen can possibly be used not only for mobility purposes but also for other energy needs in metals, chemicals and other industries. Hydrogen can also be used as a fuel to generate power through microturbines or gas turbines.

Hydrogen plays a vital role in many sectors, which helps to further development of hydrogen economy. Before moving towards to a hydrogen economy, to understand about complete value chain of hydrogen infrastructure which includes production, storage, transport, distribution and utilization at end user.

PRODUCTION ROUTES

Several technologies have been industrialized to produce hydrogen from renewable and non-renewable sources as shown in the **Fig 3**. The hydrogen represents different color coding depending on its source of raw material and production technology like brown, grey, blue and green hydrogen. Both brown and grey hydrogen production processes use fossil fuels as feedstock (coal gasification for brown, natural gas reforming for grey).

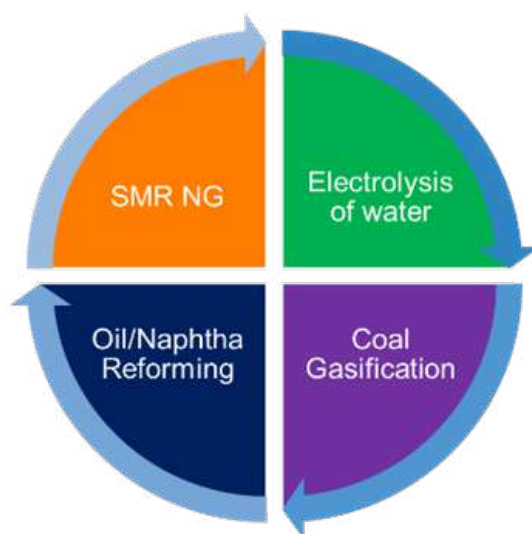


Fig. 3. Routes of hydrogen production

With these production technologies, large amount of carbon dioxide is being released to atmosphere resulting in severe damage to the environment. While Green hydrogen is produced through electrolysis of water by using renewable energy sources, which does not produce CO_2 and hence no emissions to atmosphere. But, green hydrogen is showing encouraging trends towards sustainable solutions in the long term than brown and grey hydrogen.

Steam methane reforming (SMR). This is most widely used and well-known process for commercial-scale production of grey hydrogen. Typical process conversion efficiency (natural gas to hydrogen) of this technology is 74%–85%. Today, about 96 % of global hydrogen production from this route, which offers cheapest hydrogen production cost. However, this process intakes fossil fuel as feedstock and emits high concentrations of CO_2 .

Biomass-to-hydrogen. Two types of processes are used to produce hydrogen from biomass pyrolysis and biomass gasification. The biomass pyrolysis process gives several products such as syngas ($\text{CO}+\text{H}_2$), bio-oil, biochar and carbon, charcoal. Typically, 30 kg–40 kg of biomass is required to produce one kg of hydrogen.

Biomass can be transformed into hydrogen and hydrogen-rich gases by thermochemical processes. Generally, a thermochemical process is classified as pyrolysis and gasification. Biomass gasification is the thermal decomposition of biomass occurring in the presence of oxygen at a temperature range of 200°C–1,200°C at 1 bar(g) –33 bar(g) pressure. Typical biomass gasification efficiency is 52%, but it depends on the type and quality of feedstock, type of catalyst, temperature and pressure levels, etc.

Today, many energy producers are willing to invest on carbon-free energy production technologies and are keen to replace fossil fuel-based energy production technology due to country's policy, pledge and commitment to zero emission ambition. Green hydrogen is produced from electrolysis of water and the power is drawn by non-conventional or renewable energy sources. Various types of water electrolysis such as Alkaline Water Electrolysis (AWE), Proton Exchange Membrane Electrolysis (PEM), Solid Oxide Electrolysis (SOE) and Anion Exchange Membrane Electrolysis (AEM) are used for successful and commercial production of green hydrogen.

In AWE & PEM electrolysis process oxygen is separated at anode and hydrogen at cathode under the influence of direct current. Both these technologies are producing hydrogen at megawatt scale commercially and the cost of production is decreasing continuously and exponentially due to technological advancements.

Typically, AWE & PEM cell stacks consume power in the range of 3.8 kWh/Nm³ and 4.53 kWh/Nm³, respectively. AWE stack can produce up to 3,880 Nm³/h of H₂ (~8 TPD) & capacity of PEM stack can go as high as 4,000 Nm³/h. These two technologies of AWE and PEM are dominating the current market than SOE. Anion exchange membrane (AEM) water electrolysis has several advantages which can replace the conventional noble metal electrocatalysts. AEM electrolysis is still under research and development (R&D) stage at laboratory scale and not yet commercialized. However, these technologies are available with different levels of maturity. Based on current technological maturity, global cumulative installed capacity of green hydrogen stood at 100 MW from 2010 to 2018 [3]. Each technology differs in their individual characteristics and their key performance indicators as shown in the **Fig 4**.

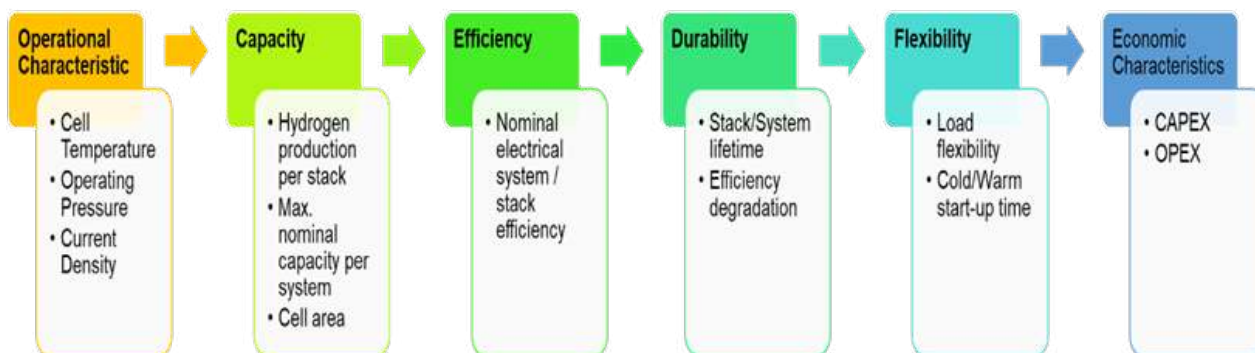


Fig. 4. Key performance indicators for electrolyzers

HYDROGEN COST

Generally, the cost of green hydrogen is a function of the price of electricity needed, the cost of the electrolyser and operating cost to run the system. Currently, green hydrogen production cost varies from US\$ 3 to 7.5 per kg of hydrogen [4]. The hydrogen cost differs due to the source of electricity price. Cost of hydrogen production with AWE / PEM electrolyzers and different power sources are depicted below;

- Grid power: 5.73 \$/kg
- Solar power: 8.96 \$/kg for larger scale and 13.55 \$/kg for small one
- Wind power: 8.01-9.1 \$/kg

But, the brown/grey hydrogen production cost varies from US\$ 0.9 to 3.2 per kg of hydrogen due to country's natural gas price variation.

Typically, CAPEX cost calculations include various components such as electrolyser cost (including the balance of plant), stack replacement, project planning, depreciation period and interest rate. OPEX costs includes direct operating costs of production



(i.e., raw materials as water, specific electricity consumption, KOH requirements, process steam, nitrogen and maintenance cost etc. are considered, without considering insurance, taxes, administration, distribution, overhead costs, etc.

Mass balances and utility requirements have been adapted from literature [5]. The hydrogen production costs analysis is based on the key assumptions;

- Specific energy consumption of electrolyser is 53 kWh per kg of hydrogen
- Capex of an electrolyser approximately US\$ 840 per kW
- 8,000 annual full load hours
- Production capacity would be 160 TPA
- 10-year life and linear depreciation
- H₂ storage cost at US\$ 0.23 per kg
- H₂ transport costs US\$ 1.73 per kg

Further, typical utilities consumption for a kilogram of hydrogen production as 10.11 m³ of pure water, 2.75 x 10⁻⁴ kg of KOH solution, 0.038 kg of process water and 0.7115 x 10⁻⁴ kg of nitrogen.

Renewable energy price has been reducing dramatically due to technology development and is seeing increased investment from major global players. In this context, Saudi Arabia, Qatar and Abu Dhabi are proving to be lowest-cost sources of renewable energy.

Renewable price varies from country to country and technology used to generate the power. In 2018, the global weighted-average Levelized Cost of Electricity (LCOE) of Solar PV, wind onshore, wind offshore, geothermal, hydro power and concentrated solar power was US\$ 85, 60, 127, 72, 47 185 per MWh, respectively [6]. **Fig. 5** depicts hydrogen cost produced from different renewables. The estimated hydrogen cost is less than US\$ 6 per kg of H₂ including storage and transport by using Hydro and Onshore wind power. However, energy producers mostly prefer solar PV and wind energy to produce green hydrogen.

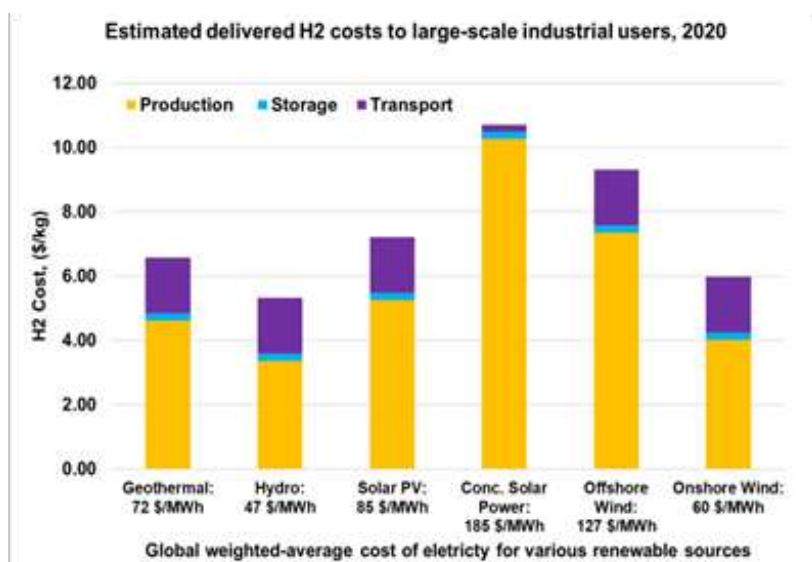


Fig. 5. Green hydrogen cost from different renewable sources

Fig. 6 depicts estimated green hydrogen costs in different regions for solar PV. It can be inferred from the **Fig. 5** that gulf region could produce lowest cost green hydrogen than other regions like India, USA, Japan, and China. Recently, the cheapest solar PV power cost about 30 \$/MWh was reported by Dubai, Abu Dhabi - Saudi Arabia. In such a scenario, Green hydrogen production cost can be as low as around US\$ 2.51 per kg of H₂, excluding storage and transportation cost, which shows cost competitiveness compared with conventional (steam methane reforming- SMR technology) hydrogen production technology. It indicates that green hydrogen takes great advantage from rapid reduction of solar PV and wind energy price.

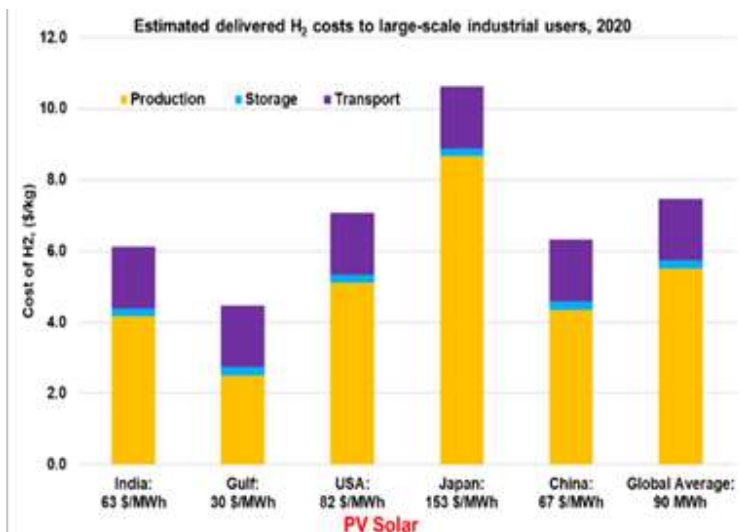


Fig. 6. Estimated green hydrogen costs in different regions for solar PV

BREAKEVEN ANALYSIS

Fig. 7 depicts break-even analysis of the green hydrogen production cost curve and to evaluate and compare the impact of the electricity price on the production costs of green hydrogen and relate it to fossil fuel based brown/grey/blue hydrogen costs. The grey colour panel shows costs of hydrogen produced from fossil fuel via SMR and coal gasification. It indicates that the cost of green hydrogen production will fall drastically due to declining costs of renewable electricity price and along with improvement and scaling up of electrolyser manufacturing. For instance, in a scenario where electricity prices are below US\$ 40 / MWh, green hydrogen cost is expected to reach cost competitiveness and can break-even in comparison with conventional production technologies.

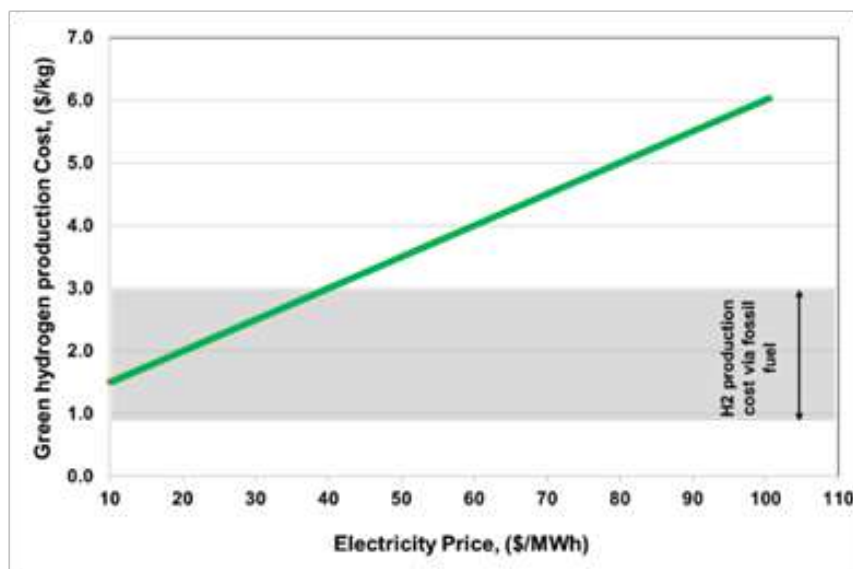


Fig. 7. Break-even analysis for green hydrogen with grey/blue hydrogen

TAKEAWAY

Hydrogen is an emerging fuel as a clean and alternative source of fuel, which is fetching newer applications such as transport fuel, industrial feedstock, building heating energy, industrial energy and industrial power (i.e. H₂ firing in Combined Cycle Power Plant) and stationary power generation. It reflects that the future of industry is green hydrogen and will enhance rapid



growth to ensure sustainable economy globally. This green hydrogen will penetrate domestic market as renewable energy growth with lower prices are happening and proactive policies frameworks encouraging sustainable growth are being promoted towards zero emission ambition. Engineering consulting firms need to play a significant role in this ambition and green hydrogen value chain of integrating various technologies for renewables, H₂ production, storage and distribution to end users.

REFERENCES

1. S Sakthivel, "Way forward to carbon-free electricity for e-mobility," Chemical Industry Digest, June 2019.
2. S Sakthivel, Hydrogen economy offers low-emissions fuel to combat air pollution, Gas Processing & LNG, pp. 25-27, July/Aug 2020.
3. IEA, Electrolyser capacity installed by year-2010-2018, IEA, Paris <https://www.iea.org/data-and-statistics/charts/electrolyser-capacity-installed-by-year-2010-2018>.
4. IEA, Hydrogen production costs by production source-2018, IEA, Paris <https://www.iea.org/data-and-statistics/charts/hydrogen-production-costs-by-production-source-2018>.
5. Kuckshinrichs W, Ketelaer T and Koj JC, Economic Analysis of Improved Alkaline Water Electrolysis. Frontiers in Energy Research, vol 5 (1), doi: 10.3389/fenrg.2017.00001, 2017.
6. IRENA (2019), Renewable Power Generation Costs in 2018, International Renewable Energy Agency, Abu Dhabi.



Green Multi-Storey Society Concept for Urban Area of India

Kapil Kukreja^{1*}, Manoj Kumar Soni², Bibekananda Mohapatra¹

National Council for Cement and Building Materials (NCB)¹

Birla Institute of Technology and Science, Pilani²

Delhi-Mathura Road (NH-2), Ballabgarh, Faridabad, Haryana

*✉ kapil.kukreja@ncbindia.com

ABSTRACT

At present, almost 34 percent of the population of India resides in urban areas which are forecasted to increase by 40.76 percent by 2030. With increasing population density in an urban area, the development of multi-storey societies is increasing rapidly. Various states and central government put a lot of effort into making policy for sustainable development of multi-storey societies which includes rainwater harvesting, solar cell installation at the roof, zero sewage treatment plant (STP) discharge, green area development, and segregated household waste management, etc. This paper highlight the use of kitchen waste for producing biomass, which can be used for cooking purpose in the multi-storey society by replacing some part of Liquid Petroleum Gas (LPG) as well as for the generation of electric power by replacing diesel in the diesel engine.

Keywords : Biogas; Kitchen waste; LPG, Diesel generator.

INTRODUCTION

At present, almost 34.47 percent of the population of India resides in urban areas which are forecasted to increase by 40.76 percent by 2030 [1-2]. With increasing population density in an urban area, the development of multi-storey societies is increasing rapidly. Various states and central government put a lot of effort into making policy for sustainable development of multistore society which includes rainwater harvesting, solar cell installation at the roof, zero STP discharge, green area development, and segregated household waste management, etc [3]. This paper highlight the use of kitchen waste as biomass, which can be used for cooking purpose in the multi-storey society by replacing some part of LPG as well as for the generation of electric power by replacing diesel in the diesel engine. Biogas when used for cooking can conserve LPG and provide a cooking solution to areas where there is higher demand. On the other way, each multi-storey apartment has the power back up and this power back is being provided by a diesel generator, the electricity unit cost while operating at DG is very high from 16 to 20 Rs/unit. In urban areas, the average LPG consumption per family per month is 12.37 kg (~400g /day/family). The calorific value of biogas is ~30 MJ/kg when compared to the calorific value of ~46.1 MJ/Kg for LPG [4]. Hence, 1 m³ of biogas may be replaced by 0.40 kg of LPG. This paper covers a case study for a multi-storey urban society located in Faridabad, Haryana, India, comprising 1600 flats and a total of 20 nos. towers.

KITCHEN WASTE AS A SOURCE FOR COOKING GAS

Municipal waste can be categorized as organic and non-organic. Kitchen waste constitutes the organic part. Treatment of kitchen waste moreover contributes towards the Indian government initiated Swachh Bharat Mission. Kitchen waste-based system turns out to be 800 times more efficient than conventional systems of biogas generation. This is because kitchen waste has a comparatively high calorific and nutritive value which is very beneficial for the microbes. This increases the methane-producing efficiency. Kitchen waste has high water content and low lignin and lingo hence, anaerobic degradation is a practical approach to produce biogas. Cellulose content makes it optimal for the digesting process. At the least, it reduces the foul smell which would be caused by decaying food waste [5]. Kitchen waste also has less solid content (organic material) as compared to cow dung so it is rapidly decomposed by the anaerobic microbes [6]. This case study was conducted for a multi-storey urban society comprising of 1600 flats (20 nos. towers). As per data collected from a number of families (2 families from each tower having the family size of 2 Adults + 2 kids), an average of 2 kg kitchen waste is being generated per family per day, hence total estimated waste generation is 3200 kg (1600 nos. flats). The main source of cooking fuel in society is LPG (in cylinders). Society was having all the facilities like rainwater harvesting, STP, developed green area, solar cell on the roof, etc.

A KVIC (Khadi and Village Industry Commission) floating drum type model (large scale plant) is proposed for the society for biogas generation as the same technology is working satisfactorily for kitchen waste-based biogas generation at Indian Institute of Technology, New Delhi [7]. Following **Fig. 1** shows the typical working of KVIC type floating drum type biogas plant:

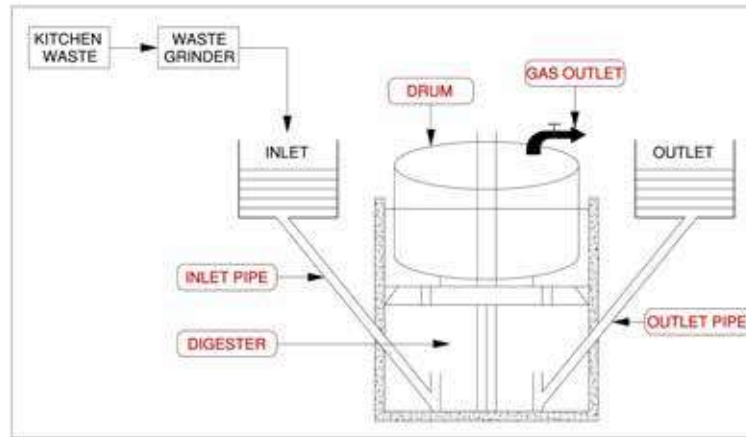


Fig. 1. Floating drum type biogas plant

Following **Table 1** Potential indicates the potential of biogas generation from 3200 kg kitchen waste.

Table 1. Potential indicates the potential of biogas generation from 3200 kg kitchen waste

Sl. No.	Description	Value	Unit	References
1	Total number of flats	1600	Nos.	
2	Tentative Kitchen waste generated	3200	kg/day	
3	Potential for biogas generation	448	m ³ /day	[8]
4	Potential for LPG replacement	179.2	kg/day	[8]
5	% of replacement total LPG by biogas	27	%	[8]

KITCHEN WASTE AS A SOURCE OF ELECTRIC POWER:

Another application of kitchen waste-based generated biogas may be for electric power generation by using it in a diesel generator. As society is having power backup by utilizing several diesel generators, where biogas can be utilized to generate the electric power and to supply the flats as power backups. Based on the data collected from society electricity bills, the average power electricity bill is ~1300 INR/month/family which comprises 150 units of electricity on-grid power @ 5.95 INR/kWh and ~28 units on Diesel generator @ 16 INR /kWh. Hence, approximately ~16% of total electric power is being fulfilled by the diesel generator which accounts for ~35% of the total bill value.

Diesel engines are based on a compression ignition system and unlike diesel, biogas cannot self-ignite. Therefore some amount of diesel is required for the ignition to occur. A diesel to biogas ratio of 2:8 is considered optimal. Besides diesel also acts as a lubricant for the fuel injectors. Biogas generated has many challenges before using as fuel in CI engines these are high CO₂ content reduces the power output, making it uneconomical as a transport fuel. It is possible to remove the CO₂ by washing the gas with water. The solution produced from washing out the CO₂ is acidic and needs careful disposal. H₂S is acidic and if not removed can cause corrosion of engine parts within a matter of hours. The generated biogas may be cleaned by passing through a high-pressure water scrubber as shown in **Fig. 2**. In the scrubber, CO₂ is dissolved in the water, while CH₄ concentration in biogas is enhanced. This was happened due to CO₂ has a greater solubility in water than CH₄. The biogas leaving the scrubber has a higher methane concentration. The water scrubber also removes harmful impurities like sulfur dioxide (SO₂) and hydrogen sulfate (H₂S). Further, the moisture from the biogas was removed by using a moisture filter. After moisture removal, biogas was further cleaned using a bag filter. After a complete cleaning, the biogas was supplied to the engine through a control valve which helps in controlling the gas flow [9] [10].

Following **Fig. 2** shows the proposed scheme, Kitchen waste generated gets ground in grinder machine which further fed to digester (Floating type). Biogas may further be fed to the water scrubber column for purification. Purified biogas can be used as

a fuel in a Diesel generator along with diesel (20% Diesel + 80% Purified biogas). As a by-product of the process, bio manure is also generated which can be used for horticulture purposes in society.

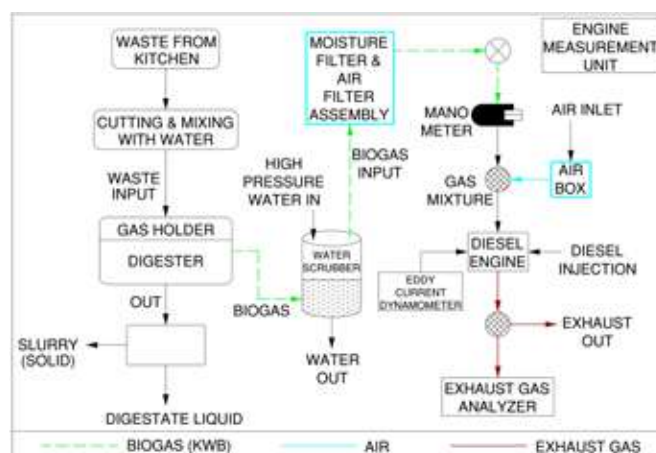


Fig. 2. Typical Scheme for Biogas generation and firing to Diesel generator [10]

The following **Table 2** indicates the potential of diesel replacement by utilizing biogas generated from kitchen waste and purifies by a water scrubbing system:

Table 2. Potential of diesel replacement by utilizing biogas

Sl. No.	Description	Value	Unit	References
1	Total number of flats	1600	Nos.	
2	Tentative Kitchen waste generated	3200	kg/day	
3	Potential for biogas generation	448	m ³ /day	[8]
4	Potential for Electric Power Generation	672	kwh/ day	[8]

PROJECT COST AND PAYBACK

As the kitchen waste generated in the flats shall be used for biogas generation, hence a very fewer logistics cost for waste collection. However, proper training for segregated waste collection is mandatory for the effectiveness of the proposal. The total estimated kitchen waste generation is 3200 kg, hence two numbers biogas generation unit comprising 1500kg/day each is proposed which will be capable to produce 2 x 210-225m³/day biogas [11]. Two numbers of the unit are considered based on the flexibility of the operation and readily available digester size in the Indian market.

The following **Table 3** indicates the estimated capital cost and required operational expenses for proposed units:

Table 3. Estimated capital cost and operational expenses for biogas plant

Description	Cost in USD	Cost in INR*	References	Remarks
Capex Expenditure	2 × 100,000	1.46 Crores	[11]	
Land Cost (2 X 300 m ²)	10,000	7.3 Lakhs	[11] [12]	Considered government circle rate of land
Total initial investment	210000	1.53 Crores		
Operational & Maintenance Cost	10320 per annum	7.5 Lakhs per annum		

* 1 USD = 73 INR

Payback on investment has been estimated for both the cases i.e. (1) Utilization of Biogas as the replacement of LPG and (2) Utilization of biogas for replacing diesel in a diesel generator.

The following **Table 4** indicates the tentative simple payback on investment while utilizing biogas as the replacement of diesel generator:



Table 4. Simple payback on investment when biogas is replacing Diesel in DG

Description	Value	Unit	Remarks
Average Electricity Supplied in society through DG	537600	kwh/annum	Based on the data collected
Total Electricity generation through biogas	241920	kwh/annum	360 days/annum running
Saving by using biogas in place of Diesel	3870720	INR	Saving at 16 INR / kwh
Operational & Maintenance Cost	750000	INR	
Net saving	~31.2	Lakhs INR/annum	
Simple Payback Period	<5.0	years	Against the investment of ~ INR 1.53 Crores

The following **Table 5** indicates the tentative simple payback on investment while utilizing biogas as the replacement of LPG:

Table 5. Simple Payback on Investment when Biogas is replacing LPG for cooking

Description	Value	Unit	Remarks
Total LPG Consumed by 1600 Flats	19792	kg/annum	
Total saving by replacing LPG by the biogas	~2725632	INR/annum	LPG Cylinder filling cost 600Rs/14.2 kg (42.25 INR/kg)
Operation and Maintenance	750000	INR/annum	From Table-III
Net Saving	~20.00	Lakhs INR/annum	
Simple Payback Period	~7.65	Years	

CONCLUSION

Waste management is a real problem in the urban city of India and when this waste can be utilized as a source of energy, it would be a win-win situation for ecological balance. Both the options for utilizing kitchen waste either in the form of cooking gas or for the generation of electricity seem beneficial, however biogas uses as electricity generation seems more lucrative with less payback time and it may further be attractive if government extends some subsidy for initial capital expenditures. If the government makes the policy to utilize this kitchen waste within the society mandatory while approving the project, just like other facilities (i.e. Rainwater harvesting, solar cell on the rooftop, green area development, etc.), it will support the implementation of this concept at a faster rate in India. Biogas generation from kitchen waste is well established technical know-how in India, hence the concept presented in this paper may easily be implemented. A builder may also explore to get the benefits of less duty and taxes on investment for the biogas plant.

REFERENCES

1. India: Degree of urbanization from 2009 to 2019, <https://www.statista.com/statistics/271312/urbanization-in-india/> (Last Accessed on 14.11.2020).
2. McKinsey Global Institute, India's urban awakening: Building inclusive cities, sustaining economic growth https://www.mckinsey.com/~media/McKinsey/Featured%20Insights/Urbanization/Urban%20awakening%20in%20India/MGI_Indias_urban_awakening_executive_summary.pdf (Last Accessed on 14.11.2020).
3. Town and Country Planning Organization, Ministry of Urban Development, GoI, <http://mohua.gov.in/upload/uploadfiles/files/MBBL.pdf> (Last Accessed on 14.11.2020).
4. TERI Energy & Environment Data Directory and Yearbook 2013/14.
5. Ziana Ziauddin1, Rajesh P, Production, and Analysis of Biogas from Kitchen Waste, International Research Journal of Engineering and Technology (IRJET), Volume: 02 Issue: 04 | July-2015.
6. Jasleen Bhatti and G.N. Tiwari, A Comparative Study of Biogas Production by Using Kitchen Waste and Water Hyacinth: A Case Study, Journal of Basic and Applied Engineering Research, Volume 2, Issue 23; October-December, 2015, pp. 2026-2029.



7. <http://web.iitd.ac.in/~kvijay/files/Biogas%20technology.pdf>, (Last Accessed on 17.11.2020)
8. <https://www.worldbiogasassociation.org/wp-content/uploads/2020/06/WBA-presentation-20-05-2020.pdf> (Last Accessed on 17.11.2020)
9. N.H.S.Ray, M.K.Mohanty and R.C.Mohanty, A Study on Application of Biogas as fuel in Compression Ignition Engines, International Journal of Innovations in Engineering and Technology (IJJET), Vol. 3 Issue 1 October 2013
10. Sohan Lal & S. K. Mohapatra, A feasibility study to utilize kitchen waste for power generation in urban areas using CI engine, Energy Sources, Part A: Recovery, Utilization, and Environmental Effects , DOI: 10.1080/15567036.2019.1604895
11. http://www.iwmi.cgiar.org/Publications/Books/PDF/resource_recovery_from_waste-133-141.pdf
12. <https://cdn.s3waas.gov.in/s305049e90fa4f5039a8cad6acbb4b2cc/uploads/2018/05/2018051770.pdf>



Effluent Treatment & Wastewater Recycling- Copper Smelter Perspective

Mary Sarker

Water & Utility Department, Mining & Metallurgy Business Unit, TATA Consulting Engineers Limited, Mumbai

✉ marys@tce.co.in

ABSTRACT

Present practice in most of the industries is to adopt different methods to reuse and recycle wastewater due to scarcity as well as restrictions on discharging effluent beyond plant boundary. This article deals with the wastewater recycling methods adopted in Copper Smelters by implementing various treatment processes for the process effluents. One case study of developing effluent treatment schemes to treat contaminated water from copper smelter process has also been elaborately discussed with merits and demerits.

Keywords : Effluent treatment; Zero liquid discharge; Wastewater recycle.

INTRODUCTION

Water supply and quality issues have become a major concern throughout the world nowadays. Freshwater supply sources are decreasing at a faster rate due to increasing population and industry worldwide. To keep sustainability of water supplies globally in the future, it is essential to find ways to conserve, and re-use it to the extent possible.

Apart from scarcity of water source, environmental issue is also an important reason to reuse and recycle waste and effluent water within the plant. Effluents discharged from various industries pollute water bodies, which results in human health problems, poisoned wildlife, and damages ecosystem. Hence now, global concerns are on the regulation and reduction of wastewater discharge from industries. In most of the countries, statutory regulations have been implemented to restrict industry and agricultural operations from discharging pollutants into surface water bodies. As a result, Zero Liquid Discharge (ZLD) concept has been conceived by many industries where the plant design is aimed to recycle all the effluent water within plant with or without treatment.

EFFLUENT TREATMENT AND WATER RECYCLE - COPPER SMELTERS

This article will discuss about the effluent treatment and wastewater recycling in copper smelter industry. In copper smelters, increasing impurities in the ore concentrate, new feed materials, along with new environmental and trade policies are increasing the importance of proper handling of impurities. As a response to this challenge, copper smelting industries along with technology suppliers in various parts of the world have developed impurity handling solutions through a wide range of technologies and strong technical expertise. With implementation of these processes, most of the impurities are discharged with water and these are the main process effluents from copper smelters.

Major Effluents

To increase efficiency in process and eliminate environmental issues, off-gas generated during smelting and converting processes in copper smelters are presently treated in wet scrubbers and cooling tower for wet gas cleaning. Because of this process, waste water is generated from primary copper smelter. From smelting process flue dust, metals mainly in the form of oxides or sulphates, will be dissolved in wastewater during the wet gas cleaning. In the flue dust from converting process, metals mainly in sulphide or metallic form, will be present as suspended particles in effluent water. These effluent flows are acidic in nature, and will comprise of a huge amount of dissolved heavy metals, specifically Cu, Fe, Zn, Pb and As. In these processes, arsenic is usually found as arsenite (As(III)) or arsenate (As(V)) inorganic oxyanions. Due to carcinogenic nature of arsenic compounds, it is of focus to reduce the exposure of arsenic-contaminated water to as low level as possible.

Here, treatment of effluent water from some of the copper smelters around the world has been described briefly.

Wastewater Treatment in Chilean Smelters

The mineral processing industry in Chile has a large impact on the economy of the country and the environmental status. The pyro metallurgic copper processing plants produce large amounts of arsenic that vaporize as arsenic trioxide. This compound is absorbed from the gas flow, and finally fixed as calcium or ferric arsenate, when the wastewater stream is treated with ferric chloride or sulphate.

A scheme of the conventional wastewater treatment process is shown in **Fig. 1**.

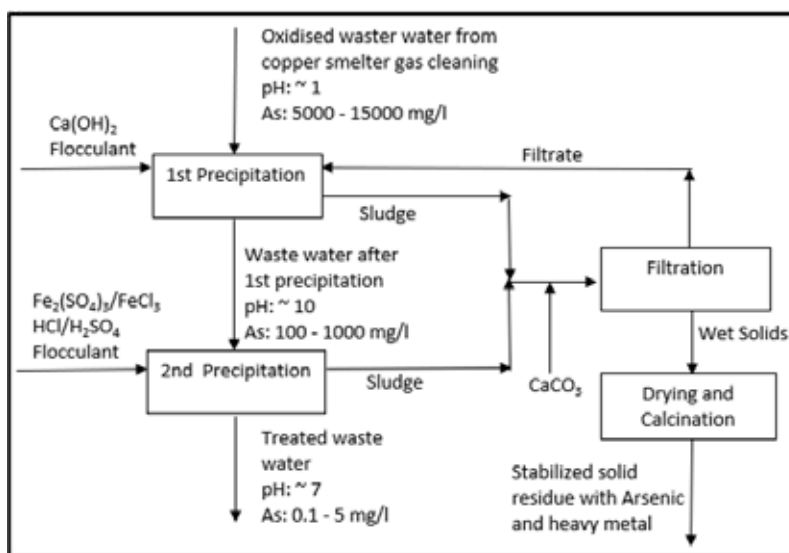


Fig. 1. Conventional Effluent treatment process

Typical composition of waste water from copper smelters are given in Table 1.

Table 1. Typical Effluent Water Quality

Parameter	Unit	Value
Flow	m ³ /hr	20 - 30
pH		~ 0
Arsenic	g/l	5 - 15
Copper	g/l	0.5 - 2
Lead	g/l	0.2 - 0.3
Antimony	g/l	0.05 - 0.1
Nickel	g/l	0.05 - 0.1
Bismuth	g/l	0.05 - 0.1
Selenium	g/l	~ 0.01
Sulphuric Acid	g/l	25 - 100

In the conventional treatment process, large amounts of solids are generated that needs to be disposed of with high costs as hazardous waste. The conventional treatment scheme usually satisfies the Chilean legislation for wastewater discharge, but it has also several disadvantages.

At the Universidad Técnica Federico Santa Maria, environmental remediation processes have been investigated for treating arsenic contaminated waste waters (Hansen et al., 2006). Especially in wastewater treatment the electrochemical processes are getting importance specially for removal of heavy metals and arsenic. This study suggested a new treatment scheme that would eliminate the disadvantages of the conventional treatment scheme. **Fig. 2** shows the proposed process that comprises of:

- a lime addition step to remove the majority of sulphates present,

- b) an electrodialysis (ED) step to separate copper from arsenic for recovery, and
- c) an electrocoagulation (EC) step to precipitate arsenic.

This scheme would eliminate the following disadvantages in the conventional copper smelter wastewater treatment scheme:

- a) The lime addition is expected to be reduced by about 50% as compared to the conventional treatment
- b) The calcium sulphate produced would contain very low amounts of arsenic and copper.
- c) Copper would be concentrated in a solution during the ED process and could be recovered by electrodepositing processes.
- d) The dosage of ferric ions during EC would be easy to control by the electric current. Consequently, the treated wastewater would contain less arsenic than the Chilean limit for arsenic concentration in waste water discharge.
- e) In the first neutralization step, lime is added until pH increases to 2. Then the electro dialysis (ED) and electro coagulation (EC) processes would further reduce the acidity of the waste water, resulting in minimal control of the final pH.

Treatment of Wastewater Copper Smelter In Serbia

Copper mining and smelting in Serbia is one of the most important producers in Central Eastern Europe since 1903. Initially, wastewater treatment plant for weak acids neutralization was designed and constructed for treating 15.300 kg/h of weak acid containing 98 kg/h of H_2SO_4 , and 153 kg/h (1%) of suspended particles in this plant.

Afterwards, new wet scrubbers and cooling tower has been installed for wet gas cleaning. To treat the generated waste water from this plant, the WWTP needs to be reconstructed. Innovating a technical solution for the WWTP was conducted by a team from University of Belgrade.

The scheme is shown in **Fig. 3**.

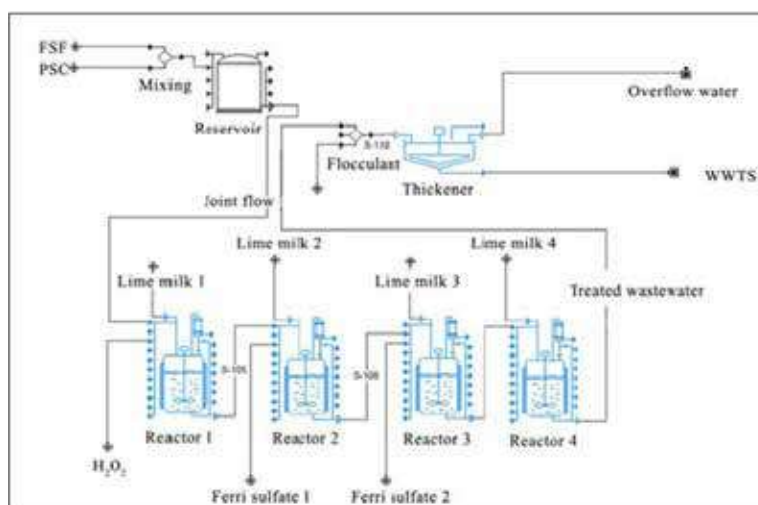


Fig. 3. Effluent treatment process in Serbia

Projected characteristics of wastewater generated in Serbian copper smelter are listed in **Table 2**.

Table 2. Effluent water quality at Serbian Smelter

Parameter	Unit	Value
Flow	m ³ /hr	8.66
pH		-0.464
Solid	% wt	1.36
Arsenic	g/l	1.37
Copper	g/l	0.53

Lead	g/l	0.45
Zinc	g/l	0.54
Iron (Fe ²⁺)	g/l	0.38
Sulphuric Acid	g/l	142.7

In pilot plant scale, the acidic wastewater was neutralized by using 13% solution of commercial grade hydrated lime, $\text{Ca}(\text{OH})_2$, in distilled water to precipitate metal ions in the form of hydroxide. Lime milk was constantly added for neutralization and the pH value and temperature of the solution was continuously monitored. After reaching the pH of 9.5, process was stopped, and possible change of pH value was monitored for the next 30 minutes.

From the wastewater treatment process 7,21 m³/hof treated water and 10.281,6 kg/h sludge underflow from the thickener will be generated. Eh-pH diagrams for the metals present in treated wastewater were done according to the projected number of reactants and target pH value and presented in Fig. 4.

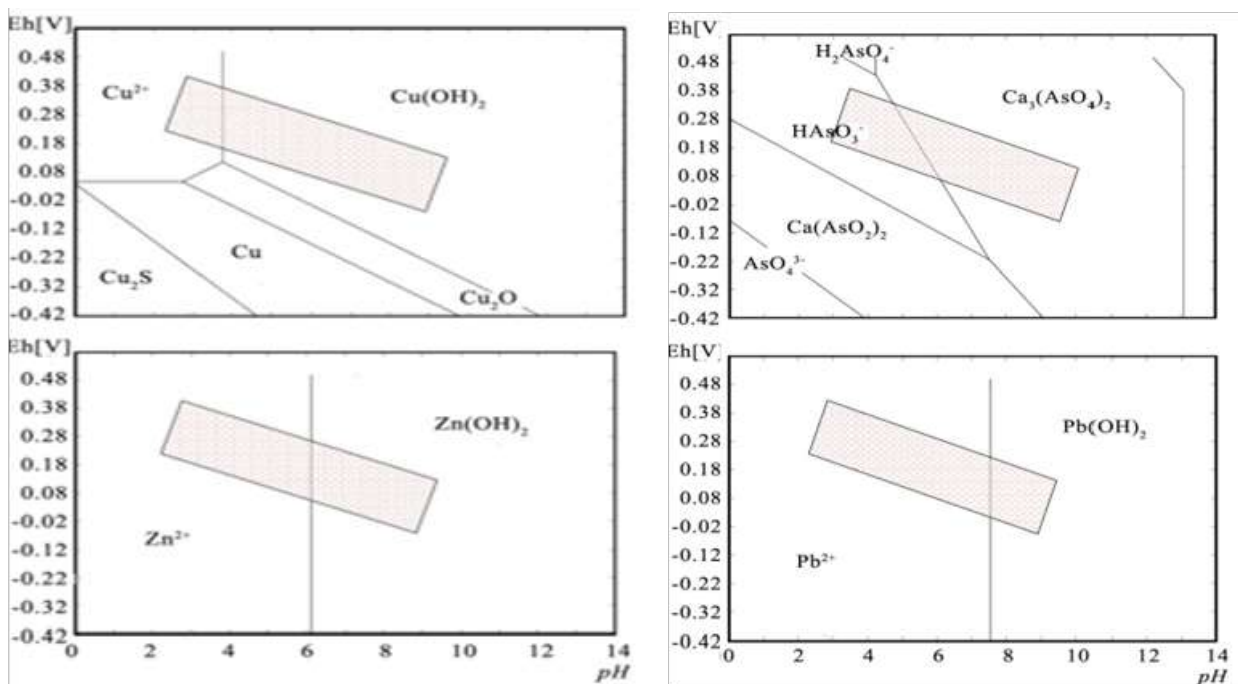


Fig. 4. Eh-pH diagram of Cu, As, Zn and Pb in treated water

Chemical composition of treated wastewater is given in Table 3. It is clear that about 99% of investigated metals (Cu, Fe, Zn, Pb and As) has been removed by applying the proposed wastewater treatment process.

Table 3. Expected treated water quality

Parameter	Unit	Value
Flow	m ³ /hr	7.21
pH		9.7
solids	% wt	< 0.1
Arsenic	mg/l	4.0
Copper	mg/l	0.01
Lead	mg/l	< 0.03
Zinc	mg/l	0.025
Iron (Fe ²⁺)	mg/l	0.014



TYPICAL CASE-STUDY

A case-study of effluent treatment scheme and recycling of wastewater has been carried out for a proposed Asian copper smelter plant.

The primary source of water for this plant is seawater. Desalination water plant is also being installed for the process water and hence significance of wastewater recycling is of higher consequence.

Source and Analysis of Effluent

a) Non-Process Wastewater

Non-process wastewater will be generated from the following sources:

- Desalination plant reject
- Sea water cooling tower blow down
- Wastewater generated from backwashing of side stream filters, pre-treatment of desalination plant and regeneration process of demineralization plant.

The cooling water for process heat exchangers are supplied from sea water cooling tower where sea water is used as make-up. The reject from desalination plant and cooling tower blow down has been considered to discharge in the sea. An option of using the cooling tower blow down as desalination plant feed has been proposed.

The wastewater generated in plant and storm water will be treated in a wastewater treatment plant consisting of neutralization and sludge separation process. The treated water will be reused in process.

b) Process Wastewater

Process wastewater are effluents generated from process plant. Proposed process and reuse of this effluent is elaborated below.

A table indicating the details of the effluents coming from the various units is shown below:

Table 4

Quality of Effluent to ETP

Description	Weak Acid	AF Effluent	PMR Effluent	EW Purge
Solids, t/h	0.02	0.00		
Total Mass, t/h	25.952	0.161	0.549	1.701
Liquid Flow, t/h	25.936	0.161	0.549	1.701
Volume, m ³ /h	24.077	0.144	0.479	1.476
Temperature, C	61.986	76.751	56.044	65.000
Moisture, %	99.937	99.986	100.0	100.0
Gypsum, t/h	0	0.00002	0	0
Wt% Gypsum	0	85.184	0	0
Composition w/w				
SO ₄	13.184	10.142	8.920	21.644
Al	0.001	0	0	0
As	0.203	0	1.092	0.347
Bi	0.0001	0	0.291	0.0001
Ca	0.0002	0.004	0	0
Cd	0.018	0	0	0
Cl	0.258	0	6.167	0.003
Cu	0.002	0	0.051	0.130



F	0.089	0	0	0
Fe	0.013	0.000	0	0
Hg	0.0004	0	0	0
Mg	0.001	0.000	0	0
Na	0.071	5.113	3.340	0.000
Ni	0.000	0	0.0002	0.526
Pb	0.006	0	0.077	0.000
Sb	0.002	0	0.177	0
Se	0.005	0	0.018	0.000
Si	0.046	0.0001	0	0
Zn	0.006	0	0	0.000

Development of Effluent Treatment Process

Initial Effluent Treatment Scheme

Initially, scheme considered consisted of:

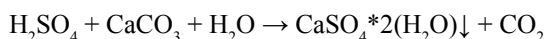
- Effluent Holding Tanks and Prefiltration

The effluents will be collected in the effluent holding (buffer) tanks and pumped to filter presses with addition of diatomite as precoat filter aid and collected solids will be discharged in the form of cake. The filtrate will be pumped into the clean gypsum precipitation reactors.

Exhaust SO₂ from the effluent collection tanks will be sent back to GCP.

- Clean Gypsum Precipitation & Filtration

Clean gypsum will be precipitated by adding calcium carbonate suspension. From the last reactor the clean gypsum slurry will flow by gravity to the clean gypsum filter feed tank from where part of will be recycled to the first reactor and the rest will be pumped into the clean gypsum filters. sulphuric acid is neutralized according to reaction:

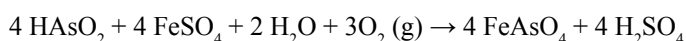


Filtrate will be pumped into the Ferric Arsenate Precipitation Reactors. One drier has been considered for drying the clean gypsum cake.

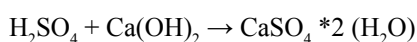
- Ferric Arsenate & Metal Hydroxide Precipitation & Filtration

Ferrous sulphate solution will be fed to the second and third precipitation reactors to precipitate the arsenic as a ferric arsenate at a pH of approximately 4.5 by adding lime milk. In the last precipitation reactor, the pH will be further raised to 10 - 11 by dosing lime milk to precipitate other metal impurities out of solution as metal hydroxides.

Ferric arsenate is precipitated according to reaction:



pH adjustment by acid neutralizing according to reaction:



From the metal hydroxide precipitation reactor, the slurry will flow by gravity to the thickener. The overflow water will flow by gravity to the thickener overflow tank from where the effluent will be pumped further to ETP internal process water usages and ZLD plant. Underflow discharge slurry of the thickener will be pumped filter presses via filter feed tank. This discharged cake is also named as dirty gypsum.

Final Treatment Plant

The Ferric arsenate thickener overflow water and PMR effluent will be sent to Zero Liquid Discharge (ZLD) for final treatment. A pre-treatment stage will be used prior to ZLD to remove metals mainly magnesium in the form of metal hydroxide precipitates by adding milk of lime. In ZLD traces of dissolved metals are removed from water to meet desired quality.

The treated water quality from the Ferric Arsenate overflow thickener will be as given below:

Table 5. Treated water quality (Initial)

Item	Unit	Max Value
Total volumetric flow	m ³ /h	52.3
Temperature	°C	37.7
TSS	mg/l	250
pH		9
SO ₄	g/l	1.5
As	mg/l	5
Cl	mg/l	474
F	mg/l	0
Hg	mg/l	0
Se	mg/l	16
Zn	mg/l	1
Cd	mg/l	10
Pb	mg/l	<1
Sb	mg/l	62
Bi	mg/l	80
Cu	mg/l	<1
Fe	mg/l	0.6
Ni	mg/l	0.05

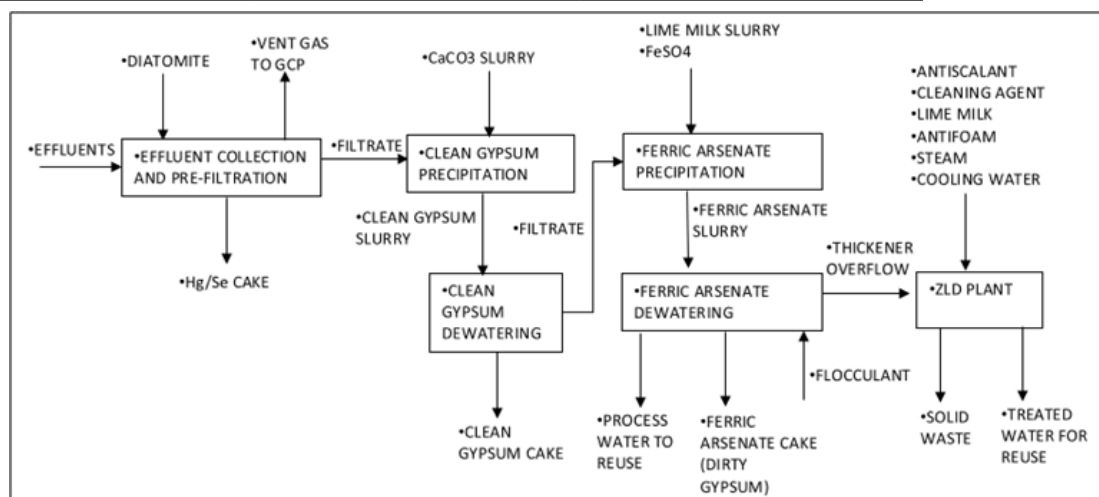


Fig. 5. Initially proposed treatment scheme

Total Dissolved Solids (TDS) in treated water by ZLD will be less than 100 ppm

Modified Effluent Treatment Scheme

To overcome the flaws in the initial process, ETP process has been modified.

Initially, Ferrous Sulphate with lime milk has been considered to be added to precipitate Arsenic as Ferric Arsenate. As it is necessary to use at least four times the amount of ferrous iron compared with the stoichiometric amount to arsenic concentration, hence huge amount of Ferrous Sulphate is required. Accordingly, a large amount of Ferric Arsenate cake thus produced is required to be disposed of suitably.

In the initial process, pH of the last reactor of Arsenic and heavy metal precipitation stage needs to be kept at 10-11 which redissolves the Arsenic.

Proposed ETP optimization process has been developed based on a software simulated mass balance prepared by expert. The proposed optimized scheme is given below:

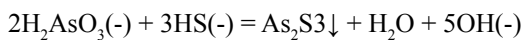
The effluent treatment plant will comprise of the following areas:

- Effluent Holding Tanks and Se/Hg Dewatering

From the holding tanks, the effluent is pumped to the thickener for settling. Overflow water from the thickener is sent to Cu-As precipitation reactors. Underflow Hg/Se slurry from the thickener is pumped to the filter press through filter feed tank with addition of diatomite as precoat filter aid.

- Cu-As Precipitation & Dewatering

Sodium Hydro-Sulphide (NaHS) will be added to the Cu-As reactors to precipitate As_2S_3 according to the following reaction:



Cu will also be precipitated as CuS. The precipitate slurry is then sent to thickener by gravity to settle the As_2S_3 precipitate. Due to high acidic nature of the solution, poisonous H_2S gas will also be produced on addition of NaHS which will be scrubbed off by NaOH.

Overflow water from the thickener is sent to clean gypsum precipitation reactors. Underflow As_2S_3 slurry from the thickener is pumped to the filter press through filter feed tank. The As_2S_3 cake produced from the filter will be mixed with heavy metal precipitate cake and sent to smelter for reuse.

- Clean Gypsum Precipitation & Dewatering

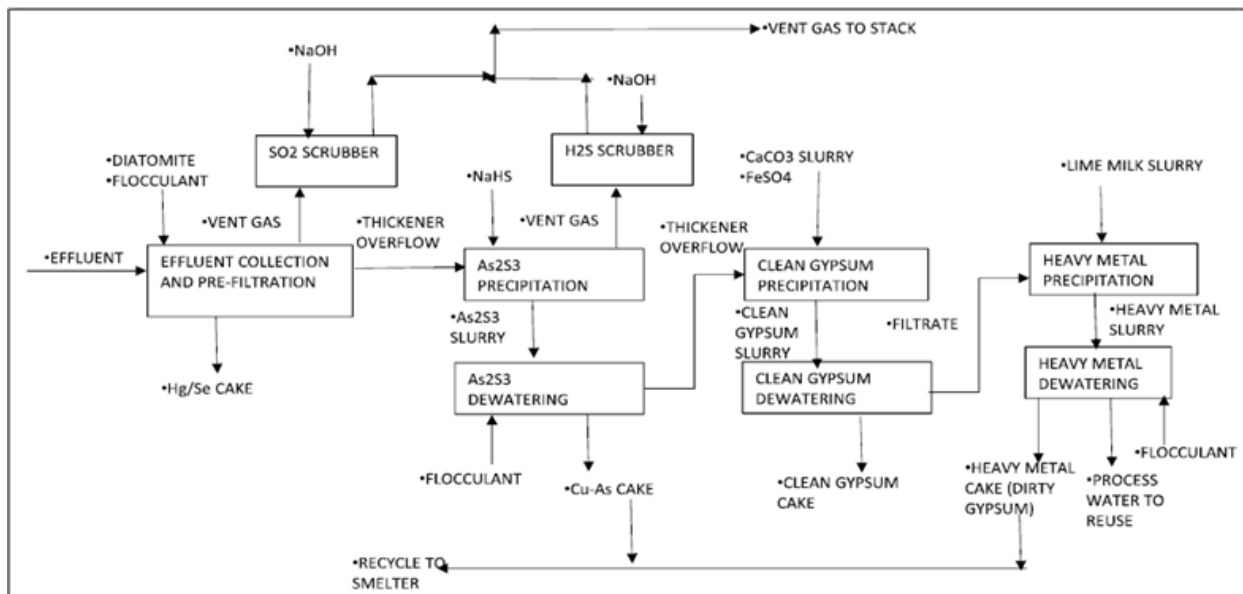
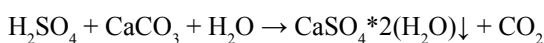


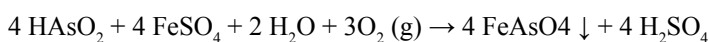
Fig. 6. Treatment process proposed as per optimization

Clean gypsum is precipitated by adding calcium carbonate slurry at 35% wt in a controlled manner, keeping pH low to avoid precipitation of impurities to the produced clean gypsum.

As a result, clean gypsum is precipitated by neutralizing Sulphuric acid according to the following reaction:



Along with Gypsum Ferric Arsenate will also be precipitated due the following reaction:





The sulphuric acid produced will be neutralized by CaCO_3 to produce gypsum. From the clean gypsum filter feed tank, the gypsum slurry is pumped to filters. The filtrate is pumped to the heavy metal precipitate flash mixing tank. The clean gypsum cake produced will be transferred to the clean gypsum storage facility adjacent to the ETP.

- Heavy Metal Precipitation and Dewatering

In the flash mixing tank, lime milk is added along with the filtrate water from clean gypsum filters and then sent to heavy metals precipitation reactors. The pH of the solution is kept at 9. The final concentration of heavy metals is expected to be near 1 mg/l. Metals are removed with lime milk according to following reaction:



The precipitate solution is then sent to thickener by gravity to settle the heavy metal precipitate.

The overflow water from the thickener is reused in the ETP and slag cooling. Underflow heavy metal slurry from the thickener is pumped to the filter press through filter feed tank. The treated water Arsenic concentration will be around 100 ppb.

The heavy metal cake produced will be mixed with As_2S_3 precipitate cake and sent to smelter.

The quality of the treated water from heavy metal thickener overflow tank is expected to be as below:

Table 6. Quality of treated water

Description	Treated effluent
Total Volume, m ³ /h	35.67
Total Mass, t/h	36.502
Liquid Flow, t/h	36.502
Temperature, C	34.890
Composition wt%	
SO ₄	1.835
As	0.00005
Bi	0.00003
Ca	0.273
Cd	0.0001
Cl	0.408
F	0.0003
Fe	0.000002
Mg	0.286
Na	0.321
Ni	0.0001
Pb	0.000002
Se	0.00005
Si	0.023
Zn	0.0001

- Further Optimization Proposed Using Bauxsol

Further optimization has been proposed using Bauxsol for acid neutralization and arsenic removal. About 10 years ago, an Australian company developed a method, the BASECONTM process, which allows the transformation of the caustic alumina refinery residue into a benign environmental remediation product, so-called BAUXSOLTM. The acid neutralizing capacity of Bauxsol is provided by a mixture of carbonate, hydroxide and hydroxycarbonate but some of these react slowly. Hence, a longer reaction time is required. This longer reaction time will be achieved by sending the mixed solution to a sedimentation pond through 21 km pipeline.

This scheme comprises of the following steps.

- Mercury selenide is removed by filtration and sent to hazardous material disposal and SO₂ scrubber is included to collect gases evolving from the influent water.
- The pH is then raised to 5.0 in 3-stages to precipitate gypsum and bismuth by adding lime stone which is termed as “normalization”.
- Arsenic will then be removed by Bauxsol or Ferrous Sulphate addition with aeration. This step is termed “stabilization”. The slurry at 14% solids and 93% gypsum would be pumped to another treatment plant for further heavy metal removal and the treated water will be used in flotation process of the captive ore concentration plant

In place of the proposed scheme of normalization process by adding lime stone slurry to produce clean gypsum precipitate, another scheme of using NaOH in also under active consideration as shown in the **Fig. 7** below.

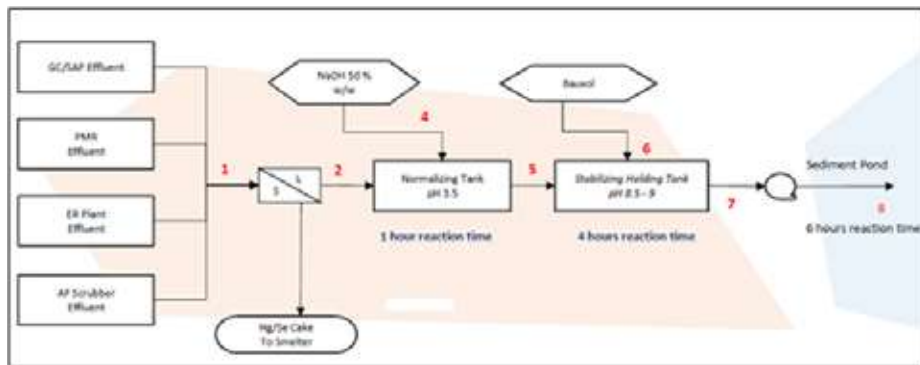


Fig. 7. Treatment process proposed using Bauxsol

Pilot testing is under progress. The scheme will be finalized after receiving the result.

Analysis of the Treatment Processes

- As per Initial Process, huge amount of Ferrous Sulphate is consumed for arsenic precipitation whereas as per proposed optimisation, very small amount of Ferrous Sulphate and NaHS is consumed for precipitating Arsenic.
- As per Initial Process, amount of Ferric Arsenate cake produced will be higher as compared to the amount of As₂S₃ and heavy metal slurry produced which will be recycled to smelter.
- In the process proposed initially, pH of the last reactor of Arsenic and heavy metal ppt stage needs to be kept at 10-11. However, after pH 9, solubility of As increase as shown in the pH vs. solubility curve (**Fig. 8**). Hence, Arsenic is re-dissolved in the solution. The concentration of Arsenic in the treated water is likely to be 5 mg/l. But Arsenic content in treated water is expected to be about 100 ppb only.

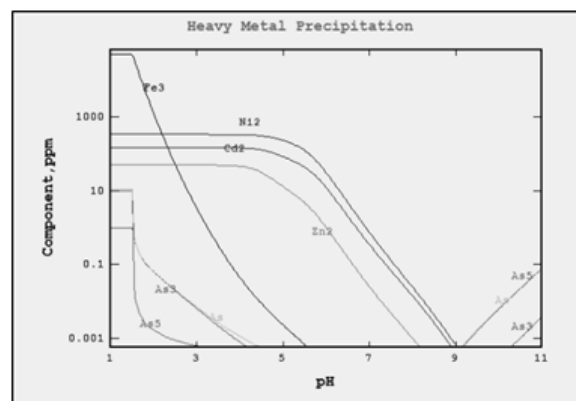


Fig. 8. Solubility vs. pH curve



- As the treated effluent water in the proposed scheme is of better quality than that proposed initially, hence the ZLD plant has been eliminated in this scheme.
- In As₂S₃ precipitation with NaHS, toxic H₂S gas will be generated. Hence, proper arrangement needs to be done during installation of the system so that no fatal incident occurs.
- In case of the optimized scheme, power consumption will be reduced by 45% as compared to the initially proposed scheme.
- Total operating cost will be reduced by 48% as compared to the initially proposed scheme.
- A capex savings of about 24% can be achieved with this optimization.

With further optimization scheme by adding Bauxsol, the arsenic cake and heavy metal precipitate steps can be eliminated. This has the beneficial effect of reducing the recirculating load of impurities. Consequently, the Electro refinery bleed drops from 1.6 to 1.0 m³/h. The arsenic level of the weak acid falls from 2.4 to 1.3 g/l.

OVERALL OUTCOME OF THE CASE STUDY

From the above study, it is clear that the proposed optimized scheme for ETP is much more effective in terms of removal of Arsenic. By-product Arsenic cake generation is also less as compared to initial process. Moreover, Capex, Reagent cost as well as power consumption is less as compared to the scheme initially proposed.

Further optimization scheme by using Bauxsol will be the most cost-effective solution as compared to the conventional treatment processes as described in this article.

REFERENCES

1. D. Radovanović, M. Ranitović, Ž. Kamberović, M. Korać, M. Gavrilovski, "Treatment of wastewater from new copper smelter RTBBor", PT TemaBroja, Article – July 2017.
2. Henrik K. Hansen, Adrián Rojo, Claudia Gutiérrez, "A new process for sustainable wastewater treatment in Chilean copper smelters", European Journal of Sustainable Development (2016).
3. Armando Valenzuela, "Arsenic Management In The Metallurgical Industry" September 2000 edition
4. J.J.P. Zijlstra, V. Bellò, R. Ruggeri and A. Teodosi, "The BAUXSOLTM Technology: An Innovative Solution For Environmental Remediation Problems", Conference Paper, January 2005.



Conservation of Topsoil at Construction Sites

Krishna Nirmalya Sen, Gollapalli Muralidhar

EHS Department, Larsen and Toubro Metallurgical and Material Handling, Kolkata

✉ knsen@lntmcl.com

ABSTRACT

Topsoil formation is a natural and slow process occurs due to wreathing rocks and the subsequent addition of organic matter from decaying plants and animals. Loss of topsoil also known as soil erosion, can have devastating effects on environment, causes for this criterion varies from natural phenomena like local climate, wind, rainfall along with human activities like agriculture, deforestation, mining, urbanization etc. Globally, nearly 10 million hectares of arable land is lost to erosion and other forms of soil degradation every year. Construction activities such as road laying, construction, pipe laying are the ones which commonly involves the disturbance of soil strata. Proper planning aided by careful execution and suitable equipment can help in handling of topsoil without degrading the physical, chemical, and biological characteristics of soil. Development of site-specific plan, stripping of topsoil with right equipment, preserving the stripped soil and restoration of the soil after the work are the key steps to achieve the conservation of topsoil.

Keywords : Topsoil; Conservation; Soil stripping; Stockpiling.

INTRODUCTION

Soil is a valuable and non-renewable resource which is central to the health and correct functioning of the natural environment, all the life forms on earth depend on soil either directly or indirectly. Globally, nearly 10 million hectares of arable land is lost to erosion and other forms of soil degradation every year[1]. Soil erosion, particularly the loss of topsoil can have irreversible effects on environment. Topsoil is a finite resource and valuable due to its fertility as it has the highest biological activity, organic matter, nutrients, and physical characteristics necessary to grow and sustain permanent vegetation. One hectare of topsoil can contain up to 5 tonnes of living organisms and as it can take more than 500 years to form a 2cm thickness, it is in practical terms non-renewable [2]. Loss of this upper layer eliminates soils natural ability to provide nutrients, regulate water flow and combat pests and diseases [3]. Soil erosion can be caused by several causes, varying from natural phenomena like local climate, wind, rainfall along with human activities like agriculture, deforestation, mining, urbanization etc. Majorly urbanization activities are damaging the capacity of soil to continue to perform in full in its broad variety of crucial eco-system functions. In addition, soil degradation has significant impacts on other areas of common interest to the community, such as food and water safety, human health, climate change, and biodiversity protection [4].

Construction activities in general have the potential to damage the soils in several ways such as soil over compaction due to through trafficking of plant or vehicles or storage of materials; Contamination of soil due to mixing soil with construction materials or waste; Accidental spillage or the use of chemicals, incorrect handling i.e. mixing different qualities of soil during handling and storage, including subsoil with topsoil. Construction and other associated activities may have a permanent negative impact on soil [3]. Soil erosion during construction is often a serious problem and left unprotected, sites will be further degraded by erosion and begin to adversely affect the surrounding environment. At, construction sites erosion is the major source of sediment because the potential for erosion on highly disturbed land is commonly 100 times greater than agricultural land [5]. Hence the soil resources at the sites to be protected and the sites to be re-vegetated for protection against off site impacts and to increase soil organic matter levels to remedy the on site damage caused by preparation.

Soil management plan plays an important role in conserving and ensuring soil sustainability during construction projects. Plan usually contains information about of areas where soil to be stripped, types of soil present, methods for stripping, locations & methods for stockpiling, restoration methods etc. In this paper, an attempt made to highlight important aspects of soil management for conservation of topsoil in construction sites.

CLEARING OF SITE AND TOPSOIL STRIPPING

Soils are particularly vulnerable to physical degradation during intensive soil handling operations such as stripping, storage and restoration. Any damage to the soil structure would reduce aeration and drainage characteristics and increase the risk of water logging and anaerobic conditions, therefore care must be taken.

Before commencing the works at construction site, areas of soil that need to be protected from construction activities, should be clearly marked out by barrier tape/fencing and exclusion signs to prevent movements across these areas. Avoid stripping topsoil from areas that will not be disturbed by the construction activities such as excavation, grading, pipe laying etc. Once re-usable soil resources have been identified within a site, topsoil can be stripped and stored carefully for beneficial reuse on or off-site.

Clearing of Site: Clearing of area where topsoil to be removed, includes but is not limited to the removal of existing vegetation, debris, rubbish and stones or boulders etc. Any large stones, waste or non-topsoil materials or soil heaps should be removed from areas to be stripped prior to topsoil stripping. Pre-treatment of area should be done to control weed and vegetation to the quantity of weed seed content and vegetation entering the storage stockpiles in order to minimise the formation of anaerobic conditions in stock piles and to preserve the topsoil quality. Depending on the type of vegetation, suitable equipment to be used to clear the vegetation. Good quality cleared vegetation can be used in the re-vegetation process at project sites and poor-quality cleared vegetation should be sent to landfill.

Topsoil Stripping: Selection of appropriate equipment and work practices is pivotal in stripping of soil. In general, excavators and dump trucks used for stripping and transportation of soil. Topsoil will normally be stripped to specific depths not exceeding 150 mm [6], as stripping the topsoil too deeply will reduce its quality and fertility due to the subsoil incorporation. Many a times, subsoil will not need to be stripped but it should be protected from damage. However, in some cases it might need to be temporarily removed to make way for haul roads or, if it is of a suitable quality, recovered and reused to manufacture a topsoil substitute. If subsoil to be removed, topsoil and subsoil must be removed in separate lifts and stockpiled in separate piles to reduce mixing soil layers when the reclamation process begins. Subsoil never should be placed or stored on top of topsoil. Extra care must be taken while handling soils of different quality and compositions, to avoid cross contamination.



Fig. 1. Stripping of topsoil

As far as possible, Topsoil stripping and stockpiling should be carried out whilst the soil is reasonably dry. Soils generally lose strength and become less resistant to damage as they become wetter; therefore, it is essential that they are stripped, handled and trafficked only in the appropriate conditions of weather, soil moisture, and with suitable machinery [7]. It is advisable to avoid stripping of soil during or after heavy rainfall or in waterlogged condition, as the properties of topsoil will degrade much more rapidly if recovered when too wet. In the event of heavy or continuous rain, stripping and handling of topsoil should be suspended and recommenced only after when the soil is moderately moist or dry. During this time, movement of large equipment over topsoil materials to be reduced to minimize compaction. If possible, planning of the site activities should be done to facilitate the soil stripping and handling during summer months in order to reduce likelihood of compaction, and other problems due to wet conditions. It is important to note that, movement of soil that is too wet or dry may result in the loss of topsoil properties.



SOIL STOCKPILING

Temporary stockpiling of soil will minimise the area required for storage and prevents damage from the weather and other construction activities. Although mechanical handling of soil would affect its physical properties, stockpiling of the soil could have the greatest effect which sometimes could be irreversible. Hence stockpiling of soils should be done with utmost care for its reuse in the later stages. Biological, chemical, and physical changes do occur, mainly as a result of anaerobic conditions within the heaps, but also as a result of mechanized handling during the stripping and stockpiling [8], so as to maintain the quality of the topsoil as near as possible to its pre-disturbance condition, the below factors should be taken into consideration while storing topsoil for longer periods.

Stockpile Location & Design & location: As far as possible, works should be planned to minimise the need any temporary storage of soils. Otherwise, depending on where the topsoil has been recovered from, available space at construction site and proposed area reuse, suitable stockpile locations to be identified as early as possible. Separate stockpiles for topsoil and subsoil must be ensured. Topsoil's should be stored in an area of the site where they can be left undisturbed and does not interfere with other construction site operations. Storage area surface should be kept clear of vegetation and any waste arising from the site progression such as construction debris and measures should be taken to prevent any infiltration of contaminants. Stockpiles should be located away from site boundaries, vehicle haul way routes, Excavation areas and any areas vulnerable to adverse effects from run-off such as water bodies, ditches etc.

The size and height of the stockpile will depend on several factors, including the amount of space available, the nature and composition of the soil, moisture content and the prevailing weather conditions. In any case stockpiles should not be stored more than 2 m in height [6], soil should be stockpiled in low mounds with lesser higher height and maximum flat surface area.

Moisture Content: Soil moisture is the major factor in deciding the size and height of the soil and the stockpile storing method. Topsoil stockpiling should be carried out whilst the soil is reasonably dry, it is less prone to compaction, and can be re-spread easily. When the soil is dry, method is form mounds of soil not exceeding 2 m height and measures should be taken to restrict any water intrusion during the storage period.

Soil stockpiled wet or when plastic in consistency is easily gets compacted by its own weight and due to the machinery handling. If stored in wet condition, due to the compaction in the core of the stockpile remains wet and anaerobic for the duration of the storage period. These conditions effect the soil quality and makes the soil difficult to handle and re-spreading. To avoid this wet soil to be reconditioned prior to stockpiling. In this method, wet soils will be spread over the surface as windrows till the topsoil is dried out. This technique minimises the amount of compaction caused by stockpiling as well as maximising the surface area of the stockpile for topsoil drying.

Storage Period: Storage period of topsoil should be kept as minimum wherever possible to reduce the impacts from compaction and the reduction of oxygen in the soil. If stockpiled over a length of time (+/-6 months), may result in total or partial loss of soil microorganisms [9] and there by greater reduction in the quality of the soil during that period. Although negative impacts would occur after two weeks, the soil could be stored carefully for up to one year before irreversible impacts are likely to occur, therefore soil should be used within 12 months [7].

Once stockpiled, the soils should be covered with plastic material to avoid erosion due to the wind or water. Stockpiles should be kept free of weeds or any other contaminants in order to safeguard the soil properties and to keep the soil in its suitable state for reuse. In addition, stockpiling soil should not cause soil erosion, pollution to watercourses or increase flooding risk to the surrounding area. Hence covering should be done to avoid erosion and weed growth.

RESTORATION OF TOPSOIL

Topsoil Preparation: If stockpiled, some level of topsoil preparation is required prior to restoration, the top 1 foot of the stockpile material should be mixed with the remainder of the stockpile to ensure that living organisms are distributed throughout the topsoil material at the time of final placement. In case of wet stockpiled soil, clumps of topsoil should be broken up during re-spreading as the clumps of topsoil would hinder root growth due to its compacted structure and often would lead to waterlogged and/or anaerobic conditions. Where quantities of topsoil are limited, it is recommended to cover the more critically disturbed areas to the proper depth, rather than covering all areas

Replacement of Topsoil: Soil properties and conditions may vary across the project site and the main objective for soil restoration is to achieve soil profiles as close to the original pre-construction state as possible. This is primarily achieved by ensuring that

the full soil profile is restored in the correct sequence of horizons, and in a state where good soil profile drainage and plant root development are achieved; and by ensuring that the reinstatement works cause minimum damage to soil structure [2]. It is critical that the reinstated soil should provide a suitable growing medium to support vegetation. During restoration, handling of topsoil when dry or slightly moist, usage of suitable equipment and less mechanical handling of soil prior to restoration damage to the soil can normally be mitigated to a large extent and good quality of soil profile can be achieved.

Loose-tipping Method: It is essential to provide a structured, un-compacted and well-aerated soil profile for the successful establishment and subsequent growth vegetation. Over compaction of soils prevents plant root growth and reduces water infiltration and the ability of excess water to drain away. It is one of the most common reasons for poor plant life and increased erosion and runoff. Therefore, while replacing the soil, it is particularly important that receiving surface is loosened prior to the application of the subsoil and/or topsoil. On the other hand, movement of heavy machineries and vehicles across the construction sites causes localised compaction, and this should be kept to a minimum. Process known as “Loose tipping method” is found to be effective, as it prevents it prevents a solid border between the soil layers, which may hinder drainage; and it remediates the compaction of the receiving surface which may have occurred during the construction phase [2].



Fig. 2. Restoration of topsoil

In this method, receiving surface is first loosened with a wing-tine ripper and soil tipped on the receiving surface and replaced with help of excavators sequentially. It is vital that the topsoil is not over-compacted during spreading. If the subsoil is stripped along with topsoil, sub soil should be replaced first followed by topsoil. Topsoil should be loosely tipped on to the areas and smoothed over by an excavator, thereby removing the need for movement of machinery over subsoil. In no case, subsoil should never be placed over or mixed with topsoil.

During the replacement, thickness of topsoil layer should be sufficient to support the plant growth, usually ranging from 75 mm to 100 mm [6]. If topsoil thickness is too deep, there is a possibility for development of anaerobic conditions due to the excess oxygen demand for breaking down of organic matter. After the replacement, leave the surface in a roughened condition to reduce erosion and facilitate establishment of permanent vegetation.

Seeding & Mulching: Seeds of approved quality and suitable for type of soil should be applied and to improve the organic content of the soil, and to assist in rebuilding soil microorganism populations. topsoil can be mixed with approved commercial or organic materials such as compost. Mulching materials consisting of straw, hay, wood shavings or sawdust can also be applied in dry condition to the topsoil for added slope protection, to create a microclimate at the seed soil interface to promote germination while controlling erosion. All the seeded and mulched areas shall be inspected periodically and maintained until the final acceptance.

Other Applications of Topsoil: If it is not feasible to stockpile the topsoil at construction site, it can be diverted to off-site for sustainable use in applications like embankment turfing, establishment of new landscapes, gardens, or other green spaces.



CONCLUSION

Each year, Millions of hectares of land is being lost to soil erosion and India is no different. With rapid urbanisations and industrialization, agricultural lands are being disturbed to facilitate infrastructural development such as roads, pipelines, railways etc. If not prevented, soil erosion will be further aggravated by the construction activities and will adversely affect the surrounding environment. Hence to minimise the soil erosion, conserve the valuable topsoil and to make the construction sites aesthetically pleasing management of soil resources is utmost important. With a detailed planning, suitable equipment and careful handling soils can be stripped, stored at construction site premises and re-instated in the later stages to achieve soil profiles as close to the original pre-construction state.

REFERENCES

1. Pimentel D, Burgess M. Soil Erosion Threatens Food Production. *Agriculture*. 2013; 3(3):443-463.
2. DEFRA (2009): Construction Code of Practice for the Sustainable Use of Soils on Construction
3. Highways Agency (2014). Preliminary environmental information report: A14 Cambridge to Huntingdon improvement scheme.
4. National Soil and Land Use Policy – for Serving Farmers and Safeguarding: The National Academy of Agricultural Sciences (NAAS)
5. Brady, N.C., and R.R. Weil. 1999. *The Nature and Properties of Soils*. 12th ed. Prentice Hall. Upper Saddle River, NJ.
6. Specifications for Road and Bridge Works: Ministry of Road Transport and Highways
7. British Standard BS3882:2007 - Specification for topsoil and requirements for use.
8. Rai, V. K., N. S. Raman, S. K. Choudhary, and S. Rai. 2014. Topsoil Management in Coal Mines: A Paradigm Shift Required in Approach. *International Journal of Innovative Research in Advanced Engineering (IJIRAE)*; Volume 1 Issue 10, pp 448-454. ISSN: 2349-2163
9. Standard Specifications for Highway Construction: Idaho Transportation Department (2018).



GIS-based Well Water Monitoring of Gunjalwadi and Velhale Villages, Maharashtra, India

Navale V B, Mhaske S Y

Department of Civil & Environment Engineering, VJTI, Mumbai, Maharashtra

✉ navale1289@gmail.com

ABSTRACT

The paper investigates; the Gunjalwadi village 20 wells and 19 wells of Velhale village are selected for well groundwater table depth monitoring. The groundwater table depth data are collected by field survey method and a Well way point location is taken from the global positioning system. The data are collected for four years from 2017 to 2020 for two seasons such as pre-monsoon and post-monsoon. The Average rainfall data are collected from the local irrigation department. The hypothesis is formulated that the rainfall and other natural parameter are influencing groundwater depth or not and later on identified it. The different thematic maps are prepared by Geographic information system such as, Soil Map, land use/land cover map, slope and contour map, well way point location map etc. The relation between groundwater depth and rainfall data is found out by linear correlation and regression model. The R^2 value indicates that the influence of rainfall on Groundwater table depth and its value greater than 0.5 indicate that there exists a strong correlation. This study is useful for sustainable groundwater resources and its management, villagers for agriculture management.

Keywords : GIS; GPS; Remote sensing; Well water depth; Linear regression.

INTRODUCTION

In the world, groundwater is important to the source of freshwater. Groundwater assists as an important source because of continued availability throughout the world and it is superior quality. The natural source of Groundwater is including rivers, lakes, Stream flow, and the reservoir. The artificial recharge included seepage from the canal, excess Agriculture, Irrigation, etc. The hydro geological process is a prerequisite for groundwater study..The water appears in wells, bore well, it derived from rain water. The groundwater present as a source of water and very less presence in the surface water. The quantity of water present is inadequate and the nature of basalt rock is impervious. Its consequence that water not gets deep percolates into the earth's surface. The aquifer parameter helps in groundwater evaluation, numerical simulation and scientific management (S.F.R. Khadri and Kanak Moharir 2016). The identity of the groundwater potential zone depends upon the number of dug well, well yield and landuse/landcover (K. Balasubramani et al. 2019). The groundwater movement, its presence and the properties of groundwater depend on the hydrogeology of the area. The optimum depth of well is 100 m for maximum yield (Sivaramakrishnan J. et al. 2015). Ground water potential zones and artificial recharge sites are identified using remote sensing and GIS (Gurav Chandrakant and Md. Babar 2019). The GIS-based different thematic maps i.e. slope, topographic position index, geology, lineament density, drainage density are useful for the Identification of groundwater potential zone (J. Qadir et al. 2019). Different Thematic maps such as runoff coefficient, drainage density, slope, and proximity the water surface bodies are prepared using by Geographical information system (Laishram Kanta Singh, et al. 2018). The multi-criteria evaluation technique is used for groundwater and resource evaluation (Rajat C. Mishra et al. 2015). The geographical information system and Finite difference method are used to develop the Numerical model for sustainable groundwater development (Mulu Sewinet Kerebin, et al. 2017). The parameters required for the sustainable development of the area are Geology, Soil, vegetation, sediments, erosion, geomorphology, groundwater, etc. (AL Homound et al 1995). Groundwater, Remote sensing, and GIS technique are used for the determination of groundwater potential zone. The three factors are considered for sustainable groundwater resource management i.e. Agriculture, Irrigation and sustainable management (William F. Ritter and

Jennifer de mooy, et al 2015). The Groundwater analysis depends on the different thematic maps such as Geology structure, Landuse/Landcover and Geomorphology (Rajat C. Mishra et al. 2015). The parameter considers for the groundwater vulnerability analysis are aquifer type, hydraulic conductivity, slope, depth to the water table, Landuse/Landcover, etc (Abdelwahde Ajdi, et al. 2018). The suitable areas for artificial groundwater recharge sites are analyzed using the Geographic Information system

and Analytical hierarchy process (AHP) (Mohammad Karamouz et al. 2018). The water-budget structure and hydrologic model for the distribution of groundwater recharge are developed (Rhsan Beigi and Frank T.C. Tsai et al. 2019). The central valley hydrologic model is used to determine how to crop type and drought impact on the groundwater (Ruopu Li et al. 2018). Nash conflict resolution method used for an artificial groundwater recharge plan (Mostafa Farhadian et al. 2017). The Rainfall, Infiltration process effect on groundwater depth. The relation between rainfall and groundwater depth is determined using regression and co-relation analysis (Sasin Jirasirilak et al. 2015). The parameter considered for groundwater vulnerability analysis is depth to water table ratio, hydraulic conductivity, closeness to the river, landuse/landcover, etc. (Abdelwaheb Aydi, et al. 2018). The different GIS-based thematic maps are used to identify groundwater potential zone such as landuse/landcover, topography, Geomorphology, Geology, etc. (Adnan Ozdemir 2011). The regression analysis and least square method are used to define the relation between the groundwater level and its fluctuation (Amit Kumar and Arvind Pandey 2016). The objective of the study is firstly to classify landuse/Landcover using by Geographical information system and then after using CARTOSAT-DEM image different thematic maps are prepared and lastly by use field survey method the well water monitoring of Gunjalwadi village and Velhale village and then after using regression and correlation model the different influencing factor on groundwater table depth are identified.

STUDY AREA

The Gunjalwadi and Velhale village belong to Sangamner Taluka in the Ahmednagar district of the region of Khandesh and Maharashtra Northern state, in India. The Geographical area of the Gunjalwadi and Velhale village is 964.97 ha. and 1558.29 ha. The Mhalungi River passing to the middle of Gunjalwadi village and also, side of Velhale village and it is a left-bank tributary of river Pravara. The dam is constructed on the Mhalungi River by using the stones in the Gunjalwadi village area and also two small weirs constructed in Velhale village. The percolation tank is constructed in 1972. The mean annual rainfall is 617mm on the year. The Study areas are selected because of Irregular rainfall, more Scarcity of water and continuous decline of the water table. The mean sea level is 509m. The total population of the Gunjalwadi and Velhale village is 7164 and 4639 respectively. Study area shown in Fig. 1.

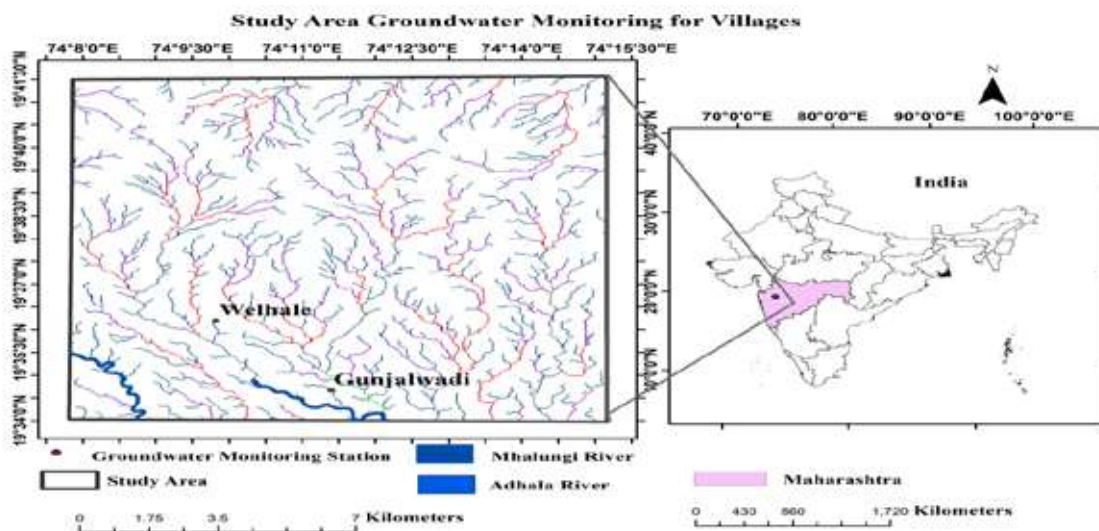


Fig. 1. Study area

DATA SOURCE AND METHODOLOGY

The Remote sensing data of the study area are collected from <http://earthexplorer.usgs.gov>. A Landsat-7 ETM+ data with a cloud-free scene data from 1st Jan to 31st June is chosen for this study, the Landsat-7 satellite data are used as primary data. Secondary data used are the Geographic information system software and is used to analyze the data and to draw the thematic map. In order to classify Land use/Land cover of the study area these images are processed in GIS with projection system WGS1984 UTM 43N, To make research accurate and more reliable the Landsat-7 images and other data such as survey of India toposheet, village development plan, population data of villages are used. The Cartosat-DEM data collected from Bhuvan India

Portal. The Water table depth data from the bottom of well collected by field survey method by using the Global positioning system. The details of the Methodology shown in **Fig. 2** of flow chart.

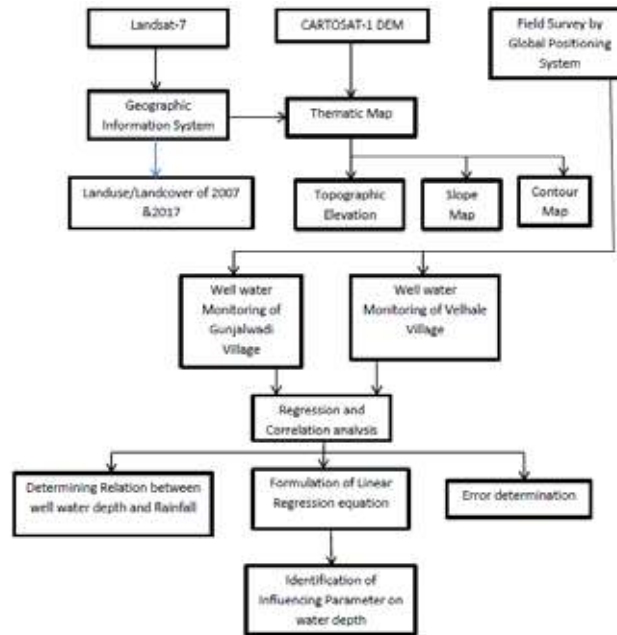


Fig. 2. Flow chart of methodology

SOIL OF STUDY AREA

The study area consists of three different type of soil. The soils of plains and valley are deep, to some extent well drained, fine, soils on gently sloping plains and valleys with moderate erosion, Moderate salinity and moderate sodicity associated with deep, well drained, fine, calcareous soils with moderate erosion. The soils of undulating land are slightly deep, somewhat excessively drained, associated with slightly deep, loamy soils on gently sloping undulating lands with severe erosion, well drained, fine, calcareous soils with moderate erosion. The soils of plains are well drained, deep, calcareous, loamy, soils on very gently sloping plains with moderate erosion, associated with well drained, moderately deep, fine, calcareous soils.

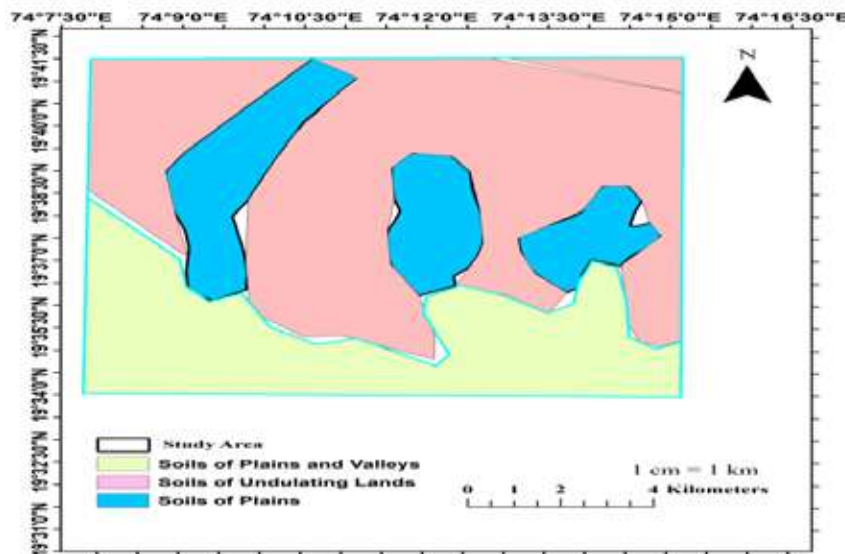


Fig. 3. Soil map

LAND USE/LAND COVER OF GUNJALWADI AND VELHALE VILLAGE

Remote Sensing Imagery data of the study area are collected from USGS earth explorer, it used for the source of primary data. The study area shape file is collected in Bhuvan India. The visual Identification purpose actual field visit and Google earth reference are taken, the training sample of respective classes is taken then maximum likelihood supervised image classification is done by GIS software. Landuse/Landcover shown in **Fig. 4** and **Fig. 5** of Gunjalwadi and Velhale village.

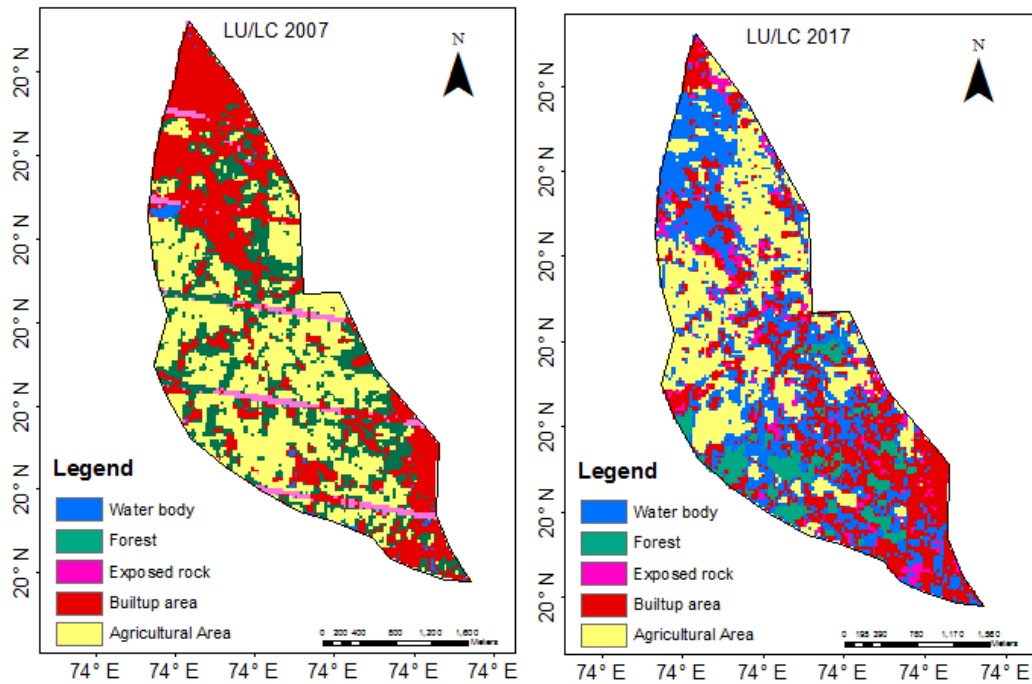


Fig. 4. Landuse/Landcover map of Gunjalwadi Village

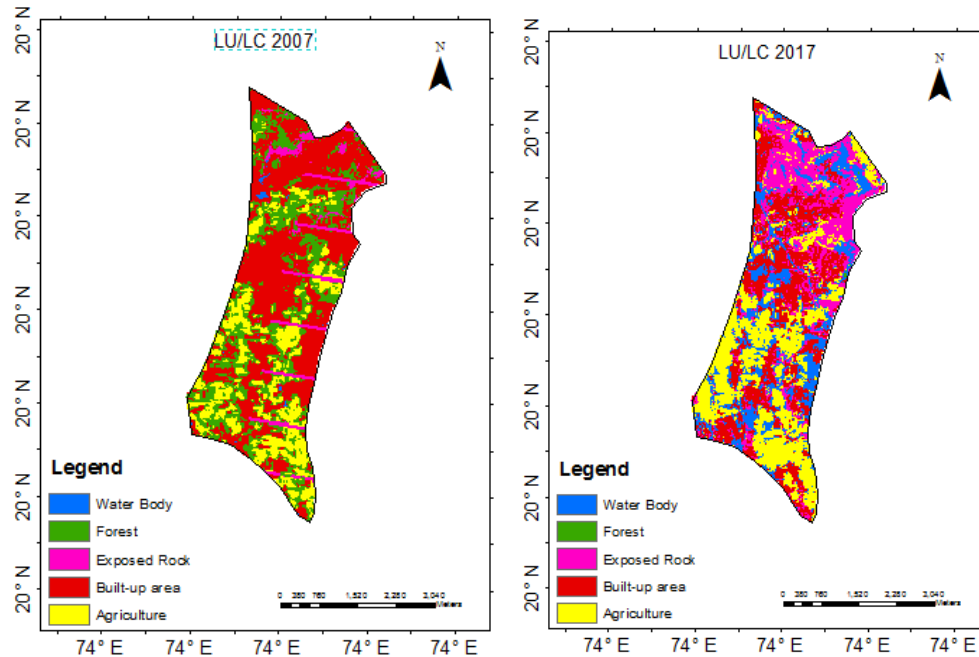


Fig. 5. Landuse/Landcover map of Velhale village

SLOPE MAP AND CONTOUR MAP OF GUNJALWADI AND VELHALE VILLAGE

The map showing different classes of slope and contour elevation is developed from the Digital Elevation Model; the prerequisite DEM data is collected from portal Bhuvan India. The Contour Interval is the elevation difference between two adjoining Contour line. The degree of slope indicates that the steepness of Terrain, the flat slope lies between 0 to 5%, the shallow slope is between 8 to 15%, moderate slope lies between 15 to 25% and the steep slope is greater than 45%. This slope layer is helpful for visualizing the nature of ground it helpful to indicate the flow of the groundwater. The contour map gives the idea of Terrain Nature. The slope map and contour map are useful to construct different soil and water conservation structure such as compound contour trenches, earthen Nala bund, percolation pond, compartment bunding, etc. Maximum contour elevation of Gunjalwadi village is 33m and the contour elevation of Velhale village is 70m and **Figs. 5 and 6** show the slope map and contour map of Gunjalwadi village and Velhale village.

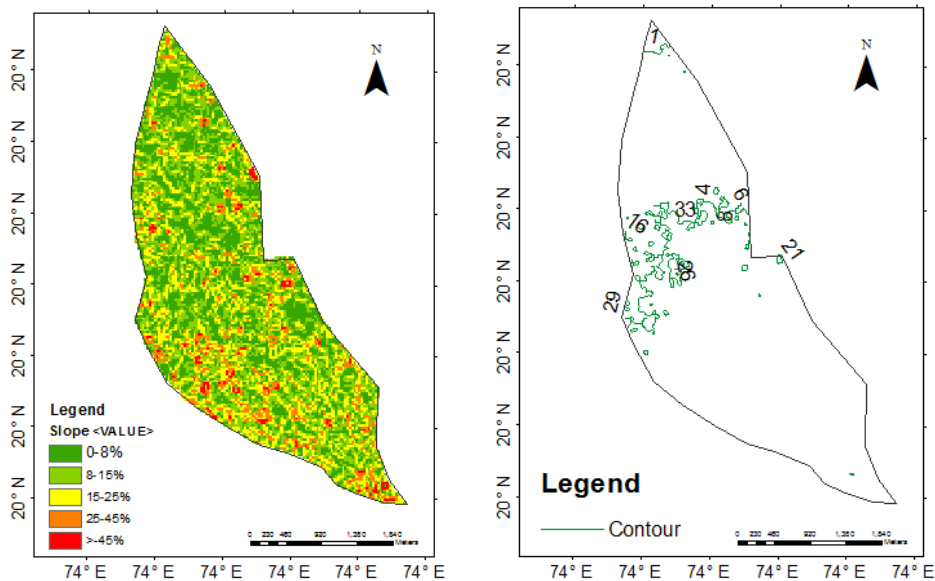


Fig. 6. Slope and contour map of Gunjalwadi Village

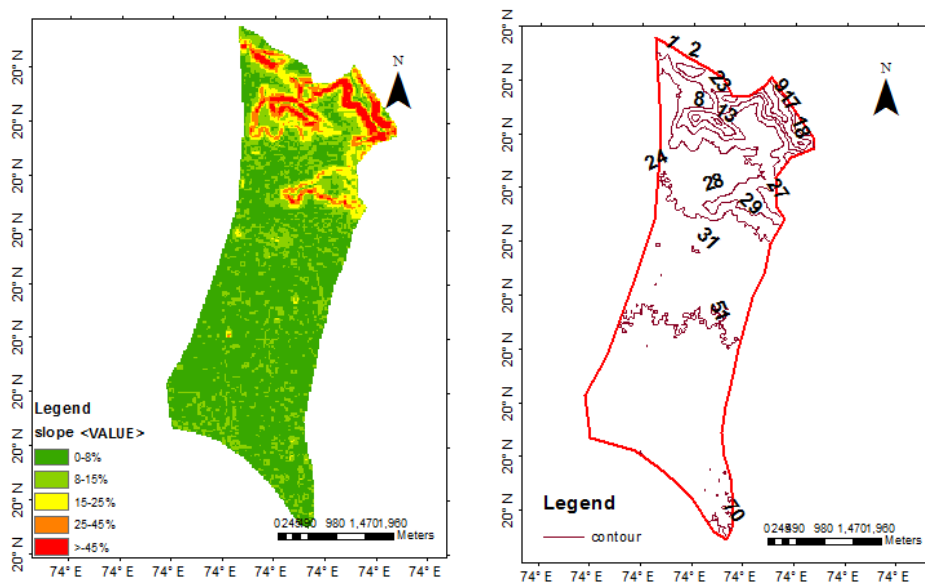


Fig. 7. Slope and contour map of Velhale Village

WELL LOCATION DETAILS OF GUNJALWADI AND VELHALE VILLAGE

The wells are located in the Gunjalwadi and Velhale village in Sangamner. In the study area, 20 well from Gunjalwadi village and 19 wells of Velhale village have been Identify for monitoring groundwater table depth. The data was collected in the pre-monsoon and post-monsoon season in the year 2017, 2018, 2019 and 2020. The latitude and the longitude of the well were taken from the android app called GPS Essential. Drilling of more well and its results in more withdrawn water for Agriculture purposes, its impact on the scarcity of water.

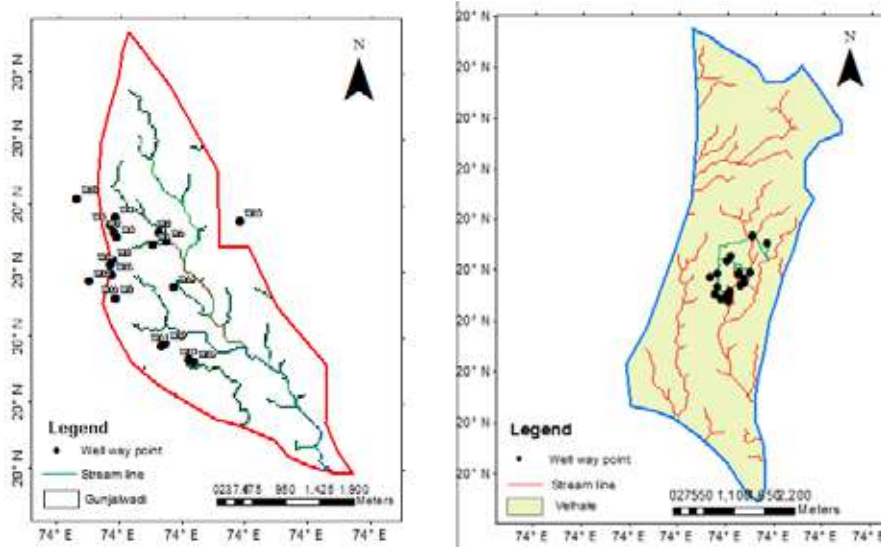


Fig. 8. Well location map of Gunjalwadi and Velhale village

WELL WATER MONITORING OF GUNJALWADI AND VELHALE VILLAGE

The **Table 1**, **Table 2** shows the linear data which include well number, depth of the well, the water level in the well. The latitude and the longitude of the well were taken in the android app called GPS Essential. The pre-monsoon data was collected in the Month of March and post-monsoon data was collected in December. The local rainfall plays an important role to recharge the groundwater table. According to the value of the groundwater table, it decrease 2017 and it increase from 2018 to 2020. In dry season i.e. month of April to May the more requirement of water, its result on pumping of well water. During the period of the dry season, the groundwater table is reduced, thus the seasonal variability also effects on water table depth.

Table 1. Well monitoring of Gunjalwadi village

Well no.	Depth of well	Premonsoon- Mean Groundwater Table(2017 to 2020)	Postmonsoon- Mean Groundwater Table(2017 to 2020)
W1	11.1	10.475	11.875
W2	13	5.875	8.575
W3	14.6	9.45	13.15
W4	13.3	3.1	6.6
W5	15	7.25	9.425
W6	16.3	5.5	9.375
W7	12.9	3.9	7.775
W8	12.7	12.5	5.95
W9	13.7	4.7	9.1
W10	18.5	6.95	11.475



W11	22.9	5.525	13.45
W12	24	4.275	8.9
W13	17	1.3	6.9
W14	16.3	5.125	8.275
W15	16.7	1.825	7.95
W16	18	3.3	10.1
W17	18.7	4.25	9.6125
W18	17.9	3.9	9.375
W19	14.6	1.275	5.175
W20	17.6	4.7	7.225

Table 2. Well monitoring of Welhale village

Well no.	Depth of well	Premonsoon- Mean Groundwater Table(2017 to 2020)	Postmonsoon- Mean Groundwater Table(2017 to 2020)
W1	15.2	0.575	2.25
W2	15.84	2.35	8.55
W3	20.11	0.925	4.575
W4	12.5	4.725	8.15
W5	19.2	8.1	12.325
W6	12.2	1.025	4.35
W7	16.2	6.7	10.9
W8	16.6	4.525	6.5
W9	14.3	4.25	7.15
W10	13.5	0.575	3.65
W11	20.2	10.675	13.625
W12	18.6	6.525	7.1
W13	12.1	1.225	3.175
W14	18	0.2725	2.85
W15	14.7	3.95	7.175
W16	21.6	4.05	5
W17	18.6	5.675	7.725
W18	17.1	7.775	9.475
W19	11.1	2.85	4.3

REGRESSION AND CORRELATION ANALYSIS

Co-relation shows the co-variation between two or more variables..If there is n variable and n-1 are the dependent variables. The regression model can be expressed as

$$X_1 = a_1 + a_2x_2 + a_3x_3 + \dots + a_nx_n$$

Where a_1 is the intercept, a_i ($i = 1, 2, 3, \dots, n$) is the multiple regression coefficients is a dependent variable X_1 ($i = 1, 2, 3, \dots, n$) be the independent variable.

RESULT AND DISCUSSION

The groundwater levels and drainage density are different in the respective villages. The drainage density of Gunjalwadi village

is 0.002066 m/m² and the drainage density of Velhale village is 0.0005345m/m². The groundwater levels are influenced by the rainfall and among that the other parameters are such as rock present, Landuse/Landcover, slope, contour, etc. The influencing parameter on groundwater level decline are less rainfall, less drainage density, less infiltration capacity of clay soil, Geology of the area, cropping pattern of the village, seasonal variability, etc. The less infiltration capacity impacts less deep percolation. The basalt rock is not permitted to the flow of water. As per the Land use/Land cover pattern of Gunjalwadi and Velhale village from 2007 to 2017 forest cover, water bodies are decreases and The area covered under an exposed rock is increasing because of the forest cover decrease. The built-up area of the village increasing slightly. The agriculture area in pre-monsoon decreases because of less availability of the rainfall. As per 2017, the Gunjalwadi Landuse/Landcover pattern percentage of Forest, Built-up, exposed rock, water body, Agriculture are 6.82%, 28.37%, 5.03%, 30.78%, and 29.06% respectively. As per 2017, the Velhale Landuse/Landcover pattern percentage of Forest, Built-up, exposed rock, water body, Agriculture are 0.051%, 27.98%, 22.53%, 19.77%, and 29.66% respectively.

Table 3. Regression equation

Station	Regression Equation
Gunjalwadi	Groundwater depth = -1828 - 0.00114* Rainfall + 0.909 Year
Velhale	Groundwater depth = -646 -0.000340* Rainfall + 0.3229 Year

Where, Coefficient of Constant are 1828 and 646

Coefficients of Rainfall are 0.00114 and 0.000340

Coefficients of Year are 0.909 and 0.3229

Table 4. The performance of validation evaluation model of Gunjalwadi and Velhale

Sr. No	Station	R ² value	R ² value (adj)	R ² value (pre)
1	Gunjalwadi	96.29%	88.88%	32.11%
2	Velhale	72.70%	18.10%	0.00%

The Pearson correlation defined the correlation between Groundwater depths; Rainfall and year are shown in table.

Table 5. Pearson correlation for Gunjalwadi

Sr. No		Groundwater Depth	Rainfall
1	Rainfall	0.485	
2	Year	0.842	0.688

Table 6. Pearson correlation for Velhale

Sr. No		Groundwater Depth	Rainfall
1	Rainfall	0.485	
2	Year	0.842	0.688

The regression model is helpful for defining the influencing of one parameter on another parameter it may be adopted for the sustainable planning of well water resources of the village area.

CONCLUSION

The statistical analysis shows the relation between groundwater table depth and rainfall. The R² value greater than 0.5 indicate that more influence of rainfall on groundwater because naturally rainfall occurring is also less and among that other natural parameter that presence of basalt rock have less pervious nature and availability of clay soil everywhere in area also have less infiltration capacity its result on deep percolation of rain water into the ground. From 2017 to 2020, the groundwater table is decreasing to increasing. In the study area avoid deforestation, soil and water conservation and sustainable groundwater resource management are required. The measure for water conservation by constructing different groundwater recharge structure need to planned depending upon Land use/Land cover, soil map, Geology map, contour map, slope map, and other



confined factors. The Remote sensing Imagery, Geographic Information system, Global positioning system, and regression and correlation analysis are the effective techniques for groundwater study.

REFERENCES

1. Kumar and A. Pandey, "Geoinformatics based groundwater potential assessment in hard rock terrain of Ranchi urban environment, Jharkhand state (India) using MCDM-AHP techniques," *Groundwater for sustainable development*, 2016, pp. 27-41.
2. G. Chandrakant and Md. Babar, "Identification of groundwater potential zones and artificial recharge sites in the Vedganga river sub-Basin using Remote Sensing and GIS Techniques," *Urbanization challenges in emerging economies*, 2019, pp.189-199.
3. J. Qadir, M. S. Bhat, A. Alam, I. Rashid, "Mapping groundwater potential zones using remote sensing and GIS approach in Himalaya, Jammu, and Kashmir," *GeoJournal*, 2019, doi.org/10.1007/s10708-019-09981- 5. (0123456789).
4. K Shahbaz, A Aftab and W Butian., "Quantifying Rainfall and Flooding Impact on Groundwater Levels in Irrigation Areas: GIS Approach," *Journal Irrigation Drain Engineering*, 2007, 133:359-367.
5. Mhaske S.Y, and Choudhury Deepankar, "GIS-GPS Based Map of soil index properties for Mumbai. *Geo- Frontiers*," 2011, vol.211, pp. 2366-2375.
6. Mhaske S.Y, Choudhury Deepankar, "GIS-based soil liquefaction susceptibility map of Mumbai city for earthquake events," *Journal of Applied Geophysics*, 2010, vol.70, pp.216–225.
7. M. S. kerebih and K. K. Ashok, "GIS-Coupled Numerical modeling for sustainable Groundwater Development: a Case study of Aynalem Well field, Ethiopia", *Journal Hydrol.Engg.*, 2017, 05017001-13.
8. S. Jirasirilak. A. Puttividhya and C. Phongesinabhichart, "GIS-Based statistical analysis of rainfall and Groundwater depth correlation in Thailand," *World Environment and water resource congress*, 2015.
9. S.F.R. Khadri, K. Moharir (2016), "Characterization of aquifer parameter in basaltic hard rock region through pumping test methods: a case study of Man River basin in Akola and Buldhana Districts Maharashtra India," *Model Earth Syst. Environment*, 2016, vol. 2:33.
10. Sainath Aher, Sambhaji Shinde, Praveen Gawali, Pragati Deshmukh and Lakshmi B. Venkata, "Spatio- temporal analysis and estimation of rainfall variability in and around upper Godavari river basin, India," *Arabian Journal of Geoscience* , 2019, vol.12, 682.



Sewage Pollution of Ground Water

Mahesh Patnaik

Indian Institute of Management Calcutta, Joka, Kolkata, West Bengal

✉ patnaikmahesh2@gmail.com

ABSTRACT

The practice of sewage disposal at Berhampur town by allowing it to flow down in open channels without any treatment on the heart and outskirts of the city has led to indiscriminate use of the Sewage for growing a variety of market garden crops and, in consequence, not only the soil and the crops but also the waters in the well (used for the domestic purposes) around the sewage channels have been polluted. A similar study was made of the water near the septic tanks in the premises of certain Industrial establishments in and around Berhampur town.

These and other results indicate the necessity for effective treatment of Sewage and similar wastes and the utilization of the treated waters to the fullest extent possible for the production of suitable crops, to prevent the pollution of groundwater, and to ensure the natural circulation of the elements of nutrition in the interests of environmental sanitation and health.

Keywords : Sewage; Pollution; Effluent; Ground water.

INTRODUCTION

The purpose of this paper is to draw attention to the extent of sewage pollution of the well waters in and around Berhampur town(Orissa) where raw Sewage has for over many years been allowed to flow down in open channels without any treatment. This is an unusual method or mode of sewage disposal that has caused pollution of the area's ground water. A few wells in the vicinity of these channels from which the waters were used for human consumption had to be abandoned recently. The problem of pollution of market garden crops irrigated with the Sewage from the channels has also been the problem.

In some localities in Berhampur town, as in the premises of some industrial establishments, septic tanks are employed for treatment of Sewage, and the water from the well dug near these areas for domestic use have also indicated sewage pollution. The effluents from some of the septic tanks have also been used for growing vegetables.

These and other conditions at Berhampur town prompted the present study in which a large number of samples of Sewage, well waters, and washing of Sewage grown crops have been examined. The results, along with the related experiments, are briefly described and discussed in this paper.

MATERIALS AND METHODS

Samples of water from 16 wells were periodically examined. These wells are located in the neighborhood of (i) the sewage channels on the outskirts and heart of the Berhampur town, (ii) the septic tanks on the campus of some industrial establishments and residential buildings.

In this connection, the samples of Sewage from the channels at Berhampur town were also analyzed.

The quality of water from the tender coconuts of the trees growing near the sewage channels was compared with the quality of water from the tender coconuts of the trees growing far away from the sewage channels. The quality of washing of vegetables (five successive washings with distilled water) grown on the effluents from the septic tank and sewage water were studied.

Sewage, effluents, well waters, washings of vegetables were analyzed for pH, turbidity, acidity, alkalinity, oxygen absorption, dissolved oxygen (DO), nitrite, and nitrate nitrogen, water-soluble phosphorus, chloride, total bacterial count and coliforms as indicated by the most probable number (MPN), biochemical oxygen demand (BOD). All items of analysis were carried out by standard methods and practices.

RESULTS

Observation on the flowing Sewage at Berhampur town.

Although the condition and practice of sewage disposal at Berhampur town were described earlier, they may be briefly considered here for a proper appraisal of the problem of water pollution at this place. In Berhampur town, the Sewage is collected through the open drains of brick masonry running on both sides of the roads and /or between two plots in row housing and ultimately disposed to two main open natural drains (nallahs) running, one on the northern fringe and one on the southern fringe of the town. This unique method of sewage disposal has been made possible by the topography of the land in and around Berhampur town.

On either side of the two main channels, the Sewage is drawn for irrigating extensive areas of land and growing a variety of crops, including market garden crops. In the streets, wells are sunk by the individual house owners on both sides of the drains to supply the water for domestic use. The buildings constructed near the main drain (nallaha) collects the water for use, as mentioned above.

A set of results of the analysis of the Sewage at the outfall for one of the channels and at various points in this channel (drain) are given in **Table 1**.

Table 1. Results of analysis of samples of sewage taken from one of the channels at different points

Sampling point (distance from the out fall in K.M)	0.0	0.5	1.0	1.5	2.0
Turbidity	142	142	142	142	142
pH	7.1	7.2	7.3	7.4	7.5
Acidity	60	55	40	40	39
Alkalinity	190	250	310	350	390
Dissolved Oxygen	0	0	0	0	0
BOD	147	185	227	182	197
NH ₃ -N	39	45	49	50	52
N ₂ -N	0	0	0	0	0
Water soluble P	6.5	6.5	6.5	7.0	7.5

Note- Results are expressed as mg/l, except turbidity and pH.

Pollution of water in the wells in the vicinity of the flowing Sewage

Over the years of the constant flow of Sewage in the channels in Berhampur town, the water table in some areas has risen. Although, as a result of filtration of Sewage through the soil, the waters in the wells dug in the area were clear, they showed large numbers of coliforms and high concentrations of nitrates, chlorides and phosphates (**Table 2**). In a few wells, the increases in these constituents intolerably affected the quality of the waters, and they were abandoned by those who had been consuming those waters. This well was later discarded by the user. Apart from these serious cases of pollution, there were other samples of water polluted to various extents as indicated by the analytical figure for ammonical nitrite and nitrate nitrogen, chloride, phosphorus, and for bacteria, including coliforms. The people who were consuming these waters complained about gastrointestinal disorders.

Table 2. Results of analysis of samples of well water as affected by the sewage flowing in the channel

Characteristics	Sewage in the channels	Sewage drawn into a pit for irrigation	A well about 3.0 Mt away from the sewage pit
Turbidity	89	7	11
pH	•	130	145
Acidity	400	420	520
Alkalinity	16	18	4



Dissolved Oxygen	150	100	16
BOD	57	54	5
NH ₄ -N	0	0	0
NO ₂ -N	0.3	0	0
Water soluble P	6.7	6.7	3.0
Chloride Cl	193.7	205.5	403.1

Note- Results are expressed as mg/l, except turbidity and pH.

Examination of the water in the tender coconuts from Trees growing near the Sewage Channel

It was thought desirable to have an idea of the effect of flowing Sewage on the quality of the water in the tender coconuts on the trees growing near the sewage channels. The qualities of the water from these coconuts were compared to the quality of the water from the tender coconuts on the trees growing in the area about 10 km away from the sewage channel. The results showed that the water from tender coconuts from the trees growing near the sewage channel contained much more nitrogen and chloride but much less phosphorous than the water from the tender coconuts from trees growing away from the sewage channel.

Effect of septic tanks on the quality of water in the wells in the neighbourhood

Samples of water were collected from 6 wells near the septic tanks on the residential buildings and from two wells near the industrial establishments and were examined. The effluent from the septic tank in the residential buildings flows down in the open brick drains running between the houses in the colony.

The effluent from the septic tank at the industrial establishment is allowed to soak through the soil in a soak pit, but this provision has not prevented the waters in the wells within a radius of one furlong from being polluted like the other well waters.

DISCUSSION

This study seems to raise a few points of special and general interest. The continuous flow of crude Sewage on the land in and around Berhampur town for a long time has naturally polluted the groundwater and also raised the water table in some areas there. Although the favorable topographical conditions have permitted such a mode of sewage disposal, this should be stopped in the interest of environmental sanitation and safe water supply. The use of Sewage for growing vegetables, including those eaten in the raw state, should also be prohibited in consideration of public health.

SUMMARY

Over 50 samples of water from the wells located in the neighborhood of channels carrying raw Sewage and in the neighborhood of septic tanks were examined and were found unfit for human consumption. Examination of crops grown on Sewage and on effluents from septic tanks showed evidence of sewage pollution.

While it is necessary to bring back the elements of plant nutrition in Sewage into the cycle of life and food, it is also necessary to treat the waste material properly before it is utilized for control of water pollution and for promotion of environmental health.

REFERENCES

1. Rechar Feachem, Michel McGarry, Duncan Mara 'Water, Wastes and Health in hot climates' John Wiley & Sons, London.
2. Dr G K Seth, R K Saraf, 'Environmental Pollution' CIPHERI, Nagpur-20. J.-G. Lu, "Title of paper with only the first word capitalized," J. Name Stand. Abbrev., in press.
3. 'Manuals of methods for examination of water, Sewage and industrial wastes' Indian Council of Medical Research, New Delhi.
4. IS 3025, Part 1 to 49: Methods of Sampling and tests (Physical and chemical) for Water and Waste water.
5. IS 4733: 1972 Methods of Sampling and Test for Sewage Effluents
6. G M Fair, J C Geyer, D A Okun 'Water and Waste Water Engineering' John Wiley & Sons, London.



Energy Audit of Waste Heat Recovery System in Indian Cement Plants - Case Studies

Prateek Sharma, M V Ramachandra Rao, Ashutosh Saxena, B N Mohapatra

Centre for Mining Environment, Plant Engineering & Operation, National Council for Cement and Building Materials, Faridabad, Haryana

✉ prateek.sharma@ncbindia.com

ABSTRACT

Almost more than 99 % of Indian cement industry is dry process based. Studies had shown that in case of wet process plants, kiln exit gas temperature is low to the tune of 180-200 °C and gases are moisture laden while in dry process, kiln exit gas temperature is more than 250 °C with negligible moisture. Hence heat input availability for waste heat recovery is much more in present scenario. Indian cement industry has buildup waste heat recovery system (WHRS) capacity of more than 400 MW and still striving to achieve more. Simultaneously cement plants, suppliers, consultants, energy auditors are looking towards energy efficiency improvements of these systems to enhance WHRS potential. National Council for Cement and Building Materials (NCCBM) has done several energy audits for WHRS of cement plants. This paper presents case studies carried out by NCCBM indicating the energy savings potential, efficiency of key WHRS equipment along with some recommendations.

Keywords : Waste heat recovery; Cooler; Preheater; Cement plant; Clinker.

INTRODUCTION

Cement industry is known to be energy intensive consuming large amount of thermal and electrical energy during clinker and cement production. Waste heat recovery (WHR) has already been identified as a green energy worldwide which has enormous potential to replace captive power along with sustainable clinker production. There are different sources of waste heat like heat in flue gas, vapour streams, convective & radiant heat, cooling water heat loss, stored heat in products leaving the process etc. [1]. Indian cement industry has a huge potential of more than 1200 MW power through WHRS with current installed capacity of more than 400 MW [2]. As per sustainability report of Shree Cement [3], it is leading in the world (excluding China) in terms of power generation through waste heat recovery with a capacity of 126 MW upto FY 18-19. Several stakeholders like Cement Manufacturers Association (CMA) and Bureau of Energy Efficiency (BEE) are working towards thriving WHR as a status of renewable power. It is known that for a 3000 tpdclinkerisation capacity, around 3 MW of power through WHRS is feasible considering Steam Rankine cycle of power generation. However, plants are looking to achieve more than the rated potential. Some of the ways adopted by cement plants to enhance power generation through waste heat recovery systems are [4]:

1. Reduction of boiler exit gas temperature by optimizing Secondary firing by conventional fuel through hot air generator to enhance the WHR potential from cooler side
2. Reduction of boiler exit gas temperature by optimization of hot air requirement for mills
3. Tapping of waste heat from stack flue gas which are at temperature from 150-200°C for additional power through WHRS at cooler side
4. Mid air tapping from cooler which enhance power generation tremendously
5. Dual mid air tapping from cooler side
6. Monitoring of energy consumption for WHRS systems through energy audits and implementation of energy saving measures.

In view of above, NCCBM has carried out several energy audits of WHRS of cement plants to enhance WHR potential and two of them are highlighted in this paper.



CASE STUDY-1

The plant is having two waste heat recovery boilers namely Preheater boiler (PH Boiler) and Air quenching cooler (AQC) Boiler. The waste air coming out of cooler vent at a temperature of 315 °C are used to heat water in the AQC boiler to produce saturated steam. This steam is then sent to PH boiler for super heating. The waste gasses coming from Preheater to PH boiler at a temperature of 395 °C are used to produce steam. This steam is then sent to turbine for power generation. A single extracting cum condensing type turbine of 2.5 MW rated capacity has been installed.

The design details of AQC Boiler and PH Boiler are given in Table 1 below:

Table 1. Design details of AQC and PH boiler

Particular	Details
Type of boiler	Waste heat recovery (water tube)
No. of boilers	Two (PH & AQC Boiler)
Cooler boiler capacity	5.0 tph
Preheater boiler capacity	10.0 tph
Inlet steam temperature of turbine	330 +/- 5 °C
Power output	2500

Performance assessment of various equipment

Preheater boiler

- Preheater boiler efficiency considering all inputs based on data analysis [5] and process measurement works out to 83.5 % which is ok[6].
- The Oxygen content at PH boiler inlet is 3.9% and at PH boiler outlet is 4.5%. The false across the PH Boiler is 3.63% which is very good.
- The false air across the PH Boiler is 3.63% which is very good.

AQC boiler

The AQC boiler efficiency is low at around 68 % because plant has reduced heating surface area by modification in order to reduce velocities to prevent damage of tubes.

Turbine

- The turbine heat rate and efficiency are found to be 3787 kcal/kWh and 22.7%.

Water cooled condenser

- The condenser efficiency is 72.6 % which is ok.
- Terminal temperature difference of condenser is 4.92 °C

Cooling Tower Assessment

- Plant is having 4 mechanical draft cooling towers and 1 jet cooling tower. Cooling tower range and approach is 13.57 and 5.5 which are ok.
- Cooling tower effectiveness is 70% which is ok.
- Plant is having 4 cooling water pumps for cooling condensate in condenser as well as for auxiliary cooling purpose. 3 pumps are in running condition and 1 pump is in standby. The efficiencies of these cooling water pumps are ok

Condensate extraction pump (CEP) water pumps assessment

Plant is having 2 CEP pumps for extracting condensate. 1 pump is in running condition and 1 pump is in standby. The performance assessment of CEP water pumps is given in **Table 2** below.

**Table 2.** Assessment of CEP water pumps

Parameters	Unit	CEP-1	CEP-2(stdby)
Power Measured	kW	6.96	7.50
Flow	m ³ /hr	22.00	20.00
Head	M	42.00	42.00
Hydraulic Power	kW	2.52	2.29
Pump shaft Power	kW	6.40	6.90
Efficiency of the pump	%	39.32	33.17

Observations:

- The efficiencies of CEP water pumps are low.

Performance assessment of Bore water pumps- Colony

The efficiencies of bore pumps in Colony are given in Table III below:

Table 3. Performance assessment of colony bore water pumps

Parameters	Unit	C-22	E-1	S-28	S-57	S-1
Power Measured	kW	14.60	10.90	18.40	10.80	11.50
Flow	m ³ /hr	16.00	12.50	15.00	7.50	21.00
Head	m	185.00	178.00	170.00	173.00	56.00
Hydraulic Power	kW	8.07	6.06	6.95	3.54	3.20
Pump shaft Power	kW	13.43	10.03	16.93	9.94	10.58
Efficiency of the pump	%	60.05	60.46	41.05	35.58	30.29

Observations:

- The efficiency of pumps S-28, S-57 and S-1 are low.

Recommendations

1) It is recommended to replace the mechanical draft cooling towers with mist cooling towers instead of jet cooling towers. The advantages of mist cooling tower over mechanical draft cooling tower and jet cooling tower as claimed by suppliers is given in **Table 4** below[7, 8]:

Table 4. Advantage of mist cooling tower over induced and jet cooling tower

Feature	Mechanical Draft Cooling Tower (MDCT)	Jet Cooling Tower (Fan less)	Louver Type Mist Cooling System (Fan less)
Approach to WBT	4 to 5 degrees.	6 to 8 degrees.	1 to 2 Degrees.
Temperature Drop	8 to 10 Degrees	6 to 8 Degrees	Regular: 12 Degrees.
Power consumed	100 HP : 100% 70 HP : 100% on Pumping & 30 HP : Fan)	100 HP : 100% 100 HP : 140% on Pumping & 00 HP : Fan)	70 HP : 70% 70 HP : 100 % on Pumping & 00 HP : Fan)
Water droplet size	5 mm	2 to 3 mm	Atomized to 5 to 50 Microns
Nozzles	Ordinary type	Ordinary Jet type	Special whirling type

The schematic diagram of mist cooling tower and outside view of Louver type are given in **Fig. 1 & Fig. 2**.

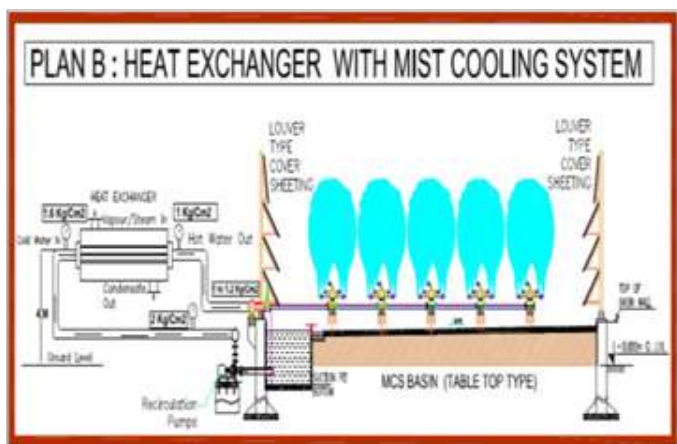


Fig. 1. Schematic diagram of mist cooling tower



Fig. 2. Outside view of Louver type

The Energy savings on account of replacing Mechanical draft cooling towers with mist cooling towers is given in **Table 5**.

Particular	Value	Unit
Power consumed by each cooling tower fan	9	kWh
Total power consumption by 3 fans	27	kWh
Annual power savings by replacing existing ID cooling tower with mist type cooling tower	213840	kWh
Payback	1.73	years

Replace CEP-1 with new efficient pump

The efficiencies of CEP water pumps (both running and standby) are low. It is recommended to change atleast one pump with high efficiency pump. The energy savings by replacing existing pump with high efficiency pump is given in Table 6.

Table 6. Energy savings by installing high efficiency pump

Particular	Value	Unit
Efficiency of the pump	39.32	%
Power consumption of pump	6.9	kWh



Efficiency of new pump	70	%
Power consumption of new pump	34	kWh
Annual savings	22968	kW
Cost of power	5.4	Rs
Monetary savings	1.2	Rs Lakhs
Investment	2.0	Rs Lakhs
Payback	24	Months

It is recommended to replace the low efficiency pumps with new high efficiency pumps. The energy savings on account of this is given in **Table 7**.

Table 7. Energy savings by installing high efficiency bore pumps

Particular	S-28	S-57	S-1	Unit
Efficiency of the pump	41	35	30.29	%
Power consumption of pump	18.4	10.8	11.5	kWh
Efficiency of new pump	70	70	70	%
Power consumption of new pump	11	5.49	5	kWh
Annual savings	54792	32009	71797	kW
Cost of power	5.4	5.4	5.4	Rs
Monetary savings	2.9	1.72	3.8	Rs Lakhs
Investment	1.0	1.0	1.0	Rs Lakhs/annum
Payback	4	7	5.5	Months

CASE STUDY-2

The plant is having 01 kiln systems equipped with 02 no of boilers one preheater boiler and one Air quenching cooler boiler. The efficiency of key equipment is tabulated below.

Performance assessment of various equipment

Preheater Boiler

The boiler efficiency of preheater boiler is

Atmospheric temperature	32	°C
Inlet temperature of PH flue-gas	350	°C
PH boiler flow	278000	kg/hr
Specific heat of air	0.245	kcal/kg °C
Energy in flue gases	21658980	kcal/hr
Radiation losses	216589.8	kcal/hr
Temperature outlet	220	°C
Raw mill outlet temp	70	°C
Energy in flue gases	12804680	kcal/hr
Heat taken for drying of materials	10216500	kcal/hr
Actual heat available for recovery	2588180	kcal/hr
Efficiency by indirect method	87.0	%



AQC Boiler

Atmospheric Temperature	32	°C
Flue gas inlet temperature	350	°C
AQC boiler flow to coal mill	19783	kg/hr
AQC boiler flow after coal mill	108000	kg/hr
Specific heat of air	0.256	
Energy in flue gases	6386688	kcal/hr
Radiation losses	5109.3504	kcal/hr
Flue gas temperature leaving AQC	260	°C
Energy recovered from flue gas leaving AQC to coal mill	455798.016	kcal/hr
Temperature of flue gas outlet	90	°C
Energy in from flue gas leaving AQC to coal mill	1169881.574	kcal/hr
Energy in flue gases out	1686528	kcal/hr
Efficiency	58.9	%

Turbine efficiency

Particular	Parameters	Average Value	Units
Turbine inlet	Flow Rate -HP steam	17.7	(TPH)
	Pressure – HP steam	24.8	Kg /cm ²
	Temperature – LP steam	335.6	oC
	Enthalpy of HP steam at turbine inlet	738.9	Kcal /Kg
	Flow Rate -LP steam	1.4	(TPH)
	Pressure – LP steam	1.1	Kg/cm ²
	Temperature – LP steam	187	oC
	Enthalpy of LP steam at turbine inlet	664.4	Kcal /Kg
Feed water pump	Feed Water Pr	38.4	Kg /cm ²
	Feed Water Temp	122.8	oC
	Feed water flow rate	18	TPH
	Enthalpy	123.19	kcal /Kg
Power generated gross	3170	kW	
Turbine heat rate	3719.64	kcal/kW	
Turbine cycle efficiency	23.1	%	

In this case both HP and LP streams are available, and both has to considered for turbine cycle calculation.

Recommendations

Operating efficiency of BFP pump is 54.07 %. This is on lower side hence it is recommended for optimization of pump discharge pressure for reducing line losses and try to operate with biasing logic as discharge pressure in auto mode with feedback from drum pressure and steam temperature. As example if drum pressure is 106 kg/cm² then set value come 114 kg/cm² for maintaining drum level in safe mode other if drum level goes to further down it will increase discharge pressure in auto mode from plus 8 kg/cm² to 9 kg/cm² and may be more. Same for steam temperature because total drum-head losses is maximum 5 kg/cm².

CONCLUSIONS

Indian cement industry has come a long way in implementing WHRS in their cement plants. Both studies indicated that that



there is enough energy savings potential in utility area like pumps and cooling tower for WHRS system in these cement plants. Similar trend has been observed for other cement plants having waste heat recovery systems. Thus there is a need to focus on utility areas with proper scheduled maintenance and replacement with suitable capacity systems wherever needed. Stand by pumps and air compressors should be utilized adequately as per the requirement. Plants are recommended to maintain boiler efficiencies above 80 % and turbine efficiency 21-23 % as well as close to design capacity for efficient plant operation.

REFERENCES

1. Bureau of Energy Efficiency. Waste heat recovery. <https://beeindia.gov.in/sites/default/files/2Ch8.pdf>
2. Saxena, A., et al., Compendium The Cement Industry India 2019, National council for cement and building materials. p. 251-260.
3. Shree Cement Limited, Expanding the sustainability horizon 15th corporate sustainability report 2018-19: p. 1-132.
4. Patil, Green energy for cement plants, in 16th NCB International Seminar on Cement, Concrete and Building Materials. 2019: New Delhi.
5. Vakkilainen, E. and P. Ahtila. Modern Method to Determine Recovery Boiler Efficiency. 2011.
6. Confederation of Indian Industry, Energy benchmarking for Indian cement industry. 2019.
7. Mist Resonance Engineering Pvt. Ltd. Mist cooling system. <https://www.mistcreation.com/mcs.html>.
8. Cooling India. High Efficiency Mist Cooling System as an Alternative to Cooling Tower. <https://www.coolingindia.in/high-efficiency-mist-cooling-system-as-an-alternative-to-cooling-tower/>.



Wealth from Waste

Bhalchandra B Bhalerao

Aquair Consulting Engineers, Nerul (West), Navi Mumbai, Maharashtra

✉ bbbhalerao@gmail.com

ABSTRACT

Pollution caused by improper waste disposal is detrimental to human health and also a burden on our limited financial resources [1]. Treatment of waste has not kept pace with increased population and increase in the industrial production. About two thirds of our waste is organic materials. This can be converted into compost or biogas – both very valuable products for an agricultural country like ours.

Anaerobic biological digestion converts up to 70% organic matter into methane rich biogas. The power requirement of the system is also very low. It shows how a liability of treatment of waste water and its cost is turned in to a profitable proposition.

Case studies for Molasses based alcohol distillery, Corn Starch factory and Milk dairy where installation of anaerobic digestion and its financial aspects have been presented. The application of anaerobic digestion processes not only reduces pollution load but is a source of income. The investment made in installation of the anaerobic digesters is source of recovered in about 2-3 years. In the subsequent period the digester is for the factory.

Keywords : Anaerobic digestion; UASB; CSTR; Corn starch; Dairy; Distillery; Payback period.

BASICS OF ANAEROBIC DIGESTION PROCESS

The fermentation process in which organic material is degraded and biogas is produced is referred to as Anaerobic digestion process [2].

The anaerobic bio-degradation of organic matter is a multi-step process. The four successive stages are namely

Hydrolysis

Acidogenesis

Acetogenesis, and,

Methanogenesis

Hydrolysis

This process is merely a surface phenomenon in which the polymeric particulates degraded through action of co enzymes to produce smaller molecules which can cross the cell barrier. During the enzymatic hydrolysis process proteins are hydrolysed to amino acids, polysaccharides to simple sugars and lipids to long chain fatty acids (LCFA).

Acidogenesis/Fermentation

During the Acidogenesis step the hydrolysis products which are relatively small soluble compounds are diffused inside the bacterial cells through cell membrane and subsequently fermented or anaerobically oxidised. The acidification products include VFA, acetate and higher organic acids such as lactic acids, ethanol and ammonia.

Acetogenesis

Intermediary acid production is converted into acetate, H_2 , and CO_2 as well as new cell material.

Methanogenesis

In this process acetate, hydrogen plus carbonate, methanol are converted into methane, CO_2 and new cell material.



Methanogenic bacteria accomplish the final stage in the overall anaerobic conversion of organic matter to methane and carbon dioxide. It is only in this step when influent COD is converted to gaseous form and automatically leaves the reactor system.

Certain substances are toxic to anaerobic process as given in **Table 1** [2].

Co-digestion with other waste, can significantly improve the waste treatment efficiency [3]

Table 1. Toxic substances to anaerobic process

pH Related toxicity	
Ammonia	1000 mg/L
VFA	1000 mg/L
Dissolved sulphides dispersed sludge to granular sludge as unionised H_2S	50-250 mg/L
Immediate toxicity	
Chlorinated compounds CCl_4 , CH_3Cl , CH_2Cl_2	1 mg/L or less
Cyanides	Highly toxic but adaptable
Formaldehyde	50-100 mg/L
Oxygen	toxic to methane formers
Concentration related	
Heavy Metals	1-10 mg/L, but generally precipitated As non-toxic metal sulphides and may cause sludge disposal problems

UASB

The Up flow Anaerobic Sludge Blanket reactor is constructed in steel for treating small volume waste water and in RCC for large volume of waste water. Waste water to be treated enters the reactor at the bottom and travels to the top from where it is discharged. The tank height is restricted to 6-8 meters. The volume of reactor depends upon the loading rate and COD load [4,5].

The unique feature of the UASB reactor is the phase separator. This device is placed at the top of the reactor and divides the reactor into a lower part, the digestion zone and an upper part the settling zone. The wastewater is introduced uniformly over the reactor floor, passes through the sludge bed and enters into the settling zone via the aperture between the phase separators.

CSTR DIGESTER

CSTR Digester consists of continuous stirred tank reactor where continuous mixing of effluent and biomass take place with the help of central and lateral agitators.

The essential feature of that the wash out of the active anaerobic bacterial biomass from the reactor is controlled by a sludge separator recycle system. The basic idea underlying the anaerobic contact process is that:

- Provide contact between the active biomass and feed.
- Utilize the digester volume effectively.
- Prevent stratification and temperature gradient
- Minimize the formation of scum layer and the deposition of sludge solids.

MEDIA BASED REACTOR

Also called Anaerobic Fixed Film Reactor (AFFR) or Fixed Film Attached Growth Reactor.

The reactor is fabricated out of mild steel sheets of various thicknesses and with protective coating inside and outside. The reactor is filled with specially designed rigid PVC media for bacterial immobilization on its surface. As the media modules have very large surface to volume ratio, large population of bacteria is available in the digester. The reactor content is kept completely mixed by re-circulating the treated spent wash up to 20 times which also helps maintain the reactor pH around 7-7.2.



The treated effluent is collected at the bottom so as to avoid short-circuiting. The bio gas is collected at the tank top dome, which is fitted with safety devices for gas pressure to be maintained within prescribed pressure limit. The bio gas is transported to a gas blower and then to the point of use such as boiler or biogas engine.

The liquid retention time in the reactor is dependent upon influent COD value. It is around 12 days for distillery effluent COD value of 100,000 mg/L. This anaerobic process will bring down the COD levels by around 70% and the organic matter so removed is converted into methane rich biogas.

DAIRY INDUSTRY

Milk & Milk Products & their manufacturing processes Operations in a Dairy [6]

Receiving

Pasteurizing

Bottling

Condensing (condensed milk production)

Dry milk manufacture

Butter making

Cheese making

Casein

Skimmed milk

Whey

Yogurt

Water Use

Water is mostly used for washing and cleaning of the tanks, bottles and equipment.

Cleaning In Place (CIP)

Equipment Cleaning

Floor Washing

Steam Generation

Cooling

Ultra-Filtration, etc.

In the following example the dairy maximum milk processed per day during the peak season is around 400,000 litres per day. The water consumption is estimated at 1200-1300 m³/day.

Sources & Quantity of Wastewater Generated [6]

Many dairies carry out only process of receiving milk, pasteurise it and bottle it for retail distribution, while many others produce one or more of the products. The wastewater volume and characteristics depends upon the type of operation carried out.

Table 2. Wastewater analysis: Dairy Effluent Analysis for milk only (no milk products)

S No.	Parameter	Raw Effluent	Effluent after Dissolved Air Floatation (DAF) & inlet to UASB
1	pH	7-8	7-8
2	COD mg/L	3200	2560
3	BOD mg/L	1600	1280



4	Oil & Grease mg/L	150	30
5	T. S. S. mg/L	1800	180
6	T. D. S. mg/L	2000	900
7	Sulphate (SO ₄)	25	25

TREATMENT PLANT –BRIEF DESCRIPTION

- Oil & Fat removal (DAF)
- Equalization of flow and characteristics of the wastewater
- pH correction
- First stage anaerobic biological treatment
- Second stage aerobic biological treatment
- Polishing treatment for removal of residual suspended matter.

The raw effluent generated at the plant is led from the last manhole to the inlet of the Effluent Treatment Plant. The combined effluent is passed through an open channel where on line flow measurement is done .

After screening, the effluent is led to a Dissolved Air Floatation (DAF) unit and then to the receiving sump. From the sump the effluent is pumped to the inlet of two fill and draw type equalization tanks provided for balancing the hydraulic and organic load fluctuations. The contents of the Equalization tank shall be kept completely mixed and agitated by diffused aeration system provided on the floor of the tank.

Once the anaerobic reactor is stabilized, it will have enough buffering capacity and pH adjustment shall not be required. The effluent after pH adjustment in the Equalization tank is pumped to the inlet of the anaerobic digester based on the Up flow Anaerobic Sludge Blanket (UASB) process and shall be uniformly distributed at the digester floor.

The gas generated in the digester rises to the top and collected by a separate piping system. The biogas is led to a gas holder and then to the point of use.

Excess sludge from the UASB digester is withdrawn through the valves to be provided at different levels in the digester, and taken to sludge pit from where it is sent to sludge drying sand beds.

The effluent from the anaerobic treatment (UASB) is further treated in Aerobic biological treatment and Polishing treatment for removal of residual suspended matter.

PAYBACK PERIOD

Table 3. Payback period for Bio gas plant for 1000 m³/day Milk dairy (2010)

1.	Basic Data for the Dairy	
	Capacity of the Dairy	400 m ³ /day
	Qty. of wastewater per day	1000 m ³ per day
	B.O.D. value of the Wastewater	1280 mg/L
	C.O.D. value of WW	2560 mg/L
	Total COD load/day 1000 x 2560 /1000	2560 kg/day
	COD destroyed = 70% of 2560=	1792 kg/d
2.	Estimated generation of Methane rich Biogas (Assuming 0.53 Cum. Biogas per Kg of C.O.D. removed 1792x 0.53=	950 Nm ³ /day
	Calorific value of Biogas (Average value)	5300 Kcal/m ³
	Total calorific value of the biogas produced 950 x5300= 50 million k Cal	5 million K Cal
3.	Equivalent furnace oil quantity with furnace oil Calorific value of 10000 Kcal/litre	5035 litres



4.	Cost of Furnace oil saved @ Rs. 25 / litre	Rs 12588 / day
5.	Yearly saving (considering 300 working days in a year for the distillery)	Rs 38 lakh /year
6.	Yearly Power, Chemicals, Manpower & Maintenance cost of the anaerobic plant	Rs 5 lakh
7.	Net yearly saving	Rs 33 lakh
8.	The estimated cost of the bio-gas generation Plant for the above capacity (Anaerobic Treatment only)	Rs 90 lakh
9.	Estimated payback period for bio-gas generation plant	2.7 years 33 months

DISTILLERY INDUSTRY

Alcohol Production from Molasses

Process Description

The main raw material for the distillery is molasses obtained from the sugar mills in the neighbourhood.

Alcohol Production process flow scheme is as follows:

Molasses is diluted with water in 1:4 ratio and the mixture fed to the Fermenter. In the Fermenter yeast is added for propagation. In the Fermenter Sludge is separated and sent for disposal. The supernatant is sent to the Analyser and then to the Rectifier column. In the Rectifier column alcohol and spent wash is generated. The alcohol is sent for recovery while the spent wash is sent for treatment in anaerobic digester. In the digester almost & 70% of COD is converted in methane rich biogas.

Table 4. Distillery spent wash characteristics

S.No	Parameter	Batch Process	Continuous Process
1	Volume (L/L alcohol)	14 – 15	10 – 12
2	Color	Dark brown	Dark brown
3	pH	3.7 – 4.5	4.0 – 4.3
4	COD mg/L	80000-100000	110000 – 130000
5	BOD mg/L	45000 – 50000	55000 – 65000
6	Total solids mg/L	90000 – 120000	130000 - 160000
7	Inorganic dissolved mg/L	30000 – 40000	35000 – 45000
8	Total volatile mg/L	60000 – 70000	60000 – 75000
9	Inorganic dissolved mg/L	30000 – 40000	35000 – 45000
10	Chlorides mg/L	5000- 6000	6000 – 7500
11	Sulphates mg/L	4000 – 8000	4500 – 8500
12	Total Nitrogen	1000 – 1200	1000 – 1400
13	Potassium mg/L	8000 – 12000	10000 – 14000
14	Phosphorous mg/L	200 – 300	300 – 500
15	Sodium mg/L	400 – 600	1400 – 1500
16	Calcium mg/L	2000 – 3500	4500 – 6000

Table 5. Basic data for system design

Sr No	Parameter	Raw Spent Wash	After anaerobic treatment
1	Quantity	600 m ³ /day	600 m ³ /day
2	BOD mg/L	41500	6500
3	COD mg/L	105000 mg/L	40000 mg/L
4	pH	4.2-5.0	6.5-7.5



Effluent Treatment Plant for a Distillery [7]:

Distillery capacity 40 kL/day
Wastewater 600 m³ /day
Wastewater COD 105000 mg/L
COD load 63000 kg/day

Civil works

1. Foundation for reactor
2. Sump for hot liquid
3. Yeast settling tank
4. Holding Ponds - 3 nos.
5. Homogenisation tank.
6. MCC Room
7. Laboratory
8. Foundations
9. Yeast sludge drying beds

Mechanical equipment

- M.S. Fabricated Reactor 27.9 mm dia. x 11m height
- PVC Media 5808 M3- Made up plain & corrugated PVC sheets
- Bio gas Blower with Motor
- Plate Heat Exchanger
- Feed Pump with Motor
- Re circulation Pump with Motor
- Filtrate Pump for Yeast drying beds

Instruments & Safety Equipments

Painting, Electrical Work M. C. C. Panel, Pipe Fabrication & laying

Instrument Panel & Instruments, etc.

PAYBACK PERIOD

Table 6. Payback period for Bio gas plant for 40 -KL Distillery (2001)

1.	Basic data assumed for the Distillery	
	Capacity of the Distillery	
	Qty. of spent wash per day	600 m ³ per day
	B.O.D. value of spent wash	41500 mg/L
	C.O.D. value of spent wash	105000 mg/L
	Total COD load/day 105000 x 600 / 1000	63000 kg/day
	COD destroyed = 70% of 63000	44100 kg/d
2.	Estimated generation of Methane rich Biogas (Assuming 0.53 Cum. Biogas per Kg of C.O.D. removed 44,100 x 0.53=	23373 Nm ³ /day



	Calorific value of Biogas (Average value)	5300 Kcal/m ³
	Total calorific value of the biogas produced $23373 \times 5300 = 7$ million kCal	124 million kCal
3.	Equivalent furnace oil quantity with furnace oil Calorific value of 10000 Kcal/litre	12400 litres
4.	Cost of Furnace oil saved @ Rs. 12 / litre	Rs 148800 / day
5.	Yearly saving (considering 300 working days in a year for the distillery)	Rs. 45 lakh /year
6.	Yearly Power, Chemicals, Manpower & Maintenance cost of the anaerobic plant $45 \times 6 = 39$ lakh	Rs 6 lakh
7.	Net yearly saving	
8.	The estimated cost of the bio-gas generation Plant for the above capacity (Anaerobic Treatment only)	Rs. 200 lakh
9.	Estimated payback period for bio-gas generation plant	5 years or 60 months

CORN STARCH INDUSTRY

Starch Production

Starch is manufactured out of corn kernel mainly adopting wet milling process.

The corn wet milling process in which the kernel is separated into its component parts, and those parts are then further subdivided and refined. Corn wet millers buy shelled corn that is delivered to the plant by truck. Incoming corn is cleaned to remove extraneous material such as pieces of cob, foreign seeds, stray metal, and fine grit. It then is conveyed to storage silos, until ready to go to the refinery.

Flow chart of Wet Milling Process is as follows:

1. Cleaning
2. Steeping- Crushing (Grinding)
3. Germ Separation -Germ Press- Germ Dryer
4. Oil Expeller
5. Fiber separation -Fiber Press –Fiber used as used as Cattle Feed
6. Gluten Separation - Gluten Dryer
7. Starch refined -Starch Slurry Drying -Dry Starch
8. Glucose making
9. Centrifuge

Wet milling gives following products --

- Starch 60%
- Gluten 8-9%
- Germ 6-7%
- Husk 22-24%

Sources of Effluent

The two main streams of effluent emanating from corn starch factory are:

1. Light steep Liquor
2. Starch Plant Waste

In addition to this, following processes and operations result in to wastewater.



3. Reactor jackets (cooling water)
4. Reactor washing
5. Filter washing
6. Drying bowl washing Vacuum pump cooling water
7. Floor washing
8. Drum washing, etc.

Wastewater characteristics

Parameter	Combined Effluent
Volume M ³ /day	290
pH	3.5 to 3.8
Oil & grease	17
Total Solids	48300
Suspended Solids	13300
COD	35000
BOD	21500
Chloride	500
Sulphate	1100
Phosphate	500
Nitrogen	1500
Total Dissolved solids	35000

ETP PERFORMANCE

The stage wise ETP performance in terms of COD & BOD reduction and the final treated effluent quality is as given in **Table 8**.

Table 8. ETP Performance

	COD In	COD Out	BOD In	BOD Out
Raw Effluent	35000	--	21500	--
After Equalization & neutralization	35000	31500	21500	19350
After anaerobic digestion	31500	7875	19350	2900
After aerobic treatment-stage 1	7875	1970	2900	145
After aerobic treatment-stage 2	2900	1450	145	100
After tertiary treatment	1970	250	--	Below 100

- Biogas production: 0.5-0.56 m³/ kg of C. O. D. Removed
- COD removed as given above 350 m³/d x (31500-7875)= 23625 mg/L== 8268 kg/day
- Bio gas production= 8368 x 0.53= 4435 m³/day on the basis of above figures.

Gas Composition

- o Methane content: 52% to 65 %
- o Hydrogen Sulphide: 1.5 % to 2.5 %
- o Carbon Dioxide: 38 % to 46 %
- o Calorific value: 5600-6000 Kcal/m³



PAYBACK PERIOD

Table 9. Payback period of the anaerobic digester (UASB)

Capacity of the starch factory: 300 Tons /day maize grinding & 150 Tons /d native food grade starch manufacture	
Quantity of combined waste water per day	350 m ³ /d
BOD value	21000 mg/day
COD value	35000 mg/L
Total COD value/d 350 x 35000/1000	12200 kg/d
COD removed @ 70%=12,200 x 0.7=8540 kg/d	8540 kg/day
Biogas generation rate per kg COD removed	0.53 m ³ /biogas/kg COD removed
Biogas generated 8540 x0.53=	4526 m ³ /d
Avg. Calorific value of biogas	5300 kL cal/m ³
Total Calorific value of biogas generated 4526 x 5300=	24 million kL calorie
Equivalent furnace oil @ 10,000 kL calorie/m ³ 24 million/10,000	2400 litres/day
Cost of furnace oil @ Rs 20/liter	2400 x 25 = 60000
Yearly saving (considering 300 working days in a year for the distillery)	Rs 120 lakh
Yearly Power, Chemicals, Manpower & Maintenance cost of the anaerobic plant	Rs 40 lakh
Net yearly saving (180-60)=120 lakh	Rs 80 lakh
Installed cost of the bio-gas generation Plant(Anaerobic Treatment only)	Rs 100 lakh
Estimated payback period for bio-gas generation plant	1.25 years or 15 months

REFERENCES

1. CPCB ENVIS-Centre on Control of Pollution Water, Air and Noise http://www.cpcbenviis.nic.in/water_pollution.control.html
2. S. J. Arceivala & S. R. Asolekar book Wastewater Treatment for pollution Control & Water Reuse, Third Edition, Tata McGraw Education Pvt. Ltd. New Delhi , Seventh Reprint (2011)
3. Makarand Ghangrekar, NPTEL Indian Institute of Technology, (IRJET) Kharagpur Volume: 02 Issue: 08 Nov-2015
4. A C Van Haandel & Gatze Lettinga book on Anaerobic Sewage Treatment A Practical Guide for Regions with Hot Climate, John Wiley & Sons (1994)
5. B.B.Bhalerao Application of UASB Technology for Waste water Treatment in India, Enviro Vision 2010 Indian Institute of Technology Bombay(IITB), November 25-27, 2010.
6. A D Patwardhan book Industrial Waste Water Treatment, second edition 2018 Published by PHI Learning Pvt. Ltd Delhi 2018.
7. Bhalerao BB, Wairagrade Madhavi (Aquair Consulting Engrs, Nagpur). Waste water treatment and disposal for molasses based alcohol distillery - Proc Natl Conf Polln Prev Contl India : IAEM, 2-3 March, 2002, Nagpur.



Design Algorithm: Solar Powered Water Supply System for Municipalities & Rural Area

Dilip Yewalekar, Manisha Kinge

Design Dept, Jain Irrigation Systems Ltd, Jalgaon, Maharashtra

✉ yewalekar.dilip@jains.com

ABSTRACT

‘WaterGems’ software is widely used to design a water supply system considering electrical motor pump sets supported by standby Diesel Generator assuming no power failure. It has been found that in many water supply projects, recurring cost of power, financial analysis & viability of projects are not evaluated and/or neglected because of Political & Social Sensitiveness. The concern article is highlighted ‘the design principles and consideration’ of Solar Powered Water Supply System along with representative financial analysis. It can be clubbed with ‘WaterGems’ software. This will help to optimize the cost of power as well as overall cost of water supply system and to take the decision of implementation.

Keywords : Solar photovoltaic; Inverters; Coagulant; Sedimentation; Filtration; Disinfectant.

INTRODUCTION

In general, water supply system has been designed from tail end to water source on per capita demand on 12 to 24 hrs basis and electrical power requirement is worked out to supply water to consumers. Same methodology is followed in ‘WaterGems’ by inserting: Nodes, Route of Water Distribution Piping, Hydrants, Water Tank, Valves, Surge Tank, Pump along with input data Water Demand, Flow & Pressure at Pump or Elevation of ESR followed by zoning of operation and ‘WaterGem’ does hydraulic analysis and gives the results of hydraulic gradient (frictional head losses) in the network. Based on the results, design engineers used to work out the power requirement and insisting of a dedicated power supply without evaluation of power costing and overall economics. Means, there is a limitations & lacuna while using ‘WaterGems’ software and whatever results obtained by ‘WaterGems’ has be accepted prejudicially.

In ‘Solar Powered Water Supply System’, design is made inversely - based on how much solar power could be harvested over the time and optimizing to meet the per capita demand. In this method, prevailing solar radiations at particular location is estimated, independent assured water source has to be identified to meet the water demand of the particular localities along with the configuration of water distribution network & ESR (Elevated Storage Reservoir).

Main components of Solar Powered Water Supply System are:

- Photovoltaic Solar Panels.
- Inverters + Control Panel.
- Intake from Raw water source.
- Coagulant plant.
- Sedimentation Plant.
- Filtration System.
- Disinfectant plant (Chlorine + Ozone Injector).
- Finished water storage (ESR/GWR).
- HDPE Main Supply Pipe.
- Water Metering.
- Control Accessories.
- House Connections.

DESIGN ENGINEERING PRINCIPLES & CONSIDERATIONS

Since solar radiation is available in a day time for generation of power, the entire water supply scheme has to be concluded in a day time only. Obviously all the design calculation is based on the fluctuation of solar radiation from morning to evening and season to season to meet the per capita demand. However, following steps have to be followed & integrated while using 'WaterGems' software to design a water supply system.

1. Collection data of average solar radiation on daily, monthly & Seasonal basis, Climatic data (temp, RH, Precipitation, Wind Speed & direction) of a particular locations. **Fig.1** is shown the potential of solar energy for India for reference.

(<http://worldclim.org/version2>; www.photovoltaic-software;

<http://apps.ecmwf.int/datasets/data/interim-full>

-daily/levtypes=sfc).



Fig. 1. Potential of Solar Energy in India -MW

2. Determine the solar PV energy output of a photovoltaic system

There are various methods and formula available to determine the solar energy. Average solar energy can be harvested to 200-300 watt/m² at various locations base on latitude and longitude. It varies from season to season and mainly affects the cloud cover and haziness. Maximum solar power can be harvested in summer season and minimum in rainy seasons due to cloudiness. Similarly in a day time solar energy is minimum in morning, maximum in noon and again minimum during evening. **Fig. 2.** shows the solar monochrome, it is very clear that the design of water supply scheme should be made corresponding to available solar radiation only.

$$E = A * r * H * PR$$

E - Gross Energy (kwhr)

A - Total area of solar panel (sqmt)

r - Solar panel yield (%)

H - Annual average irradiation on tilted panel

PR -Performance ratio, coefficient for losses (range between 0.9 and 0.5, default value = 0.75)

$$\text{NetSE} = E * L$$

NetSE- Net Solar Energy (kwhr)

L (%) = Power Losses (in Inverters, Temperature, Cables (AC/DC), Shading %, Weak Irradiation, Dust, snow fall, RH, Cloud cover & unforeseen losses)

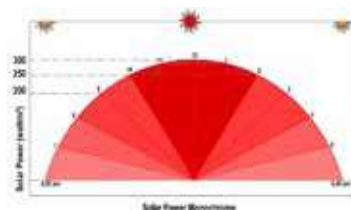


Fig. 2. Solar power monochrome

3. Hydrologic Model (Water Assessment)

Study and Assessment of assured water availability for drinking purpose year round. It can be done hydrological survey and remote sensing data. Some of data is available at remote sensing dept.

(<http://www.gislonge.com>; <http://www.india-wris.nrsc.gov.in>)

4. Raw water Testing & Assessment

Based on water test report, water treatment stages and procedure has to be decided to make it potable for drinking.

5. Estimation of KW vs Output

Output (Discharge) of water is the function of power (kw) & Head (H). It is expressed as below and can be represented as shown in **Fig. 3** for example at atmospheric head of 10 m.

$$q = kw * n * t * 360 * H^{-1}$$

q - out put (discharge) (m3 per day)

kw- estimated solar power harvested (kw/hr)

n - overall efficiency of motor (%).

t - time (hrs per day).

H - designed head (m).

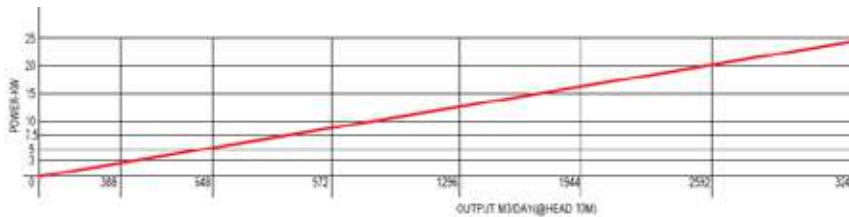


Fig. 3. Discharge as a function of power & head

6. Determine number of consumer to be catered

$$N = q / ((d+f)*e)$$

N – number of consumer.

q- out put per day (m3) or (x1000 lpd)

d- per capita demand (lpd)

e – water used efficiency (80%)(Towards water losses).

f- fire hydrant (lpd) (if required)

7. Master plan of water supply scheme

Master plan (**Fig. 4**) of water supply scheme comprising of intake structure, coagulant plant, sedimentation plant, filtration plant, disinfectant plant, finished water storage (ESR/GWR), water distributions & delivery to end consumers and should be designed adequately and harmonized to with harvested solar power.

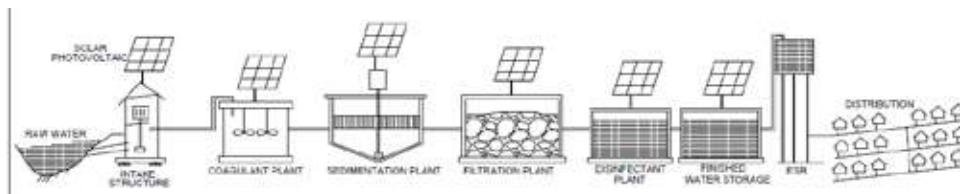


Fig. 4. Master plan of Water supply scheme



8. 'WaterGems' software to be used to design water distribution network and analyses.
9. Optimization of requirement of motor-pump-set (solar powered)
10. Photovoltaic Solar Module.
11. Techno-commercial parameters.

Representative Comparison of Conventional and Solar Powered Water Supply System

Sr	Heads	Conventional Water Supply	Solar Powered Water Supply
1.	Coverage of area (localities)	Large city.	Small clustered based or Rural
2.	Piping Network	Large size.	Smaller size.
3.	Frequency -supply	1/2/3day basis	Daily basis.
4.	Monitoring	Difficult	Easy.
5.	Maintenance	Difficult	Very easy.
6.	Traffic Obstruction	Always.	Some times.
7.	Initial investment	Very high	Substantial less
8.	Dependency on Gov electric supply	100 %.	Not at all.
9.	Risk – hazardous	Electrical Accident.	Zero Risk. Safe.
10	Pollution	Yes.	No.

CONCLUSION

India as well as countries located at equator, between Tropic of Cancer and Capricorn, are blessed with free abundant solar radiation and can harvest the solar power to meet their domestic demands as well as used dedicatedly for water supply system for municipalities and rural area.

ACKNOWLEDGMENT

Thanks to

1. WaterGems software.
2. ArcGIS.
3. Remote Sensing.
4. Various websites.
5. Solar Dept, Jain Irrigation Systems Ltd.

REFERENCES

1. Dr. Sanjay Jain, "Role of Remote Sensing & GIS in Hydrological modeling," GoogleScholar, Training program 'Advanced Technologies in Water Resource Management, Nov 2020, College of Engineering, Aurangabad.
2. Dr. Ashish Pandey, "Application of Remote Sensing & GIS in water resources," GoogleScholar, Training program 'Advanced Technologies in Water Resource Management, Nov 2020, College of Engineering, Aurangabad.
3. FAO publication 1985, "A Crop Water Evaluation Manual for India'.
4. CPHEEO manual, Ministry of Housing and Urban Affairs, Govt of India.
5. Various literatures and technical information.



Master Plan for Drought Mitigation at Jhargram District of West Bengal to Ensure Sustainable and Reliant Drinking Water Supply

P RoyChowdhury

Public Health Engineering Department, Govt. of West Bengal, Kolkata

✉ pronoyrc@gmail.com

ABSTRACT

Jhargram is a newly formed district of the state of West Bengal. The district is geographically located within the Chota Nagpur plateau area, the terrain is rocky and wooded. More than 70% of the land area of Jhargram district is located in infertile laterite zone. It is very difficult to cultivate and yield crop in that area. There is no perennial river flowing through the area and the area has extreme variation of temperature conditions between the summer and the winter months. One of the major problems of the area is water scarcity. All the eight blocks of Jhargram district are affected by severe drought like situation every year during the hot summer months of May, June even up to July. About 96.52% of the total population of the area lives in the rural sector and are financially backward and tribal people. The prevailing drought during the summer months affects agriculture and drinking water sector causing lot of hardship to the local population. Due to such natural challenges many local inhabitants have migrated to the urban areas in search of food, potable water and sustainable livelihood. This has impacted the social parameters of development, which are unsatisfactory. In this paper a brief review of the initiatives taken by the Government of West Bengal shall be made, to identify the measures taken for development of the drinking water sector in that area so that the problem of recurring drought like situation could be mitigated in a sustainable manner. It is easily understood that ensuring safe and adequate drinking water is the essential necessity of a progressive social system and any elected Government is mandated to generate these facilities to the population. Thus the intervention in the sector of improvement of drinking water through the application of proper civil engineering planning and use of alternative technology and thinking shall go a long way to instil confidence among the local population to ensure a sustainable and self reliant society.

Keywords : Drought mitigation; Self-reliance; Sustainable development; Drinking water; Water supply.

INTRODUCTION

Jhargram district is the 22nd district of west Bengal. It is located in the so called “Jungalmahal” of west Bengal. The district was formed on 4th April 2017, after splitting of the PaschimMedinipur district. The district is administratively divided into eight community development blocks. A large portion of the district is covered with wooded forest. Geographically the area is a part of the ChotaNagpur plateau which gradually slopes creating an undulating terrain with relatively infertile laterite formation and rocky soil. The area is dotted with hilly ranges of Belpahari, Kakrajhor etc. The weather condition is extreme and tropical. temperature may rise to as high as 46° C in the hot and dry months of May and June and may plummet to as low as 4°C during the chilly nights of late December or January months. Some seasonal rivers flow through the Jhargram district including Kangsabati, Subarnarekha, DulungNala, Terapheni etc. However Kangsabati and Subarnarekha are the major rivers which floods at certain locations in the rainy season but reduces to a trickle during the hot summer months and doesnot supply enough water for irrigation or drinking purpose. As per 2011 census the population of the district is 11,36,548 souls. 96.52% population lives in the village areas while 3.48% lives in the urban locality. Almost all the block areas of the Jhargram district are drought prone due to the prevailing extreme temperature condition, infertile soil and lack of dependable natural source of water supply. Every year during the three months of May, June and July severe drought like situation develops which affects agriculture, drinking water supply and the general livelihood of the people. Due to such natural hazards the affected population face lot of hardship in day to day life and the social growth and wellbeing is badly affected. In this paper a detailed discussion shall be taken up regarding the methodology to be adopted for development of a sustainable water supply for the drought prone areas of the Jhargram district during the drought affected hot summer months. Ensuring potable safe and adequate drinking water to the population is a very important marker of sustainable development towards self-reliance of the society, If the basic needs of the population such as food, drinking water, housing, health safety and employment is ensured. Thus the study in this



paper gives a deeper insight that how Civil Engineering intervention in improvement of drinking water supply sector can ensure the development of a self reliant society.

DRINKING WATER PROBLEM

One of the important markers of social development is the effective supply of sufficient quantity of appropriate quality of drinking water to the population. As per norms of Central Public Health and Environmental Engineering Organisation (CPHEEO) [1] the per capita requirement of water supply at Rural sector through house connection in 70 (Liter per Capita Per Day)lpd. This provision provides for drinking, cooking and domestic use of the household, ensuring safe drinking water and sanitary condition in the household and the locality. However provision of 70lpd drinking water supply is not an easy task to achieve in the rural sector of Jhargram where water supply is scarce and population is scattered and sparse. For ensuring an adequate and safe drinking water to the population at first it is essential to have a reliable and sustainable source of water in the area. Geologically the area is predominantly a laterite zone and having hard rock formation at relatively shallow depth. Thus there is very limited possibility of extracting ground water in sufficient and sustainable quantity through big diameter production tube well to extend the facility of drinking water to the population.

In general the state of WestBengal is a part of the Gangetic plain. The land is generally fertile and drained by perennial river Ganges. The State receives sufficient rainfall of the order of 150 to 200 cm annually and the ground water reserve is satisfactory overall. However the ground water table is exhibiting a general falling trend across certain block areas of W.B. due to over-exploitation of ground water reserve for extensive use of shallow and medium duty tubewells for increasing cultural command area through minor irrigation schemes.

The other major problem in ground water is chemical contamination of ground water by geogenic arsenic and fluoride contamination. While all the districts along the course of river Ganges including Malda, Murshidabad, Nadia, North 24 Pgs, South 24 Parganas, parts of Hooghly and Burdwan district are affected with arsenic contamination in ground water (refer figure no.1) at the shallow aquifer zones at about the depth of 60m B.G.L, other districts such as Purulia, Bankura, Birbhum, Uttar Dinajpur&DakshinDinajpur are affected by fluoride contamination in ground water(refer Figure no.2). Whereas areas nearer to the sea in South and north 24 Parganas, PurbaMedinipur& parts of Howrah district (refer figure no.3) experience saline intrusion from sea water of Bay of Bengal and experience coastal salinity problem both in surface, sub-surface and ground water. Whereas Purulia, Bankura, Jhargram and parts of Paschimmedinipur and Birbhum(refer Fig no.4) experiences drought like situation in hot summer months due to acute scarcity of drinking water. Thus the problem of drinking water in West Bengal is multifarious. The acute water scarcity in Jhargram is mostly due to non-availability of suitable water bearing aquifer.

The alluvial deposit in the Jhargram district is mostly consolidated and older alluvium. The permeability of the formation is low and does not permit dynamic movement of water. The material of the formation is not suitable for yielding substantial yield of ground water. In this area ground water is found mostly in the fissures and fractures of the rocky formation. The yield of the tubewell is limited to the water stored in the fissures, once the stored water is pumped out again it takes time to replenish the water withdrawn from the fissure, So the yield of the tubewell is intermittent and not dependable for sustainable water supply through piped water supply schemes. The population of the Jhargram district is widely scattered and there are wooded areas, so due to scattered population large lengths of pipeline is required to be laid from the water treatment plant head works to the rural habitations. This makes the distribution system costly where large lengths of pipeline are required to be laid to reach water supply to the scattered habitations.

The Kangsabati river rises in the Jabarpahar near the Jhalda district, it passes through Purulia, Bankura and enters Jhargram district near Binpur Police station. The River later splits into two and joins the Rupnarayan River near Daspur and the other branch joins the Kalghairiver and forms the Haldia River and flows into the Bay of Bengal at Haldia. The Kangasabati is a seasonal river. It flows through the northern side of Jhargram district, the soil of the flood plain of the river is marked with the characteristic of sand and silt interclarified with clay and is a good aquifer material, so the groundwater potential is high in the flood plain zone. The Subarnarekha River originates from Nagri/Piska near Ranchi in the Chota Nagpur plateau after traversing a long distance via Ranchi and eastern Singhbhum enters the Jhargram district in the North western part near Dhalbhum. The river passes by the two Blocks of Gopiballavpur-I, II, Sankrail and Nayagram blocks of Jhargram before entering PaschimMedinipur district. The Subarnarekha River has a rapidly flowing stream and sandy bed. The river has a tributary called Dulungnala which originates near Dulundiha, passes through Jamboni block, Gopiballavpur and again re-joins with Subarnarekha river in the Sankrail block. The Terefani River originates in the Banspahari Range of Jhargram after passing through Binpur, Belpahari it finally merges with Kangsabati River. There is a small Barrage on the Terefani River. All the above



rivers are seasonal rivers and the get reduced to a trickle in the hot summer months and doesnot provide any substantial and dependable water supply.

Since there is inadequacy of ground water, thus in a pursuit to mitigate the drought like situation in Jhargram district alternative thinking and technology is required to be judiciously implemented for the purpose of drought mitigation.

DROUGHT MITIGATION STRATEGY

A comprehensive strategy has been planned to generate a sustainable solution for drought mitigation of the area and for making the society self-reliant with respect to drinking water supply, which shall in the long run improve the general health, hygiene and livelihood of the rural population. It shall also prevent to a considerable extent the migration of the local population to other areas in search of succour, potable water and other prime necessities of livelihood sustenance. The strategy in general may be classified under two heads:-

- (i) Contingency Plan to meet immediate necessity
- (ii) Long term plan to be implemented within a period of three years.

The above two fold strategy has been developed after extensive study conducted at the Jhargram district. Actual survey of the water resources has been done by the officers of the Public Health Engineering Department Government of West Bengal, ground water related data has been obtained from Central Ground Water Board[2] sources and after study of the static water level fluctuation in the exploratory borings and model tubewells at the various block jurisdictions, trial bore was made in the river bed to obtain data about subsurface flow, layer chart of existing big diameter deep tubewell were studied to identify the depth of the soil stratum where it is possible to find ground water, all possible sources of water such as large water tanks which are naturally/artificially formed were also considered. The study is very elaborate in nature here only the process has been indicated for the sake of ready reference. The data of the existing hand pump tubewells with India mark-II type Deep water pump as obtained from various block offices were also utilised to get a general assessment about the availability of water resources in a particular area.

- (i) The contingency Plan:- This plan involved sketching out the area in which immediately water shall be supplied with the help of truck mounted tankers and cycle van mounted tankers at least two times a day so that the basic necessity of the population is met with respect to drinking water. The jurisdiction of the existing water supply schemes which are about 60 nos. in the district are identified and truck mounted water carriers are filled through the water columns from the head works site pump houses and water rationing is done in the affected areas with close collaboration with the local authorities. Often in the hot season there is problem of power cut thus in such situation diesel generator set hired by the department and the pump machinery is kept running for some time so that the tankers can be loaded and water supply to the population can be ensured. Before the setting of the hot summer season the yield from the tubewells are checked if the yield is less in such case it is attempted to improve the yield of the tubewell by surging the strainer of the tubewell. Phone numbers of all important officials at the block and the panchayat level is kept for close liaison. Drinking water poly pouch of 350ml is often manufactured with Mobile Water Treatment Unit (MTU) which are truck mounted units having facility of water treatment and chlorination at the rate of 4000 pouches per hour and supplied to the water scarcity areas. The outcome of this plan is to give immediate relief to the population and to instil confidence in the affected population.
- (ii) Long term Plan:- This plan is meant for permanent solution to the long staging issue, the plan involves following strategy:-
 - (a) Areas where there is less and scattered population and far away from river, stand-alone solar power operated water treatment plant has been proposed. The plant incorporates a deep tubewell with 100mm X 40mm diameter and 170m to 200m deep tubewell fitted with 0.75 HP submersible pumping machinery which is energised with solar power panel (refer figure no.5) . The water is treated through and iron removal unit which is the only quality problem in drinking water in Jhargram district. The water from the deep tubewell after passing through the iron elimination plant is chlorinated with bleaching dosing through doser type chorinator and then supplied to the population through community tanks. On either side of the plant pipeline is laid for 500m and one community tank is located every 200m fitted with 3 nos. water spout.
 - (b) In the areas which are near to the riverine belt where sufficient flow is found in the trial bore at the river bed such as Subarnarekha from there sub-surface water based piped water supply scheme has been proposed with the construction of infiltration gallery/ radial collector well[3] in the stream channel. Blocks such as Gopiballavpur-I, II and Sankrailmay be provided with such schemes.

- (c) Water from Terefeni dam during the rainy season may be stored in large pond storage and harvested so that it may supplied to the affected population during the dry months after disinfection by chlorination.
- (d) In general comprehensive rain water harvesting and ground water recharge structures are required to be constructed across the district depending upon the local geological conditions of the area to improve ground water storage.
- (e) All schools and anganwari centers to be identified and hand pump tubewells as well as water supply connection where ever feasible should be extended.

This comprehensive strategy involves a large financial allocation to the tune of Rs 500.00 crores, and it has been estimated that such as strategy which has thoroughly covered all the cojent aspects of water scarcity in that area shall go a long way in resolving the recurring drought faced by the population of Jhargram district.

CONCLUSION

There is no greater social contribution for an Engineer than providing potable drinking water in adequate quantity to the population in a free and progressive society. The problem of recurrent drought in Jhargram is a pressing problem to the human development in that area. A planned Civil engineering intervention to solve the drought problem shall go a long way to improve the social markers in that district and help to alleviate suffering of the people and develop a self-reliant society.

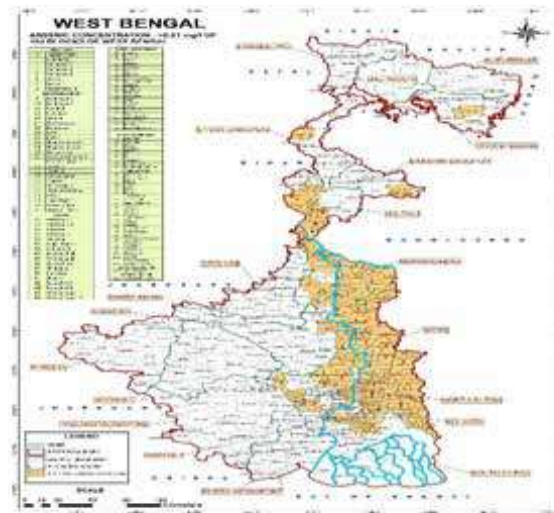


Fig. 1. Arsenic affected areas of West Bengal
(Source official Website of Public Health Engineering Dept. Govt.of WB)



Fig. 2. Fluoride affected areas of West Bengal
(Source official Website of Public Health Engineering Dept. Govt.of WB)



Fig. 3. Salinity affected areas of West Bengal
(Source official Website of Public Health Engineering Dept. Govt.of WB)



Fig. 4. Drought affected areas of West Bengal
(Source official Website of Dept. of Disaster Management, Govt.of WB)

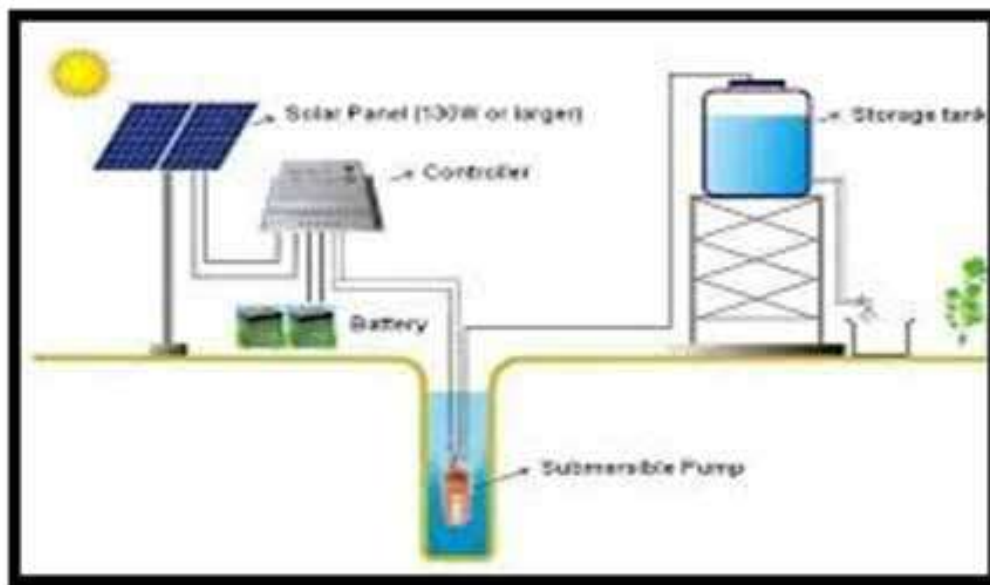


Fig. 5. Schematic view of solar photo voltaic panel with submersible pump type small community water tanks

REFERENCES

1. Manual on water supply and Treatment, Central Public Health and Environmental Engineering Organisation, Ministry of Urban Development, Government of India, New Delhi, 3rd edition, 1999, pp-11-12.
2. Ground water Data of Central Ground water Board, New Delhi, Ministry of Jalshakti, Government of India, May 2016,
3. Manual on water supply and Treatment, Central Public Health and Environmental Engineering Organisation, Ministry of Urban Development, Government of India, New Delhi, 1999, 3rd edition, pp-38-45.

Electronics & Telecommunication Engineering



Design and Analysis of Converters for Hybrid Electric Vehicle

Dr K Balachander

Department of Electrical and Electronics Engineering, Faculty of Engineering, Karpagam Academy of Higher Education Coimbatore

✉ kaybe.ind@gmail.com

ABSTRACT

The availability of petroleum resources has now decreased and more scope has been increased for vehicle applications especially in hybrid electric vehicles. Various DC-DC converters are used for automotive applications in order to achieve a better drive range and the best engine output used in the vehicle. Basic converter architecture plays a crucial role, and is the basis of controllers such as PI controllers, Fuzzy controllers, etc. The performance comparison of the CUK converter and modified converter compared to the current Boost converter is proposed in this paper, with the aid of the PI closed loop. The Simulations were compared and outcomes were analyzed. For this study, the Toyota Prius was taken as the base model. Hopefully, this will provide the electric vehicle industry with a small contribution.

Keywords : DC-DC converters; Hybrid electric vehicle; Toyota priuso, CUK converter.

INTRODUCTION

Around 93% of the present cars keep running on oil-based item, which are evaluated to be exhausted by 2050. Also, current vehicles use just 25% of the vitality discharged from oil and rest is squandered into the climate. Regardless of late endeavors to enhance eco-friendliness and lessen dangerous outflows in autos, emanations have kept on expanding consistently in the previous two decades.

For conservation of gas for future and expanding the effectiveness of vehicle an electric vehicle can be a noteworthy achievement. An electric vehicle is sans contamination and is productive at low speed conditions for the most part in high rush hour gridlock territories. In any case, battery charging is tedious. In addition, it can't give high power required by drives amid rapid conditions or in inclines of uneven territories. Fuel motor demonstrates its productivity at higher speeds in high ways and wastes a ton of vitality in urban zones. A mixture vehicle takes care of these issues by consolidating the benefits of both the frameworks and utilizations both the power sources at their proficient conditions. The target of this task goes for better use of fuel vitality and decreases reliance on non-inexhaustible assets utilizing most recent innovation. The execution includes advancement of HEV that utilizes battery and in addition fuel control for drive of vehicle.

Throughout the most recent decade, 'Feasible Development' turned into the need of global administrative bodies. So as to secure the earth, critical cuts as far as harmful discharges must be made. Also, as the world's feedstock of fossil assets bit by bit lessens, provoke moves must be made so as to build up the utilization of inexhaustible wellsprings of vitality.

The car business, a noteworthy supporter of Green House impact, is very much aware of the need to build up another innovation that would empower an ecological inviting transportation division. A few pathways are presently being investigated, in any case, the innovation that will be utilized to impel tomorrow's vehicle has not yet been chosen.

In fact, there is no accord among the partners of the business regarding which innovation will end up being the prevailing structure for what's to come. Therefore, the industry is at present in a time of change in which every single rising innovation are seeking force, support, and energy. Among all the potential choices an innovation which progressively has picked up significance is the Hybrid innovation.

ELECTRIC HYBRID VEHICLE

A half and half electric vehicle (HEV) have two kinds of vitality stockpiling units, power and fuel. Power implies that a battery (here and there helped by ultra-caps) is utilized to store the vitality, and that an electromotor (starting now and into the foreseeable future called engine) will be utilized as footing engine. Fuel implies that a tank is required, and that an Internal

Combustion Engine (ICE, starting now and into the foreseeable future called motor) is utilized to create mechanical power, or that a power module will be utilized to change over fuel to electrical vitality. In the last case, footing will be performed by the electromotor as it were. In the main case, the vehicle will have both a motor and an engine.

EXISTING BOOST CONVERTER

The Prius is a new-generation hybrid automobile that was introduced into the market by the Toyota Motor Corporation. Fig. 1 shows the Highly Integrated Vehicle Control Systems with Boost converter. As a hybrid vehicle, the Prius uses both a gasoline-powered internal combustion engine capable of delivering a peak-power output of 57 kW and a battery-powered electric motor capable of delivering a peak-power output of 50 kW as motive power sources. Combining these two-motive power sources results in improved fuel efficiency and reduced emissions compared to traditional automobiles and provides the Prius with the energy saving characteristics.

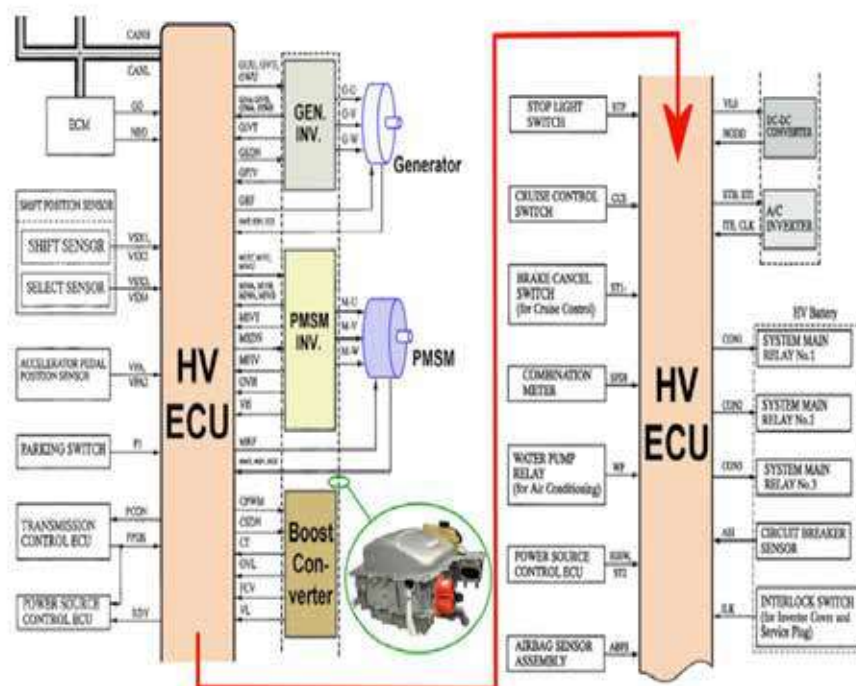


Fig. 1. Highly Integrated Vehicle Control Systems with Boost converter

Energy Saving Characteristics

- Energy-loss reduction is achieved by automatically stopping the engine when idling.
- Energy is recovered and reused by capturing kinetic energy that is normally wasted as heat during deceleration and braking. The starter and electric motor then convert this energy to electricity for use.
- Engine is able to operate at peak-efficiency speed a high percentage of the time.
- Supplementary power is provided by the electric motor during acceleration when engine efficiency is low.

PROPOSED CONVERTERS

CUK Converter

In proposed methodology suggesting using CUK converter (**Fig. 2**) instead of Boost converters. Toyota Prius had used boost converters for existing model. The CUK converter having more boosting ability and output ripple current is minimal as compared with boost converter. CUK converter can boost as well as step down the DC voltages. Which will be more useful when vehicle moving steep down. It can do step up and step-down voltages based the vehicle need. One of the drawback is size of the capacitor is somewhat more.

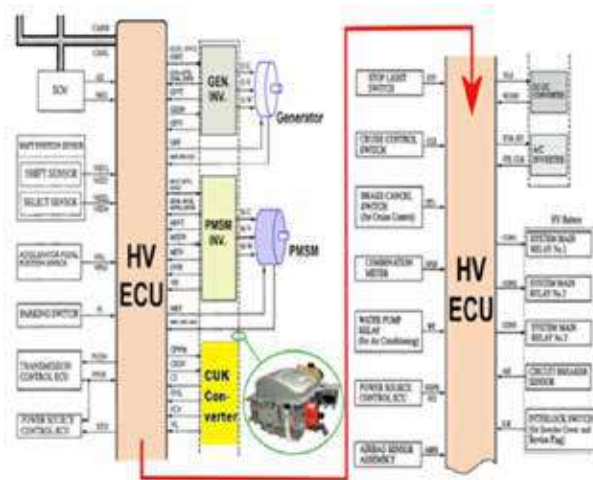


Fig. 2. Highly Integrated Vehicle Control Systems with CUK converter

The energy transfer in CUK converter depends on capacitance C_1 . The output capacitance C_2 is used to maintain output voltage constant. The advantage of CUK converter is continuous input and output current. The operation is based on capacitive energy transfer who is more efficient than inductive energy transfer.

Modified CUK Converter

In proposed system recommending utilizing Modified CUK converter rather than CUK converters. Toyota Prius had utilized CUK converters for existing model. The Modified CUK converter having all the more boosting capacity and yield swell current is insignificant as contrasted and CUK converter. Altered CUK converter can help and in addition venture down the DC voltages. Which will be increasingly helpful when vehicle moving steep down. It can do venture up and venture down voltages based the vehicle require. One of the downside is size of the capacitor is to some degree more.

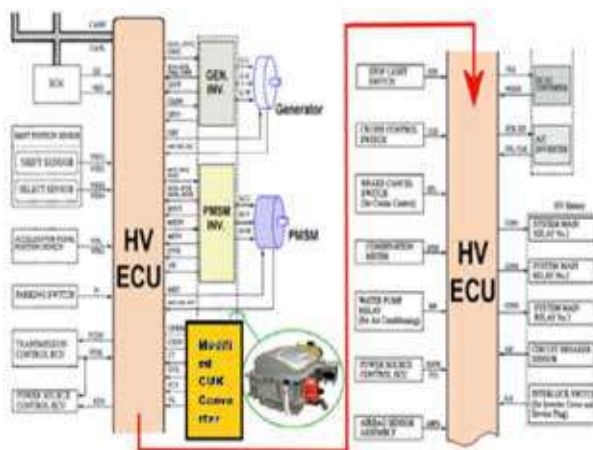


Fig. 3. Highly Integrated Vehicle Control Systems with modified CUK converter

The vitality move in Modified CUK converter relies upon capacitance C_1 . The yield capacitance C_2 is utilized to keep up yield voltage consistent. The upside of Modified CUK converter is consistent information and yield current. The activity depends on capacitive vitality exchange that is more productive than inductive vitality exchange.

RESULTS AND DISCUSSIONS

The existing system of Toyota Prius had used boost converter with PI controller for tuning. PI is the basic controller for tune the boost converter. The **Fig. 4** shows complete circuit for the simulation. A 12V (V_{in}) as input voltage and finally tuned out put voltage as 50V (V_{out}) for boost converter. Load we had used as Permanent magnet motor. Parameter used for this test had mentioned in the **Table 1**.

The below 50V output is the maximum tuned out put. When we received 50V output the error is zero. From the below diagram we can see that constant for tuning is used as 50. This helps us to tune the error. All the tuning had done based on trial and error method. When the constant value moves towards zero then error factor going to negative and output of the DC voltage having more ripples no steady state voltage observed. PI tuning factor has more importance in this simulation. The simulation Parameters used for this test had mentioned in the **Table 1**.

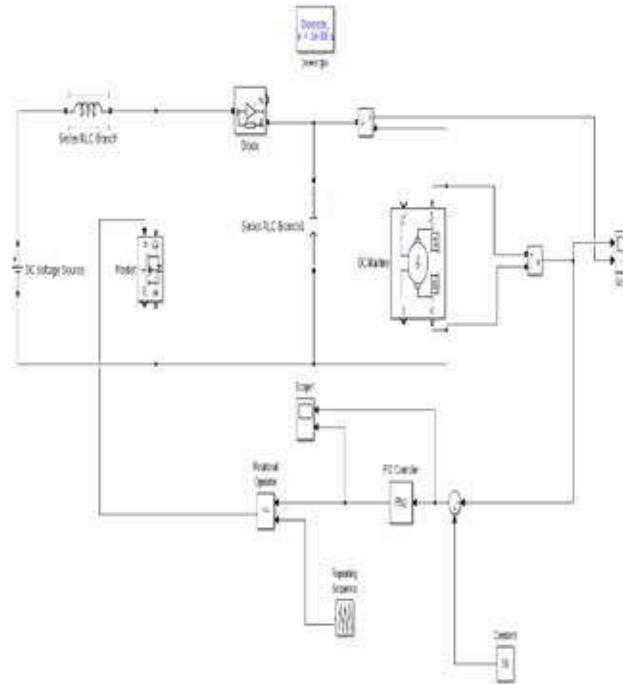


Fig. 4. Boost converter with Closed Loop PI controller (existing)

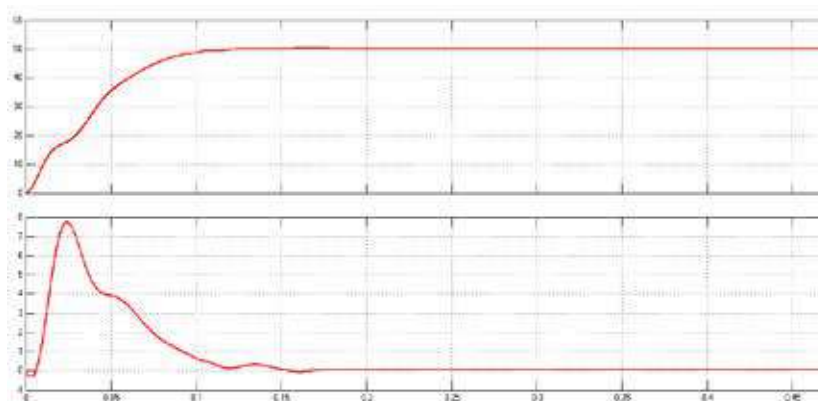


Fig. 5. Output Voltage and Current of Boost Converter (existing)

The proposed system1 of Toyota Prius had used CUK converter with PI controller for tuning. PI is the basic controller for tune the boost converter. The matlab simulation diagram (**Fig. 6**) shows complete circuit for this test. 12V (V_{in}) as input voltage and finally tuned out put voltage as 120V (V_{out}) for CUK converter. Load we had used as Permanent magnet motor. Parameter used for this test had mentioned in the **Table 1**.

The below 120V output is the maximum tuned out put. When we received 120V output the error is ~zero. From the below diagram we can see that constant for tuning is used as 148. Constant helps us to tune the error. All the tuning had done based on trial and error method. When the constant value moves towards zero then error factor going to negative and output of the DC voltage having more ripples no steady state voltage observed. PI tuning factor has more importance in this simulation. The output of CUK converter is shown in **Fig. 7**.

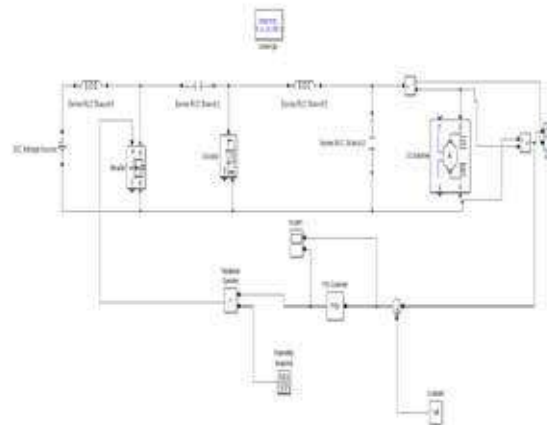


Fig. 6. CUK Converter with PI controller closed Loop (proposed1)

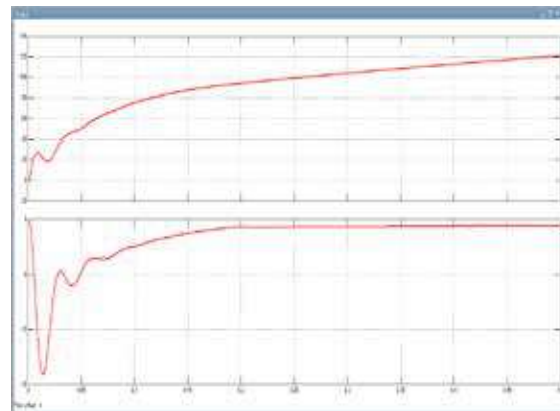


Fig. 7. Output Voltage of CUK Converter (proposed1)

Here Modified CUK converter with PI controller used for tuning. Fig. 8 shows the complete simulation diagram of modified CUK converter. For this test 12V (V_{in}) as input voltage and finally tuned out put voltage as 148V (V_{out}) for Modified CUK converter. Load we had used as Permanent magnet motor. The simulation Parameters used for this test had mentioned in the **Table 1**.

The below 148V output is the maximum tuned out put. When we received 148V output the error is \sim zero. From the below diagram we can see that constant for tuning is used as 135. Constant helps us to tune the error. All the tuning had done based on trial and error method. When the constant value moves towards zero then error factor going to negative and output of the DC voltage having more ripples no steady state voltage observed. PI tuning factor has more importance in this simulation. Fig. 9 shows the output Voltage and Current value of modified CUK converter.

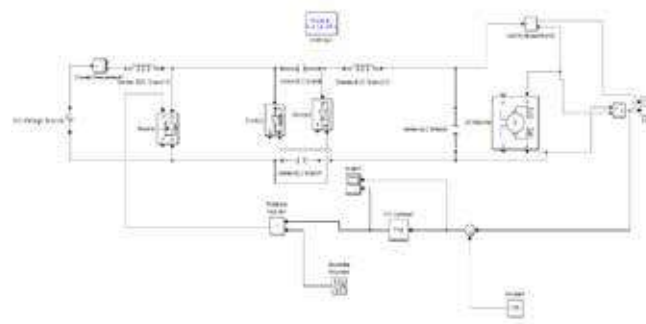


Fig. 8. Modified CUK with PI controller closed Loop (proposed2)

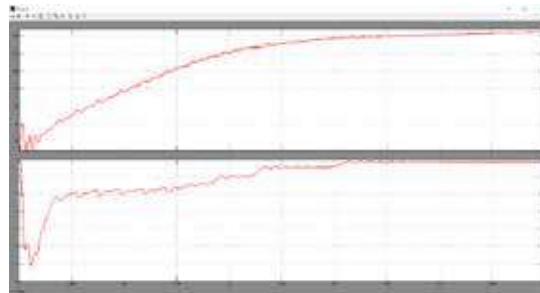


Fig. 9. Output Voltage of Modified CUK Converter (proposed2)

Table 1. Simulation Parameters

S. No.	Simulation Parameters	Value
1	Input DC Voltage	12V
2	FET resistance	0.1 ohms
3	Internal diode resistance	0.01 ohms
4	Torque Constant for Permanent Magnet Motor	1.8 N.M/A
5	Coulomb friction torque	0.1 N.m
6	Initial Speed	1 rad/sec
7	Armature resistance	0.6 ohms
8	Armature inductance	0.012 H
9	Resistance of Diode	0.001 ohms
10	Forward Voltage	0.8V
11	Snubber resistance	50 Ohms

CONCLUSION

This paper gives a far-reaching study on Toyota Prius DC-DC converter side. Existing Toyota Prius had utilized CUK converter for expanding the yield dc voltage. Toyota Prius display they had utilized CUK with PI controller. Proposed display had effectively reproduced and acquired more yield contrasted and existing model. Proposed show is modified CUK with PI controller. The better outcome (Table 2) got for proposed display by utilizing same parameter which utilized by existing model. Beneath table clarifies the yield correlation for Toyota Prius.

Table 2. Comparison of Converter Output

Converter	$V_{in}(V)$	$V_{out}(V)$
Boost	12	50
CUK	12	120
Modified CUK	12	148

From the above table and simulation results clear that Toyota Prius can use modified CUK converter with PI controller for better range extension.

FUTURE WORK

HEV assumes essential job in future on the grounds that Global warming and less accessibility of petroleum derivatives. From writing audit, we comprehended the HEV inquire about was more in 2004 time at outside nations yet after that the advancement in research was less a direct result of oil cost down. Be that as it may, in future certainly the shortage of non-renewable energy source will draw close to future, so at any rate HEV inquire about is order not so distant future.

Future work manages discovering more yield in converter side for that we need to utilize the diverse controllers or further



developed DC-DC converters. Same time advance the equipment estimate too. Enhancement of equipment and programming assumes a fundamental job for HEV in future.

REFERENCES

1. Staunton, R.H., et al., Evaluation of 2004 Toyota Prius Hybrid Electric Drive System. 2006: United States. p. Size: 4 Mb.
2. T. Q. Duong, U.S. Department of Energy, Forrestal Building/EE2G, 1000 Independence Avenue, S.W., Washington, D.C. 20585.
3. Young-Joo Lee, Alireza Khaligh, Ali Emadi, "Advanced Integrated Bidirectional AC/DC and DC/DC Converter for Plug-In Hybrid Electric Vehicles," IEEE Transactions on Vehicular Technology, vol. 58, no. 8, pp. 3970-3980, October 2009.
4. Emadi, Ali, Kaushik Rajashekara, Sheldon S. Williamson, and Srdjan M. Lukic, "Topological overview of hybrid electric and fuel cell
5. Chan, C. C., Alain Bouscayrol, and Keyu Chen, "Electric, hybrid, and fuel-cell vehicles: Architectures and modeling," IEEE Transactions on Vehicular Technology, 59, no. 2 (2010): 589-598.
6. S.A. Elankurisil, S.S. Dash, "Comparison of isolated and non-isolated bi-directional dc - dc converter for DC motor," J. of Electrical Engineering.
7. Y. Saber and G. K. Venayagamoorthy, "Plug-in vehicles and renewable energy sources for cost and emission reductions," IEEE Trans. Ind. Electron, vol. 58, no. 4, pp. 1229-1238, Apr. 2011.
8. O. Hegazy, J. Van Mierlo, and P. Lataire, "Analysis, modelling and Implementation of a multidevice interleaved DC/DC converter for fuel cell hybrid electric vehicles," IEEE Trans. Power Electron, vol. 27, no. 11, pp. 4445-4458, Nov. 2012.
9. Jong-Seob, W., R. Langari, and M. Ehsani, "An energy management and charge sustaining strategy for a parallel hybrid vehicle with CVT. IEEE Transactions on Control Systems Technology, 2005. 13(2): p. 313-20.
10. Meisel, J. An analytic foundation for the Toyota Prius THS-II powertrain with a comparison to a strong parallel hybrid-electric powertrain. in SAE 2006 World Congress. 2006. Detroit, MI.
11. Stienecker, A.W., T. Stuart, and C. Ashtiani, "An ultracapacitor circuit for reducing sulfation in lead acid batteries for Mild Hybrid Electric Vehicles. J. of Power Sources, 2006. 156(2): p. 755-762.
12. T. Q. Duong, U.S. Department of Energy, Forrestal Building/EE2G, 1000 Independence Avenue, S.W., Washington, D.C. 20585.
13. Markel, T. and A. Simpson. Energy storage systems considerations for grid-charged hybrid electric vehicles. 2005. Chicago, IL, United States: Institute of Electrical and Electronics Engineers Computer Society, Piscataway, NJ 08855-1331, United States.
14. Schupbach, R.M., et al. Design methodology of a combined battery-ultracapacitor energy storage unit for vehicle power management. 2003. Acapulco, Mexico: IEEE.
15. Cownden, R., M. Nahon, and M.A. Rosen, Modeling and Analysis of a Solid Polymer Fuel Cell System for Transportation Applications. Int. J. of Hydrogen Energy, 2001. 26(6): p. 615-623.



IoT based Smart Energy Meter Tracking using ZigBee

Dr Belsam Jeba Ananth M¹, Dr Revathi KG²

Associate Professor/ Mechatronics Engg ,SRM Institute of Science and Technology, Kattankulathur, Tamilnadu¹

Professor/ ECE ,DMI College of Engineering, Chennai, Tamilnadu²

✉ ??

ABSTRACT

In present time Electricity is the necessary thing in the world for human life. Today every home, offices, companies, industries have electricity connection. So here this project is building only for interfacing electricity energy meter with micro controllers. The main aim of the project is identifying the current meter reading and intimating the user when they are crossing the certain limit. It also identifies the power theft and auto tripping will be done. Here, Arduino is used for interfacing and the main aim of this project is to know, how much unit is obtained and the total amount of rupees has to be paid. That will be sent to the EB office for billing. Excess power usage can also be monitored. Hence, power theft can be avoided. If bill is not paid in time, then it will automatically turn off the power..

Keywords : Energy reading; Power management; Wireless sensor network; ZigBee; Arduino.

INTRODUCTION

The development of automatic metering system is presented in this paper. The power management system is consists of Zigbee Digital Power meters installed in every consumer unit and an Electricity e-Billing system at the energy provider side. The Zigbee Digital Power meter (ZPM) is a single-phase digital kWh power meter with embedded Zigbee modem which utilize the Wireless sensor network to send its power usage reading using information back to the energy provider wirelessly. At the power provider side, they have the control to change priority of the devices when power distributed in low range.

Human operator billing or prone to reading error as sometime the houses electric power meter is place in a location where it is not easily accessible. The concept of dynamic assignment of priorities to interrupts is discussed which reduces the time delay for a lower priority task which under some circumstances becomes a higher priority task. Slicing of interrupt timings is also discussed which can be used to improve the performance. The highest priority task is serviced a greater number of times and with lesser time period. Hence it need not wait for the slack time of other previously higher priority interrupts. If power will be less in grid, automatically power will be managed. Our proposed system when low power generation automatically goes to power management. All the devices controlled depends upon the priority based and timing-based control the devices when low power generation.

RELATED WORKS

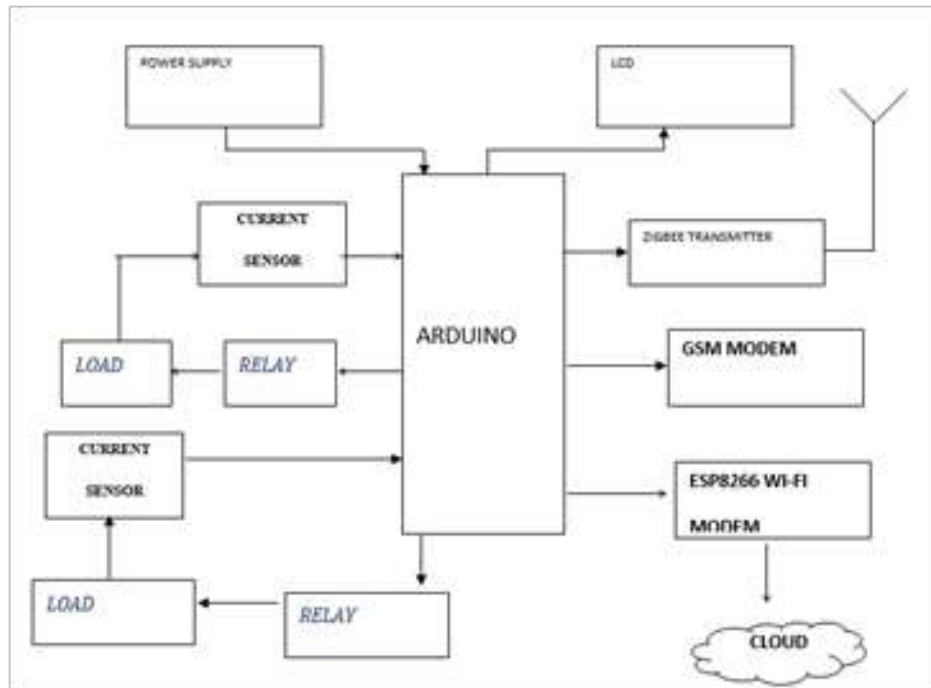
In our country Electricity Board billing system and reading of load consumption is made by man power. Sometimes the man from the Electricity Board may have made mistake on reading and sometimes the disconnected household may consume power in illegal way. To overcome these problems, we made revolution on energy metre system. The project proposed is IoT based Smart Energy Metre Tracking using Zigbee our smart energy metre will track the power consumption and send a notification to the consumer as a message they can pay the amount received on the message. If the consumer failed to pay the bill the power supplied to the consumer is disconnected by the electricity board from the remote area by tapping on the web server.

PROPOSED WORK

This block mainly consists of Sensors. Arduino Uno is interfaced with the energy meter the meter reading is measured by using Current sensors, which is connected to the load through the relay unit. The measured consumption of load is read by Arduino and also displayed on the LCD display. The consumed unit and amount for the consumption are sent to the consumer on the regular period of days by using the GSM module. The reading and data are also stored in Electricity Board server cloud by ZigBee transmitter can also be sampled by an internal ADC and the resulting codes available directly or through peripheral or

internal processor RSSI can be used internally in a wireless networking card to determine when the amount of radio energy in the channel is below a certain threshold at which point the network card is clear to send (CTS). Once the card is clear to send, a packet of information can be sent

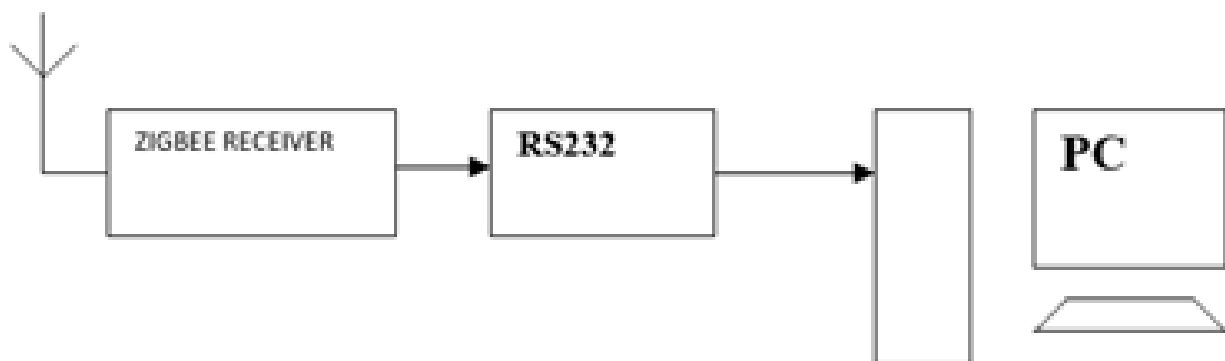
RSSI can be used internally in a wireless networking card to determine when the amount of radio energy in the channel is below a certain threshold at which point the network card is clear to send (CTS). Once the card is clear to send, a packet of information can be sent.



(Metering - side)

Fig. 1. Block diagram of Proposed System

This block diagram shown in **Fig. 1** mainly consist of Sensors. Arduino Uno is interfaced with the energy meter the meter reading is measured by using Current sensors, which is connected to the load through the relay unit. The measured consumption of load is read by Arduino and also displayed on the LCD display. The consumed unit and amount for the consumption are sent to the consumer on the regular period of days by using the GSM module. The reading and data are also stored in Electricity Board server cloud by ZigBee transmitter.



(Controlling-side)

Fig. 2. Block diagram of Proposed System

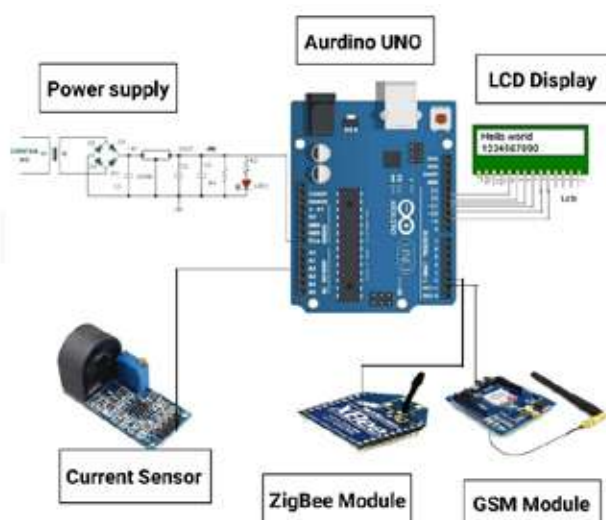


Fig. 3. Circuit Diagram of Proposed System

Fig. 3 represents the circuit diagram for the proposed system, in which GSM, GPS, and various sensors are inter-connected to Arduino. ZigBee is used to establish a wireless connection between the sensor nodes and control centres. The connection done in the hardware kit is done as per the connection in the circuit diagram, to sense the parameter of the power is calculated using the sensors connected to the connected to the Arduino. RS232 is capable of serial communication between the ZigBee receiver and the control centre. The GPS module is used to find the exact location of the fire with latitude and longitude information. The GSM module is used to digitalize the parameters sensed and transfer the information.

SIMULATION & RESULTS

Arduino is used as a microcontroller, which is used to gather the measured parameters from the sensor. Arduino has been chosen to be employed in our work because it is cost-efficient and has a flash memory of 32kb. Arduino is also a great tool for developing interactive objects and controlling the input and output of the sensors. Compared to the traditional techniques the proposed techniques using ZigBee for forest fire detection are found to be a successful Implementation. The number of false alarms is reduced and effective distinguishing of fire can be done without any damage to property and human lives. Gas sensor MQ-2 is connected to the analog pin A3 of the Arduino UNO. The output of the gas sensor is an analog value. Flame sensor LDR is connected to the analog pin A5 of Arduino UNO. The sensors are connected to the analog pins to convert the analog values into digital values. This is carried out by an ADC Converter present in the Arduino.

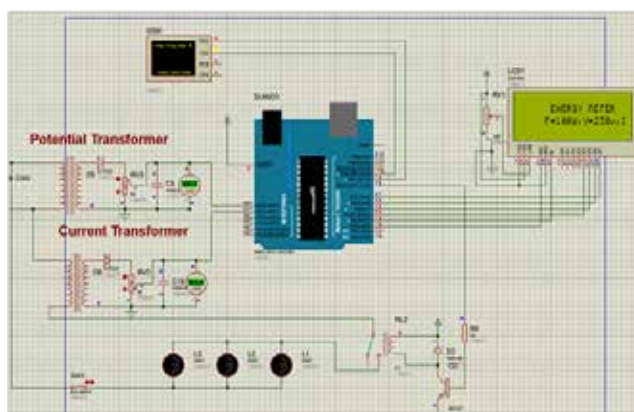


Fig. 4. Simulation Circuit Diagram

Several pins RX and TX of the Arduino are used to connect the GSM module. The TX pin of GSM is connected to RX of

Arduino and the RX pin of GSM is connected to the TX pin of Arduino. Also, the grounds of both GSM and Arduino are interconnected. The enable pin of the LCD Module is connected to the digital pin 11 of the Arduino. The LCD module is connected in 4-bit mode. The 4 data pins of the LCD are connected to the 4 digital pins of the Arduino. The register selects (RS) pin of LCD is connected to the digital pin 12.

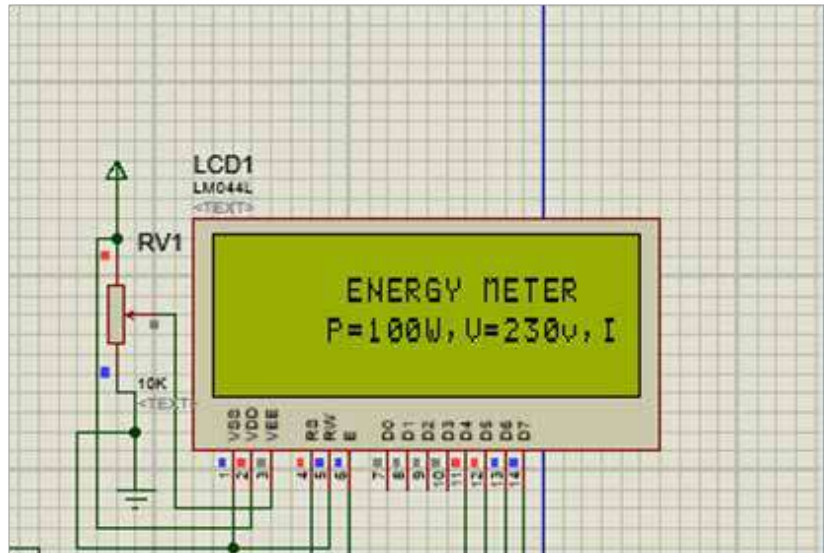


Fig. 5. Simulation output

The existing reading system in metering in our country is a time consuming and it needs a number of labors to. The proposed project will eliminate the need for labor and it is a cost efficient. The proposed system gives the information about the energy consumption on real time on IoT dashboard on mobile application and PC. The consumed load Charge billing through IoT and the notification sent as a message through GSM. This smart energy meter also provides the distributor to make disconnection or reconnect the supply from the remote area when the consumer failed to pay their bill. **Fig. 6** shows the final Hard ware kit of the proposed system



Fig. 6. Hardware kit of the proposed system



CONCLUSION

In this project, IoT based smart energy meter tracking system is very useful to read the consumption of energy in a efficient and highly accurate. It helps to Electricity Board to avoid the drift for disconnecting supply of unpaid consumers, rather it may disconnect from the remote area. The major advantage our project is the system consist of Zigbee, It is the one of the developing high level communication protocol. The system is designed with IoT which helps the system more reliable.

REFERENCE

1. Lin, C. M., & Chen, M. T.,” Design and implementation of a smart home energy saving system with active loading feature identification and power management.” IEEE 3rd International Future Energy Electronics Conference and ECCE Asia, 2017.
2. M., Abdelghani, Y., & Ghany, M. A. A. E,” Wireless IoT based metering system for energy efficient smart cites.” 29th International Conference on Microelectronics (ICM),2017.
3. S. Visalatchi, K. Kamal Sandeep,”Smart energy metering and power theft control using arduino & GSM Automated Smart Metering”, 2nd International Conference for Convergence in Technology (I2CT),2017.
4. Bibek Kanti Barman ,Shiv Nath Yadav, Shivam Kumar, Sadhan Gope,”IOT Based Smart Energy Meter for Efficient Energy Utilization in Smart Grid”2nd International Conference on Power, Energy and Environment: Towards Smart Technology (ICEPE), 2018.
5. M. Prathik, K. Anitha ,V.Anitha,”Smart Energy Meter Surveillance Using IoT”International Conference on Power, Energy, Control and Transmission Systems (ICPECTS), 2018.
6. T Ranjith ; P Sivraj,”Futurstic Smart Energy Meter – Design Based On Embedded Perspective “2018 Second International Conference on Intelligent Computing and Control Systems (ICICCS)Year: 2018, Conference Paper, Publisher: IEEE.
7. Himanshu K. Patel ,Tanish Mody ,Anshul Goyal,”Arduino Based Smart Energy Meter using GSM” 4th International Conference on Internet of Things: Smart Innovation and Usages (IoT-SIU), 2019.
8. Nanda Kishor Panda ; Mayank Senapati ; S. Meikandasivam ; D. Vijaykumar, Jaganatha Pandian,” ZigBee Based Clamp-On IoT Energy Meter”2019 9th Annual Information Technology, Electromechanical Engineering and Microelectronics Conference (IEMECON) Year: 2019, Conference Paper, Publisher: IEEE.
9. J Belwyn Samson ; K Alwin Fredrick ; M Nithin Sathiya ; R. Catherine Joy ; W Joel Wesley ; S Stanley Samuel,”Smart energy monitoring system using raseberry pi”2019 3rd International Conference on Computing Methodologies and Communication (ICCMC) Year: 2019, Conference Paper, Publisher: IEEE.

Innovative Slope Stability Monitoring Instrument for O/C

S P Singh

Chief Manager Wani Area, Nagpur, Maharashtra

✉ rsp.spsingh@gmail.com

ABSTRACT

Open cast mining is the integral part of future mining system. Open cast mine are going wider and deeper with a serious problem of stability of benches and overburden dumps. Despite of several attempts many dump and high wall failure occurred in past in different subsidiaries of CIL causing loss of life and property. There are several methods that are in vogue for slope monitoring, these include Survey Methods, Laser Based Technique, and Radar Technique for Slope Monitoring in open cast. Each method has its own merit and demerit. Slope domain involve detailed analysis of their stability, real time monitoring with best possible equipment. This paper deals with the smart sensor technology, which has been developed to solve the slope monitoring problem and give the real time information for the mode of failure of slope for the safety of men and machine working in open cast, and this instrument provide safe working environment in open cast which is the need of hour.

Keywords : Slope stability; Monitoring instrument; Opencast.

INTRODUCTION

The Real Time Slope Monitoring Device is a system designed in view to analyze strata displacement typically on the level of open cast mines. Real Time monitoring system designed on the virtue of digital embedded system with ease to handle and tough to environment. Generalized System topology can be viewed as follow.

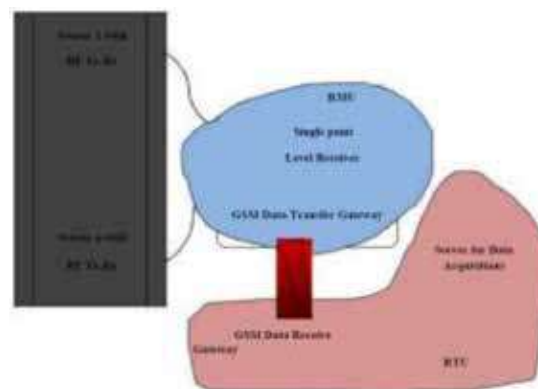


Fig. 1. System block diagram

METHODOLOGY

Real Time Monitoring Device works in three tier system with its data flow as Sensor Transmitter Unit to Remote monitoring Unit (RMU) and then Remote monitoring Unit (RMU) to Remote Terminating Unit (RTU). In this system primary focus has given to precise measurement of soil displacement in particular level of open cast mine. To measure this level, a unique motorized mechanism will in move corresponds to metal detector sensor under ABS Chamber.

This microcontroller based high time- resolute circuit will monitor the position of sensor and decode this value for further wireless transmission. As viewed in figure below sensor displacement will be measure of soil displacement. System has been develop in order to measure upward as well as downward movement below the soil, however degree of displacement can be customized and calibrated by programming software as per requirement. This displacement measure can further be decoded in

wireless frame format for transferring its value to single point receiver wireless or Remote Monitoring Unit (RMU). Localized wireless used for this system will work in license free ISM band with highly secured data encrypted system. All this system has made compatible to work with DC power supply in composed with solar system with appropriate back up.

In this Real Time Monitoring system multitransmission can be put on single level of opencast mine data of which.

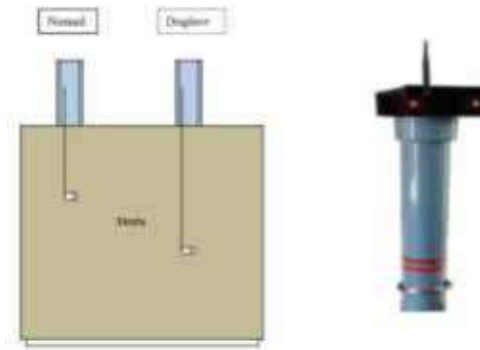


Fig. 2. Generalize mechanism sensor

Fig. 3. Developed sensor mechanism with transmitter system

All these transmitter receiver pairs are able to work in following network topology as shown in figure In these topologies, ID will be assigned to each wireless transmitter which will be decoded by receiver in “teach and learn” genetic algorithm pattern with parental orphan hypothesis, thus devices can be added or reduced at any time with attachment to single receiver.

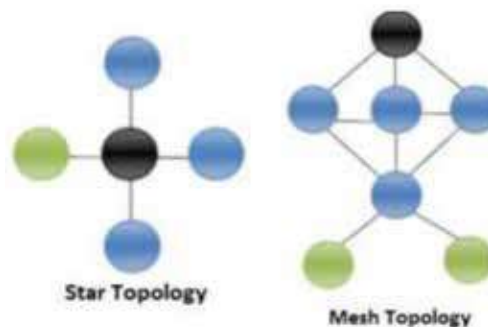


Fig. 4. Multi sensor network topologies

Next to then this data of single receiver can be further restored with temporarily assigned stack-hip management pattern in microcontroller, due to which controller system makes it feasible to transfer data in another data gateways. Data obtained from this gateway can be further processed with GSM/GPRS for RTU (Remote Terminal Unit) which will be located in central monitoring system.

Again this total system with bilateral data processing unit can be work solar back-up.



Fig. 5. RMU with RF-GSM gateway

Data transferred by RMU will be received by RTU which will be received by Remote PC with serial data transfer methods with proper data transfer rates. A single USB based connection can be used for this. This RTU will transfer all data received from multiple RMU to server with serial data interface.

Again this server can be customized with and as per client requirement for further data acquisitions. Currently this server will be compatible to all window based system for delivering SMS to mobile numbers as mention in system. This data acquisition also able to show trend in soil displacement which can further be used for any safety analytics.



Fig. 6. RTU with GUI for advance data acquisition

ENVIRONMENTAL PROTECTION

A customize robust enclosure with ABS Chamber has been used for all field based system which will be look as follows, As display above this enclosure may be equipped with battery in coal/mining fields. This this Real Time Monitoring device embedding with all digital features can be suitably used with its entire technical enhancement for open cast mining to meet its some safety requirements.



Fig. 7. ABS Chamber Compatible for Solar Mountings

INTERPRETATION

There are various instruments available over the counter for slope monitoring of dumps. Some are contact based, and some are laser based and some are radar based. Each one has its own limitations. Contact based instruments are time consuming and prone to human errors. The laser-based instruments are quite reliable but have a distance limitation and have limited capability to scan. The radar-based system is very popular but very costly both in operation and maintenance. The continuous slope monitoring device is very cheaper with respect to cost and easy in installation as well as low maintenance cost.



USEFULNESS

An immediate warning when movement occurs greatly increasing the safety of men and reducing costly damage to equipment. Real time slope monitoring system is very much useful, cheaper, reliable and efficient self-powered with solar panel arrangement fitted with adequate warning system, self-diagnosis, self-calibration, self-identification and self-adaption function.

CONCLUSION

In nutshell such real time slope monitoring system can be installed in open cast which will give warning in case of slope failure for safety of men and machine working in open cast. This device will be a real tool, very cheaper for Real time monitoring of slope in open cast.

REFERENCES

1. Logan, Kenneth Scott. "Analysis of wireless tilt meters for ground stability monitoring." (2008).



Source and Effects of Conductive Emission in the Frequency Range 2.5 to 150 kHz and Its Measurement

Y Dhayaneswaran¹, Dr A Amudha², Dr L Ashokkumar³, Y Umamaheswari¹

Research Scholar, EEE, Karpagam Academy of Higher Education, Coimbatore¹

Professor and Head, EEE, Karpagam Academy of Higher Education, Coimbatore²

Professor & Associate HOD, EEE, P S G College of Technology, Coimbatore³

✉ dhayaneswaran.y@gmail.com; ✉ amudha11@gmail.com; ✉ askipsg@gmail.com; ✉ yummyaskisan@gmail.com

ABSTRACT

In the industry or domestic appliance, inverters are being used to modernize the machines or variable speed according to the process requirements, as far as the domestic appliances to reduce power consumption inverters are used in Air conditioner, Fridge, Ceiling fans. Also, solar panels are in increasing trend for moving towards greener energy, where in inverters are used to convert the DC voltage to AC voltage. Due to this reason, conductive emission is produced in the range of 2kHz to 150kHz. The interference sources, victims and effects are discussed.

Keywords : Harmonics; EMI; Supra harmonics; 2.5 to 150 kHz.

INTRODUCTION

The research on voltage and current distortion has mainly been constrained to the frequency range up to 1 or 2 kHz. Through the years, a large amount of knowledge has been gathered here. However, the amount of research covering higher frequencies is still very limited. One of the reasons for this lack of interest is the apparent absence of well-documented cases of interference that can be clearly attributed to this frequency range. Another reason, and probably a more fundamental one, is the lack of appropriate measurement equipment for higher Frequencies. [1] A new threat to grid operators: 2kHz–150kHz emissions, or “Supra harmonics”, can burn capacitors, knock out communications and even foul up revenue meters. The biggest single source is Emissions from photo voltaic inverters. Some wind turbines, fuel cells, battery chargers can also be significant sources. Supra harmonics also affect street lighting controls, household dimmers, semiconductor manufacturing equipment, medical scanners, security systems and transportation controls.

The number of research papers dealing with supraharmics (waveform distortion in the frequency range between 2 and 150 kHz) has increased over the last years e.g. [2]. There are several reasons for this interest; an increasing number of non-linear devices in the networks that injects emission in the supraharmonic range, the use of power line communication and lack of standardization covering the range although standards’ revisions with new compatibility levels for supraharmonic disturbances are on their way. An increase in the number of malfunctions and non intentional equipment behavior due to the presence of supraharmics has been reported during the last years, for example, with power line communication (PLC), smart meter, ground leakage current switches and overload of electrolytic Capacitors.[2]

TERMINOLOGY OF WAVEFORM

The frequency range up to 150 kHz contains different classes of distortion. Based on the frequencies involved, the following classes are distinguished:

- Components at integer multiples of the power-system frequency. Waveform is distorted but periodic with the same period as the power-system frequency. These components are referred to as “integer harmonics” or “harmonics”.
- Components at non-harmonic frequencies, (inter harmonics).
- Components at frequencies less than the power-system frequency (sub harmonics). These are also a subclass of inter harmonics The component at zero frequency (dc).



- Components at any frequency between 2 and 150 kHz, referred to as “high-frequency harmonics” [9,10], “high-frequency distortion” [11] or more recently “supraharmonics” [8].

INTERFERENCE SOURCES AS PER IEC 61000-4-19

Voltage/current components due to disturbances and signalling in the frequency range 2 kHz to 150 kHz have been considered in standardization only to some limited extent. Concerning the related differential current and voltages, no immunity requirements have been set up until now and no general emission limitations have been established. In the frequency range from 2 kHz to 150 kHz, electromagnetic interference are mainly the results of:

- the operation of electrical equipment, generating non-intentional voltage/current components different from the mains frequency,
- using the mains network for intentional signal transmission, by mains communications systems.

Related voltage/current components occur with the following behaviour in the time-domain:

- with constant envelope over longer time periods, up to some minutes;
- with a non-constant envelope, with typical duration from some tens of ms to several hundreds of ms.

At present, electrical devices that seem to be mostly involved in related electromagnetic interference cases are:

As a source of disturbances:

- 1) inverters (e. g. elevator drives, ski lift drives, PV installations)
- 2) smart meters with PLC data transmission
- 3) switched mode power supplies (e. g. in compact lamps, computers, TVs)
- 4) UPS
- 5) variable speed drives
- 6) DVD players

As a victim, with degraded performance or malfunction:

- 1) smart meters with PLC data transmission
- 2) solid state meters
- 3) touch-dimmer lamps (TDL)
- 4) communication systems (e. g. Ethernet-system, ISDN-, ADSL-modems, IP network branch exchange, routers)
- 5) contact less card readers
- 6) credit card terminals
- 7) alarm systems
- 8) electronic controls (e. g. in heating systems, street lighting, traffic lights, urinals)
- 9) household appliances (e. g. steam irons, coffee machines, microwave ovens, ceramic hobs, washing machines)
- 10) notebooks (cursor position)
- 11) road vehicle smart keys
- 12) TV and radio receivers

with the following examples of degradation of performance or malfunction:

- 1) disturbed amateur radio reception of distant transmitters
- 2) electronic metering systems with

- i) incorrect display of energy supplied at the meter
- ii) communication failures/temporary loss of data transmission function due to interfering signals
- iii) failed communication due to attenuation through shunting by network user equipment

disturbances of electronic control:

- i) unintentional switching of TDLs (between light steps, OFF, ON)
- ii) unintentional switch-on and -off of street lighting
- iii) electronic clocks being fast
- iv) self-restart of household appliances up to some hours after end of intended operation phase
- v) automatic urinal water control switching to permanent operation
- vi) loss of traffic light function
- vii) incorrect operation of heating systems due to sensor faults
- viii) incorrect relay switching in ceramic hobs
- ix) insufficient heat, water loss at steam iron.

The malfunction was caused by the ripple current of the inverter, which may influence an electricity meter under certain circumstances. In most cases, such ripple currents from inverters either from house hold appliances or Solar inverters have a frequency in the range from 3 kHz to 150 kHz, stemming from the switching frequency of the inverter (several tens of kHz) and its harmonics. Emissions produced by inverters are differential mode currents, occurring in low-impedance networks.

Further investigations are needed and are under way to extend the knowledge of equipment to be considered as proven or potential sources or victims in related EMI cases and the related disturbance mechanisms. Nevertheless, the available investigation results show discontinuous voltage/current components with differential mode coupling, with transient respectively slowly repetitive character, in particular the sudden rise of an HF voltage, as the generator of such disturbances.

With regard to real power supply networks, it is to be considered that pure common mode (CM) or differential mode (DM) signals never occur, because the unsymmetrical network impedance and the impedance of the connected equipment convert DM signals to CM signals and vice versa. Therefore, for the frequency range from 2 kHz to 150 kHz, tests with continuous, unmodulated signals and with CM coupling only cannot completely cover the effects of such voltage/current components.

The below figure shows existing standards dealing with non-intentional and intentional emissions.

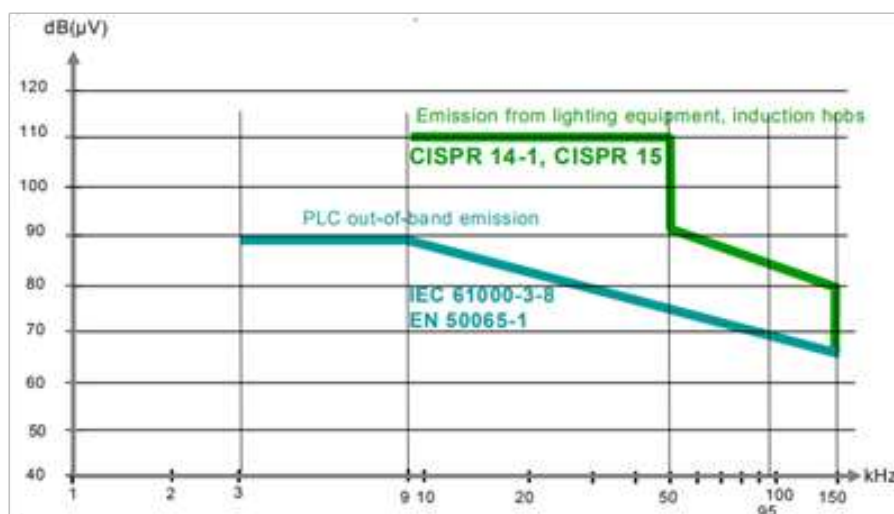


Fig. 1. Standards dealing with voltage levels due to non-intentional emissions in the frequency range 2 kHz to 150 kHz (Ref: IEC 61000-4-19)

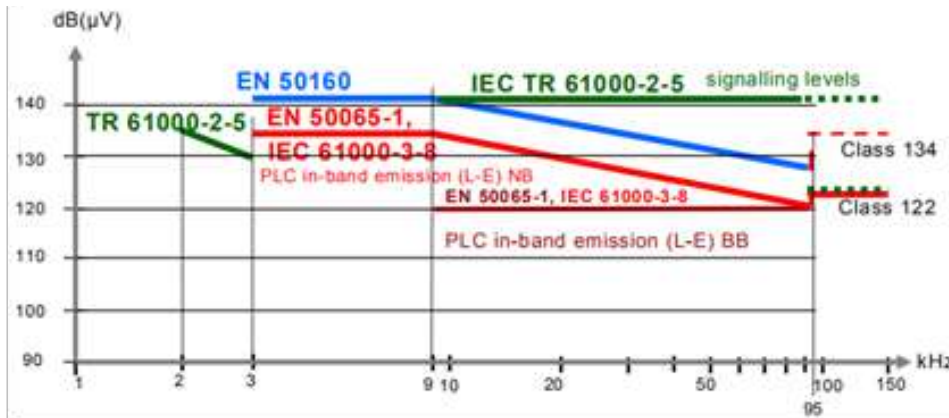


Fig. 2. Standards dealing with voltage levels due to intentional emissions in the frequency range 2 kHz to 150 kHz (Ref: IEC 61000-4-19)

HIGH FREQUENCY VOLTAGE TRANSFER TO THE GRID

Equipment that generate supra-harmonics isn't doing anything wrong in regards to regulations, but can harm other equipment. Photovoltaic inverters, fuel cells, some wind turbines, and almost all other DC to AC switching equipment generate 2kHz–150kHz forced emissions. Power supplies, variable frequency drives and other AC to DC switching devices can produce 2kHz to 150kHz leakage emissions. Power line carriers (PLC) generate emissions intentionally. For the purpose of data transmission, they provide coupling for 2kHz–150kHz across barriers in the network.

Electrical networks are designed to transfer energy at 50 or 60Hz. However, these networks can conduct at higher frequencies, up to about 150kHz. At around 100 kHz, the network impedance typically peaks, maximizing the conversion of supra-harmonic current into voltage. These conducted emissions travel through overhead lines, underground cables and building wiring. They also pass through high efficiency transformers, due to their larger-than-normal inter-winding capacitance. Power factor correction capacitors do not trap these supra-harmonic emissions, because they are often filtered to operate only at 50 or 60Hz. Power line carrier (PLC) couplers provide, by design, a low-impedance path for emissions in this frequency range. In summary, the grid is designed to move power at 50/60Hz but, unfortunately, it also carries 2kHz–150kHz fairly efficiently.

VOLTAGE AT HIGHER FREQUENCIES AS PER IEC 61000-2-4

Distortion of the voltage wave form in the frequency band above the 50th harmonic and less than 9 kHz is also represented by sinusoidal components, which can occur both at discrete frequencies and in relatively broad bands of frequencies. In the case of such higher frequency voltages, it is generally not significant whether they are harmonics or interharmonics. For a discrete frequency in the range above the 50th harmonic and up to 9 kHz, levels are expressed as the ratio u of the r.m.s. voltage at that frequency to the r.m.s. value of the fundamental component of the voltage.

For a band of frequencies above the 50th harmonic and up to 9 kHz, the levels are related to any 200 Hz bandwidth centred at frequency F , and are expressed as follows:

$$u_b = \frac{1}{V_{IN}} \times \sqrt{\frac{1}{200 \text{ Hz}} \times \int_{F-100 \text{ Hz}}^{F+100 \text{ Hz}} V^2(f) \times df}$$

where,

V_{IN} is the rated r.m.s. value of the fundamental component

$V(f)$ is the r.m.s. voltage at frequency f

F is the centre frequency of the band (the band is above the 50th harmonic)



MEASUREMENT OF INTERHARMONICS AND HARMONICS FREQUENCY RANGE UP TO 9 KHZ AS PER IEC 61000-4-7

Spectral components in the interval between two consecutive harmonic frequencies result from a signal containing interharmonic components. Interharmonic components are caused primarily by two sources:

- variations of the amplitude and/or phase angle of the fundamental component and/or of the harmonic components, e.g. inverter drives;
- power electronics circuits with switching frequencies not synchronized to the power supply frequency, for example, a.c./d.c. supplies and power factor correctors.

Possible effects are, for example:

- noise in audio amplifiers;
- additional torques on motors and generators;
- disturbed zero crossing detectors e.g. in dimmers;
- additional noise in inductive coils (magnetostriction);
- blocking or unintended operation of ripple control receivers.

Spectral components associated with interharmonic components usually vary not only in magnitude but also in frequency. A grouping of the spectral components in the interval between two consecutive harmonic components forms an interharmonic group. This grouping provides an overall value for the spectral components between two discrete harmonics, which includes the effects of fluctuations of the harmonic components.

Components in signals (currents or voltages) with frequencies from the 40th harmonic (approximately 2 kHz) but below the upper limit of the low frequency range (9 kHz) are due to several phenomena:

- pulse-width modulated control of power supplies at the mains side connection (synchronous or asynchronous with the frequency of the mains supply), for example as used in (active) power factor correction systems;
- emissions, such as mains signalling;
- feed-through from the load side or generator side of power converters to the mains system side;
- oscillations due to commutation notches. These components can be single frequency type or broadband.

The measurement of these components does not require a high resolution in the frequency domain. Instead, it is customary to group the energy of the signal to be analyzed into predefined frequency bands. For the frequency analysis, the DFT method linked to the methods described in Clause 4 is recommended.

Since one of the objectives is emission analysis in the 2 kHz to 9 kHz range, generally with small amplitudes, a suitable network impedance may be utilized to filter out the more dominant lower order harmonics. Given the use of this filter, the EUT test voltage for these 2 kHz to 9 kHz measurements can be derived directly from the low voltage network, provided the voltage is stable and within required tolerance levels and at the applicable frequency. Alternatively, a suitable power source may be used in cases where the appropriate line frequency, or correct voltage, is not available from the public low voltage network. Also, in some cases where the measuring instrument has a combination of internal filters and a sufficiently large dynamic range, the analysis in the 2 kHz to 9 kHz range might be possible without the use of the above filter.

The frequency range of external voltage and current sensors should be appropriate for measurements in the range 2 kHz to 9 kHz. In view of the low level of the signals to be measured, a band pass filter can considerably decrease the uncertainty of the measurement by attenuating the amplitudes of the fundamental and of components above 9 kHz. The attenuation for the fundamental frequency should exceed 560 times (55 dB). The sampling frequency should be chosen in accordance with the established rules of signal analysis such that frequency components up to 9 kHz inclusive can be measured. A rectangular data acquisition window with a width of 200 ms should be used, corresponding to approximately 10 (12) fundamental periods of 50 Hz (60 Hz) systems.



MEASUREMENT AS PER IEC 61000-4-30 ED 3

The measurement method available in IEC 61000-4-30 that could provide an overview, in a power quality context, of conducted voltage emissions in the 2 kHz to 150 kHz range. These emissions are presumed to be quasi-steady-state levels, although they may have amplitude modulation. The understanding of measurement methods in this frequency range is still evolving. The measurement method for 2 kHz to 150 kHz, including requirements for Class A and Class S, is under consideration. The measurement methods of IEC 61000-4-7:2002, Annex B (informative) could be considered.

One method under consideration is the method of CISPR 16-1-2. CISPR 16-1-2 emphasizes immunity and emission measurements for equipment under test (EUT), and may not be optimized for in-situ power quality measurements. For the purpose of in-situ power quality investigations and surveys, the measurement methods in CISPR 16 may be complex or expensive to implement, due to their gapless measurements and accuracy requirements. The measurement methods of CISPR 16 may provide a large amount of data in an in-situ power quality context. However, the amount of data for in-situ measurements specified by CISPR 16 may be required for coordination with levels defined by various IEC standards.

In another method, The frequency range of 9 kHz to 150 kHz could be divided into equal-width segments. The segment width could be an integer multiple of 200 Hz, preferably either 200 Hz or 2 kHz. For the purposes of this measurement method, it is acceptable to process a frequency range beyond 9 kHz to 150 kHz, for example processing the range 8 kHz to 150 kHz if a 2 kHz segment width is selected. The minimum, average, and maximum magnitude of the r.m.s. voltage in each frequency segment in the 9 kHz to 150 kHz range could be recorded during each 10/12-cycle interval. In addition, the single maximum value in any segment, on any channel, could be recorded.

The following example design demonstrates the intent of the measurement method, measurement range, and measurement uncertainty:

- The 9 kHz to 150 kHz measurements could be made on each channel through cascaded high pass and low pass filters. The high pass filter could have 2 poles, with a 3 dB point at 1.5 kHz or higher. The low pass filter could have 4 poles, with the 3 dB point at 200 kHz. The measurement range after the filters could be at least ± 50 V instantaneous, with a resolution of 12 bits or more.
- 9 kHz to 150 kHz measurements could be taken at the output of the cascaded filters at equally spaced time intervals such that 32 approximately equally-spaced measurements are taken each 10/12-cycle interval. Cross-channel synchronization is not necessary. Each measurement could consist of 512 samples taken at a sampling rate of 1,024 MHz.
- For 9 kHz to 150 kHz, the 512 samples could be processed with a Discrete Fourier Transform or equivalent, yielding 256 bins spaced at 2 kHz. The lowest 4 bins and the upper 181 bins could be discarded. The magnitudes of the remaining 71 bins contain the emissions from 8 kHz to 150 kHz. These emissions could be reported as an r.m.s. value.
- For 9 kHz to 150 kHz, at each 10/12-cycle interval, 32 sets of these 71 bins are available. At each 10/12-cycle interval, the minimum, average, and maximum value of the 32 r.m.s. magnitudes of each of these 71 bins could be reported. In addition, at each 10/12-cycle interval, a single r.m.s. maximum value of all 71 bins across all channels could be reported.

Minimum, maximum, and average values could be considered during each aggregation interval. The average r.m.s. value could be used, for example, to determine typical emissions. The maximum r.m.s. value could be used, for example, to determine worst-case emissions. The difference between the minimum and maximum values could be used, for example, to detect the presence of amplitude modulation. The single maximum r.m.s. value could be used, for example, to set worst-case 95 % limits. Measurement methods may generate a large amount of data, which, depending on the application, may need to be stored, transmitted, analysed, and/or archived. Depending on the application, the amount of data may be reduced. To reduce the amount of data, consider applying statistical methods at the measuring location such as 95 % or 99 % levels, or storing only extreme and average values, or storing detailed data only when trigger thresholds are exceeded, or other methods.

MEASUREMENT INSTRUMENT

Though many PQ measuring devices are available in the current market, to measure the PQ in the range of 2.5 to 150 KHz, the manufacturer Powerside <https://powerside.com> is producing PQube 3 meter, which measures the Supraharmonics. This monitor is certified for Class A power quality according to IEC 61000-4-30 Ed3 [2].

Also, Dranetz also makes the PQ meter to measure the Harmonics <https://www.dranetz.com>



However, other manufacturer may have that feature, which is to be studied further.

CONCLUSION

This paper has discussed about the source and effects of conductive emission in the range from 2.5kHz to 150 kHz and its measurement methods with its importance.

FUTURE WORK

The detail study needs to be done in the selective industrial grid and Solar panel connected grid in India.

REFERENCE

1. Sarah Karolina Rönnberg, et.al, “Interaction Between Narrowband Power-Line Communication and End-User Equipment”. IEEE TRANSACTIONS ON POWER DELIVERY, VOL. 26, NO. 3, JULY 2011
2. Rönnberg, S. K., “Supraharmonics in European and North American Low-Voltage Networks” 978-1-5386-5186-5/18/\$31.00 ©2018 IEEE
3. Y Dhayaneswaran et.al. “Review of electrical noise on field elements”. 978-1-61284-764-1/11/\$26.00 ©2011 IEEE
4. IEC 61000-4-7
5. IEC 61000-4-19
6. IEC 61000-4-30
7. IEC 61000-2-4
8. M. Bollen, M. Olofsson, A. Larsson, S. Rönnberg, M. Lundmark, Lundmark standards for supraharmonics (2 to 150 kHz), IEEE Electromagn. Compat. Mag. 3 (2016) 114–119.
9. B. Ekehov, S. Halen, T. Larsson, L. Palmqvist, A. Edris, D. Kidd, A.J.F. Keri, B. Mehraban, High-frequency impacts in a converter-based back-to-back tie; the Eagle Pass installation, IEEE Trans. Power Deliv. 18 (October (4)) (2003) 1410–1415.
10. H. Vahedi, A. Sheikholeslami, M. Tavakoli Bina, M. Vahedi, Review and simulation of fixed and adaptive hysteresis current control considering switching losses and high-frequency harmonics, Adv. Power Electron. 2011 (2011), Article id 397872, 6 pages.
11. A.A. Girgis, M. C. Clapp, E. B. Makram, J. Qiu, J.G. Dalton, R. C. Catoe, Measurement and characterization of harmonic and high frequency distortion for a large industrial load, IEEE Trans. Power Deliv. 5 (January (1)) (1990) 427–434.



Text Recognition of Embossed Metadata Obtained from Live Video of UAVs

Gagan Kumar Nigam, MGR, Sumit Srivastava, SE

Development and Engineering, Network Centric System, Bharat Electronics Limited, Ghaziabad

✉ gagankumarnigam@bel.co.in; ✉ sumitsrivastava@bel.co.in

ABSTRACT

Unmanned Aerial Vehicles (UAVs) are becoming a key platform for reconnaissance, target tracking and other missions of the various forces in the recent past. Most of these UAVs are operated independently with one or more UAVs looking at the same or multiple target/s and/or region/s. It is important and necessary as part of managing and monitoring the airspace, that the geo-location of these airships/UAVs are known and indicated appropriately within the larger monitoring framework in addition to identifying the friend or foe ship. In the current scenario, only the video stream from the UAV is available with related metadata embossed on it. To handle this effectively, this paper presents a SVM based machine learning model for extracting the relevant information, meta-data, from the video stream while addressing the video/image challenges posed due to analog video capture with continuously changing background and foreground information. The developed model and prototype show that the trained model performs well and achieves a text recognition level of more than 94% and is able to recognise text even when it is faint to the human eye.

Keywords : Support vector machine; Text recognition; Unmanned aerial vehicles; Video.

INTRODUCTION

Unmanned Aerial Vehicles or UAVs, are aircrafts without a pilot on board. They are remotely controlled or autonomous, ideally suited for ‘dull and dirty’ jobs in the military where they are predominantly used. UAVs are available in a wide range of sizes and few of them are used for civilian purposes as well. Professional, small UAV systems have generated interests in a wide range of monitoring applications like forest fire monitoring, traffic or crowd monitoring, disaster and damage assessment etc., in addition to its use in the military applications. UAV camera is a common payload and is used for both data collection and navigation. Any application that intends to use UAVs, can provide the aerial video and sensor data as a byproduct. The low altitude aerial perspective of the ground opens up numerous possibilities in any mapping application. However, since most of these are flown independent of each other and can interfere with the airspace management of both military and civilian airspaces, it is necessary to know their exact geo-location for any Air-Space Management. Countries like the United States have come up with road maps [1] for integrating UAVs into the civilian airspace. In India too, DGCA has released directions on operating these RPAs and a plan to integrate them. On the other hand, as these systems are at various stages of development, different vendors and manufacturers are using a range of on-board devices and software systems that limit the integration of these information in a seamless way. Also, the already operational UAVs may have limited capability for data inter-operability and exchange, limiting the information being collated within the Airspace management system. But, many of these UAVs display the sensor data as text over the camera feed and is available over the handheld or other terminals that the UAV operator uses with or without a map background. As seen in the frame capture of a video feed in Fig.1, these on-video metadata text if extracted, can provide valuable information on the geo-location of the UAV platform and the target it is viewing.

Traditionally, Optical Character Recognition (OCR) based techniques are explored primarily for typewritten text extraction in images. However, majority of the literature is focused on text extraction from digital books where background is assumed to be constant/uniform in appearance (applicable to documents) [4]. Recently, Deep Learning (DL) enabled in-the-wild text detection and recognition techniques have been proposed. However, these learning techniques require significant amount of training data and computational means both while training and inference time. Additionally, these DL solutions are more suitable for detect/recognise text in the wild with large variations in text appearance including articulated fonts and size variations [5]. Thus, in the context of problem of extracting text metadata from UAV video feed, the OCR approach is not very suitable due to existence of cluttered background in the viewing field and DL solutions seems overkill due to fixed font and text position scenario in case of

embossed text in UAV's as well as the computational and annotated data needs are high. In case of text extraction from videos, there are multiple challenges such as low resolution of video feeds, background clutter, optical saturation, noise induced by lossy video compression formats, missing frames, video jitters etc.



Fig. 1. A screen capture from a UAV video feed showing the embossed text in yellow

Hence, this paper addresses the problem of text recognition from the embossed metadata text on the video feed available from the UAVs. The paper proposes a generalized solution for meta-data text extraction from UAV video feeds which attempts to address some of the key challenges using the machine learning techniques. The key idea is to model the problem as character recognition/classification. The expected inputs to our method is assumed to be video feeds having a single color fixed font text, embedded in videos in a fixed layout and captured with stabilized camera while having minimal existence of background clutter noise as well as no large chunks of frames missing.

METHODOLOGY

Overall Framework of the Model

In order to create a Metadata Text Recognition System, input video is first separated into individual frames and layout specification is carried out. It is assumed here that each frame has a set of Analog alphanumeric strings of fixed size and color, occurring at fixed locations. Thus, the entire frame can be divided into regions and then into sub regions, where character level information can be specified. The ground truth for this data is then generated and two classifiers are trained, one for Alphabetic Characters and another for Numeric Characters. These trained models are then tested with unseen data and fine tuning is done until the performance of the models is deemed satisfactory. These models are then used to generate a frame-tagged text file output that is further converted to a video subtitle format, SRT file, so that we can overlay the recognised text and visualize it along with the video feed. **Fig. 2** illustrates the detailed model workflow.

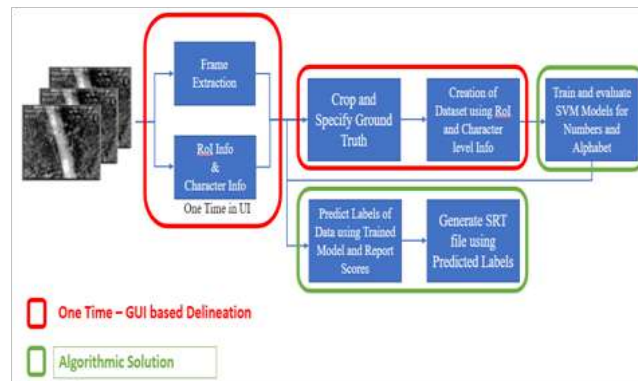


Fig. 2. Proposed model workflow

Data Description

The current experiment is performed on a video of 16 seconds (approx.) at 25fps which yields a total of 408 frames. The entire frame is divided into regions and the initial experiment is done on the top left corner region. **Fig. 3** depicts the Region of Interest (RoI) under consideration. The problem appears to be relatively structured, given that exact layout of the given text data embedded/embossed in the video feed is known beforehand. Nevertheless, there are a few challenges associated to the problem of text extraction from videos such as low resolution of video feeds, background clutter, optical saturation, noise induced by lossy video compression formats, video jitters etc.



Fig. 3. Region of interest for the current

Data Preparation

As mentioned earlier, the data is divided into alphabetic and numeric characters as the dimensions of the two types were seen to be slightly different. While both types of characters had a height of 15 pixels, alphabetic characters were broader, being 10 pixels in width and the numeric characters were slightly narrow, being 8 pixels in width. Once the characters level information is known, the datasets can be generated by specifying the ground truth of each character. In cases where the character was not perceivable clearly even by the human eye, an educated guess was made based on the inform of the prior frames. Since many of the characters remained unchanged, this task was done manually, with relative ease. As seen in **Fig. 4** there is a pronounced class imbalance, with the character '3' occurring significantly higher number of times in the cases of the numeric data. A similar case is seen with the character 'A' in the alphabetic data as seen in **Fig. 5**.

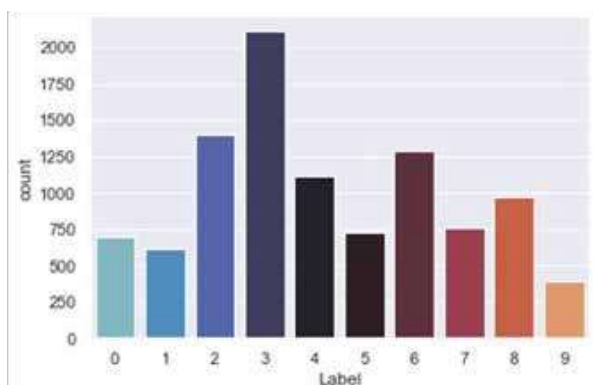


Fig. 4. Numeric Data Counts

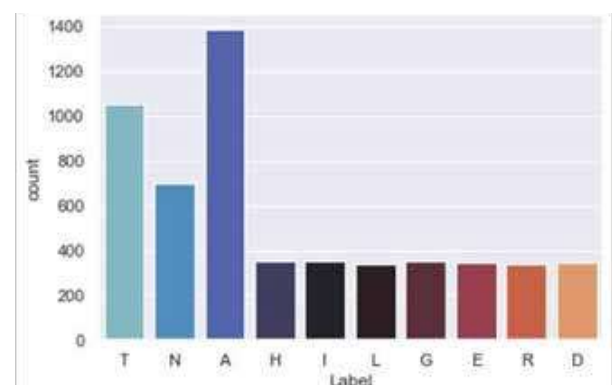


Fig. 5. Alphabetic Data Counts

Algorithm Specification

Considering the amount of data available, it was decided that the Support Vector Machine (SVM) algorithm will be used to build the classifier. SVMs are powerful Machine Learning methods which have been known to perform well in both classification and regression tasks. Fundamentally, a Support Vector Classifier (SVC) tries to divide the data in such a way that the inter-class distance is maximum, i.e., it tries to find a hyperplane which maximizes the margin between two classes.

Consider a set of vectors w_1, w_2, \dots, w_m represented as w , where 'm' is the number of dimensions, and a set of variables x_1, x_2, \dots, x_n , represented as X , where 'n' is the number of samples. When a vector w_0 is taken as the bias term 'b', the equation of the hyperplane or the decision boundary is given as:

$$f(x) = w^T X + b$$

For the sake of convenience, let us take a binary classification scenario, with +1 and -1 being the two class labels and assume for now that the data is linearly separable. The SVM finds a hyperplane such that distance between the two classes is maximized, as depicted in the Fig. 6 and the vectors responsible for determining the two boundaries are called Support Vectors. In other words, we want a case where:

$$w^T x_i + b \geq +1, \quad \text{when } y_i = +1 \quad (1)$$

$$w^T x_i + b \leq -1, \quad \text{when } y_i = -1 \quad (2)$$

or in general,

$$y_i (w^T x_i + b) \geq +1$$

The difference between the two planes is given by:

$$\frac{b+1}{\|w\|} - \frac{b-1}{\|w\|} = \frac{2}{\|w\|}$$

The aim of the SVM is to now maximize this distance. This given by the following equation, which is the SVM objective in its primal form.

$$\min_w \frac{1}{2} w^T w \quad \text{Subject to the constraint } y_i (w^T x_i + b) \geq +1 \quad (3)$$

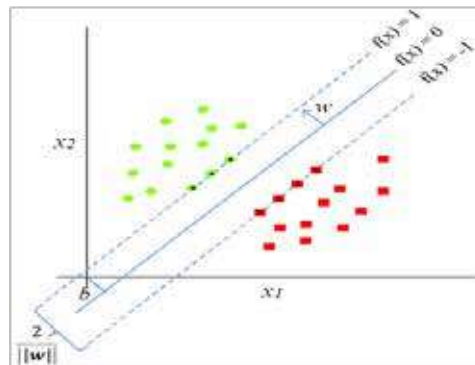


Fig. 6. Hard margin SVM Source: adapted from [2]

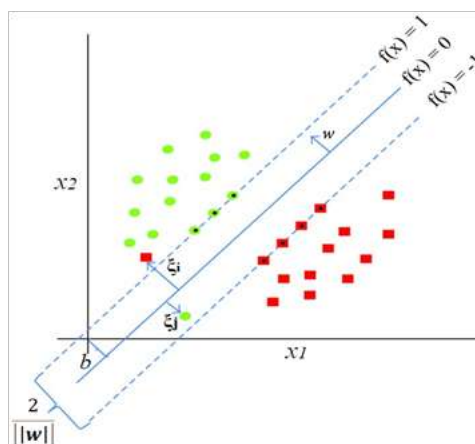


Fig. 7. Soft margin SVM source: Adapted from [2]

As mentioned earlier, this case holds good for linearly separable data but when the data is not linearly separable, we must introduce a new variable, ' ξ ' that penalizes the samples which violate the assumption of linear separability. The earlier case was known as a Hard Margin SVM, depicted in Fig. 6. The current case, with certain number of non-linearly separable instances is called a Soft Margin SVM and is depicted in Fig. 7. The equation now becomes:

$$\min_w \frac{1}{2} w^T w \quad \text{Subject to the constraint } y_i (w^T x_i + b) \geq +1 - \xi_i, \\ \text{where } \xi_i \geq 0$$

On taking the Lagrange Multiplier constant C, which balances the number of allowed violations, we get:

$$\min_w \frac{1}{2} w^T w + C \sum_{i=1}^n \xi_i$$

So far we have discussion a scenerio with only two dimensions, but in practical applications, we encounter a large number of dimensions and in most of the cases, the data is not linearly separable. In order to deal with these issues, we make use of Kernels. 'The Kernel Trick' is a method to solve non-linear problem using linear algorithms. Assume you have 2 vectors p and q, given by:

$$p = \begin{bmatrix} p_1 \\ p_2 \end{bmatrix} \text{ and } q = \begin{bmatrix} q_1 \\ q_2 \end{bmatrix}$$

Their dot product is given by:

$$(p^T \cdot q) = (p_1 q_1 + p_2 q_2)^2 \\ = \begin{bmatrix} p_1^2 \\ p_2^2 \\ \sqrt{p_1 p_2} \end{bmatrix}^T \begin{bmatrix} q_1^2 \\ q_2^2 \\ \sqrt{q_1 q_2} \end{bmatrix}$$

This dot product can be represented in the kernel form as:

$$K(p, q) = \phi(p)^T \cdot \phi(q)$$

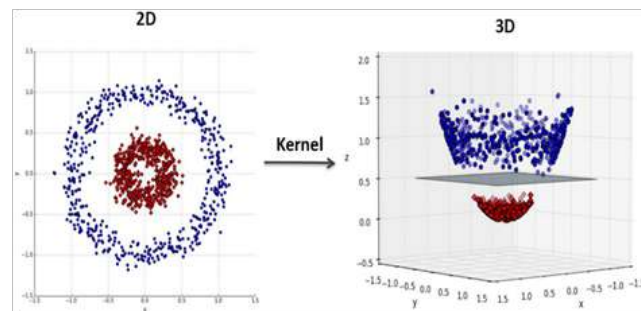


Fig. 8. Non-linear classifier using Kernel tick source: [3]

In other words, here the kernel is allowing us to compute the dot product in a new feature space without really going into that feature space. In order to kernelize the SVM, we have to write the objective in terms of a dot product, which can be achieved by converting the equation in its primal form to its dual form. To do that, we differentiate equation (3) once with respect to w and then another time with respect to b, equate them to zero and write the equations in terms of a Lagrange Multiplier ' α '.

$$w = \sum_{i=1}^n \alpha_i y_i x_i \quad (4)$$

$$\sum_{i=1}^n \alpha_i y_i x_i = 0 \quad (5)$$

On substituting (4) and (5) in (3) and simplifying, we get:

$$J(\alpha) = \max_w \left(\sum_i^n \alpha_i - \frac{1}{2} \sum_{i=1}^n \sum_{j=1}^n \alpha_i \alpha_j y_i y_j x_i^T x_j \right) \quad (6)$$

On close observation, we see that $(\alpha_i \alpha_j y_i y_j x_i^T x_j)$ the dot product of $x_i^T x_j$, multiplied with a few scalars. Thus, the equation is can now readily kernelized to the form:

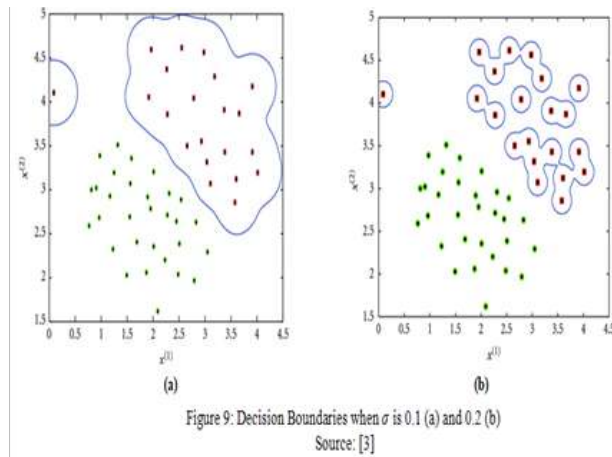
$$f(x) = \sum_i^n \alpha_i - \frac{1}{2} \sum_{i=1}^n \sum_{j=1}^n \alpha_i \alpha_j y_i y_j K(x_i, x_j)$$

In practice, α is zero for all the samples other than those which are the Support Vectors. When all the non-support vectors are removed, the maximum margin hyperplane is obtained. There are many popular kernel functions which can be used but for our experiment, we chose the Radial Basis Function (RBF) Kernel. Consider two samples x and x' in the input space.

The RBF kernel is defined as:

$$K(x, x') = e^{\left(-\frac{\|x - x'\|^2}{2\sigma^2} \right)}$$

$$K(x, x') = e^{(-\gamma \|x - x'\|^2)}$$



The hyperparameters for this method are C and γ (gamma). As discussed earlier, C is a penalty applied on the misclassified data. When the value of C is small, it shows that more misclassification is permissible, i.e., there is high bias and low variance. When the value of C is large, there is heavy penalization of misclassified data, thus indicating that there is low bias and high variance. Extremely high values of C might cause overfitting and very small values of C might cause underfitting. On the other hand, the parameter gamma helps us control the decision region. When gamma is low, the curvature of the decision boundary is low, thus giving a larger decision region. When the gamma value is very high, there is very high curvature, which results in isolated decision regions, which may lead to overfitting. **Fig. 9** depicts the plots decision boundaries obtained for different values of σ (which is inversely proportional to the root of twice of gamma).

EXPERIMENTAL RESULTS

System Setup

The experiment was performed on a 64-bit system with Window 10 OS with a RAM of 16 GB, 5 GHz processor with 6 cores. The entire code was written in python 3.7.

Model Creation

Once the data was generated, a separate dataset was created for the alphabetic and numeric characters. These datasets were divided into two portions, the first containing 90% of the data, which was used for training the model and 10% of the data was kept aside for testing. In order to find the best parameters Grid Search Cross Validation of 5-folds using various combinations of C and Gamma values to obtain the best parameters. After the search, it was C and Gamma values for the Alphabetic Data



were found to be 100 and 0.0001 and for Numeric Data, the values of C and Gamma were 10 and 0.0001. Using these values, the model was then trained and 10-fold cross-validation was performed on this training data. The mean accuracy for the Alphabetic and Numeric Model were found to be 0.99098 and 0.946525 respectively. The trained models were then tested with on the 10% of the test data and the results obtained are summarized below in the **Tables 1 & 2**.

Table 1. Summary of test alphabetic data

Character	Precision	Recall	f1 Score	Support
A	0.98	0.99	0.98	246
D	1	1	1	66
E	1	1	1	63
G	1	1	1	59
H	1	1	1	60
I	0.98	0.93	0.95	55
L	1	1	1	69
N	0.98	0.97	0.98	118
R	1	1	1	72
T	1	1	1	171
Accuracy			0.99	979
Macro Average	0.99	0.99	0.99	979
Weighted Avg	0.99	0.99	0.99	979

Table 2. Summary of test numeric data

Character	Precision	Recall	f1 Score	Support
0	0.97	1	0.93	48
1	0.97	0.95	0.96	60
2	0.95	1	0.98	81
3	0.98	0.99	0.98	136
4	0.93	0.94	0.93	67
5	0.98	1	0.99	40
6	0.92	0.91	0.91	76
7	1	0.94	0.97	67
8	0.94	0.91	0.93	56
9	1	0.83	0.91	35
Micro Average	0.95	0.95	0.95	666
Macro Average	0.95	0.95	0.95	666

Table 3. Prediction scores for alphabetic data of all frames

Character	Precision	Recall	f1 Score	Support
A	0.99	1	1	1632
D	1	1	1	408
E	1	1	1	408
G	1	1	1	408
H	1	1	1	408
I	1	0.99	0.99	408

L	1	1	1	408
N	1	1	1	816
R	1	1	1	408
T	1	1	1	1224
Accuracy	1			6528
Macro Average	1	1	1	6528
Weighted Avg	1	1	1	6528

Table 4. Prediction scores for numeric data of all frames

Character	Precision	Recall	f1 Score	Support
0	0.97	0.97	0.97	811
1	0.99	0.98	0.99	709
2	0.98	1	0.99	1664
3	0.99	0.99	0.99	2484
4	0.98	0.98	0.98	1308
5	0.99	0.98	0.99	865
6	0.98	0.98	0.98	1502
7	0.98	0.98	0.98	885
8	0.98	0.98	0.98	1146
9	0.99	0.98	0.98	458
Micro Average	0.99	0.99	0.99	11832
Macro Average	0.98	0.98	0.98	11832
Weighted Avg	0.99	0.99	0.99	11832

Prediction

Once the models were generated, they were used to perform predictions on the top left regions of all the frames. The time taken for performing character extraction and prediction for 408 frames was found to be 12.55 seconds. The predicted labels were stored in an SRT file so that they could be played along with the video for later reference. The summary of the results obtained is depicted in **Tables 3 and 4** and the confusion matrices are given in the Fig. 10A (Alphabetic Data) and **Fig. 10B** (Numeric Data).

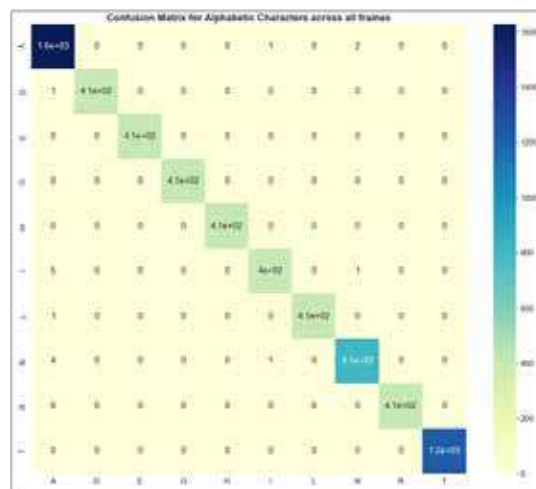


Fig 10 (A). Confusion Matrix for predictions across all frames of the Input Video for (A) Alphabetic characters

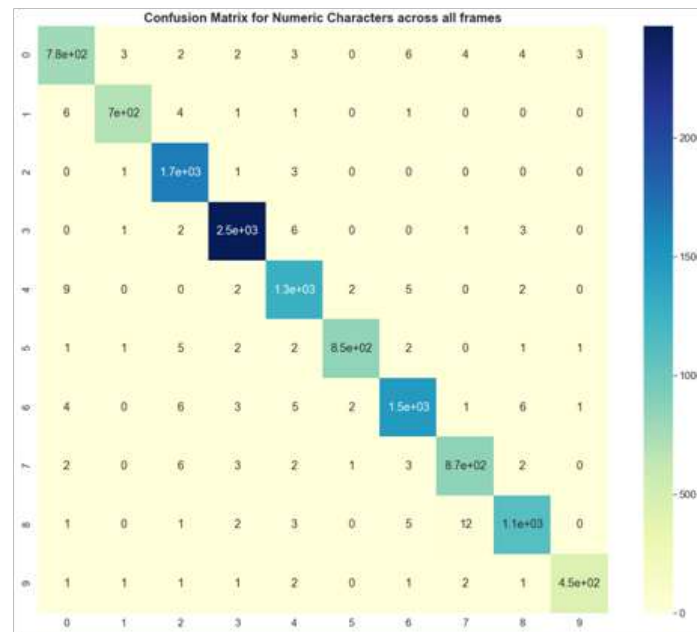


Fig.10 (B). Confusion matrix for predictions across all frames of the input video for (B) numeric characters

DISCUSSIONS

Upon observing the scores and the confusion matrix, it can be inferred that for the most part, the labels were predicted accurately. When it comes to the alphabetic data, there were some instances of misclassification between 'I', 'N' and 'A'. This could be owing to the fact that the character 'I' was very narrow compared to other characters and was placed at the corner of the character window, giving it an appearance that was somewhat similar to a portion of 'N', as seen below in the **Fig.11**. Moreover, 'I' appears very close to 'A', leading some parts of 'A' to overlap with 'I'. This coupled with the high amount of class imbalance cause by the character 'A'.

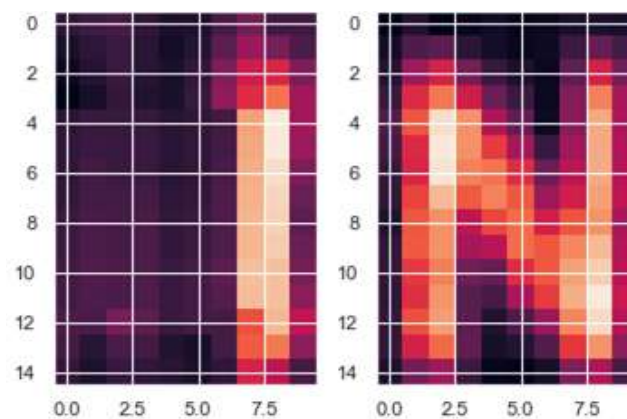
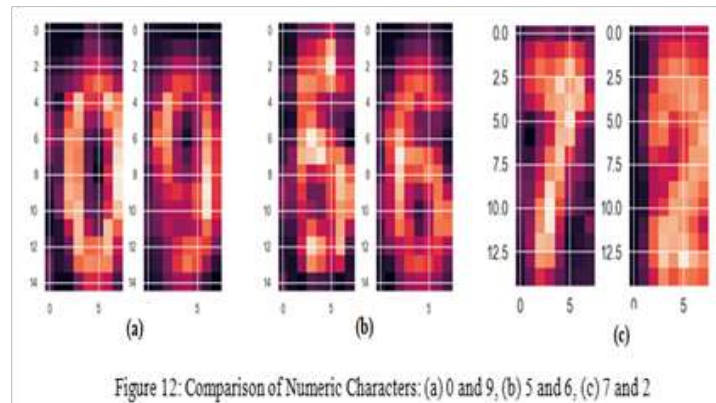
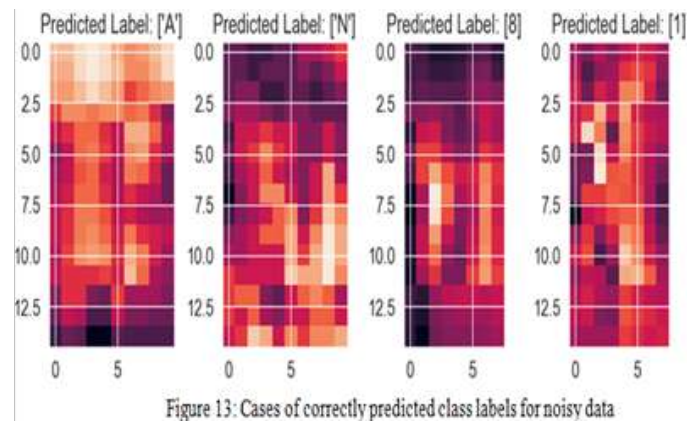


Fig. 11. Depiction of characters 'I' and 'N'

While the confusion matrix of the alphabetic data was almost diagonal in nature, there were more misclassifications seen in the numeric data. This could be attributed to the fact that most of the alphabetic characters occurred in regions with a clear background, while the numeric data had a background with a large amount of variability. Moreover, there was the same case of class imbalance with the number of instances of '3' occurring a proportionally larger number of times. Added to this is the fact that some of the characters like '0', '9' and '6' or like in the case of '3' and '8', appear to be quite similar in terms of their shape. This uncertainty is further amplified by the background noise in quiet a few cases. The **Fig. 12** depicts some of the instances where different characters appear to be similar.



Keeping in mind these difficulties, the models still performed well in cases where even the human eye could not distinguish between characters properly. This could be seen in the cases when there was a large degree of occlusion caused by the presence of clouds in the background. **Fig. 13** depicts a few examples of such cases.



Final Output

Based on the recognized text from each of the frames of the Video, the final output was generated as a time-stamped text data in the subtitle format so that it can be visualized with the input data as shown in the screen grab in **Fig. 14**. Also the metadata present in this text file can be suitable used for geo-locating the UAV and any other derived information of use for the application concerned.



Fig. 14. Recognized text for the top left corner presented as Subtitle over the video



CONCLUSIONS

The proposed model, as shown in **Fig 2** is able to successfully handle the UAV video input and do text recognition from each of the frames. Also, the performance of the current implementation is around 30ms, which is less than the rate of getting the frames from the UAV video with 25-30 fps enabling an almost real time deciphering of the text on the video. Also, since the overall performance of the Kernel SVM with an RBF Kernel classifier was quite satisfactory without the imposition of any domain constraints, especially given the quality and the quantity of data that was available for development of the solution. To further improve the algorithm performance and handle the imbalance in the support data based on the input video data itself, techniques like data augmentation will be explored. At an algorithmic level, methods like hierarchical classification models can be evaluated to see if it can help in the detection and of characters with similar shapes and appearances. In addition to this, the character recognition errors that might creep in due to video blur or background clutter, may be improved further by introducing spatial and flight path constraints based on related supplementary knowledge.

ACKNOWLEDGMENT

Arvind Kumar DGM D&E-NCS, BEL Ghaziabad and Manoj Tyagi DGM, D&E-NCS, BEL Ghaziabad for their constant support and guidance used for this research.

REFERENCES

1. Integration of Civil Unmanned Aircraft Systems (UAS) in the National Airspace System (NAS) Roadmap - First Edition (2013).
2. Mahmoudi, Abdelhak & Takerkart, Sylvain & Regragui, Fakhita & Boussaoud, Driss & Brovelli, Andrea. (2012). Review Article Multivoxel Pattern Analysis for fMRI Data: A Review. Computational and Mathematical Methods in Medicine. 14. 10.1155/2012/961257.
3. Hachimi, Marouane & Kaddoum, Georges & Gagnon, Ghyslaine & Illy, Poulmanogo. (2020). Multi-stage Jamming Attacks Detection using Deep Learning Combined with Kernelized Support Vector Machine in 5G Cloud Radio Access Networks.
4. Gupta, Maya R.; Jacobson, Nathaniel P.; Garcia, Eric K. Pattern Recognition. 40 (2): 389.OCR binarisation and image pre-processing for searching historical documents,
5. Xiaoxue Chen, Lianwen Jin, Yuanzhi Zhu, Canjie Luo, Tianwei Wang arXiv:2005.03492v1, 2020, Text Recognition in the Wild: A Survey.



Mitigate Challenges of Co-location Interference for SDR applications

Sandeep Singla, Sidharth Sarswat, Radheshyam Kumawat, Deepa Bajpai

Bharat Electronics Ltd, Panchkula, Haryana

✉ sandeepsingla@bel.co.in

ABSTRACT

In today's environment, when multiple antennas/radios are co-located and operating at same/different frequency bands, enhancing modern SDR transceiver's performance in a co-located environment with reliable communication is a real challenge. The signals from one equipment interfering & jamming the other equipment's receiver becomes common phenomenon thus reducing the real application of communication equipment. SDR radios are faced by such challenges due to multiple radios fitted on a single AFV (Armored Fighter Vehicle). In other applications the radio is used at command & control stations where there are other radios operating in same area e.g. Military Command & Control stations, Air Traffic Control Stations (ATC) etc. This co-located environment degrades the performance of SDR systems due to other equipments operating nearby and due to its own isolation problems in antenna T/R switch. This paper discusses the challenges faced due to co-location of equipments and techniques to mitigate those challenges.

Focus is also given for designing high performance Co-site module which can work as a front end module to cater the needs for co-located equipments as well as the problems in SDR systems due to isolation between transmit and receive ports of radio.

Keywords : SDR; LNA; AFV; Co-site; Tx; Rx; Limiter; Filter.

INTRODUCTION

In modern communication systems, one radio/equipment is not sufficient to cater the needs of communication. Military Command & Control (C2) platforms, Air traffic control stations, battlefield vehicles like AFV (tanks, trucks) and Naval ships require multiple radios for different kind of communication needs. Dependent upon the application scenario like redundant application or separate communication, the radios can be of same frequency range or different frequency range. Due to complexities of battlefield vehicles and control stations, space for mounting radios and their respective antenna is a challenge. This limitation leads to co-located antennas in close proximity, thus reducing the isolation between transmitter and receiver. This environment causes co-site interference in receivers [1]. The high level of power radiated from transmitter of one radio may cause high level RF coupling at receiver of any other radio. This may jam the receiver. This complex environment causes interference in the receiver chain of radio, which significantly degrades the performance of communication system. In some cases the power level may be as high as to burn the receiver LNA. The self generated noise in transceiver also degrades the performance of SDR systems. The scenarios for networked military communication environment and control stations are as shown in **Fig. 1 and Fig. 2.** [2].

There are two types of general techniques that are used to mitigate the interference caused due to co-location of equipments

1. Antenna placement optimization/Increasing distance between antennas of radios
2. Frequency separation/planning for multiple radios

First method i.e. antenna placement, is feasible in the areas where space is not a limitation and antennas can be mounted very far away. In today's scenario due to increase in complexities of communication needs and warfare vehicles like tanks, trucks and naval ships enough space to separate these antennas is not feasible.

Second method is a good technique to implement, but it imposes some limitations, which will be discussed in part II in this paper.

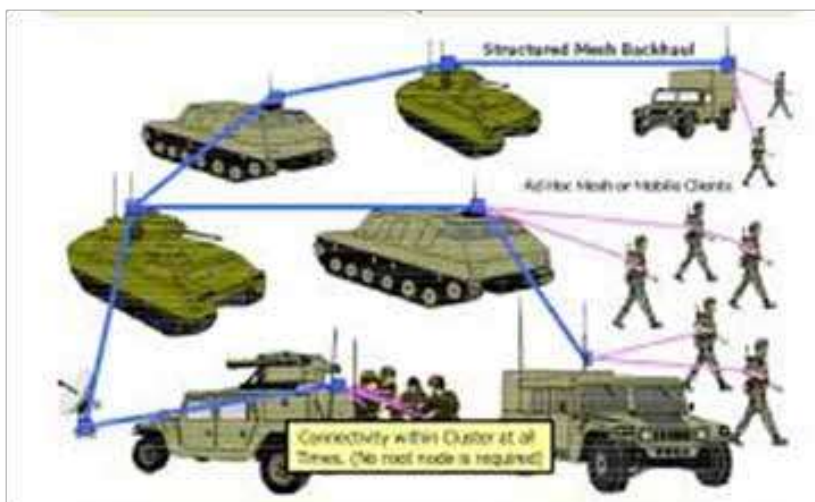


Fig. 1. Networked military communication environment



Fig. 2. Multiple antennas closely mounted at control station

To overcome the limitations of above methods, a third type of technique can be used. This technique involves filtering out all other unwanted receptions at the frequencies away from intended frequency and is named as selective filtering method.

The above selective filter also called frequency agile filter along-with transmit/receive switch, an amplifier and limiter for selective filtering is called Integrated Co-site Equipment (ICE).

Key Features of ICE:

- Reduced transmit broadband noise levels
- Suppressed harmonics, inter-modulation and spurious emissions
- Significantly enhanced receiver dynamic range
- Improved noise figure, and high signal handling and inter-modulation
- Reduced reciprocal mixing and cross-modulation
- Mitigation of receiver desensitization at close frequency spacing improves the selectivity of receiver.

Part I of this paper describes the challenges faced in today's communication environment. Part II explains the existing methods to mitigate these challenges. Part III explains the co-site interference problem and method used for mitigation. Part IV and V explains other important front end methods for saving the receiver from burnout and T/R switch isolation.



A BRIEF ABOUT EXISTING METHODS

As highlighted earlier, there are basically two methods which are used to mitigate the co-location interference. These methods with their pros and cons will be discussed in this section.

Increasing distance between radios: As we know from path loss calculations that if a transmitter is placed nearby then the received power is a function of two elements

The frequency

Distance between antennas

$$P_L \text{ (dB)} = 32.44 + 20\log_{10} f + 20\log_{10} d \quad (1)$$

Where: P_L = free space path loss in dB

f = Frequency of transmitter in MHz

d = distance b/w Tx and Rx antenna in Km

From “(1)” it is clear that the path loss is directly proportional to logarithm of the distance between transmitter and receiver antennas. If we double the distance between antennas by a factor of 2, then the path loss is increased by 6 dB. By adjusting the distance between antennas we can reach to an optimum value so that the receiver doesn't go into saturation and co-location interference is made minimal.

This method is beneficial in the areas where space is not a limitation and the antennas can be separated easily. In today's environment multiple radios are installed at same place making this a difficult task. Moreover if these radios are installed at vehicles such as tanks, trucks and warships, the space is a big limitation thus making this solution unviable.

Frequency separation/planning: As can be seen in figure 1 and 2, the radios are configured in close proximities to each other. In such applications the co-location interference caused by one radio to other can be mitigated by planning frequencies in such a manner that the operating frequency of one radio is sufficiently far from the operating frequency of other radio. This will allow the radios to have a room for filtering out the received level from other radio at later stages like front end filters and crystal filters.

The above method has following limitations:

1. It reduces effective number of channels of radio as frequency separation needs to be high
2. Even if the frequency separation is implemented, the in band transmission from nearby equipment will saturate the receiver LNA due to high receive level.
3. This method can't be implemented for the radios that are working as frequency hopping radios with high hop rates in entire frequency range

CO-LOCATION INTERFERENCE AND ITS MITIGATION FOR TRANSMITTER & RECEIVER

When there are multiple radios operating in vicinity to each other, the primary problem faced by the receiver of SDR radios is Desensitization. A condition in which the receiver is unable to process a weak signal due to noise higher than its sensitivity level. When a high power transmitter is operating at a nearby location, in addition to amplify the intended signal it generates noise which may be termed as broadband noise of transmitter. When this broadband noise is high as compared to the receiver's sensitivity, the SDR radio receiver is unable to process the signal from distant radio. A condition with broadband noise dominating the receiver sensitivity [2] is shown in **Figs. 2(a) and 2(b)**. As can be seen in **Figs 2(a) and 2(b)**, the transmitter of one radio is sending signal to receiver of other radio, when the antenna isolation between these two radios is high the broadband noise due to nearby transmitter is well below the sensitivity level of receiving radio. [3][4]. In this condition the receiver can easily process the received signal. When antenna isolation is less, the broadband noise dominates the receiver's sensitivity. In such condition the receiver fails to process the received signal from remote transmitter.

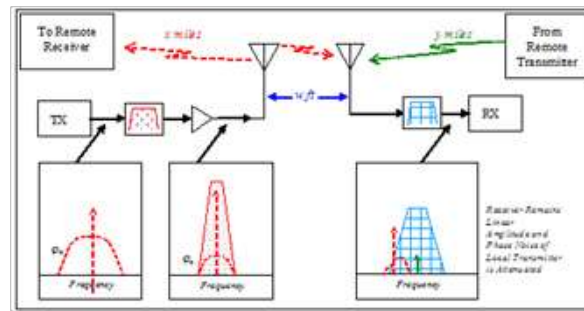


Fig. 2(a). Cosite environment for transceiver

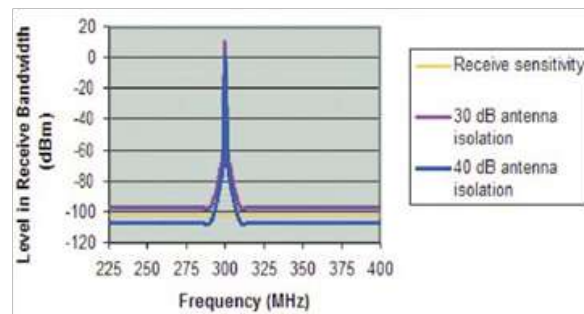


Fig. 2(b). Broadband noise effect on receiver due to antenna isolation

For example if a radio transmitter of 50W output power i.e. 47dBm is operating in close vicinity to a receiver of sensitivity of -113 dBm, the isolation between the receiver and transmitter should be minimum of 160 dB ($47 - (-113)$) for the receiver to process the received information at its sensitivity level.

To achieve above isolation the antenna distance between transmitter and receiver can be increased based on path loss calculations as described in part II of this paper. This technique is practically impossible for the applications where the antennas can't be separated physically e.g. Vehicle, Tank, Warships, Command and control stations etc. In such conditions, Selective filtering can be used to achieve the desired isolation between the two radios. Selective filtering works on the concept of band pass filtering of required signal and rejecting all other signals. Only the intended signal is allowed to pass through the filter section with a pre defined bandwidth. All other unwanted signals are attenuated from the selective filtering section.

Fig. 3 shows basic block diagram of the Integrated Co-site module that has been implemented in SDR-AFV radio to reduce the broadband noise from transmitter. In SDR applications not only receiver design should be such that it can work in co-sited environment but transmitter should also generate reduced broadband noise to make other radios work effectively.

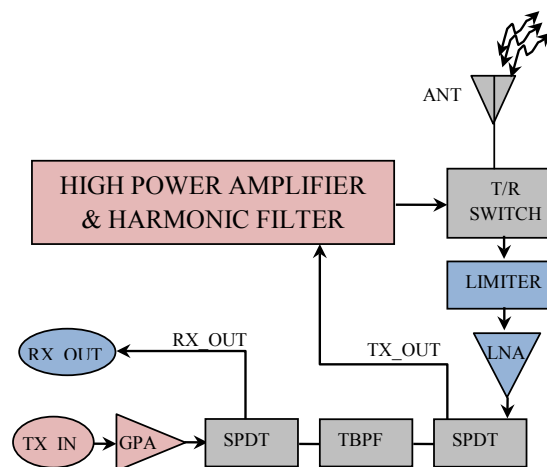


Fig. 3. Block diagram of front end module with co-site filtering

A generalized specification for the selective filter is given in **Table 1**.

Table 1. Generalized Specifications for tunable filter for co-site environments

Parameter	Value
Insertion loss	<5 dB
3 dB bandwidth	5%
40 dB Bandwidth	10%

Fig. 4 shows the response curve of selective filter section measured for SDR-AFV application in lab environment for carrier frequency of 100 MHz. This measurement is taken on vector network analyzer for standalone selective filter section. As can be seen from figure 4, the insertion loss at carrier frequency is 5.89 dB and 3 dB bandwidth is 6 MHz. The response for out of band signals is quite good (40 dB bandwidth for the signal is 74 MHz). The filter bandwidth of 5% was selected which matches with the practical result as shown in **Fig. 4**. This filter section is very effective for rejecting all signals which are different from intended frequency.

As can be seen in block diagram of figure 3, the same filter section can also be used for co-site mitigation problem in receiver chain. Let us consider that the receiver is tuned at center frequency of 100 MHz and the nearby transmitter is operating at frequency separation of 10% i.e. 110 MHz. If the receiver is receiving a required signal of -110 dBm from a distant transmitter and if selective filtering is not implemented then due to broadband noise of nearby transmitter the receiver is unable to process the information received from distant transmitter.

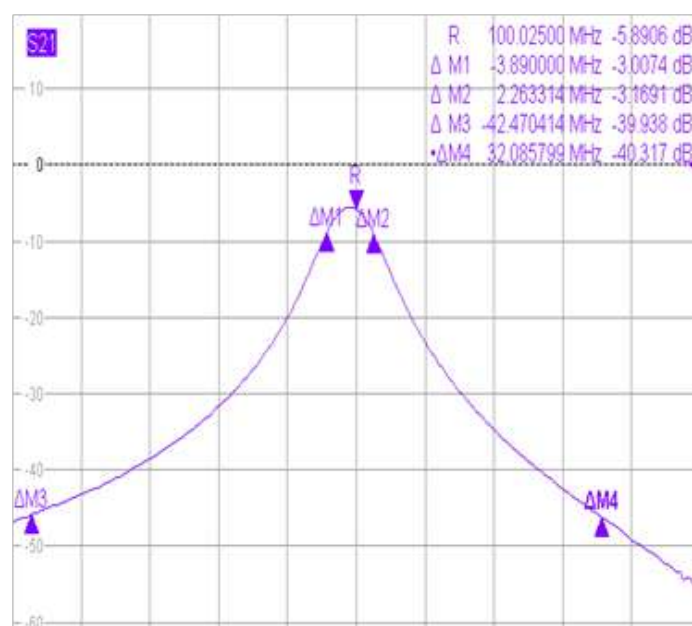


Fig. 4. Tunable filter response at 100 MHz

After implementing the selective filtering in receiver chain, the signal of nearby transmitter is attenuated by 40 dB and the receiver processes the information received from remote transmitter easily.

If more selectivity is desired then multiple selective filtering sections can be cascaded to attenuate out of band signals to the desired level. The primary disadvantage of implementing multiple filter sections is insertion loss, which can be compensated by using LNA with suitable gain profile.

SAVING THE RECEIVER FROM BURNOUT

In co-located environments the primary problem faced by the receiver LNA is excessive level from nearby transmitter. As can be calculated using “(1)” that if a 50 W transmitter is operating in vicinity of 5 m to a receiver at military vehicle, the receiver receives RF level of 16 dBm. Typical P1dB (input) value for LNA is found to be 0 dBm approx. The RF input level of 16 dBm

is too high for the receiver LNA to sustain. Thus the receiver LNA burns out due to excessive level applied at its input. To save the receiver from burnout it is necessary that some protection should be provided to receiver. An effective approach is to use limiter at the front end so that high received level beyond a specific threshold is maintained to a constant value. While selecting a limiter following parameters should be taken care of

- Frequency range
- Power handling capability
- Limiting level
- Response time
- Insertion loss

TRANSMIT/RECEIVE SWITCH & ITS ROLES

Apart from the receiver burning as discussed in part IV, it can also be saturated or damaged due to its own transmitter. When transmitter of radio is operating at high power then due to low isolation between transmit and receive port of radio, the receiver LNA can go into saturation. If the transceiver power is 50W i.e. 47 dBm and the isolation between Transmit and receive port is 30 dB, then 17 dBm power is available at the receiver port which is enough to damage the input LNA of the radio, thus in addition to limiter as discussed in part IV, the SPDT (single pole double throw) switch used for the transceiver should have as much high isolation as possible. For RF power switch, use of pin diodes is most common and high isolation can be achieved using cascaded stages of pin diode T/R switch. A basic T/R switch [5] using pin diodes is shown in **Fig. 5**. This T/R switch can be realized using few components.

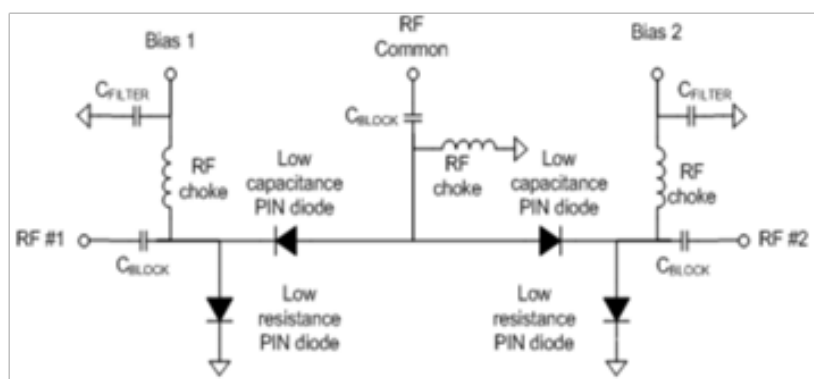


Fig. 5. basic series shunt SPDT configuration

While designing pin diode switch following parameters are taken care of

- Insertion loss:** During transmit mode, high insertion loss causes heating up of pin diodes and other circuitry. Thus designing a circuit with low insertion loss is mandatory
- Isolation:** Isolation between two ports should be as high as possible to avoid leakage of power
- Switching speed:** For high switching speed applications from tx to rx and vice versa, like SDR, high speed SPDT switch typically of order of ns or μ s should be designed

CONCLUSION

In this paper we have discussed about the co-location challenges faced in SDR radio operation in closely operated environments like AFV(tank/trucks), warships and other applications like command & control centers. The techniques like selective filtering, Limiter to save receiver burnout, High isolation T/R switch have been implemented in SDR-AFV for Indian Army. The radios were tested in rigorous and co-located environment during trials with Indian army and all radios performed without degradation in performance. The implementation of all these techniques widely improves the communication reliability which strengthens the user's operational experience.



ACKNOWLEDGEMENT

The Authors would like to thank Mrs. Prabha Goyal (GM-PK) Bharat Electronics Ltd, for her continuous support encouragement and grating permission to publish this work. Authors also like to mention the contribution from D&E team for providing all the technical support for design and realization of SDR systems. Authors would also like to thank everyone who were involved directly and indirectly involved in this work (like mechanical housing & assembly of the system)

REFERENCES

1. Zhiyao Ding, Wenwu Song, Chonghua Fang, and Yang Xu, “Suppressing cosite interference of shipboard antennas using AIC Technology”
2. Benjamin A. Culver, “Modern Co-Site RF Interference Issues and Mitigation Techniques”
3. Netcom Application note, “Co-Location Interference Mitigation; otherwise known as Cosite Mitigation”
4. Timothy A. Harrington, “Mitigating self-generated communications interference”
5. www.macom.com, “Designing with PIN Diodes: Discrete, HMIC or AlGaAs”



EMI/EMC (MIL-STD) Compliant Design for 12V/28VDC Bus to Meet Ground based Military SDR Systems

Sandeep Singla, Radheshyam Kumawat, Vikas Arora, Deepa Bajpai

Bharat Electronics Ltd, Panchkula, Haryana

✉ sandeepsingla@bel.co.in

ABSTRACT

In the era of Software defined radios, where same technology is used for all types of variants like Handheld, Manpack and Vehicular role, Military environment is the toughest form of environment. When these radios are subjected to vehicular mode of operation then more challenges are faced due to complex DC Input bus requirements for radios where multiple systems like gun, firing controls, fire mechanism of tank and all other electronic accessories share the same load. Due to all types of form factors being compatible to each other, Handheld and Manpack version SDR radios can also be used as replacement to Vehicular radio when needed. In such conditions all type of SDR form factors are required to sustain the toughest environment for reliable operation. Due to load sharing between different modules & systems and switching of reactive loads, containing a significant level of stored energy or sudden disconnection of a constant load results in surges for other equipments operating at same dc power. During engine startup of tank and firing, the voltage fluctuations are such that it may result into permanent damage to other equipment operating in the tank. The US Department of Defense created MIL-STD-1275D/E and MIL-STD-461-G to set down the requirements of electrical systems powered from a military vehicle's DC Input bus.

This paper describes the tools and techniques which can be used to save the Software defined radio from such spikes, surges and transients present at DC input bus, so that reliable communication can be established during operational life of radio. These techniques are successfully implemented in CNR MKII (SDR-AFV) radio set and reliable communication was demonstrated during rigorous testing inside T-90 tanks of Indian Army.

Keywords : SDR; MIL-STD; AFV; CNR; Surge; Spike; Transients

INTRODUCTION

Tactical communication is backbone of Military communication. For achieving reliable long range communication, apart from operational RF parameters like Transmitter power, Receiver sensitivity and environmental conditions, an important parameter is DC input bus for the radio. The power supply design of the radio should be such that it should not only introduce minimal noise into the system but save the radio from the Surges, Spikes, ESD etc. introduced into DC input bus from outside world also.

Spikes and Surges : A voltage spike is an energy-limited transient waveform having a duration less than or equal to 1 ms. These typically result from the interaction of the power delivery system wiring and switching of reactive loads or a mismatch in impedance between the wiring harness and equipment. A surge is a transient waveform having a duration greater than 1 ms and a specific wave shape, typically a rising/falling edge and a slow exponential decay for the falling edge. Surges result from the switching of reactive loads containing a significant level of stored energy or sudden disconnection of a constant load [1].

A military vehicle is a tough environment for electronics, where the potential for damaging the radio due to DC input bus fluctuations is high. U.S. Department of Defense MIL-STD-1275D/E [1] sets down the requirements for electronics when powered from a 28V supply, ensuring that electronics survive in the field. Passive components can be used for power supply surge and transient protection with disadvantages. The main disadvantage of these passive components is its bulkiness in size. SDR based communication systems are very complex as compared to traditional systems with reduction in weight and size. Also these components fail once the protection is achieved from the stringent power supply fluctuations. This requires replacement of components and reduces the availability of system in field.

In this paper, design methodology for SDR is presented for mitigating the complex DC input bus requirements. This design can

meet all types of fluctuations present at DC input bus during different stages of ground based military operation of SDRs i.e. Handheld, Manpack, Battlefield tanks and Military trucks.

Part I of this paper describes power supply challenges for ground based military SDR radios. Part II describes the modes of operation for SDR radios. Major specifications for input DC bus applicable to SDR systems are given in part III. Techniques to safeguard military SDR from complex DC bus requirements are given in Part IV and Part V, which is followed by conclusion

MODES OF OPERATION

The SDR systems operates in three types of applications viz handheld, manpack and vehicular. The most complex requirements of military SDR for DC input bus are given in MIL-STD-1275D/E. When these radios are subjected to vehicular role then there are primarily three modes of operation [1]

1. Starting Disturbances
2. Normal Mode
3. Generator Only mode

Starting Disturbances: Starting mode disturbances defines the condition where the engine is started. Starting mode disturbances are the under-voltage variations from the steady-state level and are caused by engine starter engagement and cranking. During start-up of engine and warfare events like firing from tank the DC input bus has under voltage variations known as Initial Engagement Surge (IES). During this event the 28V steady state voltage drops to as low as 6V for duration of 1 second (typical). There are other disturbances in DC input bus due to cranking in the engine which may last as long as 30 seconds. The graph of IES and cranking level disturbance is as shown in **Fig. 1**. The starting disturbance may turn off the radio during under voltage variations on input bus. Care must be taken to overcome this problem to enable reliable communication during starting disturbances.

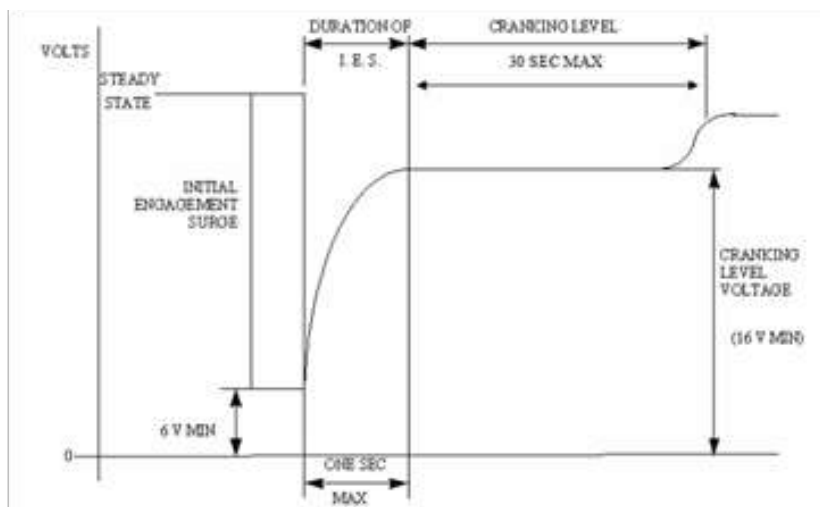


Fig. 1. Starting Disturbances as defined in US MIL-STD-1275-D

Normal Mode: Normal mode of operation is steady state operation where only inherent, natural and random changes of the system occur. In this mode both generator and battery DC supply are present. During normal mode of operation the DC input power supply has inherent surges and spikes, which may degrade the performance of the equipment.

The envelope of surges for normal mode of operation is as shown in **Fig. 2**. The surges during normal mode go to as high as 40V and as low as 18V. After the surge events the DC input bus level is maintained between 23V and 32V.

The envelope for spikes for normal mode is shown in figure 3. The spikes may go upto $\pm 250V$. The maximum energy during Spikes may go upto 15 millijoules. The duration of these spikes is 70 μs max.

These disturbances can spoil the SDR system if mitigating techniques are not implemented to safeguard the radio.

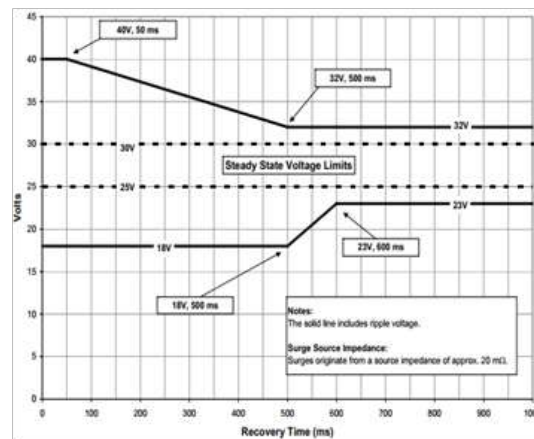


Fig. 2. Envelope of surges in normal operating mode for 28 VDC systems as defined in MIL-STD-1275-D

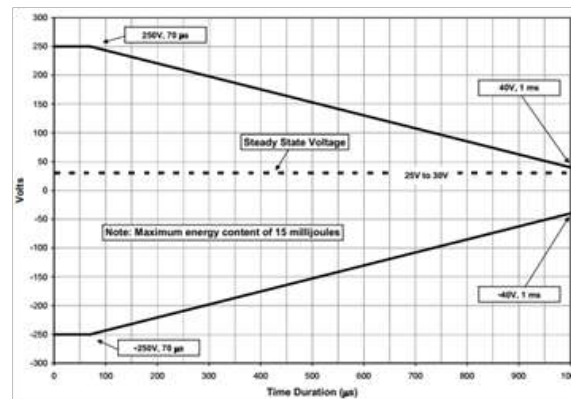


Fig. 3. Envelope of spikes in normal operating mode for 28 VDC systems as defined in MIL-STD-1275-D

Generator Only Mode: Generator only mode of operation is most challenging mode of operation. In this mode the battery of vehicle is not available for powering up the equipment, due to which all types of fluctuations introduced due to generator are sent directly to the DC input bus. The limits defined for generator only mode are very stringent as compared to the normal mode of operation. If the radio system is designed to sustain generator only mode then it can easily support Normal mode of operation for vehicular systems. The envelope for surge and spikes for generator only mode is shown in **Figs 4 and 5**, respectively.

As can be seen from **Figs 5 and 6**, that during generator only mode, the surge levels may go upto 100V while the spikes may reach upto 250V. These surge and spike levels may damage the equipment partially or permanently.

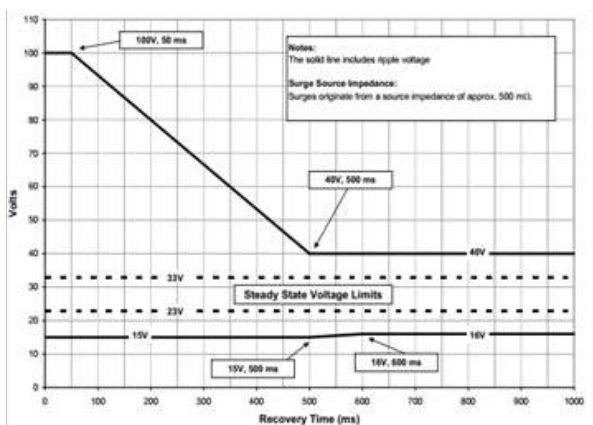


Fig. 5. Envelope of surges in generator-only operating mode for 28 VDC systems as defined in MIL-STD-1275-D

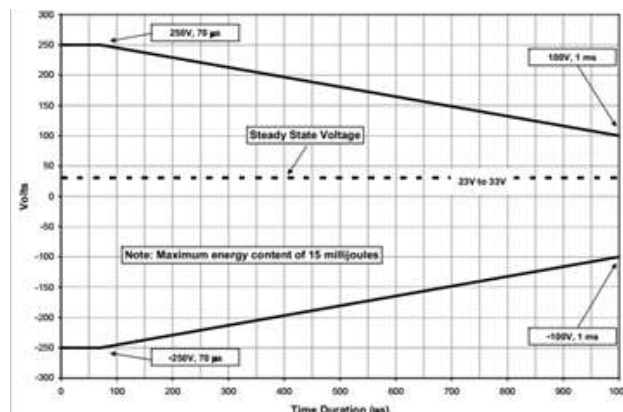


Fig. 6. Envelope of spikes in generator-only operating mode for 28 VDC systems as defined in MIL-STD-1275-D

SPECIFICATIONS FOR VEHICULAR DC INPUT BUS

Based on the requirements for ground based radio applications, Input DC bus specifications are laid down in different military standards. Vehicular radio has most stringent Input DC bus conditions as there is load sharing between different modules & systems and switching of reactive loads, containing a significant level of stored energy or sudden disconnection of a constant load results in surges for other equipments operating at same dc. Some of the critical specifications as given in MIL-STD-1275D are defined in **Table 1**.

Table 1. Specifications for vehicular radio input bus in normal operating mode and Generator only mode

Specification	Normal Operating Mode	Generator Only Mode
Steady State	25V to 30V	23V to 33V
Spikes	$\pm 250V, 70\mu s$	$\pm 250V, 70\mu s$
Surges	40V, 50ms	100V, 50ms
Ripple	$\pm 2V$	$\pm 7V$
Reverse Battery Protection	DC input current \leq Normal operating current	DC input current \leq Normal operating current

Techniques must be developed in modern SDR systems to comply to these DC input bus requirements so that reliable radio operation can be achieved. Due to all types of forms factors being compatible to each other, Handheld and Manpack version SDR radios can also be used inside vehicle, where RF output power requirement is less as compared to vehicular SDR. In such cases all specifications that are applicable for vehicular SDR also applies to Handheld and manpack SDR radios as well.

TECHNIQUES FOR COMPLYING DC INPUT BUS REQUIREMENTS FOR MILITARY APPLICATIONS

Different types of challenges are faced during radio operation in ground based applications. These challenges are specified in part II and part III in detail. The techniques to comply IES, cranking surges, spikes etc are explained here.

IES (Initial Engagement Surge) : As can be seen in **Fig. 1**, during IES the DC input bus drops to as low as 6V for 1 second. SDR systems should work without degradation in performance during this period without switching off. A simple method is to use hold up circuit using bulk capacitor that will store energy during normal operation, and restore it during power interruption [2]. A typical hold up circuit is as shown in **Fig. 7**.

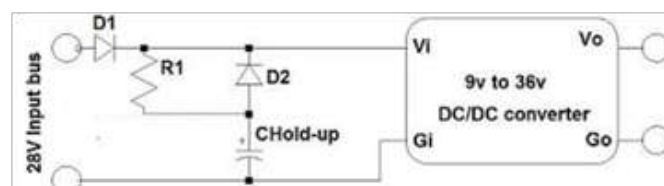


Fig. 7. Typical hold up circuit

The required C_{HOLD} value can be calculated using (1)

$$C_{HOLD} = \frac{2 \times P \times t \times 10^6}{\eta \times (V_1^2 - V_2^2)} \quad (1)$$

Where C_{HOLD} = Hold up capacitor value in μF

P = Power at load in watts

t = Hold up time required in seconds

η = Efficiency of DC-DC converter

V_1 = capacitor voltage before power drop out in Volts

V_2 = drop out voltage in Volts

For a 20W DC-DC converter operating at 28V DC bus with efficiency of 80% the required hold up capacitor value is 66845 μF . It is practically impossible to use such bulky capacitors in SDR applications. Also the In-rush current requirement of such bulky capacitor becomes very high which adds on another limitation. To mitigate this problem Hold up circuit is developed and used for SDR-AFV.

Surge/Spike/ESD protection: The most difficult form of surge and spikes are observed during generator only mode. The spikes are as high as 250V and surges are 100V. Although the level of surge is 100V, but this is more challenging as compared to 250V spikes due to its duration of existence. 250V spikes are present for a very small duration of 70 μs , while 100V surge is present for 50 ms which can damage SDR radios permanently.

Apart from surge and spikes present at DC input bus, ESD can also damage the equipment. Typical Surge waveform due to lightening and ESD are shown in **Figs 8 and 9**.

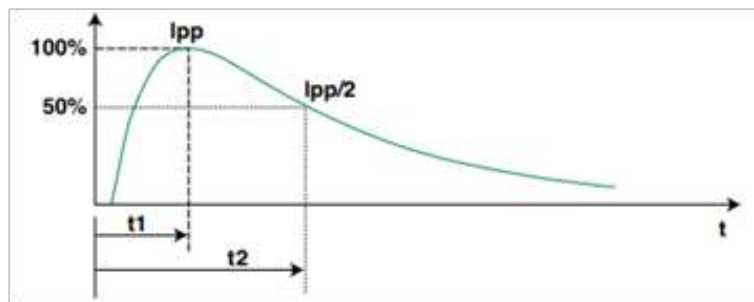


Fig. 8. Typical surge waveform due to lightening

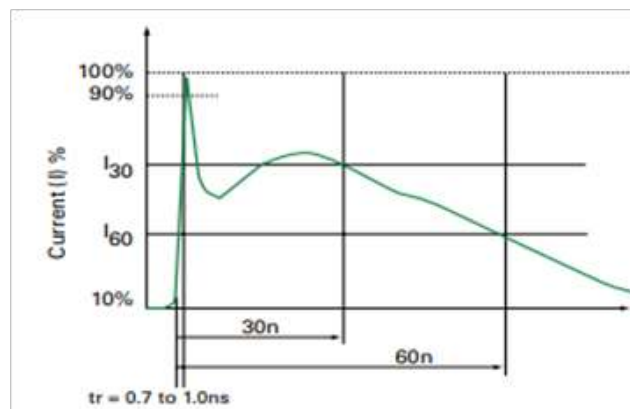


Fig. 9. Typical ESD waveform

The rise time (10% to 90%) of the surges due to events like lightening is of the order of 10 μs . The total duration of surge is of

order of 1000 μ s. This waveform is normally written as 10/1000 waveform. For ESD events the rise time and total duration becomes order of ns.

For vehicular DC input bus, the spike levels of ± 250 V are present for 70 μ s. Protection from all these transient events can be achieved by using MOV (Metal Oxide Varistors) or TVS (Transient Voltage Suppressor) diodes. TVS diodes are faster than MOV. While MOV has higher clamping voltage level, the properties degrade with time. Thus by defining the values for breakdown voltage, clamping voltage and energy of transient waveform suitable TVS diode can be used.

For protection from 100V/50ms surge, the selection of TVS diode should be such that the energy can be dissipated in diode itself without damage

The energy which is absorbed by the diode is given by [3]

$$E = \int_0^{t_p} V_c I_p dt = K V_c I_p t_p \quad (2)$$

Where

E = Absorbed energy in Joules

V_c = Clamping voltage in volts

I_p = Peak pulse Surge current in Amps

t_p = impulse duration

K = constant (0.5 to 1.4 for different transient waveforms)

The value of K is 0.5 for the rising part of waveform shown in figure 8 and 1.4 while decaying part. From eq 2 the energy absorbed by a suppression diode can be calculated for a given transient waveform.

While deciding clamping voltage for suppression diode one must be careful about the operating temperature for the equipment. The Clamping voltage for a TVS diode varies with temperature and is given by

$$V_{CT2} = V_{CT1} \times [1 + \theta_c \times (T_2 - T_1)] \quad (3)$$

Where

V_{CT1} = Clamping voltage at temperature T_1

V_{CT2} = Clamping voltage at temperature T_2

θ_c = Temperature coefficient per $^{\circ}$ C

For a TVS diode with clamping voltage of 59.8V at 25° C the new clamping voltage at 85° C becomes 63.4V using equation (3) for a θ_c of $10^{-3}/^{\circ}$ C. Thus for application requiring clamping voltage less than 60V, the TVS diode may seem suitable at 25° C, but while considering the operating temperature requirements the Clamping voltage may not be suitable to protect the circuitry.

Thus it is a good practice to devote time and make calculations for selecting TVS diode as circuit protection as the energy during ESD and lightening is quite high.

Reverse battery protection: The reverse battery protection can be given using Schottky diode in series mode. The primary disadvantage using diode in series is voltage drop and power dissipated in diode. For a Schottky diode with a voltage drop of 0.5V with equipment current of 5A, the power consumption in diode is 2.5W. Alternate solution for this problem can be P-Channel MOSFET [4] in a configuration as shown in Fig. 10.

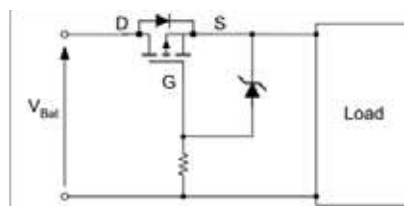


Fig. 10. Reverse battery protection using P channel MOSFET

While selecting P channel MOSFET for SDR applications, RDS and maximum current calculation should be taken into account for determining the drop across MOSFET device. The P channel MOSFET considered here [5] has RDS(ON) value as 11m Ω to 16 m Ω . Thus for an application requiring 5A current and 16 m Ω resistance dissipates as less as 0.08W, much lesser than a schottky diode. The P channel MOSFET solution has better efficiency. The zener diode is connected at Source of P channel MOSFET to protect MOSFET in case of DC input voltage beyond permitted VGS (Gate to Source voltage)

Steady State operation: Steady state operation requirements for ground based SDR systems vary between 23V to 33V for 28VDC systems. Many times primary source of DC supply is not available. The radio may be required to operate at lesser voltage levels e.g. 12V/18V/24V etc. For complying to such scenarios, design of power supply should be such that it should cover entire range of possible DC input bus requirements. For SDR systems design of power supply for 9-36V DC input bus is a good choice which can sustain the steady state requirement of 23V to 33V without any degradation in performance.

TECHNIQUES FOR COMPLYING DC INPUT BUS REQUIREMENTS FOR MIL-STD-461G

MIL-STD-461 is one of oldest standard developed by US department of defence. This standard defines the requirements of EMI/EMC specifications for any radio used for military operation. The requirements of MIL-STD-461G are listed in table II for Ground army application [6].

Table 2. Applicable requirements for ground, army equipments for MIL-STD-461G

Requirement	Description
CE102	Conducted Emissions, Radio Frequency Potentials, Power Leads
CS101	Conducted Susceptibility, Power Leads
CS114	Conducted Susceptibility, Bulk Cable Injection
CS115	Conducted Susceptibility, Bulk Cable Injection, Impulse Excitation
CS116	Conducted Susceptibility, Damped Sinusoidal Transients, Cables and Power Leads
CS118	Conducted Susceptibility, Personnel Borne Electrostatic Discharge
RE102	Radiated Emissions, Electric Field
RS103	Radiated Susceptibility, Electric Field

The power supply design can be done with an additional filter having good response from 10 KHz to 10 MHz at input of DC-DC converter. The susceptibility related requirements can be fulfilled using the methods given in part IV of this paper.

In addition to proper part selection, grounding and layout plays an important role for reducing the noise in the system. If the part selection w.r.t. quality and reliability is carefully done and PCB design does not consider grounding and layout, all effort comes down to zero. It is important that the loops should be minimized and separate ground planes to be given for dc-dc converter input and output isolation. A typical grounding method is as shown in Fig. 11.

The isolated ground can have coupling capacitor connected between both planes and decoupling capacitors shall be placed at all DC input and output bus. Common mode capacitor network should be placed to reduce noise. An additional filter at output should be used to reduce ripple and noise entering in the system to achieve better sensitivity of SDR receiver.

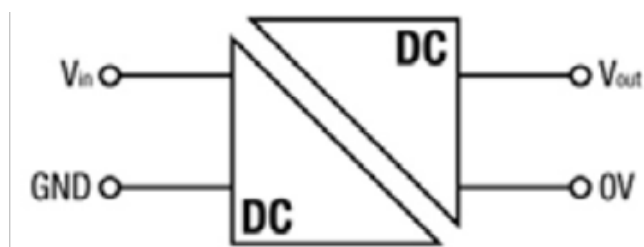


Fig. 11. Ground isolation for DC-DC converter

CONCLUSION

In this paper we have described the challenges that are faced at DC input bus for ground based SDR systems. The requirements and techniques to comply to those requirements are discussed in detail. These all methods are implemented in SDR-AFV radio



developed by Bharat Electronics Limited and demonstrated in field as well. The radios were subjected to harsh environment of Military tanks and TG (Truck/Ground) applications in field and all radios performed as per the requirements. A single form factor SDR is not limited to its intended use only, it can be used for other applications due to its flexible nature, thus it is always better to implement vehicular requirements into handheld/manpack radios to make it flexible for use in any environment.

ACKNOWLEDGEMENT

The Authors would like to thank Mrs. Prabha Goyal (GM-PK) Bharat Electronics Ltd, for her continuous support, encouragement and grating permission to publish this work. Authors also like to mention the contribution from D&E team for providing all the technical support for design and realization of ground based SDR systems. Authors would also like to thank everyone who were involved directly and indirectly involved in this work (like mechanical housing & assembly of the system)

REFERENCES

1. US Department of Defense, "MIL-STD-1275D/E".
2. Steve Taranovich, "Managing hold up/ transparency time in high reliability power supplies" edn.com.
3. Semtech, "SI97-02, Surging ideas TVS diode application note".
4. Marco Pürschel, Infineon "Automotive MOSFETs Reverse Battery Protection".
5. Datasheet of IPB110P06LM.
6. US Department of Defense, "MIL-STD-461G".



Design and Development of Forced Air Cooled Dip-brazed Chassis for Safety Critical Electronics

Prashant¹, A Karthikeyan²

Dy.Manager¹, DGM PDG/D&E- Avionics, EW&A SBU², Bharat Electronics Limited, Bangalore

✉ karthikeyana@bel.co.in

ABSTRACT

In this paper, Design and Development of forced air cooled Air Transport Rack (ATR)chassis is represented. This design of dip-brazed ATR chassis was taken up to avoid dependency on foreign OEM. There are 20 Nos of plug-in type electronics cards inside the chassis namely power supply, analog, digital cards etc. In ATR dip-brazed Chassis, individual electronics modules are often conduction-cooled to the side walls of a chassis, where heat from the module edges is dissipated to cooling air forced through finned wall ducts. This arrangement can provide a sealed compartment to protect the electronic components from various environmental factors (moisture, dust, sand, salt, etc.) while efficiently rejecting heat to platform-delivered cooling air. Overheating conditions could significantly affect the performances and durability of electronic devices. Design of a chassis with the given geometrical and thermal constraints starts with generation of the three dimensional (3D) model. Then, thermal analysis of 3D model is conducted to determine if the given heat loads can be dissipated. According to results, geometry and material of 3D modal is updated to reach optimum cooling solution. Advanced cooling solutions can reduce thermal stresses and provide the capability to both improve system reliability and accommodate higher performance components.

A study explores chassis-level air cooling limits for ruggedized military electronics enclosures constrained by pressure drop requirements and fin manufacturing capabilities. Numeric and analytic models are developed and used to define a methodology for optimizing the geometry of longitudinal folded fins included in side wall ducts to maximize the amount of heat that can be dissipated from an air-cooled chassis. To minimize the weight and enhance EMI shielding of the equipment, an aluminium dip-brazing process is used for manufacturing of chassis. Brazing process is validated using Test specimen as per standard to obtain a safety margin of critical brazed joints and validation of thermal model reduces the cost of prototype for similar chassis design projects and also reduces certification process by using analysis results to compliance to MIL-STD-810 structural and thermal requirements without any real test systems.

Keywords : ATR chassis; Thermal/CFD analysis; Dip-brazing; Validation.

INTRODUCTION

Present Electronic Product Designs for airborne EW \ Avionics applications are driven to meet stringent weight and size restrictions. Heat dissipations from the electronic components/modules are steadily increased, which leads to efficient method of electronics cooling. In today's scenario the electronic equipment must function within wide variations in ambient temperature or withstand harsh environmental conditions. Often these systems are sealed to protect against contaminant ingress and other heat source nearby. Based on the failure statistics, more than 50 percent of electronic product failures are caused by thermal-related effects. Therefore, a sound thermal design is vital to ensure high product reliability [1]. At the same time, the airborne EW \ Avionics electronic equipment is required to work in the high vibration environment for airborne application.

The traditional methods of solving the complex problems analytically holds well to provide qualitative understanding of the system behavior; however, experience shows that for the most practical problems faced by engineers, analytical solutions are barely available. Therefore, the use of numerical methods to solve the mathematical models associated with complex structure has become an essential ingredient in the design process. In order to meet product/customers' requirements and to build quality, reliability in product during the design stages it has become imperative to evaluate the design before the actual production takes place [2]. Evaluating the design at this stage reduces the overall cost in terms of time saves: number of prototypes made and elimination of design errors. It also provides opportunity to evaluate/consider alternate design approaches and arrive at the optimum design using tools like Thermal & Structural simulation tools.

DESIGN OF AIRBORNE ELECTRONIC CHASSIS

Airborne electronic Chassis is a double walled air-cooled with one long ATR size. The primary mode of cooling the electronic equipment is forced air convection. Cooling of the internal SRU's is accomplished by forced convection in the heat exchangers located in the side of the internal walls. These folded fins are incorporated in the side wall ducts to maximize the amount of heat that can be dissipated from an air cooled chassis. ECS Cooling air enters at the rear of the chassis through dedicated channels. Further, cooling air is spliced and guided in to the folded fin heat exchangers on both the side walls with minimum pressure drop. To minimize the weight of the chassis, a dip-brazing manufacturing process is adapted. The advantage of dip-brazing process is very thin sections can be joined together to form assembled part with minimum weight. The metallic portions between the four channels of the Airborne electronic Chassis consist of solid aluminium plates dip-brazed to the sides of the chassis, these partitions are provided for thermal/electromagnetic isolation between the channels [2].

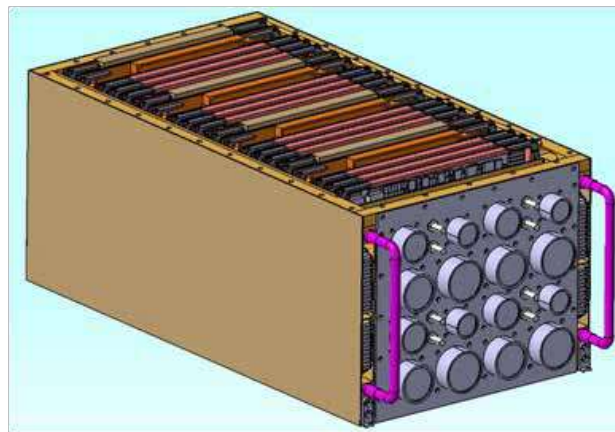


Fig. 1. CAD model of chassis

THERMAL ANALYSIS

The equation that mathematically describes general fluid motion governs conservation of mass (continuity), momentum (Newton's second law) and energy (First Law of thermodynamics). The Navier-Stokes equations are a special form of the momentum equations for Newtonian viscous flows. These non-linear, second order, partial differential equations form the mathematical foundation of viscous flow theory and CFD. An analytically derived "exact" solution to a flow problem would yield a continuous description of the field variables (i.e. the velocity components, pressure and temperature) throughout the region of flow. However the equations of fluid motion are highly non-linear, and closed-form solutions exist for only a handful of idealized cases. Instead the designer must rely on computer-based flow simulation models that calculate approximate values of the field variables at discrete points in the flow. Solutions for complex flow of engineering importance are possible only through the numerical techniques of CFD.

A CFD computer model represents a geometric region of interest called a fluid-domain, whose flow condition are known or assumed at its boundaries and whose detailed internal flow characteristics are sought. A fluid domain may be characterized as either an internal flow within solid walls or an external flow around the immersed bodies.

Finite Element CFD modeling requires the fluid domain to be discretized, i.e., spatially subdivided into a computational mesh consisting of individual elements interconnected at nodes.

Boundary Conditions

The CFD analysis evaluated the thermal performance of the chassis while operating under normal forced air cooling condition, the loss of cooling and trouble conditions without cooling air flow in variant ambient environment.

The primary mode of cooling the chassis is forced air convection. Cooling of the internal SRU's is accomplished by forced convection in the heat exchangers located in the sides of the internal walls. These efficient extended surfaces consist of 15 fins/inch. The mode of heat transfer internal to the chassis is primarily conduction. The heat from the component is transferred to the thermal ladder mounted on the PCBs. These thermal ladders are in contact with the chassis wall and thus heat is transferred to the walls. Externally the heat transfers from the chassis surface to the ambient air is by convection.

Table 1. Heat generation values of various modules

Module	Channel 1 (Watts)	Channel 2 (Watts)	Channel 3 (Watts)	Channel 4 (Watts)
Module 1	6.3/10.3	6.3/10.3	6.3/10.3	6.3/10.3
Module 2	8.7	8.7	8.7	8.7
Module 3	8.7	8.7	8.7	8.7
Module 4	8.11	8.11	8.11	8.11
Module 5	23.73	23.73	23.73	23.73
TOTAL	65.84	65.84	65.84	65.84

- a. Thermal analysis of Airborne electronic unit has been carried out under the following Test cases:-
1. Cooling air flow of 16.6g/s at 15°C till system reaches steady state at an ambient temperature of 71°C.
 2. Cooling air flow of 13.2g/s at -10°C till system reaches steady state at an ambient temperature of 71°C.
 3. Cooling air flow of 16.6g/s at 15°C till system reaches steady state and then cooling air cut off for 1 hr. at an ambient temperature of 71°C.
- b. The material property of the various components considered for analysis-
1. Chassis – Al alloy 6061-T6
 2. Folded fin Foam – Al alloy 1100-0
 3. Heat Sink/Thermal ladder– Al alloy 6061 T6
 4. Card Retainer – Al alloy 6061-T6
 5. PCB: 14 layer PCB with Polyimide as base material

Method of Modeling

3D CAD model of different concepts were taken in to CFD software. Flow volumes were created separately for all the developed concept models. Material properties for SRUs and chassis were provided. Heat dissipation on individual SRUs was applied and the total heat dissipation of airborne electronic unit is 264.3 Watts.

CFD Result and Discussion for Thermal Analysis

Case 1: Cooling air flow of 16.6g/s at 15°C till system reaches steady state at an ambient temperature of 71°C.

The above mentioned condition was simulated using the analysis software - Flow Therm and the behavior of the chassis was studied.

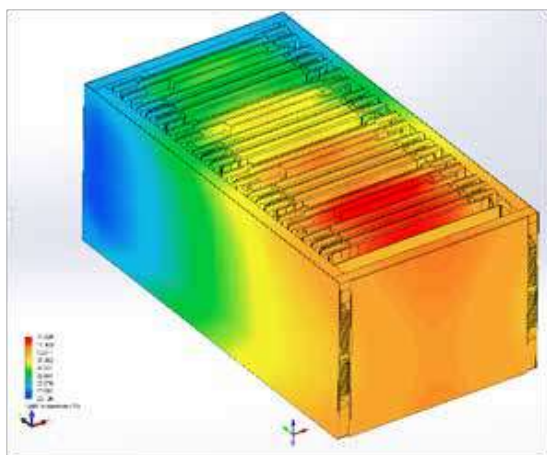
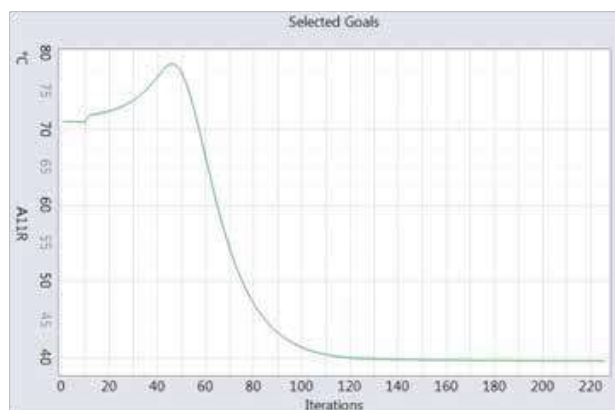


Fig. 2. Temperature distribution inside chassis during steady state analysis



Graph 1. Guide rail temperature profile for case 1.

Case 2: Cooling air flow of 13.2g/s at -10°C till system reaches steady state at an ambient temperature of 71°C.

The above mentioned condition with calculated heat transfer coefficient was simulated using the analysis software - Flow Therm and the behavior of the chassis was studied.

The maximum temperature observed in this case came in CH1. The steady state value is 32.9°C.

Case 3: Cooling air flow of 16.6g/s at 15°C till system reaches steady state and then cooling air cut off for 1 hr. at an ambient temperature of 71°C.

The maximum temperature observed in this case came in CH3 and the value is 110.2°C.

The above mentioned condition with calculated heat transfer coefficient was simulated using the analysis software – FlowTherm and the behavior of the chassis was studied. The above three cases indicates maximum card temperature of 110.2°C which is well below the Junction temperature of electronic components.

STRUCTURAL ANALYSIS OF AIRBORNE CHASSIS

ATR chassis is made of several parts that are brazed together to form single entity. The dip-brazing of the parts allow less use of fasteners during assembly. The main load carrying members of the chassis are left plate, right plate, intermediate plate and block. These parts are made of AL Alloy. The outer covers are not load carrying members hence they are made of clad sheet. The chassis can accommodate 20 SRUs and are divided into 4 identical channel. At each channel support is provided for the Motherboard PCB through divider plates made of Al Alloy. The chassis is forced convection cooled and for that purpose cooling fins are brazed on the left and right plate, material AL Alloy. The cooling fins are aligned horizontally and have air entry from rear (since the air inlet provision in the aircraft is from rear). The cooling air enters from rear and passes through the fins, absorbing the heat, and finally exits from front. This chassis is designed to dissipate 264W approx. of heat generated from cards. The chassis has 2 handle at front, ergonomically designed for lifting. It has 2 locating cup at rear, made of stainless steel, for aligning to the aircraft tray and 2 J-hook at front to lock to the tray. The j-hooks are made of forged steel material.

FE MODELING

Finite Element model created using shell elements from surfaces extracted from 3D model. To establish a proper connectivity between the surfaces adaptive meshing was used. The number of elements was decided based on the edge length and nodes are uniformly distributed. Lumped mass elements were used to represent the printed circuit board mass at specific locations. Rigid elements were created to represent the connection between the motherboard and printed circuit boards. Grouping of elements and nodes were done for easy access of FE model for any modification of elements/node properties. Combination of auto mesh and manual mesh has been taken with 'tria' and 'quad' elements. The total numbers of elements are 82510 with 100450 nodes. The individual FE models were connected and created the complete finite element assembly of the airborne electronic unit. Physical properties for different elements were created and appropriate material properties were assigned to each group of elements. Shock loads are applied at base to simulate the actual condition. Final meshed model for analysis is shown in fig.3 below. Quality index is checked for accurate results and errorless FE analysis.

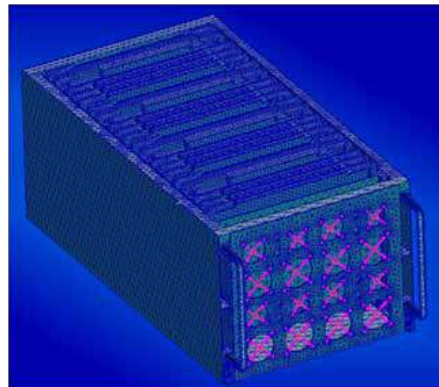


Fig. 3. F E model of an airborne electronic equipment

PRINCIPLE OF MODELLING

- The Finite Elements software used for F E modelling is MSC/Patran.
- Side panels, top , bottom cover, front panel, rear panel, side covers & partition plates meshed with TET elements.
- Bolt connections are modelled with BAR & RBE2 elements.
- Weight modelled as CONMASS elements.

NORMAL MODE ANALYSIS

Normal mode analysis was carried out with locating cup & J-hook were fixed boundary conditions.

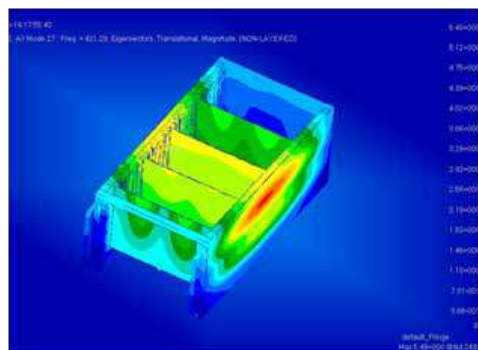


Fig. 4. Natural Frequency of Airborne Chassis 421 Hz

ACCELERATION ANALYSIS

Linear static analysis was carried out with inertial load applied in all 6 direction and locating cup & J-hook was fixed boundary conditions.

Table 2. Acceleration analysis result

Sl. No.	Load Direction	Acceleration (in 'g')	Stress (MPa)
1	Fore	6	20.1
2	Aft	12	40.3
3	Right	6.75	37.3
4	Left	6.75	37.3
5	Up	15.75	33.2
6	Down	12.75	43.6

VALIDATION OF DIP-BRAZING PROCESS

Evaluation of strength margins in structural components is a normal practice used in the design of metallic and composite structures. Mechanical, welded or adhesively bonded joints in such structures are routinely assessed for their load carrying capabilities in accordance with widely accepted engineering analysis techniques and failure criteria. Establish brazed joint allowable by testing the standard test specimens described in the AWS C3.2 specification under near pure shear and tensile loads. The brazed joints in this study were comprised of standard aluminum material dip brazed with AWS standard filler metal for aerospace application [2].

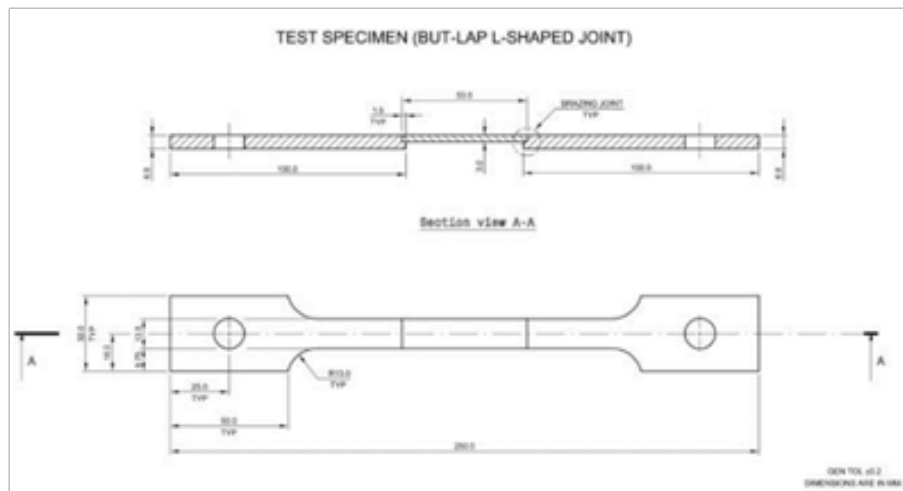
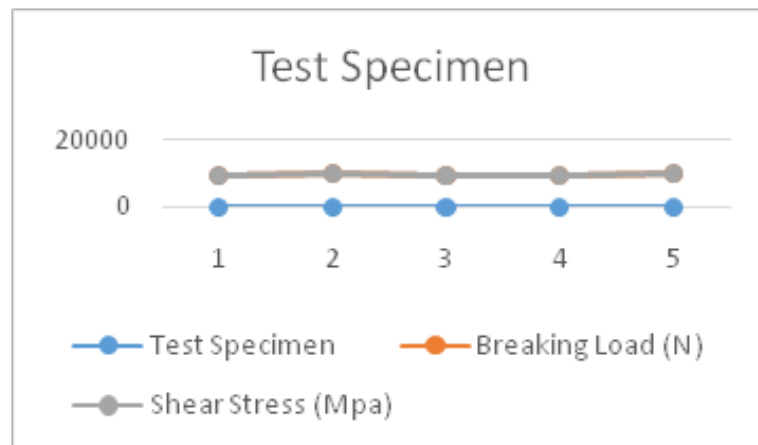


Fig. 5. Test coupon as per AWS standard

Test Result



Grpah 2. Test specimen validation plot

SUMMARY AND CONCLUSION

Design analysis of forced air Cooled dip-brazed Chassis for safety critical electronics has been presented. Design verification was completed by this simulation process using Flow-therm and MSC/Nastran Software. The integrated modelling methodology involves system level Computational Fluid Dynamics) CFD/ Computational Heat Transfer (CHT) simulation and Structural Analysis simulation. The temperature plots of the various Printed Circuit Boards, the temperature profile of the cooling air and the flow pattern of the cooling air was taken and studied. From these it was found that the temperature of the Printed Circuit Boards on which components will be mounted were well below the operating temperatures. Also it was found that inertial stress due to acceleration loads are much lower than the yield strength of the parent material. The Validation of Test specimen as per AWS standard was carried out and it is found quality of brazed joints are superior. The clearance was provided for manufacture



of prototype unit for design validation. The test results on the prototype unit were within the simulation results. Based on this the engineering design was qualified for bulk production of the airborne electronic equipment. Also successfully flight trials was completed with Indigenized chassis and CEMILAC clearance was obtained for service aircraft usage.

ACKNOWLEDGMENT

The authors would like to thank all those individuals who volunteered their time and/or resources to help carry out this work. Also special thanks to our Divisional and Business Unit heads for their encouragement support.

REFERENCES

1. Troscinski mark and Guangnan Jiang, “FLOTRAN chills out hot Aerospace Electronics” ANSYS Solutions Vol4, No2, April 2002.
2. Karthikeyan A, Product Design of Flight Control Computer using DFSS tools, Second International Conference on Electronics Warefare, EWCI-2012.
3. Hari Narayanan and SooBengKhoh, Deploying Design for Six Sigma in New Product Development, IEEE ICMIT 2008.
4. [Rohit Dev Gupta, “Integrated Thermal Analysis of An Airborne Electronic Package”, I-DEAS User conference 2006.
5. Thermal performance maps for forced air cooling of ruggedized electronics enclosures, Jesse vanengelenhoven and Gary L. Solbrekke, IPACK2007.
6. Rudhiramorrthy A, “Flow & Thermal analysis of an Avionics Computer system using I-DEAS ESC”, I-DEAS User conference 2006.
7. Evaluation of Margins of Safety in Brazed Joints, YuryFlom, Len Wang, Mollie M Powell NASA / Goddard Space Flight Center, Greenbelt, Maryland Jesse Vanengelenhoven, gary L solbrekken and Karl J L Geisler,
8. “Thermal Performance maps for forced air cooling of ruggedized electronics enclosures”, ASME, IPACK 2007.
9. Flowtherm 2018 user manual.
10. MSC\Nastran 2016 Advanced dynamic User’s guide.



Low Power ADC Design for Biomedical Implantable Devices

Aneesh K, Manoj G

Department of Electronics and Communication Engineering, Karunya Institute of Technology and Sciences, Coimbatore, Tamilnadu

✉ aneeshk.anj@gmail.com

ABSTRACT

Implantable biomedical devices play a vital role in acquisition and monitoring of critical biophysiological signals in the human body. Since these devices are in contact with critical organs, the reliability of the system is having great importance. The energy efficiency of the system has a direct impact on reliability. These devices are powered by non-rechargeable batteries which are also implanted in the body. It is found that, if the system draws more energy for operation, the battery drains faster. This leads to untimely failure of the system. Amongst the various blocks in a physiological signal monitoring system, ADC (Analog to digital convertor) operation contributes more to the power consumption. This paper discusses different low power techniques and methodologies to make the ADC more energy efficient.)

Keywords : Implantable devices; ADC; Capacitive DAC; Physiological signal acquisition; leakage power; comparator.

INTRODUCTION

The implantable microsystems like cardiac pacemaker, ICD (implantable cardioverter defibrillator)[1], cochlear implants, visual prosthesis systems, neural simulators have gained importance in today's world, since they all deal with the critical biophysiological signals. These devices are implanted in the body by surgical means. A constant monitoring of critical signals is being done by these devices and it should be active all the time. Each of these devices are powered by a non-rechargeable battery embedded in the system. The life of the battery directly depends on the energy efficiency of the device. A less efficient circuit draws more power and this leads to the sudden depletion of the battery. Frequent replacement of the battery is not advisable since it can only be done with surgical procedures. This is not only costly but also infectious to the patient. Recent studies show that, analog front-end design of such devices consume more power. The various blocks in a bio signal monitoring system are shown in Fig. 1.

Amongst these blocks, ADC (Analog to digital convertor) is found to be the major power dissipator[2]. Many types of ADC's are proposed in the past literatures like Flash type ADC, sigma- delta ADC, dual slope ADC, Pipelined ADC etc. The bio medical devices, which are discussed in this paper are dealing with electrical activities from the critical organs.

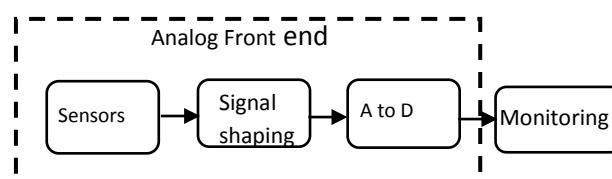


Fig. 1. Block diagram of physiological signal monitoring system

These signals are having less amplitude and they fall in low frequency spectrum (low variation). The SAR ADC with moderate speed is suitable to handle physiological information.

$$P_{\text{dynamic}} = \alpha_{\text{act}} CV^2 f \quad (1)$$

The "Equation (1)" validates the idea discussed before. Here in "(1)", α_{act} is the switching factor, C is the capacitance in the design, V is the supply voltage and f is the frequency of operation. P_{dynamic} is the dynamic power consumption in the circuit. By reducing the operating frequency, the dynamic power reduction can be achieved[3]. Thus, usage of SAR ADC with a moderate

speed helps to limit the dynamic power consumption. Moreover, in SAR ADC, all the building blocks except comparator are digital in nature. This enables the designer to incorporate advanced CMOS technology in the design, and this further contributes to the low power. The basic block diagram of an SAR ADC is shown in Fig. 2. It is made up of capacitive DAC array, sample and Hold circuit, comparator and SAR logic. The unnecessary power dissipation of each of these blocks are to be capped to propose an efficient design. Out of these major blocks, the switching dissipation in the CADC array is mainly discussed and different methods for an energy efficient technique are analyzed in this paper. This is involved in reducing “ α_{act} ” (switching activity) of the CADC array. The sample and hold arrangement are used to sample the input signal to the comparator. MOS (Metal oxide semiconductor) transistors are used as switches. The size of these switches can be kept minimum by adopting new CMOS design technologies. But the sub-micron design techniques are suffered by high amount of leakage current through it. “Fig. 3” explains the leakage mechanisms.

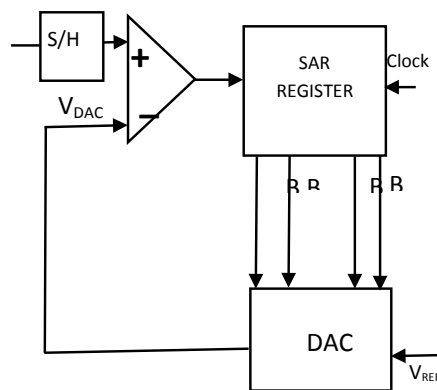


Fig. 2. Block diagram of SAR ADC

Factors to be Considered for Switch Design

Even though the switch is closed during the hold operation, output node is connected to the input side through two parameters. The first one is the drain-source leakage (modelled as R_{leak}). This is getting worse with technology scaling. The other parameter is the drain to source capacitive coupling (modelled as CC). Due to this, output voltage of the switch is degraded even when the switch is closed.

In low speed ADC, the switch leakage is a significant factor and it degrades the system performance. Another problem that is associated with the sampling switch is the charge injection. It is a leakage mechanism due to injection of charges from the channel region to both input and output sides of the switch. In this the charge injection to the output side leads to significant changes in the output voltage. This leads to nonlinear errors[4]. These effects are shown in figure 3 and figure 4. The techniques which are used to avoid these problems are

- 1) Stacked transistor arrangement to reduce the leakage current [5]
- 2) Dummy transistor arrangement to mitigate charge injection problem[6]

The above-mentioned techniques not only reduce the leakage current, but also helps to impart linearity to the switch operation.

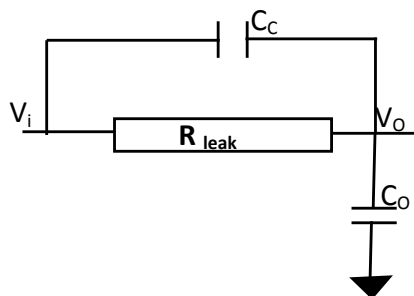


Fig. 3. Leakage mechanism in CMOS switch

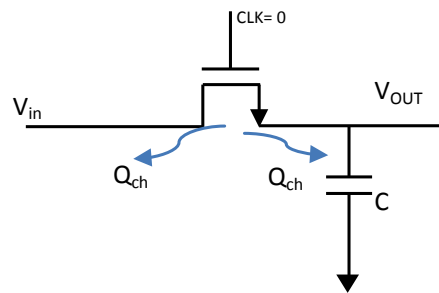


Fig. 4. Leakage mechanism in CMOS switch

This helps to avoid switch induced non linearity and offset errors. From the above discussions, it is clear that additional components or slight modifications of the conventional architecture is required for achieving power efficiency. The stacked transistor arrangement is shown in **Fig. 5**. The down side is that, it may increase the design complexity and size of the device. Hence care must be taken, in selection of the additional circuit to be incorporated. Simple and effective design is preferred in low power applications. More investigations can be done in this context.

Importance of Capacitive DAC array and Switching energy dissipation

From various literatures, it is evident that CDAC block consumes large amount of power. It consists of switches and capacitors. The values in the capacitors are updated according to the output of comparators. This involves many switching sequences to achieve the correct conversion. The relation between the switching activity and the power dissipation is given in (1).

The inevitable switching in CDAC makes it more vulnerable to dynamic power consumption. Thus, an energy efficient architecture and switching schemes are having paramount importance in DAC design. Two basic architectures available for DAC's are given below.

1): Binary weighted Capacitive array DAC: This is the conventional architecture for DAC. The capacitors in the array are controlled by the signals from the SAR logic. The values in the capacitors are updated accordingly (via charging up to supply or discharging to ground). This design is prone to high switching power dissipation[7].

2): Split Capacitor array DAC: This is a modification over the binary weighted capacitor array. Here the capacitive array is segmented in to M bit MSB (most significant bit) array and N bit LSB (least significant bit) array. The number of unit capacitors in this architecture is found to be lesser than the conventional architecture. This reduces the size and power consumption of the block. This is a more suitable architecture in low power design[8].

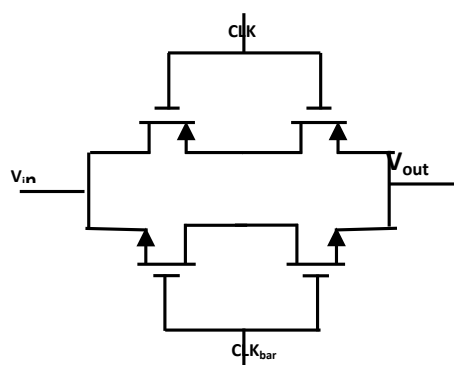


Fig. 4. Stacked transistor techniques for switches

$$E_S = CV_{ref}^2 \quad (2)$$

$$E_{stepwise} = C V_{ref}^2 / S \quad (3)$$

The various switching strategies adopted for CADAC array are listed below

- I) **Stepwise Charging:** The energy required (E_s) for updating the value of a capacitor is given in (2). The energy is directly proportional to capacitance (C) and the reference voltage (V_{ref}). The switching energy can be reduced by scaling down the voltage and the capacitance. But this may degrade the performance of the circuit. An alternate solution is enumerated in (3). In this, the capacitors are being charged in different steps[9]. This step wise charging reduces the overall switching energy dissipation by a factor (S).
- II) **Charge recycling:** It is an effective method to mitigate the switching energy dissipation in capacitive array. In this, the discharging current from one capacitor is used to charge another capacitor[8].
- III) **Hybrid Techniques:** In this method, more than one switching strategies are combined together to achieve better power performance[10]. But this may increase the circuit complexity. This problem can be nullified by combining energy efficient switching scheme with area efficient strategies (capacitor split architecture is combined with area efficient segmentation technique).
- IV) **Tri level Switching:** As shown in (2), the switching energy dissipation depends on V_{ref}

$$V_{ref} = \frac{V_{cm}}{2} \quad (4)$$

In this technique, V_{ref} (reference voltage) is selected as the half of the input common voltage (V_{cm}). This leads to considerable savings in switching power dissipation[11].

- V) **V_{cm} based Switching:** The V_{cm} is derived to be half of the reference voltage (V_{ref}). This architecture saves 97.66 % of switching energy[12]. The voltage V_{ref} is considered as positive reference and input common mode voltage V_{cm} is taken as negative reference in this case. Moreover, as per published literatures, this scheme offers better area efficiency, since it achieves 75% reduction in total number of capacitors, compared with the conventional design.
- VI) **Charge dumping switching scheme:** This scheme is superior to the previous techniques, in terms of switching and area efficiency.

Apart from these schemes, some new ideas have been proposed in the recent literatures. The comparison of various switching scheme is given in **Table 1**. In the entries, the energy efficient scheme and the charge sharing switching methods are found to be effective in terms of switching power dissipations, since they hardly dissipate any switching power. But these two schemes exhibit logic complexity in the design level. The charge sharing switching scheme offers only a 25% reduction in area compared to the conventional architecture. The bio medical implantable devices have to exhibit higher power efficiency and area efficiency. The circuit complexity of these devices should be maintained in moderate level.

Charge dumping switching scheme[13] saves 99.86% of the switching energy. This design also achieves a 93.75% of improvement in area efficiency. The logic complexity is also less compared to the state-of-the-art design. Thus, this can be adopted for ADC architecture for bio medical devices.

Selection of Capacitance value in CADAC array

The CDAC array consists of switches and unit capacitors. The selection of the value of this unit capacitor is important, when the linearity is concerned. To improve the linearity, a larger unit capacitor is preferred. Larger value of capacitor restricts the thermal noise to lower limits. The equation for calculating the thermal noise voltage is given in “(5)”

$$V_n = \frac{KT}{C} \quad (5)$$

The noise voltage is represented as V_n , K is the Boltzmann's constant and T is the temperature in Kelvin. A large unit capacitor (C_u) also introduces certain problems. This increases the total size of the CDAC array leading to additional power consumption. It necessitates more charging and discharging time, which makes the circuit operation slow. The speed of operation is not a major concern in the biophysical acquisition systems, since these signal frequencies are low. But increase in the device size is not a desirable feature for implantable devices. The selection of a small unit capacitance causes matching problems in the DAC array. One solution is to use a small unit capacitor in the design, and iron out the mismatches and offset variations using an additional calibration circuit. But this technique makes the entire design overloaded, since an additional calibration circuit

is employed in operation. Thus, a designer must evaluate the tradeoffs, and depending on the application, an optimum value of unit capacitor can be proposed. This eliminates any additional calibration techniques.

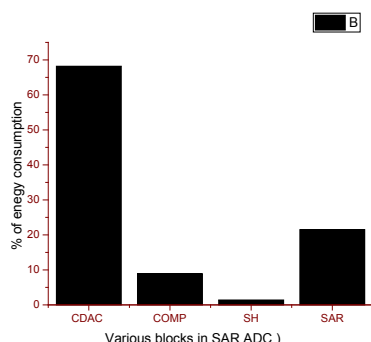


Fig. 5. Power consumed by various blocks in SAR ADC

$$C_{TDAC} \geq \frac{24KT2^{2N}}{V^2} \quad (6)$$

The minimum value of the total capacitance required for CADAC array is given in “(6)”. C_{TDAC} is the total capacitance of the CADAC array, N is the total number of bits involved and V is the supply voltage[16]. The selection of optimum capacitance should be done in such a way that, it should satisfy the relation given in “(6)”. Hence, this is a challenging task for the designer and more studies can be done on the selection procedure. The two limiting factors to be considered for DAC design are (i) Capacitive matching (ii) Thermal noise.

Capacitive matching is more troublesome in power consumption. It is found that in-efficient capacitive matching incurs power consumption in the order of 8x per added bit. The thermal noise effect causes the power consumption in the order of 4x per added bit. The value of capacitance is an important parameter that determines the above-mentioned effects.

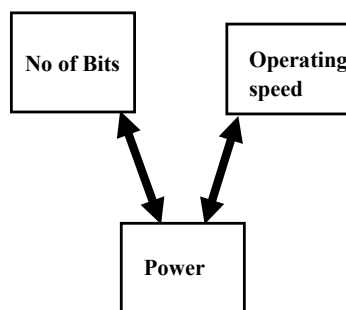


Fig. 6. Tradeoffs in ADC design [17]

Performance analysis of SAR ADC

Performance of an SAR ADC depends on the various tradeoffs associated in their design. It is shown in figure (6). The no of bits (resolution) of ADC and the power consumption is directly related. As there are a greater number of bits in the operation, the system consumes more power. Similarly, if the system operates faster, more power is being consumed. This relation is shown in “(7)”. It is the responsibility of the designer to choose amongst these tradeoffs. It depends on the application that is to be realized.

In this discussion, the required device is an implantable system which handles the physiological signals. As already discussed, these signals are in low frequency spectrum. Hence, moderate speed convertor is enough for operation. The amplitude ranges of biological signals, that are being collected are also very low. To represent low amplitude ranges, moderate number of bits (8-10) are only required. This further reduces the power requirement.

$$\text{Power} = \text{Energy} \times \text{Conversion rate} \quad (7)$$

The figure of Merit (FoM) is a number, which is used to represent the performance matrix of SAR ADC. This number reflects the design tradeoff in an efficient way. FoM's are generally higher for low speed ADC and its value decreases as the speed of ADC increases. Two types of FoM's are generally used for performance analysis in SAR ADC. They are

1): Walden figure of merit (FoM_w): This is one of the popular figures of merit that is being used to measure the ADC performance. The formulae for calculation is given in "(8)". The low resolution and moderate speed ADC's are analyzed by this method. This is regarded as the simplest FoM calculations available. But FoM_w is not suitable for ADC's with higher resolution.

2): Schreier figure of merit (FoM_s): To analyze the performance of a high speed and high-resolution ADC, (FoM_s) is preferred. It is shown in "(9)". In other words, for the system having SNDR (Signal to noise distortion ratio) greater than 50 dB, Schreier figure of merit is found to be more accurate than FoM_w .

Table 1. Comparison of switching schemes

SL NO	Switching method	% of Energy saving	Area efficiency	Complexity
1	Conventional[8]	Reference	Reference	Less
2	Trilevel [11]	96.89	75	Medium
3	Vcm- scheme based [12]	97.66	50	Medium
4	Hybrid method[10]	98.83	75	Low
5	Charge dumping scheme [13]	99.86	93.75	Medium
6	Energy efficient[14]	100	87	High
7	Charge sharing[15]	100	25	High

$$FoM_w = \frac{P}{f_s \times 2^{ENOB}} \quad (8)$$

$$FoM_s = SNDR + 10 \log \left(\frac{f_s/2}{P} \right) \quad (9)$$

The term P represents the power consumption in the ADC, ENOB is the effective number of bits, SNDR is the signal to distortion ratio and f_s is the operating frequency of the device. From these equations it is clear that, the FoM depends on ENOB and SNDR.

The SNDR is defined as the ratio of signal power to the noise power. To achieve a reasonably higher SNDR, the signal level must be kept high. Studies show that higher SNDR levels are achieved at the/ cost of more energy consumption. The ENOB is the measure of SNDR which is used to compute the actual ADC performance with ideal ADC. This value is calculated using the formulae given in "10"[18].

$$ENOB = \frac{SNDR - 176}{6.02} \quad (10)$$

For a low speed, ultra-low power ADC, FoM_w is preferred. In lower operating speeds, higher value of FoM is expected.

CONCLUSION

The early drainage of the battery in the implanted devices causes sudden failure of the system without warning. The ADC in the analog front end of the design draws major power for operation. In SAR ADC, the major power-hungry block is DAC. By incorporating efficient switching methodology, the switching energy dissipation of capacitor array can be capped. Though the advancement in scaling ensures area efficiency, the leakage power dissipation becomes a concern in sub-micro meter designs. More efficient techniques can be proposed for the suppression of leakage power. Since the implantable devices deal with the critical organs, an ultra-low power, energy efficient design is to be incorporated for improving the reliability and durability of the system.



ACKNOWLEDGMENT

This work is supported by the Ministry of Electronics & Information Technology (MeitY), Government of India, through 'Visvesvaraya PhD Scheme for Electronics & IT'.

REFERENCES

1. W. Hu, T. Nguyen, Y. T. Liu, and D. Y. C. Lie, "Ultralow-power analog front-end circuits and system design for an implantable cardioverter defibrillator (ICD)," *Proc. 2011 IEEE/NIH Life Sci. Syst. Appl. Work. LiSSA 2011*, no. ICD, pp. 34–37, 2011.
2. D. Zhang, A. Bhide, and A. Alvandpour, "A 53-nW 9.1-ENOB 1-kS/s SAR ADC in 0.13- μ m CMOS for medical implant devices," *IEEE J. Solid-State Circuits*, vol. 47, no. 7, pp. 1585–1593, 2012.
3. P. Zhao, J. McNeely, W. Kuang, N. Wang, and Z. Wang, "Design of sequential elements for low power clocking system," *IEEE Trans. Very Large Scale Integr. Syst.*, vol. 19, no. 5, pp. 914–918, 2011.
4. G. K. Balachandran and P. E. Allen, "Switched-current circuits in digital CMOS technology with low charge-injection errors," *IEEE J. Solid-State Circuits*, vol. 37, no. 10, pp. 1271–1281, 2002.
5. D. Zhang, A. K. Bhide, and A. Alvandpour, "Design of CMOS sampling switch for ultra-low power ADCs in biomedical applications," *28th Norchip Conf. NORCHIP 2010*, pp. 4–7, 2010.
6. S. A. Mahmoud, H. A. Salem, and H. M. Albalooshi, "An 8-bit , 10 KS / s , 1 . 87 μ W Successive Approximation Analog to Digital Converter in 0 . 25 μ m CMOS Technology for ECG Detection Systems," *Circuits, Syst. Signal Process.*, pp. 2419–2439, 2015.
7. J. L. McCreary, "All-MOS Charge Redistribution Analog-to-Digital Conversion Techniques—Part I," *IEEE J. Solid-State Circuits*, vol. 10, no. 6, pp. 371–379, 1975.
8. B. P. Ginsburg and A. P. Chandrakasan, "An Energy-Efficient Charge Recycling Approach for a SAR Converter With Capacitive DAC," pp. 184–187, 2005.
9. M. Van Elzakker, E. Van Tuijl, P. Geraedts, D. Schinkel, E. A. M. Klumperink, and B. Nauta, "A 10-bit charge-redistribution ADC consuming 1.9 μ W at 1 MS/s," *IEEE J. Solid-State Circuits*, vol. 45, no. 5, pp. 1007–1015, 2010.
10. L. Xie, G. Wen, J. Liu, and Y. Wang, "Energy-efficient hybrid capacitor switching scheme for SAR ADC Liangbo Xie , Guangjun Wen , Jiaxin Liu and Yao Wang," vol. 50, no. 1, pp. 22–23, 2014.
11. C. Yuan and Y. Lam, "Low-energy and area-efficient tri-level switching scheme for SAR ADC," vol. 48, no. 9, pp. 9–10, 2012.
12. Z. Zhu, Y. Xiao, and X. Song, "VCM-based monotonic capacitor switching scheme for SAR ADC," *Electron. Lett.*, vol. 49, no. 5, pp. 327–329, 2013.
13. S. H. W. Chiang, "Charge-dumping switching scheme for successive-approximation-register analogue-to-digital converters," *Electron. Lett.*, vol. 52, no. 5, pp. 348–350, 2016.
14. T. Yousefi, A. Dabbaghian, and M. Yavari, "An Energy-Efficient DAC Switching Method for SAR ADCs," *IEEE Trans. Circuits Syst. II Express Briefs*, vol. 65, no. 1, pp. 41–45, 2017.
15. M. Akbari, O. Hashemipour, M. Nazari, and F. Moradi, "A charge sharing–based switching scheme for SAR ADCs," *Int. J. Circuit Theory Appl.*, vol. 47, no. 7, pp. 1188–1198, 2019.
16. M. Boutemour, "A 3,3V 12Bits rail-to-rail ADC SAR for neuronal implant," *Proc. 8th IEEE Int. NEWCAS Conf. 2010*, pp. 5–8, 2010.
17. B. Murmann, "The Race for the Extra Decibel: A Brief Review of Current ADC Performance Trajectories," *IEEE Solid-State Circuits Mag.*, vol. 7, no. 3, pp. 58–66, 2015..
18. B. Murmann, "The Successive Approximation Register ADC : A Versatile Building Block for Ultra-Low- Power to Ultra-High-Speed Applications," no. April, pp. 78–83, 2016.



Study on Electro Magnetic Interference and Compatibility Across Various Levels and Mitigation Technique using Software

Y Uma Maheswari¹, Y Dhayaneswaran¹, Dr A Amudha², Dr L Ashokkumar³

Research Scholar, EEE, Karpagam Academy of Higher Education, Coimbatore¹

Professor and Head, EEE, Karpagam Academy of Higher Education, Coimbatore²

Professor & Associate HOD, EEE, P S G College of Technology, Coimbatore³

✉ yummyaskisan@gmail.com

ABSTRACT

In recent days testing of a product with the EMI standard using test set up is a mandatory as most of the product has the electronic circuitry which posses the high speed signals. In this paper the main objective is to study about the electromagnetic interference and compatibility across various levels and mitigation technique at various levels and to give the overview of the software tools.

Keywords : EMI; EM Simulation tools; Printed circuit board (PCB).

INTRODUCTION

Electromagnetic interference is the operational disturbance of electronic devices when the presence of electromagnetic waves caused by another device or source. Unwanted signal can be emitted by electrical or electronic circuits due to various reasons. Because of the high speed clock signals, processor noise, high switching frequency, transmission interferences, network interferences electromagnetic emission happens. Because of this performance of the signal, receiver circuit degrades. This will cause the unintended operation or malfunction of electromechanical equipments, circuits and components happen.

This paper covers the following topics:

- Basic understanding of Electro Magnetic Interference, EMI and its standard
- EMI at various levels such as component, PCB and Product levels
- Overview of Various EM Simulation tools and its gap

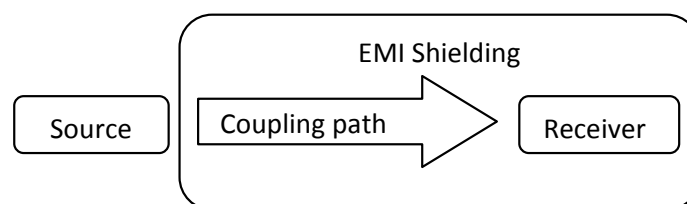


Fig. 1. Elements of the EMI

As shown in the **Fig. 1**, source generated the interference, conducted and radiated through coupling path. Due to this interference, receiver is not receiving the expected signal. Measures to be taken care both the source and transmission side or conduction path. Two most common sources of EMI are conversion of some differential signal into a common signal, which eventually gets out on an external-twisted pair cable and Ground bounce on a circuit board generating common currents on external single-ended shielded cables. Additional noise can come from internally generated radiation leaking out of the enclosure.

EMI mitigation is required for high density semiconductor packaging technology advancement with complex stacked chip and multi chip packages. This is equally important due to the other reasons such as increase of electromagnetic pollution and emerge of Internet of Things (IoT). EMI is regulated and enforced at international and national standard to overcome these problems.

Some of the bodies are

- International Electrotechnical Commission (IEC)
- Federal Communications Commission (FCC)
- Verband Deutscher Elektrotechniker (VDE)
- International Special Committee on Radio Interference (CISPR)
- IEEE -Institute of Electrical and Electronics Engineers
- Other standards organizations, including ISO, SAE and also defined a number of standards geared towards specific applications or industries.

Standards are classified as Basic standard, Generic standard, Product oriented standard and Product family oriented. They are based on the frequency band or wavelength and the testing parameters or metrics. The **Fig. 2** shows in general various frequency range with the wave length.



Fig. 2. Frequency range with wavelength

With the different frequency ranges, there are various application. The **Table 1** shows the typical communication examples with their operating frequency.

Table 1. Application and their frequency range

Description	Frequency range
Wireless	500MHz +
Wi-Fi	2.4 – 5 GHz
Bluetooth	2.4 – 2.485 GHz
4G cellular	0.7 – 2.7 GHz
5G cellular	6GHz

EMI problem arises in the high frequency, and it has to be watched at various levels to overcome the issue.

EMI AT COMPONENT LEVEL

Behaviour of an electronic component in the low frequency is differs from high frequency. For example, in the case of resistor under low frequency, it works as resistor as expected. But during the high frequency operation, the equivalent circuit will not be a resistor alone; instead some inductance effect is also added. This is same for other components also. The **Fig. 3** shows the passive components and its behaviour at high and low frequency. In resistor, at higher frequencies, however, parasitic capacitance (between windings or end-to-end) limits impedance. Capacitor impedance is actually low at resonance, which might be seen as good. But above the resonant frequency, the capacitor actually behaves like an inductor, increasing in impedance with frequency.

Selection of capacitor is important based on the operating frequency. With the lead of the capacitor, the performance will degrade. The **Table 2** shows without lead values.

EMI shielding is applicable to various component levels such as System-in-Package (SiP), System-on-Chip (SoC), Microcontrollers, Application processors, Power amplifiers, wireless modules, radio frequency modules, memory,

sensors, Digital signal Processors (DSP), Application specific integrated circuits (ASIC), Field programmable gate arrays (FPGA), Analog Digital Converters (ADC) and so on.

EMI AT PCB LEVEL

In Printed Circuit Board, there will be conducted emission and radiated emission due to the power supply and signal speed. The source of EMI is the place or module where the interference is generated. A receptor for EMI is the block being affected by the interference. PCB has various modules such as power supply, memory, filters, Synchronizer and Other components - Cable, PCB traces, Connector, Res-Ind-Cap, Switch. Each module has to be taken care for EMI issue. Two different domains are used to analyze EMI, named time and frequency domain. In time domain, signals are analyzed with respect to time. In the frequency domain, signals are analyzed with respect to frequencies. In the very high frequency signal PCB requires electronic band gap (EBG) which acts as low pass filter, which is used for mitigating EMI issues[1].

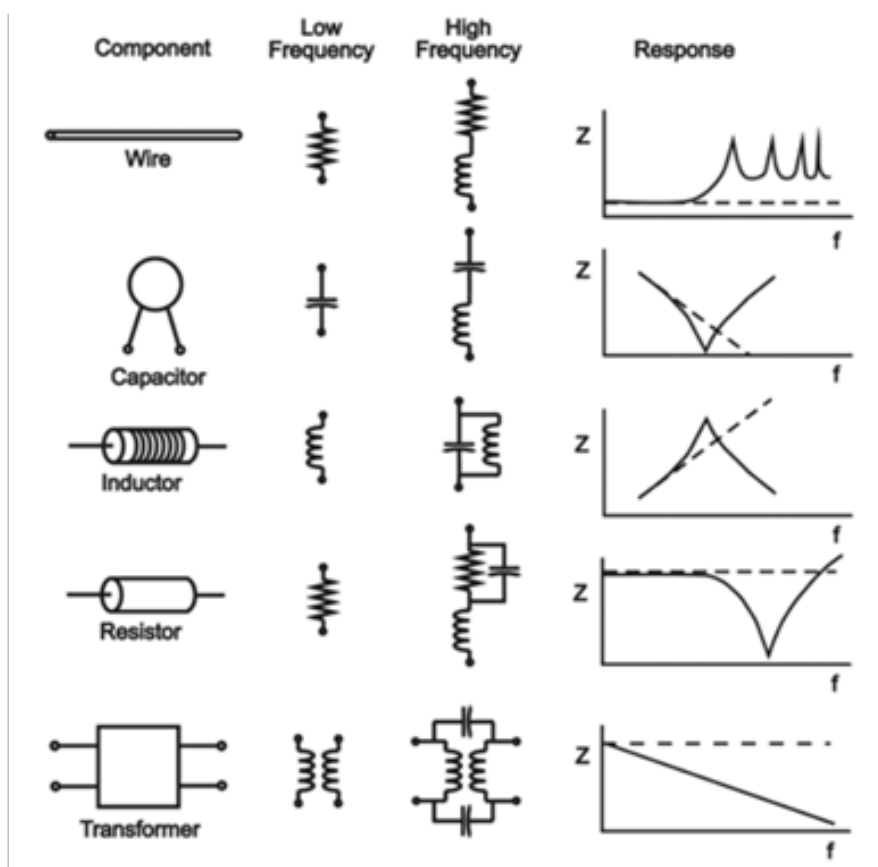


Fig. 3. Equivalent circuit of component with operation frequency

Table 2. Application and their frequency range

Type	Maximum frequency
Aluminium Electrolytic	100 kHz
Tantalum Electrolytic	1 MHz
Paper	5 MHz
Mylar	10 MHz
Polystyrene	500 MHz
Mica	500 MHz
Ceramic	1 GHz



EMI MITIGATION TECHNIQUES

Solution for the EMI issues can be applied under the following types[3].

- a) Hardware solution
- b) Software solution
- c) System level solution

a) Using Hardware: Fundamental and lower order harmonics produces the radiation. This radiation, interfere with other possible signals. Different reduction or elimination techniques can work out for Electromagnetic Interference issues. Broadly it can be done by applying the following.

- Fabric-over-Foam (FoF)
- Shielding
 - Coaxial Transmission Line Method
 - Dual TEM Cell Method
 - Rectangular Waveguide Method
 - Nested Reverberation Chamber Method
 - Shielded Box Method
 - Shielded Room Method
 - Free-Space Method
- Conductive filler CM and DM noise
- Form-in-Place
- Ferrite
- Grounding
- Bonding,
- Spatial placement of hardware
- Circuit topology modification and spread spectrum

Noise due to High frequency in power lines can be eliminated by adopting the proper filters in the circuit. EMI filters normally consist of a combination of inductors and capacitors. The requirement of capacitors and inductors is based on the node impedance where capacitors are used in high-impedance node and inductors are used in low impedance node. Enclosing the system with a conductive material completely called shielding eliminates the EMI effect. This is the costliest solution, but it works. Radio-frequency (RF) emitting devices have to be isolated to limit the propagation of their interference to nearby components. Now-a-days, the world is moving towards miniaturization, light weight, and high speeds. This becomes a challenge to overcome the problem.

b)Using software: There are various software tools available in the market to test the EMI parameters in the printed circuit board. Once the native CAD design files are imported into the tool, design rules can be checked. Prior to the simulation, EMC engineer identifies the critical nets and critical components which are most important to EMC performance. Clock signals, fast rise time or data rate data signals are called as critical nets. Critical components might be decoupling capacitors, filter components, termination resistors, etc.

c) System level solution: Optimization of the assemble level code improves the EMI related problem. This method eliminates the physical redesign of the system[2].

EMI SIMULATION

During the design-stage of EMI analysis, S-parameter (scattering parameter) model extraction in frequency domain can be done



to know transmission and reflection characteristics by finding out the amplitude and phase information of a signal. There are three types of simulators available which can be perform to find the EMI levels before manufacturing the product.

1. Electromagnetic (EM) simulators, which solve Maxwell's Equations and simulate the electric and magnetic fields at various locations in time domain or frequency domain. There are several EM simulation technologies have emerged based on Maxwell's equation. Electromagnetic full wave simulation includes the Method of Moments (MoM), Finite Element (FEM), Finite Difference Time Domain (FDTD) and The partial-element equivalent circuit (PEEC) technologies.
2. Circuit simulators, which solve the differential equations corresponding to various circuit elements and include Kirchhoff's current and voltage relationships to predict the voltages and currents at various circuit nodes, in time or frequency domains. It is a mathematical model depicting the behaviour of an actual circuit.
3. Behavioral simulators, which use models based on tables and transmission lines and other passive-element models based on transfer functions, which quickly predict the voltages and currents at various nodes, typically in the time domain.

VARIOUS EM SIMULATION TOOL

The entire EMI performance of a product is dependent on the surrounding environment and noise within block of the product. One of the main blocks is PCB. Simulation has to be done for electrical signal quality and signal propagation paths. This topic explains the various existing tools for the simulation in the market.

FEKO: This tool can be used in the industries such as telecommunications, automobile, space and defense industries. The software tool works based on the technology "Method of Moments (MoM)" for both frequency and time domain. Altair Engineering from Germany developed FEKO. FEKO includes a complete integrated cable modeling tool that permits the analysis of the radiation of cables[4].

ANSYS SIwave is a 2.5D EM simulation tool where finite element method (FEM) and the method of moments (MOM) technologies are used. This solver uses a 2-D triangular mesh and can handle very complex PCB layouts. It solves complete layouts including the traces, planes, through hole vias, metal thickness, and dielectric thickness effects. Desktop. ANSYS SIwave includes the Electronics Desktop which has a circuit simulation capabilities. The includes numerous model types such as extracted PCB S-parameter models, driver/receiver IBIS models, RLC passive component equivalent models and arbitrary input signals to perform a precise and complete circuit simulation. It produces near-field and far-field results with the corresponding excitation signal source. The final step is to connect SIwave near-field results to HFSS in order to predict radiated emissions from the enclosure. ANSYS EMIT is software tool which simulate RFI in complex environments[5].

Computer Simulation Technology (CST) CST EMC STUDIO tool is used to analyse and optimize the EMI behavior. This is one of the leading tool used by the industry. The CST "Complete Technology" approach means that CST EMC STUDIO includes a series of solvers for many different scenarios, from general purpose to specific solver in time and frequency domain. From Electronic Design Automation tools, Printed circuit Board can be imported into CST EMC STUDIO. Specialized PCB simulation tools can quickly calculate signal integrity and power integrity (SI/PI) and identify violations of EMC design rules, while the general purpose 3D solvers can simulate radiated and conducted emissions/susceptibility in detail[6].

The AWR Design Environment software tool helps RF/microwave engineers with integrated high-frequency circuit. The helps designers managing in circuit behavior of complex integrated-circuit (IC), package, and printed-circuit board (PCB) modeling, simulation, and verification[7].

PathWave EM Design - EMPro allows engineers to simulate the emissions of their circuits and components to make sure they are within the required common electromagnetic compatibility (EMC) levels. EMPro 2013 provides analysis based on finite-element-method (FEM) techniques, as well as FEM hybrid boundary conditions that boost speed and accuracy. Electromagnetic Professional (EMPro) provides a design platform for analyzing the electromagnetic effects of RF and microwave components such as high-speed IC packages, antennas, and PCB interconnects. EMPro supports a modern design, simulation and analysis environment, and time-domain and frequency-domain simulation technologies. It can be easily integrated with the leading RF and microwave circuit design environment Advanced Design System (ADS) for designing efficient and fast RF and microwave circuits[8].

Elmer is developed by CSC - IT Center for Science (CSC) as an open source multiphysical simulation software tool. It is an open source finite element software for multiphysical problems[9].

COMSOL Multiphysics® is general-purpose simulation software tool. It is used for modeling designs, devices, and processes in



all fields of engineering, manufacturing, and scientific research. AC/DC, RF, Wave Optics, Ray Optics, Plasma, Semiconductor are some of the modules[10].

XFDTD® 3D EM Simulation Software tool with powerful tools, includes a specialized FDTD solver effectively. It is a General purpose 3D EM simulation solver that simplifies analysis of a wide variety of applications[11].

Momentum is a simulator tool with 3D planar electromagnetic (EM) that enables RF and microwave designers to significantly expand the range and accuracy of their passive circuits and circuit models. The ability to analyze arbitrary shapes, on multiple layers and to consider real-world design geometries when simulating coupling and parasitic effects, makes Momentum an indispensable tool for customized passive circuit design. In this tool, it is possible to capture S-, Y-, and Z-parameters of general planar circuits. Microstrip, stripline, slotline, coplanar wave guide, and other circuit topologies can also be analyzed. Vertical Interconnect (VIA) can be simulated. Accurate result of multilayer RF/MMIC's, printed circuit boards, hybrids, and Multi-Chip Modules (MCMs) can be found in the simulation results. Table III shows the brief information among the tools[8].

Table 3. Comparison of tools

Name of the Simulation Tool	Solver overview	Product highlight	Features
FEKO	Frequency and time domain full wave solvers: MoM, FDTD, FEM and MLFMM. Unique CMA solver calculates model currents, eigenvalues, model significance and characteristic angles	EMC analysis including emissions, immunity and shielding effectiveness Wide set of hybridized methods to solve large and complex problems Special tools including windscreen antennas, arrays, cable modelling and CMA	Set up of the entire problem CAD and mesh import/export of most major formats Gerber, ODB++ and 3Di for printed circuit boards Media library with pre-defined and user-defined materials Powerful meshing algorithms EMIT interface Impedance, S-parameters measurement
ANSYS SIwave	Uses finite element method (FEM)	IBIS and IBIS-AMI SerDes Analysis Automated Decoupling Capacitor Optimization Simulation of Circuit, block diagram, State machine simulation, VHDL-AMS Integrated graphical modeling environment, Multidomain System Modeling	Power electronic device and module characterization Co-simulation with Math Works Simulink Supported ECAD Translations: Zuken, ODB++ from other packages, IPC 2581 from other packages, Altium Designer Impedance and Cross-talk Scanning
Computer Simulation Technology (CST)-SIMULIA	Uses finite element method (FEM), the finite integration technique (FIT), method of moments (MOM) and the transmission line matrix method (TLM). Various High frequency, Low frequency and pcb solvers, frequency domain solver	The sophisticated healing mechanisms, which restore the integrity of flawed or non-compliant data, are particularly important as even one corrupted element can prevent the use of the whole part.	CST Studio Suite is renowned for its superb CAD and EDA data import capabilities



AWR Design Environment	<p>Microwave Office :powerful harmonic-balance circuit simulation,</p> <p>Visual System Simulator: supports VSWR-aware modeling of RF and DSP blocks,</p> <p>AXIEM: 3D planar method-of-moments (MoM) EM analysis</p> <p>Analyst: accelerates high-frequency product development from early physical design characterization through to full 3D EM verification.</p>	<p>Faster and more accurate simulation results</p> <p>Meshing Technology</p> <p>Scripting, Customization</p>	<p>Easier 3D EM setup</p> <p>Layout/Drawing Editor – 2D/3D construction and views</p> <p>Visualization and results post - processing f Parametric Studies – Optimization, tuning, and yield analysis</p> <p>Interoperability with third-party tools covering technologies from synthesis to models and T&M.</p>
PathWave EM Design (EMPro)	<p>3D modeling and simulation environment for analyzing the 3D electromagnetic (EM) effects of high-speed and RF/microwave components.</p> <p>Uses Finite Element Method (FEM) and Difference Time Domain FDTD</p>	<p>Geometry modelling</p> <p>Port/sensor setup</p> <p>Mesh and simulation setup</p> <p>Export 3D EM component to ADS library</p>	<p>High capacity time- and frequency-domain simulation technologies</p> <p>The industry's leading RF/microwave and high-speed design environment.</p> <p>Enhancements in import HFSS designs and support for a3dcomp</p>
Elmer	<p>Open source multiphysical simulation software</p> <p>Elmer solves by the Finite Element Method (FEM).</p>	<p>Elmer includes physical models of fluid dynamics, structural mechanics, electromagnetics, heat transfer and acoustics</p> <p>Elmer has a modern programmable graphical user interface.</p>	<p>Elmer is divided into a number of separate executables that may also be used independently.</p>
COMSOL	<p>Uses FEM-based full-wave propagation</p>	<p>Boundary conditions for EM modelling</p> <p>EM specific modelling tool</p> <p>Meshing and Post processing tools</p> <p>Dedicated tools for the analysis of semiconductor device operation at the fundamental physics level.</p>	<p>Available EM modules AC/DC, RF, Wave Optics, Ray Optics, Plasma, Semiconductor</p> <p>Interfacing products for synchronising MATLAB,MS excel</p>



XFDTD	FDTD-based full-wave propagation	Powerful Flexible Modeling. Fast, Intelligent Meshing ESD Testing Simulation Circuit Element Optimizer (CEO) Circuit Co-Simulation	Parameterization & Scripting CAD and PCB Import Electrostatic Solver (ESS) Specific Absorption Rate (SAR) Power Density Superposition Circuit Element Optimization
Momentum	based on the Method of Moments (MoM) technology	Combines full-wave and quasi-static EM solvers for RF passives, high-frequency interconnects and parasitic modeling Efficient meshing, adaptive frequency sampling Able to simulate complex EM effects including skin effect, substrate effect, thick metals and multiple dielectrics	Capable of computing S-, Y-, and Z-parameter Integrated in RFPPro, ADS, Genesys and Cadence Virtuoso

GAP IN SIMULATION AND FUTURE WORK

All above mentioned tools can be used to model and simulate for a particular module. The entire modeling of a complete panel consisting of power supply, PCB, drive, motor, load etc becomes a challenge in the industry. Currently, EMC testing is done after assembling the panel. If the discrepancies are found, the process needs to be iterated till the desired results as per the standard. However in case of software, Engineer could identify issues prior production and act accordingly. Once the software results are satisfied, it can be assembled and for the verification the hardware testing can be executed.

REFERENCES

1. Bruce Archambeault, Sam Connor, "Review of Printed-Circuit-Board Level EMI/EMC Issues and Tools", IEEE TRANSACTIONS ON ELECTROMAGNETIC COMPATIBILITY, VOL. 52, NO. 2, MAY 2010
2. Shih-Vi Yuan#1, We-Bing SU#2, Hao-Ping Ho#3, "A Software Technique for EMI Optimization", 978-1-4577-1559-4/12/\$26.00 ©2012 IEEE
3. Mandeep Kaur, Shikha Kakar, Danvir Mandal, "ELECTROMAGNETIC INTERFERENCE", 978-1-4244-8679-3/11/\$26.00 ©2011 IEEE
4. <https://altairhyperworks.com/product/Feko/>
5. <https://www.ansys.com/products/electronics/ansys-siwave>
6. <https://www.3ds.com/products-services/simulia/products/cst-studio-suite/>
7. <https://www.awr.com/>
8. <https://www.keysight.com>
9. <https://www.csc.fi>
10. <https://www.comsol.co.in>
11. <https://www.rfglobalnet.com>



Comparison between Different Wavelet Transform Techniques for Indoor Optical Wireless Communication System Employing Pulse Position Modulation & On-OFF Keying

Ankita Aggarwal¹, Dr Gurmeet Kaur²

Research Scholar¹, AP Professor², Department of ECE, Punjabi University, Patiala, Punjab

✉ ankitahctm@gmail.com; ✉ farishta02@yahoo.co.in

ABSTRACT

Different types of wavelet transform methods for Optical Wireless Communication system (OWCS) are discussed in this paper. Discrete Wavelet Transform (DWT), Stationary Wavelet Transform (SWT) and combination of both i.e. DWT + SWT are implemented for various characteristics of OWCS to enhance the performance of the proposed system using Pulse-Position Modulation (PPM) and On-Off Keying (OOK) modulation.

Keywords : DWT; SWT; DWT+SWT; PPM; OOK; OWC.

INTRODUCTION

The first Wireless Communication System was made accessible, in nineteenth century. The optical wireless system basically works on three links, i.e. Line-of-sight (LOS), Non-LOS and Hybrid, where, light beams are used to carry information, which propagates through atmosphere or space. High data rate is offered by wireless system due to the availability of abundance bandwidth. The impending ability disaster for radio based networks, are resolved by Optical Wireless Communication systems. IR advancement has an enormous focal point over RF due to its suitability for short range and used effectively in the centre of source and target.

INDOOR OPTICAL WIRELESS COMMUNICATION

To give fast access to telephones, PCs, printers and computerized cameras in workplaces, malls, distribution centres and planes, a method is proposed, which uses infrared frequency is named as Communication for wireless Optical (OWC) [1]. As these frequencies cannot penetrate via walls, tethering the transmission into the room, as a consequence, made them inherently inoffensive, even as allowing reuse of identical optical carrier in an adjoining room. These links chiefly employ intensity modulation with direct modulation (IM/DD) resulting in refutation of multipath fading [2].

Here in this paper, implemented methods, reduces FLI due to artificial light in Indoor Optical System. First technique is the PPM technique, which is preferred because of the requirement of low power consumption.

Second one is the On Off Keying, which is widely used and the most admired method.

To reduce the FLI due to artificial light in indoor optical system, these two methods are discussed in this paper. Also, to measure the performance of the system SNR, efficiency and data rate, are presented here. In the previous work, DWT based scheme was discussed to lessen the upshot of FLI. In the present work two new techniques i.e. Stationary Wavelet Transform (SWT) and combination of both i.e. DWT + SWT are discussed, showing improvement over the existing one. On studying the performance of SWT and DWT+SWT in various fields, it is used to design a new IOWCS. The proposed model is designed using On-OFF Keying & Pulse Position Modulation and comparison in encoded with the existing one i.e. DWT.

DISCRETE WAVELET TRANSFORM

Wavelet analysis is used to analyse the both types of frequencies. For determining the time- frequency resolution of Wavelet Transform (WT) and Short Term Fourier transform (STFT), the window size is considered fixed for time and frequency in

STFT but not for WT. Hence WT is very beneficial & operative in analysing various types of signals. Different types of wavelet transform methods are marked in this paper for comparison.

The filter banks used by DWT for the creation of determination T-F plane have quality of both types of filters i.e. low and high pass with down sampling of both. The LP parts are then decayed into bands until satisfactory level of information is obtained. In DWT, the signal is convolved and decimated by accomplishing the choice of odd indices. If all the possible DWTs of the signal are performed, then there will be 2^j decomposition level for j levels.

STATIONARY WAVELET TRANSFORM

It is intended to defeat the absence of interpretation invariance of the DWT. Interpretation invariance is accomplished by expelling the down examples and up tests in the DWT and up examining the channel by a factor of $2^{(j-1)}$ in the j th level of the calculation. The SWT is characteristically repetitive plan as the yield of each degree of SWT contains indistinguishable number of tests from the information, so for a deterioration of N levels there is an excess of N in the wavelet coefficients [15,16]. This calculation is all the more generally known as "algorithme a trous" in French which means embedding zeros in the channels. It was presented by Holschneider [17]. The accompanying square graph portrays the advanced execution of SWT.

In SWT, the HP & LP filters are used on all level and improved on every level with the addition of extra zeroes.

SYSTEM DESIGN

Here, the designing of the planned system constructed on Stationary Wavelet transform, is described. The proposed system consist of two techniques i.e OOK and PPM. The description for both is given below:

Based on OOK

Firstly, the system is designed using OOK technique. The schematic for the same is prearranged in figure 1 and described as: an OOK generator is used as input device, which generate an OOK signal, after which it is mixed with the channel noise. AWGN noise is considered as a standard. At the receiver side, after filtering the received data using receiver filter, denoising based on wavelet transform and artificial neural network is applied. The two wavelet transform used for the proposed system are: 1. Stationary Wavelet transform (SWT), shown as solid line 2. Combination of Stationary Wavelet transform and Discrete Wavelet Transform, shown as dotted line. The NN used is BPNN. Finally, the threshold is applied to the output of ANN to achieve the desired output.

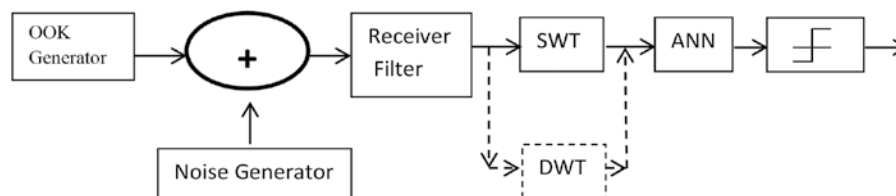


Fig 1. Schematic of planned scheme

The same process as described by the block diagram is also embodied in the form of algorithm. For the proposed system, the algorithm is presented below:

1. Generate OOK Data
2. Add AWGN
3. Match filtering
4. DWT or SWT or DWT + SWT windowed data
5. Train Neural network
6. Repeat step 1-5
7. Classify using neural network
8. Threshold network output

9. Calculate BER
10. Save
11. Check BER for particular value
 1. If yes, Train and Plot result
 2. If No, decrease AWGN and go to step 6.

The flow-sheet of the future system prearranged in **Fig 2**. Through flow chart, the step by step processing of proposed system is being described.

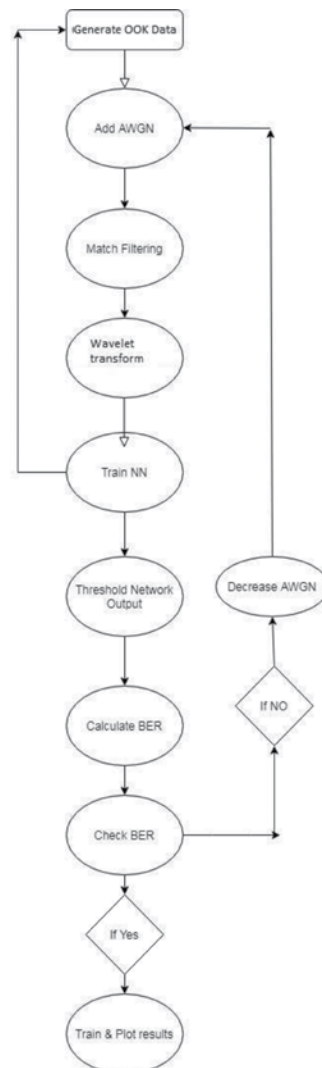


Fig. 2. Flow chart of proposed system

Based on PPM

The diagram the system is prearranged in **Fig. 3** and described as: a PPM generator is used as input device, which generate a PPM signal, after which it is mixed with the channel noise. AWGN noise is considered as a standard. At the receiver side, after filtering the received data using receiver filter, denoising based on wavelet transform and artificial neural network is applied. The wavelet transform used for the proposed system is combination of Stationary Wavelet transform and Discrete Wavelet Transform, shown as dotted lines and Stationary Wavelet Transform, represented as solid lines. The NN used is BPNN. Finally, the threshold is applied to the output of ANN to achieve the desired output.

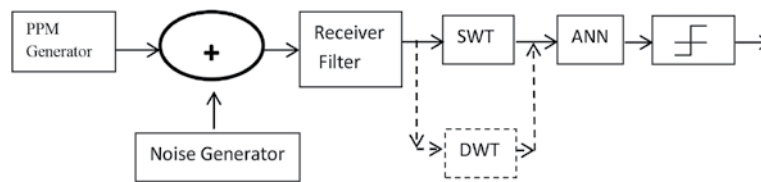


Fig. 3. Schematic of planned scheme

The same process as described by the block diagram is also embodied in the form of algorithm. For the proposed system, the algorithm is presented below:

1. Generate PPM Data
2. Add AWGN
3. Match filtering
4. DWT or SWT or DWT+SWT windowed data
5. Train Neural network
6. Repeat step 1-5
7. Classify using neural network
8. Threshold network output
9. Calculate BER
10. Save
11. Check BER for particular value
 3. If yes, Train and Plot result
 4. If No, decrease AWGN and go back

The flow-sheet of the future system is given in figure 4. Through flow chart, the step by step processing of proposed system is being described.



Fig. 4. Flow Chart of Proposed System

SIMULATIONS

The simulations are done using Matlab R2015a. The several standard parameters used for the same are prearranged below.

Table 1. Factors used for offered scheme

Factor	Used Value
Mother Wavelet	Sym ²
Window Size	3
NN Type	Back Propagation NN
Hidden Layer	1
Neurons	5(HL), 1(OL)
Transfer function	Log- Sigmoid
Threshold Data	If last value > 0.5 then „1 □ else „0 □

RESULTS AND DISCUSSIONS

Here in this section, performance of the DWT+SWT & SWT based system are specified and verified with the existing technique. Various characterizations recycled to show the enactment of the suggested organization are: change in BER vs SNR, efficiency and data rate.

SNR vs BER for OOK

To equate the smooth of wanted signal to the level of background noise, relation of noise & signal is preferred. BER & SNR, both the values are calculated for the proposed system using OOK modulation with SWT–NN, DWT–NN & SWT+DWTNN. The comparison between the two is given in **Table 2**.

Table 2. Comparison of SNR/BER for DWT & SWT Using OOK

S.NO.	SNR(dB)	BER		
		DWT	SWT	DWT+SWT
1	5.5	0.1717	0.1567	0.1567
2	8.5	0.098	0.098	0.094
3	10	0.0825	0.08	0.08
4	16	0.0535	0.02	0.05
5	19	0.0433	0.0396	0.0354
6	22	0.0418	0.0379	0.0343
7	25	0.0329	0.0319	0.03
8	28	0.0283	0.0275	0.0263

The above table shows that when SNR increases, BER decrease. As given in [6], there is enhancement in SNR vs BER for the proposed system which indicates the increase in performance. Comparison between three different methods is shown in **Table 2**. From figure it is clearly visible that for the proposed methods i.e. DWT +SWT and SWT, BER is decreased as compared to the existing one.

SNR vs BER for PPM

Both SNR & BER are calculated for the proposed system using PPM with SWT–NN, DWT–NN and DWT + SWT –NN. The comparison between the three techniques is given in **Table 3**.

Table 3: Comparison of SNR/BER for DWT & SWT using PPM

S.NO.	SNR	BER								
		DWT			SWT			DWT + SWT		
		4	8	16	4	8	16	4	8	16
1	5.5	0.1767	0.1733	0.1683	0.1725	0.1683	0.1675	0.1675	0.1658	0.1658
2	8.5	0.0975	0.096	0.096	0.096	0.096	0.0955	0.096	0.094	0.0905
3	10	0.085	0.0783	0.0779	0.0838	0.0825	0.0817	0.0725	0.0714	0.07
4	16	0.0539	0.0532	0.0517	0.052	0.0518	0.0512	0.0473	0.0473	0.0465
5	19	0.0466	0.0448	0.0433	0.0464	0.0454	0.0427	0.0425	0.0423	0.0413
6	25	0.0328	0.0314	0.0309	0.0322	0.0303	0.0278	0.0319	0.0309	0.0278
7	28	0.0291	0.029	0.0286	0.027	0.0268	0.0256	0.0263	0.0254	0.0249

From the above table, it is shown that when SNR increases, BER decrease. As given in [6], there is improvement in SNR vs BER for both the proposed systems, which indicates the growth in performance.

Efficiency for OOK

The performance of a system is better computed by calculating its efficiency. For the IOWCS, the spectral efficiency in bits/Hz is computed for DWT, SWT and DWT + SWT techniques for OOK modulation. The **Fig. 5** below shows the comparative efficiency for the both methods.

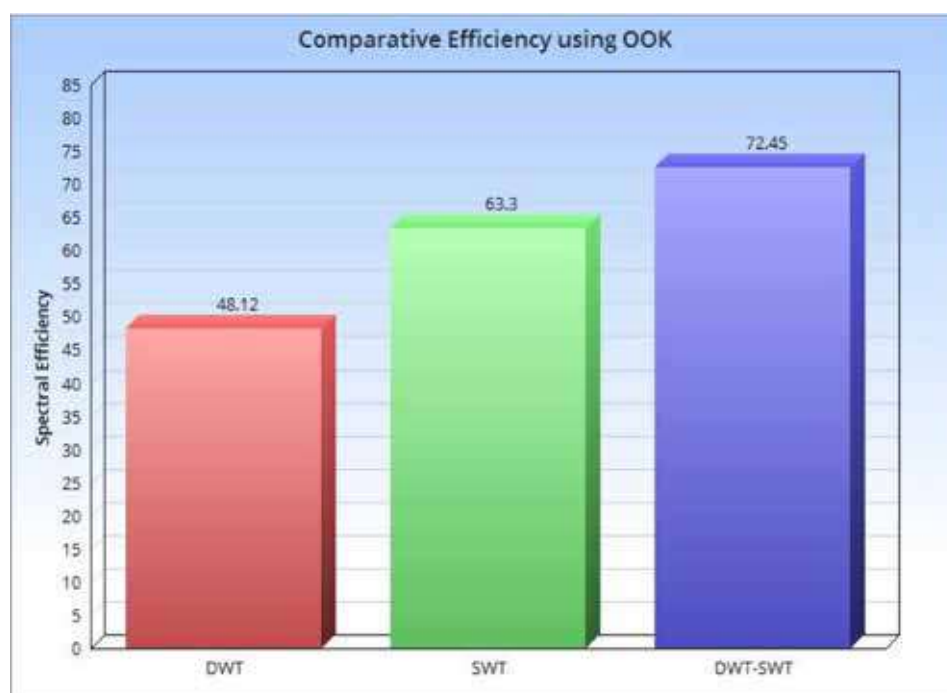


Fig. 5. Efficiency for OOK using DWT & SWT

On viewing the graph, it can be concluded that the efficiency of the offered schemes is improved than the present one, i.e. it is 72.45% for DWT + SWT, 63.3% when using only SWT and is 48.12% with existing technique.

Efficiency for PPM

Enactment of a structure is restored by calculating its efficiency. For the IOWCS, the spectral efficiency in bits/hz is computed for both DWT and SWT techniques for PPM. The **Fig. 6** shows the efficiency for PPM using DWT, for symbol length 4, 8 and 16. In figure, it is shown that the efficiency is more for PPM-16 i.e. 75.88%, which comes out 55.61% for PPM-8 and for 4-PPM it is only 42.46%.

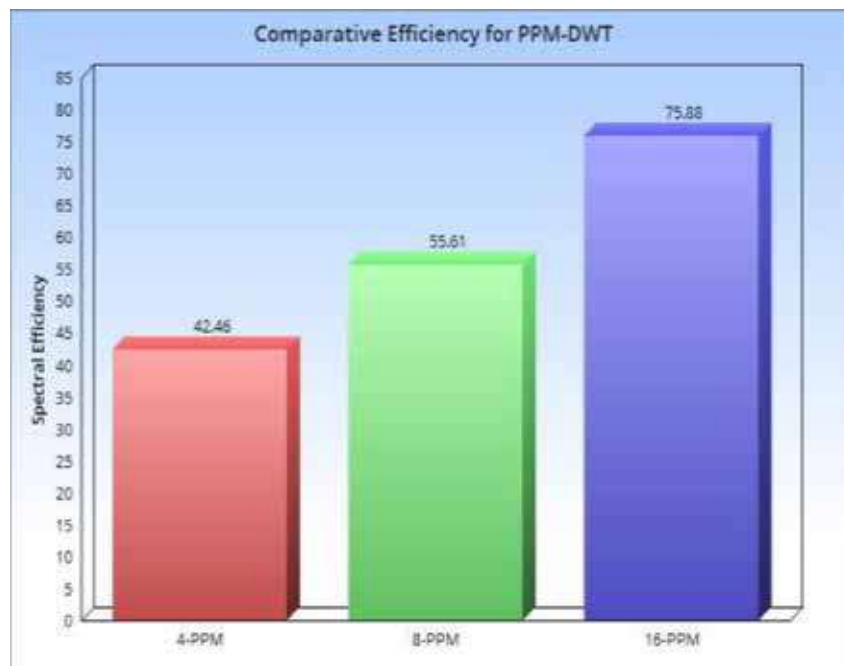


Fig. 6. Efficiency for PPM using DWT

The **Fig. 7** shows the efficiency for PPM using proposed technique SWT, for symbol length 4, 8 and 16. It is shown that the efficiency for PPM-16 is 78.94%, which is 60.92% for PPM-8 and for 4-PPM is only 46.36%.

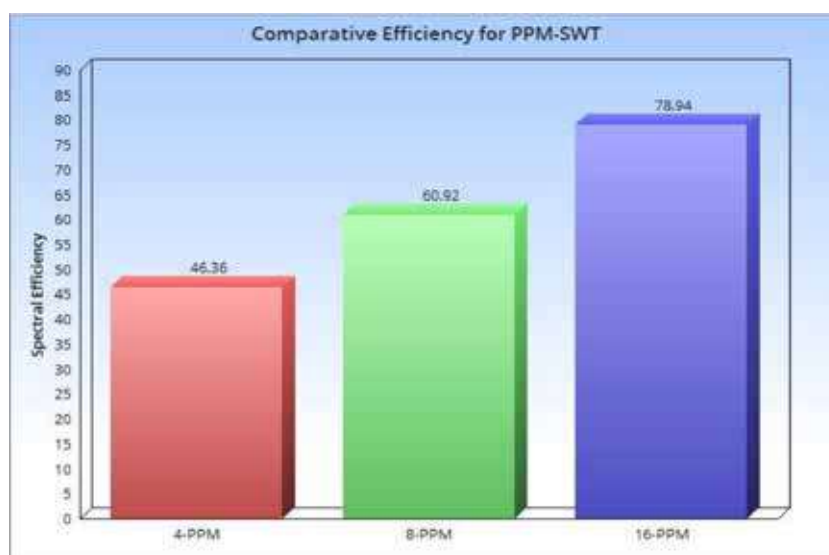


Fig. 7. Efficiency for PPM using SWT

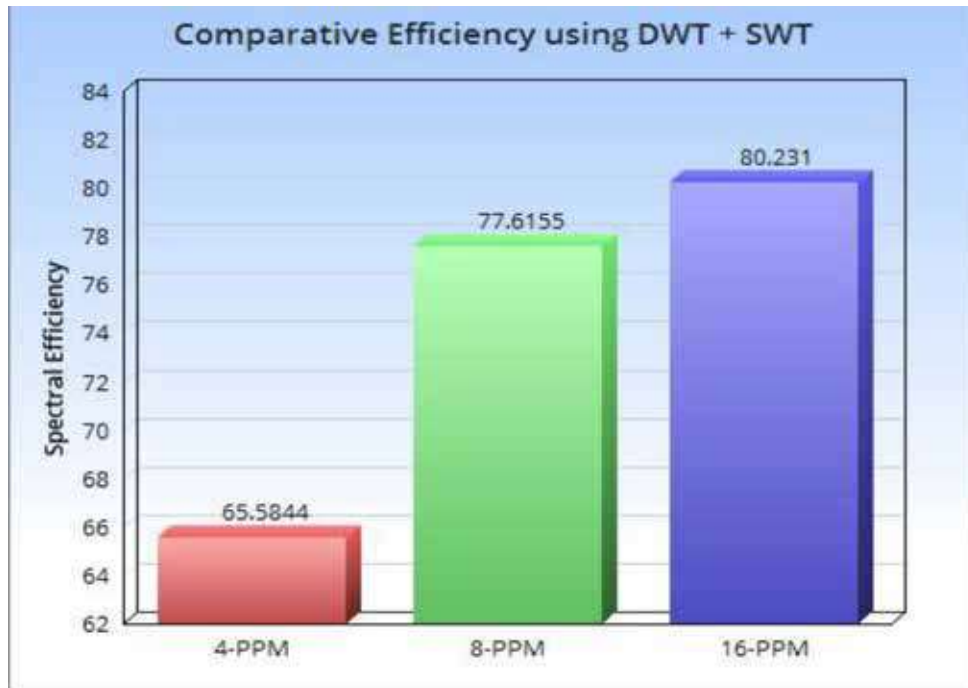


Fig. 8. Efficiency for PPM using DWT

The **Fig. 8** shows the efficiency for PPM using proposed technique DWT + SWT, for symbol length 4, 8 and 16. It is shown that the efficiency for PPM-16 is 80.231%, which is 77.62% for PPM-8 and for 4-PPM is only 65.5844%.

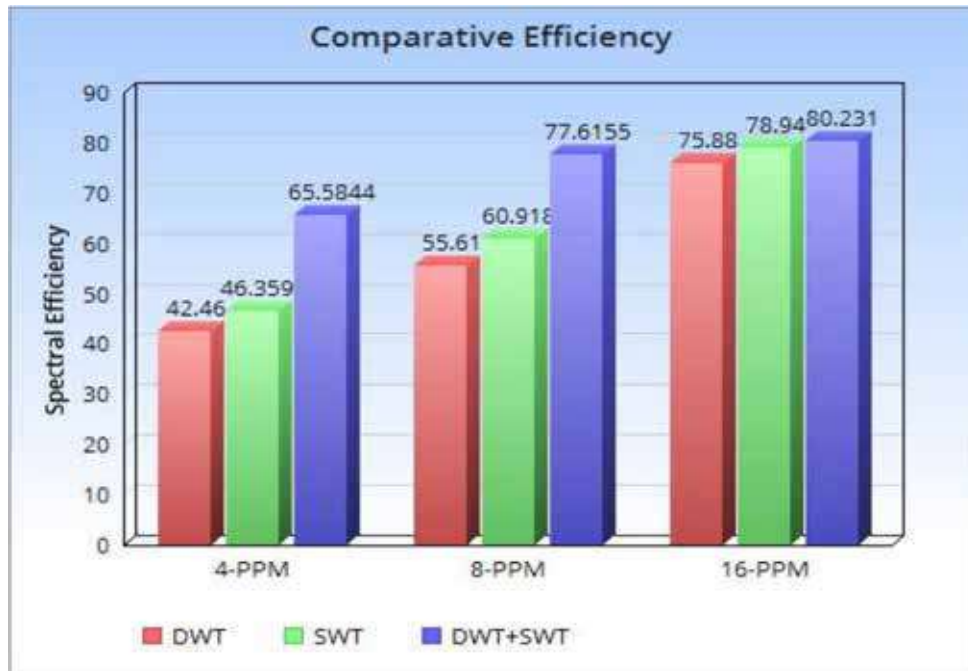


Fig. 9. Efficiency for PPM using DWT & SWT

The **Fig. 9** shows the comparative efficiency for PPM using DWT, SWT & DWT + SWT. Figure shows that the efficiency is more for PPM-16 as compared to PPM 4 and 8. On viewing the graph, it can be concluded that the efficiency of the future system is improved than the present one.

NOPR vs Data Rate

For comparison between two techniques is also made through Normalized Optical Power requirement which is defined as:

$$\text{NOPR} = \frac{\text{Optical power required to achieve a desired slot error rate}}{\text{Optical power required to achieve same slot error rate in ideal channel}}$$

The NOPR is plotted with respect to data rate, and different plots plotted using OOK & PPM are comprised of:

- NOPR, with noise only.
- NOPR, with FLI interference
- NOPR, with FLI interference and DWT denoising
- NOPR, with FLI interference and SWT denoising

Using OOK

By using first technique i.e. OOK, relation is plotted between normalized optical power and data rate. The figure 10 shows the improvement over existing technique i.e. DWT for data from 10 to 100 Mbps as given in [6] when the proposed techniques SWT and DWT + SWT are used.

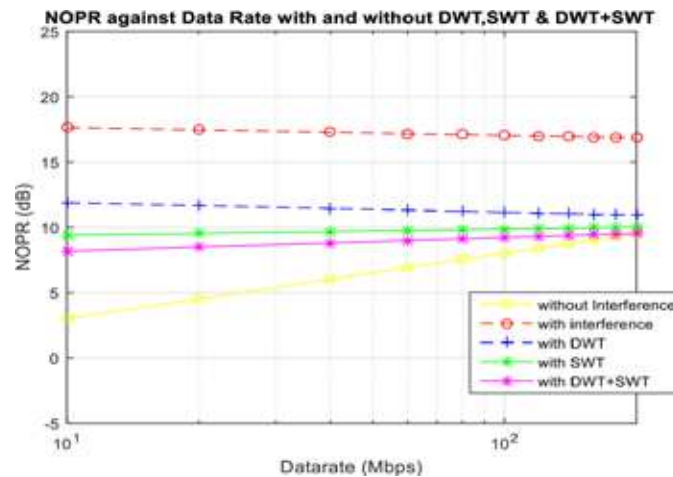


Fig. 10. NOPR vs Data rate

The same curves are plotted after increasing the data rate from Mbps to Gbps and are shown in Fig. 11.

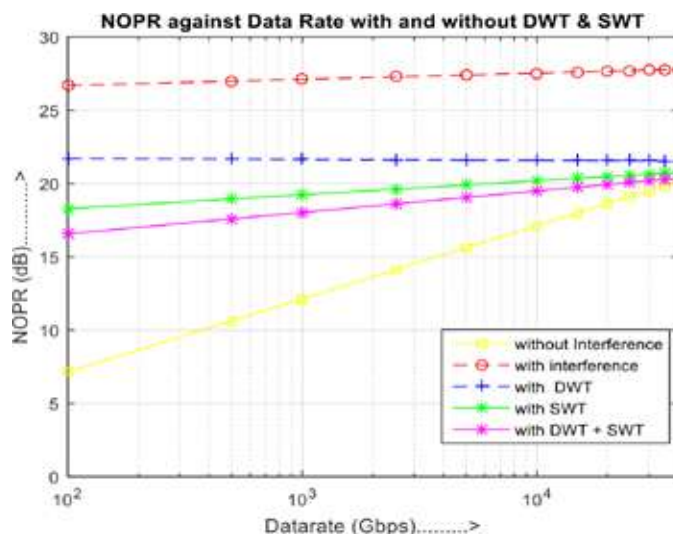


Fig. 11. NOPR vs High Data rate

On increasing data rate from 200 Mbps to 40 Gbps, the comparison is shown in **Fig. 11**, which also shows the increasing curve. It shows that with the increase in data rate, curves are still raising, and proves the improved performance of the system at high data rate too.

Using PPM

By using second technique i.e. PPM, normalized optical power and data rate are plotted for existing method and the proposed method for existing data rate and for the improved data rate too from **Fig. 12 to 17**.

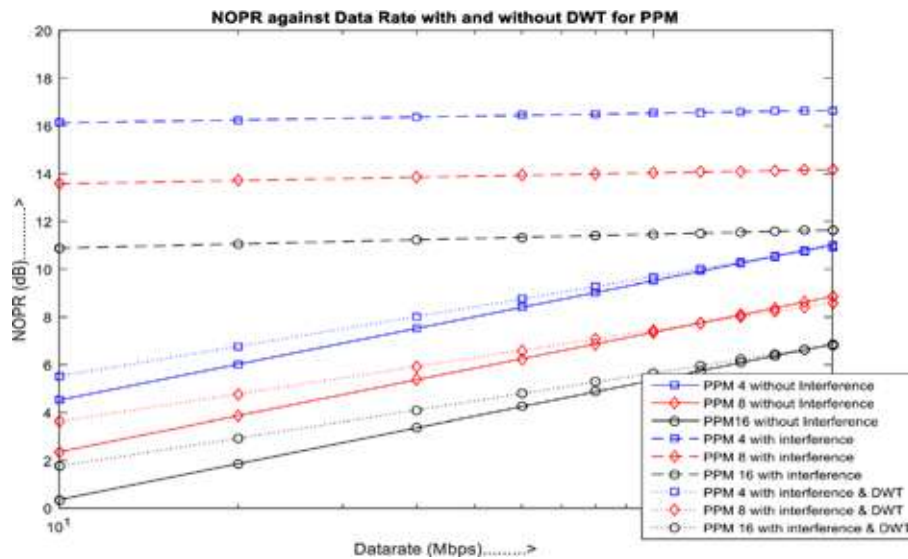


Fig. 12. NOPR against Data rate for DWT

The **Fig. 12** shows the relative plot using 4, 8 & 16 PPM for existing technique as given in [6] for data rate up to 100 Mbps only.

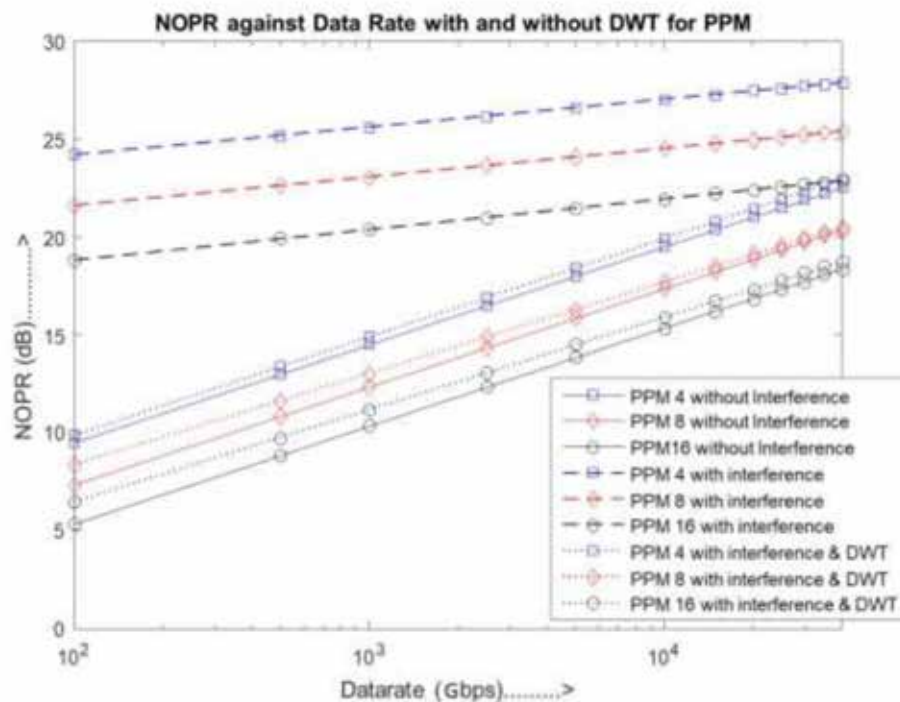


Fig. 13. NOPR against High Data rate for DWT

The Fig. 13 is plotted for the existing technique i.e. DWT but for improved data rate. As shown in figure, when data rate is increased from Mbps to Gbps, the curves try to meet, which shows the improvement as interference shows no effect.

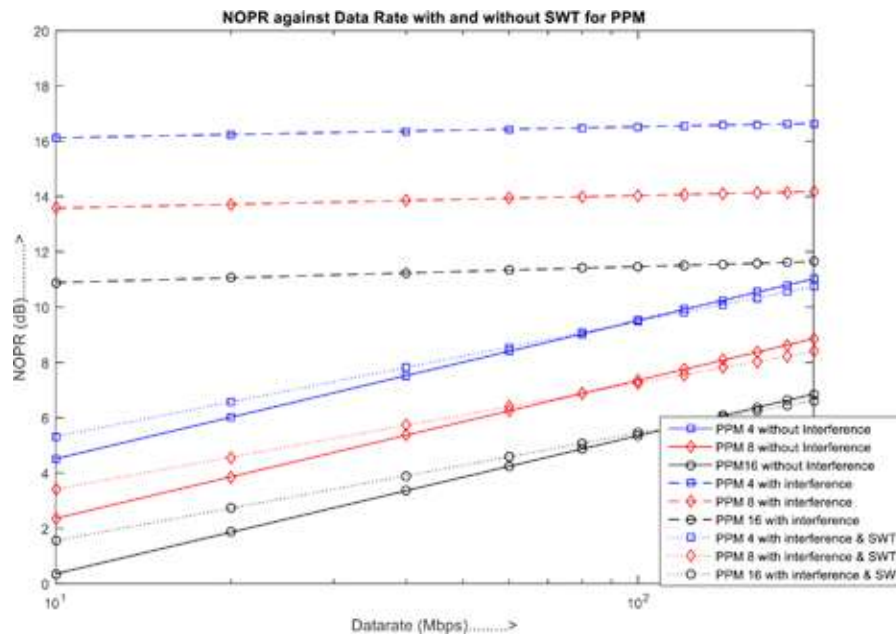


Fig. 14. NOPR against Data rate for SWT

The Fig. 14 shows the design for proposed technique for data rate up to 100 Mbps, using 4PPM, 8PPM and 16 PPM. From the figure it can be said that with SWT also, with interference, same results are obtained as obtained from DWT in Fig 12.

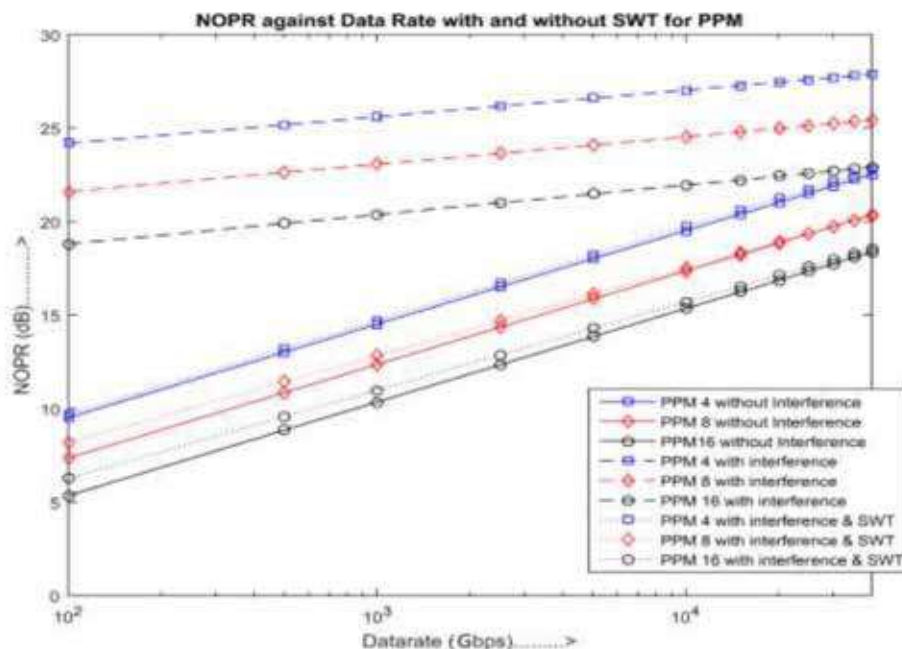


Fig. 15. NOPR against High Data rate for SWT

The Fig. 15 is plotted for the proposed technique i.e. SWT with improved data rate. As shown in figure, the same results are attained, when data rate is increased from Mbps to Gbps. It even shows the improvement over the existing technique which is given in Fig 15.

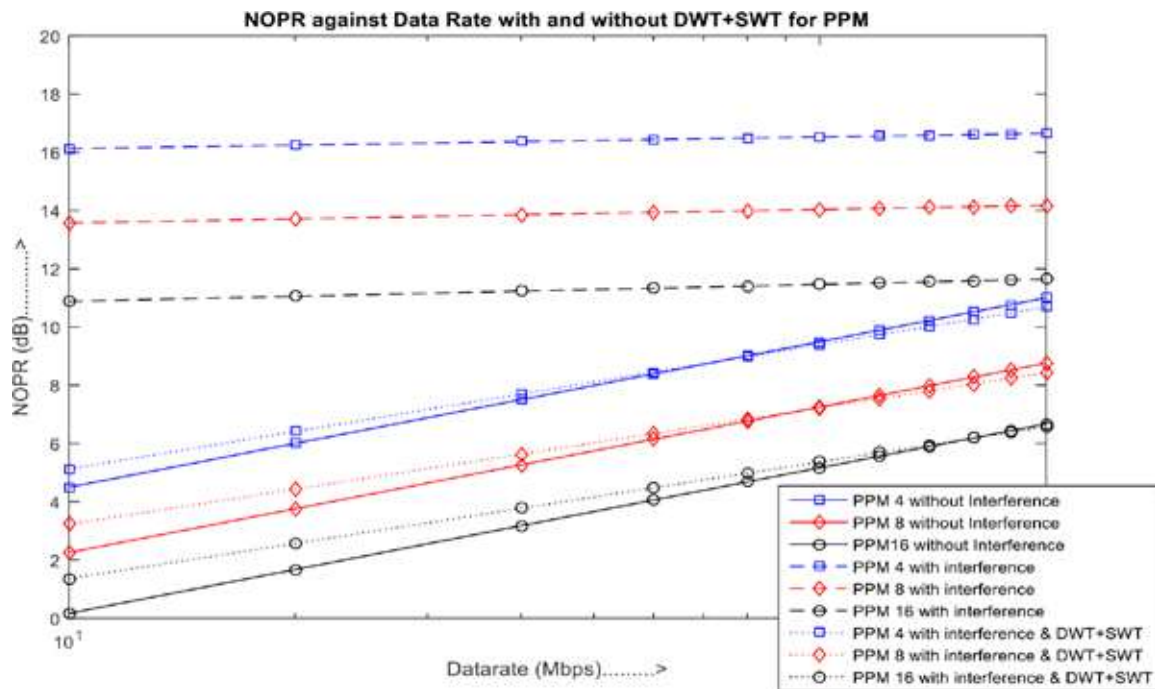


Fig. 16. NOPR against Data rate for DWT + SWT

The **Fig 16** shows the design for second proposed technique for data rate up to 100 Mbps, using 4PPM, 8PPM and 16 PPM. From the figure it can be said that with DWT+ SWT also, with interference, same results are obtained as obtained from DWT in Figure 12.

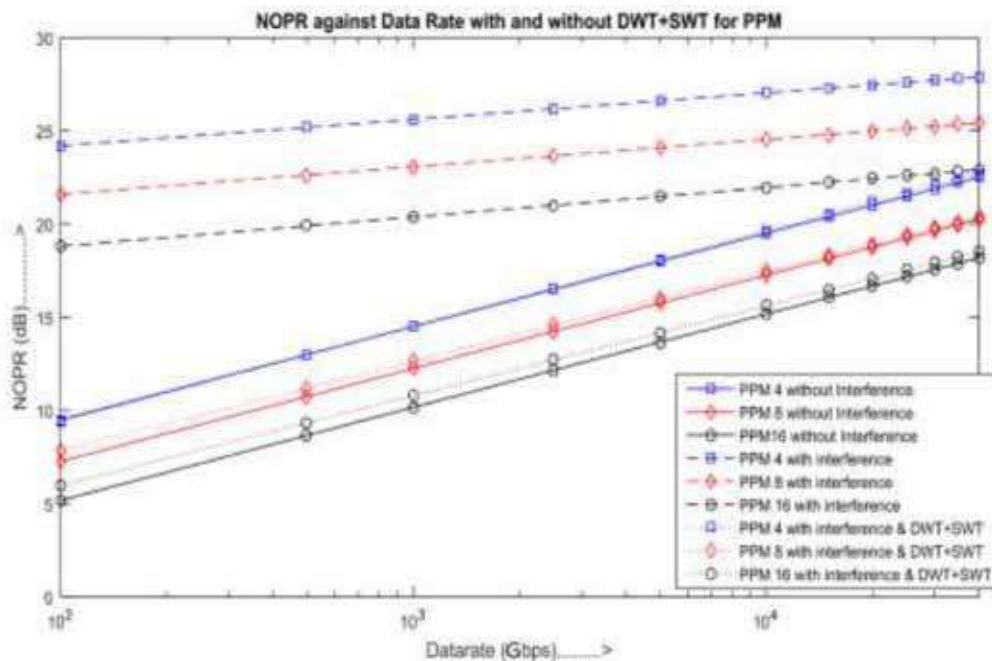


Fig. 17. NOPR against High Data rate for DWT + SWT

The **Fig. 17** is plotted for the proposed technique i.e. DWT+SWT with improved data rate. As shown in figure, the same results are attained, when data rate is increased from Mbps to Gbps. It even shows the improvement over the existing technique.

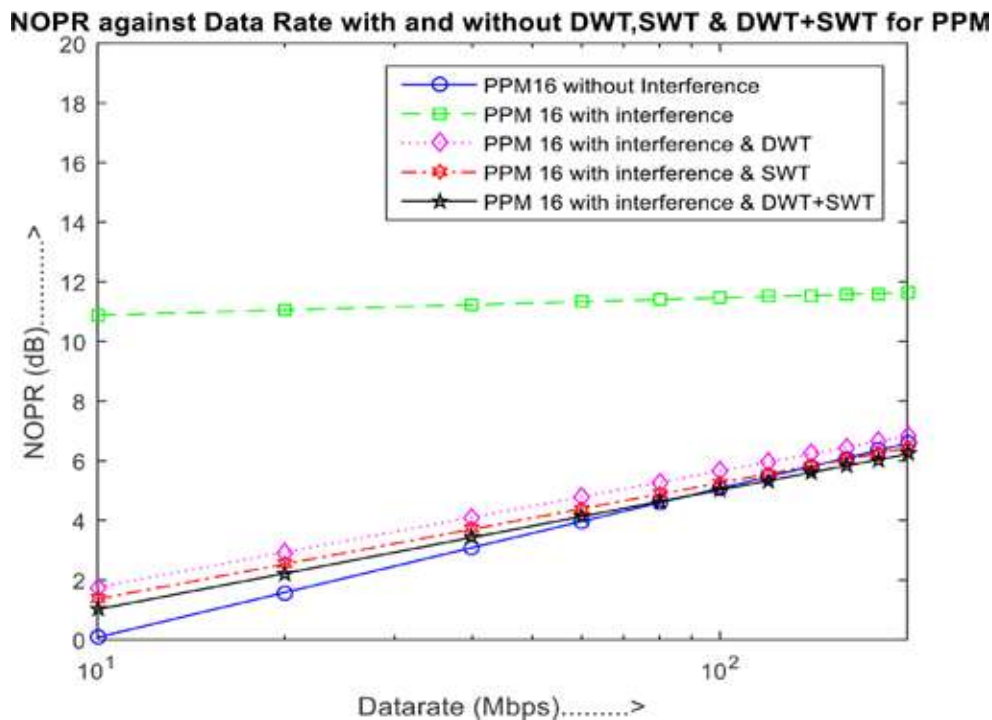


Fig. 18. Comparison between NOPR vs Data rate

The **Fig. 18** shows the comparison of existing design and proposed techniques for data rate up to 100 Mbps, using 16 PPM. From the figure it can be said that SWT and DWT+SWT with interference, approaches near to the curve having no interference, when compared with the existing one i.e. DWT.

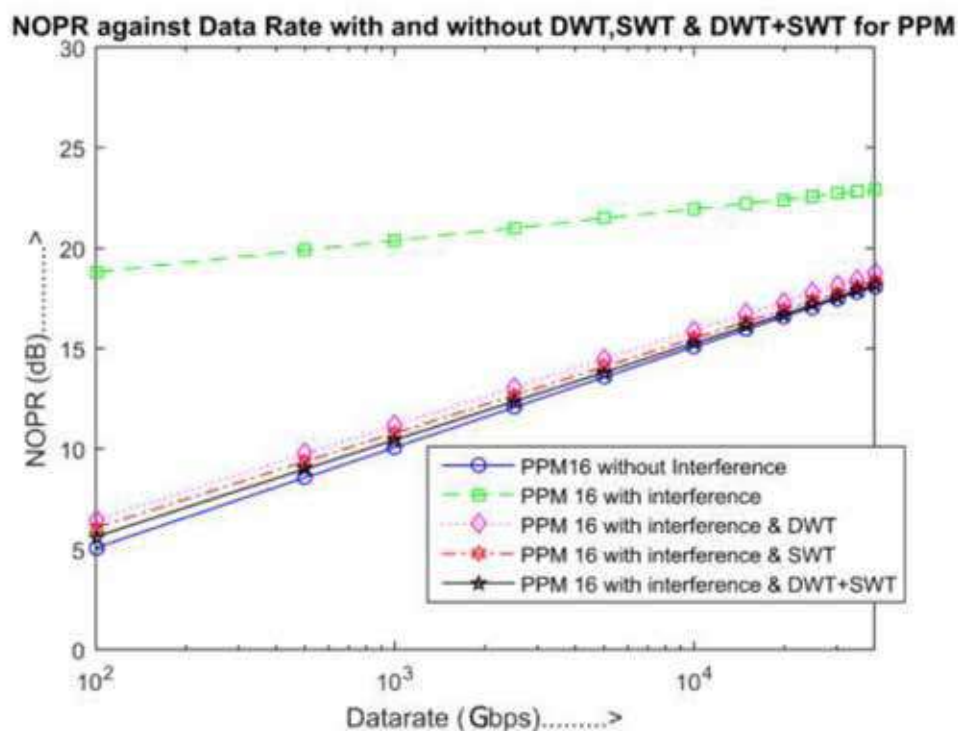


Fig. 19. Comparison between NOPR vs High Data rate



The Fig. 19 also shows the comparison of existing design and proposed techniques for the improved data rate i.e. from Mbps to 40 Gbps, using 16 PPM. Through graph, it can be concluded that, at high data rate, DWT+SWT, SWT and DWT approaches near to the each other but approaches near to the curve with no interference, hence showed improvement for improved data rate.

CONCLUSION

The Stationary wavelet transform has various applications and even shows improvement in many fields like Image processing, Signal denoising, Pattern recognition, Brain Image Classification and Pathological Brain detection. In the proposed system, same is implemented in place of DWT and where it contributes a better performance in terms of better SNR/BER, Spectral Efficiency and improved data rate for both OOK & PPM while using different Wavelet Techniques i.e. WT+SWT, SWT and DWT.

REFERENCES

1. H. Elgala, R. Mesleh & H. Haas, "Indoor Optical Wireless Communication: Potential & state of art", IEEE Communication Magazine, vol. 49, no. 9, pp 56- 62, Sep 2011.
2. F. R. Gfeller & U. Bapst, "Wireless In-Home Data Communication via Diffuse Infrared Radiation," Proceeding IEEE, vol 67, pp 1474-1485, 1979.
3. A.J.C. Morairo, R.T. Valadas & De Oliveira, A.M. Duarte, "Characterization & modeling of artificial light interference in OWC System", Proceeding of PIMRC, vol 1, pp 326-331, 1995.
4. A.C. Boucouvals, "Optical wireless Communication", IEEE Procdings on Opto electronics, vol 147, pp 279-280, 2000.
5. J.R. Barry, "Wireless Infrared Communication," Kluwer Academic Publishers, pp 79-107, Boston 1994.
6. S. Rajbhandari, Z. Ghassemlooy, M. Angelova, " Wavelet Artificial Neural Network Receiver for Indoor Optical Wireless Communication", Journal of lightwave Technology, vol. 29, no. 17, pp. 2651- 2659, 2011.
7. H.D.O. Mota, F.H. Vasconcelos, C.L.D. Castro, "A Comparison of Cycle spinning vs Stationary Wavelet Transform for the extraction of Features of a Partial Discharge Signal", IEEE Transactions on DiElectric and Electrical Insulation, Vol. 23, no. 2, pp 1107-1118, April 2016.
8. Naga Rajesh A1, Chandralingam S1, Anjaneyulu T2, Satyanarayana K3, "Denoising EOG Signal using Stationary Wavelet Transform" MEASUREMENT SCIENCE REVIEW, Volume 12, No. 2, 2012.
9. Y. Zhang, "Feature Extraction of Brain MRI by Stationary Wavelet Transform and its Applications". Journal of Biological Systems, pp 115-132. doi:10.1142/S0218339010003652.
10. Z. Dong, "Magnetic Resonance Brain Image Classification via Stationary Wavelet Transform and Generalized Eigenvalue Proximal Support Vector Machine". Journal of Medical Imaging and Health Informatics, pp 1395-1403. doi:10.1166/jmihi.2015.1542.
11. H. Prasetyo, C.H. Hsia, J.M. Guo, "Improving EDBTC Image Quality using Stationary and Decimated Wavelet Transform", International Symposium on Electronics and Smart Devices, 2019.
12. K. Kannan, S.A. Perumal, "Optimal Level of Decomposition of SWT for Region Level Fusion of Multi Focused Images",
13. S. Rajbhandari, "Application of Wavelets and Artificial Neural Network for Indoor Optical Wireless Communication Systems", PhD Thesis, School of Computing, Engineering and Information Sciences, Northumbria University, 2009.
14. http://en.wikipedia.org/wiki/discrete_wavelet_transform.
15. http://en.wikipedia.org/wiki/stationary_wavelet_transform.
16. Y. Yang, C.S. Boling, A.M. Kamboh, A.J. Mason, " Adaptive threshold Neural spike detector using Stationary wavelet transform", IEEE Transaction on Neural System & Rehabilitation Engineering, vol. 23, issue6, pp. 946-955, 2015.
17. M. Holschneider, R. Kronland-Martinet, J. Morlet and P. Tchamitchian, "A real time algorithm for signal analysis with the help of wavelet transform", in wavelets, Time-Frequency Methods and Phase Space, pp 289-297, Springer-Verlag, 1989.

Streaming Video Data from Remote Sites to Command Center under Bandwidth Constrained Environment

Anitha K M, Sampath Kumar R, Prabha Gupta, Sonu Shreshtha

Software SBU, BEL Bangalore

✉ anithakm@bel.co.in

ABSTRACT

This paper demonstrates a video surveillance algorithm for the efficient transfer of video data over RTSP session for a multisite organisation distributed in different geographic locations. The sites are organised in clusters in a hierarchical manner which are connected to their respective cluster head quarter site and all these cluster head quarter sites are connected to a single apex command and control centre (C&C).

A solution that efficiently and reliably deals with real-time buffer management for continuous live streaming for a large number of cameras spread across several locations is a challenging job in a bandwidth constrained network environment.

Keywords : Video management system; RTSP; Remote assets table; Command and control center; C&C center.

INTRODUCTION

BEL has installed its Video Management System (VMS) in one of the customer premises as part of its Enterprise Access Management System. The solution is installed in multiple sites of the client with one of the site being the command and control center.

The network has a pyramidal connectivity with (T3) being at the apex. It is connected on leased lines with all its T2 sites which are the respective cluster headquarters. The T2 sites are connected to their respective T1 sites which are the field sites through the captive client network. This is shown as **Fig. 1** Typical VMS Federated Architecture.

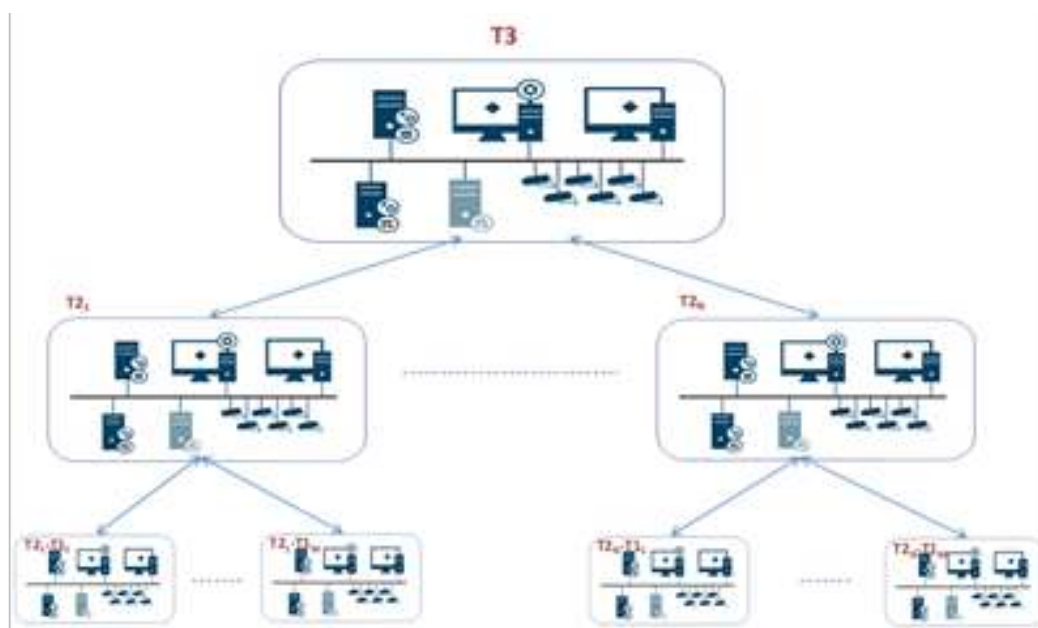


Fig. 1. Typical VMS Federated Architecture

Video Management system (VMS)

The VMS is typically comprised of cameras, management server, recording server(s) administrative client and user clients. The streaming sessions (RTSP) are created by recording server and the data base (DB) management is by the management server. The live stream of the cameras and playback of the recorded video is through the user client. In the T2 and T3 setup, there is an additional server called as the media server.

A UI is provided in the VMS to set the parent IP of the site. For each T1, the parent IP is the IP of its T2 VMS server. The parent IPs for all the T2 sites is the server IP of the T3 server at Delhi.

Camera and Server health Monitoring

Each site will send the health status of its servers and cameras to its respective parent IP periodically (5 seconds) through UDP sockets. The T2 site will receive this health packet from all its T1 sites and updates its DB (Remote Assets Table). It also consolidates the details from the available T1 sites and sends this consolidated data to T3 site along with its own health data periodically (every 10 seconds).

The T3 site will receive the consolidated health packet from all its T2 sites and updates the DB (Remote Assets Table). So at T3 at any point of time, the health status of the cameras and servers of the complete enterprise VMS is available in its DB in the Remote Assets Table. The health message flow is depicted in **Fig. 2:- Health Message Tx Rx**

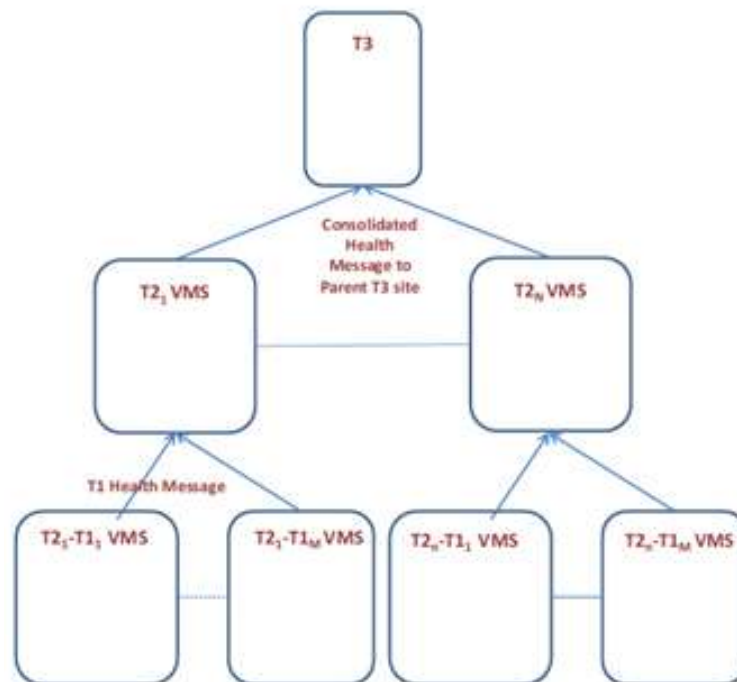


Fig. 2. Health Message Tx Rx

Remote Camera Session

At every local site, the recording server creates typically two sessions of RTSP, one for recording which is usually in the Full HD resolution at 15 FPS. The other is for the live streaming which is generally the SD resolution at 30 FPS. These sessions are consumed in the local network. In addition to this, a remote RTSP session is created which is at 4 CIF resolutions at 7 FPS. This stream is transmitted to the parent site or the T3 site on a demand basis. The resolution and the FPS for the remote RTSP session are kept low as the video data is bandwidth intensive and the customer network would get bogged down otherwise.

The Media server at T2/T3 would subscribe to the above remote session of its child server (on demand), buffer it for a few seconds and create a local RTSP session for its clients at T2/T3. The client at T2/T3 will subscribe to this session of the Media server and display the video stream of the remote sites. As the data is buffered and also streamed from the local Media server, the display is smooth and glitch free.

The client at T2 can display the remote streams of its T1 sites and the client at T3 can display the remote streams of any T1 or T2 sites.

Command And Control Center Display

At T3, there is a war room setup with a video wall. This facility is provided to view the camera stream of all its assets.

A system had to be designed by taking into account the bandwidth availability of the customer network which differs from site to site. The cluster connectivity from each T2 cluster to T3 is also not uniform. For e.g.:- The connectivity from cluster X to T3 is high whereas the connectivity from cluster Y to Delhi is very poor.

Bandwidth Constrained Streaming

Each cluster has a threshold index which indicates the number of video sessions it can stream out. This is configurable for each cluster depending on its bandwidth availability.

The T2 sites are indicated as T2 i where i can vary from 1 to N. In the case of the customer network, $N=22$.

The T1 sites for any T2 are depicted as T2i_T1j, where i can vary from 1 to N and j can vary from 1 to M. In the case of the customer network M varies from 1 to 50.

The camera at T2 site is depicted as T2i_CAMk. The camera at any T1 site is depicted as T2i_T1j_CAMk, where k can vary from 1 to P. In the case of the customer network P varies from 5 to 200.

The data read from the Remote Assets Table is read and split into bins of immediate child clusters. In the case of T3, there are N bins which represent N T2s. In the case of T2, there are M bins which represent M T1s. Each bin has online cameras from all its child sites. The concept is displayed as **Fig. 3-Distribution of camera into T2 bins at T3**.

Each of these bins has a threshold index T2i_Thl, which is the bandwidth availability of the respective T2 cluster. l varies from 1 to Q. It means that from a particular T2 cluster only T2i_Thl camera can be streamed at a time. In the case of the customer network l varies from 1 to 10.

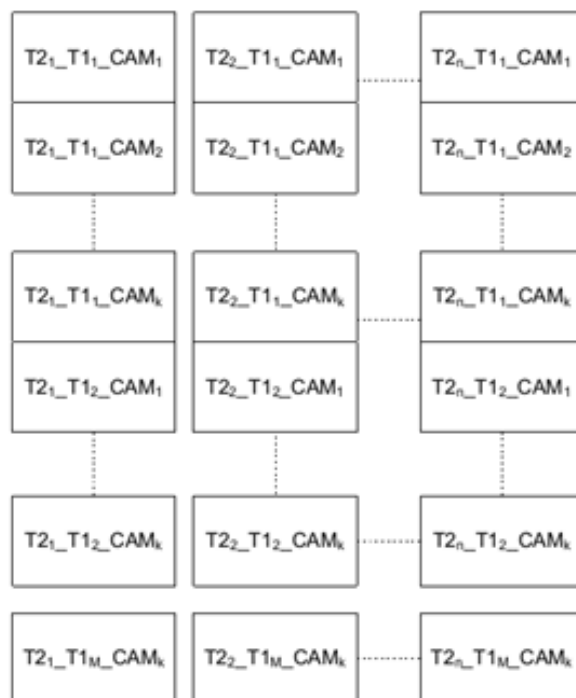


Fig. 3. Distribution of camera into T2 bins at T3

By Bandwidth analysis, it was determined that at T3, at a time T3_Thl remote sessions can be streamed. If we try to stream more than this number, the sessions were getting broken and other network traffic was getting blocked. The Input Bandwidth

Threshold at T3 site is defined as T3_Thl. It can vary as per the T3 site bandwidth availability. In the case of the customer network T3_Thl is 32

The total available cameras at the complete customer network are around 2000 to 2500. A system had to be designed that would stream T3_Thl remote cameras at T3 at a time which meant at a time the Media server at Delhi would establish remote RTSP sessions with T3_Thl cameras belonging to various remote sites. The selection of these cameras is through an algorithm.

On startup, the media server at T3 reads Remote Assets Table of the DB. It retrieves the available camera ids of online cameras from the table and creates queue with these details. The queue size would be typically around 1900 to 2000 cameras. The queue is reordered in chunks of T3_Thl elements in such a way that these elements would have a mix of camera from all the clusters.

At T3 the queue is re-ordered into T3_Thl sized chunks based on the above constraints and in the following manner

$$\sum (T2i_T1j_CAMk, \leq T2i_Thl) \leq T3_Thl$$

i = 1 to N (N = max number of T2)

j = 1 to M (M = max number of T1 under any T2)

k = 1 to P (K = max number of cameras at any site)

l = 1 to Q (Q = max number of RTSP session that can be transmitted or received across sites)

The client at the command and control center will display T3_Thl / 2 cameras in the first sweep. This will be retained on the display for Z seconds. In the case of the customer network Z is set as 300. After Z seconds these T3_Thl / 2 RTSP sessions are closed by the media server and the remaining T3_Thl / 2 sessions are displayed. At the same time, the media server will pick up the next T3_Thl / 2 cameras from the queue and creates session with the respective remote servers. This ensures that at any time T3_Thl sessions will be maintained by the media server at T3.

We display T3_Thl / 2 sessions at a time to maintain seamlessness between the sweeps. If we display all the T3_Thl sessions at a time, during the subsequent sweeps the session creation and stabilization glitches will be visible to the user.

The number of cycles

$$C = \sum (T2i_T1j_CAMk,) / (T3_Thl / 2).$$

In the case of the customer network $\sum (T2i_T1j_CAMk,) = 2000$. T3_Thl = 32.

So C = 125.

The time taken for C cycles is C * Z seconds, In the case of the customer network Z = 300 seconds, so time taken is 10.41 hours for the display of all the cameras. The concept is depicted in **Fig. 4** Display of Remote Camera streams

Once the queue is empty, it is recreated again by reading the Remote Assets Table where the latest data is available.

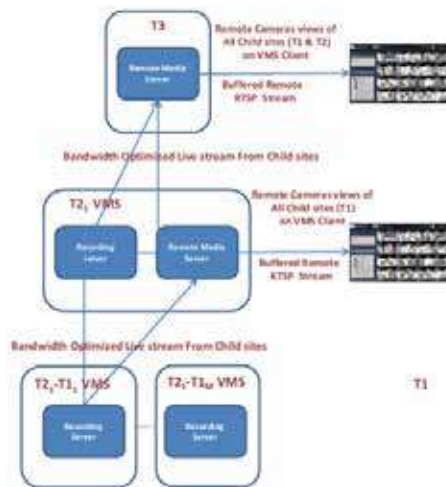


Fig. 4. Display of Remote Camera streams



A feature is also provided to view any camera from any of the remote site at Delhi on a need basis. In this case the user can select a few cameras from any cluster and can start streaming them. The system ensures that this does not exceed the T2i_Thl for the particular cluster. The remote stream would be displayed till the user stops or changes its selection.

CONCLUSION

The system displays camera stream of all remote site cameras in multi-tile layout with periodic swaps in round robin manner for 24*7, smooth and glitch free surveillance. This solution is sufficiently fault tolerant and robust with scalability of camera network to support addition of new cameras and also manages availability of network bandwidth efficiently.

REFERENCES

1. Real Time Streaming Protocol (RTSP)- <http://tools.ietf.org/html/rfc2326>.
2. Q. Lone, "Bandwidth allocation for video streams subject to an end-to-end percentile delay", MS Thesis, North Carolina State University, 2011
3. Basem Al-Madani, Anas Al-Roubaiey, and Zubair A.Baig, "Real-Time QoS-Aware Video Streaming: A Comparative and Experimental Study" Hindawi Publishing Corporation Advances in Multimedia Volume 2014, Article ID 164940.
4. D. Marpe, T Wiegand, and G J Sullivan, "The H.264/MPEG4 advanced video coding standard and its applications," IEEE Communications Magazine, vol.44, no.8, pp.134–142, 2006.



Design of Charge Pump PLL using 180nm CMOS Technology

Ashwini Desai¹, Uma Kulkarni²

Department of Electronics and communication Engg.¹, Department of Electrical and Electronics Engg.²

KLE DR. M. S. Sheshgiri College of Engineering and Technology, Udyambag, Belagavi

✉ ingalekl2000@gmail.com

ABSTRACT

Low Power with high stability is the critical factor for today's VLSI designs. Clock Systems synchronize the working of various modules that exist in a system. For any design it is essential that the clock signals must be stable and have minimum rise and fall times, specified duty cycles, and zero skew. Phased Locked loops (PLL) with low power consumption are essential to control any clock system. In this paper, we propose a Charge Pump PLL (CPPLL) design used for clock synchronization and generation. The design of CPPLL involves designing Phase Frequency Detector, a Charge pump with filter, Voltage Controlled Oscillator (VCO) and divider circuits. The proposed design is implemented in Cadence Virtuoso 6.1.5 using 180nm technology. A locking time of 757ns was achieved. The results show that the total power consumed by the CPPLL was 248 μ W excluding the divider.

Keywords : Phased locked loop; Low power; VCO, Virtuoso.

INTRODUCTION

A processor consists of many sequential and combinational circuits along with storage elements. All these circuits are interdependent and should work in synchronization with each other. Clock system ensures synchronized working of all the circuits. A good clock system design ensures that there is zero or minimal clock skew and also ensures that the clock signal has low jitter and noise. The important part or the essence of the clock system is the phase locked loop. There are several designs like APLL (Analog or Linear PLL), DPLL (Digital PLL), SPLL (Software PLL), NPLL (Neuronal PLL) and CPPLL (Charge pump PLL). CPPLL is a modification of the PLL with PFD (phase frequency detector). It has the advantage that it allows quick locking onto the phase of the input signal.

The performance matrices for today's PLLs like speed, power and area have led to drastic changes in the design of phase locked loops [1]. As the complexity and processing capability of the processor increases the complexity of designing a good and efficient PLL for a clock system also increases. A clock signal needs to be distributed to all the components of the system. The distribution should be such that each node receiving the clock signal should be in synchronous with each other and jitter free [2]. Hence necessary topologies should be employed which provide accurate clock signal to all the nodes.

Phase locked loop is a closed loop feedback system that consists of phase detector, filter and a controlled oscillator. Phase detector compares the reference signal and the feedback signal and generates phase error. Based on this phase error the oscillator either increases or decreases the oscillation frequency. PLL along with buffers help in achieving zero clock skew for a clock system. A phase detector is used to detect any phase difference (also difference in frequency) with respect to the reference signal and the feedback signal. The phase detector is followed by the loop filter. The filter output operates the oscillator. Hence the oscillator employed here is known as the voltage controlled oscillator (VCO). Owing to the lesser number of modules traditional analogue phase locked loop is being employed. Figure 1 represents PLL architecture. The phase locked loop consists of the following parts:

- Phase frequency detector/Phase Detector.
- Charge pump with LPF (Low Pass Filter).
- Voltage controlled oscillator.
- Frequency divider.

In this paper a CPPLL is designed and implemented in 180nm CMOS technology using Cadence Virtuoso 6.1.5. and is suitable for clocking systems used in low power VLSI designs.

METHODOLOGY FOR CPPLL DESIGN

Phase Locked Loop: A PLL is a controlled feedback system and consists of phase detector, filter and a controlled oscillator. It retains a fixed phase relationship between the phases of a reference clock and the output clock. PLL can track the phase changes within the designed bandwidth. A PLL multiplies a low-frequency input clock Clk_{in} and produces a high clock frequency Clk_{out} known as clock synthesis [3]. The various components of the CPPLL design are shown in **Fig. 1**.

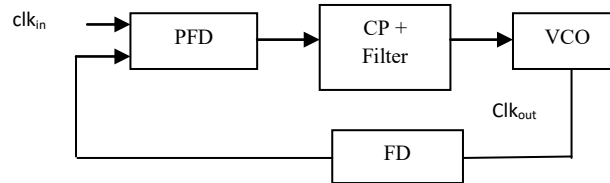


Fig. 1. CPPLL block diagram

Phase Frequency Detector Design: **Fig. 2** shows the PFD module integrated with charge pump. It has two outputs Vout and Vout1 which are not complementary. Based on whether the frequency of the input signal V_{in} is greater than the frequency of the signal at $V_{\text{in}1}$, pulses are produced at either Vout or Vout1. If frequency of both the signals is same, then the pulses are produced either on Vout or Vout1 with width equal to the phase difference between the two input signals. The PFD design is simulated for different variations of the input signals V_{in} and $V_{\text{in}1}$ considering all the corner cases. The phase and frequency difference between the two input signals are compared by PFD. Accordingly the PFD generates output signals with respect to the phase and frequency deviations.

Charge Pump and Filter: Charge pump acts as a converter. It converts the digital signal of the output of the PFD into the analog signal. It consists of two switches. A combination of charge pump and LPF offer two important advantages over the XOR/LPF designs. The capture range of the PLL is now only dependent on the VCO output characteristics and also the static phase error is zero. The closed loop transfer function of the CPPLL is given in equation 1.

$$H(s) = \frac{K_{pfd} K_{vco}}{s^2 + K_{pfd} K_{vco}} \quad (1)$$

By solving equation (1) we conclude that there are two imaginary poles as in equation 2.

$$\omega = \pm j \sqrt{K_{pfd} K_{vco}} \quad (2)$$

The instability can be avoided by adding a zero to the open loop transfer function. This is achieved by placing a resistor in series with the output capacitor. LPF is used to filter the output obtained from the phase detector. If a PFD is used then the LPF is used in conjunction with the charge pump.

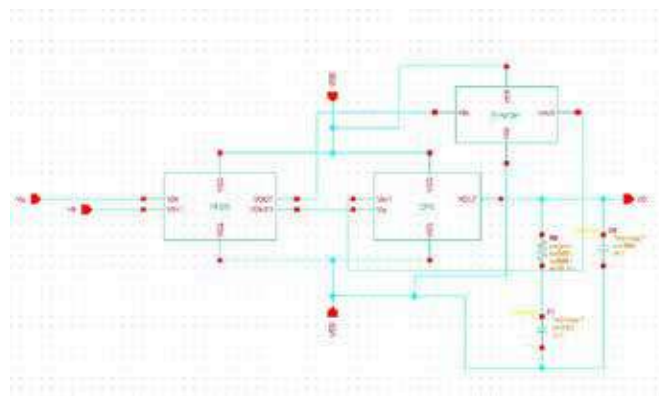


Fig. 2. Charge pump integrated with PFD

The charge pump along with the PFD is shown in **Fig. 2**. Charge pump is driven by the output pulses from the PFD. The output pulses either charges the loop filter or discharges the loop filter, accordingly the control voltage is generated [4].

Voltage Controlled Oscillator: VCO is a circuit that generates oscillations based on its control voltage. As the applied voltage increases, the oscillations increase and as the control voltage decreases, the oscillations decrease [6]. The output frequency of the VCO is given in equation 3.

$$\omega_{out} = K_{vco} V_{cont} + \omega_0 \quad (3)$$

V_{out} = Output frequency

K_{vco} = Gain of the VCO

V_{cont} = Control voltage

ω_0 = Free running frequency

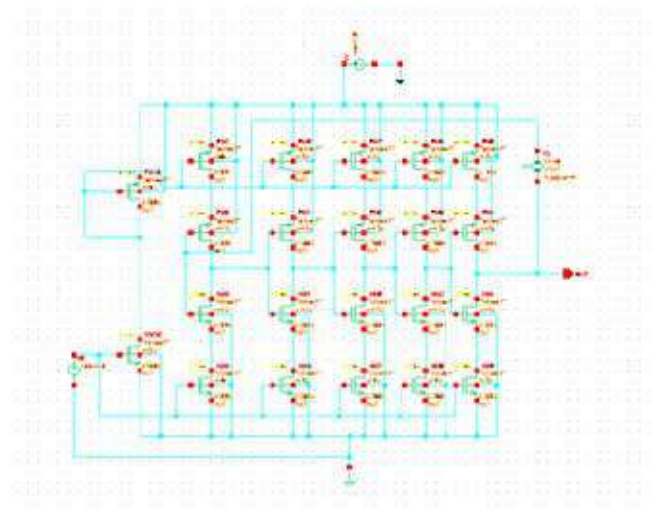


Fig. 3. Schematic of VCO.

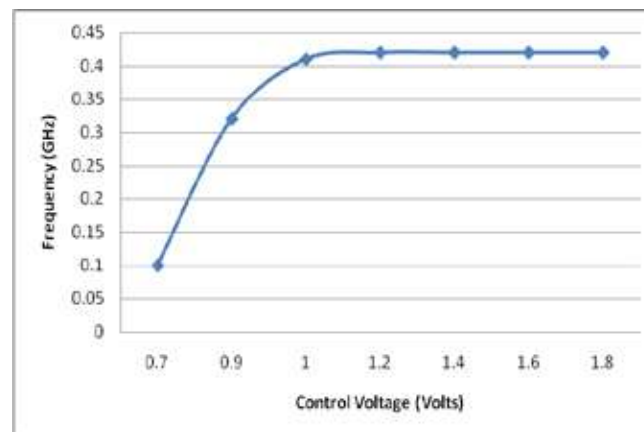


Fig. 4. VCO control voltage vs frequency

The implementations of VCO using Cadence Virtuoso in 180nm technology is shown in **Fig. 3**. The VCO was designed using five inverter stages at a DC voltage of 1.8 volts.

The VCO tuning characteristics are plotted and is shown in **Fig. 4**. It is seen that the VCO has a lock in a range of 0.35MHz to 0.43MHz with a low control voltage variation of 0.7 to 1.2V after which it stabilizes. This is achieved at low power dissipation of 176.54μW.

Frequency Divider Circuit: The VCO output will be usually much higher than that of the reference signal. Hence to reduce it and make it comparable with the reference signal, the output of the VCO must be reduced. Frequency divider circuit is used to divide the signal by a suitable factor. The design of the divider circuit is implemented for $n = 2$.

RESULTS

The modules of CPPLL were individually designed and simulated in CADENCE Virtuoso 6.1.5 using 180nm technology. The modules were integrated on obtaining satisfactory results. The simulations were verified using CADENCE Analog Design Environment with Spectre which supports for detecting and reporting circuit problems during simulation. The simulation results of the integrated CPPLL are shown in **Fig. 5**. The locking time was calculated using Virtuoso Visualization and Analysis XL and the Calculator Graphical User Interface (GUI) and a locking time of 757ns was obtained. The power dissipation of the PLL was 248 μ W which is low compared to other designs at 180nm technology [5].

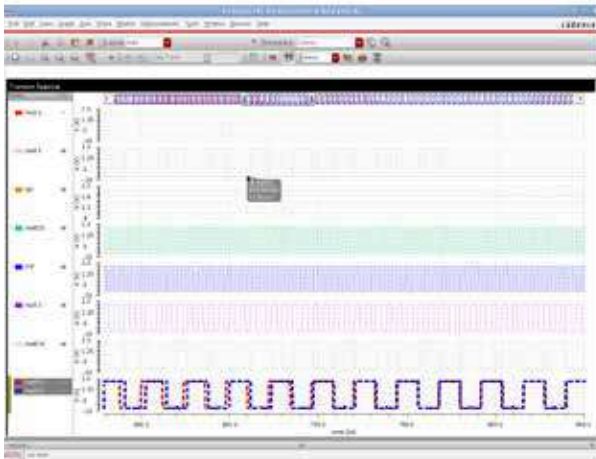


Fig. 5. PLL simulation results

The power dissipation of each of the PLL submodules was calculated using Virtuoso Visualization and Analysis XL tool and the results are shown in **Table 1**.

Table 1. Experimental results

SL.NO	PLL Submodules	Power Dissipation μ W
1	PFD	7.40
2	CP+LPF	64.06
3	VCO	176.54
4	Divider	113.1
5	PLL (Divider optional)	248.0

CONCLUSION

A low power CPPLL is successfully implemented for a processor which is under evaluation. A charge pump is designed to minimize the delay due to jitter. The current mismatch between the charging and discharging cycles is also reduced. The PFD module gives overall improvement in power consumption and increased system stability. The CPPLL is simulated in CADENCE 180nm technology and a locking time of 757ns was achieved. A stable VCO frequency range of 0.35MHz to 0.43MHz is achieved. The results show the total power consumed by the PLL is 248 μ W excluding the divider which is 7-10% less than the existing designs.

REFERENCES

1. Behzad Mesgarzadeh, Member, IEEE, and Atila Alvandpour, Senior Member, IEEE, "A Low-Power Digital DLL-Based Clock Generator in Open-Loop Mode", IEEE Journal Of Solid-State Circuits, Vol. 44, No. 7, July 2009.
2. Martin Omaña, Daniele Rossi, Daniele Giaffreda, Cecilia Metra, Fellow, IEEE, T. M. Mak, Asifur Rahman, and Simon Tam, Senior Member, IEEE, "Low-Cost On-Chip Clock Jitter Measurement Scheme", IEEE Transactions on Very Large Scale Integration (VLSI) Systems (Volume: 23 , Issue: 3 , March 2015).
3. Gande Bhargav, Govind Prasad, Srikar Datta Canchi, Badam Chanikya, "Design And Analysis Of Phase Locked Loop



- in 90nm CMOS” Thirteenth International Conference on Wireless and Optical Communications Networks (WOCN)“ published in IEEE Xplore, December 2016.
4. Akshay A. ; Divya Kiran ; Chandramohan P. ; Punithavathi Duraiswamy, “Design and analysis of Phase Locked Loop for low power wireless applications”, Conference on Emerging Devices and Smart Systems (ICEDSS), published in IEEE Xplore October 2016.
 5. S. Aditya_ and S. Moorthi, “A Low Jitter Wide Tuning range Phase Locked Loop with Low Power Consumption in 180nm CMOS Technology”, 2013 IEEE Asia Pacific Conference on Postgraduate Research in Microelectronics and Electronics (PrimeAsia).
 6. Ashish Tiwari, Renu Prabha Sahu, “ Review on Design and Analysis of Low Power PLL for Digital Applications”, International Journal for Research in Applied Science & Engineering Technology ,ISSN: 2321-9653; IC Value: 45.98; SJ Impact Factor: 6.887 Volume 6 Issue VI, June 2018.
 7. Behzad Razavi, “RF Microelectronics”, Second Edition, Pearson 2012.



A Brief Study of Optical Flip-flops based on Microring Resonator

Kankana Debnath, Srikanta Das*, Arka Roy Bin, Bishanka Brata Bhowmik

Department of Electronics and Communication Engineering, Tripura University, Agartala, Tripura

✉ srikanta.ece@tripurauniv.com

ABSTRACT

Microring resonators become the heart of the present optical communication system. Various logic circuits are implemented using microring resonator. Because of its simplicity and various good quality like low losses, low power requirement properties it has become popular. In this paper, we explain about microring resonator and studied various flip-flops like SR-flip-flop, JK-flip-flop, T-flip-flop, D-flip-flop, etc implemented using micro-ring resonator. Flip-flops are storage elements and for advanced technology storage elements become an integral part, to understand the present scenario of flip-flops using micro-ring resonators and getting ideas about our future work we surveyed various recent research papers which are included in this paper.

Keywords : MRR; Flip-flops.

INTRODUCTION

Fiber communication is an advanced technology [1] introduced in early 1980. It has become popular because of its large bandwidth, low power losses, good security, and lightweight. By using optical fiber several data can be transmitted for very long distance, it has a transmission capacity from gigabyte per second to a terabyte per second. Also, it can be used for switching and networking [2]. For these various reasons, they are used broadly not only for research purposes but also in various industries.

In recent days microring resonators are also playing a vital role because of their effective properties. Micro ring resonators are simple in structure and working principle also simple, [3] easy in fabrication and quality factor is high so it becomes more popular for various circuit designing. It has become more popular in present days because of its qualities, like-easy to cascading, small size, low losses, etc.

We know that logic gates are the basic material for any circuit. They gave different output for various sets of different inputs. Input and output of logic gates either low or high.

In this paper, our aim is to study various flip-flops based on optical microring resonator. Flip-flops are the elementary configuration of a circuit [4]. The output of flip-flops depends on the previous input & output. Flip-flops are bi-stable multivibrator; the stable state can be changed by using proper triggering. Flip-flops are memory element and simple in structure and small in size, for low power switching and processing flip-flops get more preference [5]. In optical field flip-flops store photons for a very small period of time [6]. For future in case of optical computing ultra-high bit rate, communication organizations storage devices are the most important component. Various types of flip-flops are existing, namely-

1. set-reset flip-flops
2. J-K flip-flops
3. T- flip-flops
4. D-flip-flops

THEORY OF MICRO RING RESONATOR

An optical microring resonator is a waveguide where a light source (LASER) is provided at the input of the loop by coupling and output is received.

Optical ring resonator is a group of a guided wave, and only one or two guided wave is coupled to some sort of light. More coupling is occurring if ring resonator and waveguide place close together.

The operational principle optical ring resonator is based on the theory of total internal reflection, constructive interference, optical coupling [6]. Due to its constructive interference property it constructs intensity over various round trips. In optical ring resonator some selective wavelengths are in resonance so it can work as a filter. The properties of optical ring resonator depend on- radius of the ring, basic design, gap between waveguide and ring, waveguide structure, etc. [7]

The MMR is generally made up of silicon, photonic crystal or Ga-As. In general the ring resonator has 4-ports they are input port, output port, through port and add port [8]. The simple arrangement of MRR be made up of a unidirectional coupling among a ring waveguide and linear waveguides, stand for a 4-port configuration. The radius of the MRR r and the linear waveguides are evanescently joined through coupling and a portion of the inward field is transmitted to the ring. As soon as the optical length of a roundtrip is a numeral multiple of the effective wavelength, an interference will take place within the ring known as constructive interference. Then there will be nothing at the output of MRR and it will be 'IN' resonance [9]. Light moving through the linear waveguide can couple in to the ring at different wavelengths. This coupling creates a slope which become dip at resonant wavelengths. Generally numerous wavelengths can be processed through ring, a linear waveguide can similarly cast off as a 'drop' channel, over which this resonance can out-couple producing a peak transmission [10].

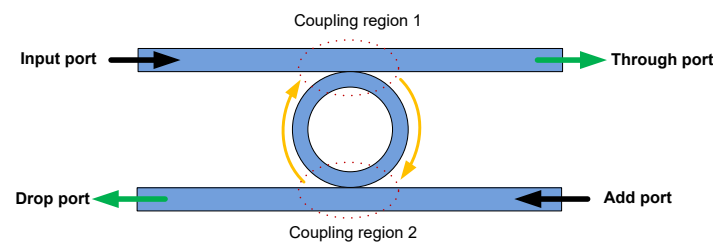


Fig. 1. Basic configuration of microring resonator with two linear waveguide

A microring resonator is a highly developed optical component with privileged circumstances of applications particularly popular at the field of switching, sensing, and routing. Ever since 1990 it has turn out to be one of the extensively cast off optical modules in the arena of optical integrated technology. It is applied to encircle light by total internal reflection, to be produced by nano or micro fabrication practices. A microring resonator generally comprises of a linear waveguide alongside with a round one, the light which confine in the straight one is combined to the round one or two straight waveguide couple by a round one.

The laser light signal propagating throughout the linear waveguide couples to the ring waveguide i.e. resonate, this happens only when the wavelength of the moving optical signal equals the total optical path length of the hole, that condition can be

$$\Delta\lambda_{\text{res}} = (\Delta n_{\text{eff}} L/m) \quad (1)$$

Here m is the mode order, L is the total length of the ring and n_{eff} is the effective refractive index.

Free spectral range states the distance between two successive resonance wavelength of the ring resonator, and it can be express as

$$\text{FSR} = \lambda^2 / 2\pi n_g R \quad (2)$$

The fraction among free spectral range and resonance wavelength known as finesse. The finesse is calculated by:

$$\text{Finesse} = \lambda_{\text{res}} / \text{FWHM} \quad (3)$$

When the light from laser move from end to end a linear waveguide, it completes the over-all no of rounded distance. Which defines the sharpness kin to the dominant frequency. Q factor of that ring can be write off as

$$\text{Q-factor} = (n_g L / \lambda) F \quad (4)$$

LITERATURE SURVEY

In 1989 C. Casper and EJ Bachns describe manufacturing and measurement of microring resonator with a small radius. By small radius, it can exhibit large FSR [11].

In 2006 , Sanjoy Mandal a*, Kamal Dasgupta planned an idea to establish transfer function in Z-domain of optical wave guide using microring resonator .They used optical coupler for designing which is constructed by take two waveguides close for overlapping their evanescent field [12].



In 2009, using micro ring optical modulator is constructed, which has low losses, high speed and simple structure. It has a property that power consumption can be reduced by reducing the radius of the wavelength. This has a benefit of assisting additional optimization of the junction doping summary to reach enhanced modulation competence while upholding a low voltage [13].

2012 all-optical SR flip-flop proposed by P.Nadimi and others which constructed using silicon-ion-insulator ring resonator. They used nonlinear characteristics and transfer matrix to analyze the continuous wave propagation and bi-stability behaviors due to the Kerr effect through microring resonator. They used dual ring resonators having the same radius, for the nonlinear and bi-stable characteristics of ring resonators the refractive index is altered when CW wavelengths are changed [14].

In 2013, J K Rakshit and others proposed a new plan to design an all-optical D flip-flop by GaAs-AlGaAs centered on a solo microring-resonator. Using an optical pump beam the micro ring resonator is modulated. When the clock pulse is applied it transform its state or else controls the information of the preceding state and holds it. In that paper, they confirmed numerical simulation and developed theoretically the typical configuration of D flip-flop. From the simulation output, they calculated different figures of merits, such as On-off ratio, fall-time and rise-time contrast fraction, amplitude modulation, ER. Since the all-optical D flip-flop used only one micro-ring-resonator for design, so it becomes easy to cascaded with integrated circuit and provide less complexity [15].

In 2014, Purnima Sethi and others proposed various designs of all-optical SR, clocked-SR, and other flip-flops along with comparators-decoder, etc by using silicon microring resonator. They designed the circuit having the properties of low power operation, high modulation, ultrafast optimization, etc. [16].

In 2017, Khathanuv Luangxaysana and others proposed a scheme to make an all-optical D flip-flop by improved single ring double waveguide resonance. The circuit consists of a coupler and one EDFA. Since improved single ring with a double waveguide resonator is used it becomes easy to cascading with other integrated circuits. In this paper they show the truth table, simulation value and results but didn't show the extinction ratio, constructive ratio, On-off ratio etc [17].

In 2017 J-k flip-flop is recommended by Gaurav Bharti & Jayanta Kumar Rakshit. On that paper, they provide numerical simulation along with the design configuration of clocked j-k flip-flop. They also describe the numerical simulation of SR, T, and D flip-flop. To design of JK flip-flop they designed a simple way so it became informal toward cascade by other combined circuits. By means of they used simply optical microring resonator so it becomes compact, they also analyzed various system parameters [18].

In 2018, photonic D flip-flop is proposed by Foo Kuilaw and others based on silicon micro ring resonator. For design D flip-flop they used rings as NAND gates and NOT gate. Two PIN photo-detectors are used at the output of the D flip-flop. T [19]

In 2019, D flip-flop is proposed using photonic crystal and the working is depends on the interference effect. The advantages of this design are – simple in structure, no need of external phase-shifter etc. [20].

In Feb 2020 D-flip-flop is proposed for using three rings instead of a single micro ring to remove the illegibility of realizing the response of the ring. Those flip-flops are cascaded for constructing a 2-bit optical down counter. Under pump pulse this flip-flop work as a switch also [20].

In 2020, all-optical D flip-flop circuit is suggested for 1.72 Tb/sec using a unique structure of line waveguide and OMRR. To understand the process of this flip-flop they change dimensions of photonic crystal. On that paper they get a bit rate of 1.72 Tb/sec and footprint is $11.4\mu\text{m} \times 6.24\mu\text{m}$ [21].

SUMMARY

A simple all optical SR flip flop constructed using nonlinear characteristics and transfer matrix to analyze the continuous wave propagation and bi-stability behaviors due to the Kerr effect through micro ring resonator. For that two MMR of having same radius are constructed parallel to each other set by linear waveguides (**Fig. 2**). For realizing the bistable behavior parameters of MRR1 and MRR2 are chosen to specific. By introducing two continuous wave signals at 1550nm and 1518 nm respectively for set and reset at two different linear waveguides bistable behaviour can be realize as MRR1 detuned to resonance wavelength and MRR2 tuned to resonance wavelength [16]. Over the years evaluating and analysing the same principle all optical several flip-flops has been proposed using different structures of ring with linear waveguides.

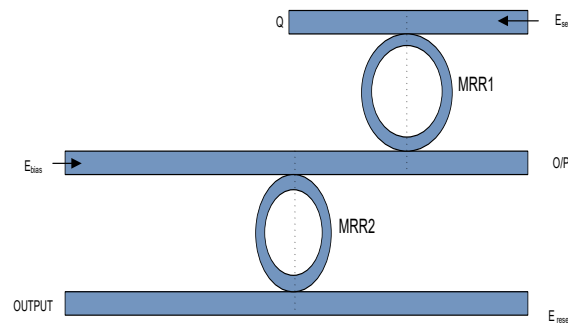


Fig. 2. A simple all optical SR flip flop taken from ref. [10]

CONCLUSION

Integrated all-optical logic circuits already have been constructed and proposed using nonlinear waveguide devices like Distributed-Bragg gratings and Mach-Zehnder interferometers [22], [23]. Mirroring resonators also have been used to build elementary logic circuits by changing the size of the proposed devices [24].

Irrespective of the robust research in this area, most efforts have not treated these gates in a combined design and functioning manner. In this paper, we describe the micro ring resonator, it's working, and some formulas related to the micro ring resonator. We also studied different research papers related to flip-flops based on micro-ring resonator. Our future aim is to construct a master-slave flip-flop utilizing micro-ring resonator. In master-slave flip-flop, two flip-flops are cascaded using an inverter in between two flip-flops. And we will try to construct various logic gates and circuits using micro ring resonator depending on wavelengths.

REFERENCES

1. Biswas, Dwaipayan. "Modern Optical Fiber: Communication Splitter." A paper from International Journal of Scientific and Research Publications 7, no. 5 (2017): 317-320.
2. [Kumar, A. Anand. Fundamentals of digital circuits. PHI Learning Pvt. Ltd., 2016.
3. Reshef, Orad, Michael G. Moebius, and Eric Mazur. "Extracting loss from asymmetric resonances in micro-ring resonators." Journal of Optics 19, no. 6 (2017): 065804.
4. Hill, M. T., A. Srivatsa, N. Calabretta, Y. Liu, H. d Waardt, G. D. Khoe, and H. J. S. Dorren. "1/spl times/2 optical packet switch using all-optical header processing." Electronics Letters 37, no. 12 (2001): 774-775.
5. Little, Brent E., Sai T. Chu, Hermann A. Haus, J. A. F. J. Foresi, and J-P. Laine. "Microring resonator channel dropping filters." Journal of lightwave technology 15, no. 6 (1997): 998-1005.
6. Bahrapour, A. R., S. Mohammad Ali Mirzaee, F. Farman, and S. S. Zakeri. "All-optical flip-flop composed of a single nonlinear passive microring coupled to two straight waveguides." Optics Communications 282, no. 3 (2009): 427-433.
7. Wooten, Frederick. Optical properties of solids. Academic press, 2013.
8. Rabus, Dominik G. Integrated ring resonators. Springer-Verlag Berlin Heidelberg, 2007.
9. Rakshit, Jayanta Kumar, Jitendra Nath Roy, and Tanay Chattopadhyay. "A theoretical study of all optical clocked D flip flop using single micro-ring resonator." Journal of Computational Electronics 13, no. 1 (2014): 278-286.
10. Rakshit, Jayanta Kumar, and Jitendra Nath Roy. "Micro-ring resonator based all-optical reconfigurable logic operations." Optics Communications 321 (2014): 38-46.
11. Caspar, C., and E-J. Bachus. "Fibre-optic micro-ring-resonator with 2 mm diameter." Electronics Letters 25, no. 22 (1989): 1506-1508.
12. Mandal, Sanjoy, Kamal Dasgupta, T. K. Basak, and S. K. Ghosh. "A generalized approach for modeling and analysis of ring-resonator performance as optical filter." Optics communications 264, no. 1 (2006): 97-104.



13. Dong, Po, Shirong Liao, Dazeng Feng, Hong Liang, Dawei Zheng, Roshanak Shafiha, Cheng-Chih Kung et al. "Low V_{pp}, ultralow-energy, compact, high-speed silicon electro-optic modulator." *Optics express* 17, no. 25 (2009): 22484-22490.
14. Nadimi, P., D. D. Caviglia, and E. Di Zitti. "Exploiting silicon-on-insulator microring resonator bistability behavior for all optical set-reset flip-flop." *International Journal of Physical and Mathematical Sciences* 6, no. 11 (2012): 1485-1489.
15. Rakshit, Jayanta Kumar, Jitendra Nath Roy, and Tanay Chattopadhyay. "Design of micro-ring resonator based all-optical parity generator and checker circuit." *Optics Communications* 303 (2013): 30-37.
16. Sethi, Purnima, and Sukhdev Roy. "Ultrafast All-Optical Flip-Flop and Binary Counter using Silicon Microring Resonators." In *International Conference on Fibre Optics and Photonics*, pp. T3A-71. Optical Society of America, 2014.
17. Luangxaysana, Khanthanou, Xaythavy Louangvilay, Khamla Non-Alisavath, S. Kanthavong and Vimontha Khieovongphachanh. "All-optical clocked D flip-flop using modified Add/Drop Resonance Ring." 2017 14th International Conference on Electrical Engineering/Electronics, Computer, Telecommunications and Information Technology (ECTI-CON) (2017): 924-928.
18. Bharti, Gaurav Kumar, and Jayanta Kumar Rakshit. "Design of all-optical JK, SR and T flip-flops using micro-ring resonator-based optical switch." *Photonic Network Communications* 35, no. 3 (2018): 381-391.
19. Law, Foo Kui, M. Rakib Uddin, and Hasnul Hashim. "Photonic D-type flip flop based on micro-ring resonator." *Optical and Quantum Electronics* 50, no. 3 (2018): 119.
20. [Rao, Dalai Gowri Sankar, Venkatrao Palacharla, Sandip Swarnakar, and Santosh Kumar. "Design of all-optical D flip-flop using photonic crystal waveguides for optical computing and networking." *Applied Optics* 59, no. 23 (2020): 7139-7143.
21. Verma, N., and D. Mishra. "New approach to design D-flip flop and two bit down counter using optical micro-ring resonator for high speed data processing." *SN Applied Sciences* 2, no. 4 (2020): 1-13.
22. Damodaran, Saranya, T. Shankar, and Rajesh Anbazhagan. "All optical clocked D flip flop for 1.72 Tb/s optical computing." *Microelectronics Journal* 103 (2020): 104865.
23. Smith, S. D. "Optical bistability, photonic logic, and optical computation." *Applied optics* 25, no. 10 (1986): 1550-1564.
24. Little, Brent E., and Sai T. Chu. "Toward very large-scale integrated photonics." *Optics and photonics news* 11, no. 11 (2000): 24.



Cybernation of Home Appliances using Raspberry PI

Yerramsetti Jaswanth, BathinaVenkateswara Rao, Kalagara V V R S Vishnu, Thejavathu Thirumalarao

Department of EEE, V R Siddhartha Engineering college, Kanuru, Vijayawada, Andhra Pradesh

✉ drbvrao@vrsiddhartha.ac.in

ABSTRACT

Monitoring, controlling and protection plays the most prominent role in any automation. However, due to factors like fast switching, ease of control, compact size and energy efficient, these devices require a system cybernation to track and diagnose. The cybernation does not affect the existing system but it adds the smart control of operation through the adaptive techniques. Three techniques were used to design the cybernation. The energy is being monitored and represented in the form of plot such that the user monitors the power consumed at each interval of time as now a days some of them are utilizing the solar power, so the power received from panels and consumed by loads are plotted. The protection and controlling are chosen to function from the same circuit with thyristor control. Therefore the Electromechanical devices used for protection such as MCB's and fuses are being replaced for the individual rooms with the proposed device. In this paper Raspberry PI used for Home Automation along with, protecting the house hold equipment to minimize the use of MCB's.

Keywords : Cybernation; Raspberry PI; Home automation; MCB.

INTRODUCTION

The electrical appliances are controlled and monitored using few gadgets such as the IR controlling, Bluetooth control, Zigbee control, iotetc[1]. all these technologies motto is to have the easy control on home appliances and the industrial appliances. The technology of hand gesture control, voice assistant control, User interface control, Infrared remote control etc[2]. The national status regarding the protection, monitoring and controlling uses the Google assistant. The home automation by using Google HOME application developed by the Google LLC, it has the control of lights, fans and electrical accessories[3]. The Google HOME application has the feasibility to add the devices to be controlled, lights such as Philips hue and wifi routers such as the TP-Link. The GE smart bulbs, Philips hue Bluetooth etc. the Google Home, chrome cast. The supported controllers such as the node mcu, raspberry pi, tinker board, nvidiajesson, msp430, stm32 boards with wifi as the communication protocol. There are various platforms such as the IFTTT[4], adafruit, ESPHOMEetc. The IFTTT platform delivers the users to have the control using smart phones.

Hemalathaet. al propose [5] home automation by using Google Assistant, explained about the appliances control using the google services by using node mcu microcontroller, but it's not feasible for custom made. Uma et.al [6] use, the efficient implementation for Internet of Things used for monitoring and controlling the home appliances via World Wide Web. It is the control of appliances without the application, it uses the webpage. Irrespective of operating system it can have the UI control. Abu Sulayman et.al [7] apply home automation using the microcontroller with an extra feature depending on time or other sensor readings such as light, temperature or sound from any device in the Home Automation network.

Rozita Teymourzadeh,[8] Malaysia home automation technology using Global System for Mobile Communication (GSM) modem to control home devices or appliances such as light, conditional system, and security system via Short Message Service (SMS) text messages is presented. PIC16F887 microcontroller with the integration of GSM provides the smart automated house system with the desired baud rate of 9600 bps. The prototype of GSM based home automation system was implemented and tested with maximum of four loads and shows the accuracy of $\geq 98\%$. Dharma singh et.al [9] Smart home automation system is a web based application that allows user to monitor home appliances using mobile devices. This system established for the entire home user after gaining access from administrator considering issue of security authentication and access control for people with special needs.

As the future depends on artificial intelligence based, the human work is replaced by the machine. In home automation homes are automated through the internet. This also comes under the category of artificial intelligence. Many authors apply the Raspberry PI for Home Automation but no one use this for protecting the house hold equipment, in this paper authors use the

Raspberry PI for Home Automation along with protecting the house hold equipment. The proposed one monitors, controls and protects the home appliances with ease of control to the user at a time. The protecting devices such as MCB and fuses all are being minimized by the proposed module.

This paper proposes the mode of operation through UI, the UI is developed in the node red, and the control button is toggled to have the manual control or the auto control. The auto control uses the raspberry pi board and uses the GPIO pins to control the appliances. The most considerable thing is that protection of electrical appliances in an industry and home are important the need of fuse is replaced by the MCB's. MCB are extensively used and these are placed in individual room control in home, the proposed one minimize or replace the fuse and MCB usage.

HARDWARE DESIGN

The Hardware design is subdivided in to three parts due to different functionality of the system, the main purpose of the system is to monitoring, protection and controlling.

Monitoring: The live data of real time power consumption is monitored continuously using voltage and current sensors. And the graph is taken with respect to time. Here a common voltage sensor for all the appliances and separate current sensors for each appliance is used. The measured values in terms of numerically and graphically shown in user mobile.

Protection: The MCB's and fuses are replaced by this system. Here the current, voltage sensors, Raspberry PI and the thyristor based relay plays a major role. As the sensor's identify the current or voltage values exceeds or fall behind some fixed threshold value then current sensor measured value processed with the help of predetermined programme in Raspberry PI then it will trigger the thyristor to turn off the supply either in single room or entire house based on the requirement. For the purpose of turn on the equipment in room, user need to change the position in his/her mobile. The entire house electrical parameters can be viewed by the user on his/her mobile.

Controlling: this includes controlling the brightness of the lights and fan speed, ON and OFF of the appliances used in the house.

IMPLEMENTATION AND WORKING

The main parts of Cybernation of home appliances are STT, TTS, PU and UI. The entire block diagram is shown in **Fig. 1**.

STT: speech (Articulation) to text converts the user speech or commands to the text through mic and such that the processing unit process the user commands to perform the necessary action.

TTS: text to speech is vice versa of STT here the raspberry pi sends the results of the user commands by converting the text to speech through speaker.

PU: the processing unit performs the tasks that are programmed, it is the assistant's brain all commands and results are analyzed by the Processing unit. The flow chart is given in **Fig. 2**.

UI: The User Interface is developed in the node red, the node red UI has several options such as dashboard, input, output, functions etc.

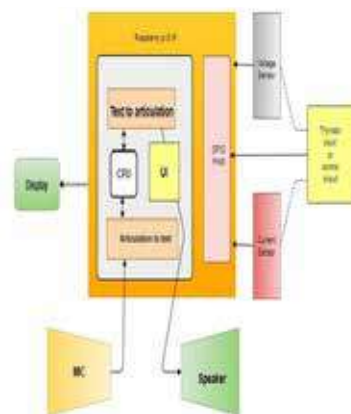


Fig. 1. Block diagram of cybernation of home appliances

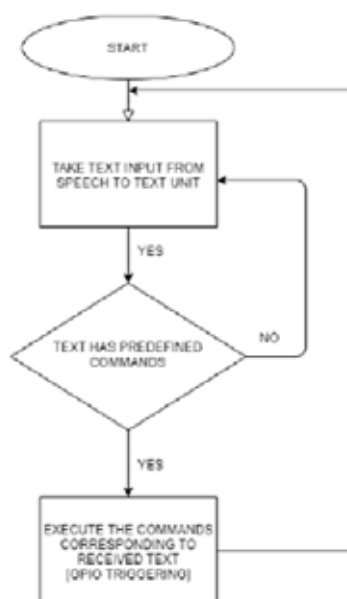


Fig. 2. Flow chart of PU

The dash board of the user mobile consists of switch, gauge, led indicator, slider, graph plot etc. From the **Fig. 3** it has been observed that user can monitor the flow of current, voltage and power consumption in his/her mobile. **Fig. 4**, shows that user can also control the brightness of light and speed of the fan from his/her mobile screen. The user commands are processed and then the actions are controlled, when the user says the a particular device to be on/off, the mic converts the user commands and it is processed in the processing unit and then the GPIO pins are triggered, the power sensor are placed for each room and they sense the power consumed by the devices and it is fed to the processor, the current sensor senses the real time current and if in case the current exceeds then the current sensor sends the trip signal to raspberry pi and such that raspberry pi trigs GPIO to be opened. This process is analogous to MCB in home, when the current settles down then the appliances or devices are ready for controlling, the data of current and voltage are being updated to the UI in which the user has the access of all appliances and the real time energy consumption at various instances is plotted.

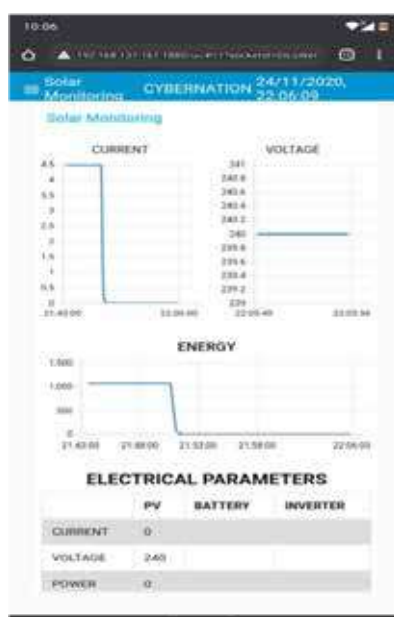


Fig. 3. Screen of the user mobile to monitor the different electrical quantities like current, voltage and energy



Fig. 4. Screen of the user mobile to control the brightness of light and speed of the fan

OPERATION AND RESULTS

1. Establish the communication between current, voltage sensors, Raspberry PI and control circuit using node red and Power monitoring and energy consumption is viewed in mobile.
2. User can select the Auto/manual mode selection in his/her mobile screen.
3. User can also use the Voice assistant control [speech recognition] for Online/Offline modes.
4. Smart light control with Study mode/ Movie or Sleep mode/General mode/scary mode
5. Fan speed control with Super Storm mode/ Storm mode/ Slow breeze/ Gentle air mode.
6. Socket and other appliances control [on/off] can also do with the help of mobile.
7. Current magnitude-based auto reclosing fuse for protecting the equipment from fault currents.
8. It is observed through the proposed methodology the user can Successful in monitoring, controlling and protection of appliances.



Fig. 5. Control circuit consist of Raspberry PI and relay unit.



Fig. 5 shows the prototype of proposed model to control the brightness of the light. This circuit consists of Raspberry PI, current sensor, mic, thyristor switch and mobile. The main advantages of this method are fast switching and smooth response, Controlling of appliance can be done at anywhere without pointing to ir receiver, ease of control and Smart control via internet/ local host, cost efficient with Compact size, save energy by adapting automation, the protecting devices such as MCB and fuses all are being replaced by the proposed module and finally it works on independent of operating system.

CONCLUSION

The device proposed is low cost, most reliable and scalable. It reduces the man power and maintenance, the developed device saves the energy when it is selected in auto mode, in auto mode the appliances are timely based. It operates according the times specified by the user or by weather conditions. In manual mode the user can have the control by voice assistant and UI control. It creates a friendly environment to the user. The device ensures an efficient and reliable operation for the existing home appliances by just adding the extra control circuit. The designed system is tested for number of times and it works effectively. The developed equipment can be used in industries and communication operations with some modifications

ACKNOWLEDGMENT

The author/s thankfully acknowledge(s) the financial support provided by The Institution of Engineers (India) for carrying out Research & Development work in this subject.

REFERENCES

1. Z. Jebroni, "Home Energy Monitoring System Towards Smart Control of Energy Consumption," GreeNets 2018, LNICST 269, pp. 40–53, 2019, p. 14.
2. J. Skovranek, M. Pies, and R. Hajovsky, "Use of the IQRf and Node-RED technology for control and visualization in an IQMESH network," IFAC-PapersOnLine, vol. 51, no. 6, pp. 295–300, 2018, doi: 10.1016/j.ifacol.2018.07.169.
3. G. Xiong, C. Chen, S. Kishore, and A. Yener, "Smart (In-home) Power Scheduling for Demand Response on the Smart Grid," p. 7.
4. P. N. Gajera and V. Gupta, "Universal Electronic Circuit Breaker," in 2020 International Conference on Power Electronics & IoT Applications in Renewable Energy and its Control (PARC), Mathura, Uttar Pradesh, India, Feb. 2020, pp. 33–36, doi: 10.1109/PARC49193.2020.236552.
5. B. Hemalatha, "Google Assistant Controlled Home Automation," JMCMS, vol. 1, no. 2, Aug. 2019, doi: 10.26782/jmcms.spl.2019.08.00035.
6. S. Uma, R. Eswari, R. Bhuvanya, and G. S. Kumar, "IoT based Voice/Text Controlled Home Appliances," Procedia Computer Science, vol. 165, pp. 232–238, 2019, doi: 10.1016/j.procs.2020.01.085.
7. "Abu Sulayman et al. - 2017 - Designing and Implementation of Home Automation", 2017 9th IEEE-GCC Conference and Exhibition (GCCCE) .
8. R. Teymourzadeh, "Smart GSM Based Home Automation System," p. 4, 2013.
9. D. S. Jat, A. S. Limbo, and C. Singh, "Voice Activity Detection-Based Home Automation System for People With Special Needs," p. 12.



Data Interoperable on DVB-S /S2 “Digital Video Broadcast” Compliant Systems

Y S Rayudu

D&E-Coastal Surveillance System/NS-2, Bharat Electronics Ltd., Bangalore

✉ rayuduys@bel.co.in

ABSTRACT

Digital Video Broadcasting DVB-S/S2 is the most successful standard adopted by most of the digital video broadcasters across the globe due to its popularity. All vendors will implement a common approach for video and audio encoding but data services implement in different ways as DVB/MPEG standards itself provides multiple approaches to accommodate multiple data services. The popular DVB -S/S2 encoders and decoder manufactures who are Tandberg and Scopus implemented the data services in two different ways. The flexibility provisioned in DVB standard resulted in data interoperable problems between different encoding and decoding systems. This article describes how BEL addressed this data interoperable issue using Intelligent Interactive Terminal without replacing the already deployed encoding or decoding systems in the field.

Keywords : DVB Digital Video Broadcast; Teletext, Coastal surveillance network; Service Information (SI), PID (Program Identifier).

INTRODUCTION

Digital Video Broadcasting DVB-S/S2 standard popularly used to provide transportation of professional quality video, associated audio and data services over the satellite media. Most of the professional broadcasters include in their RFP (Request for Proposals) that the solutions proposed should be compliant to DVB standards. DVB standards which are based on MPEG-2 and MPEG-4 standards suggest that video, audio and data required to transmit with stream types as specified in the MPEG standards. Most of the original equipment manufacturers solutions are truly compliant to DVB S/S2 standards for Video and associated Audio where as transportation of user private data is concerned, standard provide hooks only to equipment providers in order to accommodate wide number unexplored niche applications. Doordarshan which is the professional official broadcaster in India, implemented DVB-S/S2 encoding systems mostly from M/s Tandberg Encoding system due to its professionalism, and maturity of their technology though it is costly compared with other similar equipment manufactures for transportation their media content. Whereas same Doordarshan procured their receiving equipments such as IRDS (Integrated Receiver Decoders) from Ms Scopus on global tender in order to obtain competitive commercials as receiver's quantities are huge.

CASE STUDY

Bharat Electronics supplied majority of encoding systems from M/s Tandberg Encoding system and IRDS (Integrated Receiver Decoders) from Ms Scopus to Doordarshan. All these encoding & decoding systems are deployed in the field and providing video and audio services successfully (inter operable for video and audio) without any issues.

Real Problem aroused, when Doordarshan tried to transfer user private data between Tandberg encoding system and Scopus make IRD system. This experiment Doordarshan R&D team tried for exploring remote program selection of either National program or Regional program for their unmanned Very Low power TV transmitters.

Initially Doordarshan R&D wing which is responsible for identifying newer applications tried to resolve themselves user private data service feature available in the encoders and decoders. Doordarshan R&D found that private data able to transmit if both the encoders and decoders are of same make. When Encoders and decoders are of different make, private data is not able to transfer though there is no problem for video and audio. Later Doordarshan referred back above interoperable problem to Bharat Electronics as they were unable to resolve by them self and BEL has supplied both the encoding and decoding systems from different vendors by complying both the solutions are DVB compliant.



BEL in turn referred above Problem to both the vendors who provided encoding / decoding systems by claiming their solutions are DVB compliant in their compliances while procurement. For the above data interoperable problem, both the vendors tried to en-cash something more out of this problem. Tandberg advised to replace entire decoding systems supplied by M/s Scopus with their IRD's as the data is private data and their interoperable is limited to video and audio only with vested interest to enter into IRD business in addition to encoders. In similar way Scopus want to enter into Encoder business and advised to replace Tandberg encoders replaced with Scopus encoders in order to ensure transfer of user private data along with video & audio. But customer already procured good number of IRDs from Scopus and Encoders from Tandberg which are already deployed in nook and corners of India.

As problem is serious in nature, which require lot of money and efforts to replace either encoders or decoders in the field as suggested by both the vendors. BEL and Doordarshan R&D wing took more seriously as Doordarshan "Engineer in chief" was not ready to fall in the vendor traps. Finally BEL resolved same by developing Intelligent Interactive Terminal after analyzing MPEG-2 transport stream in detail and Doordarshan R&D settled to address remote program selection feature by analog audio tone method by sacrificing one audio channel and additional satellite bandwidth.

RESOLUTION OF DATA INTEROPERABLE ISSUE

DVB/MPEG compliant encoder first digitize video, audio and user private data and packetized in 188/204 bytes with suitable stream type as per syntax called in MPEG-2/4/ DVB standards. Stream type 0x01 is used for MPEG-2 (ISO 13818-2) video packets, stream type 0x02 for MPEG-1 (ISO 11172-2) audio packets, stream type 0x03 for MPEG-2 (ISO 13818-4) audio packets and stream type from 0x06 to 0xFF for transporting of user private data services in order to accommodate multiple user data services. After packetization video, audio and user data packets are multiplexed in MUX unit for further modulation and transportation. At the receiving decoding end, after demodulation extracted transport stream fed to DEMUX (De Multiplexer) which require to differentiate type of stream based upon on stream ID and suitably fed to either video decoder , audio decoder or data decoder.

Captured DVB/MPEG-2 Compliant transport streams from both Tandberg & Scopus encoders are analyzed bit by bit by mapping stream type tables and header information with reference to above standards. It was observed that both the vendors are assigned stream types as per standard in their transport streams. In spite of both the vendors transport streams are truly compliant to standards, user data from Tandberg encoding system was unable to transport through Scopus Decoders. BEL cannot take action on either vendors as both are assigned stream types of each and every packets of video audio and data are as per stream type called in PES Program elementary streams header information guidelines. Data transfer is occurring between Tandberg encoder and Tandberg decoder without any issue including private data, and similarly between Scopus encoders and decoders. Transfer data between Tandberg encoders and Scopus IRD interoperable is limited to video, audio only but unable to transfer user private data. Same behavior is occurring with M/s Scopus encoders and M/s Tandberg decoders as well.

As no solution is coming out, in spite of analyzing transport streams of either systems, further deeply transport streams were examined and found that though both are assigning as per standards. Tandberg encoder is assigning stream type as 0xFF, where as Scopus encoder is assigning stream type as 0x06 for data. Due to this difference in stream types unable to transfer private data between different make encoder and decoders though both stream types are allowed in above standard. With the above analysis, root cause of the problem got identified. These captured transport streams from either make encoders are edited offline using MPEG analyzer cum editing tool. After modification of Tandberg transport stream with 0x06 it is observed that Scopus decoder able to receive private data as well along with video, audio. Similarly it is verified with Scopus make encoder by editing stream to 0xFF. With this modifications and reasons for problems in either systems were completely understood and offline solution got evolved.

Though problem got identified and how to implement same on encoders and decoders which are already deployed in the field. This interim offline solution is might be good for technological demonstrations where as we are looking for permanent solution which required to address live requirements where each transport stream comprises of multiple programs each dynamically update its PID (Program identifies). As per MPEG standards PID values will be in the order of 4294967297 and are dynamically assigned leaving few reserved for pre defined MPEG/DVB tables.

This complexity and dynamic requirement enable to design Intelligent Interactive Terminal which will address live requirements and enable customer to implement un explored data applications without procuring additional encoders or decoders and costly satellite bandwidth.

Flow chart of Intelligent Interactive Terminal is explained in **Fig. 1**. This solution enable us to demonstrate to National to Regional changer over system at VLPT of Doordarshan from Bangalore to Delhi on live satellite network to Doordarshan “Engineer in Chief”. This is contractual requirements as well, as customer gave order to BEL since we complied including data as per tender requirements.

Table 1. Stream type assignments

Stream ID Value	Description
0x00	ITU-T ISO/IEC reserved
0x01	ISO/IEC 11172-2 (MPEG-1) Video
0x02	ITU-T Rec. H.262 ISO/IEC 13818-2 (MPEG-1) Video
0x03	ISO/IEC 11172-3 Audio
0x04	ISO/IEC 13818-3 Audio
0x05	ITU-T Rec. H.222.0 ISO/IEC 13818-1 private sections
0x06	ITU-T Rec. H.222.0 ISO/IEC 13818-1 PES packets containing private data
0x07	ISO/IEC 13522 MHEG
0x08	Annex A - DSM CC
0x09	ITU-T Rec. H.222.1
0x0A	ISO/IEC 13818-6 type A
0x0B	ISO/IEC 13818-6 type B
0x0C	ISO/IEC 13818-6 type C
0x0D	ISO/IEC 13818-6 type D
0x0E	ISO/IEC 13818-1 auxiliary
0x0F – 0x7F	ITU-T Rec. H.222.0 ISO/IEC 13818-1 reserved
0x80 -0xFF	User private data

DATA INTEROPERABILITY IMPLEMENTATION ALGORITHM

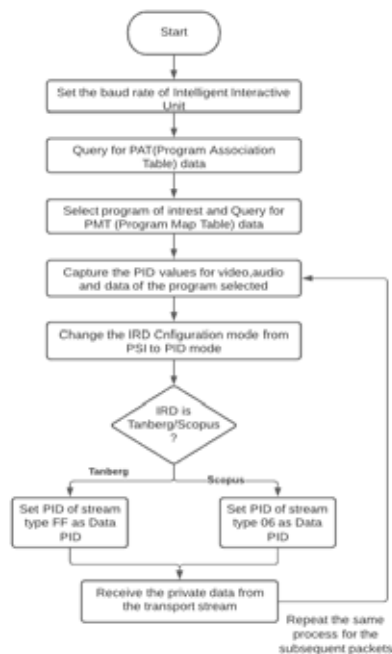


Fig. 1. Flowchart representing data interoperability implementation algorithm

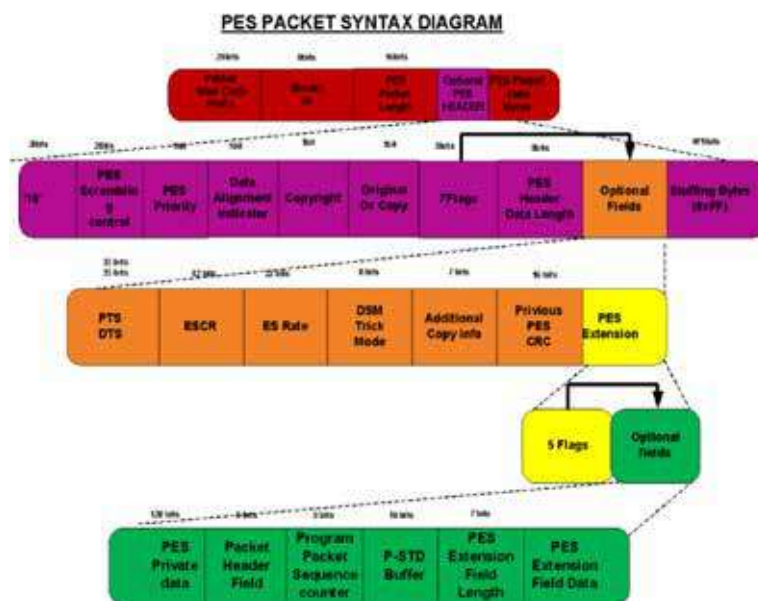


Fig. 2. PES packet syntax used in MPEG2 standards

UNEXPLORED DATA BROADCASTING APPLICATIONS ON DVB PLATFORM

Further to resolution of data interoperable solution on DVB platform, as off shoot of same solution enables to explore other Data Broadcasting applications / protocols specified by DVB such as

1. Data pipe
2. Synchronized streaming data
3. Synchronous streaming data
4. Asynchronous streaming data
5. Multiprotocol data grams
6. Data carousel
7. Object carousel

BEL was able to meet DD (Doordarshan) compliances requirements and explored data broadcasting applications in DVB platforms, one among is Print cast solution to HP Labs using Teletext, National to Regional change over in LPT/VLPT TV transmitters.

IRD with Data services is the one more offshoot of data interoperable solution which enables to use Data services in addition to conventional Video and Audio services in STB/IRD. This data services feature differentiate BEL Set top Boxes / IRDs with STB,s available in the market which were probably imported from China.BEL STB (which is also called as “BEST” Bel Set top box) as it is meeting stringent ISRO requirement of 1MSPS, VBI teletext encoding and data broadcasting in addition to video & Audio.

TELETEXT – DIGITAL DATA TRANSMISSION OVER DVB PLATFORM

The method by which ITU-R System B Teletext (ITU Recommendation BT.653), is known as EBU Teletext (see EN 300 706), may be carried in DVB bit streams. The teletext data is transmitted in the Vertical Blanking Interval (VBI) of the 625 lines PAL –B system television signal. All the 625 lines does not carry active video, Lines 6 to 22 in field 1 and 319 to 335 in field 2 are available to carry teletext data. The maximum data rate for each Teletext service is equivalent to 16 lines transmission mechanism should be capable of transmitting subtitles with accurate timing with respect to the video.

HP labs which is design house for HP worldwide products for providing concepts for building next generation innovative

products. HP labs would like to capitalize VBI teletext concept for increasing the market share of their printers by integrating STB/IRD with print cast feature to enhance student distance education program effectiveness closure to real class room. As per their research studies, most of the students retention power what they learned over distance education sessions wont last for longer duration, unless it is revised major topics and / or pictures later. With HP Labs integrated print cast unit with STB/IRD with data capability can address this issue and HP can increase their printer market share further in different market as well.

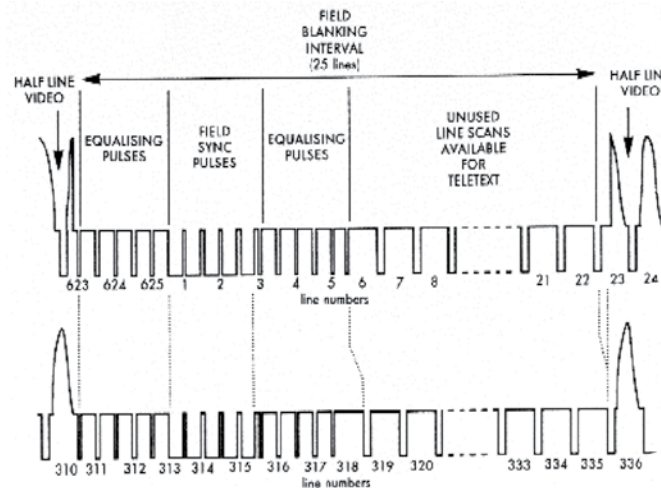


Fig. 3. Teletext data transmission in VBI interval period

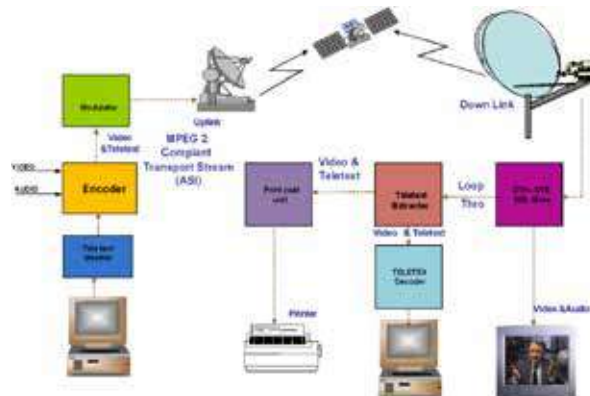


Fig.4 Distance Education through Print cast Using BEL make STB to HP Labs (APPLICATION 1)

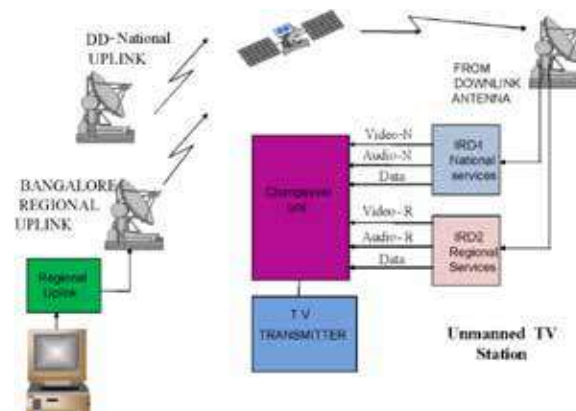


Fig. 5. Data broadcast on DVB platform regional/national program changeover (APPLICATION 2)



CONCLUSIONS

DVB platform supports good number of Data Broadcasting applications which are unexplored which designers capitalize same to find innovative applications such as print cast implementation to HP Labs.

Every standard with no exception to DVB-S/S2 standard provide hooks for developing user specific applications. Most of the vendors would like to take advantage of same to enjoy monopoly for their commercial interests, so it is required to analyze interoperable problems instead of blindly falling in the traps of the vendors.

REFERENCES

1. ETSI TS European Standard EN 300 421103 129 V1.1.1 (2013-0) Digital Video Broadcasting (DVB) [2] EN 300 421.ISO/IEC DIS 13818-1 Information technology -- Generic coding of moving pictures and associated audio information: Systems
3. EN 300 743 Digital Video Broadcasting DVB Subtitling system
4. ETR 211 DVB guidelines for implementation and usage of Service Information (SI) Service Information in DVB system.
5. EN 301 192 Specifications for Data Broadcasting TR 101 202; Implementation Guidelines for Data Broadcasting.



ML-based Constellation-rotation Correction of QPSK Signal in Optical Fiber Communication

Nitish Sinha, Satyabrata Singha, Mohua Chakraborty, Bishanka Brata Bhowmik

Department of Electronics & Communication Engineering, Tripura University, Agartala, Tripura

✉ satyabrata.ece@tripurauniv.in

ABSTRACT

We propose a machine learning (ML) based algorithm to find and correct the angle of rotation of constellation after passing through an optical fiber. The system can detect both forward and backward rotation and thus will be able to reduce the overall BER (bit error rate) of the system.

Keywords : Machine learning; QPSK; Constellation diagram; Eye diagram; BER.

INTRODUCTION

Optical fiber is a prevalent, low loss transparent fiber [1], made up of silica glass, by chemical vapor deposition [2]. These are extensively used due to their dielectric nature, low loss, and huge data transmission capacity [3]. These are basically the light equivalent of microwave wave guide, providing a higher bandwidth [1]. During the last few years, optical fibers have brought a revolution in the field of telecommunication by replacing copper cables [1]. It provides a greater bandwidth within a much cheap rate. The advent of the low loss fiber nearly five decades ago has started with less than 20dB/km at 632.8 nm [4]. From that point of time, the present scenario is long-haul communication of 850 nm multimode fiber to 1550 nm single-mode fiber (SMF). SMF and Erbium-Doped Fiber Amplifier (EDFA), jointly, have transmitted multiple wavelength channels with the help of Wavelength Division Multiplexing (WDM) [4]. In recent times, optical fiber has diverse uses, be it high-speed internet across the world, internet of things, cloud computing [5]. The advantages to cite are lower attenuation, smaller size with reduced weight. It provides electromagnetic isolation [6]. One more point regarding optical fiber communication is coherent detection which has led to severe slash in case of cost, power and density, during the last few years in the field of communication [7].

Coherent detection being far superior to direct detection, has remarkably increased the spectral efficiency as it uses the amplitude, phase, and polarization of optical carrier. Coherent modulation detection has taken its place in both metros and smaller cities. 400G ZR defined by Optical Internet working Forum (OIF) is to be used for inter-data center interconnect [7]. However, virtually, intensity modulation and direct detection (IM and DD) are used next advancement for further cost reduction. The next advanced step for optical communication is PAM-4, which replaces IM & DD for a higher bit rate. It is employed for 400G transceivers [7]. Optical fiber's bandwidth is almost 10Gbps, but there is still a constant pressure for higher bandwidth than the current 2.5, 10, and 40 Gbps scenario. The next-generation optical communication will be transmitted on one channel of 100Gbps and finally leading to 400Gbps [8]. The first bitrate hierarchy is 100 Gb/s to which IEEE Ethernet and the ITU-T optical transport network (OTN) standardization bodies have decided to effectuate standards for client and line side interfaces, respectively [7].

However, optical fiber has some disadvantages, along with its numerous advantages. The prominent ones are its losses and dispersion. Losses or attenuation have several adverse effects on performance, including reducing the system's bandwidth and overall system capacity. The notable losses are absorption loss, material or Rayleigh scattering loss, bending loss, radiation loss, coupling loss, linear and non-linear dispersion, etc.[9], linear ones being chromatic dispersion and polarization mode dispersion [5]. The non-linearities in optical fiber are a major drawback: these being, Self Phase Modulation, Cross Phase Modulation, and Four Wave Mixing [10].

The amalgamation of machine learning with optical communication is booming nowadays. There are numerous research works leading to various optical communication parameters- overview of applying machine learning in optical fiber communication [11], non-linearity mitigation [12], signal recovery [13], to name a few. Majid N. Khormuji et al. proposed a system to optimize

rotation of constellation in Raleigh fading wireless communication channel. The optimum rotation angle is found using the gradient search algorithm [14].

Our work deals with the effect of Self Phase Modulation where light experiences a phase change while traveling through an optical fiber and the phase mismatch that may happen between the transmitter laser and the laser at the receiver, which will act as a local oscillator in the coherent receiver. In this research work, mitigation of the phase change problem in optical fiber communication has been done by incorporating machine learning.

The phase rotation can cause the signal to be received incorrectly at the receiver, thus increasing the BER. In this work, we propose an ML-based algorithm to compensate for the phase rotation in optical fiber.

MACHINE LEARNING BASED ROTATION CORRECTION

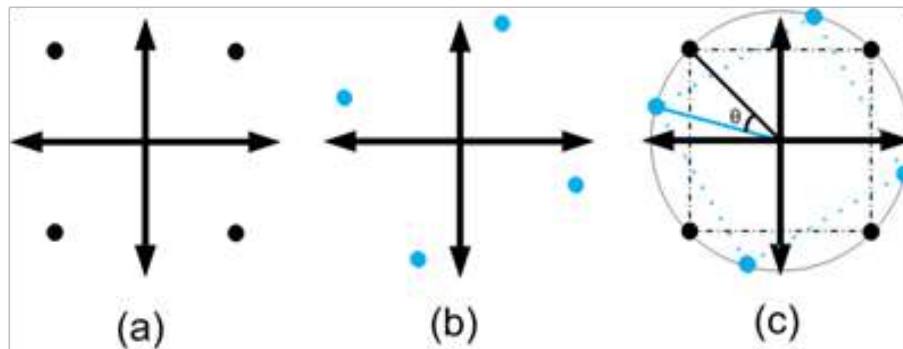


Fig. 1. QPSK signal constellation

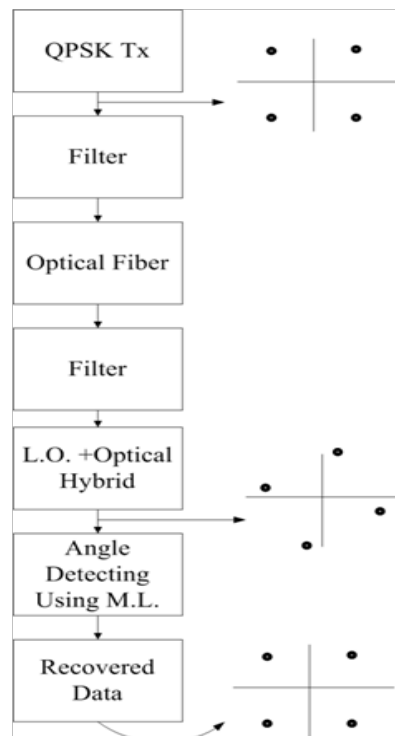


Fig. 2. Block diagram of the proposed system

A QPSK signal passed transmitted through an optical fiber. Due to fiber non-linearities, the signal constellation gets rotated by a certain angle. The local oscillator at the receiver may also introduce some phase rotation if there is any mismatch in synchronization. The smart coding algorithm can calculate the total angle by which the signal got rotated.

Fig. 1(a) is the constellation of the QPSK signal at the transmitter, **Fig. 1(b)** is the rotated constellation received. In **Fig. 1(c)**, ' θ ' is the angle by which the constellation got rotated. The signal rotation causes the eye-opening of the signal to be reduced. If it crosses a quadrant, the eye starts opening up, but BER will be increased significantly. **Fig. 2** shows the block diagram of the proposed system.

The ML algorithm is divided into three sections. In the first section, the minimum BER at which the eye-opening is maximum is calculated by rotating the constellation by 90 degrees 4 times. The corresponding angle of minimum BER is then obtained and passed on to the next section for more accurate calculation.

In the second section, the constellation is rotated by ± 10 degree in each iteration, and the angle at which eye-opening is maximum is obtained. Here ' z ' represents the eye-opening.

Similarly, in the third section, the signal is rotated by ± 1 degree. Thus, the angle obtained after the third section gives the angle by which the signal got rotated after passing through fiber and due to phase mismatch at the receiver.

SIMULATION RESULTS

To illustrate the performance of the system, a QPSK signal is sent through an optical fiber. Two bandpass filters are used at the transmitter, and the receiver has a bandwidth of 10 times and 2.5 times of modulating frequency, respectively. Results are obtained at 20 km of fiber length. The inter-symbol interference (ISI) is almost negligible at this fiber length.

Fig. 4 shows the in-phase and quadrature-phase eye-opening at the receiver before retrieving of the constellation to the original phase.

Fig. 5 shows that the constellation is rotated by a certain angle and figure shows that the signal has been rotated back to the original phase.

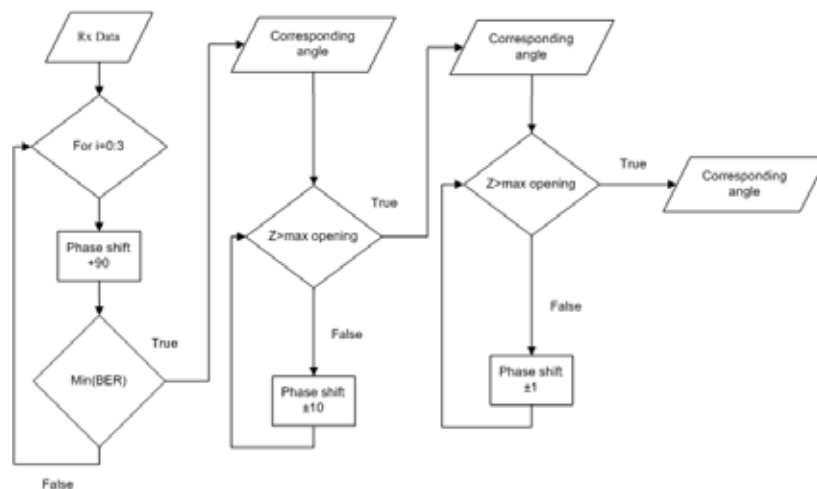


Fig. 3. ML-based algorithm to find the constellation rotation angle

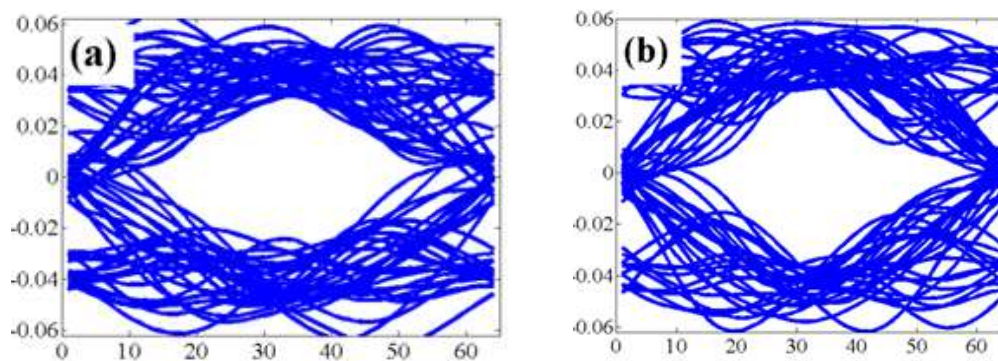


Fig. 4. Eye diagram- (a) in-phase; (b) quadrature-phase

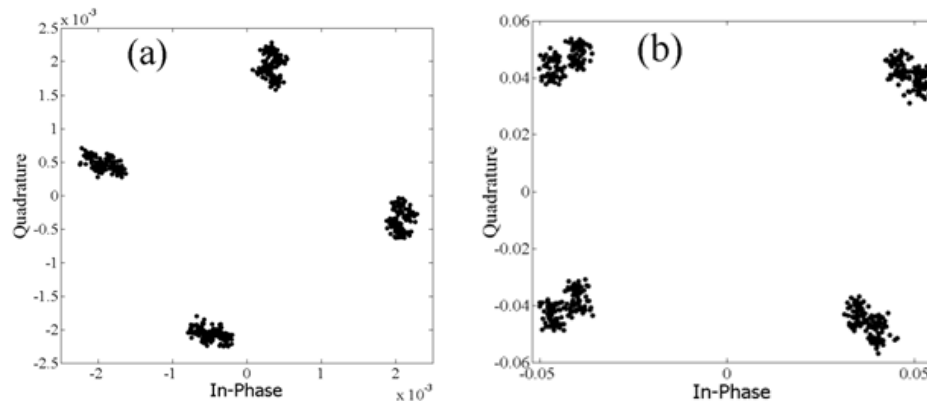


Fig. 5. Constellation diagram- (a) received data; (b) recovered data

CONCLUSION

This paper presents a new direction in mitigating the signal's constellation while passing through an optical fiber due to Self Phase Modulation, where machine learning played the key role in making it a success. The proposed method can be fruitfully used to mitigate phase change caused due to Self Phase Modulation.

REFERENCES

1. Gambling, W. A. (2000). The rise and rise of optical fibers. *IEEE journal of selected topics in quantum electronics*, 6(6), 1084-1093.
2. Oh, K., & Paek, U. C. (2012). *Silica optical fiber technology for devices and components: design, fabrication, and international standards* (Vol. 240). John Wiley & Sons.
3. Keiser, G. (2003). *Optical fiber communications*. Wiley Encyclopedia of Telecommunications.
4. Willner, A. (2019). *Optical fiber telecommunications* (Vol. 11). Academic Press.
5. Zhong, K., Zhou, X., Huo, J., Yu, C., Lu, C., & Lau, A. P. T. (2018). Digital signal processing for short-reach optical communications: A review of current technologies and future trends. *Journal of Lightwave Technology*, 36(2), 377-400.
6. Opatić, D. (2009). *Radio over fiber technology for wireless access*.
7. Kumar, S., Papen, G., Schmidtke, K., & Xie, C. (2020). Intra-data center interconnects, networking, and architectures. In *Optical Fiber Telecommunications VII* (pp. 627-672). Academic Press.
8. Lach, E., & Idler, W. (2011). Modulation formats for 100G and beyond. *Optical Fiber Technology*, 17(5), 377-386.
9. Marcuse, D. (2012). *Principles of optical fiber measurements*. Elsevier.
10. Singh, S. P., & Singh, N. (2007). Nonlinear effects in optical fibers: origin, management and applications. *progress in Electromagnetics Research*, 73, 249-275.
11. Musumeci, F., Rottondi, C., Nag, A., Macaluso, I., Zibar, D., Ruffini, M., & Tornatore, M. (2018). An overview on application of machine learning techniques in optical networks. *IEEE Communications Surveys & Tutorials*, 21(2), 1383-1408.
12. Wang, D., Zhang, M., Fu, M., Cai, Z., Li, Z., Han, H., ... & Luo, B. (2016). Nonlinearity mitigation using a machine learning detector based on k -nearest neighbors. *IEEE Photonics Technology Letters*, 28(19), 2102-2105.
13. Argyris, A., Bueno, J., & Fischer, I. (2018). Photonic machine learning implementation for signal recovery in optical communications. *Scientific reports*, 8(1), 1-13.
14. Khormuji, M. N., Rizvi, U. H., Janssen, G. J., & Slimane, S. B. (2006, October). Rotation optimization for MPSK/MQAM signal constellations over Rayleigh fading channels. In *2006 10th IEEE Singapore International Conference on Communication Systems* (pp. 1-5). IEEE.



Wavelength dependent Configurable optical AND to OR Gate based on Micro Ring Resonator loaded on Mach–Zehnder Structure

Arka Roy Bin, Srikanta Das*, kankana Debnath and Bishanka Brata Bhowmik

Department of Electronics and Communication Engineering, Tripura University, Agartala, Tripura

✉ srikanta.ece@tripurauniv.com

ABSTRACT

In this paper, we have proposed and simulated a novel wavelength dependent configurable AND to OR gates and vice-versa, using three micro ring resonator loaded in a Mach Zehnder look like structure. We have shown that two of the rings in the system of three ring operate at two different wavelengths at a time, and work as AND gate when only MRR1 and MRR2 are working at specific wavelength and as OR gate when MRR1 and MRR3 are working at another wavelength. The radius of the MRR 2 is half of MRR1 and MRR3 such that the resonance wavelength of the MRR1 and MRR3 align with each other and resonance wavelength MRR2 should have an interval twice of the other.

Keywords : MRR; Optical gates; Wavelengths, Mach–Zehnder.

INTRODUCTION

Fiber communication is an advance technology [1] introduced in early 1980. It has become popular because of large bandwidth, low power losses, good security and light weight. By using optical fiber several data can be transmitted for very long distance, it has transmission capacity from gigabyte per second to terabyte per second. Also it can be used for switching and networking [2]. For these various reasons they are used broadly not only for research purpose but also in various industries. In recent days micro ring resonators are also playing a vital role because of their effective properties. Ever since 1990 it has developed into one of the broadly cast-off optical mechanisms in the optical integrated technology. It is used to encircle light through total internal reflection, which can be generated using nano and micro fabrication methods [3]. Micro ring resonator are simple in structure and working principle also simple, easy in fabrication and quality factor is high so it becomes more popular for various circuit designing [4]. It has become more popular in present days because of its qualities, like-easy to cascading, small size, low losses etc.

We know that logic gates are the basic material for any circuit. They gave different output for various sets of different inputs. Input and output of logic gates are either low or high. Recently many logic gates are developed by using MRR, like – all optical OR/AND logic gates [5], exclusive OR and exclusive NOR [6].

In this work our aim is to construct a wavelength dependent configurable optical AND to OR gate based on micro ring resonator loaded on Mach–Zehnder look like structure. Wavelength is the distance between two peaks of a wave and if wavelength increases frequency decreases.

$$\text{Wavelength} = \text{velocity of light in the air} / \text{frequency} \quad (1)$$

For fiber optics a particular wave length is used where fiber have small transmission loss. MRR has a good property that the wave lengths (input-output) can keep in the same plane [7]. In this work we use this property to construct our desired design.

OPTICAL MICRO RING RESONATOR

An optical ring resonator is defined to be a waveguide where a light source (LASER) is provided at the input of the loop by coupling and the output is received. When light of a resonant wavelength is passed through the loop, intensity is built due to multiple adding of the constructive interference and is produced at the output. The ring resonator works on the principle of optical coupling, constructive interference and total internal reflection. The coupling in ring resonator takes place when the ring

and the waveguide are close, some light from the waveguide can couple into the ring. The distance should be less between the waveguide and the ring as closer they are the more coupling occurs. The optical ring resonator act as a filter since only some selective wavelength will be at resonance. The properties of optical ring resonator depend on- radius of the ring, basic design, gap between bus waveguide and ring waveguide structure etc. [8].

The MMR is generally made up of silicon, photonic crystal or Ga-As. In general the ring resonator has 4-ports they are input port, output port, through port and add port [9]. The simple arrangement of MRR be made up of unidirectional coupling among a ring waveguide and linear waveguides, stand for a 4-port configuration. The radius of the MRR r and the linear waveguides are evanescently joined through coupling and a portion of the inward field is transmitted to the ring. As soon as the optical length of a roundtrip is a numeral multiple of the effective wavelength, an interference will take place within the ring known as constructive interference. Then there will be nothing at the output of MRR and it will be 'IN' resonance [10]. Light moving through the linear waveguide can couple in to the linear waveguide can similarly cast off as a 'drop' channel, over which this resonance can out-couple producing a peak transmission [11].

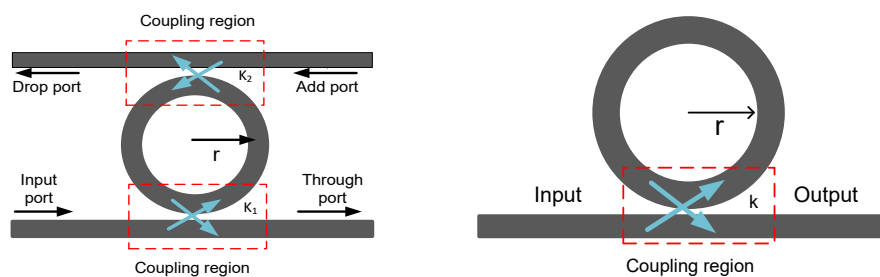


Fig. 1 Simple structure of an optical micro ring resonator. (a) Ring structure with two linear waveguide (add-drop configuration) (b) Ring structure with a linear waveguide. (All pass configuration)

Before knowing how an optical microring resonator works, we need to know the optical path length of a microring resonator. Optical length of a ring resonator with linear waveguide given below [3]

$$\text{Optical path length} = 2\pi r N_{\text{eff}} \quad (2)$$

Here, r = Radius of the ring.

N_{eff} = effective refractive index of the ring resonator's waveguide material.

The laser light signal propagating throughout the linear waveguide couples to the ring waveguide i.e. resonate, this happens only when the wavelength of the moving optical signal equals the total optical path length of the hole, that condition can be

$$\Delta\lambda_{\text{res}} = (\Delta N_{\text{eff}} L/m) \quad (3)$$

Here m is the mode order, L is the total length of the ring and N_{eff} is the effective refractive index.

Free spectral range (FSR) states the distance between two successive resonance wavelength of the ring resonator, and it can be express as

$$\text{Free spectral range} = \lambda^2 / 2\pi n_g R \quad (4)$$

From an objective point of view, the FWHM accounts for the attenuation of the optical signal propagating through the resonator by minimum of 50%. Equally the FSR and the FWHM are most important parameters to evaluate the Finesse (which denotes by F), for a resonator whose value is identical to the fraction of the FSR to the FWHM and it is written as follow:

$$\text{FSR} = \text{FSR} / \text{FWHM} \quad (5)$$

Basically from an objective of assessment, the finesse denotes 2π multiples of the no. of circular-tours completed by light which are propagating in the ring [12, 12-15].

$$\text{Finesse} = \text{FSR} / \text{FWHM} \quad (6)$$

Another parameter generally engaged to assess the performance of a resonant structure and that is the quality factor and it defined as:

$$Q - \text{factor} = (n_g L / \lambda) F \quad (7)$$

For high values of Quality factor, this explanation is the same to the one related to the system energy capacity, that is the Quality factor, which is 2π multiples of the fraction of the system energy stored above the energy which dissipated through complete of each oscillation cycle [12, 13,14]. In addition, it is likely to state the extinction ratio and it is expressed by means of a fraction, in dB.

CONFIGURATION AND OPERATION

Our propose design consists of three micro ring resonator loaded in a Mach-Zehnder like structure where, MRR 1 and MRR2 are placed serially while ring MRR3 is placed parallel with respect to MMR1 and MMR2 (as shown in **Fig. 2**). The radius of the MRR 2 is half of MRR1 and MRR3 such that the resonance wavelength of the MRR1 and MRR3 align with each other and resonance wavelength MRR2 should have an interval twice of the other. The MMR1 and MMR2 are used to find the output of an AND gate while MMR1 and MMR3 are used to find the output for OR gate while operated in λ_1 and λ_2 wavelength respectively.

When operated in λ_1 wavelength the MMR1 and MMR2 are in series connection, the laser light used as an input through the waveguide gets coupled with MMR1 and MMR2 while MMR3 is kept zero now as the laser passes through the waveguide the field gets half and gets multiplied with the transfer function of MMR1 followed by MMR2 and finally the output is received at Y and our structure works as an AND gate. While operated in λ_2 wavelength, MMR1 and MMR3 are set parallel to each other in mach-Zehnder look like structure and here MMR2 will not work at this wavelength and will remain and as it. The laser light couples with the two rings and the half field passes through the waveguide and the field gets multiplied with the transfer function of MMR1 and MMR3 and are finally added at the output port at Y an OR gate is formed. We take in consideration that the rings work as logic zero when rings are in resonance and logic one when rings are out of resonance.

All the dimension used in our design structure are considered in sensible values based on the standard dimension that has exists in the conventional optic structures. The dimension and the materials used are listed in **Table 1** [15].

Table 1.

Parameters	Value
MRR 1 radius	20 μm
MRR 2 radius	20 μm
MRR 3 radius	10 μm
Material	Silicon
Distance between MRR & linear waveguide	0.25 μm

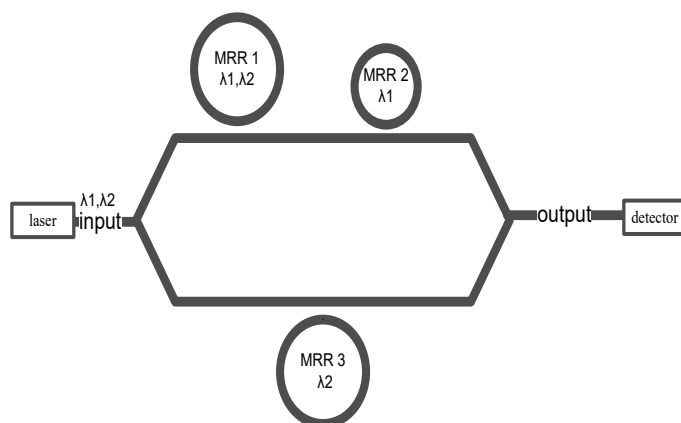


Fig. 2. Configurable optical AND to OR gate based on Micro Ring Resonator loaded on Mach-Zehnder structure

Operation of AND gate

Case 1

Ring 1 in resonance and Ring 2 in resonance. Ring 3 inactive mode, So $A=0$, $B=0$; output=0;

Case 2

Ring 1 in resonance and Ring 2 out of resonance. Ring 3 inactive mode, So $A=0$, $B=1$; output =0;

Case 3

Ring 1 out of resonance and Ring 2 in resonance Ring 3 inactive mode, So $A=1$, $B=0$; output =0;

Case 4

Ring 1 out of resonance and Ring 2 out of resonance Ring3 inactive mode, So $A=1$, $B=1$; output=1;

Operation of OR gate

Case 1

Ring 1 in resonance and Ring 3 in resonance, So $A=0$, $B=0$; output=0;

Case 2

Ring 1 in resonance and Ring 3 out of resonance So $A=0$, $B=1$; output =1;

Case 3

Ring 1 out of resonance and Ring 3 in resonance So $A=1$, $B=0$; output =1;

Case 4

Ring 1 out of resonance and Ring 3 out of resonance So $A=1$, $B=1$; output=1;

Table 2. Truth table of AND

A	B	Y
0	0	0
0	1	0
1	0	0
1	1	1

Table 2. Truth table of OR

A	B	Y
0	0	0
0	1	1
1	0	1
1	1	1

SIMULATION RESULTS

In order to demonstration the precise functioning performance of the suggested plan, the plan is created and simulated in one mathematical simulation software, called MATLAB.

A light source from laser is introduced to the mirroring and signals of measured voltage are produced by tuneable voltage source and served into the waveguide of microring.

We considered applied signal as input at MRR1 and MRR2 is at logic condition 0 when it is on a low amplitude level, whereas the signal is at logic condition 1 when it is at a high amplitude level. Correspondingly, the optical output is also considered this way where logic state is 0 when it has low amplitude level logic state is 1 when it has high level amplitude [6].

Firstly, if we consider the **Fig. 3** here MRR1 and MRR2 work as input A and Input B where two electrical input signals of digital information are fed into the MRR1 and MRR2 at λ_1 , now by analysing the amplitude level of the input A and B with the output we can see that AND gate is working properly as it gives high output only when two input pulses are high otherwise always low output.

Secondly, if we consider the fig. 4 here MRR1 and MRR3 work as input A and Input B where two electrical input signals of digital information are fed into the MRR1 and MRR3 at λ_2 , now by analysing the amplitude level of the input A and B with the output we can see that OR gate is working properly as it gives low output only when two input pulses are low otherwise always high output.

So we can conclude that our proposed design work properly as Wavelength dependent Configurable optical AND to OR gate based on Micro Ring Resonator loaded on Mach–Zehnder look like structure.

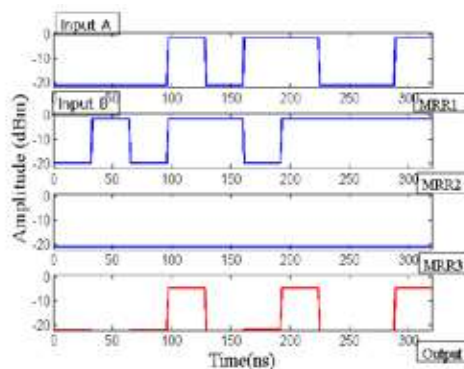


Fig. 3. Static simulation results of AND gate within timeframe when MRR 1 and MRR2 are working at λ_1 .

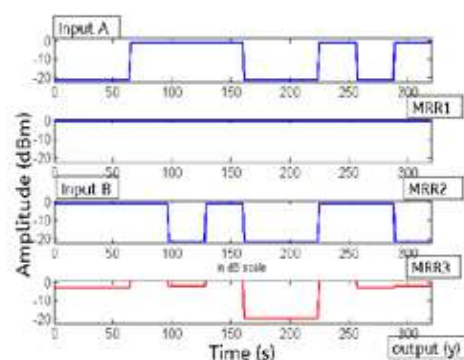


Fig. 4. Static simulation results of OR gate within timeframe when MRR 1 and MRR3 are working at λ_2 .

CONCLUSION

Integrated logic gates which are all-optical already have been proposed by using nonlinear bus waveguide devices like Distributed–Bragg gratings and Mach–Zehnder interferometers [16], [17]. Microring resonators also has been used to construct fundamental logic gates by reducing the size of the proposed devices [18].

Regardless of strong study in this arena, most exertions have not treated these gates in a combined design and functioning manner. This leads to waste of hardware resources and absence of flexibility. In this paper, we have offered and verified a novel wavelength dependent configurable AND to OR gates using three micro ring resonator loaded in a Mach zehnder look like structure. We have shown that three ring operates at two different wavelength simultaneously, and work as AND gate when only ring 1 and ring 2 are working at specific same wavelength and as OR gate when ring 1 and ring 3 are working at specific same wavelength

We trace a logical attitude and conduct a Systematic numerical analysis to originate regulation for the choice of the operating parameters, thus suitable performance standards defined for both gates are completely satisfactory. The acquired outcomes can be relevant in the manufacturing industry and specifically be of attention to companies and administrations working in the arena of optical communications [18].

As follows, an energetically emerging market is existing, which embraces the photonic components producers, the facility suppliers and the high-speed optical equipment manufacturers [19]. Our foremost objective is to propose wavelength dependent more complex devices based on logic gates, which will help in optical computing in the upcoming future [20], thus it will



leads to the formation of an ultra-high speed all-optical signal processing stage accomplished of realizing at least the similar dedicated applications as electronics [21].

REFERENCES

1. Colella, Adrienne, Mikki Hebl, and Eden King. "One hundred years of discrimination research in the Journal of Applied Psychology: A sobering synopsis." *Journal of Applied Psychology* 102, no. 3 (2017): 500.
2. Kumar, A. Anand. *Fundamentals of digital circuits*. PHI Learning Pvt. Ltd., 2016.
3. Debbarma, Papiya, Srikanta Das, and Bishanka Brata Bhowmik. "A Study of Micro-ring Resonator-Based Optical Sensor." In *Applications of Internet of Things*, pp. 59-65. Springer, Singapore, 2020.
4. Reshef, Orad, Michael G. Moebius, and Eric Mazur. "Extracting loss from asymmetric resonances in micro-ring resonators." *Journal of Optics* 19, no. 6 (2017): 065804.
5. Singh, Madan Pal, Jayanta Kumar Rakshit, Uttara Biswas, Gaurav Kumar Bharti, and Aayushi Tiwari. "Design of All-Optical OR/AND Logic Gates using Conversion of Polarization States in Single-Waveguide Coupled Ring-Resonator." In *2020 International Conference on Computational Performance Evaluation (ComPE)*, pp. 392-395. IEEE, 2020.
6. Foo Kui Law, M. Rakib Uddin, "Digital electro-optic exclusive OR and NOR gates utilizing a single micro-ring resonator", *Optik*, Volume 200, 2020, 163361
7. Roy, Jitendra Nath, and Jayanta Kumar Rakshit. "Design of micro-ring resonator-based all-optical logic shifter." *Optics Communications* 312 (2014): 73-79.
8. Wooten, Frederick. *Optical properties of solids*. Academic press, 2013.
9. Rabus, Dominik G. *Integrated ring resonators*. Springer-Verlag Berlin Heidelberg, 2007.
10. Rakshit, Jayanta Kumar, Jitendra Nath Roy, and Tanay Chattopadhyay. "A theoretical study of all optical clocked D flip flop using single micro-ring resonator." *Journal of Computational Electronics* 13, no. 1 (2014): 278-286.
11. Rakshit, Jayanta Kumar, and Jitendra Nath Roy. "Micro-ring resonator based all-optical reconfigurable logic operations." *Optics Communications* 321 (2014): 38-46.
12. Taflove, Allen. "Application of the finite-difference time-domain method to sinusoidal steady-state electromagnetic-penetration problems." *IEEE Transactions on electromagnetic compatibility* 3 (1980): 191-202.
13. Yee, Kane. "Numerical solution of initial boundary value problems involving Maxwell's equations in isotropic media." *IEEE Transactions on antennas and propagation* 14, no. 3 (1966): 302-307.
14. https://en.wikipedia.org/wiki/Finite-difference_time-domain_method.
15. Srikanta Das, Satyabrata singha, Bishanka Brata Bhowmik. "Design and simulation of Opto-fluidic sensor based on ring resonator for the quality testing of diesel oil defiled by kerosene." *Journal Tri. Math. Soc.* V20 (2019): 122-128.
16. Stegeman, George I., and Colin T. Seaton. "Nonlinear integrated optics." *Journal of applied physics* 58, no. 12 (1985): R57-R78.
17. Little, Brent E., and Sai T. Chu. "Toward very large-scale integrated photonics." *Optics and photonics news* 11, no. 11 (2000): 24.
18. 25. Little, Brent E., and Sai T. Chu. "Toward very large-scale integrated photonics." *Optics and Photonics News* 11.11 (2000): 24.
19. Heebner, John E., and Robert W. Boyd. "Enhanced all-optical switching by use of a nonlinear fiber ring resonator." *Optics letters* 24, no. 12 (1999): 847-849
20. Ibrahim, Tarek A., R. Grover, L. C. Kuo, S. Kanakaraju, L. C. Calhoun, and P. T. Ho. "All-optical AND/NAND logic gates using semiconductor microresonators." *IEEE Photonics Technology Letters* 15, no. 10 (2003): 1422-1424.
21. Kitayama, Ken-ichi, Masaya Notomi, Makoto Naruse, Koji Inoue, Satoshi Kawakami, and Atsushi Uchida. "Novel frontier of photonics for data processing—Photonic accelerator." *APL Photonics* 4, no. 9 (2019): 090901.



Soil Humidity Measurement using Microstrip Interdigital Capacitor (IDC) and Rectangular Slotted Fingers Interdigital Capacitor (RSFIDC)

Jayant Gajanan Joshi¹, Mandar P Joshi², Balwinder Singh Dhaliwal³, Shyam S Pattnaik³

Government Polytechnic, Nashik Chehedi(Bk.) Nashik, Maharashtra¹

R H Sapat College of Engineering, Management Studies and Research, Nashik, Maharashtra²

National Institute of Technical Teachers Training and Research (NITTTR), Chandigarh³

✉ jgjoshiantenna@gmail.com

ABSTRACT

In this paper, a microstrip soil humidity measurement sensors using two different configurations of IDC and RSFIDC are presented. These sensors are fabricated using glass epoxy FR4 substrate and experimental results in different humidity conditions is presented. Equivalent circuit of both configurations is analyzed and presented.

Keywords : Rectangular Slotted Fingers Inter digital Capacitor (RSFIDC); Soil humidity; Sensor; Agriculture.

INTRODUCTION

In agriculture, hydrology, cropping pattern, gardening, green house instrumentation systems, packaged food quantifying systems, and structural health monitoring (SHMs) systems it is essential to measure and estimate the water content and water retention in particular sort of soil or concrete work. Water requirement for healthy growth of crop depends upon fertilizer as well as water retention by the soil at the roots of particular crops or trees. Water supply to the crops is one of the vital factors to achieve good yield point of a farm. Water retention varies according to the type and nature of soil. Hence, it is essential to measure humidity that is water content retention by the soil needed for particular crops. Nowadays, measurement and analysis and controlling of moisture content in the soil is an important in addition to physical and chemical properties of soil. Researchers have reported various designs of sensors, microstrip patch antennas, interdigital capacitors for moisture measurement for various applications [1]-[6].

Use of rectangular microstrip patch antenna for sensing of moisture content is reported [1]-[2]. Aluminium electrode is used to measure different soil parameters [3]. Pakamas Chetpattananondh et al. proposed an inter digital capacitance-based moisture content sensor for rubber wood [4]. Paper based inductor and capacitor sensor is presented by Ee Lim Tan et al. [6] for quantifying packaged food quality. Different designs and applications of inter digital capacitor (IDC) are reported by different research groups [7]-[11]. In this research work, soil humidity measurement using two different configurations of planar sensors as conventional IDC and rectangular slotted fingers IDC capacitor (RSFIDC) is proposed. The novelty of this paper is cutting rectangular slots in the fingers of IDC. This increases the capacitance in the same design offering broader humidity measurement range. This research paper is organized into following sections. Initially, sensor design is presented in section II. Section III presents the experimental process and obtained results. Finally, the paper is concluded.

SENSOR DESIGN

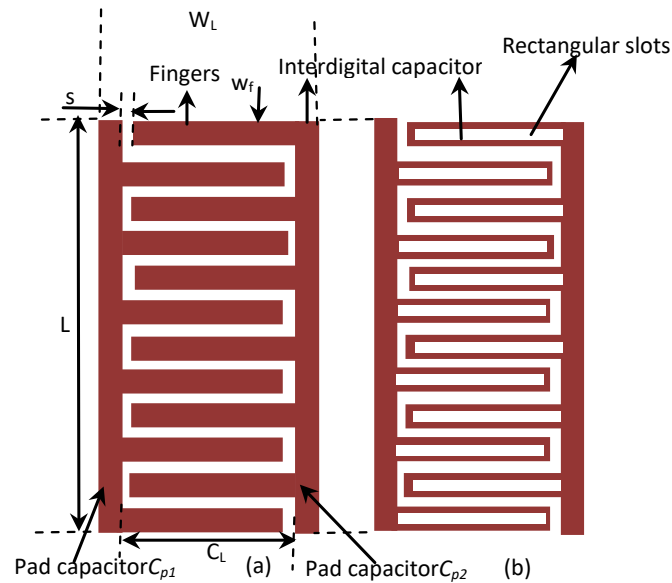


Fig. 1. Sketch and Geometrical structure of (a) Conventional interdigital capacitor (IDC) (b) Rectangular slotted fingers interdigital capacitor (RSFIDC)

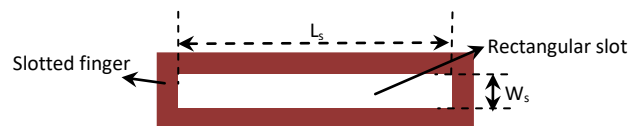


Fig. 2. Sketch and Geometrical dimensions of single slotted finger of RSFIDC

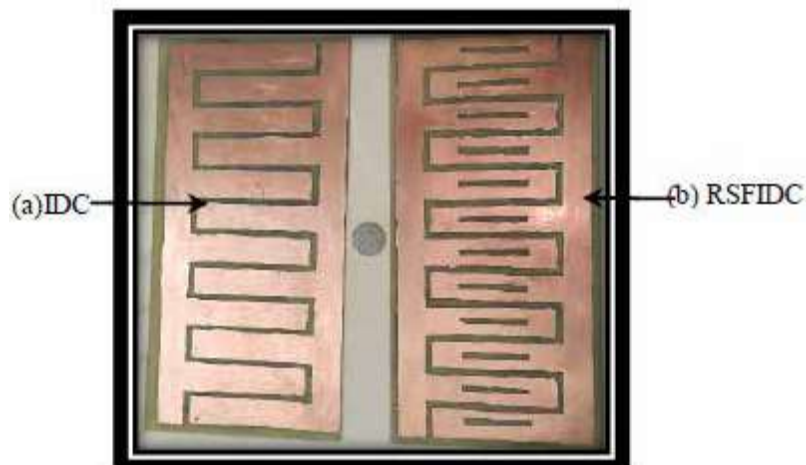


Fig. 3. Photographs of fabricated IDC & RSFIDC soil humidity sensors

FR4 glass epoxy substrate of thickness $h = 1.6$ mm and relative permittivity $\epsilon_r = 4.4$ is used to design and fabricate these microstrip soil humidity sensors by conventional PCB etching and manufacturing process. The sensor design is divided into two configurations as- M1: Design of conventional IDC soil humidity sensor and M2: Design of rectangular slotted fingers IDC (RSFIDC) soil humidity sensor. Comparatively the size of sensors is large to increase the humidity measuring capacity suitable in agriculture sector. The design details are as follows.

Configuration M1: **Fig. 1 (a)** shows the sketch and geometrical design of conventional microstrip IDC sensor. It consists of six finger pairs. The geometrical dimensions of IDC sensor are; number of finger pairs $N = 6$, finger width $w_f = 2$ cm, spacing

between the teeth's $s = 0.5\text{cm}$, IDC length $L = 29.5\text{cm}$, and $CL = 9.5\text{ cm}$. **Fig. 3** shows the photograph of fabricated IDC. WL is the width of IDC $WL = 14\text{ cm}$.

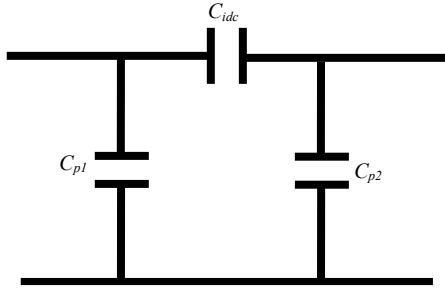


Fig. 4. Equivalent circuit diagram of IDC soil humidity sensor

Fig. 4 shows the equivalent circuit diagram of IDC. Here, inductors values are negligible hence not considered. Equation (1) is used to calculate the series capacitance (C_{idc}) of interdigitated structure. The value of C_{idc} is calculated by modifying equation expressed in [7].

$$C_{idc} = (\epsilon_0 \epsilon_r) [(N-\Delta) C_L] \quad (1)$$

where; ϵ_0 is absolute dielectric constant ($8.854 \times 10^{-12}\text{F/m}$), Δ is correction factor and estimated by (2).

$$\Delta = 0.5 (w_{eff} - w) \quad (2)$$

Here, W_{eff} is the effective corrected transmission line width and it is calculated using (3) [12]-[13].

$$W_{eff} = w + \frac{t}{\pi} \ln \ln \left\{ \frac{4e}{\sqrt{\left(\frac{t}{h}\right)^2 + \left[\frac{1}{\pi\left(\frac{w}{t} + 1.10\right)}\right]^2}} \right\} \quad (3)$$

The calculated value of C_{idc} is 70.05 pF. In the construction of IDC, pads that is two vertical lines that are connected at both end of fingers. These pads introduces parasitic capacitance with respect to ground at two ends they are called as pad capacitance (C_p)

Pad capacitance can be calculated as using (4)

$$C_p = \left[\frac{2.85 \epsilon_{eff}}{\ln \left[1 + \left(\frac{1}{2} \right) \left(\frac{8h}{w_{eff}} \right) + \sqrt{\left(\frac{8h}{w_{eff}} \right)^2 + \pi^2} \right]} \right] \times \left[\frac{C_L}{25.4 \times 10^{-3}} \right] \quad (4)$$

where; effective dielectric constant can be calculated using (5).

$$\epsilon_{eff} = \frac{(\epsilon_r + 1)}{2} + \frac{(\epsilon_r - 1)}{2} \left[1 + \frac{10h}{w} \right]^{-0.5} \quad (5)$$

Thus, the value of capacitance C_p is 0.034.

Configuration M_2 : **Fig.1 (b)** depicts the sketch and geometrical design of rectangular slotted fingers IDC soil humidity sensor. In this design, dimensions of inter-digital capacitor are kept same as per Configuration M_1 . Further, a rectangular slot of dimensions length $L_s = 5$ cm and width $W_s = 0.5$ cm is cut that is etched out in each finger hence it is called as rectangular slotted fingers IDC (RSFIDC). **Fig. 2** shows sketch and geometrical dimensions of single finger with slot. **Fig. 3** shows the photograph of fabricated RSFIDC. This rectangular slot in each finger can be modelled as resonator and adds an inductance (L_{fs}) and capacitance (C_{fs}) to the equivalent circuit of IDC. The values of L_{fs} and C_{fs} can be calculated using (6) and (7).

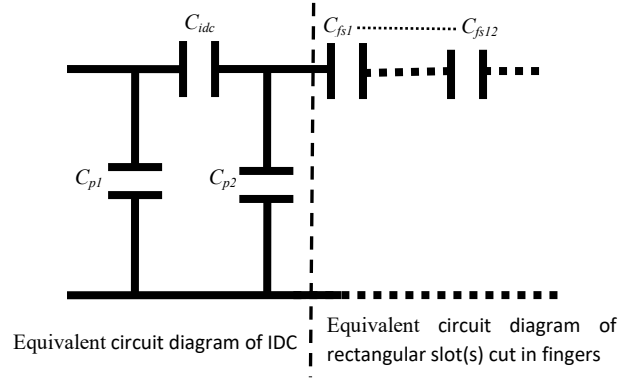


Fig. 5. Equivalent circuit diagram of RSFIDC soil humidity sensor

Fig. 5 shows the equivalent circuit diagram of RSFIDC. Dotted line shows two sections of this circuit: (1) conventional IDC indicating C_{idc} , C_{p1} and C_{p2} (2) the series capacitance(s) that gets added from finger number 1 i.e. C_{fs1} to finger number 12 i.e. C_{fs12} due to slot (s) cut in each respective finger(s). Here, the values of inductor (L_{fs}) and capacitor (C_{fs}) of rectangular slot are calculated using (6) and (7) respectively [14].

$$L_{fs} = \frac{h\pi\mu_0}{8} \left(\frac{L_s}{w_s} \right) \quad (6)$$

where; $\mu_0 = 4\pi \times 10^{-7}$ H/m

$$C_{fs} = \left(\frac{\epsilon_0 \epsilon_r L_s W_s}{h} \right) \quad (7)$$

Using (6) and (7) $L_{fs} = 0.1715$ nH and capacitor $C_{fs} = 0.000695\mu F$.

EXPERIMENTAL SETUP AND RESULTS

To detect the humidity in soil, the interdigital capacitor and rectangular slotted fingers interdigital capacitor sensors have been designed and fabricated. The experimental set up to determine the capacitance in accordance with humidity of soil is shown in photograph (s). The related capacitance was measured by using LCR meter Scientific Model SM6020. During experimentation the frequency is selected and set to 5 KHz. The sensor is connected to LCR meter for capacitance measurement. Plastic container of dimensions length = 25 cm and internal diameter = 20 cm is used for soil humidity measurement. Farm soil (Wheat/ Grapes plantation soil) is used for measurement purpose.



Fig. 6. Photographs of soil humidity measurement set up using IDC and RSFIDC

Case I Initially, the capacitance of sensors without interfacing with soil (in isolated condition) is measured and validated. It is presented in **Table 1**.

Table 1. Capacitance without contact with soil

Sl. No.	Sensor is not submerged into soil samples	
	Type of Sensor	Capacitance
1	Interdigital Capacitor (IDC)	62 pF
2	Rectangular Slotted Fingers IDC(RSFIDC)	64 pF

Case II In this case, both the sensors are directly submerged in to Black soil samples obtained from the Wheat Farm/Grapes Farm. These measurements are carried out without adding external water quantity to the soil. Table II shows the observations of capacitance without adding water.

Table 2. Capacitance of black soil

Sl. No.	Black soil at room Temperature	
	Type of Sensor	Capacitance
1	Interdigital Capacitor (IDC)	327.10 pF
2	Rectangular Slotted Fingers IDC(RSFIDC)	409 pF

Case III In this case, the pre measured water quantity is added into the same Black soil samples. Capacitance (s) is measured using both the sensors. Fig. depicts the graphical relationship between water content in the soil and the measured capacitance. The added water contents are increased in steps and measured capacitance is presented.

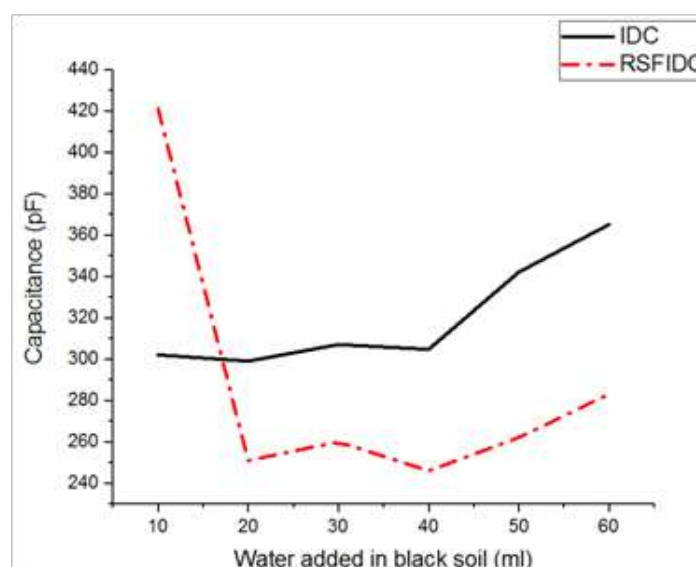


Fig. 7. Variations in capacitance in accordance with changes in water contents in the soil

Fig. 7. shows the graphical relationship between variations in capacitance in accordance with changes in water contents in the soil. This represents the variation in capacitance (s) of both the sensors.

When the soil is in humid or wet condition its dielectric constant gets changed. This variation results in changing capacitance of IDC and RSFIDC. This capacitance is measured and further it can be converted into controllable signal.

Case IV Further, the type of soil is changed by adding sand into the Black soil sample and the capacitance is measured by using same method. **Table 3** shows the values of capacitance after adding sand into Black soil.



Table 3. Capacitance of sandy soil

Sl. No.	Black soil with sand mixture	
	Type of Sensor	Capacitance
1	Interdigital Capacitor (IDC)	781 pF
2	Rectangular Slotted Fingers IDC(RSFIDC)	470 pF

When sand is added into black soil the texture of soil gets changed which in turn changes the soil humidity holding property.

CONCLUSION

In this research work, a practical approach for soil humidity measurement technique is presented. Novel method of cutting rectangular slot in IDC fingers is proposed. This cutting of slots provides better design flexibility to change the total capacitance in RSFIDC humidity sensor. There is stable relation is observed between capacitance variations and water content in the soil. This capacitance variations can be converted into digital signals and humidity in soil can be measured as well as controlled. This type of sensor will play an important role to measure soil humidity in various applications and different soil samples in region or India.

ACKNOWLEDGMENT

Dr. Jayant Gajanan Joshi is highly indebted to Shri. D. P. Nathe, Principal, Government Polytechnic, Nashik, Dr. S. D. Pabale Head of E & TC Department, and Dr. Prerana. V. Rathod Head of E & TC Department, Government Polytechnic, Nashik for their kind motivation, support and providing necessary facilities for this research work.

REFERENCES

1. A.Cataldo, G. Monti, E. De Benedetto, G.Cannazza, and L. Tarricone, "A noninvasive resonance-based method for moisture content evaluation through microstrip antennas," IEEE Transactions on instrumentation and measurement, vol.58, no.5, pp.1420-1426, May 2009.
2. K.Y.You, J.Salleh, Z. Abbas, and L.L. You, "A rectangular patch antenna technique for determination of moisture content in soil," PIER Proceedings, Cambridge, USA, July 5-8, 2010.
3. J. G. Joshi, "Measurement of soil electrical parameters using aluminium electrodes," Proceedings of 11th National Seminar on Physics and Technology of Sensors (SENSORS11) Department of Electronic Science, Pune University, India, pp.C18-1 to C18-5, February 27-March 1, 2006.
4. Pakamas Chetpattananondh, Kittikhun Thongpull, Kanadit Chetpattananondh, "Interdigital capacitance sensing of moisture content in rubber wood," Elsevier Computers and Electronics in Agriculture, vol.142, pp.545-551, 2017.
5. Qiulin Tan, Mingliang Yang, Tao Luo, Wei Liu, Chao Li, Chenyang Xue, Jun Liu, Wendong Zhang, and Jijun Xiong, "A novel interdigital capacitor pressure sensor based on LTCC technology," Hindawi Publishing Corporation, J of Sensors, vol.2014, Article ID.431503.
6. Ee Lim Tan, Wen Ni Ng, Ranyuan Shao, Brandon D. Pereles, and Keat Ghee Ong, "A wireless passive sensor for quantifying packaged food quality," Sensors, vol.7, pp.1747-1756, 2007.
7. Mohd F. Ain, Seyi S. Olokede, Yazeed M. Qasaymeh, Arjuna Marzuki, Julie J. Mohammed, Srimala Sreekantan, Sabar D. Hutagalung, Zainal A. Ahmad and Mohd. Z. Abdulla, "A novel 5.8 GHz quasi-lumped element resonator antenna," Intl. J Electron and Commun, vol.67, pp.557-563, 2013.
8. J. G. Joshi and Shyam S. Pattnaik, "Metamaterial Based Wearable Microstrip Patch Antennas," Book Title: "Handbook of Research on Progressive Trends in Wireless Communications and Networking," Chapter 20, pp. 518-556, 2014, Information Science Reference (an imprint of IGI Global), USA. DOI: 10.4018/978-1-4666-5170-8, ISBN13: 9781466651708, ISBN10: 1466651709, EISBN13: 9781466651715.



9. J.G. Joshi, and Shyam S. Pattnaik, "Polypropylene based metamaterial integrated wearable microstrip patch antenna," Proceedings of IEEE Indian Antenna Week 2013 Workshop on Advanced Antenna Technology (IEEE IAW 2013), 3-7 June, 2013, Hotel Rama International, Aurangabad, India. (DOI: 10.1109/AEMC.2013.7045103).
10. J.G. Joshi and Shyam S. Pattnaik, "Dual band wearable microstrip patch antenna," Proceedings of IEEE Indian Antenna Week 2014 Workshop on Advanced Antenna Technology (IEEE IAW 2014), 26-30 May, 2014, Hotel JW Marriot, Chandigarh, India. (Prof. Rajneesh Arora Best Research Paper Award).
11. Yafei Wang, Chang Ma, Wei Yang, and Xuehua Li, "Addition of interdigital capacitor to reduce crosstalk between non-parallel microstrip lines," Progress in electromagnetics research Letters, vol.92, pp.133-138,2020.
12. Harold A. Wheeler, "Transmission-line properties of a strip on a dielectric sheet on a plane," IEEE Transactions on microwave theory and techniques, vol. MTT-25, no.8, pp.631-647, August 1977.
13. Eric Bogatin, "Design rules for microstrip capacitance," IEEE Transactions on Components, Hybrids, and Manufacturing Technology, vol.11, no.3, pp. 253-259, 1988.
14. Mandar P. Joshi, Jayant G. Joshi , and Shyam S. Pattnaik, "Stub loaded rectangular ring shaped tri-band monopole antenna for wireless applications," Intl. J advances in microwave technology (IJAMT), vol.5, no.2, pp.227-233, May 2020.
15. Anirbid Ghosh, Jitendra Behari, and SupriyoPyne, "Dielectric Parameters of dry and wet soils at 14.89GHz," Indian J of Radio and Space Physics, vol.27, pp.130-134, June 1998.



Integrated Communication Interface with Configurable Dual Active Cellular Data Connection, Navigation and PAN Options as Generic IoT Hardware

Kiran Rawal, Harmandeep Singh, Ashish Gupta, Gurjeet Singh, Mohan Lal, Deepa Bajpai

Bharat Electronics Limited, Panchkula, Haryana

✉ kiranrawal@bel.co.in; ✉ harmandeep@bel.co.in

ABSTRACT

Broadly, Internet of Things (IoT) paradigm represents an evolving inter-networking technology which tries to reach its main goal, i.e. each and every device can be connected reliably through a network and externally controllable from any remote station. We seek to highlight the concept of realizing dual active data connection, alongwith reviewing the major protocols used for M2M following the major researches done in this direction. We seek to introduce an IoT ready hardware which may be used as an accelerated starting point for applications that require high reliability dual mode location tracking solutions. It can help the teams turn their ideas into industrial grade products quickly by delivering 70% of the prototype out-of-the-box. Then we will look forward to the scheme which makes possible the dual active data connection stable on a single device.

Keywords : IoT; M2M; LTE; Reliability.

INTRODUCTION

Asset tracking is ranked as one of the top three most in-demand applications for IoT technology. To deliver complete functionality, the web of Things is broken into a multi-stage system that has identification, sensing, communications, data processing, services, and semantics. This network of information transmission, management and delivery supports the growing demands of the IoT, including data fetching, security, and delivery. Thus, an IoT system altogether consists of 4 different components which are Sensors, Connectivity, Data Processing, and the final one being a User Interface.

Machine to machine (M2M) is direct communication between devices using any communications channel, including wired and wireless. In order to increase the reliability of M2M, dual data carriers may be employed. However, various challenges are involved in dual data connections using single processor are also discussed and implemented.

BASIC ARCHITECTURE

The utility model relates to a tracking system plug-in combining a GPS, Dual GSM AND PAN accessory. This model can be plugged in to any PC/laptop with suitable connecting arrangement on standard logic interfaces. Also, compared to other similar systems, this system has two separate GSM modems, which are able to simultaneously connect to two networks on LTE. Downfall from 4G to 3G/2G is also available in the modem. For cater for physical interference related issues, sufficient filtering and shielding mechanisms have been used and dedicated and distributed power supply has been used in the PCB design for both cellular modems instead of a common ground plane. Digital traces are routed in inner layers and are shielded by the ground plane in top and bottom layers. Reset signals are provided for both the modem signals on the combo connector. Since few frequencies from GSM can interfere with GPS signals, physical isolation has been provided. Another version of hardware is also available in which all the modules are replacable in order to cater to varying user demands. The module works from power supply ranging from 4.5V to 18V.

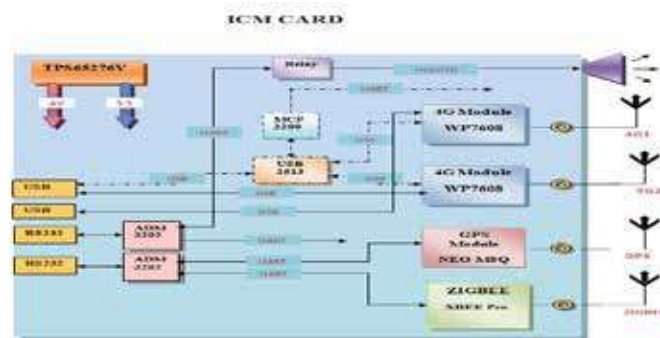


Fig. 1. Basic architecture

HARDWARE

Hardware module has been developed with single PCB design containing two cellular modems, high sensitivity navigation receiver and PAN module. Complete designed hardware module is termed as Integrated Communication Module (ICM). Since all the devices are of high freq, greater than 1 GHz, sufficient shielding and filtering options are provided for simultaneous operation of all devices. There is a rugged combination connector with various ports or connections available for configuration and accessing the required modems. Both the modems can work from a single USB interface as USB hub option is available in the PCB or from two separate USB ports, if such are available in the connecting system. This plug-in can be connected to any computing controller/processor with required interfaces available. **Fig. 2** represents the top view of PCB containing dual 4G modem, Zigbee. Design is ruggedized as visible in **Fig. 3**.



Fig. 2. PCB design



Fig. 3. Ruggedized enclosure design

HARDWARE OPTIONS

The hardware is converted to a more generic form where the LTE modems as well as the GPS and zigbee are in replaceable form factors in order to cater to varying demands of GPS receivers, cellular modems. Options with IRNSS GPS are also realized presently.



Fig. 4. Represents the generic PCB containing all replaceable modules (cellular in mini-PCIe form factor)

GSM PROTOCOLS

The AT commands are enough to transmit data over network if standalone controller (general purpose) is used with modem.

However, There are different protocols that are used for the cellular modem to connect to the network in OS based systems. The various protocols that can be used are Point to Point Protocol (PPP), Qualcomm MSM Interface (QMI), CDC-ECM, Mobile Broadband Interface Model (MBIM) Interface, etc.

Each of the above protocol has its own pros and cons. The Cellular Modems are designed to work with some specific protocols. So the protocol to be used should always be selected as per the recommendations from Modem specs.

The legacy way to connect the cellular modem is to emulate a legacy analogue modem. In this case, the modem will project one serial (TTY) interface (`/dev/ttyUSB*`) in host OS based device, which is used for both modem AT commands and data connection (PPP). In this case, on establishing network connection, the TTY device passes a single PPP datastream, and the TCP/IP protocol packets are wrapped within PPP.

The serial port speeds are more than 115200 bps. A USB-based serial port emulation may well report them. But if there is USB-based connection in actual, which most of the devices at present are, some of the details of the emulation may get ignored in serial device emulation, for example, the number of data and stop bits and the serial port speed, may be ignored, and the commands to set them can be made into no-ops. So a USB LTE modem in legacy mode may show that the `/dev/ttyUSB*` is set to 115200 bps when queried, while the actual data transfer rate can be higher.

TCP/IP and IPV6 are supported in LTE radio protocol, so it is not required to wrap TCP/IP into PPP over the radio interface. The PPP protocol is used between the host OS based device and the modem to make connection look like a legacy dial-up modem-based network connection.

The new ways to present USB-based LTE modems like QMI and MBIM have been developed. QMI is a Qualcomm proprietary protocol, and MBIM protocol specification is the output of multi-vendor efforts for standardization. These present the modems as a real network interface (`wwan0` or similar) and an additional device e.g. `/dev/cdc-wdm0` for command access.

This cuts out the PPP layer, as the TCP/IP packets are passed directly to the cellular modem for transmission over the LTE radio protocols. It removes the need for both the host PC and the cellular modem to pretend that a venerable RS-232 serial port connection exists between them, while the actual connection is USB connection. It gives a separate command channel that can be used to monitor the LTE signal strength, which may be important if the Modem is in movement while the network connection is in use.



Some of the cellular Modems are compatible with CDC-ECM protocol. CDC-ECM is the protocol which works as the Ethernet over USB protocol. This protocol is a lower overhead with higher usable bandwidth for the application. This protocol can be used for bandwidth critical applications and PPP can be used for maximum compatibility with other operating systems.

Mobile Broadband Interface Model Interface (MBIM interface) is implemented in most of the cellular modems. This is because the Microsoft request cellular module vendors to include the MBIM interface to make compatibility better with Windows 8, 8.1, 10 and later systems. The built-in connection manager of Windows also rely on MBIM interface for control of the cellular modules.

The open source Linux in-kernel driver supporting MBIM interface is also available and it is called `cdc_mbim`. The 'libmbim' library is used to communicate with the cellular devices and do required configurations to make the data connection over the cellular network.

DUAL ACTIVE CELLULAR DATA HANDLER SCRIPT

In the present hardware, both the cellular modems are used with single processor which is unique in its type in the sense that both the modems actively transmit and receive data parallelly.

In the earlier implementation of hardware, both the modems were handled with Modem Manager in RHEL 7.6. But Modem Manager solution has syncing issues with dual modems. When Modem Manager was used with qmi protocol, not all the modems respond to various queries (`qmi_wwan proxy`) sent by OS. This may cause serious problems in real time based IoT solutions. To handle this, a customized alternate of Modem Manager is developed where simplified PPP protocol is used. Two services `Modem-ppp0.service` and `Modem-ppp1.service` are running parallel which initiates two applications. The first application searches for the AT-port (`/dev/ttyUSB*`) starting from enumeration 0, i.e. in ascending order. When it connects to the AT-port, configuration of port is initiated by the application. After that the application checks the SIM availability and then initiates the dynamic algorithm for connecting to specific network. The script also dynamically caters to the changing network conditions, and ensures that modem and OS are always in sync. The APN is configured as per the ISP and PPPd is started using generic OS commands. Exclusion strategy for the other service is managed by searching for the AT ports in descending order. This also handles the case where modems get temporarily disconnected due to user behaviour or to cater to hot plugin conditions. Auto-redialling and auto-reconnection is managed by the application wherein the service reinitiates the ppp daemon whenever required.

Here both the applications are running parallel and handling modems independently. In this way, dual data connections are maintained. The application presently runs on linux, but can be easily configured to run on any OS, being derived from C code.

ZIGBEE

The hardware also has the ability to be used as a zigbee node.

Zigbee is typically used in low data rate applications where long battery life and secure networking is required. Zigbee networks are secured by 128 bit symmetric encryption keys. Zigbee has a defined rate of 250 kbit/s, best suited for intermittent data transmissions from a sensor or input device. This hardware can be used in scenarios with single co-ordinator or in a mesh topology, where all nodes work as routers.

Mesh networking is a powerful and effective way for routing data over an RF network. Range is extended by allowing data to hop node to node and reliability and resiliency is increased by "self-healing," or the ability to create alternate paths when one node fails or a connection is lost.

SENSOR INTEGRATION

Various types of sensors may be required in different applications. For example, sensors are available for measuring temperature, humidity, pressure, accelerometer, gyroscope, gas sensors, level sensors, health monitoring sensors. All these sensors are mostly available with standard interfaces. The generic hardware has the ability to connect to different sensors. If the IoT application demands connection to other devices with data on standard interfaces like TTL, USB or RS-232 ports, the hardware specifically provides these interfaces. This enhances the marketability of the hardware to adapt to varied customer requirements.



CONCLUSION

In this paper, we have described the capabilities of the generic IoT hardware. We have also described the scripts formulated to cater to increasing system reliability by simultaneously establishing two different active data connections. This module is implemented in a system designed by Bharat Electronics Limited, Panchkula and is successfully working in a field system.

REFERENCES

1. M. A. Ezechina, K. K. Okwara, C. A. U. Ugboaja. The Internet of Things (Iot): A Scalable Approach to Connecting Everything. The International Journal of Engineering and Science 4(1) (2015) 09-12.
2. Sudip Misra, P. Venkata Krishna, Harshit Agarwal, Anshima Gupta, Mohammed S. Obaidat, 2012 An Adaptive Learning Approach for Fault-Tolerant Routing in Internet of Things. IEEE Wireless Communications and Networking Conference: PHY and Fundamentals
3. M. D. Edwards, 1994, A generic hardware architecture to support the system level synthesis of digital systems, Science Direct
4. Gubbi, Jayavardhana, et al. "Internet of Things (IoT): A vision, architectural elements, and future directions." Future Generation Computer Systems 29.7 (2013): 1645-1660.

Mechanical Engineering

Designing a Proper Hoe towards Zero Loading Losses to Achieve 100% Productivity with Reduced Fuel Consumption

Rajarshi Mukherjee

A-5/5 Uttarayan Housing Estate, 102, B.T. ROAD, Kolkata, West Bengal

✉ rajarshi.mukherjee@myworldmail.org

Keywords: Back hoe; Front hoe; Motion; Loading losses; Zero loading losses.

INTRODUCTION

Hoes are one type of very important equipment in the Construction and the Mining Sectors. They are used to pick material up and load a dumper or a railway wagon towards removal and clearance of area or towards transportation to manufacturing locations. In the current world, as delivered by the Capital Equipment Industry, we have either the back hoe or the front hoe and a combination of both. All the types of currently available hoes have, based on current design standards, some type of loading losses and this paper discusses after studying the motion and loading pattern of currently available hoes, the design of a hoe that will have ZERO LOADING LOSSES, 100% productivity and much reduced fuel consumption due to nil loading losses, when considered the volume of loading done in the SPT – shortest possible time, with zero loading losses.

This paper thus delves into designing a HOE which can actually achieve zero loading losses with 100% productivity and much lower fuel consumption over the volume of loading done in the shortest possible time.

BODY

The Current Design Standards: Studying A Front Hoe and or A Back Hoe

In the modern world, globally, three types of hoes are available, the Front Hoe, the Back Hoe and a combination of the Front Hoe and the Back Hoe together in a single equipment. This paper will be having illustrations and drawings of the various types of Hoes and a write-up on exactly how and when the loading losses happen as given below.

Front Hoe

The drawing of the Front Hoe is as below, taken on the positioning of the Hoe part on the Chassis and then a description on the loading losses.

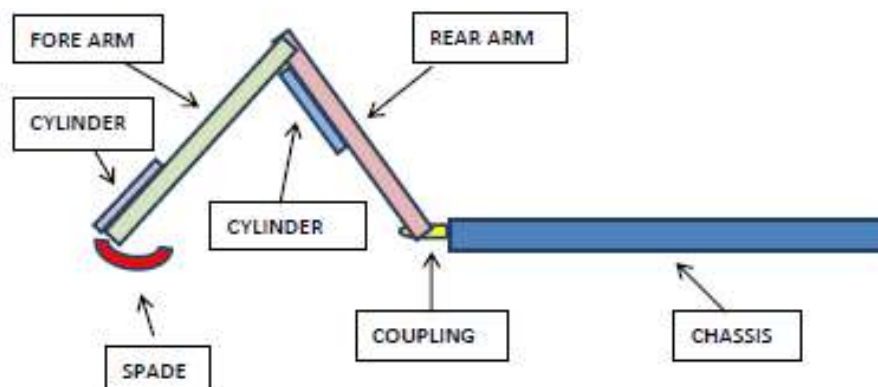


Fig. 1. Front hoe

The Front Hoe looks like above. The Coupling is welded to the Chassis. The Rear Arm is attached to the Coupling through a Non-Rotating Pin or welded. There is a Cylinder attached to the Rear Arm through coupling. The Fore Arm is attached to the

Rear Arm through a Rotating Pin. The Fore Arm has a Cylinder coupled with it at the bottom end and the Spade is coupled to the Fore Arm with a Rotating Pin with the Tube of the Cylinder coupled to the Spade.

THE STUDY OF MOTION

We retract the cylinder on the spade, it opens like a bucket and with the spade we try and do the scooping activity. On scooping, we expand the cylinder on the spade and the spade end moves up towards the front arm, and since it is a spade and not a bucket, some losses start happening here as it is a spade and load carrying portion is less. Now once this first loading loss happens on moving the spade open space towards the fore arm on expansion of the cylinder, we want to expand the retracted cylinder attached the rear arm which puts the fore arm on the upward motion, moment the fore arm with the loaded spade reached a parallel straight line with the Chassis with the load on the spade, any angle over the straight line will again start with losses as the load takes the option of laminar flow with the losses starting from the top layers from the inside end. We need to note the Elbow of the arm is at the top and if we increase the length of the rear arm, we might be able to reduce some of the losses off any angle more to the parallel straight line to the chassis, but then the loading losses due to the spade end moving towards the fore arm cannot be reduced one we start the expansion of the cylinder which connects the spade to the fore arm. If the spade is removed and a bucket provided to the front hoe, then on expansion of the front arm – bucket cylinder the open end of the bucket comes at right angle to the base of the fore arm, and any angle caused by lifting the fore arm due to the fore arm – rear arm cylinder, the losses will start happening from the inside top layers of the load due to laminar flow. Now to reduce loading losses when the cylinder movement starts on the fore arm by the cylinder attached to the rear arm, the arms can be made longer but still the loss arising off the spade cannot be eliminated when the cylinder attached to the fore arm starts its expansion motion to make the spade opening parallel to the fore arm.

BACK HOE – BUCKET ON THE OUTWARD SIDE OF THE FORE ARM

The drawing of the Back Hoe with the Bucket on the outward side of the fore arm is as below, taken on the positioning of the Hoe part on the Chassis and then a description on the loading losses.

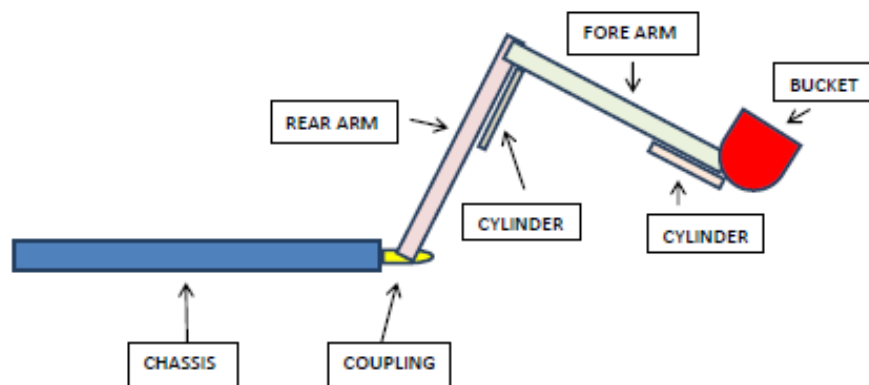


Fig. 2. Back hoe - bucket on the outward side of the fore arm

The Back Hoe – Bucket on the outward side of the fore arm looks like above. The Coupling is welded to the Chassis. The Rear Arm is attached to the Coupling through a Non-Rotating Pin or welded. There is a Cylinder attached to the Rear Arm through coupling. The Fore Arm is attached to the Rear Arm through a Rotating Pin. The Fore Arm has a Cylinder coupled with it at the bottom end and the Bucket is coupled to the Fore Arm with a Rotating Pin with the Tube of the Cylinder coupled to the Bucket.

THE STUDY OF MOTION

When we extend the cylinder on the rear arm, the forearm with a loaded bucket moves upwards while the cylinder on the fore arm, controls the movement of the bucket, from the movement of the bucket at the angle kept on construction to the open end of the bucket coming to 90 degree to the upper side of the forearm. This type of construction is not seen too much as when the fore arm moves in line parallel line to the chassis, any further an angle upwards, the load starts falling on top of the chassis and or the cabin due to laminar flow from the top end of the bucket, the only option of dropping front wards towards the outer end is full cylinder retraction, which brings the open end of the bucket at any angle below a straight line on retraction with the retraction controlling the angle to which the open end of the bucket can come down in comparison to the top flat surface of the fore arm.

BACK HOE – BUCKET ON THE INWARD SIDE OF THE FORE ARM

The drawing of the Back Hoe with the Bucket on the inward side of the fore arm is as below, taken on the positioning of the Hoe part on the Chassis and then a description on the loading losses.

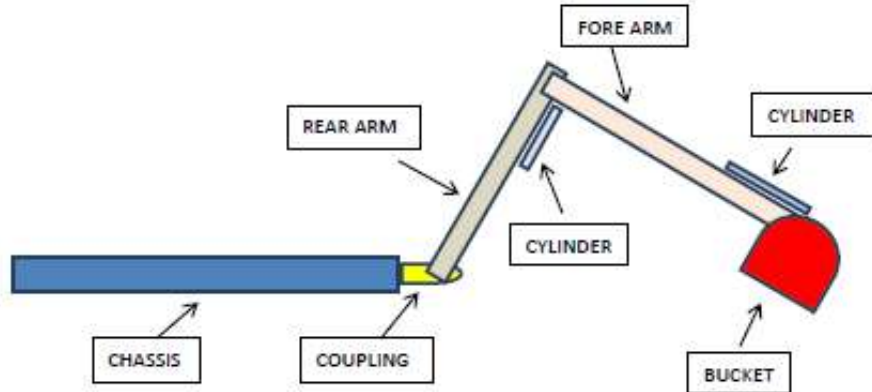


Fig. 3. Back hoe - bucket on the inward side of the fore arm

The Back Hoe – Bucket on the inward side of the fore arm looks like above. The Coupling is welded to the Chassis. The Rear Arm is attached to the Coupling through a Non-Rotating Pin or welded. There is a Cylinder attached to the Rear Arm through coupling. The Fore Arm is attached to the Rear Arm through a Rotating Pin. The Fore Arm has a Cylinder coupled with it at the top end and the Bucket is coupled to the Fore Arm with a Rotating Pin with the Tube of the Cylinder coupled to the Bucket.

THE STUDY OF MOTION

The start of motion happens with the cylinder on the rear arm fully retracted and the cylinder on the fore arm fully expanded with the bucket position like a biter – digger and the open portion of the bucket comes at right angle to the bottom face of the fore arm. Now the moment the cylinder to the rear arm is expanded and the fore arm starts lifting, the open portion of the bucket, still at right angle to the base of the fore arm picks an upward motion and the loading losses start happening with laminar flow of the top of the load and it starts at the slightest angle of lift, noting this is the more prevalent position in designing the back hoe with the bucket attached to the end of the fore arm with being intermediate to the fore arm and the chassis and actually causes the highest loading losses amongst the three types discusses so far.

THE ZERO LOADING LOSSES DESIGN OF THE HOE – THE ELBOW AT THE BOTTOM

This is not a tried and tested design in this current world and can be patented globally as well as per the design as given below. And it can be both front hoe or back hoe or both front and back hoes combined together.

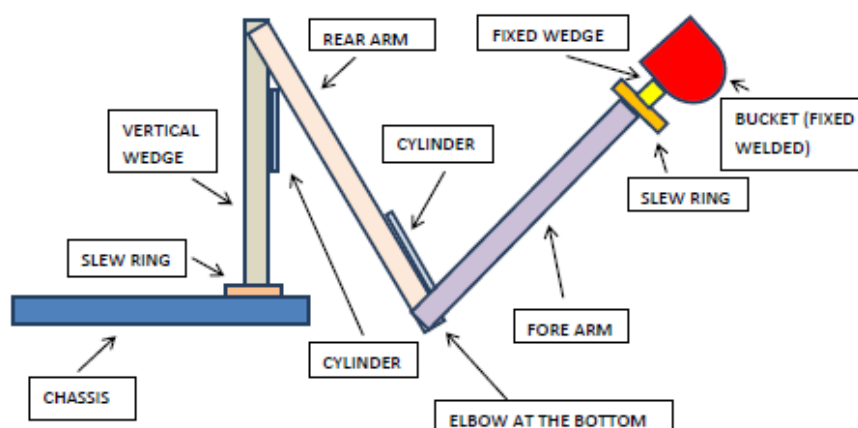


Fig. 4. The zero loading losses hoe - elbow at the bottom



The chassis can have a slew ring mounted which will allow the arms to get two seventy degrees rotated with being attached to the vertical wedge which has a cylinder attached to it to control the motion of the rear arm which has a cylinder attached to it to control the motion of the fore arm, with the elbow at the bottom. The fore arm has a slew ring attached to it to which is a fixed wedge welded with the bucket welded to the fixed wedge.

THE STUDY OF MOTION

The cylinder connecting the fore arm is expanded first, noting all hoes use Haptics in design, and since the cylinder attached to the fore arm is expanded first at the elbow at the bottom, the arms straighten out and in an in-line straight line position; the bucket is loaded with some manual spade work. Once the bucket is loaded, the cylinder attached to the rear arm starts expanding, thus lifting the straight arms till it comes ninety degree to the vertical wedge and when placed over the dumper or railway wagon, it is just needed to rotate the slew ring attached at the front end of the fore arm which causes the fixed welded bucket to turn upside down and the load can thus be dumped into the dumper or the wagon with actually ZERO LOADING LOSSES. The built to specification part rests on the vertical length of the vertical wedge so that the design specification wise vertical side wall of the dumper or the wagon can be cleared by the straightened arms at exactly ninety degree angle (with the vertical wedge) to clear the top of the side wall. A design consideration in such ways not only causes zero loading losses, it also due to such reasons causes one hundred percent productivity per lift, meaning much reduced fuel consumption and such design can be tested and patented as well.

CONCLUSION

This paper thus delves into the design of a hoe, comparatively based on all currently available hoes that actually if designed to such extent will cause zero loading losses and reduced fuel consumption with its usage in the construction and mining sectors.



Disaster Management over Indian Railways- Reliability, Operation & Safety of 140t Gottwald Crane

Narendra Kumar Verma

Retired IRSME/Ex Dy. Chief Mechanical Engineer, N Rly / Principal Supervisors Training Centre, Charbagh, Lucknow

✉ narendrakverma28@gmail.com

ABSTRACT

Safety of travelling public/human beings, goods & animals entrusted for carriage is the most important attribute of any transport system. System of train movements and avoiding accident to train is the primary concern over any Railway/transport system.

Disaster management following an accident envisages expeditious, orderly and adequate relief and rescue measures. Temporary and casual approach should be discouraged. On the basis of field experience and happenings in recent past, a well organised and planned system have been evolved for handling accidents. In odd situation due to lack of foresight and shortcomings in dealing with human situations, it became a source of public criticism. During the course of relief and rescue operations, small problems often blow up into a complex situation.

Therefore, every Railway servant and staff/officers of NDRF team are expected to be familiarised with disaster management and must acquaint themselves with the strategy to deal with accidents, particularly those involving loss of human life. Whenever safety is infringed, distress comes to travelling public with that relief operation has to be mobilised with a sense of urgency & compassion.

Indian Railways is one of the largest networks for train operation and it is the third largest in the world. Since Railways are mainly concerned with train operation carrying passengers as well as freight services. As of March 2019, the national rail network comprises 123,542 km of track over a route of 67,368 km and 7,349 stations.

In spite of main impact on safer train operation and consequent movement of rolling stock, sometimes safety is infringed due to undefined reasons.

In view of above, necessary arrangements exist over Indian Railways (as well as foreign railways) to have proper management in case of any accident occurring during train operation. Hence a setup of Accident Relief Trains (ART's) exists which is presently equipped with a 140t Gottwald make Diesel Hydraulic Breakdown Crane especially in 'A' class ART's.

Basically, ART's are equipped with MFD/Lucas van comprising of hydraulic jacks normally of 120 t capacity along with other jacks and relevant materials, equipment as recommended by Railway Board as well as zonal railways.

In addition to this since 140t Gottwald/any other make crane of same capacity is also integral part of ARTs hence its importance cannot be ignored.

In addition to hydraulic jacks, in case of major accident/disaster use of these cranes is of utmost importance because if the railway track is damaged owing to after effect of derailments or any other reason, the hydraulic jacks are normally not useful at such accident sites. So availability of heavy-duty Cranes for quicker restoration of accident sites is primarily essential.

In this paper the important features rigging of crane, operation, safety and reliability will be discussed with some design features for stability of the crane. Brief discussion about constructional details, maintenance aspects, staff deployment, propping of crane, and problems encountered during the crane working are to be discussed as a guideline to those working in the actual field. However, these details will also be equally useful where the operation of such heavy-duty cranes is essential.

Keywords: Disaster; Accident; ART's; 140t Gottwald crane; Reliability; Safety.

DISASTER MANAGEMENT

Disaster is a calamity which can lead to disruption of normal and civic system, resulting in loss of human life and property, having far reaching effect on society.



Classification

Table 1. Classification of disasters

S. No	Natural causes	Manmade causes
1	Floods	Accidents-Road, Railways, air, sea
2	Fire	Chemicals (Leakage/Explosion)
3	Lightening	Gas (Leakage/Explosion)
4	Cyclone	Wars
5	Hurricane	Terrorism
6	Tornado	Collapse of building
7	Earthquakes	Fire
8	Draught	Sabotage
9	Land slides	
10	Volcanic eruptions.	

- Safety of train movements and avoiding accidents to train is the primary concern on Indian Railways.
- Temporary & casual approach should be discouraged.
- During the course of relief and rescue operation, small problems often blow up into complex situation.
- Every Railway servant is expected to be familiarized with disaster management and must acquaint himself with the strategy to deal with accidents, particularly those involving loss of human life.

PRIORITIES

Disaster management following an accident, may it be in a block section or at a station, will have following priorities,

- To protect the affected lines.
- To save human life and alleviate sufferings.
- To provide assistance to other passengers at the site of accident.
- To protect clues.
- To protect property of both passengers and Railways (May seek assistance of RPF.)
- To ascertain the prima facie cause of accident.
- To restore through communication.
- In order to achieve efficiency, arrange to get all the relevant information of the accident promptly.

Accident aids:

- The brake van of every train carrying passengers is provided with,
 - First aid box (As personal equipment of Guard)
 - Emergency train lighting box.
 - Fire Extinguishers-two nos.
 - Portable control Telephone.
 - Stretcher
 - Wooden wedges-two /four nos.
- Details of other medical facilities e.g. local dispensaries, hospitals & medical practitioners in the vicinity of the station are maintained at all stations & displayed on a board in ASM's chamber.



RELIEF FACILITIES

Accident Relief Trains/ ART's (Breakdown trains)

- Accident relief train/ MFD/Lucas van is equipped with HRE (Hydraulic Re-railing Equipment) consisting of MFD/LUCAS make hydraulic jacks & other relevant items (Complete set) along with 140t Gottwald/Cowan Sheldon/Jessop/any other make Diesel Hydraulic Breakdown crane as an integral part of 'A' class ART.

Medical relief van & auxiliary van i.e ARME

- Medical relief van & auxiliary van i.e ARME (Accident Relief Medical Equipment van) contains mainly medical facilities with facilities for operation & HRD (Hydraulic Rescue devices) are placed in auxiliary van of ARME.
- Handpicked staffs are maintained in ready to rush position along with team of medical experts at important stations all over Indian Railways.
- Through these special trains effective and dependable relief & medical aid is made available at an accident site with least delay.
- By these measures' casualties are curtailed, dislocation to traffic is minimized and restoration work is attended quickly and debris removed expeditiously from the site.
- Through these special trains effective and dependable relief & medical aid is made available at an accident site with least delay.
- By these measures' casualties are curtailed, dislocation to traffic is minimized and restoration work is attended quickly and debris are removed expeditiously from the site.

Standardisation of ART's: For the first time, the ART (Accident Relief Trains) equipment and requirement were standardised in the year 1963. Over the last 57 years, since the last standardisation in 1963, there has been large scale dieselisation and electrification, Train loads have substantially increased and now running on BOX-N trains of 5800 t trailing load is a regular feature. Due to rapid progress in the design of rolling stocks, there are still plans to run freight trains with 7500 t & more trailing loads in near future.

Four-wheeler stock has been replaced by bogie stock with CBC's, roller bearings and now air brakes. The average speed of trains has gone up consequently the nature and extent of damages during accidents have undergone a major change Electrification of trunk routes have also contributed a major change in approach and there have been considerable developments in design of rescue equipment, hydraulic jacks and cranes as the tools and equipment provided earlier have now become redundant due to closure of steam traction.

With the passage of time and increasing speed of trains, higher axle loads and increased density of traffic, full scale Accident Relief trains with provision of 140t crane were evolved to meet the requirements. Due to above reasons heavy duty crane is essentially required as integral part of 'A' class ART's.

Brief list of Assets/equipment available in MFD/Lucas Van i.e HRE

Following specification are of Hoesch (MFD) make jacks and specifications are likely to change depending upon the lifting capacity of rolling stock.

- (i) Petrol power pack Type AA-4, Engine model GX-340 or equivalent -at least two nos. [Make Hoesch Maschinenfabrik Deutschland AG] or Diesel power pack of any make of repute.
- (ii) Telescopic Jack high lift: capacity 1200/600 KN and 600/300 KN
- (iii) Displacing Equipment:
 - (a) Rerailing bridge:-04 Nos, Material: light metal alloy (extruded)/Aluminium
 - (b) Removable top plate
 - (c) Counter Support for displacing jack-02 nos, Material steel (weight 8 kg)

This is placed into the aperture of the re-railing bridge to accommodate the head or foot of the displacing jack.



- (iv a) Step jack Lifting force -35t, height 1100mm, total stroke 825mm, stroke at the step 660mm, oil capacity 9.3 lit. Lifting point of step from Ground level-105mm
- (b) Rocker bearing support weight 16.5 kg
- (c) Lifting cable ladder with accessories.
- (d) Pressure piece (weight 6 kg)- It is a cylindrical supporting ring for multistage jacks.
- (v) Control Table -2 Nos. comprising of pump set with electric motor without control block.
 - (a) oil hydraulic axial piston pump output-8 lpm, pressure 300 Kg/Cm²
 - (b) Driving motor/electric motor output approx. 5 HP
 - (c) oil container cap.65 lits hyd. Oil, weight 126 kg.

Hand pump- for 1,2,3 connections with oil container and Pr. Gauge of oil container 10.20,30 lits mounted on a carrying frame with folding base plate for operating by two men.

Tilting Jacks

Material- steel, lifting force- 20t, constructional height-597mm, stroke 400mm, weight -57 kg, End use: for quick re-railing of a single setoff wheels of railway goods wagon up to 24t gross weight (b) Tilting jack rerailing plate and roller grid.

Hydraulic Haulage & rescue device: Material- light metal, force-25t, wt.70 Kg. This device is for a longitudinal or cross pull and is secured to the track which is suitably loaded by a vehicle.

High pressure hoses NW 10x10m long: These are the maximum pressure hose pipes 10m long for connecting between pump set and control desk/table also between control table & jacks. Pressure 500 Kg/Cm², test pressure of hose material-780 Kg/Cm². These pipes are in set of blue and red colour.

Hose Coupling-loose half with protective plugs.

Material: Thermoplast elastomer with netting inserts specially vulcanized.

Temperature Resistant (-50°C) up to (+125°C)

NW inside width 10mm, wall thickness: 3.8mm, O.D: 17.6mm

Smallest bending radius: 100mm Operating pressure: 300 bar and testing pressure 500 bar.

Mineral based Hydraulic oil characteristics: Kinematic viscosity 25 centipoise at 50°C & Sp. gravity 0.88 at 15°C, flash point 210-235 °C, solidifying point(-30°C)

In addition to above few other equipment, tool & plant are also available to facilitate the restoration work at site.

Following items are provided in auxiliary van of ARME,

- (a) Hydraulic Cutters with power pack
- (b) Hydraulic Expander/ spreader with power pack,
- (c) High pressure hoses NW 10x10m long sets.

Arrangement of gas cutting & welding along with other items to facilitate working.

Recommendations of High-level committee

Ref: Director (Safety-III) Rly Board's Letter No: 2014/safety (DM)/7/11/committee dated 17.06.2014

To upgrade the disaster management system, following recommendation have been made in co-ordination of NDRF and committee of railway officers to be added to ARMV's/ART's,

**Table 2.** Recommended items for upgradation ARMV's /ART's

S.No	Particulars	Unit	Qty
1	Life detector	Nos	01
2	Stretcher folding	Nos	09
3	MFR kits with splints	Sets	05
4	Higher capacity HRD for cutting stainless steel coaches & wagons	Nos	01(ART& ARMV each)
5	Portable plasma cutting equipment for cutting stainless steel coaches & wagons	Nos	01(ART& ARMV each)
6	Portable defibrillator	Nos	01(ART& ARMV each)
7	Abrasive cutting equipment	Set	01(ART& ARMV each)
8	Life jackets (water rescue)	Nos	100(ART)

The Indian railways first responsibility in case of accidents is to reach and extricate accident victims and organise effective trauma care. The basic principle of trauma management is speed and expediency. (There are total 13 items in recommendation, only specific items have been given here).

Stability of 140 t Gottwald Crane

- All travelling & revolving cranes should be designed for stability ensuring their safe operation without any hazard of overturning.
- Any crane should be stable in any position in operation and irrespective of its dead & live loads.
- Cranes are to be stable both when handling the rated load and without load on the hook under critical conditions involving the chance of overturning. Consequently, distinction is made between the stability under a load and the stability of the crane proper (i.e. without load).
- Stability of the crane is the ratio of the righting & tipping moments about tipping axis in terms of 'safe working load' (S.W.L) and in relation to the static tipping load.
- 'Static tipping load' is the load which, when applied to the crane hook at a given radius, would cause the crane to tip over.

Other popular methods are,

1. To define the SWL as a percentage of the static tipping load.
2. To define the stability factor, or the factor by which the SWL must be multiplied in order to obtain the tipping load. (This is reciprocal of the percentage as given at sl.1)
3. Margin of stability: Percentage of safe working load which must be added to it in order to obtain the static tipping load.

As per British stipulation 'the margin of stability' expressed as a percentage, shall not be less than,

$(\text{Maximum Stability reach} \times 12) / \text{Stability base}$

But never less than 50%, on a gradient of 1 in 40.

Stability Reach is defined as the distance of the jib head pin from the point of intersection of the nearest base line and the vertical plane passing through the centre line of the jib.

This dimension will vary for different positions of the hook in the course of one revolution during slewing, but for the purposes of calculating the stability the maximum value of these dimensions is taken. It should also be noted that the value for stability reach will also vary as the jib is derricked out, the greater values being obtained when the jib is nearest to the vertical. This is because with a jib of any given length the dynamic effect following from the jib movement is greater as the jib approaches the vertical position.

All these methods are comparable

Table 3. Stability factor

Sl. No	SWL as % of static tipping load	Stability factor	Margin of stability
1	50	2.0	100
2	66.67	1.5	50
3	75	1.33	33.33
3	85	1.175	17.7



- ❖ Coefficient of stability under a load or 'forward stability' is the ratio of the moment set up by the dead weight of all crane components with the allowance for additional forces (wind effects, inertia at starting and stopping the hoisting, slewing and travelling motions, effect of track and ground gradient), take about a tipping axis, to the moment due to the working load about the same axis.
- ❖ Stability Requirement are to be fulfilled with the jib set along, and at right angles to, the track. The latter position creates a critical condition of loading and is, consequently, relied on in stability calculations, for in most travelling cranes the gauge is shorter than the wheel base.
- ❖ The stability of railroad cranes operating without outriggers (i.e free on rail) should be ascertained taking into account the relative elevation of track rails on curves.
- ❖ The stability under a working load is always determined with the jib set at the maximum reach and treating the wind effect and terrain gradient as factors increasing the chance of overturning.
- ❖ In determining the numerical value of the coefficient of unloaded- crane stability, the boom is assumed to be positioned at the minimum outreach, the outriggers, jacks, and anchoring devices available on the crane should be omitted from calculations.
- ❖ The fuel & water tanks and fuel bunkers should be regarded as completely full, if their arrangement may detract from crane stability, otherwise they should be treated as empty.
- ❖ According to applicable codes, the minimum allowable value for both coefficients should not be less than 1.15, with no account of the stability-enhancing anchoring devices.
- ❖ Certain applicable codes also prescribe that the stability coefficient under a working load should be ascertained disregarding additional forces and track gradient. In this case, the coefficient is the ratio of the moment produced by the dead weight of crane components and counterweight about a tipping axis with no account of track gradient, to the moment produced by the maximum working load. The minimum allowable value of this stability coefficient is 1.4.

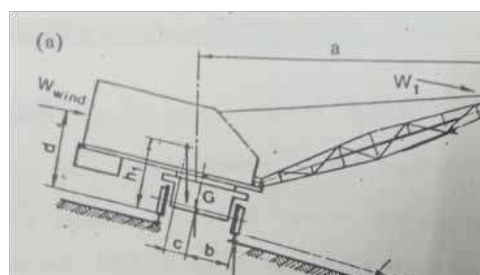


Fig. 1.

Hence static coefficient under a working load is given by,

$$K_1 = [M_G - \Sigma \text{Min} - M_{\text{Wind}}] / M_{\text{Load}} \geq 1.15$$

Where M_G = the moment produced by the dead weight of crane components and counter weight about a tipping axis with allowance for track inclination (angle α)

ΣMin = The aggregate moment due to inertia of crane components and hook load at starting and stopping crane motions including the effect of centrifugal forces set up when the crane is revolving. M_{Wind} = it is the moment from the wind pressure of the safe maximum operating value coming on the windward side of the crane and load at right angles to the tipping axis and parallel to the ground.

M_{Load} = is the moment set up by the Rated load about the same tipping axis.

A hook load with a mass Q suspended from a rope passing over the point sheave gives rise to a horizontal centrifugal force, P when the crane is revolving.

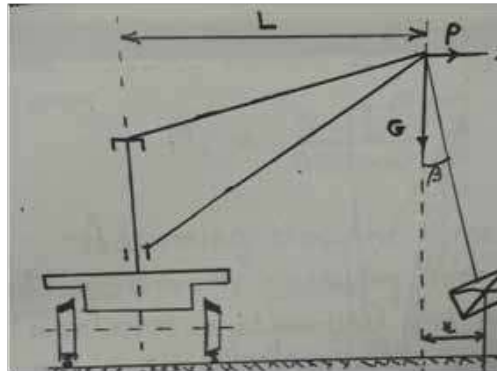


Fig. 2.

This force produces a tipping moment $MC = PH$ and is given by,

$$P = Q \omega^2 p = (Q \pi^2 n^2 p) / 30^2$$

Where n is rate of slewing in RPM Now, $p = L + x$

$$\tan \beta = P / Q g \quad x = H \tan \beta$$

$$\text{And, } p = L + H.(P/Qg)$$

Substituting the expression for p and taking $\pi^2 = g$, this centrifugal force P is given by,

$$P = (Q n^2 L) \div (900 - n^2 H)$$

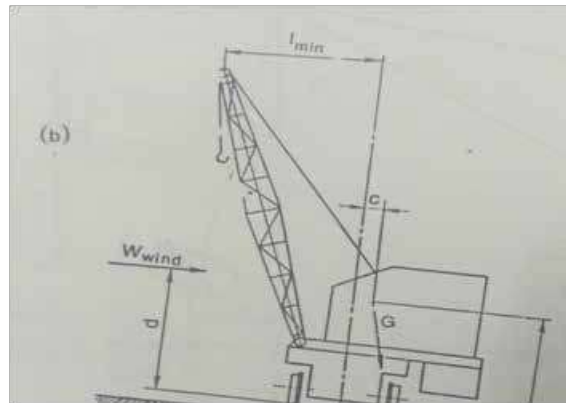
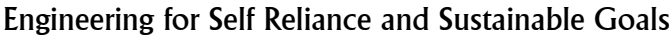


Fig. 3.


$$M_c = (Q n^2 L h) \div (900 - n^2 H)$$
$$P_{\text{Inertia}} = Qv/\tau$$

τ = period of acceleration at starting or retardation at stopping.

$$M_{\text{Inertia}} = Qv(a-b)/\tau$$
$$Q_{\text{vh}} / \tau,$$

Overtaking

[illegible]

974



Technical Specification of old model 1986 design crane (140t Gottwald)/ comparison of old & new design given in Annexure I.

Pivot distance: 7600mm Length over buffers: 13300 mm Brakes: Wheel disc brakes

Max Axle load in train order: 20t Tail radius: 5500mm

Max Propping load: 200t Min curvature: 174m

Jib: Overall length: 18000 mm (main hoist centre to jib)

Minimum working radius: 5.5m Max. working radius: 16.0m

Hoist Drive:

	Main hoist	Aux. hoist
Capacity	140t	25t
Hoist speed	5.0 (4.0 m/min New)	30 (15 m/min new)

Erection of crane- Rigging

Before starting the engine, the following oil and coolant levels should be checked once again,

- (a) Hydraulic oil level
- (b) Fuel oil level (can be checked by gauge in the operator's cab)
- (c) Oil level in gear boxes.
- (d) Engine Lubricating oil level
- (e) Radiator water level.

All stop valves of hydraulic oil lines should be in open position

Start engine & check the following,

- (a) Engine Lube oil pressure
- (b) Battery charging current (Ammeter in cab)
- (c) Pilot circuit pressure should be 30 bar
- (d) Air pressure should be 6.5 Bar plus.
- (e) Visual check of the oil line, airline water line leakages.

Axle Blocking

Basically, the bogie spring suspension is provided purely for hauling operations. When crane operation is required or self-propulsion in the crane is necessary, axle blocking is a must. i.e spring suspension is to be blocked. This means that the spring should make a solid block.

Axle blocking pressure should be 240 bar which can be ascertained with the two pressure gauges (0-600 bar) provided near the control lever on the under carriage.

Any fall in pressure caused due to leakage of oil of axle blocking cylinder, should be made up by repressurising the control lever.

Sequence of operation for axle blocking cylinder

- (i) Select oil transmission line pre-selector switch (in operator's cab) for undercarriage.
- (ii) Operate axle blocking lever until all springs are compressed against the stop. The pressure should be 240 bar approximately. When axle blocking is done, following operation take place simultaneously,
 - (a) Travelling gear engages,



- (b) Brake applies.
- (c) All side mounted display devices indicate “RED”

Erection of Boom

- (a) Pre-selector switch for oil line transmission to counterweight.
- (b) By opening the valve (on the left panel) counterweight gallsows should be raised to maximum position until the indicating lamp (in the cabin) is off.
- (c) Derrick ‘IN’ until boom heels sit on the pin.
- (d) Continue derricking ‘IN’ till ‘A’ frame is at full position
- (e) Secure ‘A’ frame pin in position.
- (f) Remove boom lock provided on the match truck trestle.
- (g) Raise boom clear of head rest(trestle) approx. 40 cms bring hook blocks under the boom head vertically either by moving the crane or Match wagon/ match truck or After raising the boom approx. 40 cms above the trestle continue derricking ‘IN’ and simultaneously both hook blocks are to be lowered till the boom head is vertically above the hook blocks.

The crane is ready for picking up the CWT(Counterweights) as per requirement or the crane is ready for operation without counterweight.

Folding of buffers: to reduce the required radius crane buffers can be folded sideways.

Propping the Crane

- (i) Switch on oil transmission line pre-selector in crane cabin to undercarriage.
- (ii) Operate lever (fitted on undercarriage) to swing out the outrigger beams as required.
- (iii) operate lever (fitted on undercarriage) to lower the propping cylinder on the stabiliser foot. Lock the stabiliser foot and the piston with pin. [it is advisable to use load distribution pads, except where space does not permit.]
- (iv) Raise the crane until the wheels sets lift clear off the rails.
- (v) Set oil transmission line pre-selectors in the crane to neutral position.
- (vi) Level the crane with the help of side mounted spirit level on the undercarriage.
- (vii) It is very important that while propping the crane no gunny bags full of sand should be placed beneath the propping base in any circumstances to avoid weak propping and sometimes likely overturning of the crane.

Counterweights

There are three counterweights of 6,14 & 18 tonnes respectively. All lie on match truck and had to be picked up as per requirements. A weight of 5.2 t lies on the chassis as base load). Following instructions have to be followed for using CWT,

- (a) Switch on boom bridging key, so that 5 metres limit switch is in circuit (by passing 5.5 m limit switch.)
- (b) Switch on Key switch which bridges safe Load Indicator (SLI). Now tge crane should not be slewed.
- (c) Pick up the CWT from match truck individually to form standard CWT condition as under,
 - (i) Half Counterweight: Only for free on rail: $18+6=24$ tonnes on gallows & 5.2t on chassis. i.e total 29.2 tonnes
 - (ii) Full CWT: $(18+6+14)+5.2=43.2$ tonnes on gallows.
- (d) Switch off Safe load indicator switch key to bring the computer safety system into the circuit. Check the correct mode of stability.
- (e) Interlock the counterweight sections and boom out to 8m radius, then slew the super structure to 180 degrees.
- (f) Set oil transmission line selector switch at ‘Counterweight’ lower counterweight gallows, mount the weights and raise the gallows to the limit position. (indication lamp goes off).



(g) Switch off boom key switch, so that 5.5 m limit switch is in circuit.

(h) Caution:

(i) Check if SLI is in operation.

(ii) correct mode of stabilisation is set on the selector switch.

(iii) Axle blocking pressure is approximately 240 bar.

A FEW DO'S & DON'TS

(a) Axle blocking pressure should be checked by a nominated person.

(b) When fixing counterweight in the crane, the crane should not be slewed unless correct propping base is selected [the mode selector on the display unit of the PAT system must show full outrigger].

(c) Before slewing, take the following action,

(d) (i) While working free on rail, 360-degree slew. No counterweight on gallows, 5.2 t counterweight should remain on the chassis.

(ii) While working free on rail, 360-degree slew. Half counterweight on gallows, 5.2 t counterweight on the chassis (24t on gallows). Jib must be beyond 8m. radius.

(e) Load charts fixed in driver's cab should be followed in toto.

(f) After gallows operation or axle blocking operation, pre- selection switch for oil transmission should be brought to 'O' position.

(g) Before starting work, make sure that computer override key and boom override key are switched to working position.

(h) Ensure counterweight indication lamps, indicating correct CWT on gallows, are in operation.

(i) Manually operated mode switch showing correct outrigger basis is operational.

(j) Important: while derigging crane after restoration work is over. bottom down boom until boom slides fully into the boom rest to the lock position. It is very important at this point to lock the hook in the boom rest. Raise counterweight gallows to full height. Fasten the 'A' frame hind bottom leg with counterweight gallows by link rope arrangements. Remove pins from 'A' frame. Boom out to give small amount of slack in derrick ropes.

(k) It is essential that while rigging and derigging, one of the staff members is deputed to watch proper setting of the rope on drum and to ensure that rope does not get out of its path.

MODIFICATION TO 'A' FRAME

This modification was basically done in old cranes of 1986 design, so that 'A' frame should not infringe OHE of the adjacent track.

Reference: RDSO/Lucknow sketch No.CR-761 'A' frame modification was done by reducing 'A' frame front leg length from 4m to 3.6m i.e reduction by 40cm.

Due to this reason, load chart had to be modified and load capacity of old crane reduced from 140t to 130 t.

To alleviate this problem further new cranes of 1997 design was introduced which has resolved the issue of 'A' frame as 'A' frame has been removed in new design of 1997

OPERATIONAL STAFF

There are total 16 technical staff to manage the crane (i.e. one supervisor presently level of Sr. Section Engineer, three diesel technicians, two crane drivers, one gunner/crane jamadar, one skilled staff to watch the props, 08- unskilled staff) [Authority Railway Board Letter No; 79/M(M&P)/175/10/vol IX/Pt-I dated 26.5.89]

Basic Operations of crane:

- Rerailing: lift, slew, derrick out, lower



- Off track: lift, derrick in. slew, lower

PAT System: Older cranes had quick release clutch, which the driver could operate in case of imminent unsafe conditions. Due to this reason newer technology was introduced by Gottwald as a precautionary measure. Hence necessity of PAT system produced by PAT GmbH was felt.

PAT system is basically microprocessor-based protection system,

- To protect crane from excessive load moment to avoid toppling of crane.
- Indicate approach of overload to avoid breakage of lifting mechanism.
- Indicate a few working parameters.

Control Unit is located below the spare seat & display is in front of driver's seat. It should be ensured that no water ingress should be there specially in rainy season to avoid damage to control unit. Proper sealing should be ensured.

Features of PAT System

- Works within safety limits given in on load charts based on (i) Maximum load moment (ii) No minimum radius restriction.
- Safety margin not known
- Reaction time of PAT 0.25 seconds (Angle of tilt $<1^\circ$)
- Reaction time of hydraulic system
- PAT disable key allows Derrick in, aux & main hoist to work.
- Power supply from 24 V battery and alternator.
- Separate micro-processor for control & display.
- Three 4KB EPROMS for control and one for display.

Table. Sensors used

Sensor	Type	Output volts	Characteristics
Load Cell	Strain gauge+ O Pamp	0-2.5V	Linear
Derrick angle	Oil damped potentiometer	(-)3.125 to (-)1.875	Non-linear
Slewing angle	Potentiometer	-0.5 to - 4.5 V (at 180°)	Linear
Counter wts.	Oil pressure switches	0-24 V	Digital

CONCLUSION

In view of all the above discussions and details available, it can be concluded that,

- Stability of the crane is an important aspect while designing the crane for actual operation at site.
- Propping of the crane is very important to avoid overturning/toppling down the crane.
- Rigging of crane should be properly done observing safety aspects and specific attention be given to do's & don'ts.
- It should always be ensured that microprocessor is working satisfactorily and it should never be bypassed as a safety aspect.
- Lifting Capacity of the crane for Railways or any other site depends on the load to be lifted by the relevant crane hence it should be chosen as per requirement of load to be lifted.
- Details of comparison of old & new design crane (140t Gottwald) are enclosed as an annexure I

REFERENCES

1. Indian Railways Institute of Mechanical & Electrical Engineering, Jamalpur, E. Rly
2. Advanced Training Institute Calcutta (ATI Dasnagar, Howrah)

3. E. Railway Workshops, Jamalpur. (Only Workshop manufacturing Diesel Hydraulic Breakdown crane Gottwald make) in Indian Railway.
4. WWW.rdsO.indianrailways.gov.in/works/uploads.
5. Error! Hyperlink reference not valid.
6. Operating & maintenance manual for 140t crane 1986 design (revised 2002)

Annexure-I

Comparison between old (1986 design) & New Design (1997) 140tonne Cranes (Gottwald)				
S.No	Sub S. No	Item	Old Design: Model No 1WDH RDSO Document reference number MP-MISC-118 (Rev-0.00)	New design: Model No 3WDH RDSO Document reference number MP-MISC-119 (Rev-0.00)
1	1	Main Power Pack	Cummins NT855R4,6 Cylinder Horizontal mounting 224KW @1800 RPM	Cummins NT855-P335,6 Cylinder vertical mounting 205 KW @1800 RPM
	2	Auxiliary power pack	Schule 10 KW@1800 RPM manual start	Kirloskar 16.9 KW @ 1800RPM electric start
2		Structure		
	1	Boom	18m long octagonal cross section	18.75m long with rectangular cross section in two sections.
	2	'A' frame	Available	Removed
	3	Gallows	Fixed	Permit the counterweight assembly to be placed at 5.5m or 6.5 m radii.
	4	Counterweight	4 pieces: 5.2t+6t+14t+18t=43.2 Tonnes	3 pieces, 8t+15t+24t=47t
	5	Slewing Ring	Internal spur gear pinion for slewing drive	External spur gear pinion for slewing drive
	6	Hydraulic oil tank	One single tank fitted in the rear portion of the super structure	Two internally connected tanks just behind the cab.
	7	Fuel tank	Annular shaped tank above the slewing ring	Box tank in the rear portion of the super structure.
	8	No. of pulleys in main hoist	Eight	Nine
	9	Bogies	Axle mounted compressor mounted outside, driven by belt drive.	Axle mounted compressor fitted inside the bogie driven by pinion meshed with the bull gear.
3		Controls		
	1	Counterweights	All control in the cab, single lever operation	All controls in the rear of the crane three lever operation.
	2	Hoists	Separate levers for main and auxiliary hoists	Single joystick for main & auxiliary hoist
	3	Rapid motion switch	Foot operated	Switch on the top of joystick for hoist operation.
4		Hand Brake System		
	1	Hand brake system	Hydraulic system for application and release of brakes	Fully pneumatic operation for hand brakes with spring loaded cylinders.
5		PAT Load Moment Indicator system		
	1	Microprocessor	Intel 8085A	Intel 8031
	2	Sensors	Derrick angle, Slew angle, Load Cell & counterweight Condition.	Derrick angle, Slew angle, Load Cell & pressure switches on pilot lines.
6		Performance Parameters		
	1	Self-propelled speed	Max 12 Km/h	Max. 20 km/h
	2	Train formation speed	Max 75 Km/h	Max 100 Km/h
	3	Main hoist speed	Max 5.0 m/min.	Max 4.0 m/min
	4	Auxiliary Hoist speed	Max 30.0 m/min.	Max 15.0 m/min.
	5	Working range	5.5m to 16m	5.5 to 17m

Experimental and Prediction Analysis of the Screening Performance of Coal in Linear and Circular Vibratory Screen

Bharath Kumar Shanmugam*, Harsha Vardhan, Govinda Raj M, Harish Hanumanthappa

Department of Mining Engineering, National Institute of Technology, Karnataka, Surathkal, Mangalore

*✉ shanmugabharathkumar@gmail.com

ABSTRACT

Screening is a process of classifying the material into different particle sizes. Screening is also a crucial process carried out during the production of clean coal. The current work investigates the screening efficiency of coal in linear and circular vibratory screen. The particle size considered in the present work was $-4+0\text{mm}$, and the screen selected was 2mm . The screening time was considered as the input parameter for screening coal. The screening was carried out for 5, 10, 15, 20, 25, 30 minutes in the vibratory screen, and respective variation in the screening efficiency was studied. From the results, it was found that there was a reduction in screening efficiency for the increase in the screening time. This was due to the high moisture content and the existence of near-size particles in the feed material. These particles have led to the progressive jam on the screen hole, which has reduced screening efficiency. Although the screening efficiency was reduced, the circular vibratory screen has yielded high efficiency of 78.54% compared with the 65.49% efficiency of the linear vibratory screen. Furthermore, prediction analysis of screening results was carried out using regression.

Keywords: Screening; Coal beneficiation; Vibratory screen; Screening efficiency; Regression.

INTRODUCTION

Screening is a process of classifying the material into different particle sizes [1, 2]. Screening has a major application in coal beneficiation [3-5]. The coal beneficiation leads to the production of clean coal, which has applications in the blast furnace. Initially, wet screening was carried out to separate coal, but it requires a large quantity of water. So, in the current work, dry screening was carried out on separating coal [6-9]. Generally, in industries, the vibratory screen with a linear vibration is used to perform dry coal screening. In the present study, coal screening efficiency was determined for 5, 10, 15, 20, 25, 30 min of screening coal. This study will result in a comparison between the performance of dry coal screening using linear vibratory screen and circular vibratory screen (newly developed).

MATERIAL USED

The feed sample was collected from JSW Steel Limited, Ballari. The size fraction selected for screening was $-4+0\text{mm}$, and the screen selected was 2mm . $-4+0\text{mm}$ coal screening with a screen hole of 2mm will result in the separation of undersize, i.e., $-2+0\text{mm}$ coal. This undersize coal has an ash content less than 10%, thereby providing suitable clean coal for blast furnace ignition. The separation of coal leads to the liberation of coal by reducing ash content [10].

EXPERIMENTAL DETAIL



Fig. 1. Linear vibratory screen

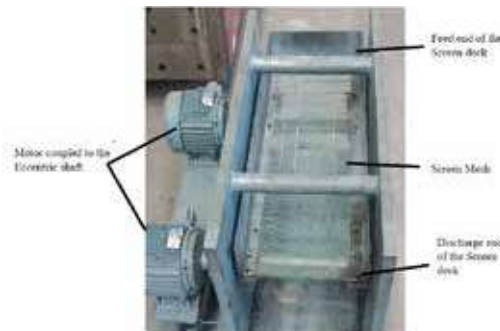


Fig. 2. Circular vibratory screen (Newly developed) [3-5, 15]

Fig. 1 and 2 show the vibratory screen with a linear vibration and the vibratory screen with a circular vibration, respectively. The feed samples were prepared with the 30% undersize and 70% oversize. During the screening, the feed samples are passed on the vibratory screen. Due to this vibration, the feed sample is classified into undersize and oversize material. The undersize will pass through the screen, and the oversize is passed through the discharge [11]. The undersize material was weighed to obtain the screening efficiency. The experimentation was carried out at a feed rate of 100Kg/hr, at an angle of 3 degrees and 8Hz frequency. The screening efficiency was obtained for 5, 10, 15, 20, 25, 30 minutes of the screening. For each experimental trial, the screening efficiency was determined by the ratio of undersize in feed which passes to the overall undersize in feed.

RESULTS AND DISCUSSION

Performance of linear vibratory screen

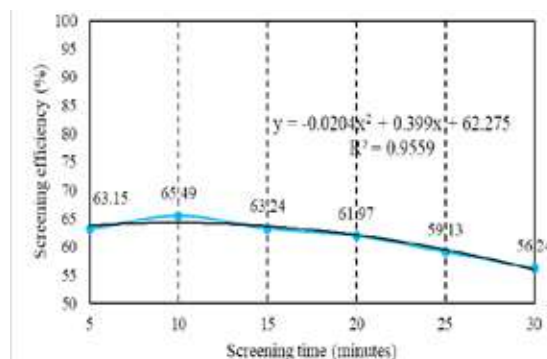


Fig. 3. Variation in screening efficiency with screening time (Linear screen)

Fig. 3 variation shows the in efficiency with screening time. The screening was carried out at 5, 10, 15, 20, 25, 30 minutes. The screening efficiency was calculated for all the trials. The screening efficiency obtained for 5 minutes was 63.15%. During this trial, it was observed that the coal material required time to settle on the screen. As the screening time was increased to 10 minutes, the highest efficiency of 65.49% was obtained. As the screening was continued further, there was a reduction in efficiency with the time. The screening efficiency was reduced to 56.24% for the screening time of 30 minutes. This reduction was due to the screen hole choking, the existence of near-size particles in the feed, and the undersize misplacement with oversize.

Due to the high moisture content and the near-size particles in feed, the coal was blocking the screen hole. This reduced the passing of undersize, leading to the undersize particle misplacement with oversize coal. To maintain highest screening efficiency, the vibratory screen has to be stopped, and the screen hole has to be cleaned with a wire brush. The stoppage of the vibratory screen will minimize the rate of production.

Performance of circular vibratory screen

In order to avoid the demerits of the existing machine, a new vibratory screen has been designed with a reduced drawback of linear vibratory screen. From literature of [12-14], it was suggested that the development of a new vibratory screen with circular vibration will reduce the drawback of linear vibratory screen. Due to the circular motion, the screen deck experiences vertical

motion. This vertical motion of the screen will incorporate the inertial force, which removes the blocked coal from the screen and reduces the screen choking. The reduced screen choking will lead to high passing of undersize through the screen and increase screening efficiency. The present authors have developed the circular vibratory screen, resulting in patent application [15].

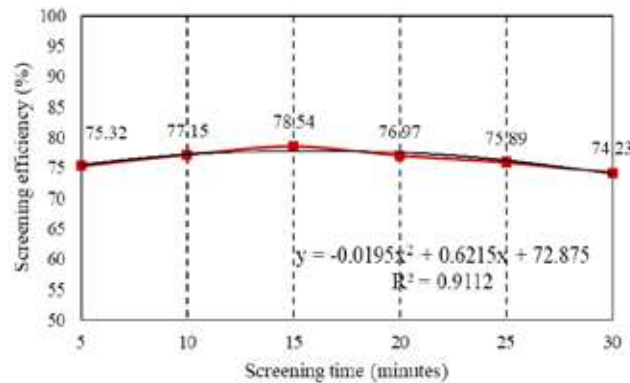


Fig. 4. Variation in screening efficiency of with screening time (circular screen)

Fig. 4 shows the variation in efficiency with screening time. The screening was carried out at 5, 10, 15, 20, 25, 30 minutes. The screening efficiency obtained for 5 minutes was 75.32%. During this trial, it was observed that the coal material required time to settle on the screen. As the screening time was increased to 15 minutes, the highest efficiency of 78.54% was obtained. As the screening was continued further, there was a reduction in efficiency with the time. The screening efficiency was reduced to 74.23% for the screening time of 30 minutes. This reduction was due to the screen hole choking, near-size particles in the feed, and the undersized particle misplacement with oversize. It was observed from Fig. 3 and 4 that the screening performance of a circular vibratory screen dominates over the performance of the linear vibratory screen. It was also observed that the screening efficiency was higher for the developed machine due to the incorporation of inertial force, which reduced screen choking. The development of this machine has led to reduced choking and a highly efficient vibratory screen. The new machine utilization will reduce stoppage and increase the vibratory screen production rate.

Regression analysis of the screening performance

Fig. 3 and 4 show the regression analysis of linear and circular vibratory screen screening performance, respectively. The regression coefficient of the linear and circular vibratory screen was 0.9559 and 0.9112, respectively. The regression coefficients are nearer to 1, which shows the maximum correlation between the prediction and experimental results. From **Fig. 3 and 4**, it was also clear that the mathematical equation developed for each vibratory screen shows the highest correlation of prediction results with the experimental results.

CONCLUSIONS

The linear vibratory screen was used for screening coal of size -4+0mm. The screening efficiency was calculated for 5, 10, 15, 20, 25, and 30 minutes. For a linear vibratory screen, the highest efficiency of 65.49% was obtained at 10 minutes. The screening efficiency was dropped to 56.24% at 30 minutes of the screening. The highest efficiency of 65.49% was obtained at 10 minutes. For the circular vibratory screen, the screening efficiency was dropped to 74.23% at 30 minutes of the screening. The highest efficiency of 78.54% was obtained at 10 minutes. The reduction of screening efficiency has occurred due to screen hole choking and the undersize particle misplacement with oversize. Due to the existence of near-size particles in feed and high moisture content, the coal was blocking the screen hole. This reduced the passing of undersize, leading to the undersize misplacement with oversize coal. Furthermore, the prediction results show that the screening results obtained for both the vibratory screen were statistically accurate and valid. From the results, it was clear that the circular vibratory screen was obtaining reduced choking by incorporating the vertical motion to the screen. The developed vibratory screen will reduce the screen choking, increases screening efficiency, and also increases productivity.

ACKNOWLEDGMENT

The present work is a collaborative work between NITK, Surathkal and JSW Steel, Ballari. The authors are thankful to the management of JSW Steels, Ballari for their support during the course of research work.



REFERENCES

1. N. Standish, "The kinetics of batch sieving," *Powder Technology*, vol. 41, no. 1, pp. 57-67, 1985.
2. K. Liu, "Some factors affecting sieving performance and efficiency," *Powder Technology*, vol. 193, pp. 208–213, 2009.
3. B. K Shanmugam, H. Vardhan, M. G. Raj, M. Kaza, R. Sah, and H. Harish, "Evaluation of a new vibrating screen for dry screening fine coal with different moisture contents," *International Journal of Coal Preparation and Utilization*, 2019.
4. B. K Shanmugam, H. Vardhan, M. G. Raj, M. Kaza, R. Sah, and H. Harish, "Screening performance of coal of different size fractions with variation in design and operational flexibilities of the new screening machine," *Energy Sources, Part A: Recovery, Utilization, and Environmental Effects*, vol. 0, no. 0, pp. 1-9, 2019.
5. B. K Shanmugam, H. Vardhan, M. G. Raj, M. Kaza, R. Sah, and H. Harish, "Experimentation and statistical prediction of screening performance of coal with different moisture content in the vibrating screen," *International Journal of Coal Preparation and Utilization*, 2020.
6. H. Hanumanthappa, H. Vardhan, M. G. Raj, M. Kaza, R. Sah, and Shanmugam, B. K, "A comparative study on a newly designed ball mill and the conventional ball mill performance with respect to the particle size distribution and recirculating load at the discharge end," *Minerals Engineering*, vol.145, no.106091, 2020.
7. H. Hanumanthappa, H. Vardhan, M. G. Raj, M. Kaza, R. Sah, and Shanmugam, B. K. "Investigation on iron ore grinding based on particle size distribution and liberation," *Trans Indian Inst Met*, 2020.
8. H. Hanumanthappa, H. Vardhan, M. G. Raj, M. Kaza, R. Sah, and Shanmugam, B. K. "Estimation of grinding time for desired particle size distribution and for hematite liberation based on ore retention time in the mill," *Mining, Metallurgy & Exploration*, 2020.
9. H Harish., H. Vardhan, M. G. Raj, M. Kaza, R. Sah, A Sinha and S. B. Kumar, "Investigation of Iron Ores Based on the Bond Grindability Test," *AIP Conference Proceedings*, vol. 2204, no. 040006, 2020.
10. M. Özer, O. M. Basha, and B. Morsi. "Coal-agglomeration processes: A review," *International Journal of Coal Preparation and Utilization*, vol.37, no.3, pp.131–67, 2017.
11. M. Soldinger, "Interrelation of stratification and passage in the screening process," *Minerals Engineering*, vol. 12, no. 5, pp. 497-516 1999.
12. B. S Kumar, Vardhan. H., Raj, M. G., Kaza, M., Sah, R., Harish, H., "Shortcomings of vibrating screen and corrective measures: A review," *International Conference on Emerging Trends in Engineering (ICETE)*, vol. 2, no. 43, pp.345–51. 2019.
13. B. S Kumar, Harsha Vardhan, M. Govinda Raj, Marutiram Kaza, Rameshwar Sah, and H. Harish, "The screening efficiency of linear vibrating screen - An experimental investigation," *AIP Conference Proceedings*. vol.2204, no. 040002, 2020.
14. R. Feller, B. Zion, J. Pagi, "Accurate sizing without cumulative screen clogging," *Jornal of Agrcultural Engineering Research*, vol. 35 no.4, pp. 235-244, 1986.
15. Shanmugam, B. K., M. Kaza, H. Vardhan, M. G. Raj, R. Sah, A. R. Choudhary, N. Onkarappa, and N. Venkategouda. "Material handling system for screening or feeding materials with high screening efficiency and energy efficiency," *Indian Patent application number*, 2018. - TEMP/E-1/53448/2018-MUM.



Satyan King-Pin-Drive for Electric Vehicles

Dr Sathyanesan T N

Former Professor of Mechanical Engineering, Govt. Engineering College, Thrissur, Kerala

✉ sathyanesantn@gmail.com

ABSTRACT

As the fossil fuel source of energy is not sustainable, Electric Vehicles on road are increasing in number day by day. In this paper, the case of driving the two front wheels with individual motor in a front wheel drive is considered. Here a new method of power transmission from the electric motor to the front wheel is discussed. The transmission is through king pin. The king pin is almost normal to road terrain but for the king-pin angles and is given the shape of a frame called Inner frame, which accommodate a bevel gear reduction unit connecting motor shaft and front wheel driving shaft. The Inner frame can turn inside an Outer frame which is attached to the vehicle body through leaf spring, shock absorber, wishbone leavers and a compression spring. The other front wheel also is kept on a similar arrangement. The two motors are energized by on-board battery pack in the vehicle and controlled by a common Control module. The steering and the brake systems are similar to the existing ones at present. This method makes the power transmission simpler and more efficient and replacement of parts easier.

Keywords: Bevel gear and bevel pinion; Stub-axle.

INTRODUCTION

To avoid the excessive use of unsustainable fossil fuel energy in vehicles, other sources of energy such as electrical energy, solar energy, nuclear energy, chemical energy (fuel cell) etc are being considered. At present there is a breakthrough in using electrical energy for propulsion of vehicles on road. The term “Electric Vehicle (EV)” refers to any vehicle that uses electric motors for propulsion. Generally electric vehicle derives its power from an on-board battery pack and so is a battery electric vehicle. An electric vehicle carrying solar panels for power is a solar vehicle. When an electric vehicle derives its power from gasoline engine, it becomes hybrid vehicle.

Electric Vehicles

Movement of a vehicle results when its wheels are powered to roll on road. In Electric Vehicle, different types of power transmission from motor to wheels are practiced. Consider a vehicle with four wheels. From a single motor power can be transmitted to the two front wheels. The two front wheels can be driven by individual motors also. Even all the four wheels can be powered by individual motors.

King Pin

In conventional design, king pin is the mechanical element connecting the stub-axle and front axle beam [1]. Steering movements to stub-axles holding the front wheel transmission shafts, are facilitated because of the king pins. The king pins in a steering system, serve the primary purpose so that the steered wheel axles have an axis to rotate (or steer) on. The king pin is the main pivot in the steering mechanism of a vehicle. Initially king pin was a steel pin on which wheel was mounted to the suspension. In modern designs, king pin may not exist physically as an actual pin, but the axis about which the steered wheel pivots is still referred to as king pin. King pin is usually made of metal and as mentioned above, it is shown here as a cylindrical pin **Fig. 1a**.

The Angles associated with king pin are [1]:-

- 1) The king pin inclination It is the angle, measured in degrees, that forms between the line passing through the steering axis and the perpendicular to the ground, looking at the vehicle from the front and is generally 7 to 8 degrees.
- 2) Camber angle Camber angle (also called wheel rake) is the tilt angle of the front wheel plane with the vertical plane. Generally does not exceed 2°.
- 3) Caster angle Caster angle is the angle between the king pin center line and the vertical through center and measured in the plane of the wheel. If the king pin center line meets the ground at a point ahead of the vertical, it is positive caster. If the point is behind the vertical, it is negative. A general value is 3°.

- 4) Negative toe, or toe out It is the front of the wheel pointing away from the centerline of the vehicle. Positive toe, or toe in, is the front of the wheel pointing towards the centerline of the vehicle. Toe in, generally does not exceed 3 mm.

All the above mentioned angles can be easily incorporated in this innovative design also.

Innovative Design

In this paper, the case of the two front wheels powered by individual motors in a front wheel drive in automobile is considered.

In this innovative design, the left and right king pins are given box-like shape called Inner frame, with upper end having a bearing for the motor shaft and lower end, a pivot pin **Fig. 1b**. This Inner frame can turn about the king pin axis in an Outer frame as shown in **Fig. 2.a** and **2.b**. This Outer frame supports the electric motor at the top and is attached to the body of vehicle through leaf spring EF, shock absorber CD and wishbone levers AB, with compression spring **Fig. 3a. b**. Here, the left motor supplies power to the left front wheel and the right motor supplies power to the right front wheel. The Outer frame is also a rectangular box-like structure covering the Inner frame partially. Both the Inner frame and the Outer frame together (or frame assembly) have the same axis as the king pin. The motor shaft, after a jaw clutch, passes through the thrust bearing at the upper end of the Inner frame and rotates in it in a bush bearing. The electric motor which is supported by the Outer frame has its axis coinciding with the king pin axis.

Extension of the motor shaft through the jaw clutch is keyed to the bevel pinion (BP) which meshes with the bevel gear (BG) keyed to the transmission shaft in the stub-axle of the Inner frame as shown in **Fig. 2.b**. Provision is provided at the bottom of the Outer frame for engaging the pivot pin of the Inner frame **Figs. 1.b, 2. a** and **2.b**. The Inner frame can turn inside the Outer frame with king pin center line as axis of rotation facilitating steering action. The axes of bevel gears intersect at 90°. Helical (or spiral) bevel gear pair provides smooth and silent operation [2]. A tie rod arm (or track rod arm) is attached to the stub-axle for steering action [1]. The speed reduction ratio of the bevel gear unit can be conveniently determined, considering motor speed, vehicle speed etc.

Vehicle Suspension

A spring system is used between the frame assembly and the vehicle body. When the vehicle moves on uneven surface of road, the spring system deflects and gives cushioning effect.

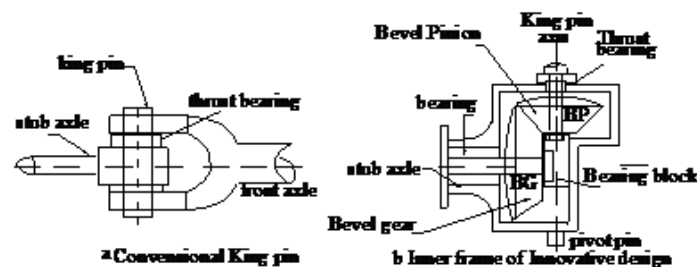


Fig. 1. a. Conventional King pin b. Inner frame

The main machine elements connecting each front frame assembly with the vehicle body are:- 1) Leaf spring, 2) Shock absorber, 3) Wishbone system, 4) Steering system and Braking system.

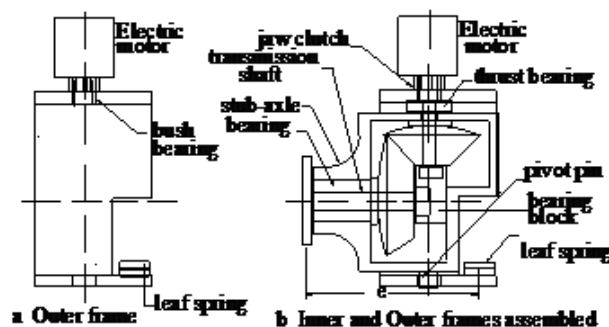


Fig. 2. a Outer frame b. Frames assembled



Leaf Spring. Semi-elliptical leaf-spring is used between front frame assembly and the vehicle body. When wheel comes across a bump, it rises and energy is stored in the leaf spring. When the wheel moves forward covering the bump the spring rebounds due to elasticity expending the energy and starts vibrating with amplitude decreasing gradually due to internal friction of spring material and friction of suspension joints. A shackle E is used at the rear end of leaf spring to compensate increase in length when leaf spring tends to straighten under load **Fig. 3b** [1].

Shock Absorber. Shock absorber absorbs the energy of shock converted into movement of the spindle by providing damping and dissipating to heat. As shock absorber is of zero resilience, it cannot support weight and so it is a damper [1]. Hydraulic type shock absorber operates on the principle that when a fluid is forced to pass through a small hole, a high resistance is developed. Shock absorber CD with coil spring is shown in **Fig.3a**.

Wishbone System. The total weight of the vehicle is transferred to the Outer frame mainly through the leaf spring. This is balanced by the upward ground reaction acting on the tire and wheel. In this design, these two forces are not collinear and so produce a moment which is balanced by wishbone system. The wishbone levers A1B1 and A2B2 are pivoted on the Outer frame and can swing about the central longitudinal beam of the vehicle [1]. The Outer frame may move inclined to the vertical direction in the transverse plane. This can be minimized by selecting proper values for wishbone lever length L and angle $\angle 1 = \phi$ **Fig.3.a**. A compression spring also is used between A1B1-A2B2 assembly and the vehicle body frame as shown in Fig.3.a.

Steering and Braking systems may be as those used in ordinary vehicle [1].

Inner and Outer Frames

The Inner frame houses the reduction unit. The bevel pinion is keyed to the electrical motor shaft extension through a jaw clutch and the bevel gear is keyed to the transmission shaft of the wheel. This Inner frame is housed in the Outer frame. Details are shown in **Figs. 5a, b, c, d, e, and f** also.

Stiffness of the front wheel assembly

Let the stiffness of the leaf spring be S_p ,

effective stiffness of the shock absorber be S_s , and

effective stiffness of compression spring be S_c Fig. 3a.

These three are in parallel,

and total effective stiffness $S = S_p + S_s + S_c$.

Dynamics of the Vehicle

Half of the total weight of the vehicle is assumed to be borne by each front wheel assembly and let it be W. Let the vehicle moving with a velocity v, takes turn on a road with radius of curvature r referred to the center line of the road **Fig. 4a**.

Centrifugal force due to weight W on the left front wheel, $CF_l = \frac{Wv^2}{g\left(r - \frac{tw}{2}\right)}$ and centrifugal force due to weight W on the right front wheel, $CF_o = \frac{Wv^2}{g\left(r + \frac{tw}{2}\right)}$, [2] where t_w is the track width **Fig. 4b**.

The total centrifugal force,

$$CF = \frac{Wv^2}{g\left(r - \frac{tw}{2}\right)} + \frac{Wv^2}{g\left(r + \frac{tw}{2}\right)} = \frac{2Wv^2.r}{g(r^2 - [tw/2]^2)} \quad (1)$$

On the point of lateral slipping, the above centrifugal force is equal to the frictional force $F_{wi} + F_{wo} = \mu \times 2W$. This gives, v^2

$$= \frac{\mu.g(r^2 - [tw/2]^2)}{r} \text{ or } v = \sqrt{\frac{\mu g(r^2 - [tw/2]^2)}{r}}$$

Here μ is the coefficient friction between wheel-tire and road surface. If track width tw is negligible in comparison with r, the velocity of vehicle on the point of lateral slipping $v = \sqrt{(\mu.g.r)}$ m/s. (2)

Considering the point of over-turning Fig. 4b and taking moment about P_o , $2 \times h \times Wv^2/gr - W \times t_w = 0$. This gives $v^2 = (gr) \times (t_w)/2h$ or $v = \sqrt{(g.r.t_w)/2h}$.m/s (3)

Now consider the case of a conventional vehicle with an IC engine on front-middle position with weight $2W$ (ie, sum of the weight of two electric motors and allied set-ups as shown in Fig. 4c). Then $CF = 2W.v^2/gr$.

The resultant of CF and $2W$, $R = \sqrt{CF^2 + (2W)^2}$.

On the point of over-turning, let resultant passes through P_o .

Taking moment about P_o , $h \times 2W.v^2/gr = (t_w/2) \times 2W$.

This gives $v^2 = g.r.t_w/2h$. Or over-turning initiates when $v = \sqrt{\frac{g.r.t_w}{2h}}$. m/s. This is same as “(3)”.

This shows that putting the weight as shown in Fig. 4b or as in Fig. 4c does not make any difference.

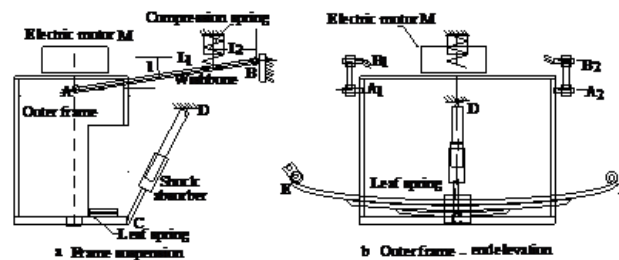


Fig. 3a. Frame suspension b. Frame end-elevation

Design details of King-pin-drive

Figures 5a and a1 give details of Inner frame. Lower end of the shaft keyed to the bevel pinion has a bearing in the Bearing block. Upper end passes through thrust bearing between the Inner and Outer frames and it has a step at thrust bearing level and increased diameter. Above the Outer frame, the shaft is coupled to the electric motor through a jaw clutch. This jaw clutch facilitates easy removal or replacement of the electric motor. The motor is kept in a guide fixed to the Outer frame.

Fig. 5 b gives the plan of Inner frame. The ‘arm’ fixed to the stub-axle is connected to the tie rod (or track rod) of steering mechanism through ball joint.

Fig. 5 c shows the elevation of Outer frame with the electric motor on the top.

Fig. 5 d is the plan of the Outer frame.

Fig. 5 e is the elevation of the assembly of Inner and Outer frames.

Fig. 5 f is the plan of the assembly of Inner and Outer frames.

Fig. 5 g is the lay-out of the electrical control system. DC power from the battery-pack is controlled in the Control module. Consider a brush less DC motor. For energizing magnetic field winding and varying the speed of the motor, AC with frequency that can be varied is required. This is obtained by an inverter. This power is supplied to motors on left and right sides. Motor speeds are sensed and fed to the module. Steering position also can be sensed and fed to the module. Many other outputs can also be sensed and controlled in the Control module.

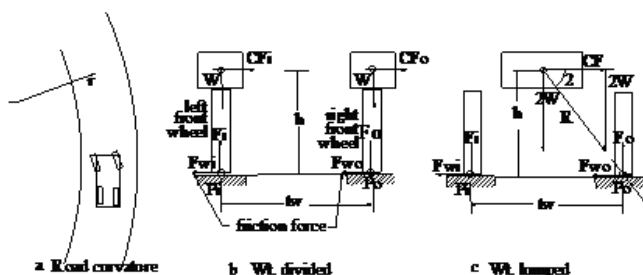


Fig. 4 a. Road curvature b. Wt. divided c. Wt. lumped

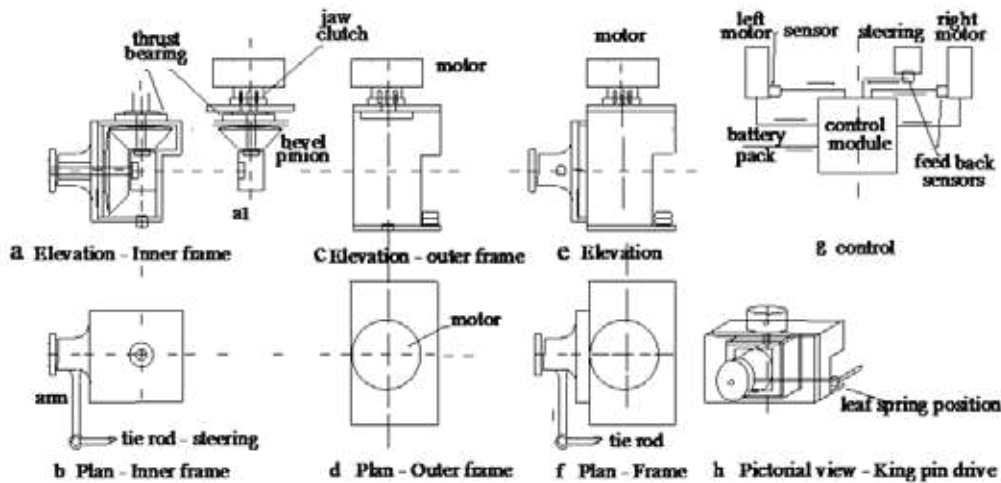


Fig. 5 a and a1-Elevation of Inner frame, b-Plan, c- Elevation of Outer frame, d-Plan, e- Elevation of assembly, f-Plan, g-Control module, h-Pictorial view.

Fig. 5 h represents a pictorial view of the left king-pin assembly. The right king-pin assembly is a similar one.

Prime mover for Electric cars or vehicles. [3]

There are different types of motors used in Electric cars or vehicles. Some of the Electric motors are:-

Interior Permanent Magnet Motors, AC Induction Motors Permanent Magnet Switched Reluctance Motor, Permanent Magnet Synchronous Motors, Interior Permanent Magnet Motor, Brush Less DC motor etc.

In some EVs the required electric power is derived from Lithium-iron cells of the order of 7000 packed in 16 boxes. If an AC motor is used, DC from the cell-packs is converted to AC. The speed of motor is proportional to frequency. Electric vehicles have less components and life 3.5 times longer than IC engine vehicles. Electric vehicles are simple and more powerful. Electric vehicles can offer full torque at zero rpm also. IC engines can operate only in a certain rpm range. So at lower speeds Electric vehicles are more powerful. Some of the advantages of Electric Vehicles over IC Engine Vehicles are high performance, higher response, no noise, no pollution at vehicle level, lower maintenance and driving cost, highly safe, single speed transmission, high torque and power, effective traction control etc. Some of the disadvantages are long charging time, low range, high cost etc.

ACKNOWLEDGEMENTS

Certified that the above manuscript titled 'SATYAN KING-PIN-DRIVE FOR ELECTRIC VEHICLE.' is my own genuine work, that there are no co-authors, that the matter contained under the title is not published till-date, and that this work did not receive any specific grant from funding agencies in the public, commercial, or not-for-profit sectors.

REFERENCES

1. KRIPAL SINGH. Automobile Engineering, Vol.1. 14th Edition 2017, Standard Publishers Distributors, 1705-B, Nai Sarak, Delhi-110006. Pp. 179-194, 218 – 226, 239, 338.
2. S S RATTAN. Theory of Machine, Third Edition, 2009, 13th reprint 2012. Tata McGraw Hill Education Private Limited, 7 West Patel Nagar, New Delhi.110 008. Pp. 560—562, P. 334.
3. ¹TAHIR AJA ZARMA, ²AHAMDU ADAMU GALADIMA and ³MARUF A.AMINU, A Review of Motors for Electric Vehicles ¹²³Department of Electrical and Electronic Engineering, Nile University of Nijeria, Abuja 1engrtahiraja@gmail.com 1tahiraja@nileuniversity.edu.ng



Efficiency Improvement of Concentrated Photovoltaic Module by way of Various Active and Passive Cooling Techniques – a Review

Yogesh Nandurkar*, R L Shrivastava, Vinod Kumar Soni³

Department of Mechanical Engineering, Yeshwantrao Chavan College of Engineering, Nagpur, Maharashtra

Senior Section Engineer, Central Railway, Nagpur, Maharashtra³

*✉ ynandurkar1@gmail.com; ✉ rlshrivastava@yahoo.com, vksoni@ycce.edu

ABSTRACT

In Multijunction tandem MJT solar cell, amount of light not converted into electricity gets transformed into heat. Waste heat play a vital role to increase the temperature of solar cell. Operating temperature of cell plays vital role in the performance of CPV System as efficiency, power output is directly proportional to operating temperature of solar cell. As operating temperature increases performance of cell decreases. Maximum power, voltage, efficiency and long life can be achieved by operating the MJT at standard test condition. Passive and active cooling techniques are popularly used to cool the cell. In Passive cooling methods extended surfaces, heat pipe and micro fins are mostly used whereas peltier effect cooling, compressed air, water jet etc. are active cooling techniques. Amalgamation of various active and passive cooling techniques reported by worldwide researchers are critically reviewed in this paper.

Keywords: Concentrated photovoltaic module; Multijunction solar cell; Cooling techniques.

NOMENCLATURE

GREEK LETTERS

A Area(m²)λ Wavelength (nm)

CR Concentration ratio (-) opt Optical

EfficiencG(λ) Spectral DNI (W/m²/nm) cell Cell Efficiency

q_{heat} Heat Power(w)

Abbreviations

Pm Maximum power output(w)

InGaAs- Indium Gallium

Pin Incident Power (w)

Arsenide

Voc Open circuit Voltage

InGaP- Indium Gallium

MJT Multi Junction Tandem

Phosphide

CPV concentrated photovoltaic

Ge- Germanium

INTRODUCTION

The Increasing worldwide demand for power, growing crude oil prices and increasing anxiety about greenhouse effect have regenerate the idea to rapidly move towards geothermal power resources. Insolation is the most promising natural energy resource available on the planet. The mechanism for converting solar energy to electrical energy have made a lot of development, minimum conversion efficiency and high capital price are the major problem to the frequent use of these technologies. To increase the performance of solar power system various techniques have been attempted over the years consistently. Solar energy is one of the world's largest unused renewable energy source. The major part of the globe community has not proper Electrical network to ingress the electricity. In electrical network it is not feasible economically to expand electric lines from power grid to remote areas; there for the CPV module are best substitute to decentralize the power source. Multijunction cells consist of more than one pair of p-n junctions. It is designed in such a way that solar energy of different wavelengths can be converted into electricity through different layers of cell as shown in **Fig. 1** Typically layers are stacked on top of each other, with light incident on the largest-band gap layer, which transmits longer wavelengths to smaller-band gap layers underneath.

MJT's are categorized as Concentrated Photovoltaic CPV, immense heat is generated through concentration. However efficiency of MJT is reported around 46% according to National Renewable Energy Laboratory (NREL 2020). If sunlight is incident on the solar cell is 300x times more than its concentration factor then and then only solar cell is economically feasible. (Cotal and Frost, 2010). Even though the amount of light not converted into electricity is converted into heat. This waste heat deteriorates both the performance and codal life of the cell.

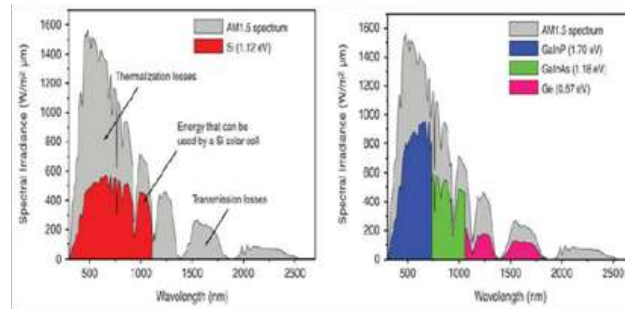


Fig. 1. Spectrum utilization through conventional PV and MJT solar cell (NREL, 2020)

The Solar cell's efficiency is defined as the ratio of the output power of solar cell to the input power of solar cell.

$$\eta_{cell} = \frac{P_{out}}{P_{in}} = \frac{P_{in}}{\int CR * A * \lambda * G(\lambda) * \eta_{opt}(\lambda) * d\lambda} \quad (1)$$

Therefore the heat power produced on the cell is

$$q_{heat} = P_{in}(1 - \eta_{cell}) \quad (2)$$

As concentration of heat flux at the surface of solar cell increases this will rapidly increases the temperature of solar cell, this will turn reduces maximum power voltage and open circuit voltage (Cotal and Sherif, 2006). It is to be observed that without any cooling arrangements, the solar cell can exceed 1000°C under 500x concentration (Cotal and Frost, 2010). This emphasizes the need of proper cooling methodology to maintain the temperature within secure operation limits as well as to keep away probability of module deterioration and insignificant performance of solar cell (Theristis and O'Donovan, 2015).

LITERATURE REVIEW

Exhaustive Endeavour are being made worldwide to decreased the operating temperature of CPV System to increase performance in terms of electrical efficiency, power output and codal life of solar cell system. There are various number of researchers have worked on cooling the CPV and PV module with various active and passive cooling techniques. some of these techniques are discussed in following section.

Peltier Effect (Active Cooling)

Fig. 2 shows schematic of the combined PV-TEC system, aluminum sheet is sandwich between TEC module and PV cell in order to extend the cooling effect at the rear surface of photovoltaic cell. Whenever solar ray incident on the uppermost surface of PV cell some amount of photon energy is transform into electric field and rest is wasted as heat through the rear and front surface of PV cell. This small amount of power output is used to place TEC module in order to give cooling effect for the PV cell.

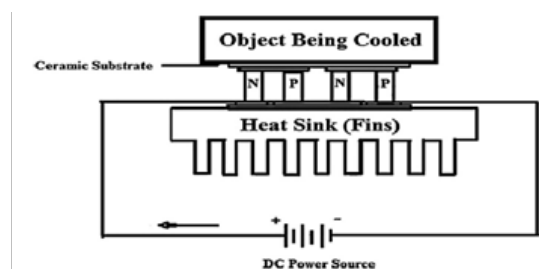


Fig. 2. Schematic of the thermoelectric cooling system (Najafi and Woodbury, 2013)

It can be observed that high cell temperature can give minimum power output for fixed solar radiation. At 3200 W/m² heat flux, if we can operate a PV cell at the temperature of 250C then it can generate 80% more power output than the cell operated at 870C. Which shows the proper use of cooling system especially at high solar radiation of concentrated photovoltaic system (Najafi and Woodbury, 2013).

Forced Cooling (Active Cooling)

Forced cooling is another alternative way of cooling PV module. **Fig. 3** shows schematic of pulsating cooling pipe arrangement on the rear side of PV panel. To dissipate heat at the top of the heat pipe a 12Volt direct current fan is used as a heat sink is shown in fig..The Power output of water cooled concentrated photovoltaic system is approximate 5 times greater than that of photovoltaic module (without cooling and concentration) (Raj.et al.,2014).

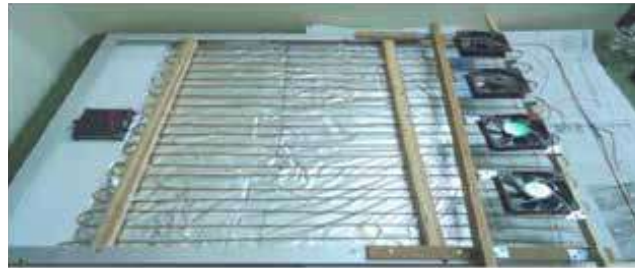


Fig. 3. Pulsating cooling pipe arrangement on the rear side of PV panel. (Raj et.al. 2014)

Natural Cooling (Passive Cooling)

Micro-fins is another alternative solution for CPV cooling. It can lower the weight of the system and at the same time maximize the thermal performance. **Fig. 4** shows cross-sectional view of the silicon wafer micro-finned and zooms on the fins. The CPV model is tested under-concentrator standard test conditions: 1000 W/m² heat flux, the cell efficiency is 42.5% and 2.20W of waste heat is produced. Worst case conditions: 1000 W/m² heat flux, the cell efficiency is 0% and 3.83W of waste heat is produced (Micheli.et.al., 2015).

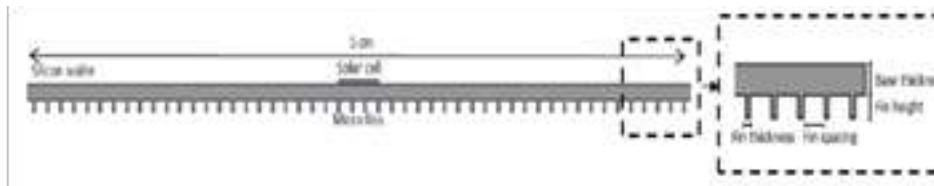


Fig. 4. schematic of silicon wafer micro-finned (Micheli.et.al., 2015)

Extended surface Cooling (Passive Cooling)

Extended surfaces are commonly used to extend transfer area to increase conventional heat transfer naturally. Fins are widely used in multiple fields where cooling is required from industrial to electronics applications.

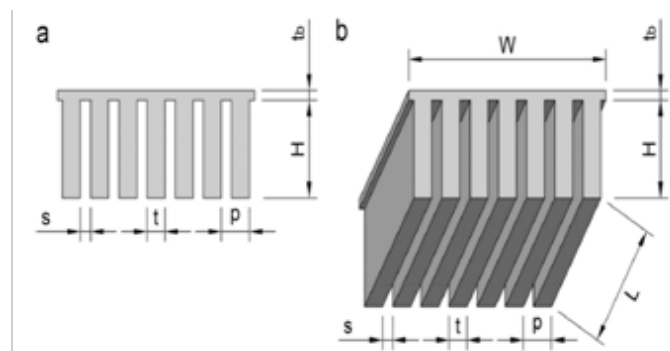


Fig. 5. Schematics of a finned heat sink (a) front view and (b) 3D rendering (Micheli.et.al.,2016).

Fig. 5. shows schematic of finned heat sink is attached at the rear side of CPV system and result shows that cell temperature goes upto 1200C without fins and cell temperature decreases upto 800C with fins under standard testing condition (Micheliet al.,2016).

Heat pipe (Passive Cooling)

At high concentration ratio single cell arrays is suitable for Heat pipe cooling , e.g. 1000 suns, and for low concentration ratio linear concentrator is suitable for Heat pipe cooling, e.g. 30 suns (Royne et al., 2005).Heat pipe with fins is used to remove heat by passive cooling. The Temperature difference between the atmospheric air and the cell was roughly 30oC (Beach and White,1981). A comparative study between forced convection water cooling for single cell system and heat pipe was conducted and observed that the cooling system of heat pipe was more efficient and effective (Farahat ,2004). Linear concentrator cooled by using heat pipe with the help of copper thermo siphon using approximate 20 incident suns on the solar cell. R-11 refrigerant is used as a operating fluid due to minimum working temperature of 400C. Passive cooling is used to remove heat to the atmosphere (Akbarzadeh and Wadowski,1996).

A concentrated photovoltaic module consist of heat pipe, back plate, saddle as shown in **Fig. 6.** A MJT cell of 500x is placed on a rear plate. The heat flux (1X) is incident 500 times with the help of Fresnel lens. High heat flux strike the solar cell and produced electric power. The some amount of waste heat passed into the heat pipe through the saddle from the cell and rejected to the atmosphere by passive cooling having temperature difference of 430C(Anderson etal.,2007).

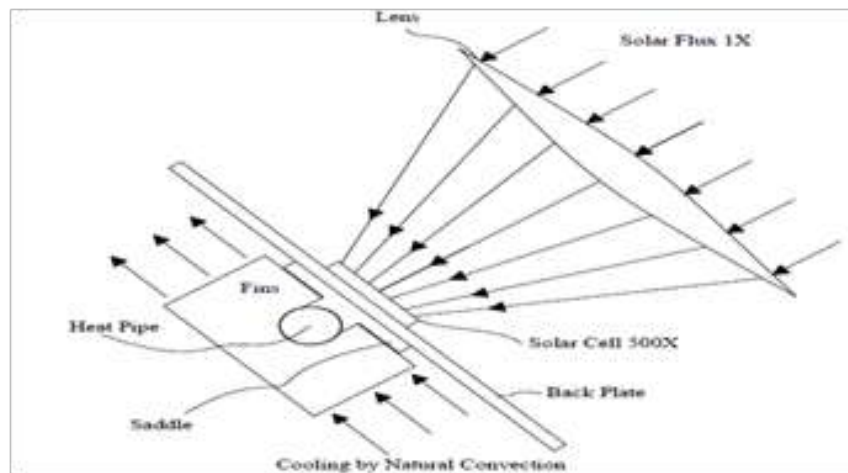


Fig. 6. Passive cooling by using Heat Pipe, Fins and Fresnel lens (Adersonet al.,2007).

AMALGAMATION OF COOLING TECHNIQUES

Cooling of solar cell is an important part of Concentrated photovoltaic system. The functioning temperature of CPV system has noticeable effect on its overall performance is well recorded. As the linearly deteriorates its performance in terms of power output, efficiency and codal life of cell. Therefore reducing the functioning temperature of CPV system can improve the electrical efficiency. Integrating various active and passive cooling techniques will improve the performance of CPV module. So many researchers have studied the various active and passive cooling techniques, but these techniques were performed on various CPV/PV system configuration and material in diverse geological condition. Therefore it is too complicated to decide which one is more productive. As a result it's field of reference to perform a experimentation with Amalgamation these various cooling methodology on one setup and to analyzed which techniques is more optimum out of them.

CONCLUSION

Solar cell performance is a function of cell operating temperature and lower temperature gives maximum efficiencies. Cell cooling is an exceptional factor when designing CPV module. When cell temperature goes on increasing it deteriorates its performance in terms of power output, efficiency and codal life of cell. Therefore maintaining the operating temperature of CPV system within STC can boost the overall performance. In natural convection extended surfaces are generally used to augment the heat from rear of CPV system. Heat pipe is most popularly used medium for passive cooling of CPV system. Micro fins on the back side of CPV system with certain time period decreases the CPV system temperature remarkably.



Forced convection requires more energy for functioning. Introducing peltier cooling device at back of CPV module and force cooling with the help of compressed air are further used to maintain the operating temperature of system. Amalgamation these methodology have remarkable effects on minimizing CPV module operating temperature result in overall performance improvement in terms of power output, electrical efficiency and codal life of cell.

FUTURE SCOPE

Various Researcher claim that codal life of cell is twice for every 100C depletion in thermic jaunt. So Amalgamation of various active and passive cooling techniques on MJT Solar cell will give optimum result.

REFERENCES

1. Cotal. H., Frost. J. "Heat transfer modeling of concentrator multijunction solar cell assemblies using finite difference techniques". .In:35th IEEE PVSC, Honolulu,HI,USA (2010).
2. Cotal. H., Sherif. R. "Temperature dependence of the IV parameters from triple junction GaInP/InGaAs/Ge concentrator solar cell." In: 4th World Conference on photovoltaic Energy Conversion, IEEE, pp.845-848 (2006).
3. Theristis, M., Odonovan,T. "Electrical-thermal analysis of III-V triple -junction solar cells under variable spectra and ambient temperatures." Solar Energy 118 (2015) 533-546 (2015).
4. Najafi, H., Woodbury,K. "Optimization of a cooling system based on Peltier effect for photovoltaic cells." Solar Energy 91 (2013) 152-160(2013).
5. Raj. A., Kumar. S., Manikandan. G., Titus. P. "An Experimental Study on the Performance of Concentrated Photovoltaic System with Cooling System for Domestic Applications." International Journal of Engineering and Advanced Technology (2014), ISSN:2249-8975(2014).
6. Micheli. L., Reddy. K., Mallick. T. "Plate micro-fins in natural convection : an opportunity for passive concentrating photovoltaic cooling." Energy Procedia 82 (2015) 301-308 (2015).
7. Micheli. L.,Fernandez. E., Almonacid. F., Mallick. T. "Performance, limits and economics perspectives for passive cooling of High Concentrator Photovoltaics." Solar Energy Materials & Solar Cells 153 (2016) 164-178.
8. Royne, A., Dey, C.,Mils, D. "Cooling Photovoltaic cells under concentrated illumination : a critical review." Solar Energy Materials & Solar Cells 86 (2005) 451-483.
9. Beach. T. and White. M. "Heat Pipe for Passive Cooling of Concentrator Solar Cells." IEEE@1981Proceedings of the 15TH Photovoltaic Specialists Conference, pp.75-85(1981).
10. Farahat .A. "Improvement in the Thermal Electric Performance of a Photovoltaic Cells by Cooling and Concentration Techniques." IEEE@2004 ISBN: 1-86043-365-0, pp. 623-628. 39th international Universities Power engineering Conference, Newyork.
11. Feldman. T.,Kenney. D. and Edenburn. W. "A Passive Heat Pipe Cooled Photovoltaic Receiver." IEEE@1981 Proceedings of the 15TH Photovoltaic Specialists Conference, pp.165-172.
12. Akbarzadeh. A. and Wadowski. T. "Heat Piped-Based Cooling System for Photovoltaic Cells Under Concentrated Solar Radiation." Applied Thermal Engineering 16(1), pp,81-87(1996).
13. Aderson,W., Tamanna,S., Sarrat,D., Dussinger,P. "Heat Pipe Cooling of Concentrating Photovoltaic (CPV) Systems." American Institute of Aeronautics and Astronautics, Advanced Cooling Technologies, Inc., Lancaster (2007), PA, 17601.
14. Ben,A., and Appelbaum, J. "Dependence of multi-junction solar cells parameters on concentration and temperature." Solar Energy Materials & Solar Cells 130 (2014) 234-240.
15. Wang, Yi., Gerger, A., Lochtefeld,A. "Design, fabrication and analysis of germanium: silicon solar cell in a multi -junction concentrator system." Solar Energy Materials & Solar Cells 108 (2013) 146-155.
16. King, R., Bhusari, D., Larrabee, D., Karam, N. "Solar Cell generation over 40% efficiency." Prog. Photovolt: Res. Appl. (2012) DOI: 10.1002/pip. 1255.
17. Shanks, K., Senthilarasu, S., Mallick, T. "Optics for Concentrating Photovoltaics : Trends , Limits and opportunities for materials and design." Renewable and Sustainable Energy Reviews 60 (2016) 394-407.



CFD Analysis of an Automotive Cabin Air Filter

Koyal V Sadaphal, Dr A S Mohite

Department of Mechanical Engineering, The Maharaja Sayajirao University of Baroda, Vadodara, Gujarat

✉ koyalvs90.com

ABSTRACT

The Air filter have been playing a significant role in an automotive air condition system. The primary function of air filter is to block the foreign particles from entering inside the automotive air-conditioned space. Controlling air pollutants in automobile cabin has become increasingly important owing to the health risks of exposure to high concentrations of harmful pollutants. This paper presents the CFD analysis for analysing the performance of the Automotive air filter with modified filter elements on the filter surface. It is observed that the filter efficiency has increased by 17% with the modified filter surface of the filter.

Keywords: Automotive air filter; CFD; Filter efficiency; Pressure drop.

INTRODUCTION

Air filter have been playing a significant role in an automotive air condition system. The primary function of air filter is to block the foreign particles from entering inside the automotive air-conditioned space. Controlling air pollutants in automobile cabin has become increasingly important owing to the health risks of exposure to high concentrations of harmful pollutants. [1, 2] Air filter is a crucial element in an automotive air condition system. In urban environments, automobiles are one of the most significant sources of airborne pollutants. The quality of air coming inside the air-conditioned space depends on the ability of the filter to trap the foreign particles. More the finer particles are blocked at air filter more pressure drop takes place. [9, 10] This pressure drop then decreases the air volume coming inside the conditioned space. Various technologies are used for the air filters so that the optimum performance can be achieved to improve the filtration, enhance economic benefits and gas adsorption efficiencies of cabin environment [7, 8]

Current advancement in air filtration technologies along with their advantages, limitations and challenges are discussed. It also covers valuable baseline information of air material to study the characteristics of cabin air quality, understanding its effect and improving it for healthy indoor air environment.

In this research paper, CFD analysis of automotive car air filter is done. Numerically, the fluid flow path and simulate the quality of fluid (air) improved (ability to filter the pollutants) by improving filter design for efficient filtration properties is done. The model comprises the different types of filter model and then the analysis is carried out for the filtration capacity of each type.

FILTER TYPES

Filter can be classified into four group that are

Low Efficiency Filter

These filters usually known as panel filters. It is typically flat panels, and mounted perpendicular to the direction of air flow. These types of filter will have below than 30% of efficiency, make it low pressure drop, low cost, good on lint, but low efficiency. This kind of filter will be used as pre filter that will installed upstream of higher efficiency filters.

Medium Efficiency Filter

Medium efficiency filters usually design as bag type or box type filters. The average ASHRAE efficiency for medium efficiency filter is between 40%- 60%. This filter will be second stage filter and effective to block 10-3 μ m of dust [3, 5, and 6]. These units filter the air passing through them at a very fine scale. They essentially are porous membranes that allow air to flow through them and used in applications where air quality is important.

High Efficiency Filter

These types of filter also usually will come as bag or box type filters. But, with average ASHRAE efficiency 80%-90% [4, 7, 9]. Usually, this filter will be the final stage filter in commercial and public building. High efficiency filter also usually recognized as pleated media panel type of bag type.

HEPA Type Filter

High efficiency particulate air (HEPA) and ultra-low penetration air (ULPA) were the best among other type. HEPA have 99.97% of efficiency for dust greater than $0.3\mu\text{m}$ in diameter, while ULPA filters have 99.999% efficiency of dust particles greater than $0.12\mu\text{m}$ diameter [10, 11, and 14]. This kind of filters frequently used in critical application

IMPORTANCE OF IAQ

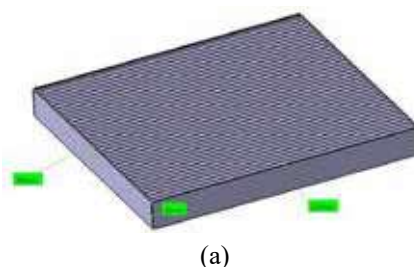
The importance of indoor air quality (IAQ) to human health is to contribute to the better work outcome and high indoor air quality. The quality of the indoor environment has a direct impact on the occupants, user's productivity. Heating Ventilation and Air Conditioning (HVAC) system consist of components such as ducts, filters, cooling coils and fans, and are used to lower outdoor and indoor particles whereby as an alternative to provide additional ventilation and lower particulate matter (PM) concentration. Efficient Filter is essential even when outdoor PM concentration are high and IAQ can be control by filter by controlling the concentration level of indoor and outdoor contamination. **Fig. 1** shows the possibilities of contamination in the cabin of an automotive. An approximately 25% reduction in PM [11] was achieved without the use of Automotive Cabin Air Filters (ACAFs) because PM adheres to the duct wall when cabin air passes through the HVAC system. However, the PM reduction performance increased to ~70% when ACAFs were used in the automobile cabin HVAC system. Thus, modern automobiles are commonly equipped with ACAF to reduce automotive cabin exposure to various airborne pollutants.

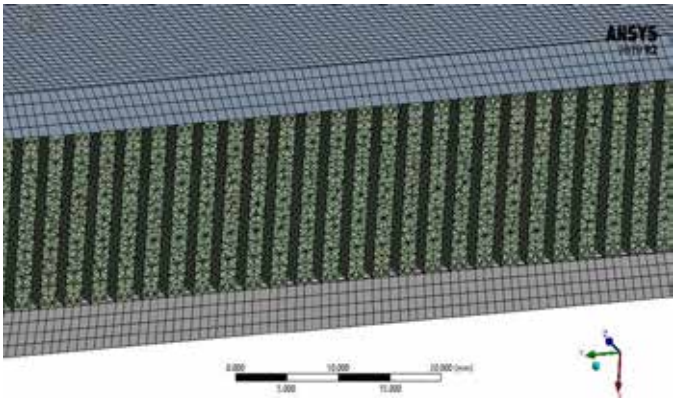


Fig. 1. The automotive cabin air filter removes harmful airborne pollutants and purifies cabin indoor air

MODELING OF AIR FILTER

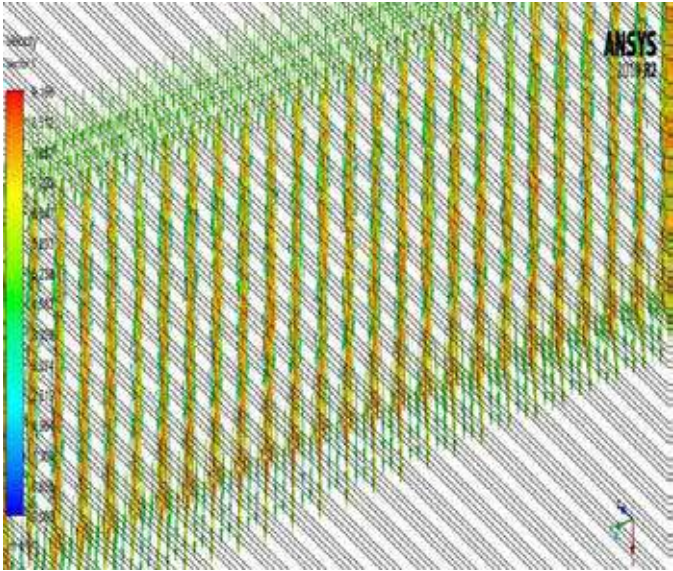
The automotive car air filter is modelled and analysed using CFD technique. The surface of the conventional automotive air filter is applied carbon particles. The activated carbon removes very effectively to greater percent of ozone. Thus, the filter is combined of two layers, one is the activated carbon granule mesh layer so as to achieve the reliable adsorption of odours and gases. To protect from fine particles and dust other layer is combined of microfiber such as polypropylene (PP), along with some kind of additives such as biocides and nano silver ions with long term stability and scientifically to be safe for humans are used. The model for basic model and modified model is shown in **Fig. 2 (a) and (b)**. Nos. of elements considered-5141304 and nodes considered-1632798. Tetrahedral type of element was used for meshing.



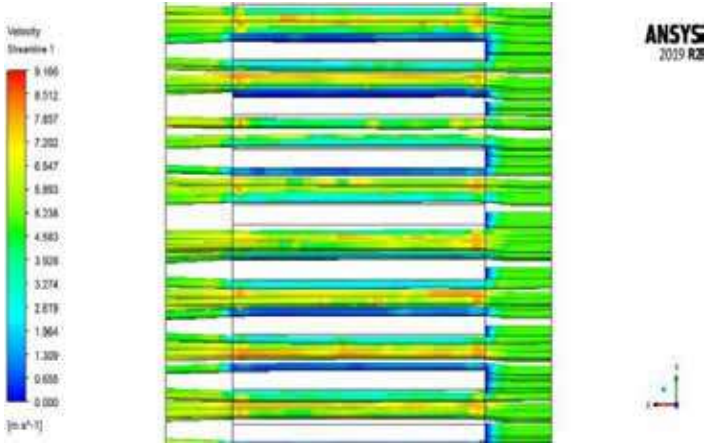


(B)

Fig. 2 a) Basic model b) Modified model

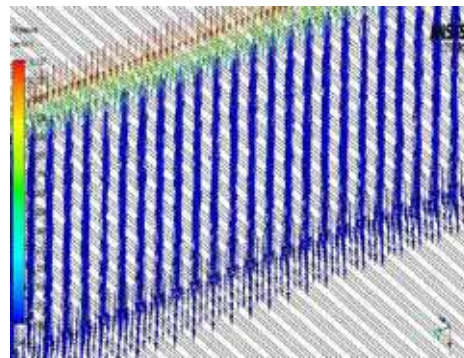


(A)

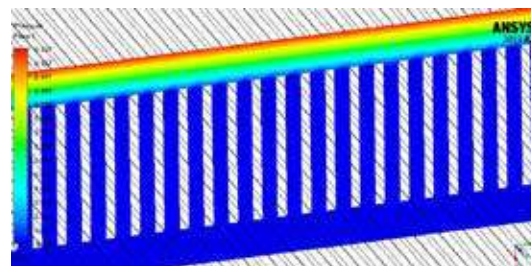


(B)

Fig. 3 (a) Velocity Vector (b) Velocity Streamline



(A)



(B)

Fig. 4 (a) Pressure Vector (b) Pressure Plane

In the Fig. 3 and Fig. 4 velocity contours and pressure contours were developed which gave the information about the maximum velocity region, maximum pressure region, streamline, vector, flow profile and re-circulation zones developed in the filter, velocity and pressure volume rendering which is difficult to visualize during experiment. Pressure vector may help to identify directional motion of fluid particles in filter domain. It can be seen internal circulation and separation zones. This is easily possible using CFD.

RESULT AND DISCUSSION

From Fig. 5 it can be observed that, existing air filter required 45-60 minutes to filter out all pollutants and provide clean air in the cabin. So much time exposure of such harmful pollutant is harmful to the occupant. Developed Carbon granules air filter required 10-12 minutes to cross hazardous pollutant level and reach in safer clean zone but caused reduction in air flow causing discomfort in cabin space. Simplifying fabrication process carbon layer cabin air filter was prepared and it required 15-18 minutes to clean air by vanishing the bad odor and PM along with increasing the air flow to about +17.29% [13] than the previously developed carbon granule filter.

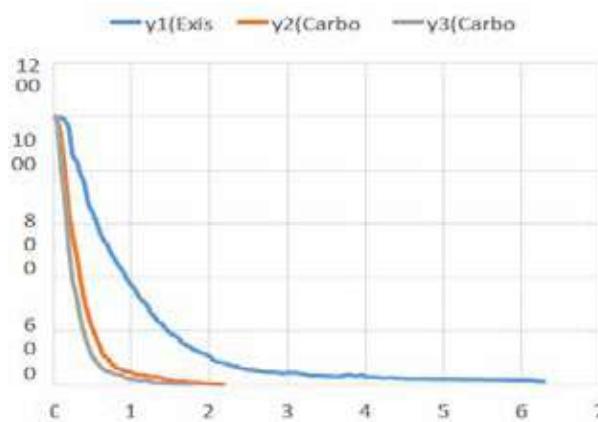


Fig. 5. Performance of filters



From this study, it can conclude that new processed carbon layer air filter is more efficient and significant to implement as it exhibited improved filtration by removable of harmful airborne particles and gases as it achieved both the objectives of suitable high efficiency filters and low-pressure drop need in the HVAC system. Thus, multilayer filter was developed with combination of layers of synthetic microfiber that is particle filter and support layer of activated carbon in order to remove gas phase indoor air pollutants such as volatile organic compounds providing.

REFERENCES

1. Yingjie Zhao, Bingrong Dai, Qi Yu, Haiqing Si, Gang Yu, "Numerical simulation study on air quality in aircraft cabins", *Journal of Environmental Sciences*, 230-240 (2016).
2. K J Heo, JW Noh, BU Lee, Y Kim, J H Jung, "Comparison of filtration performance of commercially available automotive cabin filters against various airborne pollutants", *Building and Environment* 161, 106272, (2019).
3. M A Nazarboland, X Chen, J W S Hearle, "Modelling and Simulation of filtration through woven media", *IJCST*, Vol 30 No 3, (2008).
4. Feng Z, Long Z, Chen Q, "Assessment of various CFD models for predicting airflow and pressure drop through pleated filter system", *Building and Environment*, 75, 132-141, (2014).
5. Simranjeet Kaur, Rahul Malik, "Design optimization of automotive air filter housing for minimum pressure drop", *IJEDR*, Volume 5, Issue 4, ISSN, 2321-9939, (2017).
6. Lesya V Pelyk Lviv, Volodymyr O Vasylechko, Petro O Kutsyk, Yuliya A Peleh, "Innovative filters made of polyoxadiazole fibers for industrial gas and dust emissions treatment", *Adsorption Science & Technology*, Vol. 35(9-10) 817-824, (2017).
7. Qiujian Xu, Yinping Zhanga, Jinhan Mo, Xinxiao Li, "How to Select Adsorption Material for Removing Gas Phase Indoor Air Pollutants: A New Parameter and Approach", *Indoor Built Environ*, 22, 1:30-38, (2012).
8. Cheng, Y., Tsai, C., "Factors influencing pressure drop through a dust cake during filtration", *Aerosol Sci. Technol.* 29 (4), 315-328 (1998).
9. Baumgartner, H P, Loeffler, "The collection performance of electret filters in the particle size range 10 nm-10 μ m", *Journal of Aerosol Science*, 17, 438-445 (1986).
10. Brown R C, Gray W R, Blackford, D B Bostock, "Effect of industrial aerosols on the performance of electrically charged filter material", *Annals of Occupational Hygiene*, 32, 271-294 (1988).
11. Kim K H, Sekiguchi K, Kudo S, Sakamoto K, Hata M, Furuuchi M, Otani Y, Tajima N, "Performance test of an inertial fibrous filter for ultrafine particle collection and the possible sulfate loss when using an aluminium substrate with ultrasonic extraction of ionic compounds", *Aerosol Air Qual Res* 10, 616 (2010).
12. Walsh C, Stenhouse J I, "The effect of particle size, charge, and composition on the loading characteristics of an electrically active fibrous filter material", *Journal of Aerosol Science*, 28, 307-321 (1997).
13. Ji, J.H., Bae, B.N., Kang, S.H. and Hwang, J.H, "Effect of Particle Loading on the Collection Performance of an Electret Cabin Air Filter for Submicron Aerosols" *J Aerosol Sci.* 34, 1493-1504 (2003).



Study and Analysis of Asphalt Hot Mixing Plant

Vishal K Patel, Dr A S Mohite

Department of Mechanical Engineering, The Maharaja Sayajirao University of Baroda, Vadodara, Gujarat

✉ vishalkpatel195@gmail.com

ABSTRACT

The infrastructure development is the major indicator of country's growth. If country has well developed road and building then it is in the row of developed country. The good quality road is artery of nations GDP growth. For good road and its sustainability you must have well developed and advance technology for build it. Asphalt Hot Mixing Plant is used for prepare asphalt for construct a road. It mixes hot asphalt with different sized grain. For this there are different types of Hot Mixing Plants regarding their construction, availability of source, types of used fuel, location of road making if it is remote location or else. It is used by its different volume handling capacity. Low combustion efficiency, low thermal efficiency and not properly transfer heat e.g. bypass of produced heat by burning of fuel are the major problem in Hot Mixing Plant. In this combustion efficiency is mainly depend on Nozzle. A different type of Nozzle with different nozzle angle is used for spraying fuel in plant. Nozzle is the key element which atomizes the fuel and make it sound for better combustion. By setting the stoichiometric air-fuel ratio and nozzle cone angle we can get desire output.

Keywords: Light diesel oil; Final temperature of product and exhaust gases; 45° and 60° Nozzle; Burner.

INTRODUCTION

First example of modern road construction with binder is seen in Nottingham in 1848 where tar is used as Binder. In 1858 bitumen is used as an overlay for cement concrete layer in Paris.

The use of Asphalt started thousands of years before the finding in USA. Mesopotamians are credited as the first to use asphalt to waterproof temple bath and water tanks. It was also used by Phoenicians to waterproof their merchant ships. Asphalt is first used for road building in Babylon at around 625 BC. The Romans took up the road system from Carthaginians and built roads for easier travel by the military.

Burner stability and reduction of pollution level are the main concern of designers of industrial burner and many practical combustion system. Flam stabilization is affected by several parameters such as mixing and boundary condition at the nozzle exit. Partially premixed flames are likely to be more stable than premixed flames and thus can be more attractive for practical applications.

The PM emission associated with HMA production include the criteria pollutants PM-10 (PM less than 10 micrometres in aerodynamic diameter) and PM-2.5, hazardous air pollutant (HAP) metals, and HAP organic compounds. The gaseous emission associated with HMA production include the criteria pollutants Sulphur dioxide, nitrogen oxides, carbon monoxide and volatile organic compounds as well as volatile HAP organic compounds.

The pollution problem as discuss above is only can control by the better and proper combustion of fuel. This may help in both for reducing pollutant production and good burning efficiency. Good burning efficiency reduce the fuel consumption and it is directly benefited in cost of road production. The final temperature of final product of mixture is also important for good quality of road and easy rolling and spreading. That is why the good heating effect is also important.

Fawzy El-Mahallawy, Mohy S. Mansour and Ahmed found that how the mixing and nozzle geometry effects on the flame structure and stability. In the research that they conduct shows that partially premixed flame are more stable than premixed and Non-premixed flames. An optimum level of partially premixing has been obtained for all conical nozzles at a mixing length five times the nozzle diameter. The data show also that stability can also improve by increasing the cone angle.

Imam, Yasamin and Kazem found the effect of fuel spray angle on pollutant emission in turbulent spray flames and it show that for various pattern and angle of fuel spray pollutant measured and it is for different cone angles 45°, 60° and 80° and spray

pattern of hollow and solid is increasing in spray angle reduces the co and nox emission. The cone angle 60° and hollow pattern is most suitable for heating process in their pilot furnace and condition is also favourable for minimum gas emission.

EXPERIMENTAL TEST FACILITY

Experimental Set-up

The project was performed on the hot mix plant located in Vadodara Municipal Corporation. The plant are settled by the Himalaya Pvt. Ltd and Burner used in that plant is supplied by the Shakti Burners Pvt. Ltd. The whole plant has mainly seven part mixing drum, Burner, Fuel tank, Hot Bitumen storage tank, material handling system (conveyor belt), Pollution control unit and Aggregator storage. From those all parts our focus is on Burner.

There are two types of hot mixing plant first is continuous mixing plant also known as drum mixing plant and second one is batch mixing plant. Both have its own advantages and disadvantages and particular reasons for choose one of them. The plant at which our project is done is continuous mixing type.

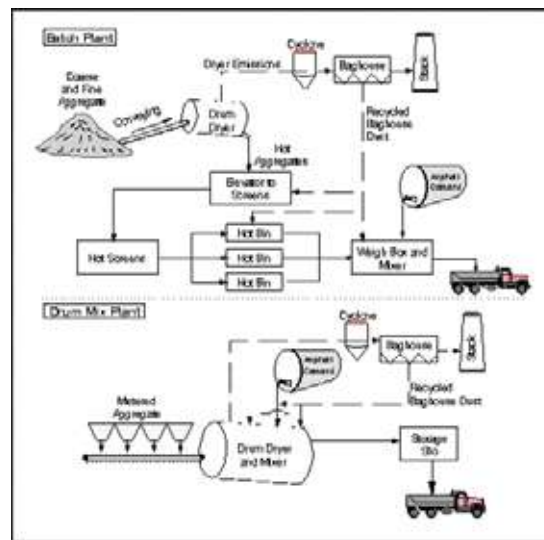


Fig. 1(a) Schematic diagram of drum mix plant



Fig. 1(b) Real image of drum mix plant

Fig. 1. Drum mix plant

Burner

Burner is the main heart of the hot mix plant. Burner is a device which produce a flame with using high pressure fuel and supplied air from compressor. It is heat input device. Burner is a device to generate a flame to heat up products using a gaseous fuel such as acetylene, natural gas and propane. Some burner have an air intake to mix the fuel gas with air to make a complete combustion.

The burner used in the project analysis is medium capacity burner. The specification of burner is given below:

1. Diffuser Disc
2. Nozzle
3. Ignition Electrodes
4. Nozzle Gun
5. Ignition Cable
6. Transformer
7. Control Box
8. Inspection Glass
9. Impeller (fan)
10. Electric Motor
11. Fire Tube
12. Air Dumper
13. Air Gate
14. Solenoid Valve
15. Oil Connecting Pipe
16. Oil Pump

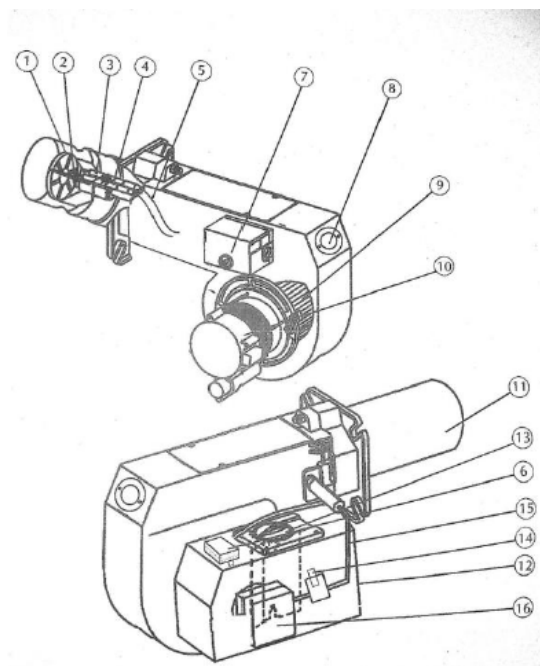


Fig. 2. Schematic diagram of burner

Nozzle Study

Separation of oil into small droplets requires the application of energy. In the case of nozzles, this energy is supplied in the form of pressure, usually from an appropriately designed motor driven pump. Pressure energy as such will not break up oil it must first be converted into velocity energy. Since energy is consumed in overcoming fluid friction, we would expect that with higher

viscosity fuels the spray angle would not be as stable as with low viscosity fuels. If the viscosity is high enough, the effective spray angle may collapse to the extent that a long, very narrow flame results.

An experiment perform on the burner with the different nozzle angle. We use two different nozzles of 45° and 60° cone angle. The study is for getting the idea of atomization and the spread of the fuel particles. These was done on the burner which is settle on the testing frame and the burner was connected by the two supply lines one is intake of LDO and second one is return line of the LDO. Return line helps to maintain the pressure and for that it supply back the further fuels to the tank.



Fig. 3(a) Spray of fuel with different nozzle angle 60° and 45° respectively



Fig. 3(b) Flame propagation by using 60° and 45° respectively

Fig. 3. Study of two different Nozzle on spray of fuel and flame propagation

The above two pictures clearly shows that the higher the degree of cone angle the higher the spray spreading the fuel and the higher the flame propagate. This experiment is helps to implementation of nozzle in hot mix plant and study the effect on the temperature gain.

Experimental Procedure

First off all for calculate the combustion efficiency we get the data of Air supply and Fuel supply and then find the Air-Fuel ratio. For calculate the air supply on different air gate position we set the burner on the test set-up and measure the air velocity with the help of Anemometer and measure the area of the delivery side. By doing this we have air flow rate at different air gate position.



Table 1. Air velocity (m/s) at different air gate position

Sl. No.	Velocity						
	V. P.	V ₁	V ₂	V ₃	V ₄	V ₅	V _{avg}
1	3	4.15	4.20	3.90	3.70	3.75	3.94
2	5	3.90	5.20	5.03	5.10	4.90	4.82
3	7	4.83	4.83	5.40	5.37	5.26	5.13
4	10	5.37	5.97	6.00	5.75	5.90	5.79

By measuring the delivery side dimensions and calculate the area,

Area: 0.015712 m²

Mass flowrate = Density×Area×Velocity

By using the above equation for all air gate position we get mass flowrate of air (\dot{m}_a in Kg/min).

$(\dot{m}_a)_1 = 4.3653$ Kg/min

$(\dot{m}_a)_2 = 5.3404$ Kg/min

$(\dot{m}_a)_3 = 5.6827$ Kg/min

$(\dot{m}_a)_4 = 6.4137$ Kg/min

And fuel supply is constant for all cases is 0.3194 Kg/min.

The specification of experiment is given below:

Mass of bitumen in the tank : 5000 Kg

Specific heat of bitumen : 2.68 KJ/Kg-K

Calorific value of LDO : 43.09 MJ/Kg

Atmosphere temperature : 37 °C

Pouring temperature : 58 °C

After getting this initial data, we measure the time require for increase the temperature for sufficient range at different Air-Fuel ratio. This time is used for calculate the total fuel consumption for increase the temperature. By this we can get the heat supply by burning of fuel for increase the temperature. Same way we can get the theoretical value of heat require to increase the same temperature for given Air-Fuel ratio. This calculation can get by the help of specific heat of bitumen at given temperature and mass of total bitumen in storage tank.

RESULT AND DISCUSSION

Time calculation for Increase Temperature

Table 2. Requirement of time for 45° nozzle

Sr. No.	Air-Fuel ratio	Time for increase ΔT_1	Time for increase ΔT_2	Time for increase ΔT_3
1	(A:F) ₁	186 sec	188 sec	198 sec
2	(A:F) ₂	179 sec	180 sec	187 sec
3	(A:F) ₃	179 sec	179 sec	183 sec
4	(A:F) ₄	171 sec	172 sec	176 sec

Table 3. Requirement of time for 60° nozzle

Sr. No.	Air-Fuel ratio	Time for increase ΔT_1	Time for increase ΔT_2	Time for increase ΔT_3
1	(A:F) ₁	178 sec	180 sec	185 sec
2	(A:F) ₂	168 sec	173 sec	177 sec
3	(A:F) ₃	165 sec	167 sec	172 sec
4	(A:F) ₄	161 sec	161 sec	163 sec



From the above two tables, we can say that the time required for the increase in same temperature is more in 45° nozzle as compared to 60° nozzle. It shows that there is some effective heating or we can say more heat transfer is done in case of 60° nozzle as compared to 45° nozzle. But as we know the heat exchanger is same for both the cases that lead the discussion towards the proper burning of fuel is done in 60° nozzle as compared to 45° nozzle.

The reason behind this data is that the 60° nozzle atomized the fuel particles very fine as compared to 45° nozzle and the spray cover area is more. That will help to proper combustion of fuel and reduce the wastage of fuel in the form of unburnt fuel particles.

The proof of less wastage of fuel in the form of unburnt fuel is found in the temperature reading of exhaust gas. The temperature of exhaust gases is lower for the 60° nozzle as compared to 45° nozzle and less for higher Air-Fuel ratio.

CONCLUSION

The result of this study on hot mix plant by using two different nozzles 45° and 60° give the knowledge of flow pattern and spread of flame in the furnace and gives the complete data of heat losses by bypassing the flue gases without heating effect.

REFERENCES

1. Fawzy el-mahallawy, Ahmed Abdelhafez, Mohy S. Mansour, "Mixing and nozzle geometry effect on flame structure and stability", Combustion Science and technology, 2007.
2. R.K.Jain, "Experimentally investigated effect of flame temperature on performance of rotary furnace". International Journal of mechanical engineering, 2014.
3. Jassim M. Abdulkarim jaff, "The effect of nozzle angle and distance between burner and burning velocity in counter flame", International journal of scientific and engineering research, volume 6, issue 9, 2015.
4. Fatih Yonar, "Evaluation of asphalt plant in term of performance: A case study", researchgate, 2010
5. Thaddaeus A. Bode, "An analysis of impact of temperature segregation in hot mix asphalt", American society of mechanical engineering, 2012.
6. Reyes Ortiz O, Berardinelli E, Alvarez A. E., Carvajal-Munoz, J.S., Fuentes, L.G., "Evaluation of hot mixture with replacement of aggregates by reclaimed asphalt pavement (RAP) material", Sciverse sciencedirect Elsevier, 2012.
7. Office of Air quality and planning and standards, "Hot mix asphalt plant emission assessment report", United States environmental protection agency, 2000.
8. D. Peinado, M. de Vega, N. García-Hernando, C. Marugán-Cruz, "Energy and exergy analysis in an asphalt rotary dryer", Research and development department Spain, 2011.
9. Km. Monu, Preeti Banger, A.K Duggal, "A review paper on Hot mix asphalt technologies", International research journal of engineering and technology, Volume 2, Issue 5, 2015.
10. Iman Abrishamchi, Yasamin khazraii, Kazem Bashirnezhad, "Effect of fuel spray angle on pollutants emissions in turbulent spray flame", International conference on chemical engineering and application, 2010.
11. Arthur H. Lefebvre, "Gas turbine combustion", Third edition, CRC press.
12. H.I.H. saravanamuttoo, G.F.C. Rogers, H. Cohen, A.C.Nix, P.V.Straznicky, "Gas turbine theory" seventh edition, pearson.



Sustainability Adaptation by Retrofitting Volatilizer in Thermal Power Plant for Co-generation of Cement and Power

C Prabhakar Reddy¹, Amiya P. Goswami²

SOET, CMR University, Bagalur, Bangalore¹

Independent Researcher²

✉ amiyagoswami@gmail.com

ABSTRACT

Fossil fuel fired thermal power plants release green-house gas (GHG) and produce fly ash as solid waste leaving disposal problem. While 27% of fly ash is consumed in cement industries and construction, rest goes for land fill contaminating soil and water on the earth. A novel semi-U shaped volatilizer is recommended to be retrofitted in the Pulverised Fuel (PF) boiler of thermal power plant for gasification under atmospheric pressure. Outgas is drawn to run a gas turbine while de-volatilized solid fuel is burnt in a boiler installed with fluidized bed to ensure complete combustion of residual carbon at lower temperature for reducing NO_x. Sand is separated out by centrifuging the de-volatilized solid fuel in mid section of the tower that allows segregation of coarse sand particles in the bottom part of the PF boiler. Admixture in the desired proportion are dosed to fly ash in the conveyor before passing into silo and bagging as cementitic material.

INTRODUCTION

The coal or lignite based power generation is affordable, but associated with green-house gas, SO_x and NO_x emission. India is committed to the global carbon-neutral movement. Consequently thermal power generation is cut down to 165 GW and policy is in place to produce renewable energy by over 50% of energy requirement to 175 GW by the turn of 2022 (INDC, 2015) from 42.5 GW as on March 2016 (CEA, 2016). However there is a further need to explore energy efficient thermal power plant designs mitigating environmental issues and simultaneously offering affordability in BRICS countries where coal and lignite deposits are available sufficient to cater for a century. In this connection authors published a patent providing new design for energy efficient with low emission while producing cement and sand for construction simultaneously [1]. Heat efficiency of a lignite based Russian boiler in thermal power plant is seen to be as low as 34%, hence investigated further [2]. Efficiency in combined cycle is known to improve substantially [3]. Fluidised bed combustion technology is known for efficient combustion with reduced emission due to lower residence time of fuel.

Apart from green-house gas, thermal power plant produces solid waste in the form of fine inorganic powder known as fly ash after combustion of coal or lignite in various proportion in the range of 7-41% depending on the source material. Fly ash disposal poses a serious environmental disorder because of its toxic elements and heavy metal affecting flora and fauna. The ash produced from these power plants are stored in wet ponds or collected in powder form using electro-static precipitators and then physically evacuated, mostly dumped as land fill while a small part of it finds use in cement plant for producing PPC cement to the maximum extent of 25%. Cement production from calcareous raw material also generates greenhouse gas both on account of decomposition of carbonates and fossil fuel used for pyro-chemical reaction at elevated temperature. One of the authors (APG) published another patent for producing cementitic material in thermal power plant head using fly ash in between 70-90% in the mixture with the counter components enabling the conversion [4]. The entire quantity of fly ash produced in thermal power plants can be converted into cement which is responsible for 7% of global anthropogenic greenhouse gas emission.

Gas turbine based combined cycle plants are the most efficient in the range of 60-63%, clean and reliable than pulverized fossil fuel based (PF) boilers commonly used in thermal power plants. The cost of power from the combined cycle gas plants is currently cheaper by about 40-50% of that obtained from pulverized coal-based plants of equal or larger scale even where coal or lignite is delivered at 60% of the price of gas [5]. The process of gasification is done separately from solid fuel to run gas turbine while unburnt portion is transferred to a fluidized bed combustor to heat up water into steam to run steam turbine (Rankine Cycle) for generating electrical energy. In addition to this, introduction of superheated steam boiler together with conventional steam drum is disclosed in a patent for operational flexibility in combined cycle electric power generation incorporating heat

recovery steam generator (HRSG) system from the outlet of gas turbines [6]. Generally, a pressurized fluidized bed combustor (PFBC) is designed for production of high pressure combustible gas in the relatively low temperature environment in the range of 850-900 °C and used directly in the gas turbine after gas cleaning inside the pressurized combustor or reactor. At such low temperature the efficiency of heat conversion in gas turbine becomes low. Furthermore, a single pressurized vessel serves both for gasification and combustion of solid component of the fuel, hence cost is higher for pressure vessel. This design being much different from the existing power plants retrofitting by partial or minor changes poses a difficulty. This deficiency can be overcome by providing a separate gasification or volatilizer and retrofitted while a gas turbine run independently that can be operated with every possible combination of pressure and temperature thus attaining flexibility and higher efficiency.

RETROFITTING

Thermal Power Plant

Fig. 1 presents a schematic view of novel thermal power plant with improved efficiency in power generating system involving gasification of solid hydrocarbon fuel e.g., coal or lignite while incorporating with an innovative process for co-generation of cement. The present system uses combined cycle and fluidized bed combustion (CCFBC) technology and processes for co-generating cement-like material for construction along with electric power from volatile matter containing carbonaceous feed using such system.

Volatilizer and Gas Turbine

The system comprises a semi-U-shaped volatilizer for cracking/ gasification of lignite/ coal at controlled temperature using preheated pulverized solid fuel as the de-volatilized residual charcoal flows through the mid-section of main PF boiler where steam is produced to run steam engines. A gas turbine engine is provided to generate power from combustion of gasified fuel from volatilizer and pressurized air mixture ensuring better economics and higher efficiency in optimized operating condition. Exhaust gas from gas turbine is re-circulated into the volatilizer for fluidization of fuel bed. Residual pressure of gas turbine exhaust allows vigorous fluidization of fuel by centrifugal action that also segregate relatively coarser and heavier sand component from fuel/ash at the bottom segment of the PF boiler. Sand can either be collected from bottom of PF boiler or used as heat storage media.

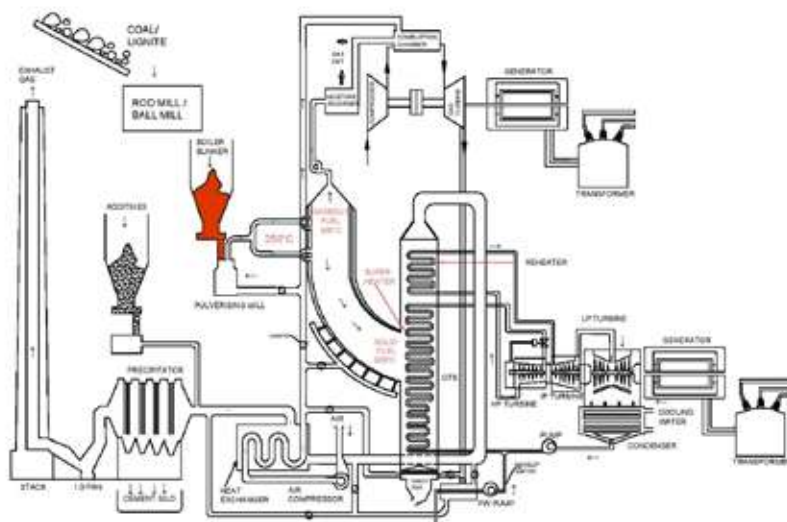


Fig. 1. General outlay of retrofitted thermal power plant

ID Fan and Recuperator

Selected additive materials are added at a controlled temperature and proportion into the flue duct or silo collecting dry fly ash from electrostatic precipitator (**Fig. 1**). Finally fly ash and additives are mixed thoroughly before packing as cementitic material for constructions. If required the cementitic material collected can be milled in a ball mill separately. A heat recovery system disposed downstream from the PF boiler to receive heat energy from flue gas for supply of preheated air to various locations as shown in **Fig. 1**.

MATERIALS

Solid Fuels: Any solid fuel with high volatile matter content such as wood, straw, lignite and coal are suitable. In order to determine the volatile matter content, the fuel is initially dried at 110 °C till constant weight is obtained. The dry fuel is placed in an electrically heated lab furnace and loss is determined by heating slowly without producing flame at 450°C with 2 hour of soak. The furnace is cooled and specimen weight is used to calculate the volatile matter content by difference. Specimen is again heated to 750°C until constant weight to determine ash content. Bulk quantity of ash was also manually produced at two stages by low temperature calcination in air without producing flame as seen in **Fig. 2** and then burning in an electrical furnace for converting to ash. The ash was sieved through 75 µm mesh to separate out sand. The ash passed through the mesh was used to mix with admixture for preparation of cement.

Admixture: Anhydrous NaOH pellets are procured from local supplier. Other chemical and minerals are also from local sources as described elsewhere [4].



Fig. 2. Showing volatile matter released upon heating lignite fuel

EXPERIMENTAL & RESULT

Fly ash produced in usual high temperature boiler contains substantially glassy phase. Crystalline phases consist of both the precipitated ones from the ash-melt formed in combustion of solid fuel and those whichever are not affected by the temperature inside the boiler. A detailed description of fly ash morphology is presented elsewhere [7]. In the present process, no glass formation is possible due to low temperature of ash formation. The crystalline mineral compounds present in the fuel can only be structurally transformed, dehydrated or decomposed partially or completely. The low temperature ash is highly porous and light in weight (low density) and fragile with high specific surface area. Usual fly ash is also light in density in spherical form like glass bubble. Glass in fly ash dissolves in alkaline environment and is said to be responsible for reactivity in geopolymer chemistry. However, alkali activated geopolymer produced from low temperature ash did not show any strength [7]. A new set of additives were developed suitably for both low and high temperature fly ash [4]. **Table 1** shows the properties of the fuel and ash investigated.

Table 1. Properties of fuel and ash

Source of ash	Volatile matter content, wt. %	Ash content, wt. %	Fraction retained over size		
			150µm	75µm	53µm
Usual lignite	46.8	6.7	0.18	0.33	0.39
High ash lignite	36.1	31.8	0.11	0.19	0.31

Preparation of Specimen

The sand fraction above 75µm size was used for preparation of mortar cube using Ultratech OPC 53 grade cement in the standard ratio of 1:3 as specified in IS 4031 Part 6. In each of the trials, five numbers of 50 mm sized cubes were prepared and strength is tested after curing for 3, 7 and 28 days as specified in the said IS in ambient condition (15-27°C). Compressive load is applied in a compression testing machine ('Datacone' make) at the load-rate of 1.8 kN/sec. Ultimate strength is



calculated by dividing load with respective area. Standard river sand is used for comparison. The average strength is calculated and presented in **Table 2**.

Table 2. Ultimate strength of mortar after specified curing period

Sand type	3 day MPa	7 day MPa	28 day MPa	Water/Cement ratio
Lignite ash sand	29.6	44.1	58.5	0.41
Coal ash sand	29.1	43.4	57.8	0.40
River sand	28.3 (27)	42.9 (37)	56.5 (53)	0.42

DISCUSSIONS

Combined cycle can increase the plant's power generating efficiency by using an indirectly heated, fluidised bed volatilizer/thermal cracker. Existing Russian designed PF boilers can be retrofitted with a low temperature volatilizer (400°C) and a gas turbine to run combined cycle. Additionally a recuperator can be installed for waste heat recovery from flue gas and hot air is provided for combustion ensuring better heat utilisation. By selecting solid fuel with high volatile matter content, the power plant can maximize the ratio of gas turbine output (Brayton Cycle) to steam turbine output (Rankine Cycle). Existing subcritical boilers are preferred due to flexibility of load variation in case of low demand when the plant has to be run within 40% of capacity.

Proposed retrofitting for co-generation of cement and power will have multiple benefits such as (a) high efficiency of combustion due to combined cycle and fluidized bed technology, (b) NO_x is less due to low combustion temperature of residual solid fuel, (c) SO_x and H₂SO₄ (sulfuric acid) is trapped before the entry into gas turbine or similar engines, hence emission is reduced and (d) no scale formation in tubes leading to long life, (e) low rank lignite/coal or fodder stock can be utilised, and (f) above all, green-house gas is cut down to save the environment. Table 2 shows that the sand can be used for construction. Manufacture of cement from fly ash will cut down green-house gas by over 200 Million tonne every year assuming 1 tonne of green-house gas for every tonne of cement. Better economy is possible compared to well known carbon capture and sequestration where the efficiency goes down by 7-8 points [8].

CONCLUSION

Existing Russian designed PF boilers can be retrofitted with a volatilizer using heat recovery for economy and a gas turbine for higher efficiency. The improved efficiency will result in lower power cost and reduced emission.

ACKNOWLEDGEMENT

Authors thank the management of Presidency University, Bangalore and NLCIL for their support in conducting the investigation. Thanks are due to Mr. Girish for his relentless effort in preparing Autocad drawings.

REFERENCES

1. A. P. Goswami, C. P. Reddy, "Co-generation of Cementitious Material in Thermal Power Plant," Emerging Technologies for Power Generating Systems, Annual Technical Volume of Mechanical Engineering Division Board, Institution of Engineers (India), vol. 2, pp. 37-41, 2017.
2. C. P. Reddy and A. P. Goswami, "Process for Co-generation of Cementitious Material and Sand with Reduced Emissions in Thermal Power Plant," Indian Patent No. 201841047645.
3. P. K. Nag, Power Plant Engineering, 3rd ed., McGraw Hill Education (India), 2013, pp. 379-396.
4. A. P. Goswami, "Additives and Methods to Convert Fly Ash into Hydraulic Cementitious Product in Thermal Power Plant," Indian Patent No. 201841005320.
5. C. Higman and M. van der Burgt, Gasification, 2nd ed., Gulf Professional Publishing, 2008, pp. 329-355.
6. J. D. Holt and G. R. Smith, "Combined Cycle Power Plant," US Patent 8726625.
7. A P Goswami, "Determining Physico-Chemical Parameters in Stronger Ambient Cured Geopolymer from Fly Ash," Advances in Cement Research, unpublished.
8. T. Wang and H. A. Long, "Techno-economic analysis of biomass/coal Co-gasification IGCC Systems with Supercritical Steam Bottom Cycle and carbon Capture," International Journal of Energy Research, vol. 34, pp. 1667-1692, March 2014.



Optimization of Cross Flow Forced Draft Air Cooled Tubular Heat Exchanger (FDAC-HE) of Fumes Extraction System in Steel Melting Plant

Vijay S Kumavat¹, Dr Arvind Mohite², Manish Khanna³, Hemant Chaudhary⁴

Department of Mechanical Engineering, Faculty of Technology & Engg., The M S University of Baroda¹

Assistant Professor, Department of Mechanical Engineering, Faculty of Technology & Engg., The M S University of Baroda²

General Manager, CMD, AM/NS India, Hazira, Surat³

Joint General Manager, FES, SMP-1, AM/NS India, Hazira, Surat⁴

✉ vs6121995@gmail.com; ✉ Mohite21@yahoo.com; ✉ Manish.khanna@amns.in; ✉ Hemant.chaudhary@amns.in

ABSTRACT

The Fumes extraction system (FES) is used in many industries to cool and remove contaminants from fumes produced by different operations in steel plants, rubber plants, melting shops, power plants etc. Water and air both types of cooling are used in the FES. The main focus is to achieve a desired outlet temperature of off-gas as high temperature off-gas damages the bags of the bag house. In this work, the authors have tried to study the effect of fan capacity of cooling air on off-gas temperature drop, overall heat transfer coefficient, maximum velocity (velocity from least free space), and pressure drop across tube banks for a module of 3m length and tube pitch equal to 1.25 to 1.5 times the outer diameter to optimize the FDAC-HE to get minimum pressure drops as well as maximum effectiveness by changing different tube banks arrangement. The combination of grey relation analysis and Taguchi design analysis ensured the optimization of both tube pitch as well as tube banks arrangement for cooling of 340000 Nm³/hr off-gas. The CFD analysis of FDAC-HE module is done to validate the excel-based numerical design calculations. The maximum difference of CFD analysis result and excel-based numerical design calculation is in range of $\pm 15\%$.

Keywords: FES; Cross flow; CFD; Air cooled heat exchanger; Forced draft.

INTRODUCTION

AM/NS Steel India Limited is one of India's leading integrated steel producers with an annual production capacity of 10 million tonnes. It has a fully integrated steel plant located at Hazira, Surat[1]. Plant of AM/NS steel has four DC EAFs which have steel production capacity of 150 tph. All the EAFs have been also equipped with FES facility which has main purpose to cool and treat the off gases generated during the steel making. The FES mainly consist moving elbow, water cooled duct, plain duct, FDAC-HE, bag house for separation of the dust particles with the gases, induced draft fan, and stack. The EAFs canopy was provided with a secondary hole to extract fumes generated during operation and discharge through a stack in the environment. FDAC-HE is used for cooling off-gas. A number of axial flow fans used for air to discharge in cross-flow towards the tubes of FDAC-HE for cooling the Off-gas. A temperature drop is around 380-400 °C means a huge amount of heat is removed (large heat exchanger is required). It is designed such that the results should be minimum overall cost (initial cost and operating cost).

Moody, L.F. et al. [2] suggest the detailed about the surface roughness design values to compute the friction factor for the calculation of pressure drop using darcy-weisbach equation. Shashi Menon, E. paper main objective is to calculate Reynolds number to classify the fluids as laminar or turbulent. Importance of friction factor and moody diagram is explained. Also provide detailed guidance of a trial and error solution to find friction factor using Colebrook-white equation.

Zukauskas et al. [3] suggest the correlation for heat transfer and pressure drop in in-line and staggered banks of tubes apply to Reynolds number between range of 1 to 2×10^6 and prandtl number from 0.7 to 104 with a wide range of relative transverse and longitudinal pitches.

R.K. Shah, Fundamental of Heat Exchanger Designing, John Wiley & Sons. USA, 2003 [4] main objective of this is to compute Heat transfer rate, effectiveness etc. and the conclusion is explained relation between heat transfer rate and effectiveness. It's



also provides detail about heat exchanger surface geometrical characteristics for both in-line and staggered arrangement of tube banks which helps in determining transverse and longitudinal pitches with a different value of the tube pitch.

In the textbook of heat transfer by J.P. Holman[5] provides data for value of overall heat transfer coefficient and correction factor for cross-flow heat exchanger with one fluid unmixed. The important correlation of NTU-Effectiveness is also given for different flow arrangement. This correlation is very fruitful in the design calculations of cross-flow forced draft air cooled tubular heat exchanger.

Gunes et al. [6] has applied Taguchi method of optimization for the design parameters of heat exchanger tube with coil wire insert. The objective of his study was to enhance heat transfer with minimum pressure drop. Chamoli[7] study on optimization of flow and surface geometrical parameters in a rectangular channel roughened with V down perforated baffles using Taguchi, which goals to improve heat transfer with minimum pressure drop. One common aspect in all of these deliberated is that most of the researchers are concentrated on enhancement of heat transfer with minimum pressure drop. The traditional Taguchi method developed by Taguchi is based on orthogonal array of experiments, which provide much reduced variance for the experiment with best setting of process control parameters, but it is not suitable for optimization of multi-objective optimization problem. In order to overcome this difficulty a new optimization method i.e. Taguchi-grey relational analysis is being adopted by the researchers for multi-objective optimization problem. Senthilkumar et al. [8] deliberated on experimental and performance analysis of cemented carbide inserts of distinct geometries using Taguchi based grey relational analysis, and the objective was to find optimum conditions, which presented a lower flank wear and surface roughness with higher material removal rate. Yeh and Tsai [9] carried out a study on optimizing the fine-pitch copper wire bonding process with multiple quality characteristics using a combination of grey-Taguchi analysis approach.

Gurbir Singh and Hemant Kumar[10] shows that CFD resolve the entire heat exchanger in discrete elements to find the temperature gradients, pressure distribution and velocity vectors. The turbulence model k-ε is used for accurate results from CFD. CFD models or packages provides the contours and data which predict the performance of the heat exchanger design and are effectively used because it has ability to obtain optimal solutions.

DESIGN OF EXPERIMENT

Grey Relational Analysis

In 1989, grey relational analysis was suggested by Deng. The optimization of process parameters which are having multi-responses is done by grey relational analysis through grey relational grade[8][9]. Taguchi method with grey relational analysis is used with multiple performance characteristics which includes the following steps:

Identification of response characteristics.

1. Numbers of levels are determining for the process parameters.
2. Appropriate orthogonal array is selected.
3. Based on the orthogonal array experiments are conducted.
4. Experiments results are normalized.
5. Grey relational coefficient is calculated by performing grey relation generation.
6. By averaging the grey relational coefficient, grey relational grade is calculated.
7. Using the grey relational grade (GRG) and statistical ANOVA (Analysis of Variance) experimental result are analysed.
8. Optimal level of process parameters is selected.
9. Through the confirmation test optimal process parameters are verified.

In grey relational analysis normalization of original sequence is calculated as follows:

$$X_i^*(k) = \frac{\max X_i(k) - X_i(k)}{\max X_i(k) - \min X_i(k)} \quad (1)$$

Where,



$X_i^*(k)$ = sequence after data processing

$X_i(k)$ = comparability sequence

In grey relational analysis deviation of sequence is calculated as follows:

$$\Delta_{oi}(k) = X_{o*}(k) - X_i^*(k) \quad (2)$$

Where,

$\Delta_{oi}(k)$ = deviation sequence.

$X_{o*}(k)$ = reference sequence.

$X_i^*(k)$ = comparability sequence.

In grey relational analysis grey relational co-efficient and grey relational grade is calculated as follows:

The grey relation co-efficient is given as follows:

$$\xi_i(k) = \frac{\Delta_{\min} + (\xi^* \Delta_{\max})}{\Delta_{oi}(k) + (\xi^* \Delta_{\max})} \quad (3)$$

Where,

$\Delta_{oi}(k)$ = deviation sequence

ξ = identification or distinguishing coefficient

The grey relation grade is given as follows:

$$\gamma_i = 1/n \sum_{k=1}^n \xi_i(k) \quad (4)$$

Where,

γ_i = grey relational grade for i^{th} experiment

n = number of performance characteristics.

Taguchi approach to design of experiment

Taguchi approach is used in present investigation, which is a prevailing design of experiment tool[6][7][11]. To determine optimum parameters this method is efficient, simple and systematic as compared to conventional methods which are too complex, expensive and number of experiments have to be carried out to study the process. Orthogonal array is used in Taguchi method to study the entire process with only a small number of experiments. However, only one factor is involved at each experiment in traditional experiments, wherein one parameter is changed while the rest are held constant. Also, traditional method fails to consider any possible interactions between the parameters. An interaction is the failure of one factor not to produce the same effect on the response at different levels of a second factor and to study all factors involved in the process. All these drawbacks are overcome in Taguchi technique. For optimization of process parameters and identifying the optimal combination of factors for the desired responses Taguchi approach is used.

Taguchi approach consist of the following steps:

Process parameters are identified.

Numbers of levels are determined for the process parameters.

Orthogonal array is selected.

Optimum level of process parameters is selected through ANOVA(Analysis of Variance) analysis.

Confirmation test is performed to verify the optimal process parameters.

Selection of orthogonal array

By using the orthogonal array the effect of different parameters on the performance characteristic can be examined. After identifying the controllable parameters affecting a process, the levels at which these should be varied decided. Detail



understanding of process is required to determine what levels of a variable to be tested, including the maximum, minimum and the current value of the parameter. Typically, in the experimental design the number of levels for all parameters is chosen to be the same to aid in the selection of the proper orthogonal array.

The present study comprises of two different input factors (V) in which each having four levels (L).

Taguchi formula for minimum number of experiments is:-

$$N_{\text{taguchi}} = 1 + V (L-1)$$

$$= 1 + 2 (4-1)$$

$$= 7$$

Orthogonal array $> N_{\text{taguchi}}$

Hence L16 orthogonal array is chosen for present analysis.

Table 1. Numerical design data for different tube pitch and tube arrangement (114.3 mm outer diameter)

Tube arrangement	Tube pitch (d_o times mm)	Pressure drop of cooling air (mm of WC)	Pressure drop of off-gas (mm of WC)	Heat capacity required (10^4) W/K	Cooling air required (10^3) m ³
30	1.25	93.5	38.4	43.8241	14.9497
30	1.35	70	47.7	53.9094	12.5658
30	1.45	60.6	57.9	66.1101	11.0053
30	1.5	60	64	74.174	10.2596
45	1.25	45.4	46.3	51.0086	12.8546
45	1.35	37.6	59	66.7301	10.8113
45	1.45	35.3	70.9	84.4715	9.6216
45	1.5	37.1	79.6	97.1268	8.906
60	1.25	93	39.2	43.7139	14.7557
60	1.35	71.3	48	52.9114	12.5701
60	1.45	61.4	57.7	65.0947	10.9967
60	1.5	63	65.3	73.4517	10.1432
90	1.25	90.5	47	47.5109	12.7555
90	1.35	70	58	59.0602	10.945
90	1.45	63.7	72.6	74.8	9.4879
90	1.5	64.8	81.6	85.4625	8.7939

Table 2. Numerical design data for different tube pitch and tube arrangement (129 mm outer diameter)

Tube arrangement	Tube pitch (d_o times mm)	Pressure drop of cooling air (mm of WC)	Pressure drop of off-gas (mm of WC)	Heat capacity required (10^4) W/K	Cooling air required (10^3) m ³
30	1.25	127.1	35.5	56.071	13.1359
30	1.35	102.5	42.6	71.9496	11.3066
30	1.45	100.8	52.4	94.6469	9.74
30	1.5	107.8	58.5	110.3799	9.0055
45	1.25	53	42.8	68.4149	11.3455
45	1.35	49.4	53.6	95.5538	9.5941
45	1.45	50.3	62.9	128.4424	8.5627
45	1.5	60.6	71.4	154.1999	7.8475
60	1.25	112.7	36.5	56.0336	12.9024



60	1.35	92.1	43.1	71.9693	11.2093
60	1.45	97.5	53.4	94.2727	9.6378
60	1.5	110.9	61.4	111.2594	8.7913
90	1.25	126.8	42.2	61.4265	11.3844
90	1.35	108.1	52.4	81.957	9.6914
90	1.45	114	67.2	112.537	8.2416
90	1.5	127.1	76.2	134.3446	7.5653

ANOVA

ANOVA can be useful for determining influence of any given input parameter from a series of experimental results which can be used to interpret experimental data. In ANOVA studies with certain test errors, it is very essential to determine error variance. Obtained values are then used to determine F-value of fisher test (F-test). The obtained variation of an experiment attributes to individual significant factor or interaction which reflects percentage contribution (P). This shows the relative power of a factor to reduce variation. The factor with substantial P plays an important role.

Taguchi's method calculates the minimum number of experiments by using formula:

$$NT = 1 + V (L-1)$$

Where,

NT = minimum number of experiments.

V = number of variables.

L = number of levels.

For ANOVA, following terminology is required to calculate.

Grand total Sum of Squares, N_i

$$= \sum_{i=1}^n \left(\frac{S}{N_i} \right)^2 \quad (5)$$

Where, n = total number of experiments

Total Sum of Squares or Total Variation (ST),

$$\sum_{i=1}^n \left(\frac{S}{N_i} \right)^2 - CF \quad (6)$$

Where, CF = Correction Factor,

$$CF = \frac{\left(\sum_{i=1}^n \frac{S}{N_i} \right)^2}{n} \quad (7)$$

Sum of square for a factor (SF),

$$S_F = \frac{F_1^2}{N_{F_1}} + \frac{F_2^2}{N_{F_2}} + \frac{F_3^2}{N_{F_3}} - CF \quad (8)$$

Where, F1, F2, F3 are sum of S/N ratio of level 1, 2, 3 respectively.

N = number of repetitions of the factor in orthogonal array.



Mean Square of Factor (Variance),

$$V_F = S_F / dof_F \quad (9)$$

Mean Square Error (Se),

$$V_E = S_E / dof_F \quad (10)$$

Where, SE = sum of square due to error;

dof_F = degree of freedom due to error.

F ratio = VF/VE

S/N ratio

In Taguchi designs, S/N ratio minimizes the effects of noise factors to reduce variability in a process by identifying control factors. Control factors are those process parameters which can be controlled. Noise factors can be control during experimentation but cannot be control during process use. In a Taguchi method, to occur variability noise factor is manipulated to force and from the results, optimum control factor settings are identified that make the process strong, or resistant to variation from the noise factors. To minimize the effects of the noise factors high value of S/N ratio identify control factor settings[6][7].

Two step optimization process is mainly used in Taguchi experiments. In step 1 to reduce variability S/N ratio identifies those control factors. In step 2 in order to move the mean to target and to have a small or no effect on the S/N ratio, those control factors are identified. Under different noise conditions how the response varies relative to the nominal or target value is measure in S/N ratio. Depending on the goal of experiment different signal to noise ratios can be chosen. There are three signal-to-noise ratios.

- Larger-the-better
- Normal-the-better
- Smaller-the-better

The S/N ratio for 'smaller-the-better' and 'normal-the-better' is calculated as,

$$\text{smaller} = -10\log((S^2 \times Y)) \quad (11)$$

$$\text{normal} = -10\log((1/n)(\sum Y^2)) \quad (12)$$

The S/N ratio for 'larger-the-better' is calculated as,

$$\text{larger} = -10\log((1/n)(\sum (1/Y^2))) \quad (13)$$

Where,

\bar{Y} = average of observed data Y.

$(S^2 \times Y)$ = variance.

n = number of observations.

Confirmation Test

The confirmation test is used to verify the essential result with the experiment results. If the optimal combination of parameters and their levels coincidentally match with one of the experiments in the orthogonal array, then the confirmatory much with one of the experiments in the orthogonal array, then the confirmatory test is not required[11].

RESULT & DISCUSSION

Analysis of Cross-flow FDAC-HE with Different Tube Pitch

Normally the tube pitch of banks is between the ranges of 1.25 to 1.5 times the outer diameter of the tube. Tube pitch is defined as the distance between the Centers of the tube hole.

The graph of fan capacity vs off-gas temperature drop, overall heat transfer coefficient, maximum velocity (velocity from least

free space), the pressure drop across tube bank for a module of 3m length and tube pitch equals to 1.25, 1.35, 1.5 times outer diameter is given below:

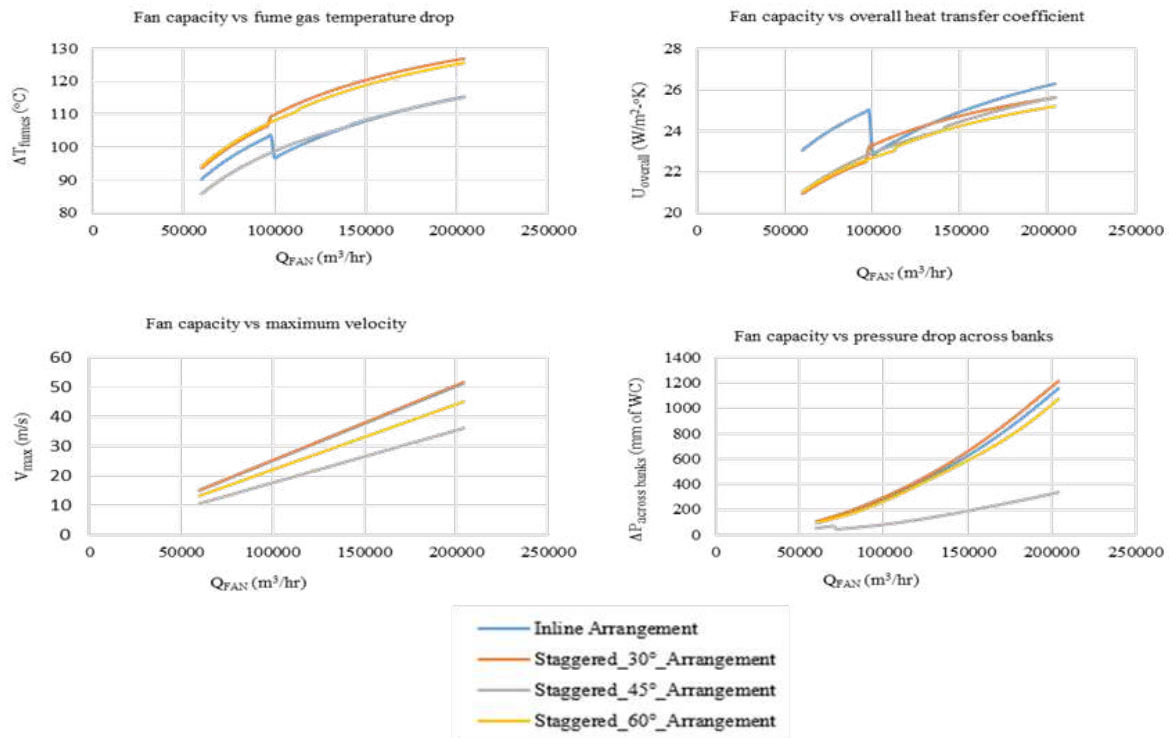


Fig. 1. Tube pitch equals to 1.25 times the tube outer diameter

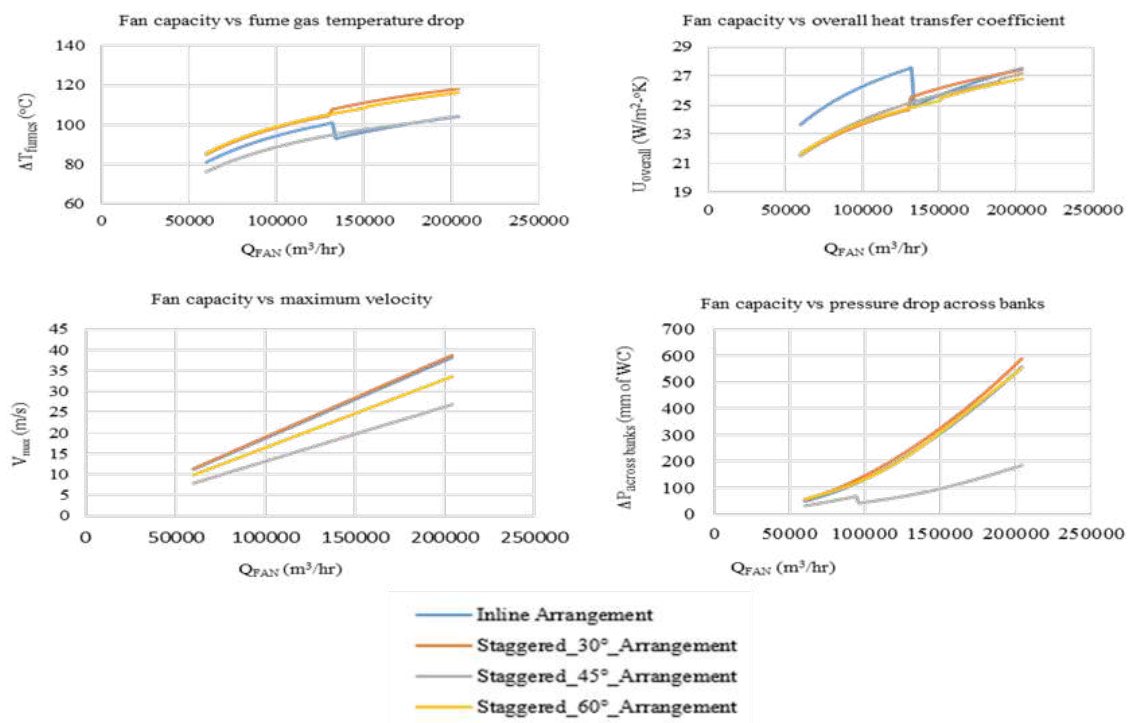


Fig. 2. Tube pitch equals to 1.35 times the tube outer diameter

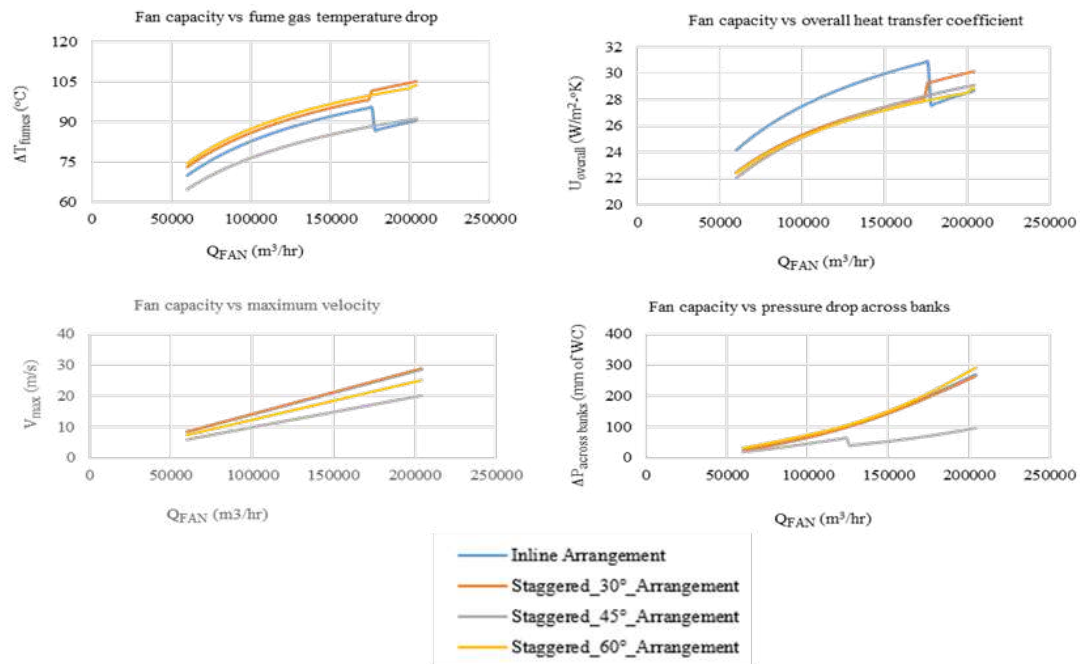


Fig. 3. Tube pitch equals to 1.5 times the tube outer diameter

Fig. 1. shows the off-gas temperature drop is maximum for staggered_30°_arrangement but the cooling area is also 15.86% more as compared to a minimum area.

Fig. 2. shows the off-gas temperature drop is maximum for staggered_60°_arrangement but the cooling area is also 17.23% more as compared to a minimum area.

Fig.3. shows the off-gas temperature drop is maximum for staggered_60°_arrangement but the cooling area is also 17.40% more as compared to a minimum area.

So overall at a minimum cooling area, more overall heat transfer coefficient, and minimum pressure drop, staggered_45°_arrangement is best for tube pitch equal to 1.25, 1.35, and 1.5 times the outer diameter for FDAC-HE.

Taguchi Method-Based Grey Relation Analysis: Plots of S-N ratio of GRG versus Tube Arrangement & Tube Pitch

The **Fig. 4** shows the value of S-N ratio is large for staggered_45°_arrangement with tube pitch equals to 1.25 time's outer diameter for both module having 129mm and 114.3mm outer diameter of tube.

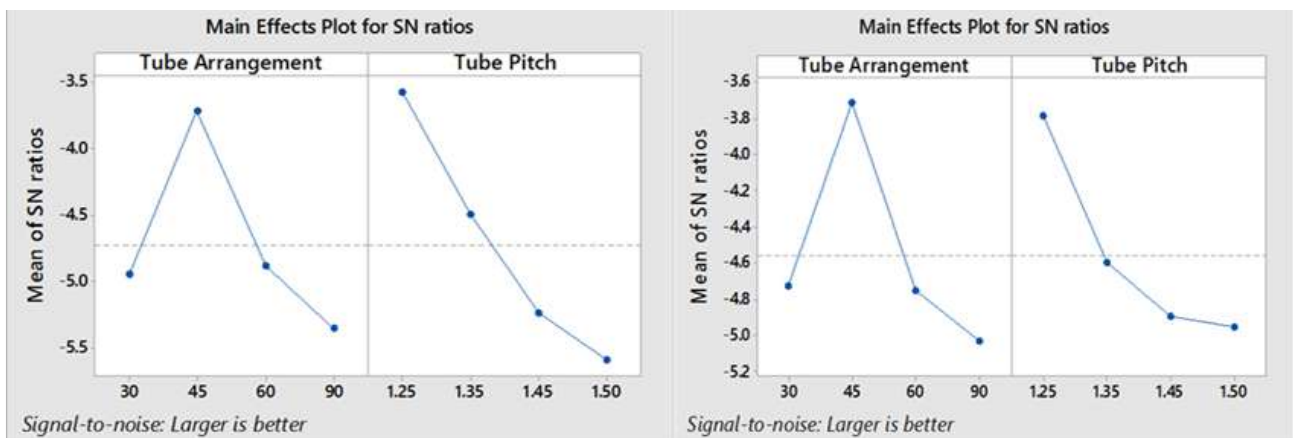


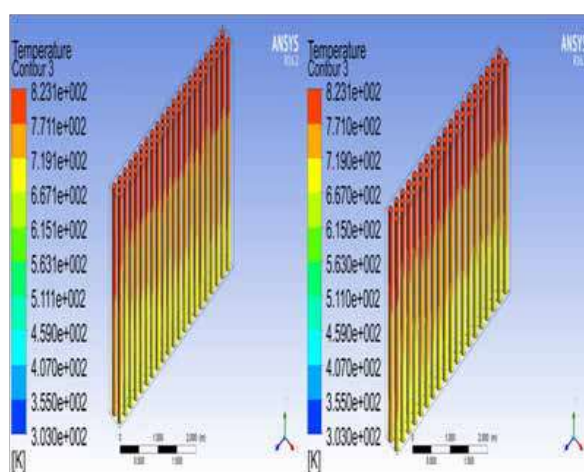
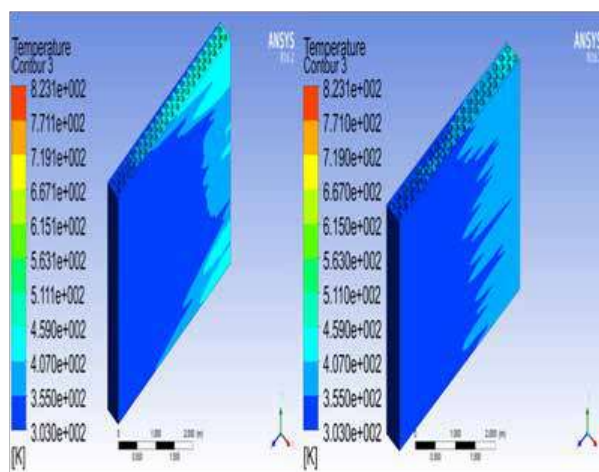
Fig. 4. S-N ratio plots of grey relational grade versus tube arrangement and tube pitch (larger is the better)

General Linear Model: GRG versus Tube Arrangement & Tube Pitch**Table 3.** ANOVA (Analysis of variance/129 mm outer diameter)

Source	DF	SS	MS	F-value	P-value	Contribution
Tube Arrangement	3	0.027944	0.009315	25.81	0.000	36.98%
Tube pitch	3	0.044353	0.014784	40.97	0.000	58.71%
Error	9	0.003247	0.000361			4.31%
Total	15	0.075545				100%

Table 4. ANOVA (Analysis of variance/114.3 mm outer diameter)

Source	DF	SS	MS	F-value	P-value	Contribution
Tube Arrangement	3	0.019342	0.006447	10.59	0.003	45.55%
Tube pitch	3	0.016728	0.005576	9.15	0.004	40.26%
Error	9	0.005482	0.000609			14.19%
Total	15	0.041552				100%

CFD contours of both module of 114.3mm and 129mm outer diameter of tube**Fig. 5.** Temperature contours of off-gas/fumes**Fig. 6.** Temperature contour of cooling air

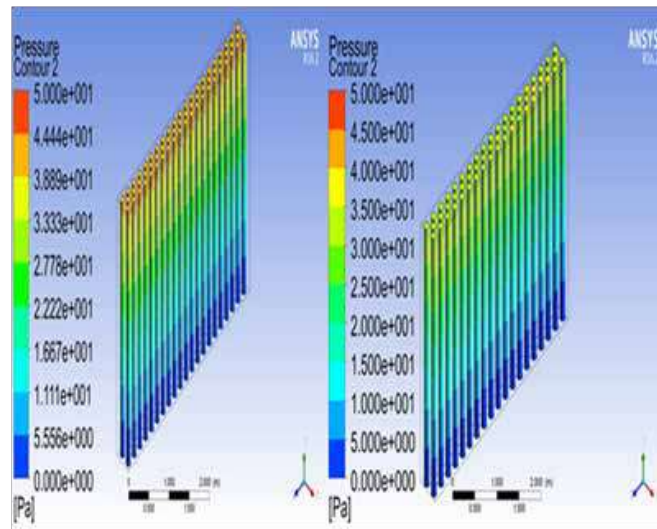


Fig. 7. Pressure contour of off-gas/fumes

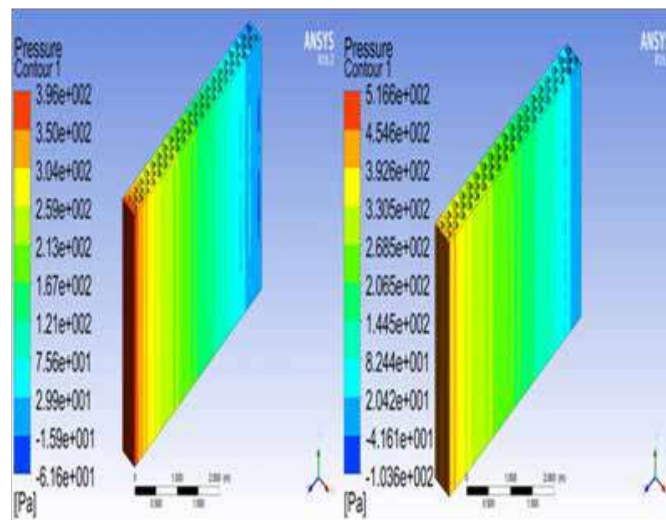


Fig. 8 Pressure contour of cooling air

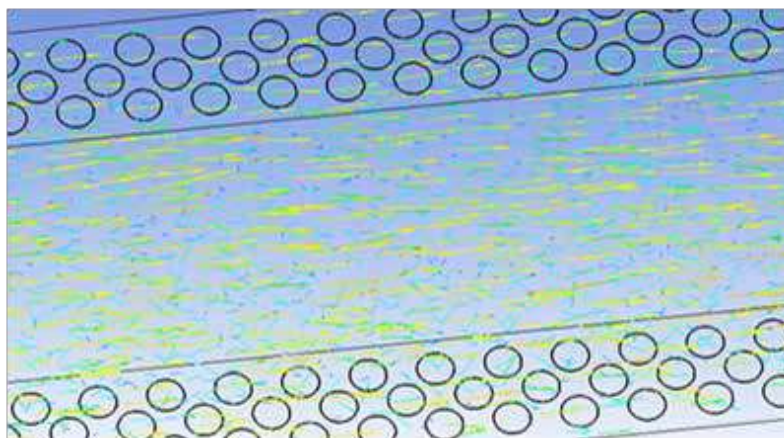


Fig. 9 Velocity vector of cooling air

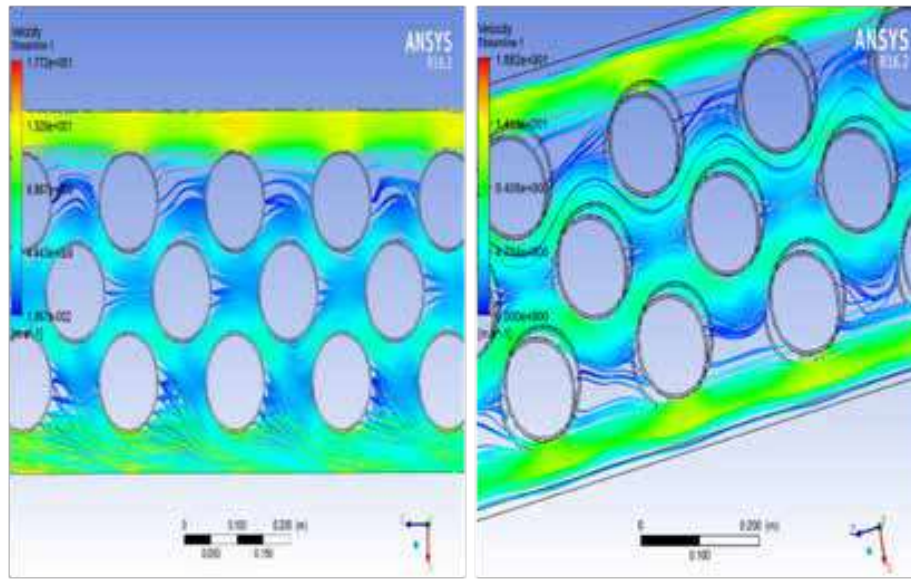


Fig. 10. Velocity streamline of cooling air

CONCLUSION

The graph of fan capacity vs off-gas temperature drop, fan capacity vs overall heat transfer coefficient, fan capacity vs maximum velocity (velocity from least free space), and fan capacity vs pressure drop across tube banks for a module of 3m length and tube pitch equal to 1.25 to 1.5 times the outer diameter of FDAC-HE shows that the value $UA_{cooling}$ product is maximum for staggered_60°_arrangement but pressure drop across tube bank is more while for staggered_45°_arrangement $UA_{cooling}$ product value is 5-10% less but at a minimum pressure drop across tube banks for a particular fan capacity. Hence the staggered_45°_arrangement is best suitable in fumes extraction system for cooling of 340000 (Nm³)/hr off-gas at the working condition of baghouse.

The Taguchi-based grey relation analysis (Fig. 11) also confirmed that the staggered_45°_arrangement and the tube pitch is equal to 1.25 times the outer diameter are the best configuration for FDAC-HE for cooling of 340000 (Nm³)/hr off-gas at the desired working condition of baghouse with a minimum pressure drops.

ANOVA shows (Table 1) the contribution of both tube pitch and tube configuration on performance of FDAC-HE is in range of 35-60%.

The CFD results of FDAC-HE module are in good agreement with the excel-based numerical design analysis model with maximum difference of $\pm 15\%$.

ACKNOWLEDGMENT

I am deeply indebted thanks to my guide Dr A. S. Mohite, Ass. Professor, Mechanical Engg. Dept., Faculty of Tech. & Engg., The M. S. University of Baroda, for his valuable guidance and encouragement. I would like to express my gratitude to my industrial guide Mr. Manish Khanna, General Manager, & Mr. Hemant Chaudhary, Joint General Manager, SMP-1 Department, AM/NS INDIA for his immense support and guidance. Last, but most importantly, I'm grateful to my parents, sister, brother, wife and family for their love, blessings and support throughout this endeavour.

REFERENCES

1. ArcelorMittal & Nippon Steel India Limited, "Fumes Extraction System," Hazira.
2. L. P. Moddy, "Friction Factors For Pipe Flow," Trans. of the ASME 66(8), pp. 671-684, 1994.
3. A. M. V. a. S. A. Zukauskas, "Heat Transfer in Banks of Tubes in Crossflow of Fluid," in Thermophysics, Vol.1., Vilnius, 1968, pp. 46-102.



4. R. K. SHAH and D. P. Sekulic, "Fundamentals of Heat Exchanger Design," 2003.
5. J. Holman, "Heat Exchanger," in Heat Transfer, 2002, pp. 521-584.
6. S. Gunes, E. Manay, E. Senyigit, V.ozceyhan, "A Taguchi approach for optimization of design parameters in a tube with coiled wire inserts," Applied Thermal Engineering, no. 31, pp. 2568-2577, 2011.
7. S. Chamoli, "A Taguchi approach for optimization of flow and geometrical parameters in a rectangular channel roughened with V down perforated baffles," Case Study Thermal Engineering, no. 5, pp. 59-69, 2015.
8. N. Senthilkumar, T. Tamizharasan, V. Anandkrishnan, "Experimental investigation and performance analysis of cemented carbide inserts of different geometries using Taguchi based grey relational analysis," Measurement 58, pp. 520-536, 2014.
9. J. Yeh, T. Tsai, "Optimizing the fine-pitch copper wire bonding process with multiple quality charecteristics using a grey-fuzzy Taguchi method," Microelectron. Reliab. 54, pp. 287-296, 2014.
10. Gurbir singh & Hemant kumar, "Computational Fluid Dynamics Analysis of Shell and Tube Heat Exchanger," Journal of Civil Engineering and Environmental Technology, vol. I, no. 3, pp. 66-70, 2014.
11. R. Shah, Fundamental of Heat Exchanger Designing, The USA: John Wiley & Sons, 2003.
12. A. A. Zukauskas, "Heat Transfer from Tubes in Crossflow," in Advance in Heat Transfer, Vol 8,, Newyork, Academic Press, 1972, pp. 93-160.
13. A. A. Zukauskas and Konvektivnyi perenos v teploobmennikakh, "Convective Transfer in Heat Exchaanger," Moscow, 1982, pp. 222-291.
14. A. Zukauskas and A. Ulinskas, "Efficiency Parameters for Heat Transfer in Tubes Banks," Heat Transfer Engineering, pp. 19-25, 2007.
15. Taguchi, G., "Taguchi techniques for quality engineering," Quality Resources, 1987.



Effect of Different Cooling Mediums on Friction Stir Welded AA6061 Alloy

Dinesh Chaudhary, Dr A S Mohite

Department of Mechanical Engineering, The Maharaja Sayajirao University of Baroda, Vadodara, Gujarat

✉ dmchaudhary1009@gmail.com

ABSTRACT

Friction Stir Welding has shown great potential to weld AA6061 heat treatable aluminium alloy. But the effectiveness of joint in FSW depends on the temperature distribution and cooling condition during welding. Hence the present study was carried out to investigate the temperature distribution in the weld zone and the effect of different cooling medium on microstructure and mechanical properties of FS-Welded AA6061 aluminium alloy. The temperatures were recorded at eight specific position by IR thermometer under same set of process parameters but different cooling medium such as Air cooling, Forced water cooling and under water cooling. Experimental results showed that by increasing the peak temperature deteriorated the mechanical properties. Similarly, on the other hand cooling medium also found to have a significant effect on mechanical properties. Tensile strength and microhardness during welding have been discussed under the presence of different cooling medium. It was found that under water cooling showed better mechanical properties compared to air cooling and forced water cooling.

Keywords: Friction stir welding; AA6061 alloy; Temperature distribution; Air cooling; Forced water cooling; Under water cooling.

INTRODUCTION

FSW is a solid-state welding technology, generally used for welding aluminum alloys [1]. Though FSW is a solid state welding process, the temperatures development during the process plays a very vital role in controlling the mechanical properties of friction stir welded joint. Hence among many issues in FSW, temperature analysis and heat transfer phenomenon during this process have been the point of focus for researchers. According to Shah and Badheka [2], during FSW of AA7075-T651 a lower heat input results in defects like pin holes and tunnel defects whereas higher heat input leads to dissolve the strengthening precipitates in the matrix which results in degradation of the mechanical properties. The same observation is reported during the study under excessively hot processing conditions by Qian et al. [3, 4]. In order to analyze the heat generation, Silva et al. [5] evaluated the different methods of temperature measurement during FSW for feedback control. They reported that location of thermocouples plays an important role for accuracy in temperature measurement inside the workpiece. Ramulu and Narayanan [6] investigated the effect of different process parameters on temperature evolution of friction stir welded AA6061-T6 and observed that peak temperature increases by increasing the shoulder diameter, plunge depth, and tool rotation speed, whereas it decreases for increasing welding speed due to lower heat input per unit length. Yau et al. [7] studied the temperature distribution study during the FSW of AA2024-T3 aluminium alloy using different thermocouple layouts. They found the higher temperatures at the finish points in the weld runs compared to the starting points which lead to cumulative heat build-up in the workpiece. They observed the higher temperature on AS compared to the RS. Keivani et al. [8] studied the effects of pin angle and preheating on temperature distribution during FSW operation and found that heat generation crucially affected by the pin angle whereas the effect of preheating on temperature distribution was minor. Rajamanickam et al. [9] studied the effect of process parameters on thermal history and mechanical properties of friction stir welded AA6061 and reported that the peak temperature at weld zone is strongly influenced by the tool rotation compared to weld speed. Fehrenbacher et al. [10-12] studied the effects of tool workpiece interface temperature on weld quality as well as improvement of quality by controlling the temperature and concluded that unequal temperature gradients are generated by variations in heat dissipation, which affects the properties of the weld and temperature may cross the permissible limit. They proposed the controlling of welding parameters such as rotational speed or axial force to maintain the weld temperature within the permissible limit in order to avoid the creation of defects by online feedback system.

Based on the literature review with respect to the thermal aspects of FSW it was found that heat generation causes annealing and reduces the hardness and strength of the material. This reduction in properties can be avoided or controlled by controlling the heat input, i.e., Peak temperature generation. Moreover, the properties can be controlled by controlling the heat output control through provision of different cooling mediums during FSW.

The present work is carried out to study the effect of different cooling mediums on temperature generation and consequently its effect on various mechanical properties of FS-Welded AA6061 alloy. Three experiments were carried out using optimal process parameter combination in the presence of three cooling mediums (Air cooling, forced water cooling and underwater cooling) were used for the present study. For each experiment, temperature profile was recorded and was studied with respect to the microstructure and mechanical properties of FS-Welded AA6061 alloy.

EXPRIMENTAL PLANT AND SET-UP

Material Detail

The material for research study was selected from literature review on FSW of aluminum alloys and keeping in mind the present requirement in manufacturing industries. The material was selected from sixth series of aluminum alloy which is AA6061 alloy. AA6061 aluminum alloy is an aluminum-based alloy often used in the aerospace industry. It is the most popular of the 6000-series aluminum alloys. However, it is difficult to fusion weld, as it is sensitive to hot cracking. The chemical composition of AA6061 is shown in **Table 1**. AA6061 material in as received condition was cut to required dimensions (100 mm×50 mm×6 mm) using Wire Electric Discharge Machining (WEDM).

Table 1. Chemical composition of AA6061

Name	Cu	Si	Fe	Mn	Mg	Zn	Ti	Al
Percentage (%)	0.15-0.40	0.40-0.80	0.0-0.70	0.0-0.15	0.8-1.20	0.0-0.25	0.0-0.15	Bal

Experimental Plan and Procedure

From the literature review, optimal combination of process parameters is used. Here same set of process parameter combination includes tool rotation speed, tool traverse speed and tool tilt angle. All the three experiments are carried out at the same tool rotation speed of 1500 RPM while the tool transverse speed is kept 50 mm/min and the tool tilt angle, that is angle between the perpendicular to the base metal and the axis of tool, is kept 1°, as shown in **Table 2**. This process parameter plays a very important role because frictional heat generation is mainly depending on the tool rotation speed and tool traverse speed.

Table 2. Experimental plan

	Tool type	Tool rotation speed (N) (RPM)	Tool traverse speed (v) (mm/min)	Tool tilt angle (A)	Cooling condition
1	Conical pin type	1500	50	1°	Air cooling
2	Conical pin type	1500	50	1°	Water cooling
3	Conical pin type	1500	50	1°	Under water cooling

For selected combination of process parameter, friction stir welding of AA6061 alloy was carried out in three different cooling condition i.e., 1) Air cooling (AC), 2) Forced water cooling (FWC), and 3) Under water cooling (UWC). Here an optimal process parameter was used for three different cooling condition. Therefore, total no of experiments in present study is equal to 3. Based on literature review, tool with conical pin is used for the present study. It is the simple tool with no features on it which yields better material flow during FSW. IR thermometer was used for recording temperature during FSW. For weld characterization the very first thing is to cut the sample form the nugget zone. To get the accuracy in measuring the tensile strength, test sample is cut by WEDM (Wire Electric Discharge Machining). The sample taken from the welded specimen is then used for carrying out various tests to check the quality of weld joints. **Fig. 1 (a-c)** shows the experimental setup for different cooling medium.



Fig. 1. Experimental setup for (a) Air cooling, (b) Forced water cooling, (c) Under water cooling

To maintain the accuracy each weld was repeated (prepared) thrice to get the average responses of temperatures. The welding was performed with a specially designed fixture made from SS304 and backing plate made of high carbon steel. During the welding process temperature data were continuously recorded at specific location on the plates using IR thermometer.

The accuracy of these thermocouples was 0.1 °C and maximum capacity of measuring was around 1030 °C. Thermocouples were placed at equal distance from the weld Centre on both sides. Temperature data collection was done with inbuilt software. The Temperatures were recorded at intervals of 2 seconds.

RESULT AND DISCUSSION

Surface appearance of welded specimens

Three experiments were carried out under each cooling mediums with same set of process parameters. The surface appearance of weld under different cooling medium is shown in **Fig. 2 (a-c)**.



Fig. 2. Appearance of FS-Welded AA6061 alloy in (a) AC, (b) FWC, (c) UWC

The surface appearance of UWC is quite better compared to AC and FWC. The reason might be the lower peak temperature in case of UWC which controls the better flow of surface material.

Peak Temperature Generation

The temperature obtained at specific locations on the specimen during FSW has been explained below. Average responses of peak temperature recorded by considering various cooling condition is shown in **Table 3**. These temperatures were recorded by placing a single IR thermometer on AS (Advancing Side).

Table 3. Peak temperature recorded during FSW of AA6061 alloy

Sample ID	Tool tilt angle (A), degrees	Tool rotation Speed (N), rpm	Tool traverse speed (v), mm/min	Average peak temperature on AS
AC	1	1500	50	385
FWC	1	1500	50	305.7
UWC	1	1500	50	271

The temperature distribution around the weld zone plays an important role in FSW since the quality of weld joint depends on the heat generation.

A lower heat input leads to defects like pin holes and tunnel defects whereas higher heat input leads to dissolution of strengthening precipitates which ultimately spoils the mechanical properties [13]. The peak temperature was found to decrease from air cooling condition to under water cooling condition, as shown in **Table 3**.

Temperature Profiles

Temperature profiles can be used to identify the heating and cooling rates. In some experiments the overall cycle time (heating plus cooling time) is less or more compared to other experiments which affect the mechanical properties. The cycle time can be increased or decreased by external agencies depending on the requirement of output results like tensile strength, hardness etc.

The temperature profile recorded by IR thermometer on AS are shown in **Fig 3**. The online measurement of temperature plays an important role in providing the real time temperature data that can be utilized as a feedback for controlling the process parameters to obtain the good quality of weld joints.

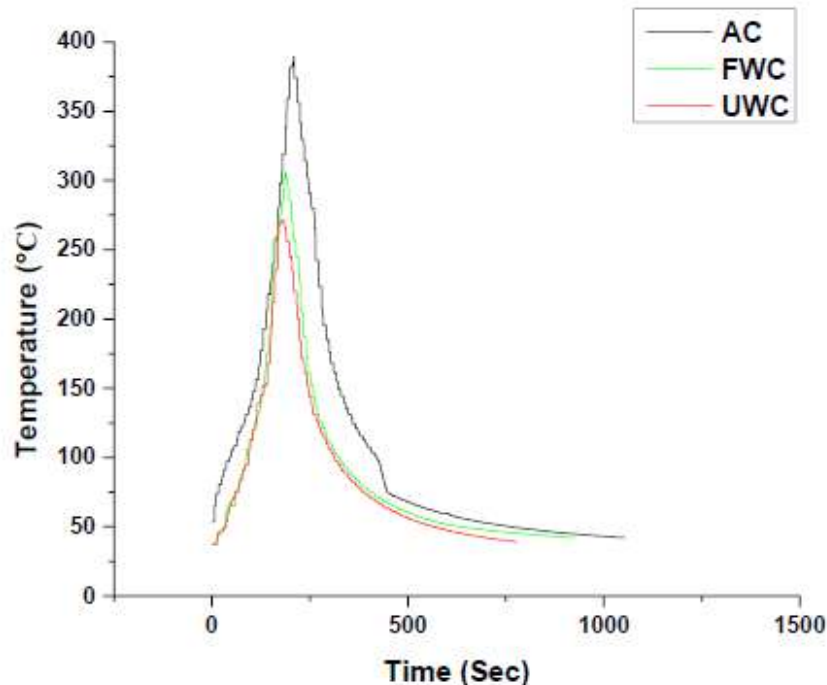


Fig. 3. Temperature profiles of FS-Welded AA6061 under different cooling mediums

It can be clearly observed from **Fig. 3** that as cooling medium changes, the peak temperature changes which consequently changes the cooling rate. The cooling rate is higher in case of UWC compared to AC and FWC.

The heating and cooling rate affects the final properties of the weld nugget. If the cooling rate is very much higher it will lead to brittle formation and hence deteriorates the properties. At the same time controlling the heating and cooling rate within certain range will yields the good weld properties. According to literature backing plate also plays a vital role in impacting heating and cooling rate but this fact is untouched in the present work and the same backing plate was used throughout the work.

It is observed that the initial rate of rise of temperature is slow and sharp for a certain period but as the tool travels towards the centre of the welding length this rate of rise of temperature increases very fast and getting fluctuated for a period of time due to sudden increases in frictional forces. Once the temperature reaches the peak level it starts decreasing steadily since the material in ahead of the rotating tool is preheated due to heat generation and hence it requires the less heat input to reach the softening temperature point. This peak temperature affects the mechanical property of the weld, especially yield strength. As the temperature increases yield strength decreases and flow of material begins [8]. The flow of material is controlled by temperature which is being controlled by process parameters. Hence proper care should be taken while choosing the optimum process parameters.

Since AA6061 aluminium alloy is precipitated strengthened alloy the peak temperature must be controlled otherwise it may lead to dissolution of strengthening precipitates which reduces the strength of the welding joint. The results of peak temperatures can be correlated with the defects occurred in the welding joint and a favourable processing window for a temperature can be produced to obtain the sound welds.

Microstructure

To study the microstructure a sample of size 10mm * 35mm was taken from the center of the welded specimen and all the samples were polished up to 1200 grit SiC papers. Final polishing was done by velvet cloth by using a diamond paste of 3 μm and 1 μm . To reveal the grain boundaries Keller's etchant was applied for 15 s on the surface of the polished sample. Optical microscopy was carried out on the specimens at different magnifications.

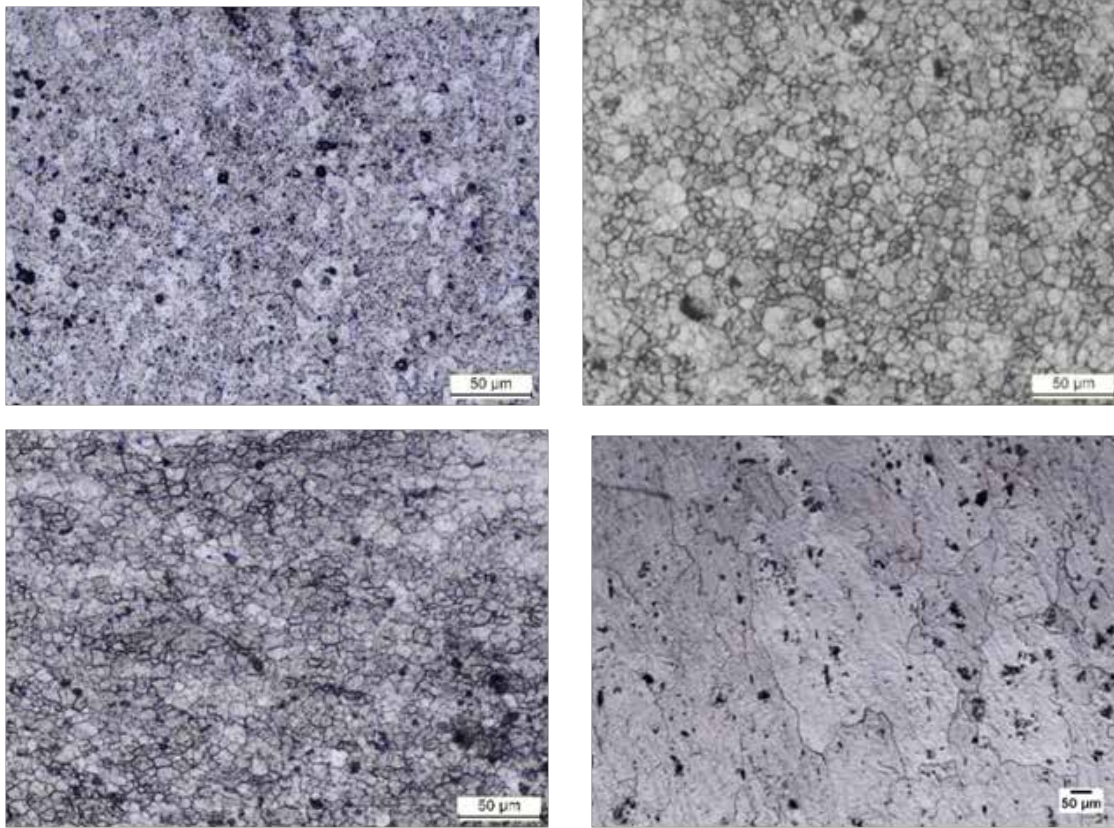


Fig. 4. Optical Micrograph for AA6061 FS-Welded in (a) AC, (b) FWC, (c) UWC, (d) AA6061 Base metal

Optical micrographs (OM) of the base metal AA6061 is shown in **Fig. 4**. Micrographs of nugget zone (NZ) under different cooling medium are shown in **Fig.4 (a-c)**. Large grains of Al matrix having an average grain size ranging from 108 to 116 μm were observed in the BM. The NZ showed dynamically recrystallized structure with refined and equiaxed grains of Al matrix because of large plastic deformation and high temperature experienced during FSW. Average grain size of Al in weld nugget zone of FSW joints is varying between 16 to 24 μm . However, grains were seeming to be larger in case of air-cooled sample, followed by FWC and UWC. The grains are very fine and smaller in case of UWC. The reason may be the lower peak temperature and higher cooling rates [14].

Microhardness

Vickers microhardness was measured on the transverse section of the weld joints. Microhardness testing was done at 300 g load and dwell time of 10s. Microhardness obtained by taking 3 indentations on nugget zone of each sample is shown in **Table 4**.

Table 4. Microhardness

Sample ID	Tilt Angle (θ), degrees	Tool rotation Speed (N), rpm	Welding Speed (v), mm/min	Avg. Temp. on AS	Avg HV at SZ
AC	1	1500	50	385	69.2
FWC	1	1500	50	305.7	87.7
UWC	1	1500	50	271	99.6

*Base metal avg. hardness- 118 HV

The Microhardness at the nugget zone for the above mentioned three samples was approaching to the hardness of the base metal. The maximum and minimum hardness value observed in the nugget zone was 99.6 HV and 69.2 HV for same set of process parameters but different cooling mediums. Therefore, it was confirmed that cooling medium plays a significant role in



FSW [15]. The hardness for AC sample, FWC sample and UWC sample was 69.2 HV, 87.7 HV and 99.6 HV respectively. It is important to note that for the same set of process parameters, the hardness was higher for UWC sample. It might be due to lower peak temperature which didn't allowed to dissolve the precipitates [16].

Tensile Strength

For tensile testing samples were taken from the transverse direction of the weld. To maintain the accuracy three tensile samples were prepared from each welded specimen according to ASTM E8 standard. Tensile tests were performed at the crosshead speed of 0.5 mm/min using the universal testing machine of 100 kN capacity at room temperature.

The average ultimate tensile strength (UTS) obtained for each specimen is shown in **Table 5**.

Table 5. Ultimate tensile strength of AA6061 FS-Welded alloy

Sample ID	Tilt Angle (θ), degrees	Tool rotation Speed (N), rpm	Welding Speed (v), mm/min	Avg. Temp. on AS	Avg. UTS (MPa)	Efficiency (η)
AC	1	1500	50	385	234.6	73.77
FWC	1	1500	50	305.7	256.8	80.75
UWC	1	1500	50	271	274.3	86.25

* Tensile strength of base metal = 318 MPa

The strength in all the samples was found lowered as compared to the base metal. The maximum UTS were found in UWC for the same set of process parameters. The effectiveness of the weld joint was also measured by the joint efficiency. There may be a presence of small size precipitates along with the Al grain size which plays an important role in improving the strength of the joint. It is important to note that the location of the fractured on the tensile specimens were found in heat affected zone (HAZ). It might be due to the larger grains and lower hardness at the HAZ. In HAZ the heat is not sufficient and hence grains become coarsen which leads to decrease the strength as well as hardness. The size of the grains observed in nugget zone was different for all cooling conditions. As the cooling improves, size of the grains reduced. The size of grain was 16 μm to 24 μm in the nugget zone whereas it was 108 μm in base metal. This decrement in grain size made the bonding between the atoms very strong and hence strength was improved in nugget zone.

Generally, for good welding joints, tensile samples should break from the HAZ due to lower hardness. It is important to note that the underwater cooled sample showed a higher tensile strength compared to air cooled and forced water cooled samples. The reason for this is the lower peak temperature generation and faster cooling in water cooled sample. The results of the tensile strength are in good agreement with the hardness [14].

CONCLUSION

The present study investigates the effect of different cooling medium on the microstructure and mechanical properties of FS-Welded AA6061 alloy. The online temperature was recorded during welding and same has been co-related with the properties. Following results can be concluded from the experiments:

- It was concluded that as the peak temperature decreases for the same set of process parameter combination, mechanical properties of FS-Welded AA6061 alloy improves.
- The thermal aspects in FSW are as important as the selection of process parameters. The effect of cooling medium of FSW is significant. As coolant improves, temperature decreases and as a result the grains remains finer which ultimately improves mechanical properties.
- Temperature was concluded higher around the center of the welding length and decreases as the tool moves away from it. However, it depends on the total length of the weld and may vary.
- It was concluded that Cooling rate increases with the improvement in coolant and its effect was observed in microstructure that more fine grains were observed in UWC compared to AC and FWC.
- It was concluded that the initial rate of rise of temperature is slow and sharp for a certain period but as the tool travels towards the center of the welding length this rate of rise of temperature increases very fast and getting fluctuated for a period of time due to sudden increases in frictional forces.



- A refined microstructure was observed after friction stir welding which helped in improving the mechanical properties of the weld. The effect of refined grains was clearly observed from the microhardness measurement that hardness was higher at the SZ and it is approaching to the base metal. The hardness was higher in case of UWC compared to AC and FWC.
- The UTS of the weld joints processes under the UWC was good compared to the joints processes in AC and FWC.

ACKNOWLEDGMENT

Authors are grateful to Government of Gujarat for funding to setup state-of-the art facilities at Manufacturing Lab at MSU Baroda. Authors also acknowledge the support of Anant Steel Mumbai for sponsoring workpiece materials for this research work.

REFERENCES

1. Thomas, W., et al., Friction stir welding. International patent application no. PCT/GB92102203 and Great Britain patent application, 1991(9125978.8).
2. Badheka, V., An experimental investigation of temperature distribution and joint properties of Al 7075 T651 friction stir welded aluminium alloys. *Procedia Technology*, 2016. 23: p. 543-550.
3. Qian, J., et al., An analytical model to optimize rotation speed and travel speed of friction stir welding for defect-free joints. *Scripta Materialia*, 2013. 68(3-4): p. 175-178.
4. Qian, J., et al., An analytical model to calculate the peak temperature for friction stir welding. *Science and Technology of Welding and Joining*, 2017. 22(6): p. 520-525.
5. Silva, A., J. De Backer, and G. Bolmsjö, Temperature measurements during friction stir welding. *The International Journal of Advanced Manufacturing Technology*, 2017. 88(9-12): p. 2899-2908.
6. Perumalla Janaki Ramulu, R.G.N. Experimental study on temperature evolution during friction stir welding of 6061-T6 Aluminum alloy. in *Design and Research Conference (AIMTDR 2014)*. 2014.
7. Yau, Y., et al., Temperature distribution study during the friction stir welding process of Al2024-T3 aluminum alloy. *International Journal of Minerals, Metallurgy, and Materials*, 2013. 20(8): p. 779-787.
8. Keivani, R., et al., Effects of pin angle and preheating on temperature distribution during friction stir welding operation. *Transactions of Nonferrous Metals Society of China*, 2013. 23(9): p. 2708-2713.
9. Rajamanickam, N., et al., Effect of process parameters on thermal history and mechanical properties of friction stir welds. *Materials & Design*, 2009. 30(7): p. 2726-2731.
10. Fehrenbacher, A., et al., Effects of tool-workpiece interface temperature on weld quality and quality improvements through temperature control in friction stir welding. *The International Journal of Advanced Manufacturing Technology*, 2014. 71(1-4): p. 165-179.
11. Fehrenbacher, A., et al., Measurement of tool-workpiece interface temperature distribution in friction stir welding. *Journal of Manufacturing Science and Engineering*, 2014. 136(2): p. 021009.
12. Fehrenbacher, A., et al., Combined temperature and force control for robotic friction stir welding. *Journal of Manufacturing Science and Engineering*, 2014. 136(2): p. 021007.
13. Khan, N.Z., A.N. Siddiquee, and Z.A. Khan, *Friction Stir Welding: Dissimilar Aluminium Alloys*. 2017: CRC Press.
14. Abnar, B., M. Kazeminezhad, and A. Kokabi, Effects of heat input in friction stir welding on microstructure and mechanical properties of AA3003-H18 plates. *Transactions of Nonferrous Metals Society of China*, 2015. 25(7): p. 2147-2155.
15. Sinhmar, S. and D. Dwivedi, Enhancement of mechanical properties and corrosion resistance of friction stir welded joint of AA6061 using water cooling. *Materials Science and Engineering: A*, 2017. 684: p. 413-422.
16. Rajamanickam, N., et al., Effect of process parameters on thermal history and mechanical properties of friction stir welds. *Materials & Design*, 2009. 30(7): p. 2726-2731.



A Vibrational Test for Chaos using 0-1 in a Vertical Axis Wind Turbine

C B Maheswaran^a, R Gopal^b, S Nadaraja Pillai^a

*Turbulence and Flow control Lab, School of Mechanical Engineering, SASTRA Deemed University, Thanjavur, Tamil Nadu^a
Centre for Nonlinear Science & Engineering, School of Electrical and Electronics Engineering, SASTRA Deemed University, Thanjavur, Tamil Nadu^b*

✉ nadarajapillai@mech.sastra.edu

ABSTRACT

Vertical axis wind turbine (VAWT) having high solidity ratio tends to exhibit nonlinear vibrations which might lead to structural failure. The 0-1 test for chaos certainly diagnoses the nonlinear vibrational behaviour and well distinguishes the periodic and chaotic signal. In our current study, the 0-1 test takes the input time series acceleration signal obtained from the VAWT and converts it to the translational variable $p(n)$ and $q(n)$. If the translational variable takes a value 0 it is understood that the vibration is periodic if the value is 1 it is chaotic. The most influencing factor for the vibrations were tip speed (ω) and pitch angle (θ). Hence an experimental vibrational study was carried by varying the tip speed and pitch angle. By applying 0-1 test, the results reveal the existence of periodic, quasi periodic and chaotic oscillations in the along wind and across wind directions. The tip speed variation was identified as an important factor responsible for the vibration in the along wind direction.

Keywords: VAWT; Tip speed(ω); Pitch angle(θ) and 0-1 test.

INTRODUCTION

The need for wind power production has been rapidly raised all over the world in the past decades. The practise of using vertical axis wind turbine is not only increasing in the urban areas but it is also predicted to provide power for small portable devices [1]. Hence it is important to study the structural stability and robustness of the VAWT. During the operation of VAWT, the changes in the flow field around the blade induces structural vibrations [2], [3]. Also, when the turbine rotates, the incident angle of the incoming wind changes continuously to induce dynamic stalling of blades. This phenomenon is responsible for inducing strong vibrations [4]. Therefore, it is a major concern to understand the nature of vibration prevailing in VAWT at different circumstances. Various studies were carried out to understand the uncertainties that were responsible for the vibrations in VAWT. One such computational study confronts the level of unpredictability in measuring the vibration response [5]. Hence, it is foremost to understand the parameters responsible for vibration. An experimental study states when the pitch angle was varied for a small VAWT, fluctuating aerodynamic load was generated which may lead to vibration in the VAWT structures [6]. The next important factor to be considered was the tip speed variation which significantly affects the dynamic behaviour of the VAWT [7], [8]. These literatures confirm the prominent factors inducing the vibrations were tip speed and pitch angle but there was no information available on how these factors affects dynamic response of VAWT. Generally, the vibrational behaviour of the wind turbine changes from periodic to chaotic when the rotor rotates at different rotational speed [9]. Since the wind turbine is subjected to different flow regimes and at different blade angles the non-linearities surrounding the turbine is still unknown. So, a research on the chaotic vibrational characteristics of the turbine is needed. Numerical studies were carried out using Lyapunov exponent to understand the non-linear dynamic response in horizontal axis wind turbine (HAWT) [10], [11]. But for better understanding the dynamic behaviour the classical chaos tool and the use of power spectra is of no use [12]. More over the experimental data contains noise signals which makes the power spectra tool not suitable [13]. The 0-1 test effectively overcomes the noisy data and also proficiently distinguish the periodic motion and chaotic motion [14], [15]. In this paper, a detailed experimental study was carried out by varying the tip speed and pitch angle in VAWT. The vibrational data obtained from this study was used in 0-1 test to identify the various dynamic states.

Experimental Setup

A small VAWT was designed for this study with a solidity ratio of 0.42. In this turbine for finding the responses at different

pitch angles a variable pitch arrangement setup was fabricated. By this the turbine pitch angle can be varied from 0° to 25° . The tip speed variation was found by placing the turbine in the axial wind blower which can produce wind speed up to 28 (m/s) and these wind speeds were calibrated prior to the experimentation. For understanding the dynamic response of VAWT a tri-axial accelerometer was attached to the shaft. The responses were taken in along wind direction and across wind direction. The sampling frequency of the accelerometer is 240Hz and the data were taken continuously for 300s. The blade tip speed was measured continuously by an optical sensor.



Fig. 1. Photograph of axial wind blower with wind turbine placed in the frontal part of the blower

Description of 0-1 test

The 0-1 test for chaos created by Gottwald and Melbourne recognizes the occasional and the clamorous conduct of the system dynamics. The 0-1 test takes any time series data as input and process the value to scalar for distinguishing the periodic and chaotic behaviour. The advantage for using 0-1 test is that no pre-processing work is required, and any noisy experimental data can be readily used [16]. In this study the given input signal (acceleration signal) $\varnothing(j)$ is translated to two variables $p(n)$ and $q(n)$ by applying 0-1 test where,

$$p(n) = \sum_{j=1}^n \varnothing(j) \cos(jc) \quad (1)$$

$$q(n) = \sum_{j=1}^n \varnothing(j) \sin(jc) \quad (2)$$

Here, c is taken as an arbitrary constant which is usually taken between $(0, 2\pi)$. 'n' corresponds to each acceleration data value ($n=1, 2, 3, \dots, N$). The translational variable in equation (1) and (2) was used to identify the different dynamics of the system. For a system to behave periodically the plot between the two translational variable appears to be bounded. For quasi periodic system the plot tends to be bounded distortedly. Finally, for a chaotic system the translational plot will be unbounded [17].

In 0-1 test to understand the development of the trajectory path, mean square displacement value was found with the help of the translational variable $D(n)$.

$$D(n) = \frac{1}{N} \sum_{j=1}^n ([p(j+n) - p(j)]^2 + [q(j+n) - q(j)]^2) \quad (3)$$

The mean square equation (3) was developed to modified mean square equation $M(n)$ for better solving the convergent factor problem.

$$M(n) = D(n) - V_{osc}(c, n) \quad (4)$$

$$\text{where, } V_{osc}(c, n) = \frac{1}{N} \sum_{j=1}^N \varnothing(j) \frac{(1 - \cos(jc))}{1 - \cos(c)} \quad (5)$$

The modified mean square value ($M(n)$ vs (n)) when plot against 'n' the modified mean displacement value almost takes a constant value while for chaotic signals the value linearly increases.

RESULTS AND DISCUSSIONS

The acceleration signal of the VAWT obtained from the experimental study was conducted for 8 blades with a turbine solidity ratio of 0.42. The base of the turbine was fixed at the frontal part of the axial blower as shown in the **Fig. 1**. The wind speed

can be varied by using a variable control motor. The time series acceleration signal was obtained for different pitch angle (θ) varying from 0° to 25° and varying tip speed ratio from 0.3(m/s) to 7(m/s). The pitch angle was varied for each 3° , for 0° to 25° . As stated earlier the time series signal were calibrated in along and across wind direction. Finally, the time series signal was taken as an input parameter for 0-1 test and were utilized to understand the various dynamics states of the VAWT system.

0-1 test plot in the across wind direction:

Fig. 2. show the different dynamic state of VAWT in the across wind directions where **Fig.2 (a)** represents the translational variable plot and Fig. 2(b) represents the modified mean square displacement. Similarly, **Fig. 2(i) (ii) and (iii)** show the 0-1 test plot for three different tip speed variation and pitch angle (θ) (0.45(m/s); $\theta=18^\circ$, 2.75(m/s); $\theta=12^\circ$ and 3.45(m/s); $\theta=9^\circ$). The translational variable plot clearly shows an unbounded plot. This confirms the system was in chaotic state even for low tip speed. This depicts that the acceleration along the across wind direction does not depend on either tip speed or the variation in pitch angle. The chaotic state of the system was further confirmed by the mean square displacement plot where the plot linearly increases. This result depicts that the across wind acceleration remains in chaotic state which is independent of tip speed and pitch angle.

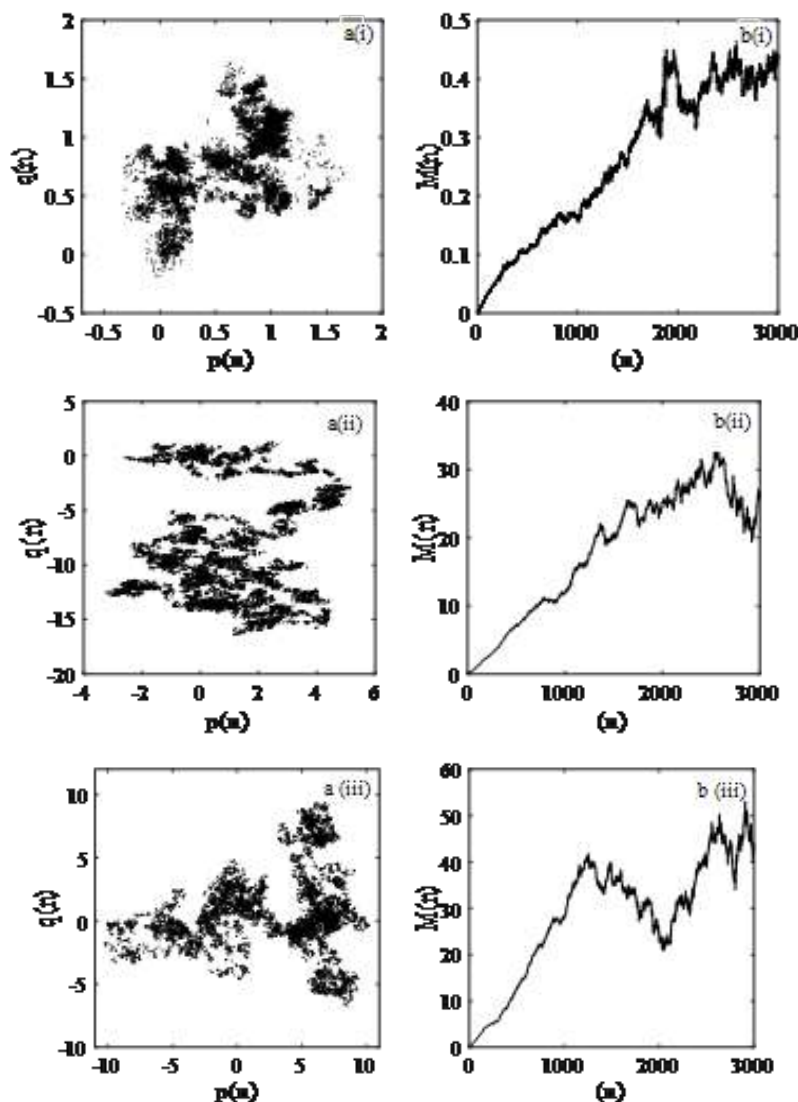


Fig. 2. 0-1 test results show the dynamic response of VAWT for X acceleration (Across wind direction) for three different turbine velocity (i)0.45(m/s) (ii)2.75(m/s) (iii)3.45 (m/s). (a) shows the translational variable plot. (b) shows the mean square displacement plot.

0-1 test plot in the along wind directions

Fig. 3 shows the different dynamical state of VAWT exists in the along wind direction. Similar to the across wind direction Fig. 3(c) represents the translational plot and 3(d) represents mean square displacement plot. For the translational plot in the Fig. 3(c)(i) the plot was well bounded which confirms the periodic oscillation ($0.45(\text{m/s})$; $\theta=18^\circ$). Further confirmation was made by Fig. 3(d)(i) which shows mean square displacement remains almost constant. For Fig. 3(ii) ($2.75(\text{m/s})$; $\theta=12^\circ$) the plot was not well bounded, and the mean square displacement plot tends to fluctuate which shows the system is in quasi periodic state. In Fig. 3(iii) it is clear that the system exhibits random translational path and further verification was done in mean square displacement plot where the plot linearly increases. This shows the chaotic oscillation takes place in VAWT along wind direction at $3.45(\text{m/s})$; $\theta=9^\circ$. Hence in the along wind direction the vibration slowly switches from periodic to chaotic which was completely influenced by the tip speed without the influence of the pitch angle.

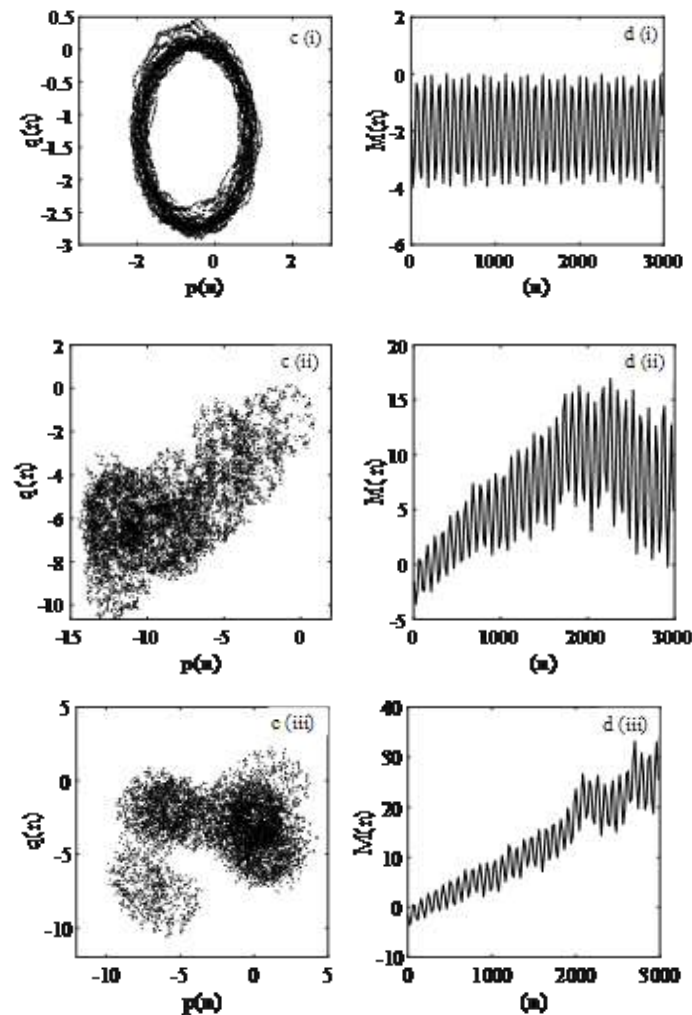


Fig. 3. 0-1 test results show the dynamic response of VAWT for Y acceleration (Along wind direction) for three turbine velocity (i) $0.45(\text{m/s})$ (ii) $2.75(\text{m/s})$ (iii) $3.45(\text{m/s})$. (a) shows the translational plot. (b) shows the Mean Square Displacement plot.

CONCLUSION

In this paper the effect of vibration in VAWT influenced by tip speed and pitch angle was analysed in detail by 0-1 test for chaos method. The vibrational signal was studied in the along wind and across wind directions for various pitch angle and tip speeds. 0-1 test identifies that in the across wind direction the VAWT exhibits chaotic oscillation even at very low tip speed, this strange phenomenon might occur because of the turbulence in the incoming wind speed and it was clear that the vibration was not



influenced by tip speed and pitch angle variation. In the along wind directions the VAWT exhibits different dynamic response like periodic, chaotic and quasi periodic oscillations. The dynamic response of VAWT changes from periodic to chaotic as the tip speed of the VAWT increases. Also, no influence of pitch angle was noted in the along wind direction. Hence when the tip speed of VAWT is greater than 3.45(m/s) the vibration behaviour of VAWT becomes chaotic independent of the pitch angle.

REFERENCES

1. Anindya Ghoshal, Mannur J. Sundaresan, *Mark J. Schulz, P FrankPai, "Structural health monitoring techniques for wind turbine blades." *Journal of Wind Engineering and Industrial Aerodynamics*. 85 (2000) 309-324.
2. Dimitrov, N., Natarajan, A., and Kelly, "M.Model of wind shear conditional on turbulence and its impact on wind turbine loads" *Wind Energy*, vol.18 1917-1931 (2015).
3. C. V. Woude, S. Narasimhan, "A study on vibration isolation for wind turbine structures", *Engineering Structures*, vol. 60, pp. 223–234, (2014).
4. Ferreira C.J.S., Kuik van G.A.M., Bussel van G.J.W and Scarano, "Visualization by PIV of dynamic stall on a vertical axis wind turbine." *Experiments in Fluids*, Vol no.46, 97–108. (2009).
5. Sha Wei, Jingshan Zhao, Qinkai Han, *Fulei Chu. "Dynamic response analysis on torsional vibrations of wind turbine geared transmission system with uncertainty." *Renewable Energy*, vol. 78 60-67, (2015).
6. Francesco Castellani, Davide Astolfi, Mauro Peppoloni, Francesco Natili, Daniele Buttà and Alexander Hirschl. "Experimental Vibration Analysis of a Small-Scale Vertical Wind Energy System for Residential Use." *Machines* (2019).
7. ImenBel Mabrouk, AbdelkhalakElHami, LassâadWalha, BacemZghal and Mohamed Haddar. "Dynamic vibrations in wind energy systems: Application to vertical axis wind turbine." *Mechanical Systems and Signal Processing*, vol 85, 396–414, (2017).
8. Yi-Xin Peng, You-Lin Xu, Sheng Zhan, Kei-Man Shum, "High-solidity straight-bladed vertical axis wind turbine: Aerodynamic force measurements." *Journal of Wind Engineering & Industrial Aerodynamics*, vol no.184, 34–48, (2019).
9. Anup KC, *Jonathan Whale, Samuel P. Evans, Philip D. Clausen. "An investigation of the impact of wind speed and turbulence on small wind turbine operation and fatigue loads". *Renewable Energy*, vol no. 146, 87-98. (2020).
10. Z.L.Zhang, M.T.Sichani, J.Li, J.B.Chen and S.R.K.Nielsen. "Non-Linear Aeroelastic Stability of Wind Turbines." *Engineering Materials*, vol no. 569-570 531-538, (2013).
11. Liming Dai, Dandan Xia, Changping Chen, "Regular and nonlinear dynamics of horizontal axis wind turbine blades subjected to fluctuating wind loads." *Energy Procedia*, vol no. 110, 529 – 536, (2017).
12. B. R. Noack and F. Obermeier, "A chaos-theoretical investigation of the wake behind a cylinder." *Z. Angew. Math. Mech.* 71, 428 (1991).
13. Feudel U., Kuznetsov S. and Pikovsky A., "Strange Nonchaotic Attractors: Dynamics Between Order and Chaos in Quasiperiodically Forced Systems," (World Scientific, Singapore) (2006).
14. R. Gopal, A. Venkatesan, and M. Lakshmanan, "Applicability of 0-1 test for strange nonchaotic attractors," *Chaos*, vol no. 23, 023123-1–023123-15, (2013).
15. S. Arunvinthan, R. Gopal, V. K. Chandrasekar, and S. Nadaraja Pillai. "Estimation of nonlinear surface pressure characteristics of aerofoil: A 0-1 test approach." *AIP Advances*, vol no.9, 055203, (2019).
16. Georg A. Gottwald and Ian Melbourne. "A New Test for Chaos in Deterministic Systems." *Proceedings: Mathematical, Physical and Engineering Sciences* 460 (2004) 603-61.
17. George A. Gottwald and *Ian Melbourne. "On the Implementation of the 0–1 Test for Chaos." *Journal on Applied Dynamical Systems* 8 (2009) 129-145.

Development of Prototype of Thermal Air Sterilizer to Combat COVID-19

Sunil Kumar Thamida^{1*}, Srikumar V R², Mohith K S¹, Amarendra Kumar Gupta¹, Vasudharani Devanatahan³
Harshini Chakravarthy³

Department of Chemical Engineering, IIT Tirupati, Andhra Pradesh¹

Opustayz Hospitality Solutions Pvt. Ltd, Thiruvananthapuram, Kerala²

Department of Biology, IISER Tirupati, Andhra Pradesh³

✉ sunil76@iittp.ac.in

ABSTRACT

This article presents an innovative technological idea related to air sterilization. In the present COVID era, it requires technology to combat the covid-19 causing corona virus present in the vicinity of positive patients. One of the means of eradicating covid-19 is to sterilize the air or decimating the corona virus in air by dry heating method. Literature has shown that this nanometer sized virus can be deactivated by heat ranging from 55 °C or above for a short duration of few seconds. General air heaters have one-pass flow pattern. In this article, the option of recycling of hot air through air blower is explored and presented as BLAAST: Blower Aided Air Sterilization by Temperature. Validation of the prototype by microbial analysis has also been included which suggests that the present technology is suitable for deployment as a Covid-19 combating device. Hence a self-reliance and make in India goals are achieved owing to a collaboration between a Start-up company and an Institute.

Keywords: Air sterilization; Recycle; Heating; Air blower; Temperature dynamics.

INTRODUCTION

COVID-19 is a new pandemic and contagious illness caused due to corona virus. This illness can even cause death in matter of 14 days if not treated properly. As there is no known or proven drug or vaccine yet. COVID-19 started being identified first in Wuhan city of China during December 2019. It started spreading to other countries. The perception is that it can spread through a chain reaction. The US Center for Disease Control and Prevention (CDC) has acknowledged on its website that COVID-19 can be spread by airborne transmission. And coronavirus droplets can remain in the air for hours.

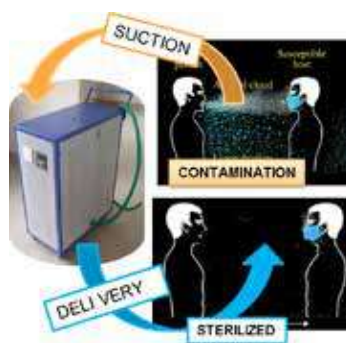


Fig. 1. Schematic representation of how an air sterilization unit will reduce contamination and infection.

Some infections can be spread by exposure to virus in small droplets and particles that can linger in the air for minutes to hours. These viruses may be able to infect people who are further than 6 feet away from the person who is infected or after that person has left the space., the CDC website says. Hence WHO and CDC recommends social distancing, usage of PPE besides hand hygiene methods to prevent the spread of infection. Hence social distancing and masks were suggested as PPE. Despite significant populace of the world adhered to these recommendations, the world has been seeing explosive growth in people testing positive and more than a million have already succumbed to Covid19. Hence an engineering intervention



based on science is imperative to counter the multi-dimensional destruction being caused now and for the future with people still struggling to adjust in the new normal which is yet to see resumption of air travel, cruises, events and save people from the killer virus. BLAAST a scientific intervention for sustained human and economic activity during covid era without any need for disinfection, isolation and quarantine, is based on air flow dynamics principles to capture the airborne contamination instantly and deactivate the coronavirus continuously based on thermal death point of all microbes using thermal energy. It is schematically shown in **Fig. 1**. But we can also look at de-activating corona virus present in air.

In this project dry heat sterilization is taken up and a prototype is developed. Air heating can be achieved through the following methods: a) Convection air heating: Convection air heating utilize gas burners for heating air by recirculating it internally. In gas-fired equipment, gas is filled into the burner and heat from the burner is distributed homogeneously by using a fan throughout the unit. Convection air heating is the most common method for air heating since the heat produced can be easily controlled. b) Infrared heating: Infrared heating utilize radiation energy emerging from light emitter panels of various wavelengths based on intensity of heating. Sheathed elements or quartz can be used to make infrared panels. c) Induction heating: electromagnetism is used in induction heating to heat a conductive component. It is accomplished by passing an electric current via an induction coil which produces an electromagnetic field. In that field, when iron or steel components are placed, resistance in the flow of electricity is introduced. Consequently, creation of energy and heat takes place in the process. d) Resistance power heating: Resistance heating is somewhat opposite of induction heating where, first, the conductive steel is heated. Here, most often the copper winding is directly heated, which then conduct the heat to the air, which is in contact with it. The equipment, which are normally used in our daily life to heat the air using above described methods are hot-air- oven, heat pump, gas-fired space heaters, electric space heaters, pallet stoves etc.

The corona virus is a nano scale particle with strong cell wall. When someone is affected with COVID-19 sneezes or coughs, the corona particles get dispersed in the air forming an aerosol. Based on terminal settling velocity, the corona particles take 5 hours to descend to the ground. In addition, because of wind blowing approximately at 20 kmph will carry the corona virus to a distance of 100 km before it touches the ground. By this time COVID-19 would have spread to a neighboring town or village. Hence it is very important to capture corona virus at the source of infected patients.

Based on all the previous factors it can be concluded that COVID-19 is air borne pandemic in addition to person-person direct contact. Therefore, it is necessary to develop methods to de-activate the corona virus surrounding the infected patient. In the perspective of COVID-19 it is found that there are no specific antibiotics or vaccines. Hence until the vaccines are produced and tested alternate means of sterilizing air can be considered as a challenging task. Not only during the COVID-19 but also during post COVID-19 there may be alternate more resistant strains of corona virus. Therefore, sterilization or de-activation of virus is important. Out of few means of sterilizing air, dry heat method is one of them. There are few literature articles indicating the temperature of the medium versus time of de-activation of SARS [1-5]. This trend has shown that for a temperature 55°C-60°C it requires very less time of the order of seconds for de-activation of the virus.

Technologies for Air Sterilization

There are a number of technologies emerging to sterilize air. For purification of HEPA filter (high efficiency particulate air filter) are widely used in the wall mounted devices. It is not a sterilizing process but only a filtration process where the particles less than 0.2µm are only allowed to pass through the HEPA filter. Therefore, the virus are not de-activated by HEPA filter. Another widely used means of sterilization is ultra- violet light. There are many commercial air sterilizers based on this technology. It also has some disadvantages from the safety point of view.

Objectives of Present Study

Compactness of the prototype:

Thermal sterilization of air requires that the flowing air to be heated for sufficient duration gives a very long pipe from the design of heat exchanger. Hence alternate design or process has to be innovated for compactness.

Suitability of recycle flow for adjusting the deactivation/retention time

As a novel idea it is proposed to have a suction blower, heater and recycle pipe in sequence and in a cyclic path. This recycle hypothesis has to be tested by building a prototype.

To examine the efficacy of the prototype as an air sterilizer

Once the prototype is built it will have an inlet and outlet for air. Before commercializing it is important to test whether the

machine is sterilizing the air. For this the air sample at exit at 55°C should be tested for microbial deactivation. If it is zero or negligible in exit air compared to ambient air then the proposed sterilizer will be very efficient.

PROPOSED PROCESS

The proposed processes are represented in a sequence as shown in **Fig. 2**. The suction requires a suction blower. Heating requires a surface heating mantle the retention and recycle sufficient volume in the pipe network. In addition to these processes there will be instruments like valves and sensors like temperature controller and flow rate measurements these sensors and instruments will help us in optimizing the operating conditions.

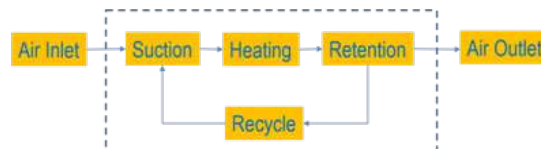


Fig. 2. Schematic of the proposed process for producing sterile air by heating method

EXPERIMENTAL DATA

The various parts of the actual prototype are indicated in **Fig. 3**. The entire prototype is mounted on a trolley with wheels for portability. The electronic gadgets and electrical switches are arranged in a wooden box for safety. The pipe lines and the heater can be insulated further to have complete safety as well as savings of energy.



Fig. 3. Prototype of the air sterilizer developed

The temperature of the exit air is monitored and plotted in **Fig. 4**. The heater was a clamp type band heater of 1000 Watts. When both blower and heater were ON, it was found that the exit air reaches the desired temperature of 55°C in a short time as compared to only blower option as can be seen from **Fig. 4**. The flow rate was about 60 LPM. With only blower ON, the air gets heated due to viscous heating or friction inside the blower. So, for the first 15 minutes the air at exit is not sterile but after 15 minutes, the exit air is sterile.

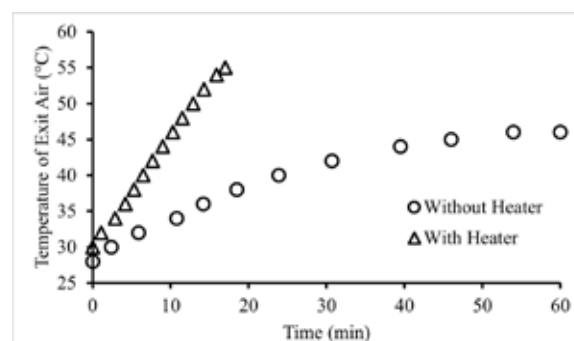


Fig. 4. Startup dynamics of temperature of exit air from BLAAST with and without Heater.



MICROBIAL VALIDATION

Agar Gel Coated Petri Dish

When an agar gel plate with suitable nutrients is exposed to contaminated air for 1 minute then incubated at 36°C gives rise to growth of microbial colonies. For sterile air there will not be any microbial colonies after 24hrs.

Solution in a conical flask containing microbe nutrients

The same procedure as above is followed with growth medium as liquid. At the end of 24 hours the optical density (OD600 with UV spectrophotometer) of the reagent liquid will indicate the microbial level.

It was found from above two tests that the exit air from BLAAST is sterile for set temperature of 55 °C or above.

DISCUSSION

Not needing of heater till 50 °C:

It was found that when the blower is switched ON without heater, the temperature gradually increased to approximately 45 – 50 °C over a time period of 60 minutes. Hence heater can be switched ON if temperature of above 50°C is required.

Effect of elbow joints on reduction of flowrate

Usually every 90° bend has a pressure drop of 45 times of the diameter in length in the prototype there are 4 bends totally. In general, if we reduce the number of sharp bends then it will result in higher flowrate, due to reduction in pressure drop.

Off shoot and error in the temperature controller

When a set point is initiated to 55 °C it was found that the temperature gradually goes to 56°C, the relay gets OFF and temperature comes down to 54 °C, again the relay gets ON making the temperature increase to 56 °C. So on an average 55±1 °C is maintained at the exit air.

Maximum time the prototype was run

The prototype was run for a long duration. No problem was found in operating the prototype.

The prototype is aptly named as BLAAST standing for Blower Aided Air Sterilization by Temperature.

FURTHER RECOMMENDATIONS

GI pipes can be replaced with aluminum pipes for reduction of weight: To reduce the weight of the machine, pipes and fittings made of aluminum can be used to replace the GI pipes.

A retention chamber for air can be incorporated: To increase the retention time for air at 55 °C, a chamber can be designed and included.

Heat recovery: A heat recovery system consisting of a double pipe heat exchanger with exit air (55 °C) can be contacted with incoming air (30 °C – 35 °C) which will reduce the exit air temperature suitable for recirculating back to the room.

Suggestions for increase in operating temperature by changing the air blower: Right now BLAAST is able to sterilize air with set point of 55 °C. In order to achieve higher temperature (100 °C) a blower with belt driven motor has to be adopted for avoiding damage to the motor.

Changing sharp bends to smooth bends for reducing the pressure drop: As discussed before, sharp bends are having high pressure drop, so to reduce the pressure drop smooth bends can be used to replace sharp bends.

COVID ERA AND POST COVID ERA APPLICATIONS

BLAAST is a unique solution as it is Safe, Versatile, Mobile, Scalable in its diverse applications like in hospitals, office spaces, factories, shopping centers, travel aggregation points like airports, hotels, restaurants, schools etc during covid and post covid era. BLAAST is capable of deactivating all airborne pathogens which makes it an all time solution to provide sterilized air in all human settings be it industrial, residential or medical environments. It can be used for a single person through targeted suction and delivery as in Medical Ventilators as well as for multiple persons in a room or large hall. AI, IoT, Remote control technologies further makes its usage convenient in residential homes which can save people from any airborne infection, solve



cross contamination problems in hospitals, integrated in HVAC systems in buildings to provide sterilized air continuously. By lowering the post sterilization temperature of air further it can become a potent replacement for Air conditioners and can be also used as Air heaters in cold weather conditions.

The present prototype BLAAST is a device that helps our Nation to achieve Self-reliance in the area of clean environment and sustainable health of the people.

ACKNOWLEDGMENT

This development project was continuously supported with ideas and motivation by Prof. K.N. Satyanarayana, Director, IIT Tirupati. This project was supported financially by Opustayz Hospitality Solutions Pvt Ltd., Bangalore & Thiruvananthapuram.

REFERENCES

1. H. Laude. "Thermal inactivation studies of a coronavirus, transmissible gastroenteritis virus." *Journal of General Virology* 56, no. 2, 235-240, 1981.
2. H. Kariwa, N. Fujii and I. Takashima, "Inactivation of SARS coronavirus by means of povidone-iodine, physical conditions, and chemical reagents," *Japanese Journal of Veterinary Research*, 52(3), 105-112, 2004.
3. L. M. Casanova, S. Jeon, W. A. Rutala, D. J. Weber and M. D. Sobsey, "Effects of air temperature and relative humidity on coronavirus survival on surfaces," *Appl. Environ. Microbiol.*, 76(9), 2712-2717, 2010.
4. K. H. Chan, J. S. Peiris, S. Y. Lam, L. L. M. Poon, K. Y. Yuen and W. H. Seto, "The effects of temperature and relative humidity on the viability of the SARS coronavirus," *Advances in virology*, 2011.
5. A. F. Henwood, Coronavirus disinfection in histopathology. *Journal of Histotechnology*, 43, no. 2, 102-104, 2020.



Design of a Centrifugal Impeller for Lean Supercharging of Motorcycle Engines

Harishankar S, Aswin A Asokan, Madhav Murali, Rejath R S, Rajesh T N

Department of Mechanical Engineering, MAR BASELIOS College of Engineering and Technology, Mar Ivanios Vidyanagar Thiruvananthapuram, Kerala

✉ harishankarsundaesan35@gmail.com

ABSTRACT

Increasing level of environmental pollution and power requirements are a great source of concern around the world. Lean supercharging is a feasible solution to increase the efficiency and to decrease the NO_x emission. This paper discusses the scope for developing an electrical centrifugal supercharger system which can replace the air filter unit of the commuter segment motorcycles for small capacity spark ignition engines. The design and analysis of the impeller of a centrifugal compressor that can be used in lean supercharging of a motorcycle engine is presented. The impeller of the centrifugal compressor consists of 7 sets of vanes with splitter. The blade profile is generated according to the required parameters and geometric constraints, using Ansys Blade GEN. The impeller is designed for a pressure ratio of 1.8 and mass flow rate of 0.015g/s of air. The vanes are backward curved at 45-degree back sweep angle. Analysis is done on the generated blade profile using Ansys CFX to study the performance of the impeller of the centrifugal compressor. The results obtained validates that a forced induction system, using a centrifugal compressor can be designed within the space limitations of a motorcycle.

Keywords: Centrifugal-compressor; supercharging; BSFC; forced induction; Ansys CFX.

INTRODUCTION

India market has always remained a fertile ground for two-wheelers. Ever-increasing acceptance for different varieties of motorcycles has attracted different global motorcycles manufacturers towards the Indian market. The automobile industry, particularly the two-wheeler segment, which is a huge beneficiary of the growth in rural consumption, is therefore poised to further consolidate India's position as the second-largest two-wheeler market in the world. As middle-income families constitute a significant portion of India's household, correspondingly small capacity commuter motorcycles constitute a major portion of India's two-wheeler market. The increase in the number of fossil fuel-powered vehicles also translates to high levels of pollution. India's air quality index(AQI) rating has always been worsening over the years, and India's metro cities are among the noisiest towns around the world. Considering these issues of global environmental threats and power crisis, India has joined the world nations in the initiative of promoting electric vehicles. The government of India has fixed a target of taking electric vehicles (EV) production up to 30 per cent of new cars and two-wheelers by 2030, from the current stand of less than 1 per cent. The scale and timing of adoption of electric motorcycles would depend on multiple factors such as nationwide public infrastructure for easy and convenient charging, mass consumer acceptance of products and cost implications. Understanding the future trends, various two-wheeler manufacturers have come up with various designs of their future electric models. But the full shift towards electric two-wheelers will have to overcome various issues like development of high energy density batteries, implementation of charging infrastructure etc. So to bridge the gap between gasoline-powered motorcycles and electric ones, battery powered electric supercharging in motorcycle engines is proposed.

The effect of air intake pressure on the fuel economy, exhaust emission is analyses by Abdullah et al. [1]. Leaner air fuel mixture extracts more energy from the combustion process. As a result, the engine performance and fuel economy are increased while the unburnt exhaust emissions components are reduced (CO₂ and NO_x emissions). Ensuring clean and good condition of air filter will maintain higher air intake pressure and absorption of polluted particles through air filter. It also helps in reducing exhaust temperature. The performance of two wheeler engines on supercharging is experimentally studied by Singh et al. [2]. The power is increased on an average about 152% more than the original engine by using a supercharger. The torque of the modified engine is highest at 7000 rpm and after that it decreases due to the fast opening and closing of valves of the engine.



The mean effective pressure of the supercharged engine is much higher. Air consumption in case of supercharged is more which increases the power of the engine.

Saini et al. [3] discussed the effect of turbocharger on the efficiency and power of the engine. It has better fuel economy and also the emissions of the engine can be controlled. Schmidt et al. [4] proposed that lean supercharging improves fuel efficiency and reduce NO_x emissions. The addition of a turbocharger system to a carbureted, naturally aspirated engine is studied by Watson et al. It was corroborated that as the fuel efficiency can be improved in a given engine by decreasing the engine capacity and by providing a turbocharger or supercharger to meet the additional power requirements. The draw through arrangement was found to be better compared to the blow through type compressor configuration [5].

Attard et al. [6] carried out performance analysis of a downsized Formula SAE engine running in a variety of Naturally Aspirated (NA) and forced induction modes. The BMEP was highest and constant power could also be achieved over half the speed range while running in the highly turbocharged mode. Various challenges faced while using a lean mixture in the development of a four-valve lean-burn engine was studied by Horie et al. [7]. It was observed that NO_x emission could be reduced to a sufficient level by improving the combustion to expand the lean limit and by developing a highly accurate air-fuel ratio control system.

The cooling of engine air at any point in the intake passageways by means of a remote thermoelectric temperature control unit is discussed by Ham [8]. The coolant circuit having a first portion contacting the thermoelectric device and second portion disposed to the engine air path. When the engine demands an increased supply of air then a reservoir of cooled liquid/gas is available to meet the demand.

Canli et al. applied pressure drops, air density and engine revolution as input parameters to calculate the variation of engine power output on introduction of an intercooler to a turbocharged engine [9]. It is found that the engine power output can be increased 154% by ideal intercooler while single turbocharger without intercooler can only increase 65%. Intercooler was observed to be helpful in decreasing the excess temperature of charge generated during turbocharging and helps reduce knocking. Came and Robinson [10] illustrates the main stages of centrifugal compressor design including the preliminary design stage. CFD analyses and validation of different impeller parameters are discussed. Jang et al. [11] carried out design and analysis of high speed brushless DC motors for centrifugal compressor. They are found to be superior in performance as they provide high efficiency and ensures fast and easy control of impeller speed.

SCOPE AND OBJECTIVE

Lean supercharging is expected to improve the combustion process by increasing the volumetric efficiency and ensuring complete combustion of available fuel. There is a scope for developing a plug and play type system that will occupy the space taken by the air filter unit of the commuter segment motorcycles.

Given the potential of lean supercharging in improving the efficiency of gasoline engines as well as easy control over the boost pressure using electric motor speed control and ease of installation, this paper studies the feasibility of designing a centrifugal compressor that can be employed for lean supercharging in motorcycle engines to improve fuel economy, while maintaining adequate power outputs.

METHODOLOGY

The complete study of this system is done in two phases, the first phase which is being discussed in this paper deals with the development and analysis of a centrifugal compressor capable of producing the required pressure and mass flow rate and the second phase involves testing of the system on a single-cylinder engine on an engine test bench.

Experimental Layout

The full model of the plug and play system uses a centrifugal compressor powered by an electric motor to supply pressurized air-fuel mixture into the combustion chamber. The system will draw air through a conical air filter, and this air is passed through the stock carburetor to produce the air fuel mixture. This air fuel mixture is then sent to the centrifugal compressor. A stepper motor is attached to the carburetor to vary the air-fuel ratio dynamically. The compressed charge is then passed on to a chamber where it is cooled. The cooling is accomplished by a pair of Peltier modules (TEC1-12715) whose cold side is attached to a heatsink, and the hot side is cooled by water cooling. Various sensors are utilized to improve the performance of the centrifugal compressor and the stepper motor to produce the optimal boost pressure and air-fuel ratio for maximum efficiency. The motors are controlled by a microcontroller which analyses the signal from various sensors in the system such as Manifold

Air Pressure(MAP)sensor, Temperature sensor, Throttle position sensor and the Oxygen sensor. The system is powered a 12V Lipo battery which can be easily coupled to the existing electrical system of the motorcycle. The **Fig. 1** represents the flow chart of the plug and play system.

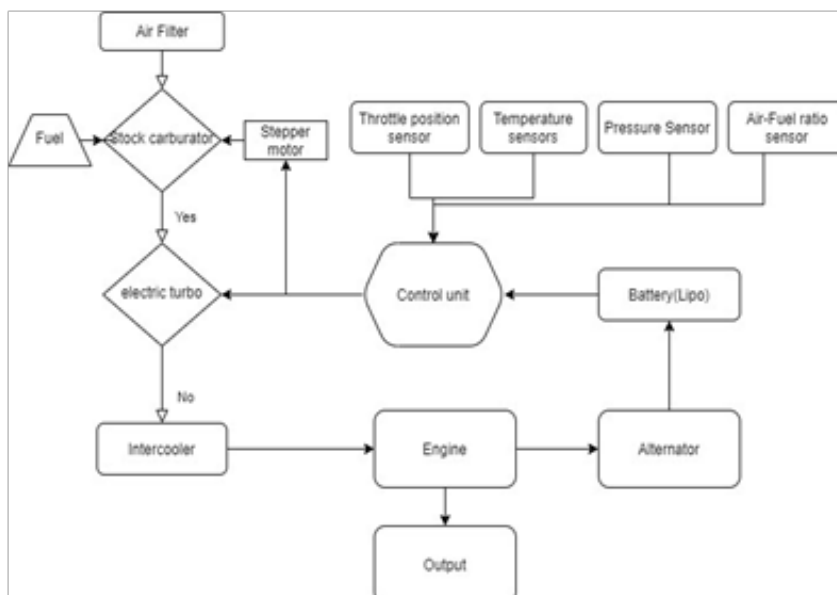


Fig. 1. flow chart of the plug and play system.

Numerical Simulation

The flow analysis through a centrifugal compressor is carried out in Ansys. The actual system was subdivided into components, which were modelled and assembled to produce the final model. The design of the centrifugal compressor is carried out using Autodesk fusion 360 software. Subdividing of the model was done so that each part can be manufactured by 3D printing.

The preliminary design of the centrifugal compressor impeller is done using Ansys Vista CCD. **Table 1** shows the input parameters supplied to the system and the results generated.

Table 1. Input for design of the centrifugal impeller

Sl. No.	Parameter	Value
1	Overall Pressure Ratio	1.8
2	Mass Flow	0.015kg/s
3	Rotational Speed	40000 rpm
4	Hub Diameter	10mm
5	Vane normal thickness	1.8mm
6	Diffuser type	Vane less
7	Axial length ratio	0.3
8	No, of main vanes	7
9	No. Of inter vanes	7
10	Back sweep angle	45
11	Rake angle	30

Blade modelling is then done using Blade Gen, and the generated blade profile can be optimized to suit the manufacturing techniques and geometrical constraints. After the blade profile is confirmed, Turbo grid is used to mesh the generated blade profile using Hybrid grid. The generated mesh has 445325 nodes and 41324 elements. **Fig. 2** shows the grid arrangement of a pair of impeller blade with splitter.



Fig 2. Mesh generated

The mesh is then exported to Ansys CFX for solving. In Ansys CFX, ‘turbo mode’ is selected, and machine type is chosen as centrifugal compressor. The axis of rotation of the impeller is defined as the z-axis at 40000 rpm. Input and output domains are pre-defined in the Turbo grid. Then the Inflow/outflow boundary templates are selected, and the solver parameters are specified. Air is selected as the fluid and steady state analysis is conducted. The boundary condition for the solver is given in **Table 2**.

Table 2. Boundary conditions for the CFX solver

Sl. No	Parameter	Condition
1	Inflow pressure	101.325kpa
2	Flow directions	Normal to boundary
3	Inflow temperature	298K
4	Outflow static pressure	150kpa
5	Wall Boundary	No slip condition

The inputs are provided and sufficient iterations are given to ensure that the solution is converged and the residue drops down to 1.E-6. The simulations are carried out for different impeller designs with varying blade profile and axial length ratios. The blade profile with the best results was selected as the optimal blade design

RESULTS AND DISCUSSIONS

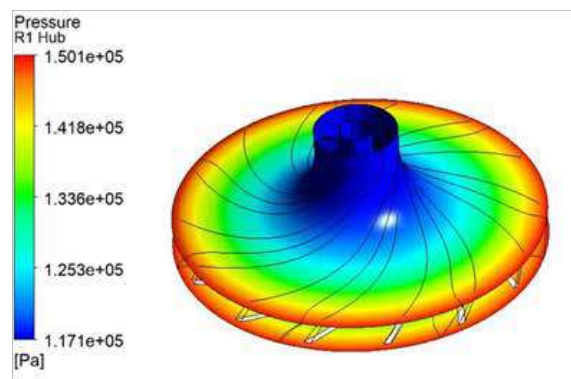


Fig 3: Pressure variation across the impeller

Fig. 3 shows the variation of pressure across the impeller. The pressure is found to increase steadily from the inlet to the exit of the centrifugal impeller. The maximum value of pressure at the exit obtained is in the range of 150kPa. The impeller is designed with increasing area in between the blades. A strong centrifugal force is imparted to the fluid as the impeller is rotating

at 40000rpm. As the fluid moves to the exit, the area gradually increase which results in the increase of pressure. Air at 101.325 kPa and 298K is drawn into the center of a rotating impeller with radial blades and is pushed toward the center by centrifugal force. This radial movement of air results in a pressure rise and the generation of kinetic energy. There is no sudden variation in pressure or any circulations developed inside the impeller and provides continuous air flow.

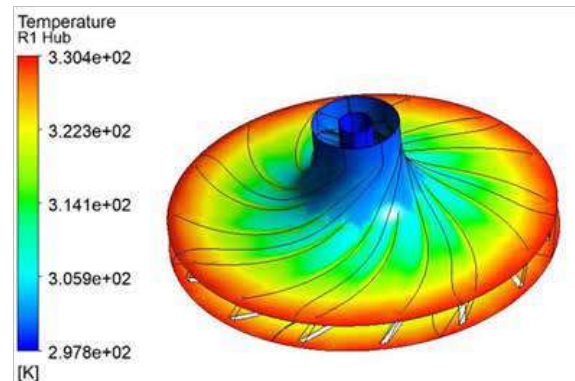


Fig. 4. Temperature variation across the impeller

Fig. 4 shows the temperature variation across the impeller of a centrifugal compressor. The temperature is found to increase steadily from the inlet to the exit of the centrifugal impeller. The maximum value of temperature at the exit obtained is in the range of 330K. The increase in the pressure of air has resulted in the subsequent rise in temperature also. This increase in the temperature of air at the inlet of engine can be lowered by using Peltier modules.

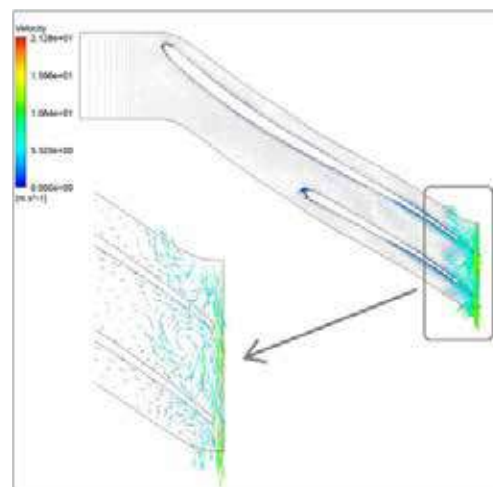


Fig. 5. Velocity vectors in a blade to blade view

Fig. 5 shows the flow velocity vectors across an impeller blade. This gives relative velocity of the fluid with respect to the rotating frame of reference. The maximum value is found to be 21.28m/s at the blade tip. It can be noted that there is some circulation developed towards the tip of the impeller blade and the splitter. This will result in reduction in energy of the compressed air and these can be reduced by fine tuning of the blades.

CONCLUSION

The design and analysis of the impeller of a centrifugal compressor that can be used in lean supercharging of a motorcycle engine is conducted. A 3D model of the impeller is developed using Ansys Vista CCD and analyzed using Ansys CFX software. The blade profile is generated according to the required parameters and geometric constraints, using Ansys Blade GEN. The impeller of the centrifugal compressor consists of 7 sets of vanes with splitter. The overall hub diameter is 100mm. The backward curved vane impeller is designed for a pressure ratio of 1.8 and mass flow rate of 0.015g/s of air. Analysis is done on the generated blade profile using Ansys CFX to study the performance of the impeller of the centrifugal compressor. At



40000rpm, the centrifugal compressor could deliver room atmospheric air compressed at 150kPa and 330K. The results obtained corroborates that a forced induction system, using a centrifugal compressor can be designed within the space limitations of a motorcycle.

REFERENCES

1. N.R.Abdullah,et al, "Effects of air intake pressure to the fuel economy and exhaust emissions on a small SI engine,"Procedia Engineering68(2013), pp.278 – 284, 2013.
2. Y. Singh, N. Singh, R. Prasad and H. Nayak, "Performance analysis of supercharging of two wheelers," IJMET ISSN, Vol-2, Issue-2, pp.63-69, 2011.
3. A.Saini, P.Shakti, H. Kulshrestha, "Turbocharged single cylinder SI engine,"IJATER IOCRSEM, pp.110-116, October 2014.
4. K.R. Schmid, "A single cylinder engine of lean supercharged operation for spark ignition engines," Scholar mine Master Theses,1982.
5. H.C. Watson, E.E.Mikins and K.Roberts and W.Bryce, "Turbo charging for fuel efficiency,"SAE Tec.Pap , pp.19-29,1983.
6. W.Attard, H.C.Watson, S.Kondaris and M.A.Khan, "Comparing the performance and limitations of a downsized Formula SAE engine in normally aspirated, supercharged and Turbocharged modes,"SAE JSAE ,2006.
7. K.Horie, K.Nishizawa, T.Ogawa, S.Akazaki, and K.Miura, "The development of a high fuel economy and high performance four-valve lean burn engine,"SAE Tec.Pap,1992.
8. D.C.Ham,"Thermoelectric vehicle engine air cooler," US Patent Application Publication Ham, April 2009.
9. E.Canli , S.Darici , M.Ozgoren,2010, "Intercooler effect on conventional super charging systems," International scientific conference 19 – 20 November 2010, GABROVO.
10. P M Came and C J Robinson, "Centrifugal compressor design," Proceedings of the institution of Mechanical Engineers, Part C: J. Mech. Eng. Sci., 1998.
11. Seok-M.Jang, Han-Wook Cho and Sang-Kyu Choi, "Design and analysis of a high-speed brushless DC motor for centrifugal compressor,"IEEE Trans. Magn, Vol 43, No.2, PP.2573-2575, June 2007.

Effect of Varying Surface Thickness on Wetting Delay and Rewetting Velocity through CFD Analysis

Monika Siyal, Chitranjan Agrawal, B L Salvi, S Jindal

Department of Mechanical Engineering, College of Technology and Engineering, Maharana Pratap University of Agriculture and Technology, Udaipur, Rajasthan

✉ monikasiyal2696@gmail.com; ✉ chitranjanagr@gmail.com

ABSTRACT

In this research paper CFD analysis is carried out on two hot horizontal surface. Two horizontal hot square plates of 0.25mm thickness and 3mm thickness at 450°C initial temperature has been quenched by round water jet of 3mm diameter. The water jet of 3mm diameter impinges perpendicular to the test section of steel. The investigations are made up to 20mm downstream location in upper sides of the stagnation point. It has been observed that during transient cooling, the wetting front velocity decreases with the rise in thickness of the plate and wetting delay increases with the rise in thickness of the plate. However rewetting velocity reduces drastically for the extreme downstream locations away from the stagnation point. and wetting delay increases drastically with the increase in thickness of the plate.

Keywords: Jet impingement; Stagnation; Rewetting; Wetting delay; CFD, Thickness.

INTRODUCTION

Water jet impingement surface cooling is being used for surface quenching in several industries due to its capability of high heat transfer rate. There are various industrial applications that require rapid surface quenching e.g., metal, nuclear, electronics. In metal industries the quick quenching is needed for controlling the surface properties, in nuclear reactor rapid cooling is part of emergency core cooling system (ECCS). During the loss of coolant accident condition the clusters of clad tubes consisting of fuel rods become over heated even after the closure of reactor. In nuclear reactor, ECCS is given to cool the overheated clad tubes to avoid the accidents. In electronics industries this technique is used for increase the life of electronic components. This technique is also utilized in various minor industrial applications e.g., cooling of different sections of the engine, cooling of turbine blades, drying of films, etc.

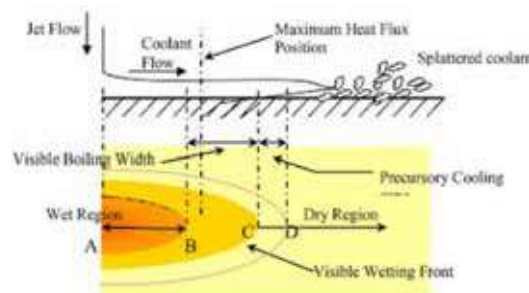


Fig. 1. Rewetting process [13]

The performance of surface quenching under transient condition is assessed on the basis of rewetting velocity or wetting front progression over the hot surface. The rewetting velocity is the measure of rapidity of surface quenching or how quickly hot surface attains the rewetting stage. The rewetting is considered as the point of sharp drop in surface temperature during transient cooling of a hot surface. In fact the sharp drop in surface temperature is the beginning of wetting front movement on the hot surface and the speed of wetting front progressing over the hot surface is known as rewetting velocity. The rewetting velocity is evaluated by determining the time taken for rewetting to occur between two marked locations on the hot surface.

In the industrial applications without performing or installing a real system of jet impingement cooling, simulation can forecast

which changes in the parameter are most vital for improving transient cooling of hot surfaces. CFD will foresee the performance of jet impingement cooling before adapting and execution in system. CFD modelling will give precise and detailed information about optimization of parameters used for jet impingement cooling. CFD modelling will save cost and turnaround time for execution in system. It will procure the reliable results also. The places which are hazardous for the humans, this technique will foresee the performance.

Objectives

1. Develop a computational fluid dynamics model for jet impingement hot surface cooling process using ANSYS software.
2. To investigate the effect of various thickness on hot surface quenching using the developed model.

MATERIALS AND METHODS

The Jet impinges on the hot horizontal surface. The diameter of jet is 3mm. The distance from the jet exit to target spacing is fixed and it is 12mm. The plate material is steel. The plate size is 50mm*50mm. In this CFD analysis jet velocity has been used- 3m/s. The coolant fluid is water. Water temperature is 24°C. the temperature of hot plate is 450°C. Thickness of the plate- 0.25mm and 3mm is considered.

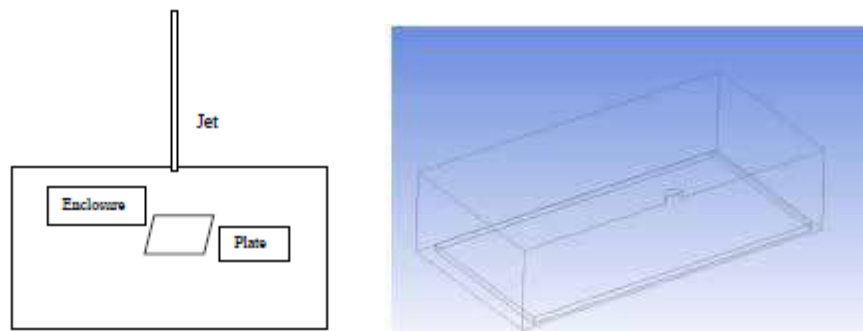


Fig. 2. Schematic diagram of jet impingement

Materials

Selection of material for plate depends upon corrosiveness of the fluid, working temperature and pressure. On studying the properties of various materials along with keeping in mind the economic viability and seeing advantage over other materials the selection of material for plate is done. The selection of material for plate is also viewed by taking into account the thermal conductivity and comparing it with various other material. From, the literature review it was found that. Therefore, the material selected for the design of plate was stainless steel, as it offers advantages over other materials. It has properties like:- great formability and durability, good tensile and yield strength and good thermal conductivity. The tensile strength of steel is comparatively high, making it highly resistant to fracture or breakage. It has ability to change shape on the application of force to it, without resulting in a fracture. This property is known as ductility, which enables it to be used in the making of different shapes and structures ranging from thin wires or large automotive parts and panels. Malleability is closely linked with ductility, and allows steel to be deformed under compression. It is long-lasting and greatly resistant to external wear and tear. Steel is a good conductor of heat and electricity. Steel is its attractive outer appearance. It is silvery in color with a shiny, lustrous outer surface. Stainless steel for instance contains nickel, molybdenum and chromium which improve its ability to resist rust.

Procedure of CFD analysis

The flow chart of the procedure of my proposed work

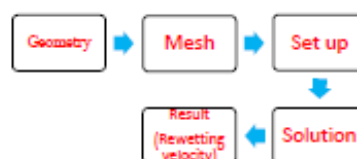


Fig. 3. Flow chart of CFD procedure

The CFD procedure for analysis of jet impingement surface cooling can be divided into six stages:

1. **Problem modeling** - It is very important to understand the problem to be simulated clearly in order to define the problem accurately. In this stage, all the necessary data required for simulation of jet impingement cooling technique will be collected and the detail about the geometry, fluid properties, flow specification, initial and boundary condition will be collected.
2. **Geometry creation** - In this stage, the geometry of domain on which simulation is performed is modelled in a Design module of the fluent. The geometry of plate and jet is be modelled in the design module. Dimensions is given to the geometry.

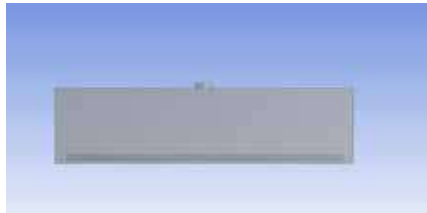


Fig. 4. Geometry

3. **Mesh generation** – In this stage, the continuous domain of geometry is sub- divided into grid of points or mesh using a series of coordinates for points in mesh which are related to each other to define the volume, also known as cell or element. It has distributed these points in flow domain which defines the position where the flow variables is be stored. The geometry is be meshed.

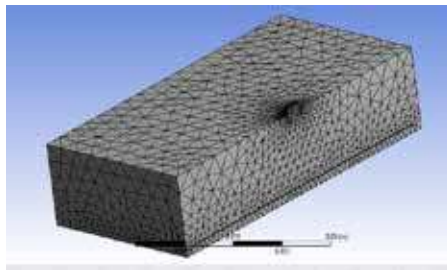


Fig. 5. Meshing

4. **Flow specifications** – When the mesh is created in the domain, boundaries of computational domain is be found and necessary boundary condition determined in initial phase is applied. These conditions are being combined with initial condition and fluid parameters specify the actual flow problem which is to be solved. The boundary conditions is be given – initial surface temperature, coolant flow rate, jet velocity, coolant temperature etc. In the setup stage there are various conditions which is assigned to the designed geometry- Type of Model like: - multiphase model, energy model, viscous model- realizable k-e standard wall function, species transport model and Type of material like:- steel, etc. and type of boundary conditions. In the boundary conditions, each part of designed geometry will be assigned boundary conditions like: - inlet velocity inlet, outlet pressure outlet.

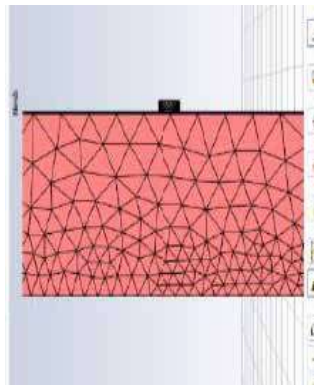


Fig. 6. Set up conditions

5. **Calculations of numerical solution** – When all the necessary information which is required for the simulation is specified, iterative calculation is performed by CFD software to arrive at a solution.
6. **Result analysis** - After the solution is obtained, we have analyzed the results to check the solution is satisfactory and to determine the required flow data. The temperature time plot is be obtained by the software and the rewetting velocity will be calculated on the basis of this plot. The complete simulation was done in ANSYS software.

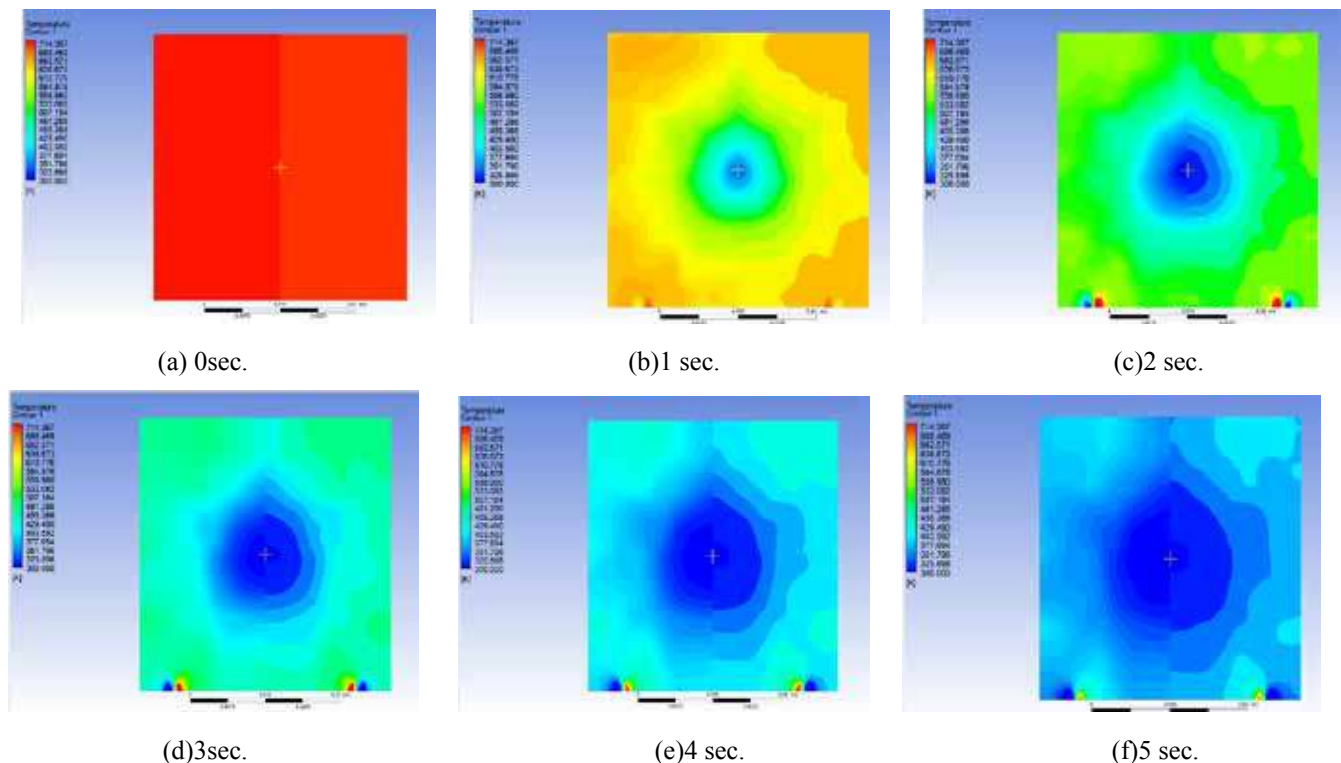
RESULTS AND DISCUSSIONS

The CFD results reported in this paper are based on water jet impingement transient cooling of hot horizontal surface. The table shows operating data for CFD analysis which is given below:-

Table 1. Operating data for CFD analysis

Parameter	Value
Initial surface temperature	450°C
Water jet temperature	24°C
Thickness of the test surface	0.25mm, 3mm
Material of the test surface	Steel
Spatial locations	0, 5, 10,15,20 mm
Jet velocity	3.0 m/s
Jet exit to target spacing	12 mm

The temperature contours that are obtained from the CFD analysis which have shown in Figure below at different time:-



(A) Temperature contours at (a) 0 sec. (b) 1 sec. (c) 2 sec. (d) 3 sec. (e) 4 sec. (f) 5 sec.

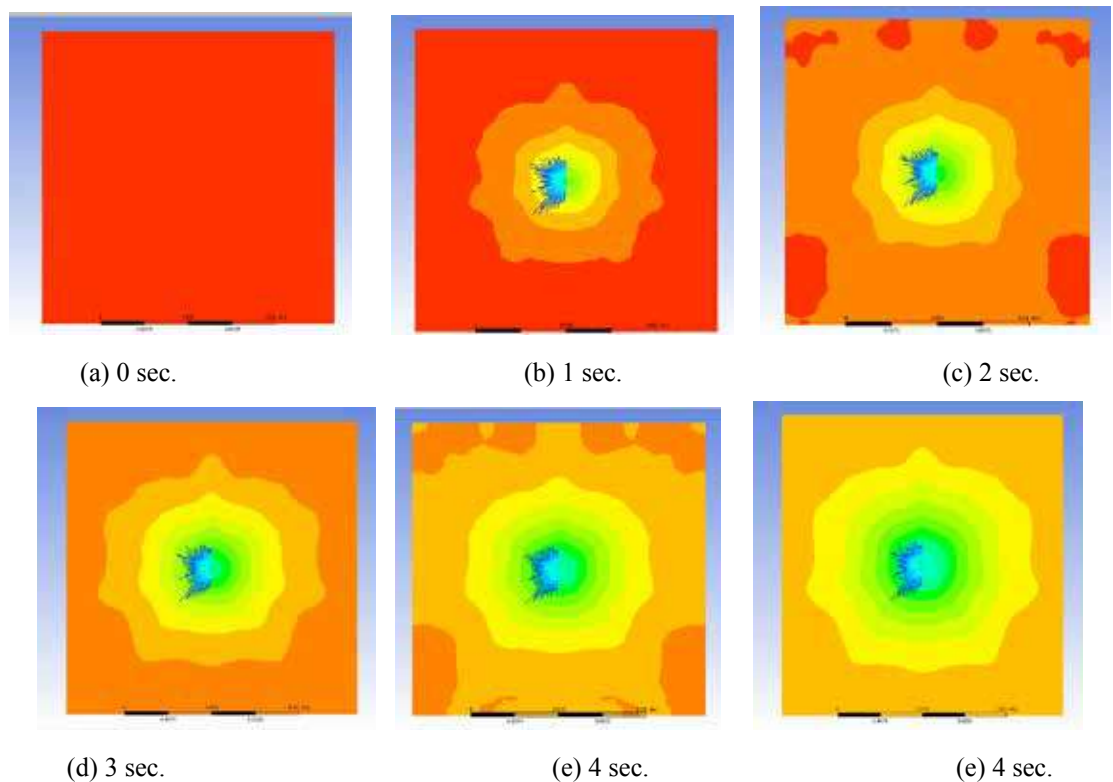


Fig. 7 (A) temperature contours for 0.25mm thickness (B) Temperature contours for 3mm thickness.

From the **Fig. 7** it has been observed that quenching occurs rapidly for thickness 0.25mm thickness than 3mm thickness.

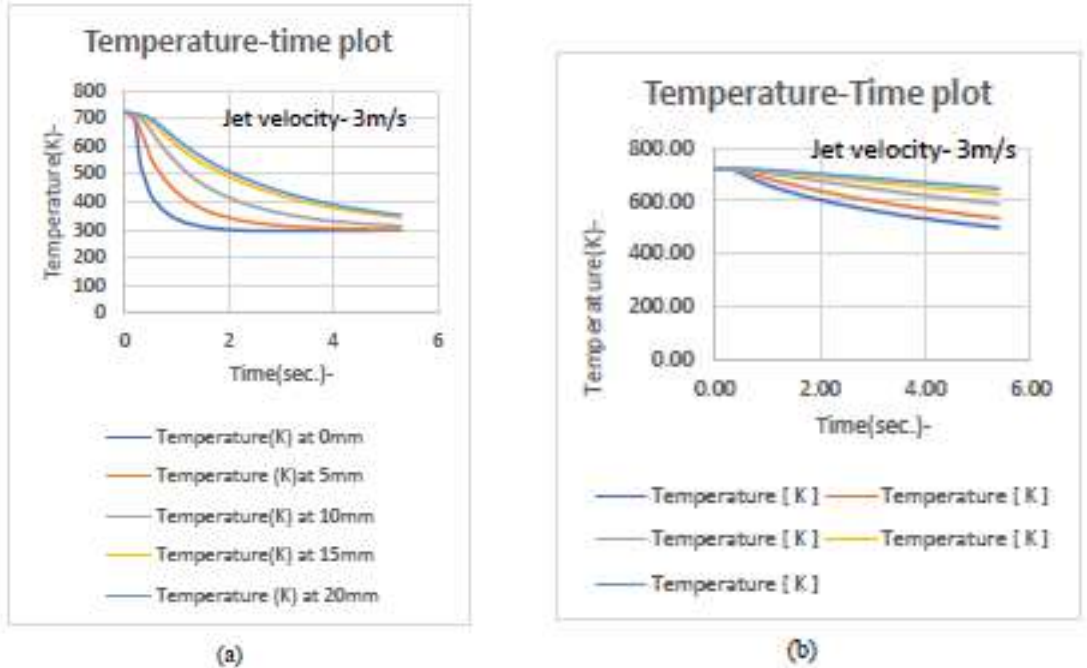


Fig. 8. Temperature-time plot for jet velocity 3m/s(a) 0.25 thickness (b) 3 mm thickness

From the **Fig. 8 (a)** the temperature time plot is for thickness 0.25mm and **Fig. 8 (b)** the temperature time plot is for thickness 3mm. quenching process is fast for thickness 0.25mm compare to 3mm thickness.

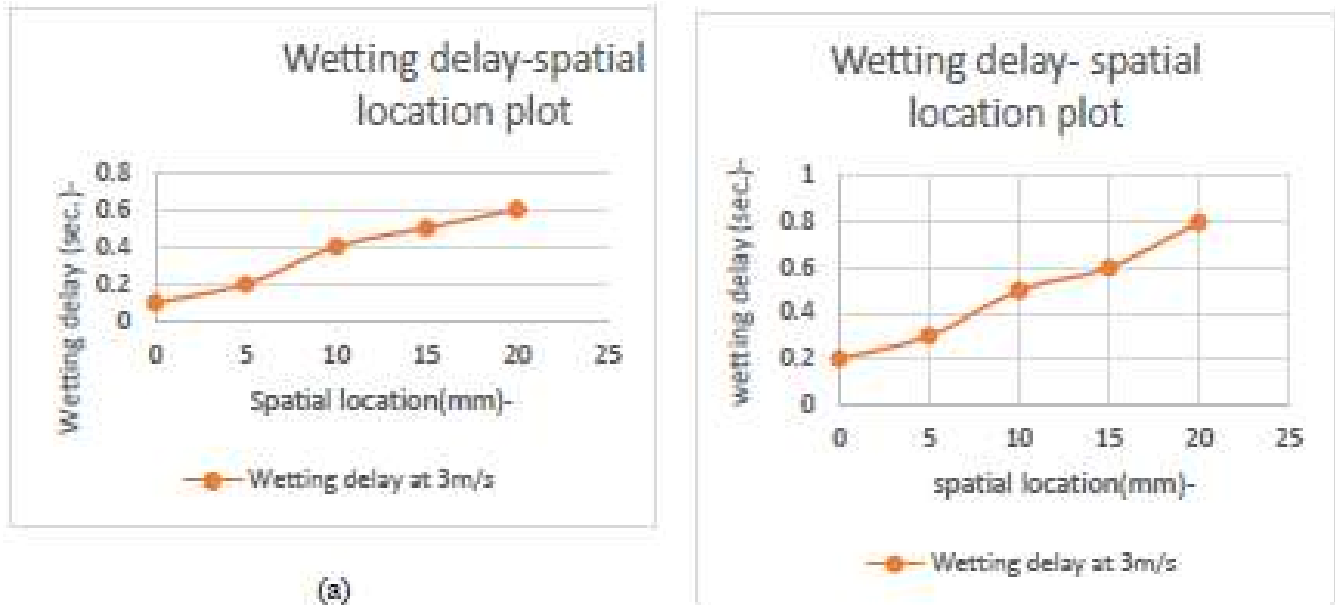


Fig. 9. Wetting delay-spatial location plot for jet velocity 3m/s (a) 0.25mm thickness (b) 3 mm thickness

In the **Fig. 9** it has been observed that when we increase the thickness then surface takes more time to cool. It has been concluded wetting delay increases when increases the thickness.

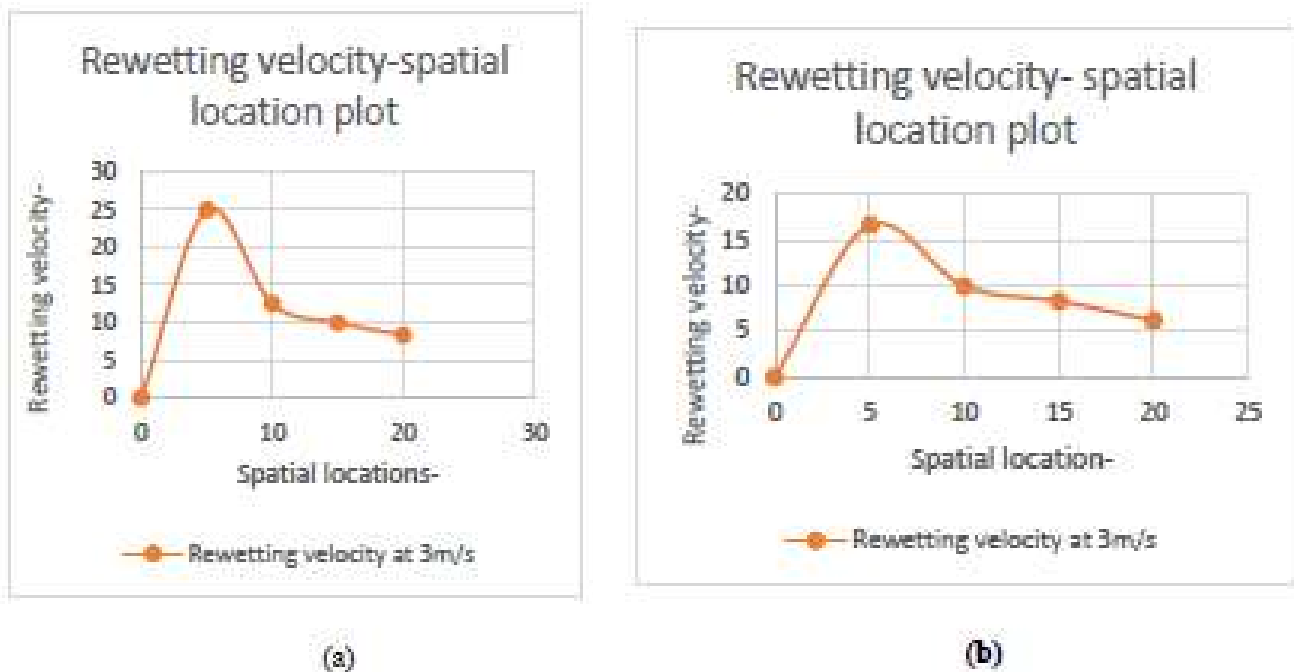


Fig. 10. Rewetting velocity-spatial location plot for jet velocity at 3m/s (a) 0.25mm thickness (b) 3mm thickness

From the **Fig. 10** it has been concluded that when we increase the thickness of the hot plate then the rewetting velocity decreases.

Validation of Model

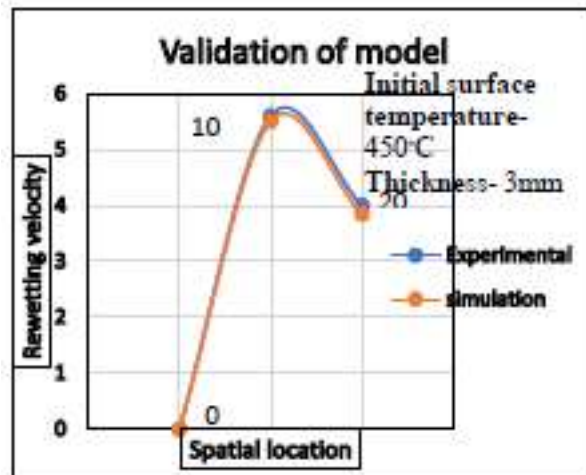


Fig. 11. Validation of model

The experimental results of (ravi et al.) are validated with the simulated results for rewetting velocity at 0mm, 10mm, 20mm. The comparison is done between simulated values of wetting front progression on the hot test surface. The experimental values are validated through CFD simulation study carried out under ANSYS fluent.

Validation of CFD model of hot test surface with experimental result is shown in the **Fig. 11**. The CFD validation for both the experimental study and for simulation study, was done for initial surface temperature 450°C and 3mm thickness. In both the cases the Rewetting velocity measured at 0mm, 10mm, 20mm are almost or nearly equal. Therefore, it can be said that there is close match in the experimental values and simulated values that was carried out for similar boundary conditions. Thus, hot test surface model is validated.

CONCLUSIONS

It has been observed that during transient cooling, the wetting front velocity increases with the rise in jet velocity and wetting delay decreases with the rise in jet velocity. However rewetting velocity reduces drastically for the extreme downstream locations away from the stagnation point. and wetting delay increases drastically with the rise in jet velocity.

ACKNOWLEDGMENT

First author is grateful to major advisor and all advisors who support in the research work.

REFERENCES

1. Akmal M, Omar AMT, Hammed MS "Experimental investigation of propagation of wetting front on curved surfaces exposed to an impinging water jet". Int J Microstruct Mater Prop 2008 vol. 3: pp.654–681.
2. Agrawal C, Kumar R, Gupta A, Chatterjee B "Determination of rewetting velocity during jet impingement cooling of hot vertical rod". J Therm Anal Calorim 2016 vol. 123: pp.861–871.
3. Mozumder AK, Woodfield PL, Islam MA, Monde M "Maximum heat flux propagation velocity during quenching by water jet impingement". Int J Heat Mass Transf 2007 vol. 50: pp.1559–1568.
4. Agrawal C, Kumar R, Gupta A, Chatterjee B "Rewetting of hot vertical rod during jet impingement surface cooling". Heat Mass Transf. 2015.
5. Ueda T, Inous N "Rewetting of a hot surface by a falling liquid film-effects of liquid sub-cooling". Int J Heat Mass Transf 1984 vol. 27: pp. 999–1005.
6. Filipovic J, Incropera FP, Viskanta R "Rewetting temperatures and velocity in a quenching experiment". Exp Heat Transf 1995 vol.8: pp.257–270.



7. Karwa N, Roisman TG, Stephan P, Tropea C “Experimental investigation of circular free-surface jet impingement quenching”: transient hydrodynamics and heat transfer. *Exp Therm Fluid Sci* 2011 vol.35: pp.1435–1443.
8. Hammad J, Mitsutake Y, Monde M “Movement of maximum heat flux and wetting front during quenching of hot cylindrical block”. *Int J Therm Sci* 2004 vol.43: pp. 743–752.
9. Raj VV “Experimental investigation on the rewetting of hot horizontal annular channels. *Int Commun Heat Mass Transf*” 1983 vol.10: pp.299–311.
10. Mitsutake Y, Monde M “Heat transfer during transient cooling of high temperature surface with an impingement jet”. *Heat Mass Transf* 2001 vol. 37: pp.321–328.
11. Dua SS, Tien CL An experimental investigation of falling-film rewetting. *Int J Heat Mass Transf* 1978 vol. 21:pp.955–965.
12. Xu F, Gadala MS “Heat transfer behavior in the impingement zone under circular water jet”. *Int J Heat Mass Transf* 2006 vol.49: pp.3785–3799.
13. Agrawal, C. “Surface quenching by jet impingement- A Review”. *Steel Research International* 2019 vol.90: pp.1-22.
14. Agrawal, C., Goherwal, D., and Singh, C. “Effect of surface thickness on the wetting front velocity during jet impingement surface cooling”. *Heat Mass Transfer*. 2016.



Energy Efficient Surfaces for Improved Performance of Heat Exchanger Through Enhanced Pool Boiling Heat Transfer: A Review

Anil S Katarkar*, Biswajit Majumder, Swapan Bhaumik

Department of Mechanical Engineering, National Institute of Technology Agartala, Tripura

*✉ anilkatarkar@gmail.com

ABSTRACT

Improvement of the performance of heat exchanger is the focal point of researchers for saving the materials, money and space. Enhancement of pool boiling heat transfer coefficient (PBHTC) through surface modification techniques have gained a lot of attention. These surface modifications can be done at various scales using different techniques. This paper presents a critical and comprehensive review of enhanced surface modification techniques for Nucleate PBHT along with an integrated discussion on their related parameters necessary for increased heat transfer characteristics. A discussion on the mechanisms for the reported improvements in boiling performance is also provided with various surface modification methods of modifying surface morphology. In the summary, a brief discussion is provided on the areas within these fields where opportunities exist to understand the behaviour in these systems better for improved performance of heat exchanger through enhanced NPBHT.

Keywords: Nucleate boiling; Heat exchanger; Surface modification techniques; Surface enhancement; Pool boiling.

INTRODUCTION

Through the years, excessive utilization of conventional energy resources has given rise to various problems for example depletion of energy resources, global warming, and climatic variations. Hence, the enhancement of energy protection and efficiency of the natural environment has become an important issue in the world [1-2]. By enhancing the performance efficiency of applications of several evaporators in the refrigeration system, heat exchangers, boilers in power plants, the effects of global warming can be mitigated [3-4]. Notably, numerous heat exchangers work on the BHT technique.

Heat transfer is one of the crucial thermo-physical phenomena and is involved in each recovery process, energy utilization and conversion. Surface morphology (enhanced surfaces) are essential for heat transfer processes in numerous engineering appliances [5]. Heat transfer enhancements want physical improvements in the heat transfer system, which will, in turn, reduce its pumping size and load (surface saving). The phase change heat transfer (PCHT) involves in almost every heat transfer application, starting from the cooling process to the heating process. The main advantage of the PCHT is its capacity to transfer a massive amount of heat energy within a reduced amount of wall superheat. In PCHT applications, the boiling and condensation phenomenon dominate (Fig. 1) these processes are like to each other in terms of variable dependency [6-7]. The boiling phenomenon is a process in which the boiling surface and the working fluid are in contact with each other.

BHT in specific is important in applications, for example, immersion cooling, power plants, two-phase, heat pipes and food process. Boiling may be defined as the change of phase from liquid to vapor accompanied by liquid-solid interface or at the formation of bubbles in a liquid. It is distinct from evaporation because of the inherently transient nature of the bubble cycle, growth, departure and nucleation of bubbles [8].

PBHT is the mode of heat transfer that happens in flooded evaporators that are used for refrigeration applications [9]. The methods for PBHT enhancement can be divided into two major types, as shown in Fig. 2. Active and passive methods. Active methods need external power input, for example, ultrasound, magnetic field, mechanical vibration. Passive methods include special surface geometries, insert devices or fluid additives for enhancement. The common passive methods involve enhanced nanofluids, surface, swirl flow device and displaced inserts. Presently, available heat-transfer enhancement devices mostly employ passive methods, due to active methods usually result in cause noise and higher cost, reliability, or safety problems [10].

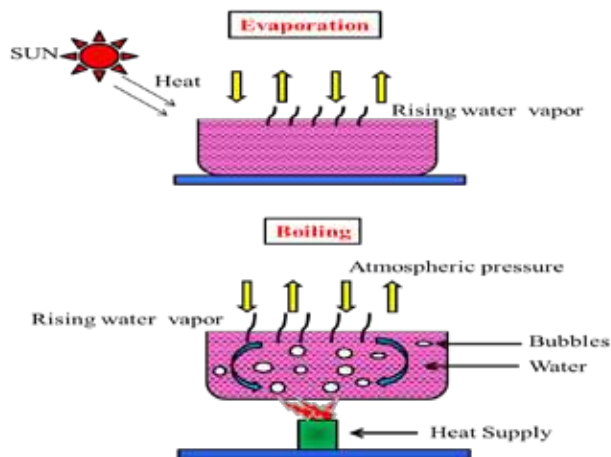


Fig. 1. Boiling phenomenon [11]

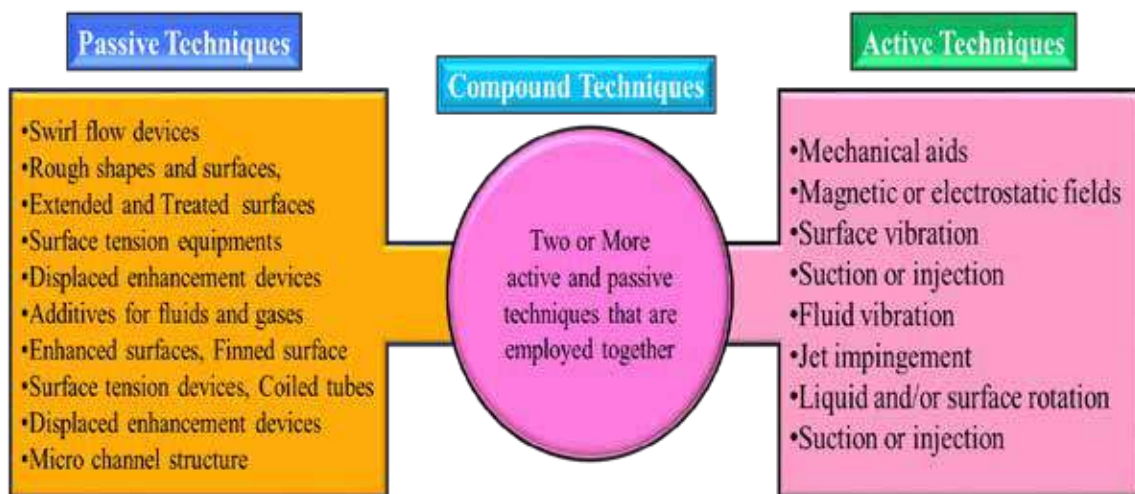


Fig. 2. Types of heat transfer improvement techniques [11]

The enhanced surface is the most widely used technique for PBHT augmentation in the refrigeration and air-conditioning company. Such as, almost all water chillers using shell-and-tube heat exchangers employ enhanced tubes. Enhanced surfaces can be used to decrease the heat exchanger size and increase efficiency and, in turn, reduce the working fluid charge [12].

This paper provides a review of PBHT on enhanced surfaces. The paper arranges with a review of the existing predictive methods for pool boiling on enhanced surfaces and suggests future work. Also In this paper, recent advances in BHT which use modified surfaces to enhance the boiling process are discussed.

Literature Review

The enhanced boiling surfaces typically have special surface geometries that give higher HTC's in terms of projected area compared with smooth (plain) surfaces. The fact that "roughness" enhances NBHT has been known since 1931 when few research studied that the BHTC for water on a rough surface is maximum as compared to a plain surface [13].

Owing to its high HTC, PBHT is inevitable in various industrial applications [14]. Boiling processes is remarkably significant in several applications [15], but elude our understanding as they involve several complicating aspects. However, the heat transfer rates related to these phenomena can be enhanced by various methods [16]. Generally, the PBHT performance can be enhanced by modifying the

- Boiling surface
- Boiling fluid

Surface modification effectively improves the heat transfer performance when the other operating conditions or the fluid are tough to modify [17]. Moreover, as a passive technique, boiling surface modification has attracted the interest of researchers around the globe. Modify surfaces result in better heat transfer performance by increasing CHF and by reduction of surface superheat. According to different phenomenological theories, this enhancement is attributed to increasing the surface area, the density of nucleation site, vapor escape paths and capillary effect to assist the liquid flow

HEAT TRANSFER ENHANCEMENT TECHNIQUES

Heat transfer enhancement techniques that are used in boiling applications contain numerous surface modification methods: artificial cavities, surface roughness and pin-fins. These techniques aim to effectively convey higher heat loads at smaller temperature differences by the following means: increase the number of active nucleation sites and increase the wetted surface area relative to the novel plain surface [18].

Micro-fin Surfaces Modification

Micro-structured fins on the surface provide small agitations in the fluid, affecting the vapor bubbles dynamic. These structures change the fluid flow improve and the heating surface area. Micro-fins can have various sizes and shapes and can be arranged in several patterns to increase heat transfer [19]. The surfaces of the micro- fin are available in different types of molds, like parallel inclined fins that are aimed to catch vapour embryos. These rectangular cross-sectional parallel vertical fins are likewise known as open microchannels, cylindrical fins as given in **Fig. 3**.

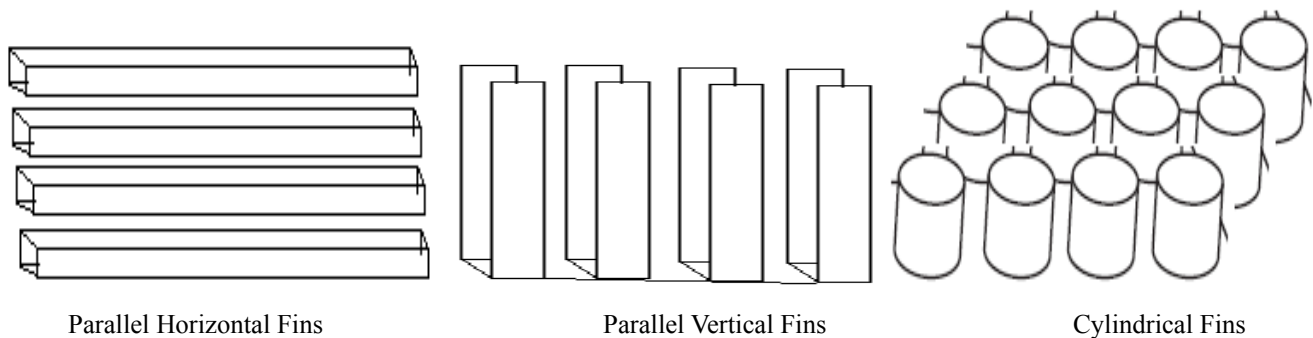


Fig. 3. Several types of micro-fins used for boiling improvement [20]

Structured Surfaces

Structured surfaces (**Fig. 4.**) are designed by lifting the base surface of a plain tube to form integral-fins and have been commercially existing since the 1930s. Further cold metal working of the integral fin produces higher-performing enhancements and more advanced. One may employ one or numerous cold-working methods (e.g., notching, rolling) using a particularly designed apparatus to form the enhanced structure that generally consists of interconnected tunnels and pores below the surface. The resulting boiling enhancement is because of both the increase in the improved bubble nucleation behaviour and the surface area.

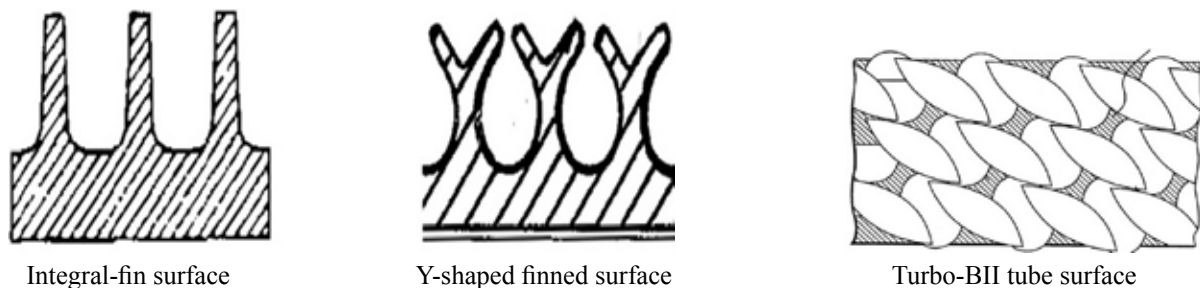


Fig. 4. Several types of structured surfaces used for boiling improvement [21].

Surface Roughness

Surface properties of boiling surfaces are considered the greatest main factors affecting BHT. Various researchers have

studied the result of surface roughness on the PBHT. Latest research efforts are focused on BHT with a roughness in complex geometries and additional complex surface exhibiting multiscale roughness. According to the previous research, roughening surface produced cavities on the heating surface generally has the tendency of increasing PBHT. In other hand, as the surface roughness increased, the temperature deference required for a given heat flux reduced. [22]. In pool boiling, surface roughness promotes the nucleation site density, which directly leads to a higher number of generated bubbles. In turn, this high bubble density augments the agitation of liquid layers above the hot surface and causes heat flux removal [23].

It is valuable outcome the effect of surface roughness on PBHT due to it is significant in the sizing/materials of heat exchangers. The growing coarseness of the heat-dispelling surface, accomplished by sandblasting, developing various small artificial cavities or by mechanical roughing, are successful methods for enhancing the performance efficiency of nucleate boiling. Fig. 5 shows the cross-section of a rough surface. Increasing the roughness of the gained by heat-dissipating surface, sandblasting, by developing numerous chemical etching synthetic holes, small mechanical hardening, is a traditional method for improving the nucleate boiling performance [24].

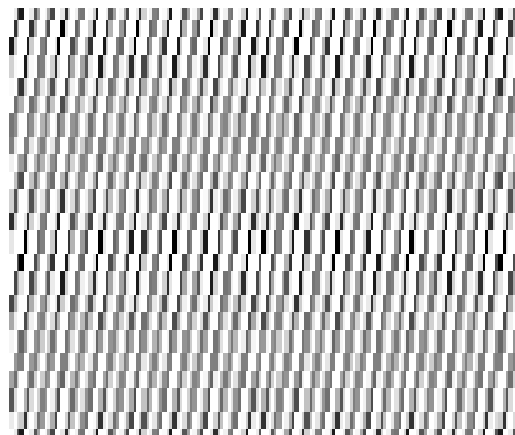
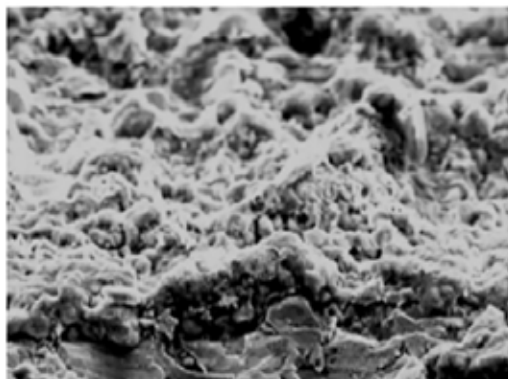


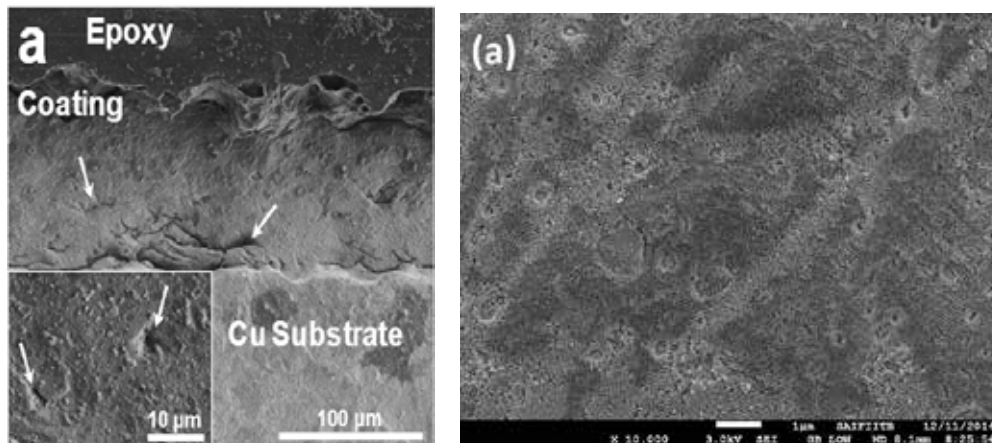
Fig. 5. Area of rough surface

Porous Surface

The enhanced BHT on porous surfaces has been of significant research interest mainly because of its numerous applications for example heat pipes, electronic equipment, boiler surfaces. Porous surface is an effective and direct way to increase the effectiveness of heat exchangers. There are several techniques proposed by researchers for boiling through porous surfaces. The porous surfaces can be created by several techniques for example welding, machining, brazing or sintering, flame spraying, electrolytic deposition, galvanizing, plasma spraying of polymers, etc. As indicated by its name, a porous surface has an interconnected porous matrix which can also increase active nucleation site density and surface area. The porous matrix can be made of either the same material as the base surface or a different one. The porous surfaces have numerous cavities that performance as nucleation sites. They proposed that once the bigger bubbles depart, the smaller nucleation cores become active. A schematic diagram of SEM images of porous surface is shown in **Fig. 6.** [25].



Cu tube surface coated [26]



CNT-Cu composite surface coatings [27] TiO_2 nanoparticles coated Cu surface [28]

Fig. 6. Several types of SEM images of Porous surface

Currently, the porous surface has appeared as a more capable approach for CHF and HTC enhancement in BHT devices. However, the significant improvement in heat transfer is attained with thinner coatings. Generally, boiling enhancement by surface modification can be mostly classified into two techniques (1) Surface modification by sandblasting machining/etching, and sintering and spraying particles (2) Surface modification by application of the surface coating (porous surface) [29-31]. In the surface coating techniques, as in numerous scientific fields in the last century, researchers are interested in using various techniques to attain superior results [32]. Numerous types techniques are used for surface coatings in boiling heat transfer based on mechanical, thermal, chemical and physical. The overview of the surface coating (porous surface) preparation techniques are shown in Fig. 7. [33-35].

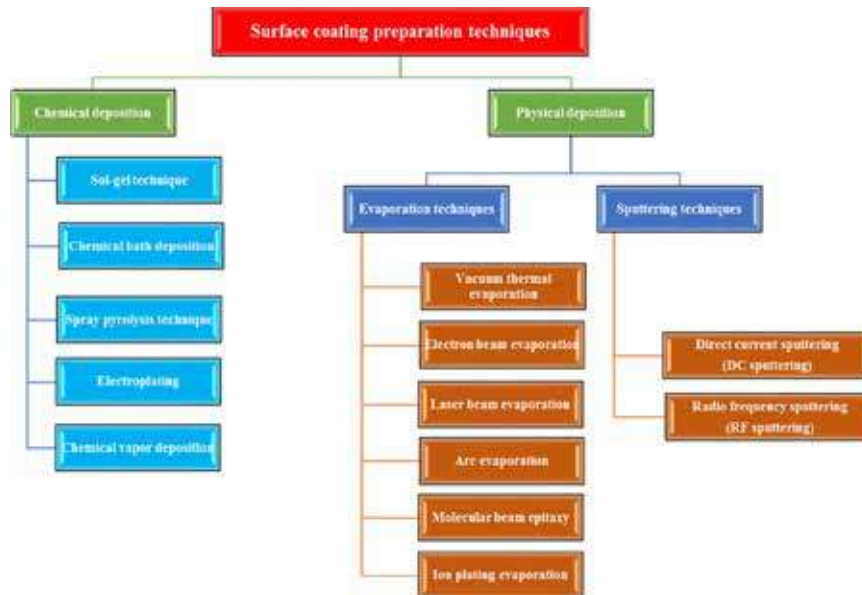


Fig. 7. The overview of the porous (Coating)surface preparation techniques [11]

Structure of Micro Channel

Microchannels are being used for heat flux (heat sinks) thermal management in electronic equipment. Micro channel surface created by using chemical process (etching, etc.) is a traditional technique for improving the nucleate boiling performance, as shown in Fig 8. Various innovative designs have been created on the channel walls to improve the thermal efficiency of mini/micro channels [36].



Fig. 8. Various types structure of micro channel surface [15]

CONCLUSIONS & RECOMMENDATIONS

This paper reviewed of enhanced surface modification techniques for NPBHT comprehensively along with related parameters necessary for increased heat transfer characteristics. Commercial use of enhanced boiling surfaces in heat exchanger has driven improvements in surface development, boiling measurements, and predictive methods to make it the leading technology for augmenting boiling heat transfer which enhances performances of heat exchangers. In the area of NPBHT, surface enhancements have aimed to modify surface wettability (hydrophobic coatings and surfactants), increase the wicking ability and surface wetting (hierarchical and micro/nanostructures structures). Researchers have studied and introduced a variety of enhanced surfaces (Micro-fin surfaces, structured surfaces, surface roughness, porous surfaces and Micro/Nanostructures surface etc.) for enhanced performance of heat exchanger where boiling process taking place. In future, it is expected that more novel surface modification techniques will be appeared in the field with sustainable measures along with different liquid combinations for better performance in applications like Air-conditioning, Refrigeration, space & nuclear and other allied fields.

REFERENCES

1. Lingnan Lin, Mark A. Kedzierski Review of low-GWP refrigerant pool boiling heat transfer on enhanced Surfaces International Journal of Heat and Mass Transfer 131 (2019) 1279–1303.
2. Manglick, R.M. Heat transfer Enhancement. In Heat Transfer Handbook; Bejan, A., Kraus, A.D., Eds.; John Wiley & Sons, Inc.: Hoboken, NJ, USA, 2003; pp. 1029–1130. ISBN 0-471-39015-1.
3. Zhang, L.; Shoji, M. Nucleation site interaction in pool boiling on the artificial surface. Int. J. Heat Mass Transf. 2003, 46, 513–522.
4. W.M. Rohsenow, J.R. Hartnett, Handbook of heat transfer, Choice Rev. Online. 36 (1999) 36-3347-36–3347. DOI: 10.5860/CHOICE.36-3347.
5. A.R. Shelke, J. Balwada, S. Sharma, A.D. Pingale, S.U. Belgamwar, J.S. Rathore, Development and characterization of Cu-Gr composite coatings by electro-codeposition technique, Mater. Today Proc. 28 (2020) 2090–2095,
6. S. Khan, M. Atieh, M. Koç, Micro-nano scale surface coating for nucleate boiling heat transfer: a critical review, Energies. 11 (2018) 3189,
7. Z. Khan, R. Shah, S. Islam, H. Jan, B. Jan, H.-U. Rasheed, A. Khan, MHD flow and heat transfer analysis in the wire coating process using elastic-viscous, Coatings 7 (2017) 15,
8. S. Mori, Y. Utaka, Critical heat flux enhancement by surface modification in a saturated pool boiling: A review, Int. J. Heat Mass Transf. 108 (2017) 2534–2557,
9. B. Shi, Y.-B. Wang, K. Chen, Pool boiling heat transfer enhancement with copper nanowire arrays, Appl. Therm. Eng. 75 (2015) 115–121,
10. S.K. Gupta, R.D. Misra, Effect of two-step electrodeposited Cu–TiO₂ nanocomposite coating on pool boiling heat transfer performance, J. Therm. Anal. Calorim. 136 (2019) 1781–1793,
11. A.S. Katarkar, B. Majumder, A.D. Pingale et al., A review on the effects of porous coating surfaces on boiling heat transfer, Materials Today: Proceedings,



12. Manglick R M 2003 Heat transfer Enhancement John Wiley & Sons Hoboken NJ USA 1029–1130.
13. B. Majumder, A. Katarkar, S. Bhaumik, Effect of structured surface on contact angle using Sessile Droplet method, IOP Conf. Ser. Mater. Sci. Eng. 814 (2020), 012034.
14. A. Mehdikhani, H. Moghadasi, H. Saffari, An experimental investigation of pool boiling augmentation using four-step electrodeposited micro/nanostructured porous surface in distilled water, Int. J. Mech.
15. Anil Katarkar, Biswajit Majumder, Swapan Bhaumik Review on Passive Heat Enhancement Techniques in Pool Boiling Heat Transfer IOP Conf. Series: Materials Science and Engineering 814 (2020) 012031.
16. Kim, H. Enhancement of critical heat flux in nucleate boiling of nanofluids: A state-of-art review. Nanoscale Res. Lett. 2011, 6, 415.
17. Liang, G.; Mudawar, I. Pool boiling critical heat flux (CHF)—Part 2: Assessment of models and correlations. Int. J. Heat Mass Transf. 2018, 117, 1368–1383.
18. Yunus A, Cengel and Afshin J G 2011 Heat and Mass Transfer McGraw-Hill Higher Education 4th ed 515-560.
19. Wen C D and Mudawar I 2004 Emissivity characteristics of roughened aluminum alloy surfaces and assessment of multispectral radiation thermometry (MRT) emissivity models Int. J. Heat Mass Transfer 47 3591–3605.
20. Mudawar I and Anderson T M 1990 Parametric investigation into the effects of pressure, subcooling, surface augmentation and choice of coolant on pool boiling in the design of cooling systems for high-power-density electronic chips, J. Electron 112 375–382.
21. Wieland-Werke Ag., GEWA-B Evaporator Tubes, 2017.
22. A. Katarkar, B. Majumder and S. Bhaumik, Effect of enhanced surfaces and materials in boiling heat transfer with HFO Refrigerants: A review, Materials Today: Proceedings,
23. Marto P J and Rohsenow W M 1966 Effects of surface conditions on nucleate pool boiling of sodium J. Heat Transfer 88 196–203.
24. Jones B J, McHale J P and Garimella S V 2009 The influence of surface roughness on nucleate pool boiling heat transfer J. Heat Transfer 131 121009.
25. A.K. Dewangan, A. Kumar, R. Kumar, Pool boiling of iso-butane and quasiazeotropic refrigerant mixture on coated surfaces, Exp. Therm. Fluid Sci. 85 (2017) 176–188.
26. A.K. Dewangan, A. Kumar, R. Kumar, Experimental study of nucleate pool boiling of R-134a and R-410a on a porous surface, Heat Transf. Eng. 40 (2019) 1249–1258.
27. Edward Joshua T. Pialago a, Oh Kyung Kwonb, Chan Woo Park a, Nucleate boiling heat transfer of R134a on cold sprayed CNTeCu composite coatings Applied Thermal Engineering 56 (2013) 112e119
28. M. Ray, S. Bhaumik, Structural properties of glancing angle deposited nanostructured surfaces for enhanced boiling heat transfer using refrigerant R-141b, Int. J. Refrig. 88 (2018) 78–90,
29. A. Katarkar, B. Majumder and S. Bhaumik, Effect of enhanced surfaces and materials in boiling heat transfer with HFO Refrigerants: A review, Materials Today: Proceedings,
30. Biswajit Majumder, Anil Katarkar, Swapan Bhaumik Effect of structured surface on contact angle using Sessile Droplet method IOP Conf. Series: Materials Science and Engineering 814 (2020) 012034 IOP Publishing
31. A.D. Pingale, S.U. Belgamwar, J.S. Rathore, The influence of grapheme nanoplatelets (GNPs) addition on the microstructure and mechanical properties of Cu-GNPs composites fabricated by electro-co-deposition and powder metallurgy, Mater. Today: Proc. 28 (2020) 2062–2067.



32. S. Mori, Y. Utaka, Critical heat flux enhancement by surface modification in a saturated pool boiling: A review, *Int. J. Heat Mass Transf.* 108 (2017) 2534–2557,
33. A.M. Rishi, S.G. Kandlikar, A. Gupta, Improved wettability of grapheme nanoplatelets (GNP)/copper porous coatings for dramatic improvements in pool boiling heat transfer, *Int. J. Heat Mass Transf.* 132 (2019) 462–472,
34. R. Parin, D. Del Col, S. Bortolin, A. Martucci, Dropwise condensation over superhydrophobic aluminium surfaces, *J. Phys. Conf. Ser.* 745 (2016),
35. E. Forrest, E. Williamson, J. Buongiorno, L.-W. Hu, M. Rubner, R. Cohen, Augmentation of nucleate boiling heat transfer and critical heat flux using nanoparticle thin-film coatings, *Int. J. Heat Mass Transf.* 53 (2010) 58–67,
36. Chinmay M. Patil & Satish G. Kandlikar (2014) Review of the Manufacturing Techniques for Porous Surfaces Used in Enhanced Pool Boiling, *Heat Transfer Engineering*, 35:10, 887-902.



Finite Element Structural Analysis of Inflatable Semicircular Air Beam

K Hans Raj^{1*}, Akash Jain², Ravi Kumar³, Arun Kumar Saxena⁴

Professor, Mechanical Engineering, Dayalbagh Educational Institute, Dayalbagh, Agra¹

Research Assistant, Mechanical Engineering, Dayalbagh Educational Institute, Dayalbagh, Agra²

PG Scholar, Mechanical Engineering, Dayalbagh Educational Institute, Dayalbagh, Agra³

Director, ADRDE (DRDO), Agra⁴

*✉ hansraj@dei.ac.in

ABSTRACT

In the recent years, structural applications with inflatable air beams or arches with advanced fabric materials have become popular. They are easily deployable, have low storage volume, light weight and are cost saving. It is highly recommended to use inflatable structures in the seismic sensitive areas as well as for temporary structures (e.g. shelters during floods and other natural calamities). Inflatable air beam is the basic element of the inflatable structures. In this work an effort is made to model inflatable beams using finite element method to understand their structural behavior. The beam is made of fibrous materials i.e. Kevlar instead of conventional material. A semicircular beam with circular cross-section made of Kevlar fabric having an identical geometry is analyzed. Finite element analysis is carried out to study air beams under different loading conditions.

Keywords: Air beam; Air inflatable structure; FEA.

INTRODUCTION

Inflatable beams or arches have various advantages over conventional material structures. Inflatable beams are made from a relatively thin skin which, unless pre-stressed has capacity to bear compressive loads. Three distinctive fields of application of inflatable structures are civil engineering, aeronautics and space applications. The objective of the work is to derive a relationship between deflection of air inflatable beams, internal pressure, properties of fabric material and geometry of inflatable beams.

Inflatable Structures provide better solution over conventional structures in terms of cost and time consumption. The main structural element used in the design of inflatable structures is an air beam. Air beams quite often utilize woven or braided fabrics of lightweight and high load carrying capabilities. An Air beam consists of high strength fabric sleeve, and a highly flexible internal bladder. When beams are inflated, they can be used as load-bearing beams. Therefore, it is necessary to investigate the interrelation between internal air pressure and base span and diameter of the air beam. In this study, a number of air beams are numerically tested with different air pressure conditions. A numerical analysis is carried out for analyzing the design of an inflatable beam. The material used is KEVLAR 49. The air beam is simulated at various pressure levels using FEM.

A series of inflatable beams are used to form a hangar. Applying cover of fabric sheet over these beams, provide a wall or roof shape structure. Analysis of the behavior of such structures with the goal of deriving a theory can be used in the design of the inflatable beam structures. The beams are placed parallel to each other and are connected only at the ends.

TYPES OF INFLATABLE STRUCTURES

There are several inflatable structures that are made by some industries. They are frequently used in seismic areas as permanent structures as well as temporary structures such as shelters[1]. There are four type of inflatable structure used in present scenario.

1. Inflatable structures made of Air beams with canopy/ cover.
2. Hybrid Inflatable structures with metal frame.
3. Inflatable structure with inflated walls, no beams.
4. Inflated structure with air beam, no continuous supply of air.

An air beam structure is used for making inflatable structure as it will allow one to construct small as well as large structures at



low cost with easy deployment. An inflatable beam relies on an overpressure to deal with externally applied compressive loads therefore the structural behavior is more influenced by the type of material, geometry and applied loads than rigid structures.

J. P. Kwake[2] developed a unique inflatable structure, invented to provide temporary structure over the top of another structure. This inflatable structure is used for covering the swimming pools, having a dome like shape. It has many advantages over conservative rigid covering structures. Structure could be effortlessly removed during summer season, when it is preferable to swim outside and can be simply stored in small space.

Yen T. Haung[3] constructed a modular dome shape structure using uniform Y-joints. The Y-joints have branch angles forming of 120, 120 and 108 deg. Y-joints are used to connect all the standardized length members and provide a desire shape like pentagonal and hexagonal structure. Y-joints make structure that are organized to form a modular dome shape structure. After inflation, all members are hardened through vulcanization and curing process to provide permanent resistance to stress and strain.

Bradley Salle[4] created inflatable truss members for designing large inflatable devices like ships and satellite decoys. The first embodiment manufactured by two MYLAR laminating sheets using a triangular pattern shape to form inflatable tubes and the sides of the material are bonded for making a cylindrical shape.

Garrett C. Sharpless [5] constructed a curved tubular inflated beam containing axial fibres and braided fibres on a elastomeric wall. The inflated tube was tape cemented on outside to reinforced the curved shape. Very small and very large tubes are constructed with a range of inflation pressures and strength of beams. A 60 feet long arch, having 123/4 inch diameter tube, for a structure 24 feet height and 30 feet wide is thus constructed.

Glen J. Brown[6], made a cylindrical air beam with a gas-retaining bladder with considerable resistance to wrinkling or buckling.

Glen J. Brown[7] manufactured an inflated tube using spiralling, high strength ribbon that is mounted on fabric skin as a structural element containing a bladder. The ribbons are mounted on outside surface equivalent to the axis of the beam/tube, which reinforced the tube against bending forces. It allowed high pressures for high structural stiffness and strength.

Eric J. McNiff [8] erected an inflatable tent which is constructed in two parts. It comprised of a frame of inflatable tubes and an optionally removable covers made of fabric material. The frame had a single inflatable continuous tubular member. It comprised of a bottom section which is connected to an upright section. The upright section is connected to one circular supporting arch segment and other end to the base section.

Gary L. Bailey[9] developed an air beam structure have unique cross-section design with reduced weight, lower inflation pressure requirements and increased rigidity. The beam structure is designed with an air impermeable fabric material having cylindrical shape. The "I" beam envelope having air impermeable walls sealed inside of cylindrical beam. A compressible material is dispersed inside the "I" beam section throughout the beam envelope. When the pressure is applied, the fabric becomes act like a rigid structure. The air beams are used in a group and it may be connected to another by fabric sheet materials to form a roof or wall structure.

CASE STUDY

Finite Element Analysis of an Inflatable Air Beam is attempted in this work to find the relation between base span to diameter of Air-beam.

A parametric CAD model (**Fig. 1 and Fig. 4**) is developed as geometric input to Finite element analysis software. Subsequently a finite element model is developed. This model enabled the study of stability, reliability and technical feasibility of the inflatable structure. Finite elements are used for static analysis to measure stresses, strains, forces and deflections to find the response of the structure in terms of the interrelation between external loads and the deflection of the beam.

This work focuses on the mechanical performance of fabric and geometry of an inflatable beam structure and the analysis part covers finite element study for determining the structural performance of the beam.

The data for the analysis has been taken from the recent inflatable air beam structures[10]. This relation helped in designing and analysing of air beams structures.

FEA OF A CYLINDRICAL ARCH BEAM

FE analysis of Inflatable air-beam structure is attempted for two different diameters.

1) 1.2 meter

2) 1 meter

CASE -1: Finite Element Structural Analysis of Inflatable Air-beam Structure at 1.2m diameter

Table 1. Data of inflatable air-beam structure at 1.2m diameter

Base span	50m
Material	Kevlar 49
Density	1.44 g/cm ³
Young Modulus	112 GPa
Poisson Ratio	0.36
Diameter	1.2m
Thickness	2mm
Surface area	297.08 m ²
Volume	0.59 m ³
Mass	849.6 kg

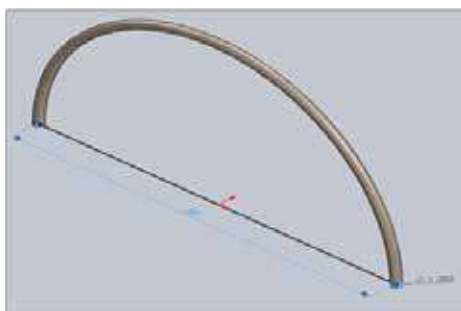


Fig. 1. Finite element model of a 50 m long cylindrical arch of 1.2m dia.

The higher mesh density influences result to be more precise and accurate though it costs more in terms of computational time. The large beam element is divided into several fine small elements. The meshing used is volume mesh as the thickness of the air beam model is small, and meshing should be finer that will provide an accurate enough solution. A structured mesh was applied to the beam. This type of meshing allows for tailoring the mesh density in two directions. In this case the number of elements around the circumference and along the length of the beam can be varied to investigate the influence of the mesh on the results.

The load used is a point load, whose value is taken around three times of inside pressure value. The value of load is taken to test at extreme conditions. Both ends of the arch beam are fixed. The inside pressure is applied as per literature. Then air beam model is meshed. The figure shows the air beam arch model that is made in ANSYS FEM software. After meshing the inside pressure is applied in the beam. Then external load is applied at the top of the beam. Finite element arch beam with inside pressure under loading is analysed.



Fig. 2. Structural deformation of dia. 1.2m beam.

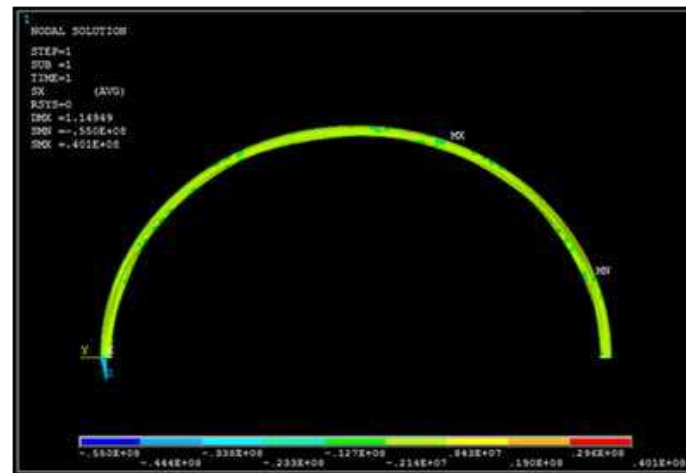


Fig. 3. Stress distribution of dia. 1.2m beam.

CASE -2 Finite Element Structural Analysis of Inflatable Air-beam Structure at 1m diameter

Table 2. Data of inflatable air-beam structure at 1m diameter

Base span	50m
Material	Kevlar 49
Density	1.44g/cm ³
Young Modulus	112 GPa
Poison Ratio	0.36
Diameter	1m
Thickness	2mm
Surface area	247.73m ²
Volume	0.49 m ³
Mass	705.6 kg

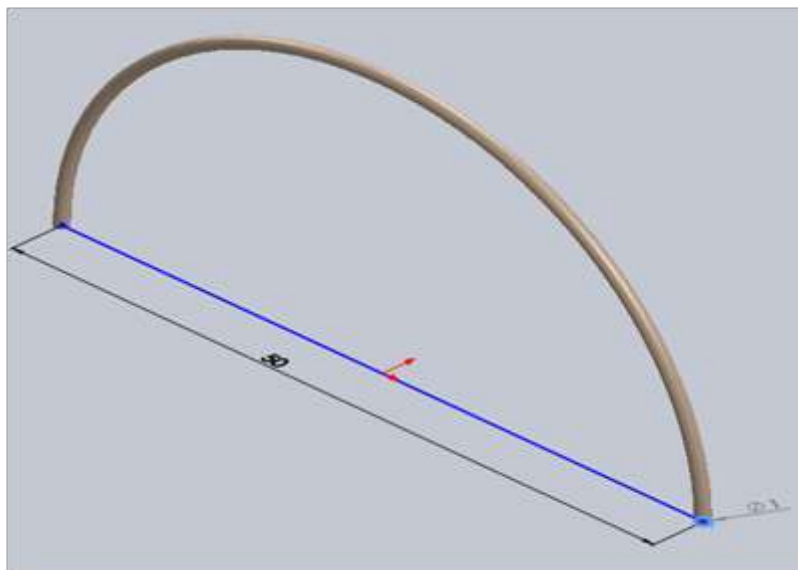


Fig.4. Finite element modelling of arch beam of 1m dia



Fig. 5. Structural deformation of dia. 1m beam

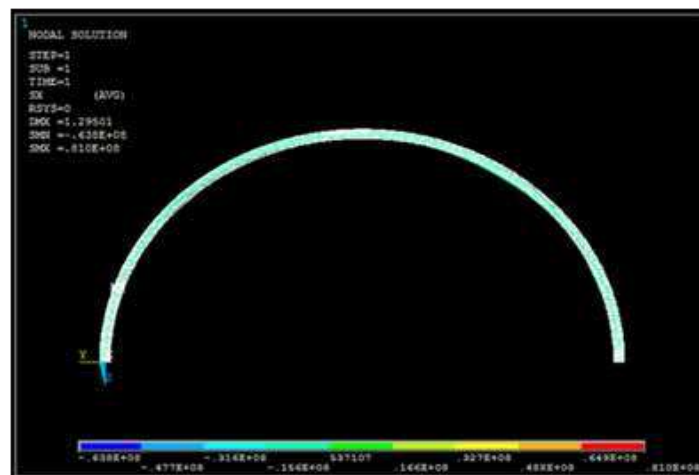


Fig. 6. Stress distribution of dia. 1m beam.

RESULTS

Table 3. Results of FEM analysis for two different diameters of air-beams

	CASE-I	CASE-II
Material	Kevlar 49	Kevlar 49
Beam diameter (in m)	1.2	1.0
Thickness(in mm)	2	2
Internal pressure(in bar)	8.7	8.7
External pressure(in MN)	2.6	2.6
Surface area (in m ²)	297.08	247.73
Mass (in Kg)	849.60	705.60
Volume(in m ³)	0.59	0.49
Min. stress(in N/m ²)	-5.50e+09	-6.38e+09
Max. stress(in N/m ²)	4.01e+09	8.10e+08
Max. Deformation (in m)	1.14949	1.29501



INTERPRETATION OF RESULTS

Figs. 1 and 4 are the geometries of air beams for diameters of 1.2m and 1m respectively. **Tables 1 and 2** indicate the data used for the beams. **Table 3**, shows the results of the finite element analysis of inflated arch beam loaded by external pressure at the top of the arch. The **Fig. 2 and Fig. 5** shows the structural deformation result from the FEM analysis. **Fig. 3 and Fig. 6** shows the stress distribution in the arch beam. The detailed FEM analysis is done on base span 50m beam. Two different diameters are analysed. Although the finite element analysis predicts the strength of the inflated beam on the higher side and it demonstrated that a problem like this can successfully be analysed using finite elements.

CONCLUSION

Inflatable structures have variety of applications and have a great potential for future. The size of Inflatable structure depends on the design of air beam. In this work the inflatable air beam structures with two diameters are analysed. The size of span is taken 50m. The air beam is mostly used in making a hangar. The inflated beams are placed in a series parallel to each other subjected to torsion and bending loads. The analysis of a single beam is presented here. These results finite element analysis of the air beam give the confidence that the design of an air inflatable structure is reliable, physically realizable and offers a cost-effective solution in case of emergencies.

REFERENCES

1. H. A. W. D. V. Ritzel, S. A. Parks, J. Crocker, "A blast and ballistic resilient temporary," p. 3459, 1888.
2. J. P. Kwake, "Inflatable structure," 1965.
3. Yen T. Huang, "Modular inflatable dome structure," 1986.
4. B. Sallee, "Inflatable truss frame," 1994.
5. A. E. Kent and C. Frank, "Curved, inflated, tubular beam," 1995.
6. G. J. Brown and G. C. Sharpless, "Braided air beam structure," 2000.
7. Glen J. Brown, "Reinforced fabric inflatable tube," 1999.
8. E. J. McNiff, "Inflatable tent," 2020.
9. R. S. W. Gary L. Bailey, "Air beam construction using differential pressure chambers," vol. 1, no. 12, 2002.
10. B. T. David Jurewicz, Glen Brown, Tom Price, Brian Gilles, Leo Lichodziejewski, Christopher Kelley, "Application of high-pressure textile inflatable structures for planetary probes," June, 2012.



Performance Characteristics of External Gear Pump with the use of Burnt Oil

Aditya Anurag Bal^{1*}, J Randhari²

M. Tech, Scholar, Mechanical Engineering Department, National Institute of Technology, Agartala, Tripura¹

Assistant Professor, Mechanical Engineering Department, Indira Gandhi Institute of Technology, Dhenkanal, Odisha²

*✉ Id-adityaanuragbal@gmail.com

ABSTRACT

The external gear pump is external rotary positive displacement pump. Gear pump provides smooth pumping action & high volumetric efficiency. It is used in industrial machine for a fluid delivery and for a cooling purpose. It is used with a wide range of fluid viscosity. In this present work with the help of external helical gear type gear pump test rig generate experimental data with the used of contaminated burnt oil as fluid medium. Setup runs at a different rpm with adjusted speed of motor through vari-o-state, which measure with the help of the tachometer. At a different rpm of gear rotor check the performance of external gear pump. The external gear pumping principle uses two rotating gears which enmesh at the suction side of pump to create a vacuum which pulls fluid into the pump. This data validates with the theoretical estimation & good agreement found.

Keywords: Contaminated burnt oil; Helical gear; External gear; Discharge pressure; Discharge flow rate.

INTRODUCTION

Pump is hydraulic machinery which is operated by use of hydraulics where liquid is a powering medium. A gear pump uses the meshing of gears to pump fluid by displacement. They are one of the most common types of pumps for hydraulic fluid power applications. Gear pumps are also widely used in chemical installations to pump high viscosity fluids. There are two main variations; external gear pumps which use two external spur gears and internal gear pumps which use an external and an internal spur gears. Gear pumps are positive displacement (or fixed displacement), meaning they pump a constant amount of fluid for each revolution[1]. Some gear pumps are designed to function as either a motor or a pump.

These hydraulic machines come across several problems during their operation if proper maintenance and repair is not carried out. Also the incorrect design of such machines may lead to unsuccessful operation. This is the reason why industries have a special maintenance department for smooth operation of the plant. Global market shows that customers want for new modifications and more flexible design in machine components, which makes the organization to concentrate more on research and development section[3]. We came across such hydraulic machine which is gear pump test rig in our institute where we found that there was a need to work on this unit. And hence all the historical data related to this gear pump test rig was collected and analyses were carried out for its improved performance.

EXPERIMENTAL WORK

System Specification

- Size of Pump: 38 cm
- Speed of Pump: 1420 rpm
- Area of Measuring Tank: 40 cm * 40 cm
- Area of reservoir tank: 25 cm* 40 cm
- Motor Efficiency = 0.8
- Standard Oil: Contaminated Burnt Oil

Gear Specification



Fig. 1. (a) Gear side view

(b) Gear side front view

The teeth on helical gears are cut at an angle to the face of the gear. When two teeth on a helical gear system engage, the contact starts at one end of the tooth and gradually spreads as the gears rotate, until the two teeth are in full engagement.

Experimental Setup

The experimental set-up consists of gear pump, in which suction side a vacuum gauge is attached while on the discharge side a pressure gauge is fitted for measurement of the delivery head. Schematic arrangement of test rig of External Gear type oil pump is shown in test rig which consists of a motor, oil sump, pressure gauge, vacuum gauge, oil reservoir, energy meter for operation. In external gear type oil pump test rig 25.4 mm pipe is used in both side suction as well as delivery side.



Fig. 2. Gear oil test

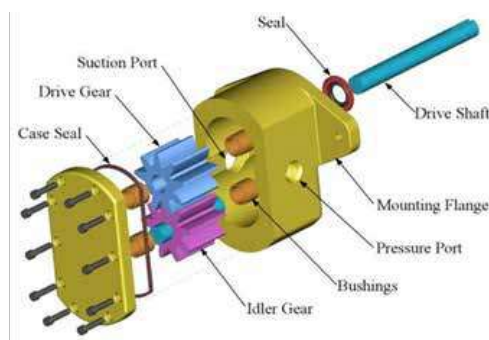


Fig. 3. Motor and pump



The modified set up consist of the following :

1. Sump tank 2. Discharge collecting tank 3. Pumping system
4. Driving system 5. Measuring system

Procedure

Start the pump and run it at a particular 'head' on it. This can be adjusted with the help of the delivery valve provided. The pressure gauge reading has to be adjusted as per valve adjustment to find out the total head on the pump. The vacuum gauge reading has to be adjusted as per valve adjustment with respect to pressure gauge to find out the total head on the pump. The time taken for 3 revolutions of energy meter disc is to be noted down. The height rise of oil in capillary tube along with time for fill up of discharge tank is to be noted down. The discharge can be calculated from the timing and height of oil rise reading taken from the reservoir tank. The input power is measured with the help of the energy meter supplied. The discharge will be slightly decreased as the working pressure increase on the pump.

Observation

Area of collecting tank= 25 cm* 40 cm = 0.1 m² Datum head= 0.45 m

RPM= 1420

Density burnt oil = 0.9 g/cm³ Motor efficiency=0.8

No. of revolutions of energy meter = 3

Use the above data to calculate discharge, input power, output power and hence calculate the efficiency and volumetric efficiency.

Table 1. Observation

S.No.	Pressure gauge (Kg/cm ²)	Vacuum gauge (mm of Hg)	Height rise of oil (cm)	Time of rise (Seconds)	Time for 3 revolution of energy disc (Seconds)
1	2	60	10.5	15.3	60
2	4	100	10	16.8	43
3	5	70	11.2	20.2	35.7

Sample Calculations

1. Actual discharge $Q = A \times h/T = \dots\dots\dots$

where A = Area of the measuring tank in meters h = Rise of oil level (say 10 cm) in meters

T = time in seconds for rise of oil level (say 10 cm)

2. Total Head = $H_d + H_s + Z = \dots\dots\dots$

H_d = Delivery Head H_s = Suction Head Z = Datum Head

3. Input = $(X/t) \times (3600) \times (1/C) \times (0.8) \text{ kW} = \dots\dots\dots$

where X= No. of revolutions of energy meter disc (say 3 rev), t = Time for Energy meter revolution disc (say 3 rev)

C = Energy meter constant

4. Output = $9.81 \times H_Q \text{ kW} = \dots\dots\dots$

5. Efficiency = Output Power/Input power = $\dots\dots\dots$

** Energy Meter Constant varies for Data 1,2,3 as 225, 200, 300 respectively in each calculation.

Sample Calculation for Data 1

P gauge = 2 kg /cm² = 196133 Pa

P vacuum = 60 mm of Hg = 7999.344 Pa



$$1. Q_{\text{actual}} = (A \cdot h) / t = (0.105 \cdot 0.1) / 15.3 = 6.863 \cdot 10^{-4} \text{ m}^3/\text{s}$$

$$2. H_{\text{total}} = H_d + H_s + Z$$

$$H_d = (\text{Gauge Density}) / (\text{Oil density} \cdot g)$$

$$= (2 \cdot 98066.5) / (900 \cdot 9.81) = 22.214 \text{ m} \quad H_s = (60 \cdot 7999.344) / (900 \cdot 9.81) = 54.362 \text{ m} \quad Z = 0.45 \text{ m}$$

$$H_{\text{total}} = 77.027 \text{ m.}$$

$$3. P_o = (W \cdot Q \cdot H) / 1000$$

$$= 900 \cdot 9.81 \cdot 6.863 \cdot 10^{-4} \cdot 77.027 = 466.733 \text{ watt} \quad 4. P_i = (X/t) \cdot 3600 \cdot (1/C) \cdot 0.8 \cdot 1000$$

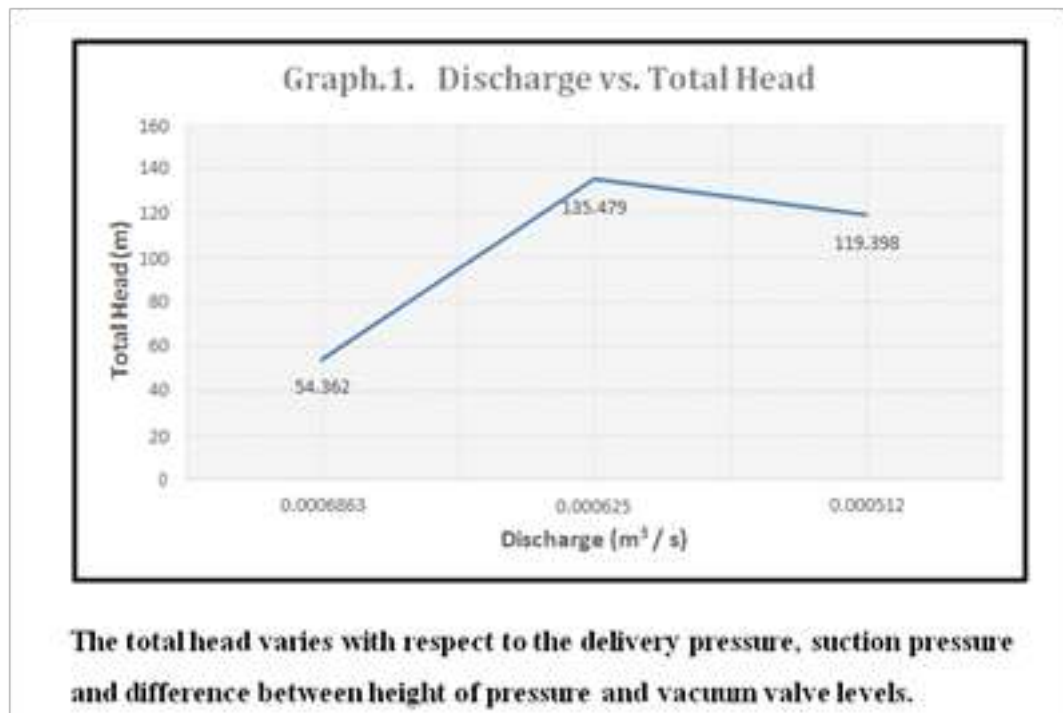
$$= (3/60) \cdot 3600 \cdot (1/225) \cdot 0.8 \cdot 1000 = 640 \text{ watt}$$

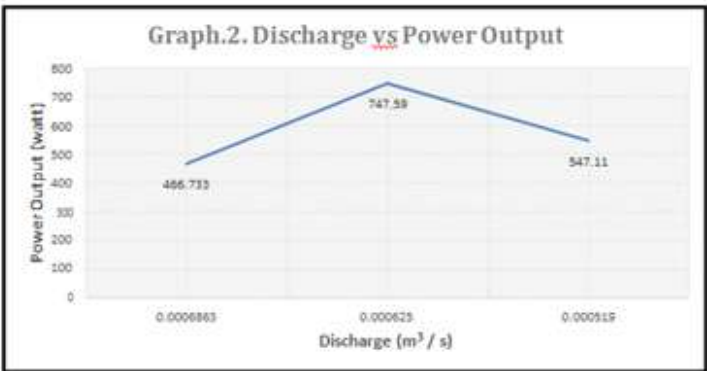
$$5. \text{Efficiency} = 72.9 \%$$

RESULTS AND DISCUSSIONS

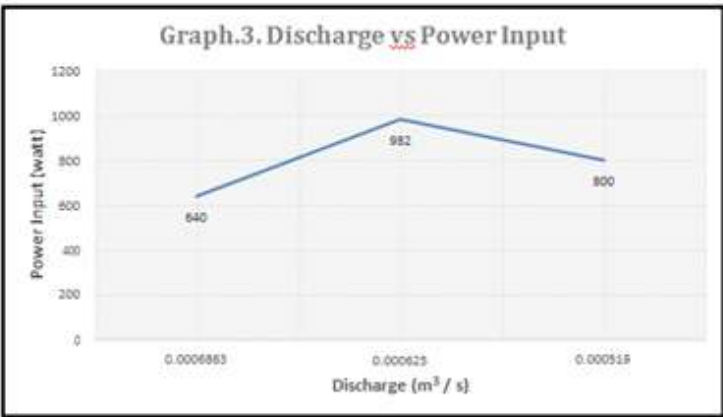
Based on the above experiment calculations carried out above we can obtain 4 graphs as shown below.

1. Graph 1 shows the relation between discharge vs total head and we found that as discharge increases to certain limit the head increases and after certain value it depreciates.
2. Graph 2 shows the relation between discharge and power output and result as discharge increases to certain limit the power output increases and after certain value it depreciates.
3. Graph 3 shows the relation between discharge and power input and result is the same.
4. Graph 4 shows the relation between discharge and efficiency and result is the same as above.

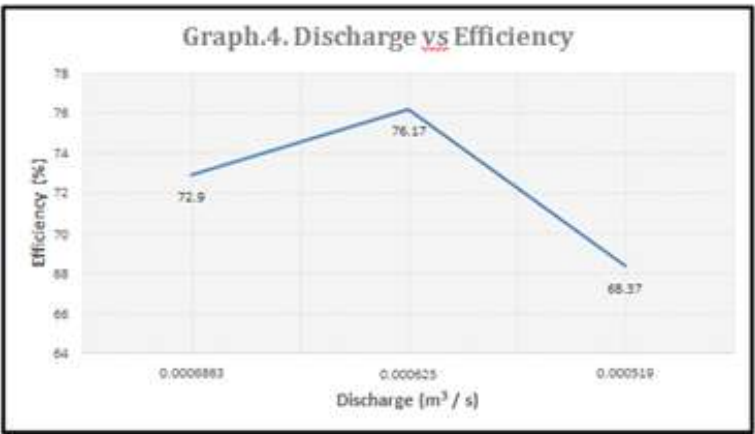




There is a change in output power produced depending on the density of the oil, the discharge rate of oil and the total head produced in setup.



Input power is affected by energy meter constant, revolution of disc, time for rise of oil level and the motor efficiency thus affecting discharge.



It is clearly seen that there is fluctuation in the efficiency of external gear pump. The efficiency is low due to the contaminant burnt oil is used and vibration of shaft, which connect the motor to the pump.



CONCLUSIONS

This study focused only on the oil flow in the suction pipe to delivery pipe and calculation of efficiency but did not consider phenomena such as cavitation, air entrainment and bubble formation. From studies it is concluded that as the rpm of gear rotor increase discharge flow rate is increase. Due to the use of burnt oil the pump efficiency decrease because of burnt oil contain less viscosity and many rust and carbon particles contamination in burnt oil.

Future studies will be extended to investigate the possibilities of cavitation, noise generation and air entrainment in the suction line, inlet ports and chambers and their effects on the pump performance. It is imperative that the amount of turbulence and entrained air is kept minimum. Entrained air can cause a reduced efficiency as well as noise and vibration.

REFERENCES

1. Rana D.A, "Performance Evaluation of External Gear Pump with The use of Burnt Oil" IJATES, Vol.03 2015.
2. Pinches, M J (2000). Kempe's Engineers Year-Book, p. 2070. Miller Freeman, Kent. ISBN 0863824420.
3. Frank Prager, Kepler as inventor, Vistas in Astronomy, Volume 18, 1975, Pages 887-889, [https://doi.org/10.1016/0083-6656\(75\)90184-1](https://doi.org/10.1016/0083-6656(75)90184-1).
4. Pellegri, M.; Vacca, A. Numerical simulation of gerotor pumps considering rotor micro-motions. *Meccanica* 2016, 52, 1851–1870.
5. Li, S.-D.; Cui, J.-K. The finite element analysis of pump body line. *Manuf. Autom.* 2011, 33, 33–37.
6. Wang, Z.-W.; Zhang, Z.-S.; Liang, W.-G.; Zhang, F. Analysis on meshing efficiency of straight conjugate internal gear pair. *Torpedo Technol.* 2013, 21, 369–374.
7. Xu, X.-Z.; Song, T.-L. Study on sliding coefficients of straight line conjugate tooth profile gear pairs. *J. Huaiyin Teach. Coll.* 2007, 3, 225–228.
8. Gao, M.-L.; Cui, J.-K.; Huang, D.-P.; Liu, S.; Zhang, L. The calculation analysis of contact ratio for straight conjugate internal gear transmission. *Fluid Mach.* 2017, 45, 28–32.
9. Hu, H.-L.; Cui, J.-K.; Xu, J.-B. Optimal design of tooth profile parameter of straight-conjugate internal gear pair. *Mech. Transm.* 2015, 39, 77–80.



Explosive Welding-The Need of Industry 4.0 for Atmanirbhar Bharat

Prabhat Kumar^{1*}, Subrata Kumar Ghosh², John Deb Barma³, S Saravanan⁴

PhD Scholar¹, Assistant Professor², Associate Professor³, Mechanical Engineering Department, National Institute of Technology, Agartala

Associate Professor⁴, Mechanical Engineering Department, Annamalai University, Chidambaram

*✉ prabhatkumar855@gmail.com

ABSTRACT

Industry 4.0 applies to nine digital industrial innovations being converged and applied: advanced robotics, additive manufacturing, virtual reality, simulation, horizontal/vertical convergence, industrial Internet, cloud computing, cyber security and Big Data and Analytics. Explosive cladding fulfilled the major challenges of industry 4.0. Explosive welding is a solid-state welding process, which uses a controlled explosive detonation to force two metals together at high pressure. In the explosive welding, two metal surfaces to be joined are kept in touch and a explosive charge is exploded against one of them. This process uses a explosive force to make an electron-sharing metallurgical connection between two metal surfaces. Explosive weld which depends on process parameters viz., explosive loading ratio, standoff distance and pre-set angle. The process parameters viz., surface preparation, stand-off distance, explosive mass, detonation energy and detonation velocity are determined through weld ability window, an analytical estimation. The explosive bonding technique has an ability to bond a variety of similar and dissimilar materials, and applied to fabricate composites such as multi-layered and wire-reinforced materials.

Keywords: Explosive welding; Industry 4.0; Weld strength.

INTRODUCTION

The age of digitalization is the Fourth Industrial Revolution, also known as Industry 4.0. Industry 4.0 applies to nine digital industrial innovations being converged and applied: advanced robotics, additive manufacturing, virtual reality, simulation, horizontal/vertical convergence, industrial Internet, cloud computing, cyber security and Big Data and Analytics. The building of railways and the invention of the steam engine caused the first industrial revolution, which lasted from about 1760 to 1840. It ushered in the mechanical manufacturing age. In the late 19th century, the second industrial revolution started and progressed into the early 20th century. Their key drivers were Henry Ford's 1913 invention of electricity and the assembly line in the automobile industry. As a result, production became much quicker, as each worker focused on only one unit of work. In the 1960s, the third industrial revolution began and was profoundly influenced by the rise of semiconductors, mainframe computers (1960s), personal computers (1970s and 1980s) and the Internet (1990s). The term Industry 4.0 reflects the fourth industrial revolution, which is characterised as a new level of organisation and control over the entire life cycle value chain of goods, based on increasingly individualised consumer requirements[1]. Industry 4.0's core goal is to meet individual consumer needs that impact areas such as order management, research research and development, commissioning of production, delivery up to use and product recycling[2]. Now, a day explosive cladding is used in various manufacturing industries such as aircraft industry, automobile industry, shipbuilding industry, etc. Because explosive welding technique has an ability to join variety of similar and dissimilar materials and also it can be created composite materials. Thus, explosive welding is need of industry 4.0.

Explosive welding is a solid-state metal joining technique employs the energy stored in a chemical explosive to clad two or more similar or dissimilar metals method together [3]. As explosive cladding process is complex, the quality of clad composite depends on the selection of process parameters viz., standoff distance, impact velocity, loading ratio and properties of explosive [4]. Explosive welding, which is termed as solid state instinctive metal joining technique, uses an explosive force to build-up an electron sharing metallurgical bond between non similar metals [5,6]. Combining of dissimilar metals is obtained through a certain critical amount of energy, which has to be spent to ensure plastic deformation and employing highly ductile and low yield strength metal as interlayer produces a strong joint [7,8]. Explosive welding is one of the important assembling technologies and is widely applied to join materials for numerous applications, such as the construction of automobiles, aircraft,

ships, gasoline pipeline and spanning bridges. Most of the solid-state welding processes can be applied to smaller shapes and thus constraining the process to produce selected components. Explosive welding offers a reliable and alternative solution to this complex problem. A small quantity of explosive can shape a tank, build a large crankshaft, has the power to weld many parts of a heat exchanger and improve the mechanical properties.

Theoretical analysis of explosive welding

Fig.1 shows the explosive welding of two dissimilar metals schematically. The top of the flyer plate is supported either parallel or with a slight angle or incidence relative to the base plate. To prevent damage from the flyer plate reacting with the chemical explosive, the top surface of the flyer plate is protected by the buffer plate.

A sheet of rubber or card board or even a thick coat of plastic paint having the same dimensions as the flyer plate may be the buffer plate. On the buffer pad, a sheet of explosive is distributed and from one end is detonated. The flyer plate collides with the base plate when detonated, obliquely creating immense pressure and temperature at the interface and causing the phenomenon of 'jetting'. The surfaces of participating metals leave two virgin clean surfaces to be pressed together to form a weld as a result of the high velocity plane. The welding has an acceptable strength equal to or greater than the strength of the weaker plate.

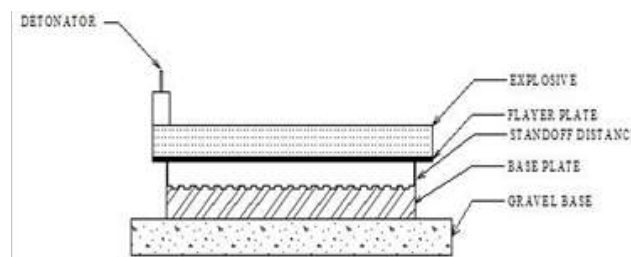


Fig. 1. Explosive welding

Basic configurations of explosive welding

In the explosive welding process two basic configurations are used parallel and inclined configurations as shown in **Figures 1 and 2**. Both of these configurations provide a standoff distance between the flyer and the base plate. To provide a distance from which the flyer plate can be accelerated to the required jetting and cladding impact velocity provide the free jet and the air between the plates with an unobstructed escape direction.

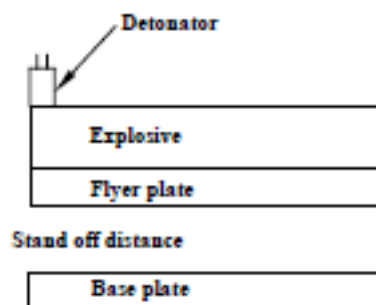


Fig. 2. Parallel configuration

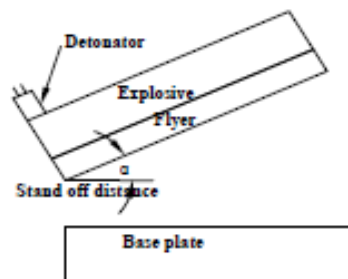


Fig. 3. Inclined configuration

In parallel configuration (**Fig. 2**), the impact velocity of the flyer plate for a given standoff distance and explosive loading will remain essentially constant over the entire weld length and is preferred when large areas are to be joined. **Fig. 3** shows the inclined configuration that is selected when an explosive with a high detonation velocity is used. Explosive characteristics, explosive loading ratio, flyer plate velocity, flyer plate thickness, base plate thickness, standoff width, anvil, surface finish and metal properties are the key parameters that define a good welding.

Explosive Welding Mechanism

It is possible to split the explosive welding process into three phases:

- (1) Explosive charge detonation
- (2) Flyer plate acceleration and deformation
- (3) Plate collision

The flyer plate, separated at an initial angle (α), moves with the velocity (V_F) upon detonation of the explosives and collapses onto the parent plate. A metallic jet is subsequently formed at the impingement line between the two plates.

As the jet sweeps away the oxide films on the surfaces of the participating metals and creates a metallurgical bond that causes the atoms of the two metals to meet at atomic scale distances, jet formation at the contact point is an essential condition for achieving a successful cladding. For interatomic bonds to be formed, the pressure produced must be sufficiently high and should last long. The time available for bonding, however is determined by the velocity of the collision point, which in turn is determined by the characteristics of the explosives. A local plastic deformation of metals at the interface is also induced by the very high pressure produced.

The pressure and the shear stress produced at the collision point are regulated by the collision velocity (V_w) and the dynamic bend angle (β).

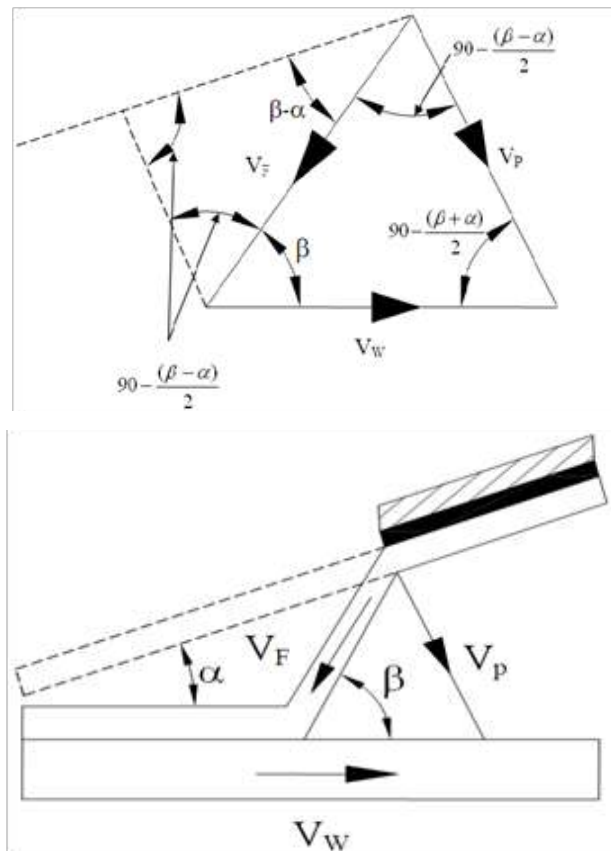


Fig. 5. Geometry of collapse of flyer plate



The advantages of explosive welding over conventional welding techniques are as follows:

- Dissimilar metals can be bonded metallurgically.
- Practically, no limitation for the size of plates to be cladded.
- Multiple layered composites and plates can be bonded in a single explosion.
- Thickness of base plate is not limited.
- Non planar objects can be successfully cladded.
- Achieves high bond strength.
- Enables welding in hostile environments.
- Maintains parent metal qualities.
- Achieves welds over large area.
- Explosive welding has the added benefit of eliminating the requirement for heat treatment, thereby saving time and making it cost effective in welding processes.

Explosive welding is generally used in industry and their application area is shown as follows:

- Chemical process vessels
- Transition joints
- Electrical applications
- Ship building
- Joining of tubes and plugging.
- Pipeline welding
- Mining
- Heat exchanger
- Clad plates for desulphurisation plants
- Joining of dissimilar metals – Aluminum to steel, Titanium alloys to Cr–Ni steel, Cu to stainless steel, Tungsten to Steel, etc.

Explosive welding has some disadvantages and their limitations are mentioned as following sentences:

- In industrial areas the use of explosives will be harshly limited by the noise and earth vibrations caused by explosion.
- The rules relating to the storage of explosives and the difficulty of preventing them from falling into unauthorized hands can well prove to be the major obstruction to the use of explosive welding.
- The metals must have high enough impact resistance, and ductility.
- Noise and blast can require operator protection, vacuum chambers, buried in sand/water.

EXPLOSIVE WELDING NEED OF INDUSTRY 4.0

The beat of the welding network beats emphatically heading into the 21st century and large projections for what's to come are commonly idealistic. It implies that welding will draw out to be utilized more later on the grounds that it has affirmed to be a beneficial and practical approach to join metals. The shopper welding business sector will keep up to give occasions to development, with home improvement and the retail foundation to help it turning into a developing business sector. It can be said that for cost-competitive reasons industry will continue to replace mechanical joining with semi automatic and automatic joining processes, giving a definite boost to welding. Development will be in elective materials, for example, plastics, composites and new alloys. Some particular portions, for example, aluminium, will become quicker than others, while the proceeding with advancements in non-metallic materials will slow a few fragments. Then again, the eventual fate of common explosives is



extremely hard to anticipate. Explosive welding method is utilized to deliver progress joints for electrical purposes, as well as different applications in the shipping industry. However, the primary market for explosive clad plates relates to the chemical industry.

CONCLUSIONS

Explosive welding plays a vital in industry 4.0 for joining of variety of similar or dissimilar materials. The following conclusions can be drawn from present study:

- In the explosive welding, two metal surfaces to be joined are kept in touch and a explosive charge is exploded against one of them. This process uses a explosive force to make an electron-sharing metallurgical connection between two metal surfaces.
- The explosion produces heat, there is no time for heat move to the metal surfaces. Accordingly, there is no apparent temperature ascend in the metals, and furthermore practically nothing dispersion happens at the interface.
- The process has been completely evolved with enormous scope applications in the manufacturing industry. Explosive welding has essentially discovered commercial application in enormous plate cladding of one metal on another, tube-to-tube plate welding, cladding one cylinder with another, plugging of exchangers, different electrical connectors, particularly those among copper and aluminum, transition pieces, particularly for pipe work in cryogenic frameworks, pipe-to-pipe welding, etc.

REFERENCES

1. M. Rubmann, M. Lorenz, P. Gerbert, M. Waldner, Industry 4.0: The Future of Productivity and Growth in Manufacturing Industries, (April 09, 2015) 1-14.
2. R. Neugebauer, S. Hippmann, M. Leis, M. Landherr, Industrie 4.0- Form the perspective of applied research, 49th CIRP conference on Manufacturing systems (CIRP-CMS 2016), 2-7.
3. F Findik, Recent developments in explosive welding, Materials and Design, 32(3), 2011, 1081-1093.
4. K Raghukandan, Analysis of the explosive cladding of cu-low carbon steel plates, Journal of Materials Processing Technology, 139 (1-3), 2003, 573-577.
5. F.Findik, Recent developments in explosive welding, Materials and Design 32 (3) (2011) 1081-1093.
6. S. Mroz, G. Stradomski, H. Dyja, A. Galka, Using the explosive cladding method for production of Mg-Al-bimetallic bars, Archives of Civil and Mechanical Engineering 15 (2) (2015) 317-323.
7. S.Saravanan , K. Raghukandan, Energy dissipation in explosive welding of dissimilar metals, Material Science Forum Vol. 673 (2011) PP 125-129.
8. Somasundaram Saravanan, Krishnamurthy Raghukandan , Kazuyuki Hokamoto, Improved microstructure and mechanical properties of dissimilar explosive cladding by means of interlayer technique archives of civil and mechanical engineering 16 (2016) 563 – 568.
9. Howes T. Explosive welding, TWI knowledge summary. UK: TWI Ltd.; 2001.
10. Crossland B. The development of explosive welding and its application in engineering. Metals Mater 1971(December):401-2.
11. Crossland B. An experimental investigation of explosive welding parameters. Metals Technol 1976;3:8.
12. Lalwaney NS. Explosive metal cladding. J Metals 1985;37(11):A92.
13. Brasher DG, Butler DJ. Explosive welding: principles and potentials. Adv Mater Process 1995;3:38.
14. Acarer M, Gulenc B, Findik F. Investigation of explosive welding parameters and their effects on microhardness and shear strength. Mater Des 2003;24(8):659.
15. Prabhat Kumar, S. Saravanan , E. Elango, K. Raghukandan, Explosive Welding of Dissimilar Metals with a Wire Mesh Interlayer, Journal of Advanced Engineering Research ISSN: 2393-8447 Volume 3, Issue 2, 2016, pp.99-102.
16. S. Saravanan , K. Raghukandan, Prabhat Kumar, Effect of wire mesh interlayer in explosive cladding of dissimilar grade aluminium plates, J. Cent. South Univ.(2019) 26: 604-611.



Analysis of Latent Heat Based IC Engine Exhaust Waste Heat Recovery System

Dr S Babu^{1*}, S A Ravi Varman², R Santhosh Mugil³

Associate Professor, Department of Mechanical Engineering, PSG College of Technology, Coimbatore¹

Project Engineer, Tata Consultancy Services, Chennai²

ME Energy Engineering, Department of Mechanical Engineering, PSG College of Technology, Coimbatore³

*✉ sjsham@gmail.com

ABSTRACT

The exhaust gas from the diesel engine exhausted to the atmosphere as waste carries approximately 30% of the heat of combustion. By providing proper Waste Heat Recovery System (WHRS), a considerable amount of heat can be saved. In the present paper, experiments are carried out to analyze the performance of thermal energy storage using PCM based compact shell and tube heat exchanger. In the current study, Paraffin RT 35 has been selected as the PCM, exhaust gas from the engine as hot fluid in tube side and water as cold fluid in shell side. The phase change in the shell- and-tube model was dominated by the effect of convective heat transfer. It is found that 0.35 kW of heat energy is saved at full load condition; it is nearly 7% of fuel power is stored as heat in the storage system, and the water can be utilized for suitable applications which are available reasonably at higher temperature.

Keywords: Phase change material; Waste heat recovery; Heat exchanger; Thermal storage; Engine exhaust gas.

NOMENCLATURE

C_p	=	Specific heat (J/kg °C)
C_{PCM}	=	Specific heat of PCM (J/kg °C)
C_{pWater}	=	Specific heat of water (J/kg °C)
C_{pl}	=	Specific heat of PCM during liquid phase (J/kg °C)
C_{ps}	=	Specific heat of PCM during solid phase (J/kg °C)
C_{pL}	=	Specific latent heat (J kg ⁻¹)
m_{PCM}	=	Mass of PCM (kg)
\dot{m}	=	Mass flow rate (kg sec ⁻¹)
ΔT	=	Temperature difference (°C)

INTRODUCTION

Energy is an important mania for the economic development of any country. The energy requirement drastically increases in the recent years because of the rapid industrial growth. A large number of industrial processes covering most industrial sectors, use significant amounts of energy in the form of heat, which are rarely, used efficiently. The methods and techniques adopted to improve energy utilization will vary depending on circumstances, but the basic principles of reducing energy cost relative to productivity will be same. Thus there is considerable scope for the use of heat exchangers and other form of heat equipment to enable waste heat to be recovered. Waste heat is generated by the way of fuel burning and then it is exhausted into the environment as a waste. Diesel engine is the one of the most efficient and versatile prime movers used in automobiles, stationary power generating plants, air compressors, construction machinery etc. Nearly about two- third of the heat generated by the engine is wasted through exhaust gas and cooling water and lost in to the surroundings. If some of this waste heat could be recovered, a considerable amount of primary fuel could be saved. Depending on the temperature level of the wasted heat and the proposed application; different heat exchangers can be employed to facility the use of recovered heat. The application

of heat recovery should be physically close to the source of waste heat for maximum benefits from recovered energy. Energy storage is needed when there is a time span between energy recovery and use. A low-cost PCM used in the thermal storage system with heat exchanger is used to collect waste heat from exhaust gas of a diesel engine and conducted an experiment utilizing waste heat as energy and recovered about 10–15% of the total waste heat for each engine load condition. The natural convective heat transfer efficiency of phase change material is somewhat low, the heat transfer efficiency drastically decreases as the PCM starts to melt and a layer of liquid matter develops. To avoid a liquid layer from developing, the space between the heat transfer surfaces where the PCM is charged should be as thin. Melting and solidification of PCM RT35 were experimentally investigated; using five various heat exchangers as heat storage systems and working at two different flow rates and two different water inlet temperatures. The obtained results are Reynolds numbers in the turbulent regime are desirable for faster phase change processes, considerable amount of the phase change time decreased (between 30% and 60%) and consequently, an increase of the average phase change power.

In this study, heat recovery system consisting of a shell and tube heat exchanger combined thermal energy storage system with PCM was designed and fabricated for waste heat recovery from diesel engine exhaust gas. Pure water is used as Heat Transfer Fluid (HTF) in both heat exchanger and thermal energy storage system. Heat energy stored in the shell and tube heat exchanger and thermal performance of heat recovery heat exchanger has been studied for various engine load conditions.

EXPERIMENTAL PROCEDURE

An experimental latent thermal energy storage unit was constructed. It has been isolated analysing the heat transfer phenomenon in the latent thermal energy storage system of the shell-and-tube type shown in **Fig. 1**. The heat exchanger system consists of a container and the HTF tubes, which are placed into the container. The heat transfer fluid flows by forced convection through the HTF tubes. The PCM has been filled within the shell space between the container and the tubes. During the engine running condition i.e. the active phase, Exhaust gas heats the PCM, the PCM melts and the heat is stored. During the discharging phase, the PCM solidifies and the stored heat is delivered to the cold fluid. It can be seen from the **Fig.1** that the HTF tubes are placed into the tube in such a way that around each of these tubes a circle can be drawn that bounds the region in which this tube exchanges the heat with the surrounding PCM. The experimental test unit consisted of two concentric tubes with 0.75 m length. The inside tube, with inner diameter of 0.016 m and outer diameter of 0.018 m, was made of mild steel while the outside tube, with inner diameter of 0.025 m and outer diameter of 0.028 m, was made of aluminium.

The PCMs having a suitable melting temperature should be selected for appropriate application. PCMs with high latent heat, high thermal conductivity and specific heat are desirable for waste heat recovery application. The thermo physical properties of paraffin wax used in the experiment are presented in **Table 1**.

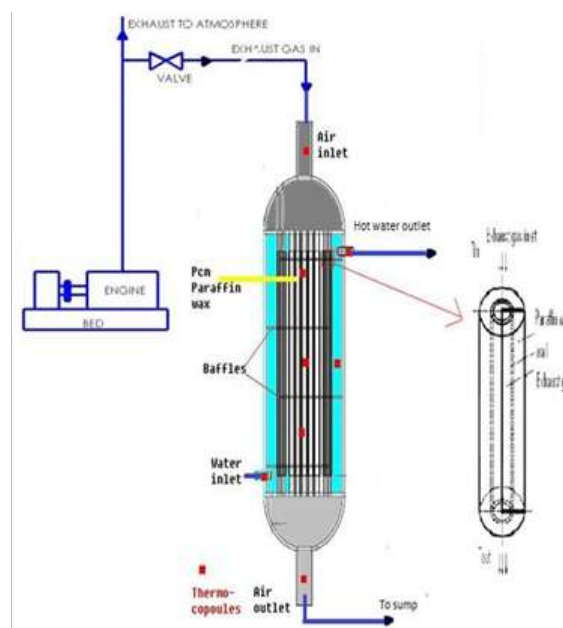


Fig. 1. Schematic diagram of integrated shell and tube heat exchanger

The values supplied by the manufacturer might be varied. Therefore, pre-characterization of PCM is recommended to get correct thermo physical properties of PCMs. Usually very small quantity of product is applied to the machine to measure the properties. Paraffin wax is the most suitable option due to its availability, non-corrosiveness, compatible melting temperatures, and low cost. Paraffin wax PCM was selected for this experiment.

Table 1. Thermo physical properties of paraffin wax

Descriptions	Value
Melting temperature	56.70C
Thermal conductivity (solid)	0.1383 W/m.0C
Thermal conductivity (liquid)	0.1383 W/m. 0C
Specific heat (solid)	2890 J/kg.K
Specific heat (liquid)	2890 J/kg.K
Density (solid)	947 kg/m ³
Density (liquid)	750 kg/m ³
Latent heat	209 kJ/kg

EXPERIMENTAL METHODOLOGY

The experiments are conducted by operating the engine at various load conditions. A few test runs are required in order to check the leakage of PCM and to calibrate the system. Charging experiment is performed when PCM comes in the solid state. The initial condition for charging is established when all thermocouples inside the paraffin shows the same temperature. During charging (melting of paraffin wax), hot air from the engine exhaust, over the melting range of PCM. The charging experiment is finished when the reading of all thermocouples is above the melting temperature range. The discharging (solidification of paraffin wax) experiment is then started with established conditions. Several experiments are conducted to check the repeatability of the results. The experiments are conducted for 25%, 50%, 75% and full load condition. The results along with the evaluated parameters are analysed and discussed in the following section.



Fig. 2. Photographic view of the experimental setup

The PCM-integrated shell and tube heat exchanger effectiveness is predicted from the energy and mass balances involved in the system. The useful energy from the exhaust gas is

$$\text{Heat gain } Q_u = m c_p (\Delta T) \quad (1)$$

The useful heat gain general equation above can be further elaborate into three equations when involved PCM. Since PCM is a phase change material, it consists of sensible heat and latent heat. The equations are as below

Heat gain when PCM is in solid state:

$$\text{Sensible heat } Q_u = \dot{m} c_{ps} (T_{s2} - T_s) \quad (2)$$

Heat gain during phase change:

$$\text{Latent heat } Q_u = m c_{pl} \quad (3)$$

Heat gain when PCM is in liquid state:

$$Q = C_{pl}(T_{L2} - T_{L1}) \quad (4)$$

The shell and tube heat exchanger operation strategy is that the experiment is to use after the engine was stopped. During the charging time heat source is the exhaust gas whereas for discharging time the heat can be obtained from PCM.

RESULTS AND DISCUSSION

The temperature variation of the exhaust gas and the water at the inlet and outlet of the Heat exchanger with respect to time for various engine load conditions (25%, 50%, 75% and full load) is shown in **Figures 3– 4**. In a diesel engine normally the temperature of exhaust gas will attain steady state within a period of 5 min at a given load. As the engine load increases the exhaust gas temperature also increases due to its higher heat release from the engine. At all loads it is observed from the water and the gas outlet temperature variation that the temperature increases at the beginning and the slope decreases when the temperature of the water attains approximately 45°C and further increases at a higher rate after a certain interval of time. It is also observed from the figures that there is a large temperature drop in the exhaust gas at all times and the increase in temperature of the water is very low since the heat capacity of the water (mwatcp.wat) is much higher than the heat capacity of the exhaust gas (mgcp.g).

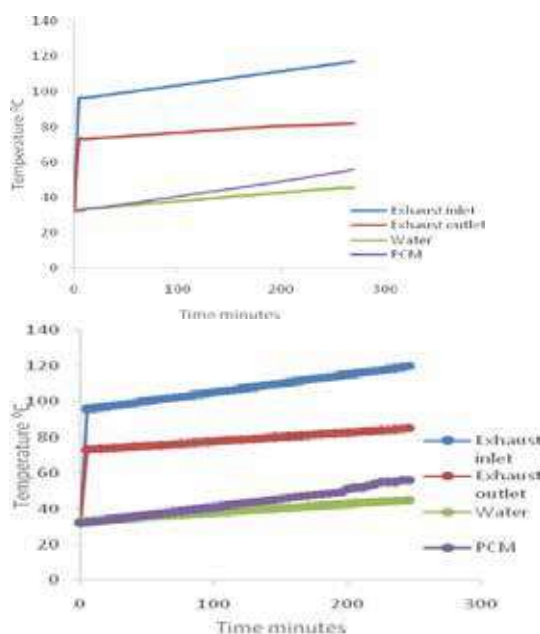
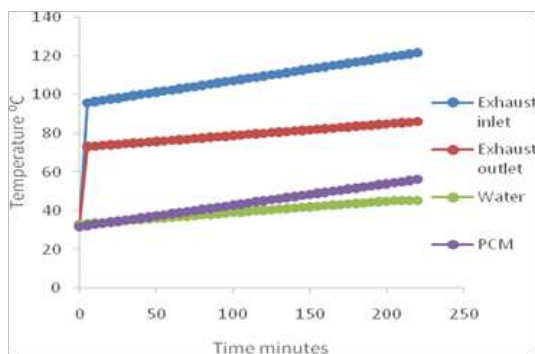


Fig. 3. Temperature variation of the exhaust gas and the water at the inlet and outlet at [a) 25% load and b) 50%load]

The time taken by the PCM to reach its melting point and the water to reach 45°C at 25%, 50%, 75% and full load are about 275, 245, 220, 190 minutes approx. Thus the charging time decreases with the load increases. The faster charging at higher loads reduces the losses encountered during the charging process.



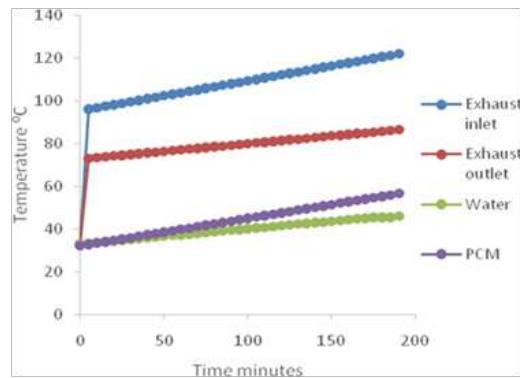


Fig. 4. Temperature variation of the exhaust gas and the water at the inlet and outlet at [a] 75% load and b) 100%]

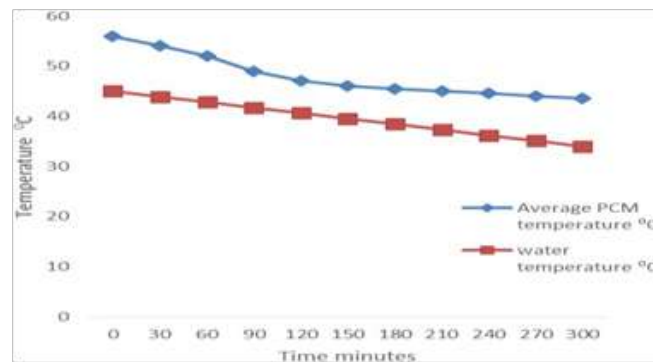


Fig. 5. Energy discharging with time intervals

Fig. 5 shows the temperature of PCM and water for different time intervals. The water temperature can be maintained for more time with proper insulation. The temperature can be maintained for about 5 hours.

The pressure drop can be calculated from the manometer reading connected at the exhaust gas inlet. The pressure drop inside the tubes through which the exhaust gas flowed need to be reasonable to avoid back pressure. **Fig. 6** shows the pressure drops inside the tubes of the heat exchangers at different loads. At 25%, 50%, 75% and 100% loads, the pressure drops were 20.4, 25.7, 27.8 and 31.3 kilo Pascal(kPa) respectively.

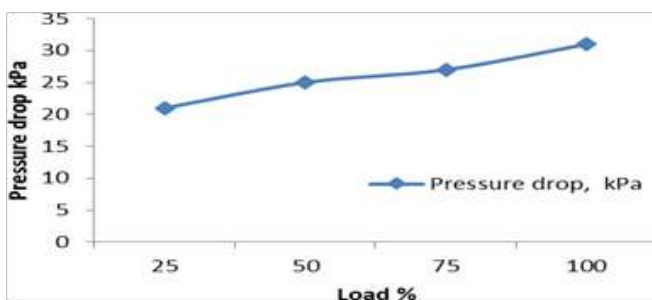


Fig. 8. Pressure drop across the heat exchanger at various loads of the engine.

CONCLUSION

The exhaust gas of a diesel engine carries a lot of heat and this energy can be recovered efficiently using Waste heat recovery system. A suitable WHR system with a large capacity of TES tank can store heat energy and this energy can be utilized for many applications like process heating etc., in industries. In the present work a shell and tube heat exchanger and a PCM based Thermal Energy Storage tank of about 80 litres were designed and fabricated and tested by integrating them with a diesel engine of capacity 3.7 kW.



The investigation has shown the following conclusions: Nearly 10–15% of total heat (that would otherwise be gone as waste) is recovered with this system. The maximum heat extracted using the heat exchanger at full load condition is around 0.35 kW.

The PCM material integration helps in retaining the heat for longer time than normal shell and tube heat exchanger. Thus, it is concluded that integrated shell and tube heat exchanger systems are a commercially viable option for waste heat recovery systems where both the hot water and filtered exhaust gas can be laundry and industrial applications.

REFERENCES

1. V. Pandiyarajan, M. Chinna Pandian, E. Malan, R. Velraj, R. V. Seeniraj, “Experimental investigation on heat recovery from diesel engine exhaust using finned shell and tube heat exchanger and thermal storage system”, *Applied Energy* (2011), Vol 88, pp77–87.
2. Jungwook Shon, Hyungik Kim, Kihyung Lee, “Improved heat storage rate for an automobile coolant waste heat recovery system using phase-change material in a fin–tube heat exchanger”, *Applied Energy* (2014), Vol 113 , pp 680–689
3. M. Medrano, M. O. Yilmaz, M. Nogués, I. Martorell, Joan Roca, Luisa F. Cabeza, “Experimental evaluation of commercial heat exchangers for use as PCM thermal storage systems”, *Applied Energy* (2009), Vol 86, pp 2047–2055.
4. S. Senthur Prabu, Asokan M.A., “A study of waste heat recovery from diesel engine exhaust using phase change material” *International Journal of Chetech Research* (2015) Vol.8, pp 711-717.
5. S. P. Raja, R. Rajavel, D. Navaneethakrishnan “Experimental Investigation Of Heat Recovery From Diesel Engine Exhaust Using Compact Heat Exchanger And Thermal Storage Using Phase Change Material(2014)IJIRSET, pp 2663-2670.
6. A. Tıp, “An experimental and numerical investigation of heat transfer during technical grade paraffin melting and solidification in a shell-and-tube latent thermal energy storage unit,” *Solar Energy* (2005), vol. 79, pp 648–660.
7. M. J. Hosseini, A. A. Ranjbar, K. Sedighi, and M. Rahimi, “A combined experimental and computational study on the melting behavior of a medium temperature phase change storage material inside shell and tube heat exchanger,” *International Communications in Heat and Mass Transfer* (2012), vol. 39, pp 1416–1424.
8. M.J. Hosseini, M. Rahimi, R. Bahrampouri, “Experimental and computational evolution of a shell and tube heat exchanger as a PCM thermal storage system “*International Communications in Heat and Mass Transfer* (2014), pp 128-136.

Materials & Metallurgical Engineering



Salvaging used Reformer Tubes for Conserving Nickel

Satish Bhagwan Kunte

BE Metallurgy from COEP, College of Engineering Pune, Maharashtra

✉ sbkunte@gmail.com

ABSTRACT

The case studies deal with salvaging of used centrifugally cast reformer tubes for an extended life. The study describes two such exercises, one dealing with HK-40 tubes and the other with HP- micro alloyed tubes. In both cases the recovery/reinstallation procedures were successful, giving good life extension. Such attempts could result in huge savings on the reformer tube inventories. It can also conserve the expensive raw material, Nickel, which can be used for other strategic applications

INTRODUCTION

It is strongly felt that we will not be able to meet the rising demand of Nickel, unless we stop the extravagant use of Nickel globally. Reformer tubes used in fertilizer and petrochemical industry is an item which uses a large quantity of Nickel. The author has an extensive experience in Manufacturing Centrifugally Cast Reformer Tubes, Testing and Inspecting the Reformer Tubes and Monitoring the health of the Reformer Tubes when they are in actual use. The author details in this paper the advantages gained in recycling the used Centrifugally Cast Reformer Tubes for conservation of Nickel. The Drawn or Extruded Reformer Tubes are commonly Salvaged or Reused after proper Solution Annealing heat treatment but Centrifugally Cast Reformer Tubes with a Dendritic Micro Structure cannot be Solution Annealed and have never been recycled. The scrapped Reformer Tubes are simply a source of Nickel for making other Nickel containing equipment. For manufacturing Reformer Tubes, all the International Standards recommend use of only fresh Nickel.

COMMONLY USED MATERIALS OF CONSTRUCTION

The industry has seen the material of Reformer Tubes change from HK40 to IN519 and now to HP- micro alloyed. The wall thickness of the Reformer Tubes reduced from about 17 mm in the past to the present about 10 mm without losing strength and other high temperature properties. This is a major advantage with respect to heat transfer; increase in volume and also with respect to the total weight of the tubes which result in series of benefits.

But, in the process, the requirement of Nickel has increased from 20% in the old HK40 tubes to 35% in the present HP- micro alloyed tubes. The attached Table shows the nominal chemical composition of HK40, IN519 and HP micro-alloyed tubes, with the approximate sound wall thickness commonly used.

Nominal Composition of Reformer Tube Alloys

Common name	C %	Cr %	Ni %	Nb %	Mn %	Si %	Other	Tube Wall thickness
HK 40	0.4	25	20	-	2 Max	2 Max	-	17 mm
IN 519	0.4	25	25	1	1.5	1.5	-	15 mm
HP Micro-alloyed	0.4	25	35	1	1	1.4	Micro alloy additions Ti, Zr, W, Cs	10 mm

This is the situation only about the reformer tubes. But in general also, the demand for Nickel is rising globally and with the current rate of consumption we may run out of fresh Nickel from Mother Earth by the end of this century.

DESIGN LIFE OF REFORMER TUBES

The reformer tubes are normally designed for a service life of 100000 running hours under normal operating conditions. The life is generally limited by creep failures. In practice there are several factors contributing to the loss of creep properties thereby making it difficult to run the tubes till the end of the desired life.



These factors are

- Thermal shocks due to tripping of the furnace.
- Localized overheating due to powdering or settling of the catalyst.
- High Thermal Gradient from top to bottom of the tubes.
- Undesired excessive firing of the burners.
- Bowing of the tubes due to restrictions in the free expansion and contraction of the tubes.
- Inadequate induced draft in the furnace.

Since accidental failure of a Reformer Tube is a very expensive affair in terms of fire hazard and production loss, the Reformer Tubes are very promptly replaced after extracting about 80 to 90% of the design life, depending on the maintenance practices being followed. The replacement could be sometimes much before that in the want of continuous running of the plant for higher production. This again means hike in the demand for Fresh Nickel beyond projection.

OPERATING CONDITIONS AND MAKING OF THE TUBES.

As per the existing norms all over the world, the Reformer Tubes are supposed to be made from fresh raw materials & no melting scrap material is allowed in the recipe. The author, being a metallurgical engineer, learnt the art of making centrifugally cast reformer tubes and other heat resistant castings in a leading foundry. The work involved planning and executing quality control at all stages of manufacturing. Spectrographic analysis of molten charge ready for pouring unto the hydraulic pressure test of the finished reformer tube assembly, to the complete satisfaction of the third party inspection agency was a routine activity.

This initial experience in the intricacies of the quality of centrifugally cast tubes has been of great help in his present responsibility, spanning a period of about twenty nine years of monitoring health, of various plant equipments in RCF. RCF is a huge fertilizer manufacturing complex, where hundreds of reformer tubes are in service in different plants. The responsibility of Plant Health Services includes, among others, monitoring the behavior and performance of Reformer Tubes & analyzing their routine and unusual failures. The author also got an opportunity to carry out entire third party inspection activity for ninety numbers of HP micro alloyed reformer tubes being manufactured for RCF in a well reputed foundry. He has thus been a witness to the gradual transition of the metallurgy of Reformer Tubes, from HK40 through IN 519 to the present HP micro alloyed, which took place gradually over the last three decades.

The reaction in the Reformer Tubes is Endothermic. The reformer furnaces in RCF are side fired. The reaction is at the peak in the top portion and it slows down towards the bottom side of the tubes. The tubes therefore tend to remain cooler at the top and to become hotter towards the bottom. If the tubes are designed to operate at TST (Tube Skin Temperature) of 870OC and if the bottom portion of any given tube is at 890OC, the top portion of the same tube could be at 820OC or 830OC or even less. Under ideal conditions the thermal gradient from top to bottom of the tubes should be at minimum level. But in practice reformers are operated sometimes with this gradient as 100OC or even more. For all practical purposes, a gradient of 20 to 30OC can be considered as very good.

Due to continuous high TST, the reformer tubes are more prone to failure in the bottom one third portions. More than 90% of the Reformer Tube failures were recorded in the bottom one third portions only. Very rarely tube failures were recorded above bottom one third regions due to localized overheating. Not a single failure was recorded in the top one third portion. As the tubes get older, they start losing their high temperature strength. The rate of losing depends largely upon their skin temperature.

NON DESTRUCTIVE TESTING OF THE REFORMER TUBES.

During the service life only the outer surface of the tubes is available for carrying out all Non Destructive testing like Microstructure, Ultrasonic Flaw Detection, Dye Penetrant Test, Magnetic Permeability Test, OD (Outer Diameter) measurement, Radiography, Soap Bubble Test etc. Out of these, the tests which tell the inside story are mainly carried out on the weld seams. The general feeling is that weld seam is the weakest portion and the cracks in the tubes originate from welds. However, many a times it has been observed that the tubes crack in the parent metal away from the weld. So the weld seam need not be treated as a part of the tube most susceptible for cracking. Secondly Reformer Tubes with only one joint and that too without using filler wire are already in use in the industry.



It is not a very common practice to carry out Radiography of the Reformer Tubes to assess the health condition and residual life. Even if radiography is carried out, it is done only for the weld seams. Ultrasonic Flaw Detection and Magnetic Permeability Tests are very commonly carried out for the entire length of the tubes. It is very tricky and difficult to co-relate the results of these tests with the residual life of the tubes. The microstructure is studied only on the outer surface of the tubes and it can not tell the story on the inside surface of the tubes. It may not be advisable to correlate the deterioration observed in the Micro Structure on outer surface of the tubes with the residual life as it may not be leading to sudden failure. The Dye Penetrant test is also done only on the weld seams and it tells about the damage that has already occurred. The soap bubble test can be done for the entire tube but it also tells about the defects that already exist.

MONITORING THE AGEING PROCESS OF THE REFORMER TUBES

The inside surface of the tubes has a machined finish but the outer surface of the as Cast Tubes has a rough shiny granular finish. As the tubes grow older, the outer surface of the tubes starts becoming smooth and gradually loses the shine. Anyone closely associated with the reformer tubes for a long time can tell the approximate age of the tubes just by examining their surface finish.

The Reformer Tubes in the present generation have a good resistance to creep. But with ageing, as they start yielding and as they gradually bulge, the surface finish starts changing. The tubes can be taken as young for the first five years of operation as they exhibit very less bulging during this period. This largely depends on the operating conditions.

The TST of the tubes has the maximum impact on their ageing process. The design of the modern Reformer furnaces is generally spacious & the possibility of the tubes receiving undesired heat flux from the neighboring tubes and from the furnace walls is minimized. Some of the tubes which run below the design TST, exhibit very less increase in the outer diameter even at the fag end of their life, whereas some tubes running at higher TST show excessive sudden bulging even in their young age. For a particular design operating pressure and temperature the manufacturer of the reformer tubes specifies the maximum allowable bulging and advises not to use the tubes beyond this bulging which is normally 2 to 3% for the HP- micro alloyed tubes.

So the warning on the tubes could be; “Best realized before 100,000 running hours or 2% bulging whichever is earlier”.

As the Reformer Tubes run hottest in the bottom one third portions, the bulging of the tubes is maximum in these regions and so are the failures. The bulging of each tube is monitored during every possible opportunity during a shutdown of the plant. Experience shows that the bulging of the tubes in top one third portions is insignificant and for assessing the residual life, the bulging of the tubes in the bottom one third portions needs to be monitored very closely. Following is the summary of the record of the measurement of the OD in bottom one third portions of all the ninety tubes in methanol reformer at RCF.

Initial OD in mm 1997	Min & Max OD 2005	Min & Max OD 2006	Min & Max OD 2007	Remarks
129.4mm to 130.2mm	130.5mm and 132.2mm	131mm and 134.6mm	131mm and 134.6mm	Tubes with more than 133 mm OD were replaced

REPLACING OLD REFORMER TUBES

The tubes showing sudden excessive bulging are more likely to fail than the tubes bulged to the same extent steadily over a long period. The tubes bulged steadily to the maximum allowable limit over a prolonged period which is substantially less than the design life, can work further as the rate of bulging is not drastic. Similarly the tubes which have bulged less than 1% but have almost lived their designed life can also give some more service. In the case of methanol reformer at RCF a life of 1,10,000 running hours has been extracted from few HK 40 tubes as their bulging was less than 1% throughout their life.

In reality no one wants to take any chances on Reformer Tubes and they are replaced in time. Slightly unhealthy and failed tubes are replaced immediately, and when the life of majority of the tubes comes to an end, all the tubes are replaced together, as no one prefers to run the reformer with a combination of fresh and old tubes. Replacement is anyway easy and preferred in modern times. Everything ultimately leads to hike in the demand for Nickel.

EXPERIMENT DONE ON USED HK 40 REFORMER TUBES

The Reformer in Methanol plant at RCF had 90 numbers of HK 40 tubes. The Reformer was of an old design and all the outlet pigtails and headers were inside the furnace. During a shutdown about 35 old damaged tubes were replaced with new HK 40 tubes as a planned activity. Due to such unavoidable partial replacements, the reformer always ran with a combination of some



very old tubes and some fresh tubes. The removed 35 tubes had only scrap value and procurement of new tubes was not planned immediately.

The failed, aged, and discarded 35 numbers of tubes were inspected thoroughly. Bulging measurements and micro structure analysis was carried out on each tube. The bottom two third portion of all these tubes was discarded, regardless of its condition. The top one third portion and about a meter extra (depending on the position of the first weld seam) of the discarded tubes was found useful from metallurgical point of view. The good portions of the discarded tubes were salvaged and ten new tubes were fabricated from these portions in-house. The bottom reducers and grid plates were salvaged from the discarded tubes. These tubes were put into service after an accidental failure of few tubes. These reconditioned tubes worked satisfactorily for about 30000 hours (four years) till all the ninety HK 40 tubes were replaced with HP- micro alloyed tubes during Revamping of the plant. This resulted in considerable cost saving and the plant could be run on full load in spite of non availability of new tubes.

SIGNIFICANCE OF THE EXPERIMENT ABOVE

This activity, never attempted before in the History of Centrifugally Cast Reformer Tube application Industry, was initially felt only as a salvaging operation for emergency use. The importance associated with the crisis for Nickel and all other expensive natural resources was not seriously taken those days as they are focused today.

EXPERIMENT DONE ON USED HP- MICRO ALLOYED REFORMER TUBES

In the same Reformer many of the same HP- micro alloyed tubes almost reached the end of their design life over a period of time. There had been accidental failures of the Reformer Tubes and the Reformer had to be operated with a combination of old and new tubes again. During a turnaround, twenty five seriously damaged tubes were replaced with new ones. The Reformer was then running with the undesired combination of some old tubes and some fresh tubes. It was planned to replace the entire reformer and the project was likely to be completed within a couple of years. Till then the Reformer had to be run with many old tubes which were installed about fourteen years old because of the difficulty and very high cost of purchasing Reformer Tubes in small quantities.

All the discarded twenty five Reformer Tubes lying in the scrap yard were therefore inspected thoroughly. Eight tubes which had developed crack and which were run in blanked condition for some time were totally discarded. The bottom half portions of the remaining seventeen tubes along with pigtail was discarded without any testing. It was planned to fabricate at least four good tubes from the seventeen top half portions of the discarded tubes. Eight good reducers and grid plates were salvaged from the scrapped tubes. The seventeen top one third portions were subjected to following tests.

1. Straightness and dimensions: The lengths were matched in such a way that the coldest end i.e. the topmost portion of the tubes becomes the bottom most portion of the new tube.
2. Bulging through out the length.
3. Microstructure study of the tubes selected at random
4. Tensile strength testing of random samples.
5. Macro structure study of sample rings selected at random.

The excessively bent portions and most of the portions of the tubes below the first weld seam were discarded. The Macro Structure did not reveal the original proportion of Equiaxed and Dendritic Columnar Grains. Some failed tubes exhibited good amount of equiaxed grains but the older tubes mostly showed columnar grains. No Macro Fissures were observed. The Microstructure analysis and the Tensile Strength values did not show any abnormal deterioration and accordingly the bulging of these portions was also to the extent of about 0.6%.

Desired lengths were measured and marked for making four new tubes. The inspection and testing norms were set just like making new tubes. The machined surface was checked with dye penetrant testing before welding and no porosity was tolerated. Welding of the selected pieces was carried out with the same WPS used for making fresh tubes. Root Dye Penetrant Test, Final Pass Dye Penetrant Test and 100% radiography was carried out. There was not much rejection in carrying out welding of the old used tubes and the weldability of the material was found well within acceptable limits. Brand new pigtails were welded to the reducers and four new tubes were made ready for Hydraulic Test. Hydro Test was carried out at the same pressure like brand new tubes. The pressure was held for a much longer time than the time specified for new tubes. There was no leakage observed.



All the fabrication, inspection, testing and witnessing was done in-house. Just making of the tubes this way does not mean Recycling Nickel. All the four Reformer Tubes Reborn from scrap material were put into service. They were subjected to real acid test as they were installed in the corners where the tubes receive maximum heat from side walls. The tubes were in service for 14 months i.e. about 10000 hours. The tubes thus contributed about 2400 tonnes of Methanol production during their second life.

CONCLUSIVE COMMENTS

All the Nickel in the Reformer Tubes does not die in the Reformer Furnace . Some more life is still left in the cold end of the Reformer Tubes. The cold end i.e. the top portion of the tubes does not get exposed to temperatures as high as the bottom portion and hence retains its original Metallurgical properties to a considerable extent. The cost for making one good tube from three used tubes is less than ten percent of the cost of new tube and the life expected from this tube could be anything between 20000 to 40000 running hours or three to five years. It will depend on how carefully the Tubes are inspected during fabrication and how carefully all the Reformers are operated as per the specified norms.

The extravagant use of Nickel or for that matter all resources by us may deprive our future generations of fresh Nickel. Salvaging Reformer Tubes this way may postpone fresh Nickel from going out of stock situation and we may escape abuses and curses from our own grand children and great grand children for our extravagancy. There is no doubt that Man is a genius creation by the Almighty. There may be new Materials of Construction invented without Nickel in it for Reformer Tubes in future by this Genius but fresh Nickel will be gone forever from the Womb of the Mother Earth.

ACKNOWLEDGEMENTS

The author is highly thankful to the RCF management for giving freedom to him for carrying out the unique exercise of salvaging used Centrifugally Cast Reformer Tubes and putting them back into service which was never attempted before in the history of Reformer Tube industry. The author is also thankful to Dr. Ellaya Perumal, Corrosion and Metallurgical consultancy, Bangalore for making the write up presentable as a technical paper by giving his valuable inputs.



Spinel Magnesium Aluminate by Sol-gel Assisted Combustion Process and Its Characterization

Soumya Mukherjee

Department of Metallurgical Engineering, Kazi Nazrul University, Asansol, West Bengal

✉ mmukherjee3@gmail.com

ABSTRACT

Utilizing precursors of Magnesium, aluminium nitrates in 1:2 molar ratios along with citric acid both as fuel and reducing agent spinel is synthesized. Initially nitrate precursors are mixed properly in distilled water followed by citric acid addition and the resultant is given mild heating in hot plate for partial combustion to obtain gel. Gel is made to dry and undergo annealing at 800°C for 5 hours to obtain the required phase. Thermal analysis is carried for the gel to determine spinelization temperature before annealing. Phase analysis by XRD is carried to determine the phase followed by bond information from FTIR analysis in terms of M-O co-ordinations. Morphology of the sample is analyzed by SEM to be uniform, spherical shape with little bit of agglomeration tendency.

Keywords: Magnesium aluminate; Spinel; Phase; FTIR; Morpholog.

INTRODUCTION

Spinel structure based Magnesium aluminate is a versatile ceramic compound and it possesses high melting point (2135°C), high temperature mechanical strength, chemically inert, good thermal shock resistance making it best suitable for metallurgical, chemical, electrochemical industrial applications. Synthesis process plays a pivotal role in controlling purity and reactivity of spinel magnesium aluminate. [1-3] Several chemicals are released in the form of toxic compounds by various operations carried in textiles, leather, refinery, plastics and chemical dye processing. Ceramic catalyst as spinel like magnesium aluminate can be used for effectively for inhibiting detrimental effects of such released toxic compounds and also to reduce environmental hazards. [4] Spinel could be viable for catalyst applications depending on certain features like high surface area, small crystallite size, more numbers of active sites are essential for effective performance. Material also possesses low coefficient of thermal expansion, resistance to acids and bases, catalytic and optical properties. [5] Spinel is fit for refractory engineering applications and mostly prepared industrially by solid state processes. Purity, morphological features of powder obtained is found to be depends on process parameters. Simplicity of the process, experimental set up is one of the attractive features of this method which involves redox reaction between nitrate ions acting as oxidant with citric acid acting as fuel and reducing agent leads to form oxide material at lower temperature. Dense bodies of spinel is produced by conventional solid state reaction, high temperature, but prolonged soaking period or reaction time causes grain growth and hard agglomerates formation. It also leads to inhomogeneity, lack of stoichiometric control which may impede the property required for high end applications. [6] Various wet techniques are carried to improve the desired properties for versatile applications and at the same time such process also reduce the sintering temperature, improvement of sinterability, proper stoichiometric control and morphology with controlled grain/crystallite size. Some of the process that are followed are as follows, hydroxide or carbonate salt precipitation [7], traditional sol-gel process [8-10], spray drying [11], freeze drying [12], mechanochemical synthesis [13, 14], hydrothermal [15, 16] and others. Amongst all the above mentioned chemical routes sol-gel process is quite popular and in the present article, sol-gel assisted combustion route is utilized to synthesize spinel magnesium aluminate followed by phase analysis, bonding and vibration analysis by FTIR along with morphological feature studies by SEM.

EXPERIMENTAL

Initially magnesium nitrate, aluminium nitrate as precursors were mixed in stoichiometric ratio gets dissolved in 5 ml deionized water followed by slow addition of anhydrous citric acid. Resultant solution was then stirred at 80°C for 3-4 hours to obtain gel powder after combustion of solution which undergoes thermal analysis to obtain the spinelization zone for phase formation. DTA/TGA analysis was carried out with: MODEL NO. : Pyris Diamond TG/DTA MAKE: PerkinElmer (Japan) with Nitrogen Atmosphere purging at a rate of (150ml/min) inside platinum crucible with alpha alumina powder as reference while the heating

rate was about 15 °C/min with sample weight of about 5 mg. Annealing of powder was carried in air at temperatures around 800°C for 5 hours to get the required spinel phase by solution combustion route. X-Ray Diffraction analysis was carried out with Bruker D8 Advance for all the samples under identical conditions with Cu K α radiation whose operating was 40 KV, 40 mA current rating with scanning rate of 1°/min and in the range $2\theta = 10-90^\circ$. For FTIR spectroscopy the sample was prepared by adding KBr to the sample to make a pellet by hydraulic pressure. One KBr pellet was also made for the reference material. SEM analysis (Hitachi S-4800, Japan) was carried to obtain the morphology of the sample after putting the powder sample on carbon tape with gold coating for better observation without any static charging effect.

RESULTS & DISCUSSION

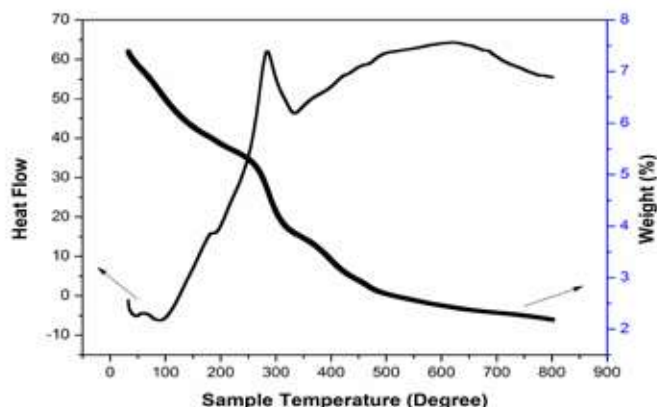


Fig. 1. DTA-TGA curve of spinel precursors with heating rate of 15°C/min

Fig. 1 indicates notable weight loss in the temperature range between 100°C to 200°C as noted from DTA-TGA curve. It is noted that there are two endothermic peaks one at at about 100°C and another one is at about 200°C in DTA. Endothermic peak at 100°C suggests removal of physically absorbed water and peak at 200°C suggests removal of structural water. There is large exothermic peak due to oxidation of organic compounds and this corresponds to 2nd weight loss with progress of scanning over temperature range. It is noted that about 350°C there is an endothermic peak due to formation of γ -alumina. At about 450°C there is another small endothermic peak which associated with decomposition of nitrates while weak broader exothermic peak which refers to start of crystallization/spinelization process within range of 500-700°C. [2]

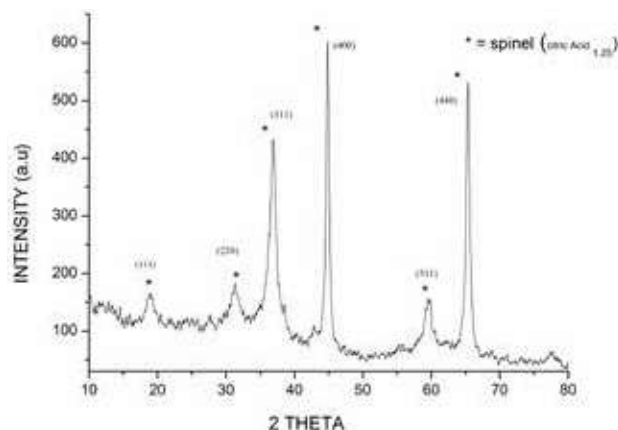


Fig. 2. XRD curve of spinel Magnesium Aluminate with scan rate of 5°/min after heating at 800°C for 5 hours.

X-ray diffraction patterns of the prepared samples annealed at 800°C is shown in **Fig. 2**. X-ray analysis exhibit complete conversion of the precursor to spinel and indicates a single phase cubic (face-centered cubic, Fd-3m with lattice size of 1.1909Å, ICDD card # 77-1193). At this temperature, the peaks of the produced powders appeared at 2θ values of 18.87°, 31.266°, 36.900°, 44.942°, 59.722°, 65.373° corresponding to diffraction planes of MgAl₂O₄ phase (111), (220), (311), (400), (511), (440), respectively. At intermediate temperature of about 800°C, a well formed crystalline MgAl₂O₄ spinel phase is

obtained. From XRD data the crystallite size of as-prepared MgAl_2O_4 particles calcined at 800°C for 5 hours is calculated using the Debye–Scherrer equation, $d = 0.9\lambda/\beta\cos\theta$ where λ is the wavelength, β is the breadth of the observed diffraction line at its half-intensity maximum, K is the so-called shape factor, which usually takes a value of about 0.9. The average crystallite size of MgAl_2O_4 spinel was calculated in diffraction plans (311), (400), (440) at 800°C . The average crystallite size was noted to be about 30 nm at 800°C annealed temperature.

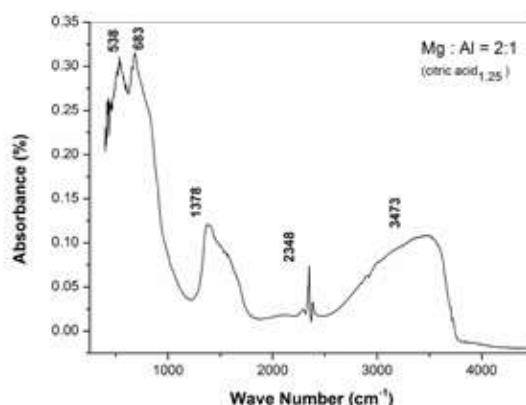


Fig. 3. FT-IR spectra of MgAl_2O_4 annealed at 800°C for 5 hours prepared using citric acid as a fuel.

The IR spectra of the sample after annealing at 800°C for 5 hours soaking period is shown in **Fig. 3** above. Two peaks presented at 535 cm^{-1} correspond with the vibrations of Al-O and another at 683 cm^{-1} correlates to Mg-O-Al vibration indicate that the crystal obtained is MgAl_2O_4 spinel. The above result is found to be in correspondence with Mostafa Y. Nassir et. al who have prepared the same by sol-gel auto combustion for photocatalytic effects. They noted spectra about 576 cm^{-1} and 747 cm^{-1} to be attributed for $[\text{AlO}_6]$ octahedral and Mg-O vibration stretching respectively for the synthesized samples. [2, 4] The broad band at 3473 cm^{-1} due to H_2O stretching vibration, indicating the existence of water absorbed in the sample and the band 2348 cm^{-1} due to the $\text{CH}_3\text{-CH}_2$ vibration. The spectra peak at 1378 cm^{-1} is observed to be corresponding to vibration modes of NO_3^- groups. Similar presence of NO_3^- groups is also noted for nanocrystalline magnesium aluminate synthesis via nitrate-citrate combustion route by Ali Saberi et.al. [6].

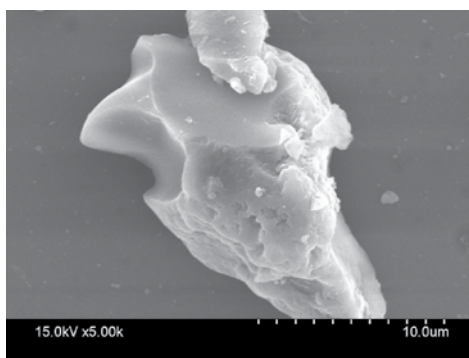


Fig 4. SEM morphology of Spinel using citric acid of 1.25 molar ratio with respect to nitrate salt after annealing at 800°C for 5 hours of soaking

From the SEM image shown (**Fig 4**) above it is noted that sample synthesized is an agglomerated chunk, with irregular polygon shape. The agglomerate is dense by nature with negligible porosity. By analysing the individual particle at higher magnification, lower resolution it can be observed that those particulates are also irregular polygon in shape but they have a very sharp corner. Morphology of the agglomerate also has roughness with irregular depth impressions. The agglomerated chunk has height of more than $18\mu\text{m}$ having width of about $9\mu\text{m}$. The individual particle is between the sizes of $0.3\mu\text{m}$ to $1\mu\text{m}$.

CONCLUSION

Sol-gel assisted combustion route is utilized to synthesize spinel Magnesium aluminate utilizing citric acid as fuel. XRD confirms the spinel phase while crystallite size is estimated to be about 30nm by Scherrers formula. Bonding features are



analysed by FTIR analysis and it exhibits M-O coordinations to be about 535 cm^{-1} correspond with the vibrations of Al-O and another at 683 cm^{-1} correlates to Mg-O-Al vibrations. Morphology from SEM executes irregular polygonal shape having dense agglomeration. Individual particulate is in between 0.3 to $1\text{ }\mu\text{m}$.

REFERENCES

1. C. Păcurariu, I. Lazău, Z. Ecsedi, R. Lazău, P. Barvinschi and G. Mărginean, "New synthesis methods of MgAl_2O_4 spinel," *Journal of the European Ceramic Society*, vol. 27, pp.707-710, 2013.
2. S. Mukherjee, "Evolution of Spinel Magnesium aluminate by combustion route using Glycine as fuel and its characterization," *International Journal of Emerging Trends in Science and Technology*, vol 6, pp 24-27, 2020.
3. S.R.Ghosh, S. Mukherjee and S. Banerjee, "Solution combustion synthesis of Alumina Spinel and its characterization," *Interceram*, vol. 67, pp 34-41, 2018.
4. Mostafa Y. Nassar, Ibrahim S. Ahmed and Ihab Samir, "A novel synthetic route for magnesium aluminate (MgAl_2O_4) nanoparticles using sol-gel auto combustion method and their photocatalytic properties," *Spectrochimica Acta Part A: Molecular and Biomolecular Spectroscopy*, vol. 131, pp 329-334, 2014.
5. S Sanjabi and A Obeydavi, "Synthesis and characterization of nanocrystalline MgAl_2O_4 spinel via modified sol-gel method," *Journal of Alloys and Compounds*, <http://dx.doi.org/10.1016/j.jallcom.2015.05.107>
6. Ali Saberi, Farhad Golestani-Fard, Hosein Sarpoolaky, Monika Willert-Porada, Thorsten Gerdes and Reinhard Simon, "Chemical synthesis of nanocrystalline magnesium aluminate spinel via nitrate-citrate combustion route," *Journal of Alloys and Compounds*, vol. 462, pp 142-146, 2008.
7. M. M. Rashad, Z. I. Zaki and H. El-Shall, "A novel approach for synthesis of nanocrystalline MgAl_2O_4 powders by co-precipitation method," *Journal of Material Science*, vol. 44, pp 2992-2998, 2009.
8. J.C. Debsikdar, "Preparation of transparent non-crystalline stoichiometric magnesium aluminate gel-monolith by the sol-gel process," *Journal of Material Science*, vol. 20, pp 4454, 1985.
9. W. Liu, J. Yang, H. Xu, Y. Wang, Sh. Hu and Ch. Xue, "Effects of chelation reactions between metal alkoxide and acetylacetone on the preparation of MgAl_2O_4 powders by sol-gel process," *Journal of Advanced Powder Technology*, vol. 24, pp 436-440, 2013.
10. Z. Haijun, J. Xiaolin, L. Zhanjie, and L. Zhenzhen, "The low temperature preparation of nanocrystalline MgAl_2O_4 spinel by citrate sol-gel process," *Journal of Material Letters*, vol. 58, pp 1625-1628, 2004.
11. X.L. Pan, S.S. Sheng, G.X. Xiong, K.M. Fang, S. Tudyka, N. Stroh and H. Brunner, "Mesoporous spinel MgAl_2O_4 prepared by in situ modification of boehmite sol particle surface: I Synthesis and characterization of the unsupported membranes," *Colloids and Surfaces A: Physicochemical and Engineering Aspects*, vol. 179, pp 163-169, 2001.
12. Ch-T. Wang, L-Sh. Lin and Sh-J. Yang, "Preparation of MgAl_2O_4 Spinel Powders via Freeze- Drying of Alkoxide Precursors," *Journal of the American Ceramic Society*, vol 75, pp 2240-2243, 1992.
13. X. Su, X. Du, S. Li and J. Li, "Synthesis of MgAl_2O_4 spinel nanoparticles using a mixture of bayerite and magnesium sulfate," *Journal of Nanoparticle Research*, vol 12, pp 1813-1819, 2010.
14. K. MacKenzie, J. Temuujin, T. Jadamba, M. Smith and P. Angerer, "Mechanochemical synthesis and sintering behavior of magnesium aluminate spinel," *Journal of Material Science*, Vol 35, pp 5529-5535, 2000.
15. M.M. Amini, M. Mirzaee and N. Sepanj, "The effect of solution chemistry on the preparation of MgAl_2O_4 by hydrothermal-assisted sol-gel processing," *Journal of Materials Research Bulletin*, vol 42, pp 563-570, 2007.
16. X. Zhang, "Hydrothermal synthesis and catalytic performance of high-surface-area mesoporous nanocrystallite MgAl_2O_4 as catalyst support," *Journal of Materials Chemistry & Physics*, vol 116, pp 415-420, 2009.



Mitigating Covid-19 induced disruption to Steel use in Construction through Engineering Solutions

Manos Kumar De, Pratip Bhattacharya

Department of Civil & Structural Engineering, Technology group and Mining & Metallurgy BU

Tata Consulting Engineers Limited, Mumbai, Maharashtra

✉ mde@tce.co.in

ABSTRACT

Construction industry is a major contributor to the economic development of a country and a primary source of employment and consumption of materials. Steel is one of the most versatile of construction materials and the construction industry is a major source of demand for this material. The economic havoc caused by the Covid-19 virus pandemic has severely affected the construction industry and the demand for steel. The uncertainty associated with controlling and eradicating the disease have caused great distress to the established systems of economic activities that contribute to growth. This article reviews the uncertainty imposed on the future of the construction industry due to the pandemic induced disruption and the subsequent effect on use of steel in construction sector. It also reviews the factors that have driven down the growth of the sector in the economic slowdown caused by imposition of lockdowns to arrest the spread of the virus. The measures planned to manage the risk and uncertainty caused due to this unprecedented phenomenon are studied. The article reviews the changing technologies that can revive the industry and improve the steel demand in the new normal era with focus on adopting digitalization and mechanization.

Keywords: Construction; Steel; Covid-19; Digitalization; Prefabrication; Modularization.

INTRODUCTION

Use of Steel in Construction

The National Steel Policy of India 2017 has envisaged 300 million tons of steel production capacity by 2030-31. The per capita consumption of steel has increased from 58.0 kg to 74.0 kg during the last five years from 2014 to 2019. As per Indian Steel Association (ISA), steel demand was set to grow by over 7.2 per cent in both 2019-20 and 2020-21 [1]. All these figures are from market trends prior to the present pandemic situation.

The increasing usage of steel in construction in both buildings and infrastructure sectors has many benefits over other materials, according to a report from the World Steel Organization [2]. The advantages of using steel in construction highlighted in the report include:

- 1) Steel can be recycled and reused innumerable times and steel manufactured contains 25% of recycled material
- 2) Higher strength of the material allows larger column spacings and lower member sizes
- 3) The lower sizes reduce material usage and lowers dead weight and foundation requirements
- 4) Higher ductility ensures better earthquake resistance
- 5) Great flexibility to combine with other building elements
- 6) Faster on-site installations using prefabricated/ pre-engineered design and construction techniques
- 7) High durability

The usage of steel of different forms and in various sectors of construction highlighted in the report are summarized in **Table 1** [2]:

Table 1. Use of steel in construction sector

Steel form/ shape	Steel usage in Construction Sectors		
	Building	Transport	Utility
Reinforcing bars	44%	60%	50%
Structural shapes, plates, rails	25%	40%	-
Pipes	-	-	50%
Sheets	31%	-	-
Non-structural steel	1%	-	-
Fixtures and Fittings	2%	-	-

Fig. 1. [2] shows the consumption figures of steel in the different sectors of construction in India

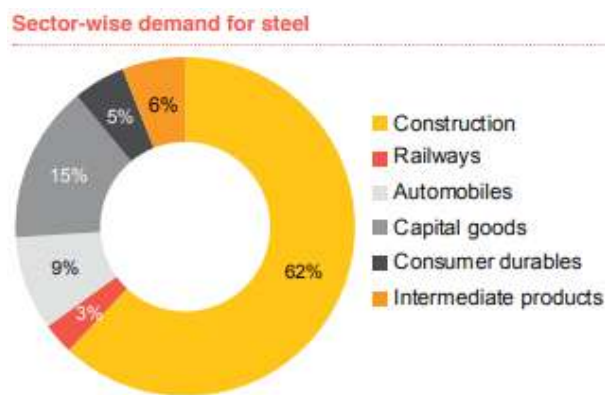


Fig. 1. Sectors of Consumption of Steel in India

As is evident from **Fig. 1**, construction sector is the biggest consumer of the steel production in India underlying the huge demand dependency of use of steel products in this sector.

Contribution of Construction industry to Economy

The share of construction industry contribution to GDP is 7.2% for China in 2019 [5], [6] and 7% for India [7]. At the time of the start of the outbreak and imposition of lockdown, total construction projects in India was worth INR 59 trillion [8] spread over 20,000 projects at 18,000 work sites according to a study by market analyst KPMG [9]. This study by KPMG [9] has also highlighted the interdependencies between the construction industry and the other sectors.

The result of this study depicted in **Fig. 2** shows the interaction of construction sector with these industries as pull factor which defines the impact of construction work on product demand and push factor which defines the effect of change in product availability on the construction sector.

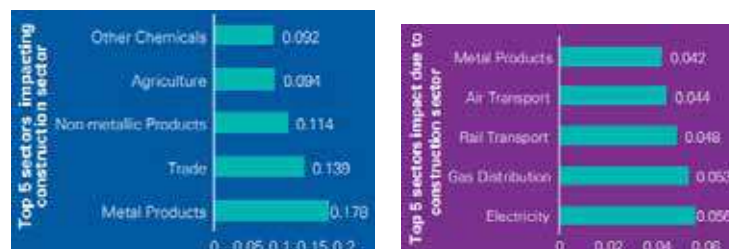


Fig. 2. Interdependency between construction sector and metal Products

While unit change in metal demand pushes construction sector by 4.2%, unit change in construction sector pulls metal industry by 17.8%, a more than four-fold effect demonstrating the significant impact of construction on the metal industry.

DOWNTURN IN CONSTRUCTION INDUSTRY

Status of Construction Industry in India

The construction industry in India was already facing numerous challenges including lack of funds, financial irregularities, regulations under the Environment Laws and the Real Estate (Regulation and Development) Act, 2016, low levels of mechanization and technology deployment at worksites, great degree of dependency on use of human workforce and low productivity rate of the workforce. Despite these challenges, the construction industry in India was on the growth path, investment in construction projects being INR 29.41 trillion with gross value add (GVA) of INR 10.51 trillion in 2019-20; this was expected to grow to investment value of INR 32.24 trillion and GVA of INR 11.02 trillion in 2020-21 at a rate of 4.9%. The various construction sectors with major contribution are infrastructure (29%), commercial (26%), industrial (19%), residential (15%) and institutional (8%).

Impact of Covid-19 on Construction Industry

The Covid-19 outbreak imposed new challenges that have dampened the base growth scenario. The report “Market Outlook of Construction post Covid-19” by Gleeds India Insights and Analytics [10] based on survey response of the construction industry indicates that the lockdown imposed caused disruption of supply chain and workforce availability at worksites and this led to complete stoppage of construction work in India. The findings are in stark contrast to the construction industry in the western world where due to large scale mechanization and better living and health facilities for the workforce, the work at site could continue.

The KPMG report [9] has studied the anticipated reduction in investment in the construction industry under various scenarios corresponding to two different periods of lockdown (short and long) and two assumed GVA growth rates (high growth rate and slow growth rate) against a baseline scenario.

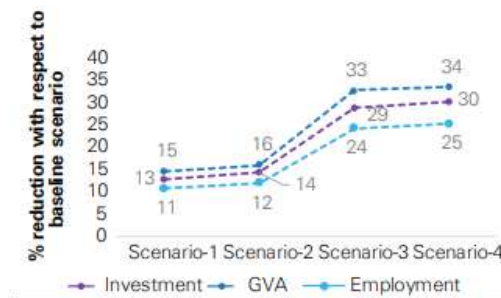


Fig. 3. Reduction in Investment, GVA, Employment from base model

As seen from Fig. 3 [9], the reduction in the construction sector varies from 11~15% in the best-case scenario (higher growth rate, shorter lockdown) to 25~34% for the worst-case scenario (longer lockdown, lower growth rate). Thus, the negative impact on the industry will further aggravate and the demand for construction materials in general including steel continue to slide without a timely cure in sight. The imposition of lockdowns to curb second wave of virus spread across Europe is a stark reminder of the future uncertainties.

The construction industry is highly sensitive to changes in economic condition and closely follows GDP trends. The pandemic induced economic downturn resulted in lower investment in construction. The pandemic also disrupted the supply chains of material and workforce in reaching construction sites resulting in reduced productivity. Productivity loss also resulted from the protocols for working in new normal conditions [15].

Impact on Steel Industry

The COVID-19 pandemic severely affected both the workforce and the supply chain of steel use for construction industry in India. The immediate effect on construction and use of steel is appreciable as seen in the previous section. The impact is expected to peak in next few months and continue further in the long term with the prevailing health uncertainty. Assuming the virus outbreak can be contained within this year, it may be anticipated that the back to normalcy will start from 2021 and may be back at pre-COVID 2019 stage in 2023 with respect to construction industry [15]. Construction projects are much more affected by volatility of such external factors compared to other sectors. The estimated four years of slump will have severe negative impact on the construction industry and its material demand. There will be different phases of lockdowns, sometime

short term, sometime long term on local basis.

Rating agency CRISIL in their report [12] had hinted at contraction of steel demand by 14-17% due to lockdown in major part of Q1-FY20 with construction activities expected to resume at end of Q1. With lockdowns continuing into Q2-FY20, the drop would further increase to 22-25% as shown in **Fig. 4**. However, with construction and automobile sectors starting to open in Q2-FY21, the demand is expected to pick up.

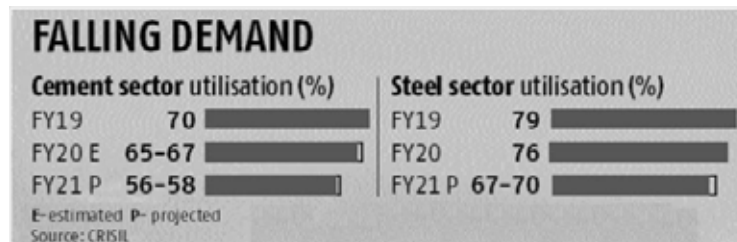


Fig. 4. Fall in demand of construction materials in India [12]

The steel demand for the construction sector is expected to fall sharply by 18% in 2020 in India as predicted by the World Steel Association while the global demand may fall by 6.4% to 1,654 MT. The Indian Steel Association (ISA) has echoed the declining trend with a forecast of 20% fall in demand in 2020 of 15.3MT from January to June and another 5-6MT from July to December compared to 2019 [16]. The major reasons stated for this falling demand are:

- 1) Stoppage of construction work in lockdown
- 2) Large change in spending patterns by the population focusing more on basic needs with downslide in real estate demand
- 3) Strong work from home (WFH) policies implemented by IT and ITES sectors leading to low demand for office spaces
- 4) Huge upsurge in online retail sales of essential commodities leading to lowering in demand for commercial outlets
- 5) Complete halt to tourism industry and related construction projects
- 6) Construction workforce leaving the site (Gleeds India survey [10] shows that 50-80% workers have left site after lockdown and is expected to return only in Q1-FY21)
- 7) Investment in construction projects falling out of favour of investors

REVIVAL OF DEMAND FOR USE OF STEEL IN CONSTRUCTION

The Indian economy counts the Steel industry as one among the eight core industries and the demand for steel shows positive correlation to the growth of economy. The Ministry of Steel recently organized a conference to chalk out additional growth path for rural steel consumption which currently stands at 19.1kg compared to the national average of 74.0 kg. The Confederation of Indian Industries (CII) has been assigned the task of identifying new rural use sectors that will include agriculture, rural infrastructure, dairy and food processing.

Trends in the revival of Steel Industry

The gradual easing of lockdown has seen increase in steel demand from automobile industry and white good sector and partial revival of government infrastructure projects [23]. This has mostly benefitted large producers with captive mines, integrated steel plants that use blast furnace route for iron making, presence of finish production units and access to export markets. Small producers faced distress due severe shortages of raw materials, increased prices, reduced manpower availability, low availability of oxygen for operating electric arc furnaces.

The need for change in Construction Industry

Multiple factors of stagnant productivity, low levels of digitization and low profitability have been the main deterrents for the poor performance of construction industry in addition to factors like fragmented work chain and high share of manual labor. Increasing demands of sustainable operation, new technologies and materials and digital tool usage are bringing in need for innovation.



The Trend for new Technologies in Construction

Various short- and long-term trends are anticipated to set in the construction industry. These include the following:

- 1) Short-term trends: Focus on increased use of digitization including use of BIM tools, digital twins and integrated construction site and workforce monitoring tools; reorganizing supply chains through build-up of inventory, new strategy for procurement of critical and long lead items and sourcing alternative suppliers.
- 2) Long-term trends: Consolidation of various construction related services and investment in IT, R&D, talent, and technology; vertical integration to improve efficiency; digitization and innovating construction systems; increase in off-site construction; promoting sustainable designs like improved energy efficiency.

Use of Digital Tools

Building Information Modelling (BIM) tools are used for creating an intelligent and integrated 3D model of the complete design, construction, operation and management processes for buildings and infrastructures. The tool enables architects, engineers and site work specialists to perform all functions in construction more efficiently through various stages of detailing from concept (LOD 100) to as-built documenting (LOD 500). The technology can be extended beyond 3D BIM to include schedule (4D), costing (5D), sustainability (6D), facility management (7D) and safety (8D). Use of BIM will eliminate many uncertainties in the various stages in life cycle of a structure. Steel structures are particularly suitable for BIM applications that can also accommodate interfaces for automated layout marking, fabrication and assembling.

Increased Mechanization and Prefabrication

Logistics and supply chain control for onsite delivery will be focal point that will drive the mechanized construction process using prefabricated units.

Technology is expected to play a major role in revising the engineering design process. Lot of focus will be on off-site manufacturing like pre-fabrication, pre-assemblies etc. Increase in off-site construction and fabricating/assembling in controlled environments will help better management of the movement and mingling of workforces from physical distancing point of view. Other off-site construction benefits include improved quality and speed benefits, and improved safety performance. Contractors will gradually push fabrication off-site and manufacturers will expand their range of prefabricated sub-assemblies. This will also lead to use of more mechanized construction to handle the large units. Large scale training and re-skilling of design professionals and workers both at shop and site will be required to bring this change in the design and construction process. Major steel makers in the country have already started manufacture of ready-to-use products like welded reinforcement mesh and custom ordered plate girder assemblies and these trends will further increase. Other manufacturers are providing design services and tools to assess the sustainability impact of steel structure construction options, benchmark the steel construction solution with market standards and integrate the solution to virtual building design tools.

Modular Design

This trend of offsite construction will enhance modularization. This entails using factory-made pre-engineered structural units along with services delivered to site as assembled structures or substantial components of a building. Modularization will improve work quality, lessen use of on-site workers, reduce erection time. The construction industry will demand more customized finished units from the fabricators rather than fabricating and assembling those units from raw/ semi-finished products at the work site. The challenges associated with this technique involve upfront finalization of all design requirements and the need for robust logistics and transport infrastructure planning and facilities. Since prefabricated units will be of larger size and special shapes, transporting these units will be a major challenge given the layout and width of roads available along most corridors. This will be more compounded considering the possible location of developing areas away from major access roads. On the other hand, this may open a new area of growth requiring establishment of road/ rail connectivity that will in turn require increase in use of steel construction products. This will all depend on the proper policy formulation and long-term development planning, but with sustainability and holistic growth in view.

Summarizing the possible scenarios, the following emerge as attention area:

- 1) Digitization, technology infusion and training
- 2) Off-site fabrication and modularization
- 3) Focus on logistic control/supply chain

- 4) Customized finished products like – tubes, profiles, cut to length materials etc.
- 5) Prefabricated reinforcement mesh

This thrust on offsite fabrication and assembly and requirement of reduced on site work will require comparatively more usage of steel. The overall figure may be lower than what would have been under pre-pandemic growth but will be more than present level of segmentation of steel and concrete as construction materials.

POLICY CHANGES TO FAST-FORWARD THE CONSTRUCTION STEEL INDUSTRY

The industry associations are urging the government and policy makers to stimulate growth in the construction industry to help it revive operations on scale. CII has suggested that government should adopt measures for timely execution and completion of projects in infrastructure sector. Other policy interventions suggested by CII include banning import of cheap scrap and defective and second grade semi-finished steel for re-rolling which pose threat to indigenous steel manufacturers.

Another industry body, the FICCI, in its report, has recommended the government to frontload investment in projects enlisted in the National Infrastructure Pipeline and allow construction activities to resume while strictly adhering to the health directives. It also recommends considering life cycle analysis (LCA) procedure for evaluating real cost of materials in construction projects where steel stands a better chance due to its higher end of life value. FICCI has suggested to declare the entire supply chain of steel manufacture and use as essential service which will allow it to function under lockdown situations. It also asked the government to give preference to indigenous steel makers for projects. As part of the announced stimulus package and considering the role of MSME sector in steel production, FICCI also recommends extending the loan moratorium to this sector. Finally, it recommends the government to develop a roadmap to transform India into steel manufacturing hub and seize the opportunity arising from disrupted supply chains in other countries to set up facilities in India.

There is uncertainty in the pricing of steel in the post pandemic market. On the one hand there is apprehension of excess stock driving market prices down in case of continued slowdown of construction. On the other hand, the Gleeds survey results shown in **Fig. 5** [10] hints at an opposing picture with 53% of the respondents predicting increase in steel costs due to lower availability of steel products especially from small scale sectors and an improving demand largely fueled by government sponsored infrastructure projects.

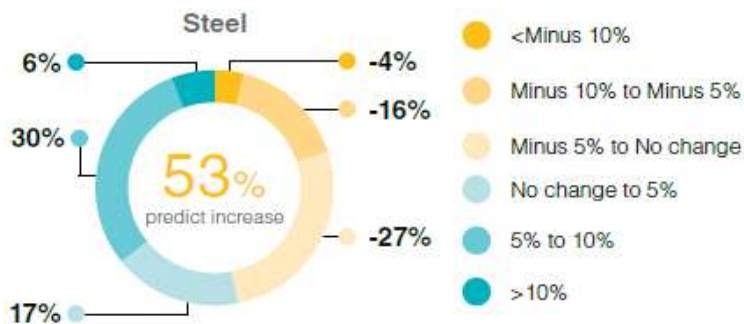


Fig. 5. Expected price change of Construction Steel [10]

The steel industry must also weather the possible dumping of steel products from foreign manufacturers since the demand in all countries had come to halt during pandemic induced lockdowns in most countries. Especially in China, there is large stockpile of steel inventory due to stoppage of exports. Globally steel price fell to USD 486/ MT in Q1-FY20 and is expected to fall further to USD 440-470/ MT in 2020 in continuation of weak demand.

CONCLUSION

In a post Covid-19 world, it may be concluded that there are clear focal areas where the consumption of steel will tend to grow, and the growth story will remain intact. Increased use of technology driven solutions for both engineering design and on-site activities will help maintain running the wheels of the construction industry. This will require increased focus on digital solutions in both the areas and integrating the overall process from concept to commissioning, operating and maintaining the facilities that will help remove some of the uncertainties. The increasing requirement for health and safety matters in the new normal will demand greater use of mechanized construction tools and processes paving the way for adoption of higher percentage of steel materials in construction.



Overall volume growth of construction may not be significant in short term but will attract more adoption of steel intensive construction. The negative impact on steel industry serving the construction sector will be less compared to other segments of the industry. The present ratio of adoption as construction material will favourably tilt towards steel as preferred material.

REFERENCES

1. India Brand Equity Foundation (<https://www.ibef.org>)
2. World Steel Organization (<https://www.worldsteel.org/steel-by-topic/steel-markets/buildings-and-infrastructure.html>)
3. PWC Report, The Indian steel industry: Growth, challenges and digital disruption by pwc and Indian Steel Association, 2019, (<https://www.pwc.in/assets/pdfs/consulting/technology/the-indian-steel-industry-growth-challenges-and-digital-disruption.pdf>)
4. S&P Global Market Intelligence (https://www.spglobal.com/marketintelligence/en/news-insights/research/metals-markets-to-rebound-after-coronavirus-epidemic-peaks-part-2?utm_medium=referral&utm_source=marketo&utm_campaign=MI-PC-MI-PC-MS-MM-MM-MIplatform-GL-200407-Mining-Microsite&utm_content=)
5. <https://asia.nikkei.com/Economy/China-s-feeble-construction-sector-dims-outlook-for-GDP-rebound>
6. <https://tradingeconomics.com/china/gdp-from-construction>
7. <https://tradingeconomics.com/india/gdp-from-construction>
8. Abinraj R.S., “India: Impact of Covid-19 on Construction and Engineering Sector”, April 2020, (<https://www.researchgate.net/publication/340966338>)
9. KPMG report “COVID-19: Assessment on economic impact on construction sector in India”, May 2020, (<https://home.kpmg/content/dam/kpmg/in/pdf/2020/05/covid-19-assessment-economic-impact-construction-sector.pdf?r>)
10. Gleeds India Insights and Analytics report, “Market Outlook of Construction post Covid-19”
11. Frank Zhong, “Economic Impact of Covid-19 outbreak in China”, Worldsteel Association Blog article, April 2020, (<https://www.worldsteel.org/media-centre/blog/2020/economic-impact-coronavirus-outbreak-china.html>)
12. CRISIL Report, “Lockdown Impact Steel Demand Likely to Slip”, April 2020, (<https://www.financialexpress.com/industry/lockdown-impact-steel-demand-likely-to-slip-by-14-17-in-fy21-says-crisil/1930646/>)
13. <https://ssmb.in>
14. <https://www.moneycontrol.com/news/opinion/reclaiming-growth-economic-recovery-tracker-5427551.html>
15. <https://www.mckinsey.com/business-functions/operations/our-insights/how-construction-can-emerge-stronger-after-coronavirus>
16. <https://www.livemint.com/industry/manufacturing/large-steel-players-stage-recovery-in-august-while-msmes-are-in-distress-11600274749062.html>



Effect of Vanadium on the Tensile Strength as a Function of Austenitizing Temperature on LHB Wheels

Smeeta Kujur^{1*}, P P Sarkar¹, Asha Bajpai²

R & D Centre for Iron and Steel, SAIL, Ranchi, Jharkhand¹

Research & Centre of Laboratory, Durgapur Steel Plant, Durgapur, West Bengal²

✉ smeetak18@sail.in

ABSTRACT

The influence of vanadium addition on the tensile strength varying austenitizing temperature at 0.49% carbon steels has been investigated. Vanadium has different effects on the tensile strength of wheel steel at different austenitizing temperatures. At lower austenitizing temperature, vanadium increases the elongation notably. On the contrary, at higher temperature, wheel steel obtains a remarkably-improved tensile strength. Therefore, for wheel steel, there exists a suitable temperature, at which vanadium addition improves strength and elongation at the same time. The phenomena above are closely connected with the dissolution and precipitation of V(C, N) in the steel.

Keywords: Wheel steel; V(C, N); Strength; Elongation; Austenitizing temperature; TS.

INTRODUCTION

Microstructures and mechanical properties of IRS R-19/93 steel depend on Vanadium behavior of dissolution, precipitation, the magnitude, size and distribution of V precipitates. V can act as both precipitation strengtheners and grain refiners depending on the composition of the wheel steel. For grain refining, the precipitates usually require being out of the solution and act by pinning austenite. At higher temperature the precipitate V (C, N) particles are bound to re-dissolve because solubility of precipitate V (C, N) particles is higher at higher temperature. When the V-bearing steel is reheated at 820°C, about 43% of V precipitates re-dissolve. It becomes almost 60% at 860°C, 78% at 900°C and 96% at 950°C [1]. Thus, total V content in the steel is divided into two parts, re-dissolved and undissolved, and their respective magnitude would strongly influence the microstructure and properties of wheel steel. Reducing the undissolved V precipitates at high reheat temperature weakens the prevention effect of V, pinning effect, on austenite grain growth. Therefore at high reheat temperature increases the austenite grain size.

Increase in austenite grain size decreases the ductility for an equivalent pearlite inter-lamellar spacing S_p [2-4]. At higher austenitizing temperature strength increases by decreasing S_p [5-7]. Decreasing the S_p effectively decreases the slip length in the ferrite, resulting in a higher strength. Fine austenite grain size has great significance for promoting final microstructure and improving toughness [8]. Further, undissolved V particles facilitate ferrite nucleation [2-4]. If there are many dispersive VN or V(C, N) particles in the matrix prior to advance of the transformation of austenite to ferrite, the transformation will be substantially accelerated and resulting into more refined transformed ferrite and higher pro-eutectoid ferrite content. The strength increases with increasing volume fraction of V(C, N) in the ferrite matrix and exhibited moderate ductility [9]. This can be related to decrease in the amount of free carbon and nitrogen due to precipitation of VC and VN [10].

In general, ferrite is the soft phase in the material and has good toughness. Compared with ferrite, pearlite has worse toughness and nearly immune to absorb impact load [1]. More ferrite in the microstructure means better impact toughness of the product. As austenitizing temperature increases, undissolved V(C, N) reduces; reducing the nucleation site of ferrite. Therefore, pro-eutectoid ferrites decrease. Hence, impact toughness reduces [1].

Indian Railways standard specification for solid forged steel wheels IRS9-93 Part 2 has given the range of mechanical properties for Rim and Web, given on **Table 1**. **Fig. 1** shows the structure of wheels' Rim and fillet. Tensile strength and hardness are important properties of wheel steel as it has strong influence on its wear. Other material parameters which are relevant to the performance include the resistance to the onset of plasticity (i.e. yield strength or proof stress) and ductility. The relationship between tensile strength and the chemistry in as-rolled pearlitic rail steel is well documented [11-15].

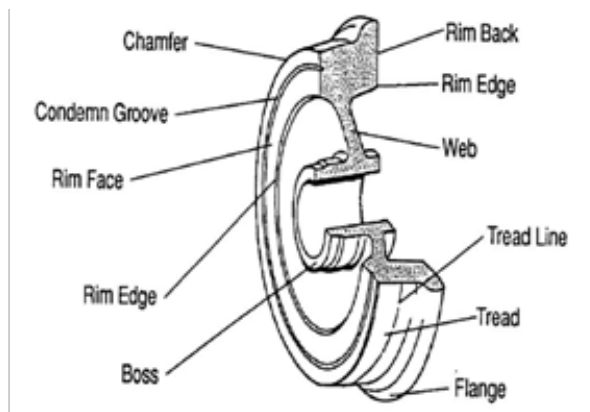


Fig. 1. Wheel structure [16]

$$TS = 227 + 803C + 87Si + 115Mn + 133Cr + 891P + 614V \quad (1)$$

Table 1. Mechanical properties according to IRS 19-93 Part 2

Mechanical properties	Tensile strength N/mm ²	Yield strength N/mm ²	Minimum Elongation, %	Hardness range BHN	Minimum Impact strength Joules
Rim	820-940	>520	14	241 to 320	Average value :17 Individual value : 12
Web	Max 760	-	16	-	-

Equation (1) describes the contribution of various micro alloying elements on the tensile strength of rail steel that undergone normal air cooling where TS = tensile strength (in MPa) and each alloying element is in weight percent.

Table 2. Chemical composition of wheel steel (in wt %)

Elements	C	Mn	P	S	Si	Cr	V
IRS R-19/93	0.52 max	0.60- 0.80	0.025 max	0.025 max	0.15-0.40	0.25 max	0.15 max
H1	0.49	0.77	0.013	0.016	0.21	0.26	0.1

EXPERIMENTAL

The manufacturing of wheels primarily involves steel making, forging, stamping and heat treatment (Rim Spraying & Tempering). These wheels are heated after hot stamping & cooling for ≥ 8 hrs. in a rotary hearth type CO gas fired furnaces (C-furnaces) to its austenitizing temperature. These wheels are rim sprayed with water in a rim quenching machine for 300 to 330 seconds depending on C contents in wheel steel and water volume (14-15 Nm³/hr). Wheels are placed on a guide cone at the centre of a rotating disc (16 rpm). The spraying system consists of a stationary Φ 2.5 “pipe ring fitted with 24 nos of flat jet nozzles. The rotation of the wheel (16 rpm) provides a uniform spray of water upon the tread only.

For this experiment a heat was were made, forged and heat treated at four different temperatures e.g. 985°C, 950°C 910°C and. Composition of the steel namely H1 is given on Table 2. For the heat treatment experiments, 6 wheel rim namely R1-R6 . Each of them was austenitized at 980°C, 950°C and 910°C and quenched in water. The detail of heat treatment has been given in Table 3. For Mechanical Properties round tension test specimen of gauge length 45mm ,diameter 10mm, radius of fillet 8mm according to ASTM E8M-04 was prepared and was tested. The microstructures of steel after heat treatments were determined by Olympus make inverted optical microscope (OM) Scanning Electron Microscope (SEM) and transmission electron microscopy (TEM, JEM-2100) analyses. Image analyzed by using Leica Application Suite- Core. 2% Nital solution was used for etching the microstructures of the steel. The microstructures were examined using TEM operating at 200 kV. Foils for the TEM analysis were cut into 2mm thickness, ground to 0.6mm by SiC abrasive paper, punched to 3mm diameter and

then thinned to perforation on a TenuPol-5 twin-jet unit with an electrolyte consisting of 90% Acetic acid + 10% perchloric acid at 25 V and current 30 amp. The types of precipitates present in steel were analyzed by Energy Dispersive Spectroscopy (EDS) attached to the TEM.

Table 3. Heat treatment details of the wheel steels

Specimen ID	Austenitizing Temp (°C)	Flow Rate (m ³ /hr)	Spray Time (min)	Type of Quench
H1T1 A	985	14.5	5	Direct
H1T1 B	985	14.5	4	Direct
H1T2	950	14.5	3	Direct
H1T3	910	14.5	5	Direct
H1T4	850	14.5	5	Direct

RESULTS & DISCUSSION

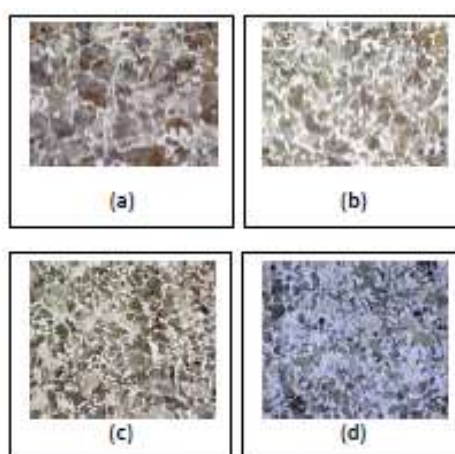


Fig. 2. Optical Micrographs of wheel steel at reheat temperature (a) 1000°C (b) 950°C (c) 900°C (d) 850°C at 500X

H1 steel having vanadium 0.10% and chromium 0.26%. Rim samples were heat treated at four temperatures 985°C, 950°C, 910°C, and 850°C and then quenched. **Figs. 2(a), (b), (c), (d)** shows the optical microstructure of wheel steel. It has pro eutectoid ferrite + pearlitic structure. For pro-eutectoid ferrite nucleation, V(C, N) should be precipitated along the prior austenite grain boundaries at the austenitizing temperature. As undissolved V(C, N) particles reported to be potent sites for the nucleation of ferrite [3]. Undissolved V(C, N) particles may be less in higher austenitizing temperature. Therefore, micrograph showed that at higher austenitizing temperature the pro-eutectoid ferrites are less as compared to the lower austenitizing temperature.

The Volume fraction of pro-eutectoid ferrite is shown in **Fig. 3(a)**. At low austenitizing temperature, more pro-eutectoid ferrite formed. With increase in austenitizing temperature the potential nucleation cores of ferrite and undissolved V(C, N) reduced, making transformed pro-eutectoid ferrite decreased.

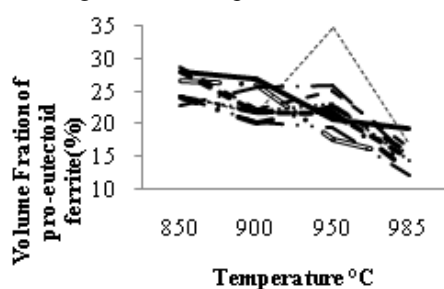


Fig 3. (a) Variation of volume fraction of pro-eutectoid ferrite for the Rim as a function of austenitizing temperature

The solubility of vanadium is high at higher temperatures, leaving undissolved V(C, N) precipitate less in quantity and promoting less pinning effect to austenite grain boundaries. Therefore, austenite grain size increases with the temperature as shown in **Figs. 2 (a), (b), (c), (d)**. Increase in austenite grain size reduces the ductility for an equivalent Sp [8]. Therefore, decrease in elongation (%) can be seen in at **Fig. 3 (b)**. **Table 4** gives the almost equivalent Spin H1 at higher austenitizing temperature. The prior austenite grain size control the distance over which flow may localize. Large grained enable flow to localize over larger distances, than fine grained [8].

In this experiment, remarkable increase of tensile strength was found at high austenitizing temperature, which was related to V precipitation strengthening. But all rims tensile strength exceeded upper limit according to standard IRS 19-93 Part 2 in spite of lowering austenitizing temperature. Lowering austenitizing temperature decreased Web T.S correspondingly. Tensile strength was higher for the high austenitizing temperature, shown in **Figs. 3(c), (d)**.

At higher temperature, almost all of Vanadium dissolved in the steel matrix [1], and during the cooling process, dispersive precipitation of V in ferrite strongly strengthened pro-eutectoid ferrite and pearlitic ferrite and thus elevated the strength [8]. Figure 4(a),(b),(c),(d) shows the typical morphology of large number of fine precipitates in the matrix of pro –eutectoid ferrite. The V(C, N) particles display different sizes of smaller particles (about 4nm) and larger particles (about 10 nm)

Table 4. Variation in Interlamellar Spacing of H1 as a function of austenitizing temperature

Austenitizing Temperature(°C)	850	900	950	985
Interlamellar spacing (μm)	0.226458	0.212324	0.24015	0.243287

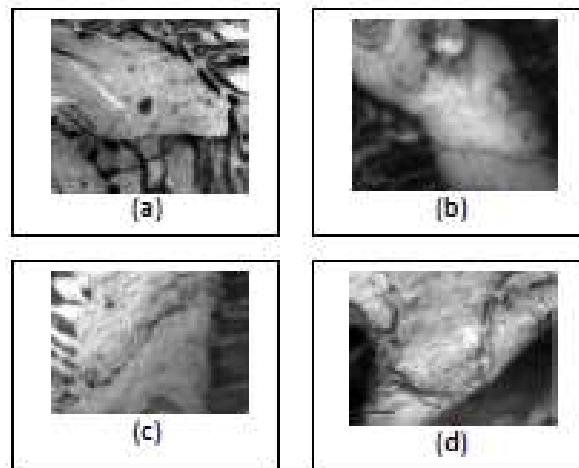


Fig. 4. Transmission Electron Micrographs of large numbers of globular V(C, N) precipitates matrix of Pro-eutectoid ferrite

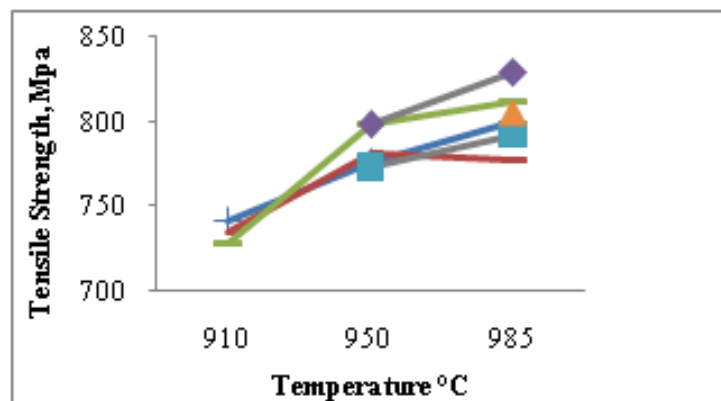


Fig. 3(d). Variation in tensile strength for the Fillet as a function of austenitizing temperature



ACKNOWLEDGEMENTS

This work was supported by the Research and development centre Iron and Steel, Steel Authority of India Limited Ranchi and Research & Centre of Laboratory, Durgapur Steel Plant, Durgapur, India. The authors would like to express their sincere thanks and gratitude to Jhon Guria, Nikhil Oraon, Roshan Ekka for support of this work.

CONCLUSION

1. Microstructure of the Vanadium alloyed wheel steel consists of Pro-eutectoid ferrite +pearlite. At higher austenitizing temperature coarse grains are found.
2. Volume fraction of pro-eutectoid ferrite found decreasing with increase in austenitizing temperature.
3. At higher austenitizing temperature elongation decreases.
4. Remarkable increase of tensile strength was found at high austenitizing temperature was related to V precipitation strengthening. All rims and fillet tensile strength exceeded upper limit according to standard IRS 19-93 Part 2 in spite of lowering austenitizing temperature.
5. Interlamellar Spacing Increase with the austenitizing Temperature.
6. Large number of V(C,N) Precipitates can be seen in the matrix of Pro-eutectoid ferrite.

REFERENCE

1. Pan Tao, Cuiyin-hui2, SuHang, ZhangYong-quan, YangCai-fu .Effect of Vanadium on the Strength and Toughness of Wheel Steel at Different Reheat Temperatures,1978,161-165.No.2003AA33 I 160
2. Shim J H, Oh Y J, Sun J Y, et al. Ferrite Nucleation Potency of Non-metallic Inclusions in Medium Carbon Steels. Acta Mater., 2001, 49:2115-2122.
3. Madariaga I, Gutierrez I. Role of theParticle-matrix Iinterface on the Nucleation ofAcicular Ferrite in a Medium Carbon MicroalloyedSteel. Acta Mater., 1999,47(3): 951-960.
4. Miyamoto G, Shinyoshi T, Yamaguchi J, et al.Crystallography of Intra-granular Ferrite Formed on(MnS+V(C, N)) Complex Precipitate in Austenite.Scripta Mater., 2003,48: 371-377
5. M. Hyzak and I. M. Bemstein: Metall. Trans. A, 1976, vol. 7A,pp. 1217-24.
6. G.T. Gray, III: Influence of Microstructure on the Fatigue Initiation and Propagation Properties of Fully Pearlitic Steels, Ph.D. Thesis,Carnegie-Mellon University, Pittsburgh, PA, 1981.
7. D.J. Alexander: Microstructural Effects on Cleavage Fracture of Pearlitic Eutectoid Steel, Ph.D. Thesis, Carnegie-Mellon University, Pittsburgh, PA, 1984.
8. Lewandowski J J, Thompson A W. The Effect of the Prior Austenite Grain Size on the Ductility of Fully Pearlitic Eutectoid Steel. Metall. Trans., 1986,Vol.17A: 461-472.
9. Batte, A.D.; Honeycombe, R.W.K. Strengthening of ferrite by vanadium carbide precipitation. Met. Sci. J. 1973, 7, 160–168.
10. Hasan Karabulut, S€uleyman G€und€uz. Effect of vanadium content on dynamic strain ageing in microalloyed medium carbon steel.Met.&Des 25.J.2004,521-527.
11. W Cahn, P. Haasen & E.J. Kramer, Constitution and properties of steel, Materials Science and Technology, Vol 7,VCH, 2005, ISBN 3527268200.
12. Kapoor and K.L. Johnson, Plastic ratchetting as a mechanism of metallic wear. Proc. R. Soc. Lond. A445, 367-381, 1994.
13. H.J. Kouwenhoven, The influence of ferrite grain size and volume fraction of pearlite on the lower yield stress and liders strain of carbon steel, Trans. ASM 62, p437, 1969.
14. F. B. Pickering, Physical metallurgy and the design of steels, 1st edition, Applied Science Publishers, 1978
15. T. Gladman, The physical metallurgy of micro-alloyed steels, 1st edition, Maney Publishers, 1997.
16. Asset Standards Authority NSW (2013), Wheel defect manual, May 2013. p.8.



Challenges for using Iron-ore as Coolant in BOF Steelmaking

Sanjay Kumar Gupta

Steel Making and Casting Group, RDCIS, SAIL, Ranchi

✉ skgupta@sail-rdcis.com

ABSTRACT

Basic Oxygen Furnace (BOF) steelmaking is an autogeneous process. The thermal balance to control excessive steel temperature is achieved by use of scrap. In present steelmaking scenario, scarcity and high cost of prime scrap has led us to explore the possibilities to use alternative coolants. The most commonly used alternative coolant is iron ore lumps due to inexpensive and easily availability. Addition of iron ore as alternate coolant is found very useful to reduce total metallic input & blowing time, to achieve higher shop productivity. However, addition of iron ore is tricky and should be added carefully. The formation of excessive slopping, increase in off gas volume, increase in hydrogen content in off gas, flame shooting are common problem arises during its addition in BOF steelmaking. In this paper, the key aspects of iron ore addition in BOF steelmaking are elucidated to substitute the scrap. The technical difficulties, challenges and essential infrastructure for the use of iron ore are explained based on the BOF blowing experiences.

INTRODUCTION

Steelmaking through BOF process is an autogenous process of conversion of blast furnace hot metal into liquid steel mainly by oxidation and subsequent removal of deemed impurities like C, Mn, S, P etc. This oxidation of impurities present in hot metal produces excess heat. High operating temperatures of the furnace is detrimental for refractory lining and also impairs certain aspects like de-phosphorization of steel. The thermal balance to control excessive steel temperature is achieved by use of scrap. It gets melted in the process and also provides metallic content to the bath. In the present context of steelmaking, scarcity and high cost of prime scrap has led us to explore the possibilities to use alternative coolants, such as iron ore lumps, pig iron, sinter, direct reduced iron, lime etc. The choice of alternative coolants used in converter is determined by availability, price and operational strategies of the shop. Iron ore, sinter etc are potential alternate coolant when charged in BOF during oxygen blowing and are integral to the thermal balance of the process and for temperature corrections.

The most commonly used alternative coolant is iron ore lumps. Since the cost of iron ore is very low compared to steel scrap, substitution of steel scrap by iron ore is helpful to reduce the production cost of steel. It is also reduced to metallic iron inside the converter, and found helpful for reduction in total metallic input. Now days, more efforts have been made to increase the iron ore usage in converter to maintain the thermal balance. Partial replacement of scrap by iron ore ~ 10 – 20 kg/t, or addition of iron ore (0.5 – 2 ton) for the temperature adjustment is general practice. Higher usage of ore requires alteration of the hot metal / scrap ratio and blowing conditions. In Steel Authority of India Limited (SAIL), the heat making with iron ore and no scrap has been established. The usage of iron ore in different SAIL plants has been given in **Table 1**. To meet the overall thermal balance, iron ore addition ~ 40 – 50 kg/ton is required. It is found techno-economically very useful to reduce total metallic input & blowing time, and to achieve higher shop productivity. In this paper, the various aspects of iron ore addition in BOF steelmaking are elucidated to substitute the scrap. The technical difficulties, challenges and essential infrastructure for the use of iron ore are explained based on the blowing experience at different steel plants of SAIL.

Table 1. Steel making operating parameters for different SAIL plant

Parameters	SMS-II, BSP	SMS-II, BSL	SMS, DSP	SMS-II, RSP	SMS, ISP
No. of BOF	3	2	3	3	3
Capacity (T)	130	300	130	150	150
Heat Weight (T)	115.5	273	119.6	155.7	151.4
HM (Kg/tcs)	1027.37	1018.4	1038.8	1007.7	1093.6

Scrap (Kg/tcs)	114.39	106.6	79.5	117.57	25.9
Iron Ore (Kg/tcs)	0.714	0.00	25.76	14.73	33.3
TMI (Kg/tcs)	1141.7	1139.5	1118.3	1125.3	1119.6

BEHAVIOR OF A TOP-BLOWN BOF STEEL MAKING

Brief Description

The primary function of the BOF steelmaking is to decarburize the hot metal using pure oxygen gas (1). In the process, > 99% pure oxygen is injected as a high-velocity jet against the surface of the hot metal, allowing penetration of the impinging jet to some depth into the metal bath (**Fig. 1**). The pure oxygen top blown BOF decarburizes hot metal from ~ 4.0%C to 0.04% carbon. Under the oxidizing conditions, the elements like Fe, Si, Mn, and P are also oxidized to form the slag. Silicon oxidation is completed in early period of blow (known as de-siliconisation period), whereas carbon removal takes place during the entire period of blow. The evaluation of bath composition (2) is shown in **Fig. 2**. Different basic fluxes like calcined lime and calcined dolomite are added to make a basic slag during the blow for refining of steel and protection of vessel refractory. **Fig. 3** shows the evaluation of slag composition (2) for BOF converter. As the blow progresses, lime (CaO) steadily dissolves in the slag and slag weight (2) increases (**Fig. 4**). The oxygen reacts directly with carbon in the hot metal to produce CO and CO₂ and escapes in the waste gas.

BOF Oxygen Blowing and Lance Height: After scrap and hot metal are charged, oxygen is supplied through a water cooled lance continuously at different lance height above liquid metal bath. The blowing rates and lance height may vary significantly from shop to shop and depend on the BOF capacity, design of lance nozzles, oxygen pressure & flow rate, quality of the oxygen supply etc. At the start of blow, lance height is kept at higher position, to avoid the possibility of lance tip contact with the scrap, to achieve the oxidizing condition and heat generating reactions. The purpose is to increase the reaction rate, dissolution rate of fluxes and early slag formation by generating higher iron oxide. Most of the reactions occur during the mid blowing period which is the longest duration and known as peak decarburization period. The lance height is kept at lower position for enhancing the decarburization rate. However, it is an empirical compromise between achieving faster carbon removal rates and proper slag making. Towards the end of the blow, lance height is kept slightly higher position to maintain fluidity and chemical reactivity of the slag by raising its FeO content.

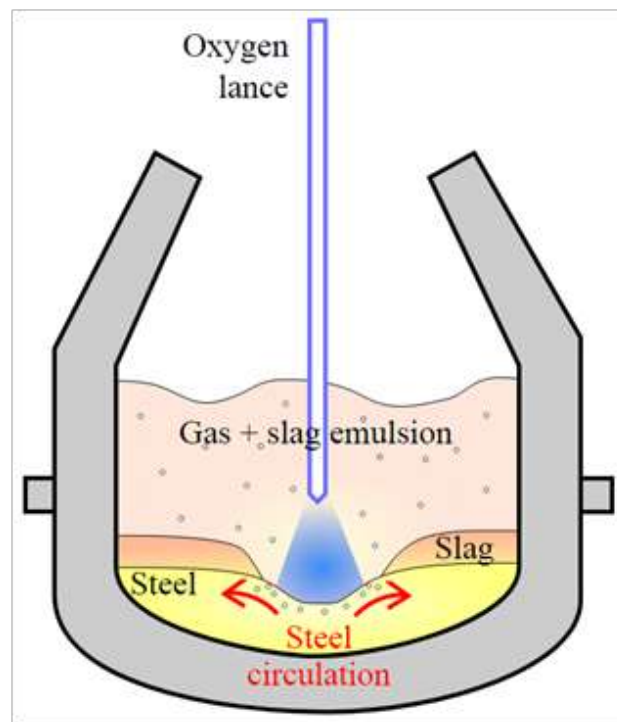


Fig. 1. Oxygen blowing in BOF converter

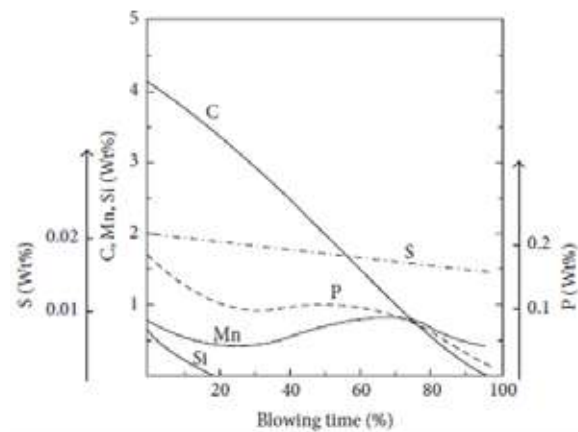


Fig. 2. Evolution of bath composition with blowing time

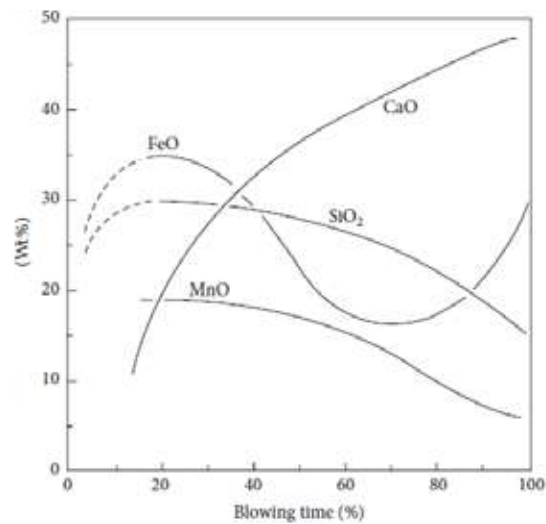


Fig. 3. Evolution of slag composition with blowing time

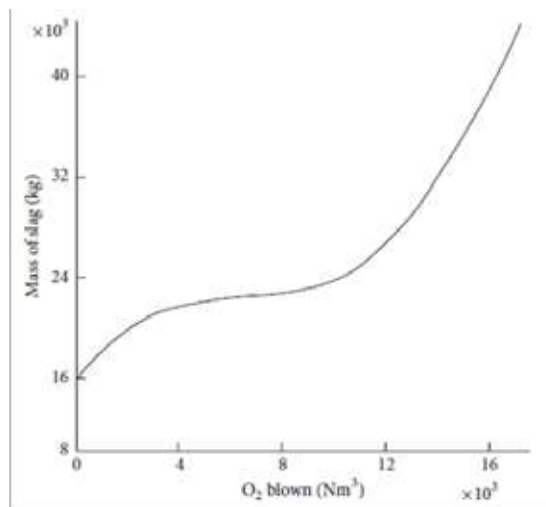


Fig. 4. Increasing mass of slag with oxygen blown



Steel scrapes as BOF coolant

Steel scrap is the most widely used coolant in converters all over the world. The commonly used scrap consists of slab and coil crop ends. Ladle and pit scrap generated inside the shop is also used; however its use is restricted to a minimum as it contains undesirable slag and refractory contamination. Scrap can be classified into two broad categories, heavy scrap and light scrap. From several model calculations and experiments in industrial heats it was shown that complete dissolution² of the charged scrap depends strongly upon the distribution of the heavy scrap such as crop and tail end of slabs and light scrap such as small sized sheets, ladle spills, ladle skull, etc. Therefore, scrap preparation is important for complete absorption of scrap into the liquid steel before the end point. Ideally, the same mix of grade and type of scrap should be used. Maintaining uniform scrap configuration becomes difficult in high production shops and leads to unpredictable turn down performance. Also at high production rates, in-house generated scrap is insufficient and the steel shops are forced to use expensive external scrap which also increases the possibility of tramp elements getting into the heat.

IRON ORE ADDITION IN BOF AS ALTERNATE COOLANT

The most commonly used alternative coolant is iron ore lumps due to inexpensive and easily availability. Addition of iron ore as alternate coolant is found very useful to reduce total metallic input & blowing time, to achieve higher shop productivity. However, addition of iron ore is tricky and should be done carefully. The formation of excessive slopping, increase in off gas volume, increase in hydrogen content in off gas, flame shooting are common problem arises during its addition in BOF steel making. To understand the genesis of associated problem, fundamental studies has been carried out for the classification of inherent properties of iron ore.

Classification of iron ore

Iron ores are natural rocks and minerals and are usually rich in iron oxides. Commercially, the most important minerals of iron are in the form of oxides, i.e. hematite (Fe_2O_3) and magnetite (Fe_3O_4). Hematite is considered to be better iron ore because of its high grade quality & lumpy nature.

Iron ore are received from different mines and accordingly their chemical composition may also differ. A list of common iron bearing minerals and its properties are furnished in **Table 2**.

Table 2. Various types of iron ore based on its chemical composition

Mineral	Chemical Composition	Fe Content (%Fe)	Color
Hematite	Alpha Fe_2O_3	70	Steel grey to red
Goethite	$\text{Fe}_2\text{O}_3 \cdot \text{H}_2\text{O}$	66.1	Brown to red
Limonite	$2\text{Fe}_2\text{O}_3 \cdot \text{H}_2\text{O}$	60	
Turgite	$2\text{Fe}_2\text{O}_3 \cdot \text{H}_2\text{O}$	66.1	Brown to red
Lepidocrosite	$\text{Fe}_2\text{O}_3 \cdot \text{H}_2\text{O}$	62	Brown to reddish brown
Maghemite	Gamma Fe_2O_3	69.9	Brown
Magnetite	Fe_3O_4	72.4	Black, blue or brown black

Chemical Composition of Iron Ores

Mining of iron ore is carried out from different mines to meet the requirement of different steel plant. Iron ores are characteristically friable in nature that result in generation of sizeable quantity of fines (<10 mm) during various stages of mining and processing. The ratio of lumps to fines produced is 2: 3. The size of lump iron ore lies in the range of +10 mm to 40 mm. The chemical compositions of iron ore lump as received from various mines are given in the **Table 3**.

Table 3. List of iron ore mines (SAIL) and production capacity

Mines (Name)	Production capacity (MTPA)	Plant to supply	Fe	SiO_2	Al_2O_3
Kiriburu	4.1	BSL	62.34	3.76	2.37
Meghatuburu	3.5	BSL	62.58	3.53	2.18



Gua	3.6	ISP	62.84	3.57	1.85
Bolani	6.2	DSP	62.47	3.05	2.06
Barsua	2.2	RSP	62.43	2.74	3.02
Dalli	4 - 5	BSP	65.11	3.9	1.50
Rajhara		BSP	64.37	4.06	1.75

Cooling efficiency for iron ore

The coolant effect of iron ore addition into converter is based upon two effects: a) Sensible heat of iron ore b) Reduction of $\text{FeO} / \text{Fe}_2\text{O}_3$. At low carbon level, reduction of ore will be suppressed and its coolant effect will be lower than at high carbon level. Heat effects of the different additions in converter are as follows:

Addition	Heat effect M.Cal/ton	% Fe	% O_2
Iron Ore,	1140	70	30
Scrap	340	99	-

The maximum cooling efficiency of iron ore is $1140 / 340 = 3.3$ times of scrap. With the decrease in iron content of ore, cooling efficiency will also be reduced due to lesser amount of chemically bonded oxygen.

Calculation of oxygen in iron ore

Iron ore contains chemically bonded oxygen and also acts as a source of oxygen in the converter. Amount of oxygen available for the process must be included in the calculation of oxygen advice. Iron ore is found in Fe_2O_3 form. So oxygen available from iron ore is 30% of its own weight. In STP, oxygen volume = $700 \times PO_2^{ore}$ Nm^3/ton

Where PO_2^{ore} = Fraction of oxygen in iron ore. It depends on iron content

$$= (3/7) * \% \text{ Feore}$$

Therefore, iron ore containing 60% Fe, PO_2^{ore} and oxygen volume are 25.71% and 180 Nm^3/ton respectively.

Moisture content of iron ore

Iron ores are hygroscopic in nature and may absorb moisture / water in the form of moisture. Due to the scarcity of iron rich haematitic ore, new mines are being developed to process ores with low iron contents or combined water. These ores normally consist of a mixture of hematite, martite, magnetite, goethite, limonite, turgite, lepidocrosite etc. The hygroscopic moisture may be evaluated by gravimetric or mass-loss methods by heating at $105 \pm 2^\circ\text{C}$. The combined water is liberated by heating at much higher temperature between $105 \pm 2^\circ\text{C}$ and $950 \pm 20^\circ\text{C}$.

The iron ores as extracted from different mines are largely different in composition and may contain a large amount of goethite, which means a higher amount of “combined water”. Comparing different iron ores, goethite is the one that has the highest surface area and thus can contain the highest amount of adsorbed water. In addition, goethite contains structural hydroxyls that are converted in water upon heating at moderate temperature $\sim 300^\circ\text{C}$. The stoichiometric loss of water according to the equation: $2\text{FeOOH} \rightarrow \text{Fe}_2\text{O}_3 + \text{H}_2\text{O}$ is $\sim 10\%$.

Literature (3) discussed the losses of mass of goethite in three different temperature ranges, and a variety of terms has been used to define these losses:

The first region up to about 150°C is named moisture, hygroscopic moisture, surface water, onset of bulk and surface dehydration, non-stoichiometric hydroxyl units (excess water), surface adsorbed water, chemisorbed surface water and adsorbed water.

The second region goes up to about $200\text{--}230^\circ\text{C}$, depending on the sample characteristics (particle size, morphology, synthetic or natural, etc.) and is named as bulk dehydration and surface dehydration / dehydroxylation, non-stoichiometric water from bulk and surface, weakly bound OH groups, surface-bound and bulk-sequestered water, loosely bound hydroxyl units, dehydration from hydrogen bonded water or dehydroxylation of surface.

The third region comprises the transformation of goethite into hematite, which is completed below 400°C . This loss of mass has been termed as structural hydroxyl, bulk dehydroxylation, intrinsic dehydroxylation, dehydroxylation, non-stoichiometric hydroxyl units, and strongly bounded water and OH groups.



Other Impurities in iron ore

Iron ore also contains certain impurities like silica, alumina, sulphur, phosphorus etc. Iron ore contains 2.5% to 4% silica which needs to be taken care during mass balance calculation to retain the required slag basicity. It contains alumina and phosphorus in the range of 1.5 – 3.0% and 0.1% max. Sulphur in the ore goes partly into the iron and steel and makes them brittle.

CHALLENGES FOR USING IRON ORE IN BOF

Foamy slag and slopping

In BOF, oxygen is injected in the steel bath for the oxidation of carbon and other impurities. During the process steel bath temperature varies from 1300 °C (hot metal temperature) to 1660°C (steel tapping temperature). Iron ore is added as coolant of steel bath. It gets melted (melting point ~ 1250 °C) completely in few seconds and joins the slag. The addition of iron ore provides an immediate increase in the oxidation potential of slag. It makes the slag excessive foaming.

The mechanism influencing slopping behaviour of the slag during oxygen steelmaking needs to be understood. The rate of reduction of FeO in the slag by carbon from iron droplets, effect of temperature on the rate of reduction of FeO by carbon and effect of the foaming properties of the slag on slopping are important. Slopping occurs when there is excessive CO evolution into highly foamable slag. The foam index depends upon the slag basicity, temperature and rate of CO generation. So, to avoid slopping, new strategies for oxygen blowing and addition of iron ore must be considered.

Release of off gas

The biggest challenge with high iron ore usage is to control the excessive slag foaming and increased exit gas flow rate. During the blowing, the gases CO & CO₂ are generated inside the converter due to oxidation of hot metal carbon by pure oxygen. At higher temperature > 1000 °C, the CO gas is quite stable. The formation of CO gas is predominant (~ 80%) compared to formation of CO₂ gas. As one molecule of oxygen produces two molecules of CO gas, an enormous volume of off gas generates during the process. The volume of off gas always remains higher than oxygen blowing rate due to formation of CO/CO₂ and mixing of atmosphere gases at converter mouth. During the de-carburisation period (i.e. middle part of BOF blowing), unexpected increase in the volume of off gas is a common phenomenon due to reduction of accumulated oxygen in the system in the form of FeO or slag metal emulsion.

Addition of iron ore accumulates oxygen in the slag to increase its oxidation potential. Depending upon the blowing profile, a sudden release of off gas may happen due to excessive CO/CO₂ gas formation inside the BOF vessel. In absence of efficient suction of the off-gases, the gases start coming out from the gap between converter mouth and skirt / hood and causes flame shooting. It is a serious safety aspect and needs to be control. An enclosure for the converters (dog house) is recommended. A high suction capacity of GCP ID fans or operating at higher designed capacity may be the alternate options.

Oxygen Consumption and Total blowing time

Oxygen available from ore is ~ 180 Nm³ per ton of ore addition. The BOF converters are designed to blow oxygen at the rate of 3 – 4 Nm³/ton/min. The total oxygen consumption varies from 50 – 60 Nm³/ton. The oxygen available from 50 kg/ton ore is 9Nm³/ton and is equivalent to 2-3 minutes of oxygen blow from the lance. The specific oxygen consumption with ore addition will definitely reduced by ~ 9 Nm³/ton for complete replacement of scrap by iron ore.

Operational difficulties during handling of iron ore

Availability and handling of iron ore particularly during rainy season is problematic. Iron ore is highly hygroscopic in nature and may absorb a huge amount of water. Iron ore cannot be used consistently in large quantities in BOF particularly in rainy season. Moisture content of iron ore causes jamming of storage bunkers, chute, and conveyor belt. Iron ore addition is always associated with dust and fumes causing environmental problem and poor working conditions.

Operating challenges for addition of Iron ore in BOF

The addition of iron ore in BOF is tricky. Addition in chunk, gives a sudden rise in off gas which may cause flame shooting. Iron ore contains a certain amount of moisture which gets dissociated at high temperature and joins the off gas. It was found that the significantly high levels of moisture content creates problem during batch or bulk charging inside the converter (during oxygen blowing) and causes the H₂ level in BOF gas to shoot up. As H₂ level in the BOF gas shoots up, it initiates blow stop action to prevent the formation of an explosive gas mixture inside the gas cleaning plant (GCP). This phenomenon limits the iron batch size to a maximum of 500 kg and thus the number of batches of iron ore increases. Moreover whenever the Iron ore is charged,



the GCP gas flow shoots up abruptly causing fugitive emissions from converter mouth as GCP by design cannot handle the suddenly increased flow rate of BOF Gas.

As a solution of this problem, a continuous or trickle feeding of iron ore is necessary for uniformity in addition. It provides a better control to achieve higher addition of iron ore in BOF. The rate of trickle feeding of iron ore can be controlled. A level of iron addition in the tune of 40 – 50 kg/tcs could be achieved easily.

CONCLUSION

The thermal balance to control excessive steel temperature is achieved by use of scrap. In the present steelmaking scenario, the scarcity and high cost of prime scrap has increased the importance to choose alternative coolants. The most commonly used alternative coolant is iron ore lumps as it is inexpensive and easily available in a steel plant. The addition of iron ore in BOF during oxygen blowing is tricky and should be done carefully. It contains chemical oxygen, moisture etc which gets liberated at higher temperature in the contact of hot metal. The formation of excessive slopping, increase in off gas volume, increase in hydrogen content in off gas, flame shooting are common problems that arise during ore addition in BOF steelmaking. The various aspects of chemical and physical conditions of iron ore have been discussed in the paper to elaborate the reason and probable remedial solution. A trickle feeding system of iron ore is useful to control flame shooting and hydrogen level in off gas within limit. Partial or full replacement of scrap has been achieved in SAIL plants. Addition of iron ore as alternate coolant is found very useful to reduce total metallic input & blowing time, to achieve higher shop productivity.

ACKNOWLEDGEMENT

The author expresses his gratitude to the management of RDCIS, SAIL for their kind support and consent for publishing this work. The author acknowledges Sri Vikash Dayal, DGM, ME&A, RDCIS for his support for providing the details of chemical composition and production of iron ore from various SAIL mines.

REFERENCES

1. Sanjay Kumar Gupta, Abdhesh Prasad, Abhinandan Chatterjee, Manoranjan Kumar, Somnath Ghosh, and Ramen Datta: "Adoption of Sinter Addition in Steelmaking Converter to Control Spitting", Journal of Metallurgy, Hindawi Publishing Corporation, Volume 2015, Article ID 187042, 5 pages.
2. B. Deo and R. Boom, Fundamentals of Steelmaking Metallurgy, Prentice Hall International (UK) Limited, 1993.
4. Geraldomagela da Costa, Katia Monteiro Novack, Megg Madonyk Cota Elias and Camila Cristina Rodrigues Ferreira da Chunha: "Quantification of moisture contents in iron and manganese ore", ISIJ International, Vol 53 (2013), No-10, PP 1732 – 1738.

Hydrothermal Synthesis and Characterization of Nanocrystalline Zinc Orthovanadate($\text{Zn}_3\text{V}_2\text{O}_8$) on Graphene Oxide Scaffolds

Lakshmana Naik R¹, H Seshagiri Rao², Pernapati Nagaraja², Bala Narsaiah T¹

Department of Chemical Engineering, JNTUA College of Engineering, Ananthapuramu, Andhra Pradesh¹

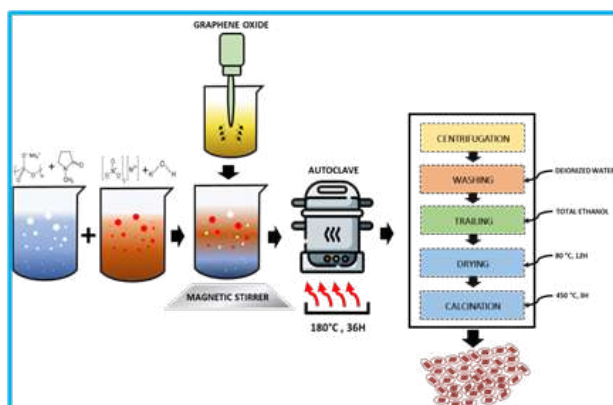
Department of Chemistry, Rajiv Gandhi University of Knowledge Technologies, Kadapa, Andhra Pradesh²

✉ lakshman2027@gmail.com; ✉ balutumma.chemengg@jntua.ac.in

ABSTRACT

Transition Metal Vanadates proved to have diversified applications in photochemical, electrochemical, energy production & storage, and fluorescence materials. Band-gap fabrication and modifying structure morphology to suit the need has been a challenging task. Nanocrystalline Zinc Orthovanadate($\text{Zn}_3\text{V}_2\text{O}_8$) crystals on Graphene Oxide scaffolds were synthesized by hydrothermal route. The structure and bonding properties of the prepared material were analysed by powder X-Ray diffraction(XRD) and Fourier transform infrared spectroscopy(FTIR). The band gap is determined by UV-visible diffuse reflectance spectroscopy (DRS), and the particle size and surface charge are analyzed by dynamic light scattering analysis. Scanning Electron Microscopy equipped with a Field Emission gun is employed to check the morphology of the material. The nanoparticles obtained were of size 37.2 nm and zeta potential of nanoparticles was found to be -25.4 mV, which indicates the dispersion and stability of the material prepared.

Keywords: Zinc orthovanadate; $\text{Zn}_3\text{V}_2\text{O}_8$; Graphene oxide; hydrothermal synthesis.



Graphical abstract of hydrothermal synthesis of $\text{Zn}_3\text{V}_2\text{O}_8$

INTRODUCTION

Transition metal vanadates are widely being used as catalyst material industrially due to low cost, abundance, the ability of vanadium to exist in variable oxidation states as MVO_4 , MV_2O_6 , MV_3O_8 , MV_2O_4 and $\text{M}_3\text{V}_2\text{O}_8$ and higher stability of the material during the catalytic activity[1]–[5]. Transition metal vanadates are well studied catalysts in photochemical, electrochemical, photo-electrochemical reactions[6]–[9]. On the other hand vanadates are also being used as organic catalyst. These compounds are also being used in super capacitors, batteries, magnetic, magneto-electric materials etc[6], [8], [9]. Hence it is proved and accepted that these materials have broadened the spectrum of energy production and storage in addition to the other industrial catalytic applications.

Among the transition metal series, titanium based compounds are counted as the best visible light photocatalysts[10], [11]. The light harvesting nature of titanium compounds have enhanced the significant usage of these materials as photocatalyst. Hence titanium vanadium oxide is assumed to be a best photo-electrocatalyst[12], [13]. Owing to the huge cost and availability of



titanium, the applications developed seldom reach the industry and hence the availability of titanium based low cost products in market is rare. Hurdles in bridging the efficiency and cost economics still exist in commercialization[14]. Zinc has been proved to mimic Titanium in energy harvesting to a considerable extent and it is economic[15]. Mixed oxides of ZnO and V_2O_5 are studied by many research groups worldwide[16]–[18]. By tailoring the composition of zinc, vanadium, oxygen, and different calcinations temperatures, a wide variety of phases as $Zn_4V_2O_9$, $Zn_2V_2O_7$ and $Zn_3V_2O_8$, etc. exists[2], [3], [5]. Among these $Zn_3V_2O_8$ is reported as a best photo harvester[2], [6]. It is also reported that Graphene Oxide offers a high surface area, better conductivity and hence tapping solar energy would be further facilitated by growing $Zn_3V_2O_8$ on graphene oxide layers[5]. However very few reports are available on the successful synthesis of $Zn_3V_2O_8$ [19]. Hence we target the hydrothermal synthesis of $Zn_3V_2O_8$ on Graphene oxide scaffolds. The prepared composites are calcinated and characterized to confirm the purity and are reported here.

Materials

Ammonium metavanadate and zinc nitrate were used as precursors of Vanadium and zinc respectively. Graphite powder, Orthophosphoric acid, sulphuric acid, sodium nitrate, hydrogen peroxide, urea, N-methyl-2-pyrrolidone, and ethanol were used for the synthesis of the composite material. All Chemicals were purchased from Sigma–Aldrich, analytical grade and used directly without purification. Double distilled water was used throughout the experiment.

Experimental section

Graphene Oxide (GO) was synthesised by Modified Hummers process as we reported in our previous article by oxidizing natural flake graphite[20]. In brief, to a mixture of sulphuric acid and phosphoric acid, graphite powder, sodium nitrate was added and stirred continuously. The mixture was cooled below 10°C and KMnO_4 was added in portions and stirring was continued for 12 hours. H_2O_2 was added to oxidize the graphite surface and metal impurities were removed by treating with 20% HCl solution. The obtained precipitate was separated, washed with ethanol and stored in DMF solution.

Zinc vanadate ($\text{Zn}_3\text{V}_2\text{O}_8$) was synthesized by a simple hydrothermal process. In a normal process, 1.323 grams of NH_4VO_3 (ammonium metavanadate) was added in 87.5 mL of N-Methyl-2-Pyrrolidone with constant magnetic stirring for 1 h (i.e. Solution A). To the above Solution A, the 8.450 grams of urea were added with constant magnetic stirring. Add approximately 3.76 grams of zinc nitrate to approximately 240 mL of water (ie solution B). The prepared solution B was added drop wise to solution A under vigorous stirring. The prepared Graphene oxide was added to the above solution with 8mg/30ml of DMF and sonicated for 15 minutes for uniform dispersion of the graphene oxide. The solution was made up to 350ml using distilled water, transferred to an autoclave lined with Teflon, sealed and heat-treated at 180°C for 36 hours. After the furnace was cooled to room temperature, the solution was centrifuged to collect the precipitate, and washed twice with distilled water and ethanol to remove impurities. The obtained precipitate was dried at 80°C in a hot air oven till it is free from moisture. The composite was calcinated in air at 450°C for 3 hours at a heating rate of 2°C min^{-1} . The calcined sample was used for further characterization.

Characterization

The bonding characteristics in the prepared nanocomposite were investigated using JASCO FTIR 4700 with ATR Pro-One accessory and TGS detector from 400cm^{-1} to 4000cm^{-1} . Crystalite size and crystal phase was identified by X-ray Diffraction technique recorded on Bruker XRD with copper $K\alpha$ as x ray source. The quantitative investigation was carried out with the software package High Score Plus, version 3.0 (PANalytical) software. Band gap was evaluated by recording reflectance spectra using JASCO UV-Visible spectrophotometer (V-660) with ISV-722 accessory and Barium sulphate was used reference material. The morphology of the prepared material was visualised using Carl Zeiss Scanning Electron Microscope (Merlin Model) equipped with Field Emission Gun. Particle size and Surface Charge density was determined using Dynamic light scattering analysis.

RESULTS AND DISCUSSION

As shown in **Fig 1** calcined nanoparticles phase purity and crystallinity were studied using X-ray diffraction. Majority of the reflection peaks was indexed to $\text{Zn}_3\text{V}_2\text{O}_8$ (The structure has been assigned an ICDS number (calculated powder diffraction data: 98-001-2846), with some weak peaks being small and broad despite the presence of Graphene oxide. The quantitative investigation was carried out with the software bundle, version 3.0, High Score Plus. The peaks locations at 2θ is 15.1, 23.2, 26.5, 29.5, 31.1, 35.05, 36.07, 43.27, 57.9, and 63.1 can be readily indexed as (020), (021), (022), (131), (040), (221), (023), (240), (025) and (420) $\text{Zn}_3\text{V}_2\text{O}_8$ bulk crystal planes respectively. Such diffraction peaks may be precisely indexed to the orthorhombic

crystalline structure of the $\text{Zn}_3\text{V}_2\text{O}_8$, not only for the peak position, but also for the relative strength of the characteristic peaks, consistent with the standard spectrum. The XRD pattern shows that the sample is a single phase without any impurity phase. This result indicates that the physical phase of $\text{Zn}_3\text{V}_2\text{O}_8$ nanoparticles actually has higher purity.

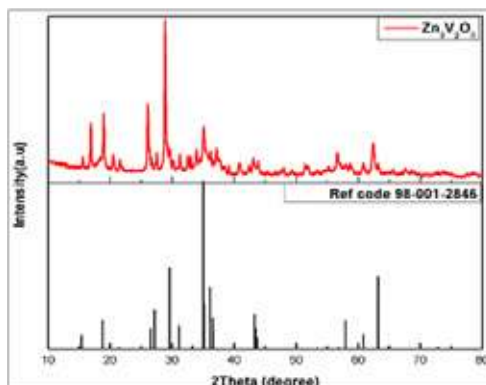


Fig. 1 XRD pattern of $\text{Zn}_3\text{V}_2\text{O}_8$

The morphologies of electrocatalyst ($\text{Zn}_3\text{V}_2\text{O}_8$) prepared via hydrothermal treatment shows that it has a prominent effect on their physical properties. The image of $\text{Zn}_3\text{V}_2\text{O}_8$ scanning electron microscopy shown in **Fig. 2** shows that the calcined metal oxide nanoparticles were dispersed uniformly and nearly spherical in shape with agglomerates.

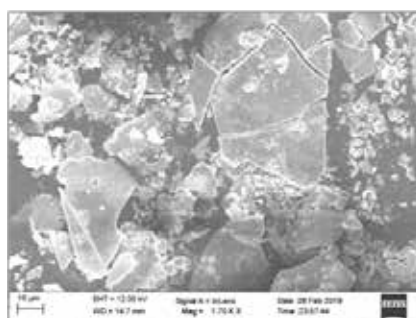


Fig. 2. Zincvanadate SEM image

The Nano electrocatalyst FTIR spectrum ($\text{Zn}_3\text{V}_2\text{O}_8$) is shown in **Fig. 3**. The FTIR spectrum of the synthesized catalyst was analysed in the wave number range of $400\text{--}4000\text{ cm}^{-1}$, and the chemical bonds and functional groups of the entire compound were determined. The spectrum shows a wide absorption peak in the range $3600\text{--}3000\text{ cm}^{-1}$ wave number which can be ascribed to the hydroxyl groups and water molecules. Vanadate stretching modes (V-O) are allocated to bands occurring between 925 and 935 cm^{-1} wave numbers. V-O-V stretching was allocated to bands between 650 and 780 cm^{-1} . The band of about 467 cm^{-1} in the FTIR spectrum is part of the inorganic stretched Zn-O system. According to records[21]–[23], the vibration band in the range of $770\text{--}650\text{ cm}^{-1}$ is attributed to $\text{V}=\text{O}$ and V-O-V. This band has been studied around 467 cm^{-1} in the FTIR band and is part of the extended mode of Zn-O, Zn -O-V, and Zn -O-Zn type bonds.

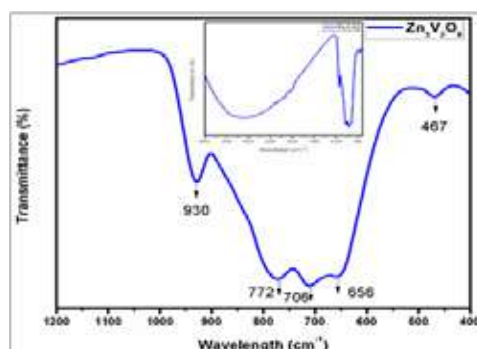


Fig. 3. (a) FTIR spectroscopy of $\text{Zn}_3\text{V}_2\text{O}_8$

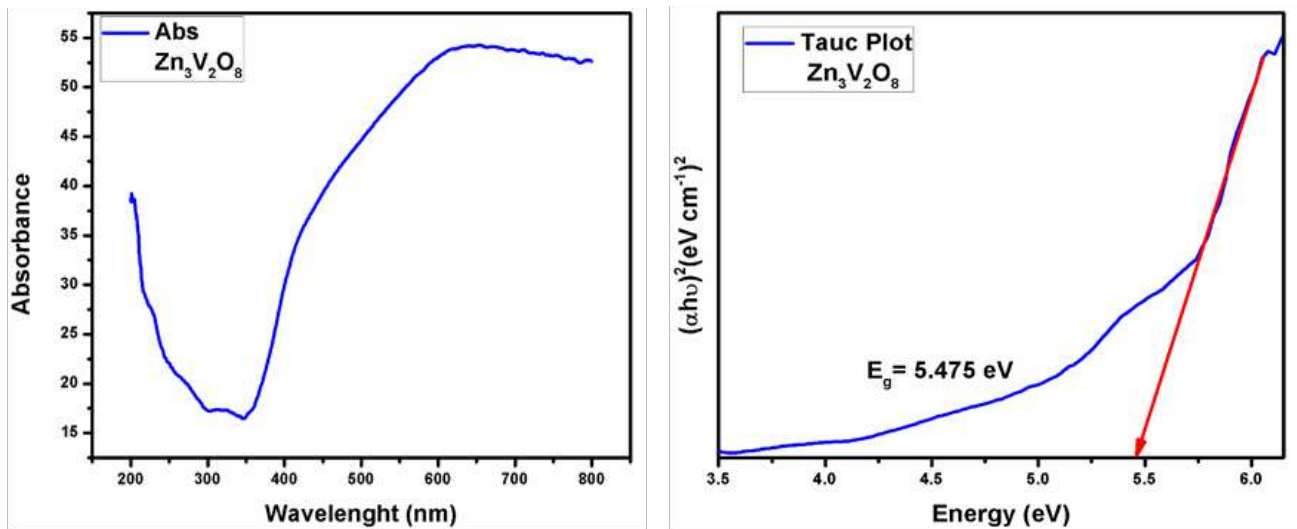


Fig. 4 (a)UV-Visible Diffuse reflectance spectra (b)Tauc plot of $(\alpha h\nu)^{1/2}$ Vs photon energy (h ν).

As shown in **Fig 4(b)**, the band gap value of the synthesized $\text{Zn}_3\text{V}_2\text{O}_8$ is determined to be 5.475 eV through the tauc diagram of $(\alpha h\nu)^{1/2}$ versus photon energy (h ν). The band gap energy (E_g) is evaluated according to the Wood Tauc theory, as shown in the **Fig 4(b)**. E_g is calculated based on the relationship of $\alpha h\nu = (h\nu - E_g)^k$, where α is the absorbance and h is Planck constant, ν is the frequency, and k is the constant related to different transitions. For the best linear relationship with a k value of 2, it indicates that there is an indirect allowed electronic transition.

As shown in **Fig 5**, the particle size distribution of $\text{Zn}_3\text{V}_2\text{O}_8$ was further confirmed by DLS. The DLS analysis reveals that the range of NPs size ($\text{Zn}_3\text{V}_2\text{O}_8$) was observed to be 14.5–300 nm in size which indicates a wide size distribution of particles with an average particle size 37.2 nm and further confirms from the SEM image as shown in **Fig 2**. The poly dispersity index (PI) of NPs was found to be 3.492.

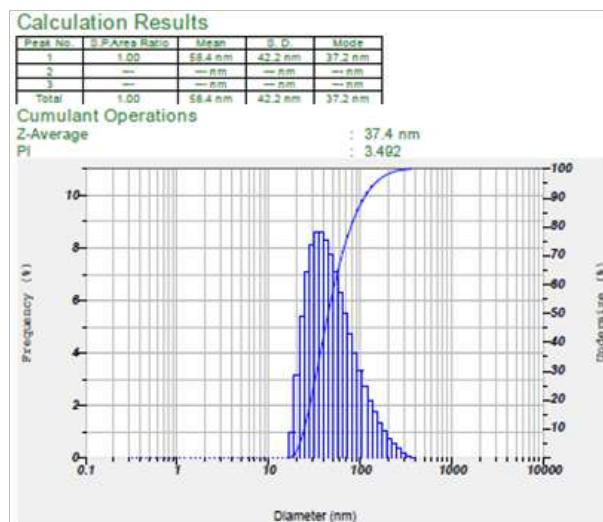


Fig. 5. Analysis of average particle size, particle size distribution and poly dispersity index of $\text{Zn}_3\text{V}_2\text{O}_8$

The value of a zeta potential value of synthesized NPs was determined by using Dynamic light scattering analysis. Zeta potential is a significant factor for determining the durability of the calcined Nano material $\text{Zn}_3\text{V}_2\text{O}_8$. In this analysis as shown in **Fig. 6**, Zeta potential of the $\text{Zn}_3\text{V}_2\text{O}_8$ was observed to be -25.4mV. High negative zeta potential indicates that $\text{Zn}_3\text{V}_2\text{O}_8$ is long lastingly stable without agglomeration and supports strong colloidal nature, high dispersion of synthesized $\text{Zn}_3\text{V}_2\text{O}_8$ due to negative-negative repulsion.

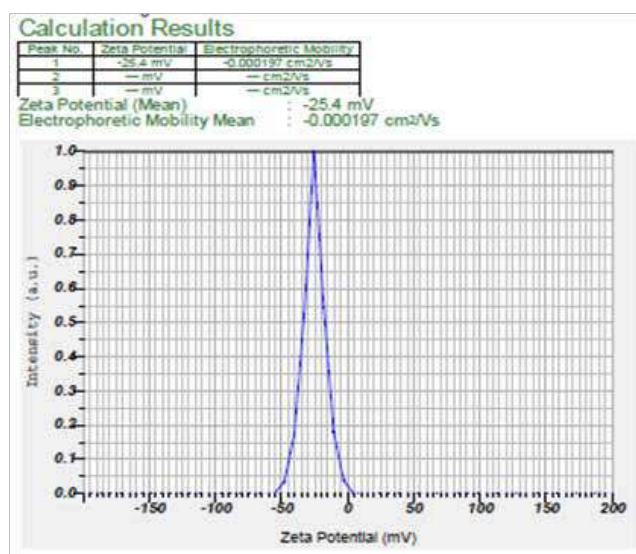


Fig. 6. Zeta potential of $\text{Zn}_3\text{V}_2\text{O}_8$

CONCLUSION

Zinc Orthovanadate nanoparticles were successfully synthesised using ammonia metavanadate as a precursor and Graphene oxide as just a conductor using a simple and easy hydrothermal process. The XRD indicates the Zinc Orthovanadate calcined orthorhombic structure at 450°C. It is evident from SEM images that the particle structure changes with rising temperatures. Finally, FTIR spectroscopy revealed the existence of V-O-V and V-O diffusion bonds of vanadium oxide and metal oxide bonds such as Zn-O, ZnO-Zn and Zn-O-V bonds. The band gap value of the synthesized $\text{Zn}_3\text{V}_2\text{O}_8$ is determined to be 5.475 eV. Characterization of electrocatalysts by analysis of particle size and Zeta potential corresponds to the formation of NPs and stability of nanoparticles. Nano particles with these unique properties such as good particle size, zeta potential, crystallite size, metal vanadate bonding etc. can exhibit excellent catalytic behavior against catalyst anode and methanol oxidation reaction in fuel cells.

REFERENCES

1. M. Birdeanu, M. Vaida, D. Ursu, and E. Fagadar-Cosma, Obtaining and characterization of $\text{Zn}_3\text{V}_2\text{O}_8$ and $\text{Mg}_3\text{V}_2\text{O}_8$ pseudo binary oxide nanomaterials by hydrothermal method, AIP Conf. Proc., vol. 1796, no. January 2017, pp. 1–5, 2017.
2. H. Sameie, A. A. Sabbagh Alvani, N. Naseri, S. Du, and F. Rosei, First-principles study on ZnV_2O_6 and $\text{Zn}_2\text{V}_2\text{O}_7$: Two new photoanode candidates for photoelectrochemical water oxidation, Ceram. Int., vol. 44, no. 6, pp. 6607–6613, 2018.
3. D. Díaz-Anichtchenko et al. Comparative study of the high-pressure behavior of ZnV_2O_6 , $\text{Zn}_2\text{V}_2\text{O}_7$, and $\text{Zn}_3\text{V}_2\text{O}_8$, J. Alloys Compd., vol. 837, 2020..
4. S. Wang, B. Liu, G. Zhi, G. Xu, Q. Wang, and J. Zhang, 2D layered mesoporous MoO_2/rGO composites for high performance anode materials in lithium-ion battery, Microporous Mesoporous Mater., vol. 246, pp. 14–23, 2017.
5. Y. Yu et al., Zinc Pyrovanadate Nanoplates Embedded in Graphene Networks with Enhanced Electrochemical Performance, Ind. Eng. Chem. Res., vol. 55, no. 11, pp. 2992–2999, 2016.
6. Q. Li et al., A High-Capacity Ammonium Vanadate Cathode for Zinc-Ion Battery, Nano-Micro Lett., vol. 12, no. 1, 2020..
7. Y. Zhang, F. Wan, S. Huang, S. Wang, Z. Niu, and J. Chen, A chemically self-charging aqueous zinc-ion battery, Nat. Commun., vol. 11, no. 1, pp. 1–10, 2020.
8. R. Tang et al., Exploring the coordination change of vanadium and structure transformation of metavanadate MgV_2O_6 under high pressure, Sci. Rep., vol. 6, no. September, pp. 1–9, 2016.
9. M. H. Alfaruqi et al., Electrochemical Zinc Intercalation in Lithium Vanadium Oxide: A High-Capacity Zinc-Ion Battery



- Cathode, *Chem. Mater.*, vol. 29, no. 4, pp. 1684–1694, 2017.
10. H. Eskandarloo and A. Badiei, Photocatalytic Application of Titania Nanoparticles for Degradation of Organic Pollutants, *Nanotechnol. Opt. Sensors*, pp. 108–132, 2015.
 11. A. T. Kuvarega, R. W. M. Krause, and B. B. Mamba, Nitrogen/palladium-codoped TiO₂ for efficient visible light photocatalytic dye degradation, *J. Phys. Chem. C*, vol. 115, no. 45, pp. 22110–22120, 2011,
 12. K. E. Dalle, J. Warnan, J. J. Leung, B. Reuillard, I. S. Karmel, and E. Reisner, Electro- and Solar-Driven Fuel Synthesis with First Row Transition Metal Complexes, *Chem. Rev.*, vol. 119, no. 4, pp. 2752–2875, 2019.
 13. D. Eisenberg, H. S. Ahn, and A. J. Bard, Enhanced photoelectrochemical water oxidation on bismuth vanadate by electrodeposition of amorphous titanium dioxide, *J. Am. Chem. Soc.*, vol. 136, no. 40, pp. 14011–14014, 2014.
 14. L. Kiran Babu, H. Seshagiri Rao, P. N. R. Kishore, and Y. V. Rami Reddy, Hydrothermal synthesis of flower-like ZnO-SiO₂ nanocomposites for solar light-induced photocatalysis and anti-bacterial applications, *Mater. Res. Express*, vol. 6, no. 8, 2019.
 15. X. Chen, Y. Li, X. Pan, D. Cortie, X. Huang, and Z. Yi, Photocatalytic oxidation of methane over silver decorated zinc oxide nanocatalysts, *Nat. Commun.*, vol. 7, no. 1, p. 12273, 2016.
 16. T. Nakajima, M. Isobe, T. Tsuchiya, Y. Ueda, and T. Manabe, Correlation between luminescence quantum efficiency and structural properties of vanadate phosphors with chained, dimerized, and isolated VO₄ tetrahedra, *J. Phys. Chem. C*, vol. 114, no. 11, pp. 5160–5167, 2010.
 17. M. Kurzawa and M. Bosacka, STUDY ON PHASE RELATIONS IN Zn₃V₂O₈ – ZnMoO₄ SYSTEM, vol. 64, pp. 1081–1085, 2001.
 18. M. Kurzawa, I. Rychlowska-Himmel, M. Bosacka, and A. Blonska-Tabero, Reinvestigation of phase equilibria in the V₂O₅-ZnO system, *J. Therm. Anal. Calorim.* vol. 64, no. 3, pp. 1113–1119, 2001.
 19. V. Mazánek et al., Ultrapure Graphene Is a Poor Electrocatalyst: Definitive Proof of the Key Role of Metallic Impurities in Graphene-Based Electrocatalysis, *ACS Nano*, vol. 13, no. 2, pp. 1574–1582, 2019.
 20. M. N. Nanoparticles and L. N. R., “Size Controlled Hydrothermal Synthesis and Characterization of Nickel Introduction : vol. 29, no. 5, pp. 10012–10018, 2020.
 21. H. Yue, G. Wang, R. Jin, Q. Wang, Y. Cui, and S. Gao, Sulfur-doped amorphous NiMoO₄ on crystalline Fe₂O₃ nanorods for enhanced lithium storage performance, *J. Mater. Chem. A*, vol. 6, no. 46, pp. 23819–23827, 2018.
 22. M. T. H. Bhuiyan et al., “Synthesis and characterization of high-quality cobalt vanadate crystals and their applications in lithium-ion batteries,” *Cogent Phys.*, vol. 3, no. 1, 2016.
 23. M. Farahmandjou, Chemical Synthesis of Vanadium Oxide (V₂O₅) Nanoparticles Prepared by Sodium Metavanadate, *J. Nanomedicine, Res.*, vol. 5, no. 1, pp. 2–5, 2017.



Study of Mechanical and Thermal Properties of ABS Reinforced with Fly Ash by using Maleic Anhydride as Coupling Agent

Bulti Kandar, Deepshikha Datta

GMR Institute of Technology, Rajam

Plastic Engineering Department, Central Institute of Plastic Engineering and Technology, Bhubaneswar

✉ deepa.datta81@gmail.com

ABSTRACT

In this study fly ash is utilized as strengthening filler in Acrylonitrile Butadiene Styrene (ABS) to create light weight composites. Fly ash is a heterogeneous side-effect material delivered in the burning procedure of coal utilized in power stations. It is a fine dark shaded powder having circular smooth particles that ascent with the pipe gases. As fly ash contains pozzolanic materials segments which reach with lime to shape cementitious materials. Acrylonitrile butadiene styrene (ABS), a terpolymer is broadly utilized building thermoplastic, known for superior item applications. The polymer has a decent mechanical property along with substance opposition, steadiness, surface appearance, and procedure capacity. Fly ash is latent empty silicate circles, a normally happening result of the consuming procedure at coal-terminated warm force plants. Fly ash as filler is principally used to decrease the heaviness of plastics, rubbers, resins, cements, and so on utilized widely as filler ointments in oil boring tasks under high warmth and high pressure conditions down the opening. Giving the upsides of decreases weight, expanded filler loadings, better stream attributes, less shrinkage and diminishes water absorption. For mechanical and thermal test ABS/FA composites material are developed with (0,5,15,25,30) wt%.

To improve the interaction between the inorganic filler and the natural fiber, the Fly ash is preheated and Maleic Anhydride is utilized as compatibilizer. The ductile and that, Fly ash joined by compatibilization prompted the slight reduction in Rigidity, Flexural quality and effect quality however generous improvement in Elastic modulus and Flexural modulus alongside warm strength of the composites. As Fly ash is ease filler by joining it in ABS decreases the expense of the item. It has also been found out that the tensile strength and flexural strength increase. But tensile modulus is found to be decrease significantly. Flexural strength of ABS increase in 70/30 wt% with flexural modulus of 5230.68. DSC studies it is observed that the melting point of virgin ABS is 130°C with enthalpy 0.1539 (J/g) and after adding 25 wt% of fly ash the temperature started to decrease and its came to 125°C In TGA studies it is shown that the final temperature of virgin ABS is a 680.2°C and the % of residue is 0.30 gm obtain. But after adding fly ash as filler of different percentage the temperature gradually increase. At 30 wt% FA the temperature increase from 436°C to 810°C and the % of residue would be 27.8 gm.

Keywords: ABS; Pozzolanic; Steadiness; Compatibilization.

INTRODUCTION

Composite materials are characterized as materials comprising of at least two parts with various properties and particular limits between them. Wood is a whiz composite of cellulose filaments in a framework of lignin[10]. The most crude artificial composite materials were straw and mud joined to shape blocks for building development. Most of composite materials utilize two constituents: a fastener or framework and a support. The fortification is more grounded and stiffer, framing such a spine, while the grid keeps the support in a set spot[10]. The fastener moreover ensures the support, which might be weak, as on account of the long glass strands utilized related to plastics to make fiber glass. Subsequently composite materials are strong multiphase materials shaped through the blend of materials with various basic, physical and chemical properties. Composites are generally utilized in such different applications as transportation, development and purchaser items.

Fly ash is commonly utilized as fortifying filler in acrylonitrile butadiene styrene (ABS) to grow light weight composites[8]. In any case, concentrate on the impact of molecule size on mechanical properties of thermoplastic-based fly ash items is exceptionally restricted. The data is essential in building up the items for elite application. This examination thinks about mechanical properties of fly ash fortified thermoplastic items made utilizing diverse molecule size[16]. The items were blended and relieved utilizing a hot press machine, before experienced a few mechanical tests and natural evaluation. The outcomes show that as the size of the fly ash molecule builds, the elastic and flexural properties of the example decline[2].



Acrylonitrile butadiene styrene (ABS), a terpolymer is broadly utilized designing thermoplastic, known for elite item applications[2]. The polymer has a decent mechanical property along with substance opposition, strength, surface appearance, and procedure capacity. Fly ash is latent empty silicate circles, a normally happening result of the consuming procedure at coal-terminated warm force plants[7]. Fly ash as filler is principally used to lessen the heaviness of plastics, rubbers, tars, concretes, and so on utilized broadly as filler greases in oil penetrating tasks under high warmth and high pressure conditions down the opening[8]. Additionally utilized as oil well solidifying, mud clay and comparable applications. Fly ash is broadly utilized in an assortment of items, including sports supplies, protection, vehicle bodies, marine specialty bodies, paints, and fire and warmth security gadgets. Giving the upsides of

decreases weight, expanded filler loadings, better stream qualities, less shrinkage and distorting and lessens water absorption[5]. In the current work, so as to improve the communication between the inorganic filler and the natural lattice, the Fly ash is preheated and Maleic Anhydride is utilized as compatibilizer. The elastic and warm properties of the composites are estimated by ASTM techniques[5]. The outcomes uncover that, Fly ash joined by compatibilization prompted the slight lessening in Elasticity, Flexural quality and effect quality yet significant improvement in Malleable modulus and Flexural modulus alongside warm solidness of the composites. As Fly ash is minimal effort filler by fusing it in ABS decreases the expense of the item.

MATERIAL USED

ABS (High Impact grade HI 121 with a Specific Gravity of 1.04 from M/s LG CHEM, India). Fly Ash (FA) average particle size of $10\mu\text{m}$ collected from Bhadrak, Emami cement plant, Orissa, India was used as filler. Muffle furnace was used for thermal treatment of FA supplied. Maleic Anhydride in pellet form by M/s Lab Chemicals, Bhubaneswar, India.

EXPERIMENTAL PROCESS

Hot Air Dry Oven

Firstly hot air dry oven is used for drying the ABS material for 2hrs for 80°C . By this process the moisture content of ABS is removed. Then it is used for further process[2].

Surface Treatments of FA

Thermal Treatment. Thermal treatment of the FA was performed at 1000°C for 1 h in muffle furnace. Once removed from furnace, FA was rapidly cooled to room temperature and it is noted as TFA hereafter[2].

Batch preparation of ABS /FA composite

Blends of ABS is prepared containing different weight percentage of FA (5, 15, 25, 30%) by using two roll mill at roll speed of 60 rpm. Temperature was maintained at 220°C for 10 mins. Subsequently the melt mixed composite is brought to room temperature and remove the sheets from two roll mill by using brass rod.

Table 1. Composition of ABS/FA composite

Sl no.	Designation	ABS(wt. in gm)	FA (wt%)	Maleic Anhydride in gm
1.	700N	600	0	3
2.	700N	600	5	3
3.	700N	600	15	3
4.	700N	600	25	3
5.	700N	600	30	3

Specimen Preparation

Molded sheets of 3 ± 0.1 mm thickness of the virgin matrix and composites were prepared using compression moulding machine at temperature of 220°C , pressure 120kg cm^{-2} and cycle time around 10 min followed by cooling to room temperature under the same pressure. Firstly, various testing samples were cut from the sheet by using knife.

RESULT AND DISCUSSION

Mechanical Properties

Tensile properties

Testing and characterization of ABS/FA Blends

The mechanical properties of ABS/FA blends are clearly shown in the given table. As it is clearly visible from the graph that tensile strength of virgin ABS is 29.8 MPa but in 70/30 wt% of ABS/FA blends tensile strength increase. As compare to virgin ABS the filler loaded ABS increase the tensile strength of ABS with tensile modulus 1913.75. But tensile modulus is found to be decrease significantly. With the help of obtained data graph is plotted and with the help of graph it can be easily recognized the nature of the graph. After testing different sample its has been observed that tensile modulus of 30 wt% FA sample is less than virgin ABS.

Table 1. Data of tensile properties

Sample designation (ABS/FA)	Tensile Strength (MPa)	Tensile modulus(MPa)
100/00	29.8	2508.78
95/5	22.05	1285.02
85/15	26.78	1575.46
75/25	28.50	1725.06
70/30	30.46	1913.75

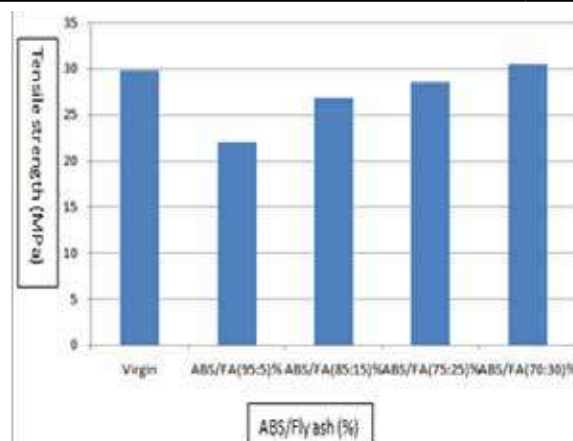


Fig 1 (a) Effect of filler loading on Tensile strength of ABS

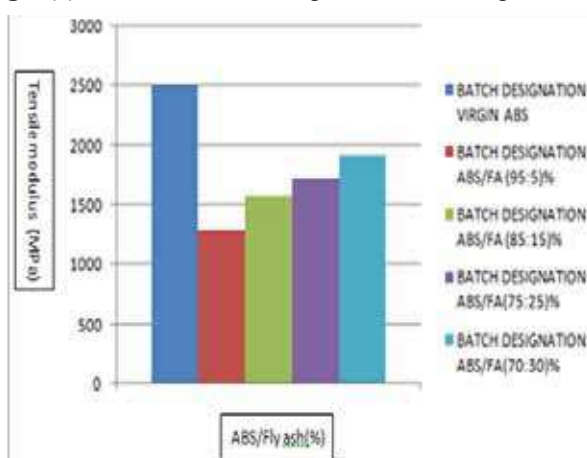


Fig 1 (b) Effect of filler loading on Tensile Modulus of ABS

Flexural Properties

Flexural strength of ABS increase in 70/30 wt% with flexural modulus of 5230.68. As from the given table we can clearly see that flexural modulus increase as compare to virgin ABS. This may be due to the effective stress transfer from the matrix to the filler at the interface. This reveals miscibility between the two components resulting in the formation of two well differentiated phases indicating moderate adhesion at the interface[5].

Table 2. Data of flexural properties

Sample designation (ABS/FA)	Flexural strength (MPa)	Flexural modulus (MPa)
100/00	46.17	2600
95/5	51.46	2963.2
85/15	57.28	3658.10
75/25	68.22	4826.78
70/30	73.24	5230.68

From the graph it can be observed the effect of filler loading on Flexural strength and flexural modulus of the different samples. At 30 wt% FA we got optimum results:

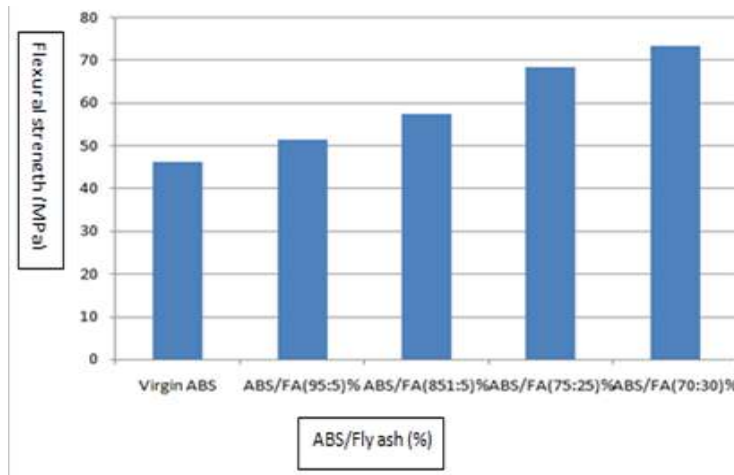


Fig. 2. (a) Effect of filler loading on Flexural strength of ABS

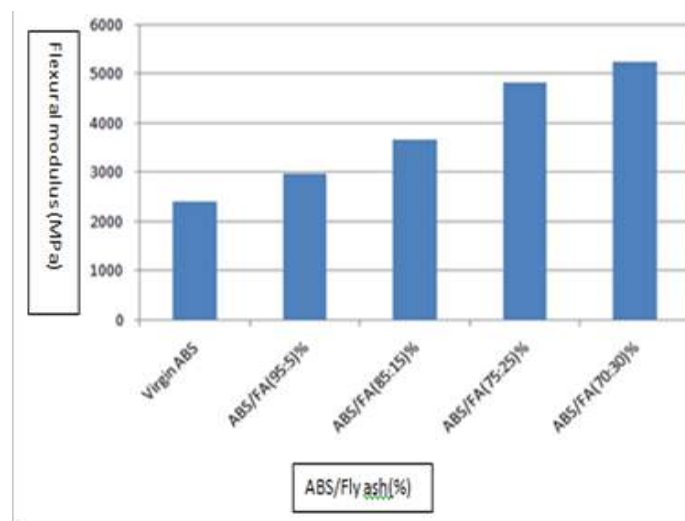


Fig. 2. (b) Effect of filler loading on Flexural modulus of ABS

Rockwell Hardness

The result of the surface mechanical test of Fly ash/ABS composites in term of hardness value with compatiblizer is presented below. Here the virgin ABS hardness value is 74.9 in L scale and by adding different % of Fly ash the hardness value increase. In 15%FA the hardness value decrease .But in 30% FA the hardness value is 76.90 in L scale. So as comparison to virgin ABS hardness value increase in 30% of FA. This is because due to compatiblizer Maleic anhydride is used with ABS.

Table 3. ABS/FA composites in terms of hardness value

Batch Designation	Hardness value(L scale)
Virgin	74.9
5% FA	75.28
15%FA	72.60
25%FA	74.71
30%FA	76.90

As this is also shown in graph as compare to other samples the 70:30 wt% ABS/FA hardness value is increased but 85:15 wt% ABS/FA batch show decrease in hardness value.

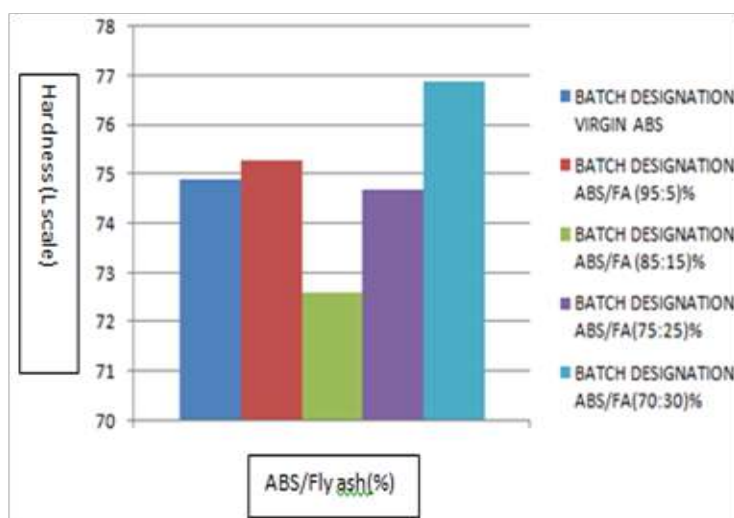


Fig. 3. (a) Effect of filler loading on Rockwell hardness test

Density

The result of the surface mechanical test of Fly ash/ABS composites in term of density value with compatiblizer is presented below. Here the virgin ABS density value is 1.038 gm/cc and by adding different % of Fly ash the density value increase. In 15%FA the hardness value increase gradually .But in 30% FA the density value is 1.209 gm/cc . So as comparison to virgin ABS density value increase in 30% of FA. This is because due to compatiblizer Maleic anhydride is used with ABS. The result of the surface mechanical test of Fly ash/ABS composites in term of density value with compatiblizer is presented below.

Table 4. ABS/FA composites in terms of density value

Batch Designation	Density (gm/cc)
Virgin	1.038
5% FA	1.065
15% FA	1.135
25% FA	1.178
30% FA	1.209

Thermal properties

DSC Test

DSC(Differential scanning calorimetry)

Measurement of temperature and enthalpies of change can be completed on very little examples in a differential scanning calorimetry (DSC). DSC thermograms of Fly ash filled ABS Blends in different wt% corresponding glass transition temperature(T_g), melting temperature (T_m)critical temperature (T_c) and heat of fusion(ΔH)values are represented in the Table.

Table 5. DSC analysis of fly ash filled ABS blend

Sample designation (ABS/FA)	Glass Transtion Temperature T_g ($^{\circ}\text{C}$)	Melting Temperature T_m ($^{\circ}\text{C}$)	Critical Temperature T_c ($^{\circ}\text{C}$)	ΔH (j/g)
Virgin	109.7	130	110	0.1539
5	108.5	129	109	1.4329
15	108.4	128	117	2.4265
25	107.8	125	126	2.821
30	106.01	136	130	3.099

This is observed from the given table is that the melting point of virgin ABS is 130°C with enthalpy 0.1539 (j/g) and after adding 25 wt% of fly ash the temperature started to decrease and its came to 125°C . But in 30 wt% of fly ash the melting temperature gradually started to increase to 136°C with heat enthalpy 3.099(j/g).The confirms the compatibilization efficiency of Maliac anhydride which increase the interfacial area and improves the stress transfer in the system[5] .The DSC thermograms of fly ash filled ABS blend composite system also exhibited constant melting.

Hence from the given observations table its can be conclude that the optimum result can be observed in 30 wt% of FA as that can be shown in below fig no.4.Here peak point temperature is in 136°C and area is 9.694 mW.

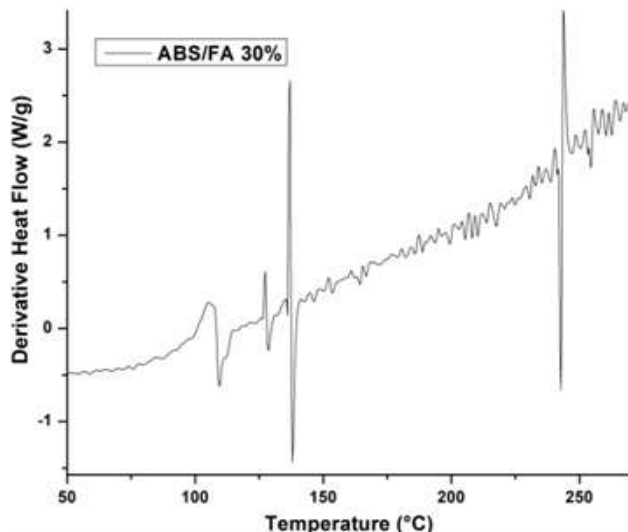


Fig 4. DSC graph of 30wt% fly ash

TGA (Thermogravimetric analysis)

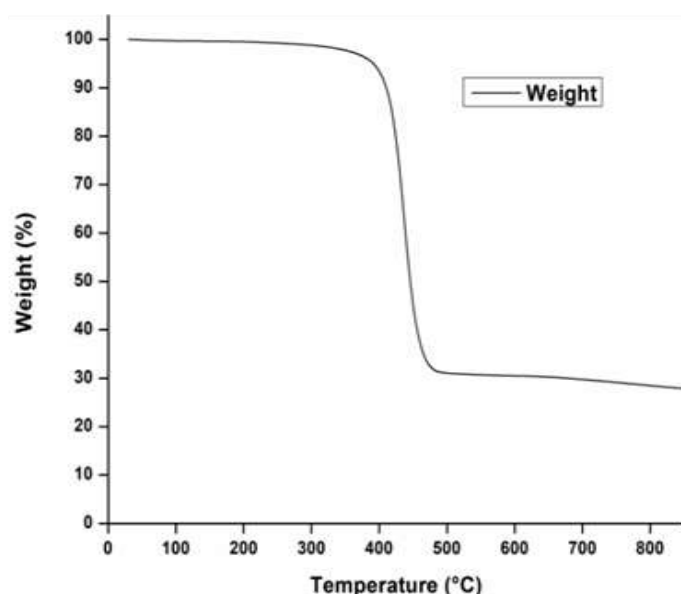
Thermo gravimetric analysis or TGA involves heating a sample to some temperature and monitoring its weight as a function of time. In general filler increase the thermal stability owing to high temperature degradation as compare with the polymeric matrix. TGA of Fly ash filled ABS Blends in different wt% corresponding initial temperature(T_i),medium temperature (T_m) and final temperature (T_f) and wt% of residue values are represented in the table In the present investigation TGA has been carried out the fly ash filled ABS composites and matrix to assess the rate of decomposition thermal stability of the sample respectively.

**Table 6.** Degradation temperature (°C) and percentage of residues of ABS/Fly ash blend

Sample Designation (ABS/ FA)	Ti (°C)	Tm (°C)	Tf (°C)	% residue
Virgin	410	425	680.2	0.30
5	415	465	728.4	10.17
15	424	478	755.0	17.28
25	430	490	786.1	22.06
30	436	496	810.2	27.8

Firstly the initial temperature of virgin ABS is 410°C and at T_m is 425°C and finale temperature is 680.2°C and the % of residue is 0.30 gm obtain. But after adding fly ash as filler of different percentage the temperature gradually increase. Here from the table it can be conclude that the optimum result will be observed at 30wt% FA sample.

From the **Fig. 5** it can be observed that the 1st degradation started at 436°C its because of degradation of ABS and 2nd partial step of degradation occurs at 496°C and their will be slightly deflection in wt% around 496°C due to due to the unburned carbon particles and volatiles around 550°C -810°C and % residue left would be 27.8 gm.

**Fig 5.** TGA graph of 30 wt% FA

CONCLUSION

ABS/FA blend compatibilised with 0.03 wt% of Maleic anhydride improves the tensile and flexural properties. It has also been found out that the tensile strength and flexural strength increase. But tensile modulus is found to be decrease significantly. Flexural strength of ABS increase in 70/30 wt% with flexural modulus of 5230.68.

This may be due to the effective stress transfer from the matrix to the filler at the interface. This reveals miscibility between the two components resulting in the formation of two well differentiated phases indicating moderate adhesion at the interface.

DSC studies it is observed the compatibilization efficiency of Maleic anhydride which increase the interfacial area and improves the stress transfer in the system.

In TGA studies it is shown that the finale temperature of virgin ABS is 680.2°C and the % of residue is 0.30 gm obtain. But after adding fly ash as filler of different percentage the temperature gradually increase. At 30 wt% FA the temperature increase from 436°C to 810°C and the % of residue would be 27.8 gm.



REFERENCES

1. N. S. Pandian "Fly ash characterization with reference to geotechnical applications." *Journal of Indian Institute of Science* 84.6 (2004): 189-216.
2. S. Bonda, S. Mohanty, S.K.. Nayak —Viscoelastic, Mechanical, and Thermal Characterization of Fly Ash-Filled ABS Composites and Comparison of Fly Ash Surface Treatments. Wiley Online Library. (wileyonlinelibrary.com). VVC 2011 Society of Plastics Engineers, POLYMER COMPOSITES —2012, 22-34.
3. J. V. Rutkowski and B. C. Levint —Acrylonitrile-Butadiene-Styrene polymers (ABS) :Pyrolysis and Combustion Products and their Toxicity-A Review of the Literature. *FIRE AND MATERIALS*, VOL. 10,93-105 (1986)
4. M.V,Deepthi , et al. "Mechanical and thermal characteristics of high density polyethylene–fly ash Cenospheres composites." *Materials & Design* 31.4 (2010): 2051-2060.
5. M. T. Bharnel , Dr. S. P. Bhosle2 "Mechanical and thermal properties of fly ash".*International Journal of Engineering Research & Technology (IJERT)* Vol. 3 Issue 2, February - 2014
6. Budrun Neher1 Md. Mahbubur Rahman Bhuiyan1 Humayun Kabir1,3 Md. Abdul Gafur2 Md. Rakibul Qadir 2Farid Ahmed1"Thermal properties of palm fiber and palm fiber-reinforced ABS composite"15 July 2015 / Accepted: 3 February 2016_ Akade'miai Kiado', Budapest, Hungary 2016.
7. MB Kulkarni, VA Bambole and PA Mahanwar" Effect of particle size of fly ash cenospheres on the properties of acrylonitrile butadiene styrene-filled composites" *Journal of Thermoplastic Composite Materials* 2014 27: 251.
8. M. I. S. Ramlan, and N. A. Shuaib"Environmental assessment and mechanical properties of acrylonitrile butadiene styrene (ABS) reinforced with fly ash filler" *AIP Conference Proceedings* 2030, 020018 (2018).
9. Haiyun Ma, Zhongbin Xu, Lifang Tong, Aiguan Gu, Zhengping Fang"Studies of ABS-graft-maleic anhydride/clay nanocomposites: Morphologies, thermal stability and flammability properties" *Institute of Polymer Composites, Zhejiang University, Hangzhou 310027, China* *Polymer Degradation and Stability* 91 (2006) 2951-2959.
10. Sateesh Bonda1, Smita Mohanty1and Sanjay Kumar Nayak1,2"Property evaluation of nanostructured fly ash-reinforced acrylonitrile butadiene styrene nanocomposites" *Journal of Thermoplastic Composite Materials* 1–16 The Author(s) 2015.
11. Kumar S and Kumar R. Mechanical activation of fly ash: effect on reaction, structure and properties of resulting geopolymer. *Ceram Int* 2011; 37(2): 533–541.
12. Paul KT, Satpathy SK, Manna I, et al. Preparation of nano structures materials from fly ash: a waste from thermal power stations, by high energy ball milling. *Nanoscale Res Lett* 2007;2(8): 397–404.
13. Paul K T, Pabi S K, Chakraborty K K, et al. Nanostructured flyash styrene butadiene rubber hybrid nanocomposites. *Polym Compos* 2009; 30(11): 1647–1656.
14. Satapathy S, Nando GB, Nag A, et al. HDPE-fly ash/nano fly ash composites. *J Appl Polym Sci* 2013; 130(6): 4558–4567.
15. Thongsang S and Sombatsompop N. Effect of filler surface treatment on properties of fly ash/NR blends. *ANTEC* 2005; 3278–3282.



Development and Applications of Forged Microalloyed Steels in India

P K Mandal

Department of Metallurgical and Materials Engineering, Amal Jyothi College of Engineering, Kanjirappally, Kerala

✉ pkmmet@yahoo.in

ABSTRACT

Microalloyed steels have become popular owing to high YS, good impact toughness and corrosion resistance repeatedly well suited for automotive and structural applications in India. Ferrite grain has a significant influence on the mechanical properties of microalloyed steels and is based on the microstructure of austenite immediately prior to the transformation of austenite to ferrite. The YS and toughness of the steels increase as the ferrite grain size decreases. The microalloyed steels were prepared through induction furnace with the addition of specified master alloys (Fe-Ti, Fe-V, Fe-Nb) during refining stage. Ferroalloy preparation by aluminothermic reduction was presumed to be simplest route to recover TiO_2 , V_2O_5 from red mud+magnetite+Al. Three microalloyed steel rods were preferred for hot forging and subsequently heat treated at 950°C and 1100°C. The heat treated samples were collected for LM analysis, inclusion analysis, CVN and tensile testing performed typically. It has to mention that HSLA steel was prepared through melting may obtain better mechanical properties. The optimum mechanical properties were achieved after normalizing treatment at 950°C likely to YS of 300 MPa, UTS of 464 MPa, ductility of 51.64%, RA of 65.89%, and notable RT impact toughness of 147 J/cm², respectively.

Keywords: Ferrite grain size; Fe-Ti; Impact strength; Microalloyed Steels; Red mud; UTS.

INTRODUCTION

The microalloying technology has been established since 1960's and later stages, due to their outstanding properties are high strength, toughness, fracture resistance, and good weldability concern used in many iron and steel industries in India. It is possible to enhance mechanical properties with minor (0.2wt.%) microalloying elements (Ti, Nb, V) [1, 2]. Hence, there is need to explore of new source for these elements contain red mud. Red mud is a waste product from alumina refinery. Red mud contains 4-8% TiO_2 with trace amounts of V and Nb. Ti is a major microalloying element in these prepared ferroalloys, and also well deoxidized and desulphurised in melts, dissolved Ti and formed strong TiN and TiC in the steel. V is an ideal microalloying element for forged quality steel as well as strong VN former which can be increased YS and decreases the particle size and volume fraction ratio. Nb is a potential ferrite strengthener as well as improved hardenability of microalloyed steels [3, 4]. Thus, mild steel scrap was used to melt with addition of FeMn and FeSi deoxidizer in an induction furnace, while with known quantities of prepared ferroalloys introduced into the melt. It is stated that high impact strength at cryogenic treatment reported for steels in the low carbon, high manganese, and vanadium microalloyed steels was developed with a mixed ferritic-pearlitic structure during forging with adequate temperature control [5, 6]. In contrary, the better toughness as well as good strength as a consequence for compensating optimum properties by the microalloying vanadium enhances precipitation hardening effect. The high titanium content microalloyed steel exhibited massive TiN particles which impart the mechanical properties. Therefore, stable precipitates likely AlN, TiN, VN are found to be most effective for austenitic grain size control in high strength low alloy (HSLA) steels [7-10]. Thus the influence of normalizing temperatures after hot forged steels on the microstructure and mechanical properties of Ti-V content microalloyed steels have been investigated.

EXPERIMENTAL PROCEDURE

Table 1. Chemical analysis of microalloyed steels (WT.%)

Steel nos.	C	Si	Mn	S	P	Cr	Ni	Ti	V	Nb	W	N	Al	Co	Fe
1	0.14	0.24	0.66	0.06	0.07	0.09	0.10	0.131	0.01	0.003	0.01	NA	0.060	-	Bal.
2	0.15	0.07	1.03	0.05	0.02	0.08	0.04	0.001	0.08	0.003	0.01	0.07	0.002	0.01	Bal.
3	0.17	1.07	0.42	0.15	0.01	0.07	-	0.330	0.05	-	-	NA	1.97	0.93	Bal.

[N.B.: Cu = 0.05-0.14wt.%, Mo=0.01-0.02wt.%]

The two types of ferroalloy were produced through aluminothermic reduction by melting and processing steps followed as shown in **Fig. 1**. Initially, the two types of charge mixture were selected such as (i) Red mud+30wt% Al, and (ii) Red mud+Magnetite ore + 30 wt% Al. Then the mixture of charge was placed in a graphite crucible and located in the muffle furnace and heated to 850°C until it was red hot. The red hot crucible brought it out and quickly triggered with magnesium powder for ignition of charging materials. During magnesium powder triggering many spattering was occurred with 40-50% yielding for ferroalloys production. It was found that slag and metal separation reasonably good for red mud contain microalloying elements. The chemical composition of different prepared ferroalloys was examined by spectroscopic analysis (wt.%): C-(1.6%), Si-(2.5-4.0%), Mn-(0.12-0.20%), P-(0.02-0.30%), S-(0.01%), Cr-(0.20-0.22%), Mo-(0.05%), Ni-(0.08%), Al-(1.4-6.6%), Co-(0.1-0.7%), Cu-(0.01%), Mg-(0.002%) Nb-(0.01%), Ti-(2.45-8.79%), V-(1.04-1.05%), rest Fe. Consequently, the three type of steels were developed by induction furnace with the addition of prepared ferroalloys. The melting was carried out in an induction furnace with the addition of FeSi and FeMn deoxidizers. The cast ingots were forged down to 15 mm round rods. The chemical analysis was confirmed by spectroscopic analysis as shown in **Table 1**. The microstructure was analyzed by light microscopy (LM) such as optical microscopy, SEM fractography with EDAX analysis. The optical microscopy was followed by mechanical polishing, then sequentially emery papers polishing, and finally etched by 2% nital. The two set of normalizing temperatures were selected for forged steels such as 950°C for 1.5h and 1100°C for 1.5h, respectively [11]. The microstructures of the ferroalloys were examined through SEM with EDAX analysis. Quantitative inclusion analysis was carried out on polished and unetched samples by an automotive image analyzer (Leica Cambridge-Q570 Particle Size Analyzer) (100X) as shown in **Fig. 4**. The average a total of six readings was taken to determine the count, volume, size distribution and aspect ratio of the inclusions. Vicker's hardness tests were performed with a load (30 kg.) with average six indentations measured for each sample. The standard Charpy V Notch (CVN) samples (10×10×55 mm³) with a notch angle of 45° and depth of 2 mm (ASTM E-23) were machined and tested with a Zwick/Roell impact tester after normalizing of forged steels and tested at room temperature (RT) as well as at 0°C to -20°C (liquid N₂) as results are shown in **Table 3** [12]. The tensile test was carried out through Instron Universal Testing Machine (UTM) with a cross head speed of 1 mm/min of 25 mm gauge length and 5 mm gauge diameter of samples ASTM E-8M) as results are shown in **Table 3**.

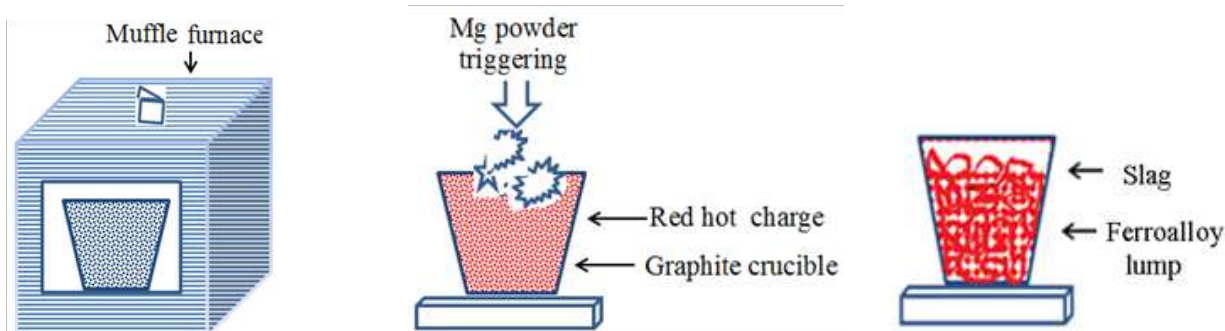


Fig. 1. Different steps had followed during ferroalloy production by aluminothermic reduction

RESULTS AND DISCUSSION

Main understanding of the temperature at the austenitic range is very important because precipitation of MX phases for designing the hot-forged conditions of the microalloyed steels. While MX interstitial phases dissolved in austenite gets bonded at a temperature (T) with the metalloid X (cubic lattice) of NaCl type as per reaction: $[M] + [X] \leftrightarrow MX$, where M→microadditions (Nb, Ti, V), X→metalloid (C, N) may be dissolved in the solid solution γ (ToK). If solubility of MX phases in the solid solution agreeing for the activation energy of their dissolving/nucleation can be presented usually as $\log[M][X] = A - B/T$, where A (value~7184-9500) and B (value~0.32-6.72) are the constants for MX phases (carbides, nitrides)[13]. **Figs 2(a, b)** shows SEM micrographs of prepared ferroalloys which may consider for clean cast composite materials are revealing several cuboids and hard TiC, VC carbides along with fine needle shape of carbide particles in matrix. While ferroalloy content magnetite ore+redmud observe thermodynamically more feasible for slag-metal separation reaction. These composite materials are main source of microalloying elements to develop Fe-Ti and Fe-V etc. Ferroalloys content Ti, V, Nb, Al, and other trace elements are Co, Ni, S, P etc. as confirmed by spectroscopic analysis. **Fig. 2(c)** shows normalized optical microscopy at 1100oC of Steel 1 with an entirely ferrite and pearlite microstructure, but few carbides are accumulated on the grain boundary regions. It is also stated that high normalizing temperature mostly ferritic grains are having tendency to coarsening as well as refined due to (Ti, Nb)(C, N) grain boundary pinning effect. Carbide formation on the grain boundary regions is vital because they help to enhance

impact strength at RT of microalloying steels[14]. Figure 2(d) shows optical microscopy of normalized at 1100°C of Steel 2 exhibited microstructure about 90% ferritic and remaining portion of pearlitic and fine carbides are embedded on the grain boundary regions. In this case grain coarsening tendency is noticeable because high Mn(1.03%) content and low Ti(0.001%) content may not encouraging for grain boundary pinning effect by microalloy nitrides. **Fig 2(e)** shows optical microscopy of normalized at 950°C of Steel 3 exhibited microstructure mostly ferritic and few pearlite and relatively more carbides are visible on grain boundary regions. In this case relatively less ferritic grain coarsening tendency is noticeable because high Si(1.07%) and high Al(1.97%) content and moderate Co(0.93%) content can promote grain boundary pinning effect due to fine carbide-nitrides precipitates in matrix. While tensile properties are better than particularly higher normalizing temperature at 1100°C. **Table 2** shows the Nb dissolution rate increases with increasing normalizing temperatures, and it completely dissolved at above 1250°C.

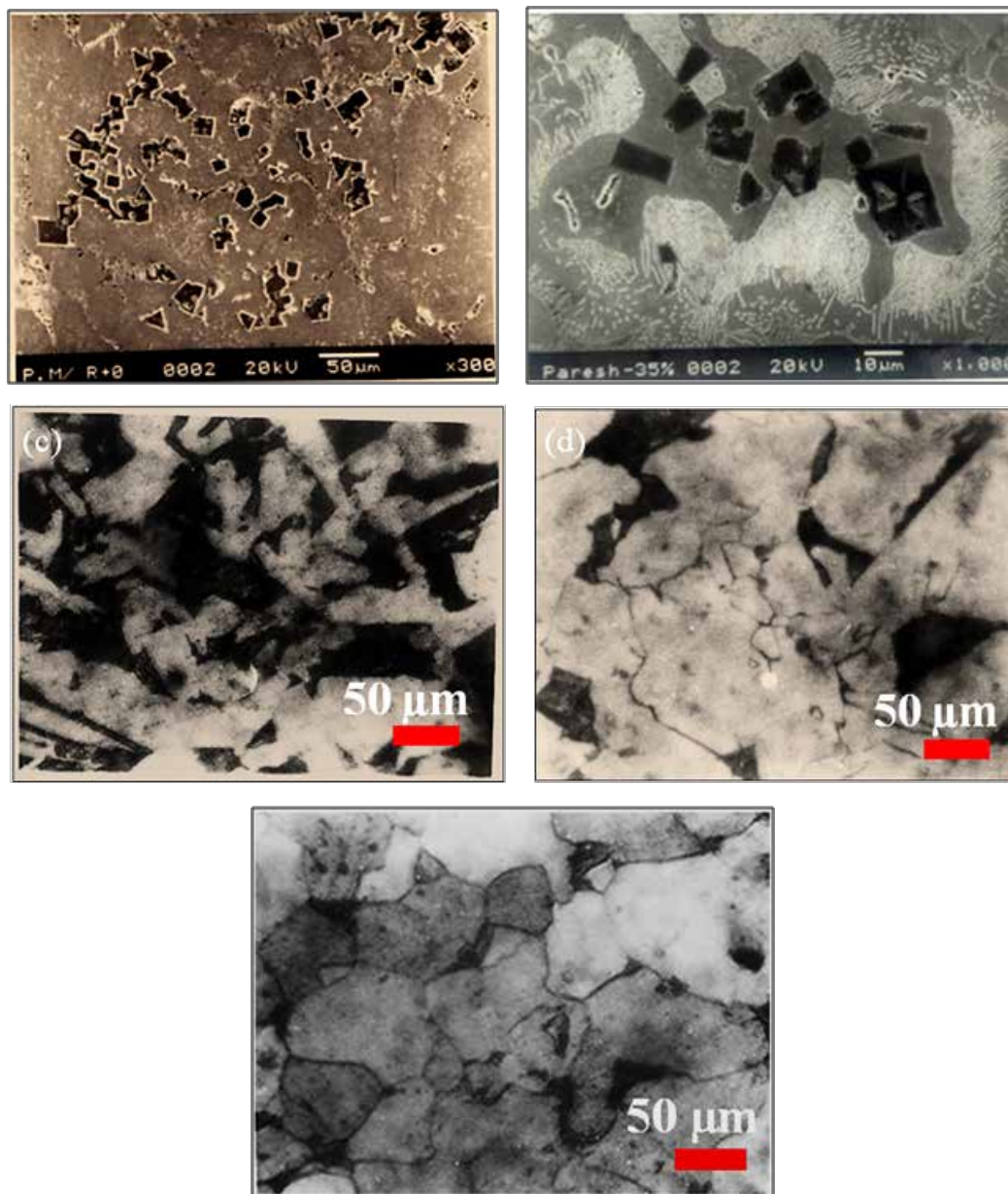


Fig. 2. The SEM micrographs showing of prepared ferroalloys:(a) Red mud+30 wt.% Al, (b) Red mud+Magnetite ore+30 wt.% Al; The optical microstructures of normalized microalloyed steels(500X):(c) Steel 1 at 1100°C/1.5h, (d) Steel 2 at 1100°C/1.5h, and (e) Steel 3 at 950°C/1.5h

Table 2. Amount of Nb dissolved in the austenite as a function of normalizing temperatures [15]

T(°C)	Nb(C, N) (wt.%) / Nb dissolved (wt.%)
900	0.002/4.3
1000	0.006/12.4
1100	0.014/30.2
1262	0.046/100

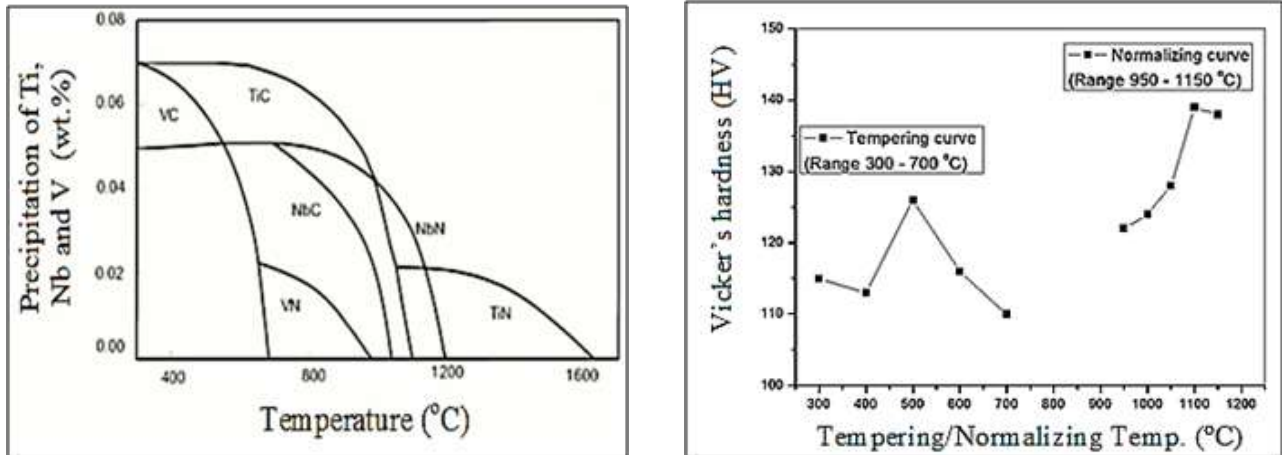
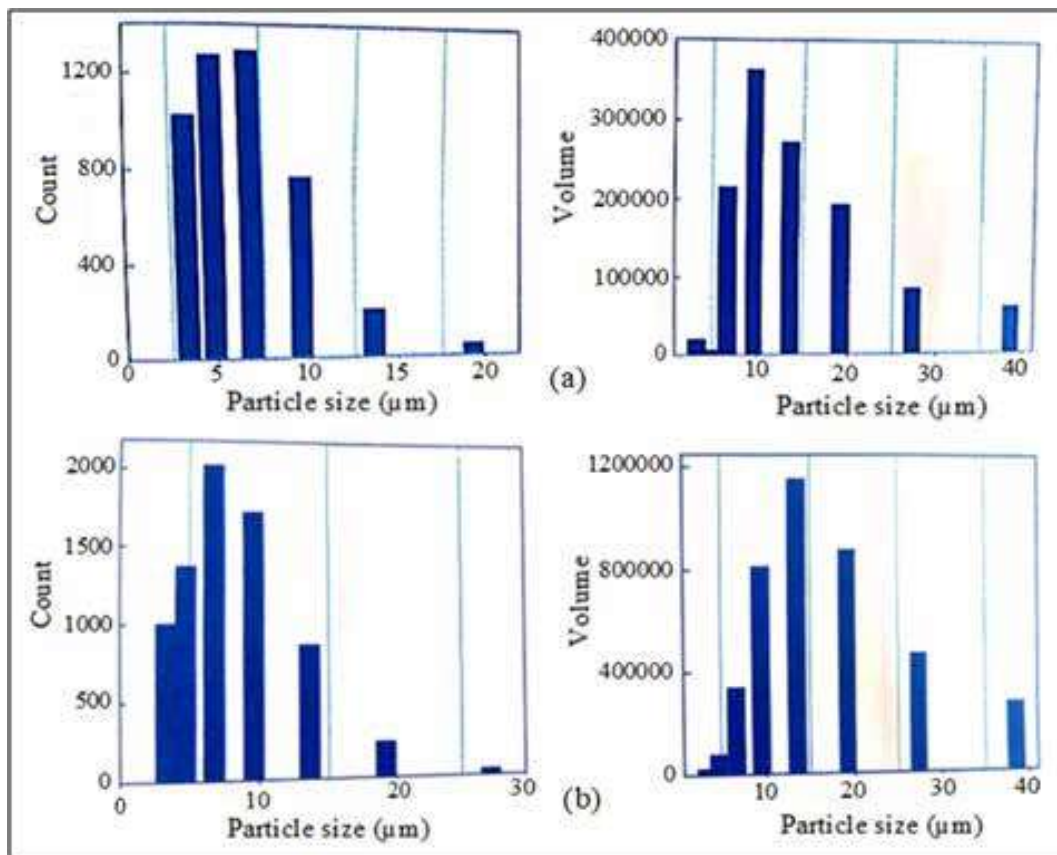


Fig. 3. (a) Showing amount of precipitates versus temperature in microalloyed steel containing minor N₂ (0.04%) content; (b) Vicker's hardness versus tempering and normalizing temperatures of microalloyed steels



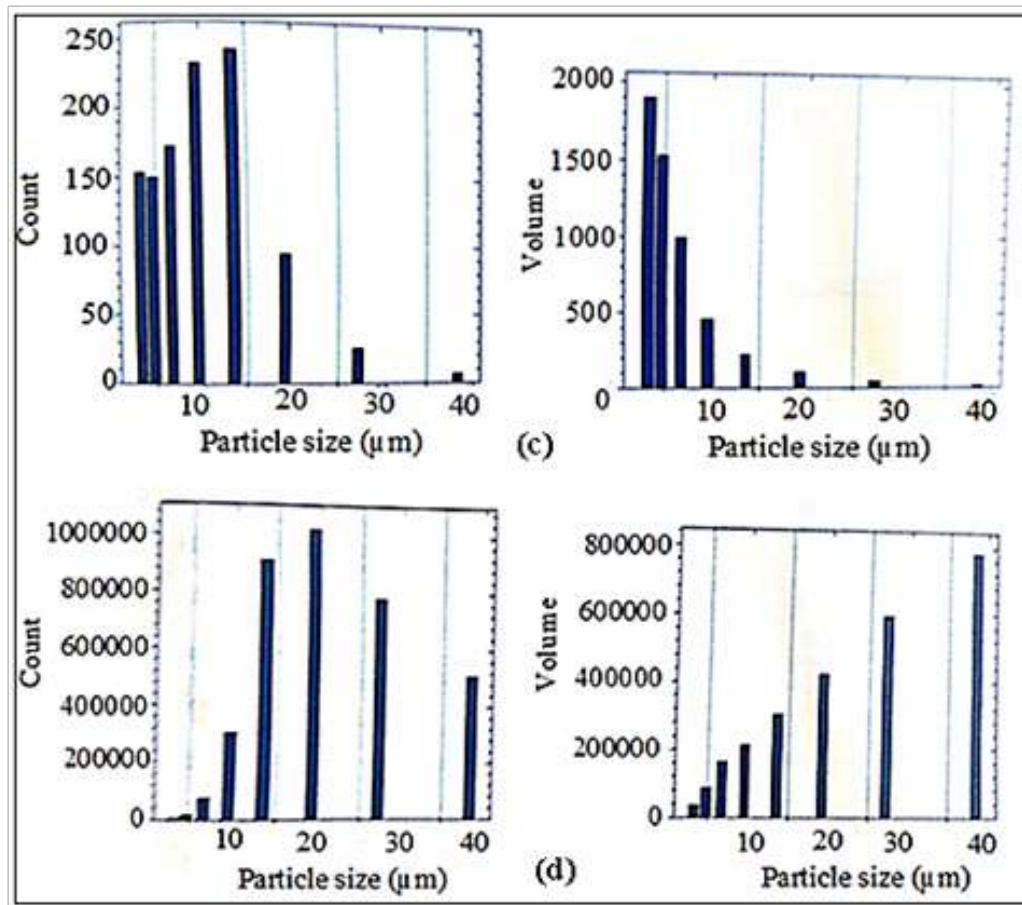
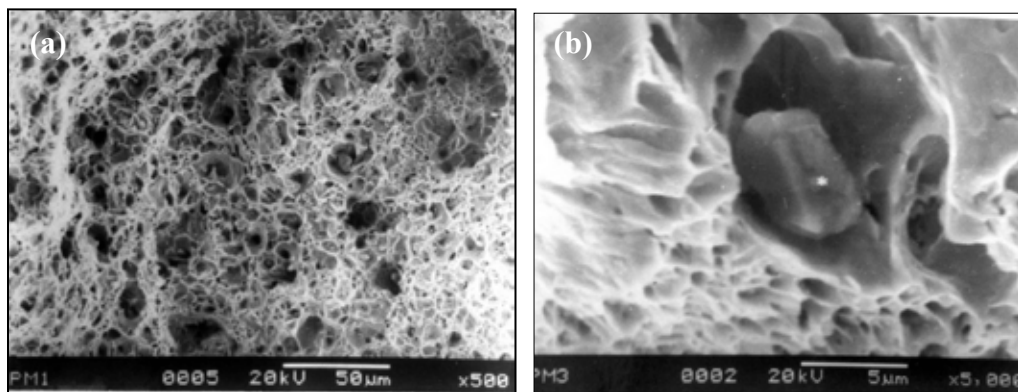


Fig. 4. Bar diagrams showing count and volume of detectable inclusions at different normalizing temperatures of microalloyed Steel 2: (a) 950°C/1.5h; (b) 1100°C/1.5h, (aspect ratio~1.5); and for Steel 3: (c) 950°C/1.5h; (d) 1100°C/1.5h, (aspect ratio~1.7)

Figure 3(a) shows the precipitation temperature range of the second phase particles depends on concentration of C, N, the type of microalloying elements. Preferable dispersive precipitates at normalizing temperature range also play an important role in designing the hot-forged steels. Figure 3(b) shows the hardness profile at various heat treated conditions such as after tempering maximum hardness reached around 126HV at 500oC. The normalizing curve shows that hardness increases steadily as the temperature rises to 1150oC. While tempering occurred at lower temperatures from 300-700oC after normalizing treatment of microalloyed steels. The normalizing curve indicated maximum hardness of 139HV at 1100oC because both the austenitic grain size and carbides formation increase on the grain boundary area as shown in optical microscopy (Fig. 2d, Fig. 2e). During analysis of inclusion count and distribution in various steels from normalizing temperatures at 950°C and 1100°C, it was observed that appreciable growth and coalescence of inclusions occur with increasing temperatures noticeably. The actual inclusions count and the total volume of inclusions may however an irregular manner. **Figs 4(a, b)** shows the effect of normalizing temperatures of Steel 2, which is a quantitative inclusion analysis on polished and unetched sample. An inclusion size varies within the $\geq 10 \mu\text{m}$ and very few inclusion sizes are within the range of 10-40 μm . In the volume vs. particle size bar diagrams indicated large numbers of inclusions varies 10-20 μm . **Figs 4(c, d)** shows the inclusion results of Steel 3, which has inclusions size mostly varied from about 3-10 μm with limited counts. In the case of inclusions volume vs. particle size bar diagrams are mostly increasing manner ~40 μm size, it may affect higher normalizing temperature at 1100°C due to coalescence of inclusions, and also increase aspect ratio with increase in heat treatment. **Fig 5(a)** shows SEM fractography characterized by ductile fracture feature, showing within the ductile-brittle transition region, large ductile zone of dimples is observed along the notch type, several inclusions also reveal possibly small size of second phase particles within dip holes. In high magnification (5000X) fractography analysis revealed inclusion contents are several oxides such as mostly TiO_2 (50.7wt.%) and Fe_2O_3 (20.2wt.%), others Al_2O_3 , SiO_2 , and MnO , etc. as shown in **Fig 5(b)**. **Table 3** shows tensile properties of Steel 1 which has exhibited better elongation of 51.64%, RA of 65.89%, and UTS of 464 MPa, YS of 300 MPa, and moderate YS/UTS ratio is

0.65. The high strength achieved due to (Ti, Nb) (C, N) phases because precipitation hardening along with restricting grain growth during normalizing temperature. In contrary, the stable TiN phase may incorporate a significant amount of V and AlN contributed strength. During hot forged and subsequently normalized at 950°C the Nb(C, N) precipitates occur in austenite region and thereby effectively retards recrystallization effectively as well as refined ferrite microstructure. Vanadium is the mostly soluble in the austenitic range and hardly affects during hot forging but rather precipitates during cooling in ferrite. These hard precipitates such as microalloying V(C, N) lead to precipitation hardening [16]. For Steel 3 shows better tensile properties for lower normalizing temperature at 950°C such as ultimate tensile strength (UTS) increase by 7.32%, yield strength (YS) increase by 30.94%, ductility increase by 24.56%, and reduction area (RA) increase by 27.27% as compared to normalizing temperature at 1100°C. It is concluded that higher normalizing temperature results in lower tensile properties perhaps grain coarsening tendency dominant for dissolution of carbides and nitrides excluding (Ti, Nb)N precipitates in matrix. For Steel 1, the impact energy is observed remarkably high of 147 J/cm² at RT and 112 J/cm² at 0°C (liquid N₂) due to mainly microalloying (~0.144wt.%) effects, high Mn content (0.66wt.%) effectively can control the sulphur in melt, fine precipitates and ferrite grains in matrix [17, 18]. Titanium content has great influence on mechanical properties due to refined grains by TiN in the austenitic range. Notable impact toughness enhances owing to the resistance capability of steel against the crack initiation and rupture. In addition, the relation between the solubility products of nitrides and carbides as a function of temperature and concentration of their micro-constituents. Specially, TiC will decrease by increasing normalizing temperature in austenitic phase [19].



Normalizing temp. at 1100°C of Steel 3	Inclusions analysis (in wt.%) of fracture surface					
	Al ₂ O ₃	SiO ₂	TiO ₂	MnO	Fe ₂ O ₃	CaO
	6.7	8.2	50.7	8.9	20.2	3.3

Fig. 5. SEM fractographs of Steel3 normalized at 1100°C: (a) low magnification (500X), (b) high magnification (5000X) with EDAX spot analysis.

Table 3. Mechanical properties of microalloyed steels

Steel nos.	Tensile properties						CVN impact energy (J/cm ²)	
	Normalizing temp. (°C)	UTS(MPa)	YS(MPa)	YS/UTS ratio	%El	%RA	At RT	At 0°C
Steel 1	950	464	300	0.65	51.64	65.89	147	112
Steel 3	950	410	362	0.88	41.20	42.24	-	-
	1100	390	250	0.64	51.32	53.76	-	-

CONCLUSIONS

- (1) The ferroalloys were prepared through aluminothermic reduction and its content sufficient amount of microalloying elements.
- (2) The HSLA steels have been developed a fine combination of strength and toughness by two different routes likely to austenitic grain size refinement through normalizing treatment after forging, and precipitation strengthening through



microalloying elements.

- (3) Microalloying elements are strong carbide formers and the formation of (Ti, V, Nb)(C, N) phases effectively restricted the grain growth and resulted in refined grains.
- (4) At high normalizing temperature of 1100oC the coalescence of inclusions may occur significantly but aspect ratio of inclusion rises simultaneously.
- (5) The impact energy has been improved in the austenitic range due to grain boundary pinning specially by TiN, VN, and AlN, etc.
- (6) The tensile properties have enhanced after normalized treatment at 950oC such as UTS increase by 7.32%, YS increase by 30.94%, ductility increase by 24.56%, and RA increase by 27.27% as compared to normalized treatment at 1100oC.

ACKNOWLEDGEMENTS

The author would like to express his sincere gratitude to Department of Metallurgical and Materials Engineering at IIT Kgp for provided laboratory facilities and guided during Master of Technology project work.

REFERENCES

1. A. Raj, B. Goswami, S.B. Kumar, A.K. Ray, High. Temp. Mater. Proc., 32, 6, pp. 517-531, (2013).
2. S. Kumar, S.K. Nath, Int. Jr. of Mat. and Met. Engg., Vol.-8, No.-9, pp. 1056-1059, (2014).
3. M. Opiela, W. Ozgowicz, Jr. of Achievements in Mat. and Manu. Engg., Vol.-55, Issue-2, pp. 759-771, (Dec. 2012)
4. G. R. Ebrahimi, H. Arabshahi, Jr. of Advanced Res. in Mech. Engg., Vol.-1, Issue-4, pp. 182-187, (2010).
5. S. Illescas, J. Fernandez, J. Asensio, M. Sanchez-Soto, J.M. Guilemany, Revista De Metalurgia, 45,6, pp. 424-431, (2009).
6. M. M. Lakhani, N. Raut, Int. Jr. of Sci. Engg. Res., Vol.- 8, Issue -2, pp. 6-9, (Feb. 2017).
7. J. Gorka, Machines, Technologies, Mat., Issue-12, pp. 24-27, (2013).
8. A. R. Khodabandeh, M. Jahazi, S. Yue, P. Bocher, ISIJ Int., Vol.-45, No.-2, pp. 272-280, (2005).
9. W. Ozgowicz, E. Kalinowska-Ozgowicz, Archives of Mat. Sci. and Engg., Vol.-32, Issue-2, pp. 89-94, (Aug. 2008)
10. J. Gorka, IOSR Jr. of Engg. (IOSRJEN), Vol.-3, Issue-11, pp. 22-28, (Nov. 2013).
11. Z. Lv, X-p. Ren, Z-h. Li, Z-m. Lu, M-m. Gao, Mat. Res. 18, 2, pp. 304-312, (2015).
12. S. K. Dua, A. Ray, D.S. Sharma, Mat. Sci. and Engg., A318, pp. 197-210, (2001).
13. Adamczyk, Jr. of Achievements in Mat. and Manu. Engg., Vol.-14, Issue-1-2, pp. 9-20, (Jan.-Feb. 2006).
14. Y. Funakawa, T. Shiozaki, K. Tomita, T. Yamamoto, E. Maeda, ISIJ Int. Vol.-44, No.-11, pp. 1945-1951, (2004).
15. A.B. Cota, O.F.L. Goncalves, A.R. Barbosa, C.A.M. Lacerda, F.G.S. Araujo, Mat. Res., Vol.-6, No.-2, pp. 117-121, (2003).
16. P. Skubisz, L. Lisiecki, T. Skowronek, A. Zak, W. Zalecki, Mat. and Tech., 50,5, pp. 783-789, (2016).
17. F. Einkhah, J. Rassizadehghani, H..Najafidejehmonfared, Nanotechnology & Applications, Vol.-1, Issue 2, pp. 1-5, (2018).
18. K. Kamei, A.G. William, L.S. Koveile, N. Ahmad, A. Chakravorty, R. Davis, IOSR Jr. of Mech. and Civil Engg. (IOSR-JMCE), Vol.-11, Issue-3, Ver.-I, pp. 17-22, (May-June 2014).
19. Hoda S. E-F., Saeed N. G., Mamdouh M. E., Jr. of Minerals and Mat. Characterization and Engg., 11, pp. 1108-1112, (2012).



Study and Development of Graphene Oxide based Hybrid Polymer Nanocomposites

Geetha Rajamani¹, Jawahar Paulraj^{2*}

Assistant Professor, Faculty of Mechanical Engineering, Velammal engineering college, Chennai, Tamil Nadu¹

Assistant Professor, Department of Mechanical Engineering, National institute of Technology, Agartala, Tripura^{2}*

✉ geeth11_r@yahoo.co.in; ✉ dr.p.jawahar@gmail.com

ABSTRACT

In this Experimental study, Graphene oxide reinforced Glass filled Nylon (GO-GFN) Hybrid nanocomposites were developed and characterized. Transmission electron microscopic studies were performed to study the dispersion of Graphene oxide in Glass filled Nylon composites. Dynamic Mechanical Analysis, Thermo gravimetric analyses were conducted on the fabricated hybrid nanocomposites to analyse the mechanical and thermal stability. Mechanical properties were investigated by tensile studies and improvements in young's modulus and tensile strength were noticed. Water absorption test was conducted to study the hydrophobic properties of the hybrid nanocomposites. The study confirms the feasibility of deploying hybrid nanocomposites for engineering applications.

Keywords: Nanocomposites; Wear analysis; Graphene oxide; Glass filled Nylon.

INTRODUCTION

In recent years, there has been an increasing commercial demand in the usage of Polymer nanocomposites to obtain hybrid properties which emerge due to the combination of several components, Reinforcements and Additives [1]. These nanocomposites offer good mechanical, optical, thermal and electrical properties [2]. The enhancement in the properties is due to the presence of nanoparticles, their state of dispersion with the polymer matrix and their interaction with the polymers [3]. Many Researchers have investigated with several polymers and nanoparticles to explore the optimal usage of these materials in various industrial and engineering applications [4]. Various research works in nanoclays, nanotubes and nanofibers have revealed the feasibility of these nanomaterials for industrial applications with some demerits reported such as the cost of these nanoparticles and processing constraints [5-10]. To overcome these demerits and to recommend a suitable nanoparticle for engineering applications, the present research work is focussed on reinforcing Graphene oxide nanopowder with Glass filled Nylon to explore the compatibility of this hybrid nanocomposites for bearing Applications. Various characterization tests were conducted on the fabricated hybrid graphene oxide reinforced glass filled Nylon (GO-GFN) nanocomposites.

EXPERIMENTAL PROCEDURE

Materials

The Graphene oxide nanopowder is purchased from United Nanotech Innovations Private Limited, Bangalore, India. Number of layers in Graphene oxide varies from 4 to 6, with a thickness of 0.7 to 2.3 nm. The ultimate carbon purity of the Graphene oxide is 99%. Graphene oxide is blended with Glass filled Nylon and drawn as wires and cut into pellets and injection moulded as Plates at Central Institute of Plastics Engineering and Technology, Guindy, Chennai.

Synthesize of Graphene Oxide –Nylon Nanocomposites

Graphene oxide and glass fibre reinforced nylon nanocomposites were synthesized by melt blending process. The materials to be blended such as glass filled nylon pellets and graphene oxide nanopowder were metered into the blend by gravimetric blending process. 0.03 wt % of graphene oxide nanopowder is added to 1 Kg of glass filled nylon through the feeder on the throat of the processing machine. The blender consists of a mixing section in which all the metered materials were mixed thoroughly to form a homogeneous blend, which is directed to flow into the processor. The processor was operated at a temperature of 300°C. At this temperature the mixture was melted completely. This molten homogeneous mixture was squeezed to flow through the orifice to form a wire. The Graphene oxide reinforced glass filled nylon wire squeezing out of the orifice is quenched in a pool

of water and subsequently cut into pellets by an automatic cutter fixed to the blending machine. The pellets are collected and injection moulded at a temperature of 256°C to form plates for mechanical and characterization testing.

Mechanical Studies

Tensile test was carried out to measure the ultimate tensile strength and elongation at break of Graphene oxide reinforced Glass filled nylon nanocomposites. The specimen is prepared according to ASTM D638 standards under ambient conditions. The test specimens were cut using press cutter of dumb – bell type as shown in **Fig. 1**. The test was conducted at a cross head speed of 5 mm/min and with a load cell of 500N. Ultimate tensile strength was found and the Youngs modulus of the hybrid polymer nanocomposite was computed from the stress – strain graph. The test was conducted at Microlabs, Chennai.

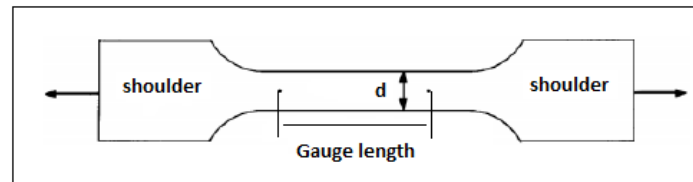


Fig. 1. Dumb – bell type specimen for tensile test

Characterization Studies

The Various Characterization tests such as Transmission electron microscopic studies , Dynamic Mechanical Analysis, Thermo gravimetric Analysis, Water Absorption Test, Density Test were conducted for the fabricated Graphene oxide reinforced Glass filled Nylon nanocomposites (GO-GFN).

Transmission Electron Microscopic Studies (TEM)

Transmission electron microscopic studies were carried out on the processed hybrid nanocomposites. The presence of the graphene oxide nano powder and the level of dispersion of the Nano powder in the glass filled nylon matrix were studied from the images obtained at different magnifications.

Dynamic Mechanical Analysis

Dynamic Mechanical Analysis (DMA) is used to study the Visco-elastic nature of the Graphene oxide reinforced Glass filled Nylon nanocomposites. The model of the Analyser used is DMS 6100, manufactured by SII Nanotechnology, Japan. The analysis is carried out at 2- point bending Dual cantilever method. The working temperature is 30oC to 200oC at a Dynamic force range of ± 10N. The test is carried out at a heating rate of 2°C/min.

Thermo Gravimetric Analysis

Thermo gravimetric Analysis (TGA) is used to study the changes in physical and chemical properties of Graphene oxide reinforced Glass filled Nylon nanocomposites as a function of increasing temperature on time with constant mass. The model of the Analyser is TG/DTA 6200, manufactured by SII Nanotechnology, Japan. The Scanning rate of the analyser is 0.01 to 150°C/min. The working temperature is 30°C – 800°C. The test is carried out at a heating rate of 20°C/min.

Water Absorption Test

The Hydrophobic or water resistant properties of the fabricated GO-GFN nanocomposites is studied using water absorption test. Sample specimens of dimensions 60mm diameter and 3 mm thickness were prepared and dried in oven. The dried samples were immersed in a water bath at room temperature and weighed periodically till no increase in weight was observed. All the samples were weighed on a weighing balance of 0.1mg precision. The increase in weight by the nanocomposite is determined by the Equation (Mt) [11],

$$M_t = \frac{W_w - W_d}{W_w} \times 100 \% \quad (1)$$

Where

W_d = weight of the dried material.

W_w = weight of the water absorbed material.

Density Test

Density is a key concept in analyzing the interaction of materials in various domains such as material sciences, engineering, and Physics etc. The theoretical density and experimental density of 0.03wt% graphene oxide infused glass filled nylon is found using rule of mixtures and archimedes principle. The theoretical density is given by,

$$\rho_{\text{the}} = v_r \rho_r (1-v_r) \rho_m \times 100 \quad (2)$$

where, ρ_{the} is the theoretical density in g/cm^3 ,

v_r is the volume of the reinforcement (GO) in cm^3 ,

ρ_r is the density of the reinforcement (GO) in g/cm^3 ,

ρ_m is the density of the matrix (GFN) in g/cm^3 .

Experimental density was found by measuring the weight of the sample in air and the weight of the sample when suspended in distilled water. By using these values, archimedes principle is applied and the experimental density is calculated and compared with the theoretical density. From the theoretical and experimental density, the percentage of porosity as follows,

$$\text{Porosity} = [(\rho_{\text{the}} - \rho_{\text{exp}}) / \rho_{\text{the}}] \times 100 \quad (3)$$

The porosity values can be used to confirm the uniform distribution and the reliability of the sample preparation method.

EXPERIMENTAL RESULTS AND DISCUSSIONS

Mechanical Tests

The tensile test was carried out in the specimen as per ASTM D638. The tensile strength was observed for the fabricated Hybrid GO-GFN nanocomposites. The test procedure was repeated for pristine nylon and Glass filled nylon nanocomposites. The results obtained were tabulated in **Table 2** and compared. From the results, it was inferred that the Graphene oxide reinforced glass filled nylon has higher tensile strength when compared to nylon and glass filled nylon systems [14]. This is due to the presence of graphene oxide which is an isotope of carbon. As Carbon imparts higher hardness and reinforcing effect, the fabricated hybrid nanocomposites possesses higher tensile strength [15]. The excellent interfacial bonding between the Graphene oxide nanolayers and glass filled nylon helps in arresting crack propagation and to withstand the higher load applied, thus enhances tensile strength of the polymer nanocomposites.

Table 2. Tensile test results

Test Parameters	Observed values		
	Nylon	GFN	GO-GFN
Ultimate tensile load (KN)	1.83	2.24	3.80
Ultimate tensile strength (N/mm^2)	40.00	47.00	82.00

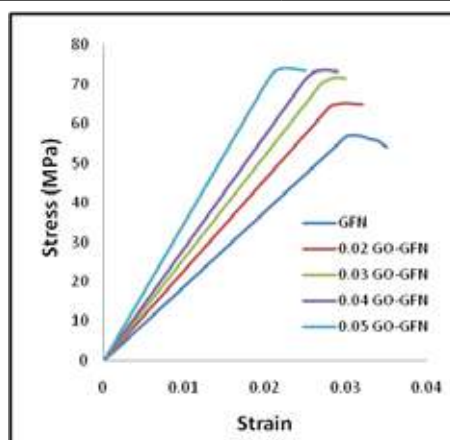


Fig. 2. Stress – strain curve for GO-GFN composite

The **Fig. 2** shows the stress strain curves of glass filled nylon and hybrid GO infused glass filled nylon nanocomposites. However the ductility is comparatively lower than that. It was also found that, the slope of the curve increases with increases in GO concentration, but the strain decreases as well. It is due to the stiffening effect of the GO in the GFN matrix. It is well corroborated with the mechanical properties, where the tensile strength increases with increase in GO concentration. Also it gives an inference about the increase in modulus as well. It was also found that the peak stress occurs for the GO concentration of 0.02 and 0.03 in glass filled nylon matrix.

Characterization Tests

Transmission Electron Microscopic Study (TEM)

The transmission electron microscopy (TEM) studies were performed in TEM instrument with an accelerating voltage of 200 KV. Graphene oxide is electronically transparent because of its very low atomic number and two-dimensional structures. The TEM image of the fabricated GO -GFN nanocomposite at various magnifications is represented in the **Fig. 3**. Since the Graphene sheet is highly stable towards electron beam, it exhibits low background in imaging mode. The TEM image at higher magnification shows multiple folds of graphene oxide sheets on the glass filled nylon matrix. The low magnification image shows 2 layers of Graphene oxide overlapping with each other. This TEM study confirmed the uniform dispersion of Graphene oxide in the glass filled nylon and also it was inferred from the study that the Graphene oxide sheets exhibited multiple layered lamellar structure with a thickness of approximately 2 to 2.5 nm. It also confirms that the nylon polymeric matrix has infused well and wound the layers of GO, which confirms the wettability and interaction of nylon matrix with the GO is good. This also assists in better improvement in mechanical properties.

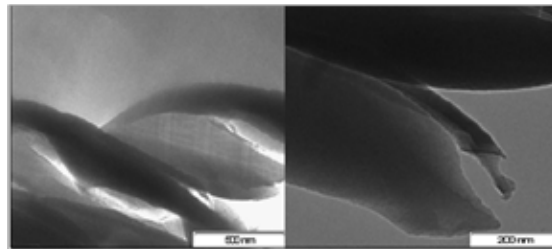


Fig. 3. Transmission Electron microscopic images of Graphene oxide reinforced Glass filled Nylon

Dynamic Mechanical Analysis

Dynamic mechanical analysis (DMA) is used to study the viscoelastic property of materials as a function of temperature or frequency when the sample is subjected to deformation under periodic loading conditions. The analysis is conducted to find the various modulus values of the 0.03wt% GO-GFN and 0.03wt% GO-N nanocomposite samples. The analysis is carried out at a temperature range of 50 to 400°C, and frequency of 1 Hz. In the **Fig. 4(a)**, the blue curve represents the storage modulus (G'), green curve represents the loss modulus (G'') and the red curve represents the loss factor ($\tan \delta$). It was observed that as the temperature increases, the loss modulus also increases and the stiffness of the GO-GFN nanocomposite decreases, which affects the storage modulus of the fabricated nanocomposites. The graph shows that at a temperature range of 180°C to 220°C, glassy to rubbery transition occurs in GO-GFN nanocomposites with 0.03wt% GO. In this region, there is a rapid change in the storage modulus slope. This region represents the glass transition temperature range of the GO-GFN nanocomposites and the sharp point of the curve indicates the glass transition temperature (T_g) of the fabricated nanocomposites. The peak of the storage modulus takes place at 216.4°C. The peak $\tan \delta$ value occurs at a temperature of 227.9°C.

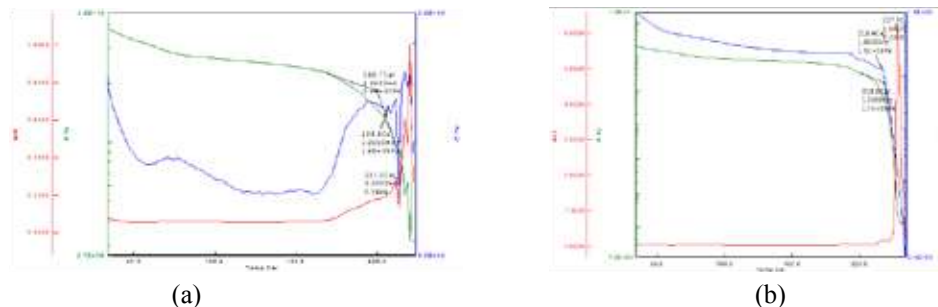


Fig. 4. Dynamic Mechanical Analysis of (a) GO-GFN hybrid nanocomposites, (b) GO-N Nanocomposites

The **Fig 4(b)** shows the dynamic mechanical analysis of 0.03wt% GO-N nanocomposite. It was inferred from the graph that the peak of the storage modulus occurred at 199.7°C and the loss modulus occurred at 206°C. The peak of the loss factor $\tan(\delta)$ occurred at 211°C. The values observed shows that the 0.03wt% GO-GFN can significantly work at higher temperatures when compared to 0.03wt% GO-N. This is attributed to the presence of glass fibers that prevents the distortion of nylon matrix significantly, which is well assisted by the infusion of 0.03wt% graphene oxide in GFN system. Good interfacial interaction by nylon part and the GO confirmed by TEM studies, improvements noted in mechanical properties by GO infusion, stiffens the GO-GFN nanocomposites and leads to improvements glass transition temperature and storage modulus as well. Hence it was confirmed, that the GO-GFN hybrid nanocomposites has enhanced Glass transition temperature due to excellent interfacial bonding of Graphene oxide with glass filled Nylon system.

Thermo gravimetric Analysis

The TG/DTA technique often referred as the thermogravimetric / Differential thermal analysis provides the measurement of change in mass of the sample under study as a function of temperature with the temperature difference of the sample and the reference curve as a function of temperature. The **Fig. 5** represents the TG/DTA curve for 0.03wt% GO-GFN nanocomposites. The blue curve represents the TG values and the black curve represents and the DTA values. The curve shows exothermic reaction with the weight loss of 50% at a temperature of 221.9°C and 16.07 μ V. the second peak occurred at a temperature of 383°C and 25.32 μ V with the weight loss of 70%. The maximum peak occurred occurred at 455°C and 9.16 μ V with the weight loss of 40%. At the temperature of 480°C, the weight loss is almost negligible and the curve follows a constant trend.

The **Fig 5(b)** shows the TG/DTA curve of 0.03wt% GO-N nanocomposites. The weight losses observed at the temperatures of 218°C, 454°C and 482°C was 75%, 72.5% and 80% respectively. At the temperature of 480°, the weight loss of the 0.03 wt% GO-N sample was 25% after which the curve followed a constant path for further increase temperature. From **Fig. 5**, it was observed that, the weight loss was significantly low for GO-GFN nanocomposite when compared to GO-N nanocomposite. This is due to the higher degree of dispersion and the excellent interfacial bonding that existed between the GO and glass fibers with the nylon matrix. The weight loss is due to the reduction of graphene Oxide containing oxygen functional groups Graphene Oxide containing oxygen functional groups analysis and thus increases the thermal stability.

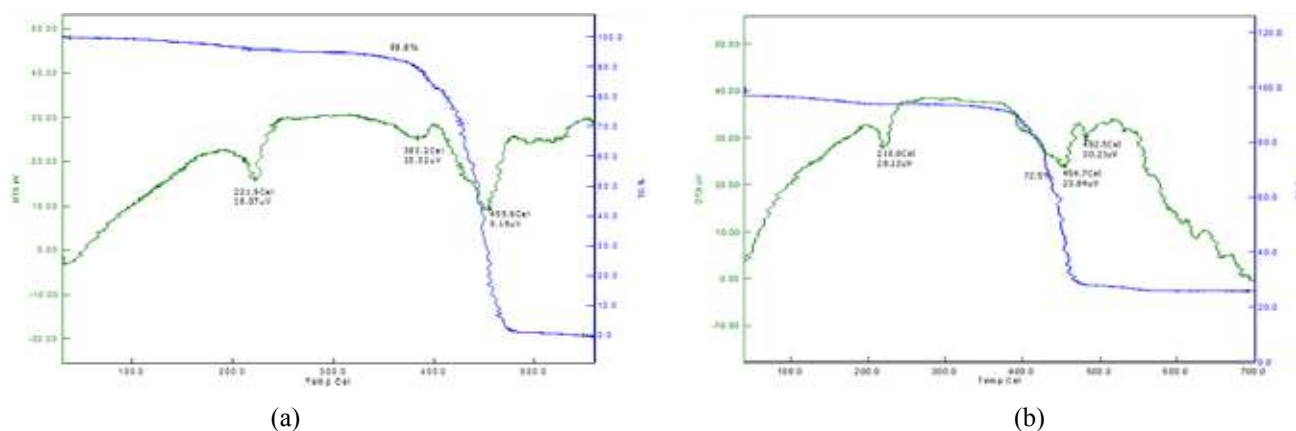


Fig. 5. Thermogravimetric analysis of (a) GO-GFN hybrid nanocomposites (b) GO-N Nanocomposites

Water Absorption Test

The water resistant property of the Hybrid GO-GFN nanocomposites was found using water absorption test. To conduct a comparative study the test was performed for Nylon, Glass filled Nylon and Graphene oxide reinforced Glass filled nylon. The test was performed till the weight of the samples achieved constant values under room temperature [16]. The **Table 3** represents the results of water absorption test.

Table 3. Water Absorption Test

Samples	NYLON	GFN	GO-GFN
Average weight of the samples measured after 6 days in gms	7.089	7.061	7.038
Fractional increment in weight	0.9829	0.5840	0.2564

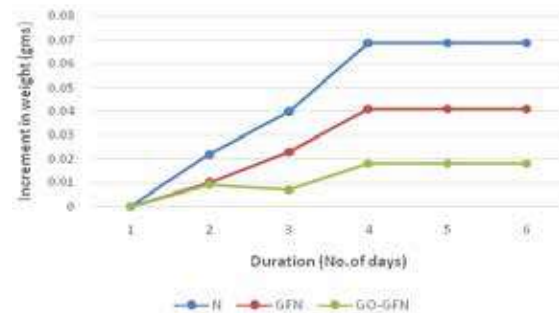


Fig. 6. Water absorption of Nylon, Glass filled Nylon, 0.03wt% GO-GFN nanocomposites

The **Fig. 6** represents the water absorption of nylon, glass filled Nylon and Graphene – oxide reinforced Glass filled nylon samples of uniform dimension and weight. The test was conducted for 6 days, out of which no appreciable weight change was observed after fourth day. It was inferred from the graph that the nanocomposites had reached the maximum limit in water absorption within four days. By comparing the water absorption capability of nylon, glass filled nylon, Graphene oxide reinforced glass filled nylon samples, the GO reinforced glass filled nylon has better water resistance capabilities. As graphene oxide is an isotope of carbon and carbon is inherently hydrophobic, the water resistance property of GO reinforced glass filled nylon was higher. The GO filler layers in the nanocomposites have decreased the diffusion path for water to penetrate deeply into the glass filled nylon polymer. This attributes to the better barrier properties of hybrid GO-GFN nanocomposites. The test performed proves that the GO had dispersed well in the Glass filled nylon without any agglomeration and assist in water absorption resistance.

Density Test

The theoretical and experimental density of 0.03wt% infused GO–GFN is found by using rule of mixtures and Archimedes principle respectively. The values of ρ_{the} and ρ_{exp} were calculated and presented in the **Table 4**.

Table 4. Theoretical and Experimental Density

Sample	ρ_{the} (g/cc)	ρ_{exp} (g/cc)
0.03wt% GO-GFN	2.371	2.369

The theoretical density of 0.03wt% GO-GFN sample coincides with the experimental density. The porosity is computed from theoretical and experimental density values, which is having a difference of 0.084 only. This confirms the less formation of pores on the 0.03wt% GO-GFN samples and corroborates the significant interfacial bonding between the GO reinforcement and GFN matrix.

Fracture Analysis

Fracture analysis was carried out to study the morphology of fractured surface using scanned electron microscope (SEM).

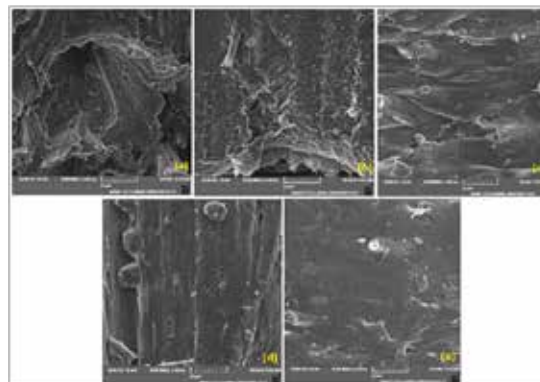


Fig. 7. Tensile fractured surface of hybrid GO - Glass filled Nylon polymer nanocomposites with (a) 0 wt.% GO, (b) 0.02 wt.% GO, (c) 0.03 wt.% GO, (d) 0.04 wt.% GO, (e) 0.05 wt.% GO



The Fig. 7 shows the scanned electron microscopic (SEM) images of tensile fractured surface of glass filled nylon with different concentrations of graphene oxide. The fractured surface of pristine glass filled nylon reveals that the mode of fracture is predominantly ductile in nature, which is evident from the surface texture of tensile fractured surface, where shearing deformations and tearing facets were noticed on the fractured surface. Nanocomposites infused with 0.02wt% and 0.03wt% GO shows no distinct interfacial cracks and micropores on the surface, which confirms that, the interfacial interaction and bonding between the glass filled nylon and graphene oxide is good and also the combined interfacial interaction between GO-Glass Fiber and Nylon is also good. Surface facets were rough and fine on nanocomposites infused with 0.02 and 0.03 wt. % GO. It also provides an inference that, cracking has occurred by passing through torturous pathway at the time of loading; hence the energy required for fracture is high and apparently contributes for significant improvement in tensile strength. With increase in GO concentration to 0.04wt% and 0.05wt%, tensile testing has shown higher tensile strength and modulus compared with Glass Filled Nylon and limited increment in properties were noticed compared with GO-GFN infused with 0.02 and 0.03 wt.% GO. The mode of fracture is ductile in nature, however less ductile compared with GFN, GO-GFN infused with 0.02 and 0.03 wt. % GO.

CONCLUSIONS

From this experimental Work presented, the following conclusions were observed,

- Hybrid Graphene oxide reinforced glass filled nylon nanocomposites was synthesized and processed to study its suitability and compatibility for engineering Applications.
- The Graphene oxide nanopowder reinforced with glass filled nylon with a very low weight percentage influences greatly the mechanical and physical properties of the hybrid nanocomposites which was confirmed by the various characterization tests conducted.
- The Density and water resistance capability of the fabricated hybrid nanocomposites were investigated. The results proved that the Hybrid nanocomposite exhibits excellent density and water resistance properties.
- Finally the investigation confirms the feasibility of the graphene oxide reinforced glass filled nylon for engineering applications.

REFERENCES

1. Pedro Henrique Cury Camargo, Kestur Gundappa Satyanarayana, Fernando Wypych, Nanocomposites: Synthesis, Structure, Properties and New Application Opportunities, Materials Research, Vol.12, No. 1, 1-39, 2009.
2. Daniel L Ciprari, Mechanical Characterization of polymer nanocomposite sand the role of interphase-Georgia Institute of Technology November 2004.
3. Xiao Huang, Freddy Boey And Hua Zhang*, A Brief Review on Graphene-Nanoparticle Composites, Cosmos, Vol. 6, No. 2 (2010) 159-166.
4. M. S. Senthil Kumar, N. Mohana Sundara Raju ,P. S. Sampath , U. Vivek, Tribological analysis of nanoclay/epoxy/glass fiber by using Taguchi's Technique, Materials and Design 70(2015) 1–9.
5. Al C. de Leon, Qiyi Chen, Napolabel B. Palaganas,Jerome O. Palaganas, Jill Manapat, Rigoberto C. Advincula, High performance polymer nanocomposites for additive manufacturing applications, (2016), doi:10.1016/j.reactfunctpolym.2016.04.010.
6. Y. Cao, G. Li, X. Li, Graphene/layered double hydroxide nanocomposite: properties, synthesis, and applications, Chemical Engineering Journal (2016), doi: <http://dx.doi.org/10.1016/j.cej.2016.01.114>.
7. M. Joshi, U. Chatterjee, Polymer nanocomposite: an advanced material for aerospace applications, Advanced Composite Materials for Aerospace Engineering. <http://dx.doi.org/10.1016/B978-0-08-100037-3.00008-0>
8. M. Galimberti, V.R. Cipolletti and M. Coombs, Applications of Clay–Polymer Nanocomposites, Developments in Clay Science, Vol. 5B. <http://dx.doi.org/10.1016/B978-0-08-098259-5.00020-2>.
9. Amir Hosein Ahmadian Hoseini, Mohammad Arjmand, Uttandaraman Sundararaj, Milana Trifkovic, Significance of interfacial interaction and agglomerates on electrical properties of polymer-carbon nanotube nanocomposites, Materials & Design 125 (2017) 126–134.



10. Gheorghe Radu Emil Maries, Processing Temperatures Influence of Three Types of Polyamide 6.6 Reinforced with Different Percentages of Fiber Glass on Some Mechanical Properties *MATERIALE PLASTICE* (52) No. 1, 2015(32-35).
11. Umit Huner, Effect of water absorption on the mechanical properties of flax fiber reinforced epoxy composites, *Advances in Science and Technology, Research Journal*, Volume 9, No. 26, June 2015, pages 1–6.
12. H Koike, K Kida, E C Santos, J Roswadowska, Y Kasima, K Kanemasu, Self Lubrication of PEEK polymer bearings in rolling contact fatigue under radial loads, *Tribology International* 49(2012) 30-38.
13. D Finney Charles, R Gnanamoorthy, Parag Ravindran, Rolling Contact fatigue behavior of Polyamide clay reinforced nanocomposite – Effect of Load and Speed, *Wear* 269, (2010), 565-571.
14. L. Stobinska^{a,b}, B. Lesiaka^a, A. Malolepszyk, M. Mazurkiewicz, B. Mierzwaa, J. Zemekd, P. Jiricekd, I. Bieloshapka, Graphene oxide and reduced Graphene oxide studied by the XRD, TEM and electron spectroscopy methods, *Journal of Electron Spectroscopy and Related Phenomena* 195 (2014) 145–154.
15. Julie Charles*, G. R. Ramkumaar, S. Azhagiri And S. Gunasekaran, FTIR And Thermal Studies On Nylon-66 and 30% Glass Fibre Reinforced Nylon-66 , ISSN: 0973-4945; CODEN ECJHAO, *E-Journal of Chemistry* ,<http://www.e-journals.net> 2009, 6(1), 23-33.
16. B Tan and N L Thomas, A Review of the Water Barrier Properties of Polymer/Clay and Polymer/Graphene Nanocomposites, *Journal of Membrane Science*,<http://dx.doi.org/10.1016/j.memsci.2016.05.026>.



Determination of Critical Temperature for Austenite to Ferrite Transformation During Hot Rolling of Low Carbon Nb-V-Ti Steel

Santosh Kumar^{1,4}, B Sunita Minz², N Mondal¹, Dr K Mukherjee^{3,4}

R&D Centre for Iron and Steel, SAIL, Ranchi, Jharkhand¹

Bokaro Steel Plant, SAIL, Bokaro Steel City, Jharkhand²

CSIR-National Metallurgical Laboratory, Jamshedpur, Jharkhand³

Academy of Scientific and Innovative Research (AcSIR), Ghaziabad, Uttar Pradesh⁴

✉ poplisk@gmail.com

ABSTRACT

Low Carbon Nb, V & Ti added Micro-alloyed steels improved mechanical properties through grain size refinement and precipitation strengthening. These steels are cold formed in complex shape and applied in automotive segment. Critical temperature like Solutionizing temperature, non-recrystallization temperature (T_{nr}), Austenite–ferrite transformation temperature (A_{r3} , A_{r1}) have important role in every step during hot rolling of micro-alloyed steel. Significant amount of deformation below the non-recrystallization temperature (T_{nr}) is given in hot strip mill to achieve an optimum combination of high productivity and combination of toughness and strength in micro-alloyed steels. Therefore, an accurate knowledge of critical temperature such as Solutionizing temperature, T_{nr} , A_{r3} , A_{r1} and the recrystallization kinetics is required.

Heat with Nb- V-Ti Microalloying was made at BSL through BOF-LHF-CC process and slabs were hot rolling. These slabs were processed under suitably designed process variables. The importance of deformation of austenite during hot rolling to influence transformation is studied. In this study, critical temperature i.e T_{nr} , A_{r3} & A_{r1} required for controlling metallurgical properties of final product is determined on a Gleeble®3500 system. The microstructure and properties were investigated. The microstructure of thermo-mechanically processed primarily consisted of polygonal ferrite (PF) and very small amount of acicular ferrite (AF) together. The ferrite predominant microstructure is fine, homogeneous and free of band structure. Yield strength levels more than 450 MPa and tensile strength levels above of 550 MPa were achieved.

INTRODUCTION

Low carbon micro-alloyed steel having a good combination of formability and weldability developed for automotive sector. These steels are cold rolled in complex shape. Micro alloying elements such as Nb, V & Ti is applied for grain refinement of ferrite and precipitation hardening of ferrite matrix. Micro alloying element Nb, V & Ti chemically react with C & N and produce carbides, nitrides and carbo-nitrides. Solubility of carbide, nitride and carbo-nitride plays an important role on effectiveness of the precipitate strengthening mechanism (Gladman T., 1997; Datta R and Mishra S, 1994). The reheating temperature above the Solutionizing temperature should be sufficient to dissolve the micro alloying precipitate, but it should not be high to cause the excessive austenite grain growth (Roy S., Chakrabarti D., and Dey G.K., 2014). A two or three stage controlled rolling schedule with single or double hold after reheating is quite a common practice to achieve the maximum grain refinement. The resulting overall effects is to control the process of recovery and recrystallization and to inhibit grain growth of the austenite. Mechanical properties of micro alloyed steels are strongly influenced by their ferrite grain structure. It is well established that a fine and uniform distribution of ferrite grains results in high strength coupled with high toughness. The evolution of the final ferrite grain structure and any precipitate population are influenced by the hot rolling draft and temperature schedule.

Factors that may affect recrystallization behaviour are strain & strain rate, temperature of deformation, initial grain size and chemical composition. Micro-alloying element first affects the critical temperature for onset of grain coarsening during reheating and subsequently the temperature at which the recrystallization process virtually stops during hot deformation of austenite. Nb has most pronounced effect i.e. retardation of the recrystallization process (Irani, Burton and Rothwell, 1967). Phenomena of retardation has been attributed to the solute drag effect, (Lucke and Detert 1957; Lucke and Stuwe 1963), and strain induced precipitation of carbo-nitride of Nb (Hiroshi and Tadakatsu, 1976; Irani, Burton and Rothwell, 1967). The point at which recrystallization stops is a complex function of the amount of deformation & temperature in each pass and composition

of the steel. Various Researcher have determined T_{nr} temperature using different laboratory experimental methods and based on finding regression empirical equations developed. The most used empirical formula is given below (Boratto F et.al, 1988; Bai D, et. al., 1996):

The commonly used Boratto equation is given as:

$$T_{nr} = 887 + 464 \times C + (6445 \times Nb - 644 \times \sqrt{Nb}) + (732 \times V - 230 \times \sqrt{V}) + 890 \times Ti + 363 \times Al - 357 \times Si \quad (1)$$

where C, Nb, V, Ti, Al, and Si are the elements in wt pct of the steel.

Another equation formulated by Bai (Bai D, et. al., 1996) incorporating both alloy content and strain is given by

$$T_{nr} = (88.1 \times \log(Nb + 0.31 \times Ti + 0.15 \times Al) + 1156) \times (\epsilon - 0.12 \dot{\epsilon} - 0.01t - 0.1) \quad (2)$$

Where, Nb, Ti, Al are the elements in wt pct of the steel and ϵ is strain, $\dot{\epsilon}$ is strain rate (/s), t is inter-pass time (in sec).

Multi-hit compression method is one of the most popular process to determine non-recrystallization temperature as reported in the literature (Homsher, and Van Tyne, 2015; Maccagn T. M., et. al., 1994; Medina and Mancilla, 1993). In multi-hit compression process, successive hot deformation is given with decreasing deformation temperatures at a specified strain per pass, strain rate, and inter-pass time. Deviation in the slope of mean flow stress (MFS) against the inverse of absolute temperature (T, K) denotes the T_{nr} (Vervynck S., Verbeken K., Thibaux P., and Houbaert Y., 2011). Multi-hit methods predict sufficiently accurate T_{nr} , but cannot provide recrystallization–precipitation interaction.

Austenite to Ferrite phase transformations ($\gamma \rightarrow \alpha$) are one of the factors that most influence steel properties. The transformation kinetics of proeutectoid ferrite in continuous cooling has been studied by several authors where the evolution of the fraction transformed to ferrite suggests that this can be predicted by an Avramilaw (Gómez, Medina and Caruana, 2003). Dilatometry is one of the classic techniques, most commonly used to determine the start and end of phase transformations in steels.

The aim of this work was to determine the critical transformation temperatures by experiment and simulation software and implement to actual hot rolling process to optimise the metallurgical properties requirement.

EXPERIMENTAL

Chemical compositions of steels used are shown in **Table 1**. The specimens having a dimension of 10 mm x 15 mm x 25 mm selected for multi-hit compression test. The austenitization temperature was set to be 1200°C which is higher than the solubility temperature of precipitates, thus assuring that the precipitates would be completely dissolved in the austenite, except Ti precipitate. Solutionizing temperature was calculated by using Thermo-Cal simulation software TCFE7 database.

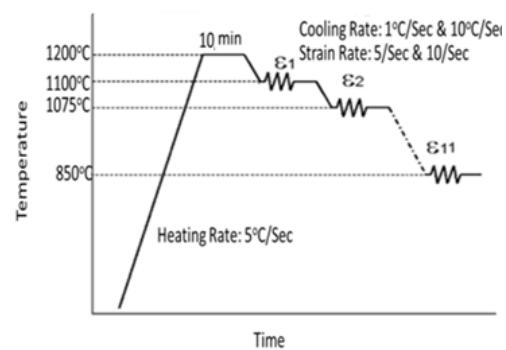
Table 1. Chemical composition of experimental steel (in % wt)

C	Mn	S	P	Si	Al	Nb	V	Ti
0.08	1.46	0.008	0.02	0.318	0.026	0.046	0.046	0.010

Laboratory set-up of Gleeble®3500 system in plain strain condition is shown in **Fig 1(a)**. For multi hit compression test, the specimens were rapidly cooled after austenitization for 10 minutes to the deformation temperature. The first deformation given at temperature 1100°C and subsequently deformation given at temperature reduced by 25°C upto 850°C keeping constant cooling rate 1°C/S & 10°C/S. The strain rate was kept 5/s & 10/s. The deformation schedule is shown in **Fig. 1b**.



(a)



(b)

Fig. 1. Deformation schedules (a) Gleeble®3500 system (b) Multi-hit compression test

Dilatometry experiments were carried out to obtain the continuous cooling transformation curve at cooling rate 10°C/s . These curves helped to determine the critical temperatures like A_{r1} and A_{r3} . The following heating, soaking and cooling parameters were adopted for the test: Heating rate: 10°C/s ; Soaking temperature: 980°C , Soaking time: 300s & Cooling rate: 10°C/s ,

Microstructures of the parent and deformed samples were examined by optical microscope (Model: Olympus GX 71). For optical observations, specimens were etched with 2% nital. Tensile test was carried out for evaluating Yield strength, Tensile strength and % elongation before fracture.

RESULTS & DISCUSSION

Solutioning temperature is predicted by using Thermo-Calc simulation software with TCFE7 database. The amount of all phases vs. temperature diagram is shown in **Fig. 3**. The dissolution temperature of Nb(CN) is $\sim 1145^{\circ}\text{C}$. Similarly, the dissolution temperature for V(CN), TiN & AlN are 775°C , $\sim 1405^{\circ}\text{C}$ & 1098°C respectively. As dissolution temperature for Nb(CN) is $\sim 1145^{\circ}\text{C}$, therefore, it is assumed that Nb(CN) will dissolve in austenite during homogenization at 1200°C during heating in Gleeble for 10 minutes.

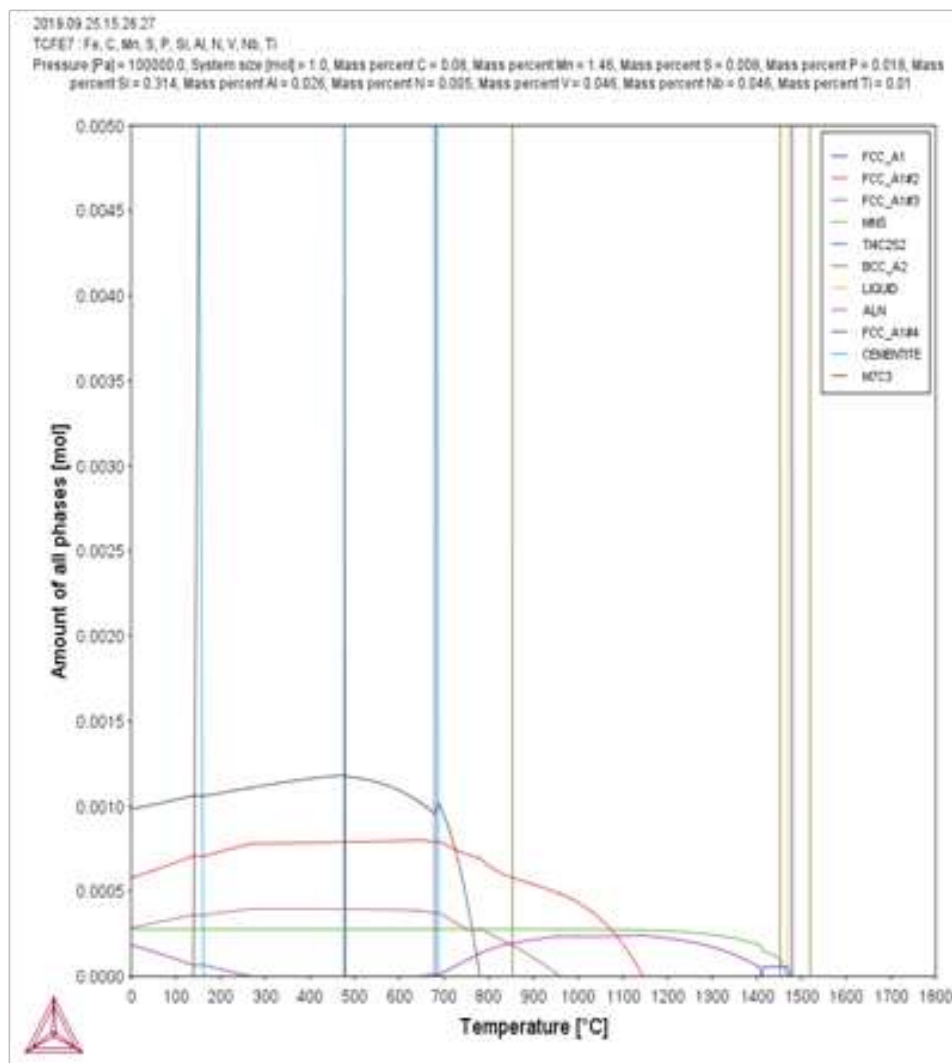


Fig. 2. Phases vs Temperature diagram plotted by Thermo-Calc simulation software (TCFe7)

Based on the data generated by Thermo-Calc, distribution of C, N, Nb & V in phases w.r.t temperature are shown in **Fig. 3**. Nb (C, N) precipitate evolves with the decrease in temperature and completed by temperature $\sim 775^{\circ}\text{C}$. Similarly, V(CN) evaluated after reaching 850°C and completed by $\sim 500^{\circ}\text{C}$.

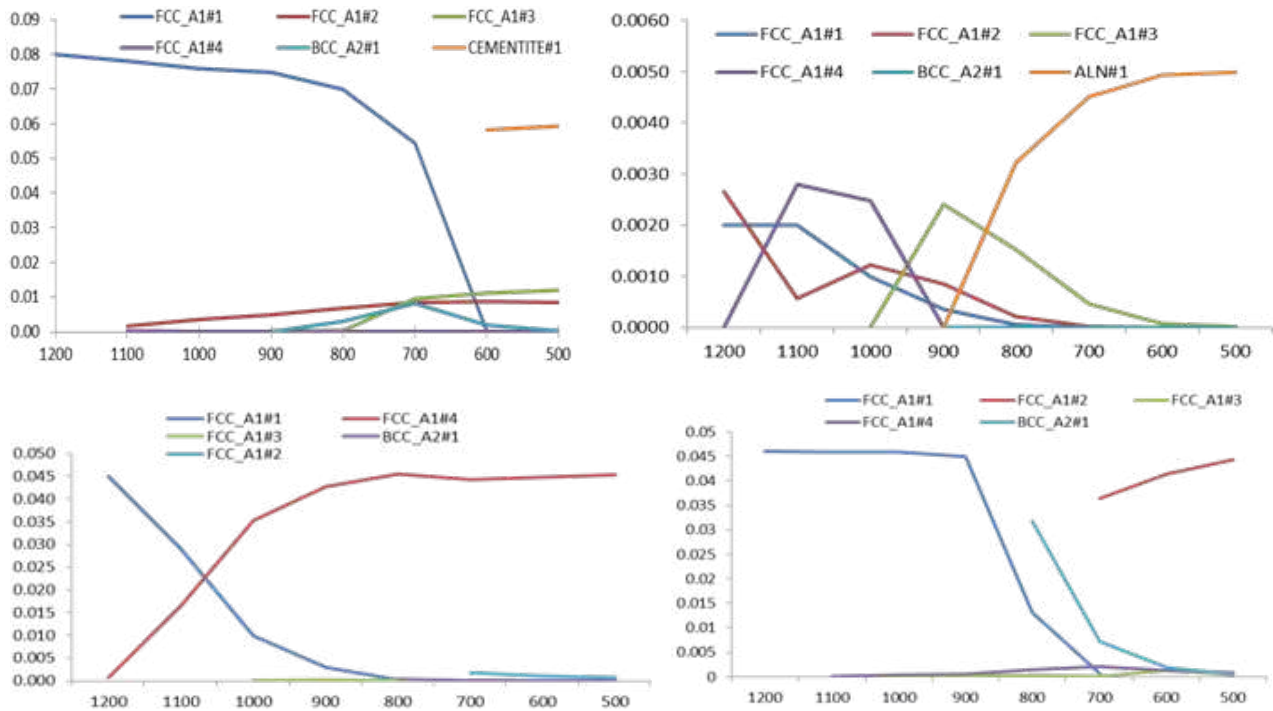


Fig. 3. C, N, Nb & V distribution in phases w.r.t temperature (data source: TCF_{Fe7}; ThermoCalc)

The non-recrystallization temperature i.e. T_{nr} of the steel was initially determined by multi-hit compression tests under plane strain compression with two cooling rate i.e. 1°C/s & 10°C/s and two strain rate i.e. 5/s and 10/s. The inter-pass time are 25 sec and 2.5 sec respective cooling rate. **Fig. 4** shows the stress–strain curves obtained with two different inter-pass times and two different strain rate. Oscillations were occurred but flow stress was linearly increasing with a decrease in temperature in all the combination of strain rate and cooling rate. Generally, the pass-to-pass oscillations are occurred due to formation of mixed microstructure formation within the T_{nr} regime as a result of competing mechanisms between hardening and recrystallization softening of austenite.

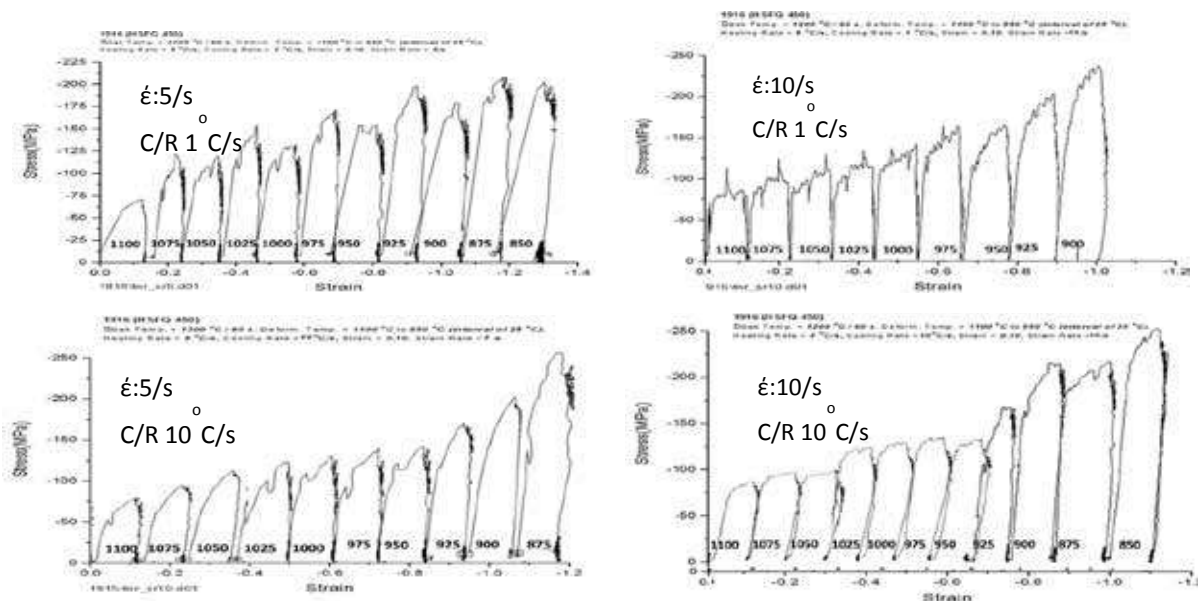


Fig. 4. True stress–strain curves of multi hit deformation test at different strain rate & cooling rate

The plot of mean flow stress (MFS) Vs. inverse of absolute temperature ($1/T, K^{-1}$) was made from the flow curve data and shown in **Fig. 5**. The deviation in the slope of the mean flow stress corresponds to the non-recrystallization temperature, T_{nr} .

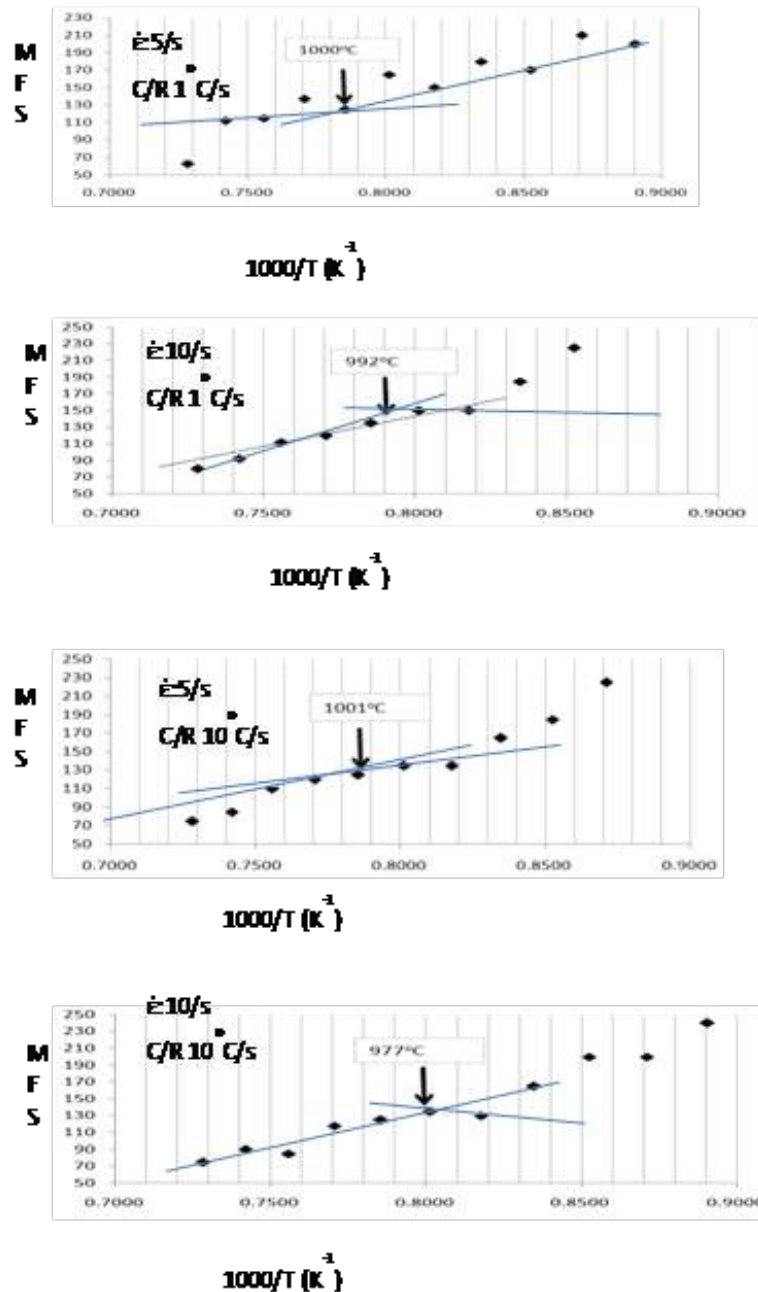


Fig. 5. MFS vs $1/T$ plot at different strain rate and cooling rate

The non-recrystallization temperature (T_{nr}) was measured by means of laboratory compression tests are compared in **Table 4**.

Table 4. Comparison of T_{nr} value

$\dot{\epsilon}: 5/s$ C/R $1^\circ C/s$	$\dot{\epsilon}: 10/s$ C/R $1^\circ C/s$	$\dot{\epsilon}: 5/s$ C/R $10^\circ C/s$	$\dot{\epsilon}: 10/s$ C/R $10^\circ C/s$
1000	992	1001	977

Fig. 6 shows the dilatometry curves obtained at cooling rates 10oC for the alloy. **Table 5** shows the Ar1and Ar3 temperatures determined from the dilatometry curve.

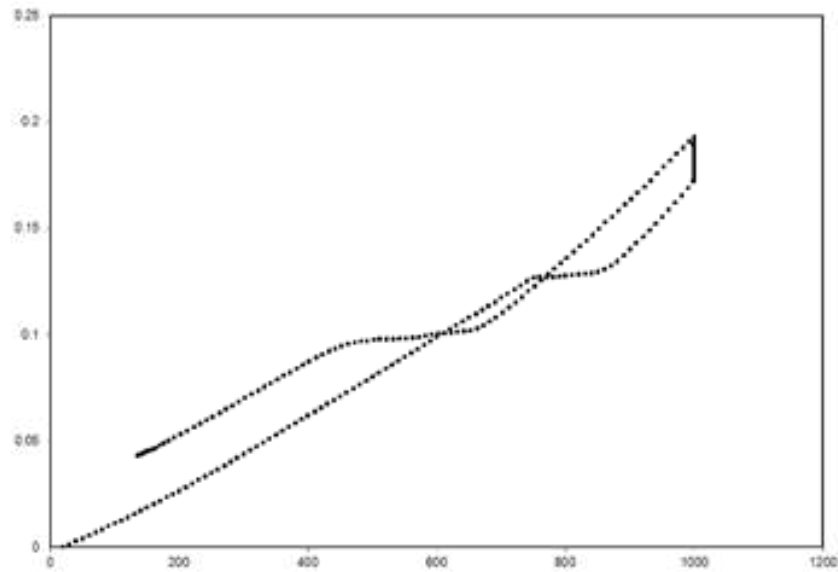


Fig. 6. Dilatometry curves

Table 5. Ar1 & Ar3 temperature for the sample alloy

Ac1	Ac3
741°C	860°C

The percentages of austenite transformed to different phases (ferrite, pearlite, bainite) have been shown in continuous cooling transformation (CCT) diagrams (**Fig. 7**).

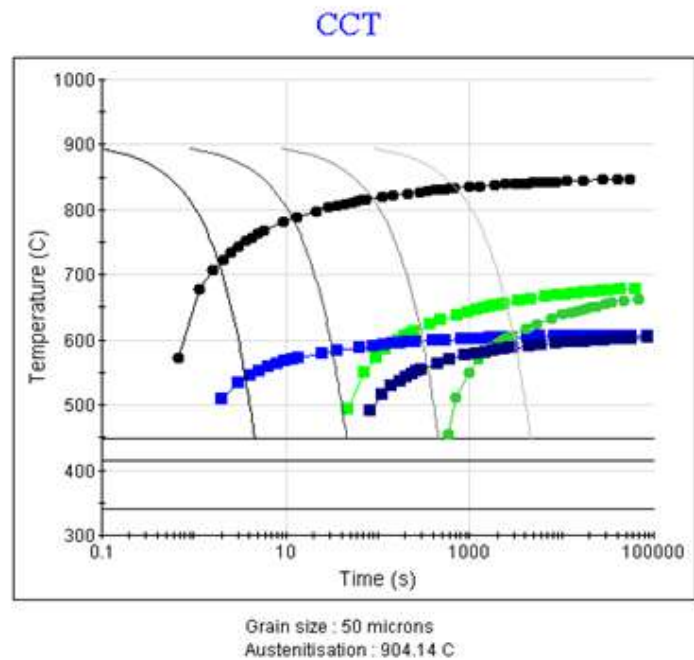


Fig 7. CCT curve of experimental alloy

The pearlite and bainite transformation start temperature at different cooling rate is charted in **Table 6**.

Table 6. Pearlite and Bainite start temperature

Cooling Rate	Pearlite 0.1%	Bainite 0.1%
100°C/S	---	566
10°C/S	504	611
1°C/S	624	620
0.1°C/S	655	620

The data observed in laboratory experiment and software simulation was:

Solutionizing Temperature of NbCN ~ 1145°C

Non-Recrystallization Temperature ~ 1000°C

Autesinite to ferrite start Temp Ar3 ~ 860°C

Autesinite to ferrite finish Temp Ar1 ~ 741°C

Based on the above experimental data, slabs were hot rolled with following parameters:

Soaking Temperature 1230-1240°C

Soaking Time 45 minutes

Roughing Mill Finish Temperature 1050-1060°C

Finishing Mill Start Temperature 960-980°C

Finishing Rolling Temperature 880°C

Coiling Temperature 600-620°C

Fig. 8 shows the Microstructure of hot rolled coil processed at above temperature and primarily consisted of polygonal ferrite (PF) and very small amount of a circular ferrite (AF) together along with around 10% pearlite. The ferrite predominant microstructure is fine, homogeneous and free of band structure.

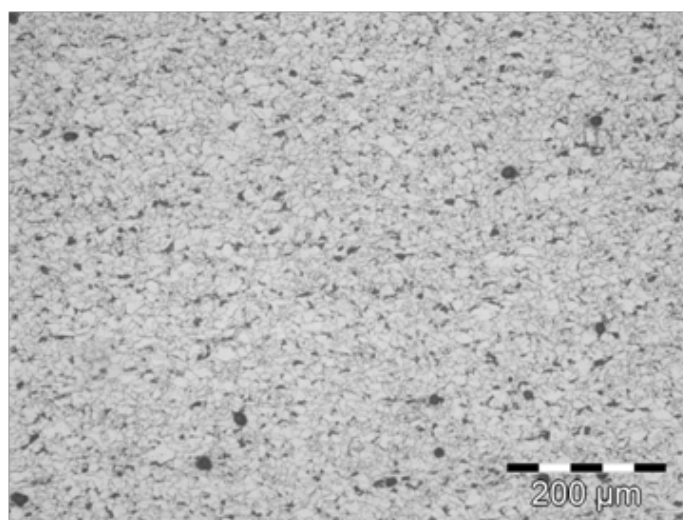


Fig. 8. Optical Microstructure

Tensile curve are shown in **Fig. 9** in which Yield strength are more than 450 MPa and tensile strength is more than 550MPa. The percentage elongation is more than 20% which indicate a very good formability with such high strength. **Table 7** shows the tensile properties.

Table 7. Tensile properties

YS	UTS	% El
532 MPa	578 MPa	24%



CONCLUSION

The critical temperature such as non-recrystallization temperature (T_{nr}), Austenite–ferrite transformation temperature (A_{r3} , A_{r1}) were measured utilizing Gleeble®3500 system in plain strain condition for selected low carbon microalloyed by multi hit compression test and dilatometry method respectively.

The microstructure of thermo-mechanically processed primarily consisted of polygonal ferrite (PF) and very small amount of acicular ferrite (AF) along with ~10% of pearlite together. The ferrite predominant microstructure is fine, homogeneous and free of band structure. Yield strength levels more than 450 MPa and tensile strength levels above of 550 MPa were achieved.

Understanding and knowledge of a critical temperature before designing a rolling process parameter helps in achieving required microstructure as well as mechanical properties.

REFERENCES

1. Bai D, et. al., 1996, Static recrystallization of Nb and Nb-B steel under continuous cooling conditions, Transactions of the ISIJ, 36(8), pp. 1084-1093.
2. Boratto F et.al, 1988, Effect of chemical composition on critical temperature of microalloyed steels, Thermec'88, Proceedings. ISIJ, pp. 383-390.
3. Datta R and Mishra S, 1994. Some new results in thermo-mechanical processing of micro-alloyed steels. Bulletin of Material Science, 17(6), pp. 643-662.
4. Gladman T., 1997, The Physical Metallurgy of Microalloyed Steels, The Institute of Materials, London, pp. 230–60.
5. Gómez M., Medina S. F. and Caruana G., 2003, Modelling of Phase Transformation Kinetics by Correction of Dilatometry Results for a Ferritic Nb-microalloyed Steel, ISIJ International, 43(8), pp. 1228–1237.
6. Hiroshi SEKINE, Tadakatsu MARUYAMA, 1976, Retardation of Recrystallization of Austenite during Hot-rolling in Nb-containing Low-carbon Steels, Trans. ISIJ, 16, pp. 427.
7. Homsher, C. N. and Van Tyne, C. J., 2015, Comparison of Two Physical Simulation Tests to Determine the No-Recrystallization Temperature in Hot Rolled Steel Plates, Materials Performance and Characterization, 4(3), pp. 1–14.
8. Irani, J. J.; Burton, D.; Jones, J. D.; Rothwell, A. B., 1967, Strong Tough Structural Steels. Special Report 104; Iron and Steel Institute: London, UK, p 110.
9. J.D. Jones, A.B. Rothwell., 1968, Deformation Under Hot Working Conditions, Iron Steel Inst., London, pp. 78-82.
10. K. Lücke and H. P. Stüwe, 1963, Recovery and Recrystallization of Metals, ed. by L. Himmel, Inter-science, New York, pp.171–210.



11. Lücke, K. & Detert, K., 1957, A quantitative theory of grain-boundary motion and recrystallization in metals in the presence of impurities., *Acta Metal.* 5, 628–637.
12. Maccagn T. M., et. al., 1994, Determination of Recrystallization Stop Temperature from Rolling Mill Logs and Comparison with Laboratory Simulation Results, *ISIJ International*, 34(11), pp. 917-922.
13. Medina S. F. and Mancilla J. E., 1993, Determination of Static Recrystallization Austenite in Microalloyed Steels, *ISIJ International*, 33(12), pp. 1257-1264.
14. Rajinikanth V., Kumar T, Mahato B., Chowdhury S G, and Sangal S, 2019, Effect of Strain-Induced Precipitation on the Austenite Non-recrystallization (T_{nr}) Behaviour of a High Niobium Microalloyed Steel, *Metall Mater Trans A*, 50, pp 5816–5838.
15. Roy S., Chakrabarti D., and Dey G.K., 2014, Austenite Grain Structures in Ti- and Nb-Containing High-Strength Low-Alloy Steel During Slab Reheating, *Materials Science Forum* 783, pp 669-673.
16. Sims R B, 1954, The Calculation of Roll Force and Torque in Hot Rolling Mills, *Proceedings of the Institution of Mechanical Engineers*, 168(1), pp. 191-200.
17. Vervynckt S., Verbeken K., Thibaux P., and Houbaert Y., 2011, Evaluation of the Austenite Recrystallization by Multideformation and Double Deformation Tests, *steel research int.* 82(4), pp 369-378.



Ag@CuO Decorated Tailored Nanostructures based CO₂ sensors: Role of n-type Semiconductors in Enhancing Heterostructured Sensor Efficiency

Shravanti Joshi

Functional Materials Laboratory, Department of Mechanical Engineering, G S Mandal's Marathwada Institute of Technology, Aurangabad, Maharashtra

✉ shravantijoshi@gmail.com

ABSTRACT

Over the past few decades, the health hazards of CO₂ have forced environmental safety bodies around the world to introduce stern policies to curb CO₂ emission from major anthropogenic sources. In this context, highly selective detection of CO₂ at low power has gained considerable interest as it is the first step towards its emission reduction. Herein, Ag-CuO/n-type semiconductors (namely ZnO, SnO₂ and BaTiO₃) are synthesized and tested for their CO₂ sensing capabilities based on chemoresistive principle. A detailed sensing study is undertaken comparing several sensor characteristics towards lower gas concentrations (~50 ppm) in dry conditions. Tailored n-type metal oxide semiconductor nanoarchitectures (ZnO, SnO₂ and BaTiO₃) were chosen based on their band-gap, work function, charge carrier concentration and other chemo-physical properties to understand their role in enhancing sensor efficiency. The sensor materials compared here can be integrated in a single unit as a multi-sensor arrays for CO₂ monitoring for varying parameters. The results demonstrated in this work are anticipated to lead way for intensified research efforts in ultrasensitive CO₂ multifunctional sensor for real industrial applications.

Keywords: CO₂ sensors; Low concentration; Chemo-resistive; Selectivity; Semiconductors.

INTRODUCTION

The Occupational Safety and Health Administration (OSHA) has recognized health hazards of CO₂ and thus has proposed stringent rules to curb its emissions. Among the many sensors documented, chemoresistive sensors are simple structured, flexible, and economic. The chemoresistive principle depends on reversible charge transfer resulting from physical and chemical adsorption between active materials and the analyte gas in the presence of oxygen [1]. Interestingly, metal oxide semiconductors (MOS) decorated with noble metal and/or metal oxides have shown high sensitivity and faster response kinetics, however in many cases at the cost of poor selectivity in the presence of various interfering gases and humidity. Few of these studies includes popular MOS such as LaOCl, CdO, CuO, SnO₂, ZnO, BaTiO₃, and so on that have been studied as possible *n-type* base matrices selected based on several parameters such as bandgap, work function, charge carrier concentration etc., [2]. However, there is no thumb rule on selection of moieties for decoration over base matrix to enhance the sensor efficiency. The bandgap of ZnO, SnO₂ and BaTiO₃ remains same but there is marked difference in the work function and the charge carrier concentration [2]. Thus, it would be interesting to study effect of these parameters on the CO₂ sensing performance and mechanism by employing sensitive layer made of *p/n* composites, wherein the *p-type* metal oxide, that is CuO remains constant. Further, selection of *p-type* oxide for decoration of *n-type* oxide is dependent on the amount of lattice matching and thermal stability of derived carbonate formed spontaneously in the presence of CO₂ gas.

Interestingly, CuO has narrow bandgap (1.2 eV), moderate work function (5.3 eV), high charge carrier concentration ($\sim 4.6 \times 10^{18} \text{ cm}^{-3}$) and has low lattice mismatching (<5%) [3]. Additionally, functionalization of *p/n* composite with metallic silver (Ag) facilitates the gas sensing phenomenon by the process of electronic/chemical sensitization and catalytic oxidation (formation of Ag/Ag₂O redox couple), thereby resulting in the increased amount of active oxygen species on the surface of the sensitive layer [4]. Silver is more effective as catalyst in expediting the CuO carbonation in the presence of CO₂ [5]. This is primarily attributed to its role as an efficient electron sink, due its characteristic ability to form large Helmholtz double layer. Furthermore, Ag over an extended period have tendency to form Ag₂O in air which promotes more intensified electron depletion layer, thus releasing trapped electrons back to base matrix through reversible reactions between Ag₂O and Ag in presence of CO₂. Moreover, Ag has

work function (4.14-4.46 eV), lower than CuO (5.3 eV) and most of the noble metal such as gold (5.1 eV), platinum (6.35 eV) and palladium (5.22 eV), thus making it preferred choice [6]. Due to this, electrons can easily be transferred from Ag to CuO, thus leading to the formation of a negatively charged accumulated layer around the Ag and CuO nanointerfaces. This process enhances the dissociative adsorption of molecular oxygen on the CuO surface, thus increasing the charge transfer dynamics between the CO₂ gas and CuO surface to form copper carbonate, which is then measured as the sensor response. In this contribution, we present a cumulative study comparing convenient approaches for repeatable and reversible CO₂ monitoring based on tailored hetero structures of Ag@CuO/n-type MOS integrated onto a transducing platform.

MATERIALS AND METHODS

Chemicals

Zinc nitrate hexahydrate (Zn(NO₃)₂·6H₂O), urea (NH₂CONH₂), tri-sodium citrate dihydrate (HOC(COONa)(CH₂COONa)₂·2H₂O), sodium hydroxide (NaOH) pellets, sodium stannate trihydrate (Na₂SnO₃·3H₂O), D-(+)-glucose monohydrate (C₆H₁₂O₆·H₂O), barium hydroxide octahydrate ((BaOH)₂·8H₂O), titanium dioxide (TiO₂), tween-80 (C₆₄H₁₂₄O₂₆), copper (II) acetate monohydrate (Cu(CO₂CH₃)₂·H₂O), polyethyleneglycol((H(OCH₂CH₂)_nOH), Mn~900-2200), silver nitrate (AgNO₃), sodium tetrahydridoborate (NaBH₄) were procured from Sigma Aldrich Chemicals. All the chemicals were of analytical reagent (AR) grade and used without any further purification. Throughout the experiments, Sartorius Stedim Biotech S.A (Model-Arium 61316) deionized water (18.2 MΩ.cm) was used.

Synthesis of ZnO, SnO₂ and BaTiO₃ Nanoarchitectures

Briefly, 3 mmol of Zn(NO₃)₂·6H₂O, 6 mmol of NH₂CONH₂ and 0.3 mmol HOC(COONa)(CH₂COONa)₂·2H₂O were dissolved in 60 mL deionized water to form solution that was transferred into a 100 mL autoclave and heated at 120°C for 6 h. Finally, ZnO powder was achieved by calcining the achieved precursor at 400°C for 2 h. For SnO₂ synthesis, 1 g of Na₂SnO₃·3H₂O was dissolved in 30 mL of deionized water to get 0.125 M stannate solution followed by addition of 2 g of D-(+)-glucose monohydrate and then kept for stirring at 50°C for 12 h. In another case, 5 mmoles of (BaOH)₂·8H₂O was dissolved in 30 mL of deionized water under magnetic stirring, followed by addition of 5 m moles of TiO₂. To this 10 mM of Tween 80 was added drop-wise using micropipette. After stirring for 20 min, the suspension was ultrasonicated and the contents were transferred to a 100 mL Teflon-lined autoclave and placed in oven. The temperature was raised to 200°C for 24 h. Thereafter, the resultant precipitate in case was suspended in deionized water and centrifuged to obtain a product that was dried in an oven at 60°C. Table 1 summarizes the chemical routes.

Table 1. Summation of sensitive materials, their morphology and the synthesis methods employed.

Material	Morphology	Method
ZnO	H.Microspheres	Hydrothermal
Pure CuO	Nano-leaves	Co-precipitation
CuO/ZnO	Interleaved Assembly	Co-precipitation
Ag@CuO/ZnO	Interleaved Assembly	Wet-impregnation
SnO ₂	H.Nanospheres	Sol-gel
CuO:Cu ₂ O	H.Flowers	Hydrothermal
CuO:Cu ₂ O/SnO ₂	H.Nanospheres	Hydrothermal
Ag@CuO:Cu ₂ O/SnO ₂	H.Nanospheres	Wet-impregnation
BaTiO ₃	Prolated Spheroids	Hydrothermal
Pure CuO	Nano-leaves	Co-precipitation
CuO/BaTiO ₃	Leaves/spheroids	Co-precipitation
Ag@CuO/BaTiO ₃	Leaves/spheroids	Wet-impregnation

Decoration with CuO Nanoparticles

The calculated quantities of n-type MOS powder was mixed with 2.143 mmoles of copper (II) acetate monohydrate to 100 mL deionized water. To this solution, 0.262 mmoles of polyethylene glycol was added. This was followed by drop wise addition



of 5 M NaOH solution until a color change from blue to black was observed. This solution was stirred magnetically for 24 h at 70°C. After completion of the reaction, the resultant mixture was centrifuged, sonicated, and washed several times to obtain a brown product.

Decoration with metallic silver

For decorating CuO/n-type MOS hetero structures with silver in 0.25 wt.%, 0.01 mmol of AgNO_3 was added to it, in 10 ml of ethanol and stirred under magnetic agitation. Thereafter, 0.04 mmol of NaBH_4 was added to reduce the silver ions to metallic silver. The resultant mixture was centrifuged, sonicated, and washed to obtain a final product that was dried at 60°C.

Characterization Techniques & Sensor Patterns

In a typical sensing experiment, ca. 10 mg of as-synthesized nanomaterial was dispersed in 10 mL of 1:1 mixture of deionized water and ethanol via ultra-sonication at room temperature. In each case, the sensor element was fabricated by dipcoating the cylindrical alumina tube provided with two platinum (Pt) electrodes for the electrical contacts into the nanomaterial suspended slurry. Nikrothal 80 wire was used as heater with coil inserted inside the alumina tube to maintain the high temperature. Prior to each sensing experiment, the sensor element was preheated at 200°C for 2-3 h in synthetic dry air to stabilize the sensor surface. The temperature was controlled by a ceramic heater coupled to a power supply utilizing K-type thermocouple placed inside the sensor chamber as a feedback for PID controller. Industrial purity grade CO_2 gas was diluted using air at a gas flow rate of 200 sccm.

RESULTS AND DISCUSSION

The materials characterization in terms of crystal structure, crystallinity, thermal stability, chemical composition, morphological evolution for Ag@CuO/n-type MOS sensors along with sensing characteristics for CO_2 concentrations ranging from 500-20,000 ppm in dry and humid conditions is detailed elsewhere [7-9]. The focus of current study is only to compare the three n-type metal oxides for their sensing capabilities and their ability to integrate in single unit as a multifunctional sensor array. These sensor arrays are fabricated with an aim to provide continuous CO_2 monitoring ranging from 40 to 400°C for 10-50 ppm gas concentrations. Usually, the sensors are fabricated for single purpose, but the sensors being studied here are anticipated to working for wide range of applications, starting from indoor monitoring to difficult environment as observed in petrochemical industries, mining and so on. **Fig. 1** shows the cycles corresponding to different concentrations of CO_2 gas that were recorded sequentially for 10, 30 and 50 ppm. Over the entire range of gas concentrations tested, the Ag@CuO/BaTiO_3 nanocomposite showed enhanced response magnitude and response/recovery times compared to ZnO and SnO_2 based nanocomposites.

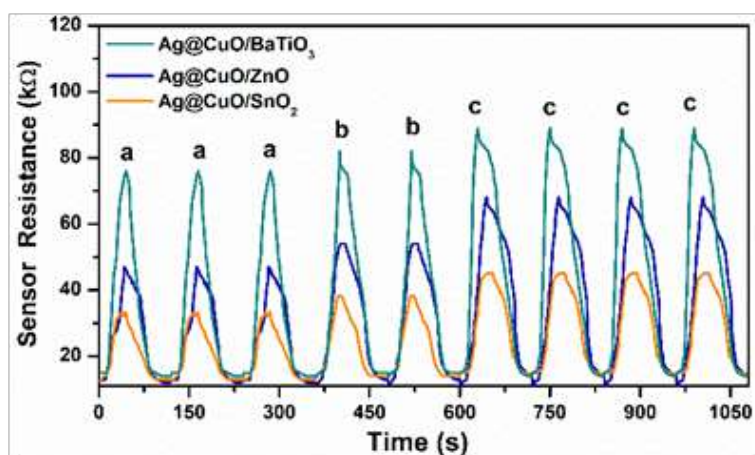


Fig. 1. Dynamic transients recorded at 120°C, 300°C and 320°C for BaTiO_3 , ZnO and SnO_2 decorated with 0.25 wt.% Ag and CuO in equimolar ratio. Here a-10 ppm, b-30 ppm, and c-50 ppm CO_2 gas concentrations in dry air

Fig. 2 illustrates the sensor response as a function of operating temperature. The formation of equal p/n junction units compared to unequal units, facilitates decreases in the energy barrier at the grain boundary of p -type and n -type oxides upon interaction of CO_2 gas effectively, that subsequently reduces the width of the depletion layer, resulting in response improvement upon exposure to CO_2 gas. **Fig. 3** exemplifies the sensor response as a function of CO_2 gas concentration. The calibration curve shows the linear dependence of sensor response on CO_2 gas concentration in the 10-50 ppm range.

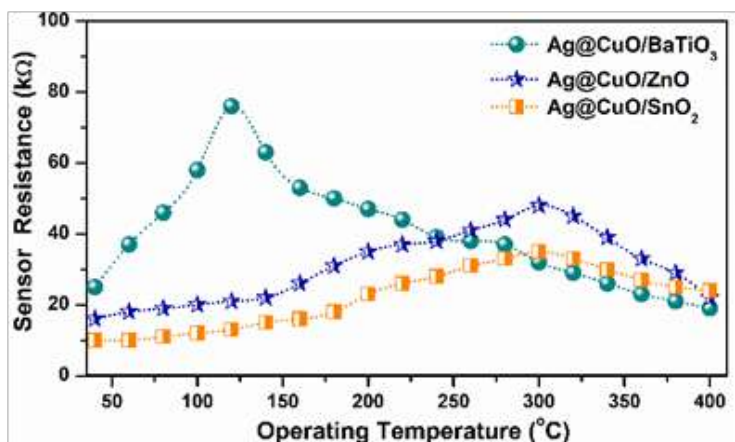


Fig. 2. Sensor response as a function of operating temperature towards 50 ppm CO₂ gas.

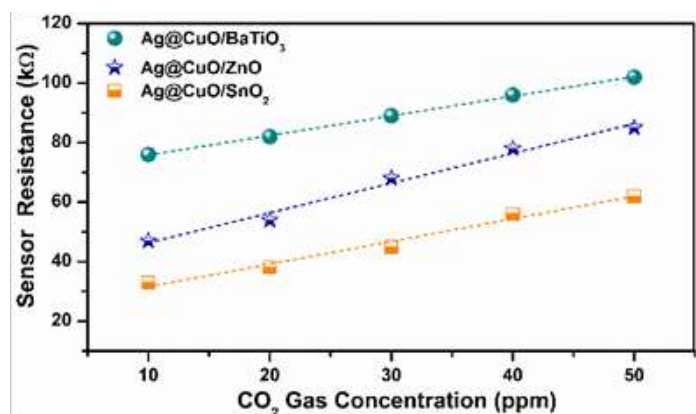


Fig. 3. Calibration curves recorded at 120°C, 300°C and 320°C for BaTiO₃, ZnO and SnO₂ decorated with 0.25 wt.% Ag and CuO in equimolar ratio.

Fig. 4 shows the longterm stability of the Ag@CuO/n-type MOS gas sensors tested towards CO₂ gas over an extended period. All three sensors exhibited good reproducibility in their sensing performance with a nearly constant response magnitude towards 50 ppm gas concentration mixed with air. Gas sensing mechanism in case of chemoresistive sensor is widely acknowledged as a surface phenomenon based on conductance modulation model[10-11]. During this phenomenon, change in resistance magnitude is observed because of physisorption of gas molecules and the interaction of these molecules with the species on the surface of the sensitive layer [9, 11].

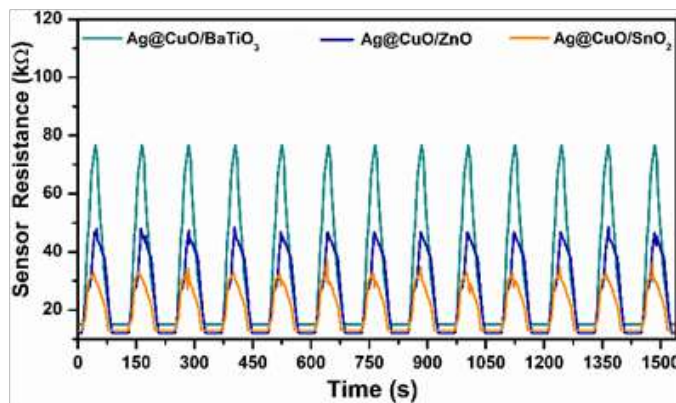


Fig. 4. Long-term stability of towards 50 ppm CO₂ gas concentration recorded at 120°C, 300°C and 320°C for BaTiO₃, ZnO and SnO₂ decorated with 0.25 wt.% Ag and CuO in equimolar ratio



Fig. 5 illustrates the multifunctional sensor arrays in a single housing. In the case of CuO/n-type nanocomposite based sensors, the sensing mechanism stems from major factors such as CuO carbonation, p/n nanointerfaces effect, reversible adsorption/desorption, and catalytic role of Ag. The utilization of n-type semiconductor as base matrix forms compatible composite with p-type semiconductor CuO owing to low lattice mismatch. Previous reports suggest that the enhancement in observed sensor response was based on the change in resistance and capacitance of CuO/n-type mixed oxide because of CuO carbonation [8-9].

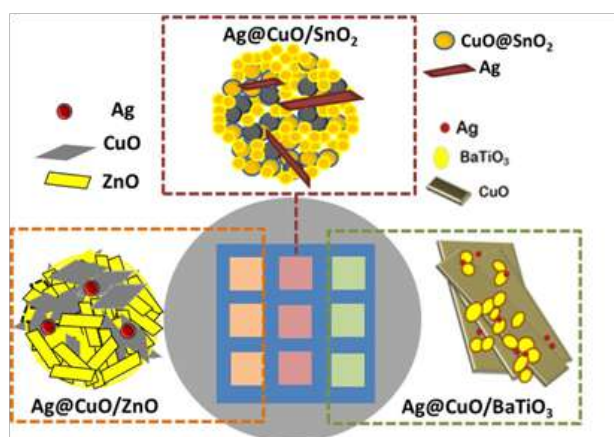


Fig. 5. Schematic representation of multi-sensor array housing the Ag@CuO/n-type metal oxide semiconductors.

Table 2. Summary of electronic properties of the *n*-type MOS

MOS	Band gap (eV)	Work Function (eV)	Charge Carrier Concentration (cm ⁻³)
ZnO	3.3	5.3	~10 ¹⁶ -10 ¹⁷
SnO ₂	3.5	4.5	~3.1×10 ¹⁷ -2.4×10 ¹⁸
BaTiO ₃	3.3	4	~7 × 10 ²¹

Table 2 summarizes few important properties of each of the n-type metal oxide. Pristine n-type metal oxide semiconductors and CuO showed negligible response to CO₂ gas and hence the formation of only CuCO₃ upon exposure does not facilitate the decomposition process, thus making it unsuitable for CO₂ sensing. Further, metal oxides such as CuO have strong affinity towards CO₂ thus, exhibiting irreversible carbonate adsorption. But in present case, these oxides at p/n interfaces are not strongly basic to allow irreversible CO₂ adsorption. Interestingly, when p-n nanocomposite is exposed to air, the molecular oxygen gets dissociatively chemisorbed in atomic form (O²⁻, O⁻) on the surface, creating electron depletion region. In presence of CO₂ gas, surface carbonation of CuO takes place which in turn reduces the adsorbed oxygen concentration and increases the acceptor density in CuO and/or n-type MOS, consequently changing the conductance of sensitive layer [5-6, 11]. As a result, the resistance of nanocomposite upon introduction of CO₂ increases and the potential barrier height between CuO and base matrix decreases. The reversible reactions in the presence and absence of target gas change the conductance of the CuO/n-type MOS layer forms the basis of the sensing mechanism [9-10].

CONCLUSIONS

In summary, we reported an important progress for selective CO₂ gas detection based on a comparative study between ZnO, SnO₂ and BaTiO₃ decorated with Ag@CuO. Enhanced CO₂ gas sensing performance in dry conditions was observed with more remarkable values for Ag@CuO/BaTiO₃ followed by Ag@CuO/ZnO nanoarchitectures. Excellent sensing performance reported here can be attributed to the synergistic combination of tailored chemical routes, gas active sites at nanointerfaces and Ag@CuO impregnation that were crucial in increasing CO₂ adsorption. Further, simple strategies and detailed insights on the oxidation states provided in the present work is likely to provide a feasible approach towards the realization of highly selectivity CO₂ sensors for a wide range of applications in environmental monitoring. Furthermore, given the ease of synthesis and sensor element fabrication, the developed chemoresistive micro-sensors can be employed as multiple sensors housed in single chamber and used for multiple applications, thus operating at various temperatures and detecting CO₂ gas at different concentrations, thereby making it feasible to almost all industrial conditions.



ACKNOWLEDGMENT

SJ acknowledges College of Science, Engineering and Health (SEH), RMIT University, Australia for financial assistance in the form of postgraduate scholarship and through the awardment of Higher Degree by Research Publication Grant. SJ is grateful to Dr. Sunkara V. Manorama from Nanomaterials Laboratory at CSIR-IICT, Hyderabad and to Dr. Samuel J. Ippolito from Mercury Laboratory, RMIT University, Australia for providing facilities to carry out the work at their respective institutes. SJ greatly acknowledge the facilities, scientific insights and the technical expertise provided by the Australian Microscopy & Microanalysis Research Facility (RMMF) at the RMIT University, Australia.

REFERENCES

1. A. Katoch, Z. U. Abideen, H. W. Kim, S. S. Kim, "Grain-Size-Tuned Highly H_2 Selective Chemiresistive Sensors Based on ZnO–SnO₂ Composite Nanofibers," ACS Applied Materials Interfaces, vol. 8, no. 4, pp. 2486–2494, January 2016.
2. S. Joshi, "Tailored Nanostructures for CO₂ Gas Sensing Applications," School of Science, RMIT University, Melbourne, PhD Thesis, Chapter 2, pp. 11-34, November 2017.
3. F. P. Koffyberg, and F. A. Benko, "A Photoelectrochemical Determination of the Position of The Conduction and Valence Band Edges of p-type CuO," Journal of Applied Physics, vol. 53, no. 2, pp. 1173, February 1982.
4. N. Yamazoe, G. Sakai and K. Shimanoe, "Oxide Semiconductor Gas Sensors," Catalysis Surveys from Asia, vol. 7, no. 1, pp. 63-75, April 2003.
5. T. Ishihara, K. Kometani, Y. Mizuhara, Y. Takita, "Improved Sensitivity of CuO–BaTiO₃ Capacitive-type CO₂ Sensor by Additives," Sensors and Actuators B Chemical, vol. 28, no. 1, pp. 49-54, July 1995.
6. M. Chelvayohan and C. H. B. Mee, "Work Function Measurements on (110), (100) and (111) Surfaces of Silver," Journal of Physics C: Solid State Physics, vol. 15, no. 10, pp. 2305, April 1982.
7. S. Joshi, S. Lanka, P. Manjula, M. V. Sunkara, S. J. Ippolito, "Chemoresistive CO₂ Gas Sensor Based on CuO–SnO₂ Heterojunction Nanocomposite Material" IEEE Xplore, 2nd International Symposium on Physics and Technology of Sensors (ISPTS-2), pp. 43-48, March 7-8, 2015, Pune, India.
8. S. Joshi, C. B. Ram Kumar, L. A. Jones, S. J. Ippolito, E. L. H. Mayes, M. V. Sunkara. "Modulating Interleaved ZnO Assembly with CuO Nanoleaves for Multifunctional Performance: Perdurable CO₂ Gas Sensor and Visible Light Catalyst" Inorganic Chemistry Frontiers, vol. 4, no. 11, pp. 1848–1861, September 2017.
9. S. Joshi, S. J. Ippolito, S. R. Periasamy, Y. M. Sabri, M. V. Sunkara. "Efficient Heterostructures of Ag@CuO/BaTiO₃ for Low-Temperature CO₂ Gas Detection: Assessing the Role of Nanointerfaces during Sensing by Operando DRIFTS Technique" ACS Applied Materials & Interfaces, vol. 9, no. 32, pp. 27014– 27026, August 2017.
10. S. Joshi, C. B. Ram Kumar, S. J. Ippolito, Y. M. Sabri, A. E. Kandjani, S. K. Bhargava, and M. V. Sunkara. "Straddled Band Aligned CuO/BaTiO₃ Heterostructures: Role of Energetics at Nanointerface in Improving Photocatalytic and CO₂ Sensing Performance" ACS Applied Nano Materials, vol. 1, no. 7, pp. 3375–3388, June 2018.
11. I. Djerdj, A. Haensch, D. Koziej, S. Pokhrel, N. Barsan, U. Weimar, and M. Niederberger, Neodymium Dioxide Carbonate as a Sensing Layer for Chemoresistive CO₂ sensing. Chemistry of Materials, vol. 21, no. 22, pp. 5375-5381, October 2009.

Mining Engineering



Retrospection of the Longwall Mining for Mass Production of Coal from Indian Underground Mines

K Nageswara Rao¹, G Budi², P K Mandal¹, A J Das¹, J Vinod Kumar¹

CSIR-Central Institute of Mining and Fuel Research, Dhanbad, Jharkhand¹

IIT-Indian School of Mines, Dhanbad, Jharkhand²

✉ nageswar7k@gmail.com

ABSTRACT

The longwall mining method is a well-known mass production mining method used to extract the coal from underground mines. Worldwide, its popularity has been grown steadily but, in India, it has not been established as much as envisaged. The Indian coal mining industry has achieved 728Mt of total coal production during the year 2018-19. The demand-supply gap of coal in India is constantly rising and every year 20%-30% of coal production is lagging behind the domestic needs. The remaining coal has been importing from other countries like Australia, Indonesia and the U.S.A etc. To make India self-reliant in coal requirement, the demand-supply gap of coal has to be reduced. It can be possible by increasing coal production from underground mines by implementing mass mining production technologies like longwall mining. So far in India, 22 underground coal mines of different collieries were introduced longwall mining technology since 1978. Some of the longwall panels among these mines have given good results and some were failed. Currently, three underground mines are practising longwall technology i.e., Adriyala Longwall Project (SCCL), Moonidih Longwall Project (BCCL) and Jhanjra Longwall Project (ECL). The strata behaviour is greatly varying in these Longwall Projects from ECL to SCCL. In this paper, an attempt is made to retrospect the Indian longwall mining for its requirement and applicability for mass production of coal from underground coal mines. Apart from this, a case study of Adriyala longwall project has been taken into consideration to find out the stability of chain pillars at a depth of 360m from the surface with numerical modelling study. Two numerical models were prepared with ANSYS software to study the stability of chain pillars, an important structure for Longwall mining. The results obtained from the numerical modelling indicates that the chain pillars are stable for long-term in both the models. The analysis will be useful for further application of Longwall mining in India.

Keywords : Longwall mining; Coal production; Sustainability; Chain pillar; Numerical modelling.

INTRODUCTION

Coal is the primary energy source for the power and steel sectors, which has been used for centuries in the world. Coal has a share of about 65% in power generation in India [1]. As per the data, India is 2nd largest thermal coal-producing country in the world and having 101Bt of proved coal reserves [2]. The coal production in India for the year 2018-19 is reported as 728Mt whereas the estimated production was as 730Mt [1]. The demand-supply gap of coal in India is constantly rising and every year 20%-30% of coal production is lagging behind the domestic needs. The remaining coal has been importing from other countries like Australia, Indonesia and the U.S.A etc. Figure 1 shows the estimated and actual coal production for the last 10 years in India [1]. Coal can be extracted either by opencast mining or underground mining. Indian coal mining industry has been operating nearly 199 underground coal mines, 212 opencast coal mines and 21 mixed coal mines [3]. Nowadays, due to lack of coal deposits at shallow depth and environmental issues, it is necessary to extract the coal from underground mines and that too at deeper depths. The coal from underground mines can be extracted either by Bord and pillar or Longwall mining methods.



Fig. 1. Estimated and actual annual coal production in India during 2009-18 [1]

Figure 2 shows the percentage of coal production lagging in India during 2009-18. To make India self-reliant in coal production, there is a need to improve underground coal production and that will be possible by successfully implementing mass mining production technologies like longwall mining. Indian coal mining industry had practised the longwall mining method much earlier in its non-mechanized and semi-mechanized forms. In 1978, the first mechanized longwall mining was introduced in Moonidih mine of BCCL with 4x280T powered support system [4].

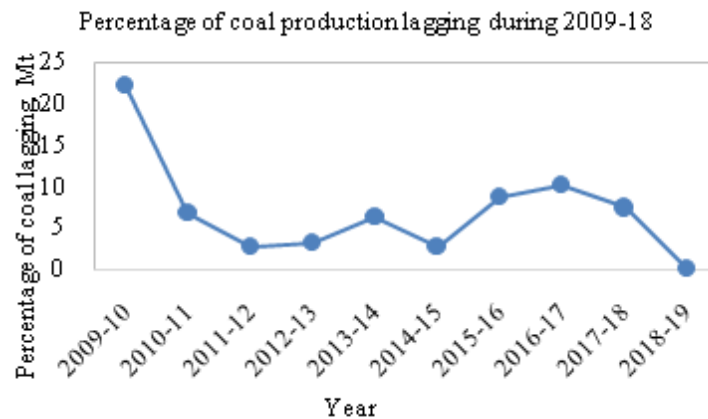


Fig. 2. The percentage of lagging in coal production in India during 2009-2018 [1]

So far, 22 underground coal mines were installed longwall technology. Among them, some were given good results and some were failed catastrophically. Currently, only three underground coal mines are operating longwall technology out of 199 underground coal mines in India. The number of coal mines which were practised longwall technology so far have been given in Table 1 [5], [6], [7] [8]. The primary reasons for the limited success of longwall mining in India is attributed to lack of knowledge about the local geology, strata behaviour and improper selection of powered support system [9].

HISTORY OF LONGWALL MINING IN INDIA

Longwall mining in India has been practising much earlier in non-mechanization and semi-machined forms. Between 1902 and 1956, a number of longwall faces were worked, some of them in developed areas with timber supports [6]. Until 1960 the longwall faces were worked with sand stowing then after caving faces were adopted. The first mechanized powered roof support face was started with a production target of 600 TPD in august 1978 at Moonidih mine in BCCL, a subsidiary of Coal India Limited (CIL) [4]. In the eighties, few more mines of Coal India Limited (CIL) were installed the Power Support Longwall (PSLW) in East Katras (BCCL), Khottadih, Seetalpur (ECL), Pathakhera (WCL) and Churcha (SECL) [6]. In Singareni Collieries Company Limited (SCCL), the first longwall panel was introduced in GDK-7 incline of Ramagundem area. So far, a total of 22 underground coal mines have been deployed longwall technology in CIL and SCCL collaboration with U.K., Russia, France and China. Figure 3 shows the annually achieved coal production in Indian coal mines upto 2011 by longwall technology since 1976 [5]. It is clear that the longwall technology has received mixed results so far but it was enabled from the data that the coal production was maximum from 1995 to 2003 with an average annual production of 4Mt.

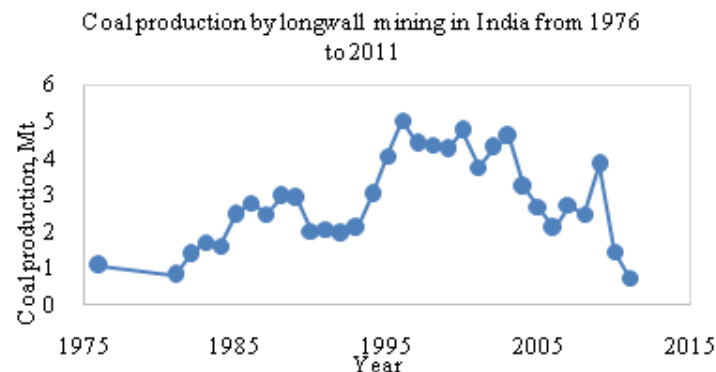


Fig. 3. Coal production by longwall mining in India from 1976 to 2011 [5]

**Table 1.** List of coal mines adopted longwall technology in India from 1978 [4], [6], [7], [8]

Colliery	Mine	Seam	Year	L*(m)	H**(m)
BCCL	Moonidih	XVII top	1978	150	400
ECL	Seetalpur	Hatnal	1982	120	550
	Dhemo Main	Borachok	1983	150	130
	Jhanjra	R-VII	1989	120	50
	Khottadih	Samla	1994	120	180-200
WCL	Pathekhera	Upper workable	1982	107	110
SCCL	GDK-7	Seam 3	1983	90	100 - 350
	VK-7	Queen	1985	124	38-382
	JK-5	Queen	1990	128	176-215
	GDK-11	Seam 1	1991	150	150-400
	GDK-10A	Seam 1	1994	105	240
	GDK-9	Seam 1	1996	108	121-133
	Adriyala	Seam 1	2013	250	360- 543
	PVK-5	Queen	1995	150	54 - 297
SECL	Churcha	Seam V	1990	154	220
	Balrampur	Passang	1998	150	45 - 55
	Rajendra	Burhar seam VI	1998	150	50-70
	New Kumda	Passang	2000	150	45 - 55

*L= Length of face, **H=Depth of workings

However, the success of longwall mining in India is limited. The longwall panels in Khottadih and Churcha failed due to underrated powered support capacity under the dynamic loading. The longwall faces of SCCL in GDK-10A, JK-5 and VK-7 had produced good results. But, the faces in GDK-7, GDK-9, GDK-11A and PVK-5 had suffered due to geological disturbances and unavailability of real-time information and data interpretation tool to take proper action [10], [11]. As the demand for coal in the country is increasing, the country is planning to exploit the coal from deeper deposits using heavy mechanized longwall panels. Some of the upcoming longwall projects in SCCL and CIL are listed in **Table 2** [12].

Table 2. Upcoming longwall projects in India [12]

Industry	Name of the mine and area
SCCL (Singareni Collieries Company Limited)	ShanthiKhani, Mandamarri area KTK-5 Incline, Bhupalpalli area RK-7 Incline, Srirampur area KTK-3, Bhupalpalli area
CIL (Coal India Limited)	Moonidih, WJ area Jhanjra, Jhanjra area Churcha, Baikunthpur area

LONGWALL MINING METHOD

The basic principle in longwall mining is to drive the gate roadways of around 1-4km of length, 2-4m of height and width of 100-250m as shown in **Fig 4**. Road headers or bolter miners are used to develop the gate roads and the roof bolts are used to support the gate roads. In the extraction process, the coal along the panel width is cut by the shearer machine and transported by armoured flexible conveyor. The face length can be supported by the powered support system with sufficient capacities of legs. The longwall panel can be extracted fully and overburden strata allowed to cave in the void called “goaf”. The extent of overlying strata fall into the extracted area varies from the immediate roof towards the surface. Based on the above criterion the overlying strata can be classified as caved, fractured and deformation zones [13]. The Indian coal measure rocks mostly belong to Barakar measures of the Gondwana formation, but still, the characteristics of the rocks vary widely from ECL to SCCL [6].

The depth of workings and powered support capacity have a greater effect on the success of longwall workings. It was found that the natural supports like gate roads, chain pillars and barrier pillars in longwall workings will play a vital role in deciding the stability of underground longwall workings. Proper designing and understanding of the behaviour of these natural supports are significant. It is imperative to say that there is a need in our country to make a proper design guideline for underground pillars beyond the depth of 300m.

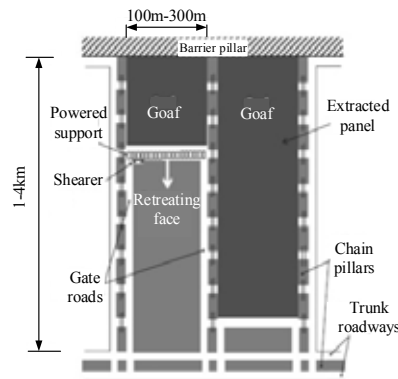


Fig. 4. The layout of generalized longwall mining (After, [14])

Powered Support System

The powered support system has a greater impact on the successful working of longwall mining technology. Therefore, it is vital to select a sufficient and suitable powered support system for longwall workings. The capacity of support system, type of supports and design characteristics are primary parameters to be decided for selection of powered support system [6]. The chronological development of support system in Indian longwall workings have adopted, can be seen as follows i.e., Timber supports, Frame type supports, conventional Chock type supports, Shield supports and Chock shield supports [4], [6].

The principal factors which influence the magnitude of the load on supports include setting load density, the height of the caving block, the distance of fracture zone ahead of the face, the overhang of goaf, the support yield characteristics, and the mechanical strength of the debris above the canopy and below the support base [15]. 2-legged shield supports were seen to induce fracturing only within the immediate 3m of roof strata. The overlying strata tended to bridge intact and the failure was occurring at approximately 25m span. In contrast, under equivalent condition, the 4-legged chock shield initiated systematic cantilever failure to a height of at least 10m over the roof horizon [6]. **Fig. 5** shows the schematic representation of 2-leg and 4-leg powered supports and their interaction with the roof and floor of the coal seam. **Table 3** indicates the different capacities of powered support system installed in underground mines and the depth of such workings in that longwall mines.

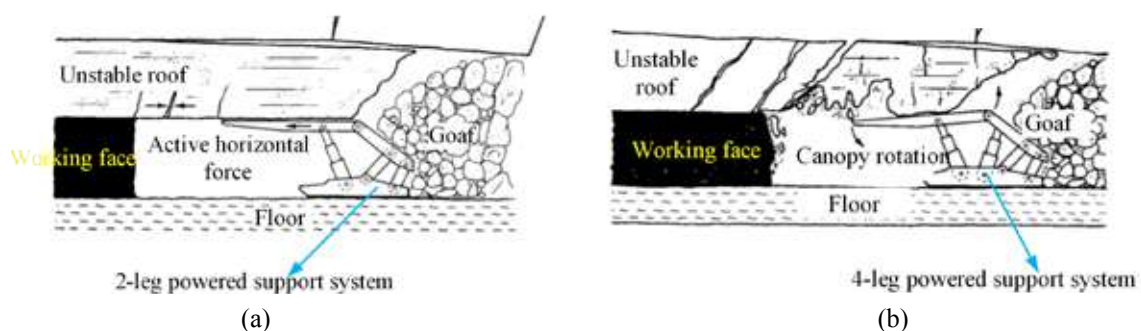


Fig. 5. The schematic representation of 2-leg and 4-leg powered support systems in longwall workings (After, [16]).

Table 3. Different capacities of powered support systems installed in Indian underground coal mines [5] [7] [8]

Mine	Powered support capacity (T)	Depth of workings (m)
Moonidih	4x280	400
Seetalpur	6x240	550
Dhemo Main	4x550	130



Jhanjra	2x314	50
Khottadih	4x476	180-200
Pathekhera	6x240	110
GDK-7	4x325	100 - 350
VK-7	4x360	38-382
JK-5	4x450	176-215
GDK-11	4x450	150-400
GDK-10A	4x750	240
GDK-9	4x750	121-133
Adriyala	2x1152	360- 543
PVK-5	4x760	54 - 297
Churcha	4x680	220
Balrampur	4x502	45 - 55
Rajendra	4x440	50-70
New Kumda	4x440	45 - 55

Estimation of support capacity for longwall face

The determination of the capacity of powered support system is depends on the likely load coming on the supports under a particular geo-mining conditions. The support capacity can be expressed in below [6].

$$\text{The Support capacity (C)} = \frac{RAK_1K_2K_3}{n} \quad (1)$$

Here,

R = desired mean load density in t/m²

A = area supported by a support system

n = efficiency to take care of inclination of legs vis-à-vis vertical resistance

K₁ = factor to take care for leakage in hydraulic system and leg circuits

K₂ = factor to take care of setting load deficiency

K₃ = factor to take care of other imperfections like premature leakage and deviations from nominal span

K₁, K₂, K₃ are the factors to take into account the deficiencies of the support system and operational imperfections.

FINDING STABILITY OF CHAIN PILLARS IN LONGWALL WORKINGS

Case study: Adriyala Longwall Project (ALP)

Adriyala Longwall Project (ALP) comes under the Ramagundam area of SCCL. Longwall mining is practicing in this mine at a varying depth of 360m to 563m from the surface having a thickness of seam is 6.5m. The working height is 3.2m and the width of the panel is about 250m. Total of 146 numbers of powered supports was installed along the face. The gate roads were developed with Road header and Bolter miner. The length of the gate roads was around 2313m and having a roadway dimension of 5m x 3.4m. **Fig. 6** is representing the layout of longwall workings in ALP. The seam is developed along the floor of maximum working height 3.2m. The rest of the coal seam of about 3.3m is composed of shaly coal, clay and some thin streaks that are considered as the immediate roof. The main roof consists of sandstone strata having a variable thickness along the panel length. The geo-mining details of the longwall panel are given in **Table 4**. Two longwall panels (Longwall Panel-I & Longwall Panel-II) were considered in this study, both were separated with chain pillars of width 45m. Between two longwall panels, one panel (longwall panel-II) was fully extracted and filled with goaf and second panel is under the extraction process. The gate roads for both these panels were developed as twin gate roads i.e. the Main Gate1 (MG1) and Tail Gate2 (TG2), because of this condition the TG2 is experiencing the cyclic and dynamic loading and double goaf effect. During the extraction process, the immediate

roof fallen immediately behind the supports and local falls were observed. From the field instrumentation data, it was observed that the main fall would occur at a distance of 83m. The front abutment zone was confined at 25m ahead of the face. The extent of fracture zone at the faces are measured in the main gate and tail gate sides and found to be 1.5-1.8m inside the face. Based on these conditions, a numerical modelling study was conducted with ANSYS software to estimate the stability of chain pillars.

Table 4. Geo-mining details of Longwall panel selected for the study

Name of the seam	1 seam
Depth	min. 360m to max. 543m
Total thickness of seam	6.5m
Face length	250m
Working section	3.2m along the floor
Supports at the face	2 x 1152 T chock shields, 146 no's
Gate roads dimensions	5mx3.4m
Average seam gradient	1 in 6
Width of barrier pillar	45m



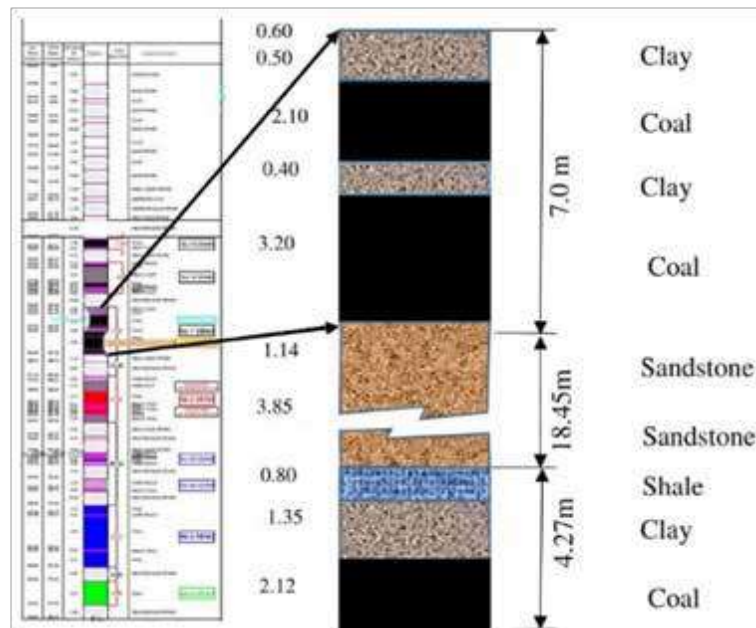
Fig. 6. The layout of longwall workings showing the selected longwall panel for the study

Development of 2-D finite element models

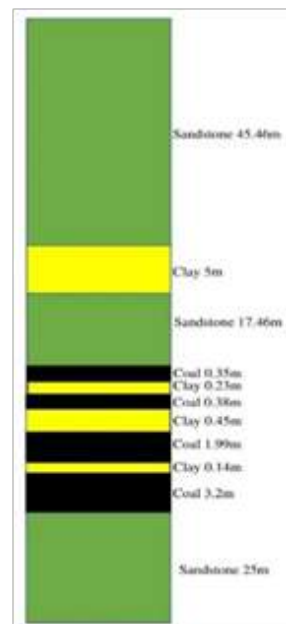
In this study, 2-D finite element models were developed with ANSYS software by considering two longwall panels which were separated by gate roads and chain pillars. The lithology as shown in **Fig. 7** and material properties as shown in **Table 5** were utilized for the development of numerical models. Two numerical models were developed as goaf on one side (only panel-1 extracted) and goaf on both sides (panel-1 and panel-2 are extracted) and both the models are represented in this paper as Model-1 and Model-2 respectively. Model-1 resembles the actual working conditions of the field. The vertical section of the longwall panel-1 and panel-2 along the panel width is taken for this study. The length of the model is 555m having panel width of 250m each, the width of gate roads is 5m and width of the barrier pillar assumed is 45m. The height of the coal seam is 3.2m and the total height of the model is 74.86m consists of 49.66m of overburden thickness and 22m of under-burden thickness. The general elastic constitutive model is applied to the models and accordingly, the material properties were assigned. The vertical load is applied uniformly along the top of the model based on working depth from the surface. In numerical models, the bottom of the model is constrained for vertical displacements, both sides along the models are constrained to horizontal displacements and horizontal pressure of $\sigma_h = 1.5\sigma_v$ is applied on vertical planes. The developed numerical models of the Model-1 and Model-2 can be seen in **Fig. 8**.

Table 5. Physico-mechanical properties used in FEM analysis

Material	Density (Kg/m ³)	Elastic modulus (GPa)	Poisson's Ratio	Compressive strength (MPa)
Coal	1500	1.535	0.35	27.5
Clay	1100	1.278	0.35	9.21
Sandstone	2147	5.132	0.28	30.59

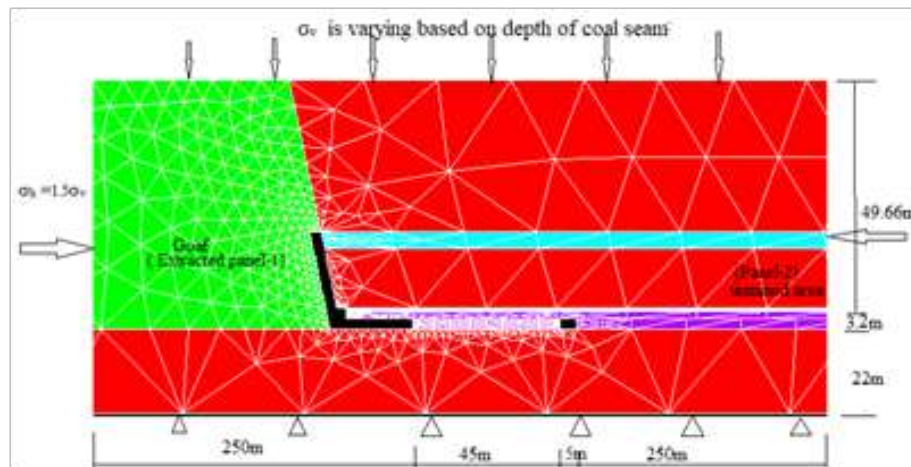


(a)

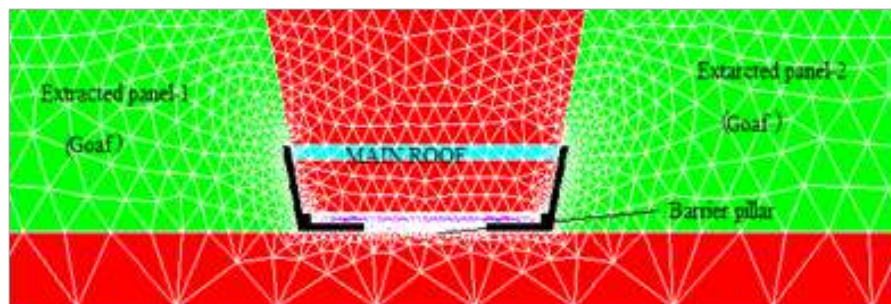


(b)

Fig. 7. (a) Typical lithology of Adriyala longwall project and (b) Lithology of ALP used in FEM models



(a)



(b)

Fig. 8. a) FEM model of goaf on one side: Model-1 (b) FEM model of goaf on both sides: Model-2

Goaf Material Properties

Caved rock mass that forms goaf plays an important role in supporting the overburden strata. The degree of compaction may occur fully or partially depending on the location of area and bulking properties of the rock strata. In this study, the goaf is considered as fully packed and material properties are considered as linear elastic and the values are presented in **Table 6** [13].

Table 6. Material properties of goaf used in FEM analysis

Goaf type	Density (Kg/m ³)	Modulus of Elasticity (MPa)	Poisson's ratio
Well packed	2100	500	0.25

Factor of safety (FoS)

As already stated earlier, the stability of the longwall workings is ensured by providing a supporting system. Natural supports like chain pillars and barrier pillars will play a vital role in supporting the longwall workings. It is important to have sufficient knowledge about the chain pillars behaviour. The stability of chain pillars can be assessed by Factor of Safety criterion (FoS) which can be defined as the ratio of the strength of pillars (S) to the stress-inducing on chain pillars (P) which can be expressed as below.

$$\text{Factor of Safety (FoS)} = \frac{\text{Pillar Strength (S)}}{\text{Pillar Stress (P)}} \quad (2)$$

In this study, CIMFR empirical equation was used to estimate the strength of chain pillars [17]. It is to be noted that the CIMFR pillar strength equation is well applicable to Indian mining conditions, after got a confidence over a couple of decades of its use

in real cases and obtained results. The average vertical stress inducing on chain pillar can be derived from numerical modelling results. CIMFR Pillar strength equation is given below

$$S = 0.27\sigma_c h^{-0.36} + \left(\frac{H}{250} + 1\right) \left(\frac{W_e}{h} - 1\right) \quad (3)$$

Here, S = Strength of chain pillar in MPa; σ_c = Compressive strength of coal in MPa; h = Height of workings in m; H = Cover depth in m; w_e = Equivalent width of pillar in m,

$$W_e = \frac{2W_1W_2}{W_1 + W_2}$$

The strength of the chain pillar has estimated by equation 3 which was found as 48.19MPa. The vertical stress inducing on the chain pillar was estimated from numerical modelling study i.e., 19.05MPa in Model-1 and 28.01 MPa in Model-2. The variation of induced stress in Model-1 and Model-2 can be seen in **Fig. 9**. From the obtained results of strength and stress of chain pillars, the FoS has found as 2.52 and 1.7 in Model-1 and Model-2 respectively. From the FoS results, it can be said that the chain pillars will provide long term stability to underground workings in Model-1 and Model-2 conditions. It is to be noted that the actual support system installed for the longwall face and gate roads has not considered in this study. However, it would be agreeable with the results obtained from the FoS of chain pillars.

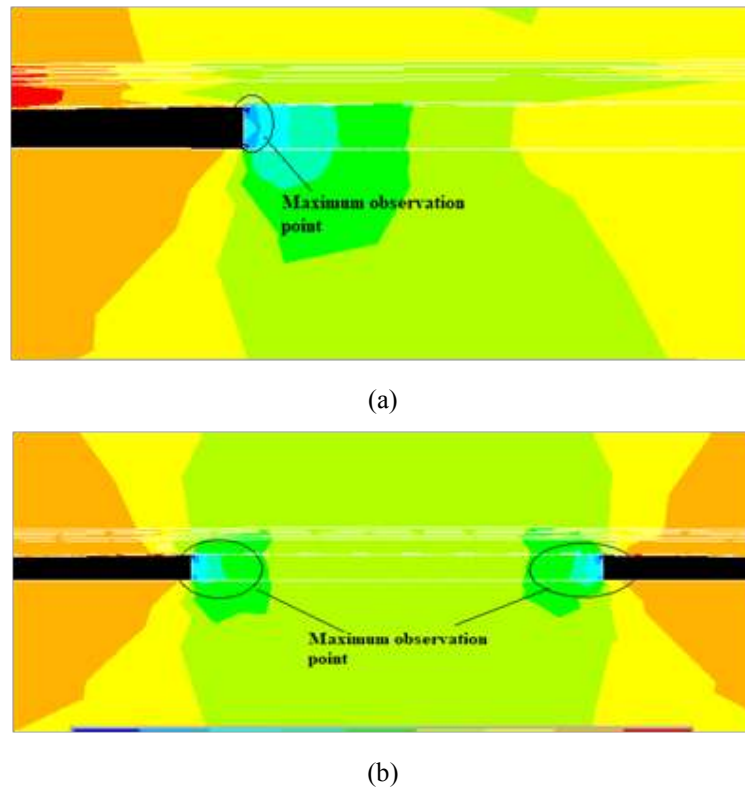


Fig. 9. (a) and (b): Induced stress variation in Model-I and Model-II and maximum observation points

CONCLUSIONS

Self-reliant India in the coal mining industry can be achievable by reducing the demand-supply gap of coal production. Despite 2nd largest thermal coal producer and 5th largest proved coal reserves in the world, India is still not matching the demand and supply of coal. Every year 20%-30% of coal is importing from other countries. As the coal reserves in the shallow depth are depleting and issues related to environmental conditions are increasing, opencast mining is not much liable to adopt for coal extraction. Therefore, it is imperative that coal mining industry has a greater opportunity to implement the mass mining technology like longwall mining to extract the coal. Although, longwall mining in India has a limited success rate in coal



production, it is a need to retrospect this method to extract the coal. The primary reasons for the limited success of longwall mining are attributed to less knowledge about the local geological conditions and strata behaviour and under-rated powered support system. Significant research work has been going on these issues and there is a scope for retrospection to longwall mining in India. A case study from Adriyala Longwall Project has been considered in this study to estimate the stability of the chain pillars, an important structure in Longwall mining, by ANSYS software. The results obtained from modelling showed that the chain pillars in Model-1 and Model-2 conditions were found to be stable for the long term.

ACKNOWLEDGEMENT

The views expressed in this manuscript of the authors and not necessarily of the organization to which they belong. The authors are expressing their gratitude to the Director CSIR-CIMFR for permitting to publish this manuscript. Thanks are due to the officials of the Adriyala Longwall Project, SCCL.

REFERENCES

1. "Annual Report," Ministry of Coal, Government of India, 2019.
2. David Turvey, "Coal in India," Australian Government, Office of the Chief Economist, Department of Industry, Innovation and Science., Australia, 2019.
3. "Coal Directory of India: Coal Statistics," Coal Controller's Organisation, Ministry of Coal, Government of India, Kolkata, 2018-19.
4. RD Singh, Principles and practices of modern coal mining., New Age International, 2005.
5. "Statistics of Mines in India," Directorate General of Mines Safety, Ministry Of Labour And Employment, Government of India, Dhanbad, 2015.
6. S K Sarkar, Mechanised longwall mining: the Indian experiences, Oxford & IBH Publ, 1998.
7. Deb D and Verma A.K, "Ground control problems in Indian longwall mines-A perspective and future research work," Journal of Mines, Metals and Fuels, pp. 178-185, 2004.
8. B Ramesh Kumar, U Siva Sankar, VNS Prasad, "Selection of Powered Roof Supports – 2-Leg Shields vis-à-vis 4-Leg Chock Shields," in International Conference on Underground Space Technology, Bangalore, India, 2011.
9. Sreenivasa Rao Islavath, Debasis Deb, Hemant Kumar, "Numerical analysis of a longwall mining cycle and development of a composite longwall index," International Journal of Rock Mechanics & Mining Sciences, pp. 43-54, 2016.
10. Verma AK, Deb D, "Analysis of chock shield support pressure using finite element method and face stability index," Min Tech (Trans Inst Min Met A), vol. 116 (2), p. 67–78., 2007.
11. Singh GSP and Singh UK., "Prediction of caving behavior of strata and optimum rating of hydraulic powered support for longwall workings,," International Journal of Rock Mechanics and Mining Sciences, vol. 47, p. 1–16., 2010.
12. Prasad SMVN., Rao SV., Kumar D and Kumar SG., "Planning and design parametres in longwall mining-a case study from SCCL mines," in Deep Excavation, Energy Resources and Production., IIT Kharagpur, 2017.
13. Peng SS and Chiang HS, Longwall mining., New York: Wiley, 1984:708.
14. Verma A. K. and Deb D, "Numerical Analysis of the Interaction between Hydraulic Powered Support and Surrounding Rock Strata at Indian Longwall Faces," international Association for Computer Methods and Advances in Geomechanics (IACMAG) , Goa, India, 2008.
15. Gupta RN and Former IW, "Interaction between roof and support on longwall faces with particular reference to support resistance," in 4th International Conference on Ground Control in Mining, West Virginia, 1985.
16. Thomas M. Barczak, "Examination of design and operation practices for longwall workings," Bureau of mines information circular, United states department of the interior, 1992.
17. SHEOREY P.R., "Design of coal pillar arrays and chain pillars," in Comprehensive Rock Engineering., Oxford, Pergamon Press, 1993, p. 631–70.



Innovative Methodologies of Carbon Sequestration for Sustainable Development of Unmineable Coal Seams

Singam Jayanthu*, Singam Jayadarshana**, Chandramohan***

Professor, Mining Engineering Department, National Institute of Technology, Rourkela, Odisha*

Centre of Excellence in Artificial Intelligence (CoE-AI)-Bhubaneswar, Odisha**

Former Joint Director-Department of Mines and Geology-Telangana***

✉ sjayanthu@yahoo.com

ABSTRACT

Many experimental trials of innovative methods of underground mining of coal deposits in various parts of India were conducted since 1980s with the experiences of about two decades and total experiences of about 34 years of the first author as scientist in premier research institutions in India. However, many limitations were observed with typical geo-mining domain in various Indian coalfields making unviable for conventional methods of extraction of the solid coal. In spite of application of various innovative technologies of mining, much of the coal remains unmineable due to complex geological conditions, greater depth covers, economic infeasibility. Also the greenhouse gas emissions, which lead to Global Warming due to burning of coal are well known. A key way to mitigate global warming is likely to be Carbon Capture and Storage (CCS), which involves storage of CO₂ emitted from power plants into geological formations. This paper presents critical review of the Enhanced Coalbed Methane Recovery (CO₂-ECBM) technology along with the status of Indian coal deposits. Emphasis is made on requirement of a highly trans-disciplinary working involving Geologists, economist, environmentalists, atmospheric scientists, mechanical, chemical, civil and mining engineers, and mathematicians including applications of Artificial Intelligence (AI), Machine Learning (ML) etc for translational Industry oriented research and academics for eco-friendly and sustainable development of unmineable coal reserves.

Keywords : Underground mining; Unmineable coal; Carbon capture; Global warming; Coal bed methane.

INTRODUCTION

Fossil fuels - coal, oil and natural gas, are presently and likely to remain the key way to meet Global Energy Requirements. Out of these fuels, Coal provides India with over 50% of its commercial energy supply and over 70% of power supply is reliant on coal (Mandal, 2007). Other economic superpowers, viz. USA and China are also heavily reliant upon Coal to meet their domestic energy needs. In this regard, two of the major constraints that could be cited for extraction and usage of coal are:

1. Despite our best technological innovations, much of the coal remains unmined in India due to techno-economic infeasibility and complex geomining conditions. The coal mining reserves of India are given in **Table 1**.

Table 1. Depth wise Gondwana coal resources of different states of India as on 1st April 2012 (GSI, 2012)

State	Resource estimate under depth			Total Reserve
	0-300m	300-600m	600-1200m	
Andhra Pradesh	9654.17	8754.74	3745.95	22154.86
Bihar	160.00	---	---	160.00
Chhattisgarh	37755.15	11609.08	1481.92	50846.15
Jharkhand	41118.05	16321.79	8703.94	80356.20**
**Jharia	-----14212.42-----			
Maharashtra	7522.32	3165.28	194.49	10882.09
Madhya Pradesh	15367.65	8656.20	352.41	24376.26
N E States	1394.66	202.00	---	1596.66

Orissa	46653.67	23086.73	1707.01	71447.41
Uttar Pradesh	1061.80	---	---	1061.80
W Bengal	13155.05	12127.36	5333.31	30615.72
Grand Total	173842.52	83923.18	21519.03	293497.15
**Jharia	-----14212.42-----			
% share	59.23	28.60	7.33	100
**Jharia	-----4.84 %-----			

2. Coal and other fossil fuels are primarily hydrocarbons and release CO₂ and other Greenhouse Gases (GHGs) on combustion. These gases allow the incoming solar radiation to penetrate through the atmosphere but do not permit the trapped heat from inside to escape through the atmosphere. Excessive concentration of such gases in the atmosphere leads to the well-known Global Warming. **Fig. 1** show how CO₂ has recently gone past the 400 ppm mark.

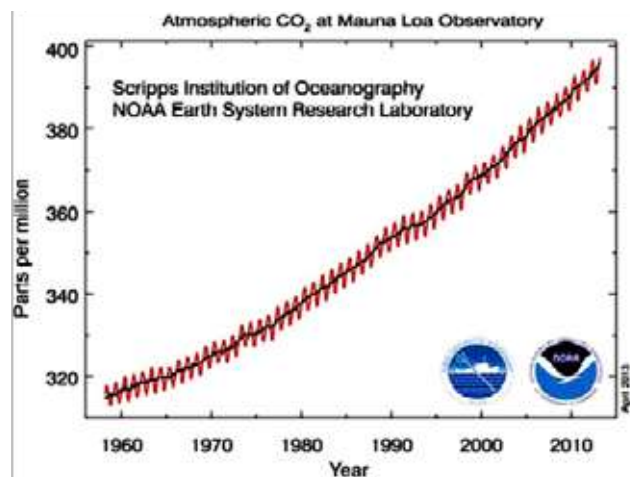


Fig. 1. Atmospheric CO₂ concentration (zigzag curve) in ppm (parts per million), measured at Mauna Loa, Hawaii represents the global mean concentration of CO₂ (Anon, 2013)

“Enhanced Coalbed Methane Recovery” (CO₂-ECBM) is a method which could be used to recover energy from very deep coal seams and the polluting impact of the GHGs could also be alleviated. The ECBM technology is a part of the larger Carbon Capture and Storage Technology (CCS), which involves storage of CO₂ from various sources into geological formations such as Basalt Formations, Deep Saline Aquifers, Depleted Oil and Gas Reserves, and Unmineable coal seams.

REASONS FOR IMPLEMENTATION OF CARBON CAPTURE AND STORAGE

Increasing GHG concentration may have an adverse impact on earthly life due to Global Warming. One way to stop it is to stop burning of fossil fuels. However, no country in history has improved its level of human development index without corresponding increase in per capita use of energy (Ghosh, 2009). It will be unrealistic for a developing country like India to stop burning coal. CCS is thus a very exciting prospect for India to continue on the path of economic growth without compromising on ecological issues.

TECHNOLOGICAL PROCESSES BEHIND CCS

The entire CCS technology is divided into three processes: Capture, Transport and Storage (IPCC, 2005; Johnsson, 2011). Enhanced Coalbed Methane Recovery is quite similar to conventional Coalbed Methane Recovery technique except that involves injection of CO₂ below ground. Since coal has more affinity towards CO₂ than towards methane, CO₂ molecules tend to get adsorbed while methane is desorbed. This methane is thereafter recovered using the normal dewatering process.

It is generally expected while making estimates or calculations that 2 molecules of CO₂ displace one molecule of methane (**Fig 2**) (Chikatmarla and Bustin, 2003). However, this ratio of CO₂ effectiveness is expected to vary according to the thermal maturity of the coal (EPRI, 1999; Stevens et al, 1998; Wong et al, 2000; Hamelinck, 2001).

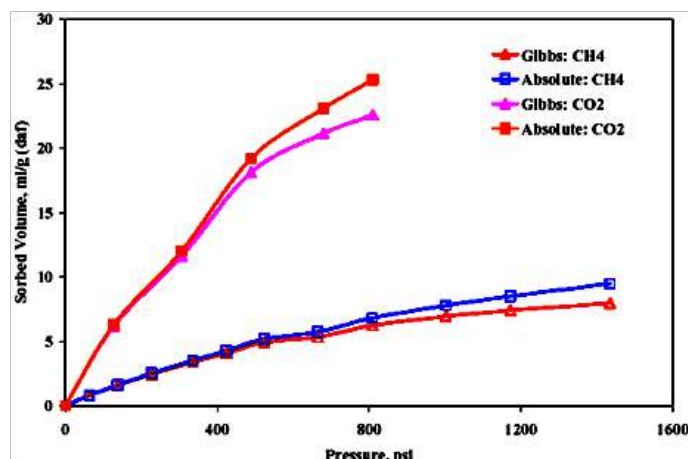


Fig. 2. Preferential adsorption of CO₂ over methane (Singh and Sinha, 2008)

CO₂ SEQUESTRATION POTENTIAL IN UNMINEABLE COAL SEAMS

International Scenario

The methane sorption capacity of coals worldwide is a thoroughly researched subject. Using 2:1 ratio, several scientists have determined various sequestration potentials. One of the first worldwide estimates of the CO₂ sequestration potential was given by Herzog (2001), in which the potential for unmineable coal seams was suggested to be of the order 10s to 100s GtC. According to the IPCC (2005), this value was 3 to 200 Giga Tonnes of CO₂ (not GtC).

As far as the two most cited India-centric studies are concerned, they give widely varying estimates of CO₂ storage potential:

1. Singh et al (2006) suggested that the storage potential is 5 Gt of CO₂.
2. Holloway et al (2008) calculated this potential to be only 0.345 Gt of CO₂.

This is so because the latter believed that coal in much of the seams could be mined out and did not take such coal seams into account. Widely contradictory views also exist in this area. Narain (2007) suggested that CO₂ storage sites are not constrained by geography or geology, while Doig (2009) suggested that there are by no means enough CO₂ storage sites in Indian Geological formations. A much greater degree of research is therefore needed in this area.

Indian Scenario

Singh and Mohanty (2013) divided the Indian coal beds into three categories and various details of the different categories are as follows (Tables 1 to 3).

Table 1. CO₂ Storage Potential in Unmineable Coal Beds in Well-delineated Coalfields (Singh and Mohanty, 2013)

Coalfield	Estimated adsorption capacity of CO ₂ (m ³ /t)	Coal Reserve (Mt)	CO ₂ storage capacity (Bm ³)	CO ₂ storage capacity (Mt)	CO ₂ storage capacity (90%) (Mt)
Singrauli	Average 20.0	37.0	0.74	1.46	1.32
MandRaigarh	Range 16.0-23.0 average 19.0	79.0	1.50	2.97	2.67
Talcher					
	Range 17.2-24.8				
Average 20.4	1017.0	20.80	41.18	37.06	
Godavari	Range 16.8-22.2				
Average 19.2	1976.0	38.02	75.28	67.75	


Table 2. CO₂ Storage Potential in Grey area coalfields (Singh and Mohanty, 2013)

Coalfield	Estimated CO ₂ adsorption capacity (m ³ /t)	Cumulative Coal seam thickness (m)	Block Area (km ²)	Coal Reserve (Bt)	CO ₂ storage capacity (Bm ³)	CO ₂ storage capacity (Mt)	CO ₂ storage capacity (90%) (Mt)
South aranpura	Range 19.5-28.0 mean 24.5	73.0	76.0	0.75	18.35	36.33	21.80
East Bokaro	Range 22.3-33.5 mean 28.1	100.0	113.0	1.53	42.90	84.94	76.45
Jharia	Range 22.0-56.0 mean 34.5	40.0	193.0	1.04	35.96	71.20	64.08
Raniganj	Range 20.8-29.0 mean 24.0	30.0	240.0	0.97	23.33	46.19	41.57
Sohagpur	Range 18.9-26.4 mean 22.6	15.0	450.0	0.91	20.59	40.76	36.69
Talcher	Range 17.2-24.8 mean 20.4	120.0	149.0	2.41	49.24	97.49	87.75

Table 3. CO₂ Storage Potential in Concealed Coal fields (Singh and Mohanty, 2013)

Coalfield	Estimated adsorption capacity (m ³ /t)	Cumulative Thickness of the coal seams (m)	Area of the block (km ²)	Coal Reserve (Bt)	CO ₂ storage capacity (Bm ³)	CO ₂ storage capacity (Mt)	CO ₂ storage capacity (90%) (Mt)
Cambay basin	Range 13.8-19.6 average 16.7	102.0	6900	63.0	1057.81	2094.45	1885.02
Barmer Sanchor Basin	Range 128-18.4 average 15.6	100.0	6700	60.0	936.00	1853.28	1667.95
W.B. Gangetic plain	Range 16.4-23.2 average 18.3	---	---	7.2	131.76	260.88	234.80
Birbhum coalfield	Range 17.2-24.8 average 20.2	100.0	312.0	4.2	85.08	168.46	151.61
Domra Panagarh	Range 18.6-25.8 average 21.8	48.0	116.0	0.751	16.39	32.45	29.20
Wardha Valley extension	Range 15.7-22.8 average 17.8	13.0	212.0	0.37	6.62	13.11	11.80
Kamptee Extension	Range 7.2-9.2 average 8.1	14.0	300	0.57	9.81	19.42	17.48

ECONOMICS OF CCS AND ECBM

Carbon Capture and Storage technology is governed by two major factors or the two eco's- ecology and economy. While it is

definitely one of the important ways to potentially reduce CO₂ emissions, it has its own share of economic penalties, similar to other clean technologies (Singh, in press).

The IPCC (2005) suggests an additional electricity cost of US\$ 0.01 to 0.05 per kilowatt-hour of electricity generated through CCS-based power plants as compared to existing power plants and US\$ 20-270 per tonne of CO₂ avoided. Another study indicates that sequestering 90% of the CO₂ from power plants would add 2¢/kWh to the busbar costs (David, 2000). All these tend to create a negative impact on the minds of economists and they prefer paying the CO₂ tax than investing in CCS. However, with Enhanced Methane Recovery, the cost of the additional methane extracted is likely to supplement these costs. According to Heddle et al (2003) ECBM technology will actually lead to a profit of US\$ 5.59/tonne of CO₂ avoided. This datum may provide a much needed boost for ECBM technology. A study on similar lines as Heddle et al (2003) can be used to judge cost effectiveness of ECBM in India as well (Fig. 3).

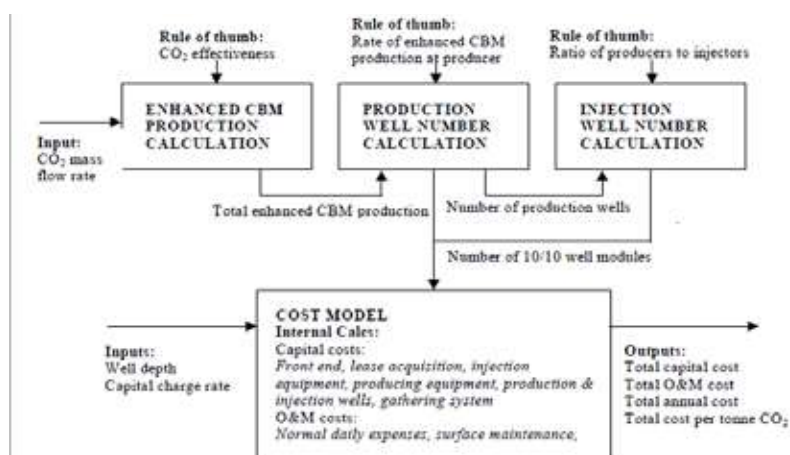


Fig. 3. ECBMR cost model overview diagram (Heddle et al, 2003)

POLICY AND REGULATORY ISSUES

Since CCS is a relatively new technology, it might require additional policy initiatives. It would not be too much to think of a new legislation for CCS activity in India. There are a variety of issues that relate to CCS demanding policy action. These pertain to:

1. Legal issues such as long-term monitoring of Stored CO₂, ownership issues, site-selection, remedial responsibility in case of accidents.
2. Social issues which include improving perception about CCS towards common people.
3. Consideration of Global Treaties such as The London Convention 1972, The London Protocol 1996 (Asthana (2008)).
4. Carbon-trading and pricing issues.

Internationally, several CCS-centred societies have developed. These include Carbon Sequestration Leadership Forum (CSLF), United Kingdom Carbon Capture and Storage Consortium (UKCCSRC), the International Energy Association Greenhouse Gas Programme (IEAGHG), the Cooperative Research Centre for Greenhouse Gas Technologies (CO2CRC) etc. In India, the Department of Science & Technology has set up the National Program on Carbon Sequestration (NCPS). Ministries which will have a major role in regulation of CCS might be those of Petroleum & Natural Gas, Coal, Power, Environment & Forests, Mines, and Science & Technology etc. Other premier bodies such as Central Electricity Regulatory Authority, Planning Commission, and Directorate General of Hydrocarbons etc. may also have a major role to play with regards to the policy formulations in this area.

CHALLENGES TO ECBM IMPLEMENTATION IN INDIA

The challenges to CCS in India which are applicable to ECBM technology are as follows:

1. CO₂ storage must be done in such a way that it ensures no leakage. Any sort of leak would not only damage the environment but also mean wastage of the money invested in the process. Carbon Dioxide leak may also lead to death of people due to



asphyxia. There exist several possible ways of leakage, e.g. during injection, transportation. Therefore, during the complete CCS course, suitable quality of the equipment of the wells, pipelines etc. must be upheld.

2. A major challenge with CCS is expected to be changing the perception of the people to accept it as a good technology. This would involve education of the people about it. Many countries such as the Netherlands and the USA have already initiated projects to make the people more aware of the CCS technology. The research community needs to reach out to the general public on the use of the technology. It must be understood that the general public must be willing to spend more for climate change abatement options and thus CCS must be made acceptable to them (Singh, in press).
3. Zoback et al (2012a) asserts that CCS technology can possibly create seismic hazards and have a tendency to create earthquakes. However, it is also worth mentioning that this has gainsaid by the response by Juanes et al (2012), which again has been refuted by the authors of the original paper (Zoback et al, 2012b).

ADVANTAGES OF ECBM

ECBM in India might be a highly beneficial technology for the following reasons:

- It will reduce hazard of Methane Explosion from Coal Mines
- It will enhance energy security for India
- It will ensure suitable use of unmineable coal
- It will provide abatement to Greenhouse Gas Effect

CONCLUSIONS

ECBM technology appears to have an exciting prospect to recover energy from unmined underground coal seams, and hence impetus need to be given for related research activities in India. CCS, in general, requires a highly trans-disciplinary working involving Geologists, economist, environmentalists, atmospheric scientists, mechanical, chemical, civil and mining engineers, and mathematicians including applications of Artificial Intelligence (AI), Machine Learning (ML) etc. Further accelerated attempts may be required to do an integrated assessment of ECBM/CCS technology in India. This should include academic institutions like NITs, IITs and other universities, CSIR Laboratories such as CIMFR, NGRI and IIP, Industries such as ONGC, BHEL, NTPC, SCCL, Coal India Limited etc.

ACKNOWLEDGEMENTS

Authors are thankful to Dr T N Singh, Former director of CMRI (Presently CIMFR) and President of Centre for Eco-friendly Mining alternatives, Dr. Ajay K. Singh, CSIR-CIMFR, Dhanbad for their consistent guidance in innovative methods of mining including coal bed methane.

REFERENCES

1. Anon, (2013), <http://www.esrl.noaa.gov/gmd/ccgg/trends>, accessed on 16.08.2013.
2. Asthana, S. (2008), Global Challenges and Cross Cutting Issues in CO₂ Capture and Storage, International Workshop on Carbon Capture & Storage in the Power Sector: R&D Priorities for India.
3. Chikatarla L, Bustin MR (2003) Sequestration potential of acid gases in Western Canadian Coals. Proceedings of the 2003 International Coalbed Methane Symposium, University of Alabama, Tuscaloosa, Alabama.
4. David, J. (2000), Economic Evaluation of Leading Technology Options for Sequestration of Carbon Dioxide, M.S. Thesis, Massachusetts Institute of Technology, Cambridge, MA.
5. Doig, A. (2009): Capturing India's Carbon: The UK's Role in Delivering Low-carbon Technology to India. A Christian Aid report based on the findings of research by the University of Edinburgh and the University of Surrey. Poverty. Christian Aid.
6. EPRI (1999), Enhanced Oil Recovery Scoping Study, Palo Alto, CA. Tech. Rep. 113836.



7. Ghosh, P. (2009), Climate Change: Is India a Solution to the Problem or a Problem to the Solution, Climate Change: Perspectives From India, 17-36.
8. GSI, (2012), Inventory of Coal and Lignite resources of India as on 01.04.2012., http://www.portal.gsi.gov.in/gsiDoc/pub/coal_resource.zip.
9. Hamelinck, C.N., A.P.C. Faaij, G.J. Ruijg, D. Jansen, H. Pagnier, F. van Bergen, K. Wolf, O. Barzandji, H. Bruining and H. Schreurs, "Potential for CO₂ sequestration and enhanced coalbed methane production in the Netherlands," [Online document], Available: <http://www.chem.uu.nl/nws/www/publica/e2001-07.pdf>
10. Heddle G., Herzog H., Klett M. (2003), The Economics of CO₂ Storage, Publication No. LFEE 2003-003 RP, MIT, USA
11. Herzog H.J. (2001), What Future for Carbon Capture and Sequestration?, Environmental Science and Technology, 35(7), 148-153
12. Holloway, S.; Garg, A.; Kapshe, M.; Deshpande, A.; Pracha, A. S.; Khan, S. R. et al. (2009): An Assessment of the CO₂ Storage Potential of the Indian Subcontinent. Energy Procedia 1(1), 2607–2613.
13. IPCC. (2005). IPCC Special Report on Carbon Dioxide Capture and Storage. Cambridge, UK: Cambridge University Press.
14. IPCC. (2005). IPCC Special Report on Carbon Dioxide Capture and Storage. Cambridge, UK: Cambridge University Press.
15. Johnsson, F. (2011). Perspectives on CO₂ Capture and Storage. Greenhouse Gas Sci Technol , 1, 119-133.
16. Juanes, R., Hager, B. H., & Herzog, H. J. (2012). No geologic evidence that seismicity causes fault leakage that would render large-scale carbon capture and storage unsuccessful. Proceedings of the National Academy of Sciences, 109(52), E3623-E3623.
17. Mandal, P. R. (2007) "Environmental Concerns of Coal Mining-Broad View in Indian Context." 7th SK Bose Memorial Lecture. ISM, Dhanbad.
18. Narain, M. (2007): Pathways to Adoption of Carbon Capture and Sequestration in India: Technologies and Policies. PhD thesis. Cambridge: MIT.
19. Singh, A. K., Mendhe, V. A., & Garg, A. (2006). CO₂ Sequestration Potential of Geological Formations of India. Proceedings of the 8th International Conference on Greenhouse Gas Technologies. Trondheim, Norway.
20. Singh, A.K. and Mohanty, D. (2013), CO₂ Storage Potential of Indian Coalfields, Proceedings of the National Workshop on Awareness and Capacity Building on Carbon Capture and Storage: Earth Processes, New Delhi, India
21. Singh, A.K. and Sinha, A. (2008), CO₂ Storage Potential in Unmineable Coal Seams in India, International Workshop on Carbon Capture & Storage in the Power Sector: R&D Priorities for India.
22. Singh, U. (in press), Carbon Capture and Storage: An Effective Way to Mitigate Global Warming, Current Science, accepted article.
23. Stevens, S. and Gale, J. (2000), "Geologic CO₂ sequestration may benefit upstream industry," Oil and Gas Journal, May 15, 2000.
24. Wong, S., W.D. Gunter and M.J. Mavor, "Economics of CO₂ sequestration in coalbed methane reservoirs," presented at the 2000 SPE/CERI Gas Technology Symposium, Calgary, Alberta, Canada, Apr. 3-5, 2000.
25. Zoback, M. D., & Gorelick, S. M. (2012a). Earthquake triggering and large-scale geologic storage of carbon dioxide. Proceedings of the National Academy of Sciences, 109(26), 10164-10168.
26. Zoback, M. D., & Gorelick, S. M. (2012b). Reply to Juanes et al.: Evidence that earthquake triggering could render long-term carbon storage unsuccessful in many regions. Proceedings of the National Academy of Sciences of the USA, 109(52), E3624.



Application of Recent Guidelines of 2020 For TARP Vis-À-Vis Design of Stable Slopes in Opencast Coal Mines-A Case Study

SingamJayanthu*, Pritiranjan Singh**, K.Sridhar Reddy***, Rishabh Lala****

* Professor, ** and ***- PhD scholars, ****-MTech Scholar

Mining Engineering Department, National Institute of Technology, Rourkela, Orissa

✉ sjayanthu@yahoo.com

ABSTRACT

This paper presents the application of recent guidelines of Directorate general of Mine safety in January 2020 for a typical coal Opencast mine. TARP suggested for the opencast coal mine is demonstrated with reference to the typical geo-mining conditions and recent data during this typical COVID19 period from opencast coal mine on monitoring the movements and numerical model studies for design of stable dump slopes and high wall slopes along with sensitivity analysis on effect of ground water. Development of proper TARP suitable for the geo-mining conditions of any opencast mine with observational approaches and meticulous monitoring and online interpretation and communication to the grass root level. Indian mining industry has recently witnessed the biggest slope stability disaster involving 23 persons under slope failure in the year 2017. Adopting a suitable TRAP will lead to self-reliant and sustainable practices with improved safety and stability of slopes.

INTRODUCTION

All geotechnical investigations aimed at collecting input design parameters, however complete, involve an inherent risk of inaccuracy. Hence, any attempt of slope stability analyses and evaluation need to be supported by a sound slope monitoring program in order to ensure the safe and smooth mining operations.

The slope monitoring method allows failures to be predicted and safe working conditions. Slope monitoring can be used to confirm failure mechanisms. The review of monitoring results, visual inspection and regular briefing of field people help to detect the onset of failure. The slope monitoring is also advisable for three consecutive wet seasons to detect any failure well in advance for the dumps, which are more than 60 m high. Initially, the monitoring can be done twice (before and after the monsoon) in a year till any movement is detected. Then the frequency can be increased to monthly basis. The interval between the monitoring stations should be decreased (5m to 10 m) in the movement zone. The monitoring should be done weekly and then daily, in this situation, to predict the date of failure in advance for the safety of men and equipment.

The main objective of slope monitoring study is to detect any instability well in advance so that any damage to men and machineries can be avoided. If the failure is unavoidable then it can be brought down in a predictable manner. The early identification of movement zones allows steps to be taken to minimize the impact of mining on stability by the implementation of correct remedial measures and at the same time provides for optimum coal extraction. The system contrasts strongly with more common 'passive' systems that frequently only record the occurrence of an event for subsequent post-mortem examination. The active monitoring system permits early and confident decision making by management for safety purposes.

The first sign of instability is a tension crack. So, it is important to carry out regular inspection to detect the development of tension cracks on the crest of the slope as well as on benches and to carry out prompt remedial measure. They may develop as a function of high stresses in the slopes. The opening of cracks will tell whether any deep - seated failure can occur or not. Tension cracks should be filled with sandstone and sealed with clay to prevent the entry of water, which may cause failure.

The rate and scale of movement in the form of velocity or what can also be termed as average velocity is another key parameter for the identification of pit slope instability. The average velocity is a derivative of the accumulated displacement based on a reference time and an assigned time window.

Prior to failure of slopes progressive, regressive and steady movement are observed. Zavodni and Broadbent (1980) have studied these movement based on empirical formula with data obtained from multiple opencast mines. Progressive stage refers to the accelerated movement till failure (**Fig 1a**), whereas in regressive stage means decelerating movement towards stabilization (**Fig 1b**). Displacement with no acceleration or deceleration is referred as steady displacement (**Fig 1c**).

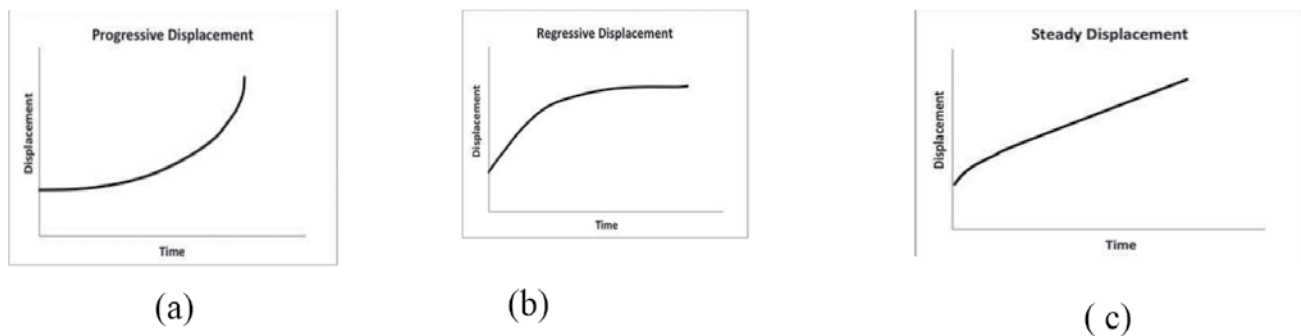


Fig. 1. a) Progressive Displacement, b-Regressive Displacement, C- Steady Displacement (Zavodni, Z.M., and Broadbent, C.D. 1980)

GEOMINING CONDITIONS-CASE STUDY

The study site(Mine A) is an opencast coal mine project situated in IB valley coalfields in Odisha. The method of mining adopted is shovel dumper combination. Drilling and blasting is done to extract the overburden material. Surface miner is engaged for extraction of coal.

Top ten nos. of seams are considered for quarrying. Opencast mining method has been adopted due to in-cropping of the coal seams at a shallow depth, OB: Coal ratio is favorable (2.59: 1) for opencast mining, and the mining by opencast method will be economical against underground method. For the above geo-mining conditions, CSM was recommended due to its precision cuttings, thereby improving the quality of mined coal especially in seams having dirt bands. There will be more than 25 benches in the mine having 255 m depth (max) in which these machines cannot be deployed exclusively due to limitation of mobility / flexibility. Hence only two seams in Rampur horizons were chosen for deployment. These machines also require wider benches which will require comparatively higher volumes of OB to be removed in the initial stages leading to higher cost of production and imbalance in equipment utilization due to subsequently decreasing OB: coal ratio. Therefore only top benches requiring lesser volume of OB handling was chosen as the place of deployment of CSM. In view of 15 seams and equal nos. of inter burden layers to be tackled, an equipment system which is capable of dealing many layers at a time (flexibility) of operations with the help of smaller units was also recommended as shovel dumper combination.

OB Dumps

The major constraint for the current FY 2020-21 is OB dump as the temporary option of the internal dumping in the previous FY 2019-2020 shall remain the major dumping site. The actual OB dump is occupied by a nearby Village which was expected to shift. But as there is much delay in acquiring the land it shall majorly affect the mine scheduling.

Hence, the OB quantity which is around 84.6 Lakh cum is proposed to be dumped internally as well as in the external OB dump area. The Internally dumped quantity shall be re-handled to the de-coaled area later.

Up to 20 June 2020, the mine excavation has gone up to about 28 m depth with four OB benches including three benches of 6 m height, and about 2 m high Top soil bench. Coal bench of about 8 m thickness is being exploited by Surface miner while the OB is removed by Shovel dumper combination. The present status of OB dump is shown in **Fig. 2**.



Fig. 2. i) Mine Plan showing three number of existing dump at mine A., (ii), (iii) ,(iv) Recent photographs of existing dumps A,B and C

Working Benches

Major coal production is done by surface miner or drilling blasting as per demand of situation. Shovel –Dumper combination is adopted for overburden removal. The prepared coal is loaded on to the trucks through front end loaders or with the help of excavators. As per the approved mining plan separate bench is suggested for coal and OB. For thicker coal seam of above 8 m it is feasible to employ surface miner. In case of thinner seams, extraction of which is not economically viable are to be segregated with OB.

NUMERICAL MODELLING

It is prudent to know the lithological units in which the slope is to be cut. Engineering properties of these litho units will influence the analysis for slope stability. The rock mass strength of lithology was appropriately reduced from laboratory test results of various samples and previous experiences of conducting simulation studies, along with data of geo-mechanical of Mine A. Properties of Overburden (OB) and rehandled Overburden (ROB) were also considered in the model. Cohesion, Friction angle, and density of OB material are 36 kPa, 310, and 1.80 gm/cc respectively. Cohesion, Friction angle, and density of coal are 300 kPa, 440, and 1.549 gm/cc, respectively. Cohesion, Friction angle, and density of sandstone are 350 kPa, 420, and 2.25 gm/cc, respectively. FLAC/SLOPE software is used for stability analysis for dump and quarry slopes. FLAC SLOPE determines the factor of safety of the slope by Shear Strength Reduction Technique. The “strength reduction technique” is typically applied in factor-of-safety calculations by progressively reducing the shear strength of the material to bring the slope to a state of limiting equilibrium. FIAC/SLOPE performs the bracketing function between the stable and unstable solutions for a given set of material properties. For a user defined strength properties FLAC/SLOPE determines the stable and unstable solutions. Then it sequentially decreases the limit between the two performing iterations till a certain level of tolerance.

Dump Slopes

The stability analysis was done considering typical vertical cross sections of the proposed pit and dump. The proposed external dump consists of two decks of 30 m each with total height of 60 m. The condition of two benches with bench angle of 37° and 30 m height of individual decks was simulated. The factor of safety estimated for the above sections is 1.67 indicating stability of dumps.

Internal dump with total height of the internal dump as 290 m was simulated with 9 benches of 30 m height and one upper bench of 20 m height comprising of 50 m high crown dump. The factor of safety estimated for the above sections indicated stability of dumps. Resultant Factor of safety of 1.34 indicates stability of internal dump. FLAC/Slope models simulated for the external and internal dumps are illustrated in **Fig. 3**.

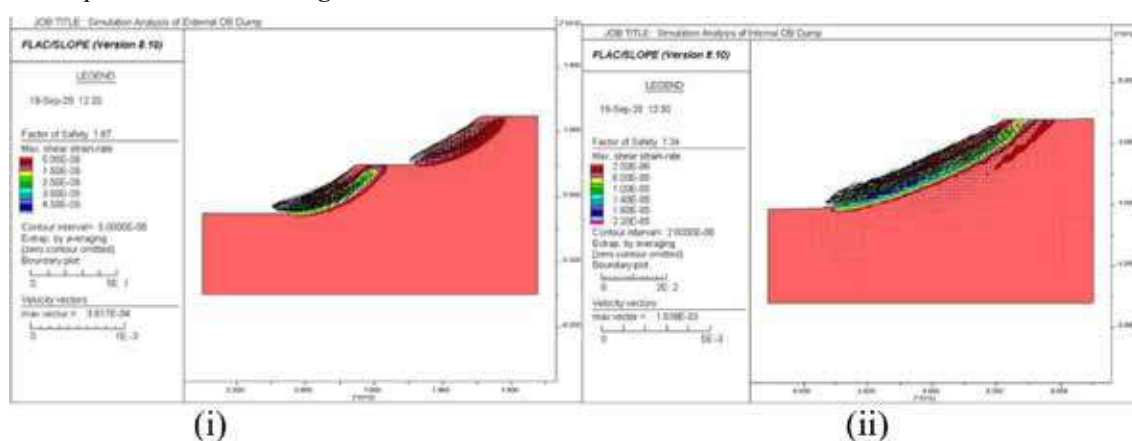


Fig. 3. i) Simulation of External Dump, ii) Simulation of Internal Dump

Bench Slopes

As per the approved mining plan Mine A project quarry cross sections in 5th year, 10th year, 20th year and final stage were analysed in FLAC/SLOPE software. During 20th year of mining operation mine will reach upto 160m from OGL. At this stage the working pit will be encountering fault plane. The effect of fault plane was also considered for deriving factor of safety. At final Stage after about 20 Years with depth of slope about 235 m, FOS with Dry and Un-drained condition of slope are 2.19, and

1.3, respectively. The stability of slopes found through numerical models are in consideration with the recent DGMS guidelines of 2020, indicating stability of permanent and temporary slopes with FOS more than 1.5, and 1.3, respectively.

Sensitivity Analysis

The sensitivity analysis was done with an aim to know the influence of water on the factor of safety. This study is highly beneficial to choose the best method of remedial measure for any critical slope. The influence of groundwater on factor of safety is remarkable. The stability analyses of highwall slope have been conducted in undrained geo-mining condition also. It is evident that the highwall slopes which may stable in drained condition with cut-off safety factor of 1.3. The factor of safety is reduced to less than 1.3 when these slopes are subjected to undrained condition. As mentioned the varying factor of safety can be seen in drained and undrained condition. However, it may be recalled that the most likely condition of the slope was already adjudged to be drained condition. The slopes are likely to be stable with available shear strength of highwall slope material in this condition. In order to avoid undrained condition, attention must be paid to avoid entry of rain/ surface water in the slope by providing suitable drainage in and around the quarry, failing which the slope can become unstable. It should be taken up well before the onset of monsoon.

Numerical analysis was performed with varying water level of 20m, 15m, 10m and 5m for a 235 deep pit. Factor of Safety found for various Water Level (from OGL) of 20m, 15m, 10m, and 5m are 1.42, 1.34, 1.29, and 1.23, respectively. This analysis shows the effect of change in factor of safety due to change in ground water level. Evidently lowest factor of safety of 1.23 was obtained with 5m water level from original ground level. Hence care must be taken to arrest accumulation of water inside high wall. Depressurization and dewatering methods may be adopted to achieve the same.

It is evident that with increase in water level there is decrease in factor of safety. **Fig. 4** shows FLAC/SLOPE models with highest and lowest assumed water level.

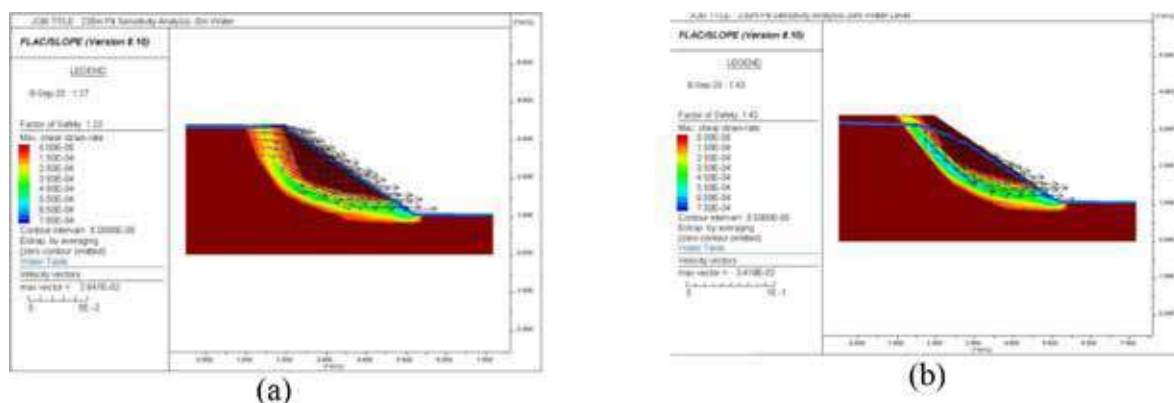


Fig. 4. Simulation of 235m deep Pit with a) 5m Water Level and b) 20 m Water level from OGL (Original ground level).

FIELD MONITORING OF SLOPE MOVEMENTS

The main objective of slope monitoring study is to detect any instability well in advance so that any damage to men and machineries can be avoided. If the failure is unavoidable then it can be brought down in a predictable manner. The early identification of movement zones allows steps to be taken to minimize the impact of mining on stability by the implementation of correct remedial measures and at the same time provides for optimum coal extraction. The system contrasts strongly with more common 'passive' systems that frequently only record the occurrence of an event for subsequent post-mortem examination. The active monitoring system permits early and confident decision making by management for safety purposes.

The first sign of instability is a tension crack. So, it is important to carry out regular inspection to detect the development of tension cracks on the crest of the slope as well as on benches and to carry out prompt remedial measure. They may develop as a function of high stresses in the slopes. The opening of cracks will tell whether any deep - seated failure can occur or not. Tension cracks should be filled with sandstone and sealed with clay to prevent the entry of water, which may cause failure.

The rate and scale of movement in the form of velocity or what can also be termed as average velocity is another key parameter for the identification of pit slope instability. The average velocity is a derivative of the accumulated displacement based on a reference time and an assigned time window. One of the most common forms of monitoring is by continuous measurement of

Reduced Level by Total stations. The change in RL w.r.t to a time window provides a broader idea about the velocity of slopes if any. Another common method of monitoring is monitoring widening of cracks by crack meter (**Fig 5a**). It is a localized form of monitoring which provide micro level observations to estimate any impending failure.

One recent development in countries such as Australia and USA is the development of Slope Stability Radar (SSR) (**Fig 5 b**). Radar technology, used widely in a variety of fields for several. SSR is now being widely used in several countries to provide real time monitoring and advance warning signals before any slope or dump failure in opencast mines. SSR system can detect and alert movements of a wall with sub-millimeter precision, with continuity, and broad area coverage. This monitoring occurs without the need of mounted reflectors on benches or walls and the radar wave adequately penetrate through rain, dust, or smoke continuously. The SSR system produces data for interpretation quickly. The radar is moved around the mine in a repeatable manner to compare movements at each site and determine problematic areas. Several case studies of SSR providing improved operational risk management of slope have been reported from different places of world during last about 20 years, and in case of any necessity with trigger levels as in Table 1 mentioned in section 5.1, this system may be adopted. The experiences of this mine regarding suitability of the system considering the technical and financial aspects is yet to be seen with reference to regular monitoring results of slope movements.



Fig. 5. a) Slope Movement Monitoring with crack meters -conventional and remote type; b) Slope Stability Radar for Slope Movement Monitoring

ANALYSIS AND TARP

Multi monitoring stations are installed on Dump A for recording the reduced level in continuous mode in a fixed interval. Observation of the monitoring stations was conducted with Total station on 16 March, 15 Apr, 4 May, 18 May, and 10 June 2020. Observations at corresponding date are shown in Figure-4. 2.5 with 254 to 266 m reduced levels. Maximum variation observed in the vertical movement was not perceptible and hovering about 1 to 6 mm in majority of the stations indicating stability of the slope. Maximum vertical movement observed was about 12 mm at the station SM-3, which may be practically attributed to settlement of the ground in the initial stages of the monitoring. Vertical movement at various monitoring stations on the OB dump. From March 2020 to First week of May 2020, accelerated movement was observed on almost all the stations; however the stability was indicated after May 2020 without any ostensible variation. **Fig. 6(a)** shows the differential movement for various monitoring stations for the above mentioned period. **Fig. 6(b)** shows the RL measurement done by total station.

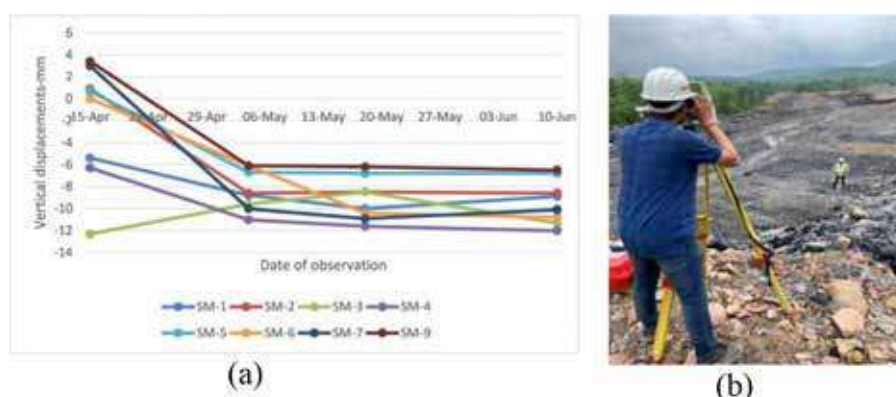


Fig. 6. a) Differential movements at various monitoring stations on the OB dump b) Total Station used for monitoring the movements of stations on dump

TARP (Trigger Action Response Plan)

Pit slope failures generally pass through several stages of movement. These stages are (Sullivan, 2007): 1. Viscoelastic response 2. Primary Creep, which may eventually stabilise, or progress to 3. Secondary Creep 4. Tertiary Creep (cracking and dislocation) 5. Collapse 6. Post collapse deformation the first two stages or “initial response” include elastic rebound, relaxation and/or dilation of the rock mass (Zavodni, 2001). Secondary creep and pre-collapse deformation is associated with yielding, softening, strength loss, localised failure and slip on structures within the rock mass.

Work conducted by Sullivan (2007) summarizes the development of pit slope movement phases and provides a holistic view of the possible stages of pit slope movement from the perspective of velocity. Sullivan (2007) proposed the classification of pit slope velocities for planning as well as for the determination of critical velocities when imminent failure is expected, as shown in **Table 1**.

Table 1. Classification of pit slope velocities for the detection of critical velocities (Sullivan 2007)

Author	Velocity(mm/day)	Period over which velocity applies (days)
Ryan and Call (1992)	12	2
	50	2
Zavodni (2001)	17	2
Zavodni (2001)	15	
Martin (1993)	10-100	
Zavodni and Broadbent (1982)	50	2
Zavodni (2001) Borax Mine	150	
Call and Nicholas (from Zavodni 2001)	300	
Savely (1993)	30-10000	
Sullivan (1993)*	1000*	<hours

Note: * Minimum instantaneous velocity immediately prior to collapse.

The table above demonstrates a typical example of slope deformation measurement as an indicator of critical velocity. The author suggest adopting a monitoring protocol able to monitor the slope deformation in real time or near real time at mm level accuracy to better understand the slope behavior. **Tables 2 and 3** suggests the trigger level and monitoring plan to be adopted by mine management.

Table 2. Trigger level and monitoring plan for slopes

Average slope Movements (mm/day)	Suggested method of monitoring	Suggested Monitoring period	Response and Control measure
< 0.1	Conventional Total Station monitoring (CSTM)	Monthly	Normal condition of slope -No appreciable response required
> 0.1	Conventional Total Station monitoring	Monthly	Initial response should start
0.1 to 15	Conventional Total Station monitoring	Fortnightly	Indicates no failure expected within 48 hours
15-50	CTSM + Crack meters/ Extensometers	Weekly	Indicates no failure expected within 24 hours
50-100	CTSM + Crack meters/ Extensometers/Other instruments	Once in two days	Indicates progressive failure
>100	Slope Stability Radar or other systems of monitoring	Daily	Clear the vicinity
>150	Slope Stability Radar or other systems of monitoring	Hourly	Stop further working and Clear the Area

**Table 3.** Frequency of monitoring plan for dump movements

Average slope Movements (mm/day)	Suggested method of monitoring			Suggested Monitoring period	Condition of slope -Response and Control measure
< 2	Conventional monitoring	Total Station		Monthly	Normal condition of slope - No appreciable response required
2-5	Conventional monitoring	Total Station		Weekly	Initial response should start
5 to 10	Conventional monitoring (CTSM)	Total Station		Once in two days	Indicates no failure expected within 48 hours
10-50	CTSM + Crack Extensometers/Other instruments	meters/		Daily	Indicates no failure expected within 24 hours
>50 mm	Slope Stability systems of monitoring	Radar or other		Continuous observation	Indicates progressive-failure Clear the vicinity

CONCLUSIONS

Recent guidelines of Directorate General of Mine safety in January 2020 for a typical coal Opencast mine are considered meticulously, and TARP is suggested with reference to the typical geo-mining conditions and recent data during this typical COVID19 period from opencast coal mine on monitoring the movements and numerical model studies for design of stable dump slopes and high wall slopes along with sensitivity analysis on effect of ground water. The analyses of factor of safety of slopes for existing slopes are found to be within prescribed safety limits. The monitoring results up to 20 June 2020, revealed the overall stability of dump slopes with practically considerable vertical displacement within 12 mm on the dump-A. However, these local movements observed from the Total Station reading is due to high moisture content of materials and deployment of HEMM near to the monitoring stations for the formation of benches in dump. The maximum horizontal movement at any station is within 14.5 mm across 19 days indicating a daily movement of 0.76 mm which is far below the critical limit proposed by various researchers, and hence the slope is considered stable.

Further analysis may be carried out in future for the Mine A with a large scale monitoring data to obtain an insight of slope movements, and analysis through Machine learning, Artificial Intelligence techniques to give more reliable guidelines on warning of failures. Development of proper TARP suitable for the geo-mining conditions of any opencast mine with observational approaches and meticulous monitoring and online interpretation and communication to the grass root level. Adopting a suitable TRAP will lead to self-reliant and sustainable practices with improved safety and stability of slopes.

REFERENCES

1. Jayanthu Singam, 2018, and 2020, Interim reports on Scientific Study On Design Of Pit And Dump Slope And Monitoring For Dulanga Coal Mining Project, Unpublished
2. Sullivan, TD 2007, 'Hydromechanical Coupling and Pit Slope Movements'
3. DGMS (Tech) Circular No 2 ,Dt 09.01.2020
4. DGMS (Tech) Circular No 3, Dt 16.01.2020
5. Approved Mining Plan, Dulang Coal Mine-NTPC
6. Adams, B.M. and T. Lucas (2011). Highwall design in intensely weathered basement rocks on the Stockton Plateau, New Zealand. Proceedings of the 2011 AusIMM NZ Branch Conference, Queenstown, NZ. AS/NZS (2004). HB 436: 2004. Risk Management Guidelines Companion to AS/NZS 4360: 2004 Standards New Zealand (note AS/NZS 4360: 2004 has now been superseded by AS/NZS ISO 31000: 2009).
7. Chiwaye, H.T. and T.R. Stacey (2010). A Comparison of limit equilibrium and numerical modelling approaches to risk analysis for open pit mining. J. Southern African Inst. of Mining and Metallurgy, Vol. 110, October 2010.
8. DME (1999). Guideline - Geotechnical Considerations in Open Pit Mines. Published by the Western Australia Department of Minerals and Energy (DME), Perth, August 1999.



9. Duncan, J. (2000). Factors of Safety and Reliability in Geotechnical Engineering. *J. Geotech. Geoenviron. Eng.*, Vol. 126, No. 4. pp. 307-316.
10. El-Ramly, H., Morgenstern, N.R., and Cruden, D.M. (2002). Probabilistic slope stability analysis for practice. *Canadian Geotechnical Journal*, Vol. 39, No. 3. pp. 665-683.
11. Gibson, W. (2011). Probabilistic Methods for Slope Analysis and Design. *Australian Geomechanics*. Vol. 46, No. 3, September 2011.
12. Hammah, R., Yacoub, T. and Curran, J. (2009). Probabilistic Slope Analysis with the Finite Element Method. *Proc. 43rd US Symp. on Rock Mechanics & 4th US-Canada Rock Mechanics Symp.*, Asheville.
13. Hammah, R., Yacoub, T., Corkum, B. and Wibowo, F. (2007). Analysis of Blocky Rock Slopes with Finite Element Shear Strength Reduction Analysis. *Proc. 1st Canada-US Rock Mechanics Symp.*, Vancouver.
14. Hoek, E. and Bray, J.W. (1981). *Rock Slope Engineering*. The Institute of Mining and Metallurgy, London, 1981. 3rd ed.
15. Kirsten, H.A.D. (1983). Significance of the Probability of Failure in Slope Engineering, *The Civil Engineer in South Africa*, Vol. 25, No. 1, 1983. pp. 17-27.
16. McMahon, B. K. (1985). Geotechnical Design in the Face of Uncertainty. E.H. Davis Memorial Lecture, *Aust. Geomechanics Journal*, November 1985.
17. Oka, Y. and Wu, T.H. (1990). System Reliability of Slope Stability. *J. Geotechnical Eng.* Vol. 116, No. 8, pp. 1185-1189.
18. Pine, R.J. (1992). Risk analysis design applications in mining geomechanics. *Trans. Inst. Min. Metall. (Sect. A)* 101: 149-158.
19. Priest, S.D. and E.T. Brown. (1983). Probabilistic stability analysis of variable rock slopes. *Trans. Inst. Min. Metall. (Sect. A)* 92: 1-12.
20. Safe Work Australia (2011). Draft Code of Practice: Ground Control in Open Pit Mines. Developed by Safe Work Australia, released July 2011. (www.safeworkaustralia.gov.au).
21. Sowers, G.F. (1979). *Introductory Soil Mechanics and Foundations: Geotechnical Engineering*, 4th Edition, Macmillan Publishing Co., Inc., New York, Collier Macmillan Publishers, London.
22. Sullivan, T.D. (2006) Pit slope design and risk – A view of the current state of the art. In: *Proc. Symp. Series S44, Stability of rock slopes in open pit mining and civil engineering situations*, 3–6 April 2006, Johannesburg, South Africa, Southern African Institute of Mining and Metallurgy, Cape Town.
23. Sullivan, T.D. (2007). Hydromechanical coupling and pit slope movements, Keynote Lecture. In: *Proc. International Symposium on Rock Slope Stability in Open Pit Mining and Civil Engineering (Slope07)*, Y. Potvin (ed), 12–14 September 2007, Perth, Australia, Australian Centre for Geomechanics, Perth, pp. 3-43.
24. Terbrugge, P. J., Wesseloo, J., Venter, J. and O.K.H. Steffen (2006). A risk consequence approach to open pit slope design. *J. Southern African Institute of Mining and Metallurgy*, Vol. 106, pp. 503-511.
25. U.S. Army Corps of Engineers (1995). Introduction to probability and reliability methods for use in geotechnical engineering. *Engineering Technical Letter 1110-2-547*, U.S. Army Corps of Engineers, Washington, D.C.
26. Varnes, D.J., (1978). Slope movement types and processes. In: *Landslides, Analysis and Control*. Special Report 176, Transportation Research Board, Washington, pp. 11-33.
27. Wesseloo, J. and Read, J. (2009). Chapter 9 - Acceptance Criteria. In: *Guidelines for Open Pit Slope Design*, J. Read and P. Stacey (eds), pp 221-236. CIRSO publishing. 496p.
28. Zavodni, Z.M. (2001). Time-Dependent Movements of Open-Pit Slopes. *SME Proceedings*, Denver, Colorado, pp. 81-87.

Marine Engineering



Design and Engineering for a Self-reliant Society in Marine Engineering

Sandeep Kumar

D-7 Parmanu Nagar Co-operative Housing Society, Sector-4, Vashi, Navi Mumbai

✉ sandeepkumar2311@gmail.com

For the marine sector, innovation led change is nothing new. Consider the impact that radar and satellite communications have had in the past one hundred years alone. But the industry now faces a tipping point, where technological developments such as autonomous and smart ships are turning the realms of science fiction into fact. At the same time, the sector is facing unprecedented cost pressures and a stricter regulatory backdrop, as environmental restrictions persist and harden.

As noted by IMO “the best package of measures for a ship to improve efficiency differs to a great extent depending upon ship type, cargoes, routes and other factors...” (MEPC.1/683). The difficulty is in determining which ones are most appropriate for a vessel and service.

In the current scenario, wide range of options exist to improve vessel efficiency, reduce fuel consumptions and lower emissions. These may be categorized into a few broad categories:

1. Hull form optimization: Issues related to the basic hull form design including selecting proper proportions, reducing resistance by optimizing the hull form and appendage design, and assessing the impact on resistance of waves and wind.
2. Energy saving devices: These are devices used to correct or improve the efficiency of propellers as well as developing technologies aimed at reducing the hull frictional resistance or using renewable energy sources (such as solar and wind energy).
3. Structural optimization and light weight construction: These concepts relate the impact of the use of high strength steel on lightship weight and energy consumption.
4. Machinery technology: Advancements in this area concentrate on the efficiency gains that are possible in the design and operation of the ship's machinery and systems. It covers main and auxiliary diesel engines, waste heat recovery and other auxiliary equipment.
5. Fuel efficiency of ships in service: This category addresses operational measures that can reduce fuel consumption. These include voyage performance management, hull and propeller condition management, optimum ship systems operation and overall energy efficiency management.

It is evident from the above that categories 1 and 3 address challenges for new vessel construction, whereas the remaining categories (2, 4 and 5) cover both new builds and existing vessels.

HULL FORM OPTIMIZATION

Improvements in the sophistication and ease of application of analytical tools and techniques for vessel design have enabled the designer to optimize and explore alternative solutions that were previously unavailable. These tools take into consideration a range of disciplines such as hydrodynamics, ship structures, and environmental and safety performance (e.g. stability, oil outflow assessment and fire control). Multi-objective and multidisciplinary optimization software packages are being developed where these various tools are linked. Economic studies (e.g., a required freight rate assessment of parametric series of designs and comparative life cycle cost assessments) are routinely applied in the design optimization process and are beneficial for assessing the relative merits of standard designs offered by shipyards.

Parameters that are to be optimized are ship size (capacity), service speed and principal dimensions. In order to minimize hull resistance and increasing propulsion efficiency, the following may be carried out:

- Optimize the fore body: Use of bulbous bows for optimizing the forebody shape (Refer **Fig 1**)



- Optimize aft body: Efforts to reduce stern waves/improve flow to propeller/avoid eddy effects
- Appendage resistance: Twin 'skeg' design
- Manoeuvring and course keeping considerations: Performance predicted through model testing in a towing tank, etc
- Hull coatings: These can lower frictional resistance and limit fouling by aquatic organisms. A saving between 1-9% fuel consumption can be had if a proper hull coating has been carried out.

ENERGY SAVING DEVICES

Different devices have been used to optimize the energy performance of ship designs. Also, recent developments have led to a series of devices aimed at reducing the hull frictional resistance/exploiting readily available natural resources, such as solar or wind energy.

This section explores a range of these devices, most of which historically concentrate on the improvement of propeller propulsion effectiveness.

Recent developments have led to a series of devices aimed at either reducing the hull frictional resistance or exploiting readily available natural resources, such as solar and wind energy.

- a) Propulsion improving devices (PIDs):
 - Wake equalizing devices : These improve the flow around the hull like Grothues Spoilers, wake equalizing ducts, stern tunnels, etc
 - Pre-swirl devices: These condition the wake flow and improve the angle of attack towards the propeller blades, eg Mewis ducts (See **Fig 2** below)
 - Post-swirl devices: These reduce the detrimental flow characteristics around the propeller and increase rudder efficiency, eg rudder bulbs, propeller boss caps, etc
 - High efficiency propellers like controllable pitch propellers (CPP), ducted propellers, Kappel propellers (modified blade tips), etc
- b) Skin friction reduction: Viscous resistance accounts for the great majority of the hull resistance in water. To reduce the same, various techniques are being tried out to varying levels of success:
 - Air cavity systems: A thin layer of air is formed and maintained over the hull flat bottom
 - Micro-bubbles: Micro-bubbles created around the hull surface in order to reduce resistance (in trial stage)
- c) Renewable energy: Wind and solar power are also being considered, especially in the generation of auxiliary power:
 - Wind energy: Rotor sails, Flettner rotors (see **Fig 3** below) are being developed. These utilize a so-called "Magnus Effect" for generating energy.
 - Solar: Solar panels have been used on some vessels (eg the NYK car carrier Auriga Leader) which is equipped with more than 300 such panels. High capital expenditure is an obvious drawback in this area.

STRUCTURAL OPTIMIZATION AND LIGHT WEIGHT CONSTRUCTION

Structural weight reductions have a great effect on required power for faster and smaller vessels like fast ferries. Structural weight optimization for large cargo vessels (displacement hulls) increases the available dead weight for a ship of the same size, thereby improving transport efficiency.

For high-speed craft, reducing the lightship through the introduction of non ferrous materials is necessary to satisfy mission requirements, and can have significant impact on fuel consumption.

FRP laminates with light weight core material as applied to high-speed craft and superstructures offer a 30 to 70 percent weight savings. Overall, application of composites has the potential of reducing lightship by 30 percent or more, which will translate into substantial fuel savings.

The cost of composites or aluminum structure for large cargo ships is prohibitive, and unlikely to be competitive to steel in the



foreseeable future. These materials are viable for high-speed craft and have potential applications for higher speed ferries and ro-ro/ropax vessels. Cost of construction, fire safety and recycling are the principal concerns.

MACHINERY TECHNOLOGY

A proper consideration of available technologies to improve the energy efficiency of main and auxiliary engines must be framed by the primary energy source – fuel. Large commercial vessels traditionally consume heavy fuel oil (HFO) also known as residual fuel oil. HFO is a byproduct of traditional refining operations and is generally very viscous containing substances that are removed from more refined (or distilled) petroleum products. Recent IMO regulations are aimed at reducing nitrogen and sulfur compounds (NO_x and SO_x) as well as CO₂ a known greenhouse gas. Reduction of CO₂ can be achieved through the reduced fuel oil consumption or greater fuel efficiency.

Reduction of NO_x is related to improvements in the combustion process. IMO has implemented a three-tier regulatory scheme to reduce NO_x emissions from shipping. The first stage of NO_x reductions, known as IMO Tier I, came into effect in 2000. The next stage, IMO Tier II, became effective in 2011 and called for a 20 percent reduction from Tier I levels. The next step, Tier III, calls for even greater reductions including an 80 percent reduction from Tier I levels when operating in emission control areas (ECAs). It is envisioned that engines will need to incorporate new innovations, possibly some sort of after treatment or cleaning system to comply with Tier III requirements. Such systems will have an adverse effect on overall efficiency.

The amount of SO_x contained in vessel emissions is directly related to the amount of sulfur in the fuel oil. IMO regulations concerning the reduction of SO_x are aimed at reducing the sulfur content of marine fuel.

Companies considering the most effective strategy for complying with IMO emissions requirements will take a holistic view at their options. Reductions of NO_x and SO_x can be achieved through use of alternate fuels such as LNG or other methane products, but capital costs are significant. Lastly, use of exhaust gas cleaning systems (scrubbers) may allow operators to continue to burn fuels with higher sulfur content, but again there is an implementation cost as well as a cost to the overall system efficiency.

A proper consideration of available technologies to improve the energy efficiency of main and auxiliary engines must be framed by the primary energy source – fuel.

- a) Prime movers – Main and auxiliary engines
 - Diesel engine energy efficiency enhancements: Electronic control engines, use of Alpha lubricators, Exhaust gas bypass systems, Variable turbocharger area (VTA), engine de-rating, etc
 - Main engine efficiency measurement instrumentation: Use of shaft power meters, mass flowmeters for fuel, etc
 - Main engine performance measurement and control: Use of computer-based systems for monitoring cylinder and fuel injection system performance are widely used, such as PMI On-line.
- b) Auxiliary equipment
 - Variable speed motors: These improve the operating efficiency of pumps and fans that operate at variable loads. This technology is especially beneficial for equipment that operate at variable loads.
- c) Waste Heat Recovery (WHR)
 - This technology can pass exhaust gases from a vessel's engines through a heat exchanger to generate steam for a turbine-driven generator. The heat energy from the exhaust gas is taken and transformed into electrical energy to reduce direct engine-fuel consumption for the propulsion system or reduce auxiliary engine needs. Energy saving potential is estimated on an average as around 8%.
 - Refer **Fig 4** below, even with high, 50% efficiency of modern low-speed engines there is still 50% of fuel input energy not being put to productive use. The possibilities are illustrated by this comparison of Sankey diagrams for Wartsila 12RT-Flex96C engines with heat recovery (left) and with high efficiency waste heat recovery plant (right), showing in this case an 11.4% gain in overall efficiency with WHR.

FUEL EFFICIENCY OF SHIPS IN SERVICE

The most direct and useful tools for improving a vessel's performance are the operational decisions made daily on how to



conduct a voyage, perform regular maintenance and monitor fuel consumption efficiencies. Accurate and regular energy use monitoring across the fleet can highlight inefficiencies and provide a mechanism for continual improvement.

a) Ship operation: Voyage performance management

- Voyage speed optimization: This has a dramatic impact on the fuel consumption because the speed is related to the propulsive power required by approximately a third or fourth power relationship. Roughly speaking this means if you double the speed you increase the power required by a factor of at least 8. Likewise, sailing at 90 percent of the design speed requires only 75 percent of the power. The corresponding reduction in total fuel consumption is offset a bit by the longer time spent to complete the voyage. So, by slowing down 10 percent the vessel can save about 20 percent in fuel for a given voyage. This significant savings makes it easy to understand why there is substantial interest in slow steaming, especially when fuel prices escalate.
- Weather routing – safe and energy efficient route selection: It selects a course from the departure port to the destination port that provides the safest passage and reliable on-time arrival while considering actual wind, wave and current conditions expected during the voyage.

b) Hull and propeller condition management: Taking care of the propeller and underwater portions of the hull is all about minimizing roughness. Regular in-service cleaning to remove fouling organisms (which are a form of roughness) is clearly beneficial unless it is carried out in a way that results in a damaged coating or one that has been ‘roughed’ up. From a fuel efficiency point of view, the emphasis should be on hull and propeller roughness management and not just on the control of fouling.

The physical micro-roughness can be increased in service by mechanical damage, failure of the applied coating (peeling, blistering, cracking, dirt inclusion, etc.), and even improper preparation of the surface and/or improper application of a new coating. For instance, overly aggressive blasting, inadequate repairs to the previously applied coating, dry over spray and uneven dry film thickness can increase the surface roughness.

For most of the present ship owners/operators, available technology is utilized to enhance energy efficiency:

a) Hull form optimization: Most company vessels have been constructed with an optimized hull form most suited to the expected operating profile during service:

- ❖ Usage of bulbous bow to reduce the wave-making resistance
- ❖ Effective external hull coatings
- ❖ Larger rudders provided resulting in increased course-keeping effectiveness

b) Energy saving devices: Many of the vessels are provided with the following energy saving devices:

- ❖ Becker-Mewis ducts

c) Machinery technology: Usually, fleet vessels have been built to “Eco-design” with the following carefully borne in mind:

- ❖ Electronic controlled engines
- ❖ Alpha lubricators
- ❖ Exhaust gas bypass systems
- ❖ Mass flow meters
- ❖ Engine auto-tuning, PMI online
- ❖ Use of variable speed motors

d) Fuel efficiency of ships in service:

- ❖ Leverage the potential of data for evaluation of vessel performance
- ❖ Regular in-service hull cleaning

The fuel or energy savings are presented in one of several ways depending on the efficiency measure:

- A reduction in specific fuel oil consumption (SFOC). This is used for measures directly related to diesel engine consumption, making the engine and/or its systems operate more efficiently.
- A reduction in propulsion fuel consumption. This is related to main engine energy use, power delivered to the propeller and overall hull resistance.
- A reduction in overall vessel fuel consumption. This includes fuel used by auxiliary engines and is related to the total fuel cost for the vessel.

When assessing the total possible savings for a vessel, it is important to keep in mind the basis for the savings for each different energy-savings measure. The application of one measure may exclude or reduce the benefit of another measure; energy-saving estimates from different measures are not cumulative.

Fuel Efficiency Incentives

One issue that transcends any measure but is critical to the selection and adoption of efficiency improvements in vessels should be mentioned at the outset. For many vessels, the vessel's owner and/or operator does not directly receive the benefit in fuel savings of efficiency measures. The benefits often accrue to the charterer who pays for the fuel. Unfortunately, this reduces the owner's incentive to invest in efficient ships.

If arrangements can be developed for the owner and/or operator to accrue direct benefits from energy efficiency investments they may lead to significantly more efficient vessels. For owners unable to share the benefit of reduced fuel costs, the largest driver for adopting these measures may be the evolving regulatory regime and their own environmental policies.

Increasing ship efficiency is a combination of multiple factors, each of which plays an important role in its own way. With lofty targets in place, there has been a consistent rise in the incentives and regulations for improving ship energy efficiency.

There is considerable potential for reducing emissions in the shipping sector. A lot of the technology is already available, and some is relatively easy to implement; slow streaming, improved voyage planning, trim optimization, hull coating and propeller cleaning. There are also a plethora of technologies available for retrofitting on existing vessels; main engine tuning, propeller and rudder upgrades, fin and duct energy saving devices, to name a few. Not all solutions can be applied to all types of ships, and individual saving measures cannot simply be added together. Current uptake of many of these technologies is limited due to the cost of implementing them and a lack of knowledge regarding their effectiveness on specific ship types/sizes/routes.

What are your thoughts about the various practices for increasing ship efficiency? Any insights on how you ensure increased efficiency in your own small way?

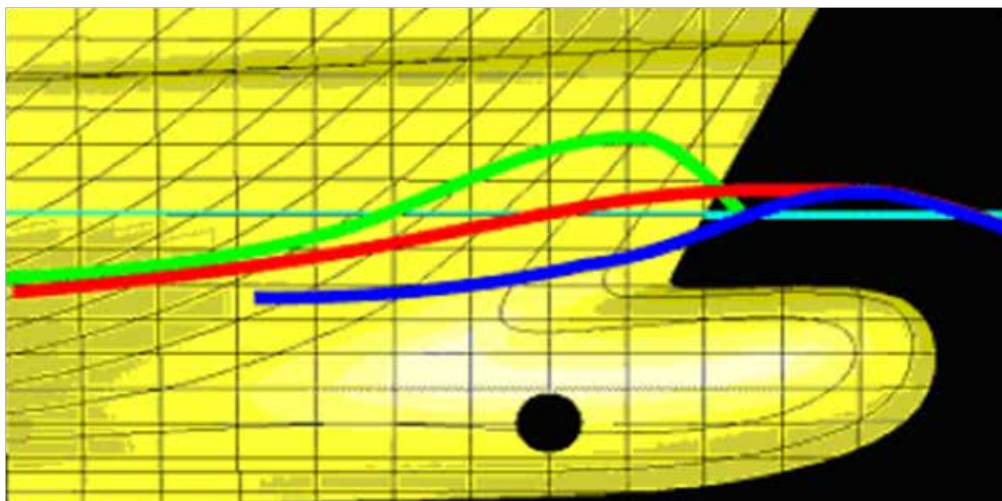


Fig. 1. Bulbous bow: The green line characterizes the ordinary bow wave of the hull. The blue line characterizes the wave formed by the bulb. The red line is the sum of these two. The altitude of the bow wave is noticeably reduced, which reduces the hull drag associated with the bow wave. This improves fuel economy and increases range.

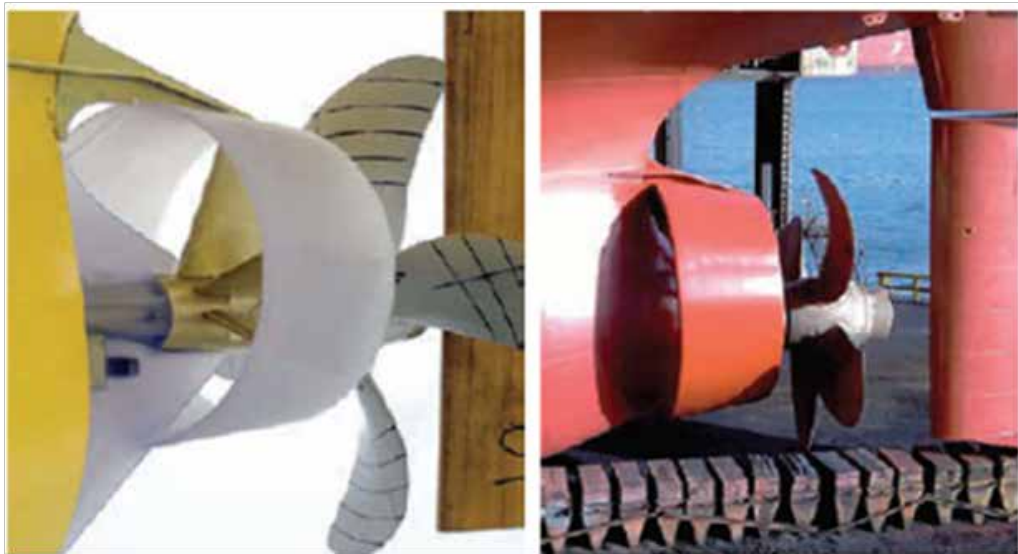


Fig. 2. Becker-Mewis Duct (an example of a “Pre-swirl” device)



Fig. 3. Rotor sails, Flettner rotors are being developed. These utilize a so-called “Magnus Effect” for generating energy

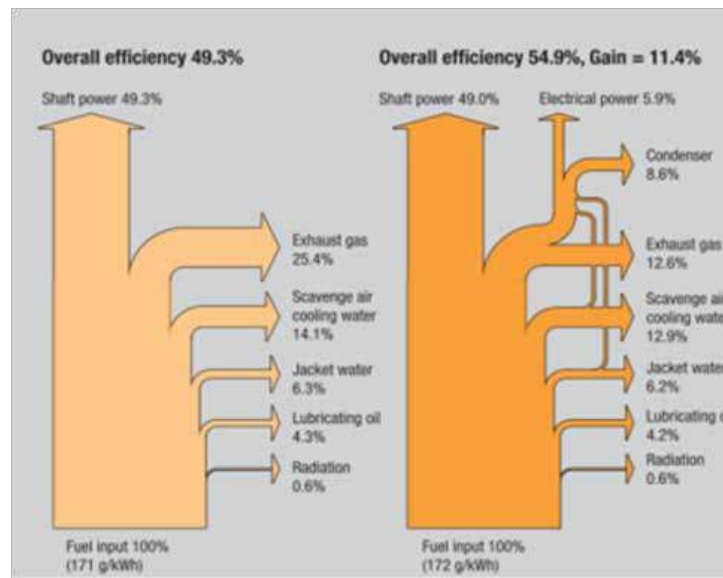


Fig. 4. Efficiency of waste heat recovery system using Sankey Diagrams

REFERENCES

- Study on energy efficiency technologies for ships // CLIMA.B3/ETU/0023r // European Commission.
- L. Larsson et. al., 2010, “The Principles of Naval Architecture Series: Ship Resistance and Flow,”.
- Specialist committee on energy saving methods – Proceedings at the 28th International Towing Tank Conference (ITTC) 2017.
- ABS Ship energy efficiency measures – Status and guidance.



Sustainable Shipping

N M C Nair

Marine Engineer, Consultant and Surveyor

✉ marinenmc@gmail.com

ABSTRACT

Sustainable Shipping is a management concept for development, applied to the shipping sector, incorporating environmental and social responsibility. The world's ocean is essential to life on our planet. It provides largest source of protein and absorbs around a quarter of our carbon dioxide emissions and most of the world's extra heat. The ocean also produces half of the world's oxygen. More than 3 Billion people depend on it for their livelihoods. The output of the global ocean economy is estimated at US\$1.5 trillion and this could more than double by 2030. Constituting more than 70% of Earth's area, and holding 95% of earth's water, the ocean contributes to the economic development of coastal and island states, whilst connecting all nations in global trade. United Nations, IMO (International Maritime Organization), Commonwealth and many others joins in the designated 17 Sustainable Development Goals 'SDG 2030' projected by UN. World over, the Shipping sector is being forced to reduce environmental and marine pollution with many strict regulations.

Keywords: UN; SDG; IMO; Shipping; Marine pollution; Environment.

INTRODUCTION

Sustainable development means 'meeting the needs of the present generation without compromising the ability of future generations to meet their own needs.'

The Sustainable Development Goals (SDGs), also known as the Global Goals, were adopted by 176 United Nations Member States as a universal call to end poverty, protect the planet and ensure that all people enjoy peace and prosperity by 2030. United Nations adopted 17 Sustainable Development Goals with 169 related targets in Sept 2015 which is for a plan of action "for the people – for the planet – for the prosperity". The three pillars of SDG are social-economic-environment. While each SDG addresses a different aspect of sustainability, the SDGs are interconnected. Therefore, some of the activities may contribute to more than one goal.



SDG 14 is "Life Below water" which aims to "Conserve and use the oceans, seas and marine resources sustainably". Oceans, seas and coastal areas form an integrated and essential component of the Earth's ecosystem and are critical to sustainable development. Oceans contribute to poverty eradication by creating sustainable livelihoods and decent work. The oceans make



human life possible with their temperature, their chemistry, their currents, their life forms. But today we are seeing nearly a third of the world's fish stocks overexploited. Oceans absorb about 30 percent of the carbon dioxide that humans produce; but we're producing more carbon dioxide than ever before and that makes the oceans more acidic—26% more, since the start of the industrial revolution. Our trash—13,000 pieces of plastic litter on every square kilometre of ocean. The Sustainable Development Goals indicate targets for managing and protecting life below water.

We need the oceans to provide more food, more jobs and more energy, so we must maintain its capacity to regulate the climate and support biodiversity. Oceans are crucial for global food security and human health & global climate. Shipping is a key user of the oceans, delivering more than 90% of world trade, and carrying millions of tourists on cruises. Fishing, Oil & Mineral exploration are other key users of the Oceans.

Oceans, seas and marine resources are being threatened, degraded or destroyed by human activities, reducing their ability to provide crucial ecosystem services. The deterioration of coastal and marine ecosystems and habitats is negatively affecting human well-being worldwide. Good governance, an enabling environment, sustainable land- and marine- based human activities, and adequate measures will be required to reduce the negative impacts on the marine environment. Plastic is one of the most dangerous man made compounds on earth. It's estimated that at least 8 million metric tons of plastic ends up in the oceans every year with detrimental impacts on species, habitat and people.

Where does this pollution come from? Where does it go? Some of the debris ends up on our beaches, some sinks, some is eaten by marine animals that mistake it for food, and some accumulates in ocean floors. Other forms of pollution that impact the health of the ocean come from a single, known sources, such as oil spills, or from accumulation of many dispersed sources, such as fertilizer from our yards & Chemical and sewage disposal.

While high-income countries generate more waste per capita, in terms of aggregate volume, developing countries produce more than half of total solid waste. Scarcity of land makes these countries' waste disposal problems acute. Rising sea levels due to global warming accelerates this scarcity.

The majority of pollutants going into the ocean come from activities on land. Natural processes and human activities along the coastlines and far inland affect the health of our ocean. One of the biggest sources is called nonpoint source pollution, which occurs as a result of runoff. Nonpoint source pollution includes many small sources, like septic tanks, cars, trucks, and boats, plus larger sources, such as farms, livestock ranches, and timber harvest areas. USA alone uses 500 million straws/day. 80% ends up in the oceans. Pollution that comes from a single source, like an oil or chemical spill, is known as point source pollution. Often these events have large impacts, but fortunately, they occur less often. Discharge from faulty or damaged factories or water and sewage treatment systems is also considered point source pollution.

As the United Nations agency responsible for developing and adopting measures to improve the safety and security of international shipping and to prevent pollution from ships, IMO (International Maritime Organization) has an integral role in meeting the targets set out in the United Nations Sustainable Development. The International Convention for the Prevention of Pollution from Ships, universally known as MARPOL, is the key treaty adopted by the International Maritime Organization.

- Pollution by Oil from ships
- Noxious liquid substances, carried in bulk
- Harmful substances carried in packaged form
- Sewage discharges into the sea
- Ship-generated Garbage- Disposal at sea
- Atmospheric pollution from ships
- Anti-fouling paints & systems used on ships,
- Transfer of alien species by ships' Ballast / de-ballast systems and
- Environmentally sound Recycling of ships.

IMO recognizes that, for its Member States and the UN system to implement the 2030 Agenda, this new framework will have to be translated into national policies and strategies taking into account cross cutting issues. As the 2030 Agenda will be implemented principally at the country level, IMO will develop and formulate innovative and targeted maritime policies to



respond to the needs of countries at the national, regional and global levels. The UN system, of which IMO is a part, is fully committed to supporting the successful implementation of the 2030 Agenda, based on the combined expertise and strengths of each entity within the system, and to ensuring universal coherence. Through increased collaboration, IMO will work to eliminate duplication and fragmentation within the system.

Shipping is an essential component of sustainable economic growth, as it is the most environmentally sound mode of transport, having the lowest carbon footprint per unit of cargo transported. Because international shipping takes place on the world's oceans, and IMO is responsible for measures to improve the safety and security of international shipping and to prevent pollution from ships, IMO's work is integral to SDG 14. IMO's objectives can be summarized as safe, secure and efficient shipping on clean oceans.

The fundamental purpose of IMO, as described in the IMO Convention, is in the conservation and sustainable use of oceans and their resources. This is reflected in the Organization's development, adoption and implementation of international law through the IMO treaty regime. This foundation is again reflected in the linkages between the IMO treaty regime and the United Nations Convention on the Law of the Sea (UNCLOS). IMO is the UNCLOS "competent organization" for navigational safety, the safety of life at sea, including the design, construction, equipment and manning of ships for safety and environmental protection, the protection of the marine environment generally, maritime security, liability and compensation for maritime casualties, and response systems for search and rescue. IMO actively addresses marine pollution and environmental incidents. Acting as the competent organization through such a broad range of activities gives IMO a considerable role in the attainment of SDG 14.

International shipping and related industries are dependent on qualified seafarers to operate ships and on shore-based personnel to support ship operations. The maritime community contributes to quality of life, particularly in developing countries, by employing 1.5 million seafarers and many more land-based personnel, thereby directly enhancing economic prosperity in local communities. The safety and security of life at sea, the protection of the marine environment and the efficient movement of global trade depend on the professionalism and competence of seafarers. The IMO International Convention on Standards of Training, Certification and Watch-keeping for Seafarer (STCW) provides universal standards of competence for seafarers and effective mechanisms for enforcing its provisions. IMO contributes to quality education by providing training activities, in particular through its technical cooperation programmes and its two maritime training institutions -the World Maritime University (WMU) and the International Maritime Law Institute (IMLI), both established by IMO. SDG 4 is on quality education and maritime training is under strict and stringent controls all over the world. Gender equality under SDG 6 is also covered with more and more women joining the merchant fleet.

IMO has developed a number of important regulations relevant to this cluster of SDGs, in particular the London Convention and Protocol (LC/LP), on the prevention of marine pollution by dumping of wastes and other matter at sea the Hong Kong Ship Recycling Convention, and the International Convention for the Prevention of Pollution from Ships (MARPOL). The LC/LP contributes to SDG 6 on the sustainable management of water by prohibiting unregulated dumping of wastes and other matter at sea. It encompasses a precautionary and risk-assessment-based approach to waste management, stressing the need to prevent, reduce and, where practicable, eliminate pollution caused by the dumping of wastes at sea.

The Hong Kong Ship Recycling Convention contributes to SDG 12 by reducing waste generation and promoting sustainable consumption. The convention is aimed at ensuring that ships do not pose any unnecessary risk to human health, safety and the environment when they are recycled at the end of their operational lives. IMO contributes to SDG 12 through the reduction of waste generation, both operational waste from ships (MARPOL) and dumping of wastes under the LC/LP. Under MARPOL Annex V, on the prevention of pollution by garbage from ships, discharging garbage into the sea is prohibited, with only a limited number of exceptions. For garbage, and several other types of waste generated on board ships, MARPOL requires port States to provide adequate reception facilities for the safe and sound management of wastes.

IMO seeks to combat climate change in a number of areas, including air pollution, energy efficiency and green house gas (GHG) emissions. IMO's global regulations and standard ensure that the maritime sector can continue to improve its efficiency, thus promoting trade and the provision of cost-effective energy across the globe. The maritime sector and IMO have a major role to play in achieving SDG 7, regarding energy efficiency in particular, and SDG 13 on climate change. IMO has worked extensively to address greenhouse gas emissions from shipping and, in 2011, adopted the first ever mandatory, global, legally binding GHG control regime for an entire industry sector, based on technical measures for new ships and operational emission reduction measures for all ships.

The shipping industry must act now in order to meet U.N. targets to cut carbon emissions by 2050. International Maritime



Organization (IMO) has said it aims to reduce overall greenhouse gas emissions from ships by 50% from 2008 levels by 2050. Carbon emissions from shipping in the six-year period to 2018 accounted for 2.9% of the world's CO₂, the latest IMO-commissioned study showed in August, adding pressure on the industry to bring levels down.

The International Chamber of Shipping (ICS), which represents more than 80% of the world merchant fleet, is among industry bodies that has proposed creating a research fund to find the right technology to meet the targets, which will also bring in governments. A 50% total cut in CO₂ by 2050 can only be achieved by improving carbon efficiency of the world fleet by around 90%. This will only be possible if a large proportion of the fleet is using commercially viable zero-carbon fuels,

A virtual meeting of the Intersessional Working Group on Reduction of GHG Emissions from Ships (ISWG-GHG 7), held during late October 2020 came up with (proposed draft amendments to the MARPOL convention, specifically Annex VI chapter 4) which will next go before the upcoming meeting of the IMO's all-important Marine Environmental Protection Committee (MEPC). The adopted measures made mandatory the Energy Efficiency Design Index (EEDI) for new ships and the Ship Energy Efficiency Management Plan (SEEMP) for all ships. These measures will require ships built in 2025 to be 30% more energy efficient than those built in 2014. IMO, with funding from the Global Environment Facility (GEF), is cooperating with the UNDP in a global effort to help the shipping industry move towards a lower carbon future, through a project entitled "Transforming the global maritime transport industry towards a low carbon future through improved energy efficiency".

The substance of the Working Group's MARPOL amendments creates a new measurement, known as the Energy Efficiency Design Index for Existing Ships (the "EEXI"), which utilizes the methodology of the Energy Efficiency Design Index ("EEDI"), a measure that's been applied to new builds since 2015, and applies it, on a one-time basis, to existing ships. The amendments also beef up the Ship Energy Efficiency Management Plan (SEEMP), which has been around since 2011.

Reduction of greenhouse gas emissions from ships

The MEPC is expected to adopt an initial strategy on the reduction of GHG emissions from ships. The initial strategy will be a framework for Member States, which is expected to set out the future vision for international shipping, the levels of ambition to reduce GHG emissions and guiding principles. The Intersessional Working Group on Reduction of GHG Emissions from Ships is expected to finalize the text of the draft initial strategy and provide a report to MEPC 72.

Implementation of sulphur 2020 limit

The 0.50% limit on sulphur in fuel oil on board ships (outside designated emission control areas or ECAs, where the limit is 0.10%) came into effect on 1 January 2020. The exception would be for ships fitted with an approved "equivalent arrangement" to meet the sulphur limit – such as an exhaust gas cleaning system (EGCS) or so-called "scrubber" – which are already permitted under regulation 4.1 of MARPOL Annex VI. Sulphur oxides (SO_x) are known to be harmful to human health, causing respiratory symptoms and lung disease. In the atmosphere, SO_x can lead to acid rain, which can harm crops, forests and aquatic species, and contributes to the acidification of the oceans.

Implementation of the Ballast Water Management Convention

The International Convention for the Control and Management of Ships' Ballast Water and Sediments, 2004 (BWM Convention), entered into force in September 2017 and has, to date, been ratified by 69 countries, representing 75.11% of world merchant shipping tonnage.

Since the date of entry into force, ships have been required to manage their ballast water to avoid the transfer of potentially invasive species. Ships are required to manage their ballast water to meet the D-1 ballast water exchange standard; or the D-2 standard, which requires ballast water management to restrict to a specified maximum the amount of viable organisms allowed to be discharged and to limit the discharge of specified indicator microbes harmful to human health.

Heavy fuel oil in the Arctic

The MEPC will consider the development of measures to reduce risks of use and carriage of heavy fuel oil as fuel by ships in Arctic waters. Currently, the use and carriage of heavy fuel oil is banned in the Antarctic under MARPOL Annex I regulation 43. It is recommended in the Polar Code that the same rules are applied in the Arctic.

Marine litter

The MEPC will be invited to consider a proposal to include a new output on its agenda, to address the issue of marine plastic litter from shipping in the context of 2030 Sustainable Development Goal 14 (SDG 14).



INDIAN SCENARIO

The vast coast line of 7550kms and the strategic location along most major shipping highways are the main advantages for Indian maritime sector unveiled a host of initiatives aimed to develop and sustaining growth of the sector. Today the country boasts of a modern ship building and shipping service sector. The “Make in India” “Athmanirbhar” and the “Sagar Mala Project” are considered to be some of the best initiatives to increase the competitiveness of Indian Maritime sector. Along with the growth, the sector should concentrate on environmental issues, and avoid or control oil spills and dumping of waste, garbage etc. into the oceans. As per the interim report submitted in June 2020, India stands at 117th rank with 61.9% performance in implementation out of 166 countries. The pandemic has slowed down the progress further. EU stands in first 10 positions with points above 80%.

REFERENCES

1. IMO SDG BROCHURE
2. November 11, 2020 by Reuters By Jonathan Saul
3. Implications of UNCLOS for IMO
4. Sustainability Challenges in Maritime Transport and Logistics Industry and Its Way Ahead Paul Tae-Woo Lee, Oh Kyoung Kwon, and Xiao Ruan Ocean College, Zhejiang University, Zhoushan 316021, China; Graduate School of Logistics, Inha University, Incheon 22212, Korea
5. Marine Engineers Review MER Sept 2020 of Institute of Marine Engineers (India).



Water Dependency Test on a Novel Method of Water Transportation at Static Conditions

Arulanantha Samy Santhiyagu, Jaikumar Mayakrishnan

Department of Automobile Engineering, Hindustan Institute of Technology and Science, Chennai, Tamilnadu

✉ ansaru2020@gmail.com

ABSTRACT

The waterway is one of the best modes of transportation that could offer a more fuel economy than other modes of transport. Buoyancy is a key term that aids in the design and production of all types of water vehicles. The load characteristics of all water vehicles are depending on the buoyancy term that can be restated as the weight density behavior of a floating object and the water. The resistance forces involving the water vehicles and ground vehicles are conversed to find the influences of the weight of the vehicle in the tractive effort required. The proposed design aims to limit the water usage to a certain level depending on the volume of the open-bottomed air vessel that can produce the required buoyancy force with the minimum possible water usage to the payload. This article builds an experimental setup that is used to describe the application of air vessel in developing a new mode of the fluid based transportation system that finds a reduction in the water usage according to the payload requirement. The experimental work reveals that the amount of water can be predetermined in this proposed water transportation that helps to establish new infrastructures for this kind of novel water transportation in the future

Keywords: Buoyancy force; Pneumatic compliances; Hydrostatic pressure; Ground guided supports; Tractive effort.

ABBREVIATIONS

R_F - the sum of tangential stresses along the wetted surface

in the direction of the motion

R_n - the Reynolds number

C_T - the total resistance coefficient of a ship

R_T - the total resistance of a ship

R = the running resistance

V = the velocity of the train

A, B, C = the coefficients determined from theoretical considerations or measurements

INTRODUCTION

This paper aims to minimize the rolling resistance of ground guided vehicles with buoyancy characteristics of boat type vehicles equipped with a defined towing path and external propulsive devices such as rope drive. In automobiles, the vertical load is carried by the suspension system, but this requirement is completely left behind the buoyancy of the water transport vehicles [1]. The equations 1, 2, 3, and 4 show that the tractive force required is the function of the resistance parameters involving the various atmospheric effects such as air and fluid flows, gravitational behavior with guidance support, and the vacuum systems.

$$R_{RL} = Fr W + 1/2 \rho V^2 C_d A + W \sin \theta \quad (1)$$

where W = weight of the vehicle, Fr = the coefficient of rolling resistance [2].

$$R = A + BV + CV^2 \quad [3], [4], [5]. \quad (2)$$

In equation 1, the components of rolling resistance and gradient resistance in the presence of weight (W) indicates the higher influence of payload and structural weight in the total resistance accounted. Whereas in equation 2, it is indirectly influencing the resistance force as it depends upon the coefficients a, b calculated. For a boat type vehicle, the following equations are used to calculate the resistance force [6].

$$C_F = 0.075 / (\log R_n - 2)^2 = R_F / [1/2 \cdot \rho \cdot S \cdot V^2] \quad (3)$$

$$C_T = R_T / [1/2 \cdot \rho \cdot S \cdot V^2] \quad (4)$$

The gradient resistance has no effects on water transport vehicles as the water has good flow property that helps to maintain the water level to be free from any slope or grade above the earth's surface. Despite this fact, there is no rolling resistance force acting directly on any part of the water vehicle at this mode of transportation since the loading compartment is surprisingly supported by the buoyancy force. Among these four equations 1, 2, 3, and 4, equations 3 and 4 are having unique parameters to calculate the total resistance forces: the density, wetted surface area, and velocity. Despite this fact, it is decided to improve the design of the water-based transportation system.

PROOF OF CONCEPT

The buoyancy force produced by water and air is in different magnitudes which makes the floating vessel oscillates under different loading conditions. From this study, it is found that the unbalanced buoyancy force of two different fluids will pay off in the end to explore a new transport mode which helps to reduce the overall tractive effort. Vehicle level control is performed through a pneumatic system, hence the application of air vessels may have more effective when designing an innovative container floating vessel [7]. According to this article, if the water depth is decreased, the heave motion will decrease, while surge motion will increase, also the natural periods of the barge in heave, roll, and pitch become larger [8]. The basic model is known as the draft adjuster. With different magnitudes of buoyancy phenomenon of water and air act on a single vessel, it is simply represented by the value of water-air buoyancy ratio as shown in **Table 1**. The total volume displacement of this model is 34 m³ when it is submerged in the water.

Table 1. Models with different ratio of [V_D / V_A]

Models	The volume of Air Can – V _A (m ³)	The volume of Draft Adjuster -V _D (m ³)	The ratio of [V _D / V _A]
Model 1	0	0.021	(No Air Can)
Model 2	0.0075	0.021	2.8
Model 3	0.020	0.021	1.05
Model 4	0.040	0.042	1

Specifications of the Air Can Models and Draft Adjuster

Draft adjuster dimensions are as follows: Length = 0.65 m; height = 0.16 m; width at the big end b₁ = 0.35 m; width at the small end b₂ = 0.30 m; area of cross-section or trapezoidal section = $\frac{1}{2} h (b_1 + b_2)$ area = 0.212 m²; volume of the draft adjuster = 0.034 m³ or 34 liters. Dimensions of the Air Vessel fitted in Model 2: Overall Height = 0.28 m; the largest radius of the Can = 0.12 m; Volume of the Can = 0.0075 m³ or 7.5 liters as shown in **Fig. 1**. Dimensions of the Air Vessel fitted in Model 3 as shown in **Fig. 2**: maximum height = 0.41 m; radius = 0.13 m; Volume = 0.020 m³ or 20 liters. In Model 4, there is two identical Air vessel of that model 4 as shown in **Fig. 3**. The total volume of the air can is 0.040 m³ or 40 liters.

Specifications of the Water Tank

The length, height, and width of the Towing Tank are 2 m, 0.5 m, and 0.71 m respectively. The volume of the tank is 0.71 m³. The air vessel can displace 40 liters of water to its surroundings or wall of the tank. The water tank is filled with water half of its total capacity.

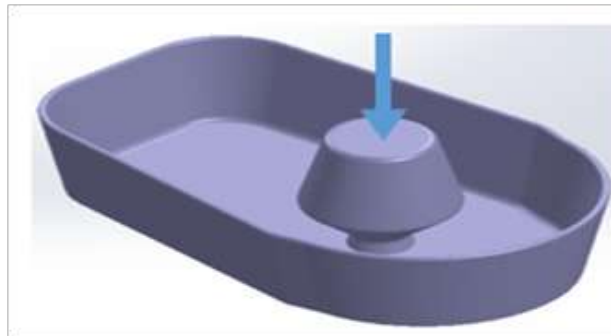


Fig. 1. Model 2 with $[VD / VA]$ ratio 2.8

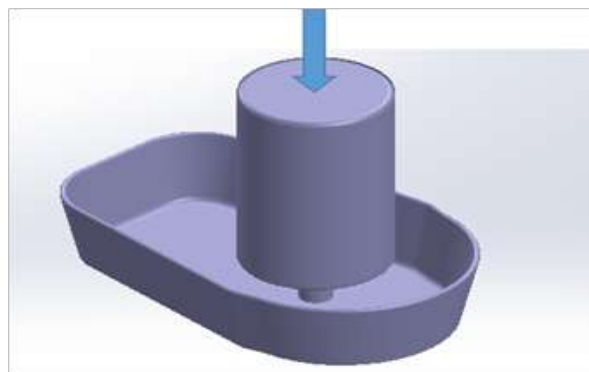


Fig. 2. Model 3 with $[VD / VA]$ ratio 1

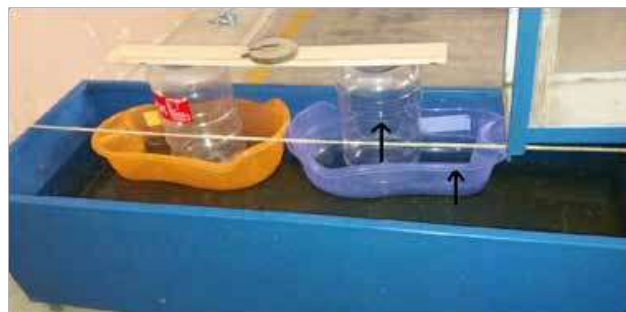


Fig. 3. Model 4 – Draft adjuster and air vessels

Test Procedure

The isothermal compression process happened in the air vessel when it is compressed by the load at the top. The volume of the water displaced when h reaches its maximum level, which is $h=0.16$ m is determined. The volume of air can + volume of trapezoidal below water line 1 is calculated for models 2, 3, and 4, the values are (34 +7.5) liters for model 2, (34+20) liters for model 2, and $[(20*2)+ (34*2)]$ liters for model 4. As shown in the experimental work in **Fig. 4**, it is determined the buoyancy force at $h=0.16$ m in model 1 is 21.8kg. Water and air are represented as the suspension materials being used for the analysis of the trim and stability characteristics of the floating vessel [9], [10], [11], [12], [13], [14]. The values for the spring stiffness and the damping co-efficient are formulated for the water by decomposing the buoyancy force into three components of space, velocity, and acceleration. The draft adjuster helps to reduce the height of the draft level of the floating vessel by balancing the two buoyancy forces of water and air with the payload only on the surface of the waterplane area of the floating vessel. This will reduce the overall fluid resistance under the waterplane area since the floating vessel oscillates on the waterplane area itself even after taking the payload at the longitudinal center of the buoyancy of the floating vessel. The payload capacity of this model is limited to 40 kg at the depth of the air vessel below the waterline reaches a maximum as indicated with an arrow mark in Fig.4 without considering the draft adjuster's capacity.



Fig.4. Experimental Setup and Static Load Test

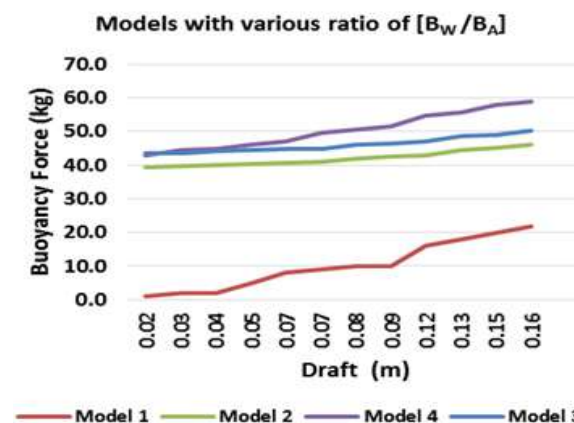
The displacement volume of the draft adjuster is taken as 0.021 m³ instead of 0.034 m³ to keep the water level the maximum. The draft adjuster has been loaded for determining the load for the draft variation within the maximum possible height in a vertical direction.

RESULTS AND DISCUSSIONS

The buoyancy assisted ride model is introduced to establish an innovative transport mode by ensuring the ride model stability concerning the heave motion of the floating vessel that helps to minimize the overall resistance force at dynamic conditions. The water tank is filled with water half of its total capacity to avoid the overflow while loading the models in the experiments. The maximum h value is assumed 0.16 m from model 1 at the static load test. The loads are varying from 2 kg to 50 kg and the loading is done in the models until h reaches 0.16 m or the draft adjuster is about to sink in the towing tank. Model 1 will be a base model, other models comparatively produce more buoyancy force. The difference in magnitude of buoyancy force for a particular mass ' m ' kg is taken as the effectiveness of the floating process. The effectiveness value has to be selected to suit the key control parameters such as pitch, roll, and sway control inputs while designing a propulsion technique. The experimental work is giving the effect of the floating process by taking mass $m = 40$ kg as shown in **Table 2**. The draft adjuster is loaded for all models till the h value reaches to 0.16 m. **Fig. 5** shows the different magnitudes of load in terms of kg for draft value ranges from 0 to 0.20 m.

Table 2. Floating effectiveness in all the Models

Models	Buoyancy Force without Air Can B_d	Buoyancy Force with Air Can BA	Effectiveness of floatation for the mass $m = 40$ kg $[B_A - B_d] / (40 \times 9.81)$
Model 1	196.2 N	-	-
Model 2	196.2 N	274.7 N	0.198
Model 3	196.2 N	392.4 N	0.5
Model 4	392.4 N	784.8 N	1


Fig. 5. Buoyancy difference in Models with Air Vessels

This shows the advantages of models 3 and 4 as these are performed well in taking more buoyancy force for a particular h value of the draft adjuster. The wave energy converter uses only a partial amount of seawater for the energy conversion process, this phenomenon raises the question that if any mechanical force can be used to produce the waves with minimum water as per the reversed wave energy theory. Reversed wave energy theory has the wave energy and mechanical energy as the output and input respectively whereas the wave energy and mechanical energy are the input and output in the wave energy converter. The wave energy content is termed as celerity in this article to elaborate on the energy content in the Rivers [15].

SUGGESTIONS FOR IMPROVEMENTS

Based on these results, the wave energy content required to produce the driving force in the current research can be determined to utilize the minimum possible amount of water in the new kind of transportation mode in the future. The author has found that the buoyancy force itself is the main reason for getting a lower resistance force in water transport vehicles. The experimental study could further improve the efficiency of the utilization of hydrostatic characteristics of water and air to float the boat type vehicles effectively to an extent. Based on the results, a new rule is derived for the payload calculation as dictated below. Payload = the weight of water which can be displaced by the Air Vessel. In other words, the minimum volume of water required for the operation will be equal to the volume of air vessel attached to the boat type vehicle. The air vessel decides the payload, for example, 1000 kg of payload requires 1 m³ of Air vessel and 1 m³ of water as the minimum water level on the towing tank/path to operate the boat type vehicle. In dynamic conditions, the water level in the towing tank/path may be increased to make the flow based on the reversed effect of the wave energy converter. It can be simply notified, wave energy transforms into mechanical energy, in turn, mechanical energy (movement of the boat) transforms into wave energy. The free-body diagram of this transportation model is represented in Fig. 6, the air pot system helps to manage the buoyancy and the weight of the boat model.

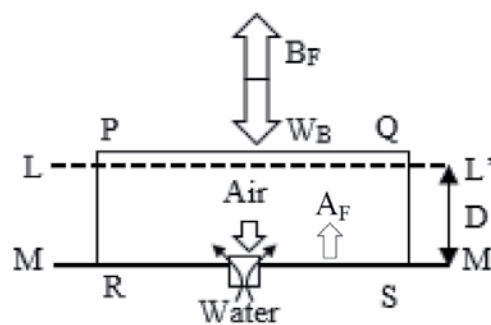


Fig. 6. Free Body Diagram of Floating Model

B_F = Water Buoyancy Force, W_B = Boat Weight

MM' = Water Level before Loading

LL' = Water Level after Loading

$PQRS$ = Air Vessel, A_F = Air Buoyancy Force

$A_F - B_F$ = Key element for levitation

The new levitation concept is established using the factor $(A_F - B_F)$ in this proposal for the effective utilization of the water for the transformation.

FUTURE WORK

The loading compartment may be supported by external guideways. The dynamic load test on a towing tank or customized water tank can be conducted as per the ITTC standard.

ACKNOWLEDGMENT

This research work is carried out in the Fluid Mechanics and Machinery Laboratory of Department of Civil Engineering, Hindustan Institute of Technology and science, Padur, Chennai, Tamil Nadu, India.



FUNDING

This research did not receive any specific grant from funding agencies in the public, commercial, or not-for-profit sectors.

REFERENCES

1. Thomas D. Gillespie, Fundamentals of Vehicle Dynamics, Society of Automotive Engineers Inc, 400 Commonwealth Drive, Warrendale PA 15096-0001.
2. S. K. Clark, 1984. Tire Rolling Resistance and Vehicle Fuel Economy, Fuel Economy, Springer Science + Business Media, New York.
3. Halvor S. Hansen, Muhammad Umer Nawaz, Nils Olsson, 2017. "Using operational data to estimate the running resistance of trains. Estimation of the resistance in a set of Norwegian tunnels", Journal of Rail Transport Planning & Management 7, 62-76.
4. Rochard, B.P., Schmid, F, "A Review of Methods to Measure and Calculate Train Resistances. Proceedings of the institution of mechanical engineers, Part F, Vol. 214, Journal of rail and rapid transit.
5. Satish Chandra and M.M. Agarwal, 2007. "RAILWAY ENGINEERING", Oxford University Press.
6. Saha G. K., Miazee M. A., 2017. "Numerical and Experimental Study of Resistance, Sinkage and Trim of a Container Ship", MARTEC 2016, Procedia Engineering 194, 67 – 73.
7. Jean-Louis BOUVIN, Xavier MOREAU, Andre BENINE-NETO, Alain OUSTALOU, Pascal SERRIER, Vincent HERNETTE, 2017. CRONE control of a pneumatic self-levelling suspension system, IFAC Papers Online 50-1, 13816–13821.
8. Takashi Kishimoto and Katsuro Kijima., 2001. "The maneuvering characteristics on tug-towed ship systems", IFAC Control Applications in Marine Systems, Scotland, UK.
9. Jinglei Yang, Zhuang Lin, Ping Li, Zhiquan Guo, Hanbing Sun, Dongmei Yang, Experimental investigations on the resistance performance of a high-speed partial air cushion supported catamaran, International Journal of Naval Architecture and Ocean Engineering, Volume 12, 2020, Pages. 38-47, doi.org/10.1016/j.ijnaoe.2019.05.004.
10. J.A.Witz, and M.H.Patel. 1987. "Control of marine vehicles with pneumatic compliances." Engineering Structures Volume 9 (Issue 2): 124-133.
11. Jang, Jinho, Soon Ho Choi, Sung MokAhn, Booki Kim, and Jong Soo Seo. 2014. "Experimental investigation of frictional resistance reduction with air layer on the hull bottom of a ship." International Journal of Naval Architecture and Ocean Engineering (Society of Naval Architects of Korea) 6 (2): 363-379.
12. Kumagai, Ichiro, Yoshiaki Takahashi, and Yuichi Murai. 2015. "Power-saving device for air bubble generation using a hydrofoil to reduce ship drag: Theory, experiments, and application to ships." Ocean Engineering (Elsevier Ltd) 95: 183-194.
13. Latorre, Dr. Robert. 1997. "Ship hull drag reduction using bottom air injection." Ocean Engineering 24 (2): 161-175.
14. Pekka Ruponen, Perttu Kurvinen, Ilkka Saisto, Jarmo Harras. (2013). Air compression in a flooded tank of a damaged ship, Ocean Engineering 57, 64–71.
15. Sokolov, S. 2020. Approximate technique for calculation the celerity of long wave in channels with complex cross section. SN Appl. Sci. 2, 231. <https://doi.org/10.1007/s42452020-2018-7>.



IoT based Oil and Gas Survey

B Kannan

Senior Engineer, McDermott Engineering, Chennai, Tamil Nadu

ABSTRACT

In Oil and Gas extraction process, seismic exploration is being widely used and well known by geophysical technique among various survey methods. Moreover, Acoustic signals and Geophones/Hydrophones data is collected and thereafter convolutional model of seismic data is made use of to understand how trace is formed under the seabed. Accordingly, for survey purpose, Artificial Intelligence system like snake Robot, Flying Drones which reduces travelling time in offshore environment is proposed in this paper. IoT (Internet of things) Controller can be fixed with Flying Drones to send live data from hydrophones to Cloud platform using satellite communication as IoT and Cyber physical system might play a vital role in the upcoming years in majority of fields. For instance, Robot can capture the temperature, pressure, wind velocity, Water depth, Humidity etc. and transmits the received data to IoT cloud environment. Digital image processing techniques is used to convert the data received at onshore station to image in addition to the above-mentioned techniques.

Keywords: Seismic exploration; Geophysical technique; Convolutional model; Snake robot artificial intelligence; IoT; Cyber physical system; Digital image processing.

INTRODUCTION

Oil and gas are extremely important natural resources for human beings. During 2008 -2009, for example the world used 150,000 l/s of Oil, the highest when compared to previous year. According to Cambridge research associates, 3.7 trillion barrels oil are left. Today global challenges require new and innovative approaches. Oil and Gas deeply buried in deep land or marine subsurface geologic structures. In order to produce oil, first we need to determine the subsurface structure that is clear and accurate image of the sub surface through large- scale data acquisition. Then oil well can be drilled for commercial purpose. The Exploration seismic method is the most widely used and well known geophysical technique for surveying method. In addition based on digital image processing acoustic wave converted and verified accordingly. Seismic method involved three stage seismic data acquisition, seismic data processing, and seismic data interpretation. The main aim of the exploration seismic method is knowledge of the distribution of wave impedance that reflects the subsurface geology. Exploration seismic typically penetrate the subsurface up to a few kilometer in depth. Basically, one records has amplitude of the reflected seismic waves and time at which such amplitudes arrived at the receiver. Then the data can be processed and interpreted using signal and image processing algorithms, which ultimately influence the decision on where to drill wells that will eventually produce hydrocarbons. The first stage in exploration seismic survey is the acquisition stage, where the seismic data are collected by an array of receivers (geophones for land and hydrophones for marine), transmitted over a narrow band- channel and stored for processing. The acquisition can be done to acquire 2D or 3D seismic data. Next comes the processing of the acquired seismic data sets. Seismic data processing involves the use of many sequential mathematical and signal processing techniques, which are blended with a somewhat subjective interpretation by an experienced geophysicist. This include seismic data processing like geometric spreading, frequency filtering, de-convolution, velocity analysis, seismic migration, and imaging. Finally, process data goes to interpretation stage. Seismic data interpretation aims to extract aims all available geologic information from the processed and imaged seismic data. Interpretation involves sophisticated image processing algorithms. Concept involved in both onshore and offshore both are same only difference (Hydrophones used in Marine environment and Geophones used in Land).

ROLE OF SURVEY

Survey like to be precise as well as accurate, in the offshore world there are added complexity for the team and the equipment. The word survey covers wide range of services includes Positioning, Geophysical surveys. Positioning offshore is provided by utilizing the multiple satellite constellations that now orbit the earth, of which the US department of defense GPS system

is the best known example. Other system are GLONASS (Russia), IRNSS (India). Geophysical surveys are carried out from vessels to acquire seismic, sonar, bathymetry, oceanographic and environmental data which is used by the hydrocarbon, telecommunications, dredging and subsea mining industries. The surveys identify drilling hazards and establish corridors for pipelines and cables as well as the seabed conditions for sub-ocean mining. This requires cutting-edge technology as the water depths vary from 5 meters to 4,000 meters – yes 4 kilometers straight down.

EXISTING SYSTEM

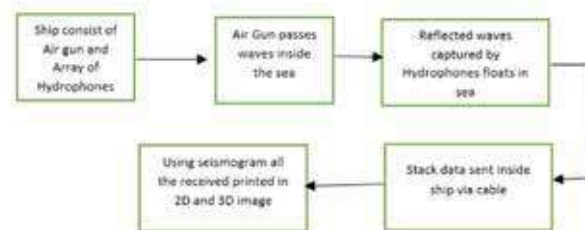


Fig 1. Basic principle of seismic method

The basic principle of Seismic method are based on determinations of the time interval that elapses between the initiation of a sound wave from detonation of a dynamite charge or other artificial shock and the arrival of the vibration impulses at a series of seismic detectors (geophones). Since the middle of the last century seismic reflection surveying has undergone rapid development and has become, arguably, the foremost method for imaging the structure of the Earth's crust referred to for more information. Reflection seismic surveys are currently widely used in a range of disciplines in academia and industry (primarily hydrocarbon exploration), with many millions of kilometres of data acquired. Refer **Figs 1-3**.

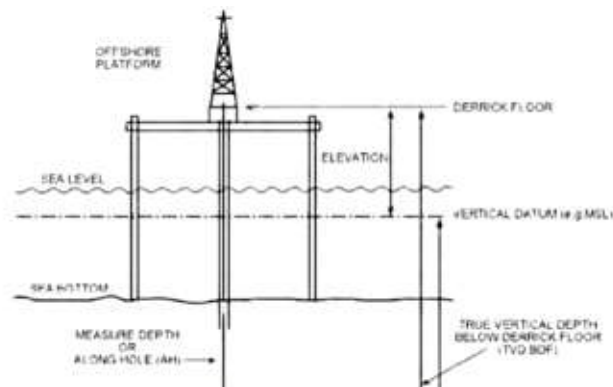


Fig -1

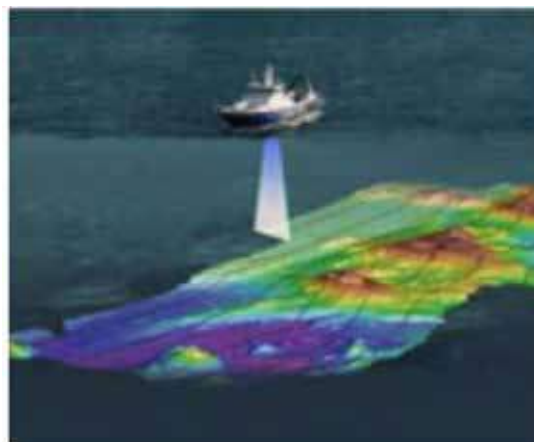
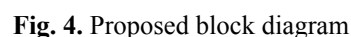


Fig -2



PROPOSED SYSTEM AI DRONE

Even a few decades back, nobody could have imagined having a video chat with their families in a different continent. Nowadays, it is a common thing. All of these is due to technology getting cheaper, and devices emerging with new and improved capabilities. People can get things done with a click on their smartphone, be it sending emails, paying bills, transferring money or booking a cab.



Apart from being used inside smart homes, IoT has a huge application area in the various industrial sectors. These solutions perform statistical and financial analysis of a company as a whole and finally provide predictions using some AI and machine learning algorithms. Since various things are continuously connecting to form an IoT, there are various disciplines that get

associated with IoT. Therefore, IoT can also be thought of as a combination of various domains. **Fig. 7** gives a representative list of some domains (most of these overlap with each other. in terms of concepts and techniques) constituting the IoT. Internet of things is just a connected system of physical things (like appliances, crop fields, plants, animals, etc.) and humans. Humans are connected to these devices using some smart objects attached to both which are capable of sending, receiving and analyzing data. These smart objects represent the entity (a human or a physical thing), it is attached to, in the network Also **Fig 5**. Shows how Drone is connected with IoT and Stacked data pushed to the Cloud platforms. List of cloud platforms are EWON, Amazon web services, SAP HANA, Siemens Mind sphere etc. By using Cloud platform all the available data in IoT device can be pulled using MQTT, HTTP Protocol via packets.

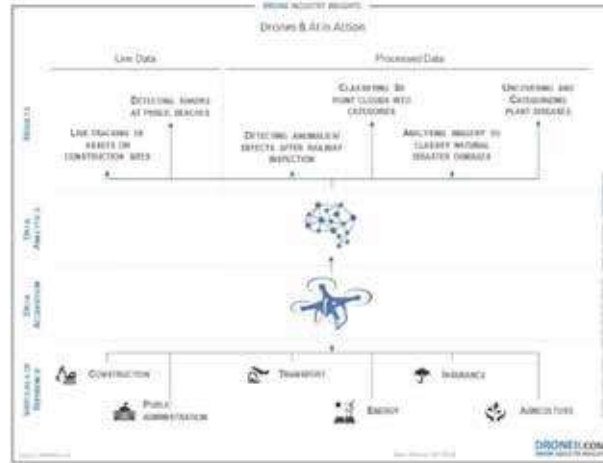


Fig 5. AI drone connected with IoT cloud

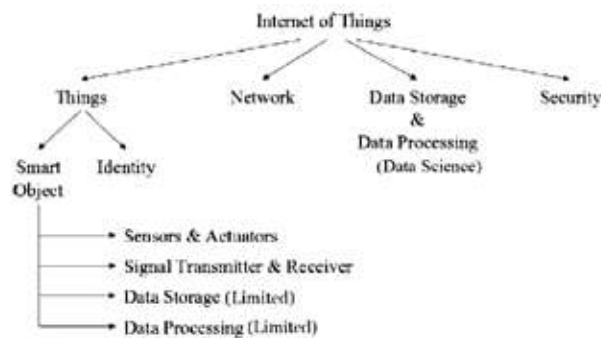


Fig 6. IoT tree

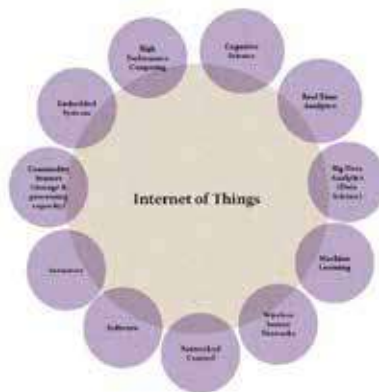


Fig 7. IoT into Different Fields.



AI Enabled IoT

IoT is a vast concept encompassing too many sensors, actuators, data storage and data processing capabilities interconnected by the Internet. Thus any IoT enabled device can sense its surroundings, transmit, store and process the data gathered and act accordingly. The last step of acting accordingly is entirely dependent on the processing step. The true smartness of an IoT service is determined by the level of processing or acting that it can perform. A non-smart IoT system will have limited capability and will be unable to evolve with the data. However, a smarter IoT system will have artificial intelligence and may serve the actual goal of automation and adaptation. In this context, few examples of existing IoT services with the working of AI behind them are Voice assistants like Alexa, Siri, Google Assistant.

CYBER PHYSICAL SYSTEM

When it was coined by Helen Gill at the National Science Foundation in the United States. CPS according to National Science Foundation (NSF) are “engineered systems that are built from, and depend upon, the seamless integration of computational algorithms and physical components”. Today it is thought of as a system that Works on and is monitored by computer-based mechanisms (built inside each component as well as in the complete system), strongly connected via the Internet and is easily accessible to its users.

SATELLITE COMMUNICATION

For offshore oil and gas, satellite communications seems made to order. It's fast, simple to use, and capable of moving huge amounts of voice, fax, and data from here to there, any place on the globe, in a fraction of a minute. Nearly everybody benefits one way or another - drillers, logging, and seismic contractors. And their clients, of course, the producers. Inmarsat A provides a high-quality phone, telex, fax and data service at transmission speeds of 9.6 kilobits per second (kbps).

GPS (Global Positioning System)

Worldwide media and scientist attention have put Unmanned Aerial Vehicles (UAVs) in the spotlight. UAV or also known as a drone is an unmanned aerial vehicle that has the main functions for intelligence, reconnaissance and surveillance. The recent developments of drone for sprayer pesticide applications and used for delivering items, for example the Amazon Prime Air, where Amazon used an octocopter to deliver items with weighs less than 5 lb or around 2.3 kg. Drone also can be used as a tool to survey a building [4], aerial photogrammetry and mapping. Recent advances also pushing drone technology to adopt a newer way of communication, such as an implementation of Mobile Edge Computing (MEC) [6], and Low Power Wide Area Network (LPWAN). Geodetic coordinate system is a coordinate system which a position defined by 3 numbers, a latitude, longitude, and altitude. A position which defined by geodetic coordinate system is a position on a globe. Latitude is a line that intersects the defined position and a line which parallel to an equator line. Longitude is a line that intersects the defined position and a line which parallel to a prime meridian line. Altitude is a distance between defined position and the ellipsoid. Our proposed method uses Air gun Outlet sensor as switch which provides information whether waves are transmitted inside the seabed. This drone will be keeping distance between sea level and drone is 10 Meter. Using ultrasonic sensor distance is measured based on same AI algorithm is developed accordingly. The system has a few features such as altitude and speed settings. Proposed system designed to be able to interact with interactive sensors. Other than that, the navigational algorithm itself could be further enhanced and fixed using a more precise and adaptive algorithm that could navigate from any distance and for any usages.

SNAKE ROBOT

Snake robots carry the potential of meeting the growing need for robotic mobility in unknown and challenging environments. These mechanisms typically consist of serially connected joint modules capable of bending in one or more planes. The many degrees of freedom of snake robots make them difficult to control, but provide traversability in irregular environments that surpasses the mobility of the more conventional wheeled, tracked and legged types of robots. Research on snake robots has been conducted for several decades. Early empirical and analytical studies of snake locomotion were reported already in the 1940s by Gray, and Hirose developed the world's first snake robot as early as 1972. In the last 20 years, the literature on snake robots has flourished enormously with numerous proposed approaches to modelling, development, and control of these mechanisms. In this paper we suggest to use snake robot in marine environment to collect the reflected waves from the sea bed. There shall be array of snake robot to collect the waves.



Fig 8. Typical Snake Robot.

CONTROL OF SNAKE ROBOT

Joint Actuation Mechanism

The articulation mechanism of each joint module (see Fig. 11) has two degrees of freedom (pitch and yaw) and consists of two links supported by bearings in a steel ring. Each link has a connection point that allows it to be connected to the next joint module by two screws. The angle of the two moving links in the joint are measured with magnetic rotary encoders (AS5043 from Austria microsystems). A magnet measuring 6 mm in diameter is attached to each link so that it rotates above the rotary encoder as shown in **Fig. 9**. Each link is driven by a Hitec servo motor (HS-5955TG) by connecting the output shaft of each motor to a worm gear (gear ratio of 1:5.71) through a steel roller chain

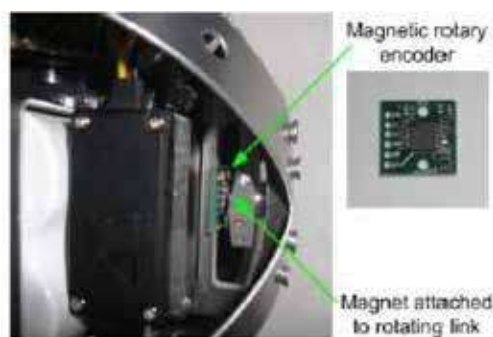


Fig 9. Magnetic Rotary Encoder for measuring the joint angles.



Fig 10. Roller chain connecting the servo motor to the worm gear

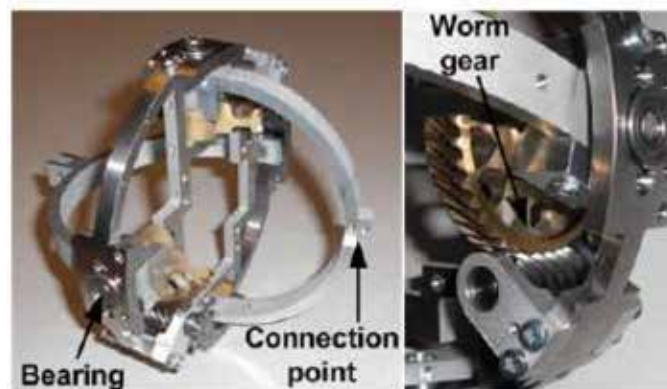


Fig 11. The articulation mechanism of the joint modules



Fig 12. The Voltage Regulation Card .Middle: The battery Charge card. Right: Joint Controller card

Controller

Each joint module is controlled by the microcontroller card shown to the right of **Fig. 12**, which is based on the Atmel microcontroller AT90CAN128. This card continuously measures the joint angles and the contact forces, and generates PWM pulses for the servo motors. The card has a CAN bus interface for communicating with the other modules of the robot refer **Fig 12**. The head is also equipped with a small wireless camera and two IR distance sensors.

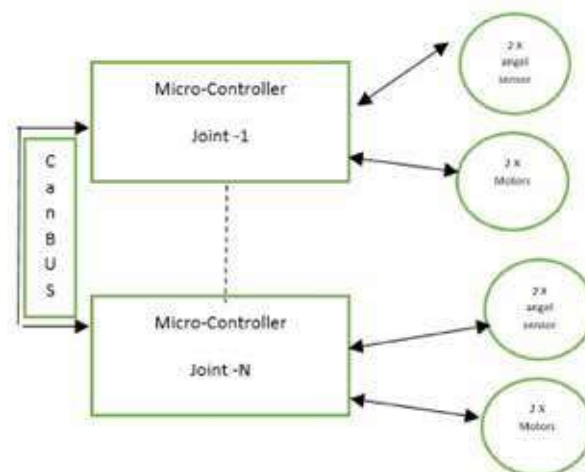


Fig 12. Data Flow between Modules

Power Supply

Each joint is powered by two serially connected Lithium Ion batteries (6.6V at about 2.3Ah), which are charged by a battery charger card (see the middle of **Fig. 12**). Regulation of the voltage to the internal components of a joint is handled by the card shown to the left of **Fig. 12**.



The exterior Gliding surface

The exterior gliding surface by covering each joint module by two hemispherical shells can be made by Inconel 625 or higher grade material to withstand in corrosive water environment. Each shell is attached to the joint mechanism by the screws.

Force sensor

Four force sensing resistors (FSRs) with diameter 13 mm are mounted on each side of a joint module to measure contact forces. A FSR is a polymer thick film device that exhibits a decrease in electrical resistance when the force applied to the sensor increases.

RESULTS AND DISCUSSION

Drone makers are collaborating with oil and gas companies to develop custom drones with data collection technology to obtain real-time insights. One of the early adopters of drones, BP, started conducting pilot studies in 2006 at its oilfields in Alaska. The studies evaluated the effectiveness of drones in monitoring gravel road conditions. This helped ensure safe and efficient movement of trucks supplying oilfield equipment to the production site. Chevron is leveraging the aerial data acquisition capabilities of drones for improving safety and productivity at oilfields. The company is applying augmented reality to drone feed for evaluating field equipment and infrastructure during inspection and monitoring operations. Chevron is also experimenting on the application of drones in the event of industrial accidents, particularly for assisting in oil spills. Apart from this drone can be used in automated data gathering, Maintenance, integrity, surveillance workflow, pipeline inspection, flare inspection.

CONCLUSION

An Offshore Industry can be replaced with Drones and Snake robot to reduce the time, man power for the Industries. In addition in Subsea system already snake robots plays vital role in installing umbilical's, riser and Flow arms under the sea. Snake robot used as a mechanic to operate the subsea system. I strongly recommend to implement ideas present in this paper practically to overcome many circumstances.

FUTURE ENHANCEMENTS

- Future work will include other testing like simulating the system using LABVIEW software.
- Need to analyze the best back up system for batteries.
- Need to analyze the best back up system for batteries.

REFERENCES

1. P Liljeback, K Y Pettersen , O Stavadahl, J T Gravdhal I., "A Review on Modelling , Implementation , and Control of Snake Robots ", Norwegian University of science and technology .
2. Ashish Ghosh , Debasrita Chakraborty, Anwesha Law " Artificial Intelligence in Internet of Things". IET Research Journals.
3. Eleni Kelasidi and Kristin Y. Pettersen Department of Engineering "Modeling of Underwater snake robots".
4. Pal Liljeback, Member IEEE, Kristin Y Pettersen, Senior member IEEE and Kristin Y Pettersen Department of Engineering "Modeling of Underwater snake robots".
5. Lin fa ; Lei wang ; Yuan Zhao, Lin liu, Yazuan zheng, Nan Zhao , Meishan Zhao , and Guohui li "Research progress in acoustical application to petroleum logging and seismic exploration ", School of engineering , XI'an' university of post and telecommunication , Xi an Shannxi, China .The james frank Institute and department of chemistry, the university of Chicago , Illinois, USA.
6. Daniel Sopher " Converting scanned images of seismic reflection data into SEG-Y format. Methodology Article.



An Overview Study of Ocean Energy Potential and Technologies in India

Geetam Saha, Dipesh Majumdar

Department of Construction Engineering, Faculty of Engineering & Technology, Jadavpur University, Kolkata

✉ dipeshce@jadavpuruniversity.in

ABSTRACT

Increasing power demands and rapid deterioration of the air quality index across majority of the urban localities of India has compelled researchers to find sustainable and harmless alternative sources of energy. Oceans have been an untapped source of energy for India since a long time. Preliminary investigation and identification of potential sites for harvesting ocean energy (OE) began in 1988 and first pilot scale wave energy plant came up in 1990. Vast research has been conducted by many researchers in the field of OE till date but still the contribution of OE is negligible towards meeting the nation's needs. OE can contribute hugely to transform the coastal areas and islands into self reliant ecosystems in terms of energy demands. This paper focuses on reassessing the OE potential of India, the available technologies for harnessing OE and stimulates research on the topics that have not been in focus so far.

Keywords: Ocean wave energy; Oscillating water column; Tidal energy conversion; Ocean thermal energy, Renewable.

INTRODUCTION

In the decade 2007-2017, India's total final consumption (TFC) of energy had increased by 50% across all sectors [1]. Increasing energy demand can be a sign of development for a developing economy like India, though the problem comes to the point that still now India falls under the list of energy deficit countries. Statistics have shown that for India the power supply deficit was 0.5% in financial year 2019-20 [2].

Also the records have shown that in financial year 2019-20, the renewable energy sector has contributed only 21.25% to the total power consumption, out of which the share of OE was almost negligible [3].

Figure 1 exhibits the graphical representation of the contribution of various types of power stations contributing to the installed power grid of India. It is clearly visible that there is huge gap between the contributions of sustainable and unsustainable energy sources.

So undoubtedly it can be said that for transforming India from a power deficit nation to a power surplus nation, it is the need of the hour to assimilate alternative power sources to main stream power grid.

Considering various factors such as scalability and sustainability which are essential for the selection of the alternative power sources, (OE) is a reliable source to ponder upon.

OE can be classified broadly into five principle forms [4]. Tidal Rise & Fall, Tidal/Ocean Currents, Waves, Salinity Gradient, and Thermal Gradient.

RELIABILITY & COMPARISON

India has a coastline of 7516.6 km [5]. Widespread presence of such marine conditions is a great advantage for India to harvest marine energy. OE harvesting technologies in India can be broadly classified under the following 3 heads.

Ocean Wave Energy (OWE)

Tidal Energy (TE)

Ocean Thermal Energy (OTE)

According to an estimate ocean and tidal currents altogether contain about 5 TW of energy and 1-10TW [6] of wave energy in

the entire ocean. Waves provide 15-20 times [7] more available energy per square meter than wind and solar energy.

OWE is far more dependable than the other alternative renewable energy sources like wind and solar energy. In terms of availability at a given site OWE is more reliable because it is available up to 90% of the time whereas availability of solar and wind energy is limited to 20-30% of the time [8].

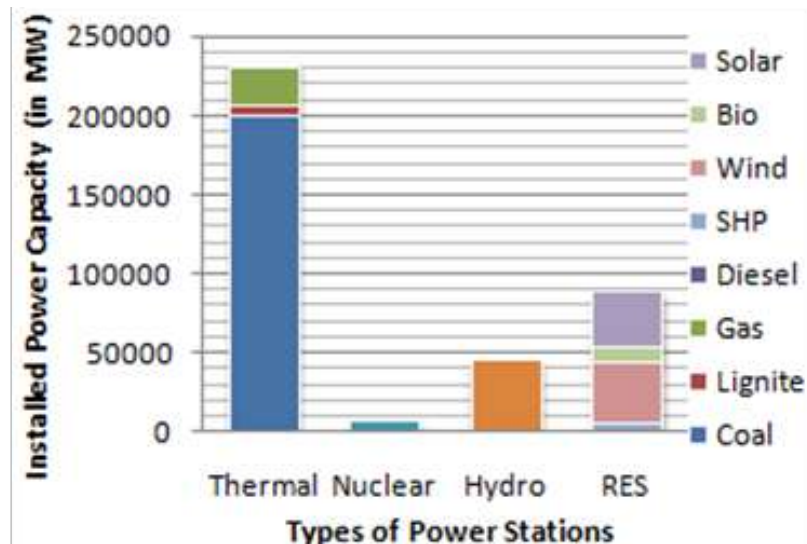


Fig 1. Installed Capacity of various types of Power Stations in India (as on 31/08/2020)

Tidal Energy harvesting under most conditions is not continuous but the timing of tides can be calculate very precisely which makes tidal energy a reliable source of energy.

In a tropical country like India, the temperature difference between free surface of the ocean and depth of around 900 m is above 20°C [9]. The fluctuation in this value is only 1°C round the year. Thus OTEC can be considered as a source to depend upon for harmless energy.

OCEAN WAVE ENERGY (OWE)

Ocean waves originate as result of energy transfer from the sun to wind and subsequently to water [7]. These waves have the capability to travel thousands of miles with little energy loss.

OWE MEASUREMENTS

Measurement of the forces acting upon the wave energy convertor (WEC) is essential for the design process. There are mainly four categories of instruments for measuring wave data. They are wave staff, sub-surface sensor, buoys and ship borne systems.

The power (P) in a wave can be expressed by the formula [10],

$$P = \frac{\rho g^2}{64\pi} H_s^2 T \quad (1)$$

Where P is in kW/m crest length, ρ is the mass density of sea water, g is the acceleration due to gravity, H_s is the significant wave height in meter and T is the wave period in seconds for actual sea state.

For precise design of underwater WEC, determination of wave power at operational depth E(d) is essential. E(d) is calculated by (2) [11], where d is depth below sea water level (SWL) and λ is wavelength.

$$E(d) = E(SWL) \cdot e^{-\frac{2\pi d}{\lambda}} \quad (2)$$

Above equation stands valid only for d greater than $(\lambda)/2$.

There are basically two approaches for energy transfer from the waves to OWE convertors. One approach is due to linear vacillating motion corresponding to change in mass of the over passing wave.

$$P_{generated} = F_{water} V_{float} = \frac{\rho_{water} H A_{float}}{g} \cdot \frac{2L_{stroke}}{T} \quad (3)$$

Equation (3) gives the power transferred to the under float from an over passing wave [7]. Where H is the wave length, A_{float} is the area of the float and L_{stroke} is the stroke length.

Second approach is power and energy transfer due to wave induced air pressurization. Oscillating water column(OWC) OWE convertors work on this approach.

$$P_{OWC} = \left(p_{air} + \frac{\rho_{air} v_{air}^2}{2} \right) \cdot v_{air} \cdot A_{duct} \quad (4)$$

Equation (4) gives power available from the airflow through the OWC outlet [7]. Where p_{air} is the pressure at the turbine, ρ_{air} is air density, v_{air} is the air flow speed at the turbine and A_{duct} is area of the turbine.

OWE HARVESTING TECHNOLOGIES: PAST & PRESENT

OWE harnessing devices can be classified into different types based on design and working principle.

Based on turbine type- Oscillating water column(OWC)

Overtopping

Based on buoy type - Tube type

Float type

Oscillating Water Column

OWC technology uses self rectifying air turbines for harnessing energy from the unidirectional flow of rotor irrespective of incident airflow directions.

For unidirectional flow of the turbine, presence of guide vanes on the downstream side of rotor introduces a loss which affects turbine's performance considerably. Vast research has been done by researchers to find an optimized air turbine design to mitigate this problem.

Fig. 2[12] depicts the variety of air turbines which are used for OWC wave energy convertors in a nutshell.

India's first OWC based wave energy plant was setup at Vizhinjam in 1990. It runs on an impulse turbine with self controlled guide vane.

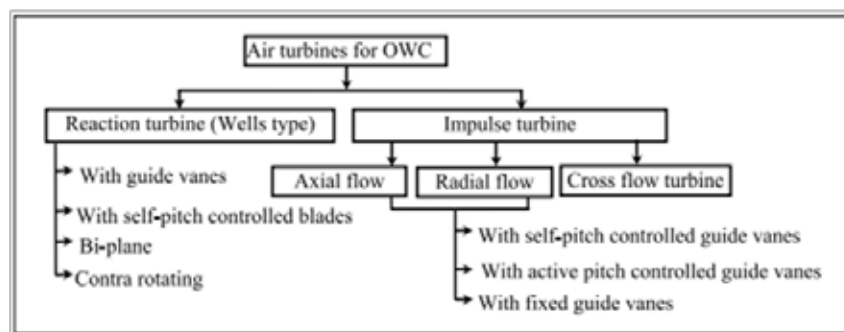


Fig. 2. Various types air turbines used for OWC WEC

Overtopping

Overtopping technology uses the concept of utilizing a variable head of water for power generation. Water from the crests of wave is captured to create a head which rises above the surrounding sea water level. This head is created by building an offshore reservoir in shallow waters. The head created is small, low head turbine is generally used for this purpose especially Kaplan turbine [13].

Buoy-Tube

Buoy-tube type WECs are moored to sea bed. As its name indicates it consists of a neutrally buoyant hollow tube. It works on the conception that pressure variations on the water surfaces induces pressure difference between tube's top and bottom causing water to flow in and out of the open ends of the tube. Piston power takeoff mechanism is preferably adopted for this purpose as rate of water flow is not rapid.

Buoy-Float

Buoy-float WEC consists of a sealed cavity which is positively buoyant. It may be sealed type or any other sort of cavity. Depending upon depth where the float is to be placed, the air and water inside the cavity is determined. The motive is to make it neutrally buoyant with respect to the depth at which it is to be placed.

Power takeoff methods for float type WEC is selected depending upon its operational depth. Linear generators are used for those float type WECs which operate at sea surface. Linear generators produce electricity from linear motion rather than rotary motion.

An inherit complication with buoy-type WEC operating at sea surface is that wave height can exceed the stroke length. In the worst case scenario, during harsh weather due to extreme wave heights damage can be caused to the WEC.

In such case a control system is used to pump air or water into the float which changes the buoyancy and save the float in case of huge wave heights.

An alternative method is utilizing a flexible hose for power generation. Due to the pressure variations induced because of passage of waves, the hose is alternatively stretched and released. This motion contraction and expansion of the tube is used to generate hydrostatic pressure which is converted into electricity.

Harnessing OWE has been the matter of concern of researchers in India since a long time. Apart from the accomplishment of establishing OWC based OWE energy in 1990, Indian researchers got a major breakthrough in 2015 by completing the sea trials of backward bent ducted buoy (BBDB).

BBDB was a floating wave power device indigenously developed, designed and fabricated at National institute of Ocean technology(NIOT).The power module on BBDB consists of a unidirectional impulse (UDI) turbine and a permanent magnet direct current generator (PMDC).Open sea trials were conducted between 2011-2015.Trials were successful. This experience ensured that floating power WECs can be made indigenously for small power requirements [14].

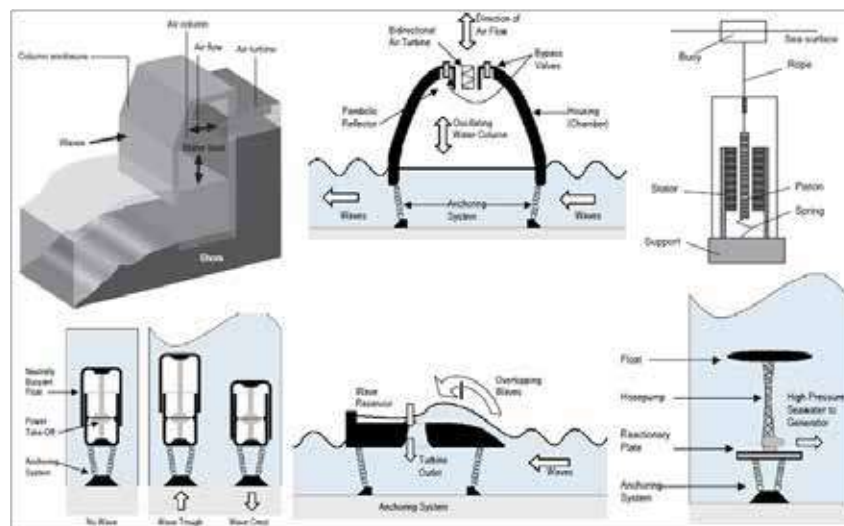


Fig 3. Various types of OWE technologies

OWE: India's potential

Presences of water bodies such as Bay of Bengal(BOB) and Arabian Sea(AS) open up huge opportunities for OWE harvesting. Wave power increases with depth from free surface along with distance from coast. Varies studies have been conducted by

various researchers and research agencies in India for measurement and estimation of OWE. Ocean engineering division of National institute of Oceanography (NIO), Goa has been collecting wave data and analyzing them for accurate estimation which helps in efficient design of indigenous OWE harvesting systems. In a study data was collected from 20 different locations (**Fig. 4**) along the Indian coastline. **Table 1** exhibits the same data [5]. Seasonal variations affect the wave characteristics considerably. In another study by NIO for computing seasonal average wave power in BOB and AS. The seasonal average wave power over the 40 years was calculated. Figure 4 [15] represents the same for pre-monsoon (February–May), southwest (SW) monsoon (June–September), and post-monsoon (October–January) along with annual mean wave power. The maximum values of average wave power during annual, pre, southwest, and post-monsoon seasons were 17.73, 13.62, 39.87, and 12.63 kW/m, respectively.

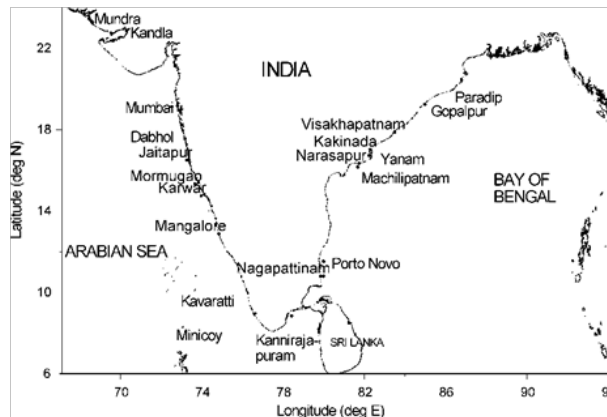


Fig. 4. Locations of Wave Measurement

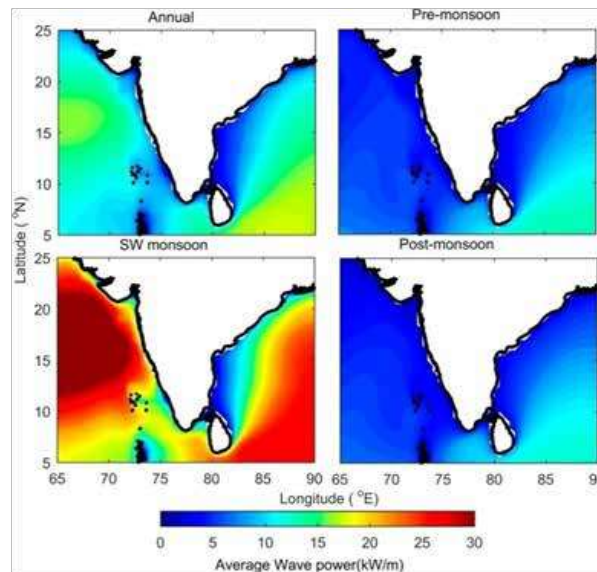


Fig. 5. Annual and seasonal mean wave power averaged over 40 years (1979 to 2018)

Table 1. Wave characteristics at various locations along Indian coastline

Location	Water depth (m)	Duration of data (month)	Range of H_s (m)	H_s for 100 year return period (m)	Predominant average wave period (s)
Mundra	18	6	0.1–2.2	4.4	2–6
Kandla	15	12	0.1–2.8	4.4	3–11



Veraval	15	4	N.A.	5.3	N.A.
Dahej	20	7	0.1–2.0	3.0	2–10
Hazira	15	7	0.1–2.9	4.2	2–14
Daman	27	7	0.1–6.0	8.0†	3–15
Umbergaon	37	6	0.2–4.8	6.6†	3–16
Vadhavan point	24	8	0.3–2.8	3.4	3–15
Bombay high	75	19	0.4–5.1	7.8	3–16
Mumbai	30	3	N.A.	5.1	N.A.
Uran	10	5	0.2–2.5	3.2	4–16
Dabhol	14	5	0.4–4.6	7.1	3–8
Ratnagiri	10	12	N.A.	3.9	N.A.
Jaitapur	16	12	0.1–3.3	5.6	3–15
Mormugao	23	12	0.3–5.9	9.7†	3–9
Mormugao	14	4	N.A.	5.1	N.A.
Karwar	16	48	N.A.	6.1	N.A.
Mangalore	13	5	N.A.	4.1	N.A.
Kavaratti	10	4	N.A.	2.1	N.A.
Kalpeni	11	12	0.2–2.3	3.1	3–12
Androth	11	12	0.3–2.5	3.6	3–9
Agatti	15	12	0.3–1.8	2.2	3–11
Minicoy	10	12	0.3–1.7	2.3	3–11
Kannirajapuram	12	12	0.3–1.9	2.3	3–9
Nagore	10	12	0.2–2.0	3.2	2–9
Pillaiperumalnallur	15	12	0.2–2.1	2.7	2–9
Porto Novo	80	6	0.3–2.1	2.8	3–12
Machalipattanam	20	8	0.5–2.3	3.0	3–15
Narasapur	10	11	0.2–4.2	4.6	4–12
Yanam	90	12	0.3–2.8	3.5	3–15
Tikkavanipalem	12	12	0.3–3.9	4.2	3–10
Visakhapatnam	17	36	N.A.	4.9	N.A.
Gopalpur	10	12	0.2–2.5	3.1	3–9
Gopalpur	15	12	0.2–3.3	4.8	4–8
Paradip	16	9	0.1–3.7	6.3	3–10
Sunderban	20	3	N.A.	2.1	N.A.



TIDAL ENERGY (TE)

Tidal energy refers to harnessing energy from fluctuation of sea surface under the influences of tides or from tidally driven currents.

Tidal motion is the result of gravitational pull of the sun and moon. It is the marine manifestation of energy fluxes existent in the earth, moon and sun system [16]. Presence of land masses complicates these energy fluxes and result in local enhancement where conditions are befitting.

TE MEASUREMENTS

An initial high expense of setting up a tidal barrage for TE harvesting is one of the primary reasons for limited presence of TE plants in the nation. But local enhancement of tidal fluxes at certain locations across the nation makes TE an economical alternative source of energy. Researchers have been working in the domain of TE harvesting because of its long life and reliability. Because of high expenses, extensive theoretical estimation and hydrodynamic modeling is essential for any detailed discussion on TE.

Tides contain both potential as well as kinetic energy.

$$E_p = 0.5 \rho g A_b \Delta h_b^2 \quad (5)$$

Equation (5) [17] gives potential energy contained in a water volume impounded in a basin, where E_p is the potential energy over a tide cycle, ρ is the density of sea water, g is the acceleration due to earth's gravity, A_b is the horizontal area of enclosed basin Δh_b is the mean tidal range in the basin.

$$E_k = 0.5 C_p g A_s V^3 \quad (6)$$

Equation (6) [17] gives the power generated by a tidal turbine from kinetic energy of the tides, where E_k the kinetic energy of the tidal stream is, C_p is the turbine power coefficient, g is acceleration due to earth's gravity, A_s is the swept area by turbine blades, V is the tidal current.

Table 2. Tidal potential across Indian coastline

Coastal region	Tidal range (m)	Typical tidal currenta (m/s)	Ave. available PE per square kilometer (MW)	Ave. available KE per square meter (W)
Khambhat	5–11	2.5	10.9	2604.3
Kutch	4–9	3.0	7.2	4500.2
South Gujarat	2–4	2.0	1.5	1333.4
Maharashtra	2–4	1.5	1.5	562.5
Karnataka	1–1.5	1.5	0.2	562.5
Kerala	1–1.5	1.5	0.2	562.5
Tamil Nadu coast	1	0.8	0.1	85.3
Andhra coast	1–2	1	0.2	166.7
Orissa coast	2–4	1.5	1.5	562.5
Sundarbans/Hooghly	4–7	2–3	7.2	2604.3

TE HARVESTING TECHNOLOGIES: PAST & PRESENT

All TE harvesting technologies can be broadly categorized into two types depending on working methodology, tidal barrage and tidal stream turbines.

Tidal Barrages

In tidal barrages, lagoons and fences the methodology is to exploit the rise and fall of sea level. Tidal barrages operate basically in two schemes single basin and multiple basin schemes. When tidal current moves towards land and away from sea it is known



as flooding while the vice versa case is known as ebbing.

In single basin power generation, 3 operational modes exist.

First ebb generation, electricity is generated only during ebb tide. This mode generates electricity for at most, 40% of the tidal range [16]. Second flood generation, in this mode all gates are kept closed during initial phase of the flood tide. Flood generation is less preferred for its detrimental effects on the environment. Third two way generations, electricity is generated in both ebb and flood tide. It enables reduced period with low power generation but generates low peak power.

Double basin power generation allows continuous power generation for a longer period but adds complexity. Till date two types of designs for double basin system are known. First or more common is the one in which a channel is used to connect to basins and the respective gates of the basin are always controlled in such a way that a head of water is created between the two basins. Second design a second smaller storage basin is created on the seaward side of primary basin from which power can be generated whatever the state of tide is.

For harnessing TE, one of the essential requisites is that the hydro turbine must work efficiently in variable and low head conditions. Generally, variable blade Kaplan turbine is employed in such circumstances [18]. A series of such turbines is generally installed at the barrages. In TE plants compact and efficient design of turbine is preferred in which generator is built into the turbine itself. Best examples of this type are bulb turbine as well as Straflo turbine.

Tidal Stream

This technology harnesses the kinetic energy of local tidal currents which an approach similar to wind turbines. Hydrokinetic turbines are employed for this purpose. Based on the principle of operation they are classified into categories such as axial-flow, cross-flow and reciprocating devices. Sea water is much denser than air so these hydrokinetic or tidal stream turbines generates more power in a given area in comparison to wind turbines.

TE: India's potential

Table 2 [17] highlights the fact that 3 regions are the most prospective in terms of TE harvesting. Those are Sunderbans, Khambat, Kutch. They have large tidal range apt for barrage type TE plant. Flow velocities are enhanced at the opening in the coastline, which is appropriate for stream type TE plant.

OCEAN THERMAL ENERGY (OTE)

OTE conversion (OTEC) exploits the temperature difference between sea surface and deep sea or ocean in pursuit to drive a thermodynamic heat engine that can generate electricity.

OTE Measurements

Hotspots for OTE are the tropical regions which lie between 20° of the equator. In these regions the surface temperature can rise up to 33°C. At a depth of about 1 km temperature 5°C. India lies between 8°4' north to 37°6' north latitude. It is clearly visible that India is a hotspot for OTE. US National Renewable Energy Laboratory estimated that 60 million km² of tropical ocean absorbs an energy equivalent to 250 billion barrels of oil/day [13].

Thermal efficiency of a heat engine can computed using (7), where W is work, T is surface water temperature, T° is deep water temperature and Q is the thermal value.

$$W = \frac{T - T^{\circ}}{T * Q} \quad (7)$$

OTE HARVESTING TECHNOLOGIES: PAST & PRESENT

OTEC plants can be classified on basis of two criteria, one is the heat engine cycle and location. On basis of heat engine cycle it can be classified into three types.

Closed Cycle

It is based on the organic Rankine power cycle. It generally uses ammonia as the working fluid. Ammonia is used because it doesn't contribute to ozone layer depletion as its other counterparts do.



Open Cycle

This method uses the warm water directly. This methods produces desalinated fresh water which can be used for drinking and irrigation purposes.

Hybrid

It combines the features of both open and closed cycle. In this method the warm sea water is flash evaporated as similar to open cycle. This steam is used to vaporize the working fluid ammonia.

Based on location OTEC plants can be classified into two types, land based and ocean based. One of the major problems with land based plant is the size of cold water pipe. Slopes are seldom larger than 15°. This leads to length of the pipe to go 1000 meters down is $\frac{1000}{\sin 15^\circ}$ or 3864 meters [19].

OTE: India's potential

As estimated by researchers for OTEC plants, the acceptable power density is 0.2 MW/km². With such spacing and allowing parasitic losses, estimated OTEC potential in India is around 180000 MW.

DEVELOPMENTS

India got its first breakthrough in OE sector when the OWC WEC started operation in 1990. As the Table III summarizes vast developments had taken place in the OE sector in last 3 decades. In 2015, successful completion of trials of BBDB empowered India for generation of offshore power as well. In this decade intense research and developments are under progress pertaining to optimization of hydrokinetic turbines and OWC turbines.

Table 3. Major developments in OE sector in India

Decade	India's milestones in OE sector
1980-1990	<ul style="list-style-type: none"> CEA had identified tidal potential in the Gulf of Kutch in Gujarat. The investigations were formally launched in 1982. The techno-economic feasibility study was completed in 1988. First wave power effort from IIT Madras .Pilot plant by GoI.
1990-2000	<ul style="list-style-type: none"> First OWC type wave energy pilot plant was installed at Vizhinjam. Generation & grid connectivity demonstrated. Hybrid BW was proposed by DOD at Thangassery and Mus point.
2000-2010	<ul style="list-style-type: none"> Horizontal axis turbine by NIOT. BBDB program started. 1MW OTEC-Installation difficulties
2010-2020	<ul style="list-style-type: none"> Kalpasar Tidal Double chamber OWC at IIT Madras-optimization BBDB Demo by NIOT Atlantis-Kutch for 50-200MW-Tidal Stream Establishment of 1 lakh litres per day LTTD plant powered by OTEC at Kavaratti Island Establishment of waste heat recovery plant at Tuticorin Thermal Power Station Development of turbines for harnessing energy from OTEC/Wave energy/Ocean currents which could be stand-alone units or used to power LTTD plants or small loads

CHALLENGES & SOLUTIONS

Despite huge potential there are a number of hindrances for OE in India. Still now there is a major disparity between theoretical, technical and practical utility of OE in India. Main limitations of OE include larger capital cost, highly movable operation and maintenance cost. A versatile OE policy is the need of the hour which focuses on both technological barrier as well as market barrier. Still now India does not have a mechanism to provide revenue stream to WEC plants. In this decade one of the crucial factors for any technology oriented decision is sustainability and self reliance. Self reliance is of utmost importance in Indian islands. Due to high cost of OE as of now grid parity is not feasible. But consideration of multiple locations for OE can introduce synergy and spatial multi users in India. Along with technological developments, the situation demands a blueprint to



commercialization of OE in India. Public private partnership can be a viable option. Despite all the challenges OE supersedes all other resources because of its sustainable and ecofriendly nature.

CONCLUSION

Above discussion clearly enunciates the fact that OE sector has major intricacies which must be focused upon, but the potentials for contribution in energy and growth are huge. Further progress needs attention on specific technological as well as market system through holistic policies and strategies. Government has a pivotal role to play in this regard.

REFERENCES

1. International Energy Agency, "India 2020: Energy Policy Review," p.21, January 2020.
2. Central Electricity Authority, "Executive Summary on Power Sector," p.7, April 2020.
3. Central Electricity Authority, "Renewable Energy Generation Data," p.1, April 2020.
4. A. Brito e Melo and J. Huckerby, "Ocean Energy System-Annual Report," The Executive Committee of Ocean Energy Systems, 2011.
5. V. Sanil Kumar, K. C. Pathak, P. Pednekar, N. S. N. Raju and R. Gowthaman, "Coastal processes along the Indian coastline," Current Science, VOL. 91, NO. 4, 25 AUGUST 2006.
6. Richard Boud, "Status and Research and Development Priorities, Wave and Marine Accessed Energy," UK Dept. of Trade and Industry (DTI), DTI Report # FES-R-132, AEAT Report # AEAT/ENV/1054, United Kingdom, 2003
7. A. Muetze and J. G. Vining, "Ocean Wave Energy Conversion - A Survey," Conference Record of the 2006 IEEE Industry Applications Conference Forty-First IAS Annual Meeting, Tampa, FL, 2006, pp. 1410-1417
8. Robin Pelc, Rod M. Fujita, "Renewable energy from the ocean", Marine Policy 26(2002), p.471-479.
9. V. Jayashankar, Purnima J., M. Ravindran, M. Mitsumori, Y. Ikegami, H. Uehara, "The Indian OTEC Program", Ocean Technology Conference Texas, May 1998
10. Prof. V.S. Raju, Prof. M. Ravindran, "Wave Energy: Potential and Programme in India", Renewable Energy, Vol 10, No. 2/3, pp.339-345, 1997
11. C. Carroll and M. Bell, Wave Energy Convertors Utilizing Pressure Differences, US Patent 6.933.6233. to Ocean Power Technologies, Inc., Patent and Trademark Office, Washington D.C., 2004.
12. Das, Tapas Kumar, et al. "Optimal Design of Air Turbines for Oscillating Water Column Wave Energy Systems: A Review." The International Journal of Ocean and Climate Systems, vol. 8, no. 1, pp. 37–49, Apr. 2017.
13. Paul Breeze, Chapter 14 - Marine Power Generation Technologies, Power Generation Technologies (Third Edition), Newnes, pp. 323-349, 2019.
14. Pattanaik B. et al., Open Sea Trials on Floating Wave Energy Device Backward Bent Ducted Buoy and Its Performance Optimization. In: Murali K., Sriram V., Samad A., Saha N. (eds) Proceedings of the Fourth International Conference in Ocean Engineering (ICOE2018). Lecture Notes in Civil Engineering, vol 23. Springer, Singapore.
15. Amrutha, M.M.; Kumar, V.S. Changes in Wave Energy in the Shelf Seas of India during the Last 40 Years Based on ERA5 Reanalysis Data. Energies 2020, 13, 115.
16. Bryden I.G. (2013) Tidal Energy. In: Kaltschmitt M., Themelis N.J., Bronicki L.Y., Söder L., Vega L.A. (eds) Renewable Energy Systems. Springer, New York, NY.
17. Murali, K. and Sundar, V. (2017) 'Reassessment of tidal energy potential in India and a decision-making tool for tidal energy technology selection', The International Journal of Ocean and Climate Systems, 8(2), pp. 85–97.
18. Paul Breeze, Chapter 9 - Tidal Barrage Power Plants, Power Generation Technologies (Third Edition), Newnes, 2019, Pages 203-217, ISBN 9780081026311.
19. Er. Prasanna Kumar Sahu, Er. Chinmaya Prasad Nanda, 2013, Indian Ocean Thermal Energy, INTERNATIONAL JOURNAL OF ENGINEERING RESEARCH & TECHNOLOGY (IJERT) Volume 02, Issue 10 (October 2013).

Production Engineering



Sustainable Manufacturing: Principles, Applications and Directions

Ashok Kumar Panda

Course Control Officer, Faculty of Electrical & Mechanical Engineering, MCEME, Secunderabad

✉ akp.eme@gmail.com

ABSTRACT

Engineering deals with several processes, because to produce a desired product or to provide required service at affordable cost and quality, we have to use certain pre-determined activities. The most prominent amongst all is day to day manufacturing in range and depth. The conventional and non-conventional manufacturing should be sustainable in Indian context or more precisely region based. The principles, applications and directions should be well legislated, regulated by single agency and proactive support from dedicated financial institutions are key to sustainable manufacturing. Equal attentions should be given to regular manufacturing like consumer goods as well as health care gadgets, agricultural support accessories, high end quality assurance tools, sensors and transducers for AI applications. The manufacturing for infrastructure requirements and defence applications need special attention for sustainable progress due to unique features. Change of political guard should not often alter the policies pertaining to manufacturing since large investments will be wasted by a simple deviation in policy. Restrictions on FDI must be removed, setting of SEZs be facilitated by Government proactive support and subsidies to be carried out for sustainable manufacturing. The rules and regulations enforced by regulators like CPCB, BEE, Labor commissions, local municipalities and RBI etc are required to be conducive for reasonable sustainable manufacturing. Continuous need analysis, skill up gradations and modernization of machineries are other key factors.

Keywords : Green manufacturing; Data analytics; Need analysis; Legislation restrictions; Vocal for local; Support systems.

INTRODUCTION

Manufacturing and associated technologies are the largest activities in present days. Starting from daily needs of food supply arrangements up to defence requirements manufacturing play a key role. Complicated areas of manufacturing like electronic hardware, nuclear and space research components, health care devices, quality assurance related non-destructive gadgets and high end sensors and transducers for automation and AI based applications always carry special attention. Further larger volume oriented manufacturing comprises transport and infrastructure sectors demands intensive environment concerns and being highly labor plus material oriented calls for need based management comprising legislated directions, applications and sustainable principles and best practices.

The requirements of manufacturing are fast changing. Emerging technologies and changing customer trends are influencing the product and service choices. Globalization of trades and near free market concepts resulting intensive competitions amongst manufacturers and traders. Legislations on green manufacturing and essence of reuse, rebuild, recycle, refurbishment and renovation should be followed in letter and spirit. Further, for sustainable manufacturing data capturing, data analytics, predictive managements reliability centered management and AI supported sensor based process monitoring requires customize developments and applications.

CRITERIA OF SUSTAINABLE MANUFACTURING

Amongst all engineering activities, manufacturing in general is the largest activity since all fields of engineering like mechanical, electrical, electronics and communication, Instrumentation, civil, computing and informatics, mining, agriculture, aerospace, architect and associated branches are involved. Further special attention to be drawn on health care instruments and quality assurance gadgets manufacturing. Keeping in view of the mentioned wide horizon of scope of manufacturing, the essential criteria for sustainable manufacturing keeping in view of principles and directions are as follows:

- Extensive need analysis of intended users, demand patterns and time bound review by professional experts are key to sustainable manufacturing.



- Adhering to all legislatures, guidelines and directives issued by Central and state governments, Pollution Control Boards, National Green Tribunal, Confederation of Indian Industries, Federation of Indian Chambers of Commerce and Industries, Ministry of Labor and Factory Inspectorate will yield desired results uninterruptedly for sustained manufacturing sooner or later.
- Setting of dedicated R & D set ups, product development and trial facilities for time bound result oriented task under direct supervision of premier establishments like CSIR, DRDO, RDSO and educational institutions of national importance. The private entities are required to be encouraged to set up own R & D or facilities in PPP model. Minimum 6 % of turnover of any commercial entity is required to be earmarked for R & D and continual improvement programs. These measures will give clear principles, directions and fruitful applications for achieving sustainable manufacturing.
- Optimization of local resources of raw material, manpower and vendor support is prime factors for sustainable manufacturing. The directions of Government on “Vocal for Local” is well justified in this context.

PRIMARY AREAS OF FOCUS

The principles, applications and directions for sustainable manufacturing calls for deliberation on under mentioned concepts as key areas:

- Use of Artificial Intelligence & big data analysis extensively to identify potential areas of customer requirements and need analysis for sustainable manufacturing.
- Application of Sensors & Telemetry in all spheres of manufacturing for real time monitoring of large scale activities which include raw material handling up to shipment of finished products .
- Technology and Technological advancements to be applied in fastest means for sustainable manufacturing keeping in view vocal for local demands and to be at par with other global manufacturing standards and requirements..
- Food security and defence requirements are the key areas of sustained manufacturing since both are capital expenditure centric. Hence professional analysis is required periodically to observe change in requirements vis a vis manufacturing preparedness to cater for renewed demands. Activation of NITI Ayog, Finance commission and related Ministries will yield planned results.
- Enhancement of quality assurance methods in particular non destructive methods for potential Green Manufacturing using best practices are to be instituted irrespective of cost involvement and reluctance from most stake holders.
- Management and handling of Natural Resources with focus on recycle, reuse & rebuild for absolute sustained manufacturing are to be brought under legislations for effective applications.
- Infrastructure development and Health care are economic burden with Engineering constraints,, hence requires definite user friendly principles, applications and directives for sustained manufacturing. The national regulators should be proactive to manufacturing related to such sectors for sustainable growth.

SUPPORT OF REGULATORS AND ENFORCEMENT AGENCIES

In reference to Indian sub continent with population factor, diversity in regions, religions and choices, the sustainable manufacturing is a tricky situation. Further the role of Government, statutory regulators and different federations to whom the manufacturers are affiliated are so intensive and diversified that norms and procedures formulated by under mentioned are potential hindrance for sustainable manufacturing. Few examples of regulators and enforcement agencies are brought out as under:

- Competition Commission of India (CCI)
- National Green Tribunal (NGT)
- Regional Labor Commission (RLC)
- Bureau of Energy Efficiency (BEE)
- Indian Electricity (I E) rules
- CII, FICCI, ASSOCHAM, NEMA etc



- Statutory commissions like NHRC, NWC etc. These regulating agencies have adequate say on various stages of manufacturing activities starting from deployment of manpower like women, working hours stipulations, industrial waste discharge management, eco aspects related to manufacturing activities, energy consumption and management criteria and safety aspects to men, material and machineries. On most instances compiling so many regulators at one point of time is a setback to sustainable manufacturing. Therefore, it is strongly recommended to institute a single regulator dealing with manufacturing as one window concept to cater for fast track progress on sustainable manufacturing.

ROLE OF FINANCIAL AND GOVERNMENT INSTITUTIONS

The range and depth of manufacturing involves number of large machineries and processes and requirement of different technical trades with different levels of skills calls for huge investment at start and to run. The periodical maintenance, replacement of machineries and up gradation of plants, machineries and specialist equipments requires steady flow of funds. We have following dedicated financial institutions to support manufacturing and allied activities:

- Small Industrial Development Bank of India (SIDBI)
- Export – Import Bank of India (EXIM Bank)
- Industrial Development Bank of India (IDBI)
- Industrial Credit & Investment Corporation of India (ICICI Bank)
- Industrial Finance Corporation of India (IFCI)
- District Industry Centre (DIC)

However, the concern is uniform policy amongst the different institutions not in place. Therefore, manufacturers are selective on financial models. Specific packages to support sustainable manufacturing with support from Government are required to be offered. The subsidies from financial institutions during lean period is justified. The infrastructural facilities like land, water and electricity and municipality supports should be provided at reasonable cost and hassle free manner for sustainable manufacturing. Without above mentioned pro active supports it is very difficult to achieve and maintain sustainable manufacturing.

ELEMENTS OF SUSTAINABLE MANUFACTURING

The prominent key elements of sustainable manufacturing are

- Self Sufficiency (AtmaNirbhar)
- Make in India (MSMEs)
- Export Orientation (Up Skill / Re skill / Soft Skill)
- Import Substitution (Alternatives / Vocal for local)
- Indigenization (Make in India / R & D augmentation / Reverse Engineering)
- Special Economy Zones (SEZs)
- Dedicated Financial and Support Institutions (EXIM, SIDBI, NABARD, ICICI,DIC,IDBI,IFC)
- Strategic planning through participative management
- Continual vendors development and support program
- Focus on Man, Material, Machineries, Methods, Motivation, Marketing, Money management to strengthen sustainable manufacturing.

CONCLUSION

The principles, applications and directions for sustainable manufacturing is a national issue which directly link with industrial growth of the country, GDP, employment status, export potential, import substitution, increase in foreign exchange reserve, ecology balance and relative position of the country in advance economic status worldwide. The infusion of the sense of requirements must be added to the secondary level course curriculum and onwards. Miniature program in respective of on job



training (OJT) should be introduced in all levels of education, to prepare future technicians to adopt the principles of sustainable manufacturing with ease and pride.

ACKNOWLEDGEMENTS

The author is deeply indebted to the Corps of Electronics and Mechanical Engineering of the Indian Army for providing a platform to work on extensive manufacturing, methodisation of effective processes, indigenization, reverse engineering applications, establishing quality assurance norms related to manufacturing and modernization aspects related to upgradation requirements over two decades.

REFERENCES

1. The author while working in Army Base Workshop with effect from 1990 to 2015 in manufacturing and production activities conceived the inputs from work experience and deliberations during participative management mechanism. No literature, books or publications of any kind referred to in developing this technical paper.



Preparing for Post Covid-19 Sustainable Manufacturing Ecosystem

Dr Goutam Sengupta

Vice Chancellor, Techno India University, West Bengal, Kolkata

✉ goutamsenguptacbs@gmail.com

ABSTRACT

The COVID-19 pandemic has exposed many gaps and weaknesses associated with our current manufacturing systems. During the last two to three decades, organizations were busy competing amongst themselves and in the process ignored the power of integration. Within the same group, the same trade, and between the countries, there were insignificant integration or visible collaboration. Furthermore, sheer competitiveness in the market-place without giving much attention to a sustainable manufacturing eco-system had led to an increasing fragmentation of knowledge along the supply chain, where the design of the product and its production became two detached processes resulting in innovations in manufacturing not getting embedded in the entire eco-system. Post COVID-19 manufacturing ecosystem shall have to address the above gaps which had left current manufacturing extremely fragile and vulnerable. Resource efficient circular manufacturing model needs to replace the current linear production system which is highly wasteful with profound environmental consequences. This article is research based combining secondary and primary researches to carve a path as to how the manufacturing industries can recover from the COVID 19 shock and bounce back stronger during the Post COVID era insulating itself from any further shock more severe than the present one.

Keywords : Paired comparison; Circular manufacturing; Collaborative manufacturing; PV/LF Synchronization; Quick Response Manufacturing (QRM).

INTRODUCTION

The COVID-19 pandemic has hit the business world in an unprecedented scale and speed. It has resulted in standstill in many businesses, work suspension in production units, disruption to global manufacturing industries and their supply networks, dwindling workforce availability and fear of extinction of specialized skills, plummeting consumer confidence in disrupted manufacturing ecosystem. This has led to acute stress on working capital for business.

Questions facing the manufacturing fraternity as global lockdown is lifted in Post COVID scenario are: How consumer behaviour may change or go for a paradigm shift?, How shall manufacturing ecosystem be affected due to changing consumer behaviour?, What shall be the emerging consumer demands?, What are the areas businesses should stress and focus on now and in the coming months to prepare for the post COVID era?

The COVID-19 crisis has revealed and exposed both the significance of and the risks associated with our current manufacturing systems. COVID 19 can be termed as a Black Swan event which shall completely disrupt the process of conventional manufacturing . It may cause the collapse of entire manufacturing ecosystems. COVID-19 is causing large scale disruption to manufacturing ecosystems globally with further impacts yet to be fully felt. There shall be scarcity of abundant capital, space, skilled workforce, raw materials and other resources needed for the manufacturing processes.

Understanding the manufacturing ecosystem integration and collaboration both upstream and downstream is critical to the continued effective management of a business' manufacturing operations. One unique attribute that differentiates this crisis from others in recent years is its worldwide effect on both demand and supply side of the manufacturing ecosystem. Furthermore the consumption pattern within the manufacturing ecosystem shall get completely disrupted. People engaged in the manufacturing process will go through a paradigm shift with respect to psychological build.

Expectation from Manufacturing Ecosystem in Post Covid 19 era:

- Half the hours of human effort in the factory

- Half the defects in the finished product
- One-third the hours of engineering effort
- Half the factory space for the same output
- A tenth or less of in-process inventories [6]

There is not an iota of doubt that there shall be gargantuan re-shuffling of manufacturing ecosystems in the post COVID-19 period. The question is how to prepare and tune the organizations for this new era so that they are ready with robust, innovative and adaptable manufacturing ecosystems sustainable enough to take on the next “Black Swan”.

Initiatives such as Industry 4.0 and others as witnessed during the pre-COVID-19 period may face a severe drag necessitating an alternate solution to emerge as an interim measure.

This article attempts to unfurl this critical challenge and throws light on some critical domains emerging through this COVID-19 scenario to better prepare the organizations in the post COVID-19 world with regard to their manufacturing ecosystems.

LITERATURE REVIEW

‘The concept of black swan events was popularized by the writer Nassim Nicholas Taleb in his book, *The Black Swan: The Impact of The Highly Improbable* (Penguin, 2008). The essence of his work is the world is severely affected by events that are rare and difficult to predict. The implications for markets and investments are compelling and need to be taken seriously’. (Investopedia, Brian J Bloch, June 25, 2019)[7]

However, the concept was challenged by Nouriel Roubini who said these are predictable vulnerabilities. “In my 2010 book, *Crisis Economics*, I defined financial crises not as the ‘black swan’ events that Nassim Nicholas Taleb described in his eponymous bestseller but as ‘white swans’. According to Taleb, black swans are events that emerge unpredictably, like a tornado, from a fat-tailed statistical distribution. But I argued that financial crises, at least, are more like hurricanes: they are the predictable result of built up economic and financial vulnerabilities and policy mistakes.” (Nouriel Roubini, *The Guardian*, International weekly edition, 19th Feb 2020)[8]

Whether we agree to either of these two philosophies, it is clear that not enough measures were taken by the nations to make the manufacturing ecosystems resilient leading to COVID-19 Manufacturing Collapse. The companies and nations were busy to create manufacturing systems for their narrow gains, going miles apart from manufacturing ecosystem global integration.

For the crisis of today, the literature review points out crisis emerging out of uncertainty of predictability of measures like social distancing. Work of Neil J Rowan, John G Laffey published in Elsevier, volume 725, July 2020 [9] highlights this uncertainty.

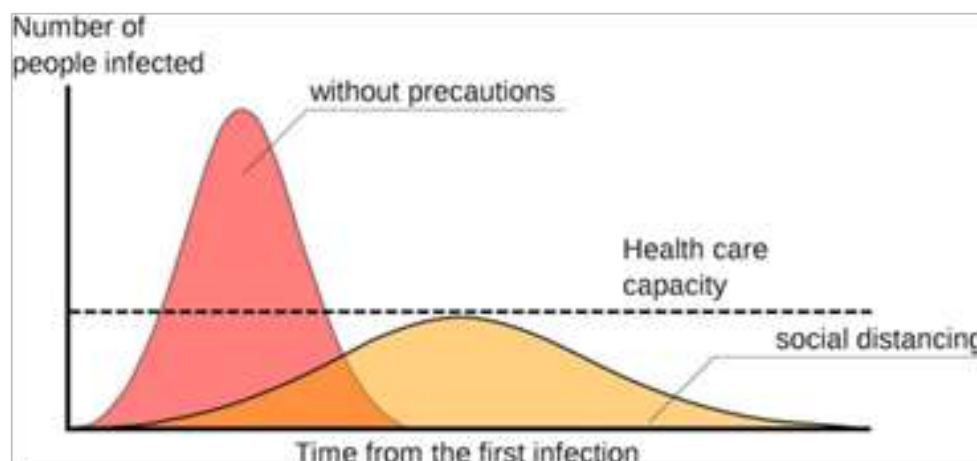


Fig. 1. COVID 19 Prognosis

#NourielRoubini is a professor at NYU’s Stern School of Business and was senior economist for international affairs in the Clinton White House’s Council of Economic Advisers. He has worked for the IMF, the US Federal Reserve and the World Bank.



Fig. 2. COVID 19 risk to Manufacturing

The above figure depicts the supply chain and manufacturing risks associated with the COVID-19 pandemic. Industries which have good inventory buffers and more number of alternate supply sources are at lower risks. Accordingly, automotive industry is at a relatively lower risk in terms of their supply chains and manufacturing ecosystem while retail and pharma are at medium risk and high tech industries are at a higher risk.

The manufacturing sector is the major contributor of GDP and employment in the secondary sector and has been recognized as an engine for vibrant growth and creator of the nation's wealth (Rele, 2020) [14]. The manufacturing sector is important in the way that it has strong linkages with other sectors, both forward and backward linkages so any impact in this sector will affect other sectors as well.

Overall, the manufacturing sector is going to be affected badly by demand–supply disruptions and global value supply chain.

COVID-19 is expected to accelerate the digital transformation in manufacturing by leveraging numerous technologies. Further, the COVID-19 impact on the manufacturing industry will create a value chain that operates like a neural network – an intensely networked set of collaborative partners aligned to a purpose-driven ecosystem. This will make the future manufacturing enterprise [10] -

- Resilient through connected, cognitive, and collaborative supply chains.
- Adaptive through an agile response to market demand by personalizing products and services.
- Purpose driven by engaging with partners across industries to deliver frictionless experience to end customers.

A more resource efficient circular manufacturing model needs to replace the current linear production systems, which are highly wasteful and polluting, by enhancing the symbiotic relationship between local consumption and production cycles to achieve sustainable production and consumption [12].

The COVID-19 crisis has exposed the fragility of the idea of separating R&D and manufacturing processes. While there is no denying the benefits generated by globalized production systems for both developed and developing countries, they have led to an increasing fragmentation of knowledge along the supply chain, where the design of the product and its production become two detached processes, eroding the connections resulting from 'learning by doing' and reducing the understanding of the resource implications of final products. Not only has this disconnection become problematic during the pandemic, the consumer's detachment from the manufacturing process also has severe implications for both innovation and the environment [12].

Post-COVID-19 economies have an opportunity to rethink manufacturing and the industrial metabolism riding a new wave of technology, which is "green" (and meets net zero or even positive carbon commitments); circular through systemic innovation; scalable; can be contextualized rapidly; enables mass customization of products; is highly adapted to specific local needs, and



builds on digital technologies and big data to enhance the traceability of processes and materials, visibility and opportunities for distributed manufacturing [12].

The post-COVID-19 period would push organisations to shift production and supply chain systems in a more sustainable way. Therefore, it is required to formulate adequate institutional and operational policies for overcoming the production losses and improving the consumption pattern, which would further boost the economy. The implications of COVID pandemic on sustainable production and consumption trends would be worthy to note, and hence, a considerable change is likely to be seen in the coming months and years. Haleem et al. (2020) [13] highlighted the various academic research areas to combat the COVID-19 pandemic; the role of sustainable manufacturing is among one of them.

The post COVID era opens an opportunity window for the sustainable business transition [1], and need to make supply and production system more resilient [2]. The COVID-19 situation creates a space for developing a flexible and resilient manufacturing system to maintaining the economic and social sustainability of the production process. Tan et al. [3] discuss the various decision support systems for developing a resilient production system. Ivanov [5] proposed a prediction model for measuring the impact of a pandemic on supply chain network and manufacturing resilience. The firm's supply chain network resilience and manufacturing resilience is required to tackle the epidemic or such disruptive events [4].

India's role post-Covid-19, particularly in the industrial sector, is a subject of great interest, hope and speculation to the rest of the world. Many believe India will emerge as one of the preferred centres for manufactured products vis-a-vis China, if not the foremost choice. This is a sensible and reasonable aspiration to have as a nation. But this is an outcome, not a strategy. The most appropriate strategy for India would be to assume greater self-control over its national value chain; embrace and enhance, what is often alluded to as the Nehruvian approach of 'core self-sufficiency', by augmenting domestic value addition in its manufacturing industry [11].

RESEARCH METHOD

The following research techniques were deployed for collection of primary data and its scientific analysis:

Delphi Technique

Paired Comparison Matrix

Decision Evaluation Matrix

There were total of 225 respondents who participated in this survey conducted during the period March 2020 to mid of April 2020. Survey was conducted maintaining social distancing protocols through webinars on digital platforms. Most of the respondents were supply chain practitioners and experts and few were from educational institutions teaching and consulting in supply chain domain. All participants remained anonymous minimizing the risk of 'bandwagon effect' or 'halo effect', allowing free expression of opinion, encouraging open critique which facilitated admission of errors while revising earlier judgements. Respondents participated in four webinars and five rounds of iterations. In the initial round, there were 120 ideas generated and at the end of fifth round it converged to twelve different proposals. Table below gives the breakup of respondents:

Table 1. Respondent Demography

Type of organizations	No. of respondents
Global Multinationals	15
Large Transnational Companies	10
National Companies	35
Consulting Companies	04
Educational Organizations	35
Operation Management Students	30
MSME Sector	96
TOTAL	225



Table 2. Results and Analysis

The proposals were tabulated under following broad headings:

Proposal No.	Proposal Description
1	PV/LF Synchronization, Waste Elimination*
2	Collaborative Manufacturing
3	Circular Manufacturing
4	Strong MSME**
5	New Technologies***
6	Multiskilling
7	Quick Response Manufacturing (QRM)& Agile Manufacturing
8	Manufacturing Strategy
9	Machine Learning & IOT
10	Scenario Building Exercise (SBE)
11	Integrated Manufacturing****
12	Automation

*: P- Product, V-Volume, L-Layout, F- Flow

** : Fuelled by relevant Quality Technology Tools (QTTs)

***: Relevant to individual industry sector and not generic Industry 4.0

****: Concept to Production to Distribution

The respondents converged to the following seven criteria for the purpose of evaluation of proposals:

Cost Effective,High Impact, High Sustainability, Ability to Absorb shocks (Black Swan), Adaptability,Ease of Implementation,Capability to cut across (industry segments)

Paired Comparison was done to arrive at weightage of each factor.

Table 3. Evaluation Matrix

Identify criteria for selection			
Identity	Criteria	Score	Rank
A	Cost effective	2	4
B	High impact	5	3
C	High sustainability	9	1
D	Ability to absorb shocks (Black Swan)	8	2
E	Adaptability	1	5
F	Ease of implementation	1	5
G	Capability to cut across (industry segments)	8	2

NB : Scores and Rank derived from Paired Comparison Table.

Table 4. Paired Comparison Criteria

Comparison	Points
Major difference	3
Medium difference	2
Minor difference	1
No difference	0



Table 5. Paired comparison table

A	B	C	D	E	F	G
	B2	C3	D2	E1	A2	G2
	B	C1	D2	B2	B1	G1
		C	C0	C2	C2	C1
			D	D2	D2	D0
				E	F1	G3
					F	G2
						G

Table 6. Decision matrix

5 point scale 5 – excellent 4- very good 3 – good 2 – fair 1 - poor	Desired criteria identities (Refer Table 3)	C	D	G	B	A	E	F	Total	Rank
Proposal Nos. (Refer Table 2)	Weightage for criteria	9	8	8	5	2	1	1		
1		4	3	5	4	3	3	3	132	5
		36	24	40	20	6	3	3		
2		5	4	5	5	4	4	3	157	2
		45	32	40	25	8	4	3		
3		5	5	5	4	4	5	3	161	1
		45	40	40	20	8	5	3		
4		4	4	4	4	2	3	2	129	6
		36	32	32	20	4	3	2		
5		4	4	4	4	5	5	4	139	4
		36	32	32	20	10	5	4		
6		3	3	3	4	2	2	2	103	11
		27	24	24	20	4	2	2		
7		4	3	4	5	2	3	2	126	7
		36	24	32	25	4	3	2		
8		2	4	4	3	2	2	2	105	10
		18	32	32	15	4	2	2		
9		4	3	4	3	2	2	3	116	9
		36	24	32	15	4	2	3		
10		3	2	4	4	2	2	2	103	11
		27	16	32	20	4	2	2		
11		4	4	5	5	4	5	4	150	3
		36	32	40	25	8	5	4		
12		4	3	4	3	3	5	4	122	8
		36	24	32	15	6	5	4		



CONCLUSION

From the detailed research study conducted and considering the ranks of the various proposals, it can be concluded that the following interventions to a large extent may prove to be effective in preparing for a post COVID-19 sustainable manufacturing ecosystem :

1. Circular Manufacturing
2. Collaborative Manufacturing
3. Integrated Manufacturing
4. New Technologies
5. PV/LF Synchronization, Waste Elimination
6. Strong MSME
7. Quick Response Manufacturing (QRM) and Agile Manufacturing

After the COVID 19 situation dissipates, the world shall see companies fall into one of two categories:

Companies that didn't do anything hoping that such disruption won't ever happen again. These companies are taking a highly risky gamble.

There will be firms that learn from this crisis, garner and implement robust interventions that shall make them well prepared when the next crisis strikes (next Black Swan) and equip them with solutions (as mentioned above) when disruptions occur.

The second group of organizations shall emerge as winners in the long run.

REFERENCES

1. M.J. Cohen, Does the COVID-19 outbreak mark the onset of a sustainable consumption transition? *Sustain. Sci. Pract. Policy* (2020), doi: 10.1080/15487733.2020.1740472 .
2. J. Sarkis, M.J. Cohen, P. Dewick, P. Schröder, A brave new world: Lessons from the COVID-19 pandemic for transitioning to sustainable supply and production, *Resour. Conserv. Recycl.* (2020), doi: 10.1016/j.resconrec.2020.104894 .
3. R.R. Tan, M.A.B. Promentilla, M.L. Tseng, Special issue: Decision support for sustainable and resilient systems, *Sustain. Prod. Consum.* (2019), doi: 10.1016/j.spc.2019.08.006 .
4. S. Hosseini, D. Ivanov, A. Dolgui, Review of quantitative methods for supply chain resilience analysis, *Transp. Res. Part E Logist. Transp. Rev.* 125 (2019) 285–307, doi: 10.1016/j.tre.2019.03.001 .
5. D. Ivanov, Predicting the impacts of epidemic outbreaks on global supply chains: A simulation-based analysis on the coronavirus outbreak (COVID- 19/SARS-CoV-2) case, *Transp. Res. Part E Logist. Transp. Rev.* 136 (2020), doi: 10.1016/j.tre.2020.101922 .
6. James P. Womack, Daniel T. Jones & Daniel Roos, “The Machine That Changed The World”.
7. Investopedia, Brian J Bloch, June 25,2019
8. NourielRoubini, The Guardian, International weekly edition, 19th Feb 2020
9. Neil J Rowan, John G Laffey published in Elsevier, volume 725, July 2020
10. <https://www.tcs.com/the-evolution-of-the-manufacturing-industry-post-covid-19>
11. <https://www.financialexpress.com/industry/manufacturing-what-india-needs-to-do-post-covid-19/1941473/>
12. <https://www.unido.org/news/why-innovative-manufacturing-and-circularity-are-key-resilient-manufacturing-industry-post-covid-19>
13. Haleem, A., Javaid, M., Vaishya, R., & Deshmukh, S. G. (2020). Areas of academic research with the impact of COVID-19. *The American Journal of Emergency Medicine*, 20, 12.
14. Rele, S. (2020). Emerging outbreaks and epidemic threats: The practicality and limitations in the development and manufacturing of treatments for Coronavirus (COVID-19). *Polymorphism*, 4, 45–52.



The Advancement of 3DBioPrinting Technology Uses as Bio-Manufacturing Process

Ranjit Barua^{1*}, Sudipto Datta¹, Pallab Datta¹, Amit Roy Chowdhury^{1,2}

Centre for Healthcare Science & Technology¹, Department of Aerospace Engg. & Applied Mechanics^{1,2}, IIST-Shibpur, Howrah, West Bengal

*✉ ranjitjgec007@gmail.com

ABSTRACT

Three-dimensional (3D) printing has quickly developed, with huge uses in the area of healthcare and bio-manufacturing engineering. One of the ultimate developments leading to three-dimensional printing was the progress the application of cells biomaterials and associate modules for the fabrication of useful alive tissues. Numerous different procedures and methods of three-dimensional bio-printing are concisely defined in this article, and applications of bio-printing for the manufacture of artificial blood vessels are described. Improvements in additive manufacturing technologies, biomaterials and tissue engineering, imaging will prime to upcoming improvements in the construction of patient-definite vascular network builds. Upcoming interdisciplinary study and inventions are projected to advance convert the areas of biomechanical and tissue engineering.

Keywords : 3DP bio-printing; Additive manufacturing; Biomaterial; Vascular network; Tissue engineering.

INTRODUCTION

3D printing (3DP) has involved growing attention through the past few years and is now applied in several industrial areas for the quick and effective fabrication of customized scaffolds and design, beyond some boundaries of traditional manufacturing methods [1]. 3DP, also recognized as additive manufacturing process which has also controlled to notable improvements in the biomedical and healthcare area, mainly in bio-manufacturing and regenerative medicine, such as it enables to “printing” of cells, tissues and organs. Advances in 3DPbioprinting have been typically inspired by the restricted accessibility of organs worldwide [2], which are required for the restoration of lost or futile tissues and organs. The utmost exciting and hard presentations for engineered soft tissues contain with cartilage, the skin [3] and hard tissues for example vascular grafts [4] cardiac tissue [5] and bones [6]

Medical exhibiting is alternative area where 3DP bioprinting is progressively being used. In medical practice, bioprinted replicas have been displayed to be suitable for surgical preparation and medical teaching [7]. The usage of 3DP printing to improve apparatuses to contribution and progress medical measures has a long track record and the CDRHFD (Centre for Devices and Radiological Health at the Food and Drug Administration) has studied and cleared numerous 3DP printed medicinal devices.

In this paper, we pointed to briefly discuss the basic mechanism and application of three dimensional bioprinting, emphasizing some key advances in the manufacture of vascular grafts and blood vessels [8].

Principles of 3D Bio-printing Process

Generally, Three-dimensional (3D) bio-printing is based on the layer-by-layer specific depositing of biological elements, living cells and biochemicals, by spatial mechanism of the engagement of functional elements of the fabricated three-dimensional construct (**Fig. 1**). Three-dimensional (3D) bio-printing is based on three major methods: (a) biomimetics or biomimicry (b) autonomous self-assembly, and (c) mini-tissue structure blocks, as defined widely somewhere else [9].

Biomimetics or biomimicry is known as the procedure of investigative properties itself, its procedures, systems and essentials in order to be stimulated and inspired for the ideal explanation of human difficulties. Combination of biomimetic constituents into a bioprinted structure has a dynamic influence on the accessory, relocation, production and purpose of both exogenous and endogenous cells. Resources have a major impact on cell accessory as well as cell shape and size, there fore allowing the mechanism of proliferation and distinction of cells in a printed scaffold [10]. Furthermore, nanoscale structures like steps, grooves and ridges, can also effect cell accessory, proliferation and cytoskeletal gathering [11]. Elsewhere these issues, cell

shape and distinction can be also moderated by the three dimensional atmosphere in a tissue-engineered paradigm [12]. A biomimicry method in 3D bioprinting of tissue materials with precise physiological purposes and characteristics involves a deep accepting of the usual tissue-exact arrangement. Independent self-assembly, correspondingly develops the embryonic organ, which is a procedure that make an exact tissue or organ in in-vitro [13]. Initially cellular objects of an evolving tissue make an extracellular matrix elements and suitable cell signals that tip to autonomous structure and modelling of the preferred tissue. Consuming independent self-assembly it is viable to apply cells for histogenesis and also to control the arrangement, functional, localization, and structural characteristics of the tissue as before explained [15]. A solid consideration of the devices of embryonic organogenesis is and the capability to influence the situations that adjust these embryonic mechanisms is vital to effectively attain this objective.

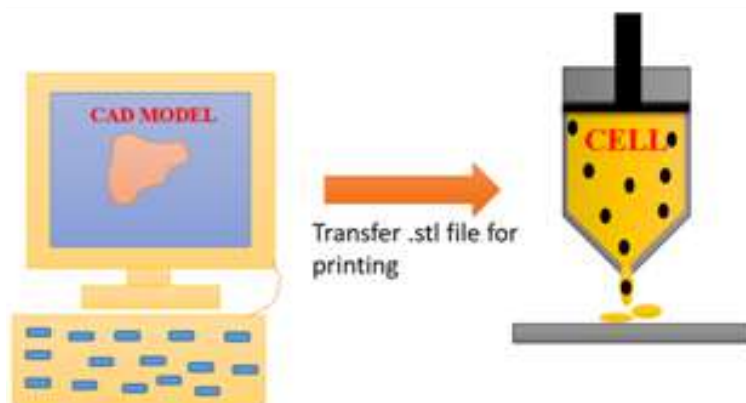


Fig. 1. Bioprinting process

Bio-manufacturing process by bio-printing

Bio-manufacturing technology is an upcoming challenging work of 'in vitro' system to fabricate the artificial organs, which is determined by two essentials: transplantation of vital organ and precise tissue replicas [16]. Now a days, three-dimensional bio-printing has been extensively applied in the creation of several organs like as artificial blood vessels, skins, hearts valve etc., it is not only a basic stage of organ replacement, but also be worked as in vitro prototypes dedicated to drug screening, pharmacokinetics, and regenerative medicine etc. Though, organs are basically complex, many bio-printing techniques are oppressed to work out the challenges of dissimilar uses [17]. That why the problem is how to select the appropriate bio-printing techniques? In this, researchers are methodically experiments and study the evolution of bio-printing, different techniques and analysis the printing biomaterials properties etc. and also grouping of three-dimensional bio-printing with an importance on the bio-printing principles and customized the bio-printers (**Fig. 2**). Different types of bio-printer are now available like extrusion-based, droplet-based, and photocuring-based bio-printer [18].

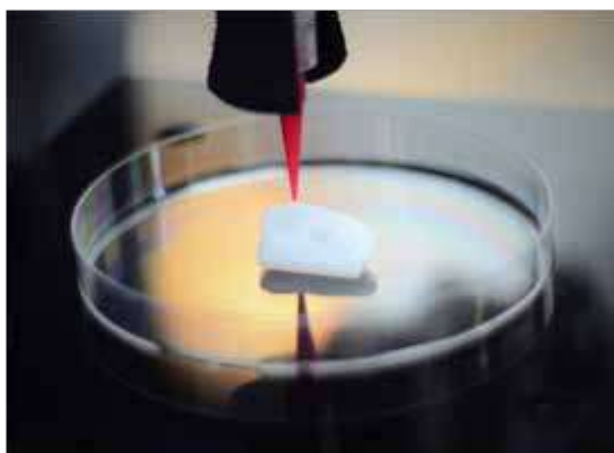


Fig. 2. Cell printing

Bioprinting of Artificial Blood Vessels

Several approaches and procedures have been planned in the works for the bio-printing techniques for cardio vascular grafts and artificial blood vessels network applying cellular or biomaterials [19]. Though several methods of three dimensional bioprinting processes are applying for biomedical and tissue engineering, also regenerative medicine area. Three main approaches are applied to fabricate the artificial blood vessel networks: (i) assembly of bulk matrices with unified vascular network as perfusable mediums, (ii) modelling of cells into line arrangements for self-assembly of unified vessel structures, and (iii) construction of free-standing tubular arrangements, which may help as artificial vascular network [20]. Bioprinted artificial blood vessel was made by gelatin and cotton candy (**Fig. 3**) [21].



Fig. 3. Artificial blood vessel

Manufacture of vascular grafts by a cellular ingredients allows the usage of organic solvents maximum printing temperature. Alternatively, cellular-based methods is relatively inspiring to accomplish three-dimensional mechanism of cell depositing on manufactured scaffold which is conceivable by consuming cellular-based methods [22][23]. Three dimensional bioprinting applying cell-laden ingredients has been displayed to create the combination of cells more effective, increase the preliminary cell filling concentration and recover the mechanism of cell spreading with single or multiple cell types [24]. A bioprinter (Itohet al.2015) was used for printing the tubular tissues (without scaffold) which have 1.5 mm internal diameter [25].

CONCLUSION

Improvements in advanced technology especially additive manufacturing technology, biomechanical engineering, tissue engineering and medical imaging techniques will develop to advance improvements in the making of patient-definite artificial blood vessel. Huge experiments continue to be require, like as specific tissue and biomaterial supplies, cell maturation and functionality and suitable innervation and blood vascular network channel. Upcoming interdisciplinary research and improvement are predictable to promote convert the areas of additive manufacturing and tissue engineering.

ACKNOWLEDGMENT

The authors would like to thanks Centre for Healthcare Science & Technology lab, IEST-Shibpur.

REFERENCES

1. Barua, R., Datta, S., Datta, P., & Chowdhury, A. R. (2019). Scaffolds and Tissue Engineering Applications by 3D Bio-Printing Process: A New Approach. In Kumar, K., & Davim, J. (Ed.), Design, Development, and Optimization of Bio-Mechatronic Engineering Products (pp. 78-99). IGI Global. <http://doi:10.4018/978-1-5225-8235-9.ch004>
2. Amaral M. Lopes M. A. Silva R. F. Santos J. D. (2002). Densification route and mechanical properties of Si₃N₄-bioglass biocomposites. Biomaterials, 23(3), 857–862. 10.1016/S0142-9612(01)00194-611771704
3. Boccaccio A. Ballini A. Pappalettere C. Tullo D. Cantore S. Desiate A. (2011). Finite element method (FEM), mechanobiology and biomimetic scaffolds in bone tissue engineering. International Journal of Biological Sciences, 7(1), 112–132. 10.7150/ijbs.7.11221278921
4. Chen G. Dong C. Yang L. Lv Y. (2015). 3D scaffolds with different stiffness but the same microstructure for bone tissue engineering. Van Den Bulcke A. I. Bogdanov B. De Rooze N. Schacht E. H. Cornelissen M. Berghmans H. (2000). Structural



- and rheological properties of methacrylamide modified gelatin hydrogels. *Biomacromolecules*, 1(1), 31–38. 10.1021/bm990017d11709840ACS Applied Materials & Interfaces, 7(29), 15790–15802. 10.1021/acsami.5b0266226151287
5. Byambaa B. Annabi N. Yue K. Trujillo-de Santiago G. Alvarez M. M. Jia W. Khademhosseini A. (2017). Bioprinted osteogenic and vasculogenic patterns for engineering 3D bone tissue. *Advanced Healthcare Materials*, 6(16), 1700015. 10.1002/adhm.20170001528524375
 6. Dehghani F. N. Annabi N. (2011). Engineering porous scaffolds using gas-based techniques. *Current Opinion in Biotechnology*, 22(5), 661–666. 10.1016/j.copbio.2011.04.00521546240
 7. Fennema E. Rivron N. Rouwkema J. van Blitterswijk C. de Boer J. (2013). Spheroid culture as a tool for creating 3D complex tissues. *Trends in Biotechnology*, 31(2), 108–115. 10.1016/j.tibtech.2012.12.00323336996
 8. Kelly D. J. Prendergast P. J. (2006). Prediction of the optimal mechanical properties for a scaffold used in osteochondral defect repair. *Tissue Engineering*, 12(9), 2509–2519. 10.1089/ten.2006.12.250916995784
 9. Liao C. J. Chen C.-F. Chen J.-H. Chiang S.-F. Lin Y.-J. Chang K.-Y. (2002). Fabrication of porous biodegradable polymer scaffolds using a solvent merging/particulate leaching method. *Journal of Biomedical Materials Research*, 59(4), 676–681. 10.1002/jbm.1003011774329
 10. Ozbolat I. T. Hospodiuk M. (2016). Current advances and future perspectives in extrusion-based bioprinting. *Biomaterials*, 76, 321–343. 10.1016/j.biomaterials.2015.10.07626561931
 11. Ting Z. (2017). Biomimetic design and fabrication of multilayered osteochondral scaffolds by low-temperature deposition manufacturing and thermal-induced phase-separation techniques. *Biofabrication*, 9(2), 25–21.28462906
 12. Zhang C. Hu Y.-Y. Cui F.-Z. Zhang S.-M. Ruan D.-K. (2006). A study on a tissue-engineered bone using rhBMP-2 induced periosteal cells with a porous nano-hydroxyapatite/collagen/poly(L-lactic acid) scaffold. *Biomedical Materials (Bristol, England)*, 1(2), 56–62. 10.1088/1748-6041/1/2/00218460757
 13. Zein I. Hutmacher D. W. Tan K. C. Teoh S. H. (2002). Fused deposition modeling of novel scaffold architectures for tissue engineering applications. *Biomaterials*, 23(4), 1169–1185. 10.1016/S0142-9612(01)00232-011791921
 14. Gross B. C. Erkal J. L. Lockwood S. Y. Chen C. Spence D. M. (2014). Evaluation of 3D printing and its potential impact on biotechnology and the chemical sciences. *Analytical Chemistry*, 86(7), 3240–3253. 10.1021/ac403397r24432804
 15. Barua, R., Datta, S., Roychowdhury, A., & Datta, P. (2019). Importance of 3D Printing Technology in Medical Fields. In Kumar, K., Zindani, D., & Davim, J. P. (Ed.), *Additive Manufacturing Technologies From an Optimization Perspective* (pp. 21-40). IGI Global. <http://doi:10.4018/978-1-5225-9167-2.ch002>
 16. Pati F. Jang J. Ha D. H. Won Kim S. Rhie J. W. Shim J. H. Cho D. W. (2014). Printing three-dimensional tissue analogues with decellularized extracellular matrix bioink. *Nature Communications*, 5(1), 3935. 10.1038/ncomms493524887553
 17. Mueller B. Kochan D. (1999). Laminated object manufacturing for rapid tooling and patternmaking in foundry industry. *Computers in Industry*, 39(1), 47–53. 10.1016/S0166-3615(98)00127-4
 18. Matsumoto K. Ishiduka T. Yamada H. Yonehara Y. Arai Y. Honda K. (2014). Clinical use of three-dimensional models of the temporomandibular joint established by rapid prototyping based on cone-beam computed tomography imaging data. *Oral Radiology*, 30(1), 98–104. 10.1007/s11282-013-0127-3
 19. Sirringhaus H. Kawase T. Friend R. H. Shimoda T. Inbasekaran M. Wu W. Woo E. P. (2000). High-resolution inkjet printing of all-polymer transistor circuits. *Science*, 290(5499), 2123–2126. 10.1126/science.290.5499.212311118142
 20. Ricci J. L. Clark E. A. Murriky A. Smay J. E. (2012). Three-dimensional printing of bone repair and replacement materials: Impact on craniofacial surgery. *The Journal of Craniofacial Surgery*, 23(1), 304–308. 10.1097/SCS.0b013e318241dc6e22337431



21. Brian J. O'Grady, Kylie M. Balotin, Allison M. Bosworth, P. Mason McClatchey, Robert M. Weinstein, Mukesh Gupta, Kara S. Poole, Leon M. Bellan, and Ethan S. Lippmann, *ACS Biomaterials Science & Engineering* 2020 6 (10), 5811-5822 DOI: 10.1021/acsbiomaterials.0c00885
22. Tschumperlin D. J. Liu F. Tager A. M. (2013). Biomechanical regulation of mesenchymal cell function. *Current Opinion in Rheumatology*, 25(1), 92–100. 10.1097/BOR.0b013e32835b13cd23114589
23. Nakamura M. Kobayashi A. Takagi F. Watanabe A. Hiruma Y. Ohuchi K. Takatani S. (2005). Biocompatible inkjet printing technique for designed seeding of individual living cells. *Tissue Engineering*, 11(11-12), 1658–1666. 10.1089/ten.2005.11.165816411811
24. Hassan W. Dong Y. Wang W. (2013). Encapsulation and 3D culture of human adipose-derived stem cells in an in-situ crosslinked hybrid hydrogel composed of peg-based hyperbranched copolymer and hyaluronic acid. *Stem Cell Research & Therapy*, 4(2), 32. 10.1186/scrt18223517589
25. Itoh M, Nakayama K, Noguchi R, Kamohara K, Furukawa K, et al. (2015) Correction: Scaffold-Free Tubular Tissues Created by a Bio-3D Printer Undergo Remodeling and Endothelialization when Implanted in Rat Aortae. *PLOS ONE* 10(12): e0145971. <https://doi.org/10.1371/journal.pone.0145971>



Challenges & Way Forward in Integration of Remote based Working Environment for a Multi-Disciplinary Engineering Design Centre

Anirban Datta^{1*}, Gautam Gangopadhyay², Sushmita Choudhury³

Department of Mechanical & Piping Engineering^{1,2}, Department of Human Resources³

Richard Design Services India Private Limited (A fully owned Subsidiary of Richard Industrial Group, USA), Sector-V, Salt Lake City, Kolkata

*✉ ani_dat@yahoo.co.in

ABSTRACT

With the outset COVID-19 pandemic globally, the extent of 'Remote Working', although not entirely a new thing for the engineering sector and already in place predominantly with software, IT and IT enabled services provider organizations, has spread its arms work methodology of core engineering organizations as well, such as engineering design centres engaged in basic & detailed engineering for power, oil & gas, petrochemical, steel & metal and sectors of heavy engineering. While the 'neo normal' phenomenon has posed enormous challenge in front of these organizations and their human resources, majority of them successfully strategized and overcome. Ultimately, this has created a new paradigm of skill development to these organizations, which would prevail as a long term intangible asset.

Keywords : Working; Neo normal; Online; Collaboration; Productivity; Communication.

INTRODUCTION

Year 2020 has shown an unprecedented challenge to the engineering sector. The COVID-19 pandemic has profoundly changed workplaces and the nature of work itself, and forced the world to recognize the advantages of a more flexible definition of "office." It has crushed the economy, wiped out crores of jobs, and caused for death of over a million people worldwide. But there are a few avenues in which the pandemic may prompt engineering fraternity to improvise, and one is "Remote Work". Thoughts triggered many, "can organizations be transformed while employees are working remotely?" The first priority of most organizations during the COVID-19 outbreak was to respond to the crisis and emphasize health, safety, essential services and, keep employees from falling sick. As Organizations were gradually coming out of this response phase, business leaders started focusing on challenges and issues to make people more agile, productive and happier while reshaping and reimagining business strategies helping the environment, and preserving infrastructure.

THE 'INITIAL SHOCK'

Working 'remotely', or referred as 'Work from Home' more colloquially, was not a new entrant for software, IT and IT enabled sectors. However, for companies who work in engineering design domain involving multiple disciplines such as civil, mechanical, piping, electrical, control & instrumentation, chemical & process, IT, project management, etc., the case was not so simple. A major cluster of these organizations are involved in delivering for projects (whether it be for power, oil & gas, steel & metal, cement, BIM sectors) which have a global collaborative environment. In many cases, the project owner may be situated in some country/continent, whereas the executor/EPC contractor, consultant and design agencies may be in some other parts of globe. In a significant number of cases, the design agencies are also split in different geographic locations, involving different time zones.

Meanwhile, the pressure on businesses to transform themselves so that they capture the next wave of productivity, speed, customer-engagement, and employee-engagement benefits kept mounting as most organizations would prefer to transform themselves under quieter conditions. Thus the prevailing COVID-19 pandemic situations pose a 'shock' to the all of the above stakeholders. From the project owners' perspective, it came as "whether the executor/EPC contractor, consultant and design agencies would be able to deliver", whereas from the perspective of agencies at other side, it emerged as "whether the client/project authority would continue with execution of the project".

And both of these perceptions had sound and logical basis!

INITIAL CHALLENGES

The first challenge, to the engineering design companies, was to build-up the confidence in the mindset of clients that the delivery would continue, through a 'Neo Normal' roadmap. To survive and thrive in this more volatile, uncertain, complex, and ambiguous world, companies were embracing agility at scale.

The next task was to set up the infrastructure, hardware, software, network connectivity and collaborative environment at the premises of individual resources. These changes across the operating model, structure, process, people, and technology seemed scary and became a mammoth task, particularly in the environment of full lockdown, as lot of statutory and regulatory guidelines had to be adhered to, amidst lack of availability of normal public systems and amenities.

Once the infrastructure was set up, the real and toughest challenge began – which is to gear up the human resources to adapt and familiarize with this 'Neo Normal' working methodology, and adhering to schedule and quality.



Fig. 1. Typical plant 3D model of a part of a refinery

In a country like India, it is practically impossible to find out a room/corner for a person to be quarantined if affected with pandemic, within a household premises, for a large number of workforces. In this context, it is ironical to find out a room/corner where one may carry out un-interrupted work.

Along with the above, there are other constraints such as interrupted electricity supply and internet connectivity.

THE STRATEGY

To emphasize on the transition journey, working from home can be stressful, and even more so when roles and operating models change. The company devoted special attention to amplified communications; to explicit support from former managers, new leaders, and specialist resources; and, overall, to creating a clear, streamlined transition journey. This transition journey consisted of both learning and applying it in practice by together defining the purposes and objectives of the new team. High-quality videos and all-company virtual meetings conveyed some of the key messages in an effective way and built a sense of community.

Remote working sounded like the business revolution which was the need of the hour but it is not something which one can simply switch to and hope for the best as it had many pros and cons with a number of challenges to overcome, as well. Thereby to respond to the business demands, working strategies and tools every business adopted to overcome these issues and reap the full benefits remote working has to offer.

Challenges for remote managers/leads:[1]

- Managing projects
- Remote collaboration
- Tracking tasks and productivity
- Working from different locations/time zones, etc.



- Dealing with language and cultural differences
- Building/maintaining trust

Challenges for remote workers:[1]

- Maximizing productivity
- Overcoming distractions
- Staying motivated
- Unplugging after work

Managing projects

Biggest challenge with remote working in a multi-disciplinary engineering design project is managing when the team is spread out across multiple locations. Whether it is a mix of in-house and remote staff or an entire team of remote workers, managers/leads are responsible for making sure meeting schedule without sacrificing quality. Managers have to be extremely cautious about the availability of resources if there is no prevailing mechanism to track and monitor whether the resource is virtually available.

Remote collaboration

The most common challenge remote teams face is collaborating from different locations. For example, how can a team of designers work on the same project when they are spread out across the country or world? When team members are under the same roof, they can interact/refer with documents, items, projects and each other without any real limitations. However, interacting with same document or working simultaneously with same plant 3D model by multiple users from remote pose substantial challenge. Also, in a typical multi-disciplinary engineering design centre executing detail engineering for complex unit of a refinery in 3D engineering & design environment, requirement of large and/or dual monitors and paper printouts for checking of drawings etc. play very crucial role in productivity and quality. However, while these are available in office premises, it is extremely difficult, and impossible in majority cases, to provide these infrastructure in the premises of individual resources. The first thing needed for remote collaboration is an effective communication channel and establishing clear operating models for teams. Simple Email correspondences does not suffice for remote team communications and it is especially important to provide every team with clear basics, such as team norms (expected behavior) and ways of communicating (tools, how to make decisions, respond, monitor and so forth). There is need of something instant, responsive and flexible. Online meeting tools have played a significant role to facilitate enhances communications. Further to this, it has been experienced that instant messaging Apps in a smart phone have played a very crucial role to open up the most effective channel of communication.

It was observed that there was even more empowerment to the teams in terms to making decisions that deliver results quickly and reduce the feedback loop.

Tracking tasks and productivity

To achieve the overall project target, it is to be ensured that all of the smaller tasks are to be completed in a timely manner. Monitoring progress of multiple remote resources on a daily basis is a daunting task. How can the manager/lead keep track of progress on individual tasks while also keeping a keen eye on project-wise progress? The common project management tools we can help to do that in a reactionary sense, i.e. they will show when team members have started tasks and finished them, but this information would only be available after these interactions take place. They would not really give the live feedback or indicate how productive team members are being while they work on tasks. To get a more real-time look at team progress, it is required to have a real-time tool which can prompt team members to provide quick “check-in” details about what they are currently working on so that the manager/lead can see what all are up to at any given time. Team members can also see what everyone else is currently working on, what they got up to yesterday, their availability status and any “blockers” that are getting in the way of completing tasks. It can also be discovered which tasks individual team members are most time-efficient with, allowing the manager/lead to assign tasks to the most suitable person. Even more important, teams must agree up front what to do when people do not behave according to expectations or things do not go as planned. The teams themselves create the norms – an approach that works better than externally imposed rules do. To focus on the important things, teams to maintain a sustainable pace, focusing as much as possible on the work immediately at hand. The key step is to visualize the flow of work from the start of remote work to the moment when a team decides that work on it is done. This approach creates transparency by helping the members of the team to act together to solve existing problems before turning to new ones

Working from different locations/time zones

One of the greatest advantages remote working gives is the ability to hire talent from around the world and transcend across geographical boundaries. The disadvantage is that much of them being in different time zones, this can put the team out of synchronization. In some cases, parts of the team could be at leisure while other parts are struggling to get things done on the other side of the world. Adding this to the freedom remote working gives the team members (maybe they have to or prefer to work in the evening shifts, for example) which guarantees that not everyone is going to be 'switched on' when exactly they are needed. The best way to solve this challenge is to set a few guidelines and norms in place for team members. Although the intention should not be to infringe on the benefits remote working has to offer, but there needs a check& balance if productivity is achievable. Tools and Mechanisms for tracking performance and progress of the project gives the Line Managers and/or the Project Managers a sense of how well and quickly things are happening and where to pay more attention. Ideally, the key members of the team are required to have a fairly regular schedule.

The weekly and daily rhythm of agile teams is to sync well in remote settings. It does not necessarily matter when they choose to work, as long as they are consistent with their planned schedule, so the manager/lead will have an idea of their availability, irrespective of whether they decide to work specific hours every week or schedule availability time for the week ahead.

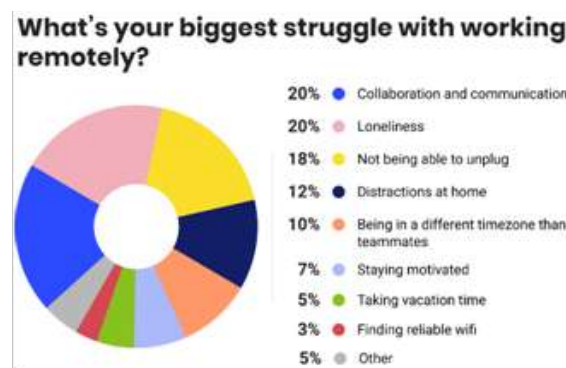


Fig. 2. Challenges associated with remote working
(Image Source: lp.buffer.com/state-of-remote-work-2020)[2]

Dealing with Language and Cultural Differences

When there is a remote team of workers from around the world, it is likely to have issues with language and cultural differences, mainly due to varying levels of English proficiency (or other business languages), but there are more specific or subtle cultural contexts that also need to be understood in terms of attitudes toward careers, families, work-life integration, and boundaries can vary greatly. Knowing the cultural dynamics of people in the team, the manager/lead would be in better position to identify which aspects of remote working are more difficult for certain members and empathize helping them to overcome those. In order to start with, it is to be ensured that no team member is criticized/demeaned on the language ability or made to feel inadequate about. Native speakers to be culturally sensitive on misunderstandings that might happen and ensure to take whatever steps possible to make them less likely/severe. Resilience is the key and Patience is crucial and making it easier for non-native speakers to understand, particularly in online platform of discussions. Also, enabling communication with video facility is extremely helpful on this. As far as communicating important/critical information are concerned, it is always better to communicate those to non-native speakers via email, so that they can read text at their own pace, read it multiple times, reading between the lines if necessary, and use a dictionary (offline/online) for any word they are not familiar with. The most important aspect for non-native speakers is to make them comfortable to ask about anything those are unclear to them without it being held against them.

Understanding how to manage cultural differences can have a huge impact on the success in coordinating the remote workforce.

Building/Maintaining Trust

There are obvious trust issues that can arise among remote teams when it cannot be seen physically what people are doing. In some cases, team members may have never met each other face-to-face and this has all kinds of subconscious effects on trust/confidence between them. For example, when working within a multi-disciplinary engineering team, it is practically



impossible to filter out issues like ‘power-failure’ or ‘network-failure’ at one or more particular locations. With following practical measures, this challenge can be eased out:

- i) Get to know each other: Team meetings in online platform, with video enabled, at least once in a day, has been extremely effective, to widen the inter-personal bond, particularly in the crisis hours of pandemic situation.
- ii) Be responsive and reliable: When team members are responsive and tasks are completed within schedule, trust typically remains high.
- iii) Promote transparency: Transparency is the essence of building the trust at every level and in each member of the team. This is achieved most efficiently through prompt and open communications, such as if some member(s) of the team are facing any issues which are typically due to external factors, those should be communicated to others so that all are apprised of the situation.
- iv) Get the right collaboration tools: Online video-conferencing platforms which are the most important collaboration tool must be selected judiciously, because although all platforms have some common elements, there are substantial issues typically associated with each of those with respect to ease of access, bandwidth, data confidentiality, etc.
- v) Create shared goals: When team members have shared goals, they have an invested interest in working together and backing up each other.
- vi) Avoid micromanagement: The manager/lead must have a check in with team members but they should avoid micromanagement themselves, as it can reduce drive, pro-activeness and improvisation by the members.
- vii) Lead by example: The manager/lead must establish to the team members that he/she is trustworthy and willing to trust them. Also, apart from coordinating & collaborating, there have to be few assignments/deliverables/milestones which the manager/lead needs to do on his own, and thus setting an example in front of other team members.

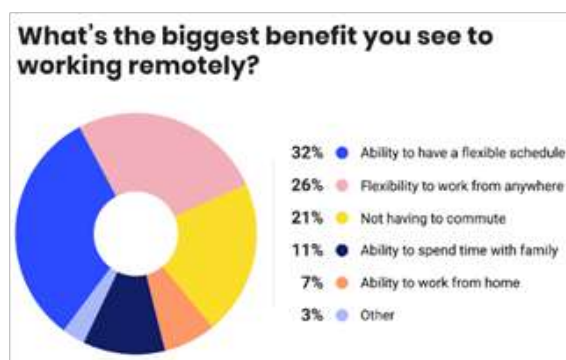


Fig. 3. Benefits associated with remote working
(Image Source: <https://lp.buffer.com/state-of-remote-work-2020>)[2]

Maximizing Productivity

Poor productivity is the worst thing for remote workers and also one of the most difficult challenges to overcome by the manager/lead as ultimately they are answerable to internal/external client. The longer it takes to complete tasks, the more they eat into one's personal life and lead the member less effective to the team. Following are some key findings from studies that look into the most common productivity killers:

- Multitasking reduces productivity by up to 40%[3]
- Humans lose focus on a single task after 5-20 minutes[4]
- It takes up to 23 minutes to regain focus after being distracted[5]

So, based on those scientific findings, here is a three-step plan to maximizing productivity:

1. Avoid multitasking: Set a single goal for each day/hour and focus to hit that target.
2. Work in short bursts: Keep focus at a higher level and increase motivation with multiple work break-downs.
3. Remove distractions: Stop unnecessary distractions from killing productivity.

Overcoming Distractions

Distractions are another group of challenges that can affect remote working severely and hinder team progress. Distractions at residential premises were the fourth most common problem reported by Buffer's 2019 State of Remote Working report. There might be issues such as power-failure, poor/nil internet connectivity, unwanted noise & sounds, to name few. Ideally, there should be a separate room dedicated to work. Also, it is extremely necessary to have a robust internet service provider with seamless connectivity as well as a back-up supply of power, notwithstanding the requirement of state-of-the-art computer hardware; however, there is always a cost factor involved.

Staying Motivated

Staying motivated is another common challenge. This is essentially an outcome being unsupervised. Without physical presence of supervisors and team members, there is less amount of pressure to get things done and a significant part of group dynamics is also not present. Appreciation and encouragement from the manager/lead through the common communication channel plays a crucial role to boost up the morale and enhance motivation level significantly.

Unplugging After Work

This is one of the worst of all the challenges associated with remote working. The best way to switch off after work is by getting everything done those are set out to do before the day is over. To ensure this, it is essential to set achievable targets for each day and routinely hit those.

THE WAR-FRONT

At the onset of Lockdown 1.0, it has been taken a couple of week's times to make the team tuned and adopt with the philosophy of remote working. It had become a daunting task for the managers/leads to percolate the necessity of open and prompt communication within the team. During the various stages of the project, practically all of the challenges mentioned above had been faced, and resolved to the extent possible. On top of those, there had been another matter of concern, which is typical for a multi-disciplinary engineering design centre, engaged in 'work-sharing' with design centres at other countries/time zones, that is smooth running of virtual private network and accessibility of engineering design & analysis software, many of which might have license server located in other continents. One of the reason was lower bandwidth, and this had been global phenomena, as people across globe enjoyed live streaming of movies, etc., thus posing hindrance to overall bandwidth availability.

Online discussions between team members, both domestic as well as abroad, at least once in day, had been extremely beneficial to overcome many of the hurdles those came into the path of project team. There had been a substantial deliberation at initial phase on selection of the appropriate collaboration platforms, as although all platforms have some common elements, there are substantial issues typicality associated with each of those with respect to ease of access, bandwidth, data confidentiality, etc. On top of that, there had been different regulations/advisories by governments/corporates at different parts of world. While the platforms which are available free of cost have been proven to be effective for a small group of people, involving lower bandwidth requirement, however with short-coming of non-availability of recording feature in many cases, and restriction with duration in some other cases, the priced online platforms have been proven to be more effective for a larger team size, having requirement of screen-sharing (e.g. starting from sharing of meeting agenda, presentation material, schedule to even live plant 3D model) involving much higher bandwidth. Even in many cases, platforms meant for webinar had to be utilized, in order to exercise a better control with respect to clarity of audio and visuals.



Fig. 4. Online collaboration



As the work process & environment became much more dependent on desktops, laptops, tablets & smartphones along with software & apps, it has been observed prominently that engineering professionals of average age group below 45 – 50 years could remain more proficient in adapting this ‘neo normal’, whilst professionals in higher age group was more posed to a struggle, however, of course with exceptions.

With subsequent phases of Lockdown and Un-Lockdown, the process became more and more streamlined. On an average, the written and oral communication skill among the baseline team members were improving gradually. Apathy to written communication had been a typical phenomenon seen among drafters, modelers and other baseline resources when working within the controlled office environment. The remote working phase played a highly positive role in inculcating these new behaviours amongst them.

WAY FORWARD

The trend of remote working, accelerated by pandemic, is likely to stay. It will profoundly change workplaces and the nature of work itself. According to a survey by a US technology research firm, the number of employees permanently working remotely globally is set to double in 2021, and percentage of permanent remote workers will rise from 16.4% to 34.4%[6], comprising of all engineering sectors, viz. core engineering, software, IT & IT enabled service providers by some way or other. Of the more than 1,000 organizations interviewed for the survey, 48.6% reported that productivity has improved since workers began working remotely, with 28.7% of respondents indicating a decline in productivity. The need to drive a holistic change is the way forward especially its human aspects - People over Process.

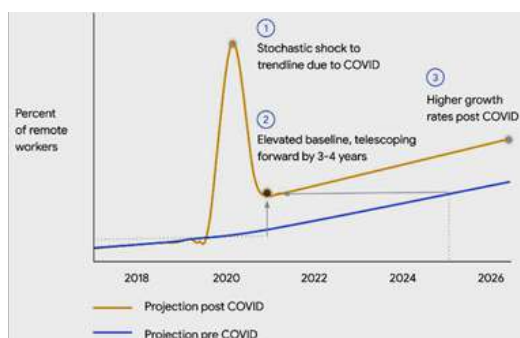


Fig. 5. Future Trend of Remote Working

(Image Source: <https://cloud.google.com/blog/products/chrome-enterprise/the-remote-work-revolution>)[7]

There would be immense requirement of ‘re-skilling’ and ‘up-skilling’ to adapt new technologies and tools, and those who would be able to improvise would emerge as front-runners. It is expected that by 2030, one billion people will need reskilling.

Change will be at the enterprise level widely, for example, the way the organization does budgeting, manages performance, and runs the technology. This requires changes across all network and functions of empowered teams, rapid decision(s) and learning cycles, a dynamic people model that ignites passion, and next-generation enabling technology. Even more important is, building agile remote teams representing a fundamental change in the culture and in expectations.

As an organization, we need to ensure that every employees’ journey of change is transformative, even life-altering – but not too disruptive. Remote work increases the need to focus double on communication, to support human-to-human interactions, and to offer practical support to people during the transition.

The coronavirus pandemic has largely served to increase the visibility of the HR agenda within the workforce, as employee well being, internal communication and alterations to the working habits of many professionals take centre stage within the strategies of many businesses. However, one key development since the start of the pandemic in the UK, remote working, could well lead to an increase in racism and prejudice, according to recent research by the Woolf Institute. The study, which was conducted by polling firm Survation, researching interfaith relations and polled over 11,700 workers within the UK, noted that workplace friendships are the key to breaking down ‘misconceptions’ within the workplace, yet currently the workforce is at risk of going “back into isolated silos,” due to widespread remote working, reported by Woolf Institute’s Founder Ed Kessler to BBC. The Woolf Institute’s research suggested that of those who work in shared offices, 76% - regardless of ethnicity - were in



a setting that is ethnically diverse. However, the research also unearthed that unemployed people are 37% more likely to only have friends from their own ethnic group. So, it is important to note that this might lead to actively open up professionals to other diverse groups, whilst the isolation caused by remote working could well reverse this.

With emphasized working models and employee expectations changing in unexpected ways since the COVID-19 pandemic, and it is very much essential to re-imagine the 'employee experience' and organizations align the business and workforce strategies in the 'NEW NORMAL'.

ACKNOWLEDGMENT

Authors acknowledge the Management of Richards Design Services, India for encouragement and support to write this paper.

REFERENCES

1. Aaron Brooks, 10 Common Remote Work Challenges, <https://www.ventureharbour.com/remote-work-challenges-solutions/>
2. The 2020 State of Remote Work, <https://lp.buffer.com/state-of-remote-work-2020>
3. American Psychological Association, March 20, 2006, Multitasking: Switching costs, <https://www.apa.org/research/action/multitask>
4. Neil A. Bradbury, Department of Physiology and Biophysics, Chicago Medical School, Rosalind Franklin University of Medicine and Science, North Chicago, Illinois, Attention span during lectures: 8 seconds, 10 minutes, or more?, *Advances in Physiology Education*, 40, 2016, pp. 509 - 513
5. Gloria Mark, Department of Informatics, University of California, Irvine, CA, USA, Daniela Gudith and Ulrich Klocke, Institute of Psychology, Humboldt University, Berlin, Germany, The Cost of Interrupted Work: More Speed and Stress, *Proceedings of the SIGCHI conference on Human Factors in Computing Systems-2008*, pp. 107 - 110
6. The World Economic Forum COVID Action Platform, The number of permanent remote workers is set to double in 2021, <https://www.weforum.org/agenda/2020/10/permanent-remote-workers-pandemic-coronavirus-covid-19-work-home/>
7. John Solomon, The future of computing showed up early, <https://cloud.google.com/blog/products/chrome-enterprise/the-remote-work-revolution>



Principles, Applications and Directions of Sustainable Manufacturing: A Case of Indian Micro, Small and Medium Enterprises (MSMEs)

Dr Om Parkash Mehta

Director, Office of the Development Commissioner (MSME), Ministry of MSME, Govt. of India, Nirman Bhawan, New Delhi

✉ drommehta@yahoo.co.in

ABSTRACT

MSMEs are the engine of growth of any country. Micro-, Small and Medium-sized Enterprises (MSMEs) make up over 90% of all firms and account, on average, for 70% of total employment and 50% of GDP. Micro-, Small and Medium-sized Enterprises Day is observed globally on 27th June every year since 2017. The objective of SDG was to produce a set of universal goals that meet the urgent environmental, political and economic challenges facing our world. 17 SDGs are designed to bring the world to several life-changing 'zeros'. Product-Evolution Process is a process for developing and commercializing an innovation or an invention in more depth. It is imperative that manufacturing industries strive for 'Sustainable Manufacturing' (SM) on their part. The waste generated during the manufacturing processes, during the use of the products and after the end of the life of the products is responsible for the degradation of the environment. Life Cycle Assessment (LCA) is the tool generally used to implement SM. Sustainable manufacturing requires that all manufacturing organisations should aim for the four activities. Zero-emission (i.e. closed-loop) manufacturing views the manufacturing system as an industrial ecosystem, and requires the reuse of wastes or by-products within the manufacturing system. It is also important to develop new processes that use less harmful materials and generate

fewer emissions. Union Ministry of MSME, Government of India runs a number of schemes to provide financial and non-financial assistance to the MSMEs across the country. These schemes mainly include registration, Credit assistance related, Credit Linked Capital Subsidy - Technology Upgradation Scheme (CLCS-TUS), Cluster Development Programme, Infrastructure assistance, Marketing assistance etc besides having a number of schemes for Khadi and Village Industries as well as Coir sector. Hon'ble Prime Minister of India Shri Narendra Modi has launched CHAMPIONS, a technology platform to empower MSMEs on 1st June 2020. The Ministry has issued a notification dated 26th June 2020 regarding revision of definition of MSMEs and process of registration. CLCS-TUS is aimed at promoting competitiveness amongst Indian Micro, Small and Medium Enterprises (MSMEs) by the way of wastage reduction through Lean Manufacturing, support for Design improvement, building awareness on Intellectual Property Rights, Zero Defect Zero Effect (ZED) Scheme, digitally empowerment of MSME through Digital MSME and to promote & support untapped creativity of individual and to promote adoption of latest technologies in manufacturing as well as knowledge based innovation MSMEs through Incubation across India. "Zero Defect Zero Effect" is a slogan coined by Hon'ble Prime Minister of India, Shri Narendra Modi. It signifies production mechanisms wherein products have no defects (Defect free) and the process through which product is made have zero adverse environmental and ecological effects (Zero effect on environment). The techniques of Lean Manufacturing enhance productivity and competitiveness by reduction of wastage in manufacturing processes, inventory management, space management, energy consumption, etc. These are some of the ways and techniques required to be adopted continuously to make a better and quality life by the masses in the world.

Keywords : MSME; SDG; SM; LCA; ZED; Product-evolution.

INTRODUCTION

Micro, Small and Medium enterprises (MSMEs) are important to almost all economies in the world, especially in developing countries. MSMEs are the engine of growth of any country. The size and importance of the MSME sector varies from country to country. In the last few decades there is an increasing recognition of the role it plays in industrial countries for their contribution in economies due to which number of MSMEs is increasing. According to the data provided by the International Council for Small Business (ICSB), formal and informal Micro-, Small and Medium-sized Enterprises (MSMEs) make up over 90% of



all firms and account, on average, for 70% of total employment and 50% of GDP. In view of their vast contribution in the economies, .Micro-, Small and Medium-sized Enterprises Day is observed globally on 27th June every year since 2017. This day is observed by the United Nations to raise public awareness of their contribution to sustainable development and the global economy. The theme of MSME day for the year 2020 has been “COVID-19: The Great Lockdown and its impact on Small Business.”

INDIAN SCENARIO OF MSME

The role of Micro, Small & Medium Enterprises (MSMEs) in the Indian economy is unique and unparalleled. The MSMEs play an important role across sectors of the economy, producing diverse range of products and services to meet demands of domestic as well as global markets. The advantages of setting MSMEs in India are many. MSMEs play a crucial role by providing large employment opportunities at comparatively lower capital cost than large industries as well as through industrialization of rural & backward areas, inter alia, reducing regional imbalances, assuring more equitable distribution of national income and wealth. It is the most important and effective sector for creation of enterprises. Entrepreneurs can expand their capabilities and horizons of empowerment comparatively with less inputs in this sector for their livelihoods besides having opportunity of being job providers and not job seekers thus to facilitate the economic growth and development of the country faster in comparison to other ventures. The MSME sector has the potential to spread industrial growth across the country and can be a major partner in the process of inclusive growth. The significant importance of the MSME sector towards driving the country's economy has thus led the Government to consider it as a priority sector. As per the National Sample Survey (NSS) 73rd round, conducted by National Sample Survey Office, Ministry of Statistics & Programme Implementation during the period 2015-16, there were 633.88 lakh unincorporated non-agriculture MSMEs in the country engaged in different economic activities (196.64 lakh in Manufacturing, 0.03 lakh in Non-captive Electricity Generation and Transmission, 230.35 lakh in Trade and 206.84 lakh in Other Services) excluding those MSMEs registered under (a) Sections 2m(i) and 2m(ii) of the Factories Act, 1948, (b) Companies Act, 1956 and (c) construction activities falling under Section F of National Industrial Classification (NIC) 2008. As per Fourth All India Census of MSME (2006-07), there were 3.62 crore MSME. The sector has grown at an annual compound rate of more than 7%. The MSME segment plays a key role in domestic manufacturing and is imperative for the success of the Make in India programme besides export potential.

SUSTAINABLE DEVELOPMENT GOALS (SDG)

The Sustainable Development Goals (SDGs) were born at the United Nations Conference on Sustainable Development in Rio de Janeiro in 2012. The objective was to produce a set of universal goals that meet the urgent environmental, political and economic challenges facing our world. The SDGs replace the Millennium Development Goals (MDGs), which started a global effort in 2000 to tackle the indignity of poverty. The MDGs established measurable, universally-agreed objectives for tackling extreme poverty and hunger, preventing deadly diseases, and expanding primary education to all children, among other development priorities. SDGs also known as the Global Goals, were adopted by all United Nations Member States in 2015 as a universal call to action to end poverty, protect the planet and ensure that all people enjoy peace and prosperity by 2030. The United Nations' 17 SDGs aim to achieve decent lives for all on a healthy planet by 2030. SDGs are integrated that is, they recognize that action in one area will affect outcomes in others, and that development must balance social, economic and environmental sustainability. Through the pledge to Leave No One Behind, countries have committed to fast-track progress for those furthest behind first. That is why the SDGs are designed to bring the world to several life-changing 'zeros', including zero poverty, hunger, AIDS and discrimination against women and girls. The creativity, knowhow, technology and financial resources from all of society is necessary to achieve the SDGs in every context. These 17 SDG include –

- Goal 1: No Poverty: End poverty in its all forms everywhere.
- Goal 2: Zero hunger: End hunger, achieve food security and improved nutrition and promote sustainable agriculture.
- Goal 3: Good Health and well-being: Ensure healthy lives and promote well-being for all at all ages.
- Goal 4: Quality Education: Ensure inclusive and equitable quality education and promote life long learning opportunities for all.
- Goal 5: Gender Equality: Achieve gender equality and power and empower all women and girls.
- Goal 6: Clean water and sanitation: Ensure availability and sustainable management of water and sanitation for all.
- Goal 7: Affordable and clean energy: Ensure access to affordable, reliable, sustainable and modern energy for all.



- Goal 8: Decent work and economic growth: Promote sustained, inclusive and sustainable economic growth, full and productive employment and decent work for all.
- Goal 9: Industry, Innovation and Infrastructure: Build resilient infrastructure, promote inclusive and sustainable industrialisation and foster innovation.
- Goal 10: Reduced inequalities: Reduce inequality within and among countries.
- Goal 11: Sustainable cities and communities: Make cities and human settlements inclusive, safe, resilient and sustainable.
- Goal 12: Responsible consumption and production: Ensure sustainable consumption and production patterns.
- Goal 13: Climate action: Take urgent action to combat climate change and its impacts.
- Goal 14: Life below water: Conserve and sustainably use the oceans, seas and marine resources for sustainable development.
- Goal 15: Life on land: Protect, restore and promote sustainable use of terrestrial ecosystem, sustainably manage forests, combat desertification and halt and reverse land degradation and halt biodiversity loss.
- Goal 16: Peace, Justice and strong institutions: Promote peaceful and inclusive societies for sustainable development, provide access to justice for all and build effective, accountable and inclusive institutions at all levels.
- Goal 17: Partnership for the goals: Strengthen the means of implementation and revitalise the global partnership for sustainable development.

PRODUCT-EVOLUTION PROCESS

It is a process for developing and commercializing an innovation or an invention in more depth. It stimulates the economic growth. Figure 1 depicts the product-evolution process. It begins with knowledge of base technology and sciences such as electronics, medical science, thermodynamics, fluid dynamics etc. and ends with products or services available for purchase in market place. The intersection of knowledge and a recognized social need that begins the product development phase is the critical point in this process. The innovation may be ordinary innovations (with little uniqueness or technology) or technological innovations (new products with significant technological advancement) and breakthrough innovations (new products with some technological change). Obviously the number of actual innovations decreases as the technology involved increases. A very apt example these days is of the availability of Covid pandemic vaccine. It is the recognized social need at Phase I in the product-evolution process. As of now the countries world over have been putting their best efforts vigorously by working day and night to develop the vaccine by making use of the technologies (Phase II- Initiation of technological innovation) and successful launch of the vaccine (Phase III- Iterative synthesis leading to invention i.e. pressing toward invention) will lead to development phase (Phase IV) and Industrial Phase (Phase V) for mass production and distribution.

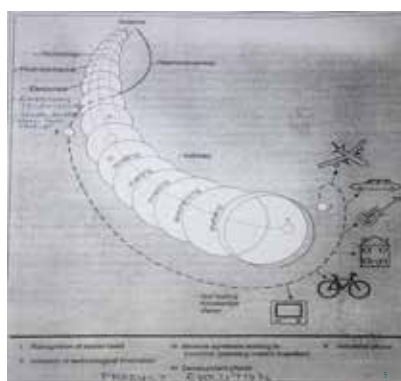


Fig. 1. Product-evolution process

ENVIRONMENTAL RESPONSIBILITY AND MSME

Environmental responsibility for manufacturing organizations is an integral part of the way product is marketed, purchased and operated. It is important to consider sustainability at all levels of the life cycle of products that are manufactured. Starting a firm and run it successfully in the existing business environment is a challenge. It has become most complex in the prevailing situation of Covid pandemic world over where each country has become shorter in its reach with the constraints of resources

and with mega cut in factors facilitating globalization e.g investment, rapid improvements in technology and liberalization of trade policies etc all in main have been shrink within the boundaries limiting to the firm levels. On the other hand there has been burden on the national economies on more consumption of their resources. It will take a long way thus to revive the growth and to sustain development of the economies. It has engendered our future generations more that they will not have access to the resources the way that we have now. The harmful effects of our consumption and its final impact on the humankind are well known. Though manufacturing systems create material wealth for humans, they consume a great amount of resources while generating a lot of waste. The waste generated during the manufacturing processes, during the use of the products and after the end of the life of the products is responsible for the degradation of the environment. Thus, minimising the resource consumption and reducing the environmental impact of manufacturing systems has become increasingly more important. Therefore, it is imperative that manufacturing industries strive for 'Sustainable Manufacturing' on their part.

SUSTAINABLE MANUFACTURING

Sustainable manufacturing (SM) or green manufacturing can be defined as a method for manufacturing that minimises waste and reduces the environmental impact. It implies application of best engineering practices that will influence the product design, process design and operational principles while also trying to maximise resource efficiency. It makes use of energy in a judicious manner for its optimum efficiency by using appropriate and advanced technology at affordable costs with reduction in wastages in each stage of product design, process, maintenance, inventory, asset management to the marketing. In other words it is required to critically examine and re-examine the life cycle analysis. Sustainable manufacturing is the most important aspect to be considered by all production engineers, not because it is a fad but a necessity as an obligation to the world we live in. Product life cycle analysis has become a tool of choice being used to establish the environmental impact of the products that we produce. Though application of PLA is time and data intensive, provides very clear avenues where engineers will be able to reduce the environmental impact. There are a number of areas within manufacturing that can be benefitted greatly by the adoption of green manufacturing practices. The three major principles to be considered are reduce the resource utilisation in the process, use environment-friendly materials, reduce all forms of waste and reuse and recycle as much material as possible to realise the goal of self-recovery capability of the earth.

SUSTAINABLE MANUFACTURING TOOLS

Life Cycle Assessment (LCA) is the tool generally used to implement SM. It is an approach to examine fully the environmental impact of different activities performed by humans including the production of goods and services by corporations. LCA can be applied for any activity that is either at national level or global level in order to identify environmental burdens resulting from the activities of a society, region or industrial sector. A schematic of the methodology employed for carrying out the LCA is given in Fig. 2.

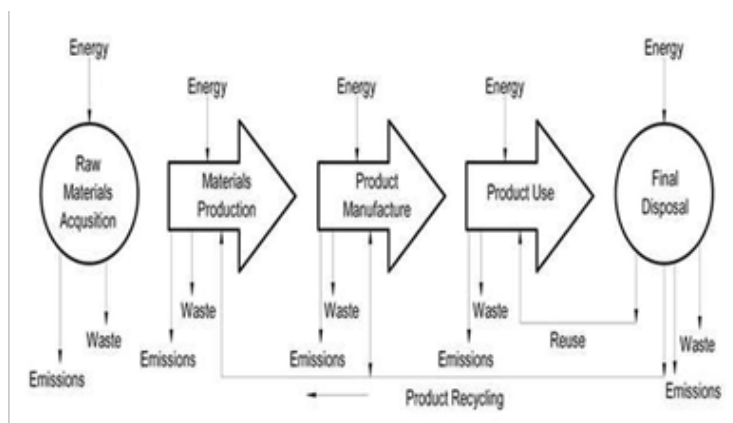


Fig. 2. Life Cycle Analysis

LCA is concerned with identifying the environmental impact of a given product or process at each of these life stages. It allows to make a quantitative comparison of the stages of a product's life, determine where the greatest environmental benefit is to be gained, and ultimately monitor the long term effect of changes in design and/or manufacturing. The ISO standards assume a process-based LCA approach and is organised into four steps: goal and scope definition, inventory analysis, impact assessment, and interpretation.

SUSTAINABLE MANUFACTURING APPROACHES

Sustainable manufacturing requires that all manufacturing organisations should aim for the four activities (Energy use reduction, Water use reduction, Emissions reduction and Waste generation reduction) that would help the environment across its entire supply chain with identified activities.



Fig. 3. Various spheres of activities in a manufacturing organisation that strive to produce sustainable manufacturing

Sustainable manufacturing should integrate sustainable activities at all levels of manufacturing – product, process and system. 3R as reduce, reuse and recycle approach is commonly followed. This may be expanded to more R's, such as, reduce, reuse, recycle, recover, redesign, remanufacturing, repurpose, refurbish, refuse, etc, as depicted in Figure 4. The reduction should always start at the source level to be more effective.

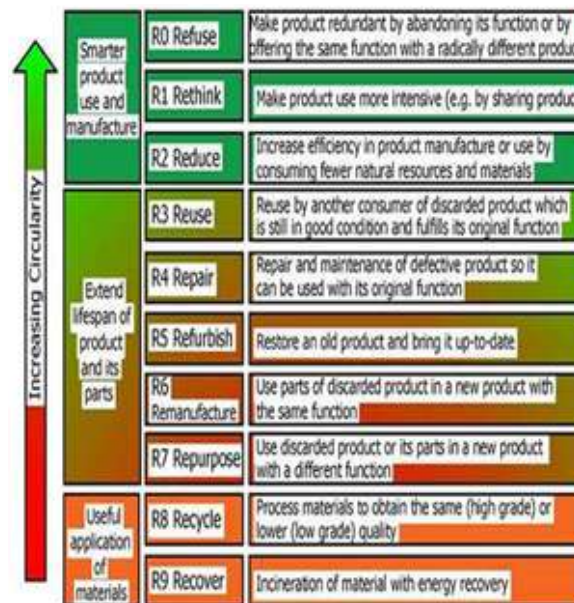


Fig. 4. Increase circularity in manufacturing to reduce the overall utilisation of the resources so that less material need to be extracted from the earth

Manufacturing processes and systems employed should consider sustainability at every level, so that there will be comprehensive adherence to sustainability principles. All the processes used are energy efficient while maintaining requisite quality. Reduce energy intensity and emissions in all operations and the supply chain. Zero-emission (i.e. closed-loop) manufacturing views the manufacturing system as an industrial ecosystem, and requires the reuse of wastes or by-products within the manufacturing system.

DEVELOP NEW GREEN PROCESSES

In addition to improving and optimising the existing processes, it will also be important to develop new processes that use less harmful materials and generate fewer emissions which can then be considered as green processes.



SOME EXAMPLES SUSTAINABLE MANUFACTURING

These include Minimum Quantity Lubrication (MQL) or equivalent dry cutting conditions, Cutting fluids based on vegetable oils in place of mineral oil-based products etc.,

MAJOR SCHEMES AND PROGRAMMES OF UNION MINISTRY OF MSME

Union Ministry of MSME, Government of India runs a number of schemes to provide financial and non-financial assistance to the MSMEs across the country. These schemes mainly include registration, Credit assistance related, Credit Linked Capital Subsidy - Technology Upgradation Scheme (CLCS-TUS) – [Erstwhile National Manufacturing Competitiveness Programme (NMCP)] (except Credit Linked Capital Subsidy component), Cluster Development Programme, Infrastructure assistance, Marketing assistance etc besides having a number of schemes for Khadi and Village Industries as well as Coir sector.

CHAMPION PORTAL, REGISTRATION AND REVISED DEFINITION OF MSME

The Ministry of MSME has recently launched Champion portal which is a unified, empowered, robust, bundled and technology driven platform for helping and promoting the Micro, Small and Medium Enterprises (MSMEs) of the country. Hon'ble Prime Minister of India Shri Narendra Modi has launched CHAMPIONS, a technology platform to empower MSMEs on 1st June 2020. The Ministry of Micro, Small and Medium Enterprises has issued a notification dated 26th June 2020 regarding revision of definition of MSMEs and process of registration. Apart from the old criteria of categorization of MSMEs on the basis of investment in Plant and Machinery/ Equipment, an additional criterion on turnover has been included. This revision is expected to pave way for strengthening and growth of the MSMEs. Particularly, the provision of excluding the exports from counting of turnover will encourage the MSMEs to export more and more without fearing to MSME enterprises. Henceforth, an enterprise is being classified as a micro, small or medium enterprise basis of the following criteria –

- (a) Micro enterprise: where the investment in plant and machinery or equipment does not exceed one crore rupees and turnover does not exceed five crore rupees;
- b) Small enterprise: where the investment in plant does not exceed ten crore rupees and turnover does not exceed fifty crore rupees; and
- (c) Medium enterprise: where the investment in plant and machinery or equipment does not exceed fifty crore rupees and turnover does not exceed two and fifty crore rupees.

To facilitate the procedure of MSME registration in accordance with the revised MSME definition, Ministry of MSME launched a new portal (<https://udyamregistration.gov.in> Udyam Registration Portal udyamregistration.gov.in) on 1st July 2020. All the schemes of the Ministry has been made online. These are available on the website of its attached office i.e. Office of the Development Commissioner (MSME) and Ministry of MSME at www.dcmsme.gov.in and www.msme.gov.in respectively.

MAJOR SCHEMES OF MSME

Ministry of MSME through the Office of the Development Commissioner (MSME) has been implementing a major scheme relating to sustainability called Credit Linked Capital Subsidy - Technology Upgradation Scheme (CLCS-TUS). The Credit Linked Capital Subsidy and Technology Upgradation Scheme (CLCS-TUS) is aimed at promoting competitiveness amongst Indian Micro, Small and Medium Enterprises (MSMEs) by the way of wastage reduction through Lean Manufacturing, support for Design improvement, building awareness on Intellectual Property Rights, Zero Defect Zero Effect (ZED) Scheme, digitally empowerment of MSME through Digital MSME and to promote & support untapped creativity of individual and to promote adoption of latest technologies in manufacturing as well as knowledge based innovation MSMEs through Incubation across India. As an illustration, two major sub-schemes Zero Defect Zero Effect (ZED) Certification and Lean Manufacturing are described as under:

ZERO DEFECT ZERO EFFECT (ZED) CERTIFICATION: AN INDIGENOUS CERTIFICATION CONCEPT FOR MSMEs

“Zero Defect Zero Effect” is a slogan coined by Hon'ble Prime Minister of India, Shri Narendra Modi. It signifies production mechanisms wherein products have no defects (Defect free) and the process through which product is made have zero adverse environmental and ecological effects (Zero effect on environment). The slogan also aims to prevent products developed from India from being rejected by the global market. The scheme provides “Financial Support to MSMEs in ZED Certification Scheme” for the benefit of MSMEs and has various components including training. It will also provide an opportunity to

units to strive to continuously improve its processes thereby aiming to move up the ZED maturity assessment model (Bronze-Silver-Gold-Diamond-Platinum). It would ensure that the larger companies investing in India have a ready-made vendor base to support their activities and an expansive base of trained human capital who can contribute to their manufacturing process without much retraining.

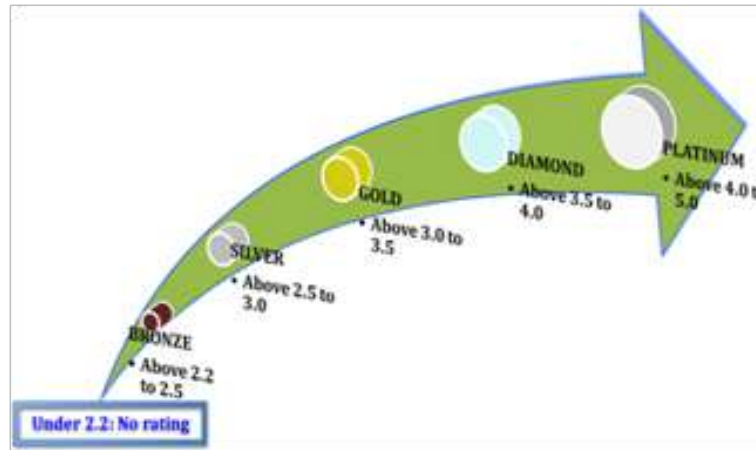


Fig. 5. Ratings in each parameter under ZED

LEAN MANUFACTURING OR LEAN PRODUCTION

Lean manufacturing or lean production, often simply “lean”, is a systematic method for waste minimization (“Muda”) within a manufacturing system without sacrificing productivity. Lean also takes into account waste created through overburden (“Muri”) and waste created through unevenness in workloads (“Mura”). Lean aims to enhance productivity by simplifying the operational structure enough to understand, perform and manage the work environment.

IMPLEMENTATION OF LEAN MANUFACTURING COMPETITIVENESS SCHEME (LMCS) UNDER CREDIT LINKED CAPITAL SUBSIDY AND TECHNOLOGY UP-GRADATION SCHEME (CLCS-TUS)

The basic rationale of the Government support to MSMEs for undertaking lean manufacturing (LM) is to enhance their productivity and competitiveness by reduction of wastage in manufacturing processes, inventory management, space management, energy consumption, etc. The LM techniques also result in reduction in rejection, standardization of processes, better layout of machines resulting in reduced transportation of products during manufacturing, etc. The implementation of LM techniques leads to cost reduction for MSMEs. It also has lot of social benefits in terms of training of labour, creation of knowledge, increased labour productivity, lower input costs to other industries, and introduction of new production equipment / methods in manufacturing and development of work culture in society. Lean Manufacturing is a set of techniques, which have evolved over a long period and are based on various minor to major breakthroughs that help in reducing cost and hence increase productivity and competitiveness. The main LM techniques include 5S System, Visual Control, Standard Operating Procedures (SOPs), Just in Time (JIT), KANBAN System, Cellular Layout, Value Stream Mapping, Poka Yoke or Mistake Proofing, Single Minutes Exchange of Dies or Quick Changeover (SMED), TPM (Total Productive Maintenance), Kaizen Blitz or Rapid Improvement Process and Other Lean Techniques on need basis, etc.

OBJECTIVES OF LEAN MANUFACTURING SCHEME

The objectives of the Scheme is to enhance the manufacturing competitiveness of MSMEs through the application of various Lean Manufacturing (LM) techniques by:- (i) Reducing waste; (ii) Increasing productivity; (iii) Introducing innovative practices for improving overall competitiveness; (iv) Inculcating good management systems; and (v) Imbibing a culture of continuous improvement. The scheme is demand driven. The general approach involves engagement of Lean Manufacturing Consultants (LMC) to work with selected MSMEs in the chosen clusters with financial support by the Government. Under the Scheme, MSMEs will be assisted in reducing their manufacturing costs through proper personnel management, better space utilization, scientific inventory management, improved process flows, reduced engineering time and so on with the application of LM techniques. The Scheme is basically a business initiative to reduce “waste” in manufacturing and is implemented with a number of components like Awareness Programme, National Workshop and visits to Lean adopted units etc.



CONCLUSION

MSMEs contribute to sustainable development and the global economy. These firms play a very important role towards meeting SDGs in each country. It is evident by the recognition being given to these units internationally. Product-evolution process, sustainable manufacturing, environment friendly production and zero tolerance in safety and quality are some of the ways and techniques required to be adopted continuously to make a better and quality life by the masses in the world. Union Ministry of MSME in India have a number of schemes to strengthen MSMEs to build their technological capability with no effect on environment in order to raise their standards.

REFERENCES

1. Entrepreneurship – The McGraw-Hill Publishing Company Limited, New Delhi by Robert D. Histrich, Michael P. Peters and Dean A. Shepherd
2. Various papers and presentations during Safety Conventions of the Institution of Engineers (India) [IE(I)], Delhi State Centre since 2014 onwards by Dr. Om Parkash Mehta, FIE(I)
3. <https://www.undp.org/content/undp/en/home/sustainable-development-goals.html>
4. www.msme.gov.in
5. www.dcmsme.gov.in
6. <https://www.industr.com/en/sustainable-manufacturing-principles-applications-and-directions-2333598>
7. <https://www.un.org/en/observances/micro-small-medium-businesses-day#:~:text=That%20is%20why%20the%20General,development%20and%20the%20global%20economy.>



Unforeseen Risks in Project Execution – A Case Study

Balakrishnan Nair

*Past. Hon. Secretary, IEI Qatar Chapter, Past. Company Representative, Petroleum Development Oman
(Ajanta, TC 28/2063, Opp. Fort High School, Fort P.O, Trivandrum*

✉ bala27_krishnan@hotmail.com

ABSTRACT

Most of the projects are confronted with delayed delivery schedules and other associated risks. Delays may not be accounted for during the initial period of project conceptualization, but slowly creep up due to various causes. The big question is how to address the risks and control it in the most effective manner to bring back the project on schedule as committed. Risks can come from liabilities, credit risk, accidents, delays, property loss, natural causes and disasters as well as deliberate attacks from an adversary. A case study of an ongoing project is highlighted in this paper which enlightens the fact once again that each project risks are unique and different mitigation techniques are required to be adapted to overcome these risks. The plight of the contracting firm who invest finance and other resources for realization of projects should be considered by customers while negotiating such eventualities as various risks are to be overcome in the process of navigating the project to a safe completion.

Keywords: Delays; Risks; Project risks; Mitigation.

INTRODUCTION

What is Project Safety Management? Safety is a state in which hazards and conditions that lead to physical, psychological, financial or material harm need to be controlled [1]. These controls are very much essential to preserve the health and well-being of management, individuals and the community.

Project Risk Management [2]

Project risk management is the process of identifying, analyzing and then responding to any risk that arises during the life cycle of a project to help the project meet its schedule. A risk is anything that potentially impacts project's timeline, performance or budget. Risk management is part of the planning process to figure out risk that might happen in the project, as an active monitoring tool and apply control measures to reduce the risk to a reasonable low level. Risk management strategies might include extensive detailed planning for each risk to ensure mitigation strategies are in place.

Effective risk management strategies include identifying the project's strengths, weaknesses, opportunities and threats. In order to ensure project's success, it is important to define how potential risks would be handled so that one can identify, mitigate or avoid problems when needed.

The three different types of risks [3] that a firm might face and needs to overcome can be classified into three types: Business Risk, Non-Business Risk, and Financial Risk.

Anything that threatens a company's ability to achieve its financial goals is considered a business risk. Business risks refers to the possibility of business making inadequate profits due to various factors - for example: changes in process, changing preferences of customers, strikes, increased competition, changes in government policy. A company may face different risks in production, risks due to irregular supply of raw materials, machinery breakdown, labor unrest, etc. In marketing, risks may arise due to fluctuations in market prices, changing trends and fashions, errors in sales forecasting, etc. In addition, there may be loss of assets of the firm due to fire, flood, earthquakes, riots or war and political unrest which may cause unwanted interruptions in the business operations.

The Business risk is classified into different types:

1. Financial Risk [4]: Financial risk is the possibility of losing money on an investment or joint venture. It concerned with a company's ability to generate sufficient cash flow to make interest payments on financing projects or ventures. Directors



often struggle to meet the demands of company operational requirement due to inadequate and sufficient funding from their customers despite timely contract completions and forced to borrow finance from institutions at exorbitant interest rates.

2. Operational Risk [5]: These risks are associated with the operational and administrative procedures of organisations. Operational risk is “the risk of a change in value caused by the fact that actual losses, incurred due to inadequate or failed internal processes, people and systems, or from external events including legal risks and differ from the expected losses”.
3. Compliance Risk (Legal Risk) [6]: These are risks associated with mandatory obligations to comply. Legal risk is the risk of financial or reputational loss that can result from lack of awareness, ambiguity in; how the regulation applies to your business, its relationships, processes, products and services.
4. Other risks: There would be different risks like natural disasters that include floods, earthquakes, tsunami and others depend upon the nature and scale of the losses.

TYPES OF PROJECT RISKS

Several types of risks that occur frequently, regardless of the specifics of the project include:

Cost: The risk of events that impact the budget, especially those that cause the project to be completed over budget. Errors in cost estimation commonly generate risk in addition to external factors.

Schedule: The risk of unplanned scheduling conflicts, such as events that cause the project to be delayed. Scope creep is a common reason for scheduling issues and project delays.

Performance: The risk of events that cause the project to produce results those are inconsistent with the project specifications.

Project Regulators: Citing previous experiences on the performance of projects, project regulators override the initial specifications floated during bid and force their way with new added requirements to contractors’ operations domain and cause enormous delays as well as huge financial risks.

Engineering Risks: Even before the engineering designs get frozen, contractors are forced to start works at site with few inputs that cause multiple risks in terms of procurement and schedule.

Steps in the Risk Management Process [7]

Project managers typically follow an ongoing risk management process which helps them identify, understand, and respond to threats and opportunities. This process contains the following steps:

Identify the risks that could potentially impact your project:

Assign ownership of each identified risk to team members who will be charged with overseeing that threat or opportunity so that they can drive the analysis to realization.

Analyze each risk to fully understand the driving factors and potential impacts: Each threat should be properly analyzed at this stage to evaluate the severity of each risk in the context of the overall project.

Prioritize project risks according to urgency and the severity of the impact they could cause:

Respond to your identified risks in accordance with your risk management approach, either by taking steps to prevent the risk event from occurring or to minimize the impact if it does occur.

Monitor your risk management strategy and make changes as needed:

Although there are clear steps in the risk management process, this should ideally be an ongoing effort. After all, the nature of risk is inherently unpredictable, and project managers should judiciously take follow up actions to adapt to changes throughout a given project.

HOW TO REDUCE AND MANAGE RISK? [8]

While it is impossible to completely eliminate risk, there are steps that project managers can take to effectively manage projects while reducing the amount of risk. Here are four tips to get started:



Create a risk management plan

A risk management plan defines the methodology for identifying and prioritizing the risk, its effect on the project, action plans to respond to risk and how it can be resolved. Developing such a plan takes time and effort, but doing this exercise very early in the planning phase can create a guideline to take the team through the execution phase of the project. Macro and micro plans are often a part of this plan, including prioritizing the project risks. Some of the risks may not be settled during implementation as it may be linked up with project start up, commissioning or operation activities for warranty.

Keep your risk register up to date

The risk register, can either be combined with risk management plan or a separate document, is a list of all possible risk events that have the potential to impact a project. This document will help to keep focused on top of potential issues. Risk register can be used to keep track of what risk events occurred, how the team responded, and whether any new risks have surfaced which were not detected initially.

Developing project management skills

Effectively managing projects and their associated risks requires strong project management skills. Project Managers should stay abreast with recent industry trends; keep attending conferences and workshops involving managing risks techniques with a proactive approach.

Risk Audit [9]: Independent technical experts carry out risk audit where risks are checked with recommendations to improve effectiveness of risk management, involving steps to check whether risks are properly identified, its extensiveness of analysis, effectiveness of mitigation plans and whether project risks may affect organizational risks.

PROJECT RISK EFFECTS – A CASE STUDY

In 2014, a refinery project was awarded to a renowned, world class and resource rich organization in the Kuwait City by their Petroleum Company, at a cost of 496 Million US Dollars with a scheduled completion slated in April 2018. It is an excellent contract involving design of civil facilities, mechanical, electrical and instrumentation works connecting green field project with an existing and operating plant involving nearly 976 tie-ins connections to be completed.

As a normal saying goes, a job award also brings numerous complex issues and any project is not a cake walk. Rejoicing will last until the job is awarded after hectic estimation work outs and tough negotiations between the customer, engineering consultants, contractors, other vendors including in-house specialists on the strategies to be evolved from contract bid stage until award.

The works started when engineering was nearly 60% completed. Consultants were given tight schedule to release the drawings to start site activities. The various risks associated with the project are given below:

- a. **Engineering Design Risks:** Design reviews including engineering reviews were restricted except for certain critical activities. Unlike other projects elsewhere, the drawings had to go through four to five revisions of reviews before an approval for Construction is reached. Nearly a year delay due to engineering approvals was registered in the contract.
- b. **Equipment Delivery:** Procurement orders for most of the equipments could not be released due to vendor confirmations and specification requirements from the customer. Eight numbers of fired heaters were ordered on an overseas vendor, but could not be installed on foundations due to approval delays from process regulators which necessitated replacement of certain project materials for installation.
- c. **Logistics Risks:** Some oversize dimensional consignments also compounded the risks. The consignment reached the port from overseas vendor after undergoing rough sea and turbulent weather causing delays. But hauling it to the work site, just 65 km from port, took enormous time due to restriction on inland travel speed of just 1 km/day from the port and inclement weather.
- d. **Subcontractor risks:** This risk is associated with payments made to subcontractor for mobilizing their resources as scheduled, but delays due to engineering drawing releases and work front releases, their compensation claims had to be settled as they paid for materials under their scope of supply.
- e. **Risks associated with Quality Assurance:** Quality assurance regulator, customer's representative, introduced upon specification changes of process materials which were once welded as per approved welding procedure specifications.



Implementation of new procedures with additional tests took time, effort and cost. A number of pipe weld joints for steam service, had to be cut and re-welded as per recommendations of the regulator who provides warranty approval for the process.

- f. Access Control Regulations: Visa rules, travel regulations and recent COVID 19 restrictions had its cascading effects on the overall execution of the project. In an average, more than 2 hours per day were affected due to these strictures.
- g. Green field and Brownfield Interface: Working in a brown field project is never easy. Frequent and unforeseen interruptions due to gas leaks or other process affects daily production. Nearly 205 days delay due to these factors was added risks in the project.
- h. Cost Over unrisks: Mitigating the above cited risks not only involve a resolution from the customer, but also result in a huge over run of the project in terms of time. The project is on its two year overrun period and is likely to reach a three year overrun. Expenditures to retain the resources including technical and administrative resources will be a huge economic burden on the management.

These types of project risks cannot be foreseen during the bid stage and contract was awarded after tough negotiations. Project risks always add delays to the project amid mounting high economic instability in the organization. Mitigating such risks is a huge task as cash flow is very important for smooth execution. Financial risk is an important factor, however cash rich the organization may be.

How these risks were addressed?

Risk mitigation processes are complex. It depends upon various factors including involvement and availability of in-house management team, vendor teams, engineering consultants, and customers. The first and foremost activity is to prepare the risk register, then segregate and initiate discussions with the concerned team for resolution. A few measures to mitigate risks in the subject project are given below:

1. Engineering and Design risks: In order to address delays on release of engineering documents, the company hired additional manpower from their engineering offices in Abu Dhabi to work. They also outsourced manpower from overseas countries to overcome the delays. Design engineers were retained to overcome delays. These measures helped the company to compress the delays to a great extent.
2. Logistics Risks: The Company adopted to cover up as much delay as possible through assembly of various appurtenances on equipments which arrived at site beyond the scheduled dates. The over dimensional consignments had to undergo internal inspections as part of contractual requirements and these delays could no longer be reduced due to confined spaces. Higher capacity cranes had to be outsourced from neighboring countries to take care of some delays.
3. Risks to Sub contractors: Delayed release of work fronts were settled with sub-contractors as it involved procurement and installation of materials. They adopted a progressive method of extending financial support by waiving contractual terms, reducing risk in terms of time.
4. Risk due to third party Regulators: This was the main threat to the contract. Scope of work was discussed and finalized during contract finalization time. The threat of quality assurance activities on carbon content presence in the weld and parental piping materials generated serious risk on time and money. The process variance in already approved welding procedures to new procedure specification was not anticipated. Regulators insisted on adopting a flexible project specific allowance weld procedure to provide warranty to the customer. For this the already welded joints had to be cut, re-welded, and non-destructive tests done including ultra-sonic testing which all were new requirements.
5. Visa and Travel Regulations: Travel regulations were imposed by the Kuwaiti Government on recruitment of expatriate workers into the country during the project execution. During the peak time nearly nine thousand people were employed. Special sanction was obtained through the customer to get commercial visa for additional mobilization of workmen on bulk basis with a condition that these workers shall not be deployed in brown field area whereas they can work in green field locations only. This necessitated swapping of personnel and fresh training sessions involving additional cost.



CONCLUSION

The risk settlement processes are in the advanced stages of finalization. The project risk management is therefore a very significant process in large value projects and requires specific and dedicated team to register risks for a very effective resolution. Project is scheduled to hit a 55% cost overrun due to the above risks.

ACKNOWLEDGEMENT

I acknowledge with gratitude the Project Planning Team of the Kuwait Refinery Project Team, for the guidance in providing an insight for preparation and submission of this paper.

REFERENCES

1. INSPQ Public Health Expertise and Reference Centre; Quebec; Definition of the Concept of Safety
2. Scott W. O'Connor; "The Project Risk Management Process/ 5 Tips for Success; North Eastern University Graduate Programme; March 25, 2020
3. EshnaVerma; Financial Risks and Types.Simplilearn; Nov 13, 2020
4. James Chen; David Kindness; "Financial Risk"; Investopedia; Corporate Finance and Debt; Sep 4, 2020
5. Wikipedia; Operational Risk
6. Wikipedia; Whalley M; "Legal Risk"; 2016
7. Scott W. O'Connor; "The Project Risk Management Process/ 5 Tips for Success; North Eastern University Graduate Programme; March 25, 2020
8. Scott W. O'Connor; "The Project Risk Management Process/ 5 Tips for Success; North Eastern University Graduate Programme; March 25, 2020
9. Lavanya, N. & Malarvizhi, T; "Risk analysis and management: a vital key to effective project management"; Paper presented at PMI® Global Congress 2008—Asia Pacific, Sydney, New South Wales, Australia. Newtown Square, PA: Project Management Institute; 03 March 2008.



Engineering Solution as Sustainable Manufacturing for Protection in Pandemic Regime

A A Panja¹, M S Patwardhan²

Life Source (India) Technology Pvt. Ltd.1., FSRE2, (MIDC, Ahmednagar1 MPKV, Rahuri2), Ahmednagar

✉ asmitapanja262@gmail.com

ABSTRACT

The COVID-19 pandemic triggered a surge in demand for facemasks to protect against disease transmission. In response to shortages, WHO and many public health authorities have been recommending 3 ply disposable face masks. Virus particles are tiny, ranging from 0.1 to 0.3 micron. A size 40-micron particle is visible with the naked eye – anything smaller, specialized equipment is required to see it. Protective masks like the 3-ply mask with nose clip and N95 are designed to prevent virus particles from flowing in and out of the mask. This study was undertaken to discuss the aspects of automation for mask manufacturing process using technological aspects. This study showed that mask is an effective solution to fight against this international surge.

Keywords: Non-woven fabric; COVID-19; 3 ply disposable face masks; Ultrasonic welding; Disinfection.

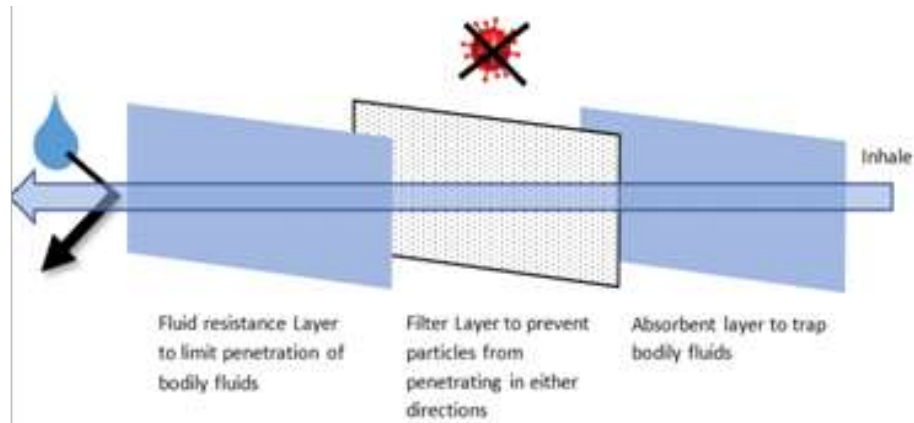
INTRODUCTION

Emerging and re-emerging infections have emerged as a threat to human health in recent decades[1]. Given how interconnected the world is today, a pathogen capable of human-to-human transmission can spark an outbreak far from where it originated. The virus causing the Middle East Respiratory Syndrome, for example, emerged in the Middle East but caused an outbreak in Korea. The world is in the midst of the COVID-19 pandemic, which is caused by the SARS-CoV-2 virus. Lockdowns and travel restrictions imposed to halt the spread of COVID-19 have led to devastating economic repercussions. The control of an infectious disease is based on knowledge of its mode of transmission. The recent COVID-19 pandemic is caused by the novel coronavirus, SARS-CoV-2, which is transmitted largely by the respiratory.[2][3]

The best nonpharmaceutical interventions against disease spread are broadly termed social or safe distancing measures, i.e., reducing close contact between individuals [4][5]. Where safe distancing is not possible, masks are the most important piece of PPE. They all serve the general purpose of providing some form of protection against contaminants in the air, ranging from pollen to chemical fumes to pathogens. The filtering capacity, and hence the level of protection against pollutants and pathogens, depends on the materials used and the engineering design. Masks made of polypropylene(PP) or coated with water-resistant materials are more effective against large virus-laden respiratory droplets and fluid spills. In addition to filtering capacity, factors such as user comfort and breath ability also vary across different models. For instance, although the tight-fitting N95 respirator has filtering capacity superior to surgical masks, they have lower breath ability and may cause discomfort after hours of wearing. Mask-wearing can be effective in the containment of communicable diseases and has thus become a new normal in many societies in the COVID-19 pandemic.[6][7]

What does 3 Ply Masksinsist ?

The 3-ply surgical mask is commonly used in the COVID-19 pandemic. It is made up of 3 different layers of nonwoven fabric with each layer having a specific function, as shown in below **Figure**. The outermost layer (Spun bond) is waterproof and helps to repel fluids such as mucosalivary droplets. The middle piece is the Melt blown filter, which prevents particles or pathogens above a certain size from penetrating in either direction. The innermost layer is made of absorbent materials (Spun bond) to trap salivary droplets from the user. This layer also absorbs the moisture from exhaled air, thus improving comfort. Together, these 3 layers effectively protect both the user and the surrounding people by limiting the penetration of particles and pathogens in both directions.



The spun bond process combines the spinning and sheet formation process into one continuous, nonwoven manufacturing system.[5]

- Extrusion is the process where the polymer is melted by heat and mechanical action of the screw
- The gear pump plays a critical role in controlling the precise volumetric flow rate of the molten polymer. This is a key step to maintain a uniform temperature of the molten polymer
- The spin pack is a die block assembly which turns the molten polymer into uniform thin filaments and is designed to be able to withstand 300°C to 400°C
- The filaments are then quenched by cool air
- After quenching, the filaments are collected together as filament web on a moving belt
- The filaments in the web are then bonded together via heat, chemical, or mechanical means to form the nonwoven fabric and collected in the winder.

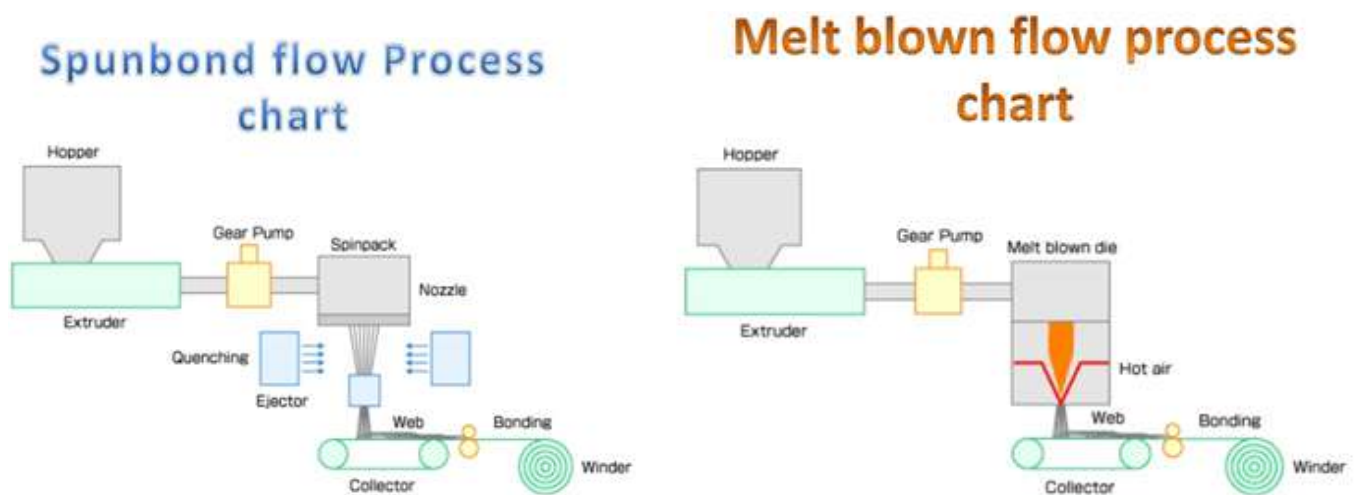


Fig 2. Spunbond and Meltblown Nonwoven fabric making process [5]

Production Capacity

For the automatic mass production of 3 ply disposable face mask, it can manufacture up to 60,000 pcs/day/machine approximately under full-time operation (24 hrs). It may reach up to 80,000 pcs/day/machine at full speed with no errors.

24 hrs = 60,000 pcs/day

1 min = 42 pcs/min

Table 1. Mask production capacity

Sr. no.	Types	No. of machines	Production capacity (Pcs)	No. of employees
1	Adult masks	8	$60,000 \times 8 = 480,000$	$2 \times 8 = 16$
2	Baby masks	2	$60,000 \times 2 = 120,000$	$2 \times 2 = 4$
3	Tie on masks	1	$60,000 \times 1 = 60,000$	$2 \times 1 = 2$
	TOTAL	11	660,000	22

METHODOLOGY**Mask Manufacturing Process****Table 2.** Overview of an automatic 3 ply mask machine

Working Process	Machine	No. of parts
Discharge Table	Auto unwinding of raw materials	1
Mask Forming Machine	Mask Blank Machine	1
Mask Feeder Machine	Ear Loop Welding Unit	2

*Ultrasonic Welding***Working Principle**

The digital ultrasonic generator can convert low frequency alternating current into high frequency alternating current and then converts electric energy into mechanical energy of high frequency vibration via the transducer. The welding head can generate thousands of high frequency vibrations per second when applied to the contact surface of the mask. Through the upper weldment, the high frequency vibrations transmit the ultrasonic energy to the welding zone where the upper and lower weldments will generate locally high temperature through mutual friction. After the ultrasonic action, the pressure lasts for few seconds, making weldments solidify and set and form strong molecular chain to achieve welding.

Advantage of ultrasonic welding –

- Intelligence environmental protection, high efficiency, safe
- This system can search and track frequency automatically with no need of manual regulation.
- No need of solvents, adhesives or other aids.

Table 3. Technical specification

Sr. No.	Parameters	Rated Values
1	Working frequency	20 ± 1
2	Maximum Power (VA)	1500
3	Rated voltage (V)	AC, 230V $\pm 10\%$, 50/60Hz
4	Overall Dimensions	310(L) * 288(W) * 143(H)
5	Weight (Kg)	5.6

**Fig. 2.** Various parts of ultrasonic welding [10]

Block Diagram of mask manufacturing process

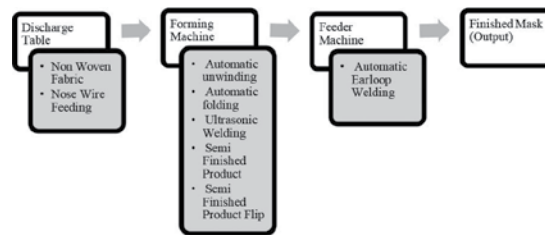


Fig. 3. Block diagram of mask production

- (i) Combine three layers of non-woven fabric:
Threedifferent PP non-woven fabric rolls and PP nose wire are placed on the fixed support on the production line and neatly stacked together.
- (ii) Auto folding mask:
To ensure that different people have the right size requirements so that the nose, mouth and chin are wrapped to the greatest extent. This is due to a folding device to achieve this purpose.Next, in order to create a crease and better processing in subsequent processes, it needs to be flattened by a roller machine.
- (iii) Weld the nose clip into three-layer non-woven fabric:
Nose clip must be pinched to the bridge of the nose when wearing, so that wearing the mask will be firm. Otherwise, without this structure, nose leak is more serious, the seal is not tight, and the protection is affected. Hence the wire is matched and conveyed along one side of the non-woven fabric, then the next edge is rolled, and the back is ultrasonically welded and the wire is welded in.
- (iv) Cut to a single mask unit:
After trimming of mask, each mask is flipped automatically and sent to Station 1 and Station 2 alternately.
- (v) Fixing the ear loopsat4 corners of the mask by spot welding with the help of ultrasonic generator:
Because in the process of wearing a mask, the hanging ear loop is in a relatively tight state for a long time. In order to strengthen the binding strength of the rope and the mask body, it is necessary to weld the four corners of the mask. During this process, the ear loop is mechanically transported pneumatically (The ear loop is pulled by the gripper, cut equally with the help of scissors). Fix the ear loop to the 4 corners of mask by ultrasonic welding.
- (vi) Automaticstacking:
After welding, masks are stacked together automatically onconveyor belt.
- (vii)Disinfection:
During the entire production process of the mask, not only the processing contact of the machine, but also the contact of many artificial links, the mask will inevitably be contaminated by bacteria. If it is an ordinary mask, it does not need to be sterilized, but for the healthcare personnel the masks are UV treated to kill the bacteria on the mask. After UV treatment, it can be packaged and shipped to medical staff.

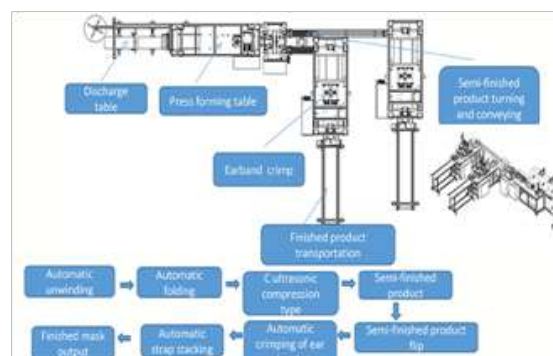


Fig. 4. Step by step procedure of manufacturing [11]



Controlling Factors–

- To ensure uniform tension of raw materials to get high quality product, if not maintained cutting of the mask would be affected.
- To control the welding quality, welding power should be maintained.
- Air pressure should be maintained (0.4 - 0.6 Pa). Less air pressure may lead to inefficient work which may affect the quality of the product.

Advantages

Machine -

1. User friendly design, ease of operation
2. Fully automated with intelligent lean production, speedy production, high level of precision
3. Stability is high, and hence low failure rate, high output
4. Strong, safe and reliable
5. Better control of raw materials

Mask

1. Comfortable to wear, soft and light weight, easy to carry
2. Hydrophobic (outer layer), Hydrophilic (inner layer)
3. Good filtering effect (protects from pollution, dust, germs and air borne contaminants)
4. Fits perfectly according to face shape of person (Unisex mask)
5. Widely used for healthcare workers, mining, pollution, construction and other industries
6. Welding quality is good, durable and reliable

Disadvantages

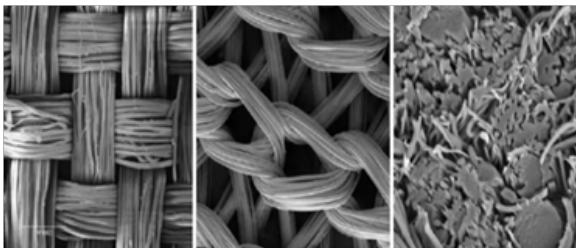
Machine –

1. Capital cost is high, more maintenance is needed
2. Ultrasonic transducer breakdown due to high frequency
3. Due to continuous work of sensors, sensors may not work efficiently.

Mask –

1. One-time use, should be disposed after 8 hours of use
2. Occurrence of fog on specs while wearing a mask
3. Wastage of material due to rejections (cutting)

Safety, Health aspect



Woven Fabric

Knit Fabric

Non - Woven



Table 4. Difference between various fabrics

Sr. No.	Product Type	Considerations
1	Woven Fabric	Openings between the yarns can cause the penetration of droplets / germs to transmit through the fabric
2	Knit type	Structure can distort once stretched across the face, creating open spaces to allow transmission
3	Non– Woven Fabric	This structure provides a blocking advantage, depending on how fibres are packed. Non – woven do not stretch in any direction

Cloth masks cannot block or filter the COVID-19 virus because it can easily flow between the openings of fabric. This helps in transmission of the virus from the wearer to others by large droplets and spray produced by a cough or sneeze or vice versa. WHO recommends to use 3 ply ear loop masks which plays a role in preventing sick people from spreading the virus when coughing or simply talking or breathing. WHO issued new guidance on the use of masks for healthy people in community settings on 6 April 2020 and health authorities are increasingly recommending the broader use of masks.

Mask Quality

In view of the fact that the quality of filter materials for medical masks is difficult to control through convenient and effective inspection methods, the standardized operation of the production quality management system is the main means for enterprises to ensure the quality of mask products. Primary medical masks can be sold in the market only after passing the test of specific items due to their characteristics of medical purposes. The testing of disposable medical mask products includes factory inspection and type inspection:

1. The factory inspection items should have at least the following items: appearance, 3-layerstructure, size (175mm*190mm), PP coated nose clips (100mm), mask earloop (180mm, 2.5mm diameter), proper welding, Fire Test and Water Test.
2. The type inspection shall be the full performance inspection of the product standard. Testing from NABL accredited lab SITRA (The South India Textile Research Association):[11]
 - BFE (Bacterial Filtration Efficiency) – 99.9%
 - Breathability (Differential Pressure, IS 16289) – 30.0 Pa/sq.cm
 - Splash Resistance (ASTM F1862) – Result at 160 mmHg (pass)
 - PFE (Particulate Filtration Efficiency at 0.3 micron) – 98%
 - Flammability – Class 1

FUTURE SCOPE [7]

The Indian medical device market valued at US\$3.5 billion in 2015 and could expand to approximately US \$4.8 billion in coming years. As India's economic, healthcare, and social landscapes evolve, its medical device market emerges as a promising opportunity.

Opportunities in the Indian market:

- India relies on imports to supply its healthcare system with medical disposables.
- Growing availability of modern healthcare to Emerging Market regions.
- Increasing potential for Pandemic Outbreaks (COVID-19 – 19, SARS, Avian Influenza, Swine Flu etc)
- The medical tourism and luxury healthcare markets are among India's fastest-growing industries.

Industry challenges in India:

- Medical device regulation in India only apply to certain product categories.



- The weak rupee makes it difficult for some medical device companies to remain profitable in this market, particularly for manufacturers competing with low-cost Chinese products.
- Significant competition from American, European, and Japanese companies.

CONCLUSION

The COVID-19 pandemic has forced the global population to adopt new ways of living, including the wearing of masks as a new norm. It has even accelerated

R&D efforts in mask materials and design to offer better protection for users against airborne pollutants and pathogens. This review therefore provides a holistic summary of the A to Z of face masks, to give readers a broad-view understanding of masks from the perspective of public health to the domains of material development. The importance of mask-wearing in preventing the spread of airborne and droplet-borne infections was discussed early in this review. Thereafter, the protection mechanism, production, and performance testing of commercial masks were described.

ACKNOWLEDGMENT

The authors would like to thank the staff of Life Source(India) Technology Pvt. Ltd. for their valuable suggestions. The authors acknowledge with thanks for fruitful discussions with Miss. Vaishnavi Kanwade and Mr. Vasant Jorawar.

REFERENCES

1. S. Y. Wong and B. H. Tan, "Megatrends in infectious diseases: the next 10 to 15 years," *Annals of the Academy of Medicine, Singapore*, vol. 48, no. 6, pp. 188-194, 2019
2. H.M. Xie and Q. Chen, "Insight into 2019 novel coronavirus – An updated interim review and lessons from SARS-CoV and MERS-CoV," *International Journal of Infectious Diseases*, vol. 94, pp. 119-124, 2020
3. W.-j. Guan, Z.-y. Ni, Y. Hu et al., "Clinical characteristics of coronavirus disease 2019 in China," *New England Journal of Medicine*, vol. 382, no. 18, pp. 1708-1720, 2020
4. S. G. Benzell, A. Collis, and C. Nicolaides, "Rationing social contact during the COVID-19 pandemic: transmission risk and social benefits of US locations," *Proceedings of the National Academy of Sciences*, vol. 117, no. 26, pp. 14642-14644, 2020
5. I. M. Hutten, "Chapter 1-Introduction to non woven filter media," in *Handbook of Nonwoven Filter Media (Second Edition)*, I.M. Hutten, Ed., pp. 1-52, Butterworth-Heinemann, Oxford, 2016
6. www.who.int accessed on 20-11-2020
7. www.ficci.in accessed on 11-10-2020
8. www.bis.gov.in accessed on 07-07-2020
9. D. K. Chu, E. A. Akl, S. Duda et al., "Physical distancing, face masks, and eye protection to prevent person-to-person transmission of SARS-CoV-2 and COVID-19: a systematic review and meta-analysis," *The Lancet*, vol. 395, no. 10242, pp. 1973-1987, 2020.
10. <https://conprofetech.cn/> accessed on 10-10-2020
11. <https://www.hugongwelds.com/news/detail43.htm> accessed on 20-11-2020



The Sustainable Manufacturing in Chennai Plastic Sacks Cluster

Dr E Bhaskaran

Joint Director (Engineering), Department of Industries and Commerce, Government of Tamil Nadu, Chennai

✉ e.bhaskaran19@gmail.com

ABSTRACT

The Sustainable Development Goal no. 8, i.e, promote sustained, inclusive and sustainable economic growth, full and productive employment and decent work for all includes workforce improvement as per Government of India and Tamil Nadu policy through cluster development approach. Plastics sacks manufacturers in Chennai have become indispensable in the form of raw-materials, employment, production and turnover including exports. The objective is to study on the Physical and Financial Performance, and to find Difference in Differences (DID) on the control variable and experimental variables on productivity after Government of India and Tamil Nadu Intervention on Plastic Cluster. Physical Performance is an increasing trend for no. of units, employment and production and also for Financial Performance like Turnover and export as per increasing CAGR. To conclude, as per DID the control group (who have not undergone Cluster Development Approach) and Treatment Group (who have undergone Cluster Development Approach) have much difference in differences on employment, production, turnover and export and there is increase in productivity due to adoption of cluster development approach by experimental group.

Keywords: SDG; Cluster development approach; Difference in differences.

INTRODUCTION

Clusters can be defined as sectoral and geographical concentration of enterprises, in particular Small and Medium Enterprises (SME), faced with common opportunities and threats [1]. The Sustainable Development Goal no. 8, i.e., promotes sustained, inclusive and sustainable economic growth, full and productive employment and decent work for all includes workforce improvement as per Government of India and Tamil Nadu policy through cluster development approach. The CFC located at Pillaipakkam Village, Sriperumbudur Taluk, Kancheepuram District in SF.No:400/2A, Kaduvancherry Road having 4.65 acres of Land and 120000 sqft of constructed area of Factory premises.

The plastic cluster in the suburbs of Chennai has been in existence for more than four decades. The cluster members manufacture wide range of plastic products through various process (injection molding, blow molding and extrusion etc.,) both for the common segment as well as for number of industries such as automotive building construction, electrical and electronics industrial medical and Packing, transportation etc. The woven sack manufacturing industry started in the last 70's of the last century in the suburbs of Chennai. The plastic woven sacks/bags manufacturing segment uses the extrusion method for manufacturing cast film and tapes for weaving fabric form which laminated or unlaminated are stitched.

TECHNICAL SURVEY

The Ministry of Micro, Small and Medium Enterprises (MSME), Government of India (GoI) has adopted the Cluster Development approach as a key strategy for enhancing the productivity and competitiveness as well as capacity building of Micro and Small Enterprises (MSEs) and their collectives in the country. [2]

The plastic woven sacks are widely used for packing various items viz

- Food products, flower, corn, grain, sues, rice, Maida, salt, animal feed.
- Chemical & fertilizer carbon, caustic soda, petards Phosphorus.
- Petrochemical Polystyrene Granules, PVC compound.
- Minerals, cement, calcium carbonate lime as sand.

NEED OF CFC IN CHENNAI

In around Chennai, Chengulpet, Kancheepuram and Thriuvallore more than 130 Micro Units having only stitching and printing facility. Small units those who are having manufacturing facility of Fabric but the production capacity are very low. Therefore Micro units depends on the Medium size units for their raw material viz., woven fabric with high fluctuations and monopolist control in the price of POLYPROPYLENE GRANUALS. The Micro players get their raw material at non competitive price, which in turn increase their production cost in the result of which they are unable to compete the business with medium and small player. Their survival is totally depends on medium and big players in plastic industry.[3]

The Micro and Small players face tough competition from the players in the medium sector as well as from neighboring states. They are unable to undertake bulk orders from the cement and fertilizer industries as well as from other industries as they are unable to reduce their present cost of production.

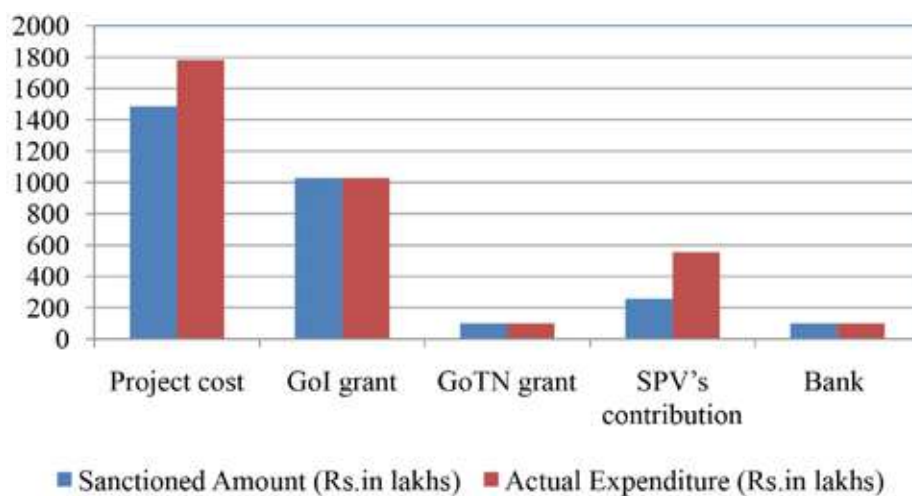
The Micro and Small players unable to enter into the markets for jumbo bags and leno bags as they do not have the facility to manufacture stronger fabric and that segment is monopolized by the medium and big players.

The demand for woven sacks by the cement, fertilizer and chemicals industries and also by other users has been increasing every year. Expanding the capacity individually by the micro and small players is not possible as capital investment required for manufacturing woven fabric will be beyond their reach.

Under these circumstances a common facility centre having high capacity extruders and weaving machines with latest technology will help the micro and small players. Many studies have been made to identify performance for Clusters under Cluster Development Approach like Match, Printing, Auto components, Leather, Plastic, Hosiery, Textile, Lorry Body Building, Pharmaceutical, Ceramic, Wet Grinder, Jewellery and Rice Mill [3]. Tamil Nadu is first to implement 24 clusters in India which includes Chennai Heavy Engineering Cluster [4]. A cluster is identified by two constituents – the product and the place, and is generally localized. [5] Many studies have been made to identify performance for Clusters under Cluster Development Approach like Match, Printing, Auto components, Leather, Plastic, Hosiery, Textile, Lorry Body Building, Pharmaceutical, Ceramic, Wet Grinder, Jewellery and Rice Mill [3]. Tamil Nadu is first to implement 24 clusters in India which includes M/S. Chennai Plastic Sacks Cluster Pvt.Ltd M/S. Chennai Plastic Sacks Cluster Pvt.Ltd [4]. A cluster is identified by two constituents – the product and the place, and is generally localized. [5]

Under Micro Small Enterprises Cluster Development Programme (MSE – CDP) they set up common facility centre for manufacturing of woven fabric which is raw material. Subsequently started one common facility centre in the name and style of M/S. Chennai Plastic Sacks Cluster Pvt.Ltd.[4]

During the month of 2010 Chennai Plastic Sacks Cluster Pvt. Ltd. incorporated in the Companies Act and purchased 4.65 acres Land in Pillaipakkam Village, Sriperumpudhur Taluk, Kanchipuram District. The project cost with Government of India (GoI), Government of Tamil Nadu (GoTN), Special Purpose Vehicle (SPVs) and Bank contribution is given in figure.



500 KVA power was activated after that, increased production from 50 Mts to 100 Mts then to 150 Mt. Now they are producing 160Mts. to 180Mts. per month which is the maximum load for the first Phase. After that 2nd phase production went up to

400Mts and it will be enhanced to 550Mts within short period. Facilities created in CFC are Testing Center, Quality Fabric, FIBC Fabric, Lamination & POPP Lamination.

OBJECTIVES OF THE STUDY

The objectives are

1. To Study the Physical and Financial Performance of Chennai Plastic Sacks Cluster (CPSC) in Kancheepuram District of Tamil Nadu before and after cluster development approach.
2. To Study the Compound annual growth rate, Descriptive Analysis, Correlation Analysis, Regression Analysis and Trend Analysis of CPSC before and after cluster development approach.
3. To study on the difference in difference on the control variable and experimental variables after Government Intervention of CPSC
4. To study on the Value Chain Analysis of the CPSC.
5. To develop Cluster Map of CPSC.

METHODOLOGY

The methodology adopted is collection of primary data from 44 Plastic Sacks Manufacturers in Kancheepuram District of Tamil Nadu, South India before (2015-16, 2016-17) Cluster Development Approach (CDAB) and after (2016-17, 2017-18) Cluster Development Approach (CDAA). Secondary data is collected from Ministry of Micro, Small and Medium Enterprises, Government of India, and Micro, Small and Medium Enterprises, Government of Tamil Nadu, Department of Industries and Commerce, Government of Tamil Nadu and Tamil Nadu Small Industries Development Corporation Limited (TANSIDCO).

The data were analyzed with Descriptive Analysis, Correlation Analysis, Regression Analysis, Trend Analysis, Compound Annual Growth Rate (CAGR), and Analysis of Variance (ANOVA) by taking No. of Units[U], Employment in numbers[E₁], Production in Mts [P], Year/time [Y] as independent variables and Turnover[T] in Crores and Export in Crores[E₂] as Dependent Variables. The Difference in Difference is also studied for Control Variable and Experimental Variables.

TECHNICAL ANALYSIS

Physical Performance

The physical performance of Plastic Cluster is shown in **Fig. 1 and Fig 2**.

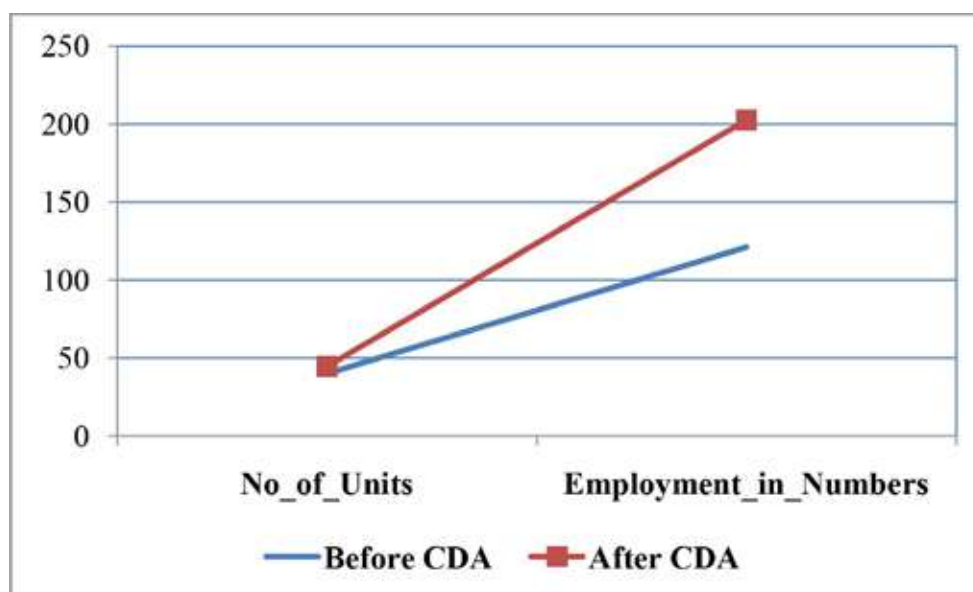


Fig. 1. Units and employment

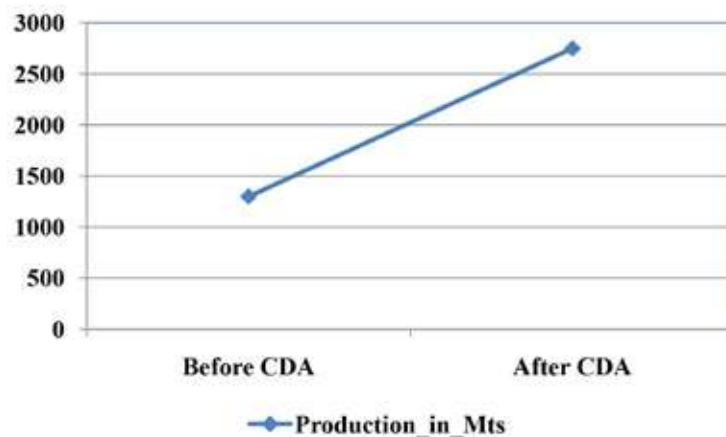


Fig. 2. Production in Meters

Physical Performance as shown in **Figs 1 and 2** is an increasing trend for no. of units with CAGR of 7.64, employment with CAGR of 34.33 and for production with CAGR of 64.27.

FINANCIAL PERFORMANCE

The financial performance of Plastic Cluster is shown in **Fig. 3**.

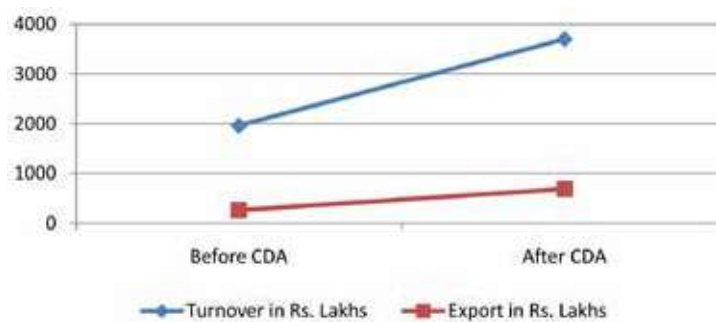


Fig. 3. Financial performance

Financial Performance as shown in 3 is an increasing trend for Turnover with CAGR of 66.89 and for export with CAGR of 53.90.

DESCRIPTIVE ANALYSIS

The Descriptive Analysis is given in **Table 1**.

The mean value of units, employment, production, turnover and exports indicates that there is growth in all variables after cluster development approach.

Table 1. Statistics

	UB	UA	E1B	E1A	PB	PA	TB	TA	E2B	E2A
Mean	41	44	141	185	1,500.00	2,433	2.95	5.08	0.82	1.57
Standard Error	3	0	26	22	351.19	584	0.62	1.52	0.44	0.38
Median	44	44	150	180	1800	1900	3.52	3.61	0.95	1.5
Standard Deviation	5	1	45	38	608.28	1,012	1.07	2.63	0.76	0.65
Sample Variance	21	0	2,001	1,425	370,000.00	1,023,333	1.14	6.92	0.58	0.43

Skewness	(2)	2	(1)	1	(1.68)	2	(1.72)	1.73	(0.77)	0.45
Range	8	1	88	75	1100	1800	1.89	4.6	1.5	1.3
Minimum	36	44	92	150	800	1800	1.72	3.52	0	0.95
Maximum	44	45	180	225	1900	3600	3.61	8.12	1.5	2.25
Sum	124	133	422	555	4500	7300	8.85	15.25	2.45	4.7
Count	3	3	3	3	3	3	3	3	3	3

Source: Computed Data.

CORRELATION ANALYSIS

The Correlation Analysis is given in **Table 2**.

Table 2. Correlations

	Before CDA					After CDA				
	U	E ₁	P	T	E ₂	U	E ₁	P	T	E ₂
U	1					1				
E ₁	0.9421	1				0.9177	1			
P	0.9966	0.9665	1			0.9988	0.9362	1		
T	0.9991	0.9554	0.9992	1		0.9999	0.9243	0.9995	1	
E ₂	0.9320	0.9996	0.9587	0.9465	1	0.9069	0.9997	0.9266	0.9139	1

Source: computed data

As per **Table 2**, there exists a significant positive relationship between no. of units, and employment, production, turnover and export after cluster development approach. Higher no. of units is associated with higher employment. Higher Production is associated with higher turnover. Higher Production is associated with export. Higher turnover are associated with higher export.

Higher dependent variables like turnover and exports are associated with higher independent variables like units, employment and production after cluster development approach.

REGRESSION ANALYSIS

The Regression Analysis is given in **Table 3**.

Sl.No	Regression Equations	R ²	p value	Result
1	$T = 7.39 - 0.33 U + 0.067 E_1$	R ² =0.89	p = 0.33	Not Significant
2	$T = -0.480 + .002 P$	R ² =0.99	p = 0.01	Significant
3	$E_2 = -1.590 + 0.017 E_1 + 0.0002 P$	R ² =1.00	p = 0.02	Significant
4	$E_2 = -7.22 + 0.20 U$	R ² =0.78	p = 0.12	Not Significant
5	$P = 1469.029 - 84.36 U + 25.47 E_1$	R ² =0.93	p = 0.27	Not Significant
6	$E_2 = -1.37 - 0.006 U + 0.02 E_1$	R ² =1.00	p = 0.01	Significant

Source: Computed Data.

Regression equation 1, in **Table 3** reveals that employment significantly predicts turnover. Regression equation 2, in table 3 reveals that production significantly predicts turnover. Regression equation 3, in table 3 reveals that production significantly predicts exports. Regression equation 4, in table 3 reveals that no. of units significantly predicts exports. Regression equation 5,

in table 3 reveals that employment significantly predicts Production. Regression equation 6, in table 3 reveals that employment significantly predicts exports.

Higher dependent variable like turnover and exports significantly predicts independent variables like units, employment and production after cluster development approach.

TREND ANALYSIS

The Trend Analysis is given in **Table 4**.

Table 4. Trend equations

Sl.No	Trend Equations	R ²	p value	Result
1	$U = 35.50 + 2.70 Y$	$R_2 = 0.69$	$p = 0.17$	Not Significant
2	$E_1 = 54.50 + 42.90 Y$	$R_2 = 0.99$	$p = 0.01$	Significant
3	$P = -100.00 + 850 Y$	$R_2 = 0.89$	$p = 0.05$	Not Significant
4	$T = -0.58 + 1.93 Y$	$R_2 = 0.83$	$p = 0.09$	Not Significant
5	$E_2 = -0.65 + 0.73 Y$	$R_2 = 0.99$	$p = 0.01$	Significant

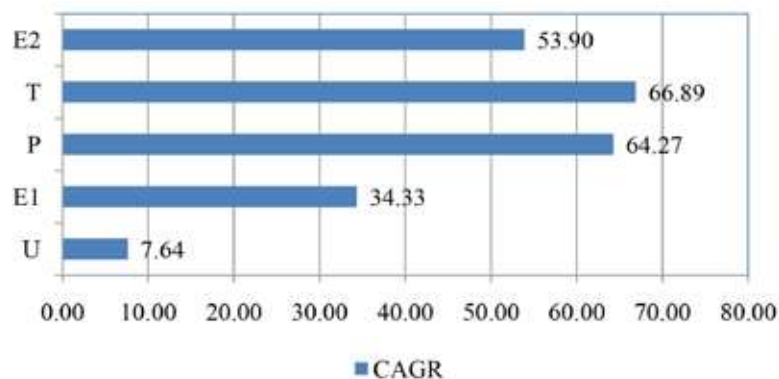
Source: Computed Data.

As per trend equation 1 in **Table 4**, an annual average increase in no. of units is 3 nos. As per trend equation 2 in table 4, an annual average increase in employment is 43 nos. As per trend equation 3 in **Table 4**, an annual average increase in production is Rs.850 Mts. As per trend equation 4 in table 4, an annual average increase in turnover is Rs. 1.93 crores. As per trend equation 4 in table 4, an annual average increase in export is Rs. 0.73 crores.

There is an annual average increases in dependent variables like turnover and exports and also there is an annual average increase in independent variables like units, employment and production after cluster development approach.

COMPOUND ANNUAL GROWTH RATE (CAGR)

The Compound Annual Growth Rate (CAGR) is given in **Fig. 4**.



Source: Plastic Cluster, Kancheepuram, Tamil Nadu and computed data

Fig. 4. Compound Annual Growth Rate (CAGR)

As per **Fig. 4**, there is increase in CAGR of No. of Units to 7.64% after Cluster Development Approach. There is increase in CAGR of employment to 34.33% after Cluster Development Approach. There is increase in CAGR of production to 64.27% after Cluster Development Approach. There is increase in CAGR of turnover to 66.89% after Cluster Development Approach. There is increase in CAGR of export to 53.90% after Cluster Development Approach.

In general the CAGR increases for both dependent variables like turnover and exports and also for independent variables like no.of units, employment and production after cluster development approach.

There is an annual average increases in dependent variables like turnover and exports and also there is an annual average increase in independent variables like units, employment and production after cluster development approach.

ANALYSIS OF VARIANCE (ONE WAY ANOVA)

The descriptive is given in **Table 5**.

Table 5. Descriptive

		N	Mean	Std. Deviation	Std. Error	95% Confidence Interval for Mean		Minimum	Maximum
						Lower Bound	Upper Bound		
U	1.00					-10.82	90.82		
	2.00	2	44.50	.707	.500	38.15	50.85	44	45
	Total	4	42.25	4.193	2.097	35.58	48.92	36	45
E ₁	1.00	2	121.00	41.012	29.000	-247.48	489.48	92	150
	2.00	2	202.50	31.820	22.500	-83.39	488.39	180	225
	Total	4	161.75	55.788	27.894	72.98	250.52	92	225
P	1.00	2	1300.0000	707.10678	500.00000	-5053.1024	7653.1024	800.00	1800.00
	2.00	2	2750.0000	1202.08153	850.00000	-8050.2740	13550.2740	1900.00	3600.00
	Total	4	2025.0000	1161.53634	580.76817	176.7365	3873.2635	800.00	3600.00
T	1.00	2	2.6200	1.27279	.90000	-8.8156	14.0556	1.72	3.52
	2.00	2	5.8650	3.18905	2.25500	-22.7875	34.5175	3.61	8.12
	Total	4	4.2425	2.72764	1.36382	-.0978	8.5828	1.72	8.12
E ₂	1.00	2	.4750	.67175	.47500	-5.5604	6.5104	.00	.95
	2.00	2	1.8750	.53033	.37500	-2.8898	6.6398	1.50	2.25
	Total	4	1.1750	.94736	.47368	-.3325	2.6825	.00	2.25

Source: Computed Data.

The one way ANOVA is given in **Table 6**.

Table 6. ANOVA

		Sum of Squares	df	Mean Square	F	Sig.
U	Between Groups	20.250	1	20.250	1.246	.380
	Within Groups	32.500	2	16.250		
	Total	52.750	3			
E ₁	Between Groups	6642.250	1	6642.250	4.930	.157
	Within Groups	2694.500	2	1347.250		
	Total	9336.750	3			
P	Between Groups	2102500.000	1	2102500.000	2.162	.279
	Within Groups	1945000.000	2	972500.000		
	Total	4047500.000	3			



T	Between Groups	10.530	1	10.530	1.786	.313
	Within Groups	11.790	2	5.895		
	Total	22.320	3			
E ₂	Between Groups	1.960	1	1.960	5.352	.147
	Within Groups	.732	2	.366		
	Total	2.693	3			

Source: Computed Data

Null Hypothesis 1: There is no significant difference in no. of units on before and after cluster development approach.

Alternate Hypothesis 1: There is significant difference in no. of units on before and after cluster development approach.

As per table 6, $p = 0.380 > 0.05$, $F = 1.246 < F_{\text{Critical}} = 18.51$, hence null hypothesis is accepted and alternate hypothesis is rejected i.e., there is no significant difference in no. of units on before and after cluster development approach. However as per table 5, M (Mean) value on CDAA = 44.50 > CDAB = 40.00 where there is significant increase in no. of units after cluster development approach.

Null Hypothesis 2: There is no significant difference in employment on before and after cluster development approach.

Alternate Hypothesis 2: There is significant difference in employment on before and after cluster development approach.

As per table 6, $p = 0.157 > 0.05$, $F = 4.930 < F_{\text{Critical}} = 18.51$, hence null hypothesis is accepted and alternate hypothesis is rejected i.e., there is no significant difference in employment on before and after cluster development approach. However as per table 5, M (Mean) value on CDAA = 202.50 > CDAB = 121.00 where there is significant increase in employment after cluster development approach.

Null Hypothesis 3: There is no significant difference in production on before and after cluster development approach.

Alternate Hypothesis 3: There is significant difference in production on before and after cluster development approach.

As per table 6, $p = 0.279 > 0.05$, $F = 2.162 < F_{\text{Critical}} = 18.51$, hence null hypothesis is accepted and alternate hypothesis is rejected i.e., there is no significant difference in production on before and after cluster development approach. However as per table 5, M (Mean) value on CDAA = 2750.00 Mts > CDAB = 1300.00 Mts where there is significant increase in production after cluster development approach.

Null Hypothesis 4: There is no significant difference in turnover on before and after cluster development approach.

Alternate Hypothesis 4: There is significant difference in turnover on before and after cluster development approach.

As per table 6, $p = 0.313 > 0.05$, $F = 1.786 < F_{\text{Critical}} = 18.51$, hence null hypothesis is accepted and alternate hypothesis is rejected i.e., there is no significant difference in turnover on before and after cluster development approach. However as per table 5, M (Mean) value on CDAA = Rs.5.87crores > CDAB = Rs.2.62 cores where there is significant increase in production after cluster development approach.

Null Hypothesis 5: There is no significant difference in export on before and after cluster development approach.

Alternate Hypothesis 5: There is significant difference in export on before and after cluster development approach.

As per table 6, $p = 0.147 > 0.05$, $F = 5.352 < F_{\text{Critical}} = 18.51$, hence null hypothesis is accepted and alternate hypothesis is rejected i.e., there is no significant difference in export on before and after cluster development approach. However as per table 5, M (Mean) value on CDAA = Rs.1.88 cores > CDAB = Rs.0.48 cores where there is significant increase in export after cluster development approach.

Paired Sample T-Test

The Paired Sample T-Test is given in **Table 7**.

Table 7. Paired samples test

		Paired Differences							
					95% Confidence Interval of the Difference				
		Mean	Std. Deviation	Std. Error Mean	Lower	Upper	t	df	Sig. (2-tailed)
Pair 1	U _A - U _B	4.50	4.95	3.500	-39.97	48.97			
Pair 2	E _{1A} - E _{1B}	81.50	9.19	6.500	-1.09	164.09			
Pair 3	P _A - P _B	1450.00	494.97	350.00	-2997.17	5897.17	4.14	1	.151
Pair 4	T _A - T _B	3.25	1.92	1.36	-13.97	20.46	2.40	1	.252
Pair 5	E _{2A} - E _{2B}	1.40	.14	.10	.12	2.67	14.00	1	.045

Source: Computed Data.

As per **Table 7**, there is increase in no. of units, employment, production, turnover and export.

Difference in Differences (DID)

The Government of India and Tamil Nadu policy on Cluster Development Approach is an important one for MSMEs. A test was conducted between control group (who have not undergone Cluster Development Approach) and Treatment Group (who have undergone Cluster Development Approach). The Treatment T for time t for employment, production, turnover and export formed is given in equation 1, 2, 3 and 4.

$$E_1 = 92 + 88 T + 58 t - 13 T t \quad (1)$$

DID = -13 where the employment in this cluster need improvement.

$$P = 800 + 1100 T + 1000 t + 700 T t \quad (2)$$

DID = 700 where the production is significant in this cluster.

$$T = 1.72 + 1.89 T + 11.8 t + 2.71 T t \quad (3)$$

DID = 1.72 where the turnover is significant in this cluster.

$$E_2 = 3.33 E - 16 + 1.5 T + 0.95 t - 0.2 T t \quad (4)$$

DID = -0.2 where the Export is significant in this cluster need improvement.

Advantages after completion of CFC

1. Reduction in raw material (PP/PE) production cost. Since the members are procuring the raw materials for their supply.
2. Reduction in the conversion cost from raw material to woven fabric.
3. The Micro units can increase their production capacity with very little investment of stitching cutting machines as they are getting their raw material (woven fabric) at a cheaper price by utilizing CFC.
4. After implementation they are expanding to newer market and product viz., PO PP Lamination bags and Jumbo bags.
5. The Micro and Small units are having capacity to take bulk orders from cement and fertilize industry by getting competitive price since they reduced the cost of Production.
6. Now they are getting Jumbo Bag Export order from South Korea & USA monthly 4 containers.
7. Increase in employment from 50 to 200 in the cluster unit and it will be increase to 350.

8. After implementation of CFC nearly 15 micro units started in and around Porur near Chennai.
9. The testing facility is utilized by all the members and is getting good quality fabric.
10. SPV members individually increasing their income and their turnover has been increased to 20% average. Apart from that all the SPV members increased their production and in the result of which total employment increased entire cluster. For example one women entrepreneur started her stitching unit during the year 2007, her turnover was Rs.50 lakhs. Before starting the CFC during the year 2015 her turnover was Rs.2.5 crore. After starting CFC 2015-2016 turnover was 3.5 crore, 2016-2017 turnover was 4.5 crore, 2017-2018 turnover was Rs.5.5 crore, 2018-2019 turnover was Rs.6.5 crore and in the same way income also increased. Labour employment also enhanced from 10 to 20 people. In this way all the members increased the business and getting more profit.
11. The CFC is servicing to Non members also. More than 62 non members are utilizing the CFC and getting different color of Fabric, High weight fabric which is not available in the market. For example a non member is getting nearly 20 MT fabrics from the CFC with low cost and supplying maximum super market in the Chennai City. He is having only stitching and printing machine only. His Capital investment is nearly Rs.35 Lakhs but doing turnover of Rs.6.00 crore per annum.
12. Every 6 months 10 to 15 employees are getting training form helper to operator, supervisor and mechanics.
13. Annual turnover of CFC has been increased to Rs.100 Crores.
14. Facilities created in CFC are shown in **Figure 5**.



Fig. 5. Facilities created in CFC

VALUE CHAIN ANALYSIS

The value-chain concept has been used to distinguish between cooperative strategies according to the type of resources pooled by the partners. This study is based on the value chain concept and integrated approach developed by researcher on cluster development as shown in **Fig. 6**.

Supportive Activities	Infrastructure Resource	With Government of Tamil Nadu through TANSIDCO and Government of India assistance created Common Facility Centre. Facilities at CFC are Ware House, Laboratory etc.				Infrastructure Interrelationships	
	Human Resource Management	Cluster based Human Resource Strategy is also implemented where the recruitment, retention, replacement, Internal Carrier Development and skill development training of individual firms is taken care of by the Cluster. Training Centre has Laboratories and Skill Development Centre to train and impart technical skills to employees					
	Technology Development Resource	Technology Awareness / Training Programmes and Technology Transfer Schemes including Joint ventures and Quality Upgradation are conducted through and thereby Technology Interrelationships has taken place. Testing Laboratory to carry out Mechanical Tests, Chemical Tests and Physical Tests for the raw materials and products. High Precision Laboratory with latest technology available in CPSC				Technology Interrelationships	
	Procurement Resource	The common raw material bank (consortia) created under Public Private Partnership (PPP) concept leads to best quality inputs with Low input costs and Just in Time (JIT) model. Industrial Estate has got raw material depot and through them the Industries has got the raw materials with less cost (10% to 20%) compared to open market.				Procurement Interrelationships	
	Primary Activities	Testing Center, Quality Fabric, FIBC Fabric, Lamination POPP Lamination.			Common Product Display Centre, Website design and development and Partnership Exchange for Business Linkages with reputed companies, Auction Centre and related international fairs and Exhibitions conducted. Visiting of Trade and Investment Delegations. Moreover Inter-firm exposure and Inter Cluster Exposure taken place in the cluster. The Members also got loan from Banks due to CDA.		
		Inbound Logistics	Operations	Outbound Logistics	Marketing / Sales	Service	
		Production Interrelationships			Marketing Interrelationships		

Source: Developed by Researcher

Source: Developed by Researcher

Fig. 6. Value chain analysis for CPSC

It has been discussed that Cluster Approach is a major motivating factor and enterprises are keen to accept the challenge to maximize their profits. Majority of enterprises are moderately satisfied with the infrastructure interrelationships, technology interrelationships, procurement interrelationships, production interrelationships and marketing interrelationships after the CDA.

CHENNAI PLASTIC SACKS CLUSTER MODEL(CPSCM)

The SPSCM as shown in fig.7, indicates the cluster level linkages of all actors namely, TIIC- Tamil Nadu Industrial Investment Corporation, SIDBI- Small Industries Development Bank of India, EXIM Bank – Export Import Bank, SIDCO- Small Industries Development Corporation, SAGOSERVE, TANSTIA- Tamil Nadu Small and Tiny Industries Association, NSIC- National Small Industries Corporation, MSMEDI- Micro, Small and Medium Enterprises Development Institute, RTC- Regional Testing

Centre, DIC- District Industries Centre, ITPO- Industrial Trade Promotion Organization, MOFPI- Ministry of Food Processing Industry involved effectively in the formation and the supporting activities of SPSC.

From the outcome of the present study, it is obvious that SPSC has significant interrelationships among the enterprises. One Location of the clusters plays a crucial role in the integrated study. Constant involvement of industrial units in the cluster will improve their performance. The costs of the industrial units have considerably reduced due to the intervention and the profit increased sizably. The policy planners can identify the parameters of industrial growth in different locations of the region using Cluster Development Approach. The outcome of Cluster Development Approach will attract the financial investors to concentrate more on specified industrial centres for investment. This will improve the economic status of the region for overall development. The SPSC Model indicates the cluster level linkages of all actors involved effectively in the formation and the supporting activities of SPSC.

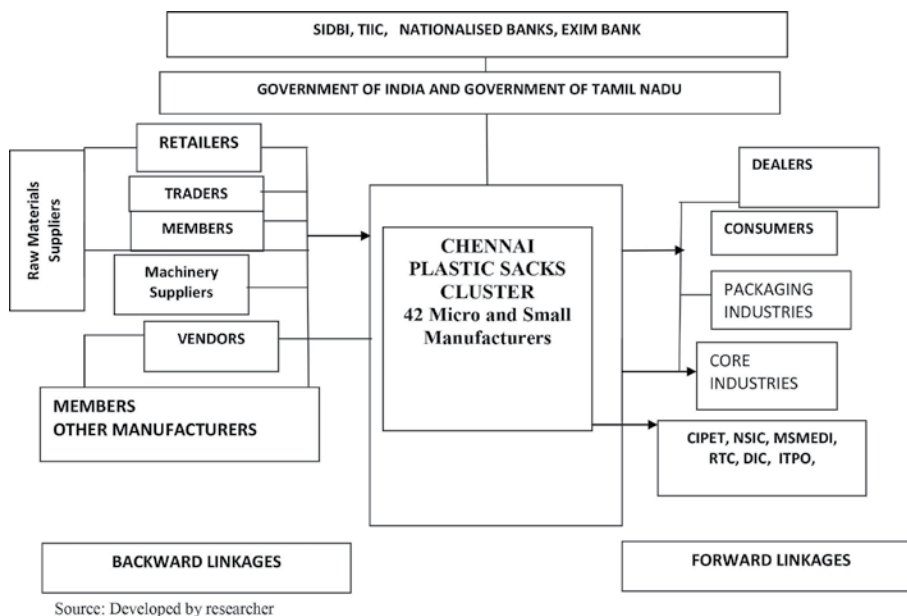


Fig. 7. Chennai plastic sacks cluster model

FINDINGS, SUGGESTIONS AND CONCLUSION

A Study conducted on the Physical and Financial Performance, and to find difference in differences on the control variable and experimental variables after Government Intervention on Plastic Cluster in Kancheepuram District of Tamil Nadu. Physical Performance is an increasing trend for no. of units, employment and production and also for Financial Performance like Turnover and export as per increasing CAGR. The mean value of units, employment, production, turnover and exports indicates that there is growth in all variables after cluster development approach. There exists a significant positive relationship between no. of units, and employment, production, turnover and export after cluster development approach. Higher no. of units is associated with higher employment. Higher Production is associated with higher turnover. Higher Production is associated with export. Higher turnover are associated with higher export.

Higher dependent variables like turnover and exports are associated with higher independent variables like units, employment and production after cluster development approach. Employment significantly predicts turnover. Production significantly predicts turnover and exports. No. of units significantly predicts exports. Employment significantly predicts Production also exports. Higher dependent variable like turnover and exports significantly predicts independent variables like units, employment and production after cluster development approach.

There is an annual average increases in dependent variables like turnover and exports and also there is an annual average increase in independent variables like units, employment and production after cluster development approach. There is significant difference in employment, production, turnover and export after cluster development approach.

The Government of India and Tamil Nadu policy on Cluster Development Approach is an important one for MSMEs. As per



DID the control group (who have not undergone Cluster Development Approach) and Treatment Group (who have undergone Cluster Development Approach) have much difference in differences on employment, production, turnover and export and this is increase in productivity due to adoption of cluster development approach by experimental group.

The cluster development is one the very good concept for developing MSE's for that GOI and GOTN are supporting through TANSIDCO as implementing agency. All the departments in the State as well as Central are very Co-operative during the implementation of the project.

REFERENCES

1. https://www.unido.org/sites/default/files/2008-05/Supplier_Networks-EN_0.pdf, p.no.3 UNIDO website assessed on 24.11.2020.
2. <http://www.dcmsme.gov.in/MSE-CDProg.htm> Ministry of MSME, Government of India website assessed on 24.11.2020.
3. http://www.indcom.tn.gov.in/pdf/MSME_Clusters.pdf p.no.7, Department of Industries and Commerce, Government of Tamil Nadu website assessed on 25.11.2020.
4. Policy Note, 2020-21, MSME Department, Government of Tamil Nadu p.no.145.
5. SME Cluster Development, A Training Manual, National Resource Centre for Cluster Development (NRCD) of School of Enterprise Development (SED), National Institute for Micro, Small and Medium Enterprises, An organization of the Ministry of MSME, Hyderabad p.no.2.

Application of AI based Models on 3D Printing Technology : Future Prospects for Additive Manufacturing

Shivam Raj, Sanjit Kumar Rajak, Ganta Sai Rahul, Rajat Gupta

Department of Mechanical Engineering, National Institute of Technology Mizoram, Aizawl, Mizoram

✉ Shivamraj00g@gmail.com

ABSTRACT

Additive manufacturing is one of the sustainable and fastest growing technologies. The convergence of Artificial Intelligence (AI) with 3D printing is the future of smart and digital manufacturing. This will turn out as an embryonic technology with potential to disrupt the manufacturing industry. In this paper an attempt has been made to analyze the possibilities of applications of AI in 3D printing innovation. With the help of AI models like neural network, decision tree etc. one can reduce the time, cost and energy required in the 3D printing process. This technology can additionally improve the productivity of the generally accessible models and furthermore recommend changes to be accomplished for a long existence of item. Further, this paper deals with the issues of 3D printing which are solved by AI models integrated with CAD software, which will bring a significant improvement in additive manufacturing system.

Keywords: Additive manufacturing; 3D printing; Artificial intelligence & CAD.

INTRODUCTION

In recent years, developing consideration has zeroed in on both the artificial intelligence and 3D printing technology. 3D printing or additive manufacturing (AM) is a cycle for making a 3D object of any shape from a 3D model or other electronic information sources through added substance measures in which progressive layers of material are set down under pc controls [1]. Hideo Kodama of Nayoga Municipal Industrial Research Institute is commonly respected to have printed the primary strong article from a computerized plan. Notwithstanding, the credit for the main 3D printer by and large goes to Charles Hull, who in 1984 planned it while working for the organization he established, 3D systems corp. Charles Hull was a pioneer of the strong imaging measure known as stereolithography and the STL (stereolithographic) document design which is as yet the most generally utilized arrangement utilized today in 3D printing [2]. He is additionally respected to have begun business quick prototyping that was simultaneous with his improvement of 3D printing. Artificial intelligence (AI) can be characterized as the hypothesis and improvement of pc frameworks ready to perform undertakings typically requiring human knowledge, for example, visual discernment, discourse acknowledgment, dynamic, and interpretation between dialects [3]. Here, this paper is keen on the dynamic capacity of AI. This property of AI empowers us to upgrade the generally accessible models to build their productivity. This paper shows how to be profited by AI for determination of material for printing various zones of the model.



Fig. 1. 3D-printer [4]



MATERIALS USED FOR 3D PRINTING

Some of the common materials used in 3D printers are :

- I. Acrylonitrile Butadiene Styrene [ABS]
- II. High Impact Polystyrene [HIPS]
- III. Poly Lactic Acid [PLA]

Acrylonitrile Butadiene Styrene [ABS]

ABS is one of the most broadly utilized materials since the initiation of 3D printing. This material is truly strong, marginally adaptable, and lightweight and can be effortlessly expelled, which makes it ideal for 3D printing. It requires less power to expel than when utilizing PLA, which is another famous 3D fiber. This reality makes expulsion simpler for little parts. The inconvenience of ABS is that it requires higher temperature. Its glass progress temperature is about 105°C and temperature around 210 -250°C is normally utilized for printing with ABS materials. Likewise another disadvantage of this material is very exceptional exhaust during printing that can be risky for pets or individuals with breathing troubles. So 3D printers should be put in very much ventilated zone. Likewise solid counsel is to abstain from taking in vapor during printing considering the expense of 3D materials ABS is the least expensive, which makes it top choice in printing networks as of recently [5].

Technical properties

- Density- 1-1.4 gm/cm³
- Dielectric constant- 3.1 to 3.2
- Dielectric Strength [Breakdown Potential]- 15-16 kV/mm [0.59-0.63 V/mil]
- Elastic modulus- 2 to 2.6 GPa
- Elongation at break- 3.5 to 50%
- Flexural modulus- 2.1 to 7.6 GPa
- Flexural strength- 72 to 97 MPa
- Heat deflection temperature at 1.82 MPa -76 to 110°C
- Heat deflection temperature at 455 KPa- 83 to 110°C
- Strength to weight ratio- 37 to 79 kN-m/kg
- Tensile strength: 37 to 110 MPa
- Thermal expansion- 81 to 95 µm/m-K
- Material Properties of Acrylonitrile Butadiene Styrene[ABS]
- Temperature - 225°C
- Flow Tweak - 0.93
- Bed Temperature - 90°C
- Bed Preparation - apply glue stick 2 layer & then abs glue 1 layer

High Impact Polystyrene [HIPS]

HIPS fiber is produced using a High Impact Polystyrene material and it is another illustration of help 3d materials. This material is all around spread in food industry for bundling. It is additionally used to pack CD plates and to create plate in medication normally this fiber has brilliant white tone and it is additionally biodegradable so there is no unfriendly impact when it is put in close contact with a human or creature body. HIPS fibers have twisting and grip issues, which can be decreased by utilizing a warmed bed during the printing. HIPS material that can likewise be utilized as help structure during the printing and afterward broke down in a drab fluid hydrocarbon arrangement. Technical properties:

- Density - 1.0 g/cm³ (62 lb/ft³)
- Dielectric Strength (Breakdown Potential) - 18 kV/mm (0.7 V/mil)



- Elastic (Young's, Tensile) Modulus - 1.9 GPa (0.28×10^6 psi)
- Elongation at Break - 40 %
- Flexural Strength - 62 MPa (9.0×10^3 psi)
- Glass Transition Temperature - 100 °C (210 °F)
- Heat of Combustion (HOC) - 43 MJ/kg
- Limiting Oxygen Index (LOI) - 18 %
- Poisson's Ratio - 0.41
- Specific Heat Capacity - 1400 J/kg-K
- Strength to Weight Ratio - 32 kN-m/kg
- Tensile Strength: Ultimate (UTS) - 32 MPa (4.6×10^3 psi)
- Thermal Conductivity - 0.22 W/m-K
- Thermal Diffusivity - 0.16
- Thermal Expansion - 80 $\mu\text{m/m-K}$
- Vicat Softening Temperature - 110 °C (230 °F)
- Water Absorption After 24 Hours - 0.08%

Material Properties of High Impact Polystyrene [HIPS]

- Temperature - 225°C
- Flow Tweak - 0.91
- Bed Temperature - 90°C
- Bed Preparation - apply glue stick 2 layer & then abs glue 1 layer

Poly Lactic Acid [PLA]

PLA (is gotten from corn and is biodegradable) is another widely used material for 3D printing technology. It is a biodegradable thermoplastic that is produced from sustainable assets. It is also easily available like other plastic materials. The other extraordinary component of PLA is its biocompatibility with a human body. The structure of PLA is harder than the one of ABS and material melts at 180 – 220°C which is lower than ABS. PLA glass progress temperature is between 60 – 65 °C, so PLA along with ABS could be some acceptable alternatives.

Technical properties

- Density - 1.3 g/cm³ (81 lb/ft³)
- Elastic (Young's, Tensile) Modulus - 2.0 to 2.6 GPa (0.29 to 0.38×10^3 psi)
- Elongation at Break - 6.0 %
- Flexural Modulus - 4.0 GPa (0.58×10^6 psi)
- Flexural Strength - 80 MPa (12×10^3 psi)
- Glass Transition Temperature - 60 °C (140 °F)
- Heat Deflection Temperature At 455 kPa (66 psi) - 65 °C (150 °F)
- Melting Onset (Solidus) - 160 °C (320 °F)
- Shear Modulus- 2.4 GPa (0.35×10^6 psi)
- Specific Heat Capacity - 1800 J/kg-K

- Strength to Weight Ratio - 38 kN-m/kg
- Tensile Strength : Ultimate (UTS) - 50 MPa (7.3×10^3 psi)
- Thermal Conductivity - 0.13 W/m-K
- Thermal Diffusivity - 0.056

Material Properties of Poly Lactic Acid [PLA]

- Temperature - 180°C
- Flow Tweak - 0.95
- Bed Temperature - 60°C
- Bed Preparation - apply glue stick 2 layer

AI MODELS USED IN 3D PRINTING

Artificial Neural Networks (ANNS)

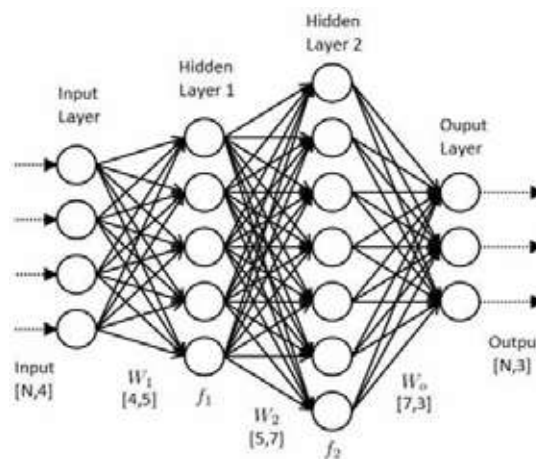


Fig. 2. Neural network AI model [6]

Artificial neural networks (ANNs), usually simply called neural networks (NNs), are computing systems vaguely inspired by the biological neural networks that constitute animal brains [7]. An ANN is based on a collection of connected units or nodes called artificial neurons, which loosely model the neurons in a biological brain. Each connection, like the synapses in a biological brain, can transmit a signal to other neurons. An artificial neuron that receives a signal then processes it and can signal neurons connected to it. The “signal” at a connection is a real number, and the output of each neuron is computed by some non-linear function of the sum of its inputs.

Decision Tree

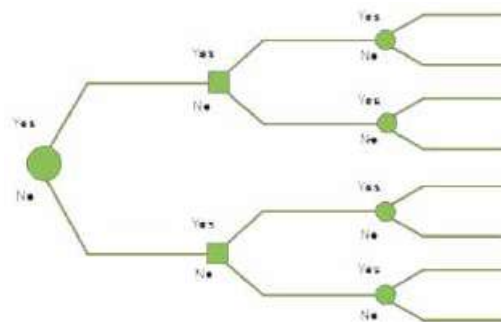


Fig. 3. Decision Tree AI Model



A decision tree is a decision support tool that uses a tree-like model of decisions and their possible consequences, including chance event outcomes, resource costs, and utility. It is one way to display an algorithm that only contains conditional control statements. Decision trees are commonly used in operations research, specifically in decision analysis, to help identify a strategy most likely to reach a goal, but are also a popular tool in machine learning [8].

DISCUSSION & CONCLUSION

Currently, people all over the world are using only one material at the time of printing the whole product but with the use of AI they can build a model which can decide which part of the product requires what kind of material for printing and then use that material for the job. This AI model is based on the data available by examining the different products on different parameters. Neural network models of AI can be used for the above purpose taking all the relevant parameters as the nodes for making a decision we can run a decision tree network parallelly which will give us the final result. A better image recognition API plugged in with the CAD software can help in redesigning of models which will require less time and energy. The models created through this methodology are expected to be cost effective and long lasting in nature.

In this paper it has been perceived how AI can change the 3D printing society and give us the adaptability to not stress over the best material for printing. This methodology will save the time by not going in hit and trial method for deciding the material and furthermore help in material conservation. Alongside in choosing materials AI can likewise be useful in the upgrading of items for better productivity and long life. AI can be integrated with CAD software to find defects that can make prediction whether a model is printable or non-printable in a 3-D model which could reduce time & material wastage. Preparing of these models may take some more time and lot of information is required for this cycle. In a more drawn-out setting, we can say that these AI models will end up being a solid and safe even in the field of 3D printing with a superior responsibility.

REFERENCES

1. Dongkeon Lee, Takashi Miyoshi, Yasuhiro Takaya and Taeho Ha, “3D Micro fabrication of Photosensitive Resin Reinforced with Ceramic Nanoparticles Using LCD Microstereolithography”, *Journal of Laser Micro/Nano engineering* Vol.1, No.2, 2006.
2. Ruben Perez Mananes, Jose Rojo-Manaute, Pablo Gil, “3D Surgical printing and pre contoured plates for acetabular fractures”, *Journal of ELSEVIER* 2016.
3. Poole, Mackworth & Goebel (1998), which provides the version that is used in this article. These authors use the term “computational intelligence” as a synonym for artificial intelligence.
4. Vinod G. Gokhare, D. N. Raut & D. K. Shinde “A Review paper on 3D-Printing Aspects and Various Processes Used in the 3D-Printing” *International Journal of Engineering Research & Technology* Published by : www.ijert.org Vol. 6 Issue 06, June – 2017.
5. Pshtiwan Shakor, Jay Sanjayan, Ali Nazari, Shami Nejadi, “Modified 3D printed powder to cement-based material and mechanical properties of cement scaffold used in 3D printing”, *Science Direct*.
6. <https://www.datasciencecentral.com/profiles/blogs/the-artificial-neural-networks-handbook-part-1>.
7. Chen, Yung-Yao; Lin, Yu-Hsiu; Kung, Chia-Ching; Chung, Ming-Han; Yen, I-Hsuan (January 2019). “Design and Implementation of Cloud Analytics-Assisted Smart Power Meters Considering Advanced Artificial Intelligence as Edge Analytics in Demand-Side Management for Smart Homes”. *Sensors*. 19 (9): 2047. doi:10.3390/s19092047. PMC 6539684. PMID 31052502.
8. Kamiński, B.; Jakubczyk, M.; Szufel, P. (2017). “A framework for sensitivity analysis of decision trees”. *Central European Journal of Operations Research*. 26 (1): 135–159. doi:10.1007/s10100-017-0479-6. PMC 5767274. PMID 29375266.



Possible Mitigation Measures for Various Hazards Associated with Cement Factories of Assam- A Discussion

Dr Sanjoy Kumar Dey¹, Dr Rajat Gupta²

Senior Inspector of Factories, Government of Assam¹, Director, NIT, Mizoram²

✉ sanjoy.deyl@gmail.com

ABSTRACT

Cement is a basic ingredient for any construction activity. Considering its wide spread use in road, building, dams and other infrastructure related activities, it has gained an ever increasing significance as a medium of development in both developed and developing nations resulting in continual increase in the production volume of Cement. Cement production is a labour intensive, resource intensive and energy intensive process. Consequently, production of Cement invariably accompanies serious Occupational health & safety (OHS) and environmental hazards. Identification of these hazards and their mitigation is indispensable in order to produce Cement in a socially, economically, occupationally and environmentally sustainable manner. And this is more important now keeping in view the Pandemic situation across the globe. This paper reviews the OHS hazards in Cement production in Assam and their possible mitigation measures thereby paving the way for the best practice in Cement production in this State.

Keywords: Occupational health and safety (OHS); Hazard mitigation; Cement dust.

INTRODUCTION

Owing to the fact that cement manufacturing is a high risk industry, workers employed therein are exposed to different health and safety hazards. Also, local and global environment are impacted by cement manufacturing. In Assam, more than thirty (30) nos. of cement factories are in operation. In addition to the various health hazards, cement workers are exposed to dust at different stages cement production such as quarrying, crushing, raw material grinding, blending, kiln burning, cement grinding and packaging. Dust exposure may lead to the lung function impairment, chronic obstructive lung disease, restrictive lung disease, pneumoconiosis and Cancer of Lungs, Stomach and Colon. Hence, ensuring safe and healthy work environment for workers engaged in cement manufacturing is an issue that is strongly linked to the overall sustainability of society and general environment of Assam.

BRIEF LITERATURE REVIEW

The dust particles less than 2μ are trapped in the lung and their settling may affect the physiology of lungs (Junge 1977). The effect of dust on the body varies with nature and duration of exposure as well as age of the persons (Chandaran & Rajkumar 2002). Silica dust causes pneumoconiosis, and skin diseases are strictly of occupational origin (Mishra & Gupta 1993). Development of cancer in Danish stone industries workers, Vermont granite shade and quarry workers due to silica exposure have been reported (Gue'ne'l et al. 1989). Cement dust is one of the major air pollutants. It consists of hazardous materials such as 1. Alkaline compounds (lime) that are corrosive to human tissue, 2. Silica that is abrasive to skin and causing damage to lung (silicosis), and 3. Chromium that can cause allergic reaction (pulmonary as well as skin). Cement dust affects three main organs, in general, like eyes, lungs and skin causing different types of respiratory, skin and eye diseases (Singh 2010). Particulate air pollution has been associated with the incidence and severity of respiratory disorder (Pope & Dockery 1992, Near et al. 1995, Peters et al. 1996).

CLASSIFICATION OF FACTORIES OF ASSAM BASED ON SAFETY AND HEALTH RISKS

There are a number of legislations regulating the safety and health in the factories of Assam. Factories Act 1948, Assam Factories Rules 1950, Manufacture, Storage and Import of Hazardous Chemicals Rules 1989, Chemical Accidents (Emergency Planning, Preparedness and Response) Rules, 1996, Hazardous and Other Wastes (Management and Transboundary Movement) Rules, 2015 are the primary statutes that regulate the different aspects of safety and health of workers employed in the factories of Assam. The factories of Assam have been categorised in accordance to the risk based priority. They are classified as follows:

- Major Accident Hazards Installations (as defined in Rule 2(6) of Chemical Accidents (Emergency Planning, Preparedness and Response) Rules, 1996.
- Factories involving Hazardous Process: (As defined under Section 2(cb) of Factories Act, 1948.
- Factories involving dangerous operations as declared under Rule 94 of the Assam Factories Rules 1950 framed under section 87 of Factories Act, 1948.
- Factories employing more than 10 workers but not coming under any of the above three categories.
- Factories employing less than 10 workers (As declared under Section 85 of the Factories Act, 1948.
- Factories under self-certification scheme as introduced vide Assam Govt. Notification No. GLR.71/2016/C/Pt/44 dated 16-03-2017.

Cement manufacturing comes under the hazardous category of industry. Number of special provisions have been incorporated in the Factories Act, 1948 (Sections 41A to 41H) to secure safety and health of persons employed in the hazardous processes

BRIEF MANUFACTURING PROCESS

Cement manufacturing consists of drying, grinding and mixing limestone and additives like iron and bauxite ore into a powder known as “raw meal”. The lime stone is collected from lime stone quarry and quarrying is usually performed by explosives. The primary ingredients used in cement production are limestone, sand, clay, bauxite and gypsum. The raw meal is heated and burned in pre-heater and kiln up to a kiln temperature of 2000C. The heated contents are then cooled by air cooling to produce a semi-finished product known as clinker. The clinker is then stored in silos after air cooling. The clinker (95%) is subsequently ground with Gypsum (5%) in cement mill to form ordinary cement. **Fig. 1** depicts schematic diagram of a typical cement manufacturing process.

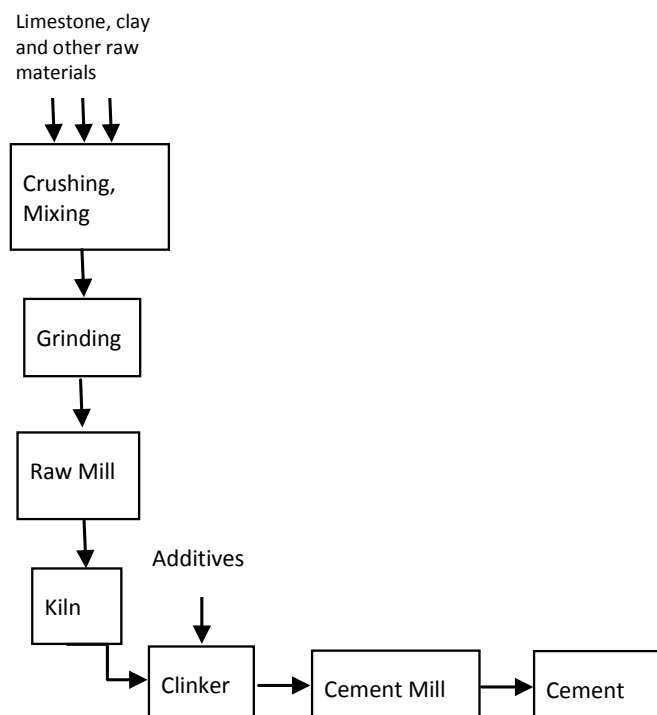


Fig. 1. Typical cement manufacturing process

SAFETY PERFORMANCE IN THE FACTORIES OF ASSAM

There are approximately eight thousand factories are running across Assam. About 30% of these factories come under hazardous category. **Table 1** provides a glimpse of the incidences occurred in the factories Assam leading to the physical injury with fatalities for five year period wef 2016 to November, 2020.

**Table 1.** Accident data in the factories of Assam (2016-2020)

Year	Number fatal accidents	Number of fatalities	Number of non-fatal accidents	Total number accidents
2016	12	12	41	53
2017	9	10	53	62
2018	12	13	35	47
2019	4	6	21	25
2020 (Up to November)	8	8	15	23

Source: Statistics cell (Chief Inspectorate of Factories, Assam, 2020)

Falling from height, electric shock, explosion, flush of hot water, entanglement with the moving machine parts, accident due to vehicular traffic inside the factory premises, burn, boiler explosion, falling flat on the ground, trapping with the running machine parts, hit by falling objects etc. are some of the causes that resulted in the accidents.

Table 2 gives the accident data in the Cement factories of Assam for the period 2016-2020 (November)

Year	Number fatal accidents	Number of fatalities	Number of non-fatal accidents	Total number accidents
2016	2	2	4	6
2017	2	2	2	4
2018	3	3	1	4
2019	Nil	Nil	1	1
2020 (Up to November)	1	1	1	2

Source: Statistics cell (Chief Inspectorate of Factories, Assam, 2020)

Falling from height, hit by vehicular traffic inside the plant, unreported health condition, trapping with the moving parts of machines particularly transmission machinery, sleeping on non-designated areas were the underlying conditions that led to these accidents.

HAZARDS ASSOCIATED TO THE CEMENT MANUFACTURING:

The processes in cement production that involve specific OHS hazards are

i) Quarrying: This involves extraction of Lime stone and other raw materials. ii) Crushing: The extracted materials are then crushed. iii) Transport: Crushed materials are then transported to the cement plants. iv) Clinker production. v) Milling processes at raw mill, coal mill and cement mill. vi) Filtering. vii) Storage. viii) Packaging/bagging. ix) Logistics or loading and delivery of finished material. x) Fuel storage. xi) Power generation.

These processes and hazard factors associated to them are presented in the **Table 3**.

Table 3. Hazard factors associated to the cement manufacturing process

Serial number	Processes involving hazards	Hazard factor
1	Quarrying	Dust and noise
2	Crushing	Noise and dust
3	Raw mill, coal mill	Toxic gases such as NO _x , SO _x , CO, CO ₂ , dust, noise, thermal pollution
4	Clinker production	Dust, high thermal radiation, toxic gases such as NO _x , SO _x , CO, CO ₂
5	Cement milling	Auxilliary materials, additives, dust and noise
6	Storage and packaging	Dust, high work load



7	Transport of materials and delivery of finished materials	Dust, noise, mishaps involving vehicular traffic inside the plant and high work loads
8	Fuel burning	Green house gases like CO and CO ₂
9	Power generation	Toxic gases such as NO _x , SO _x , CO, CO ₂ , vibration, fire and explosion

These hazard factors give rise to:

- Environmental hazard

in the form of i) Air pollution due to emission of NO_x, SO_x, Nitrogen during high temperature processes and green house gases such as CO and CO₂ emitted as result of fuel burning and ii) Particulate matters produced during raw material collection, preparation, packaging, storage and delivery.

- Respiratory hazards

Dusty environments present in cement plants can expose workers to various health complications. Inhalation of excess amounts of cement dust is a critical concern. Studies show that cement dust can enter into systemic circulation and reach various body organs including the heart, liver, spleen, bone, muscles and hair, which may affect their micro-structure and physiological performance.

In addition, following hazards are associated to cement production

- Physical hazard
 - a) Noise
 - b) Vibration
 - c) High thermal radiation
- Mechanical hazard

Mechanical hazard occurs in

- a) Revolving parts of machinery like shafts, spindles, Fly wheels etc.
 - b) Transmission machinery.
 - c) Conveyor belts, rollers.
- Fire hazard
 - a) Coal storage: Due to spontaneous ignition.
 - b) Coal conveying: Combustible nature of crushed coal poses a fire hazard in the conveying system.
 - c) Cement is a highly energy intensive industry. Therefore, hazards like fire in the lube oil, heavy duty electric equipments for generation, distribution, control and utilization electric power, electric cables etc. pose major fire hazard.
 - d) Other storages of combustible materials: Empty bag storage area poses potential fire hazard due to combustible nature of the materials.
 - e) The Rubber conveyors used to carry heated clinkers after cooling pose significant fire hazard unless they have fire resistant component.
 - Explosion hazard
 - a) Coal pulverization: Pulverising significantly reduces the mean particle size of coal, thereby increasing drastically the fire/explosion hazard potential.
 - b) Bag filters: Bag filters used in the cement mill are considered to pose high fire / explosion hazard due to smaller particle size of coal.
 - c) Electrostatic precipitators: Mixture of finely dispersed coal dust in air or CO in air can result in explosion hazard in the ESP.



- d) Storage and handling of explosives: Explosives used in the quarrying of lime stone and other raw materials should be handled and stored in proper manner in order to avoid undesirable detonation.
- e) Boilers used in the on-site captive power plants pose explosion hazard if not maintained in a prescribed manner.
- Hazard of COVID-19

Cement industry is highly labour intensive. Also, there is frequent entry and exit of Trucks and other vehicular traffic engaged in transport of raw materials and finished goods. The drivers and cleaners of these heavy vehicles on their way come into contact of people of unknown health conditions and hence, become vulnerable to the risk of getting infected. During their stay inside the plant they may come in contact with the workers / staffs of the plant and may contribute to the spreading of the virus. Further, owing to highly contractual nature of employment in cement industry a large proportion of the workers are supplied by the labour contractors. As a result, the set of workers engaged in loading and unloading operations, material handling, sweeping, cleaning and other incidental petty works keep on changing every day. This poses a very high risk of COVID infection inside the plant area.

HAZARD MITIGATION

Cement production is a hazardous process involving serious occupational safety and health hazards, environmental, physical, mechanical and fire & explosion hazards and unless these hazards are properly mitigated, shall impair the overall sustainability of cement production. Certain routine safety measures are definitely in place in the cement factories of Assam. But, in order to achieve a foolproof safety and health management system one should implement and maintain dynamic and vibrant safety and health culture. Following steps are recommended for a holistic hazard elimination/reduction measures in cement manufacturing.

General duties and responsibilities on the part of the management

- Every management shall ensure the health, safety and welfare of all workers while they are at work in the factory. Such duty shall include- (a) the provision and maintenance of plant and systems of work in the factory that are safe and without risk to health; (b) the arrangements in the factory for ensuring safety and absence of risks to health in connection with the use, handling, storage and transport of articles and substances; (c) the provisions of such information, instruction, training and supervision as are necessary to ensure the health and safety of all workers at work; (d) the maintenance of all places of work in the factory in a condition that is safe and without risks to health and the provision and maintenance of safe means of access to, and egress from every work places without any OHS risks; (e) the provision, or maintenance or monitoring of such working environment in the factory for the workers that is safe, without risk to health and adequate as regards to facilities and arrangements for their welfare at work.
- Health and safety policy:

Every management shall prepare, and, as often as may be appropriate, revise, a written statement of his general policy with respect to the health and safety of the workers at work and the organisation and arrangements for carrying out that policy.

- Fire and fire mock drill:

In every cement factory, all practicable measures shall be taken to prevent outbreak of fire and its spread, both internally and externally, and to provide and maintain- (a) safe means of escape for all persons in the event of a fire, and (b) the necessary equipment and facilities for extinguishing fire. All the workers must be familiar with the means of escape in case of fire and have been adequately trained in the routine to be followed in such cases.

- Keeping health record:

Every management of a cement factory shall- (a) maintain accurate and up-to-date health records of the workers who are exposed to chemical, toxic or any other harmful substances including cement dust.

- Periodical medical examination of workers:

Every management of cement factory shall provide for medical examination of every worker- (i) before such worker is assigned to a job in cement production, and (ii) while continuing in such job, and after he has ceased to work in such job, at least annually.

- Formation of safety committee:

Every management of cement factory shall set up a Safety Committee to promote cooperation between the workers and the management in maintaining proper safety and health at work.



- Hazard identification and Risk analysis:

Every management shall conduct regular Safety audit using third party Auditor for identification of hazard and associated risk assessment.

Dust Control

- Isolating the process producing the dust.
- Enclosing the process producing dust.
- Regular and water sprinkling to suppress airborne dust.
- Use of proper PPEs by the workers to protect eyes and skin and restrict inhalation of cement dust.

Vehicular movement

- Movement of vehicular traffic inside the plant premise should be regulated in accordance to the provision of Motor vehicle Act.

Work permit

- Job safety analysis and work permit are to be invariably followed while undertaking works involving any potential hazard.

Precautions for COVID-19

- Attention to be paid to the entering vehicles of all types with special attention to the heavy vehicles and their drivers and staffs. All the vehicles are to be disinfected before entering the plant premise. The drivers and staffs of the Trucks must be kept isolated during their stay inside the plant premise from the factory workers. As far as possible workers should be kept inside the plant.

CONCLUSION

Accidents do happen in the cement factories of Assam with fatalities. Also, there exists number of serious OHS hazards in terms of cement dust inhalation, skin exposure, noise, fire and explosion apart from mechanical, physical and environmental hazards. COVID-19 pandemic has added new challenge to the health management of the workers employed in cement factories. Therefore, ensuring healthy and safe working conditions for employees and workers is a fundamental key to corporate social responsibility, and is one of the most important issues for the cement industry. In view of the above, a vibrant, accountable and responsive safety culture needs to be introduced in the cement factories of Assam in excess of the normal safety gadgets. Elevation of the safety and health management system of the cement factories Assam to the height of a culture and not merely a routine to be followed is a need of the hour in order to achieve sustainability in cement production in Assam. Most significantly, such safety culture shall boost overall productivity of the cement production in Assam as safety and productivity in modern world are considered to move hand in hand.

REFERENCES

1. Junge, 1997. Scope-14: Saharan Dust. John Wiley & Sons, New York
2. Chandran, M. and Rajkumar, A. 2002. Morbidity and mortality among quarry and stone crusher workers of Madurai South Taluk. Nature Environment and Pollution Technology 1(2): 217-220.
3. Mishra, R.M. and Gupta, A.K. 1993. Pollution oriented occupational health problems of limestone crusher workers. Environ. Ecol., 2(3): 634-637.
4. Gue'ne'I, P., Hojberj, G. and Lynge, E. 1989. Cancer incidence among Danish stone workers. Scand. J. Work Environ. Health, 15: 265-270.
5. Singh, S., 2010. Occupational health hazards in Cement plant workers and their remedies. Nature environment and pollution technology, 9(2): 443-446.
6. Dockery, D.W and Pope, A.C. 1994. Acute respiratory effects of particulate air pollution. Annu. Rev. Public Health, 15: 107-132.
7. Factories Act, 1948.
8. Assam Factories Rules.



Framework for Skill-Based Teaching Pedagogy for Computerized Numerical Control (CNC) Machine Programmer Course

Dr Charudatta Pathak¹, Rajkumar Baghel², Sumit Dubal³, Yogendra Jain⁴, Dr Hrushikesh B Kulkarni⁵

School of Automobile Engineering¹⁻³, School of Mechatronics Engineering⁴⁻⁵, Symbiosis Skills and Professional University, Pune, Maharashtra

✉ charudatta.pathak@sspu.ac.in

ABSTRACT

Industry demands skilled employees in the domain of advanced manufacturing. As a CNC machine programmer and machinist, one should have certain skills like solid modeling, Geometric Dimensioning, and Tolerancing, knowledge of various controllers for post-processing and machining software. Traditional industrial training institutes offer CNC programmer courses; however, the candidates getting certified are not able to perform advanced-level manufacturing tasks as per the need due to the skill gap. This necessitates a need to change the teaching pedagogy so that candidates acquire skills required by the industry. To address this issue there is a need to design skill-based teaching pedagogy for CNC programmer and machinist course, keeping in mind the lacunas of conventional CNC machine programmer course. Implementation of the proposed framework reveals that defined learning outcomes are achieved along with enhancement of knowledge and skills in the candidate which is assessed through the pre and post-test and during the continuous assessment.

Keywords: Skilled based education; Skill gap; CNC machining; Teaching pedagogy; CNC programming.

INTRODUCTION

Rapid Industrialization and mass production demand automation of manufacturing operations. Computerized numerically controlled machines are developed for this purpose. CNC machine tools use software programs and controllers that provide instructions necessary to control the axis motions, spindle speeds, tool changes, etc. CNC machine tools allow multiple axes of motion simultaneously, resulting in 2D and 3D contouring ability. CNC technology also increases productivity and quality by allowing multiple parts to be produced using the same program and tooling. It offers various advantages over conventional machines like high precision, accuracy, time-saving, increase in productivity, etc.[1]

The use of CNC machine tools is increasing in the automotive industry for the manufacture of automotive components such as flywheels, wheels, gearbox cases, pistons, transmissions, and engine cylinder heads. The use of such automated machines lowers the cycle time and increases throughput for manufacturers. Thus, the rising industrial automation in India is expected to drive market growth [1].

India ranks third in implementing Manufacturing Automation [2]. The automation market size in India is expected to grow at a compound annual growth rate (CAGR) of 12% by 2023 and is expected to reach \$4.43 billion by 2023. India needs to strengthen its manufacturing sector to reach an expected GDP growth of 25% to 30% by FY 2030.

The automotive industry will account for the largest share of the overall controller market during the forecast period. CNC controllers play a key role in the development and production of quality automobile components. Fanuc, Siemens, Decal, Mitsubishi, and other companies have developed controllers for CNC machine tools. To operate and program these controllers there is a need for a highly-skilled workforce. Training to prepare a highly-skilled workforce needs systematic design of curriculum keeping skill-based education at a high priority.

Skill-based learning is about planning, implementing, and analyzing skills gained through the knowledge-based learning method. Students are motivated to think logically, analyze concepts, and apply their insights. The idea behind this innovative and most in-demand learning method is to develop learners into independent thinkers, make them industry-ready, and to prepare them for the challenges in the future.



Skill-based teaching pedagogy aims towards building the skills of the student who has already acquired knowledge through classroom lectures and encourage them to experiment and apply those concepts to strengthen the learning process. In a skill-based classroom, teachers focus on imparting education through physical activities. To help students to retain concepts, instructors plan, discuss ideas, and provide constructive feedback so that students can reflect on the skills gained in the classroom [3].

There is a mismatch between the skills that employers rely upon in their employees and the skills that job seekers possess. This mismatch makes it difficult for individuals to find jobs and for employers to find appropriately trained workers[4].

In mass production, CNC machines are used to produce high-quality components which need skilled workers to handle CNC machines. There are various agencies viz. private and government institutes which provide training programs for CNC programmers and machinists but these are found less effective as there is a lack of practical approach and desired skill set.

Various educational institutions offer a vocational course on CNC machining of duration ranges from 100 hours to 500 hours [5]. However, these courses have limited scope for learning CAD tools for the simulation, generation of CNC codes, communication skills, teamwork, and industrial safety norms. It is observed that private organizations which offer CNC programmer course charge higher fees which is not affordable to underprivileged or economically weaker sections of the society. In the traditional course, the theory is focused more with less emphasis on hands-on experience.

In the era of product customization, there is a need for skills like CAD modeling, understanding industrial drawings, handling advanced CNC machines, and writing CNC programs.

The objective of this work is to redesign the curriculum that will impart the desired skill sets along with fundamental knowledge. The main aim of the proposed framework is to impart skills to candidates to understand and interpret engineering drawings, write CNC code, simulate and execute on CNC machine and diagnose faults if any, follow safety standards, and to develop interpersonal skills.

METHODOLOGY

In the proposed methodology relevant theory aspect are taught during the demonstration session as a part of the discussion. This enables the student to understand and implement the concepts practically while doing the job. Skills component in the curriculum includes hand-on experience on measuring instruments like vernier caliper, micrometer screw gauge, edge finder, use of simulation software, handling fire and safety equipment, etc.

In the proposed, activity-based teaching approach experts have developed instructional activities for each module. **Fig. 1** shows the detailed procedure followed while developing the curriculum of the skill-based CNC Course.



Fig. 1. Steps followed in CNC programmer course



The instructional activities are expected to be followed for each module and it shall be assessed as per the checklist prepared by the instructor.

Fig. 2 shows the activities and decision making procedure to be implemented at the time of execution of the course.

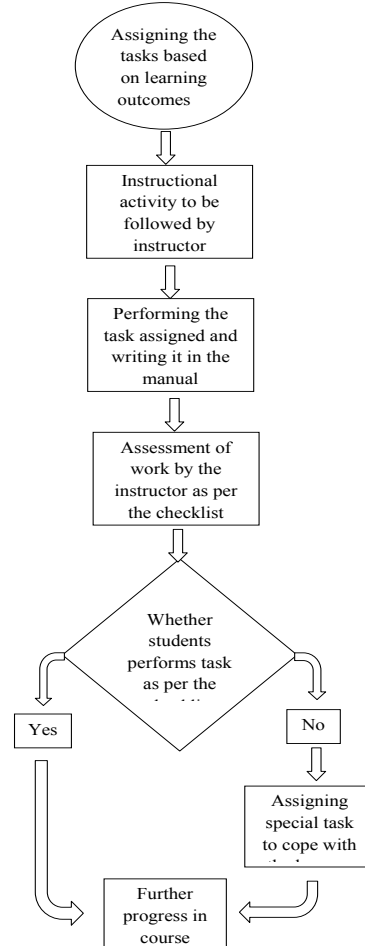


Fig. 2. Flowchart of instructional activity

During execution, the tasks shall be assigned to the students based on the learning outcomes. Students are expected to perform the tasks as per the guidelines given by the instructor. Work done by the students shall be assessed based on the checklist provided to the instructor. Based on the decision of success or failure of the student to perform the task, a special task shall be allotted to them to cope with the lacunas. To evaluate the overall performance of the student continuous assessment test, continuous assessment practical, end semester practical, and skill assessment is proposed to be carried out by industrial experts. Credits will be allotted which can be considered in further education. A certificate of completion will be provided once the student achieves the desired skill set defined in the curriculum and will get placement assistance.

CASE STUDY

In the course, structure candidates will be trained in the subjects like an engineering drawing, CAD modeling, measuring instruments, CNC machines like CNC trainer, CNC Fanuc, CNC milling trainer, CNC SINUMERIC 828D milling machine. Also soft skills like communication, behaviors, writing skills, presentation skills are included in the course.

In the machine drawing module, students shall be taught to read Industry drawing, sketching orthographic projection views, isometric view of the object, modeling of 3D objects, geometric dimensioning, and tolerances.

In the CNC programming module, students shall use various measuring instruments and also handle CNC machines primarily. Further, they will learn to write a CNC program using cut-viewer software where they can simulate the program before actual

execution. This simulation shall help them to avoid damage to the tools, work pieces, and accidents during an actual machining operation. Later on, they can handle advanced controllers like Fanuc and Sinumerik which are industry-specific and complicated to work with.

To understand the above framework a case study of a CNC program with and without a controller is explained below. Before execution on the CNC machine, the programs are simulated on the cut viewer software. Program of circular pocket milling as per FANUC controller is mentioned below,

```
N1 M03 S1500  
(STOCK/BLOCK, 100, 100, 10,0,0,10)  
(TOOL/MILL, 2,0,50,0)  
(COLOR, 255,255,255)  
N2 G90 G00 X25  
N3 X25 Y25  
N4 G01 Z-1 F50.0  
N5 G12 I2 F50.0  
N6 G01 X25 Y 25 F50  
N7 G12 I3 F50.0  
N8 G01 X25 Y 25 F50  
N9 G12 I4 F50.0  
N10 G01 X25 Y 25 F50  
N11 G12 I5 F50  
N12 G01 X25 Y 25 F50  
N13 G12 I6 F50  
N14 G01 X25 Y 25 F50  
N15 G12 I7 F50  
N16 G01 X25 Y 25 F50  
N17 G12 I8 F50.0  
N18 G00 Z25  
N19 M30
```

The above program is written using ISO G and M code to create a circular pocket of a radius of 12 mm. **Fig. 3** represents a pocket created on a square plate using cut-viewer simulation software.

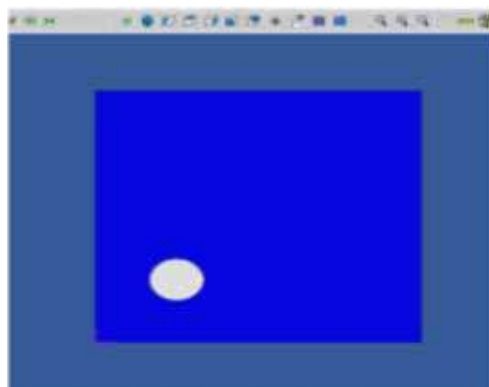


Fig. 3. Output window of cut-viewer software

Fig. 4 shows the snapshot of the Sinumerik 828D controller. Further, there is a need to select circular pocket command where some basic information about an operation like speed, feed, depth of cut, tool size, tool offset, circle radius, etc. need to enter first, and then automatic code is generated in the form of canned cycle and operation is performed.



Fig. 4. Output window of Siemens Sinumerik 828D controller

After comparing the number of lines of code generated by ISO G and M codes and Sinumeric 828D controller, it is found that the same task can be performed in different controllers using different methods. Each one is specific to its type and complexity for variation of the generated code

The course has enhanced the workability and practical knowledge of the candidates which makes them Industry ready. Working on advanced controllers like Fanuc, Sinumerik, and simulation software like cut viewer improve their confidence to work and adapt to other controllers also.

From the above case study, it is observed that without simulation software students need to write lengthy code and takes more time but with the help of simulation software code reduced to few lines, time is saved and the risk of accident and failure is minimized.

CONCLUSION

The Framework of skill-based education developed is found to be successful for enhancing technical and soft skills among the candidates.

After successful implementation of skill-based learning approach following objectives were achieved

- The course objective and the outcome maps with the NSQF level.
- Outcomes-based on instructional activities were well defined due to which implementation of the course was done efficiently and successfully.
- Learning through instructional activities made students involved in more than passive listening and greater emphasis placed on developing student skills.
- The communication and programming skills of the students were improved. This also enabled the students to understand customer's requirements and communicate effective solutions to them.

During training, students shall visit industry which will improve their knowledge and employability. Also, candidates after this course will easily adapt to the CNC machine and controller available in the Industry.

REFERENCES

1. HinsuJindal1, Rakesh kumar2, Kartik D. Kothari, "Modern Techniques in CNC Machines -A Review", International Journal of Advance Engineering and Research Development, Vol. 1, Issue 6, June 2014
2. <https://www.maiervidorno.com/industry-expertise/industrial-automation/#:~:text=Indian%20Industrial%20Automation%20Market%20is,the%20GDP%20by%20FY%202030.>
3. Skill-Based Learning and Teaching: How It Benefits the Newgen Learner <<http://www.reva.edu.in>>.
4. Anindita Sengupta, "Mismatch between Skills and Jobs in Indian Labour Market During the Post-Reform Era: Estimates with Unit Level Data", Conference on Experiences and Challenges in Measuring Income, Inequality, and Poverty in South Asia, Hooghly Women's College The University of Burdwan, November 23-25, 2017.
5. Competency-based curriculum for the module of operator CNC Milling (production & manufacturing), under Modular Employable Skills (MES) government of India ministry of skill development and entrepreneurship.



The Future of Industrial Training and Simulation

Dr Sathyanarayana A

Former Director, Air Liquide, Paris, France

✉ satya.appia@gmail.com

ABSTRACT

This paper highlights the key enablers of digital transformation, which is transforming the future of industrial training and simulation. Digital transformation of all sectors of manufacturing and process industry using Virtual / Augmented reality (AR/VR), IoT (Internet of Things) & AI (Artificial Intelligence) and Digital Twins (DT), which will transform the digital training platform to train the new generation of engineers.

Keywords: AR & VR; IoT; DT; Skill development; Training.

INTRODUCTION

The industrial training provided by the various industries for young engineers or technicians might change drastically in the future with the advent of key enablers such as:

- Digital Transformation: VR & AR Simulation
- IoT & AI
- Digital Twins and Digital Thread.

The Industry Training centers, skill development centers and technical education centers should focus on developing digital training platform which will train engineers and technicians to develop the skills and expertise required for on-job requirements.

In this paper we will look into some of the examples of Digital Training platform used in the industry and the way forward. We will highlight, especially the development in the area of Virtual and Augmented Reality, Modelling and Simulation, and Digital Twins in Digital Industrial Training.

DIGITAL TRAINING PLATFORM

The digital training platform utilizes the cutting edge process control technologies used in advanced manufacturing plants to train technicians, fresh engineers and existing workers on instruments used to monitor and control industrial processes. This will improve knowledge and skill transfer by enabling hands-on training with a real process. The key benefits are:

- Safe Environment with no damage to equipment or property and no personal injury or to the health of trainee.
- Portable, scalable and customizable training platform. Virtual simulator using Virtual or Augmented reality simulating a real environment.
- VR (Virtual reality) is a technology that combines software and hardware to setup an immersive interactive environment, simulating a real-world scenario in virtual mode.
- The simulation projects a future scenario and measures the consequences, it also allows the trainee in the decision making process by simulating several correction scenarios.
- Upskill existing staff and a new generation engineers in the latest digital technologies.

We will review two important cases in order to understand the importance of Digital Training Platform:

Virtual Reality Welding Simulator [1][2]

VR Welding simulator facilitates computer based training to novice welders to develop the required welding skills and exposure before taking on the on-job real welding process. The VR Welding simulator benefits the novice welders to develop the required

sensor motor skills, which will enable them to use welding equipment and learn basic skills effectively and safely. Another important aspect of VR Welding simulator is it acts as an evaluation tool because every simulation exercise carried out by the novice welder is recorded and reproduced for quantitative assessment. See **Fig. 1**.



Fig. 1. A VRITEX 360 Welding simulator

Pump Health Monitoring System [3]

Pumps are critical equipment in many manufacturing and process facilities and they require continuous monitoring and maintenance to ensure high availability. Any major intervention will result in shutdown of the plant, affecting the profitability of the company. It is estimated that pump accounts for 7% of total maintenance cost, if they are not monitored online. And this cost can be significantly reduced if there is an online condition monitoring of the pump.

There are several process simulation softwares available in the market, which can be used to model pump failures and train young engineers on the design aspect of pump selection, piping routing, discharge capacity and operating constraints. It can also be used to analyse possible causes of failure such as Impeller damage, seal failure, bearing wear, fire etc. It can also determine reduced efficiency over time by simulation of a degraded pump performance. Some of the monitoring system can be connected to a pump system operating in a remote location to study seal fluid level/pressure, pump discharge pressure, cavitation and vibration monitoring in order to find the root cause of pump failure. See **Fig 2**.

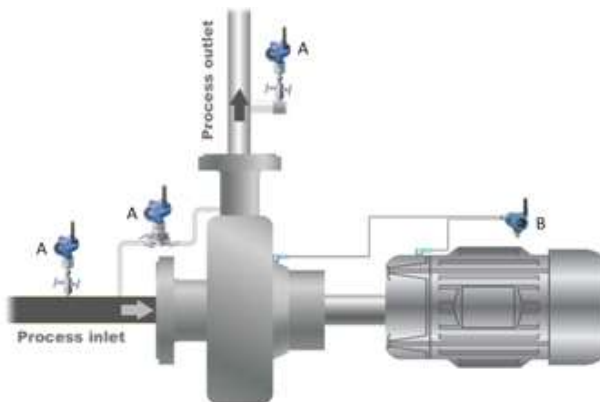


Fig. 2. Shows two accelerometers measuring vibration and peak impact on the pump and shaft.



DIGITAL TWINS (DT) [4] [5]

The concept of digital twins was first introduced by Michael Grieves in 2002, since then it has evolved with IIOT, Industrial Internet of Things.

Digital twins is a computer model that contains all the information about the system i.e. its design, manufacturing, properties, operation history, health history etc., which enables to assess the system and decision support capabilities of the system. The key benefits are:

- Decision making
- Cost reduction for testing and analysis
- Risk reduction due to monitoring and control

However, there are information and uncertainty challenges and the complication of aggregative data.

With the advent of IoT, Internet of Things, DT technology has become cost-effective to implement for large, complex and capital intensive plants. **Fig. 3** shows a Digital Twin (DT) with data flow in both directions, which imply that the digital object might also control the physical object.

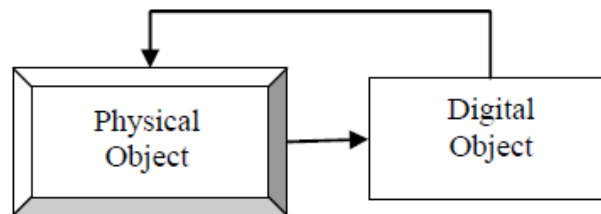


Fig 3. Digital Twin

ACKNOWLEDGMENT

I acknowledge the Institution of Engineers (India) for involving professional engineers in the area of skill development and Training.

REFERENCES

1. Byrd AP, Anderson RG, Stone R. The use of virtual welding simulators to evaluate experienced welders. *Welding journal*. 2015;94(12):389.
2. Yunus FA, Baser JA, Masran SH, Razali N, Rahim B. Virtual reality simulator developed welding technology skills. *Journal of Modern Education Review*. 2011 Oct 8;1(1):57-62.
3. 3 Innovative Ways to Improve Pump Reliability, White Paper, www.emersonprocess.com/pumps
4. Kritzinger W, Karner M, Traar G, Henjes J, Sihn W. Digital Twin in manufacturing: A categorical literature review and classification. *IFAC-PapersOnLine*. 2018 Jan 1;51(11):1016-22.
5. Madni AM, Madni CC, Lucero SD. Leveraging digital twin technology in model-based systems engineering. *Systems*. 2019 Mar;7(1):7.

Textile Engineering



Potential of Jute & Banana Blended Engineered Fabric for Technical Application

S N Chattopadhyay, N C Pan, A N Roy, Kartick K Samanta

ICAR-National Institute of Natural Fibre Engineering and Technology, Kolkata

✉ sambhu_in@yahoo.com

ABSTRACT

Jute and other lignocellulosic fibres like ramie, flax, pineapple, banana, etc are very strong and suitable for making apparel, home and technical textiles. These fibres are coarse and stiff, thus require special processing technologies to make fine and soft yarns, apposite for high value application. After apparel products, home textile occupies an important economical position in today's textile market, where natural fibres can play an imperative role due to its eco-friendliness, biodegradability, and agro-renewability. Some of the important home textiles products are bed covers, curtains, sofa covers and appliances cover, which are very sensitive to human instinct and mood. The process of pre-treatment and bleaching of jute/ banana fibres have been standardized. The fibres become finer, whiter and brighter after the chemical treatment with some loss in tensile property. Jute and banana fibres before and after bleaching were utilized for producing different blended yarns of 8 lb count with ratio of 75:25, 50:50 and 25:75; out of which the jute and banana blended yarn with ratio of 75:25 produces the maximum tensile properties. The tenacity of jute/banana blended yarn produced from the bleached fibre was always much higher than that produced from grey fibres, irrespective of blend ratios. Union fabrics have been produced using cotton yarns as warp and jute/ banana blended yarn as weft. The fabric made from jute/banana blended yarn, produced from bleached fibres, also shows better tensile properties. In order to improve the functional properties of jute /banana blended fabric to make them apposite for home textile, they were subjected to ultraviolet (UV) protection and fire retardancy treatment in an eco-friendly manner. The above fabrics were used to make bed cover, table runner, men's & women jackets etc.

Keywords: Jute; Banana; Yarn; Fabric; Colouration; Pre-treatment .

INTRODUCTION

Our country is blessed with a variety of natural fibres, some of them are commercially exploited for making different textile and non-textile items, whereas a large number of fibres are still under or non-exploited. Different lignocellulosic fibres like jute, ramie, flax, pineapple, banana, etc are very strong and suitable for making technical textiles [1-3]. These fibres are coarse and stiff, and require special processing technologies to make fine and soft yarns for making value added products [4]. Such underutilized fibres can be profitably utilized for making functional as well as home textiles. After apparel, home textiles have occupied a very important position in today's fashion market, where natural fibres can play a very important role due to its eco-friendliness. Some of the home textiles products are bed covers, curtains, sofa covers and appliances cover, which are very sensitive to human instinct and mood [1]. These products should be very contemporary and friendly to fashion designers, producers and customers. For the sustainability of these products, developments of suitable processing technologies are very important. Further-more, the process must be low energy consuming, environment friendly and pollution free [5-11]. Colouration of such products improves the aesthetic look and finishing process further imparts its functional attributes [13-14]. Look of these products can be improved by following eco-friendly wet processing technology like, bioscouring, natural dyeing, printing, etc. whereas, functional properties of these products could be improved by innovative finishing technology for soil resistance, water repellency, crease recovery and fire retardancy [11-14].

Jute is a lingo-cellulosic, biodegradable, annually renewable natural fibre. It is mainly utilised for making hessians and sackings bags for use as a packaging material since several decades, whereas banana fibres can be obtained from the unorganised sector and mainly utilised for making low value products [1,2,6,8-10]. But it has the potential for utilisation in value added technical textile items after suitable blending with other lignocellulosic fibres like jute. So, all the lignocellulosic fibres have very good opportunities to cater these new areas of home textiles. So a detailed study has been carried out at ICAR-National Institute of



Natural Fibre Engineering and Technology (NINFET), Kolkata for processing of jute and banana fibres with eco-friendly bio-catalyst, bleaching agents and colouring material for making different home textile items with improved colour yield. In this study jute and banana fibres have been characterized. The process of pre-treatment and bleaching of jute / banana fibres have been standardized. The fibres become finer, whiter and brighter after the chemical treatment with about 20% loss in tenacity. Jute and banana fibres, both grey as well as bleached, have been blended in different proportions like 75:25, 50:50 and 25:75 to produce 8 lb count yarn. Blending of jute and banana in the ratio 75:25 produces the maximum tensile properties irrespective of fibre quality i.e., bleached or grey fibres. The tenacity of jute/banana blended yarn produced from bleached fibres is much higher than that produced from grey fibres, irrespective of blend ratio. Union fabrics have been produced using cotton yarns as warp and jute/banana blended yarn as weft. The fabric made from jute/banana blended yarn produced from bleached fibres also shows better tensile properties. The bleached as well as dyed yarns were used to produce woven fabrics in handloom to develop stripe design in textile, which can be judiciously utilised for making fine table cover, bed cover, jackets, etc. as shown above. All the banana/jute/viscose fibres blended fine textile can be utilised for making home textile and life style products. In order to improve the functional properties of jute /banana blended fabric they were subjected to eco-friendly chemical treatments for improvement of UV protection and Fire retardancy. Reducing the pollution load in wet processing operations is a pressing problem for textile industry in general. Small and cottage scale textile processors in particular, as they cannot afford costly effluent treatment processes necessary to meet the waste water discharge norms [7-9, 13], the eco-friendly process agents, dyes and chemicals will not only bring down the pollution load, but will also add to the an extra value to the finished goods in such sectors [14].

MATERIALS AND METHODS

Materials

Grey jute fibre of TD3 variety in reed form and banana fibre in strand form was collected/procured and used for this study. The following chemicals of analytical grade were used in the experiment: hydrogen peroxide (30%), trisodium phosphate, sodium carbonate, acetic acid, sodium silicate, Glauber's salt and Ultravon JU (non-ionic surface active agent). Commercial cellulase enzyme, Texbio M and xylanase enzyme, Texzyme J (M/s Textan Chemicals Pvt. Ltd., Chennai) were used. The commercial finishing chemicals namely, Ecofinish 480, Ecofinish UV500 and Ecoflame CT-6 (from ECOSTAR, Tirupur, Tamilnadu) were used for functional finishing of blended textile.

Methods

Bioscouring

Raw jute fabric was treated with xylanase enzyme (Texzyme J, 2% owf), cellulase enzyme (Texbio M, 2% owf) and non-ionic surface active agent (Ultravon JU, 2 g/L) at a temperature of 50 °C for two hour, keeping the material-to-liquor ratio at 1:10 and pH 7-9. After this treatment, the temperature of the bath was raised to 90 °C and maintained at that temperature for 15 minutes after which the fabric was washed thoroughly in cold water and dried.

Bleaching

Bleaching of grey and bio-scoured jute fabrics were done in a closed vessel for 90 min at 80-85 °C, keeping the material to liquor ratio at 1:20 with hydrogen peroxide, trisodium phosphate (5 g/L), Ultravon JU (2 ml/L), sodium hydroxide (1 g/L) and sodium silicate (10 g/L). The pH of the bath was maintained at 10. After bleaching, the fabrics were washed thoroughly in cold water, neutralised with acetic acid (2 ml/L), washed again in cold water and finally dried.

Evaluation of fibre properties

Weight loss: Weight loss of the jute and banana fibres, jute/banana blended yarns and union fabric samples at the different stages of processing like bi-oscouring and bleaching were measured by gravimetric method as per IS:1383-1977.

Diameter of fibre: Evaluation of diameter of untreated jute and banana fibres were determined by using Nikon Stereo microscope (Model SMZ18).

Optical properties: The K/S value, L*, a*, b*, whiteness index on the 'HUNTER' scale, yellowness index on the 'ASTM D 1925' scale and brightness index on the 'TAPPI 452' scale of the jute and banana fibre samples were measured by the Spectrascan-5100 computerized colour matching system.

Linear Density: Linear density (i.e. fineness expressed as mass per unit length) of fibre was measured by gravimetric method.



The fibre length of 2 mm cut from different part the fibre sample was mixed and 100 of such were taken and weighed. The results were expressed in unit “Tex”. An average of three such readings was taken.

Bundle strength: The bundle tenacity of the jute and banana fibers was measure at standard condition ($65 \pm 2\%$ relative humidity and 27 ± 2 oC temperature) using NIRJAFT fibre bundle strength tester (a balance type tester) following the BIS, 1986 (f) test method.

Evaluation of yarn properties

Tensile properties: Tensile properties of yarns were evaluated as per IS: 1670-1970. For evaluation of breaking load and extension, the Instron Tensile Tester was used with 50 cm gauge length and 200 mm/min crosshead speed. The average of 60 test results was taken for each sample.

Optical properties: The K/S value, L^* , a^* , b^* , whiteness index on the ‘HUNTER’ scale, yellowness index on the ‘ASTM D 1925’ scale and brightness index on the ‘TAPPI 452’ scale of all the yarn were measured by the Spectrascan-5100 computerized colour matching system.

Evaluation of fabric properties

Grey, bioscoured and bioscoured-bleached jute/banana fabric samples were evaluated by using different standards i.e., whiteness index (HUNTER), yellowness index (ASTM D1925), brightness index (TAPPI 452), K/S value (Kubelka-Munk equation), L^* , a^* , b^* values (computer colour matching system), handle properties (IS:6490-1971) and tensile properties (ASTM D1682-1975).

RESULTS AND DISCUSSION

Jute is a lignocellulosic, biodegradable, annually renewable natural fibre. It is mainly utilised for making hessians and sackings for use as a packaging material, whereas banana fibre can be obtained from unorganised sector and mainly utilised for making low value products, but it has the potential for utilisation in value added technical textile items after suitable blending with other lignocellulosic fibres like jute. With a view towards developing eco-friendly jute / banana blended fabric with quality and high added value to cope with growing awareness of health and hygiene, the present research work has focused on pre-treatment, bleaching and blending in different proportion to produce yarns and subsequently preparation of union fabric. Jute and banana fibre samples were received from different sources and they were characterized for optical and physical properties.

Table 1. Optical properties of banana and jute fibres

Fibre	K/S value	Reflectance (%)	Whiteness Index (HUNTER)	Yellowness Index (ASTM D 1925)	Brightness Index (TAPPI 452)
Banana	1.69	19.22	53.80	44.87	23.56
Jute	2.22	15.91	50.39	52.27	19.91

It is clear from the table that banana fibres are whiter and brighter than jute fibre which is of golden colour. The fineness of both the fibres was evaluated in tex value and the diameter were also measured by micro-scope. The bundle tenacity of the fibres was also evaluated. All the values are tabulated in **Table 2**. Banana fibres are found to be coarser than jute and their bundle tenacity is similar in nature. The diameter of the fibres are shown in **Figs. 1, 2, 3**. The chemical composition of both the fibres were evaluated and tabulated in **Table 3**.

Table 2. Fineness and tenacity of banana and jute fibres

Fibre	Bundle tenac-ity (gm/tex)	Fibre fineness (tex)	Diameter (mm)
Banana	24.42	8.3	0.16-0.18
Jute	27.15	3.4	0.11

Table 3. Chemical composition of banana and jute fibres

Fibre	α -cellulose (%)	Hemicellulose (%)	Lignin (%)	Crystallinity (%)
Banana	60.70	26.12	8.7	56
Jute	61.10	18.80	13.2	67



The α -cellulose content of both the fibres is similar but lignin content is more in case of jute. All the fibre samples like bio-scoured, bio-scoured-bleached and only bleached fibres were evaluated for optical and physical properties which are tabulated in **Tables 4 and 5**.

Table 4. Optical properties of banana fibres

Sample	Whiteness Index (HUNTER)	Yellowness Index (ASTM D 1925)	Brightness Index (TAPPI 452)	K/S value	L	a	b
Control	53.80	44.87	23.56	1.69	63.22	4.43	11.35
A	58.45	41.76	28.77	1.32	69.24	3.88	17.28
B	81.32	28.95	60.38	0.60	89.33	-3.01	17.84
C	78.94	30.68	56.16	0.65	87.52	-2.83	18.54

Table 5. Physical properties of banana fibre

Sample	Bundle tenacity (gm/tex)	Fibre fineness (tex)	Diameter (mm)	Weight loss (%)
Control	24.42	8.3	0.16-0.18	-
A	20.40	6.8	0.15	6.20
B	18.30	6.0	0.14	10.04
C	19.40	6.2	0.15	14.70

Analysis of the tables revealed that wet processing of banana fibres accompanied by loss of weight with improvement of fineness, whiteness, brightness. Cumulative loss of weight of banana fibre during bio-scouring –bleaching is more than that produced by only bleaching. There is about 20% reduction of tenacity of the banana fibre after the treatment compared to control. Raw jute and banana fibres have been blended in three different proportions like 75:25, 50:50 and 25:75 and yarn of 8 jute count have been produced. Similarly bleached jute and banana fibres will be blended in different proportions and yarn will be produced. These yarns have been bioscoured and then bleached using following recipe.

(A) Bio-scouring of jute / banana blended yarns

Enzyme, Texbio M	- 2% (owf)
Enzyme, Texzyme J	- 2% (owf)
Sodium carbonate	- 0.5 g/L
Ultravon JU	- 2 g/L
Temperature	- 600C
Time	- 120 minute
pH	- 8-9
M:L ratio	- 1:10

(B) Bleaching of bio-scoured jute / banana blended yarns

Hydrogen peroxide (30%)	- 20 ml/L
Tri sodium phosphate	- 5 g/L
Sodium hydroxide	- 1 g/L
Sodium silicate	- 10 g/L
Ultravon JU	- 2 g/L
Temperature	- 80 - 850C



Time - 120 minute

pH - 10-11

M:L ratio - 1:10

Optical properties of the bleached yarns were evaluated and tabulated in **Table 6**. Similarly the physical properties were evaluated and tabulated in **Table 7**. Coding of the yarn samples were done as follows :

A- Jute / banana blended yarns in the proportion 50:50

B- Jute / banana blended yarns in the proportion 75:25

C- Jute / banana blended yarns in the proportion 25:75

Table 6. Optical properties of Jute / banana blended yarns

Sample	Whiteness Index (HUNTER)	Yellowness Index (ASTM D 1925)	Brightness Index (TAPPI 452)	L	a	b
A	71.99	33.53	45.04	81.42	-0.33	17.73
B	77.15	32.58	52.18	86.00	-1.29	18.51
C	72.74	35.35	45.75	82.41	-0.43	19.06

Table 7. Physical properties of Jute / banana blended yarns

Sample	Max. Load (N)	Max. Extension (mm)	Tenacity (cN/tex)	Strain (%)	Total Energy (mJ)	Breaking modulus (cN/tex)
A	9.97	9.08	3.80	1.49	51	261
B	16.9	9.92	6.45	1.63	84	397
C	11.5	12.1	3.96	1.99	77	201

Analysis of the **Tables 6 & 7** revealed that blending of jute and banana in the ratio 3:1 produces yarn with good tensile properties and the whiteness index of the yarn is also best in this case.

Union fabrics were produced using different jute / banana blended yarns as weft and cotton yarn as warp. Three different blended yarns were used (A) Jute / Banana:: 50:50 (B) Jute / Banana :: 75:25 (C) Jute/ Banana- 25:75. The fabrics were first bio-scoured using biocatalysts and then bleached by hot hydrogen peroxide method. The results of the optical evaluation of the samples are tabulated in **Table 8**.

Table 8. Optical properties of grey, bioscoured and bioscoured-bleached jute fabric samples

Sample	Treatment	K/S value	Whiteness Index (HUNTER)	Yellowness Index (ASTM D 1925)	Brightness Index (TAPPI 452)
A	Raw	0.93	61.33	32.24	32.68
	Bioscoured	0.88	66.59	27.88	32.82
	Bioscoured-bleached	0.21	82.43	19.20	63.06
B	Raw	0.96	60.65	32.99	31.84
	Bioscoured	-	-	-	-
	Bioscoured-bleached	0.19	82.51	16.58	63.89
C	Raw	0.73	65.52	31.45	37.42
	Bioscoured	0.78	62.92	27.43	35.39
	Bioscoured-bleached	0.21	82.66	19.43	63.90

It is found from the table-8 that the grey fabric produced from jute/ banana blended yarn using 25:75 blend ratio shows better whiteness as well as brightness. This may be due to better whiteness of the raw banana fibres. But the fabrics achieve equal



whiteness of 82 in the HUNTER scale after bioscouring followed by bleaching irrespective of the blend ratios of the yarns. Physical properties of grey and bleached fabrics were evaluated with respect to their tensile properties and handle behaviour and the results have been tabulated in **Table 9**.

Table 9. Physical properties of grey and bleached jute fabrics

Sample	Tenacity (cN/Tex)Warp Weft		Extension (mm) Warp Weft		Bending length(cm) Warp Weft		Bending modulus Warp Weft	
A _G	3.90	6.30	16.7	2.1	Warp Weft	6.19	1.05	60.0
A _b	3.26	5.40	18.6	3.48	1.26	4.13	0.41	18.52
B _G	3.92	6.43	19.6	2.5	1.60	6.16	1.21	56.58
B _b	3.21	6.24	20.0	3.7	1.16	4.00	0.52	18.40
C _G	3.76	4.86	23.0	2.0	1.60	6.26	1.12	74.75
C _b	3.61	4.39	20.0	2.7	1.33	4.78	0.46	27.15

G – Grey fabric b- bleached fabric

Analysis of the **Table 9** revealed that the tenacity of the fabric prepared from jute rich yarn is more and they also retain maximum strength after scouring and bleaching . This may be due to higher tenacity of the 25:75 (BB:BJ) blended yarn. It is also clear from the table that the fabric handle is better in case of Jute rich fabric as bending length as well as bending modulus is minimum in this case.

During this period jute and banana fibers were blended in three different proportions to produce blended yarn. Union fabrics were produced from them as follows:

Sample A : fabric using Jute/Banana (25:75) blended yarn

Sample B : fabric using Jute/Banana (50:50) blended yarn

Sample C : fabric using Jute/Banana (75:25) blended yarn

All here fabrics were bleached by conventional hot hydrogen peroxide bleaching and evaluations of optical properties of the bleached samples are tabulated in **Table 10**.

Table 10. Optical properties of bleached jute/banana blended yarns

Sample	Bleach loss (%)	K/S Value	Whiteness Index (HUNTER)	Yellowness Index (ASTM D-1925)	Brightness Index (TAPPI 45)
A	9.72	0.168	84.09	16.15	66.61
B	8.64	0.166	84.68	16.97	67.24
C	7.97	0.115	86.77	13.68	71.49

Weight loss of the fabrics during bleaching was found to be more in case of banana rich fabric whereas jute rich fabrics show more whiteness/brightness after bleaching. All these fabrics were subjected to integrated finishing using Ecofinish 480, Ecofinish UV500 and Ecoflame CT-6 by pad-dry-cure process. The optical and physical properties of the finished samples were carried out by standard testing procedure and tabulated in **Table 11** and **Table 12** respectively.

Table 11. Optical properties of different samples

Sample	K/S Value	Whiteness Index (HUNTER)	Yellowness Index (ASTM D-1925)	Brightness Index (TAPPI 45)
A	0.20	83.00	19.018	64.09
B	0.15	84.06	17.88	67.22
C	0.16	84.56	17.31	66.81

Evaluation of the results clearly indicate that integrated finishing of the samples have no detrimental effect on the optical properties of the finished fabric.

Table 12. Physical properties of different samples

Sample	Bending length (cm)		Bending modulus		Tenacity(g/tex)		Strain	
	Warp	Weft	Warp	Weft	Warp	Weft	Warp	Weft
A	3.0	136	0.56	25	2.93	4.62	25.95	4.96
B	2.5	122	0.47	23	2.93	5.27	25.72	4.06
C	2.5	97	0.49	19	3.15	4.71	25.58	3.82

Analyses of the handle property of the jute/banana blended fabrics are more drapable. This may be due to softer, finer and pliable nature of jute fibre compared to that of banana fibre. The functional proper-ties of those fabrics were evaluated by standard procedures and have been tabulated in **Table 13**. The functional properties included crease recovery, flame retardance and fire retardance properties.

Table 13. The functional properties of different fabrics

Sample	Ultra Violet Protection (UPF) rating	Limiting Oxygen Index (LOI)	Crease recovery (0) (Warp+Weft)
A	45	37	146
B	40	36	144
C	30	39	145

All the fabrics show very good fire retardance properties. Banana rich fabrics show excellent UV-protection properties but the crease recovery proper-ties are very poor in all the cases.



The scoured-bleached union fabric produced from cotton yarn in warp and jute/banana blended yarn as weft was subjected to eco-friendly dyeing using high exhaustion reactive dye (procion golden yellow HER) and natural dye extracted from manjistha by long liquor exhaustion method. The colour strength and fastness properties of the dyed fabrics were evaluated and tabulated in **Table 14**.





Value home textile products developed from banana and jute fibres.

Table 14. Optical properties of different dyed fabrics

Dye used	λ_{\max} Value	K/S	L	a	b	Wash Fastness
Reactive dye	500	12.65	56.18	6.25	74.26	3-4
Natural dye	420	1.05	67.61	14.01	15.78	3

The colour yield and wash fastness is very good in case of reactive dyeing whereas bright but light shade can be produced using natural dyes with good wash fastness properties. All these fabrics can be utilized for making home appliances, cover, curtains, upholsteries etc.

CONCLUSION

- The banana and jute fibres have been characterized. The banana fibres are found to be coarser, whiter, and brighter and contain low lignin. On the other hand jute fibre is golden yellow in colour and contains more lignin but it is finer than banana fibre.
- The process of pretreatment and bleaching of banana fibre has been standardized. The fibres become finer, whiter and brighter after the treatment with about 20% loss in tenacity.
- Jute / banana blended yarn of 8 lb could be produced from grey or bleached fibres with good tensile strength and uniformity. Blend ratio of 3:1 (jute: banana fibres) produced the best yarn. The blended yarn produced from bleached jute and bleached banana fibres are superior to that produced from grey jute and grey banana fibres.
- The blended yarn could be dyed in solid shades using eco-friendly reactive dyes. The dyed yarns were used to produce handloom fabric using jacquard design.
- Finishing of the fabrics were done using eco-friendly finishing agent to produce flame retardant as well as UV protective fabric. Integrated finishing of the samples has no detrimental effect on the optical properties of the finished fabric.



- The finished fabrics show excellent flame retardancy, UV-protection properties very much suitable for curtain and interior decoration.
- The bright colored home textile items can be produced using eco-friendly reactive and natural dyes.

ACKNOWLEDGEMENT

Authors acknowledge the Director, ICAR-NINFET and Indian Council of Agricultural Research for necessary advice and inputs.

REFERENCES

1. C Byrne, 'Technical textiles', Textiles Mag., issue 2.95, pp. 12–16, 1995.
2. S K Mukhopadhyay, 'High performance fibres', Textile Prog., 25(3/4), 1993.
3. S N Pandey, S N Chattopadhyay and N C Pan, Recent advances in resin finishing of jute and jute blended textiles, The Indian Textile Journal, CIII (10), July 1993, 30-32.
4. Wei Q.: Surface modification of textiles, Wood-head Publishing Series in Textiles No.97., ISBN 978-1-84569-419-7, UK, 2009.
5. A R Horrocks, 'Flame-retardant finishing of textiles', Rev. Prog. Coloration, 16, 62–101, 1986.
6. D S Varma, 'High performance organic fibres for industrial applications', Man-made Textiles in India, 380–386, August, 1986.
7. J Shore, Colorants and Auxiliaries, Organic Chemistry and Application Properties, Volume 1 –Colorants, The Society of Dyers and Colourists, Bradford, 1990.
8. R Jeffries, 'Clothing for work and protection', Tex-tile Asia, 1988 19(11) 72–82.
9. W C Smith, 'Protective clothing in the US', Textile Asia, 1989 20(9) 189–194.
10. P Bajaj and A K Sengupta, 'Protective clothing', Textile Prog., 1992 22(2/3/4) 1–110.
11. D B Ajgaonkar, 'Flame/Fire retardant/Thermostable clothing', Man-made Textiles India, Oct. 1994, 465–469.
12. A D R staff, 'Review of flame retardant products used in Textile wet processing', Amer. Dyestuff Repr., 1997 86(1) 15–33.
13. S N Chattopadhyay, N C Pan, A K Roy, S Saxena and A Khan, Development of natural dyed jute fabric with improved colour yield and UV protection characteristics, Journal of the Textile Institute (UK), 104(8), 2013, 808-818.
14. Bose G and Chattopadhyay S N, Ambient temperature bleaching of jute fibre – its effect on yarn properties and dyeing behaviour, IJFTR, 21 (3), 1996, 217-222.



Tensile, Impact & Dynamic Properties of Jute/E-Glass Composite by Adding Shear Thickening Fluid

Abhishek M R, Dr Suresh P M

Department of Mechanical Engineering, K S I T Research Centre, Visvesvaraya Technological University, Bengaluru

✉ abhimalasani@gmail.com

ABSTRACT

Composites are known for higher specific strength, ease of manufacturing and economical, promoting utilization of composites in many industries as structural components. Hybridization of composite drives researchers to try different combination to enhance the properties of materials and make it more efficient. In the current investigation an attempt was made to fabricate composite comprising of E – Glass/Jute as fiber with Epoxy as polymer by varying fiber fraction (Eight compositions viz. D1 – D4 & DS1 – DS4) using Hand layup technique. Mechanical properties such as Youngs Modulus, Ultimate Tensile Strength (UTS), % Elongation, Hardness, Impact Energy and Natural frequencies are evaluated for the composite developed. Also the effects of Shear Thickening Fluid (STF) composed of cornstarch in water are determined. Results indicate that Young modulus, UTS and % Elongation, Hardness, impact strength and Natural frequencies of composite decreased with increase in Jute Wt% in composite. Similar trend is observed for composite with STF, but an increment in Youngs modulus and impact strength, decrement in UTS, % Elongation. Also Hardness and Natural frequencies of composites with STF is lesser compared to composite without STF.

Keywords: E-glass; Epoxy; Hybrid composite; Jute; Natural frequency; Shear thickening fluid.

INTRODUCTION

Materials are one of the significant parameter to be considered in the manufacturing, based on which the cost of a product will be decided. The type of material used plays a vital role in the field of automotive and aerospace sector. The recent trend reveals that most of the parts which are made of conventional monolithic materials such as Steel, Aluminium etc. are being replaced by composite materials. Binding two or more materials to form newer materials of required properties are known as composite materials. Varieties of composites are available based on the nature of reinforcement and matrix material, but composites made up of fiber and resin are simple to manufacture, cost effective, lighter in weight, higher strength to weight ratio, environmental friendly and easily available in market because of which it has got higher thrust to be used in structural application. India has a greater potential to use composites made of natural fibers viz. Jute, Hemp, Sisal, banana fibers as reinforcement in composite which are bio-degradable in nature [1]–[8].

Many researchers have focused on absorption of impact forces during collision in automobiles. They adopted various sensors with artificial intelligence and machine learning methods to determine the accident in automobiles before it happen. By sensing the same STF are pushed to the projected areas to absorb impact energy [9]–[12]. By this method a significant amount of impact can be absorbed from transferring it to the body or vehicle, providing safety to the passenger.

From the above discussion, it can be concluded that composite comprising of only natural fibers as reinforcement are not fulfilling the strength requirements to be used in automotive application. On the other hand, researchers are trying for alternative methods to improve impact strength in structures.

Thus in the current investigation a combination of natural fiber viz. Jute and synthetic fiber viz. E – Glass and epoxy as polymer resin composite are developed and tested for mechanical properties. Also for the above said composite effect of addition of STF are obtained. STF is a Visco - elastic material made of cornstarch and water, which is added as fourth element in composite to improve impact strength in it [13].

MATERIALS & COMPOSITION

As discussed in the earlier section the materials selected are Jute/E – Glass and Epoxy. As a part of material procurement above said materials are obtained from Suntech fibers, Bangalore where Jute and E – Glass are having a thickness of 0.64 and 0.2 mm respectively. Mechanical properties of Jute and E – Glass are listed in **Table 1 and 2** respectively.

In this investigation composite are defined on the basis of weight fraction. The composition is composed of Epoxy 70 Wt%, Jute 5 – 20 Wt% (in step of 5 Wt%) and E – Glass 25 – 10 Wt% (in step of 5 Wt%). The detailed composition for the composition defined is listed in **Table 4**. Composites are fabricated using hand lay up technique.

Also Epoxy and hardener has been procured in the liquid form from Yuje enterprises, Bangalore. Material properties for resin are listed in the **Table 3**.

In addition to the above said composition, the effect of addition of STF was tested. STF is added to Epoxy during casting. Composition table for composite with STF are shown in **Table 5**.

Table 1. Mechanical properties of Jute

Density (g cm ⁻³)	Tensile strength (MPa)	Youngs modulus (GPa)
1.3	393	26.5

Table 2. Mechanical properties of E - Glass

Density (g cm ⁻³)	Tensile strength (MPa)	Youngs modulus (GPa)
2.55	1750	70

Table 3. Mechanical properties of Epoxy

Density (g cm ⁻³)	Tensile strength (MPa)	Youngs modulus (GPa)
1.2 -1.3	50-125	2.5-4.0

Table 4. Composition of the composite without STF

Composition	Jute Wt%	E-Glass Wt%	Epoxy Wt%
D1	5	25	70
D2	10	20	70
D3	15	15	70
D4	20	10	70

Table 5. Composition of the composite with STF

Composition	Jute Wt%	E-Glass Wt%	Epoxy Wt%
DS1	5	25	70
DS2	10	20	70
DS3	15	15	70
DS4	20	10	70

STATIC AND DYNAMIC MECHANICAL TESTING

Tension Test

One of the simple and easiest ways to assess the nature and strength of a material are to conduct tension test. In this test the materials are tailored according to the ASTM D 638 type I, mechanical properties such as Youngs modulus, UTS and ductility of the materials are determined.

Hardness Test

Composites are also tested for its hardness according to ASTM D785 [14]. According to the standards, size of the ball indenter is 6.35 mm diameter with minor and major load of 98.07 N and 980.7 N respectively for Rockwell hardness M Scale (HRM).



Charpy Impact Test

Impact is a property which requires mainly in structural application in fields like automotive and aerospace. Here Charpy impact test are conducted by pendulum type machines. The specimens are prepared according to ASTM D256.

Dynamic Mechanical Testing

Dynamic mechanical testing by using Fast Fourier Transform (FFT) analyzer is one of the methods to evaluate Mechanical properties such as Natural frequency of the materials [15]–[19]. Dynamic vibration analysis were conducted to evaluate the natural frequencies of the passenger car components [20]–[22]

RESULTS & DISCUSSION

Tension Test

Set of three specimens are prepared for each given composition to check the repeatability of the test results. **Table 6** reveals the data acquired by the tensile test. **Fig. 1** indicates the effect of variation of Jute and addition of STF.

It is evident from **Fig. 1(a)**, that small increment in values of Youngs modulus is observed between composite having with and without STF, also Youngs modulus decreases with increase in the Wt% of Jute in the composites. But **Fig. 1(b)** indicates that there is a decreasing trend in the UTS as the Wt% of Jute increases in the composite. Also UTS decreases when STF is added to the composite. This decrease in UTS is caused by poor bonding between fibers in composites.

Variation of % Elongation in the composites having with and without STF is indicated in **Fig. 1(c)**. Result indicates that % Elongation of the composite decrease as Jute Wt% in the composite increases. Addition of STF results in increase in the % Elongation of composite. This increases in the % Elongation is due to increase in Youngs modulus in the composite.

Hardness Test

From **Fig. 2**, hardness decreases with increase in the Wt% of Jute in the composite. Maximum hardness of 69 HRM was recorded for 5 Wt% of Jute in composite while least of 64 HRM for 20 Wt% for composite without STF. Hardness decreases with the addition of STF to composite from 47 HRM in 5 Wt% Jute to 42 HRM in 20 Wt% Jute. The results are tabulated in **Table 7**. It is evident from the results that the decrease in the hardness in composites having STF is due to increase in ductility (increase in % elongation).

Table 6. Results for tension test

Composite	Youngs modulus (MPa)	UTS (MPa)	% Elongation
D1	12164.0	159.4	13.0
D2	8292.6	92.9	12.1
D3	7706.0	90.0	10.5
D4	3013.0	58.3	9.4
DS1	12250.0	142.2	14.3
DS2	8951.0	92.4	12.2
DS3	7808.0	88.8	11.6
DS4	5817.6	38.4	10.5

Table 7. Hardness test results

Composition	HRM	Composition	HRM
D1	69	DS1	47
D2	67	DS2	45
D3	66	DS3	43
D4	64	DS4	42

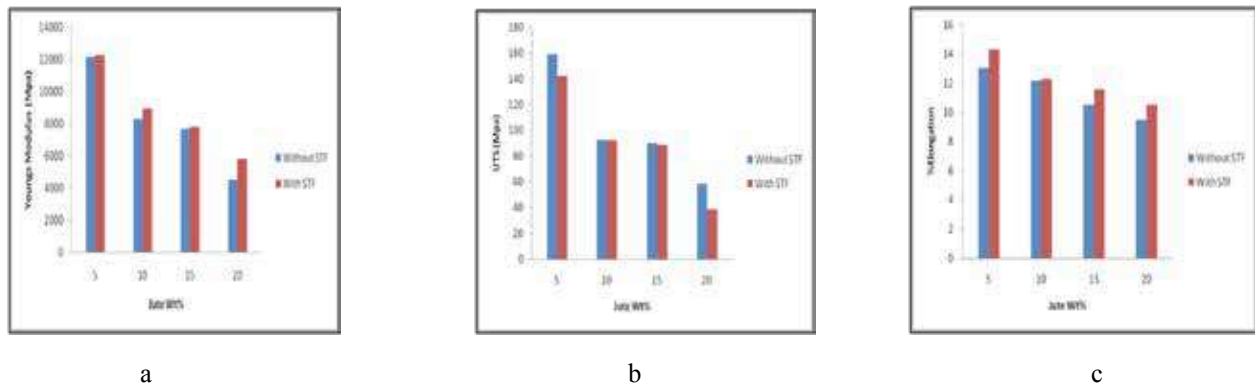


Fig. 1. Results for tension test (a) Jute Wt% vs Youngs modulus (b) Jute Wt% vs UTS (c) Jute Wt% vs % Elongation

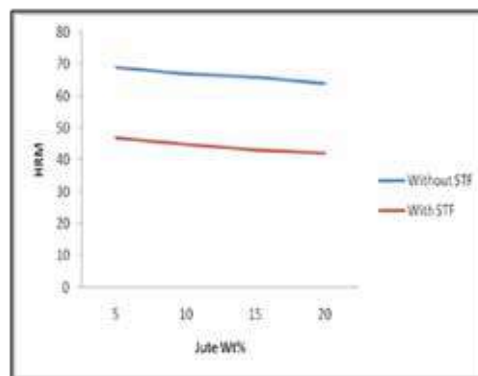


Fig. 2. Result for hardness test

Charpy Impact Test

Fig. 3 indicates impact energy of composite decreases with increase in Jute Wt% of composites. Similar trend are recorded for the composites upon adding STF, but the energy absorption capacity of composite increased. Maximum impact strength of composite for DS1 is 35 J and minimum of 20 J for D4, which indicates that addition of STF enhances the energy absorption capacity as indicated in **Table 8**.

Table 8. Impact test results

Composition	HRM	Composition	HRM
	J		J
D1	29	DS1	35
D2	25	DS2	32
D3	22	DS3	31
D4	20	DS4	26

DYNAMIC MECHANICAL TESTING

Fig. 4 shows the variation of natural frequency in the composite for mode 1, 2 and 3. It is evident from the results that higher natural frequency is obtained for 5 Wt% Jute for composite having with and without STF 105.11 Hz and 106.755 Hz respectively. Lower frequencies for 20 Wt% Jute of 40.246 Hz and 41.501 Hz for with and without STF respectively.

Natural frequencies for all other composition are tabulated in **Table 9**. It is evident that magnitude of natural frequencies decreases as Wt% of Jute increases in the composite; this is due to decreases in the stiffness of composite which are evident from Youngs modulus values as obtained from tension test.

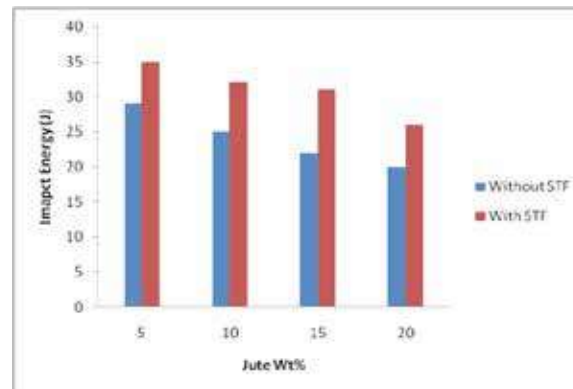


Fig. 3. Variation of impact strength vs Jute Wt%

CONCLUSION

Composites comprising E – Glass/Jute and Epoxy polymer are successfully casted by hand layup techniques for varying fiber loading condition, to evaluate the effect of Jute Wt% in composite, also composite are evaluated for the effect of addition of STF to composite. The following inferences can be stated based on the experimental results.

Youngs modulus for composites with and without STF for 5 Wt% Jute is 12250 MPa and 12164 MPa respectively, an increase of 0.7 % is achieved. Similarly for 10 Wt% Jute it is 8951 Mpa and 8292.6 Mpa respectively, an increase of 7.3 %. For 15 Wt% it is 7808 Mpa and 7706 respectively, an increase of 1.03 %. For 20 Wt% Jute it is 5817.6 Mpa and 3013 Mpa, results indicates that addition of STF to composite increases magnitude of Young modulus. But the Youngs modulus decreases as Wt% of Jute in the composite increases for the composites with and without STF.

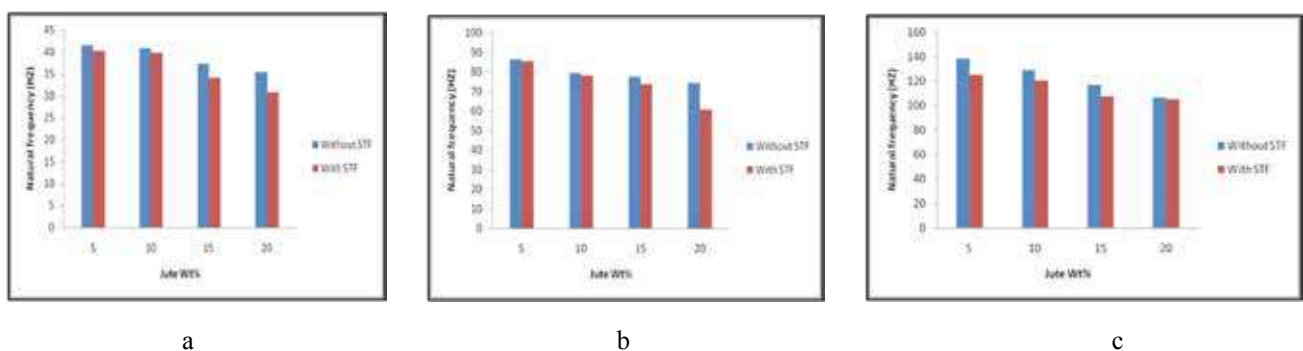


Fig. 4. Results for dynamic mechanical testing (a) mode 1 (b) mode 2 (c) mode 3

Table 9. Results for Dynamic Mechanical Test

Composite	Mode 1 (Hz)	Mode 2 (Hz)	Mode 3 (Hz)
D1	41.501	86.213	138.027
D2	40.895	79.361	128.927
D3	37.341	77.509	116.927
D4	35.428	74.442	106.755
DS1	40.246	85.512	125.110
DS2	39.827	78.210	120.553
DS3	34.141	73.563	107.875
DS4	30.899	60.752	105.110



1. UTS of the composites with STF shows decrease as compared to composite without STF. Composite having 5 Wt% Jute with and without STF is 142.2 Mpa and 159.4 Mpa respectively with an increase of 10.79%, for 10 Wt% jute, it is 92.9 Mpa and 92.4 Mpa respectively with an increase of 0.53%, for 15 Wt% Jute, it is 88.8 Mpa and 90 Mpa respectively with an increase of 1.33% and for 20 Wt% Jute it is 38.4 Mpa and 58.3 Mpa respectively with an increase of 34.13%. It indicates that with the addition of STF to composite, the UTS decreases. But the UTS of composite decreases with increase in Jute Wt% for composite with and without STF.
2. Similarly % Elongation of the composite are compared and results indicates that the addition of STF increases % Elongation indicating material is more ductile. The % Elongation of DS1 to DS4 composites were 14.32, 12.29, 11.608 and 10.532 respectively and for D1 to D4 were 13.042, 12.17, 10.5253 and 9.494 respectively. The increase in % Elongation for composites with and without STF was 8.92%, 0.97%, 9.3% and 9.8% respectively. But as the Jute Wt% in composite increases % Elongation decreases for composites with and without STF.
3. Hardness of composites decreases upon addition of STF. Hardness of composites DS1 to DS4 were 47, 45, 43 and 42 respectively and for D1 to D4 were 69, 67, 66 and 64 respectively. The decrease in hardness of composite between with and without was 31.88%, 32.83%, 34.84% and 34.37% respectively. Also the hardness of composites with and without STF decreases with increase in Jute Wt% in composite.
4. Impact strength of the composites with STF shows increment in magnitude compared to composites without STF. For composites DS1 to DS4 impact strength were 35, 32, 31 and 26 J respectively and for composite D1 to D4 were 29, 25, 22 and 20 J respectively. The increase in impact strength of composite between with and without was 17.14%, 21.87%, 29.03% and 23.07% respectively. Also the impact strength of composites with and without STF increases with increase in Jute Wt% in composite.
5. Natural frequency obtained from dynamic mechanical testing indicates that there are no significant changes due to addition of STF. Composite with STF, DS4 recorded minimum natural frequency of 30.899 Hz in Mode 1 and maximum natural frequency of 125.1107 Hz in Mode 3 for composite DS1. Composite without STF, D4 recorded minimum natural frequency of 35.428 Hz in Mode 1 and maximum natural frequency of 138.027 Hz in Mode 3 for composite D1. The natural frequency of composites with and without STF decreases with increase in Jute Wt% for all the three modes of vibration.

Comparing the results of tension, hardness, impact and dynamic mechanical tests of composites with STF reveals that enhancement in Young's modulus, % Elongation (Ductility) of material and impact strength, while suppressing its UTS, hardness and frequency.

REFERENCES

1. P. Wambua, J. Ivens, and I. Verpoest, "Natural fibres: can they replace glass in fibre reinforced plastics?," *Compos. Sci. Technol.*, vol. 63, no. 9, pp. 1259–1264, Jul. 2003, doi: 10.1016/S0266-3538(03)00096-4.
2. D. Saravana Bavan and G. Mohan Kumar, "Potential use of natural fiber composite materials in India," *J. Reinf. Plast. Compos.*, vol. 29, no. 24, pp. 3600–3613, Dec. 2010, doi: 10.1177/0731684410381151.
3. B. Nam, S. Ko, S. Kim, and D. Lee, "Weight reduction of automobile using advanced polypropylene composites," *ICCM Int. Conf. Compos. Mater.*, pp. 1–4, 2011.
4. M. M. Davoodi, S. M. Sapuan, A. Aidy, N. A. Abu Osman, A. A. Oshkour, and W. A. B. Wan Abas, "Development process of new bumper beam for passenger car: A review," *Mater. Des.*, vol. 40, pp. 304–313, 2012, doi: 10.1016/j.matdes.2012.03.060.
5. S. Dalbehera, "Study on mechanical properties of natural fiber reinforced woven jute-glass hybrid epoxy composites," *Adv. Polym. Sci. Technol.*, vol. 4, no. May, pp. 1–6, 2015, doi: 10.13140/RG.2.1.1589.6486.
6. B. D. Prasad, G. K. Reddy, and A. A. Yadav, "Mechanical Properties of Composite Material Reinforced by Jute and E-Glass Fibers," *Int. J. Emerg. Eng. Res. Technol.*, vol. 2, no. 5, pp. 135–138, 2014.
7. k sabeel ahmed A arun kumar, b palani rasan, "A car bumper application of jute-glass fiber reinforced polyester hybrid composites - a finite element approach," 2007.
8. M. Ramesh, K. Palanikumar, and K. H. Reddy, "Comparative evaluation on properties of hybrid glass fiber-sisal/jute reinforced epoxy composites," *Procedia Eng.*, vol. 51, no. NUI CONE 2012, pp. 745–750, 2013, doi: 10.1016/j.proeng.2013.01.106.



9. O. Ashtikar, A. Basangar, C. Kendurkar, M. Bahegavankar, and M. Marachakkanavar, "Smart Collision Mitigation System for Automobiles Using Shear Thickening Fluids," *SSRN Electron. J.*, vol. 2017210043, no. 201721004316, pp. 1628–1633, 2019, doi: 10.2139/ssrn.3356673.
10. X. Zhang et al., "Optimization of shear thickening fluid encapsulation technique and dynamic response of encapsulated capsules and polymeric composite," *Compos. Sci. Technol.*, vol. 170, no. April 2018, pp. 165–173, 2019, doi: 10.1016/j.compscitech.2018.11.040.
11. K. C. Chang, F. Y. Yeh, and T. W. Chen, "Feasibility study of shearing thickening fluid (STF) dampers," *ICCM Int. Conf. Compos. Mater.*, pp. 1–4, 2011.
12. M. R. Abhishek, P. M. Suresh, and H. S. Sreedhar Murthy, "Evaluation of Mechanical Properties of Jute/E-Glass Epoxy Hybrid Composites by Varying Fibre Loading with and Without Shear Thickening Fluid," *Mater. Today Proc.*, vol. 4, no. 10, pp. 10858–10862, 2017, doi: 10.1016/j.matpr.2017.08.039.
13. J. Ding, W. Li, and S. Z. Shen, "Research and Applications of Shear Thickening Fluids," *Recent Patents Mater. Sci.*, vol. 4, no. 1, pp. 43–49, Mar. 2011, doi: 10.2174/1874465611104010043.
14. R. Hardness, "ASTM D 785 Standard Test Method for Rockwell Hardness of Plastics and Electrical Insulating," no. C, pp. 8–13, 2010, doi: 10.1520/D0785-08.2.
15. A. Zak, M. Krawczul, and W. Ostachowicz, "Vibration of a Laminated Composite Plate with Closing Delamination," *J. Intell. Mater. Syst. Struct.*, vol. 12, no. August 2001, pp. 545–551, 2001, doi: 10.1106/9PFK-LXAD-9WLL-JXMG.
16. S. S. Chavan and M. M. Joshi, "Study on vibration analysis of composite plate," *Int. J. Adv. Prod. Mech. Eng.*, vol. I, no. Viii, pp. 69–76, 2015.
17. A. S. Bassiouni, R. M. Gad-Elrab, and T. H. Elmahdy, "Dynamic analysis for laminated composite beams," *Compos. Struct.*, vol. 44, no. 2–3, pp. 81–87, 1999, doi: 10.1016/S0263-8223(98)00057-9.
18. K. Senthil Kumar, I. Siva, P. Jeyaraj, J. T. Winowlin Jappes, S. C. Amico, and N. Rajini, "Synergy of fiber length and content on free vibration and damping behavior of natural fiber reinforced polyester composite beams," *Mater. Des.*, vol. 56, pp. 379–386, 2014, doi: 10.1016/j.matdes.2013.11.039.
19. I. Mishra and S. K. Sahu, "An Experimental Approach to Free Vibration Response of Woven Fiber Composite Plates under Free-Free Boundary Condition," *Int. J. Adv. Technol. Civ. Eng.*, no. 2, pp. 67–72, 2012, [Online]. Available: http://www.interscience.in/IJATCE_Vol1Iss2/paper11.pdf.
20. B. Basanth Kumar, B. T. Chandru, P. M. Suresh, and B. H. Maruthi, "Numerical and Experimental Modal Analysis of Car Door with and without Incorporating Visco-elastic Damping," *Mater. Today Proc.*, vol. 5, no. 10, pp. 22237–22244, 2018, doi: 10.1016/j.matpr.2018.06.589.
21. B. T. Chandru and P. M. Suresh, "Finite Element and Experimental Modal Analysis of Car Roof with and without damper," *Mater. Today Proc.*, vol. 4, no. 10, pp. 11237–11244, 2017, doi: 10.1016/j.matpr.2017.09.045.
22. B. T. Chandru, P. M. Suresh, J. Sathya, and B. H. Maruthi, "Modal Analysis of Car Hood with Viscoelastic Damper," *Mater. Today Proc.*, vol. 5, no. 10, pp. 22293–22302, 2018, doi: 10.1016/j.matpr.2018.06.595.



The Effect of Flow Rate on the Electrospun PEG-PVA/CNF/NCG Nano-composite Fibres

Arpita Priyadarshini Samanta^{a,b1}, Jonathan Tersur Orasugha^{b1*}, Dipankar Chattopadhyay^b
Swapan Kumar Ghosh^{*a}

Department of Jute and Fiber Technology, Institute of Jute Technology, University of Calcutta, Kolkata^a

Department of Polymer Science and Technology, University of Calcutta, Kolkata^b

*✉ ijtskg40@gmail.com; *✉ calunivjto@gmail.com

ABSTRACT

Indubitably, electrospun nanocomposites are of great interest to the material research scientist within the last decade. The utilization of bio-nanofillers is of vital importance in the field of biomaterials for advance applications. In this study, we have presented cellulose nanofibrils (CNF) nanocollagen (NCG) in PVA electrospun bionanocomposites with potentials for application in diverse niches of biomaterials. CNF was isolated from jute caddice while NCG was prepared from waste fish scales and applied as nano-reinforcement lutaraldehyde cross-linked electrospun PVA/MC/PEG bionanocomposite. The influence of the polymer solution flow-rate on the diameter of the virgin polymer blend and nanocomposites was studied. The flow-rate demonstrated a direct relationship to the final diameter of the electrospun fibres.

INTRODUCTION

Among the manufacturing processes generally adopted to fabricate nanocomposites, electrospinning is found to be a cost-effective and versatile technique involving not so severe processing conditions which also allows incorporation of various natured nanoparticles through dispersion of the nanofillers within the initiating polymer solutions [1-4].

Nano-based fibres are fabricated by several techniques including: phase separation; bicomponent extrusion [1]; Template synthesis e.g. carbon nanotubes and nanofibers [5] and/or conductive polyaniline (PANI) [6], polypyrrole (PPY) [7], drawing, melt blowing, etc. [8].

Amongst these techniques, electrospinning is a well-known approach for the electrostatic production of polymeric nanofibers [3,4]. Formhals was the first to publish patent on fabrication of artificial threads via electrospinning in 1934 [4]. Electrospinning is a smart approach for fabrication of polymeric nanofibers producing nonwoven mats having an excellent volume/area ratio [1-5]. Electrospinning adopted in this paper uses a jet of the polymer solution which is expelled from the tip of a droplet under the influence of electrostatic force of attraction [9].

Celluloses' higher crystallinity in jute fibres points to its appropriateness for the synthesis of micro or nanocellulose (MCC/NC/CNF) [11-18]. Though the major drawbacks towards the use of CNFs is its high inclination towards agglomeration as a result of the enormous amount of surface polar and hydrophilic groups.

Wide-ranging investigation has been presented with respect to the isolation of nanocellulose from diverse raw materials and their use for the preparation of polymeric nanocomposites [14-19]. The mechanical combined chemical pretreatments unto isolation have been the most utilized techniques towards obtaining NC and their application in reinforced polymeric nanocomposites [14-18].

Collagen protein is represented by a trademark space of proline-rich Gly-X-Y polypeptide having two astonishing things to see: (I) Gly is found at every 3rd buildup with the simple repeating (Gly-X-Y)_n tripeptide assemblage [20-22]; (ii) a high extent of deposits (20%) in the tripeptide successions is consistently comprised proline (X) and hydroxyproline (Y) [20-22]. The utilization of NCG as a grafted particle on the surface of CNFs towards biopharmaceutical use has been reported in literature [17].

NCs reinforced PVA composites present substantial enhancement in barrier, mechanical, and thermal properties [23]. There are reports in literature aimed at PVA application in diverse biomaterial areas, such as contact lenses, artificial organs, drug



delivery, cartilage repair, wound healing, etcetera [24,25]. PVA is biodegradable under both aerobic and anaerobic environments is prepared via hydrolysis of polyvinyl acetate as source material and is one of the most vital and significantly used synthetic polymer for medical, industrial, commercial, and nutraceutical applications [26].

More than a few approaches are known for cross-linking of PVA based compounds to fabricate 3D architectures for diverse applications in biomaterial science and technology. Crosslinking by using different chemical cross linkers like glutaraldehyde having high cross linking efficiency introduces strong bonding between the molecular segments leading to enhancement in properties like mechanical, water resistance, etc. Although natural polymers possess difficulty in electrospinning, by composite spinning nanofibres can be produced with a better compatible synthetic polymer like PVA/PEG. The parameters of the machine and polymer properties can have an impact on, i.e. the morphology and diameter of the produced nanofibers.

The goal behind this work is extraction and synthesis of CNF & nanocollagen from jute fibres and fish scales respectively following optimization of the process; characterization of the produced nanoparticles as reinforcing agent to obtain glutaraldehyde cross-linked electrospun bio-nano composites utilizing PVA/MC/PEG as matrix enhancing the property performance of the synthesized nanocomposite. However, some researchers have done work on the synthesis of microcrystalline cellulose-PVA composite using crystalline cellulose from different other resources but there is no mention on any reports regarding the nanocomposite based on CNF from jute combined with nanocollagen and PVA/PEG. Subsequently the nanocomposite fibre is manufactured using electrospinning process following an optimized process parameter and its evaluation of the properties of the synthesized. Furthermore, this work also illustrates the future scope of the application of the obtained electrospun nanocomposite in various diversified advancing biomedical fields.

MATERIALS AND METHODS

Materials

The materials utilized in this work are; CNFs were prepared as per previous work [14,15]. NCG was synthesized using waste fish-scales (WFS). Glutaraldehyde, hydrogen peroxide (H_2O_2), sodium chloride (NaCl), and sulphuric acid (H_2SO_4) were purchased from Sigma-Aldrich. WFS were collected from the market (V.I.P bazaar, Kolkata-700039), acetic acid, urea, caustic soda, and nitric acid were purchased from Merk Specialties Pvt Limited, Mumbai, India.

Preparation of CNFs and NCG

Jute caddies fibres was treated with 25% H_2SO_4 and 2% H_2O_2 solution at 80-90°C for 1 h to weaken and breaks most of the fibres down to micrometer size; filtered; washed with water to neutral, and oven-dried at 70°C to constant weigh. The microfibrers were then subjected to HNO_3 treatment at pH 4, 90°C for the elimination of lignin for 2 h; cooled to room temperature (25 °C); washed to neutral and then treated with 5% sodium chlorite at pH 4, 90 °C, for 20 min. In addition, the fibres (MCC) were washed to neutral and dried. The fibres were after wards treated with HNO_3 (49% v/v) at 90°C for 1 h and then subjected to NaOH treatment at 25°C aimed at eliminating hemicelluloses from the fibres. Lastly, the prepared CNF dispersion was then washed to neutral with water by centrifugation and freeze-drying.

For NCG synthesis, the fish scales were subjected to NaOH (2 %) treatment at 60°C for 2 h. Again, treated fish scales were then washed with H_2O to neutral and afterwards subjected to H_2O_2 (3% v/v) treatment at 70-80 °C. The material was then treated with 5% NaOH at 70°C for 1-2 h, washed to neutral, and dried to a constant weight. The dried sample was subjected to 0.5% (v/v) Acetic acid treatment for overnight, washed well with Di-water to neutral and dried. The material was then treated with 1% NaCl (wt./v) at room temperature for 3 h, washed with H_2O to neutral by centrifugation and dried and characterized accordingly.

Preparation of nanocomposite formulations

The electrospinning sample solutions preparation was carried out using an improved approach in literature [14,15]. 1% (wt./v) CNF and 1% (wt./vol) NCG suspensions was prepared with Di-water and subjected to sonication for 2 h and used for the preparation of the nanocomposite (VPB.CNF.NCG) and the virgin polymer blend (VPB). A virgin polymer formulation containing 2% (wt./vol) MC, 10% (wt./v) PVA and 5% PEG was also prepared. All samples were cross-linked with glutaraldehyde 1% (v/v). The electrospinning process was performed at 30-35 kV, 8-10 cm distance, cabin temperature of 45 °C and flow rate of 0.5-0.7 mL/h.

Characterization

Microscopy Analysis

The dried CNF, NCG dispersions (0.0005 wt.%) and the electrospun nanocomposites were analyzed using ZEISS EVO 18 scanning electron microscope (SEM).

Fourier Transform Infrared (FTIR) Spectroscopy

Fourier transform infrared spectroscopy (FTIR) was determined by direct transmittance with Perkin Elmerspectrum-2 at 32 scans with a resolution of 4 cm⁻¹ with wave number range of 4000-400 cm⁻¹.

RESULTS AND DISCUSSION

Microscopy Studies

The dimensions of nanofibrillar networked CNF (**Fig. 1a**) analyzed by SEM is ≥ 154.334 nm \times ≥ 24.156 nm (**Fig. 1ai and 1aii**). A similar networked structure for CNFs is reported by other researchers too [13-16]. CG presented a particle size of ≥ 26.7 nm (**Fig. 1b**): this kind of CG's morphology is also confirmed in literature [27]. On the other hand, it has been observed that, the diameter of the electrospun nanofibres increase with increment in the flow-rate and vice-versa as shown in **Figs. 2 & 3** as shown in **Table 1**.

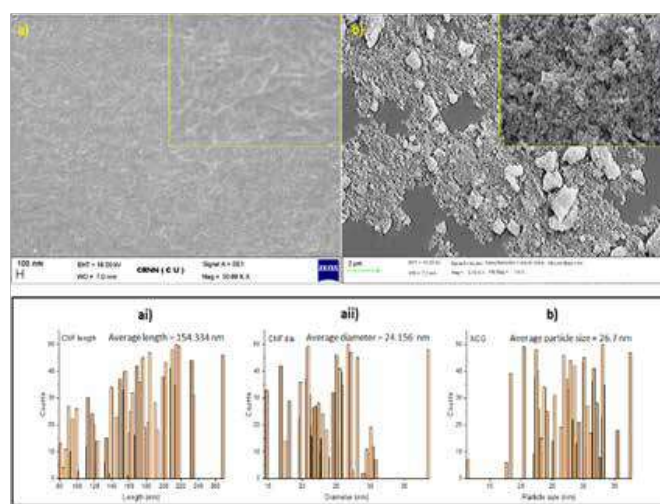


Fig. 1. a) SEM micrograph of CNF and NCF and ai, aii, and b) CNF length and diameter distribution and NCG particle distribution graphs.

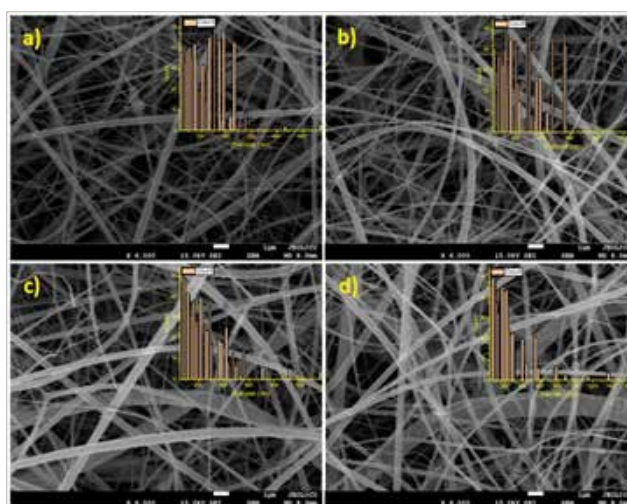


Fig. 2. SEM of the electrospun VPB fibres along with their respective diameter distribution graphs for flow-rate a) 0.5 mL, b) 0.6 mL, c) 0.7 mL, and d) 0.8 mL respectively.

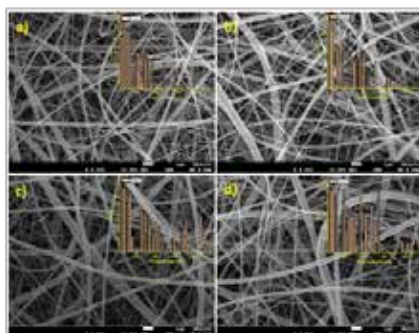


Fig. 3. SEM of electrospun VPB.CNF.NCG fibres along with their respective diameter distribution graphs for flow-rate a) 0.5 m/L, b) 0.6 m/L, c) 0.7 m/L, and d) 0.8 m/L respectively.

Table 1. Solution flow-rate, fibre diameter, and morphology of VPB, and VPB.CNF.NCG

Formulation (Composition)	Flow-rate (mL/h)	Average fibre diameter (nm)	Morphology
VPB (2% (wt./v) MC, 10% (wt./v) PVA and 5% PEG)	0.5	133.384	Networked
	0.6	232.036	networked
	0.7	303.369	Networked
	0.8	305.193	Networked
VPB.CNF.NCG (1% (wt./v) CNF and 1% (wt./v) NCG, 2% (wt./v) MC, 10% (wt./v) PVA and 5% PEG)	0.5	200.183	Networked
	0.6	312.988	Networked
	0.7	318.083	Networked
	0.8	354.812	Networked

Fourier Transform Infrared (FTIR) Spectroscopy

As represented in **Fig. 4**, jute caddice (JC) reveals peaks at 3436.21 cm⁻¹ assigned to -OH stretching, -CH stretching was observed at 2923.49 cm⁻¹, while the C-O-C stretching due to β-glucosidic linkage at 1018.25 cm⁻¹ (cellulose I peaks) [28]. C=C stretching vibrations due to aromatic lignin ring in JC at 1550 cm⁻¹ were also revealed. The peak at 1749.49 cm⁻¹ revealed ester linkage from carboxylic groups' presence in JC [15]. The absence of lignin-based peaks in MCC/CNF spectra confirm its elimination. CNF's -OH stretching peak at 3443.14 cm⁻¹ reveals the cellulose II presence [28] while -CH stretching vibration due to cellulose II in CNF is represented at 2905.35 cm⁻¹ [15]. The amide I C=O stretching along with amide A N-H stretching is revealed at 1637.37 and 3435.11 cm⁻¹ though with a shift as a result of multiple coordinate/H-bonding interface formation of the amide nitrogen [27]. The interfacial interaction between the matrices and the reinforcing fillers is confirmed by the broadening and reduction in intensity of the IR peak at around 3049-3691.97 cm⁻¹ due to multiple coordinate/H-bonds in the nanocomposites.

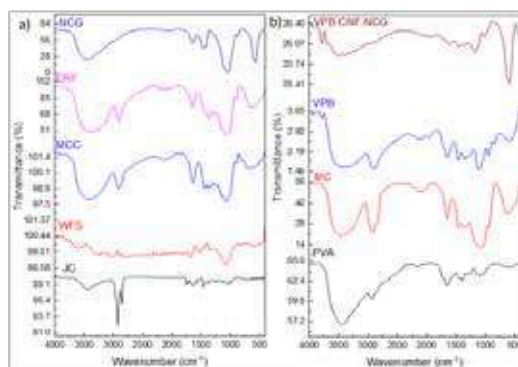


Fig. 4. FTIR spectra of JC, MCC, CNF, WFS and b) PVA, MC, electrospun VPB and VPB.CNF.NCG fibres along with their respective diameter distribution graphs



4. CONCLUSION

Jute caddies from jute industries is here used as raw material to prepare microcellulose used for CNF extraction while waste tilapia fish scales were used to prepare nanocollagen for cytocompatibility (biocompatibility) enhancement of the reinforced PVA/MC/PEG hybrid having potential for diverse biomaterial application. Here we have shown in this study that a decrease in the flow-rate of the electrospinning solution has a direct relationship with the electrospun fibre diameter which is an important factor towards the fabrication of diverse electrospun fibres where the diameter is vital factor especially in tissue scaffold engineering. We have shown here that waste jute fibres and waste fish scales can be utilized for the synthesis of novel nanomaterials for advanced application in material science. These cheap waste if utilized as proposed herewith will lead to a sustainable economy in India and the entire world.

ACKNOWLEDGMENT

The authors wish to express their gratitude to the Department of Jute and Fibre Technology, Institute of Jute Technology; Centre for Research in Nanoscience and Nanotechnology (CRNN); and the Department of Polymer Science & Technology, University of Calcutta; and the Ministry of Textiles, Govt. of India for their support.

REFERENCES

1. R.R. Hegde, A. Dahiya, M.G. Kamath, "Bicomponent Fibers," 2006. <http://www.engr.utk.edu/mse/pages/Textiles/Bicomponent%20fibers.htm>.
2. Z-M. Huang, Y.Z. Zhang, M. Kotaki, S. Ramakrishna, "A review on polymer nanofibers by electrospinning and their applications in nanocomposites", *Comp. Sci. and Tech.*, vol.63, no.15, pp. 2223-2253, 2003.
3. M. Bognitzki, W. Czado, T. Frese, A. Schaper, M. Hellwig, M. Steinhart, A. Greiner, J.H. Wendorff, "Nanostructured fibres via electrospinning", *Adv. Mat.*, vol.13, pp.70-72, 2001.
4. A. Formhals, "Process and apparatus for preparing artificial threads", US Patent 1, pp. 975 and 504, 1934.
5. H. Yang, Yan, Y. Liu, F. Zhang, R. Zhang, Y. Meng, M. Li, S. Xie, B. Tu, D. Zhao, "A Simple Melt Impregnation Method to Synthesize Ordered Mesoporous Carbon and Carbon Nanofiber Bundles with Graphitized Structure from Pitches", *The J. Phys. Chem. B*, vol.108, pp. 17320-17328, 2004.
6. X. Li, S. Tian, Y. Ping, D.H. Kim, W. Knoll, "One-step route to the fabrication of highly porous polyaniline nanofiber films by using PS-b-PVP diblock copolymers as templates", *Langmuir: the ACS J. Sur. and Coll.*, vol.21, pp. 9393-7, 2005.
7. J. Feng, J. Li, W. Lv, H. Xu, H. Yang, W. Yan, "Synthesis of polypyrrole nano-fibers with hierarchical structure and its adsorption property of Acid Red G from aqueous solution", *Synth. Met.*, vol.191, pp. 66-73, 2014.
8. M.A. Hassan, B.Y. Yeom, A. Wilkie, B. Pourdeyhimi, S.A. Khan, "Fabrication of nanofiber meltblown membranes and their filtration properties", *J. Memb. Sci.*, vol.427, pp.336-344, 2013.
9. X. Wang, B. Ding, G. Sun, M. Wang, J. Yu, "Electro-spinning/netting: A strategy for the fabrication of three-dimensional polymer nano-fiber/nets", *Prog. Mat. Sci.*, vol. 58, pp. 1173- 1243, 2013.
10. L. Ren, R. Ozisik, S.P. Kotha, "Rapid and efficient fabrication of multilevel structured silica micro-/nanofibers by centrifugal jet spinning", *J. Coll. Interf. Sci.*, vol. 425, pp. 136-142, 2014.
11. J. Cherian, J. Paulose, P. Vysakh, "Harnessing Nature's Hidden Material: Nano-Cellulose", *Mat Today: Proc.*, vol.5, pp.12609-12614, 2018.
12. J.T. Orasugh, S. Dutta, D. Das, C. Pal, A. Zaman, S. Das, K. Dutta, R. Banerjee, S.K. Ghosh, D. Chattopadhyay, "Sustained release of ketorolac tromethamine from poloxamer 407/cellulose nanofibrils graft nanocollagen based ophthalmic formulations", *Int. J. Biol. Macromol.*, vol.140, pp. 441-453, 2019.
13. J. T. Orasugh, S. Dutta, D. Das, J. Nath, C. Pal, D. Chattopadhyay, "Utilization of Cellulose Nanocrystals (CNC) Biopolymer Nanocomposites in Ophthalmic Drug Delivery System (ODDS)", *J. Nanotech. Res.*, vol. 1, pp.075-087, 2019.
14. J.T. Orasugh, N.R. Saha, D. Rana, D. Rana, G. Sarkar, M.M.R. Mollick, A.K. Chattopadhyay, B.C. Mitra, D. Mondal, S.K. Ghosh, D. Chattopadhyay, "Jute cellulose nano fibrils/hydroxypropylmethylcellulose nanocomposite: A novel material with potential for application in packaging and transdermal drug delivery system", *Ind. Crop. Prod.*, vol.112, pp.633-643,



2018.

15. J.T. Orasugh, N.R. Saha, G. Sarkar, D. Rana, R. Mishra, D. Mondal, S.K. Ghosh, D. Chattopadhyay, "Synthesis of methylcellulose/cellulose nano-crystals nanocomposites: Material properties and study of sustained release of ketorolac tromethamine", *Carbohydr. Polym.*, vol. 188, pp.168–180, 2018.
16. J.T. Orasugh, N.R. Saha, G. Sarkar, D. Rana, D. Mondal, S.K. Ghosh, D. Chattopadhyay, "A facile comparative approach towards utilization of waste cotton lint for the synthesis of nano-crystalline cellulose crystals along with acid recovery", *Int. J. Biol. Macromol.*, vol.109, pp.1246–1252, 2018.
17. J.T. Orasugh, G. Sarkar N.R. Saha, B. Das, A. Bhattacharyya, S. Das, R. Mishra, I. Roy, A. Chattoapadhyay, S.K. Ghosh, D. Chattopadhyay, "Effect of cellulose nanocrystals on the performance of drug loaded in situ gelling thermo-responsive ophthalmic formulations", *Int. J. Biol. Macromol.*, vol.124, pp.235–245, 2019.
18. J.T. Orasugh, S.K. Ghosh, D. Chattopadhyay, Edited by A.T. Nguyen, "Chapter 10: Nano-Fiber Reinforced Biocomposites", Elsevier, pp.199-233, 2020.
19. A.P. Mathew, K. Oksman, M. Sain, "Mechanical properties of biodegradable composites from poly lactic acid (PLA) and microcrystalline cellulose (MCC)", *J. Appl. Polym. Sci.*, vol.97, pp.2014–2025, 2005.
20. J. Tylingo, G. Gorczyca, S. Mania, P. Szveda, S. Milewski, "Preparation and Characterization of Porous Scaffolds from Chitosan-Collagen-Gelatin Composite", *React. Funct. Polym.*, vol.103, pp.131-140, 2016.
21. B. Brodsky, J.A.M. Ramshaw, "The collagen triple-helix structure", *Matrix Biology*, vol.15, pp.545–54, 1997.
22. J. Chang, C. Anthony Poole, "Sequestration of type VI collagen in the pericellular microenvironment of adult chondrocytes cultured in agarose" *Osteoarth. Cart.*, vol. 4, pp.275-285, 1996.
23. H. Zhang, Q. Wang, L. Li, "Dehydration of water-plasticized poly(vinyl alcohol) systems: particular behavior of isothermal mass transfer," *Polym. Int.*, vol.58 (1), pp.97–104, 2009.
24. K. Kanimozhi, S. Khaleel Basha, V. SuganthaKumari, K. Kaviyarasu, M. Maaza, "In vitro cytocompatibility of chitosan/PVA/methylcellulose – Nanocellulose nanocomposites scaffolds using L929 fibroblast cells", *Appl. Surf. Sci.*, vol.449, pp. 574–583, 2018.
25. M. Kobayashi, Y.S. Chang, M. Oka, "A two year in vivo study of polyvinyl alcohol-hydrogel (PVA-H) artificial meniscus", *Biomat.*, vol.26, pp.3243–3248, 2005.
26. N. Ben Halima, "Poly(vinyl alcohol): review of its promising applications and insights into biodegradation", *RSC Adv.*, vol.6, pp.39823–39832, 2016.
27. K. Muthumari, M. Anand, M. Maruthupandy, "Collagen Extract from Marine Finfish Scales as a Potential Mosquito Larvicide", *J. the Prot. J.*, vol. 35, pp.391–400, 2016.



Sustainability of Handlooms and Textiles for A Self Reliant India

Dr Sasmita Panda¹, Dr P L Panda²

Associate Professor & Campus Academic Coordinator, Textile Design Department, NIFT, Hyderabad¹

Ex- Founder Director, NIFT, Hyderabad²

✉ sasmita.panda@nift.ac.in

ABSTRACT

India is a country with multi cultural identity and understanding that has defined its ancient history and values. Indian handlooms and textiles just fits in with this ideology with a wide spectrum of diversified products with a more diversified technology in production, weaving culture, spectrum of region specific colors, designs, texture and other varied features with a history dating back to about 5000 years. Indeed, it has attained a heritage status with a challenging responsibility for the society not only to preserve and protect but also to sustain it for economic necessity and carry forward so as to serve the society in the domestic and global market.

This requires to undertake a well coordinated approach by the state and the corporate sector so as to preserve the languishing craft to make a mark in the over all cluttered textiles of our country with the coexistence of highly technologically advanced technology and that of out dated technology still adopted by a majority of handloom craftsmen.

The quintessential but still popular handwoven Indian saree reflects the essence of timeless style and oriental fashion, pain stakingly hand crafted draws the attention of a tradition conscious beholder but also mesmerizes with the wonderfully laid down designs and color schemes brought down from generations. But, with the onslaught of western influence in design, texture, color and fashion the handwovens have almost lost the race with its sustainability at stake.

The trend commenced with the advent of colonial rule which dumped cheap powerloom made cloth in the Indian sub-continent after which the sustainability of not only the handmade textiles but also the survival of the craft and craftsmen became the biggest concern.

It is this backdrop which compelled the father of our nation Mahatma Gandhi to give a clarion call for a “SWADESHI” movement to use locally made handwovens popularly called “KHADI” cloth along with rejection of a of host of other imported items. Perhaps, this was the first sincere movement to make the country self reliant in every aspect and prevent draining of our own resources at the cost of locally made products.

However, over a period of time, again it was observed that a host of not only textile items but also other related items are imported which are not only depriving our own manufactured items to sustain but also eating away our hard earned foreign exchange.

Hence, it is a right step adopted by the state to take up the issue of self reliant or ATMA NIRBHAR BHARAT and make the imported items in our country which is possible with the present encouragement given to the entrepreneurs to set up their own units to manufacture products as under import substitution and Make -In- India programme.

A case in point is the production of face masks and PPES (Personal Protective Equipment) which were hugely imported but now not only produced to meet the local demand but also exported to other countries. Vocal for Local. Similar steps to sustain the entire textile sector will be a welcome development for the country as a whole.

Keywords: Handlooms; Tradition; Swadeshi; AtmaNirbhar Bharat; Self reliant.

INTRODUCTION

India is a country with a multicultural identity and understanding, that has defined our ancient history and values which should be protected and preserved with not just a moral imperative but also as a economic necessity. A harmonious society preserving its art, craft and heritage of our country must be created where diversity is respected and the rights of handcraft persons be



protected without being encroaching upon their areas by flooding duplicate products. In order to revive these values and revival of this languishing handicraft a series of step need to be taken to preserve this heritage.

The enormous diversity in textiles in general and handlooms in particular with stories deeply ingrained in every piece of handcrafted textiles either design, motifs or a glimpse of traditional technology brought down from generations reflecting the grandeur of this 5000 year craft of handwoven textiles should be given priority.

However, with the passage of time and with western influence the society is gradually getting inclined to the Western influenced fashion world thereby loosing the touch with this ancient culture.

Hence, the gist of this background is that the world is changing in almost every sphere and textiles and handlooms are no different. And in order to arrest the declining trend of handlooms and handicraft sector and to sustain it should change and repeatedly change accordingly to time and trend without diluting its traditional ethos and values.

During the colonial British rule the hand weaving trade suffered its worst because of the dumping of cheap mill made textiles. These textiles mills were put up in U.K mostly in Manchester, Lancashire and other areas keeping in pace with industrial revolution of Europe. In order to prevent this, Mahatma Gandhi started his Swadeshi movement of “Khadi” cloth being hand spun and hand woven purely with manual labor and the locally available skills. This was the magnificent foundation for a self reliant India i.e AtmaNirbhar Bharat presently encouraged by the Central Government.

After Independence, our country had to take up the production of cloth in order to cater to the needs of the growing population and also to restrict the flow of our natural wealth to other countries for importing clothes from other countries. This is the time when textile industry was encouraged to set up our own textile mills in different parts of our country . The first mechanized cotton cloth textile mill was set up in 1854 but it took several years for the industry to grow and gradually a large number of textile ,mills were set up in Bombay(now Mumbai) Ahmedabad, Delhi, Kolkata, Madras(now Chennai) , Coimbatore and other potential areas. Concurrently, several programmes were launched to promote handloom industry of our country.

An observation made in the Textile Ministry’s note on the Indian Textile Industry states that it plays a major role in the economy of India contributing towards

- Generating employment for about 38 million people
- Accounting for about 4% of gross domestic product (GDP)
- Accounting for 14% of industrial products
- Accounting for 9% of excise collections
- Accounting for 18% of employment in the industrial sector
- Accounting for 16% of country’s total export earnings

The report estimates that one of every six households in the country depends on this sector directly or indirectly.

A glimpse of the Indian Handloom Industry

Indian handloom industry is antique, diverse and region specific. It is well know that the hand crafted and hand woven textiles were some of the Major attractions for earlier traders who sailed to India in the 16th century from Portugal, Holland, Britain and France. Very fine hand woven and hand painted textiles, embroidered with attractive eastern motifs, designs and colors were traded. In the eastern and southern part, Kalamkari fabrics, a typical handwoven cloth with hand painted using natural and vegetable colors, along with super fine cotton textiles were highly appreciated and procured by the traders and bartered for other western commodities. The famous “Pashmina” shawl of Kashmir also found to have attracted the western buyers for its high craftsmanship.

Although the handloom industry suffered during the colonial rule, its revival started after the country became independent in 1947. Several initiatives were taken by the Governments at the state and central level not only for its revival but also to bring its past glory and glamour and to preserve culture and tradition of our country.

A brief of the last handloom census 2009-2010 is given in **Table 1**.

**Table 1.** A brief of handloom census 2009-2010¹

Sl.no	Number of looms	23.77 lakh
1		20.66 lakh looms-Rural areas
		3.11 lakh looms-Urban areas
2	Number of looms in NER	15.5 lakh (65% of total looms)
3	Number of persons engaged in weaving and allied activities.	43.31 lakh
		36.33 lakh workers- rural areas
		6.98 lakh workers- urban areas
4	Number of adult weavers and allied workers	38.47 lakh
5	Man days worked per weaver per annum	234 days

¹Development Commissioner (Handlooms) GOI, 3rd Handloom census 2009-10

Source: GOI, MOT, DCH Report, Dated 30th December 2015

The report states out of the 38.47 lakhs number of adult weaver and allied workers in the country as stated in the table 77% are women and 23% male weavers, 10% of the weavers are from Scheduled Caste (SC), 18% of the weavers are from Scheduled Tribes (ST), 45% are from other backward classes (OBC) and 27% are from other castes. However, as per the report, there has been a very disturbing trend in the overall weaving population. There is a reduction of people engaged in handloom weaving by 22.19% over a period of thirteen years. The decline is indicated in Table no.2 given below and the reduction is 33.87% over 1995-96

Table 2. Persons engaged in handloom and allied activities²

Sl.no	Census survey report	Persons engaged in weaving and allied activities as per the census Report(in lakhs)
1	Year 1995-96	65.50
2	Year 2009-10	43.31
	Reduction in engagement	22.19
	Reduction over 1995-96	33.87%

²DCH, GOI, MOT, Report dated 10th December, 2015

Source: Development Commissioner (Handlooms), GOI

In order to find out the real position of handlooms in the field level, a self financed professionally conducted survey was undertaken in a reputed handloom cluster in Nuapatna and Maniabandha area of Cuttack district in Odisha. The survey obtained valuable data on actual position of handloom artisans, made an analysis with documented data of four handloom weavers cooperative societies of Nuapatna.

CASE STUDY

A Brief analysis of one of the societies namely Nuapatna No.2 Weavers Cooperative Society LTD, Nuapatna, District Cuttack, Odisha

- Name of the society: Nuapatna No.2 weavers' cooperative society Ltd.
- Date of registration: No.61/CU, Date: 02/06/1954

Table 3. A brief analysis of the society no 2

Sl. no.	Particulars	Years 2012-13	2013-14	2014-15
1	No. of members enrolled	405	405	405
2	No. of looms	295	295	295
3	No. of working looms	100	100	118



4	Value of production per year in rupees	Rs.45,67,000	Rs.51,50,000	Rs.81,37,000
5	Value of sales per year in rupees	Rs.43,35,000	Rs.57,75,000	Rs.84,50,000
6	Average value of production per loom per year	Rs.45,670	Rs.51,500	Rs.68,957
7	Average value of production per month per loom/weaver (sl. no 6/12)	Rs.3805	Rs.4291	Rs.5746
8*	Average earning of a weaver per month (sl.no7/2)	Rs.1902	Rs.2145	Rs.2873
9**	Average earning of a weaver per day (sl. no 8/25)	Rs.76	Rs.85	Rs.114

Source: the concerned society during the survey conducted in Dec-2015

*Assumption: 50% of the production value goes towards the wage of the weaver.

**Average working of 25 days in a month

A brief analysis of Nuapatna No.2 Weavers Cooperative Society LTD, Nuapatna

As per the statement and information supplied by the society, it was registered on Dt.02/06/1954 vide no.61/CU which is one of the oldest societies of Nuapatna (62 years old as on 02/06/2016).

However, the facts are that:

- The society has 405 No. of members enrolled
- No. of looms 295
- No. of working looms 100 in the year 2012-13, 100 in the year 2013-14 and 118 in the year 2014-15.

Further, when there are 405 members enrolled, and no. of looms stated as 295, why only 100 looms in the year 2012-13, 100 in the year 2013-14 and 118 in the year 2014-15 were working . This is almost 50%of the members enrolled and about 25% of looms working.

The capacity utilization is less than 25% and about 75% of the enrolled weavers are deprived of their livelihood and benefit from the society.

Average production marginally increased

As per the **Table 3** the value of production was about Rs.45.67lakhs in 2012-13, Rs.51.50lakhs in 2013-14 and Rs.81.37lakhs in 2014-15. Even though the number working looms in the society are about 25% of the enrolled members and about 33% of the number of looms registered, the average production increased from Rs.45.67 lakhs in 2012-13 to Rs.81.37 lakhs in 2014.

The average value of production per month per weaver works out to be Rs.3805 in 2012-13, Rs.4291 in 2013-14, and Rs.5746 in 2014-15. Assuming that the wages of a weaver is about 50% of the production cost (in Nuapatna area as told by some of the expert weavers) the average earning of a weaver per month works out as given below.

Table 4. Average daily earning of the weaver member Nuapatna No.2 Weavers Cooperative Society Ltd

Sl.no	Year	Average earning per weaver per month in rupees	Average earning per weaver per day in rupees
1	2012-13	Rs.1902	Rs.76
2	2013-14	Rs.2145	Rs.85
3	2014-15	Rs.2873	Rs.114

Source: Compiled report by the society

While in one of the oldest societies, the very skilled traditional hand weaving occupation gets on an average of only Rs.76 per day in 2012-13, Rs.85 in 2013-14 and Rs.114 per day in 2014-15, which is a cause of grave concern and is very detrimental for sustaining the hand weaving culture and tradition for long. These wages per day also includes the labor and skill put up by the entire family of the weaver as women, children even the senior citizens of the family are engaged in the preparation and other allied activities of the hand weaving trade.

Apart from this, very often efforts are put up by the entire family for more than eight hours per day. "Cest La Vie- This is life"



The main cause of concern is the very meager amount of earning for the weavers which may lead to exodus of traditional weavers to other better paying areas at the cost of loss to the culture and tradition of hand weaving profession for which sustainability of handlooms is at stake.

CONCLUSION

1. Handloom industry dates back to ancient times and encompassed several stages of development before coming to its present status
2. But, this development is found to be very inadequate in sustaining the craft longer. The massive declining trend of more than 30% in this sector speaks volumes of its present status and its sustainability in this present approach appears to be next to impossible.
3. The main reason for its down sliding appears to be that the craft is no longer able to sustain not only with the severe competition from the mechanized sector by flooding cheap imitation products but also because of very low earning by craft persons inspite of the entire family getting involved in the trade.
4. As per the professional survey conducted in 2015-16 at a handloom predominated area of Nuapatna and Maniabandha in Cuttack district of Odisha, the average monthly earning of a handloom weavers family is around 3500 (Rupees three thousand and five hundred only) which does not compare well even with the daily earning of a non-skilled daily wage earner. The daily income works out to a maximum of Rs.117 per day or even less.
5. It is, therefore imperative to focus solely on this aspect for sustaining the craft.
6. In order to sustain and develop the craft, it is therefore essential to view handlooms in a very different perspective. Instead of a holistic approach clubbing the entire textile industry with handlooms, specific region wise schemes may be made for overall improvement in the present status. Entrepreneurship in handlooms may be encouraged under Make-in-India.
7. While making region specific schemes technology development, design intervention, introduction of digital systems, value addition of products, strengthening of research and development, extensive use of traditional surface design techniques, timely supply of inputs and finance are some of the important aspects to be taken up.
8. Export market to be extensively tapped, production to be undertaken as required and timely release of export incentives are some of the other developmental work to be undertaken
9. Above all, the steps taken should be aimed at contemporising the products so as to be acceptable to the growing western world and the younger generation without dialuting the traditional essence of the products.
10. Lastly, handwovens since time immemorial have been used in various platforms including socio-cultural celebrations uniting all in enjoyment and engagement catering to the needs of all through multiple narratives. In handlooms one can see art, history, craft, craftsmanship and above all brilliance in re-engineering the woven textiles with wonderful array of exotic colors which is a source of eternal aesthetic enjoyment and intellectual recreation. It is a part of our cultural heritage which is considered as a languishing craft.

Hence, sustaining of handlooms should be taken up in all the earnestness not only for providing livelihood to millions but also to keep alive the cultural, tradition and heritage of our country and to be an active partner for building a self reliant ATMA NIRBHAR INDIA “VOCAL FOR LOCAL”.

REFERENCES

Books, Newspapers, Journals, Periodicals

1. Chambers, R & Conway G.(1992), “Sustainable rural livelihoods: Practical concepts for the 21st century”, Brighton: Institute of Development Studies, University of Sussex, IDS discussion paper; no. 296.
2. Chellappan, K(1988), “Handloom in retrospect and prospect” Co-operative perspective Co-operation, Vol.80, No.4.
3. Collins M, (2015), 'The Pros and Cons of Globalization', Forbes, accessed August 9, 2015, <http://www.forbes.com/sites/mikecollins/2015/05/06/the-pros-and-cons-of-globalization>.
4. Dantawala, M, N(1990), “Helping Hand to Handlooms”, The Tamil Nadu Journal of cooperation, Vol.82, No.3.



5. Das, N.C and Mahapatro(1986), “Development of Handloom Industry”, Deep and Deep.
6. Ghosh.S.K. and Aktar. S (2005), “Handloom Industry on the way of Extinction: An Empirical study over the Pre-Dominant Factors”, Brac University Journal, II(2):1-12.
7. Joshi, Thakur (1999), Shanti, “Women and Development: The changing scenario” Mittal Publications, New Delhi, Lok Sabha Secretariat (1989), Factual Study on ‘National Textile Policy’, Third Edition, New Delhi.
8. Misra, Sanjiv (1993), “India’s Textile Sector: A Policy Analysis”, New Delhi: Sage Publications.
9. Rajendra Nair, IAS(2002) “Handloom Exports Beyond”, Ministry of Textiles, New Delhi

Reports

- Annual Report of Ministry of Textiles, Government of India, 2011-2012
- Annual Report of Ministry of Textiles, Government of India 2012-2013
- Annual Report of Ministry of Textiles, Government of India 2013-2014
- Annual Report of Ministry of Textiles, Government of India 2014-2015
- Census Report of India(provisional), 2011
- Economic Survey of India, 2011-2012



Development of Portable Water Tank for Retting of Jute Ribbons and Root Cuttings

A K Thakur*, V B Shambhu, A Singha

ICAR-National Institute of Natural Fibre Engineering and Technology, Kolkata

*✉ drakthakur65@gmail.com

ABSTRACT

In Jute retting process, the pectinous materials are broken down into simple compounds and thus fibres are liberated from bark. The conventional retting process is dependent on many natural factors and is also a potential reason of environmental pollution. Availability of high grade good quality fibre is limited due to scarcity of high volume of free flowing water and improper retting technologies. Thus conventional retting process in ditches and ponds leads to shorter fibre length, dull colour and rough surface with increased proportion of cuttings and faults. Retting of whole plant in inadequate poor quality water yields more barky jute which is of no use in the mill. The jute mills normally discard 10-12 inches of barky jute (root cuttings) during the mechanical processing for yarn making. Ribbon retting releases less than one-third of organic matter as released by whole plant retting into the retting water and therefore ribbon retting has a major environmental and social advantage. Considering the above facts and gaps in the area of retting technology, it is visualized that the retting process of jute needs to be mechanized or semi-mechanized by developing a portable water tank with water circulation for artificial retting of jute ribbons and barky jute. Tank-retting of jute ribbons suggested that it is working satisfactorily and retted the jute-ribbons in 7-8 days without addition of any bacterial inoculums or other food supplement for bacteria.

Keywords: Jute ribbons; Retting; Artificial tank; Fibre quality.

Jute retting usually involves two distinct phases that is physical phase and biochemical phase (Paul and Bhattacharyya, 1978). The physical phase begins when the harvested plants are placed in water. The tissues absorb water and swell, ultimately split open to release soluble components into the water. In the biochemical phase, the released substances such as carbohydrates, nitrogenous compounds and salts of different kinds facilitate growth and multiplication of the microbes in the retting water prior to their entry into the reeds (Yadav et al., 2009). Retting microbes consume the non-fibrous cementing materials mainly pectin and hemicelluloses. The efficiency of retting depends on various factors such as age of the plant, quality of water including pH and temperature (Bera et al., 2009). Mature plants of above 110 days accumulate more of lignin and are hence difficult for decomposition (Banik et al., 2008). Soft and slow moving water having a pH of 6.0 to 8.0 is convenient for retting (Broker, 2007). The optimum temperature for jute retting is around 34-36°C at which the process is completed in the minimum time due to the accelerated activity of the retting micro-flora. Microbial action in retting water is highest at a depth of 15 cm from the surface of water and retting is quicker and better at this depth.

Shortage of water due to erratic and untimely rain and scarcity of river or canal water, farmers are compelled to let their jute plants to decompose in local ditches, road side muddy water bodies, canals and ponds which are generally meant for community use. The harvested jute out of traditional retting are of low quality as there is virtually no control over the water quality and temperature (Guha, 1999). This apart, results in polluting the stagnant water which subsequently becomes breeding ground of mosquitoes and thus pollutes the local environment (Mitra et al., 2006). Traditional retting also involves manual labour inside the polluted water causing irritation to skin and health hazards. Sometimes labours decline to process them owing to these reasons or they may charge a higher wage. Further, on account of poor quality jute out of the traditional retting, it fetches a lesser price and limits its use for making jute diversified products.

Thus, the conventional retting process is not only dependent on many natural factors but also is a potential reason of environmental pollution, depending on water availability and likely to result in inferior quality of jute fibre. Availability of high grade good quality fibre is limited due to scarcity of high volume of free flowing sweet water, improper retting technologies and post-harvest management that leads to shorter length, dull colour and rough surface with increased proportion of cuttings and faults (Azad et al., 2002).

Rostom Ali et al., (2015) provided information about the present status of jute retting process and identified problems on different jute retting process at the water scarce area in Bangladesh. Due to the shortage of water in harvesting period, farmers use muddy water and small canal with insufficient water for traditional retting of green jute. Several problems like environment pollution, fish cultivation, bad quality fibre, and time consuming etc. are appeared in traditional jute retting process. Therefore the traditional retting process of jute is not feasible in the water scarcity area. The appropriate technology like as ribbon retting with artificial polythene tank is needed to extend in the water scarce areas.

JUTE PLANT RETTING

The procedure to separate or extract the fibers from non-fibrous tissues and woody stem through dissolution and decomposition of pectin, gums and other mucilaginous substances is called retting (Gupta et al., 1996; Majumdar and Day, 1977). Retting of Jute is one of the important post-harvest operations which largely determine the quality of fiber. In retting process, the pectineous materials are broken down into simple compounds and thus the fibers are liberated. Fiber quality is dependent on retting in different natural conditions and duration of retting. Usually, the bottom portion of the jute plant is thick and tough which takes an extended time for retting than the middle and upper portion of the plant. Owing to high maturity index, variety and improper retting the bottom portion of un-retted bark are cut down in the mills and are known as cuttings. Apart from barky jute, some jute fibers are naturally spiky, coarse, harsh and less pliable and these fibers are known as low-grade jute and have less utility than normal jute fibers; such fibers accounts for 30-40% of the total fibers which are not suitable for spinning (Ahmed and Akhter, 2001). The prevalent practice for retting of whole jute plants and ribbons is shown as flow chart in Fig. 1.

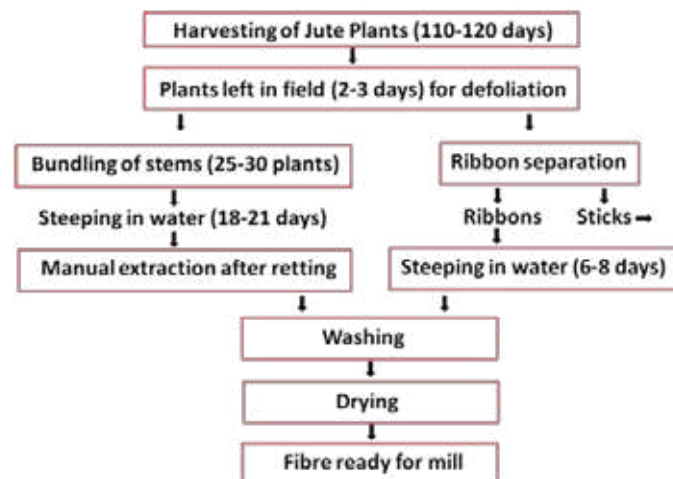


Fig. 1. Process flow for jute fibre extraction from stem retting & ribbon retting

MECHANICAL INTERVENTION IN JUTE RETTING PROCESS

Jute, mesta or other bast fibre do not directly provide us the fibre as in the case of cotton. These plants needs to be retted after harvesting in suitable medium normally water for extraction or removal of fibre from stem. So the process of retting is one of the important post harvest operation in view to obtain the quality fibre. The retting process itself is a cumbersome and labour intensive and it is becoming difficult for the farmers now a day due to scarcity of water as well as non-availability of labourers. Therefore mechanical intervention in retting operation is indispensable for minimum retting water and labour requirement. The separation of green bark or ribbons from plant stem and retting of ribbons in an artificial tank may be a suitable proposition because of the reduced requirement of water as well as labour and time. After harvesting, bundling of the plants and its transportation to the natural water body requires a maximum labour input. Further separation of fibre from retted plant stem also needs much of labour and at the same time no one is willing to do this job in tainted water because of the health risks. The ICAR-NINFET has already developed a power ribboner which is capable to extract the green bark from the whole plant leaving the plant stick un-broken and further in view to obtain the superior fibre from the ribbons, the work is undertaken to develop a suitable tank with facility of slow flowing water for quality retting of ribbons. The engineered water tank will help in determining the end point of retting of ribbons and whole plant in terms of optimum quality of fibre yield. The technology of tank-retting system for jute ribbons or barky jute may benefit the farmers, jute mills and other stake holders dealing with jute research, jute production, post harvest aspects of jute & mesta fibre.



Ribbon Retting

The traditional practice of jute retting involves placing of harvested plant bundles into a water bodies for 18-20 days. In the present environmental situation farmers are facing great difficulties in performing the retting process of jute because of the shortage of sufficient quality water. They are compelled to ret their jute crop in traditional pond, road side ditches, muddy water in their fields and this practice ultimately yield a poor quality jute fibres with more and more barky jute fibres. The longer time duration for jute plants retting in insufficient quantity of poor quality water are the major concern in view to obtain the good quality fibre. Considering the above difficulties in retting process, ribbon retting has been proved to be successful in order to reduce the retting time as well as the quantity of water and retting space. Ribbon retting is a particular method of retting based on a mechanical pre-treatment of plant stalks that allowed reducing the requirement of water, the length of retting time and the level of environmental pollution to almost one-fourth in comparison to other method that processed the whole jute plant. Ribbon-retting releases less than one-third of the organic matter released by whole plant retting into the retting water, and this is a major environmental advantage. It is observed that time required for ribbon retting is only 6-8 days. There is several advantages of ribbon retting are being noticed such as quality and yield of the fibres is considerably increased in comparison to traditional whole plant retting. Retting of whole plant in insufficient poor quality water yields more barky jute which is of no use in the mills. The jute mills normally discard 10-12 inches length of barky jute during the mechanical processing for yarn making.

Efforts have been made to develop machines and gadgets for separation of ribbons (fibrous barks) from the jute stalks. Manual and power driven decorticators and ribboner has already being developed in which ribbons is separated from the whole jute stick. A major disadvantage of the use of decorticators, from the outlook of farmer need, is the breaking of jute sticks into short pieces during the separation of ribbons from the plant. Ribboner separates bark from the stem leaving the whole stick unbroken which will be acceptable to the farmers for efficient peeling of ribbons. Earlier two mechanical devices have been developed by ICAR-NINFET for separation of ribbons from green plants of jute & mesta leaving the intact and unbroken sticks. A portable manual ribboner developed for the purpose can handle about 80 kg green plant yielding about 35 kg ribbon per hour depending upon skill and practice of operator. The power ribboner machine can handle 150-200 kg green plants of jute and mesta producing 60-80 kg ribbons per hour. A comparison of whole jute plant retting and ribbon retting is presented in **Table 1**.

Table 1. Comparative performance of whole Jute plant and Ribbon retting

Parameter	Whole plant retting	Ribbon retting
Transport of plant bundles	Stem bundles are carried from field to retting pond (35-40 ton/ha)	Ribbons having only 40 % of the weight of whole plant carried to pond after ribboning at field
Retting time	18-21 days	6-8 days
Water requirement	Approx. 25000 liter/per ton of stem	Approx. 8000 liter/per ton of stem (only ribbons)
Fibre extraction	Needs stripping and washing after proper retting	Needs only washing after complete retting
Fibre quality	Lower quality with barky cuttings due to muddy/dirty water	Good quality fibre with minimum barky roots
Quality of stick	Strength and colour of stick deteriorated during soaking	Intact stick with full strength and natural colour
Environmental impact	More than 10 tons organic matter released during retting from 1 ha plants causing environmental pollution and facilitate breeding of mosquitoes	Release of organic matter reduced by one third, therefore less environmental pollution and breeding of mosquitoes can be controlled
Economics	Costly because of involvement of large number of labourers	Relatively cheaper with mechanization through ribboner and accomplishing retting in mechanical tank

RETTING OF RIBBONS IN ARTIFICIAL TANK

Ribbon retting requires about one fourth the quantity of water as compared to the traditional practice of whole plant retting. Retting time also reduced to only 7-8 days. BJRI has developed a technique of ribbon retting in which green ribbons are arranged in the form of a ring and are retted in polythene lined artificial retting tank or ditches. Urea (0.01%) or retting effluent



is used as retting accelerator. The retting time is significantly reduced by 5-7 days though fibre quality does not improve compared to traditionally retted fibre.

CRIJAF had developed a technology of in-situ jute retting with microbial consortium. A circular micro pond of 6.5 m floor diameter and 7.5 m top diameter and 1 m deep having 1 m wide earthen embankment lined with polyethylene sheet (800 to 1000 gauge, 30 ft x 27 ft) is sufficient to ret jute/ mesta harvested from 1333.3 m² (one bigha) land. Harvested jute bundles are arranged radially up to three layers keeping base of the plants towards periphery of the pond. Microbial consortium with a cfu (108 to 1010) was then applied to the jute bundles in the pond. Under ground water was then added to the retting tank and the jute bundles are then covered with straw/aquatic weeds; and for proper immersion of the jute bundles in the water, cement bags filled with sand, brick or soil can be put above the jute bundles. After retting, the fibres have to be washed in the retting pond itself after removal of 50 % retted water and addition of fresh water in the pond.

The Chinese practice of jute retting is somewhat different. The jute plant bundles are transported to retting places which include ditches, ponds, lakes, streams and rivers.

The bundles are kept immersed under water for 5-7 days first. To prevent the floating of bundles, stones or soil are used as a weight. After this period of submersion, the plants are taken out and ribbons are extracted. Then the only ribbons are bundled and again immersed in water for retting until the fibre can be extracted from the ribbons.

Reduction of Fibre Cuttings

The hardy basal parts of jute fibres are called cuttings. This part is cut away and sold separately at a much lower price. They have a great role in the quality of fibre. The less the cuttings, the better is the quality of fibre. These cuttings are formed mainly because of the over-maturity of the plants and improper retting practices. Jute plants are thicker at the base than the top. If more time is given for retting of the basal parts, the middle and top parts become over retted and the fibres of these areas become weak. So usually retting is stopped when middle areas are retted properly. This always results in some under retted basal areas which forms cuttings. Rise and fall of flood water around base level of the plants also give rise to these cuttings. It appeared from the study that the cuttings could be greatly reduced by (i) harvesting the jute plants at right time, (ii) soaking the basal parts before steeping, (iii) malleting the basal parts before steeping, (iv) by special method of extraction, (v) separately retting the basal and top parts after cutting the plants in the middle.

Retting of Jute Ribbons in Mechanical Tank

Looking into the present status of retting process of bast fibres particularly jute, it is imperative to develop an artificial tank with some mechanical intervention such as controlled flowing water to facilitate the quality retting of jute fibre and to learn the parameters responsible for retting. There is no prior art available for the functional design and development of any style of water tank especially for the retting of jute/other bast fibres and its ribbons. No study has been reported for the retting of jute in an artificially controlled condition over physical or chemical parameters affecting the quality of retted jute fibre. Considering the above facts and gaps in the technology development to overcome the problem of retting, it is visualized that the retting process of jute needs to be mechanized or partially mechanized. Therefore in the line of above thoughts, a portable tank for retting of jute ribbons and barky jute is functionally designed and fabricated at ICAR-National Institute of Natural Fibre Engineering & Technology, Kolkata. The line diagram and photographs of the portable tank is shown in the figures 2 and 3 respectively. The material of construction of the tank is fibre reinforced plastic (FRP). The whole unit consists of three separate tanks of dimension 1.37m x 0.91m x 0.61m. All three tanks are fitted on iron frame to make as a single unit. Tanks are connected to each other with suitable pipes in order to get the desired water flow from first tank to second and third tank. A half hp water pump is also fitted at appropriate place to pump the water into first tank from third tank so that circulation of the same water is achieved. The first tank is meant for water storage and supply whereas second and third tank are for accommodating 50 kg ribbons for retting.

Ribbons were extracted from whole jute plant by using power ribboner machine. 50 kg of ribbons were suitably placed by hanging into the tank and the tank was filled with fresh water for accomplishing the retting process. Progress of retting was observed every subsequent day. The retting process completed at the end of 7th day. On completion of retting, the retted jute ribbons was taken out from the tank and they were washed using fresh water in order to remove the decomposed pectinous matters adhered to the retted ribbons and thereafter obtained clean wet jute fibres. The wet fibres were dried by hanging them over a string in open air condition. The dry jute fibre was analysed for its quality characteristics and found the quality grade of fibre as TD-3. The performance of portable tank was also evaluated for retting of root cuttings (barky jute). 25 kg barky jute was placed in the tank with fresh water in the ratio of 1:15. Bacterial culture was added to liquor mixture (water and barky jute) at

a rate of 3% and it was stirred thoroughly with the help of a stick in view to mix the culture & submerge barky jute properly in the liquor. The progress of retting of barky jute (softening of dry bark) was monitored on subsequent days and it was observed that retting was completed at the end of 4th day. After that the retted barky jute was removed from the tank and it was spread over a cemented floor for sun drying. On completion of drying process, the barky jute fibre was tested for spinning in Institute's jute mill.

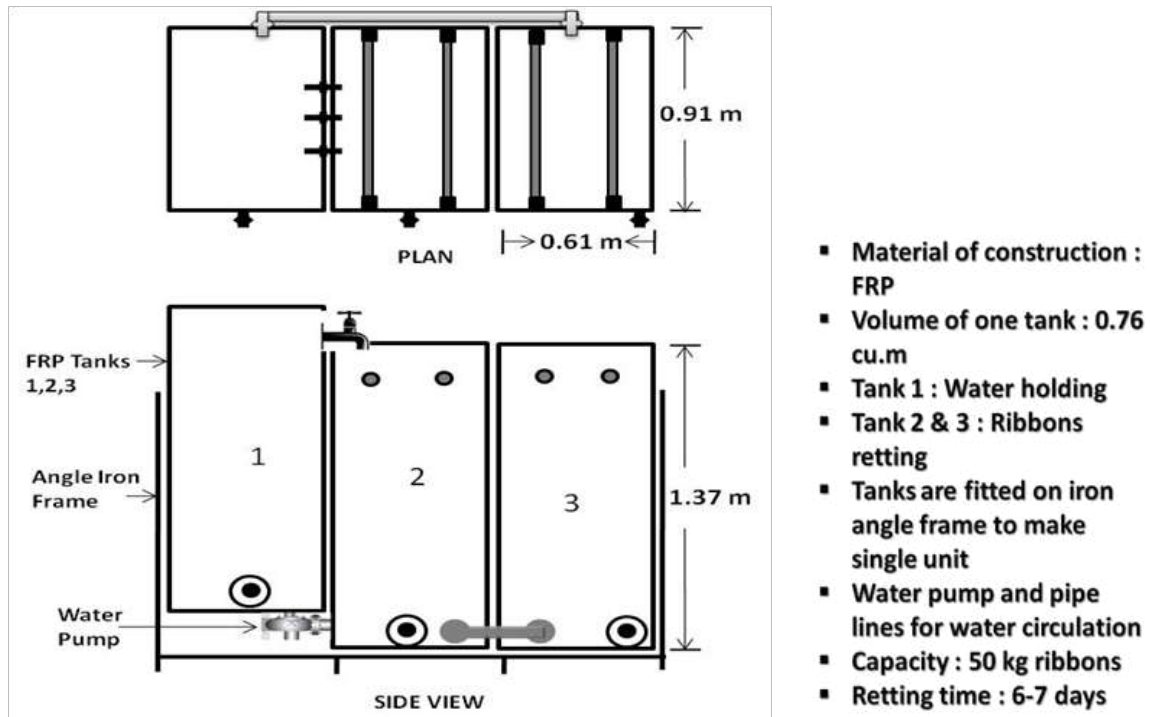


Fig. 2. Line diagram of portable water tank for retting of jute ribbons and barky jute



Fig. 3. Images of portable water tank for retting of jute ribbons and barky jute



CONCLUSION

Chief findings

- A portable water tank with water circulation mechanism has been fabricated for retting of half quintal jute ribbons and barky jute.
- Tank-retting of jute ribbons suggested that it is working satisfactorily and retted the jute-ribbons in 7-8 days without addition of any bacterial inoculums or other food supplement for bacteria.
- Quality of dry fibre obtained from portable tank-retting has been evaluated and found in the range of TD-3 & TD-4.
- Retting of barky jute (root cuttings) in tank was completed in 4 days with liquor ratio 1:15 (barky jute: water) and with addition of 3% bacterial culture. Yarn quality was found satisfactory with quality index of 70%.
- However, the up-scaling of ribbon retting tank will require the material of construction to be tough because of the increased volume of ribbons, therefore masonry tank shall be of more effective and long lasting.

REFERENCES

1. Ahmed, Z. and Akhter, F. (2001). Jute Retting: An Overview. Online J of Biological Sciences 1(7): 685-688.
2. Azad, A. K., Nabi, M. N., Choudhury, M. Z. A. (2002). Input output relationship, jute cultivation in Bangladesh. Final Report, Contact Research Project, BARC, Bangladesh Jute Research Institute, Manikmia Avenue, Dhaka, Bangladesh, 1207.
3. Banik, S., Basak, M.K., Paul, D., Nayak, P., Sardar, D., Sil, S.C., Sanpui, B.C. (2008). Ribbon retting of jute - a prospective and eco-friendly method for improvement of fibre quality. Industrial Crops and Products 17, 122-140.
4. Bera, A., Chowdhury, H., Ramasubramanian, T., Mahapatra, B.S. (2009). Seed production technology and quality assurance for raw jute. Technical Bulletin No. 26/2009, CRIJAF, Barrackpore, Kolkata.
5. Borkar, U. N. (2007). Improved method of bast fibre extraction. In: Mitra, S., Sinha, M.K., Sarkar, S. (Eds.), Training Manual of National Level Training on Improved Production Technology for Jute and Allied Fibre Crops. CRIJAF, Barrackpore, Kolkata, 30-33.
6. Guha, B. (1999). Cultural weed management in tossa jute (*Corchorus olitorius*). Annals of Agricultural Research 20(4), 406-410.
7. Gupta, P. C. D., Sardar, D. and Majumdar, A. K. (1976). Chemical retting of jute. Food Farming and Agriculture, 8: 7-9.
8. Majumdar, A. K. and Day, A. (1977). Chemical constituents of jute ribbon and the materials removed by retting. Food farming and Agriculture 21: 25-26.
9. Mitra, S., Maiti, S. N., Sarkar, S. (2006). Recommendations for jute and allied fibre crops: an endeavour of All India Network Project. CRIJAF, Barrackpore, Kolkata, 28.
10. Paul, N. B., Bhattacharyya, S. K. (1978). Effect of inoculation of harvested green jute plants with bacterial retting cultures on period of retting and quality of jute. Science and Culture 44, 379-381.
11. Rostom, A. Md., O. Kozan., Rahman, A., Islam, K. T. and Md. Iqbal Hossain (2015). Jute retting process: present practice and problems in Bangladesh. Agric Eng Int: CIGR Journal Open access at <http://www.cigrjournal.org> Vol. 17, No. 2: 243p.
12. Yadav, S., Yadav, P.K., Yadav, D., Yadav, K.D.S. (2009). Pectinlyase: A review. Process Biochemistry 44, 1-10.

Interdisciplinary



Engineering Institution for Self-reliance and Sustainable Goals

Dr S Swapna Kumar

Department of Electronics & Communication Engineering, Vidya Academy of Science & Technology, Thrissur, Kerala

✉ swapnakumar.s@vidyaacademy.ac.in

ABSTRACT

Self-reliance and sustainable development are versatile areas where the stages and its logic shows the preservation of basic values associated with a series of stages. Sustainable development needs the coherence growth without compromising the needs of the future goal. In this paper provide a critical perspective on the relationship between self-reliance and sustainable development on academic institutions to successfully steer and guide the development process in our country. The aspect of indigenous technology development based on institutions human factors and teaching practice has been examined in this proposed work. This research actively presents options open to technology self-reliance. It is clear that several attempts toward achieving self-reliance and promoting sustainable development. Adaptive technology has an important role in human capital development and explored greater values.

Keywords : Education institutions; Indigenous technology; Innovation; Sustainable.

INTRODUCTION

Self-reliance is a goal, not a policy, it takes time and right policy framework to be a self-reliant nation. The self-reliance is the ability to define self value and dependency to get the needs by self-involvement. It is the reliance of one's own effort and abilities to meet the goal. The perception of self-reliance philosophy is the power of self, creativity, and novelty of the objective without external support and meet the needs to glorify the importance of self-application (Uwem, 2016). The most vibrant example is of the Father of nation Mahatma Gandhi (1859-1948), who have shown the self-reliance mode of freedom movement of India from Britishers. The former President of India, Dr A P J Abdul Kalam stressed on higher education institutions to focus on the importance of Research and Development for it enhances the quality of teaching and learning. He made an appeal to the institutions to remember the significance of Research in Higher Education. His ideas towards, Unique, innovative, activities symbolize association of industry and academia enriches the engineering education as a whole. Engineering education faces numerous challenges of its own, including attracting and retaining for survivals (Okon, 2020). This needs broader study of self-reliance and sustainable economic developments for the success of any organization or state or country. cross-sections of strengthening the educational enterprise; by creating more effective interdisciplinary alliances with sciences and technology. So that it will enhance focus on innovation, entrepreneurship and job creation, that will promote increased public awareness and support for the engineering enterprise.

CONCEPT

As Buddha quoted, The height of the lotus depends on the depth of water. That means Opportunity is concealed with Issues and Challenges. For the success and sustainability of any domain depend on three Ds i.e, Demand-Development-Decline. The demand is the human needs and that shapes to develop the goal. The sustainability of the goal depend fulfilment. More the demand the life of the development will prolong. This is common in the technology areas. Technology is related to hardware, software, education, organizational forms and management techniques etc. (Date, 1981). It is an important tool that is self-reliance, development and mold as per the needs. India is in the process of transforming itself into a developed nation by 2020. The role of engineering and science are essentially part of the same spectrum of activity. The relationship among science, technology and engineering can be roughly described as shown in the Fig. 1.

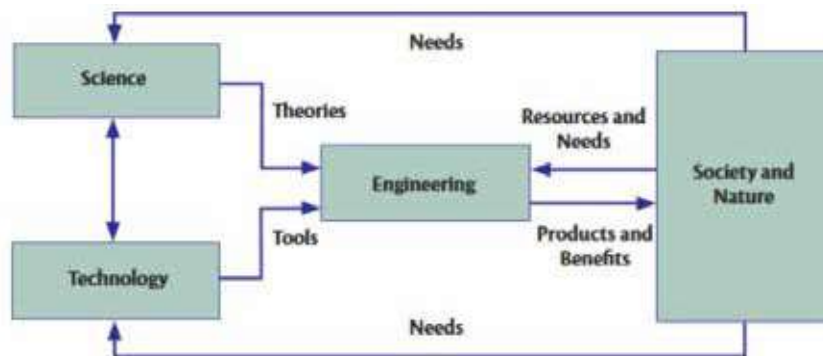


Fig. 1. Relationship among science, technology and engineering, UNESCO Report (2010)

The field of engineering uses both scientific theories and tools to create technologies and infrastructure. This is to address human, social & economic issues and challenges to overcome the needs of applications. The developments in the science and technology always creates an opportunity for engineering education sector accomplish the needs through their research and development. The technology is regarded as innovation and adaptation on technical models of behavior applied to the solution (Aminu, 1979). The strategies sheds on engineering institution for self-reliance and sustainable goals is the first step towards future of the nation on indigenous technology developments. In any medium level institutions across our country there's is need to look into following factors to improve the needs and creating an aspiration of the youth for self-reliance. Indigenous technology referred as related socially appropriate and progressive technology Baron (1978). Following factors shows the basic strategies.

- **Admission:** (In recent days a serious discussion on quality and ranking of of higher education institutions in deliberated everywhere. This is due to the poor quality primary education and quality admission. When the admission level is poor it adversely affects the employability of graduates. Here listed a relation of good inputs to output with defined process stages.)
 - Admission > Results: As per the inputs on admission the performance of the academic results and teaching will improve.
 - Good Admission > Good Teaching > Commitment > Rank Results: The chain is a related factors for developments.
 - Meritorious Admission > Creative Teaching > Research & Development > Academic Identity > Funds Inflow (Projects) > Patent: The best admission always shows the way towards the creativity ideas to build and organizes knowledge. The development will be more towards self-reliance ideas
 - Global Meritorious Admission > Creative/New development Teaching > Research & Development Projects (1st semester on-wards) > Center of Design/Consultancy/Testing > Funds Inflow (Projects/Products)
 - > Patents
- **Faculty:** (The faculty in all institutions is top notch, extremely sincere and brilliant. But due to a certain condition number of research/ project/ consultancy and contribution to a number of research papers and citations falls. The research need to be ground breaking.)
 - Faculty > Research work > Outcome Results > Publication
 - Faculty > Add-on-course > Resource person > Visit for lectures/training
- **Employability:** (In the global market fluctuations and its impact on the national GDP growth rate shows the variation in demand of employability of the country. As institutions has grown in terms of number of colleges in the state and country, to reduce gap between the quantity and quality of higher education offered for better employability.)
 - Market demand > Quality learning environment > Market needs > Employability
- **Strategic Planning:** (In the technical education institutions, just as ad- mission strategies; there is a need of proper strategic planning, appropriate guidelines, and corrective measures of all departments of institutions. It is a systematic process of envisioning a desired future, and translating The management always been on forefront in this and need to continue to mea-



sure the realistic strategic goal of all departments. More emphasis needs to put towards qualified, competent, committed, updating and suitable faculty members.)

- Vision & Mission > Strategic Objective & Measurable Values.
- Department Realistic Short/ Medium/ Long term goal > Implementation > Measurable Values.
- Analysis of Measurable Strategy > Structure Control & Feedback.
- **Academic Growth:** (Faculty-student ratio to enable healthy interaction need to quantify in terms of department objectives.)
 - Committed teachers > New and challenging question papers/assignments > Prevent rote(parrot-fashion) learning.
 - Reducing Drop outs > Remedial action > Department objective
 - Lab equipment > Experiment > For project-based assignments > Hands-on learning .
 - Collaborations with national labs, research institutions and industry R&D sectors > Student Internships/ Projects/ Recruitment after graduation.
- **Knowledge Building Teamwork:** (Emphasis on knowledge building team work is important for creativity and analytic thinking. Also on team dynamics and leadership.)
 - Students interested domain identifies > team-based classwork > Projects.
 - Tutors/Faculty > Work (splitting+combining) > Cooperation > Collaborate > Outside Competition/Techfest.
 - Students Performance evaluation index > Attend for (conferences, internships, NSS, other cultures etc.).
 - Faculty Performance evaluation index > Attend for (conferences, Workshop, Other Value-added-Service etc.).
- **Problem-based Learning:** (Engineering education is a foundation for the development of society. In today's modern world technology is changing fast and there is a need for change of engineering education towards more student centered learning methods. When technological innovations, there will be production of new goods, economic growth and human development.)
 - Students centric Education > Improve the passing rates > Value-added-Service measurable.
 - Technological innovations > New market product > Special appreciation.
- **Innovation:** (Research and Development (R&D) is an integral part of relevant appropriate technology. For self-reliance to be achieved innovations in the form of projects need to grow. The way to grow faster is to invest more is the emphasis on innovation. Scale and skill have to grow together to remain competitive in the marketplace for sustainable growth.)
 - Students interested domain identifiers > team-based real-time Projects > Real-time Projects Projects.
 - Product development > New technology development > Patent creation
- **Publication:** (The book publication and Journal publication is a scholarly contribution. The publication initiates the eagerness to write only when someone involves towards new findings.)
 - Student development > Product development > Publication
 - Faculty Project/ Research, development > Product development > Publication
 - Branded product focused > Product development > Publication
- **Resource excellence:** (The key attributes of an engineer, is to be reflected in the educational process, with sound understanding of a technical engineering discipline with an ability to analyze, solve problems and evolve innovative solutions in that discipline.)

The different training facet of Personal, Technical and professional training will lead to good placement achievements.

 - Access to alumni gatherings > Technology sharing > Department developments > Student placements.
- **Personal and training:** (Personal & training is essential for students and teachers. It is important to build up the knowledge, expertise and assistance from various agencies by visiting/ invited mode.)

- Career counselling > Students
- Technical Training > Undergraduate and Postgraduate levels
- Non technical Training > Undergraduate and Postgraduate levels
- Career counselling > Students
- Empowering women > Overall development
- Psychology minds, training > Students capacities of inquiry, creativity, technology, entrepreneurial and moral leadership.

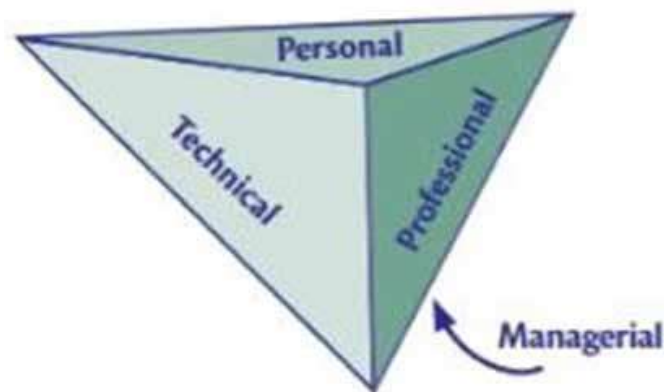


Fig. 2. Facets of engineering professional attributes, UNESCO Report (2010)

Institutions need to work collectively from all dimensions to climb the ladder progressively. The indigenous technology and subsequently self-reliance paths will lead the institutions and country towards sustainable growth.

CONCLUSION

Self-reliance and sustainable development are associated with each other that limits and preservation of environmental resources. It is clear that the self-reliance and sustainable development is a vast areas. Here the factors considered on institutions that has several attempts toward achieving self-reliance and promoting sustainable development. However, the efforts and strategies adopted seem to have yielded limited results. Self-reliance and sustainable development in Indian education system will require strong growth and a focus on institutions self-reliance development. Modern technology and latest tools has important role in academic development and needs to be explored in greater details.

REFERENCE

1. Aminu, S (1979) "Opening statement to plenary sessions: In review of some recent literature and policy statements", International Labor Re- view, 117 (5) 625 634
2. Baron, C. (1978) "Appropriate technology come of age: A review of some recent literature and policy statement", International Labor review, 117 (6) 65 72.
3. Date, A (1981) "Understanding appropriate technology. In methods for developing planning scenarios. Models and macro studies", UNESCO press, 189 200.
4. Okon Joseph Umoh , Augustine Okon Jacob, (2020) International Journal of Research and Innovation in Social Science (IJRISS), Volume IV, Issue V.
5. Uwem E. Ite, (2016) Perspectives on self-reliance and sustainable development in Nigeria, 2nd National Conference of Academic Staff Union of Polytechnics (ASUP), Rivers State, Nigeria.
6. UNESCO Report (2010), "Engineering: Issues Challenges and Opportunities for Development".



Skilling India through NSQF - A Way forward to Atmanirbhar Bharat

Dr Anil Kumar¹, Suneel Grover

State Project Administrator, SPIU-UP/TEQIP-III, Ministry of Education, Government of India, Lucknow, UP¹

Chairman, National Skill Development Forum (NSDF), The Institution of Engineers (India), Engineers Bhawan, Nigam Vihar, Shimla, HP²

✉ kr_anil3@rediffmail.com; ✉ grovers_in@yahoo.com

ABSTRACT

As India moves progressively towards becoming a global knowledge economy, it must meet the rising aspirations of its youth. This can be partially achieved through focus on advancement of skills that are relevant to the emerging economic environment. The challenge pertains not only to a huge quantitative expansion in skill training for the youth, but also to the much more important task of raising their quality.

Government of India, taking note of the requirement for skill development among students launched National Vocational Education Qualification Framework (NVEQF) which was later on assimilated into National Skills Qualifications Framework (NSQF). Various Sector Skill Councils (SSCs) are developing Qualification Packs (QPs), National Occupational Standards (NOSs) and assessment mechanisms in their respective domains, in alignment with the needs of the industry.

The Skill development is looked after by Ministry of Skill Development & Entrepreneurship (MSDE) and for education is the domain of Ministry of Education. There is missing link in terms of Credit to skill programmes, Skill Credit Bank, Credit transfer to general preprogrammed tertiary education, vertical and horizontal movement between skill programmes and university programmes. National Education Policy 2020 has the provision to address this issue of Credit Bank, Credit Transfer, mobility – both vertical and horizontal appropriately.

Keywords : Skill; Skill development; NSQF; Credit bank; Credit transfer; Horizontal and vertical movement between skill programmes and university programmes.

INTRODUCTION

Skills and knowledge are the driving forces of economic growth and social development for any country. Presently, the country faces a demand – supply mismatch, as the economy needs more ‘skilled’ workforce than that is available. In the higher education sphere, knowledge and skills are required for diverse forms of employment in the sector of education, health care manufacturing and other services. Potentially, the target group for skill development comprises all those in the labour force, including those entering the labour market for the first time, those employed in the organized sector and also those working in the unorganized sector.

A recent studies indicate that employers found just about 25% of Indian graduates are ‘employable’ in the organized sector. The informal sector which comprises 93% of the workforce has no skilling mechanism, as the skill development takes place on the job.

So, there is a need for quick reorganization of the skill development ecosystem and the promotion of which is necessary to suit to the needs of the industry to ensure enhancement of life of the population through suitable enabling mechanism of certification, credit transfer and horizontal and vertical movement.

National Skills Qualification Framework (NSQF)

The National Skills Qualification Framework (NSQF) organizes qualifications according to a series of levels of knowledge, skills and aptitude. These levels are defined in terms of learning outcomes which the learner must possess regardless of whether they were acquired through formal, non-formal or informal learning. It Provides structure for development and maintenance



of progression pathways which provide access to qualifications and assist people to move easily and readily between different education and training sectors and between those sectors and the labour market.

Features of NSQF

- Across sectors and across the country
- Short duration, focused and modular programs
- Practical hands on focus
- Delivery in the local language
- Full day, half day or week end programs
- A network of centres
- Full mobility between formal, Vocational streams of education and the Job market with multi Point Entry and Exit.

NSQF LEVEL DESCRIPTORS

NSQF LEVELS					
LEVEL	Process required	Professional knowledge	Professional skill	Core skill	Responsibility
Level 1	Persons prone to carry out process that are repetitive on regular basis require no previous practice	familiar with common trade terminology, instructional words meaning and understanding	routine and repetitive tasks safety and security measures	Reading and writing, addition subtraction personal financing, familiarity with social and religious diversity, hygiene and environment	No Responsibility always works under continuous instruction and close supervision
Level 2	Persons prone to carry out process that are repetitive on regular basis with little application of understanding, more of practice person may carry out a job which may require limited range of activities and predictable	Minimal tools Application in a limited context, understands content of work and quality	Limited service skill used in limited context, select and apply tools, assist in professional works with no variables differentiate a good and bad quality	Receive and transmit written And oral messages, basic arithmetic personal financing understanding of social political and religious diversity, hygiene and environment	No responsibility works under instruction and close supervision
Level 3		Basic process facts, and principle applied in trade employment	recall and demonstrate practical skill, routine and repetitive in narrow range of application	Communication written and oral, with minimum required clarity, skill of basic arithmetic and algebraic principles, personal banking, understanding of social and natural environment	Under close supervision Some Responsibility for own work within defined limits
Level 4	work in familiar, predictable, routine, situation of clear choice	factual knowledge of field knowledge or study	recall and demonstrate practical skill, routine and repetitive in narrow range of application, using appropriate tool, using quality Concepts	language to communicate written or oral, with required clarity, skill to basic arithmetic and algebraic principles, basic understanding of social political and natural environment	Responsibility for own work and learning
Level 5	job that requires well developed skill with clear choice of procedures familiar content	knowledge of principles, processes and general concepts, in a field of work or study	a range of Cognitive and practical Skills acquired to accomplish tasks and Solve problems by Selecting And Applying Basic methods, tools materials and information	Desired mathematical skill, understanding of social, political and some skill of collecting organizing information, communication	Responsibility for own work and learning and some responsibility for other's work and learning
Level 6	Demand wide range of specialized technical skill, clarity of knowledge and practice in broad range of activity involving standard non standard practices	factual and theoretical knowledge in broad contents within a field of work or study	a range of cognitive and practical skills required to generate solutions to specific problems in a field of work or study	Reasonably good in mathematical calculation, understanding of social, political and, reasonably good in data collecting organizing information, and logical communication	Responsibility for own work and learning and full responsibility for other's work and learning
Level 7	requires a command of wide ranging specialized theoretical and practical skill, involving variable routine and non-routine content	wide ranging factual and theoretical knowledge in broad contents within a field of work or study	wide range of cognitive and practical skills required to generate solutions to specific problems in a field of work or study	good logical and mathematical skill understanding of social political and natural environment problem solving organizing information, communication skill presentation skill	full responsibility for output of group and development
Level 8	Comprehension, cognitive, theoretical knowledge and practical skills to develop creative solutions to abstract problems. Undertakes self study, demonstrates intellectual independence, analytical rigour and good communication.			Exercise management and supervision in the context of work/study having unpredictable changes, responsible for development of self and others.	
Level 9	Advanced Knowledge and skill Critical understanding of the subject, demonstrating mastery and innovation, completion of substantial research and dissertations.			Responsible for decision making in complex technical activities, involving unpredictable study/work situations.	
Level 10	Highly specialized knowledge and problem solving skill to provide original contribution to knowledge through research and scholarship.			Responsible for strategic decisions in unpredictable complex situations of work/study.	



Horizontal and vertical mobility

For horizontal and vertical mobility to take place, the following are essential:

- Each level is linked to the ones above and below it by a series of steps. If these steps in any industry sector or academic domain are missing, the NSQF would help identify and map these missing gaps.
- The degree of lateral mobility that is considered desirable would have to be identified by the NSQF, and the same would have to be facilitated through on- going credit accumulation and transfer.

CREDITS EARNED AND CREDIT TRANSFER

- i. “Credit” is recognition that a learner has successfully completed a prior course of learning, corresponding to a qualification at a given level. The credit points give learners, employers and institutions a means of describing and comparing the learning outcomes achieved. Credits quantify learning outcomes that are subject to valid, reliable methods of assessment. The number of credits may be worked out on the basis of the number of notional learning hours that an ‘average’ learner at a specified NSQF level might expect to take to achieve the learning outcomes, including the assessment. However, this is merely a guide and no credits are added or taken away if more or less time is taken to achieve the outcomes. No credits are ‘earned’ by a learner if the learning outcomes are not achieved or, in the case of RPL, demonstrated.
- ii. Credits can be used to assist learners to transfer between programs. This can happen only when awarding bodies determine how much credit can be transferred into which of their programs. This decision will depend upon the nature/content of the learning for which the credit has been given and the requirements of the program into which transfer is being sought. This will also facilitate multiple entry and exit pathways at each level (or within a level) with the bundle of credits earned clearly certified by assessment and certification bodies which have been authorized to do so.

NSQF – APPROACH OF AICTE

Operational Methodology: Integrating VE with & Conventional Education

- Skill Knowledge Providers / Trainers (SKP) to be registered by AICTE or other authorised bodies for imparting specific skills.
- A student registers with an AICTE approved Technical Institute or any other college for a Vocational Diploma or a Vocational Degree or registers with any other Institute affiliated to any Technical Board or a University.
- The student completes the skill modules as required at various certification levels, one level at a time, acquires the necessary credits from the Skill Knowledge Provider/Trainers (SKP), and gives them on to the Institute where he is registered for a Diploma, Post Diploma or a Degree.
- These credits are transferred to the Technical Board or the University as the case may be, which compiles the Vocational Skill credits and the formal education credits and if all such credits are available as required by the certification level, then the Technical Board or the University shall award the certification at that level.
- Certification levels as required will entail the student for the award of a Vocational Degree or a Vocational Diploma or a Vocational Post Diploma.
- The candidates may enter the job market after each certification level or may continue to acquire additional credits in part time / full time mode in order to complete the requirements of Vocational Diploma, Post Diploma or a Vocational Degree.
- In all seven certification levels of ‘Knowledge and Skill’ have been identified. First two levels refer to standard IX and X at school level. These shall be with the CBSE schools or schools affiliated to State Boards and equivalent other boards.
- Each level requires 1000 hours of education and training per annum. For the vocational stream leading to a Degree or a Diploma or a Post Diploma, these hours shall have both vocational and academic component.
- A candidate shall have freedom to choose either a vocational stream or a conventional stream to reach graduation level. This multi level entry and exit system shall allow the candidate to seek employment after any level and rejoin the education as and when feasible to upgrade qualifications / skill competency.
- A student entering a Vocational stream from general stream can enter at a certain level provided the skills required at that level are acquired, from a registered SKP.



- A student who has acquired the skills through work experience, can also enter the Vocational stream at an appropriate level provided he is assessed for the skills acquired from a registered SKP.
- The qualification frame work with upward mobility is shown asunder:

DURATION AND ENTRY LEVEL QUALIFICATIONS UNDER FRAMEWORK

Certification Level	Normal Qualification	Case I		Case II	
		Vocational Qualification	Certifying Body	Vocational Qualification	Certifying Body
1	Secondary School Grade IX	Grade IX (Vocational)	School	Grade IX (Vocational)	School
2	Secondary School Grade X	Grade X (Vocational)	School	Grade X (Vocational)	School
3	Higher Secondary School Grade XI	Diploma (Vocational)	Board of Technical Education	Grade XI (Vocational)	School
4	Higher Secondary School Grade XII			Grade XII (Vocational)	School
5	1 st yr bachelors			Degree (Vocational)	University
6	2 nd yr bachelors	Advanced Diploma (Vocational)	Board of Technical Education		
7	3 rd yr bachelors				

AICTE SUGGESTED DURATIONS

Qualification	Equivalence		Skill certification Level	Competency based skill building (in Hrs) (approximate)	General learning (in Hrs.) (approximate)	Total Hrs.
IX std.	IX	IX	1	250	750	1000
X std.	X	X	2	250	750	1000
XI std.	Diploma (Vocational)	XI (Vocational)	3	400	600	1000
XII std.	Diploma (Vocational)	XII (Vocational)	4	450	550	1000
Year I	Diploma (Vocational)	Degree (Vocational)	5	550	450	1000
Year II	Advanced Diploma (Vocational)	Degree (Vocational)	6	600	400	1000
Year III	Advanced Diploma (Vocational)	Degree (Vocational)	7	750	250	1000

NSQF – UGC APPROACH

There will be full time credit-based modular programmes, wherein banking of credits for skill and general education components shall be permitted so as to enable multiple exit and entry.

The multiple entry and exit enables the learner to seek employment after any level of Award and join back as and when feasible to upgrade qualifications / skill competencies either to move higher in the job profile or in the higher educational system. This will also provide the learner an opportunity for vertical mobility to second year of B.Voc degree programme after one year diploma and to third year of B.Voc degree programme after a two year advanced diploma. The students may further move to Masters and Research degree programmes mapped at NSQF Level 8 –10.



The curriculum in each of the semester/years of the programme(s) will be a suitable mix of general education and skill development components. The General Education Component shall have 40% of the total credits and balance 60% credits shall be of Skill Component.

Skill Development Components (60% Weightage)

- Skill component of the programmes/courses shall be employment oriented. The institutions, in consultation with the industry partner(s) and based upon skills Gap analysis report published by the NSDC, industry associations, Sector Skills Councils, Government agencies etc, may decide specific Job Role(s) to be embedded in curriculum.
- The curriculum should be aligned to Qualification Packs (QPs) / National Occupational Standards (NOSs) of selected job role(s) within the industry sector(s). This would enable the students to meet the learning outcomes specified in the NOSs.
- The curricula and system of certification for the skill component should be as per the UGC guidelines for curricular aspects, assessment criteria and credit system for skill based vocational courses or as per the provisions in MHRD Skill Assessment Matrix for Vocational Advancement of Youth(SAMVAY).
- In case, NOS is not available for a specific area / job role, the university/college should get the curriculum for this developed in consultation with industry experts as provided at (ii)above.
- The curriculum should also focus on work-readiness in terms of skills in each of the three years.

General Education Component (40%Weightage)

- The general education component should adhere to the university / collegiate education norms and shall be decided by the Board of Studies of the concerned University / Autonomous College. It should lay emphasise on offering courses which provide holistic development.
- The general education component may also include the course(s) which are supportive to core trade in addition to communication skills, soft skills, ICT skills, critical thinking, problem solving, environmental studies and value education.

PROBLEMS FACING NSQF

- Unlike general academic education, where certain level of certification is required before further progression is permitted, there is no clear definition of the course curriculum within the NSQF that enables upward mobility.
- There is no connection of the tertiary level vocational courses to prior real knowledge of theory or practical experience in a vocational field.
- Efforts to introduce new Bachelor of Vocation and Bachelor of Skills courses were made, but the alignment of these courses was not completed.



- Lack of alignment between the Ministry of Education (responsible for the school level and Bachelor of Vocation courses) and the Ministry of Skill Development (responsible for non-school/non-university-related vocational courses).
- There are too many Sector Skill Councils in India and each is not comprehensive, like we have four SSCs for manufacturing but they are treated as one in World Skills courses.

The following can be done to improve skill framework in India:

- There is a need for more holistic training and to re-examine the narrow, short-term NSQF-based NSDC courses.
- NSDC should include skills in broader occupation groups, so that trainees are skilled enough to compete at the international level.
- SSCs should be consolidated in line with the National Industrial Classification of India to improve quality, outcomes, and help in directly assessing the trainee's competence. It might also bring some coherence to our skills data collection system.
- Vocational education must provide broader skills in broader occupational groups.

REFERENCES

1. Ministry of Finance notification dated 27th December, 2020 (No.8-6-2013-Invt.) on NSQF
2. AICTE guidelines on National Skill Qualification Framework (NSQF).
3. UGC Guidelines for providing Skill Based Education under NSQF.
4. "Qualifications Framework". UNESCO-UNEVOC.
5. Keevy, James; Chakroun, Borhene (2015). Level-setting and recognition of learning outcomes: The use of level descriptors in the twenty-first century. Paris, UNESCO. pp. 10, 12–13. ISBN 978-92-3-100138-3.
6. Architecture of the NVEQF, Government of India Ministry of Human Resource Development, New Delhi, dated 3 September 2012, p-7.



Self Reliance and Sustainability : An Environment Perspective

Seema Garg, Navita Mahajan

Amity University, Noida, Uttar Pradesh

✉ seemagarg1@gmail.com; ✉ navitamahajan07@gmail.com

ABSTRACT

This paper examined the relation between the self-reliance and sustainability. This study also explores the role of self-reliance in producing and maintaining a sustainable society. It results in showing its importance in the context of environment. The paper examines the meaning of self-reliance, business enterprises assuming responsibility for the consequences of their operation in the social as well as the physical environment. It is inevitable that when one goes for self-reliance, its impact on the environment will also be seen. Hence, one should evolve such a methodology where development is done with no or minimal damage to nature or sustainable development. As it is a belief that the idea of sustainable development and self-reliance are inextricably linked to each other. The paper relies upon original research by the authors and a review of studies in a variety of disciplines.

Keywords : Self reliance; Sustainability; Environment.

INTRODUCTION

Today environmental sustainability is one of the biggest issues faced by the mankind. Human beings are facing man-made environmental degradation. Increasing population along with tremendous escalation in human activities has raised several questions on the sustainability of natural resources on earth. No part on our planet is now untouched by the effect of pollution. Ever increasing human population and increment in per capita consumption has put great constraint on the natural resources. Also, urbanization, industrialization and modern agricultural practices have polluted the water resources, air and soil all around the globe. The natural resources are thus over-exploited and becoming contaminated with toxic chemicals making it difficult for the survival of future generations. Hence, there have been continuous endeavors across the globe to measure and mitigate this problem caused by human activities. At a time of soaring energy costs and fragile financial markets, executives are increasingly looking toward sustainability strategies to save money, cut emissions and, as many claim, simply to do the right thing.

SELF -RELIANCE

Self reliance is defined as the reliance on one's own powers and resources rather than relying on others. The term self-reliance was penned by Ralph Waldo Emerson in a similarly titled essay published in 1841 which stressed the trust in one's present thoughts, skills, originality, belief in own capabilities and intelligence and living from within. Means rejecting the need for external support and glorifies the importance of self-application, e.g. tilling of the land to get the "kernel of nourishing corn" (Emerson, 1841). Kripalani (1965) states that Gandhi expanded this concept to incorporate a simple life style asserting that nature produces enough for our wants, and if only everybody took enough for him/herself and nothing more, there would be no people dying of starvation in this world.

SUSTAINABILITY

The term sustainability can be defined as the avoidance of the depletion of natural resources in order to maintain an ecological balance. Sustainable means bearable and also capable of being continued at a certain level. Sustainability is made up of three major pillars: the economy, society, and the environment. These principles are also informally used as profit, people and planet. Sustainable development occurred in 1998 (Mebratu, 1998). The often-quoted Brundtland report defined sustainable development as "development that meets the needs of the present without compromising the ability of future generations to meet their own needs." (World Commission on Environment and Development, 1987).

SELF- RELIANCE AND SUSTAINABILITY

Self-reliance can be understand from a sustainability perspective ,which is crucial for such a life style to be encouraged as an alternative to the western model of development for traditional communities in developing countries in the world. This self reliance leads to short term gains and for this humans have destroyed the natural systems with great pace. But it is difficult to



estimate the impact of activities caused by humans on ecology, in term of economics and even the survivability rate of different life forms on Earth.

Sustainability in an enterprise can mean small adjustments or a major reorientation. Information technology (IT) is not itself a big part of the problem, as it is estimated to contribute only a small percentage of global carbon emissions. But it can be a big part of the solution. The optimization of the data and other operational issues such as teleporting, companies are now leveraging IT capabilities to facilitate sustainability initiatives across the enterprise in new areas, including fleet management, paperless billing, and construction and facility management, among others. Therefore responsible corporate citizens are more concerned about social and environmental aspects because only economic performance of a company is no longer consider as corporate success. Now organizations have understood that if they will not focus on sustainability, they have to pay for it in the form of tangible or intangible cost. For creating a balance between businesses and environment green practices come in existence. Going green refer to adopt knowledge and practices that are environment friendly and ecological policies and procedure that cannot harm environment and sustain a business as well as natural resources for current and future generation. After the Industrial Revolution in 1991 environment degradation is increasing day by day, whole world is concerning about environmental issues. These concerns are resulting as green management by applying eco-friendly practices in organizations. Since the Businesses are going globalized organizations are shifting their structure from financial status to sustainable efficiency-based organizations. Employee development towards going green contributes a vital role in suitability of an organization

NEED OF THE STUDY

Earlier also the environmental sciences existed and society had environmental concerns at large. They had into the considerations about the environment whether they are degrading or not. The role of environmental sciences changes with the realization that human-induced stresses on various environments and indulged in taking a dangerous toll: some types of human activities were understood as not being sustainable.

However, in some situations – and with some research questions – it can be harder to see the links between the two. These gaps become particularly apparent in reflecting on the role played by humans and their impacts on the environment. Knowing how current human activities dynamically affect tomorrow's environment is a key focus of study. In this perspective, sustainable development is the end goal, and environmental protection is a subsidiary goal. Many environmental experts focus their work on understanding environmental issues with little or no research focus on (human) development of any kind. Hence environmental practices must be included as one of the top agendas in modern day society.

OBJECTIVES

Primary objective of study is to study the concept of self reliance with sustainability and its impact on the environment. And to check whether sustainable development and self-reliance are inextricably linked to each other.

RESEARCH METHODOLOGY

This study is based on secondary data. For the fulfillment of above stated objected literature review has been done about impact of green banking on customer, employee and organization. This study helps in understanding the relationship how organizational things are connected with society.

REVIEW OF LITERATURE

In this present scenario environmental management should be the first aim of every organization (Lolan,2015). While there is enormous credit to the concept of Sustainability, Self Reliance and Environment, the concept itself serves more purpose when followed by outlining transformer like “ecological” or “agricultural” or “economic.”(John Morelli,2012). While the paths leading to environmental sustainability and self-reliance can be different for different sector specific for each county, each economy and each organization as well (Robert Godland 1995). Another school of thought (Robert Godland and Daly 1996) have segregated sustainability into three categories, social, economic and environmental. The three essential conditions for more sustainable environment and self-reliance are resource conservation technologies practices, local involvements, local groups, institutions and participation of external entities (Pretty JN 1995)

Corporates are having great control on any economy. They can lead a businesses, production as well as day to day life of people that why this become more important for corporates to adopt sustainable and environmental conducive practices. For self-reliance corporates must adopt environmentally friendly products in its' operations (Ginovsky, 2009). Environmental and Self reliable practices encourage innovation and improve resource utilization (Menon & Shivdas 2017) therefore corporates are



introducing paperless and technology-oriented process for most of their operations (Fernando and Fernando, 2016). Corporates should prepare environment friendly measures for self-reliance and sustainable reporting which include past performance, present development and future plans (Lalon 2015). With the underlying notion of sustainability being the ability to meet the needs of today while protecting and enhancing opportunities for the future and self reliance for environmental conservation the industries needs to focus further at achieving more sustainable practices (Dickson, 2010).

Rural India Towards Sustainability, Environment Self Reliance : For a country like India where 60 per cent of the population lives in villages and rural economy is one the backbone in India's GDP contribution, the self-reliance and sustainability at rural level play a key role. village level self-sufficiency in food, water, energy, sanitation, housing and other need tell us stress upon localization as the first step for moving towards globalization. If India as country really want to achieve self-sustainability and self-reliance, it needs to support a dignified livelihood in agriculture, animal husbandry, forestry, fishery, craft and small manufacturing at village level. It has to set up produce consumer links and abolishment, stop pandering to large organization, eliminate GST burdens on handmade products, providing better marketing facilities, buy back arrangement and minimum support process for primary products (The Hindu , June 5 2020). In the context of Atma Nirbhar Bharat, the task of achieving self-sustainability in agriculture. is easier than other sectors and it is not only environmentally friendly up a great level but the growing concept of organic is another boost to the sector. The first set of measure step towards it can be globally branding of Indian products making farmers aware of the quality and environmental friendly techniques.(the economics Times, May 26,2020). The success behind India's agriculture to be sustainable and self-reliant in long term lies in the fact that how much in sync with environmental friendly techniques Indian farmer is exposed to.

Discussing about the efficient systems (Azeeb J Naqvi, June 29,2020) has mentioned those practices that Government of India can frame for creating Sustainable, self-reliant environment and that is create a encourages only environmentally friendly practices. Government of India needs to think of a creative way to impose taxes. Only a strong, timely, stepwise and sincere implementation and adherence to the sustainable goals can n push India towards self-reliance that will be durable and truly effective in saving its environment as well.

Employees Towards Environmental Sustainability for Self-Reliance: Implementation of Environmental friendly measure depends on the day to day practices of employees. The workplace should have environmentally sound policies and employees should work with full efficiency of resources (Sathyapriya et al., 2013). This is also needing that organizations should maintain good human resource department which can help in developing employees' attitude towards sustainable and environmental practices (Paille et al., 2014). Environmental friendly practices related to employee have significant impact on organizational environmental performance and it will help in creating organizational citizenship (Shaumya K. & Arulrajah). Environmental and sustainable initiatives in organization would make everyday life of employees easy and less loaded and also provide greater efficiency, lower cost and help in making good relation among employees that result in for of better organization performance (Mathapati,2013).

Organizations Towards Self Reliance through Environment Sustainable Methods: Implementing environmentally friendly practices like Online channels, providing green loans, and other CSR activates etc are some the activities organizations can take up at their level to meet the goal. Organizations have started conducting energy audits, surveys, recycling the resources, reduce transportation, save water and other environmental practices that will result in cost reduction, increasing market shares and also satisfied all stakeholders (Ayeswarya,2017). For safeguard and accelerating the growth rate of economy organizations need to adopt proactive nature towards environment. Sustainable practices helps in attracting customer, build market image and get greater legitimacy (Zhixia,Husan,Mujafary & Begum 2018). Taking Environmental Initiative not only good for nature but also beneficial for organization as it help in earn carbon credits, decrease costs, and give competitive advantage (Yadav & Swaroop Pathak 2013) also help in gaining efficiency in operation, lower vulnerability and cost reduction. Go Green it is a wide concept that would lead the growth, variation & innovation in an organization (Sudhalakshmi & Chinnadorai 2014). Sustainable practices are not cost for environmental protection but in long run these practices will be beneficial for agriculture,economy, business, industries , economy (Nigamanda Biwas 2011). As a part of society organizations have some responsibility towards society and environment. When organization take their decision with the consideration of environment, sustainability, self-reliance and society, they are not only doing their responsibilities but also make it's operations smooth and effective (Bihari & Chandra,2010).

DISCUSSION

This study takes a more comprehensive assessment in sustainability survey research although, there have been other articles



published with a similar objective. From the literature and secondary data from published sources it is found that Saline soils are going to increase by 50% up to 2050 and land degradation has affected almost every country of the world. Human population is going to produce 27 billion tones of municipal solid waste by 2050 which would require great input of technology to manage and role of microorganisms will be immense. Amount of non-degradable wastes is increasing and some of the dangerous recalcitrants are accumulating in the food chains and are the cause of contamination of natural resources and extinction of species apart from causing harm to the humans. As per recent report published in Scientific Reports a mass of plastic waste named as “Great Pacific Garbage Patch” approximately 1.6 million km² in size~twice the size of Texas, is floating on the surface of Pacific ocean. Plastics are also accumulating on land and in water bodies at an unprecedented rate and we need to find a quick alternative for these harmful creations of humans. It is very important to assess the impact of human activities on the local ecosystems and the planet as a whole on a regular basis. Use of latest technologies and tools although help in the assessment of the situation but the need is to find green solutions like green manufacturing, green marketing , green banking as well. And the green solution is on the way to control this problem.

CONCLUSION

Environment degradation increasing day by day due to increase in industrialization based on self reliance.. Environmental sustainability is thus one of the biggest challenge and important targets of the present times. It catches the major attention of researchers, academicians, scholars, governments and non-government organizations involving individuals, communities, countries, continents and the globe as whole. Environmental sustainability is the main strategy against the backdrop of the growth of human population and the extensive exploitation of environment by humans. Hence the concern of modern society is that while today people are enjoying the comforts of economic development, the future generations are on the verge of confronting scarce natural resources and polluted environment and it is our most important responsibility to leave the planet as a self sustainable system providing equal opportunities of survival not only to our future generations but also to all other species co-habiting with us.

REFERENCES

1. <https://www.thrall.org/special/goinggreen.html>
2. <https://www.newbusinessage.com/Articles/view/2804>
3. <https://www.thehindu.com/society/what-does-self-reliance-really-mean-amazing-stories-emerge-from-indias-villages/article31756580.ece>
4. Morelli, John (2011) “Environmental Sustainability: A Definition for Environmental Professionals,” Journal of Environmental Sustainability: Vol. 1: Iss. 1, Article 2. DOI: 10.14448/jes.01.0002 <http://scholarworks.rit.edu/jes/vol1/iss1/2>
5. www.Econmicstimes.com
6. <https://www.mapsofindia.com/my-india/business/top-10-largest-public-sector-banks-in-india-2019#>
7. <https://www.oliveboard.in/blog/private-banks-india/>
8. http://www.cwejournal.org/wp-content/uploads/2015/09/Vol10_No3_Gree_Kan_Fig2.jpg
9. Bahl Sarita (2012). “Role of Green Banking in Sustainable Growth”, International Journal of Marketing, Financial
10. Services and Management Research, 1(2)
11. Nath, V., Nayak, N. &Goel , A. (2014). Green Banking Practices – A Review.International Journal of research In Business Management, Vol.2, No. 4, PP 45- 72
12. . Dickson, C. (2010). Promoting sustainable event practice: The role of professional associations. International Journal of Hospitality Management, 29(2), 236-244.
13. Chowdhury, S. H., Roy, S. K., Arafin, M., & Siddiquee, S. Green HR Practices and Its Impact on Employee Work Satisfaction-A Case Study on IBBL, Bangladesh.
14. Kapoor, N., Jaitly, M., & Gupta, R. (2016). Green banking: a step towards sustainable development. International Journal of Research in Management, Economics and Commerce, 7, 69-72.



15. Veena, K. & Nayana, N. (2017). A Study on Customer Perception towards Green Banking – A Special Reference to State Bank of India - Bangalore and Mysore City. *Journal of Exclusive Management Science*, 6, 02.
16. Ibe-Enwo, G., Igbudu, N., Garanti, Z., & Popoola, T. (2019). Assessing the relevance of green banking practice on bank loyalty: The mediating effect of green image and bank trust. *Sustainability*, 11(17), 4651.
17. Biswas, N. (2011). Sustainable green banking approach: The need of the hour. *Business Spectrum*, 1(1), 32-38.
18. Bhardwaj, B. R., & Malhotra, A. (2013). Green banking strategies: sustainability through corporate entrepreneurship. *Greener Journal of Business and Management Studies*, 3(4), 180-193.
19. Dharwal, M., & Agarwal, A. (2013). Green banking: An innovative initiative for sustainable development. *ACCMAN Institute of Management Article*, 2(3), 1-7.
20. Vijayasarathi, V., & Velmurugan, G. (2016). A Study on Usage of Self Service Kiosk with Special Reference to City Union Bank Pvt Ltd, Vellore Branch. *Asian Journal of Research in Banking and Finance*, 6(3), 26-30.
21. Sudhalakshmi, K., & Chinnadorai, K. (2014). Green banking practices in Indian banks. *international Journal of Management and Commerce innovations*, 2(1), 232-235.
22. Yadav, R., & Pathak, G. S. (2013). Green marketing: Initiatives in the Indian context. *Indian Journal of Marketing*, 43(10), 25-32.
23. Mebratu, D. (1998) Sustainability and sustainable development: historical and conceptual review *Environ. Impact Assess. Rev.*, 18 (1998), pp. 493-520
24. Muhamat, A. A., & Nizam bin Jaafar, M. (2010). The development of ethical banking concept amongst the Malaysian Islamic banks. *Norfaridah, The Development of Ethical Banking Concept Amongst the Malaysian Islamic Banks* (February 25, 2010). *iCAST*, 24-25.
25. Miah, M. D., Rahman, S. M., & Mamoon, M. (2020). Green banking: the case of commercial banking sector in Oman. *Environment, Development and Sustainability*, 1-17.
26. Gupta, J. (2015). Role of Green banking in Environment Sustainability-A study of selected Commercial Banks in Himachal Pradesh. *International Journal of Multidisciplinary Research and Development*, 2(8), 349-353.
27. Aizawa, M., & Yang, C. (2010). Green credit, green stimulus, green revolution? China's mobilization of banks for environmental cleanup. *The Journal of Environment & Development*, 19(2), 119-144.
28. Islam, M. S., & Das, P. C. (2013). Green banking practices in Bangladesh. *IOSR Journal of Business and Management*, 8(3), 39-44.
29. Rahman, F., & Perves, M. M. (2016). Green Banking Activities in Bangladesh: An Analysis and Summary of Initiatives of Bangladesh Bank. *Research Journal of Finance and Accounting*, 7(10), 6-7.
30. Weber, O. (2014). Social banking: Concept, definitions and practice. *Global Social Policy*, 14(2), 265-267.



Self Reliance: A Context of Sustaining Indian Automobile Industry

Rohit Radhakrishnan, Vaisakh V, Dr Nidhi M B

Department of Mechanical Engineering, Mar Baselios College of Engineering & Technology, Mar Ivanios Vidyanagar, Nalanchira P.O, Thiruvananthapuram, Kerala

✉ rohitradha123@gmail.com; ✉ vaisakhv99@gmail.com; ✉ nidhi.mb@mbcet.ac.in

ABSTRACT

Self-reliance is not a new concept as India started this journey during the independence era itself. Self-reliance and sustainable development are closely related to each other. They emphasize on the well-being of humans, the basic needs of the poor, the welfare of future generations, as well as the limits and preservation of environmental resources. The COVID-19 pandemic has forced almost every nation around the globe to think about satisfying their own demands by themselves. The paper analyses the basic principles which govern self-reliance and sustainable development taking into consideration the importance of enhancement of skill, quality and safety. It also discusses the vital role played by engineers in making the country self-reliant through sustainable methods. Since the automobile industry was not included in the Aatma Nirbhar economic package, special attention has been paid to suggest some of the ways in which the industry can move towards self-reliance and be sustainable in nature. Self-reliance cannot be achieved by the initiative from the government alone. Only the combined efforts of the government, industries and most importantly the support and participation of the people will ensure that self reliance is attained.

Keywords : Self-reliance; Sustainable development; Skill enhancement; Quality; Safety.

INTRODUCTION

Self-Reliance, a term introduced by the US philosopher Ralph Waldo Emerson in one of his essays titled the same, has been the center of discussion over the past few years [1]. In view of the COVID-19 pandemic almost every nation around the world has been forced to think about satisfying their own demands by themselves.

Self-reliance refers to the social and economic ability of an individual/community to meet their essential needs in a sustainable manner. It involves the development and strengthening of their livelihoods by allowing them to be self sufficient and independent thus improving their quality of life. [2]

Sustainability is a term that is most widely used to describe the need to minimize ecological damage and preserve natural resources. To define the sustainability problem the three pillars of sustainability i.e. economic, social, and environment play a vital role. In order to have an in depth study, sustainability can be analysed using some additional aspects like technology, politics and culture [3].

Self-reliance and sustainable development are closely related to each other. They emphasize on the welfare of human beings, the basic needs of the poor, the prospects of future generations and preservation of environmental resources. The concept of self-reliance has taken a modern turn with key focus points being creativity, originality, quality and the need to be self sufficient in all fields. One of the famous quotes of Mahatma Gandhi states:

“Nature produces enough for our wants, and if only everybody took enough for himself/herself and nothing more, there would be no people dying of starvation”.

Therefore it can be said that self- reliance mainly grows on the idea of thinking and executing tasks without the aid or influence of others. There are various definitions and interpretations available for sustainable development, the most widely used definition is that of the World Commission on Environment and Development (WCED) which defines sustainable development as “Development that meets the needs of the present without compromising the ability of future generations to meet their own needs”. The three factors affecting self-reliance are explored in the context of sustainability in this paper (**Fig. 1**).

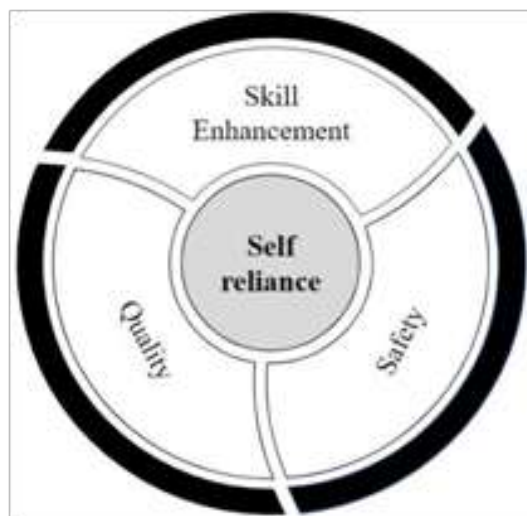


Fig. 1. Factors affecting Self-reliance

Self-reliance and Quality

Self-reliance is directly related to quality. The developed nations are dominating global markets because of their superiority in terms of innovation and product quality. Nowadays consumers select a product in terms of their quality rather than its cost. Inferior quality products are not preferred by customers, whereas top quality products are sought after even at high prices. The competitiveness of a product in the market mainly depends upon its quality. According to Dr. APJ Abdul Kalam, “The best way to achieve quality is to build it into the design.”

In order to obtain maximum quality products, India needs a strategic shift from the Quality Control (QC) approach to that of Total Quality Management (TQM) [4]. Quality Control is an inspectorial attitude to quality, whereby designated supervisors will inspect and certify quality, and the duty of deficiency free production lies with the production department. TQM is the continual process of detecting and reducing or eliminating errors in manufacturing, streamlining supply chain management, improving the customer experience, and ensuring that employees are up to speed with training. Total quality management aims to hold all parties involved in the production process accountable for the overall quality of the final product or service. Quality Management focuses on an end-to-end intervention and continuous improvement of quality and systems rather than post production inspection.

Self-reliance and Skill Enhancement

India is a country bestowed with abundant resources be it natural or human capital. To improve product quality the most important prerequisite is to instil a desire for superior quality products in the minds of people.

There is a need to improve the quality of our human capital so that its demand in the employment market increases. No country has achieved self-reliance without mass quality public education. Skill development will play a crucial part in finding avenues of employment for the qualified and the unemployed. In order to increase employment demand, the quality and skill set of our human capital needs to be improved. Skill development plays a major role in increasing job availability. In order to attain self-reliance the research and development standards should be in par with the world standards. The number of top tier educational institutions proportional to our population needs to be set up so that no potential student is deprived of their opportunities. Good quality of education is one of the first stepping stones in the path to self-reliance.

Around the world, youth is considered as the driving force behind future research and development. Unlike other countries, India has a huge wealth in terms of youth. In terms of percentage, about 65 percent of the country's population is below the age of 35. The inventory of a huge educated young population and the demographic potential allows the nation to reap the advantage of this vast human resource talent. However, to utilize the current available opportunities to its maximum, there is a need to upskill/upgrade the youth so that they are in pace with the current advances and employment requirements in technology and research. When compared with the other nations, India has immense potential of emerging as the global hub for providing skilled manpower to the rest of the world.



Self-reliance and Safety

Safety plays a vital role in ensuring self-reliance of a nation. All aspects of safety including national safety as well as industrial safety contribute to the development of a self-reliant nation. Peace and safety in a country ensures growth and development of industries as well as attracts foreign investment to the country. Industrial safety refers mainly to employee safety and it ensures a safe working environment to them thereby producing satisfied employees which in turn helps to increase productivity.

Self-reliance and Sustainable Development

As discussed earlier sustainability can be analyzed using several aspects like economy, society, environment, technology, politics and culture (**Fig. 2**).

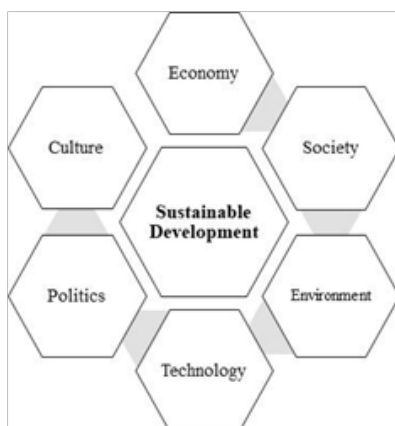


Fig. 2. Dimensions of sustainable development

Environmental Sustainability is achieved by the maintenance of the long term integrity and productivity of the planet's life support systems and environmental infrastructure. The inefficient use of natural resources can be attributed as one of the main reasons for environmental problems. In practical terms, environmental sustainability depends on sustainable use of resources, maintenance of sink functions of environmental processes, ensuring the increase in the quality and quantity of natural capital, adopting the precautionary principle and the establishment of adequate and suitable institutional frameworks for environmental protection.

Economic sustainability is achieved by adopting practices that support long-term economic growth without negatively impacting social, environmental and cultural aspects of the community. By being economically self-reliant the variation in world economic conditions will have minimal effect on the Indian economy.

A sustainable society can be defined as a society that has learned to live within the boundaries established by ecological limits. The excessive burdens upon the environment can be lowered through the practice of self-reliance and sustainable society. The nation can attain self-reliance if investors, consumers and other economic agents believe in the commitment of the political leadership and the capability of the administration to deliver.

Technology mainly refers to the study or application of industrial skills & applied sciences for optimized performance [5]. However, engineering is the method of converting resources into materials and products which advance the growth of economy and development. Therefore, wherever technology is engaged, engineering is also involved and engineering means engineers are involved. The engineers need to move faster and lead the way towards better performance, higher productivity and safety. Skilling in this direction may be envisioned to tap opportunities for nation betterment. Some government skill development organizations are NSDC, KASE, NASSCOM, Skill India Initiative etc.

Self Reliance & Sustainable Development in the Indian Automobile Sector

India is currently the fourth largest auto market in the world. The automotive industry is a major economic contributor in India. The industry supports the employment of more than 3.7 crore people and contributes to 15 percent of GST amounting to Rs 1.50 lakh crore every year. Even though this sector is of prime importance, the auto industry has been left out of the Aatma Nirbhar Bharat economic package. India has the potential of being self-reliant in various domains which include electric and fuel cell vehicles, electricity storage systems etc.

Due to the COVID-19 pandemic there has been a severe disruption in the supply chain network. In order to solve the issues occurred during the pandemic such as displaced manpower and broken supply chain, a new type of manufacturing network needs to be developed. The usage of new logistics technologies will ensure efficiency and cost effectiveness.

In order to achieve the goal of a self-reliant India, the Indian auto component industry has to focus on localizing designs and engineering. “We must stretch beyond products and focus on building sustainable designs and strive to achieve Make in India. With the frugal approach to production in India, we will have the opportunity to take on the global supply chain,” says Guenter Butschek, MD and CEO of Tata Motors.

Green Supply Chain Management (GSCM)

Environment related issues have become serious and cannot be ignored in the present day business environment. With the increasing awareness on environmental sustainability issues, manufacturing firms have, nowadays, started to think and act green.

Green supply chain management (GSCM) has emerged as an important organizational strategy in the modern day business environment [6]. It is an efficient approach to enhance manufacturing sustainability. It begins with adapting green materials, green manufacturing, green packaging and green transportation and improving operations by employing environmental solutions. Some examples of GSCM include:

1. Toyota adopted its green principles in 1992 to provide clean and safe products and also to enhance the quality life of every one through their activities. Since 1992, Toyota has been working for green procurement, environmental action plans, Hybrid vehicles, Environmental campaigns etc.
2. Pepsi-Cola saved \$44 million by switching from corrugated to reusable plastic for 1L and 20 oz. bottles thus conserving 196 million pounds of corrugated material [7].

GSCM involves the following aspects [8]

- **Green Purchasing:** GP is defined as an environmentally conscious purchasing initiative that tries to ensure that purchased products or materials meet environmental objectives set by the purchasing firm, such as reducing the sources of wastage, promoting recycling, reuse, resource reduction, and substitution of materials.
- **Green Design:** It involves the process of designing a product or a service that encourages environmental awareness.
- The two main strategies adopted by automobile companies in green design are environment conscious design (ECD) and life cycle analysis /assessment (LCA) as shown in Fig. 3 [9].
- **Green Manufacturing:** It is the type of manufacturing in which the workers use fewer natural resources, reduce pollution and waste, recycle and reuse materials, and moderate emissions in their processes.
- **Green Packaging:** It involves the use of materials and manufacturing techniques to diminish energy use and reduce the harmful impacts of packaging on the environment. It often includes biodegradable and recyclable materials as an alternative to plastic and Styrofoam.



Fig. 3. Classification of GSCM practices in automobile industry (Srivastava, 2007)



Setting up of an India Mobility R&D Protocol

While setting up a new manufacturing network there arises a need of significant investment in R&D which needs to be focussed on setting up a clear protocol that fosters innovations and solutions that are most relevant to the nation's requirements, desires and applications [10]. The solutions discovered should be apt enough so that the concerns of all sections of the society are addressed. The solutions should be equally unique and specific, so that it becomes a role model for the world to adopt.

Environmental sustainability can be achieved by imposing taxes like Congestion taxes, Environment Compensation Charge (ECC) etc. Congestion tax is implemented on private cars and vehicles to encourage more users to use public transit and reduce the number of private cars on roads during peak hours. This will significantly reduce vehicular pollution and also reduce the usage of fuel, which further leads to reduced expenditures on fuel cost.

Environment Compensation Charge (ECC) is a charge in which 1% of retail price of the vehicle is levied for the registration of diesel cars above 2000 cc.

Announcement of a fresh Auto Mission Plan

The current jump from BS IV TO BS VI was quick and most of the automobile manufacturers faced several problems in terms of design modifications as well as obtaining materials and optimising their SCM network. The need of the hour is the creation of a new Auto Mission Plan 2030. The steps involved in this process are: Creation of fresh blueprints on emissions, safety, sustainability and economic impact. Setting up development and investment plans in sync with the larger national targets.

Post-COVID Scenario

The pandemic has brought several changes in the mindset of customers. Some of the changes that will be visible in near future are:

1. Preference for personal mobility: A sense of social distancing and fear of being infected with the virus has got people preferring their own private transport instead of the public ones. This will lead to an increase in automobile sales[11].
2. The e-commerce industry has grown multitudes during the pandemic. In order to fulfill these orders, there is an increased demand for light commercial vehicles (LCVs) for facilitating logistics [12].
3. The pandemic has caused significant reduction in pollution mainly due to the concept of Work from Home. In the automobile sector, the factory workers continue to work as before, in an extremely controlled environment. The employees working from home mostly hold desk jobs.

Manufacturing of automobiles will undergo more automation and digitisation. A major part of investment will immediately go into the technology upgradation at manufacturing units adopting Industry 4.0. The implementation of remote working environments will see an improvement in productivity for the desk and office oriented jobs in the automotive industry. This will help the companies in optimising the working pattern of employees which will help in reducing operating costs.

CONCLUSION

Self-reliance and sustainable development are very closely related to each other. The inter-relationship between the factors that affect self-reliance and the dimensions of sustainable development have been established. Enhancement of skill, quality and safety play the most important roles that can guide India towards self-reliance.. Engineers play a vital role in ensuring the same. The study conducted in the automobile industry is a primary attempt at analysing the present and future situations. It also throws light into how the sector can attain self-reliance through sustainable efforts. Desired changes cannot be brought by the Government if there is an absence of public consensus. It can only be built if people are actively made to realise the damage which they are doing to the environment through their actions. Only a strong and sincere adherence to sustainable development can push India towards the goal of self-reliance that will be durable and truly effective.

REFERENCES

1. Uwem E. Ite (September 2016) 'Perspectives on Self-Reliance and Sustainable Development in Nigeria', 2nd National Conference - Academic Staff Union of Polytechnics (ASUP)
2. Book 1 WHY SELF-RELIANCE?, <https://www.unhcr.org/44bf3e252.pdf>



3. K. Jilcha, D. Kitaw, Industrial occupational safety and health innovation for sustainable development, Eng. Sci. Tech., Int. J.(2016), <http://dx.doi.org/10.1016/j.jestch.2016.10.011>
4. Abhijit Rajkhowa, Abhishek Chakravarty, India needs a Strategic Shift in its Policy on Quality to achieve self-reliance', (2020), <https://www.insidene.com/india-needs-a-strategic-shift-in-its-policy-on-quality-to-achieve-self-reliance/>
5. ErN Shyamsundar Singh, FIE, Happy Engineers' Day Engineers for a self-reliant India,(2020), <https://www.thesangaiexpress.com/Encyc/2020/9/15/Happy-Engineers-DayEngineers-for-a-self-reliant-India.html>
6. S. Luthra, D. Garg, A. Haleem, Empirical Analysis of Green Supply Chain Management Practices in Indian Automobile Industry, (2012).
7. Gyaneshwar Singh Kushwaha, Sustainable development through strategic green supply chain management, I.J.E.M.S., VOL. 1(1): 7-11.
8. Anil S. Dube, Dr.R.R.Gawande (2011), Green Supply Chain management – A literature review, International Journal of Computer Applications (0975 – 8887).
9. S. K. Srivastava (2007), Green supply-chain management: A state-of-the-art literature review, International Journal of Management Reviews, 9(1), pp. 53-80.
10. Avik Chattopadhyay, Opinion: Seven steps for Indian auto industry to be self-reliant, (2020), <https://auto.economictimes.indiatimes.com/news/industry/opinion-seven-steps-to-be-self-reliant-for-indian-auto-industry/75863931>
11. Nabeel A Khan, Auto industry from the other side of Covid-19 crisis, (2020) <https://auto.economictimes.indiatimes.com/autologue/auto-industry-from-the-other-side-of-covid-19-crisis/4165>
12. Paran Balakrishnan, Post-Covid, auto sector is on a slow recovery, (2020) <https://www.thehindubusinessline.com/opinion/columns/auto-sectors-on-a-slow-path-to-recovery/article32014662.ece>



Flamingo: Labour Management Interface System

Kushal Vilas Datrange¹, Pankit Rajesh Rana¹, Dr Anil Achyut Kunte²

Department of Civil Engineering

Student, A P Shah Institute of Technology / Mumbai University¹, Professor, A P Shah Institute of Technology / Mumbai University², Thane, Maharashtra

✉ kdatrange@gmail.com; ✉ ranapankit21@gmail.com; ✉ kunte.anil@rediffmail.com

ABSTRACT

The Indian construction industry is the second largest employment generating industry for which, major workforce is needed, after agriculture industry. It employs around 51 million people and contributes around 9% to the country's GDP. Thus, construction industry requires large amount of workforce, due to this, there is large amount of migration taking place from underdeveloped regions to developing regions as the developing regions open new avenues of opportunities in different sectors for vast work force. In the eventuality like COVID-19 pandemic more stressful conditions, develops on the resources and management of workforce. Imposition of "Lockdown" ordered, more than 53 million workers migrate to their home states, in panic, leaving a great impact on the construction industry. When the lockdown will be lifted, the need of workforce will create enormous pressure on the resource management. For this, to have controlled reversed migration of construction workers from their home states, "Labour Management Interface System" would be introduced for proper supervision and control the migration of the workers.

Keywords : Labour management; Migration; Construction industry.

INTRODUCTION

The construction industry has a very strategic and vital role in the development of a country. Currently, the construction sector continues to experience rapid growth, and these developments increase needs of the elements associated with the various construction sector. The workforce skilled and unskilled, is one of the critical aspects, on which depends execution of the construction projects. The workers migrate from their home states to other states in search of job opportunities, on completion of major agricultural activities, from rural regions to developing regions, within the country, and Middle East countries, in construction sector which employ large workforce. Accordingly, skill development programmes, balance the demand of the construction industry through trained the skilled and semi-skilled labourers and provide the trained labourers to the industry. "Skill India" and "Digital India" are correspondingly the supportive chauffeurs of this movement. The "Grameen Kaushal Yojana" designed, by the labour ministry of the central government aims at developing skill in the Indian youth by allocating Rs. 15,000 crores.

Though "Make in India" conquers eminence as an imperative objective, the upcoming path of development and growth of Indian economy reckons together with "Skilling India" and "Make in India". Under the platform of "Digital India", "Flamingo: Labour Management Interface System" is introduced, inspired from the migratory bird species Flamingos, those migrate every year to our country in the summer and head back to their respective countries after fulfilling its requisites. On the same logic this system is being conceptualized, in which the workers head back to their respective home states after their job duration at a specific location is accomplished. This system will, further, indirectly keep track and help in guiding the skilled labour, to places with better opportunities of longer duration. This system will help in controlling the rate of migration and even distribution of workforce throughout the country. Recent Skill Mapping done by the State Government of Uttar Pradesh can prove to be beneficial in implementing the system, which in turn will give the data related to the employment of various sectors, related to construction industry with their quantum of migration.

METHODOLOGY

From the **Fig. 1**, "Key Members", different stakeholders associated with the system are shown. In this, initially the workers need to register themselves with the system, with their bio data, preferred job locations and get the things attested from the police authorities from their residential jurisdiction. On the other hand, the employers i.e. builders, contractors, etc. are

supposed to enrol themselves giving authenticated information related to their project, like number of workers needed and their types, location of work, duration of work, facilities like provision of labour camp, and their health care. Certain terms and conditions shall be laid down for both the stakeholders i.e. employees and the employers on accepting or rejecting the jobs and or employees.

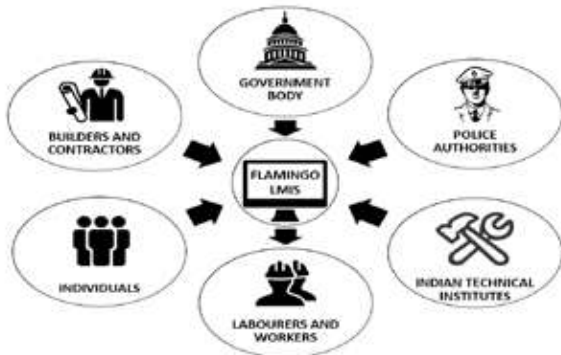


Fig. 1. Key members in Flamingo: Labour Management Interface System

For the ease of operation of this system, the help-desk (offices) will be setup at different locations throughout the country for clarification of doubts of the stakeholders, alongside online help. These help-desks will also provide information to the workers about the different job opportunities according to their job preference. In case, if any worker wish to enhance their skill, they can apply to the ITI's like technical bodies, this system will provide help in this respect.

With its user friendly interface, the workers will have freedom to choose preferences and look for different opportunities. This system, therefore, can provide the proper verification of all the workers, in respect with their background, past experience, history, etc. With this system, the digitalisation of payment as well as the employment facilities of the daily wage workers is possible which will be helpful in selecting and tracking different activities related to the different aspects of employers.

The most important thing in this system is that, the duration for stay of worker at the job location will be limited only for the stipulated period mentioned in the contract with the employer, after which they may head back to their respective home state or they will have the option to acquire new job through the portal. This will relieve the stresses of the idle resources of the urban areas to a great extent. Thus, in turn be beneficial for the development of the different regions along with the proper utilization and management of idle resources. This system will provide a great job security and safety for the workers and their families by tracking the workers current location of job at ease.

BENEFITS

For workforce

- [1] In enriching the livelihood of the workers.
- [2] Choice of selection of work locations and trades.

For other stakeholders

- [1] Recommendations from the system, on the basis of rating made by the system.
- [2] Provides updated info to employers about available workforce, opening the choice of selection, in their location.
- [3] Authenticated workforce.

RECOMMENDATIONS

- [1] Association of Government bodies will help the administration to utilize different data related to the Migration and Employment in a more efficient way.
- [2] Implementation of the system should be done through employment exchange with industry associations like CII, CEAI, ASSOCHAM, etc. helping in maintaining the database and also ensure implementation of the system at project sites.



- [3] ITI like institutions would be involved for enhancing the skills of the labour under the platform of “Skill India” initiative of the Govt. of India.
- [4] An identity proof could be generated to recognize migrants, as a stakeholder in urban development and for effective provision for the resources.

CONCLUSION

Labour Management Interface System provides a key platform for enriching the lives of workers while protecting their dignity. All the key members will be under one roof, which will provide transparency in their transactions. This system will, further, generate employment in the form for providing smooth functioning of system for different operations at different levels. Skill mapping at different stages, updating rating of workforce and of different sectors will be undertaken through this system.

Though at this stage, this system seems to be tough for understanding and implementation, especially for the workforce but, by providing proper education to the workers regarding this system through different awareness programs at different levels, with its benefits, this system can be easily implemented.

ACKNOWLEDGMENT

“Mr. Manos De, Discipline Head, Tata Consulting Engineers Limited, thanks for providing immense guidance and recommendations related to our system.”

REFERENCES

1. Ankul Pandey and Prof. D. K. Nema, “Skill Development strategy and employability of workforce in India (Make in India movement)” in Open access internal journal of science & engineering, Vol II, issue 7, 2017
2. R.B. Bhagat, Reshmi R.S., Harihar Sahoo, Archana K. Roy and Dipti Govil, “The COVID-19, Migration and Livelihood in India” International Institute for Population Sciences, April 14, 2020
3. Policy Brief, “The COVID-19, Migration and Livelihood in India: Challenges and Strategies” in International Institute for Population Sciences
4. Wheebox, “India Skills Report 2020”
5. Mr. Manos De, “Respect to our Nation Builder” Tata Consulting Engineers Limited, July 2020.



The Technical Efficiency of Unemployed Youth Employment Generation Programme in Tamil Nadu

Dr E Bhaskaran

Joint Director (Engineering), Department of Industries and Commerce, Government of Tamil Nadu, Chennai, Tamil Nadu

✉ e.bhaskaran19@gmail.com

ABSTRACT

Sustainable Development Goals of 9, the Industry, Innovation and Infrastructure is important for enterprise development. Micro, Small and Medium Enterprises Department, Government of Tamil Nadu introduced scheme namely “Unemployed Youth Employment Generation Programme (UYEGP)” which is implemented by Department of Industries and Commerce, Government of Tamil Nadu which aims to eradicate unemployment problems of socially and economically weaker section in Tamil Nadu, for educated unemployed youth to become self employed in their native places itself and to prevent the mass migration from rural areas to urban areas due to unemployment by setting up Micro Manufacturing / Service / Business enterprise. The objective is to study on technical efficiency of no. of enterprises started and subsidy released under UYEGP scheme by Government of Tamil Nadu. The methodology adopted is collection of secondary data from policy note of MSME Department. The data were analysed using Descriptive Analysis, Correlation Analysis and Data Envelopment Analysis. There is strong relationship between no. of enterprises started and subsidy released under UYEGP scheme by Government of Tamil Nadu where the correlation coefficient is 0.94 and the Technical Efficiency is 0.873. To conclude, Government of Tamil Nadu Policy on providing subsidy under UYEGP scheme to micro manufacturing, service and business enterprises is a significant one and should be increased and continued for benefit of new startups in Tamil Nadu. These enterprises should adopt cluster development approach for cost minimization and profit maximization.

Keywords : Micro enterprises; Unemployed youth employment generation programme; Data envelopment analysis; Government of Tamil Nadu policy.

INTRODUCTION

Sustainable Development Goals of 9, the Industry, Innovation and Infrastructure is important for enterprise development. The Micro, Small and Medium Enterprises Department, Government of Tamil Nadu introduced scheme namely “Unemployed Youth Employment Generation Programme (UYEGP)” which is implemented by Department of Industries and Commerce, Government of Tamil Nadu which aims to eradicate unemployment problems of socially and economically weaker section in Tamil Nadu, for educated unemployed youth to become self employed in their native places itself and to prevent the mass migration from rural areas to urban areas due to unemployment by setting up Manufacturing / Service / Business enterprise (MSB). [1]

- Scheme: For the educated unemployed youth from economically weaker sections by providing subsidy linked financial assistance
- Financial Assistance: Up to Rs.10 lakhs for Manufacturing Sector, Rs.5 lakhs for Service and Business sector provided through banks
- Eligibility: Individuals above 18 -35 years of age for General Category and 18-45 for Special Category, with minimum education of pass in 8th Std with family income not exceeding Rs.5.00 lakhs per annum
- Promoter's Contribution: 10% for General Category and 5% for Special Category (SC/ST/BC/ MBC/ Minorities/ Women/ Ex-servicemen/ DA/Transgender)
- Subsidy : 25% of the project cost subject to the maximum of Rs. 1.25 lakhs[2]



LITERATURE SURVEY

The District Task Force Committee headed by the General Manager, District Industries Centre, will select the beneficiaries through an interview process. Entrepreneur Development Programme (EDP) training will be given to the beneficiaries for Seven days by Entrepreneurship Development and Innovation Institute (EDII)[3], Tamil Nadu. Repayment schedule and moratorium shall be as per the norms of the financial Institution. For marketing support the concerned General Manager, District Industries Centre (DIC), will arrange Buyer Seller Meet, Exhibitions etc. and for land and cluster development approach entrepreneur can approach Tamil Nadu Small Industries Development Corporation (TANSIDCO) [4]. The micro enterprises development under UYEGP scheme may adopt cluster development approach [5] based on their enterprises for cost minimization and profit maximization.

OBJECTIVE OF THE STUDY

1. To study about the Descriptive Analysis of UYEGP scheme in Tamil Nadu.
2. To study about the Correlation Analysis of UYEGP scheme in Tamil Nadu.
3. To study on Technical Efficiency of UYEGP scheme in Tamil Nadu using Data Envelopment Analysis.
4. To give suggestions on further improvement in Government Policies for growth and implementation of UYEGP scheme in Tamil Nadu.

METHODOLOGY

The methodology adopted is collection of secondary data like subsidy given by Government (S) as input variable and No. of Units (U) benefitted as output variable for different districts in Tamil Nadu from 2011-12 to 2018-19 taken from policy note of MSME Department, Government of Tamil Nadu(GOTN). The data were analysed using Micro Soft Excel Data Analysis by finding, Descriptive Analysis, Correlation Analysis and Data Envelopment Analysis.

DESCRIPTIVE ANALYSIS

The descriptive analysis is given in **Table 1**.

Table 1. Descriptive analysis

	(I}S	(O)U
Max	1239.69	2055
Min	187.72	456
Average	584.3175	1183.75
SD	261.6928	370.7555

Source: Computed Data using DEA Solver

CORRELATION COEFFICIENT ANALYSIS

The correlation analysis is given in **Table 2**.

Table 2. Correlation analysis

	S	U
S	1	0.94
U	0.94	1

Source: Computed Data using DEA Solver



There is positive and high degree of relationship exists between S and U.

DATA ENVELOPMENT ANALYSIS

BCC-O Model

$$\begin{aligned} & \rightarrow \quad \rightarrow \\ \text{Max} \quad & Z_0 = \theta + \varepsilon \sum S^+ + \varepsilon \sum S^- \\ & \theta, \lambda, S^+, S^- \\ \text{Subject to} \quad & \\ & \theta Y_0 - \sum Y \lambda + S^+ = 0 \\ & \sum X \lambda + S^- = X_0 \\ & \rightarrow \\ & \sum \lambda \geq 1, \quad \lambda, S^+, S^- \geq 0 \end{aligned}$$

Model Description

The scalar variable θ appears in the primal problem is the reduction applied to all inputs of DMUs to improve efficiency. This reduction is applied simultaneously to all inputs and results in a radial movement toward the envelopment surface. The presence of non-Archimedean (Infinitesimal constant) ε in the primal objective function effectively allows the maximization over θ to pre-empt the optimization involving the slacks. Thus, the optimization can be computed in a two-stage process with

- maximal reduction of inputs being achieved first via θ
- then in the second stage movement on to the efficient frontier is achieved via the positive input and output slack variables (S^-, S^+)

Here, the constraint

$\sum \lambda \geq 1$ is known as convexity constraints, which will admit variable RTS (VRTS). The above discussion leads to form the following statement. A DMU is efficient if and only if $\theta = 1$, b) All slacks are zero. $S^- = 0$ and $S^+ = 0$.

Computing Methodology

Initially we consider 1st Engineering Cluster Enterprise as the studied DMU and the Linear Programming (LP) Model is formulated as given below

$$\begin{aligned} \text{Max } & \theta \\ \text{Subject to } & \\ & 632 \lambda_1 + 1523 \lambda_2 + \dots + 1286 \lambda_{32} \geq 1286 \quad \text{Output Constraints} \\ & 200.26 \theta - 200.26 \lambda_1 - 844.21 \lambda_2 - \dots - 567.39 \lambda_{32} \geq 0 \quad \text{Input Constraints} \\ & \lambda_1 + \lambda_2 + \dots + \lambda_{32} = 1. \\ & \lambda_1, \lambda_2, \dots, \lambda_{32} \geq 0, \theta \text{ is unrestricted.} \end{aligned}$$

By solving the above equations and continuously changing the studied DMUs the value of λ_i 's and θ_i 's for each DMU is obtained.

Efficiency Scores

The value of λ_i 's (being the weights of the districts) and θ_i 's (being the efficiency scores of the districts) were found using DEA Solver is given in the **Table 3** and the graph is given in **Fig. 1**.

As per **Table 3**, the ECI which has score $\theta_i = 1$ and rank = 1 and it is highly efficient. The efficiency and rank of ECI which has



$\theta < 1$ are also given. It has to perform well to attain 100% efficiency and rank 1. The overall technical efficiency of UYEGP Scheme is 0.873.

Table 3. Technical efficiency of engineering industry cluster

No.	DMU	Score θ_B	Rank	Reference set (lambda) λ			
1	1	0.82	25	27	1.00	28	0.00
2	2	0.90	14	3	0.03	30	0.97
3	3	1.00	1	3	1.00		
4	4	0.80	26	28	0.62	30	0.38
5	5	0.90	15	27	0.12	28	0.88
6	6	0.82	24	27	0.22	28	0.78
7	7	0.89	18	3	0.13	30	0.87
8	8	0.98	6	3	0.53	30	0.47
9	9	0.82	23	27	0.06	28	0.94
10	10	0.76	28	27	0.21	28	0.79
11	11	0.86	19	28	0.84	30	0.16
12	12	0.93	10	28	0.35	30	0.65
13	13	0.72	29	27	0.58	28	0.42
14	14	0.67	32	28	0.77	30	0.23
15	15	1.00	1	15	1.00		
16	16	0.76	27	27	0.88	28	0.12
17	17	0.83	22	27	0.40	28	0.60
18	18	0.90	16	27	0.74	28	0.26
19	19	0.69	31	28	0.46	30	0.54
20	20	0.85	21	27	0.47	28	0.53
21	21	0.93	9	27	0.03	28	0.97
22	22	0.86	20	27	0.80	28	0.20
23	23	0.91	13	28	0.73	30	0.27
24	24	0.96	7	3	0.72	30	0.28
25	25	0.95	8	28	0.63	30	0.37
26	26	0.71	30	28	0.02	30	0.98
27	27	1.00	1	27	1.00		
28	28	1.00	1	28	1.00		
29	29	0.90	17	27	0.19	28	0.81
30	30	1.00	1	30	1.00		
31	31	0.91	12	27	0.08	28	0.92
32	32	0.91	11	28	0.97	30	0.03

Source: Computed Data using DEA Solver

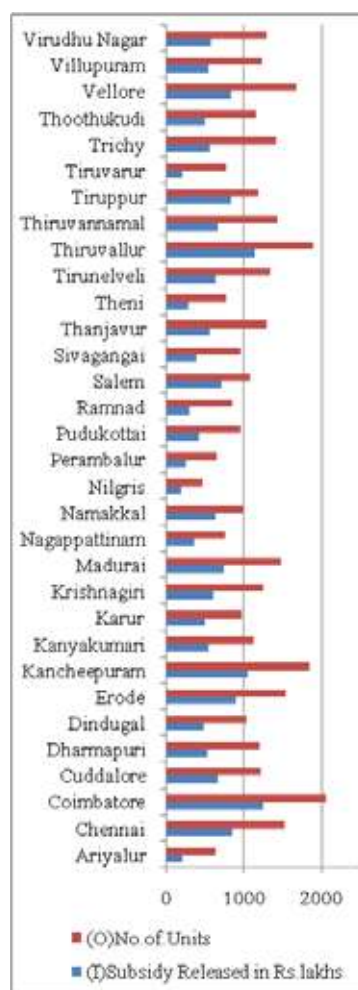


Fig. 1. Physical and Financial Performance of UYEGP

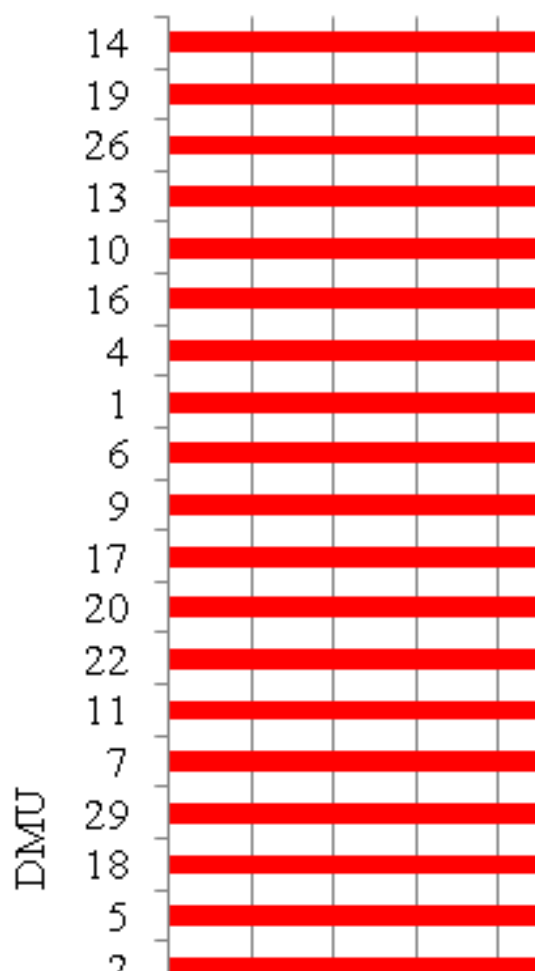


Fig. 2. Technical Efficiency

List of Enterprises under UYEGP Scheme

The lists of MSB Enterprises that can be started under UYEGP scheme are given in **Table 4**.

Table 4. List of enterprises under UYEGP scheme

Manufacturing Enterprises	Service Enterprises	Business Enterprises
Agro and Food Processing Fish and Meat Processing. Engineering and Auto Components Electrical and Electronics products Chemicals Medicine Medical equipments Solar Energy Products Energy Efficient Products Wind Mill	Consultancy Machine Repair Medical Laboratories Coaching Centres Restaurant, Catering, Event Management House Keeping Electrical Works Legal Services Civil and Plumbing Refrigeration and Airconditioning Services Building contracts Building Architecture and Drawing. Interior Decoration Employment Services Transport Services Beauty Parlour Gym, Fitness, Yoga Maintenance Service Waste Treatment Telecommunication Services Environmental services.	Export-Import Real Estate Agricultural Products Electric and Electronics Shop Auto Parts Chemicals Retail /Wholesale Wood and Wooden Furniture Hardware Readymade Garments Motor and pumps

Source: Developed by Researcher


Table 5. Technical efficiency of UYEGP

No. of DMUs	32		
Average	0.87311		
SD	0.095007		
Maximum	1		
Minimum	0.671382		
Frequency in Reference Set			
Peer set	Frequency to other DMUs		
	3	3	
	27	13	
	28	22	
	30	12	
No. of DMUs in Data =	32		
No. of DMUs with inappropriate Data =	0		
No. of evaluated DMUs =	32		
Average of scores =	0.87311		
No. of efficient DMUs =	5		
No. of inefficient DMUs =	27		
No. of over iteration DMUs =	0		

FINDINGS, SUGGESTIONS AND CONCLUSIONS

The Correlation Coefficient exposes that there is strong relationship between the studied variables. Based on the Technical Efficiency obtained using BCC model it is found there is increase in average Technical Efficiency for UYEGP Scheme and also for individual districts except few. The input and output slack variables give information about what the individual district should follow to increase their Technical Efficiency. There are increase, decrease and constant returns to scale for EIs.

It is suggested that for inclusive growth and sustainable development, these districts should increase their Units or decrease subsidy to increase Technical Efficiency. It is also suggested that the clustering of these units will strengthen infrastructure interrelationships, technology interrelationships, procurement interrelationships, production interrelationships and marketing interrelationships.

To conclude, UYEGP scheme should plan for growth according to Government of Tamil Nadu and also should get benefit out Micro, Small and Medium Industries Policy of Government of Tamil Nadu which leads to increase in productivity and efficiency of Units for sustainable business development.

REFERENCES

1. www.tn.gov.in assessed on 10.1.2020.
2. www.indcom.tn.gov.in assessed on 19.1.2020.
3. www.tansidco.in assessed on 10.2.2020
4. www.editn.in assessed on 28.3.2020
5. Bhaskaran E, (2011), "The Technical Efficiency of Chennai Auto Industry Cluster," Society of Automotive Engineers (SAE), International, Technical Paper, <http://papers.sae.org/2011-28-0100>



Role of Consulting Engineers in Mechanical Engineering on the way to Self-Reliant India

Anirban Datta¹, Tarun Kumar Ray Chaudhury²

Manager, Department of Mechanical & Piping Engineering, Richard Design Services India Private Limited, Kolkata¹

Partner, Electromech Engineers (India), Kolkata

✉ ani_dat@yahoo.co.in

ABSTRACT

Consulting Engineers, or Engineering Consultants play a very crucial role towards the development & growth of infrastructure, industry, society and environment. They may be individuals or groups – with in-depth knowledge, varying skill sets, vast experience and problem solving acumen. They contribute in development of new and renovation projects. While consulting engineers receive a great respect & honour worldwide, their roles are also associated with enormous challenges, both technological as well as non-technical. They have to cope up and overcome those not only for their own well-being, but for the society at large. In the way forward to ‘Self-Reliant’ India, consulting engineers have enormous role to set the path for emerging technologies as well as developing the next generation of engineering professionals.

Keywords : Consulting; Services; Mechanical engineering; Professional; Self-reliant.

INTRODUCTION

Engineering consultancy services have been in existence since the dawn of civilization, and is one of the oldest knowledge-based professions in the universe. Ever since the men started harnessing natural resources in the service of the mankind, the significance & importance of this profession has been increasingly realized. Engineering consultancy services required during pre-industrial revolution era were in a nascent stage and the projects were undertaken without time, money and resource constraints. However, these services have become highly complex requiring multi-disciplinary skills in view of ever increasing demands with respect to high quality, cost and schedule. This is the reason why the role of professional engineering consultant in projects is a well-established fact and their appointment is an essential requirement. Without the involvement of a professional engineering consultant, a project cannot take proper shape.[1]

Definition of Consulting Engineer

“A consulting engineer is an expert in the planning, design, and construction of both public and private infrastructures. The consulting engineering profession is aimed to benefit the whole of society, through the application of safer, cleaner, and more efficient foundations.” - The Association of Consulting Engineers of Ireland.

“A consulting engineer provides expertise and leadership in the planning, design, modification, or rehabilitation of public and private infrastructure. Consulting engineers are registered professional who practice in many disciplines, including civil, structural, sanitary, environmental, mechanical, electrical, geotechnical, chemical, industrial and agricultural engineering.” - American Council of Engineering Companies of Texas

“Consulting Engineers means the independent engineer or engineering firm or corporation employed in connection with any Project to perform and carry out the duties of the Consulting Engineer under this Indenture or any Supplemental Indenture.” - www.lawinsider.com.

Above definitions of ‘consulting engineers’, or, alternatively, ‘engineering consultants’ are correct, but not exhaustive. There are lot of other points to ponder.



Fig. 1. Execution of an industrial project

‘Consulting Engineers’ or ‘Engineering Consultants’ may be an individual, or a group of individuals – small or medium sized, or even a large organization having thousands of resources under single or multiple locations. They may be independent individual consultants/architects, retired technocrats, R&D institutions, engineering institutions, corporate houses rendering consultancy services, etc. These entities have experienced multi- disciplinary engineering man power/architects, extensive in-house engineering database, exposure to latest technological advancements, latest infrastructure facilities like computer hardware along with design & analysis software, project management software developed both in-house as well as procured externally, access to online data banks, strategic tie-ups/partnerships with leading global technology know-how suppliers/ process licensors, backup services from institutions like government and private research laboratories, reputed academic institutions, etc.

An engineering consultant plays an advisory role as client’s design engineer during project inception phase and supervisory role as owner’s site engineer during project implementation phase.[1]

ROLE OF CONSULTING ENGINEERS IN DEVELOPMENTAL PROJECTS

Consulting engineers, at all corner of the globe, are involved in designing virtually every new and renovation developmental projects, from bridges to highways to water treatment plants to power generation, transmission& distribution systems to refineries to steel & metallurgical plants. They design ventilation and electrical systems for new hospitals, hotels, shopping malls and theatres. They figure out how to build tunnels through mountains without disturbing the local wildlife, and renovate sewage treatment systems for metropolitan cities. And, of course, they solve environmental and ecological problems.

As a catalyst in the process of providing solution and problem-solving, consulting engineers lead teams of multi-disciplined professionals on complex technical projects. They also serve as expert advisors to local, state and federal government agencies, and to public sector and private industries and businesses, through the stages project inception, preliminary survey, basic engineering, specification & tendering, detailed engineering, construction supervision, project management, performance tests, trial run and commissioning.

The functions of a consulting engineer can broadly be classified as below:

- Developing/studying project techno-economic feasibility reports (TEFR) and detailed project reports (DPR) including their financial reliability and cost estimates; environmental impact assessment (EIA) and environment management plan (EMP)
- Preparing and/or reviewing mechanical, piping, structural, architectural, electrical, HVAC, fire protection system calculation, designs and drawings.
- Preparation of technical specifications & tender documents, including inviting tenders, evaluating bids and managing tendering procedures.
- Hazardous operability study (HAZOP), hazard identification (HAZID), and hazardous area classification
- Supervising and ensuring highest quality of performance standards, adhering to national & international codes & standards, regulations as well as project specification.
- Advising on repair, alteration and maintenance of existing structure/equipment/machineries.
- Offering advice on inter-disciplinary matters such as selection of plant and equipment like elevators, electricals, control system, water supply network etc.

- Act as Proof/Validation Consultant for cross-checking design in case of complex structures/systems/process to ensure complete safety and economy.



Fig. 2. Role of Consulting Engineers

In short, a consulting engineer has to ensure that the state-of-the art and cutting edge technology is used for all solutions which should be creative but at the same time environmental-friendly and economic.

Apart from technical qualifications, knowledge and expertise, a consulting engineer should have other qualities/traits for the success in his profession, some of which are:

- Considerably fair working knowledge of finance and business procedures& management.
- Importance of team spirit and human relations.
- Ability to convince clients.
- Language & communication skills when working in international projects & clients.
- Maintenance of confidentiality of information of clients and other stakeholders such as process licensors.
- Not to indulge, promote or encourage any unethical and/or unfair practice which may affect client, other stakeholders in particular and society at large.
- Have no conflict of interest in the project handled by him/her.

PROCESS OF ENGINEERING CONSULTANCY

Following **Fig. 3** depicts a typical engineering consultancy process and interrelationship of various departments in a large multi-disciplinary consultancy organization, working in the project of a large coal-based thermal power plant.

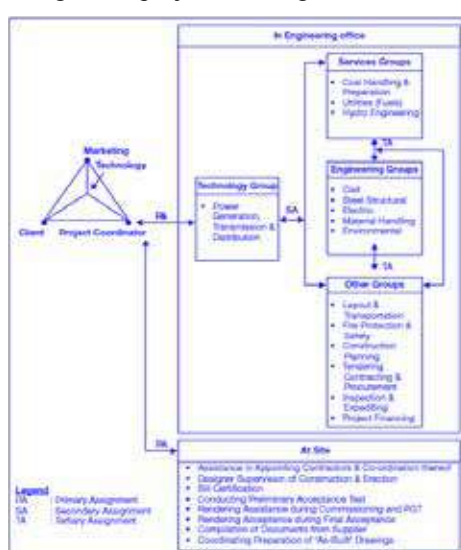


Fig. 3. Engineering consultancy process (typical work situation)[1]



Necessity of engaging consultant very early in the inception stage of a project cannot be overemphasized. Serious errors can occur in delaying such an appointment. Without having the consultant mobilized in project at the early stage, various types of hindrances have been found coming in the path of execution.

Large engineering design organizations often maintain in-house consultants on a regular payment/retainer-ship basis. While not trying to belittle their work and ability, in-house engineers may have their own set of strengths, ideas and pinpricks, while an outsider independent consultant can put in new proposals, latest concepts and be totally unbiased with their approach.

To carry out the selection of right consulting engineer(s), the client or the EPC contractor MUST have a fairly good knowledge about the consultant's experience, expertise and background. There have been cases where direction less selection created severe problems. The consultant and in-house staff with their assumed/confined outlook and knowledge are often limited by obsolete traditional practice. In third world countries the clients, hindered by financial limitations, generally try to select a consultant on lower price criteria, rather than on the basis of competence & experience, which often lead to delays and project losses. When turn-key/EPC tenders are called, contractors who do not have a strong engineering design office of their own with competent staff, generally team up with consultants with whom they have regular contact, but who may not necessarily be of the highest calibre. In such a case again the benefit of low prices which could be offered by medium-sized contractors are lost due to poor and un-economic designs emanating from less competent consultants.

On a global spectrum, the leading financial/funding organizations such as World Bank, Asian Development Bank (ADB), European Bank for Reconstruction and Development (EBRD), African Development Bank (AfDB) and others keep a roster of consulting firms and individuals, who render services in over 70 specialized fields ranging from architectural and industrial design to civil works, energy, infrastructure, aerial, hydro and geological surveys, disaster planning & management, forensic engineering, rehabilitation & resettlement planning, manpower planning, project supervision & monitoring and virtual design. In India there are a few Indian engineering organizations whose membership covers consulting engineers – both individuals as well as groups – with appropriate expertise & experience.

CHALLENGES & CONSTRAINTS BY ENGINEERING CONSULTANTS – GLOBAL & INDIAN PERSPECTIVE

The global spectrum of consulting fraternity have presented many upturns and downturns over last 50 years. It changed from the one-man show via. group of individuals to large consulting organizations providing multi-disciplinary services under a single roof and serving global clients including those in India. In last 25 years, it has practically become insignificant/unimportant whether the project location and location of consultants are in the same part of the globe or in different corners, due to the enormous advent in information technology. The concept of 'work-share' in engineering design and engineering consultancy sector has leveraged the hiring of expert(s) from any part of the world.

However, from the perspective of large consulting organizations, there have been some points of concern:

- o With emergence of Engineering, Procurement & Construction (EPC) companies who built up large pool of experts in-house, the existence of large engineering consulting firms who deal only with intangible assets like knowledge and concept have been facing gross challenge, as a major portion of clients are preferring complete solution from one window.
- o It has become a common perception among clients as well as other stakeholders that consultants attribute to delay in execution and completion of projects, as well as not adding significant value towards quality.
- o The cost of project hitting the sky due to exorbitant price charged by large consulting organizations.

World-wide, consultants, whether individuals or with organized structure, are facing challenges due to various changes, such as:[2]

- ❖ Changes in commercial practices
- ❖ Emergence of new technology, and difficulty in adapting the same
- ❖ Shift in social dimensions
- ❖ Rise in knowledge base and sophistication by clients who are placing the more and more emphasis on tight completion schedules and higher quality standards.\
- ❖ Working on too many projects simultaneously

- ❖ Shortage of working personnel as well level of experience
- ❖ Dissatisfaction among personnel over remuneration/pay package
- ❖ Not receiving payment from client in timely manner
- ❖ Large overheads in the organization

Table 1. Overall Ranking of the Problems Faced by Engineering Consultants

Sl. No.	Types of Problem	Ranking
1	Handling too many projects simultaneously	1
2	Shortage of manpower/resources	2
3	Lack of experience/skill set	5
4	Highly demanding client	4
5	Irregularity in payment from client	5
6	Lack/failure of commitment from associates	5
7	Overhead in organization	8
8	Technological obsolescence and difficulty to adapt new technology	9
9	Unsatisfied personnel over pay package	3

Following factors can play a positive role for enhancing performance of the consulting engineer(s):

- (i) Support from the top management of client's organization and participation/commitment of client's team members
- (ii) Own core-competency
- (iii) Clearly defined goals
- (iv) Methodological compatibility
- (v) Standardization of procedures



Fig. 4. Specialized service by consultants

While the perceptions and challenges indicated above have historical and logical basis, it is needless to say that still there are relevance of multi-disciplinary engineering consultancy organizations for mega projects like super critical & ultra-super critical thermal power plants, large integrated iron & steel plants, oil & gas refineries and petrochemical plants, large hydro-electric projects, etc. Therefore, it is call of the day that Indian consulting firms gear up/reorient themselves for handling such projects and show their skill and resourcefulness in competing with international consultants.

However, in a parallel route, there is silver lining for the individuals having high level of competencies to fit themselves in the engineering consultancy for medium and small scale projects; however, this needs a more pragmatic approach in India to pave way for Professional Engineer (PE) certification, so that there must be accountability associated always.

For example, as far as product & machineries manufacturing sectors are concerned, it has been seldom observed the engagement

of large consulting houses, mainly due to maintaining confidentiality by the product/process developers/licensors. However, individuals and/or smaller groups of consulting have played/would continue to play significant role, particularly in highly specialized areas like finite element analysis, vibration analysis, stress analysis, 3D modelling, BIM solutions, performance guarantee test, etc, along with emerging & new-age technologies such as Internet-of-Things (IOT), Augmented Reality (AR), Machine Learning, Cloud based engineering & design, etc.

For the next-gen engineers aspiring to shape up careers in engineering consultancy, the training has necessarily to go beyond classrooms and text books, because the field of consulting engineering is getting widened rapidly, practically day-by-day, and as such practising engineers should take in their fold the students with bright background and give them hands-on training in their organizations, thus bringing in more of the 'design office' within the classroom. The seasoned industry professionals should take up the role of 'educator-practitioner'.



Fig. 5. 'Educator-Practitioner'

As far as inculcation of engineering knowledge sharing to the society is concerned, unfortunately there are very few practicing engineering consultants in India who write present papers at engineering forums/professional bodies, or write articles in technical and professional journals, citing their practical experiences. Most of the contents come out from professors and research scholars of various universities and research institutions. It is now high time that consulting engineering professionals lead the movement and contribute in print the findings of their matured experience and knowledge for the benefit of the engineering fraternity in particular and even for the society at large. Over the next 10 years India will require around \$1.7 trillion to finance its infrastructure needs, viz. roads, ports, airports, power generation, transmission and railways etc. Needless to state that in all of these areas, consulting engineers are bound to be connected and play a significant role towards setting the path forward.

As Government of India have set a target in building rural infra-structure through Bharat Nirman in order to pave the way of rapid rural transformation, engineering consultants would play a crucial role in this endeavor. Coupled with sustainable development and emergence of 'smart technologies', the practicing engineering consultants need to lend their hand. Issues of climate change, renewables energy systems, rain-water harvesting, zero-discharge and CO₂ emissions & capture are areas where there are immense scope of engineering consultants to contribute towards Self-Reliant India.

ACKNOWLEDGMENT

Authors acknowledge the Authority of The Institution of Engineers (India) for giving opportunity to write this paper.

REFERENCES

1. Pradeep Kumar Chatterjee, Partho Pratim Chatterjee, Marketing of engineering consultancy services : a global perspective, The Technical Manager's Survival Guides, published by ASME Press, pp. 1, 2, 58.
2. Wan Zulkifli Wan Yusof, Bachan Singh, Abdul Rahim Abdul Hamid, Ngang Shue Ming, The Role of Consulting Engineers in Project Development, Issues in Construction Industry, published by Universiti Teknologi Malaysia, Chapter – 8, pp. 124–133.



Innovations, Incubation and Entrepreneurship is a Driving Force for the National Economic Development

Dr C Sendil Kumar

Addl. Chief Manger, Centre for Applied Research and Development, NLC India Ltd, Neyveli TS, Tamil Nadu

✉ sendil4kumarc@gmail.com

ABSTRACT

The unemployment is the major concern for the heavily populated countries like India. In positive sense, the human resource asset are the major advantage to India that to having with huge younger population. Major economic development is possible by using these assets effectively. The only way is making the educated youths to turn to take the self-employments. At the outset more idea becomes more innovation and creates more entrepreneurs and contributes to more GDP. This paper indicates idea of innovation, incubation and entrepreneurship and its relationship. Here, also discussed steps to increase the number of entrepreneurs. The benefits given by the Government and various provisions available also discussed.

Keywords : Innovations; Incubation; Business start -ups; Government supports for entrepreneurship.

INTRODUCTION

Though Innovation, incubation and entrepreneurship are seems to be different words, the articulate theme is one and the same. Innovation is the application of something new for a specific use. Students must be cultivated with ideology of innovating skills from childhood which will lead them to create some purposeful thought. The other two are evolution from the innovation. Definitely the “make India concept” would be fulfilled if number of entrepreneurs come forwarded to augment. Now the opportunity is available in the hands of young technocrats. The Government is providing all sorts of helps and guidance in this aspect. The growth of individual will uplift the family, geographical region and interns the country. Of course it would become as a major contributor to the GDP. This paper aims to motivate and create awareness among the young people to emerge as job creator instead of job seekers.

INNOVATIONS, INCUBATION,

Innovation implies a very sharp understanding of the reality, and a high degree of creativity. Analyses of how things are working, how best it can be improved and what are actually missing and needed. The gap & business analysis are more important for the success.

Innovation deals with

- creativity
- new products
- new production methods,
- new markets,
- new forms of organization

Incubation is a process which always involves whenever there is a need and support to entrepreneurs in developing their own business. An incubator is a place where the incubation activities are carried out and helping entrepreneur and existing small enterprises in terms of facilities and expertise, to address their needs and develop their business ideas, and transform them into sustainable realities.

Research and development are essential part in developing new products as discussed above. The country capex spending on the R&D is also one of the indicators of development of the county. In this context, the developments in self-employment segment viz., tiny, small, medium scale industries are significant contributor for the national development. It creates jobs,



demand, and run the economic cycle. Start up companies are the most dynamic in development of national economic growth. The R&D is the starting point for the innovation, incubation and for start ups, every country interested to augment the area.

A list of countries their research and development (R&D) spending in real terms are indicated in the table 1. The R&D spending in India is Rs 1,13,825.03 crore in 2017-18. India's per capita R&D expenditure has increased to PPP \$ 47.2 in 2017-18 from PPP \$ 29.2 in 2007-08. India spent 0.7% of its GDP on R&D in 2017-18, while the same among other developing BRICS countries. Though this is appreciable indicators and still the parameters shall be improved by enhancing innovation, incubation and entrepreneurship.

Table 1. List of research and development (R&D) spending by major countries

Country	Expenditure on R&D (billions of US\$) PPP	% of GDP PPP	Expenditures on R&D per capita (US\$)	Year
Israel	18.6	4.9	1,973	2018
South Korea	91.6	4.3	1,518	2014
Japan	165.7	3.2	1,297	2016
Sweden	14.2	3.2	1,468	2014
Finland	7.2	3.2	1,318	2014
Taiwan	33.7	3.1	1,384	2015
Austria	11.9	3.1	1,416	2015
Denmark	8.2	3.1	1,450	2014
Switzerland	13.1	3	1,648	2012
Germany	118.8	2.9	1,450	2016
United States	511.1	2.7	1,586	2016
Belgium	12.4	2.5	1,103	2014
China	553.4	2.2	388	2018
*India	80.4	0.7	47.2	2018

*calculated values

The process in the incubation is spelt out as below. The incubation tree is split into three categories as Pre incubation, Incubation and Post incubation [4]. The process is guided by the experts available in the incubation Centre.

Pre incubation

- Innovation evaluation
- Business plan
- Business modeling
- Training

Incubation

- Financial Plan
- Mentoring and Guidance
- Hosting
- Training
- Patenting
- Commercialization
- Applied business plan



Post incubation

- Innovation Diagnostics
- International support
- Technology out bid
- Clustering
- Business Development

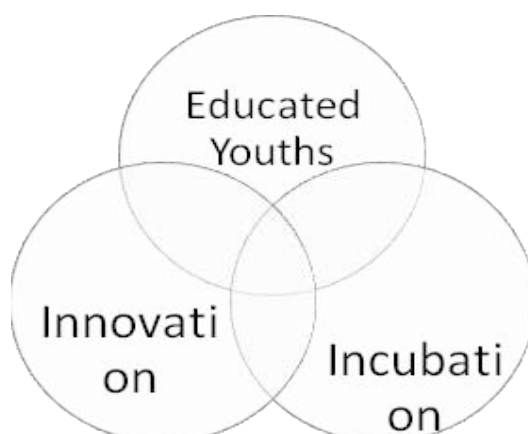


Fig. 1. Relationship Diagram for “Start-ups”

The Figure1 illustrate the formation of start ups from innovation to incubation. The educated youth community has to come forward to take up the carrier by using the potentials.

ENHANCING METHODOLOGIES

The improvement of Innovations, Incubation, and Entrepreneurship will ultimately give a positive response to social development. This development is combined responsibility of individual, academia, industries, and politics. Start ups are the key here to revive the economy and make India a self-reliant country. Start ups are not just another new business but they bring added value to society.

At state level and national level government has taken more initiatives; The Government of India has taken various initiatives for the development of this segment. Under Atal innovation mission, Atal incubation Centre are the one of the innovative idea, which develops the incubation centres in the educational institution and in the PSU industrial sectors in all over India.

To enhance the innovation skills of Science, Engineering & technological students should be trained accordingly. In curriculum itself necessary input must be provided. The sectors available and its potential scope shall be clearly defined to the Entrepreneurs. The Government policy on incubator and the facility & incentive available shall be wide spread to attract the youth communities. Various minor projects, competitions, games, related events shall be conducted to meet the challenges in the real world problem. Working and experience persons interested in starting the start ups with their valid proof of concept also be encouraged with suitable business model.

No product will shine for ever; it has its own product cycle dependent on time. Hence, the developer should always think on modification, value addition or new product. Quality and safety on the product/service is an important factor. Making profit alone will not sustain in future. The Covid-19 taught us many things. For example the holistic medicine or natural herbs are having attractive scope in near future. To make India as self-reliant and sustainable, student should come forward to be an employment provider. This attitude shall be inculcated from their child hood stage itself.

Facility available under the scheme:

1. Assistance in technology development
2. Investment assistance



3. Seed capital assistance
4. Equipment & Facility sharing
5. Assistance in procurement of equipment
6. Technological assistance
7. Dissemination assistance
8. Patenting
9. Providing space and infrastructures
10. Guidance in the business process & marketing

CONCLUSION

To shift India from developing country to the developed country, the MSME sector is one of the promising segments. India has set target of achieving more than 2 % of GDP in the R&D expenditure. This is the order of the day, to develop more MSMEs & ancillary sectors as start-ups. This would be possible by inducing more number of educated youths to take up this as a carrier option. Both State and Central Government has taken several measures to boost the sectors. Innovation, Incubation centres has been formed in all major private and public institutions as well in the PSUs. But still it requires forming more number of Incubation and Innovation centres with budgetary allocation. The education curriculum has to be accordingly formed and must be practical and project oriented one. We hope that creating awareness and motivation will enlarge the sector further. It is concluded that more number of scientific, technical and management institutions to take necessary steps for boosting the sector.

REFERENCE

1. Hanadi Mubarak, Al-Mubarak, Challenges and opportunities of innovation and incubators as a tool for knowledge-based economy, Journal of Innovation and Entrepreneurship, Jul 2017.
2. Okon Joseph Umoh, Augustine Okon Jacob, Effective Indigenous Technology for Self-Reliance and Sustainable Economic Development, International Journal of Research and Innovation in Social Science (IJRISS) |ISSN 2454-6186, Volume IV, Issue V, May 2020.
3. Siddaram, H.M. Rural-urban transformation and Economic development in India, International Journal of Research in Social Science, 1 – 14, 2017
4. The Smart Guide to Innovation-Based Incubators (IBI), Luxembourg: Publications Office of the European Union ISBN 978-92-79-14859-0, 39 pp, 2010
5. https://en.wikipedia.org/wiki/List_of_countries_by_research_and_development_spending.
6. <https://niti.gov.in/aim#> Atal Innovation Mission -NITI Aayog.
7. <https://data.worldbank.org/indicator/>



Exploring Nexus of Socio-economic-environmental Aspects for High Speed Rail Corridors Development in India

Dheeraj Joshi¹, Shikha Saini², Vivek Joshi³

Civil Engineering Department¹, Electrical Engineering Department², Ministry of Railways, Government of India
Project Unit³, National High-Speed Rail Corporation Ltd., Vadodara, Gujarat

✉ dj.utokyo@gmail.com

ABSTRACT

India being the seventh largest nation with more than a billion populations has a large and diverse, but energy inefficient transport network and India has a large potential to invest in energy efficient transport infrastructure. High Speed Rail offers comparative advantage of reduction in travel time and having low carbon footprint. Most of the previous researches which studied High Speed Railways mainly focused on economic geography or the environmental impact in terms of CO₂ emission. But for sustainable development, it is critical that an integrated socio-economic-environmental approach must be developed to implement High Speed Rail projects so that they can be well assimilated in the developing economy of India because Sustainable development is a process linking past to what we're doing now, which in turn affects outcomes of the future. This study thereby utilizes temporal statistical and spatial remote sensing data (prepared through analysing some of the major global HSR frameworks) in evaluating the nexus of existing social, economic and environmental outcomes of current HSR corridor in India and the understanding from this integrated approach is useful for transformative Sustainable High-Speed Rail Corridors Development in India with a view to enhance economic geography and improve quality of life.

Keywords : SDG; Transit oriented development; Night-lights; NDVI; Population; Urban area.

INTRODUCTION

Quality infrastructure is not only confined to infrastructure development, but it is an all-inclusive concept including factors as sustainability, safety and resilience, local job creation, and human resource development. The United Nations, Sustainable Development Goals also list “sustainable infrastructure projects” which includes efficient transportation services as one of its several objectives [1].

Banking on energy-efficient technologies and improved performance, India has a large potential to invest in energy efficient transport infrastructure. Ministry of Railways in India after Mumbai-Ahmedabad High Speed Corridor has now identified for preliminary study, new High Speed Rail Corridors for development in India namely Delhi-Jaipur-Udaipur-Ahmedabad, Mumbai-Nasik-Nagpur, Chennai-Bengaluru-Mysore, Delhi-Chandigarh-Ludhiana-Jalandhar-Amritsar and Mumbai-Pune-Hyderabad in February 2020 for preliminary study of these corridors [2], besides undertaking feasibility study for Delhi-Varanasi High Speed Corridor.

The argument for considering integration and nexus between the economic, social and environmental dimensions of sustainable development was reaffirmed at the 2012 UN Conference on Sustainable Development [3]. The word nexus stands, in general, for “a connection or series of connections linking two or more things” [4]. When governments only seek to enhance economic growth in order to reduce poverty levels, then drastic environmental impacts like climate change cannot be avoided [4,5]. Therefore, sustainability implies that any development path that leads to an overall reduction of the stocks of natural capital (or, specially, to a decline below the minimum threshold) fails to be sustainable even if other forms of capital increase [6].

LITERATURE REVIEW

HSR as an emerging alternative: Transport infrastructure is a catalyst of economic growth and development as it creates better access to markets and ideas. The history of major developed geographies such as Japan, Western Europe and the United States shows that the period of construction of transport infrastructure like railroads harmonize with the period of rapid economic growth [7]. Particularly in Japan where this economic growth further led to development of high-speed rails.



High Speed Rail is a complex system involving interplay of various elements of infrastructure, rolling stock, energy, operations, finance, human factors and managerial components [8]. But the High-Speed Rail system is more than a technical concept and the anticipated impacts from HSR are omnibus and important tool for political integration: linking territories and improving accessibility to broader geographic areas and improves quality of life of people [9].

HSR & Economy: Benefits of HSR can be significant in two ways, the first benefit accruing from time saving by travellers and secondly through addition and changes in economic activity leading to enhanced economic productivity and market expansion [10]. In the context of China, it was found the investment in HSR had positive effect on national economic growth [11]. Regional economic productivity is also affected by agglomeration and diffusion effect [12].

HSR & Environment: As there are no natural prices for environment, landscape and life, the economic analysis requires creation of artificial ones [13]. How much economic analysis is inappropriate for such elements is understood from the study of Ref. [14] wherein economic benefit of smoking was analysed in the society and suggested smokers are assets to society by calculating the costs saved on their pensions and social security. HSR is being projected as an environmentally friendly alternative to other modes of transport [9]. In European HSR emission study it was found out emission reduction in HSR and Freight Measure scenario in 2025/2030 against reference scenario (No HSR) in 2025/2030 [15].

HSR & Society: HSR requires high volume of demand to compensate for high construction costs in urban areas, which is sensitive to population density. Cities with high population along the corridor improves benefit to people through lower the cost of travel as more users are sharing the fixed cost of capacity [16].

HSR & Transit Oriented Development: Transit oriented development is a land-use and transport planning to optimise transport services by concentrating urban development around transit stations [17]. Location of HSR station is strategic for the success of the system to take advantage of the reduced travel times by passengers including access and egress. HSR stations with intramodality have the potential for attracting retail shops, hotels, business activities grouping together and also serving as remote co-working office [8]. In Mumbai, it was found the modal walking distance as 1250 m for commuters [18]. Ref. [19] suggested pedestrian radius as 500-1000m walking distance to rail station and used radius of 1000 m of rail stations for their study. Ref. [20] found the walking distance value to be 1.7 km (1.3 km for females) and 5.2 km for bicycling for deciding location of transport related facilities in urban areas in Indian cities context. Therefore, TOD buffer zone around HSR station are important for understanding the impact of HSR stations on HSR city.

Literature review for selection of indicators for the study: To compare sustainability across different societies, development of such indicators is necessary which account for holistic sustainability evaluation in a coherent and consistent manner [21].

Over half the world's population is living in urban areas but the economic performance across regions and nations is impaired by the absence of data on urban Gross Domestic Product (GDP). To overcome this scarcity of global urban information, night-time light data is used as a proxy for economic activity in urban areas [22]. Ref. [23] suggested that satellite night data are useful proxy for economic activity at spatio-temporal scales. Impact of HSR on urban economy has been investigated using night light data of Chinese cities by Ref. [12]. Therefore, night-light data is used as an economic indicator for this study.

The urbanization impact on vegetation cover is captured by Normalized Difference Vegetation Index (NDVI) trends to observe urban greening as pointed by Ref. [24] and finding trend of disturbances in city cores and subsequently help to establish alternative strategies for minimizing environmental impact. Therefore, in this study NDVI values will be utilised as environmental indicators for analysis.

As, HSR requires high volume of demand to compensate for high construction costs in urban areas, which is sensitive to population and population growth rate as identified vide Agenda 21 of the United Nations is a crucial social indicator affecting long term sustainability and has implications for elements related to education, infrastructure and employment [25]. Therefore, the population growth rate will serve as an appropriate social indicator for this study.

METHODOLOGY

Data Sources

“Rocket” locomotive reaching 50 km/h in 19th century to Tokaido Shinkansen operating at 210 km/h in 20th century. With 21st century commercial HSR speeds have seen a jump reaching speeds above 320 km/h [8] with the huge development of HSR lines from around 5000 km in the year 2000 to almost reaching 50000 km by 2020 [8, 26]. Thereby, this study examines some global HSR systems developed after the year 2000 for analysis. The data is derived for HSR corridors namely Madrid-Barcelona,

Aomori-Hokuto, Osong-Mokpo, Beijing-Shanghai and for Mumbai-Ahmedabad route for understanding nexus of indicators of social, economic and environment trends.

Night-time light data.DMSP/VIIRS data as available on Google Earth Engine Data Catalog (GEE)[27].

Landsat-7 data. ETM+ as available on GEE [27] and is used to produce NDVI composites vide eq. (1).

$$NDVI = \frac{NIR - RED}{NIR + RED} \quad (1)$$

Population growth data. Population growth data is derived from the official statistics (as available on the official census websites of each country)for the respective HSR corridor cities upto the latest census.

The rate of population growth (herein used as PGR), r , between two time points, t_1 and t_2 , is calculated as an exponential rate of growth [25] in eq (2):

$$r = 100 \ln (P_2 / P_1) / (t_2 - t_1) \quad (2)$$

Administrative boundaries. Database of Global Administrative Areas hosted on DIVA-GIS [28].

Coordinates of the HSR stations. The coordinates of the stations for linking above data is based on WGS_1984 Coordinate System hosted on Google Maps [29]. The coordinates of Mumbai-Ahmedabad HSR stations are converted from UTM coordinates to WGS84 coordinates.

Table 1. Description of data used

Data	Data Description	Year
DMSP-OLS NTL	Annual product – stable lights composite	2001-2013
NPP-VIIRS DNB	Monthly product – “vcmcfgr”	2013-2019
LANDSAT-7	Landsat 7 ETM+ sensor, SR product	2001-2019
Population	Census data	2001-2020

The general methodology and research flow is shown in **Fig. 1.** flowchart for this research study.

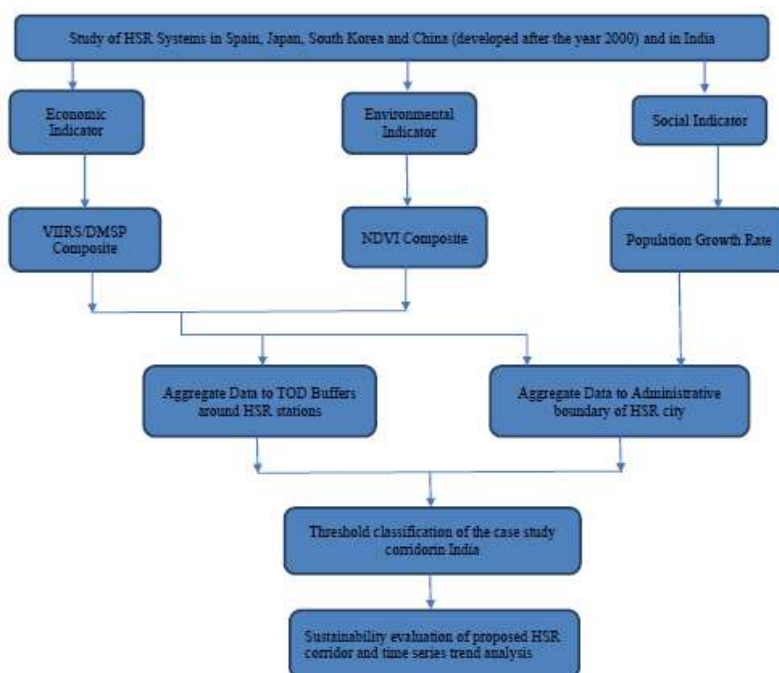


Fig. 1. Flowchart showing general methodology proposed in this study

RESULTS & DISCUSSIONS

The socio-economic-environmental indicators developed by the consolidated global HSR framework are analysed by finding the threshold through medians for night-light data, green space and population growth rate data, for the zones: HSR region and TOD buffer zones around the HSR stations.

Out of 5 global HSR corridors considered in this study, representative results for Beijing-Shanghai HSR corridor are discussed here and representative spatial data being shown in **Fig. 2**. The corridor came into operation in the year 2011 and there are total 6 stations in this corridor namely Beijing, Tianjin, Jinan, Xuzhou, Nanjing and Shanghai. In social indicators, for big cities like Beijing and Shanghai, the population growth rate (PGR) was high when HSR opened but now PGR is showing decreasing trend but for other cities it is almost constant. Most critical aspect is environmental indicator as none of the city is above threshold in any of the zones of study after HSR opened as per time series results shown in **Fig. 3 (A)** while economic performance over the years is increasing for all the zones under study over the years as per **Fig. 3 (B)**.

For Mumbai-Ahmedabad HSR corridor cities, there are total 12 stations (9 cities) in the Mumbai-Ahmedabad HSR corridor namely Mumbai, Thane, Virar, Boisar, (in Maharashtra), Vapi, Bilimora, Surat, Bharuch, Vadodara, Anand, Ahmedabad and Sabarmati (in Gujarat) with a total length of 508.17 km. The corridor will traverse 155.76 kms in the state of Maharashtra (7.04 Kms in Mumbai sub-urban, 39.66 kms in Thane district & 109.06 kms in Palghar district), 4.3 kms in union territory of Dadra & Nagar Haveli and 348.04 kms in the state of Gujarat.

The areas identified have NDVI composites value almost stable and with coming of HSR corridor and development of HSR transit stations the values may undergo change further as per **Fig. 3 (C)**. All station-cities shows economic growth above global threshold value of median nightlight and this shows that the station area is conducive for economic activities and shows promising potential for further TOD development along the HSR corridor as per **Fig. 3 (D)**.

In social indicators the official statistics shows census values up to year 2011 for which year the PGR values are computed and analysed. In the social indicator analysis, 6 out of 9 station-cities have PGR above threshold value and Mumbai city though having highest population is having lowest PGR. But the adjoining city of Thane has very high PGR showing population adjoining to big city as a result of “dispersion effect” as the night-light data is showing positive trends and NDVI values are below threshold value.

Region: Administrative boundary of the city

TOD 1: 500m buffer around station coordinates

TOD 2: 2.5Km buffer; TOD 3: 5Km buffer

TOD 4: 10Km buffer; TOD 5: 25Km buffer

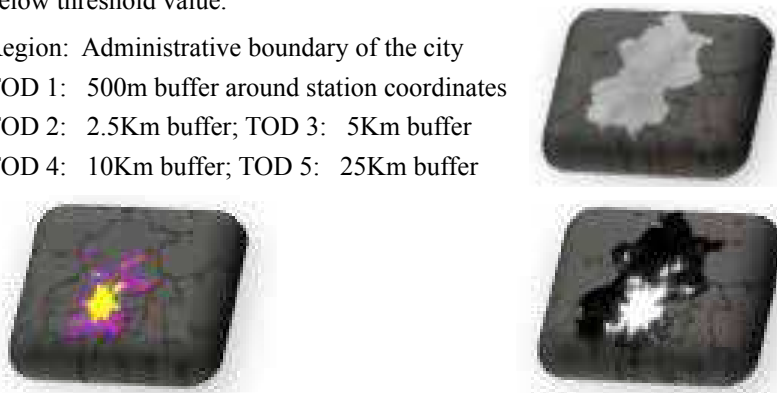
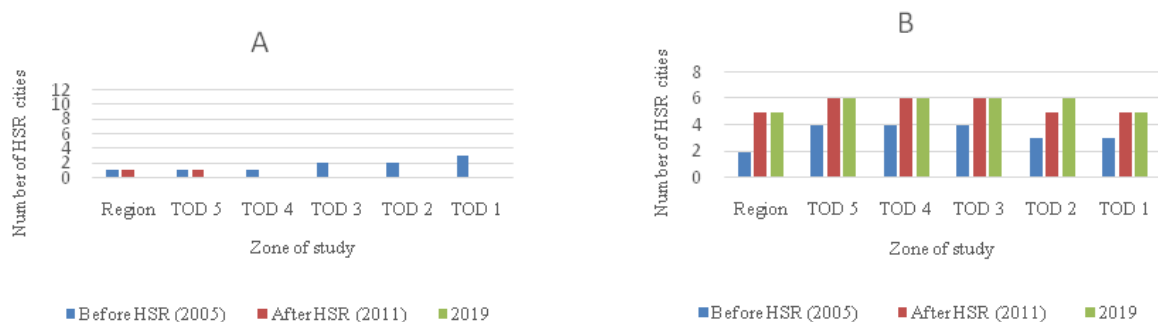


Fig. 2. (From left) Landsat-7 NDVI Image, night light image and vector image of night light (Beijing city is shown here as an example of indicators, similar exercise done for 34 other cities including their TOD zones)



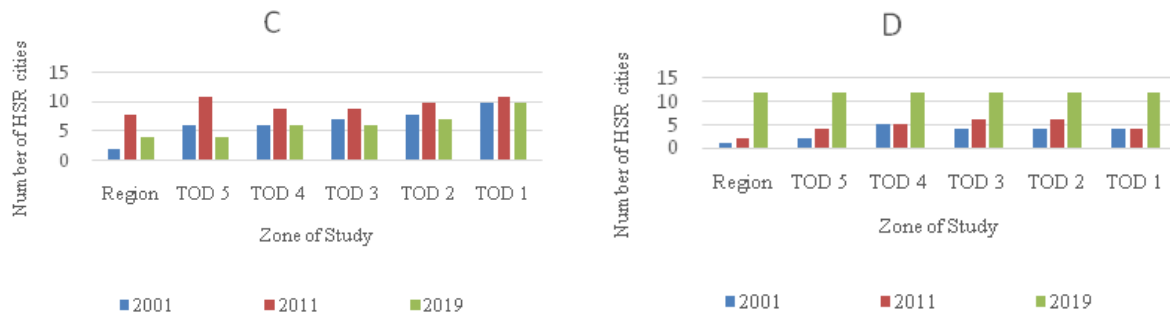


Fig. 3. (From top) A: Beijing-Shanghai HSR corridor green space evaluation; B: Beijing-Shanghai HSR corridor economic evaluation; C: MAHSR green space evaluation; D: MAHSR economic evaluation

CONCLUSION

The HSR project is strategic in bilateral relationship between India and Japan and provide ‘demonstration effect’ for Japan’s involvement in similar hi-tech infrastructure projects in Mekong River Region[1].

Apart from the above strategic issues the importance lies in sustainable development of the HSR corridor in social, environmental and economic terms so as to learn from the negatives of negative spill overs of economy as seen from the adverse environmental impact in Beijing-Shanghai HSR corridor.

Thus, through this novel integrated approach, cities and transit zones around HSR or even metro station locations can be identified where socio-economic-environmental aspects especially environmental indicator is critical especially open and green spaces around HSR stations (WHO guidelines stipulate 9m² per capita and Ministry of Urban Development [30] calls for making conscious efforts for adhering to the WHO norms) and suitable interventions can be planned through coordinated planning by urban and transport planners for sustainable development and designing right mix of economic and environmental geography. Because for sustainable development it is critical that an integrated approach must be implemented so that the upcoming infrastructure projects can be well assimilated in and supported by the developing economy of India. The understanding from this integrated approach is useful for transformative Sustainable High-Speed Rail Corridors Development in enhancing economic geography and improving quality of life.

ACKNOWLEDGMENT

The authors are grateful to the Ministry of Railways, Government of India for supporting us in this endeavour.

REFERENCES

1. Purendra Jain, 2019. “Japan’s Foreign Aid and ‘Quality’ Infrastructure Projects: The Case of the Bullet Train in India”. In: JICA-RI. No. 184.
2. Tender Document titled “Carrying out the Stage-I preliminary route development for new high-speed rail corridors for NHRCL”, February 2020. Available Online: <https://nhsrcl.in/ja/tenders/active-tenders> (accessed on 29 June 2020).
3. UN Report on Sustainable Development, 2012. Available Online: https://www.un.org/ga/search/view_doc.asp?symbol=A/CONF.216/16&Lang=E (accessed on 29 June 2020).
4. Ingrid et al, 2016. “Cross-sectoral strategies in global sustainability governance: towards a nexus approach”. In: Int Environ Agreements (2016) 16:449–464 DOI 10.1007/s10784-016-9321-1
5. Young et al, 2014. “Earth system challenges and a multi-layered approach for the sustainable development goals”. In: Post2015/UNU-IAS Policy Brief No. 1, Tokyo: UNU-IAS.
6. Gallopin, 2003. “A systems approach to sustainability and sustainable development”. In: ECLAC/ Government of the Netherlands Project NET/00/063 “Sustainability Assessment in Latin America and the Caribbean”, United Nations Publication.
7. Banerjee et al, 2012. “On the road: Access to transportation infrastructure and economic growth in China”. In: Social Science Electronic Publishing, 11 (1), 1–53. <https://doi.org/10.2139/ssrn.2018637>



8. UIC, 2018. "High Speed Rail" UIC High Speed Department. Available Online: https://uic.org/IMG/pdf/uic_high_speed_2018_ph08_web.pdf (accessed on 31 January 2020).
9. UIC, 2012. "High Speed Rail" UIC High Speed Department Available Online: https://uic.org/IMG/pdf/2012_high_speed_brochure_2012.pdf (accessed on 31 January 2020).
10. De Rus, 2012. ed. Economic Analysis of High-Speed Rail in Europe, Revised Version, Bilbao: Fundacion BBVA, 2012.
11. Zhenhua et al, 2016. "The impact of high-speed rail investment on economic analysis and environmental change in China: A dynamic CGE analysis". In: Transportation Research Part A.
12. Chunyang et al, 2020. "The impact of high-speed rails on urban economy: An investigation using night lighting data of Chinese cities". In: Research in Transportation Economics.
13. Ackerman et al, 2002. "Pricing the Priceless. Cost-Benefit Analysis of Environmental Protection". In: Georgetown Environmental Law and Policy Institute, Georgetown University Law Center. Available from: www.globalpolicy.org/socecon/encronmt/2002/CostBen2002.html
14. W. Kip Viscusi, 1994. "Cigarette Taxation and The Social Consequence of Smoking". In: National Bureau of Economic Research.
15. Akerman, J., 2011. "The role of high-speed rail in mitigating climate change – The Swedish case Europabanan from a life cycle perspective". In: Transportation Research Part D.
16. Gines et al, 2007. "Is Investment in High Speed Rail Socially Profitable?". In: Journal of Transport Economics and Policy. Volume 41, Part 1, January 2007, pp. 3–23.
17. Anna et al, 2019. "Transit-oriented development: A review of research achievements and challenges". In: Transportation Research Part A.
18. Rastogi et al, 2003. "Travel Characteristics of Commuters Accessing Transit: Case Study". In: Journal of Transportation Engineering.
19. Pongprasert et al, 2017. "Factors Affecting Residents Living near Transit stations to Use Non-Motorized Access Mode: Case study about Daily Travel in Bangkok, Thailand". In: The Journal of the Eastern Asia Society for Transportation Studies, Vol. 12.
20. Arasan et al, 1994. "Characteristics of Trips by Foot and Bicycle Modes in Indian City". In: Journal of Transportation Engineering.
21. Tracey et al, OECD Insights, 2008. In: OECD Insights: Sustainable Development – Linking economy, society and environment".
22. Charlotta et al, 2015. "Night-Time Light Data: A Good Proxy Measure for Economic Activity?". In: PLOS One.
23. Henderson et al, 2012. "Measuring Economic Growth from Outer Space". In: The American Economic Review.
24. Igor et al, 2016. "Trends in normalized difference vegetation index (NDVI) associated with urban development in northern West Siberia". In: Atmospheric Chemistry and Physics.
25. United Nations, Department of Economic and Social Affairs (DESA). Available online: https://www.un.org/esa/sustdev/natlinfo/indicators/methodology_sheets/demographics/population_growth_rate.pdf (accessed on 02 February 2020).
26. EESI, Environment and Energy Study Institute. Fact Sheet High Speed Rail Worldwide, 2018. Available Online: https://www.eesi.org/files/FactSheet_High_Speed_Rail_Worldwide.pdf (accessed on 31 January 2020).
27. Google Earth Engine Data Catalog. <https://developers.google.com/earth-engine/datasets/catalog>
28. DIVA-GIS website <https://www.diva-gis.org/gdata> (accessed on 05 February 2020, 06 February 2020, 15 February 2020 and 16 February 2020).
29. Coordinates from Google Maps: <https://www.google.com/maps>
30. Urban Greening Guidelines, Ministry of Urban Development, Government of India, 2014. Available Online: [http://mohua.gov.in/upload/uploadfiles/files/G%20G%202014\(2\).pdf](http://mohua.gov.in/upload/uploadfiles/files/G%20G%202014(2).pdf)



Prediction and Assessment of Environmental Impacts (Effects) on the Design and Arts Environment for Industry 3.0 Cotton Roller Ginning Process

Dr Vijayan Gurumurthy Iyer

Professional Engineer, A-2/31, Kendriya Vihar-II, Paruthipattu, Avadi, Chennai

✉ vijayangurumurthy@rediffmail.com

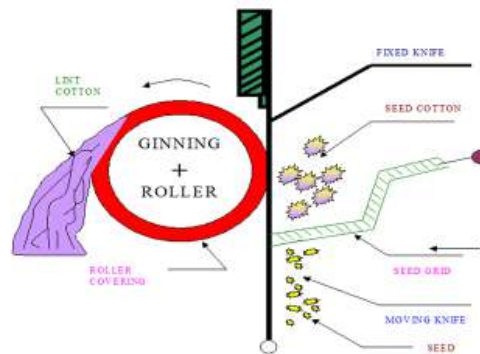
ABSTRACT

“Environmental Impact Assessment (EIA) can be defined as the systematic identification and evaluation of the potential impacts (effects) of proposed projects, plans, policies, programs, or legislative actions relative to the physical-chemical, physical-biological, biological chemical, cultural, anthropological, architectural, archaeological, socio-economical and surveillance components of the total environment. The past five decades have been characterized by passage of EIA legislation dealing with the environment, including legislation on control of land, air and water pollution, solid-and hazardous-waste management, resource conservation and recovery, and soil and ground water and surface water remediation. Coronavirus and Byssinosis Disease Impact Assessment (CIA) is investigated and discussed. Sustainable development is the artistic idea that science and humanities must live and meet their needs without compromising the efficacy and efficiency of future generations to meet their own needs. Prediction and Assessment of Environmental Impacts (Effects) on the Design and Arts Environment for Industry 3.0 Cotton Roller Ginning Process is provided. Sustainable design and arts are discussed in this research work. EIA of conventional design and arts is investigated. Sustainable design and arts environment for cotton ginning process is presented. The case study and check of strengthening of agricultural extension through sustainable entrepreneurship is discussed in this article.

Keywords: Agriculture; Arts; Cotton; Design; Environment; Entrepreneurship; Ginning; Sustainability.

INTRODUCTION

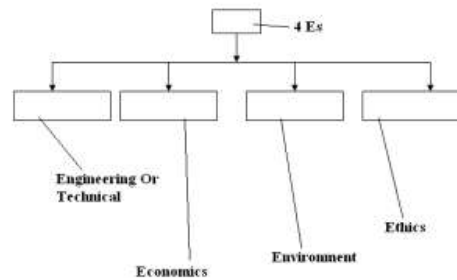
Sustainable entrepreneurship (SE) is a kind of an entrepreneurship that meets the needs of the present without compromising the ability, efficiency and values of future generations to meet their own needs. Agricultural entrepreneurs can be developed through well-conceived and well directed training programmes around thrust areas, thus advancing the frontiers of theories and practice sustainable entrepreneurship. The objectives of the study are (i) to introduce the concept of sustainable entrepreneurship in Ethiopia based on an entrepreneurial research conducted in South India, (ii) to formulate and appraise forty three number of detailed project reports (DPRs) of Diploma in Entrepreneurship and Business Management (DEBM) extension learners in eleven batches attached with the DEBM Counselor and Co-ordinator of Entrepreneurship Development Institute of India -Ahmedabad (EDI) during the research year (RY) 2007-2020, (iii) to promote policy recommendation so as to strengthen agricultural scientific and technical services focusing on Ethiopian Agricultural Extension System(EAEM). EDI has conceptualized and launched an innovative entrepreneurship development programme through distance learning and personal counseling DEBM in the year 1983. It was formerly known as Open Learning Programme on Business Entrepreneurship (OLPE) which is an one year programme through open & distance learning and personal counseling. DEBM extension learners are equipped with the knowledge, skills and motivation to set up their sustainable enterprises and function dynamically and manage successfully. DPRs put by learners are bankable projects duly investigated as per guidelines provided by EDI. All entrepreneurial business planning assessment regimes (EBPARs) have been done. The result analysis of forty three extension learners has been discussed. Agricultural green designs find that products and services are environmental advantage with sustainable production, good performance and prices. Pilot plant of a case study DPR-I on unsafe chromium from Ethiopian cotton roller ginneries and development of green design and art environment roller gin Rollers (Chrome composite Leather – cladding) for cotton gins duly investigated in a ginning factory working on McCarthy Principle is virtually investigated which has been demonstrated(Reference three figures and plates).



McCARTHY PRINCIPLE OF COTTON ROLLER GINNING PROCESS



The Most Important Considerations in Project Planning and Decision Making Process Can Be Referred To As “The Three Es”.
Sustainable Industry 4.0(Specific Industrial) , Generic 4.0 (Agriculture) and Source Specific (Municipal)



BATTERY OF DOUBLE ROLLER (DR) GINNING MACHINES



**GROUP OF OCCUPATIONALLY EXPOSED WORKERS
IN PALA HOUSE AND BEATING OF LINT COTTON**

Coronavirus and Byssinosis Disease Impact Assessment (CIA) is investigated and discussed. Low-carbon and energy-efficient agricultural technologies of agricultural hi-tech industries make important contributions to mitigating the impacts of economic growth on global warming. SE provides innovation to improve agricultural science and technology extension system and sustainable agricultural mechanization for mitigation of rural poverty in Ethiopia. This action-based research study on SE can promote policy recommendation to strengthen agricultural technical extension in Ethiopia. Coronavirus and Byssinosis Disease Impact Assessment (CIA) is investigated and discussed (Vijayan Gurumurthy Iyer, 2020) .

Entrepreneurship is a process of setting up of new enterprises to pursue opportunities. An entrepreneur, who organizes, manages, assumes risks and enjoys profits of enterprise or business successfully. Agricultural entrepreneurship is defined as a process of setting up of agricultural business at considerable risk. Sustainable entrepreneurship involves all the functions, activities, and actions associated with the perceiving of new sustainable agricultural opportunities and the creation of sustainable agricultural enterprises to pursue them. Entrepreneurs perceive new agricultural opportunities and create enterprises to pursue it (Legg , 2004). The concept of SE challenges that fosters long-term protection of the environment and its habitants as the technological developments are guided by efficiency, productivity, profitability, health and environmental impacts, resource and energy conservation, waste management, and social impacts such as public convenience, unemployment and crime (Hendry , 2004). A sustainable entrepreneur combines efficiently and effectively of six kinds of input resources can be referred to as “The six Ms” such as Man-power, Machinery, Material, Method, Money and Market in order to transform to output goods, products or services (Vijayan Gurumurthy Iyer, 2013). Agricultural entrepreneurs consider the environment in agricultural planning and decision making and to arrive at actions which are more environmentally compatible plans. The concept of sustainability is highlighted when the resources do not get depleted due to business endeavors. The expert counselor and coordinator has got an autonomy to conduct one year Diploma in Entrepreneurship and Business Management (DEBM) duly awarded by Entrepreneurship Development Institute of India (EDI) to forty three DEBM extension learners during the research year (RY) 2007-2020. Coronavirus and Byssinosis Disease Impact Assessment (CIA) is investigated and discussed. DEBM counselor has to provide the learners for necessary academic support and guidance , conduct of course work, two contact sessions, evaluation of assignments , tutorials , detailed project reports (DPR) and conduction of term end examinations . All DPRs have been formulated and appraised on agricultural green design and arts and structure of products and services.

The course is recognized by All India Council for Technical Education (AICTE), University Grants Commission (UGC) and Distance Education Council (DEC) as per reference <http://www.debm.ediindia.ac.in> ; reference agency code number 80410.

To address the need of developing new and committed agricultural entrepreneurs on a large scale, there is a need of an innovative agricultural technical extension programme through distance learning and personal counseling in Ethiopian Agricultural Extension System (EAES). A dynamic and pragmatic approach is introduced to create agricultural entrepreneurs on a large scale and to strengthen agricultural extension in Ethiopia.

Rationale and Background

Education coupled with entrepreneurship is an intricate sustainable educational process towards sustainable development that can be focused on sustainable rural development and poverty eradication in Ethiopia from the emerging enterprise spirit (Vijayan Gurumurthy Iyer, 2014). The poverty is a result of inefficient use of resources (Vijayan Gurumurthy Iyer, 2014). If it aids for sustenance, then that can be eradicated. About 88% of economic growth is created by innovation (Vijayan Gurumurthy Iyer, 2013). To achieve this degree of excellence, resources must be utilized at optimum and sustainable levels to maximize



efficiency as per the results analysis of optimum competitive and social markets (Vijayan Gurumurthy Iyer, 2014). The referred “A.K” economic model for an optimum output level of economic growth is the product of engineering or technical factor level (A) and the capital (K) (Vijayan Gurumurthy Iyer, 2014). The solution is the creation of new sustainable agricultural enterprises by innovation. The entrepreneurial idea generation is based on the concept of entrepreneurship and innovation management. The economic growth development of Ethiopia is explained by three factors which are given below:-

1. The natural increase in the accumulation of labor potential,
 2. Capital accumulation or money with which a business is being started and run,
- and
3. Technological momentum can be referred as total factor productivity (TFP) or efficiency in industrial processes.

The fundamental sustainable entrepreneurial momentum keeps the capital development dynamic which comes from the new agricultural enterprise creation process, new agricultural products or service requirement from customers, the new methods of production and processes, new transportation, and new agricultural markets and new forms of industrial organization.

Standard Production Function (SPF) is expressed as

$$Y = f(C, L)$$

Where Y=Output, C=Capital, and L=Labor

As knowledge is an important factor for the economic growth,

Standard Production Function (SPF) is modified as

$$Y = A(C, L) f(C, L)$$

‘A’ represents Knowledge on engineering or technical extension

Y = Output

C = Capital

L = Labor

f = Standard production function

(Product approach equation)

As per the given standard production function, knowledge is a decisive production variation, optimum innovation level is required in engineering or technical extension system. The solution is the application of low-carbon and energy-efficient agricultural green product designs and structures.

Materials and Methods

One year DEBM course is offered by EDI and sponsored by Friedrich-Naumann-Stiftung (FNSt)-A foundation of International repute from Germany. Professional expert counselor has conducted DEBM course independently to forty- three extension learners during the research year (RY) 2007-2014 in eleven batches as per EDI guidelines. EDI has provided guidelines to conduct the course as per the website reference <http://www.debm.ediindia.ac.in>. SE was the targeted research area. The methodology of the DEBM course includes, self-instructional study material, assignment, personal counseling through professional expert counselors and contact sessions during the course. The award of the diploma is based on assessment of the assignments, detailed project reports (DPRs) submitted by the learners and performance in the final (TEE) examination. Forty three green product design projects were submitted by DEBM learners under the research guidance of expert counselor during the given RY. List of forty-three extension learners and their academic records were uploaded in URL

<http://www.debm.ediindia.ac.in/counsellors/studentrecord/candidates.jsp>, and counsellor code number (User ID) 80410.

http://www.ediindia.org/doc/List of Institutions for website_latest.pdf serial number 68.

Website: www.ediindia.org & <http://debmcourse.blogspot.in/>



Fig. 1. Represents important elements of entrepreneurship and innovation management for setting up of sustainable enterprises through sustainable enterprise creation process.

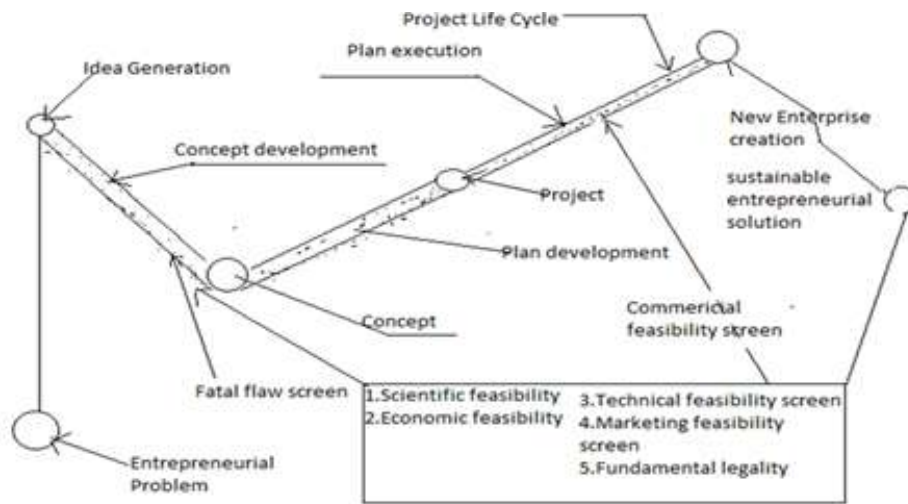


Fig. 1. Schematic representation of entrepreneurship and innovation management for sustainable enterprise creation process

All DEBM projects were screened for the five fatal flaws, namely, (i) Scientific feasibility, (ii) Economic feasibility, (iii) Technical feasibility, (iv) Marketing feasibility, and (v) Fundamental legality. The sustainable entrepreneur or a trusted member of an entrepreneurial team should need skills in ethics, accounting, law, finance, team creation and marketing aspects in order to avoid failures in the process. The sustainable entrepreneur has thorough knowledge on environmental management system (EMS) in order to skillfully bring about and manage resources efficiently to do a dedicated sustainable entrepreneurial process. EMS is a system of a continual cycle involving various processes as planning, implementing, reviewing and improving the activities for the enterprises to comply technical, economic, environmental and social obligations. EMS ensures that agricultural organizations identify and focus on improving areas where they have significant environmental and social impacts. Sustainable entrepreneurs follow the principle of process approach as depicted in **Fig. 2**. Sustainable agricultural technical extension system functions on the principle of process approach which is an activity based management system as outlined in **Fig. 2**. Monitoring, measurement and control including evaluation opportunities in extension system through process approach have been identified during the RY. Coronavirus and Byssinosis Disease Impact Assessment (CIA) is investigated and discussed.

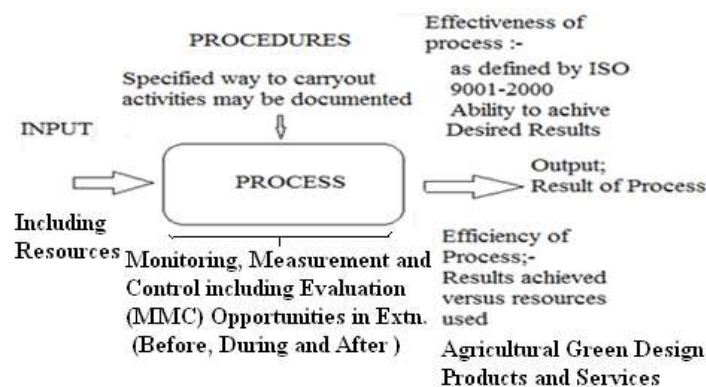


Fig. 1. Schematic representation of sustainable entrepreneurial process employed in agricultural technical extension system

In order to make the venture a dynamic and growing sustainable enterprise, the entrepreneurs have to skillfully bring about and manage resources efficiently to do dedicated sustainable entrepreneurial process. A process approach has been developed in order to bring labor, capital, technology, management, market, machineries, land and information together in new ways and to establish a new mechanism for sustainable rural development and eradicating poverty by providing scientific and technical services in agriculture. This approach enhances innovation in agricultural science and technology, improvement in

the agricultural technological extension system and advance agricultural mechanization and agricultural extension education. A methodology on eco-friendly rubberized cotton fabric roller development for cotton roller gins has been elaborated (Vijayan Gurumurthy Iyer, 2007).

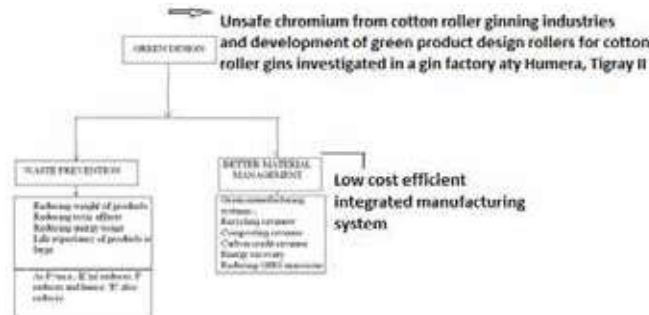


Fig. 1. Case study of DPR-1: sustainable agricultural production and quality

All projects have been scrutinized for the fatal flaws (**Fig. 3**). Case study of a DPR-I is discussed on unsafe chromium from Ethiopian cotton roller ginneries and development of green design and arts environment roller gin rollers for cotton gins duly investigated virtually in a ginning factory at Humera, Tigray II (Vijayan Gurumurthy Iyer, 2014). The study realizes the hazards of chromium contamination and pollution caused in the use of chrome composite leather-clad (CCLC) rollers commonly used in Ethiopian cotton roller ginning industries and attempts to eliminate the chromium contamination and pollution during the complete process (Vijayan Gurumurthy Iyer, 2014). The cotton roller ginning process is the mechanical separation of cotton fibres from their seeds by means of one or more rollers to which fibres adhere while the seeds are impeded and struck off or pulled loose (Gillum, 1974). Most of the cotton ginning operations are done using roller gins. The CCLC roller coverings contain about 18 000 to 30 000 mg/kg (ppm) as total chromium of trivalent and hexavalent forms which are toxic to human health (Vijayan Gurumurthy Iyer, 2007). When the seed-cotton is ginned, due to the persistent rubbing of CCLC rollers over the fixed knives, the cotton and its products get contaminated with the total chromium of trivalent and hexavalent forms. Hexavalent chromium leaks threat to cotton mill workers and to those who wear cotton garments. Cotton garments get contaminated and polluted with toxic hexavalent chromium. Consumers of cotton garments and ginning mill workers are exposed to chromium pollution and are susceptible to health hazards. Toxic effects are produced by prolonged contact with airborne or solid or liquid chromium compounds even in small quantities. There are many chromium based diseases that come out of the case industries (Vijayan Gurumurthy Iyer, 2014). Coronavirus diseases (COVID-2019) and Byssinosis diseases are investigated in cotton ginning industries.

To avert the problems in cotton ginning factories, an eco-friendly rubberized cotton fabric roller has been designed and developed. This green design and arts product has been successfully demonstrated for its performance (**Fig. 4**). The objectives of DPR-I were (1) to identify and study the environmental and health related problems existing with the present CCLC rollers employed in cotton roller ginning industries including the investigations of coronavirus diseases (COVID-19) and byssinosis synergistic diseases among occupationally exposed Indian gin and mill workers and 2) to virtual design and arts and develop green design cotton roller gin rollers for Ethiopian and Indian cotton roller gins in Seed-Cotton Roller Ginning factories and to evaluate its performance with a particular reference to technical, economical, and environmental and social aspects in cotton ginning industries as per author's sustainable design and art environment as per given below plate.



Fig. 1. Gin rollers of double roller gin are made of rubberized cotton fabric roller covering material; green design-cast study-DPR-1



RESULTS AND DISCUSSIONS

Entrepreneurial process is a set of inter-acting and inter-relating entrepreneurship activities in an organized manner. Forty-three DPRs were formulated and appraised. The study material of the DEBM course and help provided by EDI counsellors enable the extension learners to set up their own agricultural businesses. The course enables the learners to assess their entrepreneurial competencies and understand weakness and strength to start business. Overall the extension course equips learners to function dynamically and acquire the requisite knowledge and skill to plan and successfully launch their own agricultural ventures. The result analysis of all projects have been uploaded in website reference

<http://www.debm.ediindia.ac.in/counsellors/studentrecord/candidates.jsp>, and counsellor code number (User ID) 80410.

The success of a good entrepreneur is determined by a sustainable business plan development. It is an important document that provides critical aspects, basic assumptions, and financial projections regarding the business venture. It is the basic document used to interest and attract financial support. All entrepreneurial business planning assessment regimes (EBPARs) have been evaluated. A sustainable entrepreneurial agricultural venture includes four key ingredients:

1. A talented lead sustainable entrepreneur with a balanced and compatible team.
2. A technically and environmentally sound and marketable idea for a green product or service.
3. A thorough venture analysis leading to a complete sustainable business plan.
4. A clear statement of the cash required, phased over the period until the venture becomes cash flow positive and an indication of the minimum equity component.

DEBM extension learners were focused to work on agricultural green design and arts products and services oriented towards low-carbon and energy-efficient agricultural technologies during the RY. Sustainable enterprises reduce environmental impacts associated with the manufacture, use and disposal of products. The output of green products and services that are sustainable production, environmental advantages with good performance and price (Masters, 2008).

A case study of a DPR on unsafe chromium from Ethiopian cotton roller ginning industries and development of green arts and design rollers for cotton roller gins investigated in a cotton ginning factory at Humera , Tigray II , a pilot plant of which has been demonstrated. Such low-carbon and energy-efficient agricultural technologies of agricultural hi-tech industries can make important contributions to mitigate the impacts of economic growth on global warming (Vijayan Gurumurthy Iyer, 2014). SE provides innovation to improve agricultural science and technology extension system and sustainable agricultural mechanization for mitigation of rural poverty in Ethiopia (Vijayan Gurumurthy Iyer, 2014). Coronavirus and Byssinosis Disease Impact Assessment (CIA) is investigated and discussed. All DEBM extension learners were equipped with the knowledge, skills and motivation to set up their sustainable enterprises and function dynamically and manage successfully. The DEBM programme promotes the application of multidisciplinary technologies to agricultural industries and sustainable agricultural production with education and research.

All DPRs can be accessed from the reference website , <http://www.debm.ediindia.ac.in>. DPRs may also be obtained from EDI or counsellor.

As per the characteristics and assessment of DEBM extension learners, handbook cum guidelines have been prepared with respect to entrepreneurial requirements to become a sustainable agricultural entrepreneur and to set up sustainable enterprise (Vijayan Gurumurthy Iyer, 2013). All fifteen steps are not discussed however step number 6 is focused which has been considered a very important step on sustainable entrepreneurship.

Step- 1: Decision to be self-employed to become an agricultural entrepreneur and to set up an enterprise.

Step- 2 : Product and Innovative Process selection including marketing feasibility .

Step -3 : Deciding on size of the unit

Step -4 : Location of the unit

Step- 5 : Technical and financial feasibility of the unit

Step- 6 : Environmental and Social feasibility of the unit.

Step -7 : Awareness on statutory requirements including fundamental legality.



Step -8: Infrastructures for the unit

Step -9 : Working out project cost

Step -10: Provisional micro, small and medium scale industry (SSI/MSME) registration

Step- 11: Bio-data of the agricultural entrepreneur

Step- 12 :Preparation of sustainable business plan

Step- 13: Project implementation schedule (PIS)

Step -14: Project report preparation –Bankable project report

(Preliminary project report and detailed project report)

Step- 15 : Financial assistance for setting up an agricultural enterprise.

Step-16 : Environment and Sustainability Reports' assessment and evaluation.

Step-6 : Environmental and Social Feasibility including sustainability of the Project

A project may be technically and economically feasible but can be implemented only if environmentally and socially feasible. Environmental impact assessment (EIA) can be defined as the systematic identification and evaluation of the potential projects, plans, programs, or legislative actions relative to the physical-chemical, biological, cultural, and socio-economical components of the total environment. The purpose of the EIA process is to encourage the consideration of the environment in planning and decision making and to ultimately arrive at actions which are more environmentally compatible. It is important to conduct social impact assessment (SIA) and sustainability health impact assessment to avert Corona virus biochemical epidemic and pandemic disasters separately for the projects for example COVID-19 (Vijayan Gurumurthy Iyer, 2020).

This action-based research study on sustainable entrepreneurship promotes policy recommendation to strengthen agricultural extension in Ethiopia and India based on the study conducted in India (Vijayan Gurumurthy Iyer, 2013).

SUMMARY

Agricultural entrepreneurs can be developed through well-conceived and well directed training programmes around thrust areas, thus advancing the frontiers of theories and practice sustainable entrepreneurship. This action-based research and extension field study can give avenue for national development specifically to Ethiopian agricultural extension system. SE challenges and prospects that fosters long-term protection of the environment and its habitants as the technological developments are guided by efficiency, productivity, profitability, health and environmental impacts, resource and energy conservation, waste management, and social impacts such as public convenience, unemployment and crime. The development of new knowledge is an important factor for the economic growth of Ethiopia. The standard production function has indicated that knowledge is a decisive production variation. About 88% of economic growth is created by innovation. The agricultural project planning and decision making should include the integrated consideration of technical, economic, environmental, social, and other factors. The most important of these considerations can be referred to as “The four Es” (engineering or technical, economics, environment and ethics) in planning and decision making process. A project may be technically and economically feasible but can be implemented only if environmentally and socially feasible as per Coronavirus and Byssinosis Disease Impact Assessment (CIA) which is investigated and discussed. A process approach has been developed in order to bring labor, capital, technology, management, market, machineries, land and information together in new ways and to establish a new mechanism for sustainable rural development and eradicating poverty by providing scientific and technical services in agriculture. Monitoring, measurement and control including evaluation opportunities in extension system through process approach have been identified during the RY.

The objective of the DEBM extension course is “New Enterprise Creation and Management”. DEBM course develops motivation to extension learners and reinforces agricultural entrepreneurial traits with the spirit of setting up sustainable agricultural enterprises. Forty-three green design and arts projects proposed by DEBM extension learners attached with the counsellor during RY 2007-2020 have been formulated and appraised. Projects were screened for five fatal flaws, viz., (i) Scientific feasibility, (ii) Economic feasibility, (iii) Technical feasibility, (iv) Marketing feasibility, and (v) Fundamental legality. EBPAs have been evaluated. The learners have set up their own sustainable enterprises based on sustainable creation process under the research guidance of expert counsellor. Sustainable agricultural enterprises were set to focus on green design and arts products



and services that reduce environmental impacts associated with the manufacture, use and disposal of products. The results are environmental advantages with sustainable production, good performance and price. The extension learners have been duly awarded Diploma by EDI.

Education coupled with entrepreneurship is an intricate sustainable educational process towards sustainable development that can be focused on sustainable rural development and poverty eradication in Ethiopia from the emerging enterprise spirit. Agricultural cleaner technologies can produce more output than conventional technologies by causing less damage to the environment. Agricultural greener technologies as those that are less polluting, use resources in a sustainable manner, recycle more of their wastes and products and handle all residues in a more environmental acceptable way. Pilot plant of a DPR-I on unsafe chromium from Ethiopian cotton roller ginneries and development of green design and arts roller gin rollers for cotton gins virtually investigated in a ginning factory at Humera, Tigray II. This green design and art product has been successfully demonstrated for its performance.

DEBM study material and help provided by the counsellor enable the learners to set up their own agricultural enterprises. DEBM course assures the learners to assess their entrepreneurial competencies and understand weakness and strength to start business. The study can promote policy recommendation to strengthen agricultural extension in Ethiopia based on the entrepreneurial research conducted in India. The programme promotes the application of multidisciplinary technologies to agricultural industries and sustainable agricultural production with education and research. It is recommended that such kind of entrepreneurial service system with financial support is essential for sustainable development. As recommended in this paper, it is imperative that such a dynamic and pragmatic approach be implemented to create agricultural entrepreneurs on a large scale in Ethiopia. For further reading http://www.ediindia.org/doc/List of Institutions for website_latest.pdf serial number 68.

ACKNOWLEDGEMENTS

The author expresses his gratitude to Organizing Committee Secretary Mr. Elias Zerfu (Dr.) of Ethiopian Society of Rural Development and Agricultural Extension (ESRDAE) who has reviewed paper and review comments for giving an opportunity to participate in 1st Professional Conference of the ESRDAE for the theme entitled “ Strengthening of Agricultural Extension and Advisory Services for Improved of Livelihood Smallholders” held at Ethiopian Institute of Agricultural Research (EIAR) Hiruy Hall during 6-7 November 2014 in Addis Ababa, Ethiopia including presentation FDRG on 6 th November 2014 and publication of the paper in Ethiopian publication. The author is thankful to the organizers of 35 th IEC.

REFERENCES

1. Gilbert M.Masters, Wendell Ela.P (2008). Introduction to Environmental Engineering and Science , Third Edition, PHI Learning P Ltd., 610-612.
2. Gillum, N(1974). Properties of Roller Covering Materials.USDA-1490, Washington.D.C. PP.2-4.
3. Glynn.Hendry J, and Heinke Gary.W (2004). Environmental Science and Engineering, Prentice –Hall of India Private Limited, New Delhi-110001, PP. 9.
4. Iyer, Vijayan Gurumurthy (2007). Eco-Friendly Rubberized Cotton Fabric Roller Development for Cotton Roller Gins. Journal of Agricultural Safety and Health, American Society of Agricultural and Biological Engineers (ASABE), JASH 6067. 13 (1) January 1: 33- 43. 97.
5. Iyer, Vijayan Gurumurthy (2014). “Unsafe Chromium From Cotton Ginneries in Ethiopia and Development of a Rubberized Cotton Fabric Roller for Cotton Roller Gins”, In Proceeding and Abstract Book of the National Symposium on Science, Technology and Innovation for National Development , ISBN (13 digits) 978-99944-889-2-6 (STIND/2014/136) held in Wollega University during 21 and 22 March 2014 at Nekemte, South Ethiopia published by Wollega University Press Proceedings pp. 204-216 and 238 and Abstract Book pp. 49. <http://www.starjournal.org/wu-press.html>.
6. Iyer, Vijayan Gurumurthy(2014). “Toxic Tanning Without Environmental and Safety Protection in Unsafe Chromium Leather Tanneries In Ethiopia”. In Proceeding and abstract book of the National Symposium on Science , Technology and Innovation for National Development, ISBN (13 digits) 978-99944-889-2-6 (STIND/2014/136) held in Wollega University during 21 and 22 March 2014 at Nekemte, South Ethiopia Published by Wollega University Press Proceedings pp. 237 and 238 and Abstract Book pp. 46. <http://www.starjournal.org/wu-press.html>.
7. Iyer, Vijayan Gurumurthy (2014), “Education Coupled with Entrepreneurial Process Approach Towards Sustainable



- Development”, In Abstracts & Proceedings Book of the Global Conference on Contemporary Issues in Education (ISSN: 18770428) organized by the Academic World Education and Research Center, www.awer-center.org, at Las Vegas, USA during 12-14, July 2014, Published by Elsevier Ltd., <http://www.globalcenter.info/globe-edu/wp-content/uploads/2013/06/GLOBE-EDU-2014-Abstracts-Book.pdf>, pp.17 , 32-33.
8. Iyer, Vijayan Gurumurthy (2014). “Sustainable Enterprise Creation Process Towards Economic development of Ethiopia”. In Abstracts book of the First National Research Conference in Technology Transfer held during August 8-9, 2014 at Ethiopian Institute of Technology, Mekelle University, Ethiopia, Mekelle, and PP. 10-11.
 9. Iyer, Vijayan Gurumurthy (2013). “Sustainable Entrepreneurship Education is A New Dimension in Higher Technical Education for Sustainability”, In Abstracts Book of the 43 rd ISTE National Annual Convention 2013 Theme: “Empowering Technical Education to Address Sustainability and Global Competitiveness”, Sub theme: New Dimensions in Higher Technical Education for Sustainability (ISBN: 978-93-5142-315-7) Organized by Indian Society for Technical Education-T.K. Institute of Engineering & Technology, Warananagar, Tal: Panhala, Dist. Kolhapur-416 113 on 19-21 st December 2013, PP.23.
 10. John M. Legg, Kelvin G. Hinde (2004), Entrepreneurship, Context, Vision and Planning, Palgrave Macmillan 2004 Edition, PP.93-94.
 11. URL:http://www.ediindia.org/doc/List of Institutions for website_latest.pdf serial number 68.
 12. URL:<http://www.debm.ediindia.ac.in> ; Agency code number: 80410
 13. URL:<http://debm.ediindia.ac.in/counsellors/studentrecord/candidates.jsp>
 14. URL:Website: www.ediindia.org & <http://debmcourse.blogspot.in/>
 15. Vijayan Gurumurthy Iyer(2020). “Strategic Environmental Assessment (Sea) Process Towards Sustainable Toxicological Management Development for the Toxicological Industries to Achieve Business Excellence”, Journal of Emerging Trends in Engineering and Applied Sciences (JETEAS) (ISSN: 2141-7016) , 11(3):91-108, © Scholarlink Research Institute, 2020. scholarlinkinstitute/jeteas.org , https://issuu.com/vijayangurumurthyiyer/docs/strategic_environmental_assessment_online
 16. Vijayan Gurumurthy Iyer (2020). “Environmental Health Impact Assessment Of Chrome Composite Leather-Clad Rollers Used By Indian Cotton Roller Ginning Industries And Design And Development Of Eco-Friendly Alternatives”, International Journal of Emerging Trends in Health Sciences(ISSN:2547-8850) , Open Journal Systems (OJS), Volume 04, Issue 1 (2020) PP.36-67 (32 Pages) , www.ij-hs.eu Publishers: Birlisik Dunya Yenilik Arastirma ve Yayıncılık Merkezi. The Academic Event Group (TAEG) , BD Center, Turkey.
 17. Vijayan Gurumurthy Iyer (2020) . “Strategic Environmental Assessment (SEA) Process for Cotton Ginning and Textile Science and Engineering Systems Towards Inclusive Sustainable Development”, World Journal of Textile Engineering and Technology, (ISSN: 2415-5489) Open Journal Systems (OJS), Volume 6, © 2020 Scientific Array, NSCKU, Published on 02.07.2020, PP.21-38. DoI: <https://doi.org/10.31437/2415-5489.2020.06.3>
 18. Iyer, Vijayan Gurumurthy, 2020. “Environmental Impact Assessment (EIA) Educational Process for the Effective and Efficient Learning, Teaching and Sustainable Education Leadership”. Draft Program for Online Conference Presentation 11 th World Conference on Learning, Teaching, and Educational Leadership(WCLTA-2020), Abstract book page number 17. Christian University St.Petersburg, Russia , 13-15 , September 2020 , Session-II, on 13 th Sep 2020 Sunday GMT+2 Session 3 , 18:00-19:40, Organized by The Academic Events Group (TAEG) , <https://www.globalcenter.info/wclta/> PP.11.
 19. Iyer, Vijayan Gurumurthy, 2020. “Coronavirus Impact Assessment (CIA) for Control of Infection Criticality Due to Novel Coronavirus Pandemic and Epidemic Disasters”. Draft Program for online conference presentation 7 th World Conference on Health Sciences HSCI 2020, Christian University St.Petersburg , Russia , 13-15 , September 2020 , Session-II, on 13 th Sep 2020 Sunday GMT 15:40-17:30, Organized by The Academic Events Group (TAEG) , www.h-sci.org PP.12.
 20. Iyer, Vijayan Gurumurthy, 2020. 4th International Conference on Nursing “University of Barcelona , 04-05 September 2020. Investigations on Integration of Quality and Safety Management in Hospital Industries for Measurement, Monitoring and Control of Infection Criticality due to Novel Coronavirus Epidemic Disasters” , <http://www.ic-on.org/Draft> PP.10/ Program Abstract book- PP. 08. <https://www.kongreuzmani.com/4-international-congress-on-nursing-icon-2020.html>.



21. Iyer, Vijayan Gurumurthy (2020) “Webinar on Healthcare and Nursing, Nursing Virtual Summit 2020” title entitled “Integration of Quality, Safety and Sustainability Management for Hospital Industries towards Sustainable Development” held during World Healthcare and Nursing Webinar on Advances and Innovation in Healthcare and Nursing”, (WHCN), Organized By IRIS Scientific Group Final Program pp. 13, in Zoom Login ID, <https://irisscientificgroup.com/conferences/healthcare-nursing/webinar> on 22nd August 2020 at 12:00 TO 19:00 GMT , 5.30 PM TO 12: 30 PM IST, Oral Presentation of Speaker Time Zone: 16:10 -16: 30 (20 minutes) GST, 21:40 TO 22:00 IST. https://issuu.com/vijayangurumurthyiyer/docs/nursing_webinar
22. Iyer, Vijayan Gurumurthy,2020.“Strategic Environmental Assessment (Sea) Process for Sustainable Administrative and Political Sciences towards Sustainable Development”, Draft Program for Online Virtual Presentation 9 th World Congress of Administrative and Political Sciences (ADPOL-2020), Program Book 12, Abstract book page number 8. Porto, Portugal, 01-03, October 2020 , 02 October 2020 , Session-IV, 14.40-16.40, Porto Time GMT+2, Organized by The Academic Events Group (TAEG),
www.adpol.org, <https://issuu.com/vijayangurumurthyiyer/docs/adpol-draft-program>
https://issuu.com/vijayangurumurthyiyer/docs/adpol-draft-program_7150ee13099ac2
https://issuu.com/vijayangurumurthyiyer/docs/adpol_30_th_sep_2020-draft_program__1__1_
<https://issuu.com/vijayangurumurthyiyer>



Protocol Analysis for Intrusion Detection System on IoT Based Network Communication

S Ponmaniraj, Dr Amit Kumar Goel

School of Computing Science and Engineering, Galgotias University, Greater Noida, Uttar Pradesh

✉ ponmaniraj@gmail.com

ABSTRACT

Internet of Things (IoT) is the trendy technologies to make communication between machines to machines with the help of network communication principle. Many electronic devices embedding with machines are sensing the real time data and processing them for certain applications. Collected data from the sensors of the IoT devices are transferred to the centralized network places to obtain required functions to perform in the form of raw data, information, and instruction or might be the commands to control devices remotely. During the data transmission from source to target place, there will be any malfunctions can be occurred in order to modify the information or to take over the control of the connected devices from the cyber attackers. Since nobody knows the zero day attacking mechanism, easily attackers can deploy any malicious functioning codes in between end devices to perform their obligated attacks. This research paper is going to present IoT architecture, Machine to Machine communication on Cloud, Protocol analysis and Intrusion detection mechanism to avoid network based attacks.

Keywords: Constrained application protocol; Internet of Things; Intrusion detection system; Message queuing Telemetry Transport; Protocol Analysis.

INTRODUCTION

Basics of IoT

IoT is an emerging technology combined with cloud concept for data transmissions. Basically internet of things functioning on four important substances such as i) Machines or Devices; ii) Networking; iii) Data transmission; iv) Remotely access mechanism. Function of the said substances of an IoT has been done through the following component's helps; software modules, data collecting materials (Sensors), processing devices (Actuators), Data transmission mediums (Networking and Cloud). In the field of IoT, networking mechanism is used to perform data transmission over the cloud services. LoRaWan (Long Range Wide Area Network) application is used for long range data communication when any IoT device wants to share or receive their sensitive data. "Ref. [1]" discusses about LoRaWan architecture and its modulation techniques. Lora transceiver provides long range data transmission on cloud based IoT services. Without LoRa technology IoT devices cannot transfer the data to the long distance and only to the local region that can be able to communicate.

IoT architecture contains four basic elements such as Devices, Gateways, Cloud platform and Applications. Sensors and Actuators are the physical devices which are used to collect the analog data from machines or real world and convert them into machine readable format done by actuators. Through Gateways performs collect, process then share that processed information to the devices from the cloud applications. Cloud platform offers many services and mainly focuses on software as a service (SaaS) to provide actuation of the data, data analysis, managing the devices remotely etc. Applications have implemented in various ranges starting from small applications like web services to highly secured mobile applications on the dashboard access [2].

There are seven different operating system based architectures have been developed for IoT communication from simple application to more complex functional modules. They are listed as follows;

1. No – Operating System Architectures (No – OS)
2. Language Runtime Operating System Architecture (LROS)
3. Real Time Operating System (RTOS) Architecture
4. Full Operating System Architecture (F-OS)



5. Server Based Operating System Architecture (S-OS)
6. Container Operating System Architecture (C-OS)
7. Application Based Operating System Architecture (App OS)

“Ref. [3]” explains that layered architecture of IoT communication. As per the direction of International Telecommunication Union’s specifications this architecture holds five different layers for data communication with the help of different transport protocols and which is similar to ISO/OSI layer models. These layers are listed as below:

1. Application Layer
2. Middleware Layer
3. Network Layer
4. Access Layer and
5. Sensing Layer

Connection Technologies

In the very beginning of the IoT communication many technologies were used to transmit and receive data. Basically Radio Frequency Identifier tag had used to transmit the data to target device and there were no built in power supply to activate this RFID tags. This RFID aka Near Field Communication (NFC) device. It contains sensor, nano and embedded technology in itself to process and share the required information. Based on the power supplying process, RFID tags are classified into three broad categories such as i) Active; ii) Passive and iii) Semi Passive. This tag contains reader, controller, server access, antenna and a tag [4].

After RFID, Internet protocol (IP) came in to the picture for carrying data and signals in between end devices. Two broad categories of IP versions are used in internet protocol suite such as IPv4 and IPv6. This kind of protocol supports for 2¹²⁸ addresses or 85 trillions of addresses to provide for each and every devices which are connected through network and cloud services based systems. In order to provide different functions, these IP addresses divided into five different classes [5]. Those classes and ranges are as follows;

- Class A – 0 to 126
- Class B – 128 to 191
- Class C – 192 to 223
- Class D – 224 to 239
- Class E – 240 to 255

Bluetooth (standard 802.15.1) and ZigBee (standard 802.15.4) are the two most important wireless sensor protocol for data transmission up to the range 100 meters and those protocols are used in some industrial applications, Agriculture, Home automation, power systems etc. With the help of said protocols, it is possible to create personal area networks (PAN) inclusive of 8 to 10 devices [6].

GATEWAY IOT AND HARDWARE STRUCTURE

Sensor nodes and the network services are being in vital role of an IoT environment. All the real time and the devices generated data are collected and processed through sensor nodes along with actuators. Wired and wireless communication mediums such as Ethernet cable, wifi, Bluetooth etc are used in this gateway to process and share the data with cloud services [7].

As mentioned in the below figure, **Fig. 1**, IoT gateway architecture, all the sensor and actuator devices are collecting the real time data from world entities such as smoke, fire, gas, humidity and light etc and forward them through some communication protocol which are present in between gateway and sensor devices then forward them in to cloud services or to the user interface application or to the devices [8]. Docker engine takes the responsibility for all the implemented applications to be run on IoT dashboards and system devices. Also it performs verification and validation process of swarm mode worker and swarm mode manager, TLS security, Certificate authority, service discovery and load balancing of the system resources etc. There are multiple containers from the distributed services of networks will be working through some plug-in modules. At running time

those plug-in modules gets SaaS from the cloud services to make docker engine to run their applications which is implemented on various software languages. **Fig. 1**, shows that model architecture of IoT gateway process.

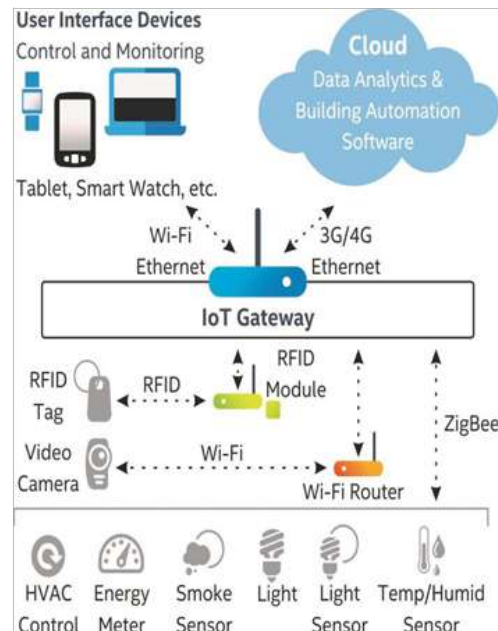


Fig. 1. IoT gateway architecture model (image source: DoI:10.1088/1757-899x/263/4/042012)

COMMUNICATION PROGRESS

Message Queue Telemetry Transport

Message queue transport telemetry (MQTT) is a light weight protocol used in IoT environment for data sharing via Publish/Subscribe techniques. It contains 2 (MB) of header information and up to 256 (MB) of payload information along with Quality of service (QoS) level. On the basis of working condition, MQTT is having four different stages as follows; i) Connecting stage, ii) Authentication stage, iii) Communication stage and iv) Termination stage. MQTT is simply acting like a broker (Server) for the subscribers or client devices. If any clients or the device machines wants to send data to the broker or server, that process is called publish and the same is done on the reverse progress is known as subscribe [9]. Any client machines are departed from the broker during communication then the subscribed message was stored in the broker's buffer till the disconnected machines get joined back to the connection and once it is joined then the broker message has been delivered to the client devices. For a normal communication MQTT standard 1883 is used and there is no security functions implied on this communication [10]. Whenever the client device wants to communicate with any broker, then the broker won't look for any kind of authentication parameters such as user name and password from those publishing devices. Broker will simply accept the non authenticated client device connections. This will lead cyber criminals to misuse the connected devices data or the connected session links for their malicious attacks.

For a secured connection, IoT environment uses MQTT standard 8883 and it is supporting the security techniques with SSL/TLS services. In this standard mode of communication, they will follow three way handshake mechanisms for the security matters. Publishing devices firstly will go for an initialization of its publishing services (Connection stage). Then broker will check for the client devices authentication parameters for identifying the reliability of the client's device (Authentication stage). Once authentication is verified then broker and publishing devices or the clients can be able to share their information through network services (Communication stage). After the requested information shared in between client devices and broker servers via publish/subscribe mode then the session will come to an end and this stage is known as termination stage. In this 8883 MQTT standard messages between the end devices will be encrypted for safety purposes.

Constrained application protocol (CoAP), Advanced message queuing protocol (AMQP), Simple sensor interface (SSI), Mosquitto and Simple/Streaming text oriented message protocol are the few protocols which are working along with MQTT to provide broker services and some other specified services on publish/subscribe mode of operations. Though MQTT protocol

is very important for an IoT environment, it has some design flaws too. Due to those design issues, MQTT protocol facing many problems during communication [11]. The following chapter deals with the challenges of MQTT protocol with respect to security, interoperability.

MQTT Security Challenges

Since the MQTT protocol is light weighted, It cannot go with more security functions such as SSL/TLS security functions. MQTT is fully based on application purposes so that it cannot hold security information in it. The topic structure maintained by MQTT is not in the structured format and because of that reason the topic structure cannot be divided into more logical small structure. This leads IoT environment not to support for scalability. When the scalability increases automatically the topic structure will get more complex and so that communication devices cannot be able to access the required topic structure.

Another drawback of MQTT is binary information format without any specific encoding information. Different manufacturers are developing their applications in their own format but they are unable to develop an application for the MQTT due to its non standard encoding format. Since MQTT uses simple binary encoding system, client's user name and passwords will be shared as plain text as anyone can easily understand. Injection of harmful messages into the MQTT is very easy and it will penetrate some malicious codes into the communicated networks and the client devices, servers as well. Since no well suited security modules inside the MQTT, receiver cannot identify the original source information of a shared data unless the message contains original data.

PROTOCOLS AND SERVICES ANALYSIS

MQTT uses the transport control protocol and internet protocol (TCP/IP) services for application process. Hyper text transport protocol (HTTP), is the important protocol for data transfer from the IoT devices to the cloud server under web services. To carry over those web services and port access, MQTT uses the TCP/IP services an application protocols. Since HTTP uses numerous tiny blocks of data information to be shared, enormous amount of protocols and data overhead transactions obtained during the data transmission. This results in performance degradation of IoT communication [12, 13]. Based on the services provided from TCP/IP along with HTTP, Few errors may occurred as follows; Transfer delay, Packet loss, low throughput and increasing of error rate etc. Unlike HTTP communication sequences of actions, MQTT is not supporting for "ACK and FINACK". Instead MQTT uses "CONNECT and CONNACK" fields in the properties field. "CONNECT/CONNACK" is the functional modules of connection establishment and Response messages. These modules contains few important flags as follows; i) Protocol name and version, ii) Keep alive time duration, iii) Properties of the data, iv) User name and Password flags, v) Packet size, vi) Will QoS and etc. **Figs. 2 (a) and (b)** shows that communication sequences of HTTP and MQTT protocols.

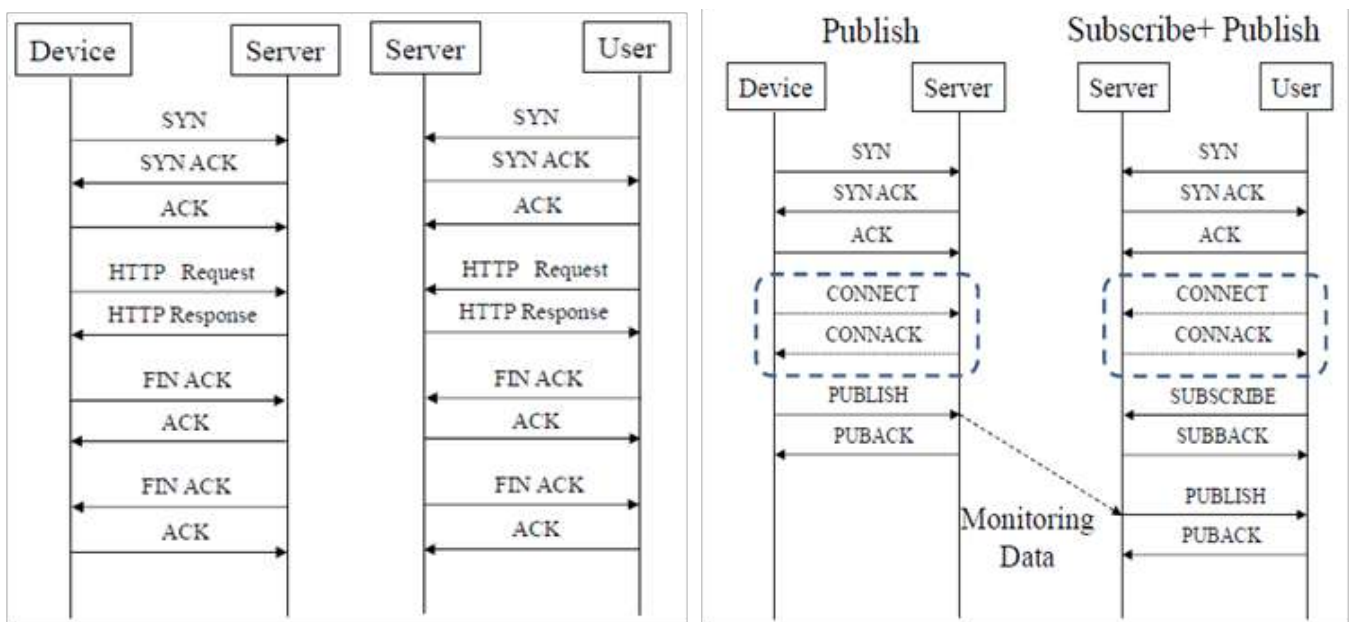


Fig. 2(a) Communication progress of HTTP **Fig. 2(b)** Communication progress of MQTT



INTRUSION DETECTION ON PROTOCOL PARAMETERS

Attacking Threats and Vulnerabilities

Threats and vulnerabilities are the loophole entry point for the hackers to intrude and attack any targeted (client) devices. Threat for a system is an event can exploit the system security easily and vulnerability is meant to be a quality of the security functions of the systems or the devices. Since IoT devices are doing data transmission on network based access, those devices security modules must be good enough to protect them from external attacks. Network vulnerabilities or the attack on a targeted system is denial of services through generating enormous requests to the system continuously. Malware or virus program performs eavesdropping the data being exchanged, stealing of data or destroying them.

Intrusion Attacks

Intrusion is the upcoming attacking methods on internet communications in order to eavesdrop any sensitive information or to attacking the targeted systems or the devices. Since MQTT is not lifting the heavy load information in order to secure data transmission, easily intruders can misuse the device data or the controlling instructions. Distributed denial of services (DDoS) is the one attack happened on video surveillance camera over the network communication and which is the first attack happened on IoT devices. “Mirai” is the name of the botnet, which attacks internet connected devices and cameras switches and routers. Since IoT devices exchanging their data on networks through their different layers, Network intrusion is playing a vital role in intrusion attacks on each layer [14]. As IoT has perception layer at the physical data transaction, Network layer responsible to routing information and application layer meant for logical control of business applications, hackers or the cyber criminals mainly targeting these layers to attack.

Intrusion attack happens via impersonating the user as legal one. Spoofing or phishing is the mechanism hackers are adopting to perform intrusion attacks. Spoofing is done on IP address, Domain Name System (DNS) and Address Resolution Protocol (ARP). IP spoofing is the technique which makes falsify header on the IP packets in order to create DDoS attacks. In ARP spoofing, local area network (LAN) systems will be compromised through their medium access control (MAC) protocol. It looks for the data to be exchanged to the LAN via MAC. DNS spoofing leads the attackers to get IP address for the domain name system which connects all the services and request made from client devices [15].

Protocol Analysis

HTTP web services collecting the sensors/actuators data and before transmitting them those data will get preprocessed with some machine learning tools and algorithms such as supervised, unsupervised machine learning algorithms to extract and classify the data based on some threshold value [16]. Mostly categorized datasets are fallen on three different groups as “Below normal”, “Normal” and “Above normal”. Docker engine deployed for running multiple micro services at IoT environment and Cloud. Virtual IoT Devices (VID) is used in running micro services and its elements. This VID is taking care of annotating the data, data exchange between devices, data validation, preprocessing, actuation and storage [17].

“In Ref. [18], authors discussed about feature extraction of the data being communicated in between end devices to mitigate some malevolent events against Domain name system, HTTP and MQTT protocols. To extract the features, TCP/IP parameters have been used. TCP/IP model of MQTT is responsible for connection reliability; hence its features are extracted and compared with well known parameters of Network intrusion detection system (NIDS) to identify the attacking patterns. Knowledge discovery data (KDD-99) dataset is the best one for intrusion detection system. Those dataset values are extracted from the TCP/IP parameters and they have found 41 important features which are to be observed on data transmission over any network links. Decision tree and Naïve bayes algorithms are used to classify the features. To secure from NIDS, the following steps must be followed;

- Collecting the data from the network traffics
- Analyze the data to classify them into groups
- After classification, find the security events which are related to the attacks
- Detect attacks and generate alarm or warning signals to the user and update report about the occurred event

Table 1, shows that KDD dataset for TCP/IP parameters. In which labels “B”, “C”, “T” and “H” meant for Basic, Content, Traffic and Host features of the TCP/IP model [19]. Those labeled features are accessed and updated every two seconds or even less than that to protect communication from intrusions. If any malicious, illegal, suspicious data or access is present on the

network link then this parameters will let know the administrator to take necessary actions against malicious event.

Table 1. KDD dataset attributes

Sr. No	Label	Attribute Name	Sr. No	Label	Attribute Name
1	B	duration	22	C	is_guest_login
2	B	protocol_type	23	T	count
3	B	service	24	T	error_rate
4	B	src_bytes	25	T	error_rate
5	B	dst_bytes	26	T	same_srv_rate
6	B	flag	27	T	diff_srv_rate
7	B	land	28	T	srv_count
8	B	wrong_fragment	29	T	srv_error_rate
9	B	urgent	30	T	srv_error_rate
10	C	hot	31	T	srv_diff_host_rate
11	C	num_failed_logins	32	H	dst_host_count
12	C	logged_in	33	H	dst_host_srv_count
13	C	num_compromised	34	H	dst_host_same_srv_rate
14	C	root_shell	35	H	dst_host_diff_srv_rate
15	C	su_attempted	36	H	dst_host_same_src_port_rate
16	C	num_root	37	H	dst_host_srv_diff_host_rate
17	C	num_file_creations	38	H	dst_host_error_rate
18	C	num_shells	39	H	dst_host_srv_error_rate
19	C	num_access_files	40	H	dst_host_error_rate
20	C	num_outbound_cmds	41	H	dst_host_srv_error_rate
21	C	is_hot_login	42	-	class

This dataset increases high intrusion detection rate and very less false alarm rate. With the help of new technologies, cyber criminal or hacker increases their attacking methods and no one security mechanism can handle this kind of zero day attacking. Still this dataset attributes helps us to increase the analyzing property of an intrusion detection system. Since these parameters are updating themselves for every 2 seconds, it gives better result in intrusion analysis.

CONCLUSION

Internet of things is the trending technology for controlling electronic devices remotely with the help of internet services. It gives new platform to the people to take their life easily and smoothly with some learning techniques. Though users are facing much problem with some security issues with IoT environment, intrusion detection helps them to come out from few attacks. Specifically network intrusion detection system (NIDS) is the one, which gives more sophisticated data transaction over the network without an apprehension of intrusion attacks. KDD dataset along with intrusion detection system can protect network communication environment, still this technology cannot bring 100% solution for any problem and intrusion detection system also just used to warn the user about newly, unauthorized network access or connectivity. IDS won't protect or prevent any network devices from an attack. With the help of raised warning alarm signals, users or administrators can take required remedial actions against vulnerabilities.

In future, tools can be implemented to increase the findings of attacking methods and by using machine learning techniques remedial actions also can be taken against intrusion attacks. Updating MQTT protocol with some light weight encryption techniques leads to data security and reliability during transmission. Password protection mechanism at the end devices also is a possible solution to protect end devices in IoT, Cloud environment.



REFERENCES

1. Fox, J., Donnellan, A., & Doumen, L., "The deployment of an IoT network infrastructure, as a localised regional service". IEEE 5th World Forum on Internet of Things (WF-IoT), 2019, doi:10.1109/wf-iot.2019.8767188.
2. Antero Taivalsaari, Tommi Mikkonen, "A Taxonomy of IoT Client Architectures", IEEE Software, 2018, P 83-88.
3. Somayya Madakam, R. Ramaswamy, Siddharth Tripathi, "Internet of Things (IoT): A Literature Review", Journal of Computer and Communications, ISSN No: 2327-5219, 2015, 164-173.
4. Want, R., "An Introduction to RFID Technology", IEEE Pervasive Computing, 5, 25-33.
5. Bicknell, "IPv6 Internet Broken", Verizon Route Prefix Length Policy, 2009.
6. Chen, X.-Y. and Jin, Z.-G., "Research on Key Technology and Applications for the Internet of Things", Physics Procedia, 33, 561-566, <http://dx.doi.org/10.1016/j.phpro.2012.05.104>
7. Zhong, C.-L., Zhu, Z., & Huang, R.-G., "Study on the IOT Architecture and Gateway Technology", 14th International Symposium on Distributed Computing and Applications for Business Engineering and Science (DCABES), 2015. doi:10.1109/dcabes.2015.56
8. Sarker, D., & Sumathy, S., "Cognitive IoT incorporating intelligence in building smart environment", IOP Conference Series: Materials Science and Engineering, 2012, 263, 042012. doi:10.1088/1757-899x/263/4/042012
9. Hunkeler, U., Truong, H. L., & Stanford-Clark, A. "MQTT-S — A publish/subscribe protocol for Wireless Sensor Networks", 3rd International Conference on Communication Systems Software and Middleware and Workshops (COMSWARE '08), 2008, doi:10.1109/comswa.2008.4554519
10. <https://internetofthingsagenda.techtarget.com/definition/MQTT-MQ-Telemetry-Transport>
11. Yassein, M. B., Shatnawi, M. Q., Aljwarneh, S., & Al-Hatmi, R., "Internet of Things: Survey and open issues of MQTT protocol". International Conference on Engineering & MIS (ICEMIS).2017, doi:10.1109/icemis.2017.8273112
12. Yokotani, T., & Sasaki, Y. "Comparison with HTTP and MQTT on required network resources for IoT". International Conference on Control, Electronics, Renewable Energy and Communications (ICCEREC), 2016, doi:10.1109/iccerec.2016.7814989
13. M. Belshe, R. Peon, M. Thomson, "Hypertext Transfer Protocol Version 2 (HTTP/2)", IETF RFC 7540, 2015
14. Chaabouni, N., Mosbah, M., Zemari, A., Sauvignac, C., & Faruki, P., "Network Intrusion Detection for IoT Security based on Learning Techniques". IEEE Communications Surveys & Tutorials, 1–1. doi:10.1109/comst.2019.2896380
15. M. Conti, N. Dragoni, and V. Lesyk, "A Survey of Man In The Middle Attacks," IEEE Communications Surveys Tutorials, vol. 18, no. 3, pp. 2027–2051, 2016.
16. Ahrabian, A., Koloza, S., Enshaeifar, S., Cheong-Took, C., & Barnaghi, P. "Data analysis as a web service: A case study using IoT sensor data". IEEE International Conference on Acoustics, Speech and Signal Processing (ICASSP), 2017. doi:10.1109/icassp.2017.7953308
17. S. K. Datta and C. Bonnet, "An edge computing architecture integrating virtual iot devices," IEEE 6th Global Conference on Consumer Electronics (GCCE), 2017, pp. 1–3, Oct 2017.
18. N. Moustafa, B. Turnbull, and K. R. Choo, "An Ensemble Intrusion Detection Technique based on proposed Statistical Flow Features for Protecting Network Traffic of Internet of Things," IEEE Internet of Things Journal, 2018, pp. 1–1.
19. Preeti Aggarwal, Sudhir Kumar Sharma, "Analysis of KDD Dataset Attributes - Class wise For Intrusion Detection", ICRTC-2015, ScienceDirect, Vol. 57, PP. 842-851.



Upliftment of Indian Economy through Sustainable Development

Vaibhav Gupta¹, Sudershan K Popli²

Engineer (Civil), RITES¹, General Manager (Civil), RITES

✉ poplisk@gmail.com

ABSTRACT

India is booming and sustainable development becomes increasingly more important. With cities generating more economic output, an increasing number of Indians are leaving rural areas to seek employment in cities. The rapid growth of cities putting number of challenges, such as increase demand of in housing, power, drinking water, public transport, health services, banking, internet, etc.

Similarly, villages are to be provided with facilities like good schools, good primary health centers, good sanitation, adequate supply of drinking water and electricity, good connectivity – both roads as well as internet. India's 65% of population still live in villages, therefore it is required to provide all facilities at par with urban areas in today's world of internet.

Therefore, it is crucial to meet the challenges of continuing growth, without destroying environment and social harmony, planning at urban and rural level for sustainable development.

Keywords : Sustainable Development Goals (SDG's); Economic sustainability; Social sustainability; Environmental sustainability.

INTRODUCTION

Sustainable development is the key for overall prosperity of the world. The word sustainable development has many definitions and the most popular definition had been coined by report of "Brundtland", which defines sustainable development as "development that meets the needs of present without compromising the ability of future generations to meet their own needs".

India has embarked on the journey to attain the Sustainable Development Goals and Economic Growth for all. Government of India launched program like Make in India, Startup India, Skill India, Digital India, etc. with the underlining principle of creating employment opportunities.

To attain the Sustainable Development Goals (SDG), India needs to focus on two aspects: Urbanization and Industrialization. The requirement at India's level is innovation in all aspects i.e. education, health, manufacturing, etc. As SDG's are interlinked, it is required to attain the indicators of one SDG, several other SDG's and their indicators also need to be evaluated and achieved.

TRANSPORTATION SYSTEM FOR SUSTAINABLE DEVELOPMENT

Transportation is the key for sustainable development. It is required to promote public transportation, improving road riding surface, tolling of expressways/Highways, improvement in vehicle technology, using renewable clean fuels.

An efficient transportation system provide social and economic opportunities and benefits results in multipliers effects such as better accessibility to markets, employment and investments.

Sustainability in the transportation sector facilitates lower income community to fulfill their transport needs. Transportation sector is the biggest employment generator in the country and its expansion will create more employment opportunities and thus the unemployment levels in the community will get reduced.

HEALTHY POPULATION FOR SUSTAINABLE DEVELOPMENT

Healthy population is the key to sustainable development. For a healthy, productive and fulfilling life, each individual should have access to a nutritious diet, safe drinking water, clean air, good sanitation facilities, health care facilities, etc. In developing countries, people are now more vulnerable, earlier they were getting disease such as material and cholera due to lack of poor



hygiene and non availability of drinking water. But now, they are getting affected by modern diseases also such as hypertension, diabetic, heart diseases, cancer, etc. The latest example is Covid-19 pandemic, whole world is suffering irrespective of the economic condition of a Country but poor countries may have to wait for months for vaccination.

India has successfully undertaking child immunization program to protect from fatal diseases. India has successfully eradicated polio by mass vaccination program. Recently Swatch Bharat program has shown results and resulted in less malaria cases due to overall improvement of environment. So to attain sustainable development a healthy population is must.

POVERTY ERADICATION FOR SUSTAINABLE LIVELIHOODS

Poverty is the root cause for hunger and malnutrition. Literacy and basic education are essential for enabling the poor individuals to avail the benefits of development initiatives and market opportunities.

India has recently launched various programs for poverty eradication such as Skill India program, Startup program, etc. The skill India program is to provide basic skills such as carpentry, masonry, electrician, driving; etc to youth to earn their livelihood. Similarly Startup program is to help the educated youths to take up their own business and generate employments. Recently, India has launched social assistance and basic needs fulfillment schemes to poor farmers. The poverty eradication ultimately will lead to sustainable livelihoods and finally leading to sustainable growth.

STRENGTHENING GOVERNANCE FOR SUSTAINABLE DEVELOPMENT

Local Level

An effective use of resources required management of resources by all stake holders. At the local level, strengthening democratic institutions such as Panchayat empowerment is leading to development at local levels. The local people's participation in local governance, committees comprising of both elected and executive members of local bodies and representatives of community groups has enable them to undertake local development activities according to community priorities.

National Level

At the National level, policies are framed and programs are implemented for sustainable development. The Government-e-Procurement (GeM) has been implemented to bring transparency in procurements. MSME has been promoted by various incentives to achieve sustainable growth. So, a multidisciplinary agency has to work as a nodal agency at national level to achieve optimal gains from several variables rather maximizing those from single one.

International

There is both a need and scope for regional and global cooperation in sustainable development. Environment, Hunger, Health, etc are major areas for international cooperation for sustainable development of the International Community.

CONCLUSIONS

The issue of sustainable development would not be a conclusive one. For every economy, it is a continued process; the efforts should never halt anywhere and anytime. Sustainable growth can be achieved with the concerted, undivided, dedicated efforts put by every country such as development of human capital, institutional & infrastructure development and innovation will go a long way in making sustainable development in the current competitive globalised environment.



Education's New Normal: Some Challenges and Much Opportunity

Dr Shilpa Tripathi

Chairman, IEI, Indore Local Centre, Professor, Department of Mechanical Engineering, Medi-Caps University, Indore

✉ slptrip@yahoo.com

March 2020 will everlastingly be known in the education community as the month when almost all the world's universities and schools get closed. By the end of the March about 185 countries had closed across the globe, affecting 90 percent of the world's students. The speed of these closures and the rapid move to distance learning has allowed little time for planning or reflection on both the potential risks to safeguard against and the potential opportunities to leverage.

The pandemic has significantly disturbed the higher education sector, which is a critical determinant of a country's economic future. Till date there is no certainty when they will reopen. This is a crucial time for the education sector—University examinations, board examinations, nursery school admissions, entrance tests of various universities and competitive examinations, among others, are all held during this period. To stop the outbreak of Covid-19 school and university closures, will not only have a short-term impact on the continuity of learning for more than 285 million young learners in India but also cause far-reaching economic and societal consequences.

The first thing affected by this closure is the structure of education and learning including teaching and assessment methodologies. Only a handful of universities could adopt online teaching methods. Most of the private and government institutions have completely shut down for not having access to e-learning solutions. Hence the students missed the opportunity of learning during this time and forced to face the economic and social stress.

There are 34 crore students in the country, more than America's population. In this a large number of Indian students, second only to China, opted for the universities abroad, especially in countries worst affected by the pandemic, USA, UK, Australia and China. Many such students have now been banned from leaving these countries. If the situation persists, in the long run, a decline in the demand for international higher education is expected.

Among many economic sectors, the higher education sector is undergoing a tectonic shift right now. The forecast done by several futurists and education technologists for long, is now happening and will happen.

The bigger apprehension in present circumstances is the upshot of the disease on the employment rate & affecting campus placements. There are chances that the corporate may withdraw the job offers or keep on hold given to young professionals which result in increase in rate of unemployment.

Is Indian Education System equipped to handle the changes?

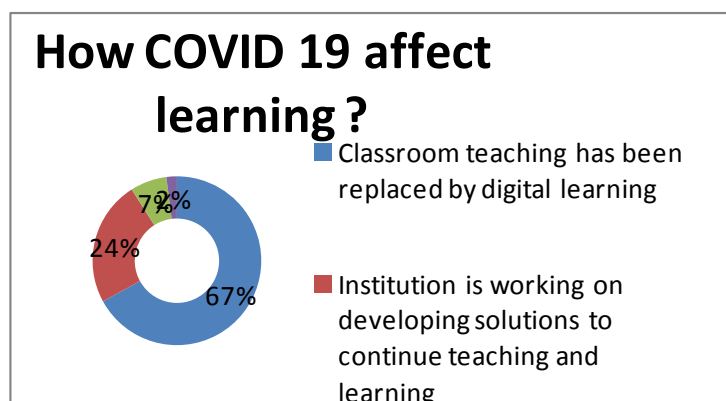


Fig. 1.

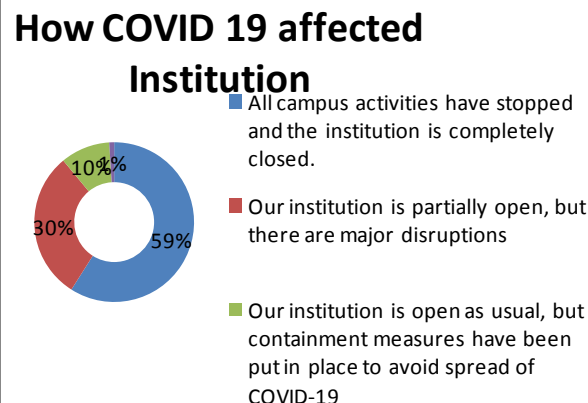


Fig. 2

The pandemic has transformed the centuries-old, chalk–talk teaching model to one driven by technology. This interruption in the delivery of education is pushing policymakers to invent the effective methodologies while ensuring the e-learning solutions and tackling the digital divide.

CHALLENGES: SHORT-MEDIUM-LONG TERM

More than 1.5 billion students and youth across the world are affected by school and university closures due to the COVID-19 outbreak which lead to the problems in carrying out the teaching and learning activities during the socio, economic, cultural and health crisis.

In India a survey has been carried out in India states-

92% of parents do not want to send their children to college /school

56% of parents will wait for at least a month after lockdown open

15% parents are thinking about home tuition

Only 8% parents are interested in sending their children

This suggests that the institutions, universities, academic leaders, administrators and students are required to think for the remote future.

We understand that the COVID-19 pandemic will change the world sooner than we know. The way our governments, institutions, organizations, and people think and function, will fundamentally change – perhaps for the long term. The online higher education has been around for more than a decade now. Unfortunately, it did not take over the conventional education system in the Pre-Covid era. When massive businesses have already moved from offline to online in the Pre-Covid era, the higher education could not move to online.

Some Challenges:

1. Distance learning will support teaching and learning approaches.

Many universities have already shifted to distance learning/online approaches, through distributing study material or using technology to aid online learning. This involves the real risk in teaching–learning process as these approaches are very timid and instructive, just asking students to sit and quietly watch videos, read documents online, or click through presentations. This may be defined as the worst form of learning for the students, sitting inactively and listening, specially for the one of poor academic background.

2. Unavailability of appropriate and quality content/teaching material for the teachers

Teachers had almost no information about the university closure due to this sudden outbreak and shifting to online teaching-learning system. Due to unavailability of teaching material, teachers have shared the content whatever they found whether good or poor quality.



3. Sudden dealing with the individual lives

During this pandemic period, everyone is experiencing this strange new world as mothers, fathers, grandparents etc. Everyone was trying to deal with their individual lives and take care of their family members too. So same is the case with the teachers, trying to find the new ways to make sure that learning continues along with the other responsibilities.

4. Safety of students

The teachers must be more mindful about the design & delivery of online teaching-learning so that fraud individuals don't get in online classes. The protection of personal contact numbers and their personal files and data is also a big challenge.

5. University closures will widen the equity gaps.

This online teaching-learning is possible only due to availability of devices and connectivity to the maximum students. At the same time, some of the students have no access to digital devices or internet connectivity at home, which leads to increase the gap between the students. Therefore, we need to ensure that every student is getting access to learning resources by making them available on every kind of device.

6. Poor experiences of teaching and learning

Some of the students will have a poor experience because they're not used to it. This will not only affect the academic score of the students but make them unhappy because the mental health effects of being isolated. And those poor experiences are really important to learn about the Do's and Don'ts.

7. Effect on the employment rate

The bigger apprehension in present scenario is the effect of the disease on the employment rate. Recent graduates in India are in fear of withdrawal of their job offers from corporate. The Centre for Monitoring Indian Economy's estimates on unemployment shot up from 8.4% in mid-March to 23% in early April and the urban unemployment rate to 30.9%.

8. Financial sustainability

Self-sponsored universities and Institutions dependent on international students for financial income will no longer be sustainable. Those institutions unable to make the shift to different models will not survive. This is also particularly true for business schools. According to the recent survey 40% of international students are considering changing their study abroad plans due to the current crisis.

EDUCATION 4.0

As the government struggles to mitigate the impact of the COVID-19 Pandemic teachers and edutech entrepreneurs across the country are bracing themselves for the 'new normal' in education.

The new, total technology-mediated education can be termed as Education 4.0 and best part is under these circumstances our educationist is trying to adopt Education 4.0

Recognizing the health hazard posed by small classrooms packed with students, the governments are also exploring how digital education and virtual learning can be expanded and made more accessible amidst this global health crisis.

The Directorate of Education in the national capital launches its pilot online learning programme — Aspiration Project (AP). The project was first launched in March to help Class 12 students continue their studies through the lockdown. Many of the online platform like courser, swayam, NPTEL etc were opened their courses free for the students.

Many of the renowned university across the globe uploaded all the lectures on YouTube, so that students could access them on their own time. The teachers were rigorously trained.

Once the vaccine is out and there is more comfort, there will be interesting 'blended' models that will emerge — online classes will happen along with offline interactions.

India's growing education sector is worth over Rs 15,000 Crore and as BARC report there has been a 30 per cent increase in the time spent on education apps since the lockdown commenced. Their aim was to widen their demographic to include audiences they had previously ignored. It has also given educators and entrepreneurs the opportunity to experiment with technology and to engage students at a more personalized level. Occasional online workshop pre-pandemic converts in to frequent Webinars, Workshops, hand on training sessions.



FACTORS INFLUENCING THE SHIFT

The long term and sustainable achievement of this shift will depend on seven major elements of online learning: -

1. Online learning is NOT a library of video lectures and e-books that converts class-notes into PDFs.
High quality digitized learning content must be created to make learning interesting and engaging. This requires an extraordinary skill set, and for the same, Universities need to collaborate with the organizations having such expertise.
2. Subject matter covered in classroom is to be delivered online, but with technology as the intermediary. Blind replication of the classroom practices will not work. It requires a great deal of understanding & application of learning science and digital pedagogy. For making this successful, every teaching faculty needs to be equipped with this knowledge of learning science or else association with experts is the way forward.
3. Classrooms have typically diverse learner groups. In classical pedagogy, the teachers and subject matter experts derive a content-context cluster as a mean of the class collective ability and past knowledge. Accordingly, the teaching-learning process is developed.
This will not and cannot work in online learning. Institutions need to spend as much time on the context for the diverse learner profiles, as on the content, and make it an integral part of program design.
4. New technologies like artificial intelligence, big data, machine learning, block chain etc. and deep learning models can help us in creating a tailored learning plans and methods.
Higher education institutions must emphasize on such upcoming technologies quickly to overcome the flows of current digital higher education.
5. Online learning is not about ONE pedagogical model but it's a cluster of various models.
It is a dedicated learning science that combines learning psychology, behavioural analytics, content delivery, and assessments to estimate and measure the individual learner's progress. Effective delivery model/mechanism can be developed with the help of experts.
6. Give importance to learning science, and not to the technology.
Many models have already being created today which looks for the use of technology and tools to improve the online 'delivery' (teacher-centric) with online 'learning' (learner-centric).

'Learning' is about gradual changes in: -

- Learner's actions and behavior
- Learners thinking and mental models
- Understanding and conceptual strengthening of the learners
- Learners ability to apply the acquired knowledge in practical situations in life, profession, or workplace

Each teaching faculty needs to be massively re-trained and oriented for teaching-learning mode. Equal importance must be given to 'learning sciences in digital media'.

7. Post COVID-19 era, offline or conventional education models will not become obsolete.
 - Emphasize on blended learning (a combination of classroom and online modes) i.e. blend the two judiciously according to the context and the content by applying the 'science of digital learning'.
 - Universities should come out from their self-memorization of knowing all and become willing to collaborate with digital learning specialists to train their teachers and re-design higher education for the newest online education world.
 - A well-funded systems/organization must be developed to improve the research projects in the current context.
 - In long run it is a unique opportunity to transform the higher education sector beyond traditional outcomes and demographics and to move forward with more blended and fully digital experience.



8. Evident digital divide

- While virtual learning opens up many possibilities for students, this digital divide and imbalance makes online education more challenging for a large number of students, particularly those from less having less infrastructural facilities. At the same time caste and gender are also seen to have an impact on access.
- According to data from the National Sample Survey report (2017-18), only 24 per cent of Indian households have an internet facility. The situation in rural areas is poor than as capered to urban areas, as only a little over 15 per cent of rural households have access to internet services.
- Low internet penetration (36 per cent as of 2019) and often unsupportive home environments makes the transition to online learning more difficult. Across India, there have been many protests by students who are unable to cope with this new normal.

OPPORTUNITIES TO LEVERAGE

1. Blended learning approaches will be tried, tested, and increasingly used.

After having done 100 percent online at the end of this period, will increase the possibility of rebalancing the mix between face-to-face and online. Teachers have started to innovate and trial with these online tools and may want to continue online pedagogies.

2. Teachers and University will receive more respect, appreciation, and support for their important role in society.

In an educational Institute the teachers and the students share a bond, a face-to-face connection and support them across their unique skills which are very difficult to replicate in a distance learning environment. Such support may not be widely available at home.

3. Quality teaching and learning materials will be better created and more widely used.

The good quality online learning tool will be developed by the reliable sources and made easily available. Connecting with educators, scientist, researchers and counsellors will become easier through this digital world letting the acquaintance with the world outside their own background.

4. Teacher collaboration will grow and help improve learning.

Teachers have come across with the big resource sharing, which can be utilized by others to improve their lecture delivery. They may be updated with current practices by forming community online, sharing the burden which will make things a bit easier.

5. This crisis will help us come together across boundaries.

It is an opportunity for the education sector to unite, form connections across countries and continents, and truly share what works in a global way and come out stronger as a country because we are fighting together, working together.

6. Developing new technologies for effective and efficient delivery.

Artificial Intelligence (AI), Block Chain, machine learning, data science will play a very important role prominent role in post-COVID learning. For example, “AI can offer support by monitoring and mapping the learning graph of students. Once the data has been acquired from an individual, it’s scrutinized using advanced analytics for generating insights like strengths and weaknesses.

7. Changing attitudes towards virtual learning

The thinking of people that learning things required contact classes has changed. The children have adopted it so beautifully. It has given the opportunity to lean many things, sitting at home.

8. Technology Driven Education –

Government of India has announced the PM eVIDYA service to encourage technology-driven education, making clear that both the Centre and states will have to increase spending on digital infrastructure for education. In year 2020-21, the Ministry of Human Resource Development budget for digital e-learning has allotted Rs 469 crore.



Modified seating arrangements change in timings and further division of the class into different sections are short term approaches but in a socially distanced post-COVID world.

“As necessity is the mother of invention, this situation may become an opportunity for teachers and learners to become more empowered, creative and innovative”

We should really appreciate this overnight shift of teachers and students so as to minimize the loss of students in terms of their learning & time, safeguarding their future endeavours. Our teachers are committed to deliver quality education despite many challenges. Online learning platforms like SWAYAM, Coursera, NPTEL and the world class universities are offering free online courses, which allow students to continue “life-long learning” and help them to reskill and upskills. India’s e-learning market is likely to expand to over 9.5 million users by 2021.

9. Building a credit-system for such learning - will be important to encourage students to leverage these courses as part of their overall education. For example, Ministry of Human Resource Development’s (MHRD)
10. Redesigning of the curriculum of current courses
11. Increase digital access, adequate IT infrastructure and improved competency set.
12. Technical infrastructure and accessibility: Infrastructure and online access are a prerequisite for shifting to distance teaching and learning.
13. Effect of COVID-19 on Industry Institute partnerships- Will learn the opportunities of getting adjust with the new normal practices followed by the industries.

CONCLUSION

In such unprecedented and uncertain times, it is normal for people to experience higher levels of stress and anxiety including teachers and students. They all need socio-emotional support to face the extra pressure of delivering and learning in a time of crisis.

In Indian perspective, a multi-pronged strategy is necessary to manage the crisis and build a flexible Indian education system in the long term.

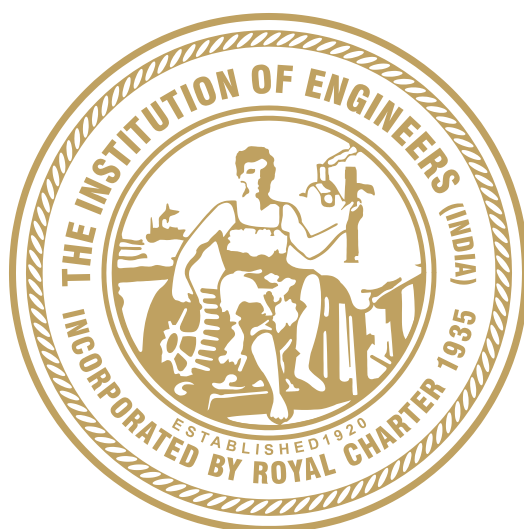
In the last few weeks higher education institutions have shown their significant capability to adapt very quickly to the crisis, with lots of flexibility without any preparations.

There are certainly lessons to be learnt to improve institutional flexibility in higher education. We need to work upon complicated risk management, on scenario planning along with the sustainable approaches.

Universities have a great opportunity to gain new legitimacy in society by demonstrating that they are a great source of knowledge and expertise for society.

In this time of crisis, a well-rounded and effective educational practice is needed for the capacity-building of future professionals. It will develop skills that will drive their employability, productivity, health, and well-being in the decades to come, and ensure the overall progress of India.

ISBN 978-81-950662-0-9
Technical Volume of
35th Indian Engineering Congress



The Institution of Engineers (India)

8 Gokhale Road, Kolkata 700020

Phone : +91 (033) 2223-8311/14/15/16, 2223-8333/34

Fax : +91 (033) 2223-8345

e-mail : technical@ieindia.org; iei.technical@gmail.com

Website : <http://www.ieindia.org>